Printed by: e48d507df5d1141@placeholder.94092.edu. Printing is for personal, private use only. No part of this book may be reproduced or transmitted without publisher's prior permission. Violators will be prosecuted.

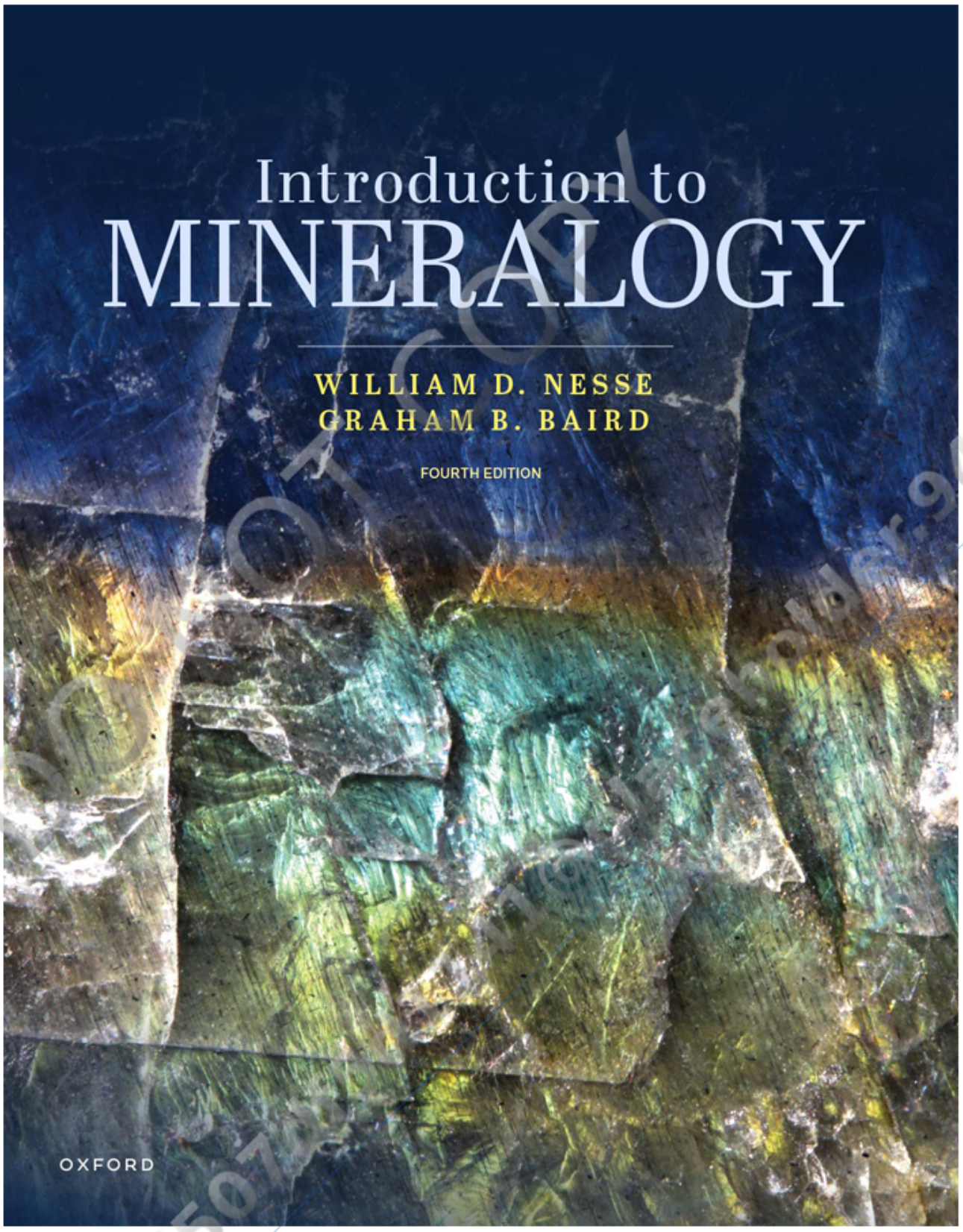

Printed by: e48d507df5d1141@placeholder.94092.edu. Printing is for personal, private use only. No part of this book may be reproduced or transmitted without publisher's prior permission. Violators will be prosecuted.

Introduction to Mineralogy

Fourth Edition

William D. Nesse
University of Northern Colorado

Graham B. Baird
University of Northern Colorado

OXFORD
UNIVERSITY PRESS

DO NOT COPY
e48d507df5d1141@placeholder.9409

Printed by: e48d507df5d1141@placeholder.94092.edu. Printing is for personal, private use only. No part of this book may be reproduced or transmitted without publisher's prior permission. Violators will be prosecuted.

OXFORD
UNIVERSITY PRESS
Oxford University Press is a department of the University of Oxford. It furthers the University's objective of excellence in research, scholarship, and education by publishing worldwide. Oxford is a registered trade mark of Oxford University Press in the UK and in certain other countries.

Published in the United States of America by Oxford University Press
198 Madison Avenue, New York, NY 10016, United States of America.

© 2024, 2017, 2012, 2000 by Oxford University Press

For titles covered by Section 112 of the US Higher Education Opportunity Act, please visit www.oup.com/us/he for the latest information about pricing and alternate formats.

All rights reserved. No part of this publication may be reproduced, stored in a retrieval system, or transmitted, in any form or by any means, without the prior permission in writing of Oxford University Press, or as expressly permitted by law, by license, or under terms agreed with the appropriate reprographics rights organization. Inquiries concerning reproduction outside the scope of the above should be sent to the Rights Department, Oxford University Press, at the address above.

You must not circulate this work in any other form and you must impose this same condition on any acquirer.

Library of Congress Control Number: 2023033486
ISBN: 978-0-19-761460-0 (print)
ISBN: 978-0-19-761462-4 (epub)

Printed by Sheridan Books, Inc., United States of America

Created on: 06 December 2024 at 4:35 a.m.

DO NOT COPY
e48d507df5d1141@placeholder.9409

Printed by: e48d507df5d1141@placeholder.94092.edu. Printing is for personal, private use only. No part of this book may be reproduced or transmitted without publisher's prior permission. Violators will be prosecuted.

Dedication

WDN: For Carl and Erik

GBB: To Mom, for improving my writing in my formative years, and to Dad, for sparking my interest in geology

DO NOT COPY
e48d507df5d1141@placeholder.9409

Printed by: e48d507df5d1141@placeholder.94092.edu. Printing is for personal, private use only. No part of this book may be reproduced or transmitted without publisher's prior permission. Violators will be prosecuted.

Contents

Part One Crystallography and Crystal Chemistry

Chapter 1 Introduction

- Minerals
- Mineraloids
- Mineralogy
- Mineral Nomenclature
- Minerals and Society
  - Gems
  - Natural Resources
  - Critical Mineral Resources
  - Conflict Minerals
  - Minerals and Health
  - Medical Uses of Minerals
- Getting Started
  - **BOX 1.1 Getting Started: Mineral Physical Properties**
- General References on Mineralogy
- References Cited and Suggestions for Additional Reading

Chapter 2 Crystallography

- Introduction
- Translational Symmetry: Two Dimensions
- Translational Symmetry: Three Dimensions
  - Space Lattices and Unit Cells
  - Bravais Lattices and Crystal Systems
- Point Symmetry
  - Reflection
  - Rotation
  - Inversion
  - Compound Symmetry Operations
  - Symmetry Notation

DO NOT COPY
e48d507df5d1141@placeholder.9409

Printed by: e48d507df5d1141@placeholder.94092.edu. Printing is for personal, private use only. No part of this book may be reproduced or transmitted without publisher's prior permission. Violators will be prosecuted.

Symmetry Notation
The 32 Point Groups
Steno's Law
Measurement of Crystal Angles
Determining Crystal System and Point Group
Space Groups
■ **BOX 2.1 Quasicrystals**
Crystal Faces
Laws of Haüy and Bravais
Miller Indices
Indices and Crystal Axes in the Hexagonal Crystal System
Determining Miller Index
Crystallographic Planes
Assigning Miller Indices by Inspection
Crystallographic Directions
Zones
Crystal Forms
Isometric Forms
Nonisometric Forms
Combining Crystal Forms
Enantiomorphous Forms and Crystals
Positive and Negative Forms
Forms in the Six Crystal Systems
Triclinic Crystal System
Monoclinic Crystal System
Orthorhombic Crystal System
Tetragonal Crystal System
Hexagonal Crystal System
Isometric Crystal System
Crystal Habit
References Cited and Suggestions for Additional Reading

Chapter 3 Crystal Chemistry

Introduction
The Nature of Chemical Elements

DO NOT COPY
e48d507df5d1141@placeholder.9409

Printed by: e48d507df5d1141@placeholder.94092.edu. Printing is for personal, private use only. No part of this book may be reproduced or transmitted without publisher's prior permission. Violators will be prosecuted.

- Nucleus
- Electrons
- Element Groupings
- Formation of Ions
- Abundance of the Elements
- Chemical Bonding
  - Valence-Related Bonding
  - Relation among Valence-Dependent Bonding
  - Conductors, Insulators, and Semiconductors
  - Bonds Involving Asymmetric Charge Distribution
- Size of Atoms and Ions
  - Oxidation State
  - Coordination
- References Cited and Suggestions for Additional Reading

Chapter 4 Crystal Structure

- Introduction
- Illustrating Mineral Structures
- Controls of Crystal Structure
  - Metallic Bonding Structure Controls
  - Covalent Bonding Structure Controls
  - Ionic Bonding Structure Controls
  - Application of Pauling's Rules
  - Structure Controls with Molecular Crystals
- Isostructural Minerals
- Polymorphism
  - Reconstructive Polymorphism
  - Displacive Polymorphism
  - Order–Disorder Polymorphism
  - Polytypism
- Mineral Classification
- Compositional Variation in Minerals
  - Substitution Solid Solution
  - Omission Substitution
  - Interstitial Substitution

DO NOT COPY
e48d507df5d1141@placeholder.9409

Printed by: e48d507df5d1141@placeholder.94092.edu. Printing is for personal, private use only. No part of this book may be reproduced or transmitted without publisher's prior permission. Violators will be prosecuted.

Interstitial Substitution
Mineral Formulas
Graphic Representation
Binary Diagrams
Ternary Diagrams
Mineral Formulas and the Unit Cell
References Cited and Suggestions for Additional Reading

Chapter 5 Mineral Growth

Introduction
Mineral Stability
Stability
Gibbs Free Energy
Mineral Reactions
Phase Diagrams
Single-Component Systems
Binary Systems
Mineral Nucleation
Homogeneous Nucleation
Heterogeneous Nucleation
Crystal Growth
Rate of Growth
Zoned Crystals
Inclusions
Structural Defects
Point Defects
Line Defects
Planar Defects
Twinning
Growth Twinning
Transformation Twinning
Deformation Twinning
Postcrystallization Processes
Ordering
Twinning

DO NOT COPY
e48d507df5d1141@placeholder.9409

Printed by: e48d507df5d1141@placeholder.94092.edu. Printing is for personal, private use only. No part of this book may be reproduced or transmitted without publisher's prior permission. Violators will be prosecuted.

- Recrystallization
- Exsolution
- Pseudomorphism
- Radioactivity and Minerals
  - ■ **BOX 5.1 Radiometric Dating**
- Mineral Evolution
- Biomineralization
  - Biologically Induced Mineralization
  - Biologically Controlled Mineralization
  - Applications
- References Cited and Suggestions for Additional Reading

Part Two Mineral Properties, Study, and Identification

Chapter 6 Physical Properties of Minerals

- Introduction
- Mass-Dependent Properties
  - Density
  - Specific Gravity
- Properties Related to Mechanical Cohesion
  - Hardness
  - Tenacity
  - Cleavage
  - Fracture
  - Parting
- Color and Luster
  - Light
  - Perception of Color
  - Mineral Luster
  - Mineral Color
  - Color from Mechanical Causes
  - Consistency of Mineral Color
  - Streak
  - Luminescence
- Magnetism

DO NOT COPY
e48d507df5d1141@placeholder.9409

Printed by: e48d507df5d1141@placeholder.94092.edu. Printing is for personal, private use only. No part of this book may be reproduced or transmitted without publisher's prior permission. Violators will be prosecuted.

-
Diamagnetism
Paramagnetism
Ferromagnetism
Ferrimagnetism
Electrical Properties
Electrical Conductivity
Piezoelectricity
Pyroelectricity
Miscellaneous Properties
References Cited and Suggestions for Additional Reading

Chapter 7 Optical Mineralogy

Introduction
Light
Light Waves
Polarized Light
Transparent and Opaque Minerals
Interaction of Light and Matter
Optically Isotropic versus Anisotropic Materials
Reflection and Refraction
Dispersion
Petrographic Microscope
Direction Conventions
Illuminator
Substage Assembly
Microscope Stage
Objective Lenses
Upper Polarizer
Bertrand Lens
Oculars
Focusing Mechanism
Accessories
Isotropic Materials
Anisotropic Minerals
Interference Phenomena

DO NOT COPY
e48d507df5d1141@placeholder.9409

Printed by: e48d507df5d1141@placeholder.94092.edu. Printing is for personal, private use only. No part of this book may be reproduced or transmitted without publisher's prior permission. Violators will be prosecuted.

Interference Phenomena
Use of the Interference Color Chart
Extinction
Function of Accessory Plates
Optical Indicatrix
Isotropic Indicatrix
Uniaxial Indicatrix
Biaxial Indicatrix
Mineral Color and Pleochroism
Isotropic Minerals
Uniaxial Minerals
Biaxial Minerals
Extinction Angle and Sign of Elongation
Extinction Angle
Sign of Elongation
Categories of Extinction
Extinction in Uniaxial Minerals
Extinction in Biaxial Minerals
Interference Figures
Uniaxial Interference Figures
Biaxial Interference Figures
Refractometry: Measurement of Index of Refraction
Immersion Method
Refractometry in Thin Section
Isotropic Minerals
Uniaxial Minerals
Biaxial Minerals
Reflected-Light Optics
Observation in Plane-Polarized Light
Observation with Crossed Polarizers
Internal Reflections
Tactics for Mineral Identification
Grain Mount Identification with Transmitted Light and Petrographic Microscope
■ **BOX 7.1 Practical Guide to Transmitted Polarized Light Thin Section Analysis**

DO NOT COPY
e48d507df5d1141@placeholder.9409

Printed by: e48d507df5d1141@placeholder.94092.edu. Printing is for personal, private use only. No part of this book may be reproduced or transmitted without publisher's prior permission. Violators will be prosecuted.

Analysis

Polished Sample Identification with Reflected Light and Petrographic Microscope

References Cited and Suggestions for Additional Reading

Chapter 8 Analytical Instrumentation and Techniques I: Crystallography

Introduction

X-Rays

X-Ray Generation

X-Ray Detection

X-Ray Diffraction

Powder X-Ray Diffraction

Sample Preparation

Instrumental Output

Data Reduction

Powder Diffraction File

Bragg Reflection Indices

Mineral Identification

Mixed Samples

Estimation of Relative Mineral Abundance

Estimation of Composition

Determining Unit Cell Parameters

Other Crystallography Instruments

Single Crystal X-Ray Diffraction

Transmission Electron Microscopy

References Cited and Suggestions for Additional Reading

Chapter 9 Analytical Instrumentation and Techniques II: Chemical Analysis of Minerals

Introduction

Analytical Methods

Wet Chemical

Electron Beam Instruments

Radiation Types

X-Ray Fluorescence

Mass Spectrometry

Conventions in Reporting Chemical Analyses

DO NOT COPY e48d507df5d1141@placeholder.9409

Printed by: e48d507df5d1141@placeholder.94092.edu. Printing is for personal, private use only. No part of this book may be reproduced or transmitted without publisher's prior permission. Violators will be prosecuted.

Major Elements

Trace Elements

Conversion of Chemical Analyses to Structural Formulas

References Cited and Suggestions for Additional Reading

Chapter 10 Strategies for Study

Introduction

■ **BOX 10.1 Introduction to Field Study and Sample Collection**

Presentation of Mineral Data

Mineral Identification Tactics

Hand-Sample Identification

Thin Section Identification

Grain Mount Identification

Sample Polishing and Identification Using Reflected Light

Scanning Electron Microscope (SEM) and Electron Microprobe (EPMA)

X-Ray Diffraction

Mineral Separation

Rock/Mineral Crushing

Sieving

Grain Washing

Density Separation

Magnetic Separation

Mineral Association

Problems in Paradise

References Cited and Suggestions for Additional Reading

Part Three Mineral Descriptions

Chapter 11 Silicates

Introduction

Silicate Structure and Classification

Silicate Chemical Formulas

Mafic versus Felsic

Igneous Rocks

Magmatic Processes

■ **BOX 11.1 Bowen's Reaction Series**

DO NOT COPY

e48d507df5d1141@placeholder.9409

Printed by: e48d507df5d1141@placeholder.94092.edu. Printing is for personal, private use only. No part of this book may be reproduced or transmitted without publisher's prior permission. Violators will be prosecuted.

Igneous Environments
Clastic Sedimentary Rocks
Sedimentary Processes
Sedimentary Environments
Metamorphic Rocks
Metamorphic Variables
Metamorphic Processes
Connecting Metamorphic Assemblage to Temperature–Pressure Conditions
Metamorphic Environments
References Cited and Suggestions for Additional Reading

Chapter 12 Framework Silicates

Introduction
Silica Group
Quartz
Tridymite
Cristobalite
Opal
BOX 12.1 Micro- and Non-Crystalline Silica
Feldspar Group
Composition
Structure
Al/Si Order–Disorder
K-Feldspar
Plagioclase
Exsolution in the Feldspars
Alkali Feldspar
Plagioclase
Other Feldspar Intergrowths
Twinning
Plagioclase
Alkali Feldspar
Microcline
Orthoclase
Sanidine

DO NOT COPY
e48d507df5d1141@placeholder.9409

Printed by: e48d507df5d1141@placeholder.94092.edu. Printing is for personal, private use only. No part of this book may be reproduced or transmitted without publisher's prior permission. Violators will be prosecuted.

- Sanidine
- Adularia
- Anorthoclase
- Feldspathoids
- Nepheline
- Leucite
- Sodalite
- Zeolite Group
- Other Framework Silicates
- Scapolite
- References Cited and Suggestions for Additional Reading

Chapter 13 Sheet Silicates

- Introduction
- Structure and Classification
- 1:1 Layer Silicates
- 2:1 Layer Silicates
- Polytypism
- *TO* Structures (1:1)
- Serpentine
- Kaolinite
- ■ **BOX 13.1 Asbestos**
- *TOT* Structures (2:1)
- Talc
- Pyrophyllite
- *TOT* + *c* Structures: Mica Minerals (2:1)
- Muscovite
- Biotite
- Lepidolite
- Glauconite
- *TOT* + *c* Structures: Brittle Micas (2:1)
- Margarite
- Clintonite
- *TOT* + *O* Structure
- Chlorite

DO NOT COPY
e48d507df5d1141@placeholder.9409

Printed by: e48d507df5d1141@placeholder.94092.edu. Printing is for personal, private use only. No part of this book may be reproduced or transmitted without publisher's prior permission. Violators will be prosecuted.

Clay Minerals
Structure and Classification
Geology of Clay
Identification
Uses
Clay in the Environment
Other Sheet Silicates
Stilpnomelane
Prehnite
Apophyllite
Chrysocolla
References Cited and Suggestions for Additional Reading

Chapter 14 Chain Silicates

Introduction
Pyroxene Group
Structure and Classification
Geology of Pyroxenes
Orthopyroxene
Pigeonite
Calcic Clinopyroxene
Aegirine, Aegirine–Augite
Jadeite
Omphacite
Spodumene
Pyroxenoids
Introduction
Wollastonite
Rhodonite
Pectolite
Amphibole Group
Structure and Classification
Geology of Amphiboles
Orthoamphibole
Cummingtonite–Grunerite

DO NOT COPY
e48d507df5d1141@placeholder.9409

Printed by: e48d507df5d1141@placeholder.94092.edu. Printing is for personal, private use only. No part of this book may be reproduced or transmitted without publisher's prior permission. Violators will be prosecuted.

Cummingtonite–Grunerite
Tremolite–Ferro-Actinolite
Hornblende
Glaucophane–Riebeckite
Other Amphiboles
References Cited and Suggestions for Additional Reading

Chapter 15 Disilicates and Ring Silicates

Disilicates
Structure and Classification
Zoisite
Clinozoisite–Epidote
Allanite
Lawsonite
Pumpellyite
Ring Silicates
Structure and Classification
Beryl
Cordierite
Tourmaline
References Cited and Suggestions for Additional Reading

Chapter 16 Orthosilicates

Introduction
Olivine
Garnet
■ **BOX 16.1 Enhanced Rock Weathering and Carbon Sequestration**
Zircon
Aluminum Silicates
Andalusite
Sillimanite
Kyanite
Staurolite
Chloritoid
Titanite (Sphene)
Topaz

DO NOT COPY
e48d507df5d1141@placeholder.9409

Printed by: e48d507df5d1141@placeholder.94092.edu. Printing is for personal, private use only. No part of this book may be reproduced or transmitted without publisher's prior permission. Violators will be prosecuted.

Topaz

Additional Orthosilicates

References Cited and Suggestions for Additional Reading

Chapter 17 Carbonates, Sulfates, Phosphates, Tungstates, Molybdates, and Borates

Structure and Classification

Carbonates

Rhombohedral Carbonates (Calcite and Dolomite Groups)

Calcite

■ **BOX 17.1 Limestone and Dolostone**

Magnesite

Siderite

Rhodochrosite

Dolomite–Ankerite

Aragonite Group

Aragonite

Witherite

Strontianite

OH-Bearing Carbonates

Malachite

Azurite

■ **BOX 17.2 Evaporites**

Sulfates

Gypsum

Anhydrite

Barite

Phosphates

Apatite

Monazite

Xenotime

Turquoise

Tungstates and Molybdates

Borates

References Cited and Suggestions for Additional Reading

Chapter 18 Oxides, Hydroxides, and Halides

DO NOT COPY

e48d507df5d1141@placeholder.9409

Printed by: e48d507df5d1141@placeholder.94092.edu. Printing is for personal, private use only. No part of this book may be reproduced or transmitted without publisher's prior permission. Violators will be prosecuted.

Chapter 18 Oxides, Hydroxides, and Halides

- Introduction
- Oxides
- X_2O Group
  - Cuprite
  - Ice
    - **BOX 18.1 Paleoclimate**
- XO Group
- XY_2O_4 Minerals
  - Spinel Group
  - Magnetite
    - **BOX 18.2 Banded Iron Formations**
  - Chromite
  - Spinel Series
  - Chrysoberyl
- X_2O_3 Group
  - Hematite
  - Corundum
  - Ilmenite
- XO_2 Group
  - Rutile
  - Cassiterite
  - Uraninite
- Hydroxides
  - Brucite
  - Iron Hydroxide Minerals
  - Aluminum Hydroxide Minerals
  - Manganese Oxide and Hydroxide Minerals
- Halides
  - Halite
  - Sylvite
  - Fluorite
- References Cited and Suggestions for Additional Reading

Chapter 19 Sulfides and Related Minerals

DO NOT COPY
e48d507df5d1141@placeholder.9409

Printed by: e48d507df5d1141@placeholder.94092.edu. Printing is for personal, private use only. No part of this book may be reproduced or transmitted without publisher's prior permission. Violators will be prosecuted.

Introduction
Crystal Chemistry and Classification
Sulfide Deposits
Hydrothermal Deposits
Supergene Processes
Sulfide Minerals
Sphalerite
Galena
Pyrrhotite
Chalcopyrite
Cinnabar
Pyrite
Marcasite
Molybdenite
Bornite
Chalcocite
Covellite
Sulfarsenides
Arsenopyrite
Arsenides
Tellurides
References Cited and Suggestions for Additional Reading

Chapter 20 Native Elements

Introduction
Metals
Gold
Silver
Copper
Metalloids
Nonmetals
Sulfur
Graphite
■ **BOX 20.1 Graphitic Carbon**
Diamond

DO NOT COPY
e48d507df5d1141@placeholder.9409

Printed by: e48d507df5d1141@placeholder.94092.edu. Printing is for personal, private use only. No part of this book may be reproduced or transmitted without publisher's prior permission. Violators will be prosecuted.

Diamond

■ **BOX 20.2 The Carbon Cycle**

References Cited and Suggestions for Additional Reading

Appendices

Appendix A Effective Ionic Radii of the Elements

Appendix B Determinative Tables

■ **TABLE B.1 Determinative Table for Nonmetallic Minerals with White, Gray, or Other Pale-Colored Streak**

■ **TABLE B.2 Nonmetallic Minerals with Distinctly Colored Streak**

■ **TABLE B.3 Minerals with Metallic and Submetallic Luster**

■ **TABLE B.4 Specific Gravity**

■ **TABLE B.5 Minerals That May Fluoresce**

■ **TABLE B.6 Selected Minerals That Are Ferromagnetic and Ferrimagnetic**

■ **TABLE B.7 Minerals That Effervesce in Dilute HCl**

■ **TABLE B.8 Color of Minerals in Thin Section and Grain Mount**

■ **TABLE B.9 Indices of Refraction of Isotropic Minerals**

■ **TABLE B.10 Indices of Refraction of Uniaxial Minerals**

■ **TABLE B.11 Indices of Refraction of Biaxial Negative Minerals Arranged in Order of Increasing n_β**

■ **TABLE B.12 Indices of Refraction of Biaxial Positive Minerals Arranged in Order of Increasing n_β**

■ **TABLE B.13 Minerals That Produce Pleochroic Halos in Surrounding Minerals**

■ **TABLE B.14 Colors Exhibited by Opaque Minerals in Polished Section Viewed in Air**

■ **TABLE B.15 Opaque or Nearly Opaque Minerals That Display Internal Reflections with Reflected Light**

Appendix C Mineral Associations

■ **TABLE C.1 Mineralogy of Common Igneous Rocks**

■ **TABLE C.2 Mineralogy of Sedimentary Rocks**

■ **TABLE C.3 Mineralogy of Common Metamorphic Rocks**

■ **TABLE C.4 Mineralogy of Hydrothermal Sulfide Deposits**

DO NOT COPY
e48d507df5d1141@placeholder.9409

Printed by: e48d507df5d1141@placeholder.94092.edu. Printing is for personal, private use only. No part of this book may be reproduced or transmitted without publisher's prior permission. Violators will be prosecuted.

Preface to the Fourth Edition

William D. Nesse
University of Northern Colorado

Graham B. Baird
University of Northern Colorado

DO NOT COPY

When Bill Nesse asked me to take over revision of *Introduction to Mineralogy*, I was apprehensive for two reasons. First, I firmly believe that it is one of the best textbooks, not just in the field of mineralogy, but in all geoscience fields. It is difficult to improve something that is already at such a high level. Second, though I have over fifteen years of experience with using *Introduction to Mineralogy* to teach mineralogy and other related courses, I'm not a mineralogist in the strict sense. (Bill reminds me that he doesn't identify as a mineralogist either.) However, a detailed knowledge of a large variety of minerals, and the techniques used to investigate them, are required for my research in the fields of structural geology, igneous and metamorphic petrology, geochronology, and tectonics. So ultimately, I was able to construct an approach to revision and improvement.

Because previous editions of the book worked so well with the structure Bill had defined, those familiar with previous editions will see that the chapter order, organized into three parts, is retained in this fourth edition. Chapters on Crystallography and Crystal Chemistry are contained within Part One, chapters on Mineral Properties, Study, and Identification are contained within Part Two, and chapters containing Mineral Descriptions are within Part Three. Also retained is the overall style and level of detail, which is aimed at teaching mineralogy to undergraduate students. Further, individual chapters are self-contained as much as possible to allow instructors to teach topics in a different order than presented.

Revisions, in part, focus on improving clarity, accuracy, organization, and readability. In particular, the definitions of bolded key terms have been revised to ensure clear, concise definitions are included with their first use. Revisions also ensure the book is up-to-date with respect to commonly used techniques and changes to society and the earth system. Chapter 1 and elsewhere was revised to better connect the importance of minerals, and geologic knowledge in general, to the reader's daily lives and society. Chapters that cover analytical instrumentation (Chapters 8 and 9) have been more thoroughly revised with improved or added discussions of single crystal X-ray diffraction, transmission electron

Printed by: e48d507df5d1141@placeholder.94092.edu. Printing is for personal, private use only. No part of this book may be reproduced or transmitted without publisher's prior permission. Violators will be prosecuted.

microscopy, scanning electron microscopy and electron microprobe, and handheld X-ray fluorescence. Also added throughout the book are a number of new box insets that cover specialty and society relevant topics, including radiometric dating, thin section analysis, field study and sample collection, Bowen's reaction series, asbestos, enhanced rock weathering and carbon sequestration, and the carbon cycle.

I'm very pleased with how the revisions turned out, and given that "writing is rewriting," I encourage any reader who finds errors, or has suggestions for improvement, to please contact me.

GBB

Greeley, Colorado

DO NOT COPY
e48d507df5d1141@placeholder.9409

Printed by: e48d507df5d1141@placeholder.94092.edu. Printing is for personal, private use only. No part of this book may be reproduced or transmitted without publisher's prior permission. Violators will be prosecuted.

Acknowledgements

Textbook revision is a huge undertaking and many helped complete the task. First, Bill Nesse must be thanked for producing such a wonderful textbook, entrusting me with its revision, and promptly replying to any inquiry I had about the book and potential approaches to improvement and revision. The following individuals are thanked for serving as *Introduction to Mineralogy 4th edition* pre-revision reviewers: David M. Jenkins, Jade Star Lackey, Jie Li, Sean Regan, Bernhardt Saini-Eidukat, Melanie Steigler, Robert Vance, and Andrew Wulff.

Further, several colleagues at the University of Northern Colorado, including Cindy Shellito, Tim Grover, Emmett Evanoff, Marian Hamilton, Bob Houser, and Melissa Weinrich, either reviewed portions of the text or provided critical information. Richard Romkee, Gabrielle Mather, and Torren Clemens helped organize and prepare figure files or compile a key terms list. Others also reviewed portions of the text or provided critical information, including Aaron Bell (University of Colorado Boulder), Jeff Chiarenzelli (St. Lawrence University), Peter Hudleston (University of Minnesota Twin Cities), David Jenkins (Binghamton University), Nigel Kelly (Bruker Nano Analytics), Ryan Kerrigan (University of Pittsburgh Johnstown), Jerry Magloughlin (Colorado State University), Kevin Mahan (University of Colorado Boulder), Rory McFadden (Gustavus Adolphus College), and Sean Regan (University of Alaska Fairbanks). I also thank everyone at Oxford University Press that helped bring the fourth edition to publication, including Tracey MacDonald, Joan Kalkut and Sukwinder Kaur. I apologize to anyone who helped with this endeavour but was inadvertently not listed.

I also must thank my family. I know that work on the revisions reduced the amount of time I've spent with them in recent years. As always, thank you Cindy, Owen, Heather, Annelise, Mom, and Dad for all your support.

DO NOT COPY
e48d507df5d1141@placeholder.9409

Printed by: e48d507df5d1141@placeholder.94092.edu. Printing is for personal, private use only. No part of this book may be reproduced or transmitted without publisher's prior permission. Violators will be prosecuted.

PART ONE

CRYSTALLOGRAPHY AND CRYSTAL CHEMISTRY

William D. Nesse
University of Northern Colorado

Graham B. Baird
University of Northern Colorado

DO NOT COPY
e48d507df5d1141@placeholder.9409

Printed by: e48d507df5d1141@placeholder.94092.edu. Printing is for personal, private use only. No part of this book may be reproduced or transmitted without publisher's prior permission. Violators will be prosecuted.

CHAPTER 1
Introduction

William D. Nesse
University of Northern Colorado

Graham B. Baird
University of Northern Colorado

DO NOT COPY

Minerals are critically important to human society. Beyond making up the majority of the planet we live on, minerals provide the raw materials needed to construct, for example, buildings, roads, bridges, smartphones, and cars. All vegetation, including the crops that we eat, grows in soil composed of minerals. Geoscientists use the chemical composition, structure, and texture of the minerals to decipher the history of the Earth and better understand such potentially devastating Earth processes as earthquakes, volcanic eruptions, and landslides. In short, if the whole Earth system and how society interacts with it is to be understood, minerals must be understood. Such knowledge is required to allow modern human society to thrive on a healthy and sustainable planet.

e48d507df5d1141@placeholder.9409

Printed by: e48d507df5d1141@placeholder.94092.edu. Printing is for personal, private use only. No part of this book may be reproduced or transmitted without publisher's prior permission. Violators will be prosecuted.

Minerals

The term **mineral** is used in a variety of ways. In the economic sense, it often means any valuable material extracted from the Earth, including coal, oil, natural gas, groundwater, iron ore, gold, dimension stone (building stone), sand, gravel, or anything else that is mined. Nutritionists use the term *mineral* to mean any of a variety of chemical compounds or elements that are important for health. In common usage, anything that is neither animal nor vegetable might be considered mineral. As the term is used in the geosciences, however, a different and more restrictive definition is applied:

> A mineral is a naturally occurring crystalline solid.

A material that is **naturally occurring** is formed by natural processes without human intervention, and it must be possible to find samples in the natural environment. Humans can artificially create many crystalline solids with the same chemical and physical properties as their natural mineral counterparts. These artificial materials are **synthetic minerals**.

Minerals must be **crystalline solids**. The atoms that form crystalline materials are arranged and chemically bonded with long-range order, which is a regular and repeating pattern (**Figure 1.1**). At the macroscopic scale, symmetrically arranged crystal faces (Chapter 2) and cleavages (Chapter 6) are clear evidence that a material is crystalline. At the microscopic scale and smaller, the ability to diffract X-rays (Chapter 8) demonstrates that a material is crystalline. The chemical bonds (Chapter 3) that hold the atoms in a regular and repeating pattern require that crystalline materials are solid (not a liquid or a gas). However, crystalline solids, under appropriate temperature–pressure conditions, can very slowly flow in a ductile manner like a fluid. An example of such behavior is demonstrated by the folds observed in some metamorphic rocks.

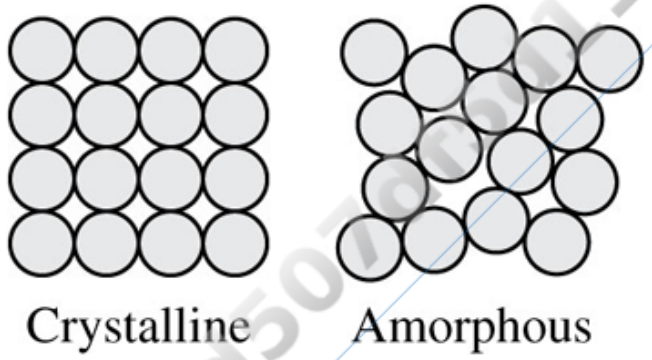

FIGURE 1.1 Simple representations that compare the highly organized atoms in a crystalline material to the relatively disorganized atomic arrangement found in an amorphous material. View larger image

DO NOT COPY
e48d507df5d1141@placeholder.94092

Printed by: e48d507df5d1141@placeholder.94092.edu. Printing is for personal, private use only. No part of this book may be reproduced or transmitted without publisher's prior permission. Violators will be prosecuted.

Not all solids are crystalline. Glass, for example, is a solid, but the atoms lack long-range atomic order, so it is considered **amorphous** or **non-crystalline** (Figure 1.1). In most cases the distinction between crystalline and non-crystalline is relatively clear, but this is not always true. No crystalline material is perfect; at the atomic scale some imperfections and disorder always are present in varying amounts, as discussed in Chapters 4 and 5.

A consequence of being crystalline, minerals have a definite or definable, but not necessarily fixed, chemical composition; thus a chemical formula may be written for any mineral. An example is the common mineral quartz (SiO_2), which is composed of silicon and oxygen in a fixed ratio (ideally) of 1:2. But the composition of many specific minerals may vary within certain limits. An example is the mineral olivine, which may be iron-rich (Fe_2SiO_4) or magnesium-rich (Mg_2SiO_4), or may have an intermediate composition (for example, $Mg_{1.4}Fe_{0.6}SiO_4$). However, the elemental proportions always work out so that the ratio (Fe + Mg):Si:O remains 2:1:4. Hence, different samples of a mineral species may have different compositions, but the variability is limited. Because minerals are crystalline and have a definite chemical composition, they also have definite physical properties. These physical properties also may vary within limits because they are controlled by the variation in chemical composition.

Some definitions of what constitutes a mineral require that it be formed by inorganic processes. This historical perspective, which probably has its roots in Aristotle's division of matter into animal, vegetable, and mineral, should no longer be used. Minerals constitute an integral part of biologic structures and processes. Obvious examples are the minerals calcite and aragonite (both $CaCO_3$ but with different structures), which are secreted to form the shells of many marine invertebrates and whose remains are a major component of the rock limestone. The mineral apatite [$Ca_5(PO_4)_3(OH,F,Cl)$] makes up a substantial portion of the teeth and bones of vertebrates. If desired, these biologically produced minerals may be called **biominerals**.

Bacteria are an integral part of many geochemical processes at or near the surface of the Earth and directly influence the growth of many minerals. For example, the pyrite (FeS_2), found in many shale and coal beds, is produced by the action of sulfate-reducing bacteria. The interaction of microbes and geologic processes is the focus of the emerging and exciting field of study called geomicrobiology. Numerous different minerals and mineraloids, or materials that almost fit the mineral definition (see section on Mineraloids) are now recognized to be produced by biologically induced and controlled mineralization processes (Weiner and Dove, 2003). Many more will undoubtedly be recognized as our understanding of these processes improves. Further, biologic processes have profoundly affected the Earth's near-surface chemical environment and therefore also have affected the types and distribution of minerals.

DO NOT COPY e48d507df5d1141@placeholder.9409

Printed by: e48d507df5d1141@placeholder.94092.edu. Printing is for personal, private use only. No part of this book may be reproduced or transmitted without publisher's prior permission. Violators will be prosecuted.

Mineraloids

Mineraloids are mineral-like materials that lack the required crystalline structure with long-range order. They generally include amorphous solids and glasses.

Many amorphous solids may possess short-range (~10–100 Å) order, but lack order at greater scales. Opal is probably the best-known example and consists of silica gel, often arranged in small spherical masses. Other similar examples include liquid crystals and most plant and animal flesh (skin and muscle, for example).

The crystalline structure of U- and Th-bearing minerals, such as zircon, may be extensively disrupted by radioactive decay of these elements. The term **metamict** is used to describe these disrupted structures, and once a mineral's structure becomes metamict, it is properly considered a mineraloid.

Natural glasses also may be considered mineraloids. Volcanic glass, called **obsidian**, is the most common example, but many exist. Solidified frictional melts called **pseudotachylite** may be produced in a fault zone during an earthquake. Meteorites, if large enough, may melt the rocks that they strike and produce an **impact melt**. Small masses of glass called **tektites** are usually interpreted to be samples of now-solidified impact melt ejected from an impact crater. Lightning, when it strikes soil or rock, may generate melt that solidifies into a **fulgurite**. **Ash glass** is the vesicle-filled, slag-like glass created by burning coal beds that melt the surrounding rock.

DO NOT COPY e48d507df5d1141@placeholder.9409

Printed by: e48d507df5d1141@placeholder.94092.edu. Printing is for personal, private use only. No part of this book may be reproduced or transmitted without publisher's prior permission. Violators will be prosecuted.

Mineralogy

Mineralogy is the study of minerals. The beginning of this particular branch of science extends back to prehistoric times. Evidence of mining and smelting minerals to extract useful metals such as copper, lead, and zinc is found in many ancient civilizations thousands of years ago.

The modern study of mineralogy can be traced back to Theophrastus (ca. 387–272 BCE) who wrote the earliest-preserved book dealing with minerals and rocks, titled *On Stones*. Some 400 years later, Pliny the Elder, who died during the 79 CE volcanic eruption of Vesuvius, provided us with an encyclopedic review of mineralogy as it applied to the metallic ores, gemstones, and pigments in use in the Roman Empire around 77 CE. Some 1500 years later (1556), the German physician and mining engineer Georg Bauer, known to us by his Latinized name Georgius Agricola, provided detailed mineral descriptions and defined physical properties, such as hardness and cleavage, that continue to provide the basis for mineral hand-sample identification.

Through the seventeenth to nineteenth centuries, a number of notable scholars provided significant advances to the science:

- **Niels Stensen (Nicholas Steno), 1638–1686, Denmark**. Demonstrated the law of constancy of interfacial angles (1669). This means that for a particular mineral species, the flat sides produced by growth always have the exact same angle relative to each other.
- **G. Werner, 1750–1817, Germany**. Standardized terminology used for mineral descriptions.
- **René-Juste Haüy, 1743–1822, France**. "Father of mathematical crystallography." Showed that crystals were constructed of numerous, stacked identical building blocks, which we now call unit cells. Also developed the idea that crystal faces have orientations that can be expressed as coordinates relative to these building blocks (Chapter 2).
- **J. J. Berzelius 1779–1848, Sweden**. Recognized that minerals are chemical compounds and provided the foundation for the chemical classification of minerals (Chapter 3).
- **William Nicol, 1768–1851, Scotland**. Invented the Nicol prism (1828), which allowed the behavior of polarized light passing through minerals to be studied and provided the foundation for optical mineralogy (Chapter 7).
- **James D. Dana, 1813–1895, Yale University**. Published the first edition of *A System of Mineralogy* in 1837. The fourth edition (1854) introduced the chemical classification of minerals that is still in use (Chapter 3).

DO NOT COPY e48d507df5d1141@placeholder.94092

Printed by: e48d507df5d1141@placeholder.94092.edu. Printing is for personal, private use only. No part of this book may be reproduced or transmitted without publisher's prior permission. Violators will be prosecuted.

classification of minerals that is still in use (Chapter 3).

- **Henry Clifton Sorby, 1826–1908**. Developed the use (along with Alfred Des Cloizeaux in France) of the petrographic microscope for studying rocks and minerals (Chapter 7).

Perhaps the most dramatic progress in understanding minerals came with the discovery of X-rays. In 1912 Max von Laue (1879–1960) demonstrated that crystals diffract X-rays (see Chapter 8), thus proving that minerals possess a regular and repeating atomic arrangement. By 1914, W. H. Bragg (1862–1942) and his son W. L. Bragg (1890–1971) in Cambridge, United Kingdom, had used X-rays to determine the **crystal structure** of minerals, or the particular repeating arrangement of atoms within minerals.

During the twentieth century a wide variety of instrumentation improved our ability to determine the chemical composition of minerals and refine our understanding of their crystal structures (see Chapter 9). In addition, petrologists and chemists immensely expanded our knowledge of the origins and behavior of minerals in a wide range of geologic environments.

DO NOT COPY
e48d507df5d1141@placeholder.9409

Printed by: e48d507df5d1141@placeholder.94092.edu. Printing is for personal, private use only. No part of this book may be reproduced or transmitted without publisher's prior permission. Violators will be prosecuted.

Mineral Nomenclature

A **mineral species** is distinguished from other minerals by a unique combination of composition (Chapter 3) and crystal structure (Chapter 4). Over 4900 mineral species have been identified, described, and named, although fewer than a hundred mineral species are common. The Commission on New Minerals, Nomenclature and Classification of the International Mineralogical Association provides criteria by which new minerals are recognized. A list of approved mineral names is available as a free Internet download from the International Mineralogical Association (www.ima-mineralogy.org). New minerals are regularly discovered, and a summary is included in each issue of the *American Mineralogist*, published by the Mineralogical Society of America (www.minsocam.org).

The criteria for new mineral species approval include the following:

- It must be a mineral as defined above.
- It must be new and not previously described and named.
- The crystallography (Chapter 2), composition (Chapter 3), and crystal structure (Chapter 4) must be determined.
- The physical (Chapter 6) and optical (Chapter 7) properties must be described.
- The geologic and geographic setting in which the mineral was found must be described.
- A **type sample** of the mineral must be preserved in an appropriate repository, such as a museum or the collection of a research institute.

A mineral may be named after an individual, a place where it is found, or in reference to its chemical composition or a significant physical property. Some minerals have names whose origins are no longer known. The origin of mineral names can be found in Mitchell (1979) and Gains and others (1997). de Fourestier (1999) provides a glossary of mineral synonyms (~35,000 of them) and obsolete mineral names are found in Bayliss (2000).

A mineral species may have more than one **mineral variety**. Different varieties of a mineral are distinguished by differences in color, habit (shape), or other properties. For example, the mineral corundum (Al_2O_3, Chapter 18) is typically gray and fairly ordinary looking. However, ruby and sapphire are varieties that can form eye-catching specimens considered to be gems (see section on Minerals and Society). Ruby is red because it contains small amounts of Cr, and sapphire is blue because it contains small amounts of Ti + Fe. The terminology for mineral varieties is not well organized and it mostly follows historical practices.

A **mineral series** is two or more minerals among which there is a range of chemical

DO NOT COPY e48d507df5d1141@placeholder.9409

Printed by: e48d507df5d1141@placeholder.94092.edu. Printing is for personal, private use only. No part of this book may be reproduced or transmitted without publisher's prior permission. Violators will be prosecuted.

A **mineral series** is two or more minerals among which there is a range of chemical compositions. An example is the olivine mineral series described above; another is the plagioclase mineral series (Chapter 12). The two end members of the plagioclase series are the minerals albite ($NaAlSi_3O_8$) and anorthite ($CaAl_2Si_2O_8$). Natural plagioclase typically has a composition intermediate between albite and anorthite.

A **mineral group** is a set of minerals with the same basic structure but different compositions. The group is generally named for one of the constituent minerals. An example is the calcite group (Chapter 17) whose general chemical formula is MCO_3, where M is a metal cation (Chapter 3).

Calcite	$CaCO_3$
Magnesite	$MgCO_3$
Rhodochrosite	$MnCO_3$
Siderite	$FeCO_3$
Smithsonite	$ZnCO_3$

Members of a mineral group also may form a mineral series, but this is not required. For example, magnesite and siderite form a mineral series because intermediate compositions are common.

The term **crystal** has been used in two ways in mineralogy. In a restricted sense, a crystal is a piece of a mineral bounded, at least in part, by regular, smooth surfaces produced during growth, called **crystal faces**. The presence of crystal faces is a direct consequence of the atoms being arranged in a regular and repeating manner in minerals. In a broader sense, however, mineralogists often use the term *crystal* for any piece of a mineral, regardless of whether it displays crystal faces. Bounding surfaces may be crystal faces, fractures, cleavages, or contacts with adjacent mineral grains. In this book, the term *crystal* is used for specimens only when crystal faces are present, while the term **mineral grain** is used when the nature of the bounding surfaces around a specimen is not specified.

DO NOT COPY
e48d507df5d1141@placeholder.9409

Printed by: e48d507df5d1141@placeholder.94092.edu. Printing is for personal, private use only. No part of this book may be reproduced or transmitted without publisher's prior permission. Violators will be prosecuted.

Minerals and Society

Gems

Many people think of gems when they think of minerals. Gems, gemstones, or precious stones are materials typically used in jewelry, often after being cut or polished. Gems are valued due to some combination of their color, luster, transparency, and rarity. Though many commonly recognized gems are minerals, not all are and no strict definition exists.

Many common minerals have gem examples, such as a particularly transparent and brightly colored tourmaline or garnet crystal. For some minerals, a specific color variety is labeled with a name recognized as a gem (see the ruby and sapphire example above). Some gems are not a single mineral; for example, jade could either be gem-quality jadeite (a pyroxene) or nephrite (an amphibole, Chapter 14). Mineraloid examples of gems include amber (fossilized tree resin) and opal, while some rocks (Chapter 5) are considered gems; the metamorphic rock lapis lazuli is an example.

Synthetic varieties of many gems exist and some “gems” are fully synthetic and do not occur naturally. An example is cubic zirconia, a relatively low-cost diamond substitute. Cubic zirconia is an isometric (see Chapter 2) form of zirconium oxide (ZrO_2), which naturally would only have a monoclinic structure and exists as the mineral baddeleyite.

Gems are a complicated topic, and given how rare they are, knowledge of gems is of little use for most scientists interested in minerals. The reader is directed to the index to find at least brief descriptions of most gem minerals and some gem mineraloids. For an in-depth discussion, interested readers are directed to dedicated books on the topic, such as O’Donoghue (2006).

Natural Resources

Without **mining** minerals and other materials out of the ground, there would be no raw materials for nearly everything that civilization builds. Rocks used to build structures are called **dimensional stone**. Another critical building material is **aggregate**, which is the sand and gravel used in, for example, concrete and asphalt. Mining of **ore** is also required. Ore is any material extracted from the Earth that can be processed to obtain a specific mineral and/or metal of value. Mining can be a polarizing topic. On one side, mining provides critical resources for societies and helps support local economies. On the other side, mining may exploit workers and/or cause significant environmental damage. It is possible to mine responsibly such that workers are treated fairly and there is virtually no environmental damage, but mining in this way typically must be done in democratic

DO NOT COPY e48d507df5d1141@placeholder.94092

Printed by: e48d507df5d1141@placeholder.94092.edu. Printing is for personal, private use only. No part of this book may be reproduced or transmitted without publisher's prior permission. Violators will be prosecuted.

countries with strong central governments. Here, laws that enforce fair worker treatment and protect the environment must be followed. Some topics associated with problematic mining are explored a bit further in the section on Conflict Minerals.

A few metals that society needs and the minerals from which they are extracted are listed in **Table 1.1**. Because the distribution of ore is uneven, it is essential for nations to globally trade these resources. The United States, for example, has large economic resources of molybdenum and gold, but little nickel or tungsten. For these and many other resources, domestic production is insufficient to meet the country's needs. American manufacturers must, therefore, purchase raw materials from worldwide sources. The same applies to manufacturers in the United Kingdom, China, Germany, Japan, and all the other countries in the world. This international trade ideally allows each country to obtain the needed resources.

TABLE 1.1 Select Metals and Some Minerals from Which They Are Extracted

Metal	Mineral	Chemical Formula	Major World Sources
Iron	Magnetite Hematite	Fe_3O_4 Fe_2O_3	Australia, Brazil, China
Copper	Chalcopyrite	Cu_5FeS_4	Chile, Peru, United States
Molybdenum	Molybdenite	MoS_2	Chile, United States, China
Lead	Galena	PbS	China, Australia, United States
Tungsten	Scheelite Wolframite	$CaWO_4$ $(Fe,Mn)WO_4$	China, Russia, Canada
Nickel	Pentlandite	$(Fe,Ni)_9S_8$	Russia, Canada, Indonesia
Aluminum	Bauxite	Mixed oxides of Al	Australia, China, Brazil
Titanium	Rutile Ilmenite	TiO_2 $FeTiO_3$	Australia, Norway, China
Zinc	Sphalerite	ZnS	China, Peru, Australia

Source: U.S. Geological Survey *Minerals Yearbook*, 2007, 2008.

Because minerals are valuable, it is not surprising that wars are fought over access to them; World War II is one example. Iron is absolutely essential to support both modern industry and a strong military. At the beginning of the war, Germany had only modest iron ore production, whereas France, Sweden, the Soviet Union, and the United Kingdom each had significantly more production (**Table 1.2**). Even tiny Luxembourg had nearly as much iron ore production as Germany. If Germany was to succeed in its military ambitions, it

DO NOT COPY e48d507df5d1141@placeholder.9409

Printed by: e48d507df5d1141@placeholder.94092.edu. Printing is for personal, private use only. No part of this book may be reproduced or transmitted without publisher's prior permission. Violators will be prosecuted.

iron ore production as Germany. If Germany was to succeed in its military ambitions, it needed to acquire at least some of the iron ore production from other sources in Europe. The German invasion of France and Luxembourg served to secure the supplies of iron from those countries. Also of great importance was the Swedish supply of iron ore in Kiruna, which was all shipped to buyers through Narvik, on the west coast of Norway. The 1940 German invasion of Norway, and particularly of Narvik, had as one strategic goal—the acquisition of those supplies from neutral Sweden. Fortunately for the United Kingdom and the other allies, the United States had abundant supplies of iron ore available for the war effort both before and after the United States entered the conflict on December 8, 1941.

TABLE 1.2 Iron Ore Production in 1937 in Select Countries

Country	Amount (million metric tons)
Luxembourg	8
Germany	10
United Kingdom	14
Sweden	15
Soviet Union	26
France	38
United States	73

Source: U.S. Geologic Survey *Minerals Yearbook*, 1939.

Critical Mineral Resources

Iron will continue to be one of the most important metals needed for society. However, society is rapidly changing because of the ever-increasing use of electronics and the need to transition away from fossil fuel energy because of the mounting problems caused by climate change (see Box 20.2). Electronics and renewable energy resources, such as wind and solar, require many metals in supplies far greater than they have ever been needed in the past, and often in quantities greater than can be produced. **Critical minerals** are those minerals that contain a metal required for some current technology. A good example is the **rare earth elements** (**REE**), which are defined as Y, Sc, and the lanthanide series of elements (La through Lu; see the periodic table).

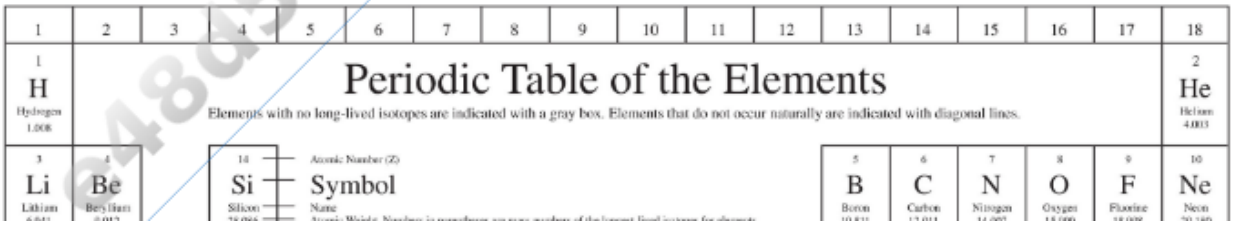

DO NOT COPY
e48d507df5d1141@placeholder.9409

Printed by: e48d507df5d1141@placeholder.94092.edu. Printing is for personal, private use only. No part of this book may be reproduced or transmitted without publisher's prior permission. Violators will be prosecuted.

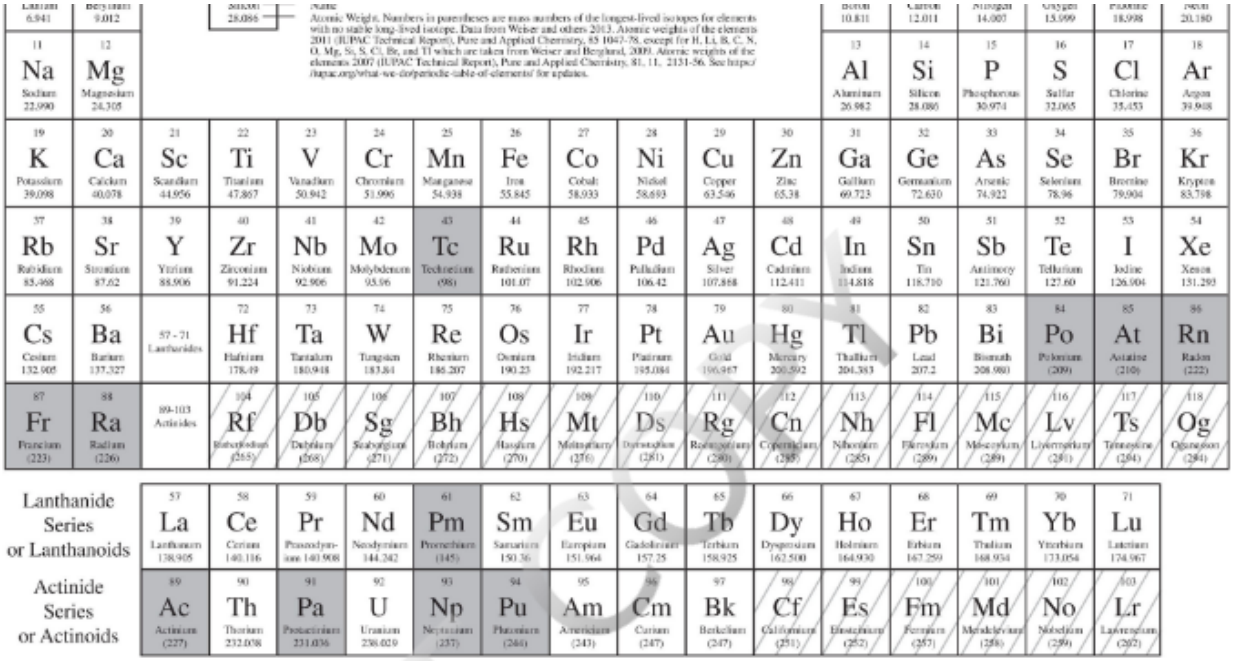

The REEs are typically extracted from high concentrations of relatively common minerals, such as monazite [$(Ce,La,Th)PO_4$], or a variety of rare minerals such as Bastnäsite [$(La,Ce,Y)CO_3F$]. Two of the REEs, Nd and Sm, are required to produce very strong magnets for electric motors and wind turbines. Flat panel displays, such as computer monitors and smartphone screens, also use Y and Eu. The typical smartphone uses some amount of many to most REEs when all its components are considered.

Currently China is the largest producer of REEs, and demand may soon exceed supply. However, there are a number of additional large deposits of REEs in the crust, most notably in the United States, Canada, and Australia, but these deposits are either not currently mined or not yet mined to a large capacity. These additional REE deposits will need to be mined as the high demand for electrics continues and as the global energy infrastructure becomes more reliant on renewable energy. More about REEs can be found in Voncken (2016).

Conflict Minerals

Conflict minerals are minerals mined to obtain profits that help fund wars or repressive regimes. So-called “blood diamonds” are one example. To maximize profits, mining is done with little regard for environmental impacts or mine worker safety, who may be effectively slaves. The source of such diamonds is often obscured and thus unknown to the consumer. Conflicts and human atrocities in Angola, Sierra Leone, Liberia, Côte d’Ivoire, and adjacent areas in Africa have been funded by diamonds extracted and sold in this way.

Critical minerals can also serve as conflict minerals. Tantalum (Ta) is a required element for capacitors, which all electronics require. The most common ore for Ta is coltan, a mineral series with end members of columbite [$(Fe,Mn)Nb_2O_6$] and tantalite

Printed by: e48d507df5d1141@placeholder.94092.edu. Printing is for personal, private use only. No part of this book may be reproduced or transmitted without publisher's prior permission. Violators will be prosecuted.

mineral series with end members of columbite [$(Fe,Mn)Nb_2O_6$] and tantalite [$(Fe,Mn)Ta_2O_6$]. The Democratic Republic of Congo (DRC) has perhaps the world's largest deposit of coltan, and mining was driven by the increased in demand for Ta and electronics.

In a scenario similar to that of blood diamonds, most DRC coltan mines are controlled by rebel forces; workers are essentially slaves and many are children. DRC government forces often do not treat workers any better, and both sides have perpetrated human atrocities. The ecological devastation associated with the mines includes the hunting of local animals for food to near extinction and groundwater contamination by radioactive elements found in the ore. Ore is often smuggled out of the country to help obscure its source, and despite efforts to trace the source of Ta, some amount obtained through exploitation of workers makes it into the world's supply chain and consumer electronics. Profits from mining fund the continued conflict between the DRC army and rebel forces. More information on conflict minerals and other conflict resources globally can be found in Burnett and Burnett (2016).

Minerals and Health

Over 2000 years ago the Greek physician Hippocrates established a correlation between disease and location, demonstrating that geological environment influences the incidence of disease. We now recognize that some of these spatial variations in disease are tied to the mineralogical composition of the soils and rocks on which we live. Selenium, for example, is an essential nutrient that is taken up by plants from the soil. Humans and animals get their selenium by eating plants, and if the soil is deficient in selenium, health problems may develop from a selenium deficiency. Too much selenium, however, may also lead to significant health problems. Many other metals sourced from minerals in the soil and bedrock are essential nutrients in small amounts but are toxic in large amounts; examples include arsenic, chromium, cobalt, copper, iron, manganese, molybdenum, nickel, tin, tungsten, vanadium, and zinc.

Other chemical elements, such as hexavalent chromium, lead, and mercury, do not have known nutritional benefits and can be quite toxic. While poisoning from natural sources of these elements has occurred, most cases of toxicity come from human-made sources. The metals are mined and used in products or industrial processes that expose people to them. Lead in paint, gasoline, and solder is a good example.

Most people can tolerate the inhalation of small amounts of mineral dust that unavoidably occurs every day. However, chronic inhalation of significant quantities of any mineral dust can be hazardous, and several minerals appear to pose particular problems. One of the most widely recognized problems is with the group of minerals referred to as **asbestos**, which form thin flexible fibers that are useful for a number of products and industrial processes (Box 13.1). The commonly used asbestos minerals are chrysotile (Chapter 13) and amphibole (Chapter 14). While the use of asbestos is now largely banned, in the past

DO NOT COPY e48d507df5d1141@placeholder.94092

Printed by: e48d507df5d1141@placeholder.94092.edu. Printing is for personal, private use only. No part of this book may be reproduced or transmitted without publisher's prior permission. Violators will be prosecuted.

asbestos minerals were used in insulation, flooring, automotive brakes, and many other products. Inhalation of the fibrous mineral particles has been documented to cause cancer and a variety of other lung-related pathologies. In response to the real and potential threat posed by asbestos, this material has been removed at considerable expense from homes, schools, and other buildings.

Quartz (Chapter 12) dust also has been documented to cause silicosis, a pathology most commonly found in miners, mill workers, and kitchen countertop fabricators exposed to high levels of dust in the work environment. The accumulation of high levels of quartz particles in the lungs leads to scarring and decreased lung function. Other pulmonary diseases, including cancer, also have been linked to silicosis.

Chronic inhalation of other mineral dusts (e.g., kaolinite, pyrophyllite, montmorillonite, and zircon) also has been documented to cause medical problems. Chronic inhalation of almost any particulate material, mineral or otherwise, should be avoided because of its potential to cause problems.

Medical Uses of Minerals

Minerals have probably been used for medical purposes since before the start of recorded history. Before the development of modern pharmaceuticals, physicians and healers had to rely on a relatively limited collection of natural materials. This included minerals in addition to materials from plants and animals. Pliny the Elder mentions the medical uses of minerals (Bostock and Riley, 1857), and the earliest textbook on mineralogy (Agricola, 1546) includes a section that describes the medical uses of minerals. Limpitlaw (2006) has documented that about 100 different minerals have been used for medicinal purposes and that some continue to be an integral part of the modern pharmacy.

Many minerals are used in folk remedies and in homeopathic and other preparations for which scientific documentation of their efficacy is notably lacking. In many cases, these uses probably do no harm and are only successful to the degree that they trigger the placebo effect. The placebo effect is based on the observation in medical trials that placebos (pills or other treatment with no active ingredient) can produce benefits. The placebo effect is a complicated process as benefits have been documented whether or not the patient knows that the treatment is a placebo. The placebo effect probably helps explain the common historical use of gemstones, beautiful crystals, and other precious or rare minerals for medical purposes. These uses still flourish, as an Internet search will readily confirm.

The most common way minerals are prepared in such treatments include ingestion of powders; drinking a “tea” or extract by soaking the mineral in water, beer, wine, or other liquid; preparing a poultice of the powdered mineral; and carrying the mineral in an amulet. Homeopathic preparations are commonly diluted to the point that only traces (or none) of the original material are present. The modern practice of wearing gemstones is

DO NOT COPY e48d507df5d1141@placeholder.9409

Printed by: e48d507df5d1141@placeholder.94092.edu. Printing is for personal, private use only. No part of this book may be reproduced or transmitted without publisher's prior permission. Violators will be prosecuted.

in part derived from ancient beliefs that the gems provided protection from, or a cure for, various ailments.

It should be noted that some of the historical medical uses of minerals were definitely hazardous to the patient's health. One example is calomel, a mercury chloride (Hg_2Cl_2). It was used to treat gastrointestinal problems, infections, and other maladies from at least 1500 up to the 1860s, but it also produced mercury poisoning. Another example is preparations made with gold, which were claimed to energize and ensure longevity. Diane de Poitiers, mistress to King Henry II of France in the sixteenth century, routinely drank an elixir made from gold and probably died from gold poisoning (Charlier and others, 2009). Lastly, lead oxides such as minium (Pb_3O_4) continue to be used as a folk remedy to treat diarrhea in certain Central American societies and can result in lead poisoning.

The reader should not infer that all medical uses of minerals are associated only with the placebo effect or are directly harmful. A significant number of minerals are routinely and productively used for modern medical purposes. These include the clay minerals (Chapter 13), zeolites (Chapter 12), and calcite (Chapter 17).

Medical uses of some minerals are mentioned as part of the descriptions in Chapters 12 through 20. The reader is cautioned that the authors do not endorse any of these uses, and that qualified physicians and pharmacists should be consulted about the appropriate treatment for any medical condition. The reader also is cautioned that mineral uses that now seem improbable may yet prove to be beneficial and vice versa.

DO NOT COPY
e48d507df5d1141@placeholder.9409

Printed by: e48d507df5d1141@placeholder.94092.edu. Printing is for personal, private use only. No part of this book may be reproduced or transmitted without publisher's prior permission. Violators will be prosecuted.

Getting Started

Students are understandably eager to get their hands on minerals in the lab as they start a course focused on minerals. However, the detailed discussion of the physical properties that provide the basis for identification of unknown samples is not presented until Chapter 6. The reason for this organization is that an understanding of mineral physical properties (habit, color, luster, streak, hardness, specific gravity, cleavage, fracture, etc.) requires an understanding of crystallography and crystal chemistry, the topics of Chapters 2 through 5. The objective of studying minerals is not simply to collect, identify, and catalog them. Much of the Earth's geologic history is recorded in the compositions, textures, associations, and spatial and temporal distributions of the minerals that compose the rocks, sediments, and soils that make up the solid Earth. Without a working knowledge of crystallography and crystal chemistry, it is not possible to accurately document and interpret the information that minerals provide.

It is assumed here that students using this text will have completed at least one college-/university-level course in introductory-level geology. Such a course should provide them with basic information about minerals, rocks, and geologic processes and environments. A review of the relevant chapters in any college-/university-level textbook that covers introductory geology is strongly recommended for all readers and will make the study of the following chapters easier and more informative. A brief review of the physical properties that are routinely used to identify mineral hand samples and the tools used is provided in **Box 1.1**.

DO NOT COPY e48d507df5d1141@placeholder.9409

BOX 1.1
Getting Started: Mineral Physical Properties

The properties used to identify minerals can be grouped into those that involve shape, mass (density and specific gravity), mechanical properties (hardness, cleavage, fracture), interaction with light (luster, color, streak), and other properties (magnetism, taste, smell, reaction with acid).

Hand Lens

For identification of minerals, a hand lens is an indispensable tool, and a good lens can last a lifetime (**Figure 1.2a**). A 10× lens is suitable for most routine work and costs between $10 and $50, depending on quality. Higher and lower magnifications also are available. The lens is held close to the eye and the sample brought up to the lens to bring the image into focus (**Figure 1.2b**). For those that wear glasses for vision correction, the hand lens can be used either with or without glasses, but experimentation is encouraged to determine what works best. In the field, a hand

Printed by: e48d507df5d1141@placeholder.94092.edu. Printing is for personal, private use only. No part of this book may be reproduced or transmitted without publisher's prior permission. Violators will be prosecuted.

experimentation is encouraged to determine what works best. In the field, a hand lens is conveniently carried on a lanyard or string around one's neck or tucked in a pocket. Close examination with a hand lens will reveal habit, mineral color, and luster, as well as cleavage and fracture. Even if unambiguous mineral identification is not possible, hand lens examination can allow the mapping of different rock units based on differences in textures and mineral assemblages. The mineral descriptions in the latter part of the book contain tips for hand lens identification of many of the common minerals.

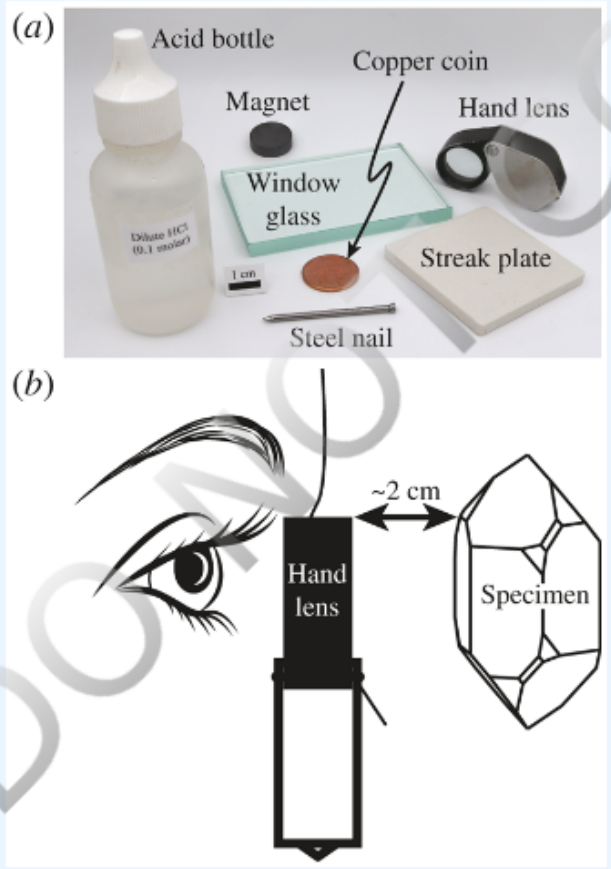

FIGURE 1.2 Mineralogy tools and use. (*a*) Basic tools used in mineral identification. (*b*) Proper use of typical 10× hand lens. View larger image

Mineral Shape

Minerals commonly form eye-catching crystals, ideally with a specific set of geometric shapes and crystal faces. For example, quartz crystals form six-sided columns with pointed ends, and pyrite commonly forms cubes with thin parallel lines, called striations, on the cube sides. These shapes can be described with specific terminology used by mineralogists—elongate, stubby, fibrous, cubic, prismatic, and so forth. The detailed study of crystals has revealed symmetrical relationships among crystal faces and has developed into the subject of crystallography. Chapter 2, on crystallography, explores mineral symmetry and establishes a coordinate system of crystal axes and an extensive nomenclature for crystals. This background allows us to systematically describe and discuss the properties of minerals.

DO NOT COPY e48d507df5d1141@placeholder.9409

Printed by: e48d507df5d1141@placeholder.94092.edu. Printing is for personal, private use only. No part of this book may be reproduced or transmitted without publisher's prior permission. Violators will be prosecuted.

systematically describe and discuss the properties of minerals.

Mass-Related Properties

Density and **specific gravity** are both closely related to mass. Density (ρ) is defined as mass (m) per volume (v):

$$\rho = m/v$$

The usual units are grams per cubic centimeter (g/cm^3). Specific gravity (G) is the ratio of the density of a material (ρ) divided by the density of water at 4°C (ρ_{H_2O}).

$$G = \frac{\rho}{\rho_{H_2O}}$$

G is unitless because it is a ratio of densities. Because the density of water at 4°C is essentially 1 g/cm^3, the numerical value for specific gravity is the same as density expressed in terms of grams per cubic centimeter. Details of how specific gravity is measured are provided in Chapter 6, but a rough estimate can be made by determining a sample's **heft**. Heft is determined by gently shaking a sample of a mineral in one's hand to get a sense of its weight, then a sample of similar size and of known specific gravity, such as quartz ($G = 2.65$), is similarly hefted to determine whether the unknown has a higher or lower specific gravity to the known sample. The controls of density are chemical composition (Chapter 3) and the manner in which the atoms that compose the mineral are packed and chemically bonded together (Chapter 4).

Mechanical Properties

Hardness (H) is a measure of the resistance of a mineral to being scratched. The Mohs scale of hardness ranks minerals from 1 for very soft, easily scratched minerals, to 10 for the hardest mineral, diamond (**Table 1.3**). To provide a standard of comparison, specific minerals are assigned to each hardness number. A mineral with hardness 5 will scratch a mineral with hardness 4 and be scratched by a mineral with hardness 6, for example. To make comparisons in the lab and field easier, mineral hardness is routinely tested with common materials of known hardness (Figure 1.2)—a fingernail (2.5), a steel nail or knife blade (~5), window glass (~5.5), and a piece of quartz (7). In the United States and Canada, a copper penny is also commonly used and has a hardness of about 3. A sharp knifepoint or metal nail can be used to scratch even small grains to estimate hardness. The identification tables at the end of this book (Appendix B) use groupings based on these values.

TABLE 1.3 Mohs Scale of Hardness

DO NOT COPY e48d507df5d1141@placeholder.94092

Printed by: e48d507df5d1141@placeholder.94092.edu. Printing is for personal, private use only. No part of this book may be reproduced or transmitted without publisher's prior permission. Violators will be prosecuted.

1	Talc
2	Gypsum
3	Calcite
4	Fluorite
5	Apatite
6	Orthoclase
7	Quartz
8	Topaz
9	Corundum
10	Diamond

Hardness is fundamentally controlled by the nature of the chemical bonds among the atoms that compose a mineral. The detailed discussion of hardness in Chapter 6 depends on an understanding of chemical bonding (Chapter 3) and crystal structure (Chapter 4). Both of these are intimately related to a mineral's symmetry (Chapter 2).

Cleavage and **fracture** both refer to the manner in which a mineral breaks. All minerals fracture when hit with a hammer or otherwise are forced to break. When a mineral fractures, it breaks on an irregular surface. If the surface is smooth and curved, like broken glass, the fracture is **conchoidal**. **Irregular**, **hackly**, and **splintery** fracture are terms that indicate increasing degree of relief ("pointiness") on the fracture surface. Only some minerals display cleavage, where the breaks are on smooth planar surfaces that are planes of weakness in a mineral. The cleavage may be described as perfect, good, fair, or poor, depending on the ease with which the cleavage can be produced, as well as how smooth and continuous the cleavage surfaces are. Minerals with cleavage may have one, two, three, or more different directions along which they break. Table B.1 in Appendix B groups minerals based on the number of cleavages. Because cleavages are planes of weakness in a mineral's structure (Chapter 4), they have crystallographic control and are identified with the nomenclature of crystallography (Chapter 2). A detailed discussion is provided in Chapter 5.

Color Properties

A mineral's **luster** and **color** are perhaps the first things that an observer notices. Luster is generally categorized as **metallic** or **nonmetallic**, that is, does the mineral look like metal or not? Whether we perceive a mineral to be metallic or nonmetallic is not a function of color—rather, it is a function of how much of the incident light is reflected, which is discussed in Chapters 6 and 7. Separate identification tables are provided in Appendix B for metallic and nonmetallic minerals. Color for minerals with a metallic luster is generally quite consistent for different samples of the mineral and

DO NOT COPY e48d507df5d1141@placeholder.9409

Printed by: e48d507df5d1141@placeholder.94092.edu. Printing is for personal, private use only. No part of this book may be reproduced or transmitted without publisher's prior permission. Violators will be prosecuted.

a metallic luster is generally quite consistent for different samples of the mineral and is therefore a useful diagnostic property—a property that can be used for mineral identification. For nonmetallic minerals, however, color can be quite variable. Quartz, for example, can be almost any color, and K-feldspar, another very common mineral, can be pink, white, gray, green, or blue. An understanding of the controls of a mineral's color requires knowledge of chemical bonding and the interaction of light with matter. These topics are covered in Chapters 3, 6, and 7.

For minerals with highly variable color, such as quartz and K-feldspar, it turns out that the color of the mineral when powdered can be quite consistent; this color is the mineral's **streak**. In most cases, the streak color is obtained by rubbing a mineral on a hard, unglazed white porcelain tile, called a streak plate (Figure 1.2). The rubbing leaves a trail of fine mineral powder from which the streak color can be determined. If a streak plate is not available, a knife blade, rock hammer, or other similar implement can be used to produce a little powder of an unknown mineral. While the streak of nonmetallic minerals is usually quite consistent regardless of variations in mineral color, it is not a particularly useful diagnostic property because the streak of most nonmetallic minerals usually is white, gray, or some other pale color. Only a few nonmetallic minerals have a distinctly colored streak (Appendix B: Table B.2).

Other Properties

A few common minerals are **magnetic**, meaning that they are attracted to a magnet (Appendix B: Table B.6; Figure 1.2). However, magnetism is much more complicated than simple attraction to a magnet, which is described in Chapter 6. Understanding these properties requires knowledge of mineral composition and of its chemical bonding (Chapter 3).

Other properties such as **taste** and **smell** are unique to certain minerals. Halite (NaCl) and sylvite (KCl) are readily soluble in water and have a salty taste; most clay minerals yield an earthy odor if moistened. Some carbonate minerals such as calcite ($CaCO_3$) and dolomite [$CaMg(CO_3)_2$] will effervesce in dilute hydrochloric acid (Figure 1.2), though dolomite must first be powdered. These properties are discussed at more length in Chapter 6. Table B.7 in Appendix B lists minerals that effervesce in dilute HCl.

Other Tools

The study of minerals is not restricted to the physical properties outlined in this section. Many mineral samples cannot be identified based on physical properties, either because the sample is too small or because the physical properties that can be measured do not lead to a unique answer. Physical properties cannot be used to determine the details of a mineral's chemistry. Other analytical tools are required and are routinely used. For purposes of identification, the petrographic microscope (Chapter 7), X-ray diffractometer (Chapter 8), and electron microprobe (Chapter 9) are workhorses in most mineral studies, and each has strengths and weaknesses. Some additional mineral chemical analysis techniques are described in Chapter 9.

DO NOT COPY e48d507df5d1141@placeholder.9409-

Printed by: e48d507df5d1141@placeholder.94092.edu. Printing is for personal, private use only. No part of this book may be reproduced or transmitted without publisher's prior permission. Violators will be prosecuted.

General References on Mineralogy

This book is intended as an introduction to the study of minerals and, of necessity, cannot include the depth of coverage provided in more specialized resources. References will be provided in each chapter to sources of additional information. However, all readers should be aware of a number of additional important sources.

Among the most important is the series of volumes by Deer and others titled *Rock-Forming Minerals*, which provides extensive information on the structure, chemistry, properties, and occurrence of common minerals. The same authors also have compiled a one-volume summary (Deer and others, 2013) that is highly recommended.

The seventh edition of *Dana's Manual of Mineralogy*, in three volumes (1942–1962), provides coverage of the physical and related properties of nonsilicate minerals, and quartz and its polymorphs. Unfortunately, much of the chemical and crystal structure information is now out of date, and volumes dealing with the silicates are not published. The eighth edition (Gains and others, 1997) provides an exhaustive compilation of minerals in one volume.

The *Handbook of Mineralogy*, in five volumes, by Anthony and others (1990–2003), provides another exhaustive compilation of mineralogical data. Separate files for each of the 3734 minerals included in the handbook may be downloaded from the Mineralogical Society of America. Strunz and Nickel (2001) provide additional data. Mineral data are widely available on the Internet as well. **Mindat.org** has one of the most comprehensive compilations, and other sources can be readily found with common Internet search tools.

The Mineralogical Society of America publishes the *Reviews in Mineralogy & Geochemistry* series, which now totals over 80 volumes. New volumes are published every year, often based on a short course offered at the society's annual meeting. Each volume typically deals in depth with a specific group of minerals or some mineral-related topic. The Mineralogical Society of America and a host of other scientific societies also publish *Elements* quarterly. Each issue presents a group of articles addressing a topical issue related to mineralogy and geochemistry.

The literature of mineralogy is published in many journals in a variety of languages. The most widely circulated English-language journals are *American Mineralogist*, published by the Mineralogical Society of America; *Canadian Mineralogist*, published by the Mineralogical Society of Canada; *Mineralogical Magazine*, published by the Mineralogical Society of Great Britain and Ireland; and *European Journal of Mineralogy*, published by Schweizerbart Science Publishers.

DO NOT COPY e48d507df5d1141@placeholder.94092

Printed by: e48d507df5d1141@placeholder.94092.edu. Printing is for personal, private use only. No part of this book may be reproduced or transmitted without publisher's prior permission. Violators will be prosecuted.

provides extensive information on the structure, chemistry, properties, and occurrence of common minerals. The same authors also have compiled a one-volume summary (Deer and others, 2013) that is highly recommended.
The seventh edition of *Dana's Manual of Mineralogy*, in three volumes (1942–1962), provides coverage of the physical and related properties of nonsilicate minerals, and quartz and its polymorphs. Unfortunately, much of the chemical and crystal structure information is now out of date, and volumes dealing with the silicates are not published. The eighth edition (Gains and others, 1997) provides an exhaustive compilation of minerals in one volume.

The *Handbook of Mineralogy*, in five volumes, by Anthony and others (1990–2003), provides another exhaustive compilation of mineralogical data. Separate files for each of the 3734 minerals included in the handbook may be downloaded from the Mineralogical Society of America. Strunz and Nickel (2001) provide additional data. Mineral data are widely available on the Internet as well. **Mindat.org** has one of the most comprehensive compilations, and other sources can be readily found with common Internet search tools.

The Mineralogical Society of America publishes the *Reviews in Mineralogy & Geochemistry* series, which now totals over 80 volumes. New volumes are published every year, often based on a short course offered at the society's annual meeting. Each volume typically deals in depth with a specific group of minerals or some mineral-related topic. The Mineralogical Society of America and a host of other scientific societies also publish *Elements* quarterly. Each issue presents a group of articles addressing a topical issue related to mineralogy and geochemistry.

The literature of mineralogy is published in many journals in a variety of languages. The most widely circulated English-language journals are *American Mineralogist*, published by the Mineralogical Society of America; *Canadian Mineralogist*, published by the Mineralogical Society of Canada; *Mineralogical Magazine*, published by the Mineralogical Society of Great Britain and Ireland; and *European Journal of Mineralogy*, published by Schweizerbart Science Publishers.

REFERENCES CITED AND SUGGESTIONS FOR ADDITIONAL READING

Agricola, G. 1546. *De natura fossilum*. Translated by M. C. Bandy and J. A. Bandy, 1955. Geological Society of America Special Paper **63**, 240 p.

Agricola, G. 1556. *De re metallica*. Translated by H. Hover, 1950. Dover Publications, New York, 638 p.

Anthony, J. W., Bideaux, R. A., Bladh, K. W., and Nichols, J. C. 1990–2003. *Handbook of Mineralogy (5 volumes)*. Mineral Data Publishing, Tucson, AZ.

DO NOT COPY e48d507df5d1141@placeholder.9409

Printed by: e48d507df5d1141@placeholder.94092.edu. Printing is for personal, private use only. No part of this book may be reproduced or transmitted without publisher's prior permission. Violators will be prosecuted.

Back, M. 2014. *Fleischer's Glossary of Mineral Species 2014*. The Mineralogical Record, Tucson, AZ, 434 p.

Bayliss, P. 2000. *Glossary of Obsolete Mineral Names*. The Mineralogical Record, Tucson, AZ, 235 p.

Blackburn, W. H., and Dennen, W. H. 1997. *Encyclopedia of Mineral Names*. Canadian Mineralogist Special Publication **1**, 368 p.

Bostock, J., and Riley, H. T. 1857. *The Natural History of Pliny*. Henry G. Bohn, London, 529 p.

Burnett, M. T. 2016. *Natural Resource Conflicts: From Blood Diamonds to Rainforest Destruction*, ABC-CLIO, Santa Barbara, CA, 911 p.

Caraballo, M. A., Michel, F. M., and Hochella, M. F., Jr. 2015. The rapid expansion of environmental mineralogy in unconventional ways: Beyond the accepted definition of a mineral, the latest technology, and using nature as our guide. *American Mineralogist* **100**, 14–25.

Carr, D. D. (ed.). 1994. *Industrial Minerals and Rocks*, 6th ed. Society for Mining, Metallurgy, and Exploration, Littleton, CO, 1196 p.

Chang, L. L. Y., Howie, R. A., and Zussman, J. 1998. *Rock-Forming Minerals, Volume 5B: Nonsilicates: Sulfates, Carbonates, Phosphates, Halides*, 2nd ed. The Geological Society, London, 383 p.

Charlier, P., Pupon, J., Huynh-Charlier, I., Saliege, J.-F., Favier, D., Keyser, C., and Ludes, B. 2009. A gold elixir of youth in the 16th century French court. *British Medical Journal* **339**, 5311.

de Fourestier, J. 1999. *Glossary of Mineral Synonyms*. Canadian Mineralogist Special Publication **2**, 448 p.

Deer, W. A., Howie, R. A., and Zussman, J. 1997. *Rock-Forming Minerals, Volume 2B: Double-Chain Silicates*, 2nd ed. The Geological Society, London, 774 p.

Deer, W. A., Howie, R. A., and Zussman, J. 2001. *Rock-Forming Minerals, Volume 1A: Orthosilicates*, 2nd ed. The Geological Society, London, 919 p.

Deer, W. A., Howie, R. A., and Zussman, J. 2001, *Rock-Forming Minerals, Volume 1B: Disilicates & Ring Silicates*, 2nd ed. The Geological Society, London, 630 p.

Deer, W. A., Howie, R. A., and Zussman, J. 2001. *Rock-Forming Minerals, Volume 2A: Single-Chain Silicates*, 2nd ed. The Geological Society, London, 678 p.

Deer, W. A., Howie, R. A., and Zussman, J. 2001. *Rock-Forming Minerals, Volume 4A: Framework Silicates: Feldspars*, 2nd ed. The Geological Society, London, 984 p.

Deer, W. A., Howie, R. A., and Zussman, J. 2009. *Rock-Forming Minerals, Volume 3B: Layered Silicates: Excluding Micas and Clay Minerals*, 2nd ed. The Geological Society, London, 314 p.

Deer, W. A., Howie, R. A., and Zussman, J. 2013. *An Introduction to Rock Forming Minerals*, 3rd ed. The Mineralogical Society, London, 498 p.

DO NOT COPY e48d507df5d1141@placeholder.9409-

Printed by: e48d507df5d1141@placeholder.94092.edu. Printing is for personal, private use only. No part of this book may be reproduced or transmitted without publisher's prior permission. Violators will be prosecuted.

Minerals, 3rd ed. The Mineralogical Society, London, 498 p.

Deer, W. A., Howie, R. A., Zussman, J., Bowles, J. F. W., and Vaughan, D. J. 2011. *Rock-Forming Minerals, Volume 5A: Non-Silicates: Oxides, Hydroxides and Sulfides*, 2nd ed. The Geological Society, London, 932 p.

Deer, W. A., Howie, R. A., Zussman, J., and Wise, W. S. 2004. *Rock-Forming Minerals, Volume 4B: Framework Silicates: Silica Minerals, Feldspathoids, and Zeolites*, 2nd ed. The Geological Society, London, 996 p.

Fleet, M. E., and Howie, R. A. 2003. *Rock-Forming Minerals, Volume 3A: Micas*, 2nd ed. The Geological Society, London, 758 p.

DO NOT COPY

e48d507df5d1141@placeholder.9409

Printed by: e48d507df5d1141@placeholder.94092.edu. Printing is for personal, private use only. No part of this book may be reproduced or transmitted without publisher's prior permission. Violators will be prosecuted.

LIST OF KEY TERMS

- aggregate
- amorphous
- asbestos
- ash glass
- biominerals
- cleavage
- color
- conchoidal
- conflict mineral
- critical mineral
- crystal
- crystal face
- crystalline solid
- crystal structure
- density
- dimensional stone
- fracture
- fulgurite
- hackly
- hardness
- heft
- impact melt
- irregular
- luster
- magnetic
- metallic
- metamict
- mineral
- mineral grain

DO NOT COPY
e48d507df5d1141@placeholder.9409

Printed by: e48d507df5d1141@placeholder.94092.edu. Printing is for personal, private use only. No part of this book may be reproduced or transmitted without publisher's prior permission. Violators will be prosecuted.

mineral grain

mineral group

mineraloid

mineral series

mineral species

mineral variety

mining

naturally occurring

non-crystalline

nonmetallic

obsidian

ore

pseudotachylite

rare earth elements

REE

smell

specific gravity

splintery

streak

synthetic mineral

taste

tektite

type sample

DO NOT COPY
e48d507df5d1141@placeholder.9409

Printed by: e48d507df5d1141@placeholder.94092.edu. Printing is for personal, private use only. No part of this book may be reproduced or transmitted without publisher's prior permission. Violators will be prosecuted.

CHAPTER 2
Crystallography

William D. Nesse
University of Northern Colorado

Graham B. Baird
University of Northern Colorado

DO NOT COPY
e48d507df5d1141@placeholder.9409

Printed by: e48d507df5d1141@placeholder.94092.edu. Printing is for personal, private use only. No part of this book may be reproduced or transmitted without publisher's prior permission. Violators will be prosecuted.

Introduction

Crystallography has an evolved terminology that describes the shape, symmetry, and crystal structure of minerals. Despite what seems to be a very dense chapter, this is only an introduction to crystallography. Not covered is much of the theoretical and mathematical foundation on which the terminology is based. For a more extensive coverage of crystallography, refer to Bloss (1971), Smith (1982), O'Keeffe and Hyde (1996), and Boisen and Gibbs (1985).

A discussion of crystallography in the second chapter of a mineralogy textbook may seem inappropriate because crystallography is often considered to be among the most challenging parts of mineralogy. It is perhaps more exciting to immediately begin reading about specific minerals and learning to use analytical tools. However, it is important to establish a framework and common nomenclature that allow the structure and properties of minerals to be described. To do this, it is essential to first understand symmetry, because symmetry is the foundation on which the study of minerals is built.

The two important questions addressed in this chapter are:

What is the symmetry of crystals and crystal structures?

What is the terminology associated with crystals and crystal structures?

In studying this chapter, it will be useful to keep the following organization in mind.

Symmetry

- Symmetry starts with **translational symmetry**, first in two dimensions and then in three dimensions. This leads to the important concepts of **unit cells**, **crystal axes**, **crystal systems**, and **Bravais lattices**.
- Next, the elements of **point symmetry** (**reflection**, **rotations**, **inversion**) that can be identified in crystal hand samples are presented. This leads to the definition of the 32 **point groups**, which are members of the six crystal systems.
- Lastly, translational symmetry is combined with point symmetry operations to define **space groups**.

Descriptive Nomenclature of Crystals

- Descriptive nomenclature of crystals establishes that **crystal faces**, or the flat sides that ideally result from crystal growth, have rational orientations relative to the **crystal lattices**. That is, a crystal lattice is like a grid of points that shows how the atomic structure gets repeated in three dimensions according to the crystal's symmetry. Crystal faces always follow planes that can be defined by whole-number intercepts through that grid.

DO NOT COPY e48d507df5d1141@placeholder.9409

Printed by: e48d507df5d1141@placeholder.94092.edu. Printing is for personal, private use only. No part of this book may be reproduced or transmitted without publisher's prior permission. Violators will be prosecuted.

- **Miller index** notation allows individual crystal faces and crystallographic planes, such as cleavage, to be identified and described numerically.
- **Crystallographic directions** and **zones** in minerals are important orientations within the repeating grid that makes up the crystal lattice. For a crystal, a zone is parallel to the orientation that multiple crystal faces intersect.
- The collection of crystal faces that make up a crystal is referred to as the **crystal form**. Crystal form terminology includes shapes such as cubes and octahedrons, as well as a variety of other shapes, such as prisms, pinacoids, and pyramids.
- For each specific point group symmetry, there is a unique set of crystal forms, this unique set of forms is a **crystal class**. Given there are 32 point groups, there are therefore 32 crystal classes, one for each point group.
- **Crystal habit** includes the terminology that covers the way mineral grains are shaped and intergrown in rocks and mineral deposits.

A conventional view is that an object with symmetry consists of two halves that are mirror images of each other. However, symmetry involves far more than just mirror images. It involves all of the ways that something can be systematically repeated in three dimensions. Because minerals have a regular and repeating atomic structure, it follows that they must display symmetry. This symmetry is manifested in the symmetrical arrangements of crystal faces and the internal structure of crystals, which in turn control cleavage and the diffraction of X-rays. It is not surprising, then, that the concepts of crystallography are built on an understanding of symmetry.

DO NOT COPY e48d507df5d1141@placeholder.9409

Printed by: e48d507df5d1141@placeholder.94092.edu. Printing is for personal, private use only. No part of this book may be reproduced or transmitted without publisher's prior permission. Violators will be prosecuted.

Translational Symmetry: Two Dimensions

Consider a dot, which could represent a collection of atoms (**Figure 2.1a**). That dot can be repeated by translating parallel to vector *a* toward the bottom of the page again and again. The result is a column of dots extending as far as desired. The dots can also be repeated by translating parallel to vector *b* at angle *γ* from the *a* direction (**Figure 2.1b**). Repeated translations parallel to *a* and *b* produce a continuous repeating pattern of dots known as a **plane lattice** in the *ab* plane. The center of each dot at the intersection of the **lattice lines** is called a **lattice node**.

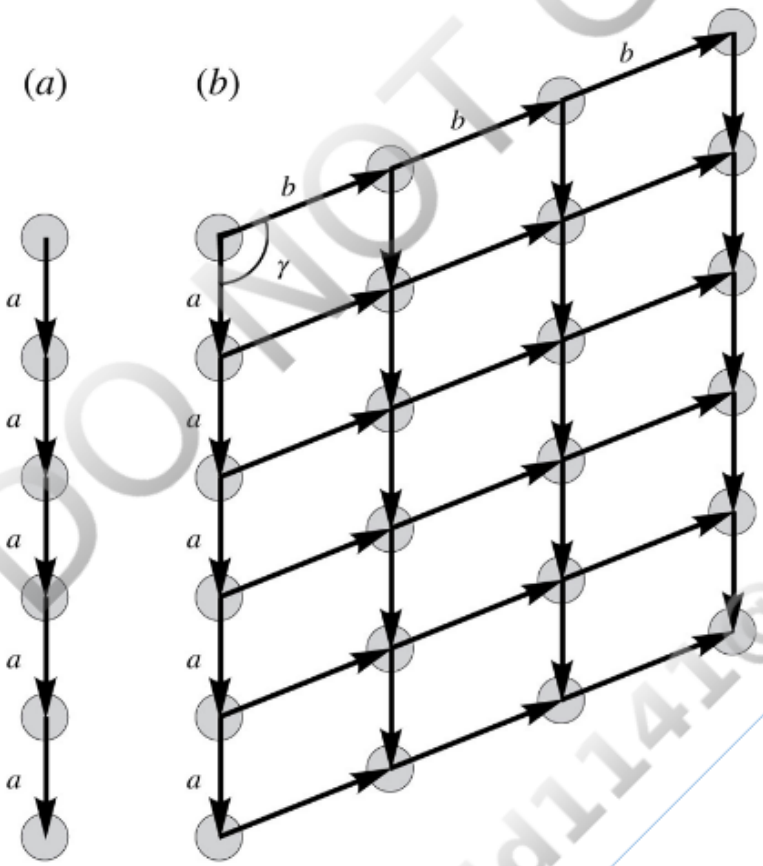

FIGURE 2.1 Simple translation to form a plane lattice. (*a*) A dot is repeated by translation distance *a* toward the bottom of the page. (*b*) Repeated translation of these dots, distance *b* at angle γ, produces a two-dimensional plane lattice. The dots represent the lattice nodes. View larger image

If the translation distance of *a* and *b* are varied, as well as the angle *γ*, there are only five different plane lattices that can be produced by simple translation in two dimensions (**Figure 2.2a**). They are the **square**, **rectangle**, **diamond**, **hexagonal**, and **oblique** plane lattices. They utilize only four fundamentally different shapes, called **unit meshes** (**Figure 2.2b**)—square, rectangle, rhombus, and parallelogram. Note that the unit mesh

DO NOT COPY e48d507df5d1141@placeholder.9409

Printed by: e48d507df5d1141@placeholder.94092.edu. Printing is for personal, private use only. No part of this book may be reproduced or transmitted without publisher's prior permission. Violators will be prosecuted.

for the diamond plane lattice is a rectangle with a node in the center, so the diamond plane lattice is also called a **centered rectangle** lattice. All but the diamond lattice have **primitive (P)** unit meshes because lattice nodes occur only at the corners. The diamond plane lattice has a **centered (C)** unit mesh because a lattice node is also at its center.

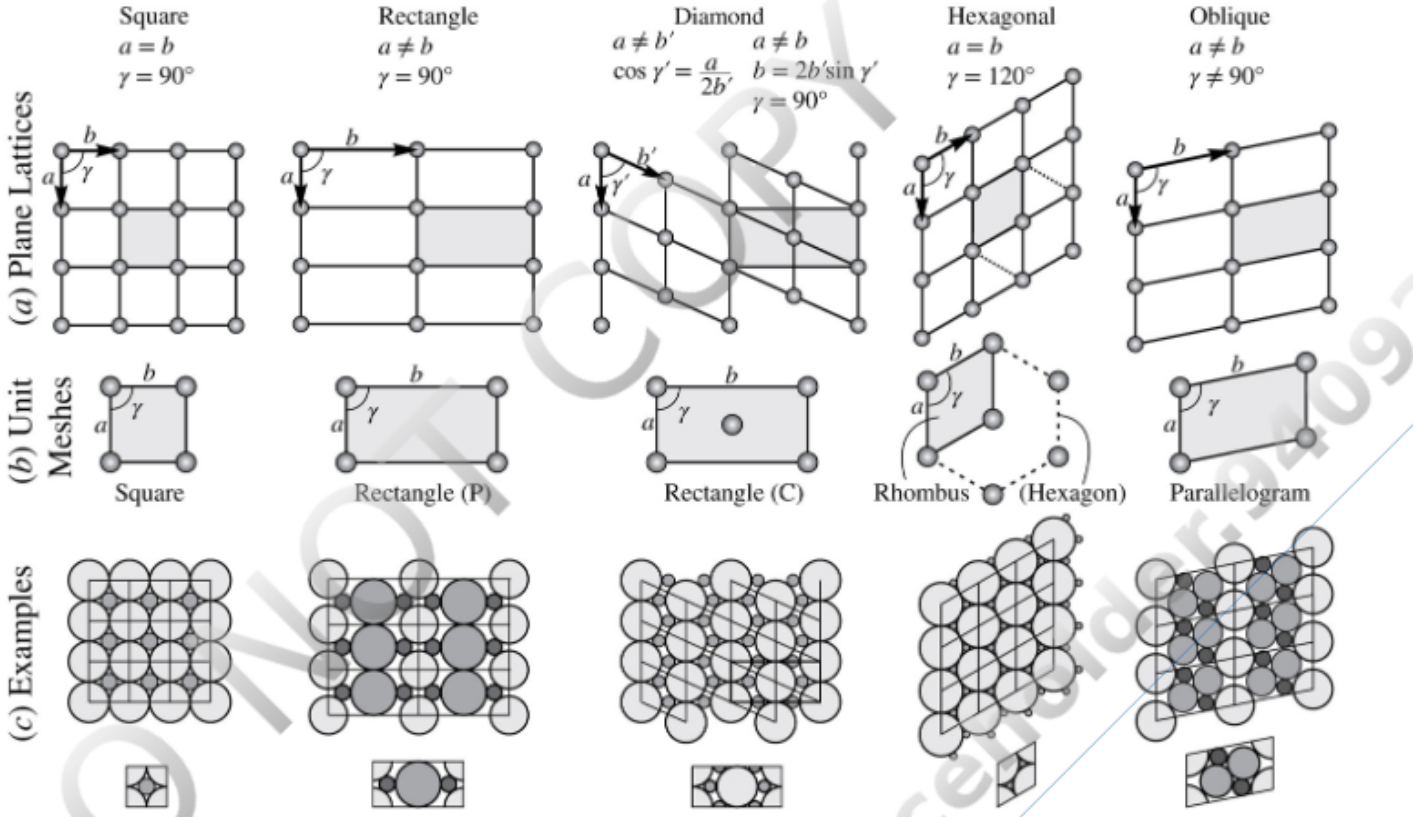

FIGURE 2.2 Plane lattices and unit meshes. (*a*) Five different plane lattices can be produced by combinations of translation in two directions. The unit meshes are shaded. (*b*) Unit meshes for the five plane lattices. A rectangle unit mesh can be used for both the rectangle and diamond plane lattice; the only difference is that the unit mesh for the diamond lattice has an additional lattice node at its center. If desired, a hexagon unit mesh (dashed lines) can be used with the hexagonal plane lattice, but the rhombus is simpler. (*c*) Examples of how hypothetical two-dimensional "atoms" might be arranged in the five plane lattices. A single unit mesh is shown below each lattice. View larger image

Unit mesh axes are parallel to the edges of the unit mesh and are labeled a and b even if they are the same length. The angle between a and b is γ. So that the unit mesh axes in the rectangle and diamond lattices can be the same ($a \neq b$, $\gamma = 90°$), the second translation vector in the diamond lattice is b' at angle γ', where $b = 2b' \sin \gamma'$.

Figure 2.2c shows how hypothetical two-dimensional "atoms" might be arranged in two-dimensional plane lattices. For each different lattice, the pattern of atoms in one unit mesh is the same as in every other unit mesh, and for every atom, a duplicate will be found in adjacent unit meshes parallel to the two translation vectors a and b.

The type of translational symmetry described here is routinely used in building brick walls and laying ceramic tile on floors and walls (**Figure 2.3**). This translational

DO NOT COPY e48d507df5d1141@placeholder.94092-

Printed by: e48d507df5d1141@placeholder.94092.edu. Printing is for personal, private use only. No part of this book may be reproduced or transmitted without publisher's prior permission. Violators will be prosecuted.

symmetry is also present in wallpaper patterns. Bricks typically are laid using either a rectangle or a centered rectangle (diamond) lattice, and square ceramic tiles are laid using a square lattice. Hexagonal ceramic tiles must be laid with a hexagonal lattice. Wallpaper typically uses square, rectangle, or centered rectangle lattices. Oblique lattices are not commonly used because walls and floors typically have square and rectangular shapes.

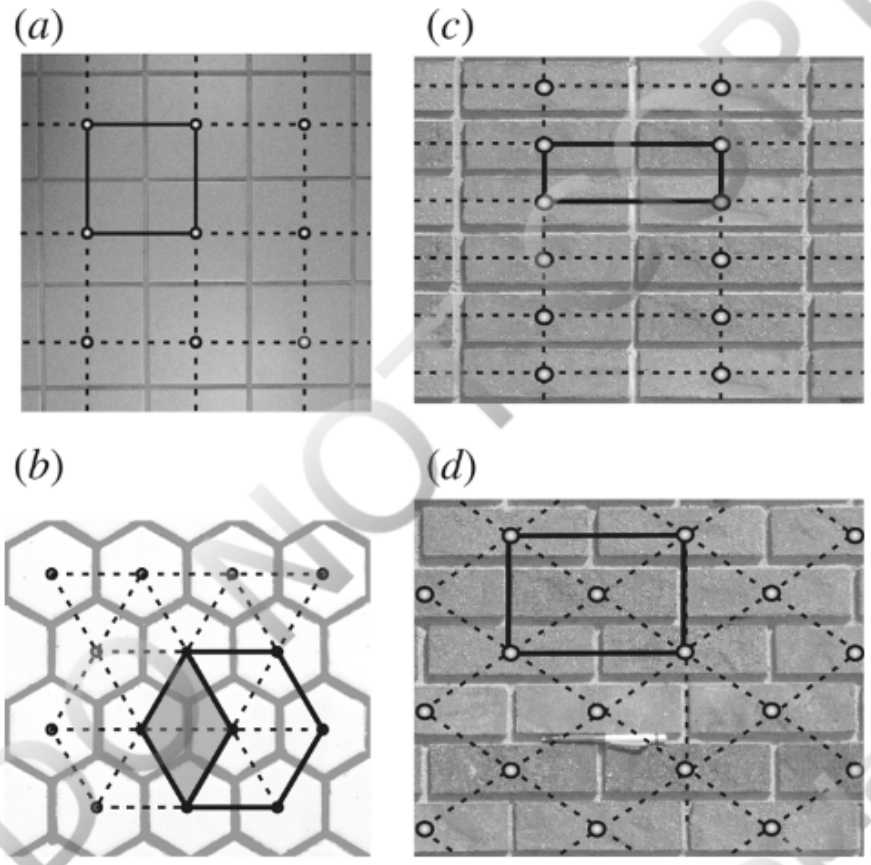

FIGURE 2.3 Plane lattices and unit meshes in everyday life. (*a*) Square ceramic tile laid in a square lattice. (*b*) Hexagonal ceramic tile laid in a hexagonal lattice. The rhombic unit mesh includes pieces sufficient to make one tile if the tile parts within the unit mesh are rearranged. (*c*) Rectangular bricks laid in a rectangular lattice. The unit mesh contains one brick. (*d*) Rectangular bricks laid in a centered rectangular (diamond) lattice. The unit mesh contains pieces sufficient to make two bricks.
View larger image

DO NOT COPY e48d507df5d1141@placeholder.9409

Printed by: e48d507df5d1141@placeholder.94092.edu. Printing is for personal, private use only. No part of this book may be reproduced or transmitted without publisher's prior permission. Violators will be prosecuted.

Translational Symmetry: Three Dimensions

Space Lattices and Unit Cells

If the two-dimensional plane lattices are systematically repeated one above the other, to allow for a translation vector in the third dimension, the result is the formation of a **space lattice** (Figure 2.4) in which lattice nodes are repeated in all three dimensions. The volume outlined by lattice nodes is known as the **unit cell**, analogous to the unit mesh in two dimensions.

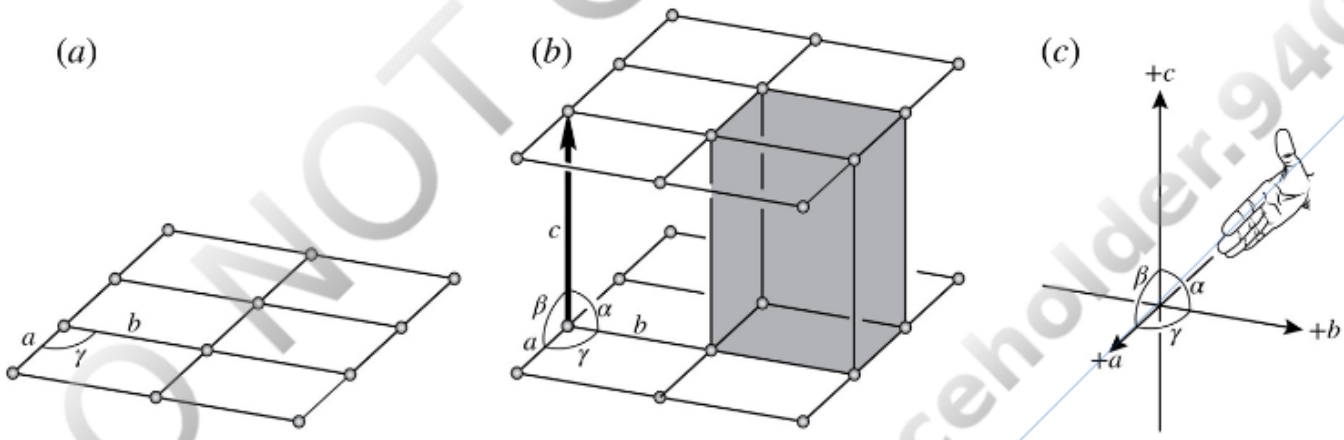

FIGURE 2.4 Space lattice. (*a*) A plane lattice with axes *a* and *b* at angle *γ*. (*b*) Translation of the lattice distance *c* at angles *α* and *β* to form a repeating pattern of lattice nodes in three dimensions. A unit cell (shaded) is the volume outlined by lattice nodes. (*c*) Crystal axes *a*, *b*, and *c* are parallel to the edges of the unit cell at angles *α*, *β*, and *γ*. A flattened right hand can be used to ensure the positive ends of the crystal axes are correctly positioned relatively to each other. View larger image

The edges of the unit cells are parallel to **crystal axes** (or crystallographic axes), which are identified as ***a***, ***b***, and ***c*** (Figure 2.4). The axes, which intersect at a point called the **origin**, have positive and negative ends. Figure 2.4c shows that a right-handed reference frame is used, where, in this sketch, positive *a* is to the front, positive *b* is to the right, and positive *c* is up. A flattened right hand with extended thumb can be used to confirm positive *a*, *b*, and *c* are correctly oriented relative to each other—the index through pinky fingers point to positive *a*, the palm faces toward positive *b*, and the thumb points toward positive *c*. The dimensions of the unit cell along the *a*, *b*, and *c* axes are the length of the translation vectors *a*, *b*, and *c*; the angles between the axes are *α*, *β*, and *γ*. Note that *α* is the angle between *b* and *c*, *β* is the angle between *a* and *c*, and *γ* is the angle between *a* and *b*.

Bravais Lattices and Crystal Systems

DO NOT COPY e48d507df5d1141@placeholder.9409

Printed by: e48d507df5d1141@placeholder.94092.edu. Printing is for personal, private use only. No part of this book may be reproduced or transmitted without publisher's prior permission. Violators will be prosecuted.

Bravais Lattices and Crystal Systems

The five plane lattices can be repeated in three dimensions to produce 14 different space lattices. These are known as the **Bravais lattices** (**Figures 2.5**–**2.9**), named for Auguste Bravais (1811–1863). These 14 Bravais lattices are divided into six groups based on the shape of the unit cell (**Figure 2.10**). Many unit cell shapes are familiar to anyone who has played with wooden blocks. They represent the shapes that can be regularly stacked together with no voids between the blocks. The six unit cell shapes are identified with the six **crystal systems**: **triclinic**, **monoclinic**, **orthorhombic**, **hexagonal**, **tetragonal**, and **isometric** (**cubic**). **Primitive (P)** unit cells contain lattice nodes only at the corners. **Body-centered (I)** unit cells contain an additional lattice node at the center. **Face-centered (C)** unit cells contain lattice nodes on the corners and on two opposite sides. **Face-centered (F)** unit cells contain lattice nodes at the corners and at the center of each face.

DO NOT COPY

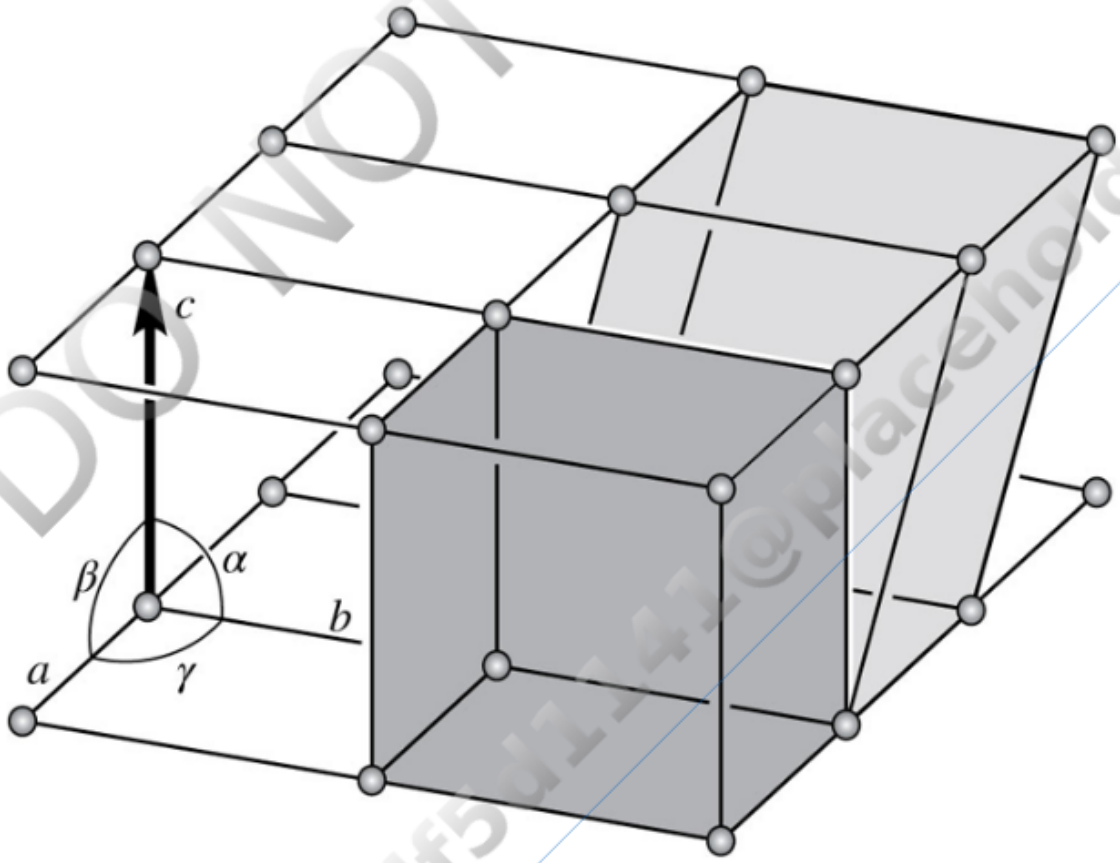

FIGURE 2.5 Triclinic Bravais lattice. An oblique plane lattice is repeated by translation distance c so that the α and β angles are not equal to 90°. Light and dark shading show two unit cell choices. Generally, the unit cell with angles closer to 90° is used, but crystal morphology and/or convenience in describing the crystal structure may dictate that a different unit cell is chosen. View larger image

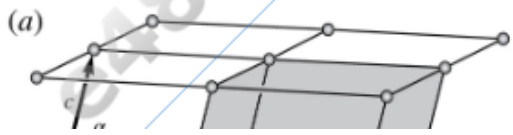

Printed by: e48d507df5d1141@placeholder.94092.edu. Printing is for personal, private use only. No part of this book may be reproduced or transmitted without publisher's prior permission. Violators will be prosecuted.

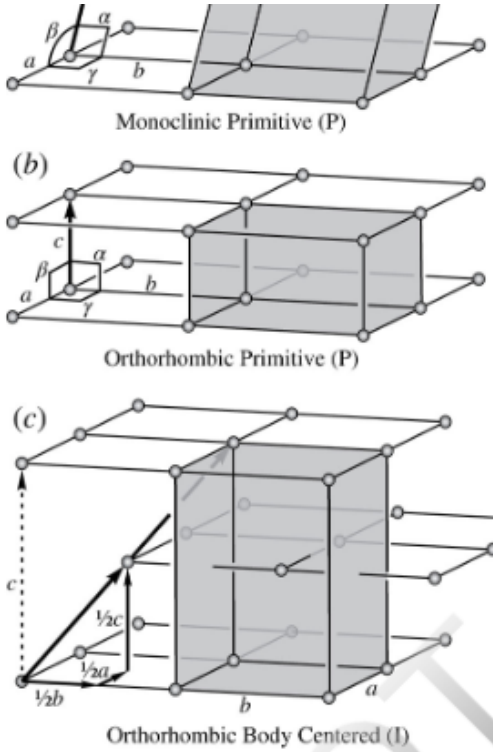

FIGURE 2.6 Bravais lattices produced by translation of a rectangle plane lattice where *a* and *b* are different lengths and angle $\gamma = 90°$. (*a*) Primitive (P) monoclinic lattice produced by translation distance *c* so angles $\alpha = 90°$ and $\beta > 90°$. (*b*) Primitive (P) orthorhombic lattice produced by translation distance *c* so that angles α and β are 90°. (*c*) Translation ½ *b* to the right, ½ *a* back, and ½ *c* up produces a body-centered orthorhombic (I) lattice. View larger image

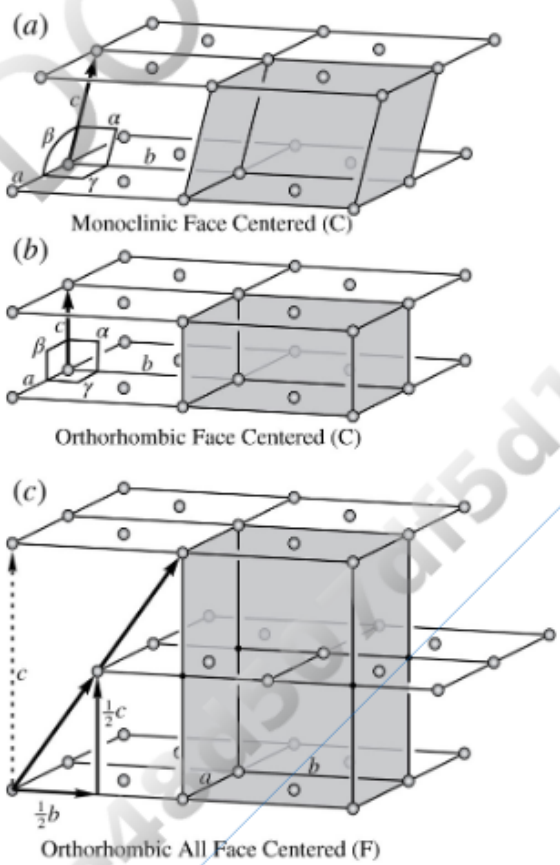

FIGURE 2.7 Bravais lattices produced by translation of a centered rectangle (diamond) plane

DO NOT COPY

Printed by: e48d507df5d1141@placeholder.94092.edu. Printing is for personal, private use only. No part of this book may be reproduced or transmitted without publisher's prior permission. Violators will be prosecuted.

FIGURE 2.7 Bravais lattices produced by translation of a centered rectangle (diamond) plane lattice where a and b are different lengths and $\gamma = 90°$. (a) Translation distance c so that $\alpha = 90°$ and $\beta > 90°$ yields a face-centered (C) monoclinic lattice. (b) Translation distance c so that $\alpha = \beta = 90°$ produces a face-centered (C) orthorhombic lattice. (c) Translation ½ b to the right and ½ c up produces an all face-centered (F) orthorhombic lattice. View larger image

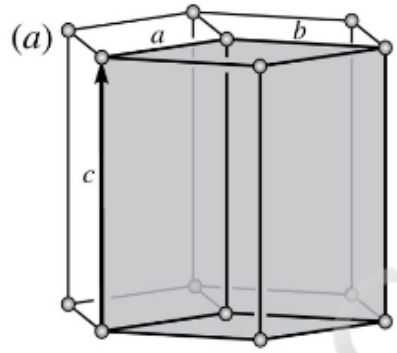

Hexagonal (P)

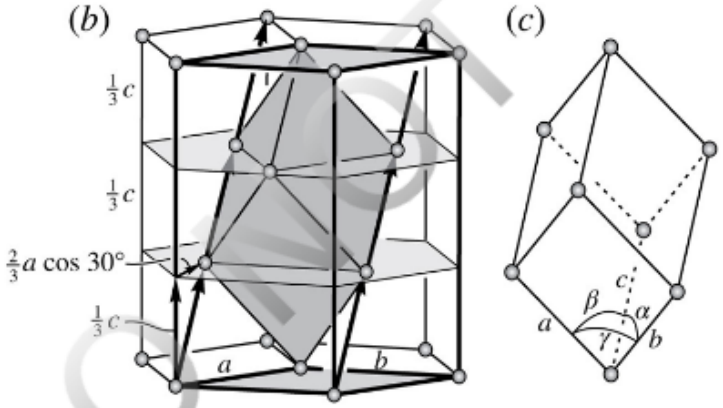

Rhombohedral (R) Rhombohedral (R)

FIGURE 2.8 Bravais lattices produced by translation of a hexagonal plane lattice. (a) Vertical translation by distance c produces a primitive hexagonal (P) lattice. The simplest unit cell is shaded. (b) Translation ⅓ c up and ⅔ a cos 30° back at right angles to the b axis produces a rhombohedral (R) lattice. The translation vector is parallel to two edges of the rhombohedron defined by the lattice nodes as shown. A unit cell that is the same as the primitive hexagonal lattice is shown with heavy lines and shading on the top and bottom. (c) A unit cell and crystal axes also can be defined by the edges of the rhombohedron ($a = b = c$, $\alpha = \beta = \gamma \neq 90°$), but this unit cell is almost never used. View larger image

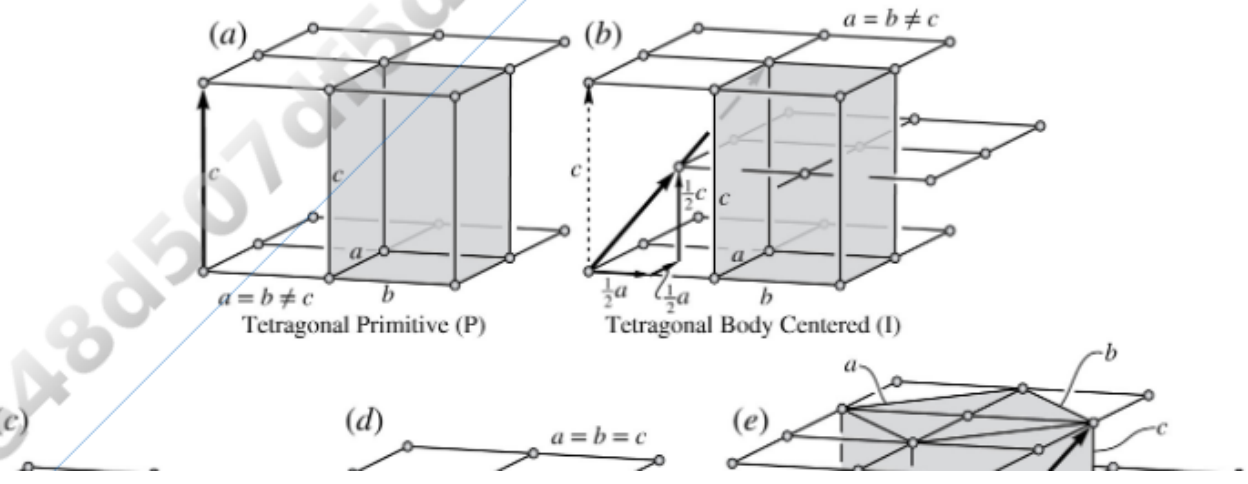

Tetragonal Primitive (P) Tetragonal Body Centered (I)

DO NOT COPY e48d507df5d1141@placeholder.9409

Printed by: e48d507df5d1141@placeholder.94092.edu. Printing is for personal, private use only. No part of this book may be reproduced or transmitted without publisher's prior permission. Violators will be prosecuted.

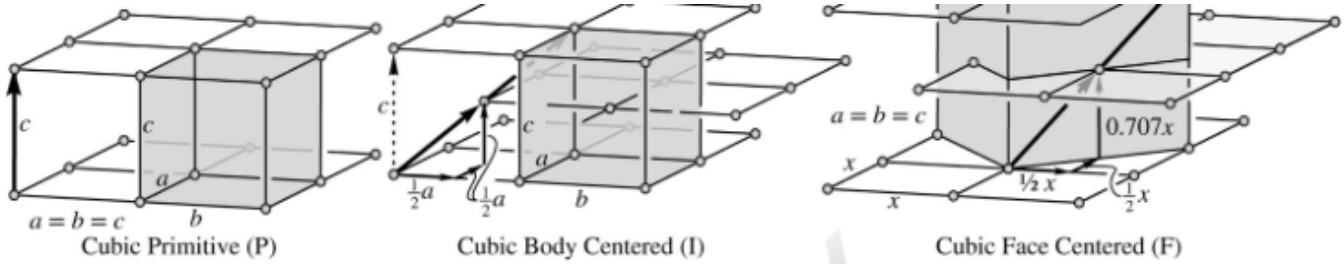

FIGURE 2.9 Bravais lattices produced by translation of a square plane lattice whose dimensions are $a = b$. (*a*) Vertical translation distance $c \neq a$ produces a primitive (P) tetragonal lattice. (*b*) Translation ½ *a* right, ½ *a* back, and ½ *c* up where $c \neq a$ produces a body-centered (I) tetragonal lattice. (*c*) Vertical translation distance $c = a$ yields a primitive (P) cubic (isometric) lattice. (*d*) Translation ½ *a* right, ½ *a* back, and ½ *a* up yields a body-centered (I) cubic lattice. (*e*) Given a square lattice whose dimensions are *x*, translation ½ *x* to the right, ½ *x* back, and 0.707 *x* up produces a face-centered (F) cubic lattice whose unit cell outline is at 45° to the lattice edges of the original plane lattice. View larger image

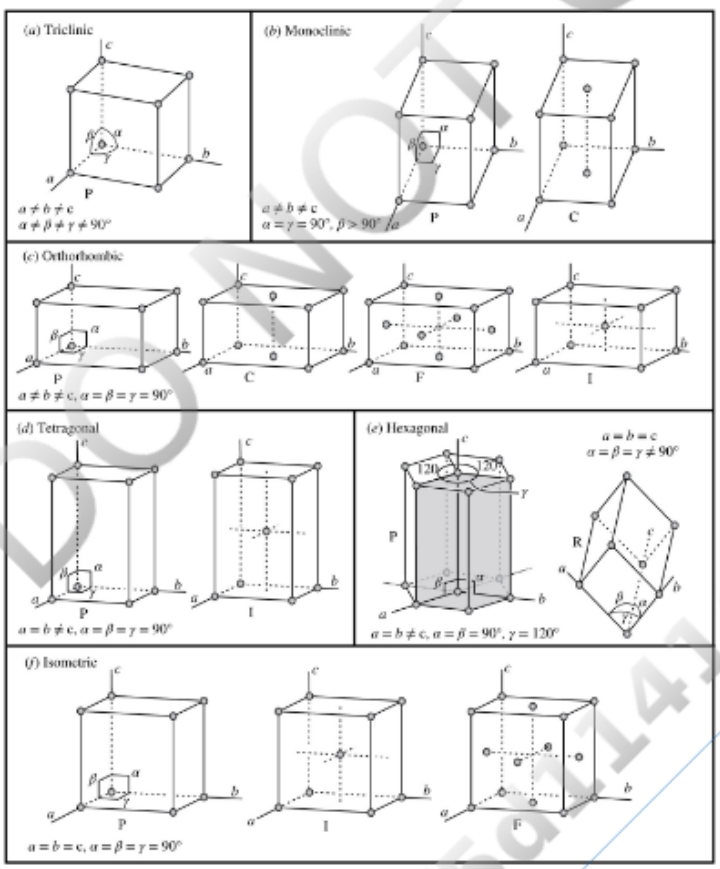

FIGURE 2.10 The 14 Bravais lattices define six different three-dimensional volumes (*a*–*f*) that correspond to the unit cells of the six crystal systems. The lengths of the three unit cell axes are *a*, *b*, and *c*, and the angles between them are *α*, *β*, and *γ*. In the notations, the ≠ sign indicates that equality of the axis lengths or angles is not required, although occasionally equality may occur by chance. The hexagonal (R) lattice shown in (*e*) is based on the rhombohedral axes shown in Figure 2.8c. A unit cell with the same geometry as the hexagonal (P) lattice shown in Figure 2.8a is far more commonly used. View larger image

Except for triclinic, each crystal system has more than one Bravais lattice. In a hand sample, it is not possible to distinguish among the Bravais lattices within a crystal system

Printed by: e48d507df5d1141@placeholder.94092.edu. Printing is for personal, private use only. No part of this book may be reproduced or transmitted without publisher's prior permission. Violators will be prosecuted.

—X-ray diffraction techniques are required. Hence, when studying the Bravais lattices, pay particular attention to the differences among the crystal systems and the geometries of the six different unit cells.

The single **triclinic Bravais lattice** is produced from the oblique plane lattice. No universally adopted convention exists to guide the assignment of crystal axes to the edges of the unit cell. Two different possible unit cells are shown in Figure 2.5. Generally the *c* axis is placed parallel to some prominent elongation (a **zone**) defined by crystal faces seen in a hand sample. The *b* axis is placed down and to the right, and the *a* axis is placed down and to the front.

> The triclinic Bravais lattice (Figure 2.5) is produced by translating an oblique plane lattice distance *c* in a direction that is not at right angles to either *a* or *b*. The unit cell dimensions (Figure 2.10a) are of different lengths and none of the angles between axes is 90° ($a \neq b \neq c$, $\alpha \neq \beta \neq \gamma \neq 90°$).

The two **monoclinic Bravais lattices** (Figure 2.10b) are derived from either a rectangle (P) or rectangle (C) plane lattice. All unit cell dimensions are of different length ($a \neq b \neq c$) and any axis may be the longest. The *b* and *c* axes are at right angles, and the *a* axis is at right angles to *b* but not to *c* ($\alpha = \gamma = 90°$, $\beta > 90°$). Note that the axes are arranged so that the angle between the positive ends of the *a* and *c* axes is greater than 90°.

> The monoclinic primitive (P) lattice is produced by translating a primitive rectangle plane lattice a distance equal to *c* so that angle $\beta > 90°$ and angle $\alpha = 90°$ (Figure 2.6a).
>
> The monoclinic centered (C) lattice is produced by translating a centered rectangle plane lattice a distance equal to *c* so that angle $\beta > 90°$ and angle $\alpha = 90°$ (Figure 2.7a).

The four **orthorhombic Bravais lattices** (Figure 2.10c) are derived from the rectangle (P) plane lattice and rectangle (C) plane lattice whose unit mesh dimensions are *a* and *b*. All three unit cell dimensions are of different length. A common convention is to assign the axes so that the *c* unit cell dimension is the smallest, *b* is the longest, and *a* is intermediate ($c < a < b$). Other conventions have been used, and in some minerals either *c* or *a* may be the longest unit cell dimension. The axes are all at right angles so $\alpha = \beta = \gamma = 90°$.

> The orthorhombic primitive (P) lattice is produced by vertical translation of a primitive rectangle lattice a distance equal to *c* (Figure 2.6b).
>
> The orthorhombic body-centered (I) lattice is produced by translating a primitive rectangle lattice a distance equal to ½ *b* right, ½ *a* back, and ½ *c* up. Every second lattice plane is aligned vertically at distance *c*, and the intermediate lattice plane places a node in the center of the unit cell (Figure 2.6b).
>
> The orthorhombic face-centered (C) lattice has nodes in the center of the top and bottom faces, and is produced by vertical translation of a centered rectangle plane lattice a distance equal to *c* at right angles to the *a*–*b* plane (Figure 2.7b). Note that if the faces with the centered node were on the front and back or on right and left faces, this also could be called an (A) or (B) face-centered lattice. The differences among A, B, and C face-centered lattices are only in how the crystal axes are labeled, which, in the orthorhombic crystal system, is not done consistently.

DO NOT COPY e48d507df5d1141@placeholder.94092

Printed by: e48d507df5d1141@placeholder.94092.edu. Printing is for personal, private use only. No part of this book may be reproduced or transmitted without publisher's prior permission. Violators will be prosecuted.

done consistently.

The orthorhombic all face-centered (F) lattice has nodes in the center of all faces. It is produced by translating a centered rectangle plane lattice a distance equal to ½ *b* right and ½ *c* up. Every second lattice plane is aligned vertically at a distance *c* (Figure 2.7c).

The two **hexagonal Bravais lattices** (Figure 2.10e) are derived from the hexagonal plane lattice whose lattice dimensions are $a = b$. The unit cell dimension perpendicular to the plane lattice is $c \neq a$. Because *a* and *b* are interchangeable, some authors prefer to designate them a_1 and a_2. See the discussion on Miller indices and crystal axes in the hexagonal crystal system later in this chapter for an alternative crystal axis geometry used in hexagonal minerals.

The primitive lattice (P) is produced by vertical translation of a hexagonal plane lattice a distance equal to *c* at right angles to the plane lattice (Figure 2.8a). The unit cell (shaded) has a rhomb-shaped cross section with internal angles of 60° and 120°.

The rhombohedral (R) lattice is produced by translating a hexagonal plane lattice on a diagonal a distance equal to $^1/^3$ *c* up and $^2/^3$ *a* cos 30° back at right angles to the *b* axis (Figure 2.8b). A primitive rhombohedral unit cell, which looks like a cube stretched or shortened along a diagonal through the center, can be constructed by connecting lattice nodes as shown. It is possible to define crystal axes along the edges of the rhombohedron (Figure 2.8c) in a manner similar to how the axes are defined in the isometric system except that the angles are not 90° ($a = b = c$, $\alpha = \beta = \gamma \neq 90°$). It is far more common, however, to define the unit cell by using the same convention as for the primitive hexagonal lattice with two axes (*a* and *b*) at 120° with *c* at right angles, as shown in Figure 2.8b. This convention is used consistently in this book and in most other references because it allows the same unit cell convention to be used for all hexagonal minerals.

The two **tetragonal Bravais lattices** are derived from the square plane lattice whose lattice dimensions are $a = b$. The unit cell dimension perpendicular to the original plane lattice is $c \neq a = b$ (Figure 2.10d). All three axes are at right angles ($\alpha = \beta = \gamma = 90°$), and the *c* axis may be either longer or shorter than the *a* and *b* axes. Note that the *a* and *b* axes are interchangeable, and some authors prefer to designate them a_1 and a_2.

The primitive (P) lattice is produced by vertically translating a square plane lattice distance *c* (Figure 2.9a).

The body-centered (I) lattice is produced by translating a square plane lattice a distance equal to ½ *a* right, ½ *a* back, and ½ *c* up. Alternate plane lattices are aligned vertically at distance *c* (Figure 2.9b).

The three **isometric Bravais lattices** are derived from the square plane lattice. Unit cell dimensions along all three axes are the same, and the axes are all at right angles (Figure 2.10f): $a = b = c$, $\alpha = \beta = \gamma = 90°$. Note that the three axes are interchangeable. For this reason, some authors prefer to use a_1, a_2, and a_3 for the three axes.

The primitive (P) lattice is produced by translating the square plane lattice distance *a* perpendicular to the plane lattice (Figure 2.9c).

The body-centered (I) lattice is produced by translating the square plane lattice along a diagonal a distance equal to ½ *a* to the right, ½ *a* to the rear, and ½ *a* up. Alternate plane

Printed by: e48d507df5d1141@placeholder.94092.edu. Printing is for personal, private use only. No part of this book may be reproduced or transmitted without publisher's prior permission. Violators will be prosecuted.

lattices are aligned vertically at distance *a* (Figure 2.9d).

The face-centered (F) lattice is produced by translating the square plane lattice (whose unit mesh dimension is *x*) a distance equal to ½ *x* to the right, ½ *x* to the rear, and $x/\sqrt{2}$ vertically (Figure 2.9e). The cubic unit cell thus produced has a lattice node in the center of each face and is at 45° to the original plane lattice. The length of each side of the unit cell is $a = b = c = \sqrt{2}x$.

DO NOT COPY
e48d507df5d1141@placeholder.9409

Printed by: e48d507df5d1141@placeholder.94092.edu. Printing is for personal, private use only. No part of this book may be reproduced or transmitted without publisher's prior permission. Violators will be prosecuted.

Point Symmetry

Point symmetry deals with how a motif, or the simplest component of a pattern, can be repeated about a point. In minerals, the motifs that are repeated may be crystal faces or a particular arrangement of atoms that makes up the structure of a mineral. The possible point symmetry operations are reflection, rotation, and inversion. For the discussion that follows, the point about which symmetry is recognized is the center of the crystal or the origin of the unit cell.

Reflection

A reflection is produced by a mirror plane, indicated by the letter *m*, that passes through a crystal structure so that the pattern on one side is a mirror image of the pattern on the other. Each point that makes up the crystal structure or crystal faces on one side of the mirror plane has a corresponding point on the opposite side of the mirror plane the same perpendicular distance from the mirror plane but in the opposite direction. **Figure 2.11** shows a monoclinic mineral with a mirror plane that contains the *a* and *c* crystal axes and is perpendicular to the *b* axis; this plane is called the *ac* plane.

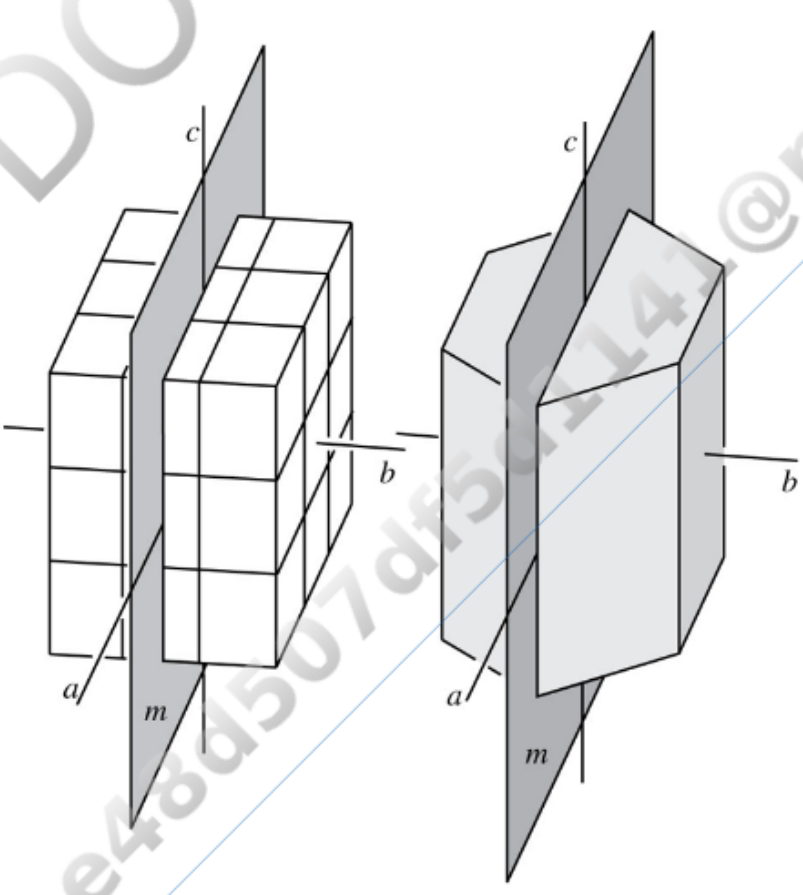

DO NOT COPY
e48d507df5d1141@placeholder.9409

Printed by: e48d507df5d1141@placeholder.94092.edu. Printing is for personal, private use only. No part of this book may be reproduced or transmitted without publisher's prior permission. Violators will be prosecuted.

FIGURE 2.11 Symmetry by a mirror (*m*) plane or reflection. The mirror plane operates on the lattice, structure, and crystal faces of the mineral. View larger image

In a given mineral, only planes in specific orientations can be mirror planes. In the monoclinic crystal system, only one mirror plane is possible, and it is usually the *ac* plane. This is similar to the human body, in which the right side is a mirror image (more or less) of the left but no other plane of symmetry is present. Triclinic minerals have no mirrors, and isometric minerals can have as many as nine different mirror planes.

Rotation

Rotational symmetry involves repeating a motif by a set of uniform rotations about an axis. The notation for a rotation is a capital letter A with a subscript indicating the number of motif repeats in 360° of rotation. The repeated motif is a wedge-shaped segment of crystal including crystal faces, lattice, and atoms. Consider the tetragonal crystal shown in **Figure 2.12**. The entire crystal can be produced by repeating a 90° wedge four times by rotations of 90° about the *c* crystal axis. This is a 4-fold rotation (A_4). The other possible rotational symmetry operations are 6-fold, 3-fold, 2-fold, and 1-fold rotations (A_6, A_3, A_2, A_1) (Figure 2.12), which involve rotations of 60°, 120°, 180°, and 360°, respectively. Note that 1-fold rotational symmetry is essentially no symmetry because it is simply rotation of an object through 360°. Because rotation of 360° brings everything back to its original position, every object has an infinite number of 1-fold symmetry axes.

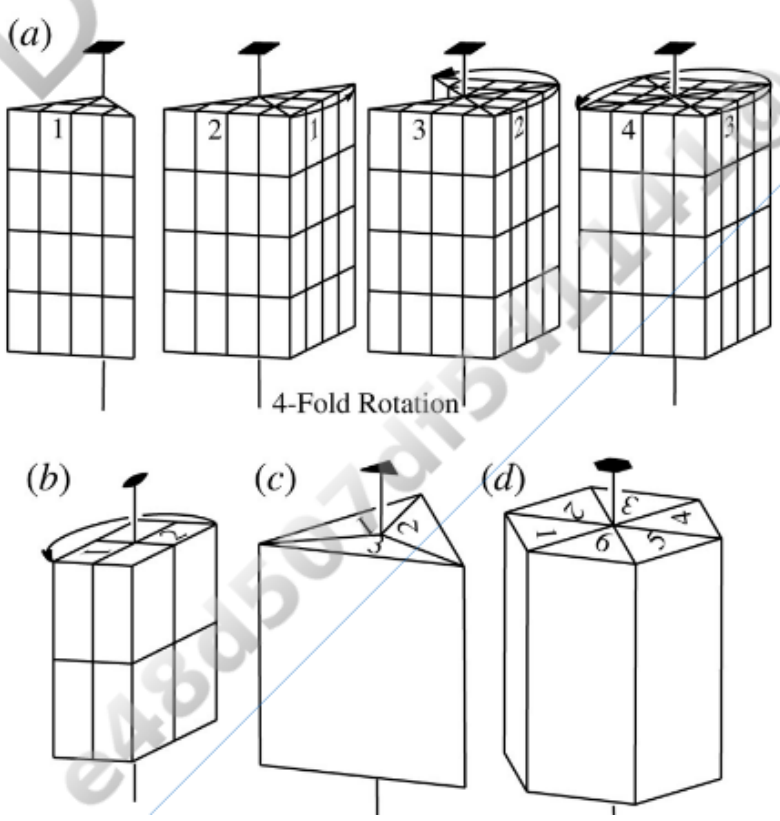

DO NOT COPY

Printed by: e48d507df5d1141@placeholder.94092.edu. Printing is for personal, private use only. No part of this book may be reproduced or transmitted without publisher's prior permission. Violators will be prosecuted.

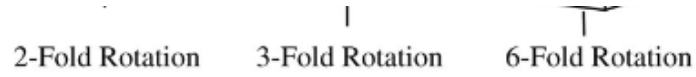

FIGURE 2.12 Rotational symmetry. (*a*) Four-fold rotation. The full crystal can be produced by repeating four wedge-shaped motifs by rotations of 90° about the rotation axis. (*b*) Two-fold rotation. The lattice and crystal faces are repeated every 180°. (*c*) Three-fold rotation. The lattice and crystal faces are repeated every 120°. (*d*) Six-fold rotation. The lattice and crystal faces are repeated every 60°. Note that different symbols label the rotation axes and include a lemon (A_2), a triangle (A_3), a square (A_4), and a hexagon (A_6). View larger image

Inversion

If a crystal has **inversion** or **center** symmetry, any line drawn through the origin will find identical features equidistant from the origin on opposite sides of the crystal. Inversion symmetry is indicated with the letter *i*. Consider the simple crystal with inversion shown in **Figure 2.13a**. A line from point *h* through the center of the crystal finds an equivalent point *h′* on the other side. Similarly, lines from *i*, *j*, and *k* all find equivalent points *i′*, *j′*, and *k′* on opposite sides of the crystal. The crystal shown in **Figure 2.13b** lacks center symmetry because lines through the crystal's center from points such as *l* do not find equivalent points on the opposite side of the crystal.

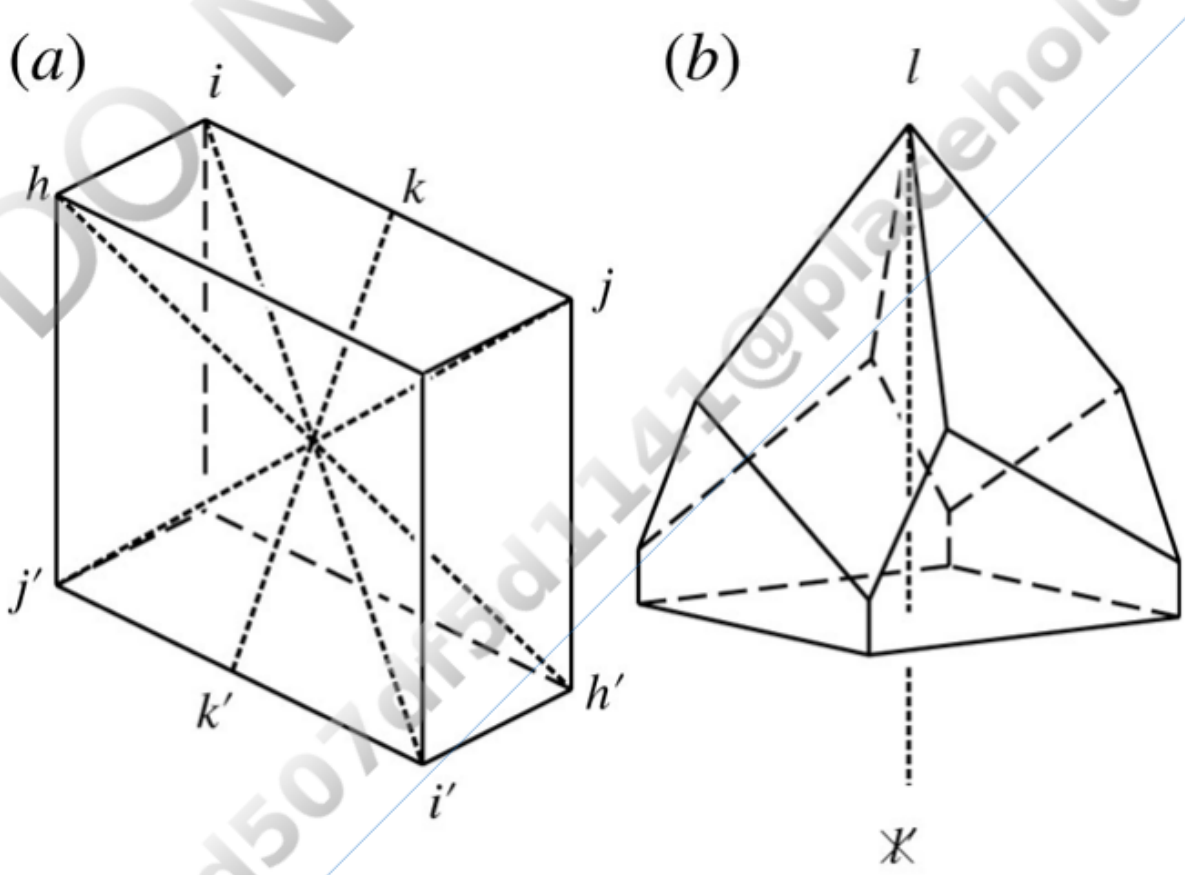

FIGURE 2.13 Inversion. (*a*) Crystal with inversion. Points *h*, *i*, *j*, and *k* all have equivalent points *h′*, *i′*, *j′*, and *k′* on the opposite side of the crystal. (*b*) Crystal without inversion. Points such as the *l* are not duplicated on the opposite side of the crystal (hence *l* is crossed out). View larger image

DO NOT COPY e48d507df5d1141@placeholder.94092

Printed by: e48d507df5d1141@placeholder.94092.edu. Printing is for personal, private use only. No part of this book may be reproduced or transmitted without publisher's prior permission. Violators will be prosecuted.

Compound Symmetry Operations

Rotation axes may be combined with inversion to produce symmetry elements called 1-, 2-, 3-, 4-, and 6-fold **rotoinversion axes**. Rotoinversion axes are indicated by a capital letter *A* with a bar (¯) over it and a subscript (1, 2, 3, 4, or 6) indicating the number of repeats in 360° of rotation, for example, $\overline{A}_4$ for a 4-fold rotoinversion.

The simplest is a 1-fold **rotoinversion** $\overline{A}_1$ ("A bar one"). Consider point *a* on the crystal shown in **Figure 2.14a**. It is repeated by rotation of 360° followed by inversion through the center to produce point *a*′. All other points on the top of the crystal are similarly reproduced on the bottom by the same process. This combination is not very useful because it is the same as a simple inversion $\left(\overline{A}_1 = i\right)$, but it demonstrates the components of rotoinversion.

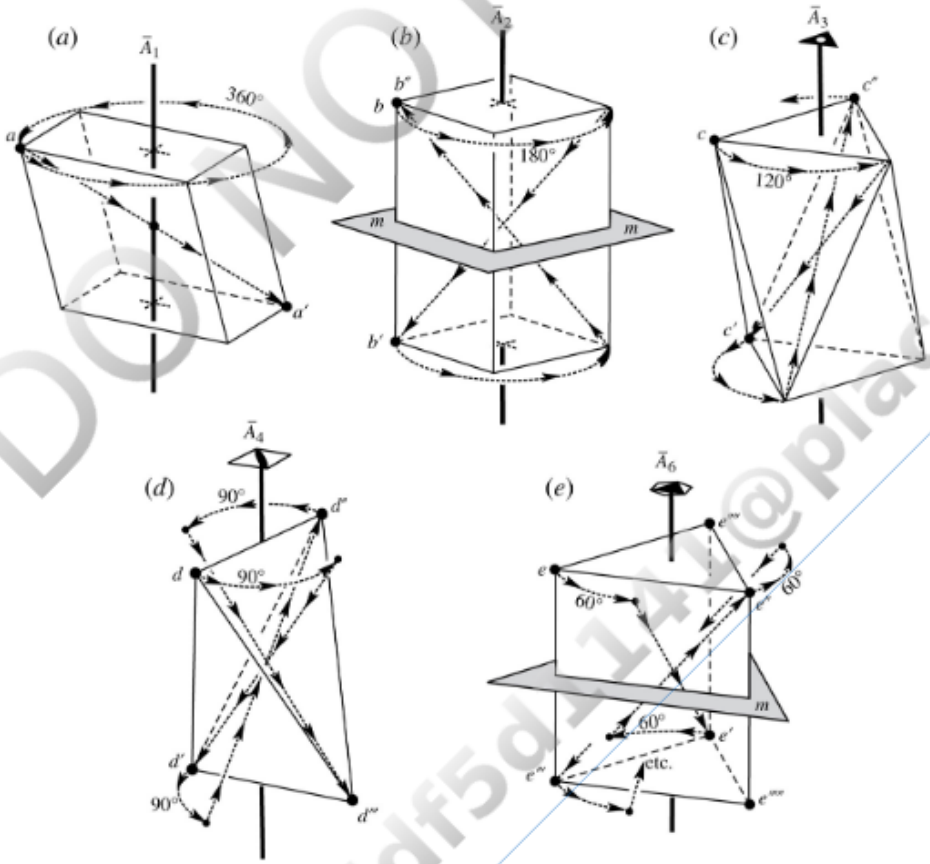

FIGURE 2.14 Rotoinversion. See text for discussion. (*a*) One-fold rotoinversion equals a simple inversion. (*b*) Two-fold rotoinversion is the same as a mirror at right angles to the rotation axis. (*c*) Three-fold rotoinversion is equivalent to a simple 3-fold rotation and inversion. (*d*) Four-fold rotoinversion is not replicated by other simpler symmetry operations. (*e*) Six-fold rotoinversion is equivalent to 3-fold rotation with a mirror at right angles. View larger image

A 2-fold rotoinversion $\left(\overline{A}_2\right)$ is produced by a rotation of 180° followed by inversion

DO NOT COPY e48d507df5d1141@placeholder.9409

Printed by: e48d507df5d1141@placeholder.94092.edu. Printing is for personal, private use only. No part of this book may be reproduced or transmitted without publisher's prior permission. Violators will be prosecuted.

through the center (**Figure 2.14b**). Consider point *b*. Rotation of 180° followed by inversion through the center produces point *b′* directly below *b*. The second 180° rotation followed by inversion produces point *b″* coincident with the original position of *b*. This result turns out to be the same as a mirror plane at right angles to the rotoinversion axis $\left(\overline{A}_2 = m\right)$.

Figure 2.14c shows a 3-fold rotoinversion $\left(\overline{A}_3\right)$. Point *c* is rotated 120° and inverted through the center to *c′*. A second rotation/inversion produces *c″* and so forth. The net result is to produce a crystal with a conventional 3-fold rotation axis that also possesses center symmetry $\left(\overline{A}_3 = A_3 + i\right)$.

The symmetry produced by 4-fold rotoinversion $\left(\overline{A}_4\right)$ cannot be duplicated with combinations of other simpler symmetry operations. It involves 90° of rotation followed by inversion through the center (**Figure 2.14d**). Point *d* gets rotated 90° and inverted to *d′*, an additional 90° rotation and inversion leads to *d″*, and so forth. The result is to produce four faces (or sets of faces) at 90° to each other that alternate between being upright and upside down.

Figure 2.14e shows that a 6-fold rotoinversion $\left(\overline{A}_6\right)$ produces the same result as a 3-fold rotation axis at right angles to a mirror $\left(\overline{A}_6 = A_3 + m\right)$. Consider point *e*. Rotation of 60° and inversion through the center produce *e′*. A second rotation and inversion produce *e″* and so forth. When completed, each point on the top of the crystal has a mirror image on the bottom.

Symmetry Notation

The notation used for symmetry is shown in **Table 2.1**. In the foregoing discussion of symmetry, **symmetry symbols** have been used to refer to symmetry operations. For example, the orthorhombic mineral shown in **Figure 2.15** contains the following symmetry.

$$i,\ 3A_2,\ 3m$$

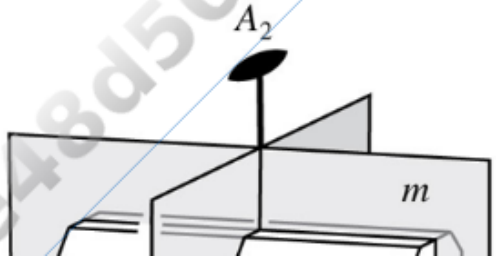

DO NOT COPY e48d507df5d1141@placeholder.9409

Printed by: e48d507df5d1141@placeholder.94092.edu. Printing is for personal, private use only. No part of this book may be reproduced or transmitted without publisher's prior permission. Violators will be prosecuted.

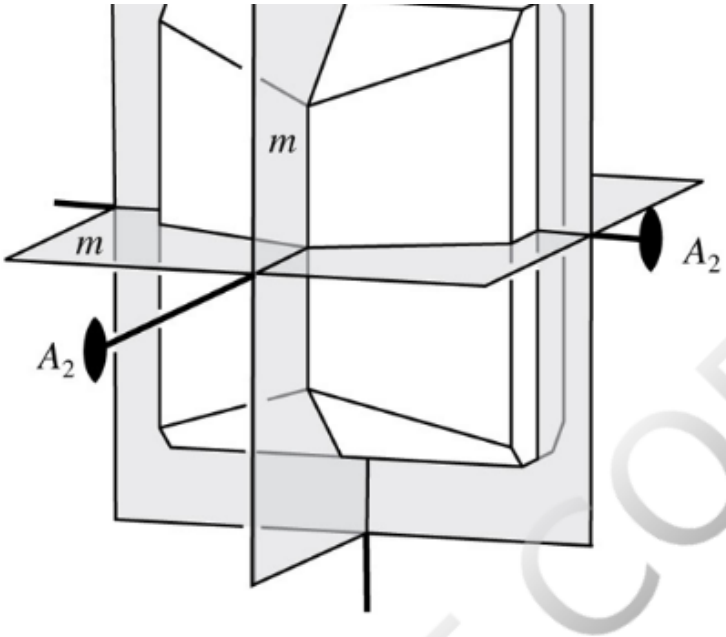

FIGURE 2.15 This orthorhombic crystal has center symmetry (i), three 2-fold axes ($3A_2$), and three mirrors ($3m$). View larger image

TABLE 2.1 Nomenclature for Symmetry Elements

Symmetry Operation	Symmetry Symbol	Hermann-Mauguin Symbol	Graphic Symbol
Mirror	m	m	n/a
Rotation Axis			
1-fold	A_1	1	n/a
2-fold	A_2	2	
3-fold	A_3	3	
4-fold	A_4	4	
6-fold	A_6	6	
Rotoinversion Axis			
1-fold	$\overline{A}_1$	$\overline{1}$	n/a
2-fold	$\overline{A}_2$	$\overline{2}$	n/a
3-fold	$\overline{A}_3$	$\overline{3}$	
4-fold	$\overline{A}_4$	$\overline{4}$	
6-fold	$\overline{A}_6$	$\overline{6}$	

DO NOT COPY e48d507df5d1141@placeholder.9409

Printed by: e48d507df5d1141@placeholder.94092.edu. Printing is for personal, private use only. No part of this book may be reproduced or transmitted without publisher's prior permission. Violators will be prosecuted.

6-fold	A_6	6	

This means that the crystal possesses inversion or center symmetry (i), three 2-fold rotation axes ($3A_2$), and three mirror planes ($3m$). The symmetry elements may be listed in any order, although for the sake of consistency it is convenient to list center first (if present), followed by rotation axes and then mirrors.

Hermann-Mauguin symbols, named for Carl Hermann (1898–1961) and Charles-Victor Mauguin (1878–1958), recognize that the symmetry elements in a mineral must be related to each other and that some symmetry operations are implied by the presence of others, and therefore, do not need to be explicitly listed. The Hermann–Mauguin notation for the symmetry of the orthorhombic mineral shown in Figure 2.15 is $2/m\ 2/m\ 2/m$. This means that there are three 2-fold axes, each perpendicular to a mirror. The presence of the three mirrors at right angles requires that the mineral have center symmetry, so it is not necessary to explicitly state that center symmetry is present. The order in which Hermann–Mauguin symbols are listed is specific to each crystal system and is described in a later section.

In the sections that follow, symmetry symbols are used to describe the specific symmetry operations and axes that a mineral may have. Hermann–Mauguin symbols are used to specifically identify each of the 32 different possible combinations of symmetry known as point groups, which are described in the next section and are used in the mineral descriptions in Chapters 12 through 20.

DO NOT COPY
e48d507df5d1141@placeholder.9409

Printed by: e48d507df5d1141@placeholder.94092.edu. Printing is for personal, private use only. No part of this book may be reproduced or transmitted without publisher's prior permission. Violators will be prosecuted.

The 32 Point Groups

As the preceding discussion implies, the symmetry elements of inversion, rotations, and mirrors may be combined in a variety of ways. However, the combinations are limited because the symmetry elements must be compatible with each other.

In two dimensions the possible symmetry elements are mirrors (m) and rotations (A_1, A_2, A_3, A_4, and A_6). Though it is alluring to consider inversion as a permissible two-dimensional operation, it would be no different than any even-fold rotation axis, and in detail, two-dimensional inversion is not exactly analogous to inversion in three dimensions. Therefore, inversion is not considered to exist in two dimensions. The symmetry elements may each be taken individually or may be combined to produce a total of 10 different two-dimension point groups (**Figure 2.16**).

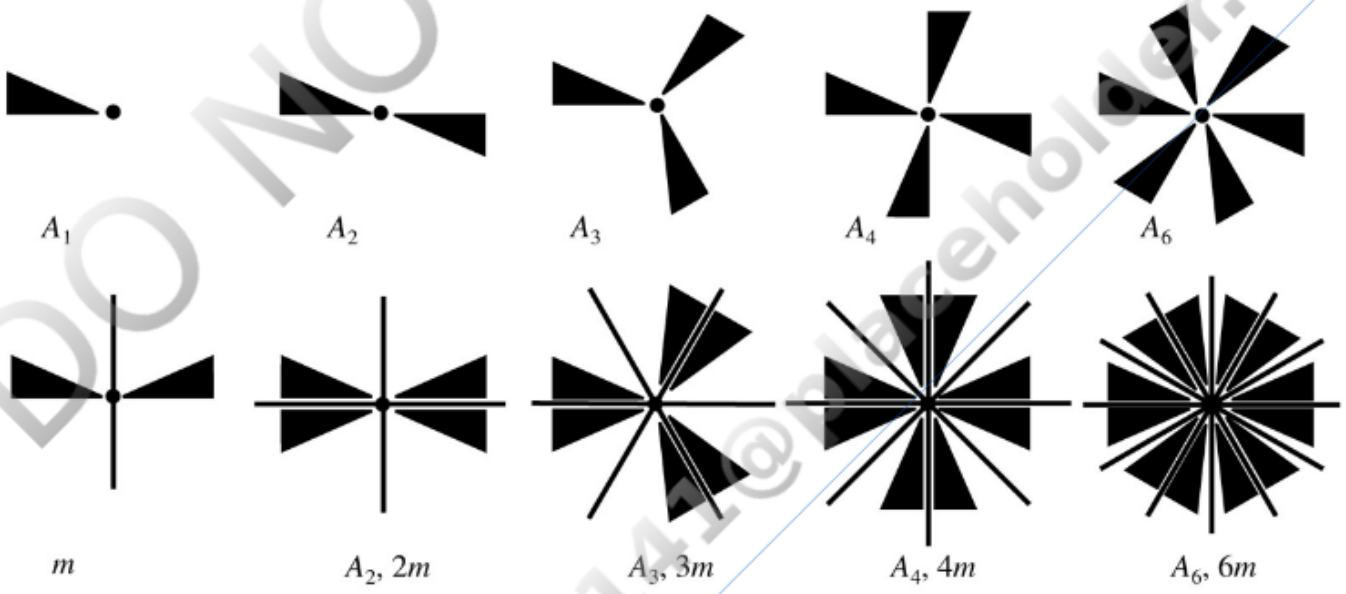

FIGURE 2.16 The 10 two-dimension point groups. View larger image

With the addition of the third dimension, inversion becomes a unique symmetry operation and the number of different combinations of symmetry increases to 32. These symmetry combinations are known as the **32 point groups**. These point groups may be grouped into the six different crystal systems based on common symmetry elements. Recall that the six crystal systems were defined earlier based on unit cell geometry generated from the Bravais lattices. **Table 2.2** shows the symmetry elements possessed by each of the different point group and the crystal system to which each belongs. By convention, the point groups are identified with Hermann–Mauguin representations of the symmetry.

TABLE 2.2 The 32 Point Groups[a]

Printed by: e48d507df5d1141@placeholder.94092.edu. Printing is for personal, private use only. No part of this book may be reproduced or transmitted without publisher's prior permission. Violators will be prosecuted.

TABLE 2.2 The 32 Point Groups

Crystal System		Point Group	Symmetry Content	Common Symmetry Elements	Crystal Axes
Triclinic		1	None (= A_1)	One-fold rotation with or without inversion.	No symmetry restrictions; prominent zone = *c*.
		$\bar{1}$	$i = A_1$		
Monoclinic		2	$1A_2$	Two-fold rotation axis and/or a single mirror.	Two-fold axis or line perpendicular to mirror = *b*, prominent zone = *c*. $\beta > 90°$.
		m	M		
		2/*m*	*i*, $1A_2$, *m*		
Orthorhombic		222	$3A_2$	Three 2-fold rotation axes or two mirrors and a 2-fold rotation axis.	The 2-fold axes or lines perpendicular to mirrors coincide with the three mutually perpendicular crystal axes; the first H–M symbol refers to the *a* crystal axis, the second to the *b* crystal axis, and the third to the *c* crystal axis.
		mm2	$1A_2$, 2*m*		
		2/*m* 2/*m* 2/*m*	*i*, $3A_2$, 3*m*		
Tetragonal		4	$1A_4$	Single 4-fold rotation or rotoinversion axis.	The 4-fold axis = *c*; the *a* and *b* crystal axes are perpendicular to *c* and coincide with A_2 axes or are perpendicular to mirrors, if present: the first H–M symbol refers to the *c* axis; if present, the second refers to the *a* and *b* crystal axes, and the third to symmetry axes that bisect the angles between *a* and *b* [110].
		$\bar{4}$	$1A_4$		
		4/*m*	*i*, $1A_4$, *m*		
		422	$1A_4$, $4A_2$		
		4mm	$1A_4$, 4*m*		
		$\bar{4}$ 2m	$1A_4$, $2A_2$, 2*m*		
		4/*m* 2/*m* 2/*m*	*i*, $1A_4$, $4A_2$, 5*m*		
Hexagonal	Trigonal Division	3	$1A_3$	One 3-fold rotation axis.	The 3-fold or 6-fold axis = *c*, the *a* and *b* crystal axes are parallel to A_2 axes or perpendicular to mirrors, if present: the first H–M symbol refers to the *c* axis; if present, the second refers to the *a* and *b* axes, and the third to
		$\bar{3}$	$1A_3 (= i + 1A_3)$		
		32	$1A_3$, $3A_2$		
		3*m*	$1A_3$, 3*m*		
		3 2 /*m*	$1A_3 (= i + 1A_3)$, $3A_2$, 3*m*		

DO NOT COPY e48d507df5d1141@placeholder.9409-

Printed by: e48d507df5d1141@placeholder.94092.edu. Printing is for personal, private use only. No part of this book may be reproduced or transmitted without publisher's prior permission. Violators will be prosecuted.

					axes, and the third to symmetry axes that bisect the angles between *a* and *b* [210].
	Hexagonal Division	6	$1A_6$	One 6-fold rotation axis.	
		$\overline{6}$	$1\,\overline{A}_6(=1A_3+m)$		
		$6/m$	i, $1A_6$, m		
		622	$1A_6$, $6A_2$		
		6mm	$1A_6$, $6m$		
		$\overline{6}\,m2$	$1\,\overline{A}_6(=1A_3+m)$, $3A_2$, $3m$		
		$6/m\ 2/m\ 2/m$	i, $1A_6$, $6A_2$, $7m$		
Isometric		23	$3A_2$, $4A_3$	Four 3-fold rotation axes; these axes are oriented to go diagonally through the center of the cubic unit cell from corner to corner.	The three 2-fold or 4-fold axes coincide with the interchangeable *a*, *b*, and *c* crystal axes; symmetry requires that these axes be at 90° to each other; the first H–M symbol refers to the symmetry on the crystal axes, the second to the long diagonals through the unit cell [111], the third to edge-to-edge diagonals through the unit cell [110].
		$2/m\,\overline{3}$	$3A_2$, $3m$, $4\,\overline{A}_3(=i+4A_3)$		
		432	$3A_4$, $4A_3$, $6A_2$		
		$\overline{4}3m$	$3\,\overline{A}_4$, $4A_3$, $6m$		
		$4/m\ \overline{3}\ 2/m$	$3A_4$, $4\,\overline{A}_3(=i+4A_3)$, $6A_2$, $9m$		

[a] H–M stands for Hermann–Mauguin; numbers in square brackets ([]) refer to Miller indices.

Assigning crystal axes relative to symmetry elements is generally fairly straightforward; that is, crystal axes may be parallel to rotation axes or in an orientation parallel or perpendicular to a mirror. The conventions adopted for orienting crystal axes relative to the symmetry axes and planes are summarized in Table 2.2. More thorough descriptions of the conventions used to orient crystal axes are included in the descriptions of the crystal systems later in this chapter.

The relation between the 32 point groups and the 14 Bravais lattices is not immediately obvious. Clearly, minerals displaying isometric point groups must utilize an isometric Bravais lattice, tetragonal point groups must utilize a tetragonal Bravais lattice, and so forth. While it is beyond the scope of this discussion to demonstrate it, the point groups from each crystal system can use any Bravais lattice from that crystal system. The single exception occurs in the hexagonal system, where only members of the trigonal division may use the rhombohedral (R) Bravais lattice. While point group symmetry may be identified from well-developed crystals, Bravais lattices cannot be identified without X-ray

DO NOT COPY

Printed by: e48d507df5d1141@placeholder.94092.edu. Printing is for personal, private use only. No part of this book may be reproduced or transmitted without publisher's prior permission. Violators will be prosecuted.

identified from well-developed crystals, Bravais lattices cannot be identified without X-ray diffraction studies.

Steno's Law

Knowledge of an unknown mineral's point group and/or crystal system often can be of great help when attempting to identify it. The point group may be determined by carefully examining well-formed crystals to identify symmetry elements. Allowance often must be made for the fact that crystals are rarely perfect and that equivalent faces may have different sizes.

Fortunately, the angles between crystal faces are remarkably consistent. This observation was originally made by Nicolas Steno (Niels Stensen) in 1669. He demonstrated that the angles between the same two faces on quartz crystals are the same for different specimens of the mineral, regardless of sample size, the size of the crystal faces, or where the crystals may have been collected. This observation has been formalized into **Steno's Law** or the **Law of Constancy of Interfacial Angles** because it applies to all minerals.

> The angles between equivalent faces on crystals of the same mineral are the same.

Measurement of Crystal Angles

A simple contact goniometer (**Figure 2.17**) allows crystal angles to be measured with reasonable accuracy. This instrument is basically a protractor with a movable arm. The bottom edge of the goniometer is placed on one crystal face and the movable arm is aligned with an adjacent face. The plane of the goniometer must be perpendicular to the crystal edge formed by the two faces. The goniometer scale has two sets of numbers, one for the internal angle between the faces and one for the complement to that angle. The internal angle is the angle between lines oriented at right angles to the two faces, and it is the angle normally reported. Note that the sum of internal angles going all the way around a crystal must equal 360°.

(*a*)

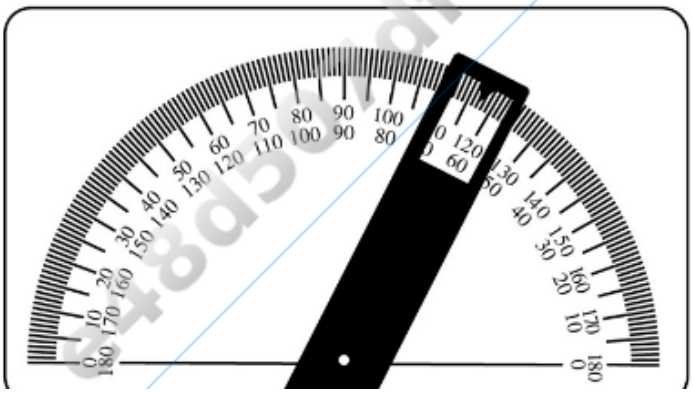

DO NOT COPY

Printed by: e48d507df5d1141@placeholder.94092.edu. Printing is for personal, private use only. No part of this book may be reproduced or transmitted without publisher's prior permission. Violators will be prosecuted.

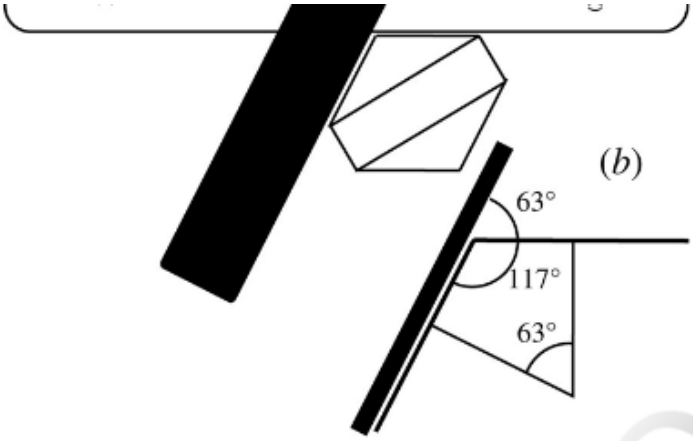

FIGURE 2.17 Contact goniometer. (*a*) The base of the goniometer is placed on one crystal face, and the cursor (movable arm) is aligned with the adjacent face. The edge between the faces must be perpendicular to the plane of the goniometer. The internal angle between the faces is read from the scale. (*b*) The internal angle (63°) is the angle between lines at right angles to the crystal faces.
View larger image

Determining Crystal System and Point Group

Assuming that well-formed crystals of a mineral are available, below is the procedure to determine the point group.

- Determine whether the mineral possesses center symmetry. To do this, select several points, such as corners, on one side of the crystal (Figure 2.13a). The crystal has center symmetry if an imaginary line from each point finds an equivalent point on the opposite side of the crystal when projected through the center.
- Identify mirror planes. Mirrors divide crystals into two mirror-image halves (**Figure 2.18a**). Angles on opposite sides of the mirror must be identical.
- Identify rotation axes. A rotation axis can be considered an axle about which the mineral rotates to repeatedly bring equivalent collections of faces into view (**Figure 2.18b**). Two-fold axes require 180° of rotation to bring duplicate sets of faces into view. Other rotations are 3-fold axes = 120°, 4-fold axes = 90°, and 6-fold axes = 60°. Refer to Figure 2.14d to see a 4-fold rotoinversion.
- Compile the combination of symmetry. The crystal in Figure 2.18 has *i*, $1A_2$, *m* and is a member of the 2/*m* point group in the monoclinic system (Table 2.2).

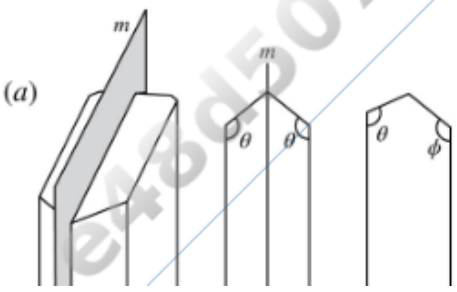

DO NOT COPY
e48d507df5d1141@placeholder.9409

Printed by: e48d507df5d1141@placeholder.94092.edu. Printing is for personal, private use only. No part of this book may be reproduced or transmitted without publisher's prior permission. Violators will be prosecuted.

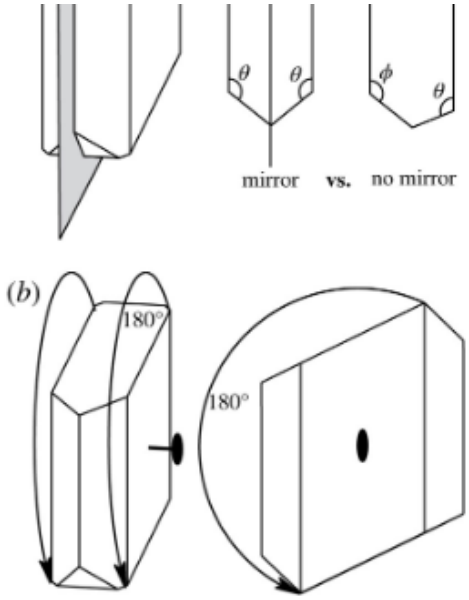

FIGURE 2.18 Determining crystal symmetry. (*a*) Mirrors split the crystal into two mirror images. Angles on opposite sides of the mirror are the same. (*b*) Rotations repeat the same collection of faces every 60°, 90°, 120°, or 180° of rotation (A_6, A_4, A_3, A_2). A 2-fold rotation is shown. View larger image

Minerals are not evenly distributed among the crystal systems and point groups (**Table 2.3**). Nearly half of all minerals are in just two point groups—monoclinic $2/m$ and orthorhombic $2/m\ 2/m\ 2/m$.

TABLE 2.3 Percentage of Minerals in Each Crystal System and Point Group

Crystal System	Point Group	Percent	Crystal System	Point Group	Percent
Triclinic 9.0%	1	1.3%	Hexagonal (trigonal division) 11.7%	3	1.0%
	$\bar{1}$	7.7%		$\bar{3}$	1.9%
Monoclinic 35.1%	2	2.0%		32	0.9%
	m	2.1%		$3m$	2.9%
	$2/m$	31.0%		$\bar{3}2/m$	5.0%
Orthorhombic 19.3%	222	2.1%	Hexagonal (hexagonal division) 7.6%	6	0.7%
	mm2	3.2%		$\bar{6}$	0.1%
	$2/m\ 2/m\ 2/m$	14.0%		$6/m$	1.5%
Tetragonal 7.7%	4	0.1%		622	0.6%
	$\bar{4}$	0.2%		6mm	0.8%

Printed by: e48d507df5d1141@placeholder.94092.edu. Printing is for personal, private use only. No part of this book may be reproduced or transmitted without publisher's prior permission. Violators will be prosecuted.

	$4/m$	1.5%		$\bar{6}m2$	0.6%
	422	0.6%		$6/m\ 2/m\ 2/m$	3.2%
	4mm	0.4%	Isometric 9.6%	23	0.6%
	$\bar{4}2m$	0.9%		$2/m\ \bar{3}$	1.4%
	$4/m\ 2/m$ $2/m$	4.1%		432	0.1%
				$\bar{4}3m$	1.6%
				$4/m\ \bar{3}\ 2/m$	5.9%

Source: Based on data compiled by WebMineral.com for minerals whose point group is known.

An alternative to the nomenclature for crystal systems shown in Table 2.2 is shown in **Table 2.4**. Using this nomenclature, minerals that have single 6-fold and 3-fold axes are assigned to the hexagonal and trigonal crystal systems respectively, producing a total of seven crystal systems—triclinic, monoclinic, orthorhombic, tetragonal, trigonal, hexagonal, and isometric. A new category, called **crystal family**, is added and the hexagonal and trigonal crystal systems are grouped into the hexagonal crystal family. The other crystal families are identical with their crystal systems.

TABLE 2.4 Alternative Crystal System Nomenclature

Crystal Family	Crystal System	Symmetry Requirements
Triclinic	Triclinic	None
Monoclinic	Monoclinic	One 2-fold rotation axis or one mirror
Orthorhombic	Orthorhombic	Three 2-fold rotation axes or two mirrors and one 2-fold rotation
Tetragonal	Tetragonal	One 4-fold rotation axis or rotary inversion
Hexagonal	Trigonal	One 3-fold rotation axis
	Hexagonal	One 6-fold rotation axis
Isometric	Isometric	Four 3-fold rotation axes

DO NOT COPY e48d507df5d1141@placeholder.9409

Printed by: e48d507df5d1141@placeholder.94092.edu. Printing is for personal, private use only. No part of this book may be reproduced or transmitted without publisher's prior permission. Violators will be prosecuted.

Space Groups

The symmetry elements of mirror, rotations, and inversion that in combination produce the 32 point groups can completely describe the symmetry observed in the distribution of crystal faces and related crystallographic features arrayed around the center of a crystal. The symmetry of simple translation in three dimensions yields the 14 Bravais lattices. The 230 **space groups** represent all the combinations of the point symmetry with translational symmetry.

Groupings of atoms that possess the symmetry of one of the 32 point groups are placed at the lattice nodes of a compatible Bravais lattice. These groupings are then duplicated over and over at each lattice node in the Bravais lattice to create the structure of the mineral. The point group symmetry must be consistent with the symmetry of the lattice. Isometric point groups can be used only with isometric lattices, tetragonal point groups with tetragonal lattices, and so forth. These combinations of point symmetry and simple translation yield 73 of the space groups.

This is not yet the full story because two additional symmetry operations called **glides** and **screws** are possible in three dimensions. Each is a compound symmetry operation consisting of a translation and either reflection or rotation.

A glide is produced by a combination of translation a specific distance and direction followed by reflection across a mirror plane called the **glide plane** (Figure 2.19a). The pattern made by footprints is the same as that produced by a glide. Footprints follow each other at a regular distance, but they alternate between the right and left feet, which are mirror images of each other.

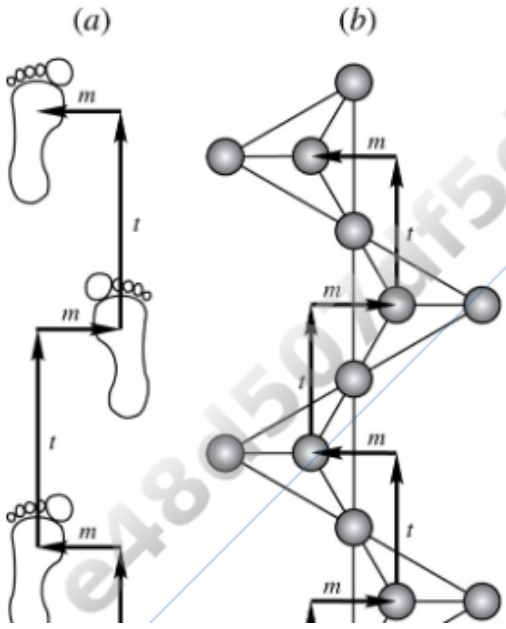

DO NOT COPY
e48d507df5d1141@placeholder.94092

Printed by: e48d507df5d1141@placeholder.94092.edu. Printing is for personal, private use only. No part of this book may be reproduced or transmitted without publisher's prior permission. Violators will be prosecuted.

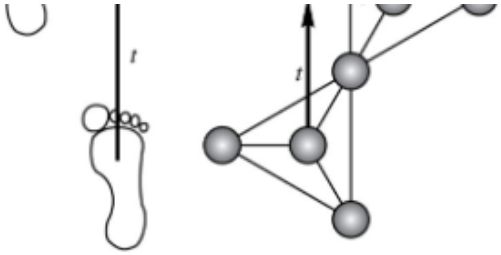

FIGURE 2.19 Glide symmetry. (*a*) Footprints repeated by a translation *t* and reflection *m*. (*b*) Chain of silicon tetrahedra (single silicon, hidden, surrounded by four oxygen ions) produced by translation *t* followed by reflection *m*. View larger image

A typical way in which glides operate in minerals is seen in the chains of silicon tetrahedra found in pyroxenes (**Figure 2.19b**). A silicon tetrahedron consists of a silicon ion surrounded by four oxygen ions in a tetrahedral arrangement. Silicon tetrahedra are strung together in long chains by sharing oxygen ions between adjacent tetrahedra (see Chapter 11). Successive tetrahedra are related to each other by translation *t* followed by reflection *m*. Glide planes, if present in a mineral, must be parallel to mirrors represented by the point group symmetry.

A screw is produced by a combination of translation a specific distance and direction followed by a rotation (**Figure 2.20**). The axis about which rotation occurs is the **screw axis**. The possible rotations are 2-fold (180°), 3-fold (120°), 4-fold (90°), and 6-fold (60°). A 4-fold screw axis, for example, repeats a 90° wedge of the crystal structure every 90° in a spiraling stepwise fashion, somewhat like the treads on a spiral staircase. The other symmetry operations present in the mineral repeat the wedges of crystal to fill in the full structure. Screw axes, if present, must be parallel to and consistent with rotation axes present in the point group symmetry.

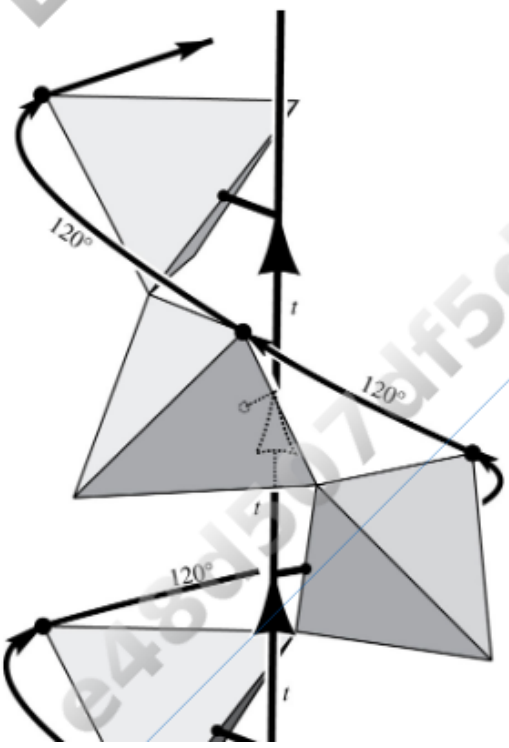

DO NOT COPY e48d507df5d1141@placeholder.9409

Printed by: e48d507df5d1141@placeholder.94092.edu. Printing is for personal, private use only. No part of this book may be reproduced or transmitted without publisher's prior permission. Violators will be prosecuted.

FIGURE 2.20 Screw axis. A 3-fold screw axis is shown. In quartz, a silicon tetrahedron is translated distance *t* and rotated 120° in spiral-staircase fashion to form a helix of tetrahedra extending along the *c* axis. Screw axes may also be 2-fold, 4-fold, or 6-fold. View larger image

The addition of screw axes and glide planes to the mix of symmetry yields an additional 157 space groups for a total of 230 possible ways of repeating a motif in three dimensions. A complete tabulation of all 230 space groups and discussion of the nomenclature used to enumerate them can be found in Bloss (1971) or O'Keeffe and Hyde (1996). Henry and Lonsdale (1952) provide an authoritative compilation and description of space groups. All minerals belong to one or another of the space groups. Although a thorough understanding of space groups is essential for anyone attempting to decipher the structural complexity of a mineral, it is beyond the scope of this text. Interested readers are encouraged to study the references cited above for additional enlightenment.

DO NOT COPY
e48d507df5d1141@placeholder.9409

Printed by: e48d507df5d1141@placeholder.94092.edu. Printing is for personal, private use only. No part of this book may be reproduced or transmitted without publisher's prior permission. Violators will be prosecuted.

Crystal Faces

Crystal faces always grow in rational orientations; that is, the orientation of a crystal face can be defined by coordinates given in whole numbers of unit cells with respect to the crystal axes. The most common faces are often parallel to the surfaces of the unit cell, that is, parallel to the principal planes through the crystal lattice. The result is that minerals with cubic unit cells often form cubic crystals, minerals with hexagonal unit cells often have hexagonal cross sections, and so forth. Crystal faces also often follow simple diagonals through the lattice.

Laws of Haüy and Bravais

The tendency of crystal faces to follow simple, rational orientations through the crystal lattice has resulted in recognition of two related laws of crystallography. The first is called the **Law of Haüy**:

> Crystal faces intercept crystal axes with unit cell coordinates of whole numbers.

The second is called the **Law of Bravais**:

> Common crystal faces are parallel to lattice planes that have high lattice-node density.

Figure 2.22 shows a primitive monoclinic lattice with several possible crystal faces. Planes *A*, *B*, and *C* (Figure 2.22a) are principal planes in the lattice and have high lattice-node density (many lattice nodes per unit of area). Based on the laws of Bravais and Haüy, crystal faces should be parallel to all three lattice planes. Plane *T* (Figure 2.22b) cuts through the lattice on a simple diagonal (*a*: *c* = 1 : 1). It makes rational intercepts on the crystal axes and has a fairly high lattice-node density, so crystal faces parallel to *T* should be fairly common. In contrast, plane *Q* (Figure 2.22c) cuts at an angle through the lattice so that it goes up one cell along *c* for every two unit cells along *a* (*a*: *c* = 2 : 1). Although it has rational intercepts on the crystal axes, the lattice-node density is low. Crystal faces parallel to *Q* probably will be small or may not exist. A simple crystal with these faces is shown in Figure 2.22d.

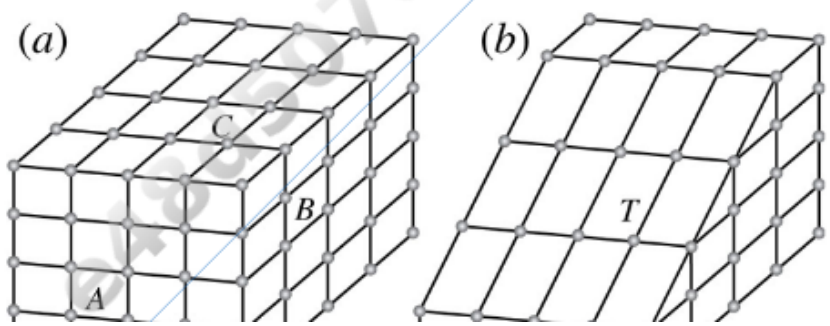

Printed by: e48d507df5d1141@placeholder.94092.edu. Printing is for personal, private use only. No part of this book may be reproduced or transmitted without publisher's prior permission. Violators will be prosecuted.

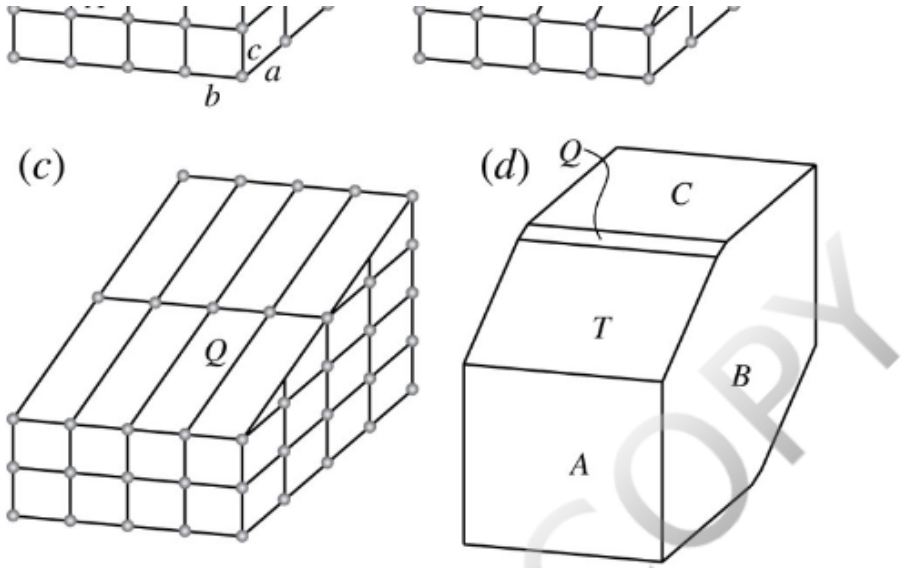

FIGURE 2.22 Primitive monoclinic lattice. Prominent crystal faces are parallel to rational planes in the lattice that have high density of lattice nodes. (*a*) Planes *A*, *B*, and *C* are parallel to the faces of the unit cell, have high lattice-node density, and are likely crystal faces. (*b*) Plane *T* has fairly high lattice-node density and is a likely crystal face. (*c*) Plane *Q* has low lattice-node density and is not a prominent crystal face. (*d*) A simple crystal with these faces. View larger image

Miller Indices

Because crystal faces have rational orientations relative to the crystal lattice, it is possible to develop an elegant shorthand system to describe the orientation of crystal faces and crystallographic planes. A **Miller index**, named for William H. Miller (1801–1880), consists of three numbers that indicate the relationship of a crystal face to the unit cell. A Miller index has the general form (*hkl*) where *h*, *k*, and *l* are integers related to the *a*, *b*, and *c* crystal axes, respectively. The numerical value of *h*, *k*, and *l* are inversely proportional to the intercepts of the crystal face or crystallographic plane with the edges of the unit cell. Miller indices are the standard way to label, for example, crystal faces and cleavage planes; therefore, a sound understanding of them is required for any in-depth treatment of minerals.

Consider a monoclinic mineral that forms a crystal with face *t* that, if extended, intersects all three crystal axes (**Figure 2.23a**). This face cuts through the lattice as shown in **Figure 2.23b** so that the numbers of unit cells out from the crystal center on *a* and *b* are both twice the number of unit cells on *c* ($a = 12$, $b = 12$, $c = 6$). For real crystals, whose unit cell dimensions are a few angstroms, it is impractical to actually determine these intercepts. Therefore, it is easiest when describing Miller indices to reference the crystal face or crystallographic plane as a parallel plane within a single unit cell, as shown in **Figure 2.23c**. Mathematically, this is done by dividing all the intercept values by the largest of the three values. The cell intercepts w_a, w_b, and w_c for face *t* within the unit cell are therefore

$w_a = 1$ $w_b = 1$ and $w_c = 1/$

DO NOT COPY

Printed by: e48d507df5d1141@placeholder.94092.edu. Printing is for personal, private use only. No part of this book may be reproduced or transmitted without publisher's prior permission. Violators will be prosecuted.

$$w_a = 1, \quad w_b = 1, \quad \text{and} \quad w_c = ½.$$

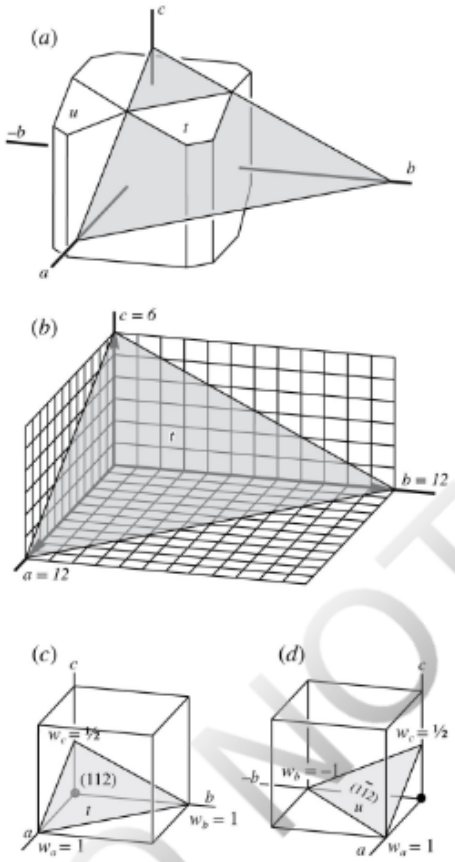

FIGURE 2.23 Miller index. (*a*) Face *t*, when extended, intersects the positive ends of all three crystal axes. (*b*) Face *t* cuts through the lattice so that it intersects the *a* and *b* crystal axes at the same number of unit cells from the origin (12 in this case) and intersects the *c* crystal axis at half that number (six). (*c*) When referenced to a single unit cell, face *t* intersects the crystal axes so that $w_a = 1$, $w_b = 1$, and $w_c = ½$. Fraction inversion results in a (112) Miller index label for this plane. (*d*) Face *u*, which intersects the negative end of *b*, intersects the crystal axes of a single unit cell at $w_a = 1$, $w_b = -1$, and $w_c = ½$. Fraction inversion results in a $(1\bar{1}2)$ Miller index label for this plane. See text for discussion. View larger image

This means that the face cuts the cell at one unit cell dimension along *a*, one unit cell dimension along *b*, and one-half a unit cell dimension along *c*. The Miller index for face *t* is simply the inverse of these values or

$$(hkl) = \frac{1}{w_a}\frac{1}{w_b}\frac{1}{w_c} = \left(\frac{1}{1}\frac{1}{1}\frac{1}{\frac{1}{2}}\right) = (112). \qquad \textbf{(2.1)}$$

The Miller index is read as "one one two." Note that calculation of Miller indices always results in at least one digit of either 1 or $\bar{1}$, because every plane considered will be within the unit cell and intersects at least one axis at a value of one unit cell.

Some faces intersect the negative end of one or more crystal axes. Consider face *u* on the

DO NOT COPY e48d507df5d1141@placeholder.9409

Printed by: e48d507df5d1141@placeholder.94092.edu. Printing is for personal, private use only. No part of this book may be reproduced or transmitted without publisher's prior permission. Violators will be prosecuted.

crystal shown in Figure 2.23. It intersects the positive ends of the a and c axes and the negative end of the b axis with cell intercepts of $w_a = 1$, $w_b = -1$, and $w_c = ½$ (**Figure 2.23d**). Its Miller index is therefore $\left(1\bar{1}2\right)$, which is read as "one negative-one two" or "one bar-one two."

Many common crystal faces are parallel to one or two of the crystal axes. Consider face v shown in **Figure 2.24**. This face intersects the a and b axes with a cell intercept of $w_a = 1$ and $w_b = 1$, but is parallel to the c axis. The value for w_c must therefore be infinity ($w_c = \infty$), because no matter how far the face goes, it never intersects the c axis. Note that anything divided by infinity is zero, so the index for this face calculated from Equation 2.1 is

$$(hkl) = \frac{1}{w_a}\frac{1}{w_b}\frac{1}{w_c} = \left(\frac{1}{1}\frac{1}{1}\frac{1}{\infty}\right) = (110)$$
$$= (\text{one one zero}).$$

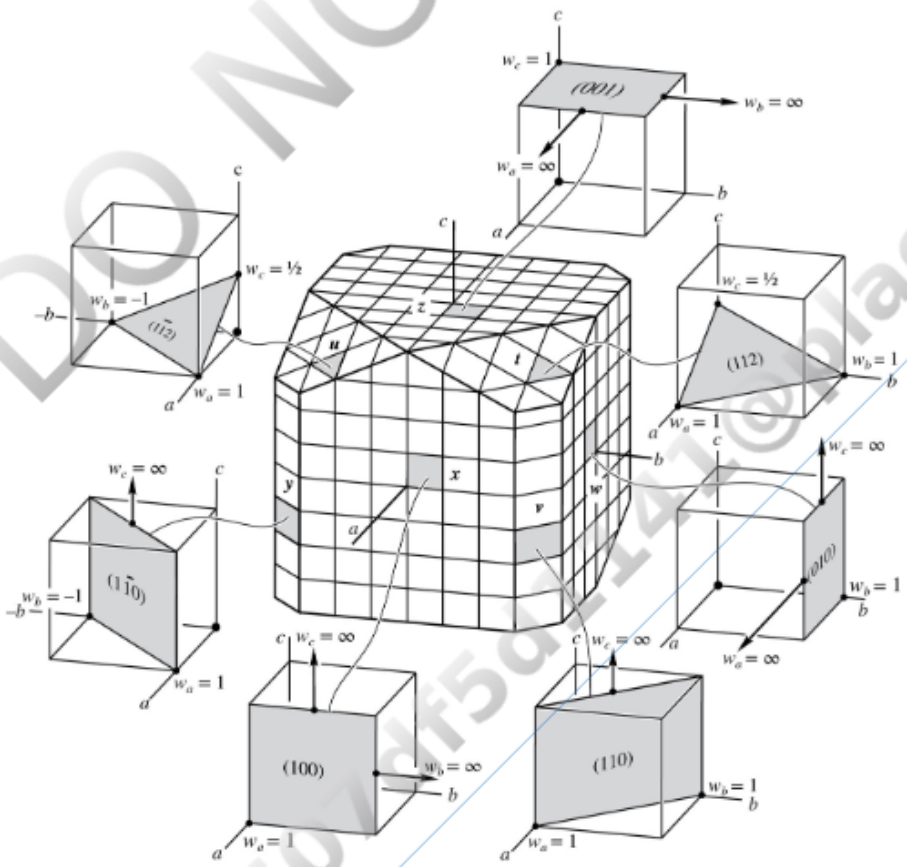

FIGURE 2.24 Miller indices for all visible faces on the crystal shown in Figure 2.23. The traces of unit cells are sketched on the crystal. See text for discussion. View larger image

Face w, which is parallel to a and c, cuts the positive end of the b axis ($w_a = \infty$, $w_b = 1$, $w_c = \infty$). Its Miller index must therefore be (010) (zero one zero). Faces x, y, and z get

Printed by: e48d507df5d1141@placeholder.94092.edu. Printing is for personal, private use only. No part of this book may be reproduced or transmitted without publisher's prior permission. Violators will be prosecuted.

Miller indices of (100), $(1\bar{1}0)$, and (001) by similar calculation. Note that if the first digit in the Miller index (h) is zero, the face is parallel to a; if the second digit (k) equals zero, the face is parallel to b; and if the third digit (l) equals zero, the face is parallel to c.

Indices and Crystal Axes in the Hexagonal Crystal System

Crystal axes and indices in the hexagonal system require some additional explanation because two common conventions are in use. One, which was described earlier (Figures 2.8 and 2.10, and Table 2.2), utilizes three axes (a, b, and c), and the other utilizes four axes (a_1, a_2, a_3, and c).

Consider the hexagonal crystal shown in **Figure 2.25a**. The a, b, and c crystal axes are located according to the three-axis convention. **Figure 2.25b** shows the unit cell intercepts of the lighter-shaded face—$w_a = 1$, $w_b = \infty$, and $w_c = \infty$. By Equation 2.1, the Miller index for this face is (100). The relation of the $(1\bar{1}0)$ face (dark shading) to a unit cell is shown in **Figure 2.25c**; note that this face cuts the negative end of the b axis. The Miller indices for the other vertical faces shown in cross section (**Figure 2.25d**) can be obtained by similar considerations. The top face of the crystal is (001) and the bottom face is $(00\bar{1})$.

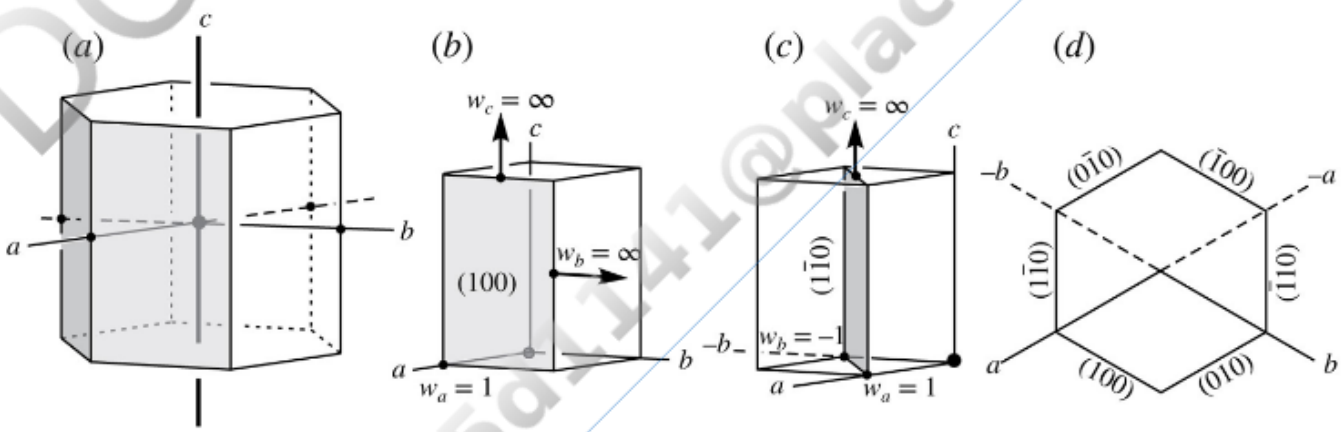

FIGURE 2.25 Miller indices in the hexagonal crystal system. (*a*) Hexagonal crystal with a, b, and c crystal axes. (*b*) Relation of light-shaded face to the unit cell. Based on unit cell intercepts, the Miller index is (100). (*c*) Relation of the dark-shaded face to a unit cell. Based on unit cell intercepts, the Miller index is $(1\,\bar{1}\,0)$. (*d*) View down the c axis with the Miller indices for all vertical faces shown. View larger image

An alternative convention uses four crystal axes in the hexagonal crystal system (**Figure 2.26**). Hexagonal crystals have three directions at 120° from each other that are typically parallel to 2-fold rotation axes and/or perpendicular to mirrors. Three crystal axes

Printed by: e48d507df5d1141@placeholder.94092.edu. Printing is for personal, private use only. No part of this book may be reproduced or transmitted without publisher's prior permission. Violators will be prosecuted.

identified as a_1, a_2, and a_3 are placed parallel to these directions. The a_1 and a_2 axes are parallel to the *a* and *b* crystal axes as defined in the preceding discussion of the hexagonal unit cell; the a_3 is at 120° to them. The *c* axis is the same in both axis conventions. The unit cell based on the four-axis convention therefore has a hexagonal cross section. The four-axis convention is widely used in many older reference works.

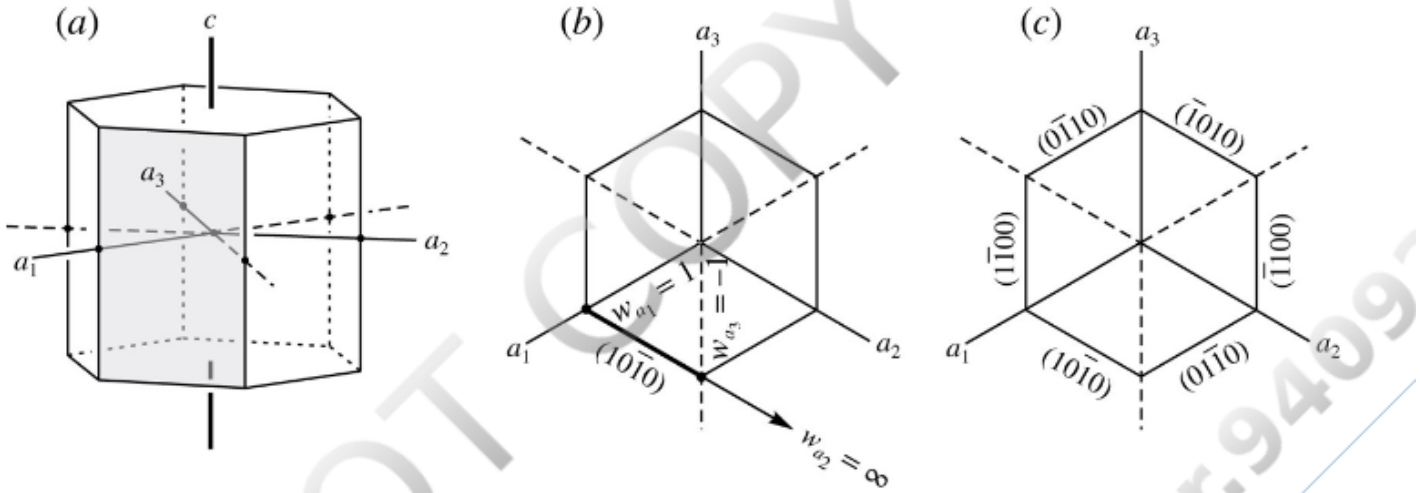

FIGURE 2.26 Miller–Bravais indices in the hexagonal crystal system. (*a*) Hexagonal crystal with a_1, a_2, a_3, and *c* crystal axes. The *a* axes are parallel to 2-fold rotation axes and are 120° from each other. The shaded face cuts the a_1 and $-a_3$ axes and is parallel to a_2 and *c*. (*b*) Top view of the unit cell showing the unit cell intercepts that yield a Miller–Bravais index of $\left(10\bar{1}0\right)$. (*c*) Top view of the crystal showing the Miller–Bravais indices for all the vertical faces. The top and bottom faces are (0001) and $\left(000\bar{1}\right)$, respectively. See text for discussion. View larger image

A modification of Miller indices was developed by Auguste Bravais to accommodate the four-axis convention, so these indices are referred to as **Miller-Bravais** indices. Because there are four crystal axes, the Miller–Bravais index contains four integers (*hkil*), which refer to the a_1, a_2, a_3, and *c* axes, respectively. Consider the shaded face on the hexagonal crystal shown in Figure 2.26a. This face is parallel to *c* and a_2, so $w_c = \infty$ and $w_{a_2} = \infty$. It cuts the positive a_1 axis at one unit cell dimension ($w_{a_1} = 1$), and the negative a_3 axis at one unit cell ($w_{a_3} = -1$). By Equation 2.1, the Miller index must be

$$(hkil) = \left(\frac{1}{1}\,\frac{1}{\infty}\,\frac{1}{\bar{1}}\,\frac{1}{\infty}\right) = \left(10\,\bar{1}0\right).$$

Because the three *a* axes are at 120°, it always works out that

$$h + k + i = 0 \qquad (2.2)$$

for all Miller–Bravais indices in the hexagonal system. The mathematical proof of this assertion can be found in Bloss (1971, pp. 53–54). Either all three of the *a* axes have 0 for

Printed by: e48d507df5d1141@placeholder.94092.edu. Printing is for personal, private use only. No part of this book may be reproduced or transmitted without publisher's prior permission. Violators will be prosecuted.

assertion can be found in Bloss (1971, pp. 53–54). Either all three of the *a* axes have 0 for an index or at least one will have a negative index and one a positive index.

Miller–Bravais indices can be converted to Miller indices by deleting the third (*i*) digit. Miller–Bravais indices may be derived from Miller indices with reference to Equation 2.2.

Determining Miller Index

Determining the Miller index for a crystal face on a real crystal requires two pieces of data: the **axial intercepts** for the crystal face and either the unit cell dimension or the **axial ratio**. Consider the crystal face (*x*) shown on the augite crystal in **Figure 2.27**.

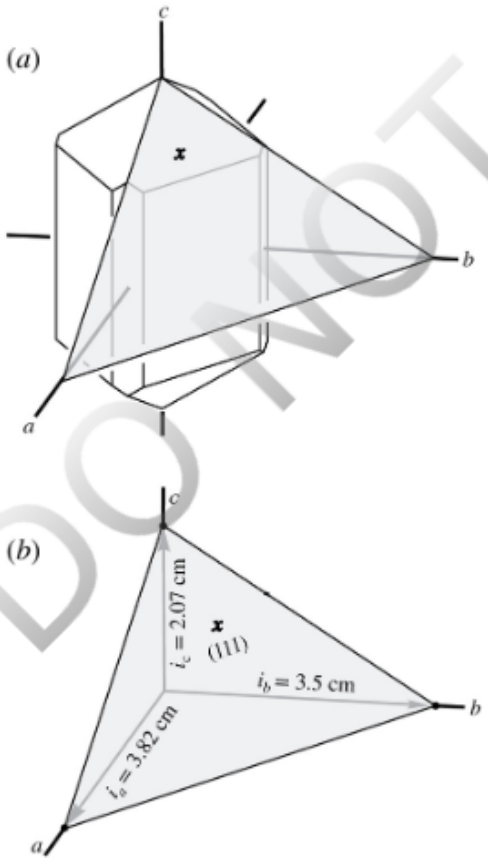

FIGURE 2.27 Calculating the Miller index for face *x* on an augite crystal. (*a*) Face *x* is extended out until it intersects all three crystal axes, as shown by the shaded plane. (*b*) The dimensions of these intersections measured from the center of the crystal are i_a = 3.82 cm, i_b = 3.5 cm, and i_c = 2.07 cm. The Miller index for this face is (111). See text for discussion. View larger image

The axial intercepts (i_a, i_b, i_c) for the face are the distances from the origin where the crystal face, when extended, crosses the crystal axes. In this case i_a = 3.82 cm, i_b = 3.5 cm, and i_c = 2.07 cm (ignoring the difficulty of actually making these measurements).

The axial ratio is calculated by dividing each unit cell dimension by the *b* unit cell dimension.

DO NOT COPY e48d507df5d1141@placeholder.9409

Printed by: e48d507df5d1141@placeholder.94092.edu. Printing is for personal, private use only. No part of this book may be reproduced or transmitted without publisher's prior permission. Violators will be prosecuted.

$$\text{axial ratio} = a : b : c = \frac{a}{b} : \frac{b}{b} : \frac{c}{b}. \tag{2.3}$$

For augite, the unit cell dimensions are $a = 9.73$ Å, $b = 8.91$ Å, and $c = 5.25$ Å, so the axial ratio is 1.09:1:0.59. The Miller index is obtained by dividing the axial ratio values (or the unit cell dimensions) by the intercept values and clearing fractions.

$$\begin{aligned}(hkl)\,\alpha\left(\frac{a}{i_a}\,\frac{b}{i_b}\,\frac{c}{i_c}\right) &= \left(\frac{1.09}{3.82}\,\frac{1}{3.50}\,\frac{0.59}{2.07}\right) \\ &= (0.29\ 0.29\ 0.29).\end{aligned} \tag{2.4}$$

Dividing by 0.29 produces the smallest available integers to yield the Miller index

$$(hkl) = (111).$$

If the Miller index and axial intercepts of a crystal face are known, the axial ratio can be calculated by rearranging Equation 2.4.

$$a : b : c = i_a h : i_b k : i_c l \tag{2.5}$$

Crystallographic Planes

Miller indices for crystallographic planes within a crystal, such as cleavage, are assigned with reference to the unit cell (Figure 2.24) in the same way that crystal faces are assigned indices. Consider the crystal shown in **Figure 2.28a**. A cleavage surface parallel to the (001) crystal face is given a Miller index of (001) because it has the same relation to the unit cell as the face. The three principal crystallographic planes in the crystal are shown in **Figure 2.28b**. They are parallel to the (100), (010), and (001) crystal faces and are assigned those Miller indices. The convention is to use Miller indices with positive integers where possible. The *bc* crystallographic plane is therefore (100) and not $(\bar{1}00)$.

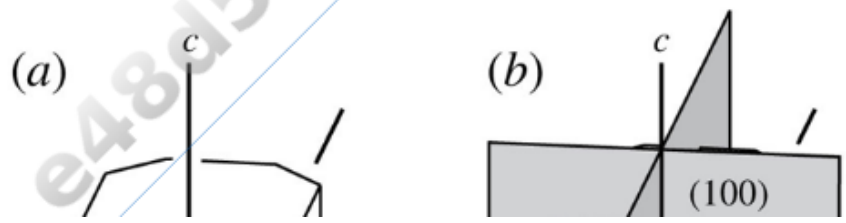

DO NOT COPY
e48d507df5d1141@placeholder.9409

Printed by: e48d507df5d1141@placeholder.94092.edu. Printing is for personal, private use only. No part of this book may be reproduced or transmitted without publisher's prior permission. Violators will be prosecuted.

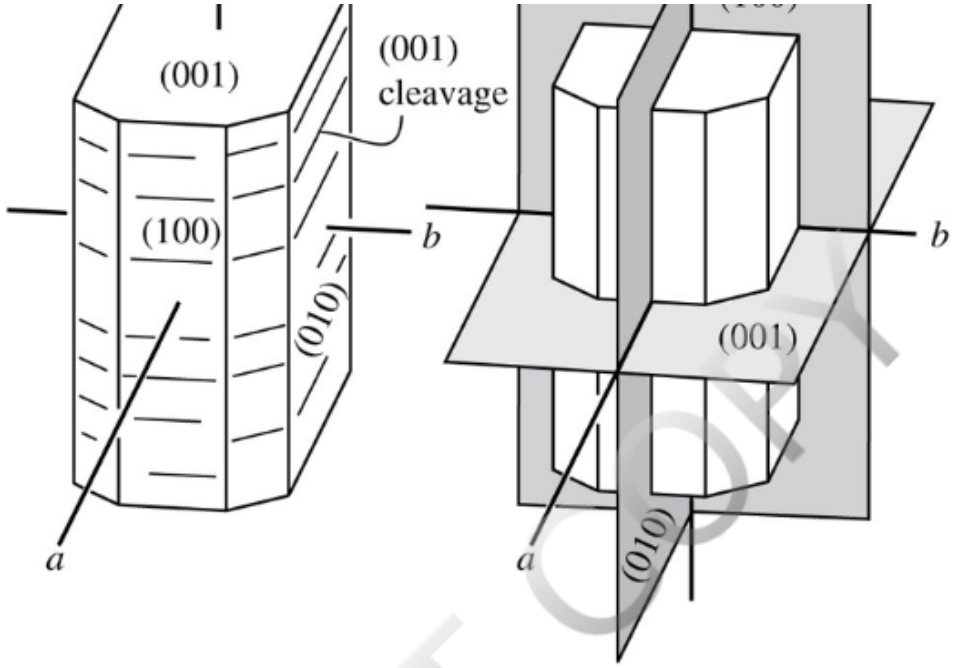

FIGURE 2.28 Crystallographic planes are assigned the same Miller index as the crystal face to which they are parallel. (*a*) A cleavage (shown with thin lines) parallel to the (001) crystal face is identified as a (001) cleavage. (*b*) The three principal crystallographic planes are parallel to the surfaces of the unit cell and the (100), (010), and (001) crystal faces. They therefore have Miller indices of (100), (010), and (001). View larger image

Assigning Miller Indices by Inspection

Fortunately, the Miller indices for the major crystal faces on many minerals can be assigned without any calculation. Because of the relationships observed in the laws of Bravais and Haüy, the integers found in Miller indices are small. Integers larger than 2 are unlikely for prominent crystal faces. Integers larger than 4 are rare even for minor faces. This makes it relatively easy to assign Miller indices to major crystal faces by inspection, at least for crystals without too many different faces.

Prominent faces that cut just one of the crystal axes have indices (100), (010), (001), $(\bar{1}00)$, $(0\bar{1}0)$, or $(00\bar{1})$. The most prominent faces that cut two axes but not the third are usually (110), (011), (101), $(0\bar{1}1)$, $(\bar{1}\bar{1}0)$, and so forth; less prominent faces are likely to have indices such as (120) or (210). The most prominent faces that cut all three axes are usually (111), $(\bar{1}\bar{1}1)$, $(1\bar{1}\bar{1})$, and so forth. The (111) face is known as the **unit face**. Note that because Miller indices are inverses of the intercepts, a larger index number for a given axis means that the intercept (distance from the origin) will be smaller (Figure 2.23).

Consider the orthorhombic crystal shown in **Figure 2.29**. Face *q* cuts the positive *a* axis and is parallel to both *b* and *c*, so its index must be (100). Similarly, face *r* cuts only the positive end of the *b* axis, so its index must be (010), and face *s* cuts only the positive end

Printed by: e48d507df5d1141@placeholder.94092.edu. Printing is for personal, private use only. No part of this book may be reproduced or transmitted without publisher's prior permission. Violators will be prosecuted.

of c axis, so its index must be (001). Prominent face t cuts the positive a and b axes and is parallel to c, so its index is (110). Face u, if extended out, would cut the positive ends of all three axes and is prominent, so its index is (111). Face v, the counterpart of u on the bottom of the crystal, cuts the negative c axis, so its index is $\left(11\bar{1}\right)$. Face w cuts the c axis closer to the origin than face u, so the index for w works out to (112). Face x, the counterpart to w on the bottom of the crystal, has index $\left(11\bar{2}\right)$.

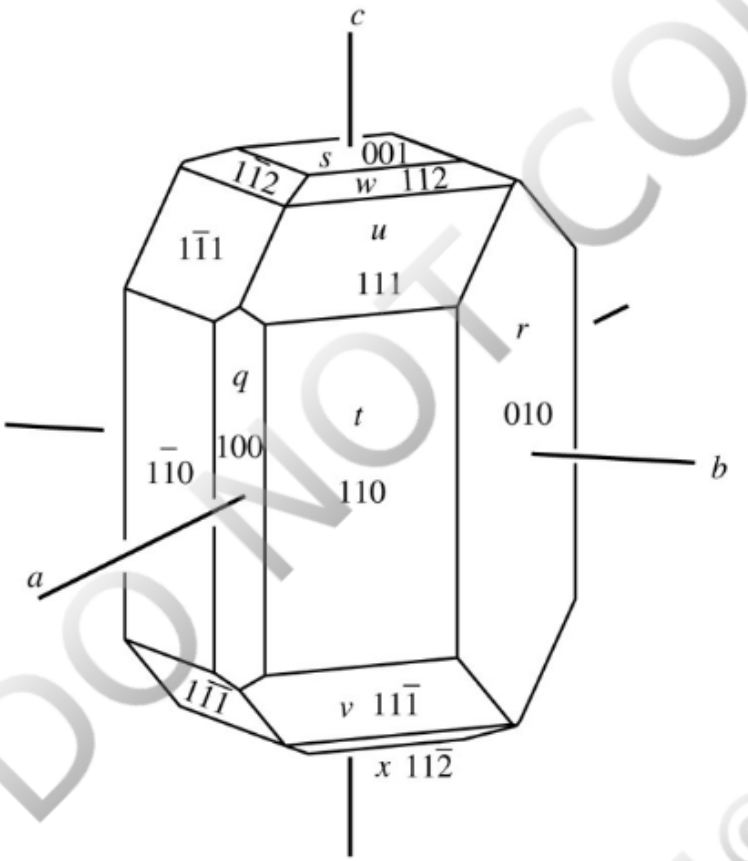

FIGURE 2.29 Assigning Miller indices by inspection. See text for discussion. View larger image

Assigning Miller indices by inspection of course is not always foolproof. Some faces with larger integers in their Miller index may, because of accidents of growth or crystal chemical requirements, be more prominent than the laws of Bravais and Haüy suggest. Further, the unit cell and crystal axes may be assigned in more than one way for some minerals, allowing published sources to assign different Miller indices to the same features on some minerals.

DO NOT COPY e48d507df5d1141@placeholder.9409

Printed by: e48d507df5d1141@placeholder.94092.edu. Printing is for personal, private use only. No part of this book may be reproduced or transmitted without publisher's prior permission. Violators will be prosecuted.

Crystallographic Directions

Crystallographic directions or linear features are identified by using integers within brackets [*uvw*]. For purposes of developing the nomenclature, consider several lines starting at the origin of the crystal lattice as shown in **Figure 2.30**. The index for each direction is determined by the coordinates of the lattice nodes through which it passes. Coordinates for lattice nodes are given in terms of unit cell dimensions (*a*, *b*, and *c*).

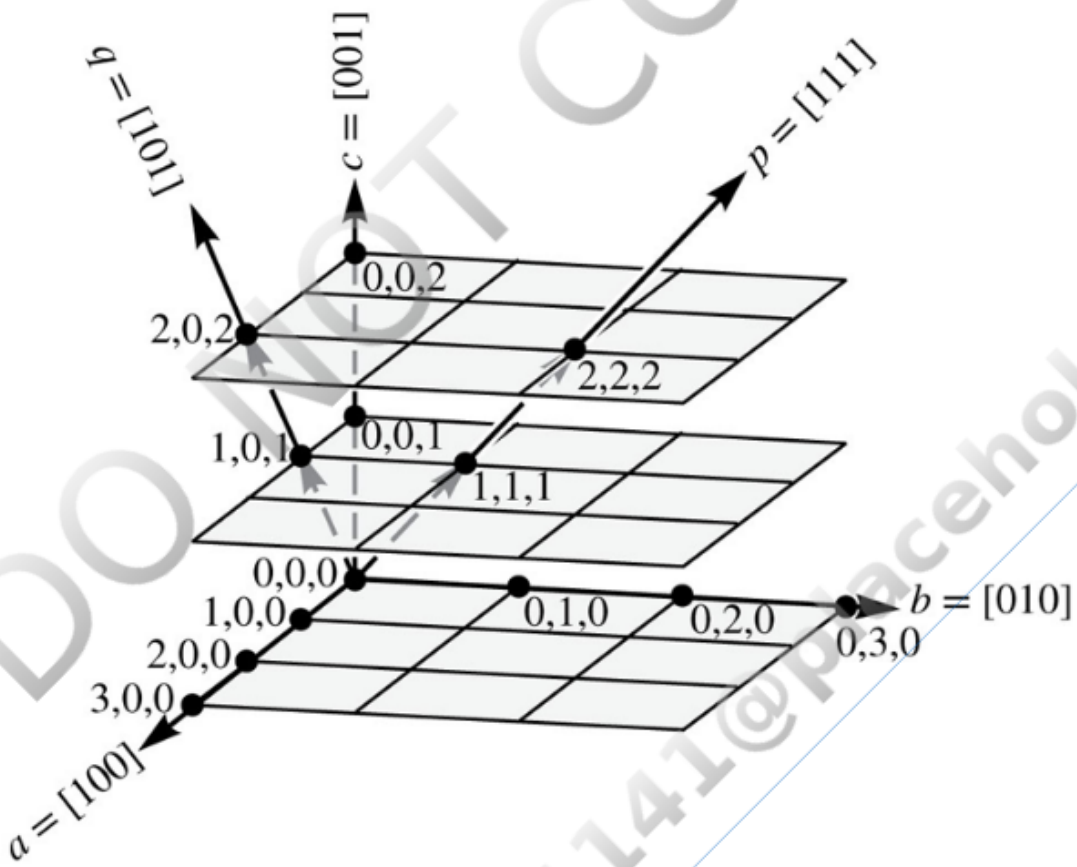

FIGURE 2.30 Crystallographic directions. Crystallographic direction [111] (line *p*) goes through lattice nodes 1,1,1 and 2,2,2, and so forth. Direction [101] (*q*) goes through lattice nodes 1,0,1 and 2,0,2. The three crystal axes *a*, *b*, and *c* are the [100], [010], and [001] crystallographic directions.
View larger image

Consider line *p* that passes through lattice coordinates 1, 1, 1; 2, 2, 2, etc. Its crystallographic direction is obtained by dividing the coordinates by their common factor. Coordinate 2, 2, 2 can be divided by 2 to yield crystallographic direction [111] for line *p*. Line *q* passes through lattice coordinates 1, 0, 1; 2, 0, 2, etc.; its index is [101]. The crystal axes, therefore, are *a* = [100], *b* = [010], and *c* = [001].

DO NOT COPY e48d507df5d1141@placeholder.9409

Printed by: e48d507df5d1141@placeholder.94092.edu. Printing is for personal, private use only. No part of this book may be reproduced or transmitted without publisher's prior permission. Violators will be prosecuted.

Zones

A **zone** is a collection of crystal faces, all of which are parallel to a common line called a **zone axis**. A zone is identified with the index of the zone axis [*uvw*]. For example, a tetragonal prism (**Figure 2.31**) constitutes a zone because the faces are all parallel to a common line (the *c* axis) through the middle of the prism. The zone axis is therefore [001]. The zone axis also is parallel to the edges defined by the intersection of the faces.

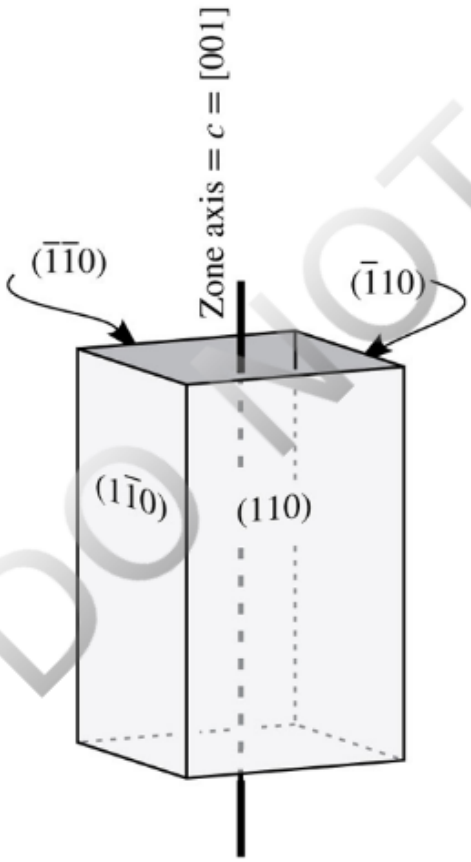

FIGURE 2.31 Crystal zone. The (110), ( ), ( ), and ( ) faces constitute a [001] zone because they intersect in edges parallel to [001] (the *c* axis), which is the zone axis. View larger image

If the Miller indices of two intersecting faces (*hkl*) and (*qrs*) in the zone are known, a simple mathematical technique allows the index of the zone axis to be calculated. Consider the ( ) and (110) faces on the prism in Figure 2.31. Write out the index for the ( ) face twice, and immediately beneath, write out the index for the (110) face twice.

DO NOT COPY e48d507df5d1141@placeholder.9409

Printed by: e48d507df5d1141@placeholder.94092.edu. Printing is for personal, private use only. No part of this book may be reproduced or transmitted without publisher's prior permission. Violators will be prosecuted.

$$\begin{array}{lll} h\,k\,l\,h\,k\,l & \text{or} & 1\,101\,10 \\ q\,r\,s\,q\,r\,s & & 110110 \end{array} \tag{2.6}$$

Cross off the first and last number in each row.

$$\begin{array}{lll} \cancel{h}\,k\,l\,h\,k\,\cancel{l} & \text{or} & \cancel{1}101\,1\cancel{0} \\ \cancel{q}\,r\,s\,q\,r\,\cancel{s} & & \cancel{1}1011\cancel{0} \end{array} \tag{2.7}$$

The zone index [*uvw*] is given by cross multiplying as follows.

$$\begin{array}{cccc} k & l & h & k \\ \diagdown\!\diagup & \diagdown\!\diagup & \diagdown\!\diagup & \\ r & s & q & r \end{array} \quad \text{or} \quad \begin{array}{cccc} \bar{1} & 0 & 1 & \bar{1} \\ \diagdown\!\diagup & \diagdown\!\diagup & \diagdown\!\diagup & \\ 1 & 0 & 1 & 1 \end{array}$$

$$\begin{array}{ccc} u & v & w \\ 0 & 0 & 2 \end{array}$$

$$u = k*s - l*r \quad \text{or} \quad -1*0 - 0*1 = 0$$

$$v = l*q - h*s \quad \text{or} \quad 0*1 - 1*0 = 0$$

$$w = h*r - k*q \quad \text{or} \quad 1*1 - 1*-1 = 0$$

Divide by 2 to reduce to the smallest possible integers:

$$[uvw] = [001]$$

DO NOT COPY e48d507df5d1141@placeholder.9409

Printed by: e48d507df5d1141@placeholder.94092.edu. Printing is for personal, private use only. No part of this book may be reproduced or transmitted without publisher's prior permission. Violators will be prosecuted.

Crystal Forms

A **crystal form** is a collection of equivalent crystal faces that are related to each other by the symmetry of the mineral. **Figure 2.32a** shows a simple orthorhombic crystal of the point group 2/*m* 2/*m* 2/*m* that is composed of two sets of equivalent faces. One set consists of the four faces related to the (011) face: (011) and $(0\bar{1}1)$ on the top and $(0\bar{1}\bar{1})$ and $(01\bar{1})$ on the bottom. The (100) and $(\bar{1}00)$ faces are the second set. Each of these sets of equivalent faces is a crystal form. For convenience, each crystal form is identified by braces { } around the *hkl* Miller index of one of the faces that compose the form. For example, {011} identifies the four faces equivalent to (011), and {100} identifies the two faces equivalent to (100).

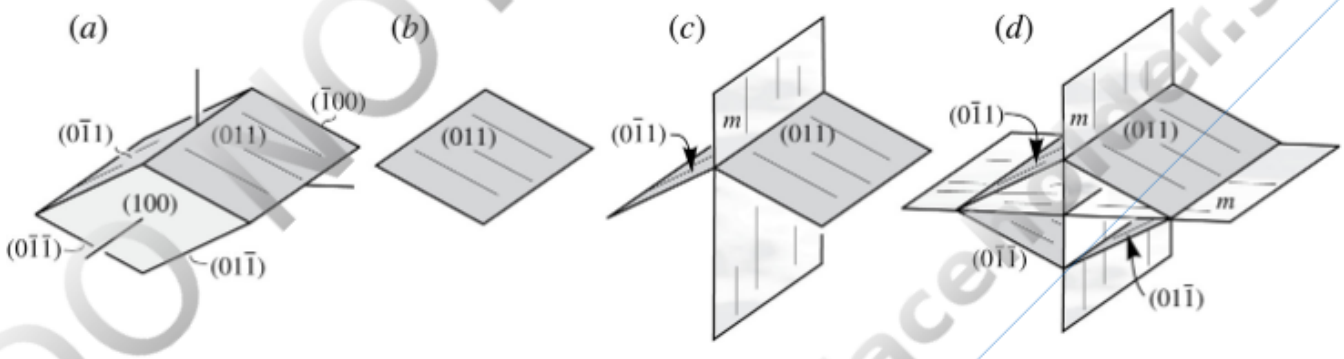

FIGURE 2.32 Crystal forms are produced by a repetition of crystal faces by symmetry operations. (*a*) A simple orthorhombic crystal. (*b*) The (011) face. (*c*) The $(0\bar{1}1)$ face is produced by reflection on the vertical mirror (*m*). (*d*) A horizontal mirror produces the $(01\bar{1})$ and $(0\bar{1}\bar{1})$ faces to complete the four faces of the {011} rhombic prism. View larger image

Given one face of a crystal form, the point symmetry operations of the crystal will replicate the face to produce all the faces of the form. Consider the (011) face on Figure 2.32a, which is shown isolated in **Figure 2.32b**. A vertical mirror *m* parallel to (010) produces a mirror image of this face with index $(0\bar{1}1)$ (**Figure 2.32c**). The horizontal mirror parallel to (001) duplicates these two faces to create the $(01\bar{1})$ and $(0\bar{1}\bar{1})$ faces (**Figure 2.32d**). This form is identified with the original face and is called a {011} rhombic prism. The (100) and $(\bar{1}00)$ faces are related to each other by the third mirror in the orthorhombic crystal, which is not shown, and create a separate form called a {100} pinacoid. Prisms, pinacoids, and other forms are discussed in the following sections.

DO NOT COPY
e48d507df5d1141@placeholder.9409

Printed by: e48d507df5d1141@placeholder.94092.edu. Printing is for personal, private use only. No part of this book may be reproduced or transmitted without publisher's prior permission. Violators will be prosecuted.

A form may be either an **open form** or a **closed form**. A closed form such as a cube entirely encloses a volume. An open form such as a prism does not entirely enclose a volume.

Isometric Forms

A total of 15 different forms, all of them closed, are possible in the isometric system (**Figure 2.33**). Of these, the most common are the cube {001}, octahedron {111}, tetrahedron {111}, and rhombic dodecahedron {110}. Note that both the octahedron and the tetrahedron have the same form symbol {111}. Although it might seem that this would produce confusion, it turns out that tetrahedrons and octahedrons are found in crystals with different point group symmetry (see Table 2.9). Pyrite and a few other structurally similar minerals may have a pyritohedron crystal form. A pyritohedron, at first glance, is very similar to a pentagonal dodecahedron (see Box 2.1); however, whereas a pentagonal dodecahedron is made of regular pentagons (consistent angle between each side), a pyritohedron does not have the same angle between each side and results in a different symmetry. When trying to determine point group symmetry, distinguishing between a pentagonal dodecahedron and a pyritohedron can be difficult, but pyrite often has striations on the pyritohedron faces which must be considered in the symmetry (see section on Nonisometric Forms).

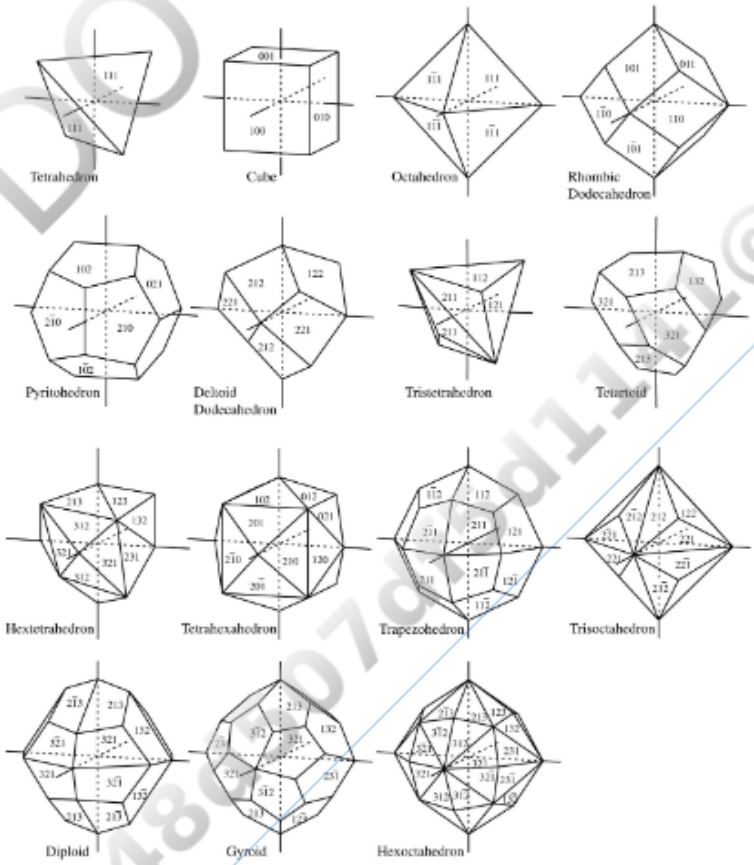

FIGURE 2.33 Crystal forms in the isometric system. View larger image

DO NOT COPY e48d507df5d1141@placeholder.9409

Printed by: e48d507df5d1141@placeholder.94092.edu. Printing is for personal, private use only. No part of this book may be reproduced or transmitted without publisher's prior permission. Violators will be prosecuted.

BOX 2.1
Quasicrystals

While traditional crystallography theory precludes crystals from having 5-fold rotational symmetry, it turns out that it is possible for **quasicrystals** to possess that symmetry (**Figure 2.21a**) and other "forbidden" symmetries such as 7-fold and 10-fold. Quasicrystals utilize the equivalent of Penrose tiling, in which differently shaped tiles are arranged systematically to continuously fill an area (**Figure 2.21b**) with 5-fold and other symmetries. While the patterns are systematic and have rotational symmetry, *they lack translational symmetry.*

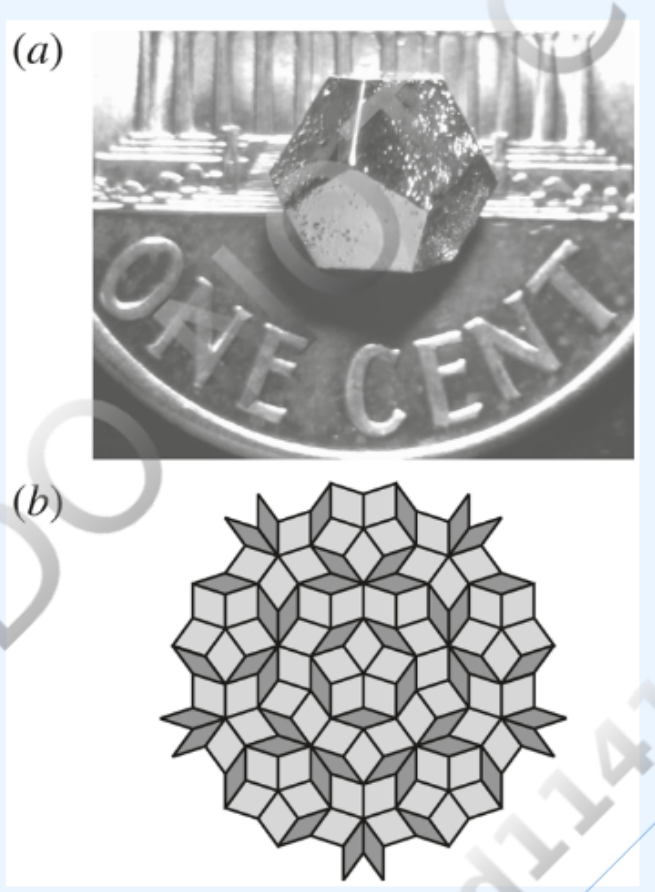

FIGURE 2.21 (*a*) A synthetic pentagonal dodecahedron quasicrystal of Ho-Mg-Zn resting on a penny coin. Unlike pyrite, which has a similar appearance, the faces of the pentagonal dodecahedron are regular pentagons, revealing the pentagonal (5-fold) rotational symmetry. Photo courtesy of Dr. Paul Canfield, Ames Laboratory, U.S. Department of Energy. (*b*) Penrose tiling using two different diamond-shaped tiles to produce pentagonal symmetry. While the pattern is systematic, it lacks translational symmetry. Photo courtesy of Dr. Paul Canfield, Ames Laboratory, U.S. Department of Energy. View larger image

Two natural quasicrystal minerals—icosahedrite ($Al_{63}Cu_{24}Fe_{13}$) and decagonite ($Al_{71}Ni_{24}Fe_5$)—have been discovered in the Khatyrka meteorite found in southeastern Chukotka, Russia. While detailed studies of their structures have not yet been done,

DO NOT COPY e48d507df5d1141@placeholder.9409

Printed by: e48d507df5d1141@placeholder.94092.edu. Printing is for personal, private use only. No part of this book may be reproduced or transmitted without publisher's prior permission. Violators will be prosecuted.

presumably a slice through one of these quasicrystals would reveal alternating clusters of atoms arranged in a pattern similar to Penrose tiling.

Nonisometric Forms

The crystal forms possible in the remaining crystal systems (tetragonal, hexagonal, orthorhombic, monoclinic, and triclinic) consist of **pedions**, **pinacoids**, **dihedrons**, **prisms**, **pyramids**, **dipyramids**, **scalenohedrons**, **trapezohedrons**, **rhombohedrons**, and **tetrahedrons** (**Figures 2.34**, **2.35**, and **2.36**). In the definition of each form, open forms are indicated with (O) and closed forms are indicated with (C).

PEDION (O): A single face with no geometrically equivalent face elsewhere on the crystal. Also known as a monohedron. No symmetry element repeats the face (Figure 2.34a).

PINACOID (O): Two parallel faces on opposite sides of the crystal related by inversion or a mirror (Figure 2.34b). Also known as a parallelohedron.

DIHEDRON (O): Two nonparallel faces. Also known as a **dome** if the two faces are related only by a mirror plane or a **sphenoid** if the two faces are related by a 2-fold rotation axis (Figure 2.34c).

PRISM (O): A collection of 3, 4, 6, 8, or 12 faces that intersects in a set of mutually parallel edges forming a tube. Faces that may close off the ends of the prism are not part of the form. Prisms are named (rhombic prism, tetragonal prism, etc.) based on the shape of the cross section (Figure 2.35).

PYRAMID (O): A collection of 3, 4, 6, 8, or 12 nonparallel faces that can intersect at a point. The different types of pyramids are named based on the shape of the cross section with the same nomenclature used for prisms (Figure 2.35). A pyramid may be either a top or a bottom depending on whether it occurs on the top of the crystal or the bottom.

DIPYRAMID (C): Two pyramids, one on each end of the crystal, with a total of 6, 8, 12, 16, or 24 faces. The two pyramids are related to each other by reflection across a mirror plane between them (Figure 2.35). The different types of dipyramids are named based on the shape of the cross section with the same nomenclature used for prisms.

TRAPEZOHEDRONS (C): Forms consisting of 6, 8, or 12 faces, each of which is a trapezoid (Figure 2.36). The faces on one end of the crystal are offset relative to the faces on the other end. Tetragonal trapezohedrons have 8 faces, 4 each on the top and bottom. Trigonal trapezohedrons have 6 faces, 3 each on the top and bottom. Both positive and negative forms are possible. Hexagonal trapezohedrons have 12 faces, 6 each on the top and bottom.

SCALENOHEDRONS (C): Forms consisting of 8 or 12 faces, each of which is a scalene triangle (Figure 2.36). The faces appear to be arranged in pairs.

RHOMBOHEDRONS (C): A form consisting of six faces, each of which is rhomb-shaped (Figure 2.36). A rhombohedron looks like a cube that has been either stretched or shortened along an axis going from corner to corner through the center.

TETRAHEDRONS (C): A form consisting of four triangular faces. In isometric crystals (Figure 2.33), each face is an equilateral triangle. In the tetragonal system (tetragonal tetrahedron) the four faces are identical isosceles triangles. In the orthorhombic system

DO NOT COPY

Printed by: e48d507df5d1141@placeholder.94092.edu. Printing is for personal, private use only. No part of this book may be reproduced or transmitted without publisher's prior permission. Violators will be prosecuted.

tetrahedron) the four faces are identical isosceles triangles. In the orthorhombic system (rhombic tetrahedron) the faces form two pairs of different isosceles triangles. The nonisometric forms are also known as disphenoids (Figure 2.36).

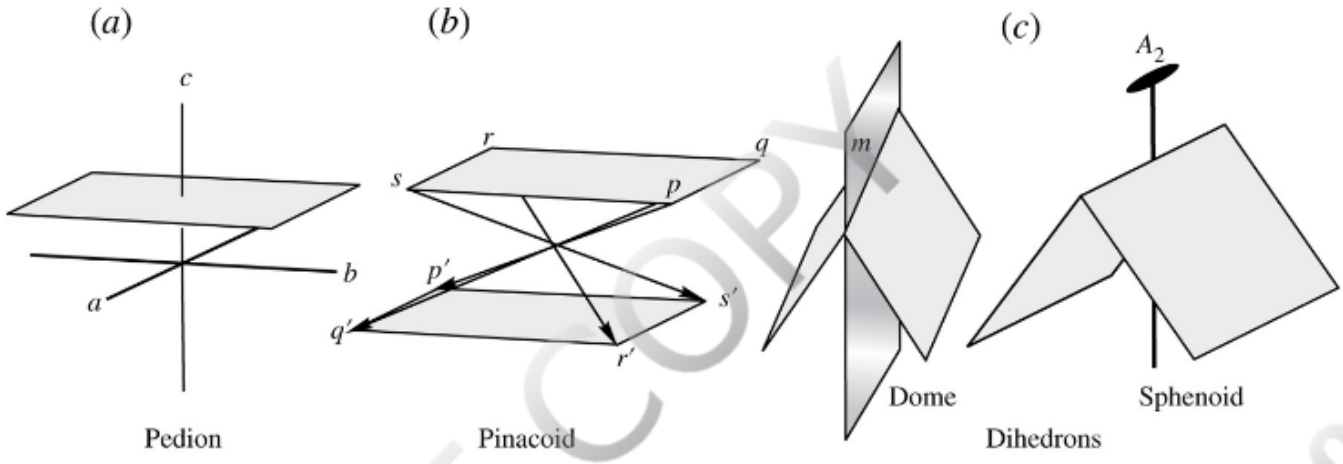

FIGURE 2.34 Crystal forms in the nonisometric crystal systems. (*a*) Pedion. (*b*) Pinacoid. (*c*) Dihedrons (dome and sphenoid). View larger image

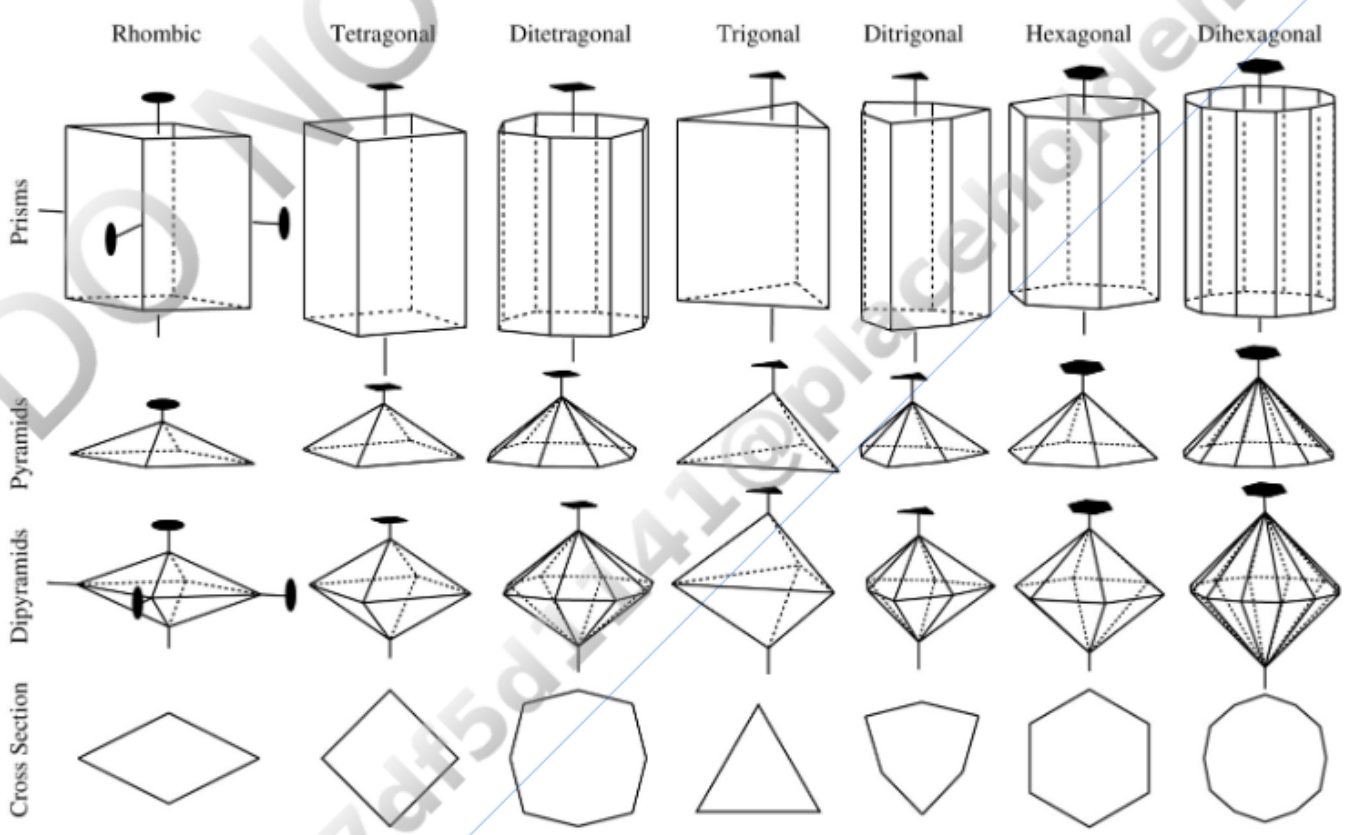

FIGURE 2.35 Crystal forms in the nonisometric crystal systems: prisms, pyramids, and dipyramids. Each form is modified by the name of the cross section shape (hexagonal prism, tetragonal pyramid, ditrigonal dipyramid, etc.). View larger image

DO NOT COPY

Printed by: e48d507df5d1141@placeholder.94092.edu. Printing is for personal, private use only. No part of this book may be reproduced or transmitted without publisher's prior permission. Violators will be prosecuted.

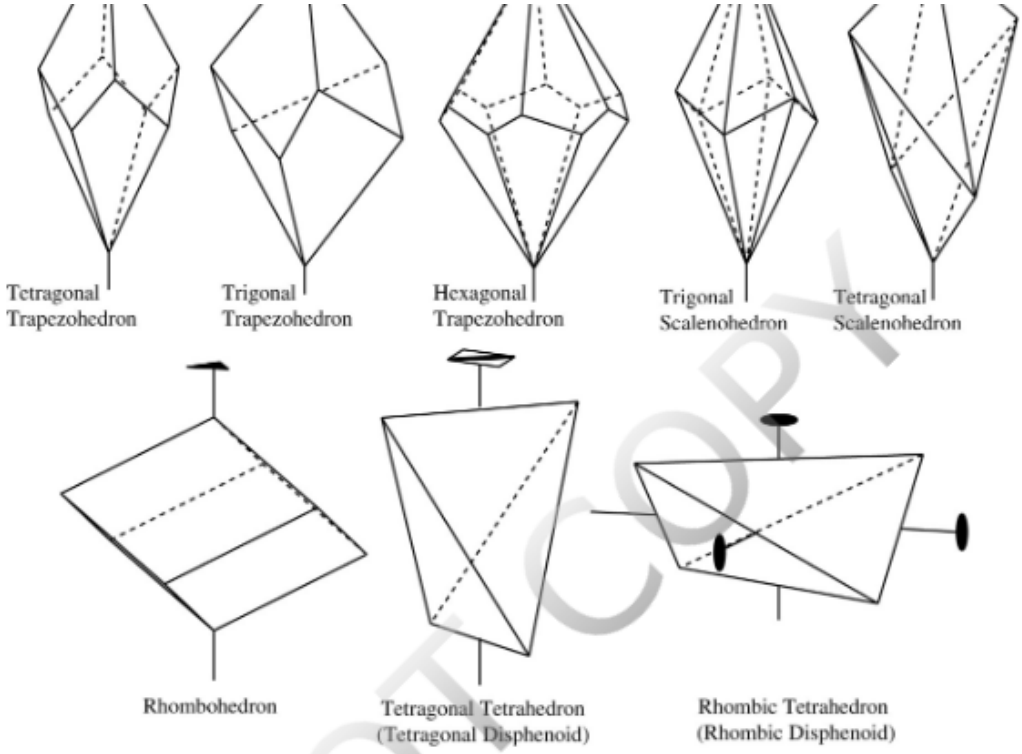

FIGURE 2.36 Crystal forms in the nonisometric crystal systems: trapezohedrons, scalenohedrons, rhombohedrons, and tetrahedrons (rhombic and tetragonal). Tetragonal trapezohedrons have 8 faces, 4 each on the top and bottom. Trigonal trapezohedrons have 6 faces, 3 each on the top and bottom. Both positive and negative forms are possible, as shown later (Figure 2.38). Hexagonal trapezohedrons have 12 faces, 6 each on the top and bottom. View larger image

Combining Crystal Forms

Simple crystals may consist of only a single closed form such as a cube or a dipyramid; more complex crystals may include several different open and/or closed forms. If a crystal consists only of open forms, at least two and sometimes three or more different open forms must be present to enclose the volume represented by the crystal.

All the forms on any given crystal must be compatible with one another. A mineral that crystallizes in the isometric crystal system may include only isometric forms, tetragonal minerals may include only tetragonal forms, and so forth. **A mineral can have only the forms that are consistent with the point group symmetry to which it belongs.** These are described shortly.

Avoid the mistake of assuming that a multifaced form is composed of several simpler forms. For example, a pinacoid is not composed of two pedions. A pinacoid consists of two and only two parallel faces related to each other by the symmetry of the mineral. Similarly, a cube consists of six equivalent faces; it is not composed of three pinacoids.

Enantiomorphous Forms and Crystals

DO NOT COPY e48d507df5d1141@placeholder.9409

Printed by: e48d507df5d1141@placeholder.94092.edu. Printing is for personal, private use only. No part of this book may be reproduced or transmitted without publisher's prior permission. Violators will be prosecuted.

Enantiomorphous forms lack center symmetry and mirrors. This makes it possible for each form to have left- and right-handed versions, like left- and right-handed gloves. The trigonal trapezohedron shown in **Figure 2.37a** is a good example. The crystal on the right displays the right-hand form {211} and the one on the left displays the left-hand form $\{3\bar{1}1\}$. Note that the crystals are mirror images of each other, and the individual trapezoidal faces of the right- and left-hand versions are also mirror images of each other. On a single crystal, only the right- or the left-hand form may be present, never both together. Different samples of the same mineral may have either form.

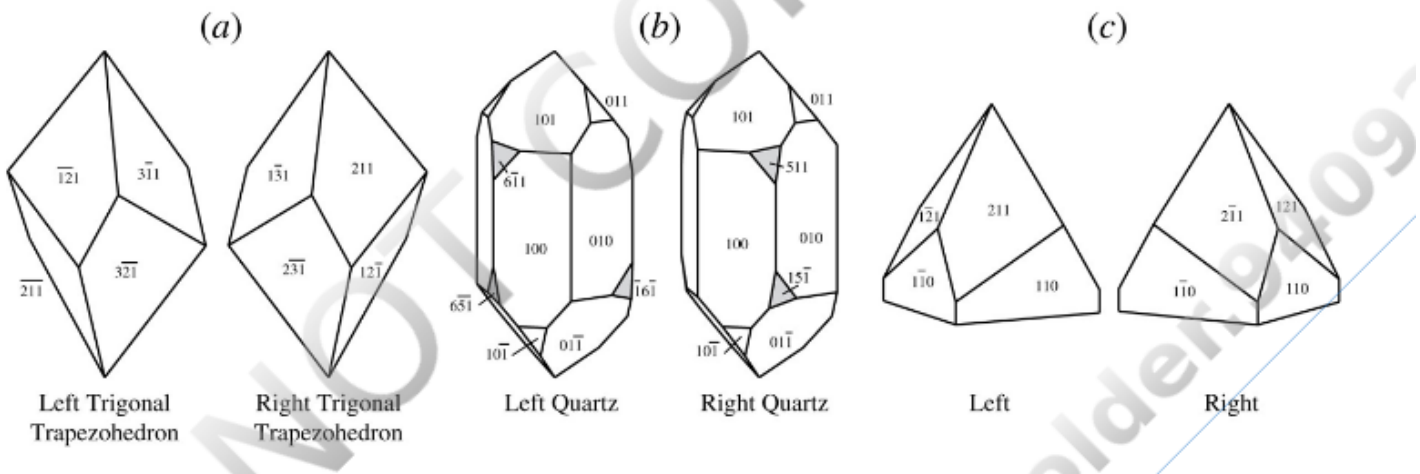

FIGURE 2.37 Enantiomorphous forms and crystals. (*a*) The right-handed {211} and left-handed $\{3\bar{1}1\}$ trigonal trapezohedron lack center or mirrors. (*b*) The right {511} and left $\{6\bar{1}1\}$ trigonal trapezohedron (small shaded faces) on right- and left-handed quartz. (*c*) Right- and left-handed crystals in the 4 point group. The {211} and $\{2\bar{1}1\}$ pyramids are not themselves enantiomorphous, but when combined with the {110} prism and $\{00\bar{1}\}$ pedion, they form right- and left-handed crystals. View larger image

The presence of an enantiomorphous form indicates that the mineral has a screw axis that is a repeating structure analogous to a spiral staircase that may spiral to either the right or left. Common quartz, for example, has a structure with either a right- or left-hand spiral. Right-hand quartz can display the {511} right-hand trigonal trapezohedron; left-hand quartz can display the $\{6\bar{1}1\}$ left-hand trapezohedron (**Figure 2.37b**). These faces are not commonly found, however.

Forms that may be enantiomorphous and the point groups in which they are found are listed in **Table 2.5**. Enantiomorphous forms are the characteristic forms in the point groups in which they are found, all of which lack center, rotoinversion, and mirrors. The 1, 2, 3, 4, and 6 point groups also lack center, rotoinversion, and mirrors and may have enantiomorphous crystals, although they will be composed of forms that are not individually enantiomorphous. **Figure 2.37c** shows enantiomorphous crystals in the 4 point group.

DO NOT COPY
e48d507df5d1141@placeholder.94092

Printed by: e48d507df5d1141@placeholder.94092.edu. Printing is for personal, private use only. No part of this book may be reproduced or transmitted without publisher's prior permission. Violators will be prosecuted.

TABLE 2.5 Enantiomorphous Forms (Figures 2.33, 2.36, and 2.37) and the Point Groups in Which They Occur

Form	Point Group
Rhombic tetrahedron (disphenoid)	222
Trigonal trapezohedron	32
Hexagonal trapezohedron	622
Tetragonal trapezohedron	422
Gyroid	23
Tetartoid	432

TABLE 2.6 Forms Found in the Point Groups and Crystal Classes of the Triclinic, Monoclinic, and Orthorhombic Crystal Systems[a]

Number of Faces	Name of Form	Triclinic			Monoclinic		Orthor	
		1 Pedial	$\bar{1}$ Pinacoidal	*m* Domatic	2 Sphenoidal	2/*m* Prismatic	*mm*2 Rhombic Pyramidal	22 Rhom Dispen
1	Pedion	X		X	X		X	
2	Pinacoid		X	X	X	X	X	X
2	Dihedron (dome)			X			X	
2	Dihedron (sphenoid)				X			
4	Prism					X	X	X
4	Rhombic tetrahedron (disphenoid)							X
4	Rhombic pyramid						X	
8	Rhombic dipyramid							

[a] The name of each crystal class is listed beneath the point group.

Positive and Negative Forms

Positive and negative varieties of a form, such as a rhombohedron, differ only in that the negative form is rotated relative to the positive form. Figure 2.38a shows a positive

DO NOT COPY e48d507df5d1141@placeholder.9409

Printed by: e48d507df5d1141@placeholder.94092.edu. Printing is for personal, private use only. No part of this book may be reproduced or transmitted without publisher's prior permission. Violators will be prosecuted.

{111} and a negative $\{1\bar{1}1\}$ tetrahedron. Note that the negative tetrahedron can be made coincident with the positive version by rotation of 90° about the *c* axis. Rhombohedrons (**Figure 2.38b**) have a single 3-fold rotation axis coincident with the *c* axis. Each face is repeated once every 120°. The positive rhombohedron is {101}. The equivalent negative rhombohedron {011} is produced by rotating the faces of the positive rhombohedron 60° about *c*. Note that the negative version of a form is produced by rotation of 60° on a 3-fold rotation axis, or 90° on a 2-fold axis or 4-fold rotoinversion axis. Forms that may have positive and negative varieties are indicated later (see Tables 2.7, 2.8, and 2.9).

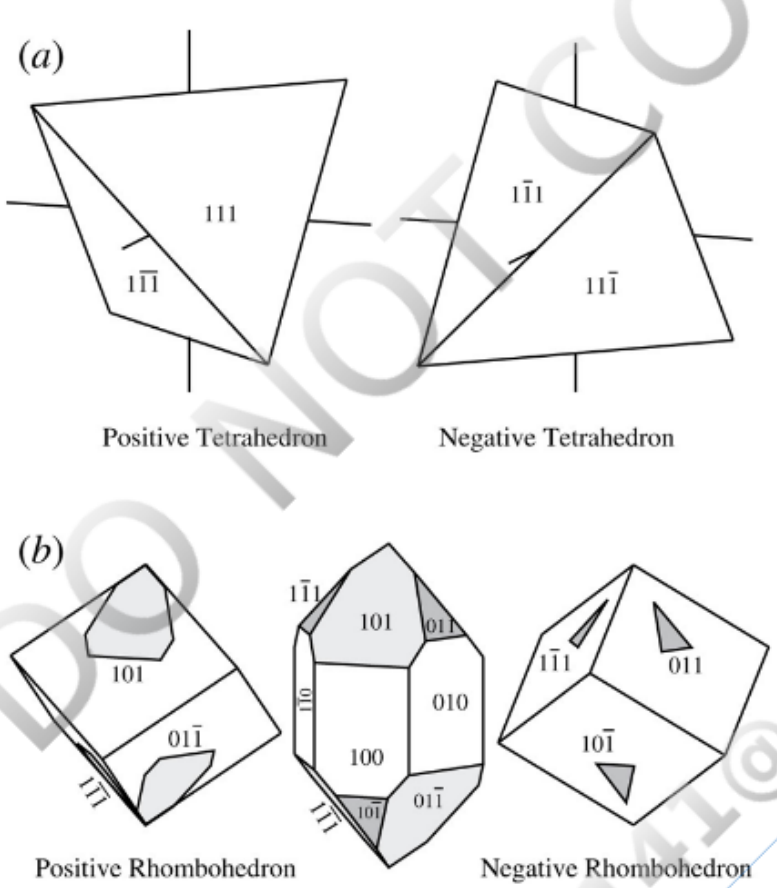

FIGURE 2.38 Positive and negative forms. (*a*) Tetrahedrons. (*b*) Quartz crystal with both positive {101} and negative {011} unit rhombohedrons. View larger image

TABLE 2.7 Forms Found in the Point Groups and Crystal Classes of the Tetragonal Crystal System[a]

Number of Faces	Name of Form	Form Symbols	Point Group				
			4 Tetragonal Pyramidal	**$\bar{4}$** Tetragonal Disphenoid	**4/*m*** Tetragonal Dipyramidal	**422** Tetragonal Trapezohedral	**4** Ditet
1	Pedion	$+\{001\}$; $-\{00\bar{1}\}$	X				

DO NOT COPY e48d507df5d1141@placeholder.9409

Printed by: e48d507df5d1141@placeholder.94092.edu. Printing is for personal, private use only. No part of this book may be reproduced or transmitted without publisher's prior permission. Violators will be prosecuted.

2	Pinacoid	{001}		X	X	X	
4	Tetragonal prism	{110}, {010}	X	X	X	X	
4	Tetragonal pyramid	{*hhl*}, {0*kl*}	X				
4	Tetragonal tetrahedron (disphenoid)	$+\{hhl\}$; $-\left\{h\bar{h}l\right\}$		X			
8	Ditetragonal prism	{*hk*0}				X	
8	Tetragonal dipyramid	{*hhl*}, {0*kl*}			X	X	
8	Tetragonal trapezohedron	{*hkl*}				X	
8	Tetragonal scalenohedron	{*hkl*}					
8	Ditetragonal pyramid	{*hkl*}					
16	Ditetragonal dipyramid	{*hkl*}					

[a] The name of each crystal class is listed beneath the point group.

TABLE 2.8 Forms Found in the Crystal Classes and Point Groups of the Hexagonal Crystal System[a]

Faces	Name of Form	Form {Generic}: {Example}	Trigonal (Rhombohedral) Division				
			3 Trigonal Pyramidal	$\bar{3}$ Rhombohedral	32 Trigonal Trapezohedral	3*m* Ditrigonal Pyramidal	T Scal
1	Pedion	{001}: $\left\{00\bar{1}\right\}$	X			X	
2	Pinacoid	{001}		X	X		
3	Trigonal prism	(*hk*0): {100}	X		X	X	
3	Trigonal pyramid	{*hkl*}: {101}	X			X	
6	Ditrigonal prism	{*hk*0}: {120}			X	X	
6	Hexagonal prism	(*hk*0): {100}		X	X	X	
6	Trigonal dipyramid	(*hkl*): {101}			X		

DO NOT COPY e48d507df5d1141@placeholder.9409

Printed by: e48d507df5d1141@placeholder.94092.edu. Printing is for personal, private use only. No part of this book may be reproduced or transmitted without publisher's prior permission. Violators will be prosecuted.

	dipyramid						
6	Rhombohedron	(*hkl*): {101}		X	X		
6	Trigonal trapezohedron	(*hkl*): {211}			X		
6	Ditrigonal pyramid	{*hkl*}: {101}				X	
6	Hexagonal pyramid	{*hkl*}: {101}				X	
12	Hexagonal dipyramid	{*hkl*}: {101}					
12	Trigonal scalenohedron	{*hkl*}: {211}					
12	Dihexagonal prism	{*hk*0}: {210}					
12	Ditrigonal dipyramid	{*hkl*}: {211}					
12	Hexagonal trapezohedron	{*hkl*}: {211}					
12	Dihexagonal pyramid	{*hkl*}: {211}					
24	Dihexagonal dipyramid	{*hkl*}: {211}					

[a] The name of each crystal class is listed beneath the point group.

TABLE 2.9 Forms Found in the Crystal Classes and Point Groups of the Isometric Crystal System[a]

Number of Faces	Name of Form	Form Symbols	Point Group				
			23 Tetartoidal	432 Gyroidal	2/*m* $\bar{3}$ Diploidal	$\bar{4}$ 3*m* Hextetrahedral	4/*m* $\bar{3}$ Hexocta
4	Tetrahedron	+{111}, $-\{1\,\bar{1}1\}$	X			X	
6	Cube (hexahedron)	{001}	X	X	X	X	X
8	Octahedron	{111}		X	X		X
12	Rhombic dodecahedron	{101}	X	X	X	X	X
12	Pentagonal dodecahedron (pyritohedron)	+{102}, −{201}	X		X		
12	Tristetrahedron	+{112}, $-\{1\,\bar{1}2\}$	X			X	

DO NOT COPY e48d507df5d1141@placeholder.9409

Printed by: e48d507df5d1141@placeholder.94092.edu. Printing is for personal, private use only. No part of this book may be reproduced or transmitted without publisher's prior permission. Violators will be prosecuted.

12	Deltoid dodecahedron	+{122}, $-\left\{1\,\bar{2}2\right\}$	X			X	
12	Tetartoid	{213}	X				
24	Tetrahexahedron	{201}		X		X	X
24	Trapezohedron	{211}		X	X		X
24	Trisoctahedron	{122}		X	X		X
24	Hextetrahedron	+{321}, $-\left\{3\bar{2}1\right\}$				X	
24	Diploid	+{321}, −{231}			X		
24	Gyroid	{321}		X			
48	Hexoctahedron	{321}					X

[a] The name of each crystal class is listed beneath the point group.

The same crystal may have both a positive and negative version of the same form. Common quartz, for example (Figure 2.38b), displays both the positive {101} and negative {011} unit rhombohedrons. One rhombohedron typically has larger faces than the other. Crystals are usually oriented so the larger set of faces is assigned to the positive rhombohedron.

Relating positive and negative crystal forms can often be done by reversing the sign of the last number of the Miller index: {101} versus $\left\{10\bar{1}\right\}$ for rhombohedrons or {111} versus $\left\{11\,\bar{1}\right\}$ for tetrahedrons. However, the negative unit rhombohedron and tetrahedron are usually identified as {011} and $\left\{1\,\bar{1}1\right\}$, respectively, because those faces cut the positive *c* axis. In some point groups, positive and negative forms are related by reversing two numbers in the Miller index—{102} versus {012} for pyritohedrons, for example.

DO NOT COPY e48d507df5d1141@placeholder.9409

Printed by: e48d507df5d1141@placeholder.94092.edu. Printing is for personal, private use only. No part of this book may be reproduced or transmitted without publisher's prior permission. Violators will be prosecuted.

Forms in the Six Crystal Systems

The forms that may occur in each of the 32 point groups within the six crystal systems are limited by the symmetry of the point group. For example, since tetragonal prisms have a single 4-fold rotation axis they can be found only in tetragonal point groups that have a single 4-fold rotation to match. Similarly, pedions, which consist of only one face, never occur in minerals with center symmetry because the inversion operation requires that an equivalent face be on the opposite side of the crystal, producing a pinacoid. Therefore, each point group has a unique set of crystal form or forms that can exist. This unique set of crystal form or forms is called a **crystal class**. There is one crystal class for each point group and the name of each crystal class is descriptive of the forms displayed by a crystal in the class.

The crystal class corresponding to each point group is illustrated and described in detail below. In the illustrations that follow, crystals are systematically oriented so that the *c* axis is vertical, *b* is to the right, and *a* is to the front.

Triclinic Crystal System

There are no symmetry constraints on the orientation of the crystal axes. Generally the *c* axis is chosen to be parallel to the dominant zone axis of the mineral, with the *b* and *a* axes parallel to crystal edges or in other rational orientations. Axes are generally oriented so that both the α and β angles are greater than 90°; in conventional illustrations of these minerals, this places the *b* axis down to the right and the *a* axis down to the front.

It is common in triclinic minerals to find that several different crystal axis orientations and unit cell geometries are in use. In some cases, crystal axis orientation and unit cell shape are established by the external geometry of the crystal faces. In other cases, crystal axis orientation is determined by detailed study of the crystal structure. The different axis conventions for a given mineral can be related to each other by appropriate mathematical or graphic manipulation. Confusion is common, however, when structural analysis is tied to one set of axes and unit cell, and descriptions of crystal faces, cleavage, or optical properties are tied to a different set of axes and unit cell. Beware—even standard reference works are not free of this particular problem.

The forms that are found in the two triclinic classes are listed in Table 2.6. Figure 2.39a shows a 1 point group crystal with **positive front** {100}, **side** {010}, and **basal** {001} pedions; **negative front** , **side** , and **basal** pedions; and the {011} pedion. Figure 2.39b shows a point group crystal with **front** {100}, **side** {010}, and **basal** {001} pinacoids; and a {011} pinacoid. Note that the two faces of a pinacoid have

DO NOT COPY e48d507df5d1141@placeholder.94092

Printed by: e48d507df5d1141@placeholder.94092.edu. Printing is for personal, private use only. No part of this book may be reproduced or transmitted without publisher's prior permission. Violators will be prosecuted.

the same Miller indices but with opposite signs. A variety of common minerals, among them plagioclase and microcline, crystallize with 1 symmetry.

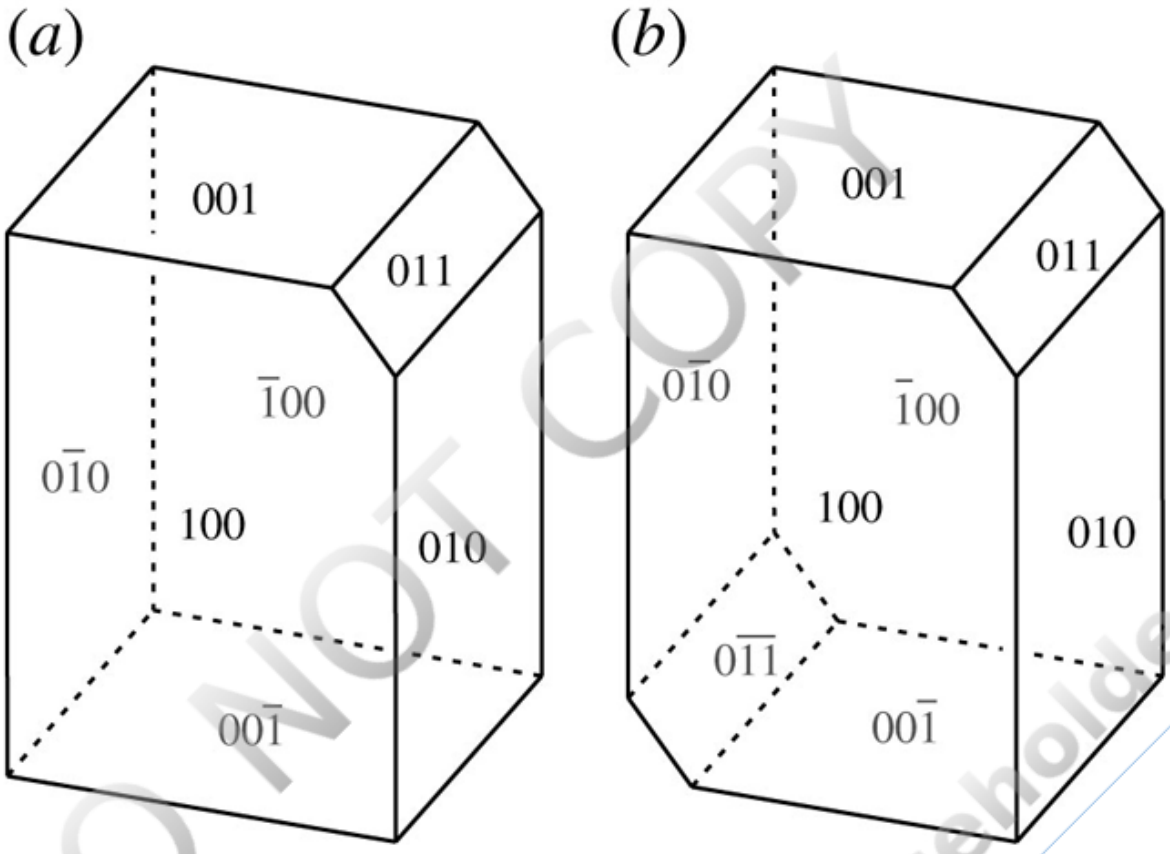

FIGURE 2.39 Forms in the triclinic crystal system. (*a*) A pedial class crystal of the 1 point group consisting of {100}, $\left\{100\right\}$, {010}, $\left\{0\,10\right\}$, {001}, $\left\{00\,1\right\}$, and {011} pedions. Note the lack of center symmetry. (*b*) A pinacoidal class crystal of the 1 point group consisting of {100}, {010}, {001}, and {011} pinacoids. View larger image

Monoclinic Crystal System

The crystal axes in the monoclinic system are most commonly oriented so that the *b* axis coincides with the 2-fold rotation axis and/or is perpendicular to the mirror plane. The *c* axis is placed parallel to a prominent zone axis and *a* is placed down and to the front so that the β angle is greater than 90°. Cleavage also may assist in establishing the orientation of the *a* and *c* axes. If a single prominent cleavage is parallel to the *b* axis, it generally is assumed to be parallel to the basal pinacoid {001}, and hence also parallel to the *a* axis. If two equivalent cleavages are symmetrically related by the mirror plane, they are usually taken to be parallel to the *c* axis. This convention for orienting the crystal axes is known as the second setting. The first setting convention places the *c* axis parallel to the 2-fold axis and *b* is parallel to a prominent zone. The second setting for monoclinic minerals will be used throughout this book and is used in all modern mineralogical literature. The forms found in monoclinic crystal systems are listed in Table 2.6. Only

Printed by: e48d507df5d1141@placeholder.94092.edu. Printing is for personal, private use only. No part of this book may be reproduced or transmitted without publisher's prior permission. Violators will be prosecuted.

minerals with 2/*m* symmetry are common (Table 2.3), and they include amphiboles, pyroxenes, micas, and many other minerals. **Figure 2.40** shows crystals with monoclinic symmetry.

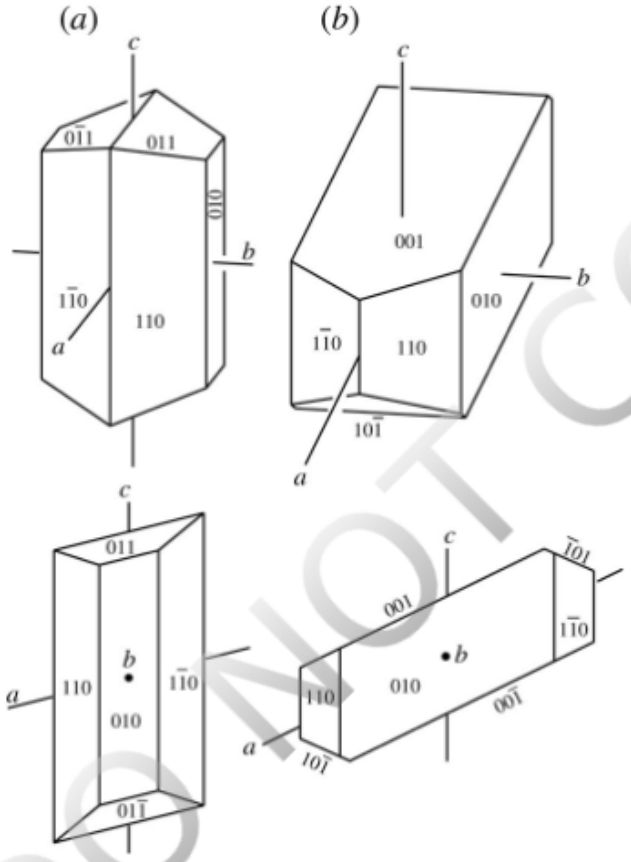

FIGURE 2.40 Monoclinic crystals. The views down the *b* axis show that the *a* and *c* axes are not at right angles. (*a*) 2/*m* point group amphibole crystal with a side {010} pinacoid and {110} and {011} prisms. (*b*) 2/*m* point group sanidine crystal with side {010}, basal {001}, and $\{10\bar{1}\}$ pinacoids; and {110} prism. View larger image

Orthorhombic Crystal System

The symmetry elements in the orthorhombic crystal system combine to produce three unique directions at right angles to each other that are parallel to the three crystal axes. The crystal axes are therefore either parallel to a 2-fold rotation axis and/or perpendicular to a mirror. Hermann–Mauguin symbols for each point group are written so that the first element refers to the *a* axis, the second to *b*, and the third to *c*. In the *mm*2 point group, for example, the *a* axis [100] is at right angles to a mirror, the *b* axis [010] is at right angles to a mirror, and the *c* axis [001] is a 2-fold rotation axis.

Except for the *mm*2 class, where the 2-fold rotation axis is taken as the *c* axis, no universally accepted convention determines which crystal axis coincides with which symmetry axis. A common procedure is to orient the crystal axes so that the unit cell dimensions are $c < a < b$. However, if a crystal has an elongate habit, the long axis may

DO NOT COPY

Printed by: e48d507df5d1141@placeholder.94092.edu. Printing is for personal, private use only. No part of this book may be reproduced or transmitted without publisher's prior permission. Violators will be prosecuted.

dimensions are $c < a < b$. However, if a crystal has an elongate habit, the long axis may be assigned to c regardless of unit cell dimensions. Similarly, the c axis may be placed perpendicular to a single prominent cleavage or to a prominent pinacoid that produces a distinctly tabular habit. Minerals with two equivalent cleavage directions (not generally at 90°) are oriented so that these prismatic cleavages are parallel to c and have the general form $\{hk0\}$. The reader is cautioned to confirm crystal axis conventions when reading the literature on orthorhombic minerals. The forms possible in the orthorhombic classes are listed in Table 2.6. **Figure 2.41** shows crystals that illustrate the different symmetry of the orthorhombic point groups. The common orthorhombic minerals all have $2/m\ 2/m\ 2/m$ symmetry (Table 2.3).

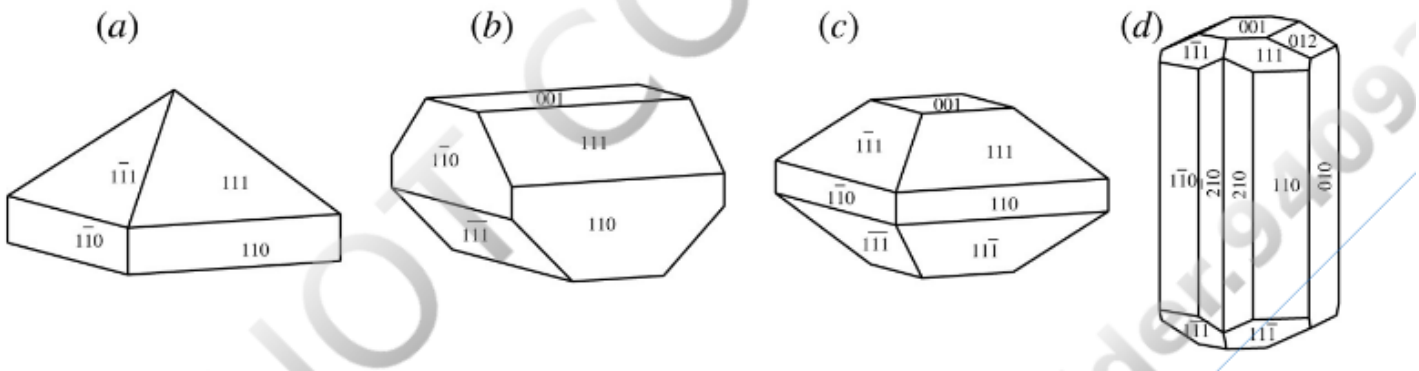

FIGURE 2.41 Orthorhombic crystals. Note how the (111), (110), and $\left(00\bar{1}\right)$ faces are duplicated to produce different forms based on the symmetry content. (*a*) *mm*2 point group crystal with a {110} rhombic prism, $\left\{00\bar{1}\right\}$ bottom pedion, and {111} rhombic pyramid. (*b*) 222 point group crystal with {111} rhombic tetrahedron (disphenoid), {110} rhombic prism, and {001} pinacoid. (*c*) $2/m\ 2/m\ 2/m$ point group crystal with a {001} pinacoid, {110} rhombic prism, and {111} rhombic dipyramid. (*d*) $2/m\ 2/m\ 2/m$ topaz crystal with {010} and {001} pinacoids; {110}, {210}, and {012} rhombic prisms, and {111} rhombic dipyramid. View larger image

Tetragonal Crystal System

All minerals in the tetragonal crystal system have a single 4-fold axis of rotation or rotoinversion that coincides with the c crystal axis. The a and b axes are at right angles to each other and coincide with 2-fold rotation axes or are perpendicular to mirror planes. The first Hermann–Mauguin symbol for the point group refers to symmetry on the c axis. The second symbols refer to symmetry tied to the a and b axes ([100] and [010]) and the third to symmetry tied to [110] and $\left[1\bar{1}0\right]$ axes at 45° to the a and b axes. In the $\bar{4}2m$ point group, the $\bar{4}$ indicates that the c axis [001] is a 4-fold rotoinversion axis, the 2 indicates that the a and b crystal axes ([100] and [010]) are 2-fold rotation axes, and the m indicates that [110] and $\left[1\bar{1}0\right]$ directions in the crystal lattice that bisect the angles between the a and b axes are perpendicular to mirrors. The forms found in the tetragonal crystal classes are listed in **Table 2.7**. Most common tetragonal minerals crystallize with $4/m\ 2/m\ 2/m$ symmetry (Table 2.3). **Figure 2.42** shows a selection of tetragonal crystals

Printed by: e48d507df5d1141@placeholder.94092.edu. Printing is for personal, private use only. No part of this book may be reproduced or transmitted without publisher's prior permission. Violators will be prosecuted.

illustrating the symmetry found in the common point groups.

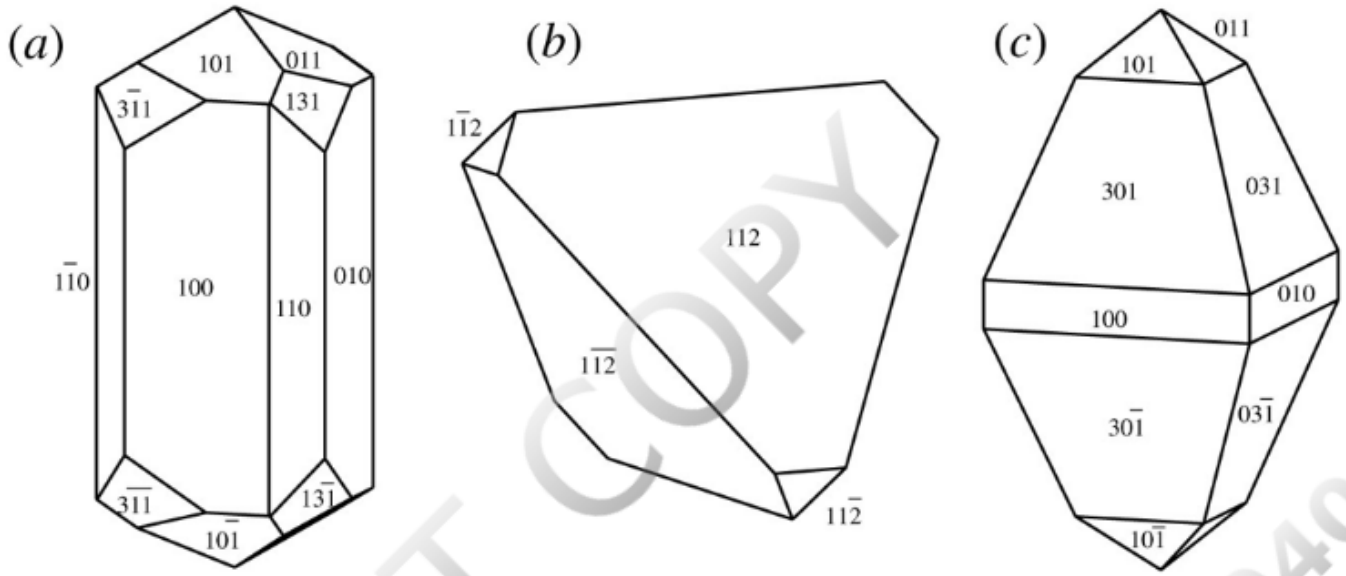

FIGURE 2.42 Tetragonal crystals. (*a*) 4/*m* scapolite crystal with {100} and {110} prisms, and {011} and {131} dipyramids. (*b*) $\bar{4}2m$ chalcopyrite crystal consisting of a positive {112} tetragonal tetrahedron (disphenoid) and a negative $\{1\ \bar{1}2\}$ tetragonal tetrahedron (smaller faces). (*c*) 4/*m* 2/*m* 2/*m* zircon crystal with {100} prism and {011} and {031} dipyramids. View larger image

Hexagonal Crystal System

The hexagonal crystal system is divided into hexagonal and trigonal (rhombohedral) divisions based on the presence of 6-fold or 3-fold symmetry, respectively. The *c* axis always is parallel to the 6- or 3-fold rotation axis. The *a* and *b* axes are arranged so that their positive ends are 120° from each other and either parallel to 2-fold rotation axes or perpendicular to mirror planes if these symmetry elements are present. The first number in the Hermann–Mauguin symmetry notation refers to symmetry tied to the *c* axis, the second to symmetry elements associated with the *a* and *b* axes ([100] and [010]), and the third to directions perpendicular to *a* and *b* ([210] and [120]).

Forms possible in each of the different hexagonal crystal classes are listed in **Table 2.8**. Many hexagonal minerals display the hexagonal prism because it is possible in all but the $\bar{6}$ and 3 point groups. Hexagonal minerals not dominated by a hexagonal prism are usually dominated by a rhombohedron or a trigonal prism. This makes distinguishing minerals in the hexagonal crystal system from other crystal systems relatively straightforward. Distinguishing among the different hexagonal point groups is often difficult, however, because faces that display reduced symmetry compared with the 6/*m* 2/*m* 2/*m* symmetry may be small or lacking. Visual inspection of real crystals often will allow differentiating only between the hexagonal and trigonal divisions based on the presence of 6-fold versus 3-fold symmetry parallel to *c*. **Figure 2.43** shows several common minerals that crystallize in the trigonal division. **Figure 2.44** shows examples of

Printed by: e48d507df5d1141@placeholder.94092.edu. Printing is for personal, private use only. No part of this book may be reproduced or transmitted without publisher's prior permission. Violators will be prosecuted.

common minerals that crystallize in the trigonal division. Figure 2.44 shows examples of minerals that crystallize in the hexagonal division.

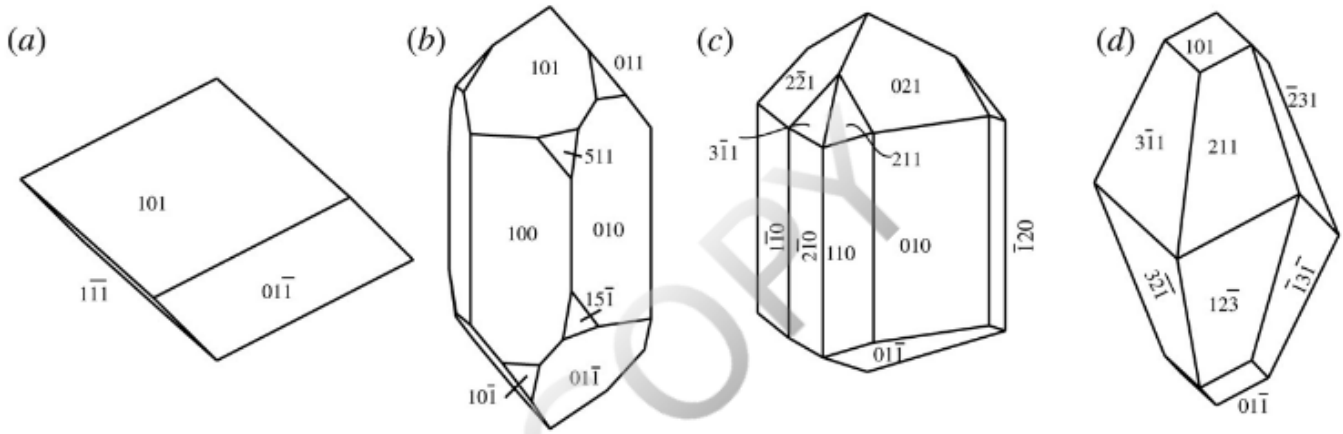

FIGURE 2.43 Crystals in the hexagonal crystal system, trigonal division. (*a*) Dolomite {101} rhombohedron in the $\bar{3}$ point group. The lack of vertical mirrors is not obvious based on these crystal faces. (*b*) 32 point group. Right-handed quartz with {100} prism, positive {101} and negative {011} rhombohedrons, and {511} trigonal scalenohedron. (*c*) 3*m* point group. Tourmaline with {021} trigonal pyramid and {211} ditrigonal pyramid on top, {110} and {010} prisms in the middle, and $\{01\,\bar{1}\}$ trigonal pyramid on the bottom. (*d*) $\bar{3}2m$ point group. Calcite crystal with {211} scalenohedron and {101} positive rhombohedron. View larger image

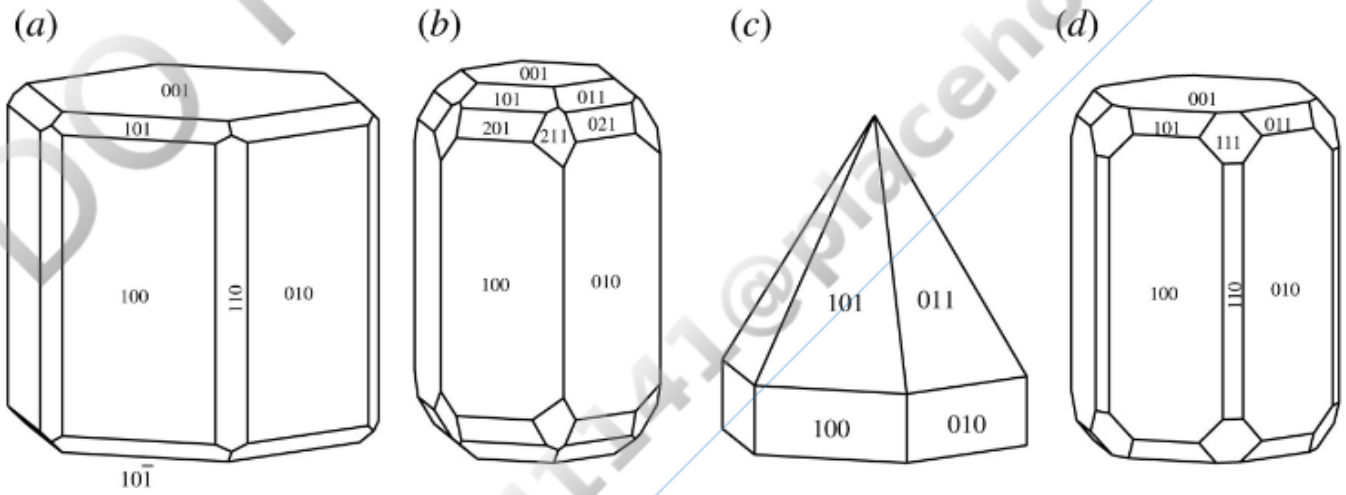

FIGURE 2.44 Crystals in the hexagonal crystal system, hexagonal division. (*a*) Nepheline (6 point group) crystals are rare, composed of {100} and {110} prisms, upper {101} and lower $\{10\bar{1}\}$ pyramids, and top {001} and bottom $\{00\bar{1}\}$ pedions. The crystal habit appears to have higher symmetry than the nepheline actually possesses. (*b*) 6/*m* apatite crystal composed of {100} prism; {101}, {201}, {211} dipyramids; and {001} pinacoid. Only the {211} dipyramid indicates that the symmetry is 6/*m*. (*c*) 6*mm* zincite crystal consists of {100} prism, {101} pyramid, and $\{00\bar{1}\}$ pedion. (*d*) 6/*m* 2/*m* 2/*m* beryl crystal with {100} and {110} prisms, {101} and {111} dipyramids, and {001} pinacoid. View larger image

Note that the trigonal scalenohedron (Figure 2.36 and Table 2.8) is referred to in some

Printed by: e48d507df5d1141@placeholder.94092.edu. Printing is for personal, private use only. No part of this book may be reproduced or transmitted without publisher's prior permission. Violators will be prosecuted.

sources as a hexagonal scalenohedron, ditrigonal scalenohedron, or hexagonal-trigonal scalenohedron. Similarly, the $\bar{3}2/m$ point group (Table 2.8) is also called the hexagonal, ditrigonal, or hexagonal-trigonal scalenohedral class. Given that the $\bar{3}2/m$ point group is a member of the trigonal division of the hexagonal crystal system, using the term *trigonal* for the form and crystal class seems less likely to cause confusion.

Isometric Crystal System

Crystals in the isometric crystal system have a cubic unit cell with three mutually perpendicular crystal axes *a*, *b*, and *c*. Note that these axes are sometimes referred to as a_1, a_2, and a_3. Three equivalent symmetry axes at right angles to each other coincide with the crystal axes. In three point groups, the crystal axes are 4-fold or 4-fold rotoinversion axes; in the remaining two point groups they are 2-fold axes. Hermann–Mauguin symbols for the point groups consist of up to three parts. The first symbol refers to the symmetry operations tied to the three crystal axes. The second refers to the three diagonal axes [111] through the cubic unit cell. The third refers to the six directions that run from the center of one edge of the unit cell to the center of the opposite edge [110]. Crystal forms found in each of the isometric crystal classes are listed in **Table 2.9** and are shown individually in Figure 2.33. Symmetry elements and selected crystal forms found in the $2/m\,\bar{3}$, $\bar{4}3m$, and $\bar{4}/m\bar{3}2/m$ point groups are shown in **Figures 2.45** through **2.48**.

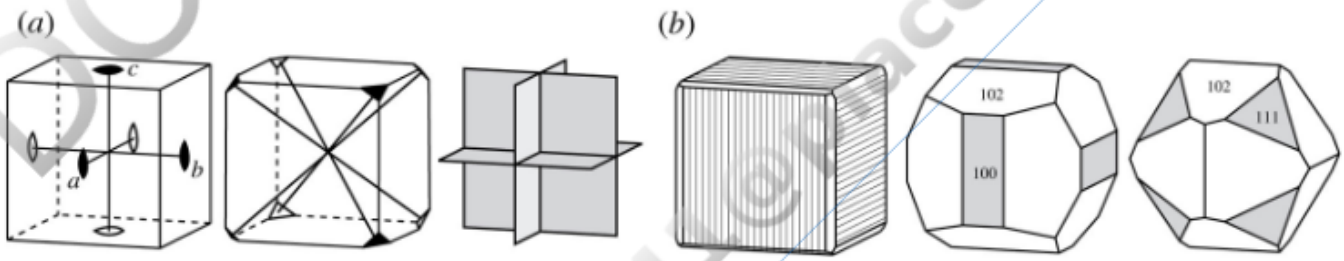

FIGURE 2.45 $2\,/\,m\,\bar{3}$ point group. (*a*) Three 2-fold axes are parallel to the crystal axes, four 3-fold axes are parallel to the long diagonals through the unit cell, and three mirror planes are parallel to the cube faces. (*b*) Striations on pyrite cube (left) are produced by interaction between the shaded cube {001} and pyritohedron {102} faces (center). Shaded octahedron {111} faces modify a pyritohedron (right). Not shown, but striations are also commonly found on pyritohedron and octahedron faces. View larger image

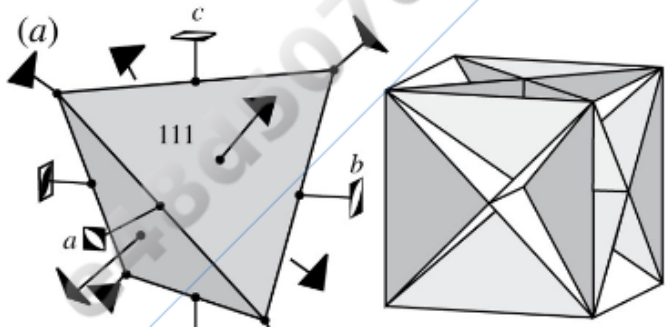

Printed by: e48d507df5d1141@placeholder.94092.edu. Printing is for personal, private use only. No part of this book may be reproduced or transmitted without publisher's prior permission. Violators will be prosecuted.

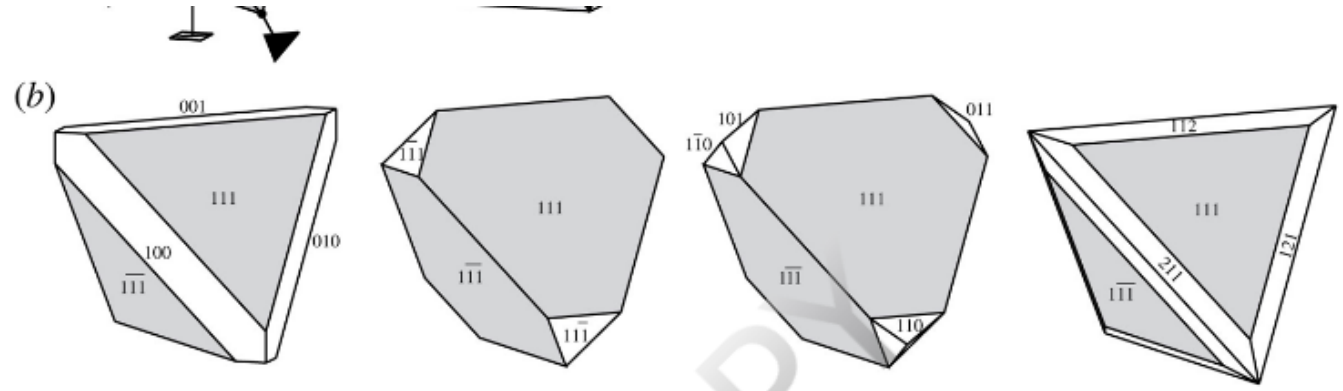

FIGURE 2.46 $\bar{4}3m$ point group. (*a*) Crystal axes (*a*, *b*, *c*) are parallel to the three 4-fold rotoinversion axes. Four 3-fold axes are parallel to the long diagonals through the cube and perpendicular to the tetrahedron crystal faces. Six mirrors are parallel to the body diagonals through the cubic unit cell. (*b*) Tetrahedrons {111} (dark) combined with (left to right) cube {001}, negative tetrahedron $\{1\bar{1}1\}$, dodecahedron {011}, and tristetrahedron {121}. View larger image

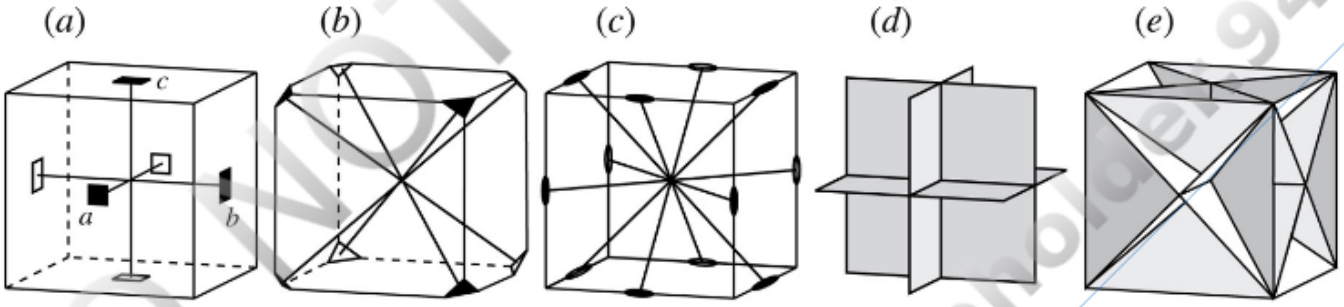

FIGURE 2.47 Symmetry elements in the $\bar{4}/m\,\bar{3}\,2/m$ point group. (*a*) Three 4-fold rotation axes are parallel to the three crystal axes. (*b*) Four 3-fold axes are parallel to the long diagonals through the cube. (*c*) Six 2-fold axes are parallel to edge-to-edge diagonals. (*d*) Three mirrors are parallel to cube faces. (*e*) Six mirrors are parallel to diagonals through the cube. View larger image

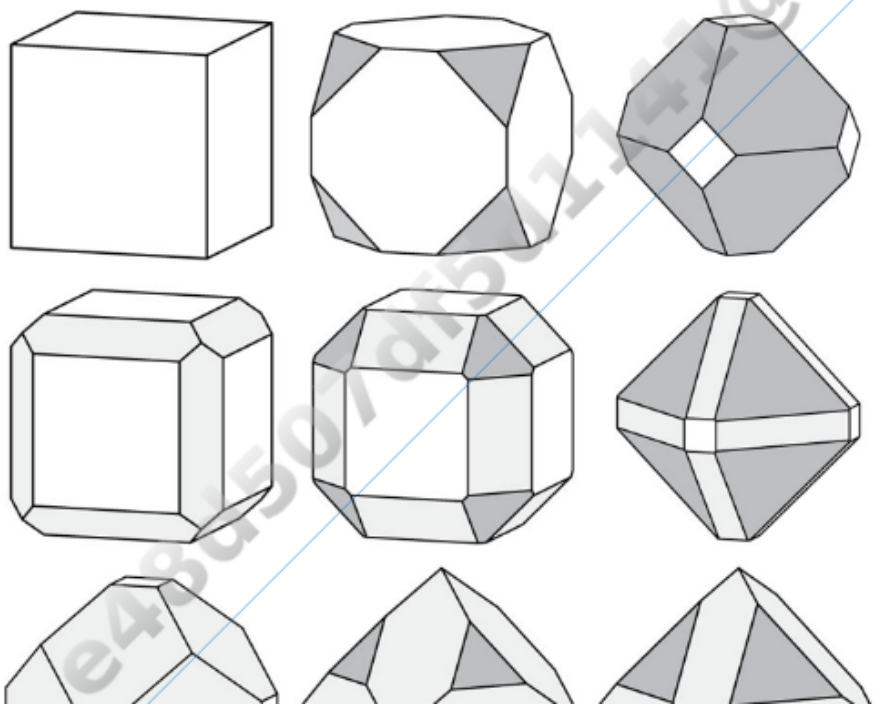

DO NOT COPY
e48d507df5d1141@placeholder.9409

Printed by: e48d507df5d1141@placeholder.94092.edu. Printing is for personal, private use only. No part of this book may be reproduced or transmitted without publisher's prior permission. Violators will be prosecuted.

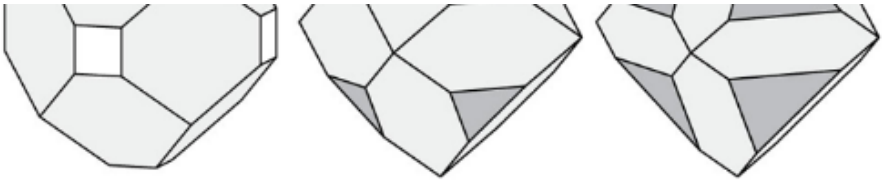

FIGURE 2.48 Various combinations of {001} cube (white), {011} dodecahedron (light), and {111} octahedron (dark) in the $\overline{4}/m\,\overline{3}\,2/m$ point group. See Table 2.9 and Figure 2.33 for additional forms that may appear. View larger image

DO NOT COPY
e48d507df5d1141@placeholder.9409

Printed by: e48d507df5d1141@placeholder.94092.edu. Printing is for personal, private use only. No part of this book may be reproduced or transmitted without publisher's prior permission. Violators will be prosecuted.

Crystal Habit

In addition to the formal crystallographic nomenclature, a variety of descriptive terminology has developed to help describe minerals and mineral aggregates. Some commonly used terms are defined here. A wide variety of additional terminology is used to describe textural features of various rock types. For a coherent description of much of this terminology, see Williams and others (1982). To fully describe any mineral grain or mineral aggregate, many terms must be applied.

Minerals may or may not display crystal faces depending on conditions of growth. Samples that display well-formed crystal faces are **euhedral**, and those without crystal faces are **anhedral**. If crystal faces are present, but are not well formed, the term **subhedral** is used (**Figure 2.49**).

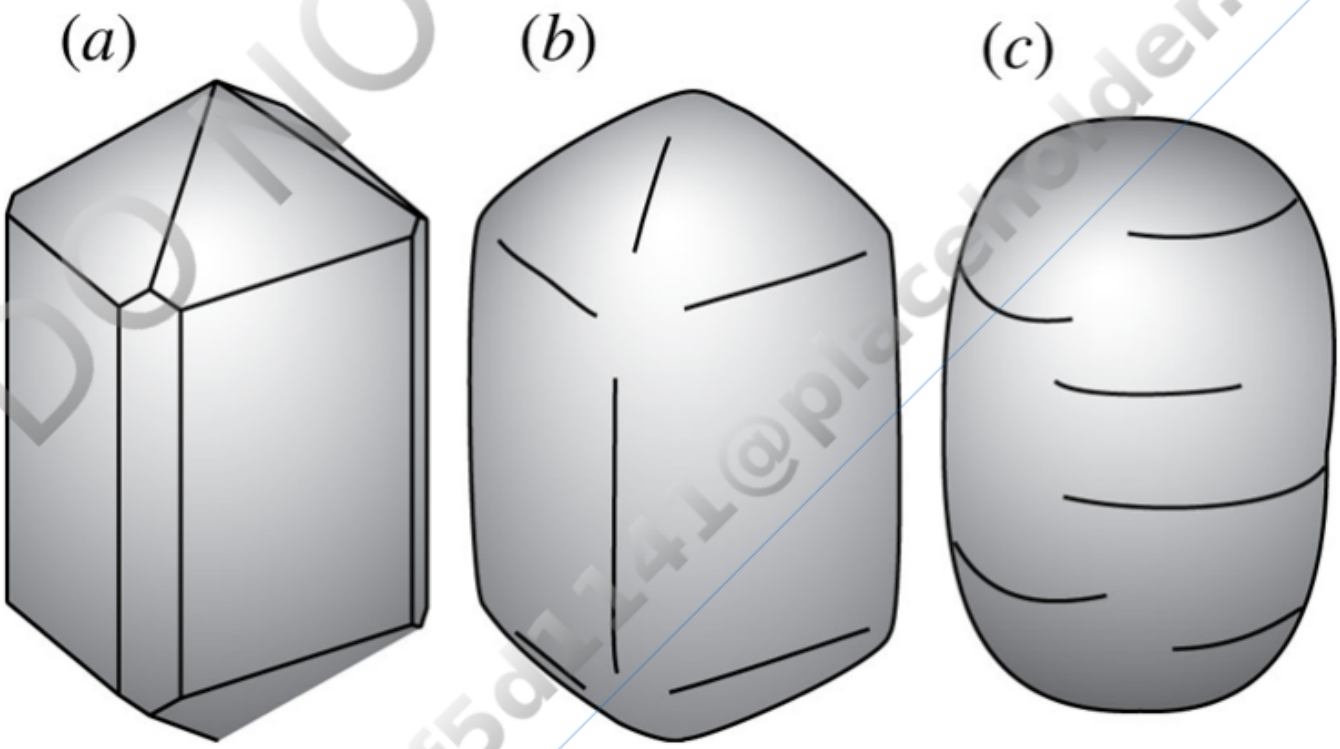

FIGURE 2.49 Degree to which crystal faces are well developed. (*a*) Euhedral. (*b*) Subhedral. (*c*) Anhedral. View larger image

Figure 2.50 shows the range of terminology used to describe the relative dimensions of individual crystals or mineral grains. These terms can be used regardless whether euhedral/anhedral, what form may be displayed, and the mineral's point group. **Equant** crystals have length, width, and height that are about the same. **Elongate**, **acicular**, and **fibrous**, **filiform**, or **capillary** crystals are progressively more elongate. **Stubby**, **platy**, and **scaly** or **micaceous** grains are progressively flatter or thinner. **Tabular** crystals are

DO NOT COPY e48d507df5d1141@placeholder.9409

Printed by: e48d507df5d1141@placeholder.94092.edu. Printing is for personal, private use only. No part of this book may be reproduced or transmitted without publisher's prior permission. Violators will be prosecuted.

and **scaly** or **micaceous** grains are progressively flatter or thinner. **Tabular** crystals are roughly book-shaped, and **bladed** crystals are relatively thin and elongate like a knife blade. **Columnar** refers to a crystal that is shaped like a column. Columnar crystals may be stubby, elongate, or acicular, for example.

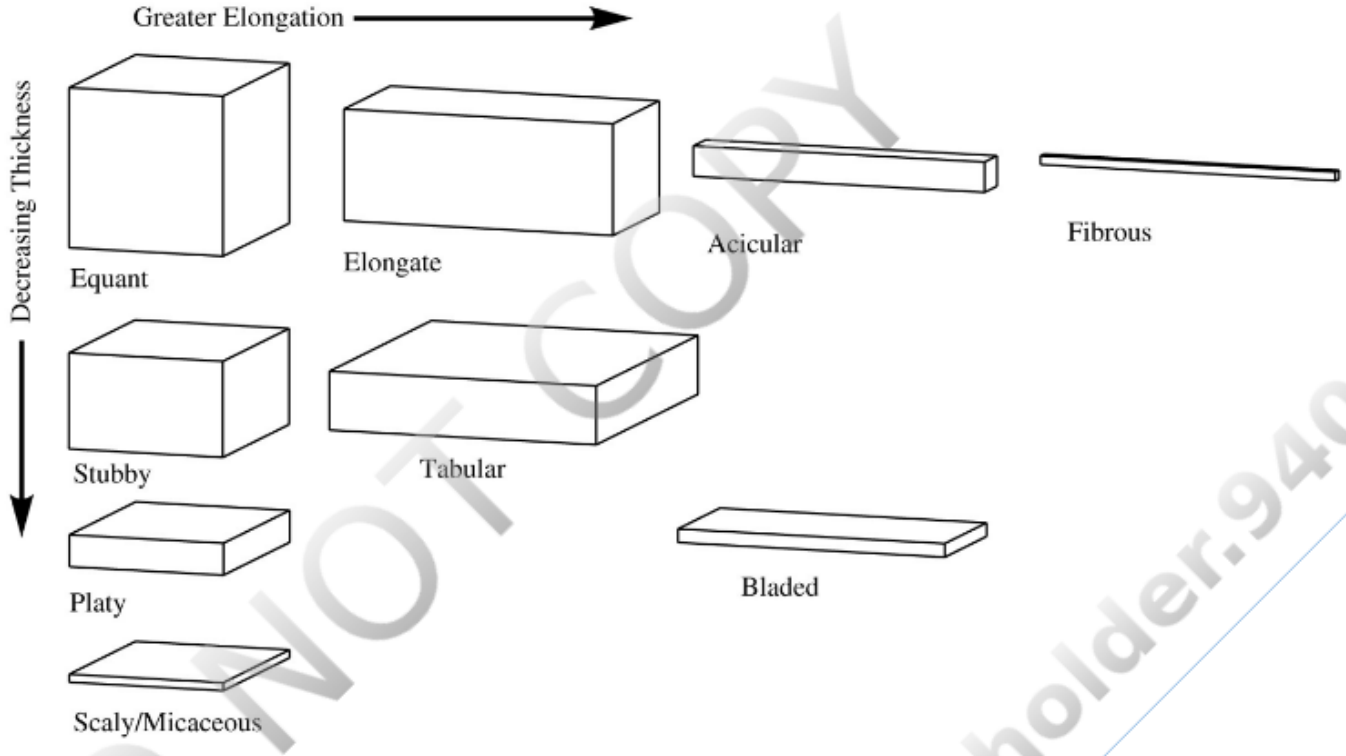

FIGURE 2.50 Nomenclature for describing the habit of individual mineral grains as a function of relative dimensions. View larger image

Figure 2.51 shows some of the systematic patterns by which mineral grains are **intergrown**, or have interlocking grain boundaries due to simultaneous growth. Equant minerals typically intergrow in a **granular** texture, and elongate minerals can form parallel or **radiating** aggregates. Platy or micaceous minerals that grow in parallel alignment are **foliated**; those that form a radiating aggregate are **plumose**.

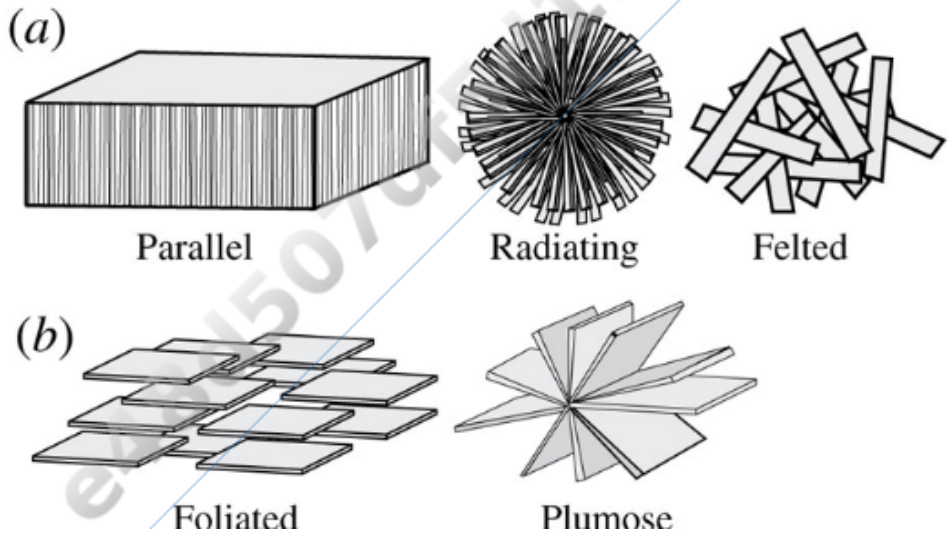

DO NOT COPY e48d507df5d1141@placeholder.9409

Printed by: e48d507df5d1141@placeholder.94092.edu. Printing is for personal, private use only. No part of this book may be reproduced or transmitted without publisher's prior permission. Violators will be prosecuted.

Foliated Plumose

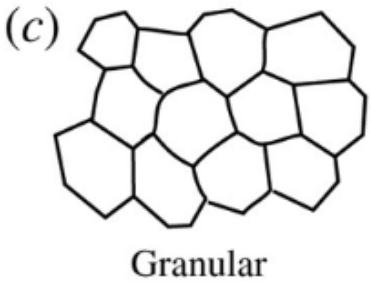

FIGURE 2.51 Patterns of mineral growth. (*a*) Elongate minerals can form parallel, radiating, or felted masses. (*b*) Platy or micaceous minerals can form foliated or plumose arrangements. (*c*) Equant minerals can form fine- to coarse-grained granular masses. View larger image

When minerals precipitate and grow on a preexisting rock surface, in a fault or fracture zone for example, the pattern of growth may take on distinctive forms (**Figure 2.52**).

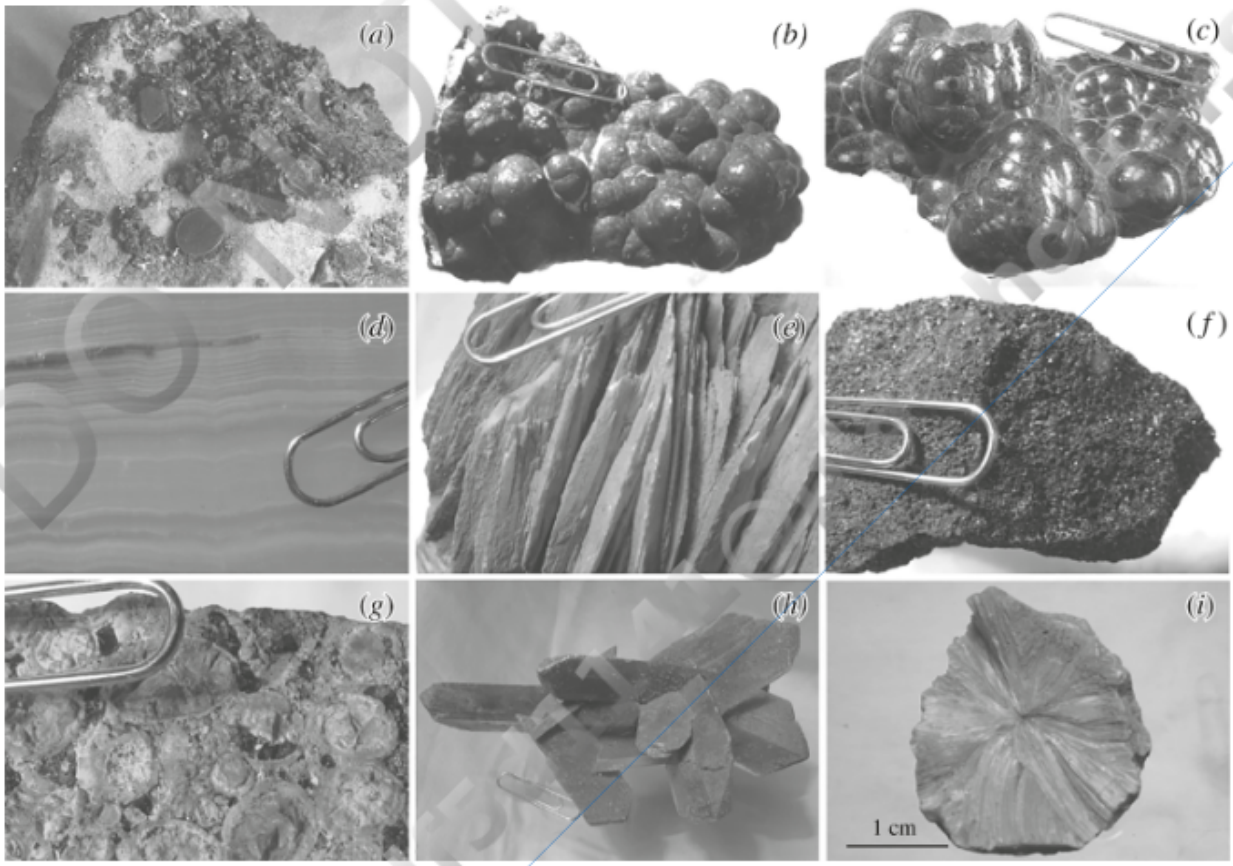

FIGURE 2.52 Habits of crystalline masses. (*a*) Drusy encrustation of sphalerite and galena on white quartz. (*b*) Botryoidal hematite. (*c*) Mammillary hematite. (*d*) Banded chalcedony. (*e*) Lamellar intergrowth of tabular barite crystals. (*f*) Granular massive chromite. (*g*) Pisolitic aluminum oxides in bauxite. (*h*) Reticulated crystals of gypsum. (*i*) Radiating concretion of barite. View larger image

Drusy	An encrustation, or coating of euhedral crystals around other minerals.
Colloform	Rounded forms usually consisting of radiating aggregates of elongate mineral grains or crystals.

Printed by: e48d507df5d1141@placeholder.94092.edu. Printing is for personal, private use only. No part of this book may be reproduced or transmitted without publisher's prior permission. Violators will be prosecuted.

Globular	A colloform mass that is roughly spherical.
Botryoidal	Overlapping colloform masses that look like a bunch of grapes.
Mammillary	Overlapping colloform masses that have the smooth rounded forms of mammary glands (e.g., a cow's udder).
Reniform	A colloform mass that is kidney shaped.

Botryoidal, mammillary, and reniform are listed in order of decreasing "lumpiness"—the dividing lines between them are poorly defined. Other terms that describe crystal shape, mineral aggregates, or distribution include the following.

Banded	Bands or layers of mineral with different color or texture.
Dendritic	Crystal aggregate has a branching form somewhat like a tree (Figure 18.9).
Skeletal	Crystals with both euhedral faces and voids that are produced by rapid growth; some dendritic crystals are also referred to as skeletal.
Prismatic	Euhedral crystals with prominent prism faces. Prismatic may also refer to cleavage faces that are parallel to prisms.
Lamellar	Composed of layers, like the pages of a book.
Massive	An aggregate of mineral grains without distinctive form or crystal faces. If individual grains are visible: granular massive. If very fine grained: compact massive.
Oolitic/Pisolitic	Roughly spherical mineral grains formed of concentric layers. Pisolites are roughly 1 cm in diameter; oolites are a few millimeters in diameter.
Reticulated	Crystals are intergrown to form an open framework.
Disseminated	Grains of a relatively low abundance mineral are isolated from each other and are evenly scattered throughout a rock or ore body.

The descriptive nomenclature is by no means restricted to these terms—almost any descriptive term may be used.

DO NOT COPY e48d507df5d1141@placeholder.9409

Printed by: e48d507df5d1141@placeholder.94092.edu. Printing is for personal, private use only. No part of this book may be reproduced or transmitted without publisher's prior permission. Violators will be prosecuted.

Botryoidal, mammillary, and reniform are listed in order of decreasing "lumpiness"—the dividing lines between them are poorly defined. Other terms that describe crystal shape, mineral aggregates, or distribution include the following.

Banded	Bands or layers of mineral with different color or texture.
Dendritic	Crystal aggregate has a branching form somewhat like a tree (Figure 18.9).
Skeletal	Crystals with both euhedral faces and voids that are produced by rapid growth; some dendritic crystals are also referred to as skeletal.
Prismatic	Euhedral crystals with prominent prism faces. Prismatic may also refer to cleavage faces that are parallel to prisms.
Lamellar	Composed of layers, like the pages of a book.
Massive	An aggregate of mineral grains without distinctive form or crystal faces. If individual grains are visible: granular massive. If very fine grained: compact massive.
Oolitic/Pisolitic	Roughly spherical mineral grains formed of concentric layers. Pisolites are roughly 1 cm in diameter; oolites are a few millimeters in diameter.
Reticulated	Crystals are intergrown to form an open framework.
Disseminated	Grains of a relatively low abundance mineral are isolated from each other and are evenly scattered throughout a rock or ore body.

The descriptive nomenclature is by no means restricted to these terms—almost any descriptive term may be used.

REFERENCES CITED AND SUGGESTIONS FOR ADDITIONAL READING

DO NOT COPY e48d507df5d1141@placeholder.9409-

Printed by: e48d507df5d1141@placeholder.94092.edu. Printing is for personal, private use only. No part of this book may be reproduced or transmitted without publisher's prior permission. Violators will be prosecuted.

LIST OF KEY TERMS

32 point groups
acicular
anhedral
axial intercept
axial ratio
banded
basal
bladed
body-centered (I)
botryoidal
Bravais lattices
capillary
center symmetry
centered rectangle (C)
closed form
colloform
columnar
crystal axes
crystal class
crystal face
crystal family
crystal form
crystal habit
crystal lattice
crystallographic direction
crystal system
cubic
dendritic
diamond

DO NOT COPY
e48d507df5d1141@placeholder.9409

Printed by: e48d507df5d1141@placeholder.94092.edu. Printing is for personal, private use only. No part of this book may be reproduced or transmitted without publisher's prior permission. Violators will be prosecuted.

diamond

dihedron

dipyramid

disseminated

dome

drusy

elongate

equant

euhedral

face-centered (C)

face-centered (F)

fibrous

filiform

foliated

glide plane

glide

globular

granular

Hermann–Mauguin

hexagonal

hexagonal Bravais lattice

intergrown

inversion symmetry

isometric

isometric Bravais lattices

lamellar

lattice line

lattice node

law of Bravais

law of constancy of interfacial angles

law of Haüy

mammillary

massive

micaceous

DO NOT COPY
e48d507df5d1141@placeholder.9409

Printed by: e48d507df5d1141@placeholder.94092.edu. Printing is for personal, private use only. No part of this book may be reproduced or transmitted without publisher's prior permission. Violators will be prosecuted.

micaceous

Miller-Bravais index

Miller index

monoclinic

monoclinic Bravais lattices

oblique

oolitic

open form

origin

orthorhombic

orthorhombic Bravais lattices

pedion

pinacoid

pisolitic

plane lattice

platy

plumose

point group

point symmetry

primitive

prismatic

prism (O)

pyramid

quasicrystals

radiating

rectangle

reflection

reniform

reticulated

rhombohedron

rotation

rotoinversion

rotoinversion axis

DO NOT COPY e48d507df5d1141@placeholder.9409

Printed by: e48d507df5d1141@placeholder.94092.edu. Printing is for personal, private use only. No part of this book may be reproduced or transmitted without publisher's prior permission. Violators will be prosecuted.

scalenohedron
scaly
screw axis
screw
skeletal
space group
space lattice
sphenoid
square
Steno's law
stubby
subhedral
symmetry symbols
tabular
tetragonal
tetragonal Bravais lattices
tetrahedron
translational symmetry
trapezohedron
triclinic
triclinic Bravais lattice
unit cell
unit face
unit mesh axes
unit mesh
zone axis
zone

DO NOT COPY
e48d507df5d1141@placeholder.9409

Printed by: e48d507df5d1141@placeholder.94092.edu. Printing is for personal, private use only. No part of this book may be reproduced or transmitted without publisher's prior permission. Violators will be prosecuted.

CHAPTER 3
Crystal Chemistry

William D. Nesse
University of Northern Colorado

Graham B. Baird
University of Northern Colorado

DO NOT COPY
e48d507df5d1141@placeholder.9409

Printed by: e48d507df5d1141@placeholder.94092.edu. Printing is for personal, private use only. No part of this book may be reproduced or transmitted without publisher's prior permission. Violators will be prosecuted.

Introduction

Because minerals are crystalline solids, they must have definite, but not necessarily fixed, chemical compositions. In this chapter some introductory chemistry is explored to provide a basis for understanding mineral compositions and properties. The following questions will be addressed.

What is the nature of chemical elements?

What is the abundance of chemical elements available to make minerals?

What mechanisms cause chemical elements to bond and form solids?

What is the size of atoms and ions?

DO NOT COPY
e48d507df5d1141@placeholder.9409

Printed by: e48d507df5d1141@placeholder.94092.edu. Printing is for personal, private use only. No part of this book may be reproduced or transmitted without publisher's prior permission. Violators will be prosecuted.

The Nature of Chemical Elements

All minerals are composed of chemical elements in various combinations. The atoms of each element are composed of the fundamental building blocks of matter: **protons**, **neutrons**, and **electrons** (Table 3.1). Other particles such as neutrinos and quarks are of great interest to atomic physicists but are not important in the present context. The **periodic table** of the elements is after the index.

TABLE 3.1 The Principal Atomic Particles

Particle	Electric Charge	Atomic Mass Units[a]
Proton	+1	1.00728
Neutron	0	1.00866
Electron	−1	0.00055

[a] 1 AMU = 1/12 the weight of a ^{12}C atom.

Nucleus

Protons and neutrons are held together in the nucleus by poorly understood strong attractive forces that overcome the otherwise normal tendency of the positively charged protons to repel each other. Each chemical element has a specific number of protons in the nucleus. The number of protons is the **atomic number** (Z) of that particular element. For example, the nucleus of hydrogen has a single proton, oxygen has 8 protons, and aluminum has 13 protons.

The number of neutrons in the nucleus of each atom is about the same as the number of protons for elements with a small atomic number, and larger than the number of protons for higher atomic numbers. The number of neutrons in the nucleus, however, varies for each element. *Each isotope of an element has a different number of neutrons*. The sum of the number of neutrons and protons is the **mass number** or atomic mass number of an atom. To distinguish among the different isotopes of an element, the mass number of the isotope is written as a superscript to the left of the atomic symbol. For example, potassium (K) is atomic number 19 ($Z = 19$), so the nucleus of every potassium atom contains 19 protons. It has three main isotopes with different numbers of neutrons in the nucleus: ^{39}K has mass number 39 with 20 neutrons, ^{40}K has mass number 40 with 21 neutrons, and ^{41}K has mass number 41 with 22 neutrons.

The **atomic mass** of an atom is the mass of the atom divided by one-twelfth the mass of a ^{12}C atom. Except for ^{12}C, the atomic mass is slightly different from the mass number for

DO NOT COPY e48d507df5d1141@placeholder.94092

Printed by: e48d507df5d1141@placeholder.94092.edu. Printing is for personal, private use only. No part of this book may be reproduced or transmitted without publisher's prior permission. Violators will be prosecuted.

^{12}C atom. Except for ^{12}C, the atomic mass is slightly different from the mass number for the atom. Because each isotope of an element has a different number of neutrons, each isotope must have a different atomic mass. The **atomic weight** of an element is the weighted average of the atomic masses of the isotopes. The weighted average takes into account the different abundances of the isotopes. For potassium, the three main isotopes (^{39}K, ^{40}K, and ^{41}K) have atomic masses of 38.964, 39.964, and 40.963 and abundances of 93.26 percent, 0.01 percent, and 6.73 percent, respectively. The weighted average of the atomic masses gives the atomic weight of 39.098. These atomic weights are reported on the periodic table of the elements (see after index).

The atomic weight of an element depends on the isotopic composition of the sample being considered. The Commission on Isotropic Abundances and Atomic Weights periodically reviews these values and recommends revisions based both on refinements of the atomic masses of the isotopes and on isotopic abundances. The isotopic abundances used by the commission are based on material likely to be available in the laboratory or used for industry, and explicitly are *not* based on the composition of the Earth or its crust or any other geological material. A recent compilation (Wieser and others, 2013) reports atomic weight ranges for 12 elements, rather than fixed values. So that students can have fixed values to use in calculations, atomic weights shown on this text's periodic table for these 12 elements are taken from the 2007 compilation (Wieser and Berglund, 2009).

The actual isotopic composition and atomic weight of any element found in rocks and minerals may differ somewhat from the "standard" values reported by the commission. For many purposes, the variations are not significant; in some cases, however, variations in the isotopic compositions of some elements in minerals are important and can provide very useful geologic information. An obvious example is radiometric dating, in which radioactive decay of uranium isotopes to isotopes of lead, for example, changes the isotopic composition of those elements in a mineral and allows the time of crystallization of the mineral to be determined (Chapter 5; Box 5.1).

A total of 118 different chemical elements have been recognized by the International Union of Pure and Applied Chemistry, but *only 83 chemical elements are available to make minerals*. Atomic numbers 98 and below are known to occur naturally; numbers 99 and above are made only in nuclear laboratories. However, 15 of the 98 naturally occurring elements are **geologically ephemeral elements**. These geologically ephemeral elements occur only in very small amounts as short-lived radioactive isotopes produced by neutron capture and/or radioactive decay involving other elements. They then decay rapidly to yet other elements. Because the radioactive decay and nuclear processes that make and subsequently destroy these elements are continuous, some is always present, but only in minute quantities. These elements are technetium (Tc, Z = 43), promethium (Pm, Z = 61), polonium (Po, Z = 84), astatine (At, Z = 85), radon (Rn, Z = 86), francium (Fr, Z = 87), radium (Ra, Z = 88), actinium (Ac, Z = 89), protactinium (Pa, Z = 91), neptunium (Np, Z = 93), plutonium (Pu, Z = 94), americium (Am, Z = 95), curium (Cm, Z = 96), berkelium (Bk, Z = 97), and californium (Cf, Z = 98).

Perhaps the rarest of these geologically ephemeral elements is berkelium. Close behind is

Printed by: e48d507df5d1141@placeholder.94092.edu. Printing is for personal, private use only. No part of this book may be reproduced or transmitted without publisher's prior permission. Violators will be prosecuted.

Perhaps the rarest of these geologically ephemeral elements is berkelium. Close behind is astatine, whose isotopes are produced from the decay of both uranium and thorium. Decay of uranium in a mineral such as uraninite (UO_2) yields atoms of astatine, which then promptly radioactively decay to form yet other chemical elements. The longest-lived isotope of astatine has a half-life of 56 seconds. It has been estimated that the total amount of natural astatine present in the Earth's crust at any time is about 30 grams, or about a teaspoonful.

Ephemeral elements with long half-lives include radium (Ra, $Z = 88$) and protactinium (Pa, $Z = 91$). The isotope ^{226}Ra, produced by ^{238}U decay, has a half-life of 1602 years, so small amounts are always present in uranium-bearing minerals. Another isotope, ^{231}Pa, produced by decay of ^{235}U, has a half-life of 32,760 years, so it could be long-lived enough to possibly be a primary chemical element in a mineral. No mineral with Pa as an essential element has been identified, so Pa is considered a geologically ephemeral element.

The list of chemical elements available to make minerals is further restricted because the noble gases that have stable isotopes—helium (He), neon (Ne), argon (Ar), krypton (Kr), and xenon (Xe)—are chemically unreactive. Isotopes of these elements are present in many minerals in small amounts because they are produced by radioactive processes involving other elements, or are present because they got included in the structure by chance. However, no minerals include them as essential elements.

It is worth noting that lead (Pb, $Z = 82$) is the element with the highest atomic number considered to have stable isotopes. Of the elements with atomic numbers greater than 82, only bismuth (Bi, $Z = 83$), thorium (Th, $Z = 90$), and uranium (U, $Z = 92$) have long-lived isotopes that become normal constituents of minerals. Long considered to be a stable isotope, ^{209}Bi has recently been found to have a half-life of 1.9×10^{19} years. Theoretical considerations suggest that all elements above atomic number 66 (dysprosium) should be radioactive, but with very long half-lives. It remains to be seen whether experiment and observation support the theory.

Additional super-heavy elements, perhaps with atomic numbers as high as 126, may have been present in the early solar system. Theory suggests that some of these elements could have sufficiently long half-lives that traces might still remain in minerals. Detection of atomic numbers 108, 111, and 122 in minerals has been reported, but additional work is needed for confirmation.

Electrons

Electrons orbit about the nucleus. In an uncharged atom, the number of electrons is equal to the number of protons. The electrons do not orbit the nucleus randomly; rather, they are systematically organized into discrete energy levels identified with four different quantum numbers: n, l, m_l, and m_s (Table 3.2). The **Pauli exclusion principle** informs us that no two electrons in an atom can have the same four quantum numbers. The four

DO NOT COPY e48d507df5d1141@placeholder.94092

Printed by: e48d507df5d1141@placeholder.94092.edu. Printing is for personal, private use only. No part of this book may be reproduced or transmitted without publisher's prior permission. Violators will be prosecuted.

us that no two electrons in an atom can have the same four quantum numbers. The four quantum numbers are something like an address, equivalent to city, street, building, and room. No two electrons can, in effect, occupy the same room.

TABLE 3.2 Relationship among Quantum Numbers[a]

Principal Quantum Number		Angular Momentum Quantum Number		Magnetic Quantum Numbers	Spin Quantum Number	
n	Shell	l	Subshell	m_l	m_s	Number of Electrons
1	K	0	s	0	$+\frac{1}{2}$	2
					$-\frac{1}{2}$	
2	L	0	s	0	$+\frac{1}{2}$	2
					$-\frac{1}{2}$	
		1	p	-1	$+\frac{1}{2}$	6
					$-\frac{1}{2}$	
				0	$+\frac{1}{2}$	
					$-\frac{1}{2}$	
				+1	$+\frac{1}{2}$	
					$-\frac{1}{2}$	

[a] Only the K and L shells ($n = 1$ and 2) are shown.

The **principal quantum number** n can have any positive integer value. The energy of an electron principally depends on n; higher n means higher energy. Because higher energy is associated with greater distance from the nucleus, the principal quantum numbers are correlated with **shells** that traditionally are identified with letters (K, L, M, N, etc.).

n	1	2	3	4	...
Shell	K	L	M	N	...

The **angular momentum quantum number** l has values between 0 and $n - 1$ and distinguishes **subshells** with different shapes (**Figure 3.1**). Although an electron can, in principle, be in any location around the nucleus of an atom, on a statistical basis it will spend most of its time within the volume represented by its subshell. The subshells are conventionally identified with letters (s, p, d, and f).

DO NOT COPY e48d507df5d1141@placeholder.9409

Printed by: e48d507df5d1141@placeholder.94092.edu. Printing is for personal, private use only. No part of this book may be reproduced or transmitted without publisher's prior permission. Violators will be prosecuted.

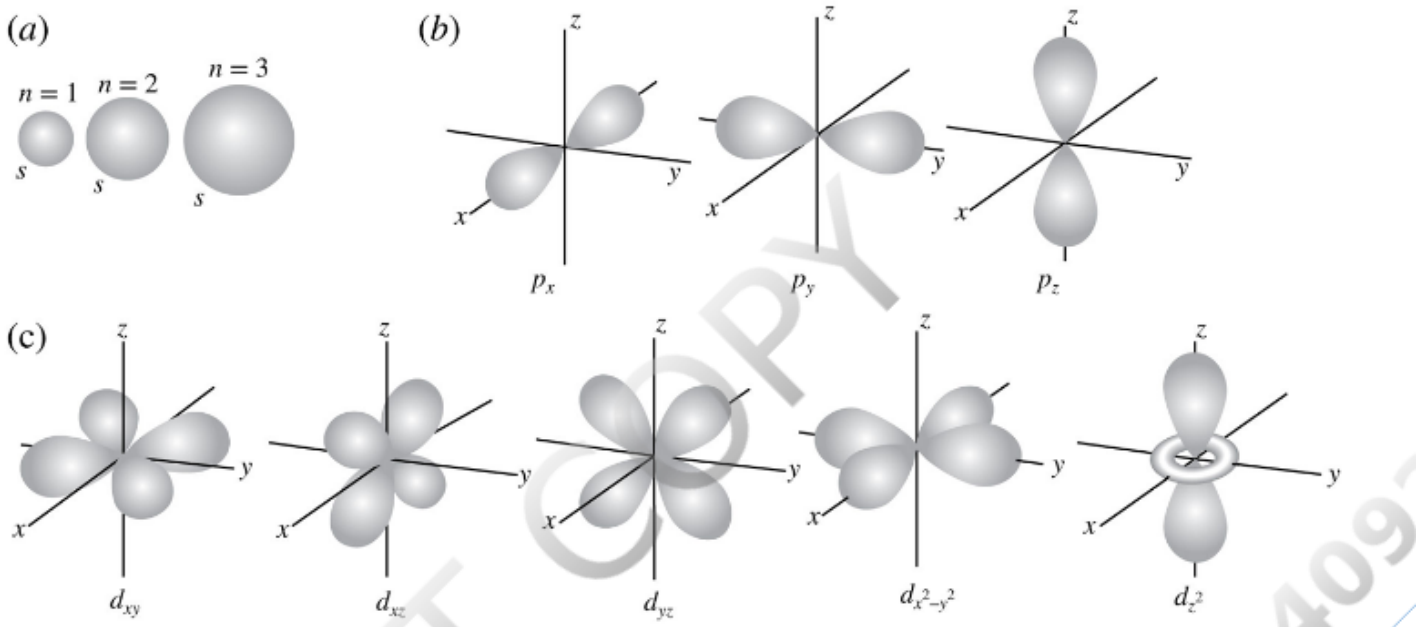

FIGURE 3.1 Geometry of orbitals in the *s*, *p*, and *d* subshells. Orbitals represent the volume around a nucleus in which an electron is most probably located. (*a*) Orbitals in the *s* subshells are spherical in all shells. (*b*) The *p* subshell contains three different bilobate orbitals oriented along orthogonal *x*, *y*, and *z* axes. (*c*) The *d* subshell contains five orbitals. The d_{xy}, d_{xz}, and d_{yz} orbitals are quadralobate and lie in the *xy*, *xz*, and *yz* planes, respectively, so that they bisect the angles between the orthogonal axes. The $d_{x^2-y^2}$ orbital forms a quadralobate shape with lobes aligned along the *x* and *y* axes. The d_{z^2} orbital forms a torus with a bilobate shape aligned along the *z* axis. View larger image

l	0	1	2	3
Subshell	*s*	*p*	*d*	*f*

The maximum subshell number within a shell is limited to $n - 1$. The *K* shell ($n = 1$) has only the *s* subshell ($l = 0$), the *L* shell ($n = 2$) can have only *s* and *p* subshells ($l = 1$), and so forth. The subshells are commonly identified with the principal quantum number of the shell and the letter associated with the subshell. For example, the *p* subshell in the *L* shell ($n = 2$) is the $2p$ subshell.

The **magnetic quantum number** m_l may have integer values between $-l$ and $+l$. It distinguishes among different **orbitals** with different orientations within a subshell. The number of orbitals within a subshell is $2l + 1$. For the *s* subshell $l = 0$, so $m_l = 0$ and the number of orbitals is 1. Because only one orientation is possible, the orbital is spherical (Figure 3.1a). In the *p* subshell $l = 1$, so the magnetic quantum numbers m_l are -1, 0, and $+1$. These are associated with three different bilobate (dumbbell-shaped) orbitals (Figure 3.1b) that lie along three mutually perpendicular axes. In the *d* subshell $l = 2$, so there are five orbitals (Figure 3.1c) distinguished with magnetic quantum numbers -2, -1, 0, $+1$, and $+2$. Four of the five orbitals within the *d* subshell are quadralobate; the fifth is bilobate with a torus (donut shape) in a plane at right angles. The *f* orbitals have

Printed by: e48d507df5d1141@placeholder.94092.edu. Printing is for personal, private use only. No part of this book may be reproduced or transmitted without publisher's prior permission. Violators will be prosecuted.

fifth is bilobate with a torus (donut shape) in a plane at right angles. The *f* orbitals have more complex geometries, which are not readily illustrated.

Each orbital can contain two electrons that are distinguished by their **spin quantum number** m_s. The possible values of m_s are $+\frac{1}{2}$ and $-\frac{1}{2}$. Electrons behave as though they were spinning on an axis, so the spin quantum numbers are generally taken to indicate a spin to the right and left, respectively. Because magnetic fields are generated by the movement of electric charge, each spinning negatively charged electron behaves like a simple magnet with north and south poles. If electron spins are balanced so that the number of right and left spins is the same, no net magnetic moment is formed. However, if electron spins are not balanced, a net magnetic moment may result, as is seen in metallic iron and the mineral magnetite.

The relative energy of the different orbitals is shown diagrammatically in **Figure 3.2**. Note that the energy level is not shown to scale. The energy difference between the inner orbitals (1*s* vs. 2*s*, for example) is large compared to the energy difference between the outer orbitals. Note also that the range of energy levels found in the subshells of the different shells overlaps. The 4*s* orbital has lower energy than the 3*d* orbital, for example. The general progression of increasing energy level is

$$1s\ 2s\ 2p\ 3s\ 3p\ 4s\ 3d\ 4p\ 5s\ 4d\ 5p\ 6s\ 4f\ 5d\ 6p\ 7s\ 6d\ 5f.$$

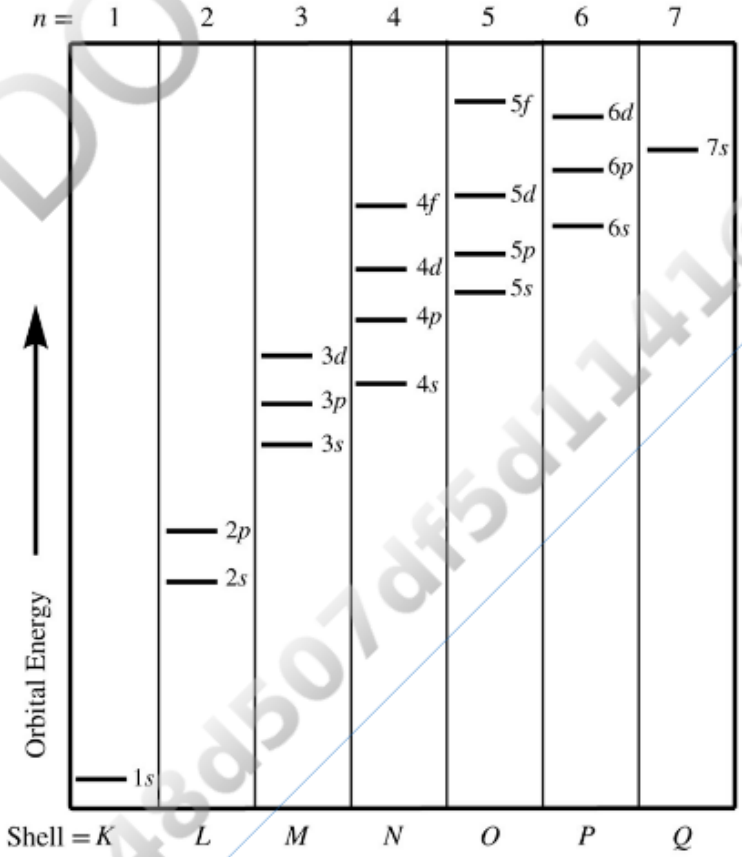

FIGURE 3.2 Relative energy level of electron subshells. Electrons fill subshells in order of

DO NOT COPY e48d507df5d1141@placeholder.9409

Printed by: e48d507df5d1141@placeholder.94092.edu. Printing is for personal, private use only. No part of this book may be reproduced or transmitted without publisher's prior permission. Violators will be prosecuted.

increasing energy level (compare to Table 3.3). View larger image

The electron configuration of uncharged atoms of the first 92 chemical elements is shown in **Table 3.3**. Note that with increasing atomic number, electrons systematically fill orbitals in order of energy level. The 1*s* orbital must be filled before electrons may occupy the 2*s* orbital, which must be filled before electrons may occupy the 2*p* orbitals, and so forth. Similarly, the 4*s* subshell has lower energy than the 3*d* subshell, so the 4*s* is filled first.

TABLE 3.3 Electron Configuration of Uncharged Atoms[a]

Atomic Number	Chemical Element	Shell/Subshell																
		K		*L*			*M*			*N*		*O*			*P*			
		1*s*	2*s*	2*p*	3*s*	3*p*	3*d*	4*s*	4*p*	4*d*	4*f*	5*s*	5*p*	5*d*	5*f*	5*g*	6*s*	6*p*
1	H	1																
2	***He***	***2***																
3	Li	2	1															
4	Be	2	2															
5	B	2	2	1														
6	C	2	2	2														
7	N	2	2	3														
8	O	2	2	4														
9	F	2	2	5														
10	***Ne***	***2***	***2***	***6***														
11	Na	2	2	6	1													
12	Mg	2	2	6	2													
13	Al	2	2	6	2	1												
14	Si	2	2	6	2	2												
15	P	2	2	6	2	3												
16	S	2	2	6	2	4												
17	Cl	2	2	6	2	5												
18	***Ar***	***2***	***2***	***6***	***2***	***6***												
19	K	2	2	6	2	6		1										
20	Ca	2	2	6	2	6		2										
21	Sc	2	2	6	2	6	1	2										

DO NOT COPY e48d507df5d1141@placeholder.94092

Printed by: e48d507df5d1141@placeholder.94092.edu. Printing is for personal, private use only. No part of this book may be reproduced or transmitted without publisher's prior permission. Violators will be prosecuted.

22	Ti	2	2	6	2	6	2	2										
23	V	2	2	6	2	6	3	2										
24	Cr	2	2	6	2	6	5	1										
25	Mn	2	2	6	2	6	5	2										
26	Fe	2	2	6	2	6	6	2										
27	Co	2	2	6	2	6	7	2										
28	Ni	2	2	6	2	6	8	2										
29	Cu	2	2	6	2	6	10	1										
30	Zn	2	2	6	2	6	10	2										
31	Ga	2	2	6	2	6	10	2	1									
32	Ge	2	2	6	2	6	10	2	2									
33	As	2	2	6	2	6	10	2	3									
34	Se	2	2	6	2	6	10	2	4									
35	Br	2	2	6	2	6	10	2	5									
36	***Kr***	***2***	***2***	***6***	***2***	***6***	***10***	***2***	***6***									
37	Rb	2	2	6	2	6	10	2	6			1						
38	Sr	2	2	6	2	6	10	2	6			2						
39	Y	2	2	6	2	6	10	2	6	1		2						
40	Zr	2	2	6	2	6	10	2	6	2		2						
41	Nb	2	2	6	2	6	10	2	6	4		1						
42	Mo	2	2	6	2	6	10	2	6	5		1						
43	Tc	2	2	6	2	6	10	2	6	5		2						
44	Ru	2	2	6	2	6	10	2	6	7		1						
45	Rh	2	2	6	2	6	10	2	6	8		1						
46	Pd	2	2	6	2	6	10	2	6	10								
47	Ag	2	2	6	2	6	10	2	6	10		1						
48	Cd	2	2	6	2	6	10	2	6	10		2						
49	In	2	2	6	2	6	10	2	6	10		2	1					
50	Sn	2	2	6	2	6	10	2	6	10		2	2					
51	Sb	2	2	6	2	6	10	2	6	10		2	3					
52	Te	2	2	6	2	6	10	2	6	10		2	4					
53	I	2	2	6	2	6	10	2	6	10		2	5					

DO NOT COPY e48d507df5d1141@placeholder.9409

Printed by: e48d507df5d1141@placeholder.94092.edu. Printing is for personal, private use only. No part of this book may be reproduced or transmitted without publisher's prior permission. Violators will be prosecuted.

53	I	2	2	6	2	6	10	2	6	10		2	5					
54	***Xe***	***2***	***2***	***6***	***2***	***6***	***10***	***2***	***6***	***10***		***2***	***6***					
55	Cs	2	2	6	2	6	10	2	6	10		2	6				1	
56	Ba	2	2	6	2	6	10	2	6	10		2	6				2	
57	La	2	2	6	2	6	10	2	6	10		2	6	1			2	
58	Ce	2	2	6	2	6	10	2	6	10	1	2	6	1			2	
59	Pr	2	2	6	2	6	10	2	6	10	2	2	6	1			2	
60	Nd	2	2	6	2	6	10	2	6	10	3	2	6	1			2	
61	Pm	2	2	6	2	6	10	2	6	10	4	2	6	1			2	
62	Sm	2	2	6	2	6	10	2	6	10	5	2	6	1			2	
63	Eu	2	2	6	2	6	10	2	6	10	6	2	6	1			2	
64	Gd	2	2	6	2	6	10	2	6	10	7	2	6	1			2	
65	Tb	2	2	6	2	6	10	2	6	10	8	2	6	1			2	
66	Dy	2	2	6	2	6	10	2	6	10	9	2	6	1			2	
67	Ho	2	2	6	2	6	10	2	6	10	10	2	6	1			2	
68	Er	2	2	6	2	6	10	2	6	10	11	2	6	1			2	
69	Tm	2	2	6	2	6	10	2	6	10	12	2	6	1			2	
70	Yb	2	2	6	2	6	10	2	6	10	13	2	6	1			2	
71	Lu	2	2	6	2	6	10	2	6	10	14	2	6	1			2	
72	Hf	2	2	6	2	6	10	2	6	10	14	2	6	2			2	
73	Ta	2	2	6	2	6	10	2	6	10	14	2	6	3			2	
74	W	2	2	6	2	6	10	2	6	10	14	2	6	4			2	
75	Re	2	2	6	2	6	10	2	6	10	14	2	6	5			2	
76	Os	2	2	6	2	6	10	2	6	10	14	2	6	6			2	
77	Ir	2	2	6	2	6	10	2	6	10	14	2	6	7			2	
78	Pt	2	2	6	2	6	10	2	6	10	14	2	6	9			1	
79	Au	2	2	6	2	6	10	2	6	10	14	2	6	10			1	
80	Hg	2	2	6	2	6	10	2	6	10	14	2	6	10			2	
81	Tl	2	2	6	2	6	10	2	6	10	14	2	6	10			2	1
82	Pb	2	2	6	2	6	10	2	6	10	14	2	6	10			2	2
83	Bi	2	2	6	2	6	10	2	6	10	14	2	6	10			2	3
84	Po	2	2	6	2	6	10	2	6	10	14	2	6	10			2	4

DO NOT COPY e48d507df5d1141@placeholder.94092

Printed by: e48d507df5d1141@placeholder.94092.edu. Printing is for personal, private use only. No part of this book may be reproduced or transmitted without publisher's prior permission. Violators will be prosecuted.

85	At	2	2	6	2	6	10	2	6	10	14	2	6	10			2	5
86	***Rn***	***2***	***2***	***6***	***2***	***6***	***10***	***2***	***6***	***10***	***14***	***2***	***6***	***10***			***2***	***6***
87	Fr	2	2	6	2	6	10	2	6	10	14	2	6	10			2	6
88	Ra	2	2	6	2	6	10	2	6	10	14	2	6	10			2	6
89	Ac	2	2	6	2	6	10	2	6	10	14	2	6	10			2	6
90	Th	2	2	6	2	6	10	2	6	10	14	2	6	10			2	6
91	Pa	2	2	6	2	6	10	2	6	10	14	2	6	10	2		2	6
92	U	2	2	6	2	6	10	2	6	10	14	2	6	10	3		2	6

[a] The noble gases are indicated in bold italics. The noble-gas core of elements is shown with light shading. The pseudo-noble-gas core of elements is shown with darker shading.

As every chemistry student learns, the elements are conveniently arranged in the periodic table, in a pattern reflecting the order in which electrons fill the orbitals in the ground state of uncharged atoms of the elements. Columns are called groups and rows are called periods. Elements in group 1 have one electron in the outer *s* subshell, those in group 2 have both electron positions in the outer *s* subshell filled, and so forth. The elements at the far right side of the table (group 18) have all of their subshells filled (Table 3.3) and are the chemically unreactive **noble gases**.

Table 3.3 shows that the electron configuration of elements exclusive of the noble gases consists of an inner shell configuration, called a core, in which all the orbital positions in each shell (*K*, *L*, *M*, etc.) are entirely filled. Additional electrons called **valence electrons** occupy subshells within shells that are not entirely filled. If the core is identical to the electron configuration of a noble gas, it is called a **noble-gas core** (light shading in Table 3.3). For example, Na has a Ne noble-gas core plus a single 3*s* valence electron, and Ca has an Ar noble-gas core plus two 4*s* valence electrons. A **pseudo-noble-gas core** consists of a noble-gas core plus an entirely filled *d* and/or *f* subshell (dark shading in Table 3.3). Arsenic (As), for example, has a pseudo-noble-gas core consisting of entirely filled 1*s*, 2*s*, 2*p*, 3*s*, 3*p*, 4*s*, and 3*d* subshells, plus three 4*p* valence electrons. Obviously, the noble gases have noble-gas cores and no valence electrons.

Element Groupings

The similarity of electronic configuration of different elements often leads to similarity in chemical behavior or properties. Based on such similarities, many elements are lumped together into formal and informal groupings. Depending on context, the groupings listed below and other groupings may be useful. Group 1 elements, not including H, are called the **alkali metals**, also referred to more simply as the **alkalis**. The most abundant alkalis found in minerals are Na and K, and alkali feldspar owes its name to the presence of these metals in its structure. Group 2 elements are called the **alkaline earth metals**.

DO NOT COPY e48d507df5d1141@placeholder.94092

Printed by: e48d507df5d1141@placeholder.94092.edu. Printing is for personal, private use only. No part of this book may be reproduced or transmitted without publisher's prior permission. Violators will be prosecuted.

Groups 3 through 12 are called the **transition metals** and these include the **lanthanide series** (atomic numbers 57–71) and the **actinide series** (atomic numbers 89–103). Other metals found in groups 13 through 16, such as Al and Pb, are sometimes called post-transition metals. Group 17 elements are called the **halogens** and group 18, as mentioned above, comprises the noble gases. **Nonmetals** typically include H, C, N, O, P, S, and Se, plus the halogens and noble gases. One of the most poorly defined groupings is the **metalloids**, or those elements that share properties of both the metals and nonmetals; these most commonly include B, Si, Ge, As, Sb, and Te. Many other groupings exists, such as the **rare earth elements** mentioned in Chapter 1, which include Sc, Y, and the lanthanides series.

Formation of Ions

Ions are atoms that have an excess or deficiency of electrons compared to the number of protons in the nucleus. **Anions** have a net negative charge because they have more electrons than protons; **cations** have a net positive charge because they have fewer electrons than protons. The charge of an ion is known as its **valence** or **oxidation state**.

Whether an element will form an anion or cation can usually be inferred from the configuration of the valence electrons. Elements will tend to gain or lose electrons to acquire the stable electron configuration displayed by the noble gases.

Neutral atoms of the metals have noble gas or pseudo-noble-gas cores and one or more valence electrons. Little energy is required to strip away the valence electrons to acquire the electron configuration of a noble gas, so the metals typically form cations.

Neutral atoms of many nonmetals have valence subshells that need only a few electrons to be filled. Hence these nonmetals have a strong affinity for electrons to fill the outer subshells and typically form anions.

Figure 3.3 shows the common oxidation states of the first 38 elements. For elements 1–20 and 31–38, the common oxidation states have a systematic pattern and reflect the pattern of filling the orbitals in the *s* and *p* subshells. For example, the increase in oxidation state from Li^+ to N^{5+} is caused by the loss of electrons from the 2*s* and 2*p* subshells required to achieve the filled-shell configuration of He. In contrast, O^{2-} and F^- gain electrons to fill the remaining sites in the 2*p* subshell and thereby acquire the stable electron configuration of Ne.

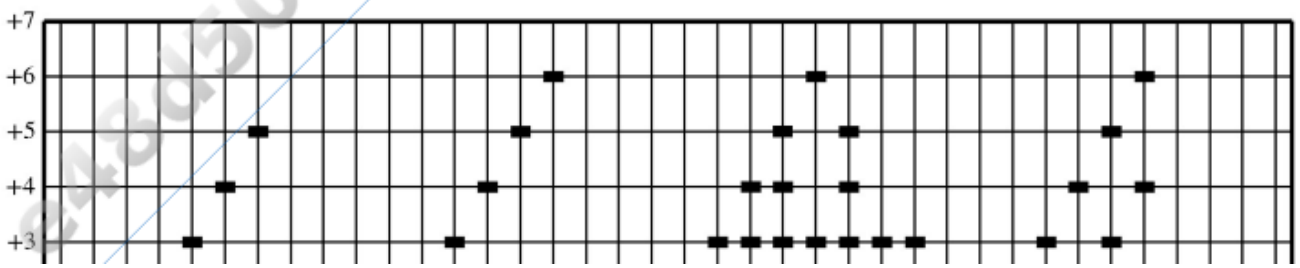

DO NOT COPY

Printed by: e48d507df5d1141@placeholder.94092.edu. Printing is for personal, private use only. No part of this book may be reproduced or transmitted without publisher's prior permission. Violators will be prosecuted.

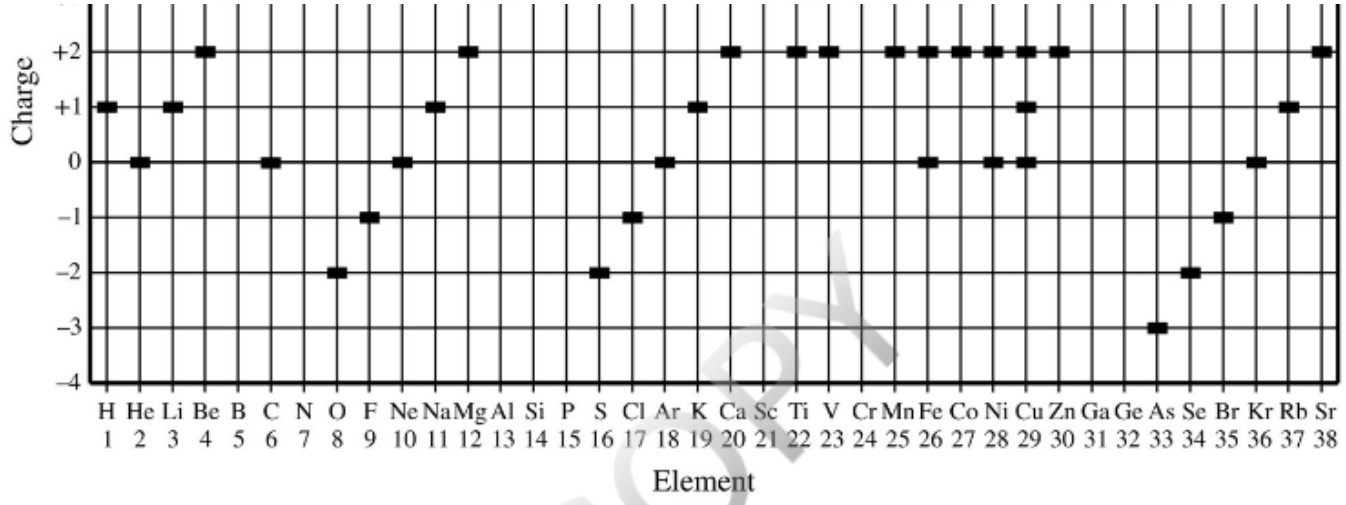

FIGURE 3.3 Common oxidation states of elements 1 through 38. View larger image

The systematic pattern breaks down for the transition metals (elements 21–30). This is because the valence electrons are in the 4*s* and 3*d* subshells. With the exception of Cr, the 4*s* subshell fills first, then the 3*d*. When electrons are removed, however, they first come from the subshell with the highest quantum number, which is the 4*s* subshell, even though this subshell has lower energy.

For Sc, Ti, and V, it is possible to remove both 4*s* electrons and one, two, and three electrons, respectively, from the 3*d* subshell to produce Sc^{3+}, Ti^{4+}, and V^{5+}, all with the electron configuration of Ar.

For atomic numbers 24–30 (Cr–Zn), both 4*s* and 3*d* electrons are available to be removed. When these elements ionize they typically lose their 4*s* electrons first. One or more of the 3*d* electrons also may be lost. As a consequence, all of these elements may have different valence states depending on how many 3*d* electrons are removed. Iron is the most notable example. It occurs both as divalent Fe^{2+}, known as **ferrous iron**, and as trivalent Fe^{3+}, known as **ferric iron**. Although Mn and Cr are most commonly divalent and trivalent, respectively, both may occur in higher oxidation states.

In summary, the oxidation state of the most common elements found in minerals (Figure 3.3) should be memorized. Note that the oxidation state for many of these elements is easily deduced from its position on the periodic table. Starting with the alkali metals, Na and K are most important and they have a 1+ oxidation state. Mg and Ca are the most important alkaline earth metals and they have a 2+ oxidation state. The transition metals are complicated, but Fe is most important and is commonly 2+, though it can be 3+ as well. Group 13, most notably Al, forms a 3+ ion, while group 14, most notably C and Si, forms 4+ ions. P is the most common group 15 element and has a 5+ oxidation state. Group 16 includes O, the most important anion for minerals at 2−, while S can both be a cation forming a 6+ charge (following the pattern for cations established above), or an anion at a 2− charge (the same as O). Halogens all form 1− ions and F and Cl are the most common. As stated above, group 18, the noble gases, does not form ions.

DO NOT COPY

Printed by: e48d507df5d1141@placeholder.94092.edu. Printing is for personal, private use only. No part of this book may be reproduced or transmitted without publisher's prior permission. Violators will be prosecuted.

Electronegativity

A measure of the propensity of an element to gain or lose electrons is conveniently provided by a value called **electronegativity**. It was defined in 1932 by Linus Pauling, who used an arbitrary scale so that lithium (Li) had an electronegativity of 1, carbon (C) an electronegativity of 2.5, and fluorine (F) an electronegativity of 4.0. Elements with low electronegativity lose their outer valence electrons readily to form cations, whereas those with high electronegativity have a strong affinity for extra electrons and tend to form anions. **Table 3.4** shows electronegativity values from Pauling (1960) for the first 38 elements.

TABLE 3.4 Electronegativity of the First 38 Elements in Their Most Common Oxidation State(s)

Z	Element	Electronegativity	*Z*	Element	Electronegativity	*Z*	Element	Electronegat
1	H	2.1	14	Si	1.8	27	Co	1.8
2	He	N/A	15	P	2.1	28	Ni	1.8
3	Li	1.0	16	S	2.5	29	Cu^{+}/Cu^{2+}	1.9/2.0
4	Be	1.5	17	Cl	3.0	30	Zn	1.6
5	B	2.0	18	Ar	N/A	31	Ga	1.6
6	C	2.5	19	K	0.8	32	Ge	1.8
7	N	3.0	20	Ca	1.0	33	As	2.0
8	O	3.5	21	Sc	1.3	34	Se	2.4
9	F	4.0	22	Ti	1.5	35	Br	2.8
10	Ne	N/A	23	V	1.6	36	Kr	N/A
11	Na	0.9	24	Cr	1.6	37	Rb	0.8
12	Mg	1.2	25	Mn	1.5	38	Sr	1.0
13	Al	1.5	26	Fe^{2+}/Fe^{3+}	1.8/1.9			

Source: Adapted from Pauling (1960). Bloch and Schatteman (1981) have somewhat different values.

At least four other electronegativity scales have been developed, but they all yield similar results. In a later section, electronegativity values are used to estimate the nature of chemical bonds. Pauling's values are more than adequate for this purpose.

DO NOT COPY e48d507df5d1141@placeholder.9409

Printed by: e48d507df5d1141@placeholder.94092.edu. Printing is for personal, private use only. No part of this book may be reproduced or transmitted without publisher's prior permission. Violators will be prosecuted.

Abundance of the Elements

Various attempts have been made to estimate the relative abundance of the chemical elements in the crust. The most influential is a compilation by Clarke and Washington (1924) who calculated an average composition based on 5159 high-quality analyses of igneous rocks. The analyzed rocks came from worldwide locations but were dominated by European and North American sources and included few samples representative of the ocean basins. With some revision and the addition of minor elements (e.g., Taylor, 1969; Mason and Moore, 1982), their values have provided the basis for the abundances shown in **Table 3.5**. Of the 83 available elements, only eight are present in substantial amounts (**Table 3.6**). These eight elements, O, Si, Al, Fe, Ca, Na, K, and Mg, collectively make up the large majority of the Earth's crust and are the elements from which most common minerals are composed.

TABLE 3.5 Abundance of the Elements in the Earth's Crust[a]

Element	Abundance	Element	Abundance	Element	Abundance	Element	Abundance
1 H	**0.14**	20 Ca	**3.6**	39 Y	33	58 Ce	60
2 He	??	21 Sc	22	40 Zr	165	59 Pr	8.2
3 Li	20	22 Ti	**0.4**	41 Nb	20	60 Nd	28
4 Be	2.8	23 V	135	42 Mo	1.5	61 Pm	??
5 B	10	24 Cr	100	43 Tc	??	62 Sm	6
6 C	200	25 Mn	**0.1**	44 Ru	0.01	63 Eu	1.2
7 N	20	26 Fe	**5.0**	45 Rh	0.005	64 Gd	5.4
8 O	**46.6**	27 Co	25	46 Pd	0.01	65 Tb	0.9
9 F	625	28 Ni	75	47 Ag	0.07	66 Dy	3
10 Ne	??	29 Cu	55	48 Cd	0.2	67 Ho	1.2
11 Na	**2.8**	30 Zn	70	49 In	0.1	68 Er	2.8
12 Mg	**2.1**	31 Ga	15	50 Sn	2	69 Tm	0.5
13 Al	**8.1**	32 Ge	1.5	51 Sb	0.2	70 Yb	3.4
14 Si	**27.7**	33 As	1.8	52 Te	0.01	71 Lu	0.5
15 P	**0.1**	34 Se	0.1	53 I	0.5	72 Hf	3

DO NOT COPY e48d507df5d1141@placeholder.9409

Printed by: e48d507df5d1141@placeholder.94092.edu. Printing is for personal, private use only. No part of this book may be reproduced or transmitted without publisher's prior permission. Violators will be prosecuted.

16 S	260	35 Br	2.5	54 Xe	??	73 Ta	2	
17 Cl	130	36 Kr	??	55 Cs	3	74 W	1.5	
18 Ar	??	37 Rb	90	56 Ba	**0.04**	75 Re	0.001	
19 K	**2.6**	38 Sr	375	57 La	30	76 0s	0.005	

Source: Adapted from Mason and Moore (1982). [a] Bold numbers are weight percent, others are parts per million; ?? signifies an unknown trace quantity.

TABLE 3.6 The Eight Most Abundant Elements in the Earth's Crust

Element	Common Oxidation State	Proportion of Earth's Crust			Oceanic Crust (wt %)	Total Earth (wt %)
		(wt %)	(atom %)	(vol %)		
O	−2	46.6	62.5	91.7	40.9	29.5
Si	+4	27.7	21.2	0.2	23.1	15.2
Al	+3	8.1	6.5	0.5	8.5	1.1
Fe	+2/+3	5.0	1.9	0.5	8.2	34.6
Ca	+2	3.6	1.9	1.5	8.1	1.1
Na	+1	2.8	2.6	2.2	2.1	0.6
K	+1	2.6	1.4	3.1	1.3	0.1
Mg	+2	2.1	1.8	0.4	4.6	12.7
Total		98.5	99.8	~100	96.8	94.9

Source: Adapted from Mason and Moore (1982).

The oceanic crust is somewhat richer in iron and magnesium than the average crust, and these values also are shown in Table 3.6. Additional elements present in the oceanic crust in significant abundance include Mn (1.0 percent) and Ti (0.9 percent).

Determining the composition of the entire Earth is even more difficult because the mantle and core cannot be sampled directly. Estimates are obtained by

- considering the Earth's mass and density distribution as determined by geophysical means,
- studying the composition of the usually basaltic magmas derived from the mantle and the samples of the mantle that sometimes arrive with the magma,
- analyzing the composition of meteorites that are presumed, in some way, to represent the material from which the Earth formed, and

DO NOT COPY e48d507df5d1141@placeholder.9409

Printed by: e48d507df5d1141@placeholder.94092.edu. Printing is for personal, private use only. No part of this book may be reproduced or transmitted without publisher's prior permission. Violators will be prosecuted.

- applying appropriate cosmological, geochemical, and petrophysical models to evaluate these data.

The values shown in Table 3.6 are approximations at best, but they clearly illustrate that the entire Earth is much richer in iron and magnesium than the crust, and lower in silicon, aluminum, potassium, sodium, and calcium. The Earth as a whole also is presumed to have substantially more nickel and sulfur than the crust.

DO NOT COPY
e48d507df5d1141@placeholder.9409

Printed by: e48d507df5d1141@placeholder.94092.edu. Printing is for personal, private use only. No part of this book may be reproduced or transmitted without publisher's prior permission. Violators will be prosecuted.

Chemical Bonding

While chemical bonding is conventionally described in terms of ionic, covalent, metallic, and electrostatic models, all chemical bonding ultimately depends on the attraction of opposite charges. The different models provide explanations for how the positive and negative charges become separated. In ionic, covalent, and metallic bonding, the distribution of electrons, with their negative charge, is dictated by the need of atoms to satisfy valence requirements and acquire the lower-energy electron configuration of noble gases. Additional bonding mechanisms include van der Waals and hydrogen bonding.

Valence-Related Bonding

Of the 83 available elements, all but the noble gases (He, Ne, Ar, Kr, and Xe) routinely bond chemically with themselves or other elements. The feature that the noble gases have in common is that all subshells are entirely filled with electrons—they lack valence electrons (Table 3.3). The lack of chemical reactivity suggests that the electron configuration displayed by the noble gases is a low-energy or stable configuration. If the other elements were to acquire the same electron configuration as one of the noble gases by gaining, losing, or sharing valence electrons, they too would be in a lower-energy, more stable configuration. All the valence-related bonding types involve mechanisms that allow elements to acquire the electron configuration of the noble gases, or failing that, a pseudo-noble-gas configuration.

Ionic Bonding

Ionic bonding is a consequence of the electrostatic attraction between cations and anions. Elements that form cations—usually metals—hold their outer electrons weakly and will easily relinquish them to acquire a stable electron configuration. Elements that form anions—usually nonmetals—hold their outer electrons tightly and readily accept additional electrons to acquire a stable electron configuration.

Consider the mineral halite (NaCl). The electron configuration of a Na atom shown in Table 3.3 has the noble-gas core of Ne with a single electron in the 3*s* subshell. If it loses that 3*s* electron, it acquires the stable electron configuration of Ne and a net charge of +1. But the Na cannot simply discard the extra electron—charge neutrality must be maintained, and that electron must go somewhere. That “somewhere” is a Cl atom, which has the 1*s*, 2*s*, 2*p*, and 3*s* orbitals completely filled but only five electrons in the 3*p* subshell. The electron lost by the Na is readily accepted by the Cl so that it can have a full complement of six 3*p* electrons. The addition of an electron to the 3*p* orbital gives Cl

DO NOT COPY e48d507df5d1141@placeholder.9409

Printed by: e48d507df5d1141@placeholder.94092.edu. Printing is for personal, private use only. No part of this book may be reproduced or transmitted without publisher's prior permission. Violators will be prosecuted.

the electron configuration of argon, and it also acquires a net −1 charge. The exchange of an electron from sodium to chlorine produces a stable electron configuration for both elements, and the sodium and chlorine end up with opposite charges and are attracted to each other.

The nature of the attractive force F_A between the oppositely charged Na^+ and Cl^- is given by the **Coulomb law** and is inversely proportional to the distance d between the center of the ions

$$F_A \propto \left(q^+\right)\left(q^-\right)/d^2 \tag{3.1}$$

where q^+ and q^- are the magnitudes of the charges on cation and ion, respectively. **Figure 3.4a** shows the magnitude of the attraction between Na^+ and Cl^-. This attraction is balanced by a **Born repulsion** produced when the electron shells of anion and cation begin to overlap. The magnitude of the Born repulsive force F_R is a negative inverse function of the distance between anion and cation

$$F_R \propto -n/d^{1+n} \tag{3.2}$$

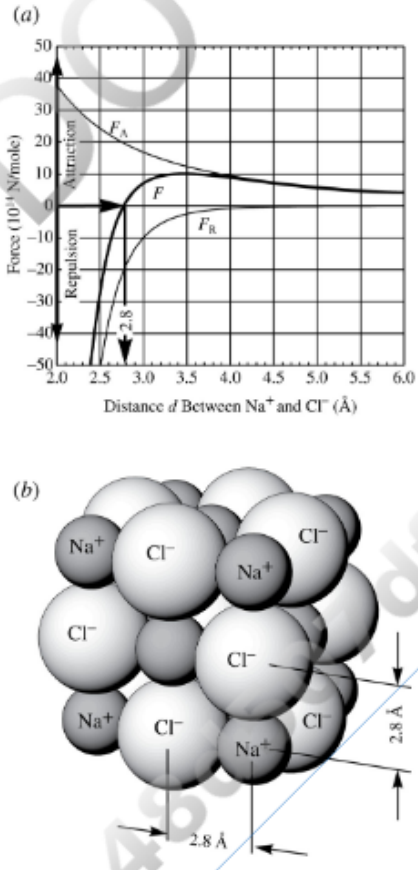

FIGURE 3.4 Ionic bonding between Na^+ and Cl^-. (*a*) The attractive F_A and repulsive F_R forces

DO NOT COPY
e48d507df5d1141@placeholder.9409

Printed by: e48d507df5d1141@placeholder.94092.edu. Printing is for personal, private use only. No part of this book may be reproduced or transmitted without publisher's prior permission. Violators will be prosecuted.

between Na^+ and Cl^- ions. The net force F is zero when the centers of the ions are at a distance of about 2.8 Å. At greater distances there is a net attraction and at a smaller distance a net repulsion. (*b*) Na^+ and Cl^- ions pack together in a face-centered cubic lattice with a spacing of about 2.8 Å.
View larger image

where n is an integer dependent on the number of filled electron shells. The repulsion exists because the electrons in the stable shells of both elements have the same charge and cannot occupy the same space. Distortion of the electron subshells involves an energy increase and therefore resistance. The magnitude of F_R for Na^+–Cl^- bonding is shown by the lower curve in Figure 3.4a.

The net force F is the sum of the attractive and repulsive forces

$$F = F_A + F_R. \tag{3.3}$$

The equilibrium distance between Na^+ and Cl^- is given where $F = 0$, which occurs at about 2.8 Å, as shown in Figure 3.4a. At greater distances, the attractive force is larger, and at smaller distances, the repulsive force is larger.

Ions bond together in ratios that ensure that the net positive charge and the net negative charge are equal. Charges must balance. For halite, this means one Na^+ for every Cl^-, and the formula is written NaCl. In the mineral fluorite there must be two F^- for every Ca^{2+}, and the formula is written CaF_2.

When bonding, ions act like charged spheres and pack together in a systematic and symmetrical manner. Positive and negative charges alternate to form an electrically neutral crystalline solid. This represents a low-energy configuration, so ionic bonding is fairly strong. Na and Cl pack together in a face-centered cubic lattice (**Figure 3.4b**) in which each Na is surrounded by six Cl and each Cl is surrounded by six Na.

Ionic-bonded crystals tend to be brittle. Attempts to deform the crystal structure and slide one part of the crystal past another will juxtapose cations against cations and anions against anions. Because like charges repel each other, ionic crystals have a strong resistance to sliding different parts of the crystal past each other. Forcing the issue may result in rupture rather than ductile deformation. Because the structures are often quite orderly, failure commonly occurs along cleavage planes.

Covalent Bonding

Covalent bonding occurs when the bonded atoms have the same affinity for their outer electrons such that electrons cannot be transferred between atoms as they are with ionic bonding. Therefore, the atoms can only acquire a stable electron configuration by sharing electrons. To share electrons, neighboring atoms must have overlapping orbitals, provided that the overlapping orbitals have no more than two electrons combined. The electrons in the overlapping orbitals are effectively shared, and this thereby satisfies the

DO NOT COPY e48d507df5d1141@placeholder.9409

Printed by: e48d507df5d1141@placeholder.94092.edu. Printing is for personal, private use only. No part of this book may be reproduced or transmitted without publisher's prior permission. Violators will be prosecuted.

electrons in the overlapping orbitals are effectively shared, and this thereby satisfies the valence requirements for both atoms. Covalent bonding tends to be strong, as demonstrated by the great hardness of diamond.

The electrostatic attraction between the atoms results from the shared electrons, on average, predominantly occupying the space between the adjacent atoms, giving that space a net negative charge. This leaves the cores of the atoms with a net positive charge. The positive and negative charges attract, thus holding the shared electrons and adjacent atoms in close proximity.

It should be evident that bonding intermediate between ionic and covalent is possible, and it turns out that bonding in most minerals displays intermediate characteristics. This is discussed in a later section.

Diamond provides a good example of covalent bonding in which adjacent orbitals overlap to form very strong bonds. It is composed of carbon that has a base-state electron configuration of $1s^2 2s^2 2p^2$ (the superscript indicates the number of electrons in the subshell). A stable noble-gas electron configuration can be obtained by either gaining four electrons to form a Ne configuration or losing four electrons to form an He configuration (Table 3.3). However, ionic bonding is not possible because all the carbon atoms have identical electron configurations and identical affinity for valence electrons. One carbon cannot receive an electron from another to form negative and positive ions. Adjacent carbon atoms can, however, share electrons so that each acquires a stable noble-gas electron configuration.

To share four electrons, four unpaired orbitals must be available. This poses a problem because in the ground-state configuration of carbon (**Figure 3.5a**), only the three $2p$ orbitals are available to share electrons; two have one electron each, and the third has none. The $1s$ and $2s$ orbitals cannot share electrons because each already contains two. To create four unpaired orbitals, **hybrid orbitals** are formed as follows.

- One of the electrons in the $2s$ orbital is promoted to the vacant $2p$ orbital; this provides four unpaired orbitals that can therefore be shared (**Figure 3.5b**).
- Because all four bonds to adjacent carbon atoms must be identical, the orbitals in the $2s$ and $2p$ subshells are hybridized into four identical sp^3 orbitals (**Figure 3.5c**). Each of these orbitals consists of a large lobe pointing in one direction and a small lobe in the opposite direction (**Figure 3.5d**). They are positioned around the nucleus so that the large lobes define the corners on a tetrahedron.

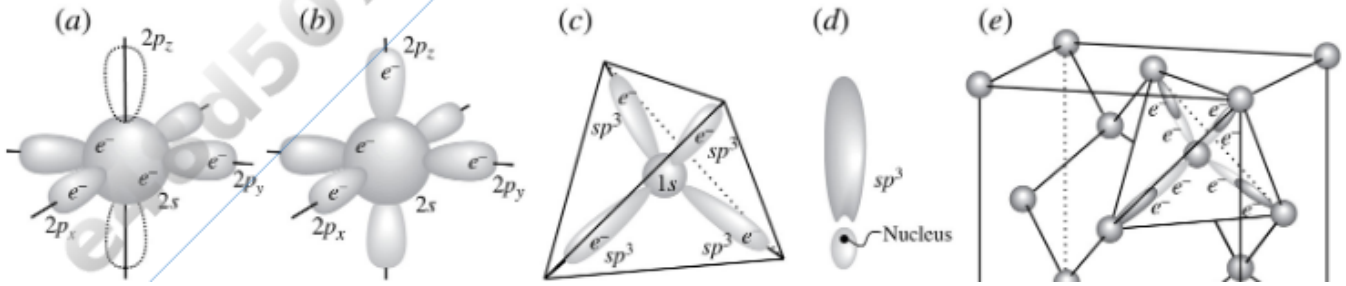

Printed by: e48d507df5d1141@placeholder.94092.edu. Printing is for personal, private use only. No part of this book may be reproduced or transmitted without publisher's prior permission. Violators will be prosecuted.

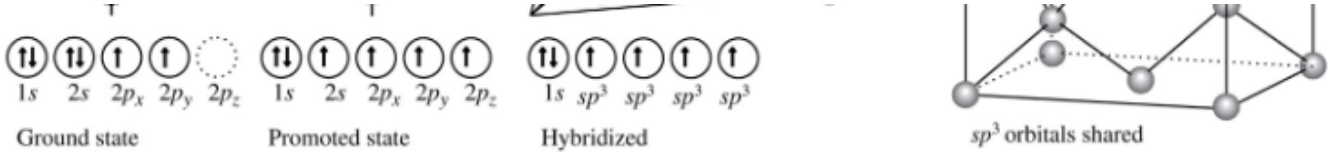

FIGURE 3.5 Formation of carbon covalent sigma (σ) bonds in diamond. (*a*) Ground-state electron configuration of carbon. The $2s$ orbital contains two electrons, the $2p_x$ and $2p_y$ orbitals each contain one electron, and the $2p_z$ orbital is vacant. (*b*) One electron from the $2s$ orbital is promoted to the $2p_z$ orbital so that four orbitals are partially filled. (*c*) Hybridization of the half-filled orbitals into four identical sp^3 orbitals arranged to point to the corners of a tetrahedron. (*d*) Each sp^3 orbital consists of a large lobe with a small lobe on the opposite side of the nucleus. The small lobes are not shown in (*c*). (*e*) Bonding of carbon atoms in diamond by sharing electrons between hybridized $2sp^3$ orbitals on adjacent atoms. Four pairs of overlapping sp^3 orbitals reaching a carbon atom are shown; similar bonds occur along each of the solid lines. The small lobes are omitted for clarity. View larger image

Each of the four sp^3 hybrid orbitals is shared with an identical hybrid orbital on each of four adjacent carbon atoms to form the continuous crystal structure of diamond (**Figure 3.5e**). Each of these covalent bonds, termed **sigma bonds (σ)**, has a high degree of symmetry about an axis parallel to the length of the orbitals that overlap end to end.

Graphite displays a different pattern of hybrid orbitals. It too is made entirely of carbon, but only $2p_x$ and $2p_y$ orbitals hybridize with the $2s$ orbital to form sp^2 hybrids. The $2p_z$ orbital is not hybridized. The carbon atoms bond to three neighbors by using the three sp^2 hybrid orbitals, forming continuous sheets of carbon (**Figure 3.6**). These three bonds are sigma bonds. The $2p_z$ orbitals, oriented at right angles to the plane of the carbon sheets, share electrons differently and form what are known as **pi bonds (π)**. With pi bonds, the orbitals overlap side to side rather than end to end, so the electrons are shared laterally.

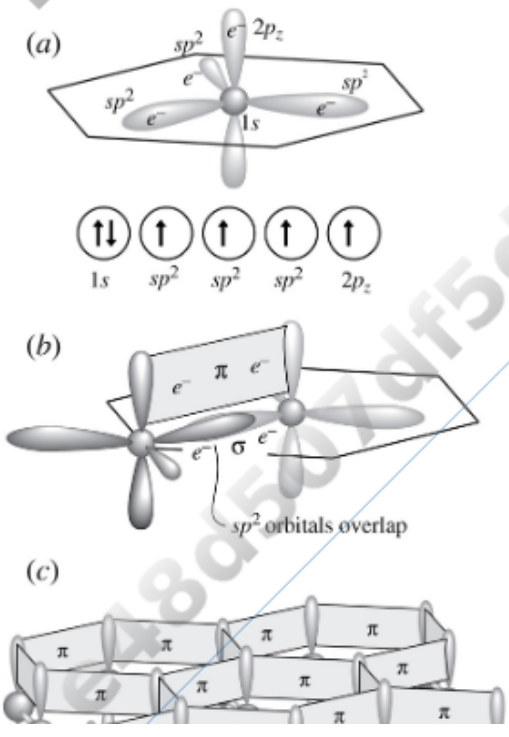

Printed by: e48d507df5d1141@placeholder.94092.edu. Printing is for personal, private use only. No part of this book may be reproduced or transmitted without publisher's prior permission. Violators will be prosecuted.

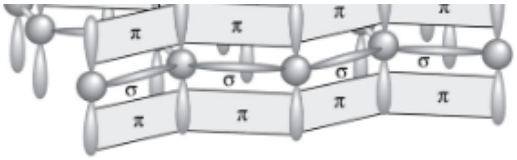

FIGURE 3.6 Formation of covalent σ and π bonds with carbon in graphite. The ground and promoted states of carbon are shown in Figure 3.5a and b. (*a*) Hybridization of orbitals forms three sp^2 orbitals with the $2p_z$ orbital at right angles. (*b*) σ Bonds form by sharing electrons between sp^2 orbitals from adjacent C atoms. π Bonds are formed by sharing electrons laterally between the $2p_z$ orbitals. (*c*) Carbon bonds to form continuous sheets. The π bonds form on both the top and bottom of the sheet, but only those in the front are shown on the bottom. View larger image

Note that each carbon atom can form pi bonds with each of its three neighbors, forming what amounts to continuous bands of electrons from the $2p_z$ orbitals above and below the sheet of carbon atoms. The electrons involved in these pi bonds are able to move from atom to atom with relative ease, effectively forming metallic bonds, which are described in the next subsection. This accounts for the fact that graphite is an electrical conductor. An applied voltage can cause these electrons to move, producing a flow of electricity along the sheets. The pi and sigma bonds within the sheets of carbon are very strong, stronger in fact than the bonds in diamond. This is because the C–C bonds in graphite are shorter than in diamond. The low hardness of graphite is a consequence of the weak van der Waals bonds that hold adjacent sheets together. Van der Waals bonds are discussed in a later section.

Some additional common hybrid orbital geometries are shown in **Figure 3.7**. All the conventional (Figure 3.1) and hybrid orbitals have specific spatial geometries. As a consequence, covalent bonding requires that atoms be placed in specific geometries so that the orbitals will overlap. The bonds are highly directional and the structures produced are often not readily described in terms of simple packing of spheres, as discussed for halite above.

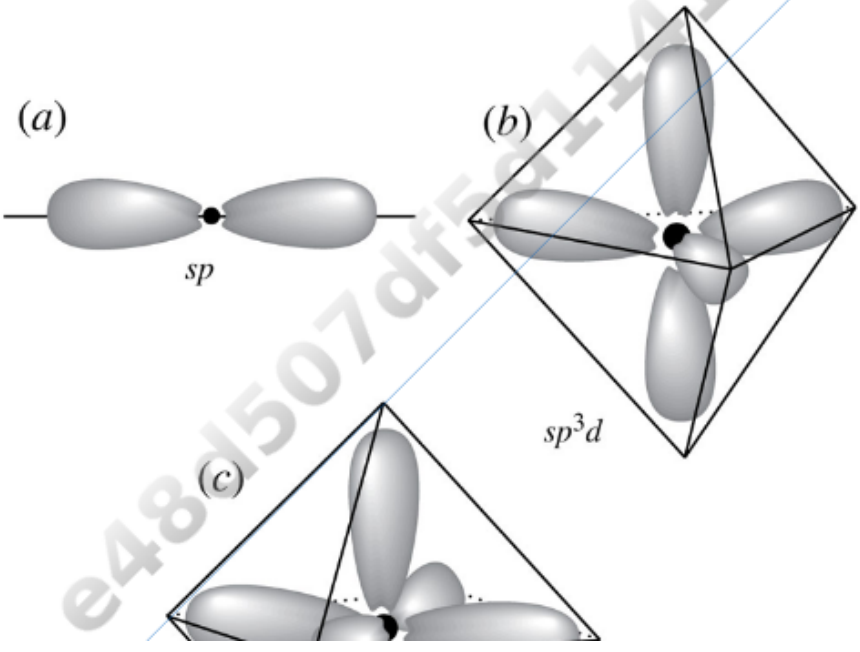

DO NOT COPY
e48d507df5d1141@placeholder.9409

Printed by: e48d507df5d1141@placeholder.94092.edu. Printing is for personal, private use only. No part of this book may be reproduced or transmitted without publisher's prior permission. Violators will be prosecuted.

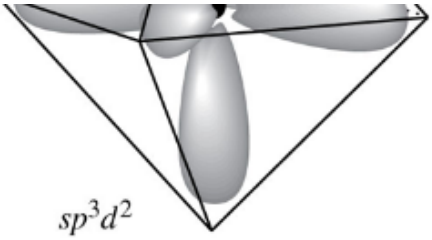

FIGURE 3.7 Hybrid orbitals. Each consists of a large and small lobe (Figure 3.5d); only the large lobe is shown. (*a*) Hybrid *sp* orbital formed from an *s* orbital and a single *p* orbital. (*b*) Hybrid sp^3d orbitals formed from an *s*, three *p*, and a *d* orbital. (*c*) Hybrid sp^3d^2 orbitals formed from an *s*, three *p*, and two *d* orbitals. View larger image

Metallic Bonding

Metallic bonding can be considered to be a type of covalent bonding in which the valence electrons are not associated with just two nuclei but are free to move from atom to atom throughout the crystal structure. In the ideal case, the metal atoms consist of positively charged spherical cores packed together to form the structure of the solid metal. Valence electrons occupy the space around the nuclei and are able to move freely. As with covalent bonding, the electrostatic attraction is produced by the valence electrons, which are, on average, most often found in the space between the adjacent atoms. The net negative charge of these electrons attracts the positively charged cores of the adjacent atoms.

The formation of metallic bonds depends on several factors. The first is that the valence electrons are held weakly. Metals, which have low electronegativity (Table 3.4), can lose their valence electrons easily. Second, metallic bonding is favored when the number of electrons that must be shared to form a noble-gas configuration is large. Sodium in its metallic form, for example, needs to share seven electrons to acquire the argon configuration. The nonmetals, in contrast, need to gain only one or two electrons to acquire a noble-gas configuration. Therefore, the nonmetals typically form covalent bonds. A third consideration is the availability of vacant energy levels into which valence electrons can readily move. This is controlled, in part, by the spacing between atoms.

Assume that the spacing between identical atoms that make up a crystal is infinite. The energy levels of the electrons within each subshell and orbital would be the same for all atoms. If the atoms are brought into proximity, their orbitals overlap. If this occurs, this might mean that two electrons with the same quantum numbers occupy the same orbital, but the Pauli exclusion principle states that this is not possible. The solution is that subshell (1*s*, 2*s*, 2*p*, etc.) energy levels, for nearby atoms, must spread out and cover a range of energies; this is called a band (**Figure 3.8**). Each electron within an energy band has a slightly different energy than all other electrons in the bonded material, such as a crystal. Given the large number of atoms found even in small crystals ($\sim 10^{22}$), the energy levels within each band are essentially continuous. The width of the energy band produced by each subshell increases as the proximity of the atoms increases. Electrons become free to migrate through the structure if the energy level of an unfilled band

DO NOT COPY e48d507df5d1141@placeholder.94092

Printed by: e48d507df5d1141@placeholder.94092.edu. Printing is for personal, private use only. No part of this book may be reproduced or transmitted without publisher's prior permission. Violators will be prosecuted.

overlaps that of a filled band or if the outer valence subshell is only partially filled.

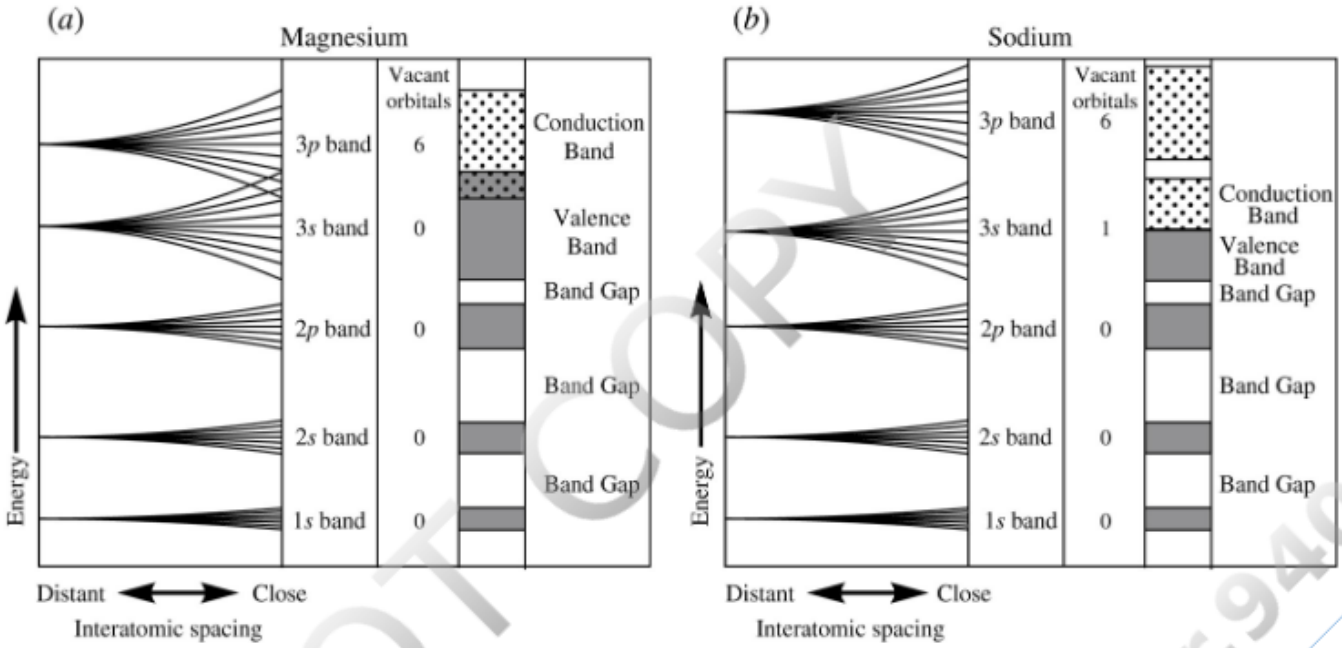

FIGURE 3.8 Energy bands form when atoms are brought into close proximity. (*a*) Magnesium. Energy levels of the 3*s* and 3*p* subshells spread into bands that overlap. Electrons from the 3*s* subshell (the valence band) can move into unoccupied energy levels of the 3*p* subshell and therefore move freely throughout the structure. (*b*) Sodium. Energy levels of electrons in the 3*s* subshell spread into a band when sodium atoms are packed together to form sodium metal but do not overlap with other bands. However, orbitals in the 3*s* subshell are only half-filled, so electrons can move into vacant energy levels and therefore move freely throughout the structure. The 3*s* subshell serves as both the valence and conduction bands. View larger image

Magnesium illustrates the overlap of an unfilled band with a filled band (Figure 3.8a). When Mg atoms are placed in close proximity, as they are in metallic magnesium, the widths of the energy bands increase so that the 3*s* and 3*p* bands overlap. Because the 3*s* orbitals are filled on all the Mg atoms, every available 3*s* energy level is occupied. The 3*p* bands, however, are vacant, so electrons from the 3*s* band are free to move into the 3*p* band, where the abundance of available energy levels allows the electrons to migrate easily through the structure. The 3*p* band is known as the **conduction band** because more energy levels are available in the band than there are electrons (none in isolated Mg atoms), and it can therefore conduct electrons through the crystal if a voltage is applied. The 3*s* band is known as the **valence band** because it provides the electrons that move into the conduction band. The inner subshells do not contribute to electrical conduction because an energy gap, known as a **band gap**, is present between bands.

The situation with Na is slightly different, because its 3*s* subshell is only half occupied. The 3*s* band that forms when Na atoms are brought together to form metallic sodium can therefore serve both as the valence band and the conduction band. Only half of the energy levels in the 3*s* band can be occupied at any one time so the remaining energy levels are available for conduction.

DO NOT COPY e48d507df5d1141@placeholder.9409-

Printed by: e48d507df5d1141@placeholder.94092.edu. Printing is for personal, private use only. No part of this book may be reproduced or transmitted without publisher's prior permission. Violators will be prosecuted.

The transition metals, such as iron, utilize both mechanisms to produce metallic bonds. The *d* subshell typically contains unfilled orbitals, so conduction can occur within the *d* bands. In addition, the energy level of the *d* band overlaps the higher *s* and *p* bands.

Because metallic bonds do not involve matching specific orbitals on adjacent atoms, the bonds are nondirectional. Metals atoms pack together in a highly symmetrical manner and are held together by the electrostatic attraction between the valence electrons and the positively charged cores of the atoms. Because the bonding is rather weak, metals tend to be relatively soft and malleable. Further, because the metal atoms have their valence requirements satisfied by the sea of valence electrons, it is very easy for one metal atom to substitute for another in the crystal structure. That is why many different metal **alloys**, which are mixtures of different metals, can be made and why it is possible to weld together pieces of metal by melting them with a torch.

The width of the energy bands increases as the atoms are brought closer together. This suggests that at sufficiently high pressure, most solids should display metallic conduction as the energy levels of the highest-filled band and next unfilled band spread sufficiently to overlap. The electrical conduction observed in the Earth's deep crust and mantle may, in part, be produced by this mechanism operating in silicate minerals, which at surface pressures are electrical insulators.

Relation among Valence-Dependent Bonding

The three valence-dependent bonding types—ionic, covalent, and metallic—all depend on acquisition of a stable electron configuration for the atoms involved. It turns out that many chemical bonds have characteristics that are intermediate between the ionic, covalent, and metallic end members. This variation can be schematically illustrated by placing the three bond types at the corners of a triangle (**Figure 3.9**).

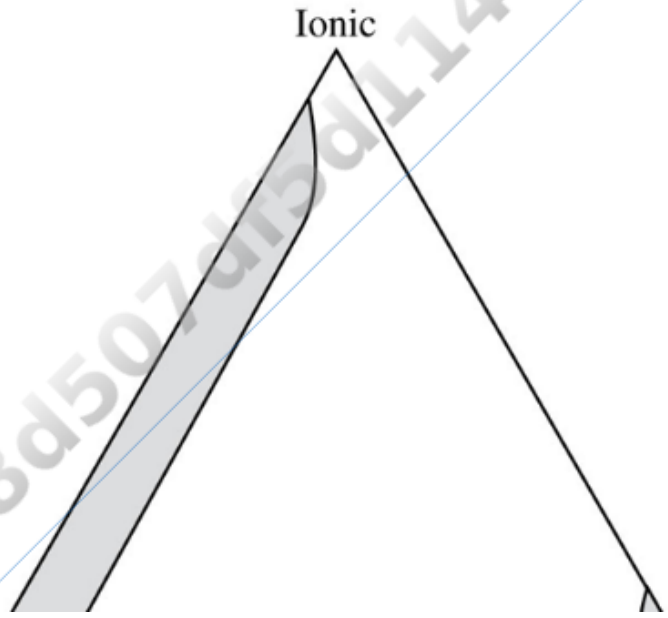

DO NOT COPY
e48d507df5d1141@placeholder.9409

Printed by: e48d507df5d1141@placeholder.94092.edu. Printing is for personal, private use only. No part of this book may be reproduced or transmitted without publisher's prior permission. Violators will be prosecuted.

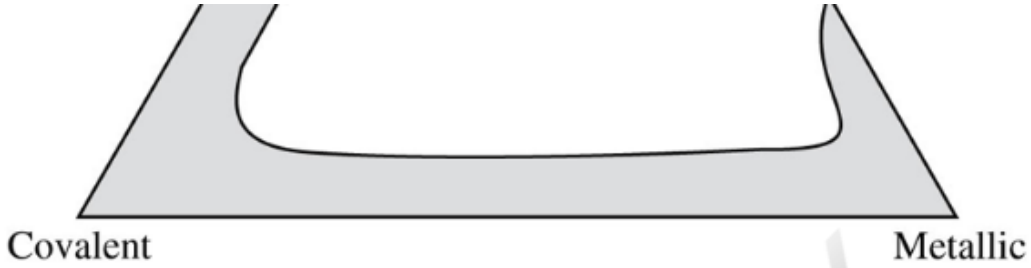

FIGURE 3.9 Range of bond character (shaded) found in valance-dependent bonding. Continuous variation exists between ionic and covalent bonds and between covalent and metallic bonds. Limited ionic character is found in metallic bonds between different metals. View larger image

The difference between ionic and covalent bonding can be considered to be a statistical question of where the valence electrons are located. With ideal ionic bonding, the valence electrons from the cation are entirely claimed by the anion, so the center of the net negative charge of the valence electrons is coincident with the center of the anion (**Figure 3.10a**). With covalent bonding, the center of net negative charge from the valence electrons is midway between adjacent atoms (**Figure 3.10b**). All gradations between these end members are possible. As the degree of ionic character increases, the center of negative charge of the valence electrons can be considered to shift from the midpoint between adjacent atoms to being more closely centered on the anions. Bonding is accomplished by the attraction between the positive cores of the atoms and negative charge of the valence electrons.

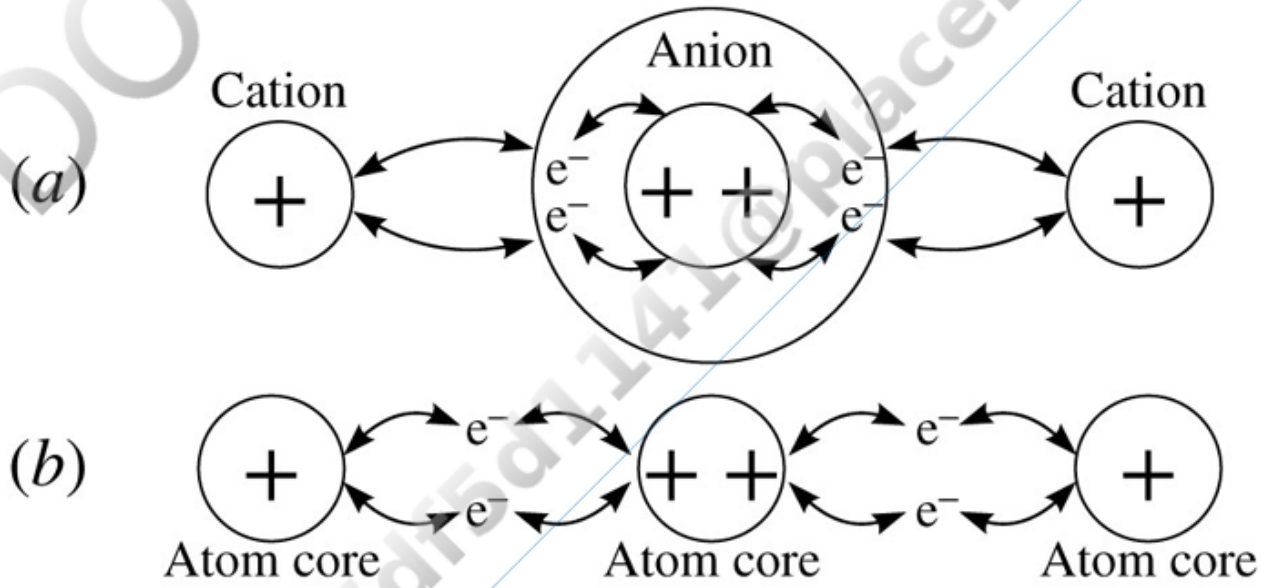

FIGURE 3.10 Conceptual model of ionic and covalent bonding. (*a*) Ionic bonding. A valence electron from each monovalent cation pairs with a valence electron from a divalent anion to satisfy valence requirements—the bonding electrons reside on the anion. Bonding is achieved because the positively charged cations are attracted to the negative charge of the valence electrons in the anion. (*b*) Covalent bonding. The bonding electron pairs are located, at least on average, between the atoms, and the atom cores each get a net positive charge. The positively charged core of each atom is attracted to the concentration of shared electrons in the space between them. In the general case where bonding is intermediate between the ionic and covalent, the average position of the valence electrons can be considered to be intermediate between being centered on the anion and being

Printed by: e48d507df5d1141@placeholder.94092.edu. Printing is for personal, private use only. No part of this book may be reproduced or transmitted without publisher's prior permission. Violators will be prosecuted.

electrons can be considered to be intermediate between being centered on the anion and being centered halfway between atoms. Adapted from Brown (2002). View larger image

Covalent bonding is usually described in terms of the explicit overlap of specific orbitals with the need to hybridize orbitals to get that match, as described earlier. The hybridization model works for cases where bonding is strongly covalent and bonding to four or fewer other atoms is involved; for bonding intermediate between ionic and covalent, where a cation may coordinate and bond with up to a dozen anions, the hybridization model does not work well.

As an approximation, values of electronegativity can be used to estimate the nature of a chemical bond. Ionic bonds require the formation of cations and anions with opposite charges. Hence, ionic bonding should be expected if the electronegativity of the elements bonding together is quite different. Covalent and metallic bonds, however, involve sharing of electrons among atoms with similar affinity for electrons and therefore a small or zero difference in electronegativity between atoms. Using this logic, Pauling (1960) devised a largely empirical relationship between the difference in electronegativity between elements and the degree of ionic character produced between those elements, shown in **Figure 3.11**. The mathematical relationship is

$$\text{Percent ionic character} = 1 - e^{-0.25(x_a - x_c)^2} \times 100. \tag{3.4}$$

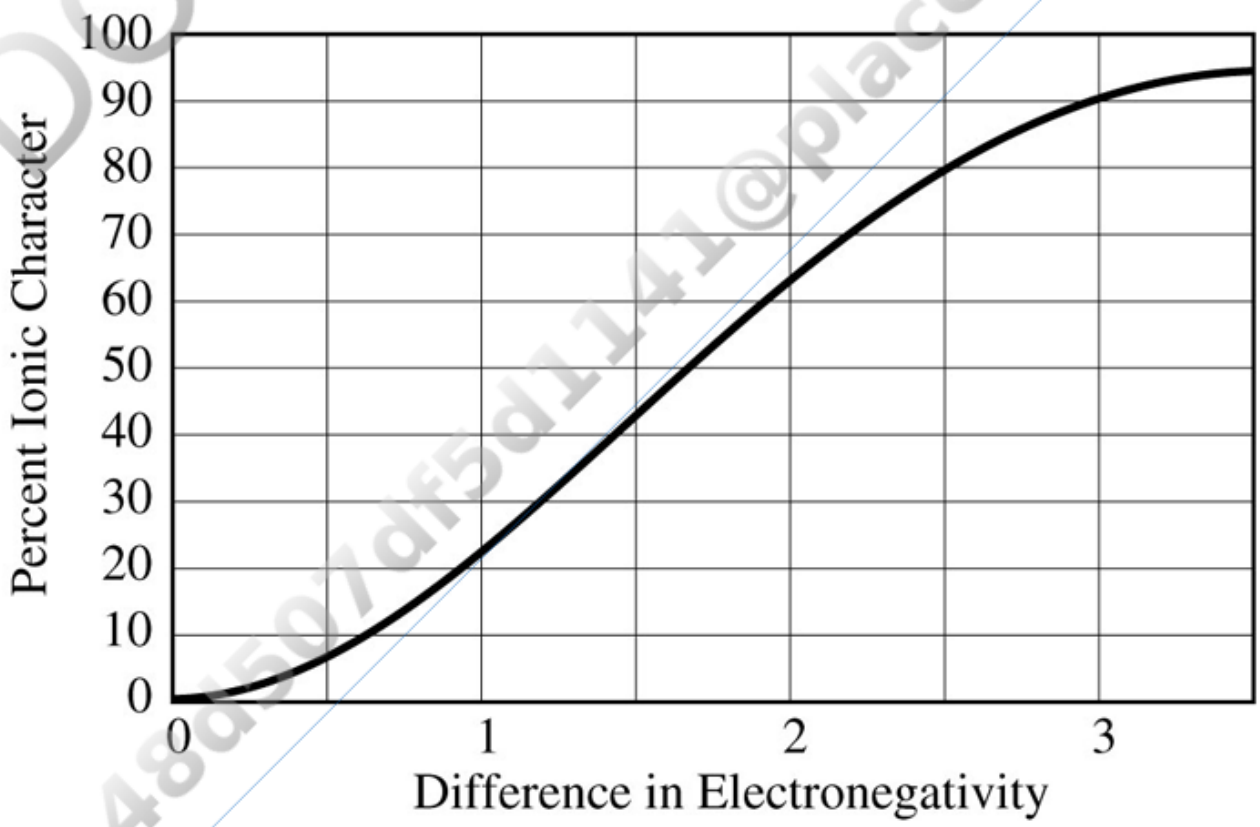

FIGURE 3.11 Curve showing the relationship between difference in electronegativity and

DO NOT COPY e48d507df5d1141@placeholder.9409

Printed by: e48d507df5d1141@placeholder.94092.edu. Printing is for personal, private use only. No part of this book may be reproduced or transmitted without publisher's prior permission. Violators will be prosecuted.

FIGURE 3.11 Curve showing the relationship between difference in electronegativity and degree of ionic character. See Table 3.4 for values of electronegativity. View larger image

Of the eight most abundant elements in the crust (Table 3.6), only oxygen forms anions, and it has an electronegativity of 3.5. The other seven elements (Si, Al, Fe, Ca, Na, K, Mg) all form cations when bonding with oxygen and have electronegativities of between 1.8 (Si) and 0.8 (K) (Table 3.4). The electronegativity difference between these cations and oxygen therefore ranges from 1.7 (Si) to 2.7 (K) and, based on Figure 3.11, bonding ranges from about 50 percent ionic (Si–O) to 80 percent ionic (K–O). The ionic bonding model therefore can serve as a reasonable first approximation for most common minerals in which oxygen is the anion.

It should be evident from Figure 3.11 and Equation 3.4 that ideal ionic bonding is not possible because the difference in electronegativity between cation and anion cannot be infinite. The maximum ionic character is about 93 percent. The Na–Cl bonding of halite, which is often used as the model for ionic bonding, is only about 67 percent ionic.

The native elements, including diamond and graphite (C), sulfur (S), gold (Au), and silver (Ag), form bonds in which the electronegativity difference is zero. These bonds cannot be ionic but may be intermediate in character between covalent and metallic. A simple number is not available to provide a measure of the relative degree of covalent versus metallic bonding. However, those native elements that have a high degree of metallic bonding (copper, gold, silver, etc.) typically have relatively low electronegativities (1.8–2.4) in addition to overlapping orbital band energies and the other factors discussed earlier. The native nonmetals (S and C) have higher electronegativities (~2.5) and favor covalent bonding.

As the degree of metallic character increases, the effective number of atoms over which valence electrons are shared increases from two atoms for covalent bonding, to the number of atoms in the crystal for metallic bonding. A limited range of bond properties extends from metallic toward ionic, usually in alloys of different metallic elements. If the two metals that form an alloy have significantly different electronegativities, the element with the higher affinity for electrons will have a higher claim on some valence electrons.

Crystals with ionic and covalent bonding have low electrical conductivity because the valence electrons are held tightly in specific orbitals. The electrical conductivity typically increases if these crystals are heated because the thermal energy increases the energy of some electrons so that they can be bumped into potential conduction bands.

Crystals with metallic bonds have high electrical conductivity because electrons are free to migrate throughout the structure in the conduction bands. The electrical conductivity of metallic bonds decreases as temperature increases because the greater thermal vibrational energy of the lattice tends to impede the migration of electrons.

Conductors, Insulators, and Semiconductors

DO NOT COPY e48d507df5d1141@placeholder.94092

Printed by: e48d507df5d1141@placeholder.94092.edu. Printing is for personal, private use only. No part of this book may be reproduced or transmitted without publisher's prior permission. Violators will be prosecuted.

The distinction between conductors, insulators, and semiconductors is important because it provides a basis for understanding the electrical properties and colors of minerals, which are discussed in Chapter 6. As shown in Figure 3.8, the energy levels of the various subshells on each atom spread into bands when the atoms are brought into close proximity in a mineral. The energy difference between the valence and conduction bands determines whether a material will be a conductor, insulator, or semiconductor.

Metallic-bonded **conductors** easily conduct electricity because the energy levels of the valence and conduction bands overlap as described earlier, and electrons can easily move between the two. **Figure 3.12a** schematically shows the abundance of electrons as a function of energy level for copper, which is an excellent electrical conductor.

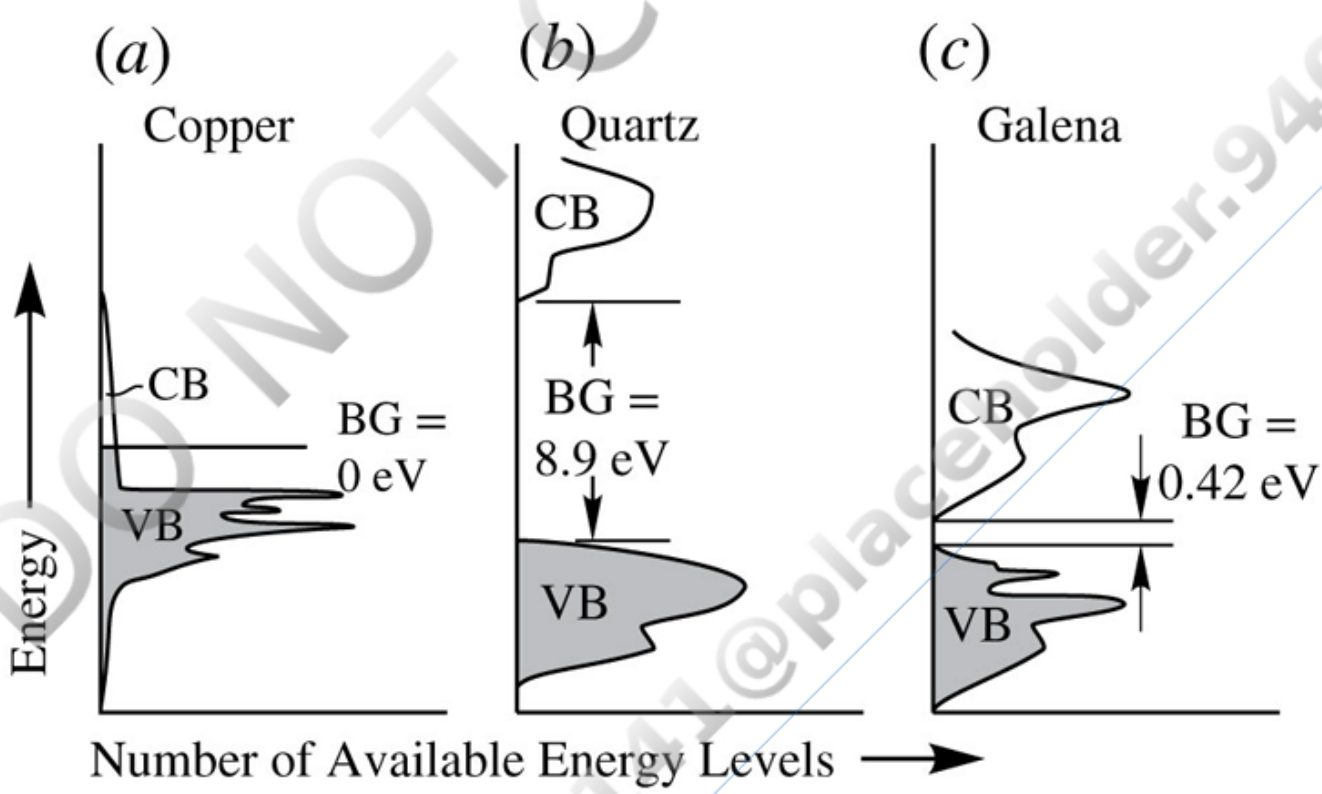

FIGURE 3.12 Band energies. Valence bands (VB) filled with electrons are shaded; the unfilled conduction bands (CB) are unshaded. (*a*) Conductor. No band gap (BG) is present between the valence and conduction bands of copper (Janak and others, 1975). (*b*) Insulator. A band gap of ~8.9 eV is present between the valence and conduction bands of quartz (Garvie and others, 2000). (*c*) Semiconductor. A band gap of only 0.42 eV is present between the valence and conduction bands of galena (Walsh, 2011). View larger image

Ionic-bonded and some covalent-bonded minerals are **insulators** and do not conduct electricity, even when a substantial voltage is applied. The energy gap between the valence band and the conduction band is large, generally greater than ~3 eV (different sources cite different values). **Figure 3.12b** shows the band structure for quartz, an insulator, which has an experimentally determined band gap of ~8.9 eV.

Some covalently bonded minerals are **semiconductors** because they have a relatively

Printed by: e48d507df5d1141@placeholder.94092.edu. Printing is for personal, private use only. No part of this book may be reproduced or transmitted without publisher's prior permission. Violators will be prosecuted.

Some covalently bonded minerals are **semiconductors** because they have a relatively small band gap between the valence and conduction bands. Light, heat, or a modest electrical voltage can promote electrons from the valence band to the conduction band. **Figure 3.12c** shows the band structure of galena, which has a band gap of only 0.42 eV.

Some materials are classified as semimetals, which are materials with a small overlap in their valence and conduction bands. Such materials have properties intermediate between that of a metal (conductor) and that of a semiconductor. Chemically they often include a metalloid, but do not universally.

Bonds Involving Asymmetric Charge Distribution

Hydrogen and **van der Waals bonding** are commonly found in minerals and depend on the development of asymmetric charge distribution. These bonds are sometimes referred to as **molecular** or **intermolecular bonds**.

Hydrogen Bonding

Ice is the most familiar mineral in which hydrogen bonding is prominent. It is composed of molecules of H_2O bonded together to form snow, hail, glaciers, and the ice cubes that cool soft drinks. Bonding occurs because the H_2O molecule is polar. Two hydrogen atoms form dominantly covalent bonds to an oxygen atom by sharing electrons with two of the oxygen's 2*p* orbitals (**Figure 3.13a**). However, because the difference in electronegativity is 1.4, the oxygen places greater claim to the electrons than do the hydrogen atoms. This produces an electrical polarity to the water molecule—positive near the two H nuclei and negative at two nodes on the opposite side of the O. The positive and negative charge concentrations are located at the corners of a tetrahedron. If temperatures are sufficiently low (<0°C), weak electrostatic attractions between the polar molecules can bond them together. In ice, this produces a hexagonal framework with each water molecule bonding to four neighbors through hydrogen bonds.

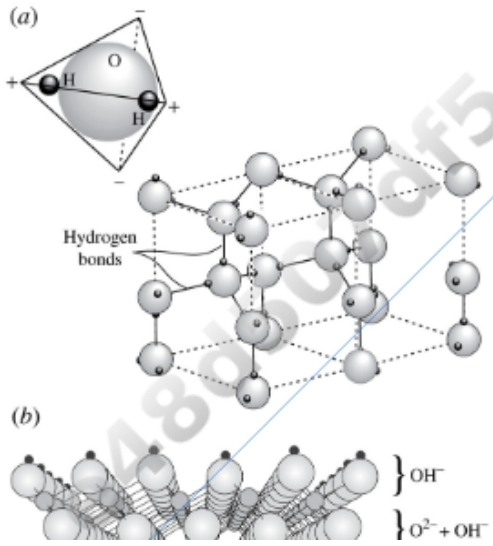

DO NOT COPY

Printed by: e48d507df5d1141@placeholder.94092.edu. Printing is for personal, private use only. No part of this book may be reproduced or transmitted without publisher's prior permission. Violators will be prosecuted.

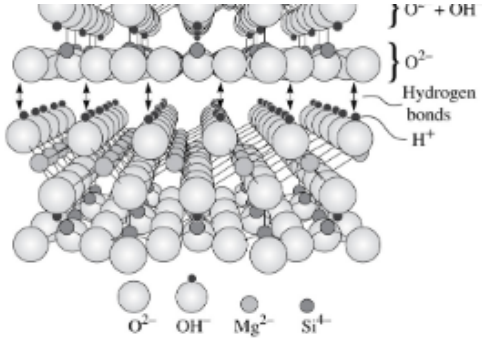

FIGURE 3.13 Hydrogen bonding. (*a*) Ice. A polar H_2O molecule is formed by covalent/ionic bonds between H and O using the 2*p* orbitals in the O. The O has greater claim on the electrons, so the H consists of little more than its positively charged nucleus, a single proton. Charge is tetrahedrally distributed—positive at the H^+ ions and negative at nodes on the opposite side of the oxygen. Each negative node on the molecule is attracted to a positive node (an H^+ ion) on an adjacent H_2O molecule to form a hydrogen bond that holds the water molecules together. Two unit cells are outlined with dashed lines. (*b*) Serpentine. The structure consists of layers made of three planes of O^{2-} and OH^- which bond with Mg^{2-} and Si^{4+} in the interstices to satisfy all valence requirements. Adjacent layers bond to each other because positively charged H^+ on the top surface of one layer face the negatively charged O^{2-} on the bottom of the adjacent layer. The opposite charges attract, producing a hydrogen bond. View larger image

Hydrogen bonds also are important in some sheet silicates (Chapter 13). Serpentine is an example. It consists of layers made of three planes of oxygen (O^{2-}) and hydroxyl (OH^-) anions. The bottom plane is all oxygen, the middle plane is mixed oxygen and hydroxyl, and the top plane is all hydroxyl (**Figure 3.13b**). Mg^{2+} and Si^{4+} occupy interstices among, and bond to, the hydroxyl and oxygen, satisfying all valence requirements. The small positively charged hydrogen cations of the OH^- on the top surface of one layer face the negatively charged oxygens anions on the bottom of the next layer. The opposite charges attract, forming hydrogen bonds between the layers.

Van der Waals Bonding

Van der Waals bonding also depends on asymmetrical charge distribution, but the asymmetry is produced in a different way. Consider graphite, whose structure consists of sheets of carbon atoms that are covalently bonded using both σ and π bonds. When the electron positions within one of these sheets of carbon atoms are averaged over a period of time, the charge on both sides of the sheet is the same. At any given instant, however, more electrons will be on one side of the sheet than the other, producing a polarization (**Figure 3.14**)—positive on one side and negative on the other. The net positive charge on one side of the sheet attracts electrons from the neighboring sheet so that the neighboring sheet also becomes polarized in the same sense. The result is a weak electrostatic attraction between the sheets produced by the short-term polarization of the sheets.

DO NOT COPY e48d507df5d1141@placeholder.94092

Printed by: e48d507df5d1141@placeholder.94092.edu. Printing is for personal, private use only. No part of this book may be reproduced or transmitted without publisher's prior permission. Violators will be prosecuted.

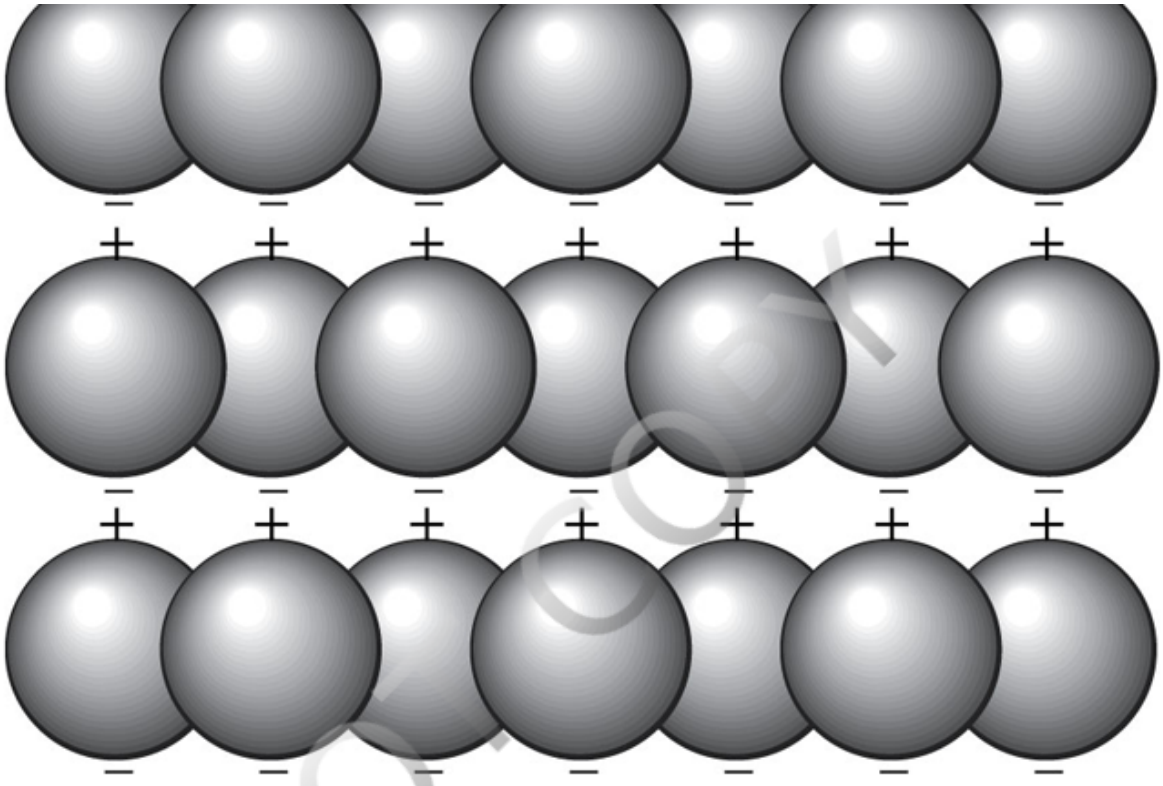

FIGURE 3.14 Van der Waals bonding. Sheets of carbon are bonded internally by π and σ covalent bonds (Figure 3.6). At any instant, more negatively charged electrons are on one side of a sheet than the other, producing a polarization. The polarization of one sheet produces a similar polarization in its neighbors. Van der Waals bonds are produced by the weak electrostatic attraction between the opposite charges on the surfaces of adjacent sheets at any instant. View larger image

Van der Waals bonding is quite weak, and minerals with it, such as graphite and talc, are typically quite soft and have a greasy feel. These properties are useful. Because graphite is soft and black, it is used to make pencil lead, and the ease with which the sheets of carbon slide past each other makes graphite a useful lubricant. Talc [$Mg_2Si_4O_{10}(OH)_2$] is widely used as a body powder (talcum powder) because it is very soft and helps prevent chafing of tender skin. The weakness of van der Waals and hydrogen bonding found in certain clay minerals also leads to a major engineering problem, known as swelling soil, which will be described in Chapter 13.

It should be evident from the preceding discussion that a mineral may have several different bonding types. Graphite, for example, has covalent σ and π bonding with intermediate covalent/metallic character, and van der Waals bonding.

DO NOT COPY e48d507df5d1141@placeholder.9409

Printed by: e48d507df5d1141@placeholder.94092.edu. Printing is for personal, private use only. No part of this book may be reproduced or transmitted without publisher's prior permission. Violators will be prosecuted.

Size of Atoms and Ions

In the section discussing chemical bonds, it was assumed that the ions behave as small hard spheres that pack together like so many differently sized marbles or ball bearings. This conceptual model for atoms and ions, although useful, has significant flaws. The volume occupied by the protons, neutrons, and electrons that form an isolated atom or ion is actually defined by the probability of finding electrons at specific locations around the nucleus. Those probabilities are not spherical, except for electrons in *s* shells, and do not have crisply defined boundaries. Some probability, however slight, always exists of finding an electron at a great distance from the nucleus. Further, chemical bonding distorts the volume within which the electrons are likely to be found and forms links or bonding pathways between adjacent atoms. The size and shape of an atom therefore depend on the nature and distribution of the other atoms with which it is bonded.

Regardless of these difficulties, it is clear that atoms and ions do pack together in crystalline solids with specific geometries and at regular distances (e.g., Figure 3.4). So, within limits, they do behave as spheres. It is therefore convenient to define the sizes of atoms and ions in terms of their **effective radius** based on the distance between the centers of adjacent atoms or ions in the crystal structure. The effective radius of an atom or ion is, in effect, the size it would have if it behaved like a small hard sphere. Appendix A contains a tabulation of effective radii for the elements under various conditions. The effective radius of an uncharged atom is the **atomic radius**, and the effective radius of an anion or cation is the **ionic radius**.

Consider a covalent- or metallic-bonded crystalline solid made of a single element. The **bond length** L between two atoms is equal to twice the effective radius R of the atoms (**Figure 3.15a**).

(3.5)

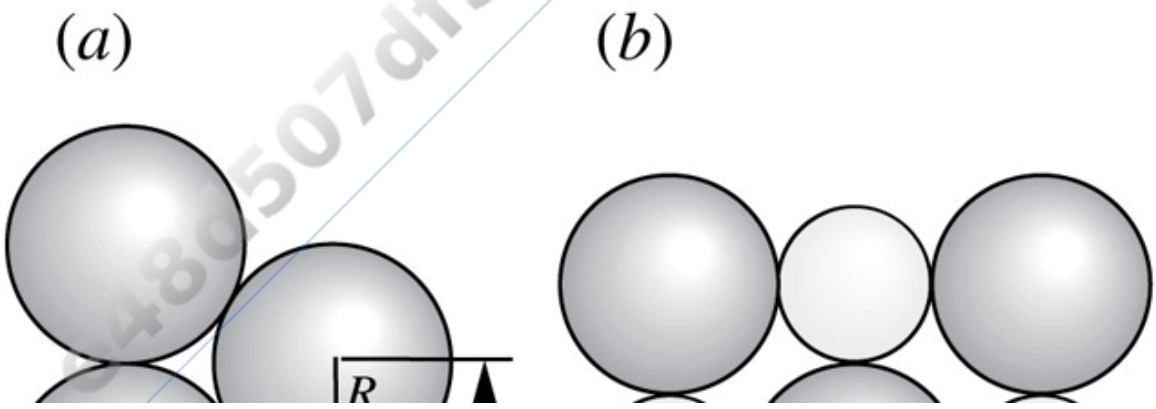

DO NOT COPY e48d507df5d1141@placeholder.9409

Printed by: e48d507df5d1141@placeholder.94092.edu. Printing is for personal, private use only. No part of this book may be reproduced or transmitted without publisher's prior permission. Violators will be prosecuted.

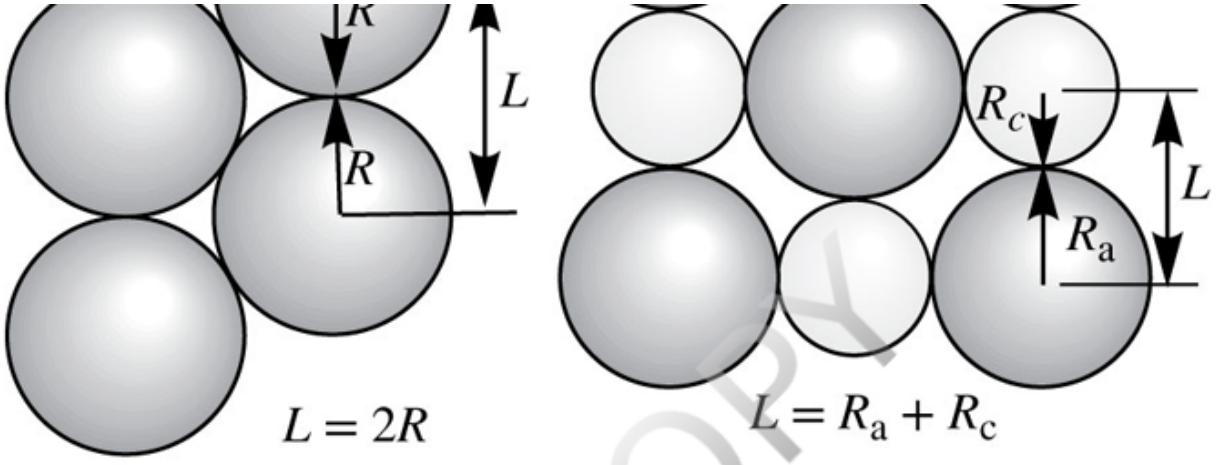

FIGURE 3.15 Bond length and effective radius. (*a*) Close-packed metal atoms of uniform size. The bond length (L) is twice the effective atomic radius R. (*b*) Anions and cations of different size. The bond length (L) is the sum of the effective ionic radii of the cation (R_c) and anion (R_a). View larger image

The techniques of X-ray diffraction (Chapter 8) make it possible to measure the bond length and therefore the sum of the effective radii of the constituent atoms. **Figure 3.16** shows the effective atomic radius for the elements exclusive of the noble gases. There are two sets of data, depending on the nature of the chemical bonds involved. For the metals and metalloids, the radii are based on metallic bonding in structures in which the atoms are closely packed so that each atom is in contact with 12 other atoms. For the nonmetals, the radii are based on single covalent bonds.

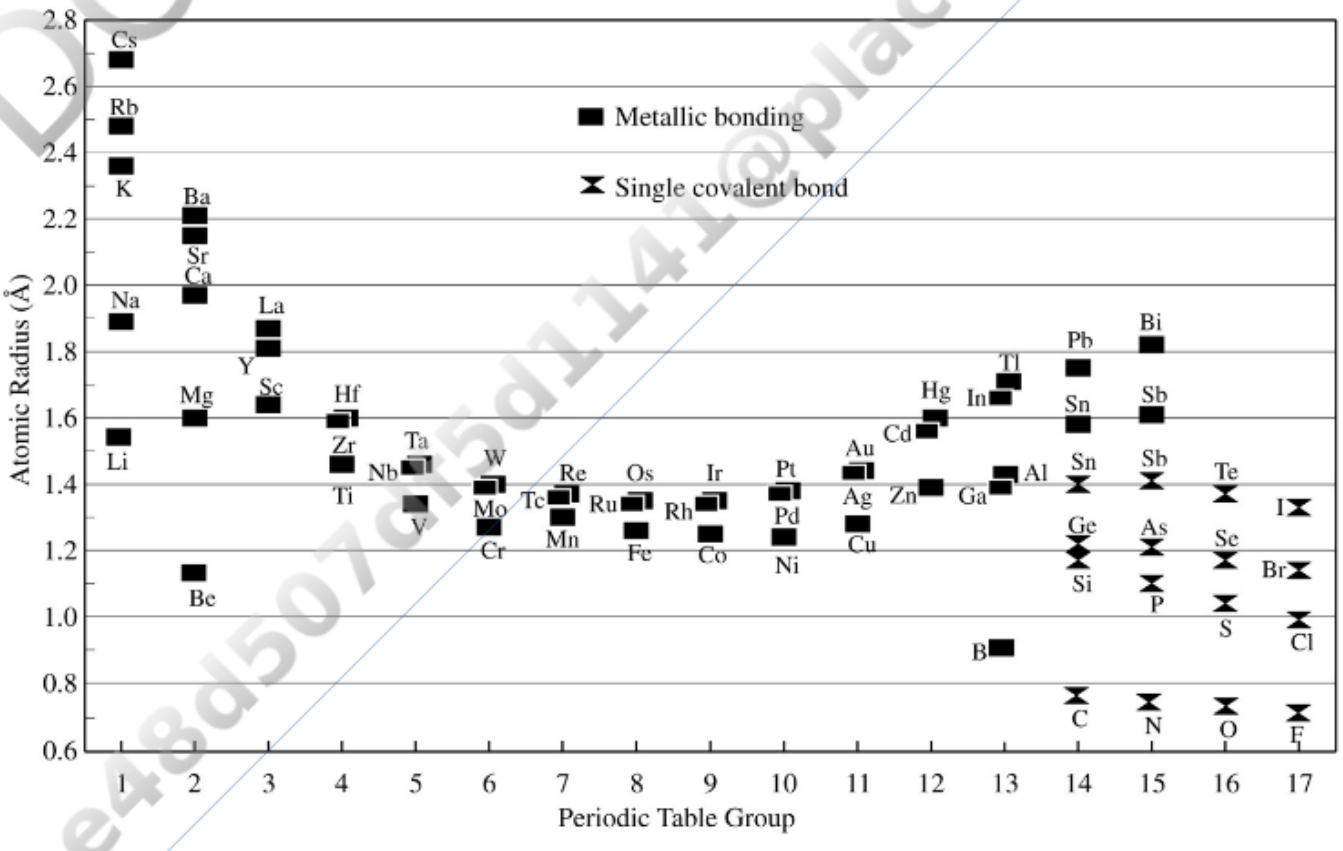

DO NOT COPY
e48d507df5d1141@placeholder.9409

Printed by: e48d507df5d1141@placeholder.94092.edu. Printing is for personal, private use only. No part of this book may be reproduced or transmitted without publisher's prior permission. Violators will be prosecuted.

FIGURE 3.16 Effective atomic radii for the elements. The lanthanide and actinide series and noble gases are omitted. Elements with metallic bonding are closely packed and in contact with 12 other atoms. Elements that do not form metallic bonds are shown for a single covalent bond. Data from Zhdanov (1965). View larger image

In an ionic-bonded crystalline solid, the bond length between the negatively charged anion and the positively charged cation is equal to the sum of the effective ionic radii of the cation R_c and of the anion R_a (**Figure 3.15b**).

$$L = R_a + R_c \tag{3.6}$$

X-ray techniques allow measurement of the length of bonds between anions and cations but cannot tell us how much of the bond length to allot to the cation and how much to the anion. However, by comparing many different structures and carefully evaluating cation–anion and anion–anion distances, it is possible to make reliable estimates of the effective ionic radii of the anions and cations.

The effective radii of the elements in their ionic configurations are shown in Figures 3.17 and 3.18 and are listed in Appendix A. These values are based on the assumption that O^{2-} has an effective ionic radius of 1.26 Å when in contact with six cations. Effective ionic radii based on 1.40 Å for O^{2-} have been widely used, but the values based on an O^{2-} radius of 1.26 Å are probably a better representation of the actual sizes of the ions and do not lead to the improbable result that some cations have negative sizes. To obtain effective ionic radii based on 1.40 Å for O^{2-}, subtract 0.14 Å from all values (except for O^{2-}) in **Figure 3.17** and Appendix A.

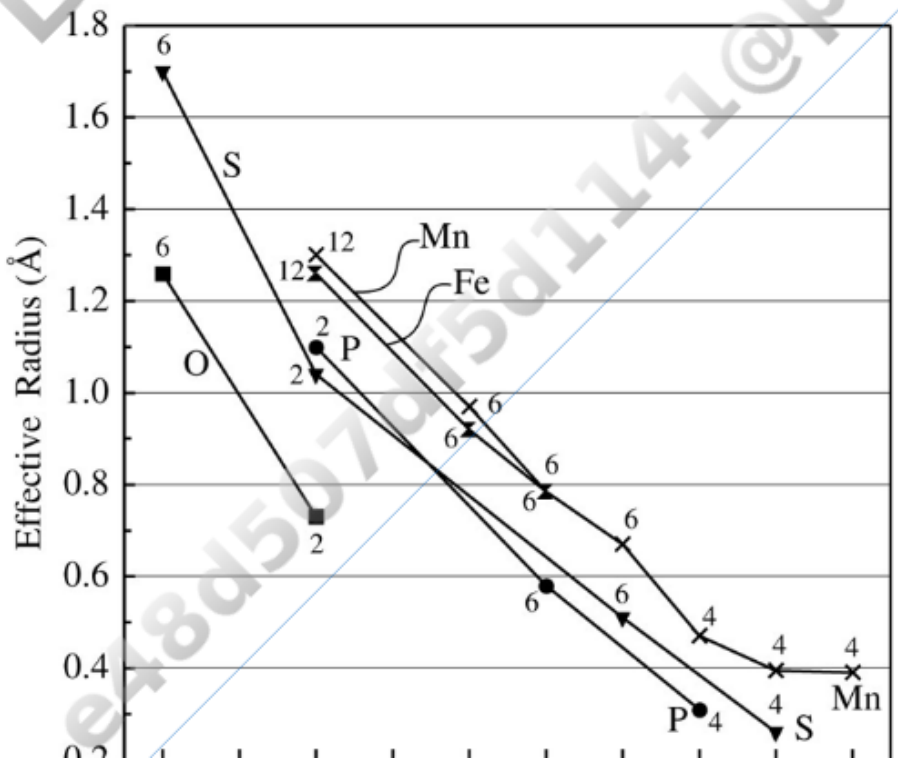

Printed by: e48d507df5d1141@placeholder.94092.edu. Printing is for personal, private use only. No part of this book may be reproduced or transmitted without publisher's prior permission. Violators will be prosecuted.

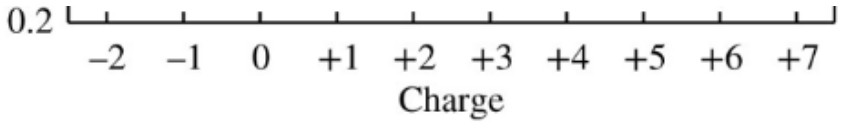

FIGURE 3.17 Effective radii as a function of oxidation state (charge) for oxygen (O), sulfur (S), phosphorus (P), manganese (Mn), and iron (Fe), elements that occur in different oxidation states. The coordination number is indicated by each symbol. Data from Appendix A and Figure 3.16. View larger image

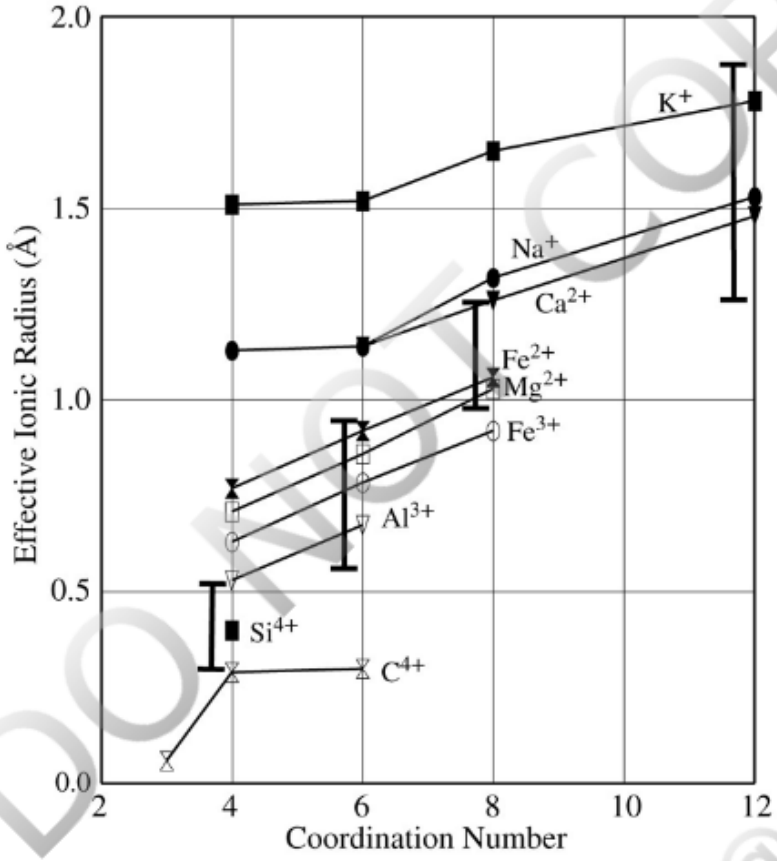

FIGURE 3.18 Effective ionic radii of the common cations as a function of coordination number. The normal ranges of cation sizes that will fit into 4-, 6-, 8-, and 12-fold coordination with oxygen are shown by bars (compare Table 4.1). Data from Appendix A. View larger image

It must be noted that the radius of oxygen varies depending on the electronegativity of the cations with which it bonds. It is larger when bonding with low-electronegativity cations and smaller when bonding with higher-electronegativity cations. Regardless, for the common cations bonded to oxygen in most minerals, the assumption of a fixed ionic radius works well when it comes to understanding the structure and chemistry of silicates and other common minerals.

The principal variables that influence effective ionic radius include the oxidation state (valence) of the ion and the number of anions in contact with the cation. The number of anions packed around the cation is called the **coordination number** (CN) and is discussed at more length in Chapter 4.

DO NOT COPY e48d507df5d1141@placeholder.9409

Printed by: e48d507df5d1141@placeholder.94092.edu. Printing is for personal, private use only. No part of this book may be reproduced or transmitted without publisher's prior permission. Violators will be prosecuted.

Oxidation State

Figure 3.17 clearly shows that effective radius is strongly controlled by charge. For a given element that may occur in more than one oxidation state, size decreases as charge becomes more positive. All cations are smaller than the equivalent uncharged atoms, and anions are larger. An increase in positive charge produces smaller ions because, for a given element, there are fewer electrons and the remaining electrons are held more tightly and close to the nucleus. Anions, with an excess of electrons, are larger than the equivalent uncharged atom because there are more electrons and the nucleus is less able to hold the additional electrons as tightly.

Coordination

Interatomic distances, and effective ionic radii, also are influenced by the number of anions with which a cation is in contact. Anions are larger than cations, so, in many minerals, the structure can be considered to consist of a framework of regularly packed anions with smaller cations tucked into the interstices, or holes, between the anions. The size of the interstices is determined by the number of anions that surround it, which is the coordination number. An extensive discussion of coordination can be found in the next chapter; but for current purposes, note that a large hole requires more anions to define its boundaries, while having fewer anions leaves a smaller hole. The arrangement of anions around a cation is typically a geometric shape called a polyhedron. A coordination number of 8, for example, involves eight anions arranged at the corners of a cube with a small space in the middle in which a small cation may reside. A coordination number of 12 involves 12 anions surrounding and in contact with a cation that is about the same size as the anions. This defines a polyhedron called a cuboctahedron. **Figure 3.18** shows that as the coordination number increases, so does the effective ionic radius of the cations occupying the hole defined by the anions. In a sense, cations expand or shrink to fill the space available. The effective ionic radii of anions also are influenced by the number of cations with which they are in contact (coordinate), but not as much as for cations.

An additional complexity that influences ionic radii is the **spin state**, which is a factor in transition metals with *d* orbitals containing four, five, six, or seven electrons. **High spin** ions have minimum pairing of electrons in the *d* orbitals; **low spin** ions have maximum pairing and are smaller (**Figure 3.19**). In general, the high spin state is preferred because having unpaired electrons represents a lower energy configuration than having paired electrons within the *d* orbital. However, some bonding geometries require hybridization that favors the low-spin configuration. Iron is the most important element that exhibits different spin states. Under crustal conditions, the high-spin configuration dominates in most minerals.

DO NOT COPY

Printed by: e48d507df5d1141@placeholder.94092.edu. Printing is for personal, private use only. No part of this book may be reproduced or transmitted without publisher's prior permission. Violators will be prosecuted.

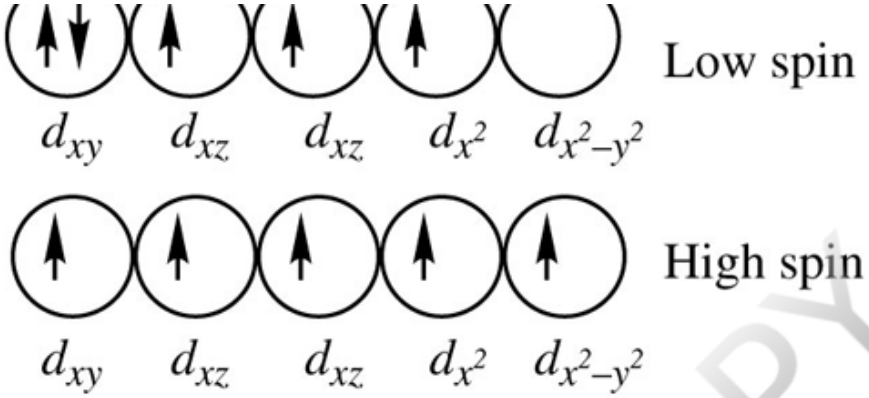

FIGURE 3.19 Spin configuration in Fe^{3+}. (*a*) Low spin. Electrons are paired in the d_{xy} orbital even though the $3d_{x^2-y^2}$ orbital is vacant. (*b*) High spin. No electrons are paired in the orbitals. View larger image

DO NOT COPY
e48d507df5d1141@placeholder.9409

Printed by: e48d507df5d1141@placeholder.94092.edu. Printing is for personal, private use only. No part of this book may be reproduced or transmitted without publisher's prior permission. Violators will be prosecuted.

(**Figure 3.19**). In general, the high spin state is preferred because having unpaired electrons represents a lower energy configuration than having paired electrons within the *d* orbital. However, some bonding geometries require hybridization that favors the low-spin configuration. Iron is the most important element that exhibits different spin states. Under crustal conditions, the high-spin configuration dominates in most minerals.

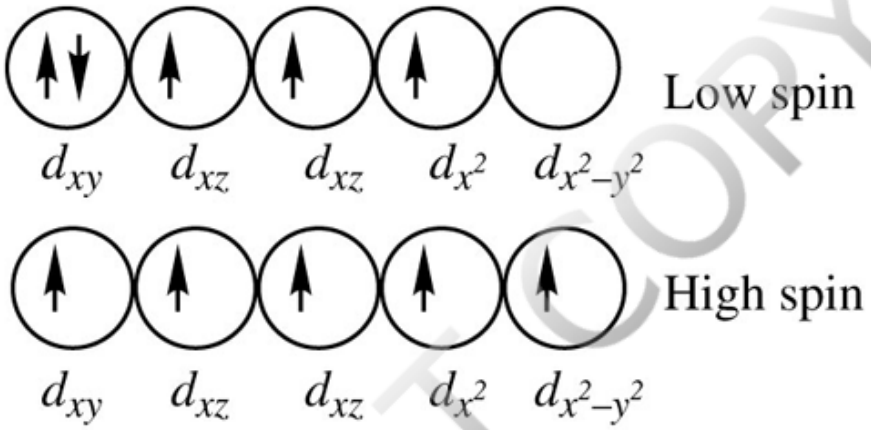

FIGURE 3.19 Spin configuration in Fe^{3+}. (*a*) Low spin. Electrons are paired in the d_{xy} orbital even though the orbital is vacant. (*b*) High spin. No electrons are paired in the orbitals. View larger image

REFERENCES CITED AND SUGGESTIONS FOR ADDITIONAL READING

Ahrens, L. A. (ed.). 1967. *Origin and Distribution of the Elements*. Pergamon Press, Oxford, 1178 p.

Bloch, A., and Schatteman, G. 1981. Quantum-defect orbital radii and the structural chemistry of simple solids, in M. O'Keefe and A. Navrotsky (eds.), *Structure and Bonding in Crystals*, Volume **1**, pp. 49–72. Academic Press, New York.

Brown, I. D. 2002. *The Chemical Bond in Inorganic Chemistry: The Bond Valence Model*. Oxford University Press, Oxford, 278 p.

Clarke, F. W., and Washington, H. S. 1924. *The Composition of the Earth's Crust. U.S. Geological Survey Professional Paper* **127**, 117 p.

Emsley, J. 2011. *Nature's Building Blocks: An A to Z Guide*. Oxford University Press, New York, 720 p.

Evans, R. C. 1966. *An Introduction to Crystal Chemistry*, 2nd ed. Cambridge University Press, Cambridge, 410 p.

Garvie, L. A. J., Rez, P., Alvarez, J. R., Buseck, P. R., Cravens, A. J., and Brydson, R. 2000. Bonding in alpha-quartz (SiO_2): A view of the unoccupied states. *American Mineralogist* **85**, 732–738.

DO NOT COPY e48d507df5d1141@placeholder.9409

Printed by: e48d507df5d1141@placeholder.94092.edu. Printing is for personal, private use only. No part of this book may be reproduced or transmitted without publisher's prior permission. Violators will be prosecuted.

Gibbs, G. V., Ross, N. L., Cox, D. F., and Rosso, K. M. 2014. Insights into the crystal chemistry of Earth materials rendered by electron density distributions: Pauling's rules revisited. American Mineralogist **99,** 1071–1084.

Janak, J. F., Williams, A. R., and Moruzzi, V. L. 1975. Self-consistent band theory of the Fermi-surface, optical, and photoemission properties of copper. *Physical Review B*, **11**, 1522–1536.

Mason, B., and Moore, C. B. 1982. *Principles of Geochemistry*, 4th ed. John Wiley & Sons, New York, 344 p.

Murrell, J. N., Kettle, S. F., and Tedder, J. M. 1985. *The Chemical Bond*. John Wiley & Sons, Chichester, UK, 333 p.

Pauling, L. 1960. *The Nature of the Chemical Bond*, 3rd ed. Cornell University Press, Ithaca, NY, 644 p.

Shannon, R. D. 1976. Revised effective ionic radii and systematic studies of interatomic distances in halides and chalcogenides. *Acta Crystallographica* **32**, 751–767.

Taylor, S. R. 1969. Abundance of chemical elements in the continental crust: A new table. *Geochimica et Cosmochimica Acta* **28**, 1273–1285.

Walsh, A. 2011. Effects of reduced dimensionality on electron structure and defect chemistry of semiconducting hybrid organic–inorganic PBS solids. *Proceedings of the Royal Society A*, **467**, 1970–1985.

Wieser, M. E., and Berglund, M. 2009. Atomic weights of the elements 2007 (IUPAC Technical Report). *Pure and Applied Chemistry* **81**, No. 11, 2131–2156.

Wieser, M. E., Holden, N., Coplen, T. B., Böhlke, J. K., Berglund, M., Brand, W. A., De Bièvre, P., Gröning, M., Loss, R. D., Meija, J., Hirata, T., Prohaska, T., Schoenbert, R., O'Connor, G., Walczyk, T., Yoneda, S., and Zhu, X.-K. 2013. Atomic weights of the elements 2011 (UIPAC Technical report). *Pure and Applied Chemistry* **85**, 1047–1078.

Zhdanov, G. S. 1965. *Crystal Physics*. Academic Press, New York, 500 p.

DO NOT COPY
e48d507df5d1141@placeholder.9409

Printed by: e48d507df5d1141@placeholder.94092.edu. Printing is for personal, private use only. No part of this book may be reproduced or transmitted without publisher's prior permission. Violators will be prosecuted.

LIST OF KEY TERMS

- actinide series
- alkali metals
- alkaline earth metals
- alkalis
- alloy
- angular momentum quantum number
- anion
- atomic mass
- atomic mass number
- atomic radius
- atomic weight
- band gap
- bond length
- cations
- conduction band
- conductor
- coordination number
- covalent bonding
- effective radius
- electronegativity
- electron
- ferric iron
- ferrous iron
- geologically ephemeral elements
- halogens
- high spin
- hybrid orbitals
- hydrogen bond
- insulators

DO NOT COPY
e48d507df5d1141@placeholder.9409

Printed by: e48d507df5d1141@placeholder.94092.edu. Printing is for personal, private use only. No part of this book may be reproduced or transmitted without publisher's prior permission. Violators will be prosecuted.

insulators
intermolecular bonds
ionic bonding
ionic radius
lanthanide series
low spin
magnetic quantum number
mass number
metallic bonding
metalloids
molecular bonds
neutron
noble-gas core
noble gases
nonmetal
orbitals
oxidation state
Pauli exclusion principle
periodic table
pi bond
principal quantum number (n)
proton
pseudo-noble-gas core
rare earth elements
semiconductor
shells
sigma bonds
spin quantum number
spin state
subshells
transition metals
valence
valence band
valence electrons

DO NOT COPY
e48d507df5d1141@placeholder.9409

Printed by: e48d507df5d1141@placeholder.94092.edu. Printing is for personal, private use only. No part of this book may be reproduced or transmitted without publisher's prior permission. Violators will be prosecuted.

valence electrons

Van der Waals bonding

DO NOT COPY

e48d507df5d1141@placeholder.9409

Printed by: e48d507df5d1141@placeholder.94092.edu. Printing is for personal, private use only. No part of this book may be reproduced or transmitted without publisher's prior permission. Violators will be prosecuted.

CHAPTER 4
Crystal Structure

William D. Nesse
University of Northern Colorado

Graham B. Baird
University of Northern Colorado

DO NOT COPY
e48d507df5d1141@placeholder.9409

Printed by: e48d507df5d1141@placeholder.94092.edu. Printing is for personal, private use only. No part of this book may be reproduced or transmitted without publisher's prior permission. Violators will be prosecuted.

Introduction

In Chapter 3 we addressed the structure of matter and the various bonding mechanisms that hold atoms together to form minerals. In this chapter we will address the following topics:

How are mineral structures illustrated?

What determines how elements combine and pack together to form minerals?

What are the structural variations of minerals?

How are minerals classified?

What controls the compositional variation of minerals?

How are mineral chemical formulas written?

How can mineral chemical compositions be graphically represented?

DO NOT COPY
e48d507df5d1141@placeholder.9409

Printed by: e48d507df5d1141@placeholder.94092.edu. Printing is for personal, private use only. No part of this book may be reproduced or transmitted without publisher's prior permission. Violators will be prosecuted.

Illustrating Mineral Structures

Recall that minerals are crystalline, meaning that their atoms are arranged into a highly order-repeating structure. Mineral structures are conveniently illustrated in a variety of different models, including as scaled spheres, ball-and-stick, polyhedra, and with coordinates.

To accurately create a "realistic" illustration of a crystal structure, it would be necessary to draw the atoms based on the irregularly shaped volumes defined by the distribution of electrons around each nucleus. This is not practical, so a reasonable compromise is to draw the atoms as scaled spheres (**Figure 4.1a**) using the atomic or ionic radii listed in Appendix A. A distinct disadvantage of this model is that the atoms occupy most of the volume and the front atoms obscure what is behind.

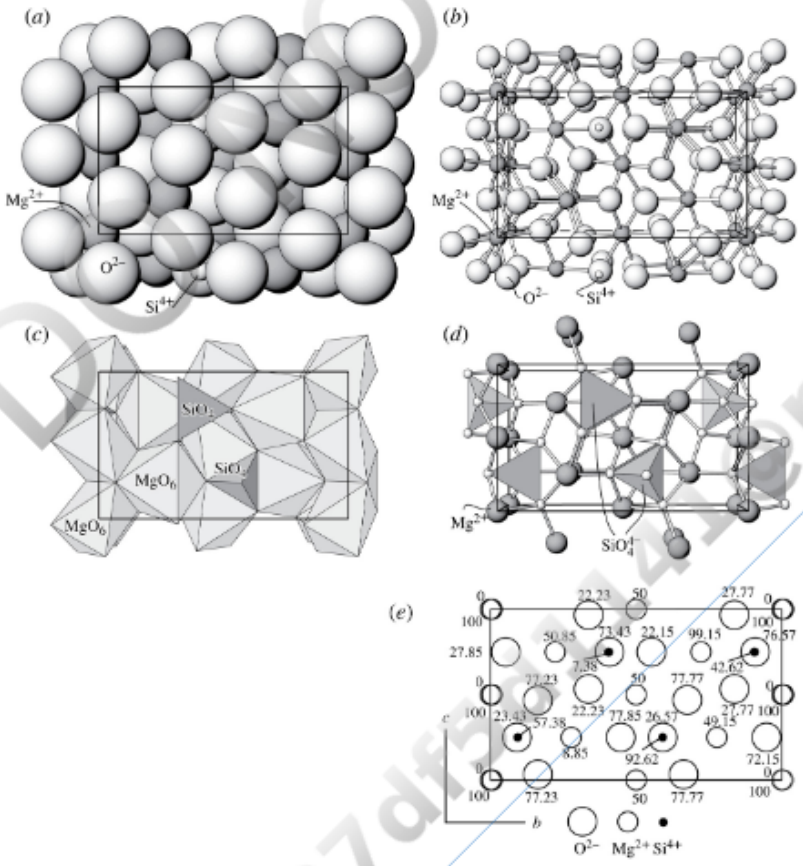

FIGURE 4.1 Illustration of olivine (Mg_2SiO_4) crystal structure viewed down the *a* axis. Each unit cell is outlined. (*a*) Scaled spheres: O^{2-} Mg^{2+}, and Si^{4+} are large, medium, and small spheres, respectively. (*b*) Ball-and-stick. Sphere size is reduced and the sticks represent bonding. (*c*) Polyhedral. Only the polyhedral framework is shown. The Si^{4+} and Mg^{2+} cations are inferred to be at the centers of the tetrahedra (dark) and octahedra (light), respectively. Oxygen anions are inferred to be at the corners of the polyhedra. (*d*) Hybrid model using both polyhedra and ball-and-stick. O^{2-} are shown as small spheres at corners of the tetrahedra. (*e*) "Mapped" structure. The height of the ions above the back surface of the unit cell is given as a percentage of the *a* unit cell dimension. The

Printed by: e48d507df5d1141@placeholder.94092.edu. Printing is for personal, private use only. No part of this book may be reproduced or transmitted without publisher's prior permission. Violators will be prosecuted.

above the back surface of the unit cell is given as a percentage of the *a* unit cell dimension. The outlines of the Mg^{2+} at the corners of the unit cell are offset slightly so that all atoms are visible.
View larger image

The ball-and-stick model (**Figure 4.1b**) reduces the size of the atoms and connects them with "sticks" so that the three-dimensional geometry can be visualized. Note that the sticks are not an accurate representation of the chemical bonds.

The polyhedral model (**Figure 4.1c**) does not show atoms; rather, the structure is represented by the coordination polyhedra, or the geometric shapes created by the anions in which the cations reside. Coordination polyhedra were introduced in Chapter 3 and are discussed later in this chapter. Anions are inferred to be located at each polyhedral corner, and the cations are in the centers of the polyhedra. Because the polyhedra in front obscure what is behind, a common tactic is to use a hybrid of the polyhedral and ball-and-stick models (**Figure 4.1d**).

The most accurate way of documenting the location of atoms in a crystal structure is to map them by using unit cell coordinates. In **Figure 4.1e**, the olivine structure is viewed down the *a* axis with the positions of the atoms projected onto the back surface of the unit cell. Here, atom location in the diagram is controlled by their *b* and *c* unit cell coordinates. The position of each atom above the back of the unit cell (the *a* coordinate) is indicated by a number representing a percentage of the unit cell. Zero means that the atom is at the back surface of the unit cell, and 49 indicates that the atom is 49 percent of the way up from the back of the unit cell.

Software such as Atoms, from Shape Software, and CrystalMaker, from CrystalMaker Software, allow illustrations of crystal structures to be readily created by using the online database of mineral structures maintained by the Mineralogical Society of America (www.minsocam.org/msa/crystal_database.html).

DO NOT COPY e48d507df5d1141@placeholder.9409

Printed by: e48d507df5d1141@placeholder.94092.edu. Printing is for personal, private use only. No part of this book may be reproduced or transmitted without publisher's prior permission. Violators will be prosecuted.

Controls of Crystal Structure

The first-order control on the structure of a mineral is the nature of the chemical bonding that holds the elements together. As we saw in Chapter 3, any given mineral may display several different bond types. Also, the valence-related bonding mechanisms represent ideal end members of what in reality is a continuum. Regardless, it is convenient to consider how bonding controls crystal structures. The three major bonding types—metallic, covalent, and ionic—will be the focus.

Metallic Bonding Structure Controls

The bonding between metals, which have low and nearly equal electronegativity, typically is metallic. Because the valence electrons are in conduction bands and are free to migrate throughout the structure, the metal atoms tend to pack together in highly ordered arrangements that minimize void space. The configurations most commonly found are based on **hexagonal closest packing** or **cubic closest packing** of spheres, often abbreviated as HCP and CCP, respectively.

Hexagonal and cubic closest packing are the most compact ways to pack spheres of equal size together. In both cases, it is convenient to consider that the spheres lie in close-packed layers (**Figure 4.2a**). The layers are stacked so that the spheres in one layer nestle in the hollows between spheres in adjacent layers (**Figure 4.2b**). The difference between hexagonal and cubic closest packing is in how the layers are arranged. In both cases, each sphere is in contact with 12 neighboring spheres, 6 from its own layer and 3 each from the layers above and below.

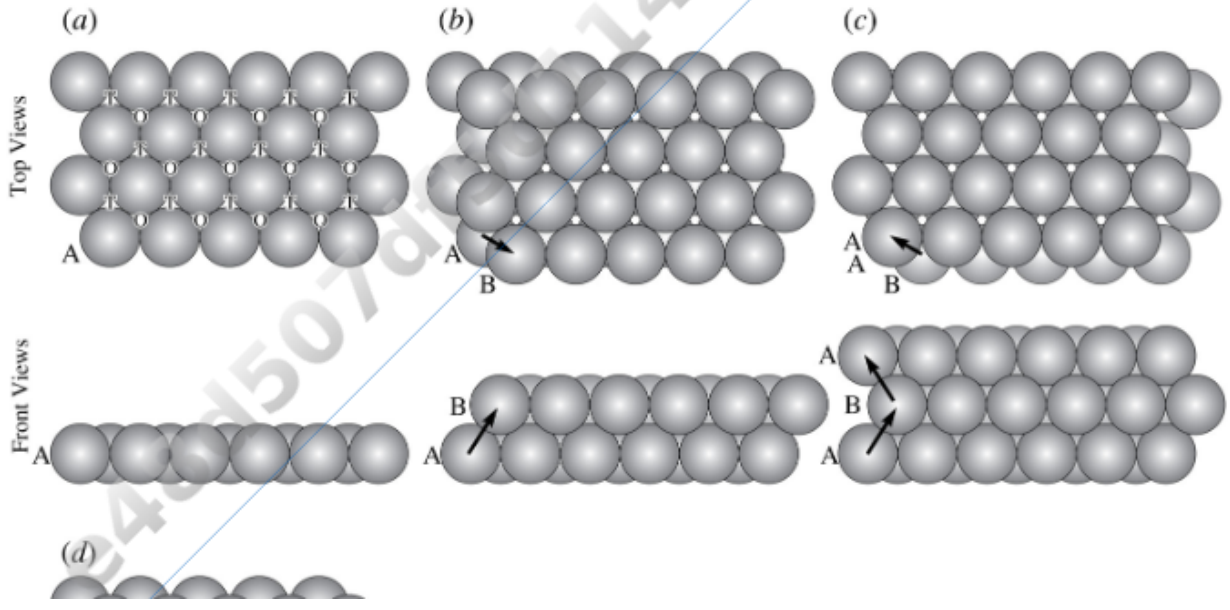

Printed by: e48d507df5d1141@placeholder.94092.edu. Printing is for personal, private use only. No part of this book may be reproduced or transmitted without publisher's prior permission. Violators will be prosecuted.

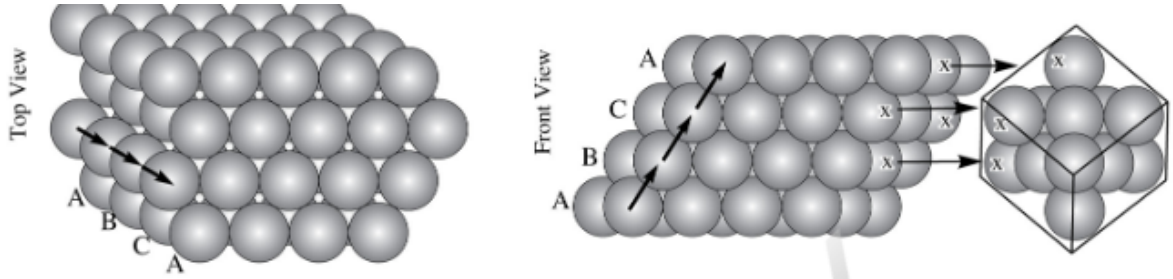

FIGURE 4.2 Closest packing of spheres. (*a*) Close-packed layer of spheres (A). Each sphere is in contact with six neighbors. The T and O sites that will be formed when the B layer is placed on top of A are indicated. (*b*) Second layer of spheres (B) stacked on top of the first so that the spheres nestle into the T sites. The T site is surrounded by four spheres and the O sites are surrounded by six spheres. (*c*) Hexagonal close packing is produced when a third layer is stacked directly above the first. The layers of spheres therefore alternate ABAB ... and are parallel to the (001) plane in the hexagonal lattice. (*d*) Cubic close packing of spheres. Instead of shifting back and forth between two positions, each successive layer is shifted in the same direction. The first two layers of spheres (A and B) are the same as with hexagonal close packing. The C layer is shifted in the same direction as B, so the C spheres are directly above the O sites in the A layer. An additional shift in the same direction places the spheres in the top layer (A) directly above those in the initial A layer. The layers of spheres therefore alternate ABCABC ... and are parallel to the (111) plane in a face-centered cubic lattice. The spheres marked *x* define the corners on one face of the cube. View larger image

In hexagonal closest packing (**Figure 4.2c**), the layers alternate between two positions. If the initial layer is considered to be in the A position, the next is in the B position, followed by A, then B, and so forth, forming what can be called an AB structure. This produces hexagonal symmetry with the planes of atoms parallel to the (001) crystallographic plane in the hexagonal lattice.

In cubic closest packing (**Figure 4.2d**), every third layer is aligned. The initial layer is A, followed by B and C, and finally A again, each shifted in the same direction. The positions of the spheres in the A layers are directly above each other. This forms an ABC structure in which the planes of atoms are parallel to the (111) crystallographic plane of a face-centered cubic lattice; the spheres are located at lattice nodes.

Many of the metals that occur as native elements (Chapter 20), including gold, silver, and copper, adopt the cubic closest packing arrangement. Metals with similar size and chemistry can be readily interchanged in this structure, forming alloys. Gold and silver, for example, have about the same size (Appendix A) and are in the same group in the periodic table of the elements, so it is possible to form gold–silver alloys with any composition intermediate between pure gold and pure silver.

A somewhat less dense arrangement, known as a **body-centered cubic packing**, is used by iron (**Figure 4.3**). In this arrangement, the atoms are placed at the nodes of a body-centered cubic lattice. Each sphere is in contact with 8, rather than 12, neighbors.

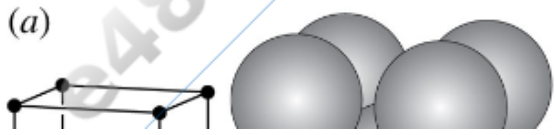

Printed by: e48d507df5d1141@placeholder.94092.edu. Printing is for personal, private use only. No part of this book may be reproduced or transmitted without publisher's prior permission. Violators will be prosecuted.

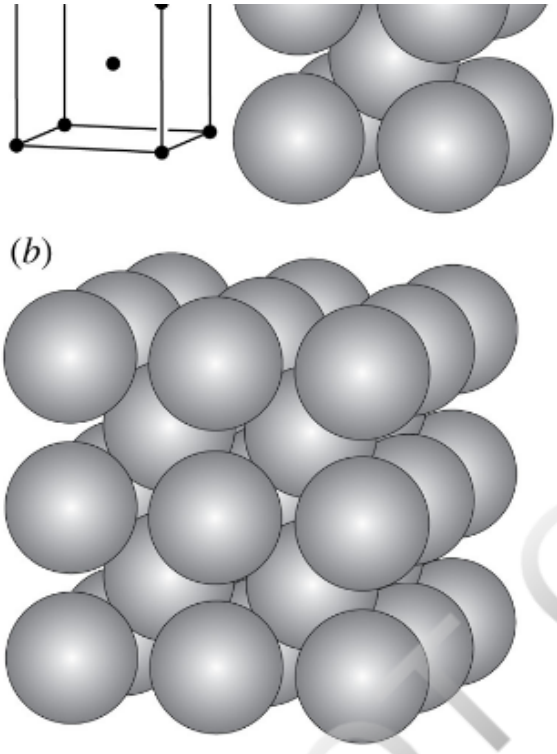

FIGURE 4.3 Body-centered cubic packing. (*a*) Body-centered lattice (left) and with atoms at each lattice node (right). (*b*) Eight unit cells. Each sphere is in contact with eight neighbors. View larger image

Because of the closeness of packing and relatively high atomic weights, most metal crystals have high density compared to ionic-bonded crystals. Minerals with metallic bonding also conduct electricity easily and are relatively malleable.

Covalent Bonding Structure Controls

Covalent bonding is typically quite strong, so covalent crystals are hard and have high melting points. The strong directional nature of covalent bonding requires that the atoms be placed in specific orientations so that orbitals can overlap. This often prevents the atoms from acquiring a close-packed arrangement. Diamond, described in Chapter 3 (Figure 3.5), is a good example.

Ionic Bonding Structure Controls

One of the most successful approaches to understanding the structure of many common minerals is based on the assumption that the anions and cations pack together as different-sized spheres. We have seen in Chapter 3 that bonding in many common minerals in which oxygen is the anion is dominantly ionic. The abundant silicate minerals such as the feldspars, pyroxenes, amphiboles, and micas are excellent examples. For these types of minerals, the bond between oxygen and silicon has about half ionic character, and the bonds between oxygen and the other common cations (Na, Mg, Al, K,

DO NOT COPY e48d507df5d1141@placeholder.9409

Printed by: e48d507df5d1141@placeholder.94092.edu. Printing is for personal, private use only. No part of this book may be reproduced or transmitted without publisher's prior permission. Violators will be prosecuted.

character, and the bonds between oxygen and the other common cations (Na, Mg, Al, K, Ca, and Fe) are even more ionic. Therefore the assumption of ionic character is reasonable.

Because ionic bonding is not directional, it also is reasonable, as a first approximation, to treat the anions and cations as spheres of consistent sizes that bond together in purely geometrical terms that are not dictated by the complexities of aligning orbitals in specific orientations required for covalent bonding. These assumptions work because they allow construction of mineral structures consistent with what is actually observed when the structures are studied in detail.

Based on these assumptions, a set of five rules, now collectively known as **Pauling's Rules**, was developed in the late 1920s.

Rule 1. The Coordination Principle

The coordination principle addresses how anions form polyhedra around cations: the specific polyhedra is controlled by the relative size of the anion and cation. As mentioned in Chapter 3, the **coordination number (CN)** is the number of anions in contact with a cation. When the bonding is dominantly ionic, each cation will attract or coordinate with (bond to and touch) as many anions as possible. The **coordination polyhedron** is the shape defined by the anions coordinating with a cation. Twelve-fold coordination (**Figure 4.4a**) is the largest common coordination number (CN = 12) and can result in a cuboctahedron polyhedron, which is not a regular polyhedron as the sides are alternating squares and triangles. The common regular coordination polyhedra are the cube (CN = 8), octahedron (CN = 6), tetrahedron (CN = 4), triangle (CN = 3), and line (CN = 2).

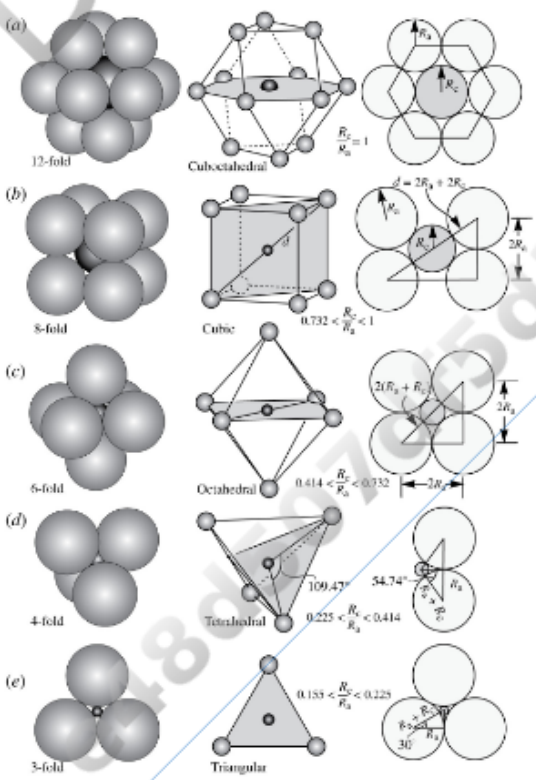

DO NOT COPY e48d507df5d1141@placeholder.94092

Printed by: e48d507df5d1141@placeholder.94092.edu. Printing is for personal, private use only. No part of this book may be reproduced or transmitted without publisher's prior permission. Violators will be prosecuted.

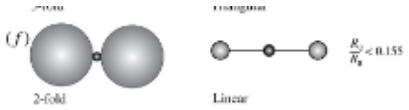

FIGURE 4.4 Coordination polyhedra. Anions with radius R_a are shown with light shading, and cations with radius R_c are dark. Left view shows cation and anions as scaled spheres. Center view shows the coordination polyhedra. Right view shows the plane through the polyhedron (shaded in center view) from which the radius ratio is calculated. See text for additional discussion. (*a*) 12-fold coordination (based on cubic closest packing), or cuboctahedral, coordination as shown. (*b*) 8-fold, or cubic, coordination. (*c*) 6-fold, or octahedral, coordination. (*d*) 4-fold, or tetrahedral, coordination. (*e*) 3-fold, or triangular, coordination. (*f*) 2-fold, or linear, coordination. View larger image

The **radius ratio** (*RR*) is a straightforward way to express the relative size difference of the cation and anion:

$$RR = R_c / R_a \tag{4.1}$$

where R_c is the cation radius and R_a is the anion radius. The minimum number of anions that will coordinate with a cation is not strictly limited, but as a general rule, cations will bond with as many anions as they can. The maximum number of anions that will coordinate with a cation, however, is limited by the need to maintain contact between the cation and surrounding anions. The range of radius ratios for the regular coordination geometries (CN = 12, 8, 6, 4, 3, and 2) is shown in **Table 4.1**.

TABLE 4.1 Radius Ratio for Common Coordination Geometries

Coordination Number	Polyhedron	Radius Ratio
12	Cuboctahedron or similar	~1
8	Cube	0.732–1
6	Octahedron	0.414–0.732
4	Tetrahedron	0.225–0.414
3	Triangle	0.155–0.225
2	Line	<0.155

12-Fold Coordination If the anion and cation are about the same size, then $RR \sim 1$. Each cation can be surrounded by no more than 12 anions (CN = 12), so each anion touches the cation. The two different ways in which 12-fold coordination can be achieved are based on cubic closest packing and hexagonal closest packing. Cubic closest packing is shown in Figure 4.4a; other polyhedra with 12-fold coordination are possible depending on the details of packing.

8-Fold Coordination If the radius ratio is less than 1, the cation is too small to maintain contact with 12 anions. With regular packing, the next smaller number of anions that can

DO NOT COPY e48d507df5d1141@placeholder.94092

Printed by: e48d507df5d1141@placeholder.94092.edu. Printing is for personal, private use only. No part of this book may be reproduced or transmitted without publisher's prior permission. Violators will be prosecuted.

contact with 12 anions. With regular packing, the next smaller number of anions that can surround and touch the cation is 8 (**Figure 4.4b**). The 8 anions arrange themselves to form a cube, so 8-fold coordination is known as **cubic coordination**. The lower limit of 8-fold coordination is achieved when the cation is small enough that the anions come in contact with each other. The radius ratio at which this happens can be calculated with the help of basic geometry. If the 8 anions that define the cube are in contact, the length of each edge of the cube is $2R_a$. The Pythagorean theorem can be used to demonstrate that the length of the long diagonal d through the center of the cube is equal to

$$d = \sqrt{3} \times 2R_a. \tag{4.2}$$

The length of d also is equal to $2R_a + 2R_c$ (Figure 4.4b) so

$$\sqrt{3} \times 2R_a = 2R_c + 2R_a. \tag{4.3}$$

Rearranging and solving for the radius ratio yields

$$\frac{R_c}{R_a} = \sqrt{3} - 1 = 0.732.$$

6-Fold Coordination If the radius ratio is less than 0.732, the cation is too small to maintain contact with eight anions, but it can maintain contact with six, down to a limiting radius ratio of 0.414. The six anions arrange themselves to form the corners of an octahedron (**Figure 4.4c**) so 6-fold coordination is known as **octahedral coordination** (not to be confused with 8-fold coordination). Note that the cation is in the center of a square defined by four anions with a single anion above and below. The length of the diagonal through the square is equal to $2R_a + 2R_c$, and also is (by Pythagoras) equal to the square root of two times the length of the sides ($2R_a$).

$$2R_a + 2R_c = \sqrt{2} \times 2R_a \tag{4.4}$$

Rearranging to solve for the radius ratio yields

$$\frac{R_c}{R_a} = \sqrt{2} - 1 = 0.414.$$

4-Fold Coordination If the radius ratio is smaller than 0.414, down to a limit of 0.225, cations are too small to maintain contact with six anions, but they can coordinate with four anions (**Figure 4.4d**). Because the four anions define the corners of a tetrahedron, 4-fold coordination is known as **tetrahedral coordination**. The lower limit of 4-fold

DO NOT COPY e48d507df5d1141@placeholder.9409

Printed by: e48d507df5d1141@placeholder.94092.edu. Printing is for personal, private use only. No part of this book may be reproduced or transmitted without publisher's prior permission. Violators will be prosecuted.

4-fold coordination is known as **tetrahedral coordination**. The lower limit of 4-fold coordination is achieved when the four anions come in contact. Because the coordination polyhedron is a tetrahedron, a triangle drawn through the centers of two anions and the cation will have an angle of 109.47° between its two equal legs. The sine of half that angle is equal to the radius of the anion divided by the sum of the anion and cation radii.

$$\sin \frac{109.47^\circ}{2} = \frac{R_a}{R_a + R_c} \tag{4.5}$$

Rearranging to solve for the radius ratio yields

$$\frac{R_c}{R_a} = \frac{1}{\sin 54.74^\circ} - 1 = 0.225.$$

3-Fold Coordination If the radius ratio is less than 0.225, down to a limit of 0.155, only three anions can maintain contact with the cation. Three-fold coordination is known as **triangular coordination**. The lower limit of 3-fold coordination is achieved when the cation is so small that the three anions come in contact (**Figure 4.4e**). The triangle produced with 3-fold coordination is an equilateral triangle so

$$\frac{R_a}{R_a + R_c} = \cos 30^\circ. \tag{4.6}$$

Rearranging to solve for the radius ratio yields

$$\frac{R_c}{R_a} = \frac{1}{\cos 30^\circ} - 1 = 0.155.$$

2-Fold Coordination Only two anions can maintain contact in **linear coordination** with a cation that is so small that the radius ratio is less than 0.155 (**Figure 4.4f**).

Other Geometries While the emphasis here is on regular coordination polyhedra, in many minerals, cations coordinate with 5, 7, 9, 10, or 11 oxygen anions. In addition, it also is common to find that the 3-, 4-, 6-, 8-, and 12-fold sites are somewhat distorted compared to the ideal geometry described earlier. Although the reasons that minerals may have structures with nonregular coordination polyhedra are numerous, they often are related either to the fact that some chemical bonds have substantial covalent character and are therefore somewhat directional, or the geometry must accommodate anionic groups such as CO_3^{2-}, SO_4^{2-}, and SiO_4^{4-}.

Common Cation Coordination Given that O^{2-} is by far the most abundant anion in

DO NOT COPY

Printed by: e48d507df5d1141@placeholder.94092.edu. Printing is for personal, private use only. No part of this book may be reproduced or transmitted without publisher's prior permission. Violators will be prosecuted.

minerals and that it has an effective ionic radius of about 1.26 Å, it is possible to predict the coordination with common cations. **Table 4.2** shows the range of cation sizes that would normally go into the coordination polyhedra and the common cations that have the appropriate sizes when coordinating with oxygen. The same ranges also are shown in Figure 3.18. Note that some of the cations fit comfortably in more than one coordination: Al^{3+} fits in both 4-fold and 6-fold coordination, Fe^{2} and Mg^{2+} have sizes appropriate for either 6-fold or 8-fold coordination, and Na^{+} and Ca^{2+} are appropriate for either 8-fold or 12-fold coordination.

TABLE 4.2 Cation Sizes for Common Coordination Polyhedra When Coordinating with O^{2-} (~1.26 Å)

Coordination	Radius Ratio	Minimum Radius (Å)	~Maximum Radius (Å)	Common Cations
12	~1.00	1.26	N/A	K^{+}, Ca^{2+}, Na^{+}
8	0.732–1.00	0.92	1.26	Fe^{2+}, Ca^{2+}, Na^{+}, Mg^{2+}
6	0.414–0.732	0.52	0.92	Al^{3+}, Fe^{2+}, Fe^{3+}, Mg^{2+}
4	0.225–0.414	0.28	0.52	Si^{4+}, Al^{3+}, S^{6+}, P^{5+}
3	0.155–0.225	0.20	0.28	C^{4+}[a]
2	<0.155	N/A	0.20	None

[a] According to Appendix A, C^{4+} has an ionic radius of 0.06 Å when in 3-fold coordination, substantially smaller than theory would suggest is appropriate. The discrepancy is probably a consequence of the fact that the C–O bond has substantial covalent character, and the simple model used here of ionically bonding spheres of different sizes is not entirely appropriate.

Many minerals have structures that are based, at least approximately, on close-packed anions. The interstices between the anions form tetrahedral (T) and octahedral (O) sites, some of which become occupied by cations. **Figure 4.5** shows how these sites are formed.

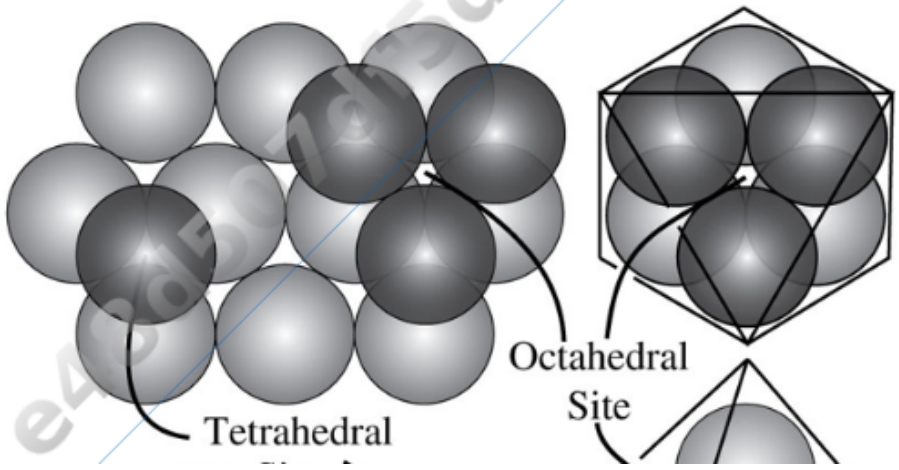

Printed by: e48d507df5d1141@placeholder.94092.edu. Printing is for personal, private use only. No part of this book may be reproduced or transmitted without publisher's prior permission. Violators will be prosecuted.

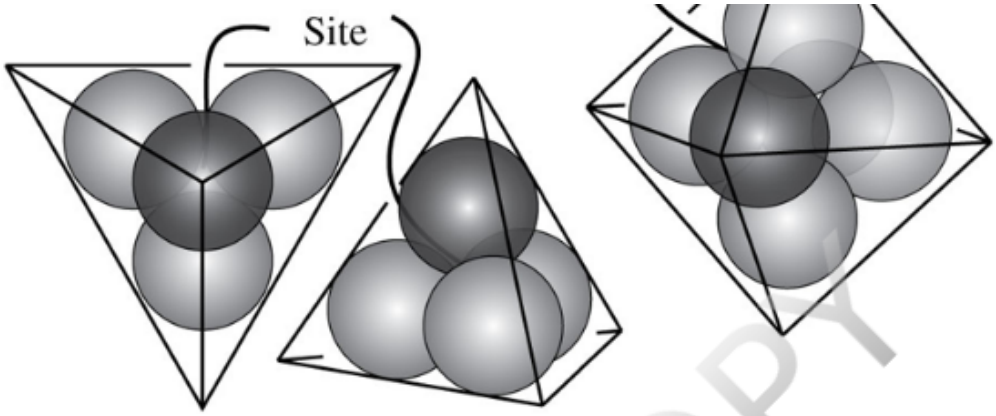

FIGURE 4.5 Tetrahedral and octahedral sites in close-packed structures. A layer of anions (light) is shown with just four anions from an adjacent layer (dark). Tetrahedral, or 4-fold, coordination sites are formed where an anion from one layer nestles into the hollow formed by three anions from the next layer. The tetrahedral site is the little opening hidden in the middle of the four anions. Octahedral, or 6-fold, coordination sites are formed where three anions from one layer nestle into three from the next. Compare Figure 4.2a, where all the tetrahedral and octahedral sites between two layers of anions are identified. View larger image

Rule 2. Electrostatic Valency Principle

For an ionic bond, the **electrostatic valence bond** (evb) is a way to determine bond strength, which is determined by the charge of a cation divided by the number of anions it is coordinated with (CN).

$$\text{evb} = \text{cation charge}/\text{CN} \tag{4.7}$$

Although this relationship seems straightforward, it leads to some interesting consequences, and it should not be overlooked that crystal structures, when all bonding is considered, must be charge neutral.

Uniform Bond Strength If all ionic bonds in a crystal have the same strength, this is called **isodesmic bonding**. Isodesmic bonding typically occurs when the mineral only has a single anion and single cation, but this can also occur for some minerals with multiple cations and/or anions. If all the cation–anion bonds are the same strength, it is impossible for any bond to occupy more than half of the anion's charge because the smallest possible coordination number is 2. Because the anion–cation bonds are all uniform, the anions tend to pack together in a highly symmetrical arrangement; often the anions have a cubic or hexagonal closest packing and the cations are situated in the interstitial space. This leads to such minerals often having highly symmetrical isometric, tetragonal, or hexagonal crystal systems.

Nonuniform Bond Strength In some structures, certain anion–cation bonds are stronger than others. The cations forming stronger bonds are small and have a high charge; C^{4+}, S^{6+}, P^{5+}, and Si^{4+} are good examples (Table 4.2 and Appendix A). Because these cations strongly bond to the anions (usually O^{2-}), the result is the formation of

Printed by: e48d507df5d1141@placeholder.94092.edu. Printing is for personal, private use only. No part of this book may be reproduced or transmitted without publisher's prior permission. Violators will be prosecuted.

these cations strongly bond to the anions (usually O^{2-}), the result is the formation of CO_3^{2-}, SO_4^{4-}, PO_4^{3-}, and SiO_4^{4-} anionic groups that serve as structural elements in the mineral's structures.

Minerals with nonuniform bond strength typically have lower symmetry than those with uniform bond strength because of the geometric complexity involved with packing the anionic groups together and coordinating with other cations. Coordination polyhedra formed between these anionic groups often are irregular. The two types of nonuniform bonding are **anisodesmic bonding** and **mesodesmic bonding**. With anisodesmic bonding, some anion–cation bonds take more than half of the anion charge; with mesodesmic bonding, some anion–cation bonds take exactly half of the anion charge.

Anisodesmic bonding is found in minerals containing small, highly charged cations. Consider the mineral calcite ($CaCO_3$), described in Chapter 17. Carbon is a small cation (Table 4.2) with a +4 charge that coordinates with three O^{2-} (**Figure 4.6**). The electrostatic valence bond (evb) strength of the C–O bonds is therefore 4/3 = 1.33. The Ca^{2+} is in 6-fold coordination with these same O^{2-} anions, with an evb of 2/6 = 1/3. Each O^{2-} bonds with two Ca^{2-} cations, so the total evb reaching each oxygen is 2. The oxygen anions are more strongly bonded to the carbon than to the calcium. As a consequence, distinct CO_3^{2-} structural anionic groups are formed. S^{6+} and P^{5+} similarly form anisodesmic SO_4^{2-} and PO_4^{3-} anionic groups.

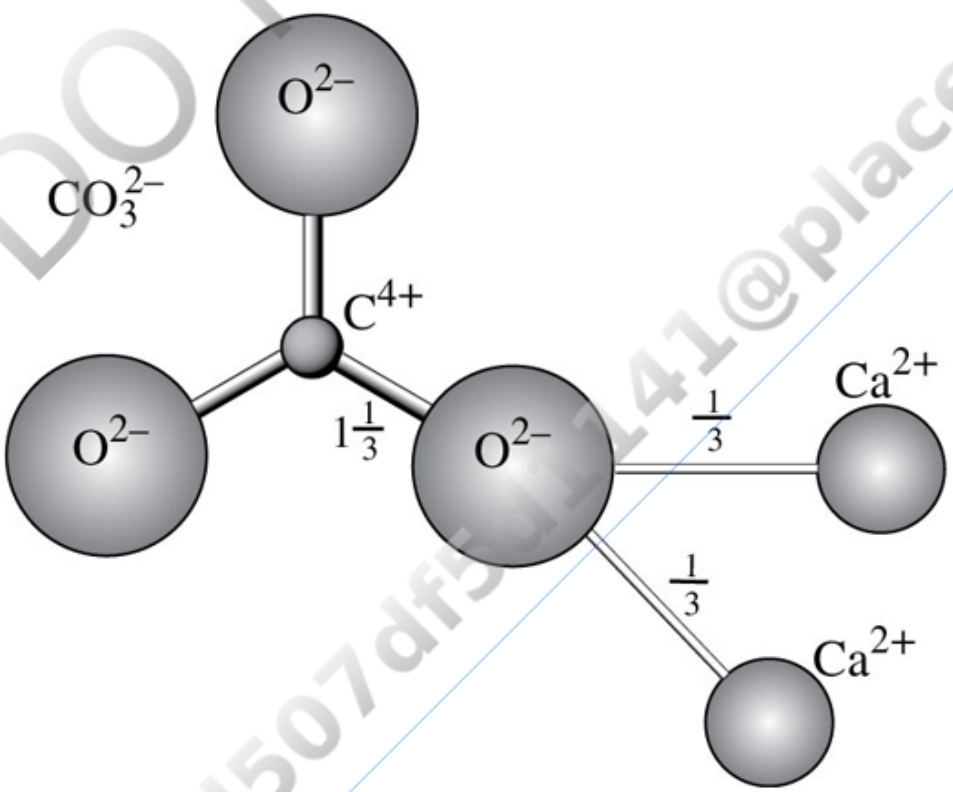

FIGURE 4.6 Anisodesmic carbonate (CO_3^{2-}) group. Each O–C bond occupies 1.33 of the available −2 charge on oxygen; only two-thirds of a charge on the oxygen is available to bond with other cations, such as Ca^{2+}. View larger image

DO NOT COPY e48d507df5d1141@placeholder.94092

Printed by: e48d507df5d1141@placeholder.94092.edu. Printing is for personal, private use only. No part of this book may be reproduced or transmitted without publisher's prior permission. Violators will be prosecuted.

Mesodesmic bonding represents a special case in which the anion–cation bond takes up exactly half of the available anion charge. The silicates provide the best example. Si^{4+} almost always coordinates with four O^{2-} in what is known as a **silicon tetrahedron** (**Figure 4.7a**). The evb strength is therefore 4/4 = 1, which is exactly half of the −2 charge on oxygen. This leaves a −1 charge on each oxygen available to bond with a second Si^{4+} by sharing an oxygen between tetrahedra (**Figure 4.7b**). Each silicon tetrahedron may share oxygen with one, two, three, or four adjacent tetrahedra, depending on how much silicon is available. The degree to which silicon tetrahedra share oxygen ions with adjacent tetrahedra and polymerize to form pairs, chains, rings, sheets, and three-dimensional frameworks provides the basis for classification of the silicate minerals (Chapter 11).

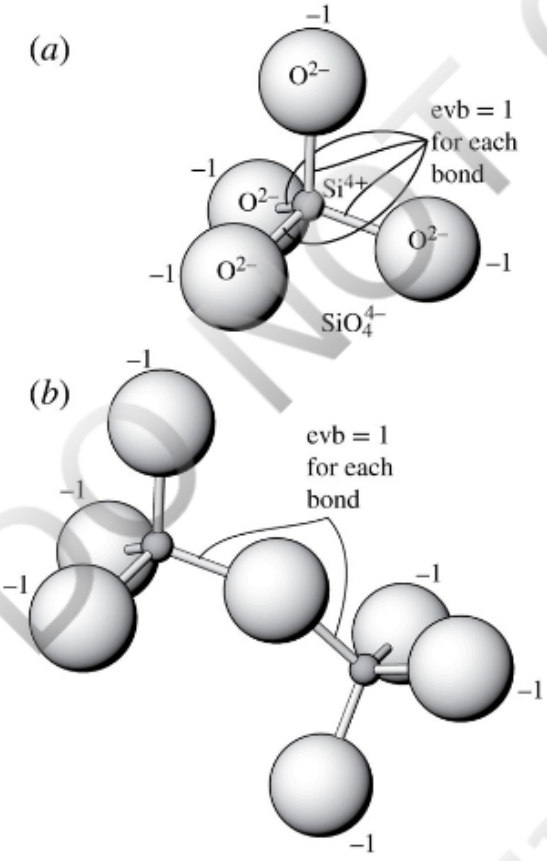

FIGURE 4.7 Mesodesmic silicon tetrahedra. (*a*) Si–O bonds occupy 1 (evb = 1) of the available −2 charge on oxygen, which is left with a net −1 charge unsatisfied. (*b*) Each oxygen can therefore bond to another Si^{4+} so that the oxygen anion is equally shared between silicon tetrahedra. A silicon tetrahedron may share one, two, three, or all four of its oxygen anions with adjacent tetrahedra.
View larger image

The oxygen in a silicon tetrahedron also may bond with other cations such as Al^{3+}, $Fe^{2+/3+}$, Mg^{2+}, and Na^{+}, depending on the relative amounts of silicon and the other cations that are available. In forsterite (Mg_2SiO_4), no oxygen from one silicon tetrahedron is shared with another, so each oxygen anion satisfies its remaining −1 charge by bonding with Mg^{2+}. The Mg^{2+} coordinates with six oxygens, so its evb will be 2/6, or 1/3. Because each Mg–O bond takes up just 1/3 of a charge, each oxygen must

DO NOT COPY e48d507df5d1141@placeholder.9409

Printed by: e48d507df5d1141@placeholder.94092.edu. Printing is for personal, private use only. No part of this book may be reproduced or transmitted without publisher's prior permission. Violators will be prosecuted.

2/6, or 1/3. Because each Mg–O bond takes up just 1/3 of a charge, each oxygen must bond with three Mg^{2+}. Of the two cations, the Si^{4+}, with evb = 1, has the stronger claim on the oxygen anions, so the silicon tetrahedron is considered the primary structural element in the mineral.

Minerals with nonuniform bond strength are classified based on the identity of the anionic group formed around the small high-charged cation; anisodesmic examples mentioned above include the CO_3^{2-}, SO_4^{4-}, and PO_4^{3-} anionic groups. The silicates with the SiO_4^{4-} anionic group are the only common mesodesmic group of minerals. The anionic groups will lead to the chemical classification of minerals.

Rule 3. Sharing of Polyhedral Elements I

Much of the focus thus far has been on the bonding and attraction between opposite-charged anions and cations. However, repulsion between like-charged ions, particularly cations, is important too. To keep cations as far apart as possible, adjacent polyhedral often only share a single anion; this ensures that the positively charged cations are kept at the greatest possible distance. **Figure 4.8** shows these relations for tetrahedra. If only a corner (single anion) is shared, the cations are 2.45 R_a apart, where R_a = anion radius. If an edge (two anions) is shared, the cations are brought to within 1.414 R_a of each other. This reduces the stability of the structure because energy is required to bring the cations into this close proximity. The lowest stability configuration involves sharing a face (three anions) between tetrahedra. This brings the cations to within 1.15R_a of each other. Similar relationships exist for other coordination polyhedra.

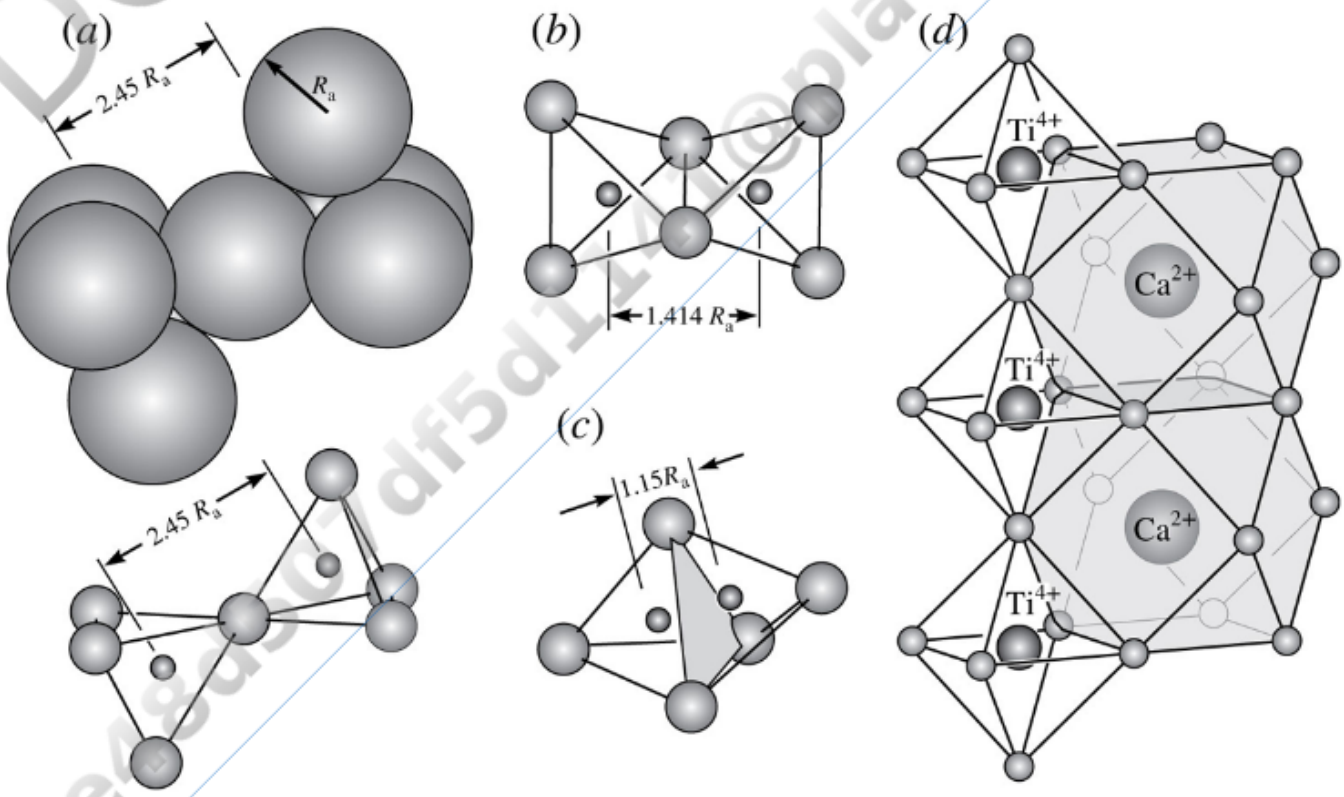

Printed by: e48d507df5d1141@placeholder.94092.edu. Printing is for personal, private use only. No part of this book may be reproduced or transmitted without publisher's prior permission. Violators will be prosecuted.

FIGURE 4.8 Sharing anions between polyhedra. (*a*) Sharing a single anion (a corner) between tetrahedra keeps the positively charged cations at a maximum distance. The upper diagram shows the anions (large) and cations (small) to scale. The lower diagram reduces the ion size to allow the tetrahedral coordination polyhedra to be more easily seen. The cations are $2.45R_a$ apart where R_a is the radius of the anion. (*b*) Sharing two anions (an edge) places the cations $1.414R_a$ apart. (*c*) Sharing three anions (a face, shaded) places the cations $1.15R_a$ apart. (*d*) In perovskite ($CaTiO_3$), the Ti^{4+} occupies octahedra that share only a single oxygen (small spheres), and Ca^{2+} occupies cuboctahedra that share four oxygen anions on common faces. View larger image

Rule 4. Sharing of Polyhedral Elements II

In structures with differently charged cations, the high-charged cations minimize the number of anions that they share between polyhedra so that the high-charged cations can be kept a maximum distance apart. The corollary is that low-charged cations are more likely to share two or more anions on edges or faces of their coordination polyhedra. Perovskite ($TiCaO_3$) illustrates this well (Figure 4.8d). The Ti^{4+} occupies octahedral (6-fold coordination) sites defined by six O^{2-} anions. These octahedra share only a single O^{2-} at a corner, thereby keeping the Ti^{4+} cations far from each other. The lower-charged Ca^{2+} is much larger and occupies cuboctahedral (12-fold coordination) sites that share four O^{2-} anions on a face. An additional consideration in some minerals follows from the second rule. Small high-charged cations (C^{4+}, S^{6+}, and P^{5+}) form low-coordination-number anisodesmic anionic groups (CO_3^{2-}, SO_4^{4-}, PO_4^{3-}) in which more than half the anion charge is occupied. This means that the anions in these anionic groups can bond only with lower-charged cations that occupy sites with higher coordination numbers.

Rule 5. Principle of Parsimony

The principle of parsimony is a statement covering the general observation (or perhaps fervent hope) that nature tends toward simplicity. The number of fundamentally different structural sites in most minerals, even those with many different chemical constituents, tends to be small. Usually the cations systematically arrange themselves into no more than four (and usually fewer) different types of coordination polyhedra and are allocated among the different polyhedra based on size and charge. Although detailed studies of some crystal structures may reveal subtle differences among different groups of tetrahedral or other sites, the observation that the anions and cations in the chemical formulas of minerals occur in small integer ratios is strong support for rule 5.

Application of Pauling's Rules

Pauling's second rule indicates that ionic minerals may be grouped into three broad categories: those with uniform bonding between anions and cations (isodesmic), those with anionic groups in which more than half of the anion charge is occupied (anisodesmic), and those with anionic groups in which half of the anion charge is occupied (mesodesmic). Let's take a look at some examples and see how Pauling's Rules

DO NOT COPY e48d507df5d1141@placeholder.94092

Printed by: e48d507df5d1141@placeholder.94092.edu. Printing is for personal, private use only. No part of this book may be reproduced or transmitted without publisher's prior permission. Violators will be prosecuted.

help explain a mineral's structure.

Uniform Bonding Example

As mentioned, if the anion–cation bonds are all uniform, the anions tend to pack together in symmetrical arrangements and the cations occupy polyhedra formed by the interstices between the anions. Some of the common structures are based on cubic closest packing, hexagonal closest packing, and body-centered cubic packing of the anions. These structures, and variants on them, are found in many minerals with simple chemistry. The structures of other, more complicated minerals are often conveniently described with reference to these simple structures.

The mineral halite (NaCl) has simple chemistry and provides a convenient example of a structure based on cubic close packing of Cl^- anions. The Cl^- anions are arranged in layers parallel to {111} in a cubic close-packed arrangement. In the NaCl structure (**Figure 4.9a**) the coordination of Na^+ is dictated by the first rule. The ionic radii of Na^+ and Cl^- are 1.16 and 1.81 Å, respectively, yielding a radius ratio of 0.64. Based on Table 4.1, Na^+ should coordinate with six Cl^-. To maintain charge balance, every one of the octahedral (6-fold) sites between the {111} layers of Cl^- must be occupied. This allows every Na^+ to bond with six Cl^- and vice versa, thus satisfying the electrostatic valency principle (second rule). Because Na^+ occupies all the available octahedral sites between the layers of Cl^-, it is necessary for the Na^+ octahedra to share edges. Because Na^+ has only a single charge, this makes edge-sharing more acceptable in the third rule. The fourth rule does not apply because only a single cation is involved; and the structure is simple with only a single cation site, so the fifth rule is satisfied.

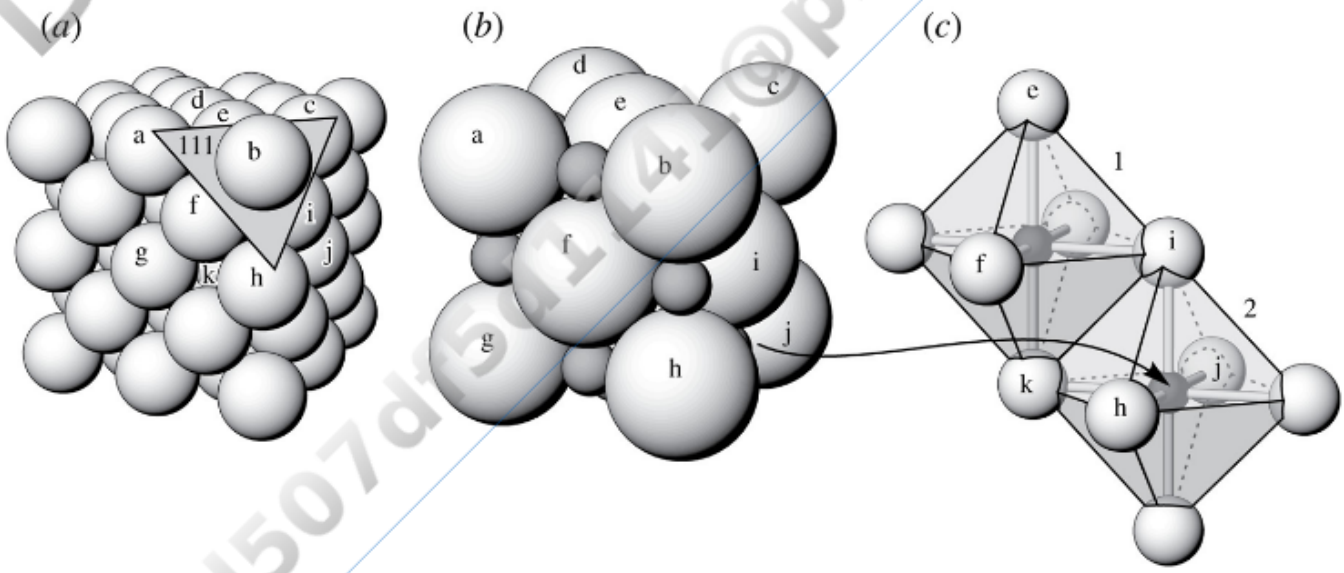

FIGURE 4.9 NaCl structure. (*a*) Layers of Cl^- anions are arranged parallel to the (111) crystallographic plane. (*b*) One unit cell showing Na^+ (dark spheres) in octahedral interstices between the Cl^-. (*c*) Octahedron 1 is formed by the Cl^- on the center of each face of the unit cell (the ions are shown at a reduced size). Octahedron 2 surrounds the Na^+ on the bottom right edge of the unit cell and includes Cl^- from adjacent unit cells. The octahedra share an edge. View larger

Printed by: e48d507df5d1141@placeholder.94092.edu. Printing is for personal, private use only. No part of this book may be reproduced or transmitted without publisher's prior permission. Violators will be prosecuted.

the unit cell and includes Cl^- from adjacent unit cells. The octahedra share an edge. View larger image

Nonuniform (Anisodesmic) Bonding Example

Anhydrite ($CaSO_4$) has an anisodesmic structure (**Figure 4.10**). S^{6+} tetrahedrally coordinates with O^{2-} (first rule). The second rule informs us that the strength of the electrostatic valence bonds reaching the S^{6+} is 6/4 = 1.5, meaning that of the −2 charge available on each oxygen, 1.5 is occupied by the sulfur and only 0.5 is available to bond with the Ca^{2+}. We know from the previous discussion on coordination that Ca^{2+} is most commonly in 8-fold coordination with oxygen. The strength of each electrostatic valence bond reaching Ca^{2+} is 2/8 = 0.25. This means that each oxygen must bond with two Ca^{2+} to satisfy its remaining 0.5 charge. This means that the SO_4^{2-} tetrahedra share oxygens with polyhedral with Ca^{2+} in 8-fold coordination. This satisfies rules 3 and 4. It turns out that ideal cubic 8-fold sites are not possible, so Ca^{2+} must settle for a somewhat distorted 8-fold site. Rule 5 is satisfied as each cation is found only in a single type of polyhedra.

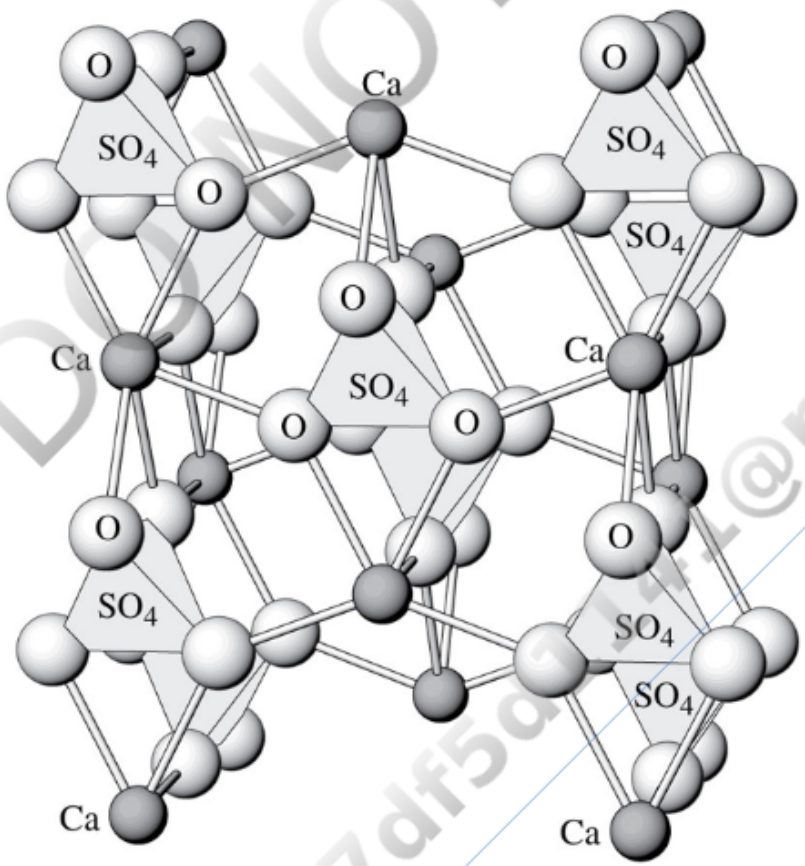

FIGURE 4.10 Anhydrite structure. Isolated SO_4^{2-} groups are bonded laterally through Ca^{2+} (dark spheres). View larger image

DO NOT COPY e48d507df5d1141@placeholder.9409

Printed by: e48d507df5d1141@placeholder.94092.edu. Printing is for personal, private use only. No part of this book may be reproduced or transmitted without publisher's prior permission. Violators will be prosecuted.

Structure Controls with Molecular Crystals

Molecular crystals consist of discrete molecules packed together in systematic ways. Each molecule in the structure is typically bonded internally with covalent bonds and therefore lacks a charge or valence with which to bond with other atoms. The forces that hold the molecules to each other are therefore limited to the relatively weak van der Waals and hydrogen bonds. Molecular crystals are therefore quite soft. The geometry of the structure is controlled by the shape and charge distribution of the individual molecules and the pattern by which they can be systematically packed together. Two examples have previously been described. Ice (H_2O) (Figure 3.13) has hydrogen bonding that holds water molecules in a hexagonal structure that controls the hexagonal shape of snowflakes. Graphite (C) (Figure 3.14) is constructed of sheets of covalent/metallic-bonded carbon that can be considered to be a molecule. The sheets of carbon are bonded to each other by van der Waals bonds.

DO NOT COPY
e48d507df5d1141@placeholder.9409

Printed by: e48d507df5d1141@placeholder.94092.edu. Printing is for personal, private use only. No part of this book may be reproduced or transmitted without publisher's prior permission. Violators will be prosecuted.

Isostructural Minerals

In the preceding discussion it was implied that different minerals may have essentially identical structures. Mineral with atoms arranged in the same crystal structure are said to be **isostructural**. Halite (NaCl) and galena (PbS), for example, are isostructural because the arrangement of Pb and S in galena is identical to the arrangement of Na and Cl in halite. The minerals are dramatically different in many physical and chemical properties, but the fact that they are isostructural is reflected in an identical symmetry, cleavage (three perfect cleavages at right angles), and crystal habits (cubes). *Isomorphism* and *isotypism* are less commonly used terms for isostructuralism.

An **isostructural group** is a group of minerals that is isostructural and also is chemically related by having the same anion or anionic group. The minerals within an isostructural group may display extensive ionic or atomic substitution, that is, more than one element may be found in the same polyhedra, or structural site, within the structure. An example of an isostructural group is the calcite group (**Table 4.3**). It is easy to conclude that the metal that differs between each member of the group resides in the same polyhedra within the structure. The calcite group is discussed in more detail Chapter 17. However, it should be emphasized that not all chemically similar minerals are isostructural; strontianite ($SrCO_3$) is not part of the calcite isostructural group.

TABLE 4.3 Calcite Isostructural Group[a]

Mineral	Formula
Calcite	$CaCO_3$
Magnesite	$MgCO_3$
Siderite	$FeCO_3$
Rhodochrosite	$MnCO_3$
Smithsonite	$ZnCO_3$

[a] All crystallize in the point group and differ only in the metal cation in the structure.

DO NOT COPY e48d507df5d1141@placeholder.9409-

Printed by: e48d507df5d1141@placeholder.94092.edu. Printing is for personal, private use only. No part of this book may be reproduced or transmitted without publisher's prior permission. Violators will be prosecuted.

Polymorphism

The ability of a chemical compound to form more than one structure is known as **polymorphism**. The different structures of a given chemical compound are known as **polymorphic forms** or **polymorphs**, and the set of different minerals with the same chemical composition is known as a **polymorphic group**. Examples of polymorphic groups are listed in **Table 4.4**.

TABLE 4.4 Common Polymorphic Mineral Groups

Chemical Composition	Mineral Name
SiO_2	α-Quartz
	β-Quartz
	α-Tridymite
	β-Tridymite
	Cristobalite
	Coesite
	Stishovite
FeS_2	Pyrite
	Marcasite
C	Graphite
	Diamond
$AlAlOSiO_4$ (generalized as Al_2SiO_5)	Andalusite
	Sillimanite
	Kyanite
$KAlSi_3O_8$	Sanidine
	Orthoclase
	Microcline

Minerals form polymorphs because most mineral structures represent a collection of compromises that balance conflicting requirements related to the attraction and repulsion of cations and anions, the fit of cations in their coordination sites, geometric requirements related to partial covalent bonding, and so forth. At a given temperature and pressure, one structure will be preferred, while at other temperatures and pressures

DO NOT COPY e48d507df5d1141@placeholder.9409

Printed by: e48d507df5d1141@placeholder.94092.edu. Printing is for personal, private use only. No part of this book may be reproduced or transmitted without publisher's prior permission. Violators will be prosecuted.

and pressure, one structure will be preferred, while at other temperatures and pressures, a different structure may be preferred, and thus the chemical compound will exist, or try to exist, with the different structure. In general, high pressures favor structures in which the atoms and ions are more tightly packed, reflected in higher mineral density. High temperature tends to favor somewhat more open, lower density structures and structures that allow greater diversity in the occupancy of specific structural sites. Because different polymorphs of the same substance exist under different sets of conditions, the presence of a given polymorph in a rock may indicate something about the conditions that formed the rock or that the rock experienced during its history.

The four different structural relationships between polymorphic forms are **reconstructive polymorphism**, **displacive polymorphism**, **order-disorder polymorphism**, and **polytypism**.

Reconstructive Polymorphism

With reconstructive polymorphism, conversion from one polymorph to another involves a major reorganization of the crystal structure. The chemical bonds that hold one structure together must be broken so that the atoms can be rearranged and bonded into the new structure. Reconstructive polymorphs need not have symmetry or structural elements in common, although the fact that the polymorphs have identical chemical compositions may lead to some structural similarities.

The structures of both diamond and graphite are described in Chapter 3 (Figures 3.5, 3.6, and 3.14). Diamond has a structure in which each carbon atom is bonded with covalent σ bonds to four neighboring carbon atoms, forming extremely hard cubic or octahedral crystals. In their most prized gem form, diamonds are perfectly clear and nearly colorless. In graphite, each carbon atom is bonded to three neighbors using a combination of σ and π bonds to form continuous sheets that are bonded to each other with van der Waals bonds. Crystals are typically very soft, black, opaque hexagonal plates. Graphite is used to make the lead in pencils. The different crystal structures of diamond and graphite clearly have a strong control on the physical properties of each mineral. The structure of diamond cannot be derived from graphite except by breaking chemical bonds and then reassembling the carbon atoms in a completely different structure.

The temperature–pressure range over which each polymorph is stable is shown in **Figure 4.11**. Note that diamond is stable only at pressures found in the mantle and that graphite is the polymorph stable at the Earth's surface. **Kimberlite** is an igneous rock in which diamond is often found and must, therefore, have originated in the mantle. The diamond found at or near the Earth's surface and mined for use in jewelry and cutting tools is **metastable**. That means that diamond does not spontaneously convert to graphite, the preferred configuration for carbon at the Earth's surface. Diamond does not automatically convert to graphite because it takes a significant amount of energy to break

DO NOT COPY

Printed by: e48d507df5d1141@placeholder.94092.edu. Printing is for personal, private use only. No part of this book may be reproduced or transmitted without publisher's prior permission. Violators will be prosecuted.

the chemical bonds holding the carbon atoms together in the diamond structure. Cooling removes energy from the system that would be needed to break diamond's bonds. This is particularly true for the fast cooling that accompanies the depressurization as the diamond-bearing kimberlite magma moves toward the surface. The fact that diamond does not automatically convert to graphite reflects one of the important features of reconstructive polymorphs. The reactions that convert one polymorph to another are quenchable. **Quenching** occurs when something is quickly cooled such that the high-temperature form is retained and does not change to the form expected for lower temperature (or pressure). Therefore, reconstructive polymorphs do not automatically convert from one structure to another with changing conditions.

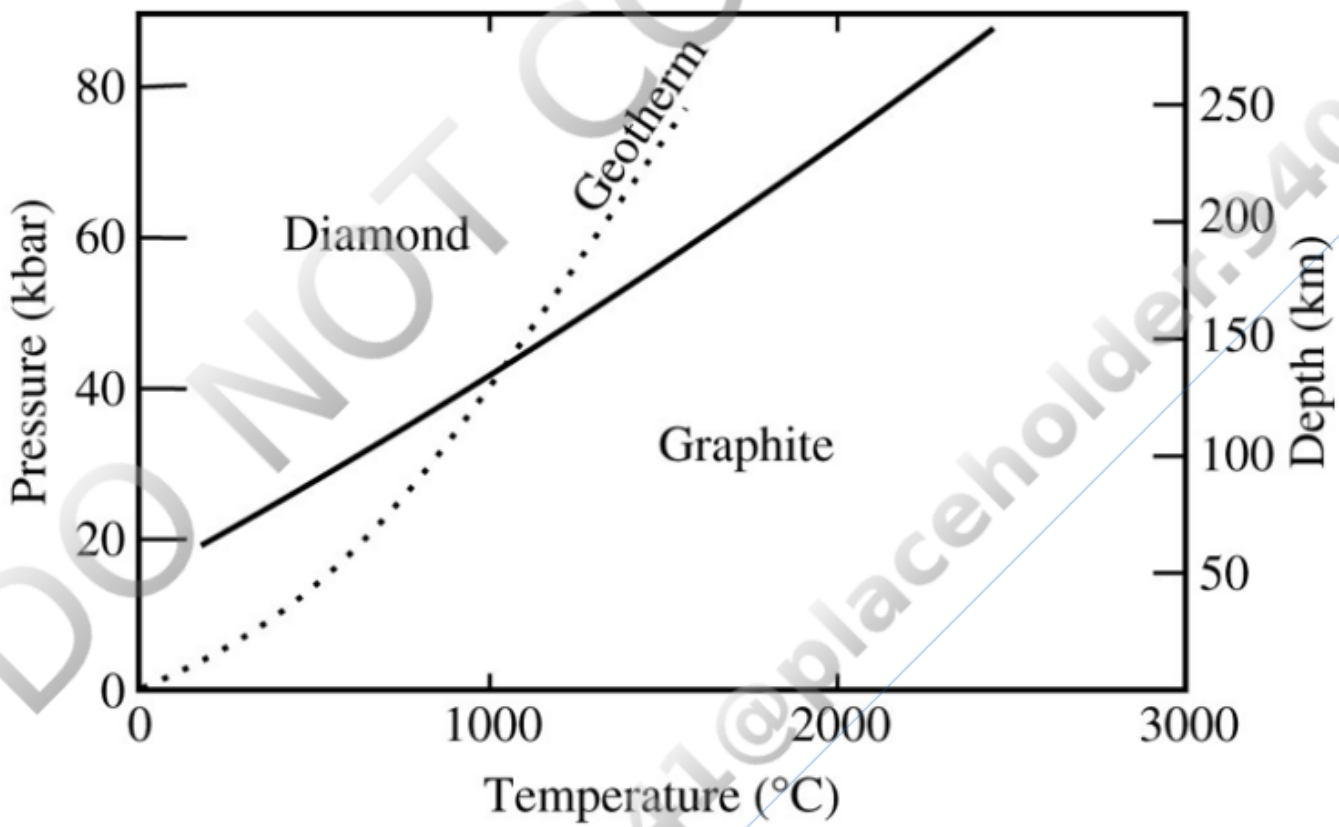

FIGURE 4.11 Diamond and graphite stability fields (Day, 2012). The geotherm tracks how pressure and temperature change with increasing depth; in this case it is shown for the rocks beneath continental shields. For this geothermal gradient, diamond is stable only at pressures greater than ~40 kilobars, which corresponds to a depth of about 125 km in the Earth's mantle.
View larger image

Displacive Polymorphism

Displacive polymorphic inversions do not involve breaking chemical bonds; the difference between polymorphs is simply a distortion or bending of the crystal structure. The relation between β-quartz and α-quartz is a good example (**Figure 4.12**). At one atmosphere pressure, β-quartz (high quartz) is stable above 573°C and has a structure consisting of a framework of silicon tetrahedra that includes 6-fold spirals (actually 6-fold

DO NOT COPY

Printed by: e48d507df5d1141@placeholder.94092.edu. Printing is for personal, private use only. No part of this book may be reproduced or transmitted without publisher's prior permission. Violators will be prosecuted.

screw axes). On cooling below 573°C, the structure undergoes an immediate, unquenchable conversion to the α-quartz (low quartz) structure in which the spirals become distorted to have 3-fold symmetry. Every time the sample is heated or cooled through the inversion temperature, the structure distorts from one structure to the other; the inversion is not quenchable—it cannot be prevented.

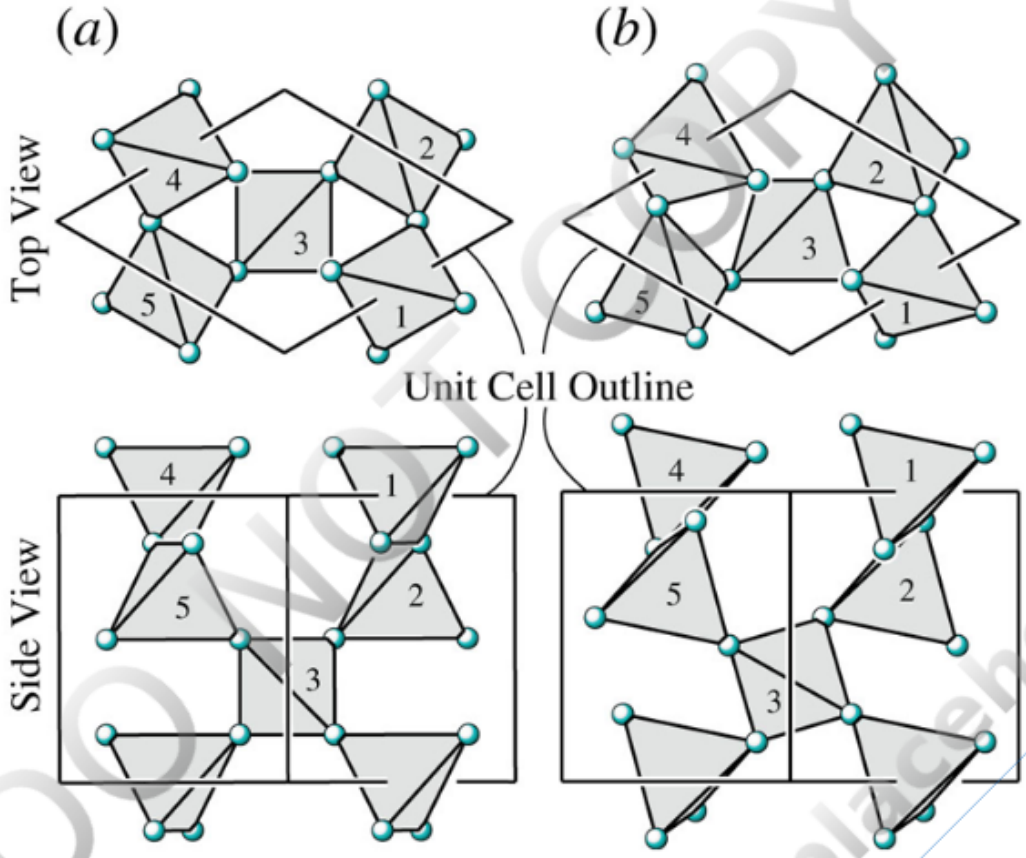

FIGURE 4.12 Structures of β-quartz and α-quartz (compare Figure 2.20). The top view looks down the c axis; the bottom view is from the side. The unit cell is outlined. (*a*) β-Quartz is the high-temperature polymorph. (*b*) α-Quartz is the low-temperature polymorph. The inversion from β-quartz to α-quartz is accomplished by a distortion that reduces the symmetry. View larger image

High-temperature forms typically have higher symmetry than low-temperature polymorphs. The crystal shape of the high-temperature polymorph will be retained on inversion to the low-temperature polymorph, though internal strains (distortion) in the crystal lattice may lead to the formation of transformation twins (segments of the crystal with different crystallographic orientation). Twinning is described in Chapter 5.

Order–Disorder Polymorphism

With order–disorder polymorphism, the mineral structure remains essentially the same. What changes is the cation distribution within different polyhedra or structural sites. If two cations X and Y can occupy two equivalent structural sites A_1 and A_2, the structure is considered disordered if there is an equal probability of finding X in either A_1 or A_2. If all

Printed by: e48d507df5d1141@placeholder.94092.edu. Printing is for personal, private use only. No part of this book may be reproduced or transmitted without publisher's prior permission. Violators will be prosecuted.

considered disordered if there is an equal probability of finding X in either A_1 or A_2. If all X cations are located in site A_1 and all Y cations are in site A_2, the structure is considered fully ordered.

Consider the mineral K-feldspar ($KAlSi_3O_8$). The three silicon and one aluminum are located in the four tetrahedral sites shown schematically in **Figure 4.13a**. The tetrahedral sites have two slightly different geometries, labeled T_1 and T_2. These sites are replicated in every unit cell in the mineral. In the completely disordered structure, represented by the high sanidine polymorph, Al is equally likely to be in any of the four sites (**Figure 4.13b**); 25 percent of these sites are filled with Al and 75 percent with Si. In the fully ordered structure, represented by the low- or maximum-microcline polymorph, all of the Al is placed in just one of the T_1 sites; the remaining T_1 and both T_2 sites contain only Si (**Figure 4.13c**). This causes a distortion to the structure and reduces the symmetry from monoclinic to triclinic. Additional ordering arrangements are possible and are discussed in the section on K-feldspar in Chapter 12.

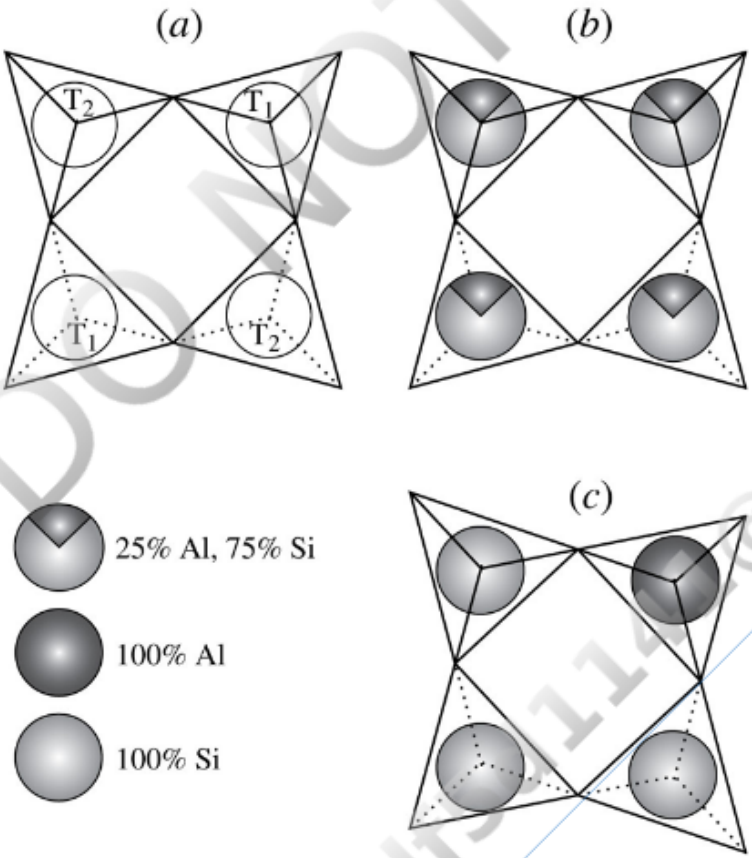

FIGURE 4.13 Order–disorder in K-feldspar ($KAlSi_3O_8$) polymorphs. (*a*) Schematic view of two up-pointing and two down-pointing tetrahedra that contain the three Si and one Al per formula unit. Two tetrahedra are T_1 sites and two are T_2 sites. (*b*) High sanidine. Al is equally likely to be in any of the four sites, so on average each contains 25 percent Al. (*c*) Maximum microcline: Al is preferentially placed in one T_1 site; Si occupies the other three sites, producing a distortion to the structure. View larger image

The degree of order in most minerals is strongly influenced by crystallization temperature and cooling history. In general, high temperatures favor crystallization with a high degree

Printed by: e48d507df5d1141@placeholder.94092.edu. Printing is for personal, private use only. No part of this book may be reproduced or transmitted without publisher's prior permission. Violators will be prosecuted.

and cooling history. In general, high temperatures favor crystallization with a high degree of disorder and low temperatures favor order. Slow cooling allows time for ions to migrate and diffuse through the crystal structure so that the different chemical elements parse themselves into the sites favored in the ordered structure; rapid cooling prevents this ordering. It should be no surprise, then, that sanidine is found in volcanic rocks, which combine high temperatures and rapid cooling. K-feldspar in plutonic igneous rocks initially crystallizes as sanidine, but slow cooling allows ordering to occur. Deep intrusions usually have sufficiently slow cooling to allow extensive ordering, so they contain microcline.

Polytypism

Polytypism is a variety of polymorphism in which the polymorphs differ only in the stacking sequence of identical sheets. **Figure 4.14** illustrates several different polytypes that can be created using a single layer. The difference between hexagonal and cubic closest packing of spheres (Figure 4.2) is another example. The sheet silicates, which include the micas and clay minerals, are an important group of minerals in which polytypism is common.

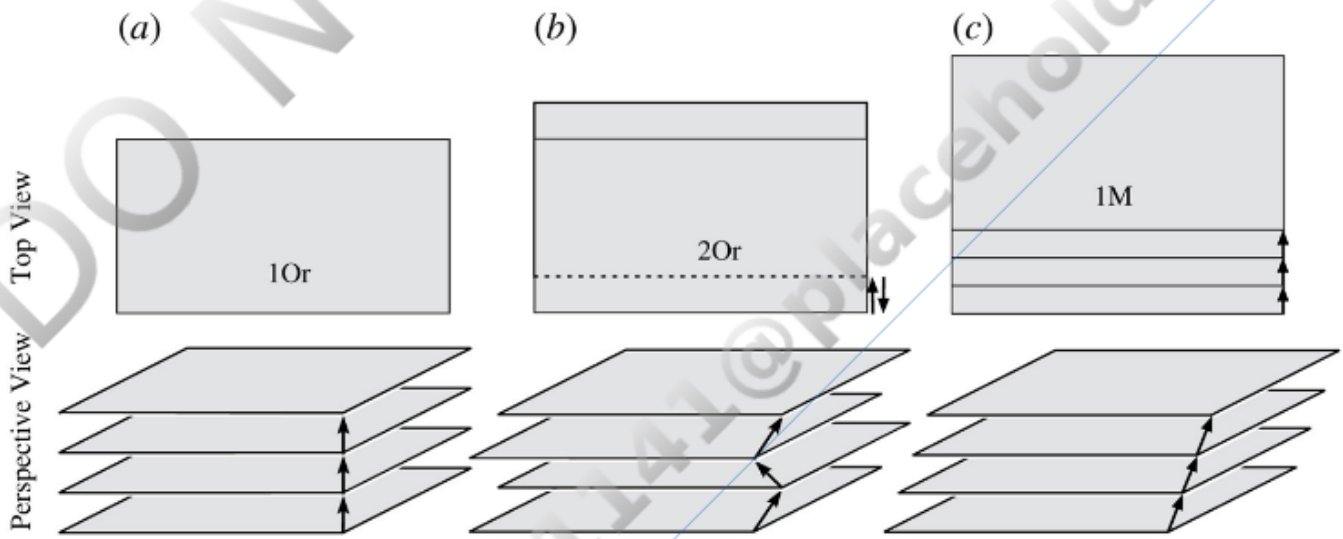

FIGURE 4.14 Polytypism involves different patterns of stacking identical sheets. The symbols used here are adapted from those used in the sheet silicates. The number in the symbol indicates the number of layers per unit cell, and the letters indicate the crystal system that results (Or = orthorhombic, M = monoclinic). (*a*) 1Or polytype with a single stacking vector at right angles to the sheets. (*b*) 2Or polytype with two stacking vectors with opposite senses. (*c*) 1M polytype with a single stacking vector at an angle to the sheets. View larger image

DO NOT COPY
e48d507df5d1141@placeholder.9409

Printed by: e48d507df5d1141@placeholder.94092.edu. Printing is for personal, private use only. No part of this book may be reproduced or transmitted without publisher's prior permission. Violators will be prosecuted.

Mineral Classification

Except for the native elements, which do not have anions, minerals are conventionally classified based on the identity of the major anion or anionic group (**Table 4.5**). This approach is consistent with normal practice in chemistry concerning the classification of inorganic chemical compounds. It also matches well with the observation that minerals with the same anion or anionic group often have clear family relations in terms of structure and physical and chemical properties. Further, the cation content of many minerals may be quite variable, whereas the anion content is typically quite limited.

TABLE 4.5 Chemical Classification of Minerals

Mineral Group	Anion or Anionic Group	Mineral Group	Anion or Anionic Group
Native elements	None	Carbonates	CO_3
Oxides	O	Nitrates	NO_3
Hydroxides	OH	Borates	BO_3, BO_4
Halides	Cl, Br, F	Chromates	CrO_4
Sulfides	S	Tungstates	WO_4
Arsenides	As	Molybdates	MoO_4
Antimonides	Sb	Phosphates	PO_4
Selenides	Se	Arsenates	AsO_4
Tellurides	Te	Vanadates	VO_4
Sulfates	SO_4	Silicates	SiO_4

This classification scheme also follows from Pauling's Rules for ionic-bonded solids. The first, third, and fourth rules inform us that we can expect the anions to define the basic structure of minerals. The second rule provides the basis for separating minerals based on whether they contain anionic groups.

Two formal classification schemes—Dana and the Strunz–Nickel—are in common use, and both follow the general arrangement shown in Table 4.5. The Dana system in its current incarnation (Gaines and others, 1997) establishes 78 mineral classes that are subdivided into types and groups. The Strunz–Nickel system (Strunz and Nickel, 2001) has 10 mineral classes that are subdivided into divisions, families, and groups. In both systems, a mineral classification is given as a series of numbers or letters.

DO NOT COPY e48d507df5d1141@placeholder.9409

Printed by: e48d507df5d1141@placeholder.94092.edu. Printing is for personal, private use only. No part of this book may be reproduced or transmitted without publisher's prior permission. Violators will be prosecuted.

Compositional Variation in Minerals

When chemical analyses of different samples of a mineral are performed, it is routinely found that they do not all have the same chemical composition. The variations may be substantial, but they ideally always fall within limits. Recall from Chapter 1 that minerals have a definite but not fixed chemical composition. **Solid solution** is the term used for when a mineral's composition varies because more than one element may be found within specific crystal structure sites.

The term *solid solution* is somewhat misleading because it is not really analogous to the familiar liquid solutions encountered in chemistry and daily life. In a liquid solution, one or more materials, the **solutes**, are mixed in variable amounts with a liquid **solvent** to form a homogeneous mixture. The solutes can be solids that dissolve, other liquids, or gases. Soda is a good example of a liquid solution. The solvent is water and the solutes are dissolved sugar, gaseous CO_2, and various organic and other compounds added to provide flavor and color. Different sodas have different solutes in different amounts.

With minerals, however, compositional variation is not a matter of mixing various solutes into a solid solvent. Rather, the compositional variation is a consequence of the ability of different elements, mostly cations, to substitute for each other within the crystal structure. The structure of an ionic-bonded mineral may be considered to be constructed of a framework of anions that form a number of distinct polyhedra or structural sites into which the cations fit. Additional sites may be vacant. Compositional variation is possible because different cations can interchangeably occupy the various sites among the anions. Additionally, in some cases different anions may be interchanged for each other. The three principal types of solid solution are **substitution solid solution**, **omission solid solution**, **and interstitial solid solution**.

The range of compositions produced by solid solution in a given mineral is known as a substitution series or a **solid solution series**. The compositional extremes of a solid solution series are known as the **end members**. End-member compositions are typically written with integer subscripts for all elements in the formula. A **continuous** or **complete solid solution series** is one in which all intermediate compositions are possible. An **incomplete** or **discontinuous solid solution series** is one in which only a limited range of compositions between the end members is possible.

Substitution Solid Solution

Substitution involves interchanging one cation for another in a structural site. Two requirements control whether substitution can occur.

DO NOT COPY e48d507df5d1141@placeholder.9409-

Printed by: e48d507df5d1141@placeholder.94092.edu. Printing is for personal, private use only. No part of this book may be reproduced or transmitted without publisher's prior permission. Violators will be prosecuted.

- Ion sizes must be similar.
- Charge neutrality must be maintained.

Size

The size requirement follows logically from Pauling's first rule and the discussion of coordination. Table 4.2 is useful for determining which of the common elements can substitute for each other based on size. For example, Si^{4+} and Al^{3+} may substitute in tetrahedral sites; Mg^{2+}, Fe^{2+}, Fe^{3+}, and Al^{3+} may substitute in octahedral sites; and Na^{+} and Ca^{2+} may substitute in 12-fold sites. Two or more elements, such as Mg^{2+} and Fe^{2+}, that can occupy or substitute for each other in the same structural site in a crystal structure are said to be diadochic. As a general rule, if the difference in ion size is less than 15 percent, extensive substitution is usually possible; if the difference in ion size is greater, substitution becomes limited.

Temperature has a substantial influence on the degree to which elements of different sizes may substitute for each other. For example, when in 8-fold coordination with oxygen, Na^{+} and K^{+} have effective ionic radii of 1.32 and 1.65 Å, a difference of about 25 percent. Only limited substitution of K^{+} for Na^{+} is likely in minerals crystallized at temperatures normally found at or near the Earth's surface. At high temperatures, however, a substantially greater tolerance of size difference is allowed. Minerals such as K-feldspar crystallized from lavas at high temperatures may display extensive Na^{+}–K^{+} substitution, meaning nearly all intermediate composition as determined by the ratio of Na to K are possible.

Because the extent of ionic substitution of dissimilar-sized cations is strongly influenced by temperature, the degree of such substitutions can be used to constrain the temperature of crystallization or recrystallization of a mineral. Further, because the extent of substitution of dissimilar-sized cations decreases with lowered temperature, samples that grew with intermediate compositions at high temperature can, on cooling, be expected to unmix into two phases or minerals—one rich in the larger cation and the other rich in the smaller cation. This type of unmixing is known as **exsolution** and is described in more detail in Chapter 5.

Charge

As mentioned above, a crystal structure must be charge neutral; therefore, charge neutrality must be maintained with any substitution of one cation for another within a structural site. The ions that substitute for each other may or may not have the same charges. If the charge of substituting cations is different, then the difference is rarely greater than 1, as this would lead to problems with maintaining charge neutrality. Simple substitution is only possible if the cations have the same charge. Coupled, omission, or interstitial substitution occurs if cation charges are different.

DO NOT COPY e48d507df5d1141@placeholder.9409

Printed by: e48d507df5d1141@placeholder.94092.edu. Printing is for personal, private use only. No part of this book may be reproduced or transmitted without publisher's prior permission. Violators will be prosecuted.

Simple Substitution

Simple substitution solid solution involves substituting cations with identical charges. If the cations also are about the same size, substitution is generally extensive. Reiterating the example from Chapter 1, the mineral olivine (**Figure 4.15a**) forms a continuous solid solution series whose end members are forsterite (Mg_2SiO_4) and fayalite (Fe_2SiO_4). Note that the subscripts for all elements in the end members are integers. The formula for olivine is conventionally written $(Mg,Fe)_2SiO_4$. The parentheses indicate that Mg^{2+} and Fe^{2+} are interchangeable in octahedral sites known as the *M* sites. Most olivine has compositions intermediate between forsterite and fayalite, such as $Mg_{1.56}Fe_{0.44}SiO_4$; note the Mg and Fe subscripts are not integers. Fe^{2+} and Mg^{2+} are diadochic: they readily substitute for each other because their radii in octahedral coordination with O^{2-} are 0.75 and 0.86 Å, respectively, and the charges are the same.

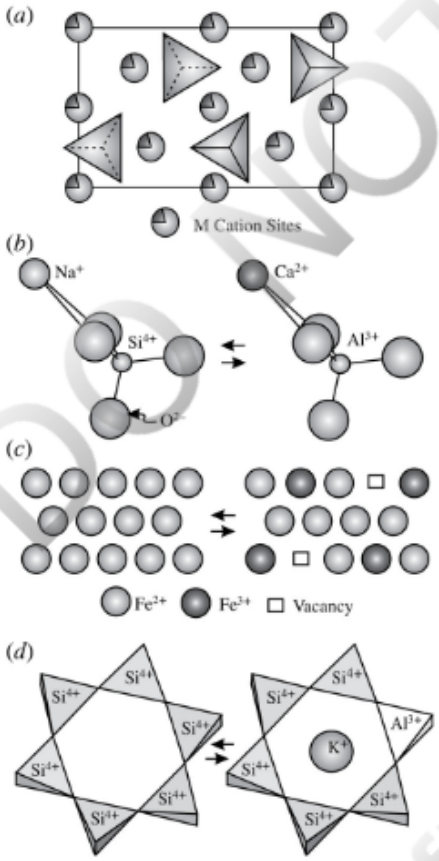

FIGURE 4.15 Solid solution. (*a*) Simple substitution in olivine, whose structure is viewed down the *a* axis. The octahedral M sites between tetrahedra may be occupied by either Mg^{2+} or Fe^{2+}. The shaded wedge shown on each M cation graphically indicates the percentage of the M sites that are occupied by Fe^{2+} (22 percent in this case). (*b*) Coupled substitution in plagioclase shown schematically. To maintain charge balance, substitution of Ca^{2+} for Na^+ is balanced by substitution of Al^{3+} for Si^{4+}. (*c*) Omission substitution of $3Fe^{2+} \Leftrightarrow 2Fe^{3+} + \square$ in pyrrhotite shown schematically. (*d*) Interstitial ionic substitution in beryl. Insertion of large monovalent cations (K^+, Na^+, Rb^+, etc.) in the open channelways defined by the rings of silicon tetrahedra is balanced by substitution of Al^{3+} for Si^{4+} in the tetrahedra. View larger image

DO NOT COPY e48d507df5d1141@placeholder.9409

Printed by: e48d507df5d1141@placeholder.94092.edu. Printing is for personal, private use only. No part of this book may be reproduced or transmitted without publisher's prior permission. Violators will be prosecuted.

Coupled Substitution

Coupled substitution maintains charge balance by coupling one substitution that increases the charge with another that reduces the charge. The mineral plagioclase is a good example (**Figure 4.15b**). The end members are albite ($NaAlSi_3O_8$) and anorthite ($CaAl_2Si_2O_8$). The Ca^{2+} and Na^+ both occupy a distorted 8-fold coordination site, and Al^{3+} and Si^{4+} both occupy tetrahedral coordination sites. Note that size considerations allow these substitutions (Table 4.2). To substitute a Ca^{2+} for a Na^+ it is necessary to also substitute an Al^{3+} for a Si^{4+}:

$$Ca^{2+} + Al^{3+} \Leftrightarrow Na^+ + Si^{4+}$$

Note that charge balance is maintained—both Ca^{2+} + Al^{3+} and Na^+ + Si^{4+} have a net charge of +5. Therefore, an example solid solution plagioclase chemical formula is $Na_{0.4}Ca_{0.6}Al_{1.6}Si_{2.4}O_8$; note how Na, Ca, Al, and Si are intermediate between the albite ($NaAlSi_3O_8$) and anorthite ($CaAl_2Si_2O_8$) end-member formulas because of the couple substitution.

In some cases coupled substitution involves only a single structural site. In the mineral corundum, Fe^{2+} + Ti^{4+} may substitute for $2Al^{3+}$ in octahedral sites. Coupled substitution also may involve both cations and anions. For example, in both biotite and hornblende, Fe^{2+} may be replaced by Fe^{3+}, balanced by replacement of OH^- by O^{2-}:

$$Fe^{2+} + OH^- \Leftrightarrow Fe^{3+} + O^{2-}$$

Omission Substitution

Omission substitution maintains charge balance when ions of different charge substitute for each other by leaving structural sites vacant or unfilled. The general relation for cations is

$$(n+1)M^{n+} \Leftrightarrow nM^{(n+1)+} + \square$$

where M^{n+} and $M^{(n+1)+}$ are the two different cations substituting for each other, n is the charge of the lower-charged cation, and □ is a vacant site that normally would be occupied by M^{n+}. Omission substitution is found in pyrrhotite (see Chapter 19). Its structure consists of hexagonal close-packed sulfur, with iron in octahedral coordination sites between the layers of sulfur. If all of the octahedral sites are occupied by Fe^{2+}, the formula is FeS. However, in most samples, some of the Fe^{2+} is replaced by Fe^{3+}. To maintain charge balance, three Fe^{2+} can be replaced by only two Fe^{3+}, leaving one site

DO NOT COPY e48d507df5d1141@placeholder.94092

Printed by: e48d507df5d1141@placeholder.94092.edu. Printing is for personal, private use only. No part of this book may be reproduced or transmitted without publisher's prior permission. Violators will be prosecuted.

maintain charge balance, three Fe^{2+} can be replaced by only two Fe^{3+}, leaving one site vacant (**Figure 4.15c**).

$$3Fe^{2+} \Leftrightarrow 2Fe^{3+} + \square$$

Up to about 13 percent of the octahedral sites in pyrrhotite can be vacant, so the formula can be written $(Fe^{2+}_{1-3x}Fe^{3+}_{2x})\square_x S$ ($x<0.13$), where x is the number of vacant octahedral sites per formula unit.

Interstitial Substitution

Interstitial substitution is a variation of coupled substitution in which charge balance is maintained by placing ions in sites that normally are vacant. Minerals whose structures provide large openings are particularly susceptible to interstitial substitution. The mineral beryl ($Al_2Be_3Si_6O_{18}$), for example, is constructed of rings of silicon tetrahedra that are stacked on top of each other to form channel-like cavities in the center of the rings (**Figure 4.15d**). Various monovalent cations, including K^+, Rb^+, and Cs^+, can be inserted into these cavities. Charge balance is maintained by substitution of Al^{3+} and Be^{2+} for Si^{4+} in tetrahedral sites:

$$\square + Si^{4+} \Leftrightarrow Al^{3+} + (K^+, Rb^+, Cs^+) \quad \text{or}$$
$$\square + Si^{4+} \Leftrightarrow Be^{2+} + 2(K^+, Rb^+, Cs^+)$$

DO NOT COPY e48d507df5d1141@placeholder.9409

Printed by: e48d507df5d1141@placeholder.94092.edu. Printing is for personal, private use only. No part of this book may be reproduced or transmitted without publisher's prior permission. Violators will be prosecuted.

Mineral Formulas

Mineral formulas are typically written to provide structural information. The basic rules for ionic solids, including minerals, are the following:

- Cations are written first, followed by the anion(s) or anionic group.
- Charges must balance. The total charge of cations must equal the total charge of anions.
- Cations in the same structural site are grouped together.
- Cations in different structural sites are listed in order of decreasing coordination number.

For historical or other reasons, these rules are not always followed, but they are nonetheless quite useful. Additional information about silicate mineral formulas is provided in Chapter 11.

The idealized formula for diopside, a common pyroxene (Chapter 14), illustrates how these rules are applied.

The cations are Ca^{2+}, Mg^{2+}, and Si^{4+}, and they coordinate with O^{2-}, which is the only anion. Charge balance can be determined by tallying the charges of cations and anions as shown in **Table 4.6**.

TABLE 4.6 Charge Balance Calculation for Diopside ($CaMgSi_2O_6$)

Cation	Charge	Stoichiometric Coefficient	Total Charge[a]
Ca	2+	1	+2
Mg	2+	1	+2
Si	4+	2	+8
O	2−	6	−12
Total			0

[a] The total charge provided by each ion is equal to the charge of the ion multiplied by the stoichiometric coefficient for the ion in the formula. The formula is balanced if the sum of the positive and negative charges equals zero.

Based on knowledge of cation size, we can anticipate that Si will be in 4-fold

DO NOT COPY e48d507df5d1141@placeholder.9409

Printed by: e48d507df5d1141@placeholder.94092.edu. Printing is for personal, private use only. No part of this book may be reproduced or transmitted without publisher's prior permission. Violators will be prosecuted.

Based on knowledge of cation size, we can anticipate that Si will be in 4-fold coordination, Mg in 6-fold coordination, and Ca in 8-fold coordination, consistent with the order in which they are written. The coordination of each cation in the formula may be explicitly indicated by placing the coordination number in Roman numerals as a superscript immediately preceding the cation in the formula.

$$^{\mathrm{VIII}}\mathrm{Ca}^{\mathrm{VI}}\mathrm{Mg}^{\mathrm{IV}}\mathrm{Si}_2\mathrm{O}_6$$

If a structural site can be occupied by multiple cations as part of a solid solution series, the interchangeable cations are grouped within parentheses. The formula here is modified to indicate that the octahedral site can hold any combination of Mg and Fe.

$$^{\mathrm{VIII}}\mathrm{Ca}^{\mathrm{VI}}(\mathrm{Mg},\ \mathrm{Fe})^{\mathrm{IV}}\mathrm{Si}_2\mathrm{O}_6$$

An alternative way of indicating composition variation is to explicitly state the degree of substitution possible.

$$^{\mathrm{VI}}(\mathrm{Mg}_{2-x}\mathrm{Fe}_x)^{\mathrm{IV}}\mathrm{SiO}_4 \quad (0 \leq x \leq 2)$$

Here the range of possible values for the coefficient x is specified. In this case, complete substitution of Fe for Mg, and vice versa, is indicated. If for a particular olivine, 22 percent of the octahedral sites are occupied by Fe^{2+} and 78 percent are occupied by Mg^{2+}, $x = 0.44$ and the formula is

$$\mathrm{Mg}_{1.56}\mathrm{Fe}_{0.44}\mathrm{SiO}_4.$$

It often is convenient to identify a mineral's composition in terms of the relative amounts of the end members. The names of the end-member compositions are often given as two-letter abbreviations. For olivine, the end members forsterite (Mg_2SiO_4) and fayalite (Fe_2SiO_4) are abbreviated as Fo and Fa, respectively. The olivine sample that contains 78 percent Mg and 22 percent Fe can be presented as $Fo_{78}Fa_{22}$ as determined by the formula:

$$\%\ \mathrm{Fo} = \frac{1.56\ (Mg\ subscript)}{2\ (total\ of\ Fe + Mg)} \times 100 = 78$$

For minerals with just two end members, just one end member may be used (e.g., Fo_{78}) because the sum of both end members (forsterite plus fayalite in olivine) must equal 100 percent.

DO NOT COPY

Printed by: e48d507df5d1141@placeholder.94092.edu. Printing is for personal, private use only. No part of this book may be reproduced or transmitted without publisher's prior permission. Violators will be prosecuted.

Graphic Representation

The techniques of mineral chemical analysis and the procedures by which chemical analyses are converted to mineral formulas are described in Chapter 9. It is convenient in many cases to graphically represent (diagram) mineral compositions derived from those analyses. There are numerous diagram possibilities, but binary and ternary diagrams are very common. For many minerals, a standard set of diagrams is often used; these diagrams are presented in Part Three.

Binary Diagrams

A binary diagram is used for minerals whose composition can be described in terms of two end members. Such compositions are represented as a point on a straight line. The ends of the line are commonly selected to be the end-member compositions of a solid solution series or other mineral or chemical species of interest. The scale along the line is mole percent of the end members. **Figure 4.16a** shows a binary diagram for olivine. The left end of the line is 100 percent forsterite (Mg_2SiO_4) and the right end is 100 percent fayalite (Fe_2SiO_4). Therefore, the right end is also 0 percent forsterite and the left end is 0 percent fayalite. The middle of the line is 50 percent of each. The composition of olivine just discussed (78 percent forsterite) is shown on the diagram, which is 78 percent of the way along the line toward the forsterite end member. **Figure 4.16b** shows use of a binary olivine diagram to illustrate the variation of density as a function of composition.

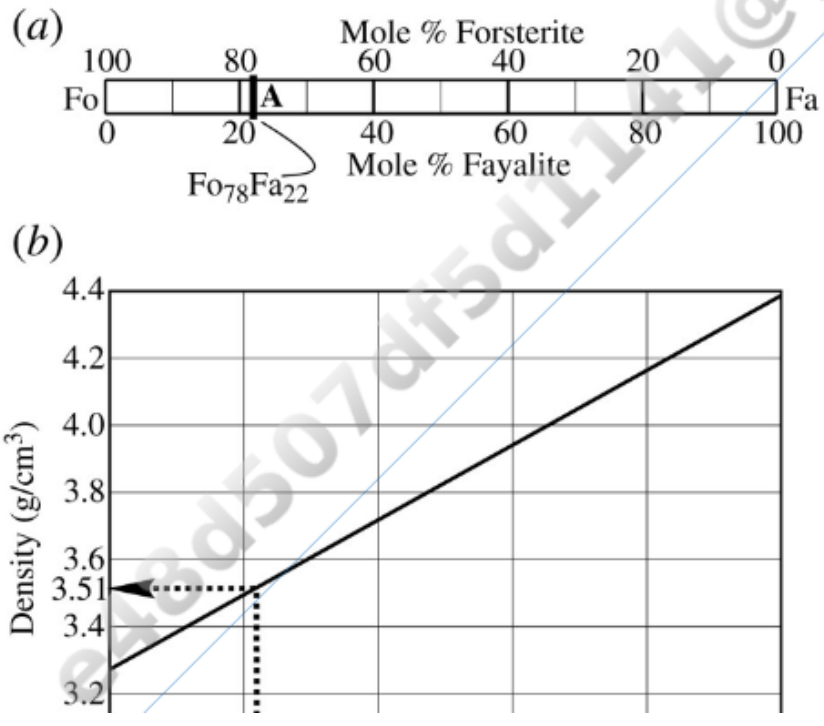

DO NOT COPY
e48d507df5d1141@placeholder.94092

Printed by: e48d507df5d1141@placeholder.94092.edu. Printing is for personal, private use only. No part of this book may be reproduced or transmitted without publisher's prior permission. Violators will be prosecuted.

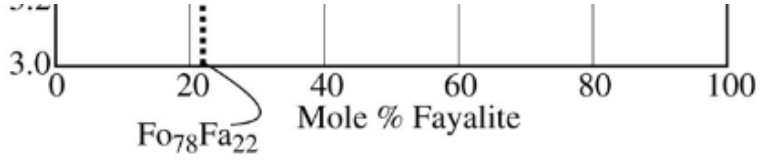

FIGURE 4.16 Binary diagrams of olivine. (*a*) The end members, forsterite (Mg_2SiO_4) and fayalite (Fe_2SiO_4), are plotted at the ends of a line. The scale is mole percent of the end members. Point A indicates a composition with 22 percent fayalite and 78 percent forsterite ($Fo_{78}Fa_{22}$). (*b*) Use of a binary composition diagram to illustrate the variation of density as a function of composition in olivine. Olivine A has a density of 3.51 g/cm^3. View larger image

Ternary Diagrams

A ternary diagram is used when there are three end-member compositions. The diagram is plotted as an equilateral triangle with an end member placed at each corner (**Figure 4.17**). Each side of the triangle is a binary diagram, and the three sets of lines that cross the diagram indicate the percentage of each end member. For example, the pyroxenes can be represented by three end members: enstatite ($Mg_2Si_2O_6$), ferrosilite ($Fe_2Si_2O_6$), and wollastonite ($Ca_2Si_2O_6$), which are represented by the symbols En, Fs, and Wo, respectively. The horizontal lines indicate the percentage of Wo: 100 percent at the top, 50 percent across the middle of the triangle, and 0 percent along the bottom edge of the triangle. The lines parallel to the triangle side opposite of Fs indicate the percentage of Fs, and the lines parallel to the triangle side opposite of En indicate the percentage of En. A mineral formula of $Mg_{0.84}Fe_{0.16}CaSi_2O_6$ is 42 percent enstatite, 8 percent ferrosilite, and 50 percent wollastonite and can be written in terms of the three end members as $En_{42}Fs_8Wo_{50}$ as determined by the formulas

$$\%\ \text{En} = \frac{0.84\ (Mg\ subscript)}{2\ (total\ of\ Mg + Fe + Ca)} \times 100 = 42$$

$$\%\ \text{Fs} = \frac{0.16\ (Fe\ subscript)}{2\ (total\ of\ Mg + Fe + Ca)} \times 100 = 8$$

$$\%\ \text{Wo} = \frac{1.0\ (Ca\ subscript)}{2\ (total\ of\ Mg + Fe + Ca)} \times 100 = 50$$

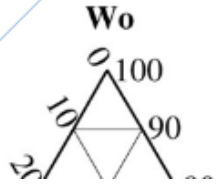

DO NOT COPY
e48d507df5d1141@placeholder.94092

Printed by: e48d507df5d1141@placeholder.94092.edu. Printing is for personal, private use only. No part of this book may be reproduced or transmitted without publisher's prior permission. Violators will be prosecuted.

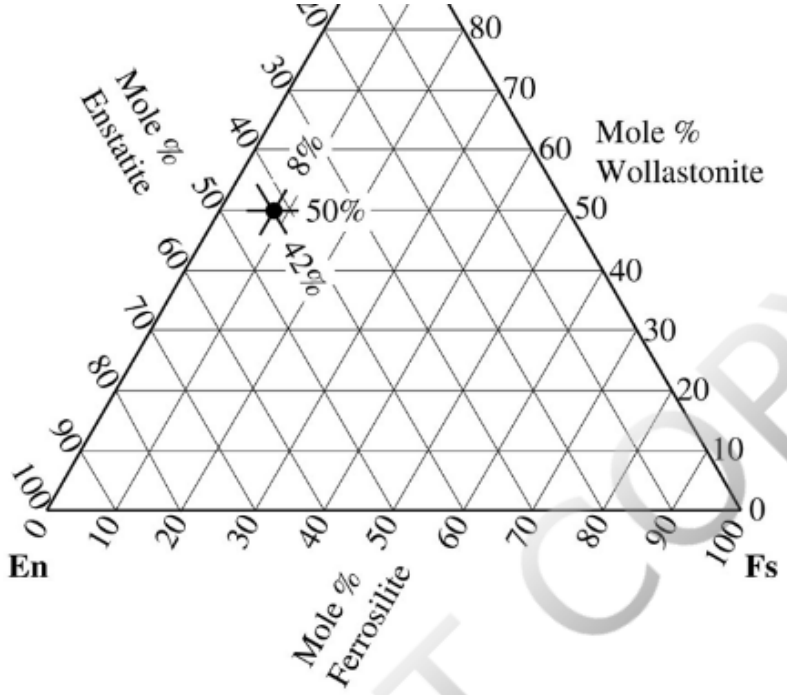

FIGURE 4.17 Pyroxene ternary diagram. The end members enstatite (En, $Mg_2Si_2O_6$), ferrosilite (Fs, $Fe_2Si_2O_6$), and wollastonite (Wo, $Ca_2Si_2O_6$) are plotted at the corners of a triangle. Three sets of lines on the diagram as labeled allow compositions to be plotted. The composition $En_{42}Fs_8Wo_{50}$ is plotted where the 50 percent Wo line intersects the 8 percent Fs and 42 percent En lines. View larger image

This composition is shown as the point where the 42 percent En line intersects the 8 percent Fo and 50 percent Wo lines.

DO NOT COPY
e48d507df5d1141@placeholder.9409

Printed by: e48d507df5d1141@placeholder.94092.edu. Printing is for personal, private use only. No part of this book may be reproduced or transmitted without publisher's prior permission. Violators will be prosecuted.

Mineral Formulas and the Unit Cell

A final point regarding mineral formulas is that although for some minerals, the mineral formula represents the sum total of atoms within the unit cell, for many minerals, this is not the case. Figure 4.1 provides forsterite ($MgSiO_4$) as an example. In representations where the location of oxygen is clearly depicted (Figure 4.1a, b, and d), it is evident that in the unit cell, there are much more than the 4 O listed in the mineral formula. In fact, there are a total of 16 O, meaning that there are 4 **formula units per unit cell**. The number of formula units per unit cell is designated by Z in the mineral entries of Part Three of this text. **Figure 4.18** provides a second, more straightforward example using the structure of cuprite (Cu_2O). Within cuprite's unit cell, the 4 Cu are obvious and indicate that $Z = 2$ for this mineral. This analysis is consistent for O as well, but fractional atoms must be considered. A total of 9 O atoms are shown in the diagram; one is located at the center and is wholly contained within the unit cell. The remaining 8 O atoms are located at the corners of the unit cell and each is shared among 8 neighboring unit cells. Therefore, only 1/8 of each O atom at the corner of the unit cell belongs to the unit cell outlined in Figure 4.18. The corner O atoms provide a total of 1 O ($8 \times 1/8 = 1$) to the unit cell depicted. Thus, with the additional whole O atom at the center of the unit cell, there is a total of 2 O per unit cell, consistent with $Z = 2$ for cuprite as stated above. In terms of mineral formulas, the cuprite unit cell contains $2 \times Cu_2O = Cu_4O_2$.

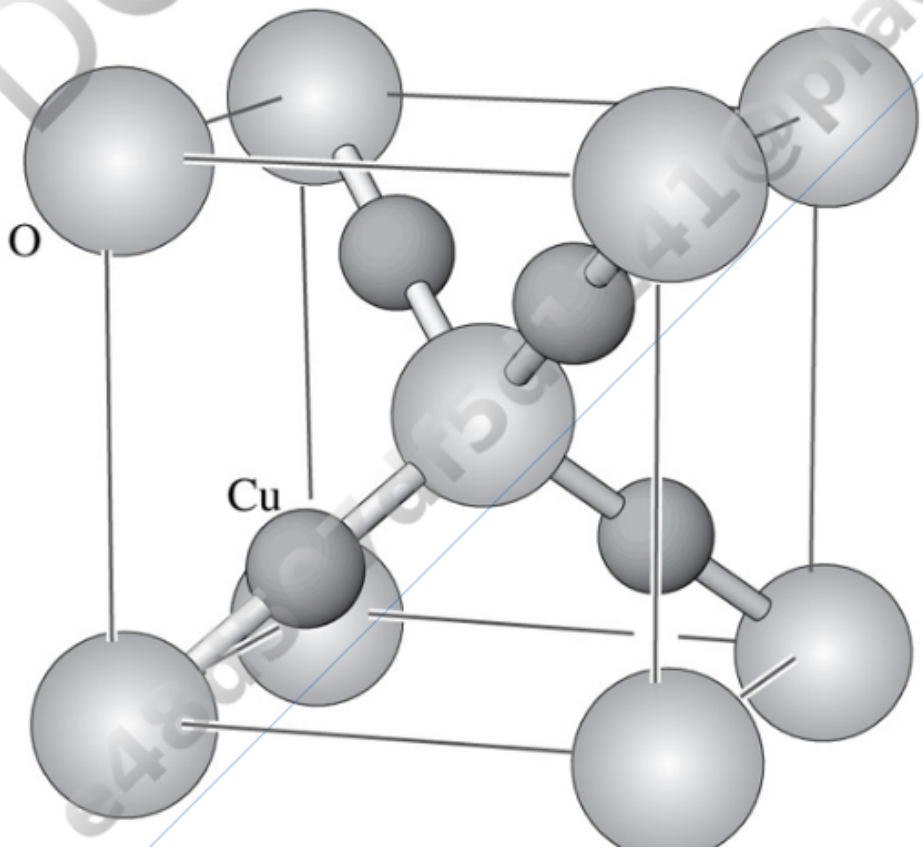

Printed by: e48d507df5d1141@placeholder.94092.edu. Printing is for personal, private use only. No part of this book may be reproduced or transmitted without publisher's prior permission. Violators will be prosecuted.

FIGURE 4.18 Cuprite structure and unit cell. Oxygen occupy the corners and center of the unit cell; Cu occupies four of the eight cube octants, or the eight smaller cubes into which any larger cube can be divided. View larger image

DO NOT COPY
e48d507df5d1141@placeholder.9409

Printed by: e48d507df5d1141@placeholder.94092.edu. Printing is for personal, private use only. No part of this book may be reproduced or transmitted without publisher's prior permission. Violators will be prosecuted.

example. In representations where the location of oxygen is clearly depicted (Figure 4.1a, b, and d), it is evident that in the unit cell, there are much more than the 4 O listed in the mineral formula. In fact, there are a total of 16 O, meaning that there are 4 **formula units per unit cell**. The number of formula units per unit cell is designated by Z in the mineral entries of Part Three of this text. **Figure 4.18** provides a second, more straightforward example using the structure of cuprite (Cu_2O). Within cuprite's unit cell, the 4 Cu are obvious and indicate that $Z = 2$ for this mineral. This analysis is consistent for O as well, but fractional atoms must be considered. A total of 9 O atoms are shown in the diagram; one is located at the center and is wholly contained within the unit cell. The remaining 8 O atoms are located at the corners of the unit cell and each is shared among 8 neighboring unit cells. Therefore, only 1/8 of each O atom at the corner of the unit cell belongs to the unit cell outlined in Figure 4.18. The corner O atoms provide a total of 1 O ($8 \times 1/8 = 1$) to the unit cell depicted. Thus, with the additional whole O atom at the center of the unit cell, there is a total of 2 O per unit cell, consistent with $Z = 2$ for cuprite as stated above. In terms of mineral formulas, the cuprite unit cell contains $2 \times Cu_2O = Cu_4O_2$.

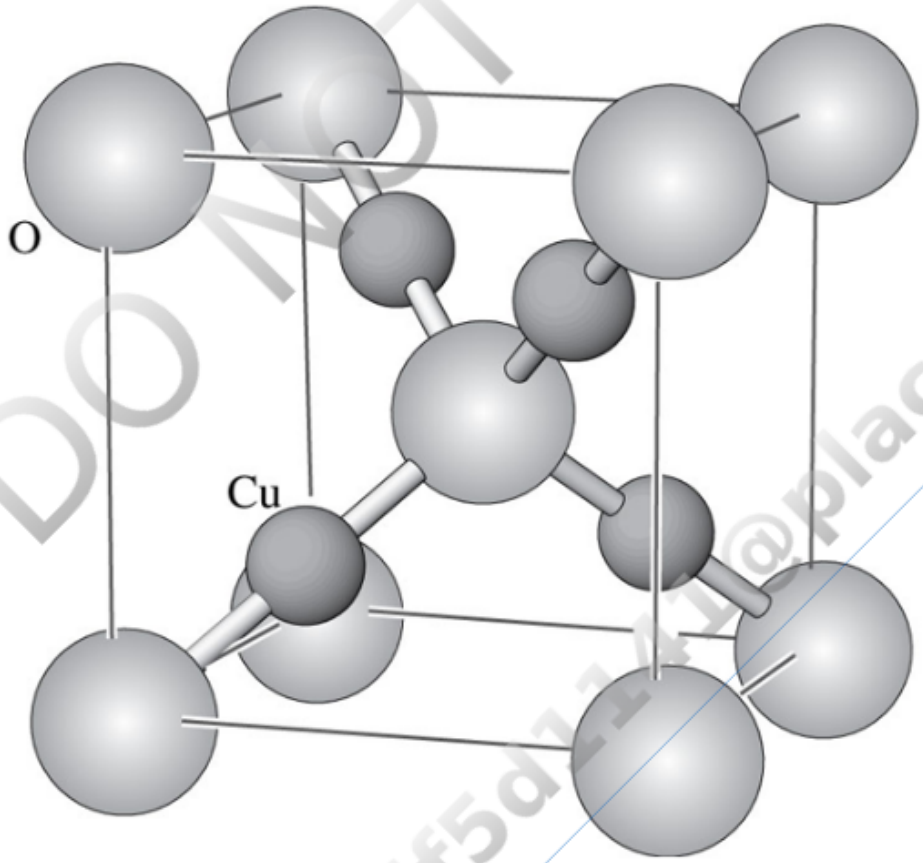

FIGURE 4.18 Cuprite structure and unit cell. Oxygen occupy the corners and center of the unit cell; Cu occupies four of the eight cube octants, or the eight smaller cubes into which any larger cube can be divided. View larger image

REFERENCES CITED AND SUGGESTIONS FOR ADDITIONAL READING

Printed by: e48d507df5d1141@placeholder.94092.edu. Printing is for personal, private use only. No part of this book may be reproduced or transmitted without publisher's prior permission. Violators will be prosecuted.

Bloss, F. D. 1971. *Crystallography and Crystal Chemistry: An Introduction*. Holt, Rinehart & Winston, New York, 545 p.

Day, H. W. 2012. A revised diamond-graphite transition curve. *American Mineralogist* **97**, 52–62.

Evans, R. C. 1966. *An Introduction to Crystal Chemistry*. Cambridge University Press, Cambridge, 410 p.

Gaines, R. V., Skinner, H. C. W., Foord, E. E., Mason, B., and Rosenzweig, A. 1997. *Dana's New Mineralogy*, 8th ed. John Wiley & Sons, New York, 1819 p.

Pauling, L. 1960. *The Nature of the Chemical Bond*, 3rd ed. Cornell University Press, Ithaca, NY, 644 p.

Putnis, A. 1992. *Introduction to Mineral Science*. Cambridge University Press, Cambridge, 457 p.

Smyth, J. R., and Bish, D. L. 1988. *Crystal Structures and Cation Sites of the Rock-Forming Minerals*. Allen & Unwin, Boston, 332 p.

Strunz, H., and Nickel, E. H. 2001. *Strunz Mineralogical Tables*, 9th ed. Schweizerbart'sche Verlagsbuchhandlung, Stuttgart, 870 p.

DO NOT COPY
e48d507df5d1141@placeholder.9409

Printed by: e48d507df5d1141@placeholder.94092.edu. Printing is for personal, private use only. No part of this book may be reproduced or transmitted without publisher's prior permission. Violators will be prosecuted.

LIST OF KEY TERMS

12-fold coordination
2-fold coordination
3-fold coordination
4-fold coordination
6-fold coordination
8-fold coordination
anisodesmic bonding
body-centered cubic packing
complete solid solution series
continuous solid solution series
coordination number
coordination polyhedron
coupled substitution
cubic closest packing
cubic coordination
discontinuous solid solution series
displacive polymorphism
electrostatic valence bond
end member
exsolution
formula units per unit cell
hexagonal closest packing
incomplete solid solution series
interstitial solid solution
isodesmic bonding
isostructural
isostructural group
kimberlite
linear coordination

DO NOT COPY
e48d507df5d1141@placeholder.9409

Printed by: e48d507df5d1141@placeholder.94092.edu. Printing is for personal, private use only. No part of this book may be reproduced or transmitted without publisher's prior permission. Violators will be prosecuted.

linear coordination

mesodesmic bonding

metastable

nonuniform bond strength

octahedral coordination

omission solid solution

order-disorder polymorphism

Pauling's rules

polymorphic forms

polymorphic group

polymorphism

polymorphs

polytypism

quenching

radius ratio

reconstructive polymorphism

silicon tetrahedron

simple substitution solid solution

solid solution

solid solution series

solute

solvent

substitution solid solution

tetrahedral coordination

triangular coordination

DO NOT COPY
e48d507df5d1141@placeholder.9409

Printed by: e48d507df5d1141@placeholder.94092.edu. Printing is for personal, private use only. No part of this book may be reproduced or transmitted without publisher's prior permission. Violators will be prosecuted.

CHAPTER 5
Mineral Growth

William D. Nesse
University of Northern Colorado

Graham B. Baird
University of Northern Colorado

DO NOT COPY
e48d507df5d1141@placeholder.9409

Printed by: e48d507df5d1141@placeholder.94092.edu. Printing is for personal, private use only. No part of this book may be reproduced or transmitted without publisher's prior permission. Violators will be prosecuted.

Introduction

Rocks are inextricably linked to minerals as most minerals reside in rocks, or **sediment**—the weathered remains of rocks. Therefore it is useful to formally define a rock.

> A rock is a naturally occurring solid cohesive aggregate of mineral grains and/or mineraloids.

Naturally occurring and *solid* are both used with the same meaning as they were for the mineral definition. *Aggregate* refers to the fact that rocks are made of more than one mineral grain. The mineral grains are stuck together—they are cohesive—such that rocks require a reasonable amount of force to break them apart. Therefore, loose sediment is not a rock. A rock can be made of multiple grains of a single mineral species; for example, some marbles are essentially composed of only calcite grains. More commonly, though, rocks are made of many different minerals, such as granite—a rock that requires approximately equal proportions of quartz, plagioclase, and alkali feldspar. Often granite also contains other minerals such as biotite, muscovite, and possibly amphibole. Rocks can be fully composed of mineraloids; obsidian is an example. But it is also common for some volcanic rocks to be a mixture of volcanic glass and mineral grains.

Many, if not most, geologic processes are fundamentally involved with or influenced by rock and sediment mineralogical changes. Mineralogical changes occur in response to geologic environment changes, which can be generalized by the **rock cycle** (Figure 5.1). For example, when a **magma** cools and crystallizes, it forms an **igneous rock** that may consist of feldspars, quartz, and other minerals. **Crystallization** is the term used when new grains of a mineral are created. When exposed by erosion to the Earth's surface environment, these minerals interact with surface waters and are converted via **chemical weathering** to clay minerals and dissolved ions released to the water. Quartz is known to be quite resistant to chemical weathering, so quartz grains from the original rock often persist in the resulting sediment. Such quartz grains are called **detrital** grains; these are nearly always reduced in size and are more rounded than the grains of the original rock because of **physical weathering**. The clay minerals and detrital grains may become, after transportation, deposition, and lithification, a layer of shale—a **sedimentary rock**. The shale may in turn be buried to a depth of 30 km or more because of plate tectonic processes, where it is subjected to metamorphic conditions of high temperature and pressure, often aided by ion-bearing aqueous fluids deep in the crust. At such conditions, the elements in the quartz and clay are used to crystallize new minerals, such as micas and feldspars through **metamorphic reactions**. **Recrystallization** also occurs, in which grains of a mineral already present, such as quartz in this case, change their shape or composition (if possible) or break down to create new grains of the same mineral. The rock is now a **metamorphic rock**, and the shale served as the metamorphic rock's **protolith**, or the rock that existed before metamorphism. The metamorphic rock, if subjected to sufficiently high temperatures, may melt to form magma that later

DO NOT COPY e48d507df5d1141@placeholder.94092

Printed by: e48d507df5d1141@placeholder.94092.edu. Printing is for personal, private use only. No part of this book may be reproduced or transmitted without publisher's prior permission. Violators will be prosecuted.

If subjected to sufficiently high temperatures, may melt to form magma that later crystallizes into a new igneous rock, completing the cycle. Igneous rocks may similarly be converted to metamorphic rocks, and metamorphic rocks may be converted into sediments and sedimentary rocks.

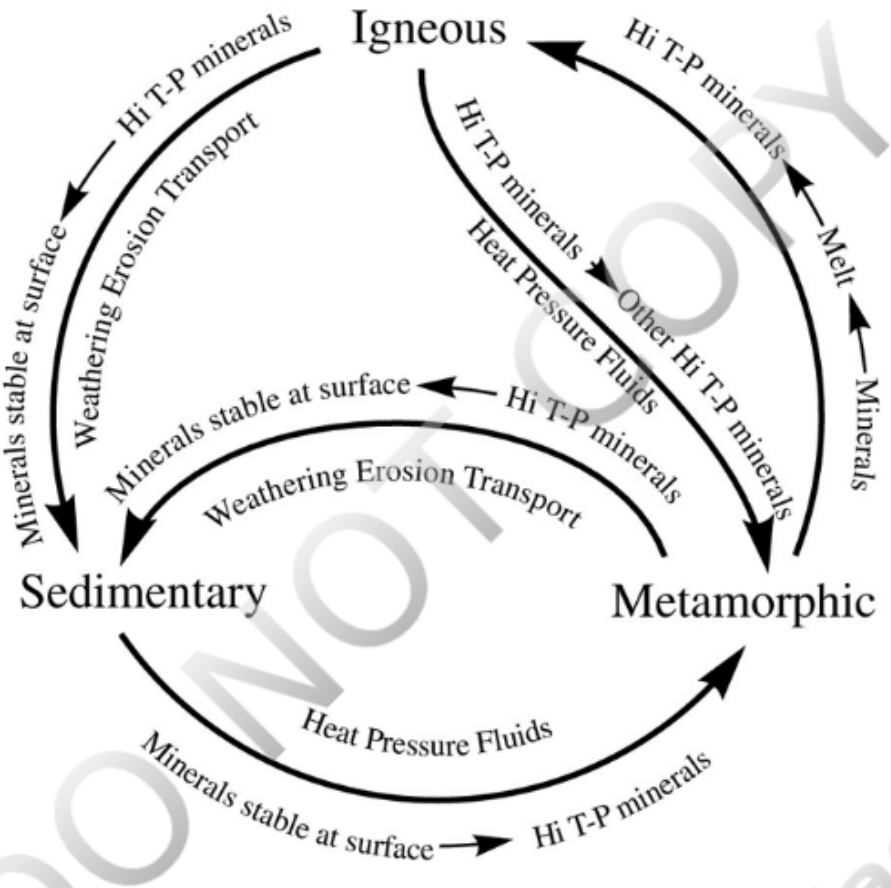

FIGURE 5.1 The rock cycle. The rock cycle fundamentally involves mineralogical changes in response to different temperature–pressure (T–P) and fluid conditions. View larger image

For each rock type, the minerals in the rock have very different origins. Most igneous rocks and their minerals are produced by the crystallization of magma. Sedimentary rocks are composed of the products of rock weathering, and the minerals could be detrital grains from the sediment source, clay minerals formed by the chemical weathering of other minerals, or minerals precipitated from ion-bearing waters. Chemical weathering initially placed the ions into such waters. Metamorphic rocks and metamorphic minerals are created by metamorphic reactions that crystallize or recrystallize the minerals, depending on whether or not the mineral existed in the protolith.

As a generalization, the temperature, pressure, chemical composition (including fluids), and rates of heating/cooling, etc. of a particular geologic environment are the primary controls on mineralogy. Because the Earth has changed over time, both independent of and directly related to biologic activity, these changes too have influence the Earth's mineralogy.

The following questions are therefore addressed in this chapter

DO NOT COPY e48d507df5d1141@placeholder.9409

Printed by: e48d507df5d1141@placeholder.94092.edu. Printing is for personal, private use only. No part of this book may be reproduced or transmitted without publisher's prior permission. Violators will be prosecuted.

The following questions are therefore addressed in this chapter.

What determines which minerals are formed?

How are phase diagrams used to interpret mineral stability and growth?

How do minerals nucleate and grow?

What types of defects are produced in mineral structures?

What changes occur in minerals after crystallization?

How has the Earth's mineralogy changed through time?

What is the role of biologic processes in mineral growth?

DO NOT COPY
e48d507df5d1141@placeholder.9409

Printed by: e48d507df5d1141@placeholder.94092.edu. Printing is for personal, private use only. No part of this book may be reproduced or transmitted without publisher's prior permission. Violators will be prosecuted.

Mineral Stability

To form a specific mineral, the first and obvious requirement is that the constituent elements must be available in the environment from which the mineral will form. The concentration of the elements in the environment is often referred to as the **bulk composition**. The formation of quartz (SiO_2), either through crystallization from a magma, during metamorphism, or by precipitation from an aqueous fluid, requires the availability of Si and O in any of those setting. Similarly, creation of pyrite (FeS_2) requires Fe and S in the environment.

Given a particular bulk composition, with specific amounts of O, Si, Al, Mg, Fe, etc., the list of minerals that might form is large; hundreds can be constructed from the five elements named. To understand which combination of minerals among the many possibilities are actually present, it is necessary to introduce two closely related concepts: **stability** and **energy**.

Stability

If two states are compared, one will be more stable if it represents a lower-energy configuration. Note that the concept of stability is always based on a comparison among different possibilities. Consider two alternative positions for a book, such this text, as shown in **Figure 5.2**: the first is on the floor and the other is 2 meters above the floor on a shelf. The relevant measure of energy for this example is gravitational potential energy, such that the higher the elevation of the book, the higher the energy. Therefore, the location on the floor is more stable because it represents a lower-energy position as it has a lower elevation. The position 2 meters above the floor on the shelf has higher energy than the one on the floor. If you hold the book 2 meters above the floor and let go, you know that the book will drop to the floor; this demonstrates that systems will spontaneously seek lower-energy states.

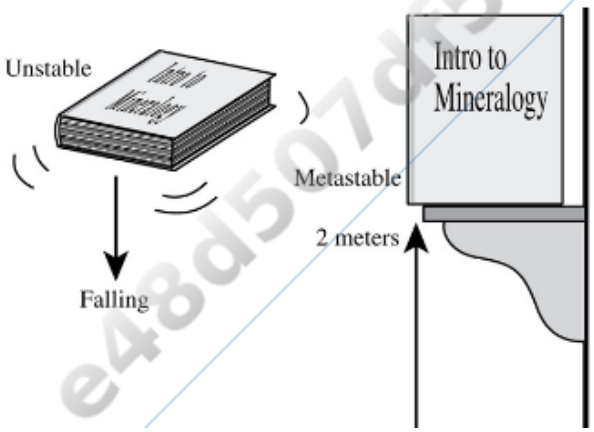

DO NOT COPY
e48d507df5d1141@placeholder.9409

Printed by: e48d507df5d1141@placeholder.94092.edu. Printing is for personal, private use only. No part of this book may be reproduced or transmitted without publisher's prior permission. Violators will be prosecuted.

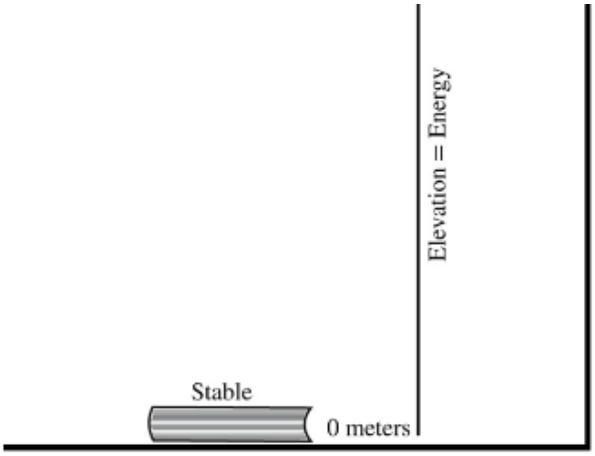

FIGURE 5.2 Stability. A book 2 meters above the floor is unstable relative to a position on the floor. If unrestrained (left, unstable book), the book will spontaneously fall to the floor. The book on the shelf is metastable relative to a position on the floor. While the floor represents a lower-energy position, activation energy, or a push of the book off the shelf, is required to allow the book to reach the low-energy floor. View larger image

Higher-energy configurations do not always spontaneously change to a lower-energy configuration. For example, consider again the book on the shelf; it has higher gravitational potential energy than one on the floor but it will not spontaneously leap off the shelf to acquire the lower-energy position—it is **metastable**. This means that the floor represents lower energy, but the book cannot drop to the floor unless energy is added in the form of a push to dislodge it from the shelf. The energy required to push the book off the shelf is called the **activation energy**, or the energy required to move a system from a metastable state to one where it will spontaneously change to a lower-energy state.

Gibbs Free Energy

Measuring the energy involved in mineralogical/chemical changes is more complex than measuring the gravitational potential energy of a book. A complete derivation of the relevant relationships is well beyond the scope of this book; only a general outline of a few important relations will be provided. Nordstrom and Munoz (1994) or Fletcher (1993) can be consulted for a thorough treatment.

The measure of energy with which to judge the stability of minerals is the **Gibbs free energy**, whose symbol is G. Units of Gibbs free energy are energy (**calories** or **joules**) per mole. One calorie is the amount of heat energy required to change the temperature of 1 g of water from 15 to 16°C. A joule (J) is 0.2390 calories.

To determine which mineral, or collection of minerals, is the lowest energy and most stable for a bulk composition at a particular temperature and pressure, it is necessary to have a common basis for comparison. The widely adopted convention is to compare among possible minerals that might exist their **Gibbs free energy of formation**, ΔG_f. The free energy of formation is the energy difference between the elements in their

Printed by: e48d507df5d1141@placeholder.94092.edu. Printing is for personal, private use only. No part of this book may be reproduced or transmitted without publisher's prior permission. Violators will be prosecuted.

The free energy of formation is the energy difference between the elements in their standard states (e.g., 298 K and 1 atmosphere [atm] pressure) and the elements when they are chemically bonded to form a mineral at the temperature and pressure of interest. Given two minerals with the same composition, such as quartz and tridymite (SiO_2), the stable mineral under specified temperature and pressure conditions is the mineral with the lowest ΔG_f. Because ΔG_f varies as a function of both temperature and pressure, under some conditions quartz has lower Gibbs free energy and is more stable, and under others, tridymite has lower Gibbs free energy and is more stable.

Mineral Reactions

Mineral transformations involve a conversion of one mineral or set of minerals to form another mineral or set of minerals. They are chemical reactions and can be dealt with by using the normal conventions of chemistry. The polymorphic transition of tridymite to form quartz can be written as

$$\begin{aligned} \text{tridymite} &= \text{quartz} \\ SiO_2 &= SiO_2. \end{aligned}$$

Note that it can be common to write such reactions twice, once using the minerals names, and again using just chemical formulas. A more complex reaction is the metamorphic reaction that forms K-feldspar and sillimanite from muscovite and quartz at fairly high temperatures.

$$\begin{aligned} \text{muscovite} + \text{quartz} &= \text{K-feldspar} \\ &\quad + \text{sillimanite} + \text{water} \\ KAl_2(AlSi_3O_{10})(OH)_2 + SiO_2 &= KAlSi_3O_8 \\ &\quad + Al_2SiO_5 + H_2O \end{aligned}$$

Both reactions are chemically balanced; the number of atoms of each element is the same for the **reactants** and the **products**. The reactant minerals are those found on the left side of the equation, while the product minerals are those found on the right.

The stability of a chemical reaction can be expressed in terms of Gibbs free energy:

$$\Delta G_{\text{reaction}} = \Delta G_{f(\text{products})} - \Delta G_{f(\text{reactants})}. \quad \textbf{(5.1)}$$

That is, the free energy of a reaction is the difference in the free energy of formation of the product minerals and the reactant minerals. If at a specific temperature–pressure (T–P) condition, $\Delta G_{\text{reaction}} < 0$, the products are more stable and the reaction can

DO NOT COPY e48d507df5d1141@placeholder.9409

Printed by: e48d507df5d1141@placeholder.94092.edu. Printing is for personal, private use only. No part of this book may be reproduced or transmitted without publisher's prior permission. Violators will be prosecuted.

P, T condition, $\Delta G_{reaction} < 0$, the products are more stable and the reaction can spontaneously occur. If $\Delta G_{reaction} > 0$, the reactants are more stable and the reaction would proceed in reverse if any products exist in the rock. If $\Delta G_{reaction} = 0$, the products and reactants have the same free energy and no net reaction would occur. In such cases, all reactants and products are stable and are said to be in **equilibrium**. In theory, a rock (or a system) is in equilibrium any time there is no net reaction or no change in the amount of each mineral species.

In most cases, rocks are made of a number of different minerals, but ion-bearing aqueous or other fluid may also be present in the interstitial space between mineral grains. For a given bulk chemical composition of rock (minerals plus fluid, if present) and specific conditions of temperature and pressure, a **stable mineral assemblage**, which is in equilibrium with the conditions, exists. The stable mineral assemblage is the collection of minerals in a rock whose aggregate free energy of formation is the lowest of all the possible mineral combinations that might be made from the chemical elements in the rock.

In practice it may be difficult to accurately determine the lowest-energy mineral configuration for a particular bulk composition of rock at a specific temperature and pressure. Databases with the free energy of formation of all relevant minerals as a function of all their possible compositional variations do exist, and specialized computer programs can be used to calculate a stable mineral assemblage. But this approach is not as easy as it might sound and is fraught with many pitfalls, particularly for trying to determine the temperature–pressure–fluids conditions a specific rock experienced. One problem is that there is no assurance that the mineral assemblage in any particular rock actually represents the lowest-energy, stable assemblage. Minerals may persist metastably for billions of years unless the activation energy is provided for reactions to proceed. This concept was introduced Chapter 4 in the discussion of the polymorphic change between diamond and graphite. Recall that the activation energy is required to trigger the conversion of metastable diamond to convert to lower-energy graphite at surface conditions. Another complication is that rocks are subjected to changes in temperature and pressure as a consequence of tectonic activity, erosion, and so forth, and the mineralogy typically does not continually change to reflect all those activities, particularly at lower temperatures. One reason for this is that these changes occur very slowly. Most igneous and metamorphic rocks, for example, consist of minerals that are unstable in the weathering environment at the Earth's surface, but because the weathering reactions are slow, more time is needed to weather the minerals completely.

Regardless, all mineralogical changes are in the direction of lower-energy, more stable mineral assemblages. One useful way of presenting this information is to use phase diagrams, which are constructed from experimental studies of mineral stability.

DO NOT COPY e48d507df5d1141@placeholder.9409

Printed by: e48d507df5d1141@placeholder.94092.edu. Printing is for personal, private use only. No part of this book may be reproduced or transmitted without publisher's prior permission. Violators will be prosecuted.

Phase Diagrams

To illustrate the stability of minerals and mineral reactions, it is convenient to use **phase diagrams**, which show, for a given set of conditions, which **phase** (or phases) represents the lowest-energy configuration of a given composition. A phase can be a specific mineral, an aqueous fluid, a melt (magma), or a gas. Ice, for example is a single phase, whereas ice in water represents two phases. We will look only at single-component and binary systems. In single-component systems, all the phases (minerals, melts, etc.) can be described with a single chemical composition. In a binary system, all the phases can be described by combinations of two chemical compositions. While rock and mineral systems with three or more components have been extensively studied, single-component and binary systems illustrate many of the important processes involved in mineral growth and stability.

In the examples that follow, it is assumed that equilibrium is maintained. This means that the real-world problems of reaction rates, metastability, and crystal nucleation and growth are ignored such that the only phases present are those with the lowest energy. In reality, to actually get crystals to grow requires significant overstepping of equilibrium conditions to provide the activation energy needed to get the chemical reactions to proceed. For example, before crystals can begin to grow, melts must be cooled significantly below the expected temperature where crystals would form (the equilibrium temperature where the free energy of crystal formation and melt are the same). A good real-world example of this is that distilled water often must be cooled to below 0°C before ice will begin to form. Crystal nucleation and growth are discussed in later sections.

There are a wide variety of phase diagrams. T–P phase diagrams were in fact introduced during the discussion of polymorphs in Chapter 4. There, the horizontal and vertical axes were temperature and pressure, respectively. Temperature is almost always presented in degrees Celsius. The unit for pressure is commonly the kilobar (kbar). Lithostatic pressure, or the pressure due to depth in the Earth's crust, increases roughly 1 kbar per 3 km depth, depending on the density of the rocks. Some sources advocate using the gigapascal (GPa) for pressure, but conversion between the two units is straightforward—1 GPa = 10 kbar. For other phase diagrams, an axis may be composition (sometimes abbreviated to *X*) where the ends of the axis represent different compositions. It is also common to have some other variable serve as an axis variable, such as Gibbs free energy. As long as a diagram presents fields that represent the stability of phases at different conditions at equilibrium, the diagram is a phase diagram.

Single-Component Systems

DO NOT COPY e48d507df5d1141@placeholder.9409

Printed by: e48d507df5d1141@placeholder.94092.edu. Printing is for personal, private use only. No part of this book may be reproduced or transmitted without publisher's prior permission. Violators will be prosecuted.

A good example of a single-component T–P phase diagram is shown in **Figure 5.3**. This diagram is specifically for the aluminum silicate polymorphs of andalusite, sillimanite, and kyanite, which all have the chemical formula of Al_2SiO_5. They are common minerals in mica schists produced by the metamorphism of shale. The free energy of formation of each mineral from aluminum, silicon, and oxygen varies as a function of both temperature and pressure and can be shown by surfaces in temperature–pressure–free energy space (Figure 5.3a). These surfaces are shown as planes for ease of illustration, but they are slightly curved. Under some conditions andalusite has the lowest free energy, while under others sillimanite or kyanite may be the lowest-energy form of Al_2SiO_5.

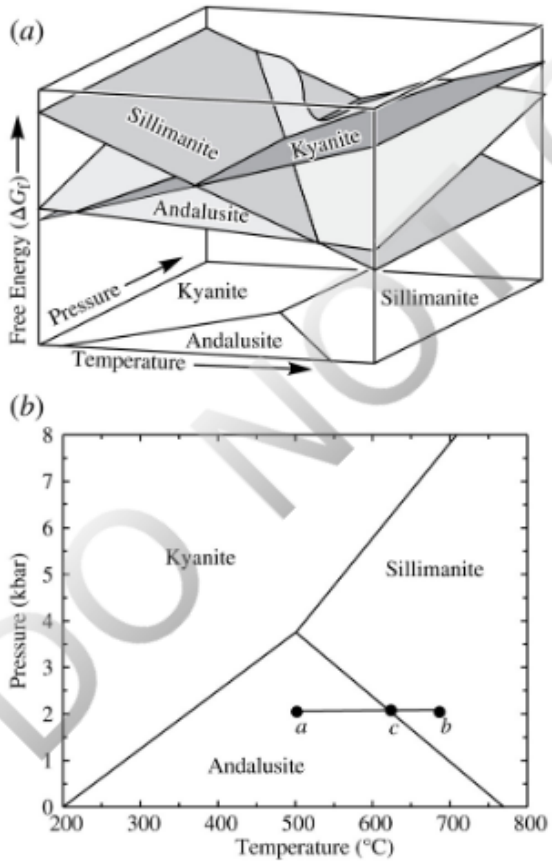

FIGURE 5.3 Aluminum silicate stability. (*a*) Schematic illustration of Gibbs free energy of formation of andalusite (light), sillimanite (intermediate), and kyanite (dark) as a function of pressure and temperature. The mineral with the lowest free energy at a specific T–P condition is the stable phase at those conditions. (*b*) T–P stability fields of the aluminum silicates. See text for discussion. Adapted from Hemingway and others (1991). View larger image

The T–P field in which each mineral is the most stable is indicated in Figure 5.3b. The stability fields are separated by lines that indicate the T–P conditions along which both minerals have the same ΔG_f and their free energy surfaces intersect. Along each line, the minerals on adjacent sides are both stable and can exist in a system in equilibrium. The one T–P condition at which all three minerals have the same ΔG_f and can exist together in equilibrium lies at the point where the three lines join. This is called the triple point.

If a metamorphic rock contains andalusite, the conditions of metamorphism can be

DO NOT COPY e48d507df5d1141@placeholder.9409

Printed by: e48d507df5d1141@placeholder.94092.edu. Printing is for personal, private use only. No part of this book may be reproduced or transmitted without publisher's prior permission. Violators will be prosecuted.

inferred to have been somewhere within the relatively low pressure and moderate temperature andalusite stability field, such as at point *a* (500°C and 2 kbar) in Figure 5.3b. If this same andalusite-bearing rock were progressively heated, for example to a temperature indicated by point *b* in the sillimanite field, sillimanite should grow as andalusite breaks down because sillimanite is the lowest-energy form of Al_2SiO_5 under the new conditions. Andalusite and sillimanite have the same ΔG_f along the line separating their stability fields (point *c*), and neither would break down to form the other at this temperature.

Binary Systems

Binary systems have two components. The components may be the chemical composition of minerals, or they may be another convenient chemical species. In the examples that follow, the components are identified with mineral species. Three examples of crystallization from a melt will be examined: one with no solid solution among the minerals, and two with solid solution. While most real rocks are more complicated in that they have more than two components, the following examples illustrate well some of the processes that dictate the crystallization of minerals from melt or the melting of a rock to produce magma.

Figure 5.4 shows the binary system diopside–anorthite at 1 atm pressure (essentially the pressure of the Earth's surface). The diagram shows the melting and crystallizing stability relations for mixtures of diopside, which is a pyroxene (Chapter 14), and anorthite, which is the calcium-rich end member of the plagioclase solid solution series (Chapter 12). No solid solution exists between diopside and anorthite.

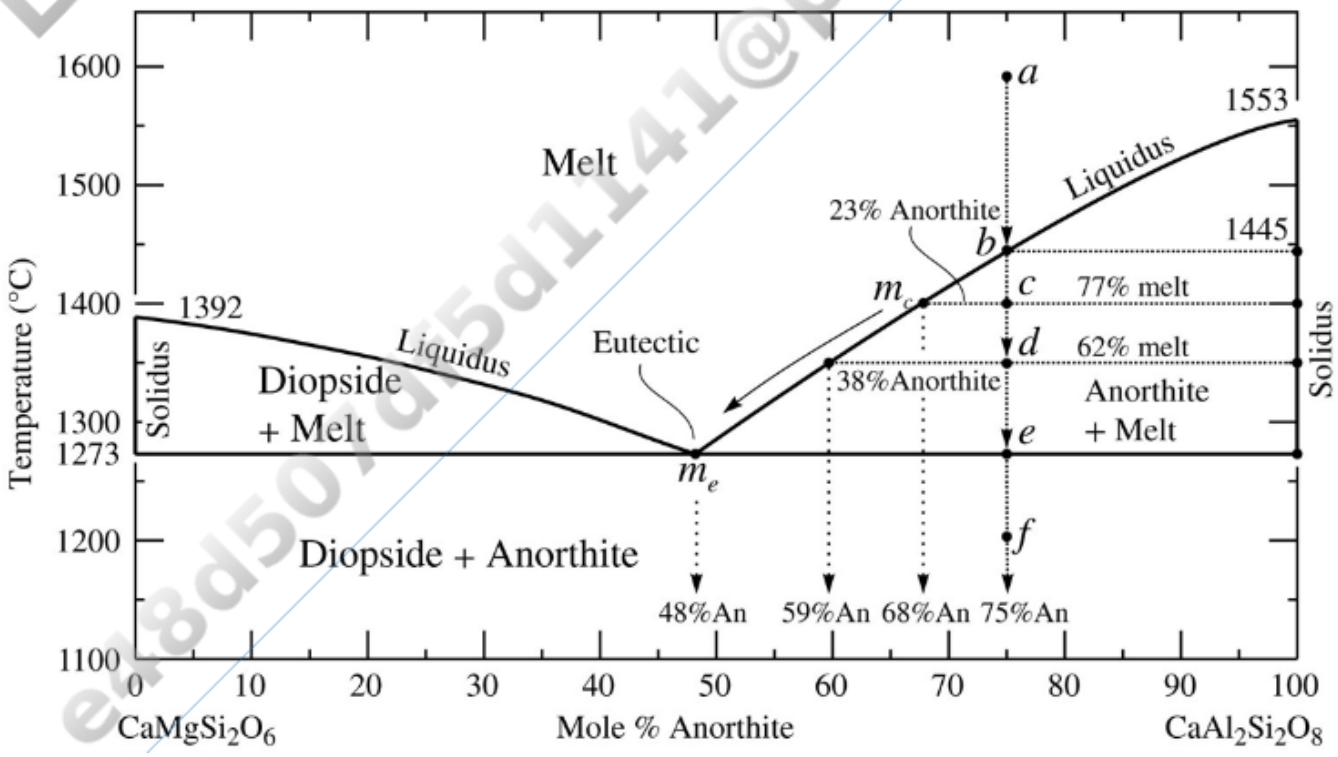

DO NOT COPY e48d507df5d1141@placeholder.94092

Printed by: e48d507df5d1141@placeholder.94092.edu. Printing is for personal, private use only. No part of this book may be reproduced or transmitted without publisher's prior permission. Violators will be prosecuted.

FIGURE 5.4 Crystallization in the system diopside (Di)–anorthite (An) at 1 atm pressure. After Osborn (1942). See text for discussion. View larger image

Pure diopside melts at 1392°C and pure anorthite melts at 1553°C. A mixture of diopside and anorthite, however, melts at a lower temperature. The two curved line segments labeled **liquidus** show the composition of liquid in equilibrium with crystals at a particular temperature. Above the liquidus curves, the system is entirely melt (magma). The heavy lines on each side of the diagram are the **solidus** lines, and they show the composition of crystals in equilibrium with liquid at a particular temperature. The solidus lines are vertical here because the compositions of diopside and anorthite do not vary as there is no solid solution. If there is solid solution, these solidus lines will be curved, as will be seen in a later section.

The roughly triangular area labeled *diopside + melt* shows the temperature–composition combinations where both melt and crystals of diopside coexist. The area labeled *anorthite + melt* shows the temperature–composition combinations where both melt and crystals of anorthite coexist. A horizontal line at a specific temperature that goes from the liquidus to the solidus in one of the crystal + melt areas is called a **tie-line**. The ends of a tie-line on the liquidus and solidus define the compositions of the crystals and melt that are in equilibrium at that temperature. The area on the diagram below 1273°C shows where all mixtures of diopside and anorthite are entirely solid.

Consider crystallization of a melt with a composition of 75 percent anorthite (An) and 25 percent diopside (Di) beginning at 1600°C, as shown by point *a* on Figure 5.4 (the percentage of the anorthite component in the melt will be identified as *X* percent An). To determine the crystallization history of melt *a*, begin by drawing a vertical dotted line through point *a* so that the bulk composition is indicated for all temperatures. At different temperatures, the system may contain various combinations of crystals and melt, but the overall bulk chemical composition of the system will remain constant. We will look at the changes that occur as the system cools under conditions of **equilibrium crystallization**. This means that, as cooling progresses, the crystals and melt remain in equilibrium with each other and the amount and composition of each represent the lowest-energy configuration available to the system under the specified conditions.

- Point *a* is in the melt field, so only melt is present. This melt will be allowed to cool until it reaches point *b*.
- Point *b* is on the liquidus line at 1445°C, which represents the equilibrium temperature where crystals have the same free energy of formation as the melt. At temperatures below this line, the anorthite + melt field is entered. That means that anorthite crystals will begin to crystallize as heat is removed if the system is to be in its lowest-energy configuration. A temperature line drawn through *b* from the solidus to the liquidus shows the compositions of melt (75 percent An) and anorthite in equilibrium with each other.

DO NOT COPY

Printed by: e48d507df5d1141@placeholder.94092.edu. Printing is for personal, private use only. No part of this book may be reproduced or transmitted without publisher's prior permission. Violators will be prosecuted.

anorthite in equilibrium with each other.

- Continued cooling to 1400°C will be accompanied by progressive crystallization and growth of more anorthite from the melt, so the proportion of the melt must decrease. The residual melt must also become progressively enriched in the diopside component. The composition of the melt (68 percent An) is given by drawing a horizontal tie-line through c to the point where it intersects the liquidus at m_c and then projecting a line down to read the composition off the horizontal axis. By the **lever rule** (**Figure 5.5**), we find the system consists of 77 percent melt and 23 percent anorthite crystals. Continued cooling to d causes more anorthite to crystallize, so that at 1350°C, the system consists of 38 percent anorthite crystals and 62 percent melt, which has a composition of 59 percent An.
- Cooling to point e at 1273°C marks the point at which diopside crystals begin to grow from the melt. Three phases (melt, anorthite crystals, and diopside crystals) are present, and these three phases can be together only at the **eutectic temperature**, which, at 1 atm pressure, is 1273°C. The composition of the melt (m_e = 48 percent An) is called the **eutectic composition** because it is defined by the **eutectic**, where the two liquidus curves meet. With continued removal of heat from the system, both anorthite and diopside crystals grow as the melt is used up. However, the temperature does not drop below 1273°C until the last of the liquid has been converted into crystals. The proportion of anorthite and diopside crystals formed is the same as the composition of the eutectic melt—48 percent anorthite crystals and 52 percent diopside crystals.
- Point f at 1200°C is in the anorthite + diopside field, meaning that the magma is now completely crystallized and consists of 75 percent anorthite crystals and 25 percent diopside crystals. Note that this is the same bulk composition that the melt started at (point a).

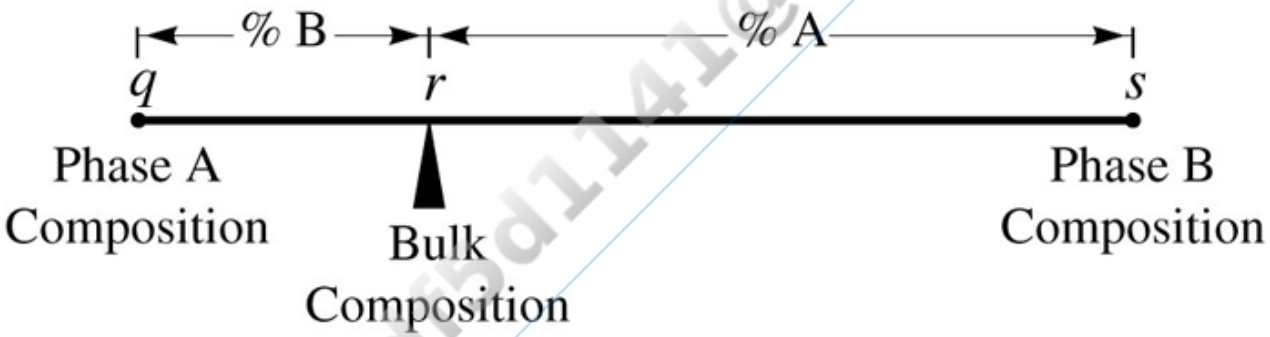

FIGURE 5.5 Lever rule. Given the bulk composition and a tie-line *qrs* between the compositions of phase A and phase B, the relative amounts of A and B are given by the relative lengths of the two line segments: %A = *rs/qs* and %B = *qr/qs*. View larger image

If crystallization begins with a diopside-rich composition to the left of the eutectic, crystallization begins with diopside, and the melt composition becomes progressively enriched in the anorthite component until it reaches the eutectic.

DO NOT COPY e48d507df5d1141@placeholder.94092

Printed by: e48d507df5d1141@placeholder.94092.edu. Printing is for personal, private use only. No part of this book may be reproduced or transmitted without publisher's prior permission. Violators will be prosecuted.

Equilibrium melting is the reverse of the crystallization sequence. Starting with a solid rock made up of 75 percent anorthite and 25 percent diopside crystals at 1200°C and adding heat will melt the rock as follows.

- At point *f* the rock is solid anorthite and diopside crystals. Heating brings it to point *e*.
- Point *e* is at the eutectic temperature (1273°C). Melting of both diopside and anorthite crystals begins to produce the eutectic melt whose composition is 48 percent An. Melting will continue until one or the other of the minerals is used up. In this case, diopside crystals are used up first because the bulk composition is to the right of the eutectic. The temperature remains at 1273°C as long as diopside, anorthite, and melt are present. Once all the diopside has been used up, the temperature can continue to increase with addition of heat.
- At point *d* anorthite continues to melt and progressively enriches the bulk melt composition in the anorthite component. At point *d* the melt is 59 percent An, and as determined by the lever rule, the amounts of anorthite crystals and melt are 38 percent and 62 percent, respectively. Continued heating to point *c* reduces the amount of anorthite crystals to 23 percent, and the melt composition is now 68 percent An.
- At point *b* the last crystals of anorthite have been melted and the bulk composition of the melt is now 75 percent An, the same as the initial bulk composition. Continued heating up to point *a* just heats up an entirely molten magma.

Figure 5.6 shows a case with continuous solid solution between two end members. In this case the mineral is olivine, which has complete solid solution between forsterite (Fo, Mg_2SiO_4) and fayalite (Fa, Fe_2SiO_4). The two curves in this binary diagram are the liquidus and the solidus. At a given temperature, the ends of a tie-line from the solidus to the liquidus indicate the composition of coexisting melt and olivine crystals. Above the liquidus, only melt is present, and below the solidus, only olivine crystals are present. Between the solidus and liquidus is the olivine + melt area.

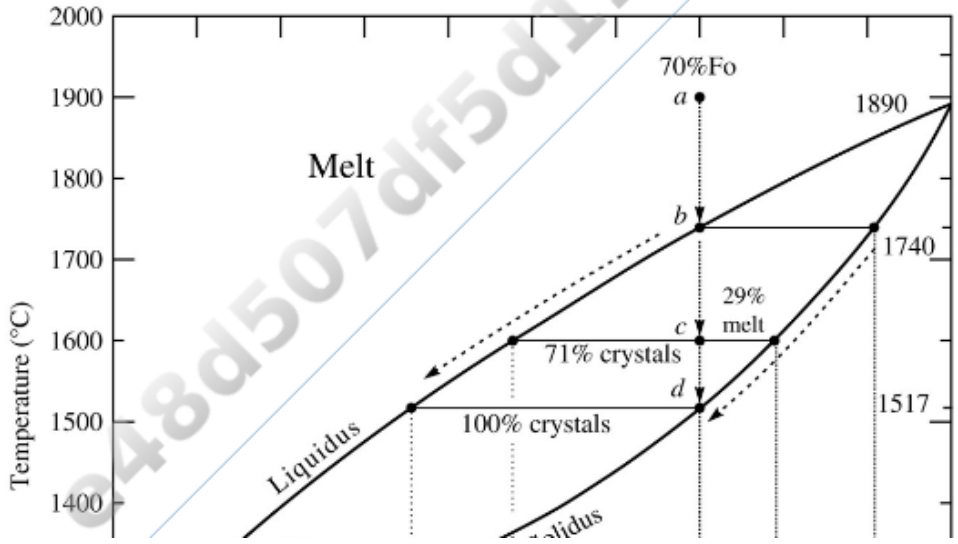

DO NOT COPY
e48d507df5d1141@placeholder.9409

Printed by: e48d507df5d1141@placeholder.94092.edu. Printing is for personal, private use only. No part of this book may be reproduced or transmitted without publisher's prior permission. Violators will be prosecuted.

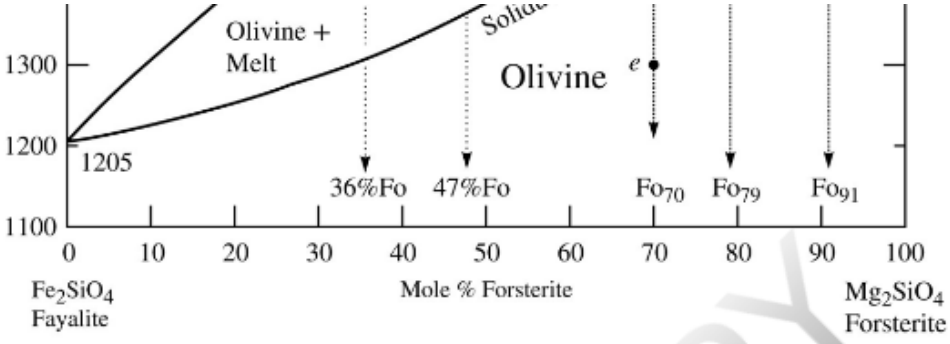

FIGURE 5.6 Olivine crystallization at 1 atm pressure. After Bowen and Schairer (1935). See text for discussion. View larger image

Consider an initial melt consisting of 70 percent forsterite and 30 percent fayalite at 1900°C (point *a*). Begin by drawing a vertical dotted line through point *a* so that the bulk composition can be tracked. Equilibrium crystallization proceeds as follows.

- Point *a* represents the composition 70 percent Fo and 30 percent Fa at a temperature of 1900°C. Because it is above the liquidus, it is entirely melt. Progressive cooling will bring the system to point *b*.
- Point *b* is on the liquidus curve, and it marks the temperature (1740°C) at which crystallization of olivine begins if equilibrium is maintained. The small, first-formed crystals of olivine have a composition of 91 percent Mg and 9 percent Fe, or Fo_{91}, given where the temperature tie-line intersects the solidus. Because these crystals are enriched in Mg relative to the melt, growth of these crystals requires that the residual melt be depleted of Mg and become richer in Fe.
- Progressive cooling to point *c* at 1600°C causes additional crystallization of olivine from the melt. The relative amounts of olivine crystals and melt are given by the lever rule: 71 percent crystals and 29 percent melt. The tie-line between the liquidus and solidus through point *c* shows that the melt now has only 47 percent of the forsterite component, and the crystals are 79 percent forsterite (Fo_{79}). If equilibrium crystallization is maintained, the first-formed crystals, and all subsequent olivine crystals, must exchange Fe and Mg with the melt via **diffusion** to also acquire the composition Fo_{79}. Diffusion is the process by which matter or energy moves from regions of relatively high concentration to regions of relatively low concentration. Particularly at high temperature, elements can diffuse through crystals, as will be discussed later in the chapter. Here the olivine crystals are relatively high in Mg and low in Fe, while the melt is relatively low in Mg but high in Fe. Therefore, Mg will diffuse from the crystals into the melt, while Fe will do the opposite. Here the extent of diffusion is dictated by equilibrium composition of the crystals and melt as shown by the tie-line ends at any temperature. That is, diffusion between crystals and melt will occur if either is not at the equilibrium composition as indicated by the solidus and liquidus for a particular temperature.
- Still more cooling to 1517°C at point *d*, accompanied by diffusion, brings the composition of all the olivine to Fo_{70}, the same as the original bulk composition of

DO NOT COPY

Printed by: e48d507df5d1141@placeholder.94092.edu. Printing is for personal, private use only. No part of this book may be reproduced or transmitted without publisher's prior permission. Violators will be prosecuted.

the melt—70 percent forsterite. At this point, crystallization is complete and no melt is left. The composition of the last drop of melt is given where the temperature tie-line intersects the liquidus—36 percent Fo in this case.

- Point *e* is in the olivine field, so the system is now entirely made of solid crystals of olivine whose composition is Fo_{70}.

Equilibrium melting tracks the melt and crystal compositions in reverse. First-formed melt has a composition of 36 percent Fo, and melting would progress until all the olivine had been consumed at 1740°C. The final melt is 70 percent Fo. In addition to the reduction of crystals while the melt proportion increases during heating, diffusion also constantly adjusts melt and crystal composition during the melting process to ensure compositional equilibrium is maintained as shown by tie-lines.

Figure 5.7 shows a T-*X* diagram where the minerals have solid solution and the added complexity of a **solvus**, a curve that defines the T–P field where two separate minerals represent the lowest-energy configuration rather than a single homogeneous solid. In this case, the minerals are K-feldspar (Ks, $KAlSi_3O_8$) and albite (Ab, $NaAlSi_3O_8$); both are feldspars (Chapter 12), and together they are referred to as alkali feldspars. The presence of water results in a substantial reduction in melting temperature compared to dry conditions (compare with Figures 5.4 and 5.6), but no water enters into either mineral.

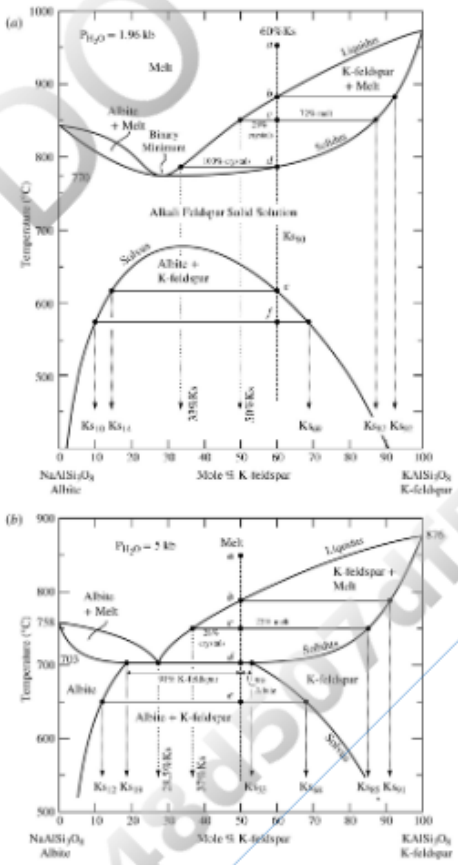

FIGURE 5.7 Alkali feldspar crystallization. (*a*) The system at 1.96 kbar water pressure (after Bowen and Tuttle, 1950; the solvus is from Thompson and Waldbaum, 1969). (*b*) The system at 5

DO NOT COPY e48d507df5d1141@placeholder.9409

Printed by: e48d507df5d1141@placeholder.94092.edu. Printing is for personal, private use only. No part of this book may be reproduced or transmitted without publisher's prior permission. Violators will be prosecuted.

Bowen and Tuttle, 1950; the solvus is from Thompson and Waldbaum, 1969). (*b*) The system at 5 kbar water pressure (Morse, 1970). See text for discussion. View larger image

From the discussion in Chapter 4, we know that K^+ and Na^+ have sizes that allow them to substitute for each other at high temperatures, but that at low temperatures, substitution is restricted, as is shown by the presence of the solvus. The position of the solvus relative to the solidus and liquidus varies with pressure.

Figure 5.7a shows the system at 1.96 kbar water pressure. The solidus and liquidus curves for both albite and K-feldspar define a K-feldspar + melt area and an albite + melt area. Each of these can be treated like a simple solid solution system shown in Figure 5.6. The point where the two segments meet in the middle at 770°C is called a **binary minimum**. The alkali feldspar field below the solidus shows that complete solid solution is possible between albite and K-feldspar at 1.96 kbar at temperatures below the binary minimum and above the top of the solvus. The solvus curve outlines the albite + K-feldspar field. A temperature tie-line from one side of the solvus to the other defines the equilibrium compositions of coexisting albite and K-feldspar at that temperature.

In Figure 5.7a consider a melt (point *a*) at 950°C whose bulk composition is 60 percent K-feldspar component and 40 percent albite component. As described for Figure 5.6, crystallization will proceed as follows.

- Crystallization of Ks_{92} crystals begins at point *b*.
- At 850°C (point *c*), Ks_{87} crystals are in equilibrium with 50 percent Ks melt, and the system consists of 28 percent crystals and 72 percent melt. Diffusion of K and Na between melt and crystals keep early-formed crystals in composition equilibrium with cooling temperatures.
- Crystallization is complete at 786°C (point *d*), and the crystals have the composition Ks_{60}, the same as the original melt. The last drops of melt have a composition of 33 percent Ks. Continued cooling of the solid, homogeneous K-feldspar crystals brings the system to the solvus at point *e*.
- Point *e* is on the solvus that bounds the albite + K-feldspar field. Below the solvus, a single homogeneous feldspar is no longer stable and will unmix into separate albite and K-feldspar phases. The first-formed albite that separates from the K-feldspar has a composition of 14 percent K and 86 percent Na, $Ks_{14}Ab_{86}$. Continued cooling to point *f* allows continued growth of progressively more Na-rich albite from K-feldspar, which becomes enriched in K through diffusion. This unmixing, or exsolution, is described at more length in a later section.

Figure 5.7b shows the same system but at 5 kbar water pressure; at this pressure, the solvus intersects the liquidus/solidus curves. Complete solid solution from albite to K-feldspar is no longer possible, and separate fields are present for both albite and K-feldspar. The point where the two liquidus curves meet is now called a eutectic, because at this temperature a liquid and two solids of different composition are in equilibrium. Consider an initial melt (*e*) with 50 percent Ks and 50 percent Ab at 850°C. Equilibrium

DO NOT COPY e48d507df5d1141@placeholder.94092

Printed by: e48d507df5d1141@placeholder.94092.edu. Printing is for personal, private use only. No part of this book may be reproduced or transmitted without publisher's prior permission. Violators will be prosecuted.

Consider an initial melt (*a*) with 50 percent Ks and 50 percent Ab at 850°C. Equilibrium crystallization would proceed as follows.

- Crystallization of K-feldspar (Ks_{91}) begins at point *b*.
- At point *c* at 750°C, Ks_{85} crystals and 37 percent Ks melt are in equilibrium, and the system consists of 28 percent crystals and 72 percent melt. As previously discussed, diffusion between crystals and melt keep both in compositional equilibrium with changing temperature. Further cooling brings the system to the eutectic at 703°C.
- Point *d* is at the eutectic temperature (compare Figure 5.4), so albite crystals start to grow in addition to K-feldspar. The last melt has composition 28.5 percent Ks, and the albite and K-feldspar have compositions of Ks_{19} and Ks_{53}, respectively. When crystallization is complete, the system will consist of 91 percent K-feldspar crystals and 9 percent albite crystals.
- Cooling to point *e* allows the already formed crystals of albite and K-feldspar to unmix. The proportions of albite and K-feldspar at any temperature are determined by using the lever rule on the tie-line for a temperature. During cooling, the albite becomes progressively Na-rich and the K-feldspar becomes progressively K-rich as Na and K are exchanged due to diffusion between the already crystallized minerals.

DO NOT COPY
e48d507df5d1141@placeholder.9409

Printed by: e48d507df5d1141@placeholder.94092.edu. Printing is for personal, private use only. No part of this book may be reproduced or transmitted without publisher's prior permission. Violators will be prosecuted.

Mineral Nucleation

The formation of mineral **embryos** or **nuclei**, or the initial cluster of atoms of a new mineral grain, may take place by either homogeneous nucleation or heterogeneous nucleation.

Homogeneous Nucleation

With homogeneous nucleation, the growth of a mineral grain requires that the appropriate atoms chemically bond to form what will become the embryo of a crystal. The embryo must then grow by progressively adding more atoms to its surface.

In any chemical system, such as a melt or an aqueous solution, the atoms are constantly moving, colliding, and bonding to form a variety of chemical combinations. Some of these combinations will have the composition and structure of a mineral that would crystallize from the melt. Most of the embryos will be small, consisting of only a few atoms, but some will be larger. In general, the abundance of embryos decreases exponentially with increasing size (**Figure 5.8a**). Whether these embryos will ultimately form nuclei from which mineral grains grow depends on both the stability of the mineral and the size of the embryos.

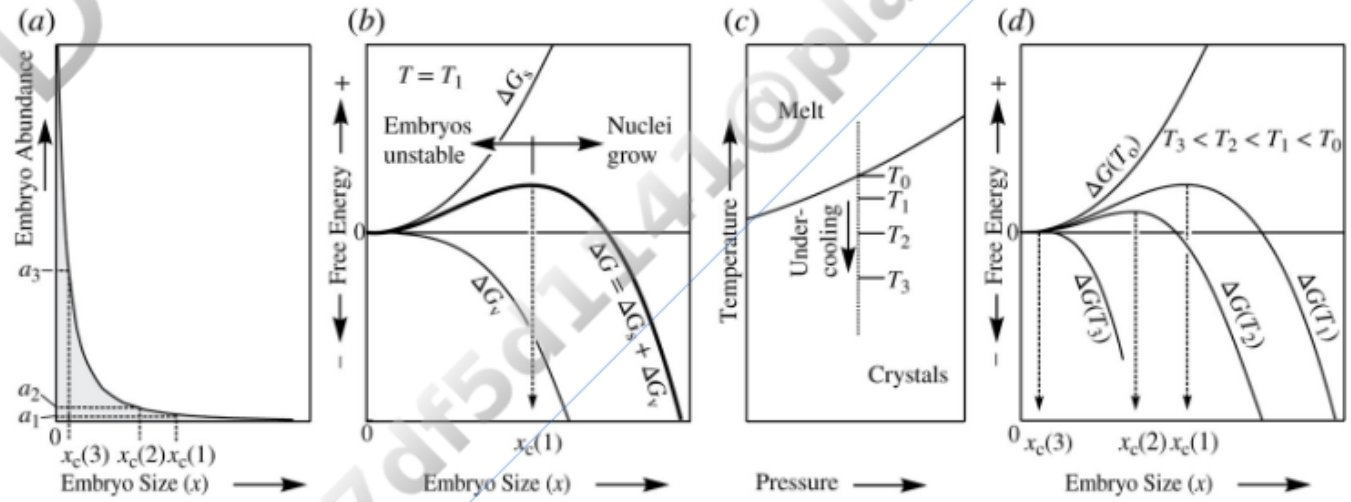

FIGURE 5.8 Formation of crystal embryo from a melt. (*a*) Abundance of different-sized crystal embryos in melt. Small embryos are much more abundant than large embryos. (*b*) The Gibbs free energy of formation ΔG of crystal embryos is the sum of the surface energy ΔG_S and ΔG_V. Only embryos larger than the critical growth radius x_c are stable with respect to the melt; additional growth reduces the energy level. Crystal embryos smaller than x_c will be resorbed spontaneously by the melt because they represent a higher-energy configuration than melt, and additional growth involves an increase in energy. (*c*) Schematic T–P plot of mineral stability with different degrees of undercooling T_0, T_1, T_2, and T_3. (*d*) The critical growth radius for different degrees of undercooling.

DO NOT COPY

Printed by: e48d507df5d1141@placeholder.94092.edu. Printing is for personal, private use only. No part of this book may be reproduced or transmitted without publisher's prior permission. Violators will be prosecuted.

See text for discussion. View larger image

The embryos cannot grow if the new mineral has a higher Gibbs free energy of formation (is less stable) than the same elements as part of a melt, a solution, or another mineral. If the embryo cannot grow, the embryos will break apart, and the constituent atoms will return to the lower-energy configuration of residing in the melt, solution, or another mineral.

At some point, however, the temperature, pressure, or fluid composition (or all three) may change so that the crystalline structure of a new mineral represents a lower-energy configuration for the atoms. This does not mean that all the embryos will immediately begin to grow into mineral grains. The complicating factor is the surface energy of the embryos. The atoms at the surface of the embryo can bond to additional atoms, that is, they have unbalanced charge, which is a high-energy configuration. The magnitude of the surface energy is proportional to the surface area.

In the discussion that follows, only crystal growth from a melt is considered, but the principles outlined here apply also to growth from an aqueous solution or from existing minerals during metamorphism. As outlined in the preceding paragraphs, the energy change involved in forming a crystal embryo from a melt includes two terms, one related to the free energy of formation of the crystal embryo and the other to the surface energy of the crystal embryo.

The first term is the free energy of formation of the crystal embryo (ΔG_v) whose volume is v

$$\Delta G_v = \left(\Delta G_{f(xl)} - \Delta G_{f(melt)}\right)v \quad \textbf{(5.2)}$$

where $\Delta G_{f(xl)}$ and $\Delta G_{f(melt)}$ are the free energy of formation of crystal and melt expressed in terms of calories or joules per unit volume of crystal. If $\Delta G_v < 0$, the chemically bonded crystalline solid represents a lower-energy configuration than the same atoms in the melt. If $\Delta G_v = 0$, the melt and the crystalline configurations have the same energy levels; they are in equilibrium. If $\Delta G_v > 0$, the melt is the lower-energy configuration.

The second term is the surface energy of the crystal embryo (ΔG_s)

$$\Delta G_s = \gamma a \quad \textbf{(5.3)}$$

where γ is the surface energy per unit area of crystal and a is the surface area of the crystal embryo. If we assume a cubic crystal whose edges are length x, the area is $6x^2$ and volume is x^3. The free energy of formation of a crystal is therefore

$$\Delta G = \Delta G_v + \Delta G_s$$

DO NOT COPY e48d507df5d1141@placeholder.9409

Printed by: e48d507df5d1141@placeholder.94092.edu. Printing is for personal, private use only. No part of this book may be reproduced or transmitted without publisher's prior permission. Violators will be prosecuted.

$$\begin{aligned} \Delta G &= \Delta G_v + \Delta G_s \\ &= \left(\Delta G_{f(xl)} - \Delta G_{f(melt)}\right)x^3 + \gamma 6x^2. \end{aligned} \tag{5.4}$$

Figure 5.8b shows the balance between the surface energy (ΔG_s) term, which is positive, and the volume term (ΔG_v), which in this case is negative because the temperature (T_1) is slightly below the equilibrium temperature (**Figure 5.8c**). If the temperature selected is above the equilibrium temperature, ΔG_v will be positive and the net free energy must be positive for all sizes of embryos.

Figure 5.8d schematically shows the free energy of formation of crystal embryos as a function of the embryo size for different degrees of undercooling below the equilibrium temperature.

- T_0 has no undercooling. This is the ideal equilibrium condition; the melt and crystalline states have exactly the same energy: $\Delta G_v = 0$. While embryos may form by chance, the surface energy ensures that ΔG of crystal growth is positive for all embryo sizes. All crystal embryos, regardless of size, are therefore unstable with respect to the melt and will break apart.
- T_1 has a small degree of undercooling. The crystalline state has a slightly lower energy than the melt, but the surface energy is very large (Figure 5.8b). Embryos smaller than the **critical growth radius**, x_c, are resorbed by the melt because the melt represents lower energy, and additional crystal growth results in a higher-energy configuration. Embryos larger than x_c can continue to grow because additional growth yields a lower-energy configuration. For crystals to grow, the chance collision and combination of atoms in the melt must therefore yield embryos larger than the critical growth radius $x_c(1)$, as shown in Figure 5.8b and Figure 5.8d. The abundance of stable embryos (a_1) is low (Figure 5.8a).
- T_2 has a moderate amount of undercooling. ΔG_v is more negative, so the surface energy term becomes less important. The critical growth radius $x_c(2)$ is smaller, and more embryos (a_2) can become stable.
- T_3 has a strong amount of undercooling. ΔG_v is quite negative, so the critical growth radius $x_c(3)$ is small and many embryos (a_3) can become stable.

The fact that crystals do not begin forming as soon as the temperature drops slightly below the equilibrium temperature indicates that melt remains metastable with respect to crystals. To get crystal growth, it is necessary to undercool the melt to provide the activation energy to overcome the high surface energy. The magnitude of the required undercooling, and therefore the activation energy, is time dependent. For slow cooling, lots of time is available and the activation energy is small. For rapid cooling, the activation energy is larger.

The significance of these observations for igneous rocks should be clear. A magma that cools very slowly at deep crustal levels will have a small degree of undercooling, and chance collisions of atoms in the melt will form few embryos that are large enough to

DO NOT COPY e48d507df5d1141@placeholder.94092

Printed by: e48d507df5d1141@placeholder.94092.edu. Printing is for personal, private use only. No part of this book may be reproduced or transmitted without publisher's prior permission. Violators will be prosecuted.

chance collisions of atoms in the melt will form few embryos that are large enough to persist. Those few embryos, however, will have the opportunity to grow over the extended duration of cooling to form the large mineral grains typically found in plutonic igneous rocks. For quickly cooling lava (magma at the surface) and magma in small, shallow intrusions, the degree of undercooling is large. Many small embryos will form by chance collisions between atoms and will therefore become stable and continue to grow. Because many crystals are growing, the size of each is limited and the resulting grain size is smaller.

Growth of a mineral from an aqueous fluid or in the solid state during metamorphism follows similar constraints. Chance combinations of elements either in solution or along the surfaces between mineral grains must form stable embryos once the stability field of a new mineral has been reached. The stable embryos then grow by the addition of successive layers of atoms to the surface. To get stable embryos requires that the equilibrium condition be overstepped to some degree.

With metamorphic rocks, grain size is not simply a matter of cooling rate. Grain size of minerals in metamorphic rocks is principally controlled by three processes. The first is the growth of new minerals as T–P conditions change. The rate of change of temperature and pressure in most metamorphic environments is quite slow. Therefore, the degree of overstepping of equilibrium conditions is small, so relatively few embryos of new mineral grains can become stable. Newly crystallized minerals in metamorphic rocks often form relatively few large crystals called **porphyroblasts**, rather than many smaller grains. It should be noted that most new mineral crystallization in metamorphic rocks occurs as the temperature increases, rather than decreases as occurs with a crystallizing magma. The second is recrystallization. Higher temperatures allow the fine grains of detrital quartz, for example, in the parent sediment or low-grade metamorphic rock to recrystallize and form fewer but larger grains. This too happens as temperature increases during metamorphism. The third process is deformation, which may distort or twist the crystal lattice of minerals (see sections on dislocations later in the chapter). Grains with distorted or twisted crystal lattices are high energy, so those grains will recrystallize into smaller grains with undistorted crystal lattices that have a relatively low energy. In extreme deformation, grains may be mechanically broken; thus their grain size is reduced.

Although they might not have realized it, grade school children and other individuals who have grown salt or sugar crystals, or used crystal-growing kits available from nature stores, have experienced the nucleation issues described here. Rapid evaporation of the water from the solution produces a relatively high degree of supersaturation and allows many embryos to become stable. The result is the formation of many small crystals. If, however, evaporation is restricted so that the degree of supersaturation is quite low, large crystals are more likely formed because only a few embryos are large enough to become stable and grow.

Heterogeneous Nucleation

Printed by: e48d507df5d1141@placeholder.94092.edu. Printing is for personal, private use only. No part of this book may be reproduced or transmitted without publisher's prior permission. Violators will be prosecuted.

Heterogeneous Nucleation

With heterogeneous nucleation, new minerals nucleate by taking advantage of the structure of an existing mineral. This avoids some of the energetic problems associated with homogeneous nucleation. If an existing mineral has a surface or structure that is similar to a new mineral, formation and growth of embryos is much easier.

Epitaxial nucleation is one variety of heterogeneous nucleation where the new mineral selectively nucleates on certain crystallographic surfaces of an existing mineral with structural similarities. A common example is the overgrowth of hematite (Fe_2O_3) on magnetite (Fe_3O_4) (**Figure 5.9**). The magnetite structure is based on cubic close-packed oxygen anions with Fe in octahedral and tetrahedral sites between close-packed layers of oxygen that extend parallel to (111). The hematite structure is based on hexagonal close-packed oxygen anions with Fe cations similarly situated between close-packed layers of oxygen parallel to (001). Recall from Figure 4.2 that hexagonal and cubic close packing differ only in the order of stacking close-packed layers of anions. Hence, hematite can readily nucleate and grow on the (111) faces of magnetite because the layer of oxygen exposed on that face is essentially identical to the layers of oxygen that are parallel to the (001) face of hematite.

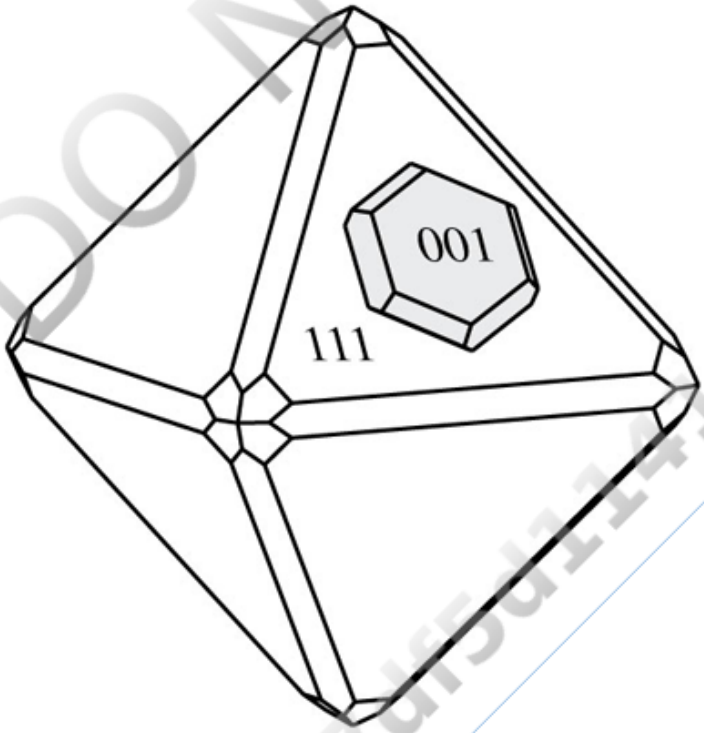

FIGURE 5.9 Epitaxial growth. Hematite crystal (shaded) may nucleate and grow on the (111) face of magnetite. See text for discussion. View larger image

Heterogeneous nucleation can also take place on structural defects such as grain boundaries and various imperfections in crystal structures (described later). In each case, formation of an embryo on these features destroys part of the defect and yields a reduction in energy level that can reduce the activation energy required to grow a

DO NOT COPY e48d507df5d1141@placeholder.9409

Printed by: e48d507df5d1141@placeholder.94092.edu. Printing is for personal, private use only. No part of this book may be reproduced or transmitted without publisher's prior permission. Violators will be prosecuted.

Crystal Growth

Once embryos have become stable, growth proceeds by adding atoms or groups of atoms to the surface of the crystal. This faces energetic problems similar to those of nucleation. Consider the process of adding atoms or some larger building block to the face of a crystal. Adding a new unit to a crystal with a planar surface (**Figure 5.10a**) is energetically difficult because the new unit stands proud of the surface and bonds only at the surface of contact. The chemical bonds that normally would stabilize the unit in the middle of the crystalline solid are missing, so there is a significant likelihood that the bond holding the unit to the surface will break and the unit will simply return to the liquid. In contrast, adding a new unit along the edge of a half-completed layer on the surface of a crystal is more likely because bonds can be made on several sides (**Figure 5.10b**). This suggests that the limiting factor in crystal growth is overcoming the energetic difficulties involved in starting a new growth layer on a crystal face. Theoretical considerations dealing with adding layers one at a time suggest that a substantial degree of undercooling or supersaturation should be needed to allow the first units of a new layer to be added so that growth can progress.

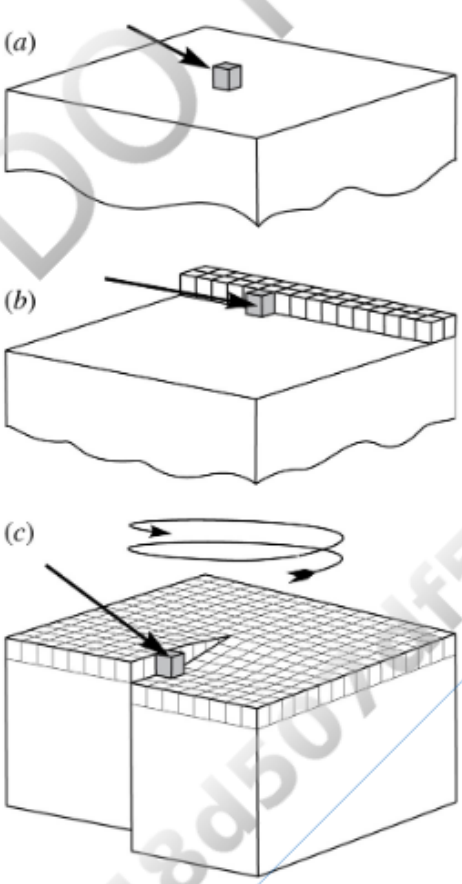

FIGURE 5.10 Growth on a crystal face. (*a*) Adding a new growth unit to a crystal face is energetically difficult because the new unit stands proud of the surface and has many unsatisfied

DO NOT COPY e48d507df5d1141@placeholder.9409

Printed by: e48d507df5d1141@placeholder.94092.edu. Printing is for personal, private use only. No part of this book may be reproduced or transmitted without publisher's prior permission. Violators will be prosecuted.

chemical bonds. (*b*) Adding a new growth unit along the edge of a partially completed layer is easier because more chemical bonds are satisfied. (*c*) Growth on a screw dislocation ensures that an edge always remains available for growth. The crystal grows by adding a continuous spiraling layer. View larger image

It turns out that real crystals grow much more easily and rapidly than this theoretical analysis suggests. The explanation appears to be that real crystals do not grow one layer at a time. Rather, growth often takes advantage of **screw dislocations** (**Figure 5.10c**). A screw dislocation is a structural defect (described in more detail in a following section) in which one part of the crystal is displaced relative to the other such that the displacement terminates in a line normal to the crystal face. The offset produces a geometric equivalent to a helix or a spiral staircase. As growth progresses, the continuously exposed edge of the screw dislocation spirals upward and always provides a favorable location for continued crystal growth.

Rate of Growth

Although it seems counterintuitive, *the slowest-growing crystal faces are the faces most likely to be present or large on a crystal.* The reason is that fast-growing faces grow themselves out of existence.

Consider the small halite crystal shown in **Figure 5.11a**, which has both octahedral {111} and cubic {001} faces. The octahedral {111} faces are parallel to layers of Na^+ and Cl^- in the structure, so growth consists of adding a layer of just Na^+ followed by a layer of just Cl^-, and so forth. For the {001} face, either Na^+ or Cl^- could be added at any time.

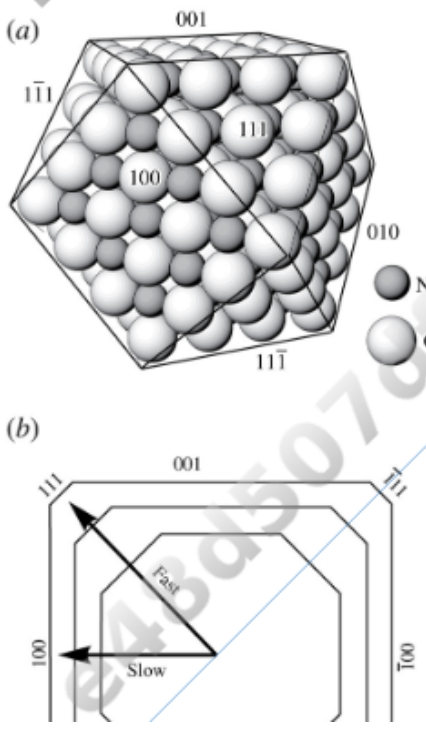

DO NOT COPY
e48d507df5d1141@placeholder.9409

Printed by: e48d507df5d1141@placeholder.94092.edu. Printing is for personal, private use only. No part of this book may be reproduced or transmitted without publisher's prior permission. Violators will be prosecuted.

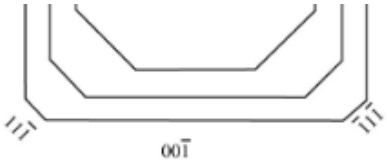

FIGURE 5.11 Slow-growing faces become larger. (*a*) The {111} crystal faces of halite are covered with either all Na^+ or all Cl^- and have a high net charge and high surface energy, which strongly attracts successive layers of Na^+ and Cl^- on such faces to produce high growth rates. The {001} faces have equal numbers of Na^+ and Cl^- with a relatively low charge and low surface energy leading to slow growth rates. (*b*) Section through the halite crystal showing {001} and {111} faces. Because growth rate on the {111} faces is higher than on the slow-growing {100} faces, the {111} faces will "grow" out of existence. View larger image

Both the Na^+ and the Cl^- are in octahedral coordination (CN = 6) in the halite structure. Using the electrostatic valency principle (Chapter 3), each ion on the {001} face is bonded to five oppositely charged ions; therefore, each ion on that face has a remaining charge of one-sixth that can be used to bond to the next oppositely charged ion added to the surface. On the {111} face, each ion is bonded to three oppositely charged ions and therefore has a remaining charge of one-half that can be used to bond ultimately to three other oppositely charged ions. Adding a new Na^+ to any face, for example, depends on random movement of a Na^+ in solution to a position close to the face where it can be attracted and bonded by the local negative charge of a Cl^-. Comparing a Cl^- on the {001} versus the {111} face, the one-half charge of the Cl^- on the {111} is much more likely to attract the Na^+ and bond to it than the one-sixth charge of the Cl^- on the {001} face; hence the {111} face will grow faster than the {001} face.

Figure 5.11b shows a cross section through a halite crystal with {001} and {111} faces. If the {111} faces grow faster, the amount of new crystal added on that face is greater for the same duration. Fast {111} growth results in those faces become progressively smaller at each instance, and ultimately they will cease to exist.

Using the electrostatic valency principle to explain the rate of growth of different crystal faces is entirely consistent with the principles of thermodynamics. Natural systems tend to change in directions that minimize their energy level. Rapid growth of high-energy faces, such as the highly charged {111} face in halite, ultimately reduces their size. The faces with low surface energy grow more slowly and are therefore larger. Minimizing the area of high-surface-energy faces and maximizing the area of low-surface-energy faces tend to ensure that the total surface energy is minimized.

The Law of Bravais (Chapter 2) also does a good job of predicting the dominant crystal faces for many minerals. Recall that the Law of Bravais states that the most prominent faces are those that intersect the greatest number of lattice nodes—that is, planes that have the most closely spaced lattice nodes. This ensures that the Miller indices for prominent faces usually consist of *hlk* values of ones and zeros. **Figure 5.12a** shows a primitive rectangular lattice looking down the *b* axis, where the *c* unit cell dimension (d_{001}) is the smallest and the *a* unit cell dimension (d_{100}) is the largest. A face parallel to (100) has lattice nodes on that face spaced d_{010} apart, which is the closest spacing

Printed by: e48d507df5d1141@placeholder.94092.edu. Printing is for personal, private use only. No part of this book may be reproduced or transmitted without publisher's prior permission. Violators will be prosecuted.

(100) has lattice nodes on that face spaced d_{001} apart, which is the closest spacing possible. Lattice nodes on faces parallel to (001) are spaced d_{100} apart, which is larger than for (100). All other faces have more widely spaced lattice nodes on the face, and the spacing between lattice planes is smaller. For example, lattice planes parallel to (102) are d_{102} apart, the smallest of the three faces considered, and lattice nodes on the face are spaced $(4d_{100}^2 + d_{001}^2)^{1/2}$ apart, the largest of the three faces. Of these three faces, (102) should be fastest growing and smallest on the crystal (if it exists), (001) should be slower growing and larger, and (100) should be the slowest growing and largest. Based on these observations, the Law of Bravais can be restated.

> The growth rate of a crystal face is, in general, inversely proportional to the interplanar spacing of that face.

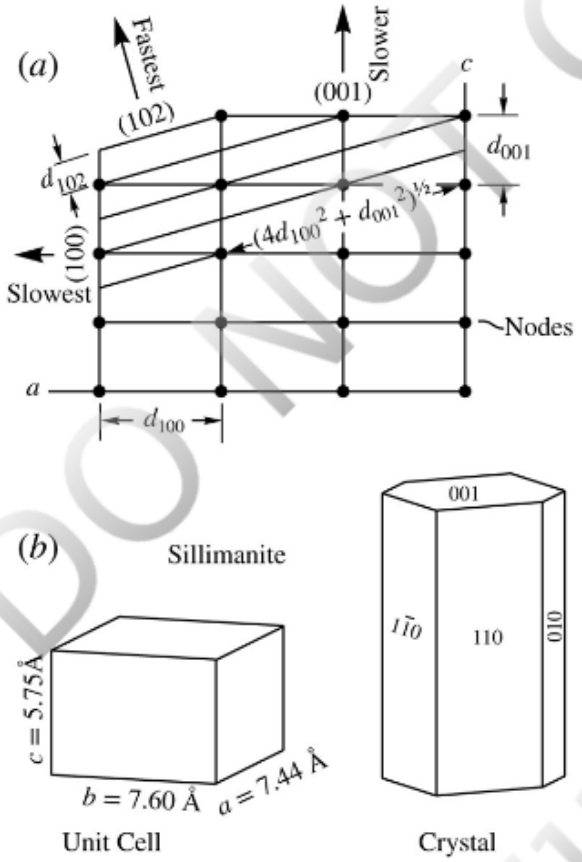

FIGURE 5.12 Growth rates of crystal faces are inversely proportional to interplanar (*d*) spacing. (*a*) Growth is fastest normal to the (102) face, slower normal to the (001) face, and slowest normal to the (100) face because $d_{102} < d_{001} < d_{100}$. Crystals should therefore be elongate parallel to the *c* axis, and the {102} faces should be small or nonexistent. (*b*) Sillimanite. The *c* unit cell dimension is smallest, so crystals are elongate parallel to the *c* axis. View larger image

Note that this leads to another seemingly counterintuitive relationship: the *longest dimension of a crystal typically is associated with the shortest unit cell dimension.* Consider the unit cell of sillimanite, shown in **Figure 5.12b**, whose *c* unit cell dimension is significantly smaller than the *a* and *b* dimensions. Because the interplanar spacing along *c* is less than along *a* and *b*, growth is fastest along the *c* axis and crystals become elongate parallel to *c*. This relationship does not always hold, but a review of the unit cell

DO NOT COPY e48d507df5d1141@placeholder.9409

Printed by: e48d507df5d1141@placeholder.94092.edu. Printing is for personal, private use only. No part of this book may be reproduced or transmitted without publisher's prior permission. Violators will be prosecuted.

elongate parallel to *c*. This relationship does not always hold, but a review of the unit cell dimensions of elongate minerals in later chapters such as zircon, tourmaline, apatite, amphibole, and andalusite, shows that the long dimension of most minerals correlates with the smallest unit cell dimension.

In Chapter 2 it was discussed that for a particular point group, there is often more than one crystal form for a mineral. If the only consideration of which crystal faces exist on a mineral specimen are the guidelines given by the charge of particular faces or the lattice plane spacing, then the observed crystal faces would largely be connected to crystal size, but this is not always the case. Additional complexity comes from the fact that pressure, temperature, and composition all play a role in the rate of crystal face growth. Diamond provides a good example. Diamond's point group is $4/m\ \bar{3}\ 2/m$, which can grow a variety of crystal forms (Table 2.9), but cubes and octahedrons are most common. Diamond laboratory growth studies (Palyanov and others, 2013; 2017) show that at low temperature, the cube crystal form is most common, meaning that the {100} faces are relatively slow growing, but at higher temperature, the octahedron form is most common, suggesting under these conditions the {111} faces are the relatively slow growing. The addition of various elements and compounds to the environment, such as Mg, Si, Ge, and H_2O, can also control growth rates and the faces found on a diamond crystal.

Zoned Crystals

Chapters 1 and 3 emphasize that minerals have definite, but not necessarily fixed, chemical compositions. For example, as discussed earlier, the relative amounts of Fe and Mg in olivine may vary in different samples. A single crystal of a solid solution mineral may similarly vary such that it is common to find that the center, or **core**, of a crystal has a different composition than the outside, or **rim**.

Because chemical composition may control mineral properties such as color, index of refraction, or other optical properties, chemical zoning may be recognized in mineral hand samples with or without the aid of a hand lens. More often, thin sections of minerals are required to observe zoning. A thin section is a very thin (0.03 mm) slice of a rock or mineral mounted on a glass microscope slide. Thin sections are examined with a petrographic microscope using techniques described in Chapter 7. **Figure 5.13** shows chemically zoned crystals of pyroxene. The presence of chemical zoning in a crystal generally indicates that chemical and/or physical conditions changed as the crystal grew.

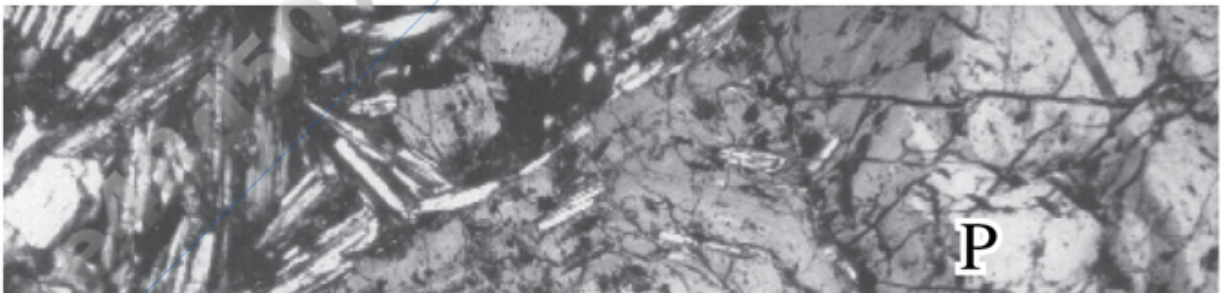

Printed by: e48d507df5d1141@placeholder.94092.edu. Printing is for personal, private use only. No part of this book may be reproduced or transmitted without publisher's prior permission. Violators will be prosecuted.

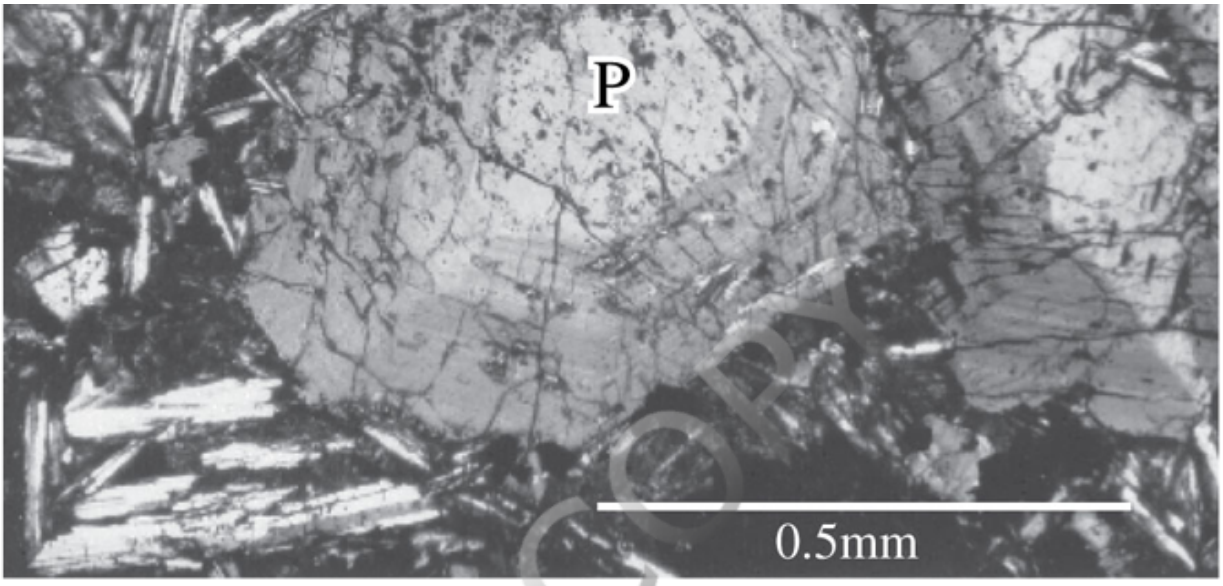

FIGURE 5.13 Photomicrograph of a thin section (see Chapter 7) showing zoned crystals of pyroxene (P) (crossed polarizers). The chemical zoning is indicated by a change in the color from the center of crystals to the rim. The slender crystals are plagioclase. See also Figure 12.12 for zoned plagioclase. View larger image

Plagioclase forms a continuous solid solution series whose end members are albite ($NaAlSi_3O_8$) and anorthite ($CaAl_2Si_2O_8$) (Chapter 4). Coupled substitution allows $Na^+ + Si^{4+}$ in albite to substitute for $Ca^{2+} + Al^{3+}$ in anorthite.

A phase diagram at 5 kbar pressure for plagioclase in the presence of water is shown in **Figure 5.14**. Compare this with Figure 5.6, which shows a similar solid solution series for olivine. Consider a sample of melted plagioclase whose composition is 55 percent anorthite (An) at a temperature of 1200°C, as shown in Figure 5.14a. Under equilibrium conditions, crystallization begins at 1100°C with growth of An_{77} plagioclase. At 1050°C, An_{68} crystals grow from a melt with a composition of 43 percent An. Crystallization is completed at 980°C, and all the plagioclase has the composition An_{55}, the same as the initial bulk composition. Diffusion allowed the exchange of Na, Si, Ca, and Al between the melt and crystals so that both maintain chemical equilibrium during cooling. The result is that, although the core of a plagioclase crystal may have initially formed with a composition of An_{77}, the core (and entire crystal) has a final composition of An_{55} when crystallization ended.

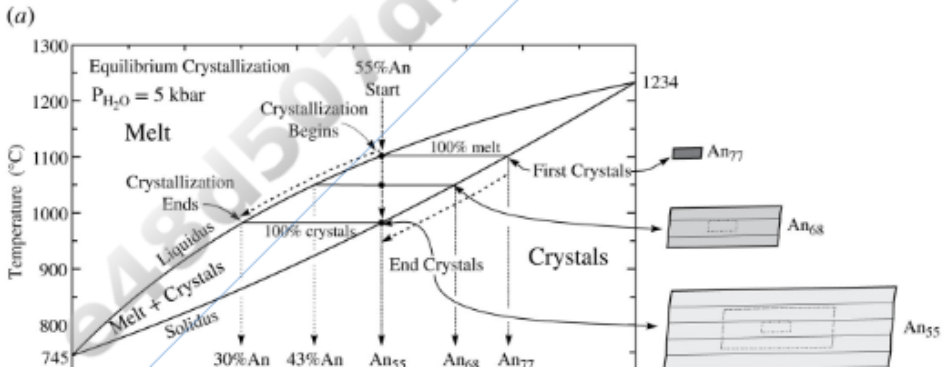

Printed by: e48d507df5d1141@placeholder.94092.edu. Printing is for personal, private use only. No part of this book may be reproduced or transmitted without publisher's prior permission. Violators will be prosecuted.

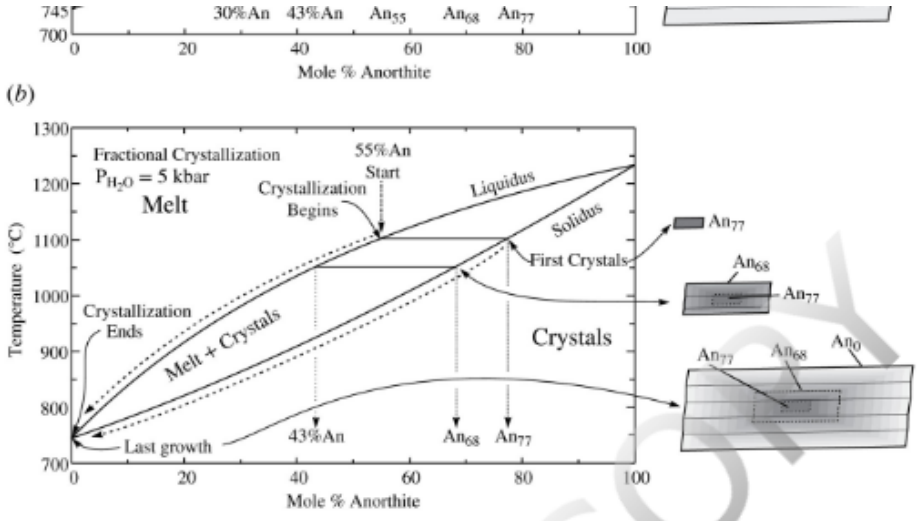

FIGURE 5.14 Plagioclase phase diagram at 5 kbar water pressure. Adapted from Yoder and others (1957). (*a*) Equilibrium crystallization. (*b*) Fractional crystallization. See text for discussion. View larger image

With **fractional crystallization**, crystals are isolated from the melt as soon as they grow, so diffusion between melt and crystals is not possible and melt and crystals cannot stay in chemical equilibrium. Temperature–composition (T–X) phase diagrams, such as Figure 5.14b, can also be used to understand fractional crystallization. Crystallization again begins at 1100°C (or slightly below, to allow for nucleation) and the first-formed crystals are An_{77}; however, if growth is rapid, diffusion cannot exchange $Na^+ + Si^{4+}$ in the melt with $Ca^{2+} + Al^{3+}$ in the crystals fast enough such that the composition of the first crystals remains unchanged with cooling. Successively more Na-rich layers of plagioclase are then grown on these cores as cooling progresses. At 1050°C, layers of An_{68} are added to the exterior of the crystals, resulting in a zoned crystal with a Ca-rich An_{77} core and a more Na-rich (An_{68}) rim. Because crystals do not interact with the melt, each increment of cooling is equivalent to starting with a new, slightly more Na-rich, bulk composition and no crystals. It is therefore possible for the melt composition to progress all the way to the Na end member (An_0), from which a last thin layer of pure albite grows on the crystals. Crystals therefore are strongly zoned, with a relatively Ca-rich core to albite on the rim. The bulk composition of the crystals, however, will on average be the same as the original bulk composition of the melt, which is still An_{55} for this example.

In almost all cases, real crystallization of solid solution minerals is intermediate between ideal equilibrium and ideal fractional crystallization. Close-to-equilibrium crystallization is most likely in deep-seated, slowly cooled intrusions, while fractional crystallization is most likely in rapidly cooled, shallow intrusions and volcanics. Whether zoned crystals are formed depends upon the diffusion rate of the relevant elements through the crystals and the amount of time available for diffusion. Diffusion through plagioclase is slow, so zoned plagioclase crystals are common, even for relatively deep-seated, slowly cooled, intrusions. The diffusion of Fe and Mg through the crystal lattice of olivine is relatively fast, so zoned olivine crystals usually are found only in volcanic rocks and shallow intrusions.

DO NOT COPY e48d507df5d1141@placeholder.94092

Printed by: e48d507df5d1141@placeholder.94092.edu. Printing is for personal, private use only. No part of this book may be reproduced or transmitted without publisher's prior permission. Violators will be prosecuted.

The preceding discussion of zoned crystals emphasizes crystallization from magmas. Zoned minerals also are common both in metamorphic rocks and in minerals grown from aqueous fluids, such as in hydrothermal mineral deposits. In all these cases, chemical zoning documents progressive growth of the mineral during periods of changing temperature, pressure, and/or chemical conditions. Zoning can therefore provide important information concerning the changing conditions under which the mineral grew.

Inclusions

When a mineral grain grows, it can engulf and completely surround a portion of its surroundings; this could be a neighboring mineral grain, a pocket of melt, or a pocket of aqueous fluid. The engulfed material is called an **inclusion**. Inclusions are common and may be abundant, but mineral grains free of inclusions are possible. Generally, inclusions are small and require a hand lens or a microscope to be seen (**Figure 5.15**).

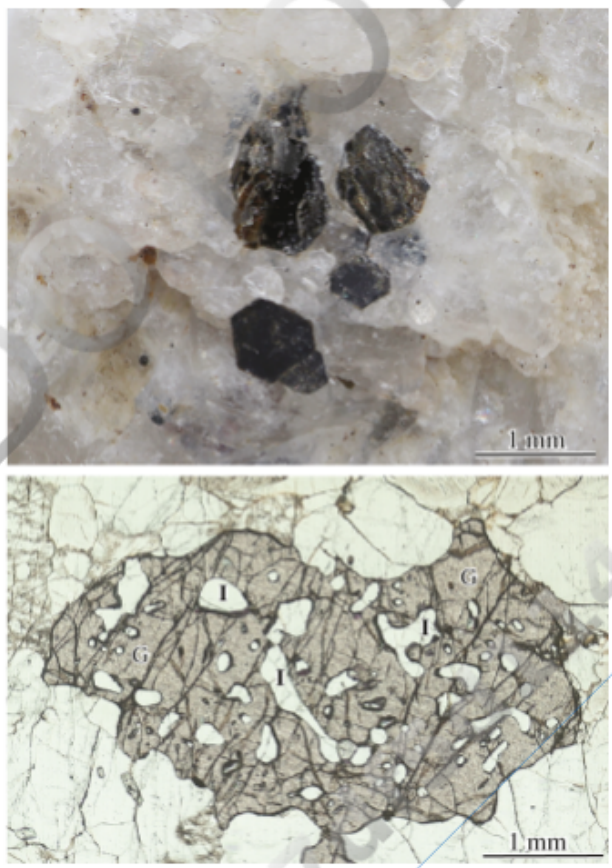

FIGURE 5.15 Examples of inclusions. (*a*) Fracture surface of a sanidine crystal as viewed through the hand lens. Four relatively large black biotite inclusions are in the image's center. Small black flecks elsewhere in the image are also biotite inclusions. (*b*) Photomicrograph of a thin section showing an anhedral garnet (G) with many irregularly shaped inclusions (I) of mostly quartz. Only three inclusions are labeled. Plane-polarized light. View larger image

Printed by: e48d507df5d1141@placeholder.94092.edu. Printing is for personal, private use only. No part of this book may be reproduced or transmitted without publisher's prior permission. Violators will be prosecuted.

Structural Defects

The ideal model of crystalline structures assumes that the regular and repeating pattern of atoms continues without flaw throughout an entire crystal. Real crystals, however, always contain a variety of irregularities or defects that can influence their properties. These defects are conveniently grouped into **point defects**, **line defects**, and **planar defects**.

Point Defects

All real crystals have point defects consisting of vacant sites, atoms out of their correct position, extraneous atoms, or substituted atoms. In general, the density of these defects is higher for crystals grown at high temperature. Defects represent disorder, and high temperatures favor disordered arrangements.

Schottky Defects

Schottky defects are vacancy defects (**Figure 5.16a**). In ionic crystals, it is necessary for vacant cation sites to be balanced by vacant anion sites to maintain charge balance. In a simple structure, such as NaCl, every vacant Na^+ site is balanced by a vacant Cl^- site. In crystals with more complex compositions, charge balance must still be maintained, but the balance between anion and cation vacancies depends on the charges of the ions. The presence of Schottky defects does not influence the stoichiometry of the mineral; the ratio of anions and cations remains the same.

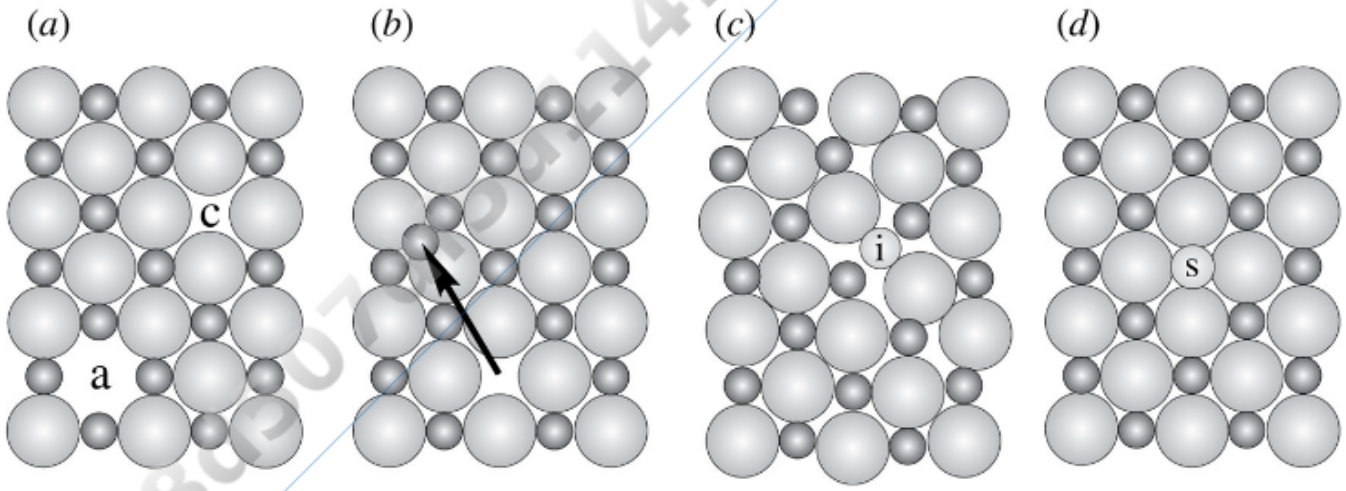

FIGURE 5.16 Point defects. (*a*) Schottky defects. A missing cation (c) is balanced by a missing anion (a). (*b*) Frenkel defects. A cation, missing from its normal structural site, is located elsewhere in the structure (arrow). (*c*) Interstitial defect. A foreign cation is located in the structure (i), presumably

DO NOT COPY e48d507df5d1141@placeholder.94092

Printed by: e48d507df5d1141@placeholder.94092.edu. Printing is for personal, private use only. No part of this book may be reproduced or transmitted without publisher's prior permission. Violators will be prosecuted.

the structure (arrow). (c) Interstitial defect. A foreign cation is located in the structure (i), presumably charge balanced elsewhere. (*d*) Substitution defect. A foreign cation (s) substitutes for a cation normally in the structure. View larger image

Frenkel Defects

Frenkel defects are mislocation defects (**Figure 5.16b**). A cation (or anion) is moved from its normal position to an alternative site that normally is not occupied. Cations are more commonly involved in Frenkel defects because they are smaller than anions. Frenkel defects do not affect charge balance or stoichiometry of minerals.

Impurity Defects

No mineral is pure in the sense of consisting only of the elements present in the ideal chemical formula. Other elements are always present, even if only in trace amounts. **Interstitial defects** are foreign atoms that occupy sites that do not normally exist in the crystal (**Figure 5.16c**). Their charge is balanced elsewhere, for example, by substituting a lower-charged cation for a higher-charged cation. A **substitution defect** (**Figure 5.16d**) is an ion that substitutes for one of the normally present ions in the ideal or pure crystal structure.

It should be evident that the identity of an impurity defect depends on first defining what constitutes the "pure" chemical composition and ideal structure for the mineral. Substitution defects are chemically and structurally the same as simple substitution and interstitial substitution solid solution varieties described in Chapter 4. The choice of whether to describe mineral compositional variation in terms of impurity defects or as solid solution depends mostly on the expectation of the mineralogist regarding the normal chemical variability of the mineral. High temperatures allow more impurities to be present because thermal vibrations of the atoms are greater, allowing atoms to occupy positions that are not possible at lower temperature.

Schottky and Frenkel defects were originally proposed to explain diffusion of atoms and ions through crystal structures. For an ion to move, it must either move into a vacant site, as in a Schottky defect, or at least temporarily occupy an interstitial position, forming a Frenkel defect. The abundance of these defects is a function of temperature; more defects are present at high temperatures. This helps explain the observation that diffusion of atoms through a crystalline solid is faster at high temperatures.

Line Defects

Rocks are often subjected to forces caused by gravity or plate motions; if the force per area, also called the **stress**, exceeds the strength of the rock, the rock will **deform**, or change in shape. In tectonic environments that involve high temperatures and pressures, the deformation typically occurs slowly and in a ductile manner such that the rock does not break. The ductile deformation can form folds that range in scale from microscopic to

DO NOT COPY e48d507df5d1141@placeholder.94092

Printed by: e48d507df5d1141@placeholder.94092.edu. Printing is for personal, private use only. No part of this book may be reproduced or transmitted without publisher's prior permission. Violators will be prosecuted.

not break. The ductile deformation can form folds that range in scale from microscopic to the dimensions of mountain ranges. Ductile deformation must occur within individual mineral grains if the rock is to ductily deform at the larger scale.

Based on extensive studies of the ductile deformation of crystalline metals, such as copper wire or the steel used in automobile bodies, it was found that crystals deform by slip along favored crystallographic planes and in specific directions. The combination of the crystallographic plane and the slip direction together define a **slip system**. In the simple orthorhombic lattice shown in **Figure 5.17**, the slip system can be described as {001}[010], meaning that slip occurs on crystallographic planes parallel to the {001} faces and that the slip direction is parallel to [010], that is, parallel to the *b* crystal axis.

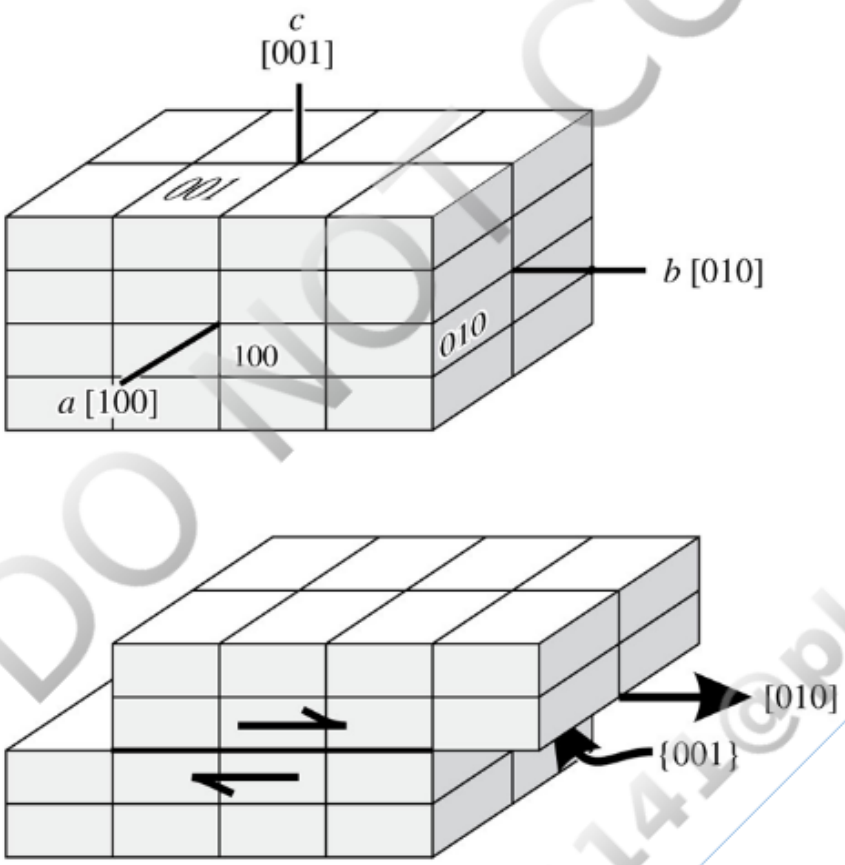

FIGURE 5.17 Slip system in a crystal lattice. Slip occurs on a crystal plane parallel to (001) and in a direction parallel to [010] (the *b* axis), so the slip system is {001}[010]. View larger image

Producing slip in a crystal by having all the bonds on a slip plane break simultaneously requires orders of magnitude more stress than that needed to ductily deform minerals experimentally. This suggests that the method of slip does not involve simultaneously breaking all bonds along the slip plane. Rather, slip propagates through a crystal so that bonds are broken only along a line defining the leading edge of the slip surface. The edges of the propagating slip surface, where bonds are broken, are known as **dislocation lines**. They define the boundary between where slip has already occurred and where it has not. There are two varieties of dislocation lines: **edge dislocations** and **screw dislocations**.

DO NOT COPY
e48d507df5d1141@placeholder.9409

Printed by: e48d507df5d1141@placeholder.94092.edu. Printing is for personal, private use only. No part of this book may be reproduced or transmitted without publisher's prior permission. Violators will be prosecuted.

In this discussion, formation of edge and screw dislocations is driven by deformation, but such dislocations can form in minerals during crystallization; recall that earlier in the chapter screw dislocations played an important role in facilitating mineral growth.

Edge Dislocation

With edge dislocations, the dislocation direction known as a **Burgers vector** is at right angles to the dislocation line (**Figure 5.18a**). The Burgers vector can be defined by starting at a point S on a lattice node and tracing a circuit around the dislocation, taking an equal number of lattice steps in opposite directions. If a dislocation is enclosed within the Burgers circuit, the circuit will not close and will finish at point F. The vector *b* between F and S is the Burgers vector, and as shown, it is at right angles to the dislocation line. With progressive deformation, the dislocation line moves through the crystal parallel to the Burgers vector, as shown in the sequence. The result is that the mineral grain has changed shape without breaking.

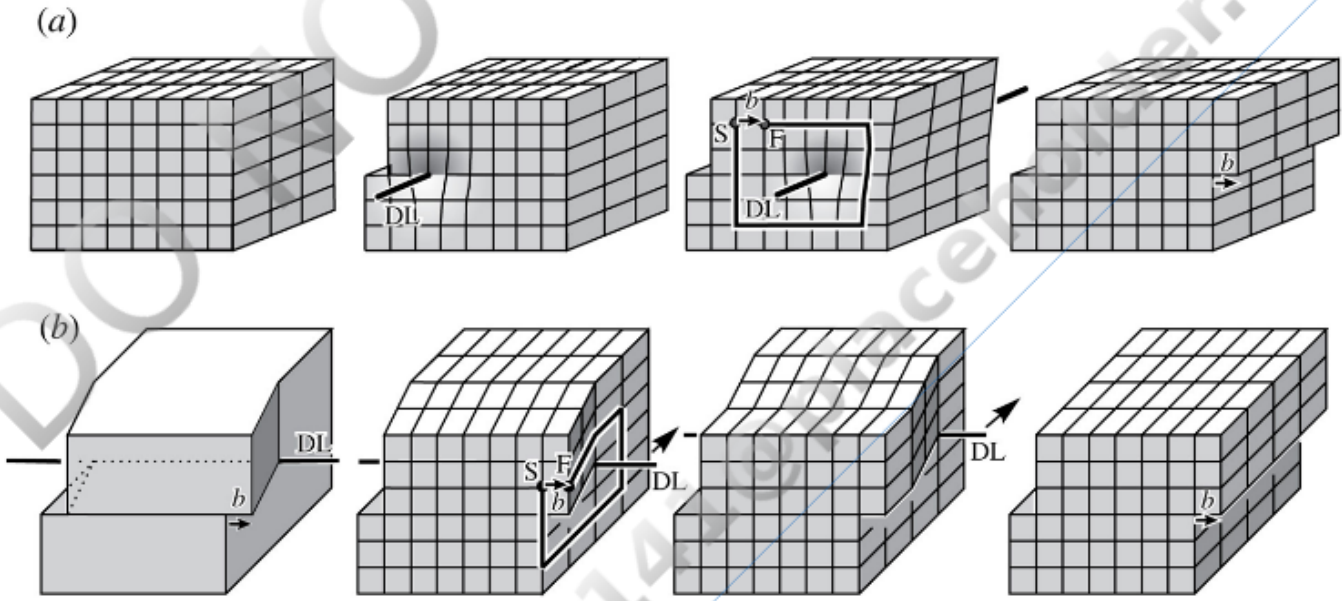

FIGURE 5.18 Dislocations. The Burgers vector *b* is defined by completing a Burgers circuit. Start at lattice position S and make a box around the dislocation, counting the same number of lattice units in opposite directions, to reach finish position F. Vector *b* between S and F is the Burgers vector. (*a*) An edge dislocation is produced by deforming the crystal as shown. The dislocation line (DL) is perpendicular to the Burgers vector and moves to the right (parallel to the Burgers vector) as deformation progresses. When the dislocation line exits the crystal on the right, the top segment of the crystal is offset relative to the bottom by a distance equal to the Burgers vector. (*b*) Screw dislocation. The dislocation line is parallel to the Burgers vector and moves to the back (perpendicular to the Burgers vector) as deformation progresses. When the dislocation line exits the crystal to the back, the top of the crystal is offset relative to the bottom by a distance equal to the Burgers vector. View larger image

Screw Dislocation

Printed by: e48d507df5d1141@placeholder.94092.edu. Printing is for personal, private use only. No part of this book may be reproduced or transmitted without publisher's prior permission. Violators will be prosecuted.

With screw dislocations, the Burgers vector is parallel to the dislocation line (**Figure 5.18b**). The applied stress produces an offset in the lattice parallel to the dislocation plane and parallel to the Burgers vector. However, as the deformation progresses, as shown in the sequence, the dislocation line moves perpendicular to the Burgers vector. Note that if the Burgers circuit continued, it would define a spiral, like the threads of a screw or a spiral staircase.

Both ends of a dislocation line must either terminate at the surface of a crystal (Figure 5.18) or form a continuous loop within a crystal (**Figure 5.19**). The nature of the dislocation line changes from edge to screw along its length, but the Burgers vector remains constant and is parallel to the offset that produces the dislocation.

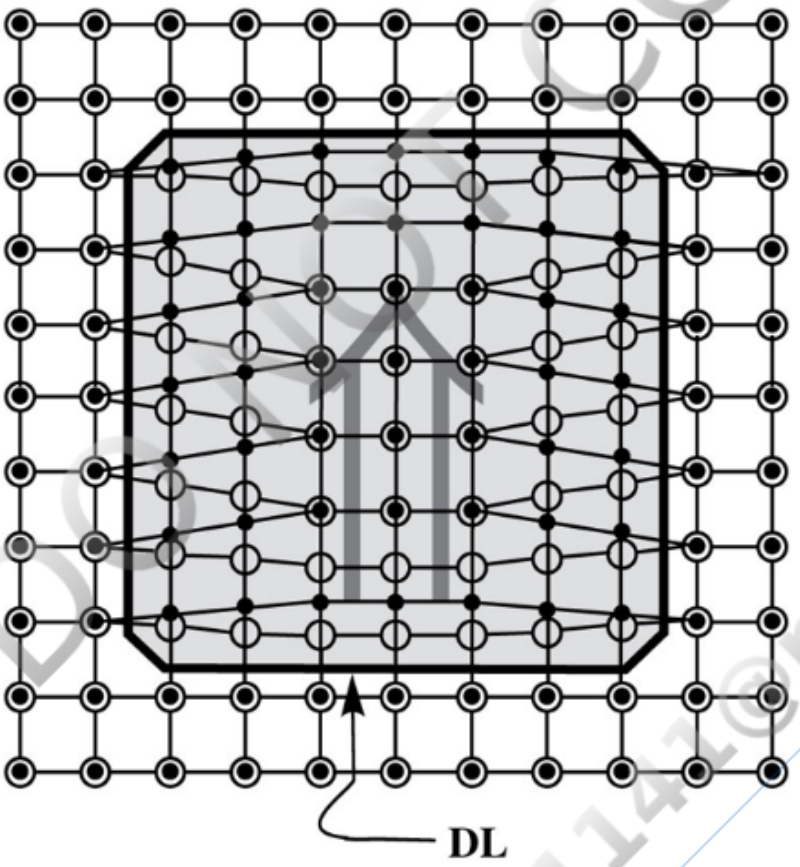

FIGURE 5.19 Unless terminated at the edge of a crystal, a dislocation line (DL) forms a continuous loop outlining a surface, equivalent to a fault, with movement parallel to the Burgers vector. The "fault surface" (shaded) between the lower layer of circles and upper layer of solid dots is bounded by screw dislocations on the sides and edge dislocations at the top and bottom. View larger image

Strongly deformed mineral grains will be a much different shape than they were prior to deformation and typically they will contain many screw and edge dislocations. One of the consequences of a high density of dislocations is that materials like metals can **work-harden**, meaning that as ductile deformation progresses, the stress needed to further deform the material increases. This is caused by dislocations in different orientations interfering with each other and inhibiting their motion. Heating a material allows the

Printed by: e48d507df5d1141@placeholder.94092.edu. Printing is for personal, private use only. No part of this book may be reproduced or transmitted without publisher's prior permission. Violators will be prosecuted.

crystal structure to rearrange itself to remove the dislocations in a process called **annealing**.

Planar Defects

Planar defects involve a mismatch of the crystal structure across a surface. The surfaces may be planar, or they may be curved in complex ways. The planar defects described here include **grain boundaries**, **stacking faults**, and **antiphase domain boundaries**.

Grain Boundaries

In the mathematical model of a crystal structure, the regular pattern of atoms continues to infinity in all directions. To an atom sitting in the middle of a crystal that is a few millimeters across, the surface of the crystal is many millions of atoms away, so from the perspective of that atom, the crystal structure does go on forever. However, all mineral grains do have a limit to their size, and the edge of the grain is called a grain boundary. Grain boundaries may be a crystal face, a fracture or cleavage surface, or the boundary between two mineral grains within a rock.

Stacking Faults

Stacking faults are produced when a layered mineral structure contains a layer that is out of sequence or position. In the hexagonal closest-packed structure shown in Figure 4.1 the layers of spheres alternate between the A and B positions to form an ABABABAB repeating pattern, whereas in cubic closest packing, the layers use a third C position to produce a repeating sequence of ABCABCABC, etc. A stacking fault would be present if a layer in the C position were inserted in a hexagonal closest-packed structure to produce a pattern ABABCABAB. Minerals that display polytypism, such as the micas and clay minerals, also commonly have stacking faults when the repeating pattern of layers is disrupted.

Antiphase Boundaries

Antiphase boundaries separate segments of a crystal, called **antiphase domains**, which are related to each other by a simple translation. Adjacent antiphase domains have the same crystallographic orientation, but there is a translational mismatch between the domains. Most antiphase boundaries are produced when crystals undergo a displacive polymorphic transition. **Figure 5.20a** schematically shows the structure of pigeonite, which is a pyroxene (Chapter 14) commonly found in mafic volcanics. The high-temperature structure contains chains of silicon tetrahedra that all have the same geometry. At lower temperatures, pigeonite goes through a displacive polymorphic transition in which the chains distort and the symmetry is reduced. The distortion, however, is accomplished by alternate layers of chains kinking in alternate directions.

DO NOT COPY e48d507df5d1141@placeholder.94092

Printed by: e48d507df5d1141@placeholder.94092.edu. Printing is for personal, private use only. No part of this book may be reproduced or transmitted without publisher's prior permission. Violators will be prosecuted.

Ideally, alternate layers of chains kink in opposite directions throughout the crystal. In practice, however, the kinking in one domain follows one pattern and in an adjacent domain it follows the opposite pattern (**Figure 5.20b**). The result is the formation of antiphase domains bounded by antiphase boundaries. The pattern in one domain can be made to match its neighbor by a simple translation.

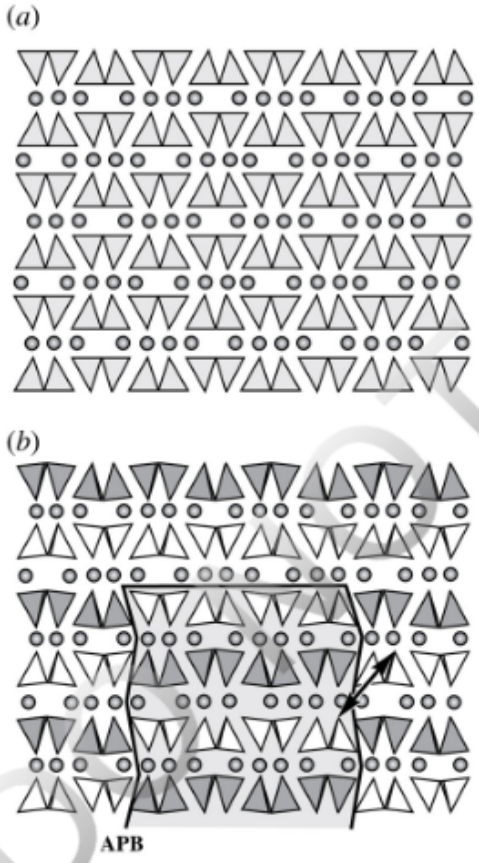

FIGURE 5.20 Antiphase boundary in pigeonite $(Mg,Fe,Ca)_2Si_2O_6$. (*a*) The high-temperature structure consists of chains of silicon tetrahedra extending in and out of the page. The chains are bonded to each other through the Mg, Fe, and Ca (circles). (*b*) Upon cooling, the chains distort, with alternate layers of chains kinking inward (darker) and outward (lighter). The pattern of kinking in one part of the crystal may differ from that in adjacent parts, resulting in the formation of an antiphase domain (shaded) bounded by an antiphase boundary (APB). The antiphase domain is related to the surrounding crystal by a translation (arrow). View larger image

Because antiphase domains have identical crystallographic orientations, they cannot be seen in hand samples or by using conventional microscopic techniques, even if the domains are sufficiently large. Imaging of natural and synthetic materials by means of transmission electron microscope techniques (Chapter 8) shows that the domains are usually highly irregular.

DO NOT COPY e48d507df5d1141@placeholder.9409

Printed by: e48d507df5d1141@placeholder.94092.edu. Printing is for personal, private use only. No part of this book may be reproduced or transmitted without publisher's prior permission. Violators will be prosecuted.

Twinning

Twinning represents a symmetrical intergrowth, or intertwining, of two or more crystal segments of the same mineral. Because the segments are joined along a surface, twinning can be considered a variety of planar structural defect. Twinning can take a variety of forms, from the intergrown cross pattern found in twinned staurolite crystals, to the finely laminated twinning seen in plagioclase. Twinning is not the same as the random intergrowth of mineral grains and crystals that invariably takes place in rock and mineral deposits (see Chapter 2).

In every case the two or more twin segments are related to each other by a symmetry operation called a **twin operation**. There are three possible twin operations: reflection, rotation, and inversion. The **twin law** that describes the twin operation includes specification of the twin operation and identification of the crystallographic plane or axis associated with the twinning.

Twinning by reflection produces two segments of crystals that are related to each other by a mirror parallel to a crystallographic plane common to both segments (**Figure 5.21a**). The mirror plane is identified by its Miller index. It must not be a plane that is normally a mirror in the untwinned crystal. The twin law is usually expressed as "reflection on {*hkl*}" or "twins on {*hkl*}," where {*hkl*} is the form symbol of the mirror plane.

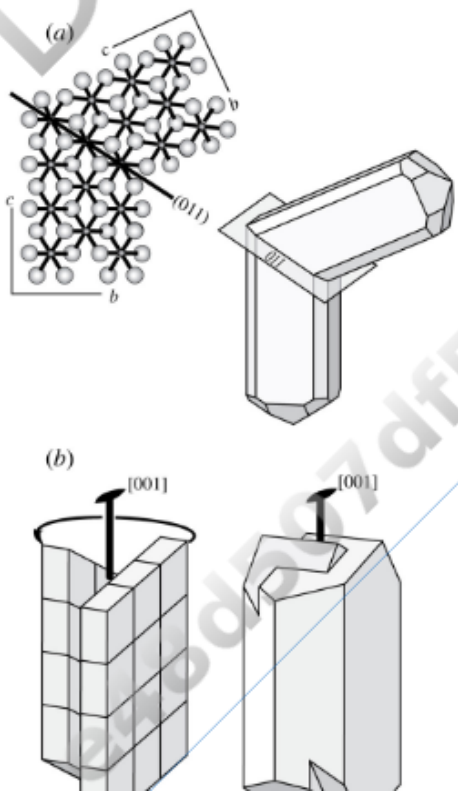

DO NOT COPY
e48d507df5d1141@placeholder.9409

Printed by: e48d507df5d1141@placeholder.94092.edu. Printing is for personal, private use only. No part of this book may be reproduced or transmitted without publisher's prior permission. Violators will be prosecuted.

FIGURE 5.21 Symmetry operations in twinning. (*a*) Twinning by reflection on {011} in rutile. (*b*) Twinning by rotation on [001] in K-feldspar to produce a Carlsbad twin. View larger image

Rotation produces two or more crystal segments related to each other by rotation on a crystallographic axis common to all segments (**Figure 5.21b**). Almost always the rotation is 2-fold (180°), although other rational rotations are possible. The rotation responsible for the twinning must not duplicate a rotation axis present in the untwinned crystal, although a twin axis may be parallel to a symmetry axis if the rotation required for twinning is not the same as the rotation required by the symmetry axis. For example, the [111] body diagonal through a cube is typically a 3-fold rotation axis. Twinning by 2-fold rotation on [111] is possible because it does not duplicate the 3-fold rotation. The twin law for a typical 180° rotation is usually expressed as "2-fold rotation on [*uvw*]," where [*uvw*] is the crystallographic axis on which rotation occurs. This may be shortened to "twinning on [*uvw*]" if 2-fold rotation is presumed. If the twin axis is defined as being perpendicular to a specific crystal plane (*hkl*), the twin law would be expressed as "2-fold rotation ⊥ (*hkl*)," where ⊥ means "perpendicular to."

With inversion twinning, the two crystal segments are related to each other by inversion through the center. In most cases, however, the processes of rotation or reflection can be used to express the same twin.

The surface along which two twin segments are joined is called the **composition surface**. In some cases the composition surface is irregular and in others it follows a rational crystallographic plane and can be indexed. If the composition surface is a smooth rational crystallographic plane, it is called a **composition plane** and is identified with its Miller index (*hkl*). If the twinning is produced by reflection, the twin plane will be the composition plane. Rotation twins may produce either a composition plane or an irregular composition surface.

Twins may be characterized by whether the twin segments appear to be intergrown or not. **Contact twins** (**Figure 5.22**) are joined on a rational composition plane, and the twin segments do not appear to be intergrown. Contact twins may be produced by either reflection or rotation. Twin segments that appear to be intergrown (**Figure 5.23**) are known as **penetration twins** and typically have irregular composition surfaces. Penetration twins are usually produced by rotation.

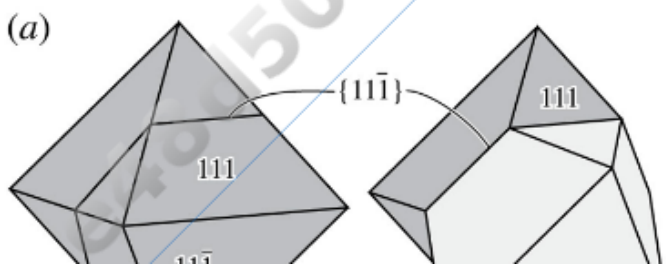

DO NOT COPY e48d507df5d1141@placeholder.94092

Printed by: e48d507df5d1141@placeholder.94092.edu. Printing is for personal, private use only. No part of this book may be reproduced or transmitted without publisher's prior permission. Violators will be prosecuted.

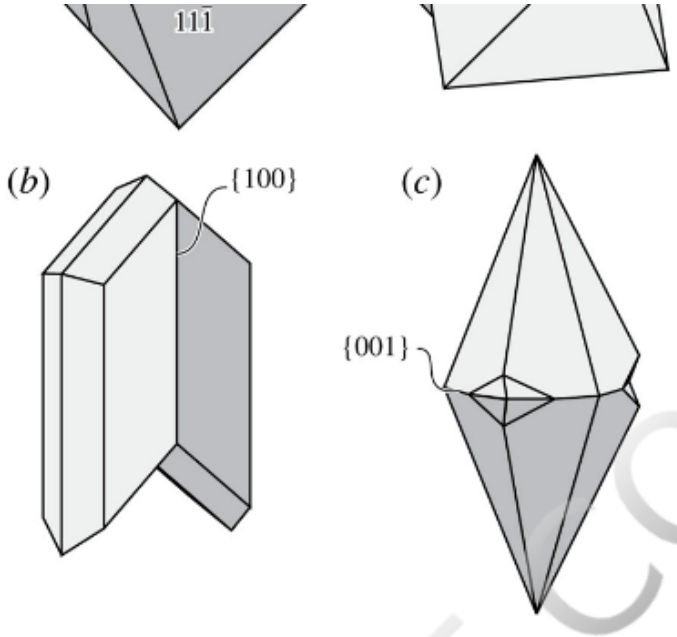

FIGURE 5.22 Contact twins. (*a*) Octahedron of spinel twinned by reflection on $\{11\,\bar{1}\}$ (spinel law). (*b*) Gypsum twinned by reflection on {100}. (*c*) Calcite twin with {001} composition plane. View larger image

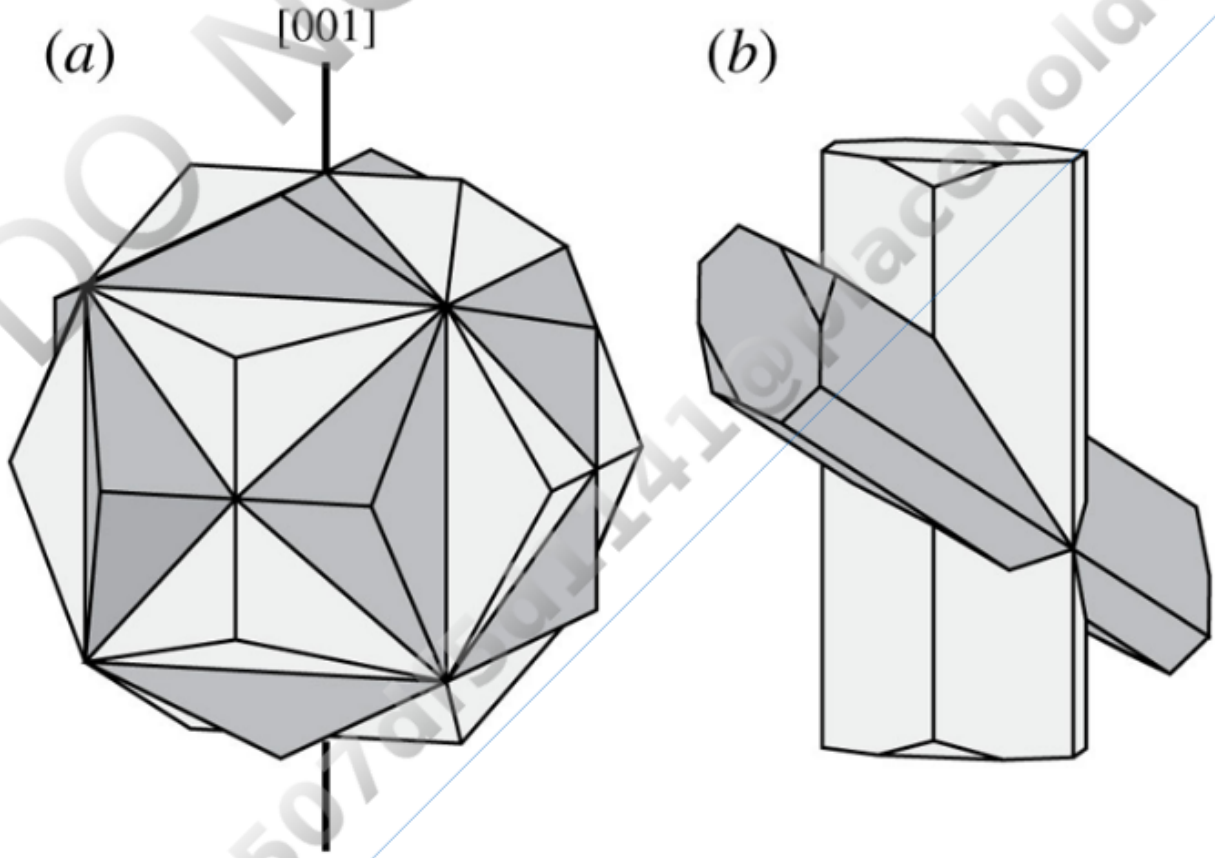

FIGURE 5.23 Penetration twins. (*a*) Pyrite "Iron Cross" twin by 90° rotation on [001]. (*b*) Staurolite twin by reflection on {231}. View larger image

Simple twins, such as those shown in Figures 5.21–5.23, are composed of just two twin segments. **Multiple twins**, however, are composed of three or more segments repeated

DO NOT COPY
e48d507df5d1141@placeholder.9409

Printed by: e48d507df5d1141@placeholder.94092.edu. Printing is for personal, private use only. No part of this book may be reproduced or transmitted without publisher's prior permission. Violators will be prosecuted.

segments. **Multiple twins**, however, are composed of three or more segments repeated by the same twin law. If the twin segments are joined on successive parallel composition planes, the result is the formation of **polysynthetic twins** (**Figure 5.24a**). Plagioclase is probably the most widely recognized mineral with polysynthetic twins. Plagioclase is triclinic, and twinning by reflection on {010} is repeated over and over, producing **lamellae**, or thin layers, in one orientation alternating with lamellae in the reflected orientation. The striations on plagioclase cleavage surfaces are produced by this twinning. If the successive composition surfaces are not parallel, a **cyclic twin** may result (**Figure 5.24b**) and can produce a twinned crystal that circles back on itself.

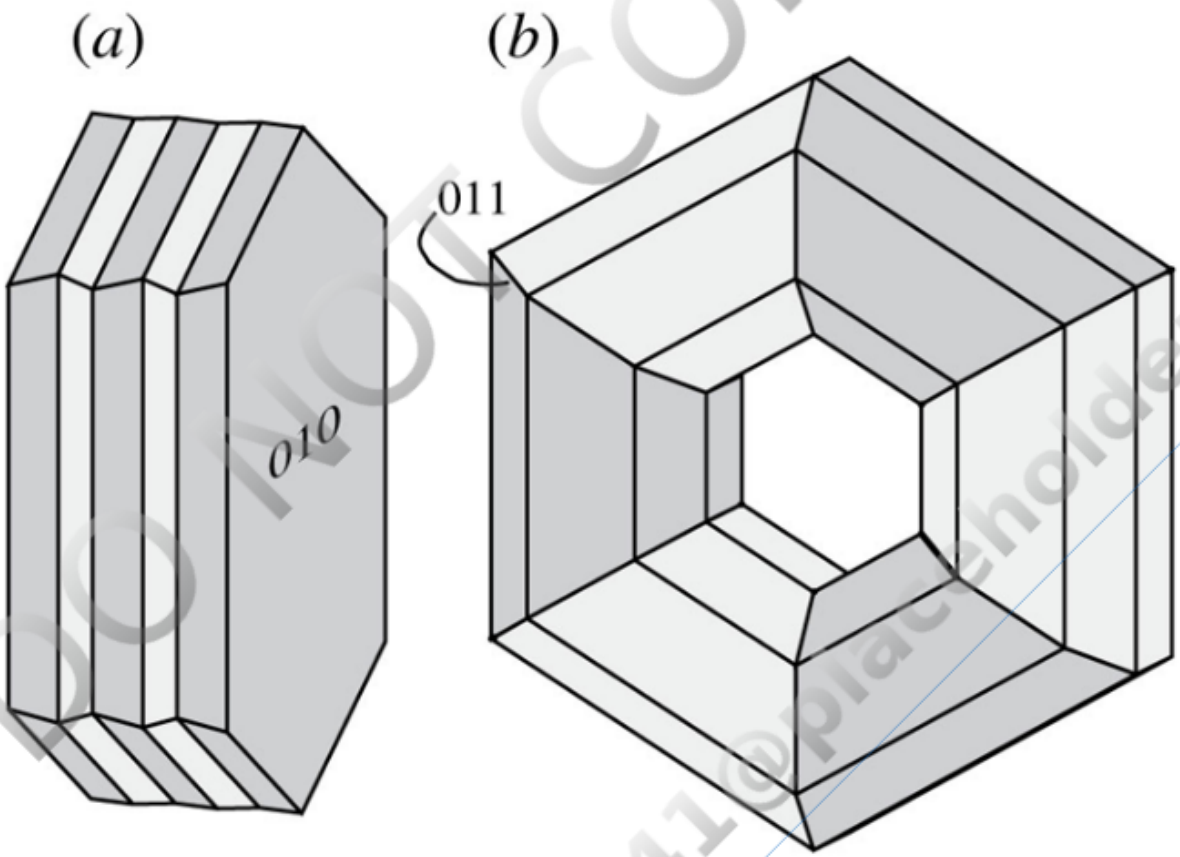

FIGURE 5.24 Multiple twins. (*a*) Polysynthetic twinning in plagioclase by repeated reflection on {010}. These twins are known as albite twins. (*b*) Cyclic twinning in rutile by repeated reflection on {011}. View larger image

Recognition of twinning, as opposed to random intergrowths of mineral grains and crystals, is not always easy. A pattern of angular embayments on crystal faces may indicate the presence of twinning, as does a systematic intergrowth pattern seen on multiple samples of the same mineral. Striations on cleavage surface may also indicate the presence of twinning. Different twin segments on the same crystal or mineral grain often can be recognized when a thin section of a mineral sample is examined with a petrographic microscope (see Chapter 7) because the different segments have different optical orientations.

Common types of twins in the different crystal systems are listed below. Certain twins in

DO NOT COPY e48d507df5d1141@placeholder.9409

Printed by: e48d507df5d1141@placeholder.94092.edu. Printing is for personal, private use only. No part of this book may be reproduced or transmitted without publisher's prior permission. Violators will be prosecuted.

Common types of twins in the different crystal systems are listed below. Certain twins in some minerals have been given names: for example, Carlsbad twins (Figure 5.21b) in the feldspars and spinel twins (Figure 5.22a) in the spinel group of minerals. These names usually apply only to the specific minerals from which they were derived.

TRICLINIC SYSTEM: There are few symmetry restrictions regarding twinning in triclinic minerals. Albite twins in plagioclase (Figure 5.24a) are an example.

MONOCLINIC SYSTEM: Twinning by reflection on the {001} and {100} planes is common, although just about any plane except {010} is possible. Because [010] is usually a 2-fold axis, twins on this axis are not found, but rotation on the *c* axis as in Carlsbad twins (Figure 5.21b) is possible.

ORTHORHOMBIC SYSTEM: Twins by reflection are common parallel to a prism face such as {110}.

TETRAGONAL SYSTEM: Typical twins involve reflection parallel to a pyramid face such as {011} producing elbow-shaped twinned crystals (Figure 5.21a).

HEXAGONAL SYSTEM: Twins by reflection parallel to one of the rhombohedral crystal face {101} or {111} are common. Twins by reflection on {001} or 2-fold rotation on {001} may be found in crystal classes with appropriate symmetry (Figure 5.22c).

ISOMETRIC SYSTEM: Twins by reflection on one of the octahedral faces are known as spinel twins because they are common in spinel (Figure 5.22a). Two-fold rotation on the [111] or [001] axes also may be found (Figure 5.23a).

The mechanisms by which twinned crystals may be produced include growth, phase transformation, and deformation.

Growth Twinning

There are many examples of penetration twins and contact twins that demonstrate twinning was established at, or soon after, the initiation of mineral growth because the twin segments are continuous all the way to the center of the crystal. The mechanisms that favor the growth of twinned crystals as opposed to untwinned crystals are poorly understood, but the systematic development of twins in some minerals suggests that the twinned geometry may represent a lower-energy configuration.

Transformation Twinning

Transformation twinning is produced as a consequence of a displacive polymorphic phase transition. The mineral leucite ($KAlSi_2O_6$), which is common in certain K-rich mafic lavas, displays transformation twinning. Leucite during growth in the lava typically forms trapezohedral crystals and crystallizes with isometric symmetry with a cubic unit cell (**Figure 5.25a**). When the temperature drops below about 665°C, the structure undergoes a displacive polymorphic transition to tetragonal symmetry with a change in unit cell dimensions.

DO NOT COPY e48d507df5d1141@placeholder.9409

Printed by: e48d507df5d1141@placeholder.94092.edu. Printing is for personal, private use only. No part of this book may be reproduced or transmitted without publisher's prior permission. Violators will be prosecuted.

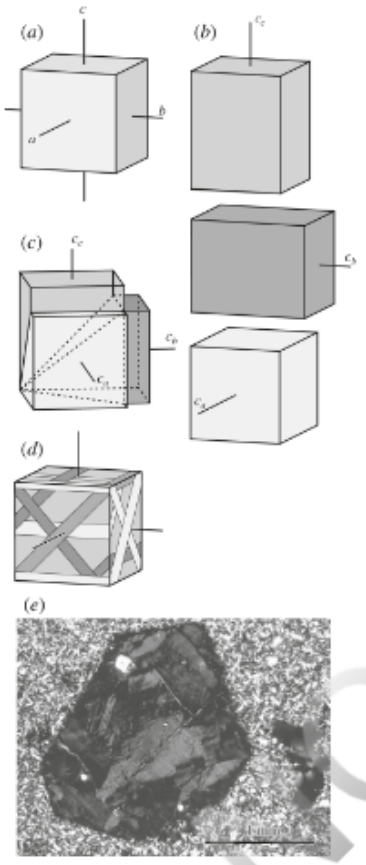

FIGURE 5.25 Transformation twinning in leucite. (*a*) The unit cell is isometric ($a = b = c$) at temperatures above 665°C. (*b*) Below 665°C the symmetry transforms to tetragonal ($a = b < c$). The tetragonal *c* axis could be parallel to either the *a*, *b*, or *c* axis (c_a, c_b, c_c) of the original crystal. When the transformation occurs, different parts of the crystal assume each of the three possible orientations. Dimensions are exaggerated. (*c*) The three orientations are related by reflection on the {101} dodecahedral faces. (*d*) Twinned crystals contain lamellae in each of the three different orientations. (*e*) Photomicrograph of a leucite phenocryst showing twin lamellae related to each other by reflection on {101}. View larger image

Because the three isometric *a*, *b*, and *c* axes are identical, there is an equal probability that any one of them will become the *c* axis of the tetragonal unit cell (**Figure 5.25b**). If the entire crystal transforms to a single tetragonal orientation, the crystal would change dimensions consistent with the new tetragonal unit cell. However, the crystal is constrained by the solid rock around it. To maintain the same external shape, different parts of the crystal convert to each of the three possible tetragonal *c* axis orientations (Figure 5.25b, c). The result are twin lamellae with each of the three different crystallographic orientations so that the dimensional changes average out, and the macroscopic shape of the crystal does not change (**Figure 5.25d**).

Deformation Twinning

Deformation twins can be produced in many minerals by the appropriate application of stress. In response to the stress, the crystal lattice is distorted to a new orientation by

Printed by: e48d507df5d1141@placeholder.94092.edu. Printing is for personal, private use only. No part of this book may be reproduced or transmitted without publisher's prior permission. Violators will be prosecuted.

stress. In response to the stress, the crystal lattice is distorted to a new orientation by coordinated displacement along successive planes (**Figure 5.26**). The process is sometimes referred to as a **glide**, and the crystallographic plane along which displacement occurs is a **glide plane**. Deformation twins are always mirror twins, and the glide plane is the mirror. Calcite is particularly easy to twin by deformation; samples may readily be twinned by the pressure of a knife blade on the edges of cleavage rhombs. Calcite in deformed rocks typically displays twin lamellae produced by glide on {102}.

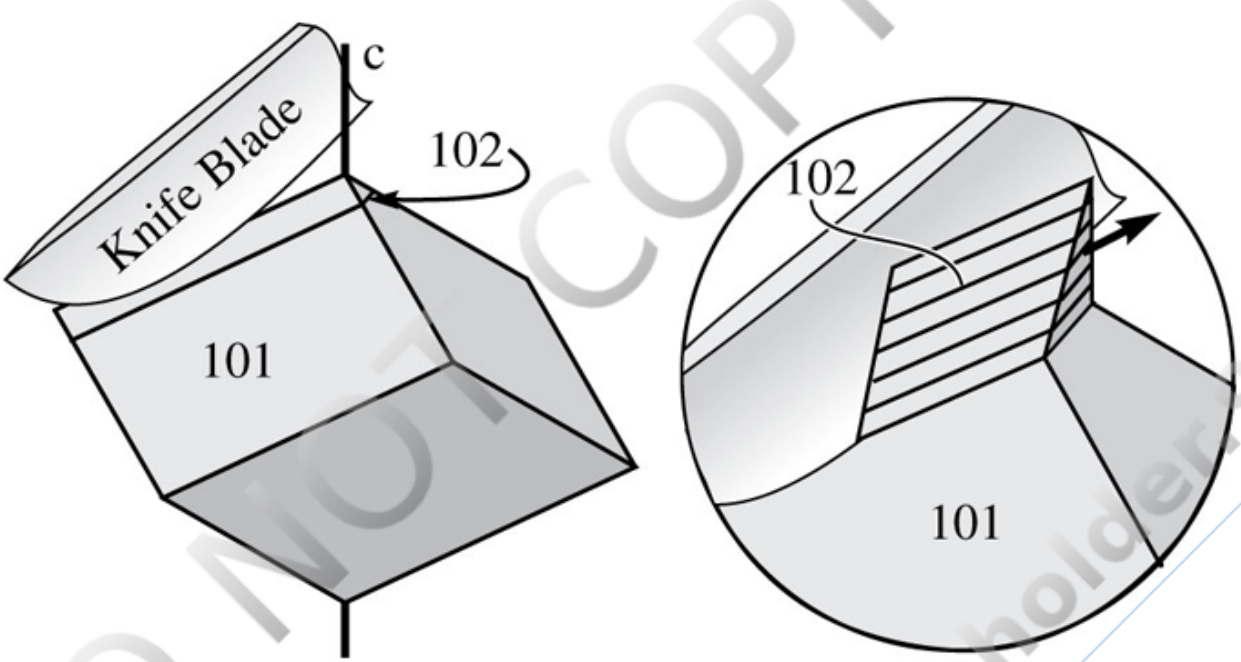

FIGURE 5.26 Deformation twinning in calcite can be produced by glide on {102} crystallographic planes. Such twinning could be artificially produced by deformation from a knife blade. View larger image

DO NOT COPY
e48d507df5d1141@placeholder.9409

Printed by: e48d507df5d1141@placeholder.94092.edu. Printing is for personal, private use only. No part of this book may be reproduced or transmitted without publisher's prior permission. Violators will be prosecuted.

Postcrystallization Processes

Once a mineral has crystallized, it may undergo a variety of changes in response to changing conditions and/or the passage of time. These changes include ordering, twinning, exsolution, recrystallization, and damage from radioactive decay.

Ordering

The concept of order–disorder in a crystal structure was discussed at some length in relation to order–disorder polymorphism in Chapter 4. Recall that in K-feldspar ($KAlSi_3O_8$), Al^{3+} and Si^{4+} are randomly distributed among tetrahedral sites at high temperature (Figure 4.13). At lower temperature, however, the Al^{3+} becomes preferentially segregated into one or two of the four available tetrahedral sites (see Chapter 4 for more detailed discussion). Ordering of Al^{3+} and Si^{4+} among the tetrahedral sites is accompanied by changes in unit cell dimension and, in some cases, symmetry. Many other minerals display order–disorder changes accompanied by unit cell changes, among them the pyroxenes and amphiboles in which Fe^{2+} and Mg^{2+} display varying degrees of ordering into octahedral sites.

Twinning

As described above, transformation twinning occurs in leucite (Figure 5.25) when it becomes polysynthetically twinned on {101} dodecahedral planes in its conversion from the high-temperature isometric symmetry to tetragonal symmetry at lower temperatures. Another example is the microcline polymorph of K-feldspar ($KAlSi_3O_8$) in slow cooling conditions developing polysynthetic twins in two directions when the symmetry changes from monoclinic to triclinic in response to $Al^{3+}-Si^{4+}$ ordering.

Recrystallization

As was previously discussed in relation to crystallization and mineral growth, the surface of a mineral represents a high-energy arrangement because the surface is charged as the continuous pattern of chemical bonds is disrupted. We therefore should anticipate that minerals will change or recrystallize in ways that minimize the total amount of surface area. In general, this can be accomplished in two ways: forming smoother grain boundaries and increasing grain size. Recrystallization in this way requires high-temperature conditions, which are commonly found during metamorphism and in igneous rocks shortly after crystallization.

DO NOT COPY e48d507df5d1141@placeholder.9409

Printed by: e48d507df5d1141@placeholder.94092.edu. Printing is for personal, private use only. No part of this book may be reproduced or transmitted without publisher's prior permission. Violators will be prosecuted.

rocks shortly after crystallization.

If the bounding surfaces between mineral grains in a rock are irregular, there is more surface area than if the boundary were smooth (**Figure 5.27a**). Hence, it is energetically advantageous to rearrange the atoms on grain boundaries to form a smooth boundary. Provided temperatures are high enough to allow diffusion, the atoms will migrate to remove protrusions and fill in embayments, resulting in smooth grain boundaries.

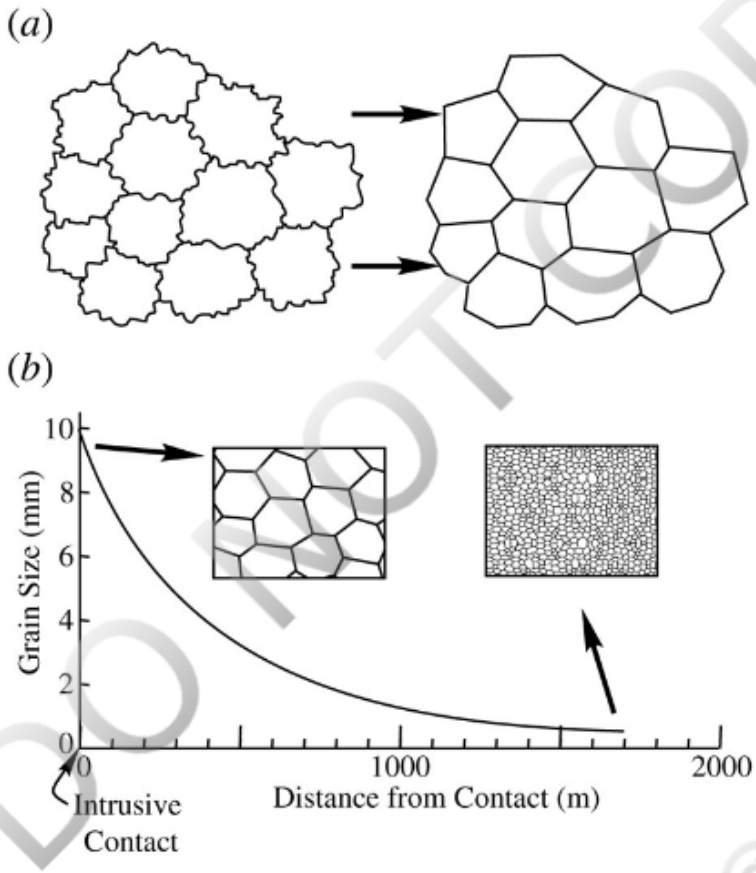

FIGURE 5.27 Recrystallization. (*a*) Recrystallization allows irregular grain boundaries to become smooth, reducing surface energy. (*b*) Average grain size of calcite in marble in a contact metamorphic aureole increases systematically toward the intrusion. Adapted from Grigor'ev (1965). Increase in grain size reduces mineral surface area and surface energy. View larger image

A rock with larger grains will have less grain boundary per unit volume than one with smaller grains. For example, total surface area of 1000 grains whose radius is 0.1 mm is 126 mm^2. If combined into a single grain whose radius is 1 mm, the surface area decreases to only 12.6 mm^2. Therefore, if the temperature is high enough, diffusion will allow some grains to grow larger by incorporating the atoms of neighboring grains of the same mineral into their structure. This removes the smallest grains. **Figure 5.27b** shows the distribution of grain size of calcite grains in marble that have been recrystallized in a contact metamorphic aureole, which is the region that experienced high temperatures due to close proximity to an igneous intrusion. Marble adjacent to the contact was subjected to higher temperature than areas at greater distances. The intrusion adjacent areas therefore had the most recrystallization and now has a much greater grain size and

DO NOT COPY e48d507df5d1141@placeholder.9409

Printed by: e48d507df5d1141@placeholder.94092.edu. Printing is for personal, private use only. No part of this book may be reproduced or transmitted without publisher's prior permission. Violators will be prosecuted.

was able to achieve a lower-energy configuration than the neighboring rock with a smaller grain size.

Other structural defects such as the screw and edge dislocations and the accompanying distortion of the crystal lattice around the dislocations described previously also represent a higher-energy configuration than if the lattice were defect-free. Again, provided that temperatures are sufficiently high, atoms will tend to rearrange themselves within the crystal lattice to remove these defects to obtain a lower-energy configuration.

Exsolution

Described in Chapter 4 are the conditions for solid solution, or substitution of one cation for another in a crystal structure. These include the requirement that the substitution must maintain electrical neutrality and that the sizes of the substituting cations must be similar. Recall that crystal structures at high temperatures are somewhat more accommodating of different-sized cations than at low temperatures. At lower temperatures, the range of possible substitution of different-sized cations is much reduced.

The alkali feldspars, whose crystallization was introduced in the section on phase diagrams earlier in this chapter (Figure 5.7), provide a good example of exsolution. The end-member compositions are albite ($NaAlSi_3O_8$) and K-feldspar ($KAlSi_3O_8$). At high temperatures, Na^+ and K^+ are readily substituted for each other, and solid solution may extend across the complete compositional range from albite to K-feldspar in the field below the solidus (Figure 5.7a). At lower temperatures a solvus is present because only limited amounts of K^+ may substitute for Na^+ in the albite structure, and vice versa in the K-feldspar structure. **Figure 5.28a** shows just the solvus at 1 kbar of water pressure. Crystallization from a melt takes place at a higher temperature at this pressure. As was described earlier, the solvus shows the temperature–composition field where two feldspars, albite and K-feldspar, represent the lowest-energy configuration. In the field outside the solvus, homogeneous alkali feldspar is the lowest-energy configuration.

(*a*) (*b*)

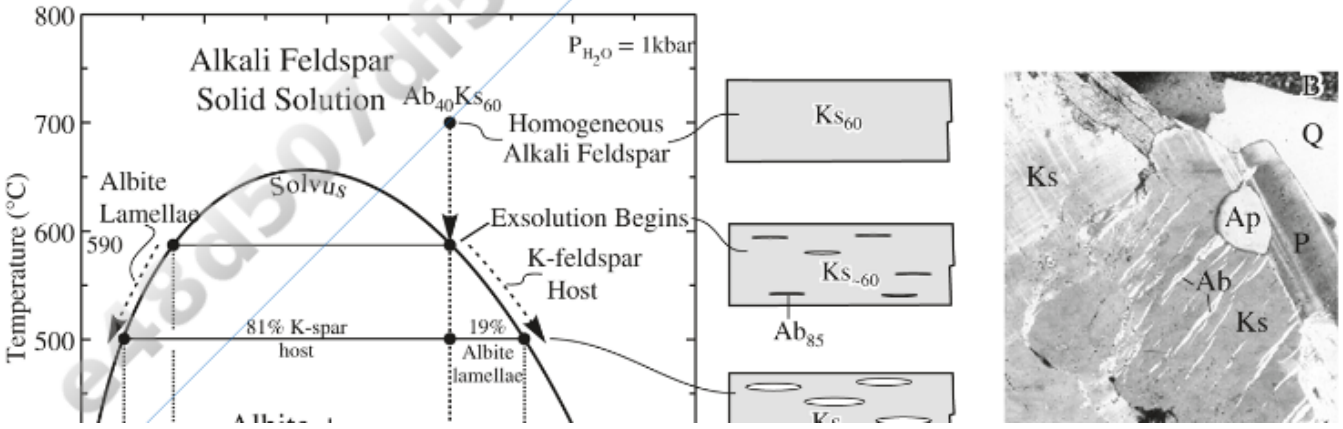

Printed by: e48d507df5d1141@placeholder.94092.edu. Printing is for personal, private use only. No part of this book may be reproduced or transmitted without publisher's prior permission. Violators will be prosecuted.

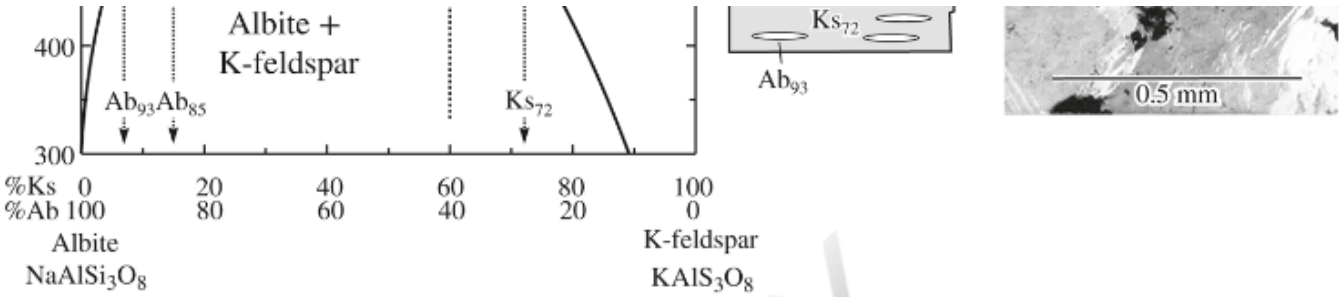

FIGURE 5.28 Exsolution in alkali feldspar. (*a*) The solvus for alkali feldspar. See text for discussion. Adapted from Smith and Parsons (1974). (*b*) Photomicrograph of a thin section of perthitic K-feldspar (Ks, center) with exsolution lamellae of albite (Ab) that extend NE–SW. Plagioclase (P), quartz (Q), apatite (Ap), and biotite (B) are also present. View larger image

Begin with an alkali feldspar that crystallized from a granitic magma and now is at 700°C. Its composition, $Ab_{40}Ks_{60}$ (40 percent Na, 60 percent K), is stable because it lies above the solvus. If this alkali feldspar is allowed to cool, the solvus will be reached at 590°C. Below that temperature, the alkali feldspar structure cannot accommodate all the Na^+. Provided time is available to allow for nucleation, domains of albite will crystallize and grow within the feldspar, which take up the excess Na^+. A tie-line at 590°C from one side of the solvus to the other shows the composition of albite ($Ab_{85}Ks_{15}$) in equilibrium with the K-feldspar. Because the structure of K-feldspar is essentially the same as that of albite, formation of albite domains within the K-feldspar requires only diffusion of Na^+ into those domains and migration of K^+ out. The albite typically forms irregular lamellae within the K-feldspar host (**Figure 5.28b**).

At lower temperatures, the amount of Na^+ allowed in the K-feldspar host progressively decreases, as does the amount of K^+ allowed in the albite. Hence, the albite-rich lamellae become larger and progressively more Na-rich, and the K-feldspar host becomes more K-rich as cooling progresses. At 500°C, the K-feldspar composition is $Ab_{28}Ks_{72}$ and the albite is $Ab_{93}Ks_7$. The relative amounts of K-feldspar host (81 percent) and albite lamellae (19 percent) are given by the lever rule (Figure 5.5).

Exsolution requires that ions migrate through the crystal structure; therefore the process is temperature and time dependent. If cooling is rapid, as with a volcanic rock or shallow intrusion, time may not be available to allow exsolution to progress to a significant degree. With slow cooling, as with deep-seated intrusions or regional metamorphism, albite exsolution lamellae within K-feldspar may be well developed.

Exsolution lamellae can range in size from microscopic to large enough to be visible in hand sample. K-feldspar with albite exsolution lamellae has a **perthitic texture**, and can be called **perthite**. Figure 5.28b is a photomicrograph of perthite. The terms **antiperthitic** or **antiperthite** are applied to an albite host with K-feldspar lamellae. **Mesoperthite** results when the feldspar composition before exsolution is intermediate between albite and K-feldspar such that after exsolution, host and lamellae are about the same proportion and cannot be distinguished.

DO NOT COPY e48d507df5d1141@placeholder.94092

Printed by: e48d507df5d1141@placeholder.94092.edu. Printing is for personal, private use only. No part of this book may be reproduced or transmitted without publisher's prior permission. Violators will be prosecuted.

Exsolution textures are common in other minerals, notably the pyroxenes (Chapter 14) and Fe–Ti oxides (Chapter 18).

Pseudomorphism

In addition to the other postcrystallization processes described here, one mineral may simply be replaced by another while preserving the external form of the original; this is called **pseudomorphism** (**Figure 5.29**). Goethite [FeO(OH)], for example, may pseudomorphically replace pyrite (FeS_2) crystals and retain the external shape of the original pyrite. This example would be called a goethite after pyrite pseudomorph. The secondary material in a pseudomorph may be either a single mineral or a collection of several minerals. **Paramorphs** result from polymorphic phase transformations in which the replacing mineral is a polymorph (same chemical composition) of the mineral being replaced.

FIGURE 5.29 Each dark feature is an aggregate of biotite grains in the shape of dodecahedrons. These biotite after garnet pseudomorphs formed when biotite replaced garnet as a result of metamorphic reactions. Rock thin sections reveal that in the cores of some biotite pseudomorphs some garnet is preserved. View larger image

Radioactivity and Minerals

Printed by: e48d507df5d1141@placeholder.94092.edu. Printing is for personal, private use only. No part of this book may be reproduced or transmitted without publisher's prior permission. Violators will be prosecuted.

Radioactive isotopes of elements are routinely incorporated into the crystal structure of many minerals, just as nonradioactive elements are. Some of the common or important radioisotopes are listed in **Table 5.1**. Of these, ^{40}K is the most abundant. It is found in all minerals containing potassium, such as K-feldspar, the micas, and some amphiboles. Radioactive isotopes of uranium and thorium are also widely distributed, though only infrequently are they abundant enough to form minerals with U or Th as major elements. In most cases, U and Th are found as minor constituents in minerals such as zircon ($ZrSiO_4$), where the U and Th substitute for Zr. ^{14}C is a common isotope found in biological material including the calcite, aragonite, and apatite that form the teeth, shells, and skeletal material of mollusks, vertebrates, and other animals. **Box 5.1** provides a brief introduction to the use of radioactive isotopes in radiometric dating.

TABLE 5.1 Selected Radioactive Isotopes Found in Common Minerals

Isotope	Ultimate Daughter Element(s)	Half-Life (years)
^{14}C	^{14}N	5730
^{40}K	^{40}Ar, ^{40}Ca	1.248×10^9
^{87}Rb	^{87}Sr	48.8×10^9
^{232}Th	^{208}Pb, ^{4}He	1.405×10^{10}
^{235}U	^{207}Pb, ^{4}He	7.038×10^8
^{238}U	^{206}Pb, ^{4}He	4.468×10^9

BOX 5.1
Radiometric Dating

Placing absolute time constraints on geologic events is called **geochronology**. There is a huge variety of geochronologic techniques, but most are based on the decay of an unstable (radioactive) parent isotope ultimately into a stable (daughter) product (Table 5.1); collectively these are **radiometric dating** techniques. Radiometric dating, when correctly applied to rocks and minerals, can constrain the timing of a wide variety of geologic events. Examples include when a rock formed, when a river cut a new canyon, when an asteroid impacted, or when two plates collided to form a mountain belt.

Historically, radiometric dating of whole rocks was typically done; this is no longer the preferred approach as single grains of particular minerals, or even zones within single grains, provide the best results. This is because contiguous crystalline material best ensures that two assumptions of radiometric dating are fulfilled. These include that no daughter is initially present and that parent and daughter have been neither added nor removed from the material dated except by radioactive decay. Because single grains of specific minerals are most widely used for radiometric dating, the first

DO NOT COPY e48d507df5d1141@placeholder.9409

Printed by: e48d507df5d1141@placeholder.94092.edu. Printing is for personal, private use only. No part of this book may be reproduced or transmitted without publisher's prior permission. Violators will be prosecuted.

step of radiometric dating most often is to crush a rock and separate its constituent minerals primarily by their density and magnetic characteristics. This isolates the specific minerals used for radiometric dating from each other and all other minerals contained in the rock. Chapter 10 covers the mineral separation process in more detail.

Let's first consider the mineral zircon ($ZrSiO_4$, Chapter 16), which often crystallizes from magma and is a common constituent of igneous rocks. Because of size and charge considerations, it is fairly easy for U and Th to substitute for Zr in zircon's crystal structure during growth, but Pb does not easily fit anywhere in the structure. This results in the zircon containing upward of 1 weight percent U and Th, while essentially no Pb (<1 ppm) is initially found in the zircon. Therefore, when the zircon is chemically or isotopically analyzed (Chapter 9), essentially all the Pb found originates from the decay of U and Th that were incorporated into the crystal when it formed. As the decay of each U and Th isotope to various isotopes of Pb occurs at a fixed and known rate (Table 5.1), it is possible to then determine how many years before the present the zircon crystallized from the magma, via the age equation

$$t = \frac{1}{\lambda} \ln\left(1 + \frac{D}{P}\right) \tag{5.9}$$

where t is years before present, ln is the natural log function, D/P is the ratio of the amount of a specific daughter isotope (D) to a specific parent (P) isotope, and λ is the decay constant of the specific parent–daughter isotope pair. The decay constant is related to the half-life ($t_{1/2}$) by the equation

$$\lambda = \frac{\ln 2}{t_{1/2}}. \tag{5.10}$$

It is possible to date zircon using three different parent–daughter pairs (Table 5.1): ^{238}U–^{206}Pb, ^{235}U–^{207}Pb, and ^{232}Th–^{208}Pb, but typically the two U–Pb parent–daughter pairs are focused on and are collectively called **U-Pb radiometric dating**. For U-bearing minerals such as zircon, calculating a date by two different parent–daughter pairs allows the assumption that no parent or daughter have been added or removed except by radioactive decay to be tested and corrected for if false. The small amounts of Pb incorporated at the time of crystallization can be corrected for as well by analysis of other Pb isotopes (^{204}Pb) not produced by radioactive decay.

Isotopic analysis and calculation of particular D/P ratios in zircon or other minerals can be done by a variety of instruments discussed in Chapter 9, including thermal ionization mass spectrometers, secondary ion mass spectrometers, or laser ablation inductively coupled plasma-mass spectrometers. The latter two have the ability to date small portions of grains, useful when a grain experiences multiple igneous and metamorphic cycles resulting in many domains or zones with different ages (**Figure**

DO NOT COPY e48d507df5d1141@placeholder.9409

Printed by: e48d507df5d1141@placeholder.94092.edu. Printing is for personal, private use only. No part of this book may be reproduced or transmitted without publisher's prior permission. Violators will be prosecuted.

metamorphic cycles resulting in many domains or zones with different ages (**Figure 5.30**).

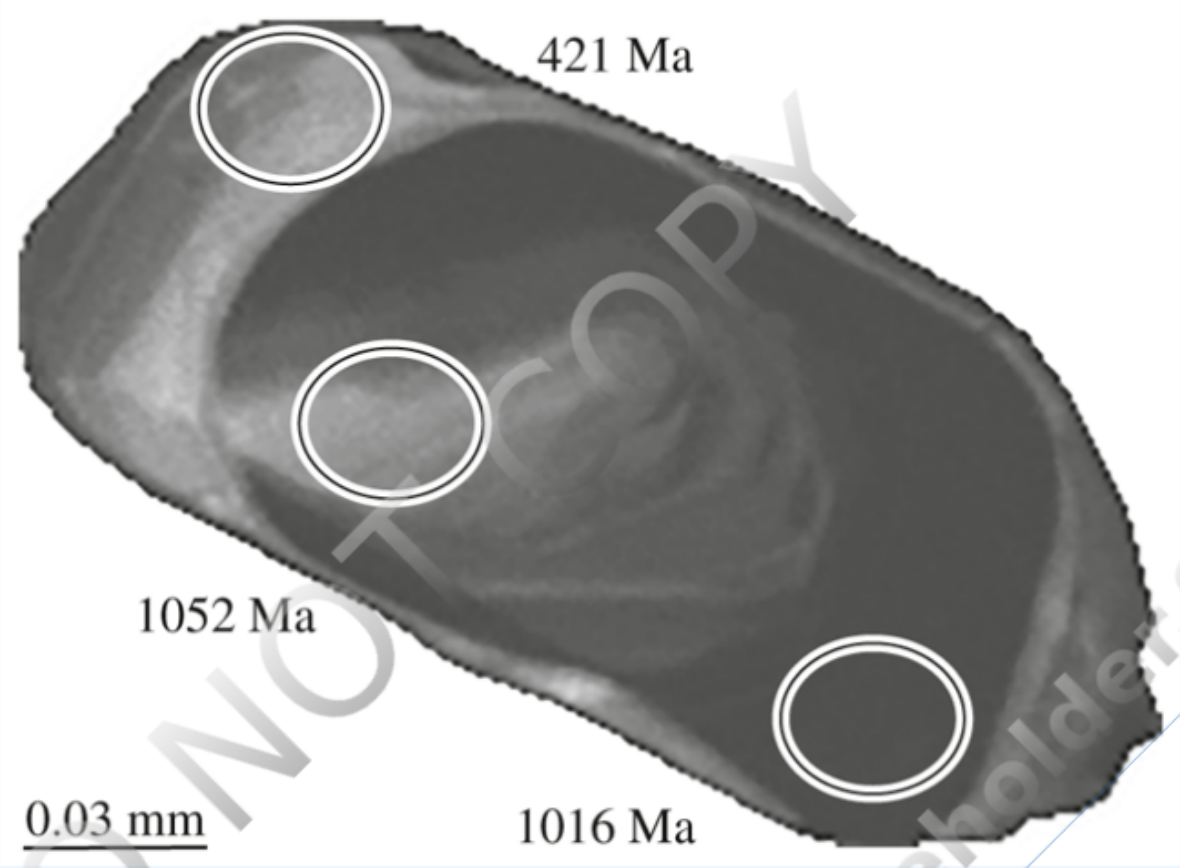

FIGURE 5.30 Cross section through a zircon crystal imaged with cathodoluminescence to highlight chemical zoning (Chapter 9). Ellipses represent spots dated by U-Pb isotopic analysis by a secondary ion mass spectrometer; the age of each spot is provided. An interpretation based on zoning characteristics is that crystallization from a magma at about 1052 Ma (millions of years before present) produced the core of the zircon, metamorphism at about 1016 Ma resulted in additional zircon growth, and lastly, the zircon grain again was placed in a crystallizing magma resulting in the growth of the rim at about 421 Ma. View larger image

Depending on the specific technique, 5 to 50 analyses of zircon grains or zones of the same age from the same rock are averaged to determine the age of a geologic event. Ideally, it is possible to constrain the age of zircon crystallization from a magma with an uncertainty of less than 1 percent. For example, for a 10-million-year-old zircon, the uncertainty regarding the accuracy of the age will be within 0.1 million years of the calculated date. For this example, the true age will fall between 9.9 and 10.1 million years old. All radiometric dates are reported with the uncertainty; in this case, as 10 ± 0.1 Ma (Ma = megaannum = millions of years before present).

Evidence from the region, outcrop, hand sample, and the zircon itself allows the conclusion that the date of zircon crystallization is the age of crystallization of the igneous rock in which it is contained. Zircon may also crystallize during metamorphism and thus provides a means to date when metamorphic events affected rocks and regions.

Though zircon is the most common mineral to be dated in this way, it is not the

Printed by: e48d507df5d1141@placeholder.94092.edu. Printing is for personal, private use only. No part of this book may be reproduced or transmitted without publisher's prior permission. Violators will be prosecuted.

Though zircon is the most common mineral to be dated in this way, it is not the only mineral that takes up U and Th and excludes Pb upon crystallization such that they can be radiometrically dated through isotopic analysis. Other minerals that can be dated this way include apatite, monazite (Chapter 17), and titanite (Chapter 16).

Many rocks contain datable minerals in at least trace quantities, but dating all of them frequently results in different ages. Often this happens because at high temperature Pb escapes from the mineral through diffusion. So as long as the mineral is above a certain temperature, no daughter is retained. The temperature below which diffusion is slow enough that the daughter is retained is called the **closure temperature**. The closure temperature is different for different minerals and isotopic systems (**Table 5.2**). For example, zircon retains Pb at temperatures below about 920°C; given that crystallization from magma and metamorphism occurs well below 920°C (typically below 700°C), every U–Pb date obtained from zircon is the age of its crystallization, be it from a magma or from metamorphism. Apatite is different; it has a closure temperature of about 420°C, so if apatite crystallizes from a magma at about 650°C, which is typical for felsic magmas, Pb is not retained until the temperature of the apatite grain (and the rock that houses it) drops below 440°C. Therefore, the U–Pb date obtained from the apatite in this scenario will be the time when it cooled through its closure temperature. Note that because of closure temperature considerations, the U–Pb date provided by apatite in this scenario will be younger than that provided by the zircon found in the same rock. Radiometric dating techniques that provide the timing of cooling are the basis for **thermochronology**, which studies the timing of cooling.

TABLE 5.2 Approximate Closure and Annealing Temperatures (°C) of Some Minerals and Isotopic Systems[a]

Mineral	U–Pb or Th–Pb	$^{40}Ar/^{39}Ar$	Fission Track	(U–Th)/He
Monazite	970		40	190
Zircon	920		320	160
Titanite	600		300	200
Apatite	420		100	50
Hornblende		520		
Muscovite		350		
Biotite		300		
K-feldspar		220		

[a] Temperatures estimated from Figure 5.18 of Reiners and others (2018) based on a 1°C/Ma cooling rate, except for the annealing temperature of monazite fission tracks (Jones et al., 2021) and titanite fission tracks (Coyle and Wagner, 1998), and the $^{40}Ar/^{39}Ar$ biotite closure temperature (Harrison and others, 1985).

Another widely used radiometric dating technique is the **$^{40}Ar/^{39}Ar$ radiometric**

Printed by: e48d507df5d1141@placeholder.94092.edu. Printing is for personal, private use only. No part of this book may be reproduced or transmitted without publisher's prior permission. Violators will be prosecuted.

Another widely used radiometric dating technique is the **$^{40}Ar/^{39}Ar$ radiometric dating** technique. It is based on the breakdown of ^{40}K to ^{40}Ar (Equations 5.7 and 5.8 above; Table 5.1). But because of the extreme difference in chemical behavior of K (an alkali metal) and Ar (a noble gas), it is not easy to analyze both isotopes in such a way as to provide a highly accurate measure of the D/P ratio needed for the age equation (Equation 5.9). Instead some of the common, nonradioactive ^{39}K in the mineral is converted to ^{39}Ar through neutron irradiation in a nuclear reactor. As the ratio of ^{40}K to ^{39}K is fixed and the irradiation process is highly controlled, the sample's ^{40}K content can be precisely known based on its ^{39}Ar content after irradiation. The $^{40}Ar/^{39}Ar$ ratio then can serve as the D/P ratio in a modified age equation. Measurement of two isotopes of Ar is substantially easier than measuring an isotope of K relative to an isotope of Ar. $^{40}Ar/^{39}Ar$ analysis can be done on portions of single grains or on multiple grains of a particular K-bearing mineral. Following irradiation, grains are heated by a laser to release the Ar, which is isotopically analyzed by a mass spectrometer.

The most common K-bearing minerals used for the $^{40}Ar/^{39}Ar$ technique include K-feldspar (Chapter 12), biotite, muscovite (Chapter 13), and hornblende (Chapter 14). Because Ar is a gas, it can escape at fairly low geologic temperatures, so the closure temperature for these minerals is generally lower than that for minerals dated by the U–Pb or Th–Pb technique (Table 5.2). Therefore, most $^{40}Ar/^{39}Ar$ dates provide the time when the mineral cooled through its closure temperature, not when the mineral crystallized.

The buildup of ^{4}He or alpha particles in minerals through alpha decay of primarily U and Th (Equation 5.5, for example; Table 5.1) is used as the basis for **(U-Th)/He radiometric dating**. Relatively low geologic temperatures allows He to escape from U- and Th-bearing minerals, so the closure temperature below which He is retained is generally 200°C or lower, depending on the mineral (Table 5.2). Therefore, all forms of (U–Th)/He dating are considered thermochronology, and they are widely utilized, for example, in understanding landscape development and modification through erosion and recent faulting.

Zircon and apatite are most widely used for (U–Th)/He thermochronology, and analysis of either typically begins with heating one or more grains with a laser, which allows the stored He to escape. The collected He is directed to a mass spectrometer for analysis. The same grain(s) are then dissolved in acid and the solution is analyzed by an inductively coupled plasma-mass spectrometer for multiple isotopes, including those of U and Th. The results of both analyses can be combined and applied to a specialized form of the age equation to determine the age of cooling of the respective mineral through its closure temperature.

Any U-bearing mineral will accumulate fission tracks when ^{238}U decays by fission. If the temperature of the mineral is sufficiently high, the damaged portion of the crystal structure will be repaired as atoms migrate back to their proper crystallographic positions through diffusion. At temperatures below the **annealing temperature** (analogous to closure temperature), however, the crystal structure is not repaired and the disrupted trails are preserved. The abundance of the fission

Printed by: e48d507df5d1141@placeholder.94092.edu. Printing is for personal, private use only. No part of this book may be reproduced or transmitted without publisher's prior permission. Violators will be prosecuted.

not repaired and the disrupted trails are preserved. The abundance of the fission tracks serves as the daughter in a specialized form of the age equation, as the number of tracks depends on both the amount of ^{238}U and how long the mineral has been below its annealing temperature. **Fission track dating** of minerals, most commonly of zircon and apatite, is based on the careful counting of etched tracks relative to the amount of ^{238}U in the grain (**Figure 5.31**). For apatite, etching is commonly done with six molar nitric acid at 20°C for about 20 seconds. The acid preferentially dissolves the disrupted crystal structure along the fission track, leaving a tube a few microns across and a maximum of 10–15 microns long that is visible with a transmitted-light microscope. Different minerals have different annealing temperatures (Table 5.2), and in general, annealing temperatures on average fall between the closure temperatures of commonly used minerals for the $^{40}Ar/^{39}Ar$ and (U–Th)/He techniques. Fission track thermochronology is similarly useful as the (U–Th)/He technique for understanding landscape uplift and erosion in tectonically active areas.

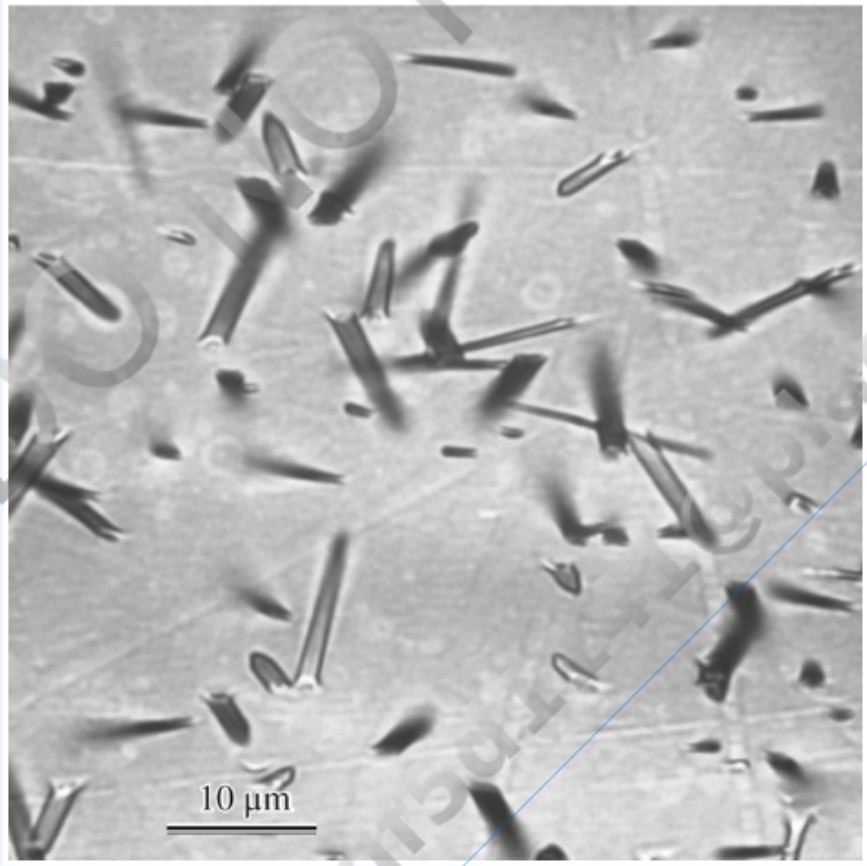

FIGURE 5.31 Transmitted-light image of etched fission tracks in apatite. The fission tracks are the randomly oriented dark features. The appearance of each fission track is controlled by its length and orientation relative to the polished grain surface. Short tracks or tracks nearly perpendicular to the surface appear as relatively small elliptical shapes; long tracks and tracks more parallel to the surface are elongate and may have a lighter central region. Image courtesy of Andrew Gleadow, University of Melbourne, Australia. View larger image

Probably the most widely referred to radiometric dating technique in popular culture

Printed by: e48d507df5d1141@placeholder.94092.edu. Printing is for personal, private use only. No part of this book may be reproduced or transmitted without publisher's prior permission. Violators will be prosecuted.

is the **^{14}C radiometric dating** technique, also called **radiocarbon dating**, but it can only be used in very specific situations. Unlike radioactive K, U, and Th isotopes, all of which were part of the material from which the Earth formed, ^{14}C is produced in the atmosphere through interactions between cosmic rays and predominantly atmospheric nitrogen. The created ^{14}C becomes part of some atmospheric CO_2, and through photosynthesis, the ^{14}C can be incorporated into carbon-bearing biological material (bones or plant material, etc.), or organisms can use some ^{14}C-bearing CO_2 to grow their calcite-based ($CaCO_3$) shells. However, ^{14}C decays relatively quickly (Table 5.1), so it is not preserved in significant amounts in these materials much older than 50,000 years. The importance of the ^{14}C dating for placing age constraints on recent geologic events or events associated with recent human history is clear, but other techniques discussed above are much more useful for most research questions requiring geochronological constraints.

Often multiple radiometric dating techniques are used to answer specific research questions regarding the timing of one or more geologic events that affected a region. All types of radiometric dating are more complex beyond the overview discussed above, and a comprehensive coverage of these and other radiometric dating techniques is found in, for example, Reiners and others (2018).

Any radioactive isotope, called the **parent** atom, will eventually **decay**, or break down, to a new atom of a different isotope or element, which is called the **daughter** atom. The decay processes include alpha decay, beta decay, positron decay, electron-capture decay, and fission. The rate of decay can be described in terms of the **half-life**, that is, the time it takes one-half of the parent atoms to decay to daughter atoms. The half-life is a fixed rate for a particular parent–daughter pair and cannot be changed by any natural geologic process (Table 5.1).

Decay Processes

In **alpha decay**, an alpha particle (α) is ejected from the nucleus of the parent atom, along with the emission of gamma (γ) rays and the release of heat. An alpha particle consists of two protons and two neutrons; it is the nucleus of a helium atom (^{4}He). Decay of the parent, therefore, produces a daughter atom whose atomic number (Z) is two less than the parent, because two protons are lost. The atomic mass number of the daughter is reduced by four because two neutrons also are lost. A typical decay is as follows.

$$^{238}_{92}\mathrm{U} \rightarrow {}^{234}_{90}\mathrm{Th} + \alpha + \gamma + \mathrm{heat} \qquad \textbf{(5.5)}$$

Ultimately the thorium will eventually decay through a series of additional steps to form $^{206}_{82}$Pb. This is one decay series utilized in multiple radiometric dating techniques (Box 5.1).

DO NOT COPY e48d507df5d1141@placeholder.9409

Printed by: e48d507df5d1141@placeholder.94092.edu. Printing is for personal, private use only. No part of this book may be reproduced or transmitted without publisher's prior permission. Violators will be prosecuted.

Beta decay is the breakdown of a neutron into a proton and an electron. The electron, or beta particle (β^-), is ejected from the nucleus along with a particle called an antineutrino ($\overline{v}$), whose mass is essentially zero. The net result is that the daughter will have an atomic number that is one larger than the parent's, but it will have the same atomic mass number because the total number of neutrons and protons have not changed. A beta decay of geological importance is as follows.

$$^{87}_{37}\text{Rb} \rightarrow {}^{87}_{38}\text{Sr} + \beta^- + \overline{v} + \text{heat} \quad \textbf{(5.6)}$$

This decay provides the basis for the Rb–Sr radiometric dating method, which is occasionally used, but other techniques are often preferred as they give better results (see Box 5.1).

Positron decay is closely related to beta decay and involves breakdown of a proton into a neutron with emission of a positron (β^+) and a neutrino. A positron is a particle like an electron but with a positive charge. The net result for the daughter is that the atomic number is one less than the parent, but atomic mass number remains the same. A small amount (~0.001 percent) of $^{40}_{19}\text{K}$ decays by positron decay to form $^{40}_{18}\text{Ar}$ as follows.

$$^{40}_{19}\text{K} \rightarrow {}^{40}_{18}\text{Ar} + \beta^+ + \overline{v} + \text{heat} \quad \textbf{(5.7)}$$

Electron capture (ec) involves capture of an electron by the nucleus so that a proton is converted to a neutron. The daughter therefore has an atomic number that is one less than the parent with no change in the atomic mass number.

$$^{40}_{19}\text{K} + \text{ec} \rightarrow {}^{40}_{18}\text{Ar} + \text{heat} \quad \textbf{(5.8)}$$

About 11 percent of $^{40}_{19}\text{K}$ decays to $^{40}_{18}\text{Ar}$ to provide the basis for the K–Ar and related $^{40}\text{Ar}/^{39}\text{Ar}$ radiometric dating techniques (see Box 5.1). The remaining ~89 percent of $^{40}_{19}\text{K}$ decays by beta decay to form $^{40}_{20}\text{Ca}$. $^{40}_{20}\text{Ca}$ is the most abundant isotope of Ca, which precludes it from serving as an effective daughter in any radiometric dating technique.

An additional decay mechanism, called **fission**, can occur predominantly with ^{238}U. This heavy nucleus occasionally will decay by spontaneously splitting, or fissioning, into two nuclei of approximately equal mass. As a consequence of the fission, a large amount of energy is released and the new nuclei fly apart at high velocity, tearing through and disrupting the crystal lattice of the host mineral. These disrupted trails, called **fission tracks**, may be observed under the microscope after a polished mineral surface has been etched with acid. Fission tracks can be used to provide time constraints on geologic events in a technique called fission track dating (see Box 5.1).

DO NOT COPY e48d507df5d1141@placeholder.9409

Printed by: e48d507df5d1141@placeholder.94092.edu. Printing is for personal, private use only. No part of this book may be reproduced or transmitted without publisher's prior permission. Violators will be prosecuted.

Radioactive Decay and Mineral Structure

One way in which radioactive decay influences minerals is that new elements are formed. In many cases, the daughter element is not the same size as the parent, nor does it have the same oxidation state. The decay of ^{40}K, for example, produces both ^{40}Ar and ^{40}Ca. In neither case is the daughter element of the same size, nor does it have the same oxidation state as the original ^{40}K; but both elements occupy structural sites that originally contained the parent ^{40}K. The ^{40}Ar is an inert gas that does not chemically bond with other elements, and its atomic radius is about 1.96 Å. The ^{40}Ca is divalent and has an ionic radius that is significantly smaller than that of K^+ in equivalent coordination (Figure 3.16). The ^{40}Ar and ^{40}Ca in the K sites are substitution defects (Figure 5.16d). Only if the temperature is high enough and sufficient time is available will either element diffuse out of the crystal.

Alpha decay has an additional structural consequence. The alpha particle, which has an atomic mass of four, is propelled at high velocity away from the decaying nucleus for distances up to about 10,000 nm (0.1 mm). Much of its energy is expended in ionizing the matter through which it passes, but as it nears the end of its trajectory, it typically dislodges several hundred atoms to form Frenkel defects (Figure 5.16b). The decayed atom also recoils for distances up to 10 nm and may dislodge its neighboring atoms, producing a small volume of disrupted crystal structure within a few atoms of the original site.

A mineral, such as zircon, that contains significant amounts of U and Th, both of which decay by alpha particle emission, can experience over 10^{15} alpha decay events per cubic centimeter over a period of several hundred million years. The result may be that the entire crystal structure of the zircon is completely disrupted. Minerals whose structures have been thoroughly disrupted by alpha decay are considered **metamict**. They do not possess long-range crystallographic order and, for all practical purposes, are glasses (amorphous). Heating to sufficiently high temperatures may allow a metamict mineral to anneal and reacquire its original crystal structure.

Metamict and partially metamict minerals may be recognized because, by comparison to unaltered minerals, their density is lower, their color may be darker, and they may be less hard. Index of refraction and other optical properties also may be influenced (see Chapter 7). Most importantly, metamict minerals do not yield characteristic X-ray diffraction peaks (see Chapter 8) because they lack long-range order. The accumulation of structural defects in the steel components of nuclear reactors from alpha (and other) radiation is also known to cause the metal to become more brittle.

Because alpha particles may travel for up to about 0.1 mm within crystalline solids, they can easily travel from the host of the radioactive element into neighboring grains. If the radioactive-element-bearing mineral, such as a zircon, is an inclusion in a mineral particularly susceptible to alpha damage, such as biotite, the result is a halo of disrupted structure around the inclusion. These radioactively disrupted zones are often visible in a

DO NOT COPY e48d507df5d1141@placeholder.9409

Printed by: e48d507df5d1141@placeholder.94092.edu. Printing is for personal, private use only. No part of this book may be reproduced or transmitted without publisher's prior permission. Violators will be prosecuted.

structure around the inclusion. These radioactively disrupted zones are often visible in a thin section when examined with a petrographic microscope (see Chapter 7) and are known as **pleochroic halos**, radiohalos, or radiation damage halos (**Figure 5.32**).

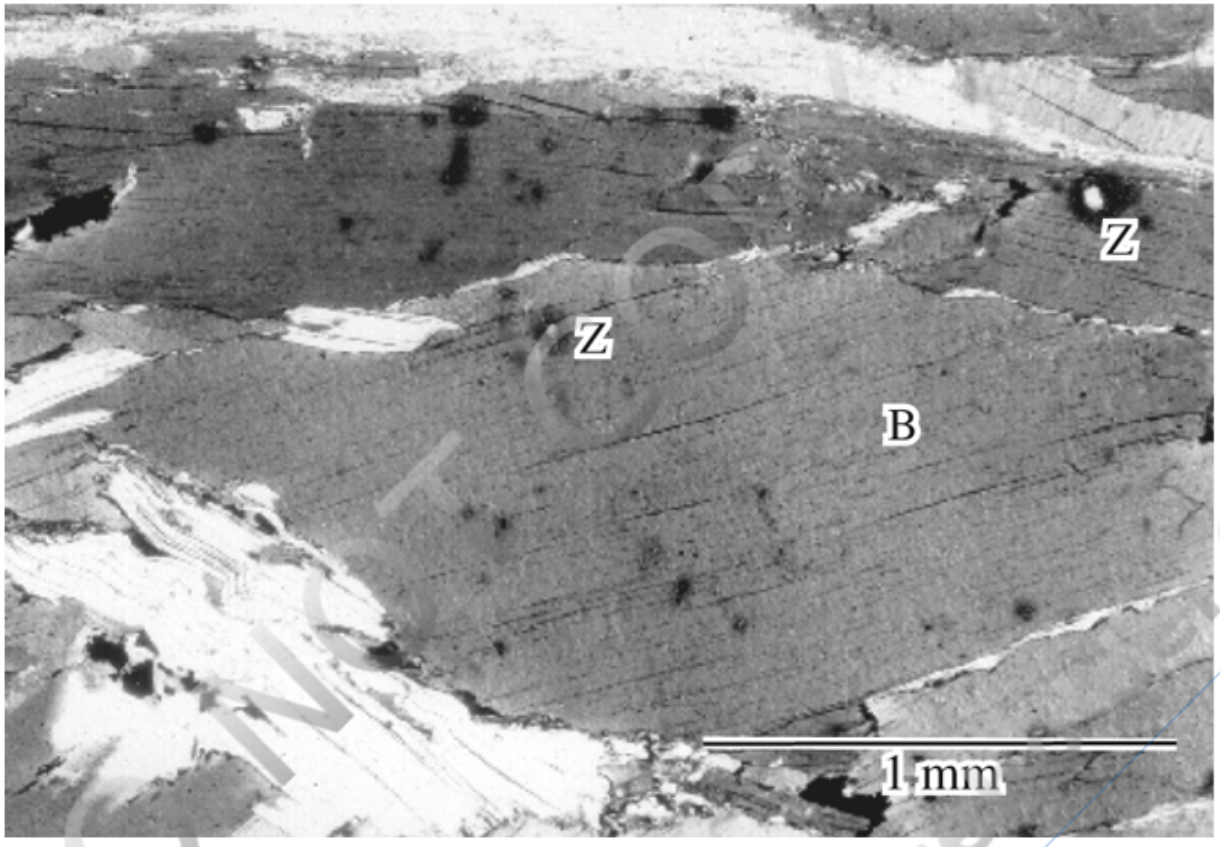

FIGURE 5.32 Photomicrograph of a thin section of mica schist showing dark pleochroic halos around radioactive zircon (Z) inclusions in biotite (B). View larger image

DO NOT COPY
e48d507df5d1141@placeholder.9409

Printed by: e48d507df5d1141@placeholder.94092.edu. Printing is for personal, private use only. No part of this book may be reproduced or transmitted without publisher's prior permission. Violators will be prosecuted.

Mineral Evolution

The suite of minerals that form the solid Earth, and particularly the minerals at or near the Earth's surface, has changed through time because the Earth itself has changed through time. Uniformitarianism and the Earth's various cycles (rock cycle, hydrologic cycle, etc.), which are routinely taught as part of introductory geology courses, can leave the impression that the Earth as we see it now is basically the same as it has always been. Although many basic Earth processes generally operate the same way since its formation at about 4.55 Ga (Ga = gigaannum = billions of years before present), it has progressively cooled. The cooling, coupled with the development of life in the Archean (~4.0–2.5 Ga), which has continuously evolved, means that the composition and rate of processes affecting the crust, sediment, water, and the atmosphere have progressively changed through time. At some point in the distant future, the Earth will have cooled enough that plate tectonics as we know it will cease to operate and another tectonic paradigm will take over. Currently, humans have drastically changed ocean and atmospheric chemistry at rates typically only associated with catastrophic events such as eruptions of supervolcanoes or meteorite impact events.

From the perspective of minerals, Earth's history can be divided into three major time periods: planetary accretion (>4.55 Ga), crust and mantle reworking (4.55–2.5 Ga), and biologically mediated mineralogy (<2.5 Ga) (Hazen and Ferry, 2010; Hazen and others, 2008). As geochemical conditions changed during these time periods, environmental conditions favor formation of some minerals over others.

During planetary accretion, the mineralogy of the primordial material that accumulated to form the Earth is probably represented by chondritic meteorites that contain olivine (Chapter 16) and pyroxene (Chapter 14), as well as a variety of less abundant minerals and carbonaceous material. Some of these minor minerals are known only from meteorites because the chemical and physical conditions needed for their formation are not found on Earth. The accumulation of chondritic material into asteroids and planetesimals changed the chemical and physical environment of the chondritic material. Chemical reactions then created new and different minerals. For the Earth, the accumulation of material was sufficient to initiate melting, and the Earth segregated into its crust, mantle, and core. Meteorites that document this melting and segregation consist of olivine crystals in an iron–nickel matrix and are called pallasites. The early crust likely was repeatedly destroyed by major impacts and then reformed. One particular impact at around 4.55 Ga separated the moon from the Earth and may have left large portions of the Earth as vast oceans of basaltic magma. Crystallization of this magma probably followed the order of Bowen's Reaction Series (see Box 11.1), with some minerals floating while others sank, so it is possible to make reasonable guesses regarding the mineralogy of the early crust, none of which survives today.

DO NOT COPY e48d507df5d1141@placeholder.94092

Printed by: e48d507df5d1141@placeholder.94092.edu. Printing is for personal, private use only. No part of this book may be reproduced or transmitted without publisher's prior permission. Violators will be prosecuted.

The next stage of crust and mantle reworking is still occurring and mostly involves melting, magmatic differentiation and fractional crystallization, volcanism, metamorphism, weathering, erosion, deposition, and lithification processes that produce and modify both oceanic and continental crust. The oceans probably were developed by 4.3 Ga, and their presence has been critical to many of the processes of crust and mantle reworking. The presence of water allowed the formation of hydroxide, hydrate, carbonate, and evaporite minerals. The generation of granitic rocks, necessary for the formation of continental crust, probably began prior to about 4.0 Ga, driven by the melting of wet basaltic crustal rocks. This process represents a substantial segregation of silicon-rich material into the Earth's crust and allowed for the production of quartz, K-feldspar, plagioclase, micas, amphiboles, and other minerals in large volumes for the first time.

The origin of life itself seems to be intimately tied to minerals in ways that remain poorly understood (see, e.g., Hazen, 2005). Both minerals and proteins and other biologic building blocks have a regular and repeating structure. The ability of mineral surfaces to adsorb and organize organic molecules may have provided one of the critical early steps in the emergence of life. Regardless, the development of life on Earth has profoundly affected the Earth's mineralogy. Hazen and Ferry (2010) argue that two-thirds of all known Earth minerals owe their existence to the environmental changes caused by life. When life first developed sometime between 3.5 and 4 Ga, the atmosphere was anoxic (no free oxygen) and may have consisted of gases similar to those emitted by modern volcanoes (including H_2O, CO_2, SO_2, CO, S_2, Cl_2, N_2, and H_2) plus ammonia (NH_3) and methane (CH_4). The earliest life appears to have included bacteria that utilized photosynthesis and released O_2 into the atmosphere as a waste product.

It took more than a billion years for bacterially generated oxygen to accumulate in the atmosphere in substantial amounts. Initially, it appears that the oxygen was consumed by weathering processes and reactions with other gases in the atmosphere. However, near the beginning of the Proterozoic (2.5 Ga), the oxygen content of the atmosphere began to increase substantially in what has been called the Great Oxidation Event. What triggered the change is unclear; but the cyanobacteria-generated oxygen accumulated in the atmosphere to high enough levels that new minerals and rocks formed. Banded iron formations (see Box 18.2), rich in magnetite or hematite, are clearly associated with this event. Of the roughly 4900 mineral species, more than half are oxidized and hydrated weathering products of other minerals, and few of these would have been stable before the Great Oxidation Event.

Hazen and Ferry (2010) argue that the number of mineral species has systematically increased over Earth history, from as few as 60 in the chondritic meteoritic material from which the Earth formed to the current number of roughly 4900. While this is probably true, it is not rigorously testable because so very few rocks formed in the Hadean (> 4.0 Ga) are preserved. Today, the oldest reliably dated rock is just slightly older than 4 Ga (Bowring and Williams, 1999).

DO NOT COPY

Printed by: e48d507df5d1141@placeholder.94092.edu. Printing is for personal, private use only. No part of this book may be reproduced or transmitted without publisher's prior permission. Violators will be prosecuted.

Because the Earth is constantly changing, the possibility of “extinct” minerals can be considered. This could happen in two ways. The first is a chemical element once present in the environment disappearing because of radioactive decay. Some physicists suggest that elements as high as atomic number 126 might have been present in the early Earth, and some of these very high atomic weight elements might have half-lives as high as 100 million years. Minerals made from these elements might have been formed but then broke down because the constituent elements decayed to stable daughter elements. The other way a mineral could go extinct is through the geologic environment needed for its formation being no longer available and no samples surviving. An “endangered” mineral might be one for which the geological environment needed for its formation is no longer available but of which samples from an earlier time are still preserved. Grew and Hazen (2014) argue this is the case for beryllium minerals.

DO NOT COPY
e48d507df5d1141@placeholder.9409

Printed by: e48d507df5d1141@placeholder.94092.edu. Printing is for personal, private use only. No part of this book may be reproduced or transmitted without publisher's prior permission. Violators will be prosecuted.

Biomineralization

Biomineralization refers to the processes by which organisms are directly involved with mineral growth. Over 55 phyla in all five kingdoms of life are involved in mineralization, and about 110 biominerals and mineraloids have been currently identified (**Table 5.3**).

TABLE 5.3 Biominerals

Mineral	Formula
Carbonates	
Aragonite	$CaCO_3$
Calcite	$CaCO_3$
Dolomite	$CaMg(CO_3)_2$
Hydrocerussite	$Pb_3(CO_3)_2(OH)_2$
Lansfordite	$MgCO_3{\cdot}5H_2O$
Magnesite	$MgCO_3$
Monohydrocalcite	$CaCO_3{\cdot}H_2O$
Nesquehonite	$MgCO_3{\cdot}3H_2O$
Rhodochrosite	$MnCO_3$
Siderite	$FeCO_3$
Strontianite	$SrCO_3$
Vaterite	$CaCO_3$
Phosphates	
Ammonium phosphate (unnamed)	$(NH_4)NaMg_2(PO_4)_2{\cdot}14H_2O$
Apatite	$Ca_5(PO_4)_3(OH,F,Cl)$
Bakhchisaraitsevite	$Na_2Mg_5(PO_4)_4{\cdot}7H_2O$
Bobierite	$Mg_3(PO_4)_2{\cdot}8H_2O$
Brushite	$CaHPO_4{\cdot}2H_2O$
Calcium pyrophosphate dihydrate*	$Ca_2P_2O_7{\cdot}2H_2O$
Carbonate–apatite	$Ca_5(PO_4,CO_3)_3(OH)$
Cystine*	$MgNH_4(PO_4){\cdot}6H_2O$
Diammonium calcium phosphate*	$(NH_4)_2Ca_2(PO_4)?$

DO NOT COPY e48d507df5d1141@placeholder.9409

Printed by: e48d507df5d1141@placeholder.94092.edu. Printing is for personal, private use only. No part of this book may be reproduced or transmitted without publisher's prior permission. Violators will be prosecuted.

Diammonium calcium phosphate*	$(NH_4)_2Ca_2(PO_4)_2$
Francolite	$Ca_{10}(PO_4)_6F_2$
Hannayite	$Mg_2(NH_4)_2H_4(PO_4)_4{\cdot}8H_2O$
Hazenite	$KNaMg_2(PO_4)_2{\cdot}14H_2O$
Magnesium ammonium phosphate hexahydrate*	$Mg_2(NH_4)(PO_4)2.6H_2O$
Magnesium hydrogen phosphate*	$MgHPO_4$
Monetite	$Ca[PO_3(OH)]$
Monosodium urate monohydrate*	$CaC_5H_3N_4O_3{\cdot}H_2O$
Newberryite	$Mg[PO_3(OH)]{\cdot}3H_2O$
Octocalcium phosphate*	$Ca_8H_2(PO_4)_6$
Struvite	$Mg(NH_4)(PO_4) \cdot 6H_2O$
Tricalcium phosphate*	$Ca_3(PO_4)_2$
Vivianite	$Fe^{2+}{}_3(PO_4)_2 \cdot 8H_2O$
Whitlockite	$Ca_{18}H_2(Mg,Fe^{2+})_2(PO_4)_{14}$
Sulfates	
Aphthitalite	$K_3Na(SO_4)_2$
Ardealite	$Ca_2[PO_3(OH)](SO_4){\cdot}4H_2O$
Barite	$BaSO_4$
Celestine	$SrSO_4$
Epsomite	$MgSO_4{\cdot}7H_2O$
Gypsum	$CaSO_4{\cdot}2H_2O$
Hexahydrite	$MgSO_4{\cdot}6H_2O$
Jarosite	$KFe^{3+}{}_3(SO_4)_2(OH)_6$
Melanterite	$FeSO_4{\cdot}7H_2O$
Schwertmannite	$Fe_8O_8SO_4(OH)_6$
Sulfides and Sulfosalts	
Acanthite	Ag_2S
Chalcocite	Cu_2S
Chalcopyrite	$CuFeS_2$
Covellite	CuS
Cubic FeS (Keilite?)	FeS
Galena	PbS
Greigite	Fe_3S_4

DO NOT COPY
e48d507df5d1141@placeholder.9409

Printed by: e48d507df5d1141@placeholder.94092.edu. Printing is for personal, private use only. No part of this book may be reproduced or transmitted without publisher's prior permission. Violators will be prosecuted.

Greigite	Fe_3S_4
Hydrotroilite	$FeS{\cdot}nH_2O$
Mackinawite	$(Fe,Ni)_9S_8$
Marcasite	FeS_2
Millerite	NiS
Pearceite	$(Ag,Cu)_{16}As_2S_{11}$
Proustite	Ag_3AsS_3
Pyrite	FeS_2
Pyrrhotite	$Fe_{1-x}S$
Sphalerite	ZnS
Wurtzite	ZnS
Arsenates	
Orpiment	As_2S_3
Realgar	AsS
Chlorides	
Atacamite	$Cu_2Cl(OH)_3$
Fluorides	
Fluorite	CaF_2
Hieratite	K_2SiF_6
Oxides	
Anatase	TiO_2
Ilmenite	$FeTiO_3$
Maghemite	γFe_2O_3
Magnetite	αFe_2O_3
Uraninite	UO_2
Hydroxides and Hydrous Oxides	
Birnessite	$Na_{0.5}Mn_2O_4{\cdot}1.5H_2O$
Ferrihydrite	$5Fe_2O_3{\cdot}9H_2O$
Goethite	$\alpha FeO(OH)$
Lepidocrocite	$\gamma FeO(OH)$
Todorokite	$(Mn,Ca,Na,K)(Mn,Mg)_6O_{12}{\cdot}3H_2O$
Other Minerals	

DO NOT COPY e48d507df5d1141@placeholder.9409

Printed by: e48d507df5d1141@placeholder.94092.edu. Printing is for personal, private use only. No part of this book may be reproduced or transmitted without publisher's prior permission. Violators will be prosecuted.

Abelsonite	$Ni^{2+}C_{31}H_{32}N_4$
Ca Malate*	$C_4H_4CaO_5$
Ca Tartrate*	$C_4H_4CaO_6$
Carpathite	$C_{24}H_{12}$
Earlandite	$Ca_3(C_6H_5O_2)_2{\cdot}4H_2O$
Glushinskite	$MgC_2O_4{\cdot}4H_2O$
Guanine	$C_5H_3(NH_2)N_4O$
Hartite	$C_{20}H_{34}$
Hoganite	$Cu(CH_3COO)_2{\cdot}H_2O$
Idrialite	$C_{22}H_{14}$
Kratochvilite	$C_{13}H_{10}$
Lindbergite	$MnC_2O_4{\cdot}2H_2O$
Manganese oxalate*	$Mn_2C_2O_4{\cdot}2H_2O$
Moolooite	$CuC_2O_4{\cdot}nH_2O$
Paceite	$CaCu(CH_3COO)_2{\cdot}6H_2O$
Sodium urate*	$C_5H_3N_4NaO_3$
Urea	$CO(NH_2)_2$
Uric acid	$C_5H_4N_4O_3$
Uricite	$C_5H_4N_4O_3$
Weddelite	$CaC_2O_4{\cdot}2H_2O$
Whewellite	$CaC_2O_4{\cdot}H_2O$
Native Elements	
Gold	Au
Sulfur	S
Silicates	
Clay	Smectite, nontronite, chlorite, Kaolinite
Mineraloids	
Amorphous calcium carbonate (at least five types)	$CaCO_3{\cdot}H_2O$ or $CaCO_3$
Amorphous calcium phosphate (at least six types)	variable
Amorphous calcium pyrophosphate	$Ca_2P_2O_7{\cdot}2H_2O$
Amorphous ilmenite	$FeTiO_3$
Amorphous iron oxide	Fe_2O_3

DO NOT COPY e48d507df5d1141@placeholder.9409

Printed by: e48d507df5d1141@placeholder.94092.edu. Printing is for personal, private use only. No part of this book may be reproduced or transmitted without publisher's prior permission. Violators will be prosecuted.

Amorphous manganese oxide	Mn_3O_4
Amorphous pyrrhotite	$Fe_{1-x}S$ ($x = 0 - 0.17$)
Amorphous silica/opal	$SiO_2 \cdot nH_2O$

Source: Adapted from Lowenstam and Weiner (1989), Zierenberg and Schiffman (1990), Skinner (2000), Weiner and Dove (2003), Konhauser (2007), Hazen and others (2008), and sources cited in Chapters 12–20 of this book.
* Not recognized as minerals by the Commission on New Minerals, Nomenclature and Classification of the International Mineralogical Association.

Biomineralization can be separated into two broad categories—**biologically induced mineralization** and **biologically controlled mineralization**. Biologically induced mineralization involves mineral precipitation as a consequence of an organism's interaction with the surrounding aqueous environment or as a byproduct of metabolic activity. Biologically controlled mineralization involves the growth of minerals that serve some physiological purpose. Undoubtedly overlap exists between the two categories, but they provide a useful reference frame.

Biologically Induced Mineralization

Biologically induced mineralization has the same requirements as any other mineral growth—the requisite chemical elements must be present, the mineral must be thermodynamically more stable than its precursors, and the activation energy to allow nucleation and growth must be available. Most biologically induced mineralization is associated with microorganisms and operates in two ways—either the cells passively provide nucleation sites for mineral growth or the cells metabolically influence the local chemical environment to promote mineral nucleation.

When a cell provides a nucleation site for a mineral, it provides a site for heterogeneous nucleation and minimizes the activation energy needed to induce crystal growth. Cell surfaces have an abundance of positively and negatively charged sites (ligands) that are capable of attracting and holding ions. The details of the organic material chemical structure dictate the spacing of positive and negative charges on the cell surface and control which ions are preferentially attracted. The process is similar to epitaxial nucleation (Figure 5.9), and a good example is provided by iron hydroxide minerals. In the simplest case, Fe^{2+}-bearing water reacts with oxygen dissolved from the atmosphere and precipitates ferrihydrite ($5Fe_2O_3 \cdot 9H_2O$, an ocher-colored mineral and a common constituent of limonite (Chapter 18). However, often one or more bacteria species in the water provide nucleation sites to trigger precipitation.

Other microorganisms can promote mineralization directly by their metabolism. The metabolism of *Chlorobium ferrooxidans* utilizes photosynthesis to oxidize Fe^{2+} to Fe^{3+}. Once oxidized, the Fe^{3+} combines with oxygen and water to precipitate as ferric hydroxide. Bog iron, iron deposits found in bogs and swamps, is a product of this type of bacterial precipitation from groundwater springs. Bog iron served as an important source

DO NOT COPY e48d507df5d1141@placeholder.9409

Printed by: e48d507df5d1141@placeholder.94092.edu. Printing is for personal, private use only. No part of this book may be reproduced or transmitted without publisher's prior permission. Violators will be prosecuted.

bacterial precipitation from groundwater springs. Bog iron served as an important source of iron in medieval Europe and colonial America. Other examples are the bacteria *Geobacter metallireducens* and *Shewanella putrefaciens*. Both oxidize organic material in sediment and reduce the Fe^{3+} in ferric hydroxides to Fe^{2+} as part of their metabolism. The reduced iron is then available to crystallize as magnetite (Fe_3O_4; Chapter 18), which forms very small grains outside the cells and can contribute to the preserved magnetism of sedimentary rocks.

The $CaCO_3$ polymorphs of calcite and aragonite (Chapter 17) are minerals formed in sedimentary environments by both biologically induced and controlled mineralization. Cyanobacteria utilize photosynthesis to induce precipitation of calcite or aragonite by the general reaction

$$Ca^{2+} + 2HCO_3^- = CaCO_3 + CH_2O + O_2.$$

CH_2O represents the organic material of cells. In environments where other divalent cations exist, the carbonate could be dolomite [$CaMg(CO_3)_2$], strontianite ($SrCO_3$), or magnesite ($MgCO_3$). Photosynthetic fixation of inorganic carbon increases the pH of the water (makes it less acidic), which decreases the solubility of calcium carbonate so that it becomes oversaturated. The surfaces of the cyanobacteria have ligands that attract and hold Ca^{2+} (or other cations) and promote heterogeneous nucleation of the carbonate minerals. Cyanobacteria and other types of algae can produce large quantities of fine-grained calcite or aragonite mud that can accumulate as limestone layers. **Stromatolites** are produced by microbial mats of cyanobacteria and other organisms that precipitate calcium carbonate.

Other minerals and mineraloids whose growth is biologically induced include dolomite, sulfates (Chapter 17), pyrite and other sulfides (Chapter 19), manganese oxides (Chapter 18), and clay minerals (Chapter 13). It is likely that many mineral alteration processes in the supergene zone of hydrothermal sulfide deposits (Chapter 19) are influenced by bacterial processes.

Biologically Controlled Mineralization

Organisms commonly utilize biologically controlled mineralization to create skeletal structures. The cation of choice is usually calcium, and the most common minerals produced are carbonates and phosphates; others include oxides and sulfides. While not a mineral, amorphous silica is abundantly produced by diatoms, radiolarians, and silicoflagellates and may subsequently crystallize as quartz, usually as a microcrystalline form, such as chert (Chapter 12). In many cases of biologically controlled mineralization, the organism expends cellular energy to concentrate the constituents (Ca, P, Fe, Mn, Si, F, etc.) needed to precipitate a mineral from an environment in which those chemical elements may be present in low concentrations.

DO NOT COPY e48d507df5d1141@placeholder.94092

Printed by: e48d507df5d1141@placeholder.94092.edu. Printing is for personal, private use only. No part of this book may be reproduced or transmitted without publisher's prior permission. Violators will be prosecuted.

Coccolithophores and **foraminifera** utilize biologically controlled mineralization to produce large quantities of $CaCO_3$. Along with mineralization by cyanobacteria and algae, these organisms are responsible for a large portion of carbonate precipitation from marine environments. Coccolithophores are unicellular algae that have been abundant in the oceans since the Jurassic (~200 Ma), but in the Cretaceous (~145 Ma) they experienced a population explosion that was associated with a worldwide accumulation of limestone. Coccolithophores grow microscopic **coccoliths** (**Figure 5.33**), which form very fine-grained micritic mud that makes up many limestones. Most species are planktonic, living in the photic zone in mid- to high-latitude coastal waters. Foraminifera are both planktonic and benthic (bottom dwelling); they secrete intricate shells that range in size from ~30 µm to >1 mm. They first appeared in the Cambrian (~540 Ma) and occupy a wide range of environments.

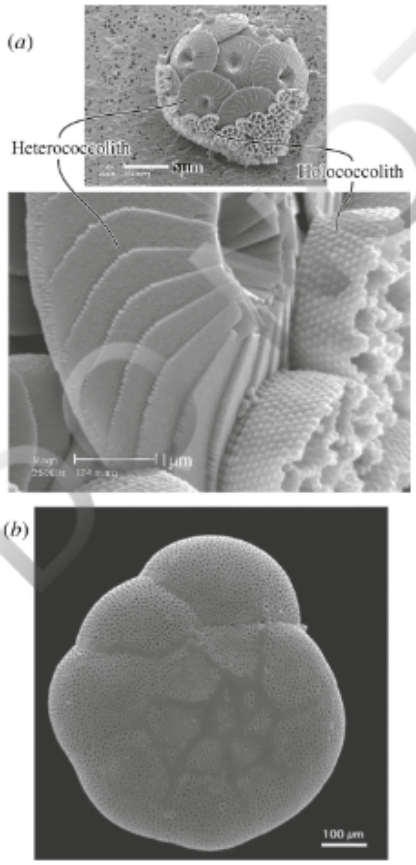

FIGURE 5.33 Coccoliths and foraminifera. (*a*) A combination coccosphere of the coccolithophore *Calcidiscus leptoporus* sp. *quadriperforatus*. Heterococcoliths and holococcoliths are formed during different phases of coccolithophore growth. Each of the individual plates in a heterococcolith consists of a single calcite crystal. Holococcoliths are made of numerous granules, each of which is a single calcite crystal. It is rare to find coccospheres with both heterococcoliths and holococcoliths. Images © Jeremy Young and Markus Geisen, The Natural History Museum London, and used by permission. (*b*) The foraminifera *Ammonia beccarii* (Thomas, E., Gapoichenko, T., Varekamp, J. C., Mecray, E. L., and Buchholtz ten Brink, J. R. 2000. Maps of benthic foraminiferal distribution and environmental changes in Long Island Sound between 1940s and 1990s. U.S. Geological Survey Open File Report OF00-304.). View larger image

DO NOT COPY e48d507df5d1141@placeholder.9409

Printed by: e48d507df5d1141@placeholder.94092.edu. Printing is for personal, private use only. No part of this book may be reproduced or transmitted without publisher's prior permission. Violators will be prosecuted.

Carbonate–apatite (Chapter 17) is the biomineral of most importance to vertebrates (Pasteris and others, 2008) because it forms the mineral content of bones and teeth. It also forms the shells of inarticulate brachiopods, two-shelled organisms found today and as fossils going back to the Cambrian. Phosphorus and calcium from dietary sources are combined in bone- and teeth-forming cells to precipitate as small platelets of apatite. The structure of bone and teeth is a composite of mineral and cellular material. Bone consists of 45 to 70 weight percent apatite and 10 weight percent water, with the remainder being collagen and other proteins. Tooth enamel, in contrast, consists of almost pure apatite. The mineral content of bones is in a constant state of dissolution and precipitation: it is entirely replaced every 5 to 10 years. Dissolution of the apatite is promoted if calcium and phosphorus are needed elsewhere in the body and dietary sources lack these elements.

Several magnetic minerals are produced by biologically controlled mineralization. One case is the presence of fine grains (nanoparticles) of magnetite on the radular teeth of the chiton (a marine mollusk), which the animal uses to grind algae and other food. The scaly-footed snail, found near hydrothermal vents in the Indian Ocean, also precipitates greigite (Fe_3S_4) on its foot, evidently as a sort of protective armor. In fact, magnetite (Fe_3O_4) and maghemite (Fe_2O_3) nanoparticles are found in a wide range of organisms including bacteria, algae, mollusks, insects, and vertebrates. In some cases, such as bacteria and insects, the magnetic particles appear to assist with navigation and maintaining orientation, but in others the function is unknown. Even the human brain contains very small particles of magnetite and maghemite, although the function, if any, remains unknown (Pósfai and Dunin-Borkowski, 2009).

Applications

The growing knowledge of the relationship between biologic activity and mineralogy has resulted in the growth of useful applications including biomining, bioremediation, and biomediated improvement of soil engineering properties.

In **biomining**, microorganisms such as *Acidithiobacillus ferrooxidans* are introduced into the ore or ore concentrate produced at a mine. Details of the process vary, but in all cases aqueous solutions containing the bacteria are introduced to the ore. As a result of the bacteria's metabolic processes, metals are released into water, which is then processed to extract the metals. This technique has been employed successfully in the extraction of copper, cobalt, nickel, zinc, and uranium. It also has been employed to remove unwanted metals from gold and silver ore. Advantages of microbial extraction processes include lower energy consumption, reduced emission of sulfur dioxide and other harmful gases, lower operating costs, and the ability to process ores with low metal content.

Bioremediation involves using plants and bacteria to remove unwanted chemicals from the environment. One example is contamination from crude oil and petroleum products, which often stick to mineral particles in the soil and are difficult to remove. Bacteria can

DO NOT COPY e48d507df5d1141@placeholder.94092

Printed by: e48d507df5d1141@placeholder.94092.edu. Printing is for personal, private use only. No part of this book may be reproduced or transmitted without publisher's prior permission. Violators will be prosecuted.

which often stick to mineral particles in the soil and are difficult to remove. Bacteria can metabolize these products and remove them. In the case of metal contamination from mine waste, bacteria and plants have been used to extract the metals from surface water by precipitation, sorption onto mineral particles, and/or uptake into plant tissue.

Biomediation can be used to improve the engineering properties of weak soils unsuitable for construction, at least in laboratory conditions. In one process studied, the metabolism of the *Sporosarcina pasteurii* bacterium causes an increase in pH of the soil pore water, which can allows calcite ($CaCO_3$) to precipitate and bind soil particles together to reduce permeability and increase strength.

DO NOT COPY
e48d507df5d1141@placeholder.9409

Printed by: e48d507df5d1141@placeholder.94092.edu. Printing is for personal, private use only. No part of this book may be reproduced or transmitted without publisher's prior permission. Violators will be prosecuted.

Applications

The growing knowledge of the relationship between biologic activity and mineralogy has resulted in the growth of useful applications including biomining, bioremediation, and biomediated improvement of soil engineering properties.

In **biomining**, microorganisms such as *Acidithiobacillus ferrooxidans* are introduced into the ore or ore concentrate produced at a mine. Details of the process vary, but in all cases aqueous solutions containing the bacteria are introduced to the ore. As a result of the bacteria's metabolic processes, metals are released into water, which is then processed to extract the metals. This technique has been employed successfully in the extraction of copper, cobalt, nickel, zinc, and uranium. It also has been employed to remove unwanted metals from gold and silver ore. Advantages of microbial extraction processes include lower energy consumption, reduced emission of sulfur dioxide and other harmful gases, lower operating costs, and the ability to process ores with low metal content.

Bioremediation involves using plants and bacteria to remove unwanted chemicals from the environment. One example is contamination from crude oil and petroleum products, which often stick to mineral particles in the soil and are difficult to remove. Bacteria can metabolize these products and remove them. In the case of metal contamination from mine waste, bacteria and plants have been used to extract the metals from surface water by precipitation, sorption onto mineral particles, and/or uptake into plant tissue.

Biomediation can be used to improve the engineering properties of weak soils unsuitable for construction, at least in laboratory conditions. In one process studied, the metabolism of the *Sporosarcina pasteurii* bacterium causes an increase in pH of the soil pore water, which can allows calcite ($CaCO_3$) to precipitate and bind soil particles together to reduce permeability and increase strength.

REFERENCES CITED AND SUGGESTIONS FOR ADDITIONAL READING

Banfield, J. F., and Nealson, K. H. (eds.). 1997. Geomicrobiology: Interactions between microbes and minerals. *Reviews in Mineralogy* **35**, 448 p.

Bard, J. P. 1986. *Microstructures of Igneous and Metamorphic Rocks. Part I: Nucleation and Crystal Growth*. D. Reidel, Dordrecht, 263 p.

Barker, A. J. 1998. *Introduction to Metamorphic Textures and Microstructures*, 2nd ed. Stanley Thornes Publishers, Cheltenham, UK, 264 p.

Bowen, N. L., and Schairer, J. F. 1935. The system MgO–FeO–SiO_2. *American Journal of Science, Series* **5, 29, 170**, 151–217.

DO NOT COPY e48d507df5d1141@placeholder.9409

Printed by: e48d507df5d1141@placeholder.94092.edu. Printing is for personal, private use only. No part of this book may be reproduced or transmitted without publisher's prior permission. Violators will be prosecuted.

Science, Series **5, 29, 170**, 151–217.

Bowen, N. L., and Tuttle, O. F. 1950. The system $NaAlSi_3O_8$–$KAlSi_3O_8$–H_2O. *Journal of Geology* **58**, 489–517.

Bowring, S. A., and Williams, I. S. 1999. Priscoan (4.00–4.03 Ga) orthogneisses from northwestern Canada. *Contributions to Mineralogy and Petrology* **134**, 3–16.

Cashman, K. V., and Ferry, J. M. 1988. Crystal size distribution (CSD) in rocks and the kinetics and dynamics of crystallizations: III. Metamorphic crystallization. *Contributions to Mineralogy and Petrology* **99**, 401–415.

Coyle, D. A., and Wagner, G. A. 1998. Positioning the titanite fission-track partial annealing zone. *Chemical Geology* **149**, 117–125.

Dickin, A. P. 2005. *Radiogenic Isotopic Geology*, 2nd ed. Cambridge University Press, Cambridge, 492 p.

Dove, P. M. 2010. The rise of skeletal biominerals. *Elements* **6**, 37–42.

Dove, P. M., De Yoreo, J. J., and Weiner, S. (eds.). 2003. Biomineralization. *Reviews in Mineralogy* **54**, 381 p.

Faure, G., and Mensing, T. M. 2005. *Isotopes, Principles and Applications*, 3rd ed. John Wiley & Sons, Hoboken, NJ, 896 p.

Fletcher, P. 1993. *Geochemical Thermodynamics for Earth Scientists*. John Wiley & Sons, New York, 464 p.

Grew, E. S., and Hazen, R. M. 2014. Beryllium mineral evolution. *American Mineralogist* **99**, 999–1021.

Grigor'ev, D. P. 1965. *Ontogeny of Minerals*. Israel Program for Scientific Translations, Jerusalem, 250 p.

Harrison, T. M., Duncan, I., and McDougall, I. 1985. Diffusion of ^{40}Ar in biotite: Temperature, pressure and compositional effects. *Geochimica et Cosmochimica Acta* **49**, 2461–2468.

Hazen, R. M. 2005. Genesis: Rocks, minerals, and the geochemical origin of life. *Elements* **1**, 135–137.

Hazen, R. M., and Ferry, J. M. 2010. Mineral evolution: Mineralogy in the fourth dimension. *Elements* **6**, 9–17.

Hazen, R. M., Papineau, D., Bleeker, W., Downs, R. T., Ferry, J. M., McCoy, T. J., Sverjensky, D. A., and Hexiong, Y. 2008. Mineral evolution. *American Mineralogist* **93**, 1693–1720.

Hemingway, B. S., Robie, R. A., Evans, H. T., Jr., and Kerrick, D. M. 1991. Heat capacities and entropies of sillimanite, fibrolite, andalusite, kyanite, and quartz and the Al_2SiO_5 phase diagram. *American Mineralogist* **76**, 1597–1613.

Hibbard, M. J. 1995. *Petrography to Petrogenesis*. Prentice Hall, Englewood Cliffs, NJ, 587 p.

Jones, S., Gleadow, A., and Kohn, B. 2021. Thermal annealing of implanted ^{252}Cf

DO NOT COPY e48d507df5d1141@placeholder.9409-

Printed by: e48d507df5d1141@placeholder.94092.edu. Printing is for personal, private use only. No part of this book may be reproduced or transmitted without publisher's prior permission. Violators will be prosecuted.

Jones, S., Gleadow, A., and Kohn, B. 2021. Thermal annealing of implanted ^{252}Cf fission tracks in monazite. *Geochronology* **3**, 89–102.

Konhauser, K. 2007. *Introduction to Geomicrobiology*. Blackwell Publishing, Malden, MA, 425 p.

Lowenstam, H. A., and Weiner, S. 1989. *On Biomineralization*. Oxford University Press, New York, 324 p.

Mann, S. 2001. *Biomineralization: Principles and Concepts in Bioinorganic Minerals Chemistry*. Oxford University Press, New York, 216 p.

McCoy, T. J. 2010. Mineralogical evolution of meteorites. *Elements* **6**, 19–23.

Morse, S. A. 1970. Alkali feldspars with water at 5 kb pressure. *Journal of Petrology* **11**, 221–251.

Nordstrom, D. K., and Munoz, J. L. 1994. *Geochemical Thermodynamics*. Blackwell Scientific, New York, 493 p.

Osborn, E. F. 1942. The system $CaSiO_3$–diopside–anorthite. *American Journal of Science* **240**, 751–788.

Palyanov, Y. N., Khokhryakov, A. F., Borzdov, Y. M., and Kupriyanov, I. N., 2013. Diamond growth and morphology under the influence of impurity adsorption. *Crystal Growth & Design* **13**, 5411–5419.

Palyanov, Y. N., Kupriyanov, I. N., Khokhryakov, A. F., and Borzdov, Y. M. 2017. High-pressure crystallization and properties of diamond from magnesium-based catalysts. *CrystEngComm* **19**, 4459–4475.

Papineau, D. 2010. Mineral environments in the earliest Earth. *Elements* **6**, 25–30.

Parmar, N., and Singh, A. 2014. *Geomicrobiology and Biogeochemistry*. Springer-Verlag, Berlin, 302 p.

Pasteris, J. D., Wopenka, B., and Valsami-Jones, E. 2008. Bone and tooth mineralization: Why apatite? *Elements* **4**, 97–104.

Pósfai, M., and Dunin-Borkowski, R. E. 2009. Magnetic nanocrystals in organisms. *Elements* **5**, 235–240.

Price, G. D., and Ross, N. L. (eds.). 1992. *The Stability of Minerals*. Chapman & Hall, London, 368 p.

Reiners, P. W., Carlson, R. W., Renne, P. R., Cooper, K. M., Granger, D. E., McLean, N. M., and Schoene, B. 2018. *Geochronology and thermochronology*. American Geophysical Union, Washington, D.C., 464 p.

Skinner, H. C. W. 2000. Minerals and human health, in D. J. Vaughn, and R. A. Wogelius (eds.), *Environmental Mineralogy*. EMU Notes in Mineralogy **2**. Eötvös University Press, Budapest, pp 383–412.

Smith, J. V., and Parsons, I. 1974. The alkali–feldspar solvus at 1 kilobar water vapour pressure. *Mineralogical Magazine* **39**, 747–767.

DO NOT COPY

Printed by: e48d507df5d1141@placeholder.94092.edu. Printing is for personal, private use only. No part of this book may be reproduced or transmitted without publisher's prior permission. Violators will be prosecuted.

Sverjensky, D. A., and Lee, H. 2010. The Great Oxidation Event and mineral diversification. *Elements* **6**, 31–36.

Thomas, E., Gapoichenko, T., Varekamp, J. C., Mecray, E. L., and Buchholtz ten Brink, J. R. 2000. Maps of benthic foraminiferal distribution and environmental changes in Long Island Sound between 1940s and 1990s. *U.S. Geological Survey Open File Report OF00-304*.

Thompson, J. B., Jr., and Waldbaum, D. R. 1969. Mixing properties of sanidine crystalline solutions: III. Calculations based on two-phase data. *American Mineralogist* **54**, 811–838.

Vaughn, D. J., and Wogelius, R. A. (eds.). 2013. *Environmental Mineralogy II*. EMU Notes in Mineralogy **13**, 489 p.

Wagner, G., and Van den Haute, P. 1992. *Fission-Track Dating*. Kluwer Academic Publishers, Boston, 285 p.

Weiner, S., and Dove, P. M. 2003. An overview of biomineralization processes and the problem of the vital effect. *Reviews in Mineralogy and Geochemistry* **54**, 1–29.

Yoder, H. S., Stewart, D. B., and Smith, J. R. 1957. Ternary feldspars. *Carnegie Institute Geophysical Laboratory Yearbook* **56**, 206–214.

Zierenberg, R. A., and Schiffman, P. 1990. Microbial control of silver mineralization at a sea-floor hydrothermal site in the northern Gorda ridge. *Nature* **348**, 155–157.

DO NOT COPY
e48d507df5d1141@placeholder.9409

Printed by: e48d507df5d1141@placeholder.94092.edu. Printing is for personal, private use only. No part of this book may be reproduced or transmitted without publisher's prior permission. Violators will be prosecuted.

LIST OF KEY TERMS

- ^{14}C radiometric dating
- $^{40}Ar/^{39}Ar$ radiometric dating
- activation energy
- alpha decay
- annealing
- annealing temperature
- antiperthite
- antiperthitic
- antiphase domain boundary
- antiphase domain
- beta decay
- binary minimum
- biologically controlled mineralization
- biologically induced mineralization
- bio-mediation
- biomineralization
- biomining
- bio-remediation
- bulk composition
- Burgers vector
- calories
- chemical weathering
- closure temperature
- coccolithophores
- coccoliths
- composition plane
- composition surface
- contact twins
- core

DO NOT COPY
e48d507df5d1141@placeholder.9409

Printed by: e48d507df5d1141@placeholder.94092.edu. Printing is for personal, private use only. No part of this book may be reproduced or transmitted without publisher's prior permission. Violators will be prosecuted.

core
critical growth radius
crystallization
cyclic twin
daughter
decay
deform
detrital
diffusion
dislocation line
edge dislocation
electron capture
embryo
Energy
epitaxial nucleation
equilibrium
equilibrium crystallization
equilibrium melting
eutectic
eutectic composition
eutectic temperature
fission
fission track dating
fission track
foraminifera
fractional crystallization
Frenkel defect
geochronology
Gibbs free energy
Gibbs free energy of formation
glide
glide plane
grain boundary
half life

DO NOT COPY
e48d507df5d1141@placeholder.9409

Printed by: e48d507df5d1141@placeholder.94092.edu. Printing is for personal, private use only. No part of this book may be reproduced or transmitted without publisher's prior permission. Violators will be prosecuted.

half-life
igneous rock
inclusion
interstitial defects
joule
lamellae
lever rule
line defect
liquidus
magma
mesoperthite
metamict
metamorphic reaction
metamorphic rock
metastable
multiple twins
nuclei
paramorph
parent
penetration twins
perthite
perthitic texture
phase
phase diagrams
physical weathering
planar defect
pleochroic halos
point defects
polysynthetic twins
porphyroblast
positron decay
products
protolith

DO NOT COPY
e48d507df5d1141@placeholder.9409

Printed by: e48d507df5d1141@placeholder.94092.edu. Printing is for personal, private use only. No part of this book may be reproduced or transmitted without publisher's prior permission. Violators will be prosecuted.

pseudomorphism
radiocarbon dating
radiometric dating
reactants
recrystallization
rim
rock cycle
rock
Schottky defect
screw dislocation
sediment
sedimentary rock
simple twins
slip system
solidus
solvus
stability
stable mineral assemblage
stacking faults
stress
stromatolites
substitution defect
thermochronology
tie-line
twin law
twinning
twin operation
U-Pb radiometric dating
(U-Th)/He radiometric dating
work-hardening

DO NOT COPY
e48d507df5d1141@placeholder.9409

Printed by: e48d507df5d1141@placeholder.94092.edu. Printing is for personal, private use only. No part of this book may be reproduced or transmitted without publisher's prior permission. Violators will be prosecuted.

PART TWO

MINERAL PROPERTIES, STUDY, AND IDENTIFICATION

William D. Nesse
University of Northern Colorado

Graham B. Baird
University of Northern Colorado

DO NOT COPY
e48d507df5d1141@placeholder.9409

Printed by: e48d507df5d1141@placeholder.94092.edu. Printing is for personal, private use only. No part of this book may be reproduced or transmitted without publisher's prior permission. Violators will be prosecuted.

CHAPTER 6
Physical Properties of Minerals

William D. Nesse
University of Northern Colorado

Graham B. Baird
University of Northern Colorado

DO NOT COPY
e48d507df5d1141@placeholder.9409

Printed by: e48d507df5d1141@placeholder.94092.edu. Printing is for personal, private use only. No part of this book may be reproduced or transmitted without publisher's prior permission. Violators will be prosecuted.

Introduction

The physical properties of minerals are controlled by their structure and chemical composition. Therefore, each mineral has a set of physical properties that can be used to identify the mineral. However, minerals with solid solution, within limits, have variation in their structure and chemistry, meaning that their physical properties can vary within limits as well. Regardless, different samples of the same mineral should display similar properties.

The physical properties of many minerals make them valuable. For example, graphite and diamond, both polymorphs of carbon, have properties that make them useful for industrial purposes. Diamond, because of its great hardness, is widely used as an abrasive and in cutting tools, and it also can be a prized gemstone because of its clarity and brilliance. Graphite, in contrast, is very soft and is used as a lubricant and as pencil lead.

It is convenient to combine physical properties into groups that depend on the mass (density and specific gravity), mechanical cohesion (hardness, tenacity, cleavage, fracture, and parting), interaction with light (luster, color, streak, and luminescence), and other properties (magnetism, electrical behavior, taste, odor, and reaction with acid).

DO NOT COPY
e48d507df5d1141@placeholder.9409

Printed by: e48d507df5d1141@placeholder.94092.edu. Printing is for personal, private use only. No part of this book may be reproduced or transmitted without publisher's prior permission. Violators will be prosecuted.

Mass-Dependent Properties

Density

Density (ρ) is defined as mass (m) per unit volume (v).

$$\rho = \frac{m}{v} \quad (6.1)$$

Density is usually expressed in units of grams per cubic centimeter (g/cm^3).

Specific Gravity

Specific gravity (G) is defined as the density of a material divided by the density of water at 4°C.

$$G = \frac{\rho_{\text{material}}}{\rho_{\text{water at 4°C}}} \quad (6.2)$$

G is unitless because it is a ratio of densities. Because the density of water at 4°C is essentially 1 g/cm^3 (actually 0.999973 g/cm^3), the numerical values of specific gravity and density are essentially identical if the latter is expressed in units of grams per cubic centimeter.

Controls on Density and Specific Gravity

Specific gravity of a mineral depends on the chemical composition and on how tightly the atoms are packed together.

The **packing index** (PI) is a convenient way to measuring how tightly the atoms in a mineral are packed together. It is defined as

$$PI = \frac{V_I}{V_C} \quad (6.3)$$

where V_C = the unit cell volume and V_I = the total volume of the atoms in the unit cell based on their ionic radii (Appendix A). This assumes that the atoms are spheres with clearly defined boundaries. As was discussed in Chapter 4, atoms are not spherical and

DO NOT COPY e48d507df5d1141@placeholder.9409

Printed by: e48d507df5d1141@placeholder.94092.edu. Printing is for personal, private use only. No part of this book may be reproduced or transmitted without publisher's prior permission. Violators will be prosecuted.

their boundaries are defined by the probabilities of where electrons will be found. Regardless, the packing index provides useful information about the degree to which a crystal structure is tightly packed or relatively open.

For most minerals, the packing index is between about 35 and 74, meaning that between 35 percent and 74 percent of the crystal structure consists of atoms. The remaining space is equivalent to porosity. Close-packed structures of uniform spheres have packing indexes of 74. The fact that most ionic minerals have packing indices less than this is an indication that the anion framework is relatively open to accommodate cations in the interstices.

As a general rule, the packing index for minerals formed at high pressure is higher than that for minerals formed at lower pressure. Kyanite is the high-pressure polymorph of Al_2SiO_5; it has a packing index of 60.1 and a specific gravity of 3.6. Andalusite, the polymorph formed at lower pressure, has a packing index of 52.3 and a specific gravity of about 3.1.

Composition also controls density and specific gravity. Minerals containing high atomic weight elements typically also have high ρ and G. If a mineral displays extensive solid solution, specific gravity typically varies systematically between the end-member values. In olivine [$(Mg,Fe)_2SiO_4$], for example, the specific gravities of the Mg and Fe end members are 3.26 and 4.39, respectively. Iron-rich varieties typically have higher specific gravity than the magnesium-rich varieties because the atomic weights of iron and magnesium are 55.85 and 24.31, respectively. The relationship is not necessarily linear, however. Intermediate compositions have specific gravities slightly higher than a straight-line relation would suggest (**Figure 6.1**).

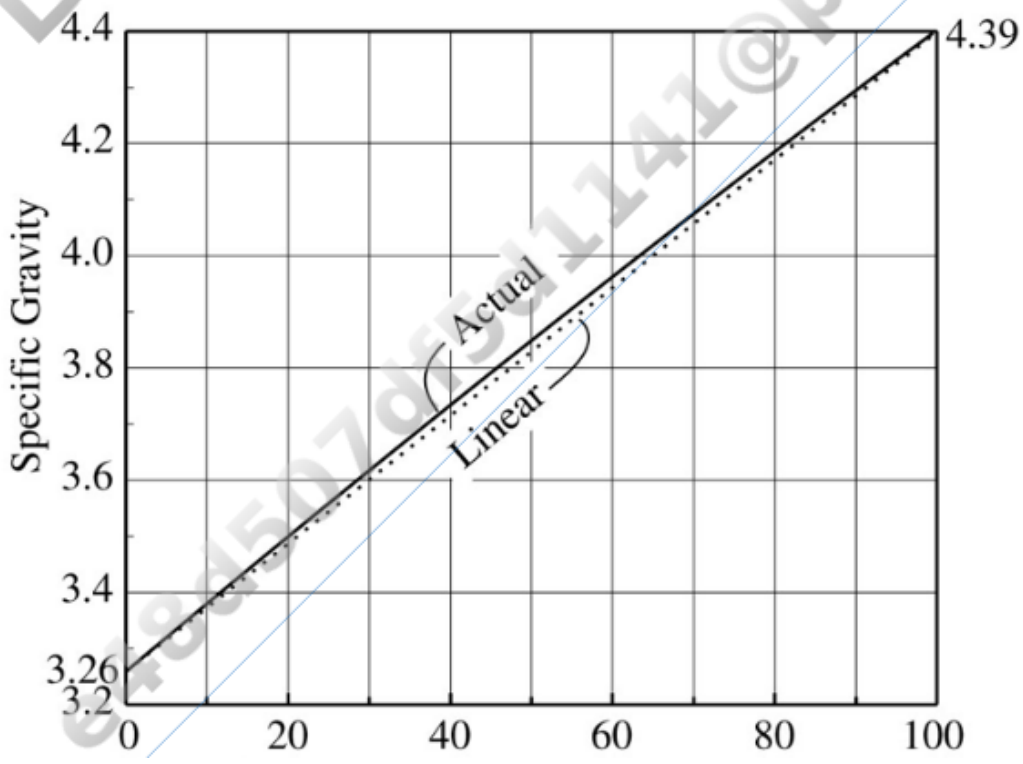

Printed by: e48d507df5d1141@placeholder.94092.edu. Printing is for personal, private use only. No part of this book may be reproduced or transmitted without publisher's prior permission. Violators will be prosecuted.

Forsterite Mg_2SiO_4 Mole % Fayalite Fayalite Fe_2SiO_4

FIGURE 6.1 Specific gravity of olivine. The dotted line assumes a linear variation in specific gravity between 3.26 for forsterite (Mg_2SiO_4) and 4.39 for fayalite (Fe_2SiO_4). The solid line is the actual specific gravity for intermediate compositions. View larger image

Measurement of Specific Gravity

A **Jolly balance** is a device that measures G for samples weighing just a few grams (**Figure 6.2a**). A sample of a mineral is first weighed in air (m_a) and then while suspended in water (m_w). The difference in these measurements ($m_a - m_w$) is, by Archimedes's principle, the weight of the water displaced by the sample. The specific gravity of the sample is

$$G = \frac{m_a}{m_a - m_w}. \quad (6.4)$$

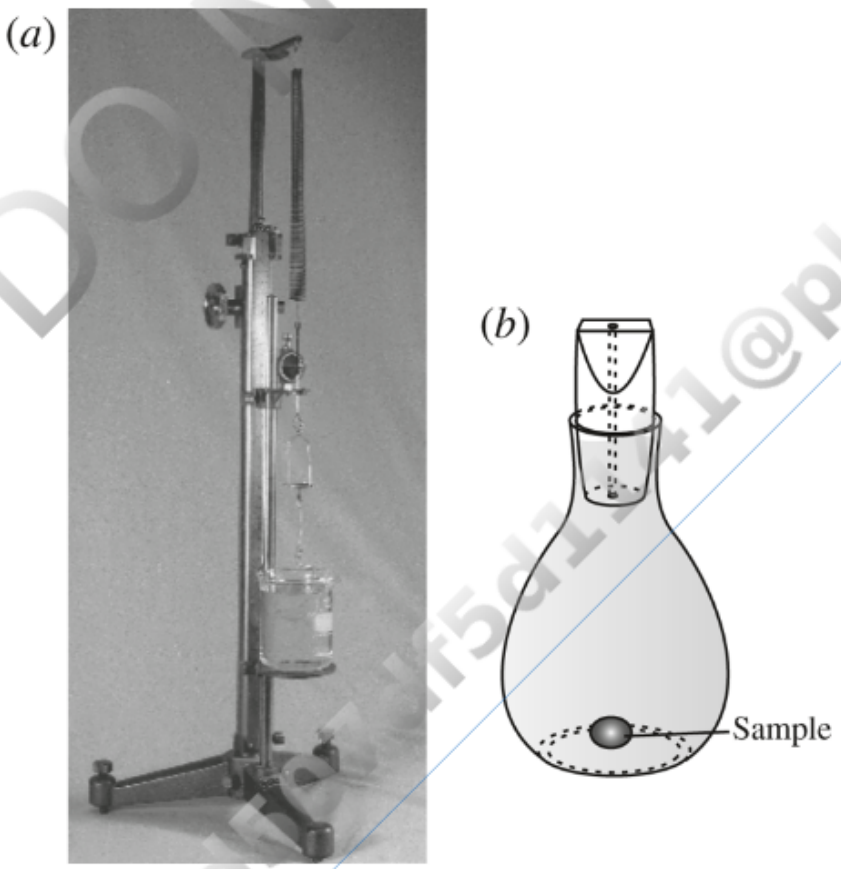

FIGURE 6.2 Apparatus to measure specific gravity. (*a*) Jolly balance; a sample of a mineral is weighed first in the upper pan and then in the lower pan, which is suspended in water. (*b*) Pycnometer. View larger image

DO NOT COPY e48d507df5d1141@placeholder.9409

Printed by: e48d507df5d1141@placeholder.94092.edu. Printing is for personal, private use only. No part of this book may be reproduced or transmitted without publisher's prior permission. Violators will be prosecuted.

A **pycnometer** (Figure 6.2b) may be used to measure specific gravity for samples too small for the Jolly balance. It is a small flask fitted with a ground-glass stopper that contains a fine hole. It is used as follows:

- Weigh the mineral grain(s) to obtain its weight (m_a).
- Weigh the pycnometer completely filled with water (m_p).
- Place samples in the pycnometer and replace the stopper, forcing water equal to the volume of the samples out of the hole so it can be removed.
- Weigh the pycnometer with sample(s) (m_{p+s}).

The weight of the water displaced from the pycnometer by the sample is equal to $m_a + m_p - m_{p+s}$, so the specific gravity is

$$G = \frac{m_a}{m_a + m_p - m_{p+s}}. \quad (6.5)$$

Another routine means of measuring specific gravity is by comparison to liquids whose specific gravity is known. Commonly used liquids are listed in Table 6.1. A sample of an unknown mineral is placed in one of these heavy liquids. If the sample sinks, its specific gravity is greater than that of the liquid, and if it floats, its specific gravity is less. If the sample neither sinks nor floats and remains suspended, the liquid and sample have the same specific gravity.

TABLE 6.1 Heavy Liquids

Liquid	Specific Gravity (~25°C)
Bromoform	2.9
Tetrabromoethane	2.97
Diiodomethane (methylene iodide)	3.31
Sodium polytungstate (SMT)	2.85
Lithium heteropolytungstate (LST)	2.9
Lithium metatungstate (LMT)	3.0

Each liquid has advantages and disadvantages. Bromoform, tetrabromethane, and diiodomethane have relatively low viscosity, which makes them easier to use, but all are quite toxic and must be used in a fume hood. The tungstate liquids are substantially less toxic, but have higher viscosities, which makes them more difficult to use. Please refer to Material Safety Data Sheets for information concerning safe handling of these materials and always follow safe laboratory procedures.

DO NOT COPY e48d507df5d1141@placeholder.9409

Printed by: e48d507df5d1141@placeholder.94092.edu. Printing is for personal, private use only. No part of this book may be reproduced or transmitted without publisher's prior permission. Violators will be prosecuted.

The density of the heavy liquids may be reduced by adding a solvent to obtain a liquid whose density matches the mineral sample. Acetone is used for bromoform, tetrabromoethane, and diiodomethane; water for the tungstates. If a known volume of the heavy liquid is weighed, its specific gravity can be calculated. The specific gravity of the diluted liquid also can be determined by dropping in samples of known specific gravity to see if they sink, float, or are suspended.

With samples that are sufficiently large, a crude but effective way of evaluating the specific gravity is by simply "**hefting**" a sample by gently shaking it in the hand and getting a sense of whether it is very heavy or light compared to the sample's size. Heft comparison between similar-sized samples of known minerals, such as quartz ($G = 2.65$), or other common minerals, help narrow down the G of sample with unknown identity. Samples that seem to be significantly heavier than a quartz sample of similar size will have much higher specific gravity than 2.65, for example. With a little practice and after some comparisons to known samples, reasonable estimates of specific gravity can be made.

DO NOT COPY
e48d507df5d1141@placeholder.9409

Printed by: e48d507df5d1141@placeholder.94092.edu. Printing is for personal, private use only. No part of this book may be reproduced or transmitted without publisher's prior permission. Violators will be prosecuted.

Properties Related to Mechanical Cohesion

All mechanical cohesion properties are related to the strength of chemical bonds that hold the mineral together. They include hardness, tenacity, cleavage, fracture, and parting.

Hardness

The ease with which a mineral may be scratched is a measure of its **hardness** (*H*). The most widely used scratch hardness scale in mineralogy is known as **Mohs scale of hardness**. It is a unitless 10-point scale, with each hardness number represented by a common mineral (**Table 6.2**). Each mineral on the list will scratch softer minerals lower on the scale and be scratched by harder minerals. The scale is no more precise than half a hardness unit. A mineral with a hardness between calcite (3) and fluorite (4), for example, has a hardness of 3.5.

TABLE 6.2 Mohs Scale of Hardness

Hardness	Mineral
1	Talc
2	Gypsum
3	Calcite
4	Fluorite
5	Apatite
6	Orthoclase
7	Quartz
8	Topaz
9	Corundum
10	Diamond

Hardness test kits consisting of scribes containing samples of minerals 1 through 9 exist. For rapid testing in the field or laboratory, common objects such as a fingernail (2.5), copper penny coin (3), knife blade (~5), window glass (5.5), and a small fragment of quartz (7) can be quite useful. The determinative tables in Appendix B are set up based on these values.

DO NOT COPY e48d507df5d1141@placeholder.94092

Printed by: e48d507df5d1141@placeholder.94092.edu. Printing is for personal, private use only. No part of this book may be reproduced or transmitted without publisher's prior permission. Violators will be prosecuted.

In practice, a mineral's hardness is determined by scratching it with materials of known hardness and vice versa. Materials of equal hardness will, with difficulty, scratch each other. Beware that a softer mineral may rub off on the surface of a harder material to leave a mark that looks like a scratch, but the mark can be rubbed off. Hardness also may be affected by weathering and other alteration, so it is important to test a fresh sample.

For some minerals, scratch hardness may vary substantially depending on crystallographic orientation (**Figure 6.3**). Kyanite (Al_2SiO_5) is a notable example. It typically forms bladed crystals that are elongate parallel to chains of edge-sharing Al octahedra. Hardness when scratched parallel to the length of crystals is 5 and at right angles is 7, reflecting weaker chemical bonding between adjacent chains than along the length of chains. Based on symmetry, the hardness of all nonisometric minerals should vary somewhat with direction, although the variation may not be easily noticed. Even isometric minerals may display some variation. Halite, for example, is slightly softer when scratched parallel to the trace of cleavage than when scratched at an angle. In all cases, the symmetry implied by hardness variation is consistent with the point group symmetry of the mineral.

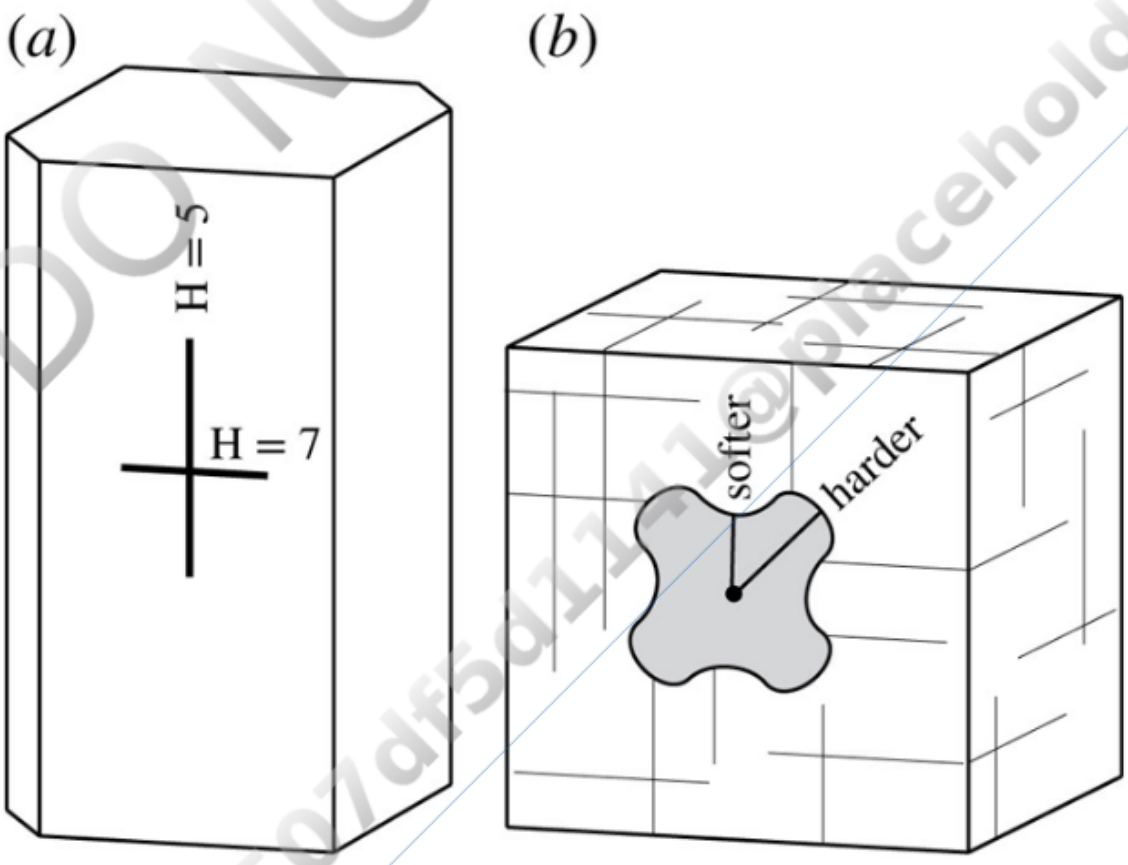

FIGURE 6.3 Variation of mineral hardness with direction. (*a*) Kyanite. Scratch hardness parallel to the length of crystals is 5 and at right angles is 7. (*b*) Halite. Scratch hardness parallel to the trace of cleavage is slightly less than hardness, at 45°. The length of a line drawn from the central dot to the edge of the shaded figure schematically shows the hardness parallel to that line. View larger image

DO NOT COPY e48d507df5d1141@placeholder.9409

Printed by: e48d507df5d1141@placeholder.94092.edu. Printing is for personal, private use only. No part of this book may be reproduced or transmitted without publisher's prior permission. Violators will be prosecuted.

An alternative and more quantitative hardness measure is **indentation hardness**. It is measured by placing a plunger with a carefully machined tip of diamond or other hard material in contact with a polished mineral surface and applying a constant load. The indentation is observed with a microscope after the plunger is removed. The depth to which the plunger penetrates the mineral is a function of the indentation hardness. Several different indentation hardness scales have been developed, based on the shape of the indenter's tip. Of these, **Vickers hardness**, which uses a pyramid-shaped indenter with a square cross section, is the most widely reported. It is commonly measured in conjunction with petrographic analysis of opaque minerals, using a reflected-light microscope. The Vickers hardness number (VHN) is the applied load in kilograms divided by the surface area of the indentation in square millimeters. VHN is somewhat variable for a given mineral depending on crystallographic orientation and the size of the load.

The relation between VHN and Mohs scratch hardness is shown in **Figure 6.4**. Note that for a given Mohs hardness, the VHN has a significant range, indicated by the width of the shaded band. Despite this variability, VHN increases systematically for Mohs hardness numbers 1 through 9 but jumps dramatically for hardness 10, reflecting the great hardness of diamond.

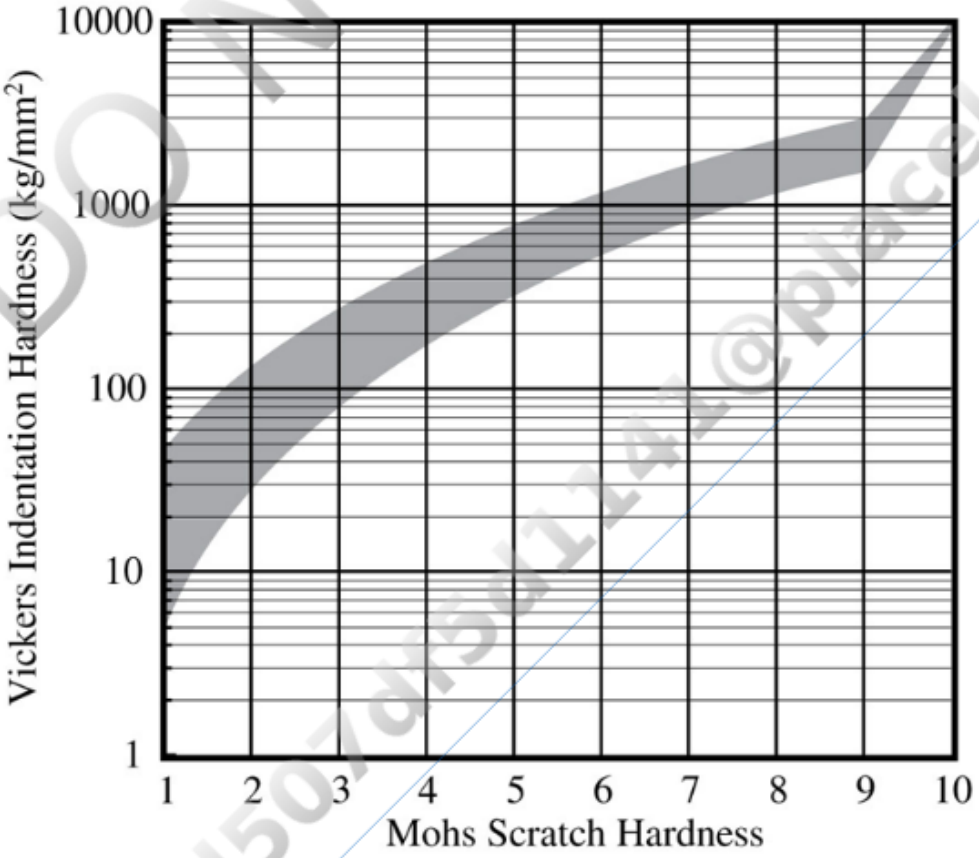

FIGURE 6.4 Approximate range of Vickers indentation hardness (shaded) as a function of Mohs scratch hardness. View larger image

Tenacity

DO NOT COPY e48d507df5d1141@placeholder.94092

Printed by: e48d507df5d1141@placeholder.94092.edu. Printing is for personal, private use only. No part of this book may be reproduced or transmitted without publisher's prior permission. Violators will be prosecuted.

Tenacity

Tenacity refers to the behavior of minerals when deformed or broken. The terms commonly applied to minerals are listed in **Table 6.3**.

TABLE 6.3 Tenacity

Term	Description
Brittle	Breaks or powders easily. Most ionic- and covalent-bonded minerals are brittle.
Malleable	May be pounded out into thin sheets. Metallic-bonded minerals may be malleable.
Ductile	May be drawn into a wire. Not easily tested. Malleable materials also may be ductile.
Sectile	May be cut smoothly with a knife. Few minerals are sectile.
Elastic	If bent, will spring back to its original position when the stress is released.
Flexible	If bent, will not spring back to its original position when the stress is released—it stays bent.

Cleavage

Many minerals have certain crystallographic planes along which chemical bonding is weaker. These weak planes along which a mineral may break are called **cleavage planes**, or **cleavages**. Because cleavages are controlled by structure and symmetry, they are always crystallographic planes and may be identified by Miller indices. For example, a cleavage plane parallel to a (100) face on a mineral is identified as a (100) cleavage surface.

Because cleavages are planes of weakness in the crystal structure, it should be possible, at least in principle, to cleave minerals into layers as thin as a unit cell that are only a few angstroms thick. Unfortunately, this cannot be practically done for most minerals; however, see the discussion of graphene in Chapter 20 for a case where it is possible.

Cleavages are typically described in terms of the crystal form (Chapter 2) to which they are parallel. Because a crystal form is a collection of essentially identical crystal faces related by the point group symmetry of the mineral, a **cleavage form** is a collection of cleavage planes related by the point group symmetry of the mineral. For example, in isometric minerals {001} cleavage signifies three cleavage directions parallel to the faces of a {001} cube [i.e., (100), (010), (001)]. In monoclinic minerals, {010} cleavage represents a single cleavage parallel to the {010} side pinacoid. The symmetry of the cleavage must, of course, be consistent with the mineral's symmetry; a monoclinic mineral will not have cubic cleavage. **Figure 6.5** shows typical cleavages for several crystal systems. *Cleavage surfaces need not be parallel to the crystal faces produced by growth.* For example, fluorite grows as {001} cubes but has {111} octahedral cleavage.

DO NOT COPY e48d507df5d1141@placeholder.9409

Printed by: e48d507df5d1141@placeholder.94092.edu. Printing is for personal, private use only. No part of this book may be reproduced or transmitted without publisher's prior permission. Violators will be prosecuted.

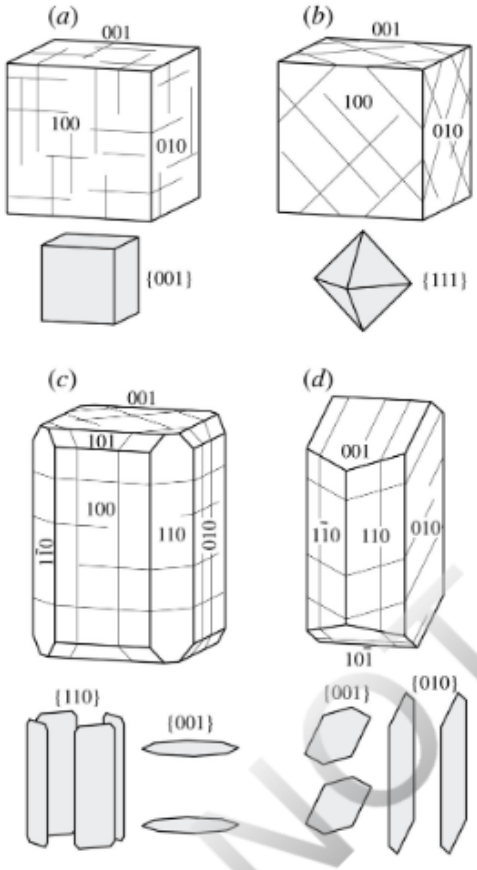

FIGURE 6.5 Cleavage. (*a*) Isometric {001} cleavage (cubic). (*b*) Isometric {111} cleavage (octahedral). (*c*) Tetrahedral {110} (prism) and {001} (pinacoid) cleavage. (*d*) Monoclinic {001} (pinacoid) and {010} (pinacoid) cleavage. View larger image

In the mineral descriptions found in Part III of this book, cleavage is described with reference to the cleavage form as described earlier. If necessary, the number of cleavages and the angles between them also may be given.

In addition to citing the Miller index symbol for the cleavage form, it is customary to describe cleavages in terms of the quality. *Quality* refers to the degree to which the cleavage surface can reflect light. **Perfect** cleavage surfaces are very flat and smooth and easily reflect light like a mirror. **Good** cleavage surfaces are interrupted by other fractures so that the surface is less continuous and light is not reflected as well as with perfect cleavage. **Fair** and **poor** are cleavage quality terms representing progressively rougher cleavage surfaces reflecting light less well. Other sources may use additional cleavage quality terms such as *imperfect*, *distinct*, and *indistinct*, which are all additional intermediate quality terms in order of decreasing quality. Unfortunately no strict definition of cleavage quality exists, but this text will only use the *perfect*, *good*, *fair*, and *poor* cleavage descriptor terms.

Fracture

Printed by: e48d507df5d1141@placeholder.94092.edu. Printing is for personal, private use only. No part of this book may be reproduced or transmitted without publisher's prior permission. Violators will be prosecuted.

Not all minerals display cleavage, as not all minerals have planes of weaker bonds within their crystal structure. Minerals without cleavage are said to have **fracture**. **Fracture surfaces** form when any mineral, even one with cleavage, is broken and the resulting surface is not crystallographically controlled. No clear distinction exists between poor cleavage and fracture; it is part of a continuum of properties. Officially olivine and tourmaline, for example, have two poor cleavages each, but these are so rarely observed that in practical terms, both minerals may be considered to only have fracture. Even though fracture does not display obvious planar surfaces, the nature of the fracture surfaces is often characteristic for some minerals. **Table 6.4** lists common terms used to describe fracture surfaces in order of increasing relief on the fracture surface.

TABLE 6.4 Fracture

Term	Description
Conchoidal	Smoothly curved as on broken plate glass
Irregular or uneven	A rough surface or one with random irregularities
Hackly	A surface with sharp-edged irregularities
Splintery	Resembles the splintery end of a broken piece of wood

Parting

Parting resembles cleavage in that a mineral may break along a regular, smooth surface. However, with parting, the mineral breaks not because of planes of weak bonds in the crystal structure, but because of some other feature in the mineral specimen. Parting is most commonly caused by twinning or exsolution lamellae (Chapter 5). As twinning or exsolution lamellae are not always present in a mineral, parting is not always present.

Partings are described in much the same manner as cleavages. A Miller index specifies the parting orientation, and terms such as *perfect* and *good* may be applied to indicate the ease with which the mineral parts. If a parting lacks strict crystallographic control, it is identified with the crystal form to which it is most closely parallel (e.g., ~{100}).

Exsolution lamellae are the most common feature that can produce parting, as the boundary between lamellae and host mineral can be a plane of weakness; the partings in the pyroxenes provide excellent examples (Chapter 14). Exsolution lamellae may have strict crystallographic control or may be in irrational crystallographic orientations.

In the past, it was common to assume that twin composition planes (Chapter 5) were planes of weakness and therefore responsible for partings. However, twin composition planes are typically quite strong and therefore not likely parting surfaces. A number of minerals where parting has been associated with twin planes are listed in **Table 6.5**. While these observations cannot be universally discounted, these examples need study

DO NOT COPY e48d507df5d1141@placeholder.9409

Printed by: e48d507df5d1141@placeholder.94092.edu. Printing is for personal, private use only. No part of this book may be reproduced or transmitted without publisher's prior permission. Violators will be prosecuted.

with modern tools. Most of these minerals can also have exsolution lamellae or other intergrowths that might produce planes of weakness. A case in point is corundum. The old literature confidently reported partings associated with rhombohedral twinning on {101}. White (1979), however, found that the {101} partings were actually produced by thin lamellae of boehmite that most likely had exsolved from the corundum.

TABLE 6.5 Common Minerals in Which Partings Have Been Associated with Twin Planes

Mineral	Presumed Twin Plane(s)	Mineral	Presumed Twin Plane(s)
Calcite	{102}	Magnetite	{111}
Cassiterite	{101}	Marcasite	{101}
Chromite	{111}	Pyrite	{011}
Corundum	{101}, {001}	Rutile	{092}, {100}
Hematite	{001}, {101}	Spinel	{111}
Ilmenite	{010}, {001}	Titanite	{221}

DO NOT COPY
e48d507df5d1141@placeholder.9409

Printed by: e48d507df5d1141@placeholder.94092.edu. Printing is for personal, private use only. No part of this book may be reproduced or transmitted without publisher's prior permission. Violators will be prosecuted.

Color and Luster

When light strikes an object, some portion of the light is absorbed, some is transmitted, and some is reflected. The balance among absorbed, transmitted, and reflected light determines our perception of color and luster. To understand how we perceive these properties, it is first necessary to acquire some background on the nature of light and how our eyes function. The nature of light will be explored in more depth in Chapter 7, particularly transmitted light through minerals.

Light

Visible light is just a small portion of the spectrum of **electromagnetic radiation** (**Figure 6.6**), which includes radio waves, cosmic rays, X-rays, etc. Although light has properties of both particles (**photons**) and waves, for present purposes it can be described by using the nomenclature and mathematics of waves. It is convenient to identify different parts of the spectrum with the wavelength of the radiation in a vacuum. Visible light has wavelengths between about 400 nm (violet light) and 700 nm (red light) (1 nm = 10^{-9}m = 10 Å). The energy of light, usually expressed in terms of electron volts (eV), increases with decreasing wavelength.

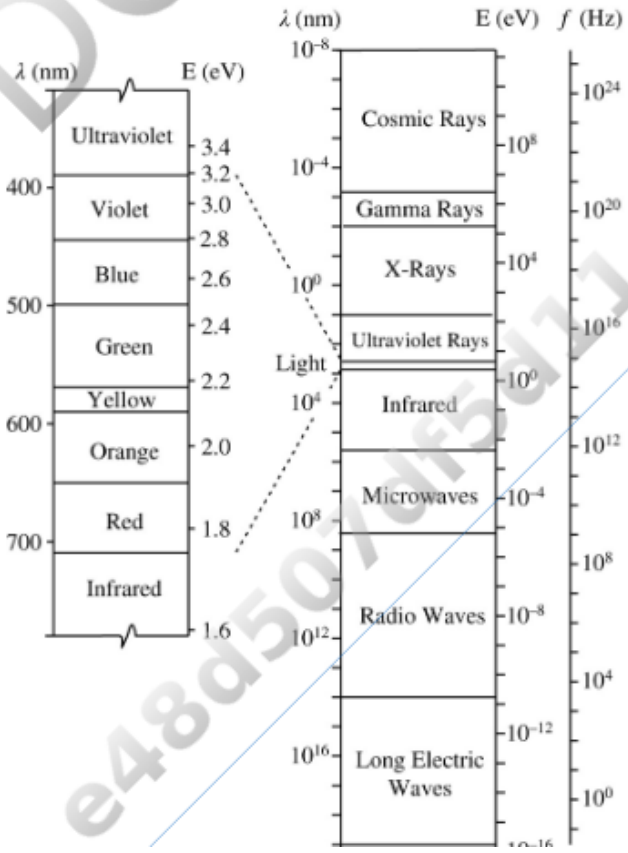

DO NOT COPY
e48d507df5d1141@placeholder.9409

Printed by: e48d507df5d1141@placeholder.94092.edu. Printing is for personal, private use only. No part of this book may be reproduced or transmitted without publisher's prior permission. Violators will be prosecuted.

FIGURE 6.6 The electromagnetic spectrum. Visible light, with wavelengths (λ) between about 400 and 700 nm and energy (E) between about 1.8 and 3.2 electron volts (eV), is a small part of the spectrum. The frequency (f) in Hertz also is shown. View larger image

Recall that the velocity of light in a vacuum is the fastest velocity possible at about 3×10^{17} nm/sec. If light enters any material, it slows down. Generally, light velocity decreases as mineral density increases. The velocity of light in a mineral is usually expressed as the mineral's **index of refraction** (n), which is the ratio of the velocity of light in a vacuum (V_v) to the velocity in the mineral (V_m).

$$n = \frac{V_v}{V_m} \tag{6.6}$$

The velocity of light in most minerals is in the range of 2 to 1.5×10^{17} nm/sec, so most minerals have indices of refraction in the range of 1.5 to 2.

Perception of Color

The human eye can discriminate the different wavelengths of visible light. Light whose wavelength in a vacuum is about 670 nm is perceived as red, 530 nm light is perceived as green, and so forth. The eye detects light by having three different color receptors that are most sensitive to wavelengths of about 660, 500, and 420 nm, corresponding to red, green, and blue-violet.

Our eyes interpret **monochromatic light**, which consists of a single wavelength, as one of the spectral colors. For example, yellow monochromatic light with a wavelength of 570 nm, stimulates the red and green receptors about equally and the blue-violet receptors very little. The brain interprets those signals to indicate that a wavelength about halfway between red and green is present and we perceive the color as yellow.

Polychromatic light consists of more than one wavelength. If polychromatic light stimulates the eye's color receptors, the combination of wavelengths is still perceived as a single color, even if the wavelength associated with that color is not present. For example, the perception of yellow can be produced by stimulating the red, green, and blue-violet color receptors with appropriate combinations of wavelengths that mimic the stimulation produced by yellow light. Televisions, computer screens, and smartphone screens take advantage of the way the eye works to allow perception of all colors by using only combinations of red, green, and blue-violet light. To confirm this, examine a white area on a computer screen with a hand lens to see the individual spots of red, green, and blue-violet. Color printing typically uses different combinations of cyan, yellow, magenta, and black ink to produce the same results.

DO NOT COPY e48d507df5d1141@placeholder.9409

Printed by: e48d507df5d1141@placeholder.94092.edu. Printing is for personal, private use only. No part of this book may be reproduced or transmitted without publisher's prior permission. Violators will be prosecuted.

The eye also is capable of perceiving combinations of wavelengths as colors that are not in the normal spectrum. If the entire visible spectrum is present, such as in light from the sun, the eye perceives it as white. The eye will also perceive various combinations of two colors called complementary light colors as white. This is because two such colors stimulate the red, green, and blue-violet color receptors about equally. Many other color sensations, such as purple and brown, have no counterpart in the visible spectrum. The sensation of purple is produced by combinations of red and violet light, whereas the sensation of brown is produced by combinations of red, blue, and yellow.

About 4 percent of the population, mostly male, have forms of color blindness that affect their perception of color because one or more of the color receptors is absent or does not function normally. For most activities, color blindness poses no significant difficulty. However, the perception of color is important in certain areas of mineralogy, particularly optical mineralogy discussed in Chapter 7, so the inability to perceive color conventionally may pose a hardship. Typically, problems with color blindness can be dealt with once they are recognized by paying closer attention to other mineral properties or by recognizing color subtleties that are not part of normal color descriptors.

Mineral Luster

Minerals can conveniently be grouped into those that are opaque and those that are transparent. Opaque materials do not transmit light, even if quite thin, whereas transparent minerals do. In general, minerals dominated by ionic and covalent bonding are transparent, whereas minerals with metallic bonding are opaque. In hand samples of minerals, we perceive this distinction in terms of **luster**, which is divided into two broad categories: **nonmetallic** and **metallic**.

Minerals with a nonmetallic luster may be quite shiny, brilliant even, but they lack the appearance of metals because they are transparent, though a thin piece of the mineral may be needed in order to demonstrate its transparency. For transparent minerals, most of the incident light passes into the mineral and as little as 5 percent of the light is reflected. The different qualities of nonmetallic luster depend on the index of refraction and texture. High index of refraction (low velocity) is associated with a more brilliant luster (**Table 6.6**).

TABLE 6.6 Varieties of Nonmetallic Luster

Luster	Description
Subvitreous	Somewhat less brilliant luster than glass; $n < 1.5$
Vitreous	The luster of glass; $1.5 < n < 2.0$
Adamantine	Exceptionally brilliant luster like that of diamond; $n > 2.0$
Resinous	Has the luster of resin; transitional to adamantine

DO NOT COPY e48d507df5d1141@placeholder.9409

Printed by: e48d507df5d1141@placeholder.94092.edu. Printing is for personal, private use only. No part of this book may be reproduced or transmitted without publisher's prior permission. Violators will be prosecuted.

Resinous	Has the luster of resin; transitional to adamantine
Dull	Surface lacks any shine
Earthy	Dull aggregates of very fine mineral grains (looks like soil)
Greasy	Luster as if covered with oil or grease; generally caused by microscopically rough surface texture
Pearly	Has an iridescent pearl-like luster; often produced by incipient development of cleavage surfaces parallel to mineral surface
Waxy	Appearance of being made out of wax
Silky	Has a subtly textured shiny appearance similar to silk; generally produced by reflection of light from the surface of aggregates composed of parallel mineral fibers

Minerals with a metallic luster reflect light like metals and typically are opaque. If about 20 percent to 50 percent of the incident light is reflected, we perceive a normal metallic luster, like that of a piece of polished gold or steel. If more than about 50 percent of the light is reflected, the metallic luster can be described as **splendent**. If less than about 20 percent of the light is reflected, the luster is **submetallic**, which is transitional to an adamantine nonmetallic luster. The details of which wavelengths are more strongly or less strongly reflected determine the color.

Mineral Color

The color of a mineral (or any other object) is our perception of the wavelengths of light that are reflected from or pass through the material to reach our eye. *Color depends on the wavelengths not absorbed by the mineral.* A red mineral looks red because it reflects or transmits red light and absorbs a substantial part of the blue end of the spectrum. A white mineral reflects essentially all of the visible spectrum to our eye. A black mineral absorbs all wavelengths.

While color has been studied in only about 10 percent of all minerals, the underlying physics of the processes controlling absorption, transmission, and emission of color is reasonably well understood. Recall from Chapter 3 that every electron around each atom in a crystal is in a specific energy level. The electrons in outer shells are typically in higher energy levels than those in the inner shells. Electromagnetic radiation (like light) passing through a mineral can be absorbed if the energy level of the radiation, which is a function of frequency, corresponds to the difference in the energy level (E) of an electron and some open higher-energy orbital. The radiation is absorbed when its energy promotes the electron into the vacant higher-energy level, leaving a lower-energy vacancy (**Figure 6.7a**). When only one or a few wavelengths of white light (containing all wavelengths) are absorbed by this orbital electron promotion, the resulting transmitted light now lacks one or more wavelength, so it will be perceived as a color.

DO NOT COPY e48d507df5d1141@placeholder.94092

Printed by: e48d507df5d1141@placeholder.94092.edu. Printing is for personal, private use only. No part of this book may be reproduced or transmitted without publisher's prior permission. Violators will be prosecuted.

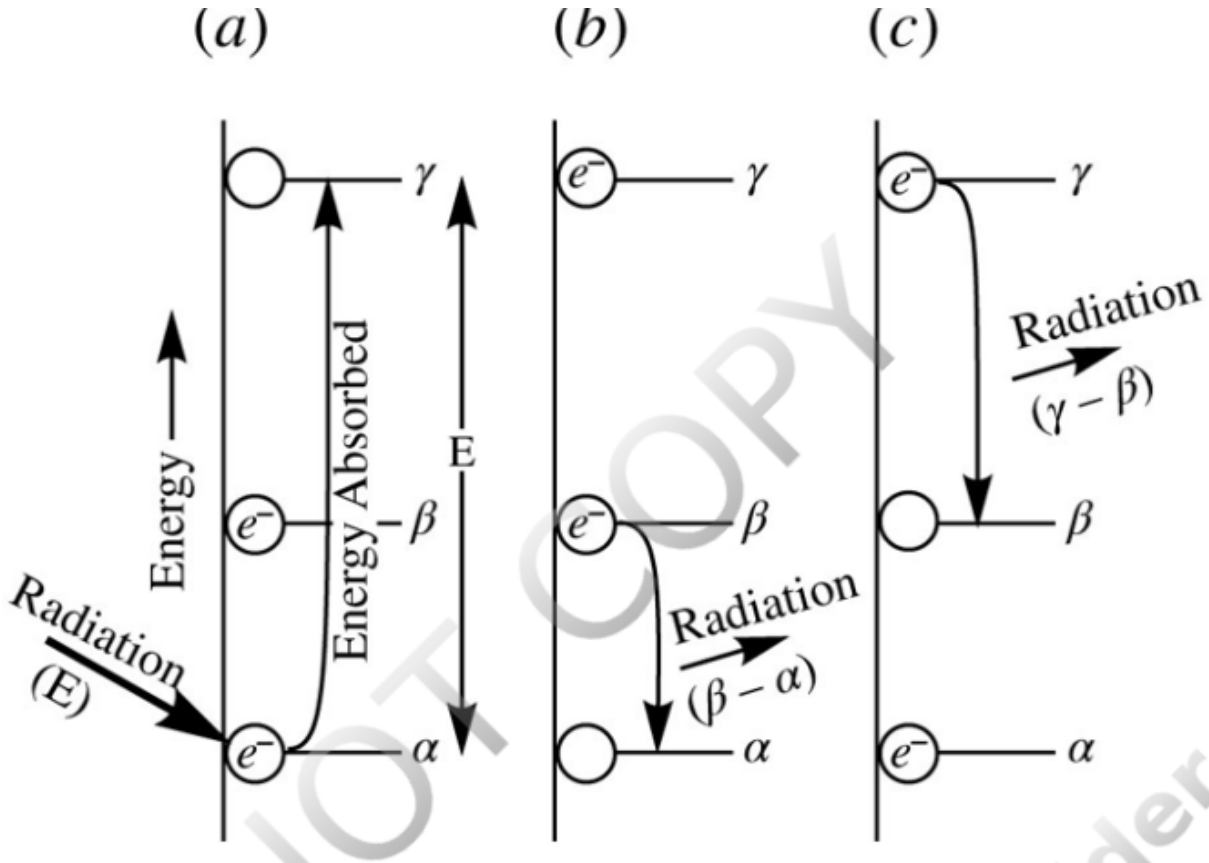

FIGURE 6.7 Absorption of electromagnetic radiation. (*a*) Electromagnetic radiation, whose energy level is *E*, excites an electron in its base energy level, *α*. If the electron can be promoted to an open energy level *γ* where the difference between *γ* and *α* is equal to *E*, the electromagnetic radiation energy will be absorbed. (*b*) An electron whose base energy level is *β* may drop into the now-vacant *α* level, releasing electromagnetic radiation whose energy is $\beta - \alpha$. (*c*) The high-energy *γ* electron now can drop into the lower-energy *β* level, releasing electromagnetic radiation whose energy is equal to $\gamma - \beta$. View larger image

When the promoted electrons fall back to their base energy levels, they re-emit electromagnetic radiation. This radiation is commonly in the infrared part of the spectrum (heat), and less commonly in the visible spectrum (**Figure 6.7b**, **c**). This process is described in a later section on photoluminescence. Processes in minerals that yield energy levels to which electrons can be promoted when visible light energy is absorbed are described by **crystal field theory**, **charge transfer transitions**, **band theory**, and **color centers**.

Crystal Field Theory

Color produced by crystal field transitions is common in ionically bonded minerals that contain cations with partially filled 3*d* orbitals. These cations include Ti, V, Cr, Mn, Fe, Co, Ni, and Cu (Table 3.3) whose outer orbitals contain unpaired electrons. Because these elements are effective in absorbing visible light energy and producing mineral colors, they are known as **chromophore elements**. Trace elements, such as those in the lanthanide series, may impart color under some circumstances. Most of the major chemical elements, including O, Si, Al, Mg, K, Ca, and Na, are not chromophores and

DO NOT COPY e48d507df5d1141@placeholder.9409

Printed by: e48d507df5d1141@placeholder.94092.edu. Printing is for personal, private use only. No part of this book may be reproduced or transmitted without publisher's prior permission. Violators will be prosecuted.

generally do not impart color to minerals. Of the chromophores, Fe is the most abundant and therefore is responsible for color in many minerals.

In a single isolated cation of one of the transition elements, all the electrons in the five orbitals in the 3*d* subshell have the same energy level (but different magnetic and spin quantum numbers) (**Figure 6.8**). When this metal cation is placed in a coordination polyhedron with anions (usually oxygen), the negative charge of the anions produces an electric field known as a **crystal field**, which interacts with the negative charge of the electrons in the orbitals around the cation. The result is that some of the orbitals in the 3*d* subshell end up with higher energy and some with lower energy with a difference of a few electron volts. This process is called **crystal field splitting**.

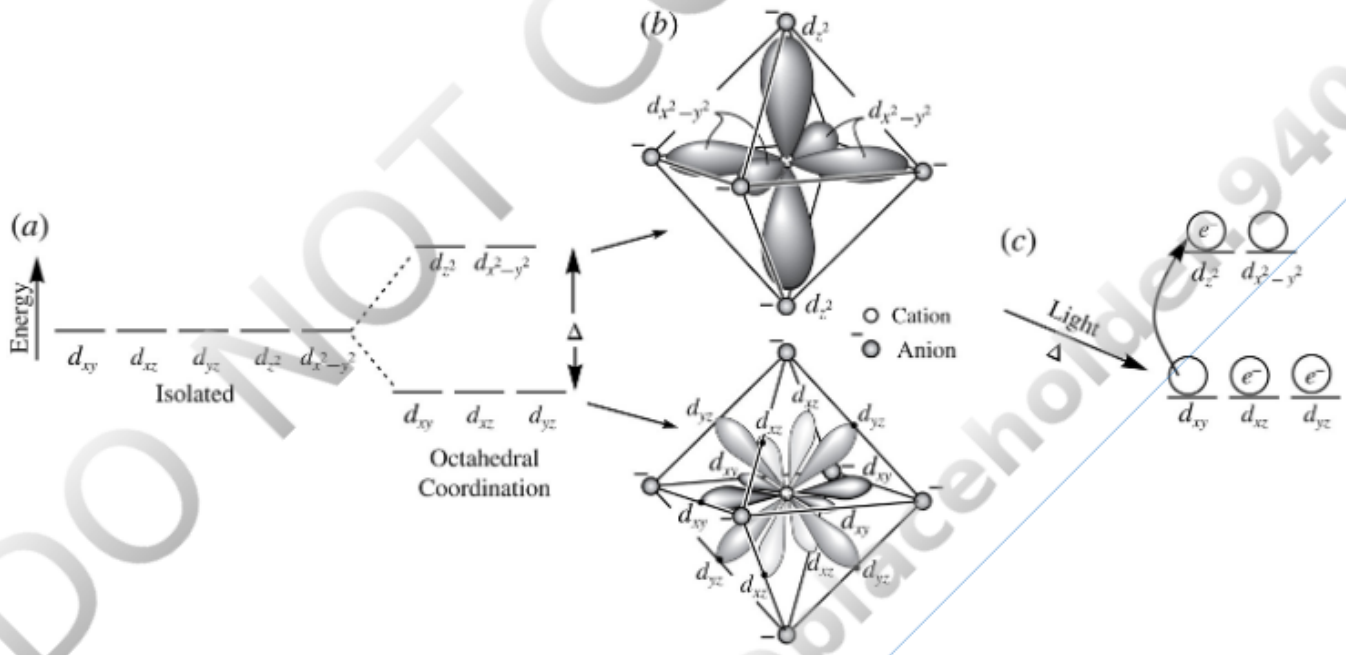

FIGURE 6.8 Crystal field splitting. (*a*) All five *d* orbitals (d_{xy}, d_{xz}, d_{yz}, d_{z^2}, and $d_{(x^2-y^2)}$) are identical in energy in an isolated transition metal cation (left). Compare with Figure 3.1. When placed in regular octahedral coordination with six anions, the *d* orbitals are split into two energy levels with an energy difference = Δ. (*b*) The d_{z^2} and $d_{(x^2-y^2)}$ orbitals are directed toward the position of the anions (top) and are forced to have higher energy because the negative charges of the anions repel the electrons. The d_{xy}, d_{xz}, and d_{yz} orbitals are directed between the anions (bottom), and have lower energy. (*c*) If incident electromagnetic energy has energy equal to Δ, it can be absorbed by promoting a lower-energy electron into a vacant higher-energy position. View larger image

Orbitals that are directed toward the anions acquire a higher energy because the negative charge of the electron(s) within these orbitals is repelled by the anions. Orbitals directed between the anions end up with lower energy. When these coordination polyhedra are combined to construct a mineral, each of the energy levels produced by crystal field splitting is spread into an energy band because the Pauli exclusion principle ensures that no two electrons in the structure can have exactly the same energy level (cf. Figure 3.8). The difference in energy between the low and high energy levels produced by crystal field splitting of 3*d* orbitals often matches the energy level of portions of the

Printed by: e48d507df5d1141@placeholder.94092.edu. Printing is for personal, private use only. No part of this book may be reproduced or transmitted without publisher's prior permission. Violators will be prosecuted.

visible light spectrum. Precisely which energy levels are available depends on the element, the details of the shape of the coordination polyhedra, and the oxidation state of the element. For example, Mn^{3+} may impart a dark pink (piemontite), pale pink (lepidolite), or green (andalusite) color.

The color of ruby is caused by crystal field splitting. Pure corundum is Al_2O_3, but in ruby, small amounts of Cr^{3+} substitute for Al^{3+}. Crystal field splitting provides excited energy levels B, C, and D, shown schematically in **Figure 6.9a**, that are about 1.9 eV, 2.23 eV, and 3.0 eV above the ground state for electrons. Incident yellow-green and violet light (λ = 550 and 400 nm, respectively) have these energy levels (Figure 6.6) and can be absorbed by promoting electrons from the ground state to the excited levels C and D. Level B is not available because of quantum mechanics considerations. The remaining wavelengths pass to our eyes and are dominated by red with some blue light. We perceive these wavelengths as a rich red color. Red fluorescence produced when the excited electrons return to their ground state is described in a later section.

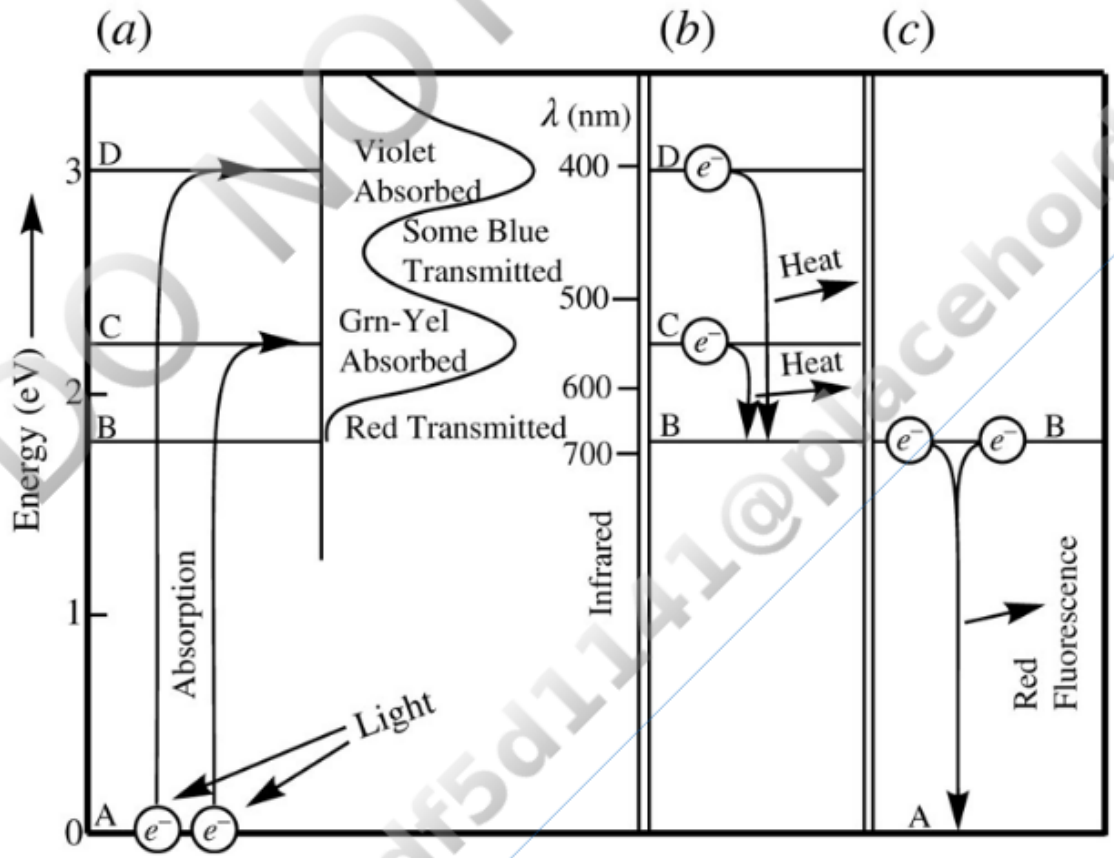

FIGURE 6.9 Light absorption in ruby. (*a*) Light with energies of about 2.23 eV and 3.0 eV can be absorbed by promoting electrons from their ground state (A) to energy levels C and D produced by crystal field splitting of Cr^{3+}. When the electrons return to their ground states, they do so by stages. (*b*) Electrons promoted to C and D fall back to the vacant B level with emission of heat. (*c*) Electrons from the B level subsequently return to A with emission of red light. Adapted from Nassau (2001).
View larger image

Charge Transfer Transitions

DO NOT COPY e48d507df5d1141@placeholder.9409

Printed by: e48d507df5d1141@placeholder.94092.edu. Printing is for personal, private use only. No part of this book may be reproduced or transmitted without publisher's prior permission. Violators will be prosecuted.

Charge transfer transitions, also known as molecular orbital transitions and intervalence charge transfers, absorb electromagnetic radiation when valence electrons are promoted to higher energy levels on adjacent ions. Charge transfers may be between two cations, between an anion and a cation, or between two anions.

With charge transfers, different ions occupy adjacent sites X and Y. Electromagnetic radiation is absorbed and promotes a lower-energy electron from ion X to a vacant higher-energy orbital on ion Y. Two common examples are transfers between Fe^{2+} and Fe^{3+}, and between Fe^{2+} and Ti^{4+}. In both cases Fe^{2+} can be considered site X. When the Fe^{2+} absorbs electromagnetic radiation and ejects an electron, it becomes Fe^{3+}. The Fe^{3+} or Ti^{4+} receives the electron, which reduces the charge by one. When the electron falls back to its original, lower-energy position, the cations revert to their original charges. In both cases the energy difference is around 1.8 eV, so light at the red end of the spectrum is absorbed and the mineral appears blue. Notable examples of color from charge transfers include the following.

- Sapphire, which is a blue gem variety of corundum (Al_2O_3), contains small amounts of Fe^{2+} and Ti^{3+} that substitute for Al^{3+}. Intervalence charge transfer between Fe^{2+} and Ti^{4+} produces the blue color.
- The Fe^{2+}–Fe^{3+} charge transfer is responsible for the black color of magnetite (Fe_3O_4) and many common mafic silicate minerals including hornblende, augite, and biotite.
- Hematite (Fe_2O_3) is deep red (when fine grained) because light energy is absorbed when an electron from an O^{2-} is transferred to an Fe^{3+}.
- Lazurite ($Na_6Ca_2[Al_6Si_6O_{24}]S_2$) is blue because adjacent sulfur atoms in different structural sites have electron energy levels that differ by a couple of electron volts. Light at the red end of the spectrum is absorbed when an electron from one sulfur atom is promoted to its neighbor.

Band Theory

Minerals with a significant degree of **metallic bonding** and **semiconductors** with a small band gap typically absorb a wide range of wavelengths and are therefore opaque. Recall from Chapter 3 that moving atoms into close proximity in a crystal involves spreading energy levels available to electrons into bands because of the Pauli exclusion principle. Energy levels of the electrons in the **valence band** are spread out so they overlap with or are close to the energy levels of the **conduction band**.

With metals (**Figure 6.10a**), no band gap is present between the valence band and the conduction band, so the entire visible spectrum can be absorbed and these materials are considered opaque. When the electrons return to their lower energy levels, some of the energy is converted to heat, and some is re-emitted as light. The efficiency of the process depends on the density of energy levels within the conduction band and on quantum

DO NOT COPY e48d507df5d1141@placeholder.9409

Printed by: e48d507df5d1141@placeholder.94092.edu. Printing is for personal, private use only. No part of this book may be reproduced or transmitted without publisher's prior permission. Violators will be prosecuted.

depends on the density of energy levels within the conduction band and on quantum mechanics considerations—not all wavelengths are equally absorbed and re-emitted.

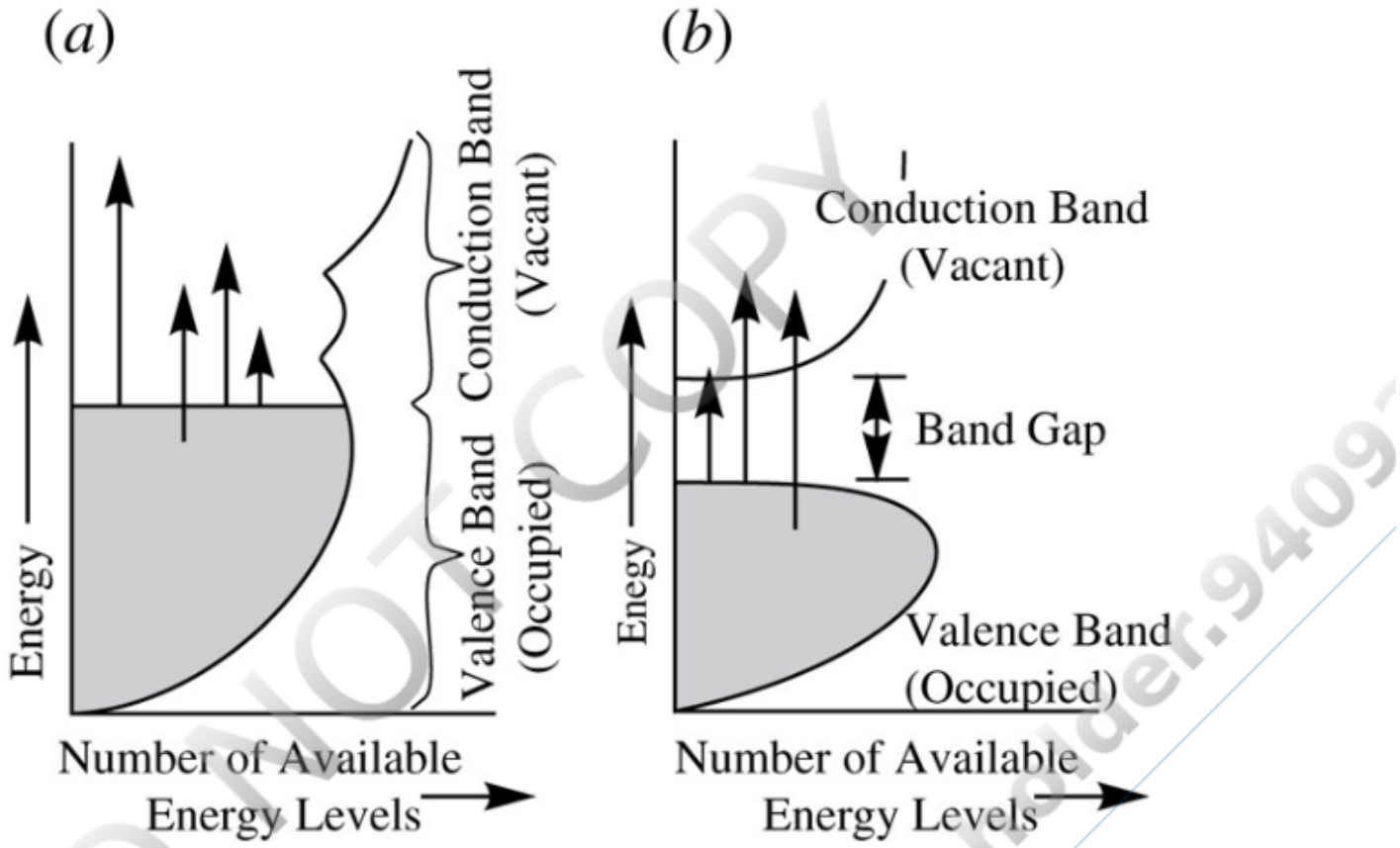

FIGURE 6.10 Band theory. (*a*) Valence bands and conduction bands do not have an energy gap between them with metallic bonding. All light is absorbed because a continuum of energy levels is available to which electrons in the valence band can be promoted. The light that is emitted as electrons return to their base energy state determines the mineral color. The emitted light is perceived as being reflected. (*b*) In semiconductors, an energy gap exists between the valence band and the conduction band. Light whose energy is greater than the band gap can be absorbed by promoting valence electrons into the conduction band. View larger image

Gold, for example, has its golden color because light at the red and yellow end of the spectrum is absorbed most strongly, and light at the blue and violet end of the spectrum is less strongly absorbed. The counterintuitive result is that the strongly absorbed light penetrates into the gold only a few hundred atoms, and these wavelengths are immediately re-emitted from the sample's surface at greater than about 80 percent efficiency (**Figure 6.11**). The re-emitted light is seen as a reflection. Light at the blue and violet end of the spectrum passes further into the gold before being absorbed. Fewer of those wavelengths are re-emitted from the surface of the sample, and more of the energy is converted to heat. If gold is pounded into extremely thin sheets (<100 nm) the light that passes through is perceived as bluish green because the red end of the spectrum is more strongly absorbed than blue-violet. Silver, in contrast, strongly absorbs and re-emits the entire visible spectrum at over 95 percent efficiency. For this reason silver is widely used as a coating for mirrors. Copper has an absorption/reflection pattern similar to gold.

DO NOT COPY e48d507df5d1141@placeholder.94092

Printed by: e48d507df5d1141@placeholder.94092.edu. Printing is for personal, private use only. No part of this book may be reproduced or transmitted without publisher's prior permission. Violators will be prosecuted.

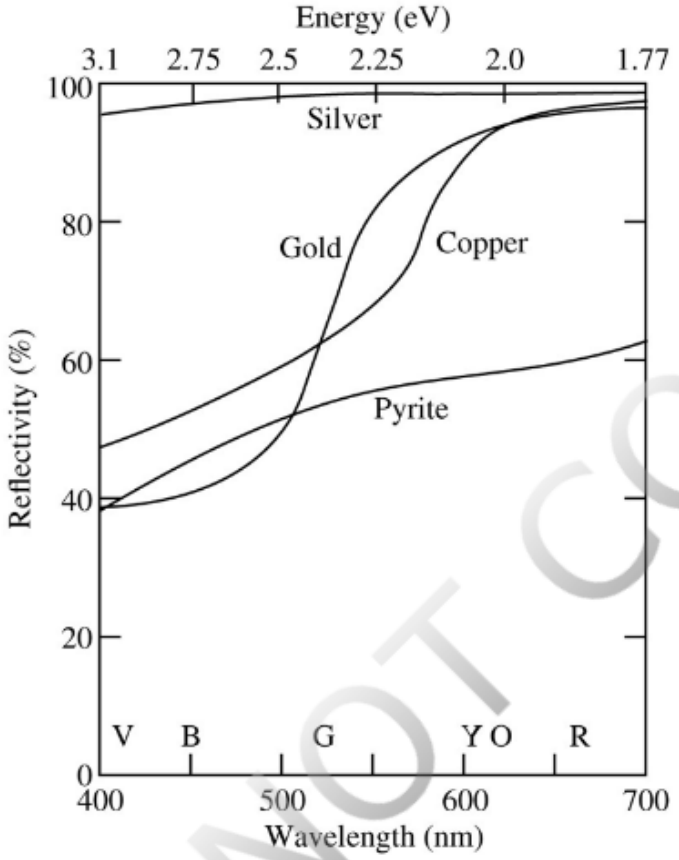

FIGURE 6.11 Reflectivity of metals and semiconductors. The most strongly absorbed wavelengths also are most strongly re-emitted. Silver absorbs and re-emits the visible spectrum with more than 95 percent efficiency. Gold and copper absorb and re-emit the red end of the spectrum more efficiently than the blue-violet end of the spectrum. Pyrite, which is a semiconductor, also has stronger absorption and re-emission at the red end of the spectrum and hence has a color similar to gold in hand sample. View larger image

Minerals with a substantial degree of covalent bonding may behave as semiconductors—sulfides are good examples. With semiconductors (**Figure 6.10b**), a gap in available electron energy levels, known as a **band gap** (E_g), exists between the conduction and valence bands. Light whose energy is greater than that of the band gap will be absorbed because it can promote electrons from the top of the valence band to vacant levels in the conduction band. If the band gap is smaller than the energy range of visible light, all the light is absorbed, and the mineral may be black or gray, like galena (PbS). Pyrite has a band gap of about 0.95 eV, so it can absorb all of the visible spectrum, but light at the red end of the spectrum is absorbed and re-emitted more strongly than at the violet end of the spectrum, similarly as with gold; hence both minerals have a similar color. If the band gap is intermediate, high-energy, short-wavelength light from the violet end of the spectrum will be absorbed, but light from the lower-energy, red end of the spectrum will not. Minerals such as cinnabar (HgS) owe their red color to this process. If the band gap is large, as in diamond (E_g ~5.5 eV), none of the visible spectrum is absorbed and the mineral is white or colorless.

Impurities in minerals with large band gaps may influence color in some cases. The blue

DO NOT COPY e48d507df5d1141@placeholder.9409

Printed by: e48d507df5d1141@placeholder.94092.edu. Printing is for personal, private use only. No part of this book may be reproduced or transmitted without publisher's prior permission. Violators will be prosecuted.

color of some diamonds is due to the presence of trace amounts of boron. Boron provides an energy level a short distance above the top of the valence band to which electrons can be promoted. This allows some light at the red end of the spectrum to be absorbed, so the diamond appears blue.

Color Centers

While crystal field transitions and charge transfer transitions depend on electrons of specific elements absorbing parts of the visible spectrum, **color centers** depend on having electrons mislocated in the structure. Some minerals whose color depends on color centers are listed in **Table 6.7**.

TABLE 6.7 Minerals with Color Centers

Mineral	Color
Amazonite (var. K-feldspar)	Blue/green
Amethyst (var. quartz)	Purple
Fluorite	Purple
Smoky quartz	Brown, black
Diamond	Green, yellow, brown, blue, pink
Topaz	Blue
Halite	Blue, yellow

Electron color centers are formed by an electron trapped in a vacant site in a crystal. Recall from Chapter 5 that crystals always contain flaws, like Frenkel defects, in which ions are missing from their normal location. If the missing ion is an anion (**Figure 6.12a**), its position may be occupied by an electron to form an electron color center. The electron occupies the vacancy (**Figure 6.12b**) when high-energy radiation is absorbed and promotes an electron from its base energy level A elsewhere in the structure, up to level F. This electron attempts to return to its original energy level, but gets trapped in the vacancy at energy level B by the positive charge of adjacent cations. Because of the interaction with the crystal field provided by adjacent cations and anions, the trapped electron has a number of specific energy levels to which it may be excited, shown as energy levels C and D. Incident light with energy E_{bd} can be absorbed and promote the electron from B to D, from which it cascades back to B via level C with emission of heat or light. If the sample is heated sufficiently to provide energy E_{be}, the electron can escape the color center and returns to its base energy level A. If the electron escapes the color center, then the mineral will lose the color created by the color center, perhaps returning to its normal white or colorless state. Re-radiating the crystal can place another electron into the vacancy to again produce a color center and the mineral's color will change accordingly.

DO NOT COPY e48d507df5d1141@placeholder.94092

Printed by: e48d507df5d1141@placeholder.94092.edu. Printing is for personal, private use only. No part of this book may be reproduced or transmitted without publisher's prior permission. Violators will be prosecuted.

accordingly.

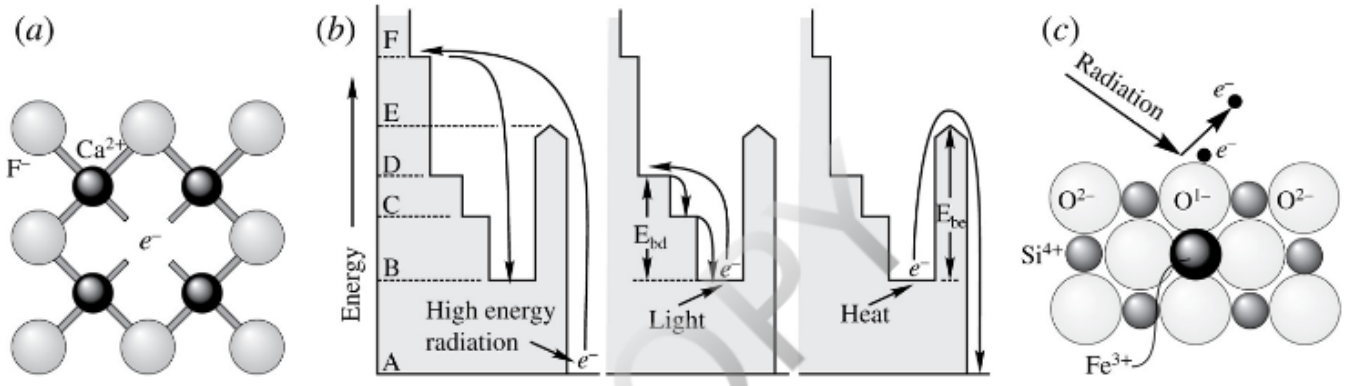

FIGURE 6.12 Color centers. (*a*) Electron color center. A F^- anion in fluorite is missing and the vacancy is occupied by an electron. (*b*) Electron color center energy structure. See text for details. (*c*) Hole color center in amethyst. See text for details. (Adapted from Nassau, 2001.) View larger image

Hole color centers are produced if an electron is missing from its normal location (**Figure 6.12c**). The purple color of amethyst, which is a variety of quartz (SiO_2), is produced when Si^{4+} is replaced by Fe^{3+}. Charge balance is maintained by including a monovalent cation such as H^+ elsewhere in the structure. The color center is produced when high-energy radiation ejects an electron from an oxygen anion bonded to the Fe^{3+}. The ejected electron gets trapped by the H^+ elsewhere in the structure, leaving the oxygen with an unpaired electron. This color center is referred to as a $[FeO_4]^{4-}$ color center because the iron coordinates with four oxygen anions, one of which is missing an electron. The energy levels provided by the hole allow light at the red end of the spectrum to be absorbed. Similar color centers in smoky quartz involving Al^{3+} are called $[AlO_4]^{4-}$ color centers.

Note that an electron center is often paired with a hole center. Either one might provide the energy levels needed to absorb light in the visible spectrum, depending on the crystal structure and the elements involved. In nature, radiation needed to form color centers comes from radioactive decay, commonly of potassium, thorium, and uranium in nearby minerals. Color centers also may be produced by exposing minerals to radiation in the laboratory, and gems such as topaz, beryl, and diamond are routinely irradiated to enhance their color and value.

Color from Mechanical Causes

In addition to being colored because of their chemical and/or structural makeup, minerals may be colored because they contain finely dispersed inclusions of other materials. Hematite (Fe_2O_3) is a widely distributed mineral that, if included in other minerals, may cause them to be various shades of red or brown. For example, jasper is a red-brown variety of fine-grained quartz (SiO_2) widely used in lapidary work. Graphite (C) may cause

DO NOT COPY e48d507df5d1141@placeholder.94092

Printed by: e48d507df5d1141@placeholder.94092.edu. Printing is for personal, private use only. No part of this book may be reproduced or transmitted without publisher's prior permission. Violators will be prosecuted.

normally white or colorless calcite ($CaCO_3$) to be black. The milky-white color of milky quartz is caused by the presence of abundant microscopic to submicroscopic inclusions of fluid, mostly water, from which the quartz originally grew.

A special mechanical phenomena is **chatoyancy**, which is seen as a silky appearance. It is produced in minerals such as satin spar gypsum ($CaSO_4 \cdot 2H_2O$) that consist of parallel fine fibers, or minerals containing abundant parallel fibrous inclusions. Closely related **asterism** is sometimes seen in corundum and quartz. Both minerals are hexagonal and may contain inclusions of fine fibrous rutile (TiO_2) that are aligned parallel to the 2-fold symmetry axes at right angles to *c*. Light scattering from these fine inclusions may be perceived to form a six-pointed star pattern (**Figure 6.13**).

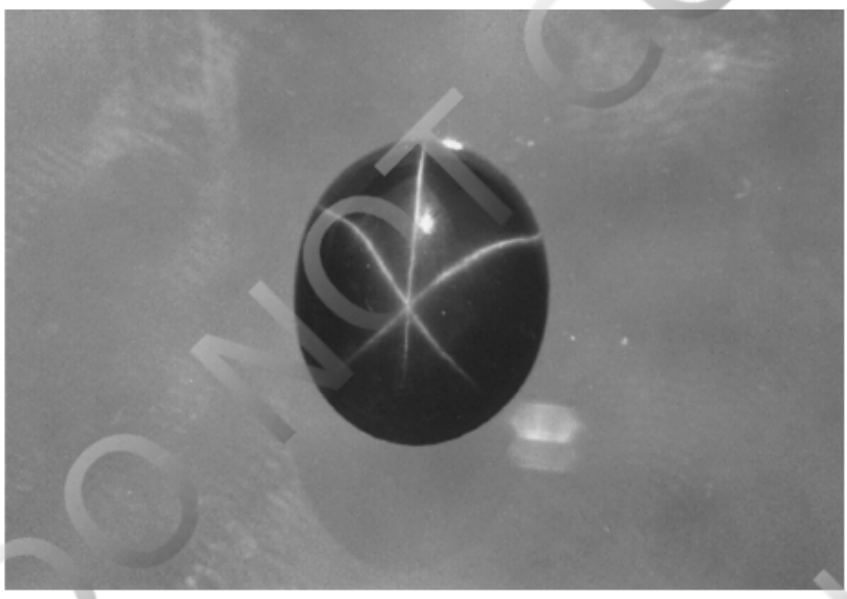

FIGURE 6.13 Photograph of star sapphire whose long dimension is 8 mm. The star pattern is due to numerous fibrous rutile (TiO_2) inclusions parallel to the hexagonally arranged 2-fold rotation axes in the host corundum. View larger image

Some minerals display flashes of varied internal color that change as the sample is moved about in the light. This "**play of color**" or **iridescence** is caused by diffraction of light on closely spaced features within the structure of the mineral. In precious opal (fire opal), the diffraction is produced by roughly uniform spheres of silica gel that are regularly packed. The dimension of the spheres corresponds with the wavelength of visible light, so they act as a diffraction grating that separates the incident polychromatic light into its different wavelengths that are dispersed in different directions. Feldspar too can have different varieties of iridescence; one variety is called moonstone. All are produced by diffraction on a closely spaced lamellar structure produced by exsolution (see Chapter 12).

Iridescence can also be seen on the oxidized surface of minerals such as pyrite, chalcopyrite, and bornite. The oxidization produces a thin layer of material that interacts with the incoming light in the same way that a film of oil on water produces iridescence.

DO NOT COPY e48d507df5d1141@placeholder.9409

Printed by: e48d507df5d1141@placeholder.94092.edu. Printing is for personal, private use only. No part of this book may be reproduced or transmitted without publisher's prior permission. Violators will be prosecuted.

Cracks inside many transparent minerals may also produce iridescent colors; this is readily observed with a hand lens.

Consistency of Mineral Color

Minerals that are opaque or that contain chromophore elements as an integral part of their chemical composition typically have consistent colors. These **idiochromatic** (self-colored) minerals may display a range of color consistent with the compositional variation displayed by the mineral.

Minerals whose color may be quite variable are termed **allochromatic** (foreign-colored) minerals. These minerals typically do not have chromophore elements as an integral part of their chemical composition and typically are fairly light colored (white or colorless), at least if pure. If not white or colorless, their color comes from color centers, trace amounts of chromophore elements, inclusions, etc. Quartz (SiO_2), for example, is colorless when pure but may be purple (amethyst) if it contains trace amounts of Fe^{3+}, pink (rose quartz) if it contains trace amounts of Ti^{4+}, or almost any color if it contains appropriately colored inclusions.

Streak

Streak is the color of a mineral when it is finely powdered. Minerals with dominantly ionic and covalent bonding tend to have fairly light-colored streaks, even if the mineral color is dark in large pieces. This is because these minerals are all relatively transparent, so only a small amount of the incident light is absorbed on passing through the fine particles of the powder. Nearly the complete spectrum is reflected back to our eye and is perceived as white or a pale color. For these minerals, even though the mineral color may vary significantly, the streak color is usually quite consistent.

The streak of minerals with metallic bonding may be richly colored or black. These minerals are typically opaque, so the incident light is strongly absorbed, even for the fine powder. Streak color may be darker than mineral color because the rough surface of the powder does a better job of absorbing incident light.

Streak color is conveniently observed by rubbing a mineral sample on a **streak plate**, which is an unglazed white porcelain tile. Streak plates have a hardness of about 6.5, so they cannot be used for harder minerals. For harder minerals, or if a streak plate is not available, the streak color may be observed by pulverizing a sample with a knife blade or rock hammer, etc.

Luminescence

DO NOT COPY e48d507df5d1141@placeholder.94092

Printed by: e48d507df5d1141@placeholder.94092.edu. Printing is for personal, private use only. No part of this book may be reproduced or transmitted without publisher's prior permission. Violators will be prosecuted.

Luminescence is a phenomenon in which a material absorbs one form of energy and then re-emits the energy as visible light. The energy source may be mechanical, thermal, or electromagnetic.

Triboluminescence

Some materials may become faintly luminous when struck, crushed, scratched, or rubbed. This **triboluminescence** is typically quite faint and requires near total darkness to be seen. The Uncompahgre Ute Native American tribe of Colorado use the triboluminescence of quartz in ceremonial rattles made of buffalo hide (Dawson, 2010). The quartz-filled rattles are shaken at night and the light generated by the quartz crystals striking each other is visible through the hide.

Thermoluminescence

If a material emits visible light energy as a consequence of being heated, it is **thermoluminescent** or **incandescent**. Thermoluminescence generally requires that the sample be exposed to light or other radiation at some point, so that electrons can be excited to higher-energy positions. These electrons may be trapped in their higher energy levels such as in a color center. Heating can provide sufficient activation energy to allow the electrons to fall back to their ground states. Thermoluminescence is generally strongest between 50 and 100°C and ceases at temperatures above 475°C. Thermoluminescence also requires near total darkness to be seen. At temperatures of about 550°C, most materials become incandescent and begin to glow dull red. Incandescence is caused when thermal excitation causes electrons to be promoted to energy levels sufficiently high that the energy released when they drop back to their ground state yields light in the visible spectrum. With increases in temperature, the incandescent color changes to yellow and eventually becomes white, as light is emitted in nearly the entire visible spectrum.

Photoluminescence

Materials that emit light in response to being exposed to visible or ultraviolet light are **photoluminescent**. The light energy that is absorbed by promoting electrons through crystal field transitions, charge transfer transitions, and color centers can be held there for a period of time. The promotion of an electron to a higher-energy position leaves vacant a lower-energy orbital from which the electron came. Eventually, a higher-energy electron will drop into the vacant orbital, and another will fill its position, and so forth, until electrons occupy the lowest set of orbitals available.

When a higher-energy electron drops into a vacant lower energy level, energy in the form of electromagnetic radiation is released (Figure 6.7). If this radiation is in the visible spectrum, the mineral is said to be **fluorescent** or **phosphorescent**. Fluorescence and phosphorescence differ only in how long it takes the electrons to return to their ground

DO NOT COPY e48d507df5d1141@placeholder.9409

Printed by: e48d507df5d1141@placeholder.94092.edu. Printing is for personal, private use only. No part of this book may be reproduced or transmitted without publisher's prior permission. Violators will be prosecuted.

states. With fluorescence, the vacant lower-energy electron positions are filled within 10^{-8} second; phosphorescence takes longer. When the incident radiation is turned off, fluorescent materials cease emitting light. Phosphorescent materials continue emitting light energy for hours or more after the exciting radiation ends.

The fluorescent/phosphorescent light has lower energy (longer wavelength) than the original exciting radiation. Hence, wavelengths in the ultraviolet range (Figure 6.6) tend to be effective in producing fluorescence in the lower-energy visible spectrum. Fluorescence is routinely observed by illuminating a mineral sample in a darkened room with either a short-wave ($\lambda \approx 254$ nm), mid-wave ($\lambda \approx 330$ nm), or long-wave ($\lambda \approx 366$ nm) ultraviolet lamp. Because our eyes are insensitive to ultraviolet light, the fluorescent light is readily observed. The different energies/wavelength of the light source may produce different fluorescent colors.

Visible light also may trigger fluorescence. The absorption of light by ruby was described earlier (Figure 6.9a). Small amounts of Cr^{3+} absorb green-yellow and violet light via crystal field transitions. When the excited electrons revert to their ground state, they cannot do so directly for reasons of quantum mechanics. Rather, they first drop to energy level B at about 1.9 eV above the ground state, with emission of infrared radiation (heat) whose energy is about 1.1 and 0.3 eV (**Figure 6.9b**). Light emission occurs when the electron drops from B back to the ground state at A (**Figure 6.9c**). This energy drop is about 1.9 eV and is the energy of red light. Hence, in addition to transmitting red light, some of the absorbed energy is reradiated as additional red light, which tends to give the ruby extra color depth and the appearance of glowing. This warmth or glow adds considerably to the appeal of ruby as a gemstone.

Over 800 minerals are known to be luminescent under some conditions, and this includes many common minerals, including feldspars, pyroxenes, amphiboles, carbonates, sulfates, etc. A comprehensive list is maintained by the Fluorescent Mineral Society (www.fluomin.org). The list of fluorescent minerals in Appendix B (Table B.5) includes only those that are consistently and distinctly fluorescent.

DO NOT COPY e48d507df5d1141@placeholder.9409

Printed by: e48d507df5d1141@placeholder.94092.edu. Printing is for personal, private use only. No part of this book may be reproduced or transmitted without publisher's prior permission. Violators will be prosecuted.

Magnetism

Magnetic fields are produced by the movement of electrons. At the atomic level, the most important movement is **electron spin**, denoted by the **spin quantum number**. Recall from Chapter 3 that each orbital may contain two electrons, but because no two electrons in an atom have precisely the same set of quantum numbers, those two electrons must have opposite spins. Each spinning electron produces a magnetic field, whose **Bohr magnetic moment** (μ_B) can be canceled by an electron in the same orbital spinning in the opposite direction.

The magnetic behavior of a mineral, therefore, depends on whether atoms have orbitals with unpaired electrons. If no element in the mineral contains unpaired electrons, the mineral is **diamagnetic**. If unpaired electrons in one or more orbitals are present, the possibilities include **paramagnetism**, **ferromagnetism**, **ferrimagnetism**, and **antiferromagnetism** (**Figure 6.14**), depending on how the magnetic moments of the atoms are oriented within the crystal structure. The most important elements that have unpaired electrons include the transition metals whose 3*d* orbitals are only partially filled (Table 3.3). Of these Fe, Mn, Ti, and Cr are the most abundant. The strength of the magnetic moment of these elements depends on how many electrons are unpaired. Fe^{3+} and Mn^{2+} have the largest magnetic moments with five unpaired 3*d* electrons each. Minerals that are ferromagnetic and ferrimagnetic display an obvious attraction to a magnet, and a list is provided in Appendix B, Table B.6.

DO NOT COPY

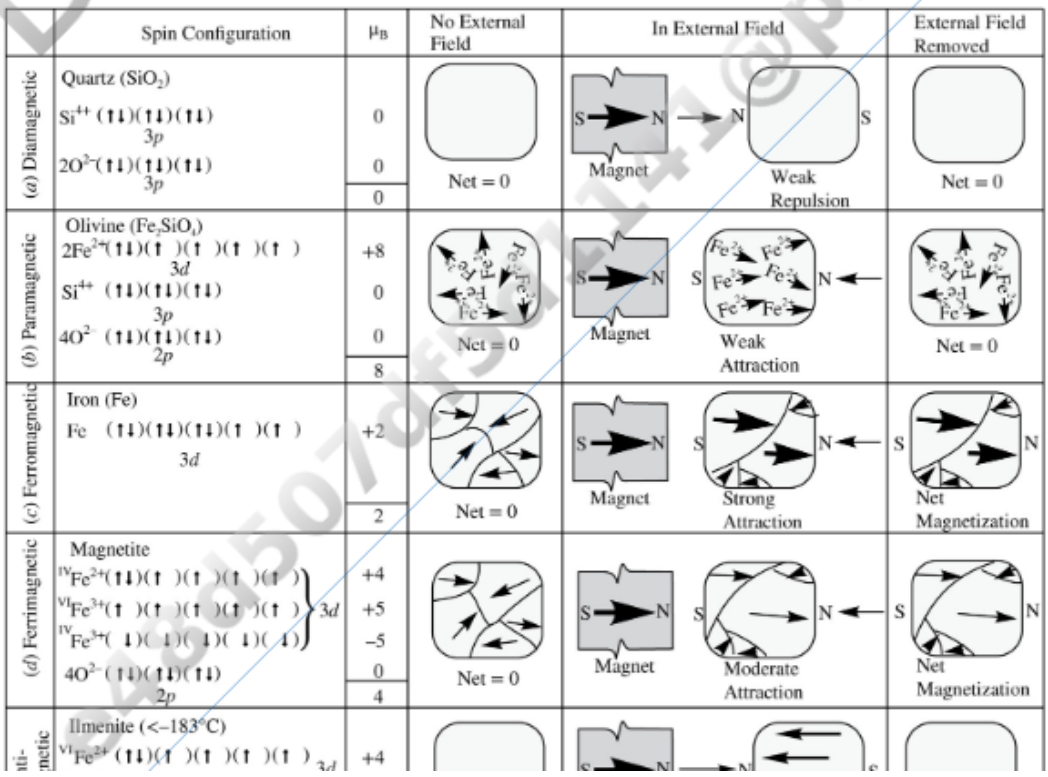

Printed by: e48d507df5d1141@placeholder.94092.edu. Printing is for personal, private use only. No part of this book may be reproduced or transmitted without publisher's prior permission. Violators will be prosecuted.

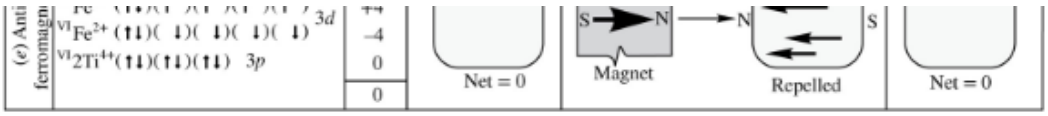

FIGURE 6.14 Magnetism. See text for discussion. (*a*) Diamagnetism in quartz. Neither Si^{4+} nor O^{2-} has unpaired electrons, so neither has a Bohr magnetic moment μ_B. (*b*) Paramagnetism in olivine. The Fe^{2+} has a net Bohr magnetic moment; but in the absence of an external magnetic field, the orientations are random. (*c*) Ferromagnetism in native iron. Each iron atom has two unpaired electrons and a Bohr magnetic moment of 2. Domains within the mineral have uniform magnetic orientation. (*d*) Ferrimagnetism in magnetite. The $^{IV}Fe^{2+}$ has a net magnetic moment and causes the magnetite to have ferromagnetic properties. (*e*) Antiferromagnetism in ilmenite below −183°C. Fe^{2+} in adjacent sites have antiparallel spins. Net magnetic moments cancel. Antiferromagnetic materials are repelled by a magnet. View larger image

Diamagnetism

In **diamagnetic** materials, all orbitals of the atoms contain paired electrons. Quartz (SiO_2) is diamagnetic. Silicon, by losing four electrons to become Si^{4+}, acquires the electron configuration of Ne, in which the 1*s*, 2*s*, and 2*p* orbitals are entirely filled (Figure 6.14a). Each oxygen gains two electrons to become O^{2-}, which also has the electron configuration of Ne. The number of "up" spin electrons is exactly balanced by the "down" spin electrons, so each ion has zero net magnetic moment and the mineral cannot have a net magnetic moment. Minerals whose atoms have acquired electron configurations of the inert gases or whose orbitals otherwise do not contain unpaired electrons are diamagnetic. In general, this excludes the transition metals, which have partially filled *d* orbitals. When placed in a magnetic field, diamagnetic minerals will actually be slightly repelled. The external magnetic field causes electrons in the mineral to move, which in turn produces a magnetic field opposing the external field.

Paramagnetism

Minerals in which the magnetic moments of the constituent atoms are not mutually aligned are **paramagnetic**. Olivine [$(Mg,Fe)_2SiO_4$], for example, contains Fe^{2+} in variable amounts. Each Fe^{2+} has a magnetic moment because each contains four unpaired electrons in the 3*d* orbitals (Figure 6.14b). These four electrons all have spins in the same direction because of Hund's Rule, which states that each orbital within a subshell gets one electron with a $+\frac{1}{2}$ quantum number (up spin) before any orbital gets a second electron with a $-\frac{1}{2}$ quantum number (down spin).

Although each Fe^{2+} has a magnetic moment, the moments do not align with each other. The net magnetic moment of all the randomly oriented Fe^{2+} is zero. If olivine is placed in a magnetic field, the orientations of the magnetic moments of the Fe^{2+} will tend to align parallel to the external field so that the sample is attracted to the magnet. Normal thermal motion of the ions in the structure randomize this alignment so the net magnetic moment and the magnetic attraction are weak. Paramagnetic minerals are not noticeably

DO NOT COPY e48d507df5d1141@placeholder.94092

Printed by: e48d507df5d1141@placeholder.94092.edu. Printing is for personal, private use only. No part of this book may be reproduced or transmitted without publisher's prior permission. Violators will be prosecuted.

moment and the magnetic attraction are weak. Paramagnetic minerals are not noticeably attracted to a handheld magnet.

The strength of the magnetic moment produced in a paramagnetic mineral is a function of the **magnetic susceptibility**, which depends on chemical composition and mineral structure. When the external magnetic field is removed, the magnetic moment of the mineral rapidly dissipates, as the magnetic moments of the constituent Fe^{2+} ions revert to random orientations. Most iron-bearing silicate minerals are paramagnetic.

Ferromagnetism

A material that is **ferromagnetic**, such as a piece of iron, is capable of retaining a magnetic polarity because the magnetic moments of the constituent atoms with unpaired electrons become systematically aligned (Figure 6.14c). An effect known as exchange coupling locks the magnetic moment of adjacent ions into parallel alignment, for reasons tied to quantum mechanics. Within a single grain of a ferromagnetic material, parallel alignment is generally restricted to microscopic volumes known as domains. Adjacent domains need not have parallel alignment. If the magnetic moments in different domains are randomly oriented, the net magnetic moment will be zero. Attraction to a magnet, however, is strong because the external field will tend to rearrange the alignment of the magnetic domains.

Exposure to an external magnetic field of sufficient strength will cause domains with magnetization parallel to the external field to expand, while other domains in unfavored orientations will shrink. The crystal therefore becomes permanently magnetized. The attraction between a ferromagnetic material and an applied magnetic field is many orders of magnitude greater than is the case for paramagnetic materials. When the external field is removed, the parallel alignment of the magnetic domains remains and the material retains its magnetic properties. Magnetizing a steel nail by consistently rubbing it with a strong magnet is a good example of this phenomenon.

Ferrimagnetism

Ferrimagnetism (Figure 6.14d) differs from ferromagnetism in that some atoms in adjacent structural sites have antiparallel magnetic moments because of exchange coupling. The magnetic moments of these atoms therefore cancel each other. Additional atoms may have unpaired electrons that can produce a magnetic moment. As long as some atoms do not have an antiparallel partner, the mineral will display ferromagnetic properties. Magnetite, which is by far the most common magnetic mineral, is ferrimagnetic. Its formula can be written as $^{IV}Fe^{3+}\uparrow {}^{VI}(Fe^{3+}\downarrow Fe^{2+}\uparrow)O_4$. The arrows in the formula indicate the magnetic spins. It consists of cubic close-packed oxygen anions with the first Fe^{3+} in tetrahedral coordination, and the second Fe^{3+} and the Fe^{2+} in octahedral coordination. Exchange coupling forces the tetrahedral and octahedral Fe^{3+} to have

DO NOT COPY e48d507df5d1141@placeholder.9409-

Printed by: e48d507df5d1141@placeholder.94092.edu. Printing is for personal, private use only. No part of this book may be reproduced or transmitted without publisher's prior permission. Violators will be prosecuted.

opposite spins, so their magnetic moments cancel. The magnetic moments of the octahedral Fe^{2+} align in adjacent sites, so magnetite can have a net magnetic moment.

The term **antiferromagnetism** is applied to materials in which antiparallel spins completely cancel to yield zero net magnetic moment. It can be considered a special case of ferrimagnetism. Among the Fe–Ti oxides, pure ilmenite ($Fe^{2+}Ti^{4+}O_3$) is antiferromagnetic below −183°C (Figure 6.14e). The Ti^{4+} lacks a magnetic moment, and the moments of Fe^{2+} in adjacent lattice planes are oriented antiparallel. Above −183°C (the Néel temperature) the antiparallel ordering is destroyed and ilmenite becomes paramagnetic. The magnetic behavior of ilmenite at room temperatures is due to nearly ubiquitous exsolution lamellae of magnetite. Hematite (Fe_2O_3) also is antiferromagnetic below −10°C, but above that temperature the opposing spin orientations of Fe^{3+} in adjacent lattice planes are not quite antiparallel. It therefore has ferrimagnetic properties and can retain a net magnetic moment.

If a magnetized ferromagnetic or ferrimagnetic mineral is heated, the strength of the magnetization gradually decreases, as the randomness imposed by thermal vibration decreases the effectiveness of exchange coupling. When a temperature known as the **Curie temperature** (T_C) is reached, all the exchange coupling is destroyed and ferromagnetic/ferrimagnetic properties are lost. Above the Curie temperature, these materials behave paramagnetically. When cooled back through the Curie temperature, minerals such as magnetite reacquire their ferromagnetic properties.

If a magnetic field, such as the Earth's, is present when ferromagnetic or ferrimagnetic minerals cool through their Curie temperature, the substances may acquire a magnetization parallel to that field. These minerals also may acquire a net magnetic moment if they crystallize below the Curie temperature in the presence of a magnetic field.

These seemingly inconsequential observations have had a profound influence on our understanding of the Earth's history. **Remnant magnetism** acquired by magnetite grains when an igneous rock cools, or by hematite during diagenesis of sediments, preserved a record of the Earth's magnetic field at the time of rock formation for millions or billions of years. Detailed study of remnant magnetism has helped document that the continents have moved relative to each other and has established that the Earth's magnetic field periodically reverses polarity. These two observations were key to building our understanding of plate tectonics.

DO NOT COPY e48d507df5d1141@placeholder.9409

Printed by: e48d507df5d1141@placeholder.94092.edu. Printing is for personal, private use only. No part of this book may be reproduced or transmitted without publisher's prior permission. Violators will be prosecuted.

Electrical Properties

Electrical Conductivity

The ability of minerals to conduct electricity depends directly on the nature of the chemical bonding. Minerals with a significant degree of metallic bonding, such as copper (**Figure 6.15a**), in which electrons can migrate freely through the crystal structure, typically easily conduct electricity, as was described in the section on metallic bonding in Chapter 3. The valence electrons are not tightly bonded to specific ions; rather, they are free to migrate through the structure. The application of an external voltage, or a changing magnetic field, provides a driving force to cause the electrons to migrate in one direction, thereby producing an electrical current. The conductivity of electrical conductors typically decreases somewhat with increasing temperature.

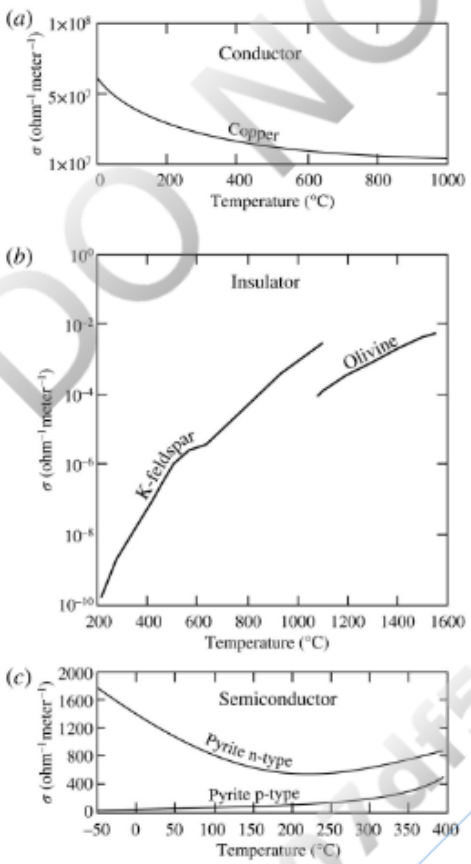

FIGURE 6.15 Electrical conductivity σ (ohm^{-1}meter^{-1}) of selected minerals. (*a*) Copper. (*b*) K-feldspar (Guseinov and Gargatsev, 2002) and olivine at 70 kbar pressure (Yousheng and others 1998). (*c*) Two samples of pyrite (Marinage, 1954). Pyrite may form both n-type and p-type semiconductors depending on details of the chemical composition. View larger image

Minerals with dominantly ionic bonding and some with covalent bonding, including most

DO NOT COPY e48d507df5d1141@placeholder.9409

Printed by: e48d507df5d1141@placeholder.94092.edu. Printing is for personal, private use only. No part of this book may be reproduced or transmitted without publisher's prior permission. Violators will be prosecuted.

silicates, are typically insulators. The electrons are tightly held by specific atoms in the structure and, therefore, are not free to move in response to an applied electrical voltage. Further, the energy gap between valence and conduction bands is large, so normal thermal vibration is not sufficient to promote significant numbers of electrons from the valence to the conduction band to allow conductivity. While conductivity of these minerals is many orders of magnitude lower than for conductors, it is not zero. For example, the conductivity of K-feldspar (**Figure 6.15b**) is more than 16 orders of magnitude less than copper at 200°C. Current flow depends on the migration of point defects in the crystal structure. Recall from Figure 5.16 that point defects include Schottky, Frenkel, and impurity defects. The movement of a cation to fill a Schottky defect, for example, involves both the transport of the charge of the cation (an electrical flow) and the formation of a new Schottky defect at the site from which the cation came. Current flow also may occur by "electron hopping" when, for example, an electron jumps from an Fe^{3+} to a neighboring Fe^{2+}. Conductivity of insulators typically increases exponentially with temperature because thermal excitation increases the mobility of point defects.

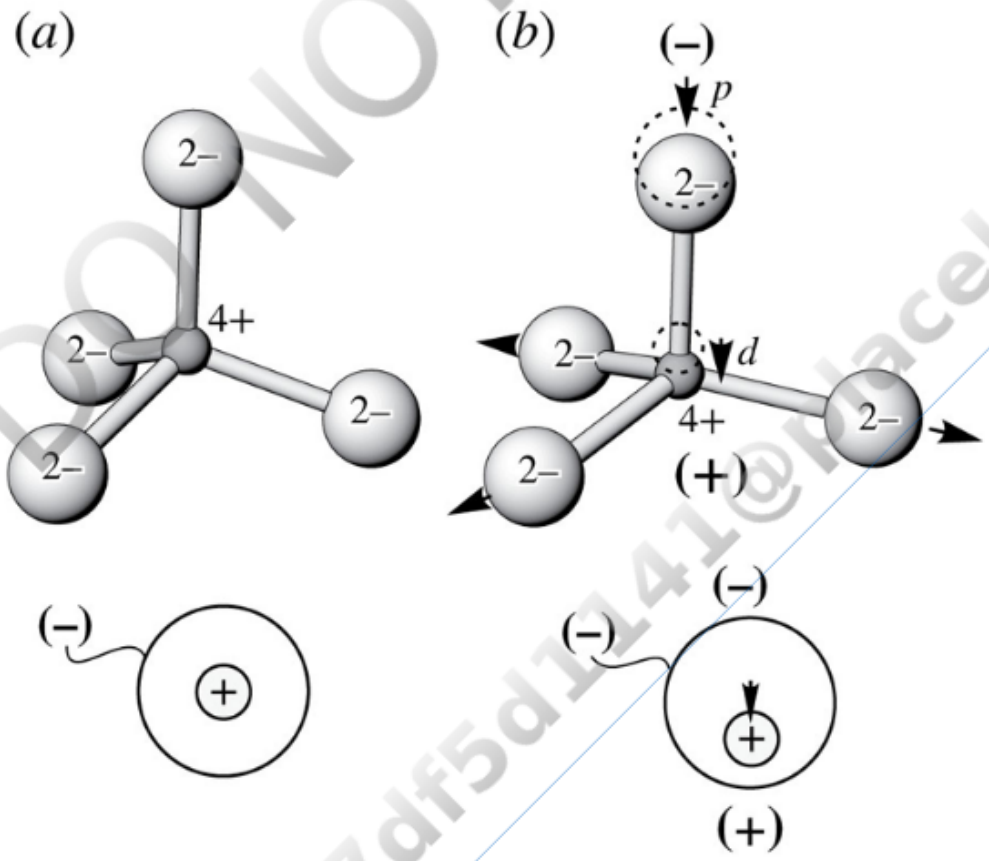

FIGURE 6.16 Piezoelectricity. (*a*) A silicon tetrahedron consists of a Si^{4+} centered within four O^{2-}. The positive charge is centered within the negative charge, as shown schematically with the two circles below. (*b*) If deformed by pressing downward at *p*, an O^{2-} and the Si^{4+} are moved downward distance *d* and the O^{2-} on the base are spread outward. Because only one O^{2-} moves down, the center of the positive charge on the Si^{4+} is moved downward relative to the center of mass of the negative charge on the four O^{2-}. This charge displacement produces a voltage, positive on the bottom, negative on top. View larger image

DO NOT COPY e48d507df5d1141@placeholder.9409

Printed by: e48d507df5d1141@placeholder.94092.edu. Printing is for personal, private use only. No part of this book may be reproduced or transmitted without publisher's prior permission. Violators will be prosecuted.

Minerals with substantial covalent bonding, such as the sulfides, are often semiconductors with conductivity intermediate between conductors and insulators. Conductivity, however, is often quite variable. Pyrite, for example, may display conductivity between roughly 1 ohm^{-1}meter^{-1} and 10,000 ohm^{-1}meter^{-1} at room temperature; galena displays a similar ~5-order-of-magnitude range. In addition to the intrinsic conduction provided when electrons are thermally excited from the valence band to the conduction band, substitution of other elements can provide electron donors (n-type semiconductor) or electron acceptors (p-type semiconductor) that facilitate electrical current flow. Electron donor elements typically have more electrons than the chemical element for which they substitute; electron acceptors have fewer. **Figure 6.15c** shows the conductivity of two samples of pyrite as a function of temperature. The relatively high conductivity of sulfides relative to silicate minerals makes it possible to explore for sulfides using geophysical techniques that involve measuring electrical properties of the bedrock.

Piezoelectricity

When deformed, certain minerals will generate a voltage so that they are positively charged on one side and negatively charged on the other. These minerals are **piezoelectric**. Common minerals that are piezoelectric include quartz (SiO_2), topaz [$Al_2SiO_4(F,OH)$], and tourmaline [$NaFe_3Al_6(BO_3)_3Si_6O_{18}(OH)_4$]. Although the piezoelectric property of these minerals does not appear to have geological significance, it has great practical use. Synthetic quartz, in particular, is widely used in electronic components and transducers.

If quartz is shortened along a 2-fold axis at right angles to *c*, it generates a voltage, positive at one end of the 2-fold axis and negative on the other; stretching reverses the polarity. **Figure 6.16** shows schematically how this works on a single silicon tetrahedron. If the tetrahedron is deformed by pushing downward on the O^{2-} labeled *p*, the Si^{4+} in the middle of the tetrahedron is forced downward distance *d* and the three base O^{2-} spread outward, but the four Si–O bonds remain about the same length. The result is a net movement of charge. One O^{2-} and the Si^{4+}, whose net charge is +2, move down distance *d* relative to the three O^{2-} on the base of the tetrahedron. Relative to the original configuration, the tetrahedron becomes positively charged on the bottom and negatively charged above. Because quartz lacks inversion symmetry, the voltage produced by this silicon tetrahedron is not counterbalanced by a reverse voltage on other tetrahedra. The entire crystal becomes positive on one side and negative on the other.

A simple transducer can be made by cutting a thin slice of quartz and mounting it so that vibrations, such as those from an old-style phonograph needle, cause the quartz to distort. Wires attached to the quartz lead to an amplifier that detects and amplifies the voltage signal.

Just as deformation of a piezoelectric crystal produces a voltage, application of a voltage

DO NOT COPY e48d507df5d1141@placeholder.9409

Printed by: e48d507df5d1141@placeholder.94092.edu. Printing is for personal, private use only. No part of this book may be reproduced or transmitted without publisher's prior permission. Violators will be prosecuted.

Just as deformation of a piezoelectric crystal produces a voltage, application of a voltage can produce a deformation. This phenomenon, called the **electrostriction** or **converse piezoelectric effect**, provides the basis for precise timing in quartz watches and tuning of modern radios. If an alternating voltage is applied to an appropriately cut wafer of quartz, the quartz will alternately expand and contract. The rate at which the quartz vibrates in response to the alternating current depends on how it is mounted and its thickness. The thinner the quartz slice, the greater the frequency of vibration. By connecting the quartz with other electronic components, it can be used to precisely control the frequency of an alternating current. Quartz watches keep track of the time by counting the oscillations of the alternating current whose frequency is fixed by the oscillating quartz. Radio tuners allow only signals whose frequency matches the oscillation of the quartz to be amplified.

Piezoelectric effects occur in nearly all crystals that lack inversion symmetry (**Table 6.8**). The one exception is the 432 point group, which lacks inversion as required, but the other components of its symmetry preclude piezoelectricity. For crystal structures with inversion symmetry, charge movement produced in one direction is canceled by a symmetrically equivalent charge movement in the opposite direction. Lack of inversion symmetry allows the 20 piezoelectric point groups to possess polar directions. A polar direction is one whose end $[uvw]$ is not symmetrically related to the opposite end $[\overline{u}\overline{v}\overline{w}]$. Recall that inversion symmetry requires that the ends of any line through a crystal must be symmetrically related; minerals with inversion symmetry may not have polar directions. Because voltage is a polar phenomena (i.e., it has a direction and a polarity defined by where the positive and negative charges are), a voltage can be generated only along polar directions.

TABLE 6.8 The 20 Piezoelectric Point Groups and 10 Pyroelectric Point Groups[a]

Crystal System	Point Group	Piezoelectric	Pyroelectric
Triclinic	1	x	x
Monoclinic	2	x	x
	m	x	x
Orthorhombic	222	x	
	$mm2$	x	x
Tetragonal	4	x	x
	$\overline{4}$	x	
	422	x	
	$4mm$	x	x
	$\overline{4}2m$	x	
Hexagonal	3	x	x

DO NOT COPY e48d507df5d1141@placeholder.9409-

Printed by: e48d507df5d1141@placeholder.94092.edu. Printing is for personal, private use only. No part of this book may be reproduced or transmitted without publisher's prior permission. Violators will be prosecuted.

	32	x	
	$3m$	x	x
	6	x	x
	$\bar{6}$	x	
	622	x	
	$6mm$	x	x
	$\bar{6}m2$	x	
Isometric	23	x	
	$\bar{4}3m$	x	

[a] All the groups lack inversion symmetry.

Pyroelectricity

A crystal is **pyroelectric** if a change in temperature causes displacement of positive and negative charges and the development of a voltage. Pyroelectricity works because heat causes distortion of the crystal lattice that displaces positive and negative charges relative to each other, much like deformation does in piezoelectricity.

Pyroelectricity is possible only in minerals with a single polar direction. These minerals lack inversion symmetry and have either no symmetry, a single mirror, or a single rotation axis (with or without mirrors parallel to that axis) (Table 6.8). This phenomenon is present only in crystals with a unique polar direction, because heat, unlike pressure, is nondirectional. Pressure can be directed along just one of several symmetrically equivalent directions, like the *a* axes in quartz, to produce the piezoelectric effect. Applying heat to quartz is equivalent to applying pressure equally in all directions, which, because of the higher symmetry of quartz, will result in canceling piezoelectric voltages. If there is a unique polar direction, heating or uniform pressure in all directions will trigger charge displacement associated with that direction and produce a voltage.

DO NOT COPY e48d507df5d1141@placeholder.9409

Printed by: e48d507df5d1141@placeholder.94092.edu. Printing is for personal, private use only. No part of this book may be reproduced or transmitted without publisher's prior permission. Violators will be prosecuted.

Miscellaneous Properties

A variety of other properties may be useful for mineral identification. They include feel, taste, odor, and reaction with acid.

Feel includes a host of perceptions, most of which involve various properties of grain size and surface texture, and therefore are only loosely related to crystal structure and/or composition. One property of feel that is associated with crystal structure is the greasy feel associated with van der Waals bonds. Recall from Chapter 3 that van der Waals bonds are very weak. A finger rubbed on the surface of a mineral such as graphite breaks these bonds and allows the mineral to smear out, producing the greasy feel.

Minerals that are readily soluble in water may have a perceptible taste. Taste is perceived if some of the mineral dissolves in saliva and activates taste receptors on the tongue. Common minerals with a distinct taste include halite (NaCl), which is salty, and sylvite (KCl), which also is salty but it is somewhat more bitter than halite. Mineral samples routinely handled in a student laboratory may acquire a salty taste from salt in hand perspiration. Great care should be taken when applying the taste test as a number of mercury- and arsenic-bearing minerals, plus other minerals such as witherite ($BaCO_3$), are hazardous, if not deadly, to ingest.

Smell too can provide useful clues regarding minerals. Most notable is the soil-like odor described as earthy or argillaceous produced by the clay group (Chapter 13) of minerals when wetted. The odor is from geosmin, a compound produced by bacteria. As most rock and mineral samples have some clay minerals on them, most produce at least a hint of earthy smell when wetted. Applying the smell test to the product of the acid test described below can be informative as well.

A characteristic of many carbonate minerals is that they may visibly react with dilute HCl. The acid is usually prepared by mixing one part concentrated HCl with nine parts water. The reaction with calcite is

The CO_2 released by the reaction causes the dilute acid to fizz or bubble. Some sulfide minerals, such as sphalerite, will release H_2S when introduced to dilute acid, which smells like rotten eggs. Pyrite and other sulfide minerals may provide a hint of a sulfur smell with the acid test as well.

Many field geologists carry a small bottle of hydrochloric acid with which to test rocks for the presence of calcite ($CaCO_3$) and dolomite [$CaMg(CO_3)_2$]. Calcite reacts vigorously

DO NOT COPY e48d507df5d1141@placeholder.94092

Printed by: e48d507df5d1141@placeholder.94092.edu. Printing is for personal, private use only. No part of this book may be reproduced or transmitted without publisher's prior permission. Violators will be prosecuted.

with the dilute acid; dolomite only shows a reaction if it is powdered. The dilute acid solution is weak enough that it does not pose a serious hazard to flesh, but clothing and eyes can be damaged. When using any caustic material, always use caution, protect your eyes, and follow Material Safety Data Sheet precautions.

DO NOT COPY
e48d507df5d1141@placeholder.9409

Printed by: e48d507df5d1141@placeholder.94092.edu. Printing is for personal, private use only. No part of this book may be reproduced or transmitted without publisher's prior permission. Violators will be prosecuted.

Miscellaneous Properties

A variety of other properties may be useful for mineral identification. They include feel, taste, odor, and reaction with acid.

Feel includes a host of perceptions, most of which involve various properties of grain size and surface texture, and therefore are only loosely related to crystal structure and/or composition. One property of feel that is associated with crystal structure is the greasy feel associated with van der Waals bonds. Recall from Chapter 3 that van der Waals bonds are very weak. A finger rubbed on the surface of a mineral such as graphite breaks these bonds and allows the mineral to smear out, producing the greasy feel.

Minerals that are readily soluble in water may have a perceptible taste. Taste is perceived if some of the mineral dissolves in saliva and activates taste receptors on the tongue. Common minerals with a distinct taste include halite (NaCl), which is salty, and sylvite (KCl), which also is salty but it is somewhat more bitter than halite. Mineral samples routinely handled in a student laboratory may acquire a salty taste from salt in hand perspiration. Great care should be taken when applying the taste test as a number of mercury- and arsenic-bearing minerals, plus other minerals such as witherite ($BaCO_3$), are hazardous, if not deadly, to ingest.

Smell too can provide useful clues regarding minerals. Most notable is the soil-like odor described as earthy or argillaceous produced by the clay group (Chapter 13) of minerals when wetted. The odor is from geosmin, a compound produced by bacteria. As most rock and mineral samples have some clay minerals on them, most produce at least a hint of earthy smell when wetted. Applying the smell test to the product of the acid test described below can be informative as well.

A characteristic of many carbonate minerals is that they may visibly react with dilute HCl. The acid is usually prepared by mixing one part concentrated HCl with nine parts water. The reaction with calcite is

The CO_2 released by the reaction causes the dilute acid to fizz or bubble. Some sulfide minerals, such as sphalerite, will release H_2S when introduced to dilute acid, which smells like rotten eggs. Pyrite and other sulfide minerals may provide a hint of a sulfur smell with the acid test as well.

Many field geologists carry a small bottle of hydrochloric acid with which to test rocks for the presence of calcite ($CaCO_3$) and dolomite [$CaMg(CO_3)_2$]. Calcite reacts vigorously

DO NOT COPY e48d507df5d1141@placeholder.94092

Printed by: e48d507df5d1141@placeholder.94092.edu. Printing is for personal, private use only. No part of this book may be reproduced or transmitted without publisher's prior permission. Violators will be prosecuted.

with the dilute acid; dolomite only shows a reaction if it is powdered. The dilute acid solution is weak enough that it does not pose a serious hazard to flesh, but clothing and eyes can be damaged. When using any caustic material, always use caution, protect your eyes, and follow Material Safety Data Sheet precautions.

REFERENCES CITED AND SUGGESTIONS FOR ADDITIONAL READING

Bannerjee, S. K. 1991. Magnetic properties of Fe-Ti oxides. *Reviews in Mineralogy*, **25**, 107–128.

Burns, R. G. 1993. *Mineralogical Applications of Crystal Field Theory*, 2nd ed. Cambridge University Press, Cambridge, 551 p.

DO NOT COPY
e48d507df5d1141@placeholder.9409

Printed by: e48d507df5d1141@placeholder.94092.edu. Printing is for personal, private use only. No part of this book may be reproduced or transmitted without publisher's prior permission. Violators will be prosecuted.

LIST OF KEY TERMS

allochromatic
antiferromagnetism
asterism
band gap
band theory
Bohr magnetic moment
charge transfer transition
chatoyancy
chromophore element
cleavage form
cleavage plane
cleavage
color centers
conduction band
converse piezoelectric effect
crystal field
crystal field splitting
crystal field theory
Curie temperature
density
diamagnetic
electromagnetic radiation
electron color centers
electron spin
electrostriction
fair
ferrimagnetism
ferromagnetism
fluorescence

DO NOT COPY
e48d507df5d1141@placeholder.9409

Printed by: e48d507df5d1141@placeholder.94092.edu. Printing is for personal, private use only. No part of this book may be reproduced or transmitted without publisher's prior permission. Violators will be prosecuted.

fluorescence
fracture
fracture surface
good
hardness
heft
hole color center
idiochromatic
incandescent
indentation hardness
index of refraction
iridescence
Jolly balance
luminescence
luster
magnetic susceptibility
metallic
metallic bonding
Mohs scale of hardness
monochromatic light
nonmetallic
packing index
paramagnetism
parting
perfect
phosphorescence
photoluminescence
photon
piezoelectric
play of color
polychromatic light
poor
pycnometer
pyroelectric

DO NOT COPY
e48d507df5d1141@placeholder.9409

Printed by: e48d507df5d1141@placeholder.94092.edu. Printing is for personal, private use only. No part of this book may be reproduced or transmitted without publisher's prior permission. Violators will be prosecuted.

pyroelectric

remnant magnetism

semiconductor

specific gravity

spin quantum number

splendent

streak

streak plate

submetallic

tenacity

thermoluminescent

triboluminescence

valence band

Vickers hardness

DO NOT COPY

e48d507df5d1141@placeholder.9409

Printed by: e48d507df5d1141@placeholder.94092.edu. Printing is for personal, private use only. No part of this book may be reproduced or transmitted without publisher's prior permission. Violators will be prosecuted.

CHAPTER 7
Optical Mineralogy

William D. Nesse
University of Northern Colorado

Graham B. Baird
University of Northern Colorado

DO NOT COPY
e48d507df5d1141@placeholder.9409

Printed by: e48d507df5d1141@placeholder.94092.edu. Printing is for personal, private use only. No part of this book may be reproduced or transmitted without publisher's prior permission. Violators will be prosecuted.

Introduction

Anyone trying to identify minerals using the standard tools (see Box 1.1 and Chapter 6) quickly learns that confident identification is not always possible and often requires data from one or more analytical techniques covered in Chapters 7, 8, and 9. Data from these techniques can also provide insights into the origins, geologic history, and significance of the mineral specimen. The petrographic microscope, covered in this chapter, provides one of the primary means of studying minerals and rocks. It is a specialized instrument that utilizes polarized light to allow measurement of a variety of optical properties that can help rapidly identify unknown minerals. The samples examined with the petrographic microscope are grain mounts and thin sections; in either case, the samples prepared are thin enough that light will transmit through most minerals.

Grain mounts are prepared by crushing a mineral sample. A few dozen grains that pass a 140-mesh sieve but not a 200-mesh sieve, producing a size range from 0.105 to 0.075 mm, are placed on a microscope slide and covered with a coverslip (**Figure 7.1a**). A dropper is used to introduce a liquid called an **immersion oil** between the slide and coverslip to surround and cover the grains. This grain mount is then placed on the microscope stage for examination. If a permanent grain mount is desired, an epoxy or other cement can be used instead of immersion oil.

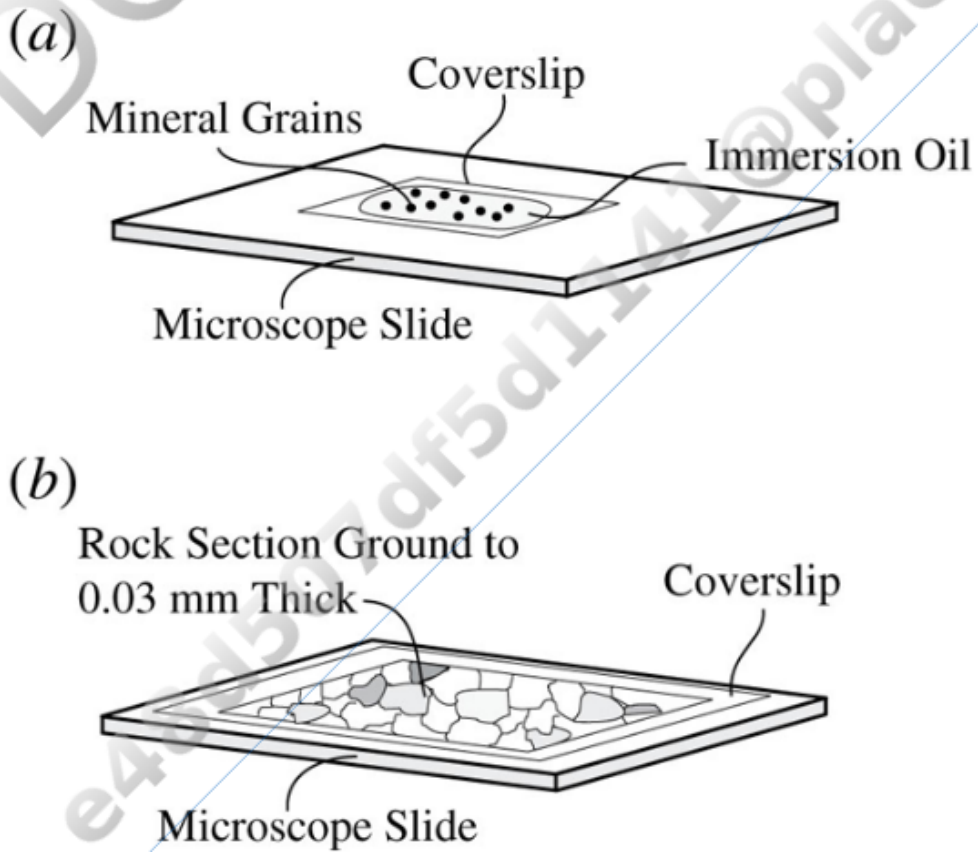

DO NOT COPY
e48d507df5d1141@placeholder.9409

Printed by: e48d507df5d1141@placeholder.94092.edu. Printing is for personal, private use only. No part of this book may be reproduced or transmitted without publisher's prior permission. Violators will be prosecuted.

FIGURE 7.1 Sample preparations for the petrographic microscope. (*a*) Grain mount. (*b*) Thin section. View larger image

Thin sections are thin slices of rock or mineral mounted on a microscope slide (**Figure 7.1b**). They are prepared by cementing a piece of rock to a microscope slide and then grinding it to its final thickness, usually 0.03 mm. The thin section is completed by cementing a coverslip in place to protect the sample. The coverslip is a thin (0.17 mm) piece of glass. If use of the scanning electron microscope or electron microprobe (Chapter 9) is needed, the coverslip is omitted and the sample is completed by carefully polishing the surface to a mirror-like shine.

DO NOT COPY
e48d507df5d1141@placeholder.9409

Printed by: e48d507df5d1141@placeholder.94092.edu. Printing is for personal, private use only. No part of this book may be reproduced or transmitted without publisher's prior permission. Violators will be prosecuted.

Light

Before discussing the details of the petrographic microscope and how to measure the optical properties, it is essential to provide additional background on the nature and properties of light beyond the introduction provided in Chapter 6.

Recall that light is a portion of the electromagnetic spectrum; as such, it is conveniently described behaving either as a wave or as a particle. In the particle paradigm, light is described as consisting of subatomic particles, called photons, which possess energy but not mass. In the wave paradigm, light is described as electromagnetic radiation (Figure 6.6) with wave properties. Because the wave theory very effectively describes the phenomena of polarization, reflection, refraction, and interference, all discussed in this chapter, light is generally treated as a wave in this chapter.

Light Waves

As the name implies, all electromagnetic radiation, such as light, has both electrical and magnetic components, all of which behave as waves. The electric and magnetic components vibrate at right angles to each other and to the direction the energy is propagating or traveling (**Figure 7.2a**). For understanding optical mineralogy, it is necessary to consider only the vibration of the electric vector that interacts with the electric character of atoms and chemical bonds in minerals. The magnetic vector interacts with minerals very little and will be ignored.

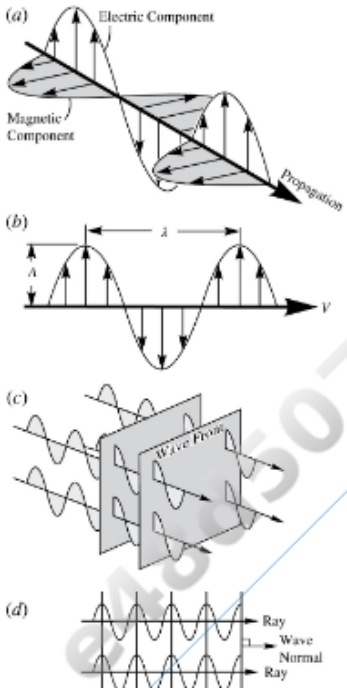

DO NOT COPY e48d507df5d1141@placeholder.9409

Printed by: e48d507df5d1141@placeholder.94092.edu. Printing is for personal, private use only. No part of this book may be reproduced or transmitted without publisher's prior permission. Violators will be prosecuted.

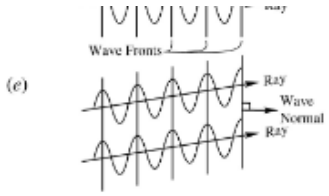

FIGURE 7.2 Electromagnetic radiation. (*a*) Electric and magnetic components of electromagnetic radiation vibrate perpendicular to the direction of propagation or travel. (*b*) Wave nomenclature. The wave travels to the right with velocity *V*. The wavelength (λ) is the distance between successive wave crests. Frequency (*f*) is the number of wave crests that pass some point per second, expressed in units of cycles per second, or hertz (Hz). Brightness of the light is proportional to the square of the amplitude (*A*). (*c*) Wave fronts connect equivalent points on adjacent waves. (*d*) In isotropic materials, the wave normal and ray directions are parallel. (*e*) In anisotropic materials, wave normal and ray directions are not parallel except for certain directions.
View larger image

The oscillating electric field can be described using the mathematics of any wave; it has **velocity** (*V*, nm/sec) and **wavelength** (λ, nm) (**Figure 7.2b**) that are related to the **frequency** [*f*, cycles/sec, or hertz (Hz)].

$$f = \frac{V}{\lambda} \tag{7.1}$$

A **wave front** is a surface that connects the same points on adjacent waves (**Figure 7.2c**). A line drawn at right angles to the wave front is a **wave normal** and represents the direction that the wave moves. A **light ray** is the propagation direction of the light energy, equivalent to the path followed by a photon, using the particle theory for light. In general, the wave normal and the path of the light ray are parallel only in materials in which light velocity is uniform in all directions (**Figure 7.2d**). If light behaves in this fashion when transmitted through a material, it is said to be **optically isotropic**. Minerals in the isometric (cubic) crystal system and amorphous materials, including glass, are isotropic. If velocity varies with direction when transmitted, as it does in all minerals not in the isometric crystal system (tetragonal, orthorhombic, monoclinic, triclinic, and hexagonal), the path followed by light rays generally is not parallel with the wave normal (**Figure 7.2e**) as discussed in later sections. This is called **optically anisotropic**.

Two light waves that vibrate at an angle to each other can be resolved into a resultant vibration direction by means of vector addition. The resultant vibration direction *R* in **Figure 7.3a** is obtained by constructing a parallelogram whose sides are parallel to the vibration directions of waves *A* and *B*. Similarly, a component of a single wave *X* (**Figure 7.3b**) may be resolved into a new vibration direction *V* at angle θ. The magnitude of *V* is given by the equation

$$V = X \cos\ (\theta). \tag{7.2}$$

DO NOT COPY e48d507df5d1141@placeholder.9409

Printed by: e48d507df5d1141@placeholder.94092.edu. Printing is for personal, private use only. No part of this book may be reproduced or transmitted without publisher's prior permission. Violators will be prosecuted.

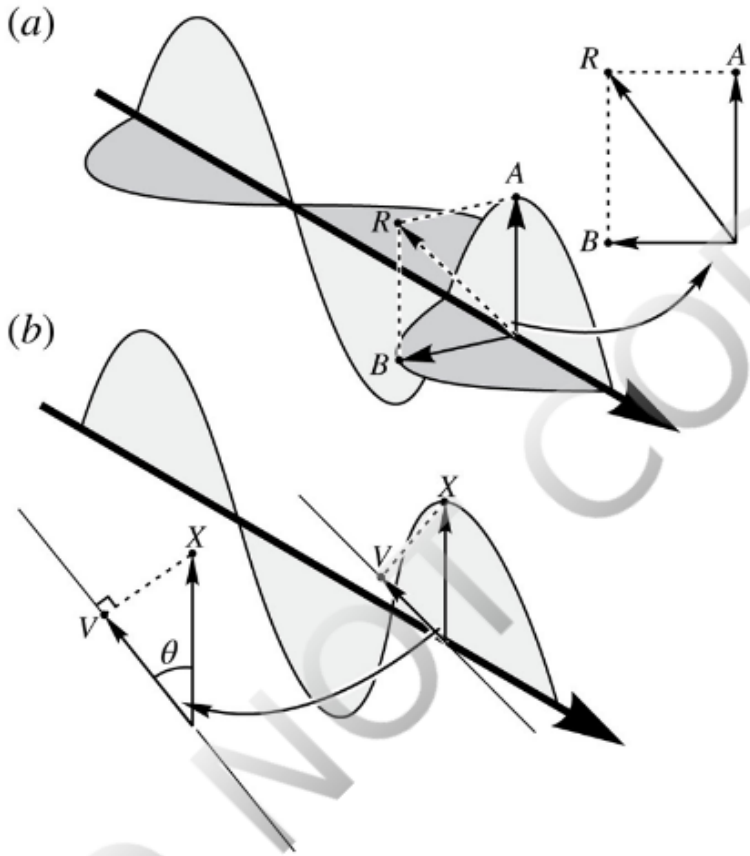

FIGURE 7.3 Vector resolution of light waves. (*a*) Waves *A* and *B* form resultant *R*. (*b*) A component *V* of wave *X* can be resolved in a new direction at angle *θ* from *X*. View larger image

Polarized Light

Ordinary sunlight or lightbulb light vibrates in all directions at right angles to the direction of propagation (**Figure 7.4a**). It is unpolarized. If the vibration of the light is constrained to a single plane, the light is **plane polarized**, and the vibration can be represented by a simple sine wave (**Figure 7.4b**).

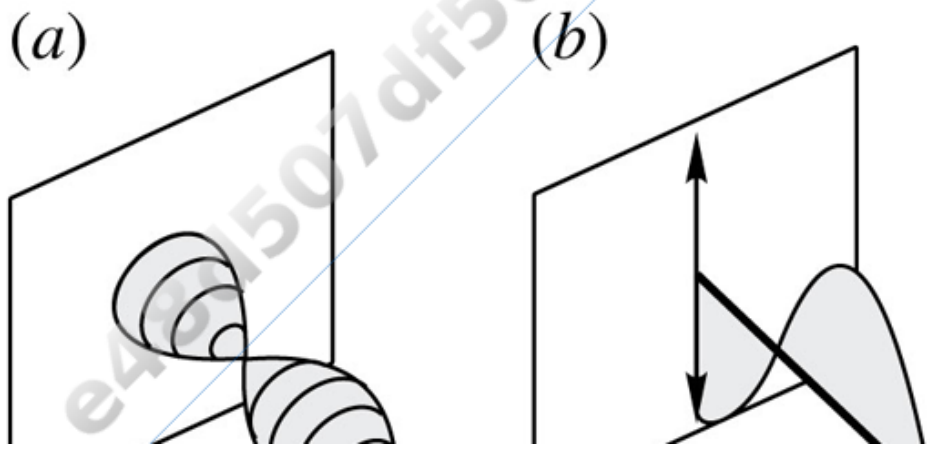

DO NOT COPY
e48d507df5d1141@placeholder.9409

Printed by: e48d507df5d1141@placeholder.94092.edu. Printing is for personal, private use only. No part of this book may be reproduced or transmitted without publisher's prior permission. Violators will be prosecuted.

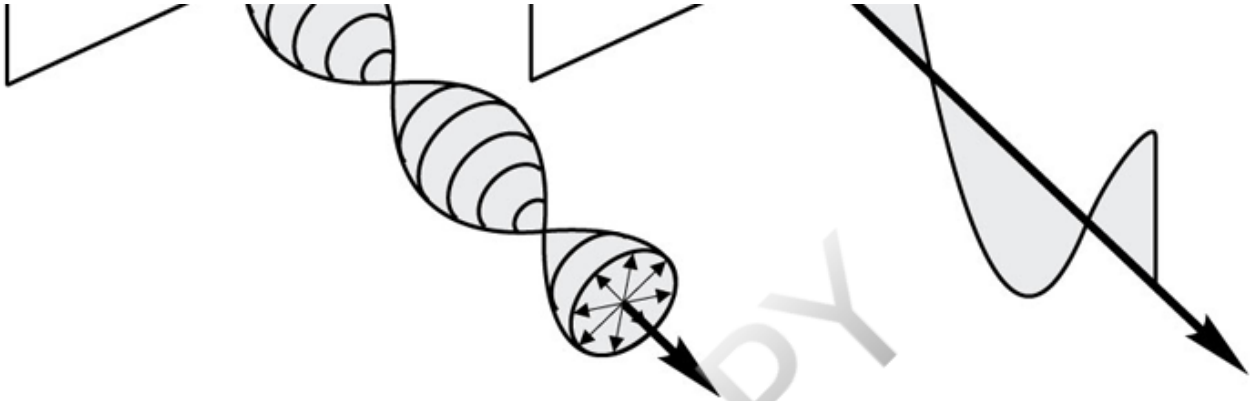

FIGURE 7.4 Polarized light. (*a*) Unpolarized light vibrates in all directions at right angles to the direction of propagation. (*b*) Plane-polarized light. The electric vector vibrates in a single plane. View larger image

Modern petrographic microscopes provide polarized light by placing a piece of **polarizing film** in the optical path. Polarizing film consists of a sheet of plastic that is optically anisotropic. When unpolarized light enters this plastic, it is split into two plane-polarized rays that vibrate at right angles to each other (much more about this is given in a later section); about half of the light energy is resolved into each ray. One of the rays is strongly absorbed by the plastic and is eliminated. The other is only weakly absorbed and passes through the plastic to emerge as plane-polarized light.

DO NOT COPY
e48d507df5d1141@placeholder.9409

Printed by: e48d507df5d1141@placeholder.94092.edu. Printing is for personal, private use only. No part of this book may be reproduced or transmitted without publisher's prior permission. Violators will be prosecuted.

Transparent and Opaque Minerals

In the following discussion, it is important to remember that the focus is on **transparent** minerals. Transparent minerals transmit light; that is, light can pass through the material at the thickness of standard thin sections (0.03 mm) or of the grains in a grain mount (about 0.1 mm). Most minerals are transparent at these thicknesses, but some minerals fully absorb light, transmitting none. These minerals will appear black in any transmitted-light microscope, which include petrographic microscopes, and are identified as **opaque** minerals. Little can be learned about opaque minerals using a petrographic microscope and transmitted light. Opaque minerals are best studied using polished samples and reflected light and/or the scanning electron microscope/electron microprobe. These alternative techniques are discussed briefly at the end of this chapter and in Chapter 9.

DO NOT COPY
e48d507df5d1141@placeholder.9409

Printed by: e48d507df5d1141@placeholder.94092.edu. Printing is for personal, private use only. No part of this book may be reproduced or transmitted without publisher's prior permission. Violators will be prosecuted.

Interaction of Light and Matter

The velocity of light transmitted through a material depends on the nature of the material and the wavelength of the light. The maximum possible velocity of light at ~3.0×10^{17} nm/sec (the "speed of light") is achieved only in a vacuum. In all other materials, light moves more slowly. The detailed explanation of why light's velocity is slower is beyond the scope of this book, but it involves the interaction of the electric vector of the light and the electric environment around each atom in the structure.

When light passes from one material to another, the frequency remains constant. When velocity decreases upon passing from air into a mineral, the wavelength must also decrease (**Figure 7.5**) to keep the frequency constant (Equation 7.1).

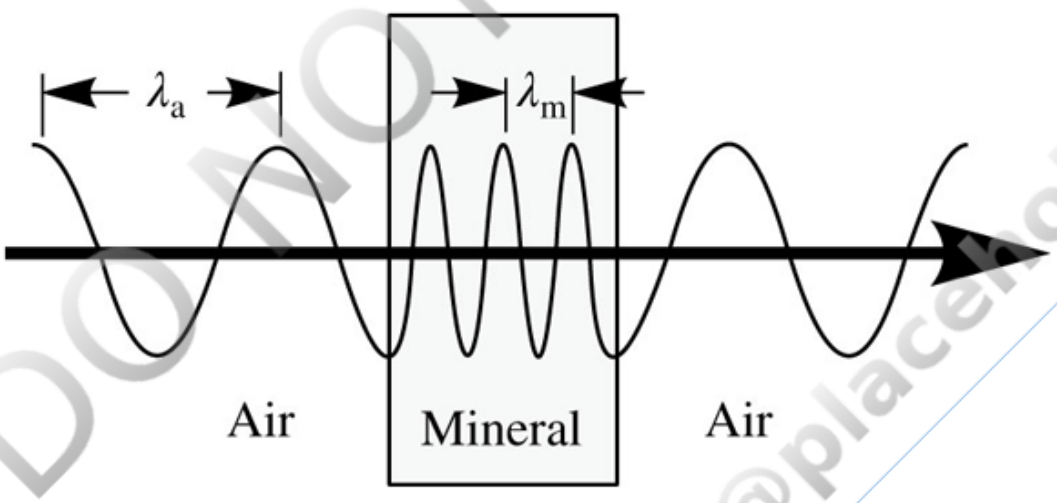

FIGURE 7.5 Light entering a mineral slows down and the wavelength (λ) decreases. View larger image

Optically Isotropic versus Anisotropic Materials

As mentioned, the velocity of light is the same in all directions in optically isotropic materials, including glass and isometric minerals. In these materials, electron density is the same in all directions, at least on average, so the strength of the electric field with which the electric vector of light interacts is also the same regardless of direction. Light velocity is therefore the same in all directions.

The velocity of light is different in different directions within optically anisotropic materials and includes tetragonal, orthorhombic, monoclinic, triclinic, and hexagonal minerals. Minerals in these crystal systems have lower symmetry than those in the isometric system, so the electron density varies with direction. The electrons of the atoms in these minerals are not able to interact with light in the same way in all directions, so

DO NOT COPY e48d507df5d1141@placeholder.9409

Printed by: e48d507df5d1141@placeholder.94092.edu. Printing is for personal, private use only. No part of this book may be reproduced or transmitted without publisher's prior permission. Violators will be prosecuted.

in these minerals are not able to interact with light in the same way in all directions, so the velocity and absorption characteristics (color) of light vary with direction. If normally isotropic solids are strained, by bending for example, some chemical bonds are stretched and others are shortened. This changes the electron density, and these materials become optically anisotropic.

Reflection and Refraction

Light reaching the boundary between two transparent materials will be both **reflected** from the surface and **refracted** into the new material. For reflected light, the angle of incidence (θ_1) and angle of reflection (θ_r) are identical (**Figure 7.6a**).

$$\theta_1 = \theta_r \tag{7.3}$$

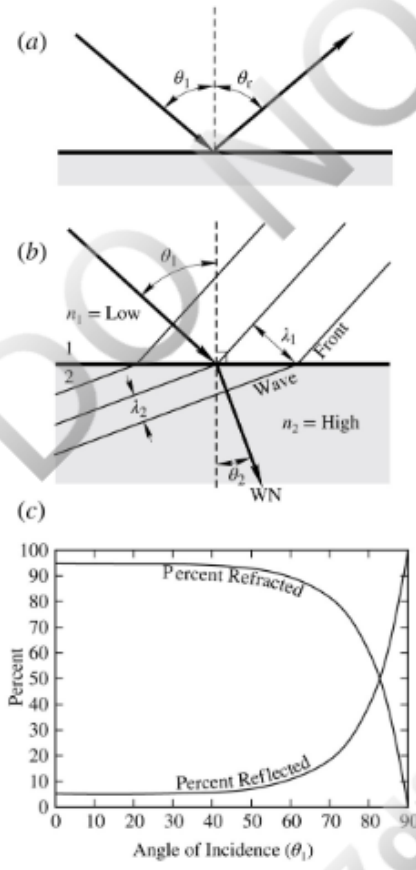

FIGURE 7.6 Reflection and refraction. (*a*) Reflection from a smooth surface. The angles of incidence (θ_1) and reflection (θ_r) are identical. (*b*) Refraction. Wave fronts one wavelength apart and the wave normal (WN) are shown for light passing from material 1 (n_1 = low index of refraction, higher velocity) to material 2 (n_2 = high index of refraction, low velocity). The wave fronts and wave normal bend at the interface because the wavelength λ_2 in the low-velocity material is shorter than the wavelength in the high-velocity material. (*c*) Relative amount of light coming from air ($n = 1$) that is reflected and refracted from the surface of a material with $n = 1.55$ as a function of the angle of incidence. View larger image

DO NOT COPY e48d507df5d1141@placeholder.9409

Printed by: e48d507df5d1141@placeholder.94092.edu. Printing is for personal, private use only. No part of this book may be reproduced or transmitted without publisher's prior permission. Violators will be prosecuted.

The light that enters the material at angles of incidence other than 0° is bent or refracted (**Figure 7.6b**).

To determine how much the light bends when passing from one material to another, it is necessary to know the **index of refraction** (n) of each material. Index of refraction is the ratio of the velocity of light in a vacuum (V_v) and the velocity of light in the material (V_m).

$$n = \frac{V_v}{V_m} \tag{7.4}$$

The angle light bends upon passing from material 1 to material 2 is given by **Snell's law**

$$\frac{\sin \theta_1}{\sin \theta_2} = \frac{n_2}{n_1} \tag{7.5}$$

where n_1 and n_2 are the indices of refraction of light in materials 1 and 2 and θ_1 and θ_2 are the angles shown in Figure 7.6b. Note that $\theta_1 = 0°$ for normal incidence to the surface and θ_1 is nearly 90° where the light glances off the surface at a very low angle.

Snell's law applies for both isotropic and anisotropic materials, provided the angles θ_1 and θ_2 are measured between the normal to the interface between the materials and the wave normals, not the rays. Recall that the wave normal and ray directions are parallel for isotropic materials but are at an angle to each other for anisotropic materials (Figure 7.2d, e).

The relative amounts of light that are reflected from and refracted into a transparent mineral depend on both the index of refraction of the material and the angle of incidence of the light. The amount that is reflected increases with higher index of refraction. Recall from Chapter 6 that mineral luster depends, in part, on the amount of reflection, and a more brilliant luster is associated with a higher index of refraction. The angle of incidence also controls how much light is reflected from a surface. If the light strikes normal to the surface (angle of incidence $\theta_1 = 0°$), reflection is a minimum, and only when the light comes in at a very shallow angle (θ_1 is close to 90°) does most of the light get reflected. The relative amounts of light that are reflected and refracted can be calculated from the Fresnel equation, which is covered in Dyer and others (2008, p. 428). **Figure 7.6c** applies the Fresnel equation to show the amount of light that is reflected and refracted at the surface of an isotropic colorless material with an index of refraction of 1.55, such as a piece of window glass. For this material, whose luster is vitreous, light striking normal to the surface ($\theta_1 = 0°$) is only about 5 percent reflected, so that 95 percent of the light enters the material. To get more than 20 percent of the light to be reflected with normal incidence, the minimum to be perceived as a metallic luster, the index of refraction must be greater than 2.6.

DO NOT COPY

Printed by: e48d507df5d1141@placeholder.94092.edu. Printing is for personal, private use only. No part of this book may be reproduced or transmitted without publisher's prior permission. Violators will be prosecuted.

Light can always be refracted from a low-index material into a high-index material because the angle of refraction is smaller than the angle of incidence. Light traveling from a high-index material into a low-index material cannot pass through the boundary if the angle of incidence is greater than the **critical angle** (CA). The critical angle is the angle of incidence that yields an angle of refraction of 90°. If the indices of refraction are known, the critical angle can be calculated as follows

$$\sin \text{CA} = \frac{n_2(low)}{n_1(high)} \tag{7.6}$$

which can be derived from Snell's law by setting θ_1 = CA and θ_2 = 90°. Consider **Figure 7.7** where wave normals *a*, *b*, *c*, and *d* in material 1 strike the boundary with material 2, which has the lower index of refraction. Wave normals *a*, *b*, and *c* strike the boundary at less than the critical angle (48.59° in this case), so some of their light is refracted into material 2 with angles of refraction greater than the angles of incidence. An angle of refraction greater than 90° is not physically possible, so wave normals such as *d*, whose angle of incidence exceeds the critical angle, experience **total internal reflection**—all the light is reflected; none enters the material with the lower index of refraction. Some of wave normals *a*, *b*, and *c* also is reflected back into material 1, with the amount increasing with the angle of incidence (Figure 7.6).

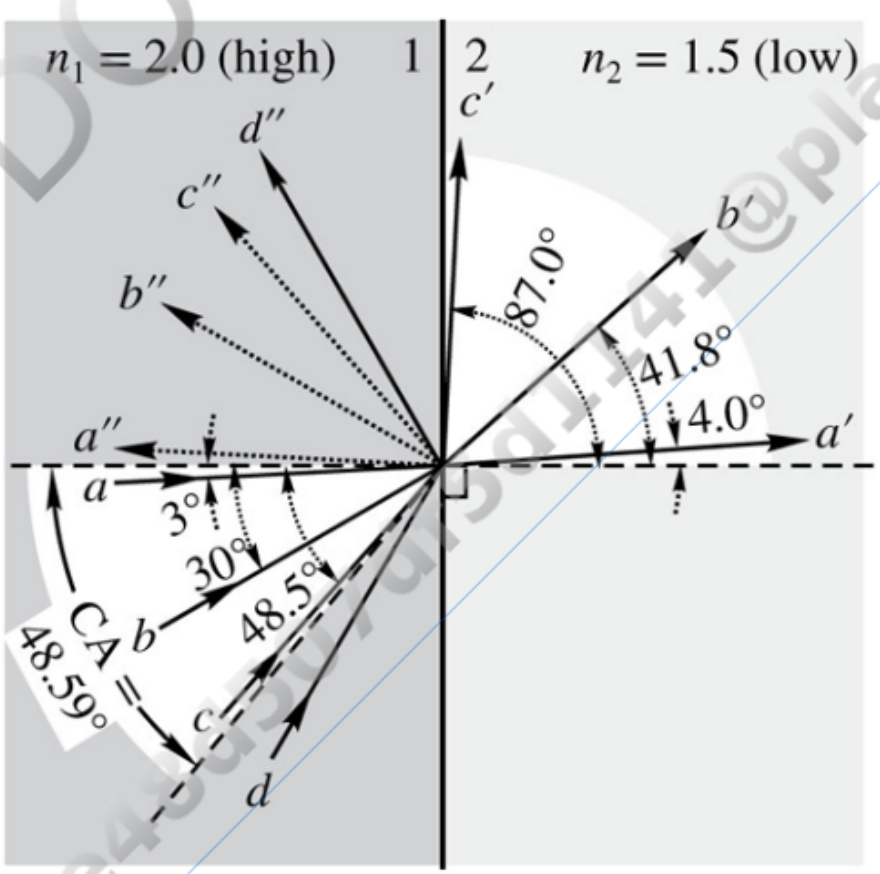

Printed by: e48d507df5d1141@placeholder.94092.edu. Printing is for personal, private use only. No part of this book may be reproduced or transmitted without publisher's prior permission. Violators will be prosecuted.

FIGURE 7.7 Critical angle and total internal reflection. Some of the light following wave normals *a*, *b*, and *c* in material 1 (n_1 = 2.0) is refracted into material 2 (n_2 = 1.5) to *a*′, *b*′, and *c*′. The angles of incidence are 3°, 30°, and 48.5°, and angles of refraction are 4.0°, 41.8°, and 87.0°, respectively, in this case. Wave normal *d*, with an angle of incidence greater than the critical angle (CA = 48.59°), is completely reflected at the boundary to *d*″. Portions of wave normals *a*, *b*, and *c* are reflected to *a*″, *b*″, and *c*″, as shown with dotted lines. The amount of reflection increases from *a* to *c* and is 100 percent for angles of incidence greater than the critical angle (Figure 7.6). View larger image

Dispersion

In most transparent minerals, violet light is more strongly refracted than red light (**Figure 7.8**); this is called **dispersion**. Normal dispersion is caused by short wavelengths having a higher index of refraction and long wavelengths having a lower index of refraction. To describe the dispersion of a material, it is necessary to report the index of refraction at several wavelengths. By convention, indices of refraction n_F, n_D, and n_C are reported for light whose wavelengths are 486, 589, and 656 nm, respectively. When only a single index of refraction is reported for a material, it is for n_D, as 589 nm light is in the middle of the visible spectrum. This index of refraction may be identified as either n_D or n.

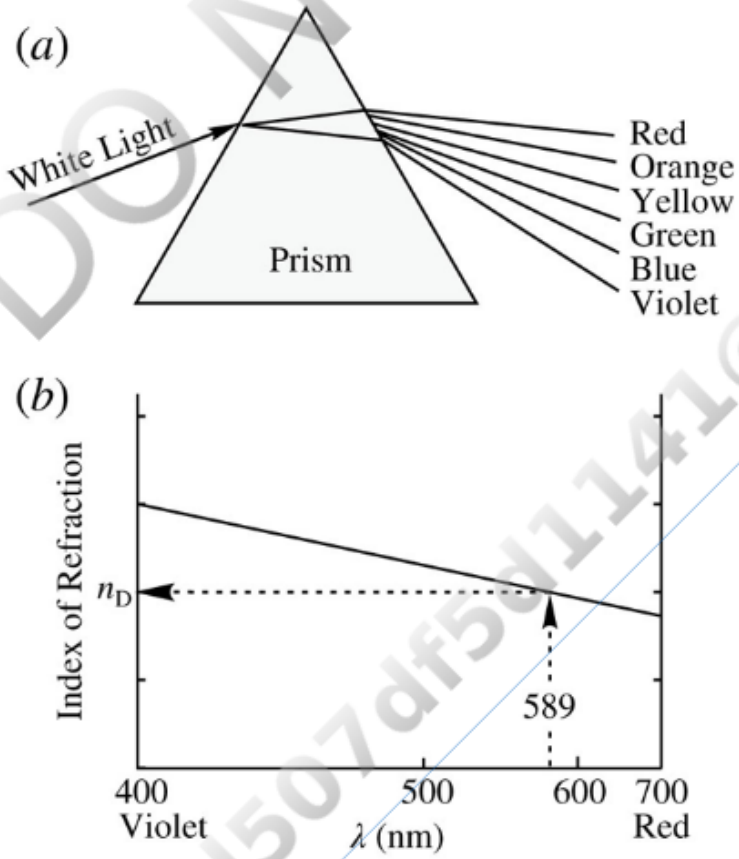

FIGURE 7.8 Dispersion. (*a*) White light is spread into its spectral colors when passed through a prism because the index of refraction for violet light is higher than for red light. (*b*) Normal dispersion of the refractive indices. Index of refraction decreases with increasing wavelength. Strongly colored minerals may display abnormal dispersion of the refractive indices (index of refraction increases with increasing wavelength) for wavelengths that are strongly absorbed by the mineral. View larger

DO NOT COPY e48d507df5d1141@placeholder.94092

Printed by: e48d507df5d1141@placeholder.94092.edu. Printing is for personal, private use only. No part of this book may be reproduced or transmitted without publisher's prior permission. Violators will be prosecuted.

Petrographic Microscope

High-quality **petrographic microscopes** are available from manufacturers such as Leica, Nikon, Zeiss, and Olympus. These instruments also are known as **polarizing light microscopes**. Although they differ in detail, all have fundamentally the same design and construction (**Figure 7.9**). From the bottom up they consist of an illuminator, substage assembly, stage, objective lenses, upper polarizer, Bertrand lens, and ocular lens(es). Focus is achieved with a focusing mechanism mounted in the microscope frame, and a slot is provided above the objective lenses for insertion of optical accessory plates.

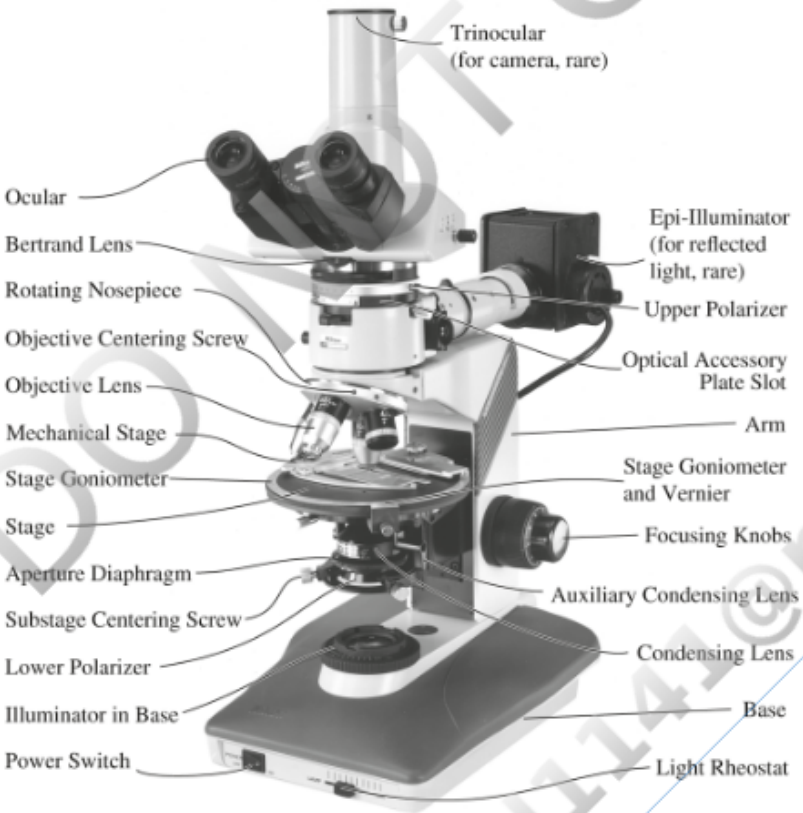

FIGURE 7.9 The petrographic microscope. Photo courtesy of Nikon Instruments Inc., Melville, New York. View larger image

Direction Conventions

Compass directions are routinely used to describe orientations relative to the microscope image. North is to the top, south to the bottom, and east and west to the right and left, respectively. The 45° positions are NE–SW and NW–SE.

DO NOT COPY e48d507df5d1141@placeholder.9409

Printed by: e48d507df5d1141@placeholder.94092.edu. Printing is for personal, private use only. No part of this book may be reproduced or transmitted without publisher's prior permission. Violators will be prosecuted.

Illuminator

The illuminator, mounted in the microscope's base, consists of a lightbulb with a rheostat control for brightness. The light is directed upward with a combination of mirrors and lenses and is filtered so that the color balance closely approximates natural sunlight.

Substage Assembly

The substage assembly typically consists of a **lower polarizer**, **condensing lens**, **auxiliary condensing lens**, and an **aperture diaphragm**. A gear mechanism may allow the substage assembly to be raised or lowered.

The lower polarizer, sometime referred to as just the polarizer, consists of optical-quality polarizing film. In many microscopes the lower polarizer may be rotated to adjust the vibration direction of the light coming up through the instrument. Polarizers may be referred to as **Nicols**, because Nicol prisms, constructed of calcite, were used in early microscopes as polarizers. The lower polarizer is typically aligned so that it passes light that vibrates E–W. In some older instruments the lower polarizer may be oriented to pass light vibrating N–S.

The condensing lens serves to concentrate and focus the light from the illuminator onto an area of the sample immediately beneath the objective lens. The illumination provided by the condensing lens is termed **orthoscopic illumination** because the light reaching the sample is nearly parallel.

The auxiliary condensing lens is mounted on a pivot so that it may be swung into or out of the optical path. Its function is to provide **conoscopic illumination**, which consists of strongly converging light. Conoscopic illumination is used to observe optical phenomena called interference figures, which are examined with the aid of the Bertrand lens and usually the highest-powered objective lens.

The aperture diaphragm is an iris diaphragm that is adjusted to control the size of the cone of light passing up through the microscope. Closing the aperture diaphragm decreases the size of the cone of light and increases the contrast in the image seen through the microscope. The aperture diaphragm is not intended to be used to adjust the intensity of illumination; instead, the illuminator rheostat should be used to adjust brightness.

Some microscopes are equipped with slots or holders in the substage assembly or base intended to hold color filters. Appropriate filters may be used to adjust the color balance of the light or to provide light of a specific wavelength.

Microscope Stage

DO NOT COPY e48d507df5d1141@placeholder.9409

Printed by: e48d507df5d1141@placeholder.94092.edu. Printing is for personal, private use only. No part of this book may be reproduced or transmitted without publisher's prior permission. Violators will be prosecuted.

Microscope Stage

The circular **stage** of the petrographic microscope is mounted on bearings so that it can be rotated smoothly. Angles of stage rotation may be measured with the **stage goniometer** and **vernier** on the outside edge of the stage. A thumbscrew or lever can be engaged on some instruments to lock the stage position.

Objective Lenses

The **objective lenses** provide the primary magnification of the optical system. Most student-model microscopes are equipped with three objective lenses with magnifications of about 2.5×, 10×, and 40×, mounted in a rotating nosepiece. Markings typically found on objective lenses include the magnification, lens type, numerical aperture, length of the microscope tube for which it is designed, and, for high-power lenses, the coverslip thickness that provides optimum performance (**Figure 7.10a**). Lenses designed for use with an optical oil between the lens and sample will be marked "oil" or "oel."

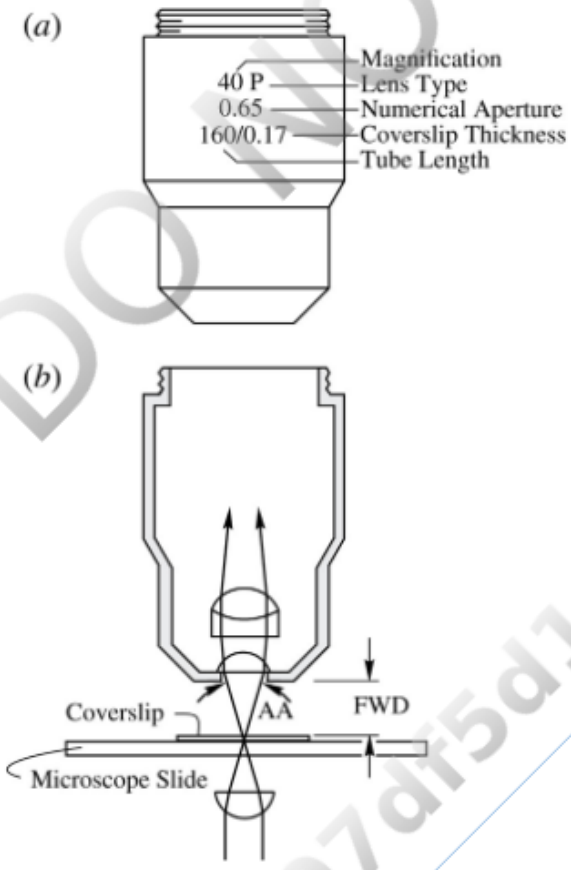

FIGURE 7.10 Objective lens. (*a*) Typical objective lens markings. P indicates that the lens is intended for use with polarized light. (*b*) The free working distance (FWD) is the distance between the end of the lens and top of the sample. Angular aperture (AA) is the size of the cone in degrees of light that the lens can accept. View larger image

The **numerical aperture** (NA) of a lens is a measure of the size of the cone of light that it can accommodate. It is given by the equation

DO NOT COPY e48d507df5d1141@placeholder.9409

Printed by: e48d507df5d1141@placeholder.94092.edu. Printing is for personal, private use only. No part of this book may be reproduced or transmitted without publisher's prior permission. Violators will be prosecuted.

it can accommodate. It is given by the equation

$$\mathrm{NA} = n \sin \frac{\mathrm{AA}}{2} \tag{7.7}$$

where n is the index of refraction of the medium between the objective lens and the sample and AA is the **angular aperture** (**Figure 7.10b**). A large numerical aperture provides greater resolving power and is possible only on lenses with a small **free working distance**, which is the distance between the end of the lens and the top of the sample. Knowledge of the numerical aperture of the high-power (e.g., 40×) lens is useful in the interpretation of optical phenomena known as interference figures. Most student-model microscopes have high-power lenses with NA = 0.65.

Upper Polarizer

The **upper polarizer**, also called the **analyzer**, is located above the objective lenses and is mounted on a slide or pivot so that it can be easily inserted into or removed from the optical path. The vibration directions of the lower and upper polarizers are conventionally set so that they are at right angles to each other. When the upper polarizer is inserted, the polarizers are said to be **crossed**; with nothing on the microscope stage, the observed microscope image is dark because the plane-polarized light that passes the lower polarizer is absorbed by the upper polarizer. If the upper polarizer is removed, the microscope image is produced by **plane light** because light from the lower polarizer is plane polarized.

Bertrand Lens

The **Bertrand lens** (also called the Amici–Bertrand lens) is a small optical element mounted just below the ocular on a pivot or slide. It is introduced into the optical path to allow the observer to view optical phenomena called interference figures, which are described in later sections. The Bertrand lens may be equipped with an iris diaphragm or a pinhole to restrict the field of view, and some manufacturers provide a focusing mechanism.

Oculars

Oculars (eyepieces) are lenses at the upper end of the microscope tube. They magnify the image provided by the objective lens and focus the light for the human eye. The magnification is usually in the range of 5× to 12×. The total magnification of the microscope is the magnification of the objective multiplied by the magnification of the ocular. With a 40× objective and a 10× ocular, the total magnification is 400×. Many

DO NOT COPY e48d507df5d1141@placeholder.9409

Printed by: e48d507df5d1141@placeholder.94092.edu. Printing is for personal, private use only. No part of this book may be reproduced or transmitted without publisher's prior permission. Violators will be prosecuted.

ocular. With a 40× objective and a 10× ocular, the total magnification is 400×. Many microscopes are equipped with binocular heads and therefore use two oculars. Often one ocular has a fixed focus while the other is adjustable by twisting it to accommodate small differences between the user's eyes. Width adjustment between binocular oculars is also provided to match the user's eye spacing.

Reticle markings that may include crosshairs and a micrometer scale are often found in the glass of one ocular; a properly adjusted microscope should have the reticle markings in sharp focus. On binocular microscopes, the ocular with fixed focus is usually equipped with the reticle markings. A small peg on the side of the ocular fits into a slot in the top of the microscope tube to ensure the crosshairs are either oriented N–S and E–W or in the 45° position. If micrometer scale is part of the reticle markings, it allows measurement of sample grain size. The micrometer scale must be calibrated for each different objective lens by comparison with a **stage micrometer**, which is a microscope slide on which a millimeter scale has been etched (**Figure 7.11**).

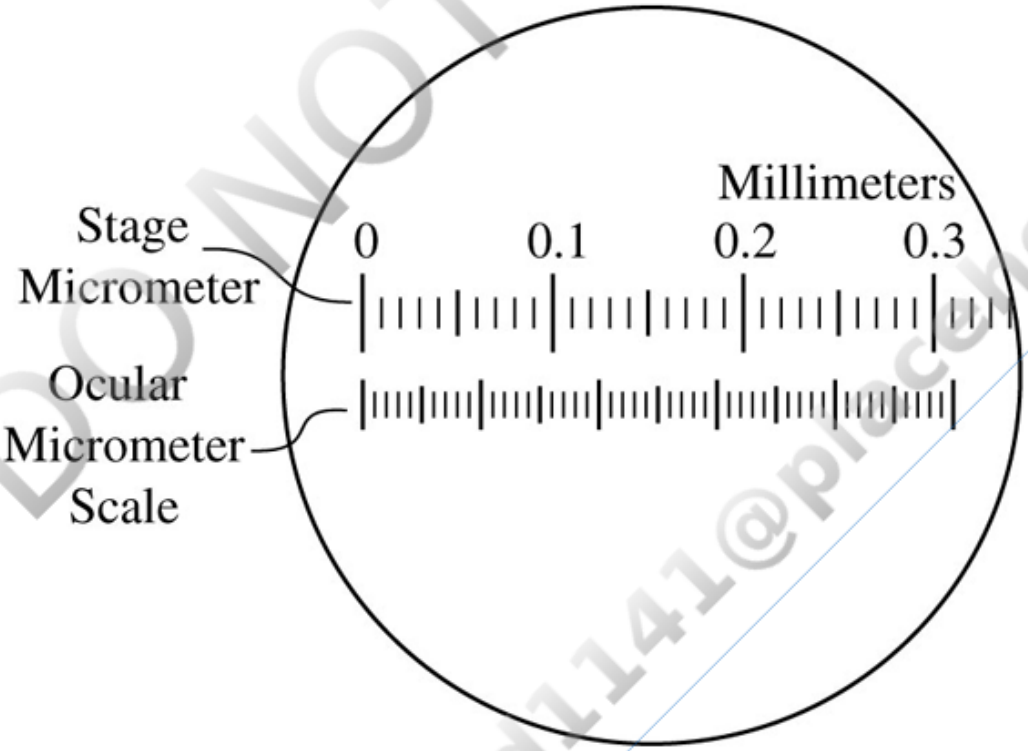

FIGURE 7.11 Calibration of an ocular micrometer scale. Fifty divisions of the ocular micrometer scale (bottom scale) equals 0.31 mm on the stage micrometer. Each ocular micrometer division must therefore equal 0.0062 mm. A separate calibration must be made for each objective lens. View larger image

Conventional oculars are designed for use without eyeglasses, and the microscope focus is adjusted to accommodate near- or farsightedness. If eyeglasses are worn, the field of view will be restricted because the eyes are kept too far from the ocular(s). Many newer microscopes are equipped with **high-eye-point oculars** that are designed for use with eyeglasses. They typically have rubber eyecups that can be flipped up for use without eyeglasses.

DO NOT COPY e48d507df5d1141@placeholder.9409

Printed by: e48d507df5d1141@placeholder.94092.edu. Printing is for personal, private use only. No part of this book may be reproduced or transmitted without publisher's prior permission. Violators will be prosecuted.

eyeglasses.

Focusing Mechanism

Both coarse and fine focusing is done in most cases by raising or lowering the stage by means of a screw or gear mechanism driven by one or two knobs. If the microscope is focused for one objective lens, it should be very nearly focused for the other lenses. When high-powered objectives with a very small free working distance are used, care must be taken to avoid collision between the sample and the lens when focusing. Fortunately, most modern-day high-powered objectives have a spring mechanism that allows compression, so contact between the lens and the sample may not result in damage.

To avoid eyestrain, accurately focus all elements of the microscope. Begin in plane light by focusing the reticle markings crosshair with nothing on the microscope stage, then focus on a sample. On binocular microscopes, similarly begin in plane light, confirm the crosshair is in focus, then focus on the sample only using the ocular with the reticle markings, and then adjust the other ocular until it is in focus. Both oculars should now be in sharp focus on the sample.

Accessories

A slot is provided immediately above the objective lens for insertion of **accessory** or **compensator plates**. They consist of a metal or plastic frame in which an optical element is mounted. The common accessory plates are the gypsum (full-wave) and mica (quarter-wave) plates. They are used to assist with measuring a variety of optical properties described in later sections.

DO NOT COPY e48d507df5d1141@placeholder.9409

Printed by: e48d507df5d1141@placeholder.94092.edu. Printing is for personal, private use only. No part of this book may be reproduced or transmitted without publisher's prior permission. Violators will be prosecuted.

Isotropic Materials

Appendix B lists the common isotropic minerals. Isotropic materials can be distinguished from anisotropic materials by inserting the upper polarizer so that the sample is between crossed polarizers. *All isotropic minerals are dark (black) between* ***crossed polarizers*** because isotropic minerals do not affect the polarization direction of the light coming from the lower polarizer. Recall that the lower and upper polarizers are arranged so that their vibration directions are at 90° to each other. From Equation 7.2 it can be seen that the vector component of incident light resolved into a direction at 90° is zero. Because the light passing through an isotropic mineral retains its original polarization, the vector component parallel to the upper polarizer is zero, so no light passes the upper polarizer. In contrast to isotropic minerals, *anisotropic minerals generally display a variety of interference colors between crossed* ***polarizers***, except in certain orientations, because the anisotropic minerals affect the polarization of the incident light, as will be described in subsequent sections.

The index of refraction is an important characteristic that controls a wide variety of optical behavior and can be used to aid in mineral identification. Appendix B lists the indices of refraction of common isometric minerals. A section on refractometry later in this chapter describes the techniques used to measure index of refraction using grain mounts.

For many minerals, the index of refraction varies depending on chemical composition, and different minerals may have the same index of refraction. Other information may therefore be needed to confirm an identification. Color in grain mount may be useful but should be used with a certain amount of care because it may be variable, as described in Chapter 6. Preparation of grain mounts involves crushing the sample, so cleavage, if a mineral has it, may control fragment shape. The common cleavages found in isometric minerals are cubic {001}, octahedral {111}, and dodecahedral {011} (**Figure 7.12**). If the sample is large enough to observe physical properties such as color, luster, cleavage, and hardness, that information can aid in the identification. If hand-sample and optical techniques do not provide an identification, X-ray diffraction techniques may be employed (Chapter 8).

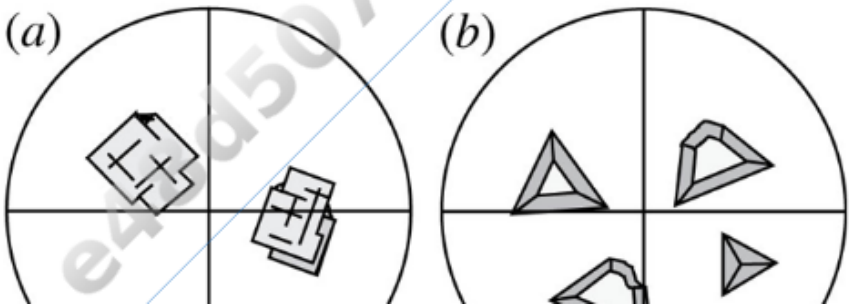

DO NOT COPY e48d507df5d1141@placeholder.9409

Printed by: e48d507df5d1141@placeholder.94092.edu. Printing is for personal, private use only. No part of this book may be reproduced or transmitted without publisher's prior permission. Violators will be prosecuted.

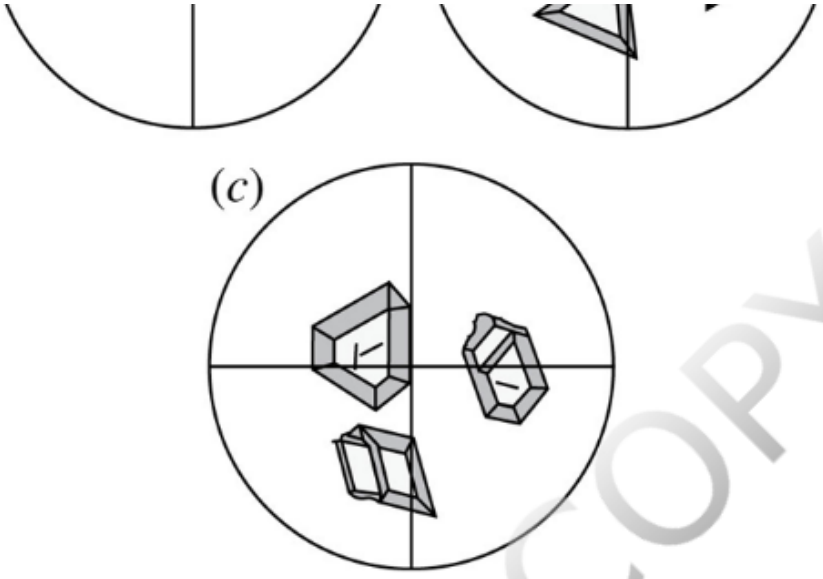

FIGURE 7.12 Cleavage in isometric minerals as seen in grain mount. (*a*) Cubic {001} cleavage. (*b*) Octahedral {111} cleavage. (*c*) Dodecahedral {011} cleavage. View larger image

In thin sections, accurate measurement of the index of refraction is not practical. Color, however, should be visible, and if crystals are euhedral or subhedral, crystal shape may be evident. The shape seen in thin section is the shape of a random slice through the crystal. Sections through cubic crystals are typically four-sided or sometimes three-sided shapes. Sections through octahedrons are usually four- or six-sided shapes, and sections through dodecahedra usually are six- or eight-sided shapes. Cleavage also may be visible as straight lines or fine cracks in the grains.

DO NOT COPY
e48d507df5d1141@placeholder.9409

Printed by: e48d507df5d1141@placeholder.94092.edu. Printing is for personal, private use only. No part of this book may be reproduced or transmitted without publisher's prior permission. Violators will be prosecuted.

Anisotropic Minerals

Optically anisotropic minerals are those in the tetragonal, hexagonal, orthorhombic, monoclinic, and triclinic crystal systems. Because the electronic environment varies with direction, light velocity also must vary with direction. As a consequence, anisotropic minerals show **double refraction**. This means that light entering an anisotropic mineral in most directions is split into two rays with different velocities. The two rays vibrate at right angles to each other. This can be demonstrated by placing a cleavage rhomb of clear calcite on a marked piece of paper (**Figure 7.13**). Two images of the markings are produced corresponding to the two rays. If the rhomb is viewed through a piece of polarizing film whose vibration direction is parallel to the short axis of the rhomb, only one image is seen. If the polarizing film is rotated 90°, only the other image is seen. The two rays must therefore be plane polarized and vibrating at right angles to each other.

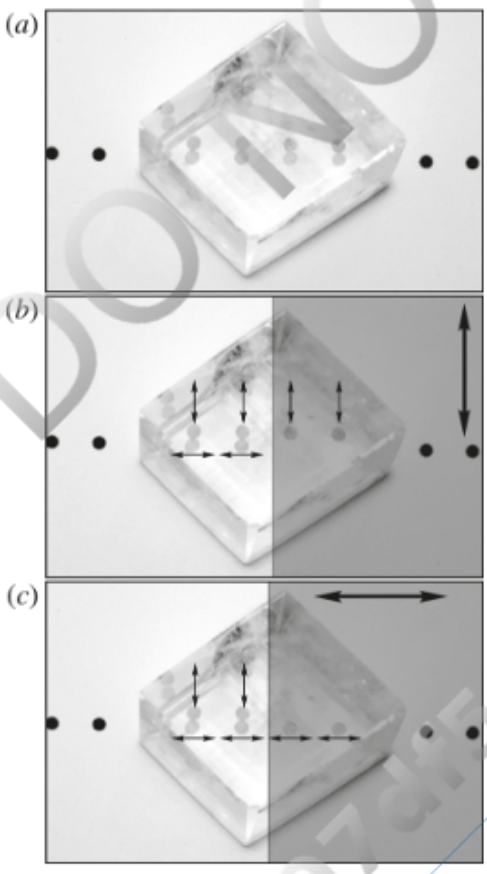

FIGURE 7.13 Double refraction of calcite. (*a*) Cleavage rhomb of clear calcite on a row of dots. Two images are produced because the light is split into two rays that vibrate at right angles to each other. (*b*) A polarizing film, whose vibration direction is parallel to the short diagonal of the rhomb, transmits one set of dots but absorbs the other. (*c*) The polarizing film is rotated 90°. The first set of dots is now absorbed, but the other is transmitted. In intermediate orientations, both sets of dots are visible but darker. View larger image

DO NOT COPY e48d507df5d1141@placeholder.9409

Printed by: e48d507df5d1141@placeholder.94092.edu. Printing is for personal, private use only. No part of this book may be reproduced or transmitted without publisher's prior permission. Violators will be prosecuted.

If the light velocity of the two rays is determined by measuring indices of refraction using techniques described later, it will be found that one ray is faster than the other. The ray with the lower index of refraction and greater velocity is called the **fast ray**, and the ray with the higher index of refraction and lower velocity is called the **slow ray**.

Every anisotropic mineral has either one or two directions, called **optic axes**, along which the light is not split into two rays. Minerals in the hexagonal and tetragonal crystal systems have one optic axis and are optically **uniaxial**. Minerals in the orthorhombic, monoclinic, and triclinic crystal systems have two optic axes and are **optically biaxial**. Uniaxial and biaxial are the two categories of **optical character**.

Interference Phenomena

When an anisotropic mineral is placed on the microscope stage between crossed polarizers, in most cases light passes the upper polarizer and the mineral displays a color. The colors seen between crossed polarizers, called **interference colors**, are produced as a consequence of light being split into two rays as it passes through the mineral. It is convenient to first consider interference with monochromatic light and then extend the discussion to polychromatic light.

Monochromatic Illumination

Consider a ray of plane-polarized light from the lower polarizer that enters an anisotropic mineral grain (**Figure 7.14**). When light enters the mineral, it is split into two rays that vibrate at right angles to each other and have different indices of refraction (different velocities). Because of the difference in index of refraction, the slow ray lags behind the fast ray. In the time it takes for the slow ray to pass through the mineral, the fast ray will have passed through the mineral plus an additional distance called the **retardation** (Δ). The retardation remains constant after the slow and fast rays have exited into the air above the mineral grain because both have the same velocity there. The magnitude of the retardation depends on the thickness of the mineral grain (d) and on the difference in index of refraction of the slow ray (n_s) and fast ray (n_f) in the mineral

$$\Delta = d(n_s - n_f) = d\,(\delta) \qquad \textbf{(7.8)}$$

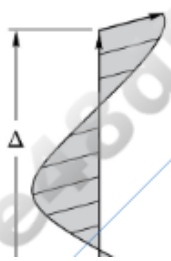

DO NOT COPY e48d507df5d1141@placeholder.94092

Printed by: e48d507df5d1141@placeholder.94092.edu. Printing is for personal, private use only. No part of this book may be reproduced or transmitted without publisher's prior permission. Violators will be prosecuted.

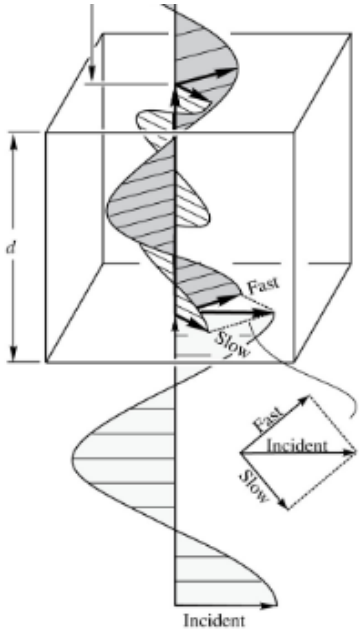

FIGURE 7.14 Development of retardation. Light entering the mineral with thickness *d* is split into slow and fast rays. In the time it takes the slow ray to pass through the mineral, the fast ray has passed through the mineral and traveled an additional distance Δ, which is the retardation. View larger image

where (δ) is the **birefringence** equal to the value ($n_s - n_f$). The numerical value of birefringence depends on the direction the light travels through the mineral. Directions parallel to an optic axis show zero birefringence, other directions show a maximum birefringence, and most show an intermediate value. *The maximum birefringence is a useful diagnostic property of minerals.*

Interference colors are produced when the slow and fast rays reach the upper polarizer and are resolved into its vibration direction. What happens depends on the magnitude of the retardation and whether the slow and fast rays are in or out of phase.

In **Figure 7.15a** the slow ray is retarded an integer number of wavelengths relative to the fast ray or

$$\Delta = i\lambda \qquad (7.9)$$

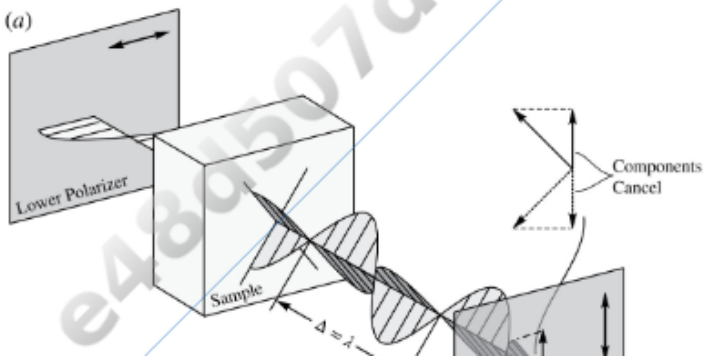

DO NOT COPY
e48d507df5d1141@placeholder.94092

Printed by: e48d507df5d1141@placeholder.94092.edu. Printing is for personal, private use only. No part of this book may be reproduced or transmitted without publisher's prior permission. Violators will be prosecuted.

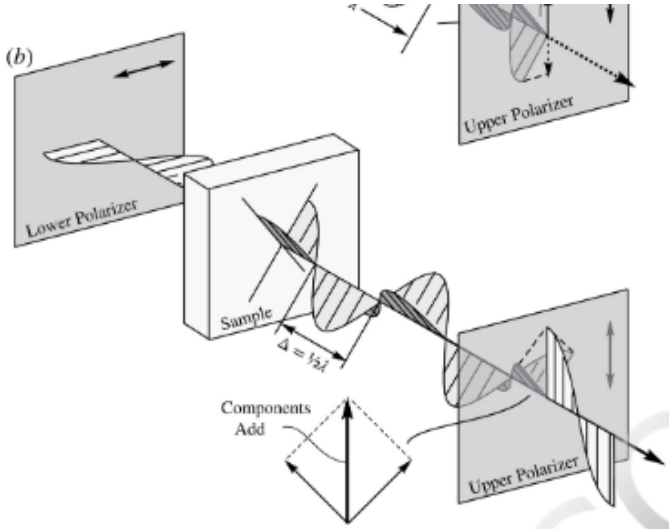

FIGURE 7.15 Interference at the upper polarizer with monochromatic light. (*a*) The retardation (Δ) is one wavelength. Vector components of the two rays resolved into the vibration direction of the upper polarizer are in opposite directions, so they cancel. No light passes and the mineral appears dark. (*b*) The retardation is one-half wavelength. Vector components of the two waves resolved into the vibration direction of the upper polarizer are in the same direction, so they constructively interfere. Light passes the upper polarizer, and the mineral appears bright. View larger image

where i is an integer and λ is the wavelength of the monochromatic light. The components of the two rays resolved into the vibration direction of the upper polarizer are of equal magnitude but in opposite directions, so they cancel each other. No light passes the upper polarizer, and the mineral grain appears dark.

In **Figure 7.15b**, the retardation is equal to one-half wavelength.

$$\Delta = \left(i + \frac{1}{2}\right)\lambda \qquad \textbf{(7.10)}$$

As before, the waves are resolved into the vibration direction of the upper polarizer. In this case, however, the resolved components are both in the same direction, so the light constructively interferes, and light passes the upper polarizer.

These relationships, in which in-phase light cancels and out-of-phase light constructively interferes, appear to be at odds with the conventional presentation of interference taught in physics and mathematics classes (in-phase adds, out-of-phase cancels). The relationships presented here are, in fact, correct because the two rays vibrate at right angles after passing through the mineral, not in the same plane. When resolved into the vibration direction of the upper polarizer they destructively or constructively interfere as described.

If the sample is wedge shaped instead of flat (**Figure 7.16a**), the thickness and retardation vary from zero at the thin end to a maximum at the thick end. When placed between crossed polarizers, areas along the wedge where retardation is equal to 0, 1, 2,

DO NOT COPY

Printed by: e48d507df5d1141@placeholder.94092.edu. Printing is for personal, private use only. No part of this book may be reproduced or transmitted without publisher's prior permission. Violators will be prosecuted.

3, etc. wavelengths ($i\lambda$) are dark, and areas where the waves have other retardations are light. The brightest illumination is where the retardation is $\left(i + \frac{1}{2}\right)\lambda$. For a colorless mineral and no losses from reflection or absorption, the percentage of light that passes the upper polarizer if the stage is rotated so that the mineral vibration directions are in the 45° positions (NE–SW, NW–SE) is given by

$$T = \left(\sin^2 \frac{180^\circ \Delta}{\lambda}\right) \times 100 \qquad \textbf{(7.11)}$$

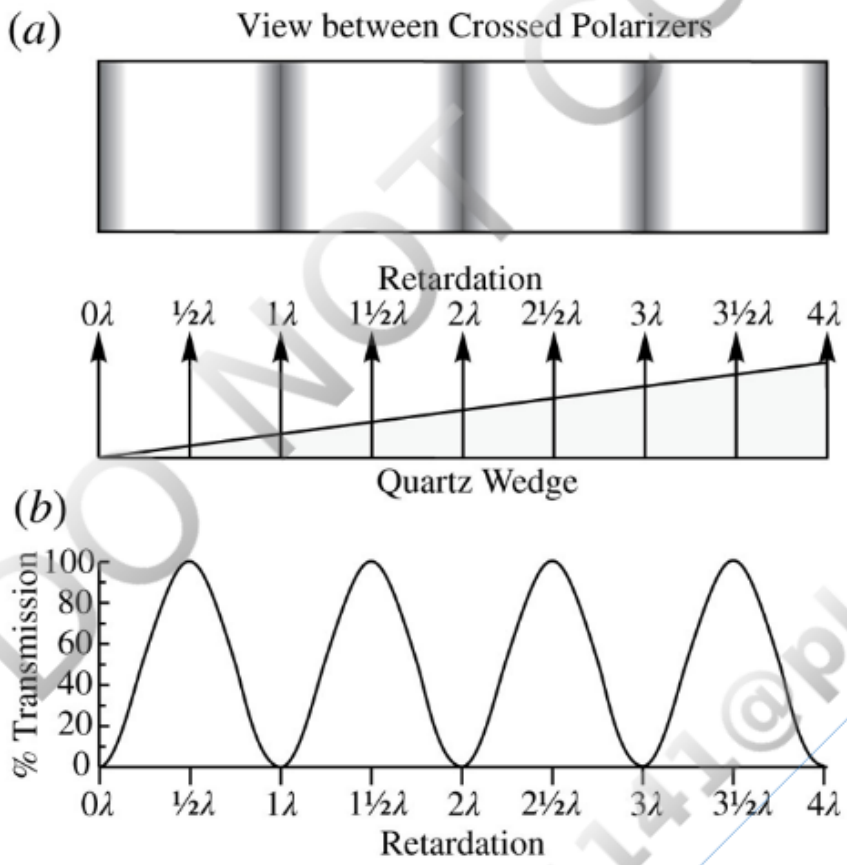

FIGURE 7.16 Interference pattern formed with a quartz wedge in monochromatic light. (*a*) Where retardation is an integer number of wavelengths, slow and fast rays destructively interfere at the upper polarizer and a dark band results. Where retardation is *i* + ½ wavelengths, the two rays constructively interfere and light passes with maximum intensity. (*b*) Percentage transmission of light by the upper polarizer, assuming ideal optical conditions. Computed from Equation 7.11. View larger image

where T is percentage transmission, Δ is the retardation (Equation 7.8), and λ is the wavelength of light being used. **Figure 7.16b** graphically illustrates this relationship for the monochromatic light passing through the quartz wedge shown in Figure 7.16a.

Polychromatic Illumination

DO NOT COPY e48d507df5d1141@placeholder.9409

Printed by: e48d507df5d1141@placeholder.94092.edu. Printing is for personal, private use only. No part of this book may be reproduced or transmitted without publisher's prior permission. Violators will be prosecuted.

With the use of white light instead of monochromatic light, all wavelengths are present, and each is split into slow and fast rays. For a given thickness of mineral, approximately the same amount of retardation is produced for all wavelengths. The two rays for some wavelengths reach the upper polarizer in phase and are canceled, and the two rays for other wavelengths reach the upper polar out of phase and are transmitted. The combination of wavelengths that passes the upper polarizer produces what we perceive as interference colors.

If an optical accessory called a **quartz wedge**, which consists of a wedge-shaped piece of quartz mounted in a holder, is placed between crossed polarizers, the sequence of colors seen in the **interference color chart**, also known as a **Michel-Lévy Chart** (Plate 1), is produced. At the thin edge of the wedge, the thickness is zero so retardation also is zero; all wavelengths cancel at the upper polarizer ($\Delta = 0\lambda$) and the color is black. As the thickness increases, the color changes to gray, white, yellow, and red and then a repeating sequence of blue, green, yellow, and red, with each repetition becoming progressively paler. The color produced at any point along the wedge depends on which wavelengths pass the upper polarizer and which are canceled. The percentage transmission for a given thickness of mineral can be calculated for each wavelength of light from Equation 7.11. These values are shown in **Figure 7.17** for three different thickness of quartz whose birefringence is 0.009.

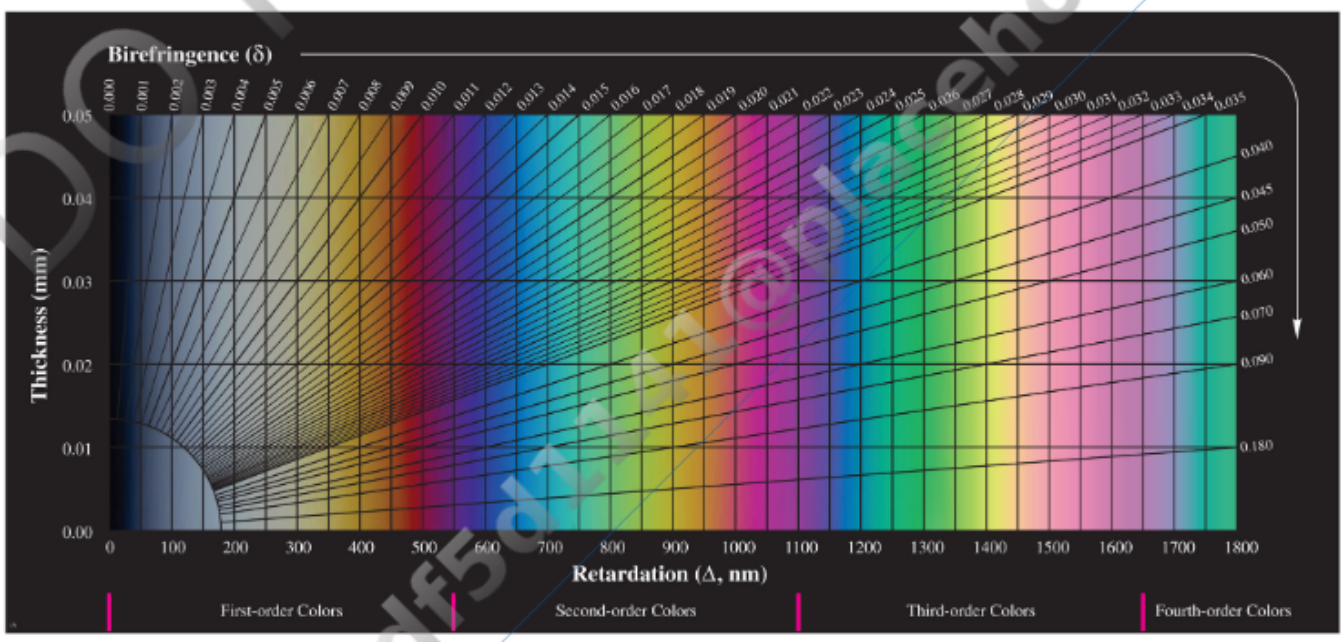

PLATE 1 Interference Color Chart. View larger image

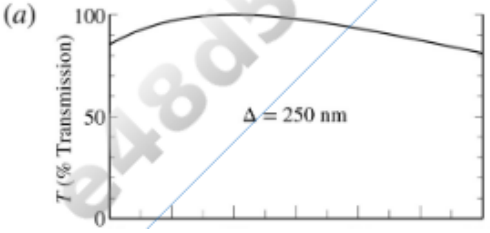

Printed by: e48d507df5d1141@placeholder.94092.edu. Printing is for personal, private use only. No part of this book may be reproduced or transmitted without publisher's prior permission. Violators will be prosecuted.

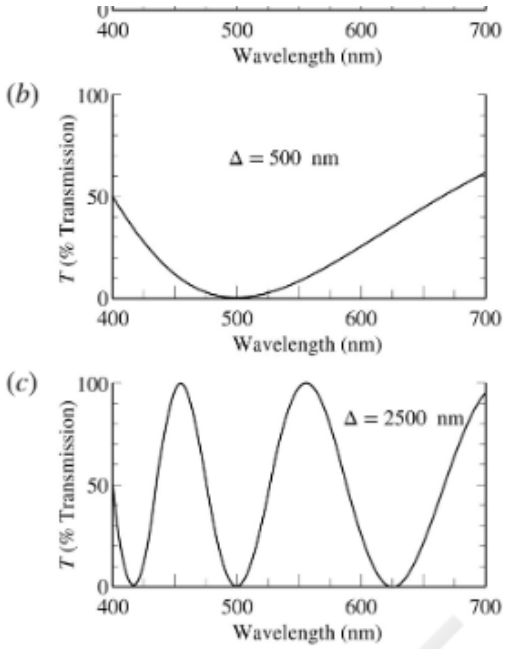

FIGURE 7.17 Formation of interference colors with polychromatic light. (*a*) Retardation for all wavelengths is 250 nm. Slow and fast rays are largely out of phase for all wavelengths, so over 80 percent of all wavelengths pass the upper polarizer to form a first-order white interference color. (*b*) Retardation for all wavelengths is 500 nm. Portions of the violet and red ends of the spectrum are transmitted and 500 nm light is entirely canceled, producing a color perceived as first-order red. (*c*) Retardation for all wavelengths is 2500 nm. Wavelengths around 417, 500, and 625 nm are canceled, and wavelengths near 455, 555, and 714 nm are passed with maximum intensity. This combination of transmitted light is perceived as an upper-order creamy white. View larger image

At the point on the quartz wedge where the thickness is 0.0278 mm (1 mm = 10^6 nm), retardation for all wavelengths is about 250 nm (Equation 7.8) and the slow and fast rays for all wavelengths are substantially out of phase. Over 80 percent of every wavelength passes the upper polar (Figure 7.17a), and the interference color appears white, with a yellowish tinge because small amounts of the red and violet ends of the spectrum are canceled at the upper polarizer.

Where the quartz is 0.056 mm thick, retardation for all wavelengths is about 500 nm. Light whose wavelength is 500 nm is canceled, as is most of the blue and green light in the middle part of the spectrum (Figure 7.17b). The remaining light that passes the upper polarizer is perceived as red with a purplish cast.

For a piece of quartz 0.278 mm thick, which is thicker than that found on most quartz wedges, retardation is about 2500 nm for all wavelengths. Light with wavelengths of 417, 500, and 625 nm are entirely canceled, and other wavelengths pass with varying intensity (Figure 7.17c). This interference color is perceived as a creamy white because a fair amount of each part of the spectrum is allowed to pass.

The interference color chart (Plate 1) shows the interference colors produced for retardations (path differences) between 0 and 1800 nm. These values are plotted along the lower edge of the diagram. This color sequence is conveniently divided into **orders**, with the breaks between orders occurring every 550 nm of retardation. First- and second-

Printed by: e48d507df5d1141@placeholder.94092.edu. Printing is for personal, private use only. No part of this book may be reproduced or transmitted without publisher's prior permission. Violators will be prosecuted.

With the breaks between orders occurring every 550 nm of retardation. First- and second-order colors are most vivid; higher-order colors are progressively more and more washed out. Above the fourth order, the colors degenerate into a creamy white.

Some minerals display interference colors not shown on the interference color chart. These **anomalous interference colors** are produced because the dispersion of refractive indices is substantially different for the slow and fast rays. This results in substantially different retardation for short-wavelength light than for long-wavelength light. A different complement of wavelengths is transmitted by the upper polarizer than if retardation were uniform for all wavelengths. Common minerals that display anomalous interference colors are listed in Appendix B. Interference color also may be influenced by mineral color. Minerals with a distinct green color, for example, will produce a green cast to their interference colors.

Use of the Interference Color Chart

The primary function of the interference color chart (Plate 1) is to allow rapid determination of retardation between the slow and fast rays. Retardation is determined by observing the interference color produced by a mineral grain in either grain mount or thin section and finding the same color on the color chart. The numerical value of retardation is read from the bottom of the chart beneath the color. If, for example, the interference color displayed by a mineral is second-order green, the retardation between slow and fast rays must be about 700 nm.

Distinguishing among similar colors in the different orders may pose some difficulty. The most direct way of determining whether a yellow interference color, for example, is first, second, or third order is to carefully observe the thin edge of the grain displaying the color. Because grains come to zero thickness at the edge, retardation also must be zero (Equation 7.8). It is therefore often possible to count interference colors inward from the edge of the grain to determine which order interference color is displayed by the majority of the grain. The red and blue colors at the transition from one order to the next form a dark band that is easily identified. Accessory plates described in a following section also may be used to determine which order of color is displayed.

Knowledge of retardation can be used to determine the thickness of a thin section if a mineral with known birefringence is present, or to determine birefringence of an unknown mineral if thickness is known.

Determining Thickness

If birefringence and retardation are known, Equation 7.8 provides the basis for determining thickness of a thin section. Quartz is an easily identified mineral that is present in many rocks. Its maximum birefringence is a consistent 0.009. The retardation that any particular quartz grain in a thin section will display depends on orientation. A grain whose c axis is parallel to the microscope stage (horizontal) will display the

DO NOT COPY e48d507df5d1141@placeholder.9409

Printed by: e48d507df5d1141@placeholder.94092.edu. Printing is for personal, private use only. No part of this book may be reproduced or transmitted without publisher's prior permission. Violators will be prosecuted.

grain whose *c* axis is parallel to the microscope stage (horizontal) will display the maximum retardation and thus the 0.009 birefringence. If the *c* axis is vertical, retardation and birefringence are zero. In all other orientations, retardation and birefringence are intermediate. Hence, to find the thickness of a quartz-bearing thin section, proceed as follows.

- Scan the slide to find grains of quartz that display the highest interference color, meaning the color furthest to the right on the interference color chart. Only these grains are oriented to display the known 0.009 birefringence.
- Identify the highest interference color displayed by the quartz and find it on the interference color chart. Read the retardation corresponding to that color from the bottom edge of the chart. If, for example, the color is first-order white with a tinge of yellow, the retardation is 270 nm.
- Calculate thickness from Equation 7.8, using 0.009 for the birefringence and the retardation determined here.

$$d = \frac{270 \text{ nm}}{0.009} = 30,000 \text{ nm} = 0.03 \text{ mm}$$

The calculation can be done graphically, directly on the interference color chart, by using the three sets of lines. Vertical lines are retardation lines, diagonal lines are birefringence lines, and horizontal lines are thickness lines (**Figure 7.18a**). Follow the vertical retardation line (i.e., the color) up to where it intersects the diagonal birefringence line (0.009). The horizontal line (0.03 mm) that passes through this intersection indicates the thickness.

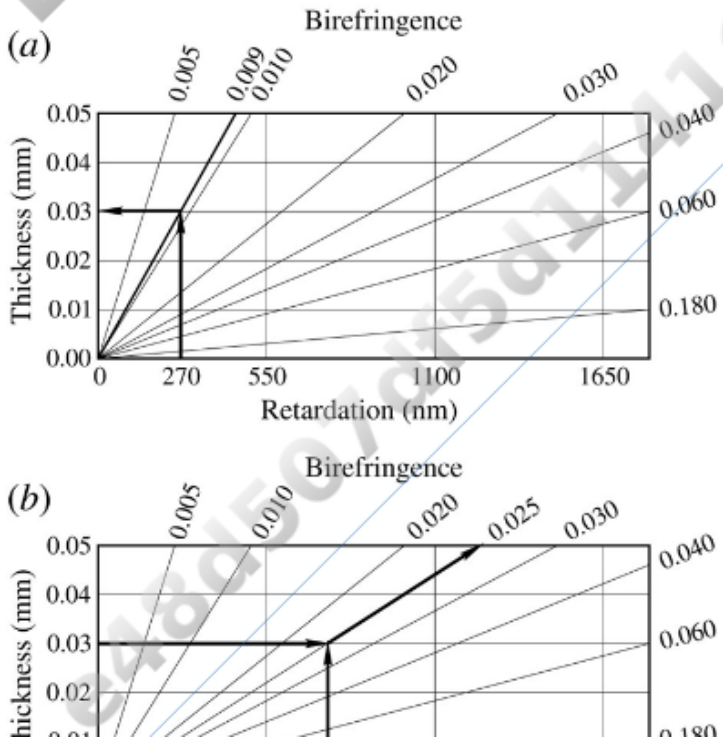

DO NOT COPY
e48d507df5d1141@placeholder.9409

Printed by: e48d507df5d1141@placeholder.94092.edu. Printing is for personal, private use only. No part of this book may be reproduced or transmitted without publisher's prior permission. Violators will be prosecuted.

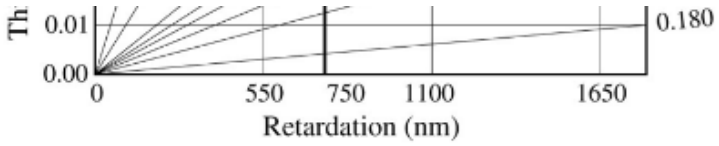

FIGURE 7.18 Use of the interference color chart (Plate 1). Horizontal lines indicate thickness, diagonal lines are for birefringence, and vertical lines indicate retardation (interference color). (*a*) Thickness is indicated by the horizontal line that goes through the point where birefringence and interference color intersect. (*b*) Birefringence is indicated by the diagonal line that goes through the intersection of interference color (retardation) and thickness. View larger image

Other minerals whose maximum birefringence is known may be used to determine thickness if quartz is not present.

Thin sections used for routine mineralogical and petrographic examination are typically 0.03 mm thick. In these thin sections, the maximum interference color displayed by quartz is first-order white with a hint of yellow. It is not uncommon for thin sections to have nonuniform thickness, thin at the edges or thick on one side, for example. Some variation does not cause problems for routine work.

Determining Birefringence

The maximum birefringence of a mineral is a very useful diagnostic property. It is easy to measure in thin sections with known thickness. Recall that the retardation displayed by a grain of a given mineral depends on how it is oriented on the stage of the microscope. A few grains will display zero retardation, a few will display the maximum retardation, and most will display intermediate values. To measure the maximum birefringence, it is necessary to search out grains that display maximum retardation as follows.

- Scan the thin section to find a grain of the unknown mineral whose interference color is highest, meaning farthest to the right on the interference color chart. Only these grains are oriented to display the maximum birefringence.
- Identify that interference color, find it on the interference color chart (Plate 1), and read the retardation corresponding to that interference color from the bottom of the chart. If, for example, the interference color is second-order yellowish green, the retardation is about 750 nm.
- Calculate the birefringence (δ) from Equation 7.8 by using the known thickness of the thin section (e.g., 0.03 mm = 3×10^4 nm), and the determined retardation.

$$\delta = \frac{\Delta}{d} = \frac{750 \text{ nm}}{3 \times 10^4 \text{ nm}} = 0.025$$

The calculation can be carried out graphically by using the lines on the interference color chart (**Figure 7.18b**). Follow the vertical retardation line corresponding to the interference color up to where it intersects the thickness line. The diagonal birefringence

DO NOT COPY e48d507df5d1141@placeholder.9409

Printed by: e48d507df5d1141@placeholder.94092.edu. Printing is for personal, private use only. No part of this book may be reproduced or transmitted without publisher's prior permission. Violators will be prosecuted.

interference color up to where it intersects the thickness line. The diagonal birefringence line that goes through this intersection indicates the birefringence.

Recognize that error exists with this method as the precise thickness of the thin section is not known, accurately recognizing interference color is difficult, and the colors on the interference color chart may be inaccurate. Further, none of the grains in the sample may be fortuitously oriented to display the maximum birefringence. Regardless of these limitations, the method provides sufficient accuracy for routine mineral identification work with the petrographic microscope. If a more accurate numerical value for birefringence is needed, the relevant indices of refraction may be measured using grain mounts and the techniques described in a later section on refractometry of uniaxial and biaxial minerals.

Extinction

Unless an optic axis is vertical with respect to the stage, all anisotropic minerals go dark or **extinct** between crossed polarizers once in every 90° of stage rotation. Extinction occurs when the vibration directions of light passing through the mineral are parallel to the vibration directions of the lower and upper polarizer (**Figure 7.19a**). No component of the incident plane-polarized light from the lower polarizer is resolved into the mineral vibration direction that is parallel to the upper polarizer (Equation 7.2). All the light passing through the mineral therefore retains its original vibration direction and is entirely absorbed at the upper polarizer.

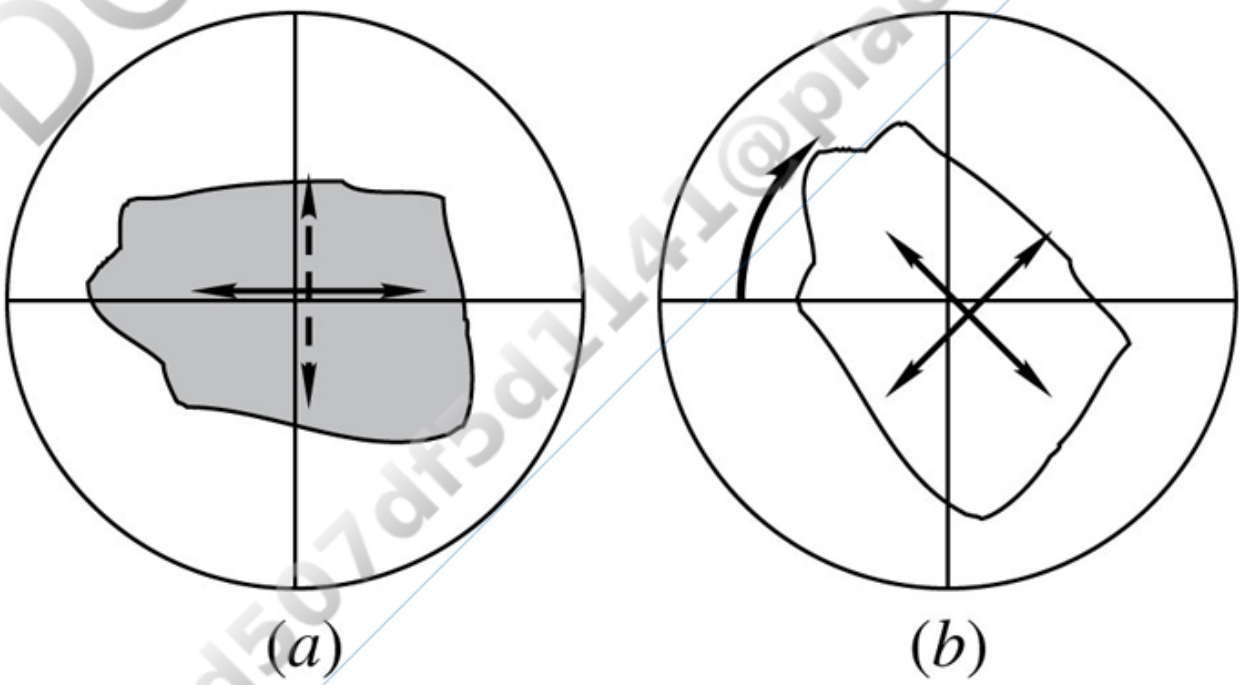

FIGURE 7.19 Extinction. (*a*) When the vibration directions of a mineral grain are parallel to the vibration directions of the lower and upper polarizer, the mineral is dark or extinct between crossed polarizers. (*b*) If the stage is rotated so that the mineral's vibration directions are not parallel to the polarizers, vector components of both rays may be resolved into the N–S vibration of the upper

DO NOT COPY
e48d507df5d1141@placeholder.94092

Printed by: e48d507df5d1141@placeholder.94092.edu. Printing is for personal, private use only. No part of this book may be reproduced or transmitted without publisher's prior permission. Violators will be prosecuted.

polarizers, vector components of both rays may be resolved into the N–S vibration of the upper polarizer so that they may interfere to form interference colors. View larger image

If the stage is rotated to place the vibration directions of the mineral in the 45° positions (**Figure 7.19b**), the plane-polarized light from the lower polarizer can be resolved into both slow and fast rays in the mineral with equal amplitude. When these rays reach the upper polarizer they interfere with each other and produce an interference color as described previously. The interference color does not change with rotation other than to get brighter and darker, because the retardation between the two rays remains constant.

The practical significance of extinction is that it allows the observer to determine the vibration directions of the two rays passing through the mineral. When extinct, mineral vibration directions are oriented N–S and E–W. An accessory plate can be used to determine which ray is slow and which is fast.

Function of Accessory Plates

The primary function of accessory plates is to determine orientation of the fast and slow rays. This information is used to determine the **sign of elongation** (described shortly) and the **optic sign** described in later sections on uniaxial and biaxial minerals. In addition, the accessory plates may help distinguish between different orders of interference colors.

The common accessory plates are the gypsum and mica plates (**Figure 7.20a**). They consist of pieces of quartz, muscovite, gypsum, or anisotropic plastic mounted in a plastic or metal holder. Because these materials are anisotropic, light passing through them is split into slow and fast rays. The optical element is carefully ground so that the accessory plate produces a known amount of retardation and is mounted so that the slow ray vibration direction is across the width of the holder and the fast ray vibration direction is parallel to the length. In most microscopes, the accessory plates slide into the optical path in a slot aligned NW–SE so that the accessory slow ray vibrates NE–SW and the fast ray vibrates NW–SE.

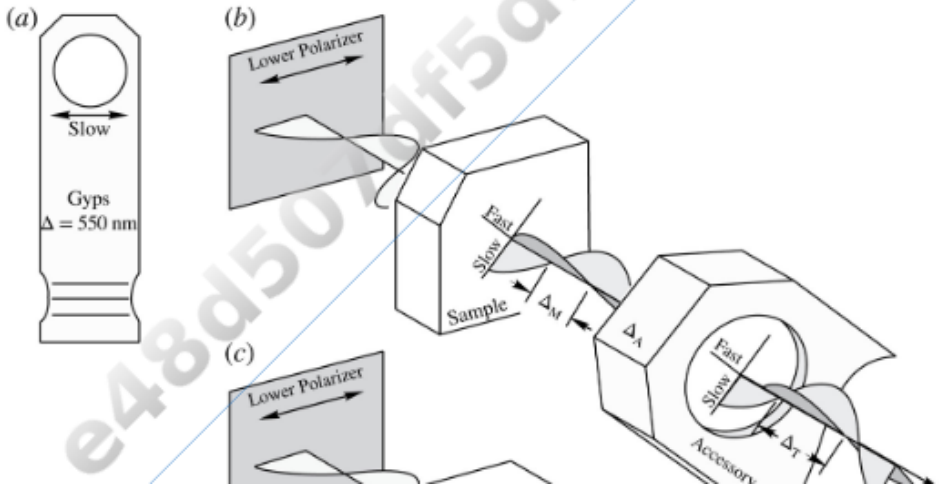

DO NOT COPY e48d507df5d1141@placeholder.9409

Printed by: e48d507df5d1141@placeholder.94092.edu. Printing is for personal, private use only. No part of this book may be reproduced or transmitted without publisher's prior permission. Violators will be prosecuted.

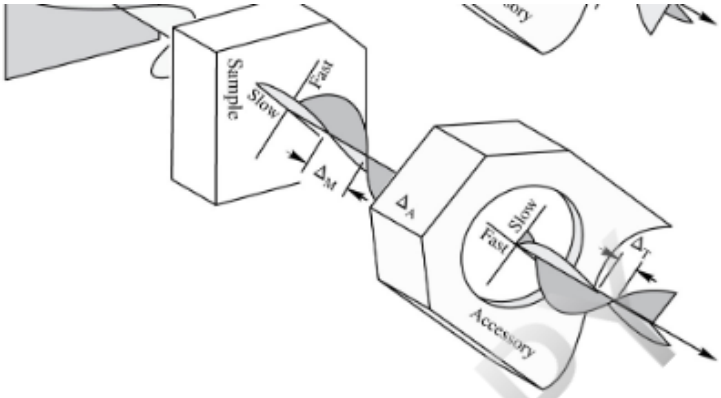

FIGURE 7.20 Compensation with an accessory plate. (*a*) Typical gypsum plate. The optical element produces a retardation Δ_A = 550 nm. The slow vibration direction is as indicated. (*b*) The mineral sample, which produces a retardation = Δ_M, is oriented so that its slow and fast ray vibration directions coincide with those of the accessory plate. The total retardation produced by sample and accessory is Δ_T, which equals $\Delta_M + \Delta_A$. (*c*) The sample is rotated so that its slow ray vibration is parallel to the fast ray vibration direction in the accessory plate. The total retardation is Δ_T, which equals $|\Delta_M - \Delta_A|$. View larger image

The **gypsum plate** also is known as a **full-wave**, **one-wavelength**, **quartz-sensitive tint**, or **first-order red plate**, and may be marked Gips, Gyps, Rot I, 1λ, Δ = 550 nm, or Δ = 537 nm. It produces 537 or 550 nm of retardation (depending on manufacturer) and if viewed with cross-polarized light it yields a distinct magenta interference color seen at the transition from first to second order (Plate 1).

The **mica plate** also is called the **quarter-wave** and **quarter-wavelength plate** and may be marked Mica, Glimmer, 1/4 λ, or Δ = 147 nm. It produces around 150 nm of retardation (depending on the manufacturer) and yields a first-order white interference color if viewed with cross-polarized light.

Consider the mineral grain shown in **Figure 7.20b**. The grain is oriented on the stage so that its vibration directions are in the 45° positions: slow NE–SW, fast NW–SE. Light passing through the mineral is split into two rays and, after passing through the mineral, the slow ray is retarded Δ_M relative to the fast ray. If the accessory plate is inserted, its slow ray vibration direction will be parallel to the slow ray vibration direction in the sample, and fast will be parallel to fast. When the slow and fast rays from the mineral enter the accessory plate, the slow ray will be retarded an additional distance equal to the retardation of the accessory plate (Δ_A), so the total retardation (Δ_T) of mineral and accessory is the sum of the two

$$\Delta_T = \Delta_M + \Delta_A \quad (7.12)$$

and the interference color increases. If the mineral produces 250 nm (first-order white) of retardation and the gypsum plate is used (Δ_A = 550 nm), the total retardation is 800 nm and the interference color observed will increase to second-order yellow. Hence,

Printed by: e48d507df5d1141@placeholder.94092.edu. Printing is for personal, private use only. No part of this book may be reproduced or transmitted without publisher's prior permission. Violators will be prosecuted.

$$\text{Retardations add} = \text{slow on slow}.$$

In **Figure 7.20c**, the mineral grain is rotated so that its fast ray vibration direction is parallel to the slow ray vibration direction of the accessory plate and vice versa. The ray that was slow in the mineral becomes the fast ray in the accessory plate. The total retardation produced by both mineral and accessory plate is the absolute value of the difference between the retardations of mineral and accessory.

$$\Delta_T = |\Delta_M - \Delta_A| \tag{7.13}$$

If the mineral produces 250 nm of retardation and the gypsum plate is used (Δ_A = 550 nm), the total retardation will be 300 nm, producing an interference color of first-order white with a yellow cast. Hence,

$$\text{Retardations subtract} = \text{slow on fast}.$$

Fast and Slow Vibration Directions

For a number of different optical measurements, it is necessary to determine which of the two vibration directions for light coming through a mineral is the fast ray and which is the slow ray. To distinguish the vibration directions, proceed as follows with crossed polarizers.

- Rotate the stage to place the selected grain in an extinction position (**Figure 7.21a**). This places the mineral's two vibration directions (*p* and *q*) N–S and E–W. Make note of the N–S crosshair line orientation on the grain, which also is parallel to the *p* vibration direction in the grain. This vibration direction could be for either the fast or the slow ray.
- Using the stage goniometer, rotate the stage 45° clockwise (**Figure 7.21b**). This rotates the *p* vibration direction into the NE–SW position. Note the interference color displayed by the grain and, from the interference color chart, record the retardation Δ_M associated with that color. In this example Δ_M = 400 nm, which is first-order yellow-orange.
- Insert an accessory plate (slow NE–SW) whose retardation is Δ_A (**Figure 7.21c**). Note the new interference color. If the retardations add, *p* is the slow vibration direction (Equation 7.12), and if they subtract, *p* is the fast vibration direction (Equation 7.13). If the accessory is the gypsum plate (Δ_A = 550 nm), addition will yield second-order yellow-orange (Δ_T = 950 nm) and subtraction will yield first-order gray (Δ_T = 150 nm). If retardations added with *p* NE–SW, they will subtract if the stage is rotated 90° to place *q* NE–SW.

DO NOT COPY

Printed by: e48d507df5d1141@placeholder.94092.edu. Printing is for personal, private use only. No part of this book may be reproduced or transmitted without publisher's prior permission. Violators will be prosecuted.

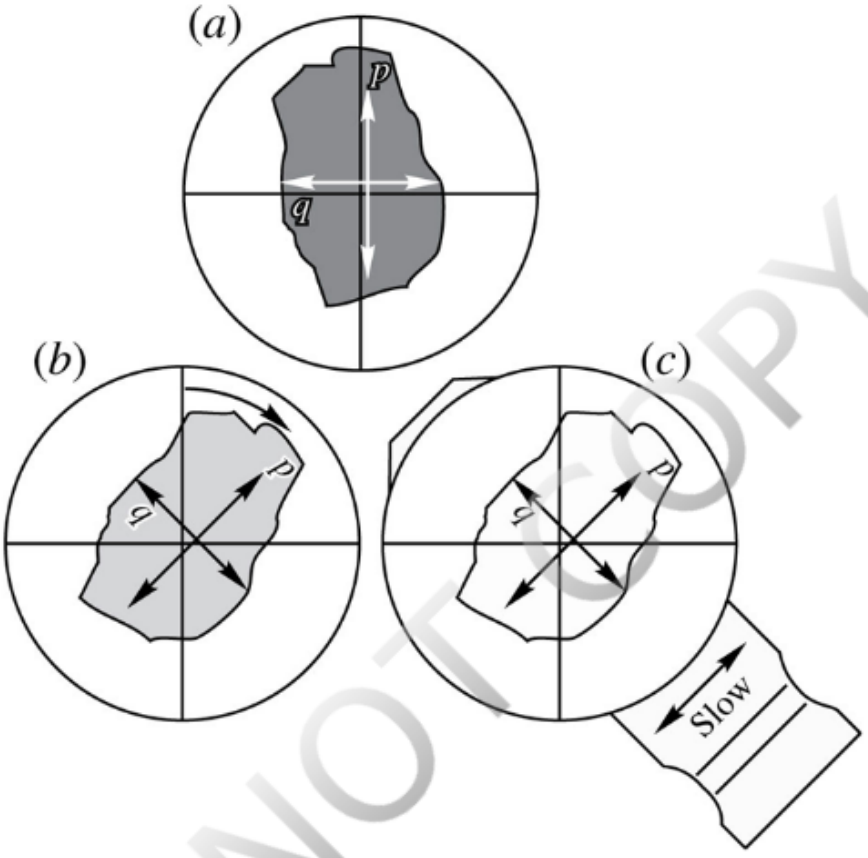

FIGURE 7.21 Determining slow and fast ray vibration directions between crossed polarizers. (*a*) Mineral grain at extinction between crossed polarizers. Vibration directions *p* and *q* in the mineral are N–S and E–W. (*b*) Mineral grain rotated 45° clockwise so that vibration direction *p* is NE–SW. (*c*) Accessory plate inserted. If retardation and interference colors add, *p* is the slow ray vibration direction; if retardations subtract, *p* is the fast ray vibration direction. View larger image

Determining Order of Interference Color

In the section on formation of interference colors, it was mentioned that accessory plates can be used in some cases to determine the order of an interference color. The gypsum plate can be used to quickly distinguish between second- and higher-order colors and to distinguish between first-order white and a high-order white. Recall that the gypsum plate either adds or subtracts retardation equal to one order of interference colors (550 nm). As the microscope stage is rotated with the gypsum plate inserted, the retardation and interference color alternates between addition and subtraction as the slow ray of the mineral is first parallel to the slow ray of the accessory plate and then parallel to the fast ray every 90°. When the mineral vibration directions are N–S and E–W, the mineral displays the magenta interference color of the gypsum plate because only one ray comes through the mineral in these orientations. A mineral displaying first-order colors between crossed polarizers will, with insertion of the gypsum plate, alternately display second- and first-order colors as retardations add and subtract as the stage is rotated. A mineral with second-order colors will, with insertion of the gypsum plate, alternately display first- and third-order colors with rotation. A high-order white interference color will not noticeably change because the different orders of high-order colors are all washed-out

DO NOT COPY e48d507df5d1141@placeholder.9409

Printed by: e48d507df5d1141@placeholder.94092.edu. Printing is for personal, private use only. No part of this book may be reproduced or transmitted without publisher's prior permission. Violators will be prosecuted.

Optical Indicatrix

A geometric figure that shows the index of refraction and vibration direction for light passing in any direction through a material is called an **optical indicatrix**. An indicatrix is constructed so that *indices of refraction are plotted as radii that are parallel to the vibration direction of the light*. Consider ray p with index of refraction $n_p = 2.0$ traveling along the Y axis in **Figure 7.22a** and vibrating parallel to the Z axis. The numerical value of this index of refraction is plotted along the positive and negative ends of the Z axis as shown. Ray q traveling along the X axis and vibrating parallel to Y has an index of refraction $n_q = 1.5$. This value is plotted along the positive and negative ends of the Y axis. If the indices of refraction for all possible light paths through the material are plotted in a similar manner, the surface of the optical indicatrix is defined. The shape of the indicatrix (**Figure 7.22b**) depends on mineral symmetry, as will be described shortly.

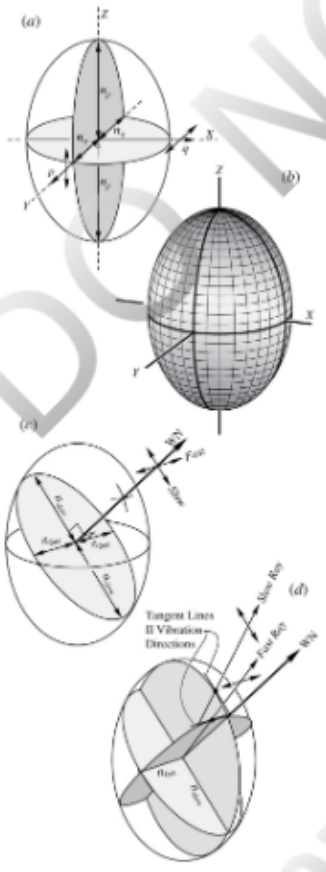

FIGURE 7.22 Optical indicatrix. (*a*) The indicatrix is constructed by plotting indices of refraction as radii parallel to the vibration direction of the light. Wave normal *p*, propagating along *Y*, vibrates parallel to the *Z* axis, so its index of refraction (n_p) is plotted as radii along *Z*. Wave normal *q*, propagating along *X*, vibrates parallel to *Y* so its index of refraction (n_q) is plotted as radii along *Y*. (*b*) The indicatrix is an ellipsoid whose shape depends on the mineral symmetry. (*c*) An indicatrix showing a wave normal direction (WN) along which the light propagates. An elliptical section through the indicatrix perpendicular to the wave normal is parallel to the wave front. The long axis of this

DO NOT COPY e48d507df5d1141@placeholder.9409

Printed by: e48d507df5d1141@placeholder.94092.edu. Printing is for personal, private use only. No part of this book may be reproduced or transmitted without publisher's prior permission. Violators will be prosecuted.

elliptical section is parallel to the slow ray vibration direction, and the radius parallel to this direction is equal to the slow ray index of refraction (n_{slow}). The short axis of the elliptical section is parallel to the fast ray vibration direction, and the radius parallel to this direction is equal to the fast ray index of refraction (n_{fast}) (*d*) Ray paths are determined by constructing tangents to the indicatrix as shown.
View larger image

The primary use of the indicatrix is to determine the indices of refraction and vibration directions of the slow and fast rays given the wave normal direction followed by the light through the mineral. While mathematical means of getting this information are available, only a conceptual understanding is needed here. The basic conceptual steps are as follows.

- Construct a section through the indicatrix at right angles to the wave normal (WN) (**Figure 7.22c**). This section is parallel to the wave front. In the general case, the section through the indicatrix is an ellipse.
- The axes of the elliptical section are parallel to the vibration directions of the slow and fast rays, and the lengths of radii parallel to those axes are equal to the indices of refraction.
- To find the ray paths, which are the paths followed by an image through the mineral such as those seen with the calcite experiment (Figure 7.13), tangents to the indicatrix are constructed parallel to the vibration directions of the slow and fast rays (**Figure 7.22d**). In the general case in which the indicatrix is a triaxial ellipsoid (all principal axes *X*, *Y*, and *Z* have different lengths or indices of refraction), both rays diverge from their associated wave normals.

Isotropic Indicatrix

Isometric minerals are isotropic. One unit cell dimension (*a*) is required to describe the unit cell and one index of refraction (*n*) is required to describe the optical properties because light velocity is uniform in all directions for a particular wavelength of light. The indicatrix is therefore a sphere (all principal axes *X*, *Y*, and *Z* have the same length or indices of refraction). All sections through the indicatrix are circles, and light is not split into two rays. Birefringence is zero.

Uniaxial Indicatrix

Tetragonal and hexagonal minerals have two different unit cell dimensions (*a* and *c*) and a high degree of symmetry about the *c* axis. Two indices of refraction are required to define the dimensions of the indicatrix, which is an ellipsoid of revolution or a spheroid (two principal axes have the same length or indices of refraction) whose axis is the *c* crystal axis (**Figure 7.23**). The radius of the indicatrix measured parallel to the *c* axis is called n_e, and the radius at right angles is called n_ω. *The maximum birefringence of uniaxial minerals is always* $|n_e - n_\omega|$

Printed by: e48d507df5d1141@placeholder.94092.edu. Printing is for personal, private use only. No part of this book may be reproduced or transmitted without publisher's prior permission. Violators will be prosecuted.

minerals is always $|n_\epsilon - n_\omega|$.

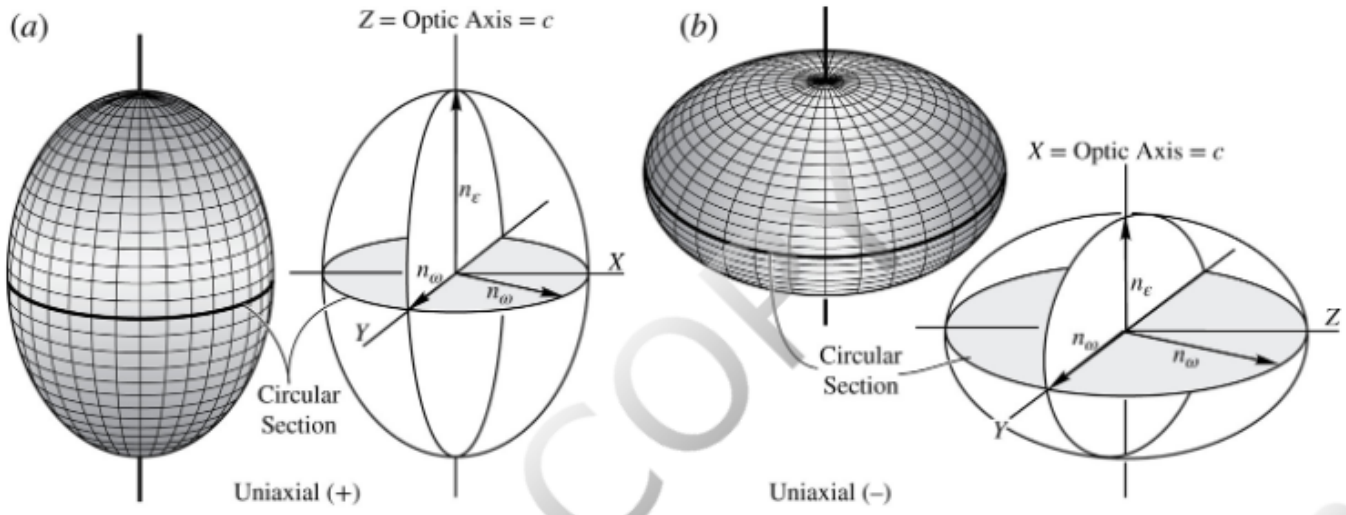

FIGURE 7.23 Uniaxial indicatrix. The circular section and a principal section are shown for each indicatrix. *X*, *Y*, and *Z* axes are included to be consistent with the convention used in biaxial minerals. (*a*) Uniaxial positive. The indicatrix is a prolate spheroid (elongated spheroid) whose axes are n_ϵ and n_ω where $n_\epsilon > n_\omega$. (*b*) Uniaxial negative. The indicatrix is an oblate spheroid (flattened spheroid) whose axes are n_ϵ and n_ω where $n_\epsilon < n_\omega$. View larger image

All vertical sections through the indicatrix that include the *c* axis are identical ellipses called **principal sections** whose axes are n_ω and n_ϵ. Random sections are ellipses whose dimensions are n_ω and n'_ϵ where n'_ϵ is between n_ω and n_ϵ. The section at right angles to the *c* axis is the **circular section** whose radius is n_ω. Because this section is a circle, light propagating along the *c* axis is not doubly refracted; the light is traveling parallel to an **optic axis**. Because hexagonal and tetragonal minerals have a single optic axis, they are called **optically uniaxial**.

Ordinary and Extraordinary Rays

As described earlier (Figure 7.13), if a cleavage rhomb of calcite is placed on a dot or other image on a piece of paper, two images appear, each composed of plane-polarized light vibrating at right angles to the other. The light passing up through the calcite can be considered to be incident at right angles. Based on Snell's law (Equation 7.5), the wave normal for this light is not bent; it remains perpendicular to the bottom surface of the rhomb.

One image (**Figure 7.24a**) is composed of light rays that refract as though they were in an isotropic material, and the ray path and wave normal are parallel. These rays are called **ordinary rays** or **ω rays**. All ordinary rays have the same velocity and index of refraction, which is n_ω, regardless of propagation direction. In calcite, $n_\omega = 1.658$. The ordinary ray vibration vector is always parallel to the (001) plane in uniaxial minerals, which is the only plane in which electron density is uniform. Regardless of propagation direction, one of the two rays produced as a consequence of double refraction in uniaxial minerals always is an ordinary ray. If the calcite rhomb is rotated about a vertical axis

DO NOT COPY e48d507df5d1141@placeholder.94092

Printed by: e48d507df5d1141@placeholder.94092.edu. Printing is for personal, private use only. No part of this book may be reproduced or transmitted without publisher's prior permission. Violators will be prosecuted.

minerals always is an ordinary ray. If the calcite rhomb is rotated about a vertical axis, the position of the ordinary ray image remains fixed.

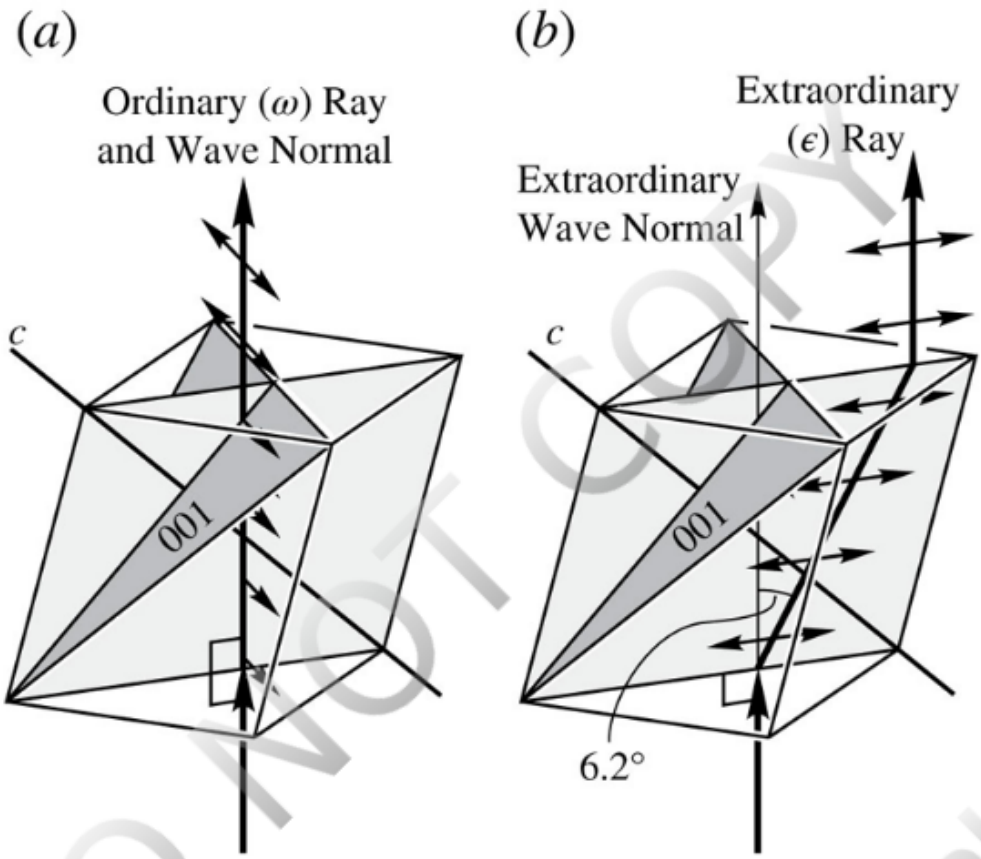

FIGURE 7.24 Ordinary and extraordinary rays. Light incident at right angles to the bottom surface of a calcite rhomb is split into two rays (Figure 7.13). (*a*) The vibration vector of ordinary ω rays is always parallel to (001) planes, and the wave normal and ray direction coincide. If the calcite rhomb is rotated about a vertical axis, the image composed of ordinary rays (ω) remains stationary. (*b*) The extraordinary (ϵ') ray direction diverges from its wave normal, and its vibration direction lies in a plane (light shading) containing the *c* axis and the two rays. If the calcite rhomb is rotated, the position of the extraordinary ray image rotates about the ordinary ray image. View larger image

The image deflected to the side is composed of light rays that behave very differently from light in isotropic materials. They are called **extraordinary rays** or **ϵ rays** because the ray path and wave normal are not parallel. The geometry shown in Figures 7.13 and 7.24b has normal incidence, so Snell's law (Equation 7.5) requires that the wave normal for the extraordinary component is not bent when incident light enters the bottom surface of the calcite rhomb; it is parallel to the ordinary ray and wave normal. However, the extraordinary ray path diverges from the wave normal. The index of refraction of extraordinary rays varies with direction between n_ω and n_ϵ, where n_ϵ may be either higher or lower than n_ω. In calcite $n_\epsilon = 1.486$. For any propagation direction except perpendicular to the *c* axis, the index of refraction of the extraordinary ray is designated n'_ϵ and is between n_ω and n_ϵ. For light whose wave normal is perpendicular to a cleavage surface of calcite (**Figure 7.24b**), the path followed by the extraordinary ray diverges at an angle of 6.2° from the wave normal direction and has an index of refraction $n'_\epsilon = 1.566$. Extraordinary rays are labeled ϵ' if their index of refraction is n'_ϵ and ϵ if their

Printed by: e48d507df5d1141@placeholder.94092.edu. Printing is for personal, private use only. No part of this book may be reproduced or transmitted without publisher's prior permission. Violators will be prosecuted.

1.566. Extraordinary rays are labeled ϵ' if their index of refraction is n'_ϵ and ϵ if their index of refraction is n_ϵ.

Optic Sign

The dimension of the indicatrix along the c axis may be either greater or less than the dimension at right angles. This provides the basis for defining **optic sign** in uniaxial minerals.

In optically positive minerals, n_ϵ is greater than n_ω; extraordinary rays are slow rays.

In optically negative minerals, n_ϵ is less than n_ω; extraordinary rays are fast rays.

Hence, the indicatrix for optically positive uniaxial minerals is a prolate spheroid (Figure 7.23a) and the indicatrix for optically negative uniaxial minerals is an oblate spheroid (Figure 7.23b).

Use of the Indicatrix

We can now examine the behavior of light passing through grains of a uniaxial mineral in different orientations in either a thin section or a grain mount as shown in **Figure 7.25**. Orthoscopic illumination is used (auxiliary condenser lens removed) so the light strikes the bottom surface of the sample more or less normal to the surface. This means that the wave normal of the light entering the mineral is not bent (Equation 7.5), and the wave front is parallel to the bottom surface of the mineral.

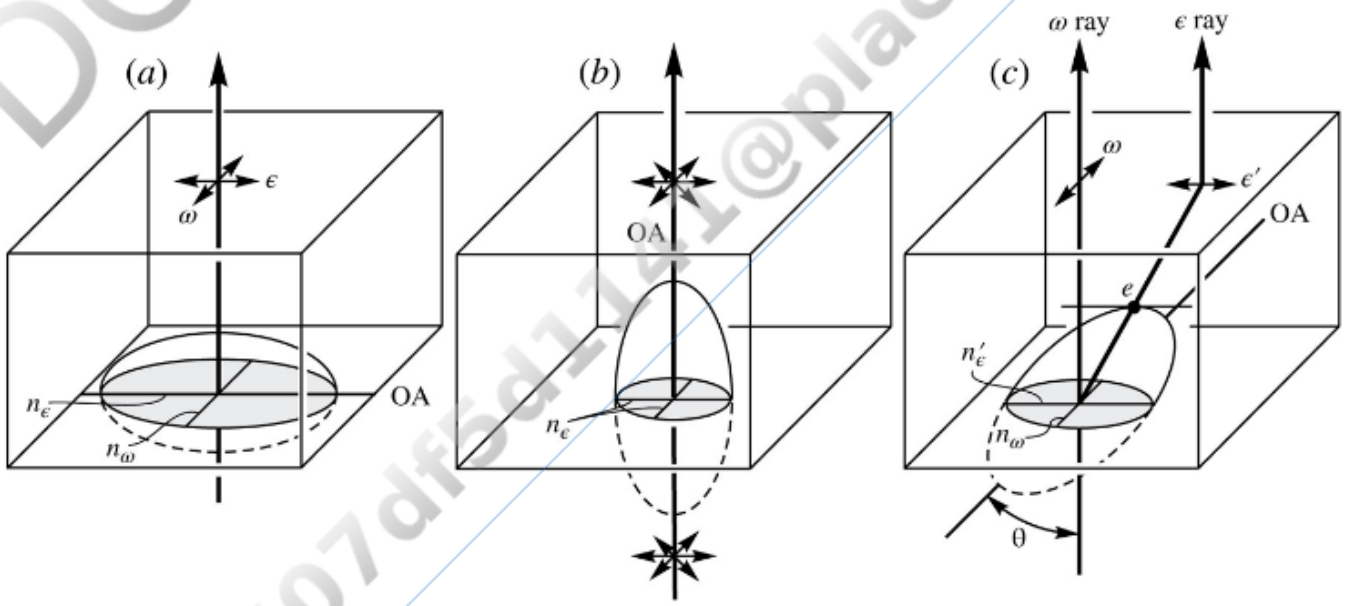

FIGURE 7.25 Behavior of uniaxial minerals in orthoscopic illumination. The optic axis is labeled OA. (*a*) Mineral grain oriented with the optic axis horizontal. The section through the indicatrix is a principal section with axes n_ω and n_ϵ. The mineral displays maximum birefringence and interference color. (*b*) Mineral grain oriented with the optic axis vertical. The section through the indicatrix is the circular section; all light passes as ordinary ray and preserves its original vibration direction. This grain displays zero birefringence and behaves like an isotropic mineral. (*c*) Mineral grain with a random orientation. The section through the indicatrix is an ellipse whose axes are n_ω and n'

DO NOT COPY e48d507df5d1141@placeholder.9409

Printed by: e48d507df5d1141@placeholder.94092.edu. Printing is for personal, private use only. No part of this book may be reproduced or transmitted without publisher's prior permission. Violators will be prosecuted.

random orientation. The section through the indicatrix is an ellipse whose axes are n_ω and n'_ϵ. Birefringence is intermediate and the ω and ϵ' rays diverge. View larger image

In Figure 7.25a the mineral sample is oriented so that its optic axis is horizontal. The mineral's indicatrix, which for convenience of illustration is assumed to be uniaxial positive, is constructed so that it is bisected by the bottom surface of the mineral grain. A wave normal is constructed through the center of the indicatrix. Because the incident light is normal to the bottom surface of the mineral, the section through the indicatrix along the bottom surface of the mineral is the section that defines the indices of refraction and vibration directions for the ordinary and extraordinary rays. Because the optic axis is horizontal, this section is a principal section, which is an ellipse whose axes are n_ω and n_ϵ as shown. The ordinary ray has index of refraction n_ω. The extraordinary ray has index of refraction n_ϵ, which is its maximum value because the mineral is optically positive. The extraordinary ray vibrates parallel to the trace of the optic axis (c axis) and the ordinary ray vibrates at right angles. Birefringence, and hence interference color, display maximum values. Note that for this specific orientation, the extraordinary ray does not behave in an extraordinary manner. The wave normal and ray directions are parallel.

In Figure 7.25b, the mineral sample is oriented so that the optic axis is vertical. The section through the indicatrix perpendicular to the wave normal is the circular section whose radius is n_ω. Light coming from below is not doubly refracted. Birefringence is zero, and the light preserves whatever vibration direction it initially had. Between crossed polarizers, this mineral grain should behave like an isotropic mineral and remain dark as the stage is rotated. In practice, however, the light from the substage condenser is moderately converging, so some light passes at a small angle to the optic axis and experiences double refraction. If the mineral has moderate or high birefringence, the mineral may display interference colors, but they will be the lowest-order color found in the sample for that mineral.

In Figure 7.25c, the mineral sample is in a random orientation so that the light path is at angle θ to the optic axis. The section through the indicatrix parallel to the bottom surface of the mineral is an ellipse whose axes are n_ω and n'_ϵ. The extraordinary ray vibrates parallel to the trace of the optic axis as seen from above; the ordinary ray vibrates at right angles. Birefringence and interference color is intermediate because n'_ϵ is intermediate between n_ω and n_ϵ. The numerical value of n'_ϵ is given by

$$n'_\epsilon = \frac{n_\omega}{\sqrt{1 + \left(\frac{n_\omega^2}{n_\epsilon^2} - 1\right) \sin^2 \theta}}. \quad (7.14)$$

The path followed by the extraordinary ray can be found by constructing a tangent to the indicatrix parallel to the extraordinary ray vibration direction (**Figure 7.26**). The

Printed by: e48d507df5d1141@placeholder.94092.edu. Printing is for personal, private use only. No part of this book may be reproduced or transmitted without publisher's prior permission. Violators will be prosecuted.

extraordinary ray, which carries the image through the calcite rhomb shown in Figures 7.13 and 7.24, goes through point E at angle ψ to the optic axis given by the equation

$$\tan \psi = \frac{n_\omega^2}{n_\epsilon^2} \cot (90 - \theta) \qquad \textbf{(7.15)}$$

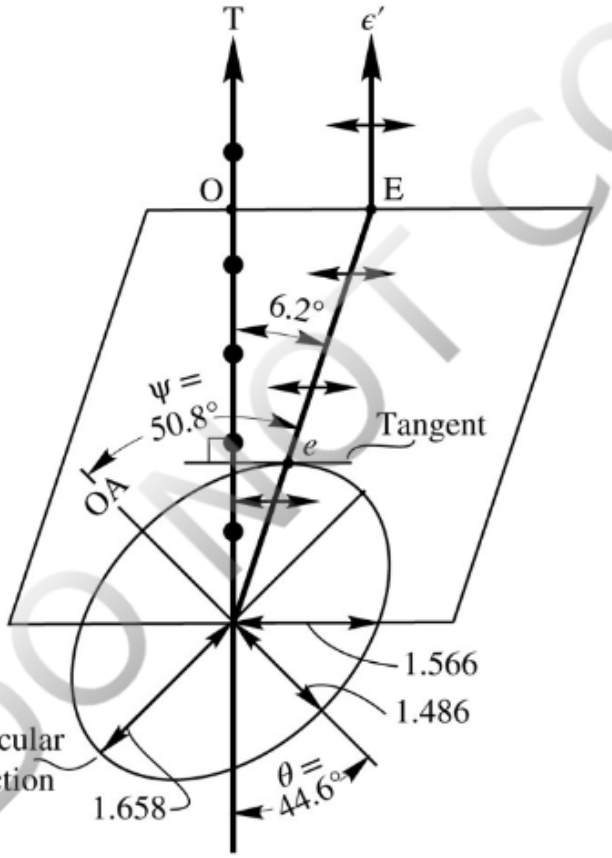

FIGURE 7.26 Calcite indicatrix construction. The ϵ' ray path is found by constructing a tangent to the indicatrix parallel to the ϵ' ray vibration direction at point e. The extraordinary image, which follows the ray, emerges from the top of the rhomb at E. A similar tangent for the ordinary ray (not shown in and out of the page) yields an ordinary ray path that coincides with the wave normal so the ordinary ray emerges at O. The dimensions of the indicatrix are not drawn to scale. View larger image

where θ is the angle between the optic axis and the wave normal. This construction helps explain the unusual behavior of the image carried by the extraordinary rays coming through a mineral such as calcite. Its application to the petrographic microscope is very limited because reflection, refraction, and interference of the light passing through minerals are best described with reference to the wave normal.

Biaxial Indicatrix

DO NOT COPY e48d507df5d1141@placeholder.9409

Printed by: e48d507df5d1141@placeholder.94092.edu. Printing is for personal, private use only. No part of this book may be reproduced or transmitted without publisher's prior permission. Violators will be prosecuted.

Orthorhombic, monoclinic, and triclinic crystal systems require three dimensions (*a*, *b*, and *c*) to describe their unit cells and three indices of refraction to define the shape of their indicatrix (Figure 7.27). The three **principal indices of refraction** are n_α, n_β, and n_γ, where $n_\alpha < n_\beta < n_\gamma$. Other conventions that may be encountered to identify the principal indices of refraction include α, β, γ; n_x, n_y, n_z; n_a, n_b, n_c; n_1, n_2, n_3; n_p, n_m, n_g; N_x, N_y, N_z; *nX*, *nY*, *nZ*; and *X*, *Y*, *Z*. *The maximum birefringence (δ) of a biaxial mineral is always* $n_\gamma - n_\alpha$.

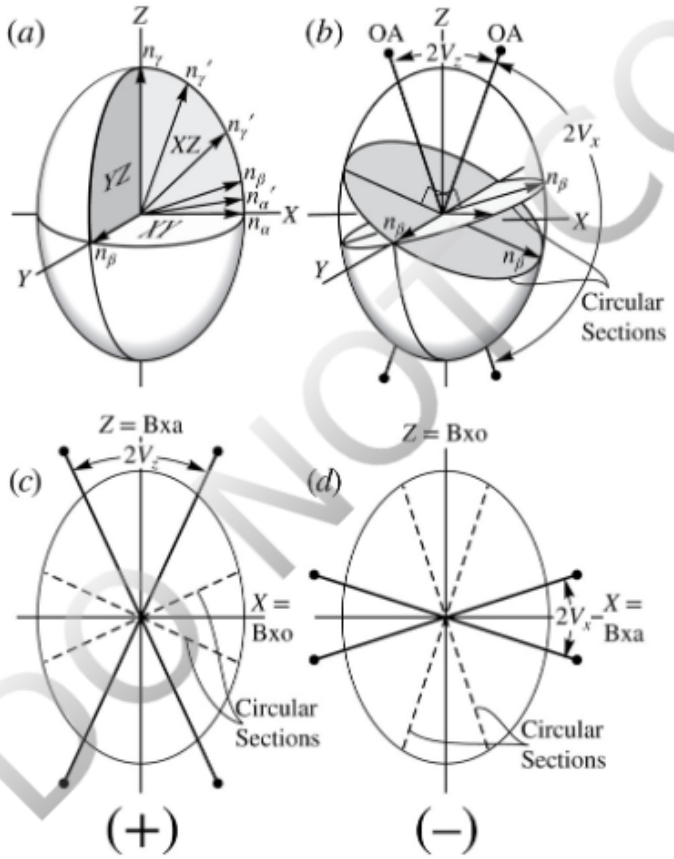

FIGURE 7.27 Biaxial indicatrix. (*a*) The indices n_α, n_β, and n_γ are plotted along the *X*, *Y*, and *Z* axes, respectively. Principal sections are the *XY*, *XZ*, and *YZ* planes. Within the *XZ* plane, radii of the ellipse vary from n_α to n_γ with certain radii equal to n_β. (*b*) Circular sections have radius n_β. The optic axes (OA) are perpendicular to the circular sections and lie in the *XZ*, or optic, plane. (*c*) Optic plane of a biaxial positive indicatrix. (*d*) Optic plane of a biaxial negative indicatrix. View larger image

The biaxial indicatrix is constructed and used much like the uniaxial indicatrix except that three indices of refraction are plotted, rather than two. The convention is to plot the three principal indices of refraction in an *X Y Z* coordinate axis system (Figure 7.27). The value of n_α is plotted along the *X* axis, n_β is plotted along the *Y* axis, and n_γ is plotted along the *Z* axis. In every case n_α is the smallest index of refraction and n_γ is the largest. The indicatrix is therefore a triaxial ellipsoid elongate along the *Z* axis and shortened along the *X* axis.

While three indices of refraction are required to describe biaxial optics, light that enters biaxial minerals is still split into two rays. As we shall see later, both of these rays behave

DO NOT COPY e48d507df5d1141@placeholder.94092

Printed by: e48d507df5d1141@placeholder.94092.edu. Printing is for personal, private use only. No part of this book may be reproduced or transmitted without publisher's prior permission. Violators will be prosecuted.

biaxial minerals is still split into two rays. As we shall see later, both of these rays behave as extraordinary rays for most propagation paths through the mineral. The wave normal and the ray diverge like the extraordinary ray in uniaxial minerals, and their indices of refraction vary with direction. We, therefore, revert to the terminology used earlier and call them the fast ray and the slow ray. The index of refraction of the fast ray is identified as n'_α where $n_\alpha < n'_\alpha < n_\beta$, and the index of refraction of the slow ray is n'_γ where $n_\beta < n'_\gamma < n_\gamma$. Rays whose indices of refraction are n_α, n_β, and n_γ are labeled α, β, and γ. Rays whose index of refraction is n'_α are labeled *fast* or α', and rays whose index of refraction is n'_γ are labeled *slow* or γ'.

The biaxial indicatrix contains three principal sections: the *XY*, *XZ*, and *YZ* planes. The *XY* section is an ellipse with axes n_α and n_β, the *XZ* section is an ellipse with axes n_α and n_γ, and the *YZ* section is an ellipse with axes n_β and n_γ. Random sections through the indicatrix are ellipses whose axes are n'_α and n'_γ.

The indicatrix has two **circular sections** with radius n_β that intersect in the *Y* axis. Consider the *XZ* plane (Figure 7.27a). It is an ellipse whose radii vary between n_α and n_γ, so radii equal to n_β must be present. Radii shorter than n_β are n'_α and those longer are n'_γ. The radius of the indicatrix along the *Y* axis also is n_β. The *Y* axis and the n_β radii in the *XZ* plane define the two circular sections (Figure 7.27b). In uniaxial minerals we saw that the circular section was perpendicular to the optic axis. In biaxial minerals, the same applies. The two **optic axes** are perpendicular to the two circular sections. The term **biaxial** is derived from the fact that two optic axes are present.

Because both optic axes lie in the *XZ* plane of the indicatrix, that plane is called the **optic plane**. The angle between the optic axes bisected by the *X* axis is called the $2V_x$ angle, and the angle between the optic axes bisected by the *Z* axis is called the $2V_z$ angle where $2V_x + 2V_z = 180°$. The *Y* axis, which is perpendicular to the optic plane, is called the **optic normal** or **ON**.

Optic Sign

The acute angle between the optic axes is called the optic angle, or **2*V* angle**. The axis (either *X* or *Z*) that bisects the optic angle is the **acute bisectrix** or **Bxa** (Figure 7.27c, d). The axis (either *Z* or *X*) that bisects the obtuse angle between the optic axes is the **obtuse bisectrix** or **Bxo**. The optic sign of biaxial minerals is defined to be consistent with the convention used with uniaxial minerals and depends on whether the *X* or *Z* indicatrix axis bisects the acute angle between the optic axes.

> If the acute bisectrix is the *X* axis, the mineral is ***optically negative***; $2V_x$ is less than 90°.
>
> If the acute bisectrix is the *Z* axis, the mineral is ***optically positive***; $2V_z$ is less than 90°.
>
> If 2V is exactly 90° so neither *X* nor *Z* is the acute bisectrix, the mineral is ***optically neutral***.

DO NOT COPY e48d507df5d1141@placeholder.9409

Printed by: e48d507df5d1141@placeholder.94092.edu. Printing is for personal, private use only. No part of this book may be reproduced or transmitted without publisher's prior permission. Violators will be prosecuted.

optically neutral.

The numerical values of n_α, n_β, n_γ, and $2V_Z$ are mathematically related by the following equation:

$$\cos^2 V_z = \frac{n_\alpha^2\left(n_\gamma^2 - n_\beta^2\right)}{n_\beta^2\left(n_\gamma^2 - n_\alpha^2\right)} \tag{7.16}$$

where V_Z is half the angle $2V_Z$.

Uniaxial indicatrixes may be considered special cases of the biaxial indicatrix. Note that if the value of n_β approaches n_α, the two circular sections converge into a single circular section in the XY plane and the two optic axes converge on the Z indicatrix axis, forming a uniaxial positive indicatrix (Figure 7.23a) where $n_\alpha = n_\omega$ and $n_\gamma = n_\epsilon$. If the value of n_β is increased so that it approaches n_γ, the two circular sections diverge away from the XY plane and close on each other in the YZ plane, and the two optic axes converge on the X axis, forming a uniaxial negative indicatrix (Figure 7.23b) where $n_\alpha = n_\epsilon$ and $n_\gamma = n_\omega$.

Crystallographic Orientation of Indicatrix Axes

The term **optic orientation** refers to the relationship between indicatrix axes and crystal axes. Because the optical properties of minerals are directly controlled by the symmetry of the crystal structure, optic orientation must be consistent with mineral symmetry.

Orthorhombic minerals have three mutually perpendicular crystallographic axes of unequal length. These crystal axes must coincide with the three indicatrix axes, and the symmetry planes in the mineral must coincide with principal sections in the indicatrix (**Figure 7.28a**). Any crystal axis may coincide with any indicatrix axis, however. The optic orientation is defined by indicating which indicatrix axis is parallel to which mineral axis. For example, in aragonite, $X = c$, $Y = a$, and $Z = b$, and in anthophyllite $X = a$, $Y = b$, and $Z = c$.

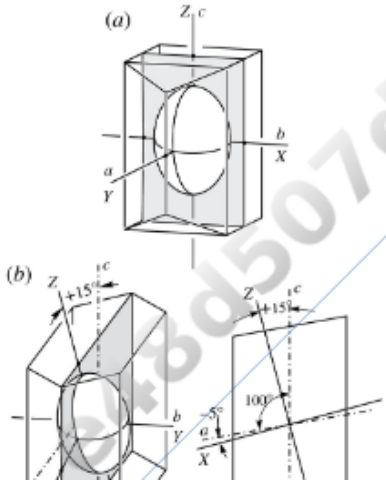

Printed by: e48d507df5d1141@placeholder.94092.edu. Printing is for personal, private use only. No part of this book may be reproduced or transmitted without publisher's prior permission. Violators will be prosecuted.

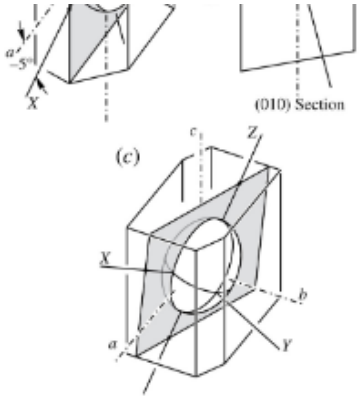

FIGURE 7.28 Relationship between crystal axes and indicatrix axes. The optic planes are shaded. (*a*) Orthorhombic. Crystal axes and indicatrix axes coincide. In this case the optic orientation is $X = b$, $Y = a$, $Z = c$. (*b*) Monoclinic. The *b* crystal axis coincides with one of the indicatrix axes. The other axes do not coincide except by chance. In this case the $X \wedge a = -5°$, $Y = b$, $Z \wedge c = +15°$. (*b*) Triclinic. None of the crystal axes coincide with indicatrix axes except by chance. View larger image

In monoclinic minerals, the *b* crystallographic axis coincides with the single 2-fold rotation axis and/or is perpendicular to the single mirror plane. The *a* and *c* crystal axes are perpendicular to *b* and intersect in an obtuse angle (β). One indicatrix axis, which could be either *X*, *Y*, or *Z*, is always parallel to the *b* crystallographic axis, and the other two lie in the {010} plane and are not parallel to either *a* or *c* except by chance (**Figure 7.28b**). The optic orientation is defined by specifying which indicatrix axis coincides with the *b* axis, as well as the angles between the other indicatrix axes and the *a* and *c* crystal axes. By convention, the angle between an indicatrix axis and either the *a* or *c* axis is a positive angle if the indicatrix axis lies in the obtuse angle between *a* and *c*, and a negative angle if the indicatrix axis lies in the acute angle. By this convention, the β angle between *a* and *c* is

$$\beta = 90^{\circ} + a \wedge (X, Y, \text{or } Z) + c \wedge (X, Y, \text{or } Z) \quad (7.17)$$

where ∧ means the angle between the axes on either side of the ∧ symbol. The optic orientation of the sample in Figure 7.28b is X ∧ $a = -5°$, Y = *b*, Z ∧ $c = +15°$. The β angle must therefore be $90° - 5° + 15° = 100°$. The reader is cautioned that other sources may define the sign of the optic orientation angles differently.

Triclinic minerals have three crystallographic axes of different lengths, none of which is at right angles. Because the only possible symmetry is center (inversion), the indicatrix axes are not constrained to be parallel to any crystal axis (**Figure 7.28c**). Although precise mathematical ways are available to specify the angles between indicatrix and crystal axes, in most cases the optic orientation is specified by indicating the approximate angle between indicatrix and crystal axes. Unfortunately, triclinic minerals may be described by using a variety of different crystal axis settings. The optic orientation

DO NOT COPY

Printed by: e48d507df5d1141@placeholder.94092.edu. Printing is for personal, private use only. No part of this book may be reproduced or transmitted without publisher's prior permission. Violators will be prosecuted.

described in different sources may therefore vary depending on which crystal axis setting is selected as a reference.

Use of the Indicatrix

The biaxial indicatrix is used in the same way as the uniaxial indicatrix. It provides information about the indices of refraction and vibration direction given the wave normal direction that light follows through a mineral. **Figure 7.29** shows a biaxial mineral cut in three different orientations. Birefringence depends on sample orientation. Birefringence is a maximum if the optic normal is vertical, minimum if an optic axis is vertical, and intermediate for other orientations.

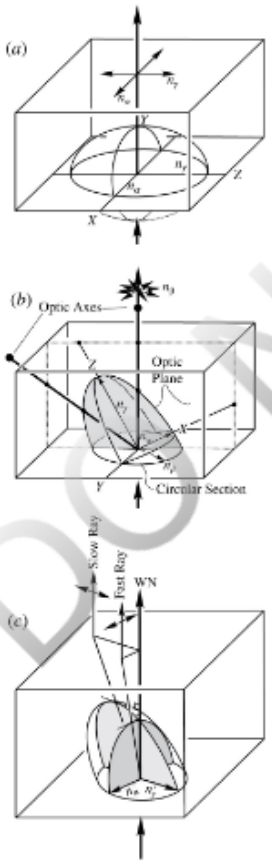

FIGURE 7.29 Behavior of biaxial minerals in orthoscopic illumination. (*a*) Optic normal (*Y*) vertical. Axes of the indicatrix section are *X* and *Z*, indices of refraction are n_α and n_γ, and birefringence is maximum. The slow ray vibrates parallel to *Z* and the fast ray vibrates parallel to *X*. (*b*) Optic axis vertical. The indicatrix section is a circle with radius n_β, birefringence is zero, and the mineral would be dark between crossed polarizers. (*c*) Random orientation. The indicatrix section yields indices of refraction n'_α and n'_γ and vibration directions as shown. Because n'_α is greater than n_α and n'_γ is less than n'_γ, birefringence is intermediate. Ray paths for both the slow and fast rays diverge from the wave normal, so both slow and fast rays are extraordinary. View larger image

DO NOT COPY e48d507df5d1141@placeholder.9409

Printed by: e48d507df5d1141@placeholder.94092.edu. Printing is for personal, private use only. No part of this book may be reproduced or transmitted without publisher's prior permission. Violators will be prosecuted.

Mineral Color and Pleochroism

Pleochroic minerals change color as the stage is rotated when the sample is observed in plane light (upper polarizer removed) (**Figure 7.30**). The color changes because the slow and fast rays are absorbed differently as they pass through the mineral and therefore have different colors. When the fast ray vibration direction is parallel to the lower polarizer, all light passes as fast ray, so the mineral displays that color. When the slow ray vibration direction is parallel to the lower polarizer, the mineral displays the color of the slow ray. If the stage is rotated to allow both slow and fast rays to come through, the perceived color is typically intermediate.

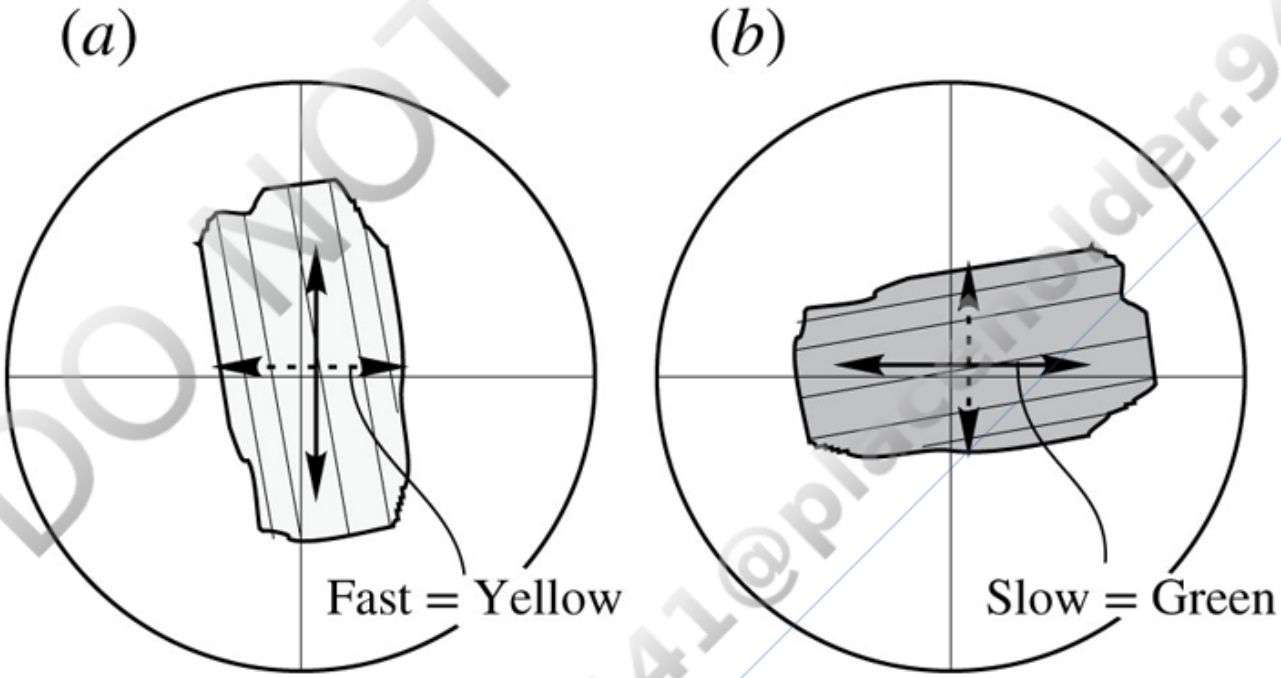

FIGURE 7.30 Pleochroism is seen in plane light. (*a*) The fast ray is yellow. When its vibration direction is parallel to the lower polarizer (E–W), the mineral is yellow. (*b*) The slow ray is green. When its vibration direction is parallel to the lower polarizer, the mineral appears green. In intermediate positions, both rays come through the mineral and color is intermediate. View larger image

Isotropic Minerals

Isotropic minerals are not pleochroic because they do not experience double refraction. In plane light, isotropic minerals display a uniform color as the stage is rotated.

Uniaxial Minerals

Printed by: e48d507df5d1141@placeholder.94092.edu. Printing is for personal, private use only. No part of this book may be reproduced or transmitted without publisher's prior permission. Violators will be prosecuted.

Colored uniaxial minerals are usually pleochroic. To describe the pleochroism, it is sufficient to identify the color of both the ω and ϵ rays. For example, the pleochroic formula of common tourmaline (schorl) is described as ω = dark green and ϵ = pale green. An alternative convention is to identify which ray is most strongly absorbed and therefore darker colored: $\omega > \epsilon$. Pleochroism may be described as strong or weak, depending on the extent of the color change and intensity of the colors. A grain oriented to display minimum retardation (lowest interference color) between crossed polarizers will, in plane light, yield the color of ω. A second grain oriented to display maximum retardation (highest interference color) between crossed polarizers will, when rotated in plane light, alternately display the colors of ϵ and ω. Because the color of ω is already known from the first grain, the color of ϵ can be determined by default.

Biaxial Minerals

To describe the pleochroism of biaxial minerals completely, it is necessary to specify three colors. One color is for light vibrating parallel to the X indicatrix axis, the second for light vibrating parallel to Y, and the third for light vibrating parallel to Z. For example, the pleochroism of hornblende can be described as X = yellow, Y = pale green, and Z = dark green. An alternative, and less informative, convention is to specify which is most strongly absorbed and therefore darkest, such as $Z > Y > X$.

A grain oriented to show minimum retardation between crossed polarizers, will, in plane light, display the color associated with Y. A grain oriented to display maximum retardation between crossed polarizers will show the colors of X and Z as the stage is rotated in plane light. Use the accessory plate to identify the slow and fast ray vibration directions. With the slow ray vibration direction parallel to the lower polar, the mineral will, in plane light, display the color associated with Z. Rotation by 90° yields the color associated with X.

DO NOT COPY e48d507df5d1141@placeholder.9409

Printed by: e48d507df5d1141@placeholder.94092.edu. Printing is for personal, private use only. No part of this book may be reproduced or transmitted without publisher's prior permission. Violators will be prosecuted.

Extinction Angle and Sign of Elongation

Extinction Angle

The angle between the length or a prominent cleavage in a mineral and a vibration direction is a diagnostic property called the **extinction angle**. It is measured in either grain mount or thin section with crossed polarizers as follows.

- Rotate the stage of the microscope until the length or cleavage of the mineral is aligned with the N–S crosshair (**Figure 7.31a**). Record the reading from the stage goniometer (g_1).
- Rotate the stage of the microscope (either clockwise or counterclockwise) until the mineral goes extinct (**Figure 7.31b**). This places either the slow or fast ray vibration direction parallel to the N–S crosshair. If the mineral is already extinct, no rotation is required. Record the new reading from the stage goniometer (g_2). The extinction angle is the difference between g_1 and g_2. If the extinction angle measured with clockwise stage rotation is EA, the extinction angle measured with counterclockwise rotation is 90° − EA. Generally it is the smaller of these two angles that is reported, although in some cases it is necessary to specifically measure the extinction angle to the slow or the fast ray vibration direction. The technique to determine which ray is which has been discussed earlier.

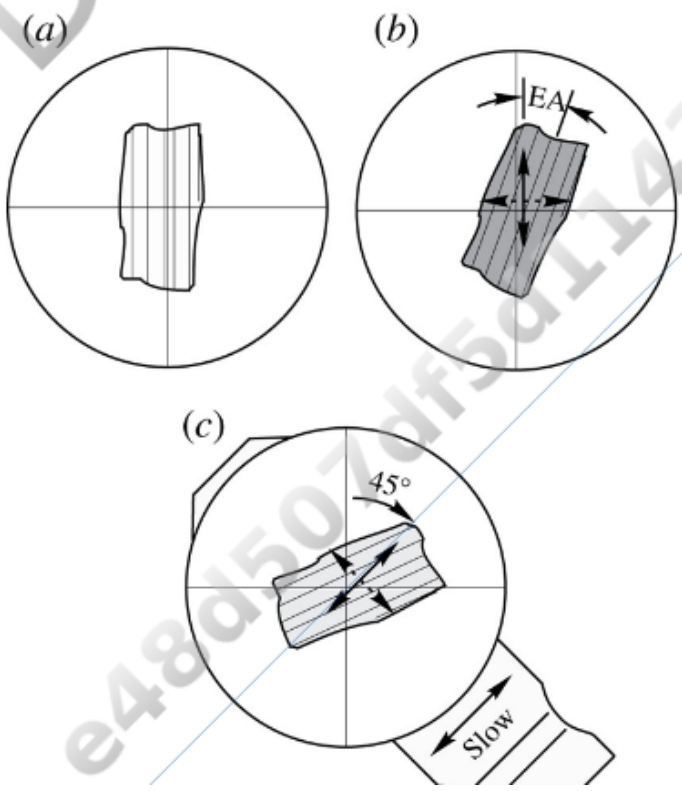

DO NOT COPY
e48d507df5d1141@placeholder.94092

Printed by: e48d507df5d1141@placeholder.94092.edu. Printing is for personal, private use only. No part of this book may be reproduced or transmitted without publisher's prior permission. Violators will be prosecuted.

FIGURE 7.31 Measurement of extinction angle and sign of elongation. Polarizers are crossed. (*a*) Grain oriented so that cleavage or length is parallel to the N–S crosshair. (*b*) Stage rotated so the grain is extinct and one vibration direction is parallel to the N–S crosshair. The extinction angle (EA) is the angle through which the stage was rotated to go from (*a*) to (*b*). (*c*) Stage rotated 45° clockwise to place the vibration direction nearest the mineral length parallel to NE–SW. Insert the accessory plate. If retardations add, the mineral is length slow; if retardations cancel, the mineral is length fast. View larger image

The extinction angle measured on a specific mineral in thin section or grain mount depends on exactly how the grain happens to be oriented in the sample. Hence, to be diagnostic, it is necessary to specify the orientation of the mineral grain on which the measurement is made. In many cases the diagnostic extinction angle is measured on grains that display maximum retardation (optic axes horizontal). In others, extinction angles are specified for certain orientations, such as resting on a cleavage surface or a cut through the mineral parallel to a specific crystallographic plane.

Sign of Elongation

The terms **length fast** and **length slow** are repeatedly encountered in the mineral descriptions in the latter part of this text. Length fast means that the fast ray vibrates more or less parallel to the length of an elongate mineral; length slow means that the slow ray vibrates more or less parallel to the length. Length fast is also called **negative elongation**; length slow is called **positive elongation**. Sign of elongation is not the same as optic sign. Optic sign is discussed in the sections on uniaxial and biaxial indicatrixes. Determine sign of elongation as follows.

- Start with the mineral extinct and with the mineral elongation or trace of cleavage so that it is less than 45° from the N–S crosshair. This generally is the position obtained after rotating to measure the extinction angle (Figure 7.31b).
- Rotate the stage 45° clockwise (**Figure 7.31c**). This places the vibration direction closest to the length or prominent cleavage NE–SW. Insert an accessory plate. If retardations add, the ray whose vibration direction is closest to the length or cleavage is the slow ray and the mineral is length slow. If retardations subtract, the ray whose vibration direction is closest to the length or cleavage is the fast ray, and the mineral is length fast.

Categories of Extinction

The four categories of extinction are parallel extinction, inclined extinction, symmetrical extinction, and no extinction angle.

DO NOT COPY e48d507df5d1141@placeholder.9409

Printed by: e48d507df5d1141@placeholder.94092.edu. Printing is for personal, private use only. No part of this book may be reproduced or transmitted without publisher's prior permission. Violators will be prosecuted.

With **parallel extinction**, the mineral is extinct when the cleavage or length is aligned parallel to one of the crosshairs (**Figure 7.32a**). The extinction angle is 0°. Either the slow ray or fast ray vibration direction may be parallel to the trace of cleavage or length of the mineral.

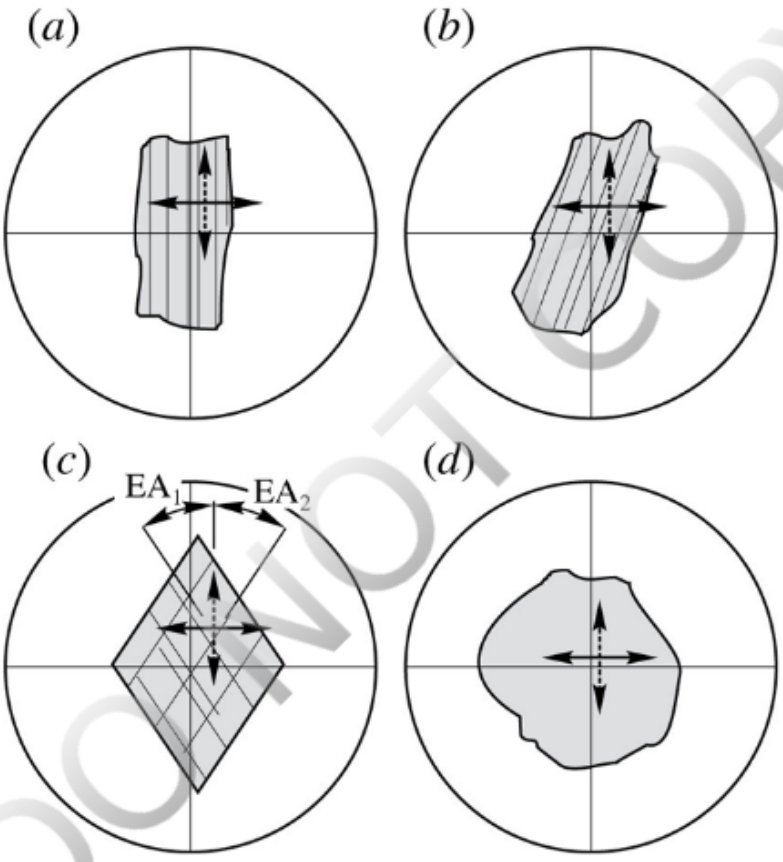

FIGURE 7.32 Categories of extinction. All grains are in extinction orientations. (*a*) Parallel extinction. The grain is extinct when the trace of cleavage or length is parallel to a crosshair. (*b*) Inclined extinction. The grain is extinct when the cleavage or length is at an angle to a crosshair. (*c*) Symmetrical extinction. Extinction angles EA_1 and EA_2 measured to the two cleavages are the same. (*d*) No extinction angle. The grain lacks cleavage or elongation from which to measure an extinction angle. View larger image

With **inclined extinction**, the mineral is extinct when the cleavage or length is at some angle to the crosshairs (**Figure 7.32b**). The extinction angle is greater than 0° and is measured as previously described. Neither vibration direction is aligned parallel to the trace of cleavage or the length of the mineral. If the slow ray vibration direction is closest to the length or trace of cleavage, the mineral is length slow; if the fast ray is closest, the mineral is length fast.

Symmetrical extinction may be observed in minerals that display either two cleavages or two distinct crystal faces (**Figure 7.32c**). If the extinction angles EA_1 and EA_2, measured from the two cleavages or crystal faces to the same vibration direction, are the same, extinction is symmetrical. To measure the extinction angles, it is most convenient to rotate the mineral to an extinction position and record the stage goniometer reading.

DO NOT COPY e48d507df5d1141@placeholder.9409

Printed by: e48d507df5d1141@placeholder.94092.edu. Printing is for personal, private use only. No part of this book may be reproduced or transmitted without publisher's prior permission. Violators will be prosecuted.

to rotate the mineral to an extinction position and record the stage goniometer reading. Then rotate clockwise to measure the extinction angle to one cleavage/crystal face. Return to the extinction position and then rotate counterclockwise to measure the second extinction angle.

Many minerals lack distinct cleavages or do not display an elongation or crystal faces. Although they go extinct once in every 90° of stage rotation, there is no cleavage, elongation, or crystal face from which to measure an extinction angle. Hence, these minerals have **no extinction angle** (**Figure 7.32d**).

In addition to these four categories of extinction angles, some mineral grains may not go uniformly extinct at the same point of stage rotation because of either deformation or chemical zoning (see Chapter 5). In many deformed rocks, mineral grains may be bent or otherwise strained so that different parts of a grain go extinct at different points of stage rotation. If the extinction follows an irregular or wavy pattern it is called **undulose extinction** or **undulatory extinction** (Figure 12.3b). Many minerals, including plagioclase, grow so that they are chemically zoned. Because extinction angle may be controlled by chemical composition in monoclinic and triclinic minerals, extinction angle may vary systematically with composition, so that the center of a grain may display one extinction angle and the rim another. A special term is not applied to this type of extinction, but minerals that display it are said to be **zoned** (Figure 5.13).

Extinction in Uniaxial Minerals

Tetragonal and many hexagonal minerals are prismatic and are either elongate or stubby parallel to the *c* axis. The common forms are prisms parallel to *c*, pinacoids perpendicular to *c*, pyramids, and related forms. Hexagonal minerals that crystallize in the trigonal group are commonly rhombohedral. Cleavages may be parallel to any of these forms (Chapter 2). A simple tetragonal mineral shown in **Figure 7.33** is cut in a variety of different orientations such as might be found in a thin section. In grain mount, individual grains are most likely to rest on one of the cleavage surfaces, although all orientations are possible. A sample with the highest birefringence will have its *c* axis parallel to the microscope stage; it will display parallel extinction to prismatic cleavage and inclined or symmetrical extinction to a rhombohedral or pyramidal cleavage. Extinction is parallel to {001} cleavage in all grain orientations.

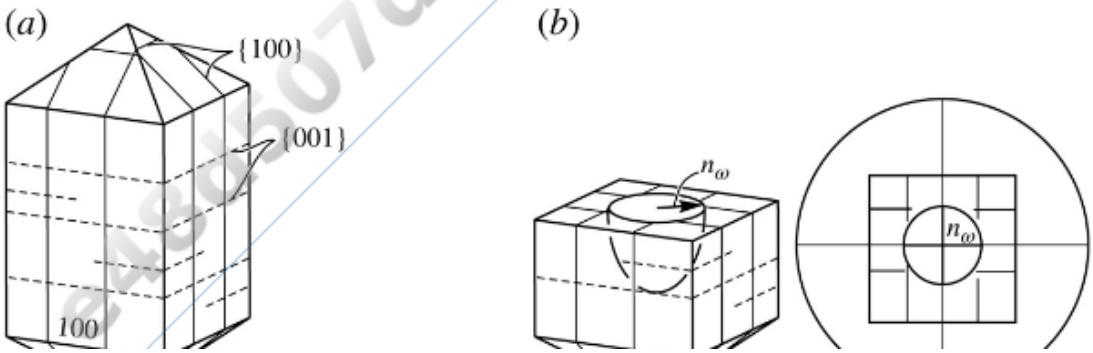

DO NOT COPY e48d507df5d1141@placeholder.94092

Printed by: e48d507df5d1141@placeholder.94092.edu. Printing is for personal, private use only. No part of this book may be reproduced or transmitted without publisher's prior permission. Violators will be prosecuted.

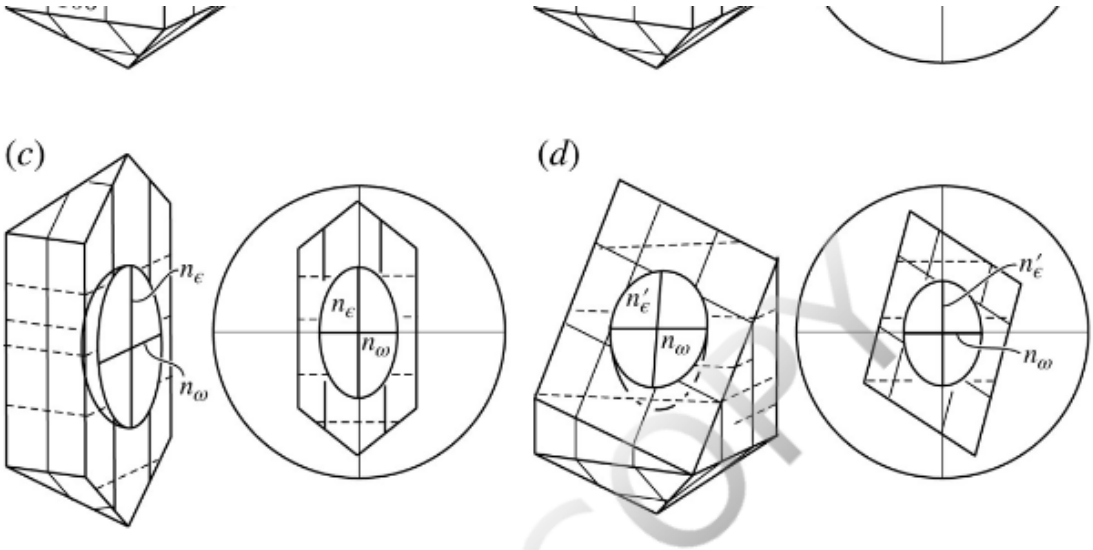

FIGURE 7.33 Extinction in a typical tetragonal mineral. (*a*) Mineral showing traces of pinacoid {001} (dashed) and prismatic {100} (solid) cleavages. (*b*) Mineral resting on the {001} cleavage with the optic axis vertical. The indicatrix section is circular, so all light passes as ordinary rays. The mineral behaves like an isotropic mineral and remains extinct with stage rotation. (*c*) Mineral oriented with optic axis horizontal. The indicatrix section is a principal section, so indices of refraction are n_ω and n_ϵ, and retardation is maximum. Extinction is parallel to the traces of both {001} and {100} cleavage. (*d*) A random cut yields a parallelogram-shaped section. Birefringence is intermediate, and extinction is parallel to the trace of {001} and inclined to the traces of the {100} cleavages. View larger image

Extinction in Biaxial Minerals

Orthorhombic minerals display parallel or symmetrical extinction in sections cut parallel to (100), (010), and (001), and inclined extinction in random orientations. Grains cut to yield maximum retardation always display parallel or symmetrical extinction. Monoclinic minerals display parallel or symmetrical extinction if {010} happens to be vertical, and inclined extinction in most other orientations (**Figure 7.34**). A common indicatrix orientation is for the *Y* indicatrix axis to be parallel to *b*. In minerals with this orientation, such as the monoclinic pyroxenes and amphiboles, grains oriented to display maximum retardation also have extinction angles that indicate the relation between the *X* and *Z* indicatrix axes and *a* and *c* crystal axes as shown. Triclinic minerals display inclined extinction in most sections because indicatrix and crystal axes need not be parallel.

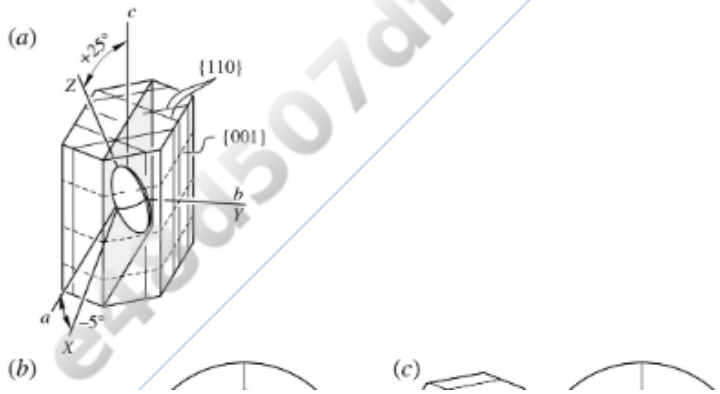

Printed by: e48d507df5d1141@placeholder.94092.edu. Printing is for personal, private use only. No part of this book may be reproduced or transmitted without publisher's prior permission. Violators will be prosecuted.

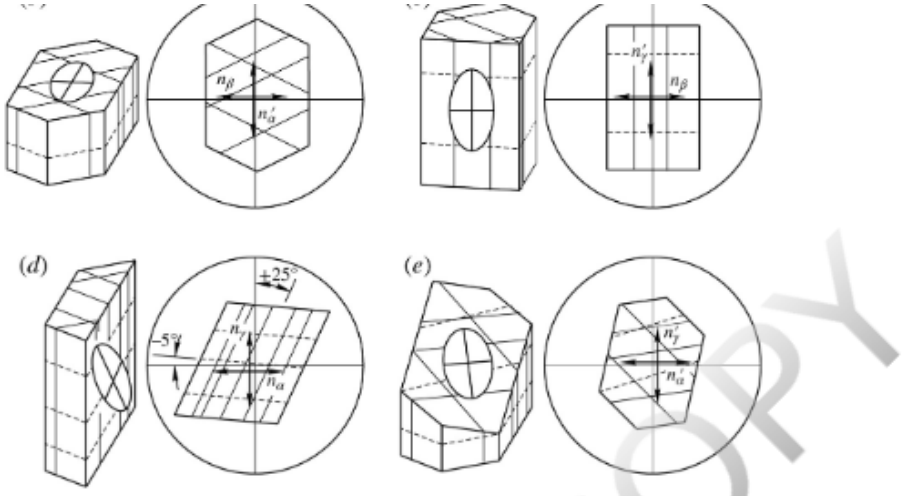

FIGURE 7.34 Extinction in monoclinic minerals. (*a*) Crystal habit showing trace of prismatic {110} (solid lines) and pinacoidal {001} (dashed lines) cleavages. The indicatrix orientation is $Y = b$, $Z \wedge c = +25°$, $X \wedge a = -5°$. (*b*) Fragment resting on the {001} cleavage. Extinction is symmetrical. (*c*) Section parallel to {100} shows parallel extinction to the trace of both cleavages. (*d*) Section parallel to {010} displays maximum retardation. Extinction is 25° (the $Z \wedge c$ angle) measured to the trace of the {110} cleavage and 5° (the $X \wedge a$ angle) measured to the trace of the {001} cleavage. (*e*) Random section: inclined extinction to all cleavage traces. View larger image

DO NOT COPY
e48d507df5d1141@placeholder.9409

Printed by: e48d507df5d1141@placeholder.94092.edu. Printing is for personal, private use only. No part of this book may be reproduced or transmitted without publisher's prior permission. Violators will be prosecuted.

Interference Figures

An **interference figure** is obtained to rapidly determine **optical character**: that is, whether a mineral is uniaxial or biaxial, and to determine the **optic sign**. If the mineral is biaxial, the $2V$ angle also may be measured. An interference figure also may be used to confirm certain mineral orientations. To view an interference figure:

- Focus on a single mineral grain with the high-power objective lens.
- Flip in the auxiliary condensing lens. Refocus if needed, and open the aperture diaphragm. Insert the upper polarizer.
- Insert the Bertrand lens. The interference figure also may be observed without the Bertrand lens by removing the ocular and looking directly down the microscope tube.

The interference figure is formed near the top surface of the objective lens and consists of a pattern of interference colors called **isochromes** on which dark bands called **isogyres** are superimposed. The nature of the interference figure and its behavior as the stage is rotated depends on the orientation of the mineral grain and whether the mineral is uniaxial or biaxial.

Uniaxial Interference Figures

Optic Axis Interference Figure

A **uniaxial optic axis interference figure** (Figure 7.35) is produced if a uniaxial mineral's optic axis is perpendicular to the microscope stage. A grain with a vertical optic axis should display the lowest interference color (retardation) of all grains in the sample. The interference figure consists of **isogyres** forming a black cross superimposed on a circular pattern of **isochromes**. The point in the center where the isogyres cross is called the **melatope**, and it marks the point of emergence of the optic axis. The interference colors increase in order outward from the melatope; those nearest the melatope are low first order. If the optic axis is exactly vertical, the interference figure does not appear to change as the stage is rotated. *The presence of a single melatope indicates that the mineral is uniaxial.* Biaxial minerals produce interference figures with two melatopes, as will be described below.

DO NOT COPY e48d507df5d1141@placeholder.9409-

Printed by: e48d507df5d1141@placeholder.94092.edu. Printing is for personal, private use only. No part of this book may be reproduced or transmitted without publisher's prior permission. Violators will be prosecuted.

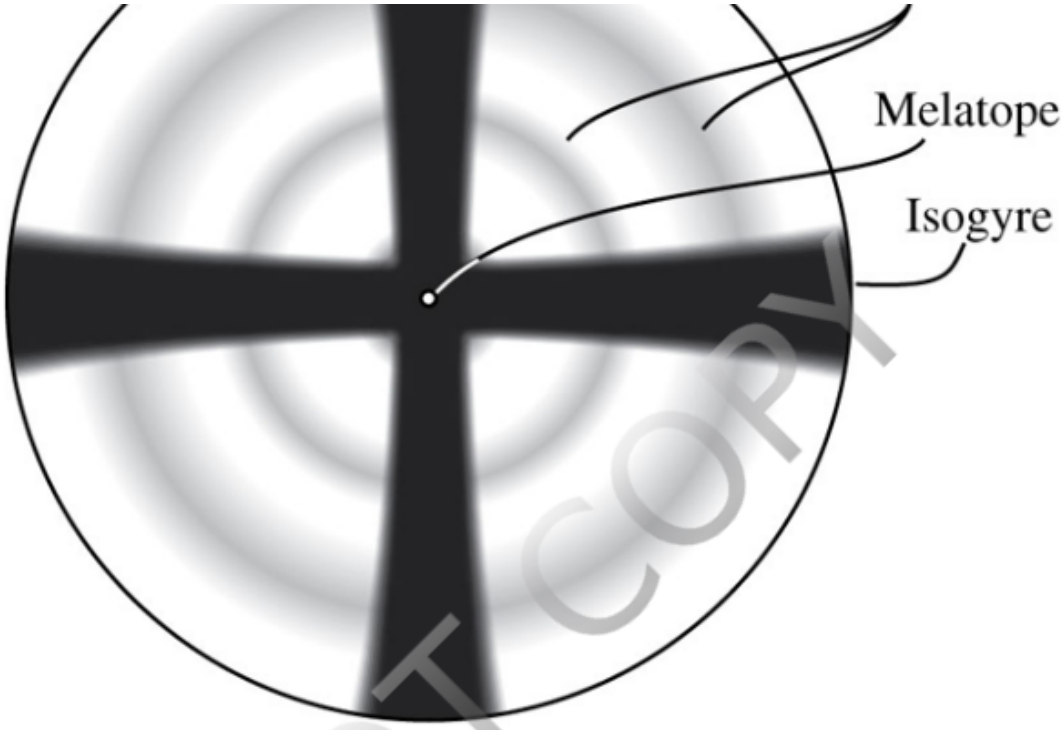

FIGURE 7.35 Uniaxial optic axis interference figure. View larger image

The formation of isochromes is shown in **Figure 7.36**. The auxiliary condensing lens provides strongly convergent light that passes through the mineral and is collected by the objective lens. Light following path 1, parallel to the optic axis, is not split into two rays and exits the mineral with zero retardation to form the melatope. Light following path 2 experiences moderate retardation because the value of n'_ϵ is close to n_ω. Light following path 3, at a greater angle to the optic axis, encounters higher birefringence and must traverse a greater distance through the mineral, so retardation is proportionately greater. The interference colors, therefore, increase outward from the melatope. Because optical properties are symmetric about the optic axis, rings of equal retardation and interference color are formed around the melatope. Minerals that are thick or have high birefringence show more isochromes than thin or low-birefringence minerals.

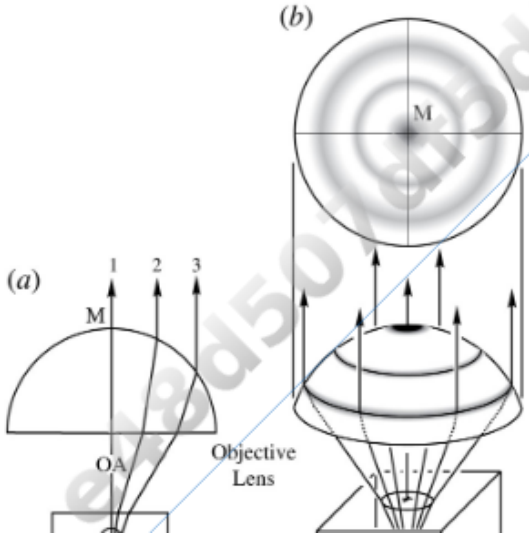

Printed by: e48d507df5d1141@placeholder.94092.edu. Printing is for personal, private use only. No part of this book may be reproduced or transmitted without publisher's prior permission. Violators will be prosecuted.

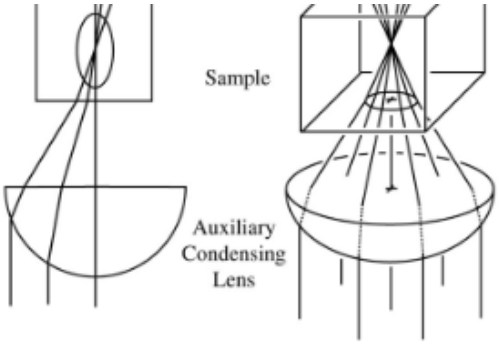

FIGURE 7.36 Formation of uniaxial isochromes. (*a*) Light following path 1, which emerges at the melatope (M), experiences zero retardation because it follows the optic axis (OA). Paths 2 and 3 produce progressively higher retardation because both birefringence and path length through the sample increase as the inclination of the path to the optic axis increases. (*b*) Optical properties are symmetric about the optic axis, so rings of equal retardation are produced about the melatope. View larger image

Isogyres are formed where vibration directions in the interference figure are N–S and E–W. They are areas of extinction. **Figure 7.37a** schematically shows the vibration directions for strongly convergent light that emerges from the center of the uniaxial indicatrix. The vibration directions are determined as described in Figure 7.22. Ordinary (ω) rays vibrate parallel to lines of latitude, and extraordinary (ϵ') rays vibrate parallel to lines of longitude on the indicatrix. These vibration directions are carried up into the interference figure (**Figure 7.37b**). Extraordinary (ϵ') rays vibrate along radial lines symmetric about the melatope and ordinary (ω) rays vibrate tangent to the circular isochromes. The isogyres are formed where the vibration directions in the interference figure are N–S and E–W. Isogyres become wider and have more diffuse edges farther from the melatope.

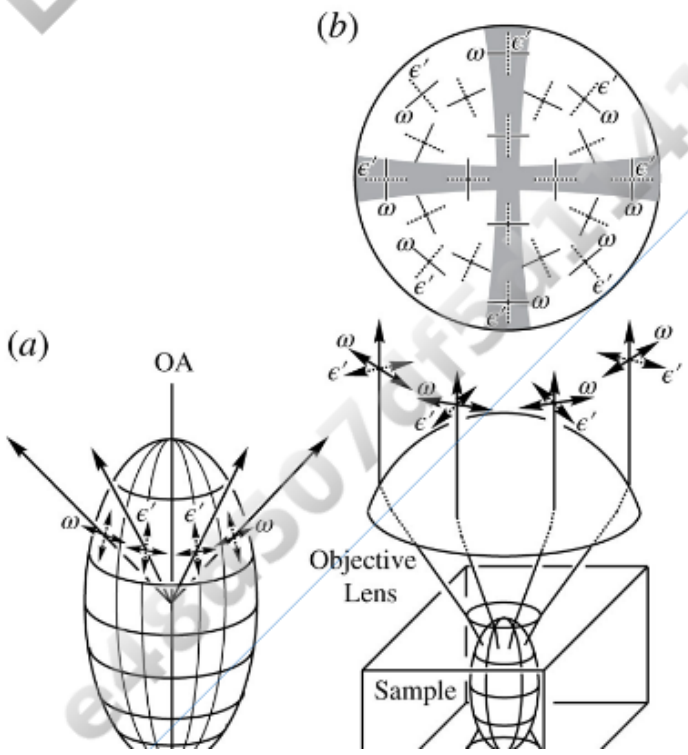

Printed by: e48d507df5d1141@placeholder.94092.edu. Printing is for personal, private use only. No part of this book may be reproduced or transmitted without publisher's prior permission. Violators will be prosecuted.

FIGURE 7.37 Formation of isogyres. (*a*) Vibration directions for light emerging from the center of a uniaxial indicatrix. Ordinary (ω) rays vibrate parallel to lines of latitude and extraordinary (ϵ') rays vibrate parallel to lines of longitude. (*b*) Strongly convergent light that passes through a mineral whose optic axis is vertical exits with a vibration pattern that is symmetric about the melatope. Extraordinary rays (ϵ') vibrate parallel to radial lines (similar to lines of longitude as seen from above), and ordinary rays (ω) vibrate tangent to the circular isochromes (similar to lines of latitude as seen from above). Isogyres form between crossed polarizers where vibration directions in the figure are parallel to the vibration directions of the lower and upper polarizers. They are areas of extinction. View larger image

Off-Center Figure

If the optic axis is inclined from the vertical, the interference figure will no longer be centered in the field of view. As long as the optic axis is within about 25° to 30° of being vertical (**Figure 7.38a**), the melatope will be visible in the field of view, and the interference figure is called an **off-center optic axis figure**. The isogyres still form a NS–EW cross centered on the melatope that swings in an arc around the field of view as the stage is rotated. As long as the melatope is present, the figure may be used to determine optical character and optic sign as is described shortly.

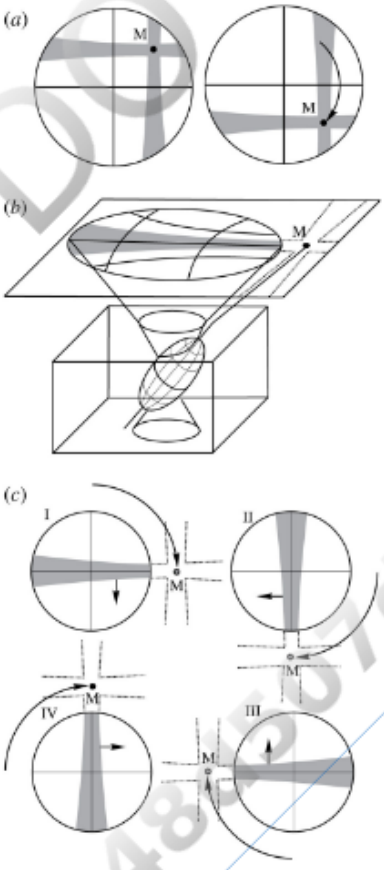

FIGURE 7.38 Off-center uniaxial interference figures. (*a*) Off-center optic axis figure. As the stage is rotated, the melatope sweeps around the field of view. Isogyres and isochromes remain

DO NOT COPY e48d507df5d1141@placeholder.9409

Printed by: e48d507df5d1141@placeholder.94092.edu. Printing is for personal, private use only. No part of this book may be reproduced or transmitted without publisher's prior permission. Violators will be prosecuted.

stage is rotated, the melatope sweeps around the field of view. Isogyres and isochromes remain centered on the melatope and the isogyres retain their essential N–S and E–W orientations. (*b*) Mineral sample with optic axis more than 30° from vertical. The melatope is out of the field of view. (*c*) Stage rotation causes isogyre arms to sweep across the field of view in sequence. The thin end of an isogyre arm points to the melatope. View larger image

If the optic axis is inclined more than about 25° to 30° from vertical (**Figure 7.38b**), the melatope will not be visible in the field of view and the figure is called an **off-center figure**. The four isogyre arms sweep across the field of view sequentially as the stage is rotated (**Figure 7.38c**). This is the interference figure most commonly encountered if grains are randomly selected. Because uniaxial and biaxial minerals may produce similar off-center interference figures, they generally cannot be used to determine either optical character or optic sign.

Optic Normal (Flash) Figure

If a mineral grain is oriented with the optic axis parallel to the microscope stage, an **optic normal interference figure** is produced (**Figure 7.39**). Mineral grains oriented to yield optic normal figures display maximum retardation. Optic normal figures are characterized by broad fuzzy isogyres that occupy nearly the entire field of view when the trace of the optic axis is either E–W or N–S. With only a few degrees of stage rotation, the isogyre splits into two segments that exit the field of view from the quadrants into which the optic axis is being rotated. Because the isogyres appear and disappear rapidly with stage rotation, these figures also are known as **flash figures**. An optic normal figure confirms that the optic axis is approximately horizontal. However, it is not routinely used to determine either optical character or optic sign because an interference figure with nearly identical appearance is produced by biaxial minerals.

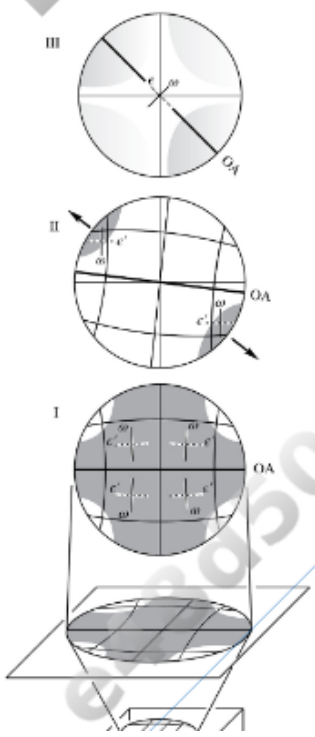

DO NOT COPY
e48d507df5d1141@placeholder.9409

Printed by: e48d507df5d1141@placeholder.94092.edu. Printing is for personal, private use only. No part of this book may be reproduced or transmitted without publisher's prior permission. Violators will be prosecuted.

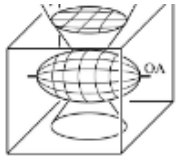

FIGURE 7.39 Uniaxial optic normal (flash) figure. The optic axis is parallel to the microscope stage. Vibration directions in the figure are derived as shown in Figure 7.37. In view I, the optic axis is exactly E–W. The isogyre is a broad, fuzzy cross because vibration directions of ω and ϵ' rays in all but the outer parts of the four quadrants are parallel to the lower and upper polarizers. In view II, the stage has been rotated a few degrees clockwise. The isogyres quickly split and exit the field of view from the quadrants into which the optic axis (OA) is being rotated (isochromes are not shown). View III shows the figure with the optic axis NW–SE. Diffuse isochromes are concave outward. The retardation decreases outward toward the NW and SE and increases outward toward the NE and SW.
View larger image

Determining Optic Sign

The optic axis interference figure is used to determine **optic sign** because the vibration directions of ordinary and extraordinary rays are known at each point in the figure (Figure 7.37). Note the interference colors in the four quadrants of the figure (**Figure 7.40a**) and determine the retardation (Δ_1) from the interference color chart (Plate 1). When an accessory plate with retardation Δ_A (slow NE–SW) is inserted, the retardations will add in two quadrants and subtract in two quadrants. Where retardations add, the new interference color will have retardation $\Delta_1 + \Delta_A$. Where retardations subtract, the new interference color will have a retardation that is the absolute value of $\Delta_1 - \Delta_A$.

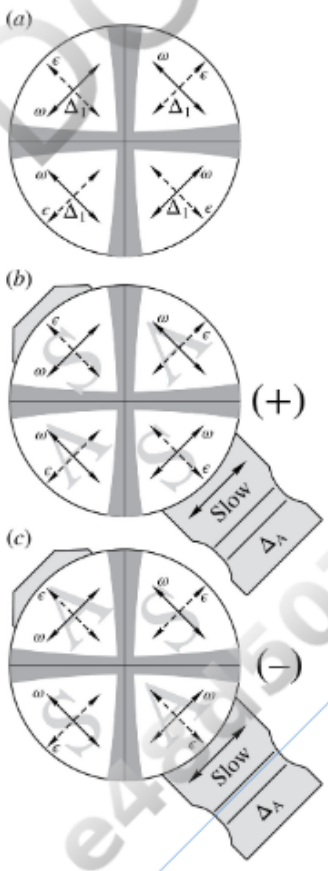

DO NOT COPY
e48d507df5d1141@placeholder.9409

Printed by: e48d507df5d1141@placeholder.94092.edu. Printing is for personal, private use only. No part of this book may be reproduced or transmitted without publisher's prior permission. Violators will be prosecuted.

FIGURE 7.40 Determining optic sign in a uniaxial optic axis interference figure. (*a*) Retardation Δ_1 is displayed in the four quadrants and the vibration directions of ordinary (ω) and extraordinary (ϵ) rays are shown. When an accessory plate with retardation Δ_A (slow NE–SW) is inserted, retardations in two quadrants will add (A) to become $\Delta_1 + \Delta_A$, and retardations in the other two quadrants will subtract (S) to become $|\Delta_1 - \Delta_A|$. (*b*) Optically positive. (*c*) Optically negative. View larger image

Consider the NW and SE quadrants where the ordinary rays vibrate NE–SW, parallel to the accessory plate slow ray. If the retardations subtract in these quadrants with insertion of the accessory plate (**Figure 7.40b**), the ordinary ray is the fast ray and the mineral is optically positive. If the retardations in the NW and SE quadrants add (**Figure 7.40c**), the ordinary ray is the slow ray and the mineral is optically negative. The interference colors in the NE and SW quadrants must change in the opposite sense because the ordinary rays vibrate NW–SE and the extraordinary rays vibrate NE–SW there. If the interference figure contains numerous isochromes, the isochrome bands will appear to shift inward in quadrants where the retardations add, as higher-order colors replace lower-order colors. In the quadrants where retardations cancel, the isochromes will shift outward as lower-order colors replace higher-order colors.

Biaxial Interference Figures

Biaxial minerals can be distinguished from uniaxial minerals by examining an interference figure on an appropriately oriented grain. The optic sign and the $2V$ angle also may be determined.

Acute Bisectrix Figure

An **acute bisectrix interference figure** (**Figure 7.41**) is obtained if the acute bisectrix (X or Z depending on optic sign) is oriented perpendicular to the microscope stage. Identifying a grain in a thin section oriented to yield an acute bisectrix interference figure is mostly a matter of chance because a correctly oriented grain will have intermediate retardation. Many grains may have to be examined before finding one in the correct orientation. Provided that $2V$ is less than about 45° to 55°, the melatopes marking the points of emergence of the optic axes will be in the field of view. The interference figure consists of isogyres that change as the stage is rotated superimposed on a field of isochromes. For study purposes, a sheet of muscovite mounted flat on a microscope slide provides an excellent acute bisectrix interference figure.

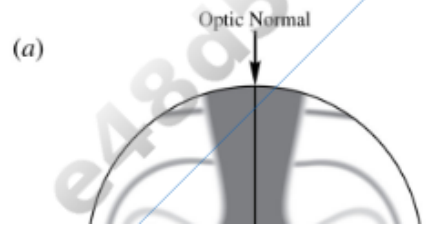

DO NOT COPY e48d507df5d1141@placeholder.9409

Printed by: e48d507df5d1141@placeholder.94092.edu. Printing is for personal, private use only. No part of this book may be reproduced or transmitted without publisher's prior permission. Violators will be prosecuted.

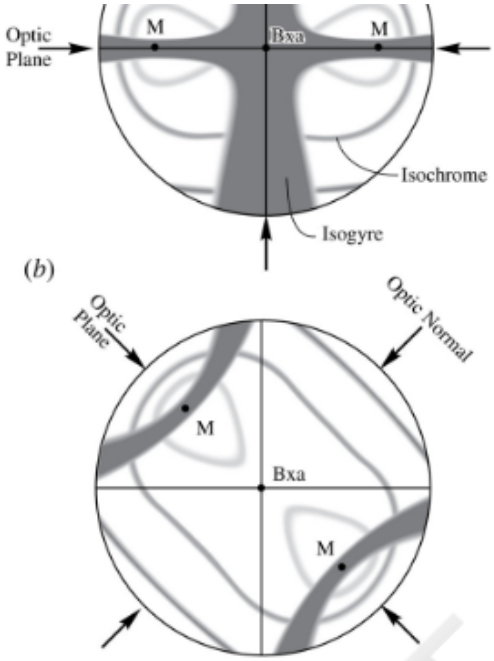

FIGURE 7.41 Biaxial acute bisectrix interference figure. The melatopes (M) mark the points of emergence of the optic axes, and the acute bisectrix (Bxa) is in the center of the field of view. Isochromes form an oval or figure-eight pattern centered on the melatopes. The isogyre pattern depends on stage rotation. (*a*) The isogyres form a cross-shaped pattern when the trace of the optic plane is oriented E–W. (*b*) Optic plane rotated to a 45° position. With rotation from (*a*) to (*b*), the isogyres split and move across the field of view to form the two arc-shaped segments centered on the melatopes. View larger image

The isochromes form an oval or figure-eight pattern about the melatopes (**Figure 7.42**). Only light that follows the optic axes experiences zero retardation. Light experiences increasing birefringence for paths inclined to the optic axes, so retardation must increase away from the melatopes to form the oval pattern. Minerals that are thick or have high birefringence display more isochromes than thin or low-birefringence minerals; this is because retardation and interference color are dependent on both thickness and birefringence (Equation 7.8). The pattern of isochromes remains fixed relative to the melatopes as the stage is rotated.

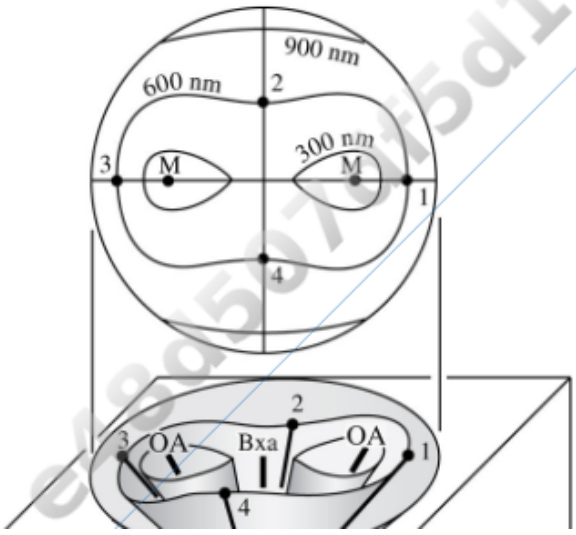

DO NOT COPY

Printed by: e48d507df5d1141@placeholder.94092.edu. Printing is for personal, private use only. No part of this book may be reproduced or transmitted without publisher's prior permission. Violators will be prosecuted.

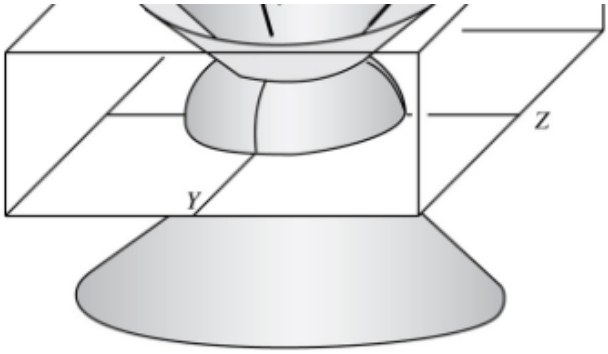

FIGURE 7.42 Formation of biaxial isochromes. Light following the optic axes emerges at the melatopes (M) with zero retardation. Light following paths within the flattened cone outlined by rays 1, 2, 3, and 4 develops the same retardation by the time each ray has exited the top of the mineral. Light inclined further from the optic axes develops greater retardation, and light following paths inclined less to the optic axes develops less. Isochromes are formed in the interference figure along bands of equal retardation. View larger image

The isogyres form a pattern that changes as the stage is rotated. Vibration directions in the figure can be derived in the same manner employed for uniaxial figures. **Figure 7.43a** shows the indicatrix for a biaxial negative mineral. Note that if the optic angle ($2V$) approaches zero, the indicatrix and the vibration directions approach those of a uniaxial negative mineral. Vibration directions for a number of light paths are projected onto the top surface of the mineral and into the interference figure (**Figure 7.43b**).

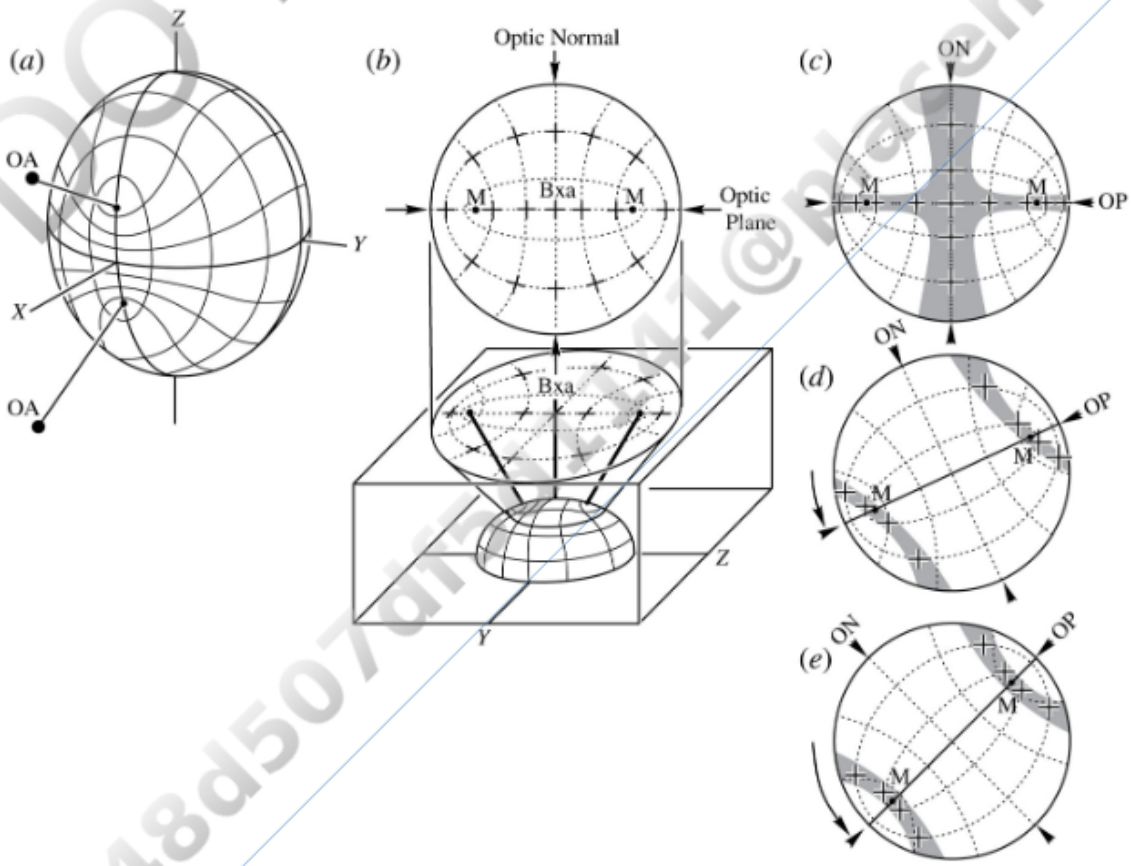

FIGURE 7.43 Formation of biaxial isogyres. (*a*) Vibration directions for all paths emerging from the biaxial indicatrix are determined as described in Figure 7.22 and are projected onto the

Printed by: e48d507df5d1141@placeholder.94092.edu. Printing is for personal, private use only. No part of this book may be reproduced or transmitted without publisher's prior permission. Violators will be prosecuted.

the biaxial indicatrix are determined as described in Figure 7.22 and are projected onto the indicatrix. (*b*) Vibration directions for a number of light paths have been projected onto the upper surface of the mineral grain and are shown in the interference figure. Isogyres are areas of extinction where vibration directions in the interference figure are N–S and E–W. (*c*) Optic plane oriented E–W. The isogyres form a cross that is wider along the trace of the optic normal (ON) and is thin at the melatopes (M). (*d*) With a few degrees of stage rotation, the isogyres split into two segments that pivot about the position of the melatopes. (*e*) Optic plane NE–SW. Isogyres form hyperbolas centered on the melatopes. View larger image

If the optic plane is oriented E–W (**Figure 7.43c**) or N–S, the isogyres, defined by areas in the figure where vibration directions are N–S and E–W, form a cross. The arm parallel to the trace of the optic normal is somewhat wider than the isogyre parallel to the trace of the optic plane. The positions of the melatopes are marked by a narrowing of the isogyres. This narrowing may be obscured in minerals with low birefringence because the low first-order gray interference color in the vicinity of the melatope may be indistinguishable from the extinction area of the isogyre.

If the optic plane is rotated away from E–W (or N–S), the cross-shaped isogyre splits into two separate isogyre segments that appear to pivot about the positions of the melatopes (**Figure 7.43d**). When the trace of the optic plane is placed in a 45° position, the isogyres form hyperbolic arcs whose vertices are the melatopes (**Figure 7.43e**). The isogyres are narrowest at the melatopes and fan out somewhat toward the edge of the field of view.

Optic Axis Figure

An optic axis interference figure is produced when one of the optic axes is vertical. Grains in this orientation display zero or minimum retardation so they are relatively easy to identify. The melatope corresponding to an optic axis is centered in the field of view. The other melatope may be in the field of view if $2V$ is less than roughly 25° to 30°; otherwise it will be outside the field of view. If $2V$ is small, the interference figure looks like an off-center acute bisectrix figure (**Figure 7.44a**).

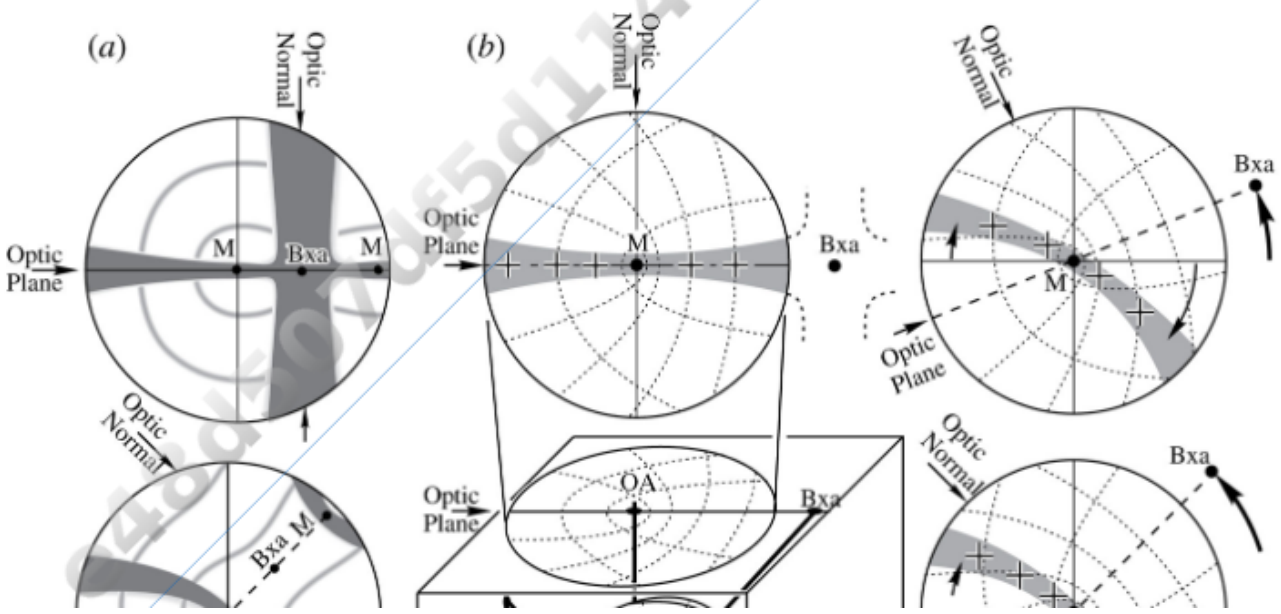

Printed by: e48d507df5d1141@placeholder.94092.edu. Printing is for personal, private use only. No part of this book may be reproduced or transmitted without publisher's prior permission. Violators will be prosecuted.

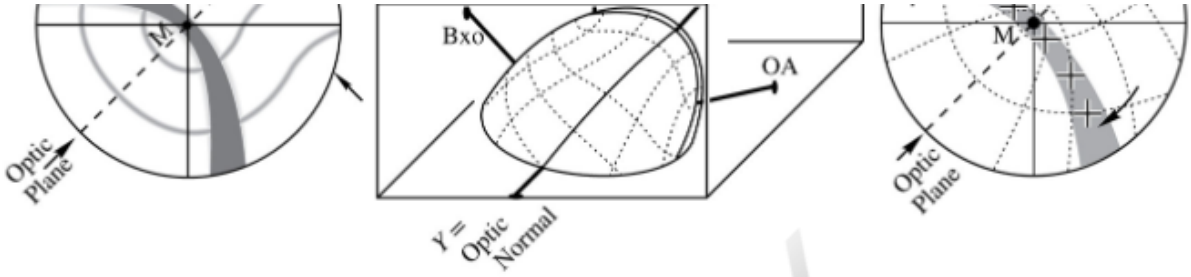

FIGURE 7.44 Biaxial optic axis interference figure. (*a*) 2*V* less than about 30°. The second melatope is in the field of view, and the figure looks like an off-center acute bisectrix figure. Isochromes are shown. (*b*) Larger 2*V*. The second melatope is out of the field of view. The dashed lines show vibration directions; isochromes are not shown. The view on the left shows the indicatrix orientation and interference figure with the optic plane oriented E–W. The views on the right show the isogyre motion as the stage is rotated counterclockwise. Note that isogyres pivot in a sense opposite to the stage rotation direction. View larger image

If 2*V* is greater than about 50° to 60°, the pattern shown in **Figure 7.44b** is seen. When the optic plane is oriented N–S or E–W, only a single arm of the cross pattern is visible in the field of view. It narrows somewhat at the position of the melatope and is straight, parallel to the trace of the optic plane. If the stage is rotated clockwise, the isogyre pivots about the melatope counterclockwise and vice versa. When the trace of the optic plane is in a 45° position, the isogyre shows a maximum curvature. The position of the acute bisectrix lies on the convex side of the isogyre. For 2*V* between roughly 25° and 60°, the Bxa will be in the field of view, so some portion of the broad isogyre along the trace of the optic normal will be seen when the optic plane is N–S or E–W.

Obtuse Bisectrix Figure

Obtuse bisectrix interference figures (**Figure 7.45**) are produced if the obtuse bisectrix is oriented perpendicular to the microscope stage. In a thin section, finding grains to display an obtuse bisectrix figure is mostly a matter of chance because retardation for these grains is intermediate. Many grains may have to be examined before finding one with the Bxo vertical. Obtuse bisectrix figures are not usually used to measure optical properties. Because the angle between the Bxo and the optic axes must be greater than 45°, the melatopes will be outside the field of view. The pattern of isochromes and geometry of vibration directions are essentially the same as for the acute bisectrix figure, except that the melatopes are well out of the field of view. The isogyres form a cross pattern if the optic plane is E–W or N–S. Typically 5° to 15° of stage rotation is required to cause the isogyres to leave the field of view. Note that for 2*V* of nearly 90°, the obtuse and acute bisectrix figures are very similar. If 2*V* is small, the obtuse bisectrix figure looks much like an optic normal figure.

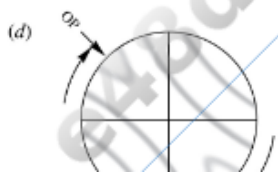

Printed by: e48d507df5d1141@placeholder.94092.edu. Printing is for personal, private use only. No part of this book may be reproduced or transmitted without publisher's prior permission. Violators will be prosecuted.

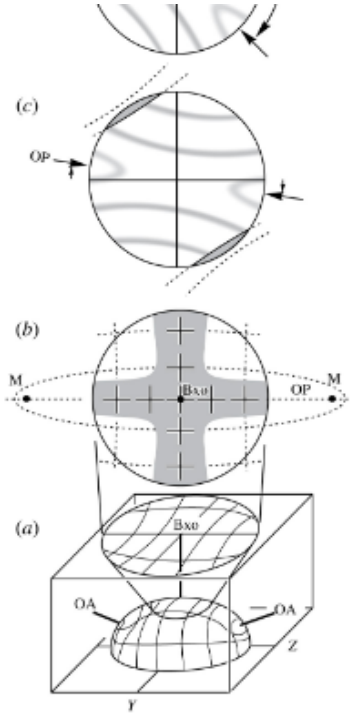

FIGURE 7.45 Obtuse bisectrix interference figure. (*a*) Pattern of vibration directions in the interference figure. (*b*) With the optic plane E–W, the isogyres form a broad cross. Melatopes are well out of the field of view. Compare with the acute bisectrix figure in Figure 7.41. (*c*) Less than ~15° of stage rotation causes the isogyres to exit the field of view. The pattern of isochromes is similar to that formed in an acute bisectrix figure. (*d*) With the optic plane in a 45° position, the field is occupied only by isochromes. View larger image

Optic Normal (Flash) Figure

Optic normal or flash figures are produced when the optic normal is vertical. Grains oriented to produce this figure display maximum retardation because the *X* and *Z* indicatrix axes are horizontal. The pattern of vibration directions in the figure is nearly rectilinear (**Figure 7.46a**) and is very similar to that seen with uniaxial flash figures (Figure 7.39). When the *X* and *Z* indicatrix axes are N–S and E–W, the field of view is occupied by a broad, fuzzy isogyre because vibration directions in all but the outer edges of the quadrants are N–S and E–W. If the stage is rotated a few degrees (**Figure 7.46b**), the isogyre splits into two curved segments that exit the field of view from the quadrants into which the acute bisectrix is being rotated. For minerals with 2*V* of nearly 90°, the diffuse cross-shaped isogyre simply dissolves as the stage is rotated. The amount of rotation required to cause the isogyres to completely leave the field of view is typically less than 5°. Optic normal figures are not routinely used to measure optical information, although they do confirm that the optic plane is parallel to the microscope stage.

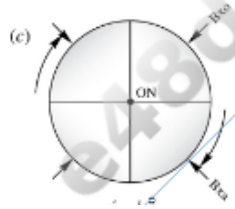

Printed by: e48d507df5d1141@placeholder.94092.edu. Printing is for personal, private use only. No part of this book may be reproduced or transmitted without publisher's prior permission. Violators will be prosecuted.

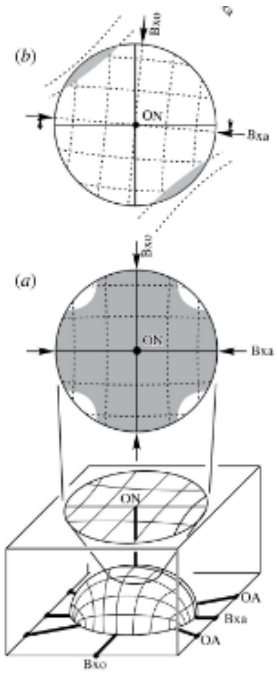

FIGURE 7.46 Optic normal (flash) interference figure. The optic normal (ON) emerges in the center of the figure. (*a*) With the Bxa and Bxo E–W and N–S, the field is occupied by a broad fuzzy cross. Only the outer edges of the four quadrants are not extinct. (*b*) Isogyres split and exit the field with a few degrees of stage rotation. The isogyres exit from the quadrants into which the trace of the Bxa is being rotated. (*c*). Isochrome pattern. No isogyres are present with traces of the Bxo and Bxa in 45° positions. The interference color in the middle of the figure is the same as that displayed by the grain in orthoscopic illumination. Colors increase outward in all four quadrants. View larger image

Off-Center Figure

Grains in random orientations display off-center interference figures whose pattern of isogyres and isochromes depends on the details of orientation. A typical figure is shown in **Figure 7.47**. As the stage is rotated, the isochrome pattern pivots about the center of the field of view, and isogyres sweep sequentially across the field of view. The wide end of the isogyre sweeps across the field more rapidly than the thin end, and the sense of isogyre rotation is counter to the direction of stage rotation. Unless a melatope or the acute bisectrix is by chance in the field of view, off-center figures are of no particular value in interpreting $2V$ or determining the optic sign. However, the fact that the isogyre does not remain parallel to the N–S or E–W as it sweeps across the field of view does indicate that the mineral is biaxial, not uniaxial (compare Figure 7.38c).

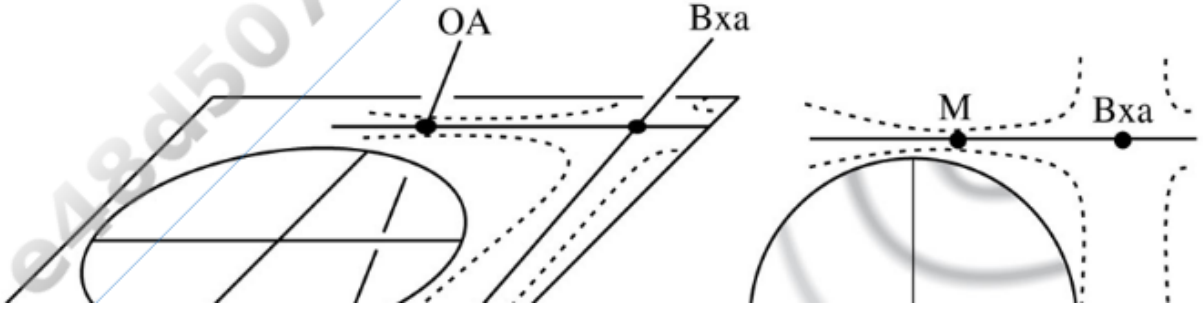

Printed by: e48d507df5d1141@placeholder.94092.edu. Printing is for personal, private use only. No part of this book may be reproduced or transmitted without publisher's prior permission. Violators will be prosecuted.

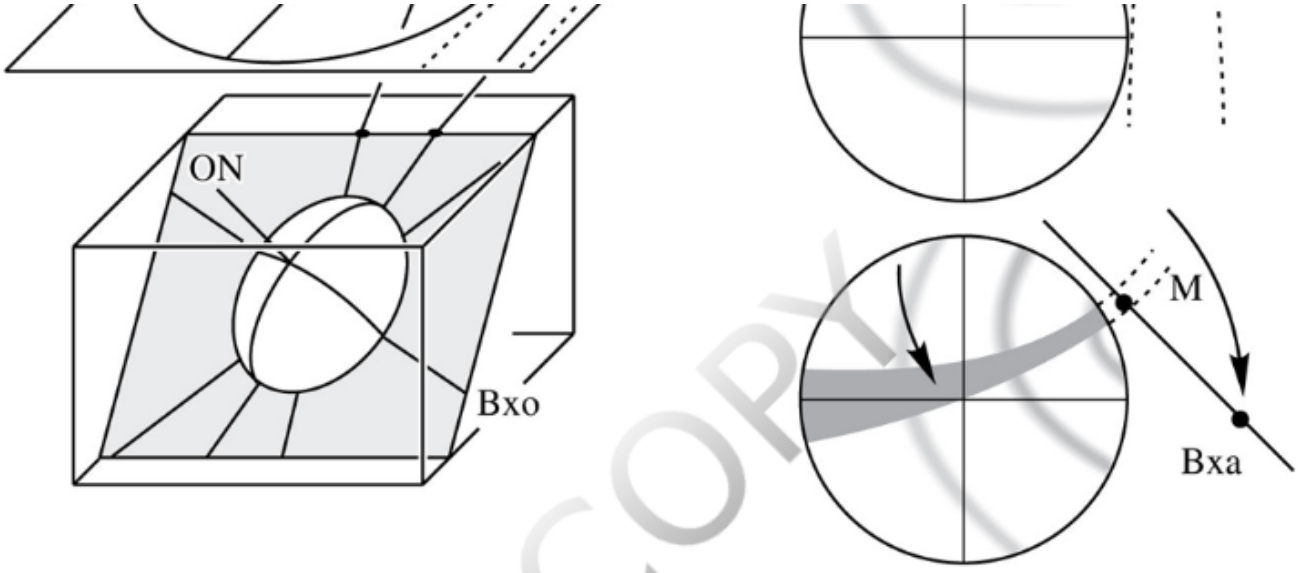

FIGURE 7.47 Biaxial interference figure for randomly oriented grain. As the stage is rotated, isogyres sweep sequentially across the field but are not parallel to the crosshairs. View larger image

DO NOT COPY
e48d507df5d1141@placeholder.9409

Printed by: e48d507df5d1141@placeholder.94092.edu. Printing is for personal, private use only. No part of this book may be reproduced or transmitted without publisher's prior permission. Violators will be prosecuted.

Determining Optic Sign

Determining optic sign is done with acute bisectrix and optic axis figures. Although optic axis figures are easiest to obtain and are used most commonly for routine work, it is easiest to illustrate the process of determining optic sign by using an acute bisectrix figure with modest $2V$.

Of the two rays of light that propagate along the acute bisectrix and emerge in the center of an acute bisectrix figure, one vibrates parallel to the Y axis (the optic normal) and has index of refraction n_β. The other vibrates parallel to the obtuse bisectrix (Bxo) along the trace of the optic plane and has index of refraction n_{Bxo}. If the mineral is optically positive, the Bxo is the X axis and $n_{\text{Bxo}} = n_\alpha$. If the mineral is optically negative, the Bxo is the Z axis and $n_{\text{Bxo}} = n_\gamma$. The task, therefore, is to determine whether the ray vibrating parallel to the trace of the optic plane in the center of the field of view is the fast ray or the slow ray. If it is fast, the mineral is optically positive, and if it is slow, the mineral is optically negative. The procedure is as follows (**Figure 7.48**).

- Obtain an acute bisectrix interference. Finding an appropriately oriented grain is a matter of luck, because many orientations may display the same intermediate retardation.
- Rotate the stage so that the trace of the optic plane is NE–SW. Near the center of the figure, the ray vibrating NE–SW vibrates parallel to the Bxo and has index of refraction n_{Bxo}. The ray vibrating NW–SE vibrates parallel to Y and has index n_β. Note the interference color in the center of the figure and determine the retardation Δ_1 that it indicates from the interference color chart (Plate 1).
- Insert the accessory plate with retardation Δ_A (slow NE–SW) and note the change in interference color in the central part of the figure to determine whether n_{Bxo} is fast or slow compared to n_β. If retardations add, the new interference color will indicate a retardation of $\Delta_1 + \Delta_A$. If retardations subtract, the new interference color will indicate a retardation of $|\Delta_1 - \Delta_A|$.
- Interpretation. If the new interference color between the melatopes indicates that retardations subtract, the ray vibrating parallel to the Bxo must be the fast ray with index n_α, so the Bxo is the X axis, the Bxa must be the Z axis, and the mineral is optically positive (Figure 7.48a). If the new interference color between the melatopes indicates that retardations add, the ray vibrating parallel to the Bxo must be the slow ray with index n_γ, so the Bxo is the Z axis, the Bxa must be the X axis, and the mineral is optically negative (Figure 7.48b). Interference colors outside the melatopes change opposite to the change seen between the melatopes. If the trace of the optic plane is placed NW–SE, the areas of addition and subtraction will be reversed.

(a) (b)

DO NOT COPY e48d507df5d1141@placeholder.9409

Printed by: e48d507df5d1141@placeholder.94092.edu. Printing is for personal, private use only. No part of this book may be reproduced or transmitted without publisher's prior permission. Violators will be prosecuted.

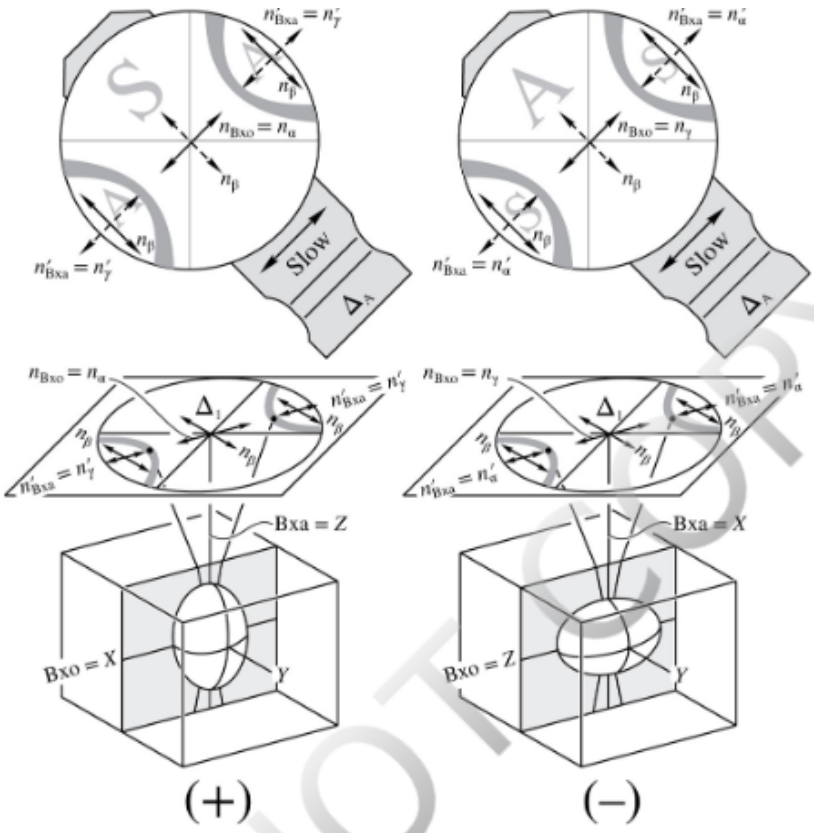

FIGURE 7.48 Determining optic sign in acute bisectrix interference figures. The trace of the optic plane is NE–SW. In the center of the field of view, the retardation is Δ_1, and the NW–SE ray vibrates parallel to the optic normal Y and has index of refraction n_β. Insert an accessory plate with retardation Δ_A (slow NE–SW) and note the change in interference color. (If the optic plane is NW–SE, the color changes are reversed.) (*a*) Optically positive. The ray vibrating NE–SW in the center of the figure vibrates parallel to X = Bxo, has index of refraction n_α, and is the fast ray compared to n_β, so retardations subtract to become $|\Delta_1 - \Delta_A|$. Outside the isogyres, the ray vibrating NE–SW has index of refraction n'_γ, which is the slow ray compared to n_β, so retardations add. (*b*) Optically negative. The ray vibrating NE–SW in the center of the figure vibrates parallel to Z = Bxo, has index of refraction n_γ, and is the slow ray compared to n_β, so retardations add to become $\Delta_1 + \Delta_A$. Outside the isogyres, the ray vibrating NE–SW has index of refraction n'_α, which is the fast ray compared to n_β, so retardations subtract. View larger image

Optic axis interference figures are usually easier to obtain because appropriately oriented grains display the lowest-order interference color. If $2V$ is small enough that both melatopes are in the field of view, the figure can be treated the same as an acute bisectrix figure. If only one melatope is visible, the figure can be considered to be half of an acute bisectrix figure.

- Start with the isogyre along either the N–S or the E–W crosshair.
- Rotate the stage to place the trace of the optic plane NE–SW with the isogyre convex to the NE. This places the Bxa in the NE quadrant (**Figure 7.49**). Depending on original grain orientation, either 45°, 135°, 225°, or 315° of clockwise rotation may be required. This figure can now be interpreted just like the SW half of the acute bisectrix figure shown in Figure 7.48. The optic sign can be interpreted with the Bxa in any of the four quadrants by comparison with the appropriate portion of a full acute bisectrix figure with the same optic plane

Printed by: e48d507df5d1141@placeholder.94092.edu. Printing is for personal, private use only. No part of this book may be reproduced or transmitted without publisher's prior permission. Violators will be prosecuted.

appropriate portion of a full acute bisectrix figure with the same optic plane orientation. If $2V$ is nearly 90°, the isogyre will be nearly straight and it may not be possible to determine the position of the Bxa. In this case the optic sign may be recorded as neutral, with $2V$ of around 90°.

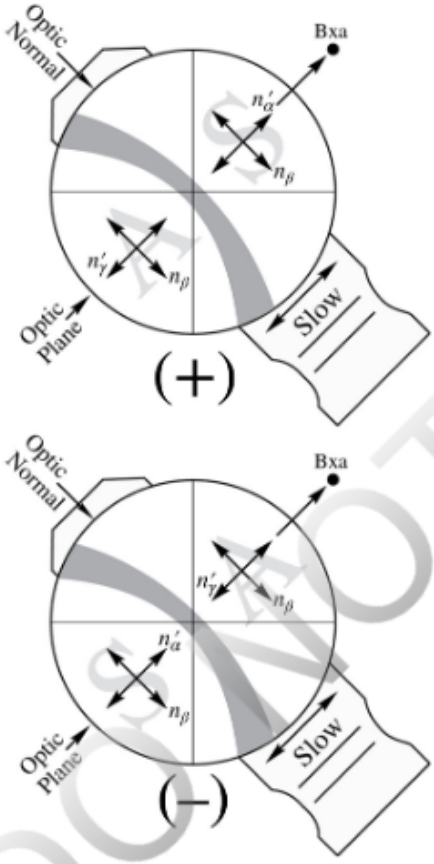

FIGURE 7.49 Determining optic sign with an optic axis figure. The trace of the optic plane is parallel to the slow ray vibration direction in the accessory plate. Retardations subtract (S) on the convex side of the isogyre for optically positive minerals and add (A) for negative. If the optic plane is oriented NW–SE, the color changes are reversed. View larger image

Determining 2V

Figure 7.50 shows the paths followed by light waves that propagate parallel to the optic axes in a crystal cut so that the acute bisectrix is vertical. Light following the optic axes has index of refraction n_β and is refracted when it enters the air above the mineral plate. The angle between the refracted optic axes is a larger angle known as ***2E***, or the **apparent optic angle**. Assuming that the material between the mineral and the objective lens is air ($n \approx 1$), the relationship between $2V$ and $2E$ is

$$\sin E = n_\beta \sin V. \tag{7.18}$$

M M

Printed by: e48d507df5d1141@placeholder.94092.edu. Printing is for personal, private use only. No part of this book may be reproduced or transmitted without publisher's prior permission. Violators will be prosecuted.

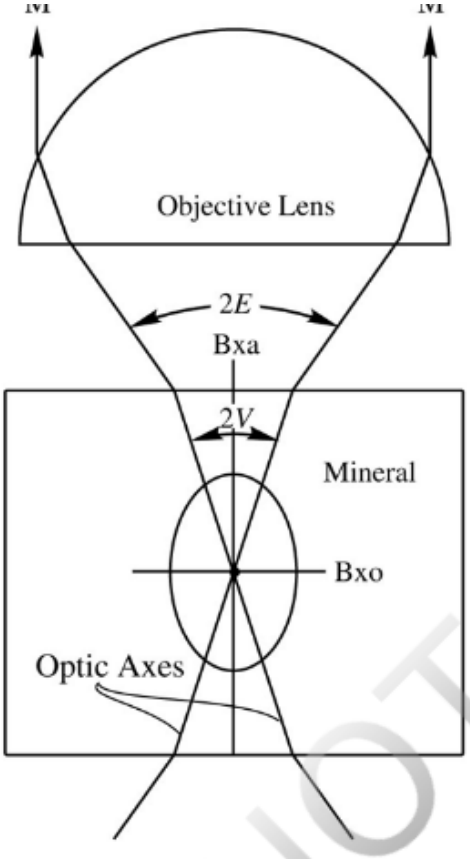

FIGURE 7.50 $2E$ versus $2V$. The angle between the optic axes is $2V$ within the mineral. Light following the optic axes is refracted as it exits the mineral to form the apparent optic angle $2E$. The position of the melatopes in an acute bisectrix interference figure depends on the value of $2E$. View larger image

The spacing between the melatopes in an acute bisectrix figure depends on the value of $2E$. For the melatopes to be at the edge of the field of view, the angular aperture of the objective lens (Figure 7.10) must equal $2E$. Hence, for a given objective lens and value of n_β, the largest $2V$ angle ($2V_{max}$) that still allows the melatopes to be within the field of view (**Table 7.1**) can be determined by combining Equations 7.7 and 7.18.

$$\text{NA} = n_\beta \sin V_{max} \quad \textbf{(7.19)}$$

TABLE 7.1 $2V$ angle ($2V_{max}$) for Melatopes at the Edge of the Field of View for Different Values of n_β and Numerical Apertures of 0.65 and 0.85

n_β	$2V_{max}$	
	NA = 0.65	NA = 0.85
1.40	55°	75°
1.50	51°	69°
1.60	48°	64°

Printed by: e48d507df5d1141@placeholder.94092.edu. Printing is for personal, private use only. No part of this book may be reproduced or transmitted without publisher's prior permission. Violators will be prosecuted.

1.70	45°	60°
1.80	42°	56°

Figure 7.51 shows acute bisectrix interference figures for different values of $2V$ assuming that $n_\beta = 1.60$ and that the numerical aperture of the objective lens is 0.65 or 0.85. Because most biaxial minerals have indices of refraction that fall in the range 1.50–1.70, these figures can be used to estimate $2V$ to within 10 or 15°, which is adequate for routine work.

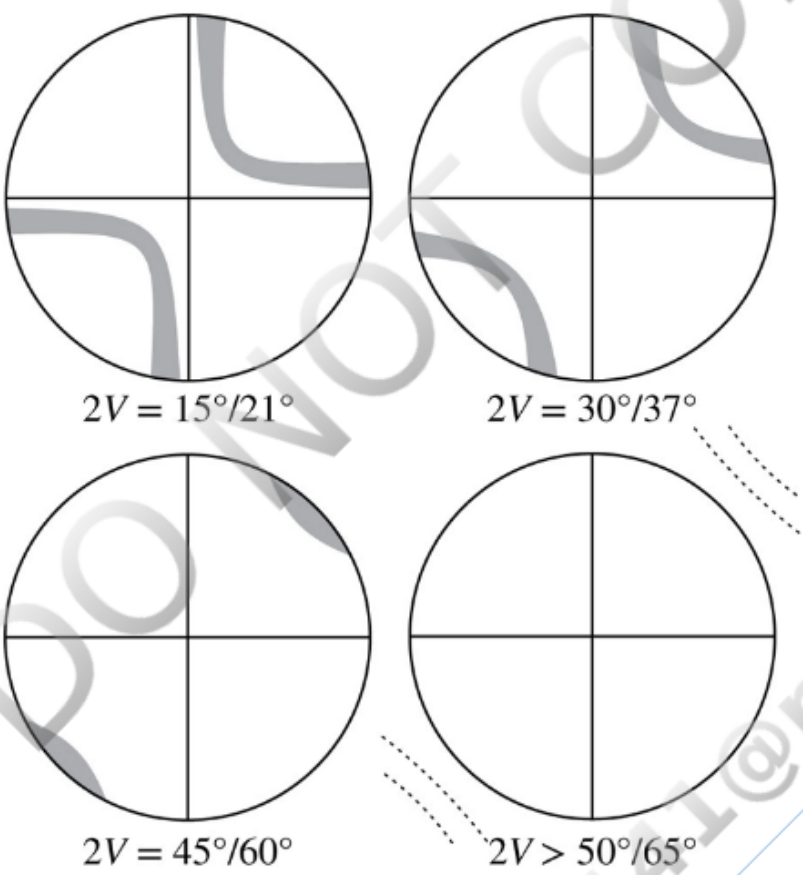

FIGURE 7.51 Rapid estimation of $2V$ based on separation of isogyres in acute bisectrix interference figures. The positions of the isogyres are shown for $n_\beta = 1.60$. Two values of $2V$ are given, the first for objective lenses with NA = 0.65, the second for NA = 0.85. View larger image

A more convenient method of estimating $2V$ uses an optic axis interference figure. This method depends on the observation that the curvature of an isogyre when the trace of the optic plane is in a 45° position depends on the value of $2V$ (**Figure 7.52**). If $2V$ is 90°, the isogyre forms a straight line, and for smaller values of $2V$, the isogyre is progressively more curved. If $2V$ is less than about 25–30°, both melatopes will be in the field of view and an estimate of optic angle can be made based on the distance between the melatopes. For $2V$ of less than 5°, the distance between the melatopes is quite small, and the figure looks like a uniaxial figure except for a small gap between the isogyres in the middle. To accurately orient the figure to place the trace of the optic plane in a 45°

DO NOT COPY e48d507df5d1141@placeholder.9409

Printed by: e48d507df5d1141@placeholder.94092.edu. Printing is for personal, private use only. No part of this book may be reproduced or transmitted without publisher's prior permission. Violators will be prosecuted.

position, proceed as follows.

- Obtain an optic axis figure. Appropriately oriented grains display low or zero retardation. Off-center figures can be used, but accuracy suffers.
- Rotate the stage to place the isogyre N–S. This places the trace of the optic plane N–S. Unless the melatope is exactly centered, the isogyre will be somewhat to the right or left of the N–S crosshair.
- Rotate the stage 45° clockwise, using the stage goniometer to measure the angle. The trace of the optic plane is now NE–SW and the curvature of the isogyre can be compared with Figure 7.52. The isogyre may be convex to the NE or the SW depending on whether the Bxa is to the NE or SW, respectively. If the isogyre is convex to the SW, 180° of stage rotation places the Bxa in the NE quadrant, which duplicates the orientation used to determine optic sign in Figure 7.49.

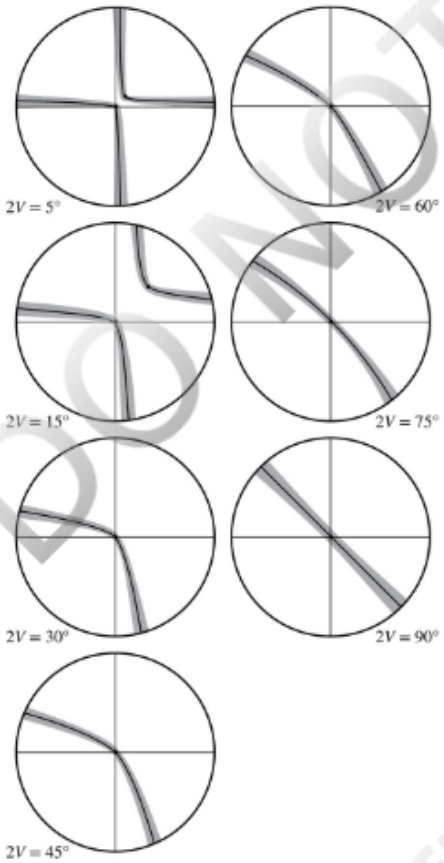

FIGURE 7.52 Isogyre curvature in biaxial optic axis interference figures with the optic plane aligned NE–SW. The geometry shown here assumes $n_\beta = 1.60$ and NA = 0.65 but will work for $NA_1 = 0.85$ and other values of n_β with little loss of accuracy. Compare Figure 7.51. View larger image

Dispersion Effects

The values of n_α, n_β, and n_γ vary for different wavelengths of light just as the index of refraction of isotropic minerals varies. Consequently, the values of $2V$ and the orientation of the indicatrix can be expected to vary for different wavelengths of light. Variation in

DO NOT COPY e48d507df5d1141@placeholder.9409

Printed by: e48d507df5d1141@placeholder.94092.edu. Printing is for personal, private use only. No part of this book may be reproduced or transmitted without publisher's prior permission. Violators will be prosecuted.

the size of $2V$ is called **optic axis dispersion**, and variation in the orientation of the indicatrix is called **indicatrix dispersion**, or **bisectrix dispersion**. If this dispersion is sufficiently strong, color fringes may be visible along the isogyres in interference figures. The dispersion is termed weak, moderate, or strong, depending on how noticeable the color fringes are.

Orthorhombic minerals can display only optic axis dispersion because the indicatrix axes are fixed parallel to the crystallographic axes. Although exceptions exist, the orientation of the optic plane in most orthorhombic minerals is the same for all wavelengths. If $2V$ for light at the red end of the spectrum is larger than $2V$ for light at the violet end, the dispersion is described as $r > v$, and if $2V$ for violet light is larger than for red light, the dispersion is described as $v > r$. The formation of the color fringes is shown in **Figure 7.53**. Note that the red fringe is found where the melatopes for violet light are located and the blue fringe is found where the melatopes for red light are located.

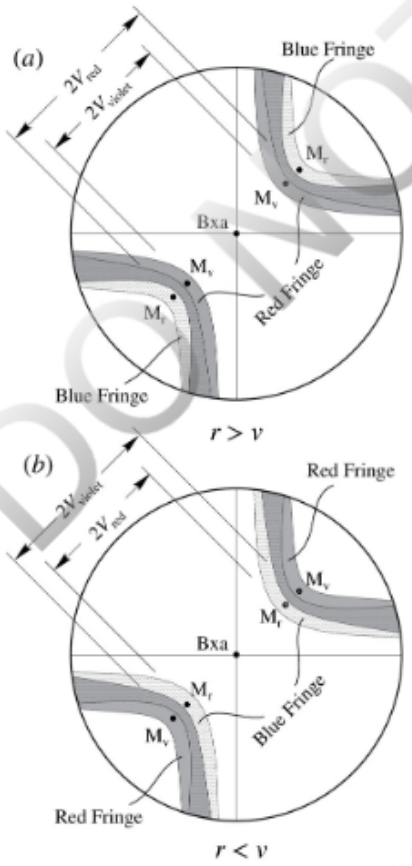

FIGURE 7.53 Optic axis dispersion: M_V and M_r are the melatopes for violet and red light, respectively. The isogyre for violet light (shaded) marks the area where no violet light comes through. The isogyre for red light (stippled) marks the area where no red light comes through. Red fringes are therefore produced where blue and violet light are lacking, and the blue fringe is produced where red light is lacking. The areas of overlap represent the normal isogyres. (*a*) $2V$ for red light is greater than $2V$ for violet light ($r > v$). (*b*) $2V$ for red light is less than $2V$ for violet light ($r < v$). The widths of the colored fringes are exaggerated here. View larger image

In addition to optic axis dispersion, monoclinic minerals may display indicatrix dispersion because the indicatrix is free to rotate about the *b* crystal axis for different wavelengths

DO NOT COPY e48d507df5d1141@placeholder.9409

Printed by: e48d507df5d1141@placeholder.94092.edu. Printing is for personal, private use only. No part of this book may be reproduced or transmitted without publisher's prior permission. Violators will be prosecuted.

because the indicatrix is free to rotate about the *b* crystal axis for different wavelengths of light. Three types of indicatrix dispersion are possible, depending on which indicatrix axis coincides with the *b* axis. **Inclined dispersion** is produced when the optic normal (*Y*) is parallel to the *b* axis. The orientation of *Y* is fixed for all wavelengths, but the *X* and *Z* are free to rotate within the {010} plane, which serves as the optic plane for all wavelengths. Color fringes are symmetrical across the trace of the optic plane in acute bisectrix figures. **Horizontal** or **parallel dispersion** is produced when the obtuse bisectrix is parallel to the *b* axis. The optic planes for different wavelengths pivot about the *b* axis so the position of the Bxa for red light emerges at a different point in the {010} plane than the Bxa for violet light. Color fringes are symmetrical across the trace of the optic normal in acute bisectrix figures. **Crossed bisectrix dispersion** is produced when the acute bisectrix is parallel to the *b* axis. The optic plane pivots about the Bxa, but because the *b* axis is vertical in this acute bisectrix figure, the color fringes are symmetrical by 2-fold rotation about the Bxa.

DO NOT COPY
e48d507df5d1141@placeholder.9409

Printed by: e48d507df5d1141@placeholder.94092.edu. Printing is for personal, private use only. No part of this book may be reproduced or transmitted without publisher's prior permission. Violators will be prosecuted.

Refractometry: Measurement of Index of Refraction

Immersion Method

Refractometry refers to measurement of indices of refraction. The simplest and most convenient method in mineralogy is the **immersion method**. With this method, grain mounts of an unknown transparent mineral are prepared, and the index of refraction of the mineral is identified by comparing it to the known index of refraction of an immersion oil. Immersion oil sets are commercially available, and a typical set consists of a number of small bottles of immersion oil with indices of refraction ranging from about 1.4 to 1.8 in increments of 0.002, 0.004, or 0.005. This range covers the indices of refraction for most minerals. Indices of refraction may be measured to accuracies of about ±0.003 using white light for illumination.

For routine work, relief and the Becke line method provide a means of comparing the index of refraction of mineral and immersion oil. For additional techniques, refer to Nesse (2013), Bloss (1961), and references therein.

Relief

The degree to which mineral grains stand out from the immersion oil or other mounting medium is called **relief** (**Figure 7.54**). If the indices of oil and mineral are not the same, light is refracted on passing from oil to mineral and the mineral appears to stand out. If the indices of refraction of oil and mineral are the same, light is not refracted at oil–mineral boundaries and the mineral does not appear to stand out. Relief may be described as high, moderate, or low (**Figure 7.55**). The approximate differences of index of refraction between mineral and immersion oil is indicated by these categories: **high relief** > 0.12, **moderate relief** between 0.12 and 0.04, and **low relief** < 0.04. Note that the relief of anisotropic minerals in both grain mount and thin section may change as the stage is rotated in plane light, particularly if the mineral has moderate to high birefringence. This is because the slow and fast rays have different indices of refraction and therefore display different relief, depending on which ray is dominant.

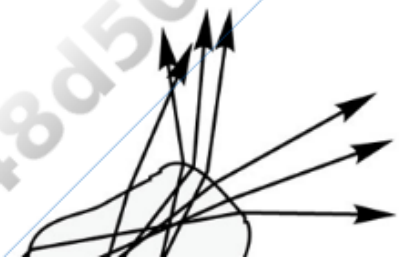

DO NOT COPY e48d507df5d1141@placeholder.94092

Printed by: e48d507df5d1141@placeholder.94092.edu. Printing is for personal, private use only. No part of this book may be reproduced or transmitted without publisher's prior permission. Violators will be prosecuted.

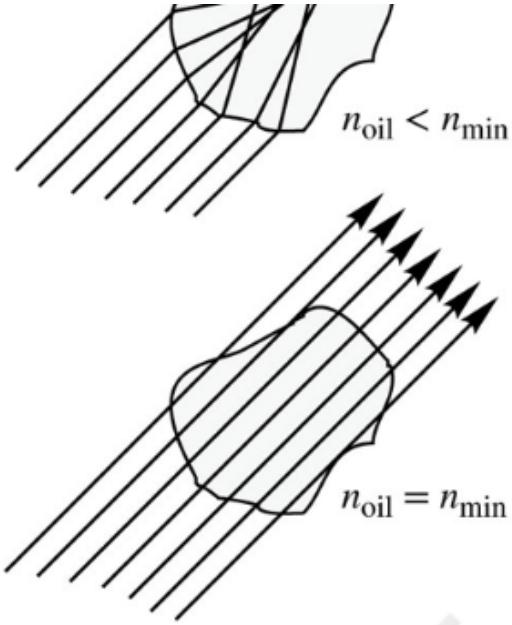

FIGURE 7.54 Formation of relief in grain mount. If indices of refraction of oil and mineral are different, light is refracted at the mineral–oil boundary and the grain stands out. If the indices of refraction are the same, light passes the mineral–oil boundary without refraction and the mineral grain does not stand out. View larger image

FIGURE 7.55 High, moderate, and low relief. View larger image

If the index of refraction of the mineral is higher than the oil, the mineral has **positive relief**, and if it is lower, the mineral has **negative relief**. However, in both cases, the

Printed by: e48d507df5d1141@placeholder.94092.edu. Printing is for personal, private use only. No part of this book may be reproduced or transmitted without publisher's prior permission. Violators will be prosecuted.

mineral will appear to stand out from the oil to the same degree.

Becke Line Method

The **Becke line** method is used to distinguish between positive and negative relief. The Becke line (**Figure 7.56**) consists of a band or rim of light along the edge of a grain. The Becke line is most easily seen when using the medium-power objective if the image is slightly out of focus and the aperture diaphragm is closed somewhat. If the stage of the microscope is lowered so that the distance between the sample and objective lens is increased, the Becke line moves into the material with the higher index of refraction. The formation of the Becke line depends on both the lens effect and the internal reflection effect.

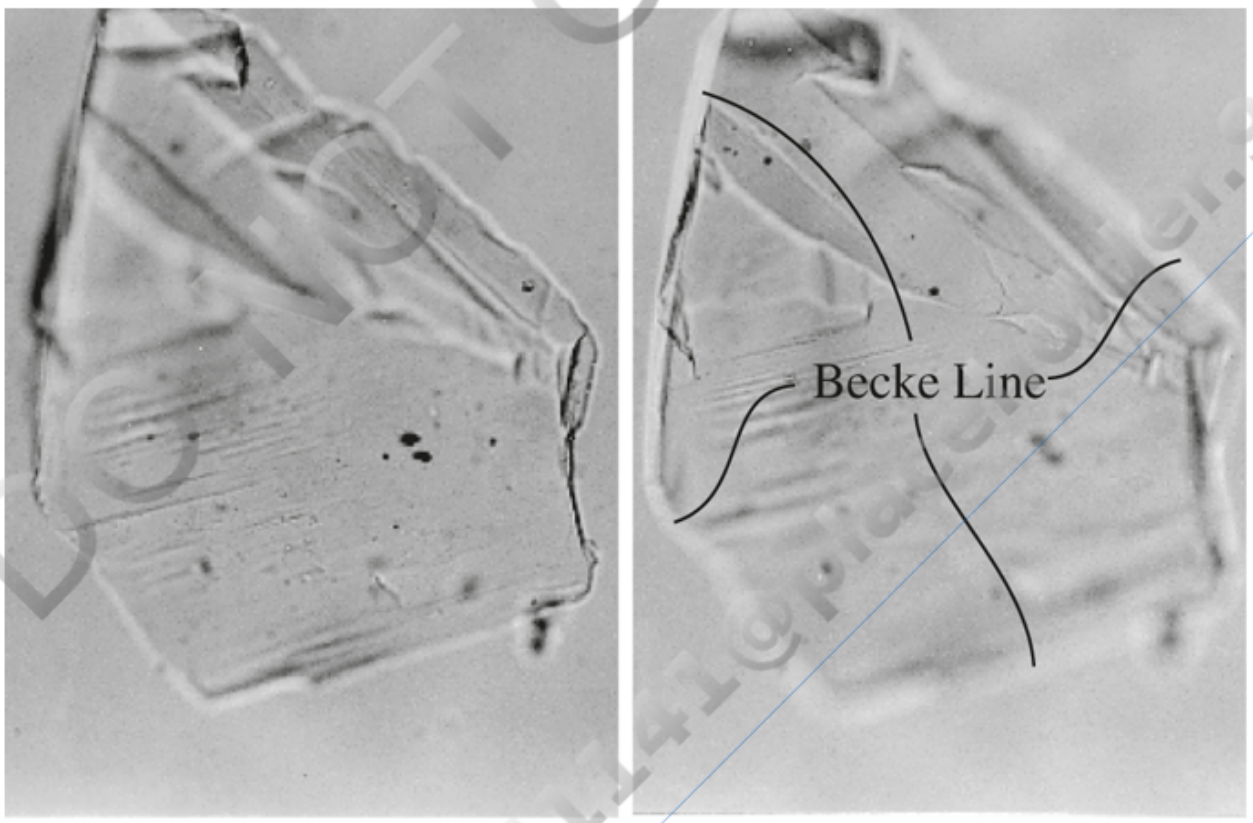

FIGURE 7.56 The Becke line. (*Left*) Microscope focused on a grain of fluorite that shows moderate relief. (*Right*) Microscope stage lowered. The Becke line is a thin band of light that moves into the medium with the higher index of refraction, which in this case is the immersion oil. View larger image

The lens effect depends on the observation that most mineral fragments are thinner on the edges than in the center and act as crude lenses (**Figure 7.57**). If the mineral has a higher index of refraction than the immersion oil, the grains act as converging lenses to concentrate light toward the center of the grain. If the grains have a lower index of refraction than the immersion oil, they act as diverging lenses and light is concentrated in the immersion oil.

Printed by: e48d507df5d1141@placeholder.94092.edu. Printing is for personal, private use only. No part of this book may be reproduced or transmitted without publisher's prior permission. Violators will be prosecuted.

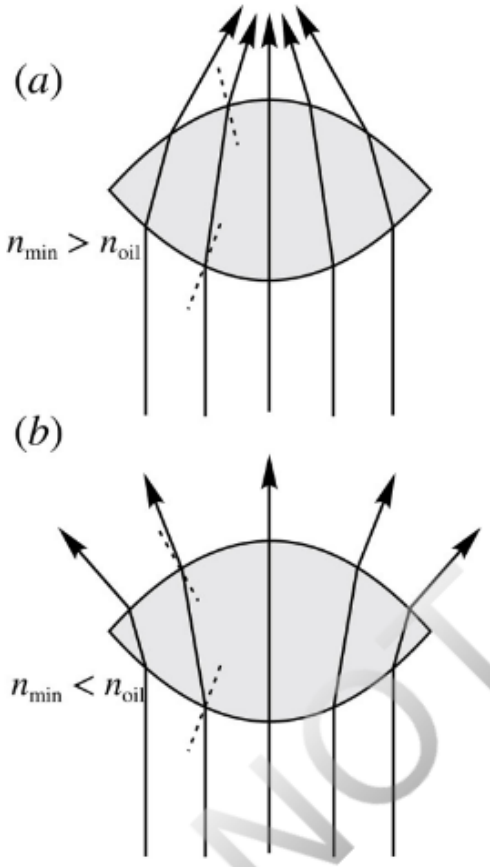

FIGURE 7.57 Formation of the Becke line by the lens effect. Light is refracted toward the normal on passing into a material with higher index of refraction and away from the normal when passing into a material with lower index of refraction as predicted by Snell's law (Equation 7.5). (*a*) $n_{mineral} > n_{oil}$. The grain acts as a crude converging lens, concentrating light above the mineral. (*b*) $n_{mineral} < n_{oil}$. The grain acts as a crude diverging lens, refracting light away from the center of the grain. View larger image

The internal reflection effect depends on the requirement that the edges of grains must be vertical at some point. Moderately converging light from below impinges on the vertical boundary and may be internally reflected or refracted, depending on the angle of incidence and indices of refraction. As can be seen in **Figure 7.58**, the result of the refraction and internal reflection is to concentrate light into a thin band in the material with the higher index of refraction.

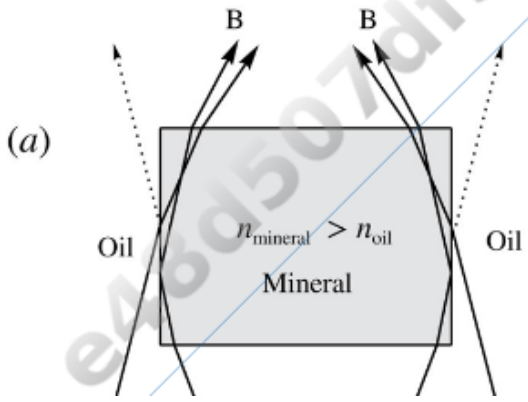

Printed by: e48d507df5d1141@placeholder.94092.edu. Printing is for personal, private use only. No part of this book may be reproduced or transmitted without publisher's prior permission. Violators will be prosecuted.

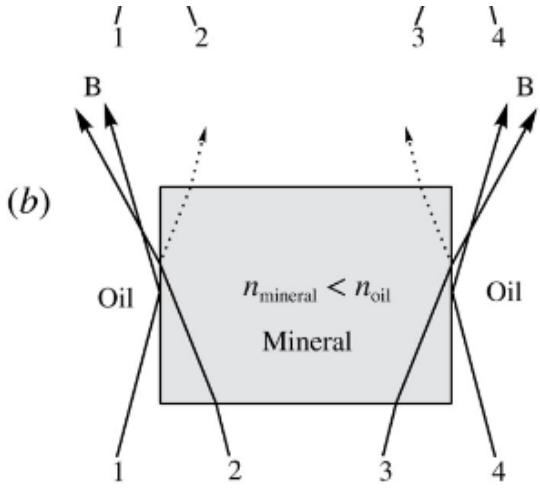

FIGURE 7.58 Formation of the Becke line by internal reflection at vertical grain boundaries. The Becke line (B) consists of a concentration of light above the mineral–oil boundary in the material with the higher index of refraction. (*a*) $n_{minerals} > n_{oil}$. Some of rays 1 and 4 are reflected (dotted lines) at the vertical mineral boundary, and some are refracted into the mineral (shaded) even for shallow angles of incidence (compare Figure 7.6c). Rays 2 and 3 strike the mineral–oil interface at greater than the critical angle and are internally reflected in the mineral (compare Figure 7.7). (*b*) $n_{mineral} < n_{oil}$. Rays 1 and 4 strike the vertical mineral–oil boundary at greater than the critical angle and are totally reflected back into the oil. Some of rays 2 and 3 are refracted into the oil. View larger image

Both the lens and internal reflection effects concentrate light into the material with the higher index of refraction in the area above the mineral grain, in effect forming a cone of light propagating up from the edge of the mineral (**Figure 7.59**). If the mineral has the higher index of refraction, the cone converges above the mineral, and if the immersion oil has the higher index of refraction, the cone diverges above the mineral. With the microscope crisply focused on a grain, the Becke line is coincident with the edge of the grain or may disappear. As the stage is lowered, the concentration of light near the top of the grain that forms the Becke line is brought into focus. Hence, *as the stage is lowered, the Becke line appears to move into the material with the higher index of refraction.* The opposite is true if the stage is raised.

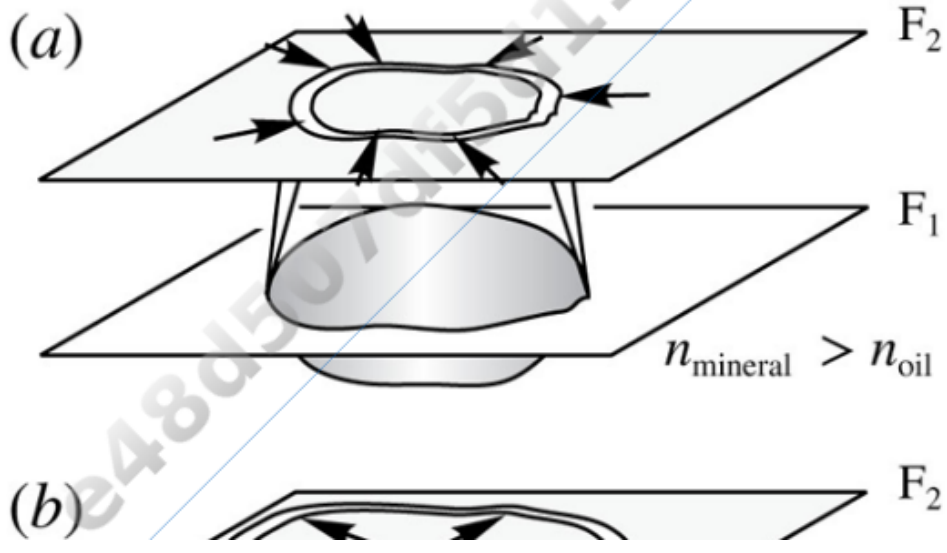

DO NOT COPY

Printed by: e48d507df5d1141@placeholder.94092.edu. Printing is for personal, private use only. No part of this book may be reproduced or transmitted without publisher's prior permission. Violators will be prosecuted.

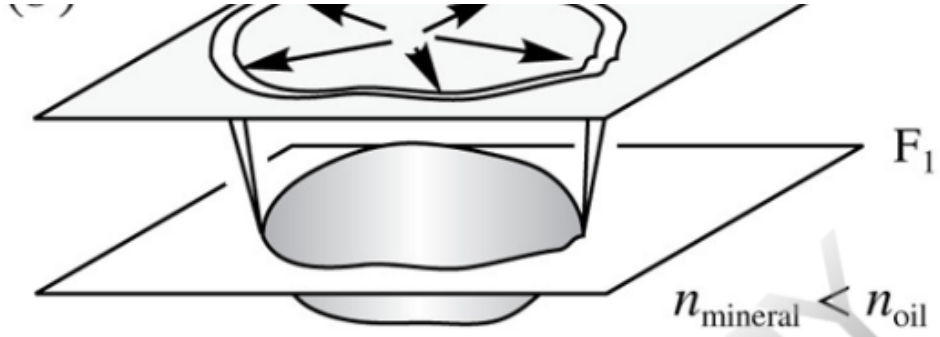

FIGURE 7.59 Movement of the Becke line as the stage is lowered. The Becke line may be considered to consist of a cone of light that extends upward from the mineral grain. If $n_{mineral} > n_{oil}$, the cone converges upward, and if $n_{mineral} < n_{oil}$, the cone diverges upward. If the stage is lowered, the plane of focus goes from F_1 to F_2 and the Becke line appears to move toward the material with the higher index of refraction. (*a*) $n_{mineral} > n_{oil}$. (*b*) $n_{mineral} < n_{oil}$. View larger image

Dispersion Effects

The dispersion of immersion oil is greater than the dispersion of most minerals, so it is possible to produce a match of index of refraction for only one wavelength of light. Ideally, the object is to produce a match for light whose wavelength is 589 nm because that is the wavelength for which indices of refraction are usually reported.

If the dispersion curves for mineral and immersion oil intersect in the visible spectrum (**Figure 7.60**), the oil will have higher indices of refraction for wavelengths shorter than the match, and the mineral will have higher indices of refraction for longer wavelengths. This results in the formation of two Becke lines, one for the shorter wavelengths and one for the longer. When the stage is lowered, the Becke line composed of shorter wavelengths will move into the immersion oil, and the Becke line composed of longer wavelengths will move into the mineral. The color of the two Becke lines depends on the wavelength at which the dispersion curves cross. The relationships are summarized in **Table 7.2**.

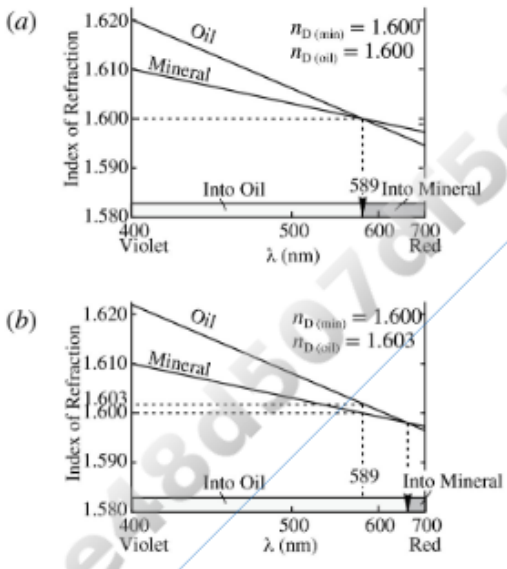

DO NOT COPY
e48d507df5d1141@placeholder.9409

Printed by: e48d507df5d1141@placeholder.94092.edu. Printing is for personal, private use only. No part of this book may be reproduced or transmitted without publisher's prior permission. Violators will be prosecuted.

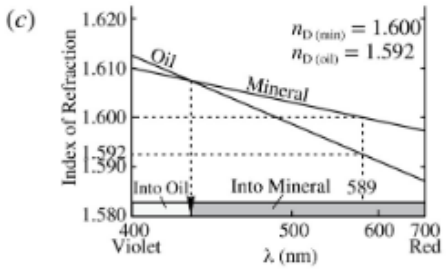

FIGURE 7.60 Formation of colored Becke lines. Immersion oil typically has higher dispersion than minerals. (*a*) Indices of refraction of oil and mineral matched at light whose wavelength is 589 nm. The mineral has higher index of refraction for longer wavelengths, so these wavelengths, perceived as yellowish orange, go into the mineral as the stage is lowered. The immersion oil has higher index of refraction for shorter wavelengths, and this bluish light forms a Becke line that goes into the oil. (*b*) Indices of oil and mineral are matched near the red end of the spectrum. The mineral has higher index of refraction for red light, and the oil for all other wavelengths, perceived as bluish white. When the stage is lowered, a red Becke line moves into the mineral, and bluish white into the oil. (*c*) Indices of oil and mineral match near the blue end of the spectrum. The oil has higher index of refraction for blue and violet light, the mineral for the rest of the spectrum. When the stage is lowered, a blue-violet Becke line moves into the oil, and yellowish white into the mineral. View larger image

TABLE 7.2 Becke Line Relationships When the Microscope Stage Is Lowered

Condition	Observation	Interpretation
n_{oil} higher for all wavelengths	White line into oil	$n_{D(oil)} >> n_{D(mineral)}$
$n_{oil} = n_{min}$ for orange/red light	Red line into mineral, bluish-white line into oil	$n_{D(oil)} > n_{D(mineral)}$
$n_{oil} = n_{min}$ for yellow light (589 nm)	Yellowish-orange line into mineral, pale blue line into oil	$n_{D(oil)} = n_{D(mineral)}$
$n_{oil} = n_{min}$ for blue light	Yellowish-white line into mineral, blue-violet line into oil	$n_{D(oil)} < n_{D(mineral)}$
n_{oil} lower for all wavelengths	White line into mineral	$n_{D(oil)} << n_{D(mineral)}$

Practical Considerations

Determining the index of refraction of an unknown mineral by using grain mount techniques can be tedious and frustrating unless it is approached systematically. The method recommended here involves successively bracketing the index of the unknown mineral until a match can be obtained with an immersion oil.

- Prepare a grain mount as described at the beginning of the chapter, using an immersion oil in the middle of the available range. Examine the grains with the microscope to determine the relief. Use the Becke line method to determine whether the mineral has a higher or lower index of refraction than the immersion oil. If the index of the mineral is higher than the oil, all lower indices of refraction can be eliminated from consideration. If the index of the mineral is lower than the

DO NOT COPY e48d507df5d1141@placeholder.9409

Printed by: e48d507df5d1141@placeholder.94092.edu. Printing is for personal, private use only. No part of this book may be reproduced or transmitted without publisher's prior permission. Violators will be prosecuted.

can be eliminated from consideration. If the index of the mineral is lower than the oil, all higher indices of refraction can be eliminated.

- Prepare a second grain mount using an immersion oil somewhere in the remaining range of possible indices of refraction. Use the relief of the mineral in the first grain mount as a guide in selecting the second oil. The object is to bracket the index of refraction of the mineral so that one oil is higher and the other lower than the index of refraction of the mineral. Examine the relief of the grains in the second grain mount and use the Becke line method to determine whether the mineral has an index of refraction higher or lower than the oil.
- Prepare a third grain mount using an immersion oil somewhere in the middle of the now much-reduced range of possible indices, using relief seen in the first two grain mounts as a guide in selecting the oil whose index of refraction is close to that of the mineral. If the first two oils did not bracket the index of the mineral and relief was high in the second oil, it may be advisable to use an oil at the extreme end of the available range to determine whether the mineral actually falls within the range of available oil.
- Make additional grain mounts, in each case selecting an oil to split the range of possible indices, until a match is obtained. With practice, a match can be obtained with as few as four or five grain mounts.

Refractometry in Thin Section

It is not practical to accurately determine indices of refraction of minerals in thin section with a petrographic microscope, but it is possible to make estimates or establish limits. The index of an unknown mineral can be compared to the index of refraction of the cement or to other known minerals in the thin section. The index of refraction of the cement depends on the manufacturer, but is usually about 1.540. Relief provides an estimate of how close the index of a mineral is to the cement. Becke lines formed at mineral–cement and mineral–mineral boundaries can be interpreted as described earlier to provide rough estimates of the index of refraction of an unknown mineral. Plate 2 organizes minerals based on relief in thin section, optical character, optic sign, and birefringence.

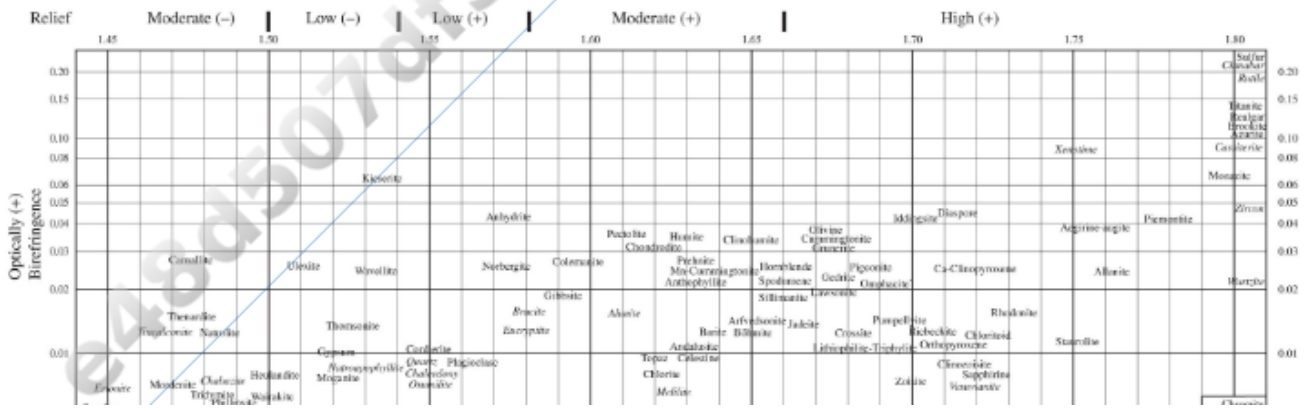

DO NOT COPY e48d507df5d1141@placeholder.94092

Printed by: e48d507df5d1141@placeholder.94092.edu. Printing is for personal, private use only. No part of this book may be reproduced or transmitted without publisher's prior permission. Violators will be prosecuted.

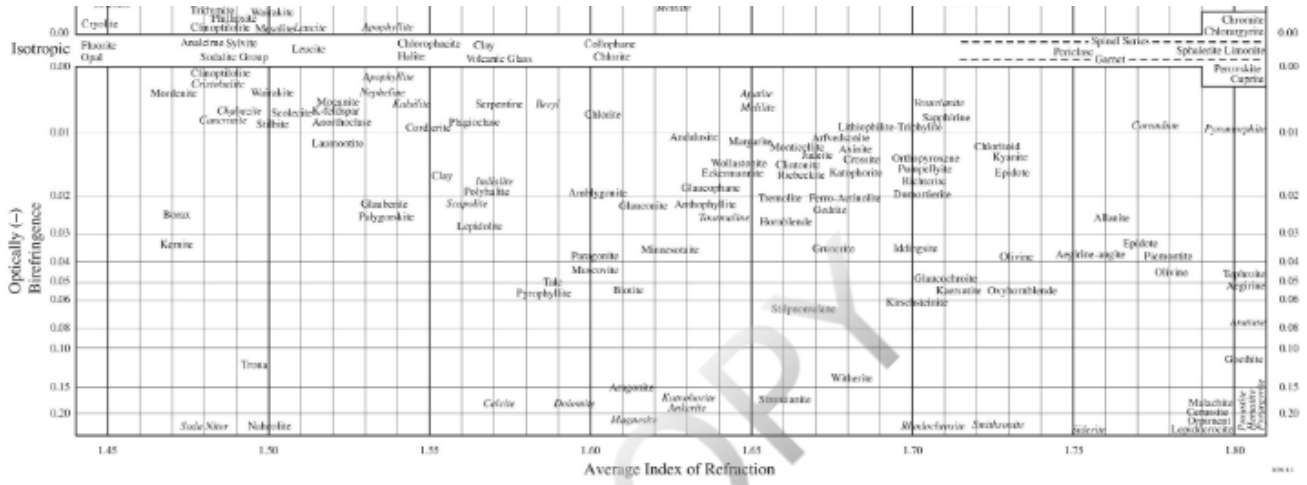

PLATE 2 Birefringence vs. Average Index of Refraction. View larger image

Isotropic Minerals

Identification of isotropic minerals requires measurement of one index of refraction. This is done by means of the technique described earlier.

Uniaxial Minerals

Identification of uniaxial minerals may be done by measuring both n_ω and n_ϵ. From these values the birefringence may be calculated ($\delta = |n_\omega - n_\epsilon|$). To begin, obtain an optic axis interference figure on a suitable grain (low interference color), confirm that the mineral is uniaxial, and determine the optic sign. Measurement of the two indices of refraction requires that grains in specific orientations be selected so that each index of refraction can be measured independently. It is generally most convenient to measure n_ω first and then measure n_ϵ. To measure n_ω and n_ϵ in grain mount, proceed as follows.

- Measure n_ω. Select a grain oriented to pass all light as ordinary ray. Two techniques are available:
  a. Cross the polarizers and search for a grain of the mineral whose optic axis is vertical. A grain in this orientation will display the lowest-order interference color and ideally will remain uniformly dark with stage rotation. All the light propagating along the optic axis passes as ordinary ray with index of refraction n_ω. To confirm that the optic axis is vertical, obtain an interference figure. The melatope should be near the center of the field of view. Determine optic sign if that has not already been done. If grains in this orientation cannot be found, use the second method.
  b. Pick any grain. As long as the mineral is uniaxial, one ray must pass with index of refraction n_ω. The trick is to rotate the stage of the microscope to place a grain in one of its extinction positions so that the ordinary ray vibration direction is parallel to the lower polarizer. Use an accessory plate to identify

DO NOT COPY e48d507df5d1141@placeholder.9409

Printed by: e48d507df5d1141@placeholder.94092.edu. Printing is for personal, private use only. No part of this book may be reproduced or transmitted without publisher's prior permission. Violators will be prosecuted.

direction is parallel to the lower polarizer. Use an accessory plate to identify the slow and fast ray vibration directions (Figure 7.21) in the grain. The appropriate vibration direction is then placed parallel to the lower polarizer (slow if optically negative or fast if optically positive) so that all light passes as ordinary ray.

Once the ordinary ray vibration direction has been placed parallel to the lower polarizer, n_ω can be compared with the index of refraction of the immersion oil using relief and the Becke line. Repeat with new grain mounts by using different immersion oils until a match is obtained.

- Measure n_ϵ. Accurate measurement of n_ϵ requires grains oriented so that the optic axis is horizontal. Grains in random orientations can yield only values for n'_ϵ, which is intermediate between n_ω and n_ϵ. To find appropriately oriented grains, scan the grain mount between crossed polarizers to find a grain of the unknown that displays the highest interference color. This grain should have its optic axis approximately parallel to the microscope stage. A symmetrical optic normal (flash) interference figure confirms that the optic axis is horizontal. If the mineral is optically positive, the ϵ ray is the slow ray, and if the mineral is negative, the ϵ ray is the fast ray. Identify the ϵ ray vibration direction and place it parallel to the lower polarizer with the aid of the accessory plate as follows.
  a. From an extinction position, rotate the stage 45° clockwise. Insert an accessory plate to determine which of the two rays is slow and which is fast as described earlier (Figure 7.21).
  b. Rotate the stage 45° clockwise or counterclockwise as required to place the slow ray (for positive) or fast ray (for negative) vibration direction parallel to the lower polarizer (lower polarizer E–W).

Once the stage has been rotated so that the grain passes only ϵ rays, the value of n_ϵ can be compared with the index of refraction of the immersion oil by using relief and Becke line methods. Prepare additional grain mounts with different immersion oils as needed to obtain a match.

Biaxial Minerals

Three indices of refraction (n_α, n_β, and n_γ) must be measured for biaxial minerals. Measurement of n_β requires that grains with an optic axis vertical be found, and measurement of n_α and n_γ requires that grains with the optic normal vertical be found. The procedure is as follows.

- Measure n_β
  a. With orthoscopic illumination and crossed polarizers, scan the grain mount to find a grain of the unknown that displays the lowest-order interference color. This grain should have the optic axis vertical, so that all light passes with

DO NOT COPY e48d507df5d1141@placeholder.94092

Printed by: e48d507df5d1141@placeholder.94092.edu. Printing is for personal, private use only. No part of this book may be reproduced or transmitted without publisher's prior permission. Violators will be prosecuted.

index n_β. Confirm the orientation by obtaining an interference figure, and determine optic sign and $2V$ if not already done.

b. Remove the upper polarizer and use relief and the Becke line to compare n_β with the immersion oil. Repeat, using the bracketing technique described earlier, until a match is obtained.

- Measure n_α
  a. With orthoscopic illumination and crossed polarizers, scan the grain mount to find a grain of the unknown that displays the highest interference color. This grain should have the optic normal vertical, so that the two rays pass with indices or n_α and n_γ. Correctly oriented grains yield optic normal (flash) figures.
  b. In orthoscopic illumination, determine which vibration direction is the fast ray with index of refraction n_α by using an accessory plate (Figure 7.21). Rotate the fast ray vibration direction to be parallel to the lower polarizer vibration direction so that all light passes with index of refraction n_α.
  c. Remove the upper polarizer and compare n_α with the immersion oil.
  d. Repeat, using the bracketing technique described earlier, until a match is obtained.
- Measure n_γ
  a. With orthoscopic illumination and crossed polarizers, scan the grain mount to find a grain of the unknown that displays the highest interference color. This grain should have the optic normal vertical, so that the two rays pass with indices or n_α and n_γ. Correctly oriented grains yield optic normal (flash) figures.
  b. In orthoscopic illumination, determine which vibration direction is the slow ray with index of refraction n_γ by using an accessory plate (Figure 7.21). Rotate the slow ray vibration direction to be parallel to the lower polarizer vibration direction so that all light passes with index of refraction n_γ.
  c. Remove the upper polarizer and compare n_γ with the immersion oil.
  d. Repeat, using the bracketing techniques described earlier, until a match is obtained.

Time can be saved by comparing all three indices of refraction with each immersion oil. Once n_β has been determined, oils needed to match n_α and n_γ can be selected based on knowledge of the birefringence, $2V$, and comparisons made in earlier oils. Note that grains used to compare n_α can be rotated 90° to compare n_γ.

DO NOT COPY
e48d507df5d1141@placeholder.9409

Printed by: e48d507df5d1141@placeholder.94092.edu. Printing is for personal, private use only. No part of this book may be reproduced or transmitted without publisher's prior permission. Violators will be prosecuted.

Reflected-Light Optics

Opaque minerals can be identified by optical methods only with the use of a reflected-light microscope and polished samples. Student petrographic microscopes are rarely equipped with reflecting-light capabilities, so only a brief summary of basic concepts is presented here. Interested readers are encouraged to pursue the subject with books such as Ineson (1989), Craig and Vaughn (1994), and Ixer (1990).

Samples for reflected-light work may be thin sections or rock/mineral samples mounted in an epoxy plug. The surface is polished to a mirror shine with progressively finer abrasives, and no coverslip is used. Polished thin sections are convenient because they can be used for transmitted-light microscopy, reflected-light microscopy, and scanning electron microscope or electron microprobe analysis.

One common geometry used for reflected-light microscopes is to adapt a conventional petrographic microscope by the addition of an epi-illuminator (Figure 7.9). This illuminator is mounted above the objective lenses and is equipped with optical elements so that a beam of polarized light passes down through the objective onto the top surface of the sample. Reflected light passes back up through the objective to the observer. The upper polarizer (analyzer) can be inserted into the optical path to determine whether the polarization of the incident light is affected by reflection on the mineral.

Observation in Plane-Polarized Light

(The analyzer is removed from the optical path.)

Color and Reflection Pleochroism

The color seen in plane-polarized light coming from the epi-illuminator depends on the specific colors of light that are absorbed and reflected by the mineral. Isometric opaque minerals display the same color regardless of sample orientation. All others may display reflection pleochroism, which is a color change observed as the stage is rotated. Tetragonal and hexagonal minerals whose *c* axis is vertical will not display reflection pleochroism. It is important to note the similarity to the behavior of light in transparent minerals.

Reflectance and Bireflectance

Reflectance (*R*) is a measure of the percentage of the incident light that is reflected from a mineral's surface. If some wavelengths are more strongly reflected than others, the

DO NOT COPY e48d507df5d1141@placeholder.9409-

Printed by: e48d507df5d1141@placeholder.94092.edu. Printing is for personal, private use only. No part of this book may be reproduced or transmitted without publisher's prior permission. Violators will be prosecuted.

mineral will be colored. If the mineral is anisotropic (not in the isometric crystal system) the reflectance may vary depending on the orientation of the plane-polarized light relative to crystallographic directions. These bireflectant minerals change brightness with rotation of the microscope stage in plane light. Bireflectant minerals also may display reflection pleochroism.

Observation with Crossed Polarizers

(The analyzer is inserted into the optical path.)

Isotropism versus Anisotropism

Opaque isometric minerals will have isotropic behavior with cross-polarized light—they remain uniformly dark or black with rotation. Hexagonal and tetragonal minerals whose *c* axis is vertical also will show the same effect. Plane-polarized light impinging on the surface of an anisotropic opaque mineral will be reflected as two plane-polarized rays that vibrate at right angles to each other, analogous to the way light is split into two rays on passing through a transparent anisotropic mineral. When this light reaches the analyzer, it can be resolved into components that pass through and reach the observer. Anisotropic minerals (all but isometric system) therefore may show variations in the intensity of color or illumination with rotation for most orientations. The strength of the anisotropy is described as ranging from very weak to very strong.

Polarization Colors

The polarization color is the color observed with cross-polarized light; in a crude way, it is analogous to interference colors seen with transparent minerals.

Internal Reflections

If the mineral is not entirely opaque, light may pass some distance into the mineral that is then reflected back to the surface by a crack or other imperfection. Internal reflections therefore show as small areas that are somewhat brighter than their surroundings. Only minerals with some degree of transparency may show them. Normally transparent minerals (carbonates, silicates, etc.) usually display internal reflections but low reflectance.

Selected properties of opaque minerals are listed in Appendix B and are included with the mineral descriptions in Chapters 18 through 20.

DO NOT COPY e48d507df5d1141@placeholder.9409-

Printed by: e48d507df5d1141@placeholder.94092.edu. Printing is for personal, private use only. No part of this book may be reproduced or transmitted without publisher's prior permission. Violators will be prosecuted.

Tactics for Mineral Identification

Chapter 10 provides a more comprehensive approach to rock and mineral study, which typically requires analysis with a petrographic microscope. The sections that follow focus on procedures that can be applied to thin sections with transmitted polarized light (**Box 7.1**) or grains mounts, or polished samples with reflected light. In all cases, analysis requires a systematic approach tempered with common sense and familiarity with a variety of common rocks and minerals. With practice, optical data can be rapidly measured, but because of small grain size, lack of grains in appropriate orientations, alteration, or other complications, it may not be possible to measure all the optical properties that might be desired. For routine work, however, identification often can be made with incomplete data, and for many minerals only selected data are needed to confirm a tentative identification.

DO NOT COPY e48d507df5d1141@placeholder.9409

BOX 7.1

Practical Guide to Transmitted Polarized Light Thin Section Analysis

When augmented by information gathered from hand sample or geologic setting, identification of minerals based on their optical properties can be quite rapid, as information from as few as one optical property may be sufficient for identification. This single optical property can be initially targeted while paying little attention to other, less informative optical properties. However, this takes experience, and typically to identify a mineral or to produce a full petrographic description, a systematic approach utilizing all optical properties must be followed. Below is a recommended comprehensive procedure.

- Begin in plane-polarized light (analyzer is pulled out). Scan the slide to get a sense of the main characteristics of the rock, including grain size and general texture and characteristics of a number of minerals. For each mineral, systematically record the following optical properties using multiple objective powers as necessary.
  a. Color. *Mineral color can only be determined in plane-polarized light.* Remember that the petrographic microscope uses transmitted light, so if the mineral appears white, it means that the light from the illuminator was not changed in color when it passed through the mineral and the mineral's color is said to be colorless. If a mineral transmits no light (all light is absorbed by the mineral), it appears black in plane-polarized light and the mineral is said to be opaque (**Figure 7.61a**). If the specific identity of an opaque mineral is needed, further analysis requires a polished thin section and reflected-light techniques or the scanning electron

Printed by: e48d507df5d1141@placeholder.94092.edu. Printing is for personal, private use only. No part of this book may be reproduced or transmitted without publisher's prior permission. Violators will be prosecuted.

microscope/electron microprobe, all covered in other parts of this and other chapters.

b. Pleochroism (if any). Rotate the stage and observe whether the mineral changes in color with rotation (**Figure 7.61b–d**). If so, the mineral is pleochroic. Make note of the range of colors displayed using multiple grains.

c. Relief. Relief is identified by the relative amount a mineral grain appears to be raised three-dimensionally compared to neighboring grains. If a mineral's boundary appears dark, then the mineral has high relief (**Figure 7.62a**). Cleavage and fracture surfaces of high-relief minerals may also appear particularly dark. Relief can be accentuated by closing the aperture diaphragm. Air bubbles in the thin section epoxy/cement generally appear as high-relief circular features; they should be ignored (**Figure 7.63a**).

d. Nature of cleavage and/or fracture. Cleavage appears as dark parallel lines (cracks) in the mineral grain (Figure 7.61b–d; **Figure 7.63b–c**). Fracture appears as dark curving or irregular cracks in the mineral (**Figure 7.62a**).

e. Mineral habit, textures, zoning, alteration, and twinning should all be described. Cross-polarized light may help to determine some of these properties depending on the mineral and sample, but plane-polarized light should be used first. Description of habit will include a variety of multiple descriptors including euhedral, subhedral, anhedral, equant, elongate, and acicular (Chapter 2). The particular habit displayed by an individual grain may be controlled by orientation, so multiple grains must be observed such that a three-dimensional picture of grain shape can be constructed and described. Other important descriptors for habit and texture includes a mineral's average and maximum grain size, whether it has inclusions and/or exsolution lamellae, if non-equant grains are aligned or not, and how grains may be intergrown with neighboring grains. Zoning can be identified by a change in mineral color across a grain (Figure 7.63c; Chapter 5), but for colorless minerals, often cross-polarized light is needed to identify zoning. Alteration is identified by whether a mineral appears to be partially replaced by another mineral (**Figure 7.63d–e**). If a grain is euhedral and twinned, it may be possible by grain shape to identify twinning. More commonly, for anisotropic minerals, twinning is identified with cross-polarized light when different parts of a grain go extinct at different angles of rotation (**Figure 7.63f**).

- Once all the information from plane-polarized light observation has been collected, move to cross-polarized light (insert the analyzer).

  a. For transparent minerals (not opaque), determine whether the mineral is isotropic or anisotropic. Isotropic minerals are fully extinct (black) with stage rotation in cross-polarized light (Figure 7.62b). Remember, though it is not a mineral, glass is also isotropic. During thin section preparation, it is possible for grains to be plucked out, leaving an isotropic hole because

DO NOT COPY e48d507df5d1141@placeholder.9409-

Printed by: e48d507df5d1141@placeholder.94092.edu. Printing is for personal, private use only. No part of this book may be reproduced or transmitted without publisher's prior permission. Violators will be prosecuted.

is possible for grains to be plucked out, leaving an isotropic hole because epoxy/cement and glass are all isotropic. Anisotropic minerals display interference colors and go extinct four times with 360° of rotation. *Interference color is a distinctly different optical property than mineral color; interference color can only be determined in cross-polarized light.* Keep in mind that some grains of anisotropic minerals may be oriented such that the view is parallel to an optic axis and thus will be extinct even with stage rotation and therefore behave as if isotropic. Because only anisotropic grains in this special orientation have this behavior, multiple grains must be observed to determine whether the mineral is isotropic or anisotropic.

- If a mineral is isotropic, go to the identification tables (Appendix B) and mineral descriptions to complete the identification.
- If the mineral is anisotropic:
  a. Scan the slide to find a grain of the unknown mineral displaying the lowest interference color. Obtain an interference figure.
     1. If uniaxial: (a) Determine optic sign. (b) Return to orthoscopic illumination and plane light and record the color associated with ω and the relief associated with n_ω.
     2. If biaxial: (a) Determine optic sign, $2V$, and dispersion characteristics, if any. (b) Rotate the stage to place the optic plane at right angles to the lower polarizer direction. Return to orthoscopic illumination and plane light and observe the color associated with Y and record the relief of the mineral associated with n_β. Check the Becke line to determine whether n_β is greater or less than the index of refraction of epoxy/cement, if adjacent to epoxy/cement. If the grain is not adjacent to epoxy/cement, quartz can substitute for epoxy/cement, as it typically has an index of refraction very close to that of epoxy/cement (see step c below).

  b. Scan the slide to find a grain of the unknown displaying the highest interference color.
     1. Determine maximum birefringence based on interference color and thin section thickness.
     2. If the mineral is elongate or has cleavage, measure the extinction angle and determine sign of elongation.
     3. Record the color and relief associated with n_ϵ (uniaxial) or n_α and n_γ (biaxial). Use the accessory plate to distinguish the appropriate vibration directions.
     4. If crystallographic directions can be recognized, determine optic orientation of biaxial minerals.

  c. Go to the identification tables and mineral descriptions to determine the identity of the mineral. The chart (Plate 2) printed behind the interference

DO NOT COPY e48d507df5d1141@placeholder.9409-

Printed by: e48d507df5d1141@placeholder.94092.edu. Printing is for personal, private use only. No part of this book may be reproduced or transmitted without publisher's prior permission. Violators will be prosecuted.

color chart provides a convenient starting point. Use the other figures and tables in Appendix B as needed to help refine the possibilities. Note that Plate 2, Table B.11, and the mineral descriptions in the latter part of the text all refer to relief in thin section. It is assumed that the epoxy/cement used in thin section has an index of refraction of 1.540. Some epoxy/cements may have an index of refraction either higher or lower than 1.540, so relief seen with these cements may be different than reported here. If in doubt about an epoxy/cement's index of refraction, consult the manufacturer, or prepare a grain mount of fragments of cured epoxy/cement and measure it by using the immersion method.

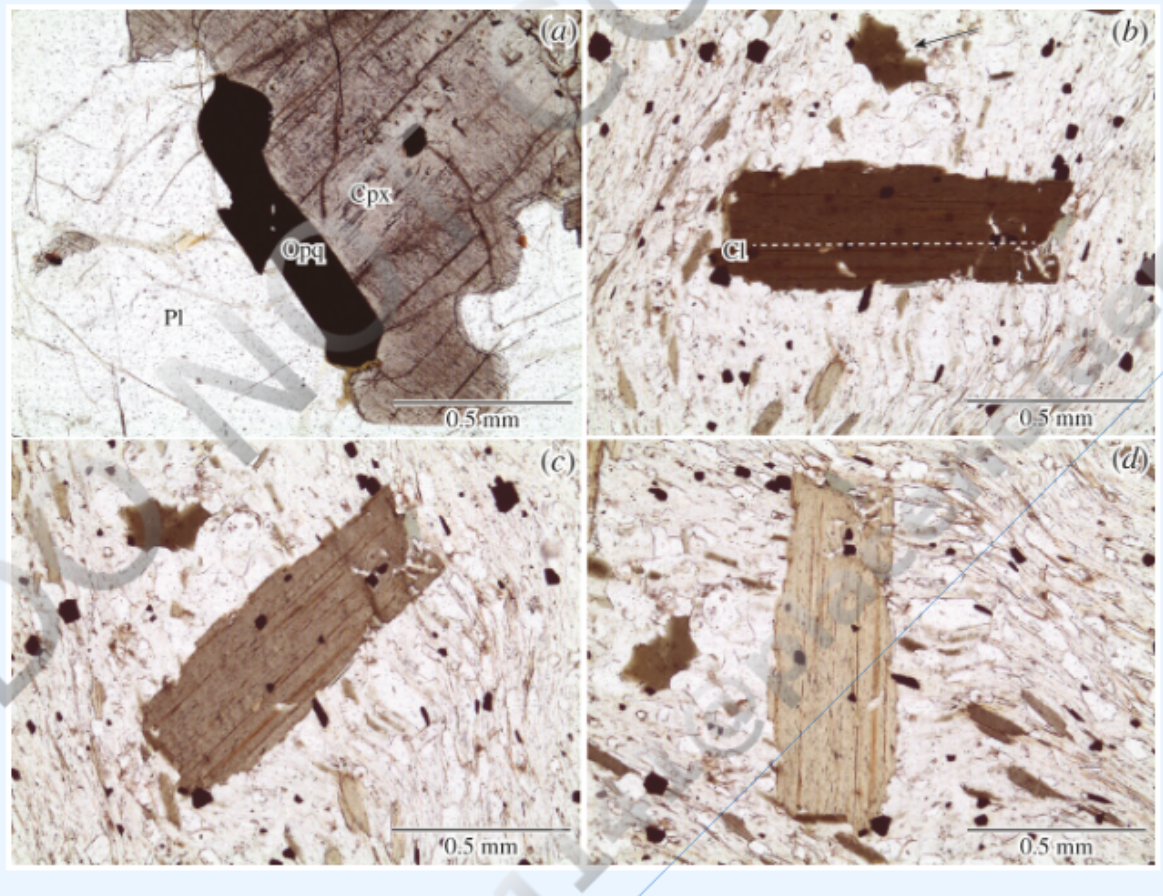

FIGURE 7.61 Photomicrographs highlighting various optical properties and features seen in thin section. (*a*) Mineral color (plane-polarized light). Plagioclase (Pl) is colorless, clinopyroxene (cpx) is colored, and the mineral that transmits no light (appears black) is said to be opaque (Opq). (*b*) (*c*) (*d*) Pleochroism in biotite (plane-polarized light). For most petrographic microscopes, if biotite cleavage (Cl) is horizontal, biotite displays a dark color; during a 90° rotation the color changes to a light version of the dark color. Some pleochroic minerals can change to a different color entirely with rotation and do not just cycle between light and dark versions of the same color. Arrow marks biotite grain viewed nearly down the *c* axis as indicated by no visible cleavage. This grain does not show pleochroism, emphasizing how optical properties vary with grain orientation. View larger image

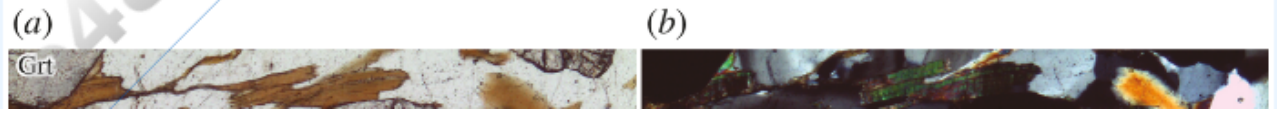

Printed by: e48d507df5d1141@placeholder.94092.edu. Printing is for personal, private use only. No part of this book may be reproduced or transmitted without publisher's prior permission. Violators will be prosecuted.

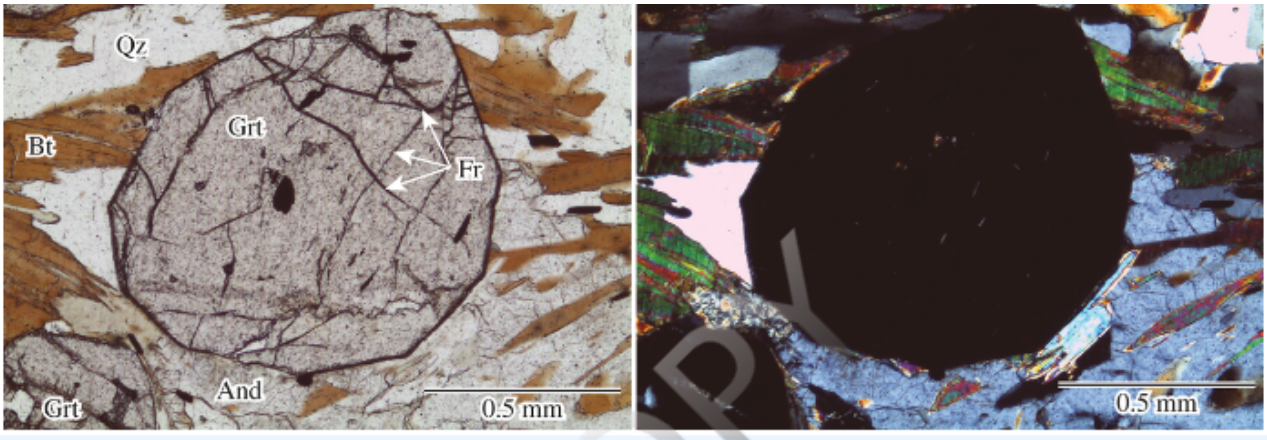

FIGURE 7.62 Relief and isotropic vs. anisotropic optical properties. (*a*) Plane-polarized light. Garnet (Grt) displays high relief, emphasized by its dark euhedral grain boundaries and dark fractures (Fr). Andalusite (And) and biotite (Bt) are moderate relief, and quartz (Qz) is low relief. (*b*) Cross-polarized light of the same area shown in (*a*). Garnet is isotropic, so it is black between crossed polarizers, no matter the orientation. Andalusite, biotite, and quartz all display interference colors. View larger image

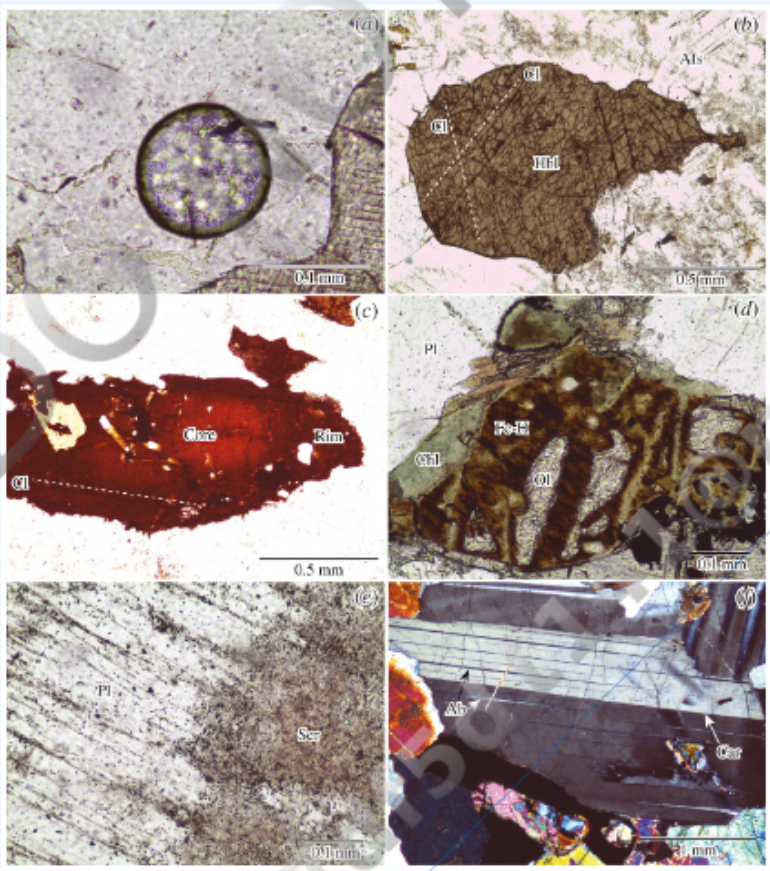

FIGURE 7.63 Photomicrographs highlighting various optical properties and features seen in thin section. (*a*) Circular, high-relief air bubble in thin section epoxy (plane-polarized light). (*b*) High-relief hornblende (Hbl) grain surrounded by alkali feldspar (Afs). The view is nearly down the *c* axis of the hornblende grain, so the angle between the two cleavages (Cl) is close to the true 56° and 124° (plane-polarized light). Compare with (*c*). (*c*) The colored hornblende grain has its *c* axis parallel to the plane of the thin section, so only one cleavage (Cl) is visible (plane-polarized light). Compare with (*b*). The hornblende is also zoned with a lighter-colored core surrounded by a darker rim. (*d*) An olivine grain (Ol) partially altered to Fe-hydroxides (Fe-

DO NOT COPY e48d507df5d1141@placeholder.94092

Printed by: e48d507df5d1141@placeholder.94092.edu. Printing is for personal, private use only. No part of this book may be reproduced or transmitted without publisher's prior permission. Violators will be prosecuted.

H, probably goethite and/or lepidocrocite) and chlorite (Chl). Alteration pattern suggests factures helped facilitate alteration. Plagioclase (Pl) surrounds the altered olivine grain. Plane-polarized light. (*e*) Plagioclase (Pl) altered to sericite (Ser). Cleavage planes are accentuated by sericite alteration. Plane-polarized light. (*f*) Cross-polarized light image of two types of twinning in plagioclase. Carlsbad twin composition surface (Car) cuts the grain in approximately half such that at this orientation, half the grain is near extinction and the other half is not. Closely spaced composition surfaces of albite twins (Ab) produce thin zones that are either extinct or not. View larger image

In all cases, to identify and describe minerals optically, proceed as follows.

- Examine the hand sample of the mineral to determine as many of the following characteristics as possible: color, luster, streak, hardness, cleavage/fracture, specific gravity, mineral habit. Provide a tentative identification or list of possibilities based on this information.
- Based on the identity of associated minerals, rock type, or type of mineral deposit, modify the tentative list of minerals that the unknown might be. Appendix C lists common mineral associations in different rock types and mineral deposits.
- Prepare a thin section, grain mount, or polished thin section or epoxy grain mount.

Grain Mount Identification with Transmitted Light and Petrographic Microscope

Grain mounts of an unknown mineral are useful because they are quicker to prepare than a thin section and they provide accurate numerical values of indices of refraction, birefringence, and related optical variables. From these data, it may be possible to estimate chemical composition or confirm an identity that was uncertain in thin section or hand sample. It is generally necessary to separate grains of the unknown (transparent) mineral from others that may be in the sample prior to preparing the mount. Refer to Chapter 10 for a summary of mineral separation procedures. In handling grain mounts, be careful to avoid getting immersion oil on lenses and working parts of the microscope. To identify an unknown mineral in grain mount, proceed as follows.

- Scan the slide to observe as many of the following properties about the unknown mineral as possible: relief relative to immersion oil, whether isotropic or anisotropic, nature of twinning (if present), nature of cleavage and fracture, and alteration.
- If it is isotropic, use the Becke line to compare the indices of refraction of immersion oil and mineral. Use different immersion oils to prepare additional grain mounts until an index of refraction match is obtained between the mineral and oil. Use the bracketing technique described earlier in this chapter.
- If it is anisotropic:

Printed by: e48d507df5d1141@placeholder.94092.edu. Printing is for personal, private use only. No part of this book may be reproduced or transmitted without publisher's prior permission. Violators will be prosecuted.

- If it is anisotropic:
  a. Scan the slide to find a grain of the unknown with the lowest interference color. Obtain an interference figure.
     1. If it is uniaxial: (a) Determine optic sign. (b) Return to orthoscopic illumination and plane light and record the color associated with ω and the relief associated with n_ω. Check the Becke line to determine whether n_ω is greater or less than the index of refraction of the oil.
     2. If it is biaxial: (a) Determine optic sign, $2V$, and dispersion characteristics, if any. (b) Rotate the stage to place the optic plane at right angles to the lower polarizer direction. Return to orthoscopic illumination and plane light and observe the color associated with Y and record the relief of the mineral associated with n_β. Check the Becke line to determine whether n_β is greater or less than the index of refraction of oil.
  b. Scan the slide to find a grain of the unknown displaying the highest interference color.
     1. If the mineral forms elongate fragments because of cleavage, measure the extinction angle and determine sign of elongation.
     2. Record the color and relief associated with n_ϵ (uniaxial) or n_α and n_γ (biaxial). Use the accessory plate to distinguish the appropriate vibration directions.
  c. Prepare additional grain mounts to find index of refraction matches for n_ω and n_ϵ (uniaxial) or n_α, n_β, and n_γ (biaxial) following the procedures described in detail earlier.
  d. Go to the identification tables (Appendix B) and mineral descriptions to identify the unknown.

Polished Sample Identification with Reflected Light and Petrographic Microscope

Proficiency in identification of minerals with a standard reflecting-light microscope depends on experience gained from study of many samples. Unlike transmitted-light optics, in which it is possible to make quantitative measurements, most of the reflective-light optical properties are qualitative. Begin by scanning the polished section both in plane light and with crossed polarizers to note intergrowth textures, colors, alteration, or other features that distinguish among different opaque minerals in the sample. Then proceed systematically to observe the following for each mineral.

- In plane light (analyzer removed):
  a. Color of the mineral
  b. Reflectance. Try to distinguish among very low (like quartz or epoxy), low (like magnetite), moderate (like galena), and high (like pyrite).
  c. Bireflectance and reflectance pleochroism

DO NOT COPY e48d507df5d1141@placeholder.9409

Printed by: e48d507df5d1141@placeholder.94092.edu. Printing is for personal, private use only. No part of this book may be reproduced or transmitted without publisher's prior permission. Violators will be prosecuted.

   c. Bireflectance and reflectance pleochroism

- With crossed polarizers (analyzer inserted):
   a. Isotropism versus anisotropism
   b. Polarization colors
   c. Internal reflections

Based on these observations, refer to the tables in Appendix B and the mineral descriptions to work out the identification.

DO NOT COPY
e48d507df5d1141@placeholder.9409

Printed by: e48d507df5d1141@placeholder.94092.edu. Printing is for personal, private use only. No part of this book may be reproduced or transmitted without publisher's prior permission. Violators will be prosecuted.

Isotropism versus anisotropism

- Polarization colors
- Internal reflections

Based on these observations, refer to the tables in Appendix B and the mineral descriptions to work out the identification.

REFERENCES CITED AND SUGGESTIONS FOR ADDITIONAL READING

Bloss, F. D. 1961. *An Introduction to the Methods of Optical Crystallography*. Holt, Rinehart & Winston, New York, 294 p.

Bloss, F. D. 1981. *The Spindle Stage: Principles and Practice*. Cambridge University Press, Cambridge, 340 p.

Craig, J. R., and Vaughn, J. D. 1994. *Ore Microscopy and Ore Petrography*, 2nd ed. John Wiley & Sons, New York, 434 p.

Dyer, M. D., Gunter, M. E., and Tasa, D. 2008. *Mineralogy and Optical Mineralogy*. Mineralogical Society of America, Chantilly, VA, 708 p.

Humphries, D. W. 1992. *The Preparation of Thin Sections of Rocks, Minerals, and Ceramics*. Oxford University Press, Oxford, 83 p.

Ineson, P. R. 1989. *Introduction to Practical Ore Microscopy*. Longman Scientific & Technical, Essex, UK, 181 p.

Ixer, R. A. 1990. *Atlas of Opaque and Ore Minerals in Their Associations*. Van Nostrand Reinhold, New York, 208 p.

Mertie, J. B., Jr. 1942. Nomograms of optic angle formulae. *American Mineralogist* **27**, 538–551.

Nesse, W. D. 2013. *Introduction to Optical Mineralogy*, 4th ed. Oxford University Press, New York, 361 p.

DO NOT COPY e48d507df5d1141@placeholder.9409

Printed by: e48d507df5d1141@placeholder.94092.edu. Printing is for personal, private use only. No part of this book may be reproduced or transmitted without publisher's prior permission. Violators will be prosecuted.

LIST OF KEY TERMS

$2E$

$2V$ angle

$2V_x$

$2V_z$

accessory plates

acute bisectrix

acute bisectrix interference figure

analyzer

angular aperture

anomalous interference colors

aperture diaphragm

apparent optic angle

auxiliary condensing lens

Becke line

Bertrand lens

biaxial

birefringence

bisectrix dispersion

Bxa

Bxo

circular section

compensator plates

condensing lens

conoscopic illumination

critical angle

Crossed

crossed bisectrix dispersion

crossed polarizers

dispersion

DO NOT COPY e48d507df5d1141@placeholder.9409

Printed by: e48d507df5d1141@placeholder.94092.edu. Printing is for personal, private use only. No part of this book may be reproduced or transmitted without publisher's prior permission. Violators will be prosecuted.

dispersion
double refraction
extinct
extinction angle
extraordinary ray
fast ray
first-order red plate
flash figure
free working distance
frequency
full-wave plate
grain mounts
gypsum plate
high-eye-point oculars
high relief
horizontal dispersion
immersion method
immersion oil
inclined dispersion
inclined extinction
index of refraction
indicatrix dispersion
interference color chart
interference colors
interference figure
isochromes
isogyres
length fast
length slow
light ray
lower polarizer
low relief
melatope
mica plate

DO NOT COPY
e48d507df5d1141@placeholder.9409

Printed by: e48d507df5d1141@placeholder.94092.edu. Printing is for personal, private use only. No part of this book may be reproduced or transmitted without publisher's prior permission. Violators will be prosecuted.

mica plate
Michel-Lévy chart
moderate relief
negative elongation
negative relief
Nicols
no extinction angle
numerical aperture
objective lens
obtuse bisectrix
ocular
off-center figure
off-center optic axis figure
ON
one-wavelength plate
opaque
optical character
optical indicatrix
optically anisotropic
optically biaxial
optically isotropic
optically negative
optically neutral
optically positive
optically uniaxial
optic axis
optic axis dispersion
optic normal
optic normal interference figure
optic orientation
optic plane
optic sign
Orders

DO NOT COPY
e48d507df5d1141@placeholder.9409

Printed by: e48d507df5d1141@placeholder.94092.edu. Printing is for personal, private use only. No part of this book may be reproduced or transmitted without publisher's prior permission. Violators will be prosecuted.

ordinary ray

orthoscopic illumination

parallel dispersion

parallel extinction

petrographic microscope

plane light

plane polarized

pleochroic

polarizer

polarizing film

polarizing light microscope

positive elongation

positive relief

principal indices of refraction

Principal sections

quarter-wave

quarter-wavelength plate

quartz-sensitive tint

quartz wedge

reflected

refracted

refractometry

relief

retardation

reticle markings

sign of elongation

slow ray

Snell’s law

stage

stage goniometer

stage micrometer

symmetrical extinction

thin section

DO NOT COPY
e48d507df5d1141@placeholder.9409

Printed by: e48d507df5d1141@placeholder.94092.edu. Printing is for personal, private use only. No part of this book may be reproduced or transmitted without publisher's prior permission. Violators will be prosecuted.

total internal reflection

transparent

undulatory extinction

undulose extinction

uniaxial

upper polarizer

velocity

vernier

wave front

wavelength

wave normal

zoned crystals

ω ray

ϵ ray

DO NOT COPY

e48d507df5d1141@placeholder.9409

Printed by: e48d507df5d1141@placeholder.94092.edu. Printing is for personal, private use only. No part of this book may be reproduced or transmitted without publisher's prior permission. Violators will be prosecuted.

CHAPTER 8

Analytical Instrumentation and Techniques I: Crystallography

William D. Nesse
University of Northern Colorado

Graham B. Baird
University of Northern Colorado

DO NOT COPY
e48d507df5d1141@placeholder.9409

Printed by: e48d507df5d1141@placeholder.94092.edu. Printing is for personal, private use only. No part of this book may be reproduced or transmitted without publisher's prior permission. Violators will be prosecuted.

Introduction

There are two basic classes of analytical instruments or techniques used to investigate minerals or other similar materials. One qualitatively or quantitatively determines sample composition. The other investigates the crystal structure (crystallography) of crystalline materials. Placing all analytical instruments into one of these two classes is somewhat simplistic as some instruments are capable of directly analyzing both composition and crystal structure. Further, it may be possible to indirectly determine composition from crystal structure if their relationship is particularly well known for a material. This chapter and Chapter 9 cover the common analytical instruments and techniques used to determine crystal structure and composition. This information may allow sample identification or help determine the geologic history of a sample.

Up to this point, it has been emphasized that chemical, physical, and optical properties of minerals indicate that minerals must be constructed of regular and repeating arrays of atoms. Determining how the atoms are arranged is done by a detailed study of how X-rays interact with a mineral's crystal structure by diffraction. The instruments that use X-ray diffraction are called **X-ray diffractometers** or **XRD** (**Figure 8.1**). Electrons can similarly be diffracted by a crystalline material, and instruments that use electron diffraction will be discussed toward the end of the chapter.

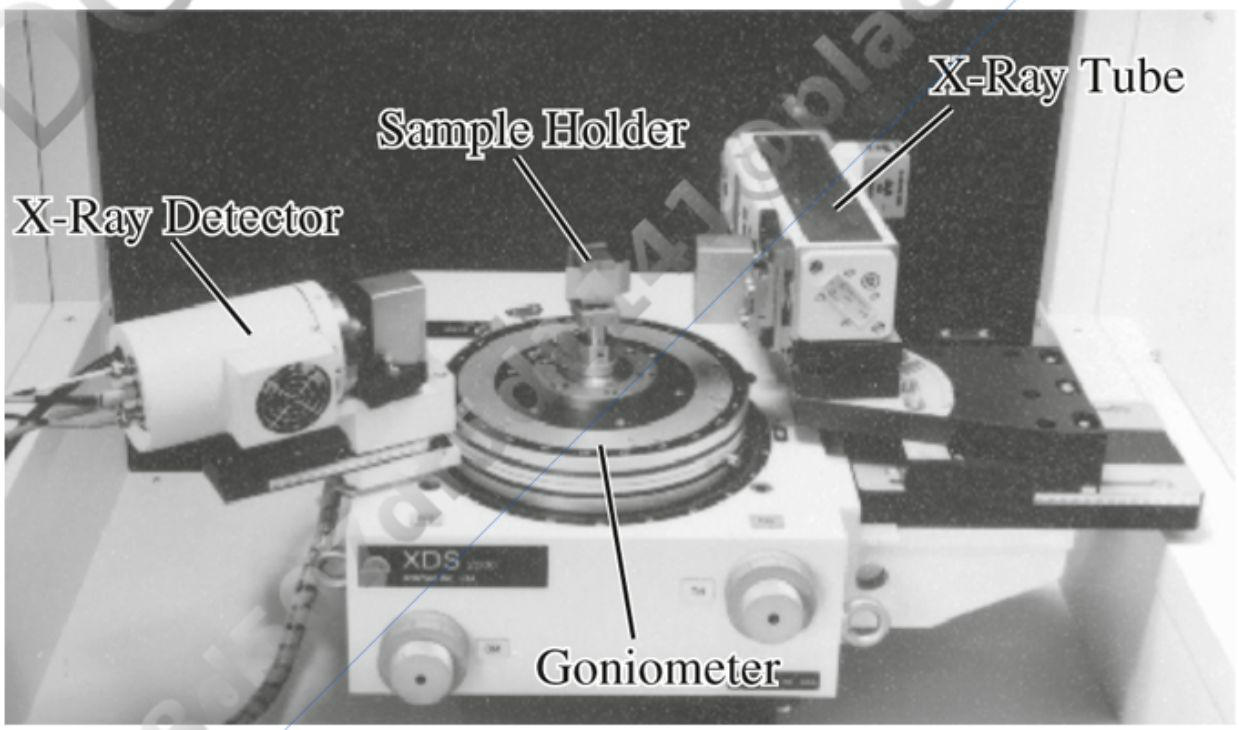

FIGURE 8.1 X-ray diffractometer. The principal components are an X-ray tube, sample holder, and an X-ray detector. X-rays are produced in the X-ray tube and directed to the sample on the holder; the X-ray detector then records the X-rays after they interacted with the sample. Sample and

Printed by: e48d507df5d1141@placeholder.94092.edu. Printing is for personal, private use only. No part of this book may be reproduced or transmitted without publisher's prior permission. Violators will be prosecuted.

holder, the X-ray detector then records the X-rays after they interacted with the sample. Sample and detector are mounted on the goniometer, which allows both to be synchronously rotated through angles θ and 2θ, respectively. Additional components include power supplies, controls, and electronics to allow the output of the detector to be recorded and displayed. Because X-rays can be very hazardous, an enclosure, shields, and other safety devices (not shown) are provided to prevent the operator from being exposed to X-rays. Photo courtesy of Scintag, Inc. View larger image

DO NOT COPY
e48d507df5d1141@placeholder.9409

Printed by: e48d507df5d1141@placeholder.94092.edu. Printing is for personal, private use only. No part of this book may be reproduced or transmitted without publisher's prior permission. Violators will be prosecuted.

X-Rays

Similar to visible light discussed in Chapters 6 and 7, **X-rays** are part of the continuous electromagnetic spectrum (Figure 6.6) whose wavelengths are between 0.1 and 10 angstroms (Å; 1 Å = 0.1 nm = 10^{-10} m).

X-Ray Generation

In a conventional X-ray diffractometer, X-rays are generated in a cathode ray tube (**Figure 8.2**). Free electrons are produced by heating a filament called the cathode (similar to the filament in an incandescent light bulb) to a high temperature. These negatively charged electrons are accelerated to high energy to form a beam by applying a voltage of several tens of kilovolts between the filament and the target or anode. Each electron in the beam has an energy in electron volts (eV), which is its charge, *e*, times the accelerating voltage, *V*. If the electrons have sufficient energy, a spectrum of both continuous and characteristic X-rays (**Figure 8.3a**) are produced when the beam electrons interact with the atoms of the target.

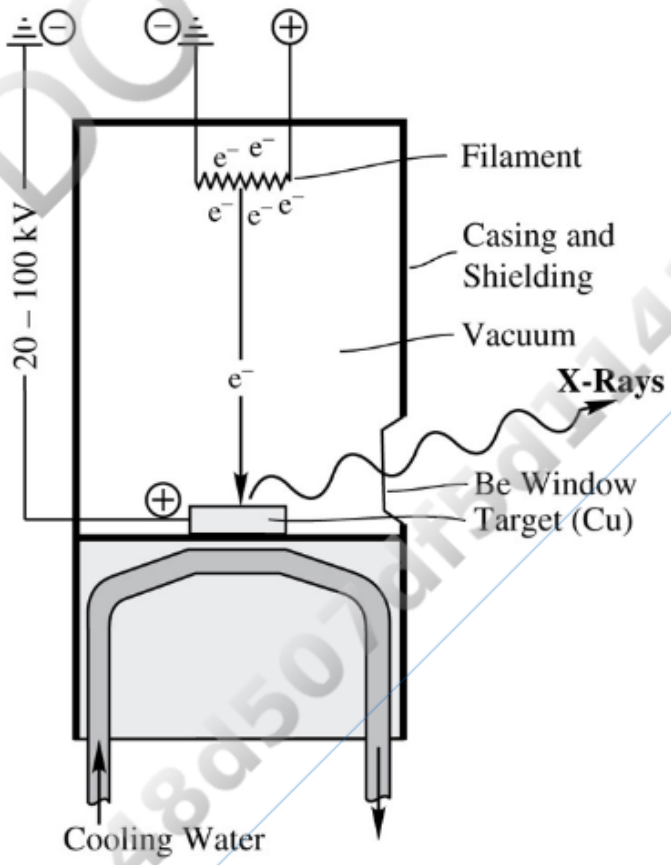

FIGURE 8.2 X-ray tube. The cathode filament is heated so that it emits electrons. A voltage of

DO NOT COPY e48d507df5d1141@placeholder.94092

Printed by: e48d507df5d1141@placeholder.94092.edu. Printing is for personal, private use only. No part of this book may be reproduced or transmitted without publisher's prior permission. Violators will be prosecuted.

20 to 100 kV is maintained between the filament and the target (the anode) to accelerate the electrons as a beam toward the target. When these high-energy electrons strike atoms in the target, X-rays are generated and exit through a thin beryllium window in the tube. The target is most commonly copper or molybdenum. View larger image

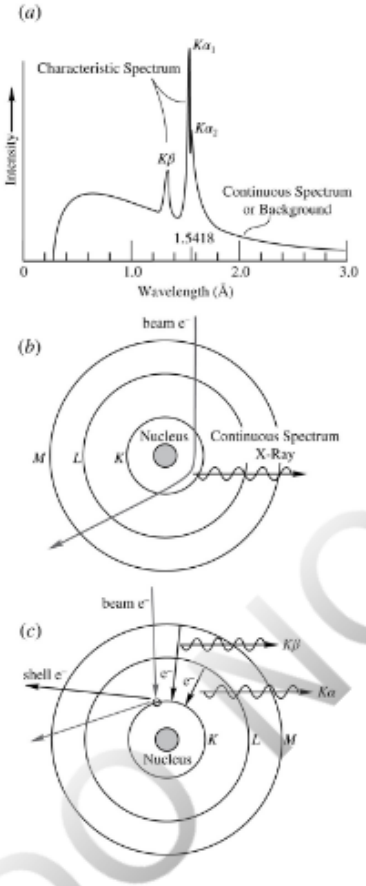

FIGURE 8.3 X-ray spectra. (*a*) Intensity of X-rays emitted by a copper target operated at 50 kV. The characteristic X-ray spectrum (peaks) is superimposed on the continuous spectrum. (*b*) Beam electron deflection (scattering) by a nucleus in the target results in the emission of a continuous spectrum X-ray. (*c*) The characteristic X-ray spectrum is produced when electrons are dislodged from the *K* shell (or other inner shells) and electrons from outer shells drop in energy to occupy the vacancy. View larger image

Continuous X-Ray Spectrum (background)

The **continuous spectrum** of X-rays (Figure 8.3a), or *Bremsstrahlung* (German for "braking radiation") is produced when the negatively charged electrons enter the target and are slowed, deflected, or halted by attraction to the positively charged nuclei of nearby atoms in the target (**Figure 8.3b**). Each of these interactions decrease the beam electron's energy, so in response it must release electromagnetic radiation, which includes a wide range of X-ray wavelengths and heat. In general, the wavelength of X-rays produced in this way is fairly random, so about an equal number of X-rays are produced for any particular wavelength. The exception is that the accelerating voltage (*kV*, kilovolts) determines the highest-energy X-rays with the shortest wavelength (λ_s, angstroms) that can be produced:

DO NOT COPY e48d507df5d1141@placeholder.9409

Printed by: e48d507df5d1141@placeholder.94092.edu. Printing is for personal, private use only. No part of this book may be reproduced or transmitted without publisher's prior permission. Violators will be prosecuted.

$$\lambda_s = \frac{12.4}{kV}. \tag{8.1}$$

So for a 50 kV accelerating voltage, the minimum wavelength produced in this fashion is 0.248 Å, as shown in Figure 8.3a.

Unfortunately, the continuous spectrum is equivalent to background noise and is not much use because X-rays of a single wavelength are needed for X-ray diffraction; hence the continuous spectrum is often referred to as **background**.

Characteristic X-Ray Spectrum

The **characteristic X-ray spectrum** (Figure 8.3a) is produced when a beam electron dislodge a tightly held K shell electron from a target atom (Table 3.2, Figure 3.2, **Figure 8.3c**). Almost immediately, an electron from an outer, higher-energy shell decreases in energy and replaces the missing K shell electron. When the outer shell electron drops in energy, it emits radiation of an energy equal to the energy difference, ΔE, between the outer shell where the orbital electron originated and the K shell it moved to. The wavelength (in angstroms) of the emitted X-rays is

$$\lambda = \frac{ch}{\Delta E} = \frac{12.4}{\Delta E} \tag{8.2}$$

where c is the speed of light and h is Planck's constant. As Figure 8.3c shows, electrons most commonly drop from the L and M shells to produce **characteristic X-ray** wavelengths known as $K\alpha$ and $K\beta$. Considering all the wavelengths of X-rays produced (Figure 8.3a), many more X-rays of the characteristic wavelengths are produced and therefore appear as **peaks** above the background, signifying their high abundance or intensity. Because the specific energy of the orbital electrons is controlled by the element, the wavelengths of $K\alpha$ and $K\beta$ shown here are specific to Cu, the material of the target. Hence their wavelength is *characteristic* of Cu. It is important to remember that depending on the atomic number, an element may have few shells or it may have many; the more shells it has, the more characteristic X-rays of differing wavelengths can be produced, and each wavelength corresponds to a specific drop in energy an electron can take from an outer shell to an inner shell. For the sake of simplicity, the discussion only focuses on the characteristic X-rays produced by electrons dropping in energy to fill the K shell.

By Equation 8.2, $K\beta$ radiation must have a shorter wavelength than $K\alpha$ because ΔE for the M–K shell transition is greater than for the L–K shell transition. L–K transitions are much more common than M–K transitions that generate characteristic X-rays, so the $K\alpha$ peak is typically about 10 times as intense as $K\beta$. Close inspection of the $K\alpha$ peak shows it actually consists of two peaks, called $K\alpha_1$ and $K\alpha_2$, and these result from sub-orbitals

DO NOT COPY e48d507df5d1141@placeholder.94092

Printed by: e48d507df5d1141@placeholder.94092.edu. Printing is for personal, private use only. No part of this book may be reproduced or transmitted without publisher's prior permission. Violators will be prosecuted.

actually consists of two peaks, called $K\alpha_1$ and $K\alpha_2$, and these result from sub-orbitals within the L shell having slightly different energies; hence an electron that originates from one sub-orbital or another will produce a characteristic X-ray of slightly higher or lower wavelength when it drops down to the K shell. The combined $K\alpha$ peak, which is a result of **peak overlap**, is often referred to as $K\overline{\alpha}$.

Monochromatic X-Rays

Effective use of X-rays in an X-ray diffractometer requires that approximately monochromatic (single-wavelength) X-rays be used. Because the $K\overline{\alpha}$ peak has the greatest intensity, it is most commonly used, and $K\beta$ and much of the continuous spectrum must be removed. This is traditionally done either by filtering or by passing the X-ray beam exiting the X-ray tube through a monochromator. Filters are pieces of metal foil that preferentially absorb some wavelengths of X-rays a great deal and absorb others very little. A piece of nickel foil is usually used with copper-target radiation to eliminate the $K\beta$ peak and much of the background. A monochromator is a carefully oriented crystal plate whose interatomic spacing is appropriate to diffract and pass along the $K\alpha$ radiation but not other wavelengths (see discussion of diffraction).

Any filter or monochromator reduces the number of X-rays of the desired wavelength, so use of too many in an attempt to make the X-rays monochromatic will result in too few X-rays for the instrument to collect meaningful data. An additional strategy is to use a solid-state detector that is tuned to only record a narrow range of wavelengths that includes the desired $K\alpha$ radiation. Regardless of the applied strategies, the X-rays used in a diffractometer are never strictly monochromatic. This is exemplified by the characteristic X-ray peaks having some width, indicating the peak covers a range of wavelengths; this occurs for a variety of reasons, including characteristic X-rays having their wavelengths changed slightly by interactions with the target, tube window, filters, etc. For the $K\overline{\alpha}$ peak, it covers a greater range of wavelengths than might be expected for a characteristic X-ray because of the above-mentioned peak overlap between the two closely spaced $K\alpha_1$ and $K\alpha_2$ peaks. Unfortunately, even with advanced, modern-day instruments, it difficult to isolate just the $K\alpha_1$ peak.

Of the elements employed as the target in X-ray tubes used for X-ray diffraction (**Table 8.1**), copper is the most common, and all have overlap between their $K\alpha_1$ and $K\alpha_2$ peaks. The weighted average wavelength of the two peaks that make up $K\overline{\alpha}$ is typically used in calculations. For Cu, $K\overline{\alpha}$ is 1.5418 Å, but different instruments filter X-rays slightly differently and may use a slightly different Cu$K\overline{\alpha}$ value than reported here.

TABLE 8.1 Characteristic Wavelengths (Å) of Metals Commonly Used as Targets in X-ray Tubes[a]

	Metal				
	Mo	Cu	Co	Fe	Cr

DO NOT COPY e48d507df5d1141@placeholder.9409

Printed by: e48d507df5d1141@placeholder.94092.edu. Printing is for personal, private use only. No part of this book may be reproduced or transmitted without publisher's prior permission. Violators will be prosecuted.

$K\beta$	0.63225	1.38217	1.62073	1.75653	2.08479
$K\alpha_1$	0.70926	1.54051	1.78892	1.93597	2.28962
$K\alpha_2$	0.71354	1.54433	1.79279	1.93991	2.29351
$K\overline{\alpha}$	0.7107	1.5418	1.7902	1.9373	2.2909

[a] $K\overline{\alpha}$ is the weighted average of $K\alpha_1$ and $K\alpha_2$.

X-Ray Detection

X-rays may be detected either photographically or electronically. In the early and mid-twentieth century, photographic film was widely used to document the diffraction of X-rays by minerals. These photographic technologies are now largely obsolete and are replaced by electronic detection technologies.

The commonly used electronic detectors in X-ray diffractometers are scintillation counters, gas-proportional counters, and solid-state devices. In a scintillation counter, a crystal plate called a scintillator emits a brief flash of light when struck by an X-ray photon. This flash of light is electronically detected and yields a brief spike of electrical current that signifies an X-ray entered the detector, which is called a count. Gas-proportional counters consist of a hollow metal tube filled with a gas. A voltage of ~1.5 kV is maintained between the tube and a thin wire along its axis. X-ray photons passing through the detector produce ions of the gas by dislodging electrons. The electrons move to the positively charged wire while the ions move to the case. The resulting pulse of electric current is recorded as a count. Solid-state detectors, which are based on semiconductor technology, convert the energy of X-ray photons that strike the detector directly to an electrical pulse. Their operation requires cooling, which was originally done by liquid nitrogen, but today it can be done by a solid-state Peltier device. All detector types are very sensitive, and their output is easily interpreted by a computer for immediate analysis and plotting.

DO NOT COPY e48d507df5d1141@placeholder.9409

Printed by: e48d507df5d1141@placeholder.94092.edu. Printing is for personal, private use only. No part of this book may be reproduced or transmitted without publisher's prior permission. Violators will be prosecuted.

X-Ray Diffraction

The wavelength of X-rays used in X-ray diffractometers is around 1 or 2 Å, which is similar to the spacing of atoms in the structure of most minerals. The similarity in dimensions means that X-rays are diffracted by the regularly spaced atoms that make up a crystal. Based on an analysis of this diffraction in three dimensions, it can be shown that the layers of atoms "reflect" the beam of X-rays only when the incident X-ray's angle θ is appropriate. Consider **Figure 8.4**. Rays 1 and 2 are incident to the layers of atoms at angle θ. Note that the angle θ is defined differently than in the discussion of reflection and refraction of light in Chapters 6 and 7. The planes of atoms are spaced distance d apart. Diffracted X-rays from each plane of atoms will be in phase only if the angle θ is such that the additional distance pqr traveled by wave 2 is equal to an integer number of wavelengths

$$(8.3)$$

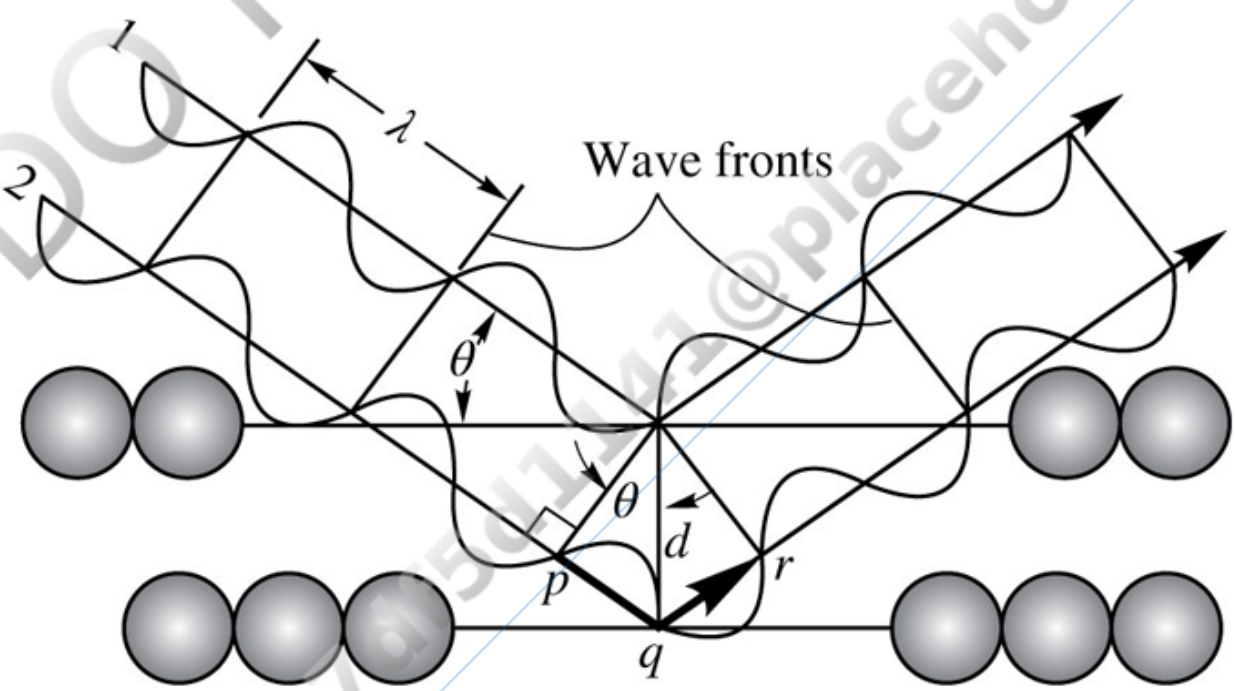

FIGURE 8.4 Diffraction from parallel planes of atoms (atoms not shown where the X-ray rays are drawn). Rays 1 and 2 interact with layers of atoms that are distance d apart. Constructive interference ("reflection") of the X-rays diffracted from these layers is possible only if the angle of incidence θ is such that the distance pqr is an integer number of wavelengths. View larger image

where n is an integer and λ is the wavelength of the X-rays. The distance pqr is twice distance pq, which is related to the interplanar spacing d by the equation

Printed by: e48d507df5d1141@placeholder.94092.edu. Printing is for personal, private use only. No part of this book may be reproduced or transmitted without publisher's prior permission. Violators will be prosecuted.

distance *pq*, which is related to the interplanar spacing *d* by the equation

$$pq = d \sin \theta \tag{8.4}$$

or

$$pqr = 2pq = 2d \sin \theta. \tag{8.5}$$

Combining Equations 8.3 and 8.5 yields

$$n\lambda = 2d \sin \theta. \tag{8.6}$$

This relationship is the **Bragg equation** (or **Bragg's Law**). When Bragg's Law is satisfied, the X-rays will continue in their new orientation after diffraction because the waves are in phase, which results in constructive interference. When Bragg's Law is not satisfied, the X-rays will be out of phase after interaction with the crystal lattice planes and therefore will not continue because of deconstructive interference between the waves. The references given at the end of the chapter offer a more complete derivation and explanation of diffraction.

In Figure 8.4, the distance *pqr*, which produces constructive interference between rays 1 and 2, is equal to one wavelength. However, constructive interference also will occur when *pqr* is equal to any integer number of wavelengths. For this reason, the integer *n* is included on the left side of the Bragg equation.

For example, the {111} planes of atoms in halite (NaCl) have a ***d*-spacing** or interplanar spacing of d_{111} = 3.2555 Å. If $\mathrm{Cu}K\alpha$ radiation is used, λ = 1.5418 Å. Solution of the Bragg equation for n = 1 yields a reflection at θ = 13.70°. This is a **first-order reflection** because n = 1. For n = 2, a **second-order reflection** is produced at 28.27°. **Third-** and **fourth-order reflections** for n = 3 and n = 4 are at 45.27° and 71.30°, respectively. Reflections higher than the fourth order are not possible for {111} because θ cannot exceed 90°.

Reflection of X-rays from planes of atoms as a result of diffraction in a crystal structure is possible only if the grain happens to be correctly oriented. For an unknown mineral whose *d*-spacings are unknown, the chances of placing a single grain in the X-ray beam in an orientation to yield a reflection in a single attempt is nearly impossible. Furthering the complexity, each mineral has many different atomic planes ({100}, {010}, {001}, {111}, {110}, etc.) that may diffract X-rays, but not all diffract from a particular grain at any time given the geometric constraints of diffraction. Therefore, to measure all the different *d*-spacings in a mineral with a single crystal, it would be necessary to systematically rotate the sample and detector so that a wide range of orientations are sampled. This is done with a **single crystal X-ray diffractometer** and requires mounting a single, pure

DO NOT COPY e48d507df5d1141@placeholder.94092

Printed by: e48d507df5d1141@placeholder.94092.edu. Printing is for personal, private use only. No part of this book may be reproduced or transmitted without publisher's prior permission. Violators will be prosecuted.

crystal that is a few tens to hundreds of microns across onto a sample holder and systematically rotating the crystal in the X-ray beam in three dimensions. Such instruments are understandably very expensive; however, they are typically not needed for general mineralogical investigations (see section on powder X-ray diffraction). A much simpler solution for routine work is to create a sample of a huge number of (small) grains of a single mineral collectively in every possible orientation, which is the basis of **powder X-ray diffraction**.

DO NOT COPY
e48d507df5d1141@placeholder.9409

Printed by: e48d507df5d1141@placeholder.94092.edu. Printing is for personal, private use only. No part of this book may be reproduced or transmitted without publisher's prior permission. Violators will be prosecuted.

Powder X-Ray Diffraction

Powder X-ray diffraction is a powerful and convenient technique for identifying minerals, and given its relatively low cost, it is generally commonplace at higher education institutions. It is not routine to determine the details of crystal structures by powder X-ray diffraction; other techniques discussed later are typically better. In addition to the fact that the technique uses a more affordable instrument, samples with small crystal size such as clays and zeolites, which usually occur in very fine-grained aggregates, work well with powder X-ray diffraction.

Sample Preparation

Powder X-ray diffraction samples consist of finely ground powder prepared by crushing a few tenths of a gram or more of the unknown mineral in a mortar. Relatively pure samples of the unknown are preferred, but mixtures of minerals also may be analyzed. Grains that pass through a 200-mesh (< 0.074 mm) or 400-mesh (< 0.037 mm) sieve are adhered to a glass microscope slide, packed into a well in a plastic or metal sample holder, or otherwise mounted on a holder of similar size (**Figure 8.5**). Grains in the sample should be as randomly oriented as possible for most identification purposes. For certain analyses of clay minerals, however, the single prominent cleavage needs to be aligned parallel to the surface of the sample holder.

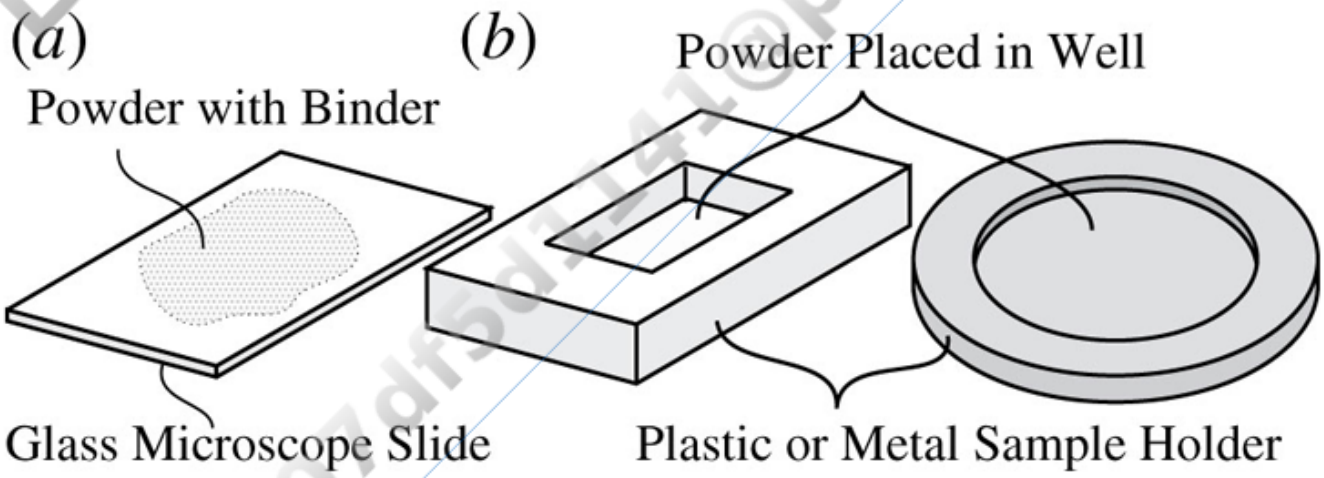

FIGURE 8.5 Sample holders for routine powder diffraction work. (*a*) Mineral powder adhered to a 26 × 47 mm glass microscope slide. (*b*) Powder is placed into the well of a plastic or metal mount. Sample holders of other types may be used, depending on the design of the instrument. Many instruments have a sample stage that allows multiple samples to be loaded and run sequentially.
View larger image

Printed by: e48d507df5d1141@placeholder.94092.edu. Printing is for personal, private use only. No part of this book may be reproduced or transmitted without publisher's prior permission. Violators will be prosecuted.

The sample is mounted in the X-ray diffractometer on a holder that pivots relative to the X-ray tube to allow the angle of incidence θ of the X-ray beam to be varied from zero up to nearly 90°. The X-ray detector is mounted on a concentric goniometer that moves at twice the angular speed between sample and X-ray tube, so that the detector is at the angle 2θ required to record reflections.

Instrumental Output

For routine identification work using Cu$K\overline{\alpha}$ radiation, the detector is moved through a 2θ angle of about 5° to 70°. This allows the instrument to detect reflections from atomic planes in a mineral whose d-spacing ranges from about 17.7 to 1.34 Å. Larger 2θ angles generally pick up only higher-order reflections or minor reflections from atomic planes with Miller indices containing relatively large integers. Smaller angles may be used if desired, but diffractometers should not be set to 0° because the intense beam coming directly from the X-ray tube may damage some detectors.

The sample and detector are rotated through the desired range of θ and 2θ angles, respectively (**Figure 8.6a**), and the intensity of the reflected X-rays is continuously recorded electronically in a computer. A peak in the intensity of the diffracted X-rays indicates that the mineral possesses atomic planes whose d-spacing is appropriate to reflect X-rays for that particular angle θ by Equation 8.6. Because ideally the powdered sample contains grains in all orientations, each of the different sets of atomic planes that are capable of diffracting X-rays will produce an X-ray peak at the appropriate angle as the detector is moved through its range of 2θ. The intensity of the diffracted X-rays for each peak, called the peak height, is also controlled by mineral structure as some atomic planes are more effective than others at reflecting X-rays or are more common due to symmetry.

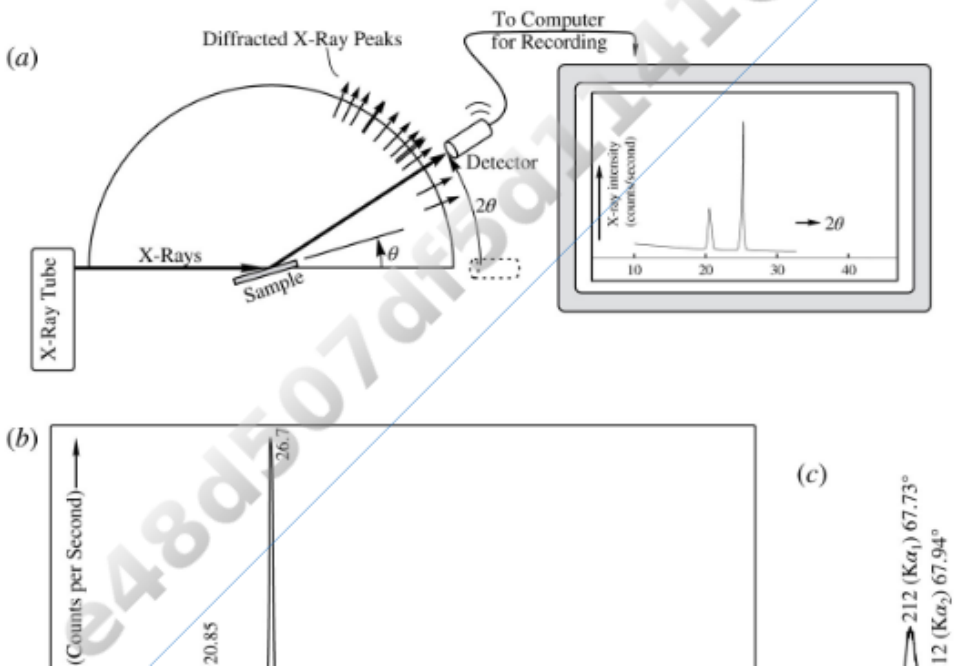

Printed by: e48d507df5d1141@placeholder.94092.edu. Printing is for personal, private use only. No part of this book may be reproduced or transmitted without publisher's prior permission. Violators will be prosecuted.

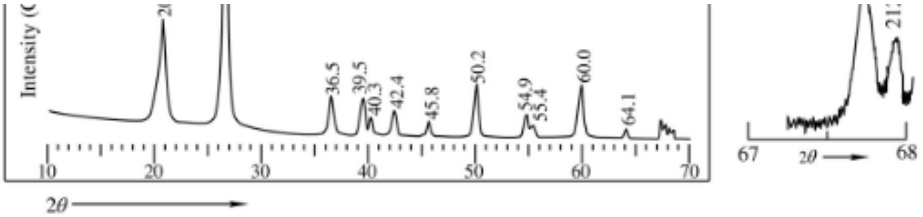

FIGURE 8.6 Collection of a powder diffraction pattern for quartz. (*a*) As the detector moves through its range of 2θ, the sample moves through angle θ, and the intensity of the diffracted X-rays is recorded as a line plot in a computer and displayed on a screen. Each reflection from the mineral is recorded as a peak on the screen at its 2θ position. (*b*) On the output X-ray profile, the horizontal axis is the 2θ angle, and the vertical scale is the intensity of diffracted X-rays, usually in terms of counts per second (cps). (*c*) Because $K\overline{\alpha}$ radiation consists of two different peaks, $K\alpha_1$ and $K\alpha_2$, each atomic plane actually produces two reflections. The peak for the $K\alpha_1$ wavelength has higher intensity than that of $K\alpha_2$. At small values of 2θ, the $K\alpha_2$ reflection may show as a slight bulge on the side of the diffraction peak created by the larger $K\alpha_1$ peak. At larger 2θ, the peaks can be distinguished. The $K\alpha_2$ peak will be on the larger 2θ side of the $K\alpha_1$ peak, as is shown for reflections from the {212} plane in quartz. View larger image

A diffractometer record for quartz is shown in **Figure 8.6b**, and a number of high-intensity X-ray peaks are obvious and correspond to a particular *d*-spacing in the crystal structure. Between the peaks, a relatively low number of X-rays are collected by the detector; this too is called background (see Figure 8.6) and is generated by X-rays randomly reaching the X-ray detector. Each peak has some width because the X-ray beam is not exactly monochromatic (see Figure 8.6), so Bragg's Law will be satisfied over a small range of angles as the X-ray beam has a small range of wavelengths. Further, because $K\overline{\alpha}$ is in fact the combination of two X-ray peaks, at small and intermediate values of 2θ, large peaks may show as a slight bulge on the side due to the presence of $K\alpha_2$. At large values of 2θ (**Figure 8.6c**), two peaks may be readily identified, one for $K\alpha_1$ and another at slightly higher 2θ at about half the intensity for $K\alpha_2$. With quartz, for example, the {100} peak occurs at 26.64° for Cu$K\alpha_1$ and 26.70° for Cu$K\alpha_2$, a difference of only 0.06°, so it generally appears as a single symmetrical peak. However, the peak for {212} occurs at 67.73° for Cu$K\alpha_1$ and 67.94° for Cu$K\alpha_2$, a more readily observed difference of 0.21°. A well-aligned and properly calibrated X-ray diffractometer will be able to distinguish these peaks. As long as the two peaks show a substantial degree of overlap, the combined peak is treated as a single entity and the *d*-spacing is calculated by using the weighted average wavelength of $K\overline{\alpha}$ (Table 8.1).

Data Reduction

The data extracted from the diffraction profile are the 2θ angle and the intensity of each peak (**Table 8.2**). The 2θ angle is conventionally chosen to be the arithmetic center of the peak at a point either one-half or two-thirds of the way up between its base and top (**Figure 8.7**). The intensity measure (*I*) may be either **peak height intensity** or **integrated intensity**. Peak height intensity is mostly commonly used, and it is simply the height of the peak above the background level. For example, adjacent to a peak with a

DO NOT COPY e48d507df5d1141@placeholder.94092

Printed by: e48d507df5d1141@placeholder.94092.edu. Printing is for personal, private use only. No part of this book may be reproduced or transmitted without publisher's prior permission. Violators will be prosecuted.

height of 3784 counts per second (cps), the average background is 123 cps; therefore the peak height intensity is 3661 cps. Integrated intensity is the area of the peak, equivalent to the total number of counts that produced it. For manual methods, the area of a peak can be approximated by assuming that it is an isosceles triangle. Computer systems can account for the actual peak shape and can calculate areas with considerable precision.

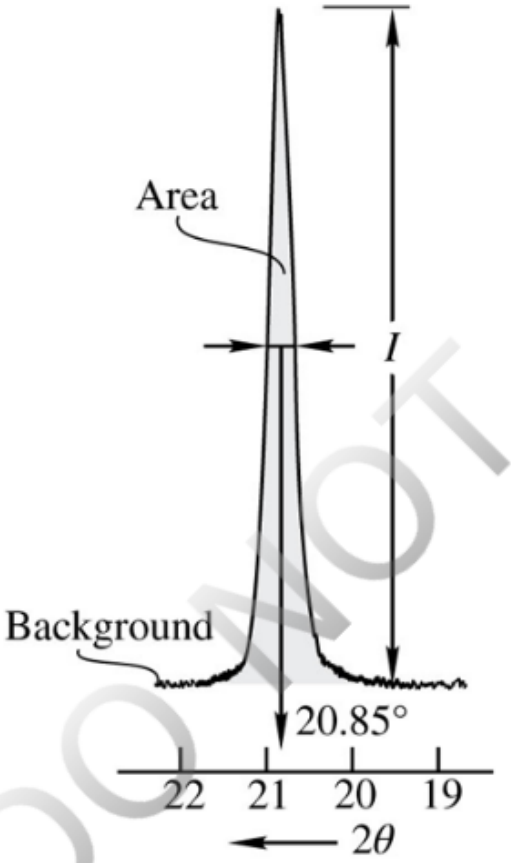

FIGURE 8.7 Recording data from the diffraction pattern: 2θ is taken as the center of the peak measured halfway from the base to the peak. Peak height (I) is the height of the peak above the background level. Integrated peak height is less commonly used and is the area of the peak (shaded). View larger image

TABLE 8.2 Data Reduction from X-Ray Diffraction Pattern Shown in Figure 8.6[a]

2θ	I (kcps)	I/I_1	d(Å)
20.9	2.8	31	4.25
26.7	9.0	100	3.34
36.5	1.0	11	2.46
39.5	1.0	11	2.28
40.3	0.4	4	2.24
42.4	0.7	8	2.13

DO NOT COPY e48d507df5d1141@placeholder.9409

Printed by: e48d507df5d1141@placeholder.94092.edu. Printing is for personal, private use only. No part of this book may be reproduced or transmitted without publisher's prior permission. Violators will be prosecuted.

45.8	0.4	4	1.98
50.2	1.4	16	1.82
54.9	0.6	7	1.67
55.4	0.3	3	1.66
60.0	1.4	16	1.54
64.1	0.3	3	1.45

[a] The values of 2θ and I are recorded for each peak from the X-ray diffraction profile. kcps—thousands of counts per second after background subtraction. The value of d is calculated from Equation 8.6 and the value of I/I_1 from Equation 8.7, where I_1 is the intensity of the highest peak.

From these data, d-spacings and relative intensity values are calculated. The d-spacing for each peak is calculated from Equation 8.6 assuming $n = 1$. Relative intensity is the ratio of the intensity of the peak (I) divided by the intensity of the highest peak (I_1).

$$\text{Relative intensity} = I/I_1 \times 100 \tag{8.7}$$

Because each mineral has its own structure and unit cell dimensions, each has its own set of atomic planes at specific d-spacings that is capable of diffracting X-rays. Identification of an unknown mineral is therefore based on comparison of the set of d-spacings and the reflection intensities of the unknown sample with d-spacing and intensity data for known minerals.

Powder Diffraction File

X-ray diffraction data for minerals and other compounds are compiled by the International Centre for Diffraction Data (www.icdd.com;12 Campus Boulevard, Newtown Square, PA 19073–3273, USA). This compilation, known as the **Powder Diffraction File** (PDF), is available in most university and industrial laboratories using X-ray diffraction and has been published in different formats. Initially it consisted of a collection of paper index cards, or equivalent images on microfiche or published in books. The information was once available in CD-ROM form too. Now the information is contained within software used for mineral identification and analysis (**Figure 8.8**). In each entry the d-spacing data are systematically presented along with selected crystallographic, physical property, and optical data.

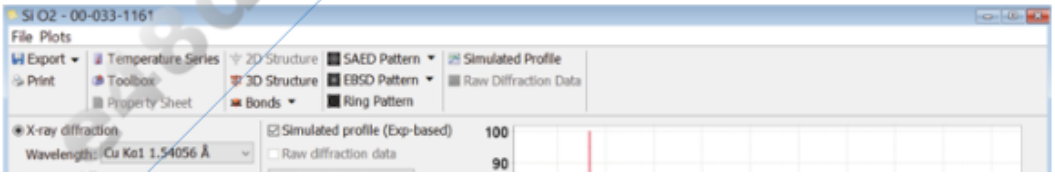

Printed by: e48d507df5d1141@placeholder.94092.edu. Printing is for personal, private use only. No part of this book may be reproduced or transmitted without publisher's prior permission. Violators will be prosecuted.

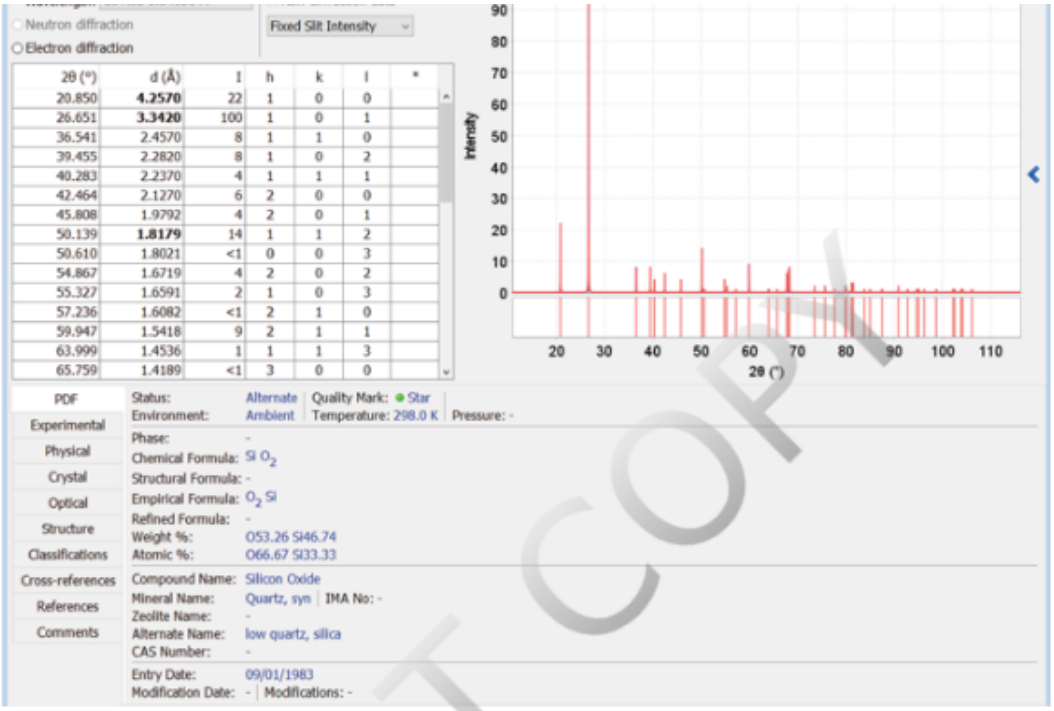

FIGURE 8.8 Powder Diffraction File. The three *d* values [d (Å)] in bold are for the three most intense peaks. Below this on the left side are the reference(s) from which the data was taken, crystallographic data, optical and physical property data, and additional information. The columns on the right include relative intensity (I, which is $I/I_1 \times 100$) and Bragg reflection index for the crystal plane producing the reflection (h, k, and l). These data are listed in order of decreasing *d*-spacing and increasing 2θ. © Joint Committee on Powder Diffraction Standards—International Centre for Diffraction Data. View larger image

Bragg Reflection Indices

The values shown in the hkl columns on a PDF entry are **Bragg reflection indices**. They are related to the actual Miller index (*hkl*) of the reflecting surface in the mineral by the value *n* in the Bragg equation (Equation 8.6).

$$\text{Bragg reflection index} = nh\ nk\ nl \qquad \textbf{(8.8)}$$

In calculating the *d*-spacings from the experimental data, it is assumed that $n = 1$. This is both reasonable and necessary. The first-order reflections, with $n = 1$, are typically strongest, and until the calculations have been completed and the mineral has been identified, it is not known which reflections are actually first order and which are higher order ($n > 1$). It is therefore assumed that all reflections are first order, and we accept the fact that *d*-spacings calculated this way may not actually be present in the mineral.

For example, in quartz (Figure 8.8) the {100} planes are 4.26 Å apart (with rounding). If Cu$K\overline{\alpha}$ radiation is used (about 1.54 Å), this plane produces a first-order reflection at $2\theta = 20.85°$, a second-order reflection at $2\theta = 42.46°$, and a third-order reflection at $2\theta = 65.76°$. If it is assumed that the latter two reflections are actually first-order reflections,

DO NOT COPY e48d507df5d1141@placeholder.9409

Printed by: e48d507df5d1141@placeholder.94092.edu. Printing is for personal, private use only. No part of this book may be reproduced or transmitted without publisher's prior permission. Violators will be prosecuted.

then Equation 8.6 yields hypothetical *d*-spacings of 2.127 and 1.419 Å, respectively. These *d*-spacings are one-half and one-third of the actual {100} spacings that are producing the reflections and are equivalent to hypothetical {200} and {300} planes (recall that Miller indices are inversely related to the actual dimensions).

The *d*-spacings of the first three orders of reflections from the {100} plane in quartz are therefore identified as d_{100}, d_{200}, and d_{300}. The Bragg reflection indices are shown without {} or () to avoid confusing them with Miller indices. The common factor, 1, 2, and 3, respectively, in the index indicates the order of the reflection. For example, d_{202} actually represents a second-order reflection from the {101} plane. If, in calculating *d*-spacings from an experimental pattern, two or more *d* values are related by factors of 2, 3, or 4, it is likely that they represent several orders of reflections from the same lattice plane in the mineral.

A complicating factor is that some minerals may have real *d*-spacings such as {200} and {300} that are one-half and one-third of the {100} *d*-spacing. These interatomic planes will produce first-order reflections at the same 2θ angle as the second- and third-order reflections from {100}. Distinguishing higher-order reflections from first-order reflections of the same *d*-spacing of a different plane can only be confidently done with crystal structures that have been fully defined, which typically requires data from single crystals X-ray diffraction or other techniques.

Mineral Identification

Prior to the widespread use of computers, it was necessary to manually compare the experimental data with *d*-spacing and intensity data for thousands of minerals in the PDF. To speed the process, the PDF data were compiled in systematic ways to make searching efficient. Search manuals published by the International Center for Diffraction Data based on the **Hanawalt** and **Fink search methods** may be found on the dusty shelves in the back of many labs. Computers now handle this task with speed and (hopefully) precision by identifying diffraction peaks and intensities, and calculating *d*-spacings and relative intensity values. These values are then compared with values for all of the minerals in the PDF, and a list of matches or near matches is provided in a matter of seconds.

A certain amount of caution is required when using computer-based search methods, however. Despite expectations based on television and movies, computer searches rarely provide an unambiguous identity for an unknown mineral. Rather, they typically yield a list of possibilities from which to choose. That list of possibilities is strongly influenced by details of the search parameters that the operator specifies in the software. Knowledge of the possible identity of an unknown sample based on physical and optical properties, rock type, associated minerals, etc., will help greatly in determining the correct identity. It also is essential to manually compare the experimental data with the values for a possible match to ensure that they really are the same and to account for discrepancies.

DO NOT COPY e48d507df5d1141@placeholder.9409

Printed by: e48d507df5d1141@placeholder.94092.edu. Printing is for personal, private use only. No part of this book may be reproduced or transmitted without publisher's prior permission. Violators will be prosecuted.

Computers are extremely fast and can search through large quantities of data, but they are no better than the quality of the data and instructions provided to them. The results they provide must be evaluated with sound geologic and scientific judgment.

Sources of Error

Powder X-ray diffraction is fairly straightforward but is subject to certain errors or problems, including the following.

- Amorphous sample. Only crystalline material can diffract X-rays; if a purely amorphous solid is analyzed, only background will be observed in the X-ray profile with no prominent X-ray peaks. However, this could be useful information as it demonstrates the sample is not a mineral and is not crystalline.
- Instrumental errors. Such errors include misalignment of the instrument and problems with sample orientation and position in the instrument. Computer-based systems can introduce errors as a result of improper calibration and software problems that can puzzle their operators. Instrumental errors may, at least in part, be identified by analyzing a sample whose *d*-spacings are accurately known, such as quartz, fluorite, or another mineral. Depending on the situation, some of the known material may be added directly to the sample of unknown identity prior to analysis to ensure the instrument is operating correctly.
- Sample preferred orientations. Minerals with a prominent cleavage tend to acquire a preferred orientation when mounted on/in the sample holder. Intensity values may, therefore, be significantly different than if a random grain orientation were obtained. Techniques to maximize randomness are described in the references at the end of this chapter. Intensity also is greatly affected if the samples are not ground small enough; below 0.010 mm is best.
- Sample purity. If a sample is not pure and contains two or more different crystalline materials, each material will produce X-ray peaks in the profile. Unless it is known that the sample is mixed (see section on mixed samples), then identification is impossible. Small amounts (a few percent) of contamination from a second mineral is usually not a problem because the peaks produced by the contaminant will be very small and will not be used for identification.
- Variation. Even with instruments that are running correctly, multiple runs on the same sample inevitably yield slightly different peak heights and 2θ positions. Particularly with computer systems, this variation may lead to incorrect interpretation of the data. The consequences of errors at small values of 2θ are substantially greater than for large values. A 0.4° error in reading 2θ at 5° produces a 1.31Å error in the value of *d*. A similar error at 50° produces only a 0.014 Å error.

An additional complication is that not all the peaks for the *d*-spacings shown in the PDF for a mineral will necessarily appear in the record of an X-ray diffraction run. The reasons

DO NOT COPY

Printed by: e48d507df5d1141@placeholder.94092.edu. Printing is for personal, private use only. No part of this book may be reproduced or transmitted without publisher's prior permission. Violators will be prosecuted.

for a mineral will necessarily appear in the record of an X-ray diffraction run. The reasons include variations in instrumental setup and grain size of the sample, and problems with preferred orientation. The missing peaks are typically those with low relative intensity values, but their absence can add considerable ambiguity to the identification process. A further complication is that many minerals display significant compositional variation that can influence *d*-spacing and intensity values. If the PDF file is for a sample whose composition is significantly different from the sample being studied, *d*-spacings may be different enough to prevent easy identification. Prior knowledge of the likely identity of the unknown can do a great deal to minimize these problems. Note, however, that variation in *d*-spacing can be used in some cases to help estimate mineral composition, as mentioned at the beginning of the chapter.

Mixed Samples

X-ray diffraction methods make it possible to identify the individual minerals in mixed rock or mineral samples. Details of the method depend on the software used. The diffraction pattern produced with mixed samples includes peaks for all the different minerals, with intensities that are roughly proportional to the amounts of the minerals present. The usual procedure is to identify one of the minerals and then remove from the list of *d*-spacings all that belong to that mineral. Intensity values for the remaining peaks are recalculated and used to identify subsequent minerals.

This procedure is complicated because peaks for different minerals may overlap, and weak diffraction peaks from one mineral may be masked by nearby larger peaks from another. Prior knowledge of the probable mineralogy of the sample can obviously greatly simplify the procedure.

Estimation of Relative Mineral Abundance

Estimates of the relative abundance of minerals in a mixture can be based on the intensity of X-ray diffraction peaks for the different minerals. For minerals such as the clays, which typically occur in various mixtures that cannot be separated, this may provide the only means of determining their relative amounts. Calibration can be difficult because X-ray intensity can depend fairly strongly on the details of sample preparation and the absorption properties of the constituent minerals. A starting point is preparation of a series of mixtures of known composition to provide a calibration based on the intensity values of one or more peaks from each mineral. If the calibration samples and the unknown are prepared under the same set of conditions, reasonable accuracy may be obtained.

Estimation of Composition

DO NOT COPY e48d507df5d1141@placeholder.9409

Printed by: e48d507df5d1141@placeholder.94092.edu. Printing is for personal, private use only. No part of this book may be reproduced or transmitted without publisher's prior permission. Violators will be prosecuted.

Many minerals display significant solid solution. Because the constituent ions that substitute for each other in the structure typically differ in size, the unit cell dimensions and the *d*-spacing between various atomic planes vary with composition. Diagrams useful for estimating composition based on *d*-space variation are included with the description of selected minerals in the latter part of this book. However, if composition must be known to a high degree, then use of instruments and other techniques that directly measure composition is required and is covered in Chapter 9.

DO NOT COPY
e48d507df5d1141@placeholder.9409

Printed by: e48d507df5d1141@placeholder.94092.edu. Printing is for personal, private use only. No part of this book may be reproduced or transmitted without publisher's prior permission. Violators will be prosecuted.

Determining Unit Cell Parameters

The mathematical relationships between unit cell parameters and the d_{hkl} values are shown in **Table 8.3**. The number of independent *d*-spacing determinations required to calculate the unit cell parameters is equal to the number of unit cell parameters. With orthorhombic minerals, for example, three different *d*-spacing measurements such as d_{100}, d_{111}, and d_{010} are required to determine the *a*, *b*, and *c* unit cell dimensions, by simultaneous solution of the equation for orthorhombic minerals for each of the three different *d*-spacings and *hkl* values. Triclinic minerals have six different unit cell parameters (*a*, *b*, *c*, *α*, *β*, *γ*) and require six different *d*-spacings. Finding the one set of *a*, *b*, *c*, *α*, *β*, *γ* values that best fits the actual diffraction data with minimum error is a task easily done by computers.

TABLE 8.3 Relation between d_{hkl} and Unit Cell Parameters[a]

Crystal System		Number of Independent d_{hkl} Measurements Needed
Isometric		1
Tetragonal		2
Hexagonal		2
Orthorhombic		3
Monoclinic		4
Triclinic		6

[a] The values *h*, *k*, and *l* are reflection indices; *a*, *b*, and *c* are unit cell dimensions; *a*, *β*, and *γ* are the angles between crystal axes.

DO NOT COPY e48d507df5d1141@placeholder.9409

Printed by: e48d507df5d1141@placeholder.94092.edu. Printing is for personal, private use only. No part of this book may be reproduced or transmitted without publisher's prior permission. Violators will be prosecuted.

Other Crystallography Instruments

Despite its commonality, relative ease of use, and practicality for helping to identify minerals, powder X-ray diffraction is not the preferred instrument for determining crystal structures. Much of the data needed to determine crystal structures come from either single crystal X-ray diffraction or from **transmission electron microscopy**.

Single Crystal X-Ray Diffraction

As mentioned above, a single crystal X-ray diffractometer uses just a single crystal to generate a diffraction pattern. Though the main components of the instrument are largely the same as the powder X-ray diffractometer (**Figure 8.9a**), but because only a single crystal is used, there are some important differences. Overall, the X-ray tube is largely the same and generates a monochromatic beam of X-rays directed toward the sample; however, the beam is more finely focused using a long collimator, as the sample size is much smaller. The sample holder is substantially different as it is required to firmly hold a single crystal of a few tens to hundreds of microns across. During analysis, the sample holder arm rotates on two axes and the crystal is spun on a third axis. This allows the crystal to be positioned within the beam at all possible three-dimensional orientations. The detector is a screen of about 100 cm^2 that digitally records the beams of diffracted X-rays. A beam block is located between the sample and the screen opposite of the collimator. The beam block intercepts the beam X-rays that travel through or around the sample without diffraction; this is an intense X-ray beam that can damage or overwhelm the detector.

(a)

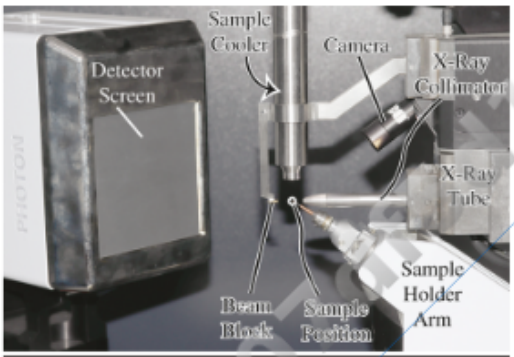

(b)

DO NOT COPY
e48d507df5d1141@placeholder.94092

Printed by: e48d507df5d1141@placeholder.94092.edu. Printing is for personal, private use only. No part of this book may be reproduced or transmitted without publisher's prior permission. Violators will be prosecuted.

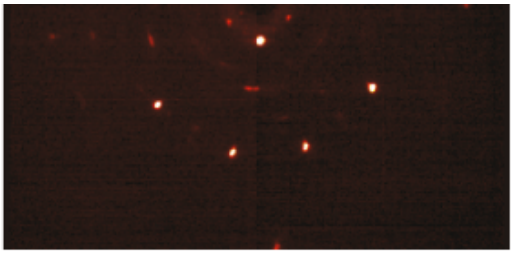

FIGURE 8.9 Single crystal X-ray diffraction. (*a*) Main components of a single crystal X-ray diffractometer. The instrument is a Bruker D8 QUEST at the University of Northern Colorado. The camera ensures the sample is properly positioned, and the sample cooler allows study of *d*-space changes with changing temperature. See text for details. (*b*) Example diffraction pattern from a potassium iodide crystal, which is isostructural with halite (NaCl). Bright spots are Bragg reflections from particular planes of atoms. View larger image

During analysis, diffraction patterns are collected as the sample is rotated to different positions. For this technique, a diffraction pattern is a series of spots, where each spot represents a reflection of the beam from a plane of atoms of specific spacing following Bragg's Law (**Figure 8.9b**). Given a systematic approach to changing the sample orientation and relating the diffraction patterns collected at each orientation, it is possible to determine the crystal structure in a matter of hours. Determining crystal structure is largely driven by software routines and significant computer processing power. Prior to the availability of computer-automated instruments, determining crystal structure was an extremely arduous task.

Given that the single crystal X-ray diffractometer is much more complicated from both a mechanical and a computer/software perspective, they cost many times more than a powder X-ray diffractometer. Single crystal X-ray diffractometers are also a much more specialized instrument, best suited for determine the crystal structure of novel materials. Therefore, single crystal X-ray diffractometers are generally not used by the typical mineralogist as the crystal structure of all common minerals has already been determined with great detail and precision.

Transmission Electron Microscopy

Transmission electron microscopy or a **transmission electron microscope** (**TEM**) (**Figure 8.10**), as the name implies, uses electrons that are transmitted through a very thin sample. Using the wave behavior of electrons, the beam's electrons may be diffracted following Bragg's Law. Beam electrons are also scattered by interactions with the sample's atoms following the same phenomenon as that depicted in Figure 8.3b. As a result of scattering and diffraction, multiple data types can be collected with a transmission electron microscope, which can lead to determining the crystal structure of minerals, but it can be used to image non-crystalline materials as well.

(*a*) (*b*) Filament

DO NOT COPY e48d507df5d1141@placeholder.9409

Printed by: e48d507df5d1141@placeholder.94092.edu. Printing is for personal, private use only. No part of this book may be reproduced or transmitted without publisher's prior permission. Violators will be prosecuted.

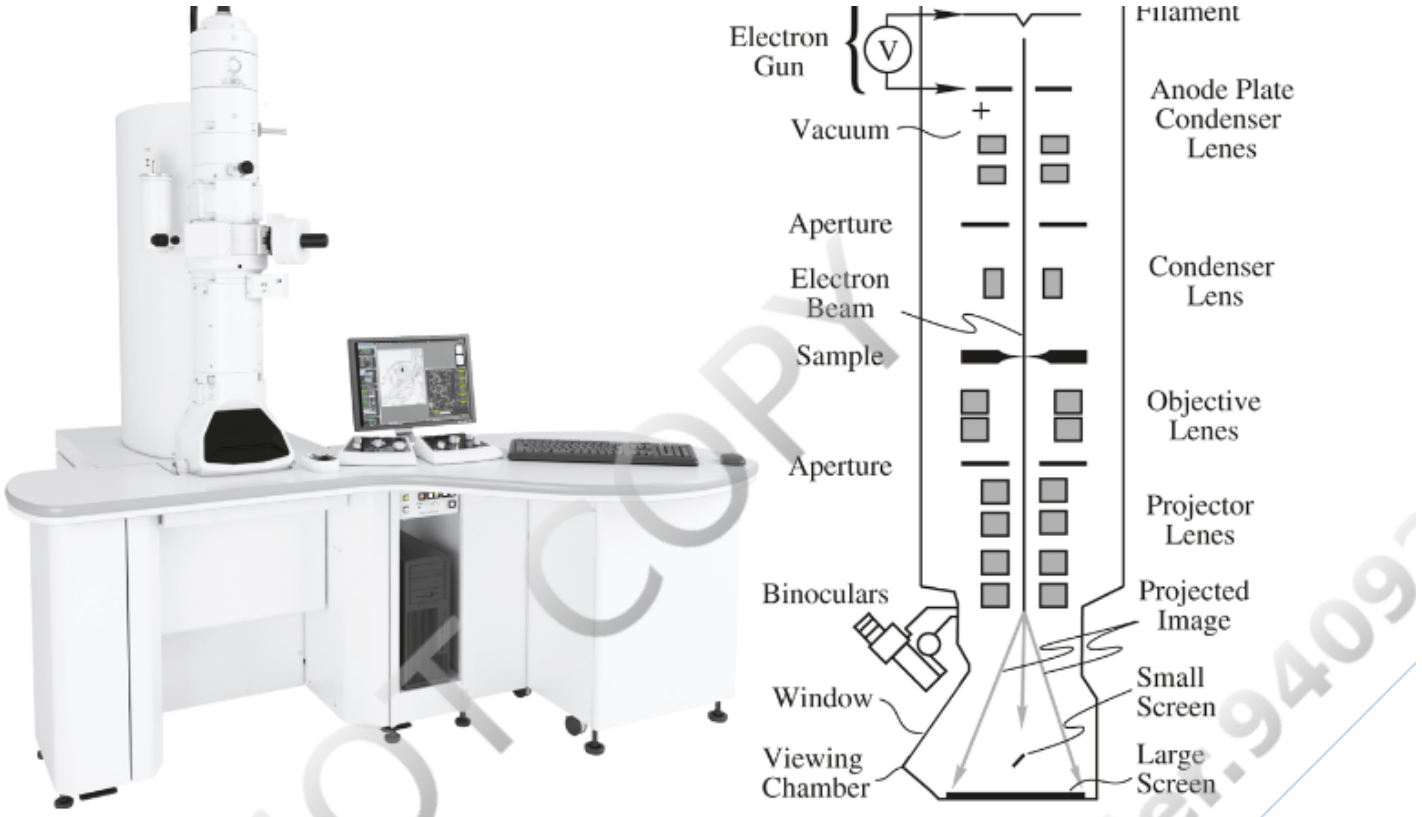

FIGURE 8.10 Transmission electron microscope. (*a*) A typical transmission electron microscope. Image courtesy of JEOL USA. (*b*) Schematic diagram showing the major components of a transmission electron microscope column, shown in the upper-left portion of (*a*). Image courtesy of JEOL USA. View larger image

Creating an "electron transparent" sample on the order of tens of nanometers thick can be difficult. One approach is to use nanoscale particles as the sample, but larger samples can be thinned through chemical or mechanical means. These very thin and small single or multiple crystals are typically supported on a 3-mm circular carbon film and/or a mesh made of a grid of metal wires. The electron beam is directed through the sample and between the wires that make up the support mesh. The grid is placed within a sample holder that can tilt and rotate the sample, so the orientation of the sample can be controlled similar to single crystal X-ray diffraction.

X-rays can travel through air relatively unaffected; in contrast, electron beams are strongly scattered and dissipated by the presence of air. Therefore, the interior of a transmission electron microscope must be in a high vacuum, maintained by a variety of vacuum pumps.

An electron beam is generated in the same or a similar way as in the X-ray tube of an X-ray diffractometer, by use of a tungsten filament cathode. A lanthanum hexaborate (LaB_6, called "lab-six") cathode, however, produces a higher-quality beam and lasts longer. Alternatively, a cold field emission electron gun that generations electrons from the very sharp tip of a tungsten element by a high voltage potential may be also used. Regardless, the generated electron beam is focused and directed toward the sample by a series of apertures and electrical coils that serve as electromagnetic lenses. The beam then

Printed by: e48d507df5d1141@placeholder.94092.edu. Printing is for personal, private use only. No part of this book may be reproduced or transmitted without publisher's prior permission. Violators will be prosecuted.

apertures and electrical coils that serve as electromagnetic lenses. The beam then interacts with the sample by diffraction and scattering. The diffracted and scattered electrons that exit the back of the sample are focused onto a screen for viewing by additional apertures and electromagnetic lenses (Figure 8.10b).

Transmission electron microscopes have a number of operational modes depending on the specific instrument and the type of data needed. The TEM can be used to generate a diffraction pattern that is essentially identical to the pattern produced by a single crystal X-ray diffractometer (Figure 8.9b). A possible advantage of transmission electron diffraction patterns is that the pattern is from a sample region that is only a few nanometers across; a disadvantage is that the spatial accuracy of the diffraction pattern is not as good as in single crystal X-ray diffraction. Crystal structures determined through transmission electron diffraction have greater uncertainty than those produced by single crystal X-ray diffraction.

Transmission electron microscopes can also collect very high magnification images and can resolve features less than a nanometer in size (**Figure 8.11a**). This degree of magnification and resolution allows atomic structure to be directly imaged. How such images are created is very complex and is rooted in the wave interference between transmitted and diffracted electrons. Bright areas in such images (**Figure 8.11b**), depending on instrument and sample conditions, may or may not be the location of atoms in the structure. Regardless, no other technique can provide such detailed information regarding the crystal structure at such a small scale.

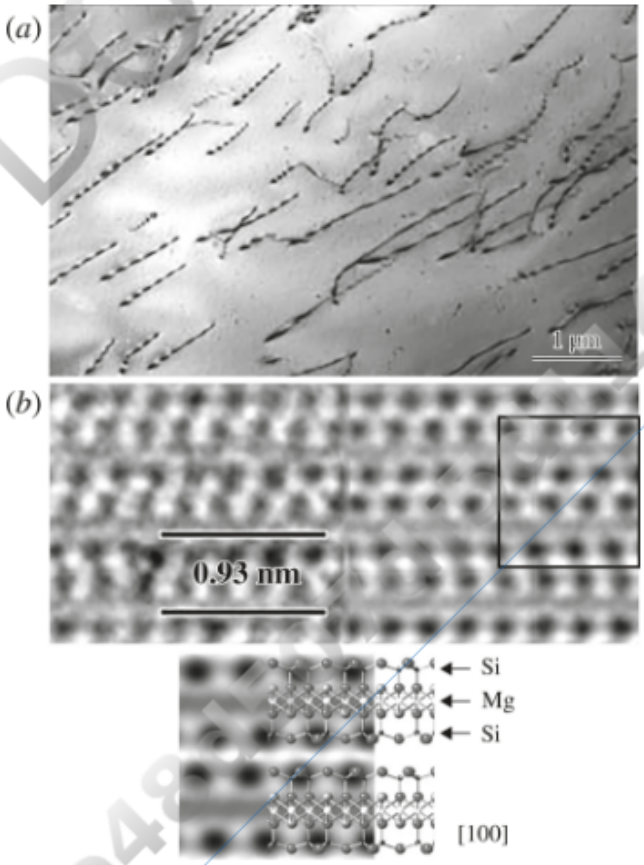

FIGURE 8.11 Example images collected by a transmission electron microscope. (a) Bright-field

Printed by: e48d507df5d1141@placeholder.94092.edu. Printing is for personal, private use only. No part of this book may be reproduced or transmitted without publisher's prior permission. Violators will be prosecuted.

FIGURE 8.11 Example images collected by a transmission electron microscope. (*a*) Bright-field image of quartz; dislocations (Chapter 5) appear as the black lines (© Morales, L. F. G., Mainprice, D., Lloyd, G. E., and Law, R. D., 2011, Crystal fabric development and slip systems in a quartz mylonite: an approach via transmission electron microscopy and viscoplastic self-consistent modelling, in Prior, D. J., Rutter, E. H. and Tatham, D. J. (eds) Deformation Mechanisms, Rheology and Tectonics: Microstructures, Mechanics and Anisotropy. Geological Society, London, Special Publications, 360, 151–174). (*b*) High-resolution phase-contrast transmission electron microscope image of talc. At the upper left is the raw image; at the upper right is a filtered image. A computer simulation produced the lower image with the incident electrons in the [100] direction. Note that the computer simulation matches the image within the box in the upper right; therefore atom locations within the crystal structure as shown can be connected to the phase-contrast image (Kogure, T., Kameda, J., Matsui, T., and Miyawaki, R. 2006. Stacking structure in disordered talc: Interpretation of its X-ray diffraction pattern by using pattern simulation and high-resolution transmission electron microscopy. American Mineralogist 91). View larger image

DO NOT COPY
e48d507df5d1141@placeholder.9409

Printed by: e48d507df5d1141@placeholder.94092.edu. Printing is for personal, private use only. No part of this book may be reproduced or transmitted without publisher's prior permission. Violators will be prosecuted.

region that is only a few nanometers across; a disadvantage is that the spatial accuracy of the diffraction pattern is not as good as in single crystal X-ray diffraction. Crystal structures determined through transmission electron diffraction have greater uncertainty than those produced by single crystal X-ray diffraction.

Transmission electron microscopes can also collect very high magnification images and can resolve features less than a nanometer in size (**Figure 8.11a**). This degree of magnification and resolution allows atomic structure to be directly imaged. How such images are created is very complex and is rooted in the wave interference between transmitted and diffracted electrons. Bright areas in such images (**Figure 8.11b**), depending on instrument and sample conditions, may or may not be the location of atoms in the structure. Regardless, no other technique can provide such detailed information regarding the crystal structure at such a small scale.

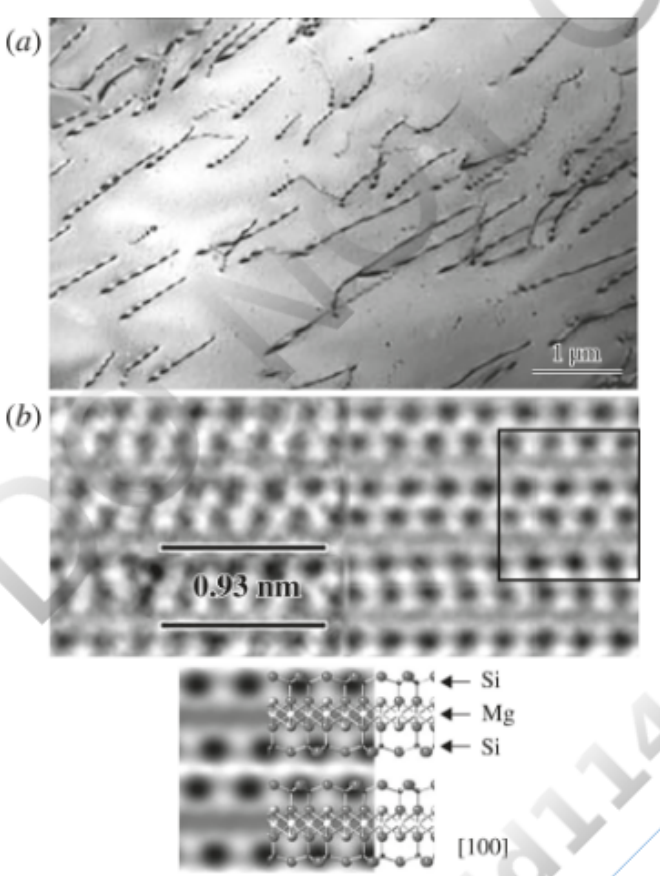

FIGURE 8.11 Example images collected by a transmission electron microscope. (*a*) Bright-field image of quartz; dislocations (Chapter 5) appear as the black lines (© Morales, L. F. G., Mainprice, D., Lloyd, G. E., and Law, R. D., 2011, Crystal fabric development and slip systems in a quartz mylonite: an approach via transmission electron microscopy and viscoplastic self-consistent modelling, in Prior, D. J., Rutter, E. H. and Tatham, D. J. (eds) Deformation Mechanisms, Rheology and Tectonics: Microstructures, Mechanics and Anisotropy. Geological Society, London, Special Publications, 360, 151–174). (*b*) High-resolution phase-contrast transmission electron microscope image of talc. At the upper left is the raw image; at the upper right is a filtered image. A computer simulation produced the lower image with the incident electrons in the [100] direction. Note that the computer simulation matches the image within the box in the upper right; therefore atom locations within the crystal structure as shown can be connected to the phase-contrast image (Kogure, T., Kameda, J., Matsui, T., and Miyawaki, R. 2006. Stacking structure in disordered talc: Interpretation of its X-ray diffraction pattern by using pattern simulation and high-resolution transmission electron microscopy. American

DO NOT COPY e48d507df5d1141@placeholder.9409

Printed by: e48d507df5d1141@placeholder.94092.edu. Printing is for personal, private use only. No part of this book may be reproduced or transmitted without publisher's prior permission. Violators will be prosecuted.

pattern by using pattern simulation and high-resolution transmission electron microscopy. American Mineralogist 91). View larger image

REFERENCES CITED AND SUGGESTIONS FOR ADDITIONAL READING

Alderton, D. 2021. *X-ray Diffraction (XRD). Encyclopedia of Geology*, 2nd ed. Elsevier Ltd., 520–531.

Azaroff, L. V. 1968. *Elements of X-ray Crystallography*. McGraw-Hill, New York, 610 p.

Bish, D. L., and Post, J. E. (eds.). 1989. *Modern Powder Diffraction. Reviews in Mineralogy*, **Volume 20**. Mineralogical Society of America, Washington, DC, 369 p.

Hawkes, P. W., and Spence, J. C. H. 2019. *Handbook of Microscopy*. Springer, Cham, Switzerland, 1543 p.

Klug, H. P., and Alexander, L. E. 1974. *X-ray Diffraction Procedures*, 2nd ed. John Wiley & Sons, New York, 966 p.

Kogure, T., Kameda, J., Matsui, T., and Miyawaki, R. 2006. Stacking structure in disordered talc: Interpretation of its X-ray diffraction pattern by using pattern simulation and high-resolution transmission electron microscopy. *American Mineralogist* **91**, 1363–1370.

Lavina, B., Dera, P., and Downs, R. T. 2014. Modern X-ray diffraction methods in mineralogy and geosciences. *Reviews in Mineralogy and Geochemistry* **78**, 1–21.

Lee, M. R. 2010. Transmission electron microscopy (TEM) of Earth and planetary materials: A review. *Mineralogical Magazine* **74**, No. 1, 1–27.

Moore, D. M., and Reynolds, R. C., Jr. 1997. *X-ray Diffraction and the Identification of Clay Minerals*. Oxford University Press, Oxford, 378 p.

Morales, L. F. G., Mainprice, D., Lloyd, G. E., and Law, R. D. 2011. Crystal fabric development and slip systems in a quartz mylonite: An approach via transmission electron microscopy and viscoplastic self-consistent modelling, in D. J. Prior, E. H. Rutter, and D. J. Tatham (eds.), *Deformation Mechanisms, Rheology and Tectonics: Microstructures, Mechanics and Anisotropy*, pp. 151–174. Geological Society, London, Special Publications, **360**.

Pecharsky, V. K., and Zavalij, P. Y. 2009. *Fundamentals of Powder Diffraction and Structural Characterization of Materials*. Springer, New York. 741 p.

Suryanarayana, C., and Norton, M. G. 1998. *X-ray Diffraction, a Practical Approach*. Plenum Press, New York. 273 p.

DO NOT COPY e48d507df5d1141@placeholder.9409

Printed by: e48d507df5d1141@placeholder.94092.edu. Printing is for personal, private use only. No part of this book may be reproduced or transmitted without publisher's prior permission. Violators will be prosecuted.

LIST OF KEY TERMS

- background
- Bragg equation
- Bragg reflection indices
- Bragg's law
- characteristic X-Ray
- characteristic X-ray spectrum
- continuous spectrum
- *d*-spacing
- Fink search method
- first-order reflection
- fourth-order reflection
- Hanawalt method
- integrated intensity
- peak height intensity
- peak overlap
- peak
- powder diffraction file
- powder X-ray diffraction
- second-order reflection
- single-crystal X-ray diffraction
- TEM
- third-order reflection
- transmission electron microscope
- X-ray diffractometer
- X-rays
- XRD

DO NOT COPY
e48d507df5d1141@placeholder.9409

Printed by: e48d507df5d1141@placeholder.94092.edu. Printing is for personal, private use only. No part of this book may be reproduced or transmitted without publisher's prior permission. Violators will be prosecuted.

CHAPTER 9

Analytical Instrumentation and Techniques II: Chemical Analysis of Minerals

William D. Nesse
University of Northern Colorado

Graham B. Baird
University of Northern Colorado

DO NOT COPY
e48d507df5d1141@placeholder.9409

Printed by: e48d507df5d1141@placeholder.94092.edu. Printing is for personal, private use only. No part of this book may be reproduced or transmitted without publisher's prior permission. Violators will be prosecuted.

Introduction

To understand any mineral, it is essential to know the chemical composition. The common analytical methods that determine mineral (and rock) compositions are wet chemical methods, electron beam microanalysis, X-ray fluorescence (XRF) spectroscopy, and mass spectrometry. Many institutions of higher education have instrumentation capable of mineral (and rock) chemical analysis. Depending on the quality of data needed, however, instrumentation at a commercial or research laboratory may be needed; fortunately using such labs is often relatively affordable. Most techniques provide mineral chemistry in terms of oxide weight percent. The end of the chapter describes how these raw chemical analyses are converted into the chemical formulas that we normally associate with minerals.

DO NOT COPY
e48d507df5d1141@placeholder.9409

Printed by: e48d507df5d1141@placeholder.94092.edu. Printing is for personal, private use only. No part of this book may be reproduced or transmitted without publisher's prior permission. Violators will be prosecuted.

Analytical Methods

Wet Chemical

Most science students get some exposure to wet chemical techniques as part of introductory chemistry laboratory activities in high school and college. These techniques are diverse, but all begin with dissolving or digesting a sample in a solvent, which for geological materials often is one or more acids, including HCl, HNO_4, and HF. Once the sample is dissolved, various reagents are added to allow gravimetric, colorimetric, titration, and related analyses of the different elements. Jeffery (1975) describes many standard techniques. Wet chemical techniques are no longer commonly used for geological materials. Procedures are slow, require great skill, and only provide an average composition for all of the material digested. Wet chemical analyses also do not allow different parts of zoned minerals to be analyzed separately, and it is impossible to differentiate between a mineral and any small inclusions that it may contain.

Electron Beam Instruments

There are two closely related instruments that use an electron beam to chemically analyze a tens of micron area of a mineral; these are the **electron microprobe** (or **electron probe microanalyzer** [**EPMA**]) and the **scanning electron microscope** (**SEM**) (**Figure 9.1**). The SEM became commercially available in the 1960s and originally was solely used for imaging samples at magnifications much greater than possible with light. Unlike light microscope images, SEM images (and now EPMA images too) have a great depth of field and relatively high magnifications that typically range from 5× to 300,000×. By comparison, the magnification of a typical petrographic microscope (Chapter 7) is from 25× to 400×. The EPMA became commercially available in the 1950s and was originally intended only for chemical analysis.

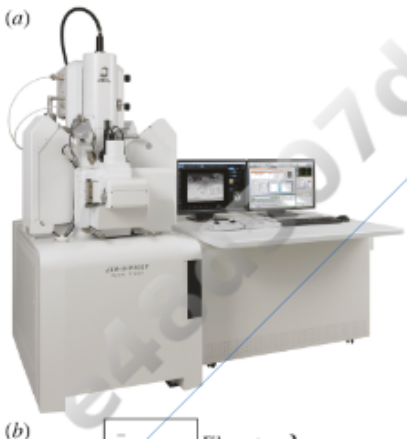

DO NOT COPY e48d507df5d1141@placeholder.9409

Printed by: e48d507df5d1141@placeholder.94092.edu. Printing is for personal, private use only. No part of this book may be reproduced or transmitted without publisher's prior permission. Violators will be prosecuted.

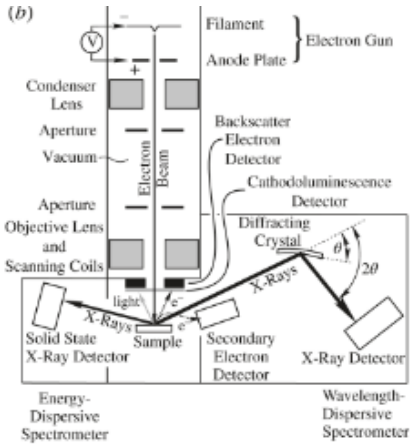

FIGURE 9.1 Electron microprobes and scanning electron microscopes. (*a*) An electron microprobe. Scanning electron microscopes look very similar. Image courtesy of JEOL USA. (*b*) Schematic diagram showing the major components of both electron microprobes and scanning electron microscopes. See text for additional discussion. View larger image

The interaction between electrons in a beam focused on a sample and the sample's atoms produce a variety of radiations emitted from the sample surface. Depending on the radiation detectors an instrument is equipped with, those radiations can be used for imaging and/or chemical analysis. The general difference between EPMAs and SEMs lies with their detectors. However, these instruments are increasingly becoming similar, since the chemical analysis capability of the SEM is ever improving, as are the imaging capabilities of the EPMA.

The transmission electron microscope discussed in Chapter 8 has many similarities to the SEM and EPMA, as it too uses an electron beam that interacts with the sample. Recall that the interior of the transmission electron microscope is under vacuum maintained by multiple pumps. This is true of the SEM/EPMA as well, since air scatters and blocks the electron beam and some of the generated radiations.

Major differences between the transmission electron microscope and the SEM/EPMA are the sample and data types. Recall that transmission electron microscope samples must be very thin and allow transmission of electrons through the sample. Transmission electron microscope data reveal information about the sample's crystal structure, and they can also produce atomic-scale images. In contrast, SEM/EPMAs are generally not useful for determining crystal structure or for imaging features much smaller than a 0.5 microns; therefore, atomic-scale images are not possible with SEM/EPMA. But the magnifications routinely used by SEM/EPMAs are more than adequate for standard investigations of typical rock and mineral specimens.

SEM/EPMA samples are most commonly conventional petrographic thin sections prepared without a coverslip or a mineral sample mounted in epoxy (Figure 7.1; **Figure 9.2a**). For some applications, unpolished samples or loose grains may be used (**Figure 9.3**), but if reliable chemical analysis is needed, the sample must be flat and carefully polished to minimize surface irregularities that might influence the emitted radiations from the sample surface. Samples are coated with a conductive material, commonly

DO NOT COPY

Printed by: e48d507df5d1141@placeholder.94092.edu. Printing is for personal, private use only. No part of this book may be reproduced or transmitted without publisher's prior permission. Violators will be prosecuted.

from the sample surface. Samples are coated with a conductive material, commonly carbon or gold, so beam electrons can be conducted away from the sample surface. A buildup of electrons on the surface would deflect the beam and render imaging or chemical analysis impossible.

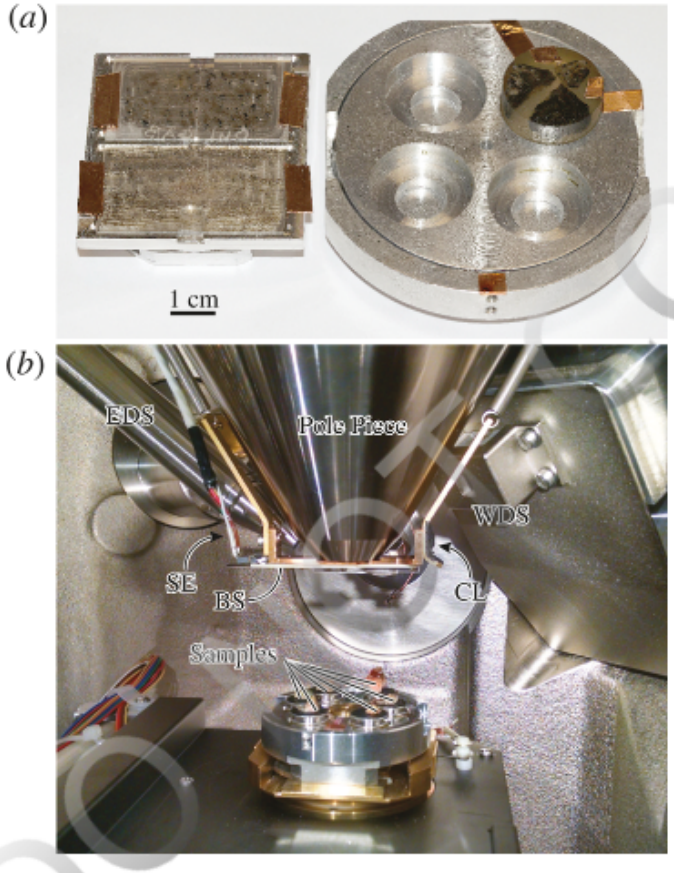

FIGURE 9.2 Scanning electron microscope and electron microprobe samples and chamber interior. (*a*) Polished samples mounted on a sample holder. On the left are two thin sections; on the right are rock fragments mounted in epoxy. The thin, about 15-nanometer, carbon coat on samples tint the samples a light gray. Here, samples are held to the holders with conductive tape. (*b*) Sample chamber. Six samples are on the stage, which will be raised to be about 1–2 cm from the pole piece for imaging and analysis. BS—Backscatter electron detector; SE—secondary electron detector (behind pole piece); EDS—energy-dispersive spectrometer; WDS—wavelength-dispersive spectrometer; CL—cathodoluminescence detector (behind pole piece). The sample chamber is evacuated by a vacuum pump after samples are loaded. View larger image

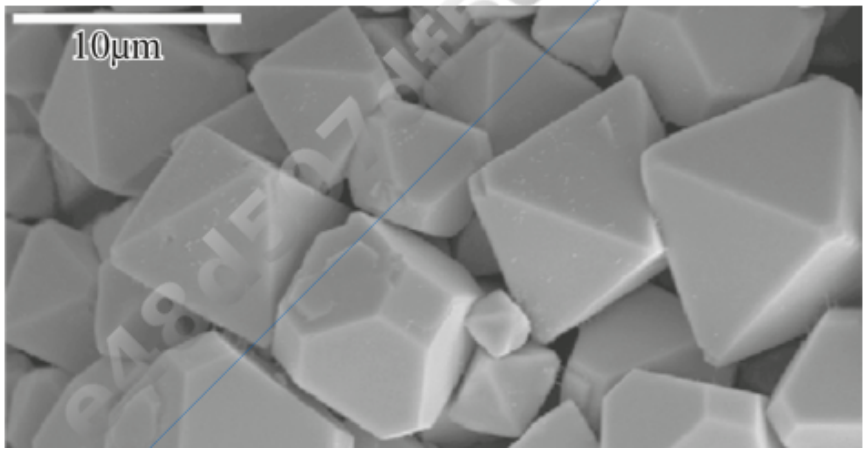

Printed by: e48d507df5d1141@placeholder.94092.edu. Printing is for personal, private use only. No part of this book may be reproduced or transmitted without publisher's prior permission. Violators will be prosecuted.

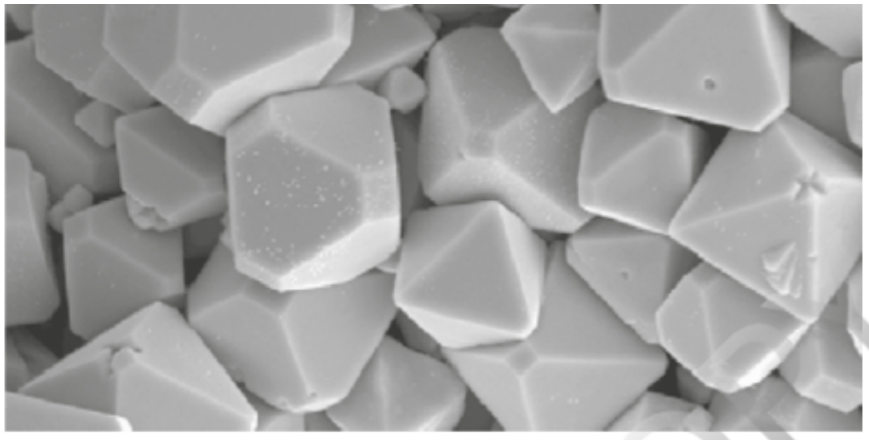

FIGURE 9.3 Secondary electron image of pyrite grains from alluvium of the Canadian River, Oklahoma. The loose grains of this sample allow crystal form to be studied. Most of the crystals are octahedrons or octahedrons modified by cubes. © George N. Breit, Michele L.W. Tuttle, Isabelle M. Cozzarelli, Scott C. Christenson, Jeanne B. Jaeschke, David L. Fey, and Cyrus J. Berry 2005. Results of Chemical and Isotopic Analyses of Sediment and Water from Alluvium of the Canadian River near a Closed Municipal Landfill, Norman, Oklahoma. U.S. Geological Survey. View larger image

Electron beam generation is essentially identical to that of transmission electron microscopes and commonly uses a thermionic source with a tungsten filament or a LaB_6 element, or a field emission source with a sharpened tungsten element. The beam has two key characteristics, called operating conditions, important for imaging and chemical analysis; both are controlled by the instrument's electron gun. This includes the accelerating voltage, which is the energy of beam electrons, and the beam current, which is the number of electrons within the beam. Most SEMs and EPMAs, when used for mineral and rock imaging and chemical analysis, use an accelerating voltage of about 15 keV and a beam current of 20 nanoamps. Following beam generation in the electron gun, the beam is focused onto the sample through a series of apertures and electromagnetic lenses, as with the transmission electron microscope.

Sample images are produced by rastering (scanning) the beam across an area on the sample. As the beam is scanned, the x–y coordinates of the beam position are recorded with the intensity of the signal from one or more of the detectors. The coordinates are combined with the signal intensity to produce an image, where bright areas indicate the detector collected more signal for that location on the sample and dark areas indicate less. For chemical analysis, the beam is typically focused on a single spot on a mineral grain in the sample and detectors collect signal that can be converted to mineral composition.

Radiation Types

When an electron beam interacts with a material, a number of radiations are produced from a small volume within the sample, called the excitation volume (**Figure 9.4**). Some of the radiations used in SEM/EPMA already have been discusses in context of X-ray generation for X-ray diffraction techniques (Chapter 8), but they will be described again

Printed by: e48d507df5d1141@placeholder.94092.edu. Printing is for personal, private use only. No part of this book may be reproduced or transmitted without publisher's prior permission. Violators will be prosecuted.

generation for X-ray diffraction techniques (Chapter 8), but they will be described again below. Each radiation type is detected by a specific detector and each type provides information regarding the sample surface topography or composition.

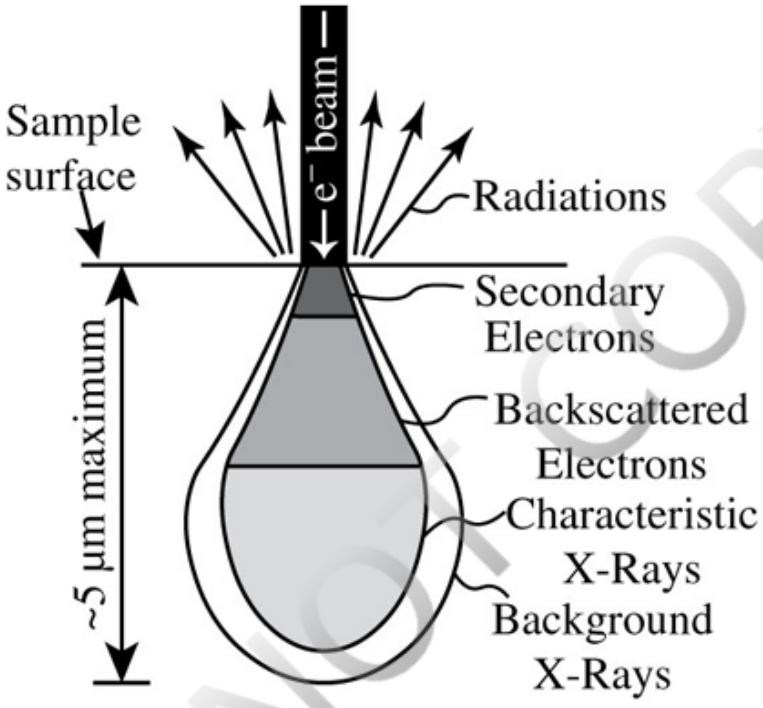

FIGURE 9.4 Excitation volume within a scanning electron microscope or electron microprobe sample showing the approximate extent within that volume from which some of the radiations originate. Size of the excitation volume depends on the instrumental operating conditions and the nature of the sample. For most typical operating conditions and geologic samples, the excitation volume extends to a maximum depth of about 5 µm. View larger image

Secondary Electrons

Secondary electrons are produced when a beam electron removes an orbital shell electron from a sample atom (Figure 8.3c). The released orbital electron, now called a secondary electron, may escape the surface of the sample. Any orbital from any element could serve as the source of the secondary electron. Secondary electrons are very low energy, which means that only those generated only within the top tens of nanometers may escape the sample and reach the detector (Figure 9.4). The secondary electron detector is placed to the side of the sample just above its surface and has a voltage applied across it (Figures 9.1b, 9.2b). The voltage creates an electric field that attracts the secondary electrons for detection. The low energy of secondary electrons means their emission is strongly influenced by the surface topography of a sample. Sharp peaks with multiple sides allow more secondary electron to escape and thus will appear bright; when the beam enters a deep crack, no secondary electrons escape and thus cracks appear dark (**Figure 9.5d**). Surfaces that face the detector also will appear brighter as secondary electrons escaping those surfaces are more easily collected by the detector (Figure 9.3). Composition also controls the number of secondary electrons emitted. Materials with high average atomic number generate more secondary electrons and

Printed by: e48d507df5d1141@placeholder.94092.edu. Printing is for personal, private use only. No part of this book may be reproduced or transmitted without publisher's prior permission. Violators will be prosecuted.

appear brighter overall.

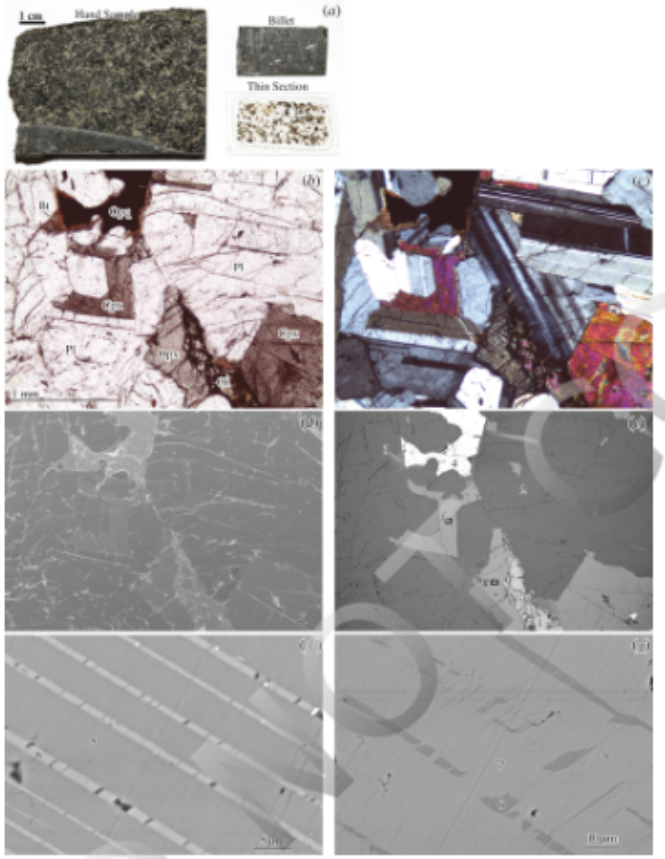

FIGURE 9.5 Hand sample to thin section and scanning electron microscope/electron microprobe analysis. (*a*) Hand sample and thin section of a gabbro sample. (*b*) Plane-polarized light image of the box shown on the thin section in (*a*). The major minerals are plagioclase (Pl), clinopyroxene (Cpx), orthopyroxene (Opx), olivine (Ol), biotite (Bt), and an opaque mineral (Opq). The opaque mineral will be revealed to be ilmenite (Ilm) with chemical analysis. (*c*) Cross-polarized light image of (*b*). (*d*) Secondary electron image of (*b*); the cracks and pits that persist after polishing are highlighted by light edges, but average atomic number of different minerals does affect the intensity of secondary electrons somewhat (brighter from higher average atomic number). (*e*) Backscattered electron image (BEI) of (*b*); cracks and pits are less obvious compared to (*d*) and appear as black features. Average atomic number of minerals controls the brightness of minerals strongly; plagioclase has the lowest average atomic number and lowest brightness of all minerals in the image. Numbers are the location of wavelength-dispersive spectrometer (WDS) analysis (results are shown in Table 9.2). Boxes are shown in (*f*) and (*g*). (*f*) BEI close-up of clinopyroxene that reveals orthopyroxene exsolution lamellae (bright) not easily observable in other images shown. The numbers are locations of WDS analysis (results are shown in Table 9.2). (*g*) BEI close-up of orthopyroxene that highlights the clinopyroxene exsolution lamellae (dark), which are also observable in (*c*). The numbers are locations of WDS analysis (results are shown in Table 9.2). View larger image

Backscattered Electrons

Backscattered electrons are beam electrons that are deflected by the atoms of the sample through one or more interactions such that the beam electron, now called a backscattered electron, escapes the surface of the sample (Figure 8.3b). The backscattered electron detector is placed immediately above the sample and detects the

Printed by: e48d507df5d1141@placeholder.94092.edu. Printing is for personal, private use only. No part of this book may be reproduced or transmitted without publisher's prior permission. Violators will be prosecuted.

number of electrons emitted from the sample surface (Figure 9.1b, 9.2b). Backscatter electron have higher energy than secondary electrons so they are not strongly attracted by the field of the secondary electron detector. The higher energy of backscatter electrons also means that they may originate from a greater depth within the sample, up to perhaps a micron (Figure 9.4). As a result, surface topography does not affect the emission of backscatter electrons much, and the number emitted is most sensitive to the average atomic number of the material, much more so than for secondary electrons. The higher the average atomic number, the more backscattered electrons are emitted and the brighter that material will appear in an image (**Figure 9.5e**, **f**, **g**).

Cathodoluminescence

When an electron beam interacts with a sample, electrons in the valence band of a sample atom can be promoted to a conduction band (see Chapter 6). Eventually the vacancy in the valence band can be filled by a promoted conduction band electron. When the electron drops in energy levels in this way, it must give off energy equal to the energy difference between the conduction band and the valence band. If the energy difference is in the visible light portion of the electromagnetic spectrum, this light is detectable with the naked eye (if bright enough) and is called **cathodoluminescence** or **CL**. Some SEM/EPMAs may be equipped with CL detectors that can detect this light. The detectors may be either monochromatic, resulting in grayscale images (**Figure 9.6**), or color detectors, resulting in true color CL images of the sample. Controlling whether CL occurs, its brightness, and its color can be complicated, but some controlling factors are sample chemistry, crystal structure, and defects in the crystal structure. CL can highlight very subtle chemistry differences across minerals grains not visible by other techniques and can provide insight into crystal structure defects.

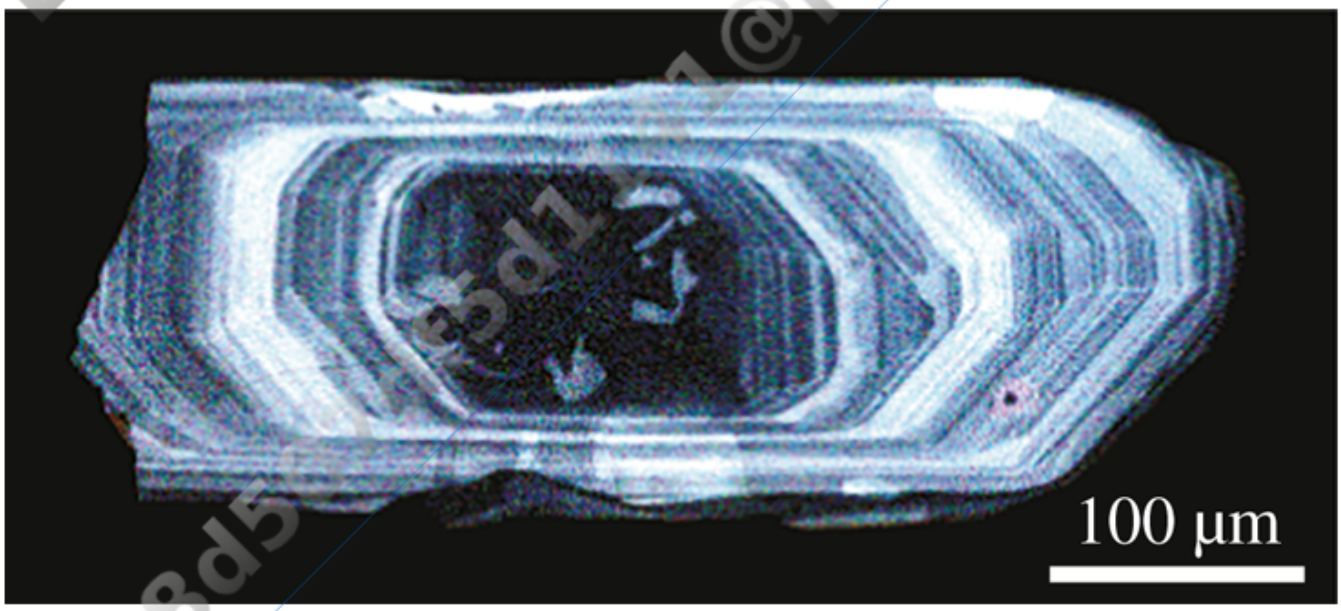

FIGURE 9.6 Cathodoluminescence image of a zircon grain. The grain was extracted from the host rock, mounted in epoxy, and ground and polished so that a cross section through the center of the grain could be imaged. Zircon zoning patterns, controlled by slight changes in chemistry, are

Printed by: e48d507df5d1141@placeholder.94092.edu. Printing is for personal, private use only. No part of this book may be reproduced or transmitted without publisher's prior permission. Violators will be prosecuted.

the grain could be imaged. Zircon zoning patterns, controlled by slight changes in chemistry, are often only observable by cathodoluminescence and are key information used for interpreting the origin and history of the grain (Box 5.1). This grain has a dark core surrounded by oscillatory zoning. View larger image

Characteristic X-Rays

As described in Chapter 8, a number of different types of X-rays are generated when an electron beam interacts with a material. Continuous spectrum or background X-rays are of a wide variety of wavelengths and energies and are predominantly generated with each deflection of a beam electron by the sample's atoms (Figure 8.3a, b). More importantly, characteristic X-rays are generated when an inner orbital electron is ejected from an atom within the sample (Figure 8.3c). The vacant orbital is quickly filled by an electron from a higher-energy orbital. As the electron drops in energy to fill the inner orbital vacancy, it emits an X-ray with energy equal to the difference in energy of the two orbitals. Because the energy of each orbital is specific to the electron configuration of that element, the energy and wavelength of the X-ray given off by this process is characteristic of the element that produced it (Figure 8.3a).

Recall that the energy (E, keV) and wavelength (λ, Å) of any electromagnetic radiation is tied to each other by the equation

$$E = hc/\lambda \tag{9.1}$$

where h is Planck's constant (4.13567×10^{-18} keV · s) and c is the speed of light in a vacuum (2.997924×10^{18}Å/s).

Any element with at least a K and L shell are capable of producing characteristic X-rays. This includes all elements of atomic number 3 (Li) or higher—H and He cannot produce characteristic X-rays. Elements heavier than Ne have more shells and therefore can produce more different characteristic X-rays, as every combination of inner orbital electron shell vacancies filled by any higher orbital electron results in a different characteristic X-ray.

Specific characteristic X-rays, sometimes referred to as X-ray lines, are given labels depending on the two orbital shells involved in generating the X-ray. The first letter indicates which shell had an orbital electron removed by the beam electron: K, L, or M, etc. Following the shell letter is a Greek letter indicating the source of the higher-energy electron. One shell higher in energy is designated by α, two shells higher is designated by β, etc. Additionally, sometimes it is necessary to distinguish different wavelength and energy characteristic X-rays produced by electrons moving from and to specific subshells; these are indicated by numerical subscripts. Not all have the same likelihood of being produced, depending on the details of the orbitals involved and the beam's accelerating voltage (see Chapter 8).

DO NOT COPY e48d507df5d1141@placeholder.9409

Printed by: e48d507df5d1141@placeholder.94092.edu. Printing is for personal, private use only. No part of this book may be reproduced or transmitted without publisher's prior permission. Violators will be prosecuted.

There are two types of X-ray detectors that SEMs and EPMAs may have. One distinguishes X-rays by their energy; these are called **energy-dispersive X-ray spectrometers**, or **EDS** (Figure 9.1b, 9.2b). Both SEMs and EPMAs are nearly universally equipped with EDS. The second type of detector distinguishes X-rays by their wavelength; these are called **wavelength-dispersive X-ray spectrometers**, or **WDS** (Figures 9.1b, 9.2b). SEMs only rarely have WDS, but EPMAs universally have multiple WDS.

EDS uses a single solid-state detector that records all the X-rays coming from the sample and distinguishes their energies. A computer then plots the data on an intensity versus energy plot (**Figure 9.7**), where intensity is usually given in counts or counts per second, while energy is in kiloeletron volts (keV). Most software that operates the EDS also identifies the element that produced high-intensity peaks of a particular energy.

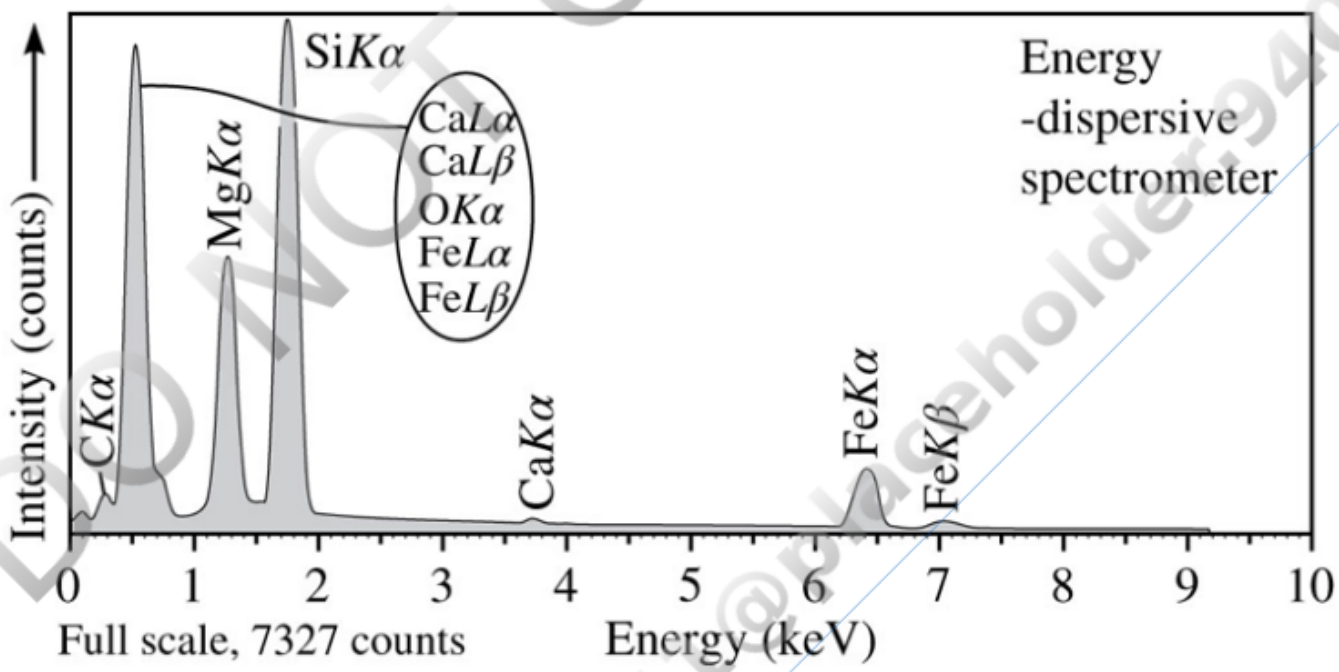

FIGURE 9.7 Energy-dispersive X-ray spectra from orthopyroxene; compare with Figure 9.8. Note that Al was not detected by the energy-dispersive spectrometer, and that the peak at about 0.5 keV includes characteristic spectra from oxygen, iron, and calcium. The small carbon *Kα* peak is from the carbon coating on the sample. View larger image

WDS uses a geometry similar to an X-ray diffractometer (Chapter 8). X-rays coming from the sample are diffracted by a diffracting crystal whose *d*-spacing is known. The diffracting crystal is set at angle θ from the Bragg equation (Equation 8.6) required to diffract a characteristic X-ray wavelength of an element in the sample, Mg *Kα*, for example. The detector is positioned at 2θ such that it only receives X-rays of that specific wavelength. The detector, usually a proportional counter, scintillation counter, or solid-state detector, similar to those used with X-ray diffraction, records the intensity of the X-rays emitted by the sample and sends the output to a computer for processing and display.

Printed by: e48d507df5d1141@placeholder.94092.edu. Printing is for personal, private use only. No part of this book may be reproduced or transmitted without publisher's prior permission. Violators will be prosecuted.

Because WDS can only detect a single X-ray wavelength at a time, EPMAs are equipped with several wavelength-dispersive spectrometers to allow simultaneous analysis of multiple elements. The *d*-spacing of the diffracting crystals dictates the range of wavelengths that a spectrometer can detect. To enable a wide range of wavelengths that encompass the characteristic X-rays produced by all elements, different spectrometers are equipped with multiple, different diffracting crystals (**Figure 9.8**).

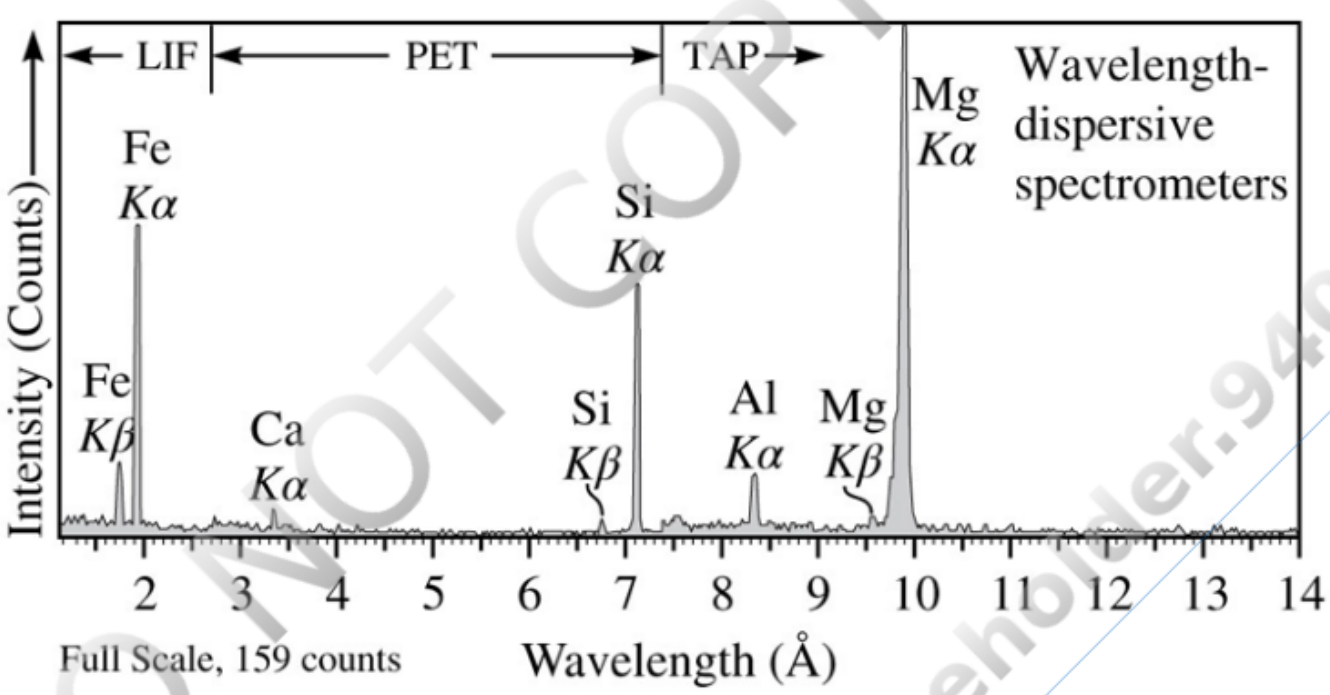

FIGURE 9.8 Wavelength-dispersive X-ray spectra for the same orthopyroxene analyzed by energy-dispersive spectrometry and presented in Figure 9.7. The wavelength ranges of the different diffracting crystals are indicated (LIF—lithium fluoride, PET—pentaerythritol, TAP—thallium acid pthalate). Note that this spectrometer is more sensitive and is able to more easily detect Al. View larger image

Chemical Analysis

SEMs and EPMAs can simply be used to identify minerals, which is often possible by determining the presence or absence of particular elements in a mineral; this is called **qualitative analysis**. Figures 9.7 and 9.8 each provides a simple qualitative analyses. As EDS is capable of simultaneously collecting an entire range of X-ray energies that the elements in a sample might produce, EDS is therefore often the preferred method of qualitative analysis for mineral identification. An experienced researcher can identify most common minerals from only a few seconds of collecting an EDS spectrum (Figure 9.7). For WDS, it might take half an hour to generate an analogous spectrum covering the characteristic X-rays for all elements that might be present as each crystal type, and their detector would have to be moved to each θ and 2θ positions (Figure 9.8).

If a precise composition of a sample is needed, then **quantitative analysis** is required. Quantitative analysis involves comparing the intensity of characteristic X-rays emitted

DO NOT COPY e48d507df5d1141@placeholder.9409

Printed by: e48d507df5d1141@placeholder.94092.edu. Printing is for personal, private use only. No part of this book may be reproduced or transmitted without publisher's prior permission. Violators will be prosecuted.

from an unknown sample to those emitted from **standards**, which are samples with a known composition. This comparison is then run through a complex routine that provides a variety of corrections, resulting in a highly accurate and complete chemical analysis of the sample. In the best cases, the reported concentration of each element may be accurate to within approximately 0.1 percent of the true concentration.

Though most elements produce multiple characteristic X-rays of differing energy and wavelength, only one for each element present in the sample is needed for quantitative analysis. An element's highest-intensity characteristic X-ray with an energy of 1–10 keV is generally chosen, except for light elements with characteristic X-ray energies less than 1 keV. Following this guideline, generally the $K\alpha$ characteristic X-ray is used for elements up to about atomic number 30 (Zn). $L\alpha$ characteristic X-rays are used for atomic numbers in the general range of 30–75 (Zn–Re), while $M\alpha$ characteristic X-rays are used for elements heavier than about atomic number 75. However, which characteristic X-ray is used depends on whether it happens to have the same or similar energy and wavelength as another characteristic X-ray produced by another element within the sample. In such cases, a different characteristic X-ray must be chosen for chemical analysis for both elements.

Table 9.1 shows a number of high-intensity characteristic X-rays produced by some elements abundant in common minerals. In this table, highlighted in bold are the characteristic X-ray lines typically used for quantitative analysis. Note that the Mn $K\beta$ and the Fe $K\alpha$ lines are close enough in energy (and wavelength), that neither EDS nor WDS can distinguish them; therefore, the Fe $K\beta$ characteristic X-ray is used for analysis to avoid this overlap problem. The S $K\alpha$ and Pb $M\alpha_1$ characteristic X-rays are also close in energy (and wavelength); though EDS typically lacks the resolution to separate them, WDS has a higher resolution and is able resolve these characteristic X-rays as separate from one another. A similar example is shown in **Figure 9.9** for S and Mo.

TABLE 9.1 Preferred Characteristic X-Rays Used for Quantitative Analysis of Elements Found in Common Minerals[a]

Element	$K\alpha$	$K\beta$	$L\alpha_1$	$M\alpha_1$
F	**0.677**			
Na	**1.041**			
Mg	**1.254**			
Al	**1.487**			
Si	**1.740**	1.838		
P	**2.015**	2.142		
S	**2.307**	2.468		
Cl	**2.622**	2.817		

DO NOT COPY e48d507df5d1141@placeholder.9409

Printed by: e48d507df5d1141@placeholder.94092.edu. Printing is for personal, private use only. No part of this book may be reproduced or transmitted without publisher's prior permission. Violators will be prosecuted.

K	**3.312**	3.589		
Ca	**3.690**	4.012	0.341	
Ti	**4.508**	4.931	0.452	
Mn	**5.895**	6.492	0.636	
Fe	6.400	**7.059**	0.704	
Pb	74.228	85.357	10.549	**2.346**

[a] Some characteristic X-ray energies listed are an average of two closely spaced characteristic X-rays from the same element. Characteristic X-rays in bold are often used for quantitative analysis.

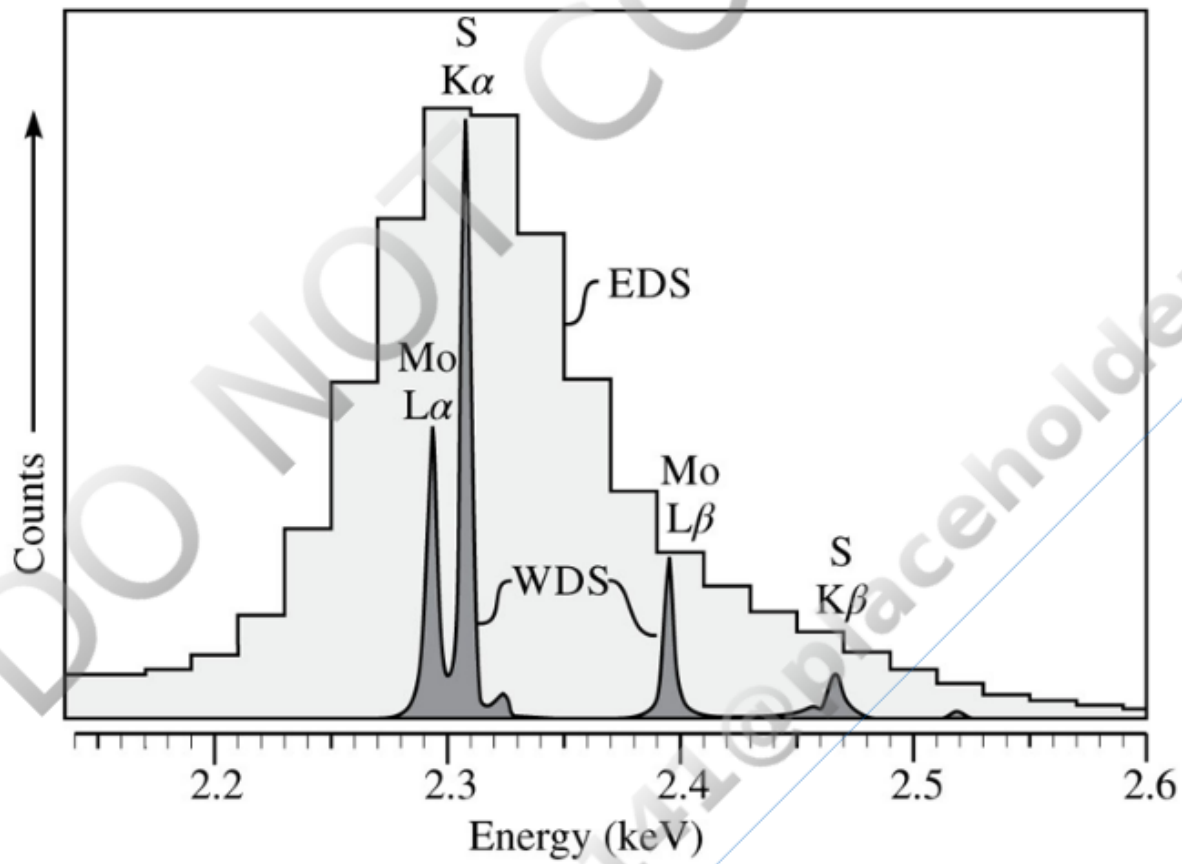

FIGURE 9.9 Comparison of energy-dispersive (EDS) and wavelength-dispersive (WDS) scans on molybdenite. The energy-dispersive spectrometer merges all the peaks for sulfur and molybdenum into a single broad peak that does not allow the two elements to be distinguished. The wavelength-dispersive spectrometer clearly distinguishes each peak of the characteristic spectra. View larger image

Elemental abundance within the sample has the greatest control over the intensity of characteristic X-rays. The higher the weight percent of that element in the sample, the more characteristic X-rays are produced for that element. Quantitative analysis requires that standards are similarly analyzed during the same analysis session to establish the intensity of characteristic X-rays produced for a particular composition. There are many factors that also slightly influence the number characteristic X-rays produced, and all must be accounted for if the quantitative analysis is to be accurate. These include the

DO NOT COPY e48d507df5d1141@placeholder.9409

Printed by: e48d507df5d1141@placeholder.94092.edu. Printing is for personal, private use only. No part of this book may be reproduced or transmitted without publisher's prior permission. Violators will be prosecuted.

must be accounted for if the quantitative analysis is to be accurate. These include the number of background X-rays produced, differences in the overall chemistry between standards and unknown samples, and slight differences in the electron beam between standard and unknown analysis. All these factors are combined in a complex correction routine handled by software and result in a complete quantitative analysis of the sample. Given the power of modern computers, this correction routine takes less than a second after all X-ray intensity data have been collected.

Generally, WDS is the preferred spectrometer for quantitative analysis. Though a slower technique, it is much more precise, as demonstrated by its ability to separate closely spaced characteristic X-rays (Figure 9.9) and identify low concentration elements (cf. Figure 9.7 and 9.8). However, for some elements, EDS can provide analysis precision that rivals that of WDS; therefore, an approach used by some labs is to use a combination of EDS and WDS simultaneously for quantitative analysis. EDS is used for those elements for which high precision results are possible, while the relatively slow WDS detectors are reserved for the elements that require WDS for high precision. Typically, after standards have been analyzed, it takes less than 10 minutes to conduct a single quantitative analysis on an unknown.

All minerals in the gabbro sample presented in Figure 9.5 were quantitatively analyzed with WDS on an electron microprobe, and the results are listed in **Table 9.2**. Note that oxygen is determined through charge balance, as this is more accurate than directly measuring its concentration. The analyses are generally of high quality, despite not totaling to exactly 100 percent. All chemical analyses are subject to some error, which may include uncorrected changes in instrument operation during the analysis session, inaccuracies in standard compositions, analysis locations with unseen inclusions or surface irregularities, random differences in X-ray generation and detection, and/or elements missing from the analysis.

TABLE 9.2 Wavelength-Dispersive Quantitative Analysis of Minerals in a Gabbro Sample (Figure 9.5)[a]

Analysis	1	2	3	4	5	6	7	8
Mineral	Ol	Pl	Bt	Ilm	Cpx host	Opx lamellae	Opx host	Cpx lamellae
SiO_2	35.22	54.61	40.30	0.00	52.18	51.50	52.67	53.36
TiO_2	0.06	0.07	3.12	48.78	0.56	0.45	0.22	0.22
Al_2O_3	0.00	28.62	14.72	0.02	1.57	1.11	0.57	0.56
Cr_2O_3	0.01	0.00	0.09	0.08	0.05	0.03	0.00	0.02
FeO	39.59	0.32	8.59	45.66	10.84	15.56	22.98	21.89
NiO	0.07	0.02	0.08	0.00	0.02	0.03	0.04	0.01
MnO	0.51	0.01	0.03	0.45	0.30	0.36	0.52	0.44

DO NOT COPY e48d507df5d1141@placeholder.9409

Printed by: e48d507df5d1141@placeholder.94092.edu. Printing is for personal, private use only. No part of this book may be reproduced or transmitted without publisher's prior permission. Violators will be prosecuted.

MnO	0.31	0.01	0.03	0.45	0.30	0.30	0.32	0.44
MgO	24.58	0.03	19.89	2.42	13.33	14.96	20.93	20.36
CaO	0.07	11.06	0.11	0.01	20.80	14.56	1.88	3.27
Na_2O	0.00	4.84	0.19	0.00	0.24	0.15	0.01	0.03
K_2O	0.01	0.44	9.57	0.01	0.00	0.00	0.00	0.00
Cl	0.01	0.00	0.18	0.00	0.00	0.00	0.00	0.00
F	0.00	0.00	1.86	0.00	0.00	0.00	0.00	0.01
Total	100.13	100.02	98.73	97.43	99.89	98.71	99.82	100.17

[a] Pl—plagioclase; Cpx—clinopyroxene; Opx—orthopyroxene; Ol—olivine; Bt—biotite; Ilm—ilmenite.

It is important to realize that using characteristic X-rays for quantitative analysis, no matter the details of the analysis, cannot distinguish different oxidation states of elements, a common issue for iron (Fe^{3+} vs. Fe^{2+}). Another limitation is that different elemental isotopes cannot be distinguished. Further, depending on the details of the spectrometers used, some of the lightest elements cannot be detected even though they produce characteristic X-rays; these may include, Li, Be, and B, and perhaps others when very old instruments are used. Recall that H and He do not produce characteristic X-rays and hence cannot be analyzed.

Though nearly all of the data in Table 9.2 are of high quality, there are some complexities. Biotite (Chapter 13) contains OH as part of its structure, as H cannot be analyzed; analysis of any mineral containing H will be below 100 percent, reflecting its presence. For ilmenite, the analysis assumes all iron is Fe^{2+} because valence cannot be determined, but this ilmenite likely contains some Fe^{3+}, which results in a total a few percentage points below 100 percent. Routines exist that estimate the amount of Fe^{3+} for such minerals and can correct this issue. The orthopyroxene lamellae in the clinopyroxene host (analysis 6) also has a slightly low total. The lamellae are very thin (Figure 9.5f), and the excitation volume likely extended into the host clinopyroxene; therefore the analysis is of a mixture of orthopyroxene and clinopyroxene. Mixed analyses such as this often lead to low totals, and this analysis is likely not useful as it does not provide the chemistry of the lamellae alone.

Additional considerations regarding quantitative chemical analyses include **detection limits**, or the minimum amount of an element that must be present to allow a precise analysis. Detection limits are generally about 0.001 weight percent for WDS, but only 0.5–1 weight percent for EDS. Detection limits can vary substantially depending on the instrument, the detector used, the operating conditions, and the length of analysis time. Longer analysis times for both spectrometers increase the ability to get precise analyses on low concentrations. For any oxide on Table 9.2 reported with a weight percent of 0.00, either this reflects a concentration that is detectable but too low to be shown after rounding, or the concentration is lower than the detection limit.

DO NOT COPY e48d507df5d1141@placeholder.94092

Printed by: e48d507df5d1141@placeholder.94092.edu. Printing is for personal, private use only. No part of this book may be reproduced or transmitted without publisher's prior permission. Violators will be prosecuted.

With both qualitative and quantitative analysis, a little caution is always needed because software may fail to properly identify the elements based on peaks, correctly identify peak overlaps, or correctly suggest standards and how an analysis should be done. Typically only well-trained instrument operators with years of experience using an EPMA can provide high-quality quantitative analyses. Generally, SEMs, even if equipped with WDS, can provide no better than **semi-quantitative** analyses that must be normalized to a total of exactly 100 percent in order to provide an approximate concentration of each elements. SEMs typically are not designed with all the necessary considerations needed for high-quality quantitative analysis. However, for many applications, a semi-quantitative analysis provides a wealth of information. For this reason, transmission electron microscopes are often equipped with EDS as well to provide semi-quantitative analyses that help in determining the chemistry of the sample.

X-Ray Chemical Maps

Quantitative chemical analyses are very useful, as they provide a precise chemistry for a very small portion of a sample. However, a possible limitation is that with only a few analyses, it can be difficult to determine whether the composition changes across mineral grains or whether all grains of the same mineral have the same composition. Collecting hundreds of analyses could be one solution to this problem, but it would be extremely tedious to conduct all these analyses. An easier solution is to collect **X-ray chemical maps**. An X-ray chemical map is an image similar to a secondary electron or backscattered electron image, but it is collected with either WDS or EDS, where the brightness reflects the intensity of a characteristic X-rays from a particular element from across an area (**Figure 9.10**). X-ray chemical maps are very informative regarding the distribution of elements across a sample. While the X-ray chemical map is always grayscale upon collection, it is conventional to use image editing software to add color to highlight variation.

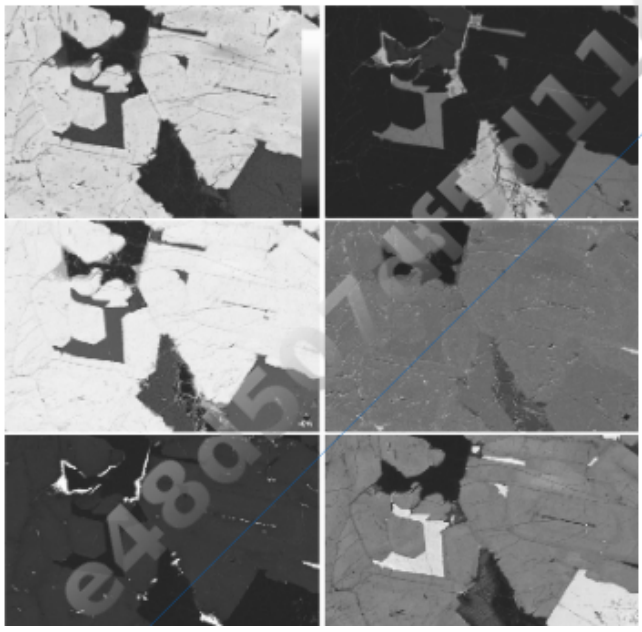

DO NOT COPY e48d507df5d1141@placeholder.94092

Printed by: e48d507df5d1141@placeholder.94092.edu. Printing is for personal, private use only. No part of this book may be reproduced or transmitted without publisher's prior permission. Violators will be prosecuted.

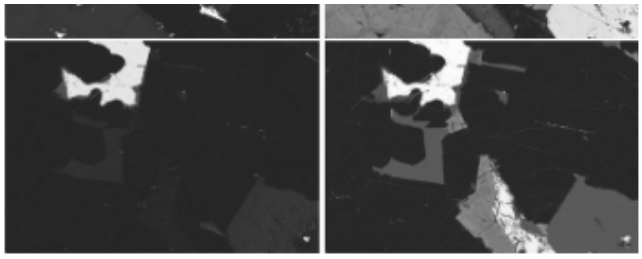

FIGURE 9.10 X-ray chemical maps. Maps cover the same area as shown in Figure 9.5b–e. For all maps, brighter indicates higher relative concentration of the element as labeled. Brightness of images has been scaled to highlight features. Note that minerals with high concentration of particular elements matches the quantitative analysis (Table 9.2). View larger image

X-Ray Fluorescence

The **X-ray fluorescence spectrometer** (**XRF**) (**Figure 9.11**) is generally similar to the SEM/EPMA and allows qualitative and quantitative chemical analysis of samples by use of EDS or WDS, but differences exist. One is that characteristic X-rays from sample elements are generated through excitation by a primary beam of high-energy background and characteristic X-rays emitted by an X-ray tube. Target metals within the X-ray tube vary depending on the instrument and application, but Mo, Rh, Pd, and W are the most common. Another difference is that sample preparation may be different, but this too may vary depending on the sample, instrument, and desired type of analysis. XRF is traditionally known for obtaining bulk chemical analysis of heterogeneous samples such as rocks, but before analysis, the rock must be appropriately prepared. One way is to finely grind the rock into a powder and compact it (a procedure called pressing), into a disk-shaped pellet. A second preparation method **fuses** the rock, which is the process of melting the rock and quenching it, or solidifying it into a glass. The fused sample is also disk shaped but is called a bead. Either method ensures the sample is homogeneous such that all elements interact with the primary X-ray beam in proportions representative of the whole rock.

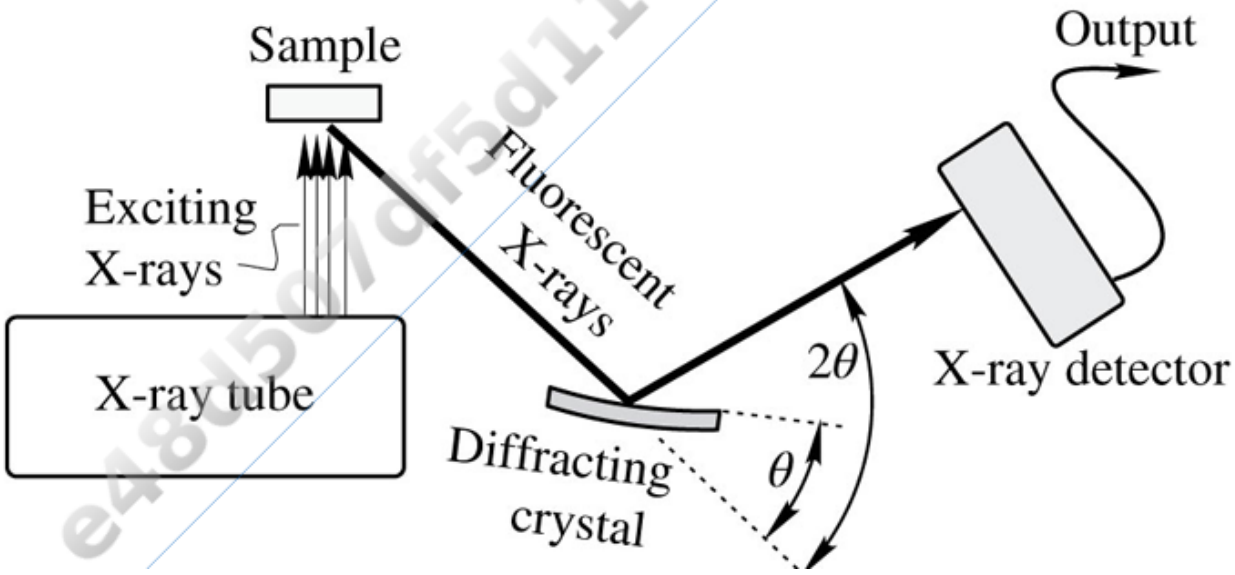

DO NOT COPY
e48d507df5d1141@placeholder.9409

Printed by: e48d507df5d1141@placeholder.94092.edu. Printing is for personal, private use only. No part of this book may be reproduced or transmitted without publisher's prior permission. Violators will be prosecuted.

FIGURE 9.11 X-ray fluorescence spectrometer. Background and characteristic X-rays from the X-ray tube cause elements in the sample to generate their characteristic X-rays. Chemical analysis is done by either wavelength- or energy-dispersive spectrometers; here a wavelength-dispersive spectrometer is shown. View larger image

The beam of some XRFs, often called micro-XRF (or μXRF) can be finely focused down to perhaps 20 μm or smaller. The small beam can then be scanned across the sample to generate chemical maps of rocks and minerals similar to those generated by the SEM/EPMA (Figure 9.10). For chemical maps, it is best that the sample surface is flat; however, samples need not be polished as they are for SEM/EPMA, and no carbon coating is necessary because X-rays are not charged. If grain size is greater than the excitation volume of the primary X-ray beam (similar to Figure 9.4), then quantitative chemical analysis of individual minerals is possible with μXRF.

For quantitative chemical analysis, similar to SEM/EPMA, the instrument is calibrated with standards of known composition. XRF detection limits, as little as 1 ppm (0.0001 weight percent) for some elements, are often lower than those of SEM/EPMA because the background spectra is generally lower.

The environment between the X-ray tube, sample, and WDS need not be under vacuum, but a vacuum must be used if analysis of the lightest elements (C, N, O, F, Ne, and Na) is needed, as the atmosphere will block the low-energy characteristic X-rays from these elements. If a vacuum is not used, typically Mg is the lightest element that can be analyzed by XRF. If a sample cannot withstand a vacuum, the atmosphere can be displaced (purged) with He, which allows elements as light as F to be detected and analyzed. Elements lighter than C typically cannot be analyzed by any XRF.

Handheld XRF

Technological advances have allowed X-ray tubes, X-ray spectrometers (specifically EDS), batteries, and powerful computers to become small enough that an entire XRF instrument can fit in a handheld unit (**Figure 9.12**). These instruments are typically referred to as handheld XRF (hXRF) or portable XRF, but other names exist. Fitting such a complex instrument into such a small size, combined with fairly large analysis areas (typically 3–8 mm in diameter), and samples often being quite complex (having rough surfaces and/or are heterogeneous) limits the ability for true quantitative analyses of rocks and minerals with hXRF if no sample preparation has been done (e.g., ensuring a flat surface). Because a vacuum between the X-ray tube, sample, and detector is impossible for hXRF, analysis of elements lighter than Mg is impossible. Some

DO NOT COPY e48d507df5d1141@placeholder.9409

Printed by: e48d507df5d1141@placeholder.94092.edu. Printing is for personal, private use only. No part of this book may be reproduced or transmitted without publisher's prior permission. Violators will be prosecuted.

instruments are capable of purging some of the atmosphere with He, but this requires an He canister attached to the hXRF. Even with He purging, analysis of only F or heavier elements is possible. Even with these limitations, such handheld units have become indispensable for providing rapid (under one minute) chemical information of samples in the mining, environmental remediation, and metallurgical industries in field settings or at locations far from a laboratory with more precise equipment.

FIGURE 9.12 Handheld X-ray fluorescence spectrometer analyzing a sample of galena (PbS). The instrument is the Bruker Tracer 5 owned by the University of Northern Colorado. View larger image

Mass Spectrometry

Mass spectrometry is another method capable of determining rock and mineral chemistry, often with extremely low detection limits—down to the parts per million or even lower than parts per billion levels in specialized cases. Mass spectrometers also have the ability to analyze the isotopic composition of a sample. Therefore, nearly all radiometric dating techniques require analysis by mass spectrometry (see Box 5.1). Similarly, paleoclimate studies relying on oxygen isotope analysis must too use a mass spectrometer (see Box 18.1). Some key components and geometry of one common type of mass spectrometer are schematically shown in **Figure 9.13**. Mass spectrometry begins with vaporizing and ionizing the sample. This can be done in a number of different ways for solid rock and mineral samples, and each method is typically identified by a name and

Printed by: e48d507df5d1141@placeholder.94092.edu. Printing is for personal, private use only. No part of this book may be reproduced or transmitted without publisher's prior permission. Violators will be prosecuted.

for solid rock and mineral samples, and each method is typically identified by a name and acronym.

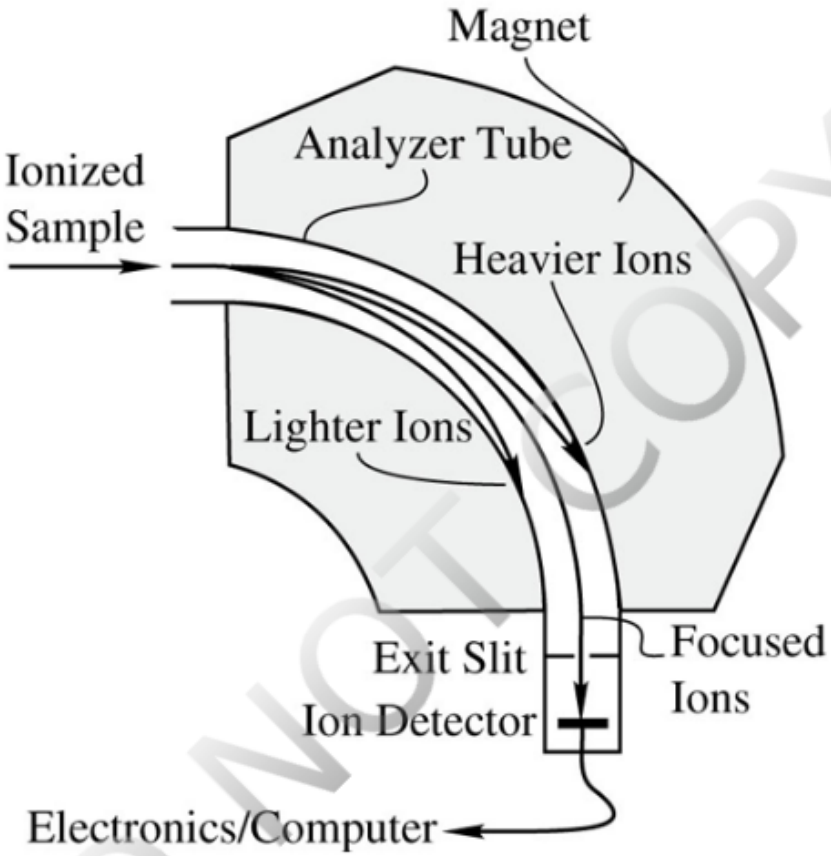

FIGURE 9.13 Schematic of typical mass spectrometer magnet and detector. A single collector mass spectrometer is depicted. View larger image

One way to form vaporized and ionized sample begins with dissolving (digesting) a sample in acid; this could be a whole rock or one or more grains of a mineral. The acidic solution is then introduced into a plasma torch, called an inductively coupled plasma, which vaporizes and ionizes the sample atoms in the solution. This technique is called inductively coupled plasma-mass spectrometry, or ICP-MS.

A second method generates sample vapor by use of a strong pulsing laser. The laser is generally focused to a diameter of 10–50 μm on a sample surface, such as part of a mineral grain. The laser is powerful enough to vaporize or ablate the sample, leaving a pit tens of microns deep. The resulting sample vapor is then carried through a tube by He or Ar gas to an inductively coupled plasma torch, where it is ionized. This technique is called laser ablation–inductively coupled plasma–mass spectrometry or LA-ICP-MS.

In another method similar to laser ablation, a tens of microns diameter beam of primary ions is focused on a solid sample surface; this is also most commonly done on specific locations within a mineral grain. For geologic samples, the primary ion beam is often O_2^- or Cs^+. The primary ion beam vaporizes and ionizes the sample in a single step. The sample ions are called secondary ions to distinguish them from the primary ion beam. The resulting pit generated by the primary ion beam is very small, at only a few

Printed by: e48d507df5d1141@placeholder.94092.edu. Printing is for personal, private use only. No part of this book may be reproduced or transmitted without publisher's prior permission. Violators will be prosecuted.

The resulting pit generated by the primary ion beam is very small, at only a few nanometers deep. This technique is called secondary ion mass spectrometry, or SIMS. Many students may come across the acronym SHRIMP in reference to the instrument used in some geochronologic studies; SHRIMP stands for sensitive high-resolution ion microprobe and is simply a particular type of SIMS.

The last common way to generate vaporized and ionized sample is by thermal ionization; hence, the technique is called thermal ionization mass spectrometry, or TIMS. With TIMS, the sample is initially prepared by acid digestion; the sample solution is then chemically purified so that only the elements of interest remain. The purified sample is deposited and dried on a millimeter-thick filament of a high–melting point and nonreactive metal, such as Re. The filament is then heated in a vacuum to several hundred degrees Celsius, which ionizes the sample.

With all the techniques listed above, once the sample ions are formed, because they are charged, they can be accelerated and focused into a beam through the influence of electrostatic fields. The beam of sample ions is directed into the analyzer tube, where ions with different mass to charge ratios are spatially separated.

Each instrument used in the techniques discussed above has its own complexities and specialized components, but for most, separation of the ionized particles traveling along the analyzer tube occurs by a strong magnet. The strong magnet deflects the path of the charged ions, and the amount that an ion is deflected depends on its mass. Light elements or isotopes are deflected more than heavy ones. By carefully adjusting the strength of the magnetic field and other instrumental settings, different atomic weight ions (isotopes) can be focused on the detector at the end of the analyzer tube. The number of ions striking the detector can be measured because each ion strike produces a detectable electric current. The abundance of the ion or isotope striking the detector is interpreted by computers and electronics based on the strength of the electric current relative to measurement of standards. Mass spectrometers may have only one detector, in which case the instrument and magnet must be tuned to the mass of every element or isotope needing analysis. Mass spectrometers with multiple collectors also exist; these can analyze many elements or isotopes simultaneously, one for each detector.

DO NOT COPY
e48d507df5d1141@placeholder.9409

Printed by: e48d507df5d1141@placeholder.94092.edu. Printing is for personal, private use only. No part of this book may be reproduced or transmitted without publisher's prior permission. Violators will be prosecuted.

Conventions in Reporting Chemical Analyses

Major Elements

Chemical analyses showing the major elemental composition of minerals are typically reported in terms of weight percent of the constituents. An analysis of arsenopyrite, for example, might be reported as 34.30 percent Fe, 46.01 percent As, and 19.69 percent S. For the majority of minerals that contain oxygen as the principal anion, major element analyses are reported in terms of the weight percent of metal oxides, plus perhaps water and additional anions.

Table 9.3 shows a biotite analysis. In this analysis, and in essentially all others that report results in terms of neutral charged oxides, the amount of oxygen in the sample is not actually measured. Rather, weight percent of the cations is measured, and then the amount of oxygen required by the stoichiometry to balance the charge of the cations is added. Not all of this oxygen may actually be present if other anion species such as F and Cl are in the sample; a correction is discussed shortly. It should not be inferred that separate oxide species actually exist in the mineral as structural entities.

TABLE 9.3 Chemical Analysis of a Biotite Sample

Compound	Weight Percent
SiO_2	39.14
Al_2O_3	13.10
TiO_2	4.27
FeO	5.05
Fe_2O_3	12.94
MgO	12.75
MnO	0.14
CaO	1.64
Na_2O	0.70
K_2O	6.55
F	1.11
H_2O^+	2.41
H_2O^-	0.58

DO NOT COPY e48d507df5d1141@placeholder.9409

Printed by: e48d507df5d1141@placeholder.94092.edu. Printing is for personal, private use only. No part of this book may be reproduced or transmitted without publisher's prior permission. Violators will be prosecuted.

Total	100.38
O ≡ F, Cl	0.46
Total (with F & Cl replacement of O)	99.92

Water may be reported as H_2O^- and H_2O^+. The value reported as H_2O^- represents actual molecular water in the sample that is adsorbed onto the surface of mineral grains or occupies small voids. It is not part of the crystal structure. H_2O^- is typically detected by determining the weight loss caused by heating the sample to 100–110°C for a period of time. H_2O^+ is inferred to represent hydrogen that is part of a mineral structure but not necessarily in the form of water molecules. Water analyses are not usually very reliable and are typically available only with wet chemical techniques.

F and Cl are the additional anions usually included in chemical analyses. Their presence requires a correction to the amount of oxygen presumed to be in the sample as part of the metal oxide species. For every two F^- or Cl^- atoms actually in the sample, one O^{2-} must be deleted. The correction is therefore

$$\begin{aligned} \mathrm{O{\equiv}F,\ Cl} &= \left(\mathrm{wt\,\%\ Cl}\frac{\mathrm{aw\ O}}{2\,\mathrm{aw\ Cl}} + \mathrm{wt\,\%\ F}\frac{\mathrm{aw\ O}}{2\,\mathrm{aw\ F}}\right) \\ &= (0.226\ \ \mathrm{wt\,\%\ Cl} + 0.421\ \ \mathrm{wt\,\%\ F}) \end{aligned} \tag{9.2}$$

where wt% Cl and wt% F are the weight percent of Cl and F, respectively, in the analysis, and aw refers to the atomic weight of the element.

The total of the different constituents in a chemical analysis rarely sums to exactly 100 percent. The degree to which the total differs from 100 percent is an indication of analytical errors and, if the total is less than 100 percent, may indicate that some elements were not detected. Even if the total comes to nearly 100 percent, the possibility of multiple errors that almost exactly offset each other must be considered.

Trace Elements

Trace element analyses of minerals and rocks are usually reported in parts per million of elements, or in some cases parts per million of the oxide of the element. Trace elements either substitute in small amounts for one of the major cations in the structure or are in sites not normally occupied in the ideal crystal structure of the mineral. They form substitutional or interstitial defects (Chapter 4). A typical analysis is shown in **Table 9.4**.

TABLE 9.4 Typical Trace Element Analysis of a Pyroxene

Element	Parts per Million (ppm)

DO NOT COPY e48d507df5d1141@placeholder.9409

Printed by: e48d507df5d1141@placeholder.94092.edu. Printing is for personal, private use only. No part of this book may be reproduced or transmitted without publisher's prior permission. Violators will be prosecuted.

Element	Parts per Million (ppm)
Sr	5.67
Y	10.8
Zr	20.4
La	0.554
Ce	2.48
Nd	2.45
Sm	0.856
Eu	0.317
Dy	1.60
Er	0.835
Yb	0.791

Source: Data from Papike and others (1995).

A common tactic to allow easy comparison among different data sets is to normalize trace element data by using a common standard. The rare earth elements, for example, are commonly normalized by dividing the observed analysis with the elemental composition of an average chondrite (Anders and Grevesse, 1989). A chondrite is a type of primitive meteorite that is inferred, in some sense, to be representative of the bulk chemistry of the solar system as a whole.

DO NOT COPY e48d507df5d1141@placeholder.9409

Printed by: e48d507df5d1141@placeholder.94092.edu. Printing is for personal, private use only. No part of this book may be reproduced or transmitted without publisher's prior permission. Violators will be prosecuted.

Conversion of Chemical Analyses to Structural Formulas

Converting a chemical analysis into a mineral's structural formula is a relatively straightforward procedure that can be done manually, which is tedious, or with the aid of spreadsheet software. Similar calculations are routinely done as part of all introductory chemistry classes. **Table 9.5** illustrates the calculation for a pyroxene whose general formula is $M2M1T_2O_6$, where M2 represents the cations in 8-fold (cubic) coordination, M1 represents the cations in 6-fold (octahedral) coordination, T represents the cations in 4-fold (tetrahedral) coordination, and O represents oxygen (see Chapters 4 and 14). Columns 1 and 2 present the chemical analysis. Note that the analysis sums to 100.12 weight percent, suggesting a small analytical error. For purposes of calculation, we assume that the sample weighs 100.12 g; the weight percent values can then be considered equal to the number of grams of each oxide species. Column 3 shows the molecular weight (grams per mole) of the oxide species based on the atomic weight of the cation and oxygen. **Table 9.6** lists the molecular weight of the common oxides. The molecular weight of the oxide is simply the sum of the atomic weights of the elements on the periodic table. For example, for SiO_2, Si weights 28.086, and O weights 15.999 (remember two O are in SiO_2); therefore SiO_2 weights 28.086+2*15.999 = 60.08 grams per mole when rounded to two decimal places. The calculations in Table 9.5 are accomplished as follows; take care to avoid rounding the figures until all calculations are complete:

COLUMN 4: Calculate the number of moles of each oxide species by dividing the weight percent value (column 2) by the molecular weight of the oxide (column 3).

COLUMN 5: Calculate moles of oxygen in each oxide species based on the stoichiometry. For example, moles of oxygen from SiO_2 are twice the moles of oxide (column 4) because SiO_2 has two oxygen atoms. The total moles of oxygen in the sample (2.74030 in this case) are summed at the bottom of column 5.

COLUMN 6: Calculate moles of cation in each oxide species based on the stoichiometry. For example, the number of moles of Si is the same as the moles of SiO_2 as there is only one Si in SiO_2, whereas the number of moles of Al is twice the number of moles of Al_2O_3 as there are two Al in Al_2O_3. At this point the chemical formula can be written (rounded to three decimal places):

COLUMN 7: In this column the formula is recalculated so that it is based on the number of oxygen anions used in the structural formula. For pyroxene this is six. First calculate the *factor* by dividing the number of oxygens per formula by the moles of

DO NOT COPY e48d507df5d1141@placeholder.9409-

Printed by: e48d507df5d1141@placeholder.94092.edu. Printing is for personal, private use only. No part of this book may be reproduced or transmitted without publisher's prior permission. Violators will be prosecuted.

oxygen at the bottom of column 5. In this case the *factor* is 6/2.74030 = 2.18954. Cations on the basis of 6 O are then calculated by multiplying the moles of cations (column 6) by the *factor*.

COLUMN 8: Cations are segregated into different structural sites based on knowledge of the mineral structure. In this pyroxene, three sites are available, one for each coordination number (see column 6), which now will be listed as a roman numeral superscript preceding the site: ^{VIII}M2, ^{VI}M1, and ^{IV}T. In general, for silicates, all the Si and some of the Al are placed in the ^{IV}T site, and the remaining Al and the other cations are placed in other site(s). In this case, the ^{IV}T site is assigned 1.961 Si and 0.039 Al to make a total of 2.000—consistent with the general formula above. The remaining 2.001 cations must occupy the 6- and 8-fold sites (M1 and M2 in the formula). As a first approximation, we will assume that Na and Ca, which are the largest cations, occupy the M2 site and the remaining cations occupy M1. This yields 1.053 cations in the M1 site and 0.948 cation in M2, which is very close to the site occupancy in the ideal formula. Based on this assumption, the formula can now be written:

$$\underset{^{VIII}M2_{0.948}}{(Na_{0.019}Ca_{0.929})}\underset{^{VI}M1_{1.053}}{(Mn_{0.002}Fe_{0.091}Mg_{0.907}Cr_{0.026}Ti_{0.005}Al_{0.021})}\underset{^{IV}T_{2.000}}{(Al_{0.039}Si_{1.961})}\underset{O_6}{O_6}$$

TABLE 9.5 Recalculation of a Pyroxene Analysis

1	2	3	4	5	6	7	8		
	Weight Percent	Molecular Weight	Moles Oxide	Moles Oxygen	Moles Cation	Cations on Basis of Six O	Structural Allocation		
SiO_2	53.8	60.08	0.89547	1.79095	0.89547	1.961	1.961	2.00	^{IV}T
Al_2O_3	1.4	101.96	0.01373	0.04119	0.02746	0.060	0.039		
							0.021	1.053	^{VI}M1
TiO_2	0.18	79.90	0.00225	0.00451	0.00225	0.005	0.005		
Cr_2O_3	0.9	151.99	0.00592	0.01776	0.01184	0.026	0.026		
MgO	16.7	40.30	0.41439	0.41439	0.41439	0.907	0.907		
FeO	3.0	71.84	0.04176	0.04176	0.04176	0.091	0.091		
MnO	0.07	70.94	0.00099	0.00099	0.00099	0.002	0.002		
CaO	23.8	56.08	0.42439	0.42439	0.42439	0.929	0.929	0.948	^{VIII}M2
Na_2O	0.27	61.98	0.00436	0.00436	0.00871	0.019	0.019		
Total	100.12			2.74030	Factor = 2.18954				

TABLE 9.6 Molecular Weight of Common Oxide Species

Oxide	Molecular Weight	Oxide	Molecular Weight

DO NOT COPY e48d507df5d1141@placeholder.9409

Printed by: e48d507df5d1141@placeholder.94092.edu. Printing is for personal, private use only. No part of this book may be reproduced or transmitted without publisher's prior permission. Violators will be prosecuted.

Oxide	Molecular Weight	Oxide	Molecular Weight
H_2O	18.02	K_2O	94.20
CO_2	44.01	CaO	56.08
Na_2O	61.98	Cr_2O_3	151.99
MgO	40.30	MnO	70.94
Al_2O_3	101.96	FeO	71.84
SiO_2	60.08	Fe_2O_3	159.69

It is probable that about 0.05 of the cations assigned to the 6-fold M1 site are actually in the 8-fold M2 site. All but the Al are sufficiently large to occupy an 8-fold site (Figure 3.18, Table 4.2, and Appendix A). Without detailed structural information, however, it is not possible to know how much of which element to assign to the 8-fold site.

These data can be further manipulated to show the relative amounts of the end-member compositions for minerals that display significant solid solution. For pyroxenes, the standard end members are wollastonite (Wo, $Ca_2Si_2O_6$), enstatite (En, $Mg_2Si_2O_6$), and ferrosilite (Fs, $Fe_2Si_2O_6$). The relative amounts of the end members are therefore equivalent to the relative amounts of Ca, Mg, and Fe. Hence,

$$\% \ \mathrm{Wo} = \mathrm{Ca}/(\mathrm{Ca}+\mathrm{Mg}+\mathrm{Fe}) = 0.929/1.927 = 48.2\%$$
$$\% \ \mathrm{En} = \mathrm{Mg}/(\mathrm{Ca}+\mathrm{Mg}+\mathrm{Fe}) = 0.907/1.927 = 47.1\%$$
$$\% \ \mathrm{Fs} = \mathrm{Fe}/(\mathrm{Ca}+\mathrm{Mg}+\mathrm{Fe}) = 0.091/1.927 = 4.7\%$$

The remaining cations (Cr, Ti, Mn, etc.) are ignored in this calculation. See Chapter 4 for more information on chemical formulas and graphical representation of mineral chemistry.

DO NOT COPY e48d507df5d1141@placeholder.9409

Printed by: e48d507df5d1141@placeholder.94092.edu. Printing is for personal, private use only. No part of this book may be reproduced or transmitted without publisher's prior permission. Violators will be prosecuted.

COLUMN 7: In this column the formula is recalculated so that it is based on the number of oxygen anions used in the structural formula. For pyroxene this is six. First calculate the *factor* by dividing the number of oxygens per formula by the moles of oxygen at the bottom of column 5. In this case the *factor* is 6/2.74030 = 2.18954. Cations on the basis of 6 O are then calculated by multiplying the moles of cations (column 6) by the *factor*.

- **COLUMN 8:** Cations are segregated into different structural sites based on knowledge of the mineral structure. In this pyroxene, three sites are available, one for each coordination number (see column 6), which now will be listed as a roman numeral superscript preceding the site: $^{VIII}M2$, $^{VI}M1$, and ^{IV}T. In general, for silicates, all the Si and some of the Al are placed in the ^{IV}T site, and the remaining Al and the other cations are placed in other site(s). In this case, the ^{IV}T site is assigned 1.961 Si and 0.039 Al to make a total of 2.000—consistent with the general formula above. The remaining 2.001 cations must occupy the 6- and 8-fold sites (M1 and M2 in the formula). As a first approximation, we will assume that Na and Ca, which are the largest cations, occupy the M2 site and the remaining cations occupy M1. This yields 1.053 cations in the M1 site and 0.948 cation in M2, which is very close to the site occupancy in the ideal formula. Based on this assumption, the formula can now be written:

$$\underset{^{VIII}M2_{0.948}}{(Na_{0.019}Ca_{0.929})}\underset{^{VI}M1_{1.053}}{(Mn_{0.002}Fe_{0.091}Mg_{0.907}Cr_{0.026}Ti_{0.005}Al_{0.021})}\underset{^{IV}T_{2.000}}{(Al_{0.039}Si_{1.961})}\underset{O_6}{O_6}$$

TABLE 9.5 Recalculation of a Pyroxene Analysis

1	2	3	4	5	6	7	8		
	Weight Percent	Molecular Weight	Moles Oxide	Moles Oxygen	Moles Cation	Cations on Basis of Six O	Structural Allocation		
SiO_2	53.8	60.08	0.89547	1.79095	0.89547	1.961	1.961	2.00	^{IV}T
Al_2O_3	1.4	101.96	0.01373	0.04119	0.02746	0.060	0.039		
							0.021	1.053	$^{VI}M1$
TiO_2	0.18	79.90	0.00225	0.00451	0.00225	0.005	0.005		
Cr_2O_3	0.9	151.99	0.00592	0.01776	0.01184	0.026	0.026		
MgO	16.7	40.30	0.41439	0.41439	0.41439	0.907	0.907		
FeO	3.0	71.84	0.04176	0.04176	0.04176	0.091	0.091		
MnO	0.07	70.94	0.00099	0.00099	0.00099	0.002	0.002		
CaO	23.8	56.08	0.42439	0.42439	0.42439	0.929	0.929	0.948	$^{VIII}M2$
Na_2O	0.27	61.98	0.00436	0.00436	0.00871	0.019	0.019		
Total	100.12			2.74030	Factor = 2.18954				

TABLE 9.6 Molecular Weight of Common Oxide Species

DO NOT COPY e48d507df5d1141@placeholder.9409

Printed by: e48d507df5d1141@placeholder.94092.edu. Printing is for personal, private use only. No part of this book may be reproduced or transmitted without publisher's prior permission. Violators will be prosecuted.

TABLE 9.6 Molecular Weight of Common Oxide Species

Oxide	Molecular Weight	Oxide	Molecular Weight
H_2O	18.02	K_2O	94.20
CO_2	44.01	CaO	56.08
Na_2O	61.98	Cr_2O_3	151.99
MgO	40.30	MnO	70.94
Al_2O_3	101.96	FeO	71.84
SiO_2	60.08	Fe_2O_3	159.69

It is probable that about 0.05 of the cations assigned to the 6-fold M1 site are actually in the 8-fold M2 site. All but the Al are sufficiently large to occupy an 8-fold site (Figure 3.18, Table 4.2, and Appendix A). Without detailed structural information, however, it is not possible to know how much of which element to assign to the 8-fold site.

These data can be further manipulated to show the relative amounts of the end-member compositions for minerals that display significant solid solution. For pyroxenes, the standard end members are wollastonite (Wo, $Ca_2Si_2O_6$), enstatite (En, $Mg_2Si_2O_6$), and ferrosilite (Fs, $Fe_2Si_2O_6$). The relative amounts of the end members are therefore equivalent to the relative amounts of Ca, Mg, and Fe. Hence,

$$\% \ \mathrm{Wo} = \mathrm{Ca}/(\mathrm{Ca}+\mathrm{Mg}+\mathrm{Fe}) = 0.929/1.927 = 48.2\%$$
$$\% \ \mathrm{En} = \mathrm{Mg}/(\mathrm{Ca}+\mathrm{Mg}+\mathrm{Fe}) = 0.907/1.927 = 47.1\%$$
$$\% \ \mathrm{Fs} = \mathrm{Fe}/(\mathrm{Ca}+\mathrm{Mg}+\mathrm{Fe}) = 0.091/1.927 = 4.7\%$$

The remaining cations (Cr, Ti, Mn, etc.) are ignored in this calculation. See Chapter 4 for more information on chemical formulas and graphical representation of mineral chemistry.

REFERENCES CITED AND SUGGESTIONS FOR ADDITIONAL READING

Anders, E., and Grevesse, N. 1989. Abundances of the elements: Meteorite and solar. *Geochimica et Cosmochimica Acta* **53**, 197–214.

Fenter, P., Rivers, M., Sturchio, M., and Sutton, W. (eds.). 2002. *Applications of Synchrotron Radiation in Low-Temperature Geochemistry and Environmental Science.* Reviews in Mineralogy **49**, 579 p.

Hawthorne, F. C. (ed.). 1988. *Spectroscopic Methods in Mineralogy and Geology.*

DO NOT COPY e48d507df5d1141@placeholder.9409

Printed by: e48d507df5d1141@placeholder.94092.edu. Printing is for personal, private use only. No part of this book may be reproduced or transmitted without publisher's prior permission. Violators will be prosecuted.

Reviews in Mineralogy, 18. Mineralogical Society of America, Washington, DC, 698 p.

Jeffery, P. G. 1975. *Chemical Methods of Rock Analysis*, 2nd ed. Pergamon Press, Oxford, 533 p.

Johnson, W. M., and Maxwell. J. A. 1981. *Rock and Mineral Analysis*, 2nd ed. John Wiley & Sons, New York, 489 p.

Margui, E., and Grieken, R. V. 2013. *X-Ray Fluorescence Spectrometry and Related Techniques: An Introduction*, Momentum Press, New York, 162 p.

Papike, J. J., Spilde, M. N., Fowler, G. W., and McCallum, I. S. 1995. SIMS studies of planetary cumulates: Orthopyroxene from the Stillwater Complex, Montana. *American Mineralogist* **80**, 1208–1221.

Reed, S. J. B. 2005. *Electron Microprobe Analysis and Scanning Electron Microscopy in Geology*. Cambridge University Press, Cambridge, 189 p.

Reeves, R. D., and Brooks, R. R. 1978. *Trace Element Analysis of Geological Materials*. John Wiley & Sons, New York, 421 p.

Skoog, D. A., and Leary, J. J. 1992. *Principles of Instrumental Analysis*. Saunders College Publishing, Fort Worth, TX, 700 p.

Wenk, H.-R. (ed.). 2006. *Neutron Scattering in Earth Sciences. Reviews in Mineralogy & Geochemistry* **63**, 471 p.

DO NOT COPY
e48d507df5d1141@placeholder.9409

Printed by: e48d507df5d1141@placeholder.94092.edu. Printing is for personal, private use only. No part of this book may be reproduced or transmitted without publisher's prior permission. Violators will be prosecuted.

LIST OF KEY TERMS

backscattered electrons
cathodoluminescence (CL)
detection limit
EDS
electron microprobe
electron probe microanalyzer
energy-dispersive X-ray spectrometer
EPMA
fuse
mass spectrometry
qualitative analysis
quantitative analysis
scanning electron microscope
secondary electrons
SEM
semi-quantitative
standard
wavelength-dispersive X-ray spectrometer
WDS
X-ray chemical map
X-ray fluorescence spectrometer
XRF

DO NOT COPY
e48d507df5d1141@placeholder.9409

Printed by: e48d507df5d1141@placeholder.94092.edu. Printing is for personal, private use only. No part of this book may be reproduced or transmitted without publisher's prior permission. Violators will be prosecuted.

CHAPTER 10
Strategies for Study

William D. Nesse
University of Northern Colorado

Graham B. Baird
University of Northern Colorado

DO NOT COPY
e48d507df5d1141@placeholder.9409

Printed by: e48d507df5d1141@placeholder.94092.edu. Printing is for personal, private use only. No part of this book may be reproduced or transmitted without publisher's prior permission. Violators will be prosecuted.

Introduction

The preceding four chapters describe a variety of techniques used to study minerals. The objective of this chapter is to provide systematic guidance directing a detailed investigation of a mineral. In most cases, mineral identification is done first, because without an identity, further study is impractical. Therefore, this guidance is principally intended to lead to an identification. Parts of the previous four chapters provide more detail of the discussed procedures and techniques. Additional information about many laboratory procedures can be found in Hutchison (1974), Zussman (1967), and Humphries (1992).

The study of minerals should start in the field (**Box 10.1**). Field research or fieldwork is important because it provides the geological context, which is often required for identification. Further, the need for mineral identification and further study is often driven by questions pertaining to the origin of the rocks and minerals in a region. For many common minerals, field identification with the aid of a hand lens is relatively easy with appropriate experience. If hand lens use and physical properties obtained through simple tests (Box 1.1; Chapter 6) still do not lead to an identification, or more analyses are needed, sample collection allows for further rock and/or mineral analysis in a laboratory (Box 10.1).

BOX 10.1
Introduction to Field Study and Sample Collection

Investigation of any rock or mineral, if possible, starts with outcrop observation. Initially this is done at a distance, typically 10 to 30 meters away. From this distance, it is determined whether one or more rock type exists, the overall color of each, the nature of the contact between the different rock types, the details of any rock layering, and other observations that can lead to identification of the rocks in the outcrop. Once all the important observations are made at a distance, the researcher systematically moves closer and laterally along the outcrop. Near the outcrop it may be possible to observe and study individual mineral grains. For each mineral, the researcher notes its color, size, habit, distribution, alignment, abundance (by way of a volume percent), and the details of cleavage, fracture, and/or crystal faces, etc. Hand lens study of rocks and minerals is mandatory and is often done last as it provides the most narrow and magnified view. A test kit (Box 1.1; Figure 1.2) or other field instrumentation may be used to provide mineral physical properties or other needed information.

All observations should be recorded in a **field notebook** (**Figure 10.1**). Any notes can be augmented by **photographs** and **sketches** that highlight important

DO NOT COPY e48d507df5d1141@placeholder.9409

Printed by: e48d507df5d1141@placeholder.94092.edu. Printing is for personal, private use only. No part of this book may be reproduced or transmitted without publisher's prior permission. Violators will be prosecuted.

observations, including those not easily described in words. When possible, photos should include an object of known size to provide a sense of scale, such as a person, a rock hammer, a hand lens, or a pen or pencil (**Figure 10.2**). Sketches too should include a scale, which could be an approximate scale bar. All photos and sketches should be described in the field notebook; the description should include the orientation of view plus the key features. Sketches can be annotated with text, labels, arrows, and so on that help highlight features. It is not uncommon for a researcher to photograph and sketch exactly the same view to ensure that all features are well shown.

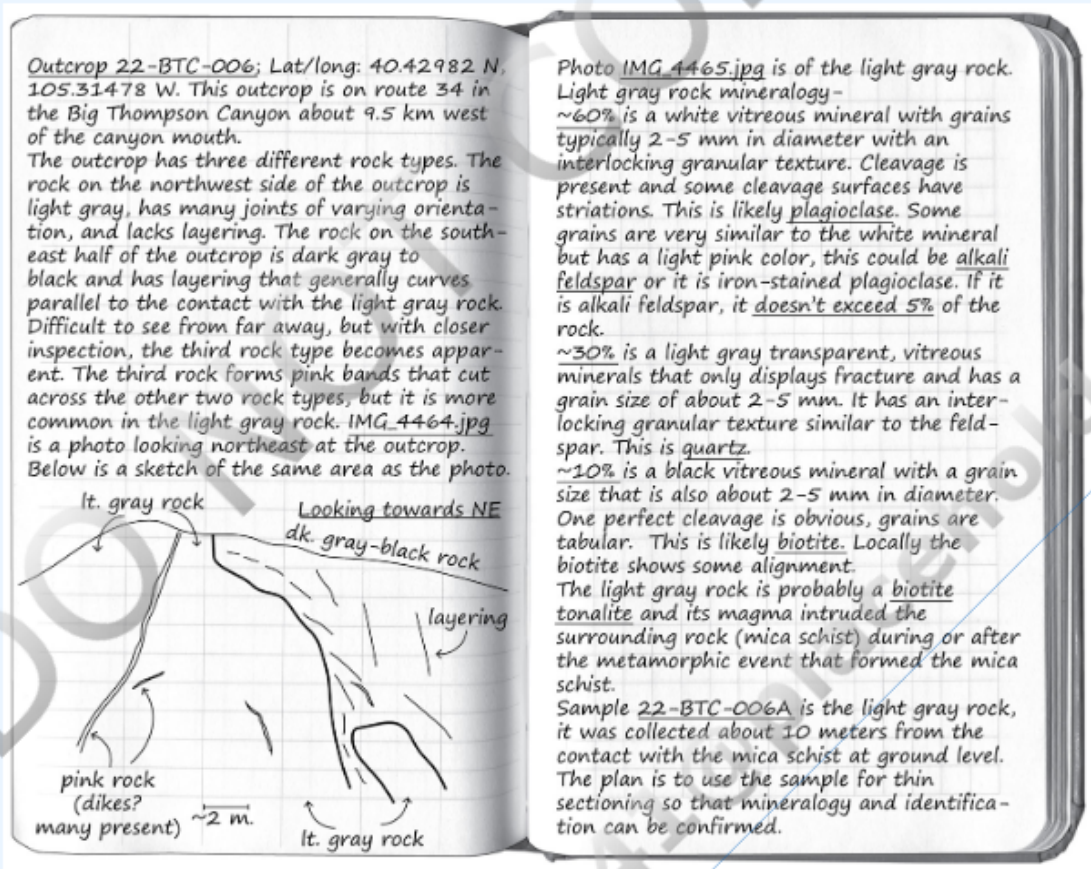

FIGURE 10.1 Example outcrop description entry in a field notebook. Only the notes that cover the outcrop general description and the light gray rock are shown. Underlining can be used to highlight important components, such as photographs, collected samples, and key observations. Figure 10.2 provides a photograph of the outcrop. Figure 10.4 is a photograph of the collected sample. View larger image

Printed by: e48d507df5d1141@placeholder.94092.edu. Printing is for personal, private use only. No part of this book may be reproduced or transmitted without publisher's prior permission. Violators will be prosecuted.

FIGURE 10.2 Photograph of the outcrop described by field notes and the sketch in Figure 10.1. Road marker in the lower right, about 1.5 meters tall, provides scale. View larger image

One of the primary goals of outcrop study is to identify the rock(s) present and their minerals. The systematic approach described above often leads to identification in the field, but this may not always be possible. In such cases, narrowing down the options can greatly aid further study. For example, just constraining the rock to belonging to one of the three rock types (igneous, sedimentary, or metamorphic) is very useful, as this greatly limits the list of possible minerals present because of mineral associations (Appendix C; Chapter 11). Similarly, for unidentifiable minerals, limiting the options based on cleavage or crystal form, for example, can be very useful.

Sample collection allows continued laboratory study of both identified and unidentified rocks and minerals without having to travel back to the site of collection. Sample collection is straightforward and typically involves removing a representative sample directly from the outcrop. The term *representative* is important and means that the collected sample should only, or mostly, include the rock or mineral of interest. For example, if the minerals in a granite will be used to determine the magma source that produced the rock, the sample must be pristine and exclude alteration or discoloration caused by weathering or by fluid migration along joints. However, if the alteration needs further study, then the sample must include the alteration. Often a rock hammer and chisel are used for sample removal (**Figure 10.3**). The collection of loose samples not directly from the outcrop is often discouraged; loose samples may have been transported from elsewhere by either humans or natural processes.

Printed by: e48d507df5d1141@placeholder.94092.edu. Printing is for personal, private use only. No part of this book may be reproduced or transmitted without publisher's prior permission. Violators will be prosecuted.

FIGURE 10.3 Sample collection directly from the outcrop aided by a hammer and chisel.
View larger image

Samples should be placed in a bag or a box and labeled with the date of collection; a unique sample label; the location of collection, including geographic coordinates such as latitude and longitude; the name of the collector; and perhaps a quick description of why the sample was collected (**Figure 10.4**). This information is recorded in the field notebook with additional information regarding the sample, such as exactly where in the outcrop the sample was collected.

DO NOT COPY

Printed by: e48d507df5d1141@placeholder.94092.edu. Printing is for personal, private use only. No part of this book may be reproduced or transmitted without publisher's prior permission. Violators will be prosecuted.

FIGURE 10.4 Collected sample. The sample description is recorded in the field notes (Figure 10.1) and on the bag label. Samples should be marked with a label using a permanent marker, shown for scale (14 cm). Canvas bags (shown) are often used to hold samples, but any sturdy bag or box can be used. View larger image

Sample size depends on the planned laboratory analyses. For most typical rocks and minerals, samples about 10 cm in diameter (called “fist sized”) provide plenty of material for thin sectioning, with the remaining intact sample used as a reference sample. Samples at least 30 cm in diameter may be required for radiometric dating (see Box 5.1), if the grain size is unusually large, or if some other planned analysis requires a large sample. **Oriented samples**, which have been marked with registration lines that allow the sample to be reoriented exactly as it was in the outcrop, may be necessary for certain petrologic and structural geologic studies. See Prior et al. (1987) for more information.

Other additions to the notebook during outcrop study often includes the best or most probable interpretations regarding the origins, history, and significance of the rock and its minerals based on the data collected thus far. With the interpretations, any planned laboratory analyses for the collected samples that may answer any outstanding questions should also be listed. Extensive field work experience and a clearly defined purpose will streamline field studies and the details included in the field notebook.

From collected samples, thin sections are almost always produced and studied with a petrographic microscope (Chapter 7). This can help determine mineral identifications and provide information about textural relations among minerals. This may be followed by oil immersion and X-ray diffraction study (Chapter 8) of selected grains to confirm an identification. If the sample is very fine grained, or if a quick estimate of mineral composition is needed, the scanning electron microscope (Chapter 9) is very useful. Electron microprobe analysis (Chapter 9) can provide detailed information about mineral composition. The results of these studies provide the raw materials for many petrological studies.

DO NOT COPY e48d507df5d1141@placeholder.9409-

Printed by: e48d507df5d1141@placeholder.94092.edu. Printing is for personal, private use only. No part of this book may be reproduced or transmitted without publisher's prior permission. Violators will be prosecuted.

Presentation of Mineral Data

To allow identification, the field- and laboratory-collected data often are compared to the descriptions and data on more than 100 common minerals provided in Chapters 12 through 20. These chapters are organized based on the chemical classification of the minerals. Silicates are presented first because they are by far the most abundant group of minerals. Data and descriptive information for each mineral are organized systematically, so that it is easy to find specific information.

Some of the information for tremolite–ferro-actinolite (Chapter 14; **Figure 10.5**) is used as an example and is typical of how the data are presented. Each mineral description begins with a summary of numerical data including the chemical formula, crystallography (crystal system, point group, unit cell dimensions), formula units per unit cell (Z), hardness (H), and specific gravity (G). This is followed by optical data including optical class (isotropic, uniaxial, biaxial), optic sign (+ or −), indices of refraction, birefringence (δ), and $2V_X$ for biaxial minerals.

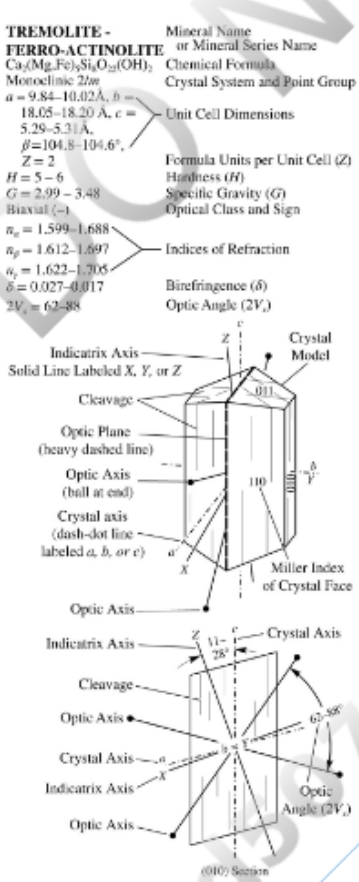

FIGURE 10.5 Presentation of mineral data. View larger image

Near the numerical data, one or more line drawings depicting a typical crystal model are

DO NOT COPY e48d507df5d1141@placeholder.94092

Printed by: e48d507df5d1141@placeholder.94092.edu. Printing is for personal, private use only. No part of this book may be reproduced or transmitted without publisher's prior permission. Violators will be prosecuted.

provided. Miller indices are shown for some faces, the traces of cleavages are shown with fine lines, and crystal axes are shown with dash-dot lines. For biaxial minerals, the trace of the optic plane is shown with a heavy dashed line, optic axes are shown with a solid line with a ball at the end, and optical indicatrix axes are solid lines labeled *X*, *Y*, and *Z*.

In many cases a drawing of a section through the crystal is provided, showing the relationships among crystal outline, crystal axes, cleavage, and indicatrix axes. This section helps visualize extinction angle relationships as seen in thin section. In the example shown for tremolite-ferro-actinolite, the extinction angle between the slow ray (parallel to *Z*) and the trace of cleavage in sections cut parallel to (010) is 11–28°. In this case the (010) section will display maximum birefringence because the *X* and *Z* indicatrix axes are in this plane.

The written material on each mineral presents information on structure, composition, form and twinning, cleavage, color, optical characteristics, alteration, distinguishing features, occurrence, and uses. Various diagrams and photographs also may be included.

DO NOT COPY
e48d507df5d1141@placeholder.9409

Printed by: e48d507df5d1141@placeholder.94092.edu. Printing is for personal, private use only. No part of this book may be reproduced or transmitted without publisher's prior permission. Violators will be prosecuted.

Mineral Identification Tactics

It is common in many introductory mineralogy courses to provide large, relatively pure samples of minerals for study. This makes it easy to observe and measure all of the normal hand-sample properties that may lead to a correct identification. In most geological work, however, minerals do not present themselves as large, easily identified samples. They are part of a rock or mineral deposit and intergrown with other minerals so that not all of their physical properties can be observed. Field identification, therefore, often depends on focusing on selected properties that distinguish similar minerals from each other. Knowledge of likely mineral associations (Appendix C) will suggest the identity of some minerals that can be confirmed by later laboratory study. Skill in identifying minerals comes with experience gained by examining many rocks and mineral deposits both in the field and laboratory settings.

Hand-Sample Identification

Hand-sample identification of an unknown mineral depends on systematically identifying the physical properties described in Chapter 6: color, luster, streak, specific gravity, hardness, cleavage/fracture, and so forth. Although identification based on these relatively crude and imprecise properties may seem haphazard, they yield remarkably good results when applied systematically, but success is by no means guaranteed. Careful examination with a hand lens or binocular microscope is essentially required. Proceed as follows.

- Observe and record crystal habit or grain shape. If crystals are well developed (euhedral), determine or narrow down the crystal system to which the mineral belongs based on symmetry and the geometry of the crystals.
- Observe and record color, luster, and streak. Use a streak plate if it is available; otherwise just crush a bit of the sample.
- Carefully examine the mineral to determine whether it has cleavage, and if so, in how many different directions and the angles between them. To do this, a hand lens or binocular microscope is nearly always required. Fine grains may reveal cleavage by a flash or sparkle when moved. Be alert to the possibility that what appears to be a cleavage may actually be a parting. On noncleavage surfaces, observe and record the nature of the fracture. Crushing a bit of sample can aid in investigating cleavage and fracture.
- Measure the hardness by scratching the sample with a fingernail ($H = 2.5$), copper penny ($H = 3$), knife blade ($H = 5$), glass ($H = 5.5$), and/or piece of quartz ($H = 7$). Also scratch the scratch tester of known hardness with the sample to confirm

DO NOT COPY e48d507df5d1141@placeholder.9409

Printed by: e48d507df5d1141@placeholder.94092.edu. Printing is for personal, private use only. No part of this book may be reproduced or transmitted without publisher's prior permission. Violators will be prosecuted.

results. Be careful, as minerals that have suffered some alteration may be softer than normal. Record the hardness by the range of possible values. For example, if a sample scratches a penny but not a knife blade, record the hardness as 3–5, meaning the hardness may be 3, 4, or 5.

- Apply other tests as necessary, including:

  Estimate the specific gravity by hefting the sample, if it is large enough.

  Determine whether the sample is strongly, weakly, or not attracted to a magnet.

  Determine whether the sample effervesces in hydrochloric acid when powdered or not.

  Determine whether the sample has a notable smell when wetted or introduced to hydrochloric acid.

This provides the basic data for use with Tables B.1, B.2, or B.3 in Appendix B, which may lead to an identity, or more commonly, a short list of possibilities for most of the common minerals. Table B.1 is for minerals with nonmetallic luster and white, gray, or pale-colored streak. Table B.2 is for minerals with nonmetallic luster and distinctly colored streak. Table B.3 is for minerals with metallic or submetallic luster. Within each table, minerals are grouped based on hardness, whether cleavage is prominent, and their color. Within Table B.1, cleavable minerals are further separated into groups based on the number of cleavages. Relatively common minerals are indicated with bold type.

Begin with the appropriate table based on luster and streak. The combination of hardness, cleavage, and color will yield a relatively short list of possible minerals. Combine the lists for one, two, and three or more cleavages on Table B.1 if the number of cleavages cannot be determined with certainty. The list of possible minerals may be shortened if specific gravity is precisely measured (Chapter 6; Figure 6.2) by using Table B.4, which lists minerals in order of increasing specific gravity. *The objective here is to acquire a list of possibilities; identification should await study of the more detailed information contained in the descriptions of these possible minerals in Chapters 12 through 20*. Some prior knowledge of the likely mineralogy of the sample based on association (Appendix C; Chapter 11) can greatly expedite the process.

Unfortunately, mineral identification often is not the highly organized step-by-step process implied here. Physical properties show substantial variability and, because of grain size or other difficulties, it may not be possible to determine some properties. Not infrequently, these difficulties make it impossible to identify a sample using hand-sample techniques, and X-ray diffraction, optical properties, scanning electron microscope, or other means must be used.

In practice, the apparent ease with which experienced mineralogists and mineral collectors recognize minerals depends on a subjective summation of the physical properties and a variety of other subtle cues. Clues from the rock that houses the mineral

Printed by: e48d507df5d1141@placeholder.94092.edu. Printing is for personal, private use only. No part of this book may be reproduced or transmitted without publisher's prior permission. Violators will be prosecuted.

and the geologic setting are often vitally important too. Once familiarity has been gained with a mineral, identification may be possible on sight or with the application of one or two diagnostic tests that distinguish among similar minerals. Regardless, if correct identification is critical, most mineralogists confirm hand-sample identifications with optical properties, X-ray diffraction, chemical analysis, or other techniques.

Thin Section Identification

Examination of thin sections provides one of the most productive means of studying rocks. Thin sections are slices of rock about 0.03 mm thick mounted on glass microscope slides (Figure 7.1). Consult Humphries (1992) and Murphy (1986) for additional information concerning specific preparation techniques. While various machines are available to speed the process and improve accuracy and consistency, the basic preparation process is as follows.

- A chip of rock, also called a billet, slightly smaller than a microscope slide is cut from a hand sample. Standard petrographic slides are 27 mm × 46 mm.
- If the sample is porous and/or friable (easily broken), it should be impregnated with an epoxy. Sample impregnation begins with immersing the sample in a small container of liquid epoxy and placing it under vacuum in a vacuum chamber. This removes air from pores in the sample. When the vacuum is broken, epoxy is forced into the pores. The epoxy is allowed to cure.
- The side of the rock chip to be glued to the microscope slide is ground smooth and flat, beginning with coarse abrasive and finishing with 600-grit abrasive for typical thin sections.
- The rock chip is glued to a clean microscope slide by using an epoxy, UV-setting adhesive, or other cement.
- When the epoxy is cured, surplus rock is cut off with a diamond trim saw and the thin section is ground to its final thickness, usually 0.03 mm. Though specialized machines may be used, final grinding to the correct thickness is usually done by hand. The interference color (see Chapter 7 and Plate 1) of quartz or other mineral in the sample is used to determine thickness.
- If desired, the thin section may be stained for K-feldspar, plagioclase, carbonate minerals, and others. Hutchison (1974), Bailey and Stevens (1960), Boone and Wheeler (1968), Houghton (1980), and Ruperto and others (1964) provide instructions.
- The sample is completed either by cementing a coverslip in place or by polishing the surface to a mirror finish. Polishing is required for study by reflected light or for use with a scanning electron microscope or electron microprobe (see section on Scanning Electron Microscope [SEM] and Electron Microprobe [EPMA]).

Tactics to measure optical properties and identify minerals in thin section are described

DO NOT COPY e48d507df5d1141@placeholder.9409

Printed by: e48d507df5d1141@placeholder.94092.edu. Printing is for personal, private use only. No part of this book may be reproduced or transmitted without publisher's prior permission. Violators will be prosecuted.

Tactics to measure optical properties and identify minerals in thin section are described in Box 7.1.

Grain Mount Identification

Grain mounts are prepared and examined as follows.

- Separate, crush, sieve, and clean grains as described in the next section. The −100/+170 or −140/+200 mesh ranges work well.
- Sprinkle a few dozen grains on a microscope slide and cover with a piece of coverslip. To immerse the grains, place a small drop of immersion oil next to the coverslip; it will be drawn under by capillary action.

Tactics to measure optical properties and identify minerals in grain mount are described at the end of Chapter 7.

Sample Polishing and Identification Using Reflected Light

Polished samples may be either polished thin sections or samples mounted in epoxy and polished. Polishing is accomplished by progressively grinding the surface with finer and finer abrasives. Grinding through 1000-grit abrasive is commonly done on a rotating lap wheel with abrasive disks or powdered abrasive. Finer abrasives, including aluminum oxide and diamond pastes, are usually applied to a fabric disk mounted on a rotating lapping wheel. Careful sample cleaning between use of different abrasives must be done to avoid contaminating one lapping disk with coarser abrasive from another. Details of polishing procedures depend on the equipment that is available and the particular sample, but for typical rock and mineral samples, polishing for about five minutes each sequentially using 15 µm, 9 µm, 5 µm, 3 µm, and 1 µm diamond pastes should result in a mirror-like smooth sample surface.

Procedures for observing optical properties with reflected light are described in Chapter 7.

Scanning Electron Microscope (SEM) and Electron Microprobe (EPMA)

The general procedure for analyzing polished samples with a scanning electron microscope (SEM) or electron microprobe (EPMA) is to first image the sample using backscattered electrons. Using backscattered electron, each mineral should have a different brightness as each mineral should have a different average atomic number. Energy dispersive spectra on selected minerals can be obtained in as little as five seconds

DO NOT COPY e48d507df5d1141@placeholder.9409

Printed by: e48d507df5d1141@placeholder.94092.edu. Printing is for personal, private use only. No part of this book may be reproduced or transmitted without publisher's prior permission. Violators will be prosecuted.

Energy dispersive spectra on selected minerals can be obtained in as little as five seconds each to quickly determine their major element chemistry. This may be followed by precise chemical analysis using the wavelength-dispersive spectrometers found on EPMAs. Element mapping and cathodoluminescence images can help document chemical zoning, mineral textures, and mineral growth histories. See Chapter 9 for more information.

X-Ray Diffraction

X-ray diffraction is routinely used to confirm an identity made with hand-sample or optical techniques or to identify minerals whose grain size is too fine for either of these methods. The material used for X-ray diffraction may be the fine-grained material left over from grain mount preparation or other material that has been selected. An absolutely pure sample is not needed, but excessive contamination can lead to difficulty when interpreting the data.

The sample consists of a finely ground powder of the unknown mineral mounted as described in Chapter 8. See Chapter 8 for more detail.

DO NOT COPY
e48d507df5d1141@placeholder.9409

Printed by: e48d507df5d1141@placeholder.94092.edu. Printing is for personal, private use only. No part of this book may be reproduced or transmitted without publisher's prior permission. Violators will be prosecuted.

Mineral Separation

The techniques employed for mineral separation depend on the amount of material needed and its purity. Radiometric dating (see Box 5.1) often requires upward of a gram of a datable mineral that has been separated from all other minerals. Zircon, for example, is often only a trace accessory mineral in most rocks, which means a few kilograms of rock must be processed to obtain the required sample. The routine methods of mineral separation include rock crushing, sieving, density separation, magnetic separation, and picking by hand. Which methods are used and their order varies depending on the mineral(s) sought, amount needed, grain size, and abundance. These same techniques are widely used in the mining industry on very large scales to obtain extremely pure ore mineral samples.

Rock/Mineral Crushing

No matter the amount of sample crushed, adequate equipment must always be used to protect eyes and ears; prevent dust inhalation (via an appropriate respirator); and perhaps to protect hands, feet, face, and so on. The purpose of crushing a sample is either to ensure individual minerals are separate from each other or to produce the small grains that are required for various analyses.

A small sample of crushed rock can be obtained by breaking apart a rock with hammer and chisel and crushing the sample with a piston-type percussion mortar (**Figure 10.6a**). If grains are small and only a few are needed, a dental pick or similar probe can be used to break out and hand pick the desired grains with the aid of a binocular microscope or hand lens.

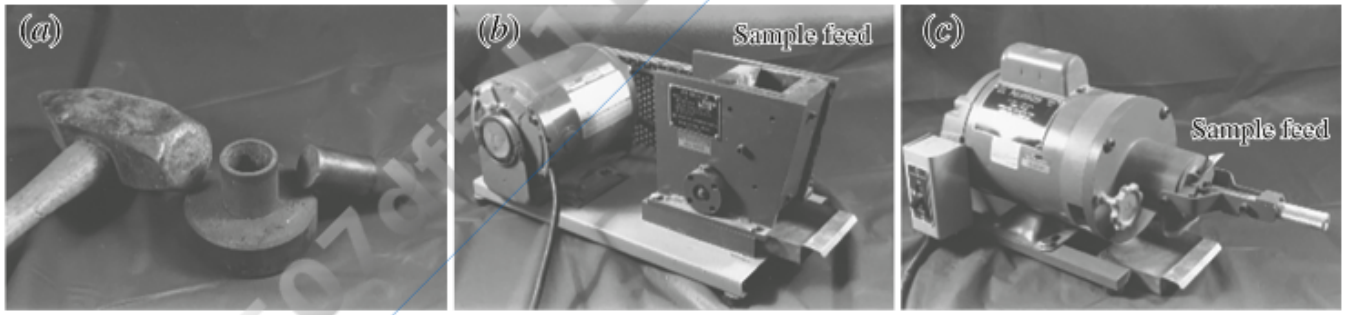

FIGURE 10.6 Crushing tools. (*a*) Piston-type percussion steel mortar and pestle. The mortar accepts samples upward of about 2 cm in diameter. The sample is crushed by placing the pestle on top of the sample in the mortar and tapping the pestle down against the sample with a hammer. (*b*) Laboratory jaw crusher. This relatively small jaw crusher accepts samples upward of about 2 cm in diameter; larger version can crush samples upward of tens of decimeters in diameter. A jaw crusher crushes samples by moving a plate toward and away an immovable plate, similar to the motion of

Printed by: e48d507df5d1141@placeholder.94092.edu. Printing is for personal, private use only. No part of this book may be reproduced or transmitted without publisher's prior permission. Violators will be prosecuted.

jaws of a feeding animal. (*c*) Rotary mill. The sample is fed into the chute and is crushed between rotating plates. This small mill accepts samples upward of about 5 mm in diameter; larger versions can crush samples upward of 1–2 cm in diameter. View larger image

If a large amount of sample is needed, a variety of tools are available to crush samples. Often a rock saw, hammer and chisel, and/or hydraulic press designed to break rocks are used to reduce the size of large samples such that they will fit into the feed hopper of crushing tools. Jaw crushers can reduce rocks to particles as small as a few millimeters, and rotary or disc mills can produce substantially finer grains (**Figure 10.6b**, **c**). Often samples will be processed initially by jaw crusher to reduce the grain size enough so that final grinding to the desired size can be done by a rotary or disc mill. Any crushing equipment must be thoroughly cleaned between different samples to avoid contamination. As a general rule, crushing igneous and metamorphic rocks should produce fragments between one-fourth and one-tenth the average grain size of the rock to ensure that most grains are monomineralic (are composed of a single mineral). Grain size of trace accessory minerals used for radiometric dating is often much smaller than the rock grain size, often 50–500 microns.

Crushing clastic sedimentary rocks requires some care because the shape of detrital grains may need to be preserved. As long as the rock is not strongly indurated (lithified), disaggregation can be accomplished in a steel mortar and pestle, or even by hand. In some cases, calcareous cement can be removed or weakened by soaking in dilute acid. Some fine-grained sedimentary rocks such as shale and mudstone may be mixed with water and disaggregated (broken apart) in a kitchen blender.

Sieving

Crushed samples may be sieved to select grains with the desired size. **Table 10.1** shows common sieve sizes. Particles that pass a 100-mesh sieve and collect on the 170-mesh sieve, or that pass a 140-mesh sieve and collect on the 200-mesh sieve, are commonly used. Sieved grains should be examined with a binocular microscope to confirm that each grain is monomineralic. If not, a finer-sized fraction may be required. Sieves come in different diameters; small sample volumes can be quickly sieved with 3-inch diameter sieves (**Figure 10.7**); large sample volumes can be sieved by 8- to 10-inch diameter sieves with or without use of automated shakers.

TABLE 10.1 Sieve Openings

ASTM[a] Number	Openings (mm)
80	0.180
100	0.150
120	0.125

Printed by: e48d507df5d1141@placeholder.94092.edu. Printing is for personal, private use only. No part of this book may be reproduced or transmitted without publisher's prior permission. Violators will be prosecuted.

140	0.106
170	0.090
200	0.075
230	0.063
270	0.053
325	0.045
400	0.038
450	0.032

[a] American Society for Testing and Materials.

FIGURE 10.7 Sieve used with small samples. On the left is a sieve, constructed of a brass ring with brass wire mesh that only allows grains of a certain size to pass. Usually two sieves of different sizes are stacked (larger size on top) with a lid and base (on right). Sample is added to the top sieve in the stack, the lid is placed, and the whole stack is shaken until no more sample passes through the sieves. View larger image

Grain Washing

For small samples totaling a few tens of grams, crushed and sieved material may need to be washed to remove fine dust from the particle surfaces. This can be done by placing the selected grains into a beaker. Tap water (or distilled water) is added to the beaker and thoroughly agitated, suspending the finest material. The water holding the suspended

Printed by: e48d507df5d1141@placeholder.94092.edu. Printing is for personal, private use only. No part of this book may be reproduced or transmitted without publisher's prior permission. Violators will be prosecuted.

thoroughly agitated, suspending the finest material. The water holding the suspended material can then be decanted (poured off). This procedure is repeated several times until all of the fines are removed. Wet grains are then transferred to a watch glass or poured into funnel with filter paper and are left to dry. Acetone or alcohol may be used instead of water to decrease the drying time.

Density Separation

There are two basic methods for separating grains by density. One method employs the varying behavior of different density minerals in flowing water. The second method employs heavy liquids in which dense minerals sink and light minerals float.

A gold pan is a simple tool that separates minerals by the first method. Mineral grains are placed in the pan and agitated by shaking the pan; this places the grains in suspension. During agitation, dense minerals migrate to the bottom of the pan. As agitation stops, lighter minerals are deposited on top of the dense minerals. Water is then washed over the grains to remove the light minerals on top. The process is repeated until the heaviest minerals are left. Shaker tables, also called wash tables, work in the same way but on a large scale, and often the process is automated (**Figure 10.8**). Mineral grains are introduced at one end of the table by an automated feeder, and water constantly washes across the table surface as it shakes. The table surface has either grooves or ridges that catch the dense minerals while the water washes the light minerals over the ridges or across the grooves. The ridges or grooves direct the heavy minerals to a specific location on the edge of the table where they are collected.

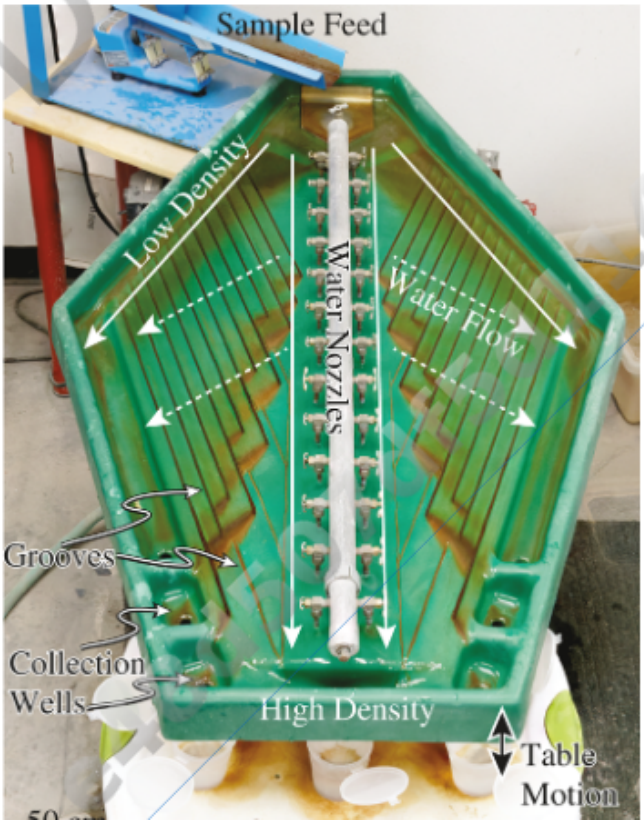

DO NOT COPY

Printed by: e48d507df5d1141@placeholder.94092.edu. Printing is for personal, private use only. No part of this book may be reproduced or transmitted without publisher's prior permission. Violators will be prosecuted.

FIGURE 10.8 Shaker table. For this type of table, sample is added to the table at the top of the image by a feed hopper, and water from water nozzles along the table center washes lighter grains to the side while the table shakes back and forth. Dense grains are caught in grooves and are directed to the collection wells at the bottom of the table. View larger image

There are a variety of heavy liquids of varying density routinely used to separate minerals based on their density (Table 6.1). The organic liquids—bromoform, tetrabromoethane, and diiodomethane—are toxic and must be used in a fume hood. The tungstate products are much less toxic, but their higher viscosity means that the separation process takes longer. Refer to Material Safety Data Sheets for appropriate safety precautions to be employed with all these materials.

The density of a heavy liquid can be adjusted by dilution with a solvent so that it lies between the densities of the minerals to be separated. The organic liquids may be diluted with acetone or certain other organic solvents. The tungstate products may be diluted with water. Lithium heteropolytungstate (LST) density also can be varied by changing the temperature. The density of the modified heavy liquid may be determined by weighing a known volume of the liquid or by comparison with aerometers, which are spheres with a known density.

Density separation by a heavy liquid is done with a separatory funnel in which both the heavy liquid and sample are placed (**Figure 10.9**). Low- and high-density minerals float and sink, respectively; periodic stirring helps produce a good separation. When separation is complete, the valve (stopcock) at the bottom of the separatory funnel is opened just so that the high-density minerals and part of the liquid can drain. The high-density minerals are retained on a filter paper in a funnel and the liquid passes into a beaker for reuse. The low-density minerals are subsequently drained and collected on a fresh filter paper. Many laboratories employ a centrifuge to increase the speed and efficiency of separation, particularly when the tungstate liquids are used.

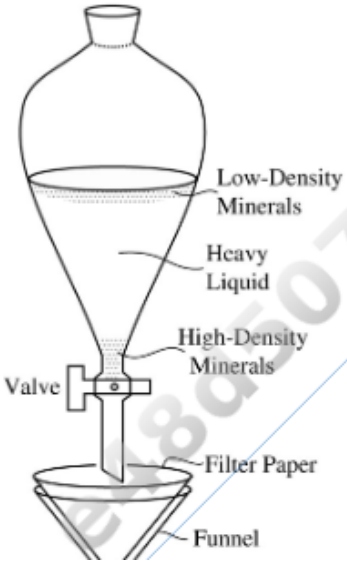

DO NOT COPY
e48d507df5d1141@placeholder.9409

Printed by: e48d507df5d1141@placeholder.94092.edu. Printing is for personal, private use only. No part of this book may be reproduced or transmitted without publisher's prior permission. Violators will be prosecuted.

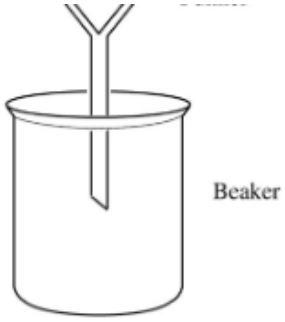

FIGURE 10.9 Separatory funnel setup. View larger image

Grains on the filter papers are washed with the appropriate solvent to remove traces of the heavy liquid. Additional separation among minerals in each density fraction may be accomplished with different heavy liquids.

Because heavy liquids are expensive, they are recovered from mixtures and from waste produced by washing grains and the apparatus. For the tungstate products, simple evaporation in an open container will remove the water. More complex reverse-osmosis apparatus may be used if large volumes are involved. Bromoform and methylene iodide are "washed" with distilled water several times. Because acetone is soluble in water, but bromoform and methylene iodide are not, water extracts acetone from the heavy liquid. The water, which floats on the heavy liquid, is decanted after each washing.

Heavy liquids only work well with small samples, so for large samples, wash tables are employed first to reduce the sample size to include a general range of densities. Precise density separation by heavy liquids can then be done on the reduced sample size.

Magnetic Separation

A very simple magnetic separation technique uses an ordinary magnet wrapped in a sheet of plastic. The crushed and sieved sample is spread on a piece of paper and the plastic-wrapped magnet is moved over or through the grains to pull off magnetite and other strongly ferro- or ferrimagnetic minerals. The magnetic grains are retrieved by stripping the plastic from the magnet over a clean piece of paper. This simple technique is typically necessary before further separation by either of the Frantz magnetic separation techniques discussed next, as strongly ferro- or ferrimagnetic minerals can clog the instrument.

A **Frantz® Magnetic Barrier Laboratory Separator** is available in many laboratories and can be used to separate paramagnetic minerals based on their magnetic susceptibilities and to separate paramagnetic from diamagnetic minerals (Chapter 6). The instrument consists of a chute positioned between the poles of a strong electromagnet. Mineral grains are placed into the feed hopper and a vibrator agitates the grains so they flow freely into the inclined chute. The inclined chute is also tilted to the side such that gravity pulls the grains down the chute and to the low side. An

DO NOT COPY e48d507df5d1141@placeholder.94092

Printed by: e48d507df5d1141@placeholder.94092.edu. Printing is for personal, private use only. No part of this book may be reproduced or transmitted without publisher's prior permission. Violators will be prosecuted.

electromagnet produces a magnetic field that causes paramagnetic minerals to be pulled to the high side of the chute. A splitting ridge divides the minerals into two populations that are collected in separate containers. Different mineral fractions are separated by running the sample through the apparatus using progressively higher magnetic field strengths and by adjusting the inclination and tilt of the chute. The mineral fraction left after the paramagnetic minerals have been removed usually consists of diamagnetic quartz and feldspar. The closely related **Frantz® Magnetic Barrier Laboratory Separator** is a significant refinement and allows more precise separations among paramagnetic minerals and also among diamagnetic and weakly paramagnetic minerals.

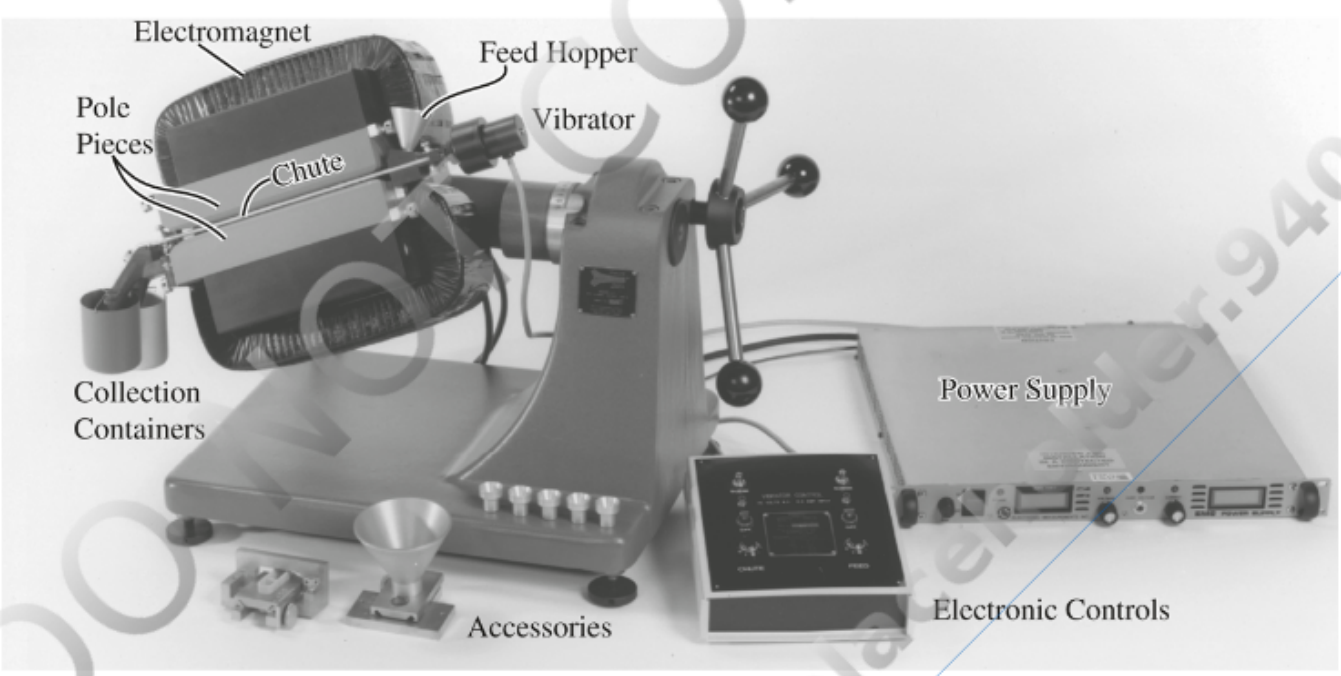

FIGURE 10.10 Frantz® Magnetic Barrier Laboratory Separator. The closely related Frantz® Magnetic Barrier Laboratory Separator provides improved capabilities and appears much similar but with a different feed hopper and chute. Photo courtesy of S. G. Frantz Company. View larger image

DO NOT COPY e48d507df5d1141@placeholder.9409-

Printed by: e48d507df5d1141@placeholder.94092.edu. Printing is for personal, private use only. No part of this book may be reproduced or transmitted without publisher's prior permission. Violators will be prosecuted.

Mineral Association

Mineral associations are never random. Some mineral combinations are very common and form certain rock types or mineral deposits, and other mineral combinations are rarely found. Therefore, knowledge of common rock mineralogy and of mineral deposits can aid in making educated guesses about the possible identity of an unknown mineral. Further, knowledge of mineral associations can suggest the presence of a mineral that otherwise might be overlooked.

A certain amount of caution is required when using mineral associations because it may be possible to overlook the presence of an unusual mineral in a rock or mineral deposit. Often unusual minerals have important implications regarding the history and origin of the rock.

The lists of mineral associations in Appendix C show the minerals likely found in a variety of common rock and mineral deposits. The list is not intended to be exhaustive and does not contain the unusual associations that can confound and delight geologists, nor does it contain any alteration or weathering products that may be present. Chapter 11 and the mineral entries (Chapters 11–20) provide context for and the meaning of many mineral associations.

DO NOT COPY e48d507df5d1141@placeholder.9409

Printed by: e48d507df5d1141@placeholder.94092.edu. Printing is for personal, private use only. No part of this book may be reproduced or transmitted without publisher's prior permission. Violators will be prosecuted.

Problems in Paradise

Mineral identification is often difficult. Some of the common problems encountered include the following.

INSUFFICIENT DATA AND COSTS: For many mineral specimens, it may not be possible to identify the mineral based on easily obtained physical properties, hand lens use, and mineral associations. Thin sections, the equipment needed to fabricate them, and petrographic microscopes all are very costly. Unfortunately, though petrographic analysis is an essentially required investigation technique, it may not be available. For some samples, even petrographic analysis might not provide the needed data. Data from scanning electron microscope or electron microprobe imaging, mineral chemistry, isotopic analysis, and/or X-ray diffraction may be required, but such analytical instruments maybe inaccessible as typically they are only available to those with direct connections to an analytical or university laboratory. Even if access is available, the cost of their use can be quite high.

ALTERATION: Alteration, from either weathering or hydrothermal processes, may affect mineral color, luster, specific gravity, and hardness. In many cases, alteration converts the primary mineral to various fine-grained phyllosilicate and oxide minerals whose presence may be indicated by a cloudy or chalky appearance; red, yellow, orange, or brown staining; or anomalous softness. In thin section and grain mount, the altering minerals similarly make minerals appear cloudy or speckled, and stain grains red, yellow, orange, or brown. In rare instances, some alteration products may be sufficiently coarse grained to be identified.

MIXTURES: It is not uncommon for two or more minerals to be intimately intergrown, making it impossible to obtain relatively pure material for standard hand sample analysis. In such situations, the sample bulk physical properties are not those of any of the constituent minerals. The nature of the intergrowth is generally evident in thin section, and individual constituents may be identified by using microscopic or X-ray techniques.

INCONSISTENCIES IN CRYSTAL AXES: In orthorhombic, monoclinic, and triclinic minerals, crystal axes may be assigned in several different ways. The convention adopted in this book is to assign axes based on external morphology. However, in some X-ray structural studies, it is convenient to assign axes differently. This has led to a substantial amount of confusion in the literature, where optical and physical properties are described based on one set of crystal axes, while the structure is described using crystal axes in another orientation. Even authoritative sources such as the series of reference works by Deer and others (1997–2011) and Anthony and others (1990–2003) are not immune to this problem. A concerted effort has been made to use consistent crystal axis orientations for all properties in the mineral descriptions, but the reader is cautioned that problems may persist and that care must be exercised when comparing data from different sources.

POORLY CONSTRAINED PROPERTIES: Most of the optical and physical properties reported in this and other standard mineralogy resources are based on observations and reports from over a century ago. These data are uncritically repeated in each new text or reference work, with a few additions or modifications based on new measurements gleaned from the literature. Old errors are perpetuated and new, often unrepresentative data are added. As a general rule, data from the reference works by Deer and others (1997–2011)

DO NOT COPY e48d507df5d1141@placeholder.94092

Printed by: e48d507df5d1141@placeholder.94092.edu. Printing is for personal, private use only. No part of this book may be reproduced or transmitted without publisher's prior permission. Violators will be prosecuted.

added. As a general rule, data from the reference works by Deer and others (1997–2011) and/or Anthony and others (1990–2003) are used here, but other sources were used where deemed appropriate. Because of the significant time required to systematically verify and update the mineralogical data, it has not been attempted. However, in a few instances, the authors of this text have simplified descriptor terms or have changed the reported properties such that they are consistent with specimens they have encountered. Regardless, it is certainly possible to find examples of inconsistencies in a mineral's properties and its description.

DO NOT COPY
e48d507df5d1141@placeholder.9409

Printed by: e48d507df5d1141@placeholder.94092.edu. Printing is for personal, private use only. No part of this book may be reproduced or transmitted without publisher's prior permission. Violators will be prosecuted.

ALTERATION: Alteration, from either weathering or hydrothermal processes, may affect mineral color, luster, specific gravity, and hardness. In many cases, alteration converts the primary mineral to various fine-grained phyllosilicate and oxide minerals whose presence may be indicated by a cloudy or chalky appearance; red, yellow, orange, or brown staining; or anomalous softness. In thin section and grain mount, the altering minerals similarly make minerals appear cloudy or speckled, and stain grains red, yellow, orange, or brown. In rare instances, some alteration products may be sufficiently coarse grained to be identified.

MIXTURES: It is not uncommon for two or more minerals to be intimately intergrown, making it impossible to obtain relatively pure material for standard hand sample analysis. In such situations, the sample bulk physical properties are not those of any of the constituent minerals. The nature of the intergrowth is generally evident in thin section, and individual constituents may be identified by using microscopic or X-ray techniques.

INCONSISTENCIES IN CRYSTAL AXES: In orthorhombic, monoclinic, and triclinic minerals, crystal axes may be assigned in several different ways. The convention adopted in this book is to assign axes based on external morphology. However, in some X-ray structural studies, it is convenient to assign axes differently. This has led to a substantial amount of confusion in the literature, where optical and physical properties are described based on one set of crystal axes, while the structure is described using crystal axes in another orientation. Even authoritative sources such as the series of reference works by Deer and others (1997–2011) and Anthony and others (1990–2003) are not immune to this problem. A concerted effort has been made to use consistent crystal axis orientations for all properties in the mineral descriptions, but the reader is cautioned that problems may persist and that care must be exercised when comparing data from different sources.

POORLY CONSTRAINED PROPERTIES: Most of the optical and physical properties reported in this and other standard mineralogy resources are based on observations and reports from over a century ago. These data are uncritically repeated in each new text or reference work, with a few additions or modifications based on new measurements gleaned from the literature. Old errors are perpetuated and new, often unrepresentative data are added. As a general rule, data from the reference works by Deer and others (1997–2011) and/or Anthony and others (1990–2003) are used here, but other sources were used where deemed appropriate. Because of the significant time required to systematically verify and update the mineralogical data, it has not been attempted. However, in a few instances, the authors of this text have simplified descriptor terms or have changed the reported properties such that they are consistent with specimens they have encountered. Regardless, it is certainly possible to find examples of inconsistencies in a mineral's properties and its description.

REFERENCES CITED AND SUGGESTIONS FOR ADDITIONAL READING

DO NOT COPY e48d507df5d1141@placeholder.9409

Printed by: e48d507df5d1141@placeholder.94092.edu. Printing is for personal, private use only. No part of this book may be reproduced or transmitted without publisher's prior permission. Violators will be prosecuted.

Anthony, J. W., Bideaux, R. A., Bladh, K. W., and Nichols, M. C. 1990–2003. *Handbook of Mineralogy* (5 volumes). Mineral Data Publishing, Tucson, AZ.

Bailey, E. H., and Stevens, R. E. 1960. Selective staining of K-feldspar and plagioclase on rock slabs and thin sections. *American Mineralogist* **45**, 1020–1025.

Boone, G. M., and Wheeler, E. P. II. 1968. Staining for cordierite and feldspars in thin section. *American Mineralogist* **53**, 327–331.

Deer, W. A., Howie, R. A., and Zussman, J. 1997–2011. *Rock-Forming Minerals* (5 volumes). Geological Society, London.

Fleischer, M., Wilcox, R. E., and Matzko, J. J. 1984. *Microscopic Determination of the Nonopaque Minerals*. U.S. Geological Survey Bulletin 1627, 453 p.

Houghton, H. F. 1980. Refined techniques for staining plagioclase and alkali-feldspars in thin section. *Journal of Sedimentary Petrology* **50**, 629–631.

Humphries, D. W. 1992. *The Preparation of Thin Sections of Rocks, Minerals, and Ceramics*. Oxford University Press, New York, 83 p.

Hutchison, C. S. 1974. *Laboratory Handbook of Petrographic Techniques*. John Wiley & Sons, New York, 527 p.

Murphy, C. P. 1986. *Thin Section Preparation of Soils and Sediments*. A B Academic Publishers, Berkhamsted, UK, 149 p.

Nesse, W. D. 2013. *Introduction to Optical Mineralogy*, 4th ed. Oxford University Press, New York, 361 p.

Phillips, W. R., and Griffen, D. T. 1981. *Optical Mineralogy, the Nonopaque Minerals*. W. H. Freeman, San Francisco, 677 p.

Prior, D. J., Knipe, R. J., Bates, M. P., Grant, N. T., Law, R. D., Lloyd, G. E., Welbon, A., Agar, S. M., Brodie, K. H., Maddock, R. H., Rutter, E. H., White, S. H., Bell, T. H., Ferguson, C. C., and Wheeler, J. 1987. Orientation of specimens: Essential data for all fields of geology. *Geology* **15**, 829–831.

Ruperto, V. L., Stevens, R. E., and Normans, M. B. 1964. Staining of plagioclase feldspars and other minerals with F.D. and C. No. 2. U.S. *Geological Survey Professional Paper* **501B**, B152–B153.

Troger, W. E. 1979. *Optical Determination of Rock-Forming Minerals, Part I: Determinative Tables*. English edition of the 4th German edition by H. U. Bambaur, F. Taborgzky, and H. D. Trochim. Schwiezerbart'sche Verlagsbuchhandlung, Stuttgart, 1988 p.

Zussman, J. 1967. *Physical Methods in Determinative Mineralogy*. Academic Press, London, 514 p.

DO NOT COPY e48d507df5d1141@placeholder.9409-

Printed by: e48d507df5d1141@placeholder.94092.edu. Printing is for personal, private use only. No part of this book may be reproduced or transmitted without publisher's prior permission. Violators will be prosecuted.

LIST OF KEY TERMS

alteration

field notebook

Frantz Isodynamic Magnetic Separator

Frantz Magnetic Barrier Separator

oriented sample

photograph

sample

sketch

DO NOT COPY

e48d507df5d1141@placeholder.9409

Printed by: e48d507df5d1141@placeholder.94092.edu. Printing is for personal, private use only. No part of this book may be reproduced or transmitted without publisher's prior permission. Violators will be prosecuted.

PART THREE

MINERAL DESCRIPTIONS

William D. Nesse
University of Northern Colorado

Graham B. Baird
University of Northern Colorado

DO NOT COPY
e48d507df5d1141@placeholder.9409

Printed by: e48d507df5d1141@placeholder.94092.edu. Printing is for personal, private use only. No part of this book may be reproduced or transmitted without publisher's prior permission. Violators will be prosecuted.

CHAPTER 11
Silicates

William D. Nesse
University of Northern Colorado

Graham B. Baird
University of Northern Colorado

DO NOT COPY
e48d507df5d1141@placeholder.9409

Printed by: e48d507df5d1141@placeholder.94092.edu. Printing is for personal, private use only. No part of this book may be reproduced or transmitted without publisher's prior permission. Violators will be prosecuted.

Introduction

The silicate minerals are by far the most abundant group of minerals in the Earth's crust and therefore this text includes an extensive discussion of their structure, chemistry, properties, and occurrences. The abundance of the silicates should be no surprise given that oxygen and silicon are the most abundant elements in the crust (Chapter 3). In general, silicate minerals can hold a wealth of information regarding how a rock was formed, the likelihood of a nearby ore deposit, or some of the controls of surface and groundwater chemistry for an area.

A few silicates are used as precious or semiprecious gemstones. Quartz, for example, can form exquisite crystals that appeal to mineral collectors and many children and adults alike. Most silicates, however, are drab and ordinary looking, which makes them easy to ignore. In general, few silicates draw attention as a few flecks of gold tend to do, but silicates too can contain elements of economic importance. Quartz, beryl, and zircon are mined as sources of Si, Be, and Zr, respectively. Quartz and many other silicates are used as **industrial minerals**, valued not for their elemental content but for their physical or chemical properties. For example, quartz is used as an abrasive, such as in sandpaper, while feldspars are a major raw material for ceramics. Silicates also make agriculture possible. The soil in which everything from artichokes to zucchini grows is composed dominantly of silicate minerals, mostly quartz and clays.

This chapter provides an introduction to the structural classification of the silicates and summarizes some of the major features of the important rock groups that are composed dominantly of silicate minerals. The coverage here is necessarily superficial. More detailed descriptions of silicate structure and classification can be found in succeeding chapters. The sources listed at the end of the chapter provide additional information on petrography and petrology of igneous, sedimentary, and metamorphic rocks.

DO NOT COPY e48d507df5d1141@placeholder.9409

Printed by: e48d507df5d1141@placeholder.94092.edu. Printing is for personal, private use only. No part of this book may be reproduced or transmitted without publisher's prior permission. Violators will be prosecuted.

Silicate Structure and Classification

The basic building block of all silicate minerals is the silicon tetrahedron (**Figure 11.1**). Si^{4+} is a relatively small cation and conveniently fits in tetrahedral coordination with O^{2-} (refer to the discussion on coordination in Chapter 4). It consists of four O^{2-} anions arranged to occupy the corners of a tetrahedron with a Si^{4+} in the center. An isolated silicon tetrahedron therefore has a net −4 charge. This has profound consequences for the structure of silicate minerals. Recall from the discussion of Pauling's second rule in Chapter 4 that the silicon tetrahedron has mesodesmic bonds. This means each O^{2-} has one of its two valence charges satisfied by bonding with the Si^{4+} at the center of the tetrahedron. The remaining −1 charge is available to bond with an Si^{4+} in the center of another tetrahedron. In effect, silicon tetrahedra may **polymerize**, or bond together in various fashions. The extent and geometry of silicon tetrahedron polymerization provides the basis for the structural classification of the silicate minerals.

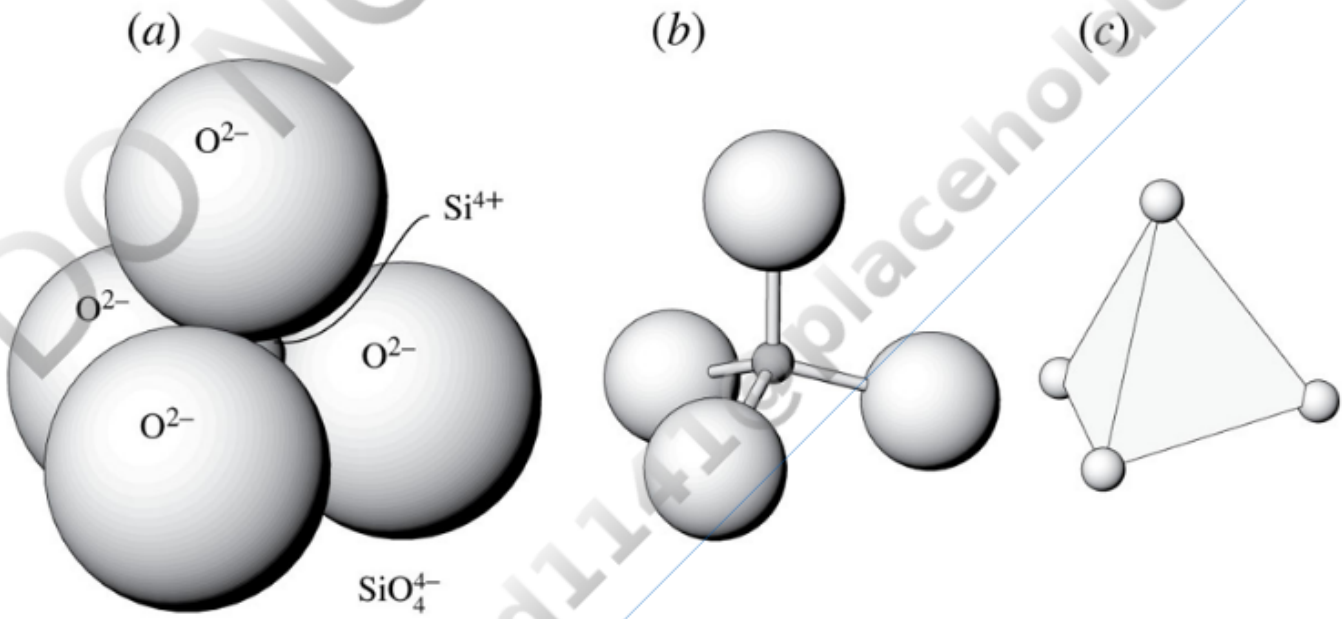

FIGURE 11.1 A silicon tetrahedron consists of four O^{2-} forming a tetrahedral coordination polyhedron around a Si^{4+}. (*a*) Silicon and oxygen as scaled spheres. (*b*) Ball-and-stick representation with silicon and oxygen sizes reduced by half. (*c*) Oxygen anions shown as small spheres at corners of tetrahedron. View larger image

Table 11.1 lists the essential characteristics of the different groups of silicate structures, and **Figure 11.2** shows the basic configuration of the silicon tetrahedra in those structures. The classification used here is conventional. Consult Liebau (1985) for detailed discussion of other schemes that can and have been used to classify silicates.

DO NOT COPY e48d507df5d1141@placeholder.9409

Printed by: e48d507df5d1141@placeholder.94092.edu. Printing is for personal, private use only. No part of this book may be reproduced or transmitted without publisher's prior permission. Violators will be prosecuted.

TABLE 11.1 Silicate Classification[a]

Silicate Class	Number of O^{2-} Shared per Tetrahedron	Z:O Ratio	Structural Configuration
Orthosilicates	0	1:4	Isolated tetrahedra
Disilicates	1	2:7	Double tetrahedra
Ring silicates	2	1:3	Rings of tetrahedra
Chain silicates			Chains of tetrahedra
Single chain	2	1:3	
Double chain	2 or 3	4:11	
Sheet silicates	3	2:5	Sheets of tetrahedra
Framework silicates	4	1:2	Framework of tetrahedra

[a] Z refers to the cation(s), usually Si^{4+}, and also Al^{3+}, that occupy the tetrahedral sites.

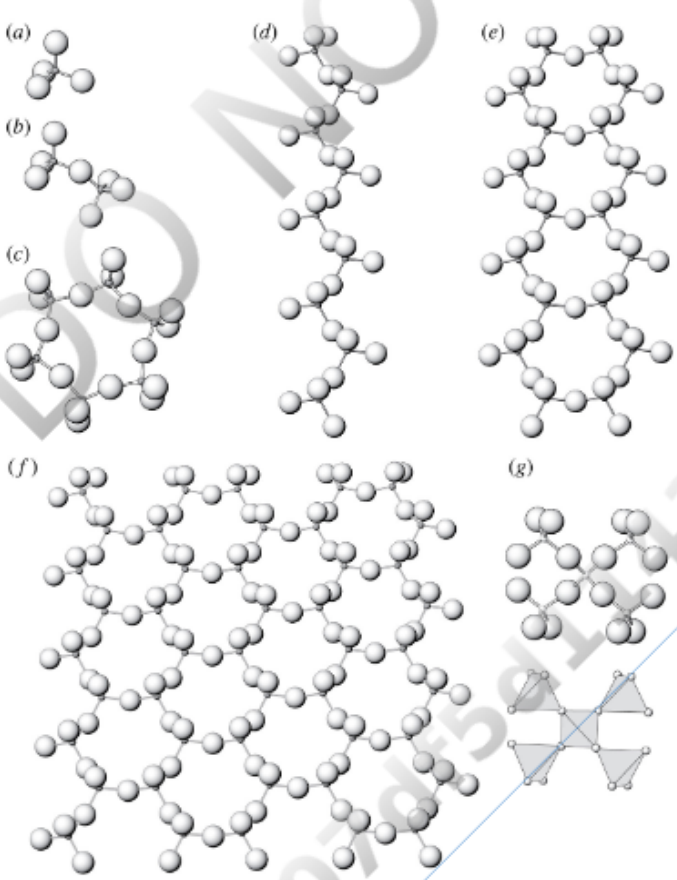

FIGURE 11.2 Silicate structures. (*a*) Orthosilicates. The basic building block is a single tetrahedron. (*b*) Disilicates. A single oxygen is shared between two tetrahedra. (*c*) Ring silicates. Tetrahedra share two oxygen each to form rings. (*d*) Single-chain silicates. Two oxygen are shared per tetrahedron. (*e*) Double-chain silicates. Tetrahedra share two and/or three oxygens. (*f*) Sheet silicates. Three oxygen per tetrahedron are shared to form continuous sheets. (*g*) Framework silicates. All four oxygens on the central tetrahedron are shared with adjacent tetrahedra, as shown in the ball-and-stick and polyhedra diagrams. While not shown, the oxygens in the outer four

DO NOT COPY
e48d507df5d1141@placeholder.9409

Printed by: e48d507df5d1141@placeholder.94092.edu. Printing is for personal, private use only. No part of this book may be reproduced or transmitted without publisher's prior permission. Violators will be prosecuted.

tetrahedra are shared with additional tetrahedra to form a three-dimensional framework. View larger image

The least degree of polymerization is found in the **orthosilicates**—no oxygen anions are shared between adjacent tetrahedra, so technically, no polymerization exists. The silicon tetrahedra form isolated structural entities whose net negative charge is balanced by bonding with other cations such as Mg^{2+}, Fe^{2+}, and Al^{3+}. Sharing of a single O^{2-} between two silicon tetrahedra produces the **disilicates**. In the **ring silicates**, the tetrahedra share two O^{2-} each and form rings, usually with six members. Two O^{2-} per tetrahedron are shared in the single-chain group of the **chain silicates**; in the double-chain group, some tetrahedra share two O^{2-} and others share three. Three O^{2-} per tetrahedron are shared to form continuous sheets in the **sheet silicates**. In the **framework silicates**, all four O^{2-} on each tetrahedron are shared with adjacent tetrahedra to form a three-dimensional framework. The following alternative terminology is used in some sources.

Orthosilicates = Nesosilicates

Disilicates = Sorosilicates

Ring silicates = Cyclosilicates

Chain silicates = Inosilicates

Sheet silicates = Phyllosilicates

Framework silicates = Tectosilicates

Except for quartz (SiO_2) and its polymorphs, the structures produced by the tetrahedra in their various polymerized configurations have a net negative charge. Cations are therefore required to balance charges and to effectively serve as the “mortar” that holds the silicate tetrahedron structures (single tetrahedra, chains, rings, etc.) together. **Table 11.2** lists the common minerals in each silicate class, and the following chapters describes the structural details.

TABLE 11.2 Common Silicate Minerals

Mineral or Mineral Group	Chemical Formula
Orthosilicates	
Olivine	$(Mg,Fe)_2SiO_4$
Zircon	$ZrSiO_4$
Garnet	$X_3Y_2(SiO_4)_3$
Aluminum silicates	$AlAlOSiO_4$ or Al_2SiO_5
Staurolite	$Al_9Fe_2(SiO_4)_4O_6(OH)_2$
Chloritoid	$(Fe^{2+},Mg,Mn)_2(Al,Fe^{3+})\ Al_3O_2(SiO_4)_2(OH)_4$
Topaz	$Al_2(SiO_4)(F,OH)_2$

DO NOT COPY e48d507df5d1141@placeholder.9409

Printed by: e48d507df5d1141@placeholder.94092.edu. Printing is for personal, private use only. No part of this book may be reproduced or transmitted without publisher's prior permission. Violators will be prosecuted.

Topaz	$Al_2(SiO_4)(F,OH)_2$
Titanite	$CaTiOSiO_4$ or $CaTiSiO_5$
Disilicates	
Epidote group	$Ca_2Al_2(Al,Fe^{3+})[SiO_4][Si_2O_7]$
Lawsonite	$CaAl_2(Si_2O_7)(OH)_2{\cdot}H_2O$
Pumpellyite	$Ca_2MgAl_2[SiO_4][Si_2O_7](OH)_2{\cdot}H_2O$
Ring silicates	
Tourmaline	$Na(Mg,Fe,Li,Al)_3Al_6[Si_6O_{18}]\ (BO_3)_3(O,OH,F)_4$
Beryl[a]	$Al_2Be_3Si_6O_{18}$
Cordierite[a]	$Mg_2Al_3[AlSi_5]O_{18}$
Chain silicates	
Orthopyroxene	$(Mg,Fe)_2Si_2O_6$
Ca-Clinopyroxene	$Ca(Mg,Fe)Si_2O_6$
Orthoamphibole	$(Mg,Fe)_7Si_8O_{22}(OH)_2$
Ca-Clinoamphibole (hornblende)	$Ca_2\ (Mg,Fe)_5Si_8O_{22}(OH)_2$
Sheet silicates	
Clay minerals	Various
Serpentine	$Mg_3Si_2O_5(OH)_4$
Pyrophyllite	$Al_2Si_4O_{10}(OH)_2$
Talc	$Mg_3Si_4O_{10}(OH)_2$
Muscovite	$KAl_2(AlSi_3O_{10})(OH)_2$
Biotite	$K(Mg,Fe)_3(AlSi_3O_{10})(OH)_2$
Margarite	$CaAl_2(Al_2Si_2O_{10})(OH)_2$
Clintonite	$CaMg_2Al(Al_3SiO_{10})(OH)_2$
Chlorite group	$(Mg,Fe,Al)_3(Si,Al)_4O_{10}(OH)_2 \cdot (Mg,Fe,Al)_3(OH)_6$
Framework silicates	
Silica group (quartz, tridymite, cristobalite)	SiO_2
Feldspars	
Potassium feldspar	$KAlSi_3O_8$
Plagioclase	$NaAlSi_3O_8{-}CaAl_2Si_2O_8$
Feldspathoids	
Leucite	$KAlSi_2O_6$

DO NOT COPY e48d507df5d1141@placeholder.9409

Printed by: e48d507df5d1141@placeholder.94092.edu. Printing is for personal, private use only. No part of this book may be reproduced or transmitted without publisher's prior permission. Violators will be prosecuted.

Nepheline	$Na_3K(Al_4Si_4O_{16})$
Sodalite	$Na_8[Al_6Si_6O_{24}]Cl_2$
Scapolite	$Na_4Al_3Si_9O_{24}Cl–Ca_4Al_6Si_6O_{24}CO_3$
Zeolite group	$M_xD_y(Al_{x+2y}Si_{n-x-2y}O_{2n})mH_2O$

[a] Beryl and cordierite also may be considered framework silicates.

DO NOT COPY
e48d507df5d1141@placeholder.9409

Printed by: e48d507df5d1141@placeholder.94092.edu. Printing is for personal, private use only. No part of this book may be reproduced or transmitted without publisher's prior permission. Violators will be prosecuted.

Silicate Chemical Formulas

Chemical formulas (Chapter 4) for silicates are typically written to provide information about crystal structure, with cations listed in order of decreasing coordination number. A general silicate formula is

$$W_aX_bY_cO_d(Z_eO_f)A_g \quad (11.1)$$

The capital letters used as placeholders within the formula can vary depending on the mineral's convention and how simple or complex is the connection between the mineral structure and the formula. For example, B may be used instead of X for some minerals, and M1 may label both a place in the formula and a structural site. Regardless, here, the W cations are large and usually are in 10 to 12 coordination, and X cations are in ~8-fold coordination. The coordination polyhedra for W and X are often irregular. The Y cations are in 6-fold (octahedral) coordination. Z represents the silicon plus other cations, usually aluminum, that occupy 4-fold (tetrahedral) sites. The Z:O ratio can help identify the silicate class (Table 11.1). Consider the example mineral chemical formulas listed in Table 11.2; see how many have a Si:O ratio consistent with the listed Z:O ratio in Table 11.1. Some minerals, however, have alternative formulas (titanite, for example) or can have Al present in the tetrahedron (the feldspars, for example); either may obscure the mineral's silicate class. In hydrous silicates such as the sheet silicates, the hydroxyl (OH^-) or other large anions such as F^- and Cl^- are listed as part of A at the end of the formula. Disilicates and orthosilicates commonly have more oxygen than is needed to account for the silicon–aluminum tetrahedra, and this oxygen may be listed separately after Y or be included as part of A. **Table 11.3** shows how this applies to several common silicates. Silicate formulas presented in this book largely follow these rules, but the reader is cautioned that these rules are not always followed in the literature, for historical or other reasons.

TABLE 11.3 Silicate Chemical Formulas Using the General Formula (Equation 11.1)

Mineral	W	X	Y	O	Z_eO_f	A	Formula
Fayalite			Fe_2		SiO_4		Fe_2SiO_4
Diopside		Ca	Mg		Si_2O_6		$CaMgSi_2O_6$
Edenite	Na	Ca_2	Mg_5		$AlSi_7O_{22}$	$(OH)_2$	$NaCa_2Mg_5(AlSi_7O_{22})(OH)_2$
Muscovite	K		Al_2		$AlSi_3O_{10}$	$(OH)_2$	$KAl_2(AlSi_3O_{10})(OH)_2$
Epidote	Ca_2		Al_2Fe^{3+}		$(Si_2O_7)(SiO_4)$	O(OH)	$Ca_2Al_2Fe^{3+}(Si_2O_7)(SiO_4)O(OH)$

Printed by: e48d507df5d1141@placeholder.94092.edu. Printing is for personal, private use only. No part of this book may be reproduced or transmitted without publisher's prior permission. Violators will be prosecuted.

Mafic Versus Felsic

For purposes of general discussion it is convenient to separate the common silicate minerals into two broad groups, mafic and felsic.

Mafic silicates are those that contain magnesium and/or iron as major constituents. The name is derived from these elements—*ma* from *ma*gnesium and *f* from the Latin word for iron, *ferrum*. The common mafic silicates include olivine, pyroxenes, amphiboles, and biotite. They tend to be fairly dark colored, with some exceptions. Rocks in which they are abundant are therefore usually dark colored, and hence the rock may be called mafic as well. Mafic rocks also are fairly low in Si; therefore, silicon tetrahedra polymerization tends to be less, so mafic rocks may be dominated by orthosilicates (olivine) or chain silicates (pyroxenes and amphiboles) only.

The felsic minerals include those that lack Mg and Fe as major constituents. They include the feldspars (from which the name was derived), quartz, muscovite, and feldspathoids. Rocks rich in these minerals may be called felsic. Felsic rocks are often high in Si, so silicon tetrahedral polymerization can be more extensive and complex; sheet (muscovite) and framework silicates (quartz and feldspar) are most common for this reason too. However, an important complicating factor is that Al may occupy some tetrahedral sites in silicate minerals. Hence, framework silicates such as plagioclase and nepheline can be found in some relatively low-silicon rocks (gabbro and syenite, for example), but only if Al is available to occupy some of the tetrahedral sites.

For purposes of general discussion, it is convenient to group silicate-dominated rocks into four broad categories based on the amount of SiO_2 in the **bulk chemical analysis** (the whole rock).

FELSIC: >65% SiO_2

INTERMEDIATE: 55–65% SiO_2

MAFIC: 45–55% SiO_2

ULTRAMAFIC: <45% SiO_2

Some sources place the breaks at 52 percent and 63 percent SiO_2. Regardless, these four categories are predominantly used for considering the classification of igneous rocks.

DO NOT COPY e48d507df5d1141@placeholder.9409-

Printed by: e48d507df5d1141@placeholder.94092.edu. Printing is for personal, private use only. No part of this book may be reproduced or transmitted without publisher's prior permission. Violators will be prosecuted.

Igneous Rocks

The silicate minerals found in abundance in igneous rocks include a relatively small selection: quartz, K-feldspar, plagioclase, muscovite, biotite, Ca-clinoamphibole (e.g., hornblende), Ca-clinopyroxene (e.g., augite), orthopyroxene, and olivine. The relative amounts of these minerals, plus one additional group—the feldspathoids—provide the mineralogical framework within which igneous rocks are classified.

Figure 11.3 shows the conventional classification scheme for igneous rocks, which is based on the relative amounts of quartz, K-feldspar, plagioclase, and feldspathoids. Note that quartz and feldspathoid minerals are mutually exclusive; they are not normally found together. Most igneous rocks will have additional minerals in fairly low proportions in addition to the quartz, K-feldspar, plagioclase, and feldspathoids used to classify the rock; these additional minerals are called **accessory minerals**. Accessory minerals may be used to modify a rock's name, as in, biotite granite. For this rock, because it is a granite, quartz, K-feldspar, and plagioclase must be in the proportions outlined in Figure 11.3, but the rock additionally has biotite.

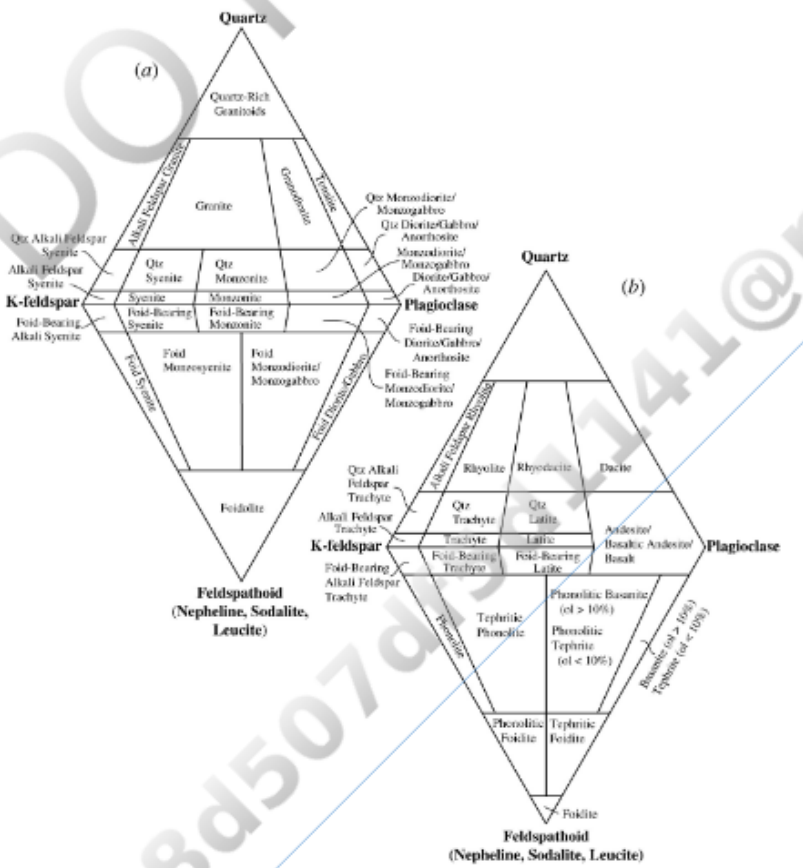

FIGURE 11.3 Classification of igneous rocks. Classification is based on the relative amounts (volume percentages) of quartz, K-feldspar, plagioclase, and feldspathoids (nepheline, sodalite, leucite). Other minerals are ignored. (*a*) Plutonic rocks. (*b*) Volcanic rocks. Adapted from Streckheisen

DO NOT COPY e48d507df5d1141@placeholder.94092

Printed by: e48d507df5d1141@placeholder.94092.edu. Printing is for personal, private use only. No part of this book may be reproduced or transmitted without publisher's prior permission. Violators will be prosecuted.

leucite). Other minerals are ignored. (*a*) Plutonic rocks. (*b*) Volcanic rocks. Adapted from Streckheisen (1976) and Le Maitre and others (2002). View larger image

The classification in Figure 11.3 is not universally accepted and has significant weaknesses, but it serves as a common point of reference. The classification distinguishes between plutonic rocks (usually coarse grained) and volcanic rocks (usually fine grained), and this distinction often requires specific observations made in the field or other information.

The classification in Figure 11.3 is based on the **modal mineralogy**, that is, the volume percent of each mineral in the rock. This normally is determined by "point counting" the rock. Point counting is done on a thin section with a petrographic microscope. The slide is moved in increments beneath the crosshairs with the aid of a mechanical stage (Figure 7.9) that holds the slide and allows it to be moved systematically by turning small knobs. The mineral beneath the crosshair after each movement is identified and tallied.

The fine grain size of volcanic rocks usually precludes the accurate determination of their modal mineralogy, so Figure 11.3b cannot easily be used in practice. Various classification schemes based on the bulk chemical analysis of volcanic rocks are in common use and are described in Philpotts and Ague (2009) and most other texts on igneous petrology. **Figure 11.4** shows one of these classifications based on the relative amount of SiO_2 and alkalis ($Na_2O + K_2O$). Another common method of classifying fine-grained volcanic rocks is to calculate the **normative mineralogy** based on the chemical analysis. The normative mineralogy is the collection of minerals that could possibly be created from the bulk chemistry, given certain assumptions concerning distribution of elements among the minerals. Refer to Philpotts and Ague (2009) or other igneous petrology books for the details of normative calculations.

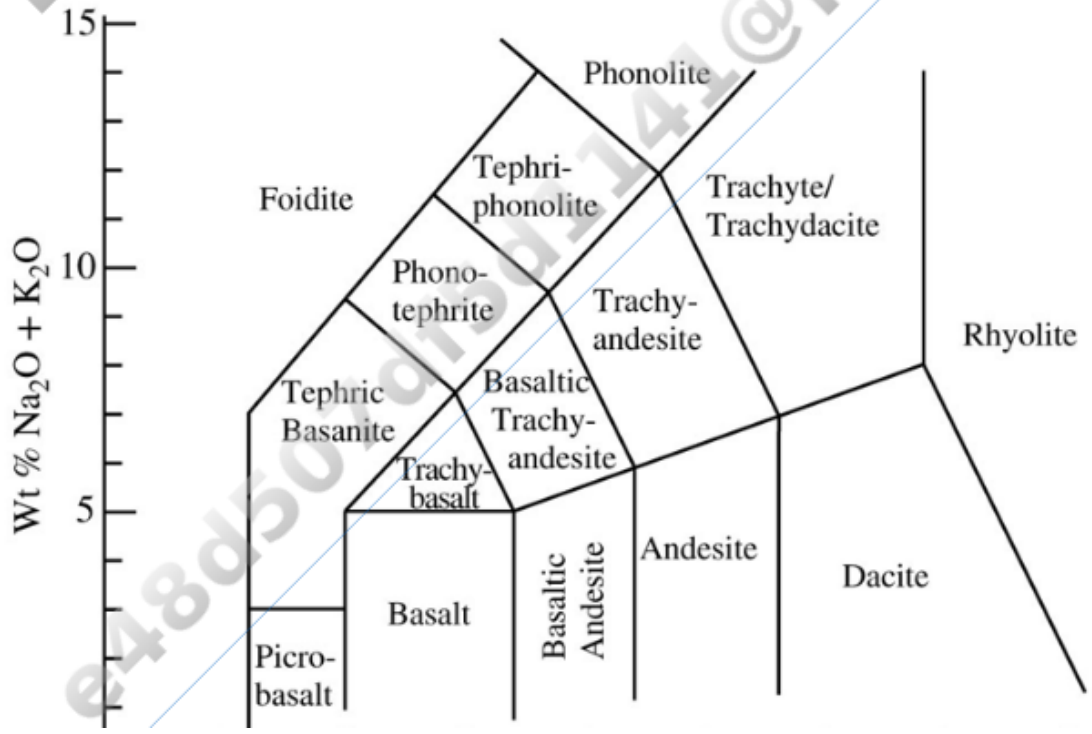

Printed by: e48d507df5d1141@placeholder.94092.edu. Printing is for personal, private use only. No part of this book may be reproduced or transmitted without publisher's prior permission. Violators will be prosecuted.

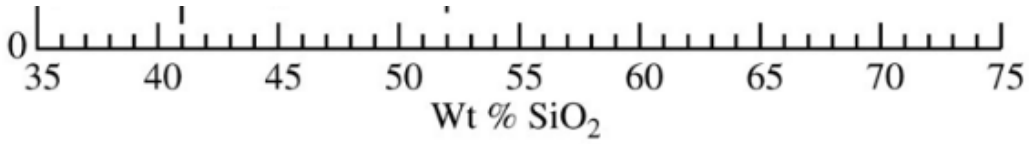

FIGURE 11.4 Chemical classification of volcanic rocks based on weight percent of SiO_2 and $Na_2O + K_2O$. Based upon Le Bas and others (1986). View larger image

Note that a number of the fields on the right side of Figure 11.3a contain two or more names—quartz monzodiorite and quartz monzogabbro, or quartz diorite, quartz gabbro, and quartz anorthosite, for example. **Table 11.4** shows criteria to distinguish diorite and gabbro as shown on the diagram. Anorthosite is distinguished from the others because it is composed of more than 90 percent plagioclase.

TABLE 11.4 Criteria to Distinguish between Diorite and Gabbro or Related Rocks (Figure 11.3)[a]

Criteria	Diorite	Gabbro
Plagioclase composition	< 50% Ca (< An_{50})	> 50% Ca (> An_{50})
Dominant mafic mineral	Amphibole	Pyroxene
Associated rocks	Granodiorite/granite	Other mafic/ultramafic varieties
Wt % SiO_2	> 55%	< 55%

[a] Figure 11.5 shows the classification of mafic, ultramafic, and related rocks.

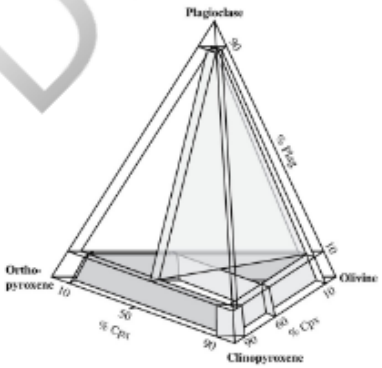

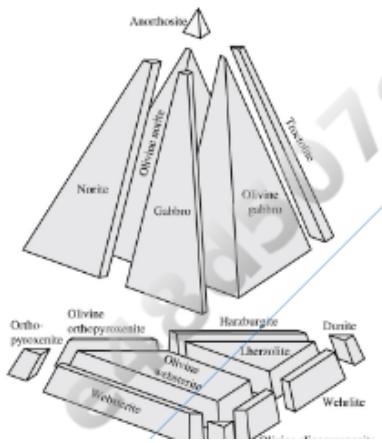

DO NOT COPY e48d507df5d1141@placeholder.9409

Printed by: e48d507df5d1141@placeholder.94092.edu. Printing is for personal, private use only. No part of this book may be reproduced or transmitted without publisher's prior permission. Violators will be prosecuted.

FIGURE 11.5 Classification of plutonic igneous rocks lacking significant amounts of quartz, K-feldspar, or feldspathoids. Adapted from Streckheisen (1976) and Le Maitre and others (2002). View larger image

In general, major minerals found in mafic and ultramafic igneous rocks include plagioclase, Ca-clinopyroxene, orthopyroxene, olivine, and hornblende (but only in rare cases). Therefore, classifying these rocks using Figure 11.3 is not practical because of the lack of quartz, K-feldspar, and perhaps plagioclase. **Figure 11.5** shows one means of classifying these rocks based on the relative amounts of plagioclase, orthopyroxene, clinopyroxene, and olivine. This diagram includes gabbro and related rocks (gabbro, norite, olivine gabbro, olivine norite), pyroxenites (orthopyroxenite, clinopyroxenite, websterite, olivine orthopyroxenite, olivine clinopyroxenite), peridotites (lherzolite, wehrlite, harzbergite, dunite), anorthosite, and troctolite. Ultramafic igneous rocks make up the vast majority of the mantle. In the crust, ultramafic mantle xenoliths can be carried to the surface in basaltic lava. Though rare, larger volumes of ultramafic mantle rocks are found in **ophiolites**, which are complete packages of ocean sediments, oceanic crust, and the underlying mantle that has been thrust onto continental crust during convergent plate tectonics.

Classifying intermediate igneous rocks is generally more straightforward than classifying mafic or ultramafic rocks, and examples include diorite, quartz diorite, and related intrusives, and andesitic volcanic rocks. For these rocks, plagioclase is abundant, and K-feldspar and quartz are fairly minor or absent; hornblende is often the most common accessory mineral, although biotite and/or some pyroxene also may be present.

Classifying felsic rocks can be straightforward as well. The felsic rocks include granite, granodiorite, rhyolite, rhyodacite, and similar types. Common accessory minerals include biotite, muscovite, and/or hornblende.

Rocks that do not fit conveniently in the felsic/intermediate/mafic/ultramafic groupings are not abundant. However, two groups are worthy of mention here—alkaline igneous rocks and anorthosites. The alkaline igneous rocks include syenite, monzonite, trachyte, latite, phonolite, and feldspathoid-bearing rocks, shown in Figure 11.3. Their compositional characteristic is an abundance of K and Na (alkali elements). Because Si is not sufficiently abundant to allow quartz to form, these rocks are often referred to as silica undersaturated. Common minerals include K-feldspar, plagioclase, and one or more feldspathoids (nepheline, sodalite, and leucite). Mafic minerals include amphiboles, pyroxenes, and biotite.

Anorthosite most commonly occurs in batholith-sized bodies, most of which were emplaced in the Proterozoic crust around roughly 1.45 to 1.1 billion years ago. This rock type is composed of plagioclase with minor amounts of pyroxene and olivine. It is common to find large bodies of orthopyroxene syenite or related alkali-rich rock associated with anorthosite. The nature and source of the magma from which anorthosite

DO NOT COPY e48d507df5d1141@placeholder.94092-

Printed by: e48d507df5d1141@placeholder.94092.edu. Printing is for personal, private use only. No part of this book may be reproduced or transmitted without publisher's prior permission. Violators will be prosecuted.

associated with anorthosite. The nature and source of the magma from which anorthosite forms remains a topic of focused research. It is generally believed that large anorthosite batholiths result from mantle-derived mafic magma crystallizing plagioclase. The plagioclase then floats to the top of the magma chamber to create a nearly pure plagioclase body with minor amounts of magma left between plagioclase grains. The mixture of plagioclase with melt is able to migrate further up into the crust because of its low density before final crystallization. The associated orthopyroxene syenite or related alkali-rich rock are thought to be derived from crustal melts created by the high temperatures of the nearby mafic magma and anorthosite.

Another rock type that does not fit well into the above classification is pegmatite. Pegmatite bodies (**Figure 11.6**) have a wide range of sizes and shapes, though roughly dike-shaped bodies less than a meter to tens of meters thick are quite common. Most are compositionally zoned, often with a quartz-rich core.

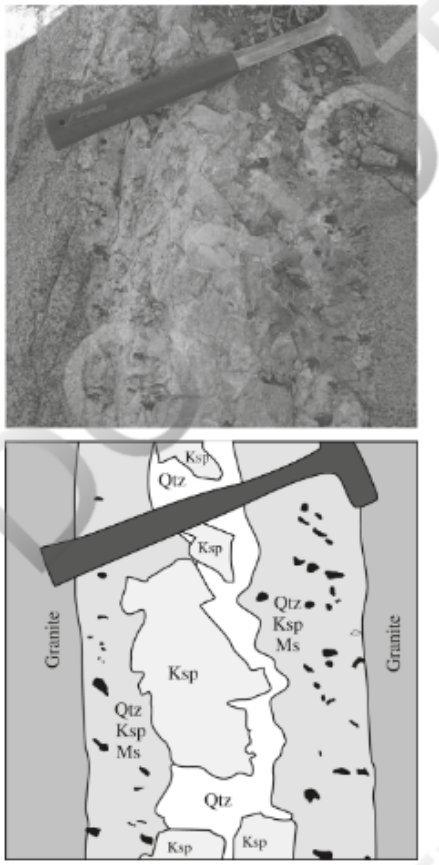

FIGURE 11.6 This small pegmatite dike (*top*) that has intruded Precambrian granite is compositionally zoned. The outer zones consist of intergrown quartz (Qtz), K-feldspar (Ksp), and muscovite (Ms) with scattered tourmaline grains (black). The central zone consists of large K-feldspar grains (some are euhedral) and large masses of quartz. The mineral zoning documents the sequence of crystallization of the magma from the margin of the intrusion to the center. The sketch at the bottom shows the major components. View larger image

Strictly speaking, pegmatite refers to an igneous rock with a grain size larger than 3 cm and does not imply a composition or specific rock type. However, the most commonly found pegmatites are associated with granitic intrusions. They are interpreted to form

Printed by: e48d507df5d1141@placeholder.94092.edu. Printing is for personal, private use only. No part of this book may be reproduced or transmitted without publisher's prior permission. Violators will be prosecuted.

found pegmatites are associated with granitic intrusions. They are interpreted to form from the water-rich last residual magma in a crystallizing granitic pluton. Compared to a typical felsic magma, the high concentration of water (and possibly other elements; see the section on magmatic processes) inhibits crystal nucleation but increases diffusion within the magma. This means new crystals form with great difficulty, but once formed, the crystals grow very easily and can reach very large sizes. In extreme cases, individual crystals up to 7 or 8 meters long have been found.

Introductory geology students often infer that the extremely coarse grain size means that the magma from which pegmatites crystallized must have cooled extremely slowly. However, this is probably not the case; as described, crystallization may actually be fairly rapid. Other arguments include that pegmatites cannot have cooled more slowly than the associated plutonic granitic magmas from which they were derived, and they often form small intrusive bodies that cannot retain heat for long.

The major minerals of pegmatites are quartz, K-feldspar, Na-rich plagioclase, muscovite, and biotite; mineralogically, they are, or are similar to, granite. Therefore, such rocks technically should be called granite pegmatite, granitic pegmatite, felsic pegmatite, and so on. However in practice, they are commonly just called pegmatite without any indication of composition.

In addition to water, a variety of less common elements (Li, B, Be, F, P, U, etc.) can also be concentrated in the magma. Therefore, granitic pegmatites crystallize in a rather unusual environment; therefore, a variety of uncommon minerals atypical of igneous rocks may form, including tourmaline, beryl, garnet, spodumene, and lepidolite. Additional minerals are listed in Table C.1 in Appendix C.

Granitic pegmatites are economically important because the minerals found in them are the primary source of beryllium, lithium, rare earth elements, and other elements society needs. Pegmatites also can be the source of industrial minerals such as feldspar and the large muscovite crystals historically used for windows.

One more special igneous rock texture requires discussion. A **porphyritic** texture consists of large, often euhedral grains, called **phenocrysts**, surrounded by a finer-grained **groundmass** or matrix. For some volcanic rocks, the groundmass may be obsidian or have a large glass component. The rock should be classified according to the groundmass grain size. Most igneous rocks show some variation in grain size from grain to grain, but only when the rock has an easily identifiable proportion of grains distinctly larger than a groundmass is the texture labeled as porphyritic. Regardless of whether or not an igneous rock is labeled a porphyry, any grain larger than the surrounding material as at any scale, including as observed in thin section, can be called a phenocryst. Porphyries may indicate a change in crystallization conditions, such as slow cooling followed by fast cooling as produced by the eruption of crystallizing magma from a deep magma chamber, but porphyries can also form from a magma chamber that experienced no change in conditions—some minerals have a tendency to grow larger than others in certain situations.

DO NOT COPY e48d507df5d1141@placeholder.94092

Printed by: e48d507df5d1141@placeholder.94092.edu. Printing is for personal, private use only. No part of this book may be reproduced or transmitted without publisher's prior permission. Violators will be prosecuted.

Magmatic Processes

There are a variety of magmatic processes that control the composition of a forming magma or change the magma composition once formed. As a result, a full spectrum of igneous rock compositions, with their corresponding mineralogy, is possible. The discussion below introduces the main processes, but books with dedicated sections on igneous petrology should be consulted for additional details. Bowen's reaction series (**Box 11.1**) continues to be a useful entry point into understanding more complex igneous processes.

DO NOT COPY

BOX 11.1
Bowen's Reaction Series

In the early 1900s, petrologist N. L. Bowen conducted a series of experiments in which he created magmas with various compositions and allowed each to cool slowly and crystallize. At different temperatures during crystallization, he would quench (rapidly cool) the experiment. When quenched, the remaining melt would convert to glass. The glass and crystal mixture provided a picture of the crystallization process at the temperature of quenching. With repeated experiments of varying composition and quenching temperature, Bowen created a reaction series (e.g., Bowen, 1922) that outlined which minerals crystallized first from the cooling magma at high temperatures and which minerals subsequently would crystallize at lower temperatures (**Figure 11.7**). Of the minerals included in the series, plagioclase has the most complicated behavior and crystallizes over a large temperature range with other minerals. Over this range, plagioclase composition varied from Ca-rich at high temperature to progressively more Na-rich at lower temperatures (see Chapters 5 and 12 for more detail).

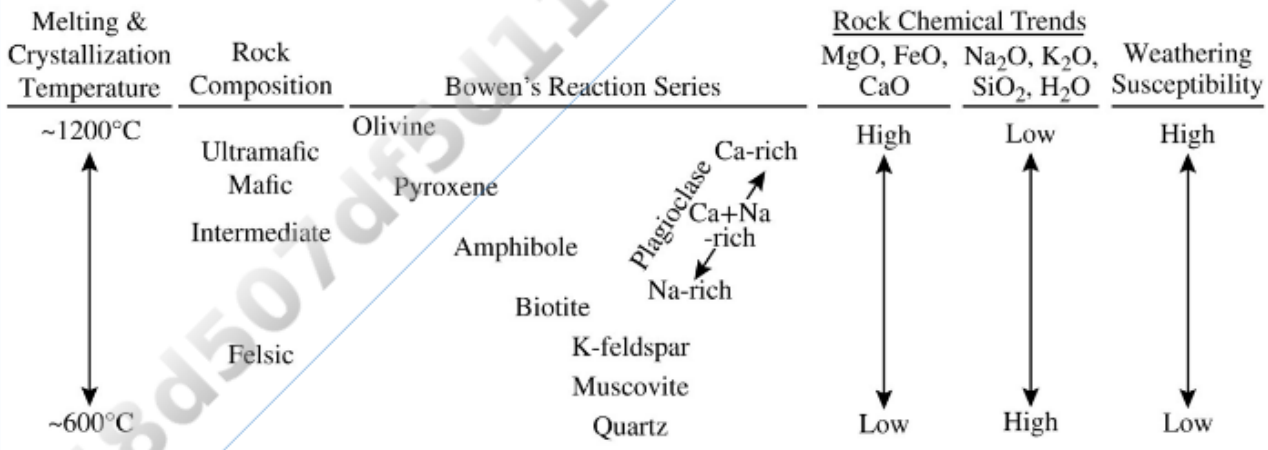

FIGURE 11.7 Bowen's reaction series simplified and connected to mineral melting and crystallization temperatures, rock chemical trends, and mineral weathering susceptibilities.

Printed by: e48d507df5d1141@placeholder.94092.edu. Printing is for personal, private use only. No part of this book may be reproduced or transmitted without publisher's prior permission. Violators will be prosecuted.

View larger image

Beyond generalizing a common order for mineral crystallization, the series also provides an approximate melting temperature and order for the included minerals upon heating. Bowen's reaction series also provides some guidance as to what minerals are likely found in different igneous rock compositions (**Table 11.5**). The ultramafic through felsic rock composition classifications are shown next to the series in Figure 11.7; spacing is not equal for the classification, as they are placed approximately in the center of the range of minerals that may compose a majority of the rock or serve as important accessory minerals. See Table 11.5 for more details.

TABLE 11.5 Bowen's Reaction Series Mineral Commonality in Igneous Rocks[a]

Rock Classification	Orthosilicate	Chain Silicates		Sheet Silicates		Framework			
		Single	Double			Plagioclase			
	Olivine	Pyroxene	Amphibole	Biotite	Muscovite	Ca-rich	Ca- + Na-rich	Na-rich	f
Ultramafic	M	M				A			
Mafic	A	M				M			
Intermediate		A	A	A	A		M		
Felsic			A	A	A			M	

[a] M—major; A—accessory or minor mineral.

The progression in the mineralogy from ultramafic to felsic igneous rocks is interrelated with the predictable and expected progression of major oxide concentrations for these compositions. At the ultramafic end of the spectrum, igneous rocks are high in MgO, FeO, and CaO, which all become lower for progressively more felsic rocks. The concentrations of Na_2O, K_2O, SiO_2, and H_2O all increase for the ultramafic to felsic progression. Such trends are easily connected to the abundance of mafic minerals and Ca-rich plagioclase in mafic igneous rocks and the abundance of quartz and K-feldspar and scarcity of mafic minerals in felsic rocks. The trend in H_2O is less obvious but is very important. Mafic and ultramafic magmas typically have very little H_2O, which explains why ultramafic and mafic igneous rocks are typically devoid of hydrous minerals such as amphibole and biotite (Table 11.5).

Bowen's reaction series also organizes and provides excellent examples for all but a few of the different types of silicate minerals. Olivine, an orthosilicate, represents the simplest silicate mineral structure. Moving down the series, the silicate structures become progressively more complicated: pyroxene is a single-chain silicate, amphibole is a double-chain silicate, and biotite is a sheet silicate (Table 11.5). The

DO NOT COPY

Printed by: e48d507df5d1141@placeholder.94092.edu. Printing is for personal, private use only. No part of this book may be reproduced or transmitted without publisher's prior permission. Violators will be prosecuted.

pattern is imperfect because the feldspars, all framework silicates, are likely present in all compositions of igneous rocks, and the bottom half of the diagram alternates between framework silicates (the feldspars and quartz) and sheet silicates (biotite and muscovite).

Lastly, mineral weathering susceptibility is largely tied to the prevalence of strong Si–O and Al–O bonds in the mineral. Such bonds are progressively more common in more complex types of silicates. Therefore, Bowen's reaction series also is a valuable guide to the relative weathering susceptibility of these common minerals. This pattern is also referred to as the Goldich dissolution series, named for S. S. Goldich (1938), who first recognized that Bowen's reaction series also organized the minerals by weathering susceptibility.

As Bowen's reaction series is about 100 years old, there have been countless additional experiments and computer models that explore the crystallization of magma, the melting of rocks, igneous rock chemical trends, and the weathering of minerals. These studies collectively have built a more robust understanding of such processes (see Chapter 5 and other parts of this chapter, for example). Despite being arguable too simple to describe these complex processes well, Bowen's reaction series remains a powerful tool for remembering a number of key relationships and trends regarding many common rocks and minerals. Because of this, it continues to be a key component of a variety of university-level geology-focused courses.

Melting

Because magma is derived from melting of preexisting rocks, it follows that the composition of the rock melted must strongly control the composition of the magma. In a simple model, felsic magmas are derived from melting of relatively felsic continental crust, and mafic magmas are derived from melting of the ultramafic mantle.

A complicating factor is that most rocks do not melt all at once; they only **partially melt**, and when they do, they melt incongruently. This means that when a rock melts, the melt produced does not have the same composition as the original rock. In such cases it is important to remember that the sum of melt plus the residual unmelted rock must equal the composition of the original rock prior to melting. **Incongruent melting** of rocks often occurs over a range of temperatures, and melt and residual rock change in composition as temperature and extent of melting changes. This provides a mechanism to produce melts of different composition from the same parent rock if melting occurs in stages and the melt is removed after each stage. This is called **fractional melting**. In general, when many silicate rocks are partially melted, the melt has a higher silica content than the parent rock and the residual rock becomes depleted in silica. Fractional melting therefore yields a relatively silica-rich magma first, followed by a series of progressively less silica-rich magmas.

Magmatic Differentiation

DO NOT COPY e48d507df5d1141@placeholder.94092

Printed by: e48d507df5d1141@placeholder.94092.edu. Printing is for personal, private use only. No part of this book may be reproduced or transmitted without publisher's prior permission. Violators will be prosecuted.

Magmatic Differentiation

It is possible for a magma, once formed, to be emplaced or erupted without further modification and form a rock of the same composition as the initial magma. Often, however, a variety of processes operate on the magma to yield a great diversity of resulting rocks. These **magmatic differentiation** processes include the following.

- **Fractional crystallization**, which occurs when crystals settle to the bottom of a magma chamber (most common) or float to the top (see discussion of anorthosites above), thus separating the crystals from the magma.
- **Magma mixing** occurs when magmas of different composition mix and produce a magma with a composition intermediate between the two initials magmas. An added complexity is that some magmas cannot mix when placed in the same magma chamber. In those cases they remain separate and do not mix, in a manner similar to the behavior of oil and water, leading to **magma mingling**.
- **Assimilation**, or the addition of material from the **country rock** or walls of the magma chamber.

Fractional Crystallization

Just as rocks do not typically melt at a single temperature, magmas do not crystallize at a single temperature. During cooling, minerals generally crystallize in order: first one mineral begins to grow, followed by another at a lower temperature, and so forth (see Box 11.1). Note that crystallization temperatures for minerals certainly overlap, but a progression in mineral crystallization does occur. Because the crystals growing from a magma rarely have the same composition as the magma, the composition of the residual magma changes or evolves as crystallization progresses. The crystallization of plagioclase described in Chapter 5 provides a good example. If the crystals stay with the magma from which they are growing, the resulting igneous rock will have the same composition as the parent magma. If, however, the crystals can be removed from the magma as the crystals grow, fractional crystallization occurs.

Consider a crystallizing magma chamber at some depth that will experience fractional crystallization. If the crystals are more dense than the magma, they will tend to settle through the magma and accumulate on the magma chamber floor. Magma near the top of the magma chamber will, over time, become depleted in the elements being taken up by the settling crystals while becoming enriched in the remainder of elements. If batches of magma are periodically removed from the magma chamber by eruption from a volcano, for example, the composition of each batch of magma should differ and the rock formed from each will have a different mineralogy.

A sequence of compositionally diverse magmas produced by fractional crystallization is called a **fractionation series**. The accumulation of crystals on the magma chamber floor becomes a separate igneous rock called a **cumulate**. Fractionation series usually produce progressively more Si-rich magmas with time; hence, younger rocks in a fractionation series often are more Si-rich

DO NOT COPY e48d507df5d1141@placeholder.9409

Printed by: e48d507df5d1141@placeholder.94092.edu. Printing is for personal, private use only. No part of this book may be reproduced or transmitted without publisher's prior permission. Violators will be prosecuted.

fractionation series often are more Si-rich.

Magma Mixing

Magmas with different compositions can and do mix with each other. Scenarios in which this can happen include the following.

- Mafic magma produced in the mantle may pool in the more Si-rich lower crust. Heat from the crystallizing magma melts the crustal rocks to produce a Si-rich magma that may, under some circumstances, mix with the mafic melt.
- Fresh magma may be injected into a magma chamber that has already experienced crystallization and differentiation. The fresh and old magma may mix.

Assimilation

Magmas cannot exist in isolation from the country rock in which they are contained. Invariably country rocks are of a different composition than the magma, so as country rock material interacts with the magma through assimilation, the magma's composition changes. The nature of the interaction may be complex and can include direct melting of country rock, dissolution of select country rock minerals, or chemical exchange with country rock minerals. The nature of the chemical change in the magma depends on details of the interaction, but generally assimilation makes magmas more felsic.

Igneous Environments

It was recognized fairly early in the study of igneous rocks that certain rock types are commonly associated with each other, while others rarely or never occur together. The plate tectonic paradigm has provided a useful means of explaining these observations.

Mid-ocean Ridges

Mid-ocean ridges are the sites of the most prolific magma generation on Earth. Here, mantle rocks rise beneath the ridges in response to the divergence of the adjoining plates. Pressure decreases on the mantle as it rises, which causes **decompression melting** of the ultramafic mantle, yielding mafic magma because of partial and incongruent melting processes. This mafic magma erupts onto the ocean floor along the mid-ocean ridge or solidifies in shallow magma chambers and dikes to form the majority of oceanic crust. Over time, newly formed oceanic crust is carried laterally away from the mid-ocean ridge by continued plate motion and ultimately returns to the mantle in subduction zones. During this journey, sedimentary rocks are generated on top and become part of the oceanic crust.

At mid-ocean ridges, fractional crystallization, magma mixing, and assimilation do not occur to a great extent, so almost all the rocks formed at the mid-ocean ridge are mafic and of similar composition and mineralogically consist mostly of plagioclase and

DO NOT COPY e48d507df5d1141@placeholder.94092

Printed by: e48d507df5d1141@placeholder.94092.edu. Printing is for personal, private use only. No part of this book may be reproduced or transmitted without publisher's prior permission. Violators will be prosecuted.

and of similar composition and mineralogically consist mostly of plagioclase and pyroxene, and usually a small amount of olivine.

Oceanic Hot Spots

An additional common oceanic association occurs at intraplate volcanic centers, such as Hawaii. Such volcanic centers are positioned over rising columns of mantle called hot spots. As with mid-ocean ridges, pressure in the rising column of mantle decreases, leading to decompression melting. Melting is similarly partial and incongruent such that the melt generated from the ultramafic mantle is mafic in composition. Substantial quantities of magma can be generated and emplaced into the oceanic crust to crystallize into gabbro or related rocks, or it may extrude onto the sea floor and build an oceanic plateau or sometimes a volcanic edifice large enough to project above sea level.

Subduction Zones

Convergent plate boundaries with subduction zones also are prolific sites for magma generation. The abundant volcanic centers that girdle the Pacific Ocean basin, for example, are testimony to the capacity for magma generation in the upper mantle and crust above subduction zones. Most of the magmas result from melting of the wedge of mantle above the downgoing slab of oceanic crust. As the downgoing slab is metamorphosed, the slab releases water that moves up into the overlying mantle, where it decreases the melting point of the ultramafic mantle such that it melts. This is called **flux melting**, the most common resulting melt is mafic in composition. However, the nature of the magmas depends significantly on the local conditions associated with the subduction zone. Minor amounts of melt may also be generated from subducted sediments or the mafic oceanic crust, oceanic plateaus, and so on. These melt contributions can modify the subduction zone melt composition but, if present at all, are rarely very large. The mafic subduction zone melt, as long as it remains less dense than the surrounding rock, then migrates upward out of the mantle and into the crust. During its ascent, it may experience significant magmatic differentiation. Ultimately a substantial amount of magma is added to the crust above a subduction zone, some of which reaches the surface to build volcanic features.

The resulting band of plutonic and volcanic rocks created above a subduction zone is called an arc. Arcs can form on oceanic crust above the subduction zone, which often results in a chain of volcanic islands called an island arc. Or, an arc can form on continental crust above a subduction zone; the resulting volcanic mountain belt is called a continental arc. On average, arc igneous rocks worldwide are intermediate in composition, although the igneous rocks associated with each magmatic center almost always have a variety of compositions controlled by specific initial melt composition and the extent of magma evolution from fractional crystallization, magma mixing, and assimilation that occurs as it migrates upward. Typically, the earliest-erupted arc lavas are mafic. Over time, the erupted lavas become progressively more felsic with more extensive fractional crystallization and assimilation and result in abundant intermediate

DO NOT COPY

Printed by: e48d507df5d1141@placeholder.94092.edu. Printing is for personal, private use only. No part of this book may be reproduced or transmitted without publisher's prior permission. Violators will be prosecuted.

extensive fractional crystallization and assimilation and result in abundant intermediate and, in some cases, felsic compositions. Felsic igneous rocks usually occur less often in island arc environments; however, in continental arcs, felsic compositions may make up a substantial amount of the rocks owing to more extensive fractional crystallization and assimilation due to continental crust being thicker and more felsic compared to the island arc setting.

For arc rocks, andesite and diorite are quite common. Hornblende is a common accessory phase in both of these or similar composition rocks such as basaltic andesite, dacite, and granodiorite. However, accessory phases also can be quite diverse: olivine and pyroxene may occur if the rock is more mafic and/or the magma was fairly dry, or biotite may occur alone or together with hornblende if the rock is slightly more felsic and/or the magma was fairly wet.

Continental Collision

Ultimately, subduction will close an ocean basin and collision of two land masses will result. The collision of two land masses of which neither can subduct means that subduction ends, and with it, flux melting of the mantle and arc magmatism both end. However, continental collisions can still generate large quantities of igneous rocks.

During continental collision, the crust continues to thicken vertically because of deformation that shortens the crust horizontally through faulting and folding. As the crust thickens, the lower crust increases in temperature because the upper crust acts as an insulating layer that does not allow much escape of mantle heat, plus heat is added from nearby intrusions, and heat is generated by the breakdown of radioactive elements (mostly K, Th, and U). Temperatures in the lower crust can therefore reach above 650°C, which is sufficient to melt most rocks found in continental crust. As the continental crust, on average, is intermediate to felsic in composition, fractional incongruent melting here results in felsic magmas. These magmas generally do not migrate to the surface to form volcanic features, as evidenced by the lack of active volcanoes in the Himalayas—the site of an active continental collision. Interestingly, the aluminum content of felsic melts generated from continental collision tends to be much higher than that of subduction zone felsic melts. So, granite and related rocks formed from collision often have biotite and/or muscovite as accessory minerals, though hornblende is possible. For felsic rocks with the highest Al content, accessory minerals such as garnet, an aluminum silicate, and/or cordierite may be present.

Intracontinental Rifting and Hot Spots

Continental flood basalts are found in many areas of the world, formed by great quantities of basaltic magma that erupted over geologically very short time periods. Individual lava flows may be a few meters to over 100 meters thick and may extend for over 100 km. Some are Precambrian; others are Tertiary or Quaternary in age. Examples include the Miocene Columbia River basalts in Washington, Idaho, and Oregon; the latest

DO NOT COPY

Printed by: e48d507df5d1141@placeholder.94092.edu. Printing is for personal, private use only. No part of this book may be reproduced or transmitted without publisher's prior permission. Violators will be prosecuted.

Cretaceous Deccan basalts in India; and Precambrian Keweenawan basalts found mostly in Minnesota, Wisconsin, and Michigan. The Keweenawan basalts may have formed because North America started to rift, while the Deccan and Columbia River basalts may be related to continental hot spots. The Columbia River basalts may have been the first magmatism associated with the hot spot now located under Yellowstone National Park, located at the junction of Idaho, Montana, and Wyoming. Regardless, in all cases the mafic magma was generated because of mantle decompression melting in a similar fashion to what occurs at mid-ocean ridges.

Layered mafic intrusions are large mafic bodies found within continental crust. The average composition of these intrusions is about the same as a typical basalt. Fractional crystallization of olivine, pyroxene, plagioclase, and other minerals results in the formation of mineralogically distinct layers as sequentially one group of crystals settles onto the magma chamber floor, followed by another group, and so on. Layers range in thickness from millimeters to hundreds of meters within bodies that can be several kilometers to hundreds of kilometers long. Most large, layered igneous intrusives are Precambrian, and they are the primary source of the so-called platinum group elements, which include Pt, Pd, Rh, Ir, Ru, and Os, but other metals such as Ni and Cr can also be extracted. Many appear to have been formed within a rifting or hot spot environment as discussed above. Some, such as the Sudbury body in Ontario, Canada, are located within large meteorite impact craters.

Alkaline igneous rocks can also be associated with intracontinental rift and hot spot systems. They are generally not voluminous and tend to be quite diverse compositionally. Their magmas appear to be derived by melting the upper mantle, but complex crustal interaction and contamination may also occur. Rocks include syenite, phonolite, and other feldspathoid-bearing rocks.

At both intracontinental rifting and hot spots, more typical granite/rhyolite type rocks commonly occur and may be widespread. This is particularly true at the active Yellowstone hot spot. The felsic magma is produced by crustal melting driven by the heat input from the mafic magmatism. The magmatism at intracontinental rifts and hot spots is often said to be bimodal, as both mafic and felsic compositions exist while intermediate compositions are lacking.

DO NOT COPY e48d507df5d1141@placeholder.9409

Printed by: e48d507df5d1141@placeholder.94092.edu. Printing is for personal, private use only. No part of this book may be reproduced or transmitted without publisher's prior permission. Violators will be prosecuted.

Clastic Sedimentary Rocks

Clastic sedimentary rocks are formed by the accumulation and subsequent lithification of mineral and rock particles derived by weathering and eroding preexisting rocks exposed at the Earth's surface. Other terms applied to clastic sediments are *terrigenous*, *siliciclastic*, *detrital*, and *fragmental*. Whatever the term used for them, these rocks are always stratified or layered. Mineralogically, clastic sedimentary rocks are composed dominantly of silicate minerals. A simplified classification of clastic sedimentary rocks, based upon grain size, is shown in **Table 11.6**.

TABLE 11.6 Simplified Classification of Clastic Sedimentary Rocks

Particle Name		Grain Size (diameter in millimeters)	Rock Type
Gravel	Boulder	256	Conglomerate (if particles are rounded) Breccia (if particles are angular)
	Cobble	64	
	Pebble	4	
	Granule	2	
Sand	Very coarse sand	1	Sandstone (see Figure 11.8)
	Coarse sand	0.5	
	Medium sand	0.25	
	Fine sand	0.125	
	Very fine sand	0.062	
Mud	Coarse silt	0.031	Mudstone (if lacks fissility) Shale (if fissile) Siltstone (if dominantly silt sized) Claystone (if dominantly clay sized)
	Medium silt	0.016	
	Fine silt	0.008	
	Very fine silt	0.004	
	Clay sized		

Conglomerates and breccias are differentiated by the degree to which the pebbles, cobbles, and boulders are rounded by physical weathering—conglomerates are composed of rounded clasts; breccias are angular. They can be further subdivided based on grain

DO NOT COPY e48d507df5d1141@placeholder.9409

Printed by: e48d507df5d1141@placeholder.94092.edu. Printing is for personal, private use only. No part of this book may be reproduced or transmitted without publisher's prior permission. Violators will be prosecuted.

of rounded clasts; breccias are angular. They can be further subdivided based on grain size and the nature of the particles—quartz pebble conglomerate, chert cobble breccia, and so forth.

Among the sandstones, a distinction can be made between framework grains and matrix. Framework grains are sand particles—usually quartz, feldspar, or lithic fragments. Lithic fragments are recognizable pieces of rock consisting of multiple mineral grains. Matrix consists of clay or other fine-grained minerals between the sand grains. Sandstones with less than 15 percent matrix are **arenites** (Figure 11.8a); those with 15 to 75 percent matrix are **wackes** (Figure 11.8b).

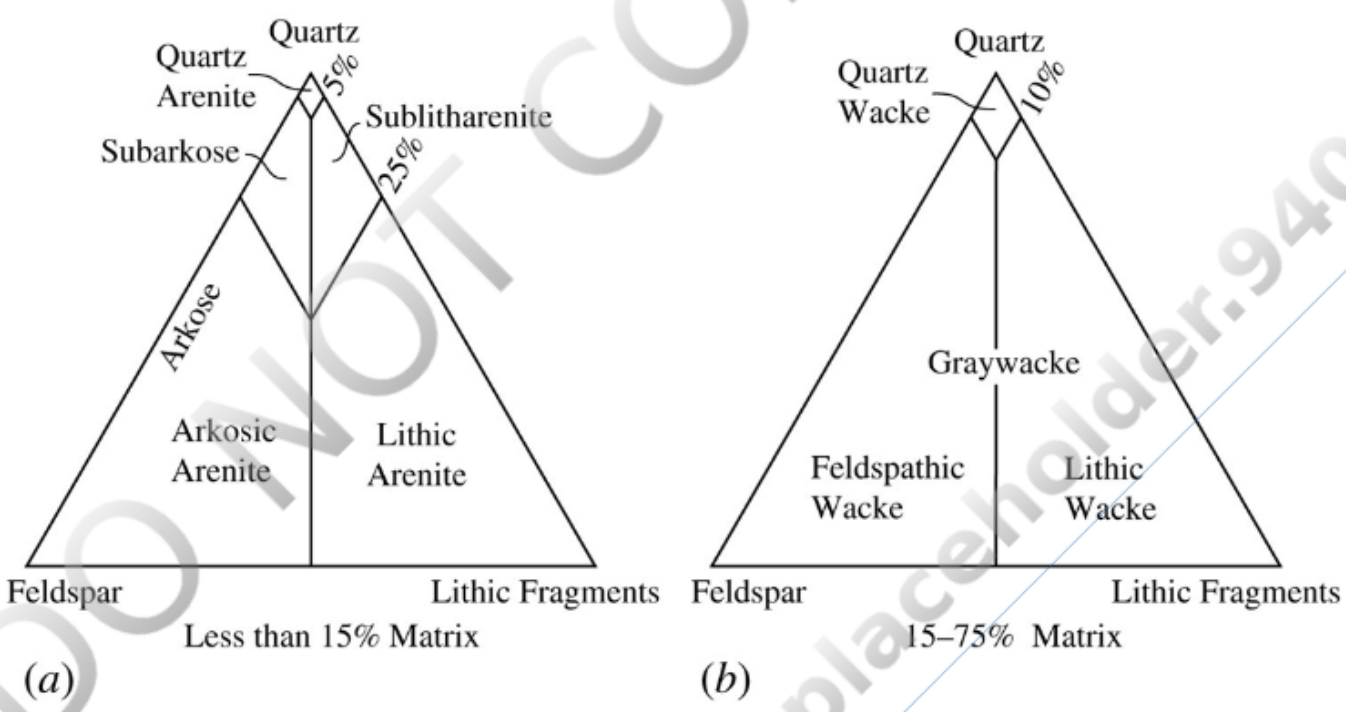

FIGURE 11.8 Classification of sandstones based on quartz, feldspar (K-feldspar + plagioclase), and lithic fragment content of the sand-sized particles. (*a*) *Arenites* have less than 15 percent matrix material (clay, fine quartz, etc.). *Arkose* is a common term for rocks with mostly quartz and feldspar grains. (*b*) *Wackes* have 15 percent or more matrix material. *Graywacke* is a more generic term applied to wackes with substantial amounts of quartz, feldspar, and lithic fragments. Modified from Dott (1964). View larger image

Silt- and clay-sized particles collectively are called mud, in reference to the slurry that can be made from silt and clay mixed with water. **Mud rock** is a generic term for all sedimentary rocks composed of over 75 percent mud-sized particles. The term **siltstone** is used if the particles are dominantly silt sized (distinctly gritty if ground between teeth); **claystone**, if the particles are dominantly clay sized (smooth if ground between teeth); **shale**, if the rock is fissile (breaks approximately parallel to bedding), and **mudstone**, if the rock is not fissile. The terminology for mud rocks has repeatedly been redefined and modified, and consensus has not developed around the details of a single nomenclature.

One source of confusion in mud rock nomenclature is that the term *clay* is used in three different ways. The first refers to a sediment or rock (e.g., claystone) that has the

Printed by: e48d507df5d1141@placeholder.94092.edu. Printing is for personal, private use only. No part of this book may be reproduced or transmitted without publisher's prior permission. Violators will be prosecuted.

different ways. The first refers to a sediment or rock (e.g., claystone) that has the property of being plastic when mixed with an appropriate amount of water. The second refers to a size—clay-sized particles are less than about 0.004 mm in diameter. The third refers to a group of hydrous sheet silicate minerals, collectively called clay minerals, which are responsible for the plastic behavior of clay. Most clay (the sediment) is made of clay-sized particles, but not all, and most of the clay-sized fraction of sedimentary material is composed of clay minerals, but again, not all. Quartz and other minerals are often present. Similarly, clay minerals may be part of the silt-sized fraction of some sediments. In this book, *clay* refers to the rock or sediment; *clay sized* refers to the size of mineral particles, regardless of mineralogy; and *clay mineral* refers to the group of hydrous sheet silicate minerals that give plasticity to clay, regardless of size.

Sedimentary Processes

The mineralogy of clastic sedimentary rocks depends both on the mineralogy of the rocks found in the source area of the sediment and on the processes of weathering, transport, deposition, and **diagenesis**. Diagenesis includes the lithification of sediments into rock, plus other chemical and physical changes to the sediment or rock that might occur due to burial, interactions with water in the material, and microbial activity.

Physical weathering serves to break rocks into smaller and smaller particles. The processes include frost wedging, biological activity (including geologists with rock hammers), exfoliation, and so forth. If physical weathering were the only weathering process, the mineralogy of sediment would be the same as that of the rocks being weathered.

Chemical weathering produces mineralogical changes that can be summarized as

$$\begin{aligned}&\text{Silicates} + \text{water} + \text{H}^+ \\ &= \text{clay minerals} + \text{quartz} + \text{ions in solution}.\end{aligned} \tag{11.2}$$

The water in most cases is meteoric, meaning that it originates as precipitation (rain, snow, etc.) that has fallen onto the ground and eventually becomes part of the groundwater supply. The H^+ is mostly from carbonic acid (H_2CO_3), produced as a consequence of dissolving atmospheric CO_2 in the water. Some H^+ also comes from organic acids produced by microbial activity and the decomposition of organic material in the soil, or from sulfuric acid (H_2SO_4) produced from sulfur emitted into the atmosphere by volcanoes or from industrial processes.

Typical reactions that can produce clays such as kaolinite and montmorillonite involve the breakdown of minerals such as K-feldspar and pyroxene.

$$2\text{KAlSiO}_3\text{O}_8 + 2\text{H}^+ + 9\text{H}_2\text{O}$$

DO NOT COPY e48d507df5d1141@placeholder.94092

Printed by: e48d507df5d1141@placeholder.94092.edu. Printing is for personal, private use only. No part of this book may be reproduced or transmitted without publisher's prior permission. Violators will be prosecuted.

$$\underset{\text{K-feldspar}}{2KAlSi_3O_8} + 2H^+ + 9H_2O = \underset{\text{kaolinite}}{Al_2Si_2O_5(OH)_4} + 4H_4SiO_4 + 2K^+ \quad (11.3)$$

$$p\text{Ca(Mg,Fe,Al)(Si,Al)}_2\text{O}_6 + q\text{H}_2\text{O} + r\text{H}^+ = \underset{\text{pyroxene}}{\quad} \underset{\text{montmorillonite}}{s(\text{Ca})_{0.5}(\text{Al}_5\,\text{Mg})(\text{Si}_4\text{O}_{10})_3(\text{OH})_6 \cdot n\text{H}_2\text{O}} + t\text{FeO} \cdot \text{OH} + u\text{Ca}^{2+} + v\text{H}_4\text{SiO}_4 \quad (11.4)$$

goethite

The H_4SiO_4 represents silica in solution that, in many cases, may be incorporated into the structure of clay minerals produced by weathering of other minerals in the same rock. The values of *p*, *q*, *r*, etc. in Equation 11.4 depend on the exact composition of the pyroxene. Some silicate minerals are more susceptible to chemical weathering than others (Box 11.1 and Figure 11.7).

Microorganisms are intimately involved in many weathering processes (Konhauser, 2007). Freshly exposed rock is rapidly colonized by bacteria, algae, fungi, and lichens, because the minerals provide a rich source of bioessential elements. Fungi that colonize rock surfaces send filaments into cracks, cleavages, and along grain boundaries. These both pry mineral grains apart and etch or pit mineral surfaces. Bacteria also coat mineral surfaces with extracellular polymers including polysaccharides and proteins, which may make the rock surface slippery when wet. These polymers retain water and thus increase the time available for water to chemically react with mineral surfaces. Microbes accelerate mineral dissolution by producing organic acids, which are metabolism byproducts or are purposely released to liberate nutrients from the minerals. The cellular surfaces of microbes may also serve as sites where clay and other minerals nucleate. These biologic processes work together with the other processes of physical and chemical weathering to accelerate weathering of rocks and the formation of soils.

Clay minerals (see Chapter 13) have many different structures and compositions. The nature of the silicate minerals being weathered and the details of the chemical environment control which clay mineral is produced. Time also plays a significant role because weathering is often progressive—one group of clay minerals initially forms, but with time, the clay minerals may progressively change to other clay minerals.

Iron from mafic minerals may be incorporated into the structure of some clay minerals, or iron can also form iron hydroxide minerals that stain the weathered rock various shades of red or brown. This discoloration is often simply called iron staining. Goethite formed by

DO NOT COPY

Printed by: e48d507df5d1141@placeholder.94092.edu. Printing is for personal, private use only. No part of this book may be reproduced or transmitted without publisher's prior permission. Violators will be prosecuted.

the weathering of pyroxene is an example (Equation 11.4).

Transport, most commonly by streams, but also by wind, waves, and other processes, produces both continued chemical weathering and progressive reduction of grain size. Near the source, sediment derived from igneous and metamorphic rocks may contain quartz and abundant plagioclase, K-feldspar, muscovite, biotite, and hornblende. With transport, all but quartz progressively break down to yield clay, as described earlier. Eventually, the sediment deposited into the ocean from an extensive river system typically consists dominantly of quartz and clay. Continued weathering also promotes a reduction of grain size because weathered minerals lose strength and hardness. Similarly, the physical abrasion that occurs during transport promotes chemical weathering because chemical reaction rates increase as grain size decreases.

Transportation also segregates grains based on grain size, shape, and specific gravity. In marine environments, this results in clay-rich mud deposition in areas with low water velocity—offshore, for example. Sand, composed of quartz, with or without feldspars and lithic fragments, may be deposited in higher-energy environments, such as beaches. In fluvial environments, clay-rich mud is deposited in overbank areas, and the quartz-rich sand and larger grain sizes are deposited in active channels.

The term **compositional maturity** refers to the degree to which sediment lacks both feldspar and lithic fragments or other easily weathered materials. A compositionally mature sandstone, for example, consists almost exclusively of quartz grains, and a compositionally mature mud rock consists dominantly of quartz and clay. A compositionally immature sediment, on the other hand, contains substantial amounts of feldspar and/or lithic fragments. In general, intense weathering in the source area and/or extensive transport produce compositionally mature sediment.

Quartz, feldspars, and clay are the most abundant minerals found in sediment, but others may be found in small amounts. Because many of these other minerals have specific gravities greater than either quartz, clay, or the feldspars, they have collectively been referred to as **heavy minerals**. Some heavy minerals may be major constituents of source area rocks, while others only as trace accessory minerals. Common heavy minerals and their relative susceptibility to weathering are listed in **Table 11.7**.

TABLE 11.7 Heavy Minerals Commonly Found in Clastic Sediments[a]

Stability	Minerals
Extremely stable (weathers slowly)	**Zircon, tourmaline**, rutile
Stable	**Garnet (low-Fe), staurolite, biotite,** magnetite, ilmenite, apatite, monazite
Moderately stable	**Epidote, kyanite, garnet (Fe), sillimanite, titanite, zoisite**
Unstable	**Amphibole, pyroxene, andalusite**

DO NOT COPY e48d507df5d1141@placeholder.94092

Printed by: e48d507df5d1141@placeholder.94092.edu. Printing is for personal, private use only. No part of this book may be reproduced or transmitted without publisher's prior permission. Violators will be prosecuted.

Very unstable (weathers quickly)	**Olivine**

[a] Silicates are in bold type.

Source: Adapted from Pettijohn and others (1987).

The net result of all weathering and transportation processes is a progressive reduction of grain size, production of clay minerals while quartz persists, and winnowing (separation) of minerals based on grain size, specific gravity, and shape. It should be no surprise that the most abundant sedimentary rocks are mud rocks, composed dominantly of clay minerals and quartz, with minor amounts of feldspar. The clay minerals are produced by the breakdown of other minerals, and the quartz is largely derived from the parent rocks. Feldspars and lithic fragments are usually a major constituent of clastic sedimentary rocks only if the sediment is close to its source and/or has been weathered little.

Once deposited, the mineralogy of sediments continues to evolve during diagenesis. Mineralogical changes that may take place include the following.

- Alteration: Primary feldspars and other minerals in the sediment may break down to form clay minerals or zeolites. This process may release silica, which can precipitate to form a cementing agent. The fine-grained clay and zeolite may also serve as a binder holding larger grains together.
- Dissolution: Some minerals may dissolve into the pore fluid over time.
- Recrystallization: Small grains may combine by recrystallization to form larger grains. Some minerals may be dissolved at one location and reprecipitated elsewhere.
- Precipitation: Ions in solution can precipitate either as new minerals or as additions to existing minerals. The silica that cements many arenites typically forms overgrowths on existing quartz grains. Calcite cement precipitates from pore water. Other minerals that may form by diagenetic processes include the feldspars, gypsum, anhydrite, iron hydroxides, and pyrite.
- Changes in clay mineralogy: The clay minerals evolve and (re)crystallize with time and burial. The detailed clay mineralogy of a sediment after many millions of years may be quite different than when the sediment was originally deposited. These processes are described in more detail in Chapter 13.

Sedimentary Environments

The depositional environments of clastic sediment can be broadly grouped into terrestrial, transitional, and marine (**Table 11.8**). The large majority of preserved sedimentary rocks were deposited in marine or transitional environments, although most

Printed by: e48d507df5d1141@placeholder.94092.edu. Printing is for personal, private use only. No part of this book may be reproduced or transmitted without publisher's prior permission. Violators will be prosecuted.

of the sediment undoubtedly spent time as deposits in, or passed through, terrestrial environments.

TABLE 11.8 Sedimentary Environments

Terrestrial	Transitional	Marine
Alluvial fan and fan delta	Deltaic	Sublittoral (continental shelf)
Fluvial (stream)	Littoral (beach)	Bathyal marine fan (continental slope)
Lacustrine (lake)	Tidal	Abyssal plain
Glacial	Estuarian	
Eolian (wind)		

Sandstones are among the most useful sedimentary rocks when it comes to recording the nature of the source area, which is referred to as the **provenance** of the sediment. **Figure 11.9** shows, in a general way, the mineralogy of sandstones derived from different tectonic environments. The corners of the ternary diagram are the relative amounts of framework grains: Q includes quartz grains and polycrystalline grains of quartzite and chert, F includes feldspar grains (K-feldspar + plagioclase), and L includes polycrystalline lithic grains of igneous, metamorphic, and sedimentary origin that are not quartzite or chert. The diagram distinguishes sand derived from continental craton, magmatic arcs, and recycled orogens (mountain belts).

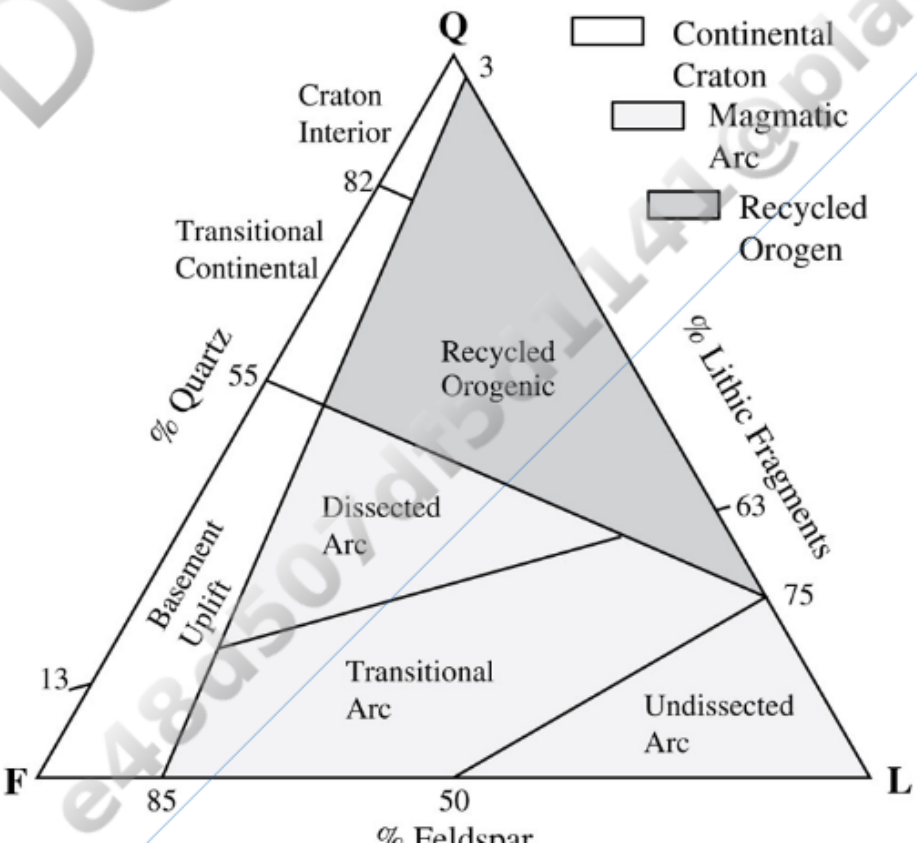

Printed by: e48d507df5d1141@placeholder.94092.edu. Printing is for personal, private use only. No part of this book may be reproduced or transmitted without publisher's prior permission. Violators will be prosecuted.

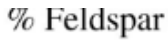

FIGURE 11.9 Mineralogy of framework grains in sandstone derived from different tectonic settings. Q=quartz, F=feldspar, L=lithic fragments. Adapted from Dickinson and others (1983). See text for additional discussion. View larger image

Three sediment sources are recognized within continental environments with exposed plutonic igneous and metamorphic rocks. The most quartz-rich sediment is from continental craton interiors with low relief. Erosion is slow relative to weathering, so that feldspars and other less stable minerals are broken down. The feldspar-rich sediments are derived from areas of substantial basement uplift where erosion is fast relative to weathering, so that feldspars are not extensively weathered. The transitional continental environment is intermediate between these two extremes.

Within magmatic arcs, the source rocks are dominantly andesitic volcanic rocks, with intermediate to felsic intrusives at depth. Sand derived from this environment is dominated by feldspars and lithic fragments; quartz is not particularly abundant. Sands with the most abundant lithic fragments are derived from volcanic arcs that have not experienced extensive erosional dissection. Deeply dissected arcs expose the felsic intrusives at depth and tend to produce sands with more feldspar and quartz. Transitional arc environments are intermediate between these extremes.

Recycled orogenic sand is derived from sedimentary rocks exposed in orogenic belts such as the Cordilleran fold-and-thrust belt that extends from northwestern Canada and through the western United States. These rocks may be metamorphosed to some degree and some volcanic rocks may be present, but felsic intrusives are largely not exposed. Because igneous rocks are not major contributors to the sediment, feldspars are not abundant.

The boundaries drawn on Figure 11.9 are in reality gradational. Sand deposited in any particular environment may be derived from a variety of areas with different tectonic characteristics and rock types. However, the diagram makes the important point that geological setting and tectonics can play a major role in determining the mineralogy of sediment.

DO NOT COPY e48d507df5d1141@placeholder.9409

Printed by: e48d507df5d1141@placeholder.94092.edu. Printing is for personal, private use only. No part of this book may be reproduced or transmitted without publisher's prior permission. Violators will be prosecuted.

Metamorphic Rocks

Metamorphic rocks are those that experienced mineralogical, textural, and/or compositional changes, usually as the result of heat, pressure, chemically reactive fluids, and/or deformation. The classification of common metamorphic rocks (**Table 11.9**), like igneous rocks, can be fairly straightforward, but there are a number of complexities. A metamorphic rock name may be based on mineralogy, but also **texture** can be used for naming. Texture includes the rock's grain size and presence or absence of foliation. **Foliation** can have two separate but related forms. One way foliation is produced is by the alignment of inequant minerals. Micas, because they form platy crystals, can produce a well-developed foliation known as **schistosity** if coarse grained (one can see individual grains without a hand lens) or **slaty cleavage** if fine grained (one cannot see the grains). Rocks with schistosity or slaty cleavage break easily along the foliation because it is parallel to the perfect cleavage of the micas. A foliation also can be formed by alternating lighter- and darker-colored layers in the rock. Because it is common in gneiss, compositional layering is also known as **gneissic foliation** (also called gneissic layering, gneissose structure, etc.).

TABLE 11.9 Classification of Common Metamorphic Rocks

Criteria	Rock Type	Comments
Defined based on texture		
Foliated	Slate	Very fine grained with dull luster on well-developed foliation surfaces; sheet silicates usually abundant
	Phyllite	Fine grained with silky luster on well-developed foliation surfaces; sheet silicates usually abundant
	Schist	Coarse grained with abundant inequant minerals such as micas that are aligned to produce a foliation
	Gneiss	Coarse grained with layering of light- and dark-colored minerals; roughly equant minerals such as quartz and feldspar are dominant
	Migmatite (gneiss)	Identical description to that of a gneiss, but the term migmatite is used *only* when it is know that the rock partially melted during metamorphism, including for rare varieties that are unfoliated
Not foliated	Hornfels	Fine grained and not foliated; inequant minerals like sheet silicates may be abundant
	Granofels	Coarse grained and not foliated; often dominated by equant minerals such as quartz and feldspars
Defined based on mineralogy	Quartzite	Primarily quartz; commonly derived from quartz-rich sandstone, but any nearly pure quartz rock can serve as a protolith; may have a small amount of micas defining a foliation, or may be unfoliated

DO NOT COPY e48d507df5d1141@placeholder.9409

Printed by: e48d507df5d1141@placeholder.94092.edu. Printing is for personal, private use only. No part of this book may be reproduced or transmitted without publisher's prior permission. Violators will be prosecuted.

	Amphibolite	Abundant amphibole such as hornblende; derived from mafic igneous rocks or closely related sediment; if well-foliated and contains hornblende, may be referred to as hornblende schist
	Marble	Primarily calcite or dolomite; derived from limestone or dolostone; may or may not have a foliation
	Skarn	Abundant calc-silicate minerals (Ca-bearing silicates) such as amphibole, pyroxene, garnet, wollastonite, and epidote, and/or olivine, calcite, and dolomite; magnetite may be abundant in some cases; derived from limestone/dolostone metamorphosed adjacent to felsic intrusive; if foliated, may be referred to as a calc-silicate gneiss
	Serpentinite	Abundant serpentine minerals (antigorite, chrysotile); derived from mafic or ultramafic igneous rocks; may or may not have a foliation
	Greenstone or greenschist	Low-grade metamorphosed mafic meta-igneous rock whose green color is derived from chlorite, amphibole, and/or epidote; greenstone is not foliation; greenschist is foliated
	Blueschist	Medium-grade metamorphosed mafic meta-igneous rock whose blue color is derived from glaucophane, a blue amphibole; kyanite may also be common in this rock and may also be blue. Rock may be coarse or fine grained; may be foliated or not foliated
	Eclogite	High-grade metamorphosed mafic meta-igneous rock with omphacite (Ca-Na pyroxene) and garnet, which imparts an alternating green-red rock color; must lack plagioclase. Because of its grade, nearly universally it is coarse grained and may be foliated or not foliated
	Granulite	High-grade metamorphic rock with no or very little OH-bearing minerals such as biotite, muscovite, or amphibole; therefore they are typically dominated by pyroxene and plagioclase with or without garnet. Because of its grade, nearly universally it is coarse grained; may be foliated or not foliated

Schistosity and slaty cleavage are often produced because the rock experienced ductile deformation during metamorphism, which causes the inequant minerals to align during metamorphism. Gneissic foliation can be created in a number of ways, and it may not be obvious how it was formed. Some gneissic foliation may be layers that existed in the protolith that are still observable, though often they have been modified by deformation. Gneissic foliation may also be created during metamorphism by the rock partially melting or by the injection of melt. Lastly, gneiss foliation may be produced by extreme deformation that has flattened more equant protolith features, such as large feldspar grains.

For rock types defined based on texture, additional modifiers are usually applied to specify some aspect of the mineralogy. An example is muscovite biotite garnet schist, which is a well-foliated rock mostly composed of muscovite, biotite, and garnet. Minerals are generally listed in order of decreasing abundance. Another example of a metamorphic rock name is quartz microcline plagioclase biotite gneiss.

Additionally, if the identity of the parent rock is evident, a metamorphic rock may be referred to by adding the term *meta-* to the parent rock name: meta-rhyolite, meta-graywacke, and so forth. Because of this and because a metamorphic rock can be named

Printed by: e48d507df5d1141@placeholder.94092.edu. Printing is for personal, private use only. No part of this book may be reproduced or transmitted without publisher's prior permission. Violators will be prosecuted.

for its texture or its mineralogy, a metamorphic rock may have multiple acceptable names.

Sometimes, the relative amount of T–P (temperature–pressure) may be referred to when discussing metamorphic rocks. A **low-grade** metamorphic rock formed under relatively low T–P conditions, perhaps 350°C and 3 kbar, while a **high-grade** metamorphic rock formed under relatively high T–P conditions, perhaps 650°C and 10 kbar. A **medium-grade** metamorphic rock experienced intermediate T–P conditions, between those of a low-grade and a high-grade rock. This will be discussed in greater detail later in the chapter.

Metamorphic Variables

One of the primary objectives in studying metamorphic rocks is to determine the conditions a metamorphic rock experienced, and from that information, it may be possible to deduce something about the tectonic history of the rock or answer some other geologic question of importance. For any metamorphic rock, the bulk composition of the protolith is of primary importance. For example even if subjected to the same metamorphic grade (T–P conditions) and fluid conditions, shale and a limestone protoliths will produce distinctly different metamorphic mineralogies, and therefore, distinctly different metamorphic rocks. Temperature, pressure, and fluid conditions may be considered external agents that act on rocks and produce metamorphic changes.

These internal and external variables also affect sedimentary and igneous rocks, so, the distinction between what rocks or conditions that should be classified as metamorphic or not is not exactly clear. The lower temperature limit of metamorphism is generally, and somewhat arbitrarily, taken to be 200°C. Mineralogical changes taking place at lower temperatures are considered to be part of sedimentary diagenesis, although diagenesis and metamorphism are clearly part of a continuum of changes that rocks experience as temperatures increase. Though mantle rocks are generally classified as igneous (see Table 11.9), they experience high T–P conditions consistent with metamorphism and their mineralogy and textures are produced by ongoing processes in the solid state, so they should be considered metamorphic. The upper temperature limit of metamorphism is also poorly defined. Migmatite (Table 11.9) is a rock that straddles the igneous and metamorphic realm. When migmatite forms, both an igneous component (the partial melt) and a metamorphic component (a solid, unmelted portion) exist. Migmatite is generally considered to be a metamorphic rock. The reality is that there are no strict boundaries between the processes or variables that control igneous, sedimentary, or metamorphic rock formation.

Temperature is perhaps the most important external control on metamorphism because most metamorphic reactions require high diffusion rates (see Chapter 5), and diffusion rates are positively correlated to temperature. The temperature also controls what metamorphic minerals might form: at higher temperatures, some metamorphic minerals

DO NOT COPY e48d507df5d1141@placeholder.94092

Printed by: e48d507df5d1141@placeholder.94092.edu. Printing is for personal, private use only. No part of this book may be reproduced or transmitted without publisher's prior permission. Violators will be prosecuted.

metamorphic minerals might form; at higher temperatures, some metamorphic minerals will form over others. The source of the thermal energy may be a nearby igneous intrusion or more extensive regional sources, such as heat from the mantle that may be related to crustal depth or from the breakdown of radioactive elements in the rocks.

Like temperature, pressure also controls metamorphism. For example, high pressure favors the formation of high-density minerals with more tightly packed atomic structures. Metamorphic pressure is the lithostatic pressure (P), or the pressure due to the weight of the overlying rock, which is given by

$$P = \rho g h \tag{11.5}$$

where ρ (kg/m^3) is the density of the overlying rock, g (9.8 m/sec^2) is the acceleration of gravity, and h (m) is the depth. Units of pressure are pascals (1 Pa): 1 Pa = 1 kg m^{-1} sec^{-2}. For geological purposes, pressure is often reported in gigapascals (GPa = 10^9 Pa) or kilobars (kbar): 1 kbar = 0.1 × 10^9 Pa. **Table 11.10** gives the lithostatic pressure produced if the overlying rock is granite, basalt, or peridotite. In general, pressure at the base of continental crust 40-km thick is approximately 10–11 kbar, as most continental crust is approximately granitic in composition.

TABLE 11.10 Lithostatic Pressure Produced by Different Rock Types

Rock Type	Density (kg/m^3)	kbar/km	km/kbar
Granite	2700	0.264	3.8
Basalt	3000	0.294	3.4
Peridotite	3300	0.323	3.1

Lithostatic pressure is generally considered to be hydrostatic, meaning that it is equal in all directions. In actively forming orogenic (mountain) belts, an additional deviatoric stress is usually present from the collision of plates. The deviatoric stress is the measure to which the pressure is not equal in all directions. The magnitude is generally not large—probably in the range of a few bars to no more than 100 bars—so it does not significantly affect the pressure stability of minerals in metamorphic rocks. However, the deviatoric stress is responsible for the extensive deformation experienced by many metamorphic terranes. The results of deformation include the formation of foliation, folding, and so on, so commonly found in metamorphic rocks. Typically covered in a structural geology course, detailed study of metamorphic rock deformation provides a crucial link to understanding the tectonic environment that formed the metamorphic rocks.

Fluids can also affect metamorphism. Prior to metamorphism, most rocks contain an aqueous fluid along grain boundaries and in pore space. The composition of this fluid can be important, for example, the stability of the mixes is reduced, meaning they will

DO NOT COPY e48d507df5d1141@placeholder.94092

Printed by: e48d507df5d1141@placeholder.94092.edu. Printing is for personal, private use only. No part of this book may be reproduced or transmitted without publisher's prior permission. Violators will be prosecuted.

be important; for example, the stability of the micas is reduced, meaning they will breakdown at lower temperatures, if the aqueous pore fluid contains CO_2, CH_4, or other chemical species. Similarly, carbonate minerals can be stable at high temperatures only if the pore fluid contains high levels of CO_2. Fluids are often driven out of rocks with increasing temperatures, but more fluid can be generated by the breakdown of hydrous minerals (containing OH^- or H_2O) such as the clays, micas, and amphiboles. Fluids may be added from external sources, and any fluid created or moving into or out of the rock can also add or remove important cations, such as Fe, Mg, Ca, and so on, which will influence the metamorphic minerals produced. The presence or absence of rock fluid has significant control on what happens as metamorphism ends and T–P conditions decrease, as will be discussed below.

It is also important to remember that metamorphism is a highly dynamic process—temperature, pressure, and fluid conditions are ever changing. As a rock is buried during convergent tectonics, the pressure increases nearly instantaneously, as shown in Equation 11.5. Temperature, however, takes time to increase, as the conduction of heat through rock is slow. After peak conditions are reached (for rock studied by geologists at the surface), the rock is brought back to the surface, often because of surface erosion. During this return journey, the T–P will decrease. Tracking the T–P changes for this rock through time results in a clockwise **T–P loop**, which is presumed to be the most common type of T–P loop for rocks metamorphosed during convergent tectonics (**Figure 11.10**). Such loops may be separated into 4 portions. The **prograde path** is the period of increasing T–P while the rock is being buried, then the **peak pressure** is reach when the rock is at its greatest depth. Following peak pressure the rock continues to heat, but rock depth and pressure decease due to erosion. This is followed by the **peak temperature** conditions, which are often considered to be the **peak metamorphic conditions** recorded by the minerals in the rock. Lastly, both temperature and pressure decrease as metamorphism ends and erosion continues; this is called the **retrograde path**. Construction of T–P paths is difficult as evidence for the **prograde metamorphism**, or the metamorphic changes that occur during the prograde path, may be completely removed by peak metamorphism; likewise, **retrograde metamorphism** may completely remove any evidence of the peak metamorphic conditions.

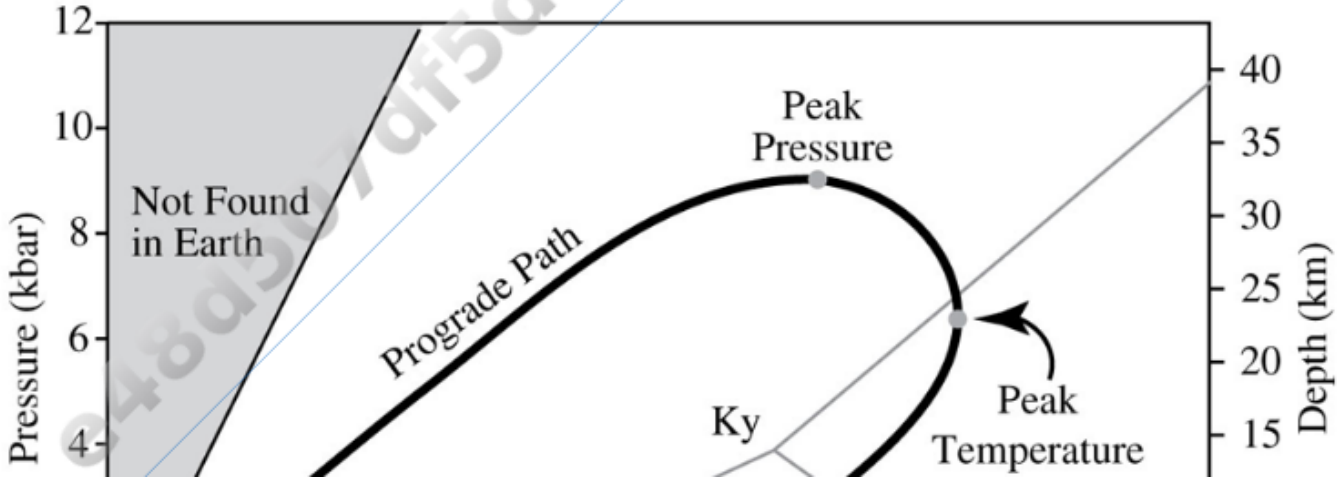

Printed by: e48d507df5d1141@placeholder.94092.edu. Printing is for personal, private use only. No part of this book may be reproduced or transmitted without publisher's prior permission. Violators will be prosecuted.

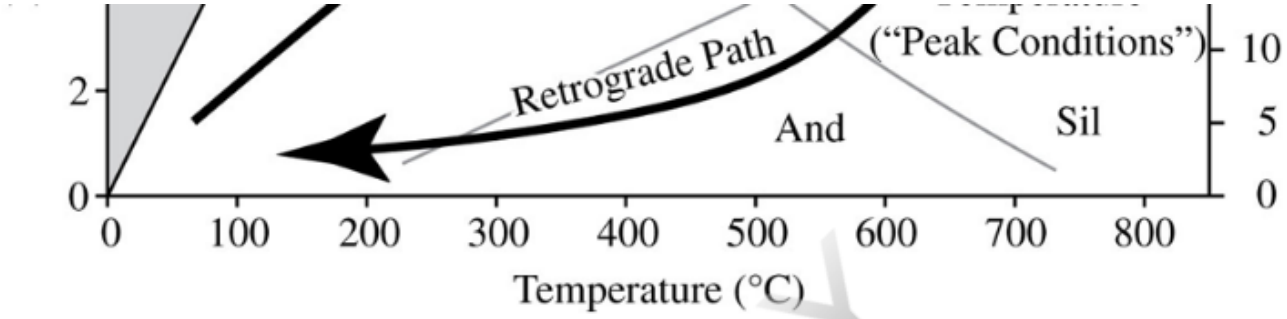

FIGURE 11.10 Generalized temperature and pressure loop for a rock buried by convergent tectonics and brought back to the surface by erosion. Important components of the loop are labeled. Stability fields of the aluminum silicates (Al_2SiO_5: andalusite [And], sillimanite [Sil], and kyanite [Ky]) are shown for reference. View larger image

Metamorphic Processes

During metamorphism, as depicted by the T–P loop of Figure 11.10, rocks go through a variety of changes. Many of these changes have been introduced in Chapter 5, but they will be covered here again. The changes include recrystallization, new mineral growth, textural changes, and compositional changes.

Recrystallization involves size and shape changes of the existing grains in a rock. Many small grains of a mineral have much greater surface area and energy than a single large grain. Minerals will tend to recrystallize to produce a smaller number of large grains to reduce the surface energy (Figure 5.27). Diffusion rates will be high in rocks subjected to high temperatures, which allows recrystallization.

If during metamorphism minerals are intensely deformed and recrystallized, for example, in a shear zone or ductile fault, this recrystallization is called **dynamic recrystallization** and will reduce the grain size. The size reduction occurs because the deformation creates mineral grains with deformed crystal lattices, which energetically is not preferred. Therefore, deformed grains will recrystallize into numerous smaller grains whose lattices are unstrained (not deformed), which is preferable. If deformation ends but metamorphic conditions persist, subsequent recrystallization allows the fine grains to coalesce to form larger grains. Grain size of deforming rocks is controlled by the balance between dynamic recrystallization, causing grain size reduction, and high-temperature recrystallization, causing an increase in grain size.

As most regional metamorphism is caused by rocks migrating to deeper crustal levels during convergent tectonics, it is obvious that this will impose a deviatoric stress on the rock. The deformation caused by the deviatoric stress aligns platy minerals, like the micas, resulting in a foliation. Most often the alignment occurs as mica (re)crystallizes, but blocky minerals like feldspars may rotate during deformation without recrystallization and contribute to the foliation as well. In a simple model, the aligned minerals and foliation will be perpendicular to the direction of greatest shortening in the rock.

DO NOT COPY

Printed by: e48d507df5d1141@placeholder.94092.edu. Printing is for personal, private use only. No part of this book may be reproduced or transmitted without publisher's prior permission. Violators will be prosecuted.

As discussed in Chapter 5, new mineral crystallization during metamorphism involves replacement of less stable, high-energy minerals with low-energy minerals that are more stable under the current T–P conditions. For example, a mica schist with chlorite and muscovite moves along a prograde T–P path as it is buried; at some point the T–P is sufficiently high that the chlorite and muscovite become unstable and chemically react to form more stable staurolite, biotite, and quartz, as detailed in the following reaction.

$$\begin{aligned} &17(Mg,Fe)_3Si_4O_{10}(OH)_2 \cdot (Mg,Fe)_3(OH)_6 \\ &\quad +30KAl_2\,AlSi_3\,O_{10}(OH)_2 \\ &= 6Al_9Fe_2(AlO_4)(SiO_4)_3O_6(OH)_2 \\ &\quad +30K(Mg,Fe)_3\,AlSi_3\,O_{10}(OH)_2 + 50SiO_2 + 62H_2O \\ &17\ \text{Chlorite} + 30\ \text{muscovite} \\ &\quad = 6\ \text{staurolite} + 30\ \text{biotite} + 50\ \text{quartz} + 62\ H_2O \end{aligned} \tag{11.6}$$

The reaction will progress, or continue, until either the chlorite or the muscovite is used up.

A **mineral assemblage** is the collection of minerals found in a particular rock. The term is also used to refer to the reactant mineral assemblage and product mineral assemblage of a particular mineral reaction. In Reaction 11.6, chlorite + muscovite is the reactant mineral assemblage and is stable at lower temperatures. Staurolite + biotite + quartz is the product mineral assemblage that is stable at higher temperatures. Note that muscovite may be stable at higher temperatures with staurolite + biotite + quartz, but not with chlorite, and that quartz and biotite may be stable with chlorite and muscovite at lower temperatures, but not with staurolite. This emphasizes that all reactants must be present in order for the reaction to occur (providing T–P is also appropriate) and that the elements needed for new minerals must come from the breakdown of previously existing minerals.

From a textural perspective, Reaction 11.6 does not simply replace small grains of chlorite and muscovite with similar-sized grains of staurolite, biotite, and quartz. The newly grown staurolite commonly forms large porphyroblasts, and the new biotite and quartz form much larger grains than the original grains of chlorite and muscovite. The net result is often a complete overhaul of the rock texture and a substantial increase in grain size of both newly crystallized minerals and the recrystallized preexisting minerals. As discussed above, this is true as long as deformation is not significant, which may lead to dynamic recrystallization and grain size reduction.

Reaction 11.6 also demonstrates well that water is often released during metamorphic reactions. This water may migrate to areas of low pressure, such as the Earth's surface. Thin veins of quartz found in many metamorphic terranes often are interpreted to be de-watering channels along which quartz precipitated as the fluid escaped. It is typically

DO NOT COPY e48d507df5d1141@placeholder.9409

Printed by: e48d507df5d1141@placeholder.94092.edu. Printing is for personal, private use only. No part of this book may be reproduced or transmitted without publisher's prior permission. Violators will be prosecuted.

watering channels along which quartz precipitated as the fluid escaped. It is typically assumed that the escape of fluids, except for the loss of the fluids themselves, does not otherwise change the rock's bulk composition.

However, in certain metamorphic scenarios, fluids derived from external sources may change the bulk composition of a rock in a process called **metasomatism**, by both dissolving some components and contributing others. An example of a metasomatic metamorphic scenario is the generation of skarns (Table 11.9). The protolith of a skarn is a limestone; here it is assumed to be made of pure calcite ($CaCO_3$). If no metasomatism occurs, the metamorphism of the limestone should yield a marble, also made of pure calcite, just as described in an introductory geology course. But skarns consist of calc-silicate minerals (Ca-bearing silicates) such as amphibole, pyroxene, garnet, wollastonite, and epidote, and they can also contain magnetite, olivine, and dolomite. Collectively, in addition to Ca, the calc-silicate and other minerals are variably rich in, for example, Mg, Fe, Al, and Si. These elements, needed to produce the metamorphic minerals, must come from an external fluid source because the protolith lacks them. Skarns are typically found next to felsic intrusions. Magmatic fluids given off by the crystallizing intrusion are a likely source of the added elements causing the metasomatism.

During metamorphism, it is often assumed that prograde mineral reactions maintain equilibrium with the changing T–P because of the large amount of time involved in metamorphic processes. It has been demonstrated that this assumption is largely correct. However, it is important to note that this is not necessarily always the case. All chemical reactions require some degree of overstepping to proceed, and some mineral reactions will require more overstepping than others. Further, metamorphism involves continuous changes in T–P conditions; mineral reactions are constantly progressing as the minerals in the rock attempt to maintain equilibrium with the changing conditions. Carlson and others (2015) provide a very useful review of the role of reaction kinetics, or the rate at which chemical reactions progress, when evaluating metamorphic processes.

There are several key ideas regarding metamorphism; first, except in rare metasomatic cases, apart from fluid escape, rocks do not change in composition during metamorphism. Second, deformation often accompanies metamorphism, which produces a foliation in the rock. Third, metamorphic rock grain size is controlled by the balance between deformation-driven dynamic recrystallization that reduces grain size and crystallization and recrystallization that increase grain size. Fourth, T–P slowly changes. Fifth, the mineral assemblage is constantly changing to maintain the most stable configuration with changing T–P.

The fifth point raises an important question. If the minerals in a metamorphic rock are constantly reacting with each other in order to obtain the most stable configuration, why, when a geologist finds a metamorphic rock at the surface long after its metamorphism, does the rock retain minerals representative of peak metamorphic conditions? There are several things to consider to solve this apparent conundrum. Figure 11.10 shows that once peak temperature is reached, the rock will begin its retrograde path with decreasing T–P. As diffusion allows metamorphic reactions and temperature directly

Printed by: e48d507df5d1141@placeholder.94092.edu. Printing is for personal, private use only. No part of this book may be reproduced or transmitted without publisher's prior permission. Violators will be prosecuted.

decreasing T–P. As diffusion allows metamorphic reactions and temperature directly controls diffusion, decreasing the temperature progressively slows the rate of metamorphic reactions along the retrograde path until reactions are unable to generate an assemblage representative of the lowering T–P conditions. Also, the loss of water from a rock during metamorphism cannot be ignored. If water is lost, then Reaction 11.6, for example, cannot occur in reverse along the retrograde path. That is, water is required to form chlorite and muscovite (lower-grade assemblage) from biotite, staurolite, and quartz (higher-grade assemblage). If water is unavailable, the reaction cannot proceed. Therefore, the drop in temperature, which slows reactions, plus the loss of water means that metamorphic reactions on the retrograde path do not occur and the rock will keep the mineral assemblage representative of peak (temperature) conditions. If, however, water is added to the rock along the retrograde path, retrograde reactions may proceed and the peak assemblage will be lost to a retrograde assemblage. Identification of such a scenario is difficult and may be more common than currently identified. If this is the case, then many rocks may have experienced much higher-grade conditions than what the evidence shows. This is all part of the challenge and/or joy of working with metamorphic rocks.

Connecting Metamorphic Assemblage to Temperature–Pressure Conditions

Thus far our treatment of metamorphic rocks has been very qualitative; that is, we have only distinguished relative metamorphic grade. **Figure 11.11a** shows one division of T–P space into very low-, low-, medium-, and high-grade metamorphism. Therefore, additional tools are needed to better indicate specific T–P conditions from the metamorphic assemblage. Because bulk rock composition plays an integral role in what metamorphic minerals are possible, it is impossible to establish universal guidelines regarding what minerals indicate specific T–P conditions. In all cases it is important to establish or assume that the metamorphic assemblage was formed by the rock achieving equilibrium at some T–P conditions. Based on the discussion above, as long as retrograde metamorphism has not occurred, the metamorphic assemblage often records conditions near the peak temperature.

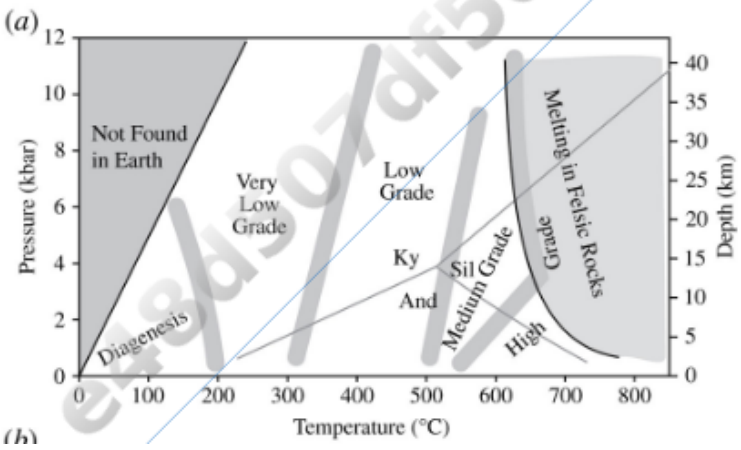

Printed by: e48d507df5d1141@placeholder.94092.edu. Printing is for personal, private use only. No part of this book may be reproduced or transmitted without publisher's prior permission. Violators will be prosecuted.

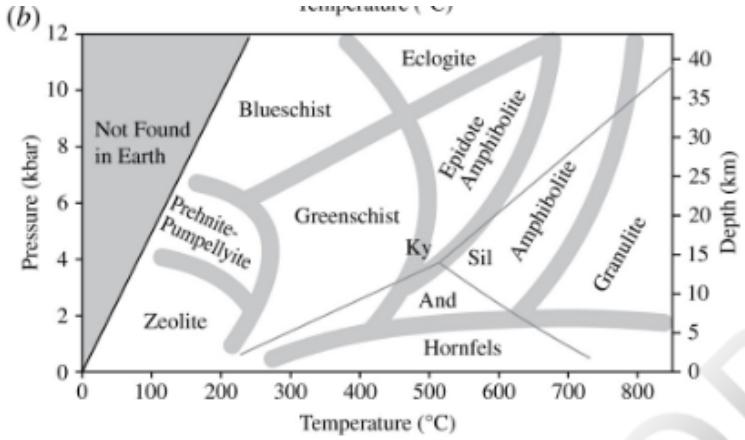

FIGURE 11.11 Metamorphic grade and facies boundaries. Stability fields of the aluminum silicates (Al_2SiO_5: andalusite [And], sillimanite [Sil], and kyanite [Ky]) are shown for reference. (*a*) Metamorphic grade, adapted from Winkler (1976). (*b*) Approximate temperature–pressure fields of the nine principal metamorphic facies. Adapted from Spear (1993) and Winter (2010). View larger image

Mafic Rocks

Mafic metamorphic rocks are derived from basaltic volcanics and gabbroic intrusions or closely related immature sediments. For such rocks, the **metamorphic facies** works well to connect a metamorphic assemblage to a range of T–P conditions that might have formed it. A metamorphic facies is a set of minerals commonly found in metamorphosed mafic rocks. Extensive work has connected the assemblage to a range of T–P conditions that formed the assemblage. **Figure 11.11b** labels nine different assemblages or facies; modifications to these and additional facies have been proposed. Mineralogy of the facies are listed in **Table 11.11**, and more detailed lists of metamorphic minerals are listed in Table C.3 in Appendix C.

TABLE 11.11 Mineralogy of Metamorphic Facies for Mafic Rocks

Facies	Characteristic Mineralogy
Hornfels	Mineralogy is poorly defined and may not be distinct.
Zeolite	Zeolites, usually laumontite, wairakite, or analcime
Prehnite-pumpellyite	Prehnite, pumpellyite
Greenschist	Chlorite, albite, epidote/zoisite ±[a] actinolite
Epidote-amphibolite	Plagioclase, hornblende, epidote ± garnet
Amphibolite	Plagioclase, hornblende ± garnet
Granulite	Orthopyroxene, plagioclase ± Ca-clinopyroxene, hornblende, garnet
Blueschist	Glaucophane, lawsonite, epidote
Eclogite	Omphacite, garnet ± kyanite, no plagioclase

DO NOT COPY
e48d507df5d1141@placeholder.9409

Printed by: e48d507df5d1141@placeholder.94092.edu. Printing is for personal, private use only. No part of this book may be reproduced or transmitted without publisher's prior permission. Violators will be prosecuted.

[a] ± indicates that the following mineral may or may not exist in the assemblage.

A point of confusion sometimes is that a number of specific metamorphic rock types share the same name as a metamorphic facies. Indeed, those facies are named for the metamorphosed mafic rock that is produced by those conditions, so care should be taken with such terms to be clear whether a specific metamorphic rock, a specific set of T–P conditions, or a specific metamorphic assemblage is meant. The metamorphic facies diagram and the aluminum silicate stability fields provide a widely used T–P reference frame for metamorphism, so even when a rock is not mafic or does not have the appropriate bulk chemistry to yield any of the aluminum silicates during metamorphism they often serve as the backdrop to discussions regarding the specific T–P conditions of a rock or region.

Pelites (and Psammites)

Pelitic metamorphic rocks are derived from mud rocks. **Psammitic** metamorphic rocks are derived from a rock intermediate between sandstone and mudstone. Generally most contain enough mud that metamorphically they behave similar to true pelites; hence, they are included in this discussion.

Because mud rocks contain Al-rich clay minerals, pelitic rocks commonly contain Al-bearing minerals such as muscovite, biotite, garnet, staurolite, cordierite, and the aluminum silicates, in addition to quartz and plagioclase (Table C.3 in Appendix C). K-feldspar may be present in high-grade rocks. Details of which minerals are present at any particular T–P condition depend, as always, on the bulk composition of the rock. A common sequence of mineral assemblages found in pelitic rocks connected to relative metamorphic grade is shown in **Table 11.12**.

TABLE 11.12 Typical Mineral Zones in Pelitic Rocks[a]

Grade	Index Mineral	Mineral Zone	Common Mineral Assemblage
Very low	Chlorite	Chlorite	Chlorite, muscovite, albite, quartz
Low	Biotite	Biotite	Biotite, muscovite, plagioclase, quartz, ± chloritoid, chlorite
	Garnet	Garnet	Biotite, muscovite, garnet, plagioclase, quartz, ± cordierite, garnet
Medium	Staurolite	Staurolite	Biotite, muscovite, staurolite, plagioclase, quartz, ± cordierite, garnet
	Andalusite or kyanite	Andalusite/kyanite	Biotite, muscovite, andalusite or kyanite, plagioclase, quartz, ± cordierite, garnet
	Sillimanite	Sillimanite	Biotite, muscovite, sillimanite, plagioclase, quartz, ± garnet

DO NOT COPY e48d507df5d1141@placeholder.9409

Printed by: e48d507df5d1141@placeholder.94092.edu. Printing is for personal, private use only. No part of this book may be reproduced or transmitted without publisher's prior permission. Violators will be prosecuted.

High	K-feldspar	K-feldspar–illimanite	Biotite, K-feldspar, sillimanite, plagioclase, quartz

[a] The mineral assemblage may vary depending on the bulk composition of the rocks involved.

Geologists mapping metamorphic terranes routinely find that they can, within a particular group of rocks, identify boundaries delineating the first appearance of specific minerals with increasing metamorphic grade called **index minerals** (Table 11.12). These boundaries are called **mineral zone boundaries**, and each zone is identified by the appearance of an index mineral (e.g., biotite-in or garnet-in). The term **isograd** is also applied to these boundaries. The rocks between successive mineral zone boundaries are a **mineral zone**. Similar boundaries may define the last appearance of minerals and are named based on the mineral being lost (e.g., chlorite-out or andalusite-out). Although this approach can certainly be done with mafic compositions, it is particularly useful for pelite compositions, as the index minerals often form large porphyroblasts, which, with the aid of a hand lens, makes mapping out index minerals a fairly easy task. Table 11.12 contains the index minerals and mineral zones for pelitic rocks. **Figure 11.12** provides an example where index minerals and mineral zones have been mapped. Other minerals found in pelitic rocks are listed in Table C.3 in Appendix C.

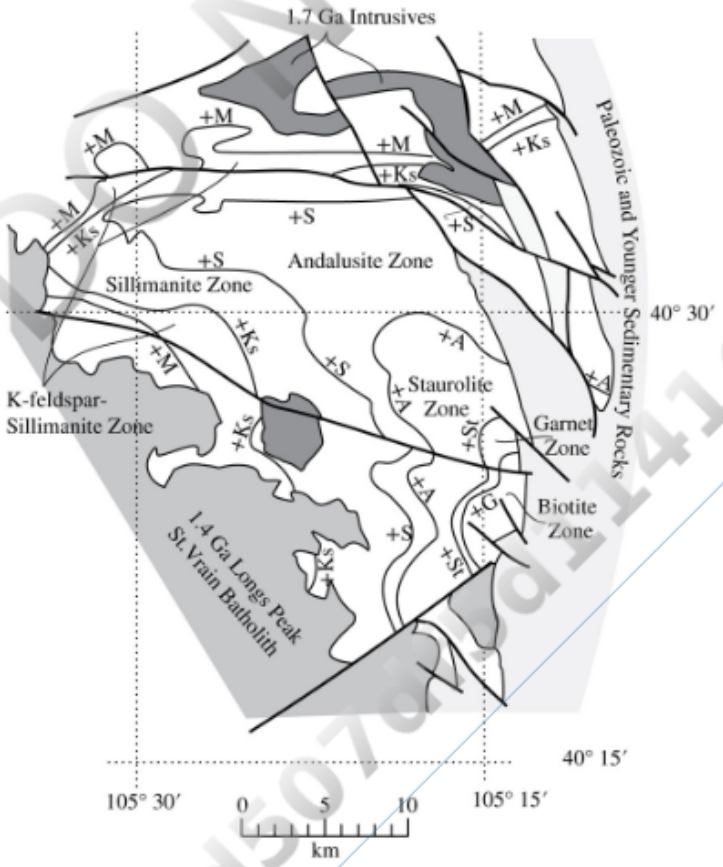

FIGURE 11.12 Metamorphic zones in Proterozoic pelitic/psammitic metamorphic rocks (no shading) of the northeastern Front Range, Colorado. The lowest-grade, biotite-zone rocks are in the southeastern part of the area. Chlorite-zone rocks are not exposed. Mapped mineral zone boundaries include garnet-in (+G), staurolite-in (+St), andalusite-in (+A), sillimanite-in (+S), and K-feldspar + sillimanite-in (+Ks). Rocks on the high-grade side of the +M boundary were partially melted during

DO NOT COPY e48d507df5d1141@placeholder.94092

Printed by: e48d507df5d1141@placeholder.94092.edu. Printing is for personal, private use only. No part of this book may be reproduced or transmitted without publisher's prior permission. Violators will be prosecuted.

sillimanite-in (+Ks). Rocks on the high-grade side of the +M boundary were partially melted during metamorphism and are migmatites. The sillimanite boundary is associated with the loss of andalusite, and the K-feldspar boundary is associated with the loss of muscovite (though muscovite produced during retrograde metamorphism may exist). Faults and shear zones are shown with heavy lines. View larger image

The introduction of an index mineral such as staurolite in pelitic rocks must be produced by a metamorphic reaction such as Reaction 11.6. Through careful mapping and thin section analysis, it is often possible to identify the reactant and product mineral assemblages on opposite sides of a mineral zone boundary. Mineral-in boundaries are often associated with mineral-out boundaries; therefore, the lost mineral must be involved in the reaction producing the new mineral. With Reaction 11.6, a chlorite-out boundary could be associated with the staurolite-in boundary.

Calc-silicate Rocks

Many sedimentary rocks contain minor to substantial amounts of carbonate minerals. The original mineralogy usually consists of quartz, clay, calcite ($CaCO_3$), and/or dolomite [$CaMg(CO_3)_2$]. When metamorphosed, these rocks undergo mineral reactions to produce minerals containing both Ca and Si; hence the term *calc-silicate*. An entire spectrum of mineralogy is possible, depending on the relative amounts of carbonates and silicates in the parent rock, temperature, pressure, fluid composition, and whether these rocks have been metasomatized. Common minerals found in these rocks are listed in Table C.3 in Appendix C. Calcite and dolomite are found in most calc-silicate rocks. Low-grade rocks may contain talc and Mg-biotite; increasing temperature usually involves introduction of amphiboles, pyroxenes, Ca-garnet, scapolite, and perhaps Mg-rich olivine. Members of the epidote group are common.

Metamorphic Environments

A variety of different and somewhat overlapping terms have been developed to describe the different environments that form metamorphic rocks. These include terminology based on the local geological setting, plate tectonic environment, and the balance between heating and deformation.

Terminology based on the local geological setting is perhaps the least obscure, because the nature of the metamorphism usually can be determined with a relatively modest amount of field work. The most important metamorphic types as follows.

- **Contact metamorphism**. Metamorphism in the immediate vicinity of an igneous intrusion that serves as the source of the heat. Some sources use the analogous term *thermal metamorphism*. The metamorphosed rocks typically form an aureole, ranging in thickness from a few millimeters to several kilometers around the intrusion, with the grade of metamorphism decreasing outward. Metamorphism is commonly not associated with extensive deformation

DO NOT COPY e48d507df5d1141@placeholder.9409

Printed by: e48d507df5d1141@placeholder.94092.edu. Printing is for personal, private use only. No part of this book may be reproduced or transmitted without publisher's prior permission. Violators will be prosecuted.

commonly not associated with extensive deformation.

- **Regional metamorphism**. Metamorphism involving large volumes of rocks, usually in orogenic belts. Some sources use the analogous term *dynamothermal metamorphism*. Igneous intrusions may be common, but metamorphism is not restricted to aureoles. Pressure is controlled by the weight of the overlying rock—the deeper the rock, the higher the pressure. Mantle heat largely controls the temperature—generally the deeper the rock, the higher the temperature—but temperature may be in part controlled by the amount of heat generated by radioactive decay; the number of igneous intrusions nearby; or, if faulting places hotter or colder rocks nearby. If deformation affected the region, which is commonly the case, deformation and metamorphism usually occurred at close to the same time.
- **Hydrothermal metamorphism**. Metamorphism produced by the flow of hot aqueous solutions into and through rocks. The source of the heat is usually an igneous intrusion. The flow of water commonly is concentrated along fault and fracture zones, or in the volume of rocks adjacent to and above an intrusion. Hydrothermal metamorphism is commonly associated with the formation of hydrothermal mineral deposits as well as metasomatism.

Some literature sources also identify other types of metamorphism, but these are ill-defined, incorrectly equate deformation to metamorphism, are not really distinct from the above, or are very rare. The following is just an abbreviated list of other types of metamorphism. Burial metamorphism is described as metamorphism that occurs at the bottom of a very deep sedimentary basin. The distinction between burial metamorphism and diagenesis is not clear, and it may be described as regional metamorphism that lacks deformation and magmatism, but regional metamorphism in a mountain belt can also lack these. Shock metamorphism is created by the impact of a meteorite. Identification of ultra-high-pressure metamorphic minerals, such as coesite or stishovite, or other features unique to impacts are usually required to demonstrate that shock metamorphism affected an area. Regardless, it is very rare. Lastly, seafloor metamorphism occurs at mid-ocean ridges where hydrothermal fluids alter the newly formed basalt and gabbro to greenschist, greenstone, or perhaps serpentinite. This is just a specific type of hydrothermal metamorphism.

Regional metamorphic environments also can be described in terms of their plate tectonic environment or setting (**Figure 11.13**). High-pressure/low-temperature metamorphism is typically produced in subduction zones or other areas where rapid overthrusting moves rocks rapidly to substantial depth; this typically results in blueschist or eclogite facies conditions. Low-pressure/high-temperature metamorphism is typical of areas of high heat flow, such as island arcs. Most commonly, the resulting metamorphic facies conditions tend to be low-pressure conditions within the greenschist, amphibolite, and granulite facies. The broad range of intermediate metamorphic conditions between metamorphism in subduction zones and island arcs is typically found in continental arcs and continental collisions. Most commonly, the resulting conditions tend to be moderate

Printed by: e48d507df5d1141@placeholder.94092.edu. Printing is for personal, private use only. No part of this book may be reproduced or transmitted without publisher's prior permission. Violators will be prosecuted.

or higher-pressure regions within the greenschist, epidote-amphibolite, amphibolite, and granulite metamorphic facies.

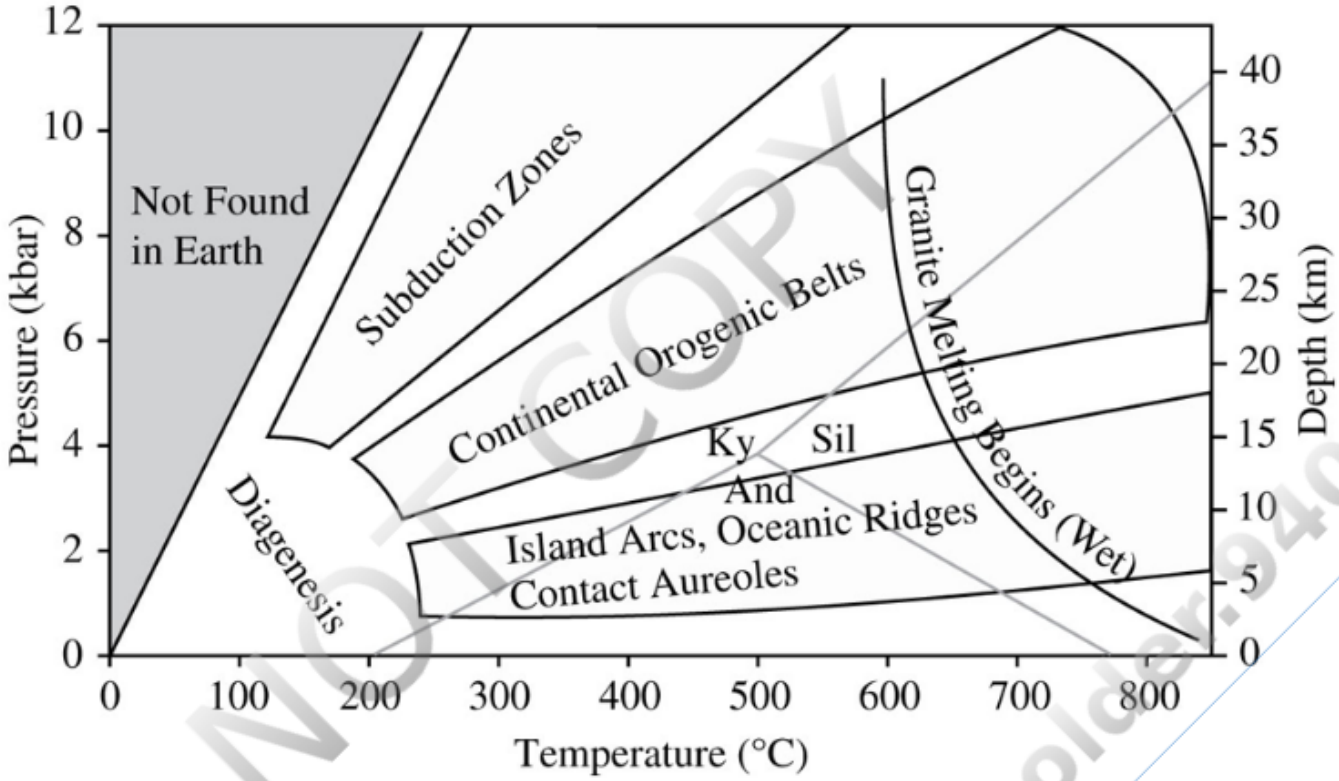

FIGURE 11.13 T–P conditions found in different tectonic environments. Adapted from Spear (1993). View larger image

Rounding out the connection between metamorphic facies conditions and metamorphic environments, hydrothermal metamorphism at mid-ocean ridges and contact metamorphic aureoles around intrusion in the upper crust tend to be hornfels facies conditions or low-pressure conditions within the greenschist, amphibolite, and granulite facies. Zeolite and prehnite-pumpellyite metamorphic facies conditions are collectively referred to as sub-greenschist facies metamorphism. Both of these overlap conditions that may be attributed to diagenesis, and neither can be connected to any particular local geologic setting or type of plate tectonic setting. Generally identification and characterizing such low-grade metamorphism is difficult.

DO NOT COPY e48d507df5d1141@placeholder.9409

Printed by: e48d507df5d1141@placeholder.94092.edu. Printing is for personal, private use only. No part of this book may be reproduced or transmitted without publisher's prior permission. Violators will be prosecuted.

Rounding out the connection between metamorphic facies conditions and metamorphic environments, hydrothermal metamorphism at mid-ocean ridges and contact metamorphic aureoles around intrusion in the upper crust tend to be hornfels facies conditions or low-pressure conditions within the greenschist, amphibolite, and granulite facies. Zeolite and prehnite-pumpellyite metamorphic facies conditions are collectively referred to as sub-greenschist facies metamorphism. Both of these overlap conditions that may be attributed to diagenesis, and neither can be connected to any particular local geologic setting or type of plate tectonic setting. Generally identification and characterizing such low-grade metamorphism is difficult.

REFERENCES CITED AND SUGGESTIONS FOR ADDITIONAL READING

Best, M. G. 2003. *Igneous and Metamorphic Petrology*, 2nd ed. Blackwell Science, Cambridge, MA, 727 p.

Boggs, S. 2009. *Petrology of Sedimentary Rocks*, 2nd ed. Cambridge University Press, New York, 599 p.

Bowen, N. L. 1922. The reaction principle in petrogenesis. *The Journal of Geology* **30**, 177–198.

Bucher, K., Frey, J., and Bucher-Nurminen, K. 2002. *Petrogenesis of Metamorphic Rocks*, 6th ed. Springer-Verlag, New York, 341 p.

Carlson, W. D., Pattison, D. R. M., and Caddick, M. J. 2015. Beyond the equilibrium paradigm: How considerations of kinetics enhances metamorphic interpretation. *American Mineralogist* **100**, 1659–1667.

Dickinson, W. R., Beard, L. S., Brakenridge, G. R., Erjavec, J. L., Ferguson, R. C., Inman, K. F., Knepp, R. A., Lindberg, F. A., and Rybert, P. T. 1983. Provenance of North American Phanerozoic sandstones in relation to tectonic setting. *Geological Society of America Bulletin* **94**, 222–235.

Dott, R. L., Jr. 1964. Wacke, graywacke, and matrix—What approach to immature sandstone classification? *Journal of Sedimentary Petrology* **34**, 625–632.

Frost, B. R., and Frost, C. D. 2014. *Essentials of Igneous and Metamorphic Petrology*. Cambridge University Press, New York, 303 p.

Gill, R. 2010. *Igneous Rocks and Processes*. Wiley-Blackwell, Chichester, UK, 428 p.

Goldich, S. S. 1938. A study in rock-weathering. *The Journal of Geology* **46**, 17–58.

Griffen, D. T. 1992. *Silicate Crystal Chemistry*. Oxford University Press, New York, 442 p.

Kerrick, D. M. 1990. *The Al_2SiO_5 Polymorphs. Reviews in Mineralogy* **22**, 406 p.

Konhauser, K. 2007. *Introduction to Geomicrobiology*. Blackwell, Malden, MA, 425 p.

DO NOT COPY e48d507df5d1141@placeholder.9409

Printed by: e48d507df5d1141@placeholder.94092.edu. Printing is for personal, private use only. No part of this book may be reproduced or transmitted without publisher's prior permission. Violators will be prosecuted.

Kretz, R. 1994. *Metamorphic Crystallization*. John Wiley & Sons, New York, 507 p.

Le Bas, M. J., Le Maitre, R. W., Streckheisen, A. L., and Zanettin, B. 1986. Chemical classification of volcanic rocks based on the total alkali–silica diagram. *Journal of Petrology* **27**, 745–750.

Le Maitre, R. W., Streckheisen, A., Zanettin, B., Le Bas, M. J., Bonin, B., Bateman, P., Bellieni, G., Dudek, A., Efremova, S., Keller, J., Lameyre, J., Sabine, P. A., Schmid, R., Sørensen, H., and Wooley, A. R. (eds.). 2002. *Igneous Rocks: A Classification and Glossary of Terms*, 2nd ed. Cambridge University Press, Cambridge, 236 p.

Liebau, F. 1985. *Structural Chemistry of Silicates, Structure, Bonding and Classification*. Springer-Verlag, Berlin, 347 p.

London, D., and Morgan, G. B., VI. 2012. The pegmatite puzzle. *Elements* **8**, 263–268.

Pettijohn, F. J., Potter, P. E., and Siever, R. 1987. *Sand and Sandstone*, 2nd ed. Springer-Verlag, New York, 553 p.

Philpotts, A. R., and Ague, J. J. 2009. *Principles of Igneous and Metamorphic Petrology*, 2nd ed. Cambridge University Press, Cambridge, 667 p.

Ribbe, P. H. (ed.). 1982. *Orthosilicates*, 2nd ed. *Reviews in Mineralogy* **5**, 450 p.

Spear, F. S. 1993. *Metamorphic Phase Equilibria and Pressure–Temperature–Time Paths*. Mineralogical Society of America, Washington, DC, 799 p.

Streckheisen, A. L. 1976. To each plutonic rock its proper name. *Earth Science Reviews* **12**, 1–33.

Tucker, M. E. 2001. *Sedimentary Petrology: An Introduction to the Origin of Sedimentary Rocks*, 3rd ed. Blackwell, Malden, MA, 262 p.

Turner, F. J. 1981. *Metamorphic Petrology*, 2nd ed. McGraw-Hill, New York, 524 p.

Vernon, R. H., and Clarke, G. L. 2008. *Principles of Metamorphic Petrology*. Cambridge University Press, Cambridge, 446 p.

Williams, H., Turner, F. J., and Gilbert, C. M. 1982. *Petrography*, 2nd ed. W. H. Freeman, San Francisco, 626 p.

Winkler, S. J. F. 1976. *Petrogenesis of Metamorphic Rocks*, 4th ed. Springer-Verlag, New York, 334 p.

Winter, J. D. 2010. *Principles of Igneous and Metamorphic Petrology*, 2nd ed. Prentice Hall, Upper Saddle River, NJ, 720 p.

DO NOT COPY
e48d507df5d1141@placeholder.9409

Printed by: e48d507df5d1141@placeholder.94092.edu. Printing is for personal, private use only. No part of this book may be reproduced or transmitted without publisher's prior permission. Violators will be prosecuted.

LIST OF KEY TERMS

- accessory mineral
- arenite
- assimilation
- bulk chemical analysis
- chain silicates
- claystone
- compositional maturity
- contact metamorphism
- continental flood basalts
- country rock
- cumulate
- decompression melting
- diagenesis
- disilicates
- dynamic recrystallization
- flux melting
- foliation
- fractional crystallization
- fractional melting
- fractionation series
- framework silicates
- gneissic foliation
- groundmass
- heavy minerals
- high-grade
- hydrothermal metamorphism
- incongruent melting
- index mineral
- industrial minerals

DO NOT COPY
e48d507df5d1141@placeholder.9409

Printed by: e48d507df5d1141@placeholder.94092.edu. Printing is for personal, private use only. No part of this book may be reproduced or transmitted without publisher's prior permission. Violators will be prosecuted.

industrial minerals
isograd
layered mafic intrusion
low-grade
magma mingling
magma mixing
magmatic differentiation
medium-grade
metamorphic facies
metasomatism
mineral assemblage
mineral zone
mineral zone boundary
modal mineralogy
mud rock
mudstone
normative mineralogy
ophiolites
orthosilicates
partial melting
peak metamorphic conditions
peak pressure
peak temperature
pelite
phenocryst
polymerize
porphyritic
prograde metamorphism
prograde path
provenance
psammite
regional metamorphism
retrograde metamorphism
retrograde path

DO NOT COPY
e48d507df5d1141@placeholder.9409

Printed by: e48d507df5d1141@placeholder.94092.edu. Printing is for personal, private use only. No part of this book may be reproduced or transmitted without publisher's prior permission. Violators will be prosecuted.

retrograde path

ring silicates

schistosity

shale

sheet silicates

siltstone

slaty cleavage

texture

T–P loop

wackes

DO NOT COPY

e48d507df5d1141@placeholder.9409

Printed by: e48d507df5d1141@placeholder.94092.edu. Printing is for personal, private use only. No part of this book may be reproduced or transmitted without publisher's prior permission. Violators will be prosecuted.

CHAPTER 12
Framework Silicates

William D. Nesse
University of Northern Colorado

Graham B. Baird
University of Northern Colorado

DO NOT COPY
e48d507df5d1141@placeholder.9409

Printed by: e48d507df5d1141@placeholder.94092.edu. Printing is for personal, private use only. No part of this book may be reproduced or transmitted without publisher's prior permission. Violators will be prosecuted.

Introduction

More than two-thirds of the Earth's crust is composed of framework silicate minerals. The common framework silicates are listed in **Table 12.1**. Of these, quartz, plagioclase, and the alkali feldspars are by far the most abundant.

TABLE 12.1 Common Framework Silicate Minerals[a]

Mineral	Igneous				Sedimentary		Metamorphic		
	Felsic	Intermediate	Mafic	Alkaline	Clastic	Chemical and Biologic	Pelitic	Mafic	Calc-silicate
Silica group	M	M			M	A	M		
Plagioclase	M	M	M	M	M		M	M	
Alkali Feldspar	M	M		M	M		M		
Nepheline				M					
Sodalite				M					
Leucite				M					
Zeolite group			A				M	M	
Scapolite							A	M	M

[a] M, major or common; A, accessory or minor mineral, or heavy mineral fraction of clastic sediments.

The structure of all framework silicates is based on the TO_4 tetrahedra where T is Si^{4+} or Al^{3+} and each of the four oxygen anions is shared with another tetrahedron. The fact that every O^{2-} is shared between two tetrahedra, coupled with the mutual repulsion of the high-charged cations in those tetrahedra, ensures that the structure of the framework silicates is fairly open. The open structure has some interesting ramifications for both the composition and physical properties of framework silicates.

The open structure of framework silicates can easily accommodate large cations such as Ca^{2+}, Na^{+}, and K^{+}. These large cations do not readily fit into structures based on close-packed anions in which the largest coordination site is octahedral (6-fold). To accommodate the positive charge of these large cations, usually Al^{3+} substitutes for Si^{4+} in the tetrahedral (T) sites. Only in the silica group of minerals are all the tetrahedra occupied by Si^{4+}. We will see later in the discussion that the very open structure of the

DO NOT COPY e48d507df5d1141@placeholder.94092

Printed by: e48d507df5d1141@placeholder.94092.edu. Printing is for personal, private use only. No part of this book may be reproduced or transmitted without publisher's prior permission. Violators will be prosecuted.

zeolite group leads to some interesting and useful chemical properties.

The open structure also means that the specific gravity for most framework silicates is significantly lower than for minerals whose anion arrangement can be approximated by close packing. Quartz (SiO_2), for example, has a specific gravity of 2.65, whereas forsterite olivine (Mg_2SiO_4), with a structure of cubic close packing of the oxygen anions, has a specific gravity of 3.27, even though Mg has a lower atomic mass than Si. Because the structure is fairly open, the framework silicates tend not to be stable at high pressures. This means that framework silicates are minerals generally restricted to the Earth's crust, and often the shallow crust.

DO NOT COPY
e48d507df5d1141@placeholder.9409

Printed by: e48d507df5d1141@placeholder.94092.edu. Printing is for personal, private use only. No part of this book may be reproduced or transmitted without publisher's prior permission. Violators will be prosecuted.

Silica Group

The silica group (Table 12.2) includes about a dozen natural and synthetic polymorphic varieties of SiO_2. Of these, quartz, tridymite, and cristobalite are the common polymorphs, and they are the only ones described here. Stishovite and coesite are quite rare, as might be inferred from the stability fields shown in Figure 12.1. They are found only where extremely high pressures have been obtained; both can be found with shocked quartz in rocks that were affected by a meteorite impact. Shocked quartz is quartz with microscopic lamellae that are only formed by deformation from a meteorite impact. Coesite additionally can be found, often with diamond, in rocks which have been subducted deep into the mantle and metamorphosed at ultra–high-pressure conditions.

TABLE 12.2 Silica Polymorphs

Polymorph	Crystal System	Specific Gravity
α-Quartz	Hexagonal (rhombohedral)	2.65
β-Quartz	Hexagonal (hexagonal)	2.53
α-Tridymite	Orthorhombic	2.26
β-Tridymite	Hexagonal	2.22
α-Cristobalite	Tetragonal	2.32
β-Cristobalite	Isometric	2.2
Coesite	Monoclinic	3.01
Stishovite	Tetragonal	4.35
Moganite	Monoclinic	2.62

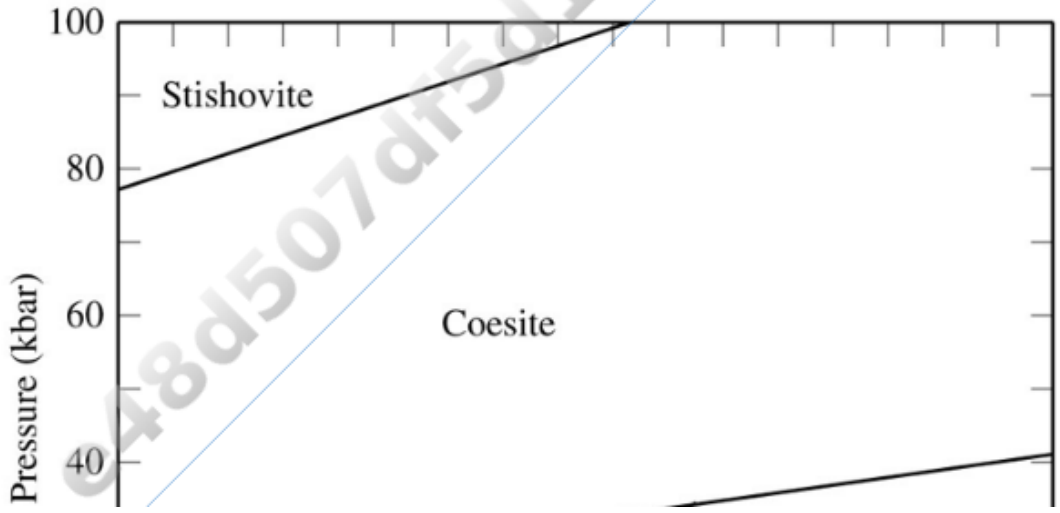

DO NOT COPY
e48d507df5d1141@placeholder.9409

Printed by: e48d507df5d1141@placeholder.94092.edu. Printing is for personal, private use only. No part of this book may be reproduced or transmitted without publisher's prior permission. Violators will be prosecuted.

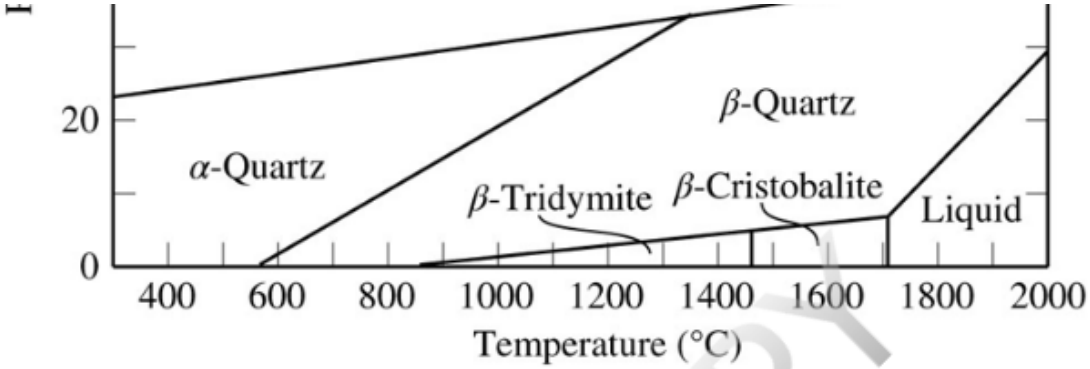

FIGURE 12.1 Stability fields of the silica minerals. Adapted from Griffen (1992). View larger image

Quartz, tridymite, and cristobalite have their own distinct structures (described later), and conversion from one to the other requires breaking of chemical bonds—they are reconstructive polymorphs. In addition, the structures of quartz, tridymite, and cristobalite each have α (low) and β (high) varieties. The α and β varieties of each mineral are displacive polymorphs, related by a distortion in the crystal lattice. In each case, the β polymorph has higher symmetry and is stable at higher temperatures than the α polymorph.

The forms of quartz, tridymite, and cristobalite at room temperature are all the α varieties. Quartz may grow as either the α or β variety, depending on the temperature and pressure as shown in Figure 12.1. With cooling, β-quartz will convert by a displacive polymorphic transition to α-quartz as described in Chapter 5. Tridymite and cristobalite grow originally only as the β varieties. Primary α-tridymite and α-cristobalite do not normally grow because there is no T–P field where they are the lowest-energy polymorph. With cooling, both β-tridymite and β-cristobalite convert by a displacive polymorphic transition to lower-energy α-tridymite and α-cristobalite that can be preserved because the reconstructive polymorphic transition to the even lower-energy quartz is very slow. For a more complete survey of the silica minerals, refer to Heaney and others (1994).

Quartz

$$SiO_2$$

$$\text{Hexagonal, trigonal}$$
$$\text{division } 32$$

$$a = 4.914 \text{ Å},$$
$$c = 5.405 \text{ Å}, \ Z = 3$$

$$H = 7$$

$$G = 2.65$$

DO NOT COPY e48d507df5d1141@placeholder.9409

Printed by: e48d507df5d1141@placeholder.94092.edu. Printing is for personal, private use only. No part of this book may be reproduced or transmitted without publisher's prior permission. Violators will be prosecuted.

Uniaxial (+)

$n_\omega = 1.544$

$n_\epsilon = 1.553$

$\delta = 0.009$

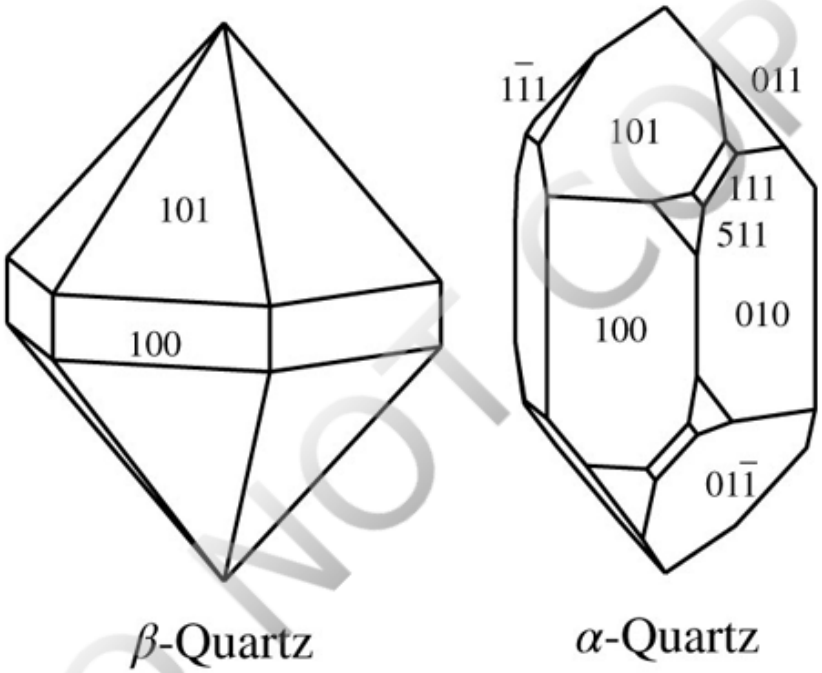

β-Quartz α-Quartz

Structure **Figure 12.2** shows the structure of quartz. Silicon tetrahedra are arranged to form interlocking spirals parallel to the *c* axis. Because the spirals may be either right- or left-handed, quartz forms enantiomorphous right- and left-handed crystals (Chapter 2). In β-quartz the spirals produce 6-fold rotational symmetry (actually a 6-fold screw axis) reflected in the hexagonal symmetry of the crystal shown above. With cooling through about ~573°C (at 1 atm), the β-quartz structure kinks so that the spirals are reduced to 3-fold symmetry and the point group symmetry is reduced to 32, forming α-quartz.

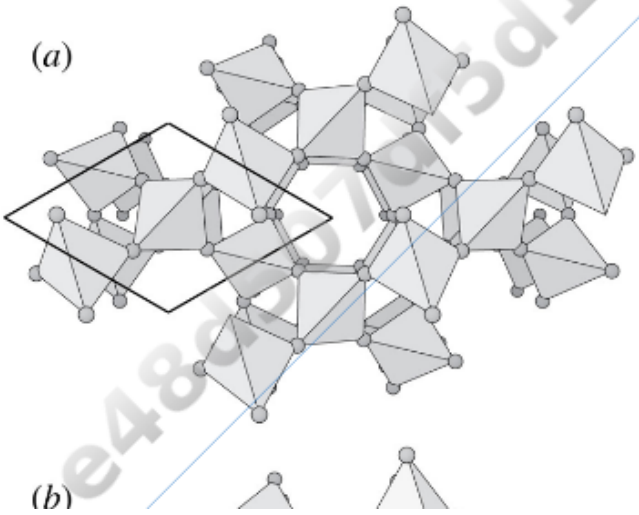

DO NOT COPY
e48d507df5d1141@placeholder.9409

Printed by: e48d507df5d1141@placeholder.94092.edu. Printing is for personal, private use only. No part of this book may be reproduced or transmitted without publisher's prior permission. Violators will be prosecuted.

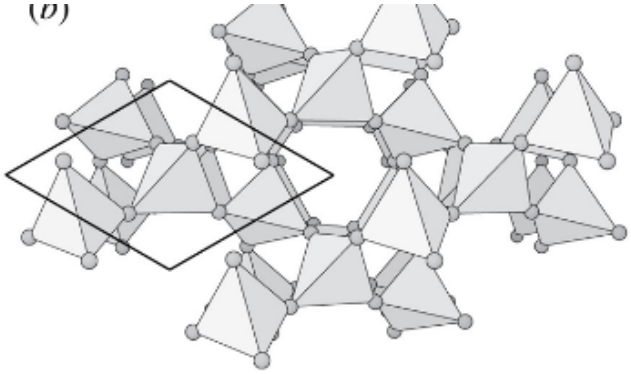

FIGURE 12.2 Quartz structure viewed down the *c* axis. A unit cell outline is shown. Silica tetrahedra link together to form spirals that extend parallel to the *c* axis (Figure 4.12). (*a*) *β*-quartz. The spirals produce hexagonal symmetry. (*b*) *α*-quartz. The structure is distorted, reducing symmetry to 3-fold. View larger image

Composition Most quartz is relatively pure SiO_2, although trace amounts of other elements may be present. The most common is substitution of small amounts of Al^{3+} and Fe^{3+} for Si^{4+}. Charge neutrality is maintained by inserting appropriate amounts of Fe^{3+}, Na^+, Li^+, or K^+ interstitially, or adding H^+, which bonds to O^{2-} to form OH^-. The amount of Ti^{4+} that can substitute for Si^{4+} is dependent on temperature and pressure and provides the basis for the TitaniQ thermobarometer (Thomas et al., 2010).

Form and Twinning Quartz commonly forms anhedral grains in both igneous and metamorphic rocks (**Figure 12.3**). Detrital grains are approximately equant. Crystals of *α*-quartz are usually prismatic {100} terminated with the positive {101} and negative {111} rhombohedrons, one of which is usually more prominent than the other. Phenocrysts that originally grow as *β*-quartz crystals are typically stubby prisms terminated with a {101} dipyramid. With cooling, the *β*-quartz inverts to *α*-quartz, but the crystals retain the external habit of the original *β*-quartz. Deformed quartz may display a pattern of **undulose extinction** or **undulatory extinction** seen in thin section with the petrographic microscope (Figure 12.3b). As the stage is rotated, areas of extinction appear to sweep across deformed grains in an irregular or wavy manner.

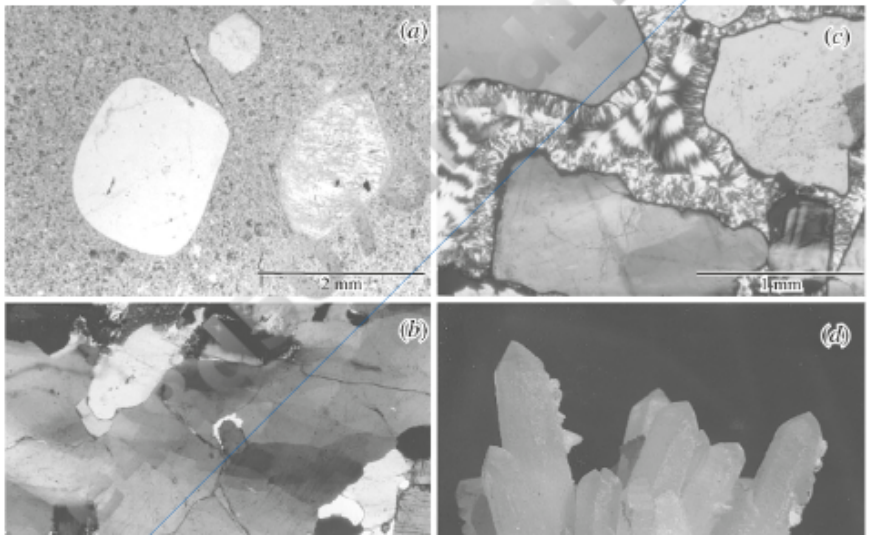

Printed by: e48d507df5d1141@placeholder.94092.edu. Printing is for personal, private use only. No part of this book may be reproduced or transmitted without publisher's prior permission. Violators will be prosecuted.

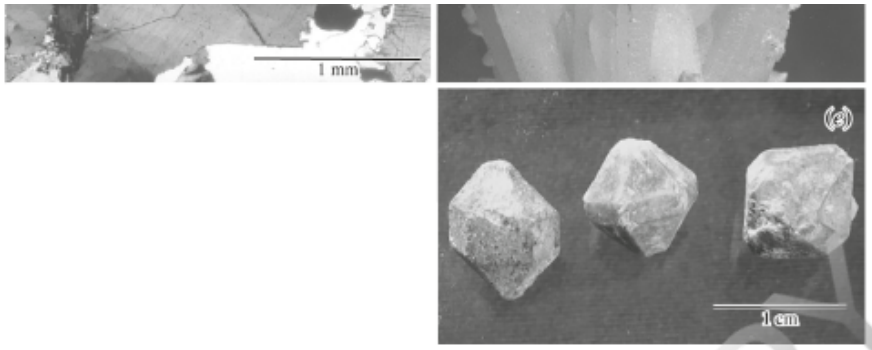

FIGURE 12.3 Quartz. (*a*) Rounded quartz (left) phenocryst in rhyodacite. The other phenocrysts are altered plagioclase. Plane light. (*b*) Undulatory anhedral quartz in deformed granite. Crossed polarizers. (*c*) Feathery-appearing chalcedony cementing quartz and microcline grains in a sandstone. Crossed polarizers. (*d*) Quartz crystals. Field of view is about 10 cm wide. (*e*) *β*-quartz crystals (now *α*-quartz). View larger image

There are a variety of quartz–feldspar intergrowths described in the feldspar section.

Quartz very commonly has Dauphiné and Brazil twins, but this is not visible in standard thin section, and only visible in hand samples if the small (511) or (111) faces are anomalously repeated or the sample is etched with hydrofluoric acid. Dauphiné twins (60° rotation on *c*) form penetration twins with complexly intergrown domains. Brazil twins (reflection on {110} with {110} composition planes) form penetration twins with a triangular and lamellar structure. A combination of both twins is also common. Japan twins, which form an elbow-shaped crystal with {111} as the composition plane, are uncommon.

Cleavage None. Conchoidal fracture. Brittle.

Color Properties

Luster: Vitreous.

Color: Colorless or gray is most common, but almost any color is possible. For a survey of the complex causes of color in quartz, refer to Rossman (1994) and Nassau (2001). **Table 12.3** shows the common varieties.

TABLE 12.3 Quartz Varieties

Variety	Color	Cause
Rock crystal	Clear	N/A
Amethyst	Violet or purple	$[FeO_4]^{4-}$ hole color centers
Smoky quartz	Smoky brown to black	$[AlO_4]^{4-}$ hole color centers
Citrine	Yellow	Related to Fe content, color centers produced by radiation, or some

DO NOT COPY e48d507df5d1141@placeholder.9409

Printed by: e48d507df5d1141@placeholder.94092.edu. Printing is for personal, private use only. No part of this book may be reproduced or transmitted without publisher's prior permission. Violators will be prosecuted.

		combination
Rose quartz	Pink	Commonly caused by very fine inclusions of pink fibers similar to dumortierite [$Al_{27}O_6(BO_3)_4(SiO_4)_{12}(OH)_3$]
Milky quartz	Milky white	Abundant minute fluid inclusions

Streak: White.

Color in Thin Section: Colorless.

Pleochroism: None.

Optical Characteristics

Relief in Thin Section: Low positive.

Optic Orientation: Crystals are length slow; fibers in chalcedony are length fast or length slow. Deformed quartz shows undulatory extinction (Figure 12.3b).

Indices of Refraction and Birefringence: Almost no variation for coarsely crystalline varieties.

Interference Figure: Basal sections yield a uniaxial positive figure. Undulatory quartz and some amethyst and smoky quartz may yield a biaxial figure with a small $2V$ angle.

Alteration Not normally altered. Very stable in the weathering environment.

Distinguishing Features

Hand Sample: Coarsely crystalline samples are distinguished by hardness, conchoidal fracture, and luster. Crystals are quite distinctive. Beryl has a higher specific gravity, has a fair to poor {001} cleavage, and is usually a shade of blue or green. Microcrystalline quartz is distinguished from other minerals by its hardness; opal is softer and has a lower specific gravity than microcrystalline quartz. As seen with a hand lens, quartz forms anhedral, equant, gray, glassy grains without cleavage in many common rock types. It may be ductily deformed into ribbons. Associated feldspars are commonly white or pink and display cleavage.

Thin Section/Grain Mount: Recognized by low relief, low birefringence, and lack of cleavage or twinning. Orthoclase and sanidine are biaxial, have cleavage, and may show a single Carlsbad twin plane. Plagioclase is biaxial, has cleavage, and is usually polysynthetically twinned. Any feldspar may show alteration (Figure 12.3a); quartz essentially never shows alteration. If not authigenic (formed during diagenesis), microcline shows its distinctive “tartan plaid” twinning. Cordierite closely resembles quartz but is biaxial and may show distinctive pinite alteration. Beryl is optically negative and has higher indices of refraction. The feldspars and cordierite may be distinguished from quartz by a variety of staining techniques that can be used with thin sections or rock

DO NOT COPY

Printed by: e48d507df5d1141@placeholder.94092.edu. Printing is for personal, private use only. No part of this book may be reproduced or transmitted without publisher's prior permission. Violators will be prosecuted.

from quartz by a variety of staining techniques that can be used with thin sections or rock slabs (Bailey and Stevens, 1960; Ruperto and others, 1964; Boone and Wheeler, 1968; Haughton, 1980).

Microcrystalline quartz may have a cloudy appearance in thin section or grain mount.

Occurrence Quartz is a very common mineral found in a wide variety of geological environments. It is abundant in felsic to intermediate intrusive and extrusive igneous rocks such as granitic pegmatite, granite, granodiorite, quartz diorite, rhyolite, rhyodacite, and dacite, and may be found in small amounts in diorite, gabbro, syenite, and volcanic equivalents. In metamorphic rocks it is abundant in slate, phyllite, schist, gneiss, and quartzite of various types. Because it is stable in the weathering environment, quartz is a major constituent in many clastic sedimentary rocks and may serve as a cementing agent, often in the form of chalcedony. While quartz is not itself a biomineral, it may crystallize from opal precipitated by diatoms and other organisms. Chert layers found in limestone are commonly derived from biogenic amorphous silica, either by direct crystallization or indirectly, by dissolution of the amorphous silica into the pore water of sediment and subsequent precipitation of quartz from the pore water. Chert commonly replaces the carbonate minerals of the host limestone. Quartz is also very common in hydrothermal veins that may or may not contain ore minerals, and also in replacement deposits, which are ore deposits formed by the replacement of carbonate rock with ore and other minerals. Quartz in these setting may exist as well-formed, euhedral crystals, or as microcrystalline and massive varieties as well. Regardless, in ore deposits, quartz is generally considered a **gangue** (pronounced “gang”) mineral—an economically worthless mineral.

Use Quartz is widely used in many industries. Relatively pure quartz sandstone is quarried to provide the raw materials for making glass and to serve as the source of elemental silicon. The applications for silicon include the manufacture of semiconductors for the electronics industry; silicone rubber caulking compound is used to seal around doors, windows, and bathtubs in residential homes. Quartz also is widely used as an abrasive or polish; a filler in plastics, paints, and related materials; and, in the form of sand, as aggregate in asphalt, mortar, and concrete. Synthetic quartz is used in the electronics industry to make electronic oscillators and pressure-sensing devices.

Quartz also is widely used as a semiprecious gemstone in the jewelry industry. Followers of “New Age spiritualism” may ascribe mystical, spiritual, and healing properties to quartz crystals, which are worn as pendants, earrings, or other ornaments. Historically, quartz was used in cures for gastrointestinal, skin, nervous system, insect bite, and other problems, particularly in the Middle Ages. Amethyst derives its name in Greek (*amethystos*) from the belief that it prevented drunkenness, perhaps because its color is similar to the color of red wine. Unfortunately, none of these therapeutic claims is supported by scientific evidence.

Tiger’s eye is an amber-colored chatoyant semiprecious gemstone. There is debate regarding how it is formed. Initial interpretations suggest pseudomorphic replacement of

Printed by: e48d507df5d1141@placeholder.94092.edu. Printing is for personal, private use only. No part of this book may be reproduced or transmitted without publisher's prior permission. Violators will be prosecuted.

crocidolite fibers (asbestos) by quartz, with the amber color created by small amounts of hematite and goethite—products of crocidolite alteration. However, a new interpretation proposes that both the crocidolite and quartz formed together during repeated cycles of crack formation and growth of crocidolite and quartz fibers into the crack from fluids, but this new model is controversial (Heaney and Fisher, 2003; Gutzmer et al., 2004; Heaney and Fisher, 2004).

Comments Although a very common and widespread mineral, quartz can pose a health risk if present as dust in substantial quantities (Chapter 1). The International Agency for Research on Cancer lists crystalline silica dust, which includes quartz dust, as a human carcinogen. Chronic inhalation of quartz dust can lead to silicosis, a pathology that, among other things, involves scarring of lung tissue and impaired lung function. Industrial health and safety regulations in most Western countries include requirements for dust suppression in industries such as mining and quarrying, where exposure to quartz dust is likely.

Tridymite

$$SiO_2$$

Orthorhombic

(222) (pseudohexagonal)

$$a = 9.88\ \text{Å},\ b = 17.1\ \text{Å},$$
$$c = 16.3\ \text{Å},\ Z = 64$$

$$H = 7$$

$$G = 2.27$$

Biaxial (+)

$$n_\alpha = 1.468 - 1.482$$

$$n_\beta = 1.470 - 1.484$$

$$n_\gamma = 1.474 - 1.486$$

$$\delta = 0.002 - 0.004$$

$$2V_z = 40 - 90^\circ$$

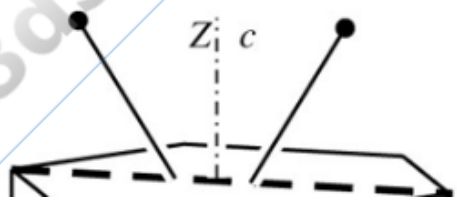

DO NOT COPY
e48d507df5d1141@placeholder.9409

Printed by: e48d507df5d1141@placeholder.94092.edu. Printing is for personal, private use only. No part of this book may be reproduced or transmitted without publisher's prior permission. Violators will be prosecuted.

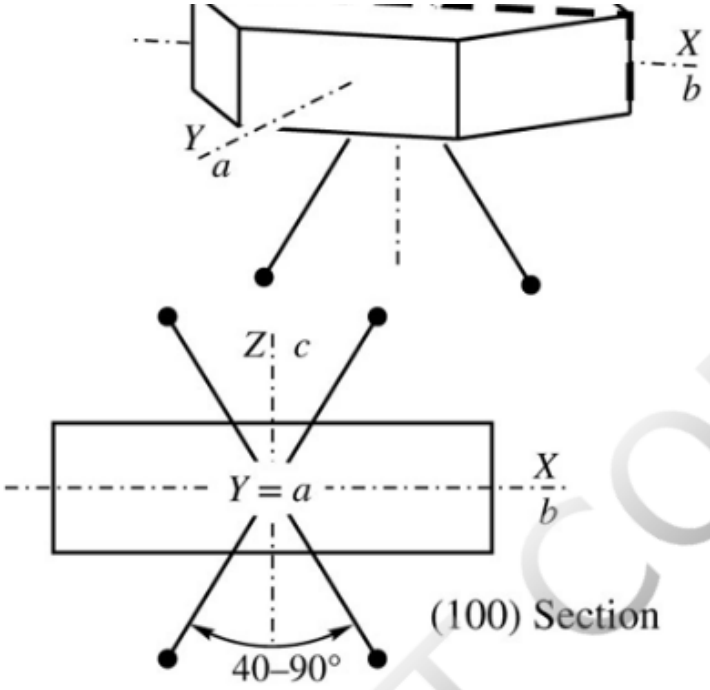

(100) Section

Structure Tridymite structure consists of stacked sheets of silicon tetrahedra. The tetrahedra within each sheet form six-member rings with the tetrahedra pointing alternately up and down. Sheets are joined by sharing oxygen anions between the tetrahedra pointing up in one sheet and the tetrahedra pointing down on the overlying sheet. As viewed down the *c* axis, the rings of tetrahedra within each sheet line up one above the other. The result is the formation of a three-dimensional framework of tetrahedra in which every oxygen anion is shared between two tetrahedra.

The high-temperature *β*-tridymite structure is hexagonal. With cooling, the structure distorts slightly and the hexagonal symmetry is lost. Low-temperature tridymite varieties with orthorhombic, monoclinic, and triclinic symmetry have been described. All tridymite at room temperature is one of these polymorphic varieties.

Composition Ideally the composition is SiO_2, but the fairly open structure can accommodate varying amounts of Na^+, K^+, and Ca^{2+}, with electrostatic charge balance maintained by substituting Al^{3+} for Si^{4+}.

Form and Twinning Crystals are typically pseudohexagonal platelets dominated by the {100} prism and {001} pinacoid. Tridymite also may form radiating or spherical aggregates or be anhedral granular.

The process of converting from hexagonal *β*-tridymite to lower symmetry typically causes crystals to be twinned on {106}. Tridymite derives its name from the fact that twins often are composed of three wedge-shaped segments.

Cleavage None. Conchoidal fracture. Brittle.

Color Properties

DO NOT COPY

Printed by: e48d507df5d1141@placeholder.94092.edu. Printing is for personal, private use only. No part of this book may be reproduced or transmitted without publisher's prior permission. Violators will be prosecuted.

Luster: Vitreous.

Color: Colorless, gray, white.

Streak: White.

Color in Thin Section: Colorless.

Pleochroism: None.

Optical Characteristics

Relief in Thin Section: Moderate negative.

Optic Orientation: $X = b$, $Y = a$, $Z = c$.

Indices of Refraction and Birefringence: Indices of pure synthetic tridymite are $n_\alpha = 1.469$, $n_\beta = 1.469$, $n_\gamma = 1.473$. Indices of refraction increase modestly with increasing Ca, Na, and K content. Birefringence is low (0.002–0.004), so interference colors in standard thin section are no higher than first-order gray.

Interference Figure: Biaxial positive with $2V$ between 40° and 90° but usually around 70°. $2V$ may be different in different segments of a twinned crystal.

Alteration Tridymite at room temperature is always a pseudomorph (paramorph) after β-tridymite. Tridymite also may be pseudomorphically replaced by quartz, either as single crystals or as aggregates. The c axis orientation of the replacing quartz generally does not coincide with the c axis of the original tridymite.

Distinguishing Features

Hand Sample: The crystal habit is characteristic, but it is not possible to distinguish tridymite from a quartz pseudomorph after tridymite in hand sample.

Thin Section/Grain Mount: Crystal habit, low birefringence, low indices of refraction, and twinning are characteristic. Quartz has higher birefringence and indices of refraction, and is uniaxial. Cristobalite is uniaxial or essentially isotropic.

Occurrence Tridymite is found in felsic to intermediate extrusive and shallow intrusive igneous rocks. It may form phenocrysts, be part of the groundmass, or form small crystals lining vesicles or other voids. It also is found in vesicles in basaltic lavas and in the contact metamorphic zones adjacent to basaltic intrusions; it has been reported in stony meteorites.

Use None.

Cristobalite

DO NOT COPY
e48d507df5d1141@placeholder.94092

Printed by: e48d507df5d1141@placeholder.94092.edu. Printing is for personal, private use only. No part of this book may be reproduced or transmitted without publisher's prior permission. Violators will be prosecuted.

SiO_2

Tetragonal

(422) (pseudoisometric)

$a = 4.971$ Å, $c = 6.928$ Å, $Z = 4$

$H = 6.5$

$G = 2.32 - 2.36$

Uniaxial $(-)$

$n_\omega = 1.486 - 1.488$

$n_\epsilon = 1.482 - 1.484$

$\delta = 0.002 - 0.004$

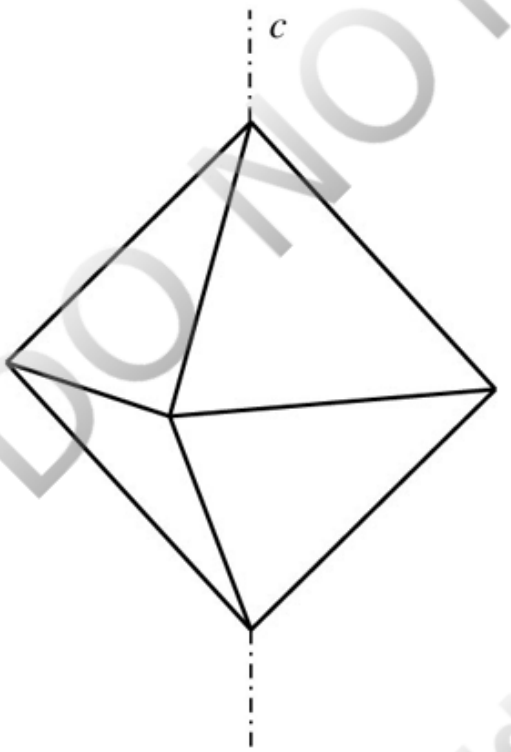

Structure Like tridymite, the structure of cristobalite consists of sheets of silicon tetrahedra arranged in 6-fold rings whose tetrahedra point alternately up and down. Sheets are tied together by sharing oxygen anions between the up tetrahedra on one sheet and the down tetrahedra on the overlying sheet. The cristobalite structure differs in that the rings in adjacent sheets do not line up with each other but are offset, so that the up tetrahedra in one sheet are over the centers of the rings in the sheet below. If the arrangement of tetrahedra in tridymite is equivalent to hexagonal close packing with sheets parallel to {001}, then the tetrahedral arrangement in cristobalite is equivalent to cubic close packing with the sheets parallel to {111}. At high temperatures, the structure

DO NOT COPY e48d507df5d1141@placeholder.9409

Printed by: e48d507df5d1141@placeholder.94092.edu. Printing is for personal, private use only. No part of this book may be reproduced or transmitted without publisher's prior permission. Violators will be prosecuted.

of β-cristobalite is isometric, but cooling below 268°C allows a slight distortion of the lattice and conversion to the tetragonal symmetry of α-cristobalite. This conversion is accompanied by twinning.

Composition The ideal composition is SiO_2, but the open structure allows interstitial substitution of Na^+, Ca^{2+}, K^+, or other cations whose electrostatic charge is balanced by substituting Al^{3+} for Si^{4+}.

Form and Twinning Crystals are typically octahedrons, rarely cubes. Also dendritic and skeletal, or intergrown with K-feldspar forming a radial pattern in spherulites produced by volcanic glass **devitrification**. Devitrification is the breakdown of an amorphous material into a crystalline material. All cristobalite at room temperature is actually a pseudomorph of α-cristobalite after β-cristobalite. Cristobalite also may be fibrous with length-slow fibers, usually consisting of distorted cristobalite/tridymite, that are sometimes called lussatite, and length-fast fibers that are called lussatine. In a confusing bit of terminology, these terms also are applied to the opal samples that contain fibrous cristobalite.

Multiple twins on {111} are produced during the conversion from β- to α-cristobalite. The *c* axis in the different lamellae in the tetragonal structure follows one of the three original *a* axes in the high-temperature isometric structure.

Cleavage None. Brittle.

Color Properties

Luster: Vitreous.

Color: Colorless to white or pale yellowish white.

Streak: White.

Color in Thin Section: Colorless.

Pleochroism: None.

Optical Characteristics

Relief in Thin Section: Moderate negative.

Optic Orientation: One of the *a* axes in β-cristobalite becomes the *c* axis in α-cristobalite after inversion and is therefore the optic axis. Fibers are usually length slow, less commonly length fast, and display parallel extinction in most cases.

Indices of Refraction and Birefringence: Indices of refraction vary within a small range, and birefringence is quite low (0.002–0.004), so interference colors in standard thin section are no higher than lower first-order gray, and for many orientations, cristobalite may appear nearly isotropic.

DO NOT COPY e48d507df5d1141@placeholder.9409

Printed by: e48d507df5d1141@placeholder.94092.edu. Printing is for personal, private use only. No part of this book may be reproduced or transmitted without publisher's prior permission. Violators will be prosecuted.

Interference Figure: Fine grain size and low birefringence make obtaining good figures difficult. Most cristobalite is uniaxial negative, but biaxial varieties with small $2V$ have been reported.

Alteration Cristobalite may be pseudomorphically replaced by quartz or may pseudomorphically replace tridymite.

Distinguishing Features

Hand Sample: Difficult to identify with certainty in hand sample because of fine grain size and complications related to pseudomorphic relations. It resembles quartz and tridymite, but with a different crystal habit.

Thin Section/Grain Mount: Crystal habit, indices of refraction, and low birefringence are characteristic, as is its presence in spherulites. Tridymite is biaxial and has somewhat higher negative relief. Quartz has higher birefringence and is uniaxial positive. X-ray techniques are often needed to identify fine-grained material.

Occurrence Cristobalite may form phenocrysts or groundmass minerals in some felsic lavas. Cristobalite is more common as grains lining cavities and vesicles in volcanic rocks and shallow intrusions in association with topaz, garnet, tridymite, and other minerals. It also is a common constituent of the material routinely identified as opal. Cristobalite has been found in meteorites and in sandstone that has been fused by contact with high-temperature magma or by underground coal fires.

Use None.

Opal

$SiO_2 \cdot nH_2O$

Amorphous

$H = 5.5–6.5$

$G = 2.0–2.25$

Isotropic

$n = 1.43–1.46$

Structure See **Box 12.1**.

BOX 12.1
Micro- and Non-Crystalline Silica

DO NOT COPY e48d507df5d1141@placeholder.9409-

Printed by: e48d507df5d1141@placeholder.94092.edu. Printing is for personal, private use only. No part of this book may be reproduced or transmitted without publisher's prior permission. Violators will be prosecuted.

Common geological materials with microcrystalline varieties of silica include the following.

Chalcedony: A rock or deposit composed dominantly of fibrous quartz and moganite.

Chert: A rock composed dominantly of finely granular quartz, plus small and variable amounts of fibrous quartz, moganite, and opaline material.

Opal: A deposit composed of hydrous silica that either is non-crystalline or forms disordered cristobalite/tridymite.

Microcrystalline Quartz

Quartz forms three microcrystalline textural varieties—micro-quartz, chalcedonite, and quartzine.

Micro-quartz consists of roughly equant grains fine enough that individual grains are too small to be distinguished with a binocular microscope. The term is used to distinguish granular quartz from fibrous quartz and moganite in chalcedony and chert. Larger grains of quartz in these materials could be called macro-quartz.

Chalcedonite is fibrous quartz whose fibers are elongate perpendicular to *c* along the [110] direction. It typically forms tightly packed radial or parallel aggregates. The fibers twist along their length so that the *c* axis sweeps out in a helix (like a spiral staircase). As seen in thin section between crossed polarizers, chalcedonite fibers show maximum birefringence when the *c* axis is horizontal and minimum when *c* is closest to vertical. The bands of light and dark along the length of fibers produce a distinctive feathery appearance typically seen in chalcedony (Figure 12.3c). *Chalcedonite* is a term originally introduced by Michel-Lévy and Munier-Chalmas (1892) for length-fast quartz fibers, but it fell into disuse by the middle of the twentieth century, replaced by *length-fast chalcedony*. However, *chalcedonite* is preferred here because it avoids using the term *chalcedony* as both a lithologic and mineralogical term, and because *chalcedonite* has precedence.

Quartzine is another term introduced by Michel-Lévy and Munier-Chalmas (1892) for quartz fibers that are elongate parallel to *c* and are optically length slow. Quartzine fibers do not twist, so they do not display the feathery appearance of chalcedonite. The term *quartzine* continues to be used. It is also referred to as *length-slow chalcedony*, but this term presents the same problems as *length-fast chalcedony*, so *quartzine* is preferred.

Most chemical analysis of chalcedony (the rock) show the presence of water trapped either in submicroscopic pore spaces between fibers of chalcedonite and moganite or in the form of hydroxyl in the quartz structure. The pore space lowers the specific gravity to 2.57–2.64 and also reduces the index of refraction compared to common quartz. The fine fibrous structure produces a luster that is dull vitreous to greasy.

Numerous names have been applied to microcrystalline varieties of quartz used

Printed by: e48d507df5d1141@placeholder.94092.edu. Printing is for personal, private use only. No part of this book may be reproduced or transmitted without publisher's prior permission. Violators will be prosecuted.

for lapidary work. A few of the common terms include

Jasper: Red or brown microcrystalline quartz (usually chert)

Flint: Black or dark gray microcrystalline quartz (usually chert)

Agate: Microcrystalline silica (often chalcedony) with color bands or irregular color patches; often translucent (Figure 2.52d)

Moganite

Michel-Lévy and Munier-Chalmas (1892) originally identified additional length-slow fibers in chalcedony that they called lutecite. Over the succeeding decades, the term *lutecite* fell into disfavor because it was not thought to be distinct from chalcedonite and quartzine. However, it has been shown that lutecite is the silica polymorph moganite, first characterized in 1976 and now recognized by the Commission on New Minerals, Nomenclature and Classification. Moganite forms length-slow fibers in chalcedony and chert, and may make up over 75 percent of some samples. Optically it is biaxial, but fine grain size generally prevents anything but the sign of elongation from being recognized. It is, therefore, difficult to distinguish from quartzine. Identification generally requires careful X-ray diffraction study.

Opal

Opal is conventionally identified as a mineraloid, but it would be better to consider it a geological deposit or rock composed of non-crystalline and microcrystalline varieties of silica. The major varieties are opal-A, opal-CT, and opal-C, and they are typically distinguished using X-ray diffraction techniques.

Opal-A is non-crystalline and occurs in two general varieties. Opal-AN is usually hydrous silica glass without obvious structure. Opal-AG, which is more abundant, is composed of spherical non-crystalline silica masses—water fills the interstices (**Figure 12.4a**). If the spheres have uniform diameters from ~150 to 300 nm and pack together in an orderly way, they will diffract light and produce the beautiful play of colors seen in precious opal. Individual spheres have either a concentric or radial structure, suggesting progressive deposition around a nucleus.

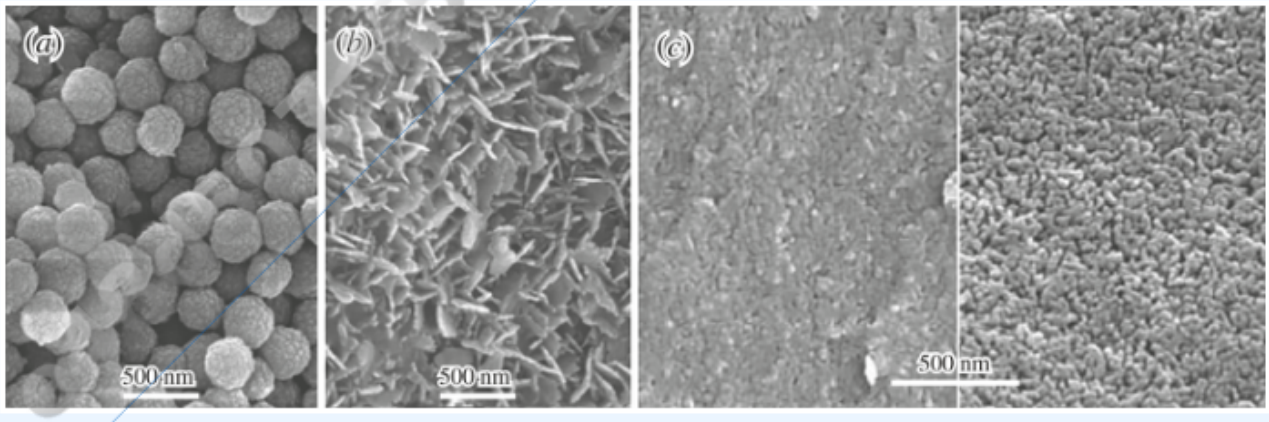

DO NOT COPY

Printed by: e48d507df5d1141@placeholder.94092.edu. Printing is for personal, private use only. No part of this book may be reproduced or transmitted without publisher's prior permission. Violators will be prosecuted.

FIGURE 12.4 Opal microstructure. (*a*) Randomly packed spheres of silica in common white opal-A. Spheres may have a concentric or radial structure. In opal-CT, similar spheres made of cristobalite/tridymite nanoparticles and platelets are called lepispheres. (*b*) Opal-CT made of random platelets, each roughly 25 nm × 300 nm. Each platelet is made of numerous ~25 nm nanograins of cristobalite/tridymite. (*c*) Opal-CT (fire opal). The left image shows a freshly broken surface. If etched with HF (right image), the structure consisting of randomly packed nanoparticles of cristobalite/tridymite is revealed. © Dr. Eloïse Gaillou / Nantes Université.
View larger image

Opal-CT is formed of abundant ~25 nm crystal plates or "nanograins." The nanograins are made of disordered cristobalite/tridymite in which domains of each structure are present. As seen with the scanning electron microscope, much opal-CT consists of random aggregates of nanograins without obvious structure (**Figure 12.4c**). The nanograins also may clump together to form larger fibers or platelets (**Figure 12.4b**). Fibers, arranged in bundles, may be ~ 25 nm in diameter and more than 4 µm long. Platelets are typically 25 nm thick and ~100–300 nm across and may arrange themselves into spherical structures called lepispheres that range from 100 nm to 20 µm in diameter. Small lepispheres may consist of intersecting platelets and resemble barite roses (Figure 17.16), and larger ones are masses of platelets. The lepispheres are capable of diffracting light if their size is appropriate and they are regularly packed together. Most opal-CT is microscopically isotropic, but some consists of parallel or radiating aggregates of length-slow fibers sometimes referred to as lussatite. The fibers are formed of disordered cristobalite/tridymite.

Opal-C is similar to opal-CT, except that cristobalite dominates. It is often considered to be opal-CT in which the nanograins have recrystallized, removing most of the tridymite component. In some cases it is made of length-fast fibers of cristobalite, which is sometimes referred to as lussatine.

The milky-white body color, called opalescence, seen in some opal is caused by Mie scattering of light by opal particles. The same scattering process causes clouds to appear white. The beautiful play of colors seen in gem opal is a diffraction effect produced when the lepispheres are of uniform size and systematically arranged. Reddish fire opal is colored by hydrous iron oxide.

Composition Variable amounts of water may be present, either in the void spaces or incorporated in some manner in the silica. Heating or long exposure to air may cause dehydration and cracking.

Form and Twinning Opal forms colloform and encrusting masses, vein fillings, or irregular masses. It may be the cementing agent in sandstone or may replace organic material, as in petrified wood. Opal also forms the skeletons of diatoms, radiolarians, and silicoflagellates, which may be abundant in lacustrine and marine waters.

Cleavage None. Conchoidal fracture. Brittle.

Color Properties

Printed by: e48d507df5d1141@placeholder.94092.edu. Printing is for personal, private use only. No part of this book may be reproduced or transmitted without publisher's prior permission. Violators will be prosecuted.

Color Properties

Luster: Vitreous to waxy.

Color: Colorless, gray, white, blue, green, red, and so forth. Gem material may display a beautiful play of colors; fluorescence is common.

Streak: White.

Color in Thin Section: Colorless.

Pleochroism: None.

Optical Characteristics

Relief in Thin Section: Moderate negative.

Indices of Refraction: Index of refraction decreases with increasing water content.

Alteration With dehydration and crystallization, opal converts to microcrystalline quartz, such as chert. The opal shells of microorganisms may be replaced by pyrite.

Distinguishing Features

Hand Sample: Opal resembles microcrystalline quartz but has lower hardness and lower specific gravity. The play of colors, if present, is distinctive.

Thin Section/Grain Mount: Opal usually is isotropic and cloudy, but may display low birefringence or be fibrous. Analcime and volcanic glass have higher indices of refraction. Fluorite has distinct cleavage.

Occurrence Opal is common in voids in volcanic rocks and shallow intrusions, and may replace part of the rock. It is precipitated both from groundwater and from hydrothermal solutions. Opal is found in sedimentary rocks as a cementing agent and may replace shells, wood fiber, or other organic material. Opal also is deposited around geysers and hot springs as geyserite or siliceous sinter.

Opal is a biomineraloid and is precipitated by microorganisms, including over 1800 species of modern diatoms, species of silicoflagellates, and by radiolarian; all form elaborate shells. Sponges also form siliceous spicules. In almost all cases silica is undersaturated in the water, so organisms must expend cellular energy to concentrate silica to the point it can precipitate. When the organisms die, the siliceous shells settle to the bottom, where they accumulate as siliceous ooze, which may later crystallize to form chert. In favorable conditions, such as freshwater lakes in volcanic terranes, diatoms may accumulate in sufficient volumes that they can later be mined as diatomaceous earth.

Use Opal with a play of color is used as a gemstone, and colored varieties are commonly used for lapidary purposes. Diatomaceous earth has numerous uses, including as a polishing compound, a filtration agent in water treatment plants, a sorbent to clean up

DO NOT COPY

Printed by: e48d507df5d1141@placeholder.94092.edu. Printing is for personal, private use only. No part of this book may be reproduced or transmitted without publisher's prior permission. Violators will be prosecuted.

Feldspar Group

The feldspars are the most abundant minerals in the Earth's crust. They are found in nearly all igneous rocks and most metamorphic rocks, and are an important constituent of many sedimentary rocks and sediments. Additional information about these important minerals can be found in Smith and Brown (1988) and Ribbe (1983).

Composition

The feldspars include three principal compositional end members: K-feldspar ($KAlSi_3O_8$), albite ($NaAlSi_3O_8$), and anorthite ($CaAl_2Si_2O_8$), whose abbreviations are Ks, Ab, and An, respectively. The abbreviation Or is commonly used to indicate K-feldspar, but this usage is not followed here to avoid the unwanted inference that Or refers to orthoclase, which is a specific variety of alkali feldspar. As is shown in **Figure 12.5**, only compositions between albite and anorthite, and between K-feldspar and albite, are found. The former feldspars are known as plagioclase and the latter as alkali feldspars.

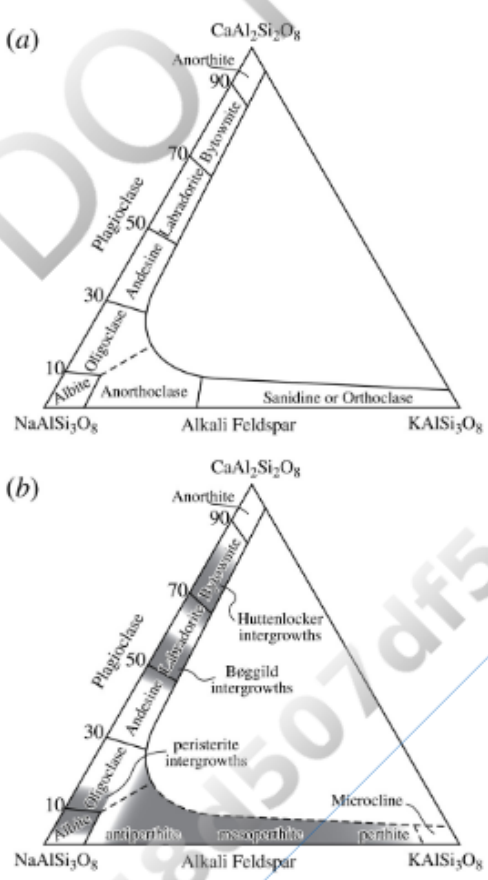

FIGURE 12.5 Simplified composition range of common feldspar; see text for details. (*a*) At high temperature there is continuous solid solution for both plagioclase and the alkali feldspars. (*b*) With slow cooling, exsolution occurs across multiple feldspar compositions (shaded regions). Plagioclase

DO NOT COPY e48d507df5d1141@placeholder.94092

Printed by: e48d507df5d1141@placeholder.94092.edu. Printing is for personal, private use only. No part of this book may be reproduced or transmitted without publisher's prior permission. Violators will be prosecuted.

slow cooling, exsolution occurs across multiple feldspar compositions (shaded regions). Plagioclase intergrowths are submicroscopic and are only visible with a transmission electron microscope. High-temperature alkali feldspars exsolve to form antiperthite, mesoperthite, or perthite, depending on composition. For these, exsolution lamellae are typically visible in thin section or perhaps hand sample. Exsolution composition ranges are approximate. View larger image

As was discussed in Chapter 4, the plagioclase feldspars represent a continuous solid solution series, at least at high temperatures, accomplished by coupled substitution. Albite is at one end of the series and anorthite at the other. Ca^{2+} can substitute for Na^{+} because they are about the same size; charge neutrality is maintained by substituting Al^{3+} for Si^{4+}. Because relatively little K^{+} is included in plagioclase, the composition is often described in terms of the percentage of the anorthite (An) end member, with the presumption that the remainder is dominantly albite (Ab), so that An + Ab = 100. The composition of plagioclase with 35 mol percent Ca^{2+} and 65 mol percent Na^{+} is An_{35}, for example. The plagioclase feldspars are conventionally separated into six different named composition ranges.

Albite	An_0–An_{10}
Oligoclase	An_{10}–An_{30}
Andesine	An_{30}–An_{50}
Labradorite	An_{50}–An_{70}
Bytownite	An_{70}–An_{90}
Anorthite	An_{90}–An_{100}

Continuous solid solution in the alkali feldspar series is possible because K^{+} and Na^{+} have the same charge, but it is limited to high temperatures because the sizes of these cations are significantly different. The lack of compositions intermediate between K-feldspar and anorthite under any geological conditions is caused by Ca^{2+} and K^{+} having substantially different sizes and also a different charge.

Structure

The structure of the feldspars consists of a framework of corner-sharing Si and Al tetrahedra. The tetrahedra are arranged to form four-member rings (**Figure 12.6a**), with the apex of two of the tetrahedra pointing “up” and two pointing “down,” parallel to the *a* axis. One of the “up” and one of the “down” tetrahedra are T_1 sites; the others are T_2 sites. The rings are joined to other rings by sharing oxygen anions to form crankshaft-like chains that extend parallel to *a* (**Figure 12.6b**). These chains are in turn joined laterally to other chains by sharing the remaining oxygen anions (**Figure 12.6c**). This results in the formation of sites between chains that can contain large cations such as Ca^{2+}, Na^{+}, and K^{+}. These cations are coordinated with nine oxygen anions

DO NOT COPY e48d507df5d1141@placeholder.9409

Printed by: e48d507df5d1141@placeholder.94092.edu. Printing is for personal, private use only. No part of this book may be reproduced or transmitted without publisher's prior permission. Violators will be prosecuted.

and K^+. These cations are coordinated with nine oxygen anions.

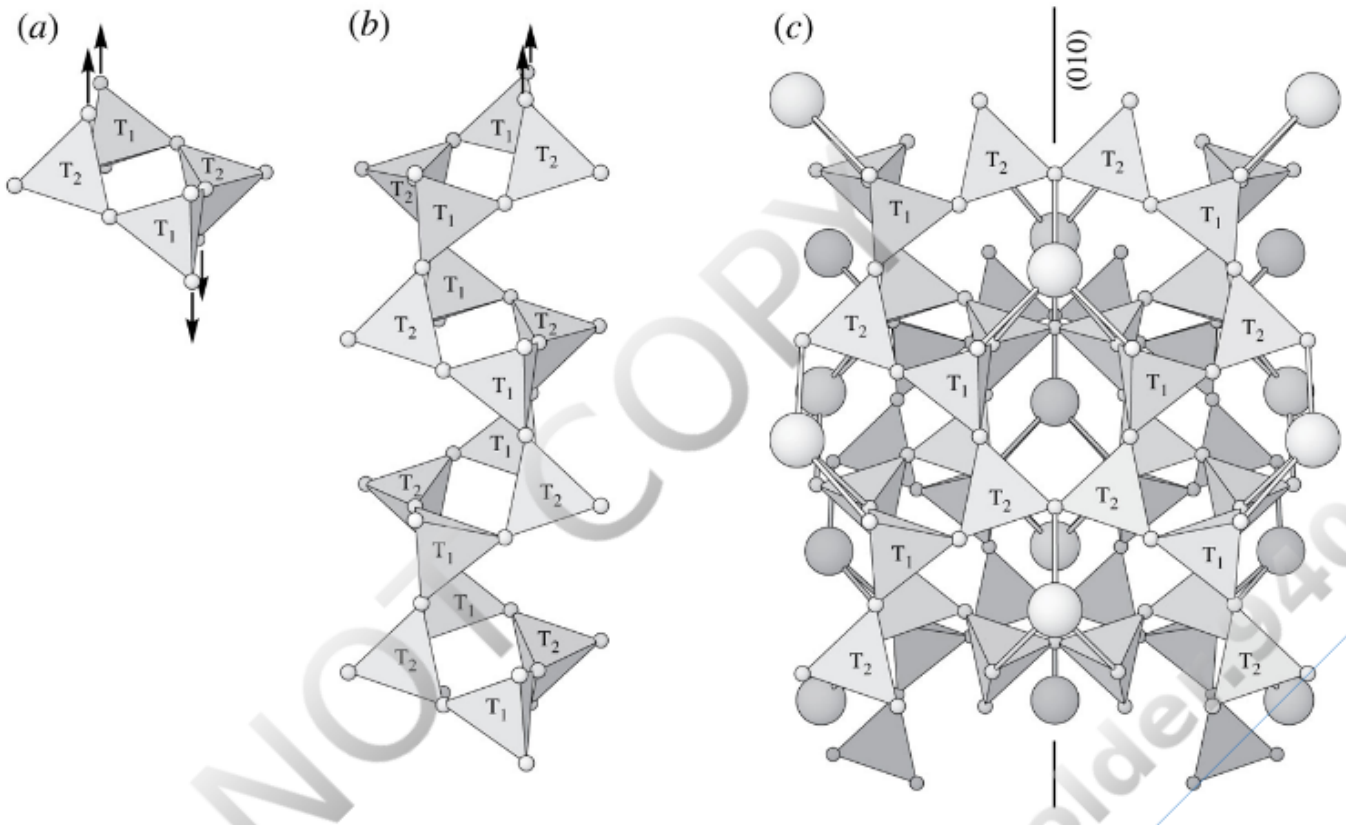

FIGURE 12.6 Idealized feldspar structure: T_1 and T_2 refer to different tetrahedral sites. View is perpendicular to the (001) plane; the same view is used in Figure 12.7. (*a*) Four-member ring of silicon tetrahedra containing two nonequivalent tetrahedral sites, T_1 and T_2. (*b*) The four-member rings share O^{2-} anions to form a crankshaft-like chain of silicon tetrahedra extending parallel to *a*. (*c*) Chains are cross-linked by sharing the remaining oxygen anions on each tetrahedron to form large coordination sites occupied by Ca^{2+}, Na^+, or K^+ (large spheres). View larger image

Al/Si Order–Disorder

The way in which Si^{4+} and Al^{3+} are distributed in the T_1 and T_2 tetrahedral sites leads to the distinction among different order–disorder polymorphs (Chapter 4) of the feldspars and has significant consequences for the exsolution structures of plagioclase. Four different modes of ordering are possible (**Table 12.4**, **Figure 12.7**). Modes I, II, and III are available to K-feldspar and albite, which have an Al:Si ratio of 1:3, and Mode IV is found in anorthite, which has an Al:Si ratio of 2:2.

MODE I: Al and Si randomly distributed in tetrahedral sites

MODE II: Al preferentially located in half the T_1 sites

MODE III: Al preferentially located in just one T_1 site

MODE IV: Al and Si occupy alternating tetrahedra

Printed by: e48d507df5d1141@placeholder.94092.edu. Printing is for personal, private use only. No part of this book may be reproduced or transmitted without publisher's prior permission. Violators will be prosecuted.

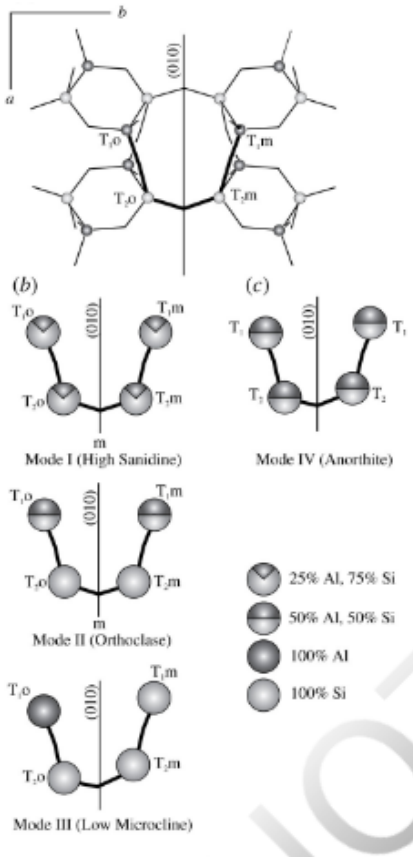

FIGURE 12.7 Ordering of Al and Si in tetrahedral sites in the feldspars. (*a*) Sketch showing the location of the T_1 (dark spheres) and T_2 (light spheres) cations within tetrahedra. The "o" and "m" identify sites on opposite sides of the (010) plane. Compare with Figure 12.6c. (*b*) Alkali feldspars, which have an Al:Si ratio of 1:3. In Mode I ordering, Al and Si are randomly distributed in the T_1 and T_2 sites so 25 percent of each site is occupied by Al^{3+} and a mirror plane exists parallel to {010}. The "o" and "m" sites are structurally identical. In Mode II ordering, the T_1 sites are half occupied by Al and half by Si. The T_2 sites contain only Si. This ordering preserves the {010} mirror, so the "o" and "m" sites are structurally identical and orthoclase is ideally monoclinic. In Mode III ordering, all of the Al is in the T_1o site, and the T_1m, T_2o, and T_2m sites contain only Si^{4+}. The {010} mirror is destroyed, and the "o" and "m" sites are structurally different. The structure distorts slightly, and symmetry is reduced to triclinic. (*c*) Anorthite, in which the Al:Si ratio is 2:2. Al and Si occupy alternating tetrahedral sites, so T_1 and T_2 sites are occupied, on average, with half Al and half Si. See text for additional discussion. View larger image

TABLE 12.4 Modes of Al:Si Ordering in Tetrahedral Sites in the Feldspars[a]

Ordering Mode	Al:Si Ratio	Description	$t_1o + t_1m$
Mode I	1:3 Alkali feldspar (Figure 12.7b)	Complete disorder; Al is equally likely to be in any of the four tetrahedral sites; on average, 25% of each of the four tetrahedral sites (T_1o, T_1m, T_2o, T_2m) is occupied by Al and 75% occupied by Si	0.5
Mode II		All of the Al is in the two T_1 sites; none is in the T_2 sites; the T_1o and T_1m, sites are, on average, 50% occupied by Al and 50% occupied by Si; the T_2 sites contain only Si	1.0
Mode III		All of the Al is concentrated in just the T_1o site, so its occupancy is 100% Al; the other three sites (T_1m, T_2o, T_2m) contain only Si; this is the highest degree of ordering available	1.0

DO NOT COPY e48d507df5d1141@placeholder.9409

Printed by: e48d507df5d1141@placeholder.94092.edu. Printing is for personal, private use only. No part of this book may be reproduced or transmitted without publisher's prior permission. Violators will be prosecuted.

		available	
Mode IV	2:2 Anorthite (Figure 12.7c)	The only way to avoid having Al in adjacent tetrahedra is to have a systematic alternation of Al and Si in the tetrahedral sites: Al is therefore in one-half of each of the T_1o, T_1m, T_2o, and T_2m sites	N/A

[a] The fractions of the T_1o and T_1m sites occupied by Al^{3+} are t_1o and t_1m, respectively.

K-Feldspar

Consider first the K-feldspars, which have an Al:Si ratio of 1:3, and occur in three polymorphs: sanidine, orthoclase, and microcline. Al and Si may order in the tetrahedral sites by modes I, II, and III.

Mode I ordering, that is, complete disorder, is displayed in the idealized high sanidine structure (Figure 12.7b), which is approached only at temperatures greater than roughly 1000°C. Because, on average, the two T_1 and two T_2 sites have the same occupancy, a plane of symmetry parallel to {010} is present between adjacent crankshaft-like chains. The structure is therefore monoclinic and the *c* axis is inclined at roughly 116° to the {001} plane. Most K-feldspar, except that grown at relatively low temperature in hydrothermal systems or as a result of diagenesis in sediments (adularia), originally crystallizes with a sanidine structure and a high degree of disorder in the distribution of Al and Si in the tetrahedral sites.

Mode III ordering, which is the most ordered Al/Si distribution possible in the alkali feldspars, is approached in the low or maximum microcline structure. This highly ordered structure can be produced by slow cooling in plutonic igneous or deep metamorphic conditions. The Al and Si, which originally were more or less randomly distributed in the tetrahedral sites, diffuse through the lattice to preferentially place all or most of the Al^{3+} in just the T_1o site (Figure 12.7b). The T_1m or the T_2 sites contain only Si^{4+}. This destroys the mirror plane and results in a slight distortion of the lattice, so microcline is triclinic.

The triclinic structure of microcline can be related to the original monoclinic structure of sanidine in one of four different but equally likely ways, depending on exactly which complement of T_1 sites in the crystal structure happens to accumulate the Al. When progressive ordering of Al and Si triggers the conversion from monoclinic to the slightly distorted triclinic microcline structure at around roughly 450°C, different parts of the crystal adopt one or another of the four possible orientations. Two of the orientations are related to each other by reflection on the {010} plane, and the other two are related by rotation about the *b* axis. Recall that different segments of crystals related by a symmetry operation are twins (Chapter 4). In the feldspars, twinning with {010} as a twin plane is called **albite twinning**, and twinning with the *b* axis as a rotation axis is called **pericline twinning**. Microcline that has been produced by ordering of an originally monoclinic K-feldspar always displays a combination of polysynthetic albite and pericline twinning. Twinning is discussed in more detail later.

DO NOT COPY e48d507df5d1141@placeholder.94092

Printed by: e48d507df5d1141@placeholder.94092.edu. Printing is for personal, private use only. No part of this book may be reproduced or transmitted without publisher's prior permission. Violators will be prosecuted.

Twinning is discussed in more detail later.

Ideally, orthoclase would be ordered according to Mode II, in which the Al preferentially is located in the two T_1 sites (Figure 12.7b). Reality, however, is more complicated. Real orthoclase displays a combination of Mode II and Mode III ordering and can be considered to represent an intermediate degree of ordering between sanidine and microcline. The transition with cooling from sanidine to orthoclase is accompanied by a systematic increase in Mode II ordering as Al^{3+} diffuses out of the T_2 sites and into the T_1 sites. However, the distribution is not even between the T_1o and T_1m sites; the T_1o site is favored. This produces some inconsistency because any ordering according to Mode III should produce a triclinic structure and orthoclase is monoclinic, at least macroscopically. The resolution to this problem is based on the recognition that most orthoclase is actually triclinic at the atomic scale, but polysynthetically twinned like microcline. The individual twin domains are submicroscopic, so the structure averages out to be macroscopically monoclinic.

The practical significance of this discussion of Al/Si order–disorder in K-feldspar is that it can inform geologists about the thermal history of the rocks containing K-feldspar. Sanidine-bearing rocks must have cooled rapidly from high temperature, called **quenching**, to prevent Al/Si ordering from occurring. Rocks containing low microcline with grid twinning must have been subjected to an extended period of slow cooling to allow the extensive Al/Si ordering. Orthoclase indicates the rock cooled at a relatively moderate rate. A quick means of estimating the degree of Al/Si order in K-feldspar is provided by measuring the $2V$ angle (see section on Plagioclase). X-ray diffraction techniques are described by Kroll and Ribbe (1983).

Plagioclase

The pattern of ordering of Al and Si in the tetrahedral sites in plagioclase depends on composition and leads to some complications not immediately evident.

Na-rich plagioclase displays modes I, II, and III order–disorder characteristics in the same way as K-feldspar. Monalbite is the high-temperature Na-plagioclase. It is monoclinic, like sanidine, and has a high degree of Al/Si disorder (Mode I ordering) in the tetrahedral sites. On cooling, it polymorphically converts to a triclinic structure at a temperature of around 980°C. Two different processes are involved in the monoclinic to triclinic conversion.

The first mechanism that leads to triclinic symmetry is a collapse or distortion of the structure (**Figure 12.8**). Na^+ is a loose fit in its structural site (which easily holds the larger K^+ in K-feldspar). At very high temperatures, the energetic vibration of the Na^+ is sufficient to effectively prop the structural site open to preserve monoclinic symmetry. With cooling, however, some of the oxygen anions collapse in toward the Na^+ and the structure distorts from monoclinic to triclinic. Triclinic Na-plagioclase with a high degree

Printed by: e48d507df5d1141@placeholder.94092.edu. Printing is for personal, private use only. No part of this book may be reproduced or transmitted without publisher's prior permission. Violators will be prosecuted.

of Al/Si disorder like sanidine is known as analbite, but it is not normally found in nature.

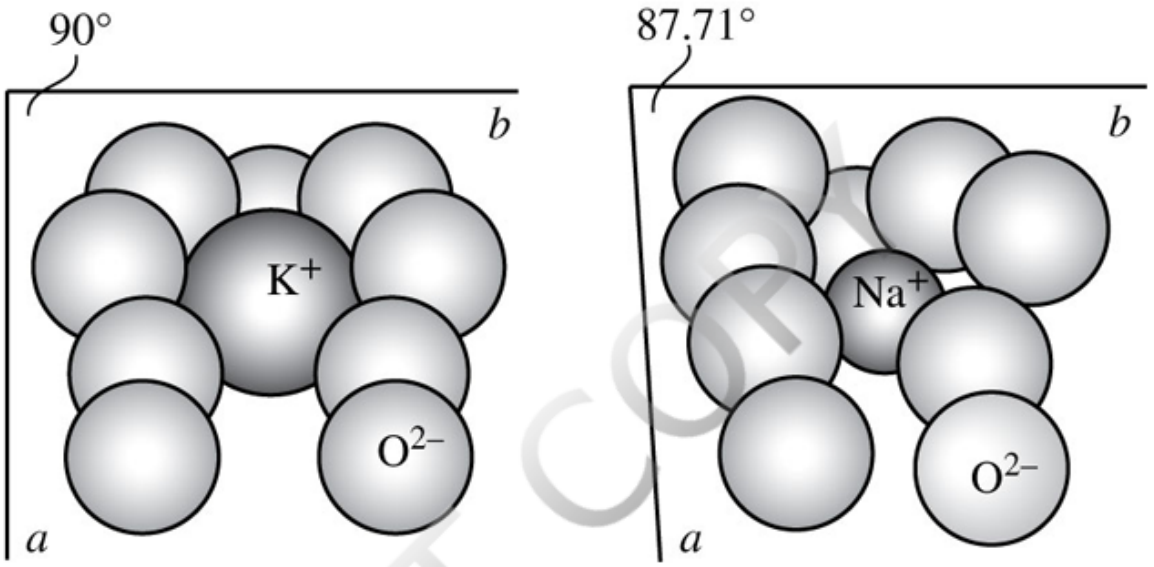

FIGURE 12.8 Arrangement of oxygen anions about K^+ in sanidine (left) and the distorted or collapsed arrangement around Na^+ in albite (right). The angle between the *a* and *b* axes in sanidine is 90°, allowing for monoclinic symmetry. In the albite structure $\gamma = 87.71°$, so symmetry is reduced to triclinic. Only at high temperatures is the vibrational energy of Na^+ in albite sufficient to keep the "cage" in which it resides from collapsing. View larger image

The second process that causes the structure to become triclinic with cooling is the preferential ordering of Al into the T_1o sites according to the Mode III ordering mechanism described earlier. While some Mode II ordering occurs, Mode III is dominant. Triclinic Na-plagioclase with only a modest amount of Al/Si ordering is called high albite, and if highly ordered it is called low albite.

The Al/Si ordering associated with converting from high albite to low albite apparently progresses fairly easily so that the high albite structure is preserved only in volcanic rocks. Samples from both shallow and deep intrusions and metamorphic rocks are typically well-ordered low albite. Samples with an intermediate degree of order are uncommon.

Ca-plagioclase (anorthite) follows Mode IV ordering (Figure 12.7c) because it contains equal numbers of Al and Si in the tetrahedral sites. The structure is apparently triclinic for all geologically normal conditions because Ca^{2+} is too small to keep its structural site propped open to maintain the monoclinic symmetry of the idealized feldspar structure. With Mode IV ordering, Al and Si tend to distribute themselves to avoid having Al in adjacent tetrahedra. This is known as the "aluminum avoidance principle." Within a given crankshaft-like chain (Figure 12.6b), placing the Al and Si in alternate tetrahedra will, for example, ensure that all T_1 sites contain Al and all T_2 sites contain Si. In adjacent chains, however, the T_1 and T_2 site occupancy must be reversed because T_2 tetrahedra bond to T_2 tetrahedra across the (010) plane (look in the center of Figure 12.6c). The net result is that T_1 and T_2 sites, on average, contain half Al and half Si. Mode IV ordering is possible

Printed by: e48d507df5d1141@placeholder.94092.edu. Printing is for personal, private use only. No part of this book may be reproduced or transmitted without publisher's prior permission. Violators will be prosecuted.

only in feldspars with near-equal amounts of Al and Si.

Plagioclase with an intermediate Na–Ca composition poses a problem because it is not possible to have a linear variation in Al/Si order between low albite (Mode III with all the Al in one site) and anorthite (Mode IV with Al and Si in alternating sites) without violating the aluminum avoidance principle. What happens in most cases is that ordering triggers the formation of submicroscopic domains, usually a few tens of angstroms across, alternating between relatively Na-rich plagioclase and Ca-rich plagioclase. The Al/Si tetrahedral framework is continuous, but the Na-rich domains have Mode III ordering and the Ca-rich domains have Mode IV ordering. Most plagioclase with compositions between ~An_{20} and An_{70} has this submicroscopic structure and is known as “e” plagioclase.

Exsolution in the Feldspars

Both alkali feldspar and plagioclase may exsolve as they cool after crystallization (Chapter 5). The driving force of the exsolution and the textures that result are somewhat different in the two types of feldspar.

Alkali Feldspar

Exsolution in the alkali feldspars was described in Chapter 5. Exsolution occurs because Na^+ and K^+ have significantly different ionic radii (1.32 vs. 1.65 Å). With cooling after crystallization, both the amount of Na^+ permissible in the K-feldspar structure and the amount of K^+ permissible in albite decrease. This is shown in Figure 5.28a. As the result of exsolution, lamellae of albite formed within a K-feldspar host crystals define what is known as a **perthitic texture** (**Figure 12.9**). Albite with exsolved K-feldspar lamellae is known as **antiperthite**. If the proportions of lamellae and host are nearly equal and cannot be distinguished, the term **mesoperthite** can be used (Figure 12.5).

Development of exsolution lamellae depends, in large part, on the rate at which the alkali feldspar cooled after crystallization. Even sanidine and orthoclase in volcanic rocks undergo some exsolution, but rapid cooling typically ensures that the lamellae are very small, and in hand sample, will appear homogeneous. In all cases, if the exsolution textures can only be seen in thin section, then the prefix *micro* can be used—**microperthite**, for example (Figure 12.9b). If lamellae are submicroscopic, identified only through X-ray diffraction or transmission electron microscope techniques, the prefix *crypto* can be used—**cryptoperthite**, for example.

(*a*) 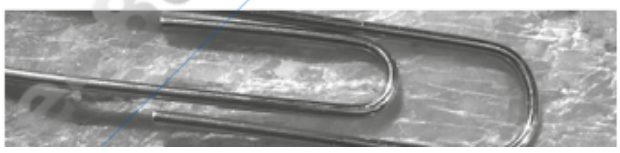

DO NOT COPY

Printed by: e48d507df5d1141@placeholder.94092.edu. Printing is for personal, private use only. No part of this book may be reproduced or transmitted without publisher's prior permission. Violators will be prosecuted.

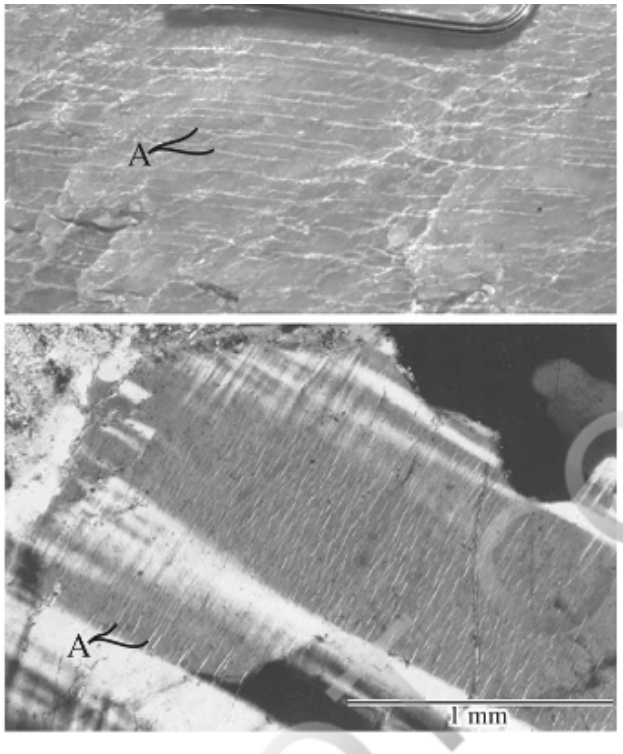

FIGURE 12.9 Perthitic exsolution. (*a*) Hand sample. Thin netlike or branching layers of albite (A) in microcline extend roughly parallel to the paper clip. (*b*) Thin section. Light thin irregular blebs (inclusions) of albite extending NE are visible in microcline (crossed polarizers). The sample also displays "tartan plaid" twinning, with relatively thick twin lamellae with diffuse borders extending NW–SE and NE–SW (cf. Figure 12.20b). View larger image

Plutonic igneous and metamorphic rocks cool at a sufficiently slow rate to allow development of larger exsolution lamellae that may be visible with a hand lens, or commonly, even in hand sample. Microcline is much more prone to developing visible exsolution lamellae than either orthoclase or sanidine. In detail, the exsolution lamellae of albite may form a braided, netlike, vein, patchy, or irregular pattern in the host K-feldspar (Figure 12.9a). Alkali feldspar known as moonstone displays a diffuse milky-white to pale-blue iridescence produced by interaction of light with submicroscopic exsolution lamellae. A comprehensive review of alkali feldspar intergrowths is provided by Parsons and others (2015).

Plagioclase

The exsolution textures in plagioclase are more subtle and depend on order–disorder considerations, not the ionic radii of the cations. Exsolution occurs because of incompatibilities in the Al/Si ordering modes in albite and anorthite described earlier. Depending on the bulk plagioclase composition, **peristerite**, **Bøggild**, or **Huttenlocher** intergrowths may be produced (Figure 12.5b). In most cases these intergrowths are not visible either in hand sample or microscopically as the thickness of the repeating lamellae may be about the same as the wavelength of visible light (i.e., several hundred nanometers). Lamellae of this scale therefore can serve as a diffraction grating, which

Printed by: e48d507df5d1141@placeholder.94092.edu. Printing is for personal, private use only. No part of this book may be reproduced or transmitted without publisher's prior permission. Violators will be prosecuted.

can cause plagioclase to be **chatoyant** or **iridescent**, a feature sometimes referred to as **labradorescence** or **schiller** (see this book's cover). The term *moonstone* is sometimes also applied to these samples.

Peristerite intergrowths are produced in plagioclase whose bulk composition falls in the range An_2 to ~An_{17}. One set of lamellae consists of nearly pure albite ($An_{0–2}$) ordered with all Al in just one of the T_1 sites (i.e., Mode III ordering). The other set of lamellae consists of an "e" plagioclase whose composition is ~$An_{20–25}$ (oligoclase).

Bøggild intergrowths are produced in bulk compositions between about An_{46} and An_{60} and consist of lamellae of andesine (~An_{44}) and labradorite (~An_{58}). Both sets of lamellae consist of "e" plagioclase.

Huttenlocher intergrowths are produced in anorthite-rich plagioclase whose bulk composition falls in the approximate range An_{65}–An_{85} and consist of lamellae of labradorite (~An_{68}) and bytownite (~An_{88}). The labradorite consists of "e" plagioclase, and the bytownite is ordered according to the anorthite model (Mode IV).

Other Feldspar Intergrowths

In addition to the exsolution textures, the feldspars are commonly found as part of intergrowth textures with other minerals. These include myrmekite, granophyre, graphic intergrowths, and (anti)rapakivi textures.

Myrmekite (**Figure 12.10a**) is the intergrowth of vermicular (wormlike) quartz in sodic plagioclase. It is visible only in thin section and is most common at the contact between K-feldspar and plagioclase in plutonic igneous rocks. Development of myrmekite evidently takes place after magmatic crystallization is complete, but the details of the mechanism are subject to some debate.

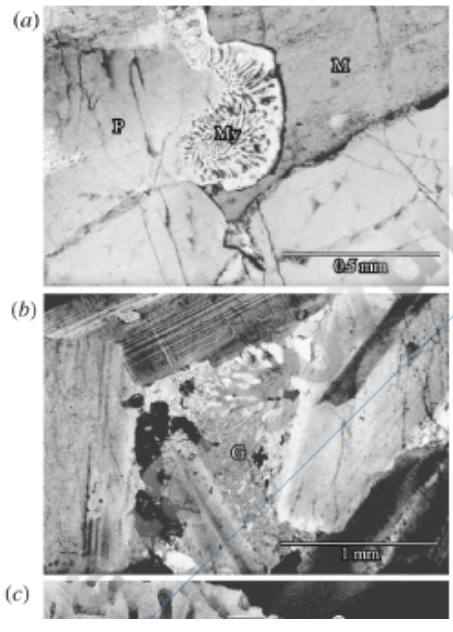

DO NOT COPY

Printed by: e48d507df5d1141@placeholder.94092.edu. Printing is for personal, private use only. No part of this book may be reproduced or transmitted without publisher's prior permission. Violators will be prosecuted.

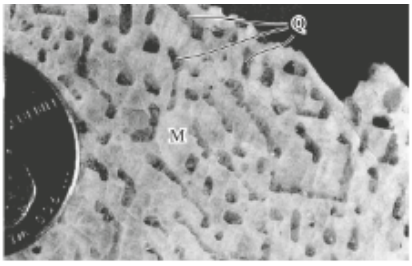

FIGURE 12.10 Quartz–feldspar intergrowths. (*a*) Myrmekite (My) consists of irregular quartz grains (dark) in plagioclase (light) seen at the contact between plagioclase (P) and microcline (M). Crossed polarizers. (*b*) Granophyre (G) in the space between plagioclase laths in norite. Crossed polarizers. (*c*) Graphic intergrowth of quartz (Q) and microcline (M) from a pegmatite. View larger image

Granophyric intergrowths (**Figure 12.10b**) involve irregular, often vermicular quartz intergrown with feldspar (usually K-feldspar or sodic plagioclase). These intergrowths are most common in the interstices between larger, earlier-formed grains, and evidently represent simultaneous crystallization of quartz and feldspar from the last residual melt in an igneous rock.

Graphic intergrowths (**Figure 12.10c**) are found most commonly in granitic pegmatite. A rock containing graphic intergrowths is sometimes referred to as a graphic granite. In this intergrowth, large crystals of perthitic K-feldspar enclose triangular to irregular quartz inclusions, which also may form an irregular branching network. The name originates from the quartz appearing to form something similar to hieroglyphs; here the term *graph* means to draw. Simultaneous crystallization of quartz and K-feldspar at a eutectic (Chapter 5) produces the intergrowth.

A **rapakivi** texture is produced when rims of sodic plagioclase mantle a phenocryst of alkali feldspar, usually in felsic intrusive rocks. An **antirapakivi** texture is produced when a rim of alkali feldspar crystallizes on a phenocryst of plagioclase.

Twinning

About 20 different twin laws have been identified in feldspars but only albite, pericline, Carlsbad, Baveno, and Manebach twins are common. Albite and pericline twins are polysynthetic and the others are single twins.

Polysynthetic albite and pericline twins are nearly ubiquitous in triclinic feldspars, but are not possible in the monoclinic feldspars. Albite twins (**Figure 12.11a**) are produced by reflection on {010}, and composition planes are parallel to that crystal plane. Pericline twins (**Figure 12.11b**) are produced by 2-fold rotation on [010] (the *b* axis). The position of the composition plane in most plagioclase is roughly parallel to {001}, but it varies significantly with composition, degree of Al/Si order, and temperature and pressure at the time of formation. In microcline, the composition plane gets to within about 15° of being parallel to {100}. Both twins may be produced by growth and by deformation. In

DO NOT COPY e48d507df5d1141@placeholder.9409

Printed by: e48d507df5d1141@placeholder.94092.edu. Printing is for personal, private use only. No part of this book may be reproduced or transmitted without publisher's prior permission. Violators will be prosecuted.

addition, both twins are readily produced as part of the monoclinic–triclinic transformation that accompanies cooling and ordering of Al and Si in tetrahedral sites, as described earlier. The absence of these twins in adularia is taken to indicate that this feldspar originally grew with triclinic symmetry below the temperature of the monoclinic–triclinic transformation.

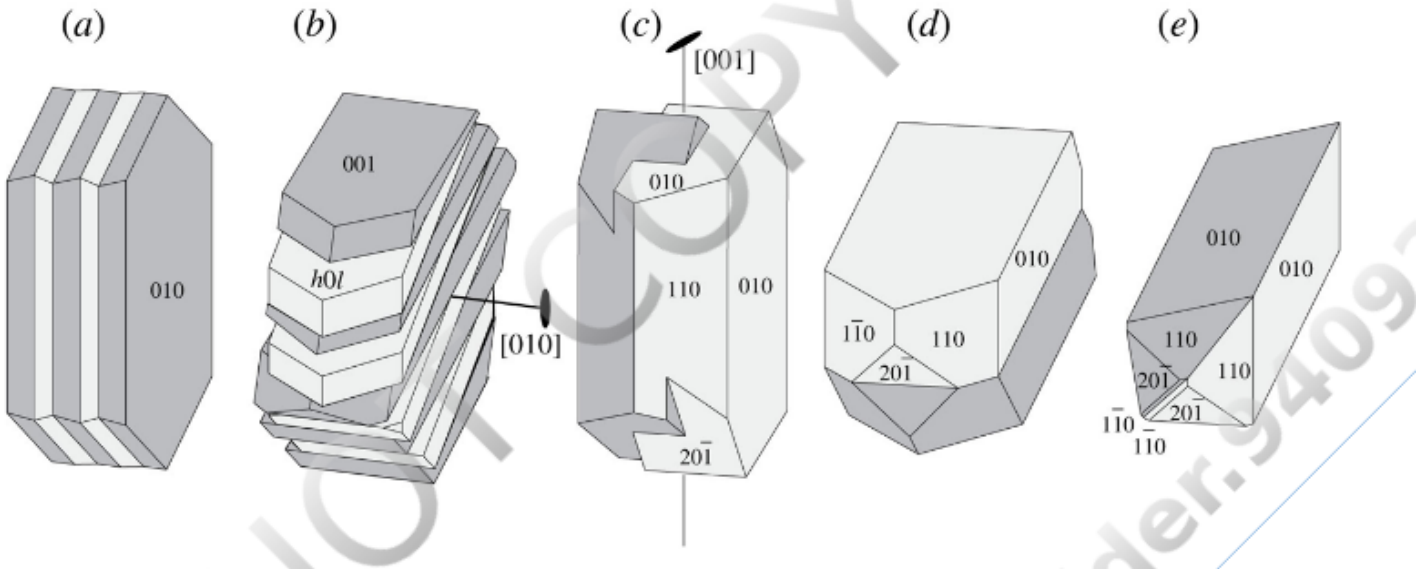

FIGURE 12.11 Common twins in the feldspars. (*a*) Albite twins on {010}. (*b*) Pericline twins produced by rotation on [010]. (*c*) Carlsbad twins produced by rotation on [001]. (*d*) Manebach twins by reflection on {001}. (*e*) Baveno twins produced by reflection on {021}. In the triclinic varieties, twinning is also possible on $\{0\bar{2}1\}$. View larger image

Carlsbad, Baveno, and Manebach twins are all single twins. Carlsbad twins (**Figure 12.11c**) are by far the most common and are produced by 2-fold rotation on [001] (the *c* axis) to yield penetration twins with a slightly irregular composition plane parallel to {010}. Manebach and Baveno twins (**Figure 12.11d** and **e**) are produced by reflection on {001} and {021}, respectively. All three twins are possible in both monoclinic and triclinic crystals and are produced only by growth.

Plagioclase

$$NaAlSi_3O_8 - CaAl_2Si_2O_8$$

Triclinic $\bar{1}$ (pseudomonoclinic)

Low albite : $a = 8.137$ Å, $b = 12.785$ Å, $c = 7.158$ Å,
$\alpha = 94.26^\circ$, $\beta = 116.60^\circ$, $\gamma = 87.71^\circ$, $Z = 4$

Anorthite : $a = 8.177$ Å, $b = 12.877$ Å, $c = 14.169$ Å,
$\alpha = 93.17^\circ$, $\beta = 115.85^\circ$, $\gamma = 92.22^\circ$, $Z = 8$

DO NOT COPY e48d507df5d1141@placeholder.9409-

Printed by: e48d507df5d1141@placeholder.94092.edu. Printing is for personal, private use only. No part of this book may be reproduced or transmitted without publisher's prior permission. Violators will be prosecuted.

$$H = 6 - 6.5$$

$$G = 2.60\ (\text{Ab}) - 2.76\ (\text{An})$$

$$\text{Biaxial}\ (+\ \text{or}\ -)$$

$$n_\alpha = 1.527 - 1.577$$

$$n_\beta = 1.531 - 1.585$$

$$n_\gamma = 1.534 - 1.590$$

$$\delta = 0.007 - 0.013$$

$$2V_x = 45 - 102^\circ\ (\text{high plagioclase})$$

$$2V_x = 75 - 102^\circ\ (\text{low plagioclase})$$

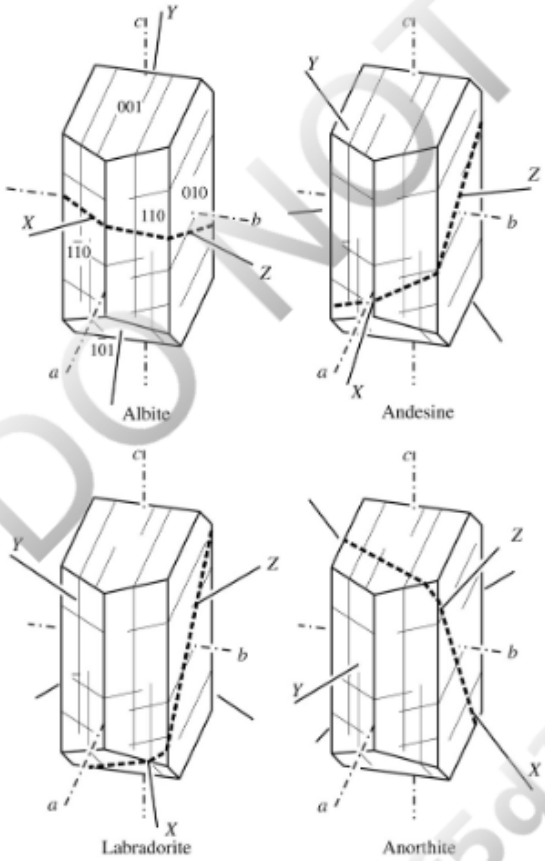

Form and Twinning Plagioclase occurs commonly as both euhedral and anhedral grains (**Figure 12.12**). As most plagioclase crystallizes in the monoclinic system, but converts to triclinic upon cooling, crystals typically appear monoclinic, hence the pseudomonoclinic symmetry descriptor listed above. Crystals are tabular parallel to {010} and elongate parallel to the *c* or *a* axis. Cross sections are more or less rectangular. Cleavelandite is a variety of albite that forms very platy crystals parallel to {010}.

(*a*)

DO NOT COPY e48d507df5d1141@placeholder.9409

Printed by: e48d507df5d1141@placeholder.94092.edu. Printing is for personal, private use only. No part of this book may be reproduced or transmitted without publisher's prior permission. Violators will be prosecuted.

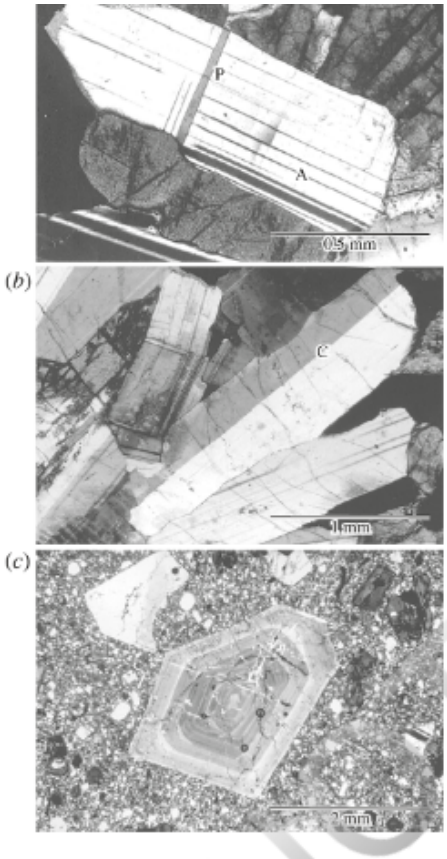

FIGURE 12.12 Plagioclase in thin section. Cross-polarized light. (*a*) Albite twin lamellae (A) extend NW–SE, and pericline twin lamellae (P) extend NE–SW. (*b*) Large grain in the center displays a Carlsbad twin (C) that divides the grain into right and left portions. (*c*) Phenocryst with oscillatory zoning. View larger image

Chemical zoning is common, particularly in volcanics and shallow intrusions, and is identified by a variation in the extinction angle from one zone to another. Zoning is considered normal if it changes smoothly from a more calcic core to a more sodic rim; the core usually has a larger extinction angle. Reverse zoning is the opposite. Oscillatory zoning involves a rhythmic alternation between calcic and sodic zones usually superimposed on an overall trend from a more calcic core to a more sodic rim (Chapter 5).

Twinning is very common. Polysynthetic albite {010} and pericline [010] twins are present in most grains, provided they are sufficiently large. In hand sample the systematic alternation of albite twin lamellae may be recognized by what appear to be fine striations on basal {001} cleavage surfaces. In thin section, albite twins are recognized by parallel lamellae that may be cut at intervals with pericline twin lamellae at a high angle. Carlsbad twins [001] are also quite common in igneous rocks, but are not reported in metamorphic rocks. Manebach {001} and Baveno {021} twins are less common.

Cleavage Basal {001} cleavage is perfect and {010} cleavage is good. They intersect at an angle of 93–94°. A poor cleavage on {110} is not normally seen in either hand sample or thin section. Cleavage tends to control fragment orientation in grain mounts. In thin

Printed by: e48d507df5d1141@placeholder.94092.edu. Printing is for personal, private use only. No part of this book may be reproduced or transmitted without publisher's prior permission. Violators will be prosecuted.

section, the cleavage may not be obvious unless the aperture diaphragm is stopped down to emphasize what little relief there is, and is most noticeable along the sample's edge where stress associated with slide preparation is more likely to fracture grains. Conchoidal to uneven fracture. Brittle.

Color Properties

Luster: Vitreous; chatoyant varieties may be pearly.

Color: White and gray are most common, also bluish, greenish, yellowish, or reddish. Varieties called moonstone display a beautiful chatoyance or iridescence related to peristerite, Bøggild, or Huttenlocher intergrowths.

Streak: White.

Color in Thin Section: Colorless in thin section and grain mount. Some may be clouded because of partial alteration to sericite or clay or may appear pale reddish, brownish, or gray because of fine Fe–Ti oxide inclusions.

Pleochroism: None.

Optical Characteristics

Relief in Thin Section: Low positive or negative.

Optic Orientation: Varies systematically with composition and provides the basis for several techniques of determining the composition. Indicatrix axes and crystal axes do not coincide, so extinction is inclined to crystal faces and cleavage traces in most orientations.

Indices of Refraction and Birefringence: Indices of refraction increase systematically with Ca content (**Figure 12.13**), and if measured accurately, can provide a useful estimate of composition. Birefringence varies between 0.007 and 0.013, but the change is too small to be of use in estimating composition. Maximum interference colors in thin section are usually first-order gray or white. Only for very calcic plagioclase will first-order yellow colors be seen.

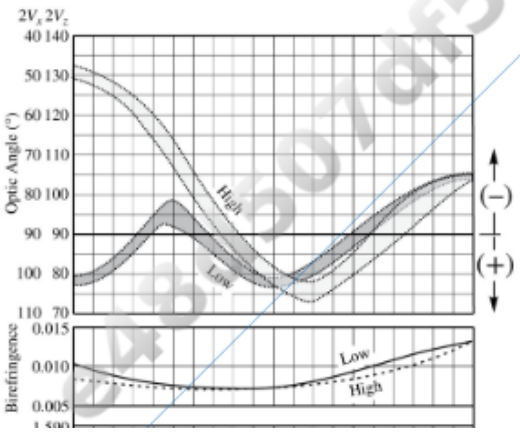

DO NOT COPY

Printed by: e48d507df5d1141@placeholder.94092.edu. Printing is for personal, private use only. No part of this book may be reproduced or transmitted without publisher's prior permission. Violators will be prosecuted.

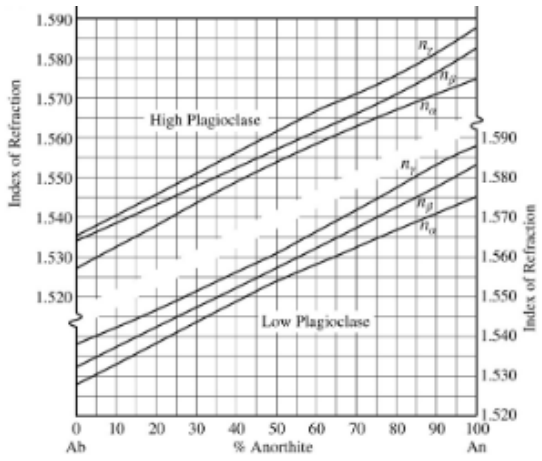

FIGURE 12.13 Optical properties of low (plutonic) and high (volcanic) plagioclase. Adapted from Smith (1958) and Burri and others (1967). View larger image

Interference Figure: $2V$ varies systematically with composition (Figure 12.13), but has a distinctly different pattern for high and low varieties. The $2V$ angle by itself cannot be used to estimate composition, but it may be used to resolve ambiguity in other techniques. Fine lamellar twinning or exsolution may make usable figures difficult to obtain in some cases. Optic axis dispersion is weak, usually $v > r$, but also $r > v$.

Alteration Plagioclase is commonly partly altered to sericite (fine-grained white mica), clay, or zeolites. Alteration may be uniformly distributed or may be concentrated along twin lamellae or in the core of grains. Other alteration products include scapolite, calcite, pyrophyllite, and sausserite (a fine-grained aggregate of epidote group minerals, albite, sericite, and other minerals).

Distinguishing Features

Hand Sample: Hardness and cleavage distinguish feldspars from other silicates. Striations produced by albite twinning and seen on the perfect {001} cleavage surfaces distinguish plagioclase from alkali feldspar. Striations are usually obvious on large unaltered samples, and for smaller grains, careful examination with a hand lens while moving and rotating the sample to get light to reflect from cleavage surfaces will usually reveal the striations. In mafic igneous rocks with abundant dark pyroxene, plagioclase may appear dark colored or black, except on weathered surfaces where grains often appear white or gray. In coarse-grained igneous rocks that contain both plagioclase and alkali feldspar, the plagioclase may be white or gray, and the alkali feldspar pale pink, though not always. In felsic gneisses, plagioclase typically forms white or gray anhedral grains and may be difficult to distinguish from alkali feldspar. Careful examination with a hand lens may reveal the striations on plagioclase cleavage surfaces. In clastic sediments, plagioclase typically forms equant white/gray grains with cleavage. Weathered/altered grains appear chalky.

Thin Section/Grain Mount: Low relief, lack of color, biaxial character, and polysynthetic twinning distinguish plagioclase from most other silicates. Cordierite may display similar

DO NOT COPY

Printed by: e48d507df5d1141@placeholder.94092.edu. Printing is for personal, private use only. No part of this book may be reproduced or transmitted without publisher's prior permission. Violators will be prosecuted.

twinning, but it alters to pinite (see cordierite entry, Chapter 15), and the twins may display a radial pattern in certain orientations. Cordierite also commonly contains pleochroic halos around radioactive inclusions such as zircon, and it has less obvious cleavage. Untwinned plagioclase, particularly in low-grade pelitic metamorphic rocks, may resemble quartz and can easily be overlooked. However, quartz is uniaxial, lacks cleavage, and usually lacks the incipient alteration or cloudiness common in plagioclase. Microcline twins with the same twin laws as plagioclase but the albite and pericline twin lamellae in microcline are irregular, fuzzy, and tend to pinch and swell, forming a "tartan plaid" pattern (see Figure 12.20b). In many volcanic rocks, plagioclase in the groundmass forms very small grains called microlites. The microlites typically are elongate along the *a* axis and may be too small to reveal albite or pericline twinning.

A number of staining techniques have been developed to aid with rapid hand-sample and thin section identification of plagioclase, alkali feldspar, and other minerals with similar appearance (e.g., Bailey and Stevens, 1960; Ruperto and others, 1964; Boone and Wheeler, 1968; and Haughton, 1980). Feldspar staining techniques have fallen out of favor for simple mineral identification because the required materials are highly hazardous, and a variety of analytical instrument or other techniques can fairly quickly and easily aid in identification.

Determining Composition It is not possible in hand sample to determine composition, but plausible guesses can be made based on the rock type in which the plagioclase is found (**Table 12.5**). Several optical techniques have been developed to allow composition to be estimated to within a few percent anorthite. If knowledge of composition is important, optical techniques should be supplemented with various analytical techniques such as electron microprobe (Chapter 9).

TABLE 12.5 Plagioclase Composition in Common Igneous Rock Types

Rock Type	Plagioclase Composition
Felsic (granitic pegmatite/granite/rhyolite/granodiorite/dacite/etc.)	Albite or oligoclase
Intermediate (andesite/diorite and related)	Andesine
Mafic (basalt/gabbro and related)	Labradorite

Grain Mount: The most accurate method depends on measurement of n_α, n_β, and n_γ and comparison with Figure 12.13. However, cleavage tends to control fragment orientation, making it difficult to find grains in appropriate orientations. The Tsuboi method works around this problem and can accurately determine the composition for plutonic plagioclase. To use the Tsuboi method, proceed as follows.

- Prepare a grain mount of crushed plagioclase (Chapter 10).
- By examination, select a fragment lying on either cleavage surface; it does not matter which.

Printed by: e48d507df5d1141@placeholder.94092.edu. Printing is for personal, private use only. No part of this book may be reproduced or transmitted without publisher's prior permission. Violators will be prosecuted.

matter which.

- Cross the polarizers and rotate the grain to extinction with the fast ray parallel to the lower polarizer vibration direction. Use the accessory plate to determine which ray is fast (Chapter 7).
- In plane light, compare the index of refraction n'_α with the index of refraction of the oil.
- Repeat, using different immersion oils, until a match is obtained.
- Use **Figure 12.14** to determine the composition. If n'_α is measured to an accuracy of ±0.001, accuracy of ±1 percent An content is possible in the range An_{20} to An_{60}, and ±3 percent An outside that range. The accuracy for volcanic rocks is probably no better than ±5 percent An. A significant complication is that plagioclase often is chemically zoned, so grains from a crushed sample of a single crystal may contain a range of compositions.

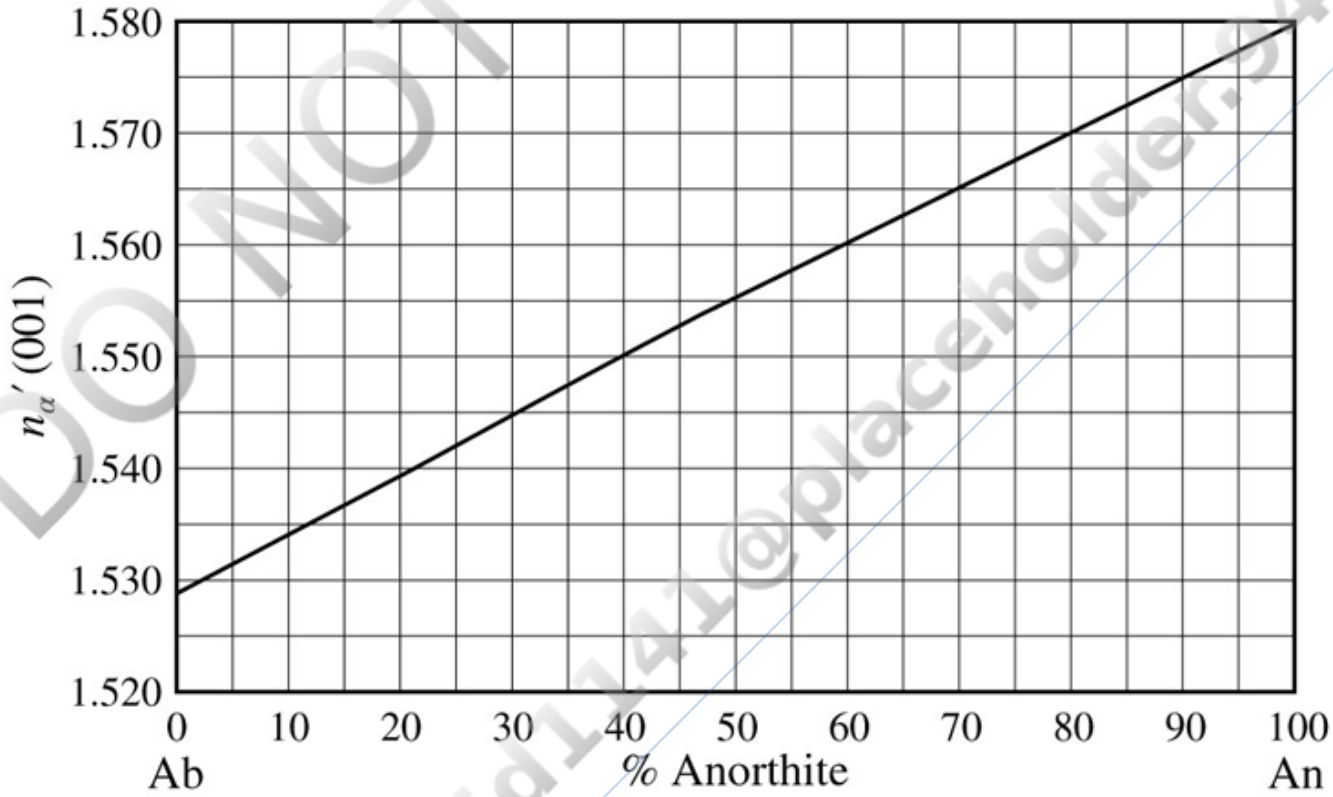

FIGURE 12.14 Index of refraction of the fast ray (n'_α) for plagioclase fragments lying on cleavages. The diagram is constructed for fragments on (001) cleavage surfaces but also may be used for fragments on (010) cleavage surfaces. After Morse (1968). View larger image

Thin Section: The **Michel-Lévy** and **Carlsbad-albite** methods are used to determine the composition of plagioclase in thin section. They depend on the fact that optical orientation of plagioclase varies systematically with composition. Both methods involve measurement of extinction angles to the trace of the {010} composition plane of albite twin lamellae, and require selection of grains oriented so that the {010} crystallographic plane is vertical (i.e., the *b* crystal axis is horizontal).

DO NOT COPY e48d507df5d1141@placeholder.94092

Printed by: e48d507df5d1141@placeholder.94092.edu. Printing is for personal, private use only. No part of this book may be reproduced or transmitted without publisher's prior permission. Violators will be prosecuted.

plane is vertical (i.e., the *b* crystal axis is horizontal).

The Michel-Lévy method requires measurement of a half-dozen or more grains in the sample to find a maximum value of the extinction angle between {010} and the trace of the fast ray vibration direction. A number of grains must be measured because the extinction angle varies depending on grain orientation and it is necessary to find a grain in the correct orientation to yield the maximum extinction angle. To use the Michel-Lévy method (**Figure 12.15**), proceed as follows.

1. Scan the slide to find a grain with the {010} composition plane between albite twin lamellae vertical. Usable grains have the following characteristics.
   - Composition planes between lamellae are crisp and sharp. If {010} is inclined significantly, the lamellae will be fuzzy and the position of the boundaries will shift laterally when focus is raised and lowered while viewed with the high-power objective.
   - All twin lamellae have essentially the same interference color between crossed polarizers when placed parallel to the N–S and in the 45° position. If the two sets of lamellae have different interference colors, either {010} is not vertical or the twins are pericline twins. If the grain is divided in half so lamellae on one side are all one color and lamellae on the other half are a different color, the boundary between the two sides is a Carlsbad twin and the Carlsbad–albite method should be used.
2. Between crossed polarizers, start with the composition plane between twin lamellae parallel to N–S. Rotate clockwise to bring one set of lamellae to extinction and record the extinction angle a_1. Return the composition plane to N–S, then rotate counterclockwise to bring the other set of lamellae to extinction and record the extinction angle a_2. If the two extinction angles differ by 4° or less, record their average. If the two extinction angles differ by more than 4°, discard the readings and find a new grain to measure because {010} is not vertical. In most cases, the extinction angle between the trace of {010} and the fast ray vibration direction is less than 45°, but for calcic plagioclase, it may be larger. To identify the fast ray vibration direction within one set of lamellae, begin by rotating the grain to bring those lamellae to extinction. Then rotate 45° clockwise from the extinction position and insert the gypsum plate (slow NE–SW). If the retardations in the lamellae in question subtract (usually to produce first-order yellow), then the fast ray in those lamellae was correctly placed N–S at extinction. If the colors increase (usually to second-order blue), the slow ray was N–S in the extinction position, and rotation in the opposite direction is needed to bring the fast ray vibration direction in the set of lamellae N–S in the extinction position.
3. Repeat for a half-dozen or more grains (more is better). Because only the maximum average extinction angle is useful, time can be saved by quickly moving on if the first angle measured on a grain is less than the largest average measurement taken on other grains.
4. The composition is determined from **Figure 12.16**. The maximum average

DO NOT COPY

Printed by: e48d507df5d1141@placeholder.94092.edu. Printing is for personal, private use only. No part of this book may be reproduced or transmitted without publisher's prior permission. Violators will be prosecuted.

1. Scan the slide to find a grain with the {010} composition plane between albite twin lamellae vertical. Usable grains have the following characteristics.
   - Composition planes between lamellae are crisp and sharp. If {010} is inclined significantly, the lamellae will be fuzzy and the position of the boundaries will shift laterally when focus is raised and lowered while viewed with the high-power objective.
   - All twin lamellae have essentially the same interference color between crossed polarizers when placed parallel to the N–S and in the 45° position. If the two sets of lamellae have different interference colors, either {010} is not vertical or the twins are pericline twins. If the grain is divided in half so lamellae on one side are all one color and lamellae on the other half are a different color, the boundary between the two sides is a Carlsbad twin and the Carlsbad–albite method should be used.
2. Between crossed polarizers, start with the composition plane between twin lamellae parallel to N–S. Rotate clockwise to bring one set of lamellae to extinction and record the extinction angle a_1. Return the composition plane to N–S, then rotate counterclockwise to bring the other set of lamellae to extinction and record the extinction angle a_2. If the two extinction angles differ by 4° or less, record their average. If the two extinction angles differ by more than 4°, discard the readings and find a new grain to measure because {010} is not vertical. In most cases, the extinction angle between the trace of {010} and the fast ray vibration direction is less than 45°, but for calcic plagioclase, it may be larger. To identify the fast ray vibration direction within one set of lamellae, begin by rotating the grain to bring those lamellae to extinction. Then rotate 45° clockwise from the extinction position and insert the gypsum plate (slow NE–SW). If the retardations in the lamellae in question subtract (usually to produce first-order yellow), then the fast ray in those lamellae was correctly placed N–S at extinction. If the colors increase (usually to second-order blue), the slow ray was N–S in the extinction position, and rotation in the opposite direction is needed to bring the fast ray vibration direction in the set of lamellae N–S in the extinction position.
3. Repeat for a half-dozen or more grains (more is better). Because only the maximum average extinction angle is useful, time can be saved by quickly moving on if the first angle measured on a grain is less than the largest average measurement taken on other grains.
4. The composition is determined from **Figure 12.16**. The maximum average extinction angle is plotted on the vertical axis; composition is plotted along the horizontal axis. Different curves are provided for high (volcanic) and low (plutonic) plagioclase. For angles less than about 18°, the curves indicate two possible compositions: one less than An_{20} (plutonic) or An_{12} (volcanic) and the other higher. The distinction between the two possibilities can be made based on indices of refraction and optic sign (Figure 12.13).

DO NOT COPY

Printed by: e48d507df5d1141@placeholder.94092.edu. Printing is for personal, private use only. No part of this book may be reproduced or transmitted without publisher's prior permission. Violators will be prosecuted.

$$\mathrm{An}_0 - \mathrm{An}_{20} : \text{Optically } (+), n_a < 1.538$$
$$\mathrm{An}_{20} - \mathrm{An}_{35} : \text{Optically } (-), n_a > 1.538$$

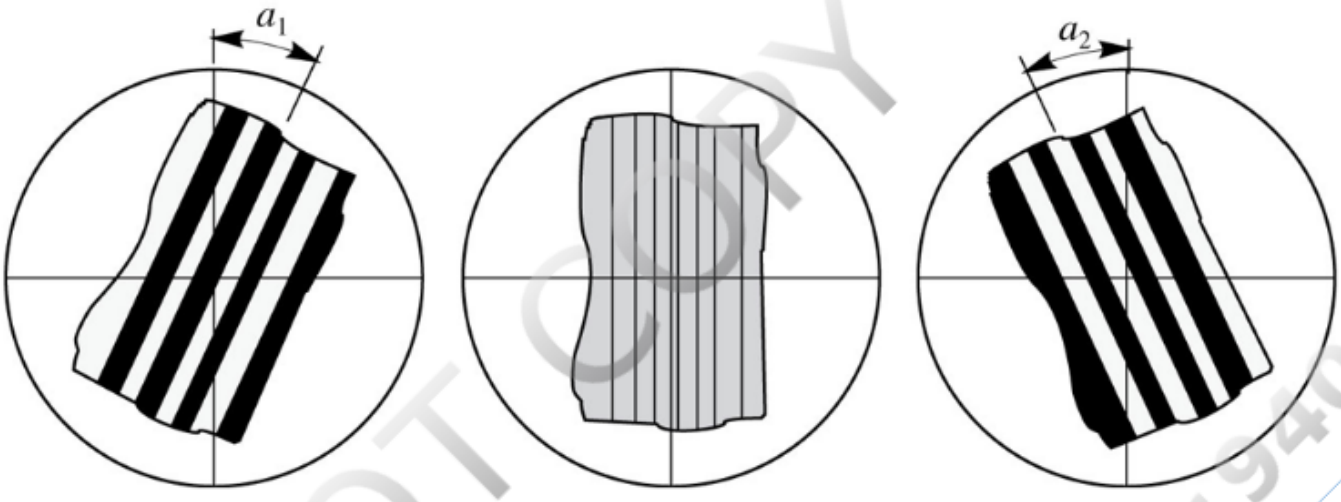

FIGURE 12.15 Michel-Lévy method. Extinction angles a_1 and a_2 are measured to the fast ray vibration direction in their respective sets of albite twin lamellae. The two angles are averaged. A half-dozen or more grains are measured, and the largest average extinction angle is used to estimate the plagioclase composition from Figure 12.16. View larger image

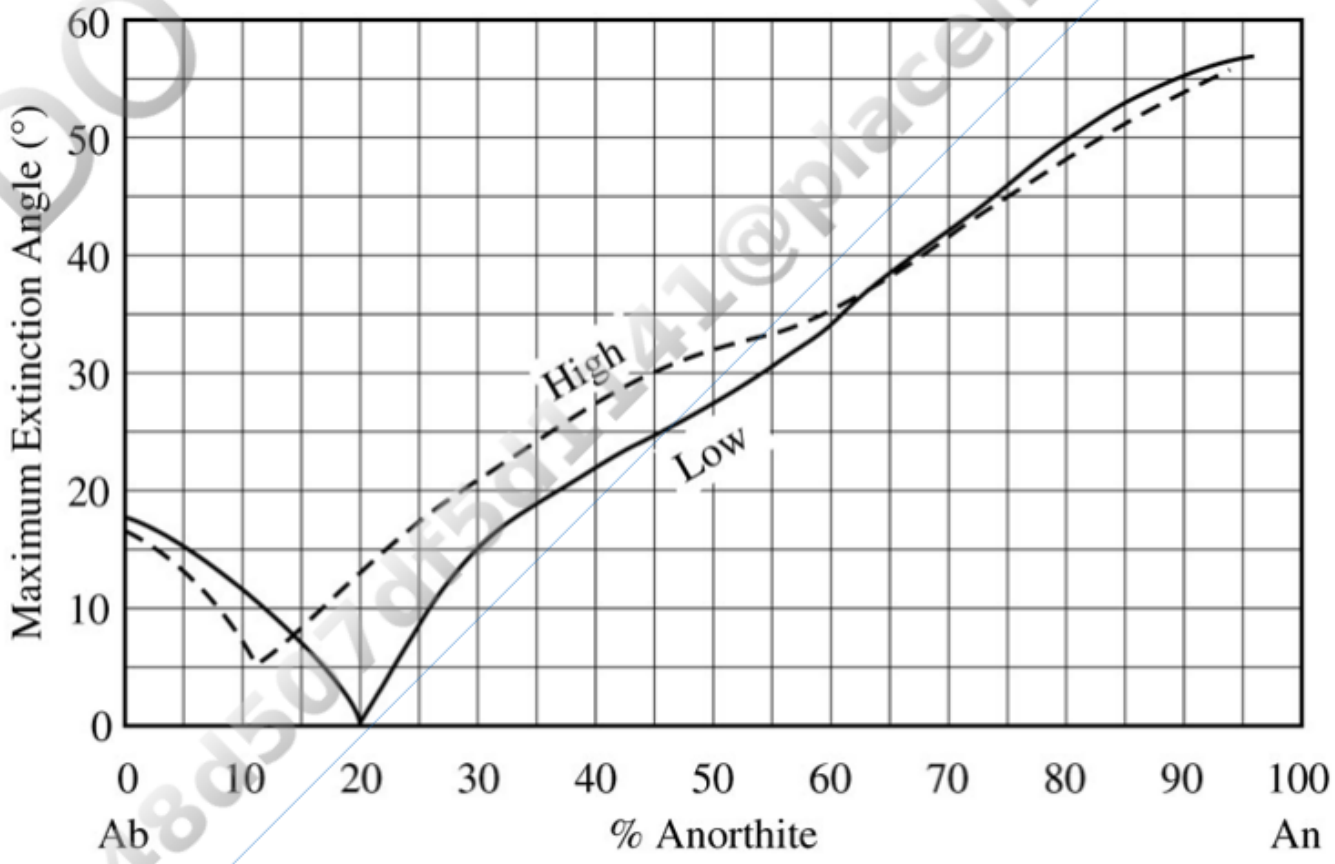

FIGURE 12.16 Diagram for use with the Michel-Lévy method. The maximum extinction angle to albite twin lamellae in sections cut perpendicular to {010} is plotted on the vertical axis:

Printed by: e48d507df5d1141@placeholder.94092.edu. Printing is for personal, private use only. No part of this book may be reproduced or transmitted without publisher's prior permission. Violators will be prosecuted.

albite twin lamellae in sections cut perpendicular to {010} is plotted on the vertical axis; composition is the horizontal axis. The dashed curve is for high (volcanic) plagioclase, and the solid curve for low (plutonic) plagioclase. See text for additional discussion. Based on curves of Tobi and Kroll (1975). View larger image

Note that 1.538 is about the same as the index of refraction of many, but not all, commonly used thin section epoxies. Provided the index of refraction of the epoxy is known to be about 1.538, the two possibilities can be distinguished by comparing n_α with n_{cement}. To do this, find a plagioclase grain with maximum birefringence whose edge is in contact with epoxy along a hole in the slide or along the edge. Rotate the stage to place the portion of the grain in contact with epoxy to an extinction position with the fast ray (n_α) vibration direction parallel to the vibration direction of the lower polarizer. Use the accessory plate to identify fast and slow ray vibration directions. Remove the upper polarizer and compare n_α with n_{cement} using the Becke line method.

Accuracy of the method for low plagioclase is roughly ±5 percent anorthite content up to about An_{60} and worse at higher An content. The accuracy is probably significantly worse with volcanic plagioclase.

The Carlsbad–albite method is closely related to the Michel-Lévy method, but only one properly oriented grain is needed to obtain a composition. The procedure is as follows (**Figure 12.17**).

1. Select a grain with both albite and Carlsbad twinning that is oriented with the {010} composition planes between albite twins vertical. Appropriately oriented grains have the following characteristics.
   - The albite twin lamellae are crisp and sharp, indicating that {010} is vertical (see Michel-Lévy method).
   - When the twin lamellae are placed in the N–S and 45° positions, the Carlsbad twin separates the grain into two segments with different interference colors, but the albite lamellae within each segment have essentially the same colors. The composition plane of the Carlsbad twin may be slightly irregular (not a straight line).
2. On the left half of the Carlsbad twin, measure the extinction angles from the albite twin lamellae to the fast ray vibration direction in each albite lamellae set as described in the Michel-Lévy method. Average the two readings provided they differ by less than 4°. If they differ by more, discard the readings and find another grain.
3. On the right half of the Carlsbad twin, measure the extinction angles from the albite twin lamellae to the fast ray vibration direction in each albite lamellae set in the same manner and average the readings. The 4° rule still applies.
4. The composition is obtained from **Figure 12.18a** for low plagioclase and **Figure 12.18b** for high plagioclase. The solid lines are for the larger of the two average extinction angles found in steps 2 and 3; the dashed line is for the smaller. The point where the two curves intersect indicates the composition, which is read from

DO NOT COPY

Printed by: e48d507df5d1141@placeholder.94092.edu. Printing is for personal, private use only. No part of this book may be reproduced or transmitted without publisher's prior permission. Violators will be prosecuted.

point where the two curves intersect indicates the composition, which is read from the bottom of the diagram. The vertical axis indicates the inclination of the *c* axis to the stage of the microscope.

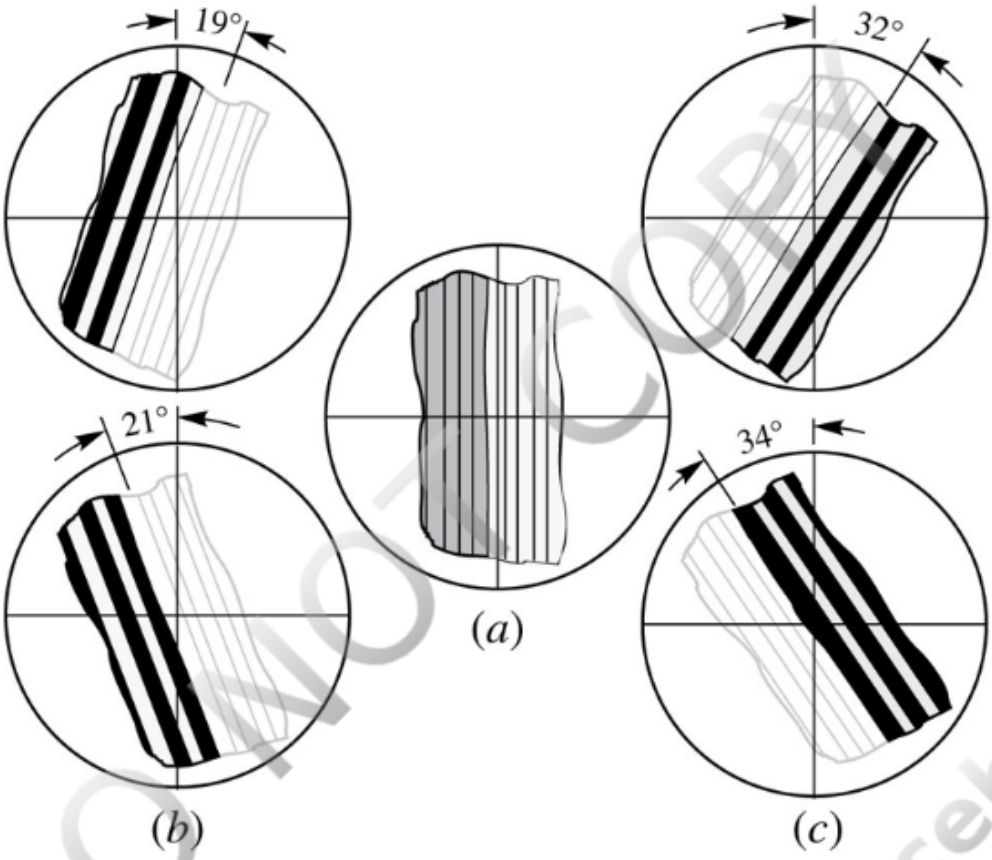

FIGURE 12.17 Carlsbad–albite method. (*a*) Grain with twin lamellae N–S between crossed polarizers. The two sides of the Carlsbad twin show different colors, but the albite lamellae within each side are uniform. (*b*) Extinction angles measured to the fast ray vibration direction in the albite lamellae on the left side of the Carlsbad twin. The average extinction angle in this case is 20°. (*c*) Extinction angles measured to the fast ray vibration direction in the albite lamellae on the right side of the Carlsbad twin. The average extinction angle in this case is 33°. The composition of the plagioclase (An_{60}) is determined from Figure 12.18a. View larger image

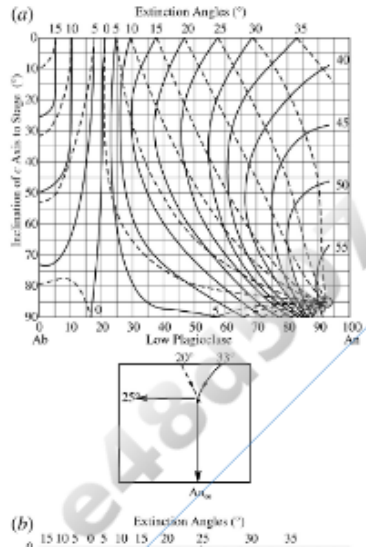

Printed by: e48d507df5d1141@placeholder.94092.edu. Printing is for personal, private use only. No part of this book may be reproduced or transmitted without publisher's prior permission. Violators will be prosecuted.

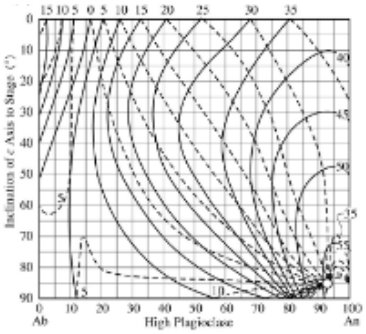

FIGURE 12.18 Diagrams for use with the Carlsbad–albite method. Solid lines are for the larger extinction angle, and dashed lines for the smaller extinction angle (Figure 12.17). See text for additional discussion. (*a*) Low plagioclase. A composition of An_{60} is indicated for a smaller extinction angle of 20° and a larger angle of 33°, and the *c* axis of the grain is inclined 25° from the microscope stage. (*b*) High plagioclase. From Tobi and Kroll (1975). View larger image

For extinction angles less than about 20°, there are two or three sets of curves, so the same set of readings may produce several intersections, indicating several possible compositions. For example, with high plagioclase, if the smaller average extinction angle is 10° and the larger is 15°, intersections can be found at An_1 (upper left), An_{29} (top at left center), and An_{66} (bottom at right center), but only one is correct. For relatively albite-rich compositions, the ambiguity is resolved in the same way described for the Michel-Lévy method. For more calcic possibilities, additional grains can be measured to determine which is correct.

Occurrence Plagioclase is the most common and abundant mineral group in the Earth's crust. As described in Chapter 11, it is abundant in many igneous and metamorphic rocks and is common as a detrital mineral in many sedimentary rocks. The plagioclase compositions found in common igneous rocks are listed in Table 12.5. The plagioclase in pelitic metamorphic rocks is usually albite if subjected to relatively low-grade metamorphism and oligoclase or andesine in medium- and high-grade environments. Fairly pure anorthite may be found in metamorphosed carbonates and amphibolite.

In sedimentary rocks, plagioclase occurs as detrital grains, but it will likely be cloudy etc. from the effects of weathering and diagenetic processes.

Use Aggregate commonly contains plagioclase. Plagioclase also is a major constituent in many of the rocks that are cut and polished to make countertops, facing stone for buildings, and headstones. Plagioclase may also be used in powdered form as a filler in paint, plastic, and rubber, and in the manufacture of glass and ceramics. Although not currently economic, plagioclase, in the form of large intrusive bodies of anorthosite, has the potential to be a significant source of aluminum.

Alkali Feldspar

$$(K, Na)\,AlSi_3\,O_8$$

Printed by: e48d507df5d1141@placeholder.94092.edu. Printing is for personal, private use only. No part of this book may be reproduced or transmitted without publisher's prior permission. Violators will be prosecuted.

$$H = 6 - 6.5$$

$$G = 2.55 - 2.63$$

Sanidine, Orthoclase, Microcline, Adularia

Biaxial (−)

$$n_\alpha = 1.514 - 1.526$$

$$n_\beta = 1.518 - 1.530$$

$$n_\gamma = 1.521 - 1.533$$

$$\delta = 0.005 - 0.008$$

$$2V_x = \text{See individual descriptions.}$$

Anorthoclase

Biaxial (−)

$$n_\alpha = 1.519 - 1.529$$

$$n_\beta = 1.524 - 1.534$$

$$n_\gamma = 1.527 - 1.536$$

$$\delta = 0.005 - 0.008$$

$$2V_x = 42 - 52^\circ$$

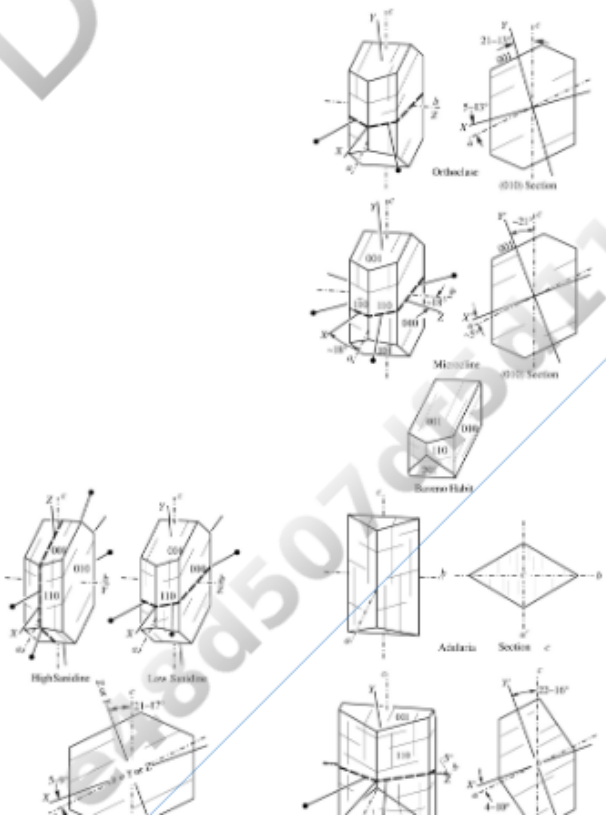

DO NOT COPY

e48d507df5d1141@placeholder.9409

Printed by: e48d507df5d1141@placeholder.94092.edu. Printing is for personal, private use only. No part of this book may be reproduced or transmitted without publisher's prior permission. Violators will be prosecuted.

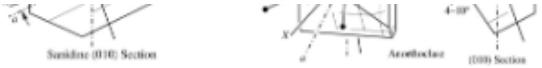

The terminology of the alkali feldspars has evolved over several centuries and is not as well defined as might be desired. The problem is that the four varieties of alkali feldspar (microcline, orthoclase, sanidine, and adularia) were originally recognized based on physical and optical properties and occurrences. These distinctions were not always built on structural or chemical considerations. We now know, for example, that much of the material traditionally identified as monoclinic orthoclase is, as has been described, triclinic, but is submicroscopically twinned so that it appears morphologically and optically monoclinic. Regardless, nothing is likely to replace the old terminology. For current purposes, the distinctions among the alkali feldspars are based on optical and physical properties as follows.

> **MICROCLINE:** Optically triclinic K-feldspar characterized by its distinctive cross-hatched twin pattern. The optic plane is nearly perpendicular to (010) and $2V_x$ is typically greater than 65°, though smaller values are possible.
>
> **ORTHOCLASE:** Optically monoclinic alkali feldspar with $2V_x$ greater than 40° and the optic plane perpendicular to (010).
>
> **LOW SANIDINE:** Optically monoclinic alkali feldspar with $2V_x$ between 0° and 40° and the optic plane perpendicular to (010).
>
> **HIGH SANIDINE:** Optically monoclinic alkali feldspar with $2V_x$ between 0° and 40° and the optic plane parallel to (010).
>
> **ADULARIA:** K-feldspar produced by authigenic or low-temperature hydrothermal processes in which the {110} prism is dominant. It is structurally similar to microcline but without the grid twinning produced by conversion from monoclinic to triclinic symmetry.
>
> **ANORTHOCLASE:** Optically triclinic sodic alkali feldspar characterized by grid twinning similar to microcline but on a finer scale, and with $2V_x$ less than 52°; found in volcanics and shallow intrusions. The composition typically lies between $Ab_{63}Ks_{27}$ and $Ab_{90}Ks_{10}$.

It turns out that $2V$ and indices of refraction in alkali feldspar vary systematically with the degree of order of Al and Si in tetrahedral sites (**Figure 12.19**). A convenient means of expressing that order is to sum the occupancy of Al in the T_1o and T_1m structural sites, which are two of the four available tetrahedral structural sites (Figure 12.7 and Table 12.4). The fraction of the T_1o site containing Al is t_1o, and the fraction of the T_1m site containing Al is t_1m. In completely disordered high sanidine, Al is equally likely to be in the T_1o and T_1m sites. Because alkali feldspar has one Al for every three Si in the tetrahedral sites, each tetrahedral site will be, on average, one-quarter occupied by Al, so $t_1o + t_1m = 0.25 + 0.25 = 0.50$. In completely ordered low microcline, all of the Al is in the T_1o site and none is in the T_1m site, so $t_1o + t_1m = 1.0 + 0 = 1.0$. Similarly, ordering according to the orthoclase model (Mode II ordering) puts all of the Al equally in the T_1o

Printed by: e48d507df5d1141@placeholder.94092.edu. Printing is for personal, private use only. No part of this book may be reproduced or transmitted without publisher's prior permission. Violators will be prosecuted.

and T_1m structural sites; each is half occupied by Al, so $t_1o + t_1m = 0.5 + 0.5 = 1.0$. This accounts for the fact that orthoclase and microcline have substantial overlap on the diagram and emphasizes the point that the nature of the ordering mechanism cannot be determined by optical and physical properties.

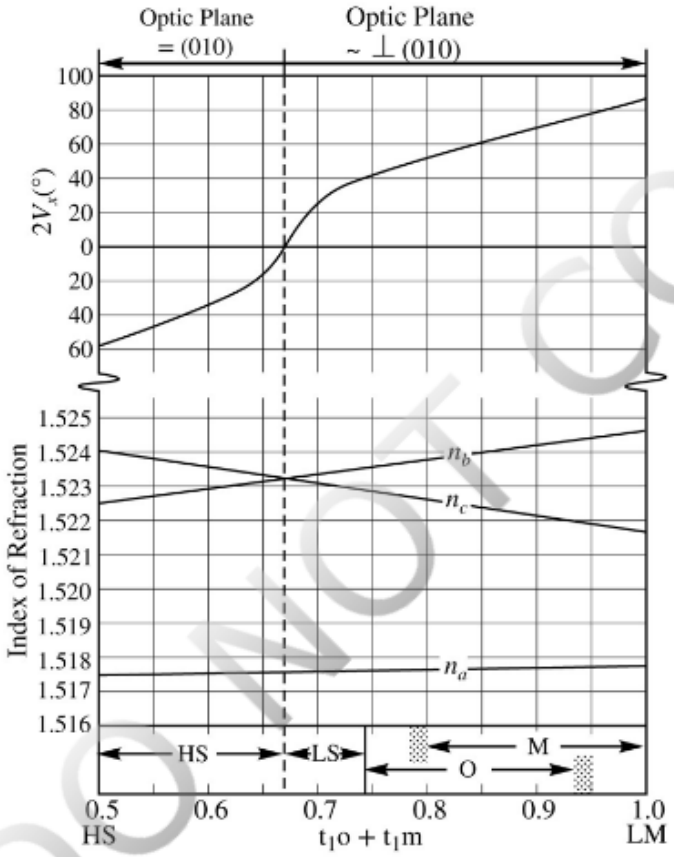

FIGURE 12.19 Variation of $2V_x$ and indices of refraction for common alkali feldspar as a function of the degree of Si–Al order. The occupancies of Al in the T_1o and T_1m tetrahedral sites are t_1o and t_1m, respectively. If Al and Si are randomly distributed among the tetrahedral sites, as in high sanidine (HS), then one-quarter of the T_1o and one-quarter of the T_1m sites are filled with Al: $t_1o + t_1m = 0.50$. If all Al is in the T_1o site, then $t_1o + t_1m = 1.00$ as in low microcline (LM). The principal indices of refraction n_a, n_b, and n_c are for light vibrating most nearly parallel to the *a*, *b*, and *c* crystal axes, respectively. The approximate ranges of high sanidine (HS), low sanidine (LS), orthoclase (O), and microcline (M) are indicated. After Su and others (1984). View larger image

Distinguishing Features in Hand Sample Cleavage at ~90°, hardness, and color distinguish feldspars from most other silicates. Lack of striations on cleavage surfaces distinguishes alkali feldspar from plagioclase, and the two commonly have somewhat different colors in the rocks in which they occur together. Close study with a hand lens while moving the sample will help reveal the cleavage surfaces; when the incident light reflects from them it may be possible to see striations, which is usually attributed to plagioclase. See, however, the discussion of anorthoclase above and below. Further, a lack of observed striations with a hand lens should not be used as definitive evidence the specimen is alkali feldspar, as striations may be difficult to see. Presence of exsolution lamellae, at any scale, however, does universally indicate the feldspar is alkali feldspar, but not all alkali feldspar exsolve. Associated quartz usually is gray and glassy without

DO NOT COPY e48d507df5d1141@placeholder.9409

Printed by: e48d507df5d1141@placeholder.94092.edu. Printing is for personal, private use only. No part of this book may be reproduced or transmitted without publisher's prior permission. Violators will be prosecuted.

but not all alkali feldspar exsolve. Associated quartz usually is gray and glassy without cleavage.

The different varieties of alkali feldspar cannot reliably be distinguished in hand sample. It is often best to use the generic term *alkali feldspar* for all varieties until optical, X-ray, or other techniques provide additional information. However, geological occurrence and selected properties can provide guidance as to which variety is most likely. Clear alkali feldspar phenocrysts in volcanics and shallow intrusions are usually sanidine. Phenocrysts and groundmass grains of microcline and orthoclase usually appear white or pink in intermediate and deep intrusions. Amazonite is a variety of K-feldspar that ranges in color from blue to green; it is almost always microcline. Alkali feldspar in regional metamorphic rocks is usually microcline—the pink color may be present in felsic gneisses and related rocks, but not always. The feldspar in immature sediments reflects the nature of the provenance; plagioclase is slightly more susceptible to weathering than alkali feldspar, and weathered feldspar may be white or chalky. If visible, exsolution lamellae indicate alkali feldspar, which is most likely microcline hosted. Many sedimentary grains are too small to allow the criteria listed above to be useful, but mounting sediment in epoxy such that a thin section could be produced, or polishing for use with a scanning electron microscope or election microprobe, could provide the data needed for identification.

Use Alkali feldspar, like plagioclase, is a major mineral in many of the rock types used as aggregate and dimension stone. Its industrial uses are in glassmaking and in the manufacture of ceramics including dinnerware, floor tiles, plumbing fixtures, and electrical insulators. Alkali feldspar also is used, in powdered form, as a filler in products including paints, plastic, and rubber. Its only legitimate medical use is in dental ceramics; historically, however, alkali feldspar has been used to treat bladder and kidney problems.

Microcline

Triclinic $\overline{1}$ (pseudomonoclinic)

$$a = 8.578\ \text{Å},\ b = 12.960\ \text{Å},\ c = 7.211\ \text{Å},$$
$$\alpha = 90.65^\circ,\ \beta = 115.96^\circ,\ \gamma = 87.65^\circ,\ Z = 4$$
$$2V_x = \text{-}65 - 88^\circ$$

Form and Twinning Figure 12.20a-b shows examples of microcline. Microcline is common as anhedral and euhedral grains in many igneous and metamorphic rocks. Crystals are elongate parallel to *c* and tabular parallel to the {010} form, or may display the Baveno habit, which is elongate parallel to *a*. {201} faces may be common, but are only shown on the Baveno habit crystal model diagram for the alkali feldspars.

(a)

Printed by: e48d507df5d1141@placeholder.94092.edu. Printing is for personal, private use only. No part of this book may be reproduced or transmitted without publisher's prior permission. Violators will be prosecuted.

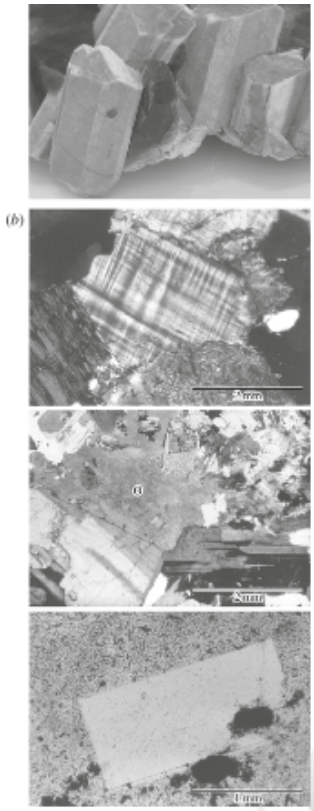

FIGURE 12.20 Alkali feldspar. (*a*) Perthitic microcline crystals with quartz (dark). (*b*) Photomicrographs. (*Top*) Thin section of granite showing microcline with "tartan plaid" albite and pericline twinning. Crossed polarizers. (*Middle*) Orthoclase (O) in granite. Crossed polarizers. (*Bottom*) Sanidine phenocryst in rhyolite. Plane light. View larger image

Polysynthetic twins according to the albite and pericline laws are characteristic of microcline that has inverted from monoclinic symmetry and produces a distinctive cross-hatched or "tartan plaid" pattern seen in thin section. The contacts between lamellae are diffuse, and the lamellae appear to pinch and swell, and are discontinuous. The composition plane for the albite twins is {010}. The composition plane for the pericline twins contains the *b* axis and is commonly inclined about 35° to {010} and may be as close as 12°. Carlsbad twins are also common, particularly in phenocrysts from igneous rocks. Baveno, Manebach, and other twins also occur. The polysynthetic twins are not evident in hand sample.

Cleavage Perfect on {001} and good on {010} at an angle of ~90.6°. Uneven fracture. Brittle.

Color Properties

Luster: Vitreous.

Color: White, pink, and salmon red are most common, also pale yellow. The blue and green color of amazonite requires small amounts of both Pb and water. High-energy radiation from either a natural or laboratory source is then needed to form the color centers. Heating destroys the color centers and re-irradiation returns them. If samples are heated above about 500°C long enough to drive off the water, radiation cannot form

DO NOT COPY e48d507df5d1141@placeholder.9409

Printed by: e48d507df5d1141@placeholder.94092.edu. Printing is for personal, private use only. No part of this book may be reproduced or transmitted without publisher's prior permission. Violators will be prosecuted.

are heated above about 500°C long enough to drive off the water, radiation cannot form the color centers and the color is permanently lost.

Streak: White.

Color in Thin Section: Colorless.

Pleochroism: None.

Optical Characteristics

Relief in Thin Section: Low negative.

Optic Orientation: $X \wedge a$ 18°, $Y \wedge c$ 18°, $Z \wedge b$ 18°.

Indices of Refraction and Birefringence: Fully ordered low microcline has indices of refraction $n_\alpha = 1.518$, $n_\beta = 1.522$, $n_\gamma = 1.525$, and the indices appear to vary systematically with degree of Al/Si order (Figure 12.19). Birefringence is usually about 0.007, so interference colors are no higher than first-order white in standard thin sections.

Interference Figure: Biaxial negative with $2V$ usually greater than about 65°, most often 70–85°, but as small as 35° is possible. Optic axis dispersion is weak; $r > v$. Twinning may make good interference figures difficult to obtain. Fragments on cleavage surfaces yield strongly off-center figures.

Alteration Microcline is commonly altered to sericite and clay.

Distinguishing Features

Hand Sample: See alkali feldspar introductory material earlier in the chapter.

Thin Section/Grain Mount: The "tartan plaid" twinning pattern is characteristic. Unlike plagioclase, the twin lamellae typically have fuzzy boundaries and tend to pinch and swell irregularly.

Occurrence Microcline is commonly found in granite, granodiorite, syenite, granitic pegmatite, and related plutonic igneous rocks, and in fairly high-grade pelitic metamorphic rocks. It is not found in volcanic rocks except as part of a xenolith.

Because microcline is fairly stable in the weathering environment, it is a common constituent of detrital sedimentary rocks. It is not uncommon for overgrowths of authigenic K-feldspar to develop on detrital grains.

Orthoclase

Monoclinic $2/m$

DO NOT COPY e48d507df5d1141@placeholder.9409

Printed by: e48d507df5d1141@placeholder.94092.edu. Printing is for personal, private use only. No part of this book may be reproduced or transmitted without publisher's prior permission. Violators will be prosecuted.

$$a = 8.563\ \text{Å},\ b = 12.963\ \text{Å},\ c = 7.299\ \text{Å},$$
$$\beta = 116.07^{\circ},\ Z = 4$$

$$2V_x\ = 40 - \text{-}\ 70^{\circ}$$

Form and Twinning Orthoclase is common as anhedral and euhedral grains in felsic igneous rocks (Figure 12.20). Crystals are elongate parallel to *c* with the {010} form prominent, or may display the Baveno habit, which is elongate parallel to *a*. {201} faces may be common, but are only shown in the microcline Baveno habit diagram of the alkali feldspar crystal models. Some orthoclase may show exsolution lamellae, and most have lamellae at a submicroscopic scale.

Carlsbad twins are common, particularly in phenocrysts found in igneous rocks. Baveno and Manebach twins are less common. Polysynthetic albite and pericline twins are not visible.

Cleavage Perfect cleavage on {001} and good cleavage on {010} intersect at 90°. Uneven to conchoidal fracture. Brittle.

Color Properties

Luster: Vitreous.

Color: White, gray, pink, pale yellow; may display schiller or opalescence; infrequently blue or green.

Streak: White.

Color in Thin Section: Colorless.

Pleochroism: None.

Optical Characteristics

Relief in Thin Section: Low negative.

Optic Orientation: $X \wedge a$ =+5° to +13°, $Y \wedge c$ = +21° to +13 °, $Z = b$.

Indices of Refraction and Birefringence: Indices of refraction vary in a small range with degree of Al/Si order (Figure 12.19). An increase in Na content produces a slight increase in indices of refraction, but the degree of Al/Si ordering is more important. Birefringence is low (~0.007), so interference colors in standard thin section are no higher than first-order white.

Interference Figure: $2V_x$ varies systematically with degree of Al/Si order (Figure 12.19) and increases slightly with Na content. The convention adopted here is to use $2V_x = 40°$ as the dividing line between orthoclase and low sanidine. Orthoclase may have a $2V$ angle as large as 85°, but it is usually less than 70°. Fragments lying on {001} and {010}

DO NOT COPY e48d507df5d1141@placeholder.9409

Printed by: e48d507df5d1141@placeholder.94092.edu. Printing is for personal, private use only. No part of this book may be reproduced or transmitted without publisher's prior permission. Violators will be prosecuted.

cleavages yield off-center obtuse bisectrix and flash figures, respectively. Optic axis dispersion is $r > v$.

Comments: Orthoclase commonly displays a slight cloudiness produced by minor alteration.

Alteration The common alteration products are sericite and clay.

Distinguishing Features

Hand Sample: See alkali feldspar introductory material earlier in the chapter.

Thin Section/Grain Mount: Lack of polysynthetic twins as either striations seen in hand sample or those seen in thin section distinguishes orthoclase from plagioclase and microcline, and the $2V$ angle and optic orientation distinguish it from sanidine. Anhedral orthoclase is readily mistaken for quartz, but orthoclase has negative relief in standard thin section, has cleavage, is biaxial, and often displays a slight cloudiness.

Occurrence Orthoclase is very common in granite, granodiorite, syenite, and related felsic rocks, particularly in shallow intrusions. Sanidine is more common in volcanic rocks, and microcline is more common in deep intrusions. Orthoclase also is found in contact and regional metamorphic rocks, and as detrital grains in clastic sediments.

Sanidine

Monoclinic $2/m$

$$a = 8.603\ \text{Å},\ b = 13.036\ \text{Å},\ c = 7.174\ \text{Å},$$
$$\beta = 116.03^\circ,\ Z = 4$$
$$2V_x = 0 - 40^\circ\ [\text{OP} \perp (010)]\ 0 - 47^\circ\ [\text{OP}\ ||(010)]$$

Form and Twinning Sanidine is common as phenocrysts that are tabular parallel to {010} and somewhat elongate parallel to *a* (Figure 12.20). Larger crystals tend to be elongate parallel to *c*. {201} faces may be common, but are only shown in the microcline Baveno habit crystal models diagram for the alkali feldspars. Cross sections tend to be square, rectangular, or six sided. Acicular crystals are common in felsic volcanic glass and in **spherulites**, sphere-shaped radiating masses of crystal produced by glass devitrification. Zoning, expressed as variation in birefringence, is fairly common. Twinning according to the Carlsbad law, which divides crystals into two segments, is common; Baveno and Manebach twins are less common.

Cleavage Perfect cleavage on {001} and good cleavage on {010} intersect at right angles. Fragments tend to lie on cleavage surfaces. Uneven to conchoidal fracture. Brittle.

Color Properties

DO NOT COPY e48d507df5d1141@placeholder.9409

Printed by: e48d507df5d1141@placeholder.94092.edu. Printing is for personal, private use only. No part of this book may be reproduced or transmitted without publisher's prior permission. Violators will be prosecuted.

Color Properties

Luster: Vitreous.

Color: Colorless to white.

Streak: White.

Color in Thin Section: Colorless.

Pleochroism: None.

Optical Characteristics

Relief in Thin Section: Low negative.

Optic Orientation: Two optic orientations are possible. In high sanidine, the optic plane is parallel to {010} with $X \wedge a = +5°$, $Y = b$, and $Z \wedge c = +21°$. Low sanidine is oriented like orthoclase with the optic plane perpendicular to {010} and $X \wedge a = +5°$ to $+ 9°$, $Y \wedge c = +21°$ to $+17°$, and $Z = b$. Grains elongate parallel to a are length fast.

Indices of Refraction and Birefringence: Indices of refraction vary systematically with the degree of Al/Si order (Figure 12.19). Indices of refraction increase moderately with Na content, but the variation is not substantial for common compositions. Birefringence is low (0.005–0.008), so interference colors in standard thin section are no higher than first-order white.

Interference Figure: $2V_x$ for low sanidine decreases with decreasing Al/Si order from 40° to 0° with the optic plane perpendicular to (010). In high sanidine, the optic plane is parallel to (010) and $2V_x$ increases to as much as 47° with decreasing order. The low sanidine orientation is more common. Provided the trace of (010) can be recognized, either as the composition plane of a Carlsbad twin or based on crystal habit and cleavage, low and high sanidine can be distinguished in thin section. Find a grain that yields a figure (e.g., an acute bisectrix figure) from which the trace of the optic plane can be recognized. Return to plane light and observe whether the trace of the optic plane is parallel or at right angles to the trace of (010). Optic axis dispersion is $r > v$ for low sanidine and $r < v$ for high sanidine.

Alteration Sericite and clay are the common alteration products.

Distinguishing Features

Hand Sample: See alkali feldspar introductory material earlier in the chapter.

Thin Section/Grain Mount: Lack of polysynthetic twinning as either striations seen in hand sample or those seen in thin section distinguishes sanidine from microcline and plagioclase. The distinction between orthoclase, low sanidine, and high sanidine is based solely on $2V$ angle and optic orientation. Quartz has a similar appearance, but has positive relief in standard thin section and is uniaxial.

DO NOT COPY e48d507df5d1141@placeholder.94092

Printed by: e48d507df5d1141@placeholder.94092.edu. Printing is for personal, private use only. No part of this book may be reproduced or transmitted without publisher's prior permission. Violators will be prosecuted.

positive relief in standard thin section and is uniaxial.

Occurrence Sanidine is the common alkali feldspar in silicic volcanic rocks such as rhyolite, rhyodacite, phonolite, and trachyte, and in dikes and other shallow intrusions of the same composition. Most sanidine has between 20 percent and 60 percent Na and is usually cryptoperthitic. Compositions with more than about 60 percent Na are triclinic anorthoclase. Terrigenous sediments may contain sanidine, but microcline and orthoclase are more common.

Adularia

This variety of K-feldspar is not strictly defined based on its physical or structural properties but on the basis of habit and occurrence. Crystals are elongate parallel to c and are dominated by the {110} prism. In most cases adularia crystallizes at low temperatures (less than about 450°C) in hydrothermal systems in veins or as a replacement after other minerals, or is produced authigenically during diagenesis of sediments. It is commonly triclinic but also may be monoclinic, and some crystals may contain domains of both symmetries. The degree of Al/Si order is variable. Indices of refraction, $2V$, and related optical properties are similar to microcline and orthoclase but can be quite variable. Triclinic varieties lack the grid twinning produced by the polymorphic transition from monoclinic to triclinic, presumably because they grew originally with triclinic symmetry.

Anorthoclase

Triclinic $\overline{1}$ (pseudomonoclinic)

$$a = 8.287\ \text{Å},\ b = 12.972\ \text{Å},\ c = 7.156\ \text{Å},$$
$$\alpha = 91.05^\circ,\ \beta = 116.26^\circ,\ \gamma = 90.15^\circ,\ Z = 4$$
$$2V_x = 42 - 52^\circ$$

Form and Twinning Crystals tend to be tabular, bladed or elongate parallel to the c axis; anhedral grains and microlites are common. Complex twinning according to the albite {010} and pericline {h01} laws are characteristic.

Cleavage Perfect {001} and good {010} cleavages, like the other feldspars, intersect at an angle of about 91°.

Color Properties

Luster: Vitreous.

Color: Colorless; also white, pale yellow, red, green.

DO NOT COPY e48d507df5d1141@placeholder.9409

Printed by: e48d507df5d1141@placeholder.94092.edu. Printing is for personal, private use only. No part of this book may be reproduced or transmitted without publisher's prior permission. Violators will be prosecuted.

Streak: White.

Color in Thin Section: Colorless.

Pleochroism: None.

Optical Characteristics

Relief in Thin Section: Low negative.

Optic Orientation: $X \wedge a \approx +4°$ to $+10°$, $Y \wedge c \approx +16°$ to $+22°$, $Z \wedge b \approx 5°$

Indices of Refraction and Birefringence: Indices of refraction increase with Na content. Birefringence is low (0.005–0.008), like the other alkali feldspars.

Interference Figure: Anorthoclase is biaxial negative with $2V_x$ less than about 52°. Complex twining may make good figures difficult to obtain.

Alteration Alters to sericite and clay, like the other feldspars.

Distinguishing Features

Hand Sample: Anorthoclase cannot reliably be distinguished from the other feldspars in hand sample. The colorless crystals most closely resemble sanidine. Orthoclase and microcline are more typically colored. Striations on cleavage surfaces from albite twinning may be visible but are often too closely spaced to be reliably seen.

Thin Section: The combined albite and pericline twins most closely resemble microcline, but the lamellae are usually finer and the $2V$ is smaller and the occurrence is different.

Occurrence Anorthoclase is found in Na-rich felsic volcanics such as alkali rhyolite, trachyte, phonolite, and equivalent shallow intrusions.

DO NOT COPY
e48d507df5d1141@placeholder.9409

Printed by: e48d507df5d1141@placeholder.94092.edu. Printing is for personal, private use only. No part of this book may be reproduced or transmitted without publisher's prior permission. Violators will be prosecuted.

Feldspathoids

As the name implies, the feldspathoids are similar to the feldspars in both structure and physical properties. The common feldspathoid minerals include nepheline, leucite, and the sodalite group. Nepheline is by far the most abundant. Chemically the feldspathoids are distinguished from the feldspars by having less silica relative to the amount of Na and K. As a consequence, they are rarely, if ever, found in primary association with quartz. Using leucite as an example, it can be generalized that feldspathoids would react with quartz to form a feldspar, in this case K-feldspar:

The principal occurrence of feldspathoids is in alkali-rich, silica-poor igneous rocks. Because magmas of these compositions are uncommon, the feldspathoids also are uncommon.

The structure of the feldspathoids is similar to the feldspars and consists of four- and six-member rings linked laterally to form a three-dimensional tetrahedral framework. The presence of six-member rings requires that the structures be somewhat more open than the feldspars, so the specific gravity of these minerals is less. The cavities created in the framework of tetrahedra are occupied by Na^+ and/or K^+, and in the sodalite group by anions and anionic groups including Cl^-, SO_4^{2-}, and S^{2-}.

Nepheline

Å Å

DO NOT COPY e48d507df5d1141@placeholder.9409

Printed by: e48d507df5d1141@placeholder.94092.edu. Printing is for personal, private use only. No part of this book may be reproduced or transmitted without publisher's prior permission. Violators will be prosecuted.

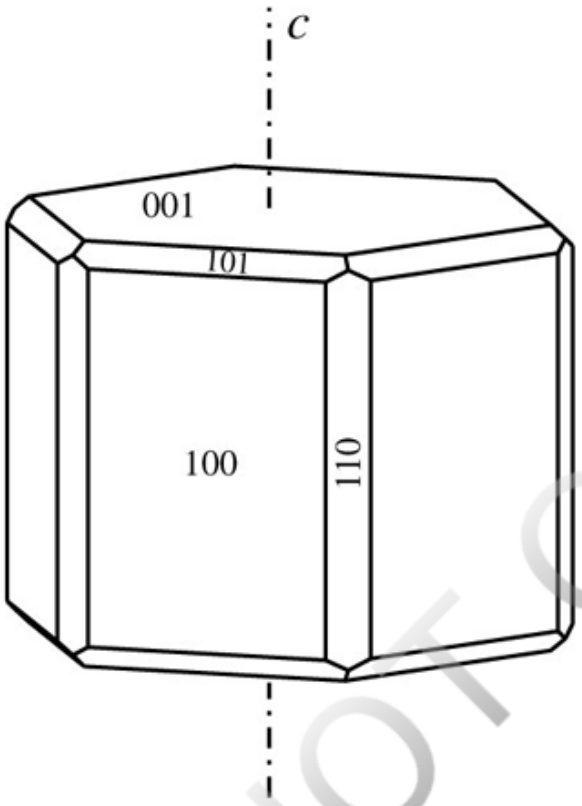

Structure The structure is similar to tridymite and consists of alternating layers of Si/Al tetrahedra arranged in rings with tetrahedra alternately pointing up and down. The "up" tetrahedra contain Si^{4+} and the "down" tetrahedra contain Al^{3+}. The "up" tetrahedra share oxygen anions with the "down" tetrahedra from the sheet above. This avoids placing Al^{3+} in adjacent tetrahedra according to the aluminum avoidance principle (see discussion in feldspar section). The Na^+ and K^+ cations are located in the middle of the 6-fold tetrahedral rings. The framework is distorted somewhat compared to the ideal tridymite structure, so that of four sites in the middle of the 6-fold rings, three are smaller and one larger. The three smaller sites contain Na^+ and the larger site contains K^+.

Composition At high temperature, extensive solid solution extends to kalsilite ($K_4Al_4Si_4O_{16}$), but at most magmatic conditions, intermediate compositions are not possible and nepheline typically has close to a 3:1 Na:K ratio. Kalsilite exsolution lamellae may be present. An excess of Si^4 over Al^{3+} is usually balanced by vacancies in the sites occupied by Na and K. Small amounts of Ca may substitute for Na and K.

Form and Twinning Uncommon crystals form blocky hexagonal prisms terminated with a basal pinacoid. More common as anhedral masses, particularly in plutonic rocks (**Figure 12.21**).

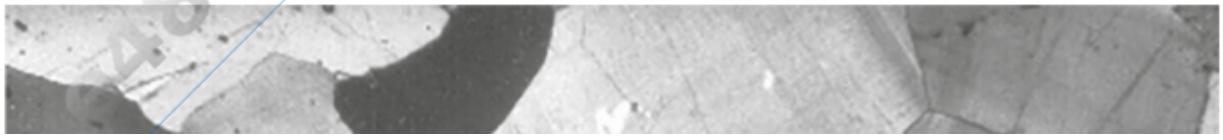

Printed by: e48d507df5d1141@placeholder.94092.edu. Printing is for personal, private use only. No part of this book may be reproduced or transmitted without publisher's prior permission. Violators will be prosecuted.

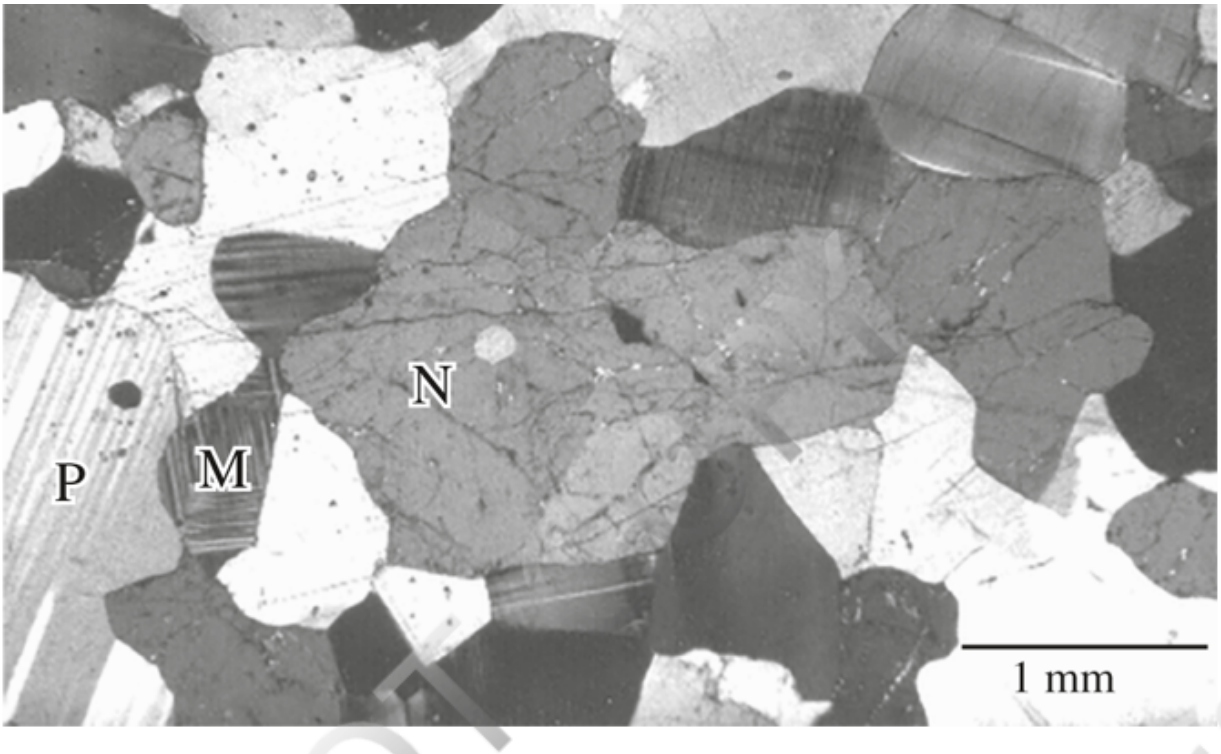

FIGURE 12.21 Photomicrograph of nepheline (N) in thin section with plagioclase (P) and microcline (M) in nepheline syenite. Crossed polarizers. View larger image

Twins on {010}, {010}, {112}, and {335} are possible but not normally seen in either hand sample or thin section.

Cleavage Poor cleavage on {100} and {001}. Subconchoidal fracture. Brittle.

Color Properties

Luster: Subvitreous to somewhat greasy.

Color: White or gray.

Streak: White.

Color in Thin Section: Colorless.

Pleochroism: None.

Optical Characteristics

Relief in Thin Section: Low positive most common, also low negative.

Optic Orientation: Uniaxial, so the optic axis is *c*. Longitudinal sections through elongate crystals are length fast with parallel extinction.

Indices of Refraction and Birefringence: Substitution of K^+ for Na^+ produces a slight increase in refractive indices. Most nepheline has indices of refraction above 1.54, so it shows low positive relief in standard thin section. Birefringence is low, so the maximum

DO NOT e48d507df5d1141@placeholder.9409

Printed by: e48d507df5d1141@placeholder.94092.edu. Printing is for personal, private use only. No part of this book may be reproduced or transmitted without publisher's prior permission. Violators will be prosecuted.

interference color seen in thin section is middle first-order gray. Kalsilite has indices of refraction $n_\omega = 1.540$, $n_\epsilon = 1.535$.

Interference Figure: Uniaxial negative, but slight separation of isogyres may be seen in some samples. Owing to low birefringence, isogyres tend to be fairly broad and fuzzy in standard thin section. Ca-rich samples may be optically positive.

Alteration Nepheline may alter to clay minerals, analcime, sodalite, calcite, and cancrinite.

Distinguishing Features

Hand Sample: Resembles quartz but is softer; has a somewhat greasy luster and poor cleavage.

Thin Section/Grain Mount: Resembles the feldspars but is uniaxial, lacks good cleavage and twinning, and has lower birefringence. Quartz is uniaxial positive and lacks the clouding common in nepheline.

Occurrence Nepheline is a common mineral in alkali-rich, silicon-poor plutonic and volcanic igneous rocks such as nepheline syenite, foidite, and phonolite. Associated minerals often include alkali feldspar, Na-rich plagioclase, biotite, and sodic and sodic–calcic amphibole and/or pyroxene. It also may be associated with leucite and sodalite. Cancrinite [$Na_6Ca_2Al_6Si_6O_{24}(CO_3)_2$] is a zeolite-like mineral, colorless, white, or pale yellow in hand sample, that is commonly associated with nepheline. Cancrinite is uniaxial (−), $n_\omega = 1.507$–1.528, $n_\epsilon = 1.495$–1.503, $\delta = 0.012$–0.025, $H = 5$–6, $G = 2.42$–2.51 with perfect {100} cleavage. Nepheline almost never occurs as a primary mineral in quartz-bearing rocks. Nepheline also may be found in some contact-metamorphosed rocks adjacent to alkali-rich intrusions, presumably as a result of sodium metasomatism.

Use Nepheline, generally as a constituent mineral in nepheline syenite, has fairly extensive industrial uses. Nepheline syenite, which typically also contains alkali feldspar and plagioclase as major minerals, is crushed, and Fe–Mg-bearing minerals are magnetically removed. The resulting material is pulverized and used in the manufacture of glass and ceramics. It also may be used as an extender or filler in the manufacture of paints, plastic, and foam rubber. The high aluminum content makes nepheline a potential source of metallic aluminum, but bauxite remains a more economic viable source except for a few locations in Russia.

Leucite

$$KAlSi_2O_6$$

Tetragonal $4/m$ (pseudoisometric)

$a = 13.05$ Å, $c = 13.75$ Å, $Z = 16$

DO NOT COPY e48d507df5d1141@placeholder.9409

Printed by: e48d507df5d1141@placeholder.94092.edu. Printing is for personal, private use only. No part of this book may be reproduced or transmitted without publisher's prior permission. Violators will be prosecuted.

$a = 13.05$ Å, $c = 13.75$ Å, $Z = 16$

$H = 5.5 - 6$

$G = 2.45 - 2.50$

Uniaxial (+)

$n_\omega = 1.508 - 1.511$

$n_\epsilon = 1.509 - 1.511$

$\delta = 0.000 - 0.001$

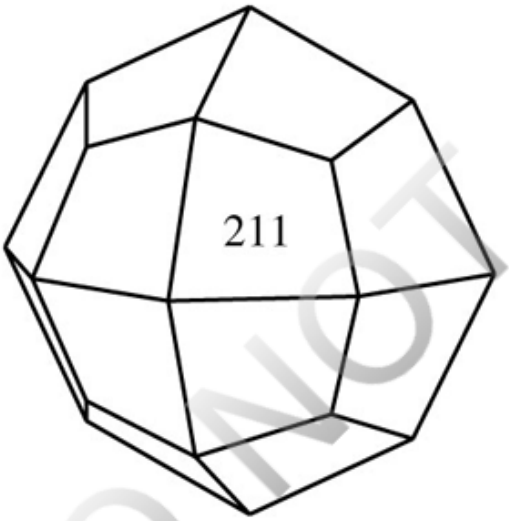

Structure The structure is an open framework of four- and six-member rings of Si/Al tetrahedra with K^+ cations occupying large openings within this framework. Above about 625°C the structure is isometric, but below that temperature it distorts to tetragonal, with the *c* axis of the tetragonal structure following one of the three crystal axes in the original isometric structure.

Composition Most leucite is relatively pure $KAlSi_2O_6$, but small amounts of Na^+ may replace K^+ and Fe^{3+} may replace Al^{3+}.

Form and Twinning Leucite commonly occurs as equant trapezohedral crystals that show eight-sided to nearly round cross sections. It also occurs as small microlites and skeletal or anhedral grains in the groundmass of volcanic rocks. Inclusions of other minerals are common. The transformation from isometric to tetragonal symmetry that accompanies cooling results in multiple twins on {110}. Twins are not visible in hand sample but appear as a complex pattern of concentric lamellae or lamellae that intersect at roughly 60° in thin section (Figure 5.25).

Cleavage Poor pseudododecahedral cleavage {110} is not normally seen and does not tend to control fragment orientation. Conchoidal fracture. Brittle.

Color Properties

DO NOT COPY e48d507df5d1141@placeholder.9409

Printed by: e48d507df5d1141@placeholder.94092.edu. Printing is for personal, private use only. No part of this book may be reproduced or transmitted without publisher's prior permission. Violators will be prosecuted.

Luster: Vitreous.

Color: White or gray.

Streak: White.

Color in Thin Section: Colorless.

Pleochroism: None.

Optical Characteristics

Relief in Thin Section: Low negative.

Optic Orientation: The optic axis coincides with one of the original *a* axes in the isometric structure.

Indices of Refraction and Birefringence: Indices of refraction show little variation. Birefringence is very low, and small grains appear nearly isotropic in thin section.

Interference Figure: Complex twinning and low birefringence make interference figures difficult to obtain and interpret in thin section. The optic sign is usually positive.

Alteration Leucite may alter to analcime or pseudoleucite, which is a mixture of nepheline and K-feldspar.

Distinguishing Features

Hand Sample: Crystal habit and occurrence are characteristic. Analcime is similar but typically occurs as a cavity-filling mineral, not as a phenocryst.

Thin Section/Grain Mount: Low birefringence, crystal habit, and complex twinning are diagnostic. Analcime and members of the sodalite group have higher indices of refraction, are isotropic, and lack the complex twinning.

Occurrence Leucite is an uncommon mineral found in potassium-rich mafic lavas and associated shallow intrusions. It is commonly associated with plagioclase, nepheline, sanidine, clinopyroxene, and sodic or sodic–calcic amphiboles. Leucite weathers readily and is not commonly preserved in sediments.

Use Leucite is used in the manufacture of ceramics used in dental prostheses.

Sodalite

Isometric $\bar{4}3m$

$Na_8Al_6Si_6O_{24}Cl_2$

DO NOT COPY e48d507df5d1141@placeholder.9409

Printed by: e48d507df5d1141@placeholder.94092.edu. Printing is for personal, private use only. No part of this book may be reproduced or transmitted without publisher's prior permission. Violators will be prosecuted.

$$a = 8.870 - 8.882 \text{ Å}, \ Z = 1$$

$$H = 5.5 - 6$$

$$G = 2.27 - 2.33$$

$$\text{Isotropic}$$

$$n = 1.483 - 1.487$$

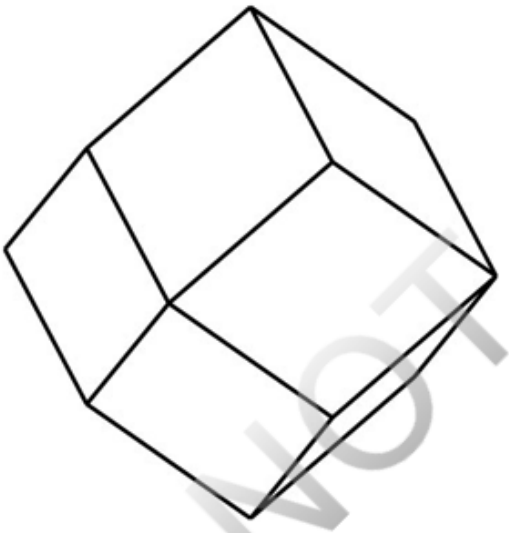

Structure The structure consists of an open tetrahedral framework, similar to the zeolites, that contains fairly large open cavities. The tetrahedra contain the Al^{3+} and Si^{4+} in an alternating pattern. The Cl^- anions, each surrounded by four Na^+ cations, occupy the large cavities.

Composition Sodalite is a member of the sodalite group, which also includes nosean [$Na_8(Al_6Si_6O_{24})SO_4 \cdot H_2O$], haüyne [$Na_6Ca_2(Al_6Si_6O_{24})SO_4$], and lazurite [$Na_6Ca_2(Al_6Si_6O_{24})S_2$]. Lazurite usually contains some Cl^-. Most sodalite is relatively close to its ideal composition. The blue color of lazurite is attributed to charge transfer between sulfur atoms that occupy three different structural sites and therefore have different electron energy levels.

Form and Twinning Crystals, usually dodecahedrons, are rare. Usually massive or as anhedral grains. Twins on {111} are common but are only recognized if the external crystal shape provides evidence for it, in which case crystals may form pseudohexagonal prisms elongate on [111].

Cleavage {110} poor. Uneven to conchoidal fracture. Brittle.

Color Properties

Luster: Vitreous.

Color: Commonly light to dark blue; also gray, colorless, white, yellow, or green; may

Printed by: e48d507df5d1141@placeholder.94092.edu. Printing is for personal, private use only. No part of this book may be reproduced or transmitted without publisher's prior permission. Violators will be prosecuted.

Color: Commonly light to dark blue; also gray, colorless, white, yellow, or green; may fluoresce.

Streak: White. The streak of lazurite may be blue.

Color in Thin Section: Colorless or very pale blue; color may be patchy. Haüyne may be more distinctly blue.

Pleochroism: None.

Optical Characteristics

Relief in Thin Section: Moderate negative.

Indices of Refraction and Birefringence: The index of refraction of nosean is 1.470–1.495 and of haüyne is 1.494–1.510. Sodalite may be weakly birefringent around inclusions.

Alteration Members of the sodalite group may alter to zeolites (often fibrous), clay, calcite, or cancrinite.

Distinguishing Features

Hand Sample: Distinguished by blue color. If not blue, sodalite may be difficult to distinguish from analcime and leucite. Members of the sodalite group are not readily distinguished from each other in hand sample.

Thin Section/Grain Mount: Members of the sodalite group are distinguished by their isotropic character, low index of refraction, and occurrence. Leucite is anisotropic and has distinctive twinning. Garnet has much higher indices of refraction. Fluorite has an even lower index of refraction and good cleavage. Analcime has poor cubic cleavage and is not blue, but is otherwise similar. The members of the sodalite group may be difficult to distinguish based on optical properties, but sodalite is colorless, lacks abundant inclusions, and is the only member usually found in plutonic rocks. Nosean and haüyne commonly contain inclusions, and haüyne is usually bluish in thin section.

Occurrence Members of the sodalite group are found in silica-poor, alkali-rich igneous rocks. Plutonic igneous rocks such as syenite are more likely to contain nepheline. Volcanic rocks such as phonolite, alkali basalt, and feldspathoidal basalt may contain sodalite, nosean, or haüyne. Both sodalite and lazurite may be found in contact-metamorphosed carbonate rocks. Lapis lazuli is a derived by contact metamorphism of limestone and consists of lazurite, pyroxene, calcite, and other silicates. It owes its blue color to the lazurite. When polished, lapis lazuli can be visually strikingly, particularly if it contains disseminated pyrite.

Use The blue color of sodalite-bearing rocks makes it valuable as a dimension stone used to face buildings and for other decorative purposes. It has been used as a folk medicine treatment for diabetes.

DO NOT COPY e48d507df5d1141@placeholder.9409

Printed by: e48d507df5d1141@placeholder.94092.edu. Printing is for personal, private use only. No part of this book may be reproduced or transmitted without publisher's prior permission. Violators will be prosecuted.

Zeolite Group

The zeolite group contains over 100 naturally occurring members and roughly 600 additional synthetic zeolites with no natural counterpart. Zeolites are the largest single group of silicate minerals and constitute major rock-forming minerals in some environments. Prior to the 1960s, zeolites were considered to be a relatively minor mineral group, represented mostly by crystals occupying vesicles and other voids in basaltic and andesitic volcanic rocks. However, the introduction of the scanning electron microscope and sophisticated X-ray diffraction techniques demonstrated that zeolites can compose a major part of certain sedimentary and metamorphic rocks and are abundant in hydrothermally altered volcanic rocks. The fine grain size of zeolites, however, makes identification and characterization difficult. In the past, much of this fine-grained material was misidentified as clay. Occurrences in vesicles and vugs in volcanic rocks are best known to mineralogists because only here are crystals large enough to be examined in hand sample or microscopically. For more information on this group of minerals, refer to Gottardi and Galli (1985), Bish and Ming (2001), or Tschernich (1992). Some of the more common zeolites are listed in **Table 12.6**.

TABLE 12.6 Physical Properties of Selected Zeolite Minerals

Mineral	Formula	Crystal System	Habit	*H*	*G*	Cleav
Analcime	$NaAlSi_2O_6 \cdot H_2O$	Isometric a = 13.72	Trapezoidal crystals	5–5.5	2.25	{001} poor
Chabazite	$(Ca, Na_2, K_2)_2Al_4Si_8O_{24} \cdot 12H_2O$	Triclinic (pseudohexagonal) $a \cong b \cong c$ =9.40–9.45 α = 94.18–94.33° β = 94.08–94.36° γ = 94.07–94.45°	Rhombs that are nearly cubic	4.5	2.05–2.20	{101} distin
Clinoptilolite	$(Ca, Na_2, K_2)_3Al_6Si_{30}O_{72} \cdot 21H_2O$	Monoclinic a = 17.63 b = 17.94	Tabular, radiating aggregates	3.5–4	2.16	{010} perfe

DO NOT COPY e48d507df5d1141@placeholder.9409

Printed by: e48d507df5d1141@placeholder.94092.edu. Printing is for personal, private use only. No part of this book may be reproduced or transmitted without publisher's prior permission. Violators will be prosecuted.

		c = 7.40 β = 116.39°				
Erionite	$(K_2,Na_2,Ca,Mg)_4Al_8Si_{28}O_{72}\cdot 28H_2O$	Hexagonal a = 13.21 c = 15.04	Fibrous	3.5–4	2.08	Poor prism
Heulandite	$NaCa_4Al_9Si_{27}O_{72}\cdot 24H_2O$	Monoclinic a = 7.955 b = 17.95 c = 7.435 β = 91.74°	Tabular to equant	3.5–4	2.20	{010} perfe
Laumontite	$CaAl_2Si_4O_{12}\cdot 4H_2O$	Monoclinic a = 14.72 b = 13.08 c = 7.76 β = 112.01°	Prismatic	3.5–4	2.3	{010} {110} perfe {011} imper
Mesolite	$Na_2Ca_2Al_6Si_9O_{30}\cdot 8H_2O$	Orthorhombic a = 18.40 b = 56.66 c = 6.54	Prismatic to fibrous, radiating aggregates	5	2.26	{110} perfe
Mordenite	$(Ca, Na_2, K_2)Al_2Si_{10}O_{24}\cdot 7H_2O$	Orthorhombic a = 18.05 b = 20.40 c = 7.50	Fibrous, radiating, or felted	3–4	2.13	{100} perfe {010} distin
Natrolite	$Na_2Al_2Si_3O_{10}\cdot 2H_2O$	Orthorhombic a = 18.27 b = 18.61 c = 6.59	Prismatic to acicular, radiating aggregates	5	2.25	{110} perfe
Phillipsite	$K_2(Ca,Na_2)_2Al_6Si_{10}O_{32}\cdot 12H_2O$	Monoclinic a = 9.87 b = 14.30	Prismatic, pseudo-orthorhombic	4–4.5	2.20	{010} {100} distin

DO NOT COPY
e48d507df5d1141@placeholder.9409-

Printed by: e48d507df5d1141@placeholder.94092.edu. Printing is for personal, private use only. No part of this book may be reproduced or transmitted without publisher's prior permission. Violators will be prosecuted.

		c = 8.67 β = 124.2°				
Scolecite	$CaAl_2Si_3O_{10}\cdot 3H_2O$	Monoclinic a = 18.51 b = 18.98 c = 6.53 β = 90.64°	Prismatic, radiating aggregates	5	2.26	{110} perfe
Stilbite	$Na_2Ca_4Al_{10}Si_{26}O_{72}\cdot 30H_2O$	Monoclinic a = 13.6 b = 18.2 c = 22.4 β = 128.2°	Tabular, sheathlike aggregates	3.5–4	2.19	{010} perfe
Thomsonite	$NaCa_2Al_5Si_5O_{20}\cdot 6H_2O$	Orthorhombic a = 13.09 b = 13.05 c = 13.23	Prismatic or lamellar rosettes or radiating aggregates	5	2.35	{100} perfe {010} good
Wairakite	$CaAl_2Si_4O_{12}\cdot 2H_2O$	Monoclinic (pseudocubic) a = 13.69 b = 13.64 c = 13.56 β = 90.5°	Trapezoidal crystals	5.5–6	2.27	?

Composition and Structure Zeolites are hydrated framework silicates with a general formula

$$M_xD_y(Al_{x+2y}Si_{n-x-2y}O_{2n})\cdot mH_2O$$

where the ratio of Si to Al varies from 1:1 to 6:1. The M and D cations make up the charge deficiency associated with having Al^{3+} rather than Si^{4+} in the tetrahedral sites. M is usually monovalent Na or K and D is Ca, Mg, or other divalent cations. The M and D stoichiometric amounts are therefore dependent on the amount of Al^{3+}. Water content is variable.

DO NOT COPY e48d507df5d1141@placeholder.94092

Printed by: e48d507df5d1141@placeholder.94092.edu. Printing is for personal, private use only. No part of this book may be reproduced or transmitted without publisher's prior permission. Violators will be prosecuted.

The structures of zeolites consist of relatively stable open frameworks of Al/Si tetrahedra (**Figure 12.22**) that link together to form open channels and voids with different geometries for different species. The water molecules and the mono- and divalent cations occupy the voids in the framework structure and are weakly bonded. This leads to some interesting and useful properties described in the following subsections.

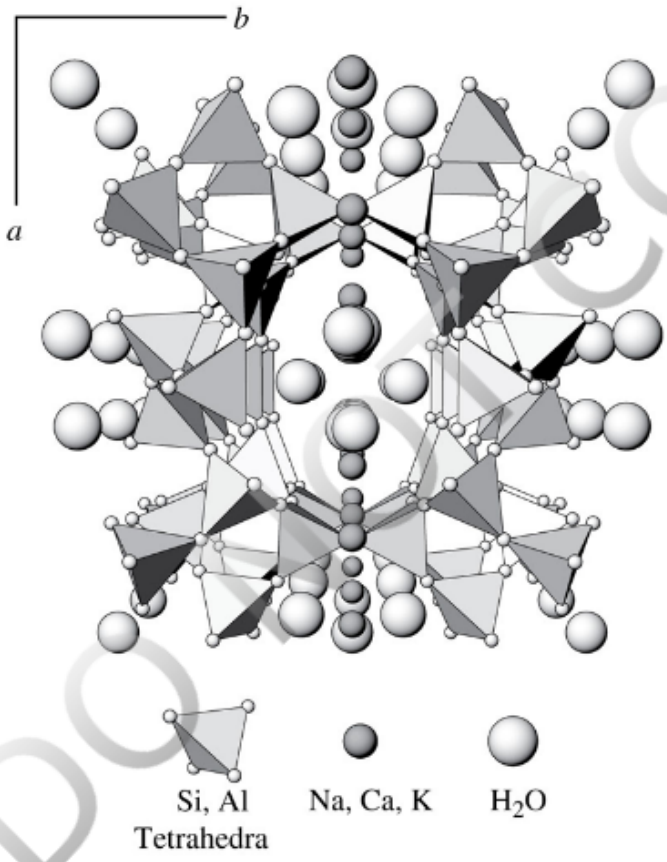

FIGURE 12.22 Typical zeolite structure. Heulandite viewed down the *c* axis. The open channels provide space for water molecules and mono- and divalent cations. Structural data from Gunter and others (1994). View larger image

Physical Properties In their most common occurrences, zeolites are too fine grained to allow identification by physical properties. Only in cases where large crystals have formed in vesicles or other voids in mafic lava flows are zeolites sufficiently large to be identified without X-ray or related techniques. The physical properties of selected zeolite minerals are listed in Table 12.6. Of these, chabazite, natrolite, heulandite, analcime, thomsonite, and stilbite are relatively common as large crystals. These minerals have a vitreous luster and white streak, and are typically white or colorless, or they may display pastel shades of yellow, pink, brown, or green. Specific gravity and hardness also vary within relatively narrow ranges. Identification is therefore made principally on the basis of habit.

ANALCIME: Equant trapezohedral crystals

CHABAZITE: Rhombohedral (pseudocubic) crystals

DO NOT COPY e48d507df5d1141@placeholder.9409

Printed by: e48d507df5d1141@placeholder.94092.edu. Printing is for personal, private use only. No part of this book may be reproduced or transmitted without publisher's prior permission. Violators will be prosecuted.

CHABAZITE: Rhombohedral (pseudocubic) crystals

HEULANDITE: Platy crystals with perfect {010} cleavage; often with a coffin-shaped cross section

NATROLITE: Slender prismatic or acicular crystals that may form radiating aggregates; also fibrous

STILBITE: Platy crystals tabular on {010} with good cleavage; often forms aggregates of aligned grains that resemble a sheaf

THOMSONITE: Acicular, prismatic, or bladed crystals, often in spherical, botryoidal, or columnar aggregates and masses that may be color zoned

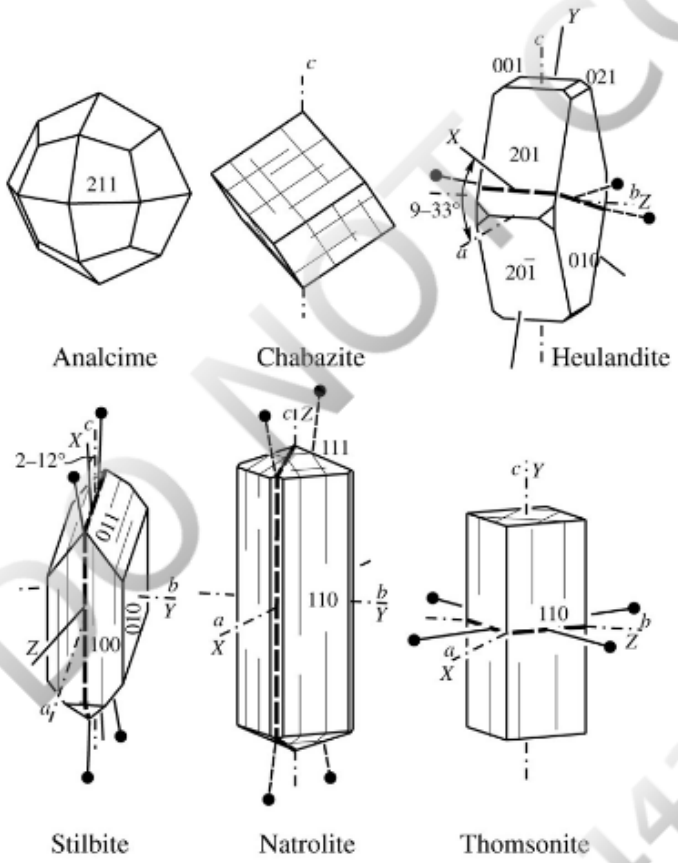

Positive identification in most cases requires X-ray diffraction study. **Figure 12.23** shows SEM image of selected zeolites.

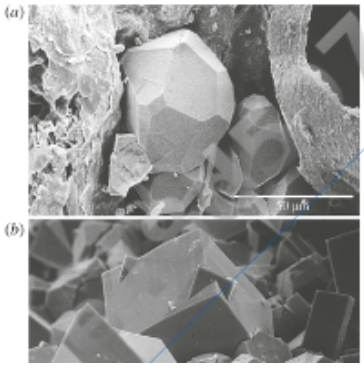

Printed by: e48d507df5d1141@placeholder.94092.edu. Printing is for personal, private use only. No part of this book may be reproduced or transmitted without publisher's prior permission. Violators will be prosecuted.

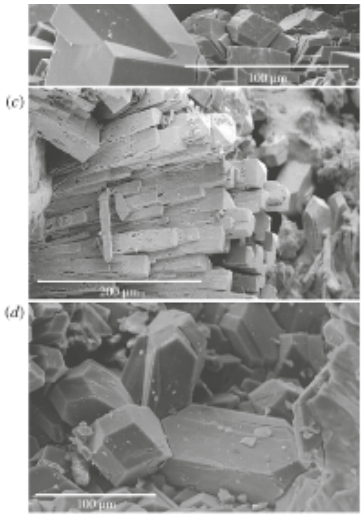

FIGURE 12.23 Scanning electron microscope images of zeolites from altered basaltic tuff, northeast Jordan. (*a*) Analcime. (*b*) Chabazite displaying penetration twins. (*c*) Natrolite crystals showing perforations. Note the pyramidal terminations on some crystals. (*d*) Phillipsite. © Ibrahim, K. M. (2004) Mineralogy and chemistry of natrolite from Jordan. Clay Minerals 39, 47–55. View larger image

Optical Characteristics Table 12.7 shows optical properties for selected zeolites. Note that the optical properties display substantial overlap and may vary depending on the degree of hydration. All have low indices of refraction, usually less than the thin section epoxy; have low birefringence; and are colorless in thin section and grain mount. It may be difficult to distinguish among different species based solely on optical properties.

TABLE 12.7 Optical Properties of Selected Zeolites

Mineral	Optical Class and Sign	Index of Refraction	Birefringence	$2V(°)$	Optical Orientation
Analcime	Isotropic	n = 1.479–1.493			
Chabazite	Uniaxial or biaxial (−) or (+)	n_α = 1.460–1.513 n_γ = 1.462–1.515	0.002–0.010	0–~30	The Bxa is ~ c in biaxial varieties
Clinoptilolite	Biaxial (−) or (+)	n_α = 1.476–1.491 n_β = 1.471–1.493 n_γ = 1.479–1.497	0.003–0.006	$2V_x$ = small to large	$Y = b$, $Z \wedge a$ = +30° to +45°
Heulandite	Biaxial (+)	n_α = 1.487–	0.001–0.011	0–70,	$X \wedge$ a = +9° to + 33°, $Y \wedge$

DO NOT COPY e48d507df5d1141@placeholder.9409

Printed by: e48d507df5d1141@placeholder.94092.edu. Printing is for personal, private use only. No part of this book may be reproduced or transmitted without publisher's prior permission. Violators will be prosecuted.

		1.505 n_β = 1.487–1.507 n_γ = 1.488–1.515		usually ~30	c = −8° to −32°, Z = b; the cleavage trace is length fast
Laumontite	Biaxial (−)	n_α = 1.502–1.514 n_β = 1.512–1.524 n_γ = 1.514–1.525	0.008–0.016	25–47	$X \wedge a$ = +30° to +62°, $Y \wedge b$, $Z \wedge c$ = −8° to −40°
Natrolite	Biaxial (+)	n_α = 1.473–1.490 n_β = 1.476–1.491 n_γ = 1.485–1.502	0.012–0.013	0–64	$X = a$, $Y = b$, $Z = c$; fibers and cleavage fragments are length slow
Stilbite	Biaxial (−)	n_α = 1.482–1.500 n_β = 1.489–1.507 n_γ = 1.493–1.513	0.006–0.014	30–49	$X \wedge c$ = +2° to +12°, $Y \cong b$, $Z \wedge a$ = +26° to +36°; elongate grains are length fast
Thomsonite	Biaxial (+)	n_α = 1.497–1.530 n_β = I.513–1.533 n_γ = 1.518–1.544	0.006–0.021	41–75	$X = a$, $Y = c$, $Z = b$; fibers and cleavage fragments may be length fast or slow

Alteration Zeolite minerals may alter to clay or to other zeolites.

Occurrence Zeolites are widely but irregularly distributed. In the large majority of occurrences, zeolites are secondary, meaning that they are produced by alteration of some precursor mineral or minerals. Only analcime occurs as a primary magmatic mineral, in which occurrence it typically forms late-crystallizing grains occupying the interstices between other minerals in basalts, phonolites, and related rocks.

The environments in which zeolites are produced by alteration include the following,

DO NOT COPY e48d507df5d1141@placeholder.9409

Printed by: e48d507df5d1141@placeholder.94092.edu. Printing is for personal, private use only. No part of this book may be reproduced or transmitted without publisher's prior permission. Violators will be prosecuted.

ordered roughly by depth of burial.

- Weathering under high pH conditions
- Sedimentary diagenesis, especially of volcanic ash in saline lakes or certain deep marine environments
- Alteration associated with percolating groundwater
- Hydrothermal alteration associated with igneous activity
- Contact metamorphism
- Burial and low-grade regional metamorphism

The most extensive zeolite deposits are found in altered felsic volcanic ash flow sheets and related volcanic rocks, most commonly of late-Mesozoic and Cenozoic age. Zeolitization may be accomplished by percolating groundwater, a hydrothermal circulation system, or contact metamorphism. Volcanic ash deposited in saline lakes also is particularly prone to zeolite alteration. The zeolites commonly formed by alteration include clinoptilolite, chabazite, mordenite, erionite, and phillipsite. The grain size is almost always submicroscopic.

Heulandite, chabazite, natrolite, and stilbite are the most common zeolites to occur as vesicle and other void-space fillings in basaltic volcanics. These crystals may be large and they appear to have crystallized from circulating groundwater, whether or not driven by a thermal system.

Burial and low-grade regional metamorphism of graywacke and related sedimentary rocks derived from andesitic to basaltic sources may produce heulandite and analcime at lower temperatures. Laumontite appears at greater depth and higher temperatures. Similar metamorphism of more felsic rocks typically produces a mineralogical progression in which clinoptilolite and/or mordenite appear first, followed by analcime, which in turn is replaced by albite with increasing depth of burial. The grain size of these rocks is almost always very fine.

Normal chemical weathering of felsic volcanic rocks can produce zeolites when the pH is quite high. This occurs in saline alkali-rich soils, which are usually found only in arid or semiarid environments.

To a significant degree, zeolite composition is controlled by the chemistry of the original rock. Zeolites that develop in mafic rocks with relatively low silica content tend to have low Si:Al ratios, and include thomsonite and scolecite. High-silica zeolites such as mordenite and clinoptilolite tend to occur in altered felsic rocks. Zeolites with an intermediate Si:Al composition such as chabazite, analcime, and phillipsite may be found in rocks of diverse compositions.

Use Zeolites are widely used in many industrial and other processes. Most of these uses depend on the unique structural and chemical behavior of these minerals. Many zeolite-

Printed by: e48d507df5d1141@placeholder.94092.edu. Printing is for personal, private use only. No part of this book may be reproduced or transmitted without publisher's prior permission. Violators will be prosecuted.

like materials have been synthesized to take advantage of these properties, and use of these materials is very extensive.

At room temperature, the structural voids in zeolites can be entirely occupied by water molecules and the M and D cations. With higher temperatures the water is released, and above 300 or 400°C, zeolites will have lost most of their water. In many zeolites, this moderate heating does not destroy the framework structure, and upon cooling the voids can again fill with water. This property makes zeolites useful as **desiccants**, or materials used to remove humidity. The zeolites are heated to drive off the water and then are exposed to gases such as carbon dioxide, refrigerator and air conditioner refrigerant, and various organic chemicals used for industrial purposes such that the zeolites will remove the unwanted water.

The fact that zeolites have large open frameworks also makes them useful as molecular sieves. Similar to their use as a desiccant, they are heated to drive off their water, and then they are exposed to some material. Molecules small enough to enter the channels are adsorbed into the zeolite and larger molecules are excluded. For example, mordenite can be used in this way to selectively remove nitrogen from air to produce a gas that is up to 95 percent oxygen.

Zeolites can also be used as cation-exchange agents, which is one of their most important industrial uses. The M and D cations in the voids and channels are loosely bound and can be exchanged for other cations under appropriate conditions. One of the earliest cation-exchange applications was to treat water to reduce its “hardness.” Hard water contains substantial quantities of Ca^{2+} cations (usually in the form of dissolved $CaCO_3$) that prevent soaps and detergents from lathering properly and leaves clothes still dirty after being washed. A synthetic Na-bearing zeolite similar to natrolite is exposed to the hard water and exchanges $2Na^+$ for Ca^{2+} in the water. The Na^+ added to the water does not prevent soap from lathering. Once the zeolite has been saturated with Ca^{2+}, it is exposed to a strong NaCl solution. The Na^+ replaces the Ca^{2+} and prepares the zeolite to be used again.

Other zeolite cation-exchange applications include removing heavy metals from mine drainage and industrial waste, and dangerous isotopes from radioactive waste. Similarly, zeolites may be used to remove undesirable metals (Cd, Cu, Pb, and Zn) from soils and reduce their availability to plants. One of the more important ion-exchange applications involves the ability of clinoptilolite and mordenite to adsorb ammonium (NH_4^+) ions. Because ammonia is generated in substantial quantities from animal and human waste, these zeolites are used to treat wastewater from sewage treatment plants and from agricultural operations. They also are used to control ammonia in fish farm water and to control odor in cat litter.

In agriculture, zeolites are used as a soil conditioner to improve soil moisture retention, increase cation-exchange capability, and buffer acidic soils. Their adsorptive capability makes them useful as a slow-release medium for nitrogen fertilizer and as a carrier for herbicides, pesticides, and fungicides. Clinoptilolite has been added to feed for chickens

DO NOT COPY e48d507df5d1141@placeholder.94092

Printed by: e48d507df5d1141@placeholder.94092.edu. Printing is for personal, private use only. No part of this book may be reproduced or transmitted without publisher's prior permission. Violators will be prosecuted.

herbicides, pesticides, and fungicides. Clinoptilolite has been added to feed for chickens, turkeys, pigs, and cattle to improve feed efficiency and to reduce diarrhea and related health problems. It has the additional benefit of producing a less odoriferous excrement by adsorbing ammonia. This manure may also have improved nitrogen release properties as a fertilizer.

Zeolites, or their synthetic analogs, are also widely used as catalysts in chemical processes, such as in petroleum refining. They are also used as a sorbent to clean oil spills and as a filler in some paper products. Despite wide application, industrial use of natural zeolites is often limited by the entrenched use of other techniques. Also, synthetic zeolites may be preferred as they can be better tailored to specific tasks.

Zeolites have been advocated as treatments for a wide variety of medical conditions including cancer, gastrointestinal problems, diabetes, and detoxification, and it is possible that some uses may prove to be valid. A notable success that has received approval from the U.S. Food and Drug Administration is the use of a synthetic zeolite as a blood-clotting agent to prevent blood loss on the battlefield and in trauma centers.

Although most zeolite minerals appear to be environmentally benign, there are exceptions. The most notable is erionite, which is fibrous. It appears to pose a significant risk of mesothelioma cancer and other respiratory pathologies, very similar to asbestiform minerals (Ross and others, 1993). See Box 13.1 for more information on asbestos.

DO NOT COPY
e48d507df5d1141@placeholder.9409

Printed by: e48d507df5d1141@placeholder.94092.edu. Printing is for personal, private use only. No part of this book may be reproduced or transmitted without publisher's prior permission. Violators will be prosecuted.

Other Framework Silicates

Scapolite

DO NOT COPY

Å Å

Å Å

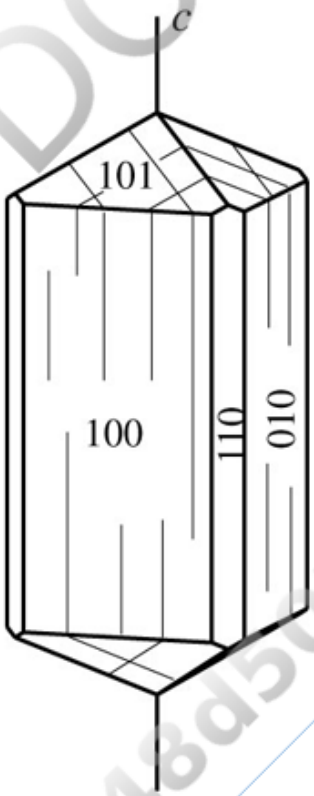

Structure Scapolite structure consists of four-member rings of Si/Al tetrahedra that are

Printed by: e48d507df5d1141@placeholder.94092.edu. Printing is for personal, private use only. No part of this book may be reproduced or transmitted without publisher's prior permission. Violators will be prosecuted.

Structure Scapolite structure consists of four-member rings of Si/Al tetrahedra that are linked together to form chains parallel to the *c* axis. These chains are in turn linked laterally through other four-member tetrahedral rings. The Ca^{2+}, Na^{+}, Cl^{-}, and CO_3^{2-} occupy voids formed in this open structure. The structure is similar to the feldspathoids, and some sources classify scapolite as a feldspathoid.

Composition Scapolite forms a solid solution series extending from meionite to marialite, although most samples have intermediate compositions. The substitution scheme is coupled with $Na^{+} + Si^{4+}$ substituting for $Ca^{2+} + Al^{3+}$, similar to plagioclase, or $Na^{+} + Cl^{-}$ substituting for $Ca^{2+} + CO_3^{2-}$. SO_4^{2-} or OH^{-} may substitute for CO_3^{2-} or Cl^{-}.

Form and Twinning Crystals are prismatic, usually with flat pyramidal terminations. Commonly as anhedral grains, granular clusters, or columnar aggregates. Some grains may be **poikilitic**, meaning that they are relatively large with abundant inclusions of associated minerals. Twinning is not reported.

Cleavage Good cleavages parallel to the {110} faces intersect at 90°. A second set of fair cleavages is parallel to {100} and 45° to the {110} cleavages. Fragment shape tends to be controlled by cleavage. Uneven to conchoidal fracture. Brittle.

Color Properties

Luster: Vitreous.

Color: White, gray, or greenish; less commonly, shades of pink, yellow, and blue. Commonly fluoresces orange to bright yellow in UV light.

Streak: White.

Color in Thin Section: Colorless.

Pleochroism: None.

Optical Characteristics

Relief in Thin Section: Low to moderate positive.

Optic Orientation: Because scapolite is tetragonal, the *c* axis is the optic axis. The traces of cleavage in longitudinal sections and cleavage fragments both show parallel extinction and are length fast.

Indices of Refraction and Birefringence: Birefringence increases linearly from about 0 to 0.040 with increasing meionite content.

Interference Figure: Scapolite is uniaxial negative, but biaxial samples with $2V < 10°$ have been reported.

Alteration Scapolite may be replaced by aggregates containing sericite, calcite, chlorite, epidote, zeolites, or other minerals.

DO NOT COPY e48d507df5d1141@placeholder.9409

Printed by: e48d507df5d1141@placeholder.94092.edu. Printing is for personal, private use only. No part of this book may be reproduced or transmitted without publisher's prior permission. Violators will be prosecuted.

Distinguishing Features

Hand Sample: Characterized by prismatic crystals with square cross sections and cleavages at 45°. Resembles feldspars, but the cleavages have a fibrous appearance.

Thin Section/Grain Mount: Distinguished from feldspar by uniaxial character and from quartz by optic sign and higher birefringence. Cordierite is biaxial. Nepheline has lower birefringence and less well-developed cleavage.

Occurrence Scapolite is found in both contact and regional metamorphic rocks with generally calcareous sedimentary mafic protoliths. In skarn deposits and marble derived from calcareous sedimentary rocks, scapolite is often associated with calcite and calc-silicate minerals such as titanite, garnet, diopside, and actinolite. In amphibolite and related mafic rocks, scapolite is associated with hornblende, calcic clinopyroxene, epidote, and titanite. It may replace plagioclase in hydrothermally altered mafic igneous rocks. Scapolite also is found in granulites and less commonly in pelitic and psammitic regional metamorphic rocks. It infrequently is found in veins cutting regional metamorphic rocks or shallow intrusions, in some pegmatites, and ejected volcanic blocks.

Use Scapolite has no industrial uses, but colorless crystals have been used as gemstones.

DO NOT COPY
e48d507df5d1141@placeholder.9409

Printed by: e48d507df5d1141@placeholder.94092.edu. Printing is for personal, private use only. No part of this book may be reproduced or transmitted without publisher's prior permission. Violators will be prosecuted.

Color in Thin Section: Colorless.
Pleochroism: None.

Optical Characteristics

Relief in Thin Section: Low to moderate positive.

Optic Orientation: Because scapolite is tetragonal, the *c* axis is the optic axis. The traces of cleavage in longitudinal sections and cleavage fragments both show parallel extinction and are length fast.

Indices of Refraction and Birefringence: Birefringence increases linearly from about 0 to 0.040 with increasing meionite content.

Interference Figure: Scapolite is uniaxial negative, but biaxial samples with $2V < 10°$ have been reported.

Alteration Scapolite may be replaced by aggregates containing sericite, calcite, chlorite, epidote, zeolites, or other minerals.

Distinguishing Features

Hand Sample: Characterized by prismatic crystals with square cross sections and cleavages at 45°. Resembles feldspars, but the cleavages have a fibrous appearance.

Thin Section/Grain Mount: Distinguished from feldspar by uniaxial character and from quartz by optic sign and higher birefringence. Cordierite is biaxial. Nepheline has lower birefringence and less well-developed cleavage.

Occurrence Scapolite is found in both contact and regional metamorphic rocks with generally calcareous sedimentary mafic protoliths. In skarn deposits and marble derived from calcareous sedimentary rocks, scapolite is often associated with calcite and calc-silicate minerals such as titanite, garnet, diopside, and actinolite. In amphibolite and related mafic rocks, scapolite is associated with hornblende, calcic clinopyroxene, epidote, and titanite. It may replace plagioclase in hydrothermally altered mafic igneous rocks. Scapolite also is found in granulites and less commonly in pelitic and psammitic regional metamorphic rocks. It infrequently is found in veins cutting regional metamorphic rocks or shallow intrusions, in some pegmatites, and ejected volcanic blocks.

Use Scapolite has no industrial uses, but colorless crystals have been used as gemstones.

REFERENCES CITED AND SUGGESTIONS FOR ADDITIONAL READING

DO NOT COPY
e48d507df5d1141@placeholder.9409

Printed by: e48d507df5d1141@placeholder.94092.edu. Printing is for personal, private use only. No part of this book may be reproduced or transmitted without publisher's prior permission. Violators will be prosecuted.

Bailey E. H., and Stevens, R. E. 1960. Selective staining of K-feldspar and plagioclase on rock slabs and thin sections. *American Mineralogist* **45**, 1020–1025.

Bish, D. L., and Ming, D. W. 2001. *Natural Zeolites: Occurrence, Properties, Applications. Reviews in Mineralogy and Geochemistry* **45**, 654 p.

Boone, G. M., and Wheeler, E. P., II. 1968. Staining for cordierite and feldspars in thin section. *American Mineralogist* **53**, 327–331.

Burri, C., Parker, R. L., and Wenk, E. 1967. *Die optische Orientierung der Plagioklase*. Birkhauser Verlag, Basel, 333 p.

Deer, W. A., Howie, R. A., and Zussman, J. 2001. *Rock-Forming Minerals, Volume 4A: Feldspars*, 2nd ed. The Geological Society, London, 992 p.

Flörke, O. W., Graetsch, H., Martin, B., Röller, K., and Wirth, R. 1991. Nomenclature of micro- and non-crystalline silica minerals, based on structure and microstructure. *Neues Jarbuch der Mineralogie, Abhandlungen* **163**, 19–42.

Frondel, C. 1982. Structural hydroxyl in chalcedony (type B quartz). *American Mineralogist* **67**, 1248–1257.

Gaillou, E., Fritsch, E., Aguilar-Reyes, B., Rondeau, B., Post, J., Barreau, A., and Ostroumov, M. 2008. Common gem opal: An investigation of micro- to nano-structure. *American Mineralogist* **93**, 1865–1873.

Gottardi, T., and Galli, E. 1985. *Natural Zeolites*. Springer-Verlag, Berlin, 409 p.

Graetsch, H. 1994. Structural characteristics of opaline and microcrystalline silica minerals. *Reviews in Mineralogy* **29**, 209–232.

Graziani, G., and Lucchesi, S. 1982. Thermal behavior of scapolites. *American Mineralogist* **67**, 1229–1241.

Griffen, D. T. 1992. *Silicate Crystal Chemistry*. Oxford University Press, New York, 442 p.

Gunter, M. E., Armbruster, T., Kohler, T., and Knowles, C. R. 1994. Crystal structure and optical properties of Na- and Pb-exchanged heulandite-group zeolites. *American Mineralogist* **79**, 675–682.

Guthrie, G. D., Jr., and Mossman, B. T. 1993. Health Effects of Mineral Dust. *Reviews in Mineralogy* **28**, 584 p.

Gutzmer, J., Beukes, N. J., Cairncross, B. 2004. New interpretation of the origin of tiger's eye: Comment and Reply: COMMENT. *Geology* **32,** No. 1, e44–e45.

Haughton, H. F. 1980. Refined techniques for staining plagioclase and alkali-feldspars in thin section. *Journal of Sedimentary Petrology* **50**, 629–631.

Heaney, P. J., and Fisher, D. M. 2003. New interpretation of the origin of tiger's eye. *Geology* **31**, No. 4, 323–326.

Heaney, P. J., and Fisher, D. M. 2004. New interpretation of the origin of tiger's eye:

DO NOT COPY e48d507df5d1141@placeholder.9409-

Printed by: e48d507df5d1141@placeholder.94092.edu. Printing is for personal, private use only. No part of this book may be reproduced or transmitted without publisher's prior permission. Violators will be prosecuted.

Heaney, P. J., and Fisher, D. A. 2004. New interpretation of the origin of tiger's eye. Comment and Reply: REPLY. *Geology* **32, No.** 1, e45.

Heaney, P. J., and Post, J. E. 1992. The widespread distribution of a novel silica polymorph in microcrystalline quartz varieties. *Science* **255**, 441–443.

Heaney, P. J., Prewitt, C. T., and Gibbs, G. V. 1994. *Silica, Physical Behavior, Geochemical and Material Applications. Reviews in Mineralogy* **29**, 606 p.

Howie, R. A., Deer, W. A., Wise, W. S., and Zussman, J. 2004. *Rock-Forming Minerals, Volume 4B: Silica Minerals*, 2nd ed. The Geological Society, London, 982 p.

Kroll, H., and Ribbe, P. H. 1983. Lattice parameters, composition and Al, Si order in alkali feldspar, 2nd ed. *Reviews in Mineralogy* **2**, 57–100.

Michel-Lévy, A., and Munier-Chalmas, C. P. E. 1892. Memoire sur diverses formes affectees par le reseau elementaire du quartz. *Bulletin de la Société Française de Minéralogie* **15**, 159–190 + 4 plates.

Miehe, G., and Graetsch, H. 1992. Crystal structure of moganite: A new structure type for silica. *European Journal of Mineralogy* **4**, 693–706.

DO NOT COPY
e48d507df5d1141@placeholder.9409

Printed by: e48d507df5d1141@placeholder.94092.edu. Printing is for personal, private use only. No part of this book may be reproduced or transmitted without publisher's prior permission. Violators will be prosecuted.

LIST OF KEY TERMS

albite twinning
antiperthite
antirapakivi
Bøggild intergrowth
Carlsbad–albite method
chatoyant
composition
cryptoperthite
desiccant
devitrification
gangue
granophyric
graphic
Huttenlocher
iridescence
labradorescence
mesoperthite
Michel-Lévy method
microperthite
myrmekite
pericline twinning
peristerite
perthitic texture
physical properties
poikilitic
quenching
rapakivi
schiller
spherulite

DO NOT COPY
e48d507df5d1141@placeholder.9409

Printed by: e48d507df5d1141@placeholder.94092.edu. Printing is for personal, private use only. No part of this book may be reproduced or transmitted without publisher's prior permission. Violators will be prosecuted.

spherulite

structure

undulatory extinction

undulose extinction

DO NOT COPY

e48d507df5d1141@placeholder.9409

Printed by: e48d507df5d1141@placeholder.94092.edu. Printing is for personal, private use only. No part of this book may be reproduced or transmitted without publisher's prior permission. Violators will be prosecuted.

CHAPTER 13
Sheet Silicates

William D. Nesse
University of Northern Colorado

Graham B. Baird
University of Northern Colorado

DO NOT COPY
e48d507df5d1141@placeholder.9409

Printed by: e48d507df5d1141@placeholder.94092.edu. Printing is for personal, private use only. No part of this book may be reproduced or transmitted without publisher's prior permission. Violators will be prosecuted.

Introduction

Sheet silicates are abundant and important minerals, particularly in geological environments at or within about 20 km of the Earth's surface. They are common in intermediate and felsic igneous rocks and in many metamorphic rocks and are abundant in many sediments and sedimentary rocks, particularly if fine grained. All are hydrous, meaning that hydrogen is included in the structure, usually bonded to oxygen to form OH^-. Sheet silicates are also called **phyllosilicates**, a term derived from *phyllon*, a Greek word meaning "leaf," which refers to nearly all members of the group having a flaky or platy habit. For additional information about the sheet silicates, please refer to Bailey (1984, 1988), Velde (1995), and Mottana and others (2002).

DO NOT COPY
e48d507df5d1141@placeholder.9409

Printed by: e48d507df5d1141@placeholder.94092.edu. Printing is for personal, private use only. No part of this book may be reproduced or transmitted without publisher's prior permission. Violators will be prosecuted.

Structure and Classification

Sheet silicates are constructed of sheets of two different types: *O* or octahedral sheets, and *T* or tetrahedral sheets. Octahedral and tetrahedral sheets are joined together to form layers. The layers are in turn stacked and bonded together to form the repeating unit structure of the mineral. The volume between adjacent layers, called the **interlayer**, may be vacant, or it may contain cations and/or water. The single perfect cleavage characteristic of most sheet silicates is controlled by the weak bonding between layers. Note that the terms *sheet*, *layer*, and *unit structure* are used with quite specific meanings outlined here and are not interchangeable.

Octahedral (*O*) sheets (**Figure 13.1**) consist of two planes of the OH^- anionic group. The octahedral sites formed between the OH^- anionic groups are occupied in most cases by either divalent cations such as Fe^{2+} and Mg^{2+}, or trivalent cations such as Al^{3+} and Fe^{3+}. If the cations are divalent, three (= tri) out of three octahedral sites are occupied, forming a **trioctahedral** sheet with a general formula $X_3(OH)_6$ (**Figure 13.2a**). Because brucite [$Mg_3(OH)_6$] is a mineral constructed only of such sheets, trioctahedral sheets are sometimes referred to as brucite sheets. If the cations are trivalent, two (= di) out of three octahedral sites are occupied, and one is vacant, forming a **dioctahedral** sheet with a general formula $X_2(OH)_6$ (**Figure 13.2b**). Because gibbsite [$Al_2(OH)_6$] is a mineral constructed only of this type of sheet, dioctahedral sheets are sometimes referred to as gibbsite sheets. *Note that the "di" and "tri" refer to the occupancy of the octahedral sites, not the charge of the cations.* The cation charge for three octahedral sites is +6 in both trioctahedral and dioctahedral sheets, and the net charge of the sheets is zero. Successive sheets in both brucite and gibbsite are therefore bonded with weak electrostatic bonds.

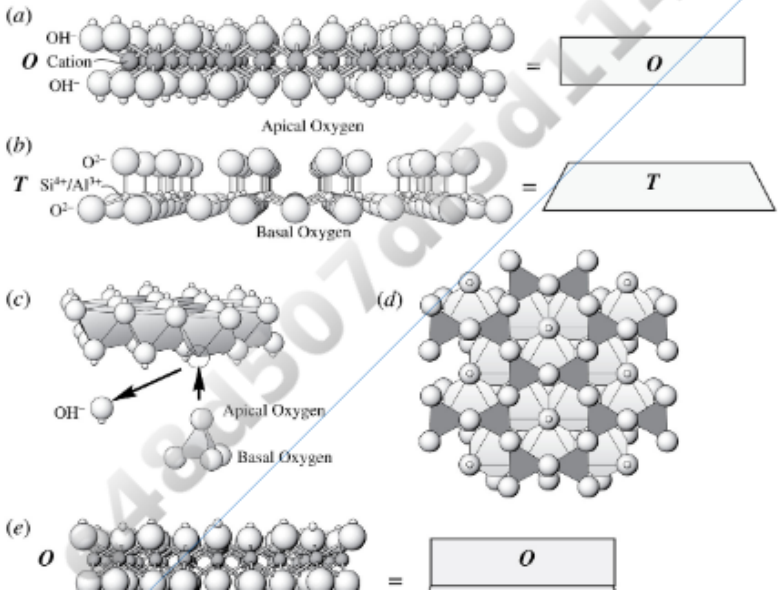

DO NOT COPY

Printed by: e48d507df5d1141@placeholder.94092.edu. Printing is for personal, private use only. No part of this book may be reproduced or transmitted without publisher's prior permission. Violators will be prosecuted.

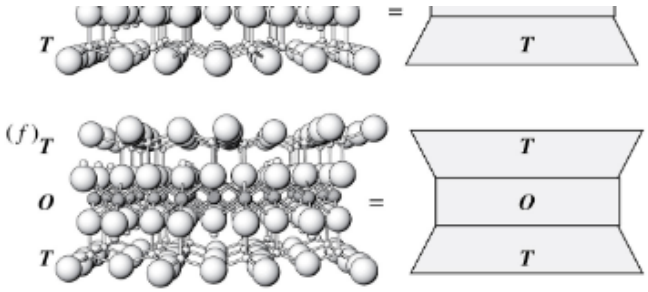

FIGURE 13.1 Sheet silicate sheets and layers. (*a*) An octahedral (*O*) sheet consists of two close-packed planes of OH^- with di- or trivalent cations occupying octahedral sites in between. The side view of an octahedral sheet is schematically represented by a rectangle. (*b*) A tetrahedral (*T*) sheet commonly consists of Si or Al tetrahedra; each tetrahedra shares three oxygen atoms with neighboring tetrahedra to form a continuous hexagonal mesh (cf. Figure 11.2f). The side view of a tetrahedral sheet is schematically represented by a trapezoid. (*c*) Combining a tetrahedral sheet with an octahedral sheet requires that an octahedral sheet OH^- is replaced by the apical oxygen of each tetrahedron. (*d*) Sheet-perpendicular view of a tetrahedral sheet combined with an octahedral sheet. The apical oxygens on the tetrahedra (dark shading) point away from the viewer and substitute for OH^- on the top of the octahedral sheet. The octahedra are shown with light shading. Note the openings formed in the center of the hexagonal rings of tetrahedra. (*e*) Side view of the bonded tetrahedral-octahedral sheets, forming a 1:1 or *TO* layer that is three layers of O^{2-}/OH^- thick. (*f*) Two tetrahedral sheets may bond on opposite sides of an octahedral sheet to form a 2:1 or *TOT* layer that is four layers of O^{2-}/OH^- thick. View larger image

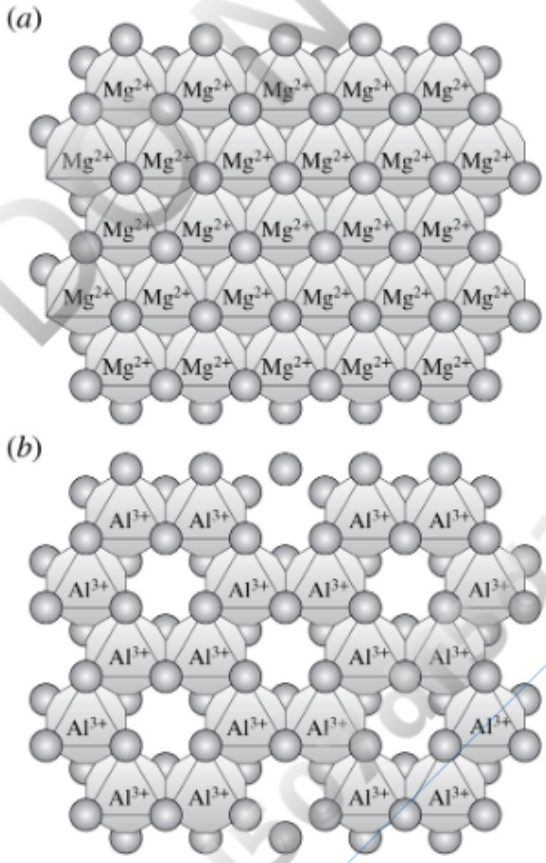

FIGURE 13.2 Schematic plan view of trioctahedral and dioctahedral sheets. (*a*) Trioctahedral. Divalent cations (usually Mg^{2+} or Fe^{2+}) occupy all (three out of three) octahedral sites. (*b*) Dioctahedral. Trivalent cations (usually Al^{3+}) occupy two-thirds of the potential octahedral sites. View larger image

DO NOT COPY e48d507df5d1141@placeholder.94092

Printed by: e48d507df5d1141@placeholder.94092.edu. Printing is for personal, private use only. No part of this book may be reproduced or transmitted without publisher's prior permission. Violators will be prosecuted.

As should be expected, site occupancy influences unit cell dimensions. In the dioctahedral sheet silicates, the *b* unit cell dimension is usually about 9 Å, whereas in the trioctahedral sheet silicates, *b* is usually about 9.2 Å. This can be measured by powder X-ray diffraction using the 060 reflection *d*-spacing. This reflection is one-sixth of the *b* dimension, or about 1.5 and 1.53 Å, respectively. Optical properties often differ between di- and trioctahedral sheet silicates. Most dioctahedral sheet silicates have an optic plane parallel to (100), whereas trioctahedral sheet silicates have an optic plane parallel to (010).

Tetrahedral (*T*) sheets (Figure 13.1b) consist of tetrahedrally coordinated cations, usually Si^{4+}, Al^{3+}, or less commonly Fe^{3+}, with a formula of Z_2O_5, where Z represents the cations. The tetrahedra are arranged in a mesh of 6-fold rings so that three O^{2-} on each tetrahedron are shared with adjacent tetrahedra (Figure 11.2f). The three shared oxygens are known as the basal oxygens, and the fourth, unshared oxygen is known as the apical oxygen. A tetrahedral sheet is therefore two oxygen atoms thick. If the cation is Si, the tetrahedral sheet is $Si_2O_5^{2-}$; substitution of Al^{3+} or Fe^{3+} for Si^{4+} increases the sheet's net negative charge.

The 6-fold symmetry of the tetrahedral ring mesh controls the nearly hexagonal shape of sheet-parallel cross sections of most sheet silicates (Figure 13.1d). However, for many such minerals, if a relatively thick euhedral specimen is considered, it is obvious that the sides of crystals are not perpendicular to the basal cleavage (parallel to the sheets), indicating the mineral does not have hexagonal symmetry. Most common sheet silicates are monoclinic, but the term *pseudohexagonal* may be appropriate given the sheet-parallel hexagonal shape so commonly observed (see Polytypism).

Tetrahedral sheets are always bonded to an octahedral sheet. This is done by sharing the apical oxygen of the tetrahedral sheet with the octahedral sheet (Figure 13.1c, d). This requires that an OH^- from the octahedral sheet is substituted by the apical oxygen.

The combination of one tetrahedral and an octahedral sheet is called a *TO* or 1:1 layer (Figure 13.1e) and consists of three planes of anions. On one side are the basal oxygen anions of the tetrahedral sheet and on the other are OH^--anionic groups of the octahedral sheet. The middle plane contains both octahedral sheet OH^- and tetrahedral sheet apical O^{2-}. The bonding of a *T* and an *O* sheet can be represented by the following equation to form a dioctahedral *TO* layer.

$$1T \text{ sheet} + 1O \text{ sheet} = TO \text{ layer} + \text{hydroxyl}$$
$$Si_2O_5^{2-} + Al_2(OH)_6 = Al_2Si_2O_5(OH)_4 + 2(OH)^-$$

The equivalent trioctahedral *TO* layer is $Mg_3Si_2O_5(OH)_4$.

A *TOT* or 2:1 layer is formed by joining a tetrahedral sheet to both sides of an octahedral

Printed by: e48d507df5d1141@placeholder.94092.edu. Printing is for personal, private use only. No part of this book may be reproduced or transmitted without publisher's prior permission. Violators will be prosecuted.

sheet (Figure 13.1f). These layers consist of four planes of anions. The outer two planes are the basal oxygen atoms of the tetrahedral sheets. The middle two planes contain both octahedral sheet OH^- and tetrahedral sheet apical O^{2-}. The bonding of two *T* layers and one *O* layer to form a dioctahedral *TOT* layer can be represented by the following equation

$$2T \text{ sheets} + 1O \text{ sheet} = TOT \text{ layer} + \text{hydroxyl}$$
$$2\left(Si_2O_5{}^{2-}\right) + Al_2(OH)_6 = Al_2Si_4O_{10}(OH)_2 + 4(OH)^-.$$

The equivalent trioctahedral layer is $Mg_3Si_4O_{10}(OH)_2$.

The *TO* and *TOT* layers are bound together in various ways to create the vast majority of the sheet silicates.

1:1 Layer Silicates

In the 1:1 group, the unit structure consists of repeating *TO* layers (**Figure 13.3a**, **Table 13.1**). The dioctahedral version is kaolinite [$Al_2Si_2O_5(OH)_4$], and the trioctahedral version is serpentine [$Mg_3Si_2O_5(OH)_4$]. Because 1:1 layers are electrically neutral, bonding between layers depends on weak electrostatic bonds, mostly hydrogen bonds. The result is that all 1:1 layer silicates are soft. The **layer repeat distance**, or the thickness of the package of layers that is repeated in the sheet silicate, is typically about 7 Å, so the *c* unit cell dimension is usually about 7 or 14 Å, depending on whether the unit cell is one or two layers thick.

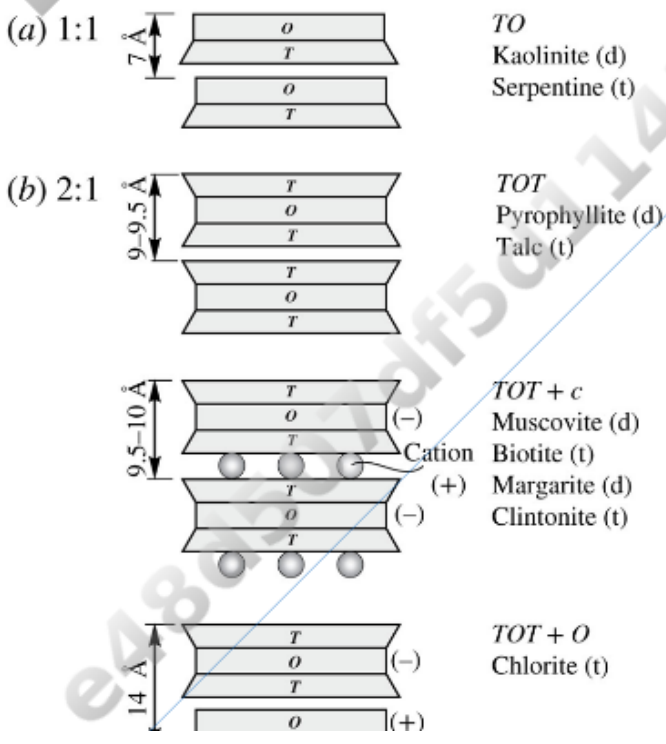

DO NOT COPY
e48d507df5d1141@placeholder.9409

Printed by: e48d507df5d1141@placeholder.94092.edu. Printing is for personal, private use only. No part of this book may be reproduced or transmitted without publisher's prior permission. Violators will be prosecuted.

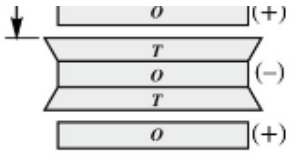

FIGURE 13.3 Schematic sheet silicate unit structures. Dioctahedral minerals are indicated with (d) and trioctahedral with (t). (*a*) 1:1 layer silicates. *TO* layers are bonded to each other with weak electrostatic bonds. (*b*) 2:1 layer silicates. Successive uncharged *TOT* layers are bonded together with weak electrostatic bonds (*TOT*, top). *TOT* layers with a net negative charge are bonded through interlayer cations (*TOT* + *c*, middle) or through *O* sheets with a net positive charge (*TOT* + *O*, bottom). View larger image

TABLE 13.1 Common Sheet Silicate Minerals

Group	Structure	Octahedral Sheet	Layer Composition	Interlayer	Unit Structure
1:1	*TO*	Dioctahedral	$Al_2Si_2O_5(OH)_4$	None	$Al_2Si_2O_5(OH)_4$
		Trioctahedral	$Mg_3Si_2O_5(OH)_4$	None	$Mg_3Si_2O_5(OH)_4$
2:1	*TOT*	Dioctahedral	$Al_2 Si_4O_{10}(OH)_2$	None	$Al_2Si_4O_{10}(OH)_2$
		Trioctahedral	$Mg_3Si_4O_{10}(OH)_2$	None	$Mg_3Si_4O_{10}(OH)_2$
	TOT + *c*	Dioctahedral	$Al_2AlSi_3O_{10}(OH)_2^{1-}$	K^+	$KAl_2AlSi_3O_{10}(OH)_2$
		Trioctahedral	$(Mg,Fe)_3AlSi_3O_{10}(OH)_2^{1-}$	K^+	$K(Mg,Fe)_3AlSi_3O_{10}(OH)$
	TOT + *c*	Dioctahedral	$Al_2Al_2Si_2O_{10}(OH)_2^{2-}$	Ca^{2+}	$CaAl_2Al_2Si_2O_{10}(OH)_2$
		Trioctahedral	$Mg_2Al(Al_3SiO_{10})(OH)_2^{2-}$	Ca^{2+}	$CaMg_2Al(Al_3SiO_{10})(OH)_2$
	TOT + *O*	Dioctahedral	$Mg_3(Si,Al)_4O_{10}(OH)_2^{1-}$	$(Mg,Al)_3(OH)_6^{1+}$	$Mg_3(Si,Al)_4O_{10}(OH)_2 \cdot (Mg,Al)_3(OH)_6$

2:1 Layer Silicates

The 2:1 layer silicates are constructed of repeating *TOT* layers. As just described, dioctahedral and trioctahedral *TOT* layers are electrically neutral; recall, however, that cations may substitute in octahedral and tetrahedral sites and change the net layer charge. The most important is substitution of Al^{3+} for Si^{4+} in tetrahedral sites so that *TOT* layers can have a net negative charge. The varieties of 2:1 structures depend on whether the *TOT* layers have a net negative charge, and if so, what is placed in the interlayer sites to balance the charge (**Figure 13.3b**).

TOT Structure

Talc and pyrophyllite (Table 13.1) are constructed of trioctahedral and dioctahedral *TOT* layers, respectively. Si^{4+} occupies all tetrahedral sites, so the *TOT* layers are electrically neutral, and bonding between adjacent *TOT* layers depends on van der Waals bonds. The

DO NOT COPY e48d507df5d1141@placeholder.94092

Printed by: e48d507df5d1141@placeholder.94092.edu. Printing is for personal, private use only. No part of this book may be reproduced or transmitted without publisher's prior permission. Violators will be prosecuted.

neutral, and bonding between adjacent *TOT* layers depends on van der Waals bonds. The unit structure therefore consists only of successive *TOT* layers. No additional cations are required to maintain charge balance. The weak interlayer bonding is responsible for the softness ($H = 1$) and waxy or greasy feel of both pyrophyllite and talc. The repeat distance of *TOT* layers in the unit structure is typically between 9 and 9.5 Å. The *c* unit cell dimension is therefore between 9 and 9.5 Å, or twice that dimension if the unit cell is two layers thick.

TOT + c Structure

Minerals with the *TOT* + *c* structure include the micas and a less common group of minerals called the brittle micas. The structure consists of *TOT* layers with some tetrahedral sites occupied by Al^{3+} rather than Si^{4+}. In the micas, the ratio of Al^{3+} to Si^{4+} in tetrahedral sites is 1:3. Dioctahedral *TOT* layers have the formula $Al_2(AlSi_3O_{10})(OH)_2{}^{1-}$; trioctahedral *TOT* layers have the formula $Mg_3(AlSi_3O_{10})(OH)_2{}^{1-}$ (Table 13.1). The net negative charge of these *TOT* layers is balanced by large monovalent cations such as K^+ found between the layers to form muscovite.

$$TOT\ \text{layer} + \text{interlayer}\ \ \text{cation}\ (c) = \text{unit}\ \ \text{structure}$$
$$\mathrm{Al_2(AlSi_3\,O_{10})(OH)_2{}^{1-} + K^+ =}$$
$$\mathrm{KAl_2(AlSi_3\,O_{10})(OH)_2(muscovite)}$$

The equivalent trioctahedral mica is $KMg_3(AlSi_3O_{10})(OH)_2$, which is phlogopite, a compositional end member of biotite. The interlayer cations are situated in the centers of the tetrahedra rings (Figures 13.1d and 11.2f) in the tetrahedral sheets. Because bonding between adjacent *TOT* layers includes both van der Waals bonds and stronger ionic bonds involving the interlayer cations, the hardness of micas is usually between 2 and 3. The layer repeat distance is usually between 9.5 and 10 Å, slightly larger than the *TOT* structure because of the addition of interlayer cations.

The brittle micas are constructed in the same way as the micas except that more tetrahedra are occupied by Al^{3+} rather than Si^{4+}. In margarite, half the tetrahedral sites are occupied by Al^{3+} so the *TOT* layers are $Al_2(Al_2Si_2O_{10})(OH)_2{}^{2-}$. To make up the net charge deficiency of −2, divalent cations, usually Ca^{2+}, occupy the interlayer sites.

$$TOT\ \ \text{layer} + \text{interlayer}\ \ \text{cation}\ \ (c) + TOT\ \ \text{unit}\ \ \text{structure}$$
$$\mathrm{Al_2(Al_2\,Si_2\,O_{10})(OH)_2{}^{2-} + Ca^{2+} =}$$
$$\mathrm{CaAl_2(Al_2\,Si_2\,O_{10})(OH)_2(margarite)}$$

The equivalent trioctahedral brittle mica would be $CaMg_3(Al_2Si_2O_{10})(OH)_2$, but this composition is not found. The most common trioctahedral brittle mica is clintonite, $\sim CaMg_2Al(Al_3SiO_{10})(OH)_2$. Roughly one-third of the octahedral sites contain Al^{3+}; the charge excess is balanced by substitution of additional Al^{3+} for Si^{4+} in tetrahedral sites.

DO NOT COPY e48d507df5d1141@placeholder.9409

Printed by: e48d507df5d1141@placeholder.94092.edu. Printing is for personal, private use only. No part of this book may be reproduced or transmitted without publisher's prior permission. Violators will be prosecuted.

TOT + O Structures

The *TOT* + *O* layer silicates are also known as 2:1 + 1 layer silicates; the chlorite group provides the most common examples. Conceptually, the structure can be derived from talc with the addition of an octahedral sheet (a brucite-like sheet) between the *TOT* layers.

$$\text{Talc-like layer} + \text{brucite-like sheet} = \text{chlorite unit structure}$$
$$Mg_3\,Si_4O_{10}(OH)_2 \;+\; Mg_3\,(OH)_6 =$$
$$Mg_3\,Si_4O_{10}(OH)_2 \cdot Mg_3\,(OH)_6$$

The contents of the *TOT* layer and the *O* sheet are written separately in the formula to emphasize that the two units are structurally distinct. The thickness of the combined *TOT* + *O* unit is about 14 Å, or about 9.5 Å for the *TOT* layer and about 4.5 Å for the *O* sheet.

In practice, the *TOT* layers in chlorite have a net negative charge because Al^{3+} substitutes for about a third of the Si^{4+} in the tetrahedral sites within the *TOT* layers, similar to the micas. In contrast, the interlayer octahedral sheet has a net positive charge produced by substitution of Al^{3+} and some Fe^{3+} for octahedrally coordinated divalent cations. The net negative charge on the *TOT* layer is balanced by the net positive charge on the interlayer *O* sheet. This results in somewhat stronger bonding between layers than would be expected if the layers were electrically neutral and bonded only with van der Waals bonds. The hardness of chlorite is 2–3, about the same as the micas.

Polytypism

The layer silicates have various polytypes controlled by the pattern in which adjacent layers are stacked. The micas provide a convenient example. Within a *TOT* layer, the top tetrahedral sheet must be offset relative to the bottom tetrahedral sheet so that the apical oxygen align with anion sites of the central octahedral sheet (**Figure 13.4a**). This offset can be directed along any of the three pseudohexagonal axes of the tetrahedral sheet. Adjacent *TOT* layers are aligned by the interlayer cations that must fit in the middle of the hexagonal rings of adjacent tetrahedral sheets. If the offset direction of successive *TOT* layers repeats itself in a systematic way, the periodicity along the *c* axis direction will be some multiple of the ~9.5° to 10 Å layer thickness. It turns out that six different polytypes are possible in the micas, with repeat distances along the *c* axis that range from ~10 Å (one *TOT* layer) to ~60 Å (six *TOT* layers). Of these, the most common are the $1M$ and $2M_1$ polytypes. In the $1M$ polytype, successive layers show the same direction of offset, and the unit cell is one *TOT* layer thick (**Figure 13.4b**). In the $2M_1$ polytype, the successive layers have offset vectors at 120°, and the unit cell is two *TOT* layers thick. Both have monoclinic symmetry.

(*a*)

DO NOT COPY

Printed by: e48d507df5d1141@placeholder.94092.edu. Printing is for personal, private use only. No part of this book may be reproduced or transmitted without publisher's prior permission. Violators will be prosecuted.

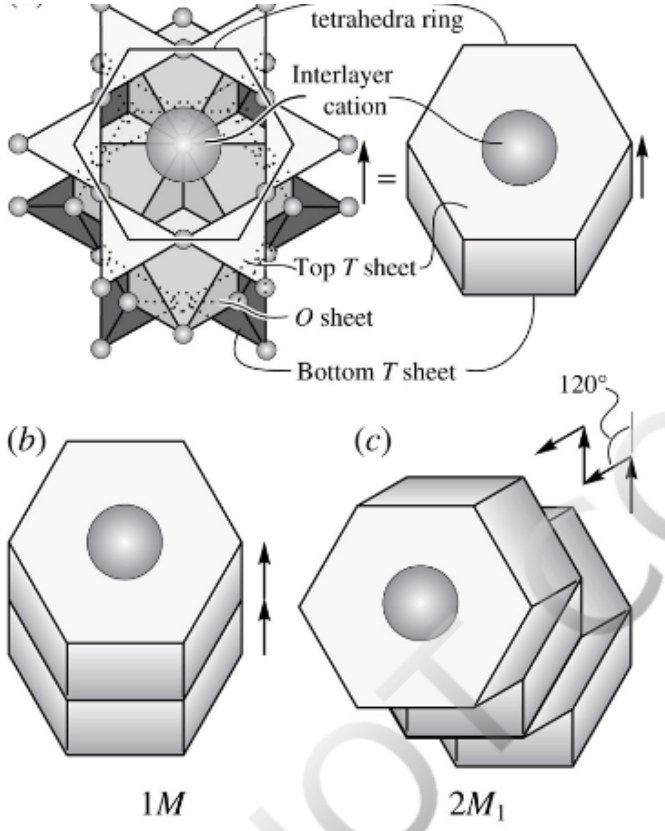

FIGURE 13.4 Polytypism in the micas. (*a*) In a *TOT* layer, the top *T* sheet must be offset relative to the bottom *T* sheet. Four octahedra from the octahedral sheet (*O*) are shown with a single ring of tetrahedra from the tetrahedral (*T*) sheets on the top (light shading) and bottom (dark shading). Adjacent *TOT* layers are aligned to each other by the interlayer cation that fits in the center of the tetrahedra rings. The shape on the right schematically represents the position of the tetrahedra rings on bottom and top. (*b*) 1*M* polytype. Adjacent *TOT* layers have the same direction of offset. (*c*) $2M_1$ polytype. The offset direction in adjacent *TOT* layers is at 120°, and the repeat distance is two layers.
View larger image

DO NOT COPY e48d507df5d1141@placeholder.9409

Printed by: e48d507df5d1141@placeholder.94092.edu. Printing is for personal, private use only. No part of this book may be reproduced or transmitted without publisher's prior permission. Violators will be prosecuted.

TO Structures (1:1)

Serpentine

DO NOT COPY

Å Å

Å

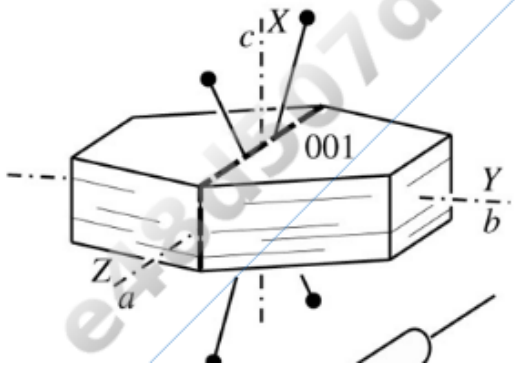

Printed by: e48d507df5d1141@placeholder.94092.edu. Printing is for personal, private use only. No part of this book may be reproduced or transmitted without publisher's prior permission. Violators will be prosecuted.

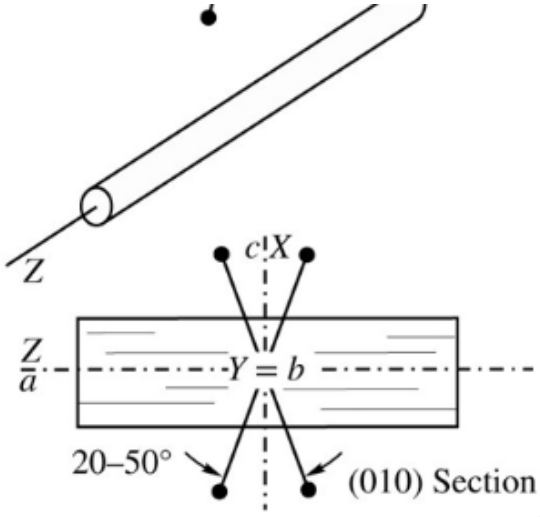

Structure The three varieties of serpentine are all trioctahedral *TO* sheet silicates. A problem with the ideal dioctahedral *TO* layer structure is that the lateral dimensions of the tetrahedral and octahedral sheets differ somewhat. The *a* and *b* dimensions of the trioctahedral sheets are about 5.4 and 9.3 Å, respectively, compared to about 5.0 and 8.7 Å for the tetrahedral sheets. The different varieties of serpentine correspond to the different ways the dimensional mismatch is accommodated.

CHRYSOTILE: The mismatch is accommodated by allowing the layers to curve (**Figure 13.5a**). As the layers grow, they curve into hollow fibers elongate parallel to *a*.

ANTIGORITE: The tetrahedral sheets are continuous, but periodically there is a reversal in the direction that the apical oxygens face and the side on which the octahedral sheet is bonded (**Figure 13.5b**). This yields a periodic reversal in the sense of curvature of the *TO* layers so that they remain essentially flat.

LIZARDITE: The pattern of tetrahedra in the *T* sheet is distorted so that it matches the *O* sheet (**Figure 13.5c**). In addition, substitution of Al^{3+} for Si^{4+} in tetrahedral sites increases its dimensions, and substitution of Al^{3+} for Mg^{2+} in octahedral sites decreases its dimensions so that the layer dimensions are more similar. Note that these coupled substitutions retain electric neutrality for the *TO* layer.

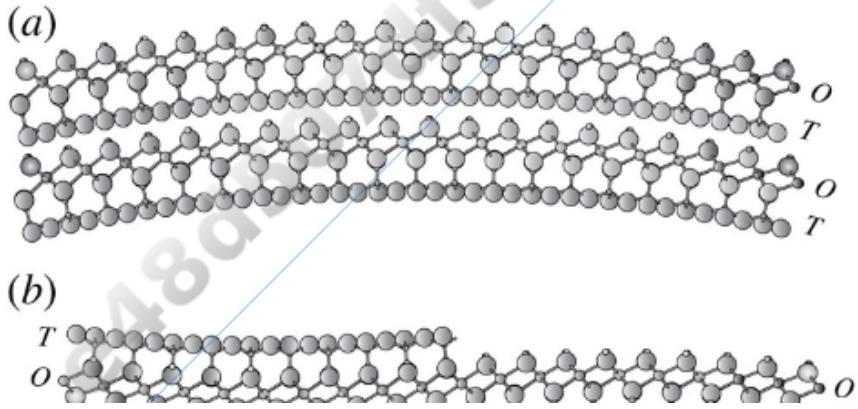

Printed by: e48d507df5d1141@placeholder.94092.edu. Printing is for personal, private use only. No part of this book may be reproduced or transmitted without publisher's prior permission. Violators will be prosecuted.

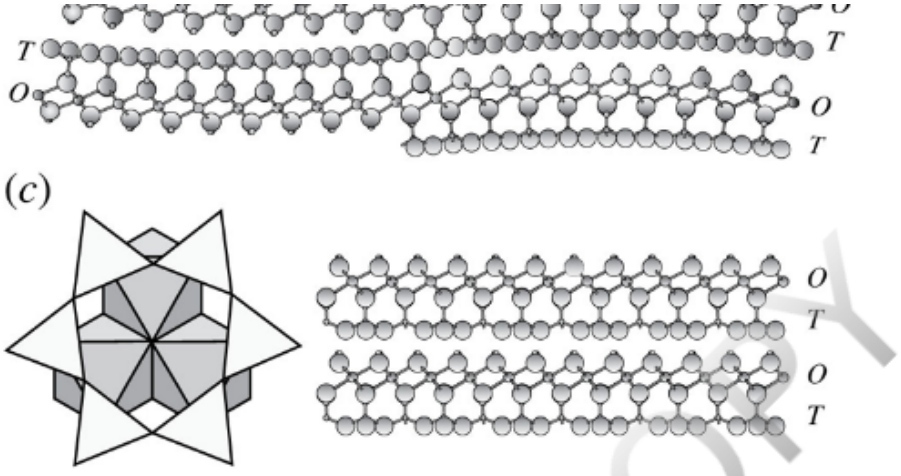

FIGURE 13.5 Serpentine structures. All are based on dioctahedral *TO* layers. (*a*) Chrysotile. Mismatch in the lateral dimensions of *T* and *O* sheets is accommodated by curving the *TO* layers so that they curve into fibers as they grow. (*b*) Antigorite. Continuous *TO* sheets contain reversals in the tetrahedra-facing direction. (*c*) Lizardite. The tetrahedra mesh (light shading) is distorted from its ideal hexagonal geometry to match the dimensions of the octahedral sheet. *TO* layers are relatively flat. View larger image

Composition Most serpentine is close to the ideal composition. Some substitution of Al^{3+} for Si^{4+}, or Al^{3+}, Fe^{3+}, or Fe^{2+} for Mg^{2+} may occur.

Form and Twinning See **Figure 13.6**. Chrysotile forms fine silky fibers in veins or matted masses. Fibers are elongate parallel to *a*. Individual fibers are submicroscopic, with diameters of 220 to 270 Å. Fibers are hollow tubes with an opening of about 70 Å across. The tube may be empty or may contain amorphous material. In many cases, what appears to be individual chrysotile fibers are actually parallel aggregates of many fibers. Lizardite is the most common serpentine variety and usually forms fine-grained greenish masses. Antigorite may be more or less micaceous and can form scaly or foliated masses. The different varieties may be intergrown. Habit is not a good guide for distinguishing between antigorite and lizardite.

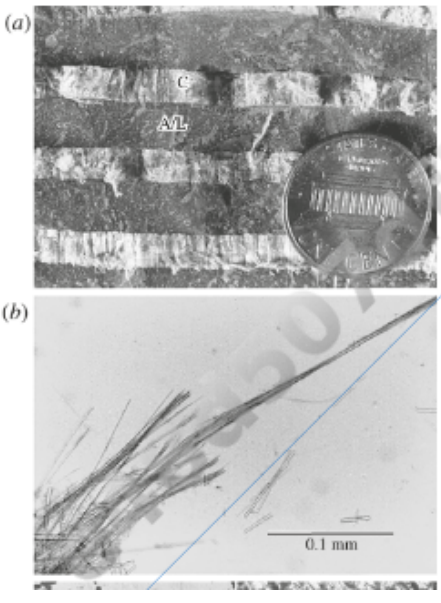

DO NOT COPY

Printed by: e48d507df5d1141@placeholder.94092.edu. Printing is for personal, private use only. No part of this book may be reproduced or transmitted without publisher's prior permission. Violators will be prosecuted.

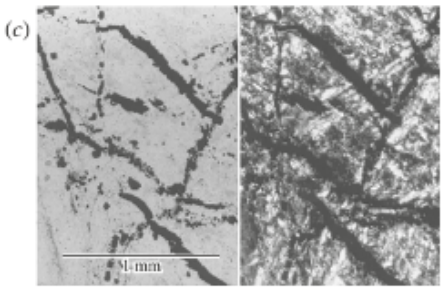

FIGURE 13.6 Serpentine. (*a*) Hand sample in which veins of cross-fiber chrysotile (C) alternate with antigorite/lizardite (A/L). (*b*) Fibers of chrysotile in grain mount. (*c*) Thin section of antigorite/lizardite. Plane light (*left*) and crossed polarizers (*right*). Note the abundance of opaque magnetite inclusions derived from Fe in the olivine and pyroxene that were altered to form the serpentine. View larger image

Each variety may occur in different polytypes. Identifiable twins are rare.

Cleavage Perfect {001} cleavage is visible only in antigorite. Chrysotile fibers are easily separated and are flexible.

Color Properties

Luster: Greasy or waxy in massive varieties, silky in chrysotile.

Color: Shades of green. Chrysotile is most commonly yellowish green, white, or gray. Lizardite and antigorite are commonly light to medium green but variable. Color, in part, is controlled by associated minerals. Magnetite may color samples gray, brown, or black, and hematite may yield shades of brown or red.

Streak: White.

Color in Thin Section: Colorless to pale green.

Pleochroism: Weak, from colorless to pale green or yellow-green. Fine-grained varieties may not be discernibly pleochroic because of random grain orientation. Chrysotile fibers are usually darker when aligned parallel to the vibration direction of the lower polarizer.

Optical Characteristics

Relief in Thin Section: Generally low to moderate positive; also low negative.

Optic Orientation: The slow ray vibration direction is generally parallel to fiber length in chrysotile, which shows parallel extinction. In antigorite $X \approx c$, $Y \approx b$, $Z \approx a$, also $X \approx c$, $Y \approx a$, $Z \approx b$, so the trace of cleavage is always length slow. The optic plane may be parallel to either {010} or {100}.

Indices of Refraction and Birefringence: Indices of refraction increase with Fe and Al content. Birefringence is low, and maximum interference color in thin section is rarely above first-order gray or white. The interference color may be anomalous. The mean index of refraction of lizardite is usually 1.54–1.55, and antigorite is slightly higher but

DO NOT COPY e48d507df5d1141@placeholder.9409

Printed by: e48d507df5d1141@placeholder.94092.edu. Printing is for personal, private use only. No part of this book may be reproduced or transmitted without publisher's prior permission. Violators will be prosecuted.

index of refraction of lizardite is usually 1.54–1.55, and antigorite is slightly higher but with substantial overlap. The indices of refraction of chrysotile are generally n_α = 1.532–1.549 and n_γ = 1.545–1.556.

Interference Figure: Usually difficult to obtain because of grain size. Basal sections of antigorite yield biaxial negative figures with $2V_x$ between roughly 20° and 50°. Optic axis dispersion may be either $r > v$ or $r < v$.

Comments: Chrysotile is distinctive because of its fibrous nature, but antigorite and lizardite cannot reliably be distinguished optically.

Alteration Oxidation of associated magnetite may stain serpentinite brown or yellow. Serpentine may be altered to chlorite or replaced by quartz.

Distinguishing Features

Hand Sample: The fibrous nature of chrysotile is distinctive. The fibrous amphiboles have different occurrences and are usually either blue or brown. They also grind to a powder in a mortar, whereas chrysotile forms a matted aggregate. Lizardite and antigorite usually form fine-grained green masses that cannot be distinguished from each other except with X-ray diffraction techniques. Chlorite also forms foliated green masses, but is more likely to be coarse grained and is commonly found as a constituent of metamorphosed sediments, whereas the serpentine minerals are found in altered mafic and ultramafic rocks.

Thin Section/Grain Mount: The fibrous amphiboles are distinguished from chrysotile by their higher birefringence and indices of refraction. Chlorite is more strongly pleochroic than antigorite, and brucite is uniaxial.

Occurrence Serpentine is commonly formed by hydrothermal alteration of mafic and ultramafic rocks, such as peridotite and pyroxenite, which contain olivine and pyroxene. The serpentine-rich rock known as serpentinite consists of masses of green antigorite/lizardite that may be cut by veins of chrysotile. Because serpentine contains relatively little iron, the iron content of the original olivine and pyroxene usually results in the formation of fine-grained magnetite disseminated through the serpentinite. The associated minerals may include talc, calcite, brucite, chlorite, magnetite, and chromite. One of the interesting byproducts of serpentization mineral reactions is the production of hydrogen and methane. These gases may provide the basis for a thriving microbial community, such as in deep-sea hydrothermal vents and hot springs. Serpentine also may be found in contact-metamorphosed carbonate rocks in association with calcite, dolomite, forsterite, magnesite, and calc-silicate minerals.

Use The fibrous nature, low thermal conductivity, and incombustibility of chrysotile have historically made it a valuable industrial mineral, and it is the most common of the minerals collectively known as asbestos (Chapter 1; **Box 13.1**). Chrysotile has been widely used in the automotive industry for the manufacture of brake shoes and clutch facings. When mixed with a binder, chrysotile has been used as a fireproof insulation on

DO NOT COPY e48d507df5d1141@placeholder.94092

Printed by: e48d507df5d1141@placeholder.94092.edu. Printing is for personal, private use only. No part of this book may be reproduced or transmitted without publisher's prior permission. Violators will be prosecuted.

facings. When mixed with a binder, chrysotile has been used as a fireproof insulation on boilers and heating pipes, and it has been used as a reinforcing fiber in floor tiles, acoustic ceiling tiles, plastics, roofing materials, adhesives, and a wide variety of other industrial and construction materials. It also can be made into a felt or woven into a fabric. Chrysotile accounts for about 98 percent of the current world production of asbestos; fibrous amphiboles (Chapter 14) are the remainder.

BOX 13.1

Asbestos

Asbestos is an industrial product made from at least one of a number of minerals that can crystallize into very long, hair-like fibers. This fibrous habit is called **asbestiform**, and the officially recognized asbestos minerals (in the United States) are chrysotile, tremolite, actinolite, anthophyllite, crocidolite (asbestiform riebeckite), and amosite (asbestiform cummingtonite–grunerite). Chrysotile is a sheet silicate (serpentine), while the rest are amphiboles (Chapter 14). Asbestos minerals are generally found in metamorphosed mafic and ultramafic rocks, but some varieties have been found in deposits of talc, vermiculite, and iron, plus other rock types, such as marbles.

Interest in asbestiform minerals stems from their high tensile strength, flexibility, low thermal conductivity, and incombustibility. These properties allow the fibers to be woven into cloth or manufactured into other materials that are effective insulators and/or fireproofing materials. Asbestos has been used in drywall, floor and ceiling tile, roofing materials, automotive parts, and so on.

Asbestos use became widespread by 1900, with chrysotile making up about 90 percent of varieties used. However, during the first half of the twentieth century, evidence that asbestos can pose a significant health risk emerged from studies of those with chronic exposure to high levels of asbestos dust. The exposure typically occurred in occupational settings, such as asbestos mining and milling, but chronic nonoccupational exposure from mine tailings and related settings also can pose a risk (e.g., Lee and others, 2021). More recently, evidence seems to suggest that merely living near rocks that likely contain asbestos, called naturally occurring asbestos, may also pose a health risk (e.g., Pan and others, 1999; Scarselli and others, 2021).

Some of these finds are debated (Ilgren, 2004), and the exact cause of asbestos-related disease is still unclear (e.g., Cui and others, 2019). It has been argued that only the amphibole varieties pose a health risk, but more recent work demonstrates that even chrysotile can cause the same diseases as the other varieties (Kanarek, 2011).

The pathologies linked to asbestos include the following.

- Lung cancer, particularly among smokers
- Mesothelioma, an otherwise rare cancer of the pleural lining of the lung cavity
- Asbestosis, a scarring of the lung tissue associated with asbestos fibers
- Pleural plaques, a localized scarring of the tissue lining the lung cavity

DO NOT COPY e48d507df5d1141@placeholder.9409-

Printed by: e48d507df5d1141@placeholder.94092.edu. Printing is for personal, private use only. No part of this book may be reproduced or transmitted without publisher's prior permission. Violators will be prosecuted.

A slight increase in the risk of cancer of the larynx, stomach, colon, and lymphoid tissues

Therefore, use of asbestos was banned in many countries in the last quarter of the twentieth century, though a handful of countries still continue its use, such as India, China, and Russia.

Though the topic of asbestos appears to be fairly straightforward in regard to what it is and its dangers, there actually is a great deal of uncertainty and controversy. First, only the six minerals identified above are regulated as asbestos in the United States. Other amphiboles varieties, such as richterite, can be asbestiform, or some other mineral entirely can be asbestiform as well. At least some of these other asbestiform minerals likely have similar health affects to those listed above, but they remain unregulated (Clintenbeard and others, 2002; Lee and others, 2008).

Criteria used to identify asbestos is also unclear and is possibly misleading. The United States Occupational Safety and Health Administration (OSHA, standard number 1910.1001) regulates fiber exposure to the listed minerals above and defines a fiber as at least 5 μm in length with a length to width ratio of 3:1. This criteria is problematic; it does not distinguish between an asbestiform fiber produced by growth of the mineral and a fiber produced by being cleaved from a large grain. Amphiboles have two cleavages oriented about 60° to each other (Chapter 14), which allows them easily break into fragments that fit the listed fiber criteria. Some argue that there appears to be no evidence that fibers of asbestos minerals formed by cleaving are any more dangerous than common rock dust (Ilgren, 2004), but this is not believed by all (c.f. Finkelstein, 2012). It is important to note that common rock dust does pose health risks; see the discussions of silicosis in Chapters 1 and 12, for example. Likely, certain properties are produced when asbestos minerals grow in the asbestiform that are not present if a grain of the same size and dimensions is produced by cleaving from a larger grain.

Confident identification of asbestos mineralogy and whether fibers are asbestiform or are formed through cleaving requires one or more of the following techniques or instruments: petrographic microscope (Chapter 7), X-ray diffraction (Chapter 8), transmission electron microscopy (Chapter 8), and scanning electron microscopy/electron microprobe (Chapter 9). Also routinely used is the phase-contrast microscope, which modifies a grain's brightness by its refractive index. In general, confident fiber identification in asbestos studies that may aid in risk determination is difficult and time consuming and requires extensive expertise.

Over the years, billions of dollars have been spent to remove asbestos from homes, schools, factories, and office buildings in an attempt to mitigate risk. A complicating and often overlooked factor in these efforts is that regulatory actions and reports in the public media may fail to distinguish among the different materials that pose significantly different health risks. Either the material is not truly asbestiform or it is asbestiform but removal creates a greater risk than leaving the material in place, based on its form or location (e.g., Lee et al., 2008).

In summary, there is no doubt that asbestiform chrysotile and amphiboles (and

Printed by: e48d507df5d1141@placeholder.94092.edu. Printing is for personal, private use only. No part of this book may be reproduced or transmitted without publisher's prior permission. Violators will be prosecuted.

In summary, there is no doubt that asbestiform chrysotile and amphiboles (and likely others similar materials) pose a significant health risk and exposure should be avoided. However, current regulations fail to distinguish between asbestos materials that pose significant risk from materials that carry the same health risks as common rock dust. Further, more work is needed to establish the relative risks of different asbestos types based on the details of exposure. Such information is necessary to better define appropriate actions based the material and potential for exposure. For additional discussion of asbestos, consult Guthrie and Mossman (1993), Clintenbeard and others (2002), Gunter and others (2007), and Lee and others (2008).

Kaolinite

Kaolinite, like serpentine, has a *TO* structure, but it is a clay mineral, so it is described in a later section on the clay mineral group.

DO NOT COPY
e48d507df5d1141@placeholder.9409

Printed by: e48d507df5d1141@placeholder.94092.edu. Printing is for personal, private use only. No part of this book may be reproduced or transmitted without publisher's prior permission. Violators will be prosecuted.

TOT Structures (2:1)

Talc

Å Å

Å

DO NOT COPY

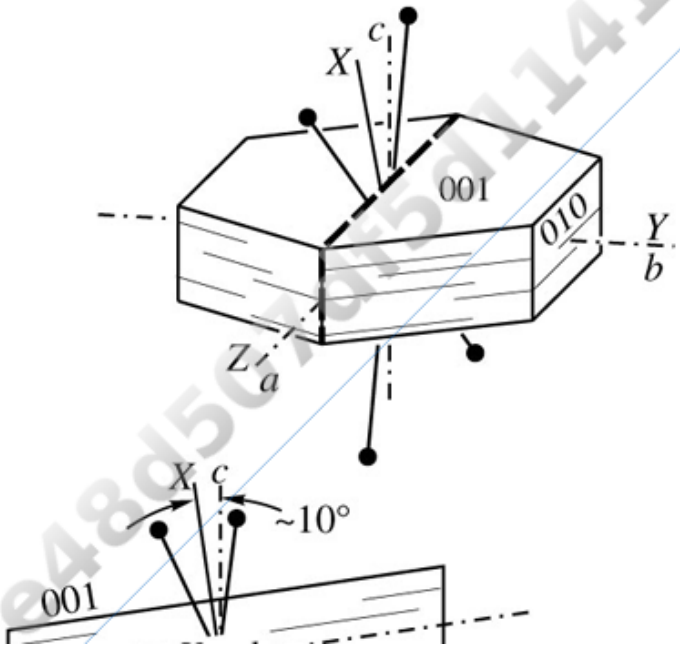

Printed by: e48d507df5d1141@placeholder.94092.edu. Printing is for personal, private use only. No part of this book may be reproduced or transmitted without publisher's prior permission. Violators will be prosecuted.

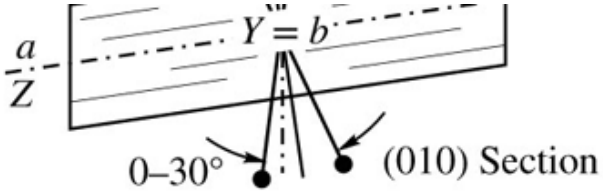

Composition The composition of most talc is relatively close to the ideal formula, with minor substitution of Fe, Mn, or other cations for Mg in the octahedral sites and of Al for Si in the tetrahedral sites. The Fe-bearing analog of talc is minnesotaite [$Fe_3Si_4O_{10}(OH)_2$], which is found in metamorphic iron formations.

Form and Twinning Talc forms foliated, radiating, or randomly oriented aggregates of irregular flakes or fibers resembling the micas. Talc has a waxy feel and is sectile. Individual flakes are easily bent but are not elastic. Fine-grained compact and massive varieties are sometimes referred to as steatite.

Cleavage {001} perfect. Sectile. Thin fragments flexible but not elastic.

Color Properties

Luster: Pearly to somewhat greasy.

Color: White, light to dark green, brown.

Streak: White.

Color in Thin Section: Colorless.

Pleochroism: None.

Optical Characteristics

Relief in Thin Section: Low to moderate positive.

Optic Orientation: $X \wedge c \approx +10°$, $Y \approx b$, $Z \approx a$, optic plane = (010).

Indices of Refraction and Birefringence: Indices of refraction increase with increasing Fe content. Birefringence is strong, and the maximum interference color seen in thin section is usually third order. Basal sections and fragments lying on the cleavage display low birefringence because n_β and n_γ are nearly the same. Minnesotaite has indices of refraction in the vicinity of $n_\alpha = 1.592$, $n_\beta = 1.622$, and $n_\gamma = 1.623$.

Interference figure: Cleavage flakes and basal sections yield essentially centered acute bisectrix figures with $2V_x = 0–30°$. Optic axis dispersion is weak to moderate, $r > v$.

Alteration Talc may alter to chlorite.

Distinguishing Features

DO NOT COPY e48d507df5d1141@placeholder.9409

Printed by: e48d507df5d1141@placeholder.94092.edu. Printing is for personal, private use only. No part of this book may be reproduced or transmitted without publisher's prior permission. Violators will be prosecuted.

Hand Sample: Characterized by softness, micaceous habit, and waxy feel. X-ray diffraction may be required to distinguish talc from pyrophyllite.

Thin Section/Grain Mount: Similar to muscovite and pyrophyllite, but with smaller $2V$. Phlogopite has higher indices of refraction, has stronger relief in thin section, and is usually pale brown. Brucite is uniaxial positive and often shows anomalous interference colors and lower birefringence. Minnesotaite has higher indices of refraction, is weakly colored in shades of pale yellow and green, has a small $2V$, and is typically fibrous.

Occurrence Talc is found in hydrothermally altered mafic and ultramafic rocks in association with serpentine, magnesite, and relict grains of olivine and pyroxene. It also forms in the metamorphism of siliceous dolomite, where it may be associated with calcite, dolomite, tremolite, and related calc-silicate minerals. Talc is a major constituent of talc schist derived by metamorphism of mafic igneous rocks or mafic volcaniclastic sedimentary rocks. These rocks also may contain magnetite, tremolite, chlorite, anthophyllite, or serpentine.

Use Talc is a versatile mineral used in a wide variety of industrial and consumer products. Industrial applications include use as a filler and colorant in paint, plastics, rubber, paper, and various caulking and roofing compounds, and as a lubricant. Talc is sprinkled on asphalt roofing shingles to keep the shingles from sticking together during transport and storage. It also is an ingredient in certain ceramic products. Consumer products that contain talc include cosmetic products such as lipstick, facial products, antiperspirant sticks, and various creams and lotions. Talc, in the form of talcum powder, is a major ingredient in a wide variety of baby, body, and foot powders available at any drug store. Some studies have claimed correlations between chronic talc exposure and cancer, though the risk may be from associated asbestiform minerals, not the talc. Talc is approved by the U.S. Food and Drug Administration for use in preventing the recurrence of pleural effusions, an abnormal collection of fluid between the thin layers of tissue (pleura) lining the lung and the wall of the chest cavity.

Pyrophyllite

$$Al_2(Si_4O_{10})(OH)_2$$

$$\text{Monoclinic } 2/m$$

$$a = \text{ - } 5.17 \text{ Å},\ b = \text{ - } 8.96 \text{ Å},$$
$$c = \text{ - } 18.68 \text{ Å},\ \beta = \text{ - } 100^\circ,$$
$$Z = 4$$

$$\text{Triclinic } \left(\bar{1} \text{ or } 1\right)$$

$$a = \text{ - } 5.16 \text{ Å},\ b = \text{ - } 8.96 \text{ Å},$$

DO NOT COPY e48d507df5d1141@placeholder.9409

Printed by: e48d507df5d1141@placeholder.94092.edu. Printing is for personal, private use only. No part of this book may be reproduced or transmitted without publisher's prior permission. Violators will be prosecuted.

$$c = \text{ - } 9.35\ \text{Å},\ \alpha = \text{ - } 91^\circ,$$
$$\beta = \text{ - } 100^\circ,\ \gamma = \text{ - } 90^\circ,\ Z = 2$$

$$H = 1 - 2$$

$$G = 2.65 - 2.90$$

$$\text{Biaxial } (-)$$

$$n_\alpha = 1.552 - 1.556$$

$$n_\beta = 1.586 - 1.589$$

$$n_\gamma = 1.596 - 1.601$$

$$\delta = 0.043 - \text{ - } 0.05$$

$$2V_x = 53 - 62^\circ$$

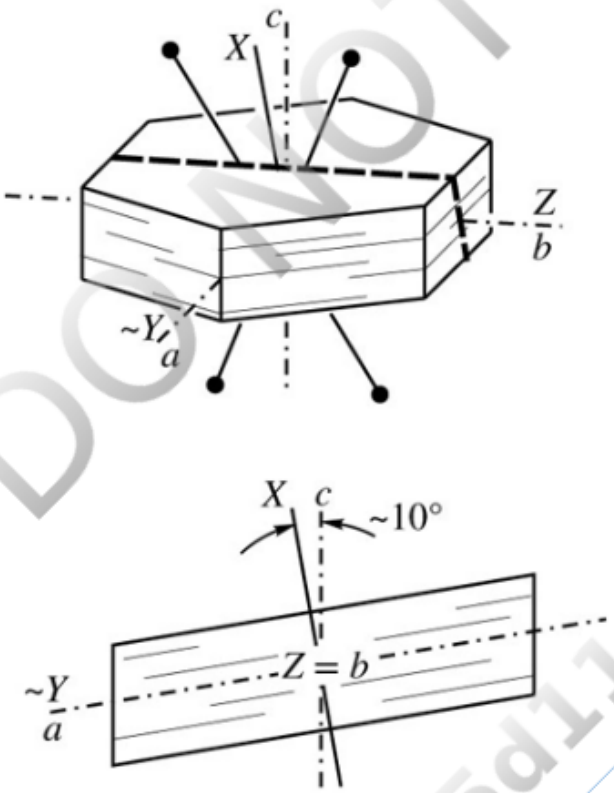

(010) Section

Structure The most common structure is monoclinic and the unit cell is two *TOT* layers thick. The stacking sequence of *TOT* layers in the triclinic polytype is somewhat different and results in a unit cell that is one *TOT* layer thick.

Composition The composition is usually close to the ideal formula, with the most common substitutions being Al^{3+} for Si^{4+} and Mg^{2+}, Fe^{2+}, Fe^{3+}, or Ti^{4+} for Al^{3+}. Minor Ca^{2+}, Na^{+}, or K^{+} may be present, presumably in interlayer sites.

DO NOT COPY e48d507df5d1141@placeholder.9409

Printed by: e48d507df5d1141@placeholder.94092.edu. Printing is for personal, private use only. No part of this book may be reproduced or transmitted without publisher's prior permission. Violators will be prosecuted.

Form and Twinning Pyrophyllite is commonly found as foliated, radiating, columnar, or massive aggregates of mica-like flakes. Also fibrous. Individual grains may be easily bent. Twins are not generally observed.

Cleavage As with the micas, perfect {001} cleavage controls fragment orientation. Folia are flexible but not elastic. Masses are somewhat sectile.

Color Properties

Luster: Pearly to dull.

Color: White, pale blue, yellow, grayish, or brownish green.

Streak: White.

Color in Thin Section: Colorless.

Pleochroism: None.

Optical Characteristics

Relief in Thin Section: Low to moderate positive.

Optic Orientation: $X \wedge c \approx +10°$, $Y = a$, $Z = b$.

Indices of Refraction and Birefringence: Indices of refraction vary within a small range and birefringence is high (~0.05).

Interference Figure: Cleavage fragments and basal sections yield nearly centered acute bisectrix figures with $2V_x = 53–62°$. Optic axis dispersion is weak, $r > v$.

Alteration Not readily altered.

Distinguishing Features

Hand Sample: Distinguished from muscovite by being softer, having a greasy or waxy luster and feel, and because cleavage flakes are not elastic. Pyrophyllite is difficult to distinguish from talc in hand sample and may require either optical or X-ray tests to confirm the identity.

Thin Section/Grain Mount: Distinguished from muscovite and talc by higher $2V$ and from kaolinite and other clay minerals by higher birefringence.

Occurrence Pyrophyllite is a relatively uncommon mineral that occurs in moderately low-grade, Al-rich metamorphic rocks such as metapelites, metabauxite, or quartzite, or as a result of hydrothermal alteration of aluminous minerals such as the feldspars, muscovite, aluminum silicates, corundum, or topaz.

Use Pyrophyllite's most common use is in the manufacturing of **refractory** materials, or

DO NOT COPY e48d507df5d1141@placeholder.9409

Printed by: e48d507df5d1141@placeholder.94092.edu. Printing is for personal, private use only. No part of this book may be reproduced or transmitted without publisher's prior permission. Violators will be prosecuted.

materials with a very high melting point. Such refractory materials are used to line kilns, furnaces, and ladles in foundries and related industries. Pyrophyllite is also used to manufacture ceramics, including wall and floor tile, pottery, china, and porcelain plumbing fixtures. Finely ground pyrophyllite is used as a carrier for pesticides or as a blending agent in animal feeds or fertilizers. Commercial applications include use as a filler in paint, plastics, cements, and construction materials such as gypsum wallboard. Pyrophyllite also is used in cosmetics.

DO NOT COPY
e48d507df5d1141@placeholder.9409

Printed by: e48d507df5d1141@placeholder.94092.edu. Printing is for personal, private use only. No part of this book may be reproduced or transmitted without publisher's prior permission. Violators will be prosecuted.

TOT + c Structures: Mica Minerals (2:1)

Micas make up about 4 percent of the Earth's crust and are found in igneous, sedimentary, and metamorphic rocks. The current recommended classification (Rieder and others, 1998) identifies 11 dioctahedral and 16 trioctahedral mica end members. Of the dioctahedral micas, only muscovite and paragonite are at all common. Of the trioctahedral micas, only the biotite and lepidolite series are common. Both glauconite and illite can be considered to be interlayer-cation-deficient dioctahedral micas. Glauconite is described with the micas, and illite is described with the clay minerals in a later section. Lithium can be an important constituent in many micas, but it cannot be detected or is not analyzed for with conventional analysis techniques (Chapter 9). Techniques to estimate Li content of micas based on the other constituents identified in electron microprobe analyses are described by Tischendorf and others (1997).

Muscovite

DO NOT COPY
e48d507df5d1141@placeholder.9409

Printed by: e48d507df5d1141@placeholder.94092.edu. Printing is for personal, private use only. No part of this book may be reproduced or transmitted without publisher's prior permission. Violators will be prosecuted.

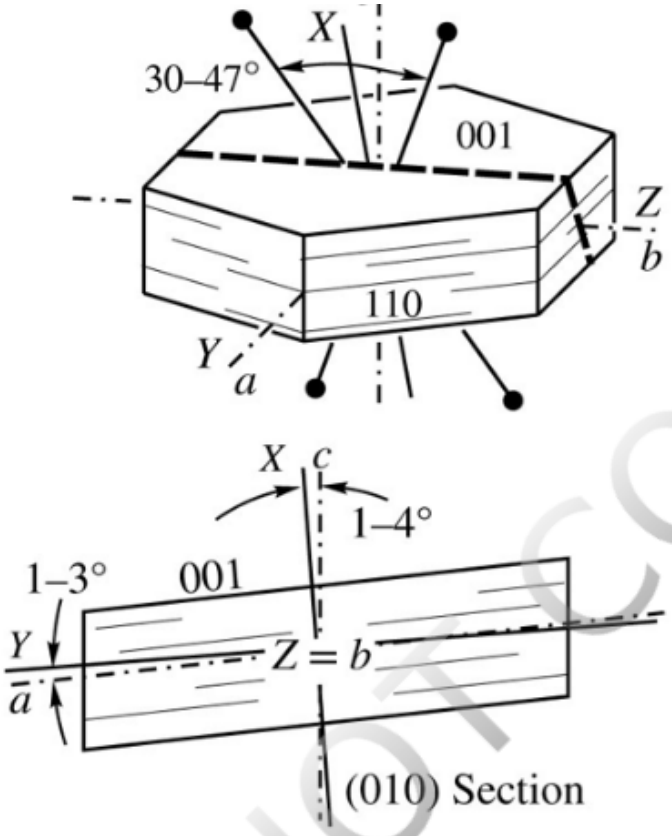

Structure The large majority of muscovite has a unit cell that is two *TOT* layers thick, consisting of the $2M_1$ polytype (Figure 13.4c). Some fine-grained muscovite from low-grade metamorphic rocks or sediments has a unit cell that is only one *TOT* layer thick and is known as a $1M$ polytype (Figure 13.4b).

Composition The common substitutions include the following.

For K	Na, Rb, Cs, Ca, Ba
For $^{[VI]}$Al	Mg, Fe^{2+}, Fe^{3+}, Mn, Li, Cr, Ti, V
For (OH)	F, Cl
Tetrahedral site	$AlSi_3$ to $Al_{0.5}Si_{3.5}$

Paragonite $[NaAl_2(AlSi_3O_{10})(OH)_2]$ is the sodium analog of muscovite; but because of differences in the sizes of Na and K cations, solid solution is limited to no more than about 10 percent Na in muscovite and 20 percent K in paragonite. In X-ray powder diffraction patterns of muscovite, d_{002} decreases with increasing Na content, reflecting its smaller size, and the d_{060} dimension increases with substitution of Al for Si in tetrahedral sites. The term phengite is applied to muscovite with Si greater than three atoms per formula units. Such compositions require that Mg^{2+} or Fe^{2+} substitute for Al^{3+} to compensate for the higher charge of the additional Si. For all muscovites, F commonly replaces some of the OH, but usually in amounts less than about 20 percent. Chlorine is restricted to less than about 1 percent of the OH sites.

Form and Twinning See **Figure 13.7**. Well-formed tabular crystals with

Printed by: e48d507df5d1141@placeholder.94092.edu. Printing is for personal, private use only. No part of this book may be reproduced or transmitted without publisher's prior permission. Violators will be prosecuted.

pseudohexagonal outlines are common in granitic pegmatite and may be referred to as "books" of muscovite in reference to the thin cleavage sheets that can be readily peeled from the crystal like the pages of a book. Muscovite is more commonly found as micaceous flakes or tablets with irregular outlines, tabular parallel to {001}. Sericite is a name given to fine-grained white mica, usually muscovite or paragonite, commonly produced by the hydrothermal alteration of feldspars or other K- and/or Al-bearing minerals (Figure 7.63e).

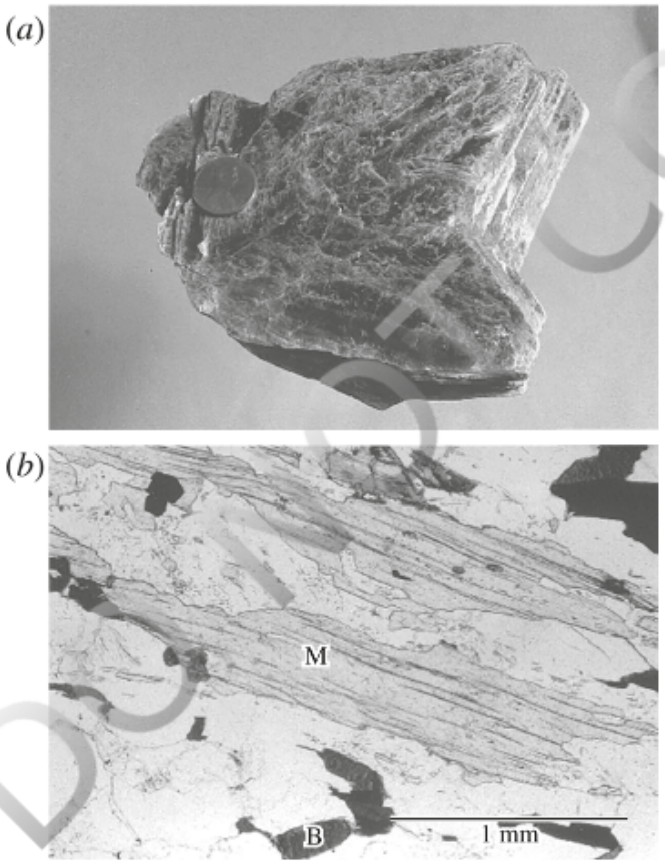

FIGURE 13.7 Muscovite. (*a*) Muscovite "book" with [310] twin from a granitic pegmatite. (*b*) Photomicrograph of muscovite (M) with dark biotite (B) and colorless quartz in a mica schist. View larger image

Twins by rotation on [310] with a {001} composition plane are not commonly seen except in large well-formed crystals from granitic pegmatites (Figure 13.7a).

Cleavage Perfect cleavage on {001} strongly controls fragment orientation. Individual cleavage folia are flexible and elastic.

Color Properties

Luster: Vitreous.

Color: Colorless or light shades of green, red, or brown. The edges of muscovite books may appear quite dark, particularly when grains are viewed as part of the rock in which they are found.

DO NOT COPY e48d507df5d1141@placeholder.9409

Printed by: e48d507df5d1141@placeholder.94092.edu. Printing is for personal, private use only. No part of this book may be reproduced or transmitted without publisher's prior permission. Violators will be prosecuted.

they are found.

Streak: White.

Color in Thin Section: Colorless.

Pleochroism: None.

Optical Characteristics

Relief in Thin Section: Modest positive, changes somewhat with rotation.

Optic Orientation: $X \wedge c = +1° - +4°$, $Y \wedge a = +1° - +3°$, $Z = b$.

Indices of Refraction and Birefringence: Relatively pure muscovite has indices of refraction at the lower end of the range given above. Substitution of Fe, Mg, Ti, Mn, Cr, and V causes indices of refraction to increase. Substitution of Li causes indices of refraction to decrease. Birefringence is high; interference colors in thin section may be as high as third order, and vivid colors of the second order are typical. Paragonite has indices of refraction $n_\alpha = 1.564–1.580$, $n_\beta = 1.594–1.609$, $n_\gamma = 1.594–1.618$, $\delta = 0.028–0.038$.

Interference Figure: $2V_x$ is between 28° and 47°; relatively pure muscovite has a $2V_x$ in the upper end of this range. Cleavage fragments yield nearly centered acute bisectrix figures. In thin section, good figures are yielded by grains that do not display cleavage and have lower to middle first-order colors. To the uninitiated, these grains do not look particularly like muscovite. Optic axis dispersion is noticeable with $r > v$. Paragonite is biaxial negative with $2V_x = 0–40°$.

Alteration Not readily altered, but may be converted to clay minerals by weathering.

Distinguishing Features

Hand Sample: Habit and perfect cleavage producing elastic folia distinguish the micas from most other minerals. Biotite, unless very rich in Mg (phlogopite), is usually much darker colored. Pyrophyllite and talc have a greasy luster and feel and are softer. Chlorite is distinctly green and has inelastic cleavage folia. The perfect cleavage and silvery-white color is usually visible with a hand lens even in small grains in rocks and sediment. If only the edges of grains are visible, their dark color may lead to misidentification as biotite or hornblende. Roughing up the edge of a grain with a sharp knifepoint helps resolve any ambiguity. Paragonite and some lepidolite have the same hand-sample properties, and the term white mica may be used as a generic term for any of them.

Thin Section/Grain Mount: Muscovite is distinguished from most biotite by lack of color. Mg-rich biotite (phlogopite) may be nearly colorless but has smaller $2V$. Talc and pyrophyllite are distinguished by having smaller and larger $2V$, respectively. A distinctive feature of muscovite and biotite is a speckled appearance seen near extinction that is called **"bird's-eye" extinction** in reference to a similar pattern seen in sugar maple

DO NOT COPY e48d507df5d1141@placeholder.94092

Printed by: e48d507df5d1141@placeholder.94092.edu. Printing is for personal, private use only. No part of this book may be reproduced or transmitted without publisher's prior permission. Violators will be prosecuted.

wood (*Acer saccharum*) cut parallel to the grain. The bird's-eye extinction pattern is due to pitting of the grain surface caused by the grinding needed for thin section fabrication. Paragonite has very similar optical properties, and X-ray or staining techniques (Laduron, 1971) may be needed to distinguish them.

Occurrence Muscovite is a very common mineral found in igneous, metamorphic, and sedimentary rocks. In igneous rocks, it is a common constituent of granitic pegmatite, granite, granodiorite, aplite, and related felsic rocks. It is somewhat less common in felsic volcanic rocks. Sericite is widespread in many igneous rocks, produced by the hydrothermal or late-stage magmatic alteration of feldspars and other minerals. The alteration may be selective, replacing only the cores of plagioclase grains or selected twin lamellae. Muscovite is a constituent of a wide variety of metamorphic rocks including slate, phyllite, schist, gneiss, hornfels, and quartzite, which are produced by metamorphism of common sedimentary rocks. Clastic sediments derived from igneous and metamorphic rock terranes and not subjected to extensive weathering or transport often contain muscovite. It is therefore a common mineral in arkosic sandstone and related clastic sedimentary rocks.

Paragonite can be found in low- to medium-grade regional metamorphic rocks and is probably more abundant than often thought, as it is commonly misidentified as muscovite. With increasing metamorphic pressures, muscovite compositions become more Si-rich, such that muscovite found in rocks subjected to the blueschist or eclogite metamorphic facies conditions is usually identified as phengite with Si > 3 atoms per formula unit. The correlation between muscovite Si content and pressure is strong enough that it has been used to calculate metamorphic pressures (Coggon and Holland, 2002).

Use One of the earliest uses for muscovite was as a substitute for glass because thin-cleaved sheets are transparent. It is still used, though infrequently, for viewing windows in industrial furnaces and ovens. It is now widely used in electronics and industrial applications. Muscovite sheets and ground muscovite are used in the electronics industry to make components as diverse as capacitors, transistors, insulators, and the windows on microwave tubes used in microwave ovens. Industrial applications include use as a filler in plastic, paint, and wallboard cement; coatings on wallpaper to produce a silky luster; mold-release agents in the manufacture of automobile tires; and in drilling mud. Consumer products that contain muscovite include nail polish, lipstick, and eye shadow. The subtle luster seen in many colored cosmetic creams is from pulverized muscovite. The use of muscovite as a treatment for colitis and other problems associated with the digestive tract has been studied in rats, particularly in China.

Biotite

$$K(Fe, Mg)_3 AlSi_3 O_{10}(OH)_2$$

DO NOT COPY e48d507df5d1141@placeholder.9409

Printed by: e48d507df5d1141@placeholder.94092.edu. Printing is for personal, private use only. No part of this book may be reproduced or transmitted without publisher's prior permission. Violators will be prosecuted.

Monoclinic $2/m$

$a = \text{ - } 5.3$ Å, $b = \text{ - } 9.2$ Å,
$c = \text{ - } 10.3$ Å, $\beta = \text{ - } 100^\circ$,
$Z = 2$

$H = 2 - 3$

$G = 2.7 - 3.3$

Biaxial $(-)$

$n_\alpha = 1.522 - 1.625$

$n_\beta = 1.548 - 1.696$

$n_\gamma = 1.549 - 1.696$

$\delta = 0.03 - 0.07$

$2V_x = 0 - 25^\circ$

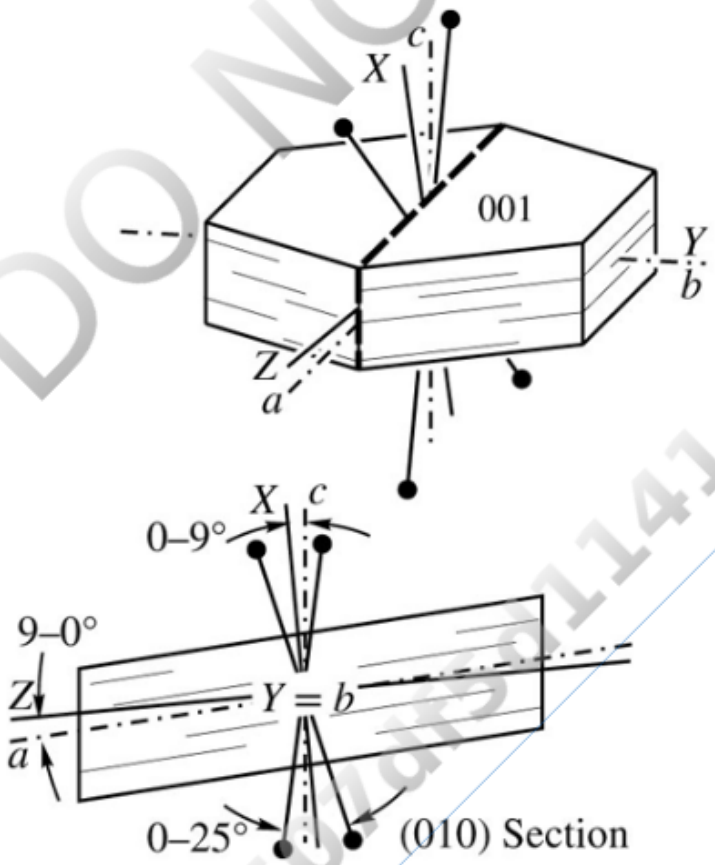

Structure Most biotite consists of the 1*M* polytype (Figure 13.4b), meaning that the unit cell is one *TOT* layer thick. Polytypes that are two or three *TOT* layers thick are known.

Composition The composition variation can be represented by four end members (**Figure 13.8**):

DO NOT COPY
e48d507df5d1141@placeholder.9409

Printed by: e48d507df5d1141@placeholder.94092.edu. Printing is for personal, private use only. No part of this book may be reproduced or transmitted without publisher's prior permission. Violators will be prosecuted.

(Figure 13.8):

$$KFe_3(AlSi_3O_{10})(OH)_2 : \text{Annite}$$

$$KMg_3(AlSi_3O_{10})(OH)_2 : \text{Phlogopite}$$

$$KFe_2Al(Al_2Si_2O_{10})(OH)_2 : \text{Siderophyllite}$$

$$KMg_2Al(Al_2Si_2O_{10})(OH)_2 : \text{Eastonite}$$

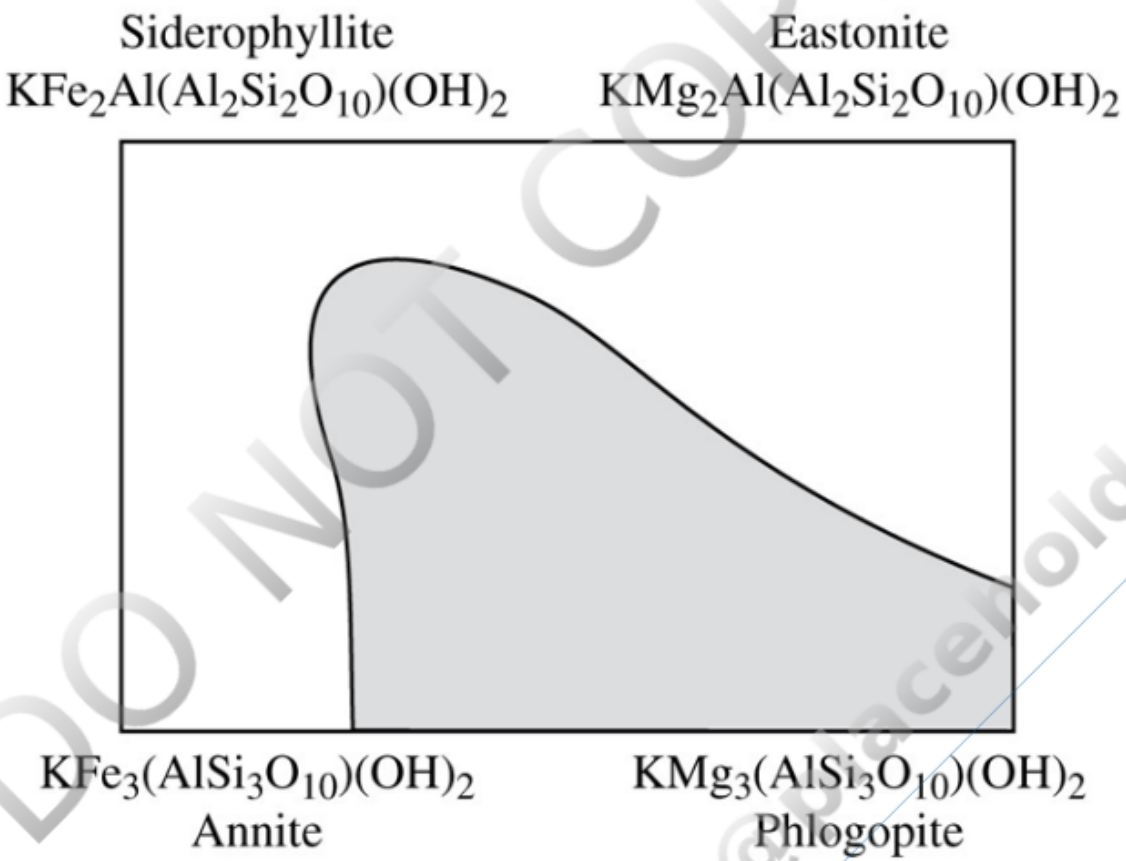

FIGURE 13.8 Compositional range of common biotite (shaded). Adapted from Deer and others (1992). View larger image

Other substitutions include Na and, to a lesser degree, Ca, Ba, Rb, and Cs for K, and substantial amounts of F and some Cl for OH. Samples with substantial amounts of Fe^{3+} substituting in the octahedral sites balanced by substituting O for OH in the hydroxyl sites are known as oxybiotite.

Form and Twinning See **Figure 13.9**. Crystals are usually tabular with a pseudohexagonal outline and are relatively common, particularly in felsic volcanic rocks. Also found as micaceous or tabular grains or grains with irregular shapes. Twins with {001} composition planes are possible but not usually observed.

(*a*)

DO NOT COPY e48d507df5d1141@placeholder.9409

Printed by: e48d507df5d1141@placeholder.94092.edu. Printing is for personal, private use only. No part of this book may be reproduced or transmitted without publisher's prior permission. Violators will be prosecuted.

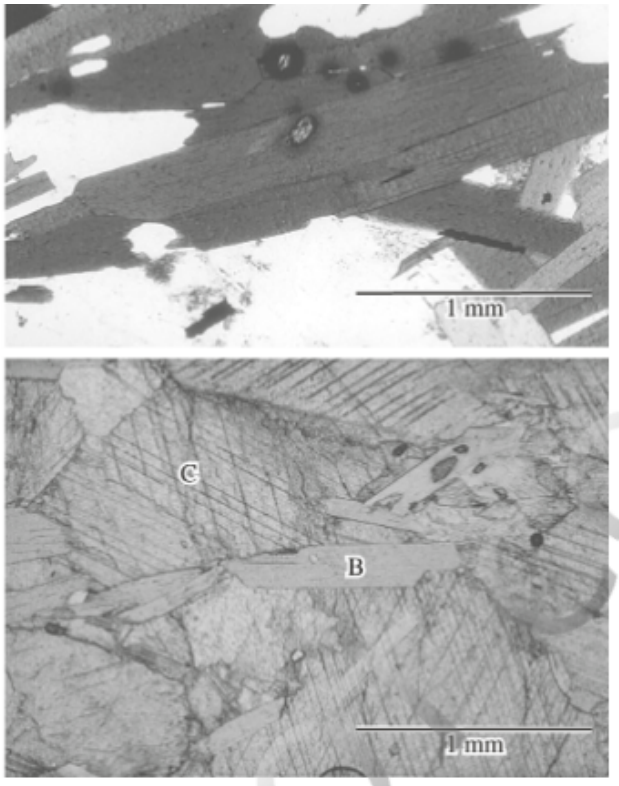

FIGURE 13.9 Biotite. (*a*) Foliated biotite grains in mica schist. Note the dark pleochroic halos around radioactive inclusions. (*b*) Pale grains of phlogopite-rich biotite (B) with calcite (C) in marble.
View larger image

Cleavage Perfect {001} cleavage produces thin elastic folia.

Color Properties

Luster: Vitreous.

Color: Most commonly black or dark brown, sometimes greenish or reddish brown. Phlogopite-rich biotite may be light brown to nearly colorless.

Streak: White or gray.

Color in Thin Section: Typically brown, brownish green, or reddish brown and strongly pleochroic. Phlogopite-rich biotite may be pale brown to nearly colorless.

Pleochroism: Usually strongly pleochroic with $Z \approx Y > X$, so grains are darker when the trace of cleavage is parallel to the lower polarizer vibration direction. The common colors are X = colorless, light tan, pale greenish brown, pale green; $Y \approx Z$ = brown, olive-brown, dark green, dark red-brown. The intensity of color generally increases with increasing iron content. Cleavage flakes and basal sections yield darker colors with little pleochroism. Pleochroic halos are common around minerals, such as zircon, containing radioactive elements (Figures 5.32 and 13.9).

Optical Characteristics

DO NOT COPY e48d507df5d1141@placeholder.9409

Printed by: e48d507df5d1141@placeholder.94092.edu. Printing is for personal, private use only. No part of this book may be reproduced or transmitted without publisher's prior permission. Violators will be prosecuted.

Relief in Thin Section: Moderate to moderately high positive, low if Mg-rich.

Optic Orientation: $X \wedge c = 0° - +9°$, $Y = b$, $Z = a$.

Indices of Refraction and Birefringence: n_γ increases approximately linearly from about 1.55 to 1.70 as mole percent octahedral Fe increases from 0 to 100 percent, but this relationship is not tightly constrained. Birefringence is strong and yields maximum interference colors in the third or even fourth order, but these colors are usually masked by the mineral color. Cleavage flakes and sections cut parallel to {001} show low birefringence.

Interference Figure: Cleavage flakes and sections cut parallel to {001} yield nearly centered acute bisectrix figures with several orders of isochromes and small $2V$. Some biotite may have $2V$ of 0°, meaning that it is sensibly uniaxial. Optic axis dispersion is weak, usually $r < v$, less commonly $r > v$ for Mg-rich varieties.

Alteration Biotite commonly alters to chlorite, which may mantle grains or be interleaved along cleavage traces (Figure 13.12). Biotite also may alter to clay minerals, including vermiculite and sericite, Fe–Ti oxides, and epidote.

Distinguishing Features

Hand Sample: Dark color and micaceous habit with one perfect cleavage distinguish biotite. Phlogopite may be light brown or tan. Small grains in sediment may appear gold colored, particularly to the uninitiated when panning for gold. Grains seen in cross section may be mistaken for hornblende, but careful examination with a hand lens will reveal that only one cleavage is present, and a sharp knifepoint can be used to test hardness.

Thin Section/Grain Mount: Dark color, strong pleochroism, high birefringence, common bird's eye extinction, and micaceous habit distinguish biotite. Light-colored phlogopite resembles muscovite but has a smaller $2V$. Chlorite is more distinctly green, has lower birefringence, and usually displays anomalous interference colors. Stilpnomelane is similar but lacks bird's-eye extinction and has a second cleavage at nearly right angles to the basal cleavage.

Occurrence Biotite is a very common mineral. In igneous rocks it is characteristic of felsic rocks such as granite, granodiorite, quartz diorite, pegmatite, syenite, nepheline syenite, rhyolite, rhyodacite, dacite, and phonolite. It also is found as a late-stage magmatic product in more mafic rocks including diorite, gabbro, norite, and anorthosite. Mg-rich biotite (phlogopite) is found in peridotite and other ultramafic varieties.

In metamorphic rocks, biotite is very common in a wide variety of hornfels, phyllites, schists, and gneisses and may persist from greenschist to upper amphibolite facies. Mg-rich biotite is also found in marble and related metamorphosed carbonate-rich rocks.

Biotite also is a relatively common detrital mineral, particularly in immature sediments,

DO NOT COPY e48d507df5d1141@placeholder.9409

Printed by: e48d507df5d1141@placeholder.94092.edu. Printing is for personal, private use only. No part of this book may be reproduced or transmitted without publisher's prior permission. Violators will be prosecuted.

Biotite also is a relatively common detrital mineral, particularly in immature sediments, but it converts to clay minerals with extended weathering and transport.

Use Biotite has few commercial uses, but vermiculite, most of which is a hydrated alteration product of biotite, has numerous applications. Alteration, accomplished either by weathering or hydrothermal processes, results in leaching of interlayer K cations and replacement with Ca, Mg, and H_2O, with ion exchanges in other sites as needed to maintain charge neutrality. As a result of adding the interlayer water, vermiculite is prone to dramatic expansion when heated. It owes its name to the observation that books of vermiculite, when heated, expand into wormlike shapes. For most applications, the vermiculite is heated to force it to expand, producing a low-density product that looks like dirty fluffed-up biotite. Expanded vermiculite is used as an insulation material, a filler in gypsum wallboard or other construction materials, and in a variety of other industrial applications. The most frequently encountered use is as an additive in potting soil.

Lepidolite

$$K(Li, Al)_3(Si, Al)_4O_{10}(F, OH)_2$$

Monoclinic $2/m$

$a = 5.209$ Å, $b = 9.011$ Å,
$c = 10.149$ Å, $\beta = 100.77^\circ$,
$Z = 2$

$H = 2.5$ on {001} cleavage surfaces, - 3 to 4 at right angles

$G = 2.8 - 2.9$

Biaxial (−)

$n_\alpha = 1.524 - 1.548$

$n_\beta = 1.543 - 1.585$

$n_\gamma = 1.545 - 1.587$

$\delta = 0.018 - 0.039$

$2V_x = 0 - 58^\circ$

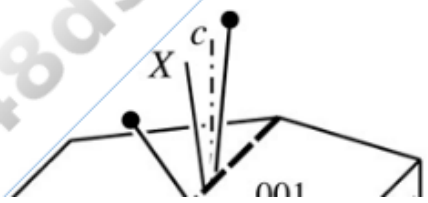

DO NOT COPY
e48d507df5d1141@placeholder.9409

Printed by: e48d507df5d1141@placeholder.94092.edu. Printing is for personal, private use only. No part of this book may be reproduced or transmitted without publisher's prior permission. Violators will be prosecuted.

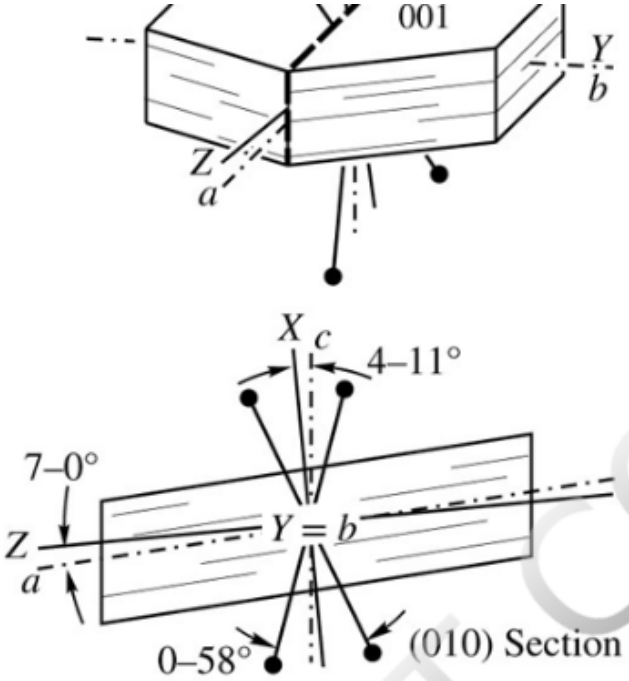

Structure Lepidolite is considered a trioctahedral mica in which the octahedral sites are occupied by Li^{1+} and Al^{3+}. The common polytypes are the $1M$ and $2M_2$ (similar to the $2M_1$ in Figure 13.4), except the offset vector is at 60° rather than 120°.

Composition The ideal end-member compositions of lepidolite are polylithionite [$KLi_2AlSi_4O_{10}(F)_2$] and trilithionite [$KLi_{1.5}Al_{1.5}AlSi_3O_{10}(F)_2$]. Most lepidolite has five out of six of the octahedral sites occupied, but compositions intermediate between lepidolite and muscovite are not uncommon (**Figure 13.10**). Interlayered mixtures of trioctahedral lepidolite and dioctahedral muscovite may account for compositions intermediate between lepidolite and muscovite. Considerable amounts of Na, Rb, and Cs may substitute for K, and Fe, Mg, and Mn may enter octahedral sites. OH and F readily substitute for each other. The lilac or pink color of lepidolite is usually a consequence of small amounts of Mn^{3+}.

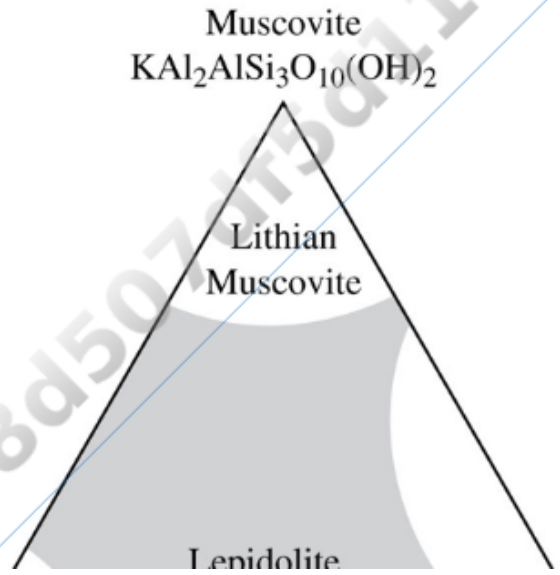

Printed by: e48d507df5d1141@placeholder.94092.edu. Printing is for personal, private use only. No part of this book may be reproduced or transmitted without publisher's prior permission. Violators will be prosecuted.

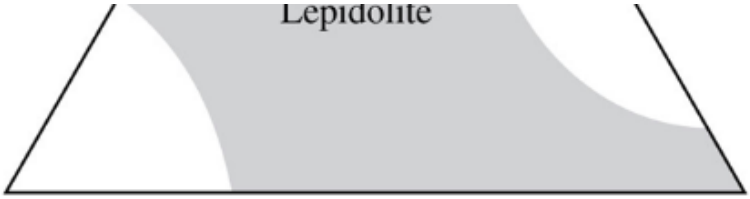

FIGURE 13.10 Lepidolite composition. The common range is shown with the shaded area. View larger image

Form and Twinning Lepidolite is micaceous and commonly forms scaly–granular masses, less commonly as large cleavable plates. Twins by rotation on [310] with a {001} composition plane are uncommon and not generally observed in hand sample.

Cleavage Perfect cleavage on {001}, like the other micas. Individual cleavage folia are flexible and elastic.

Color Properties

Luster: Vitreous.

Color: Usually some shade of lilac or pink, also purple, rose-red, violet-gray, yellowish, white, or colorless.

Streak: White.

Color in Thin Section: Usually colorless; less commonly pale pink.

Pleochroism: If present, pleochroism is X = almost colorless, $Y = Z$ = pink, pale violet.

Optical Characteristics

Relief in Thin Section: Low to moderate positive, which may change with stage rotation. The value of n_α is less than 1.540 for some samples, so relief may be low negative for some grain orientations.

Optic Orientation: $X \wedge c = +11°$ to $+4°$, $Y = b$, $Z \wedge c = 0°$ to $+7°$.

Indices of Refraction and Birefringence: Optical properties vary, mostly depending on the amount of Mn and Fe^{3+} rather than with Li content. In general, higher indices of refraction are associated with higher iron content; most lepidolite has indices of refraction in the middle of the ranges above. Birefringence is moderately high, and bright colors of the second order are typical in thin section.

Interference Figure: Cleavage flakes yield nearly centered acute bisectrix interference figures with $2V_x$ usually between 30° and 50°. Optic axis dispersion is $r > v$.

DO NOT COPY e48d507df5d1141@placeholder.9409

Printed by: e48d507df5d1141@placeholder.94092.edu. Printing is for personal, private use only. No part of this book may be reproduced or transmitted without publisher's prior permission. Violators will be prosecuted.

Alteration Not readily altered.

Distinguishing Features

Hand Sample: The micaceous habit and pink color are usually diagnostic. However, rose-colored muscovite is very similar, and X-ray diffraction or chemical tests may be required to distinguish between the two minerals. Unfortunately, standard electron microprobe and X-ray fluorescence analyses are not capable of detecting Li because of its low atomic weight.

Thin Section: Lepidolite closely resembles muscovite but has lower indices of refraction and lower birefringence. If present, the pale pink pleochroism is a useful diagnostic property.

Occurrence Lepidolite is the most common Li-bearing mineral and is usually found in Li-bearing granitic pegmatites associated with other Li-bearing minerals such as spodumene and amblygonite. Other associated minerals include quartz, feldspars, tourmaline, beryl, and topaz. Lepidolite may be formed by direct crystallization from Li-rich pegmatitic fluids, by metasomatic replacement of previously crystallized biotite or muscovite, or by reaction between K-feldspar and Li-rich pegmatitic fluids. It has infrequently been found in high-temperature hydrothermal deposits and in granitic igneous rocks.

Use Lepidolite has been mined as a source of lithium, although most lithium is derived from spodumene or from Li-bearing brines. Lepidolite has a number of historical uses as a pharmaceutical and is currently used in the preparation of various homeopathic remedies, but it is not approved for any use by the U.S. Food and Drug Administration.

Glauconite

$$(\mathrm{K, Ca, Na})_{1.6}(\mathrm{Fe}^{3+}, \mathrm{Al, Mg, Fe}^{2+})_4$$
$$\mathrm{Si}_{7.3}\mathrm{Al}_{0.7}\mathrm{O}_{20}(\mathrm{OH})_4$$

$$\text{Monoclinic } 2/m$$

$$a = \text{ - } 5.23 \text{ Å},\ b = \text{ - } 9.06 \text{ Å},$$
$$c = \text{ - } 10.15 \text{ Å},\ \beta = \text{ - } 101^\circ,$$
$$Z = 1$$

$$H = 2$$

$$G = 2.4 - 2.95$$

$$\text{Biaxial } (-)$$

$$n_\alpha = 1.59 - 1.61$$

$$n_\beta = 1.61 - 1.64$$

DO NOT COPY e48d507df5d1141@placeholder.94092

Printed by: e48d507df5d1141@placeholder.94092.edu. Printing is for personal, private use only. No part of this book may be reproduced or transmitted without publisher's prior permission. Violators will be prosecuted.

$$n_\beta = 1.61 - 1.64$$

$$n_\gamma = 1.61 - 1.64$$

$$\delta = \text{ - } 0.02 - 0.03$$

$$2V_x = 0 - 20^\circ$$

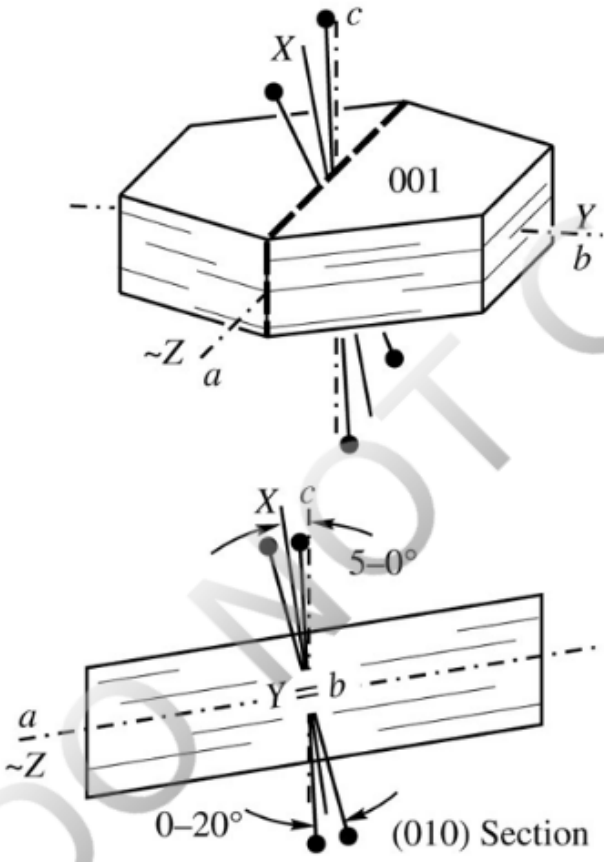

Structure and Composition Glauconite is a dioctahedral layer silicate whose structure is similar to that of muscovite. In contrast to muscovite, the octahedral sites of glauconite contain Fe^{3+} as the most abundant cation, along with some Mg^{2+}, Fe^{2+}, and Al^{3+}. The Al^{3+} content of the tetrahedral sites is lower than in muscovite to compensate for divalent cations in octahedral sites. Glauconite can be considered a clay mineral similar to illite (see later discussion of clay minerals), but its distinctive common occurrence warrants a separate description. Some glauconite contains layers of expanding clay structure. Celadonite is a similar mineral with less octahedral Fe^{3+} and Al^{3+}, more octahedral Mg^{2+} and Fe^{2+}, and less tetrahedral Al^{3+}.

Form and Twinning See **Figure 13.11**. Glauconite most commonly forms small green pellets or granules in sedimentary rocks, or forms casts of foraminifera or other microfossils. In most cases, these are all composed of aggregates of fine, irregular flakes. Celadonite is usually found as radiating masses in vesicles and other voids in basaltic igneous rocks. No twinning is reported.

DO NOT COPY e48d507df5d1141@placeholder.9409

Printed by: e48d507df5d1141@placeholder.94092.edu. Printing is for personal, private use only. No part of this book may be reproduced or transmitted without publisher's prior permission. Violators will be prosecuted.

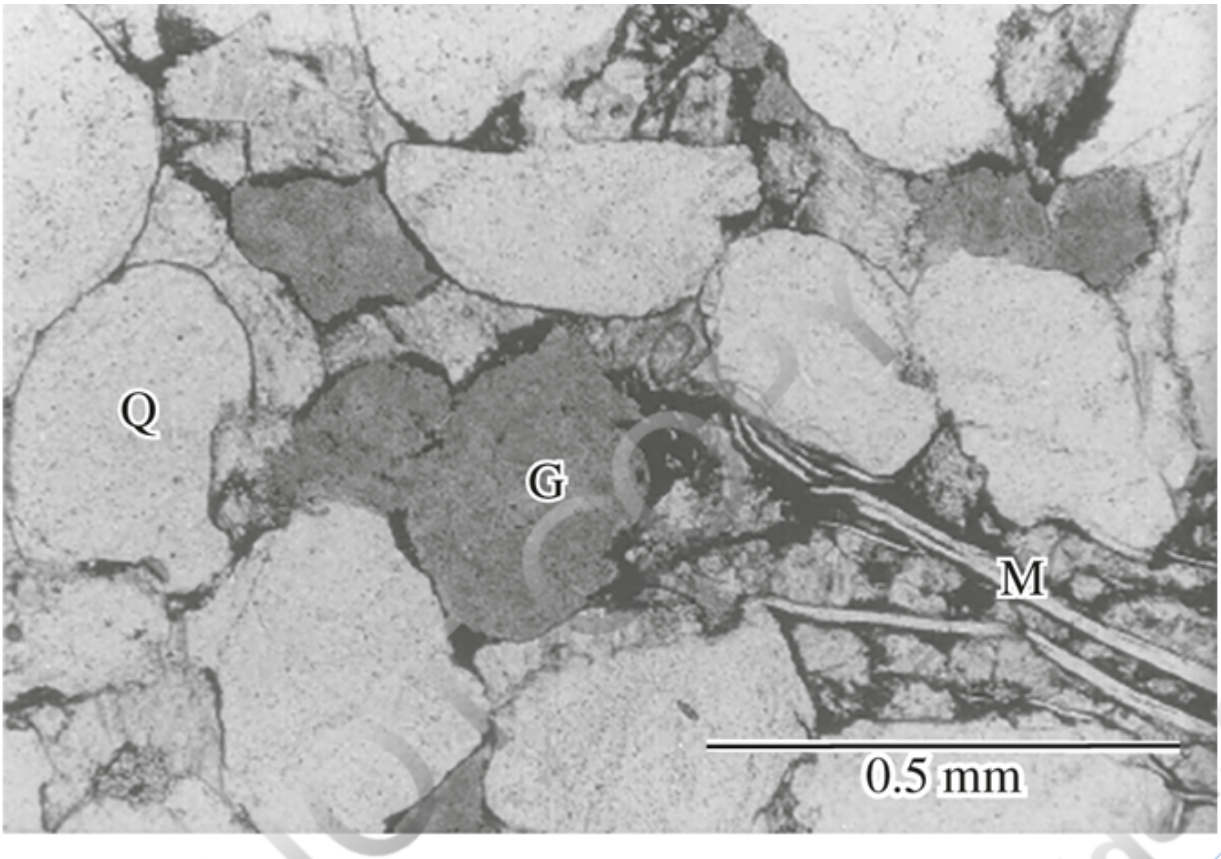

FIGURE 13.11 Glauconite pellets (G) with rounded quartz (Q) grains and elongate detrital muscovite (M). Calcite forms the cement between grains, and the opaque mineral is hematite. View larger image

Cleavage Perfect {001} cleavage, like the other micas.

Color Properties

Luster: Earthy or dull.

Color: Green or blue-green, sometimes with reddish limonite stains.

Streak: Dull green.

Color in Thin Section: Usually green.

Pleochroism: X = yellowish green to green; $Y = Z$ = green, bluish green, darker yellowish green.

Optical Characteristics

Relief in Thin Section: Moderate positive.

Optic Orientation: $X \wedge a = +5° - +10°$, $Y = b$, $Z \sim c$.

Indices of Refraction and Birefringence: Indices of refraction increase with Fe content and decrease with increasing fraction of expanding clay structure. Maximum second-order interference colors are usually masked by the mineral color.

Printed by: e48d507df5d1141@placeholder.94092.edu. Printing is for personal, private use only. No part of this book may be reproduced or transmitted without publisher's prior permission. Violators will be prosecuted.

order interference colors are usually masked by the mineral color.

Interference Figure: Fine grain size usually precludes obtaining good interference figures. Basal sections and cleavage fragments should yield approximately centered optically negative acute bisectrix figures with small $2V_x$, $r > v$.

Alteration Reddish or yellowish limonitic staining due to weathering is common in glauconite.

Distinguishing Features

Hand Sample: The distinctive occurrence and green color are characteristic, but green pellets in sedimentary rocks are not necessarily glauconite. Chlorite forms similar pellets.

Thin Section/Grain Mount: Occurrence and green color are distinctive. Chlorite in similar pellets has lower birefringence.

Occurrence Glauconite characteristically forms small rounded pellets in clastic sediments deposited in marine conditions. If abundant, these pellets give sediments a green color, hence the term *greensand*. Limestone and **marls** also may contain glauconite pellets. Marl is a sedimentary rock with approximately equal proportions of clay and carbonate. Celadonite typically fills vesicles and other voids in basaltic volcanics.

Use In the past, glauconite was used as a fertilizer to provide K for forage crops, but this use decreased in the late 1800s with the development of **potash** from other sources. Potash is a general name for any K-bearing, water-soluble materials generally used as a fertilizer. During the 1940s and 1950s, glauconite was reintroduced as a soil amendment, and it has, at times, been used in the manufacture of bricks and as a colorant to make green glass. Its principal current uses are in water treatment and as a soil amendment. In water treatment it is used to remove soluble iron and manganese salts and hydrogen sulfide. For this purpose, glauconite pellets are extracted and processed to give them a manganese dioxide coating. As a soil amendment, glauconite releases potassium slowly to aid plant growth, loosens clayey soil, and improves water retention.

DO NOT COPY e48d507df5d1141@placeholder.9409

Printed by: e48d507df5d1141@placeholder.94092.edu. Printing is for personal, private use only. No part of this book may be reproduced or transmitted without publisher's prior permission. Violators will be prosecuted.

TOT + *c* Structures: Brittle Micas (2:1)

Margarite

Å Å

Å

DO NOT COPY

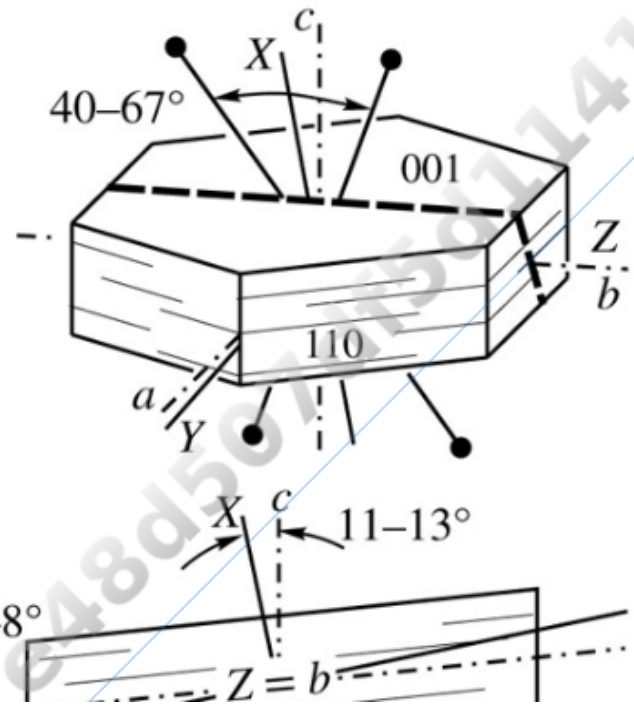

Printed by: e48d507df5d1141@placeholder.94092.edu. Printing is for personal, private use only. No part of this book may be reproduced or transmitted without publisher's prior permission. Violators will be prosecuted.

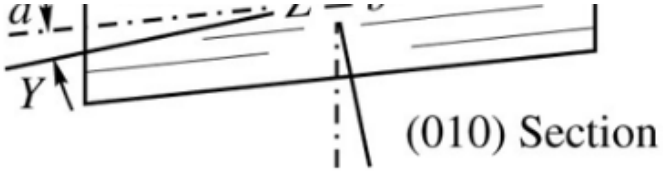

Composition Up to 30 percent Na^{+} may substitute for Ca^{2+} with charge balance maintained principally by increasing the Si:Al ratio in tetrahedral sites.

Form and Twinning Margarite has a micaceous habit, forming platy or scaly aggregates and foliated masses. Intergrowths with muscovite or paragonite are not uncommon.

Cleavage Perfect {001}. Cleavage folia are brittle.

Color Properties

Luster: Vitreous to pearly.

Color: Grayish pink, pale yellow, or pale green.

Streak: White.

Color in Thin Section: Colorless.

Pleochroism: None.

Optical Characteristics

Relief in Thin Section: Moderately high positive.

Optic Orientation: $X \wedge c = +11°$ to $+13°$, $Y \wedge a = -6°$ to $-8°$, $Z = b$. Maximum extinction angle to the trace of cleavage is therefore 6–8° and the cleavage trace is length slow.

Indices of Refraction and Birefringence: Indices of refraction decrease with substitution of Na for Ca. Birefringence is relatively low, so maximum interference color in standard thin section is usually no higher than first-order yellow.

Interference Figure: Cleavage flakes and sections parallel to {001} yield nearly centered acute bisectrix figures with strong optic axis dispersion, $r < v$. $2V$ decreases with substitution of Na for Ca.

Alteration Margarite may alter to clay minerals.

Distinguishing Features

Hand Sample: Greater hardness and brittle character distinguish margarite from muscovite and other similar sheet silicates.

Thin Section/Grain Mount: Similar to muscovite but with higher indices of refraction and lower birefringence. Chlorite and chloritoid are green and pleochroic.

DO NOT COPY
e48d507df5d1141@placeholder.9409

Printed by: e48d507df5d1141@placeholder.94092.edu. Printing is for personal, private use only. No part of this book may be reproduced or transmitted without publisher's prior permission. Violators will be prosecuted.

lower birefringence. Chlorite and chloritoid are green and pleochroic.

Occurrence Most commonly as a prograde metamorphic mineral in aluminous pelitic rocks and metamorphosed marls. Also found in metamorphosed basalts and anorthosites where the Ca and Al are derived from original plagioclase. Margarite also may pseudomorphically replace aluminous minerals such as andalusite and corundum in metamorphic pelites.

Use None.

Clintonite

$$\mathrm{CaMg_2\,Al(Al_3SiO_{10})(OH)_2}$$

$$\text{Monoclinic } 2/m$$

$$a = 5.204\ \text{Å},\ b = 9.026\ \text{Å},$$
$$c = 9.812\ \text{Å},\ \beta = 100.3^\circ,$$
$$Z = 2$$

$$H = 3.5 \text{ on } \{001\},\ 6 \perp \{001\}$$

$$G = 3.0 - 3.1$$

$$\text{Biaxial } (-)$$

$$n_\alpha = 1.643 - 1.648$$

$$n_\beta = 1.655 - 1.662$$

$$n_\gamma = 1.655 - 1.663$$

$$\delta = 0.012 - 0.015$$

$$2V_x = 0 - 33^\circ$$

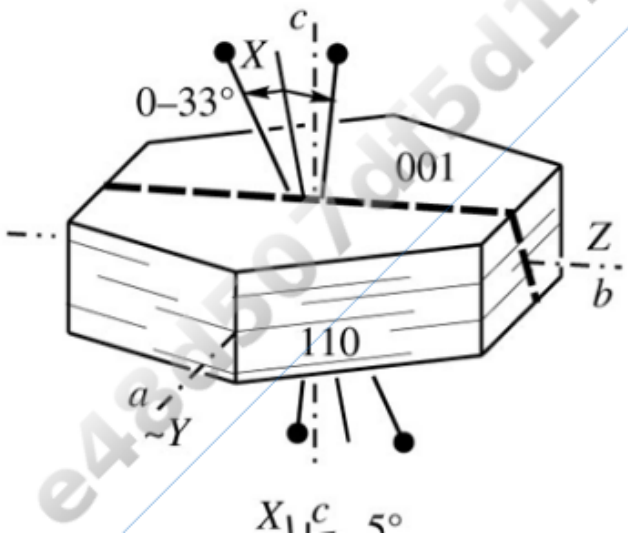

DO NOT COPY
e48d507df5d1141@placeholder.9409

Printed by: e48d507df5d1141@placeholder.94092.edu. Printing is for personal, private use only. No part of this book may be reproduced or transmitted without publisher's prior permission. Violators will be prosecuted.

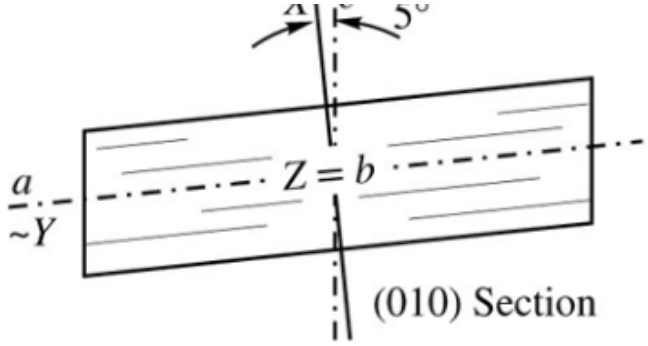

Composition Most clintonite has a composition fairly close to the ideal formula; some have a higher Si:Al ratio in the tetrahedral sites and a correspondingly lower Al content in octahedral sites. Some Fe may substitute for Mg, and F may substitute in substantial quantities for OH.

Form and Twinning Clintonite has a typical micaceous habit, forming irregular platy grains or platy aggregates. Twins with {001} composition planes are not common.

Cleavage Perfect {001} cleavage, but not as good as muscovite or biotite. Folia are brittle.

Color Properties

Luster: Vitreous, pearly to submetallic.

Color: Colorless, yellow, green, reddish brown.

Streak: White.

Color in Thin Section: Colorless or pale brown.

Pleochroism: Moderate with X = colorless, light orange, yellow, or reddish brown; $Y \approx Z$ = pale brown, pale green, $X < Y \approx Z$. Sections are darker when the trace of cleavage is parallel to the lower polarizer vibration direction.

Optical Characteristics

Relief in Thin Section: Moderately high positive.

Optic Orientation: $X \wedge c = +5°$, $Y \approx a$, $Z = b$, also $X \wedge c = +10°$, $Y = b$, $Z \approx a$.

Indices of Refraction and Birefringence: The range of indices of refraction is small, with Fe-bearing samples having higher values. Maximum interference color in thin section is first-order yellow.

Interference Figure: Cleavage fragments and sections parallel to {001} show no cleavage and low birefringence and yield centered acute bisectrix figures with small $2V$. Optic axis dispersion is weak; $r < v$.

DO NOT COPY
e48d507df5d1141@placeholder.9409

Printed by: e48d507df5d1141@placeholder.94092.edu. Printing is for personal, private use only. No part of this book may be reproduced or transmitted without publisher's prior permission. Violators will be prosecuted.

Alteration Clintonite may alter to clay minerals.

Distinguishing Features

Hand Sample: Resembles muscovite and phlogopite, but both are softer and cleavage folia are not brittle.

Thin Section/Grain Mount: Has lower birefringence than either muscovite or phlogopite, and chloritoid has larger $2V$ and is usually optically positive and more distinctly green. Chlorite is more distinctly green, has lower relief, has lower birefringence, and may be optically positive. Margarite has a larger $2V$.

Occurrence Clintonite is found in chlorite or talc schist and in metamorphosed carbonate-rich rocks.

Use None.

DO NOT COPY
e48d507df5d1141@placeholder.9409

Printed by: e48d507df5d1141@placeholder.94092.edu. Printing is for personal, private use only. No part of this book may be reproduced or transmitted without publisher's prior permission. Violators will be prosecuted.

TOT + O Structure

Chlorite

Å Å Å

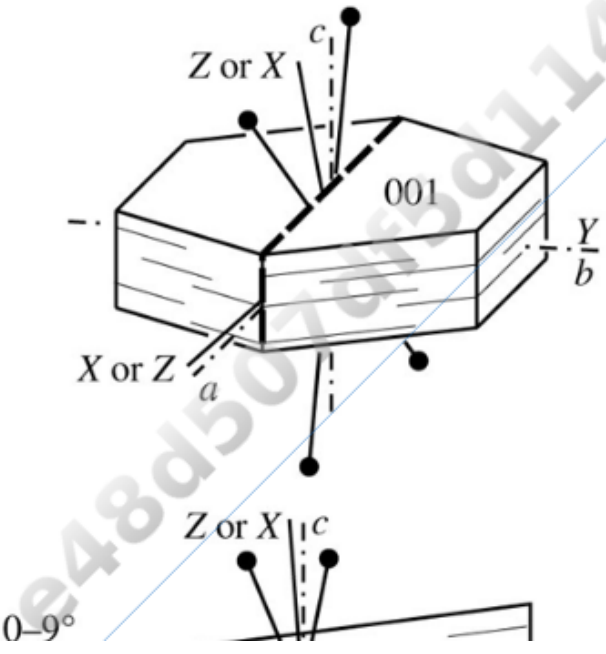

DO NOT COPY
e48d507df5d1141@placeholder.9409

Printed by: e48d507df5d1141@placeholder.94092.edu. Printing is for personal, private use only. No part of this book may be reproduced or transmitted without publisher's prior permission. Violators will be prosecuted.

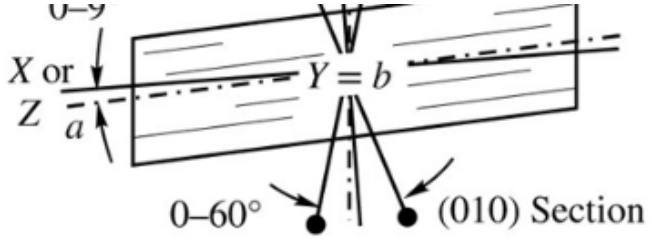

Structure Chlorite has the *TOT + O* structure described above. In common chlorite, both octahedral sheets are trioctahedral, meaning that all octahedral sites are occupied, usually by Mg, Fe, or Al. However, in some varieties either or both of the octahedral sheets may be dioctahedral. These uncommon varieties are not considered here.

Composition The principal substitutions are of Mg, Fe^{2+}, Fe^{3+}, and Al in octahedral sites, and Si and Al in tetrahedral sites as described earlier. Continuous solid solution extends from Mg-rich chlorite (clinochlore) to Fe-rich chlorite (chamosite). Substitution of minor amounts of Mn and Cr in octahedral sites also is common.

Form and Twinning See **Figure 13.12**. Most commonly it occurs as fine-grained scaly or foliated massive aggregates or isolated micaceous grains. Well-formed platy crystals with hexagonal outline are uncommon. Chlorite also may partially or completely replace other Mg/Fe-bearing minerals. Chlorite is a common constituent of the clay mineral fraction of soil and clastic sediments, and may form oolitic or spherulitic balls similar to glauconite in some sedimentary rocks. Twins with {001} composition planes are not uncommon but are difficult to recognize.

(*a*)

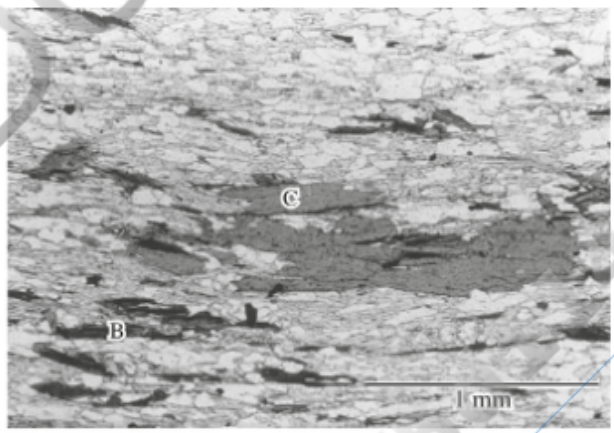

(*b*)

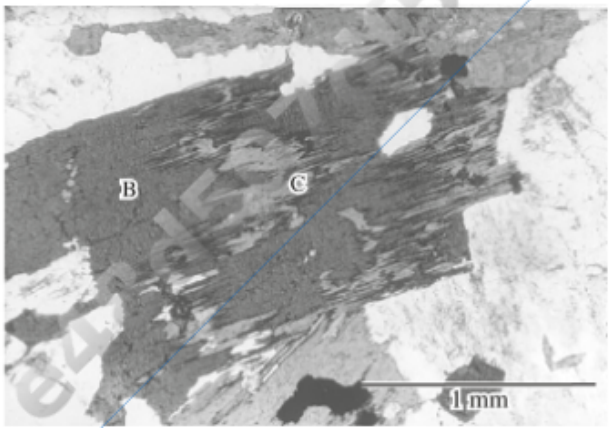

Printed by: e48d507df5d1141@placeholder.94092.edu. Printing is for personal, private use only. No part of this book may be reproduced or transmitted without publisher's prior permission. Violators will be prosecuted.

FIGURE 13.12 Chlorite. (*a*) Foliated chlorite grains (C) with biotite (B) in a thin section of moderately low-grade pelitic schist. The finer-grained matrix includes scaly chlorite and muscovite, and clear quartz. (*b*) Chlorite (C) alteration along cleavage traces in biotite (B) in a thin section of granodiorite. View larger image

Cleavage Perfect {001}. Folia are flexible but inelastic.

Color Properties

Luster: Vitreous to somewhat pearly, waxy, or dull.

Color: Various shades of green, infrequently yellow, white, pink, or rose-red.

Streak: Greenish white to white.

Color in Thin Section: Usually very pale to medium green.

Pleochroism: Moderate with shades of green. For optically positive varieties $X \approx Y > Z$: $X \approx Y$ = pale green, green, brownish green; Z = colorless, pale green, pale yellowish green. For optically negative varieties $X < Y \approx Z$: X = colorless, pale green, pale yellowish green; $Y \approx Z$ = pale green, green, brownish green.

Optical Characteristics

Relief in Thin Section: Moderate to moderately high positive.

Optic Orientation: The optic plane is normally parallel to (010) and the acute bisectrix is nearly perpendicular to (001). For optically positive varieties $X \approx a$, $Y = b$, $Z \approx c$, and the trace of cleavage is length fast. For optically negative varieties $X \approx c$, $Y = b$, $Z \approx a$, and the trace of cleavage is length slow.

Indices of Refraction and Birefringence: Indices of refraction linearly increase from about 1.58 to 1.67 with mole percent (Fe+Mn+Cr)/(Fe+Mn+Cr+Mg) over the range of 0–100; below about 50, chlorite is optically positive and length fast; below about 50, it is optically negative and length slow. Birefringence is usually low, so interference colors are rarely higher than first-order white or yellow in standard thin section. Anomalous brownish interference colors are common in optically positive varieties, and anomalous bluish or purplish interference colors are common in optically negative varieties.

Interference Figure: Cleavage flakes and sections parallel to {001} yield centered acute bisectrix figures. Optic sign can be used to distinguish between low and high Fe + Mn + Cr content, but there are many exceptions. Some may be essentially uniaxial. Optic axis dispersion is usually $r < v$. As noted earlier, the sign of elongation may be used to establish optic sign.

Alteration Oxidation may produce iron stains, and chlorite may weather to clay minerals, but otherwise it is fairly resistant to alteration.

DO NOT COPY

Printed by: e48d507df5d1141@placeholder.94092.edu. Printing is for personal, private use only. No part of this book may be reproduced or transmitted without publisher's prior permission. Violators will be prosecuted.

Distinguishing Features

Hand Sample: Green color, inelastic folia, and hardness distinguish chlorite from other sheet silicates. Small grain size in chlorite schists and related rocks generally makes individual grains difficult to distinguish, even with a hand lens, but the green color generally indicates the presence of chlorite.

Thin Section/Grain Mount: Distinguished from muscovite and biotite by green color, pleochroism, and weak birefringence. Serpentine usually has lower refractive indices and is less pleochroic. In soils and sediments, chlorite is indistinguishable from other clay minerals and must be identified with X-ray diffraction techniques.

Occurrence Chlorite is a common and widespread mineral. It is a major rock-forming mineral in low- and medium-grade pelitic and mafic metamorphic rocks; the green in greenschist facies rocks predominantly comes from chlorite. It is also common in many igneous rocks, usually derived by alteration of primary Mg/Fe-bearing minerals such as biotite and hornblende. Chlorite also is a common product of weathering and is widespread in soil, clay mineral–bearing sediments, and sedimentary rocks.

Use By itself, chlorite does not have significant industrial uses. Rocks such as chlorite schist may occasionally be used as construction stone or for decorative purposes. However, chlorite is a common constituent of clay and therefore appears in a wide variety of industrial and consumer applications described in the following section on clay minerals.

DO NOT COPY
e48d507df5d1141@placeholder.9409

Printed by: e48d507df5d1141@placeholder.94092.edu. Printing is for personal, private use only. No part of this book may be reproduced or transmitted without publisher's prior permission. Violators will be prosecuted.

Clay Minerals

The term *clay* has been used in different ways. Geologists originally applied the term to the fine-grained fraction of sediment and sedimentary rocks, typically defined as particles whose diameter is less than 1/256 mm (~0.004 mm). This size was chosen because particles this small or smaller cannot be identified with conventional optical or physical methods. Sediment made dominantly of these fine particles are now referred to as clay sized. Once X-ray diffraction techniques developed, it was discovered that the minerals in clay-sized sediment that imparted plasticity to this material were mostly sheet silicates, so the term *clay mineral* has come to refer to those minerals that are an important component of clay-sized material. The terminology used here is as follows.

> **CLAY**: Sediment or rock (claystone) composed dominantly of fine-grained minerals. Clay generally is plastic when mixed with an appropriate amount of water and will harden when dried or fired.
>
> **CLAY SIZED**: Particles whose diameter is less than 0.004 mm.
>
> **CLAY MINERAL:** The group of minerals that impart plasticity to clay when wet and that also occur in soils, sediments, sedimentary rocks, and weathered or altered rocks. These minerals are mostly, but not exclusively, sheet silicates.
>
> **ARGILLACEOUS**: Rock or sediment containing significant amounts of clay minerals.

This leads to two possible sources of confusion. The first is that clay-sized sediment includes not only clay minerals but a variety of others, most commonly quartz, but also carbonates, zeolites, iron oxides, and others. Second, while we commonly think of clay minerals as being fine grained, size is not strictly a requirement. Chlorite, for example, is abundant in many samples of clay and soil, and also a common mineral found in low- to medium-grade metamorphic rocks. It is the same mineral in both environments. Note, however, that the unique properties of clay are partly related to the small particle size and high surface area of the mineral grains. Coarse-grained clay minerals will not have the same mechanical properties as fine-grained material.

The following minerals included in this section are clay minerals.

KAOLINITE: $Al_2Si_2O_5(OH)_4$

SMECTITE: $\sim Ca_{0.17}(Al,Mg,Fe)_2(Si,Al)_4O_{10}(OH)_2 \cdot nH_2O$

ILLITE: $\sim K_{0.8}Al_2(Al_{0.8}Si_{3.2})(OH)_2$

VERMICULITE: $\sim (Mg,Ca)_{0.3}(Mg,Fe^{2+},Fe^{3+},Al)_3(Si,Al)_4O_{10}(OH)_2$

CHLORITE: $(Mg,Fe,Al)_3(Si,Al)_4O_{10}(OH)_2 \cdot (Mg,Fe,Al)_3(OH)_6$

	Kaolinite	Illite	Smectite	Vermiculite	Chlorite

DO NOT COPY e48d507df5d1141@placeholder.9409

Printed by: e48d507df5d1141@placeholder.94092.edu. Printing is for personal, private use only. No part of this book may be reproduced or transmitted without publisher's prior permission. Violators will be prosecuted.

	Kaolinite	Illite	Smectite	Vermiculite	Chlorite
a (Å)	5.15	5.2	5.2	5.3	5.3
b (Å)	8.95	9.0	9.1	9.25	9.2
c (Å)	7.4	10.0	~10–15	14.4	14.3
β (°)	104.8	~90	~90	~97	97
Z	2	2	2	2	2
Point group	1	2/m	2/m	2/m	2/m

Physical and optical properties are listed in **Table 13.2**.

TABLE 13.2 Properties of Clay Minerals

Mineral	H	G	Class and Sign	$2V_x$°	n_α	n_β	n_γ	δ
Kaolinite	2–2.5	2.61–2.68	Biaxial (−)	24–50	1.553–1.565	1.559–1.596	1.560–1.570	0.005–0.007
Smectite	1–2	~2–3	Biaxial (−)	Small	1.48–1.61	1.50–1.64	1.50–1.64	0.01–0.04
Illite	1–2	2.6–2.9	Biaxial (−)	<10	1.54–1.57	1.57–1.61	1.57–1.61	~0.03
Vermiculite	1–2	~2.3	Biaxial (−)	0–18	1.520–1.564	1.530–1.583	1.530–1.583	0.02–0.03
Chlorite	2–3	2.6–3.3	Biaxial (−) or (+)	$2V_x$ = 0–40	1.55–1.67	1.55–1.69	1.55–1.69	0.000–0.015
				$2V_z$ = 0–60				

Form and Twinning See **Figure 13.13**. Generally too fine grained to allow recognition of grains in hand sample or with light microscopes. Scanning electron microscopes reveal that most clay particles are platy, though some are bladed to ribbon shaped.

Cleavage Perfect {001}.

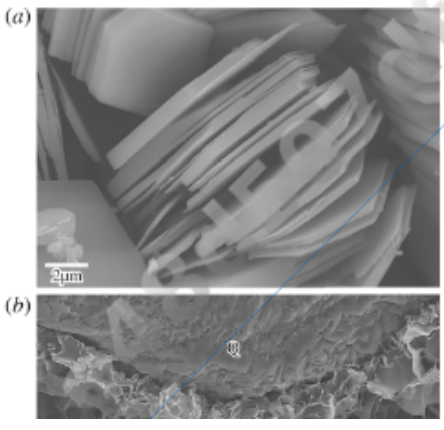

Printed by: e48d507df5d1141@placeholder.94092.edu. Printing is for personal, private use only. No part of this book may be reproduced or transmitted without publisher's prior permission. Violators will be prosecuted.

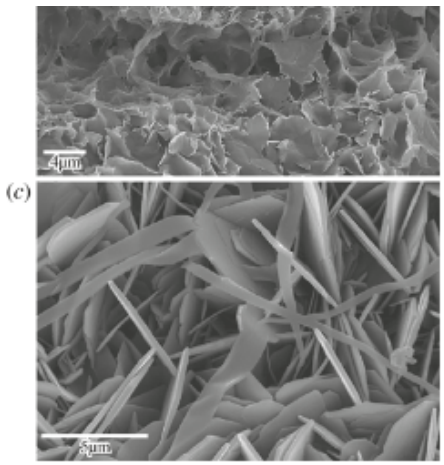

FIGURE 13.13 SEM images of clay minerals. (*a*) Kaolinite platelets in Jurassic sandstone, North Sea. (*b*) Dioctahedral smectite lining pores in Ordovician sandstone, Oman. The grain at top is quartz (Q). (*c*) Pseudohexagonal platelets of chlorite intergrown with ribbons of illite; Garn Formation, North Sea. Images courtesy of Evelyn Delbos, The James Hutton Institute, and reproduced from the "Images of Clay Archive" of the Mineralogical Society of Great Britain & Ireland and The Clay Minerals Society. Used by permission. View larger image

Color Properties

Luster: Earthy.

Color: White, gray, tan, brown.

Streak: White.

Color in Thin Section: Typically very fine-grained gray or brown earthy aggregates.

Pleochroism: None.

Optical Characteristics (Table 13.2)

Relief in Thin Section: Low to moderate positive or negative.

Comments: Clay minerals are too fine grained to allow optical properties to be measured. Coarse-grained samples of essentially the same material include chlorite, serpentine, talc, pyrophyllite, and glauconite, which were described separately earlier, and vermiculite, which is briefly described in the section on biotite as well as below.

Structure and Classification

The structure of the sheet silicate clay minerals is shown in **Figure 13.14**. The commonly used classification divides clays into 1:1 clays constructed of repeating *TO* layers, usually with basal layer spacing of about 7 Å, and 2:1 clays constructed of repeating *TOT* layers with a basal layer spacing of either about 10 or 14 Å. An additional group, called mixed-layer clays, may include combinations of any of these components interlayered in a

DO NOT COPY e48d507df5d1141@placeholder.9409

Printed by: e48d507df5d1141@placeholder.94092.edu. Printing is for personal, private use only. No part of this book may be reproduced or transmitted without publisher's prior permission. Violators will be prosecuted.

variety of ways. Layer repeat distance is measured by means of X-ray diffraction techniques, which are outlined below.

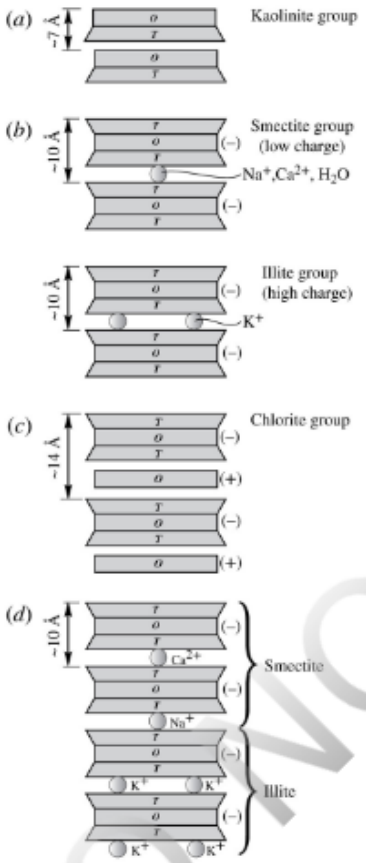

FIGURE 13.14 Clay mineral structure. Refer also to Figures 13.1 and 13.3. (*a*) 7 Å clays have 1:1 or *TO* structures. (*b*) 10 Å clays have 2:1 or *TOT* + *c* structures. The *TOT* layers in the smectite group have a relatively low charge and require fewer Na^+ or Ca^{2+} cations in the interlayer sites. In the illite group, *TOT* layers have a higher negative charge and require more cations in the interlayer sites to maintain charge balance. (*c*) 14 Å clays have the chlorite structure in which octahedral sheets with a positive charge occupy the interlayer between negatively charged *TOT* layers. (*d*) A common mixed-layer clay contains both smectite and illite layers. View larger image

1:1 Clay Minerals

The structure of 1:1 clays consists of repeating *TO* layers bonded with weak electrostatic bonds (Figure 13.14a). This group includes dioctahedral kaolinite $Al_2Si_2O_5(OH)_4$ (Figure 13.3) and trioctahedral serpentine, described earlier. Dickite and nacrite are polymorphs of kaolinite related by different repeating patterns for stacking the layers. The basal layer spacing of the kaolinite group is typically about 7 Å, although halloysite $[Al_2Si_2O_5(OH)_4 \cdot 2H_2O]$ has an ~10 Å layer repeat distance because a single layer of water molecules occupies the interlayer position. Halloysite layers have a strong tendency to roll up into cylinders and typically adopt a fibrous habit. Interlayer water is readily lost on heating.

2:1 Clay Minerals

DO NOT COPY e48d507df5d1141@placeholder.9409

Printed by: e48d507df5d1141@placeholder.94092.edu. Printing is for personal, private use only. No part of this book may be reproduced or transmitted without publisher's prior permission. Violators will be prosecuted.

The 2:1 clays are constructed of repeating *TOT* layers. The *TOT* layers have a net negative charge that is less than one per formula unit, which requires placement of cations between layers, forming an interlayer, to maintain charge balance. Two groups of 2:1 clays, with layer repeat distance of about 10 and 14 Å, are distinguished by the nature of the interlayer and correspond to the *TOT* + *c* and *TOT* + *O* structures described earlier.

In the 10 Å clays (Figure 13.14b), the *TOT* layer charge is balanced with interlayer cations, usually K, Na, or Ca; they have a *TOT* + *c* structure and are similar to the micas. The 10 Å clays can be separated into low-charge and high-charge groups depending on the net charge of the *TOT* layers and the substitution mechanism that produces the charge.

The net negative charge of the *TOT* layers in the low-charge group is usually between about 0.2 and 0.6 per formula unit and is commonly around 0.33. Ca and Na are the usual interlayer cations. The most abundant group of these minerals, collectively known as smectite, may be either dioctahedral or trioctahedral. In dioctahedral smectite, the *TOT*-layer charge is the result of either substitution of Al^{3+} for Si^{4+} in tetrahedral sites or substitution of divalent cations (usually Mg^{2+}) for Al^{3+} in octahedral sites. In the less common trioctahedral varieties, the *TOT*-layer charge results from substitution of Al^{3+} for Si^{4+} in tetrahedral sites. The relatively low layer charge of smectite coupled with the presence of cations in only about a third of the interlayer sites allows water to move into the interlayers, causing the structure to expand. Smectite with a single layer of water molecules between *TOT* layers has a basal layer spacing of about 12.5 Å, and with two layers of water molecules, about 15.2 Å. The water can be introduced and removed reversibly from smectite at room temperature in response to changing moisture content in the soil or rock. Only when the smectite is thoroughly dried is the layer repeat distance approximately 10 Å.

In the high-charge group, the *TOT* layers have a net negative charge of between 0.8 and 1.0 per formula unit, mostly as a result of substitution of Al^{3+} for Si^{4+} in tetrahedral sites. The clay minerals in this group include illite and glauconite–celadonite. All are dioctahedral, and the interlayer cation is dominantly K^+. Because structure and composition are nearly the same as muscovite, these clays have been called “mica-like.” Collectively they are known as the illite group. The presence of between 0.8 and 1.0 K^+ cation per formula unit in interlayer sites ensures that the layers are bonded to each other fairly strongly. Water molecules do not easily enter the interlayer because most interlayer cation sites are occupied and interlayer bonding is stronger, so members of the illite group do not swell when moistened.

A third group of 10 Å clays is called vermiculite (see the Use section under Biotite). It is usually produced by alteration of biotite, or less commonly chlorite. Vermiculite is an expanding clay, like the smectite group, but has a higher negative layer charge, usually around 0.6 per formula unit. The changes that accompany alteration of biotite to

DO NOT COPY

Printed by: e48d507df5d1141@placeholder.94092.edu. Printing is for personal, private use only. No part of this book may be reproduced or transmitted without publisher's prior permission. Violators will be prosecuted.

vermiculite are oxidation of some Fe^{2+} to Fe^{3+} in octahedral sites, which decreases the net negative charge of the *TOT* layer from 1.0 to about 0.6 per formula unit. To compensate for the reduction of negative charge in the *TOT* layer, some K^+ cations are stripped from interlayer sites. Additional K^+ is exchanged for Mg^{2+} or Ca^{2+} and water is introduced into the interlayer, often structurally bonded to the interlayer cations. The water in the interlayer expands the structure so that at room temperature conditions the layer repeat distance is about 14.4 Å. Only when heated to drive off the water does the structure collapse to about 10 Å layer repeat distance.

The 14 Å clays (Figure 13.14c) have the chlorite structure (*TOT* + *O*) and are called chlorite. The interlayer is an octahedral sheet (a plane of cations bonded in octahedral coordination with two planes of OH) with a net positive charge. The chlorite that occurs in clays may be either tri- or dioctahedral, unlike most coarsely crystalline chlorite, which is trioctahedral.

Mixed-Layer Clay Minerals

Natural clays rarely correspond fully to the end members just described. Most contain, to one degree or another, combinations of kaolinite-like, illite-like, smectite-like, vermiculite-like, and/or chlorite-like layers. In some cases the different layer types alternate in a regular manner; in others, they appear random (Figure 13.14d). The reader should not infer that mixed-layer clays are mechanical mixtures of two or more types of clay. The interlayering occurs at the unit cell level. Mixed-layer clays are classified by combining the names of the constituent layers. Illite/smectite contains layers of both illite and smectite, for example, and is probably the most common variety. Chlorite/smectite is also common.

Additional Clay Minerals

Palygorskite [$(Mg,Al)_2Si_4O_{10}(OH)\cdot 4H_2O$] and sepiolite [$Mg_4Si_6O_{15}(OH_2)\cdot 6H_2O$] (**Table 13.3**) are additional clay minerals with complex structures that form fibrous grains. Palygorskite may form fibrous mats known as mountain leather, and sepiolite may form fine-grained masses, known as meerschaum, that can be carved. They are formed by weathering and alteration of Mg-bearing rocks, and are common constituents of soil and sediment.

TABLE 13.3 Properties of Palygorskite and Sepiolite

Palygorskite	Sepiolite
Earthy to waxy: White, gray, yellowish, gray-green; colorless in thin section	Earthy to waxy: Gray, white, yellowish; colorless or gray in thin section
H = 2–2.5	H = 2–2.5
G = 1.0–2.6	G > 2

Printed by: e48d507df5d1141@placeholder.94092.edu. Printing is for personal, private use only. No part of this book may be reproduced or transmitted without publisher's prior permission. Violators will be prosecuted.

n_α = 1.522–1.528	n_α = 1.515–1.520
n_β = 1.530–1.546	n_β = unknown
n_γ = 1.533–1.548	n_γ = 1.525–1.529
δ = 0.011–0.020	δ = 0.009–0.010
Biaxial (−), $2V_x$ = 30–61°	Biaxial (−) $2V_x$ = 0–50°

Geology of Clay

Clay minerals form as the result of the interaction of silicate rock and water under conditions of relatively low temperature.

$$\begin{aligned}&\text{Rock} + \text{water} + \text{ions in solution}\\ &= \text{clay minerals} \pm \text{other minerals} + \text{ions in solution}\end{aligned}$$

The hydrolysis of K-feldspar is a simple example of this process.

$$\begin{aligned}&\text{K-feldspar} + \text{hydrogen ion} + \text{water}\\ &= \text{kaolinite} + \text{potassium ion} + \text{quartz}\\ &2\,KAlSi_3O_8 + 2H^+ + H_2O\\ &= Al_2Si_2O_5(OH)_4 + 2K^+ + 4SiO_2\end{aligned}$$

The environments in which clay minerals are formed are all near the Earth's surface and include weathering and soil formation, sediment transport and deposition, sediment compaction and diagenesis, and hydrothermal alteration. Clay minerals are therefore abundant in weathered rock, soil, fine-grained clastic sediment and sedimentary rocks, and hydrothermally altered rocks. The clay minerals that form in any particular environment depend on the nature of the parent rock, temperature, availability and chemistry of the water, and time. For a summary of these considerations, consult Velde (1995) or Weaver (1989). Above ~200°C (400°C in some hydrothermal conditions), clay minerals are converted by metamorphic processes into coarser-grained chlorite, micas, and other minerals.

Once formed, clay minerals change or recrystallize in response to changing environmental conditions. A common example is the conversion of smectite into illite during diagenesis. The clay produced by normal weathering of common silicate rocks and subsequent transport tends to be fairly rich in smectite. Hence, most clay-rich sediment, when first deposited, is rich in smectite and has relatively little illite. With burial, however, the amount of illite layers in the clay structure systematically increases as the smectite recrystallizes (**Figure 13.15**). This pattern is found in many sedimentary basins

DO NOT COPY e48d507df5d1141@placeholder.9409

Printed by: e48d507df5d1141@placeholder.94092.edu. Printing is for personal, private use only. No part of this book may be reproduced or transmitted without publisher's prior permission. Violators will be prosecuted.

smectite recrystallizes (**Figure 13.15**). This pattern is found in many sedimentary basins. The temperature within basins at which illite layers begin to appear ranges from about 50°C to 100°C, and the conversion progresses over a temperature interval of 35°C to 100°C. Note that conversion of smectite to illite is possible only if a source of K is available. In many cases, fine-grained detrital K-feldspar in the sediment is consumed to provide the necessary K, and the extent of conversion of smectite to illite is limited by the availability of this K-feldspar. Other changes that occur with increasing depth include an increase in the amount of chlorite and a decrease in the amount of kaolinite.

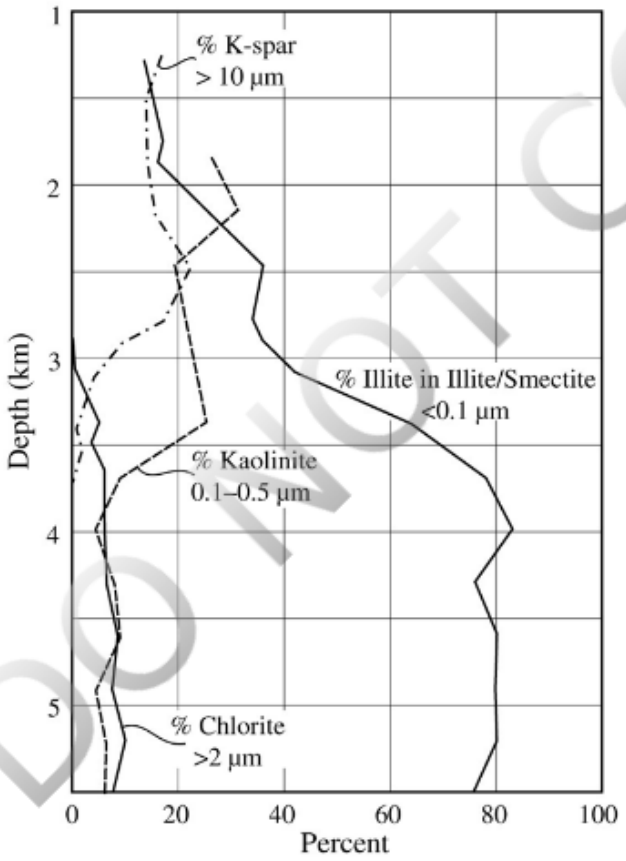

FIGURE 13.15 Clay mineralogy in selected size fractions of Miocene–Oligocene sediment in the Gulf Coast of the United States. See text for additional discussion. Adapted from Hower and others (1976). View larger image

Soil mineralogy also is influenced by climate. Intense weathering in wet climates tends to favor formation of kaolinite plus oxide minerals such as gibbsite, whereas dry temperate climates favor smectite. With progressive weathering, smectite may convert to illite/smectite and then to illite.

Bacteria are ubiquitous in weathering, transport, and diagenetic environments, and are capable of playing a role in the production of clay minerals. Bacteria cellular surfaces appear to be favorable sites for precipitation of clay with various compositions, morphologies, and structure.

Clay minerals have long been ubiquitous in Earth's near-surface environments except in

DO NOT COPY
e48d507df5d1141@placeholder.9409

Printed by: e48d507df5d1141@placeholder.94092.edu. Printing is for personal, private use only. No part of this book may be reproduced or transmitted without publisher's prior permission. Violators will be prosecuted.

the early high-temperature stage of planet formation. The nature and relative abundance of clay minerals undoubtedly evolved over time in response to the Earth's chemical and biologic evolution, but direct evidence is lacking for much of Earth's history because the record has been destroyed by normal erosion, burial, alteration, and tectonic activity. For more information on clay mineral evolution, see Hazen and others (2013).

Identification

Because most clay minerals occur as submicroscopic grains, identification is not usually possible with conventional hand sample or microscopic techniques. Therefore, the physical and optical properties listed are not particularly useful. Plasticity of wet soil or sediment is an indication that clay is present. The addition of any moisture, perhaps simply from lightly breathing on an argillaceous sample, will release the earthy odor that we associate with moist soil. The odor may be an indication of clay minerals. See Chapter 6 for more information on clay mineral odor.

In most cases, clay mineral identification depends on a combination of scanning electron microscope and X-ray diffraction (XRD; Chapter 8) techniques. The scanning electron microscope (Chapter 9) provides information about habit and chemistry of individual grains. Welton (2003) provides an excellent overview of scanning electron microscope techniques applied to sedimentary rocks. The basic outline of XRD procedures used for clay identification is provided below. For more details, consult Brindley (1980), Starkey et al. (1984), and Moore and Reynolds (1997).

Identification of clay minerals through powder XRD analysis can rarely be done by a single XRD analysis. Therefore, clay mineral samples are typically split into identical subsamples, where each is analyzed multiple times using a variety of treatments. For example, one subsample is air dried and analyzed with the powder XRD, then it is heated and reanalyzed. Another subsample maybe air dried, analyzed, then glycolated and reanalyzed. The *d*-spacing of the {00*l*} and other interplanar spacings are measured after each treatment (**Table 13.4**), and the identity of the mineral(s) in the sample can, with luck and experience, be deduced from that information. Mixed-layer clays pose additional complexity that is beyond the scope of this presentation. A description of the basic treatments are as follows.

DISAGGREGATE THE ROCK/SOIL: A variety of equipment and techniques can be used depending on the nature of the sample and the equipment available. Samples should be crushed, not ground.

SEPARATE THE CLAY FROM OTHER MINERALS: A common technique is to thoroughly mix the disaggregated sample with water in a kitchen-type blender, and then decant (pour off) the cloudy liquid, which contains the clay.

CHEMICAL PRETREATMENT: Chemical pretreatment is not always necessary, but it can be done to remove iron oxides and organic matter. Or clays can be saturated with selected cations (e.g., Mg) by soaking in an appropriate solution. See the references listed above for more details regarding the procedure and purpose of such treatments

DO NOT COPY e48d507df5d1141@placeholder.94092

Printed by: e48d507df5d1141@placeholder.94092.edu. Printing is for personal, private use only. No part of this book may be reproduced or transmitted without publisher's prior permission. Violators will be prosecuted.

listed above for more details regarding the procedure and purpose of such treatments.

PARTICLE-SIZE SEPARATION: Usually done by centrifuging the clay–water mixture. The size fraction remaining in the water can be controlled by varying the centrifuge run time. The smallest size fraction, which will be the last material to fall to the bottom during centrifuging, is used for XRD analysis.

SAMPLE PREPARATION: Initial powder XRD analysis typically involves using a sample where (ideally) all clay grains are oriented with {001} parallel to the surface of the sample holder. Such oriented samples are simply prepared by placing the clay–water mixture on a sample holder and allowing it to air dry. Multiple sample holders, constituting different subsamples, can be prepared in an identical fashion from a single sample.

HEATING: Heating a sample to 400°C for at least 30 minutes and analyzing as quickly as possible afterward produces changes in {00*l*} *d*-spacing for some clays (Table 13.4). Heating to 550°C for at least 60 minutes should fuse kaolinite into an amorphous glass, while chlorite will remain crystalline. Be aware that heating may damage sample holders and the method does not always distinguish between kaolinite and chlorite.

GLYCOLATING: Ethylene glycol (used in automobile antifreeze) readily enters the interlayer sites in smectite and expands the layer repeat distance to about 16.9 Å (Table 13.4). Ethylene glycol is hazardous, so work with it should be done in a fume hood with personal protective equipment. The preferred method of glycolating a sample is to add ethylene glycol into the bottom of a lidded laboratory casserole dish. The prepared sample is then suspended above the ethylene glycol on a small platform. The lid is secured and the dish with the sample and ethylene glycol is heated to 60°C for at least eight hours. The sample is then analyzed immediately following removal from the lidded dish. A quicker, but less effective methods is to drip a 1:1 mixture of ethyl alcohol and ethylene glycol on to the prepared sample and let it soak for a few minutes. Draw off any excess liquid with the corner of a laboratory tissue and then analyze.

TABLE 13.4 Clay Mineral Identification[a]

Clay Mineral Group	Air Dried	Heated	Glycolated
Kaolinite group	7.16	7.16	7.16
Smectite group	~15 (variable)	~10	16.9
Illite group	10.1	10.1	10.1
Vermiculite	14.4	~10	14.4
Chlorite	14.2	14.2	14.2

[a] The values are the *d*-spacing in angstroms for {00*l*} planes measured with X-ray diffraction techniques.

Uses

Clay has been used since before recorded history and continues to be used in a wide variety of industrial and commercial products. Kaolinite, for example, occurs in nearly

DO NOT COPY e48d507df5d1141@placeholder.94092

Printed by: e48d507df5d1141@placeholder.94092.edu. Printing is for personal, private use only. No part of this book may be reproduced or transmitted without publisher's prior permission. Violators will be prosecuted.

half of the manufactured products in daily use. Uses for clay include the following.

PAPER COATING AND FILLER: The paper on which this is printed contains kaolinite.

DRILLING MUD ADDITIVE: Used for drilling oil/gas wells.

CERAMICS: Probably the earliest use of clay, and an enduring one.

FILLER: Used in rubber, plastics, caulking compound, paint, and related products.

COSMETICS: Both as a filler and as a colorant.

REFRACTORY PRODUCTS: Including firebrick and foundry sand.

BUILDING PRODUCTS: Including bricks and adobe.

PORTLAND CEMENT: Clay in pulverized shale minerals is an essential component.

ABSORBENTS: Used to absorb oil and other chemicals in industrial settings and as cat litter.

FOOD: Certain types of clay are approved food additives.

PHARMACEUTICALS: Clays have been used for medical purposes since ancient times. Many uses continue today, and new applications are still being found. Williams and others (2009) provide a useful review.

Clay in the Environment

Clay minerals have a very important environmental role. They provide enormous benefits but also pose significant risks.

Clay minerals are a major constituent of soils. Plants have evolved to take advantage of the chemical behavior of clay minerals. These include the ability to adsorb and/or release various molecules, including water and nitrogen compounds that plants can use. A good case can be made that clay minerals provide the interface between the solid Earth and all life.

Clay mineral–rich rocks and soil also pose substantial engineering problems. Slopes made of clay mineral–rich materials are not stable and are susceptible to mass wasting, such as soil creep or slumping. Soils rich in smectite are capable of shrinking when dried and swelling when wet. These swelling soils can extensively damage the foundations of buildings, roadways, and other infrastructure as they change in size during wet and dry cycles. Some of the most serious problems posed by swelling clays come from sediment containing marine deposited volcanic ash. This volcanic ash, which may alter to montmorillonite, a smectite group clay, can have a very high potential for shrinking and swelling. Such altered ash beds are referred to as **bentonite** beds, but the term *bentonite* has been more generally applied to rocks containing abundant swelling clays as well.

Clays have been used extensively for environmental protection and remediation. A typical use is the installation of a clay layer a meter or so thick beneath a new waste dump or

DO NOT COPY e48d507df5d1141@placeholder.9409

Printed by: e48d507df5d1141@placeholder.94092.edu. Printing is for personal, private use only. No part of this book may be reproduced or transmitted without publisher's prior permission. Violators will be prosecuted.

containment pond. The clay layer prevents migration of contaminated water into the groundwater supply. Similar clay caps may be installed over existing dumps to prevent infiltration of water into the dump where it could become contaminated. Clays may also be used to absorb contaminants from industrial waste water or from other contaminated water supplies.

Clay minerals have also played a role in human health for millennia. Medicinal uses of clay were described by Aristotle (fourth century BCE), and new uses continue to be found. Some current health-related uses of clay are in geophagy and pelotherapy, and as antibacterials and as carriers for drugs (Williams and Hiller, 2015).

Geophagy is the practice of deliberately eating Earth materials. In modern society, geophagy may be considered aberrant behavior, and it can certainly be a manifestation of mental illness in some cases. However, geophagy has been a common practice since ancient times and continues today in many parts of the world, including the southeastern United States. Many minerals are involved in geophagy (Limpitlaw, 2010), but the clay minerals are perhaps the most common. The clay may be powdered, or formed into tablets, disks, or other shapes. An Internet search will yield numerous sources for edible clays. It may be unclear if a seller has taken the appropriate precautions to ensure a safe product, but clay is routinely sold in grocery stores, pharmacies, and markets in many parts of the world. The adverse health consequences of eating clay can include blockage of the lower intestine, nutrient deficiency, nutrient excesses, damage to the teeth and gums, poisoning, and parasitic invasions. However, geophagy also can be beneficial, and the clay may serve as a source of nutrients (e.g., K, Na, and Fe), calm upset stomachs, and control diarrhea. There is still much unknown regarding the benefits and the adverse consequences of eating Earth materials.

Pelotherapy is the application of muds (peloids) to the skin to treat rheumatic disorders, osteoarthritis, infections, sciatica, skin disorders, and a variety of other conditions. A wide range of claims are made regarding the efficacy of these treatments, and people pay large sums of money for the pelotherapy in health and beauty spas in many parts of the world. Clay is also used in a number of folk remedies, such as applying mud or clay to a bee sting to (presumably) absorb some of the venom; use of clay in these ways has not been thoroughly tested.

It is now recognized that some clays have antibacterial properties and are capable of killing a wide range of human pathogens, including antibiotic-resistant bacteria. The clays that have displayed antibacterial properties contain expandable clay minerals (e.g., smectite) and soluble Fe^{2+} and Al^{3+}. The dried clay is mixed with distilled water and exposed to the bacteria. The Fe^{2+} and Al^{3+} that goes into solution disrupt cellular metabolic functions and kill the bacteria.

A relatively recent development is to use clay minerals in wound dressings to stop severe bleeding. Of the clays tested, kaolinite was the most effective in promoting clotting, and was as effective as zeolite (Chapter 12), but with substantially less tissue damage at the application site.

Printed by: e48d507df5d1141@placeholder.94092.edu. Printing is for personal, private use only. No part of this book may be reproduced or transmitted without publisher's prior permission. Violators will be prosecuted.

application site.

Conventional applications of clay minerals in medications include use both as an inert filler and as active ingredients. Kaopectate® is a well-known antidiarrheal medication that originally was a mixture of kaolinite and pectin. The kaolinite was replaced with attapulgite (palygorskite) in the 1980s, and the product is now formulated with bismuth subsalicylate. Kaolinite-based preparations are still available in some parts of the world and are routinely used in veterinary medicine.

DO NOT COPY
e48d507df5d1141@placeholder.9409

Printed by: e48d507df5d1141@placeholder.94092.edu. Printing is for personal, private use only. No part of this book may be reproduced or transmitted without publisher's prior permission. Violators will be prosecuted.

Other Sheet Silicates

Stilpnomelane

Å
Å
Å

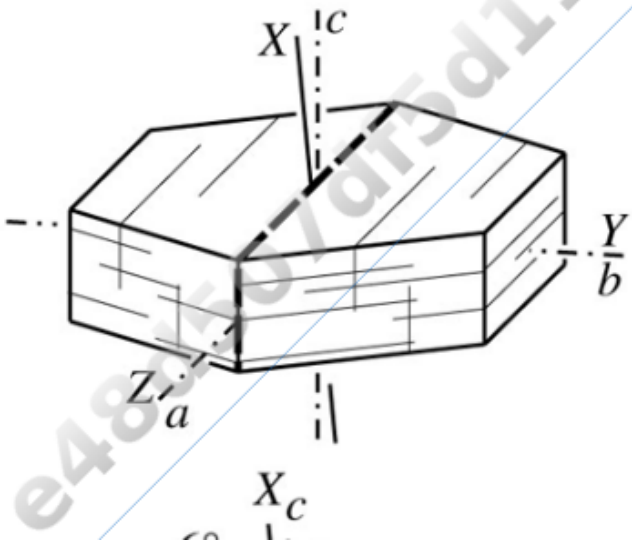

DO NOT COPY
e48d507df5d1141@placeholder.9409

Printed by: e48d507df5d1141@placeholder.94092.edu. Printing is for personal, private use only. No part of this book may be reproduced or transmitted without publisher's prior permission. Violators will be prosecuted.

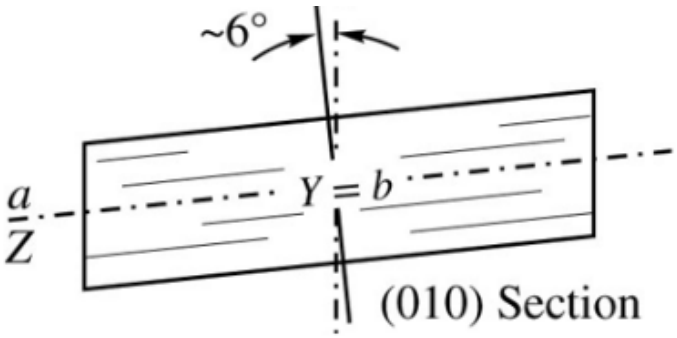

Structure In the common *TOT* sheet silicates, the tetrahedral *T* sheet apical oxygens point toward, and are shared with, a continuous octahedral *O* sheet. In stilpnomelane, groups of tetrahedra point away from the octahedral sheet (**Figure 13.16**). These outward-pointing apical oxygen anions are shared with similar outward-pointing tetrahedra on adjacent *TOT* layers and provide relatively strong bonding between layers.

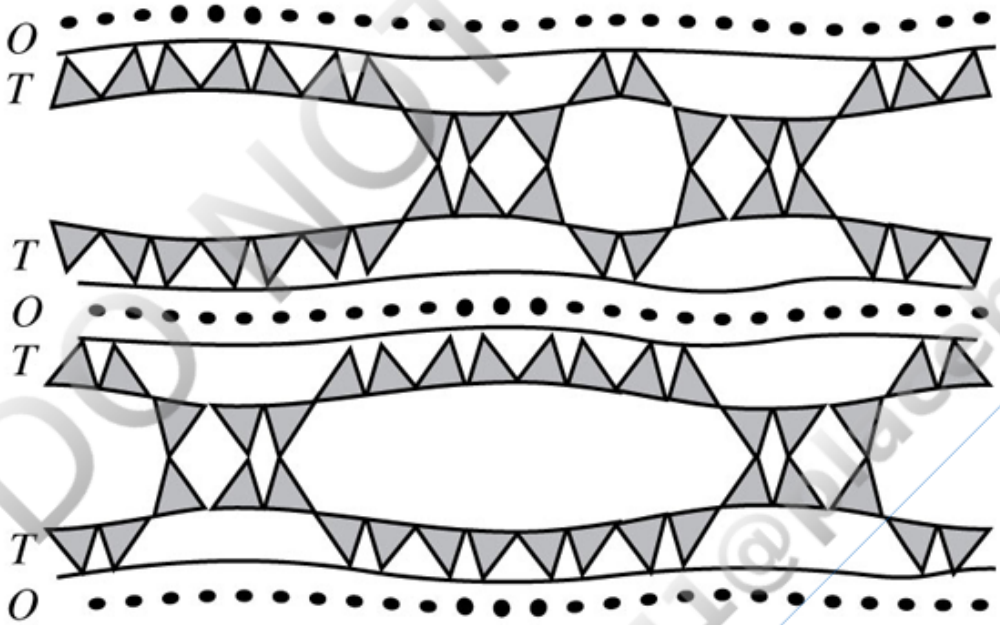

FIGURE 13.16 Idealized structure of stilpnomelane. Some tetrahedra point outward from the *TOT* layers and share oxygen anions with similar tetrahedra from adjacent *TOT* layers. Adapted from Guggenheim and Eggleton (1987). View larger image

Composition Stilpnomelane displays substantial compositional variation, principally in the relative amount of Fe^{2+}, Fe^{3+}, and Mg in octahedral sites. Substitution of Fe^{3+} is coupled with replacing OH^- with O^{2-} to maintain charge balance.

Form and Twinning See **Figure 13.17**. It is micaceous, like most sheet silicates. Grains may be arranged in foliated, sheaflike, or radiating aggregates, or interlayered with chlorite or other micaceous minerals. No twinning is reported.

Printed by: e48d507df5d1141@placeholder.94092.edu. Printing is for personal, private use only. No part of this book may be reproduced or transmitted without publisher's prior permission. Violators will be prosecuted.

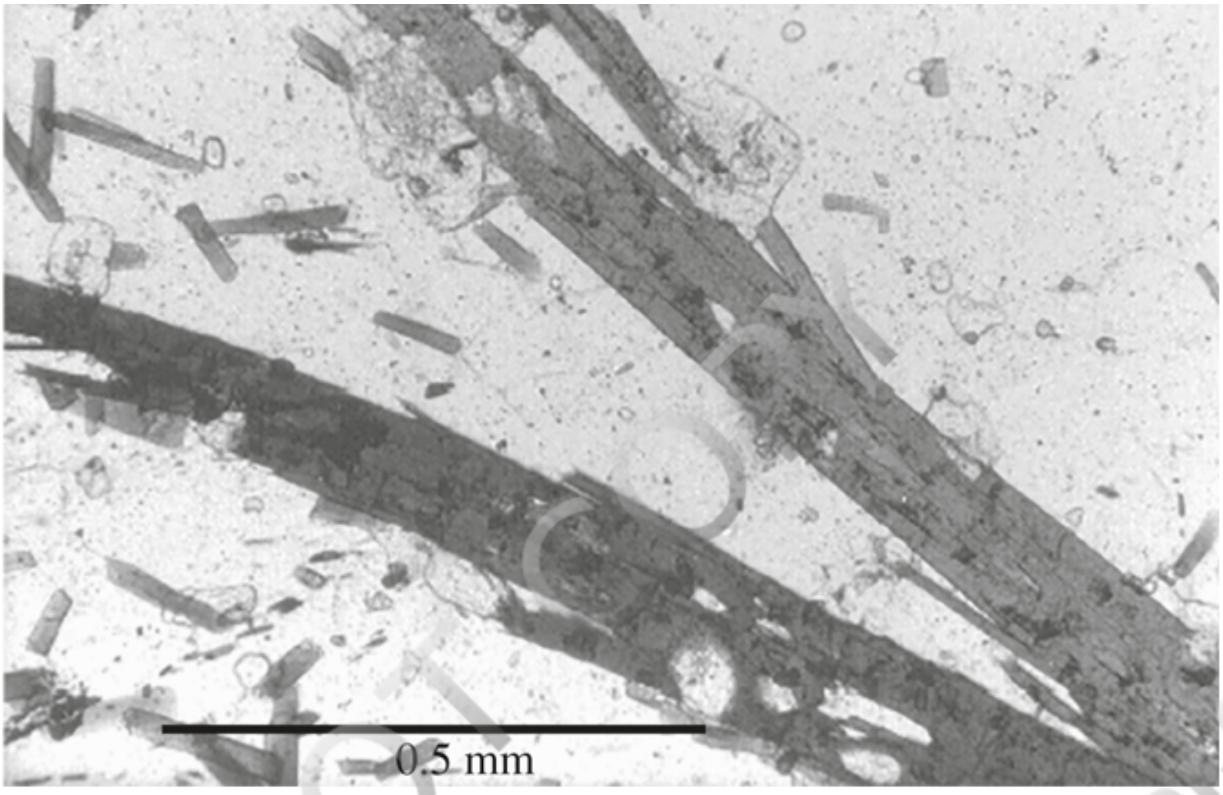

FIGURE 13.17 Stilpnomelane grains in a stilpnomelane schist. View larger image

Cleavage A perfect cleavage on {001} is not as perfect as for the micas. Fair cleavage on {010} intersects {001} at 90°.

Color Properties

Luster: Vitreous to pearly on cleavage surfaces; may be submetallic.

Color: Golden brown, reddish brown, dark green, black.

Streak: White to tan.

Color in Thin Section: Pale yellow, brown, or green.

Pleochroism: Distinct with $Z \approx Y > X$: X = pale yellow to golden yellow; $Y \approx Z$ = brown, reddish brown, greenish brown, black. Sections are darker when the trace of cleavage is parallel to the vibration direction of the lower polarizer.

Optical Characteristics

Relief in Thin Section: High positive, may change with rotation.

Optic Orientation: $X \wedge c = \sim+6°$, $Y = b$, $Z \wedge a = \sim0°$; the trace of cleavage is length slow.

Indices of Refraction and Birefringence: Increase with Fe^{3+} content.

Interference Figure: Stilpnomelane is effectively uniaxial negative. Cleavage fragments yield nearly centered optic axis figures.

Printed by: e48d507df5d1141@placeholder.94092.edu. Printing is for personal, private use only. No part of this book may be reproduced or transmitted without publisher's prior permission. Violators will be prosecuted.

yield nearly centered optic axis figures.

Alteration Stilpnomelane may alter to chlorite, iron oxides, and clay.

Distinguishing Features

Hand Sample: Similar to biotite, but the basal cleavage is less perfect and stilpnomelane has a second cleavage at 90°.

Thin Section/Grain Mount: Resembles biotite, but biotite has $2V$ up to 25° and lacks the second cleavage. Also, stilpnomelane lacks the distinctive mottling or bird's-eye extinction seen with biotite. Birefringence of Fe^{3+}-rich stilpnomelane is higher than that of biotite.

Occurrence Fairly common in low-grade regional metamorphic rocks (greenschists) along with chlorite, albite, and muscovite. Also in blueschist regional metamorphic rocks associated with glaucophane, calcite, epidote group minerals, and pumpellyite. Stilpnomelane also may be found in metamorphosed iron formations.

Use None.

Prehnite

$$\mathrm{Ca_2Al(AlSi_3\,O_{10})(OH)_2}$$

$$\text{Orthorhombic } mm2$$

$$a = 4.646 \text{ Å},\ b = 5.491 \text{ Å},$$
$$c = 18.52 \text{ Å},\ Z = 2$$

$$H = 6 - 6.5$$

$$G = 2.80 - 2.95$$

$$\text{Biaxial } (+)$$

$$n_\alpha = 1.610 - 1.637$$

$$n_\beta = 1.615 - 1.647$$

$$n_\gamma = 1.632 - 1.670$$

$$\delta = 0.020 - 0.035$$

$$2V_z = 64 - 70^\circ$$

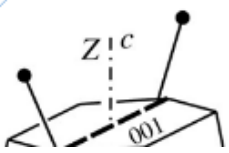

DO NOT COPY
e48d507df5d1141@placeholder.9409

Printed by: e48d507df5d1141@placeholder.94092.edu. Printing is for personal, private use only. No part of this book may be reproduced or transmitted without publisher's prior permission. Violators will be prosecuted.

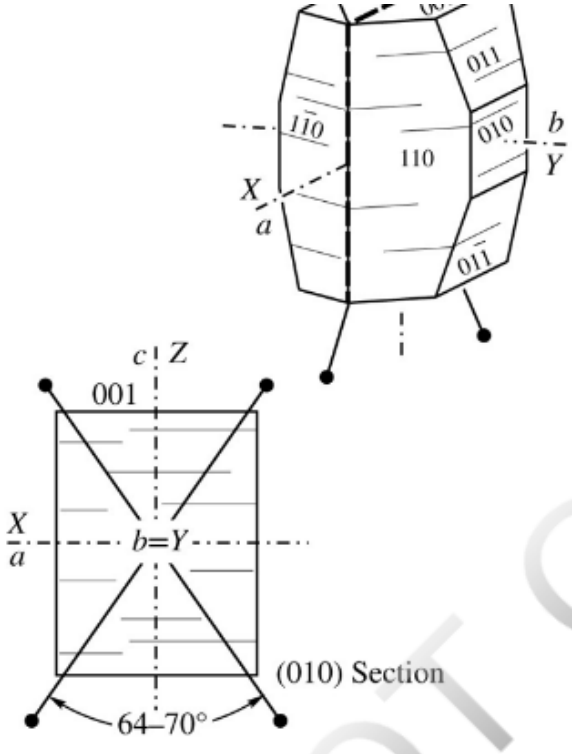

Structure The structure consists of complex sheets of Si^{4+} and Al^{3+} tetrahedra parallel to {001}. Some tetrahedra share all four oxygen ions, and some share only two. Ca^{2+} is in 7-fold coordination and Al^{3+} is in 6-fold coordination with oxygen from the tetrahedra and additional OH^- between the layers serve to bind adjacent sheets together.

Composition Some Fe^{3+} may substitute for Al^{3+}; otherwise the composition is usually fairly close to the ideal formula.

Form and Twinning Commonly occurs as lamellar or columnar masses and also as radiating, globular, fanlike, or sheaflike aggregates. A pattern resembling a bow tie is common in which adjacent grains are joined on surfaces nearly parallel to {001}. Crystals are uncommon and are either columnar parallel to *c* or tabular parallel to {001}. Fine lamellar twinning is reported, but is not common.

Cleavage Good {001} cleavage and poor cleavage parallel to {110} faces. The basal cleavage tends to control fragment orientation. Uneven fracture. Brittle.

Color Properties

Luster: Vitreous, somewhat pearly on {001}.

Color: Light to dark green, white, yellow, gray, pink; may slowly fade on exposure to light.

Streak: White.

Color in Thin Section: Colorless.

Pleochroism: None.

DO NOT COPY

Printed by: e48d507df5d1141@placeholder.94092.edu. Printing is for personal, private use only. No part of this book may be reproduced or transmitted without publisher's prior permission. Violators will be prosecuted.

Optical Characteristics

Relief in Thin Section: Moderately high positive.

Optic Orientation: $X = a$, $Y = b$, $Z = c$.

Indices of Refraction and Birefringence: Increase with Fe^{3+} content. Low-Fe samples are most common and have values near the lower end of the range given above. Interference colors may be anomalous.

Interference Figure: Biaxial (+) with a fairly large $2V_z$ (64–70°); the optic axis dispersion is weak; $r > v$.

Alteration Prehnite may alter to chlorite or zeolite minerals.

Distinguishing Features

Hand Sample: The green color and single good cleavage aid identification. The sheaflike or globular/radiating aggregates are fairly distinctive.

Thin Section/Grain Mount: Lawsonite and pumpellyite have higher indices of refraction and lower birefringence. Epidote, with birefringence similar to that of prehnite, typically has a greenish color in thin section and has higher indices of refraction. The bow-tie structure, if present, is distinctive.

Occurrence Prehnite is found in **amygdules** (a vesicle filled with secondary minerals), veins, or other cavities in mafic to intermediate igneous rocks, often in association with zeolites and calcite. Contact-metamorphosed impure limestones and marls may also contain prehnite associated with calcite, wollastonite, garnet, tremolite, or other calc-silicate minerals. The most abundant occurrence, however, is as a constituent in low-grade regional metamorphic rocks derived from graywacke, basalt, or other mafic to intermediate rocks. Associated minerals include lawsonite, pumpellyite, albite, epidote group minerals, chlorite, and zeolites. Small masses of prehnite have been found along the cleavage in biotite from granitic rocks.

Use Prehnite has been used as an ornamental material or semiprecious gem.

Apophyllite

$$KCa_4Si_8O_{20}(F, OH) \cdot 8H_2O$$

Tetragonal $(4/m\ 2/m\ 2/m)$

$$a = 8.963\ \text{Å},\ c = 15.804\ \text{Å},\ Z = 2$$

$$H = 4.5 - 5$$

$$G = 2.33 - 2.37$$

DO NOT COPY e48d507df5d1141@placeholder.9409

Printed by: e48d507df5d1141@placeholder.94092.edu. Printing is for personal, private use only. No part of this book may be reproduced or transmitted without publisher's prior permission. Violators will be prosecuted.

$$G = 2.33 - 2.37$$

$$\text{Uniaxial } (+) \text{ or } (-)$$

$$n_\omega = 1.531 - 1.542$$

$$n_\epsilon = 1.533 - 1.543$$

$$\delta = 0.000 - 0.003$$

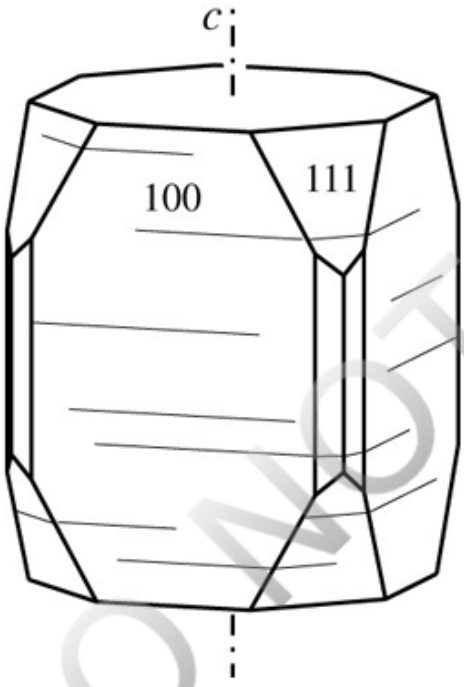

Structure The structure consists of 4-fold rings of Si tetrahedra linked together to form kinked sheets parallel to (001). The K, Ca, F, OH, and H_2O are located between these sheets.

Composition Compositions extend from hydroxyapophyllite to fluorapophyllite, which contain all OH and F, respectively. Most apophyllite is relatively fluorine-rich. Natroapophyllite contains Na instead of K and is orthorhombic.

Form and Twinning Crystals are square in cross section and may resemble cubes modified by octahedrons; also platy parallel to (001) or granular massive. Rare twins on {111}.

Cleavage Perfect cleavage on {001} and poor on {110}.

Color Properties

Luster: Vitreous, pearly on {001} cleavage surfaces.

Color: Colorless, white, gray, or a pale shade of pink, green, or yellow.

Streak: White.

DO NOT COPY e48d507df5d1141@placeholder.9409

Printed by: e48d507df5d1141@placeholder.94092.edu. Printing is for personal, private use only. No part of this book may be reproduced or transmitted without publisher's prior permission. Violators will be prosecuted.

Color in Thin Section: Colorless.

Pleochroism: None.

Optical Characteristics

Relief in Thin Section: Low negative or positive.

Optic Orientation: Apophyllite is uniaxial, so the trace of the {001} cleavage always shows parallel extinction and is length fast for optically positive samples and length slow for optically negative samples.

Indices of Refraction and Birefringence: Indices of refraction decrease with increasing substitution of F for OH. Birefringence is low, and interference colors are often anomalous.

Interference Figure: Apophyllite is usually uniaxial negative, less commonly positive. Biaxial varieties with $2V$ up to 60° have been reported.

Alteration Apophyllite may alter to clay minerals, calcite, opal, or quartz.

Distinguishing Features

Hand Sample: Distinguished from associated zeolites by crystal habit, basal cleavage, and pearly luster on cleavage surfaces.

Thin Section: Apophyllite has higher indices of refraction than the zeolites, with which it may be associated, and has a perfect basal cleavage. Interference colors are commonly anomalous. Natroapophyllite is biaxial positive with $2V_z = 32°$, $n_\alpha = 1.536$, $n_\beta = 1.538$, and $n_\gamma = 1.544$, $\delta = 0.008$.

Occurrence Apophyllite most commonly occurs in amygdules, cavities, and veins in basaltic rocks in association with zeolites, prehnite, pectolite, and calcite. It is also found in the contact aureole around granitic intrusions and in metamorphosed limestone or other calc-silicate rock. It may form from alteration of wollastonite.

Use None.

Chrysocolla

$$(Cu, Al)_2H_2Si_2O_5 \cdot nH_2O$$

Orthorhombic (?)

$$a = 5.72 \text{ Å to } 5.92 \text{ Å},$$
$$b = 17.7 \text{ Å to } 18.0 \text{ Å},$$

DO NOT COPY e48d507df5d1141@placeholder.9409

Printed by: e48d507df5d1141@placeholder.94092.edu. Printing is for personal, private use only. No part of this book may be reproduced or transmitted without publisher's prior permission. Violators will be prosecuted.

$c = 8.00$ Å to 8.28 Å,
$Z = ?$

$H =$ - 2 – 4

$G = 1.93 - 2.4$

Biaxial (−)?

$n_\alpha = 1.575 - 1.585$

$n_\beta = 1.597$

$n_\gamma = 1.598 - 1.635$

$\delta = 0.023 - 0.050$
$2V = ?$

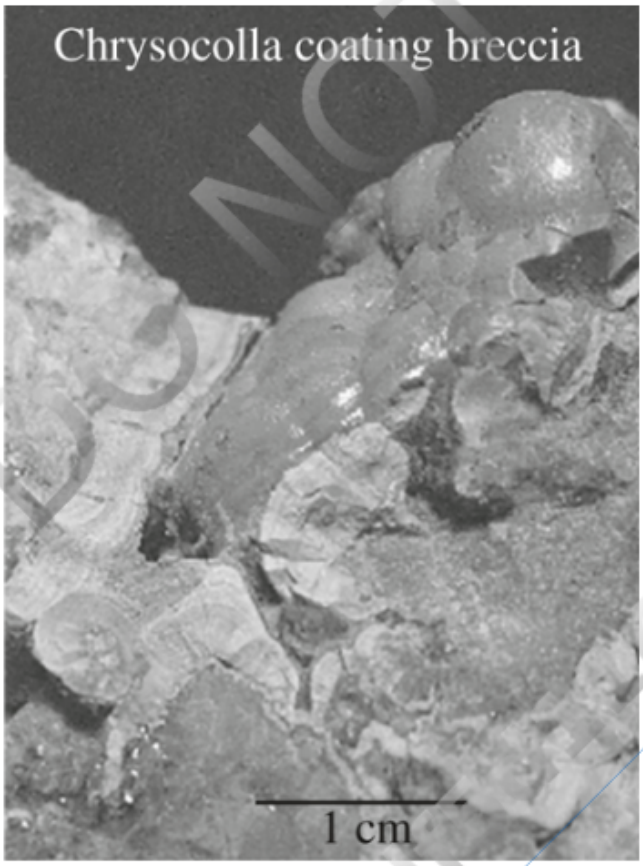

Structure The structure is poorly defined and is often amorphous, hence the question marks for various characteristics above and below. At least some contains silicon tetrahedral sheets and is therefore grouped here with the sheet silicates.

Composition Cu and Al are approximately in the ratio of 3:1.

Form and Twinning Typically forms botryoidal and encrusting masses; often cryptogranular. Rare crystals are acicular.

DO NOT COPY e48d507df5d1141@placeholder.9409

Printed by: e48d507df5d1141@placeholder.94092.edu. Printing is for personal, private use only. No part of this book may be reproduced or transmitted without publisher's prior permission. Violators will be prosecuted.

Cleavage Conchoidal fracture.

Color Properties

Luster: Usually earthy, also vitreous, waxy or dull waxy.

Color: Blue, blue-green, or green; brown or black if impure.

Streak: White or pale greenish if relatively pure.

Color in Thin Section: If not too fine grained to observe, colorless to pale blue-green.

Pleochroism: Reported colorless to pale blue-green.

Optical Characteristics

Relief in Thin Section: Moderate positive.

Optic Orientation: ?

Indices of Refraction and Birefringence: Generally so fine grained that measurement is impractical.

Interference Figure: Too fine grained to allow interference figures to be observed. Based on the reported indices of refraction, $2V_z$ should be 24°.

Alteration No consistent alteration.

Distinguishing Features

Hand Sample: Resembles turquoise but has lower hardness. Most samples will adhere to the tip of the tongue, whereas turquoise will not.

Thin Section: Amorphous/microgranular nature makes thin section identification impractical.

Occurrence Chrysocolla occurs in the oxidized portion of Cu-bearing sulfide mineral deposits.

Use Minor ore of copper. May be used as a semiprecious gem, particularly if intergrown with chalcedony to increase hardness.

DO NOT COPY
e48d507df5d1141@placeholder.9409

Printed by: e48d507df5d1141@placeholder.94092.edu. Printing is for personal, private use only. No part of this book may be reproduced or transmitted without publisher's prior permission. Violators will be prosecuted.

Interference Figure: Apophyllite is usually uniaxial negative, less commonly positive. Biaxial varieties with $2V$ up to 60° have been reported.
Alteration Apophyllite may alter to clay minerals, calcite, opal, or quartz.

Distinguishing Features

Hand Sample: Distinguished from associated zeolites by crystal habit, basal cleavage, and pearly luster on cleavage surfaces.

Thin Section: Apophyllite has higher indices of refraction than the zeolites, with which it may be associated, and has a perfect basal cleavage. Interference colors are commonly anomalous. Natroapophyllite is biaxial positive with $2V_z = 32°$, $n_\alpha = 1.536$, $n_\beta = 1.538$, and $n_\gamma = 1.544$, $\delta = 0.008$.

Occurrence Apophyllite most commonly occurs in amygdules, cavities, and veins in basaltic rocks in association with zeolites, prehnite, pectolite, and calcite. It is also found in the contact aureole around granitic intrusions and in metamorphosed limestone or other calc-silicate rock. It may form from alteration of wollastonite.

Use None.

Chrysocolla

Å Å
Å Å
Å Å

DO NOT COPY
e48d507df5d1141@placeholder.9409

Printed by: e48d507df5d1141@placeholder.94092.edu. Printing is for personal, private use only. No part of this book may be reproduced or transmitted without publisher's prior permission. Violators will be prosecuted.

Structure The structure is poorly defined and is often amorphous, hence the question marks for various characteristics above and below. At least some contains silicon tetrahedral sheets and is therefore grouped here with the sheet silicates.

Composition Cu and Al are approximately in the ratio of 3:1.

Form and Twinning Typically forms botryoidal and encrusting masses; often cryptogranular. Rare crystals are acicular.

Cleavage Conchoidal fracture.

Color Properties

Luster: Usually earthy, also vitreous, waxy or dull waxy.

Color: Blue, blue-green, or green; brown or black if impure.

Streak: White or pale greenish if relatively pure.

Color in Thin Section: If not too fine grained to observe, colorless to pale blue-green.

Pleochroism: Reported colorless to pale blue-green.

Optical Characteristics

Relief in Thin Section: Moderate positive.

DO NOT COPY e48d507df5d1141@placeholder.9409

Printed by: e48d507df5d1141@placeholder.94092.edu. Printing is for personal, private use only. No part of this book may be reproduced or transmitted without publisher's prior permission. Violators will be prosecuted.

Relief in Thin Section: Moderate positive.

Optic Orientation: ?

Indices of Refraction and Birefringence: Generally so fine grained that measurement is impractical.

Interference Figure: Too fine grained to allow interference figures to be observed. Based on the reported indices of refraction, $2V_z$ should be 24°.

Alteration No consistent alteration.

Distinguishing Features

Hand Sample: Resembles turquoise but has lower hardness. Most samples will adhere to the tip of the tongue, whereas turquoise will not.

Thin Section: Amorphous/microgranular nature makes thin section identification impractical.

Occurrence Chrysocolla occurs in the oxidized portion of Cu-bearing sulfide mineral deposits.

Use Minor ore of copper. May be used as a semiprecious gem, particularly if intergrown with chalcedony to increase hardness.

DO NOT COPY

REFERENCES CITED AND SUGGESTIONS FOR ADDITIONAL READING

Albee, A. L. 1962. Relationships between the mineral association, chemical composition and physical properties of the chlorite series. *American Mineralogist* **47**, 851–870.

Bailey, S. W. (ed.). 1984. *Micas. Reviews in Mineralogy* **13**, 584 p.

Bailey, S. W. (ed.). 1988. *Hydrous Sheet Silicates (Exclusive of Micas).* Reviews in Mineralogy **19**, 755 p.

Balan, E., Calas, G., and Bish, D. L. 2014. Kaolin-group minerals: from hydrogen-bonded layers to environmental recorders. *Elements* **10**, 183–188.

Brindley, G. W. 1980. Quantitative X-ray analysis of clays, in G. W. Brindley and G. Brown (eds.), *Crystal Structures of Clay Minerals and Their X-Ray Identification.* Monograph No. 5, pp. 411–438. Mineralogical Society, London.

Clinkenbeard, J. P., Churchill, R. K., and Lee, K. (eds.) 2002. Guidelines for geologic investigations of naturally occurring asbestos in California, *California Geological Survey Special Publication* **124**, 69 p.

Printed by: e48d507df5d1141@placeholder.94092.edu. Printing is for personal, private use only. No part of this book may be reproduced or transmitted without publisher's prior permission. Violators will be prosecuted.

Coggon, R., and Holland, T. J., B. 2002. Mixing properties of phengitic micas and revised garnet-phengite thermobarometers. *Journal of Metamorphic Geology* **20**, 683–696.

Cui, Y., Zha, Y., Li, T., Bai, J., Tang, L., Deng, J., He, R., Dong, F., and Zhang, Q. 2019. Oxidative effects of lungs in Wistar rats caused by long-term exposure to four kinds of China representative chrysotile. *Environmental Science and Pollution Research* **26**, 18708–18718.

Deer, W. A., Howie, R. A., and Zussman, J. 1992. *The Rock Forming Minerals*, 2nd ed. Longman Group Ltd., London, 696 p.

Deer, W. A., Howie, R. A., and Zussman, J. 2009. *Rock-Forming Minerals, Volume 3B: Layered Silicates: Excluding Micas and Clay Minerals*, 2nd ed. The Geological Society, London, 320 p.

Finkelstein, M. M. 2012. Malignant mesothelioma incidence among talc miners and millers in New York State. *American Journal of Industrial Medicine* **55**, 863–868.

Fleet, M. E., and Howie, R. A. 2004. *Rock-Forming Minerals, Volume 3A: Micas*, 2nd ed. The Geological Society, London, 780 p.

Guggenheim, S., and Eggleton, R. A. 1987. Modulated 2:1 layer silicates: Review, systematics, and predictions. *American Mineralogist* **72**, 724–738.

Gunter, M. E., Belluso, E., and Mottana, A. 2007. Amphiboles: Environmental and health concerns. *Reviews in Mineralogy and Geochemistry* **67**, 453–516.

Guthrie, G. D., Jr., and Mossman, B. T. 1993. *Health effects of mineral dusts*. Reviews in Mineralogy **28**, 584 p.

Hazen, R. M., Sverjensky, D. A., Azzolini, D., Bish, D. L., Elmore, S. C., Hinnov, L., and Milliken, R. E. 2013. Clay mineral evolution. *American Mineralogist* **98**, 207–229.

Hower, J., Eslinger, E. V., Hower, M. E., and Perry, E. A. 1976. Mechanism of burial metamorphism of argillaceous sediment: 1. Mineralogical and chemical evidence. *Geological Society of America Bulletin* **87**, 725–737.

Kanarek, M. S. 2011. Mesothelioma from chrysotile asbestos: Update. *Annals of Epidemiology* **21**, No. 9, 688–697.

Ilgren, E. B. 2004. The biology of cleavage fragments: A brief synthesis and analysis of current knowledge. *Indoor and Built Environment* **13**, 343–356.

Laduron, D. M. 1971. A staining method for distinguishing paragonite from muscovite in thin section. *American Mineralogist* **56**, 1117–1119.

Lee, R. J., Strohmeier, B. R., Bunker, K. L., and Van Orden, D. R. 2008. Naturally occurring asbestos—A recurring public policy challenge. *Journal of Hazardous Material* **153**, 1–21.

Lee, S., Kang, D., Kim, Y., Kim, Y.-J., and Kim, S.-Y. 2021. Activity-based exposure levels and cancer risk assessment due to naturally occurring asbestos for the residents near abandoned asbestos mines in South Korea. *International Journal of Environmental*

DO NOT COPY

Printed by: e48d507df5d1141@placeholder.94092.edu. Printing is for personal, private use only. No part of this book may be reproduced or transmitted without publisher's prior permission. Violators will be prosecuted.

abandoned asbestos mines in South Korea. *International Journal of Environmental Research and Public Health* **18**, 1–12.

Limpitlaw, U. G. 2010. Ingestion of Earth materials for health by humans and animals. *International Geology Review* **52**, 726–744.

McCollom, T. M., and Seewald, J. S. 2013. Serpentinites, hydrogen, and life. *Elements* **9**, 129–134.

Moore, D. M., and Reynolds, R. C., Jr. 1997. *X-Ray Diffraction and the Identification and Analysis of Clay Minerals*, 2nd ed. Oxford University Press, New York, 378 p.

Morrison, K. D., Misra, R., and Williams, L. B. 2016. Unearthing the antibacterial mechanism of medicinal clay: A geochemical approach to combating antibiotic resistance. *Scientific Reports* **6**, 19043; doi: 10.1038/srep 19043.

Mottana, A., Sassi, F. P., Thompson, J. B., Jr., and Guggenheim, S. (eds.). 2002. *Micas: Crystal Chemistry and Metamorphic Petrology. Reviews in Mineralogy and Geochemistry* **46**, 499 p.

Pan, X.-l., Day, H. W., Wang, W., Beckett, L. A., and Schenker, M. B. 1999. Residential proximity to naturally occurring asbestos and mesothelioma risk in California. *American Journal of Respiratory and Critical Care Medicine* **172**, 1019–1025.

Rieder, M., Cavazzini, G., D'Yakonov, Y. S., Frank-Kamenetskii, V. A., Gottard, G., Guggenheim, S., Koval, P. V., Müller, G., Neiva, A. M. R., Radoslovich, E. W., Robert, J. L., Sassi, F. P., Hiroshi, T., Weiss, Z., and Wones, D. R. 1998. Nomenclature of the micas. *The Canadian Mineralogist* **36**, 41–48.

Skinner, H. C. W., Ross, M., and Frondel, C. 1988. *Asbestos and Other Fibrous Minerals: Mineralogy, Crystal Chemistry and Health Effects*. Oxford University Press, New York, 204 p.

Scarselli, A., Marinaccio, A., and Iavicoli, S. 2021. Ophiolitic outcrops, naturally occurring asbestos exposure and mortality risk from malignant mesothelioma in Calabria (Southern Italy). *Public Health* **195**, 57–60.

Starkey, H. C., Blackmon, P. D., and Hauff, P. L. 1984. *The routine mineralogical analysis of clay-bearing samples*. U.S. Geological Survey Bulletin 1563, 32 p.

Tischendorf, G., Gottesmann, B., Förster, H.-J., and Trumbull, R. B. 1997. On Li-bearing micas: Estimating Li from electron microprobe analyses and an improved diagram for graphical representation. *Mineralogical Magazine* **61**, 809–834.

Velde, B. (ed.). 1995. *Origin and Mineralogy of Clays*. Springer-Verlag, Berlin, 334 p.

Weaver, C. E. 1989. *Clays, Muds and Shales*. Elsevier Science Publishers, Amsterdam, 819 p.

Welton, J. E. 2003. *SEM Petrology Atlas: Methods in Exploration Series No. 4*. American Association of Petroleum Geologists, Tulsa, OK, 240 p.

Williams, L. B., Haydel, S. E., and Ferrell, R. E., Jr. 2009. Bentonite, Bandaids, and borborygmi. *Elements* **5**, 99–104.

DO NOT COPY e48d507df5d1141@placeholder.94092

Printed by: e48d507df5d1141@placeholder.94092.edu. Printing is for personal, private use only. No part of this book may be reproduced or transmitted without publisher's prior permission. Violators will be prosecuted.

Williams, L. B., and Hiller, S. 2015. Kaolins and health: From first grade to first aid. *Elements* **10**, 207–211.

DO NOT COPY

e48d507df5d1141@placeholder.9409

Printed by: e48d507df5d1141@placeholder.94092.edu. Printing is for personal, private use only. No part of this book may be reproduced or transmitted without publisher's prior permission. Violators will be prosecuted.

LIST OF KEY TERMS

amygdules
argillaceous
asbestiform
bentonite
bird’s-eye extinction
clay
clay-sized
dioctahedral
interlayer
layer repeat distance
marl
phyllosilicate
potash
refractory
trioctahedral

DO NOT COPY
e48d507df5d1141@placeholder.9409

Printed by: e48d507df5d1141@placeholder.94092.edu. Printing is for personal, private use only. No part of this book may be reproduced or transmitted without publisher's prior permission. Violators will be prosecuted.

CHAPTER 14
Chain Silicates

William D. Nesse
University of Northern Colorado

Graham B. Baird
University of Northern Colorado

DO NOT COPY
e48d507df5d1141@placeholder.9409

Printed by: e48d507df5d1141@placeholder.94092.edu. Printing is for personal, private use only. No part of this book may be reproduced or transmitted without publisher's prior permission. Violators will be prosecuted.

Introduction

The chain silicates are common Fe/Mg-bearing silicates represented by two principal groups, the pyroxenes and the amphiboles. The pyroxenes and the amphiboles are constructed, respectively, of single and double chains of silicon tetrahedra (see Chapter 11). In terms of abundance, the pyroxenes are among the most common minerals, given the abundance of pyroxene in mafic and related rocks that make up oceanic crust. Although not as abundant as the pyroxenes, the amphiboles are very common minerals in a wide variety of intermediate igneous and metamorphic rocks. The pyroxenoids are relatively uncommon minerals with structures that are closely related to the pyroxene group.

DO NOT COPY
e48d507df5d1141@placeholder.9409

Printed by: e48d507df5d1141@placeholder.94092.edu. Printing is for personal, private use only. No part of this book may be reproduced or transmitted without publisher's prior permission. Violators will be prosecuted.

Pyroxene Group

Structure and Classification

Pyroxenes, with a general formula of $M2M1T_2O_6$, are constructed of single chains of tetrahedra (**Figure 14.1**) that extend parallel to the *c* axis. The T cations in the tetrahedra are most commonly Si^{4+}, although some may be Al^{3+}. The chains are stacked in the *a* direction in an alternating fashion so that bases of tetrahedra face bases and unshared apical oxygens face unshared oxygens. The M2 cations occupy the M2 structural sites between the bases of the tetrahedra in somewhat distorted 6- or 8-fold coordination, depending on how the chains are stacked and the size of the cation that occupies the site. M1 cations occupy the 6-fold (octahedral) M1 structural sites between the apical oxygens on the points of adjacent chains. The chains of tetrahedra in many pyroxenes are kinked somewhat (Figure 14.1e) so that the tetrahedra match up with the somewhat distorted octahedra that contain the M1 cations.

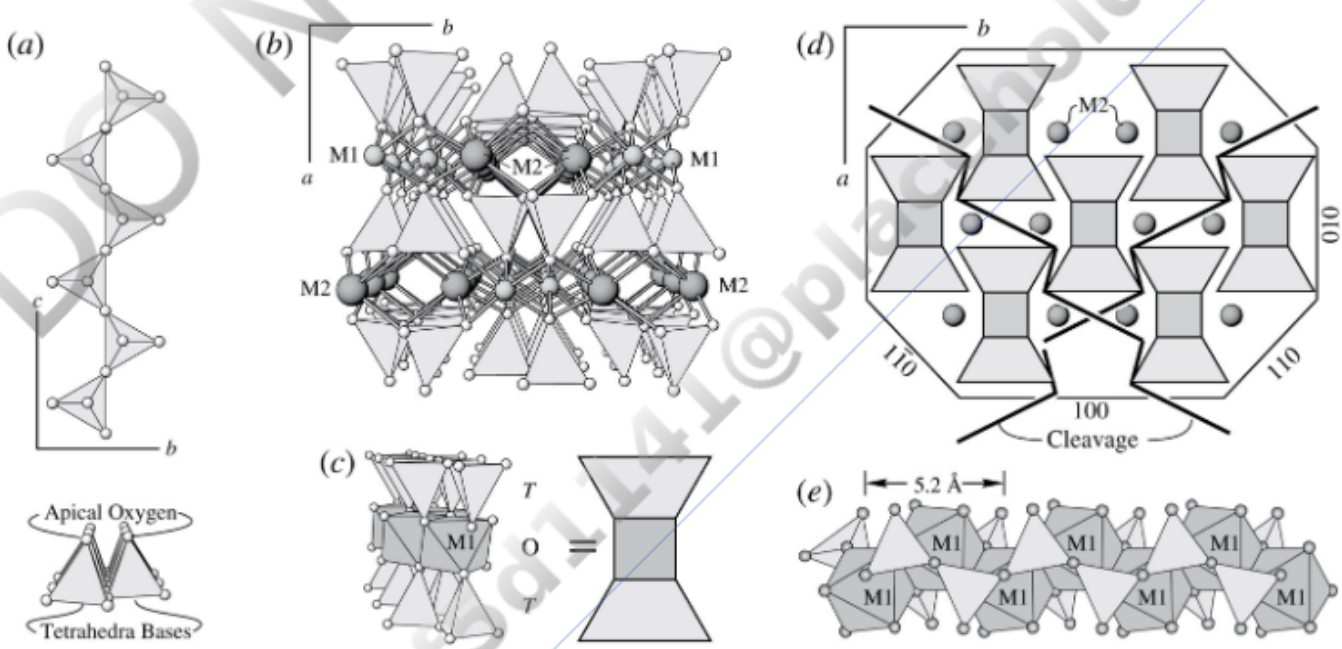

FIGURE 14.1 Pyroxene structure. (*a*) Top and end views of an idealized single chain of silicon tetrahedra. (*b*) Chains are stacked in alternating fashion to form 6-fold coordinated M1 sites between the unshared apical oxygens of the tetrahedra and 6- to 8-fold coordinated M2 sites between the bases. (*c*) Two chains and the intervening octahedral M1 sites form a structural *TOT* "I-beam." (*d*) View similar to (*b*) but with I-beams shown. Cleavage at about 87° and 93° between the I-beams is parallel to the {110} faces in the monoclinic unit cell. (*e*) In pyroxenes, the tetrahedra chains are typically kinked, rather than straight, as shown in this top view of an enstatite *TOT* I-beam. The repeat distance along chains is two tetrahedra at about 5.2 Å. Compare with Figure 14.7a. View larger image

Printed by: e48d507df5d1141@placeholder.94092.edu. Printing is for personal, private use only. No part of this book may be reproduced or transmitted without publisher's prior permission. Violators will be prosecuted.

It is convenient to treat a pair of tetrahedral chains and the octahedrally coordinated M1 site between the apical oxygens as a structural unit. This unit is often referred to as an "I-beam" because of its similarity to the cross section of a steel I-beam. Note the relationship to the *TOT* layers in the sheet silicates shown earlier (Figure 13.1). The *TOT* I-beams are stacked in an interlocking fashion to form the structure of the pyroxene group. M2 sites are found between the tetrahedral chain bases and have 6- or 8-fold coordination determined by how the adjacent I-beams line up. If they line up to produce 6-fold coordination M2 sites, the structure has orthorhombic symmetry, and if the alignment yields 8-fold coordination sites, the symmetry is monoclinic.

This structure typically produces blocky prismatic crystals elongate along *c* with square or approximately octagonal cross sections. Cleavage splits between the I-beams and produces two directions at about 87° and 93°, which is characteristic of the pyroxenes.

Pyroxene classification is based on the occupancy of the M2 site and symmetry (**Table 14.1**). The composition of most common pyroxenes can be shown on a triangular diagram (**Figure 14.2a**) whose vertices are $Ca_2Si_2O_6$ (wollastonite), $Mg_2Si_2O_6$ (enstatite), and $Fe_2Si_2O_6$ (ferrosilite). Wollastonite, enstatite, and ferrosilite are abbreviated Wo, En, and Fs, respectively. The three groups of common pyroxenes are orthopyroxene (opx), low-Ca-clinopyroxene (pigeonite), and Ca-clinopyroxene (cpx). While wollastonite is one of the vertices on the diagram, its structure is somewhat different and it is classified as a pyroxenoid, not a pyroxene, with its formula often reported as $CaSiO_3$. Diopside (Di) and hedenbergite (Hd) are the Mg and Fe compositional end members of pyroxenes containing 50% Ca relative to the total amount of Fe+Mg+Ca. Ideally Ca only occupies the M2 site. In some texts, the Ca–Fe–Mg pyroxene classification is presented as a quadrilateral only with Di–Hd–Fs–En end members shown. Solid solution pyroxenes reasonably close in composition to these end members may be identified by the end member name.

TABLE 14.1 Pyroxene Classification[a]

Group	M2	M1	T_2O_6	Mineral(s)	Symmetry	Comment
Magnesium–iron	Mg, Fe	Mg, Fe	Si_2O_6	Enstatite–Ferrosilite	Orthorhombic	Orthopyroxene (opx)
	Mg, Fe, Ca	Mg, Fe	Si_2O_6	Pigeonite	Monoclinic	Low-Ca-clinopyroxene
Calcium	Ca	Mg, Fe	Si_2O_6	Diopside–Hedenbergite		Ca-clinopyroxene (Ca-cpx or cpx)
		Mg, Fe, Al	$(Si,Al)_2O_6$	Augite		
Calcium–sodium	Ca, Na	Mg, Fe^{2+}, Al, Fe^{3+}	Si_2O_6	Omphacite		Sodic–calcic clinopyroxene

DO NOT COPY e48d507df5d1141@placeholder.94092

Printed by: e48d507df5d1141@placeholder.94092.edu. Printing is for personal, private use only. No part of this book may be reproduced or transmitted without publisher's prior permission. Violators will be prosecuted.

		Mg, Fe^{2+}, Fe^{3+}	Si_2O_6	Aegirine–Augite		
Sodium	Na	Al	Si_2O_6	Jadeite		Sodic clinopyroxene
		Fe^{3+}	Si_2O_6	Aegirine		
Lithium	Li	Al	Si_2O_6	Spodumene		Lithium clinopyroxene

[a] Based on the general formula $M2M1T_2O_6$, where M2 cations occupy the M2 structural site, M1 cations occupy the M1 structural site, and T cations occupy the tetrahedral site.

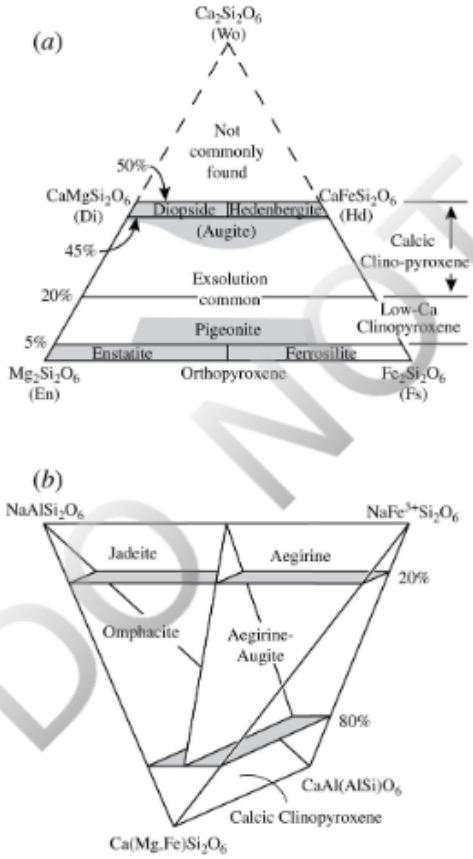

FIGURE 14.2 Pyroxene classification; see text for details. (*a*) Calcic and iron–magnesium pyroxenes. The percentages on the left side refer to the amount of Ca relative to Fe + Mg + Ca. The common compositions are shaded. (*b*) Sodic and sodic–calcic pyroxenes. View larger image

Orthopyroxene (opx) can be considered a simple solid solution series between enstatite ($Mg_2Si_2O_6$) and ferrosilite ($Fe_2Si_2O_6$). As the name implies, orthopyroxene is orthorhombic. Both the M1 and M2 sites are octahedral and both can contain Mg and Fe, but the larger Fe cations are concentrated in the somewhat larger M2 sites.

Low-Ca-clinopyroxene (pigeonite) typically has somewhat more Ca than orthopyroxene, but solid solution does not extend to Ca-clinopyroxene. Most M2 structural sites between the bases of the tetrahedra are occupied by Fe and Mg; some are occupied by Ca. The M1 site is occupied by Mg and Fe.

DO NOT COPY e48d507df5d1141@placeholder.9409

Printed by: e48d507df5d1141@placeholder.94092.edu. Printing is for personal, private use only. No part of this book may be reproduced or transmitted without publisher's prior permission. Violators will be prosecuted.

Ca-clinopyroxene (cpx) includes compositions that extend from diopside ($CaMgSi_2O_6$) to hedenbergite ($CaFeSi_2O_6$). The M2 sites contain mostly Ca and the M1 sites contain mostly Mg and Fe. The most abundant Ca-clinopyroxene is augite, in which some Al substitutes both in the M1 sites and for Si in tetrahedral sites, and some Na, Fe, or Mg substitutes for Ca in the M2 site. Augite therefore does not strictly lie in the composition plane defined by Wo–Fs–En, so parentheses have been placed around it in Figure 14.2a, and its location is based on its Ca–Fe–Mg content.

The composition space for the sodium-bearing clinopyroxenes is shown in **Figure 14.2b**. Extensive solid solution is possible between the sodic, sodic–calcic, and calcic clinopyroxenes. The common compositions fall in two ranges. One includes aegirine and aegirine–augite, and the second includes jadeite and omphacite. Those groupings are used in the mineral descriptions that follow.

Pyroxene species can be distinguished from each other only with difficulty in hand sample, and then based mostly on color and occurrence. Orthopyroxenes and pigeonite are most commonly brown; pigeonite is usually restricted to volcanic rocks. Ca-clinopyroxenes and sodic pyroxenes are commonly shades of dark green or are black. Light-green pyroxene in metamorphosed carbonate is usually diopside. Optical properties can help distinguish among the various species, but if knowledge of composition is important, chemical analysis is essential (Chapter 9). **Figure 14.3** shows photomicrographs of pyroxenes in thin section.

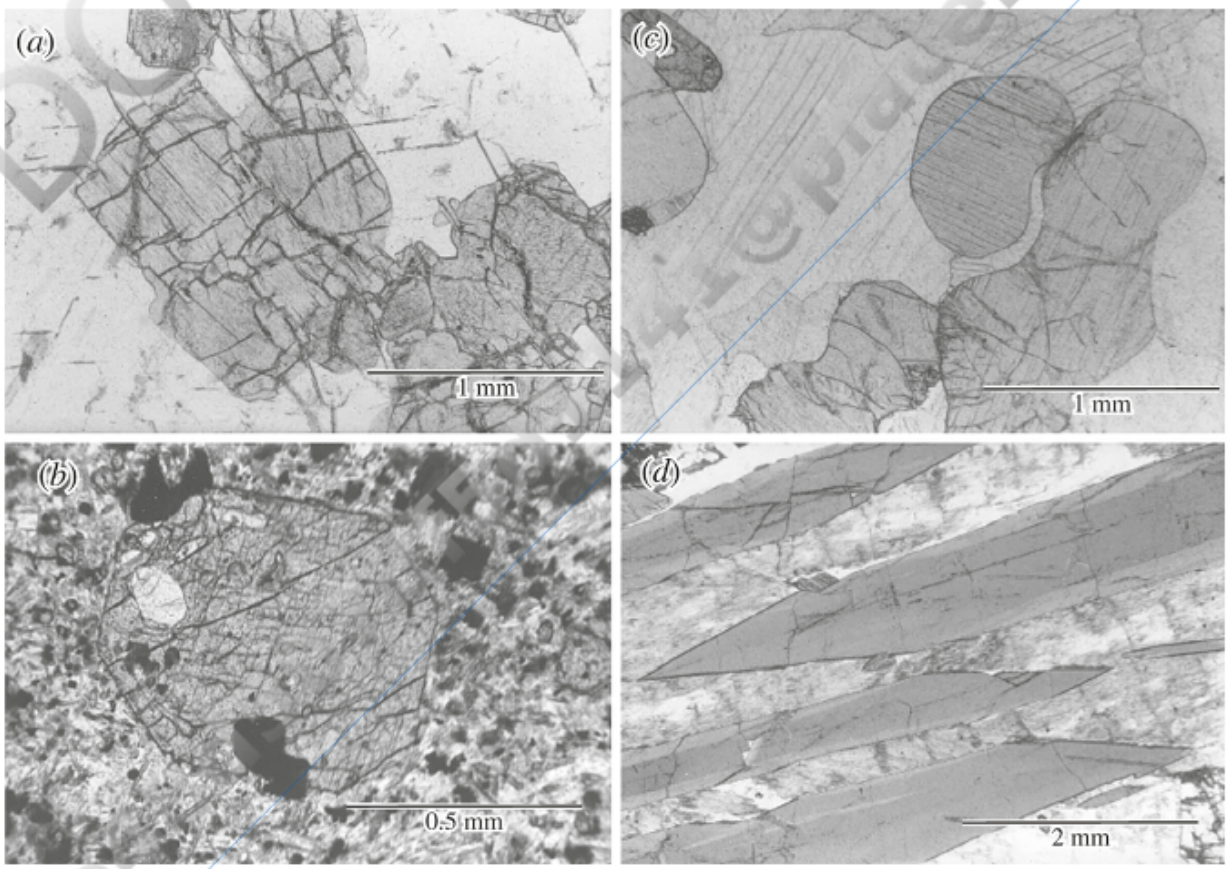

FIGURE 14.3 Photomicrographs of pyroxene in thin section. (*a*) Anhedral orthopyroxene in

Printed by: e48d507df5d1141@placeholder.94092.edu. Printing is for personal, private use only. No part of this book may be reproduced or transmitted without publisher's prior permission. Violators will be prosecuted.

FIGURE 14.3 Photomicrographs of pyroxene in thin section. (*a*) Anhedral orthopyroxene in norite. (*b*) Euhedral augite phenocryst in basalt. (*c*) Rounded diopside in marble. (*d*) Zoned aegirine in syenite. View larger image

Geology of Pyroxenes

Igneous

The most common pyroxenes in igneous rocks are augite, pigeonite, and orthopyroxene. The rocks in which they are found are intermediate to mafic (andesite, diorite, basalt, gabbro, etc.), and the associated minerals include plagioclase, olivine, and hornblende. It is common to find both augite and either pigeonite or orthopyroxene in the same rock.

Of the three common igneous pyroxenes, augite is the most abundant. It typically forms blocky prismatic crystals or roughly equant grains, depending on when in the crystallization sequence it grew. Crystals are usually enriched in Mg relative to the melt from which they grew; therefore the melt becomes enriched in Fe during crystallization. This change in magma composition commonly results in zoned crystals with more Mg-rich cores and Fe-rich rims.

With cooling, the amount of Mg/Fe that can substitute for Ca in the M2 site of augite becomes progressively more limited. Exsolution lamellae of low-Ca pyroxene or orthopyroxene (**Figure 14.4a**) form in the augite such that the host becomes progressively richer in Ca in a manner analogous to the way that albite lamellae exsolve from alkali feldspar with cooling (Figure 5.28). Pigeonite lamellae are usually oriented roughly parallel to (001) of the host augite. Orthopyroxene lamellae are usually oriented roughly parallel to (100). In most cases, the pigeonite lamellae will convert to orthopyroxene on cooling, as is described below.

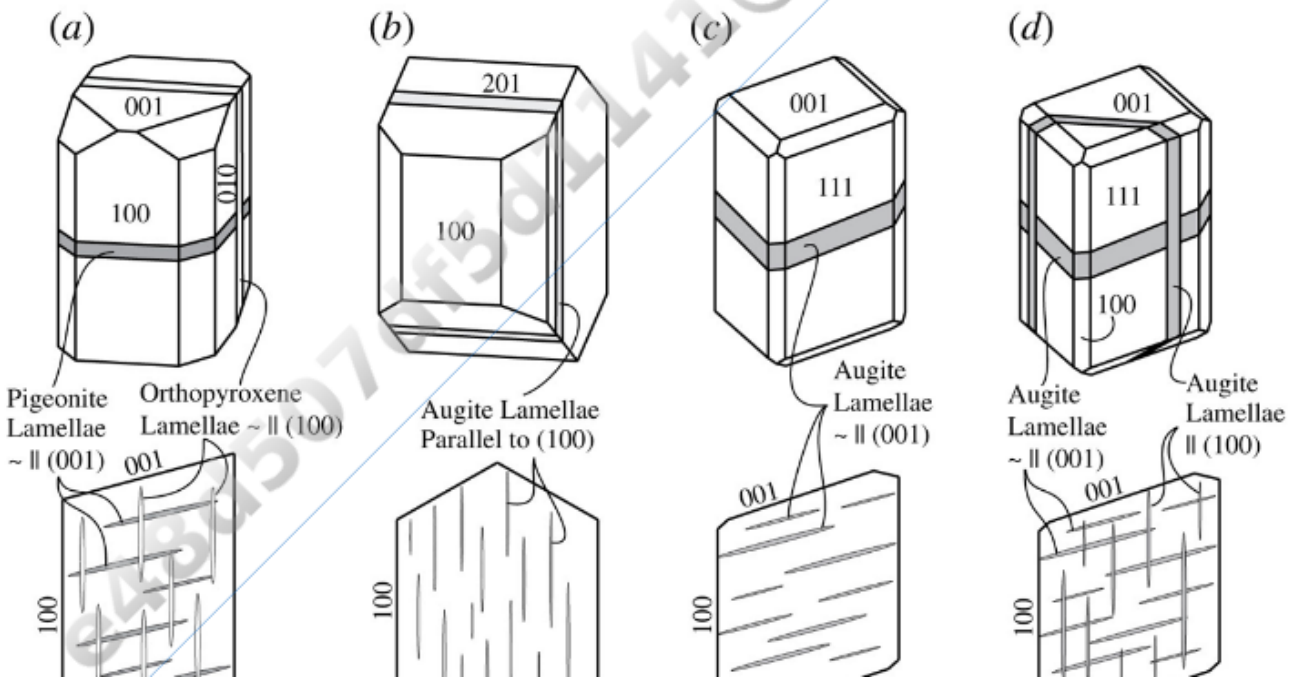

DO NOT COPY
e48d507df5d1141@placeholder.94092

Printed by: e48d507df5d1141@placeholder.94092.edu. Printing is for personal, private use only. No part of this book may be reproduced or transmitted without publisher's prior permission. Violators will be prosecuted.

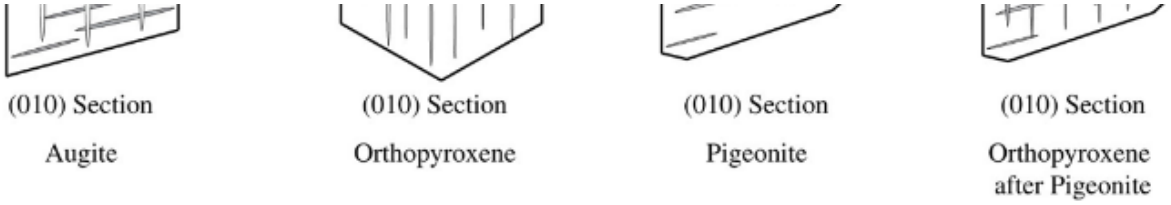

FIGURE 14.4 Exsolution lamellae may be responsible for partings in pyroxene. (*a*) Augite. Pigeonite may exsolve as lamellae roughly parallel to (001); the exact orientation depends on composition and temperature. The pigeonite converts to orthopyroxene with slow cooling. Primary orthopyroxene lamellae may exsolve parallel to (100). (*b*) Primary orthopyroxene. Lamellae of augite develop parallel to (100) of the orthopyroxene. (*c*) Pigeonite. Augite lamellae may exsolve roughly parallel to (001). The exact orientation depends on temperature and composition. (*d*) Orthopyroxene converted from pigeonite (inverted pigeonite). Unless cooled rapidly, pigeonite converts to orthopyroxene. The (001) lamellae of augite in the original pigeonite are preserved, and additional lamellae of augite develop parallel to (100) of the orthopyroxene. View larger image

Orthopyroxene may crystallize from fairly typical mafic magmas and rarely from more felsic varieties such as dacite, diorite, granodiorite, tonalite, and granite. It may be a common phenocryst in andesitic volcanics. At high temperatures, orthopyroxene may accommodate more Ca in the M2 sites than at low temperatures. With slow cooling, the excess Ca is expelled to form exsolution lamellae of augite parallel to (100) (**Figure 14.4b**).

Pigeonite also is a common mineral to grow from mafic magmas and may have up to about 10% Ca in the M2 sites at high temperatures. With cooling, some of this Ca is expelled from the M2 sites and forms exsolution lamellae of Ca-clinopyroxene (augite) roughly parallel to (001) of the host pigeonite (**Figure 14.4c**). If cooling is not too fast, pigeonite transforms to orthopyroxene at temperatures below ~1100°C for Mg-rich pigeonite or ~950°C for Fe-rich pigeonite. Pigeonite is preserved only in quickly cooled volcanic rocks.

The conversion from pigeonite to orthopyroxene may trigger the formation of a second set of exsolution lamellae because orthopyroxene cannot contain as much Ca as pigeonite can. The excess Ca forms lamellae of augite parallel to the (100) planes of the new orthopyroxene (**Figure 14.4d**). Orthopyroxene that originally grew as pigeonite crystals may therefore contain two different sets of exsolution lamellae of augite, one roughly parallel to (001) of the original pigeonite and another parallel to (100) of the orthopyroxene. Orthopyroxene inferred to have originally crystallized as pigeonite may be called inverted pigeonite.

Parting, controlled by exsolution lamellae, may be common for the pyroxenes.

Aegirine and aegirine–augite are less common and are found most often in alkali-rich igneous rocks such as syenite, nepheline syenite, and phonolite. Growth of these minerals requires the combination of high Na and modest to low Si and therefore are not found in the more common granite, granodiorite, diorite, and gabbro or their volcanic equivalents.

Spodumene, with its high Li content, is generally restricted to Li-bearing granitic

DO NOT COPY e48d507df5d1141@placeholder.94092

Printed by: e48d507df5d1141@placeholder.94092.edu. Printing is for personal, private use only. No part of this book may be reproduced or transmitted without publisher's prior permission. Violators will be prosecuted.

Spodumene, with its high Li content, is generally restricted to Li-bearing granitic pegmatites. Gigantic crystals of spodumene, up to 10 meters long, have been mined for their Li content from pegmatites in the Black Hills of South Dakota.

Metamorphic

Calcic clinopyroxenes are found both in metamorphosed carbonate rocks and in metamorphosed mafic rocks. The clinopyroxene in metamorphosed carbonates usually is fairly diopside-rich, reflecting the abundance of Ca and Mg derived from calcite and dolomite. Associated minerals include calcite, dolomite, tremolite/actinolite, members of the epidote group, and olivine. Metamorphism of hydrous mafic minerals such as hornblende and biotite to sufficiently high temperatures can cause these minerals to break down through dehydration reactions to produce Ca-clinopyroxene and orthopyroxene, respectively. For mafic rocks, granulite facies metamorphism can be indicated by the presence of both orthopyroxene and Ca-clinopyroxene.

The sodic and sodic–calcic clinopyroxenes have fairly restricted occurrences in metamorphic rocks. Jadeite is restricted to metagraywacke, blueschists, and related rocks that have been subjected to high pressures but only modest temperatures. This combination of conditions occurs in the blueschist metamorphic facies most often found in subduction zone environments (Chapter 11). Omphacite, with its higher Ca content, may be found in the higher temperature–pressure conditions such as those within the eclogite facies also within subduction zones or at the base of tectonically thickened crust.

Sedimentary

Pyroxenes, being **anhydrous** (lacking OH^-), are not particularly stable in the weathering environment and readily alter to clay minerals. Pyroxene is therefore a major constituent of sediments derived from pyroxene-bearing rocks only if chemical weathering is limited. Once deposited, normal diagenetic processes usually convert pyroxene to clay minerals. Any pyroxene that is preserved in the heavy mineral fraction of sediment, however, may be useful in determining the provenance of the sediment.

Orthopyroxene

$$(Mg, Fe)_2Si_2O_6$$

$$\text{Orthorhombic } 2/m\ 2/m\ 2/m$$

$$a = 18.22 - 18.43\ \text{Å},$$
$$b = 8.81 - 9.08\ \text{Å},$$
$$c = 5.17 - 5.24\ \text{Å},\ Z = 8$$

$$H = 5 - 6$$

$$G = 3.21 - 3.96$$

DO NOT COPY e48d507df5d1141@placeholder.9409

Printed by: e48d507df5d1141@placeholder.94092.edu. Printing is for personal, private use only. No part of this book may be reproduced or transmitted without publisher's prior permission. Violators will be prosecuted.

$$G = 3.21 - 3.96$$

$$\text{Biaxial } (+ \text{ or } -)$$

$$n_\alpha = 1.649 - 1.768$$

$$n_\beta = 1.653 - 1.770$$

$$n_\gamma = 1.657 - 1.788$$

$$\delta = 0.007 - 0.020$$

$$2V_x = 50 - 132^\circ$$

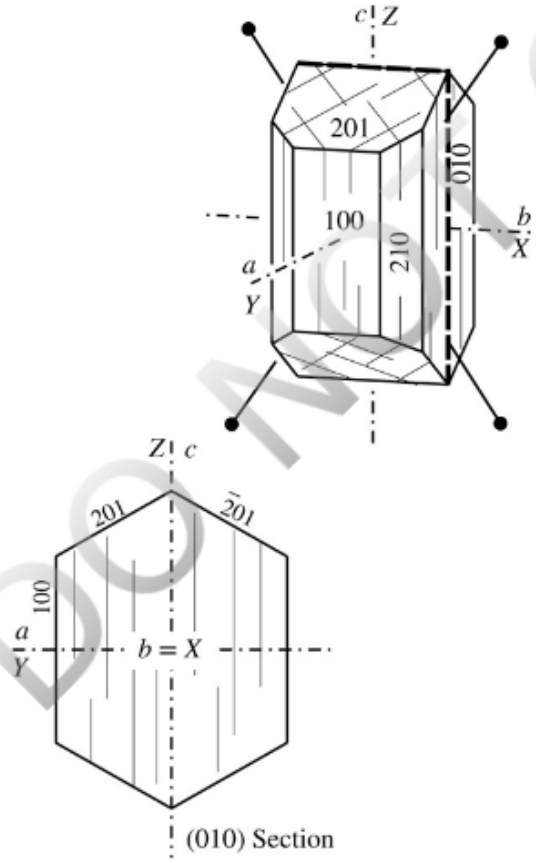

Composition The principal chemical variation is substitution of Mg and Fe in the M1 and M2 sites (Figures 14.2 and 14.5). Most orthopyroxene falls in the enstatite range. Up to 10% or 15% of other cations including Al, Mn, Ti, Cr, and Ca may be present in some cases. The common abbreviation for orthopyroxene is opx. In the past, orthopyroxene compositions have been divided into additional named ranges that included enstatite (En_{100-88}), bronzite (En_{88-70}), hypersthene (En_{70-50}), ferrohypersthene (En_{50-30}), eulite (En_{30-12}), and orthoferrosilite (En_{12-0}). Use of these names is no longer recommended by the Commission on New Minerals, Nomenclature and Classification of the International Mineralogical Association. Instead, it is common to refer to solid solution orthopyroxene with En_{100-50} as enstatite and En_{50-0} as ferrosilite (Figures 14.2 and 14.5).

Printed by: e48d507df5d1141@placeholder.94092.edu. Printing is for personal, private use only. No part of this book may be reproduced or transmitted without publisher's prior permission. Violators will be prosecuted.

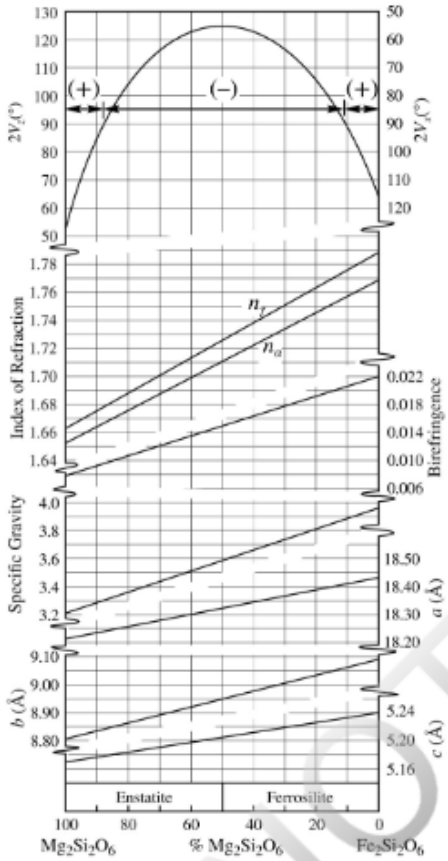

FIGURE 14.5 Optical properties, specific gravity, and unit cell dimensions of orthopyroxene. Adapted from Leake (1968), Jaffe and others (1975, 1978), and Deer and others (1978). View larger image

Form and Twinning See Figure 14.3a. Euhedral crystals are stubby prisms with four- or eight-sided cross sections. Longitudinal sections are usually roughly rectangular. Anhedral and irregular grains also are common. Late-growing orthopyroxene may form highly irregular grains that occupy the interstices among other earlier-formed mineral grains or entirely enclose them. Exsolution lamellae of augite (Figure 14.4) may be thin and tabular; or, they may pinch and swell, or form irregular rows of blebs (rounded, equant to elongate inclusions). Exsolution lamellae are not usually seen in hand sample but control the partings.

Cleavage Good cleavage on {210}; like the other pyroxenes, cleavage intersects at angles of 88° and 92°. A parting that bisects the cleavages may be present parallel to (100). For orthopyroxene that has converted from pigeonite, a second parting approximately parallel to (001) of the original pigeonite also may be present. Uneven fracture. Brittle.

Color Properties

Luster: Vitreous, some enstatite compositions may be submetallic.

Color: Mg-rich varieties most often brown or greenish brown; also white, tan, or green. Fe-rich varieties are green, dark brown, or greenish black.

DO NOT COPY e48d507df5d1141@placeholder.9409

Printed by: e48d507df5d1141@placeholder.94092.edu. Printing is for personal, private use only. No part of this book may be reproduced or transmitted without publisher's prior permission. Violators will be prosecuted.

Streak: White to gray.

Color in Thin Section: Varies with composition. Mg-rich enstatite is colorless or with very pale pinkish to greenish pleochroism; more Fe-rich varieties are darker colored with reddish to greenish pleochroism.

Pleochroism: If present, pleochroism is $X < Y < Z$, stronger with higher Fe content: X = colorless, pink, brownish pink, pale yellow; Y = colorless, light brown, yellow, pinkish yellow, greenish yellow; Z = colorless, light green, gray-green, green, bluish green.

Optical Characteristics

Relief in Thin Section: Moderately high to high positive.

Optic Orientation: $X = b$, $Y = a$, $Z = c$. Extinction is parallel in longitudinal sections and symmetrical in basal sections. Crystals are length slow.

Indices of Refraction and Birefringence: Vary systematically (**Figure 14.5**).

Interference Figure: $2V$ varies systematically with composition (Figure 14.5). Mg-rich enstatite and Fe-rich ferrosilite are both optically positive; intermediate compositions are negative. Optic axis dispersion measured about the X axis is $r > v$, weak to strong.

Comments: The value of $2V$ measured in thin section can be used to estimate composition to within 5–10 mol % Mg. Measurement of indices of refraction in grain mount provides greater accuracy.

Alteration Opx readily alters to serpentine, talc, fine-grained pale amphibole, or other silicates.

Distinguishing Features

Hand Sample: Nearly right-angle cleavage and stubby or nearly equant crystals distinguish pyroxenes from amphiboles. Amphibole cleavage is generally better than in the pyroxenes, and amphibole crystals tend to be elongate. The (100) parting that intersects the cleavages at about 45° may be confusing to the inexperienced. Brown color may distinguish orthopyroxene from clinopyroxene. The submetallic luster of some enstatitic orthopyroxene is quite distinctive. High-iron varieties may be indistinguishable from Ca-clinopyroxene.

Thin Section/Grain Mount: Orthopyroxene is distinguished from pigeonite and Ca-clinopyroxene by having lower birefringence, parallel extinction in longitudinal sections, and pale pink to green pleochroism, if present. Andalusite may appear similar to enstatite but lacks the ~90° cleavage and is optically negative. The occurrences for andalusite and enstatite are distinctly different.

Occurrence Common in mafic and ultramafic igneous rocks (gabbro, norite, peridotite,

DO NOT COPY e48d507df5d1141@placeholder.9409

Printed by: e48d507df5d1141@placeholder.94092.edu. Printing is for personal, private use only. No part of this book may be reproduced or transmitted without publisher's prior permission. Violators will be prosecuted.

pyroxenite, etc.) associated with Ca-clinopyroxene, plagioclase, and olivine. Orthopyroxene with intermediate or higher iron content may be found in diorite, or even some syenite or granite. Basalt and andesite often contain orthopyroxene phenocrysts. Very high-grade metamorphic rocks of the granulite facies may also contain orthopyroxene. Associated minerals may include feldspars, Ca-clinopyroxene, hornblende, biotite, and garnet.

Use No significant economic uses. Rocks containing orthopyroxene are sometimes used for dimension stone or decorative purposes. Occasionally used as a minor gemstone.

Pigeonite

$$(\mathrm{Ma, Fe, Ca})(\mathrm{Mg, Fe})\mathrm{Si_2O_6}$$

$$\text{Monoclinic } 2/m$$

$$a = 9.71 \text{ Å},\ b = 8.95 \text{ Å},$$
$$c = 5.24 \text{ Å},$$
$$\beta = 108.5^\circ,\ Z = 4$$

$$H = 6$$

$$G = 3.17 - 3.46$$

$$\text{Biaxial } (+)$$

$$n_\alpha = 1.682 - 1.732$$

$$n_\beta = 1.684 - 1.732$$

$$n_\gamma = 1.705 - 1.757$$

$$\delta = 0.023 - 0.029$$

$$2V_z = 0 - 32^\circ$$

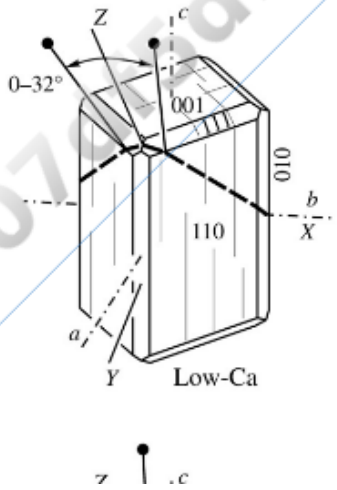

DO NOT COPY
e48d507df5d1141@placeholder.9409

Printed by: e48d507df5d1141@placeholder.94092.edu. Printing is for personal, private use only. No part of this book may be reproduced or transmitted without publisher's prior permission. Violators will be prosecuted.

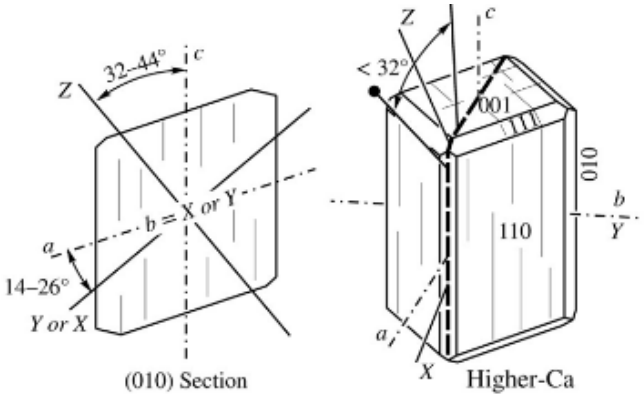

Composition Pigeonite is the common low-calcium clinopyroxene. Typically between 10% and 30% of the M2 sites are filled with Ca, with the remainder filled with Fe and Mg. The M1 site is filled almost exclusively with Mg and Fe. Most pigeonite has a Mg:Fe ratio of between 70:30 and 30:70. Minor Na, Ti, Cr, Al, and Fe^{3+} may be present. High temperature of formation favors higher Ca content. Slow cooling allows Ca to migrate out of the structure to form exsolution lamellae of Ca-clinopyroxene (Figure 14.4).

Form and Twinning Crystals are prismatic and somewhat elongate parallel to *c*. Cross sections are square or eight sided. Longitudinal sections are rectangular. In mafic and intermediate volcanic rocks it may form groundmass grains. Lamellae of exsolved augite (Figure 14.4) are common roughly parallel to (001) in pigeonite preserved in shallow intrusions but are not usually seen in hand sample. Compositional zoning may be identified in thin section by variations in color, extinction angle, or birefringence. Pigeonite may be mantled by augite.

Cleavage Good {110}, like the other pyroxenes at 87° and 93°. Partings on {100} and ~{001}. Fracture uneven. Brittle.

Color Properties

Luster: Vitreous.

Color: Brown, greenish brown, black.

Streak: Light to dark gray.

Color in Thin Section: Colorless, pale brownish green, pale yellowish green.

Pleochroism: Absent or weak: X = colorless, pale greenish brown, yellow; Y = pale brown, greenish brown; Z = colorless, pale yellow, pale green.

Optical Characteristics

Relief in Thin Section: High positive.

Optic Orientation: Low-Ca pigeonite: $X = b$, $Y \wedge a = -14°$ to $-26°$, $Z \wedge c = +32°$ to $+44°$, optic plane normal to (010). With increasing Ca content, the $2V$ angle closes on Z and

DO NOT COPY e48d507df5d1141@placeholder.9409

Printed by: e48d507df5d1141@placeholder.94092.edu. Printing is for personal, private use only. No part of this book may be reproduced or transmitted without publisher's prior permission. Violators will be prosecuted.

then opens in the (010) plane so that $X \wedge a = -22°$ to $-26°$, $Y = b$, $Z \wedge c = +40°$ to $+44°$, to optic plane = (010). The extinction angle to the trace of cleavage in (010) sections is between 32° and 44°.

Indices of Refraction and Birefringence: Increase with increasing Fe content. Interference colors in standard thin section range up to lower or middle second order.

Interference Figure: Biaxial negative with a small $2V$. Optic axis dispersion is weak, either $r > v$ or $r < v$.

Alteration Most pigeonite in plutonic rocks converts to orthopyroxene on cooling. Alteration products include fine-grained amphibole, serpentine, talc, or chlorite.

Distinguishing Features

Hand Sample: Color, cleavage, and habit distinguish pigeonite as a pyroxene. Augite is usually black. Both pigeonite and orthopyroxene are commonly brown, so distinguishing between them in hand sample may not be possible. Amphibole cleavage is generally better than in the pyroxenes, and crystals tend to be elongate.

Thin Section/Grain Mount: Distinguished from the other pyroxenes by a smaller optic angle. Olivine has higher birefringence and no cleavage.

Occurrence Pigeonite is found in dacitic, andesitic, and basaltic volcanic rocks as groundmass grains or phenocrysts. It commonly crystallizes in mafic to intermediate intrusions, but converts to orthopyroxene on cooling. Only shallow intrusions are likely to preserve pigeonite. Metamorphism of iron formations at sufficiently high temperatures may yield pigeonite, but most subsequently converts to orthopyroxene.

Use None.

Calcic Clinopyroxene

$$\text{Diopside } CaMgSi_2O_6$$

$$a = 9.75\ \text{Å},\ b = 8.90\ \text{Å},\ c = 5.25\ \text{Å},\ \beta = 105.6^\circ,\ Z = 4$$

$$\text{Hedenbergite } CaFeSi_2O_6$$

$$a = 9.85\ \text{Å},\ b = 9.03\ \text{Å},\ c = 5.24\ \text{Å},\ \beta = 104.8^\circ,\ Z = 4$$

$$\text{Augite } (Ca, Na)(Mg, Fe, Al, Ti)$$

DO NOT COPY e48d507df5d1141@placeholder.9409

Printed by: e48d507df5d1141@placeholder.94092.edu. Printing is for personal, private use only. No part of this book may be reproduced or transmitted without publisher's prior permission. Violators will be prosecuted.

$(Si, Al)_2O_6$

$a = \text{ - } 9.7$ Å, $b = \text{ - } 8.8$ Å,

$c = \text{ - } 5.3$ Å,

$\beta = 106.9^\circ$, $Z = 4$

Monoclinic $2/m$

$H = 5.5 - 6$

$G = 3.19 - 3.56$

Biaxial $(+)$

$n_\alpha = 1.664 - 1.745$

$n_\beta = 1.672 - 1.753$

$n_\gamma = 1.694 - 1.771$

$\delta = 0.018 - 0.034$

$2V_z = 25 - 70^\circ$

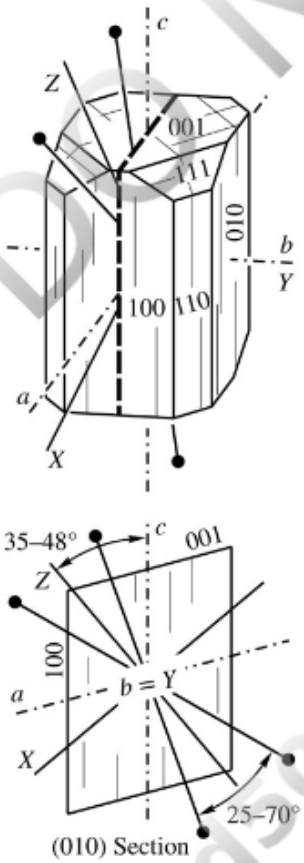

Composition There is complete solid solution among the Ca-rich clinopyroxenes. Pyroxene between the diopside–hedenbergite end members (Figure 14.2a), whose M2 site contains nearly all Ca, is generally restricted to metamorphic rocks. Most igneous

DO NOT COPY e48d507df5d1141@placeholder.9409

Printed by: e48d507df5d1141@placeholder.94092.edu. Printing is for personal, private use only. No part of this book may be reproduced or transmitted without publisher's prior permission. Violators will be prosecuted.

site contains nearly all Ca, is generally restricted to metamorphic rocks. Most igneous Ca-clinopyroxene has somewhat less Ca and more Fe/Mg in the M2 site and contains significant Al, both in tetrahedral and octahedral (M1) sites. This pyroxene is conventionally called augite. Various schemes have been applied to divide calcic clinopyroxene into compositional ranges; however, given the diversity of composition and the inability to accurately deduce composition based on physical or optical properties, the term *calcic clinopyroxene* (Ca-cpx or cpx) may be used for all varieties of Ca-rich clinopyroxene. Extensive solid solution toward the Na-rich clinopyroxenes is also possible, and most augite contains some Na substituting for Ca. Ti-bearing augite is called titanian augite, but some refer to this as titanoaugite.

The amount of Ca in the ~8-fold M2 sites is, in part, a function of temperature. High temperature allows more extensive substitution of Fe/Mg for Ca. With cooling, lamellae of pigeonite or orthopyroxene are exsolved to allow the Ca-cpx to become more Ca-rich. Pigeonite lamellae form roughly parallel to (001) of the augite and orthopyroxene lamellae are parallel to (100) (Figure 14.4). The exact orientation of the (001) lamellae depends on temperature. Exsolution lamellae are not usually obvious in hand sample, but control partings.

Form and Twinning Figure 14.3b. Crystals are usually stubby prisms elongate parallel to *c* with four- or eight-sided cross sections. Also as granular masses and anhedral grains that range from equant to highly irregular and may enclose associated minerals. Overgrowths of hornblende are relatively common. Compositional zoning may be visible in thin section and is identified by variations in color or birefringence (Figure 5.13).

Single and multiple twins with {100} composition planes are fairly common, as are multiple twins on {001}. Although visible in thin section, twins are not usually evident in hand sample. The combination of twinning and exsolution lamellae may produce a herringbone pattern in certain orientations in thin sections.

Cleavage Fair to good cleavage on {110} intersects at 87° and 93°. {100} and {001} partings may be distinct. Fracture uneven. Brittle.

Color Properties

Luster: Vitreous.

Color: Pale green (Mg-rich) to black (Fe-rich), usually dark green, greenish black, or brownish black.

Streak: White or gray.

Color in Thin Section: Colorless, gray, pale green, pale brown, or brownish green. Color zoning is fairly common, particularly in Fe- and Ti-rich varieties, and may form a distinctive "hourglass" pattern consisting of four triangular segments radiating from the center of the crystal.

Pleochroism: Fe-rich samples may be weakly pleochroic, X = pale green, bluish green, Y

Printed by: e48d507df5d1141@placeholder.94092.edu. Printing is for personal, private use only. No part of this book may be reproduced or transmitted without publisher's prior permission. Violators will be prosecuted.

Pleochroism: Fe-rich samples may be weakly pleochroic: X = pale green, bluish green; Y = pale greenish brown, green, bluish green; Z = pale brownish green, green, yellowish green. Titanian augite is more distinctly colored in shades of brown and violet.

Optical Characteristics

Relief in Thin Section: High positive.

Optic Orientation: $X \wedge a = -20°$ to $-33°$, $Y = b$, $Z \wedge c = +35°$ to $+48°$.

Indices of Refraction and Birefringence: Indices of refraction increase with Fe + Mn content but have too much variability to be used to estimate composition. Birefringence generally increases with increasing Fe content.

Interference Figure: The $2V_z$ angle increases with increasing Ca content. The common range of $2V_z$ is 50° ± 10°. Optic axis dispersion is weak to strong, usually $r > v$.

Alteration Calcic clinopyroxenes commonly alter to fine-grained, light-colored amphibole (uralite) and to chlorite, serpentine, biotite, carbonates, or clay.

Distinguishing Features

Hand Sample: Dark color, approximately right-angle cleavage, and hardness distinguish pyroxene from most other silicates, but distinguishing among different pyroxenes is often not possible. Be cautious as partings are common and may be more distinct than the cleavage. Hornblende tends to be more elongate and has better cleavage at 56° and 124°. Diopside is usually light green and is distinguished from olivine in metamorphosed carbonates by having cleavage.

Thin Section/Grain Mount: Distinguished from opx by higher birefringence, inclined extinction in (010) sections, and smaller $2V$. Pigeonite has a smaller $2V$, and jadeite has a larger $2V$. The other Na-rich clinopyroxenes (aegirine, aegirine–augite, omphacite) are usually more distinctly green and have larger $2V$. Olivine nearly always lacks identifiable cleavage and has higher birefringence. Wollastonite has lower indices of refraction and birefringence, is colorless, and has better and more cleavages.

Occurrence Augite is common in mafic intrusions of gabbro, pyroxenite, anorthosite, norite, and peridotite. Fe-rich augite may be found in more silicic rocks such as diorite and granodiorite. Basaltic and andesitic volcanics also commonly contain augite. Cr-rich diopside is common in ultramafic rocks such as kimberlite.

In metamorphic rocks, augite can be found in amphibolite, granulite and related rocks. Skarns, marble, and other metamorphosed carbonate rocks commonly contain fairly diopside-rich compositions in association with tremolite–actinolite, grossular garnet, epidote, wollastonite, forsterite, calcite, and dolomite.

Use Diopside is a component of some ceramic products, including those used for dental applications. It also has been used as a gemstone.

DO NOT COPY e48d507df5d1141@placeholder.9409

Printed by: e48d507df5d1141@placeholder.94092.edu. Printing is for personal, private use only. No part of this book may be reproduced or transmitted without publisher's prior permission. Violators will be prosecuted.

applications. It also has been used as a gemstone.

Aegirine, Aegirine-Augite

$$\text{Aegirine}: \ NaFe^{3+}Si_2O_6$$

$$\text{Aegirine} - \text{Augite}$$

$$(Na, Ca)(Fe^{3+}, Fe^{2+}, Mg)Si_2O_6$$

$$\text{Monoclinic } 2/m$$

$$a = 9.7 \text{ Å}, \ b = 8.8 \text{ Å},$$
$$c = 5.3 \text{ Å}, \ \beta = 105 - 107.5^\circ,$$
$$Z = 4$$

$$H = 6$$

$$G = 3.40 - 3.60$$

$$\text{Biaxial } (+ \text{ or } -)$$

$$n_\alpha = 1.700 - 1.776$$

$$n_\beta = 1.710 - 1.820$$

$$n_\gamma = 1.730 - 1.836$$

$$\delta = 0.028 - 0.060$$

$$2V_x = 60 - 110^\circ$$

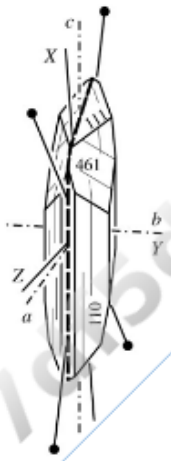

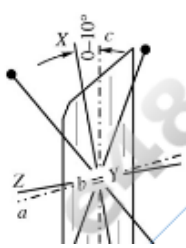

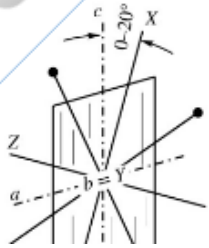

DO NOT COPY
e48d507df5d1141@placeholder.9409

Printed by: e48d507df5d1141@placeholder.94092.edu. Printing is for personal, private use only. No part of this book may be reproduced or transmitted without publisher's prior permission. Violators will be prosecuted.

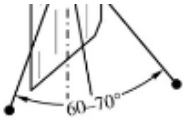

(010) Section Aegirine

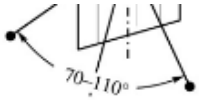

(010) Section Aegirine-Augite

Composition The principal substitutions are $NaFe^{3+}$ for $Ca(Mg,Fe^{2+})$ in the M1 and M2 structural sites. Solid solution extends to the Ca-clinopyroxenes. Limited amounts of Al may substitute in octahedral M1 sites, and almost no Al substitutes for Si in tetrahedral sites. The division between aegirine and aegirine–augite is taken here (Figure 14.2b) to be 80 mol % Fe^{3+} in the octahedral M1 site, and the boundary between aegirine–augite and augite is taken at 20 mol % Fe^{3+} in the octahedral M1 site. In the past, the term *acmite* was used interchangeably with *aegirine*. *Acmite* also has been used in a more restricted sense for brownish samples of sodic pyroxene that have sharply pointed crystals; the term *aegirine* was used for stubby crystals of green to black sodic pyroxene. The current convention is to abandon the term *acmite* and to use *aegirine* for all.

Form and Twinning Aegirine may have sharply pointed terminations (Figure 14.3d) or blocky prismatic crystals; aegirine–augite usually forms stubby prismatic crystals similar to augite. Also fibrous and as anhedral grains. Rounded intergrowths (**spongy** texture) with riebeckite may be found. Simple and lamellar twinning on {100} is common.

Cleavage Good {110} cleavage at 87° and 93°, also a {100} parting. Uneven fracture. Brittle.

Color Properties

Luster: Vitreous.

Color: Dark green to greenish black or reddish brown, less commonly brown or yellowish green.

Streak: White or gray.

Color in Thin Section: Pale to dark green or yellowish green, darker with higher Fe^{3+} content. Color zoning may be evident with crystal rims darker than cores.

Pleochroism: Distinct with X = emerald-green, dark green, bright green; Y = grass-green, yellowish green, yellow; Z = brownish green, green, yellowish brown, yellow.

Optical Characteristics

Relief in Thin Section: High positive.

Optic Orientation: $X \wedge c = +10°$ to $-20°$, $Y = b$, $Z \wedge a = +7°$ to $+36°$.

Indices of Refraction and Birefringence: Increase with Fe^{3+} content (**Figure 14.6**). The scatter in the data is probably due to variations in $Mg:Fe^{2+}$. High interference colors may be masked by mineral color.

DO NOT COPY e48d507df5d1141@placeholder.94092

Printed by: e48d507df5d1141@placeholder.94092.edu. Printing is for personal, private use only. No part of this book may be reproduced or transmitted without publisher's prior permission. Violators will be prosecuted.

be masked by mineral color.

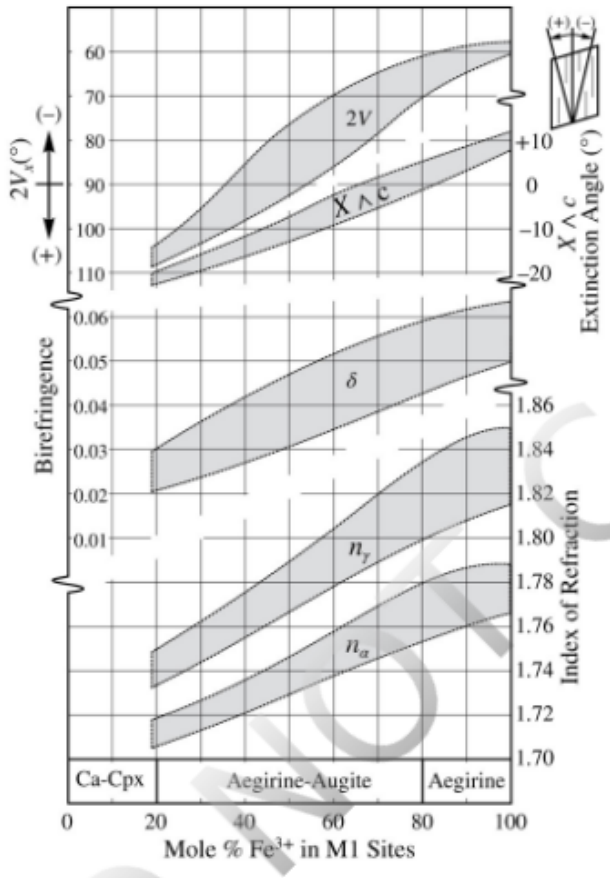

FIGURE 14.6 Variation of optical properties of aegirine and aegirine–augite with Fe^{3+} content. Data from Larsen (1942), Sabine (1950), Nolan (1969), and Deer and others (1978). View larger image

Interference Figure: $2V$ varies systematically with Fe^{3+} content (Figure 14.6). Samples with more than roughly 50% to 55% Fe^{3+} are optically negative; less Fe^{3+}-rich compositions are positive. Optic axis dispersion is moderate to strong, $r > v$.

Alteration The common alteration is fine-grained amphibole (uralite) or chlorite.

Distinguishing Features

Hand Sample: Distinguished as a pyroxene by color, cleavage, and hardness. Long slender crystals can be mistaken for hornblende, but hornblende has better cleavage at 56° and 124°. Aegirine and aegirine–augite cannot reliably be distinguished from other pyroxenes in hand sample.

Thin Section/Grain Mount: Aegirine and aegirine–augite are distinguished from other pyroxenes by color and pleochroism, smaller extinction angle in (010) sections, length fast characteristic, and higher indices of refraction and birefringence. The $2V$ angle is larger than for most other pyroxenes, and samples may be optically positive or negative. The distinction between aegirine and aegirine–augite can be made based on a combination of indices of refraction, extinction angle in (010) section, birefringence, and

DO NOT COPY e48d507df5d1141@placeholder.9409

Printed by: e48d507df5d1141@placeholder.94092.edu. Printing is for personal, private use only. No part of this book may be reproduced or transmitted without publisher's prior permission. Violators will be prosecuted.

combination of indices of refraction, extinction angle in (010) section, birefringence, and $2V$. Aegirine is generally darker than aegirine–augite. Amphiboles have cleavage at 56° and 124° and are length slow. Epidote shows only one good cleavage and generally is lighter colored.

Occurrence Aegirine and aegirine–augite are typical minerals of alkali-rich magmas. Typical occurrences include alkali granite, syenite, nepheline syenite, and phonolite. Associated minerals include K-feldspar, Na-amphiboles, and either feldspathoids or quartz. Carbonatites and their associated alkali-rich silicate magmas also may crystallize aegirine or aegirine–augite, and Na-rich fluids derived from carbonatites may replace biotite or hornblende in the country rock with these pyroxenes as a consequence of a process called fenitization. Occurrences in metamorphic rocks are generally restricted to blueschists and related rocks.

Use None.

Jadeite

$$\mathrm{NaAlSi_2O_6}$$

$$\text{Monoclinic } 2/m$$

$$a = 9.4\ \text{Å},\ b = 8.6\ \text{Å},\ c = 5.2\ \text{Å},$$
$$\beta = 107.6^\circ,\ Z = 4$$

$$H = 6$$

$$G = 3.24 - 3.43$$

$$\text{Biaxial } (+) \text{ or } (-)$$

$$n_\alpha = 1.640 - 1.681$$

$$n_\beta = 1.645 - 1.684$$

$$n_\gamma = 1.652 - 1.692$$

$$\delta = 0.006 - 0.021$$

$$2V_z = 60 - 96^\circ$$

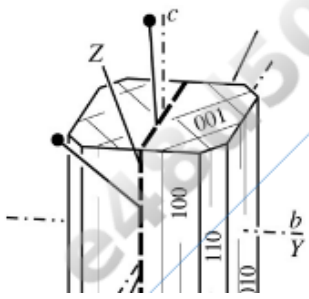

DO NOT COPY
e48d507df5d1141@placeholder.9409

Printed by: e48d507df5d1141@placeholder.94092.edu. Printing is for personal, private use only. No part of this book may be reproduced or transmitted without publisher's prior permission. Violators will be prosecuted.

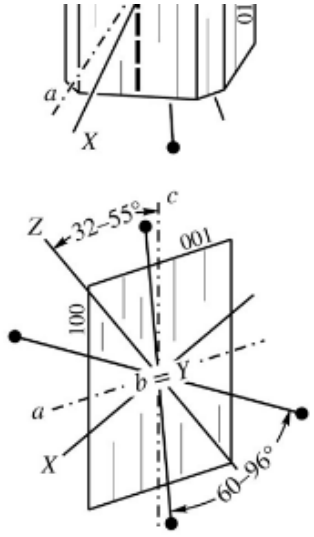

(010) Section

Composition Most jadeite is fairly close to the ideal formula. The principal variation is substitution of Ca^{2+} for up to 20% of the Na^{+} in the M2 sites between the bases of the tetrahedra. Charge balance is maintained by substituting a divalent cation such as Mg^{2+} or Fe^{2+} for Al^{3+} in the M1 sites. Some Fe^{3+} also may substitute for Al^{3+}. Omphacite is compositionally intermediate between jadeite and augite, but the three species are not part of a solid solution series. Omphacite has a slightly different structure than either jadeite or augite.

Form and Twinning Crystals are stubby to elongate prisms with four- or eight-sided cross sections. Jadeite is most common as anhedral grains and as aggregates of acicular to fibrous grains. Simple and lamellar twins on {001} and {100} are sometimes seen in thin section but are not evident in hand sample.

Cleavage Good cleavage on {110}; like the other pyroxenes intersects at 87° and 93°. A parting on {100} is reported but not common. Splintery fracture. Fibrous masses are very tough.

DO NOT COPY
e48d507df5d1141@placeholder.9409

Printed by: e48d507df5d1141@placeholder.94092.edu. Printing is for personal, private use only. No part of this book may be reproduced or transmitted without publisher's prior permission. Violators will be prosecuted.

Color Properties

Luster: Vitreous.

Color: Light to medium green; also white, colorless, greenish blue. Rarely blue or violet.

Streak: White.

Color in Thin Section: Colorless. Grains in grain mount may be pale green.

Pleochroism: None in thin section, weak pale yellow to green pleochroism in grain mount.

Optical Characteristics

Relief in Thin Section: Moderately high positive.

Optic Orientation: $X \wedge a = -14°$ to $-37°$, $Y = b$, $Z \wedge c = +32°$ to $+55°$.

Indices of Refraction and Birefringence: Indices of refraction increase with Fe^{3+}, Ca, and Mg. Birefringence is usually in the range 0.012 to 0.018, so maximum interference colors in thin section are first-order yellow or red. High Fe^{3+} may cause anomalous interference colors and lower birefringence.

Interference Figure: $2V_z$ averages around 70°, larger than for many pyroxenes. Optic axis dispersion is weak to very strong, $r > v$.

Alteration Jadeite may be replaced by amphibole, or less commonly, by analcime or nepheline.

Distinguishing Features

Hand Sample: Massive varieties are distinguished by green color and toughness. Polished surfaces of nephrite have a somewhat oily luster; jadeite is vitreous. Granular material in metagraywacke may be difficult to recognize and distinguish in hand sample.

Thin Section/Grain Mount: Jadeite has lower indices of refraction than other pyroxenes. Omphacite has higher birefringence and aegirine and aegirine–augite have higher birefringence and are more distinctly green. Jadeite with anomalous interference colors resembles zoisite, but zoisite has higher indices of refraction and parallel extinction in principal sections. Tremolite has a smaller extinction angle in (010) sections and has typical amphibole cleavage.

Occurrence Jadeite is restricted to metamorphic rocks subjected to relatively high pressures and moderate temperatures, often blueschist and eclogite metamorphic facies. Typical occurrences are in glaucophane schist, metagraywacke, and related rocks. It may occur as nearly monomineralic pods or veins or as disseminated grains. The commonly associated minerals are albite, glaucophane, lawsonite, quartz, chlorite, garnet, zoisite, tremolite, calcite, aragonite, and mica. The following typical metamorphic reaction may

DO NOT COPY e48d507df5d1141@placeholder.94092

Printed by: e48d507df5d1141@placeholder.94092.edu. Printing is for personal, private use only. No part of this book may be reproduced or transmitted without publisher's prior permission. Violators will be prosecuted.

tremolite, calcite, aragonite, and micas. The following typical metamorphic reaction may produce jadeite at the expense of plagioclase.

$$\begin{aligned}&\text{Plagioclase} + \text{water}\\&\quad = \text{jadeite} + \text{lawsonite} + \text{quartz}\\&2\,\mathrm{Na_{0.5}\,Ca_{0.5}\,Al_{1.5}\,Si_{2.5}\,O_8} + \mathrm{H_2O}\\&\quad = \mathrm{NaAlSi_2O_6} + \mathrm{CaAl_2\,Si_2\,O_7(OH)_2 \cdot H_2O} + \mathrm{SiO_2}\end{aligned}$$

With increasing temperature, more Ca may substitute for Na in the M2 site, so in equivalent higher-grade rocks, the pyroxene may be omphacite.

Use Jadeite is the principal mineral in jade, which is used for decorative purposes and jewelry. The interlocking crystals of jadeite in jade make the material quite tough. The term *jade* also is used for a very similar-looking material composed of felted amphibole crystals. Amphibole jade is also called nephrite. The material sold as jade may be either material, or in some cases, almost anything green. Historically, jadeite has been used to treat a wide range of human maladies and it continues to be used in Chinese folk medicine.

Omphacite

$$(\mathrm{Ca, Na})\left(\mathrm{Mg, Fe^{2+}, Fe^{3+}, Al}\right)\mathrm{Si_2O_6}$$

$$\text{Monoclinic } 2/m$$

$$a = 9.45 - 9.68\ \text{Å},$$
$$b = 8.57 - 8.90\ \text{Å},$$
$$c = 5.23 - 5.28\ \text{Å},$$
$$\beta = 105 - 108^\circ,\ Z = 4$$

$$H = 5 - 6$$

$$G = 3.16 - 3.43$$

$$\text{Biaxial } (+)$$

$$n_\alpha = 1.662 - 1.701$$
$$n_\beta = 1.670 - 1.712$$
$$n_\gamma = 1.685 - 1.723$$

$$\delta = 0.012 - 0.028$$

$$2V_z = 56 - 84^\circ$$

DO NOT COPY
e48d507df5d1141@placeholder.9409

Printed by: e48d507df5d1141@placeholder.94092.edu. Printing is for personal, private use only. No part of this book may be reproduced or transmitted without publisher's prior permission. Violators will be prosecuted.

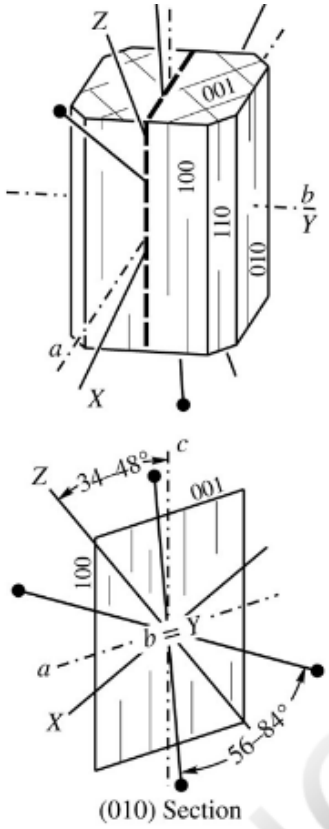

(010) Section

Composition Omphacite is compositionally intermediate between augite and jadeite (Figure 14.2b) but has slightly different structure. The M2 site is occupied by between 20% and 80% Na; the rest is occupied by Ca. The occupancy of the M1 sites by trivalent cations is about equal to the Na content in M2 sites to maintain charge balance, and Al^{3+} generally exceeds Fe^{3+}. The rest of the M1 sites are occupied by Mg and Fe^{2+}.

Form and Twinning Crystals are stubby prisms with four- or eight-sided cross sections. More common as anhedral grains. Simple and lamellar twinning on {100} is common.

Cleavage Good cleavage on {110}, like the other pyroxenes intersects at 87° and 93°. Parting on {100}. Uneven to conchoidal fracture. Brittle.

Color Properties

Luster: Vitreous to silky.

Color: Green or dark green.

Streak: Gray.

Color in Thin Section: Colorless to pale green.

Pleochroism: Weakly pleochroic: X = colorless, Y = very pale green, Z = very pale green to blue-green.

Optical Characteristics

DO NOT COPY
e48d507df5d1141@placeholder.9409

Printed by: e48d507df5d1141@placeholder.94092.edu. Printing is for personal, private use only. No part of this book may be reproduced or transmitted without publisher's prior permission. Violators will be prosecuted.

Relief in Thin Section: High positive.

Optic Orientation: $X \wedge a = -18°$ to $-33°$, $Y = b$, $Z \wedge c = +34°$ to $+48°$.

Indices of Refraction and Birefringence: Indices of refraction generally increase with Fe^{3+} content, but with considerable variability. Birefringence is moderate, so maximum interference colors in thin section are usually upper first to lower second order.

Interference Figure: The normal range for $2V_Z$ is between 60° and 75°, although the full range is larger. Optic axis dispersion is moderate, $r > v$ or $r < v$.

Alteration Alteration to fine-grained fibrous green amphibole is common. Omphacite may break down to a spongy to **symplectic** (inclusions look like worms) intergrowth of diopside and plagioclase.

Distinguishing Features

Hand Sample: Recognized as a pyroxene based on color, cleavage, and hardness. Amphiboles have better cleavage at 56° and 124°. Omphacite cannot reliably be distinguished from other pyroxenes in hand sample.

Thin Section/Grain Mount: Distinguished from the Ca-clinopyroxenes by larger $2V$ and from jadeite by darker color, and higher indices of refraction and birefringence. Aegirine and aegirine–augite are more distinctly colored and have higher indices of refraction and smaller extinction angles in (010) section.

Occurrence Omphacite is a characteristic mineral of rocks formed in high-pressure conditions such as those of the blueschist and eclogite metamorphic facies found in subduction zones and at the base of tectonically thickened crust. Common rocks containing omphacite include blueschist, eclogite, metagraywacke, and related rocks; it may also be found in granulites. Associated minerals include garnet, kyanite, glaucophane, and lawsonite.

Use None.

Spodumene

$$LiAlSi_2O_6$$

$$\text{Monoclinic } 2/m$$

$$a = 9.45 \text{ Å},\ b = 8.39 \text{ Å},$$
$$c = 5.215 \text{ Å},\ \beta = 110^\circ,\ Z = 4$$

$$H = 6.5 - 7$$

$$G = 3.03 - 3.23$$

DO NOT COPY e48d507df5d1141@placeholder.9409

Printed by: e48d507df5d1141@placeholder.94092.edu. Printing is for personal, private use only. No part of this book may be reproduced or transmitted without publisher's prior permission. Violators will be prosecuted.

Biaxial (+)

$$n_\alpha = 1.648 - 1.668$$

$$n_\beta = 1.655 - 1.671$$

$$n_\gamma = 1.662 - 1.682$$

$$\delta = 0.014 - 0.027$$

$$2V_z = 58 - 68^\circ$$

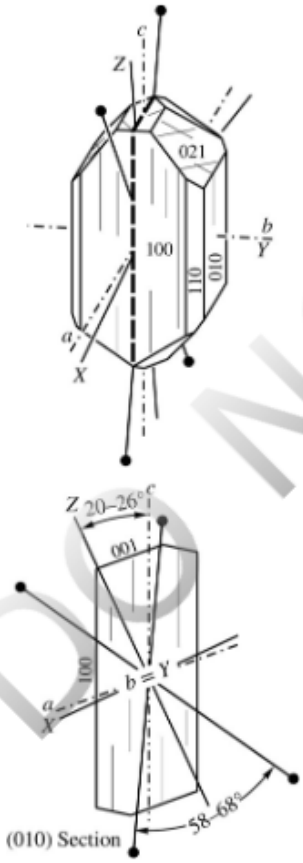

Composition Spodumene shows little compositional variation. Minor amounts of Na^+ and K^+ may substitute for Li^+ in the M2 sites, and Fe^{3+} may substitute for Al^{3+} in M1 sites. Trace amounts of other elements are common.

Form and Twinning Crystals are prismatic with roughly octagonal cross sections. Also as blade-like acicular crystals and granular masses. Crystals in some pegmatites may be very large.

Cleavage Good cleavage on {100} at 87° and 93°, like the other pyroxenes. {100} parting. Uneven to subconchoidal fracture. Brittle.

Color Properties

Luster Vitreous

DO NOT COPY e48d507df5d1141@placeholder.9409

Printed by: e48d507df5d1141@placeholder.94092.edu. Printing is for personal, private use only. No part of this book may be reproduced or transmitted without publisher's prior permission. Violators will be prosecuted.

Luster: Vitreous.

Color: White or grayish white, also pale shades of blue, green, and yellow. Fluoresces yellow, orange, or pink under both long-wave and short-wave ultraviolet light.

Streak: White.

Color in Thin Section: Colorless.

Pleochroism: None.

Optical Characteristics

Relief in Thin Section: Moderately high positive.

Optic Orientation: $X \wedge a = 0°$ to $-6°$, $Y = b$, $Z \wedge c = +20°$ to $+26°$.

Indices of Refraction and Birefringence: Indices of refraction vary within a small range. Substitution of Na for Li causes indices of refraction to decrease; substitution of Fe^{3+} for Al increases both indices of refraction and birefringence.

Interference Figure: $2V_z$ varies in a small range (58°–68°). Optic axis dispersion is $r < v$.

Alteration Spodumene is readily altered to Li-mica, albite, and eucryptite ($LiAlSiO_4$), which is uniaxial (+), colorless, granular or prismatic, with $n_\omega = 1.572$ and $n = 1.586$.

Distinguishing Features

Hand Sample: Light color, prismatic crystals, hardness, and cleavage distinguish it from other likely minerals in pegmatites. The combination of cleavage and parting may make spodumene resemble tremolite, but tremolite has only two cleavages and they are at 56° and 124°.

Thin Section/Grain Mount: Occurrence in pegmatites and small extinction angle distinguish it from other pyroxenes. Aegirine has a similar extinction angle, but has a very different occurrence and is colored. Higher indices of refraction quickly distinguish spodumene from feldspars.

Occurrence Spodumene is generally restricted to Li-bearing pegmatite. It is commonly associated with quartz, K-feldspar, plagioclase, tourmaline, beryl, and lepidolite (Li-mica).

Use About a quarter of world production of lithium comes from spodumene; two-thirds from Li-bearing brines; about 7% from hectorite, a Li-bearing smectite clay; and small amounts from lepidolite. Li has numerous uses, including in pharmaceuticals, ceramics, lubricants, and most notably, the batteries that power many electronic devices. Historically, spodumene was used to treat mental health issues, and it may have been effective. Modern medicine uses Li-based compounds to treat bipolar disorder and depression.

DO NOT COPY e48d507df5d1141@placeholder.9409

Printed by: e48d507df5d1141@placeholder.94092.edu. Printing is for personal, private use only. No part of this book may be reproduced or transmitted without publisher's prior permission. Violators will be prosecuted.

Pyroxenoids

Introduction

The pyroxenoid group differs from the pyroxenes principally in that the chains of silicon tetrahedra are distorted or twisted (**Figure 14.7**). In the pyroxenes, the repeat distance along the chains is two tetrahedra, or about 5.2 Å, which is the *c* unit cell dimension. In the pyroxenoids, the repeat distance is three or more tetrahedra. Cations in distorted octahedral coordination tie the chains together, as in the pyroxenes.

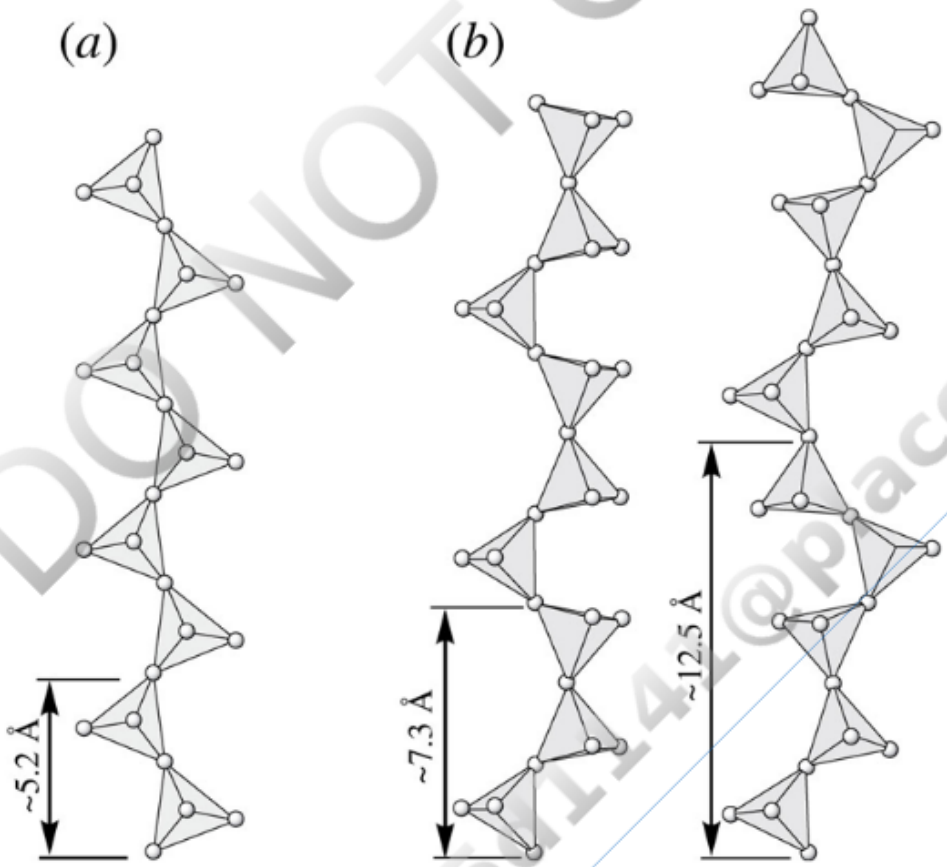

FIGURE 14.7 Chain structure of pyroxenes and pyroxenoids. (*a*) Pyroxenes have a repeat of two silicon tetrahedra at a distance of about 5.2 Å. Diopside is shown here, compare with enstatite in Figure 14.1e. (*b*) Pyroxenoids have a repeat of three or more tetrahedra. Cations in distorted octahedral coordination tie chains together as in the pyroxenes. Wollastonite (*left*) has a repeat of three silicon tetrahedra at a distance of about 7.3 Å. Rhodenite (*right*) has a repeat of five silicon tetrahedra at about 12.5 Å. View larger image

Wollastonite

Printed by: e48d507df5d1141@placeholder.94092.edu. Printing is for personal, private use only. No part of this book may be reproduced or transmitted without publisher's prior permission. Violators will be prosecuted.

$CaSiO_3$

Triclinic 1

$a = 7.94$ Å, $b = 7.32$ Å, $c = 7.07$ Å,
$\alpha = 90.03^\circ$, $\beta = 95.37^\circ$,
$\gamma = 103.43^\circ$, $Z = 6$

$H = 4.5 - 5$

$G = 2.86 - 3.09$

Biaxial (−)

$n_\alpha = 1.616 - 1.645$

$n_\beta = 1.628 - 1.652$

$n_\gamma = 1.631 - 1.656$

$\delta = 0.013 - 0.017$

$2V_x = 36 - 60^\circ$

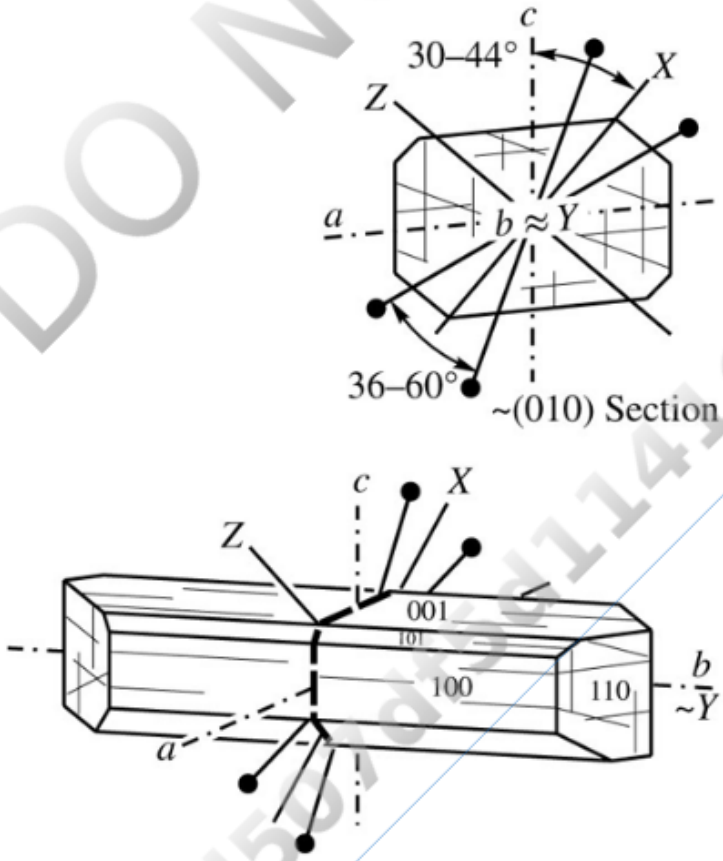

Structure The wollastonite structure consists of kinked chains of silicon tetrahedra (Figure 14.7b) that extend parallel to the *b* axis with a repeat of three tetrahedra at about 7.3 Å. Chains are linked with Ca^{2+} in three different octahedral sites, so the formula could be given as $CaCaCa(SiO_3)_3$. Alternatively, the formula may be given as $Ca_3Si_3O_9$.

DO NOT COPY
e48d507df5d1141@placeholder.9409

Printed by: e48d507df5d1141@placeholder.94092.edu. Printing is for personal, private use only. No part of this book may be reproduced or transmitted without publisher's prior permission. Violators will be prosecuted.

could be given as $CaCaCa(SiO_3)_3$. Alternatively, the formula may be given as $Ca_2Si_2O_6$, particularly when used to represent a compositional end member for pyroxenes (Figure 14.2a). Two common polytypes are wollastonite-Tc and wollastonite-2M, which are related by details of how adjacent chains are positioned relative to each other. Data for wollastonite-Tc are presented here. Pseudowollastonite is a high-temperature polymorph with three-fold rings of silicon tetrahedra.

Composition Most wollastonite is relatively pure $CaSiO_3$, but both Mn and Fe^{2+} may substitute for Ca.

Form and Twinning Wollastonite is usually bladed, columnar, or fibrous with grains elongate parallel to *b* and flattened parallel to {100} or {001}. Twins with {100} composition planes are common, but are not visible in hand sample.

Cleavage A single perfect cleavage on {100} and good cleavages on {001} and $\{\bar{1}02\}$ produce splintery cleavage fragments. The angle between the {100} and {001} cleavages is 84.5° and between {100} and $\{\bar{1}02\}$ is 70°. Uneven fracture. Brittle.

Color Properties

Luster: Vitreous.

Color: White, gray, or pale green. Some may be fluorescent.

Streak: White.

Color in Thin Section: Colorless.

Pleochroism: None.

Optical Characteristics

Relief in Thin Section: Moderate to moderately high positive.

Optic Orientation: $X \wedge c = -30°$ to $-44°$, $Y \wedge b \approx 0°$, $Z \wedge a = +35°$ to $+49°$, optic plane ~ (010). Cleavage fragments and the trace of cleavage are length slow or length fast, depending on orientation, because *Y* is parallel to fiber length.

Indices of Refraction and Birefringence: Pure wollastonite has indices of refraction near the lower end of the range given above. Indices of refraction increase with Fe and Mn content. Maximum interference color in thin section is upper first order.

Interference Figure: Most wollastonite has $2V$ of about 40°; larger values are for Fe-bearing samples. Optic axis dispersion is weak to moderate, $r > v$.

Alteration Pectolite, calcite, or other Ca-rich minerals may replace wollastonite.

Distinguishing Features

DO NOT COPY e48d507df5d1141@placeholder.9409

Printed by: e48d507df5d1141@placeholder.94092.edu. Printing is for personal, private use only. No part of this book may be reproduced or transmitted without publisher's prior permission. Violators will be prosecuted.

Distinguishing Features

Hand Sample: Resembles tremolite, with which it is often associated, but it has different cleavage. The different varieties of wollastonite can be distinguished only with X-ray diffraction techniques.

Thin Section/Grain Mount: Resembles tremolite and pectolite, but both have higher birefringence and are consistently length slow. Pyroxene such as diopside has higher relief, is optically positive, and rarely displays a bladed or elongate habit.

Occurrence Wollastonite is a common mineral in metamorphosed limestone and dolomite. Associated minerals include calcite, dolomite, other calc-silicate minerals (tremolite, members of the epidote group, grossular, diopside, etc.), and other Ca–Mg silicates. Occurrences in some alkalic igneous rocks have been reported.

Use Wollastonite, because it has an acicular habit when crushed, has replaced chrysotile asbestos in some industrial applications such as fire-resistant interior and exterior construction board, siding, roofing tile, and insulation. Paints and other coatings may contain wollastonite to improve workability and color brightness, and to increase film strength. The plastics industry uses wollastonite as a filler and to improve the working property of plastic during manufacturing processes. It also is used in ceramics, including bioceramics, and as a flux in metallurgical processes.

Comments Because processing wollastonite produces splintery fibers, the mineral has come under scrutiny as a possible health risk, similar to the asbestos minerals (Box 13.1). The available studies suggest that wollastonite, if inhaled, does not pose an unusual health hazard beyond that of normal rock dust.

Rhodonite

$$\mathrm{MnSiO_3}$$

$$\text{Triclinic } \bar{1}$$

$$a = 9.758\ \text{Å},$$
$$b = 10.499\ \text{Å},$$
$$c = 12.205\ \text{Å},$$
$$\alpha = 108.98^\circ,$$
$$\beta = 102.92^\circ,$$
$$\gamma = 82.52^\circ,$$
$$Z = 20$$

$$H = 5.5 - 6.5$$

$$G = 3.57 - 3.76$$

DO NOT COPY e48d507df5d1141@placeholder.94092

Printed by: e48d507df5d1141@placeholder.94092.edu. Printing is for personal, private use only. No part of this book may be reproduced or transmitted without publisher's prior permission. Violators will be prosecuted.

Biaxial (+)

$$n_\alpha = 1.711 - 1.734$$

$$n_\beta = 1.715 - 1.739$$

$$n_\gamma = 1.724 - 1.748$$

$$\delta = 0.011 - 0.017$$

$$2V_z = 63 - 87^\circ$$

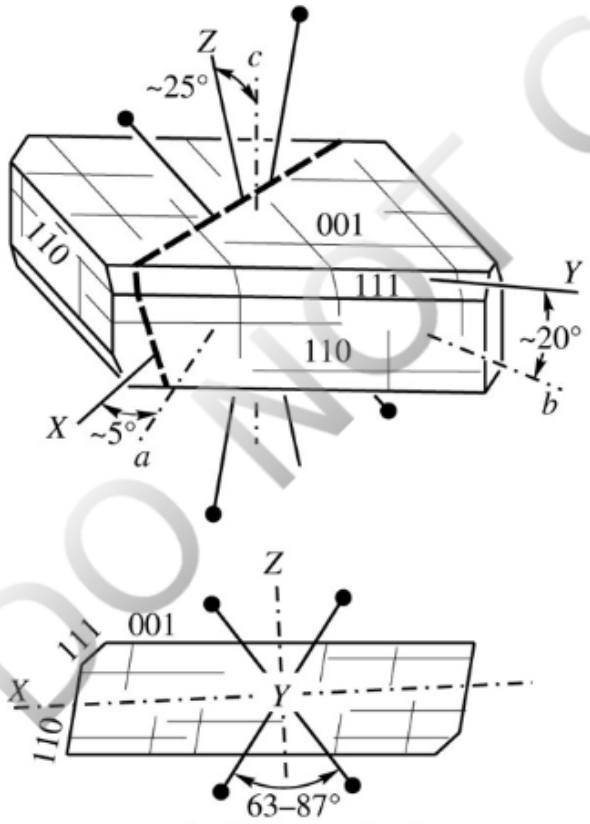

Max. Birefringence Section

Structure The structure consists of distorted chains of silicon tetrahedra (Figure 14.7b) tied laterally through Mn in octahedral coordination.

Composition Up to 20% of the Mn may be replaced by Ca and/or Mg/Fe.

Form and Twinning Rhodonite usually occurs in massive granular aggregates or anhedral grains. Crystals are tabular parallel to (001). Lamellar twins with (010) composition planes are not common and not evident in hand sample.

Cleavage Two perfect cleavages on {110} and $\{\bar{1}10\}$, and a fair cleavage on {001}. The angle between the perfect cleavages is 92.5°. Conchoidal to uneven fracture. Brittle.

Color Properties

DO NOT COPY e48d507df5d1141@placeholder.9409

Printed by: e48d507df5d1141@placeholder.94092.edu. Printing is for personal, private use only. No part of this book may be reproduced or transmitted without publisher's prior permission. Violators will be prosecuted.

Color Properties

Luster: Vitreous.

Color: Pink, rose-red, or red-brown.

Streak: White.

Color in Thin Section: Colorless to pale pink.

Pleochroism: Weak: X = yellowish red, Y = pinkish red, Z = pale yellowish red.

Optical Characteristics

Relief in Thin Section: High positive.

Optic Orientation: $X \wedge a \approx 5°$, $Y \wedge b \approx 20°$, $Z \wedge c \approx 25°$, the optic plane is roughly parallel to (010).

Indices of Refraction and Birefringence: Indices of refraction decrease with increasing Ca content. The maximum interference color in thin section is upper first-order yellow or red.

Interference Figure: $2V$ increases slightly with increased Ca content. Optic axis dispersion is weak, $r < v$, crossed bisectrix dispersion may be distinct.

Alteration Rhodonite may alter to rhodochrosite or Mn-oxides and hydroxides.

Distinguishing Features

Hand Sample: Characterized by pink color and nearly right-angle cleavage. Dark alteration/weathering products that include Mn-oxides may mask the mineral color. Rhodochrosite is softer, has rhombohedral cleavage, and reacts with acid.

Thin Section/Grain Mount: Pale pink color, if present. Bustamite [$(Ca,Mn)SiO_3$] and pyroxmangite [$(Mn,Fe)SiO_3$] are similar minerals. Pyroxmangite has higher birefringence, and bustamite is optically negative with $2V$ less than 60°.

Occurrence Generally restricted to Mn-bearing hydrothermal systems and skarn deposits. It commonly is associated with other Mn minerals, such as rhodochrosite and pyrolusite, as well as quartz, other carbonates, and a variety of sulfide minerals.

Use The pink to red color makes it useful as a decorative stone and in the lapidary arts.

Pectolite

$$Ca_2NaH(SiO_3)_3$$

Triclinic, $\bar{1}$

DO NOT COPY

Printed by: e48d507df5d1141@placeholder.94092.edu. Printing is for personal, private use only. No part of this book may be reproduced or transmitted without publisher's prior permission. Violators will be prosecuted.

Triclinic 1

$a = 7.99$ Å,

$b = 7.04$ Å,

$c = 7.02$ Å,

$\alpha = 90.52^\circ$,

$\beta = 95.18^\circ$,

$\gamma = 102.47^\circ$,

$Z = 2$

$H = 4.5 - 5$

$G = 2.86 - 2.90$

Biaxial (+)

$n_\alpha = 1.592 - 1.610$

$n_\beta = 1.603 - 1.615$

$n_\gamma = 1.630 - 1.645$

$\delta = 0.026 - 0.039$

$2V_z = 50 - 63^\circ$

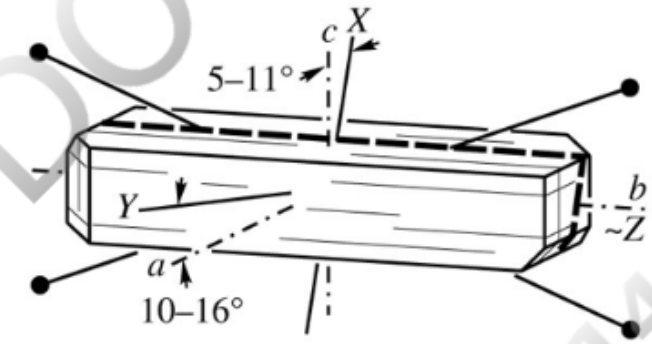

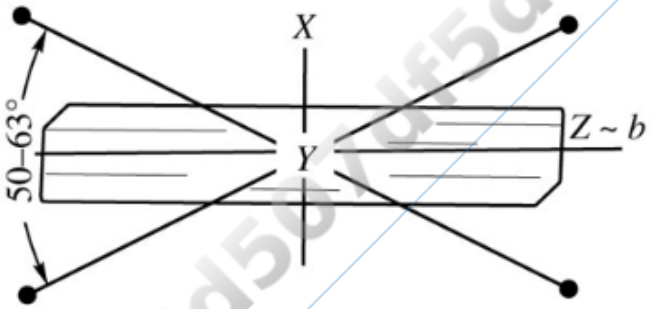

Max. Birefringence Section
~(100)

DO NOT COPY
e48d507df5d1141@placeholder.9409

Printed by: e48d507df5d1141@placeholder.94092.edu. Printing is for personal, private use only. No part of this book may be reproduced or transmitted without publisher's prior permission. Violators will be prosecuted.

Structure Distorted chains of silicon tetrahedra similar to the pyroxenoids are linked laterally by Ca and Na cations.

Composition Most pectolite is near the ideal composition. Mn may substitute for Ca in some samples.

Form and Twinning See **Figure 14.8**. Pectolite commonly forms radiating groups or compact masses of acicular crystals elongate along *b*. Twins with {100} composition planes are rare.

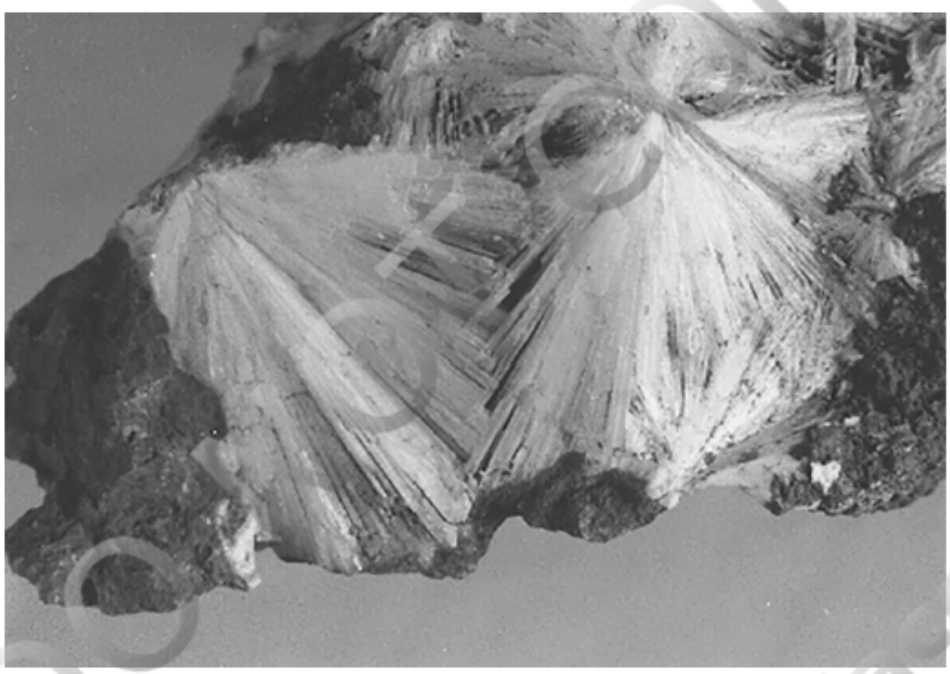

FIGURE 14.8 Photograph of radiating masses of pectolite. Field of view is about 10 cm wide.
View larger image

Cleavage Perfect cleavages on {100} and {001} intersect at 95°.

Color Properties

Luster: Vitreous.

Color: White, colorless.

Streak: White.

Color in Thin Section: Colorless.

Pleochroism: None.

Optical Characteristics

Relief in Thin Section: Moderate positive.

DO NOT COPY e48d507df5d1141@placeholder.9409

Printed by: e48d507df5d1141@placeholder.94092.edu. Printing is for personal, private use only. No part of this book may be reproduced or transmitted without publisher's prior permission. Violators will be prosecuted.

Optic Orientation: $X \wedge c = -5°$ to $-11°$, $Y \wedge a = +10°$ to $+16°$, $Z \approx b$, optic plane is nearly parallel to (100). Cleavage fragments and trace of cleavage in thin section are length slow.

Indices of Refraction and Birefringence: Substitution of Mn for Ca causes indices of refraction to increase. Interference colors in thin section are up to upper second order.

Interference Figure: $2V$ varies in a modest range for most samples, though values as small as 35° have been reported, probably as a consequence of substitution of Mn. Optic axis dispersion is weak, $r > v$ or $r < v$.

Alteration Pectolite may be replaced by pale pink stevensite, which is an Mg-rich clay mineral in the smectite group.

Distinguishing Features

Hand Sample: Resembles wollastonite and acicular zeolites such as natrolite. Wollastonite is not common as radiating masses in altered volcanics, and natrolite is more likely to form slender radiating crystals, as opposed to radiating masses.

Thin Section/Grain Mount: Pectolite has higher birefringence than most zeolites, with which it is commonly associated. Wollastonite has lower birefringence and displays both length fast and length slow sign of elongation.

Occurrence Pectolite is most common as an amygdule and cavity filling in basalt flows, diabase dikes, and related rocks. Associated minerals include zeolites and calcite. Pectolite may also be found in serpentinites, as a primary mineral in alkalic igneous rocks such as nepheline syenite, and in skarns or other Ca-rich metamorphic rocks.

Use None.

DO NOT COPY e48d507df5d1141@placeholder.9409

Printed by: e48d507df5d1141@placeholder.94092.edu. Printing is for personal, private use only. No part of this book may be reproduced or transmitted without publisher's prior permission. Violators will be prosecuted.

Amphibole Group

Structure and Classification

Amphibole structure and classification are generally similar to those of the pyroxenes, but a bit more complex. The basic building block consists of a double chain of silicon tetrahedra (Figures 11.2e and 14.9a). These chains extend parallel to the *c* crystal axis and are stacked in an alternating fashion, like the pyroxenes. Bases of tetrahedra face each other, and the unshared apical oxygens on tetrahedra face each other (Figure 14.9b, c, d). This geometry produces five different structural sites between the chains. Octahedral M1, M2, and M3 sites are between the points of the chains; larger M4 and A sites are between the bases.

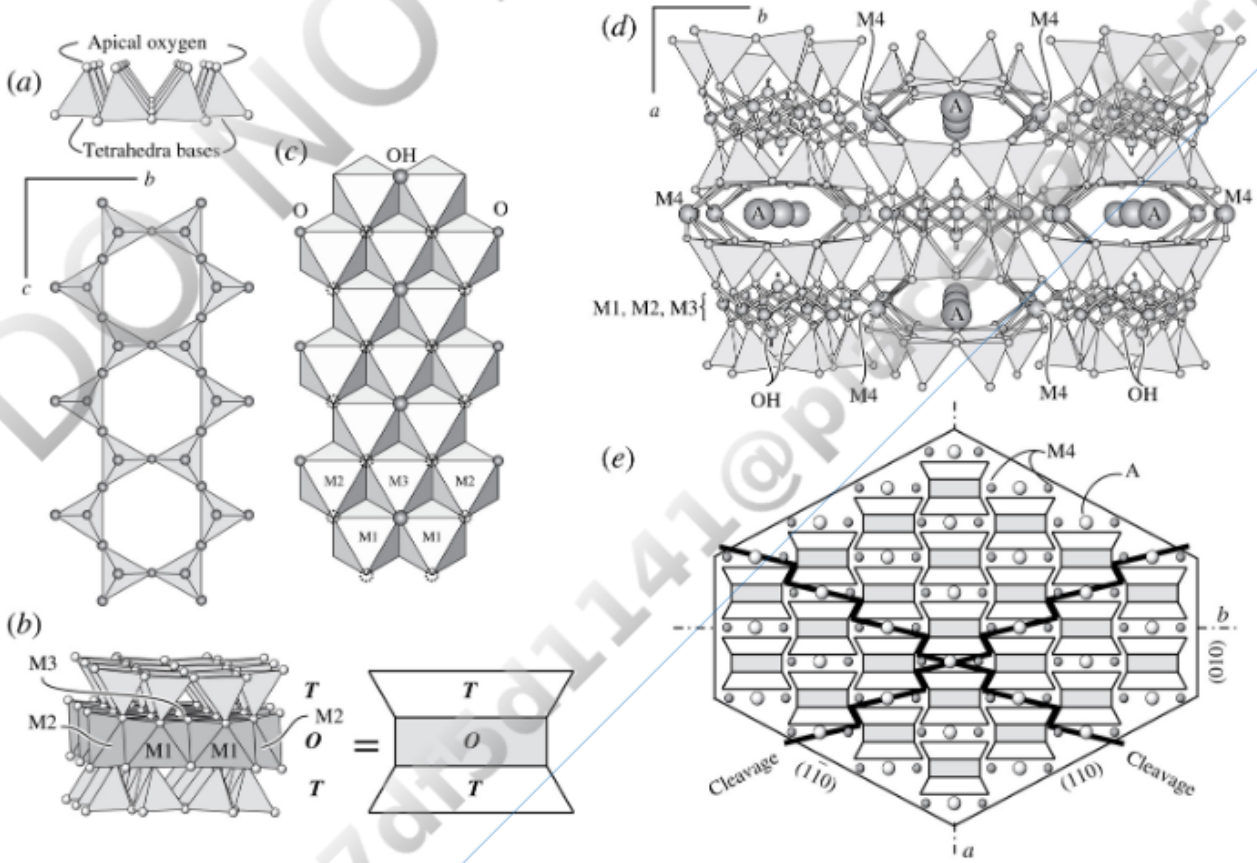

FIGURE 14.9 Amphibole structure. (*a*) Top and end views of an idealized double chain of tetrahedra. (*b*) Two chains of tetrahedra (*T*) are arranged facing each other forming octahedral (*O*) M1, M2, and M3 sites in between. The cross-section shape of this *TOT* strip, or I-beam, is shown to the right. (*c*) Top view of the octahedral layer showing distribution of M1, M2, and M3 sites. O and OH that are not shared with a tetrahedral chain are shown as filled spheres on the top surface of the octahedrons. O that are shared with a tetrahedral chain are shown as dotted circles. (*d*) *TOT* strips extend parallel to the *c* axis and are stacked in the *a* direction to produce M4 and A sites between the bases of the tetrahedra. The M1, M2, and M3 cations are shown, rather than their coordination

Printed by: e48d507df5d1141@placeholder.94092.edu. Printing is for personal, private use only. No part of this book may be reproduced or transmitted without publisher's prior permission. Violators will be prosecuted.

polyhedra. (*e*) View down the *c* axis showing the arrangement of *TOT* strips (I-beams) and their relation to the typical amphibole cross section. Cleavage between chains parallel to (110) and $(1\bar{1}0)$ is at about 56° and 124°. View larger image

Two chains with intervening cations in octahedral M1, M2, and M3 sites form a structure analogous to a strip of a *TOT* layer in the layer silicates or a double-wide version of the I-beam discussed with the pyroxenes (Figure 14.9b). These *TOT* strips are stacked together and bonded through cations in the M4 and A sites to form the amphibole structure (Figure 14.9d). Cleavage occurs between the *TOT* strips (Figure 14.9e). Because the *TOT* strips in the amphiboles are wider than the equivalent I-beams in the pyroxenes, cleavage is at about 56° and 124°, rather than nearly at right angles. Another difference is that cleavage in the amphiboles is better developed and is of higher quality than in the pyroxenes.

The amphiboles have a general formula

$$A_{0-1}B_2C_5T_8O_{22}W_2$$

where

A = **Na**, □, K, Ca, Li

B = **Na**, **Ca**, **Fe^{2+}**, **Mg**, Mn^{2+}, Li

C = **Mg**, **Fe^{2+}**, **Al**, **Fe^{3+}**, Mn^{2+}, Mn^{3+}, Ti^{4+}, Li

T = **Si**, **Al**, Ti^{4+}

W = **$(OH)^-$**, **F^-**, **Cl^-**, **or O^{2-}**

Bold type indicates the more common occupants; □ indicates a vacancy. The A cations occupy the A structural sites (**Figure 14.9**); in some amphiboles, the A site is filled, and in others it is partially or entirely vacant. The two B cations are located in the M4 sites. These are analogous to the M2 sites in pyroxenes and may have either 8- or 6-fold coordination, depending on exactly how the *TOT* strips are arranged relative to each other. If 8-fold, the B cations are usually Ca^{2+} or Na^+, and if 6-fold, the B cations are Mg^{2+} or Fe^{2+}. The five C cations occupy the octahedral M1, M2, and M3 sites, which are the octahedral sites in the middle of the *TOT* strips. The eight T sites are tetrahedral and usually contain Si and some Al. The W in the formula signifies additional anions, most commonly $(OH)^-$. If all the M sites are filled with the same element, Mg for example, the B and C cations will be combined in the formula, in this case resulting in a formula of $Mg_7Si_8O_{22}(OH_2)$. Amphiboles are a hydrous mineral because they can contain a hydroxyl group.

The above paragraphs begin to hint at the chemical complexity of the amphiboles, which results in many solid solution end members. Most amphiboles are an intermediate

DO NOT COPY e48d507df5d1141@placeholder.9409

Printed by: e48d507df5d1141@placeholder.94092.edu. Printing is for personal, private use only. No part of this book may be reproduced or transmitted without publisher's prior permission. Violators will be prosecuted.

composition between multiple end members. This is a significant challenge when working with amphiboles, compounded by the fact that physical and optical properties do not vary in a systematic way with composition, so precise amphibole classification is not possible from hand sample and thin section work alone. Regardless, anyone requiring basic knowledge of the amphiboles (which is anyone who deals with rock, minerals, sediment, or soil!) should be comfortable with the classification scheme discussed below and understand the common amphiboles. Much effort has gone into presenting a balanced discussion between practicality, accuracy, and understandability. If a more detailed discussion of amphibole classification is needed, consult Hawthorne et al. (2012) and references therein.

The most recent amphibole classification scheme as defined by the Commission on New Minerals, Nomenclature and Classification of the International Mineralogical Association is published in Hawthorne et al. (2012). Because of the chemical complexity of the amphiboles, the scheme requires high-quality electron microprobe chemical analyses (Chapter 9); unfortunately, even with such data, classification may be difficult.

Difficulties arise because the microprobe cannot distinguish between Fe^{2+} and Fe^{3+}, nor can it routinely detect chemical elements lighter than fluorine ($Z = 9$), such as lithium ($Z = 3$), which is now recognized as possibly an important constituent. These elements can be analyzed by using secondary ion and laser ablation mass spectrometry techniques (Chapter 9), but such instruments are not nearly as widely available as the electron microprobe. None of these instruments are capable of analyzing for hydrogen ($Z = 1$), which too is a very important amphibole constituent. X-ray diffraction techniques (Chapter 8) can distinguish amphiboles from most other minerals, but they generally cannot identify the specific type of amphibole as the crystal structures of the various types are too similar. An additional issue is that even with a high-quality electron microprobe chemical analysis, classification realistically requires a computer program or complex spreadsheet.

The abbreviated classification shown in **Table 14.2** includes the majority of common amphiboles. The four main groups are classified primarily on the identity of the B cations in the M4 structural sites (Figure 14.9). Each of these amphibole groups has a structural and compositional analog in the pyroxenes (Table 14.1). Like the pyroxenes, the amphiboles can be divided into those that are orthorhombic—the orthoamphiboles—and those that are monoclinic—the clinoamphiboles.

TABLE 14.2 Abbreviated Amphibole Classification of Four Common Amphiboles with Examples, Based on the General Formula $A_{0\text{-}1}B_2C_5T_8O_{22}W_2$[a]

Group	A (A site)	B_2 (M4 site)	C_5 (M1, M2, and M3 sites)	$T_8O_{22}(OH)_2$	Mineral or Mineral Series	Symmetry
Iron–magnesium		$(Mg,Fe)_2$	$(Mg,Fe)_5$	$Si_8O_{22}(OH)_2$	Anthophyllite–ferro-anthophyllite	Orthorhombi

Printed by: e48d507df5d1141@placeholder.94092.edu. Printing is for personal, private use only. No part of this book may be reproduced or transmitted without publisher's prior permission. Violators will be prosecuted.

					anthophyllite	
		$(Mg,Fe)_2$	$(Mg,Fe)_3Al_2$	$Al_2Si_6O_{22}(OH)_2$	Gedrite–ferro-gedrite	
		$(Mg,Fe)_2$	$(Mg,Fe,Ca)_5$	$Si_8O_{22}(OH)_2$	Cummingtonite–grunerite	Monoclinic
Calcic		Ca_2	$(Mg,Fe)_5$	$Si_8O_{22}(OH)_2$	Tremolite–ferro-actinolite	
	$(Na,K)_{0-1}$	Ca_2	$(Mg,Fe^{2+},Fe^{3+},Al)_5$	$(Si,Al)_8O_{22}(OH)_2$	Hornblende	
Sodic–calcic	Na	CaNa	$(Mg,Fe)_5$	$Si_8O_{22}(OH)_2$	Richterite–ferro-richterite	
Sodic		Na_2	$(Mg,Fe^{2+})_3(Al,Fe^{3+})_2$	$Si_8O_{22}(OH)_2$	Glaucophane–riebeckite	

[a] W is assumed to be (OH).

Source: Adapted from Hawthorne and others (2012).

Beyond some of the substitutions implied by the compositions listed in Table 14.2, there are other substitutions that greatly complicate the amphibole compositions provided. Simple substitutions that involve cations of the same charge are listed in **Table 14.3**. Coupled substitutions that involve cations of different charge in two or more sites are listed in **Table 14.4**, where □ = vacancy. These substitution schemes can be used individually or in combination. For example, substitution of Al^{3+} for Si^{4+} can be balanced by inserting some Na^+ in the W site combined with substituting some Al^{3+} for Mg^{2+} in octahedral sites. This results in many amphiboles containing a dozen or more different elements.

TABLE 14.3 Simple Substitutions in the Amphiboles

Formula	Structural Site	Cations
A	A	Na^+, K^+
B	M4	Ca^{2+}, Mg^{2+}, Fe^{2+}
C	M1, M2, M3	Mg^{2+}, Fe^{2+}
C	M1, M2, M3	Al^{3+}, Fe^{3+}
T	Tetrahedral	Si^{4+}, Ti^{4+}

As a start, such complex compositions will be ignored such that some common ortho- and clinoamphiboles can be shown on a ternary diagram whose vertices are $Mg_7Si_8O_{22}(OH)_2$, $Fe_7Si_8O_{22}(OH)_2$, and $Ca_7Si_8O_{22}(OH)_2$, assuming the A site is vacant and the W site only has OH (**Figure 14.10**). Note that $Ca_7Si_8O_{22}(OH)_2$ as a mineral does not exist, and compositions close to this hypothetical end member are unlikely. Therefore, the Mg–Fe–Ca classification diagram maybe presented as a quadrilateral with end members of

DO NOT COPY e48d507df5d1141@placeholder.9409-

Printed by: e48d507df5d1141@placeholder.94092.edu. Printing is for personal, private use only. No part of this book may be reproduced or transmitted without publisher's prior permission. Violators will be prosecuted.

Ca classification diagram may be presented as a quadrilateral with end members of $Ca_2Mg_5Si_8O_{22}(OH)_2$, $Ca_2Fe_5Si_8O_{22}(OH)_2$, $Fe_7Si_8O_{22}(OH)_2$, and $Mg_7Si_8O_{22}(OH)_2$. Though this diagram is insufficient to classify many of the most common amphiboles, it provides an understanding of the most important amphiboles, helps relates the amphiboles to the pyroxenes, and provides a reference frame for amphiboles that cannot be classified by such a diagram.

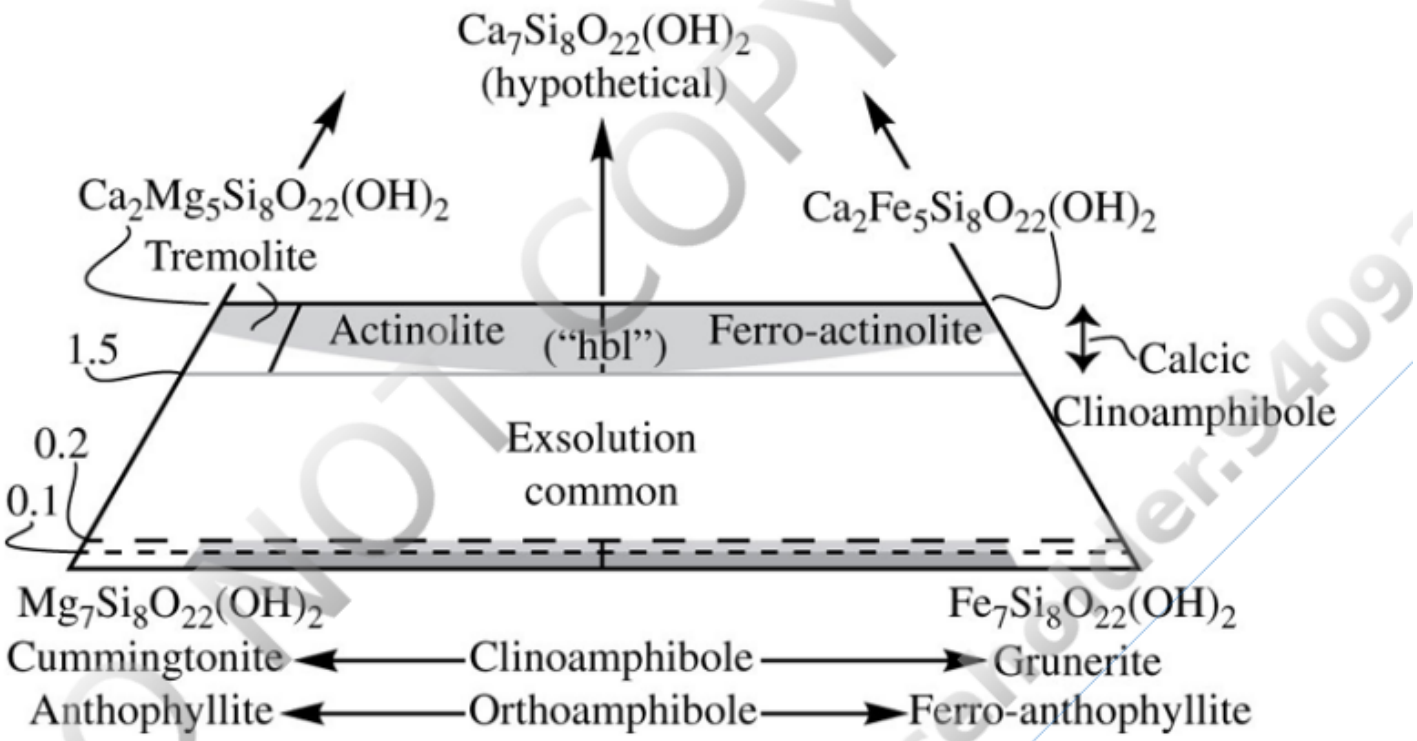

FIGURE 14.10 Fe–Mg–Ca amphiboles; common compositions are shown with shading. Decimal numbers on the left side mark various Ca compositions in atoms per formula units. ("hbl") is the approximate composition of some minerals often informally identified as hornblende, but such minerals often contain appreciable Al, Na, K, and Fe^{3+}, so they do not strictly lie in the plane of this composition diagram. See text for details. View larger image

As with the pyroxenes, first considered will be the orthorhombic amphiboles. For orthoamphiboles, simple substitution between Fe and Mg within all four M sites is common. Anthophyllite is the Mg-rich end member [$Mg_7Si_8O_{22}(OH)_2$] and ferro-anthophyllite is the Fe-rich end member [$Fe_7Si_8O_{22}(OH)_2$]; intermediate compositions are classified as one of the end members with the division between the two occurring where Fe and Mg proportions are equal. Compositions close the end members are rarer and most have less than 0.1 atoms per formula unit of Ca. These orthoamphiboles are most similar to the orthopyroxenes.

A second series of orthoamphiboles exist but do not appear in Figure 14.10 as they contain appreciable Al in the M1, M2, M3, and tetrahedral sites via the coupled substitution of $2(Fe^{2+},Mg^{2+})\rightarrow 2Al^{3+}$ in the M1, M2, and M3 sites and $2Si^{4+}\rightarrow 2Al^{3+}$ in the tetrahedral site. These orthoamphiboles, of course, also possess Fe–Mg solid solution and result in end members of gedrite [$Mg_5Al_2Si_6Al_2O_{22}(OH)_2$] and ferro-gedrite [$Fe_5Al_2Si_6Al_2O_{22}(OH)_2$].

Printed by: e48d507df5d1141@placeholder.94092.edu. Printing is for personal, private use only. No part of this book may be reproduced or transmitted without publisher's prior permission. Violators will be prosecuted.

$[Fe_5Al_2Si_6Al_2O_{22}(OH)_2]$.

Sometimes identified as polymorphic with the anthophyllite–ferro-anthophyllite series is the clinoamphibole series of cummingtonite–grunerite. This series has, for most common specimens, a similar range in Fe–Mg ratios as the orthoamphiboles, but may possess slightly higher Ca contents of up to 0.2 atoms per formula unit. Overall, the cummingtonite–grunerite series is comparable to the pyroxene pigeonite.

Calcic clinoamphiboles typically have Ca contents above 1.5 atoms per formula unit, and with the ubiquitous Fe–Mg substitution, yield the end members of tremolite $[Ca_2Mg_5Si_8O_{22}(OH)_2]$ and ferro-actinolite $[Ca_2Fe_5Si_8O_{22}(OH)_2]$. Actinolite is a recognized intermediate member of this series, with Mg content ranging from about 4.5 to 2.5 atoms per formula unit. The tremolite–ferro-actinolite series is comparable to the diopside-hedenbergite calcic clinopyroxene series.

The calcic clinoamphiboles are the most common amphiboles, and they display considerable diversity of composition. As an introduction to these other calcic clinoamphiboles, the composition of the tremolite–ferro-actinolite series $[Ca_2(Mg,Fe)_5Si_8O_{22}(OH)_2]$ is a good starting point. First, apply the coupled Al substitution that resulted in the gedrite–ferro-gedrite series from the anthophyllite–ferro-anthophyllite series described, but this is done only once for each formula site involved. This leads to an Al-bearing calcic clinoamphibole composition of $Ca_2(Mg,Fe)_4AlSi_7AlO_{22}(OH)_2$, which is the magnesio-hornblende–ferro-hornblende series.

Although perhaps difficult to understand given its wide use, the term hornblende by itself is not a specific amphibole; instead it refers to any number of dark green to black calcic and sodic–calcic clinoamphiboles, many of which are quite common. Given the difficulty of distinguishing all the specific, officially recognized amphibole varieties that fit this description, *hornblende* is the term used to generally classify such specimens when high-quality electron microprobe analyses are not available. It is not strictly accurate to define the composition hornblende on the Ca–Fe–Mg amphibole composition diagram (Figure 14.10), but dark green and black specimens of actinolite and ferro-actinolite may be generalized as hornblende; this is indicated by the ("hbl") designation on Figure 14.10. More accurately, hornblende should have appreciable Al, but Al content is impossible to determine without analytical instrumentation, and some sources do include the tremolite–ferro-actinolite series in the broader group of minerals referred to as hornblende. See the hornblende entry in this chapter for more details. Hornblende is fairly comparable to the calcic clinopyroxene augite, but augite is a recognized type of pyroxene, while hornblende is a general term and has much more chemical diversity.

If high-quality electron microprobe analysis is lacking, knowledge regarding host rock type, combined with amphibole physical and optical properties, may allow the identity of a particular amphibole specimen to be determined. The Mg–Fe amphiboles found in mafic metamorphic rocks usually are brown; anthophyllite and gedrite are the most common varieties. Sodic amphiboles are usually blue; glaucophane is found in blueschists, and riebeckite in alkalic igneous rocks. Most common are calcic and sodic–calcic amphiboles,

Printed by: e48d507df5d1141@placeholder.94092.edu. Printing is for personal, private use only. No part of this book may be reproduced or transmitted without publisher's prior permission. Violators will be prosecuted.

which are dark green to black, and until the chemistry is known, classifying them as hornblende is appropriate. White or pale green amphibole in metamorphosed carbonates is usually tremolite. Optical properties allow some additional refinement in classification, but the properties of the calcic and sodic–calcic amphiboles overlap substantially. If knowledge of composition is important, then analysis by electron microprobe or another analytical technique is required. **Figure 14.11** shows some common amphiboles.

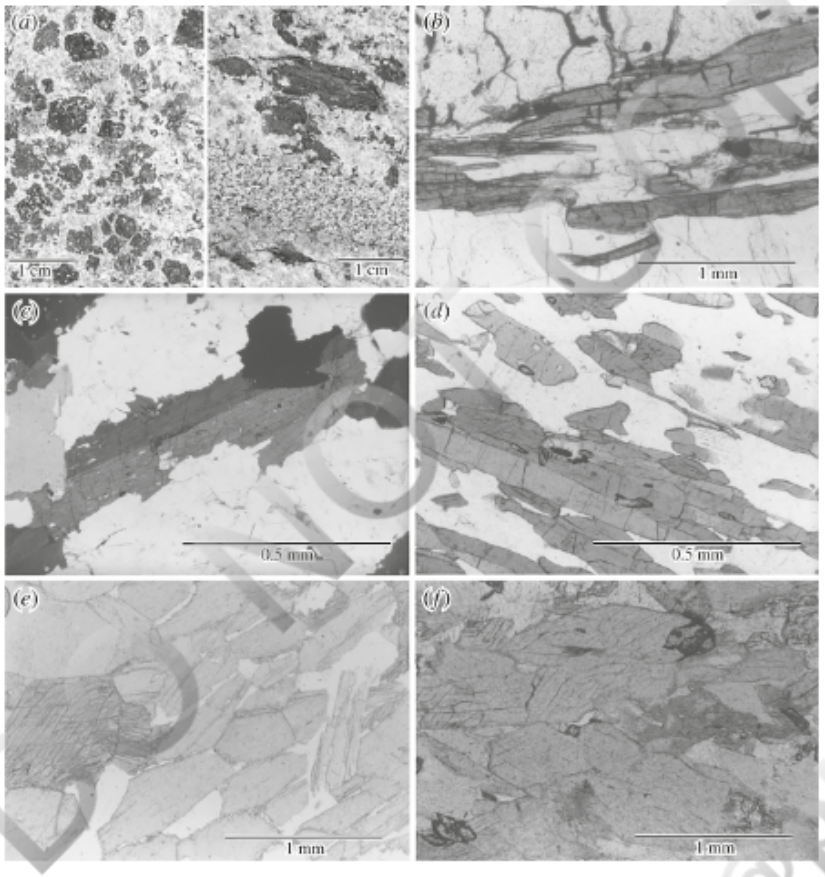

FIGURE 14.11 Common amphiboles. (*a*) Hornblende in outcrop. (*left*) Most grains are subhedral to euhedral with *c* axes parallel to the view direction; some grains display {110} and {010} crystal faces defining an irregular hexagon. (*right*) Grain *c* axes are parallel to the image. (*b*) Plane-polarized light photomicrograph of anthophyllite with cloudy cordierite (*top*) and quartz. (*c*) Plane-polarized light photomicrograph of hornblende in granodiorite. Note the twin. (*d*) Plane-polarized light photomicrograph of hornblende in amphibolite. (*e*) Plane-polarized light photomicrograph of tremolite in marble. Note that the grain on the left edge of the image is oriented with its *c* axis parallel to the view direction and clearly displays the 56° and 124° {110} cleavages. (*f*) Plane-polarized light photomicrograph of glaucophane in glaucophane schist. The small high-relief grains at the lower left and upper right are titanite. View larger image

Geology of Amphiboles

To understand the distribution of amphiboles, it is first necessary to recognize that they are hydrous, which means that amphiboles are not stable in anhydrous environments. We can also expect that very high temperatures will cause amphibole dehydration and breakdown to form anhydrous minerals like the pyroxenes. Further, the amphiboles have

Printed by: e48d507df5d1141@placeholder.94092.edu. Printing is for personal, private use only. No part of this book may be reproduced or transmitted without publisher's prior permission. Violators will be prosecuted.

a higher Si:O ratio (4:11) than either the pyroxenes or olivine, so they should be found more often Si-rich rocks than either of those minerals. These considerations lead to the following generalizations; of course many exceptions exist.

- Amphiboles are not normally abundant in mafic and ultramafic igneous rocks. These magmas have a relatively low silicon content, have little dissolved water, and crystallize at high temperatures. If present, amphiboles usually crystallize late in the magmatic history, when the residual melt is enriched both in Si and H_2O and temperatures are lower. Overgrowths of amphibole on pyroxene in mafic and ultramafic igneous rocks are fairly common.
- Amphiboles, particularly calcic and sodic–calcic varieties, should be common in intermediate to felsic igneous rocks. These magmas typically contain significant amounts of dissolved water and intermediate to high Si contents. Whether amphibole or biotite is the major Mg/Fe-bearing mineral in these rocks is determined, in part, by the abundance of K (for biotite) versus Na/Ca (for amphibole). As a general guideline, amphibole is typical in intermediate igneous rocks such as diorite, granodiorite, andesite, and dacite, whereas biotite is more common in felsic varieties.
- Amphiboles are common in rocks with intermediate to mafic compositions subjected to metamorphism. The pore fluid accompanying metamorphism under these conditions usually is water-rich, because water is available from the breakdown of hydrous minerals such as the micas and chlorite during prograde metamorphism. Actinolite commonly forms during greenschist facies metamorphism, particularly if the rock is fairly mafic. Actinolite is green and may be one of the minerals that impart a green color to greenschist facies metamorphic rocks. Amphibolite facies metamorphism gets its name from the abundant amphibole, typically hornblende, in metamorphosed mafic rocks. At very high temperatures, amphiboles break down by dehydration to produce the pyroxenes typical of granulite facies metamorphism.

Exsolution in the amphiboles is complex and pervasive. In general, high temperatures favor more extensive solid solution among the diverse amphibole end members, and cooling restricts the stable compositional ranges and triggers exsolution lamellae to develop. In the orthoamphiboles, exsolution lamellae of gedrite in anthophyllite, and vice versa, are very common. In the clinoamphiboles, it is common to find exsolution lamellae of cummingtonite develop from both calcic and sodic varieties. Actinolite lamellae also may exsolve from hornblende, and vice versa. While very common, the exsolution lamellae frequently are submicroscopic and require transmission electron microscope techniques to be observed.

Orthoamphibole

Anthophyllite – Ferro-anthophyllite

DO NOT COPY e48d507df5d1141@placeholder.9409

Printed by: e48d507df5d1141@placeholder.94092.edu. Printing is for personal, private use only. No part of this book may be reproduced or transmitted without publisher's prior permission. Violators will be prosecuted.

Anthophyllite – Ferro-anthophyllite
(anthophyllite series) : $(Mg,Fe)_2$
$(Mg,Fe)_5Si_8O_{22}(OH)$

$a = 18.54$ Å, $b = 18.03$ Å,
$c = 5.28$ Å, $Z = 4$

Gedrite – Ferro-gedrite
(gedrite series) :
$(Mg,Fe)_2(Mg,Fe)_3$
$Al_2Si_6Al_2O_{22}(OH)_2$

$a = 18.53 - 18.60$ Å,
$b = 17.74 - 17.89$ Å,
$c = 5.25 - 5.28$ Å, $Z = 4$

Orthorhombic $2/m\ 2/m\ 2/m$

$H = 5.5 - 6$

$G = 2.85 - 3.57$

Biaxial (+ or −)

$n_\alpha = 1.587 - 1.694$

$n_\beta = 1.602 - 1.710$

$n_\gamma = 1.613 - 1.722$

$\delta = 0.013 - 0.028$

$2V_x = 65 - 122^\circ$ (anthophyllite)

$2V_x = 72 - 133^\circ$ (gedrite)

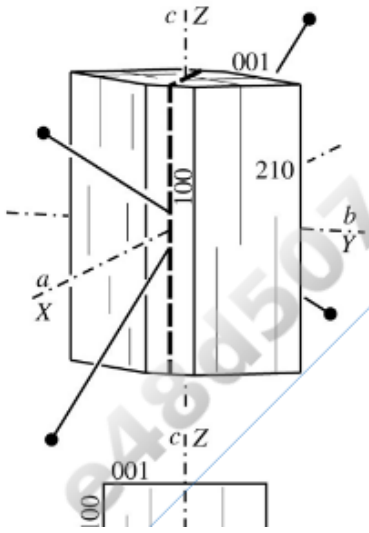

DO NOT COPY
e48d507df5d1141@placeholder.9409

Printed by: e48d507df5d1141@placeholder.94092.edu. Printing is for personal, private use only. No part of this book may be reproduced or transmitted without publisher's prior permission. Violators will be prosecuted.

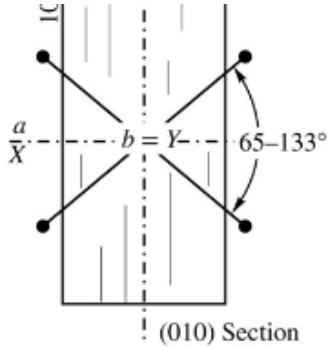

Composition See Figure 14.10 and associated text above. Ca content is typically less than 0.1 atoms per formula unit. Gedrite–ferro-gedrite may contain some Na in the A site, which remains vacant in anthophyllite. At high temperatures, it appears that the anthophyllite series and gedrite series are part of a continuous solid solution series. At lower temperatures, however, a solvus exists so that lamellae of gedrite–ferro-gedrite may exsolve parallel to (010) and (120) in anthophyllite–ferro-anthophyllite, and vice versa.

Form and Twinning See Figure 14.11. Orthoamphiboles are common as euhedral to subhedral columnar, bladed, or acicular crystals with the diamond-shaped cross section typical of amphiboles. Also found as coarse to fine radiating aggregates and as an asbestiform variety (Box 13.1). Exsolution lamellae of each orthoamphibole series in the other are always present, although the lamellae may be submicroscopic. Twins are not reported.

Cleavage Perfect {210}, like all amphiboles (the Miller index is different from other amphiboles because the *a* unit cell dimension in the orthoamphiboles is twice that of the clinoamphiboles). Also good cleavage on {100} and {010}, unlike the clinoamphiboles. Irregular fracture. Brittle. Fibers are elastic.

Color Properties

Luster: Vitreous.

Color: Clove brown, less commonly gray, grayish brown, yellowish brown, brownish green, or white.

Streak: Gray.

Color in Thin Section: Colorless to pale brown, grayish brown or greenish brown; darker with higher Fe content.

Pleochroism: Weak with $Z \geq Y \geq X$: X = colorless, pale yellow, pale grayish brown, yellowish green; Y = colorless, pale yellow, pale grayish brown, yellowish green; Z = pale grayish brown, purplish brown, grayish green. Grains are darkest when the long dimension (*c* axis) is parallel to the vibration direction of the lower polarizer.

Optical Characteristics

DO NOT COPY e48d507df5d1141@placeholder.9409

Printed by: e48d507df5d1141@placeholder.94092.edu. Printing is for personal, private use only. No part of this book may be reproduced or transmitted without publisher's prior permission. Violators will be prosecuted.

Optical Characteristics

Relief in Thin Section: Moderate to high positive.

Optic Orientation: $X = a$, $Y = b$, $Z = c$, trace of cleavage, and elongate grains are length slow.

Indices of Refraction and Birefringence: Indices of refraction for both mineral series increase fairly systematically with Fe content. The gedrite series has slightly higher birefringence than the anthophyllite series, but the ranges overlap.

Interference Figure: Both minerals have a large $2V$ and may be optically positive or negative. $2V$ for the anthophyllite series appears to vary reasonably consistently with composition, and common Mg-rich samples are most commonly optically negative. The $2V$ data for gedrite have no clear trend with composition and can be either positive or negative. Study using modern chemical and structural analyses is needed to clarify optical properties. Optic axis dispersion is weak to moderate, $r > v$ if negative, $r < v$ if positive.

Alteration Fine-grained serpentine, talc, chlorite, or other sheet silicates are the usual alteration products.

Distinguishing Features

Hand Sample: Brown color may distinguish orthoamphibole from hornblende and related greenish-black clinoamphiboles. Cummingtonite–grunerite, however, often is quite similar in hand sample. Cleavage at 56° and 124° distinguishes the amphiboles from pyroxenes.

Thin Section/Grain Mount: Parallel extinction in longitudinal sections distinguishes orthoamphibole from all clinoamphiboles, including cummingtonite–grunerite. Cummingtonite–grunerite also commonly has lamellar twins. Sillimanite is colorless and has a single cleavage seen in basal sections. The two orthoamphiboles are quite similar, but the gedrite series has higher indices of refraction. In addition, exsolution lamellae of the gedrite series may be very fine and difficult to see in anthophyllite series minerals, whereas, if host and lamellae are reversed, the lamellae are more commonly large enough to be visible.

Occurrence Both occur in metamorphosed mafic rocks of medium to high grade and are unknown in igneous rocks. Cordierite is a very commonly associated mineral; others include garnet, aluminum silicates, plagioclase, and sometimes staurolite. The protolith for anthophyllite–cordierite gneiss layers that are fairly common in Proterozoic metamorphic terranes is something of an enigma. Such rocks do not have a composition of any normal igneous, sedimentary, or metamorphic rocks. A likely explanation for this rock is that they are metamorphosed mafic rocks that have been metasomatized by seawater.

Use Fibrous varieties have been used as a form of asbestos, but this use is limited.

DO NOT COPY e48d507df5d1141@placeholder.9409

Printed by: e48d507df5d1141@placeholder.94092.edu. Printing is for personal, private use only. No part of this book may be reproduced or transmitted without publisher's prior permission. Violators will be prosecuted.

Fibrous anthophyllite series amphibole has been implicated in the health risks that are associated with other asbestos minerals. See additional discussion in Box 13.1.

Cummingtonite–Grunerite

$$(Mg, Fe)_2(Mg, Fe)_5Si_8O_{22}(OH)_2$$

Monoclinic $2/m$

$a = 9.52 - 9.56$ Å, $b = 18.14 - 8.39$ Å,
$c = 5.31 - 5.34$ Å, $\beta = 102.1^\circ$, $Z = 2$

$H = 5 - 6$

$G = 3.10 - 3.60$

Biaxial $(+$ or $-)$

$n_\alpha = 1.630 - 1.686$

$n_\beta = 1.638 - 1.709$

$n_\gamma = 1.655 - 1.729$

$\delta = 0.020 - 0.045$

$2V_z = 65 - 98^\circ$

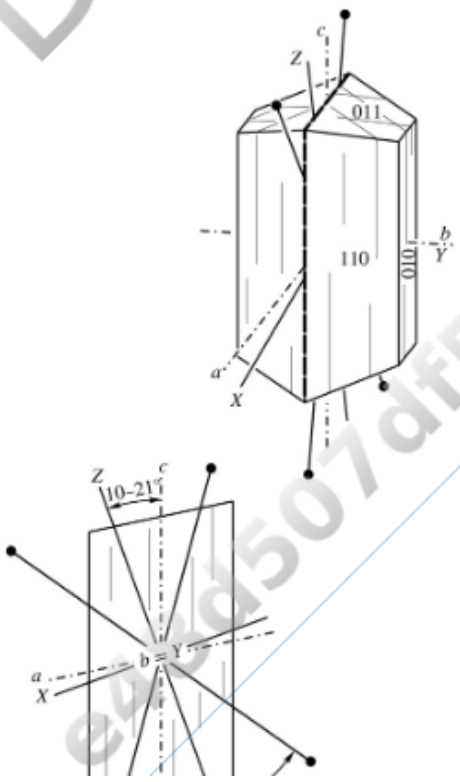

DO NOT COPY
e48d507df5d1141@placeholder.9409

Printed by: e48d507df5d1141@placeholder.94092.edu. Printing is for personal, private use only. No part of this book may be reproduced or transmitted without publisher's prior permission. Violators will be prosecuted.

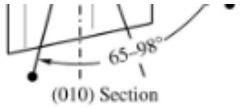

Composition See Figure 14.10 and associated text above. Minerals in the cummingtonite–grunerite solid solution series may contain small amounts of Ca, usually no more than 0.2 atoms per formula unit—somewhat more than in the orthoamphiboles.

Form and Twinning Usually columnar, bladed, or acicular and elongate parallel to *c*; also parallel or radiating aggregates. Basal sections have the diamond shape of amphiboles. Fibrous variety are called amosite or montasite (Box 13.1). Simple or lamellar twinning on {100} is common. Exsolution lamellae of calcic clinopyroxene parallel to {100} and $\{10\bar{1}\}$ are common but may be too fine to see.

Cleavage Very good {110} cleavage that intersects at 56° and 124°, like the other amphiboles. Brittle.

Color Properties

Luster: Vitreous.

Color: Dark brown to dark green, gray, tan.

Streak: White.

Color in Thin Section: Colorless to pale green or brown, darker with higher Fe content.

Pleochroism: Weak pleochroism in colored varieties: X = colorless, pale yellow; Y = pale yellow, pale brown; Z = pale green, pale brown.

Optical Characteristics

Relief in Thin Section: Moderately high to high positive.

Optic Orientation: $X \wedge a = +2°$ to $-9°$, $Y = b$, $X \wedge c = +10°$ to $+21°$, trace of cleavage and crystal length (= c axis) are length slow. The $Z \wedge c$ extinction angle varies fairly systematically with composition (**Figure 14.12**).

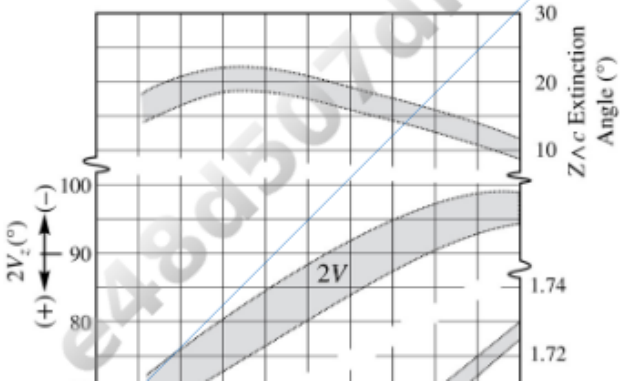

DO NOT COPY
e48d507df5d1141@placeholder.9409

Printed by: e48d507df5d1141@placeholder.94092.edu. Printing is for personal, private use only. No part of this book may be reproduced or transmitted without publisher's prior permission. Violators will be prosecuted.

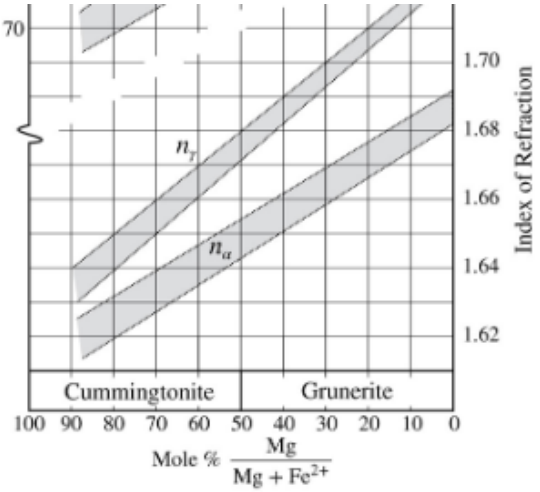

FIGURE 14.12 Optical properties of cummingtonite–grunerite. Data from Winchell (1938), Deer and others (1963, 1997), and Klein (1964). View larger image

Indices of Refraction and Birefringence: Indices of refraction decrease systematically with Mg content, as does the birefringence (Figure 14.12).

Interference Figure: $2V$ varies systematically with Mg content; grunerite is usually optically negative, cummingtonite is usually optically positive. Optic axis dispersion is weak: $r > v$ for grunerite, $r < v$ for cummingtonite.

Alteration Overgrowths of hornblende are not uncommon, and thin lamellae of hornblende may exsolve under conditions of slow cooling. Alteration to chlorite, talc, or serpentine minerals is possible.

Distinguishing Features

Hand Sample: Distinguished as an amphibole by habit and cleavage. Brown varieties closely resemble orthoamphibole; green varieties closely resemble the calcic clinoamphiboles. A firm identification requires optical or other tests.

Thin Section/Grain Mount: Cummingtonite–grunerite is most similar to orthoamphibole and tremolite–ferro-actinolite in thin section. Orthoamphiboles display parallel extinction in (010) sections, whereas cummingtonite–grunerite has inclined extinction, somewhat higher birefringence, and prevalence of fine polysynthetic twinning. A positive optic sign distinguishes cummingtonite from members of the tremolite–ferro-actinolite series, and the occurrences of the two amphibole groups are different.

Occurrence Cummingtonite–grunerite occurs in metamorphosed mafic and ultramafic rocks, sometimes with an orthoamphibole with which it is easily confused, particularly in hand sample. Cummingtonite–grunerite also may be found in granitic gneiss, hornfels, and granulite. Associated minerals include orthoamphibole, cordierite, garnet, plagioclase, hornblende, and biotite. Cummingtonite is occasionally found in intermediate volcanic rocks, diorite, gabbro, norite, and skarns. Grunerite may be found in metamorphosed iron-rich sediments along with magnetite, quartz, and other iron oxides

DO NOT COPY e48d507df5d1141@placeholder.9409

Printed by: e48d507df5d1141@placeholder.94092.edu. Printing is for personal, private use only. No part of this book may be reproduced or transmitted without publisher's prior permission. Violators will be prosecuted.

metamorphosed iron-rich sediments along with magnetite, quartz, and other iron oxides and silicates.

Use The asbestiform variety (amosite/montasite) has been used as asbestos in some industrial applications, but mining has been limited to South Africa, so distribution is not wide. It has been implicated in the health risks associated with asbestos. See Box 13.1 for more information.

Tremolite–Ferro-Actinolite

$$\mathrm{Ca_2(Mg,Fe)_5Si_8O_{22}(OH)_2}$$

$$\text{Monoclinic } 2/m$$

$$a = 9.84 - 10.02\ \text{Å},$$
$$b = 18.05 - 18.20\ \text{Å},$$
$$c = 5.29 - 5.31\ \text{Å},$$
$$\beta = 104.8 - 104.6^\circ,\ Z = 2$$

$$H = 5 - 6$$

$$G = 2.99 - 3.48$$

$$\text{Biaxial } (-)$$

$$n_\alpha = 1.599 - 1.688$$
$$n_\beta = 1.612 - 1.697$$
$$n_\gamma = 1.622 - 1.705$$

$$\delta = 0.017 - 0.027$$

$$2V_x = 62 - 88^\circ$$

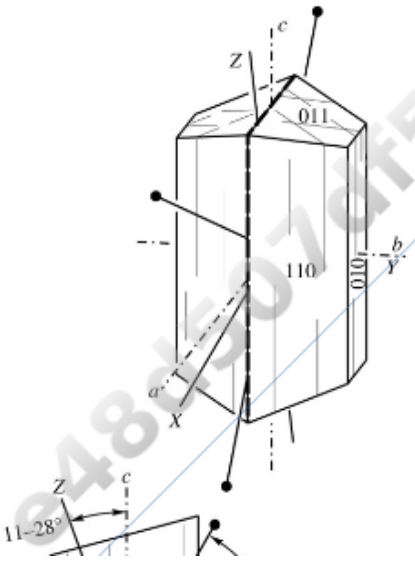

DO NOT COPY
e48d507df5d1141@placeholder.9409

Printed by: e48d507df5d1141@placeholder.94092.edu. Printing is for personal, private use only. No part of this book may be reproduced or transmitted without publisher's prior permission. Violators will be prosecuted.

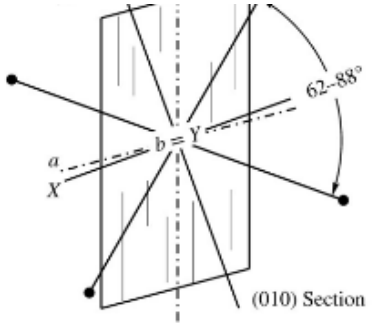

Composition Tremolite and ferro-actinolite represent an Mg–Fe solid solution series, with little substitution of Al^{3+} in either octahedral or tetrahedral sites. Compositions with more than 90% Mg are tremolite, between 90% and 50% Mg are actinolite, and less than 50% Mg are ferro-actinolite. See Figure 14.10 and associated text above. Compositions in the ferro-actinolite range are less common. There is some debate about whether solid solution extends continuously between hornblende and tremolite–ferro-actinolite. The fact that both tremolite and hornblende coexist in the same rocks and that exsolution lamellae of one may be found in the other suggest that solid solution is not continuous, at least under some conditions of temperature, pressure, and/or composition.

Form and Twinning Commonly occurs as columnar, bladed, or acicular crystals elongate parallel to the *c* axis; also fibrous or asbestiform. Basal sections are diamond shaped. Simple and lamellar twins with {100} composition planes are common; lamellar twins on {001} are rare. A variety of jade composed of interlocking fibers of actinolite is called nephrite. Exsolution lamellae of cummingtonite parallel to {100} and $\{10\bar{1}\}$ are common, but may be too fine to see. The {100} lamellae probably control parting, if present. Additional submicroscopic exsolution lamellae of hornblende approximately parallel to $(13\bar{2})$ and $(1\bar{3}2)$ also may be present.

Cleavage Good cleavage on {110} intersects at 56° and 124°. Parting on {100}. Irregular fracture. Brittle. Fibrous aggregates of nephrite jade can be quite tough.

Color Properties

Luster: Vitreous.

Color: White, gray, pale green, dark green, darker with Fe content.

Streak: White.

Color in Thin Section: Colorless (tremolite) to deep green (ferro-actinolite).

Pleochroism: Tremolite has none. Actinolite and ferro-actinolite: $X \leq Y < Z$; X = colorless, pale yellowish green, pale green; Y = pale yellowish green, pale green; Z = pale green, green, bluish green, dark green.

Optical Characteristics

Printed by: e48d507df5d1141@placeholder.94092.edu. Printing is for personal, private use only. No part of this book may be reproduced or transmitted without publisher's prior permission. Violators will be prosecuted.

Optical Characteristics

Relief in Thin Section: Moderate to high positive.

Optic Orientation: $X \wedge a = +4°$ to $-13°$, $Y = b$, $Z \wedge c = +11°$ to $+28°$. The $Z \wedge c$ extinction angle seen in (010) sections decreases with increasing Fe content above about 25% ferro-actinolite.

Indices of Refraction and Birefringence: Indices of refraction increase with Fe content, and the maximum birefringence, seen in (010) sections, yields interference colors in the upper first to middle second order.

Interference Figure: The entire series is optically negative, with $2V$ decreasing with increasing Fe content. Optic axis dispersion is weak, $r < v$.

Alteration Chlorite, talc, and carbonates are the common alteration products.

Distinguishing Features

Hand Sample: Cleavage, hardness, and habit indicate that it is an amphibole. The white to light green color of tremolite and some actinolite distinguishes them from hornblende. Dark green actinolite and ferro-actinolite cannot be distinguished from hornblende.

Thin Section/Grain Mount: Pale color distinguishes tremolite and actinolite from hornblende. Colored samples closely resemble hornblende. If the identity is in doubt, use the term *calcic clinoamphibole*. Colorless varieties of richterite also are quite similar.

Occurrence Tremolite and actinolite are common minerals in contact and regionally metamorphosed limestone, dolomite, and other calcareous sediments. The commonly associated minerals include calcite, dolomite, forsterite, garnet, diopside, wollastonite, talc, and members of the epidote group.

Tremolite and actinolite also occur in low-grade regionally metamorphosed mafic and ultramafic igneous rocks. Associated minerals include talc, carbonates, antigorite, epidote group, and chlorite. Ferro-actinolite is restricted to metamorphosed iron formations where it may be associated with calcite, dolomite, and cummingtonite.

Pyroxene in mafic and ultramafic igneous rocks commonly alters to uralite, which consists of fine-grained, light-colored amphibole, usually presumed to be tremolite–ferro-actinolite.

Use Compact massive nephrite, which usually consists of finely intergrown acicular crystals, can be used as a decorative stone and may be sold as a variety of jade. Fibrous tremolite may be used as an asbestos mineral and has been implicated, along with chrysotile and other amphibole asbestos minerals, as a health hazard. See Box 13.1.

Hornblende

DO NOT COPY e48d507df5d1141@placeholder.94092

Printed by: e48d507df5d1141@placeholder.94092.edu. Printing is for personal, private use only. No part of this book may be reproduced or transmitted without publisher's prior permission. Violators will be prosecuted.

$$(\mathrm{Na,K})_{0-1}\mathrm{Ca_2}\left(\mathrm{Mg,Fe^{2+},Fe^{3+},Al}\right)_5(\mathrm{Si,Al})_8\mathrm{O_{22}(OH)_2}$$

$$\text{Monoclinice } 2/m$$

$$a = \text{-}\ 9.9\ \text{Å},\ b = \text{-}\ 18.0\ \text{Å},\ c = \text{-}\ 5.3\ \text{Å},\ \beta = \text{-}\ 105.5^\circ,\ Z = 2$$

$$H = 5 - 6$$

$$G = 3.02 - 3.59$$

$$\text{Biaxial } (+ \text{ or } -)$$

$$n_\alpha = 1.60 - 1.70$$

$$n_\beta = 1.61 - 1.71$$

$$n_\gamma = 1.62 - 1.73$$

$$\delta = 0.014 - 0.034$$

$$2V_x = 35 - 130^\circ$$

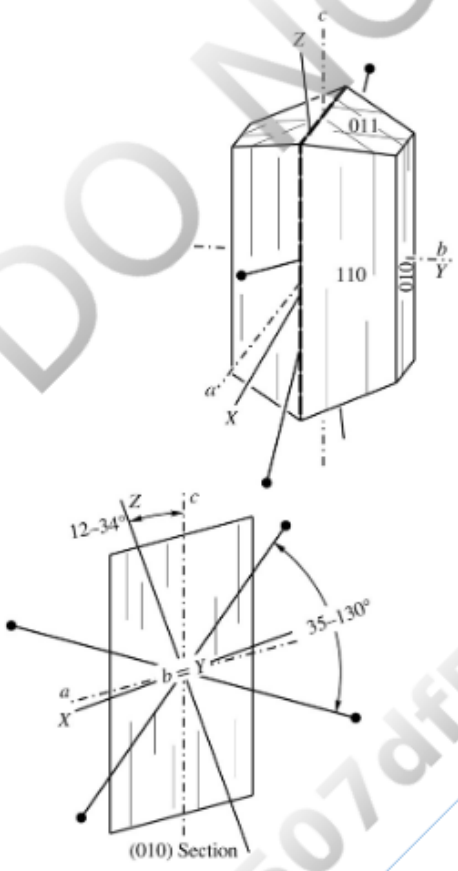

Composition Hornblende displays considerable variation in composition. In comparison to tremolite–ferro-actinolite, hornblende often contains significant Na and K in the A site, and Fe^{3+} and Al^{3+} in the octahedral M1, M2, and M3 sites. Charge balance is maintained by substituting Al^{3+} for Si^{4+} in tetrahedral sites (Table 14.4) up to about $Al_{2.25}Si_{5.75}$. The

DO NOT COPY
e48d507df5d1141@placeholder.9409

Printed by: e48d507df5d1141@placeholder.94092.edu. Printing is for personal, private use only. No part of this book may be reproduced or transmitted without publisher's prior permission. Violators will be prosecuted.

material collectively called hornblende here includes members of the following series.

MAGNESIO-HORNBLENDE–FERRO-HORNBLENDE: $Ca_2(Mg,Fe^{2+})_4AlSi_7AlO_{22}(OH)_2$

TSCHERMAKITE–FERRO-TSCHERMAKITE: $Ca_2(Mg,Fe^{2+})_3Al_2Si_6Al_2O_{22}(OH)_2$

EDENITE–FERRO-EDENITE: $NaCa_2(Mg,Fe^{2+})_5Si_7AlO_{22}(OH)_2$

PARGASITE–FERRO-PARGASITE: $NaCa_2(Mg,Fe^{2+})_4AlSi_6Al_2O_{22}(OH)_2$

MAGNESIO-HASTINGSITE–HASTINGSITE: $NaCa_2(Mg,Fe^{2+})_4Fe^{3+}Si_6Al_2O_{22}(OH)_2$

TABLE 14.4 Selected Coupled Substitution Schemes in Clinoamphiboles

A	B	C	T	=	A	B	C	T
□			Si^{4+}	=	Na^+			Al^{3+}
		(Fe^{2+},Mg^{2+})	Si^{4+}	=			(Al^{3+},Fe^{3+})	Al^{3+}
□	Ca_2^{2+}			=	Na^+	Na^+		
□	Ca^{2+}	(Fe^{2+},Mg^{2+})		=	Na^+	Na_2^+	Al^{3+}	

Additionally, Ti, Mn, and Cr may substitute in M1, M2, and M3 sites, and O, F, and Cl may substitute for (OH). Oxyhornblende is a variety in which most of the Fe has been oxidized to the trivalent state, with charge balance maintained by substituting O^{2-} for $(OH)^-$. If knowledge of composition is important, electron microprobe analysis is required; optical, physical, and X-ray methods are not sufficient.

Form and Twinning Crystals are usually slender prismatic to bladed, and elongate parallel to *c* (Figure 14.11a, c, d). Cross sections are diamond shaped, bounded by the {110} prism and {010} pinacoid. Also in anhedral to highly irregular grains, and in fibrous masses that may mantle or replace pyroxene. {100} simple and lamellar twins are common. Cummingtonite exsolution lamellae parallel to {100} and $\{10\bar{1}\}$ are common but may be too fine to see. The {100} lamellae probably control the parting, if present. Additional submicroscopic exsolution lamellae of actinolite approximately parallel to $\{13\bar{2}\}$ and $\{1\bar{3}\bar{2}\}$ may also be present.

Cleavage Good on {110} intersects at about 56° and 124°. Fragments are usually elongate. Parting on {100}. Irregular fracture. Brittle.

Color Properties

Luster: Vitreous.

Color: Most commonly green, dark green, black, also brown.

Streak: Gray to greenish gray.

Printed by: e48d507df5d1141@placeholder.94092.edu. Printing is for personal, private use only. No part of this book may be reproduced or transmitted without publisher's prior permission. Violators will be prosecuted.

Streak: Gray to greenish gray.

Color in Thin Section: Distinctly colored, usually in shades of green, bluish green, or brown. Oxyhornblende is brown.

Pleochroism: Distinct, usually $Z > Y > X$, less commonly $Y > Z > X$. Green varieties are usually X = pale yellow, yellowish green, light blue-green; Y = green, yellowish green, gray-green; Z = dark green, dark blue-green, dark gray-green. Brown varieties are usually X = yellow, greenish yellow, light greenish brown; Y = yellowish brown, brown, reddish brown; Z = grayish brown, brown, reddish brown. Zoning may be evident in thin section.

Optical Characteristics

Relief in Thin Section: Moderate to high positive.

Optic Orientation: $X \wedge a = +3°$ to $-9°$, $Y = b$, $Z \wedge c = +12°$ to $+ 34°$ optic plane = (010). The trace of cleavage and cleavage fragments are length slow.

Indices of Refraction and Birefringence: Indices of refraction increase with Fe content. Most common hornblende has indices of refraction in the range $n_\alpha = 1.655 \pm 0.010$, $n_\beta = 1.665 \pm 0.010$, and $n_\gamma = 1.675 \pm 0.015$ with birefringence between 0.018 and 0.025. Mineral color may mask interference color.

Interference Figure: Common hornblende is optically negative, with $2V_x = 75° \pm 10°$. $2V_x$ decreases with Fe content. Optic axis dispersion is moderate, either $r > v$ or $r < v$.

DO NOT COPY e48d507df5d1141@placeholder.9409

Printed by: e48d507df5d1141@placeholder.94092.edu. Printing is for personal, private use only. No part of this book may be reproduced or transmitted without publisher's prior permission. Violators will be prosecuted.

Much pargasite and some tschermakite and edenite are optically positive with a large 2*V*.
Alteration Hornblende may be altered to biotite, chlorite, or other Fe–Mg silicates.

Distinguishing Features

Hand Sample: Habit, cleavage, and hardness distinguish hornblende as an amphibole and not pyroxene. The dark green to black color usually distinguishes hornblende from other amphiboles, although some other varieties also may have the same color. Biotite has only one cleavage and is platy.

Thin Section/Grain Mount: Green color, distinct pleochroism, cleavage, and inclined extinction in (010) sections distinguish hornblende from most other minerals. Aegirine and aegirine–augite have cleavage at nearly right angles in basal sections and usually have higher birefringence. The properties of actinolite and hornblende overlap. Oxyhornblende may resemble biotite, but has inclined extinction and larger 2*V*.

Occurrence Hornblende may be found in a wide variety of igneous rocks but is a characteristic mineral of intermediate varieties including diorite, granodiorite, andesite, and dacite. It also may be a late-crystallizing mineral in mafic rocks such as gabbro or norite, and is not uncommon in granitic/rhyolitic rocks, syenite, and phonolite. Oxyhornblende is generally restricted to volcanic rocks. Primary pyroxene in mafic igneous rocks may alter to aggregates of fine amphibole called uralite. Uralite more commonly consists of tremolite–ferro-actinolite, but it can be hornblende. Alteration usually begins along grain boundaries or cracks. Recrystallization may yield optically continuous masses of amphibole.

Hornblende is common in medium- and high-grade metamorphic rocks including metamorphosed mafic rocks such as amphibolite. In general, the amount of Al in both tetrahedral and octahedral sites and the Na content of the A site increase with increasing grade of metamorphism. Marble, skarns, and other metamorphosed carbonate rocks also may contain hornblende, but tremolite–actinolite is more common in these rocks.

Use Except as a constituent of decorative or dimension stone, hornblende has no significant industrial use.

Glaucophane–Riebeckite

Å Å
Å

DO NOT COPY e48d507df5d1141@placeholder.9409

Printed by: e48d507df5d1141@placeholder.94092.edu. Printing is for personal, private use only. No part of this book may be reproduced or transmitted without publisher's prior permission. Violators will be prosecuted.

$$c = 5.30 - 5.33 \text{ Å}, \ \beta = 103.6^\circ, \ Z = 2$$

$$H = 5 - 6$$

$$G = 3.05 - 3.50$$

$$\text{Biaxial } (+ \text{ or } -)$$

$$n_\alpha = 1.594 - 1.701$$

$$n_\beta = 1.612 - 1.711$$

$$n_\gamma = 1.618 - 1.717$$

$$\delta = 0.006 - 0.023$$

$$2V: \text{ Glaucophane } 2V_x = 10 - 50^\circ$$

$$\text{Riebeckite}: 2V_z = 0 - 135^\circ$$

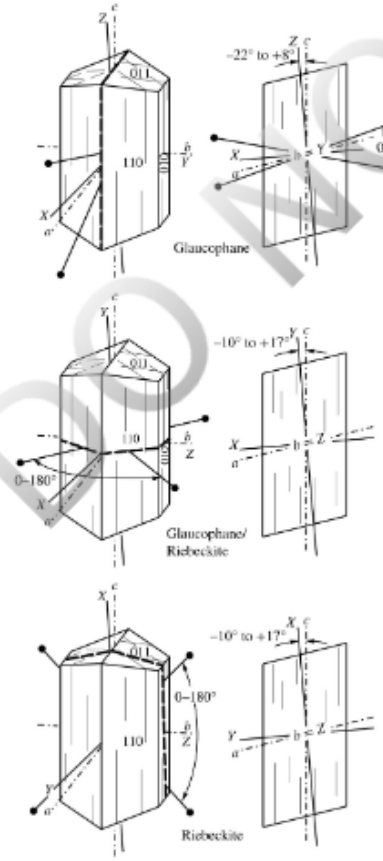

Composition The composition fields for the sodic amphiboles are shown in **Figure 14.13**. The principal substitutions are Fe^{2+} for Mg and Fe^{3+} for Al, which are represented by the two axes of the diagram. Compositions between 30% and 70% Fe^{3+} historically was known as crossite, but Hawthorne and others (2012) recommend that the division between glaucophane and riebeckite be placed at 50% Fe^{3+}. Solid solution extends toward the sodic–calcic amphiboles and arfvedsonite.

DO NOT COPY e48d507df5d1141@placeholder.9409

Printed by: e48d507df5d1141@placeholder.94092.edu. Printing is for personal, private use only. No part of this book may be reproduced or transmitted without publisher's prior permission. Violators will be prosecuted.

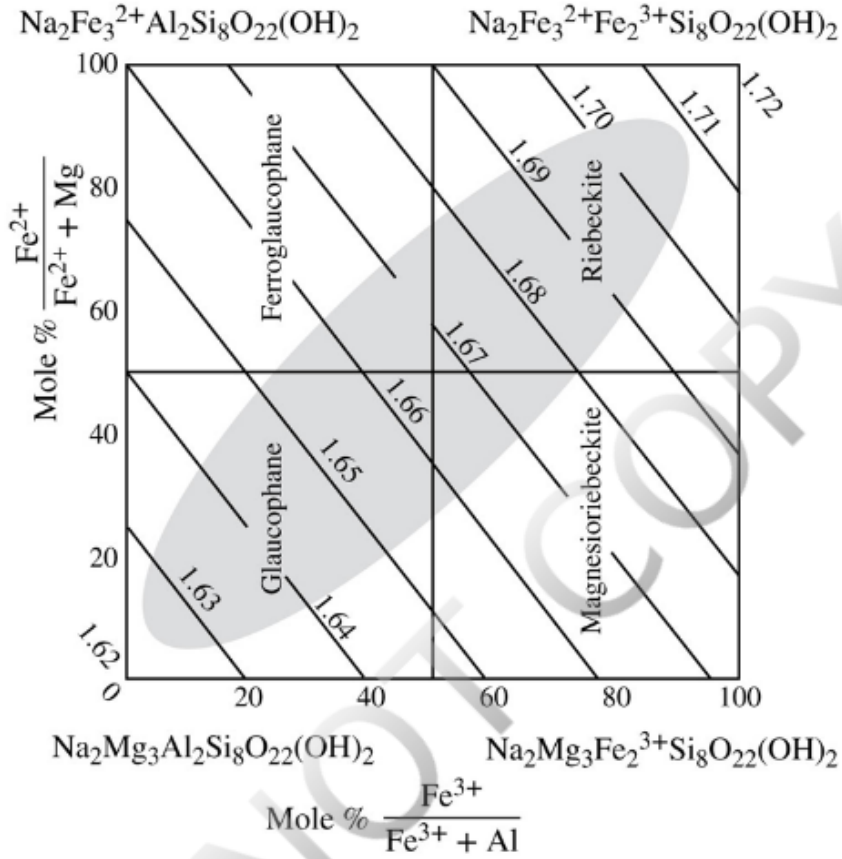

FIGURE 14.13 Composition and variation of n_γ for the sodic amphiboles. Compositions found in blueschist and related rocks fall in the shaded field extending from glaucophane to riebeckite. Compositions found in metamorphosed iron formations and alkalic igneous rocks usually fall in the riebeckite and magnesio-riebeckite fields. Data from Deer and others (1963), Borg (1967), Coleman and Papike (1968), and Ernst and Wai (1970). View larger image

Form and Twinning Glaucophane commonly forms bladed to slender prismatic crystals and may also be fibrous or granular (Figure 14.11f). Riebeckite commonly forms slender bladed or prismatic crystals, with or without terminations. Grains may be irregular or may enclose associated minerals. Asbestiform riebeckite, known as crocidolite, is common in metamorphosed iron formations (Box 13.1). Simple and lamellar twinning on {100}. Extremely fine lamellae of Ca-amphibole are found parallel to {100} and $\{\bar{2}01\}$, and cummingtonite exsolution lamellae have been found parallel to $\{28\bar{1}\}$ and $\{2\bar{8}1\}$. The {100} lamellae are probably responsible for parting, if present.

Cleavage Good cleavage on {110} intersects at 56° and 124°. Parting on {100}. Conchoidal to uneven fracture. Brittle. Fibers are flexible.

Color Properties

Luster: Vitreous.

Color: Lavender-blue, blue, dark blue, gray, or black; darker with increasing iron content.

Printed by: e48d507df5d1141@placeholder.94092.edu. Printing is for personal, private use only. No part of this book may be reproduced or transmitted without publisher's prior permission. Violators will be prosecuted.

Streak: White to gray.

Color in Thin Section: Glaucophane is pale to medium blue; riebeckite is dark blue.

Pleochroism: Distinct. Glaucophane: X = colorless, pale blue, yellow; Y = lavender-blue, bluish green; Z = blue, greenish blue, violet. Riebeckite: X = dark blue; Y = indigo-blue, grayish blue; Z = blue, yellowish green, yellowish brown; magnesio-riebeckite tends to be lighter. Grains are darkest when the long dimension (c axis) is parallel to the vibration direction of the lower polarizer.

Optical Characteristics

Relief in Thin Section: Moderate to moderately high positive.

Optic Orientation: The position of the indicatrix axes remains nearly fixed for all compositions, with one nearly parallel to c, one parallel to b, and one nearly parallel to a. The relative lengths of the indicatrix axes and the position of the optic plane change fairly systematically with increasing Fe content. In most glaucophane, the optic plane is parallel to (010). With increasing Fe content, the optic angle closes on the axis near a (X), then opens again in a plane nearly parallel to (001), as shown in the glaucophane/riebeckite crystal diagram. With additional Fe, the optic angle closes about the indicatrix axis parallel to b (Z) and then opens again in an optic plane nearly parallel to (100). The latter orientation is typical of most riebeckite. The indicatrix axis closest to c makes an angle with c of +17° to −22°; the extinction angle in (010) sections is therefore less than 22°. The trace of cleavage is length slow in most glaucophane, length fast in most riebeckite, and either length slow or length fast, depending on grain orientation, for intermediate compositions.

Indices of Refraction and Birefringence: Indices of refraction increase with Fe content (Figure 14.13).

Interference Figure: Glaucophane is usually biaxial negative with moderate to small $2V$. Intermediate compositions may be either negative or positive, with almost any $2V$. Riebeckite is usually optically negative; magnesio-riebeckite may be optically positive. Optic axis dispersion in glaucophane is weak, $r < v$. Riebeckite shows strong optic axis dispersion, $r < v$ or $r > v$.

Alteration Glaucophane may be altered to other amphiboles, and riebeckite is sometimes altered to iron oxides and carbonates. Fibrous riebeckite partially replaced by quartz is called tiger's eye and is used in lapidary work. See section on quartz (Chapter 12) for additional information.

Distinguishing Features

Hand Sample: Distinguished from the other amphiboles by the distinct blue color. Sodalite is usually massive granular and lacks good cleavage. Crocidolite is distinguished from other asbestos minerals by its blue color.

DO NOT COPY e48d507df5d1141@placeholder.94092

Printed by: e48d507df5d1141@placeholder.94092.edu. Printing is for personal, private use only. No part of this book may be reproduced or transmitted without publisher's prior permission. Violators will be prosecuted.

from other asbestos minerals by its blue color.

Thin Section/Grain Mount: The blue pleochroism distinguishes the sodic amphiboles from other amphiboles. Glaucophane is usually length slow; riebeckite is usually length fast. Intermediate compositions, however, could be either length fast or length slow. Blue tourmaline is darkest when the length is perpendicular to the vibration direction of the lower polarizer.

Occurrence Glaucophane is characteristic of high-pressure, low-temperature regional metamorphic rocks of the blueschist and eclogite facies. Some rocks colored blue by their glaucophane content are called blueschists. Associated minerals include lawsonite, pumpellyite, chlorite, albite, quartz, jadeite, garnet, and members of the epidote group. Riebeckite is found in alkali-rich igneous rocks such as syenite, nepheline syenite, and alkali granite. Crocidolite, which is asbestiform riebeckite, is found in metamorphosed iron formations.

Use A few percent of the world's asbestos production is crocidolite, most of which is mined in South Africa. Some of this material, known as tiger's eye, has been partially replaced by quartz. It displays a very attractive chatoyancy when cut and polished. See also section on quartz (Chapter 12) for additional information on tiger's eye.

Comments Crocidolite asbestos appears to be a more significant health risk than the more commonly used chrysotile. Refer to the discussion on health risks of asbestos minerals in Box 13.1.

Other Amphiboles

The properties of some of the less common sodic and sodic–calcic amphiboles are summarized in **Table 14.5**. Note that most are various shades of dark green in hand sample and therefore cannot normally be distinguished from hornblende. Optical properties and occurrence provide some aid in identification.

TABLE 14.5 Properties of Less Common Amphiboles[a]

Name	Composition	Color	Color in Thin Section	$2V_x^\circ$	n_α	n_β	n_γ
Kaersutite	$NaCa_2(Mg_3TiAl)Si_6Al_2O_{22}O_2$	Brown or black	Yellowish, reddish, or greenish brown	66–84	1.670–1.707	1.690–1.741	1.700 1.772
Richterite	$Na(CaNa)Mg_5Si_8O_{22}(OH)_2$	Brown, reddish brown, or green	Colorless to yellow or violet	64–87	1.605–1.685	1.615–1.700	1.622 1.712
Katophorite	$Na(CaNa)Mg_4AlSi_7AlO_{22}(OH)_2$	Rose-	Yellow.	0–70	1.639–	1.658–	1.660

Printed by: e48d507df5d1141@placeholder.94092.edu. Printing is for personal, private use only. No part of this book may be reproduced or transmitted without publisher's prior permission. Violators will be prosecuted.

Katophorite	$Na(CaNa)Mg_4AlSi_7AlO_{22}(OH)_2$	Rose-red, dark red-brown to bluish black	Yellow, reddish brown, bluish green	0–70	1.639–1.681	1.658–1.688	1.660 1.690
Arfvedsonite–eckermannite	$NaNa_2(Mg,Fe)_4(Fe^{3+},Al)Si_8O_{22}(OH)_2$	Dark bluish green, greenish black or black	Pale bluish green, yellowish green, brownish green, gray-green, or gray-violet	0–100?	1.612–1.700	1.625–1.709	1.630 1.710

[a] All have H = 5–6, G = 2.9–3.5, and are monoclinic.

The occurrences of these amphibole varieties are as follows.

KAERSUTITE: Alkalic volcanic rocks such as trachybasalt and trachyandesite, and in intrusions such as syenite and lamphrophyre dikes.

RICHTERITE: Metamorphosed carbonate rocks such as marble and skarn deposits. It is likely that some material conventionally identified as tremolite is actually richterite.

KATOPHORITE: Alkalic volcanic rocks such as trachyte and phonolite.

ARFVEDSONITE AND ECKERMANNITE: Usually in alkali-rich igneous rocks such as alkali granite, nepheline syenite, syenite, trachyte, and phonolite. Sodic pyroxene may form parallel intergrowths.

DO NOT COPY e48d507df5d1141@placeholder.9409

Printed by: e48d507df5d1141@placeholder.94092.edu. Printing is for personal, private use only. No part of this book may be reproduced or transmitted without publisher's prior permission. Violators will be prosecuted.

and lacks good cleavage. Crocidolite is distinguished from other asbestos minerals by its blue color.

Thin Section/Grain Mount: The blue pleochroism distinguishes the sodic amphiboles from other amphiboles. Glaucophane is usually length slow; riebeckite is usually length fast. Intermediate compositions, however, could be either length fast or length slow. Blue tourmaline is darkest when the length is perpendicular to the vibration direction of the lower polarizer.

Occurrence Glaucophane is characteristic of high-pressure, low-temperature regional metamorphic rocks of the blueschist and eclogite facies. Some rocks colored blue by their glaucophane content are called blueschists. Associated minerals include lawsonite, pumpellyite, chlorite, albite, quartz, jadeite, garnet, and members of the epidote group. Riebeckite is found in alkali-rich igneous rocks such as syenite, nepheline syenite, and alkali granite. Crocidolite, which is asbestiform riebeckite, is found in metamorphosed iron formations.

Use A few percent of the world's asbestos production is crocidolite, most of which is mined in South Africa. Some of this material, known as tiger's eye, has been partially replaced by quartz. It displays a very attractive chatoyancy when cut and polished. See also section on quartz (Chapter 12) for additional information on tiger's eye.

Comments Crocidolite asbestos appears to be a more significant health risk than the more commonly used chrysotile. Refer to the discussion on health risks of asbestos minerals in Box 13.1.

Other Amphiboles

The properties of some of the less common sodic and sodic–calcic amphiboles are summarized in **Table 14.5**. Note that most are various shades of dark green in hand sample and therefore cannot normally be distinguished from hornblende. Optical properties and occurrence provide some aid in identification.

TABLE 14.5 Properties of Less Common Amphiboles[a]

Name	Composition	Color	Color in Thin Section	$2V_x°$	n_α	n_β	n_γ
Kaersutite	$NaCa_2(Mg_3TiAl)Si_6Al_2O_{22}O_2$	Brown or black	Yellowish, reddish, or greenish brown	66–84	1.670–1.707	1.690–1.741	1.700 1.772
Richterite	$Na(CaNa)Mg_5Si_8O_{22}(OH)_2$	Brown, reddish brown,	Colorless to yellow or violet	64–87	1.605–1.685	1.615–1.700	1.622 1.712

DO NOT COPY e48d507df5d1141@placeholder.94092-

Printed by: e48d507df5d1141@placeholder.94092.edu. Printing is for personal, private use only. No part of this book may be reproduced or transmitted without publisher's prior permission. Violators will be prosecuted.

		or green					
Katophorite	$Na(CaNa)Mg_4AlSi_7AlO_{22}(OH)_2$	Rose-red, dark red-brown to bluish black	Yellow, reddish brown, bluish green	0–70	1.639–1.681	1.658–1.688	1.660 1.690
Arfvedsonite–eckermannite	$NaNa_2(Mg,Fe)_4(Fe^{3+},Al)Si_8O_{22}(OH)_2$	Dark bluish green, greenish black or black	Pale bluish green, yellowish green, brownish green, gray-green, or gray-violet	0–100?	1.612–1.700	1.625–1.709	1.630 1.710

[a] All have $H = 5–6$, $G = 2.9–3.5$, and are monoclinic.

The occurrences of these amphibole varieties are as follows.

KAERSUTITE: Alkalic volcanic rocks such as trachybasalt and trachyandesite, and in intrusions such as syenite and lamphrophyre dikes.

RICHTERITE: Metamorphosed carbonate rocks such as marble and skarn deposits. It is likely that some material conventionally identified as tremolite is actually richterite.

KATOPHORITE: Alkalic volcanic rocks such as trachyte and phonolite.

ARFVEDSONITE AND ECKERMANNITE: Usually in alkali-rich igneous rocks such as alkali granite, nepheline syenite, syenite, trachyte, and phonolite. Sodic pyroxene may form parallel intergrowths.

REFERENCES CITED AND SUGGESTIONS FOR ADDITIONAL READING

Borg, I. Y. 1967. Optical properties and cell parameters in the glaucophane–riebeckite series. *Contributions to Mineralogy and Petrology* **15**, 67–92.

Coleman, R. G., and Papike, J. J. 1968. Alkali amphibole of the Cazadero, California. *Journal of Petrology* **9**, 105–122.

Deer, W. A., Howie, R. A., and Zussman, J. 1963. *Rock-Forming Minerals, Volume 2: Chain Silicates*. Longman, London, 379 p.

Deer, W. A., Howie, R. A., and Zussman, J. 1978. *Rock-Forming Minerals, Volume 2A: Single-Chain Silicates*. John Wiley & Sons, New York, 668 p.

Deer, W.A., Howie, R.A., and Zussman, J. 1992. *The Rock Forming Minerals*, 2nd ed.

DO NOT COPY e48d507df5d1141@placeholder.9409

Printed by: e48d507df5d1141@placeholder.94092.edu. Printing is for personal, private use only. No part of this book may be reproduced or transmitted without publisher's prior permission. Violators will be prosecuted.

John Wiley & Sons, New York, 696 p.

Deer, W. A., Howie, R. A., and Zussman, J. 1997. *Rock-Forming Minerals, Volume 2B: Double-Chain Silicates*, 2nd ed. The Geological Society, London, 784 p.

Deer, W. A., Howie, R. A., and Zussman, J. 2001. *Rock Forming Minerals, Volume 2A: Single Chain Silicates*, 2nd ed. The Geological Society, London, 668 p.

Ernst, W. G., and Wai, C. M. 1970. Mossbauer, infrared, X-ray and optical study of cation ordering and dehydrogenation in natural and heat-treated sodic amphiboles. *American Mineralogist* **55**, 1226–1258.

Essene, E. J., and Fyfe, W. S. 1967. Omphacite in Californian metamorphic rocks. *Contributions to Mineralogy and Petrology* **15**, 1–23.

Hawthorne, F. C., Oberti, R., Harlow, G. E., Maresch, W. V., Martin, R. F., Schumacher, J. C., and Welch, M. D. 2012. Nomenclature of the amphibole supergroup. *American Mineralogist* **97**, 2031–2048.

Hawthorne, F. C., Oberti, R., Ventura, G. D., and Mottana, A. (eds.). 2007. *Amphiboles: Crystal Chemistry, Occurrence, and Health Issues. Reviews in Mineralogy and Geochemistry* **67**, 545 p.

Hess, H. H. 1949. Chemical composition and optical properties of common clinopyroxenes. *American Mineralogist* **34**, 621–626.

Jaffe, H. W., Robinson, P., and Tracey R. J. 1975. Orientation of pigeonite exsolution lamellae in metamorphic augite: Correlation with composition and calculated optimal phase boundaries. *American Mineralogist* **60**, 9–28.

Jaffe, H. W., Robinson, P., and Tracey, R. J. 1978. Orthoferrosilite and other iron-rich pyroxenes in microperthite gneiss of the Mount Marcy area, Adirondack Mountains. *American Mineralogist* **63**, 1116–1136.

Klein, C. 1964. Cummingtonite–grunerite series: A chemical, optical and X-ray study. *American Mineralogist* **49**, 963–982.

Larsen, E. S. 1942. *Alkali Rocks of Iron Hill, Gunnison County, Colorado*. U.S. Geological Survey Professional Paper 197a.

Leake, B. E. 1968. Optical properties and composition in the orthopyroxene series. *Mineralogical Magazine* **36**, 745–747.

Monchoux, P., and Roux, L. 1975. Les amphiboles orthor-hombiques, riches en aluminium et magnesium, des amphibolites a sapphirine des Pyrenees. *Bulletin de la Societe Francaise de Mineralogie et de Cristallographie* **75**, 166–170.

Morimoto, N. 1988. Nomenclature of pyroxenes. *American Mineralogist* **73**, 1123–1133.

Nolan, J. 1969. Physical properties of synthetic and natural pyroxenes in the system diopside–hedenbergite–acmite. *Mineralogical Magazine* **37**, 216–229.

Rabbitt, J. C. 1948. A new study of the anthophyllite series. *American Mineralogist* **33**, 263–323.

DO NOT COPY e48d507df5d1141@placeholder.9409

Printed by: e48d507df5d1141@placeholder.94092.edu. Printing is for personal, private use only. No part of this book may be reproduced or transmitted without publisher's prior permission. Violators will be prosecuted.

263–323.

Sabine, P. A. 1950. The optical properties and composition of the acmitic pyroxenes. *Mineralogical Magazine* **29**, 113–125.

Verkouteren, J. R., and Wylie, A. G. 2000. The tremolite–actinolite-ferro-actinolite series: Systematic relationships among cell parameters, composition, optical properties, and habit, and evidence of discontinuities. *American Mineralogist* **85**, 1239–1254.

Winchell, A. N. 1938. The anthophyllite and cummingtonite–grunerite series. *American Mineralogist* **23**, 329–333.

DO NOT COPY

e48d507df5d1141@placeholder.9409

Printed by: e48d507df5d1141@placeholder.94092.edu. Printing is for personal, private use only. No part of this book may be reproduced or transmitted without publisher's prior permission. Violators will be prosecuted.

LIST OF KEY TERMS

anhydrous

spongy

symplectite

DO NOT COPY

e48d507df5d1141@placeholder.9409

Printed by: e48d507df5d1141@placeholder.94092.edu. Printing is for personal, private use only. No part of this book may be reproduced or transmitted without publisher's prior permission. Violators will be prosecuted.

CHAPTER 15
Disilicates and Ring Silicates

William D. Nesse
University of Northern Colorado

Graham B. Baird
University of Northern Colorado

DO NOT COPY
e48d507df5d1141@placeholder.9409

Printed by: e48d507df5d1141@placeholder.94092.edu. Printing is for personal, private use only. No part of this book may be reproduced or transmitted without publisher's prior permission. Violators will be prosecuted.

Disilicates

The disilicates are a relatively small group of minerals that are quite widely distributed. Members of the epidote group (zoisite, clinozoisite, epidote, and allanite) in particular are very common accessory minerals in a wide variety of igneous and metamorphic rocks, and are a frequent constituent of the heavy mineral fraction of clastic sediments.

Structure and Classification

As described in Chapter 11, the characteristic feature of disilicates is a pair of silicon tetrahedra that share a single oxygen (**Figure 15.1a**). All disilicates, therefore, contain Si_2O_7 in the formula. Although the basic silicate structure is a double tetrahedron, the structure of most disilicates is more conveniently described in terms of chains of edge-sharing aluminum octahedra. These chains are linked laterally through the double tetrahedra, other cations, and, in some cases, single tetrahedra. They are structurally quite similar to the aluminum silicates, staurolite, and chloritoid, all of which are constructed of chains of edge-sharing aluminum octahedra linked laterally with single silicon tetrahedra, rather than double tetrahedra.

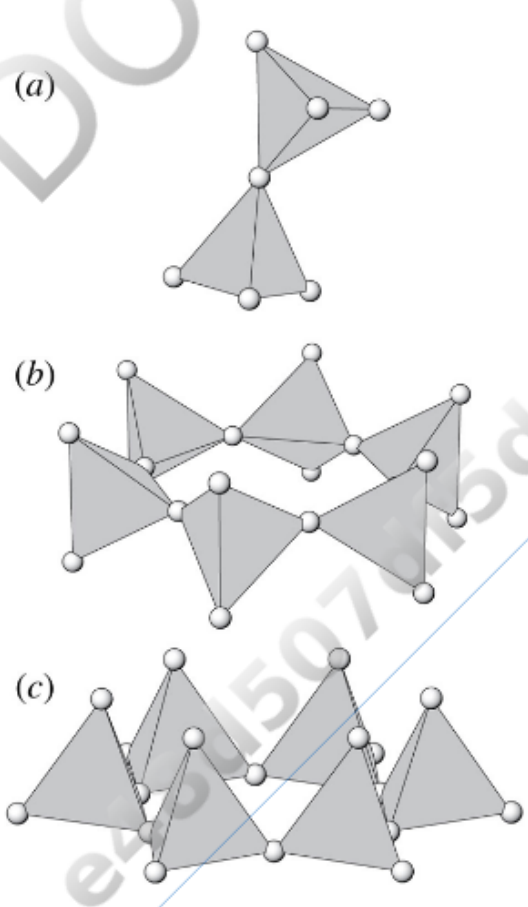

DO NOT COPY
e48d507df5d1141@placeholder.9409

Printed by: e48d507df5d1141@placeholder.94092.edu. Printing is for personal, private use only. No part of this book may be reproduced or transmitted without publisher's prior permission. Violators will be prosecuted.

FIGURE 15.1 Structural elements in disilicates and ring silicates. (*a*) Double silicon tetrahedra. (*b*) Six-member tetrahedral ring found in beryl and cordierite. (*c*) Six-member tetrahedral ring found in tourmaline. View larger image

The epidote group of minerals (**Table 15.1**) is currently defined (Armbruster and others, 2006) as monoclinic disilicate minerals with the general formula $W_2Y_3(Si_2O_7)(SiO_4)O(OH)$. The W cations occupy two sites, W1 and W2, and the Y cations occupy three different octahedral sites, M1, M2, and M3. The cations that commonly occupy these sites are as follows.

W1 = Ca

W2 = Ca, Pb, Sr, or rare earth elements

M1 = Al, Fe, Mg, Mn

M2 = Al

M3 = Al, Fe^{3+}, Mn^{3+}, V^{3+}, Cr^{3+}

TABLE 15.1 Epidote Group Minerals[a]

Mineral	W1	W2	M1	M2	M3	Composition	Symmetry
Zoisite	Ca	Ca	Al	Al	Al	$Ca_2Al_3[Si_2O_7][SiO_4]O(OH)$	Orthorhombic
Clinozoisite–Epidote	Ca	Ca	Al	Al	Al,Fe^{3+}	$Ca_2Al_2(Al,Fe^{3+})[Si_2O_7][SiO_4]O(OH)$	Monoclinic
Allanite	Ca	Ca,Mn,Ce, La,Y,Th	Al,Fe^{3+}	Al	Fe^{2+},Fe^{3+},Ti	$(Ca,Mn,Ce,La,Y,Th)_2(Al,Fe^{3+})Al(Fe^{2+},Fe^{3+},Ti)[Si_2O_7][SiO_4]O(OH)$	Monoclinic

[a] W1, W2, M1, M2, and M3 are structural sites (Figure 15.2).

In addition, F^- may substitute for the extra O^{2-}, and O^{2-} may substitute for OH. The structure consists of two different chains of octahedra (**Figure 15.2a**). One is a simple edge-sharing chain whose octahedral sites are designated M2. The H in the chemical formula is attached to O anions in this chain. The second is an edge-sharing chain of M1 octahedra with additional M3 octahedra attached on alternate sides along its length. The M2 sites in the simple chain usually contain only Al. In the M1/M3 chains, the M1 sites contain mostly Al, and the M3 sites contain most of the non-Al cations, usually Fe or Mn, plus the remaining Al. The two chains are arranged in an alternating fashion and extend parallel to the *b* axis. These chains are linked laterally through single (SiO_4) and double (Si_2O_7) tetrahedra, both of which share oxygen anions with the octahedra (**Figure 15.2b**). The combination of octahedral chains extending parallel to *b* and the cross-linking tetrahedra produces cavities (W sites) with distorted 7- to 11-fold coordination that contain larger cations, usually Ca (**Figure 15.2c**). It should be no surprise that the cleavage in these minerals is between the chains and that most are elongate parallel to

DO NOT COPY e48d507df5d1141@placeholder.9409

Printed by: e48d507df5d1141@placeholder.94092.edu. Printing is for personal, private use only. No part of this book may be reproduced or transmitted without publisher's prior permission. Violators will be prosecuted.

the *b* axis. While zoisite, polymorphic with clinozoisite, is "officially" excluded from the epidote group because it is orthorhombic, it is included in this discussion and Table 15.1 because its structure is related to the epidote structure by a twinlike repeat of the unit cell along *a* (**Figure 15.2d**).

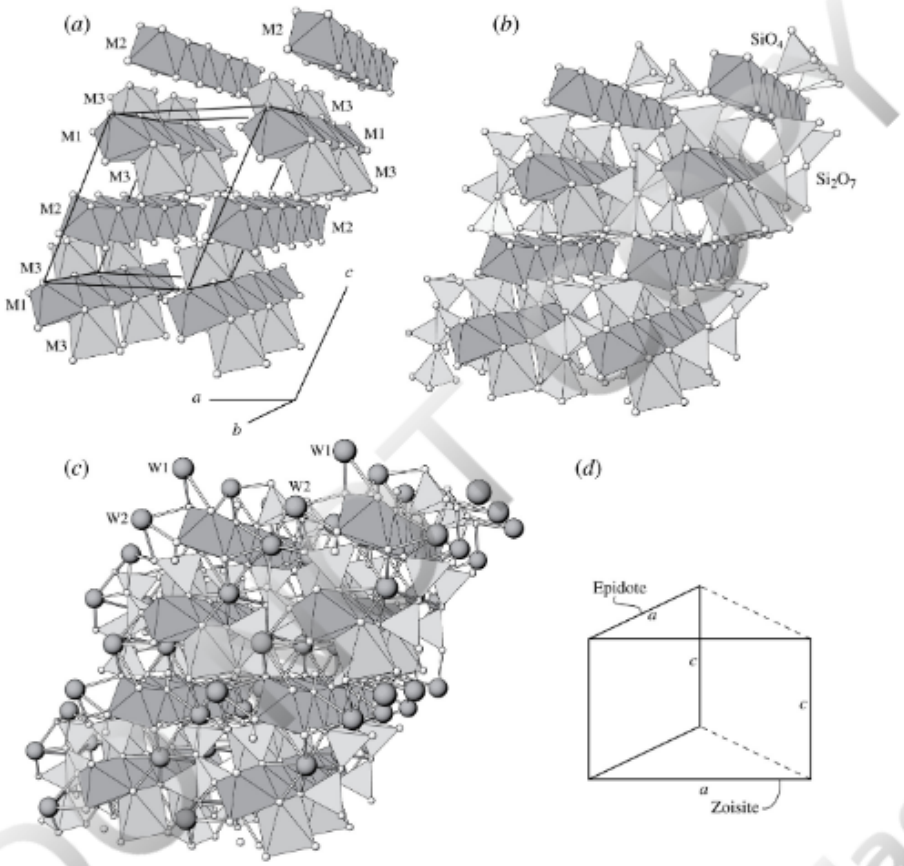

FIGURE 15.2 Structure of the epidote group. See text for additional discussion. (*a*) Chains of octahedra extend parallel to *b*. The outline of one unit cell is shown. M2 octahedra form simple chains; M1 octahedra form chains with M3 octahedra on alternate sides. (*b*) Same image as (*a*), but additionally with silicon tetrahedra. Single and double silicon tetrahedra cross-link the octahedral chains. (*c*) Same image as (*b*), but with W cations added. Large W1 and W2 cations in 7- to 11-fold coordination occupy interstices between octahedra and tetrahedra. (*d*) The orthorhombic zoisite unit cell is related to the monoclinic epidote unit cell by a twinlike doubling of the epidote unit cell along *a*. View is looking down the *b* axis. View larger image

The other disilicates described here, pumpellyite and lawsonite, have structures similar to the epidote group. Both have octahedral chains that extend parallel to *b*. In pumpellyite, both single and double tetrahedra provide the cross-links between octahedral chains. In lawsonite, only double tetrahedra are available to do the cross-linking. Properties of some less common disilicates are listed in **Table 15.2**.

TABLE 15.2 Properties of Less Common Disilicates and Ring Silicates

	Piemontite	Melilite	Vesuvianite
Composition	$Ca_2(Al,Mn^{3+},Fe^{3+})_3$	$(Ca,Na)_2(Mg,Al)(Si,Al)_2O_7$	$Ca_{19}(Al,Mg)_{13}B_{0-5}$

Printed by: e48d507df5d1141@placeholder.94092.edu. Printing is for personal, private use only. No part of this book may be reproduced or transmitted without publisher's prior permission. Violators will be prosecuted.

Composition	$Si_2O_7SiO_4O(OH)$		$Si_{18}O_{68}(OH,O,F)_{10}$
Crystal system and habit	Monoclinic: columnar, bladed, or acicular crystals; anhedral grains and aggregates	Tetragonal: tabular crystals with square, rectangle, or octagon cross sections; anhedral grains; often with rodlike inclusions parallel to c	Tetragonal: stubby prisms; also anhedral grains or grains in columnar or radial patterns
Color	Reddish brown, black, light streak; vitreous	Colorless, honey yellow, gray-green, brown, green-brown, white streak; vitreous to resinous	Yellow, green, brown, light streak; vitreous
Color in thin section	Yellow, pink, violet, red, $X < Y < Z$	Colorless to pale yellow	Colorless to pale yellow or green
Sign and $2V$	Biaxial (+) or (−), $2V_z$ = 64–106°	Uniaxial (−) or (+)	Uniaxial (−)
Indices of refraction	n_α = 1.730–1.794 n_β = 1.740–1.807 n_γ = 1.762–1.829	n_ω = 1.629–1.669 n_ϵ = 1.616–1.661	n_ω = 1.703–1.752 n_ϵ = 1.700–1.746
δ	0.025–0.073	0.000–0.011	0.001–0.009
Physical	H = 6–6.5, G = 3.38–3.61	H = 5–6, G = 2.94–3.07	H = 6–7, G = 3.32–3.34
Cleavage	{001} perfect	{001} poor	{110} very poor
Occurrence	Epidote group: hydrothermal systems, Mn-bearing metamorphic rocks	Silica-poor mafic volcanic rocks	Contact-metamorphosed limestone, altered mafic rocks, nepheline syenite

Zoisite

$$Ca_2Al_3[Si_2O_7][SiO_4]\ O\ (OH)$$

$$\text{Orthorhombic}\ \ 2/m\ 2/m\ 2/m$$

$$a = 16.19\ \text{Å},\ b = 5.55,\ c = 10.03\ \text{Å},\ Z = 4$$

$$H = 6 - 7$$

$$G = 3.15 - 3.37$$

$$\text{Biaxial}\ (+)$$

$$n_\alpha = 1.685 - 1.705$$

$$n_\beta = 1.688 - 1.710$$

$$n_\gamma = 1.697 - 1.725$$

$$\delta = 0.005 - 0.020$$

$$2V_z = 0 - 69^\circ$$

DO NOT COPY e48d507df5d1141@placeholder.9409-

Printed by: e48d507df5d1141@placeholder.94092.edu. Printing is for personal, private use only. No part of this book may be reproduced or transmitted without publisher's prior permission. Violators will be prosecuted.

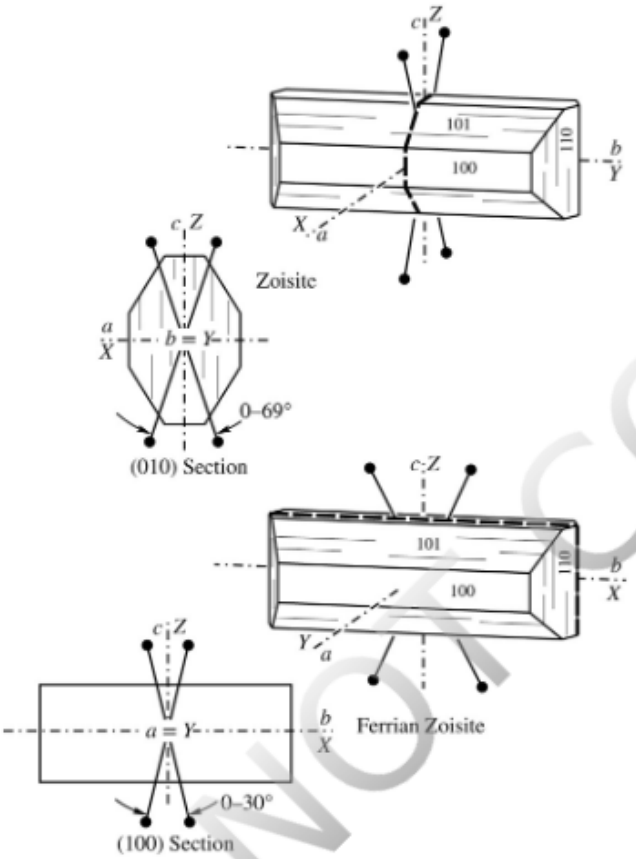

Composition Most zoisite is relatively close to the composition given here. Less than about 8% of octahedral sites may be occupied by Fe^{3+}; the monoclinic clinozoisite–epidote structure is favored for higher Fe contents. Thulite is a pink variety with up to 2% of octahedral sites occupied by Mn. Compositional zoning in Fe content is common.

Form and Twinning It is common as anhedral grains and granular aggregates. Crystals are columnar, prismatic, or acicular parallel to the *b* axis. Oriented intergrowths with epidote are possible. Twinning is not reported.

Cleavage Perfect {100} and poor {001} cleavage. Uneven to conchoidal fracture. Brittle.

Color Properties

Luster: Vitreous.

Color: White, gray, greenish brown, greenish gray, or pink (thulite).

Streak: White.

Color in Thin Section: Colorless to pale pink (thulite).

Pleochroism: Thulite is X = pale pink, pink; Y = colorless or pale pink; Z = pale yellow.

Optical Characteristics

DO NOT COPY
e48d507df5d1141@placeholder.9409

Printed by: e48d507df5d1141@placeholder.94092.edu. Printing is for personal, private use only. No part of this book may be reproduced or transmitted without publisher's prior permission. Violators will be prosecuted.

Relief in Thin Section: High positive.

Optic Orientation: Two orientations depend on composition. Low-iron (≤3%) zoisite has $X = a$, $Y = b$, $Z = c$, optic plane = (010). More Fe-rich ferrian zoisite has $X = b$, $Y = a$, $Z = c$, optic plane = (100). The trace of cleavage, cleavage fragments, and length of elongate crystals are length fast in ferrian zoisite, and either length fast or length slow in zoisite.

Indices of Refraction and Birefringence: Both indices of refraction and birefringence increase with Fe and Mn content. Interference colors for all but the most Fe-rich varieties are lower than mid–first order and are usually anomalously blue or greenish yellow. Zoning may be expressed by variation of birefringence.

Interference Figure: Increasing Fe content causes the 2V angle to close from about 50° to 0° on the *c* axis in the (010) plane for zoisite and open from 0° to over 60° in the (100) plane for ferrian zoisite. Optic axis dispersion is strong, $r > v$ in zoisite, $r < v$ in ferrian zoisite.

Alteration Not commonly altered.

Distinguishing Features

Hand Sample: Grayish color and a single well-developed cleavage distinguish zoisite from amphiboles. Clinozoisite and epidote are usually distinctly green.

Thin Section/Grain Mount: Distinguished by high relief, low birefringence, and parallel extinction to the trace of cleavage in sections cut perpendicular to *b* and in cleavage fragments. Interference colors usually are anomalous. Clinozoisite has inclined extinction in sections cut perpendicular to *b*. Epidote has higher birefringence, has inclined extinction, and usually displays patchy greenish pleochroism. In small grains, however, cleavage may not be evident. Apatite forms elongate crystals with hexagonal cross sections and is uniaxial negative. Pink andalusite resembles thulite, but is biaxial negative and has lower indices of refraction and relief.

Occurrence Zoisite is common in medium-grade metamorphic rocks derived from Ca-rich sedimentary rocks such as calcareous shale, calcareous sandstone, and limestone, and in amphibolite derived from mafic igneous rocks. It is less common in blueschists and eclogite. Hydrothermal alteration of plagioclase may yield a fine-grained material called saussurite composed of albite, zoisite or clinozoisite, sericite, and other silicates.

Use Tanzanite is a gem variety of zoisite from Tanzania that contains small amounts of V^{3+}, which gives it a reddish brown color. Heat treatment to 400–600°C causes oxidation to V^{4+}, which produces a deep blue to violet color. Thulite also is used as a gem, and notable samples are found in Norway.

Clinozoisite–Epidote

DO NOT COPY e48d507df5d1141@placeholder.9409

Printed by: e48d507df5d1141@placeholder.94092.edu. Printing is for personal, private use only. No part of this book may be reproduced or transmitted without publisher's prior permission. Violators will be prosecuted.

$$Ca_2Al_2(Al, Fe^{3+})$$
$$[Si_2O_7][SiO_4]\ O\ (OH)$$

Monoclinic $2/m$

$a = 8.88 - 8.89$ Å,
$b = 5.58 - 5.63$ Å,
$c = 10.16 - 10.15$ Å,
$\beta = 115.5 - 115.4^\circ$,
$Z = 2$

$H = 6 - 7$

$G = 3.21 - 3.49$

Biaxial (+ or −)

$n_\alpha = 1.703 - 1.751$

$n_\beta = 1.707 - 1.784$

$n_\gamma = 1.709 - 1.797$

$\delta = 0.004 - 0.049$

$2V_z = 14 - 90^\circ$

$2V_x = 90 - 64^\circ$

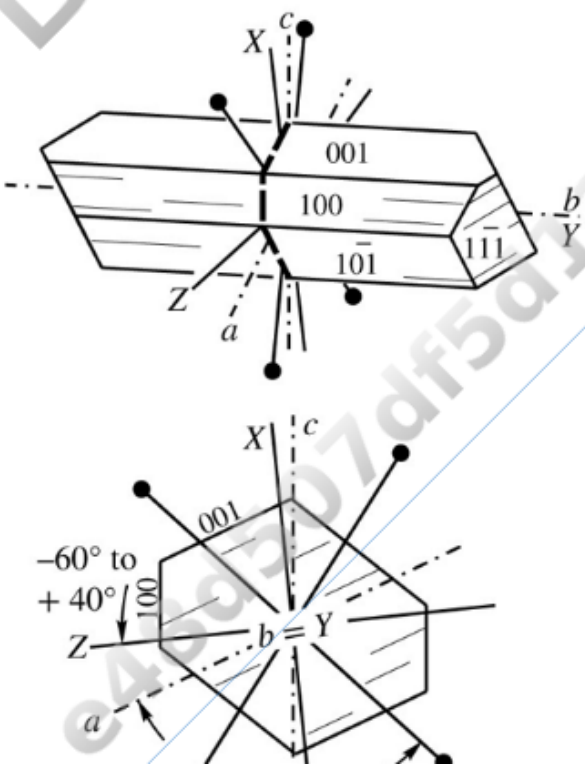

DO NOT COPY
e48d507df5d1141@placeholder.9409

Printed by: e48d507df5d1141@placeholder.94092.edu. Printing is for personal, private use only. No part of this book may be reproduced or transmitted without publisher's prior permission. Violators will be prosecuted.

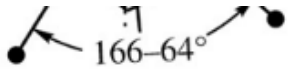

(010) Section

The ideal composition of clinozoisite is usually reported as $Ca_2Al_2Al[Si_2O_7][SiO_4]O(OH)$, and epidote as $Ca_2Al_2Fe^{3+}[Si_2O_7][SiO_4]O(OH)$; they form a solid solution series. Substitution of Al^{3+} and Fe^{3+} occurs mostly in the M3 site; the M1 and M2 sites contain dominantly Al^{3+}. Pure epidote should ideally have 33.3% Fe^{3+}—one Fe^{3+} in the M3 site and an Al^{3+} each in the M1 and M2 sites. Natural epidote, however, may have up to about 35% Fe^{3+}, indicating that some Fe^{3+} may enter the M1 and/or M2 sites; some Fe^{2+} may substitute for Ca^{2+} in the W sites. Defining epidote composition based on the ratio of total Fe^{3+} to total Al^{3+} leads to the result that samples with more than 33.3% Fe^{3+} may be considered to have more than 100% epidote. The division between epidote and clinozoisite has traditionally been taken as the change in optic sign that occurs between 30% and 45% epidote (10–15% octahedral Fe^{3+}). However, the Commission on New Minerals, Nomenclature and Classification of the International Mineralogical Association now recommends that the dividing line be placed at 50% epidote, or 16.7% octahedral Fe^{3+}. Most natural clinozoisite contains more than about 8% octahedral Fe^{3+}; lower iron content favors formation of orthorhombic zoisite. Substitution of Mn^{3+} in octahedral sites yields piemontite. Some Fe^{2+} may substitute for Ca^{2+} in the W sites. Tawmanite is a rare Cr^{3+}-bearing member of the epidote group.

Form and Twinning See **Figure 15.3**. Epidote and clinozoisite are common as anhedral grains and granular aggregates. Crystals are columnar, bladed, or acicular and elongate parallel to *b*. Columnar and radial aggregates are relatively common. Sections through crystals are usually six sided or rectangular. Detrital grains are rounded or platy parallel to the cleavage. Zoisite may form oriented intergrowths with epidote, and epidote may form overgrowths on brown allanite cores. {100} lamellar twins are not common.

(*a*)

(*b*)

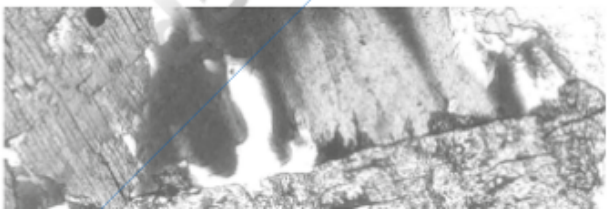

DO NOT COPY e48d507df5d1141@placeholder.94092

Printed by: e48d507df5d1141@placeholder.94092.edu. Printing is for personal, private use only. No part of this book may be reproduced or transmitted without publisher's prior permission. Violators will be prosecuted.

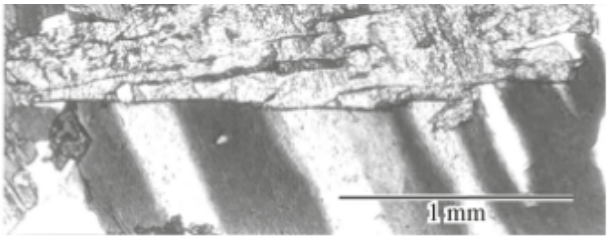

FIGURE 15.3 Epidote. (*a*) Euhedral 2 cm crystal. (*b*) Photomicrograph of a thin section of granodiorite showing of epidote (*center*) enclosed in biotite that is partially replaced by chlorite. Hornblende is at the upper left (plane light). View larger image

Cleavage {001} perfect. Small grain size may preclude observing it in either hand sample or thin section. Uneven fracture. Brittle.

Color Properties

Luster: Vitreous.

Color: Clinozoisite: pale green to gray; epidote: pistachio-green, yellowish green, green, black.

Streak: White.

Color in Thin Section: Clinozoisite: colorless; epidote: yellowish green.

Pleochroism: $Y > Z > X$, X = colorless, pale green, pale yellow; Y = yellowish green; Z = colorless, pale yellowish green. The color may be patchy or concentric. Even small amounts of Mn may produce the pink colors characteristic of piemontite.

Optical Characteristics

Relief in Thin Section: High positive.

Optic Orientation: Optic orientation varies with composition. In all cases $Y = b$ and the optic plane is (010). The $Z \wedge a$ extinction angle between the slow ray and the trace of cleavage in (010) sections varies from as much as −60° for low-Fe clinozoisite to +40° for high-Fe epidote. Most clinozoisite has $Z \wedge a = 0°$ to +30° and most epidote has $Z \wedge a =$ +25° to +40°.

Indices of Refraction and Birefringence: Increase fairly systematically with Fe^{3+} content (**Figure 15.4**). Clinozoisite usually displays a maximum of first-order colors in thin section; interference colors often are anomalously blue or greenish yellow. Epidote displays higher interference colors, and, in grains oriented to display low-order colors, the interference colors also may be anomalously blue or greenish yellow.

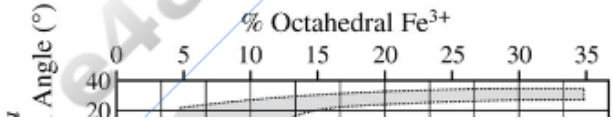

Printed by: e48d507df5d1141@placeholder.94092.edu. Printing is for personal, private use only. No part of this book may be reproduced or transmitted without publisher's prior permission. Violators will be prosecuted.

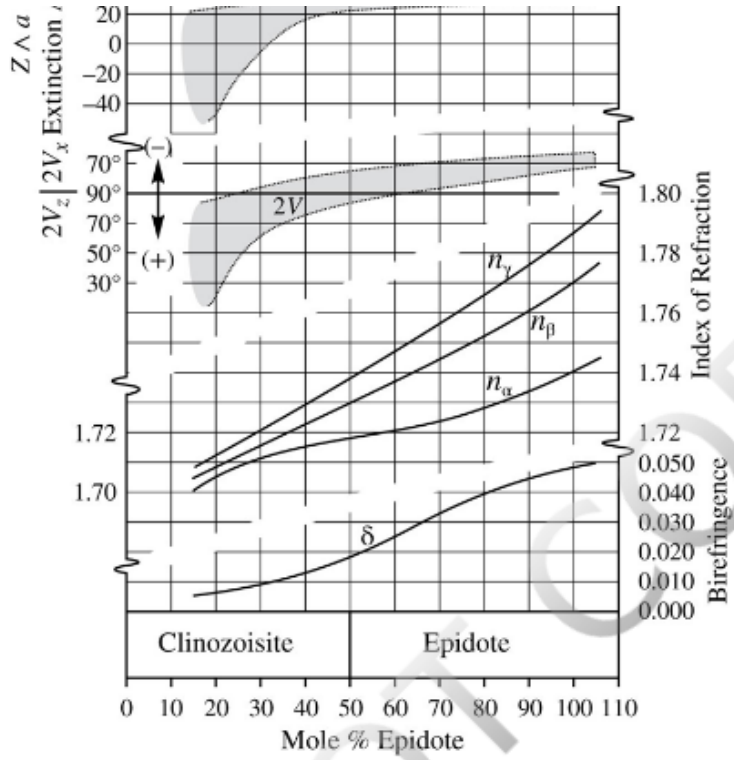

FIGURE 15.4 Optical properties of clinozoisite–epidote. Compiled from Johnston (1949), Deer and others (1962), Myer (1965), Strens (1966), and Hormann and Raith (1971), with modifications after Franz and Liebscher (2004). Indices of refraction and birefringence have some scatter about the lines shown. View larger image

Interference Figure: $2V$ varies with Fe^{3+} content but with considerable variability. Clinozoisite $2V_z$ is between 14° and ~100°, usually greater than 65°. Epidote is optically negative with $2V_x$ between ~90° and 64°. Optic axis dispersion is usually strong, $r < v$ for clinozoisite or $r > v$ for epidote. Inclined bisectrix dispersion also may be strong and may reverse the positions of the color fringes expected from the optic axis dispersion.

Alteration No consistent alteration. Clinozoisite and epidote are relatively resistant in the weathering environment, so both are common detrital grains in clastic sediments.

Distinguishing Features

Hand Sample: The distinctive green color and single cleavage are characteristic. Students often confuse granular masses of epidote with olivine, but olivine lacks cleavage and, except for metamorphosed carbonates, has different occurrences. Massive epidote also tends to have a more intense green or pistachio-green color compared to olivine.

Thin Section/Grain Mount: Clinozoisite is distinguished from epidote by lower birefringence, different optic sign, and lack of green color. Allanite is usually brown and piemontite pink. Zoisite and pumpellyite both resemble clinozoisite, but zoisite has parallel extinction in (010) sections, and colorless pumpellyite has lower indices of refraction and higher birefringence. Hornblende has two cleavages, lower indices of refraction and birefringence, and more fully saturated green color. The small size of many grains may make positive identification difficult in thin section.

DO NOT COPY e48d507df5d1141@placeholder.9409

Printed by: e48d507df5d1141@placeholder.94092.edu. Printing is for personal, private use only. No part of this book may be reproduced or transmitted without publisher's prior permission. Violators will be prosecuted.

grains may make positive identification difficult in thin section.

Occurrence Epidote and clinozoisite are common accessory minerals in a wide variety of regional and contact metamorphic rocks including pelites, metacarbonates, and felsic to mafic meta-igneous rocks. Clinozoisite is favored in aluminous rocks and epidote in more iron-rich rocks. Many igneous rocks contain epidote or clinozoisite as accessory minerals, and epidote is common in hydrothermal systems or as the result of deuteric alteration, which occurs when minerals crystallized from a magma react with late residual water-rich fluids to produce new minerals. Alteration along fault and fracture systems often yields epidote. Because epidote and clinozoisite are fairly resistant in the weathering environment, they are common constituents of the heavy mineral fraction of many clastic sediments.

Use Sometimes used as a semiprecious gem.

Allanite

$$(\mathrm{Ca, Mn, Ce, La, Y, Th})_2(\mathrm{Al, Fe^{3+}})$$
$$\mathrm{Al(Fe^{2+}, Fe^{3+}, Ti)}$$
$$[\mathrm{Si_2O_7}][\mathrm{SiO_4}]\ \mathrm{O}\ (\mathrm{OH})$$

$$\text{Monoclinic } 2/m$$

$$a = 8.93\ \text{Å},\ b = 5.77\ \text{Å},$$
$$c = 10.16\ \text{Å},\ \beta = 114.7^\circ,$$
$$Z = 2$$

$$H = 5 - 6.5$$

$$G = 3.4 - 4.2$$
$$(\text{lower if metamict})$$

$$\text{Biaxial } (+ \text{ or } -)$$

$$n_\alpha = 1.690 - 1.813$$

$$n_\beta = 1.700 - 1.857$$

$$n_\gamma = 1.706 - 1.891$$

$$\delta = 0.013 - 0.036$$

$$2V_x = 40 - 90^\circ\ (\text{negative})$$

$$2V_z = 90 - 57^\circ\ (\text{positive})$$

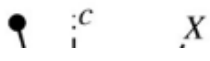

DO NOT COPY
e48d507df5d1141@placeholder.9409

Printed by: e48d507df5d1141@placeholder.94092.edu. Printing is for personal, private use only. No part of this book may be reproduced or transmitted without publisher's prior permission. Violators will be prosecuted.

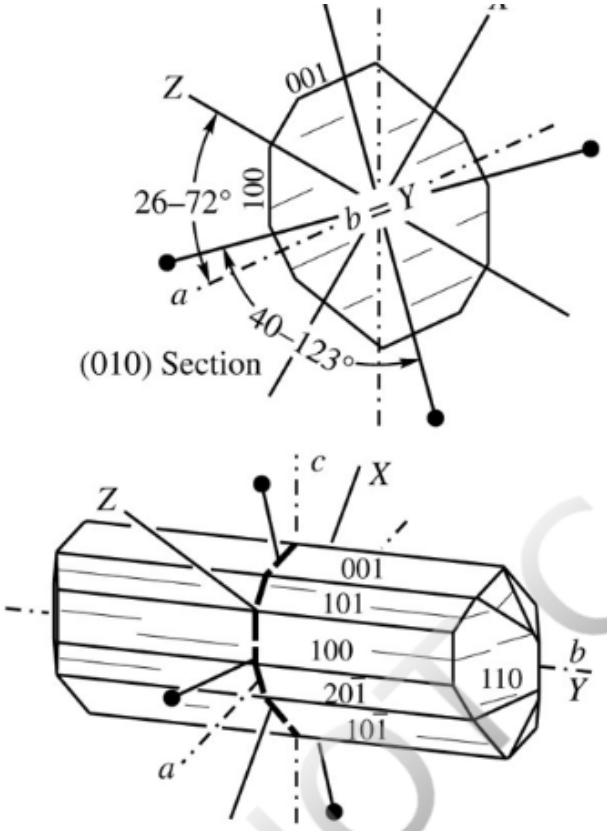

Composition The principal compositional variation is substitution of trivalent Ce, La, Y, and other rare earth elements for Ca^{2+}. Charge balance is maintained by substituting Fe^{2+} for Al^{3+}; allanite is the only member of the epidote group with significant amounts of ferrous iron. Th and U are also usually present in significant amounts, substituting for Ca. The structure may become metamict, as radioactive elements contained in the structure decay over time.

Form and Twinning It often occurs as anhedral or subhedral equant grains. Crystals are columnar, bladed, or acicular and elongate parallel to the *b* axis. Because allanite contains substantial amounts of radioactive elements, pleochroic halos may develop around allanite grains enclosed in biotite, chlorite, hornblende, or other minerals. Overgrowths of epidote on allanite are common. Twinning on {100} is not common.

Cleavage Good on {001}, poor on {100} and {110}. Uneven to conchoidal fracture. Brittle.

Color Properties

Luster: Vitreous, resinous to submetallic.

Color: Light brown to black.

Streak: Gray.

Color in Thin Section: Usually brownish yellow to brown, also colorless or greenish.

DO NOT COPY e48d507df5d1141@placeholder.9409

Printed by: e48d507df5d1141@placeholder.94092.edu. Printing is for personal, private use only. No part of this book may be reproduced or transmitted without publisher's prior permission. Violators will be prosecuted.

Pleochroism: Distinct in shades of brown or, less commonly, green: X = reddish brown; Y = dark brown, brownish yellow; Z = dark reddish brown, greenish brown. Metamict varieties are nonpleochroic.

Optical Characteristics

Relief in Thin Section: High to very high positive, metamict varieties may be low.

Optic Orientation: Usually $X \wedge c = -1°$ to $-47°$, $Y = b$, Z $\wedge$ $a = +26°$ to $+72°$. (010) sections show highest birefringence and the Z $\wedge$ a extinction angle to the trace of cleavage, if visible.

Indices of Refraction and Birefringence: Indices of refraction increase with Fe and rare earth element content. Strongly metamict varieties may be isotropic, with an index of refraction as low as 1.54. Chemical zoning may be expressed by variation in birefringence, which is usually no higher than mid–second order in standard thin sections.

Interference Figure: Allanite is usually biaxial negative with $2V$ between 40° and 90°; optically positive varieties with $2V$ between 90° and 57° are less common. Optic axis dispersion is usually strong, $r > v$ or $r < v$. Strong mineral color may make interference figures difficult to interpret.

Alteration Metamict allanite is relatively common. Becoming metamict involves an increase in volume, so surrounding grains may develop cracks that radiate away from the allanite grain.

Distinguishing Features

Hand Sample: Dark color, submetallic or resinous luster, and association with granitic rocks. Firm identification may require other techniques. Strongly metamict varieties will not yield X-ray diffraction peaks because the crystal is largely amorphous.

Thin Section/Grain Mount: Nonmetamict samples are distinguished from other epidote group minerals by brown color. Metamict samples are optically isotropic, and surrounding minerals may contain cracks radiating from the allanite. Garnet has a higher index of refraction than metamict allanite.

Occurrence Allanite is a common accessory mineral in felsic igneous rocks such as granite, granodiorite, monzonite, syenite, and some equivalent volcanic rocks. Granitic pegmatite may contain large masses. It is commonly associated with biotite, hornblende, or other mafic silicate minerals. Allanite also may be found in skarn deposits or other metamorphosed carbonate rocks, and in amphibolite or granitic gneiss.

Use Potentially a source for metallic cerium, though monazite is more commonly source. Cerium is used in the “flints” in cigarette lighters and is used in the lining of self-cleaning ovens to improve the oxidation of food residue.

DO NOT COPY e48d507df5d1141@placeholder.94092

Printed by: e48d507df5d1141@placeholder.94092.edu. Printing is for personal, private use only. No part of this book may be reproduced or transmitted without publisher's prior permission. Violators will be prosecuted.

Lawsonite

$$\mathrm{CaAl_2(Si_2O_7)(OH)_2 \cdot H_2O}$$

$$\text{Orthorhombic } 2/m\ 2/m\ 2/m$$

$$a = 8.80\ \text{Å},\ b = 5.85\ \text{Å},$$
$$c = 13.1\ \text{Å},\ Z = 4$$

$$H = 6$$

$$G = 3.05 - 3.12$$

$$\text{Biaxial } (+)$$

$$n_\alpha = 1.663 - 1.665$$

$$n_\beta = 1.672 - 1.675$$

$$n_\gamma = 1.682 - 1.686$$

$$\delta = 0.019 - 0.021$$

$$2V_z = 76 - 87^\circ$$

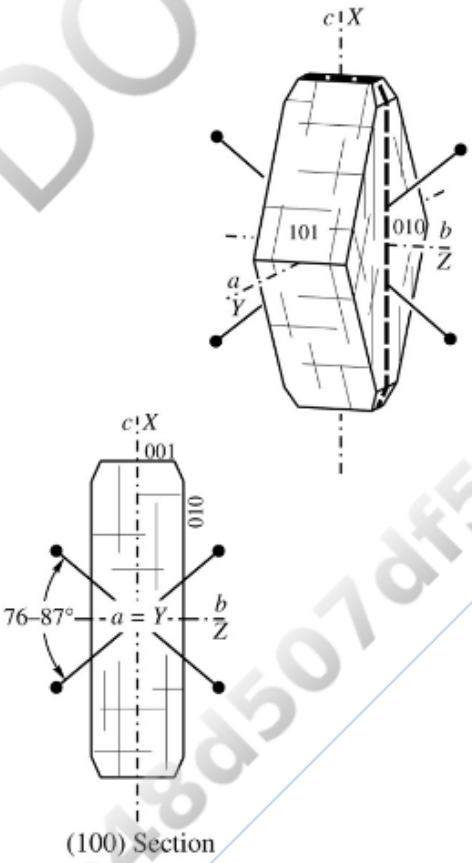

(100) Section

DO NOT COPY
e48d507df5d1141@placeholder.9409

Printed by: e48d507df5d1141@placeholder.94092.edu. Printing is for personal, private use only. No part of this book may be reproduced or transmitted without publisher's prior permission. Violators will be prosecuted.

Composition Lawsonite shows little deviation from the ideal formula given above. Minor amounts of Fe, Ti, or Mg may replace Al, and minor amounts of Na may replace Ca.

Form and Twinning See **Figure 15.5**. Crystals are usually tabular on {010} with a prismatic cross section. Also as anhedral grains and granular masses. May be acicular parallel to the *b* axis. Simple or lamellar twinning with twin planes parallel to the {101} prism faces is common.

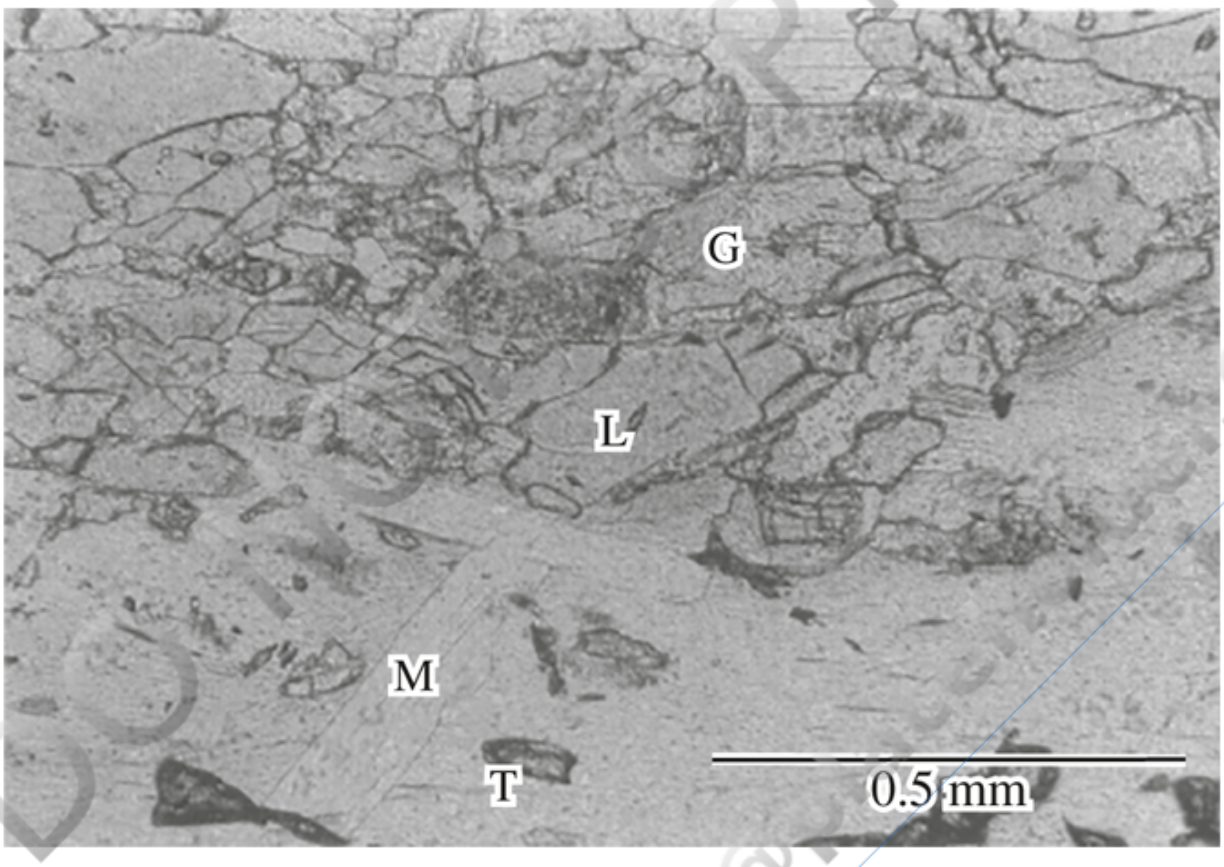

FIGURE 15.5 Photomicrograph of thin section of glaucophane schist with lawsonite (L), phengitic muscovite (M), glaucophane (G), and high-relief titanite (T) in plane light. View larger image

Cleavage Perfect cleavages on {100} and {010} intersect at right angles. Poor cleavages parallel to the {101} prism faces intersect at 67°. Uneven to conchoidal fracture. Brittle.

Color Properties

Luster: Vitreous to greasy.

Color: Colorless, white, bluish green, bluish gray.

Streak: White.

Color in Thin Section: Colorless, sometimes weakly bluish green.

Pleochroism: Not usually pleochroic. Grain mounts may be weakly pleochroic: X = light

Printed by: e48d507df5d1141@placeholder.94092.edu. Printing is for personal, private use only. No part of this book may be reproduced or transmitted without publisher's prior permission. Violators will be prosecuted.

blue or brownish yellow; *Y* = yellow, yellowish green, blue-green; *Z* = colorless or light yellow.

Optical Characteristics

Relief in Thin Section: Moderately high positive.

Optic Orientation: $X = c$, $Y = a$, $Z = b$.

Indices of Refraction and Birefringence: Little variation in either. Interference colors in standard thin sections range up to first-order red.

Interference Figure: Cleavage fragments on the {010} cleavage yield acute bisectrix figures with large $2V$. Optic axis dispersion is very strong, $r > v$.

Alteration Lawsonite may be replaced by pumpellyite as part of normal metamorphic mineral reactions.

Distinguishing Features

Hand Sample: Crystals, if present, are distinctive. Multiple cleavages distinguish lawsonite from zoisite and clinozoisite.

Thin Section/Grain Mount: Lawsonite resembles zoisite and clinozoisite but has two well-developed cleavages, has common twinning, and lacks anomalous interference colors. In (010) sections that display maximum birefringence, clinozoisite has inclined extinction and lawsonite should have symmetrical extinction to the {101} cleavages if they happen to be visible. Andalusite has lower birefringence and is usually optically negative.

Occurrence Lawsonite is a common mineral in glaucophane schist and related low- to medium-temperature, high-pressure metamorphic rocks subjected to blueschist and eclogite metamorphic facies. It commonly is associated with glaucophane, pumpellyite, jadeite, chlorite, and albite-rich plagioclase. Lawsonite is also found in metamorphosed gabbro, diabase, and related mafic rocks, and is infrequently found in marble and chlorite schist.

Use None.

Pumpellyite

$$Ca_2MgAl_2[SiO_4][Si_2O_7](OH)_2 \cdot H_2O$$

Monoclinic $2/m$

$a = 8.83$ Å, $b = 5.90$ Å,

$c = 19.17$ Å, $\beta = 97.1°$

DO NOT COPY e48d507df5d1141@placeholder.9409

Printed by: e48d507df5d1141@placeholder.94092.edu. Printing is for personal, private use only. No part of this book may be reproduced or transmitted without publisher's prior permission. Violators will be prosecuted.

$$c = 19.17 \text{ Å}, \ \beta = 97.1^\circ,$$
$$Z = 4$$

$$H = 5 - 6$$

$$G = 3.16 - 3.25$$

$$\text{Biaxial } (+ \text{ or } -)$$

$$n_\alpha = 1.665 - 1.710$$

$$n_\beta = 1.670 - 1.720$$

$$n_\gamma = 1.683 - 1.726$$

$$\delta = 0.008 - 0.020$$

$$2V_z = 7 - 110^\circ$$

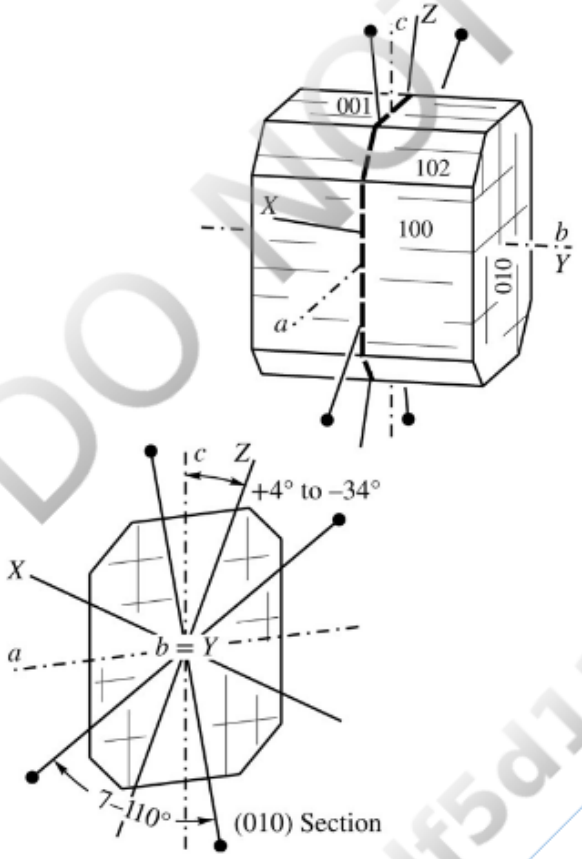

Composition The principal compositional variation is substitution of Fe^{3+} for Al, and Fe^{2+}, Fe^{3+}, and Al for Mg. Some Na or K may also substitute for Ca.

Form and Twinning Crystals are columnar, bladed, or acicular, and elongate parallel to *b*. Pumpellyite more commonly forms subhedral to anhedral grains or radiating, subparallel, or randomly oriented aggregates of elongate to fibrous grains. Twins with irregular composition planes parallel to {100} and {001} are common and may yield 4-fold sectors in appropriately cut sections.

DO NOT COPY e48d507df5d1141@placeholder.9409

Printed by: e48d507df5d1141@placeholder.94092.edu. Printing is for personal, private use only. No part of this book may be reproduced or transmitted without publisher's prior permission. Violators will be prosecuted.

fold sectors in appropriately cut sections.

Cleavage Good cleavage on {001} and fair cleavage on {100} intersect at 97°. Brittle.

Color Properties

Luster: Vitreous.

Color: Green, bluish green, brown, or greenish black.

Streak: White or gray.

Color in Thin Section: Colorless, green, yellow, or brown; darker colors are associated with higher Fe content.

Pleochroism: Colored varieties are distinctly pleochroic $Y > Z \geq X$: X = colorless, yellow, brownish, or greenish yellow; Y = light green, green, blue-green, brownish yellow; Z = yellow, brownish yellow, or reddish brown.

Optical Characteristics

Relief in Thin Section: High positive.

Optic Orientation: $X \wedge a = +4°$ to $+32°$, $Y = b$, $Z \wedge c = +4°$ to $-34°$. The trace of cleavage in longitudinal sections (parallel to b) and cleavage fragments may be either length fast or length slow, and show parallel extinction. In grains cut perpendicular to b that show maximum birefringence, the maximum extinction angle to the {001} cleavage is between 4° and 32°, with the larger values associated with higher Fe content. In some Fe-rich samples, the positions of the Z and Y indicatrix axes are reversed.

Indices of Refraction and Birefringence: Increase with Fe content. Interference colors are no higher than upper first order for most samples and are often anomalously blue or yellowish brown.

Interference Figure: Most pumpellyite is optically positive, and $2V$ increases with iron content. Some high-Fe samples are optically negative with large $2V$. Optic axis dispersion is very strong, $r < v$. Also weak inclined bisectrix dispersion.

Alteration Pumpellyite does not display consistent alteration but may show metamorphic reaction relations with associated minerals.

Distinguishing Features

Hand Sample: Closely resembles members of the epidote group but has two cleavages; some samples have a darker color. X-ray diffraction may be needed for positive identification.

Thin Section/Grain Mount: Weakly colored pumpellyite resembles zoisite and clinozoisite. Zoisite has lower birefringence and shows parallel extinction to cleavage in (010)

DO NOT COPY e48d507df5d1141@placeholder.9409

Printed by: e48d507df5d1141@placeholder.94092.edu. Printing is for personal, private use only. No part of this book may be reproduced or transmitted without publisher's prior permission. Violators will be prosecuted.

sections. Clinozoisite has higher indices of refraction and lower birefringence. Colored pumpellyite resembles epidote, but the latter is optically negative. Chlorite may have similar color and anomalous interference colors but has lower birefringence and indices of refraction. Lawsonite has lower indices of refraction, parallel extinction in grains that yield maximum birefringence, better cleavage, and generally is colorless or bluish.

Occurrence Pumpellyite can be an indicator mineral for the low-grade prehnite-pumpellyite metamorphic facies, which may occur through hydrothermal alteration of mafic igneous rocks at mid-ocean ridges. Here the pumpellyite may fill vesicles. Pumpellyite is also a common mineral in glaucophane schist and related low-temperature/high-pressure metamorphic rocks subjected to the blueschist metamorphic facies conditions. Associated minerals include glaucophane, lawsonite, clinozoisite, epidote, chlorite, actinolite, and calcite. Skarns and related metamorphosed carbonate rocks infrequently contain pumpellyite. It may be a detrital mineral in sediment derived from pumpellyite-bearing rocks, and in such cases it is easily misidentified as epidote.

Use None.

DO NOT COPY
e48d507df5d1141@placeholder.9409

Printed by: e48d507df5d1141@placeholder.94092.edu. Printing is for personal, private use only. No part of this book may be reproduced or transmitted without publisher's prior permission. Violators will be prosecuted.

Ring Silicates

Structure and Classification

The ring silicates are a small group of minerals with only three common species: beryl, cordierite, and tourmaline. Except for a slight distortion in the lattice of cordierite, beryl and cordierite are isostructural. The structure of all three minerals is based on 6-fold rings of silicon and aluminum tetrahedra (**Figure 15.1b**, **c**) that are stacked to form columns. Adjacent columns of 6-fold rings are cross-linked through other cations. Additional cations and/or anions may occupy the center of the columns.

Axinite (**Table 15.3**) has a structure that does not fall neatly in the conventional silicate classification but is included with the ring silicates based on the presence of rectangular 6-fold rings of tetrahedra. Crystals and masses of axinite can be found in contact-metamorphosed carbonate rocks and also in altered mafic igneous rocks; associated minerals may include prehnite, datolite, zoisite, tourmaline, vesuvianite, calcite, and actinolite. Axinite less commonly occurs in greenschist facies regional metamorphic rocks associated with pumpellyite.

TABLE 15.3 Properties of Axinite

Composition	$Ca_4(Fe^{2+},Mg,Mn^{2+},Zn)_2Al_4B_2Si_8O_{30}(OH)_2$
Crystal system and habit	Triclinic: wedge-shaped, bladed, or tabular crystals; radiating clusters of grains or granular aggregates
Color	Lilac-brown, yellowish, colorless; vitreous
Color in thin section	Colorless, pale yellow, violet; weak pleochroism
Sign and 2*V*	Biaxial (−), 63–90°
Indices of refraction	n_α = 1.565–1.694 n_β =1.660–1.701 n_γ = 1.668–1.706
δ	0.009–0.016
Physical	H = 6.5–7, G = 3.18–3.43
Cleavage	{100} perfect

Beryl

DO NOT COPY e48d507df5d1141@placeholder.9409

Printed by: e48d507df5d1141@placeholder.94092.edu. Printing is for personal, private use only. No part of this book may be reproduced or transmitted without publisher's prior permission. Violators will be prosecuted.

Hexagonal $6/m\,2/m\,2/m$

$a = 9.20 - 9.27$ Å,
$c = 9.19 - 9.25$ Å, $Z = 2$

$H = 7.5 - 8$

$G = 2.63 - 2.97$ (increases with alkali content)

Uniaxial $(-)$

$n_\omega = 1.560 - 1.610$

$n_\epsilon = 1.557 - 1.599$

$\delta = 0.003 - 0.009$

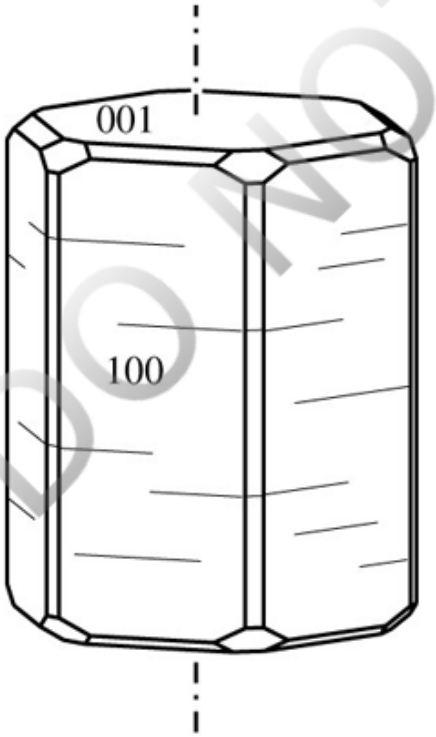

Structure In the beryl structure (**Figure 15.6**), the tetrahedra in the 6-fold rings are arranged so that the plane of the ring also is a plane of symmetry of the constituent tetrahedra (Figure 15.1b). Tetrahedra rings are stacked to form columns so that successive rings are rotated relative to the rings above and below. This allows the oxygen anions from one tetrahedral ring to fit in the gap between oxygen anions in the adjacent rings. Each column of rings therefore consists of two concentric cylinders of oxygens. These columns of rings extend parallel to the c axis and are stacked next to each other in a hexagonal array. Beryllium occupies distorted 4-fold sites formed by oxygen anions from adjacent columns of rings, and links the rings laterally and vertically. Al occupies distorted 6-fold sites formed by oxygen anions from three adjacent columns of rings. The

DO NOT COPY e48d507df5d1141@placeholder.9409

Printed by: e48d507df5d1141@placeholder.94092.edu. Printing is for personal, private use only. No part of this book may be reproduced or transmitted without publisher's prior permission. Violators will be prosecuted.

formula is conventionally written with the Be first—$Be_3Al_2Si_6O_{18}$—but this violates the convention of arranging the cations in order of decreasing coordination number.

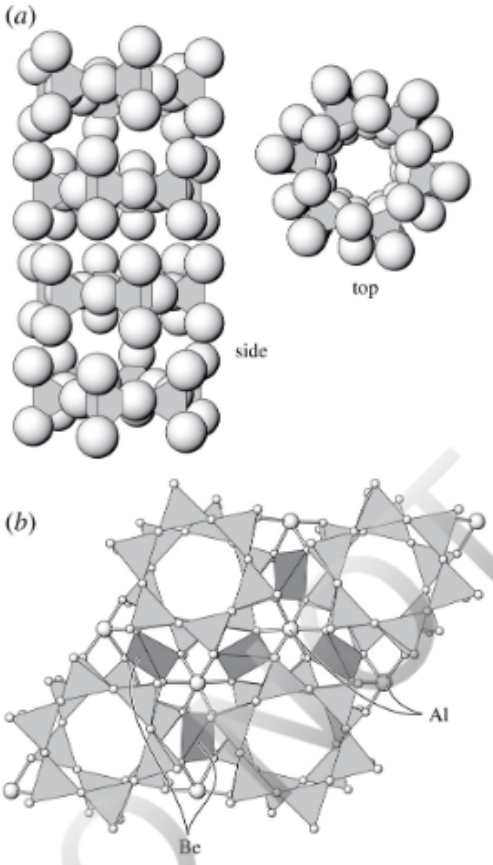

FIGURE 15.6 Structure of beryl. (*a*) Side and top view of column structure. The oxygen anions are drawn at about 70% of full size. (*b*) Columns of tetrahedral rings are cross-linked through Be in tetrahedral coordination (dark tetrahedra) and through Al in octahedral coordination. View down the *c* axis, with oxygen anions drawn as small spheres. View larger image

The combination of tetrahedra rings and cross-linking Be tetrahedra actually forms a three-dimensional framework in which each oxygen anion on every tetrahedra is shared with another tetrahedra. In a strict sense, beryl may therefore be considered a framework silicate. Because the rings are the dominant structural element, beryl is grouped with the ring silicates here.

Composition The primary compositional variation is in the presence of alkali ions including Li, Na, K, Rb, and Cs. Li may substitute for either Al or Be, but the other cations are mostly located in the center of the channels in the middle of the stacked rings (Figure 4.15d). Water and/or CO_2 molecules also may be located in the channels. Charge surplus associated with cations in the channels is probably balanced by substituting Fe^{2+}, Li^+, or Mg^{2+} for Al^{3+} in octahedral sites or by leaving vacancies in the Be sites. Crystal field splitting involving small amounts of Cr^{3+} substituting for Al^{3+} is responsible for the green color of emerald. Iron in different valence states and structural locations controls the color of blue-green aquamarine and yellow golden beryl. Minor Mn^{2+} and Mn^{3+} produce the pink color of morganite and red color of red beryl, respectively.

DO NOT COPY e48d507df5d1141@placeholder.9409

Printed by: e48d507df5d1141@placeholder.94092.edu. Printing is for personal, private use only. No part of this book may be reproduced or transmitted without publisher's prior permission. Violators will be prosecuted.

the pink color of morganite and red color of red beryl, respectively.

Form and Twinning See **Figure 15.7**. Crystals are relatively common and form {100} hexagonal prisms with blunt terminations, usually consisting only of {001} pinacoids. Some crystals taper from one end to the other. Crystals also occur as tabular hexagonal prisms, and anhedral or interstitial grains. Small needles may form radiating masses. Inclusions may form bands parallel to prism faces.

FIGURE 15.7 Beryl crystal from a granitic pegmatite. View larger image

Cleavage Poor {001} cleavage. Conchoidal to uneven fracture. Brittle.

Color Properties

Luster: Vitreous.

Color: Bluish green, blue, green, greenish yellow, yellow, colorless.

Streak: White.

Color in Thin Section: Colorless.

Pleochroism: None.

Optical Characteristics

Relief in Thin Section: Low to moderate positive.

Optic Orientation: Longitudinal sections parallel to *c* are length fast and show parallel extinction.

DO NOT COPY e48d507df5d1141@placeholder.9409

Printed by: e48d507df5d1141@placeholder.94092.edu. Printing is for personal, private use only. No part of this book may be reproduced or transmitted without publisher's prior permission. Violators will be prosecuted.

Indices of Refraction and Birefringence: Show a general increase with alkali content, but with considerable variability. Beryl typically has indices of refraction $n_\omega = 1.580 \pm 0.005$ and $n_\epsilon = 1.575 \pm 0.005$. Chemical zoning may be expressed by variation in the birefringence between the center and edge of grains.

Interference Figure: Basal sections yield centered optic axis figures. Strain of the crystal structure may produce biaxial figures with $2V$ up to 17° and variable optic orientation.

Alteration The usual alteration products of beryl are clay minerals or sericite.

Distinguishing Features

Hand Sample: Crystal habit, hardness, and color are distinctive. Apatite is softer, and quartz is softer and has a lower specific gravity.

Thin Section/Grain Mount: Both quartz and nepheline resemble beryl, but beryl has higher indices of refraction. Quartz is optically positive and length slow. Apatite has higher indices of refraction. Nepheline shows negative relief in standard thin sections ($n_{\text{cement}} = 1.540$) and is not found in the quartz-rich granitic pegmatites and granite where beryl is most frequently found.

Occurrence Beryl and other beryllium-bearing minerals are only found in rocks younger than about 3.0 Ga and no beryllium-bearing minerals are found in meteorites. The restricted occurrence of beryllium-bearing minerals throughout Earth's history is due to beryllium being the least abundant of the light elements. Therefore, beryllium must be significantly concentrated compared to its primordial abundance in order for beryllium-bearing minerals to form. Geologic processes responsible for concentrating beryllium may have needed some 1.5 billion years to produce concentrations high enough to result in beryllium-bearing minerals in a few select environments within continental crust.

Beryl is a common mineral in granitic pegmatite and typically is associated with quartz, K-feldspar, albite, muscovite, biotite, and tourmaline. Beryl is less common in granite and can be infrequently found in nepheline syenite. High-temperature hydrothermal veins may contain beryl associated with tin and tungsten minerals. Contact metasomatism of gneiss, schist, or carbonate rocks also may produce beryl.

Use Beryl is the primary source for metallic beryllium. Beryllium has properties similar to aluminum and is often alloyed with copper to improve strength and hardness; such alloys have many specialty uses. Beryllium is also widely used as X-ray–transparent windows such as those on X-ray tubes (Chapter 8). Beryl is also an important gemstone. The more common blue-green variety is known as aquamarine and is most commonly found in pegmatites. Green Cr-bearing beryl is known as emerald, and most is mined from metamorphosed carbonate rocks. High-quality emerald can be extremely valuable. Other gem varieties include pink to red morganite and yellow golden beryl. Beryl, probably because of its gemstone status, had many historical medical uses, particularly in the Middle Ages.

DO NOT COPY e48d507df5d1141@placeholder.94092

Printed by: e48d507df5d1141@placeholder.94092.edu. Printing is for personal, private use only. No part of this book may be reproduced or transmitted without publisher's prior permission. Violators will be prosecuted.

Cordierite

$$Mg_2\,Al_3[AlSi_5]\,O_{18}$$

Orthorhombic
(pseudohexagonal)
$2/m\ 2/m\ 2/m$

$a = 17.08$ Å,
$b = 9.73$ Å,
$c = 9.36$ Å

$Z = 4$

$H = 7$

$G = 2.53 - 2.78$

Biaxial (+ or −)

$n_\alpha = 1.527 - 1.560$

$n_\beta = 1.532 - 1.574$

$n_\gamma = 1.537 - 1.578$

$\delta = 0.005 - 0.017$

$2V_x = 35 - 106^\circ$

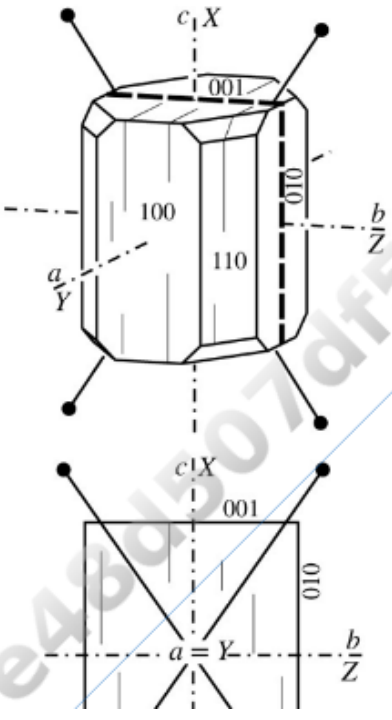

DO NOT COPY
e48d507df5d1141@placeholder.9409

Printed by: e48d507df5d1141@placeholder.94092.edu. Printing is for personal, private use only. No part of this book may be reproduced or transmitted without publisher's prior permission. Violators will be prosecuted.

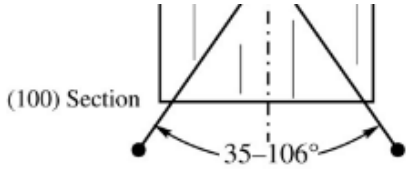

Structure The cordierite structure is essentially the same as beryl (Figure 15.6) with Mg in place of Al in octahedral sites, and Al instead of Be in cross-linking tetrahedral sites. One of six of the tetrahedra in the rings must be occupied by Al to provide charge balance. This distorts the rings and reduces the symmetry to orthorhombic. As in beryl, all tetrahedra are linked by sharing oxygens to form a three-dimensional framework, and cordierite in a strict sense should be classified as a framework silicate. It is included here because the rings are the dominant structural element.

Composition The principal compositional variation is substitution of Fe^{2+} for Mg in octahedral sites, although most cordierite is fairly Mg-rich. Fe^{3+} may substitute for Al. The channels in the centers of the rings may contain variable amounts of H_2O and CO_2, and small amounts of large alkali ions, usually Na or K.

Form and Twinning **Figure 15.8**. Cordierite most commonly occurs as anhedral to highly irregular porphyroblastic grains, often with numerous inclusions of quartz, opaque grains, or other minerals. Less commonly as hexagonal prismatic crystals. Lamellar and cyclic twins are common, but not visible in hand sample. The twin planes are {110} and {130}. Basal sections in thin sections reveal a radial or cyclic pattern with roughly hexagonal symmetry. Twins in longitudinal section may resemble twins seen in plagioclase. Cordierite in high-grade metamorphic rocks is more likely to be twinned than from medium-grade rocks.

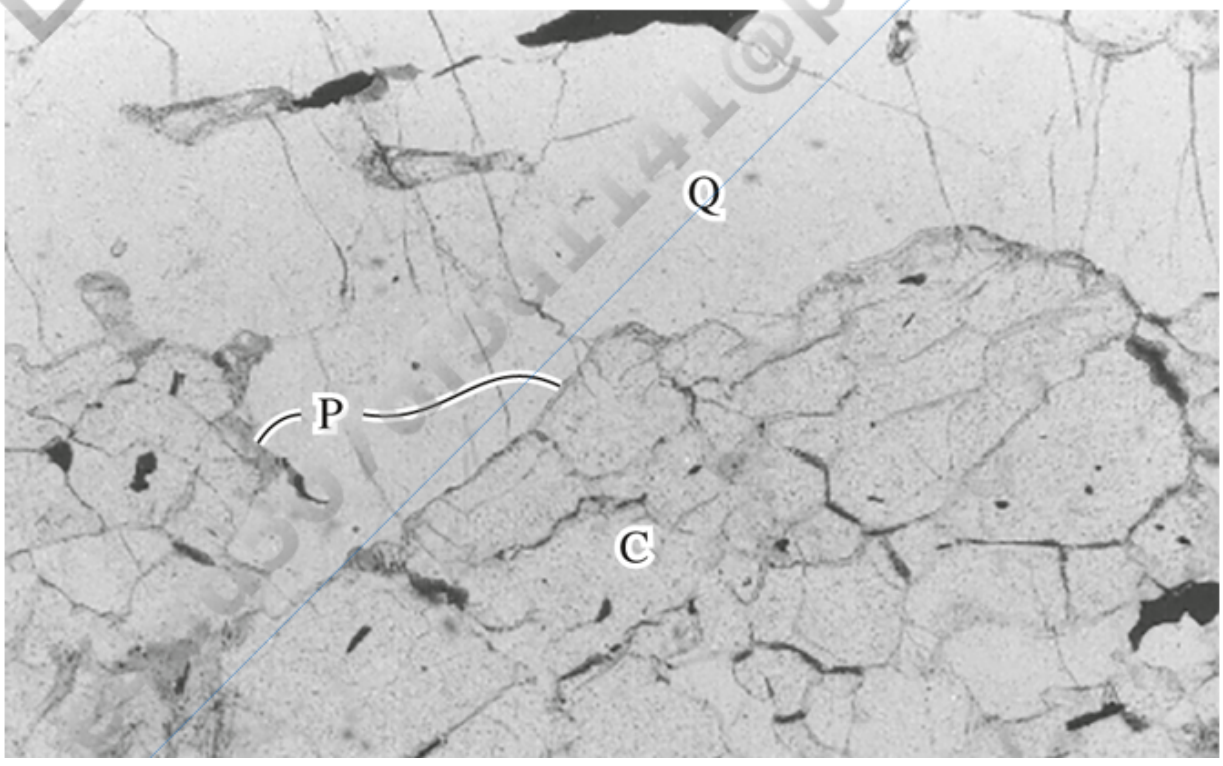

Printed by: e48d507df5d1141@placeholder.94092.edu. Printing is for personal, private use only. No part of this book may be reproduced or transmitted without publisher's prior permission. Violators will be prosecuted.

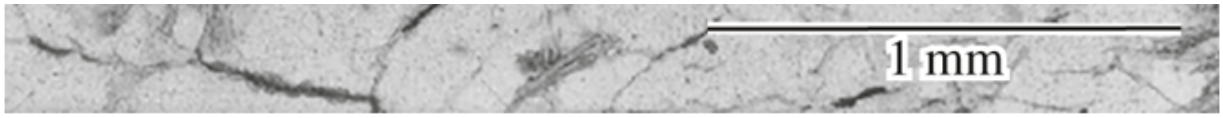

FIGURE 15.8 Photomicrograph of thin section of anthophyllite–cordierite gneiss showing cordierite (C) and quartz (Q) in plane light. Note that the cordierite has minor pinite (P) alteration at the edge of grains and is slightly cloudy because of fine opaque inclusions. View larger image

Cleavage Fair cleavage on {010} and poor cleavage on {100} and {001}. Cleavage is usually not obvious in hand sample or thin section. Subconchoidal fracture. Brittle.

Color Properties

Luster: Vitreous.

Color: Gray, grayish blue, blue, indigo-blue, or pale violet.

Streak: White.

Color in Thin Section: Colorless to very pale blue; darker colors are associated with Fe content.

Pleochroism: Usually none in thin section; grain mounts may be distinctly pleochroic. Colored samples are $Y > Z > X$: X = colorless, pale yellow, pale green; Y = pale blue to violet; Z = pale blue.

Optical Characteristics

Relief in Thin Section: Low negative or positive.

Optic Orientation: $X = c$, $Y = a$, $Z = b$. Elongate crystals are length fast.

Indices of Refraction and Birefringence: Indices of refraction increase with Fe content and also with H_2O content in channels.

Interference Figure: Most cordierite is biaxial negative with $2V$ between 40° and 90°. High water and Na content yield the lower $2V$ angles. Some cordierite is biaxial positive with large $2V$. Optic axis dispersion is weak, usually $r < v$.

Comment Yellowish halos around radioactive minerals, such as zircon, are quite common.

Alteration Cordierite is readily altered to pinite, which is a fine-grained greenish or yellowish aggregate of chlorite, muscovite, and other silicates. The alteration may develop along cracks and grain margins, leaving ragged remnants of cordierite in a matrix of pinite.

Distinguishing Features

Hand Sample: Resembles quartz but is more distinctly blue or pale violet. Corundum is

DO NOT COPY e48d507df5d1141@placeholder.9409

Printed by: e48d507df5d1141@placeholder.94092.edu. Printing is for personal, private use only. No part of this book may be reproduced or transmitted without publisher's prior permission. Violators will be prosecuted.

Hand Sample: Resembles quartz but is more distinctly blue or pale violet. Corundum is harder. Small anhedral grains in metamorphic rocks may be difficult to distinguish from quartz, particularly if the bluish color is not evident. Porphyroblasts in pelitic metamorphic rocks may stand out on weathered surfaces; but distinguishing among cordierite, andalusite, and staurolite is not always possible, particularly if the minerals are anhedral and significantly altered. Cordierite is much less likely to form euhedral crystals than either staurolite or andalusite. Staurolite is brown and, if euhedral, has a prismatic crystal habit and often displays cross-shaped twins. Euhedral andalusite is typically prismatic, with an approximately square cross section, and the cross-shaped inclusion pattern seen on basal sections of chiastolite (variety of andalusite) is distinctly different. Unaltered andalusite may be pinkish, whereas cordierite is more typically blue. Pinite alteration of cordierite may significantly reduce the hardness.

Thin Section/Grain Mount: Closely resembles quartz and orthoclase, or if twinned, plagioclase. Quartz is uniaxial, lacks alteration products such as pinite, and in many metamorphic rocks may display undulatory extinction that is distinct. Orthoclase has more distinct cleavage and has lower indices of refraction than thin section epoxy (n_{epoxy} = 1.540). Twinned cordierite resembles plagioclase, but plagioclase has more distinct cleavage and lacks radial twinning. Yellowish halos are common in cordierite around zircon grains or other minerals containing radioactive elements. Similar halos are not found in quartz or feldspars. Cordierite also may contain fine, dustlike inclusions of opaque minerals, or numerous rounded inclusions of quartz. Thin sections may be stained to distinguish cordierite from the feldspars (Boone and Wheeler, 1968).

Occurrence Cordierite is a common mineral in medium- and high-grade pelitic metamorphic rocks. Cordierite is common as porphyroblasts in hornfels found in contact metamorphic zones. In regional metamorphic rocks, cordierite may form porphyroblasts or anhedral grains similar in size and shape to quartz and feldspar. Associated minerals include chlorite, andalusite, sillimanite, kyanite, staurolite, muscovite, biotite, garnet, and chloritoid. Cordierite is also common in certain mafic metamorphic rocks associated with orthoamphibole such as in anthophyllite–cordierite gneiss (see Chapter 14). Igneous rocks of mafic to felsic compositions may contain cordierite if significantly Al-rich.

Use A blue gem variety is called iolite. The low thermal expansion of cordierite makes it useful as a ceramic. However, ceramics with the composition of cordierite are most commonly made by using talc [$Mg_2Si_4O_{10}(OH)_2$], alumina (Al_2O_3), and SiO_2 as starting materials.

Tourmaline

$$\mathrm{Na(Mg, Fe, Li, Al)_3Al_6}$$
$$\mathrm{[Si_6O_{18}](BO_3)_3(O, OH, F)_4}$$

Hexagonal (trigonal) $3m$

DO NOT COPY e48d507df5d1141@placeholder.9409

Printed by: e48d507df5d1141@placeholder.94092.edu. Printing is for personal, private use only. No part of this book may be reproduced or transmitted without publisher's prior permission. Violators will be prosecuted.

$$a = 15.8 - 16.0 \text{ Å},$$
$$c = 7.1 - 7.25 \text{ Å}, \ Z = 3$$
$$H = 7$$
$$G = 2.90 - 3.22$$
$$\text{Uniaxial } (-)$$
$$n_\omega = 1.631 - 1.698$$
$$n_\epsilon = 1.610 - 1.675$$
$$\delta = 0.015 - 0.035$$

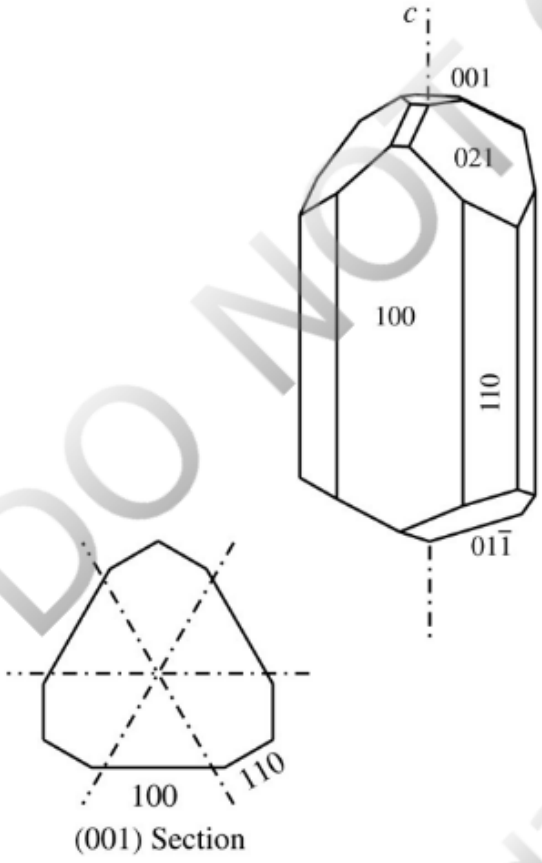

(001) Section

Structure The tourmaline structure (**Figure 15.9**) is somewhat more complicated than that of beryl. The tetrahedra in the rings are arranged so that their bases lie along a common plane resulting in one corner of each tetrahedron pointing perpendicular from that plane (Figure 15.1c). These tetrahedral rings combine with a set of three octahedra (X sites) constructed of O and OH arranged to form a triangle, and a site containing large cations (W sites), to form columns that extend parallel to *c*. All tetrahedral rings are arranged to point in the same direction. Adjacent columns are stacked next to each other in a hexagonal array. Additional cations in octahedral coordination (Y sites) cross-link between columns. Boron cations are coordinated with three oxygen anions to form triangular groups nestled into the columns of tetrahedra and octahedra. Because the

DO NOT COPY e48d507df5d1141@placeholder.9409

Printed by: e48d507df5d1141@placeholder.94092.edu. Printing is for personal, private use only. No part of this book may be reproduced or transmitted without publisher's prior permission. Violators will be prosecuted.

tetrahedra within the rings all point in the same direction, tourmaline lacks center symmetry and may be piezoelectric. Further, the triangular grouping of octahedra and boron triangles within columns reduces the symmetry to trigonal, rather than hexagonal.

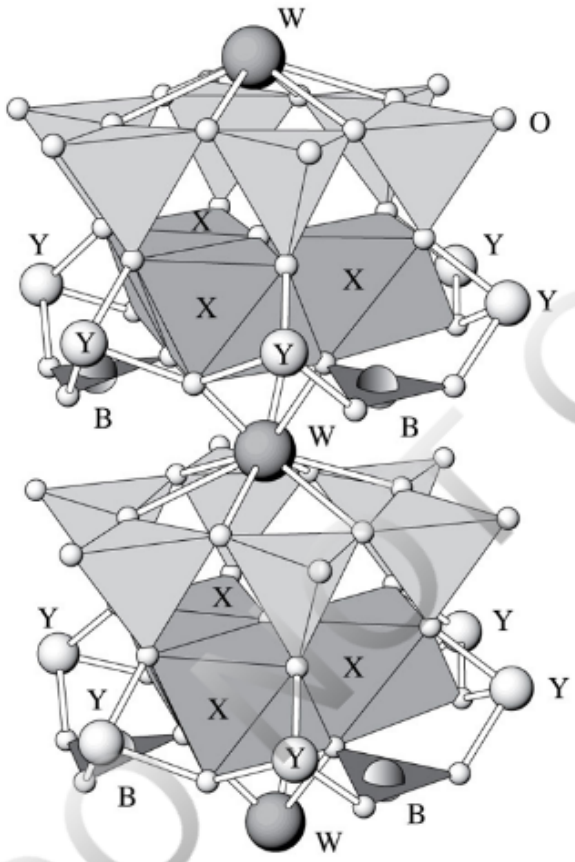

FIGURE 15.9 Tourmaline structure consisting of tetrahedral rings, triangular groups of octahedra (X), and large cation sites (W) along the axis of the column. Boron (B) is situated in triangular coordination along the edges of the columns. Columns are stacked adjacent to each other and are cross-linked through octahedrally coordinated Y cations. View larger image

Composition Tourmaline exhibits great diversity in its composition and is a major reservoir of boron in the Earth's crust. The general formula may be given as $WX_3Y_6[Si_6O_{18}](BO_3)_3(O,OH,F)_4$. The W cations are usually Na, less commonly Ca or K. The X cations are most commonly Mg and Fe, less commonly Mn, Li, and Al. The Y cations are most commonly Al, less commonly Fe^{3+} or Mg. The normal compositional range lies among the following end members; schorl-rich tourmaline is most common.

SCHORL: $NaFe_3Al_6[Si_6O_{18}](BO_3)_3(O,OH,F)_4$

DRAVITE: $NaMg_3Al_6[Si_6O_{18}](BO_3)_3(O,OH,F)_4$

ELBAITE: $Na(Li,Al)_3Al_6[Si_6O_{18}](BO_3)_3(O,OH,F)_4$

The compositional complexity makes it a useful mineral to record the changing physical and chemical conditions during rock formation. Chemical zoning is usually expressed by variations in color seen in hand sample and thin section, and indices of refraction or birefringence seen in thin section.

DO NOT COPY e48d507df5d1141@placeholder.9409

Printed by: e48d507df5d1141@placeholder.94092.edu. Printing is for personal, private use only. No part of this book may be reproduced or transmitted without publisher's prior permission. Violators will be prosecuted.

birefringence seen in thin section.

Form and Twinning See **Figure 15.10**. Crystals are quite common and usually form striated prisms that are stubby to elongate parallel to *c*. The combination of a dominant {100} trigonal prism with a subordinate {110} hexagonal prism may give crystals a somewhat rounded triangular appearance. Terminations are usually fairly blunt and consist of combinations of trigonal pyramids that are generally different on opposite ends of the crystal because center symmetry is lacking. Fractures roughly perpendicular to crystal length may be filled with quartz, feldspar, or micas. Twinning is rare on {101} and {401}.

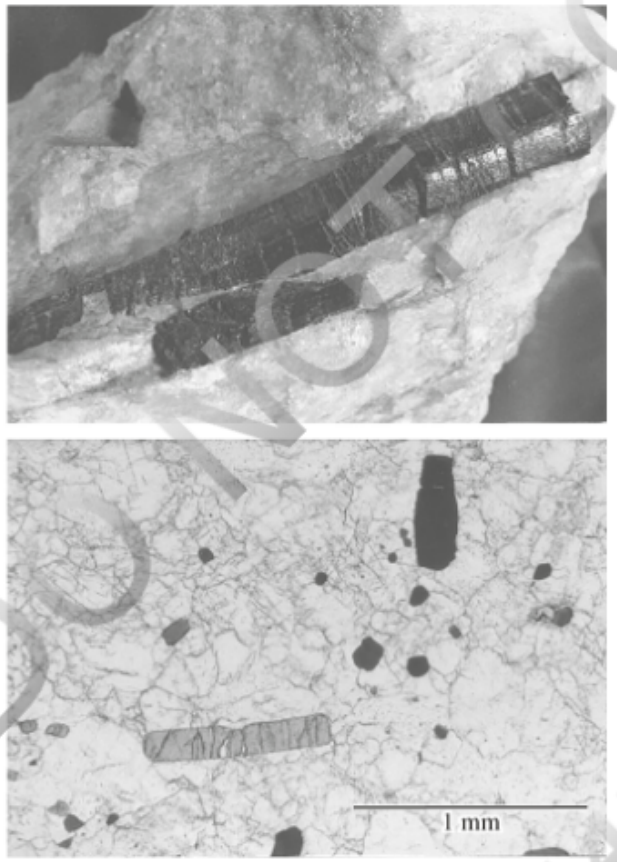

FIGURE 15.10 Tourmaline. (*a*) Elongate crystals with fractures roughly perpendicular to the length, found in a felsic pegmatite. The field of view is about 20 cm wide. (*b*) Thin section showing tourmaline crystals in a metaquartzite in plane light. The ordinary ray is dark and extraordinary ray is light colored. The grain oriented N–S and the basal sections are dark; the grain oriented E–W, which is parallel to the lower polarizer vibration direction, is light. View larger image

Cleavage Cleavages on {110} and {101} are very poor. Fracture is conchoidal. Brittle.

Color Properties

Luster: Vitreous.

Color: The myriad of tourmaline colors are caused by crystal field splitting of chromophore elements (Fe, Mn, Ti, V, Cr, Cu), intervalence charge transfer, color centers, and radiation effects. Samples with abundant Fe^{2+}, Mn^{2+}, and/or Ti^{4+} like schorl are

DO NOT COPY e48d507df5d1141@placeholder.9409

Printed by: e48d507df5d1141@placeholder.94092.edu. Printing is for personal, private use only. No part of this book may be reproduced or transmitted without publisher's prior permission. Violators will be prosecuted.

and radiation effects. Samples with abundant Fe^{2+}, Mn^{2+}, and/or Ti^{4+}, like schorl, are black. Dravite tends to be brown, and elbaite-rich tourmaline is brightly colored red, blue, green, or yellow. Almost any color is possible.

Streak: White to gray.

Color in Thin Section: Highly variable and consistently pleochroic. Schorl displays shades of blue, green, and gray, less commonly pink. Dravite-rich samples are light brown, yellow, or colorless. Elbaite-rich samples are light colored to colorless. In general, color intensity increases with Fe content. Concentric color zoning is common.

Pleochroism: Tourmaline is consistently strongly pleochroic with $\omega \gg \epsilon$, so elongate crystals are darkest when the long dimension is perpendicular to the vibration direction of the lower polarizer, and basal sections are dark.

Optical Characteristics

Relief in Thin Section: Moderate to high positive.

Optic Orientation: Longitudinal sections show parallel extinction and are length fast.

Indices of Refraction and Birefringence: Increase with increasing Fe + Mn content, but the wide diversity of composition precludes using optical properties to estimate composition.

Interference Figure: Basal sections that will yield uniaxial negative figures remain uniformly colored with rotation in plane light. The dark color may make figures difficult to interpret.

Alteration Tourmaline may alter to various phyllosilicates, including sericite, chlorite, and lepidolite (Li-mica). It is fairly stable in the weathering environment.

Distinguishing Features

Hand Sample: Columnar crystals with rounded triangular cross sections and vertical striae are characteristic. Common schorl resembles hornblende, but tourmaline lacks good cleavage and the crystal form is distinctly different.

Thin Section/Grain Mount: Crystal habit, distinct pleochroism, and moderate birefringence distinguish tourmaline. Biotite and hornblende may display similar colors, but have different crystal habits and are darkest when their long dimension is aligned parallel to the vibration direction of the lower polarizer. Hornblende has inclined extinction. Light-colored tourmaline may resemble topaz, apatite, or corundum, but topaz is biaxial, apatite has lower birefringence, and corundum has higher indices of refraction.

Occurrence Tourmaline is by far the most common boron-bearing mineral; its presence therefore requires ample concentrations of the element in the magma, protolith, or fluid that facilitated its growth. Schorl is by far the most common tourmaline and can be a

DO NOT COPY e48d507df5d1141@placeholder.9409

Printed by: e48d507df5d1141@placeholder.94092.edu. Printing is for personal, private use only. No part of this book may be reproduced or transmitted without publisher's prior permission. Violators will be prosecuted.

characteristic mineral in granitic pegmatites. It can also be an accessory mineral in granite, granodiorite, and related felsic igneous rocks. Rocks that have been hydrothermally altered adjacent to pegmatite and related felsic intrusions may contain abundant tourmaline. Tourmaline is also a common accessory mineral in schist, gneiss, quartzite, and phyllite. Dravite-rich tourmaline may be found in metasomatically altered limestone and dolomite in contact metamorphic zones. Because tourmaline is relatively resistant in the weathering environment, it is a common constituent in the heavy mineral fraction of clastic sediments; it may also crystallize under diagenetic conditions as fine prismatic grains or as overgrowths on detrital grains. The October 2011 issue of *Elements* magazine has a number of excellent articles on tourmaline.

Use Tourmaline is used as a gemstone. Green varieties are referred to as tourmaline or Brazilian emerald, pink or red stones may be called rubellite, and blue varieties may be called indicolite. Zoned crystals with red interiors and green rims are called watermelon tourmaline. Piezoelectric properties allow tourmaline to be used in the manufacture of pressure gauges and other electronic components. Tourmaline has historically been used for a variety of folk medicine purposes, probably because it forms beautiful crystals. Modern applications include use in skin care products that explicitly appeal to tourmaline's identity as a gemstone. It is probably no more or less harmful than any of the other skin creams and cosmetics used by people.

DO NOT COPY
e48d507df5d1141@placeholder.9409

Printed by: e48d507df5d1141@placeholder.94092.edu. Printing is for personal, private use only. No part of this book may be reproduced or transmitted without publisher's prior permission. Violators will be prosecuted.

lacks good cleavage and the crystal form is distinctly different.
Thin Section/Grain Mount: Crystal habit, distinct pleochroism, and moderate birefringence distinguish tourmaline. Biotite and hornblende may display similar colors, but have different crystal habits and are darkest when their long dimension is aligned parallel to the vibration direction of the lower polarizer. Hornblende has inclined extinction. Light-colored tourmaline may resemble topaz, apatite, or corundum, but topaz is biaxial, apatite has lower birefringence, and corundum has higher indices of refraction.

Occurrence Tourmaline is by far the most common boron-bearing mineral; its presence therefore requires ample concentrations of the element in the magma, protolith, or fluid that facilitated its growth. Schorl is by far the most common tourmaline and can be a characteristic mineral in granitic pegmatites. It can also be an accessory mineral in granite, granodiorite, and related felsic igneous rocks. Rocks that have been hydrothermally altered adjacent to pegmatite and related felsic intrusions may contain abundant tourmaline. Tourmaline is also a common accessory mineral in schist, gneiss, quartzite, and phyllite. Dravite-rich tourmaline may be found in metasomatically altered limestone and dolomite in contact metamorphic zones. Because tourmaline is relatively resistant in the weathering environment, it is a common constituent in the heavy mineral fraction of clastic sediments; it may also crystallize under diagenetic conditions as fine prismatic grains or as overgrowths on detrital grains. The October 2011 issue of *Elements* magazine has a number of excellent articles on tourmaline.

Use Tourmaline is used as a gemstone. Green varieties are referred to as tourmaline or Brazilian emerald, pink or red stones may be called rubellite, and blue varieties may be called indicolite. Zoned crystals with red interiors and green rims are called watermelon tourmaline. Piezoelectric properties allow tourmaline to be used in the manufacture of pressure gauges and other electronic components. Tourmaline has historically been used for a variety of folk medicine purposes, probably because it forms beautiful crystals. Modern applications include use in skin care products that explicitly appeal to tourmaline's identity as a gemstone. It is probably no more or less harmful than any of the other skin creams and cosmetics used by people.

REFERENCES CITED AND SUGGESTIONS FOR ADDITIONAL READING

Armbruster, T., Bonazzi, P., Akasaka, M., Bermanec, V., Chopin, C., Giere, R., Heuss-Assbichler, S., Liebscher, A., Menchetti, S., Pan, Y., and Pasero, M. 2006. Recommended nomenclature of epidote group minerals. *European Journal of Mineralogy* **18**, 551–567.

Boone, G. M., and Wheeler, E. P., II. 1968. Staining for cordierite and feldspars in thin section. *American Mineralogist* **53**, 327–331.

DO NOT COPY e48d507df5d1141@placeholder.9409-

Printed by: e48d507df5d1141@placeholder.94092.edu. Printing is for personal, private use only. No part of this book may be reproduced or transmitted without publisher's prior permission. Violators will be prosecuted.

Deer, W. A., Howie, R. A., and Zussman, J. 1962. *Rock-Forming Minerals, Volume 1: Ortho- and Ring Silicates*. Longman, London, 333 p.

Deer, W. A., Howie, R.A., and Zussman, J. 2001. *Rock-Forming Minerals, Volume 1B: Disilicates & Ring Silicates*, 2nd ed. The Geological Society, London, 630 p.

Franz, G., and Liebscher, A. 2004. Physical and chemical properties of the epidote minerals—An introduction. *Reviews in Mineralogy & Geochemistry* **56**, 1–82.

Henry, D. J., Novak, M., Hawthorne, F. C., Ertl, A., Dutrow, B. L., Uher, P., and Pezzotta, F. 2011. Nomenclature of the tourmaline-supergroup minerals. *American Mineralogist* **96**, 895–913.

Hormann, P. K., and Raith, M. 1971. Optisch Daten, Gitterkonstanten, Dichte and magnetische Suszeptibilität von Al-Fe (III) Epidoten. *Neues Jahrbuch für Mineralogie Abhandlungen* **116**, 41–60.

Johnston, R. W. 1949. Clinozoisite from Camaderry Mountain, Co. Wicklow. *Mineralogical Magazine* **28**, 505–515.

Liebscher, A., and Franz, G. (eds.). 2004. *Epidotes. Reviews in Mineralogy & Geochemistry* **56**, 628 p.

Myer, G. H. 1965. X-ray determination curve for epidote. *American Journal of Science* **263**, 78–86.

Strens, R. G. J. 1966. Properties of the Al–Fe–Mn epidotes. *Mineralogical Magazine* **35**, 928–944.

DO NOT COPY e48d507df5d1141@placeholder.9409

Printed by: e48d507df5d1141@placeholder.94092.edu. Printing is for personal, private use only. No part of this book may be reproduced or transmitted without publisher's prior permission. Violators will be prosecuted.

CHAPTER 16
Orthosilicates

William D. Nesse
University of Northern Colorado

Graham B. Baird
University of Northern Colorado

DO NOT COPY
e48d507df5d1141@placeholder.9409

Printed by: e48d507df5d1141@placeholder.94092.edu. Printing is for personal, private use only. No part of this book may be reproduced or transmitted without publisher's prior permission. Violators will be prosecuted.

Introduction

The common orthosilicates are listed in **Table 16.1**. Note that for all chemical formulas, the Z:O ratio is 1:4, consistent with the ratio required by the structure. These minerals may be divided into two groups. The first includes olivine, garnet, and zircon, in which all of the oxygen is part of a silicon tetrahedron. The second includes the aluminum silicate polymorphs, staurolite, chloritoid, topaz, and titanite. In these minerals, cations such as Al^{3+} or Ti^{4+} coordinate with O and/or OH that are not part of a silicon tetrahedron. This accounts for the extra anions in the chemical formulas. Additional information on the orthosilicates is provided by Ribbe (1982) and Deer and others (2001).

TABLE 16.1 Common Orthosilicate Minerals[a]

Mineral		Formula	Igneous			
			Felsic	Intermediate	Mafic	Feldspathoid
Olivine		$(Mg,Fe)_2SiO_4$			M	
Zircon		$ZrSiO_4$	A	A	A	A
Garnet	Pyrope	$Mg_3Al_2(SiO_4)_3$				
	Almandine	$Fe_3Al_2(SiO_4)_3$				
	Spessartine	$Mn_3Al_2(SiO_4)_3$	A			
	Grossular/Andradite	$Ca_3(Al, Fe)_2(SiO_4)_3$				
Al Silicates	Andalusite	$AlAlOSiO_4$ or Al_2SiO_5				
	Sillimanite		A	A		A
	Kyanite					
Staurolite		$Al_9Fe_2[(Si,Al)O_4]_4O_6(OH)_2$				
Chloritoid		$(Fe^{2+},Mg,Mn)_2(Al,Fe^{3+})Al_3O_2(SiO_4)_2(OH)_4$				
Topaz		$Al_2(SiO_4)(F,OH)_2$	A			
Titanite		$CaTiOSiO_4$ or $CaTiSiO_5$	A	A	A	A

[a] M = major or common; A = accessory, minor, or heavy mineral fraction of terrigenous sediments.

The basic structure of all of the first group of orthosilicates consists of isolated silicon tetrahedra bonded laterally through various other cations (Ca, Mg, Fe, Al, etc.) held in

DO NOT COPY e48d507df5d1141@placeholder.9409

Printed by: e48d507df5d1141@placeholder.94092.edu. Printing is for personal, private use only. No part of this book may be reproduced or transmitted without publisher's prior permission. Violators will be prosecuted.

octahedral or higher coordination with the oxygen anions of the silicon tetrahedra. The differences in the structures depend on the size and charge for the other cations.

The structures of the second group of orthosilicates are more conveniently described in terms of the polyhedral framework defined by cations other than Si. A high-charged cation, usually Al^{3+} or Ti^{4+}, is a major constituent of these minerals. A typical arrangement is for these cations to form chains or sheets of edge-sharing octahedra, or chains of corner-sharing octahedra. These chains or sheets are linked laterally through silicon in tetrahedral coordination and, if present, other cations. Members of the epidote group, lawsonite, and pumpellyite, described in Chapter 15, all have structures with similar characteristics.

Titanite is the only common member of the second group that is not Al-rich. When found, it serves as an important repository for Ti in a wide variety of igneous and metamorphic rocks. The abundance of aluminum in the others means that they are found only in Al-rich rocks. For the aluminum silicates, staurolite, and chloritoid, this often means pelitic metamorphic rocks, but the aluminum silicates can also be found in Al-rich igneous rocks. For topaz, which is fluorine bearing, this means F-bearing felsic igneous rocks and granitic pegmatites, some hydrothermal environments, and occasionally metamorphic rocks.

Olivine

$$(Mg, Fe)_2SiO_4$$

$$\text{Forsterite (Fo)}: \ Mg_2SiO_4$$

$$\text{Fayalite (Fa)}: \ Fe_2SiO_4$$

$$\text{Orthorhombic } (2/m\ 2/m\ 2/m)$$

$$\text{Fo}: \ a = 4.75 \text{ Å},\ b = 10.20 \text{ Å},\ c = 5.98 \text{ Å},\ Z = 4$$

$$\text{Fa}: \ a = 4.82 \text{ Å},\ b = 10.48 \text{ Å},\ c = 6.09 \text{ Å},\ Z = 4$$

$$H = 6.5 - 7$$

$$G = 3.22 - 4.39$$

$$\text{Biaxial } (+ \text{ or } -)$$

$$n_\alpha = 1.635 - 1.827$$

DO NOT COPY e48d507df5d1141@placeholder.9409

Printed by: e48d507df5d1141@placeholder.94092.edu. Printing is for personal, private use only. No part of this book may be reproduced or transmitted without publisher's prior permission. Violators will be prosecuted.

$$n_\beta = 1.651 - 1.869$$

$$n_\gamma = 1.670 - 1.879$$

$$\delta = 0.035 - 0.052$$

$$2V_x = 46 - 98^\circ$$

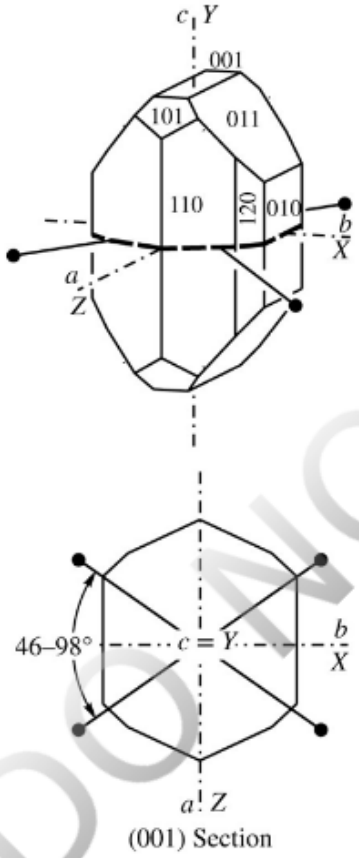

(001) Section

DO NOT COPY

Structure The structure may be visualized as a somewhat distorted hexagonally close-packed array of oxygen with one-eighth of the tetrahedral sites occupied by Si^{4+} and one-half of the octahedral sites occupied by divalent cations (**Figures** 4.1, **16.1**). The Si^{4+} cations share oxygen with adjacent octahedra, but not with other tetrahedra. In the ideal structure, all the octahedral sites would be identical, but in practice, two different sites are developed. The M1 sites that form edge-sharing chains are stretched parallel to the *c* axis, which keeps the cations within the octahedra farther apart (Pauling's Rule 3, Chapter 4). The M2 sites that are affixed to the sides of these chains are somewhat less distorted. The net result of this distortion is a decrease of symmetry from the ideal hexagonal to orthorhombic, and crystals tend to be somewhat elongate parallel to the *c* axis.

Composition Complete solid solution exists between the forsterite (Fo) (Mg_2SiO_4) and fayalite (Fa) (Fe_2SiO_4) end members, although most olivine tends to be relatively forsterite-rich. Mn also may freely substitute in the octahedral sites to form the tephroite (Te) (Mn_2SiO_4) end member, but most common olivine contains little Mn and may be

Printed by: e48d507df5d1141@placeholder.94092.edu. Printing is for personal, private use only. No part of this book may be reproduced or transmitted without publisher's prior permission. Violators will be prosecuted.

treated as a simple forsterite–fayalite solid solution series. Because Fe and Mg have different ionic radii and atomic masses, many physical and optical properties vary systematically with composition (**Figure 16.2**) and accurate measurement of one or several of these properties can provide an estimate of composition.

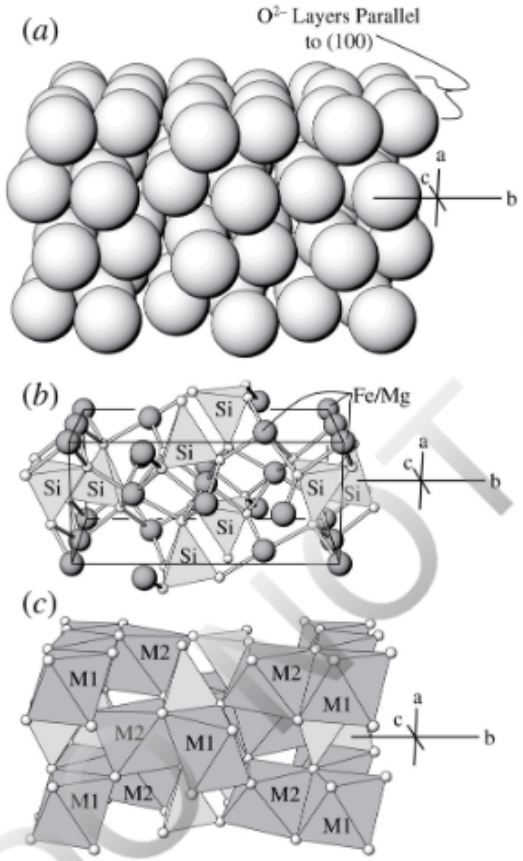

FIGURE 16.1 Olivine structure. (*a*) Oxygen anions form a somewhat loose and distorted hexagonal close-packed array with layers parallel to (100). The distortion reduces symmetry to orthorhombic. (*b*) Silicon tetrahedra point alternately up and down relative to the {100} plane and are tied laterally through Mg/Fe cations in octahedral coordination. Oxygen anions are shown as the smallest spheres; some of the oxygen anions shown in (*a*) have been omitted. The unit cell is shown. (*c*) M1 octahedral sites form edge-sharing chains that extend parallel to the *c* axis. M2 sites are attached to the sides of the M1 chains. All of the oxygen anions shown in (*a*) appear here as small spheres. See also Figure 4.1. View larger image

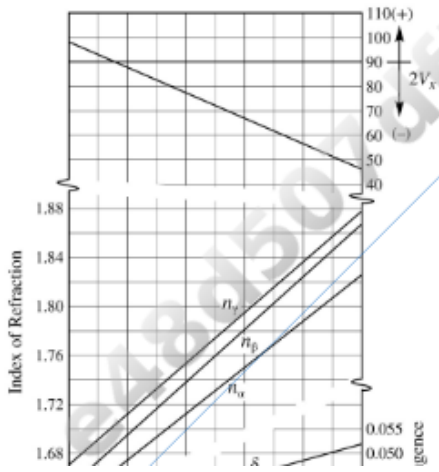

Printed by: e48d507df5d1141@placeholder.94092.edu. Printing is for personal, private use only. No part of this book may be reproduced or transmitted without publisher's prior permission. Violators will be prosecuted.

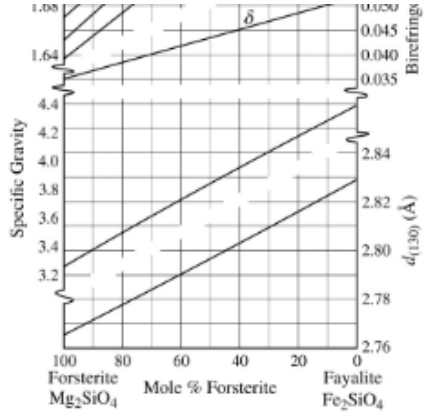

FIGURE 16.2 Specific gravity, $d_{(130)}$, and optical properties of olivine. View larger image

When olivine grows from magma, the first-formed crystals are more Mg-rich than the magma (Figure 5.6). The result is that the residual magma becomes progressively enriched in Fe as olivine crystals grow. Unless equilibrium conditions are maintained, olivine crystals become zoned, with cores more Mg-rich than rims. Refer to Chapter 5 for additional information.

Form and Twinning See **Figure 16.3**. Olivine typically forms anhedral equant grains or aggregates of grains in plutonic igneous rocks and metamorphosed carbonate-bearing rocks. Euhedral crystals are more common in volcanic rocks and tend to be slightly elongate parallel to *c* and flattened along *a* or *b*. Uncommon twins include simple or multiple twins with diffuse boundaries on {100}, {011}, or {012}.

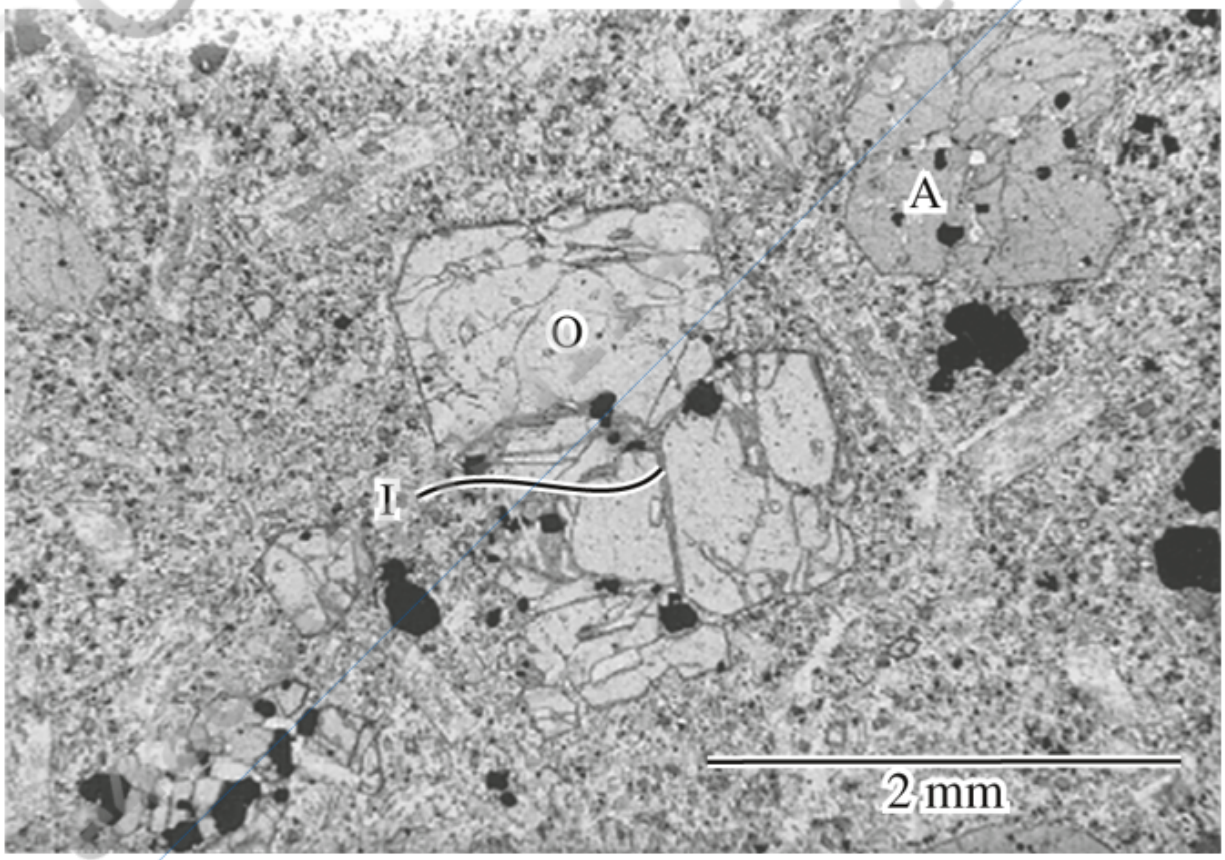

Printed by: e48d507df5d1141@placeholder.94092.edu. Printing is for personal, private use only. No part of this book may be reproduced or transmitted without publisher's prior permission. Violators will be prosecuted.

FIGURE 16.3 Olivine phenocryst (O) in basaltic dike. Note the alteration to iddingsite (I) along grain boundaries and cracks (cf. Figure 7.63d). The phenocryst at the upper right is augite (A). Plane light. View larger image

Cleavage Poor on {010} and {110}, usually not seen. Conchoidal fracture. Brittle.

Color Properties

Luster: Vitreous.

Color: Olive to yellowish green, darker with increasing Fe.

Streak: White.

Color in Thin Section: Colorless, Fe-rich varieties may be yellowish.

Pleochroism: Colored varieties: $X = Z$ = pale yellow, Y = orange-yellow.

Optical Characteristics

Relief in Thin Section: High positive.

Optic Orientation: $X = b$, $Y = c$, $Z = a$. Elongate crystals show parallel extinction and may be either length fast or length slow, depending on orientation.

Indices of Refraction and Birefringence: Vary systematically with Fe content (Figure 16.2).

Interference Figure: $2V$ varies systematically with Fe content (Figure 16.2). The $2V$ angle for olivine from volcanic rocks may be somewhat smaller than that for olivine of the same composition from plutonic rocks. Optic axis dispersion is weak with $r < v$ if optically positive and $r > v$ if negative.

Comments: Chemical zoning (Mg-rich core, more Fe-rich rim) may be recognized by variation in interference color. In sections cut parallel to (001) the rim will have higher interference color than the core, and in sections parallel to (100) the opposite is true.

Alteration Olivine commonly alters to distinctive products visible in thin section (Figures 16.3 and 7.63d). Iddingsite and chlorophaeite are combinations of various minerals and not subject to rigorous identification. Iddingsite is the term given to fine-grained reddish- to yellowish-brown material that usually contains a combination of goethite, clay, chlorite, quartz, talc, and other minerals. Despite the fact that it is an aggregate, iddingsite may display birefringence of 0.04–0.05 with $n_{low} \approx 1.70$ and $n_{high} \approx 1.75$. The brownish color usually masks the interference color. Chlorophaeite is an essentially isotropic orangish to greenish material composed of some combination of iron oxide/hydroxide, chlorite, and other low-birefringence silicates. Its index of refraction is roughly 1.5–1.6. Alteration to serpentine (chrysotile or antigorite) also is common. Olivine from igneous rocks may be mantled by pyroxene or hornblende as the result of normal magmatic reactions between

DO NOT COPY e48d507df5d1141@placeholder.9409

Printed by: e48d507df5d1141@placeholder.94092.edu. Printing is for personal, private use only. No part of this book may be reproduced or transmitted without publisher's prior permission. Violators will be prosecuted.

mantled by pyroxene or hornblende as the result of normal magmatic reactions between olivine and the melt.

Distinguishing Features

Hand Sample: Distinguished by yellowish-green or green color, vitreous luster, conchoidal fracture, and granular nature. May be confused with epidote, which usually has a richer green or pistachio-green color and cleavage. Greenish quartz also may appear similar, but quartz occurs in distinctly different rocks.

Thin Section/Grain Mount: High birefringence, distinctive fracturing, lack of cleavage, and alteration products are distinctive. Pyroxenes have lower birefringence, cleavage, simple or lamellar twinning, and for the monoclinic varieties, inclined extinction in maximum birefringence sections. Epidote has cleavage, has inclined extinction, is optically negative, and may display a patchy pistachio-green color.

Occurrence Because of how easily it weathers, olivine is rarely found in clastic sedimentary rocks, except for very immature sediments deposited near source rocks containing olivine. It is, however, common in mafic and ultramafic igneous rocks associated with Ca-rich plagioclase, Ca-clinopyroxene, and orthopyroxene. Metamorphosed carbonates may contain relatively pure forsterite in association with calcite, dolomite, diopside, epidote group minerals, grossular garnet, tremolite, and related Ca–Mg-bearing minerals. For nearly all igneous and metamorphic rocks, quartz and olivine are not found together. For igneous rocks, if the magma is dry and high enough in SiO_2 to form quartz, then pyroxene would crystallize. This can be generalized by the following reaction of forsterite with quartz, producing enstatite:

$$Mg_2SiO_4 + SiO_2 \rightarrow Mg_2Si_2O_6$$

However, this generalization is not always true. The exception are olivine-bearing granites, usually referred to as fayalitic granites. As the name suggests, Fe-rich fayalite can be found with quartz, but magma compositions that crystallize fayalite and quartz together are uncommon.

Discussion Under sufficiently high pressures, such as those obtained in the Earth's mantle, olivine is not stable relative to two different high-pressure polymorphic structures. Both high-pressure polymorphs are about 6% more dense than olivine and are based on cubic close packing of oxygen rather than hexagonal close packing. They are approximately isostructural with the mineral spinel and are therefore known as β-spinel and γ-spinel. Si is in tetrahedral coordination and Mg/Fe is in octahedral coordination; they differ only in details of site occupancy. The seismic velocity increase at around 400-km depth in the mantle may be caused by the change from the olivine structure to the spinel structure. Further, it has been argued (Green and Burnley, 1989; Iidaka and Suetsuga, 1992) that deep earthquakes in subduction zones are triggered by the reconstructive polymorphic transition of olivine to the spinel structure.

DO NOT COPY e48d507df5d1141@placeholder.9409

Printed by: e48d507df5d1141@placeholder.94092.edu. Printing is for personal, private use only. No part of this book may be reproduced or transmitted without publisher's prior permission. Violators will be prosecuted.

reconstructive polymorphic transition of olivine to the spinel structure.

Uses See **Box 16.1** regarding the use of olivine and mafic or ultramafic rocks in CO_2 sequestration.

BOX 16.1
Enhanced Rock Weathering and Carbon Sequestration

Research has investigated whether it is viable to use olivine for enhanced rock weathering and atmospheric CO_2 sequestration. Enhanced rock weathering is the artificial increase in the rate of chemical weathering. This is typically done by mining and grinding rock, resulting in a significant increase in rock and mineral surface area available for chemical weathering by the atmosphere and water. If this is done to silicate minerals, the chemical weathering reaction uses and stores atmospheric CO_2, thus sequestering the CO_2 by removing it from the atmosphere. Of the common silicate minerals, olivine by far weathers the fastest (see Box 11.1). It chemically weathers by the following reaction:

$$\begin{aligned} &Mg_2SiO_4 + 4H_2O + 4CO_2 \\ &\rightarrow 2\,Mg^{2+} + 4HCO^{3-} + H_4SiO_4 \end{aligned} \quad \textbf{(16.1)}$$

Here olivine is generalized as the forsterite end member and atmospheric CO_2 is dissolved in water (rain, fresh surface water, or seawater). The products of this weathering reaction are ions dissolved in water (here, Mg^{2+}), bicarbonate (HCO^{3-}) dissolved in water, and dissolved Si in the form of orthosilicic acid (H_4SiO_4). See Box 20.2 for further discussion of the carbon cycle and additional reactions involving these and other similarly produced weathering products. The key result of the reaction is the conversion of atmospheric CO_2 into dissolved bicarbonate; some of the bicarbonate is used by various organisms to form calcite ($CaCO_3$) shells (see Chapter 5). If the calcite is incorporated into rock, the CO_2 used by Equation 16.1 is effectively sequestered into a potentially long-term reservoir—removing it and keeping it out of the atmosphere.

Research is currently underway to assess whether developing large-scale mining and grinding projects using dunite (nearly pure olivine rock; see Chapter 11) or other olivine-rich rocks is a viable strategy for reducing atmospheric CO_2 and mitigating human-caused climate change. Ideally, 1.25 tons of CO_2 could be sequestered for every ton of olivine weathered. However, the weathering process is relatively slow. In order for the reaction to proceed quickly enough as to have an impact on atmospheric CO_2 in the following decades, the ground olivine must have a very fine grain size of tens of microns and it must be weathered in warm, wet climates. Proposed locations to spread the ground olivine include equatorial beaches and rain forests. Another option is to spread the material across the open ocean or use it as an agricultural fertilizer. But in these settings some of the material may not become fully

DO NOT COPY e48d507df5d1141@placeholder.9409-

Printed by: e48d507df5d1141@placeholder.94092.edu. Printing is for personal, private use only. No part of this book may be reproduced or transmitted without publisher's prior permission. Violators will be prosecuted.

agricultural fertilizer. But in these settings some of the material may not become fully weathered, or it may be weathered more slowly, particularly outside of tropical regions.

Mining, grinding, and transporting the olivine or olivine-rich rock requires fossil fuel burning, which of course results in additional atmospheric CO_2 and reduces the net amount of CO_2 sequestered. If it were transported 1000 km, there would be an estimated 30 percent loss in the amount of CO_2 sequestered. This transportation distance is likely a minimum as olivine-rich rocks are somewhat rare on land.

Some estimates put the minimum cost of this CO_2 sequestration technique at about $50 per metric ton of CO_2 removed. Based on current estimates, other less-expensive means of CO_2 sequestration include improved forestry management, improved agricultural techniques, and reforestation. Further, enhanced rock weathering would alter local and ocean pH and chemistry, and other side effects likely exist but have yet to be fully explored. The infrastructure (mines, mills, container ships, trucks, etc.) also do not exist to generate and distribute the gigatons of ground olivine needed annually to counter-balance CO_2 emissions by any meaningful amount (tens of percent per year), but this method could be used at a much smaller scale in local, more feasible settings as part of a range of carbon sequestration strategies employed to combat climate change.

More information on using olivine in enhanced rock weathering and carbon sequestration techniques can be found in Schuiling and Krijgsman (2006), Hangx and Spiers (2009), Köhler and others (2010), Montserrat and others (2017), and Andrews and Taylor (2019).

Clear green olivine, known as peridot, is a minor gemstone; some of the finest material comes from the island of Zebirget in the Red Sea. Presumably because of its appeal as a gemstone, peridot has historically been used to treat gastrointestinal problems and other maladies. It is used in industry to make molds for certain types of casting procedures in foundries, and infrequently as an abrasive. Some dental ceramics contain forsterite as a strengthening agent.

Garnet

$$X_3Y_2(SiO_4)_3$$

Isometric $4/m\,\bar{3}\,2/m$

$a = 11.46 - 12.05$ Å,

$Z = 8$

$H = 6.5 - 7$

$G = 3.1 - 4.2$

Isotropic

DO NOT COPY e48d507df5d1141@placeholder.9409

Printed by: e48d507df5d1141@placeholder.94092.edu. Printing is for personal, private use only. No part of this book may be reproduced or transmitted without publisher's prior permission. Violators will be prosecuted.

Isotropic

$n = 1.714 - 1.890$

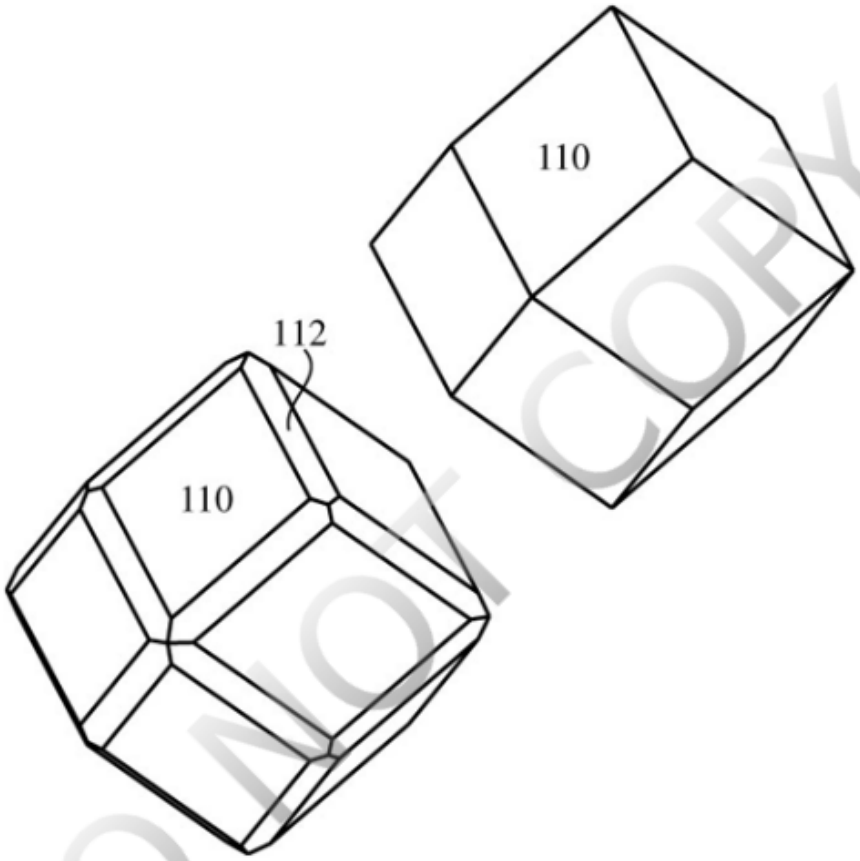

Structure The structure of garnet consists of isolated silicon tetrahedra bonded laterally through cations in 6-fold and 8-fold coordination (**Figure 16.4**). Si tetrahedra and Y octahedra share single oxygen anions to form chains extending parallel to each of the *a* axes. The spaces between these chains are distorted 8-fold sites occupied by the X cations.

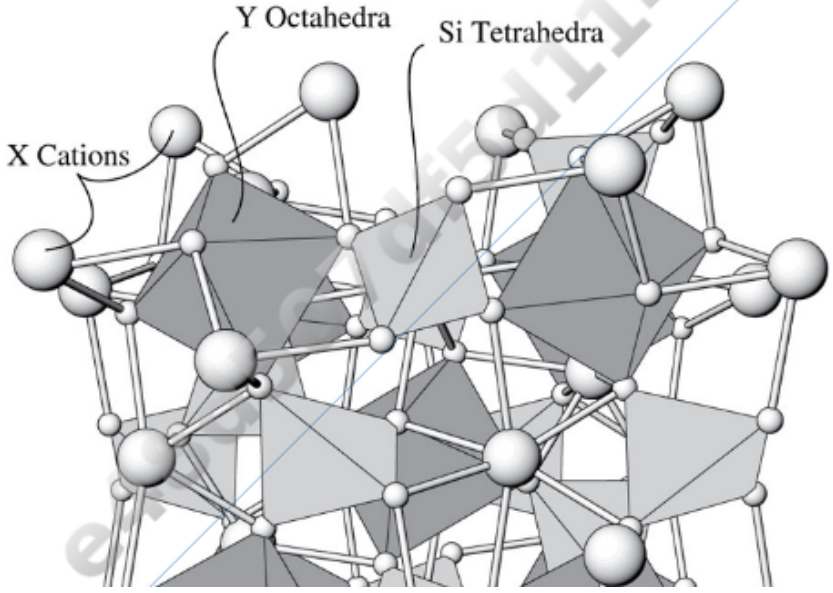

DO NOT COPY

Printed by: e48d507df5d1141@placeholder.94092.edu. Printing is for personal, private use only. No part of this book may be reproduced or transmitted without publisher's prior permission. Violators will be prosecuted.

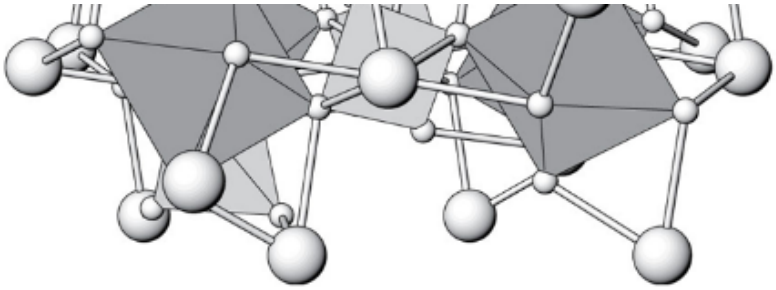

FIGURE 16.4 Garnet structure. Isolated silicon tetrahedra share single oxygen anions with Y cations in 6-fold coordination. The spaces between are distorted 8-fold sites occupied by the larger X cations. View larger image

Composition A total of 32 species of garnet have been approved by the International Mineralogical Association, and more are likely to be added. Of these, 20 are silicates; the rest are oxides, halides, hydroxides, vanadates, and arsenates that utilize the garnet structure—that is, they are isostructural.

The common garnet end-member compositions are shown in **Table 16.2**. Traditionally these have been grouped into the pyralspite (pyrope, almandine, spessartine), and grandite (grossular, andradite, hydrogrossular) groups. With inclusion of the rare Cr-bearing garnet uvarovite [$Ca_2Cr_3(SiO_4)_3$], the grandite group becomes the ugrandite group. However, the Commission on New Minerals, Nomenclature and Classification of the International Mineralogical Association (Grew and others, 2013) recommends that these group names be abandoned because they do not follow current group-naming conventions.

TABLE 16.2 Garnet

Group	End Member	Composition	*n*		*G* (calc)	*a* (Å)
			Pure Synthetic	Normal Range		
Pyralspite	Pyrope	$Mg_3Al_2(SiO_4)_3$	1.714	1.720–1.770	3.582	11.46
	Almandine	$Fe_3Al_2(SiO_4)_3$	1.830	1.770–1.820	4.315	11.53
	Spessartine	$Mn_3Al_2(SiO_4)_3$	1.800	1.790–1.810	4.197	11.62
Grandite	Grossular	$Ca_3Al_2(SiO_4)_3$	1.734	1.735–1.770	3.594	11.85
	Andradite	$Ca_3Fe_2^{3+}(SiO_4)_3$	1.877	1.850–1.890	3.859	12.05
	Hydrogrossular	$Ca_3Al_2(SiO_4)_{3-x}(OH)_{4x}$	—	1.675–1.734	3.1–3.6	Varies

Regardless, the pyralspite and grandite groupings are useful in considering the compositions of most common garnets. In the pyralspite group, the Y cation is Al^{3+}, and solid solution is extensive among these end members, though most have compositions that fall between Mg^{2+}

Printed by: e48d507df5d1141@placeholder.94092.edu. Printing is for personal, private use only. No part of this book may be reproduced or transmitted without publisher's prior permission. Violators will be prosecuted.

that fall between pyrope and almandine, or between almandine and spessartine. Ca^{2+} occupies the X site in the grandite group, and solid solution is continuous between grossular and andradite. Hydrogrossular is similar to grossular except that one Si^{4+} is missing from a tetrahedral site. Charge balance is maintained by bonding a H^{+} to each of the four oxygens surrounding the vacant site.

Garnet with a general composition $(Mg,Fe,Ca)_3Al_2(SiO_4)_3$, intermediate between the two groups, is found in high temperature (>700°C) metamorphic rocks. The size difference between Ca^{2+} and Mg^{2+}/Fe^{2+} suggests that exsolution could occur at lower temperatures, forming grossular lamellae within an almandine garnet, for example. At least at the microscopic scale, most garnet does not display obvious exsolution lamellae, though being isotropic, lamellae would be difficult to recognize. However, lamellae parallel to {110} have been reported, and it is likely that exsolution lamellae are responsible for the {110} parting reported in the literature.

The ideal isometric symmetry may be reduced to orthorhombic or triclinic in some garnets, particularly members of the grandite group, by a combination of ordering of Al^{3+} and Fe^{3+} in the octahedral sites and by distortions caused by the hydrogrossular substitution. Heating, which destroys the ordering, causes these garnets to revert to isometric symmetry.

Form and Twinning See **Figure 16.5**. Garnet typically forms euhedral to subhedral crystals composed of dodecahedral {110} and/or trapezohedral {112} faces. In thin section, these crystals usually yield six- or eight-sided shapes. Granular or irregular masses are not uncommon. Isotropic garnet does not display twinning. Anomalously birefringent varieties often display transformation twins that form a pattern of six or more wedge-shaped sectors radiating from the grain's center or a tweedlike intersecting pattern of twin lamellae.

(*a*)

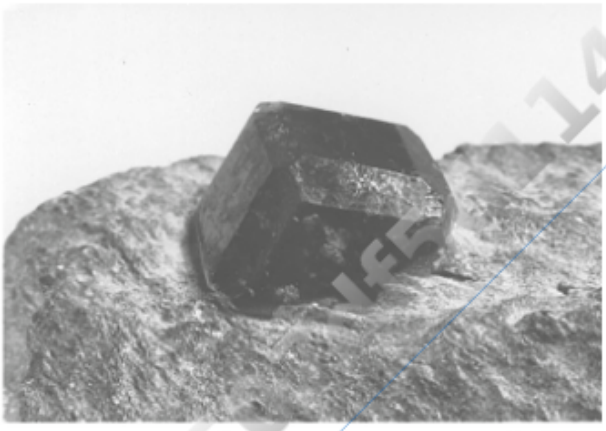

(*b*)

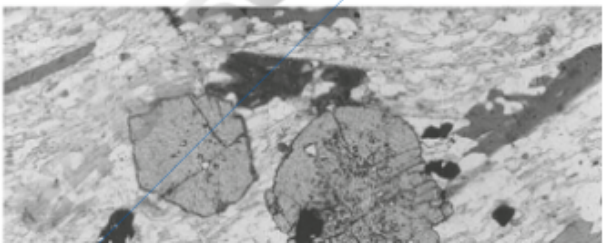

DO NOT COPY

Printed by: e48d507df5d1141@placeholder.94092.edu. Printing is for personal, private use only. No part of this book may be reproduced or transmitted without publisher's prior permission. Violators will be prosecuted.

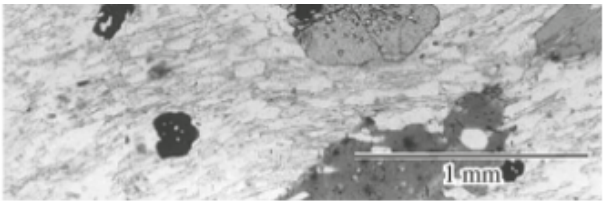

FIGURE 16.5 Garnet. (*a*) 2-cm garnet crystal in mica schist. (*b*) Photomicrograph of garnet porphyroblasts in mica schist. The larger dark grains are biotite, and the finer grains in the groundmass are quartz, plagioclase, muscovite, and chlorite. Plane light. View larger image

Cleavage None. Uncommon parting on {110}, irregular conchoidal fracture with many angular corners and edges. Brittle.

Color Properties

Luster: Vitreous.

Color: Pyrope, almandine, spessartine: wine-red to reddish brown, also black, orange, dark pink, brown. Grossular and hydrogrossular: green, colorless, pink, brown. Andradite: yellow, green, brown, black. The diversity of color is controlled mostly by the presence of chromophore elements (Fe, Mn, Cr, etc.) in the X and Y structural sites. Oxygen to metal (Fe) charge transfer transitions are responsible for the brown color of pyrope-almandine garnets. Small amounts of Cr^{3+} in the Y site provides two transitions that absorb light and produce the purple-red color of pyrope.

Streak: White.

Color in Thin Section and Grain Mount: Pale version of the hand-sample color.

Optical Characteristics

Relief in Thin Section: High positive.

Optic Orientation: Typical pyralspite garnet is isotropic, but grandite garnets and some spessartine may be anomalously anisotropic, consistent with their reduced symmetry.

Indices of Refraction: Varies systematically with composition in the two groups. For pyralspite, almandine has the highest index of refraction and specific gravity. For grandite, andradite has the highest index of refraction and specific gravity.

Interference Figure: The anomalously birefringent varieties have variable optical orientation and may be uniaxial or biaxial with variable 2*V*.

Alteration Garnet may alter to chlorite, or occasionally to other minerals such as hornblende, epidote, or iron oxide. Garnet is commonly involved in a variety of mineral reactions in metamorphic rocks and may display reaction or replacement textures with other minerals (Figure 5.29).

DO NOT COPY e48d507df5d1141@placeholder.9409

Printed by: e48d507df5d1141@placeholder.94092.edu. Printing is for personal, private use only. No part of this book may be reproduced or transmitted without publisher's prior permission. Violators will be prosecuted.

Distinguishing Features

Hand Sample: Crystal habit, hardness, and color distinguish garnet in hand sample.

Thin Section/Grain Mount: Recognized based on isotropic habit, crystal habit, and high relief. The grandite group from metamorphosed carbonate-bearing rocks may be anomalously birefringent. Spinel is distinctly green or brown, occurs as octahedrons, and often has a somewhat lower index of refraction. Basal sections of apatite in thin section may be confused with garnet but have lower relief and yield uniaxial interference figures.

Occurrence The occurrence and identity of associated minerals are fairly reliable guides to the variety of garnet. Pyrope is generally limited to ultramafic igneous rocks and the serpentinites derived from them. Almandine-rich garnet is the typical garnet in mica schist and gneiss. Spessartine and compositions intermediate between spessartine and almandine are found in particularly Al-rich compositions of felsic igneous rocks such as pegmatite, granite, and rhyolite. Grossular and andradite are the typical garnets found in metamorphosed carbonate-rich rocks associated with calcite, dolomite, tremolite, diopside, wollastonite, and epidote. Hydrogrossular is an uncommon variety found in metamorphosed carbonate rocks.

Comments Garnet is a characteristic mineral of many metamorphic rocks. The chemical composition of the almandine-rich garnet found in mica schist is influenced by the temperature, pressure, and related conditions at the time of growth. If garnet growth spanned some period of time during which temperature and pressure changed, it may acquire chemical zoning that reflects those changing conditions. Detailed microprobe analysis of the chemical zoning in garnet and associated minerals can therefore be used to infer the time–temperature–pressure history of the rocks containing the garnet. Additionally, garnet can be dated using the ^{176}Lu–^{176}Hf and ^{147}Sm–^{143}Nd radioactive parent and stable daughter isotope pairs (see Box 5.1). This further increases its utility in unraveling the history of metamorphic terranes. The December 2013 issue of *Elements* has a number of excellent review articles.

Use Garnet is used as a semiprecious gemstone. The irregular fracture paired with its hardness makes garnet valuable as an abrasive, particularly for sandpaper. Also used in filters to help purify water in wastewater treatment plants. Probably because of its eye-catching, well-formed crystals, garnet found application in early medical practice; in Roman times it was believed that garnet tied with camel hair would “harden the spleen.”

Zircon

$$\mathrm{ZrSiO_4}$$

$$\text{Tetragonal } 4/m\ 2/m\ 2/m$$

$$a = 6.61\ \text{Å},\ c = 5.98\ \text{Å},\ Z = 4$$

DO NOT COPY e48d507df5d1141@placeholder.9409

Printed by: e48d507df5d1141@placeholder.94092.edu. Printing is for personal, private use only. No part of this book may be reproduced or transmitted without publisher's prior permission. Violators will be prosecuted.

$$H = 7.5$$

$$G = 4.68$$

$$\text{Uniaxial } (+)$$

$$n_\omega = 1.920 - 1.960$$

$$n_\epsilon = 1.967 - 2.015$$

$$\delta = 0.036 - 0.065$$

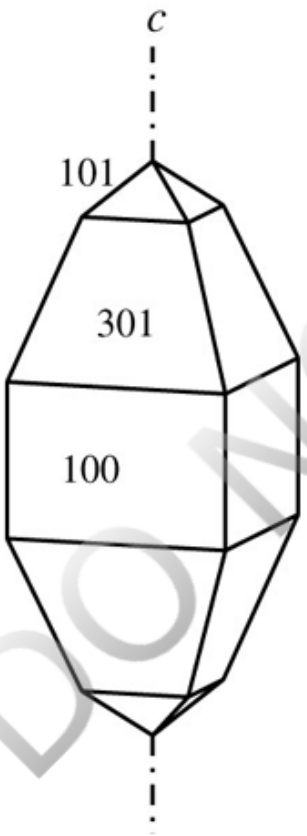

Structure Zr^{4+} is a relatively large cation (Appendix A) and fits comfortably in 8-fold coordination. The structure can be considered to consist of chains parallel to *c* in which Si tetrahedra alternate with Zr in 8-fold coordination.

Composition Zircon always contains some hafnium (Hf), and continuous solid solution extends to the rare mineral hafnon ($HfSiO_4$). Over 50 elements have been identified in zircon, including the rare earth elements, uranium, and thorium. Radioactive decay of uranium and thorium may cause the structure to become metamict (see Chapter 5).

Form and Twinning See **Figure 16.6**. Most grains are microscopic tetragonal prismatic crystals elongate along the *c* axis with dipyramidal terminations. Euhedral overgrowths may develop on subhedral or rounded cores (Figures 5.30 and 9.6). Detrital zircon may be euhedral to rounded, depending on the amount of transport. Zircon is not usually twinned, but twinning on {111} has been reported.

DO NOT COPY
e48d507df5d1141@placeholder.9409

Printed by: e48d507df5d1141@placeholder.94092.edu. Printing is for personal, private use only. No part of this book may be reproduced or transmitted without publisher's prior permission. Violators will be prosecuted.

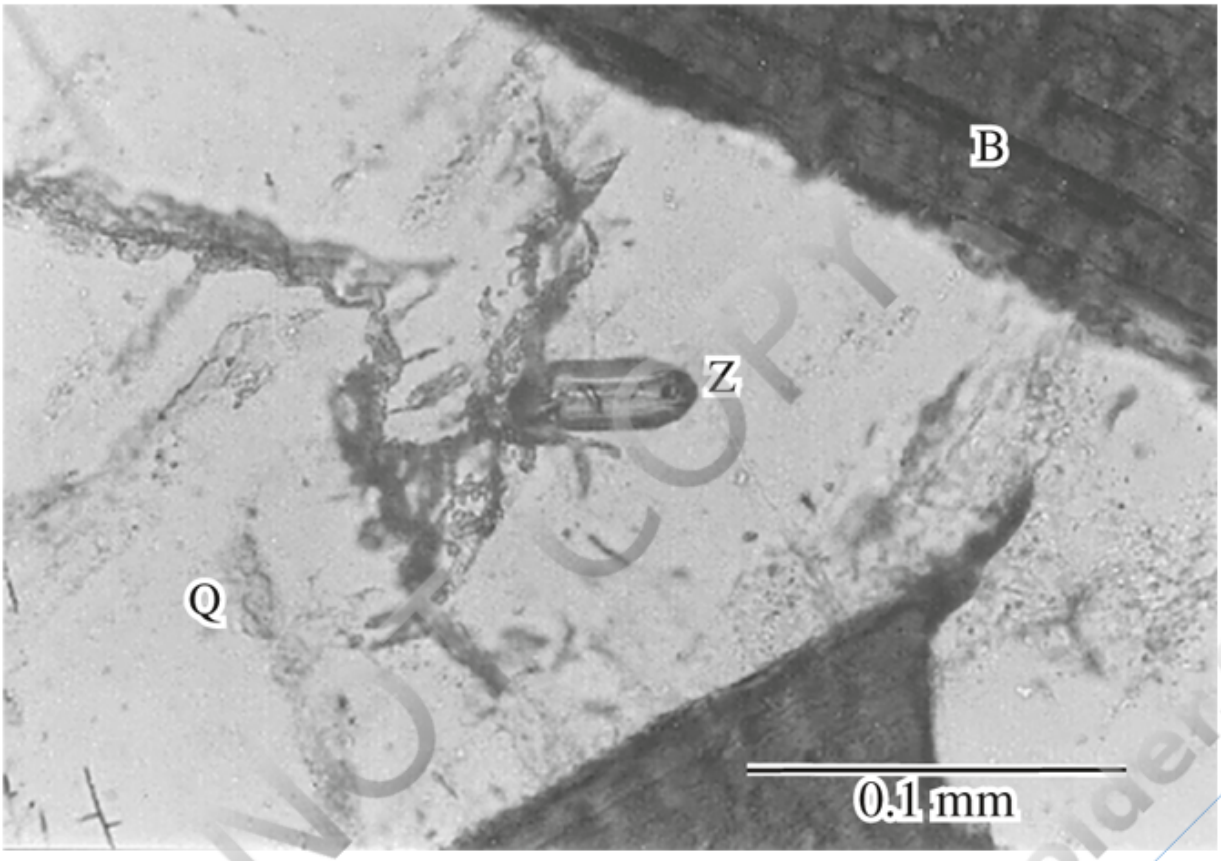

FIGURE 16.6 Photomicrograph of a thin section of granite showing a small zircon crystal (Z) in quartz (Q). The dark mineral is biotite (B). Plane light. View larger image

Color Properties

Luster: Vitreous to adamantine; greasy if metamict.

Color: Grayish, yellowish, or reddish brown; less commonly colorless, yellow, gray, pink, or bluish green. Thermoluminescent, cathodoluminescent; may fluoresce under UV light.

Streak: White.

Color in Thin Section: Colorless to pale brown, although high relief and small grain size may make color difficult to recognize. Some samples may be cloudy or may show concentric color zoning or patchy color.

Pleochroism: Weak pleochroism ($\omega < \epsilon$) of colored varieties is more likely to be visible in grain mount.

Cleavage Prismatic {110} and pyramidal {111} cleavages are poor and not usually seen in either hand sample or thin section, nor do they tend to control orientation in grain mount. Conchoidal fracture. Brittle.

Optical Characteristics

DO NOT COPY e48d507df5d1141@placeholder.9409

Printed by: e48d507df5d1141@placeholder.94092.edu. Printing is for personal, private use only. No part of this book may be reproduced or transmitted without publisher's prior permission. Violators will be prosecuted.

Relief in Thin Section: Very high positive.

Optic Orientation: Crystals are length slow and show parallel extinction in longitudinal sections or as grains in a grain mount.

Indices of Refraction and Birefringence: Natural zircon that is not metamict has indices of refraction n_ω = 1.924–1.934, n_ε = 1.970–1.977, and δ = 0.036–0.053. High-Hf zircon has higher indices. Metamict zircon has lower indices and birefringence and, if strongly metamict, may be isotropic with an index of around 1.80. The interference color of relatively fresh zircon ranges up to third and fourth order in thin section.

Interference Figure: Small grain size often precludes obtaining an interference figure. Basal sections yield uniaxial positive optic axis figures with numerous isochromes. Metamict varieties are usually essentially isotropic, but may yield anomalous biaxial figures with small 2*V*.

Alteration Except for becoming metamict because of U and Th radioactive decay, zircon is quite stable and neither weathers nor alters to other minerals.

Distinguishing Features

Hand Sample: While present in many different rock types as an accessory mineral, zircon is rarely seen in hand samples because of its small grain size. In uncommon cases of large or abundant grains, it is recognized by its crystal habit and hardness.

Thin Section/Grain Mount: Usually recognized as small, elongate, high-relief grains with bright interference colors included in other minerals. Zircon may produce dark halos in surrounding minerals such as biotite, cordierite, and hornblende because of U and Th radioactive decay. Rutile is darker colored, displays good cleavage if grains are large enough, and has higher indices of refraction and birefringence. Titanite has a different habit, is biaxial, and has higher birefringence. Xenotime (YPO_4) is a similar mineral that is isostructural with zircon but has higher birefringence (0.070–0.107) and lower indices of refraction (n_ω = 1.690–1.724, n_ε = 1.760–1.827).

Occurrence Zircon is widely distributed in many igneous, clastic sedimentary, and metamorphic rocks, but usually only as microscopic crystals. In mafic igneous and metamorphic rocks it tends to be rare, requiring a higher silica content than these rocks offer. The presence of appreciable quartz in such rocks can be used as an indicator of sufficient silica for zircon growth. Because it is durable in the weathering environment, zircon is common in the heavy mineral fraction of sediments. If these sediments are subsequently melted, detrital zircon grains can be preserved as grains in the igneous rocks produced from those melts. These zircon grains that have gone through the full rock cycle will often acquire overgrowths of fresh zircon mantling the old detrital cores (Figure 5.30).

Use Zircon is unique in that it is both a source of metals and used as an industrial mineral. It is the principal source of metallic zirconium and hafnium, and also a source

DO NOT COPY e48d507df5d1141@placeholder.94092

Printed by: e48d507df5d1141@placeholder.94092.edu. Printing is for personal, private use only. No part of this book may be reproduced or transmitted without publisher's prior permission. Violators will be prosecuted.

mineral. It is the principal source of metallic zirconium and hafnium, and also a source for rare earth elements. Zirconium is used in nuclear reactors and is alloyed to produce metals very resistant to heat and corrosion. As an industrial mineral, zircon is used in the manufacture of refractory bricks and as a foundry sand used in making castings. Most of the commercially produced zircon comes from modern or ancient beach **placer deposits**. Placer deposits are high concentrations of dense minerals in clastic sediments and sedimentary rocks formed through the selective transport and deposition of sediment. Australia produces most of the world's zircon, followed by South Africa and the United States. Zircon also may be used as a gemstone. Cubic zirconia, which is widely used in inexpensive jewelry, is a synthetic zirconium oxide often made from zirconium extracted from zircon. Other forms of zirconium oxide are used as dental crowns.

Comments Zircon is one of the most important minerals used for constructing the geologic history of an area or for the Earth as a whole (see Box 5.1). Zircon readily grows from intermediate to felsic magmas and can grow or recrystallize during metamorphism. It is physically and chemically resistant to erosion, so zircon weathered from rocks is preserved in clastic sediments and sedimentary rocks. When it grows or recrystallizes, U^{4+} substitutes for Zr^{4+} in abundances of a few hundred parts per million, while essentially no Pb is incorporated. Further, diffusion of elements into and out of zircon is slow. Therefore, zircon is an ideal mineral for radiometric dating using the U-Pb method. This method can be applied to whole grains or portions of grains with multiple domains of different ages. U-Pb radiometric dating requires sophisticated technology but produces remarkably precise ages. Decay of U also results in the progressive development of fission tracks and the accumulation of ^{4}He. These products can be used to constrain rock cooling history. In summary, zircon can be used to date pluton crystallization, metamorphism, rock cooling, the maximum age of sediment deposition, and it can track sediment sources based on the distribution of detrital zircon ages. Zircon also has considerable value because of the trace elements that it contains. The trace elements can help document rock melting and magma crystallization; in addition, they can help constrain models of crustal formation and evolution. **Table 16.3** lists some of these and other uses for zircon; Box 5.1 details its use with constraining the timing of geologic events.

TABLE 16.3 Application of Zircon to Geologic Problems

Chemistry	Application
U and Th substitution for Zr^{4+}, Pb decay product	U–Pb and Th–Pb geochronology, age of igneous rock crystallization, age of medium- to high-grade metamorphism, age of sediment deposition and identification of sediment sources (Box 5.1)
U and Th substitution for Zr^{4+}, fission tracks and He decay products	Fission track and (U–Th)/He thermochronology, determination of exhumation and landscape development (Box 5.1)
U and Th substitution for Zr^{4+}	Determine cause zircon growth (igneous or metamorphic) through U/Th ratios
Hf^{4+} substitution for Zr^{4+}	Investigate continental growth and magma source (crust vs. mantle)

Printed by: e48d507df5d1141@placeholder.94092.edu. Printing is for personal, private use only. No part of this book may be reproduced or transmitted without publisher's prior permission. Violators will be prosecuted.

Hf^{4+} substitution for Zr^{4+}	Investigate continental growth and magma source (crust vs. mantle) through Hf isotopes
Ti^{4+} substitution for Si^{4+}	Temperature of zircon growth through Ti in zircon thermometry (e.g., Ferry and Watson, 2007)
Rare earth elements substitution for Zr^{4+}	Reconstruct magmatic histories, fingerprint magmatic sources, determine metamorphic reaction history
Oxygen isotope composition	Document the contribution of sediment and crust to magma sources; examine crustal recycling
Melt inclusions	Magma composition from which zircon crystallized

Source: Adapted from Hanchar and Hoskins (2003) and Harley and Kelly (2007).

DO NOT COPY
e48d507df5d1141@placeholder.9409

Printed by: e48d507df5d1141@placeholder.94092.edu. Printing is for personal, private use only. No part of this book may be reproduced or transmitted without publisher's prior permission. Violators will be prosecuted.

Aluminum Silicates

The **aluminum silicate polymorphs** andalusite, sillimanite, and kyanite ($AlAlOSiO_4$) are common minerals in pelitic metamorphic rocks, but they can also be found in other rock types. In some sources they are referred to as the **aluminosilicate polymorphs**. The formula is usually given as Al_2SiO_5; however, writing the formula as $AlAlOSiO_4$ demonstrates that these minerals are orthosilicates and that there are two distinct Al structural sites.

Structure Andalusite, sillimanite, and kyanite are reconstructive polymorphs whose structures can be described in terms of edge-sharing chains of aluminum octahedra that are linked laterally through Si and Al. The structures differ in the details of Al coordination, chain geometry, and the manner in which Si and Al link adjacent chains. Note that these structures are quite similar to those of epidote, lawsonite, pumpellyite, and staurolite.

In andalusite, edge-sharing chains of Al^{3+} octahedra extend parallel to the *c* axis and are bonded laterally through pairs of Al^{3+} in distorted 5-fold coordination and Si^{4+} in tetrahedral coordination (**Figure 16.7a**). The formula can therefore be expressed as $^{VI}Al^{V}AlO^{IV}SiO_4$, where the superscripts refer to the coordination of the cations. The structure is relatively open, and andalusite has the lowest specific gravity (3.13–3.16) of the polymorphs. Relatively weak linkages between chains allow cleavage parallel to the {110} faces.

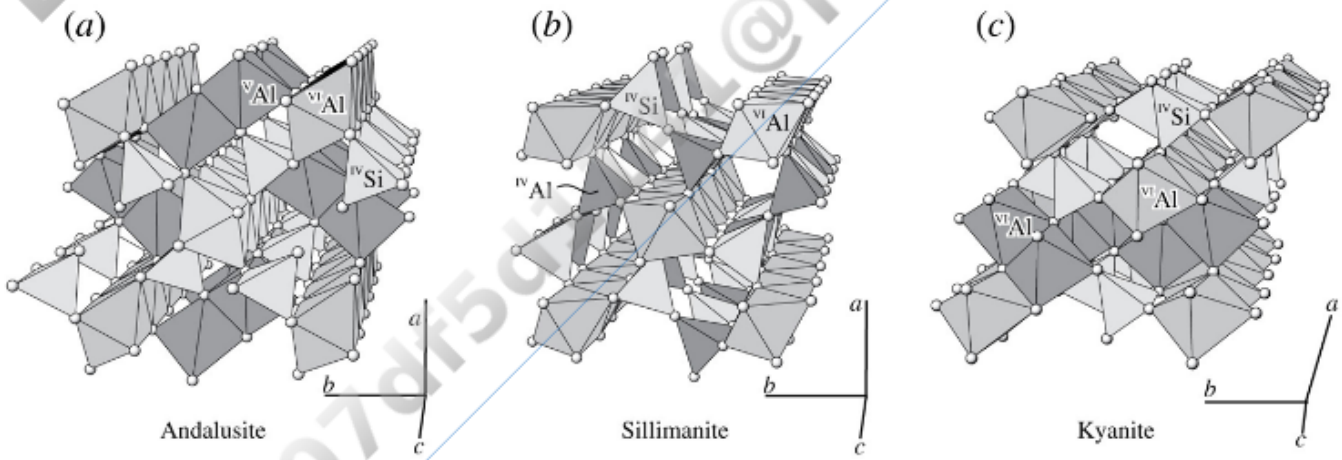

FIGURE 16.7 Structure of the aluminum silicates. (*a*) Andalusite. Edge-sharing chains of $^{VI}Al^{3+}$ octahedra (medium shading) extend parallel to *c* and are bonded laterally through pairs of $^{V}Al^{3+}$ in irregular 5-fold coordination (dark), and single $^{IV}Si^{4+}$ tetrahedra (light). (*b*) Sillimanite. Edge-sharing chains of $^{VI}Al^{3+}$ octahedra (medium shading) extend parallel to *c* and are bonded laterally through alternating $^{IV}Al^{3+}$ (dark) and $^{IV}Si^{4+}$ (light) tetrahedra. (*c*) Kyanite. Straight chains of $^{VI}Al^{3+}$ octahedra (medium shading) extend parallel to *c* and are bonded laterally through zigzag chains of $^{VI}Al^{3+}$ octahedra (dark) and $^{IV}Si^{4+}$ (light) in tetrahedral coordination. View larger image

DO NOT COPY e48d507df5d1141@placeholder.94092

Printed by: e48d507df5d1141@placeholder.94092.edu. Printing is for personal, private use only. No part of this book may be reproduced or transmitted without publisher's prior permission. Violators will be prosecuted.

octahedra (dark) and Si (light) in tetrahedral coordination. View larger image

The structure of sillimanite consists of chains of edge-sharing Al^{3+} octahedra parallel to *c* that are linked laterally through Al^{3+} and Si^{4+}, both in tetrahedral coordination (**Figure 16.7b**). Its formula, including the coordination, is $^{VI}Al^{IV}AlO^{IV}SiO_4$. Ideally the Al^{3+} and Si^{4+} occupy alternating tetrahedra (i.e., they are ordered), but some degree of randomness or disorder in the distribution of these elements is possible.

The structure of kyanite has a distorted cubic close-packed array of oxygen with Al^{3+} occupying 40% of the octahedral sites and Si^{4+} occupying 10% of the tetrahedral sites. This close-packed structure yields the highest specific gravity of the polymorphs (G = 3.53–3.67), so it should be no surprise that kyanite is the polymorph stable at high pressure. Half the aluminum is distributed in the octahedral sites to form zigzag chains parallel to the *c* axis and the other half in octahedra that form straight chains. Silicon in tetrahedral coordination links the chains together (**Figure 16.7c**). The structural formula can be written as $^{VI}Al^{VI}AlO^{IV}SiO_4$. Kyanite is notable because it displays a significant difference in scratch hardness, depending on direction (Figure 6.3). When scratched parallel to the *c* axis, it is significantly softer than when scratched at a right angle. This is presumably because bonds within the octahedral chains are stronger than the bonds that tie adjacent chains to each other. When kyanite is scratched parallel to the chains that extend parallel to *c*, adjacent chains are easily split apart. When scratched at a right angle, the stronger bonds along the length of the chains must be broken.

Occurrence The aluminum silicate polymorphs are most commonly characteristic minerals of medium- and high-grade pelitic metamorphic rocks such as mica schist, biotite gneiss, and hornfels. Recall that pelitic metamorphic rocks are derived from mudstone and shale sedimentary rocks, which, because they are clay-rich, tend to contain substantial amounts of Al.

Each polymorph has a specific temperature–pressure (T–P) range over which it is stable, so these minerals have been used extensively to establish the metamorphic T–P conditions to which rocks containing them have been subjected. The T–P stability of the aluminum silicates has been repeatedly studied and more than 15 different diagrams have been published. Figure 16.8 shows a recent determination that is consistent with field relationships and can be used with reasonable confidence. Minor diagram revisions have been published and additional refinement is likely. Problems with establishing the T–P stability fields of the polymorphs include order–disorder in sillimanite and small compositional variations of the minerals. The Al–Si order–disorder in sillimanite is not particularly important, but it appears that small amounts of Fe and/or Mn entering the structure of andalusite may have a significant effect on the range of its stability. A good summary of the mineralogy of the aluminum silicate minerals is provided by Kerrick (1990).

DO NOT COPY e48d507df5d1141@placeholder.94092

Printed by: e48d507df5d1141@placeholder.94092.edu. Printing is for personal, private use only. No part of this book may be reproduced or transmitted without publisher's prior permission. Violators will be prosecuted.

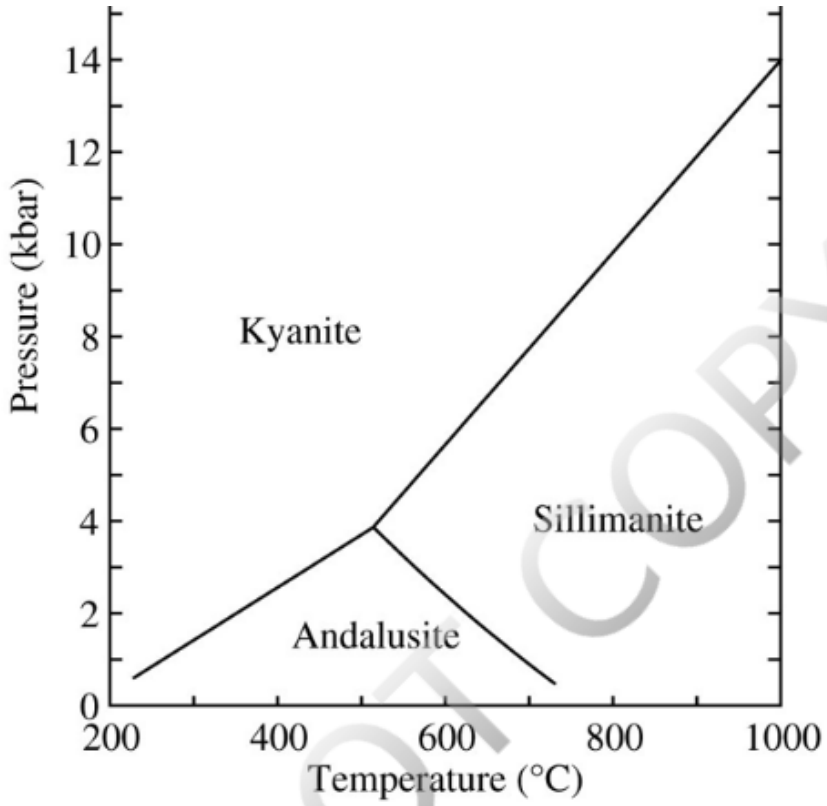

FIGURE 16.8 Aluminum silicate stability fields. From Hemingway and others (1991). View larger image

Andalusite is stable at relatively low temperatures and pressures and is commonly found in contact metamorphic aureoles of shallow and intermediate-depth intrusions and in rocks subjected to medium-grade metamorphism at relatively low pressures. Sillimanite is found in rocks that have been subjected to higher temperatures, and kyanite is characteristic of rocks subjected to relatively high pressures. These minerals may, depending on grade of metamorphism and bulk chemistry of the rocks, be associated with cordierite, staurolite, garnet, chlorite, muscovite, biotite, chloritoid, K-feldspar, and plagioclase. For rocks subjected to the blueschist or eclogite metamorphic facies, the associated minerals include pyrope-rich garnet, omphacite, jadeite, lawsonite, and glaucophane. Kyanite can be blue in such settings, and with glaucophane, can help color blueschists and related rocks blue. All three polymorphs are less commonly found in Al-rich felsic igneous rocks. A considerable literature has developed debating whether these occurrences represent primary magmatic crystallization, are the result of post-magmatic crystallization processes (i.e., metamorphism), or are **xenocrysts**, which are foreign crystals introduced into the magma from the surrounding country rock (similar to xenoliths) or from the magma's source rock. One root of this debate derives from the faulty assumption that the aluminum silicates are "metamorphic minerals" and that occurrences in igneous rocks are anomalous. Although each case must be evaluated based on field, textural, chemical, and related evidence, there is no compelling reason that these minerals should not crystallize directly from Al-rich magma. Sillimanite, in particular, appears to be a common accessory mineral in Al-rich granitic rocks.

All three polymorphs locally can be important detrital minerals, although they are not

DO NOT COPY

Printed by: e48d507df5d1141@placeholder.94092.edu. Printing is for personal, private use only. No part of this book may be reproduced or transmitted without publisher's prior permission. Violators will be prosecuted.

All three polymorphs locally can be important detrital minerals, although they are not particularly stable in the weathering environment.

Use Heating the aluminum silicates to high temperatures can cause them to convert to mullite [$Al_6Si_2O_{13}$] plus quartz. Mullite has a structure similar to that of sillimanite and is quite refractory. Mullitized aluminum silicate is used to manufacture refractory materials such as high-alumina bricks and related products used to line blast furnaces, ladles, and kilns, and in similar applications requiring resistance to high temperatures. Sillimanite is least commonly used for this purpose because it is usually fine grained and therefore difficult and expensive to extract from rocks. It also requires higher temperatures (and more money) to mullitize. The choice between andalusite and kyanite depends on availability and on details of the requirements for the specific application. Andalusite, and to a lesser degree kyanite, are used in the manufacture of certain ceramic products, abrasives, and filler materials. The largest commercial deposits of andalusite in the world are in South Africa, where it is extracted from aluminum-rich pelitic metamorphic rocks and from detrital deposits derived from these rocks. Of the three polymorphs, only kyanite has historically been used for medical purposes (stress reduction, throat problems), probably because its bladed blue crystals are more striking and likely to trigger the placebo effect. The chiastolite variety of andalusite (see section on andalusite), which contains a cross-shaped pattern, is sometimes used in jewelry and has religious significance to some people.

Andalusite

$$^{VI}Al^{V}AlO^{IV}SiO_4 \text{ or } Al_2SiO_5$$

$$\text{Orthorhombic } 2/m\ 2/m\ 2/m$$

$$a = 7.79 \text{ Å},\ b = 7.91 \text{ Å},$$
$$c = 5.56 \text{ Å},\ Z = 4$$

$$H = 6.5 - 7.5$$

$$G = 3.13 - 3.16$$

$$\text{Biaxial } (-)$$

$$n_\alpha = 1.629 - 1.640$$

$$n_\beta = 1.634 - 1.645$$

$$n_\gamma = 1.638 - 1.650$$

$$\delta = 0.009 - 0.013$$

$$2V_x = 71 - 88^\circ$$

DO NOT COPY e48d507df5d1141@placeholder.9409

Printed by: e48d507df5d1141@placeholder.94092.edu. Printing is for personal, private use only. No part of this book may be reproduced or transmitted without publisher's prior permission. Violators will be prosecuted.

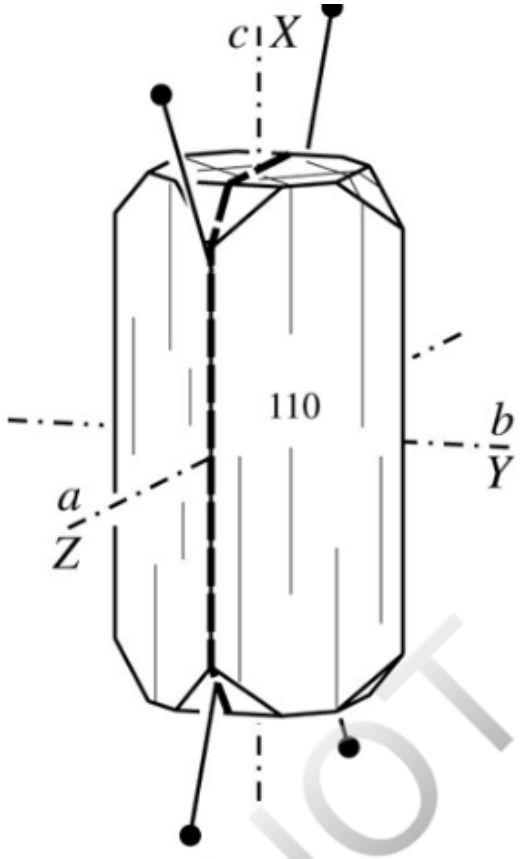

Composition Most andalusite is relatively pure Al_2SiO_5, although significant Mn^{3+} and Fe^{3+} may substitute for Al^{3+} in octahedral sites. Extensive solid solution to kanonaite ($MnAlOSiO_4$) is possible.

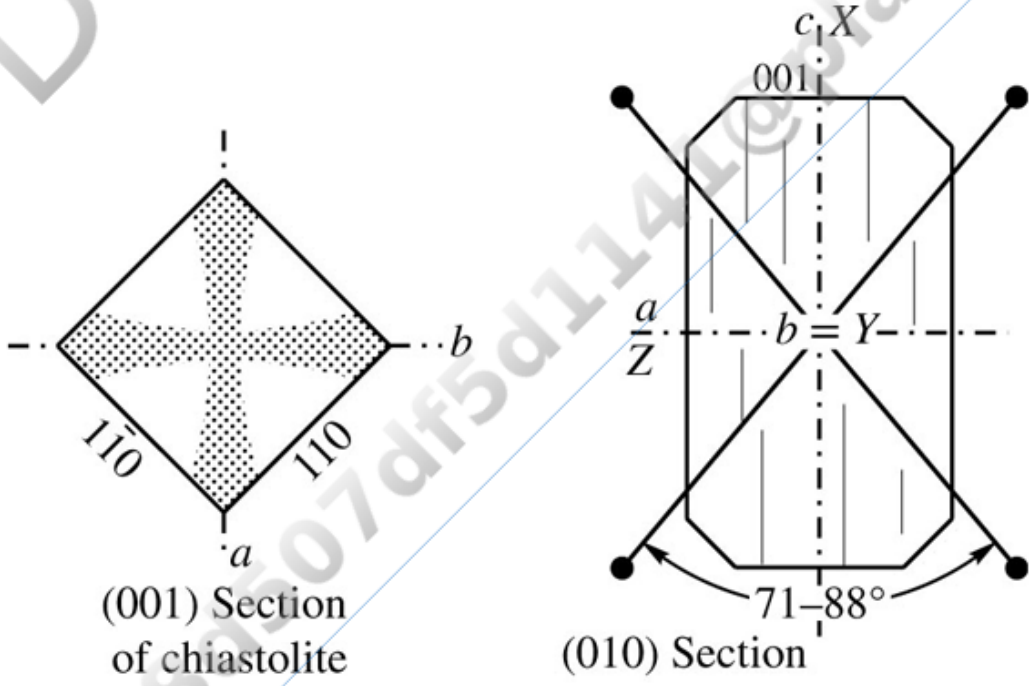

Form and Twinning See Figure 16.9. Andalusite commonly forms porphyroblasts in medium-grade mica schist. These crystals are usually prismatic {110} and elongate

DO NOT COPY

Printed by: e48d507df5d1141@placeholder.94092.edu. Printing is for personal, private use only. No part of this book may be reproduced or transmitted without publisher's prior permission. Violators will be prosecuted.

medium-grade mica schist. These crystals are usually prismatic {110} and elongate parallel to *c* with a nearly square cross section. A variety called chiastolite contains dark carbonaceous inclusions that form a cross along the diagonals of the prism. Andalusite also forms anhedral grains and irregular masses. Numerous inclusions of quartz, fine opaques, or other minerals are common but are usually visible only in thin section. Twinning on {101} is rare.

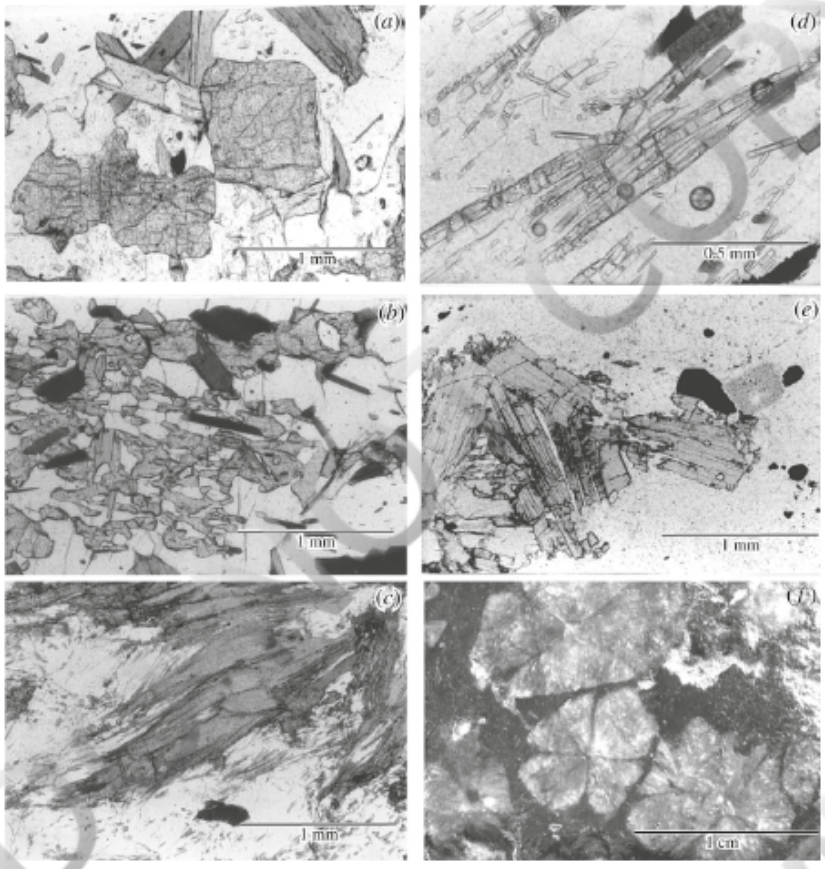

FIGURE 16.9 Aluminum silicates in mica schist. (*a*) Blocky andalusite crystal in thin section. (*b*) Strongly sieved (inclusion-rich) andalusite porphyroblast (high relief) in thin section. (*c*) Fibrolitic sillimanite mass in thin section. (*d*) Elongate prismatic crystals of sillimanite in thin section. (*e*) Bladed kyanite in thin section. (*f*) Hand sample showing cross-shaped pattern of inclusions in basal sections of chiastolite. All thin sections plane light. View larger image

Cleavage Good {110} prismatic cleavages are nearly at right angles and are parallel to prism faces in cross sections, but may not be evident in hand sample, particularly if the sample is altered. Cleavage on {100} is poor and not usually evident. Uneven to subconchoidal fracture. Brittle.

Color Properties

Luster: Vitreous.

Color: Pink, white, pinkish brown, violet, or gray; darker colors are associated with high Mn and Fe.

Streak: White

Printed by: e48d507df5d1141@placeholder.94092.edu. Printing is for personal, private use only. No part of this book may be reproduced or transmitted without publisher's prior permission. Violators will be prosecuted.

Streak: White.

Color in Thin Section: Usually colorless in thin section or grain mount, less frequently with a pale pink or green cast.

Pleochroism: Weak in colored varieties: X = reddish pink, $Y = Z$ = greenish yellow.

Optical Characteristics

Relief in Thin Section: Moderately high positive.

Optic Orientation: $X = c$, $Y = b$, $Z = a$, optic plane = (010). Length fast with parallel extinction to trace of cleavage and crystal faces in longitudinal sections, symmetrical extinction in basal sections. Samples with $Mn^{3+} + Fe^{3+} > 6.5$ mol % are length slow, $X = a$, $Y = b$, $Z = c$, and are biaxial positive.

Indices of Refraction and Birefringence: Indices of refraction increase with substitution of $Mn^{3+} + Fe^{3+}$ for Al^{3+}. Most andalusite has birefringence in the range 0.009–0.013, which gives it first-order gray and white interference colors in standard thin sections. Birefringence decreases to nearly zero at $Mn^{3+} + Fe^{3+} \approx 6.5$ mol % and increases above that point.

Interference Figure: Most andalusite is biaxial negative with $2V > 80°$. Basal sections yield acute bisectrix figures with the melatopes outside the field of view. Cleavage fragments yield strongly off-center obtuse bisectrix figures. Optic axis dispersion is weak, $r < v$ or occasionally $r > v$. Andalusite with more than ~6.5 mol % $Mn^{3+} + Fe^{3+}$ is optically positive with $2V_z$ between 65° and 85°. In the composition range where the transition from optically positive to negative is made, $2V$ is quite variable.

Alteration Andalusite may alter to sericite or to chlorite or other sheet silicates. It is commonly involved in metamorphic mineral reactions and may show reaction relations with minerals such as cordierite, staurolite, garnet, sillimanite, and kyanite.

Distinguishing Features

Hand Sample: Porphyroblasts in pelitic metamorphic rocks may be euhedral or may form highly irregular grains riddled with quartz inclusions. Other porphyroblasts with which andalusite may be confused, particularly if altered, include cordierite, staurolite, and kyanite. The habit of euhedral crystals is distinctive, particularly of the chiastolite variety, as is the pinkish color of some samples. Staurolite is brown and forms cross-shaped twins. Kyanite is bladed and may be blue, at least in patches, and the difference in hardness across and parallel to the length of crystals is distinctive. Anhedral cordierite with abundant quartz inclusions may appear to be similar but is more typically blue, not pink. The hardness of altered andalusite may be substantially reduced.

Thin Section: Moderately high relief, large $2V$, and length fast character. Sillimanite is biaxial +, length slow, and has higher birefringence and a slender prismatic to fibrous

DO NOT COPY e48d507df5d1141@placeholder.94092

Printed by: e48d507df5d1141@placeholder.94092.edu. Printing is for personal, private use only. No part of this book may be reproduced or transmitted without publisher's prior permission. Violators will be prosecuted.

habit. Kyanite has inclined extinction and higher birefringence. Staurolite has a distinct honey yellow color and higher indices of refraction. Orthopyroxene may have higher birefringence, is length slow, and has a different occurrence. Apatite is uniaxial, and has lower birefringence and slightly anomalous interference colors.

Sillimanite

$$^{VI}Al^{IV}AlO^{IV}SiO_4 \text{ or } Al_2SiO_5$$

$$\text{Orthorhombic } 2/m\ 2/m\ 2/m$$

$$a = 7.488\ \text{Å},\ b = 7.681\ \text{Å},$$
$$c = 5.777\ \text{Å},\ Z = 4$$

$$H = 6.5 - 7.5$$

$$G = 3.23 - 3.27$$

$$\text{Biaxial } (+)$$

$$n_\alpha = 1.653 - 1.661$$

$$n_\beta = 1.657 - 1.662$$

$$n_\gamma = 1.672 - 1.683$$

$$\delta = 0.018 - 0.022$$

$$2V_z = 20 - 30^\circ$$

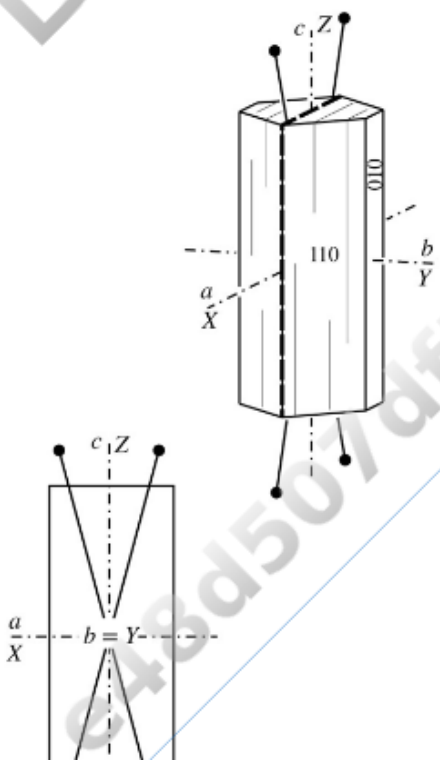

DO NOT COPY
e48d507df5d1141@placeholder.9409

Printed by: e48d507df5d1141@placeholder.94092.edu. Printing is for personal, private use only. No part of this book may be reproduced or transmitted without publisher's prior permission. Violators will be prosecuted.

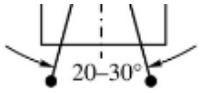

(010) Section

Composition Most sillimanite is relatively pure Al_2SiO_5, although minor amounts of Fe^{3+}, Cr^{3+}, or Ti^{4+} may be present.

Form and Twinning See Figure 16.9. Sillimanite commonly forms slender prismatic or fine fibrous crystals. Masses of fine fibrous crystals are called fibrolite. These masses may form swirled or matted aggregates a few millimeters to a centimeter across. Cross sections through crystals are usually approximately diamond shaped.

Cleavage Perfect on {010}, apparently between the chains of aluminum octahedra. Uneven fracture. Brittle. Fibrous aggregates may be tough.

Color Properties

Luster: Vitreous.

Color: Colorless or white, less commonly yellow, brown, or blue.

Streak: White.

Color in Thin Section and Grain Mount: Usually colorless, although matted fibrolite masses may be pale brown.

Pleochroism: Not usually pleochroic. Pleochroism for dark-colored varieties and thick fragments is listed in Table 16.4.

TABLE 16.4 Pleochroism in Sillimanite[a]

Hand-Sample Color	*X*	*Y*	*Z*
Yellow	Yellow	Green-yellow	Colorless
Brown	Colorless or pale yellow	Colorless or pale yellow	Violet-brown
Blue	Colorless or pale yellow	Colorless or pale yellow	Blue

[a] Most sillimanite in thin section is not visibly pleochroic.

Optical Characteristics

Relief in Thin Section: High positive.

Optic Orientation: $X = a$, $Y = b$, $Z = c$, optic plane {010}. Elongate grains show parallel extinction and are length slow.

Indices of Refraction and Birefringence: Indices of refraction show little variation. In thin section, interference colors are up to lower second order. Fine fibrolite fibers show lower

DO NOT COPY e48d507df5d1141@placeholder.9409

Printed by: e48d507df5d1141@placeholder.94092.edu. Printing is for personal, private use only. No part of this book may be reproduced or transmitted without publisher's prior permission. Violators will be prosecuted.

section, interference colors are up to lower second order. Fine fibrolite fibers show lower interference colors because they are thinner than a standard thin section.

Interference Figure: Basal sections of crystals of sufficient size yield acute bisectrix interference figures with $2V$ between 20° and 30°. Fragments on the {010} cleavage yield flash figures. Optic axis dispersion is strong, $r > v$.

Alteration Sillimanite may alter to sericite and may show reaction relations with associated minerals.

Distinguishing Features

Hand Sample: Slender crystals or fibrous clots in medium- and high-grade pelitic metamorphic rocks are characteristic. The fibrous nature of fibrolite is visible with a hand lens; it is not uncommon for fibrolite clots to be partially replaced by muscovite. Sillimanite resembles wollastonite and tremolite but has only one cleavage and a different occurrence.

Thin Section: Distinguished by high relief, moderate birefringence, parallel extinction, and slender prismatic or fibrous crystal habit. Kyanite has inclined extinction and is biaxial negative with a large $2V$. Tremolite displays typical amphibole cleavage and inclined extinction. Wollastonite is biaxial negative and has three cleavage directions. Fine fibers of sillimanite found in granitic rocks are often erroneously identified as rutile.

Kyanite

$$^{VI}Al^{VI}AlOSiO_4 \text{ or } Al_2SiO_5$$

$$\text{Triclinic } \bar{1}$$

$$a = 7.126 \text{ Å}, \ b = 7.852 \text{ Å},$$
$$c = 5.572 \text{ Å}, \ \alpha = 89.99^\circ,$$
$$\beta = 101.11^\circ, \ \gamma = 106.03^\circ,$$
$$Z = 4$$

$$H = \ \sim 5 \text{ parallel toc}, \ \sim 7$$
$$\text{at right angles on } \{100\}$$
$$\text{cleavage surfaces}$$

$$G = 3.53 - 3.67$$

$$\text{Biaxial } (-)$$

$$n_\alpha = 1.710 - 1.718$$

$$n_\beta = 1.719 - 1.725$$

DO NOT COPY e48d507df5d1141@placeholder.9409

Printed by: e48d507df5d1141@placeholder.94092.edu. Printing is for personal, private use only. No part of this book may be reproduced or transmitted without publisher's prior permission. Violators will be prosecuted.

$$n_\gamma = 1.724 - 1.734$$

$$\delta = 0.012 - 0.016$$

$$2V_x = 78 - 84^\circ$$

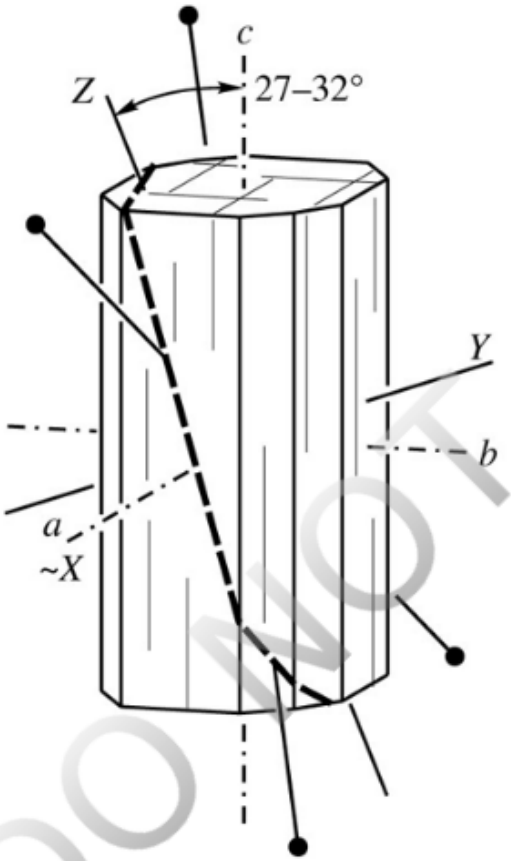

DO NOT COPY

Composition Most kyanite is relatively pure Al_2SiO_5, although minor substitution of Fe^{3+}, Ti^{4+}, or Cr^{3+} may be present.

Form and Twinning Figure 16.9e. Kyanite commonly forms elongate bladed or columnar crystals that may appear to be bent or twisted. Single or multiple twins with {100} composition planes are common; multiple twins on {001} are less common. Twinning is generally not obvious in hand sample.

Cleavage Perfect on {100}, good on {010}, where {100} ∧ {010} = 79°. Cleavage fragments may be splintery. A basal parting on {001} may be conspicuous, cutting at about 85° to the length of crystals. Splintery fracture. Brittle.

Color Properties

Luster: Vitreous.

Color: Patchy blue, gray, or white, less commonly light green. The blue color is interpreted to be caused by intervalence charge transfer between Fe^{2+} and Ti^{4+}.

Printed by: e48d507df5d1141@placeholder.94092.edu. Printing is for personal, private use only. No part of this book may be reproduced or transmitted without publisher's prior permission. Violators will be prosecuted.

Streak: White.

Color in Thin Section: Usually colorless, though some may show patchy light blue colors. Color may be more distinctive in grain mount.

Pleochroism: Weak if colored, $X < Y < Z$: X = colorless, Y = light violet-blue, Z = light cobalt-blue.

Optical Characteristics

Relief in Thin Section: High positive.

Optic Orientation: The optic plane is nearly at right angles to (100). $Z \wedge c$ and $Y \wedge b$ are both about +27° to +32° and $X \wedge a$ is only a few degrees. The maximum extinction angle of about 30° is obtained on grains or cleavage fragments with {100} parallel to the microscope stage. Basal sections yield extinction angles of less than 3°, and sections parallel to {010} yield extinction angles of around 7°. Both prismatic crystals and cleavage fragments are length slow.

Indices of Refraction and Birefringence: Indices of refraction vary in a small range. In thin section the 0.012–0.016 birefringence produces first-order interference colors. Fragments on cleavage surfaces in grain mounts yield intermediate birefringence.

Interference Figure: Grains in thin section and fragments with (100) horizontal yield acute bisectrix interference figures with the melatopes outside the field of view. Optic axis dispersion is weak, $r > v$.

Alteration Kyanite may alter to sericite or to chlorite or other phyllosilicates. Reaction textures with other aluminous minerals such as andalusite, sillimanite, staurolite, cordierite, or garnet are not uncommon.

Distinguishing Features

Hand Sample: Distinguished by bladed habit, color, cleavage, and distinct variation of scratch hardness with direction.

Thin Section/Grain Mount: Different habit, higher indices of refraction, inclined extinction, optical character, and sign of elongation distinguish kyanite from andalusite and sillimanite.

Staurolite

$$Al_9Fe_2[(Si, Al)O_4]_4O_6(OH)_2$$

$$\text{Monoclinic (pseudo} - \text{orthorhombic)}\ 2/m$$

$$a = 7.863 - 7.871\ \text{Å},$$

DO NOT COPY e48d507df5d1141@placeholder.9409

Printed by: e48d507df5d1141@placeholder.94092.edu. Printing is for personal, private use only. No part of this book may be reproduced or transmitted without publisher's prior permission. Violators will be prosecuted.

$$b = 16.534 - 16.613 \text{ Å},$$
$$c = 5.632 - 5.663 \text{ Å},$$
$$\beta = 90.00 - 90.45^\circ,\ Z = 2$$

$$H = 7 - 7.5$$

$$G = 3.74 - 3.83$$

$$\text{Biaxial } (+)$$

$$n_\alpha = 1.736 - 1.747$$
$$n_\beta = 1.740 - 1.754$$
$$n_\gamma = 1.745 - 1.762$$

$$\delta = 0.009 - 0.015$$

$$2V_z = 80 - 90^\circ$$

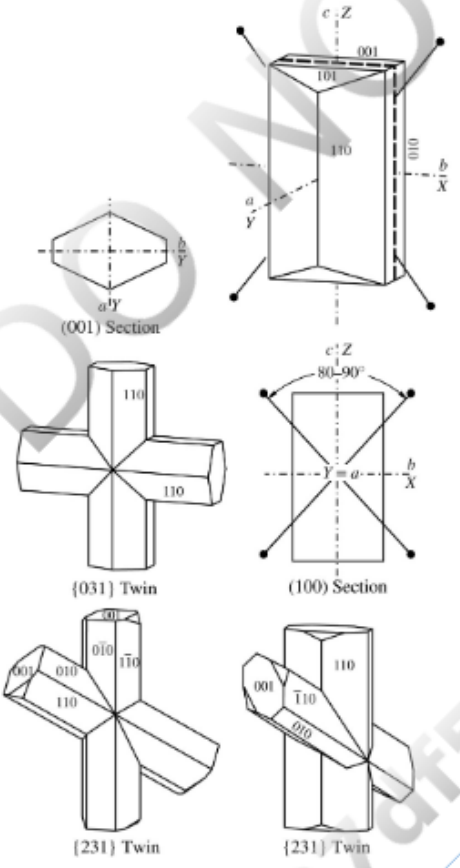

Structure The structure of staurolite is based on slightly distorted cubic close-packed oxygen and hydroxyl with cations in both octahedral and tetrahedral sites. A general formula for staurolite can be given $Y_9Z'_2(Z''O_4)_4O_6A_2$. The Y cations occupy four different octahedral sites, Y1, Y2, Y3, and Y4. The Y1, Y2, and Y3 cations form octahedral chains that extend parallel to the *c* axis; the Y4 cations occupy octahedra that link between the chains. The tetrahedral Z′ sites are nestled into one of the octahedral chains so that they

DO NOT COPY e48d507df5d1141@placeholder.9409

Printed by: e48d507df5d1141@placeholder.94092.edu. Printing is for personal, private use only. No part of this book may be reproduced or transmitted without publisher's prior permission. Violators will be prosecuted.

chains. The tetrahedral Z″ sites are nestled into one of the octahedral chains so that they share faces with adjacent octahedra. This is rather unusual, because it contains mostly Fe^{2+}, which is a relatively large cation. The Z″ tetrahedra contain Si^{4+} and a little Al^{3+}, and they link between the octahedral chains. The octahedral chains are very similar to those found in kyanite, which makes it easy for kyanite to epitaxially nucleate on staurolite—intergrowths of these minerals are common.

Composition The chemical formula for staurolite is reported in different sources in a variety of ways, depending on how much of the chemical variability is represented. A complicating factor is that more than half of the Y3 and Y4 sites are commonly vacant. The usual occupancy of these sites is (□ = a vacancy):

Y1	Al, Fe^{3+}, Cr, V, Mg, Ti
Y2	Al, Fe^{3+}, Cr, V, Mg, Ti
Y3	Al, Mg, □
Y4	Fe^{2+}, Mg, □
Z′	Fe^{2+}, Zn, Co, Mg, Li, Al, Mn^{2+}, Fe^{3+}(?), □
Z″	Si, Al
A	OH, F, O.

The Y1, Y2, and Y3 octahedral sites contain dominantly Al; the Y4 and Z′ sites contain mostly Fe^{2+}. The formula for staurolite is conventionally written with the occupancy of the Z′ sites placed first (e.g., $Fe_2Al_9[(Si,Al)O_4]_4O_6(OH)_2$), but this violates the convention of listing cations in order of decreasing coordination number (Chapter 11). The Z′ cations (usually Fe^{2+}) are listed after the Y cations here to indicate that they are in tetrahedral coordination.

Form and Twinning See Figure 16.10. Crystals are commonly prismatic and elongate parallel to *c*, with the {110} and {101} prisms and {010} and {001} pinacoids the dominant forms. The name staurolite is derived from the Greek for *cross* in reference to the common cross-shaped penetration twins. Twinning on {031} produces a cross at 90°, and on {231} produces a cross at about 60°; neither is obvious in thin section unless fortuitously cut.

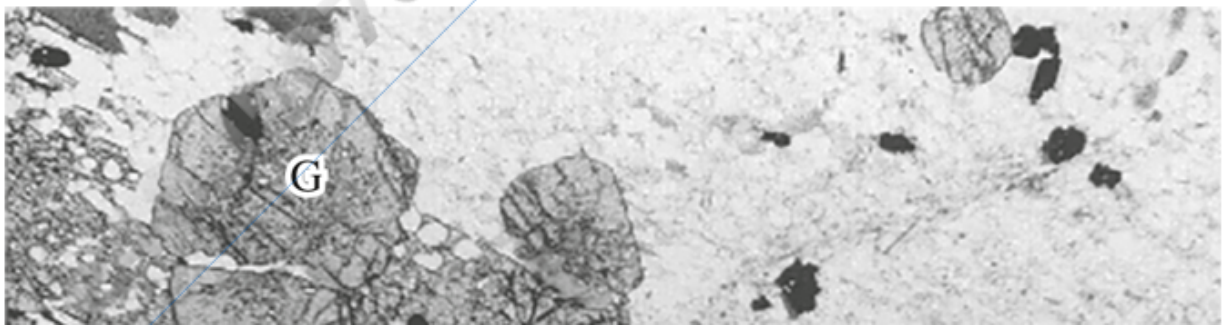

DO NOT COPY

Printed by: e48d507df5d1141@placeholder.94092.edu. Printing is for personal, private use only. No part of this book may be reproduced or transmitted without publisher's prior permission. Violators will be prosecuted.

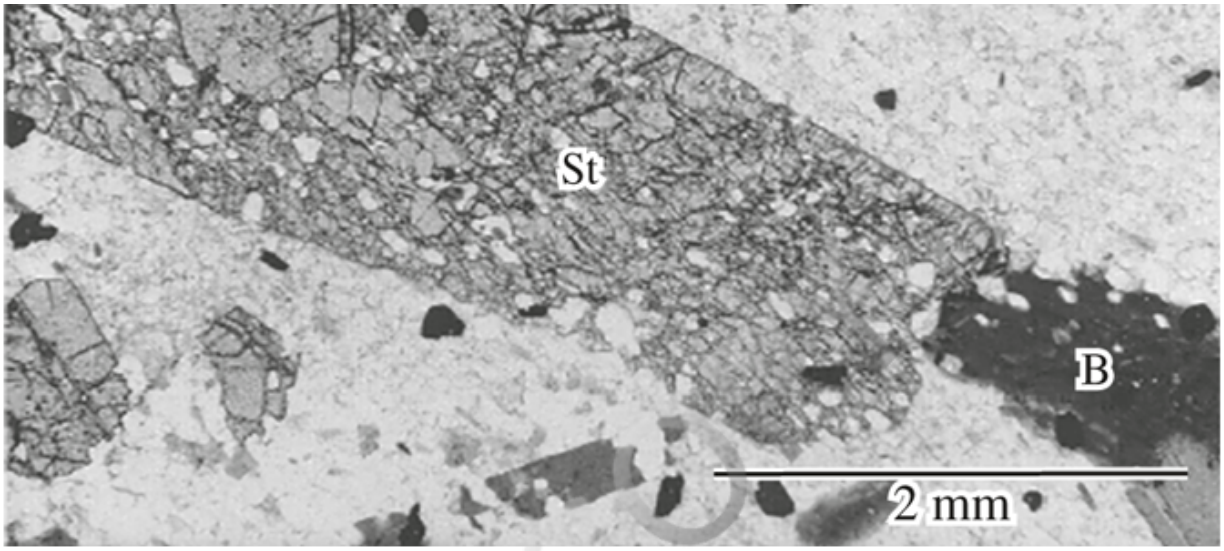

FIGURE 16.10 Sieved (inclusion filled) staurolite porphyroblast (St) with porphyroblasts of garnet (G) and biotite (B) in thin section of mica schist. Plane light. View larger image

Cleavage A relatively poor cleavage on {010} is usually not observed in hand sample or thin section and does not tend to control orientation in grain mount. Subconchoidal fracture is typical; it is brittle.

Color Properties

Luster: Vitreous.

Color: Brown, with reddish, yellowish, or blackish cast.

Streak: Gray.

Color in Thin Section: Pale honey yellow or tan in thin section; darker in grain mounts. Some may show sector zoning.

Pleochroism: Distinct with X = colorless or pale yellow, Y = pale yellow to yellowish brown, Z = golden yellow to reddish brown.

Optical Characteristics

Relief in Thin Section: High positive.

Optic Orientation: $X = b$, $Y = a$, $Z = c$, optic plane = (100).

Indices of Refraction and Birefringence: Indices of refraction increase with iron content. In thin section the first-order white interference color may appear somewhat yellowish because of mineral color. Infrequently the interference colors may be anomalously bluish.

Interference Figure: $2V_z$ increases with decreasing iron content and in some, $2V_z$ may exceed 90°. Optic axis dispersion is weak to moderate, $r > v$. Basal sections yield acute bisectrix figures with melatopes well out of the field of view.

DO NOT COPY e48d507df5d1141@placeholder.94092

Printed by: e48d507df5d1141@placeholder.94092.edu. Printing is for personal, private use only. No part of this book may be reproduced or transmitted without publisher's prior permission. Violators will be prosecuted.

Alteration Staurolite may alter to sericite or chlorite. Staurolite is involved in a variety of metamorphic mineral reactions and therefore may display reaction relations with associated minerals such as andalusite, kyanite, garnet, and cordierite.

Distinguishing Features

Hand Sample: Crystal habit, characteristic twins, and brown color are distinctive.

Thin Section/Grain Mount: Color, pleochroism, relief, and habit make staurolite relatively distinctive. It may resemble brown tourmaline, but tourmaline is uniaxial and is darkest when its long axis is perpendicular to the vibration direction of the lower polarizer, whereas staurolite is the opposite.

Occurrence Staurolite is a common mineral in medium-grade pelitic metamorphic rocks and may be associated with garnet, cordierite, chloritoid, aluminum silicates, muscovite, and biotite. Staurolite is common in the heavy mineral fraction of sediments derived from pelitic metamorphic rocks.

Use In industry it is restricted to use as an abrasive, usually in sandblasting applications, where its hardness is an advantage. Well-formed twinned crystals are used to make pendants and earrings that are sold with names such as “fairy stones” or “tears of Christ.”

Chloritoid

$$(Fe^{2+}, Mg, Mn)_2(Al, Fe^{3+})$$
$$Al_3O_2(SiO_4)_2(OH)_4$$

Monoclinic $2/m$ (also triclinic)
pseudohexagonal

$$a = 9.50\ \text{Å},\ b = 5.50\ \text{Å},$$
$$c = 18.22\ \text{Å},$$
$$\beta = 101.95^\circ,\ Z = 4$$

$$H = 6.5$$

$$G = 3.46 - 3.80$$

Biaxial (+ or −)

$$n_\alpha = 1.705 - 1.730$$

$$n_\beta = 1.708 - 1.734$$

$$n_\gamma = 1.712 - 1.740$$

DO NOT COPY e48d507df5d1141@placeholder.94092

Printed by: e48d507df5d1141@placeholder.94092.edu. Printing is for personal, private use only. No part of this book may be reproduced or transmitted without publisher's prior permission. Violators will be prosecuted.

$$\delta = 0.005 - 0.022, \text{ usually } 0.010 - 0.012$$

$$2V_z = 36 - 72^\circ \text{ (monoclinic)}$$

$$2V_x, = 55 - 88^\circ \text{ (triclinic)}$$

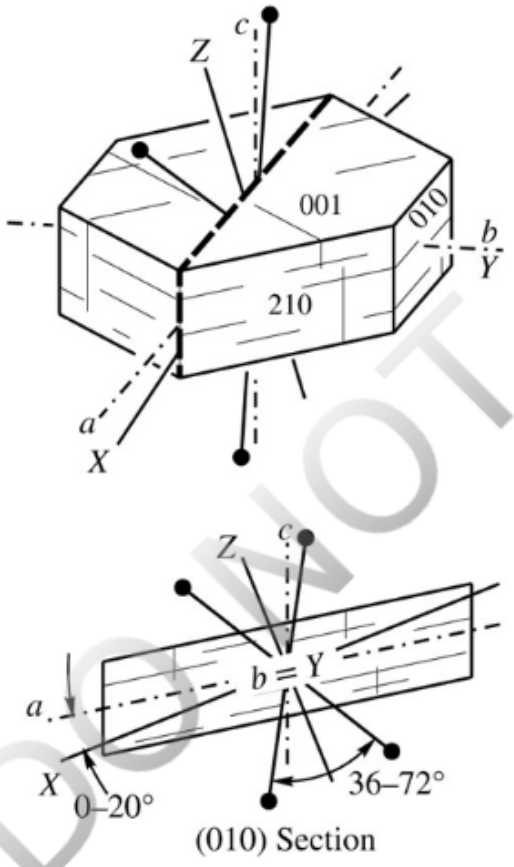

(010) Section

Structure Chloritoid resembles the micas and, like them, has a layered structure. With chloritoid, however, the sheetlike structure is defined by the distribution of cations in octahedral coordination (Figure 16.11). Two types of octahedral layers are present. One consists of two layers of O with octahedrally coordinated Al in between. The second consists of two layers of (O + OH) with octahedrally coordinated Fe + Al in between. These octahedral layers are tied to each other through Si^{4+} in tetrahedral coordination with O from the octahedral layers. Several different polytypes, including triclinic varieties, are possible because the octahedral layers can be stacked in different arrangements.

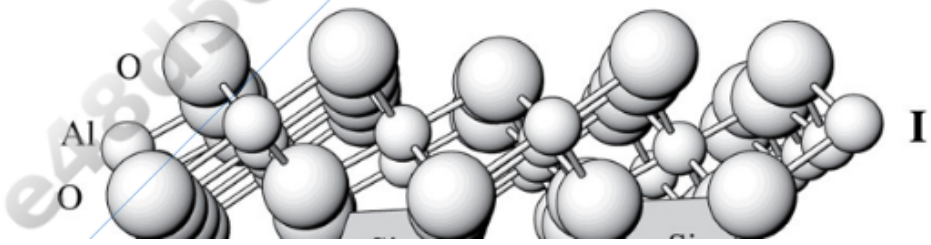

I

Printed by: e48d507df5d1141@placeholder.94092.edu. Printing is for personal, private use only. No part of this book may be reproduced or transmitted without publisher's prior permission. Violators will be prosecuted.

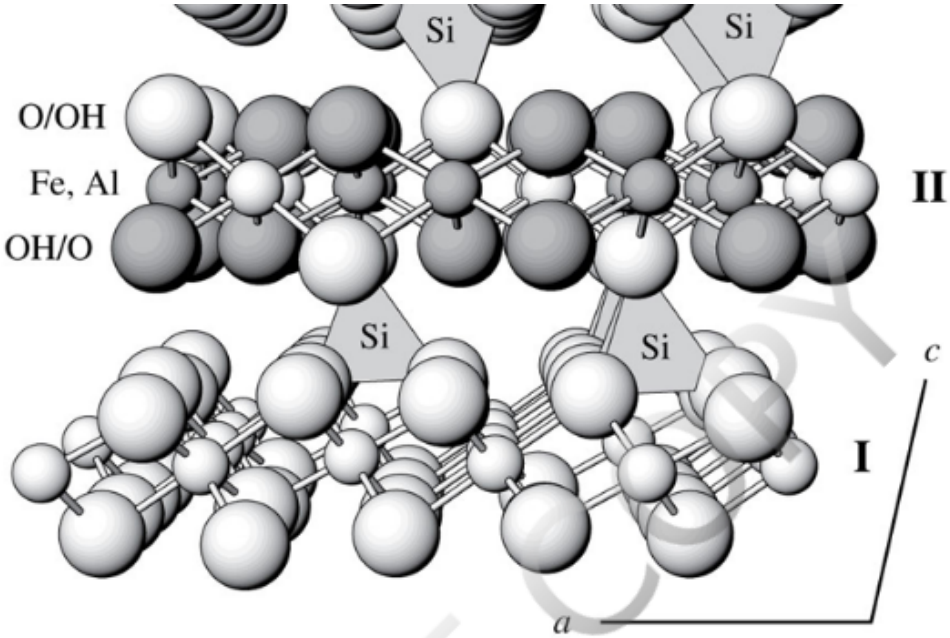

FIGURE 16.11 Chloritoid structure. Octahedral layer I contains Al^{3+} sandwiched between two sheets of O. Octahedral layer II contains Fe^{2+} (small dark spheres) and Al^{3+} sandwiched between sheets of O and OH (large dark spheres). Si^{4+} occupies isolated tetrahedral sites between alternating layers I and II. View larger image

Composition The ideal formula is $Fe^{2+}{}_2AlAl_3O_2(SiO_4)_2(OH)_4$, but some Fe^{3+} substitutes for Al^{3+}, and Mg^{2+} and Mn^{2+} typically substitute for Fe^{2+}, although most chloritoid is Fe-rich. The Mn-rich variety of chloritoid is called ottrelite.

Form and Twinning See Figure 16.12. Crystals are usually platy parallel to {001} with a roughly hexagonal basal section. Often foliated like the micas. Random cuts through porphyroblasts are usually rectangular. Lamellar twinning on {001} is common. Chloritoid commonly contains inclusions of associated minerals, particularly quartz.

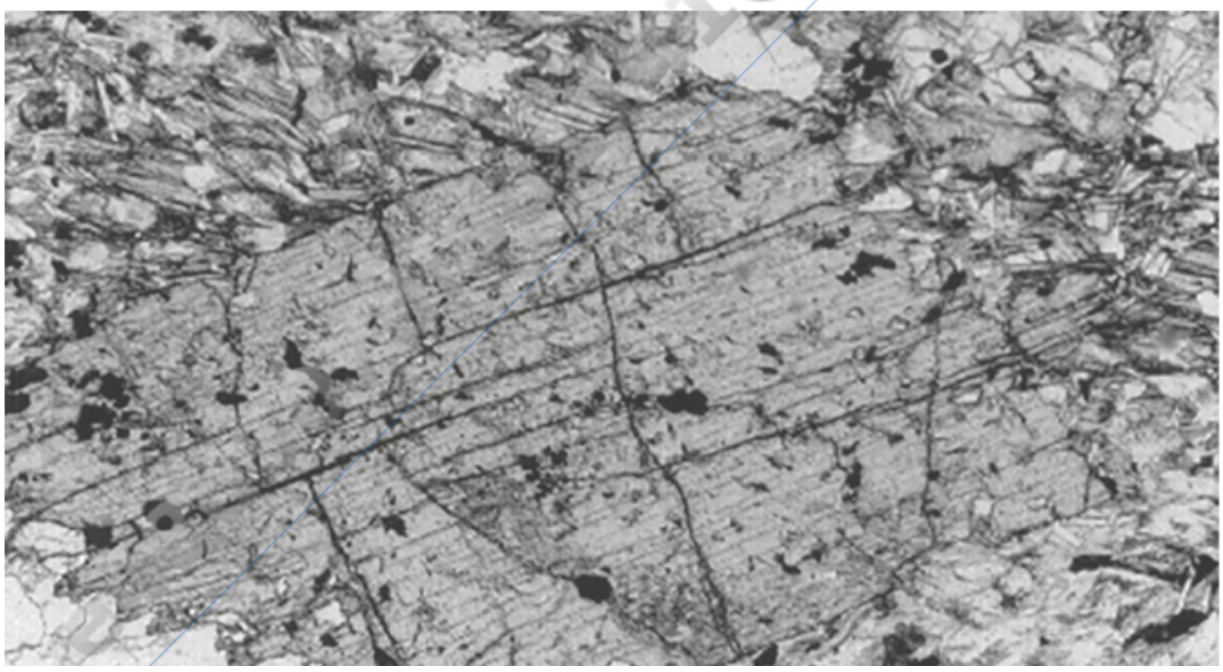

Printed by: e48d507df5d1141@placeholder.94092.edu. Printing is for personal, private use only. No part of this book may be reproduced or transmitted without publisher's prior permission. Violators will be prosecuted.

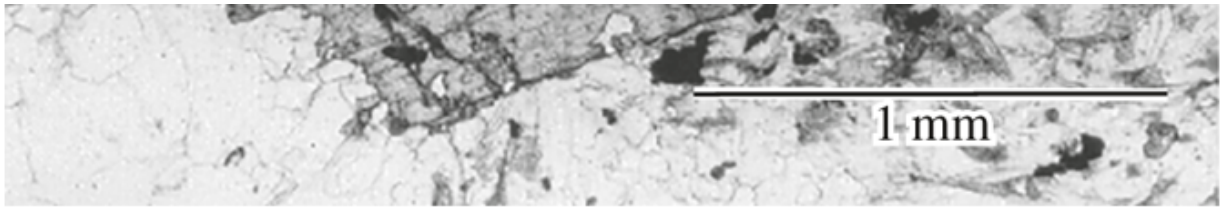

FIGURE 16.12 Photomicrograph of chloritoid in a thin section of schist. Plane light. View larger image

Cleavage A cleavage on {001} is parallel to the sheets in the structure, but is less perfect than in the micas. Prismatic cleavage on {210} is fair to poor. A parting is possible on {010}. The {001} cleavage strongly controls fragment orientation. Cleavage flakes are brittle.

Color Properties

Luster: Somewhat pearly on cleavage surfaces.

Color: Dark gray, greenish gray, greenish black; distinctly green in thin plates.

Streak: White, grayish, or slightly greenish.

Color in Thin Section: Green to colorless.

Pleochroism: Distinct: X = green or gray-green; Y = blue-gray, indigo, or blue-green; Z = colorless, yellow, or pale green. Color zoning with an hourglass pattern is common.

Optical Characteristics

Relief in Thin Section: High positive.

Optic Orientation: Variable. Y or $X \wedge a <\sim +20°$, X or $Y = b$, $Z \wedge c = +2°$ to $+30°$ for monoclinic varieties. Triclinic varieties are similar. The trace of cleavage is length fast and extinction is usually inclined between 0° and 20°, depending on the specific optic orientation of the grain and how it is oriented.

Indices of Refraction and Birefringence: Mn- and Mg-rich varieties have lower indices of refraction than Fe-rich varieties; substitution of Fe^{3+} for Al^{3+} tends to increase indices of refraction but it is not sufficiently systematic to allow composition to be estimated. Birefringence is usually 0.010–0.012, so maximum interference color in thin section is up to pale first-order yellow. Some varieties have higher birefringence and interference colors that are often anomalous.

Interference Figure: Because Z is nearly normal to the basal cleavage, cleavage fragments yield nearly centered acute bisectrix figures if positive or obtuse bisectrix figures if negative. Different samples from the same locality may display different values of $2V$ because of differences in stacking of the octahedral layers. Monoclinic varieties are usually optically positive, and triclinic varieties are usually optically negative. Optic axis

DO NOT COPY e48d507df5d1141@placeholder.9409

Printed by: e48d507df5d1141@placeholder.94092.edu. Printing is for personal, private use only. No part of this book may be reproduced or transmitted without publisher's prior permission. Violators will be prosecuted.

usually optically positive, and triclinic varieties are usually optically negative. Optic axis dispersion is strong, $r > v$, but may be quite variable in different grains from the same sample.

Alteration Chloritoid may alter to chlorite, sericite, or clay. It may display metamorphic mineral reaction relations with the minerals with which it is associated.

Distinguishing Features

Hand Sample: Strongly resembles chlorite and can be difficult to distinguish in hand sample.

Thin Section/Grain Mount: Closely resembles chlorite and may resemble green biotite. Biotite has higher birefringence and nearly parallel extinction. Chlorite has lower indices of refraction and relief, and most chlorite varieties have nearly parallel extinction. If present, the hourglass structure in chloritoid is characteristic.

Occurrence Chloritoid is common as porphyroblasts in low- to medium-grade regionally metamorphosed rocks such as mica, chlorite, and glaucophane schists, phyllite, and quartzite. It often is associated with aluminum silicates, garnet, chlorite, muscovite, and staurolite. Hydrothermal processes may form chloritoid in quartz–carbonate veins and in hydrothermally altered rocks, and it may be associated with corundum in emery deposits (rocks rich in corundum).

Use None.

Titanite (sphene)

$$\mathrm{CaTiOSiO_4} \text{ or } \mathrm{CaTiSiO_5}$$

$$\text{Monoclinic } 2/m$$

$$a = 6.555 \text{ Å},\ b = 8.707 \text{ Å},\ c = 7.445 \text{ Å},$$
$$\beta = 119.9^\circ,\ Z = 4$$

$$H = 5 - 5.5$$

$$G = 3.48 - 3.60$$

$$\text{Biaxial } (+)$$

$$n_\alpha = 1.843 - 1.950$$

$$n_\beta = 1.870 - 2.034$$

$$n_\gamma = 1.943 - 2.110$$

$$\delta = 0.100 - 0.192$$

$$2V_z = 17 - 40^\circ$$

DO NOT COPY e48d507df5d1141@placeholder.9409

Printed by: e48d507df5d1141@placeholder.94092.edu. Printing is for personal, private use only. No part of this book may be reproduced or transmitted without publisher's prior permission. Violators will be prosecuted.

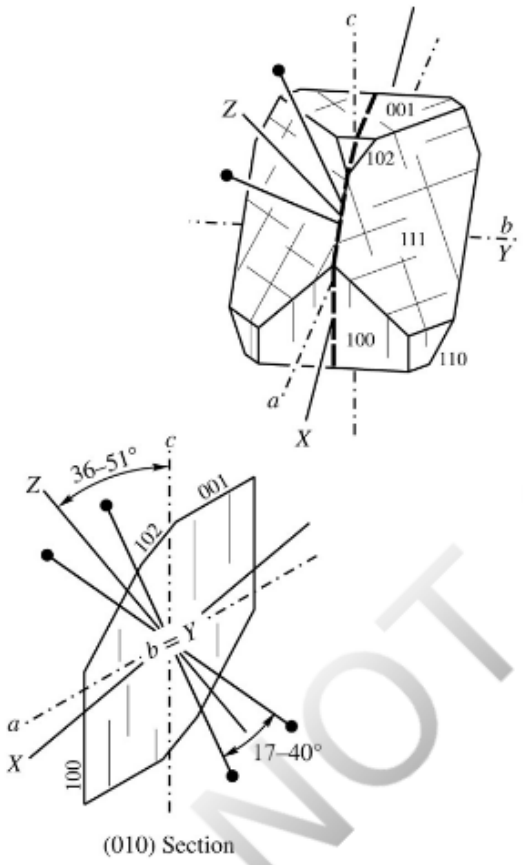

Structure The structure of titanite consists of kinked chains of corner-sharing TiO_6^{8-} octahedra that run parallel to [101] (between the *a* and *c* axes). These chains are held together laterally through Si^{4+} in tetrahedral coordination and Ca^{2+} in irregular 7-fold coordination. Note that the crystal setting used here is based on external morphology. Structural studies usually place *a* parallel to the octahedral chains and *c* parallel to $-a$ as defined here.

Composition Both Al^{3+} and Fe^{3+} may substitute for Ti^{4+}, usually coupled with substitution of OH^- or F^- for O^{2-} to maintain charge balance. Uranium, thorium, and a variety of rare earth elements may substitute for Ca^{2+} in small amounts.

Form and Twinning Wedge-shaped crystals with {111} and {110} prisms and {100} and {001} pinacoids are common; cross sections in thin section usually are diamond shaped (Figure 16.13). Grains are typically small and often are not visible in hand samples of the rocks in which titanite occurs. Also common are somewhat rounded to irregular grains. Simple twins on {100} are not uncommon and may be expressed in thin section as a composition plane along the long diagonal of diamond-shaped sections. Lamellar twinning on {221} is less common.

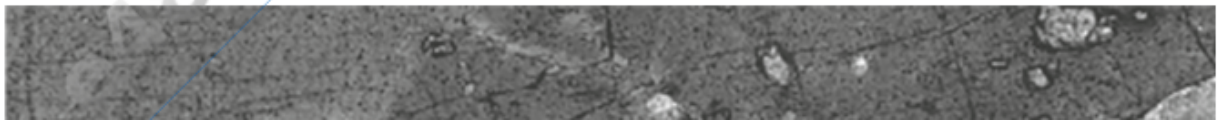

DO NOT COPY

Printed by: e48d507df5d1141@placeholder.94092.edu. Printing is for personal, private use only. No part of this book may be reproduced or transmitted without publisher's prior permission. Violators will be prosecuted.

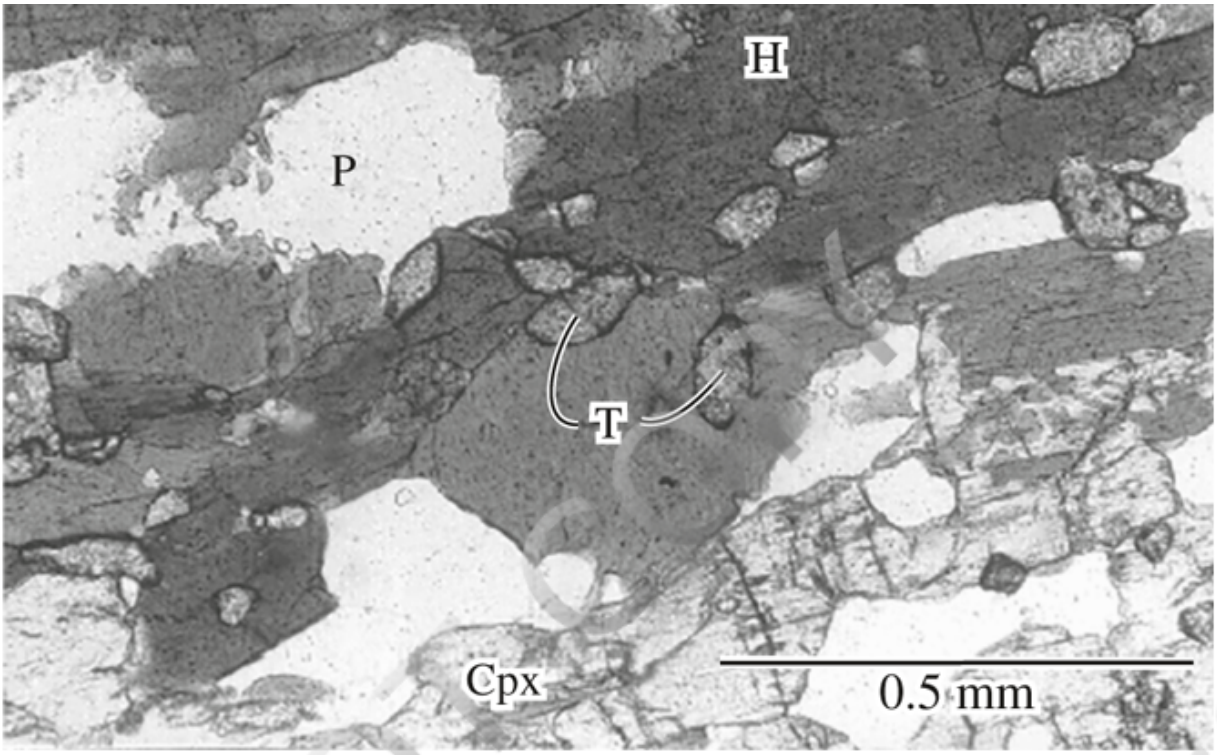

FIGURE 16.13 Photomicrograph of subhedral to anhedral titanite (T) grains with hornblende (H), plagioclase (P), and Ca-clinopyroxene (Cpx) in a thin section of an amphibolite. Plane light. View larger image

Cleavage Fair to good prismatic {110} cleavage is not obvious in thin section but may control fragment orientation. Unlike the other orthosilicates, this cleavage is not parallel to the octahedral chains. Rather, it cuts across the chains in such a way as to avoid cutting Si–O bonds. A parting parallel to {221} may be prominent. This parting has

DO NOT COPY
e48d507df5d1141@placeholder.9409

Printed by: e48d507df5d1141@placeholder.94092.edu. Printing is for personal, private use only. No part of this book may be reproduced or transmitted without publisher's prior permission. Violators will be prosecuted.

been associated with the {221} twins, though it is possible that it is associated with exsolved lamellae of anatase (TiO_2 polymorph). Exsolution lamellae of coesite and quartz also have been reported.

Color Properties

Luster: Adamantine, vitreous, to resinous.

Color: Brown, gray, green, yellow, red, black.

Streak: White.

Color in Thin Section: Shades of brown or yellowish brown, less commonly colorless.

Pleochroism: Nonpleochroic to weakly pleochroic, $X < Y < Z$: X = colorless to pale yellow; Y = yellowish brown, pink, or greenish yellow; Z = orangish brown, greenish brown, green, or red.

Optical Characteristics

Relief in Thin Section: Very high positive.

Optic Orientation: $X \wedge a = -6°$ to $-21°$, $Y = b$, $Z \wedge c = +36°$ to $+15°$.

Indices of Refraction and Birefringence: Neither appears to vary systematically with composition. Extreme birefringence yields upper-order white interference colors in thin section and grain mount, but interference color may be masked by mineral color. Strong dispersion may prevent complete extinction in white light for some sample orientations.

Interference Figure: Figures are biaxial positive with numerous isochromes and small to moderate $2V$. Optic axis dispersion is very strong, $r > v$; inclined dispersion is weak. Fragments on the {110} cleavage yield off-center figures.

Alteration The usual alteration product of titanite is an aggregate of titanium oxides, quartz, and other minerals known as leucoxene, which in hand sample may appear earthy white or yellow-white, and in thin section may be nearly opaque. Titanite may be produced by alteration of biotite or clinopyroxene.

Distinguishing Features

Hand Sample: Titanite is characterized by luster and crystal habit in the infrequent occurrences where crystals are large enough to work with. Hardness is less than staurolite and greater than sphalerite.

Thin Section/Grain Mount: Very high relief, extreme birefringence, and habit are characteristic.

Occurrence Titanite is a common accessory mineral in a wide variety of igneous rocks,

DO NOT COPY e48d507df5d1141@placeholder.9409

Printed by: e48d507df5d1141@placeholder.94092.edu. Printing is for personal, private use only. No part of this book may be reproduced or transmitted without publisher's prior permission. Violators will be prosecuted.

in which it may be the dominant Ti-bearing mineral. In metamorphic rocks it is most common in relatively mafic varieties such as amphibolite. Titanite is also found in the heavy mineral fraction of clastic sediments.

Use Titanite is a minor ore of titanium.

Comment The name titanite is in reference to the mineral's titanium content. Titanite historically was also commonly referred to as **sphene**, which is based on the ancient Greek word for "wedge," in reference to its wedge-shaped crystals. However, in the 1980s the name *titanite* was formally designated. Though a discredited name, *sphene* remains popular with some, but it should be avoided. Titanite is commonly used for radiometric dating because of its U content; see Box 5.1.

Topaz

$$Al_2SiO_4(F, OH)_2$$

$$\text{Orthorhombic } 2/m\ 2/m\ 2/m$$

$$a = 4.65\ \text{Å},\ b = 8.80\ \text{Å},$$
$$c = 8.39\ \text{Å},\ Z = 4$$

$$H = 8$$

$$G = 3.49 - 3.57$$

$$\text{Biaxial } (+)$$

$$n_\alpha = 1.606 - 1.635$$

$$n_\beta = 1.609 - 1.637$$

$$n_\gamma = 1.616 - 1.644$$

$$\delta = 0.008 - 0.011$$

$$2V_z = 44 - 68^\circ$$

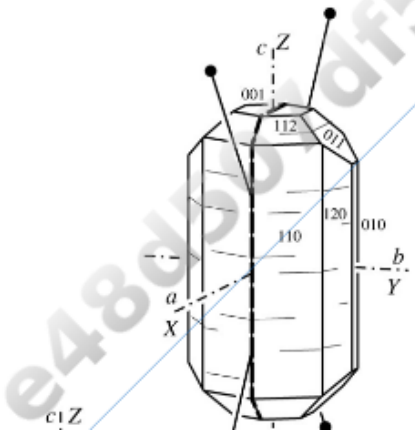

DO NOT COPY
e48d507df5d1141@placeholder.9409

Printed by: e48d507df5d1141@placeholder.94092.edu. Printing is for personal, private use only. No part of this book may be reproduced or transmitted without publisher's prior permission. Violators will be prosecuted.

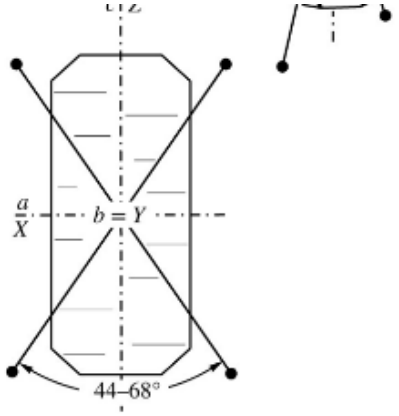

(010) Section

Structure The structure is based on close-packed sheets of O alternating with sheets of $(F,OH)_2O$ parallel to (010). Al^{3+} is distributed in octahedral sites between these sheets to form crankshaft-like chains of edge-sharing octahedra parallel to *c* that are cross-linked through Si^{4+} in tetrahedral coordination.

Composition The only significant compositional variation is in the relative amounts of F and OH.

Form and Twinning Crystals are usually stubby to elongate prisms parallel to the *c* axis (Figure 16.14). Basal sections range from nearly square to a rounded diamond shape with eight faces. Anhedral grains and irregular masses are also common. Detrital grains tend to be platy parallel to the basal cleavage. Twins on {010} are rare.

(*a*)

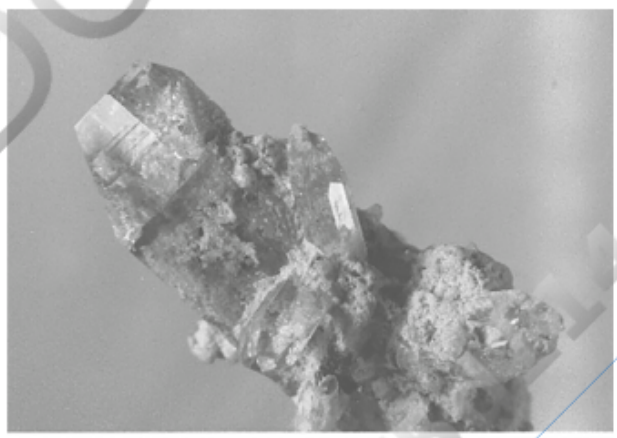

(*b*)

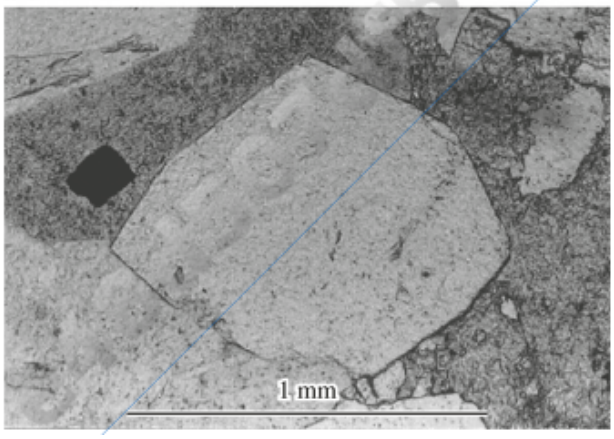

DO NOT COPY

Printed by: e48d507df5d1141@placeholder.94092.edu. Printing is for personal, private use only. No part of this book may be reproduced or transmitted without publisher's prior permission. Violators will be prosecuted.

FIGURE 16.14 Topaz. (*a*) Topaz crystal. (*b*) Photomicrograph of basal section of topaz in thin section. Plane light. View larger image

Cleavage The basal cleavage {001} is perfect and is the only plane that can cut through the structure without breaking the relatively strong Si–O bonds. Subconchoidal to uneven fracture. Brittle.

Color Properties

Luster: Vitreous.

Color: Most often colorless or gray but may be yellow, pink, red, brown, green, blue, or violet. Coloration often due to radiation-induced color centers and/or trace amounts of transition metals. A blue color, more intense than most natural blue topaz, can be produced by irradiation followed by heat treatment.

Streak: White.

Color in Thin Section: Colorless. Thick fragments in grain mount may be a pale version of the hand sample color.

Pleochroism: Weak in colored samples: $X =$ $Y =$ shades of yellow and $Z =$ shades of pink.

Optical Characteristics

Relief in Thin Section: Moderate positive.

Optic Orientation: $X = a$, $Y = b$, $Z = c$, optic plane = (010). Trace of cleavage shows parallel extinction in longitudinal sections and is length fast.

Indices of Refraction and Birefringence: Indices of refraction systematically decrease over the range of 15 to 21 wt % F. Maximum interference color in standard thin section is first-order white with a tinge of yellow. Fragments resting on a cleavage surface display birefringence of about 0.003.

Interference Figure: $2V_z$ increases systematically over the range of 15 to 21 wt % F. Basal sections yield centered acute bisectrix figures. Optic axis dispersion is distinct with $r > v$.

Alteration Relatively stable in the weathering environment. May hydrothermally alter to sericite, clay, or fluorite.

Distinguishing Features

Hand Sample: Resembles quartz but is distinguished by crystal habit, basal cleavage, high specific gravity, and hardness.

Thin Section/Grain Mount: Resembles quartz but has higher relief in thin section, is biaxial, and has cleavage

DO NOT COPY e48d507df5d1141@placeholder.9409

Printed by: e48d507df5d1141@placeholder.94092.edu. Printing is for personal, private use only. No part of this book may be reproduced or transmitted without publisher's prior permission. Violators will be prosecuted.

biaxial, and has cleavage.

Occurrence Generally rare, but occurs most commonly in both volcanic and intrusive felsic igneous rocks. Well-formed crystals may occupy vesicles or other cavities in rhyolitic volcanics, and large masses may be found in granitic pegmatites. Topaz also is found in hydrothermal tungsten, tin, molybdenum, or gold mineral deposits, in hydrothermally altered rocks adjacent to granitic intrusions, and infrequently in metamorphic quartzite and schist. Because it is relatively stable in the weathering environment, topaz is not uncommon in the heavy mineral fraction of sediments if topaz-bearing rocks are present in the sediment source region.

Use Colorless, yellow, brown, or pink topaz may be used as a gemstone. The color of most blue topaz has been induced by radiation and heat treatment. Probably because topaz is valued as a gemstone, it has historically been used for the treatment of eye problems, gout, poisons, and gastrointestinal upset.

DO NOT COPY
e48d507df5d1141@placeholder.9409

Printed by: e48d507df5d1141@placeholder.94092.edu. Printing is for personal, private use only. No part of this book may be reproduced or transmitted without publisher's prior permission. Violators will be prosecuted.

Additional Orthosilicates

Additional orthosilicate minerals include dumortierite, chondrodite, monticellite, and datolite. Table 16.5 lists their properties.

TABLE 16.5 Properties of Less Common Orthosilicates

	Dumortierite	Chondrodite	Monticellite	Datolite
Composition	$Al_7(BO_3)(SiO_4)_3O_3$	$2(Mg_2SiO_4)\cdot Mg(F,OH)_2$	$CaMgSiO_4$	$CaBSiO_4(OH)$
Crystal system	Orthorhombic	Monoclinic	Orthorhombic	Monoclinic
Color	Blue, greenish blue, violet, purple, brown; vitreous	Yellow, brown, red, grayish green; may fluoresce	Colorless, white, pale greenish gray, yellowish gray	Colorless to white, often w/greenish cast; commonly fluorescent
Color in thin section	Deep to pale blue; pleochroic	Pale yellow to colorless; pleochroic	Colorless	Colorless
Sign and 2*V*	Biaxial (−), 13–55°	Biaxial (+), 50–85°	Biaxial (−), 69–88°	Biaxial (−), 72–75°
Indices of refraction	n_α = 1.659–1.686 n_β = 1.684–1.722 n_γ = 1.686–1.723	n_α = 1.592–1.617 n_β = 1.602–1.635 n_γ = 1.621–1.646	n_α = 1.638–1.654 n_β = 1.648–1.664 n_γ = 1.650–1.674	n_α = 1.622–1.626 n_β = 1.649–1.654 n_γ = 1.666–1.670
δ	0.011–0.037	0.028–0.034	0.012–0.020	0.044–0.046
Physical	*H* = 7–8.5 *G* = 3.21–3.41 Cyclic twins on {110}	*H* = 6.5 *G* = 3.16–3.26 {001} simple and lamellar twins	*H* = 5–5.5 *G* = 3.03–3.27 {031} cyclic twins produce 6-point star	*H* = 5–5.5 *G* = 2.96–3.00
Cleavage	{100} good, {110} poor	{100} poor	{010} poor/fair	None; conchoidal to uneven fracture

Dumortierite is a relatively uncommon mineral found in granitic pegmatite, aplite, quartz

DO NOT COPY e48d507df5d1141@placeholder.9409

Printed by: e48d507df5d1141@placeholder.94092.edu. Printing is for personal, private use only. No part of this book may be reproduced or transmitted without publisher's prior permission. Violators will be prosecuted.

veins, and hydrothermally altered rocks. It also occurs in medium- to high-grade gneiss, schist, and quartzite in association with other aluminous minerals. Fine dumortierite needles may be responsible for the pink color of some rose quartz. It forms acicular or fibrous grains and fibrous masses. The fibrous habit and blue color are distinctive, both in hand sample and in thin section. It may be confused for a blue amphibole, but blue amphiboles have inclined extinction.

Chondrodite is the most common member of the humite group, whose members are

Norbergite	$Mg_2SiO_4 \cdot Mg(F,OH)_2$
Chondrodite	$2(Mg_2SiO_4) \cdot Mg(F,OH)_2$
Humite	$3(Mg_2SiO_4) \cdot Mg(F,OH)_2$
Clinohumite	$4(Mg_2SiO_4) \cdot Mg(F,OH)_2$

These minerals are found in contact-metamorphosed dolomitic limestone in association with calcite, dolomite, tremolite, grossular, wollastonite, olivine, monticellite, graphite, phlogopite, spinel, and pyrrhotite. Their structure consists of layers of an olivine-like structure parallel to (100) that alternate with layers with a brucite-like structure. The olivine-like layers are one, two, three, and four layers thick in the different minerals, as is indicated by their formulas. Fe^{2+}, Mn^{2+}, and Ti may substitute for Mg, and Al may substitute for Si in limited amounts. They usually form rounded or irregular grains or granular masses. Crystals are often platy, but they have diverse habits. Chondrodite may resemble forsterite but is more typically light yellow or red, where forsterite is green. It is distinguished from forsterite in thin section by lower birefringence, smaller $2V$, and pale yellow pleochroism.

Monticellite is another mineral found in metamorphosed dolomitic limestone in association with calcite, dolomite, tremolite, diopside, forsterite, wollastonite, humite group, and related calc-silicate minerals. The structure is the same as olivine, with half the octahedral sites occupied by Ca rather than Mg. Some Fe^{2+} may substitute for Mg, and continuous solid solution is possible to kirschsteinite ($CaFeSiO_4$). Monticellite typically forms anhedral, equant, or irregular grains. Crystals are elongate on *c*. Monticellite may resemble both forsterite and the humite group in hand sample but forsterite is typically green and chondrodite is light yellow to red. In thin section, monticellite is distinguished from forsterite by lower birefringence and from diopside by being optically negative with a larger $2V$ and poorer cleavage. Members of the humite group are all optically positive.

Datolite is most commonly a secondary mineral found in amygdules and other voids in basalt and related rocks. Crystals are typically short prismatic to roughly equant. Datolite also forms botryoidal and globular masses and may be compact massive. It is characterized by its pale green color and crystals with many faces.

DO NOT COPY

Printed by: e48d507df5d1141@placeholder.94092.edu. Printing is for personal, private use only. No part of this book may be reproduced or transmitted without publisher's prior permission. Violators will be prosecuted.

Additional Orthosilicates

Additional orthosilicate minerals include dumortierite, chondrodite, monticellite, and datolite. Table 16.5 lists their properties.

TABLE 16.5 Properties of Less Common Orthosilicates

	Dumortierite	Chondrodite	Monticellite	Datolite
Composition	$Al_7(BO_3)(SiO_4)_3O_3$	$2(Mg_2SiO_4)\cdot Mg(F,OH)_2$	$CaMgSiO_4$	$CaBSiO_4(OH)$
Crystal system	Orthorhombic	Monoclinic	Orthorhombic	Monoclinic
Color	Blue, greenish blue, violet, purple, brown; vitreous	Yellow, brown, red, grayish green; may fluoresce	Colorless, white, pale greenish gray, yellowish gray	Colorless to white, often w/greenish cast; commonly fluorescent
Color in thin section	Deep to pale blue; pleochroic	Pale yellow to colorless; pleochroic	Colorless	Colorless
Sign and 2*V*	Biaxial (−), 13–55°	Biaxial (+), 50–85°	Biaxial (−), 69–88°	Biaxial (−), 72–75°
Indices of refraction	n_α = 1.659–1.686 n_β = 1.684–1.722 n_γ = 1.686–1.723	n_α = 1.592–1.617 n_β = 1.602–1.635 n_γ = 1.621–1.646	n_α = 1.638–1.654 n_β = 1.648–1.664 n_γ = 1.650–1.674	n_α = 1.622–1.626 n_β = 1.649–1.654 n_γ = 1.666–1.670
δ	0.011–0.037	0.028–0.034	0.012–0.020	0.044–0.046
Physical	*H* = 7–8.5 *G* = 3.21–3.41 Cyclic twins on {110}	*H* = 6.5 *G* = 3.16–3.26 {001} simple and lamellar twins	*H* = 5–5.5 *G* = 3.03–3.27 {031} cyclic twins produce 6-point star	*H* = 5–5.5 *G* = 2.96–3.00
Cleavage	{100} good, {110} poor	{100} poor	{010} poor/fair	None; conchoidal to uneven fracture

Dumortierite is a relatively uncommon mineral found in granitic pegmatite, aplite, quartz

DO NOT COPY e48d507df5d1141@placeholder.9409-

Printed by: e48d507df5d1141@placeholder.94092.edu. Printing is for personal, private use only. No part of this book may be reproduced or transmitted without publisher's prior permission. Violators will be prosecuted.

veins, and hydrothermally altered rocks. It also occurs in medium- to high-grade gneiss, schist, and quartzite in association with other aluminous minerals. Fine dumortierite needles may be responsible for the pink color of some rose quartz. It forms acicular or fibrous grains and fibrous masses. The fibrous habit and blue color are distinctive, both in hand sample and in thin section. It may be confused for a blue amphibole, but blue amphiboles have inclined extinction.

Chondrodite is the most common member of the humite group, whose members are

Norbergite	$Mg_2SiO_4 \cdot Mg(F,OH)_2$
Chondrodite	$2(Mg_2SiO_4) \cdot Mg(F,OH)_2$
Humite	$3(Mg_2SiO_4) \cdot Mg(F,OH)_2$
Clinohumite	$4(Mg_2SiO_4) \cdot Mg(F,OH)_2$

These minerals are found in contact-metamorphosed dolomitic limestone in association with calcite, dolomite, tremolite, grossular, wollastonite, olivine, monticellite, graphite, phlogopite, spinel, and pyrrhotite. Their structure consists of layers of an olivine-like structure parallel to (100) that alternate with layers with a brucite-like structure. The olivine-like layers are one, two, three, and four layers thick in the different minerals, as is indicated by their formulas. Fe^{2+}, Mn^{2+}, and Ti may substitute for Mg, and Al may substitute for Si in limited amounts. They usually form rounded or irregular grains or granular masses. Crystals are often platy, but they have diverse habits. Chondrodite may resemble forsterite but is more typically light yellow or red, where forsterite is green. It is distinguished from forsterite in thin section by lower birefringence, smaller $2V$, and pale yellow pleochroism.

Monticellite is another mineral found in metamorphosed dolomitic limestone in association with calcite, dolomite, tremolite, diopside, forsterite, wollastonite, humite group, and related calc-silicate minerals. The structure is the same as olivine, with half the octahedral sites occupied by Ca rather than Mg. Some Fe^{2+} may substitute for Mg, and continuous solid solution is possible to kirschsteinite ($CaFeSiO_4$). Monticellite typically forms anhedral, equant, or irregular grains. Crystals are elongate on *c*. Monticellite may resemble both forsterite and the humite group in hand sample but forsterite is typically green and chondrodite is light yellow to red. In thin section, monticellite is distinguished from forsterite by lower birefringence and from diopside by being optically negative with a larger $2V$ and poorer cleavage. Members of the humite group are all optically positive.

Datolite is most commonly a secondary mineral found in amygdules and other voids in basalt and related rocks. Crystals are typically short prismatic to roughly equant. Datolite also forms botryoidal and globular masses and may be compact massive. It is characterized by its pale green color and crystals with many faces.

DO NOT COPY

Printed by: e48d507df5d1141@placeholder.94092.edu. Printing is for personal, private use only. No part of this book may be reproduced or transmitted without publisher's prior permission. Violators will be prosecuted.

REFERENCES CITED AND SUGGESTIONS FOR ADDITIONAL READING

Andrews, M. G., and Taylor, L. L. 2019. Combating climate change through enhanced weathering of agricultural soils. *Elements* **15**, 253–258.

Deer, W. A., Howie, R. A., and Zussman, J. 2001. *Rock-Forming Minerals, Volume 1A: Orthosilicates*, 2nd ed. The Geological Society, London, 919 p.

Ferry, J. M., and Watson, E. B. 2007. New thermodynamic models and revised calibrations for the Ti-in-zircon and Zr-in-rutile thermometers. *Contributions to Mineralogy and Petrology* **154**, 429–437.

Green, H. W., II, and Burnley, P. C. 1989. A new self-organizing mechanism for deep-focus earthquakes. *Nature* **341**, 733–737.

Grew, E. S., Locock, A. J., Mills, S. J., Galuskina, I. O., Galuskin, E. V., and Hålenius, U. 2013. Nomenclature of the garnet supergroup. *American Mineralogist* **98**, 785–811.

Griffen, D. T. 1992. *Silicate Crystal Chemistry*. Oxford University Press, New York, 442 p.

Hanchar, J. M., and Hoskins, P. W. O. (eds.). 2003. *Zircon. Reviews in Mineralogy and Geochemistry* **53**, 500 p.

Hangx, S. J. T., and C. J. Spiers, 2009. Coastal spreading of olivine to control atmospheric CO_2 concentrations: A critical analysis of viability. *International Journal of Greenhouse Gas Control* **3**, No. 6, 757–767.

Harley, S. L., and Kelly, N. M. 2007. Zircon: Tiny but timely. *Elements* **3**, 13–18.

Hawthorne, F. C., Ungaretti, L., Oberti, R., Caucia, F., and Callegari, A. 1993. The crystal chemistry of staurolite. I. Crystal structure and site populations. *The Canadian Mineralogist* **31**, 551–582.

Hemingway, B. S., Robie, R. A., Evans, H. T., Jr., and Kerrick, D. M. 1991. Heat capacities and entropies of sillimanite, fibrolite, andalusite, kyanite, and quartz and the Al_2SiO_5 phase diagram. *American Mineralogist* **76**, 1597–1613.

Iidaka, T., and Suetsuga, D. 1992. Seismological evidence for metastable olivine inside a subducting slab. *Nature* **356**, 593–595.

Kerrick, D. M. 1990. *The Al_2SiO_5 Polymorphs. Reviews in Mineralogy* **22**, 406 p.

Köhler, P., Hartmann, J., and Wolf-Gladrow, D. A. 2010. Geoengineering potential of artificially enhanced silicate weathering of olivine. *PNAS* **107**, No. 47, 20228–20233.

Liebau, F. 1985. *Structural Chemistry of Silicates, Structure, Bonding and Classification*. Springer-Verlag, Berlin, 347 p.

Louisnathan, S. J., and Smith, J. V. 1968. Cell dimensions of olivine. *Mineralogical*

DO NOT COPY e48d507df5d1141@placeholder.94092

Printed by: e48d507df5d1141@placeholder.94092.edu. Printing is for personal, private use only. No part of this book may be reproduced or transmitted without publisher's prior permission. Violators will be prosecuted.

Magazine **36**, 1123–1134.

Montserrat, F., Renforth, P., Hartmann, J., Leermakers, M., Knops, P., and Meysman, F. J. R. 2017. Olivine dissolution in seawater: Implications for CO_2 sequestration through enhanced weathering in coastal environments. *Environmental Science & Technology* **51**, 7, 3960–3972.

Ribbe, P. H. (ed.). 1982. *Orthosilicates*, 2nd ed. Reviews in Mineralogy **5**, 450 p.

Ribbe, P. H., and Rosenberg, P. 1971. Optical and X-ray determinative methods for fluorine in topaz. *American Mineralogist* **56**, 1812–1821.

Schuiling, R. D., and Krijgsman, P. 2006. Enhanced weathering: An effective and cheap tool to sequester CO_2. *Climatic Change* **74**, 349–354.

Spear, F. S. 1993. *Metamorphic Phase Equilibria and Pressure–Temperature–Time Paths*. Mineralogical Society of America, Washington, DC, 719 p.

Winchell, H. 1958. The composition and physical properties of garnet. *American Mineralogist* **42**, 595–600.

DO NOT COPY

e48d507df5d1141@placeholder.9409

Printed by: e48d507df5d1141@placeholder.94092.edu. Printing is for personal, private use only. No part of this book may be reproduced or transmitted without publisher's prior permission. Violators will be prosecuted.

LIST OF KEY TERMS

aluminosilicate polymorph

aluminum silicate polymorphs

placer deposit

sphenoid

xenocryst

DO NOT COPY

e48d507df5d1141@placeholder.9409

Printed by: e48d507df5d1141@placeholder.94092.edu. Printing is for personal, private use only. No part of this book may be reproduced or transmitted without publisher's prior permission. Violators will be prosecuted.

CHAPTER 17

Carbonates, Sulfates, Phosphates, Tungstates, Molybdates, and Borates

William D. Nesse
University of Northern Colorado

Graham B. Baird
University of Northern Colorado

DO NOT COPY
e48d507df5d1141@placeholder.9409

Printed by: e48d507df5d1141@placeholder.94092.edu. Printing is for personal, private use only. No part of this book may be reproduced or transmitted without publisher's prior permission. Violators will be prosecuted.

Structure and Classification

The minerals described in this chapter all have structures based on anionic groups that have a net −2 to −5 charge.

CARBONATES: CO_3^{2-}

SULFATES: SO_4^{2-}

PHOSPHATES: PO_4^{3-}

TUNGSTATES: WO_4^{2-}

MOLYBDATES: MoO_4^{2-}

BORATES: BO_3^{3-}, BO_4^{5-}, and others

For the mineral groups listed, for all but the borates the cation in each anionic group takes up more than half of oxygen's charge. The minerals with these anionic groups are therefore anisodesmic (Chapter 3), and the anionic groups must be treated as discrete structural elements. The carbonate group consists of three oxygens in triangular arrangement around the central carbon. For the sulfates, phosphates, tungstates, and molybdates, the anionic group is a tetrahedron with oxygen at the corners and the cation in the center. In the borates, which are included in this chapter for convenience, the B^{3+} may coordinate with either three or four O^{2-} or OH^- anions to form a variety of complex structures.

DO NOT COPY
e48d507df5d1141@placeholder.9409

Printed by: e48d507df5d1141@placeholder.94092.edu. Printing is for personal, private use only. No part of this book may be reproduced or transmitted without publisher's prior permission. Violators will be prosecuted.

Carbonates

The essential structural element in all carbonate minerals is the CO_3^{2-} anionic group (Figure 17.1). In this anionic group, carbon has a +4 charge and takes up two-thirds of the net −6 charge of the three oxygen. The oxygen is therefore more strongly bonded to the C^{4+} cation than to any other cations in the mineral structure. Further, an oxygen in the CO_3^{2-} group cannot also be shared with another CO_3^{2-} group. Therefore, the structure of all carbonates must be based on CO_3^{2-} groups that are bonded laterally through various cations. In some cases additional OH^- groups or other anionic components may be present.

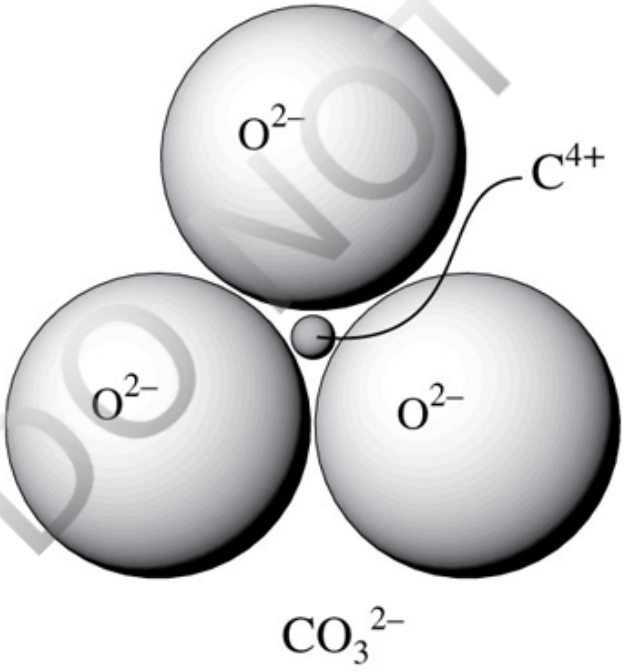

FIGURE 17.1 CO_3^{2-} anionic groups. A carbon cation is situated at the center of three oxygen anions. View larger image

The common carbonate minerals can be divided into the calcite group, dolomite group, aragonite group, and a hydrated carbonate group (Table 17.1). The calcite and dolomite groups share essentially the same structure and collectively are called the **rhombohedral carbonates**, because they have rhombohedral symmetry. Additional carbonate minerals are listed in Table 17.2.

TABLE 17.1 Major Groups of Carbonate Minerals

Calcite Group		Dolomite Group		Aragonite Group		OH-Bearing Group	
Calcite	$CaCO_3$	Dolomite	$CaMg(CO_3)_2$	Aragonite	$CaCO_3$	Azurite	$Cu_3(CO_3)_2(OH)_2$

DO NOT COPY e48d507df5d1141@placeholder.9409

Printed by: e48d507df5d1141@placeholder.94092.edu. Printing is for personal, private use only. No part of this book may be reproduced or transmitted without publisher's prior permission. Violators will be prosecuted.

Calcite	$CaCO_3$	Dolomite	$CaMg(CO_3)_2$	Aragonite	$CaCO_3$	Azurite	$Cu_3(CO_3)_2(OH)_2$
Magnesite	$MgCO_3$	Ankerite	$Ca(Mg,Fe)(CO_3)_2$	Witherite	$BaCO_3$	Malachite	$Cu_2CO_3(OH)$
Rhodochrosite	$MnCO_3$	Kutnohorite	$CaMn(CO_3)_2$	Strontianite	$SrCO_3$		
Siderite	$FeCO_3$			Cerussite	$PbCO_3$		
Smithsonite	$ZnCO_3$						

TABLE 17.2 Properties of Less Common Carbonate Minerals

Mineral	Unit Cell	Physical Properties[a]	Optics	Comments
Cerussite $PbCO_3$	Orthorhombic $2/m\ 2/m\ 2/m$ $a = 5.15$ $b = 8.47$ $c = 6.11$ $Z = 4$	H: 3–3.5 G: 6.55 Cl: {110}g, {021}pr Tw: {110}, {130}, cyclic C: Gray, colorless St: White L: Adamantine	$n_\alpha = 1.803$ $n_\beta = 2.074$ $n_\gamma = 2.076$ $\delta = 0.273$ Biaxial (−) $2V = 9°$ $r > v$, strong Colorless	Crystals variable, often tabular||(010) or acicular on c or a; found in oxidized zone of Pb-bearing hydrothermal sulfide deposits; effervesces in dilute HCl; formerly used as white pigment in lead paints
Kutnohorite $CaMn(CO_3)_2$	Hexagonal (rhombohedral) $a = 4.85$ $c = 16.34$ $Z = 3$	H: 3.5–4 G: 3.12 Cl: {101}pf Tw: {001}, {102} C: White, pink St: White L: Vitreous	$n_\omega = 1.727$ $n_\epsilon = 1.535$ $\delta = 0.192$ Uniaxial (−) Colorless	Associated with other Mn minerals in hydrothermal deposits and sediments; effervesces in dilute HCl if powdered
Nahcolite $NaHCO_3$	Monoclinic $2/m$ $a = 7.48$ $b = 9.69$	H: 2.5 G: 2.16–2.21 Cl: {101}pf,	$n_\alpha = 1.377$ $n_\beta = 1.503$	Forms grains elongate on c and granular massive aggregates; easily soluble in water; most common in evaporite deposits from saline lakes, as an

DO NOT COPY
e48d507df5d1141@placeholder.9409

Printed by: e48d507df5d1141@placeholder.94092.edu. Printing is for personal, private use only. No part of this book may be reproduced or transmitted without publisher's prior permission. Violators will be prosecuted.

	$c = 3.48$ $Z = 4$ $\beta = 93.4°$ X ^ $c = +27°$, $Y = b$, Z ^ $a = -24°$	{111} and {100}g Tw: {101} common C: White, gray St: White L: Vitreous	1.503 $n_\gamma = 1.583$ $\delta = 0.206$ Biaxial (−) $2V = 75°$ $r < v$, weak Colorless	from saline lakes, as an efflorescence, or in hot spring deposits; effervesces in dilute HCl; active ingredient in baking soda, also known as sodium bicarbonate
Smithsonite $ZnCO_3$	Hexagonal (rhombohedral) $a = 4.653$ $c = 15.026$ $Z = 6$	H: 4–4.5 G: 4.30–4.45 Cl: {101}pf Tw: N/A C: Dirty brown, also colorless, green, blue, pink St: White L: Vitreous to pearly	$n_\omega = 1.850$ $n_\varepsilon = 1.625$ $\delta = 0.225$ Uniaxial (−) Colorless	Rhombohedral or scalenohedral crystals; often forms reniform masses, encrustations, or granular masses; found as a secondary mineral in the oxidized portion of Zn-bearing hydrothermal sulfide deposits; effervesces in dilute HCl
Trona $Na_3H(CO_3)_2{\cdot}2H_2O$	Monoclinic $2/m$ $a = 20.11$ $b = 3.49$ $c = 10.31$ $\beta = 103°$ $Z = 4$ $X = b$, Y ^ $c = +7°$, Z ^ $a = +7°$	H: 2.5–3 G: 2.11–2.13 Cl: {100}pf, $\{\bar{1}11\}$, {001}pr Tw: None C: Gray, yellowish white, also colorless, white, yellow, light brown St: White L: Vitreous	$n_\alpha = 1.416$ $n_\beta = 1.494$ $n_\gamma = 1.542$ $\delta = 0.126$ Biaxial (−) $2V = 75°$ $r < v$, distinct Colorless	Fibrous or columnar || b, bladed || {001}, massive; found in evaporite deposits from saline lakes and as soil efflorescence; effervesces in dilute HCl; soluble in water; alkaline taste; mined and refined into sodium bicarbonate; see nahcolite above

[a] Cl = cleavage (pf = perfect, g = good, pr = poor), Tw = twinning, C = color, St = streak, L = luster

DO NOT COPY e48d507df5d1141@placeholder.94092

Printed by: e48d507df5d1141@placeholder.94092.edu. Printing is for personal, private use only. No part of this book may be reproduced or transmitted without publisher's prior permission. Violators will be prosecuted.

Rhombohedral Carbonates (Calcite and Dolomite Groups)

The structure of the rhombohedral carbonates can be derived from the halite structure, with CO_3 groups in place of Cl and M^{2+} in place of Na (Figure 17.2). The cube is shortened along one of its 3-fold axes to form a rhombohedron, and the plane of the triangular CO_3 groups is perpendicular to this axis, which becomes the *c* axis. As a result of this geometry, the CO_3 groups form layers perpendicular to the *c* axis. Each layer of CO_3 groups effectively consists of a simple close-packed layer of oxygen anions with C occupying selected triangular-coordination sites within the layer. Successive layers are offset so that the position of the C is equivalent to cubic close packing (i.e., their position is repeated in every third layer). Although the position of the C atoms is repeated in every third CO_3 layer, the corners of the triangular CO_3 groups alternate by a mirror plane every layer. The result is that an exact duplicate layer of CO_3 groups is repeated only every sixth layer. The unit cell must be six CO_3 layers thick or about 15 to 17 Å along the *c* axis.

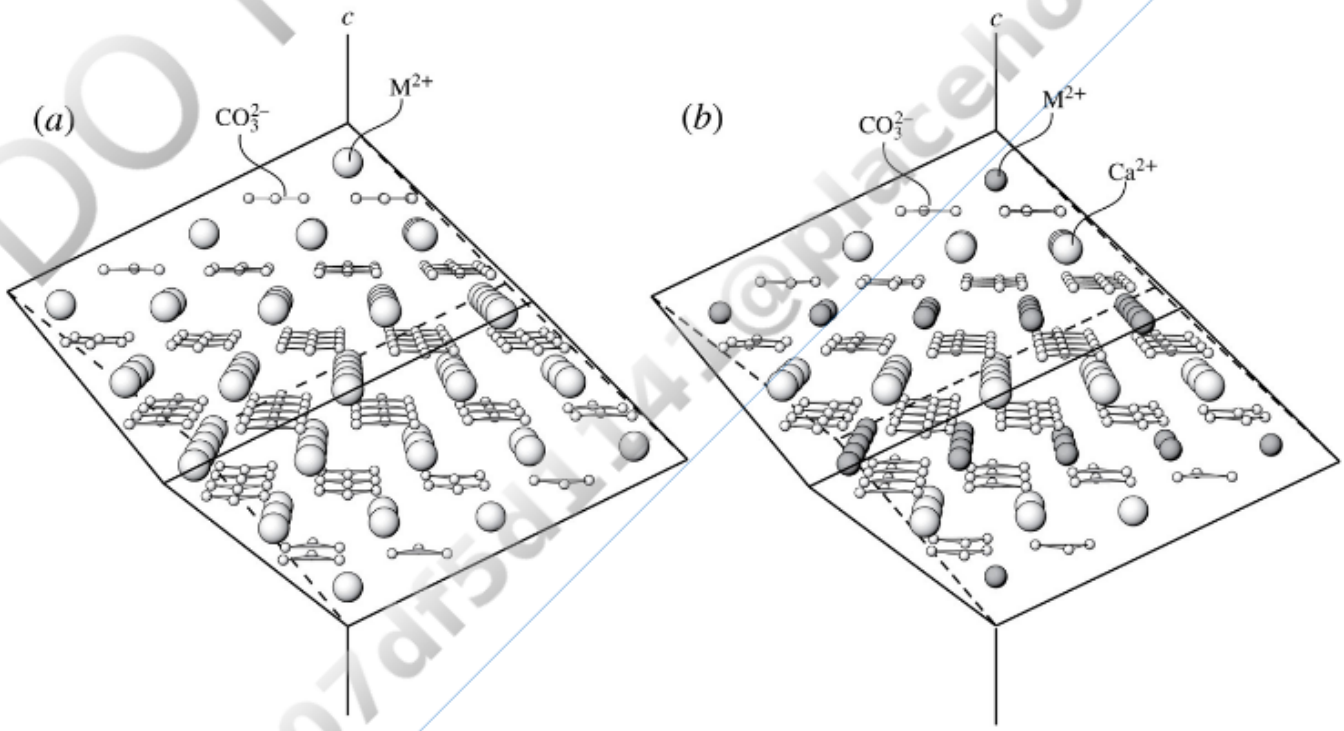

FIGURE 17.2 Structure of the rhombohedral carbonates. O^{2-} anions at the corners of triangular CO_3^{2-} groups are shown as small spheres. (*a*) In the calcite structure, CO_3 groups form sheets parallel to {001} separated by octahedrally coordinated cations (M^{2+} = Ca, Mg, Mn, Fe, or Zn). Note that the direction the CO_3 groups "point" alternates every other sheet. (*b*) In the dolomite structure, layers of larger Ca cations alternate with layers of smaller metal cations (M^{2+} = Mg, Fe, or Mn). View larger image

Printed by: e48d507df5d1141@placeholder.94092.edu. Printing is for personal, private use only. No part of this book may be reproduced or transmitted without publisher's prior permission. Violators will be prosecuted.

Divalent cations (M^{2+} = Ca, Mg, Mn, Fe, or Zn) occupy octahedral (6-fold) sites between the layers. Each oxygen anion therefore coordinates with one C cation within its layer, one divalent cation above it, and one below. In the calcite group, the octahedral sites are all occupied by the same cation(s) (Figure 17.2a). The dolomite group must accommodate two distinctly different-sized cations, one of which is Ca. This is accomplished by having layers of Ca alternate with layers of smaller Mg, Fe, or Mn (M^{2+} in Figure 17.2b).

Solid solution among the end members of the calcite group is controlled largely by ionic radii (Appendix A). Solid solution between magnesite (Mg, 0.86 Å) and siderite (Fe^{2+}, 0.92 Å) is complete, as is solid solution between siderite and rhodochrosite (Mn, 0.96 Å). Solid solution between magnesite and rhodochrosite is somewhat limited. Solid solution between smithsonite, siderite, and rhodochrosite is largely complete. Ca, however, is substantially larger (1.14 Å) than the other metals found in calcite group minerals, so calcite shows only limited solid solution with the Mg, Fe, Zn, and Mn carbonates. Ca is the largest cation that routinely fits into the 6-fold site, and it also fits in the larger coordination site provided in the aragonite structure, such that calcite and aragonite are polymorphs.

Solid solution among the members of the dolomite group is also possible. Dolomite [$CaMg(CO_3)_2$] and ankerite [$Ca(Mg,Fe)(CO_3)_2$] form a solid solution series, and some Mn may substitute for either Fe or Mg. There is little substitution of other cations for the Ca.

Based on the layered structure, it might be reasonable to suspect that cleavage in these carbonates is between the layers of CO_3 groups, i.e., {001} cleavage. However, that is not the case because bonding from the CO_3 to the layers of divalent cations is substantially stronger than bonds between CO_3 groups within CO_3 layers. Because CO_3 groups are offset from one CO_3 layer to the next, the cleavage is inclined to the *c* axis, and the three cleavage directions define a rhomb whose surfaces are parallel to the three edges of the triangular carbonate groups.

This discussion leads to a problem with nomenclature in the rhombohedral carbonates. The prominent cleavage has conventionally been considered a unit face with {101} ($\{10\,\bar{1}1\}$ for those using the Miller–Bravais convention) as an index, consistent with the laws of Bravais and Haüy (Chapter 2). The problem is that this convention requires a unit cell along *c* that is one-fourth the dimension actually measured in X-ray diffraction studies (*c* = 15–17 Å), or alternatively, an *a* dimension that is four times its actual ~5 Å dimension. The thoughtful reader might reasonably suggest that Miller indices should be reassigned based on the correct unit cell to yield {104} as the index for the cleavage. That, however, would lead to confusion in the comparison of data from different sources. The practice followed here is to use the conventional Miller indices and report both the actual unit cell dimensions and unit cell dimensions consistent with the Miller indices. In comparing information from different sources, readers are cautioned to confirm the unit cell convention used.

DO NOT COPY e48d507df5d1141@placeholder.9409

Printed by: e48d507df5d1141@placeholder.94092.edu. Printing is for personal, private use only. No part of this book may be reproduced or transmitted without publisher's prior permission. Violators will be prosecuted.

Calcite

$CaCO_3$

Hexagonal (rhombohedral) $\bar{3}\ 2/m$

$a = 4.990$ Å, $c = 17.060$ Å, $Z = 6$
($a = 19.960$ Å, $c = 17.060$ Å, $Z = 96$ to be consistent with Miller indices)

$H = 3$ on cleavage (varies with direction), 2.5 on {001}

$G = 2.71$

Uniaxial (−)

$n_\omega = 1.658$

$n_\epsilon = 1.486$

$\delta = 0.172$

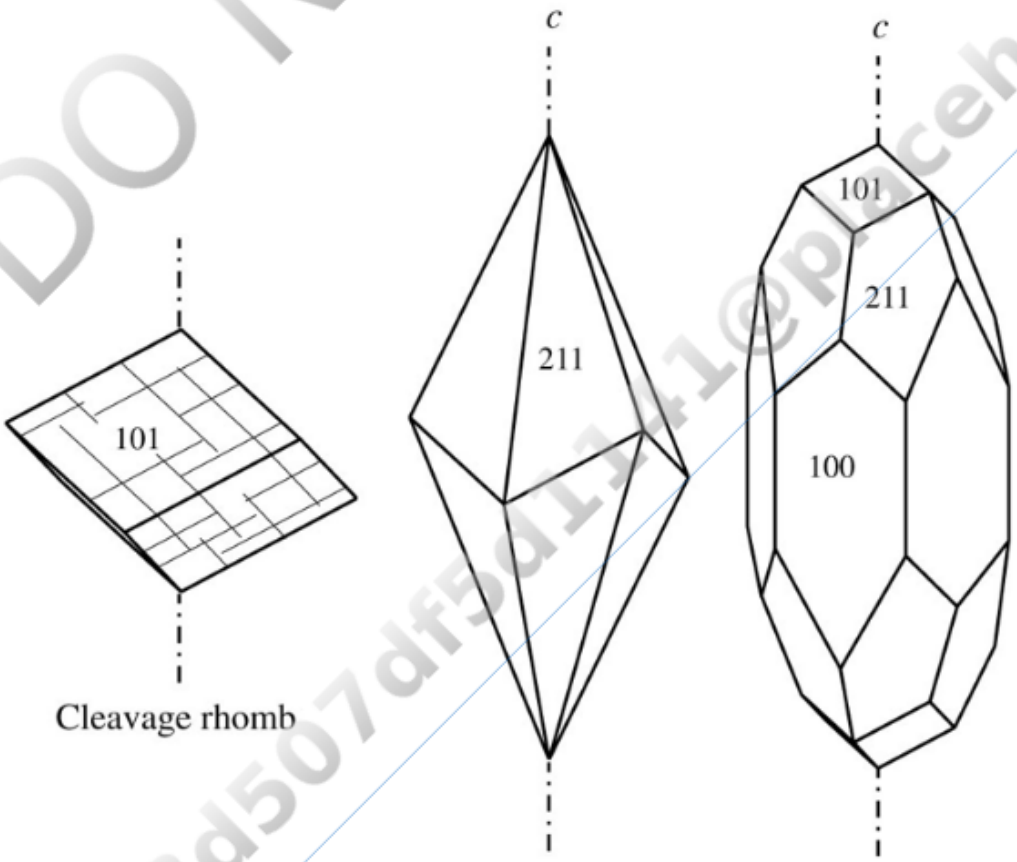

Composition Most calcite, particularly if formed in a sedimentary environment, is nearly pure $CaCO_3$. Crystallization at elevated temperatures allows some Mg, Fe, Mn, or Zn to

DO NOT COPY
e48d507df5d1141@placeholder.9409

Printed by: e48d507df5d1141@placeholder.94092.edu. Printing is for personal, private use only. No part of this book may be reproduced or transmitted without publisher's prior permission. Violators will be prosecuted.

substitute for Ca; Mg is the most common. Since lower temperature restricts the amount of Mg that the structure can accommodate, it is not uncommon to find exsolution lamellae of dolomite in calcite. Some larger cations such as Ba or Sr also may substitute for Ca.

Form and Twinning Calcite displays a wide variety of forms, but most crystals display some combinations of scalenohedrons, prisms, and rhombohedrons (Figure 17.3). The most common are the {211} scalenohedron, {100} prism, and {101} rhombohedron. Rhombohedrons, when present, usually modify other more prominent forms and simple rhombohedrons by themselves are not particularly common. Crystals in which the {211} scalenohedron dominate are sometimes referred to as dogtooth spar. The calcite in limestone usually forms fine anhedral grains. In marble and related metamorphic rocks, calcite is usually equant and interlocking (granular). Calcite that makes up fossil shells or thin veins may have a fibrous or columnar habit. High-quality clear calcite is referred to as Iceland spar.

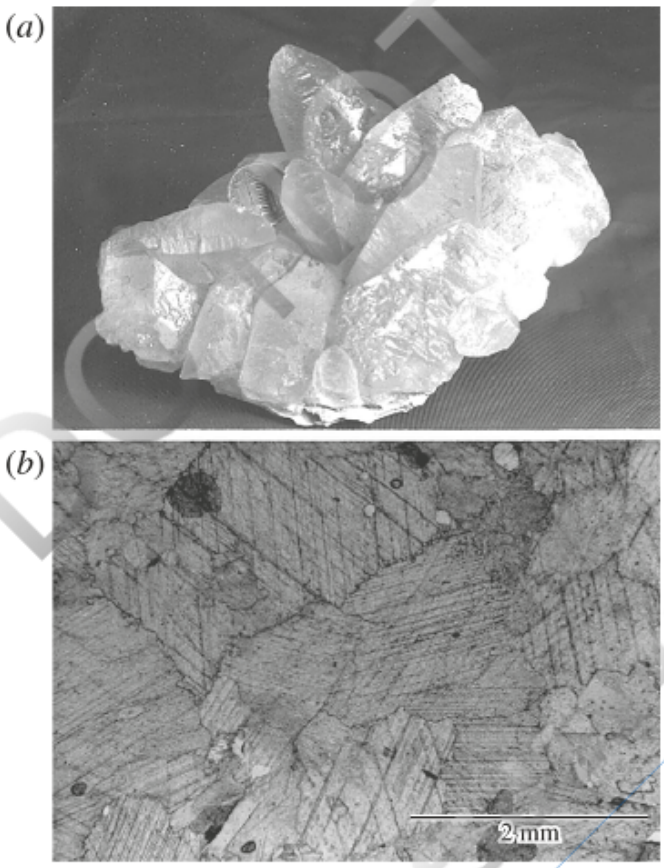

FIGURE 17.3 Calcite. (*a*) Calcite crystals. Field of view is about 20 cm wide. (*b*) Photomicrograph of calcite in marble. Plane light. View larger image

Lamellar twins on the negative rhombohedron {012} are common and will be parallel to the edge or along the long diagonal between faces of cleavage rhombs (Figure 17.4). Etching the face of a cleavage rhomb with dilute acid may reveal the presence of these twins. These twins are commonly produced as a result of deformation, and detailed study of their orientation may indicate the nature of the stresses that produced the deformation. The pressure of a knife blade on one of the obtuse edges of a cleavage

Printed by: e48d507df5d1141@placeholder.94092.edu. Printing is for personal, private use only. No part of this book may be reproduced or transmitted without publisher's prior permission. Violators will be prosecuted.

deformation. The pressure of a knife blade on one of the obtuse edges of a cleavage rhomb may be sufficient to cause twinning (Figure 5.26). Samples also may be twinned as a result of cutting or grinding in the preparation of thin sections or when samples are crushed to prepare grain mounts. Simple twins with {001} composition planes also are common. Twins on {101} are infrequent.

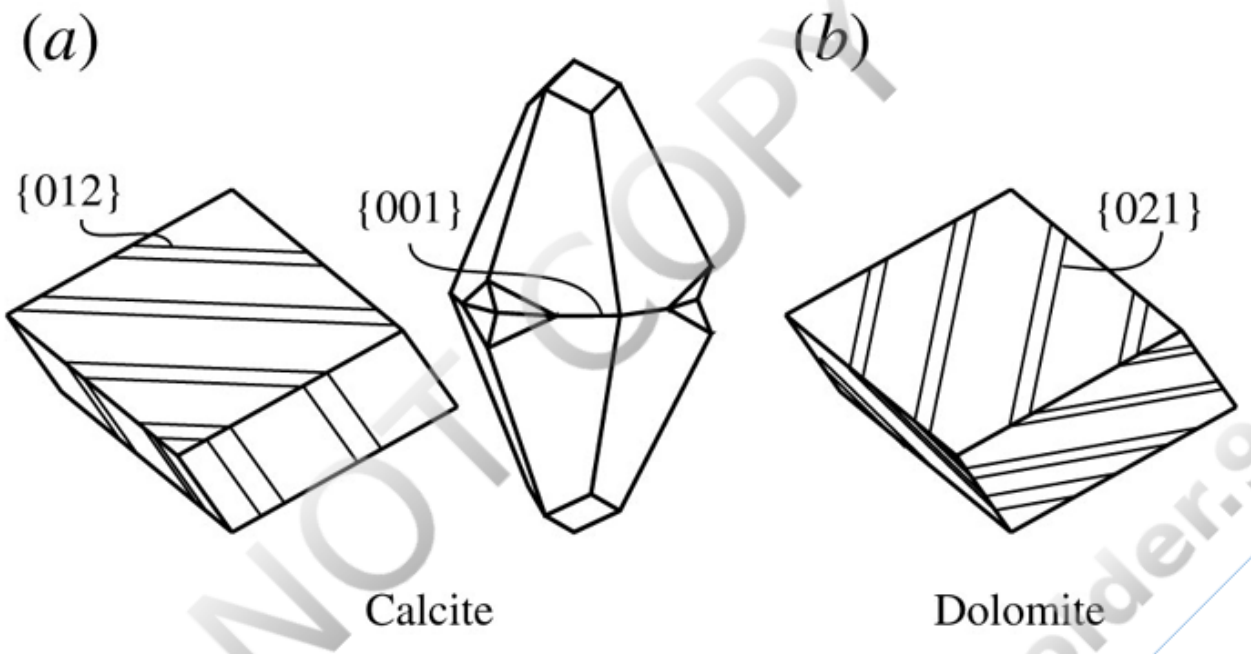

FIGURE 17.4 Twins in rhombohedral carbonates. (*a*) Lamellar {012} twins may be parallel to rhomb face edges or parallel to the long diagonal. Simple {001} twins may form distinctive crystals. (*b*) Dolomite. Lamellar {021} twins may be parallel to either the short or the long diagonal between rhombohedral cleavage traces. View larger image

Cleavage {101} Rhombohedral cleavage is perfect. The angle between cleavages is 74.9°. A parting on {012} has been associated in the old literature with twin planes in that orientation. As noted in Chapter 6, twin planes are not likely to be planes of weakness and calcite does display exsolution lamellae of dolomite, so this parting deserves study using modern tools. Fracture is conchoidal but is difficult to produce. Brittle.

Color Properties

Luster: Vitreous; earthy if very fine grained.

Color: Colorless, white, or gray most commonly, but almost any color is possible, depending on the presence of impurities or fine disseminated inclusions.

Streak: White.

Color in Thin Section: Colorless.

Other: May fluoresce under UV light. Trace amounts of Mn^{2+}, for example, can provide energy levels to which electrons can be promoted with absorption of ultraviolet light.

DO NOT COPY e48d507df5d1141@placeholder.9409

Printed by: e48d507df5d1141@placeholder.94092.edu. Printing is for personal, private use only. No part of this book may be reproduced or transmitted without publisher's prior permission. Violators will be prosecuted.

When these electrons return to their base energy levels, orange-red light is emitted. Many other elements, including Pb, may produce fluorescence.

Optical Characteristics

Relief in Thin Section: Moderate negative to high positive; changes with rotation.

Optic Orientation: Extinction is inclined or symmetrical to cleavage traces and parallel to the length of elongate crystals. The fast ray vibrates parallel to the short diagonal of rhombohedral faces and traces of rhombohedral cleavage. The angle between the fast ray (ϵ') and the trace of {012} twin lamellae is greater than about 55° in sections cut so that one of the cleavage surfaces is nearly horizontal.

Indices of Refraction and Birefringence: Indices of refraction vary systematically with composition (Figure 17.5). The index $n'_{\epsilon\{101\}}$ for fragments lying on a cleavage surface is 1.566 for pure calcite. Because birefringence is extreme (0.172), interference colors in standard thin section are usually upper-order creamy white even if the optic axis is close to vertical. Twin lamellae may be identified as pastel bands of pink or green, and zones in which twin lamellae overlap may not go entirely extinct with stage rotation. Unless the optic axis is close to vertical, grains usually display a distinct change of relief with stage rotation, lower when the short diagonal of the rhomb is parallel to the lower polarizer vibration direction.

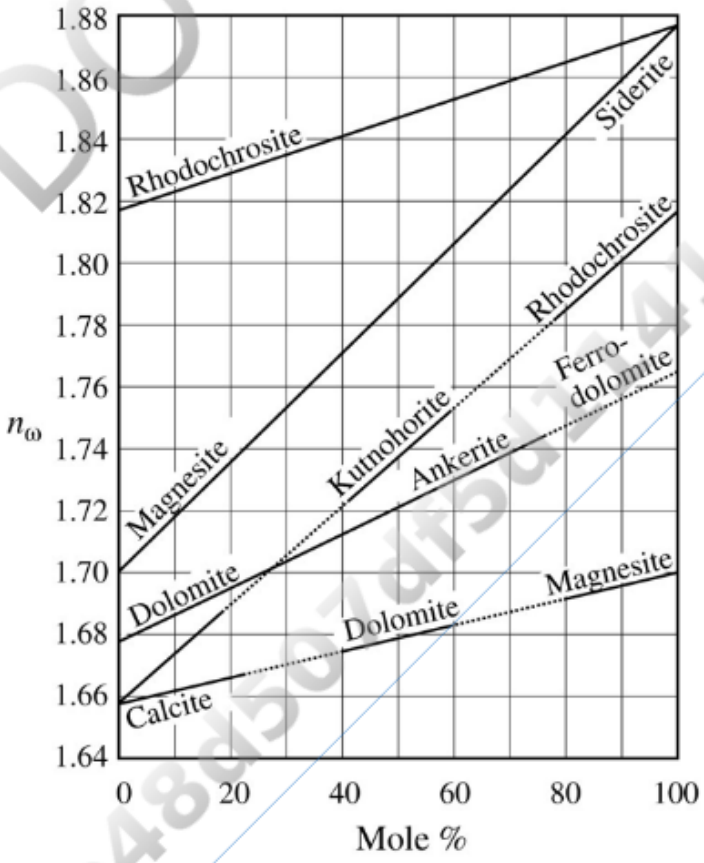

FIGURE 17.5 Index of refraction n_ω in the rhombohedral carbonates. After Kennedy (1947).

Printed by: e48d507df5d1141@placeholder.94092.edu. Printing is for personal, private use only. No part of this book may be reproduced or transmitted without publisher's prior permission. Violators will be prosecuted.

FIGURE 19.5 Index of refraction n_ω in the rhombohedral carbonates. After Kennedy (1947).
View larger image

Interference Figure: Uniaxial negative with numerous isochromes and thin, well-defined isogyres. Some calcite, particularly from metamorphic rocks, may be biaxial negative with $2V$ up to about 15°.

Alteration Calcite may be replaced by dolomite through diagenetic processes or replaced by quartz, opal, iron, manganese oxides, or other minerals, resulting in pseudomorphs. It is soluble in many natural waters and may be removed from rocks by dissolution.

Distinguishing Features

Hand Sample: Recognized by hardness, rhombohedral cleavage, and by effervescing in dilute HCl (1 part concentrated HCl, 9 parts water). Dolomite has a higher specific gravity and does not vigorously effervesce with cold dilute HCl unless powdered. Aragonite, which reacts vigorously with dilute cold HCl, has higher specific gravity than calcite.

Thin Section/Grain Mount: Cleavage, extreme birefringence, and relief change with rotation distinguish the rhombohedral carbonates from most other minerals. The orthorhombic carbonates (aragonite group) are biaxial and lack rhombohedral cleavage. Index of refraction measurement in grain mount will unambiguously distinguish calcite from dolomite and from the other rhombohedral carbonates. Use the following criteria to help distinguish between calcite and dolomite in common carbonate rocks.

- Calcite is more commonly twinned, and lamellae are not parallel to the short diagonal of the rhomb.
- Dolomite more commonly forms euhedral rhombs in limestone and dolomite; it may be cloudy or stained with iron oxides.
- Dolomite has higher refractive indices.
- Staining techniques (Friedman, 1959; Warne, 1962; Wolfe and others, 1967) can speed identification in both hand sample and thin section.

Occurrence Calcite is a very common and widespread mineral. It is an important constituent in many clastic sedimentary rocks as a cementing agent or as fossil fragments. Calcite forms by chemical precipitation from water in many different environments (marine, lacustrine, groundwater, hydrothermal, etc.) and is an important biomineral (Chapters 1 and 5). It is produced by both biologically controlled and biologically induced processes. Biologically controlled mineralization yields the shells of many marine invertebrates including mollusks, foraminifera, and coccoliths. A good example of biologically induced mineralization is the dramatic “whiting” events seen in subtropical marine waters and saline lakes (Robbins and Blackwelder, 1992). Whitings originate with blooms of plankton, which induce the crystallization of calcite and aragonite crystals on their cellular surfaces. The abundance of fine carbonate crystals

DO NOT COPY e48d507df5d1141@placeholder.94092

Printed by: e48d507df5d1141@placeholder.94092.edu. Printing is for personal, private use only. No part of this book may be reproduced or transmitted without publisher's prior permission. Violators will be prosecuted.

aragonite crystals on their cellular surface. The abundance of fine carbonate crystals gives the water its white color. Calcite and aragonite produced in this manner may be a major contributor to the mass of limestone deposited in carbonate bank environments (**Box 17.1**). Calcite also is a major mineral in evaporite deposits, which are described in Box 17.2. Calcite is common in metamorphic rocks derived from carbonate-bearing sediments and is the major mineral in marble, where it may be associated with diopside, tremolite, olivine, garnet, epidote, wollastonite, and other calc-silicate minerals. Calcite in igneous rocks is relatively rare, but may be found in silica-poor, alkali-rich igneous rocks containing nepheline or other feldspathoids, as vesicle fillings in volcanic rocks, or as a major mineral in rare calcite-rich intrusions called carbonatites. Hydrothermal mineral deposits commonly contain calcite as a gangue mineral, and it may fill fractures and form eye-catching crystals. It is common as a joint coating or fracture filling in almost any rock and may be formed by the alteration of Ca-bearing minerals such as plagioclase.

BOX 17.1
Limestone and Dolostone

Most limestone is deposited in shallow marine environments in locations without a substantial contribution of clastic sediment. Most of the calcite is produced by biologic activity. The foundation of biologic activity is photosynthesis, so most calcite production is limited to the photic zone. The photic zone is the upper part of the ocean that receives sunlight, which is generally less than about 100 meters deep. Within the photic zone, the most abundant photosynthetic activity is within a few tens of meters of the surface, and it is here that calcite-producing organisms thrive. These organisms include mollusks, corals, brachiopods, crinoids, bryozoans, and other marine invertebrates that precipitate carbonate shells. Also included are many single-celled organisms such as coccolithophores, foraminifera, and various bacteria and algae. The species involved have, of course, changed over the course of geologic time.

Many limestone layers contain significant amounts of dolomite, and a carbonate rock consisting of over 75 percent dolomite is considered a dolostone. Dolomite, however, does not usually precipitate directly from seawater, and most dolostones contain fossils that indicate a normal marine environment that deposited calcite. In most cases, therefore, the formation of major dolostone layers and dolomitic limestone is the result of post-deposition diagenesis of the original calcite in a limestone. Details of the process by which dolomite replaces calcite in limestone beds have been the subject of considerable debate. The traditional explanations involve processes by which the pore water in limestone provides Mg^{2+} to produce the recrystallization of calcite to dolomite. The pore water may be either normal seawater or a brine produced by some degree of evaporation of seawater. However, recent studies (e.g., Wright, 1999; Sánchez-Román and others, 2008) show that dolomite growth may be mediated by both sulfate-reducing and aerobic bacteria. This

Printed by: e48d507df5d1141@placeholder.94092.edu. Printing is for personal, private use only. No part of this book may be reproduced or transmitted without publisher's prior permission. Violators will be prosecuted.

suggests the possibility that dolomitization may be partly or largely a biologically driven process.

BOX 17.2
Evaporites

Evaporite deposits form by evaporation-driven precipitation of minerals from ion-saturated surface or near-surface waters. Often evaporate deposits are quite thick, indicating long periods of evaporation. Such deposits are economically important as they can house large quantities of, for example, halite and gypsum. Some deposits are also enriched in other minerals of economic importance such as borax (and other B-bearing minerals), epsomite, trona, and Li-bearing minerals. Lithium may also be extracted from brines found in actively forming evaporite deposits.

Common environments that form evaporite deposits are saline lakes, playas, restricted basins, and sabkhas. Saline lakes, or closed basin lakes, are lakes without an outlet such that water leaves the system only through evaporation. Playas are dry lake beds that are covered with water only after large storms; shortly after such events the water evaporates (Figure 17.11). Restricted basins are regions within an ocean with only limited communication to the open ocean. Evaporation exceeds water input, leading to crystallization of evaporite minerals. Sabkhas are low-lying areas adjacent to an ocean. High tides occasionally invade sabkhas, and the added water soon evaporates. Additional complexity may exist for playas and sabkhas if capillary action draws groundwater to the surface, leading to deposition of other minerals upon evaporation.

FIGURE 17.11 A view of Desert Peak across Bonneville Salt Flats, a playa in western Utah. View larger image

The minerals in evaporite deposits are all relatively water soluble, and Table 17.3 lists the common ones. For marine waters, the most abundant cations are Na^+, Ca^{2+}, Mg^{2+}, and K^+, and the most abundant anions are Cl^-, SO_4^{2-}, and HCO_3^-. Evaporating seawater therefore dominantly precipitates chlorides, sulfates, and carbonates. These minerals do not form all at once or even in the same location, depending on the

DO NOT COPY e48d507df5d1141@placeholder.94092-

Printed by: e48d507df5d1141@placeholder.94092.edu. Printing is for personal, private use only. No part of this book may be reproduced or transmitted without publisher's prior permission. Violators will be prosecuted.

minerals do not form all at once or even in the same location, depending on the details of the particular environment. If normal seawater evaporates, the minerals precipitate in the following sequence:

Calcite→Gypsum→Anhydrite→Glauberite→Halite→Polyhalite→Epsomite→other bitterns

TABLE 17.3 Select Minerals Formed in Evaporite Deposits

Carbonates		Sulfates		Halides		Borates
Aragonite	$CaCO_3$	Anhydrite	$CaSO_4$	Carnallite	$KMgCl_3 \cdot 6H_2O$	Borax
Calcite	$CaCO_3$	Epsomite	$MgSO_4 \cdot 7H_2O$	Halite	NaCl	Colemanite
Dolomite	$CaMg(CO_3)_2$	Glauberite	$Na_2Ca(SO_4)_2$	Sylvite	KCl	Kernite
Magnesite	$MgCO_3$	Gypsum	$CaSO_4 \cdot 2H_2O$			Tincalconite
Nahcolite	$NaHCO_3$	Kieserite	$MgSO_4 \cdot H_2O$			Ulexite
Trona	$Na_3H(CO_3)_2 \cdot 2H_2O$	Polyhalite	$K_2MgCa_2(SO_4)_4 \cdot 2H_2O$			
		Thenardite	Na_2SO_4			

Halite constitutes most of the minerals by volume because Na^+ and Cl^- are by far the most abundant ions in seawater. Bitterns are the most soluble minerals that precipitate after halite and include, for example, sylvite and carnallite.

In actual marine evaporite systems, the crystallization sequences can be quite complex. In restricted basins, water from open marine sources, rivers, rain/snow, and/or groundwater is continually added, and evaporation waxes and wanes with the seasons and changing climate. Additionally, as restricted basins fill with evaporite minerals, there is also a variable flux of clastic sediment. Further, sea level may change and tectonic activity can change basin geometry. Regardless, marine evaporite systems are dominated by limestone, gypsum beds, and rock salt, with variable amounts of clastic sediment. In some environments, primary anhydrite may be precipitated rather than gypsum.

The evaporite mineral chemistry of saline lakes and playas depends on the chemistry of the water fed into them from surrounding areas, which is largely controlled by the local bedrock and geology, but biologic and chemical processes can also influence the details of evaporite deposition. Consequently, the evaporite minerals in those environments may differ significantly from marine systems and can vary regionally. For example, saline lakes in the Eocene Green River basin in Wyoming had high levels of Na^+ and HCO_3^- and precipitated thick beds of trona and other sodium carbonate minerals. Saline lakes in Death Valley, California, are enriched in boron, presumably from thermal springs and other hydrothermal sources, so a suite of borate minerals resulted.

Warren (2006) can be consulted for additional information regarding evaporite deposits.

DO NOT COPY e48d507df5d1141@placeholder.94092

Printed by: e48d507df5d1141@placeholder.94092.edu. Printing is for personal, private use only. No part of this book may be reproduced or transmitted without publisher's prior permission. Violators will be prosecuted.

Use Calcite is a very important industrial mineral. It is an essential raw material in the manufacture of **portland cement** and **mortar**. Intense heating of calcite drives off CO_2 and produces CaO, which is known as **quicklime**. The reaction is as follows.

$$CaCO_3 + \text{heat} \rightarrow CaO + CO_2$$

This process is called **calcination**. Quicklime is mixed with sand and water to form mortar, which sets or hardens by chemical reaction between the CaO and the water to crystallize various Ca-hydroxides. Mortar is used to bind building materials such as bricks and rocks together. Most mortar used now also includes substantial amounts of portland cement.

Portland cement is a similar, but chemically more complex material than quicklime. Portland cement is made by mixing and pulverizing calcite, usually in the form of limestone, with a silicon- and aluminum-rich rock (usually shale) that contains some iron. The mixture is calcinated by intense heating to form a mixture of Ca-silicates and aluminates. Upon cooling this mixture is finely ground again to form portland cement. This gray powder is mixed with sand, gravel, and water to form concrete that hardens or cures by chemical reactions and crystallization, including forming various Ca-bearing hydroxides. Concrete is by far the most widely used building material both currently and historically.

Manufacturing of portland cement and quicklime is a significant contributor to the human-caused increase of atmospheric CO_2. Both the calcination reaction and the fossil fuel burning required to manufacture the products generate the CO_2 (see Box 20.2 for more information on how this CO_2 alters the Earth's carbon cycle). New methods of cement/concrete curing use CO_2. The CO_2 is injected into the cement when mixed with water and results in the formation of some amount of $CaCO_3$ instead of various hydroxides and provides a way to sequester carbon as part of the curing process. Currently, this curing method does not appear to produce a net decrease in atmospheric CO_2. However, in the future this process may decrease atmospheric CO_2 if the amount of fossil fuel consumed to make cement/concrete in this way can be reduced (Ravikumar and others, 2021).

Quicklime and hydrated lime [$Ca(OH)_2$, also produced from calcite] are widely used in the steel industry as a flux, in paper manufacture, wastewater treatment, industrial flue gas desulfurization, soil stabilization, asphalt manufacture, and sugar refining, and as a soil amendment. Hydrated lime also is used as a mild abrasive in kitchen and bath cleaners.

Oxygen isotopes from calcite-rich deep-sea sediments provide important information regarding paleoclimate as far back as 70 Ma. See Box 18.1 for more details.

Calcite is used as a pharmaceutical. Several commercial antacids are simply pulverized

DO NOT COPY e48d507df5d1141@placeholder.94092

Printed by: e48d507df5d1141@placeholder.94092.edu. Printing is for personal, private use only. No part of this book may be reproduced or transmitted without publisher's prior permission. Violators will be prosecuted.

Calcite is used as a pharmaceutical. Several commercial antacids are simply pulverized calcite, as are some of the calcium supplements that women in particular are encouraged to take to decrease bone loss associated with osteoporosis. The calcium in vitamin tablets also is commonly delivered by calcite. Pulverized calcite is added to cattle feeds to help improve digestion and is included in poultry feed to maintain high-quality egg shells.

Calcite is a major constituent of marble, which is widely used in the creation of monuments and sculpture, and as dimension stone for architectural purposes. Unfortunately, marble, which is easily cut, shaped, and polished with basic tools, is readily degraded when exposed to the elements. Rain, which is naturally acidic because of dissolved CO_2, will dissolve calcite. Surface alteration of marble to softer gypsum is produced by calcite reacting with sulfate atmospheric pollutants often derived from burning sulfur-bearing coal or other fuels. During the alteration, black particles (often also pollutants) are trapped in the gypsum crust as it forms, resulting in black streaking on the marble surface. The gypsum crust can peel off, resulting in further damage to the marble structure.

Magnesite

$$\mathrm{MgCO_3}$$

$$\text{Hexagonal (rhombohedral) } \bar{3}\ 2\ /\ m$$

$$a = 4.63\ \text{Å},\quad c = 15.01\ \text{Å},$$
$$Z = 6\ (a = 18.53\ \text{Å},\ c = 15.01\ \text{Å},\ Z = 96 \text{ to be consistent with Miller indices})$$

$$H = 3.5 - 4.5$$

$$G = 2.98 \text{ (pure)}$$

$$\text{Uniaxial } (-)$$

$$n_\omega = 1.700$$

$$n_\epsilon = 1.509$$

$$\delta = 0.191$$

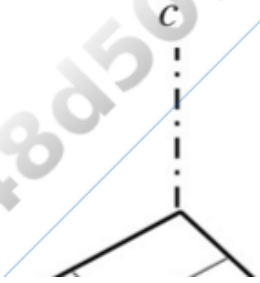

DO NOT COPY
e48d507df5d1141@placeholder.9409

Printed by: e48d507df5d1141@placeholder.94092.edu. Printing is for personal, private use only. No part of this book may be reproduced or transmitted without publisher's prior permission. Violators will be prosecuted.

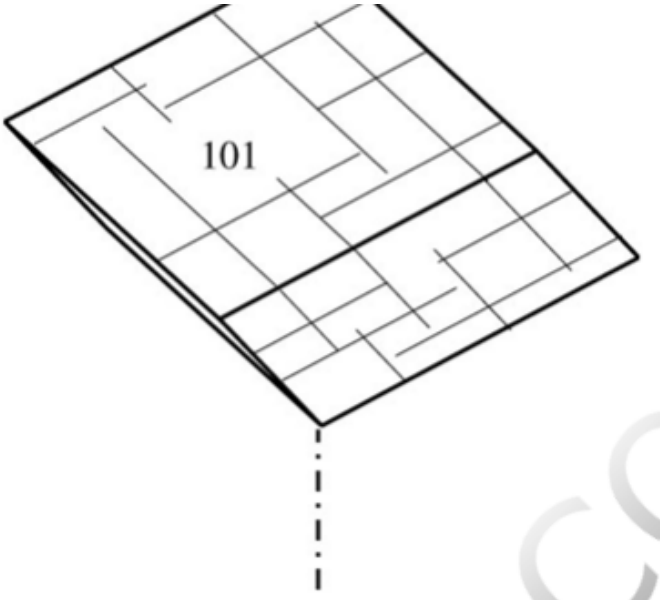

Composition Solid solution is complete between magnesite and siderite ($FeCO_3$), and substantial but incomplete between magnesite and rhodochrosite ($MnCO_3$), consistent with what should be expected based on the sizes of the cations (see earlier in this chapter and Chapter 4). Substitution of Ca for Mg is limited.

Form and Twinning Crystals are usually rhombs, but are uncommon. More commonly found as compact granular aggregates or as earthy masses. Some fine-grained masses may contain intergrown siliceous material and look somewhat like porcelain. Twins by translation gliding on {001} in the [100] direction may occur.

Cleavage Perfect {101} cleavage, like the other rhombohedral carbonates. The angle between cleavages is 72.6°. Conchoidal fracture. Brittle.

Color Properties

Luster: Vitreous.

Color: White, gray, or colorless. Fe-bearing samples may be yellow or brown.

Streak: White.

Color in Thin Section: Colorless.

Optical Characteristics

Relief in Thin Section: Low negative to high positive, marked change with rotation.

Optic Orientation: Extinction is inclined or symmetrical to cleavage traces.

Indices of Refraction and Birefringence: Indices of refraction increase with Fe and Mn content (Figure 17.5). Birefringence is extreme, so interference colors in thin section are upper-order creamy white for most grain orientations. The index of refraction $n'_{\epsilon\{101\}}$ for

DO NOT COPY e48d507df5d1141@placeholder.94092

Printed by: e48d507df5d1141@placeholder.94092.edu. Printing is for personal, private use only. No part of this book may be reproduced or transmitted without publisher's prior permission. Violators will be prosecuted.

fragments lying on {101} cleavage surfaces is 1.602 for pure magnesite, higher for Fe-bearing samples.

Interference Figure: Basal sections yield uniaxial negative figures with numerous isochromes.

Alteration Magnesite has no systematic alteration, but Fe-bearing samples may display reddish stains or may be altered to iron oxides and hydroxides.

Distinguishing Features

Hand Sample: Similar to dolomite, it reacts vigorously with dilute HCl only if powdered. Magnesite has a higher specific gravity than dolomite. White massive varieties resemble chert but are softer. Intergrown siliceous material (opal, chalcedony) may make the hardness greater than 4.5.

Thin Section/Grain Mount: Resembles calcite and dolomite but lacks twin lamellae and has higher indices of refraction.

Occurrence The most common occurrence is in altered or metamorphosed Mg-rich igneous rocks such as peridotite, pyroxenite, or dunite. It is reported infrequently from evaporite deposits (see Box 17.2) either as a direct precipitate or as the result of later diagenetic alteration of preexisting carbonate minerals. It also may be a gangue mineral in hydrothermal mineral deposits. Some of the major commercial magnesite deposits are hosted in sedimentary dolomite layers and appear to have been produced by hydrothermal replacement of dolomite by magnesite. It also is a relatively uncommon biomineral and may precipitate by a process of biologically induced mineralization on cyanobacteria in waters with sufficient dissolved Mg (Thompson and Ferris, 1990).

Use Magnesite may be used as an ore mineral for the production of metallic Mg and other Mg compounds, but most Mg currently comes from brines and seawater. The major use of magnesite is as a source for MgO (dead-burned magnesite) used in the manufacture of refractory materials. MgO is produced through magnesite calcination (heating to drive off CO_2). Natural MgO is the mineral periclase.

Siderite

$$FeCO_3$$

Hexagonal (rhombohedral) $\bar{3}\ 2/m$

$a = 4.69$ Å, $c = 15.38$ Å, $Z = 6$
($a = 18.77$ Å, $c = 15.38$ Å,
$Z = 96$ to be consistent
with Miller indices)

DO NOT COPY e48d507df5d1141@placeholder.9409

Printed by: e48d507df5d1141@placeholder.94092.edu. Printing is for personal, private use only. No part of this book may be reproduced or transmitted without publisher's prior permission. Violators will be prosecuted.

$$H = 4 - 4.5$$

$$G = 3.96 \text{ (lower w/ Mg or Mn)}$$

$$\text{Uniaxial } (-)$$

$$n_\omega = 1.875$$

$$n_\epsilon = 1.635$$

$$\delta = 0.240$$

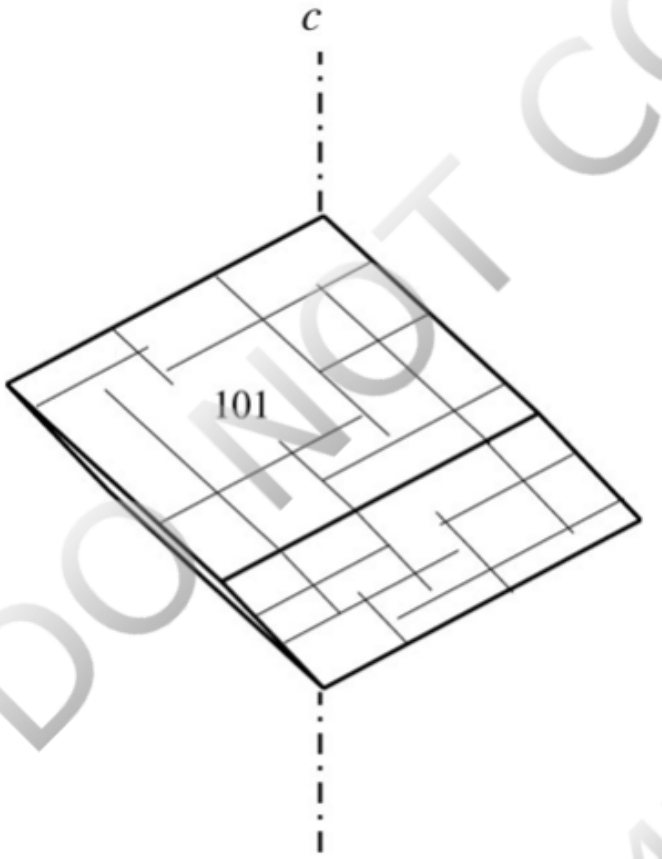

DO NOT COPY

Composition Complete solid solution extends to magnesite and to rhodochrosite. Substitution of Ca for Fe is limited to no more than 10% or 15% because of difference in cation size.

Form and Twinning Crystals are commonly {101} rhombohedrons, sometimes modified by a {001} basal pinacoid. More common as granular aggregates. Also found as oolites or as nodular and botyroidal forms consisting of radiating fibers or acicular grains. May form lamellar twins on {012} similar to calcite, or less frequently, single twins by reflection on {001}.

Cleavage Perfect {101} cleavage like the other rhombohedral carbonates. The angle between cleavages is 73°. Uneven to conchoidal fracture. Brittle.

Color Properties

Printed by: e48d507df5d1141@placeholder.94092.edu. Printing is for personal, private use only. No part of this book may be reproduced or transmitted without publisher's prior permission. Violators will be prosecuted.

Color Properties

Luster: Vitreous.

Color: Usually some shade of light to dark yellowish, reddish or grayish brown.

Streak: White.

Color in Thin Section: Colorless or pale yellowish brown.

Pleochroism: Colored varieties pleochroic $\epsilon < \omega$, so samples are darker when the long diagonal between cleavages is parallel to the vibration direction of the lower polarizer.

Optical Characteristics

Relief in Thin Section: Moderate to high positive, changes with rotation.

Optic Orientation: Extinction is inclined or symmetrical to cleavage traces and the short diagonal between cleavages is length fast.

Indices of Refraction and Birefringence: Decrease with Mg and Mn content (Figure 17.5). The index of refraction $n'_{\epsilon\{101\}}$ for fragments lying on {101} cleavage surfaces is 1.748 for pure siderite, lower for Mg- and Mn-bearing samples.

Interference Figure: Basal sections yield uniaxial negative figures with numerous isochromes.

Alteration Siderite is commonly altered to iron oxides and hydroxides (goethite, hematite, etc.). Pseudomorphs of these minerals after siderite are relatively common.

Distinguishing Features

Hand Sample: Distinguished from other rhombohedral carbonates by color and high specific gravity. It effervesces vigorously in dilute HCl only if powdered.

Thin Section/Grain Mount: Indices of refraction are higher than the other rhombohedral carbonates, and both ω and ϵ rays have indices of refraction higher than the epoxy commonly used in thin sections (~1.540), unlike calcite, dolomite, or magnesite. Siderite commonly has lamellar twinning that magnesite lacks.

Occurrence Siderite may occur as concretionary or oolitic forms in bedded Fe-rich sedimentary rocks called clay ironstones. It also is a constituent in metamorphosed iron formations. Hydrothermal systems often precipitate siderite as a gangue mineral. Larger masses may be produced by hydrothermal alteration of limestone. It also is a relatively uncommon biomineral (Chapter 5).

Use In some areas it is used as an iron ore. It also can be used as a raw material in the manufacture of iron oxide and hydroxide pigments, which are widely used in paints, cosmetics, and other products where red or brown colors are desired.

DO NOT COPY e48d507df5d1141@placeholder.94092

Printed by: e48d507df5d1141@placeholder.94092.edu. Printing is for personal, private use only. No part of this book may be reproduced or transmitted without publisher's prior permission. Violators will be prosecuted.

cosmetics, and other products where red or brown colors are desired.

Rhodochrosite

$MnCO_3$

Hexagonal (rhombohedral) $\bar{3}\,2/m$

$a = 4.77$ Å, $c = 15.66$ Å, $Z = 6$

($a = 19.07$ Å, $c = 15.66$ Å,
$Z = 96$ to be consistent
with Miller indices)

$H = 3.5 - 4$

$G = 3.70$ (higher with Fe,
lower with Mg)

Uniaxial (−)

$n_\omega = 1.816$

$n_\epsilon = 1.597$

$\delta = 0.219$

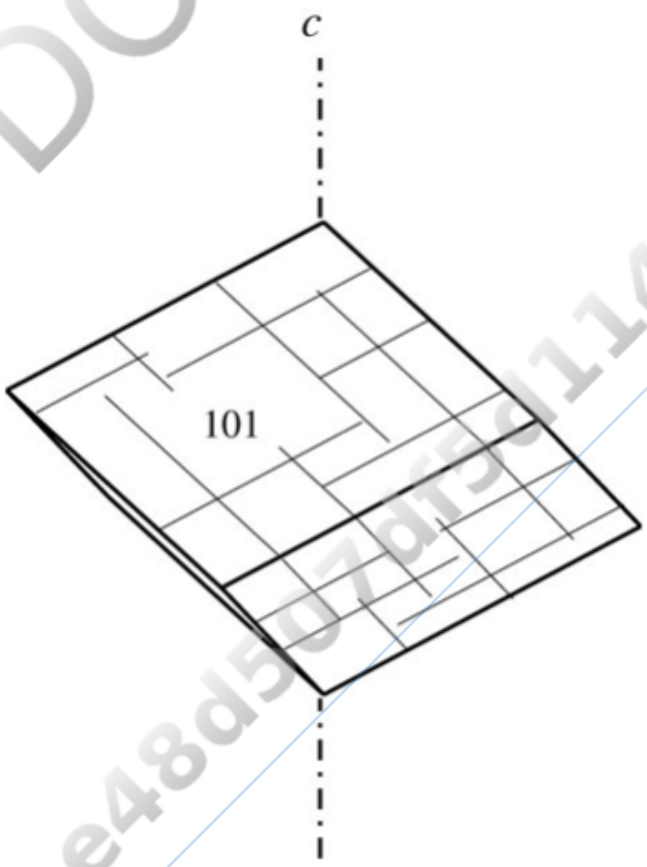

DO NOT COPY
e48d507df5d1141@placeholder.9409

Printed by: e48d507df5d1141@placeholder.94092.edu. Printing is for personal, private use only. No part of this book may be reproduced or transmitted without publisher's prior permission. Violators will be prosecuted.

Composition Rhodochrosite displays complete solid solution to siderite, and limited solid solution to magnesite. Some Ca may substitute for Mn. Kutnohorite [$CaMn(CO_3)_2$], with the dolomite structure, is compositionally intermediate between rhodochrosite and calcite.

Form and Twinning Rare crystals are {101} rhombohedrons (Figure 17.6), which may have curved faces similar to dolomite. More commonly as cleavable masses, granular encrustations, or fine-grained masses. Lamellar twinning on {012}, like calcite, is uncommon.

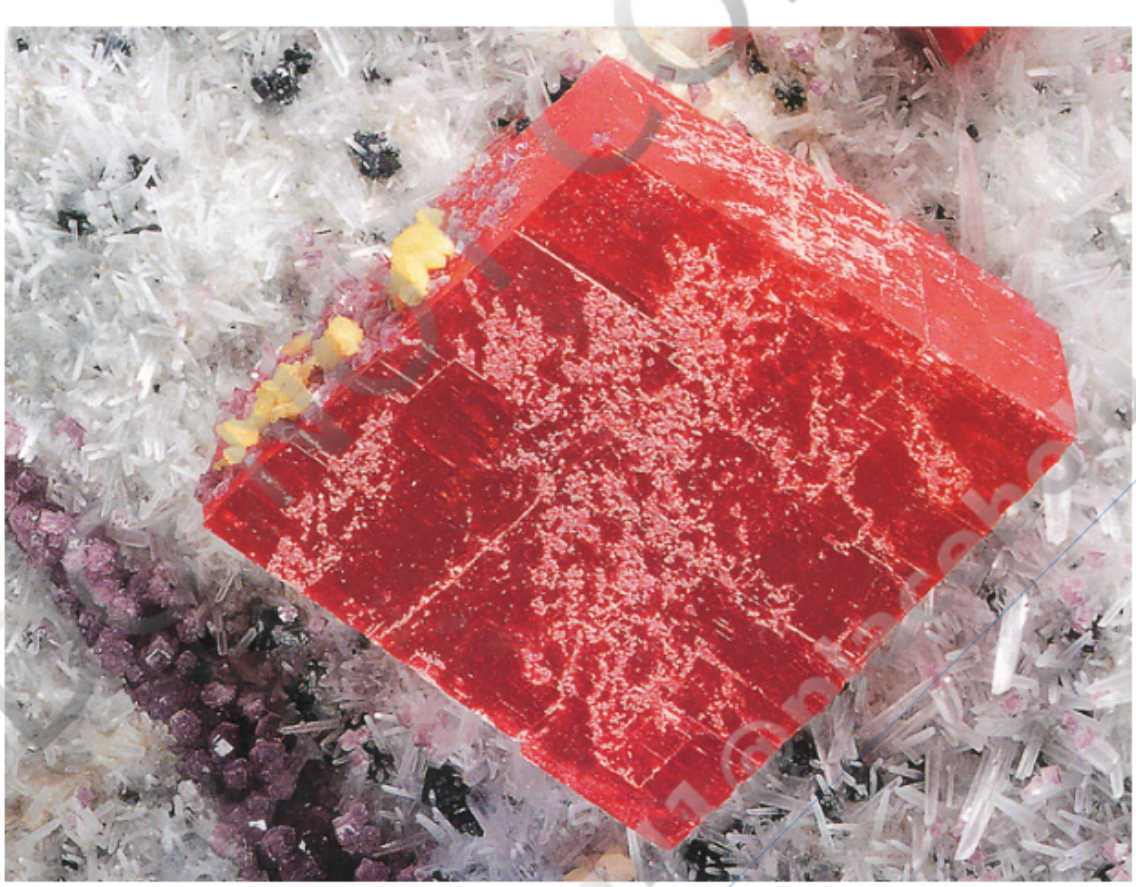

FIGURE 17.6 The Alma King, at 16.5 cm across, is perhaps the largest rhodochrosite crystal in a collection. It is from the Sweethome Mine, Park County, Colorado. The acicular white crystals are quartz, the dark grains are sphalerite, and the equant crystals (lower left) are fluorite. © Denver Museum of Nature and Science. View larger image

Cleavage Perfect {101} rhombohedral cleavage, like the other rhombohedral carbonates. The angle between cleavages is 73°. Uneven to conchoidal fracture. Brittle.

Color Properties

Luster: Vitreous.

Color: Usually pink or red, also yellow, gray, or brown. The typical pink color is produced because Mn^{2+} has a strong, narrow absorption band for light at 412 nm and broad,

Printed by: e48d507df5d1141@placeholder.94092.edu. Printing is for personal, private use only. No part of this book may be reproduced or transmitted without publisher's prior permission. Violators will be prosecuted.

because Mn^{2+} has a strong, narrow absorption band for light at 412 nm and broad, weaker absorption at around 450 nm and 550 nm; the red end of the spectrum passes with little absorption.

Streak: White.

Color in Thin Section: Colorless or pale pink; some samples may display color zoning.

Pleochroism: Colored varieties are pleochroic in shades of pink with $\omega > \epsilon$, so color is darkest when the long diagonal between cleavage traces is parallel to the vibration direction of the lower polarizer.

Optical Characteristics

Relief in Thin Section: Moderate to high positive; changes with rotation.

Optic Orientation: Extinction is inclined or symmetrical to cleavage traces. The fast ray vibration direction is parallel to the short diagonal between cleavage traces.

Indices of Refraction and Birefringence: Indices of refraction vary systematically with composition (Figure 17.5). The index of refraction $n'_{\epsilon\{101\}}$ for fragments lying on {101} cleavage surfaces is 1.702 for pure rhodochrosite, higher for Fe-bearing samples, and lower for Mg-bearing samples. In zoned samples, darker-colored areas usually have higher indices of refraction. Birefringence is extreme and produces creamy upper-order white interference colors in thin section and grain mount, even if the optic axis is nearly vertical.

Interference Figure: Uniaxial negative optic axis figures display numerous isochromes and isogyres that flare substantially toward the edge of the figure.

Alteration Rhodochrosite may alter to dark-colored Mn-oxide and hydroxide minerals or may be replaced by quartz or other minerals to form pseudomorphs.

Distinguishing Features

Hand Sample: Pink to red color and rhombohedral cleavage are characteristic. Effervesces in dilute HCl only if powdered, like dolomite.

Thin Section/Grain Mount: Distinguished from the other rhombohedral carbonates by indices of refraction, pink color, if present, and association with other Mn-bearing minerals.

Occurrence Rhodochrosite is usually restricted to hydrothermal vein and replacement deposits. It is often associated with sulfide minerals, other carbonates, barite, fluorite, rhodonite, and quartz. It also is an uncommon biomineral (Chapter 5).

Use Rhodochrosite is a minor ore of Mn. Good crystals can be highly valued by mineral collectors.

DO NOT COPY e48d507df5d1141@placeholder.9409

Printed by: e48d507df5d1141@placeholder.94092.edu. Printing is for personal, private use only. No part of this book may be reproduced or transmitted without publisher's prior permission. Violators will be prosecuted.

Dolomite–Ankerite

Hexagonal (rhombohedral) $\bar{3}$

Uniaxial (−)

Dolomite : $CaMg(CO_3)_2$

$a = 4.80$ Å, $c = 15.98$ Å,
$Z = 3$ ($a = 19.21$ Å,
$c = 15.98$ Å, $Z = 48$
to be consistent with
Miller indices)

$n_\omega = 1.679 - 1.690$

$n_\epsilon = 1.500 - 1.510$

$\delta = 0.179 - 0.182$

Ankerite : $Ca(Mg, Fe)(CO_3)_2$

$a =$ -4.82 Å, $c =$ -16.10 Å, $Z = 3$
($a =$ -19.28 Å, $c =$ -16.10 Å,
$Z = 48$ to be consistent
with Miller indices)

$n_\omega = 1.690 - 1.750$

$n_\epsilon = 1.510 - 1.548$

$\delta = 0.182 - 0.202$

$H = 3.5 - 4$

$G = 2.86$ (dolomite) to 3.10 (ankerite)

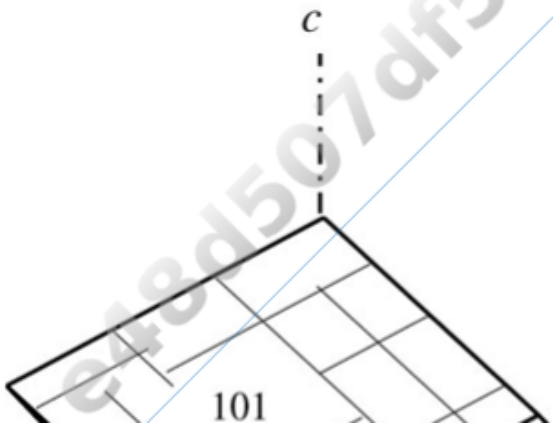

DO NOT COPY
e48d507df5d1141@placeholder.9409

Printed by: e48d507df5d1141@placeholder.94092.edu. Printing is for personal, private use only. No part of this book may be reproduced or transmitted without publisher's prior permission. Violators will be prosecuted.

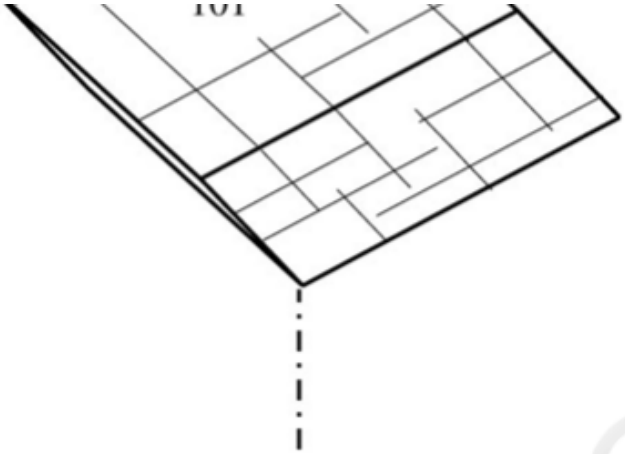

Composition Dolomite and ankerite are part of a solid solution series whose end members are $CaMg(CO_3)_2$ and $CaFe(CO_3)_2$ (ferrodolomite). Dolomite is taken here to include samples with less than 20 mol % ferrodolomite component. More Fe-rich samples are considered ankerite. Samples with more than about 75% ferrodolomite component have not been found in nature. Mn may substitute for Mg/Fe, and extensive solid solution toward kutnohorite [$CaMn(CO_3)_2$] is possible.

Form and Twinning Crystals are {101} rhombohedrons that may have curved or saddle-shaped faces (Figure 17.7). More common as coarse- to fine-grained aggregates. Infrequently as fibrous or columnar aggregates, or as oolites. Lamellar twins on {021} are moderately common. Lamellae may be parallel to either the short or long diagonal between rhombohedral cleavage traces (Figure 17.4).

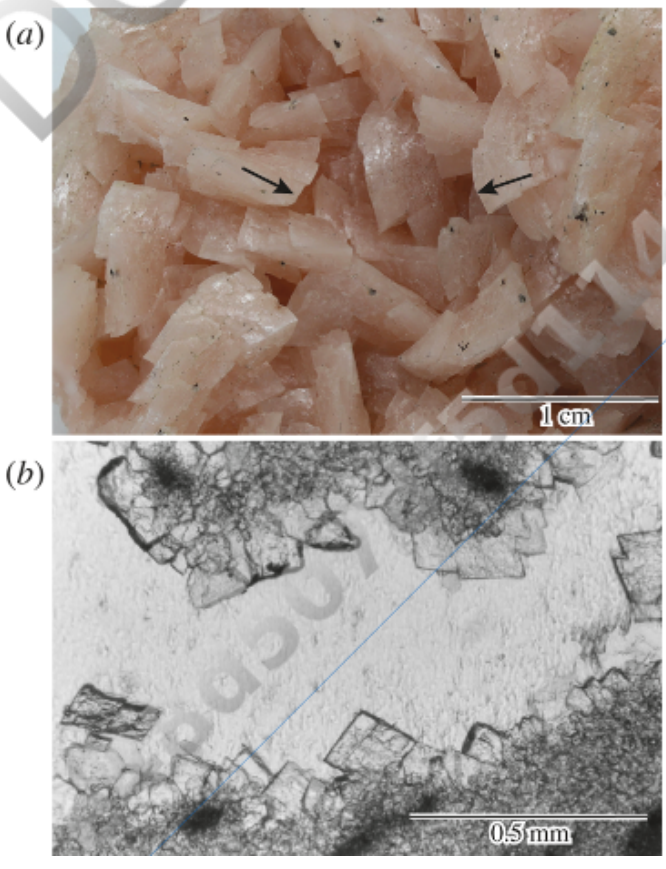

DO NOT COPY

Printed by: e48d507df5d1141@placeholder.94092.edu. Printing is for personal, private use only. No part of this book may be reproduced or transmitted without publisher's prior permission. Violators will be prosecuted.

FIGURE 17.7 Dolomite. (*a*) Dolomite crystals. Note the curved crystal faces (arrows). (*b*) Photomicrograph showing dolomite rhombs lining a void in a thin section of limestone. View larger image

Cleavage Perfect {101} cleavage like the other rhombohedral carbonates. The angle between cleavages is ~74°. Subconchoidal fracture. Brittle.

Color Properties

Luster: Vitreous.

Color: Dolomite is colorless, white, or gray, often tinged with yellow or brown; ankerite may be white, yellow, yellowish brown or brown, rarely gray or blue.

Streak: White.

Color in Thin Section: Colorless.

Optical Characteristics

Relief in Thin Section: Low negative to high positive, changes with rotation.

Optic Orientation: Extinction is symmetrical or inclined to the trace of cleavage. The fast ray vibration direction is parallel to the short diagonal between cleavages.

Indices of Refraction and Birefringence: Indices of refraction increase with Fe content (Figure 17.5). Fragments of pure dolomite lying on a cleavage surface show $n'_{\epsilon\{101\}}=1.58$. Birefringence is extreme, so interference colors in both thin section and grain mount are upper-order creamy white, even if the optic axis is nearly vertical.

Interference Figure: Basal sections yield uniaxial negative figures with numerous isochromes.

Alteration Dolomite and ankerite may be pseudomorphically replaced by other carbonates, quartz, pyrite, iron oxides, or other minerals. Iron-rich samples may be brownish because of oxidation or weathering.

Distinguishing Features

Hand Sample: Dolomite closely resembles calcite, from which it is most easily distinguished because dolomite effervesces vigorously in dilute HCl only if powdered. Dolomite and ankerite are also far more likely than calcite to form rhombohedral crystals, and these crystals may have curved faces. A brownish or yellowish color suggests, but does not demonstrate, that the sample is ankerite and not dolomite. Ankerite and siderite can be distinguished based on specific gravity.

Thin Section/Grain Mount: Dolomite closely resembles calcite. See the calcite description

DO NOT COPY e48d507df5d1141@placeholder.9409

Printed by: e48d507df5d1141@placeholder.94092.edu. Printing is for personal, private use only. No part of this book may be reproduced or transmitted without publisher's prior permission. Violators will be prosecuted.

Thin Section/Grain Mount: Dolomite closely resembles calcite. See the calcite description for criteria by which they may be distinguished. Index of refraction can be used to estimate composition in dolomite–ankerite solid solutions (Figure 17.5) and to distinguish among the rhombohedral carbonates.

Occurrence Dolomite is quite common and typically is found as a major constituent of sedimentary dolostone, which, unfortunately, also is referred to as dolomite. Dolostone is generally considered to be formed from the diagenetic alteration of calcite in limestone to dolomite (Box 17.1). Precipitation of sedimentary dolomite directly from saline waters generally requires special conditions of high alkalinity, high Mg:Ca ratio, and supersaturation found only in environments dominated by evaporation (Box 17.2), including closed basin lakes, playas (dry lake beds), or sabkhas (supratidal sandflat or mudflat). In at least some cases, the precipitation of dolomite is mediated by bacteria (e.g., Sánchez-Román and others, 2008). The replacement of calcite by dolomite generally produces pore space in the original limestone that may allow dolostone beds to serve as the reservoir rock for petroleum deposits. Dolomite and ankerite are both common gangue minerals in hydrothermal vein and replacement deposits. Ankerite also may be found as veins or joint filling in shale, clay ironstones, and coal beds. Carbonatites, which are unusual igneous bodies composed largely of carbonate minerals, may contain either dolomite or ankerite along with calcite. Metamorphic rocks that contain dolomite include marble, calc-silicate gneiss, skarn, and related rocks derived from limestone, dolostone, and other carbonate-rich sediments. Associated minerals include calcite, tremolite, diopside, and garnet. If dolomite is the dominant mineral in a metamorphic rock, it may be referred to as a dolomitic marble. Ankerite may be found in metamorphic iron formations and other metamorphic rocks derived from Fe-rich sediments.

Use Dolomite is a potential ore mineral for metallic Mg, but most Mg currently is extracted from seawater. Industrial uses are numerous and include glassmaking, flue gas desulfurization, wastewater treatment, and metallurgical fluxing. Dolomite is used to manufacture portland cement, and in the production of MgO for use in refractories and CaO for lime. Agricultural applications include use as a soil amendment and as a feed additive for cattle and poultry. Dolostone is commonly crushed and used as aggregate in concrete, asphalt, and similar applications. Cut into blocks and sheets, dolostone is used as dimension stone in the construction industry and to make monuments. Dolomite is sold as a dietary supplement, similar to calcite, and it provides both dietary calcium and magnesium. It also can serve as an antacid.

DO NOT COPY e48d507df5d1141@placeholder.9409-

Printed by: e48d507df5d1141@placeholder.94092.edu. Printing is for personal, private use only. No part of this book may be reproduced or transmitted without publisher's prior permission. Violators will be prosecuted.

Aragonite Group

The orthorhombic carbonates are aragonite, witherite, and strontianite (Table 17.1). Cerussite is fairly rare and its properties are given in Table 17.2. The orthorhombic aragonite structure is favored for cations whose radius in octahedral coordination is larger than roughly 1.1 Å; the calcite structure is favored for smaller cations. Because Ca^{2+} has an ionic radius of 1.14 Å in octahedral coordination, it may fit in either structure. To accommodate the larger cations, the aragonite structure provides distorted 9-fold coordination sites arranged between corrugated layers of CO_3 groups that are parallel to {001} (Figure 17.8). The corrugations in the carbonate layers are produced by having rows of CO_3 groups extending parallel to *a* that are alternately above and below the average plane of the layer. The larger cations are distributed in a manner equivalent to slightly distorted hexagonal close packing, accounting for the fact that members of the group have pseudohexagonal symmetry.

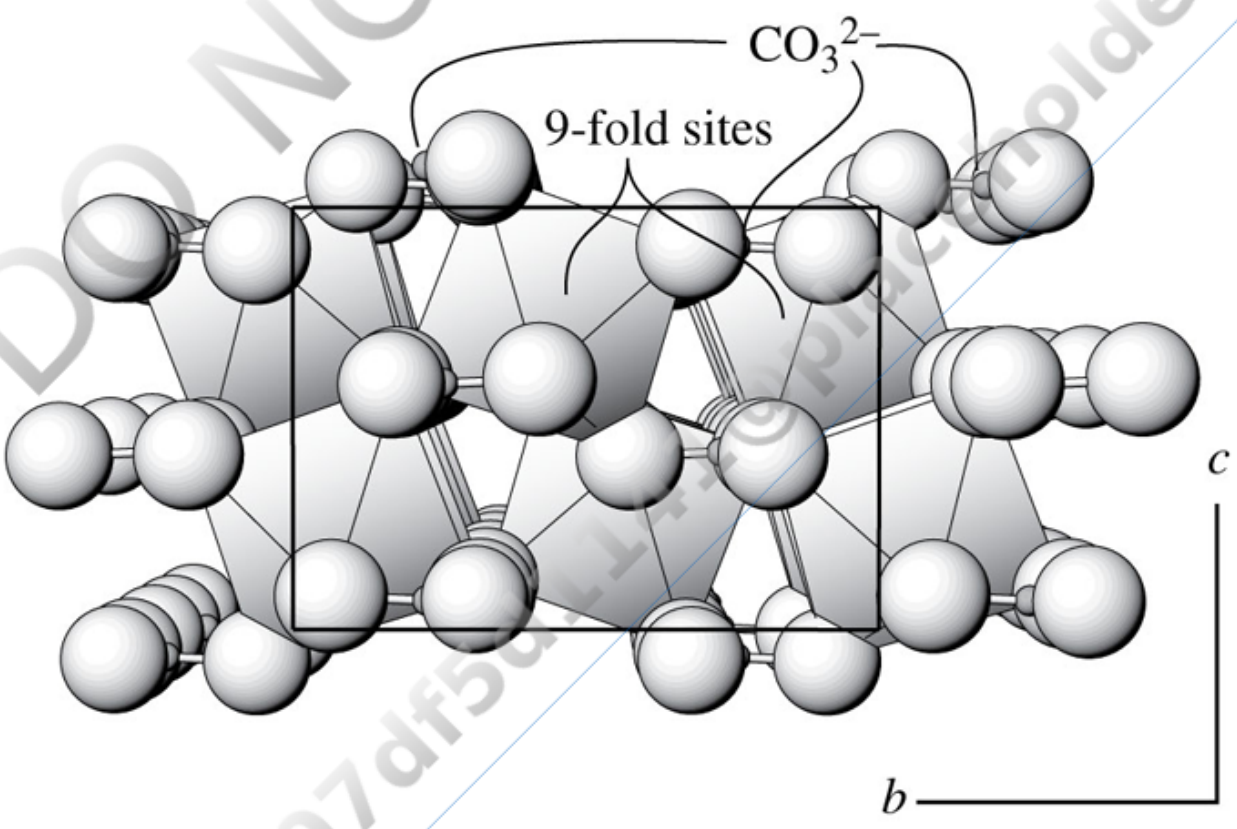

FIGURE 17.8 Aragonite structure. Triangular CO_3^{2-} groups are arranged in rows parallel to *a* (into the page). Oxygen anions are shown as larger spheres and carbon cations as small spheres. Large cations such as Ca^{2+}, Ba^{2+}, Sr^{2+}, or Pb^{2+} occupy 9-fold coordination sites between the CO_3^{2-} groups. A unit cell is outlined. View larger image

Aragonite

DO NOT COPY e48d507df5d1141@placeholder.94092

Printed by: e48d507df5d1141@placeholder.94092.edu. Printing is for personal, private use only. No part of this book may be reproduced or transmitted without publisher's prior permission. Violators will be prosecuted.

Aragonite

$$CaCO_3$$

$$\text{Orthorhombic } 2/m\ 2/m\ 2/m$$

$$a = 4.96\ \text{Å},\ b = 7.97\ \text{Å},$$
$$c = 5.74\ \text{Å},\ Z = 4$$

$$H = 3.5 - 4$$

$$G = 2.94 - 2.95$$

$$\text{Biaxial } (-)$$

$$n_\alpha = 1.530$$

$$n_\beta = 1.680$$

$$n_\gamma = 1.685$$

$$\delta = 0.155$$

$$2V_x = 18^\circ$$

DO NOT COPY

e48d507df5d1141@placeholder.9409

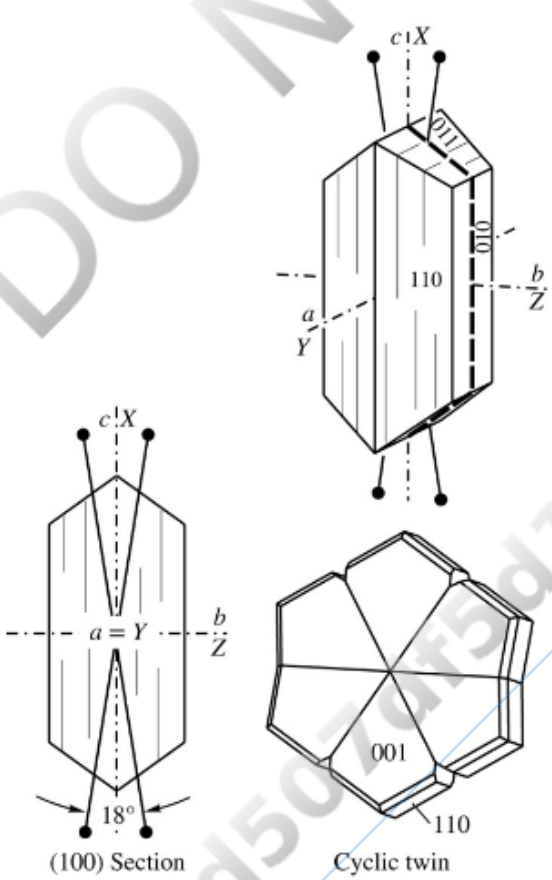

(100) Section Cyclic twin

Composition Most aragonite is relatively pure $CaCO_3$. Minor amounts of Sr or Pb may substitute for Ca in some samples. The amount of Sr substituting for Ca in aragonite from fossil scleractinian corals has been used to infer sea-surface temperatures at the time the

Printed by: e48d507df5d1141@placeholder.94092.edu. Printing is for personal, private use only. No part of this book may be reproduced or transmitted without publisher's prior permission. Violators will be prosecuted.

fossil scleractinian corals has been used to infer sea-surface temperatures at the time the corals grew their aragonite skeleton.

Form and Twinning Common as radiating or columnar aggregates of grains elongate along *c*. Crystals often have penetration twins on {110} to form columnar cyclic twinned crystals with pseudohexagonal outlines and vertical striae (Figure 17.9). Some twinned crystals may be platy parallel to {001}. {100} twinning also may be polysynthetic. Shells of marine invertebrates may be composed of aragonite, and some cave formations (stalactites, stalagmites, etc.) are composed of aragonite.

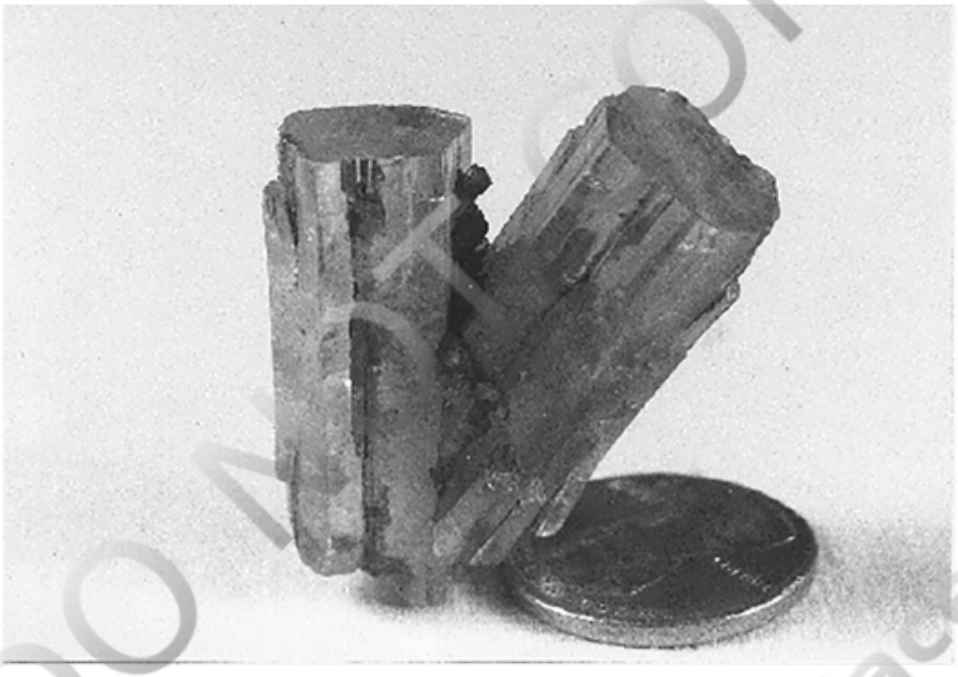

FIGURE 17.9 Aragonite crystals. View larger image

Cleavage Good {010} and poor {110} cleavage. Subconchoidal fracture. Brittle.

Color Properties

Luster: Vitreous.

Color: Colorless or white.

Streak: White.

Color in Thin Section: Colorless.

Other: Trace amounts of Mn^{2+} may cause red fluorescence under UV light. Sm, Dy, and U also may trigger fluorescence.

Optical Characteristics

Relief in Thin Section: Low negative to high positive; changes with stage rotation.

DO NOT COPY e48d507df5d1141@placeholder.9409

Printed by: e48d507df5d1141@placeholder.94092.edu. Printing is for personal, private use only. No part of this book may be reproduced or transmitted without publisher's prior permission. Violators will be prosecuted.

Optic Orientation: $X = c$, $Y = a$, $Z = b$, optic plane = (100). Extinction is parallel to crystal elongation (c axis) in principal sections and the trace of cleavage is length fast.

Indices of Refraction and Birefringence: Indices of refraction have little variation. Sr reduces and Pb increases indices of refraction. Birefringence is extreme and produces creamy upper-order colors, even if an optic axis is close to vertical.

Interference Figure: Basal sections yield centered acute bisectrix figures with numerous isochromes and small (18°) $2V$. Optic axis dispersion is weak, $r < v$.

Alteration Aragonite commonly inverts to its polymorph calcite, and pseudomorphs of calcite after aragonite are common. Aragonite also may be replaced by dolomite.

Distinguishing Features

Hand Sample: Easily confused with calcite. Aragonite reacts with vigorous effervescence in dilute HCl, particularly if fine grained, but lacks good rhombohedral cleavage, has a different crystal habit, and is more dense than calcite. The other members of the aragonite group have higher specific gravity.

Thin Section/Grain Mount: Resembles calcite but lacks rhombohedral cleavage, is biaxial, and has slightly higher indices of refraction. Strained calcite may, however, also be biaxial with small $2V$. X-ray diffraction techniques may be required if fine grained. Staining techniques (Friedman, 1959) may also distinguish between calcite and aragonite.

Occurrence Aragonite occurs in carbonate-bearing high-pressure blueschist and eclogite facies metamorphic rocks associated with glaucophane, lawsonite, pumpellyite, and related minerals. The temperature–pressure stability fields of calcite and aragonite are shown in Figure 17.10. Despite having a high-pressure stability field, aragonite often crystallizes metastably under low-pressure, near-surface conditions. Cave and hot spring deposits (stalactites, stalagmites, tuffa, etc.) may be composed of aragonite. It may also precipitate directly from warm seawater as fine needles and form ooliths in calcareous muds. Some shale deposits may contain large well-formed crystals apparently crystallized from pore water. Aragonite is a significant biomineral (Chapter 5) produced by mineralization that can be either controlled or induced biologically to produce the shells of many marine invertebrates, including mollusks and corals. Aragonite may also precipitate on the surfaces of plankton in subtropical marine waters and may contribute to the whiting events described in the section on calcite. Metastable (biologically mediated?) crystallization of aragonite in evaporite deposits (see Box 17.2) is fairly common, but inversion to calcite usually occurs rapidly. In igneous rocks, aragonite may be found as vesicle and cavity fillings in basalt and andesite. Aragonite is reported in the oxidized zone of hydrothermal sulfide deposits and in iron-rich sediments associated with siderite and iron oxides.

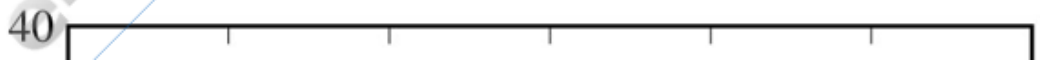

DO NOT COPY

Printed by: e48d507df5d1141@placeholder.94092.edu. Printing is for personal, private use only. No part of this book may be reproduced or transmitted without publisher's prior permission. Violators will be prosecuted.

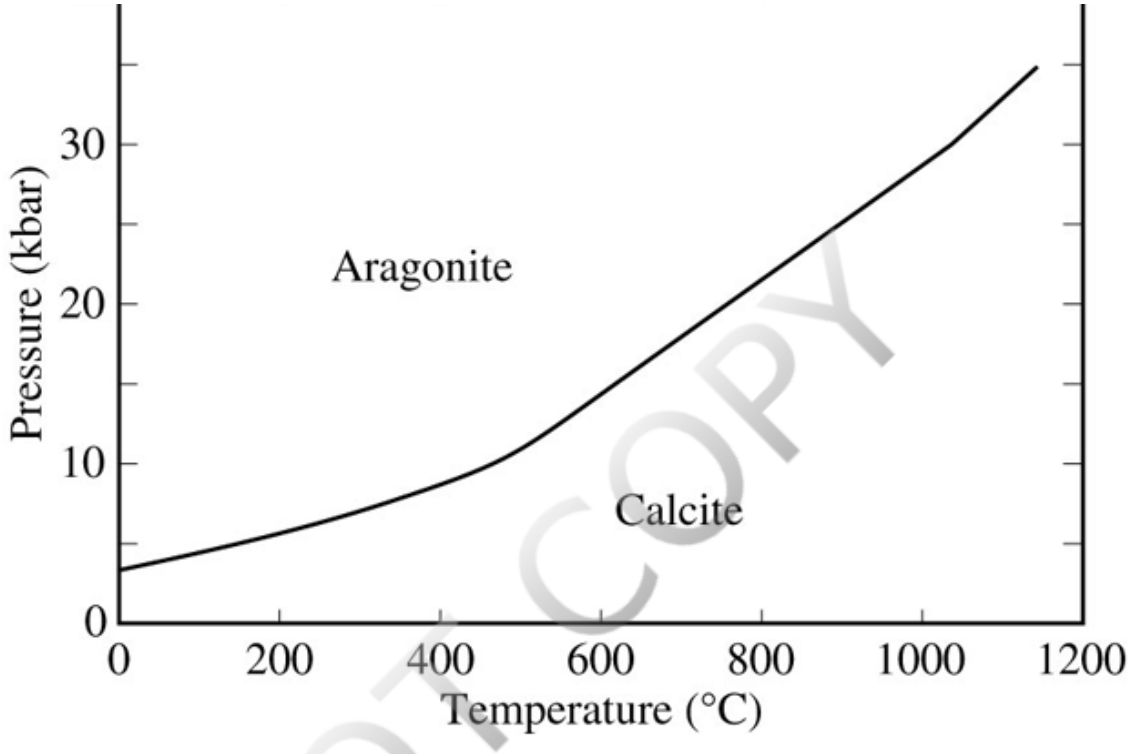

FIGURE 17.10 Temperature–pressure stability fields of calcite and aragonite. After Carlson (1980). View larger image

Use Aragonite could potentially have many of the same uses as calcite, but the lack of large deposits and the abundance of calcite in limestone and related rocks ensure that aragonite has little industrial use. Pearls are made, at least in part, of aragonite and have historically been valuable gems. Mother-of-pearl, which also contains aragonite, is used extensively in the decoration of guitars and other stringed instruments. Both pearls and mother-of-pearl have found their way into the medical practice of some cultures, including Chinese traditional medicine and the traditional Ayurvedic medicine of India. King Charles VI (1368–1422) of France reportedly took ground-up pearls as a treatment for his melancholy and episodes of insanity. The treatment did not appear to work, as he suffered from psychoses until his death. Followers of New Age spiritualism may ascribe spiritual, healing, or mystical powers to aragonite crystals.

Witherite

$$BaCO_3$$

$$\text{Orthorhombic } 2/m\ 2/m\ 2/m$$

$$a = 5.31\ \text{Å},\ b = 8.90\ \text{Å},$$
$$c = 6.43\ \text{Å},\ Z = 4$$

$$H = 3.5$$

$$G = 4.29 - 4.32$$

DO NOT COPY
e48d507df5d1141@placeholder.9409

Printed by: e48d507df5d1141@placeholder.94092.edu. Printing is for personal, private use only. No part of this book may be reproduced or transmitted without publisher's prior permission. Violators will be prosecuted.

Biaxial (−)

$n_\alpha = 1.529$

$n_\beta = 1.676$

$n_\gamma = 1.677$

$\delta = 0.148$

$2V_x = 16^\circ$

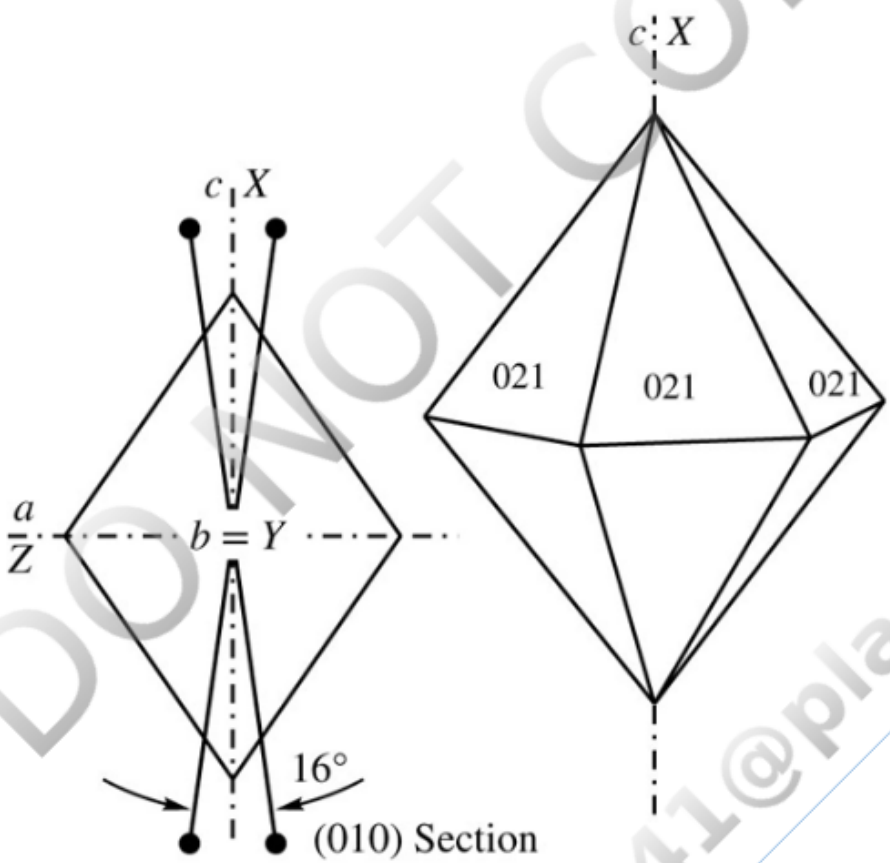

Composition Most witherite is close to pure $BaCO_3$, but minor substitution of Ca, Sr, or Mg for Ba may occur.

Form and Twinning Crystals are stubby pseudohexagonal dipyramids, the result of cyclic twinning on {110} that is always present. Granular, columnar, or fibrous aggregates also occur, and some may have rounded or botryoidal shapes.

Cleavage Good cleavage on {010} and poor cleavages on {110} and {012}.

Color Properties

Luster: Vitreous.

Color: Colorless, white, or light grayish or yellowish brown.

DO NOT COPY
e48d507df5d1141@placeholder.9409

Printed by: e48d507df5d1141@placeholder.94092.edu. Printing is for personal, private use only. No part of this book may be reproduced or transmitted without publisher's prior permission. Violators will be prosecuted.

Streak: White.

Color in Thin Section: Colorless.

Optical Characteristics

Relief in Thin Section: Low negative to high positive; may change with stage rotation.

Optic Orientation: $X = c$, $Y = b$, $Z = a$, optic plane = (010). Extinction is parallel to {010} cleavage traces in principal sections.

Indices of Refraction and Birefringence: Refractive indices have little variation. Birefringence is extreme, so interference colors in grain mount and thin section are upper-order creamy white for most grain orientations.

Interference Figure: Basal sections yield acute bisectrix figures with numerous isochromes and small (16°) $2V$. Optic axis dispersion is weak, $r > v$.

Alteration Witherite may alter to barite or may be an alteration product after barite.

Distinguishing Features

Hand Sample: Effervesces vigorously in dilute HCl, which distinguishes it from barite. Aragonite has a lower specific gravity. The green color barium gives to a flame is distinctive.

Thin Section/Grain Mount: Distinguished from rhombohedral carbonates by lack of rhombohedral cleavage and biaxial character. Indices of refraction are slightly higher than aragonite and strontianite, and lower than cerussite.

Occurrence This relatively uncommon mineral is most frequently found in hydrothermal sulfide deposits hosted in limestone or other calcareous sediment. It is usually associated with galena and barite.

Use Witherite is used as an ore mineral for barium, which has numerous industrial uses. Economic witherite deposits are far less common than barite deposits, so the latter mineral is a substantially more common source of barium.

Comment Witherite is the active ingredient in some rat poisons, and it is dangerous for humans to ingest. Do not perform a taste test if there is any possibility that the mineral may be witherite.

Strontianite

$SrCO_3$

Orthorhombic $2 / m\ 2 / m\ 2 / m$

DO NOT COPY e48d507df5d1141@placeholder.9409

Printed by: e48d507df5d1141@placeholder.94092.edu. Printing is for personal, private use only. No part of this book may be reproduced or transmitted without publisher's prior permission. Violators will be prosecuted.

Orthorhombic $2 / m\ 2 / m\ 2 / m$

$a = 5.11$ Å, $b = 8.42$ Å,

$c = 6.03$ Å, $Z = 4$

$H = 3.5$

$G = 3.75$

Biaxial $(-)$

$n_\alpha = 1.517 - 1.525$

$n_\beta = 1.663 - 1.686$

$n_\gamma = 1.667 - 1.690$

$\delta = 0.148 - 0.165$

$2V_x = 7 - 10^\circ$

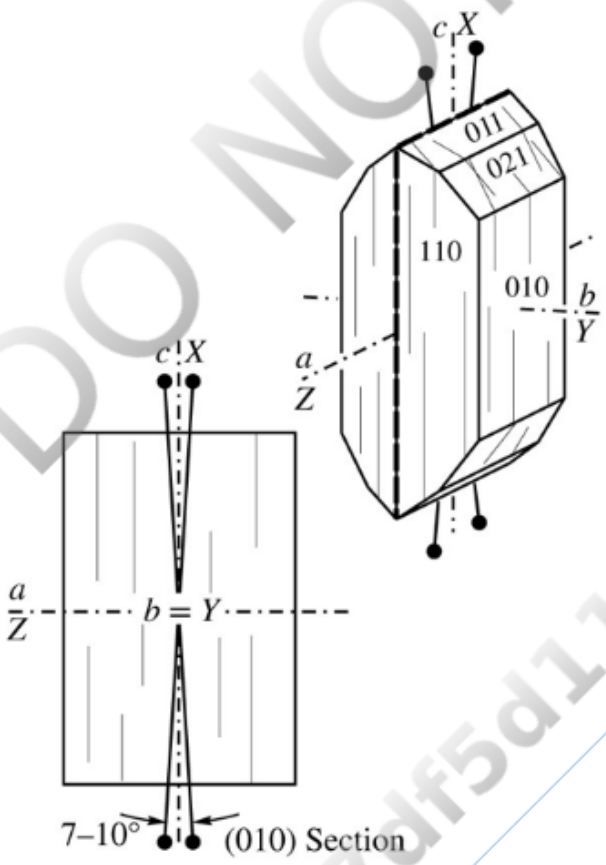

Composition Most strontianite contains up to about 20% Ca substituting for Sr. Some Ba also may substitute for Sr.

Form and Twinning Usually granular massive or as aggregates of columnar, fibrous, or acicular grains. Crystals are elongate parallel to c and often are composed of cyclic twins on {110}, like aragonite, yielding a pseudohexagonal cross section. Twins may be single, cyclic, or polysynthetic.

DO NOT COPY
e48d507df5d1141@placeholder.9409

Printed by: e48d507df5d1141@placeholder.94092.edu. Printing is for personal, private use only. No part of this book may be reproduced or transmitted without publisher's prior permission. Violators will be prosecuted.

cyclic, or polysynthetic.

Cleavage Good {110} prismatic cleavage in two directions intersect at about 64°. Uneven fracture. Brittle.

Color Properties

Luster: Vitreous.

Color: Colorless or white; also yellow, greenish, or brownish.

Streak: White.

Color in Thin Section: Colorless.

Optical Characteristics

Relief in Thin Section: Low negative to high positive, depending on orientation. May change with rotation.

Optic Orientation: $X = c$, $Y = b$, $Z = a$, optic plane = (010). Longitudinal sections and elongate cleavage fragments are length fast with parallel extinction. Extinction in basal sections is symmetrical.

Indices of Refraction and Birefringence: Indices of refraction increase with Ca and Ba content. Birefringence is extreme, so interference colors are high-order creamy white for most grain orientations.

Interference Figure: Basal sections yield centered acute bisectrix figures with small $2V$. Optic axis dispersion is weak, $r < v$.

Alteration Strontianite may be altered to celestine.

Distinguishing Features

Hand Sample: Effervesces vigorously in dilute HCl, which distinguishes it from celestine (Table 17.4). High specific gravity distinguishes strontianite from aragonite. The crimson color that Sr produces in a flame is distinctive (dissolve a bit of the sample in HCl, then introduce to a clean flame).

Thin Section/Grain Mount: Resembles the other orthorhombic carbonates. Aragonite, witherite, and cerussite have higher indices of refraction.

Occurrence Most commonly found in veins and masses in limestone deposited by hydrothermal solutions. Also found in hydrothermal sulfide deposits. Strontianite is a biomineral and is found in scleractinian coral along with aragonite.

Use Strontianite is an ore mineral for strontium, but celestine ($SrSO_4$) deposits are more economic to exploit, so little strontium is produced from strontianite. A major use of

DO NOT COPY e48d507df5d1141@placeholder.9409

Printed by: e48d507df5d1141@placeholder.94092.edu. Printing is for personal, private use only. No part of this book may be reproduced or transmitted without publisher's prior permission. Violators will be prosecuted.

strontium has been in the faceplate glass on cathode ray tubes, specifically including old-style television sets and computer monitors. The strontium is added to provide shielding from the X-rays produced in all cathode ray tubes and to improve the optical quality of the glass. Strontium is used in the manufacture of ceramics and in permanent ceramic magnets. Fireworks and other pyrotechnics commonly use strontium compounds to provide brilliant red colors. Strontium chloride is used in toothpaste for sensitive teeth, and strontium phosphate is used in the manufacture of fluorescent lights.

DO NOT COPY
e48d507df5d1141@placeholder.9409

Printed by: e48d507df5d1141@placeholder.94092.edu. Printing is for personal, private use only. No part of this book may be reproduced or transmitted without publisher's prior permission. Violators will be prosecuted.

OH-Bearing Carbonates

Azurite and malachite are the only common OH-bearing carbonate minerals (Table 17.1) and they are typically restricted to the oxidized portion of copper-bearing hydrothermal sulfide mineral deposits. Both have striking colors such that they are commonly found in mineral collections. Two other hydrated carbonates, typically found in marine and saline lake evaporite deposits, are summarized in Table 17.2.

Malachite

Å Å

Å

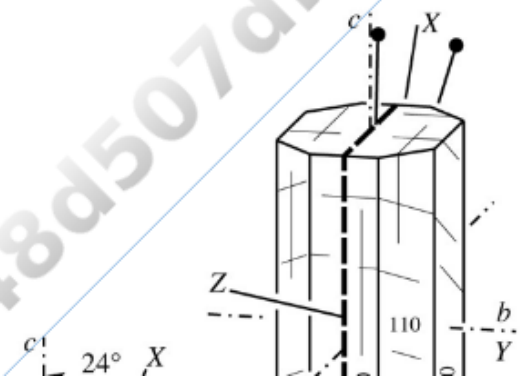

DO NOT COPY
e48d507df5d1141@placeholder.9409

Printed by: e48d507df5d1141@placeholder.94092.edu. Printing is for personal, private use only. No part of this book may be reproduced or transmitted without publisher's prior permission. Violators will be prosecuted.

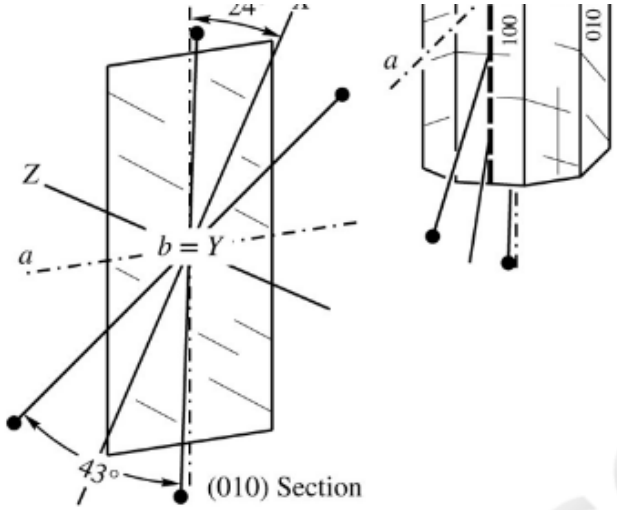

Structure The structure consists of chains of $CuO_2(OH)_4$ and $CuO_4(OH)_2$ octahedra that extend parallel to the *c* axis. CO_3 groups tie the chains together laterally.

Composition Malachite shows relatively little compositional variation.

Form and Twinning Malachite is most commonly found as massive encrusting or botryoidal forms with concentric color banding consisting of parallel fibrous grains. Also granular or earthy. {100} twins are common.

Cleavage Perfect $\{201\}$ cleavage is rarely seen because grain size is typically too small; fair cleavage on {010}. Subconchoidal to uneven fracture. Brittle.

Color Properties

Luster: Adamantine to vitreous on crystals, also silky if fibrous. Fine granular material may be earthy.

Color: Vivid green.

Streak: Pale green.

Color in Thin Section: Green.

Pleochroism: $X < Y < Z$: X = nearly colorless or pale green; Y = yellowish green; Z = dark green.

Optical Characteristics

Relief in Thin Section: High positive.

Optic Orientation: $X \wedge c = -24°$, $Y = b$, $Z \wedge a = +32°$, optic plane = {010}. Elongate grains and fibers have inclined extinction and are length fast.

Indices of Refraction and Birefringence: Birefringence is extreme, but high-order creamy white interference color will be masked by mineral color.

DO NOT COPY
e48d507df5d1141@placeholder.9409

Printed by: e48d507df5d1141@placeholder.94092.edu. Printing is for personal, private use only. No part of this book may be reproduced or transmitted without publisher's prior permission. Violators will be prosecuted.

white interference color will be masked by mineral color.

Interference Figure: Fragments on the $\{\bar{2}01\}$ cleavage yield nearly centered acute bisectrix figures with numerous isochromes.

Alteration Malachite may alter to azurite or cuprite.

Distinguishing Features

Hand Sample: Bright green color and vigorous effervescence in dilute HCl are diagnostic.

Thin Section/Grain Mount: Green color and habit are characteristic.

Occurrence Malachite is a common mineral in the near-surface, oxidized portion of Cu-bearing hydrothermal sulfide mineral deposits (Figure 19.3, Table 19.4). It is typically associated with azurite and generally is produced when primary Cu sulfide minerals, such as chalcopyrite, are oxidized and altered by acidic water percolating down from the surface. The copper may be reprecipitated as copper carbonate and copper oxide minerals in the area above the water table. The carbonate component may be acquired from CO_2 dissolved in meteoric water or from carbonate minerals in the host rock.

Use Used as a minor ore of copper. The brilliant green color makes it valuable as a decorative stone and for use in jewelry. The use of malachite for medicinal purposes goes back at least 5000 years; it has been used for a wide variety of maladies, including epilepsy, anemia, bleeding, arthritis, influenza, and gastrointestinal disorders. Copper is an essential nutrient, and small amounts of copper compounds—usually $CuSO_4$ (chalcocyanite) or CuO (tenorite)—are included in many multivitamin supplements. While copper is an essential nutrient in small amounts, high levels can pose significant health risks. Being a carbonate, malachite will dissolve in acidic gastric juices, and some portion of the copper can then become available for uptake by the body. Ingestion of malachite or other Cu-bearing minerals could, therefore, be hazardous. Malachite is also an antimicrobial agent effective against at least *Staphylococcus aureus*.

Azurite

$$Cu_3(CO_3)_2(OH)_2$$

$$\text{Monoclinic } 2/m$$

$$a = 4.97 \text{ Å}, \ b = 5.84 \text{ Å},$$
$$c = 10.29 \text{ Å},$$
$$\beta = 92.4^\circ, \ Z = 2$$

$$H = 3.5 - 4$$

$$G = 3.77$$

DO NOT COPY e48d507df5d1141@placeholder.9409

Printed by: e48d507df5d1141@placeholder.94092.edu. Printing is for personal, private use only. No part of this book may be reproduced or transmitted without publisher's prior permission. Violators will be prosecuted.

Biaxial (+)

$n_\alpha = 1.730$

$n_\beta = 1.756$

$n_\gamma = 1.836$

$\delta = 0.106$

$2V_z = 68^\circ$

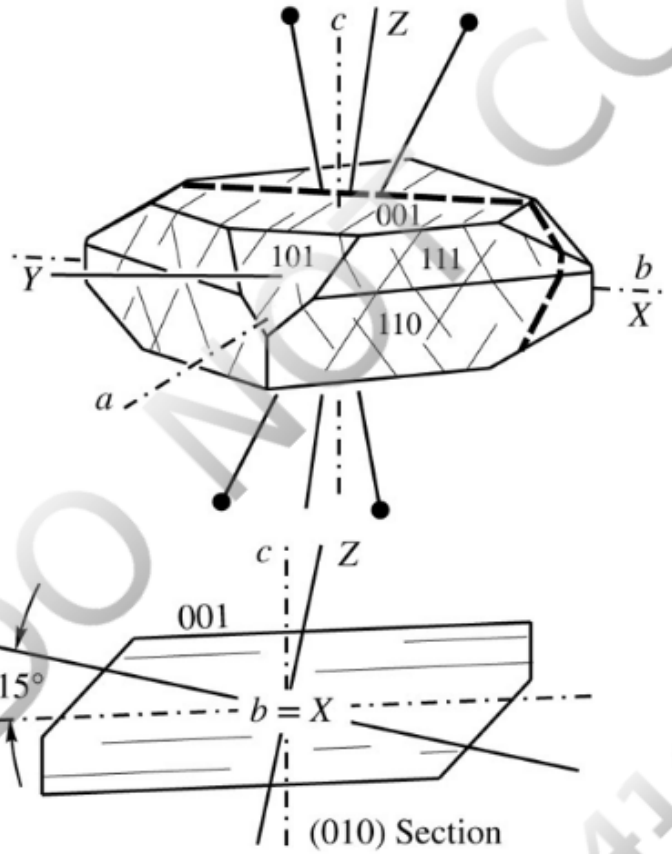

Structure The structure of azurite is complex, with Cu coordinating with two O and two OH forming a square. These square groups are linked to form chains parallel to *b* and cross-linked with CO_3 groups.

Composition Usually relatively close to the composition given by the formula.

Form and Twinning Crystals are varied, often tabular parallel to (001), or short prismatic parallel to *c* with many modifying forms. Most common as encrusting or rounded masses that may be color banded with individual bands consisting of radiating or parallel masses of acicular grains.

Cleavage Perfect {011}, fair {100}, and poor {110} cleavage. Conchoidal fracture. Brittle.

DO NOT COPY
e48d507df5d1141@placeholder.9409

Printed by: e48d507df5d1141@placeholder.94092.edu. Printing is for personal, private use only. No part of this book may be reproduced or transmitted without publisher's prior permission. Violators will be prosecuted.

Color Properties

Luster: Vitreous. Fibrous varieties may be silky; earthy if fine grained.

Color: Azure blue.

Streak: Blue, lighter than mineral color.

Color in Thin Section: Blue.

Pleochroism: Weak: X = clear blue, Y = azure blue, Z = dark blue or blue-violet.

Optical Characteristics

Relief in Thin Section: High positive.

Optic Orientation: $X = b$, $Y \wedge a = +15°$, $Z \wedge c = -12°$, optic plane $\perp$ (010). Crystals elongate on c are length slow.

Indices of Refraction and Birefringence: Indices of refraction vary little. Birefringence is extreme, but the upper-order creamy white interference color is masked by mineral color.

Interference Figure: Biaxial positive with moderately large $2V$. Optic axis dispersion is $r > v$, also horizontal dispersion.

Alteration Azurite may be replaced by malachite.

Distinguishing Features

Hand Sample: Vivid blue color and effervescence in dilute HCl are characteristic.

Thin Section/Grain Mount: Distinguished by blue color and indices of refraction.

Occurrence Azurite is a common mineral in the near-surface oxidized portion of Cu-bearing hydrothermal sulfide mineral deposits (Figure 19.3, Table 19.4). It is typically associated with malachite and generally is produced when primary Cu sulfide minerals, such as chalcopyrite, are oxidized and altered by acidic water percolating down from the surface. The copper may be reprecipitated as copper carbonate and copper oxide minerals in the area above the water table. The carbonate component may be acquired from CO_2 dissolved in meteoric water or from carbonate minerals in the host rock of the mineral deposit.

Use A minor ore of copper. Azurite also may be used for decorative purposes, and when pulverized, has been used as a pigment. Azurite has been used in homeopathic treatments and, probably because of its eye-catching color, has a history of use in folk remedies.

DO NOT COPY e48d507df5d1141@placeholder.9409

Printed by: e48d507df5d1141@placeholder.94092.edu. Printing is for personal, private use only. No part of this book may be reproduced or transmitted without publisher's prior permission. Violators will be prosecuted.

Sulfates

Sulfur is somewhat unusual in that it serves as an anion in the sulfide minerals and as a cation in the sulfates. In the sulfates, sulfur atoms lose all six of their outer electrons, four from the 3*p* and two from the 3*s* subshells (Table 3.3). These small high-charged cations coordinate with four oxygen anions to form SO_4^{2-} groups. Of the available eight negative charges on the four oxygen anions, six are taken by the sulfur. Sulfur–oxygen bonds are therefore far stronger than bonds between oxygen and any other cations. These structures are anisodesmic, and the SO_4^{2-} groups are discrete structural elements that bond laterally through other cations in the sulfate minerals (Figure 17.12). Only three common sulfate minerals (gypsum, anhydrite, and barite) are described in detail here. Additional sulfate minerals are listed in Table 17.4.

TABLE 17.4 Properties of Less Common Sulfate Minerals[a]

Mineral	Unit Cell	Physical Properties[a]	Optical Properties	Comments
Alunite $KAl_3(SO_4)_2(OH)_6$	Hexagonal (rhombohedral) 3m $a = 6.97$ $c = 17.38$ $Z = 3$	*H*: 3.5–4, *G*:2.6–2.9 Cl: {001}g, {102}pr Tw: None C: White or gray, also reddish St: White L: Vitreous	n_ω 1.568–1.620 n_ϵ 1.590–1.641 $\delta = 0.020$–0.023 Uniaxial (+) Colorless	Crystals tabular {001} or rhombs; usually fine-grained granular, plumose or flaky aggregates or disseminated grains; massive varieties resemble limestone; common in hydrothermally altered felsic to intermediate volcanic rocks
Antlerite $Cu_3SO_4(OH)_4$	Orthorhombic 2/*m* 2/*m* 2/*m* $a = 8.25$ $b = 12.01$ $c = 6.04$ $Z = 4$ $X = b$, $Y = a$, $Z = c$	*H*: 3.5, *G*: 3.88–3.94 Cl: {010}pf, {100}pr C: Light to dark green St: Paler green L: Vitreous	$n_\alpha = 1.726$ $n_\beta = 1.738$ $n_\gamma = 1.789$ $\delta = 0.063$ Biaxial (+) $2V = 53°$, $r < v$, v. strong X = yellow-green, Y =	Crystals thick tabular on {010}, equant or short prismatic on *c*; also cross-fiber grains, acicular, or granular; found in the oxidized portion of Cu-bearing hydrothermal sulfide deposits, usually in arid regions

DO NOT COPY e48d507df5d1141@placeholder.9409

Printed by: e48d507df5d1141@placeholder.94092.edu. Printing is for personal, private use only. No part of this book may be reproduced or transmitted without publisher's prior permission. Violators will be prosecuted.

			green, Y = blue-green, Z = green	
Celestine $SrSO_4$	Orthorhombic $2/m\ 2/m\ 2/m$ $a = 8.36$ $b = 5.35$ $c = 6.87$ $Z = 4$ $X = c$, $Y = b$, $Z = a$	H: 3–3.5, G: 3.96 Cl: {001}pf, {210}g, {010}pr Tw: Rare C: Colorless, white, pale blue, reddish, greenish, brownish St: white L: vitreous	$n_\alpha = 1.621$ $n_\beta = 1.623$ $n_\gamma = 1.630$ $\delta = 0.009$ Biaxial (+) $2V = 50°$, $r < v$ Colorless	Similar to barite; found in cavities and veins and as disseminated grains in limestone or dolostone; also in marine evaporite deposits, hydrothermal veins, and as a biomineral; principal source of Sr
Epsomite $MgSO_4 \cdot 7H_2O$	Orthorhombic 222 $a = 11.876$ $b = 12.002$ $c = 6.859$ Z = 4 $X = a$, $Y = c$ $Z = b$	H: 2–2.5, G: 1.68 Cl: {010}pf, {101}p, conchoidal fracture Tw: {110} rare C: Colorless, white, pale pink, pale green St: White L: Vitreous, silky if fibrous	$n_\alpha = 1.432$ $n_\beta = 1.455$ $n_\gamma = 1.461$ $\delta = 0.029$ Biaxial (−) $2V = 52°$, $r < v$, weak Colorless	Rare as prismatic crystals; typically fibrous crusts, reniform or botryoidal masses, or woolly efflorescences; found in evaporite deposits from saline lakes, as an efflorescence on soil, in mines, and around fumaroles; dehydrates readily in dry air; minor biomineral; Epsom salt is the common name
Glauberite $Na_2Ca(SO_4)_2$	Monoclinic $2/m$ $a = 9.99$ $b = 8.19$ $c = 8.41$ $\beta = 112.2°$ $Z = 4$ $X \wedge c = +30°$, $Y = b$	H: 2.5–3, G: 2.75–2.85 Cl: {001}pf, {110}pr C: Gray, yellow, colorless St: White L: Vitreous	$n_\alpha = 1.515$ $n_\beta = 1.535$ $n_\gamma = 1.536$ $\delta = 0.021$ Biaxial (−) $2V = 7°$, $r > v$, strong Colorless	Variable habit; tabular on {001}, prismatic [110], or dipyramid-like; slight saline taste; found in marine and saline lake evaporite deposits, fumarole deposits, and as amygdule filling

DO NOT COPY

Printed by: e48d507df5d1141@placeholder.94092.edu. Printing is for personal, private use only. No part of this book may be reproduced or transmitted without publisher's prior permission. Violators will be prosecuted.

Kieserite $MgSO_4 \cdot H_2O$	Monoclinic $2/m$ $a = 6.89$ $b = 7.69$ $c = 7.52$ $\beta = 116°$ $Z = 4$ $Z \wedge c = +77°$, $Y = b$	H: 3.5, G: 2.57 Cl: {110} and {111}pf, $\{\bar{1}11\}$, $\{\bar{1}01\}$ and {011} fair Tw: {001} rare C: Colorless, white, gray, pale yellow St: White L: Vitreous	$n_\alpha = 1.520$ $n_\beta = 1.533$ $n_\gamma = 1.584$ $\delta = 0.064$ Biaxial (+) $2V = 55°$, $r > v$, moderate Colorless	Massive coarse to fine crystalline; found in marine evaporite deposits with halite, polyhalite, anhydrite, etc.
Polyhalite $K_2MgCa_2(SO_4)_4 \cdot 2H_2O$	Triclinic $\bar{1}$ $a = 6.95$ $b = 8.89$ $c = 6.95$ $\alpha = 104°$ $\beta = 114° = 101°$ $Z = 1$	H: 3.5, G: 2.78 Cl: $\{10\bar{1}\}$pf, {010} parting Tw: {010}, {100} common, polysynthetic C: Colorless, white, gray, salmon St: White L: Vitreous	$n_\alpha = 1.547$ $n_\beta = 1.562$ $n_\gamma = 1.567$ $\delta = 0.020$ Biaxial (−) $2V = 62–70°$, $r < v$ Colorless	Rare crystals are tabular on {010} or elongate on c, more commonly massive, also fibrous or foliated; found in marine evaporite deposits with halite and anhydrite, also in fumarole deposits
Thenardite Na_2SO_4	Orthorhombic $2/m\ 2/m\ 2/m$ $a = 9.75$ $b = 12.29$ $c = 5.85$ $Z = 8$ $X = c$, $Y = b$, $Z = a$	H: 2.5–3, G: 2.67 CI: {010}pf, {101}g, {100}pr Tw: {100} common cruciform, also {011} C: Colorless, white, gray, yellow, brown, red St: White L: Vitreous, somewhat	$n_\alpha = 1.469$ $n_\beta = 1.475$ $n_\gamma = 1.484$ $\delta = 0.015$ Biaxial (+) $2V = 83°$, $r > v$, weak Colorless	Soluble in water, tastes faintly salty; crystals are {111} dipyramids with additional faces, or tabular parallel to {010}, rarely prismatic on a; found in evaporite deposits from saline lakes, as an efflorescence on soil and around fumaroles

DO NOT COPY
e48d507df5d1141@placeholder.94092-

Printed by: e48d507df5d1141@placeholder.94092.edu. Printing is for personal, private use only. No part of this book may be reproduced or transmitted without publisher's prior permission. Violators will be prosecuted.

		somewhat resinous		

[a] CI = cleavage (pf = perfect, g = good, pr = poor), C = color, Tw = twinning, St = streak, L = luster.

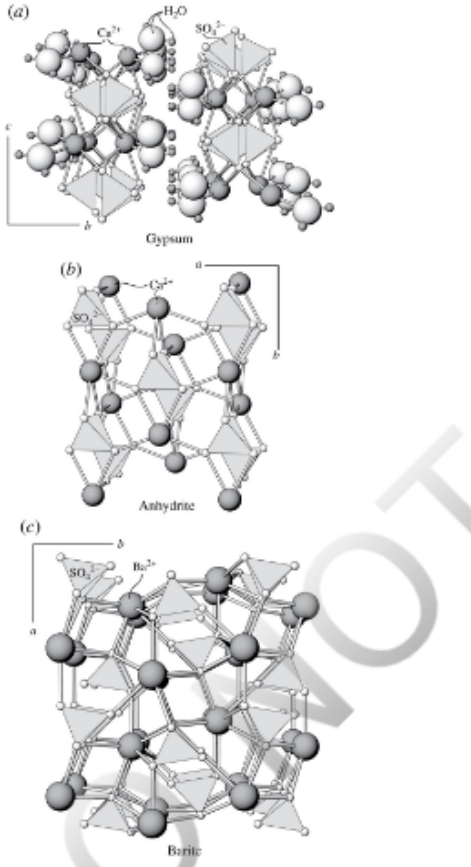

FIGURE 17.12 Structure of sulfate minerals. SO_4^{2-} groups are shown with oxygen anions as light-colored small spheres. (*a*) Gypsum viewed down the *a* axis. Cleavage on {010} splits along the layers of water molecules on the sides of the $CaSO_4$ layers. Hydrogen is shown as small dark spheres. (*b*) Anhydrite viewed down the *c* axis. (*c*) Barite viewed down the *c* axis. View larger image

Gypsum

$$CaSO_4 \cdot 2H_2O$$

$$\text{Monoclinic } 2/m$$

$$a = 6.52\ \text{Å},\ b = 15.18\ \text{Å},$$
$$c = 6.29\ \text{Å},\ \beta = 127.4^\circ,\ Z = 4$$

$$H = 2 \text{ on } \{010\} \text{ cleavage}$$

$$G = 2.30 - 2.37$$

$$\text{Biaxial } (+)$$

$$n_\alpha = 1.519 - 1.521$$

DO NOT COPY e48d507df5d1141@placeholder.9409

Printed by: e48d507df5d1141@placeholder.94092.edu. Printing is for personal, private use only. No part of this book may be reproduced or transmitted without publisher's prior permission. Violators will be prosecuted.

$$n_\beta = 1.522 - 1.526$$

$$n_\gamma = 1.529 - 1.531$$

$$\delta = 0.010$$

$$2V_z = 58^\circ$$

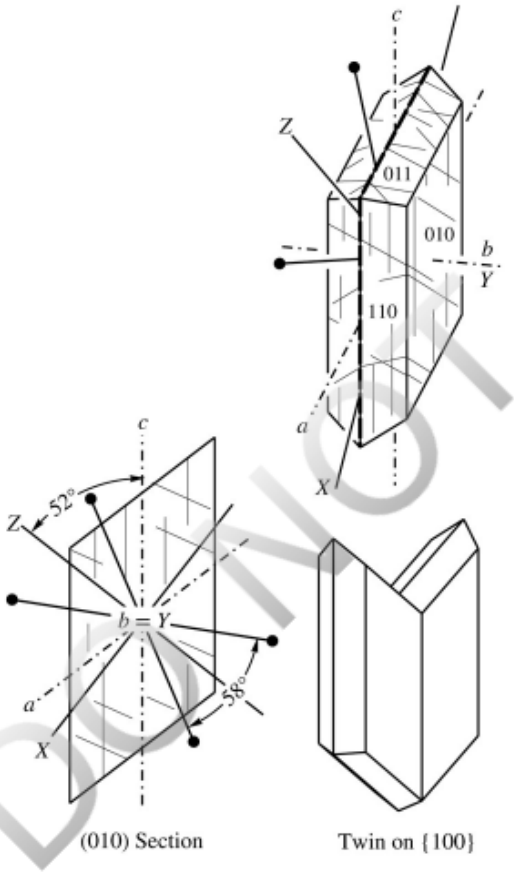

Structure The structure consists of strongly bonded layers of SO_4^{2-} + Ca^{2+} parallel to (010) alternating with layers of H_2O molecules (Figure 17.12a). Hydrogen bonding holds the H_2O molecules to the $CaSO_4$ layers and allows for the perfect cleavage on {010}. The strongest linkages within layers are parallel to the *c* axis, which corresponds to the length of fibers in satin spar. Each Ca^{2+} is coordinated with six O^{2-} from the SO_4^{2-} groups and two O^{2-} from water molecules.

Several unit cell conventions for gypsum are in common usage. The one used here lets the common prisms be the {011} and {110} prisms that are parallel to the *a* and *c* crystal axes, respectively.

Composition Deviation from the ideal formula is usually restricted to limited substitution of Sr or Ba for Ca.

Form and Twinning Crystals have a variety of habits, but most are tabular parallel to (010), less commonly prismatic or acicular parallel to the *c* crystal axis (Figure 17.13).

DO NOT COPY e48d507df5d1141@placeholder.9409

Printed by: e48d507df5d1141@placeholder.94092.edu. Printing is for personal, private use only. No part of this book may be reproduced or transmitted without publisher's prior permission. Violators will be prosecuted.

Simple contact twins on {100} are common and may form "swallowtail" twins. Twins on {001} are less common. Prismatic crystals may be curved, and tabular crystals and cleavage sheets may be bent in certain directions with relative ease. Granular or foliated masses are quite common. Gypsum has three varieties. Large euhedral crystals are known as selenite. Satin spar consists of parallel aggregates of fibrous gypsum and may fill veins. Granular massive rock gypsum is known as alabaster if white or light colored.

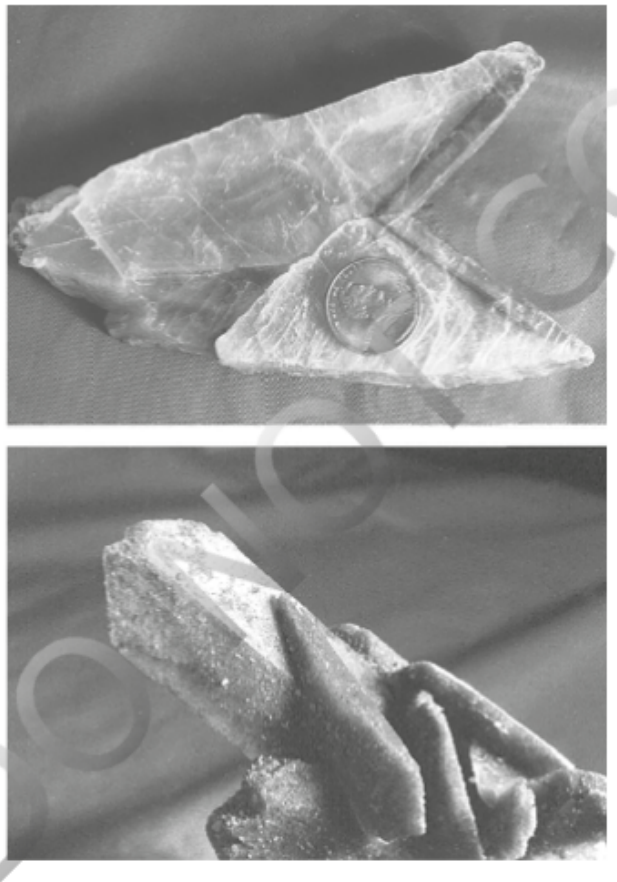

FIGURE 17.13 Gypsum. (*a*) Selenite with a swallowtail twin. U.S. penny is about 2 cm in diameter. (*b*) Bladed crystals. Field of view is about 10 cm across. View larger image

Cleavage Three cleavage forms in four directions. Perfect {010} cleavage dominates fragment shape. A second cleavage on {100} is good. Two good cleavages parallel to the $\{\bar{1}11\}$ prism intersect at angles of 42° and 138°. Cleavage folia are flexible in certain directions, but not elastic. Brittle.

Color Properties

Luster: Vitreous, cleavage surfaces may be pearly; satin spar is silky.

Color: Usually colorless or white; less commonly pale shades of gray, red, yellow, brown, or blue.

Streak: White.

DO NOT COPY e48d507df5d1141@placeholder.9409

Printed by: e48d507df5d1141@placeholder.94092.edu. Printing is for personal, private use only. No part of this book may be reproduced or transmitted without publisher's prior permission. Violators will be prosecuted.

Color in Thin Section: Colorless.

Optical Characteristics

Relief in Thin Section: Low negative.

Optic Orientation: $X \wedge a = -15°$, $Y = b$, $Z \wedge c = +52°$, optic plane = (010). The trace of the prominent {010} cleavage is either length fast or length slow, depending on grain orientation. Fragments on the {010} cleavage display 38° inclined extinction to the trace of {100} cleavage, with the fast ray closer to the cleavage.

Indices of Refraction and Birefringence: Refractive indices are less than the cement usually used in thin sections; interference colors are about the same as quartz (first-order gray or white).

Interference Figure: The $2V$ angle is about 58° at room temperature but decreases to 0° at 91°C. Above that temperature, $2V$ opens into an optic plane perpendicular to (010). Optic axis dispersion is strong, $r > v$, as is inclined bisectrix dispersion. Fragments on {010} cleavage yield flash figures.

Alteration Replacement of gypsum by quartz, opal, calcite, or celestine may produce pseudomorphs. Gypsum often is produced by hydrating sedimentary beds of anhydrite.

Distinguishing Features

Hand Sample: Characterized by hardness and four different cleavage surfaces. Anhydrite has higher specific gravity, cleavages at 90°, and often a subtle purplish cast to its color.

Thin Section/Grain Mount: Gypsum may be confused with anhydrite or barite. Both anhydrite and barite have higher birefringence, higher indices of refraction, and either parallel or symmetrical extinction in principal sections.

Occurrence Gypsum is a very common mineral in marine evaporite deposits (Box 17.2) and may be associated with halite, sylvite, calcite, dolomite, and anhydrite, as well as clay and silicate detrital grains. Biologically induced mineralization of gypsum by cyanobacteria has been documented in alkaline lakes (Thompson and Ferris, 1990) and undoubtedly takes place in evaporite deposits. The stability relationship between gypsum and anhydrite is shown in Figure 17.14. Gypsum is the stable phase in most evaporite environments, although under high salinity conditions or high temperatures, anhydrite may be the stable phase. Both anhydrite and gypsum may crystallize metastably; kinetic and biomineralization processes may dictate which crystallizes. In many evaporite deposits, gypsum is the primary mineral, but with burial and increase in temperature and pressure, the gypsum commonly dehydrates and recrystallizes as anhydrite at depths of a few meters up to a kilometer. Subsequent uplift and erosion to bring the evaporite material back to the surface may allow the secondary anhydrite to become hydrated and recrystallize back to gypsum. This latter hydration involves an increase in volume, so original bedding may be crumpled or disrupted as a consequence.

DO NOT COPY

Printed by: e48d507df5d1141@placeholder.94092.edu. Printing is for personal, private use only. No part of this book may be reproduced or transmitted without publisher's prior permission. Violators will be prosecuted.

original bedding may be crumpled or disrupted as a consequence.

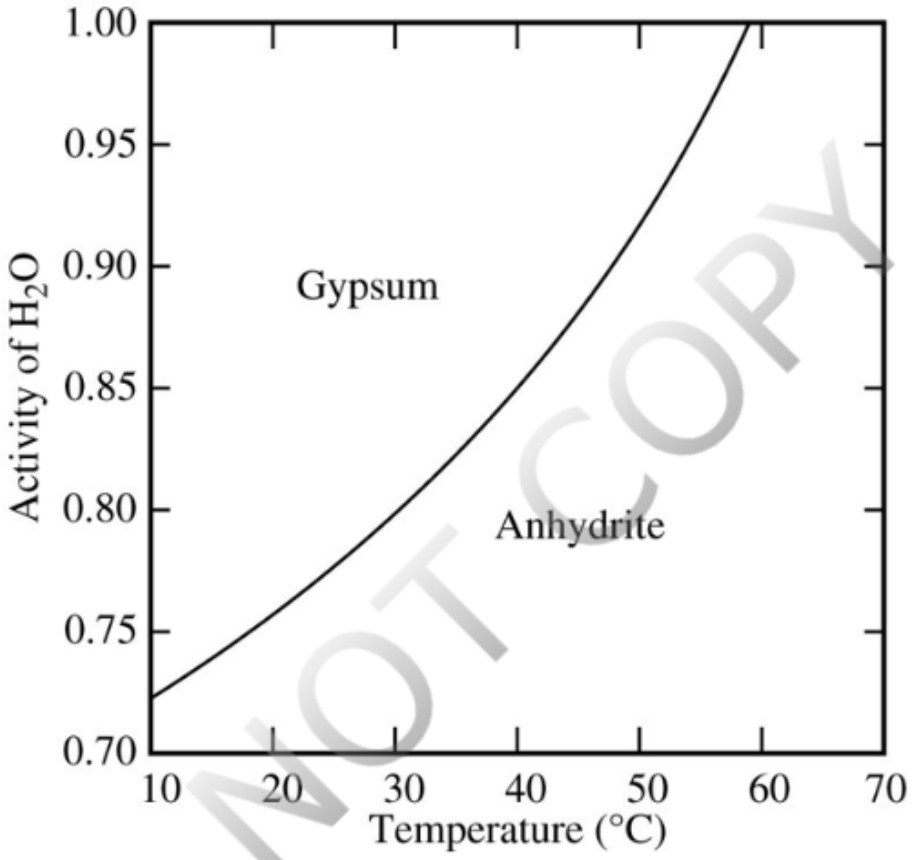

FIGURE 17.14 Stability of gypsum and anhydrite at 1 atm. Decreasing activity of water is produced by increasing salinity. © Hardie, L. A. (1967). The gypsum-anhydrite equilibrium at one atmosphere pressure, American Mineralogist, Volume 52. View larger image

Gypsum also crystallizes in desert soils from evaporation. Gypsum may also precipitate around fumaroles or volcanic vents. Infrequently it is found in the near-surface oxidized zone of hydrothermal sulfide deposits (Figure 19.3, Table 19.4).

The largest crystals ever discovered are purportedly the gypsum crystals more than 11 meters long found in a cave in Chihuahua, Mexico. The cave was temporally drained as part of mining activities, which led to their discovery in 2000; mining has since ended there and the cave has again filled with water.

Use Gypsum is one of the earlier minerals to be exploited by people; its use goes back at least 5000 years. About 70% of the gypsum now mined goes to manufacture gypsum wallboard, also known as sheetrock or drywall. Gypsum wallboard is used to cover interior walls of most houses, apartments, and offices in North America and in many other parts of the world. To make wallboard, gypsum is calcined in a process similar to that for making quicklime (see Calcite section above), which involves heating to drive off part of the water and then grinding to form a material called stucco (a similar material is plaster of Paris). Stucco is mixed with water, reinforcing fibers, and other additives to form a thick slurry that is extruded and wrapped with heavy paper to make wallboard. This material sets or hardens by recrystallizing to form gypsum. When cured, it forms a

DO NOT COPY e48d507df5d1141@placeholder.9409

Printed by: e48d507df5d1141@placeholder.94092.edu. Printing is for personal, private use only. No part of this book may be reproduced or transmitted without publisher's prior permission. Violators will be prosecuted.

This material sets or hardens by recrystallizing to form gypsum. When cured, it forms a stiff panel that is attached to interior wall framing with screws or nails. Joints between panels are finished with strips of mesh or heavy paper set in a plaster-like compound.

Gypsum also is used in portland cement (see Calcite section above) to control the setting rate, and as a soil amendment to improve soil structure and workability, provide sulfur and calcium to plants, and control the availability of other soil nutrients. Calcined gypsum has medical applications. It is used as a dietary supplement to provide needed sulfur for both people and animals, to make casts to support broken bones, and as a special casting plaster to make dental molds. Additional medical applications of gypsum include treatment of periodontal disease, bone grafting, antibiotic delivery, and oral hygiene. In Roman times, gypsum was mixed with rock salt to combat halitosis.

Alabaster, which is fine-grained white gypsum, is used as an ornamental stone and for sculpture, but its softness restricts its utility.

Anhydrite

$$\mathrm{CaSO_4}$$

$$\text{Orthorhombic } 2/m\ 2/m\ 2/m$$

$$a = 6.99\ \text{Å},\ b = 7.00\ \text{Å},$$
$$c = 6.24\ \text{Å},\ Z = 4$$

$$H = 3 - 3.5$$

$$G = 2.9 - 3.0$$

$$\text{Biaxial } (+)$$

$$n_\alpha = 1.569 - 1.574$$

$$n_\beta = 1.574 - 1.579$$

$$n_\gamma = 1.609 - 1.618$$

$$\delta = 0.040 - 0.044$$

$$2V_z = 42 - 44^\circ$$

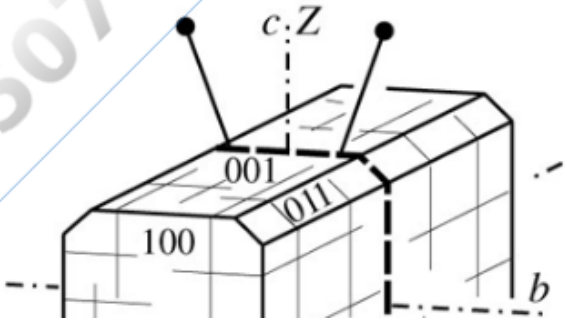

DO NOT COPY
e48d507df5d1141@placeholder.9409

Printed by: e48d507df5d1141@placeholder.94092.edu. Printing is for personal, private use only. No part of this book may be reproduced or transmitted without publisher's prior permission. Violators will be prosecuted.

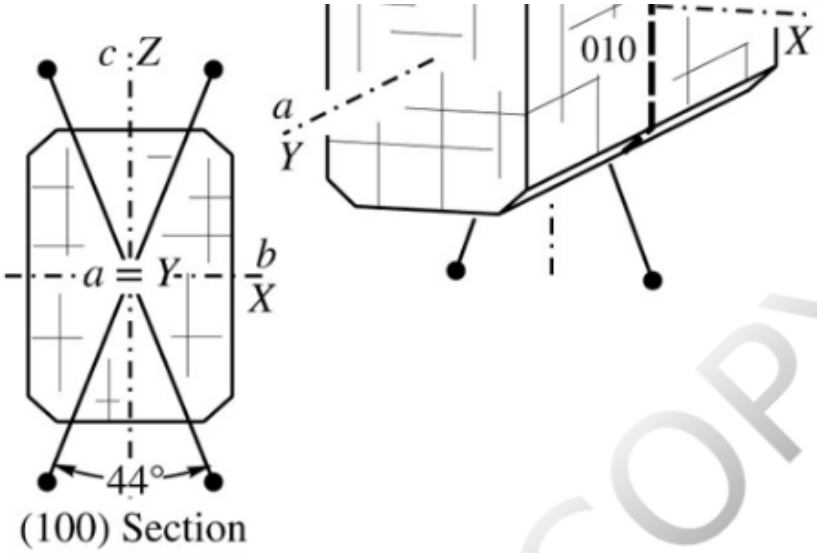

(100) Section

Structure The structure (Figure 17.12b) consists of sulfate groups arrayed in a regular fashion, defining planes parallel to (100), (010), and (001). Ca^{2+} cations occupy somewhat irregular 8-fold sites among the sulfate groups, and are arrayed so that sulfate and Ca ions alternate parallel to the *c* axis. Cleavage develops between the planes of sulfate anionic groups.

Composition Most anhydrite is close to the ideal composition, but small amounts of Sr or Ba may substitute for Ca.

Form and Twinning Anhydrite forms blocky crystals or crystals tabular parallel to {100}, {010}, or {001} (Figure 17.15). Masses of anhedral grains are much more common; fibrous or radiating aggregates are less common. Simple or repeated twins on {011} are fairly common.

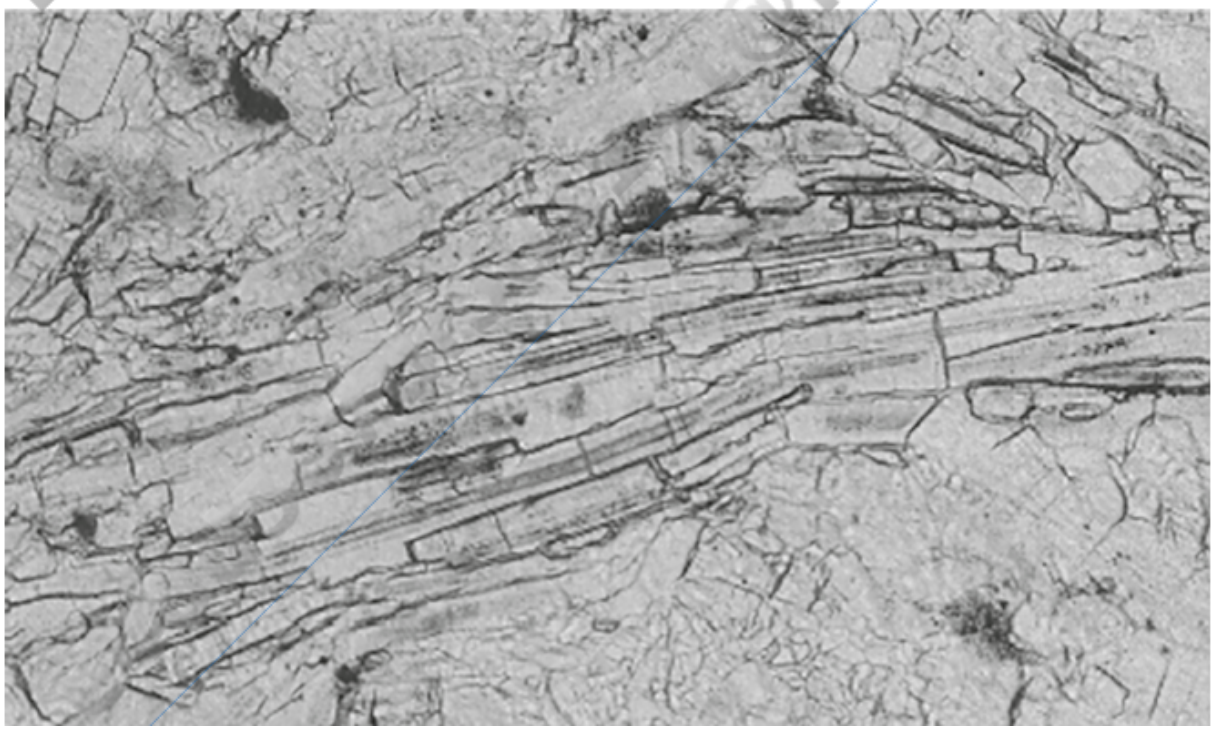

DO NOT COPY

Printed by: e48d507df5d1141@placeholder.94092.edu. Printing is for personal, private use only. No part of this book may be reproduced or transmitted without publisher's prior permission. Violators will be prosecuted.

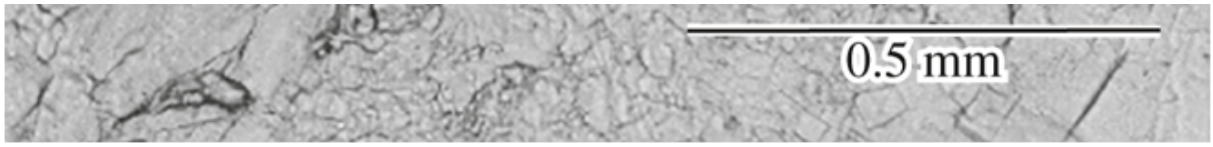

FIGURE 17.15 Photomicrograph of a thin section of bedded anhydrite. Plane light. View larger image

Cleavage Three cleavage directions at right angles: {010} perfect, {100} very good, and {001} good. Uneven to splintery fracture. Brittle.

Color Properties

Luster: Vitreous.

Color: Colorless, white, or gray, sometimes with a slight bluish cast; less commonly blue, red, or brown.

Streak: White.

Color in Thin Section: Colorless.

Optical Characteristics

Relief in Thin Section: Moderate positive.

Optic Orientation: $X = b$, $Y = a$, $Z = c$, optic plane = (100).

Indices of Refraction and Birefringence: Refractive indices show little variation. Maximum birefringence is displayed by (100) sections and interference colors in standard thin section range up to lower third order.

Interference Figure: (001) sections and cleavage fragments yield centered acute bisectrix figures. Optic axis dispersion is distinct, $r < v$.

Alteration Anhydrite commonly becomes hydrated to form gypsum. Alteration is accompanied by a volume increase that may cause bedding in the anhydrite layer to deform, resulting in folding. Anhydrite may be pseudomorphically replaced by quartz, calcite, dolomite, gypsum, and other minerals.

Distinguishing Features

Hand Sample: Most closely resembles gypsum but has three cleavages at right angles as well as greater hardness and specific gravity; may have a subtle bluish cast to its color. Barite has higher specific gravity, and calcite effervesces vigorously in dilute HCl.

Thin Section/Grain Mount: Higher birefringence and indices of refraction distinguish anhydrite from gypsum. Barite has higher indices of refraction and lower birefringence.

Occurrence Anhydrite most commonly occurs in marine evaporite deposits. Associated

DO NOT COPY e48d507df5d1141@placeholder.9409

Printed by: e48d507df5d1141@placeholder.94092.edu. Printing is for personal, private use only. No part of this book may be reproduced or transmitted without publisher's prior permission. Violators will be prosecuted.

Occurrence Anhydrite most commonly occurs in marine evaporite deposits. Associated minerals include calcite, dolomite, gypsum, and halite. It apparently may either precipitate directly from seawater or be produced by dehydration of gypsum. See Box 17.2 on evaporite deposits and the gypsum mineral entry above for more information. Anhydrite is also found in hydrothermally altered limestone and dolostone, and in the near-surface, oxidized portion of hydrothermal sulfide deposits. Primary magmatic anhydrite is not common but has been reported in intermediate volcanic rocks.

Use Anhydrite is used as a soil amendment and is mixed with portland cement to control the rate of curing. Anhydrite has been used as a source of sulfur to make sulfuric acid and other sulfur compounds, but other sources for sulfur, including gypsum, are usually more economic. Calcium sulfate is used as a carrier for antibiotics and for bone grafting, among other medical applications. In many cases, however, it is not clear whether anhydrite or gypsum is the mineral actually used.

Barite

$$\mathrm{BaSO_4}$$

$$\text{Orthorhombic } 2/m\ 2/m\ 2/m$$

$$a = 8.88\ \text{Å},\ b = 5.45\ \text{Å},$$
$$c = 7.15\ \text{Å},\ Z = 4$$

$$H = 2.5 - 3.5$$

$$G = 4.5$$

$$\text{Biaxial } (+)$$

$$n_\alpha = 1.634 - 1.637$$

$$n_\beta = 1.636 - 1.639$$

$$n_\gamma = 1.646 - 1.649$$

$$\delta = 0.012$$

$$2V_z = 36 - 40^\circ$$

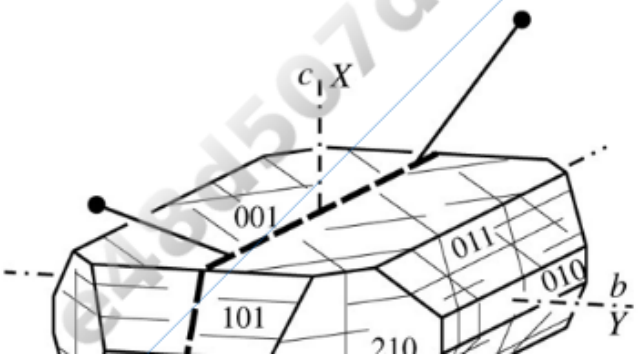

DO NOT COPY
e48d507df5d1141@placeholder.9409

Printed by: e48d507df5d1141@placeholder.94092.edu. Printing is for personal, private use only. No part of this book may be reproduced or transmitted without publisher's prior permission. Violators will be prosecuted.

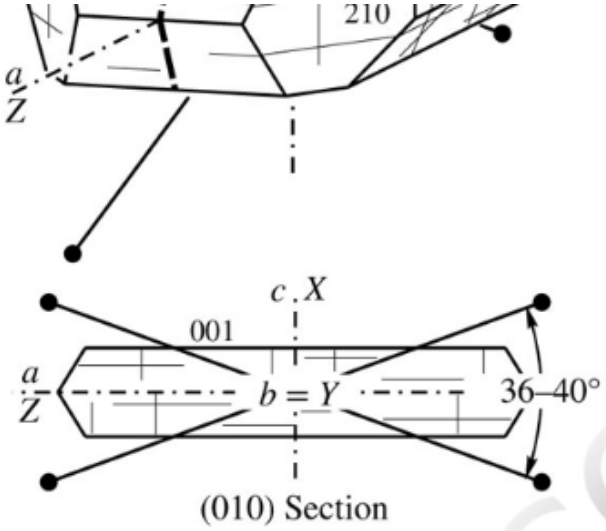

(010) Section

Structure Sulfate anionic groups are arranged in planes parallel to (010) so that oxygens form 12-fold coordination sites for Ba^{2+} cations within the same planes (Figure 17.12c).

Composition Most barite is close to ideal composition, but complete solid solution extends to celestine ($SrSO_4$) and some substitution of Pb and Ca for Ba is possible.

Form and Twinning Crystals are tabular parallel to (001), or less frequently prismatic parallel to *a* or *b* crystal axes (Figure 17.16). Crystals often are intergrown to form rosettes or platy aggregates. Barite also forms granular aggregates, cleavable masses, and concretionary masses of radial fibers. Deformation-induced twins on {110} are possible; otherwise it is not usually twinned.

(*a*)

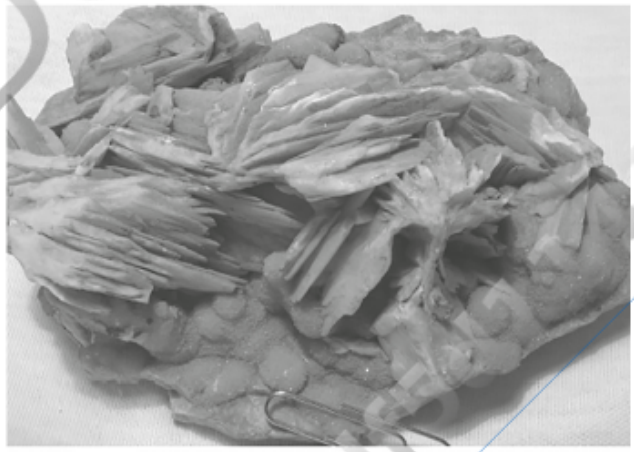

(*b*)

DO NOT COPY

Printed by: e48d507df5d1141@placeholder.94092.edu. Printing is for personal, private use only. No part of this book may be reproduced or transmitted without publisher's prior permission. Violators will be prosecuted.

FIGURE 17.16 Barite. (*a*) Intergrown platy barite crystals with mammillary masses of quartz (near paper clip). Width of paper clip is about 7 mm. (*b*) Two intergrown barite roses that formed as concretionary masses in sedimentary rocks. Width of paper clip is about 7 mm. View larger image

Cleavage Four cleavage surfaces: two very good cleavages on {210} intersect at 78°, a fair to good cleavage on {010}, and a perfect cleavage on {001} that intersects the other three at 90°. Uneven fracture. Brittle.

Color Properties

Luster: Vitreous.

Color: White, pale yellow, gray, pale green, pale blue, red, brown. Radiation-induced color centers appear to be responsible for the color of blue and yellow barite, and possibly other colors as well.

Streak: White.

Color in Thin Section: Colorless.

Optical Characteristics

Relief in Thin Section: Moderately high positive.

Optic Orientation: $X = c$, $Y = b$, $Z = a$, optic plane = (010). Sections cut parallel to *c* show parallel extinction, and basal sections and fragments on the {001} cleavage show symmetrical extinction to the prismatic cleavage. Fibrous and prismatic crystals are usually elongate parallel to *a* and are length slow. Crystals elongate parallel to *b* may be either length fast or length slow, depending on orientation.

Indices of Refraction and Birefringence: Indices of refraction decrease slightly with Sr content and increase with Pb content. Interference color in standard thin section is no higher than first-order yellow.

Interference Figure: (100) sections yield centered acute bisectrix figures with moderate $2V$. Optic axis dispersion is weak, $r < v$.

Alteration Barite may be altered to witherite ($BaCO_3$) or may be replaced by minerals such as quartz, calcite, dolomite, or pyrite.

Distinguishing Features

Hand Sample: The specific gravity, which is unusually high for a nonmetallic mineral, distinguishes barite from other minerals with similar appearance. Anhydrite has three cleavages at right angles, and the carbonates all react with dilute HCl. Celestine, which is isostructural with barite, has lower specific gravity.

DO NOT COPY e48d507df5d1141@placeholder.9409

Printed by: e48d507df5d1141@placeholder.94092.edu. Printing is for personal, private use only. No part of this book may be reproduced or transmitted without publisher's prior permission. Violators will be prosecuted.

Thin Section/Grain Mount: Resembles gypsum but has higher indices of refraction and inclined extinction in most sections. Celestine has larger $2V$ and lower indices of refraction.

Occurrence Barite is a common gangue mineral in hydrothermal mineral deposits in association with galena, sphalerite, pyrite, quartz, fluorite, and carbonates. It also occurs as concretionary masses and veins in shale, limestone, sandstone, and other sedimentary rocks. Barite rosettes (Figure 17.16) formed in an evaporative environment can be called desert roses, but gypsum can similarly form rosettes and are also called desert roses. Carbonatites may contain barite as a primary magmatic mineral. Barite is an uncommon biomineral (Chapter 5).

Use Barite is the primary ore mineral from which barium is extracted. Most barite, however, is mined as an industrial mineral and used in applications that take advantage of the high specific gravity. The majority is used in the petroleum industry as a component of drilling "mud" in oil and gas wells. Drilling mud is pumped down the center of the drill rod and exits through the drill bit as a well is drilled. The mud lubricates the bit and also carries rock cuttings from the bottom of the drill hole up to the surface. Pulverized barite is added to the drilling mud to increase its density and prevent high-pressure gas encountered during drilling from blowing the mud out of the drill hole and venting to the surface, where it could accidentally ignite.

Barite and barium compounds derived from it have over 2000 industrial uses. These include glassmaking, paper and playing card manufacture, and ceramics; as a high-density filler in plastics, rubber and related materials; and as a pigment. People may swallow substantial quantities of chemically purified $BaSO_4$ (blanc fixe) to allow certain portions of the gastrointestinal tract to be more visible in X-ray images.

DO NOT COPY e48d507df5d1141@placeholder.9409

Printed by: e48d507df5d1141@placeholder.94092.edu. Printing is for personal, private use only. No part of this book may be reproduced or transmitted without publisher's prior permission. Violators will be prosecuted.

Phosphates

The key structural element of phosphate minerals is the presence of tetrahedral PO_4^{3-} anionic groups. The phosphorus ions have a +5 charge, so phosphate groups are anisodesmic; the oxygen anions are more strongly bonded to the P^{5+} than to other cations in the mineral. The PO_4^{3-} groups must be treated as structural units. Only a few phosphate minerals are routinely encountered. Apatite is a widespread accessory mineral in many rocks, and monazite and xenotime are common in pelitic metamorphic rocks and are fairly common in granitic rocks. For all, they are typically identified only in thin section. Turquoise, although actually fairly rare, is widely used as a decorative stone in jewelry. Less common phosphate and closely related vanadate minerals are listed in Table 17.5.

TABLE 17.5 Less Common Phosphate and Vanadate Minerals

Mineral	Unit Cell	Physical Properties[a]	Optical Properties	Comments
Amblygonite $LiA1(PO_4)F$	Triclinic $a = 5.18$ $b = 7.11$ $c = 5.03$ $\alpha = 112°, \beta = 97.8°, \gamma = 68.3°$ $Z = 2$ $X \wedge b = 30–40°$, $Y \wedge a = 15–20°$, $Z \wedge c = 20°–30°$	H: 5.5–6 G: 3.0–3.1 Cl: {100}pf, {110}g fair, {001}pr Tw: common C: White; less commonly beige, pink, greenish, gray St: White L: Vitreous to greasy	$n_\alpha = 1.575–1.595$ $n_\beta = 1.587–1.610$ $n_\gamma = 1.590–1.622$ $\delta = 0.014–0.027$ Biaxial (−) $2V = 50–90°$ $r < v$, weak Colorless	Crystals are stubby prisms, often rough, and may be very large; found in Li-bearing granitic pegmatites
Autunite $Ca(UO_2)_2(PO_4)_2 \cdot 10–12H_2O$	Tetragonal $4/m\ 2/m\ 2/m$ $a = 7.0$ $c = 20.7$ $Z = 2$	H: 2–2.5 G: 3.1–3.2 Cl: {001}pf, {100}pr Tw: {110}	$n_\omega = 1.577$ $n_\varepsilon = 1.554$ $\delta = 0.023$ Uniaxial (−) ω = pale	Crystals thin and tabular on {001}; commonly forms scaly or earthy aggregates in the near-surface oxidized zone of sediment-hosted

DO NOT COPY e48d507df5d1141@placeholder.9409

Printed by: e48d507df5d1141@placeholder.94092.edu. Printing is for personal, private use only. No part of this book may be reproduced or transmitted without publisher's prior permission. Violators will be prosecuted.

		C: Bright yellow St: Yellow L: Vitreous Fluoresces yellowish green in UV light	ω = pale yellow, ϵ = yellow	uranium deposits and U-bearing veins and pegmatites
Carnotite $K_2(UO_2)_2(VO_4)_2 \cdot 3H_2O$	Monoclinic $2/m$ a = 10.47 b = 8.41 c = 6.91 β = 103.7° Z = 2 $X \sim c$, $Y = b$, $Z \sim a$	H: soft G: 4.7–5.0 Cl: {001}pf Tw: ?? C: Bright yellow, lemon-yellow St: Yellow L: Earthy; pearly, or silky if coarse	n_α = 1.75–1.78 n_β = 1.90–2.06 n_γ = 1.92–2.08 δ = 0.17–0.30 Biaxial (−) $2V$ = 43–60° X = colorless, $Y = Z$ = yellow	Usually fine-grained earthy masses or scaly grains; found in sediment-hosted uranium deposits and as an alteration on other U-bearing minerals, mined for its U and V content
Lithiophilite–triphylite $Li(Mn, Fe)PO_4$	Orthorhombic $2/m$ $2/m$ $2/m$ a = 4.86 b = 10.36 c = 6.01 Z = 4 $X = a$ or c, $Y = c$ or a, $Z = b$	H: 4.5–5 G: 3.34–3.58 Cl: {001}pf, {010}g, {110}pr Tw: N/A C: bluish or greenish gray (triph.), light-dark brown, salmon (lith.) St: White, gray L: Vitreous to subresinous	n_α = 1.670–1.705 n_β = 1.677–1.710 n_γ = 1.684–1.720 δ = 0.007–0.015 Biaxial (+ or −) $2V_Z$ = 0–180° $r < v$ or $r > v$ strong Colorless to pale pink	Crystals prismatic parallel to c; more common as cleavable masses; found in Li-bearing granitic pegmatites
Pyromorphite $Pb_5(PO_4)_3Cl$	Hexagonal $6/m$ a = 9.97 c = 7.32	H: 3.5–4 G: 7.04 Cl: {101}pr	n_ω = 2.058 n_ϵ = 2.048 δ = 0.010	Isostructural with apatite; crystals are hexagonal prisms; often in reniform, globular, fibrous, or granular

DO NOT COPY e48d507df5d1141@placeholder.9409-

Printed by: e48d507df5d1141@placeholder.94092.edu. Printing is for personal, private use only. No part of this book may be reproduced or transmitted without publisher's prior permission. Violators will be prosecuted.

	Z =2	Tw: {112} rare C: Green, yellow, brown St: White L: Resinous to subadamantine	Uniaxial (−) Colorless or pale tints of hand-sample color $\omega < \epsilon$	fibrous, or granular masses; found in the near-surface oxidized portion of Pb-bearing sulfide deposits
Wavellite $Al_3(OH)_3(PO_4)_2 \cdot 5H_2O$	Orthorhombic $2/m\ 2/m\ 2/m$ a = 9.62 b = 17.34 c = 6.99 Z = 4 $X = b$, $Y = a$, $Z = c$	H: 3.5–4 G: 2.32–2.37 Cl: {110}pf, {10l}g, {010}fair Tw: ?? Cl: White, greenish white, green, yellow, brown St: White L: Vitreous to pearly	n_α = 1.518–1.535 n_β = 1.526–1.543 n_γ = 1.545–1.561 δ = 0.025–0.027 Biaxial (+) $2V$ = 72° $r > v$ weak Colorless or pale: X = blue, green; Y = yellow-brown; Z = pale brown, pale yellow, colorless	Usually radiating or encrusting aggregates of acicular crystals elongate on c; found as a fairly common secondary mineral deposited by hydrothermal solutions in many rock types including low-grade Al-rich metamorphic rocks, phosphate deposits, massive limonite, and in hydrothermal veins with cassiterite and other phosphates

[a] Cl = cleavage (pf = perfect, g = good, pr = poor), C = color, Tw = twinning, St = streak, L = luster.

Apatite

$$Ca_5(PO_4)_3(OH, F, Cl)$$

$$\text{Hexagonal } 6/m$$

$$a = 9.32 - 9.64 \text{ Å},$$

$$c = 6.78 - 6.90 \text{ Å},\ Z = 2$$

$$H = 5$$

$$G = 3.1 - 3.35$$

$$\text{Uniaxial } (-)$$

DO NOT COPY
e48d507df5d1141@placeholder.9409-

Printed by: e48d507df5d1141@placeholder.94092.edu. Printing is for personal, private use only. No part of this book may be reproduced or transmitted without publisher's prior permission. Violators will be prosecuted.

$$n_\omega = 1.629 - 1.667$$

$$n_\epsilon = 1.624 - 1.666$$

$$\delta = 0.001 - 0.007$$

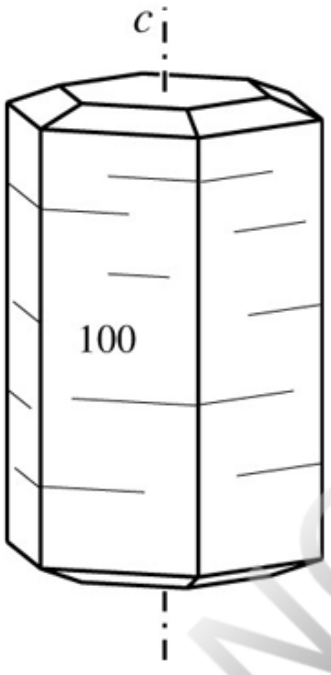

Structure The structure consists of PO_4^{3-} groups bonded laterally through Ca^{2+} (Figure 17.17). Half the Ca^{2+} is in distorted 6-fold coordination, and the other half is in distorted 7-fold coordination with O from the phosphate groups and additional OH, F, and/or Cl.

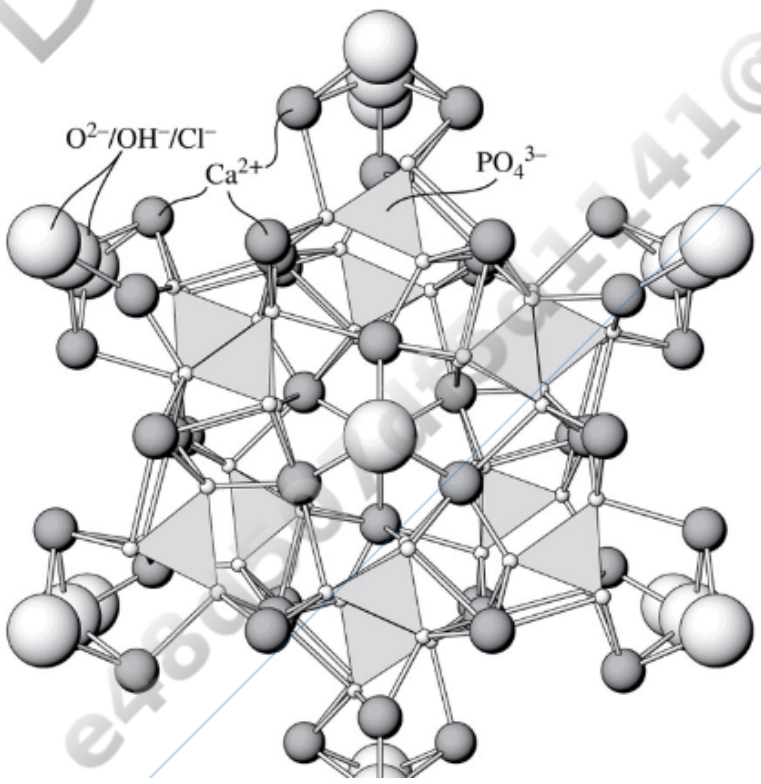

DO NOT COPY
e48d507df5d1141@placeholder.9409

Printed by: e48d507df5d1141@placeholder.94092.edu. Printing is for personal, private use only. No part of this book may be reproduced or transmitted without publisher's prior permission. Violators will be prosecuted.

FIGURE 17.17 Structure of apatite viewed down the *c* axis. The hexagonal symmetry is evident. View larger image

Composition The principal compositional variation is in the relative amounts of OH, F, and Cl. The end members are fluorapatite [$Ca_5(PO_4)_3F$], hydroxylapatite [$Ca_5(PO_4)_3OH$], and chlorapatite [$Ca_5(PO_4)_3Cl$]. Most apatite has compositions that lie between fluorapatite and hydroxylapatite, with more F than OH. Tetrahedral CO_3OH^{3-} groups can evidently replace some PO_4^{3-} tetrahedra, particularly in the apatite found in bones and teeth. The term *carbonate–apatite* has been applied to these minerals, but that term is now discredited. *Dahllite* and *francolite* are additional discredited terms for carbonate–apatite with dominantly OH^- and F^-, respectively, in the hydroxyl sites. Phosphate tetrahedra also may be replaced by SO_4^{2-}, SiO_4^{4-}, or CrO_4^{2-}. Charge balance is maintained by substituting Na^+ for Ca^{2+} or, for example, by substituting a sulfate group and a silicate group for two phosphate groups. Trace amounts of U, V, Mn, and Fe commonly are present. The term *collophane* is given to fine-grained or cryptocrystalline apatite with usually a small amount of calcite found in phosphate rock and fossil bone.

Form and Twinning Crystals are common, but are usually small, and consist of hexagonal prisms terminated with {001} pinacoid and/or {101} dipyramid. Longitudinal sections through crystals are usually elongate-rectangular. Apatite also forms anhedral grains (Figure 17.18) and granular or columnar aggregates. Collophane is usually brown and forms colloform, encrusting, spherulitic, oolitic, and related structures and is a major constituent of some fossil bone. Twins are rare on {111} or {103}.

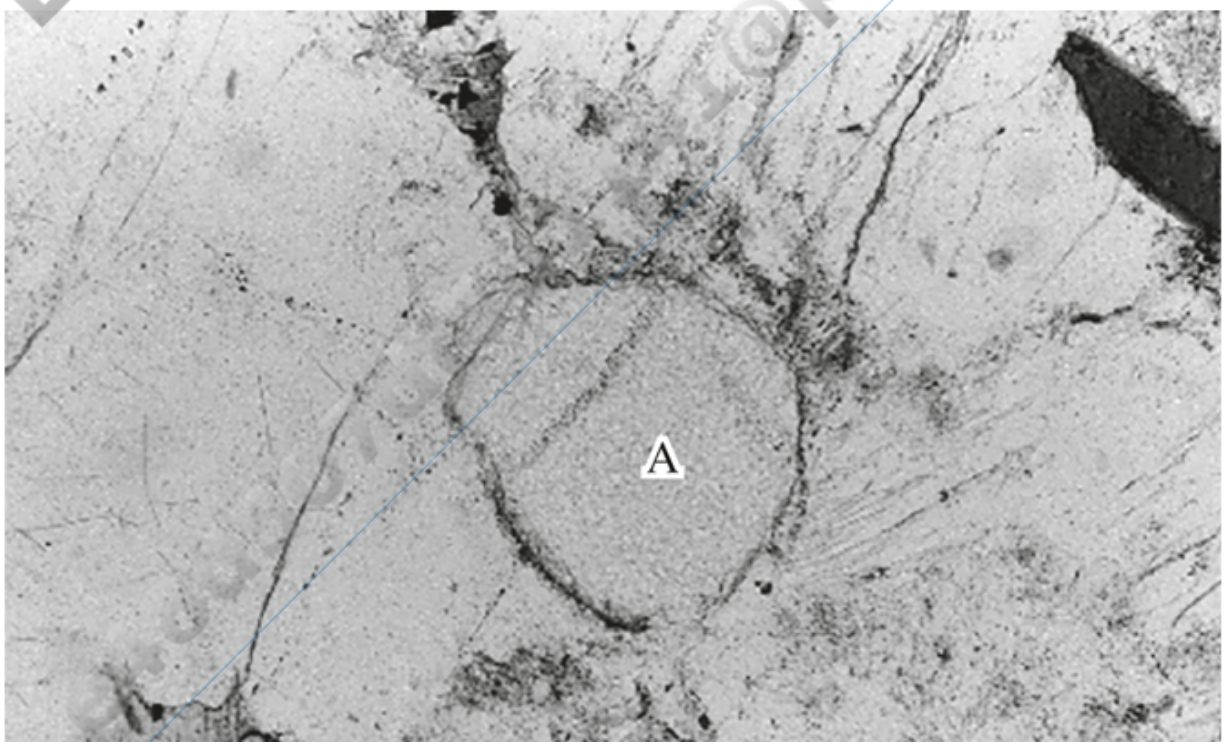

Printed by: e48d507df5d1141@placeholder.94092.edu. Printing is for personal, private use only. No part of this book may be reproduced or transmitted without publisher's prior permission. Violators will be prosecuted.

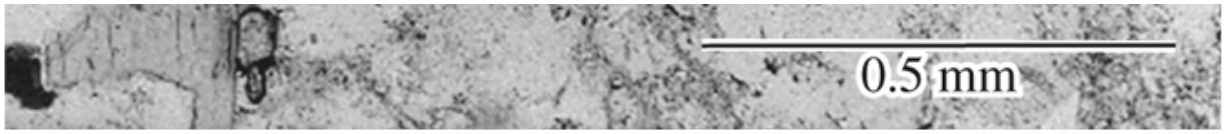

FIGURE 17.18 Photomicrograph of apatite in thin section. View larger image

Cleavage Poor cleavage on {001} is not usually visible in hand sample, but may be visible in thin section if a grain displays a longitudinal section. Cleavage does not have a strong control on fragment orientation in grain mount. Conchoidal to uneven fracture. Brittle.

Color Properties

Luster: Vitreous.

Color: Most commonly grayish blue-green, also green, yellow, yellowish green, brown, blue, pink, violet, orange, etc. Collophane is brown.

Streak: White.

Color in Thin Section: Colorless. Strongly colored samples may display a pale version of the hand-sample color. Collophane is brown.

Pleochroism: Colored varieties may be weakly pleochroic $\epsilon > \omega$, so elongate grains are darker when aligned with the vibration direction of the lower polarizer.

Optical Characteristics

Relief in Thin Section: Moderately high positive.

Optic Orientation: Elongate grains are length fast and show parallel extinction.

Indices of Refraction and Birefringence: Indices of refraction vary with composition but with considerable variability. n_ω of fluorapatite is 1.633, n_ω of hydroxylapatite is about 1.650, and n_ω of chlorapatite is 1.667. Chlorapatite has the lowest δ at about 0.001, δ of fluorapatite is about 0.004, and δ of hydroxylapatite is about 0.007. Common apatite has indices of refraction in the range n_ω = 1.633–1.650 and n_ϵ = 1.629–1.647 with δ = 0.003–0.005. Carbonate–apatite has indices of refraction n_ω = 1.603–1.638, n_ϵ = 1.598–1.619 with δ = 0.007–0.017. Collophane may be essentially isotropic.

Interference Figure: Basal sections in thin section yield uniaxial negative interference figures with diffuse isogyres on a first-order gray field. Small grain size may make interference figures difficult to obtain in thin section. Some samples, particularly carbonate–apatite, may be biaxial negative with $2V$ up to 20°.

Alteration Apatite is relatively stable in most geological environments and not readily altered. Pseudomorphs of clay, turquoise, serpentine, or other phosphate minerals have been reported.

DO NOT COPY e48d507df5d1141@placeholder.9409

Printed by: e48d507df5d1141@placeholder.94092.edu. Printing is for personal, private use only. No part of this book may be reproduced or transmitted without publisher's prior permission. Violators will be prosecuted.

been reported.

Distinguishing Features

Hand Sample: Color, crystal habit, and hardness are diagnostic. Beryl is harder and usually lacks dipyramid terminations.

Thin Section/Grain Mount: Distinguished by moderately high relief and low birefringence. In thin section it usually displays a slightly pebbly or pitted surface texture with subtle pastel color highlights in plane light. In contrast to apatite, garnet is isotropic, and topaz, sillimanite, and andalusite have higher birefringence and are biaxial. Further, zoisite has higher relief and usually displays anomalous interference colors, while beryl has lower refractive indices. Colored varieties may resemble tourmaline, but apatite is darker in plane light when the long dimension of grains is aligned parallel to the lower polarizer vibration direction.

Occurrence Apatite is a very common accessory mineral in a wide variety of igneous and metamorphic rocks and is the most common phosphate mineral. Grains are usually small and visible only in thin section. Only in granitic pegmatites and in skarns, marble, and calc-silicate gneiss derived from carbonate-rich sediment is apatite likely to be coarsely crystalline. Economic quantities of apatite are sometimes found in nepheline syenite and related rocks, and in carbonatites.

Apatite is common as detrital grains in clastic sedimentary rocks, usually as oval to somewhat elongate grains. Chlorapatite and carbonate–apatite are the major constituents of collophane in phosphatic limestone, shale, and ironstone and in some nearly pure phosphate beds. The apatite in these rocks may be derived from the skeletal remains of fish and other vertebrates or may be precipitated from seawater. Bone fragments and fish scales often serve as the nuclei for precipitation of secondary apatite.

Use Apatite, usually as collophane in sedimentary rocks, but also from some igneous sources, is a source of phosphate. Phosphate is used in fertilizer and for other industrial purposes including fluorescent light bulbs, lasers, and environmental remediation. Fluorine also can be extracted from apatite and is used to treat drinking water and in other industrial processes including aluminum refining. Additional byproducts that may be extracted from apatite during processing include rare earth elements, U, and V. Sometimes the calcium is also extracted. Apatite is a minor gemstone.

Comments Apatite is a very important biomineral because vertebrate bones and teeth are composed dominantly of carbonate–apatite (see Chapter 5 for more information). For browsing animals, the fact that their teeth are made of apatite with a hardness of 5 poses a significant problem. Quartz, with a hardness of 7, is contained within the dirt and dust that is ingested along with grass and other plants eaten by cattle, horses, rodents, and other herbivores. This quartz can grind teeth down. Strategies that have developed by evolutionary processes to deal with this problem include replacing teeth as they wear out (elephants), continually growing the teeth (rodents), and providing large teeth with lots of mass to wear away (horses). Modern biomedical applications are numerous and

DO NOT COPY

Printed by: e48d507df5d1141@placeholder.94092.edu. Printing is for personal, private use only. No part of this book may be reproduced or transmitted without publisher's prior permission. Violators will be prosecuted.

of mass to wear away (horses). Modern biomedical applications are numerous and include use in cements, ceramics, coatings on implants, and bone grafting.

A total of 42 different approved minerals, known collectively as the apatite supergroup, utilize the apatite structure, including arsenates, vanadates, silicates, silicoborates, sulfates, and other phosphates (Hughes and Rakovan, 2015). More than half of all the geologically available chemical elements can be found in these minerals, documenting the degree to which the apatite structure can accommodate a wide range of different cations and anions. As a consequence, apatite is a very useful mineral to document changing fluid compositions in igneous and metamorphic environments. In addition, apatite is amenable to multiple radiometric dating techniques [U–Pb, (U–Th)/He, and fission track dating]. See Box 5.1 for more information, as well as Chew and Spikings (2015). The June 2015 issue of the journal *Elements* contains a number of additional relevant articles regarding apatite.

Monazite

$$(\mathrm{Ce, La, Th})\mathrm{PO_4}$$

$$\text{Monoclinic } 2/m$$

$$a = 6.78\ \text{Å},$$
$$b = 7.00\ \text{Å},$$
$$c = 6.45\ \text{Å},$$
$$\beta = 104^\circ,\ Z = 4$$

$$H = 5$$

$$G = 5.0 - 5.3$$

$$\text{Biaxial } (+)$$

$$n_\alpha = 1.772 - 1.800$$
$$n_\beta = 1.778 - 1.801$$
$$n_\gamma = 1.823 - 1.860$$
$$\delta = 0.045 - 0.075$$
$$2V_z = 6 - 26^\circ$$

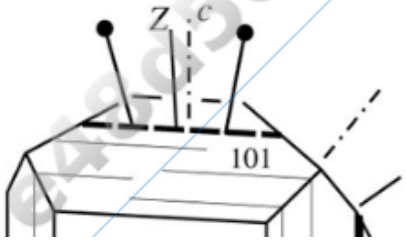

DO NOT COPY
e48d507df5d1141@placeholder.9409

Printed by: e48d507df5d1141@placeholder.94092.edu. Printing is for personal, private use only. No part of this book may be reproduced or transmitted without publisher's prior permission. Violators will be prosecuted.

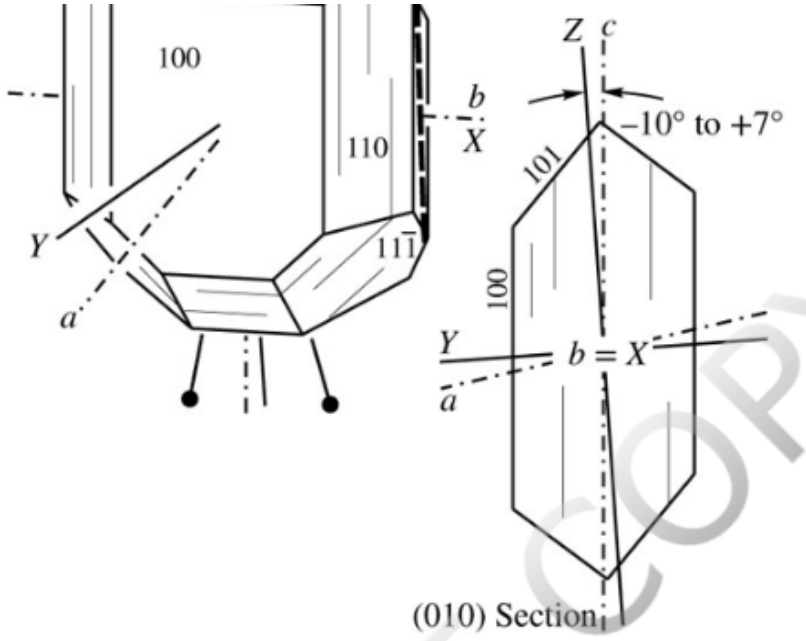

(010) Section

Structure The structure consists of slightly distorted PO_4 tetrahedra bonded laterally through rare earth element cations in 9-fold coordination with oxygen from the tetrahedra.

Composition Any of the rare earth elements, in particular the light rare earth elements (La through Eu), may occupy the 9-fold sites, but Ce and La are usually the most abundant. Between 4% and 12% of the 9-fold sites are usually occupied by Th, and some samples have up to about 30%. Minor U is also usually present. Si and S may substitute for some of the P in the tetrahedra. The high abundance of Th and U suggests that most monazite grains should be metamict. While monazite almost always shows some radiation damage, it is never to the degree predicted by its Th and U content. Nasdala et al. (2020) explored this issue and determined that "alpha-assisted annealing" limits the total amount of radiation damage. ^{4}He ions generated from the breakdown of Th and U aid in healing radiation damage, even at low temperatures.

Form and Twinning Crystals are usually small, nearly equant, flattened parallel to {100}, or elongate parallel to *b*. Simple twins on {100} are common and lamellar twinning on {001} is rare.

Cleavage A single cleavage on {100} is good, a second at right angles on {010} is fair to poor; parting on {001}. Altered samples display the cleavage more clearly in thin section. Conchoidal to uneven fracture. Brittle.

Color Properties

Luster: Resinous to waxy.

Color: Yellow, reddish yellow, or reddish brown.

Streak: White.

DO NOT COPY e48d507df5d1141@placeholder.9409

Printed by: e48d507df5d1141@placeholder.94092.edu. Printing is for personal, private use only. No part of this book may be reproduced or transmitted without publisher's prior permission. Violators will be prosecuted.

Color in Thin Section: Yellow or colorless.

Pleochroism: Weak, $Y > X \approx Z$: X = colorless or pale yellow, Y = yellow or dark yellow, Z = greenish yellow.

Optical Characteristics

Relief in Thin Section: High positive.

Optic Orientation: $X = b$, $Y \wedge a = +7°$ to $+24°$, $Z \wedge c = +7°$ to $-10°$, optic plane $\perp$ (010). The extinction angle seen in (010) sections is less than 10° to the trace of {100} cleavage, which is length slow. Fragments on the {100} cleavage show parallel extinction to the trace of {010} cleavage if displayed.

Indices of Refraction and Birefringence: Indices of refraction generally increase with Th content and decrease with alteration. Interference colors in standard thin section range up to third and fourth orders. Fragments on the {100} cleavage display maximum birefringence.

Interference Figure: Basal sections yield nearly centered acute bisectrix figures with small $2V$ and numerous isochromes. Optic axis dispersion is weak, $r < v$, or rarely $r > v$. Horizontal bisectrix dispersion is weak.

Alteration Monazite is relatively stable in the weathering environment. Alteration to a brown limonite-like material along cleavages and grain margins may occur, and some grains are clouded by fine opaque particles.

Distinguishing Features

Hand Sample: Specimens large enough to be seen in hand sample are uncommon. Monazite is distinguished from zircon by different crystal habit and lower hardness, and from titanite by greater specific gravity. X-ray diffraction or chemical analysis are usually required on small grains to confirm identity.

Thin Section/Grain Mount: Recognized by high birefringence, high relief in thin section, and pale yellow color. Staurolite is more distinctly pleochroic and has much lower birefringence. Small grains may resemble zircon, titanite, xenotime, or members of the epidote group. Zircon is uniaxial and not usually colored. Epidote has larger $2V$ and birefringence is often lower. Titanite is more strongly colored, has larger $2V$, and extreme optic axis dispersion. Xenotime has higher birefringence and is uniaxial. Because monazite contains radioactive elements, it may produce pleochroic halos in enclosing biotite, hornblende, cordierite, or other minerals, but so may zircon, titanite, xenotime, and allanite. Backscatter images or X-ray maps obtained by an electron microprobe or an SEM can be used to locate the very small grains that may be present in some samples, and is often the only practical means of locating and identifying all small accessory mineral grains.

DO NOT COPY e48d507df5d1141@placeholder.9409

Printed by: e48d507df5d1141@placeholder.94092.edu. Printing is for personal, private use only. No part of this book may be reproduced or transmitted without publisher's prior permission. Violators will be prosecuted.

Occurrence Monazite is an accessory mineral in granite, granitic pegmatite, syenite, and carbonatites. Because it is stable in the weathering environment, monazite may be part of the heavy mineral fraction of clastic sediments. It is infrequently found in hydrothermal vein deposits. In metamorphic rocks it is found in metamorphosed dolostone and in mica schists, gneiss, and granulites.

Use Monazite is one of the primary sources for Th, Ce, and other rare earth elements. Most economic deposits are placers, usually located on beaches. Cerium is used in lighter flints, glass, automobile catalytic converters, and a variety of other products including the mantles used in gas lanterns. Thorium is also used in the mantles used in gas lanterns and has been used as a fuel in nuclear reactors. Thorium also has a variety of applications in electronic equipment. Cerium oxide is used as an abrasive to polish glass and can be used to remove the fine scratches left by windshield wipers on automobile windshields.

Because monazite typically contains radioactive elements, it has become an attractive target for radiometric dating, both by traditional U–Pb isotopic analysis (see Box 5.1) but also by chemical analysis with an electron microprobe (Allaz et al., 2020). Electron microprobe dating is possible because most monazite contains no Pb upon crystallization. For a review of the issues associated with monazite geochronologic studies, consult Catlos (2013).

Xenotime

$$YPO_4$$

$$\text{Tetragonal } 4/m\,2/m\,2/m$$

$$a = 6.89\ \text{Å},\ c = 6.03\ \text{Å},\ Z = 4$$

$$H = 4 - 5$$

$$G = 4.3 - 5.1\ (4.28\ \text{calc. for pure } YPO_4)$$

$$\text{Uniaxial } (+)$$

$$n_\omega = 1.690 - 1.724$$

$$n_\epsilon = 1.760 - 1.827$$

$$\delta = 0.070 - 0.107$$

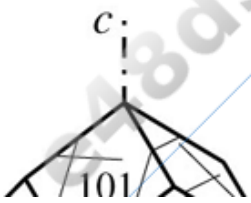

DO NOT COPY
e48d507df5d1141@placeholder.9409

Printed by: e48d507df5d1141@placeholder.94092.edu. Printing is for personal, private use only. No part of this book may be reproduced or transmitted without publisher's prior permission. Violators will be prosecuted.

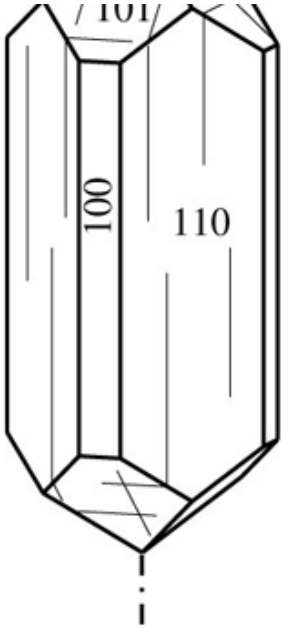

Structure The structure consists of PO_4^{3-} tetrahedra bonded through Y^{3+} (yttrium) in strongly distorted 8-fold coordination with oxygen anions from the tetrahedra. Xenotime is isostructural with zircon.

Composition Rare earth elements, particularly the heavy rare earth elements (Gd through Lu), may substitute for Y along with small amounts of Ca, Zr, Th, or U. P^{5+} may be replaced by Si^{4+} to a limited extent to maintain charge balance when Zr^{4+} or U^{4+} substitutes for Y^{3+}.

Form and Twinning Crystals are elongate tetragonal prisms resembling zircon; also found as radial aggregates or rosettes. Detrital grains are usually elongate and somewhat rounded.

Cleavage Good prismatic cleavages on {110} intersect at 90° but tend not to have a strong control on fragment orientation. Uneven to splintery fracture. Brittle.

Color Properties

Luster: Vitreous to resinous.

Color: Yellowish to reddish brown, less commonly yellow, gray, salmon pink, or shades of green.

Streak: Pale brown, or shades of yellow or red.

Color in Thin Section: Colorless, yellow, or pale brown.

Pleochroism: Weak, ω = pale pink, yellowish brown, or yellow; ϵ = pale brownish yellow, grayish brown, or greenish. Grains are darker with their long dimension parallel to the vibration direction of the lower polarizer.

DO NOT COPY
e48d507df5d1141@placeholder.9409

Printed by: e48d507df5d1141@placeholder.94092.edu. Printing is for personal, private use only. No part of this book may be reproduced or transmitted without publisher's prior permission. Violators will be prosecuted.

Optical Characteristics

Relief in Thin Section: High positive.

Optic Orientation: Parallel extinction to crystal length and cleavage traces in longitudinal sections.

Indices of Refraction and Birefringence: Indices of refraction probably increase with substitution of Th for Y. Birefringence is very strong and yields high-order creamy white colors in standard thin section. Interference colors may be masked by mineral color.

Interference Figure: Small grain size may make interference figures difficult to obtain. Basal sections yield uniaxial positive figures with numerous isochromes.

Alteration Xenotime is not readily altered.

Distinguishing Features

Hand Sample: Closely resembles zircon but has inferior hardness and cleavage at right angles.

Thin Section/Grain Mount: Small grains in thin section may be difficult to distinguish from zircon, monazite, titanite, and rutile. Zircon has higher indices of refraction and lower birefringence. Monazite is biaxial and has inclined extinction, higher relief, lower birefringence, and a different habit. Titanite has a different habit, is biaxial, and has higher relief. Rutile has higher relief and is darker colored. Indices of refraction measured in grain mount will generally resolve ambiguities: zircon, monazite, titanite, and rutile all have higher indices of refraction. An electron microprobe or scanning electron microscope may be required to identify small grains.

Occurrence Xenotime is a fairly common accessory mineral in granite, granodiorite, syenite, granitic pegmatite, and related rocks. It frequently is misidentified as zircon. In metamorphic rocks it may be found in mica schists and gneiss, or, less commonly, in marble. Xenotime is found as detrital grains in placer deposits, in beach sands, and as a heavy mineral in sandstone and related clastic sedimentary rocks.

Use Placer deposits of xenotime are a source of Y. Yttrium is used to manufacture phosphors used in fluorescent lights, cathode ray tube televisions and computer monitors, light-emitting diodes (LEDs), and in zirconia ceramics. Xenotime can be dated by an electron microprobe similar to how monazite is dated (Allaz et al., 2020).

Turquoise

$$CuAl_6(PO_4)_4(OH)_8 \cdot 4H_2O$$

Triclinic $\bar{1}$

DO NOT COPY e48d507df5d1141@placeholder.9409

Printed by: e48d507df5d1141@placeholder.94092.edu. Printing is for personal, private use only. No part of this book may be reproduced or transmitted without publisher's prior permission. Violators will be prosecuted.

$$a = 7.48\ \text{Å},\ b = 9.95\ \text{Å},$$
$$c = 7.69\ \text{Å},\ \alpha = 111.6^\circ,$$
$$\beta = 115.4^\circ,\ \gamma = 69.4^\circ,\ Z = 1$$

$$H = 5 - 6$$

$$G = 2.6 - 2.8$$

$$\text{Biaxial } (+)$$

$$n_\alpha = 1.61$$

$$n_\beta = 1.62$$

$$n_\gamma = 1.65$$

$$\delta = 0.04$$

$$2V_z = 40^\circ$$

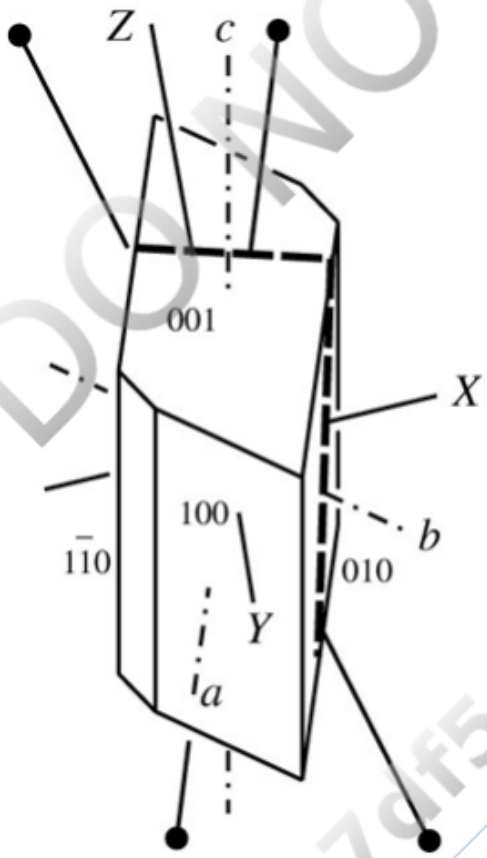

Structure Phosphate groups are linked laterally through Al in 6-fold coordination with O from the phosphate groups and additional OH. Cu occupies relatively open voids in the structure and coordinates with 4 OH and two H_2O molecules.

Composition Substitution of Fe^{3+} for Al^{3+} forms a continuous solid solution series between turquoise and chalcosiderite [$CuFe_6(PO_4)_4(OH)_8{\cdot}4H_2O$]. Most samples, however,

DO NOT COPY
e48d507df5d1141@placeholder.9409

Printed by: e48d507df5d1141@placeholder.94092.edu. Printing is for personal, private use only. No part of this book may be reproduced or transmitted without publisher's prior permission. Violators will be prosecuted.

are near the turquoise end of the series.

Form and Twinning Usually fine grained and massive, filling veins or forming reniform, stalactitic, or encrusting forms. Also as disseminated grains.

Cleavage Perfect {001} and good {010} cleavage is rarely seen because of fine grain size. Conchoidal to smooth fracture on massive material. Brittle.

Color Properties

Luster: Waxy on fractured surfaces, vitreous if polished.

Color: Turquoise-green, also sky-blue, apple-green, or greenish gray.

Streak: White or greenish white.

Color in Thin Section: Pale blue or green.

Pleochroism: $X \sim$ colorless, $Z =$ pale blue to pale green.

Optical Characteristics

Relief in Thin Section: Moderately positive.

Optic Orientation: $X \wedge b = 50°$, $Y \wedge a = 41°$, $Z \wedge c = 32°$.

Indices of Refraction and Birefringence: Indices of refraction probably increase with Fe content, but are not documented.

Interference Figure: Fine grain size will generally preclude obtaining interference figures. $2V_Z$ is reported as 40° with strong optic axis dispersion, $r < v$.

Alteration Being produced in Cu-bearing hydrothermal systems, turquoise is subject to replacement by other minerals as part of normal dissolution/precipitation processes.

Distinguishing Features

Hand Sample: The blue-green color is distinctive. Chrysocolla is similar but is softer (2–4) and has the property of adhering to the tongue when touched gently.

Thin Section/Grain Mount: Color and occurrence are distinctive. Chrysocolla has lower indices of refraction.

Occurrence Turquoise is found in hydrothermally altered volcanic rocks, usually related to copper mineralization.

Use Turquoise is used as a decorative stone in jewelry and in a wide variety of other art and craft objects. Material of inferior quality may be stabilized with epoxy or have the color artificially enhanced. Imitation turquoise exists and is made of almost anything with an appropriate color. Given its use as a gemstone, it is perhaps surprising that turquoise

DO NOT COPY e48d507df5d1141@placeholder.9409

Printed by: e48d507df5d1141@placeholder.94092.edu. Printing is for personal, private use only. No part of this book may be reproduced or transmitted without publisher's prior permission. Violators will be prosecuted.

Tungstates and Molybdates

Both W and Mo cations have a +6 charge in the tungstate and molybdate minerals. Both the tungstate and molybdate anionic groups consist of four oxygens that form a tetrahedral coordination site for W or Mo. However, both W^{6+} and Mo^{6+}, at 0.56 and 0.55 Å, respectively, are somewhat large for a normal tetrahedral site, so the four oxygen anions do not form a regular tetrahedron. Because the W and Mo cations have a high charge, they command more than half of the available anion charge. Tungstates and molybdates are anisodesmic (Chapter 4) and the WO_4^{2-} and MoO_4^{2-} tetrahedra form discrete anionic groups in mineral structures.

The more common tungstate and molybdate minerals are listed in Table 17.6, and crystal habit is shown in Figure 17.19. Because W^{6+} and Mo^{6+} have the same charge and similar size, they may substitute for each other in some minerals. Scheelite forms a solid solution series with powellite ($CaMoO_4$), and wulfenite forms a solid solution series with stolzite ($PbWO_4$).

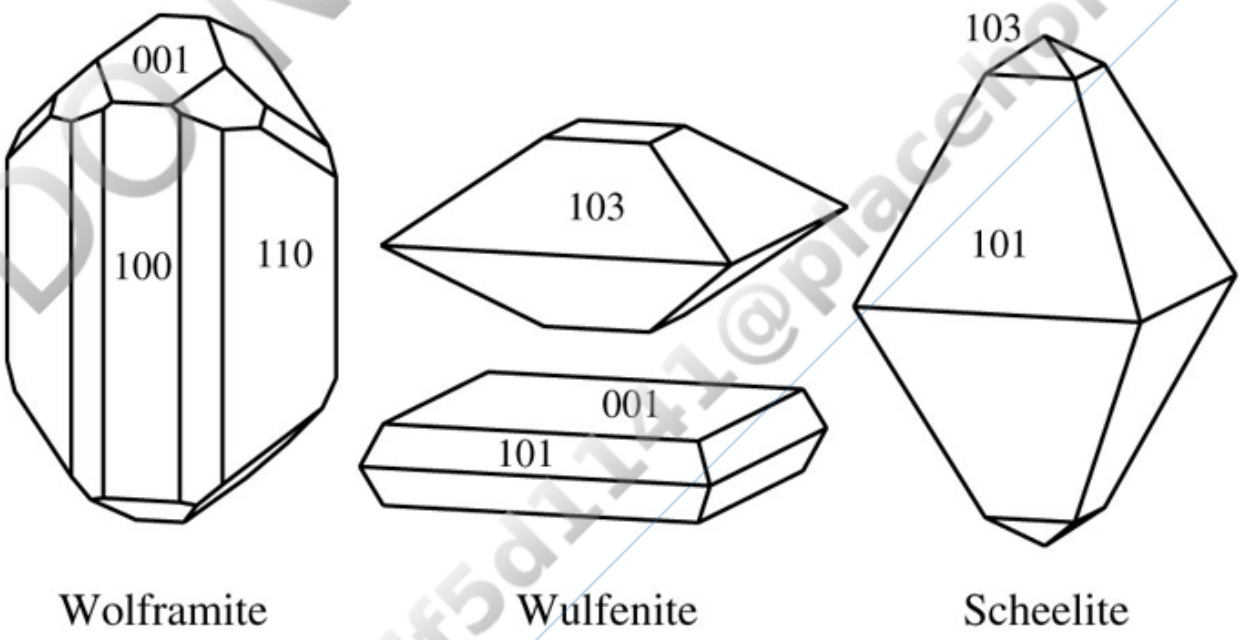

FIGURE 17.19 Crystal habit of wolframite, wulfenite, and scheelite. View larger image

TABLE 17.6 Tungstates and Molybdates

Mineral	Unit Cell	Physical Properties[a]	Optical Properties	Comments
Scheelite $CaWO_4$	Tetragonal $4/m$	*H*: 4.5–5 *G*: 5.9–6.1	$n_\omega = 1.921$ $n_\epsilon = 1.938$	Crystals usually elongate tetragonal dipyramids; commonly massive granular or columnar; found in skarn

DO NOT COPY e48d507df5d1141@placeholder.94092

Printed by: e48d507df5d1141@placeholder.94092.edu. Printing is for personal, private use only. No part of this book may be reproduced or transmitted without publisher's prior permission. Violators will be prosecuted.

	$a = 1.92$ $c = 1.94$ $Z = 4$	G: 5.9–6.1 Cl: {101}g Tw: {110} contact and penetration C: White, yellowish, or brownish St: White L: Vitreous Fluoresces bluish white in short-wave UV light	$n_\epsilon = 1.938$ $\delta = 0.017$ Uniaxial (+) Colorless	granular or columnar; found in skarn deposits formed by contact metamorphism of limestone adjacent to granitic intrusive; also hydrothermal veins; an important ore mineral for tungsten
Wolframite $(Fe,Mn)WO_4$	Monoclinic $2/m$ $a = 4.77$ $b = 5.71$ $c = 4.98$ $\beta = 90.5°$ $Z = 2$ $X = b$, $Z \wedge c = 17°$ to $21°$	H: 4–4.5 G: 7.1–7.5 Cl: {010}pf Tw: Common {100} contact C: Brownish black to iron-black St: Reddish brown to brownish black L: Submetallic	$n_\alpha = 2.17–2.31$ $n_\beta = 2.22–2.40$ $n_\gamma = 2.30–2.46$ $\delta = 0.13–0.15$ Biaxial (+) $2V = 73–79°$ X = Yellow, orange; Y = Greenish yellow, red-brown; Z = Olive, dark red-brown	Crystals common: short prismatic parallel to c and flattened on {100}; also granular massive, columnar, or lamellar; found in granitic pegmatites and hydrothermal veins
Wulfenite $PbMoO_4$	Tetragonal 4 $a = 5.44$ $c = 12.11$ $Z = 4$	H: 3 G: 6.5–7.0 Cl: {010}g Tw: {001} C: Yellow, orange, or red; also gray or white	$n_\omega = 2.405$ $n_\epsilon = 2.283$ $\delta = 0.122$ Uniaxial (−) Yellow to pale orange, $\omega > \epsilon$	Crystals tabular on {001}, often very thin, less commonly pyramidal or dipyramidal if twinned; found in the near-surface oxidized portion of Pb- and Mo-bearing hydrothermal sulfide deposits

DO NOT COPY
e48d507df5d1141@placeholder.9409-

Printed by: e48d507df5d1141@placeholder.94092.edu. Printing is for personal, private use only. No part of this book may be reproduced or transmitted without publisher's prior permission. Violators will be prosecuted.

		white St: White L: Vitreous to adamantine		

[a] Cl = cleavage (pf = perfect, g = good), Tw = twinning, C = color, St = streak, L = luster.

Wolframite displays continuous solid solution between the hübnerite ($MnWO_4$) and ferberite ($FeWO_4$) end members. Members of the solid solution series are generally restricted to high-temperature hydrothermal vein systems in association with sulfides (pyrrhotite, pyrite, sphalerite, arsenopyrite), cassiterite, scheelite, topaz, magnetite, and/or hematite, or in quartz or pegmatitic vein systems closely associated with granitic intrusive rocks.

Scheelite may be found in carbonate rocks that have been contact metamorphosed by intrusive granitic rocks. Associated minerals include carbonates, diopside, garnet, tremolite, wollastonite, and other calc-silicate minerals. Scheelite also is found, often with wolframite, in high-temperature, quartz-rich hydrothermal vein systems that typically are closely associated with granitic intrusions. Other associated minerals include topaz, fluorite, albite, sulfides (pyrite, pyrrhotite, molybdenite, chalcopyrite, etc.), tourmaline, and apatite.

Wolframite and scheelite together are the principal source for the world's tungsten. This important element is alloyed with iron to make high-strength steel. The filament in conventional incandescent light bulbs is metallic tungsten. Tungsten carbide, whose hardness is exceeded only by diamond, is used to make durable cutting tools for many industrial applications and is also used as an abrasive.

Wulfenite commonly forms eye-catching tabular crystals in the near-surface oxidized zone of Pb-bearing hydrothermal sulfide deposits. It has been used as a minor source of molybdenum, which is used as an alloying agent in high-strength steel and in lubricants.

DO NOT COPY
e48d507df5d1141@placeholder.9409

Printed by: e48d507df5d1141@placeholder.94092.edu. Printing is for personal, private use only. No part of this book may be reproduced or transmitted without publisher's prior permission. Violators will be prosecuted.

Borates

The most common building block of the borates is the triangular BO_3^{3-} group. Each B^{3+} commands one of the available two negative charges on each O. That means that the borates are mesodesmic (Chapter 4); each oxygen may be shared with another borate group to form doublets, chains, rings, and so forth, similar to the silicates. B^{3+} may also form triangular $BO_2(OH)^{2-}$ groups, as in borax. Additional structural elements found in borates are tetrahedral BO_4^{5-}, BO_3OH^{4-}, and $BO_2(OH)_2^{3-}$ groups. The triangular and tetrahedral groups can be linked together to form a variety of complex structures.

The borate minerals are, with few exceptions, found in evaporite deposits from playas and saline lakes (Box 17.2). Boron-containing deposits are typically formed in tectonically active terranes associated with plate boundaries and abundant volcanism. Because boron does not fit in the structure of common igneous silicate minerals (tourmaline is not considered a common igneous silicate mineral), it is concentrated in late residual magmatic liquids. Thermal springs and other hydrothermal waters associated with the volcanism presumably carry the boron from these late magmatic liquids to the surface.

Precipitation of borate minerals may be in an apron adjacent to a hot spring or on playa lake beds in response to seasonal evaporation. Borate minerals are typically interbedded with lacustrine sediment and volcanic ash, and may grade laterally into shallow-water lacustrine limestone. Because borate minerals are fairly water soluble, they are not found in wet climates. Notable occurrences include the arid intermontane valleys in southeastern California, Tibet, and Turkey, and in the Andes mountains of Peru, Bolivia, Argentina, and Chile.

Of the 150 or so borates that have been identified, borax, ulexite, colemanite, kernite, and tincalconite are the most common; their properties are listed in Table 17.7. Crystal habits of borax and colemanite are shown in Figure 17.20. Minerals that may be associated with borates in playa and saline lake evaporite deposits include halite, sylvite, gypsum, anhydrite, trona, nahcolite, thenardite, glauberite, polyhalite, and kieserite.

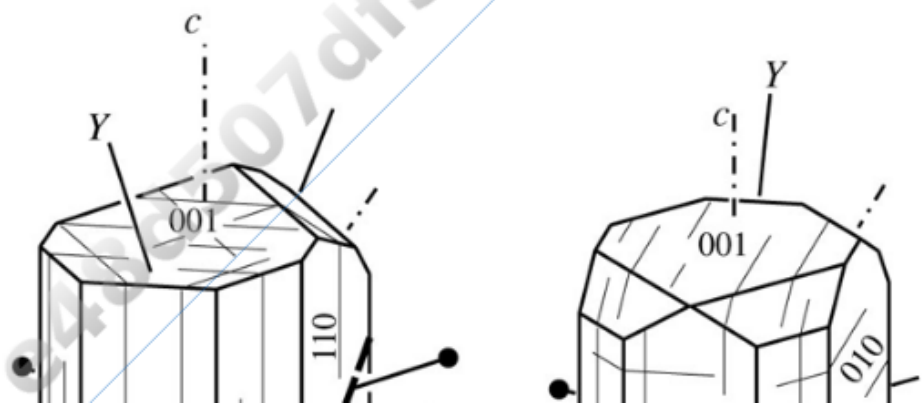

DO NOT COPY

Printed by: e48d507df5d1141@placeholder.94092.edu. Printing is for personal, private use only. No part of this book may be reproduced or transmitted without publisher's prior permission. Violators will be prosecuted.

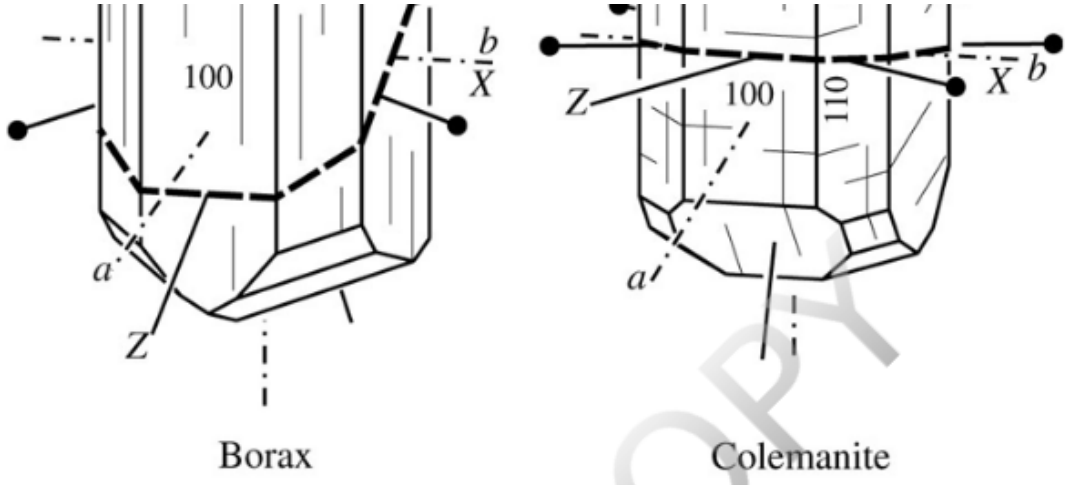

FIGURE 17.20 Crystal habit of borax and colemanite. View larger image

TABLE 17.7 Borate Minerals

Mineral	Unit Cell	Physical Properties[a]	Optical Properties	Comments
Borax $Na_2[BO(OH)]_2[BO_2(OH)]_2{\cdot}8H_2O$	Monoclinic 2/*m* $a = 11.86$ $b = 10.67$ $c = 12.20$ $\beta = 106.6°$ $Z = 4$ $Y \wedge c =$ +33° to 36°, $X = b$	*H*: 2–2.5 *G*: 1.71 Cl: {l00}pf, {110}g Tw: {100} rare C: White or gray, may be greenish or bluish St: White L: Vitreous	$n_\alpha = 1.447$ $n_\beta = 1.469$ $n_\gamma = 1.472$ $\delta = 0.025$ Biaxial (−) $2V = 39–40°$ $r > v$, strong Colorless	Soluble in water, slightly alkaline taste; crystals stubby prisms with 8-sided cross sections; commonly as granular aggregates; found in saline lake and playa evaporite deposits; readily alters by dehydration to crumbly tincalconite on exposure to air
Colemanite $Ca_2B_6O_{11}{\cdot}5H_2O$	Monoclinic 2/m $a = 8.74$ $b = 11.26$ $c = 6.10$ $\beta = 110.1°$ $Z = 2$ $Y \wedge c =$ −6°, $X = b$	*H*: 4–4.5 *G*: 2.42 Cl: {010}pf, {100}g Tw: None reported C: White, colorless, gray, or yellowish St: White	$n_\alpha = 1.586$ $n_\beta = 1.592$ $n_\gamma = 1.614$ $\delta = 0.028$ Biaxial (+) $2V = 56°$ $r < v$, weak Colorless	Decrepitates (breaks up and makes noise) with heating; crystals stubby prisms; common as granular or cleavable masses; found in evaporite deposits from playas and saline lakes

DO NOT COPY
e48d507df5d1141@placeholder.9409

Printed by: e48d507df5d1141@placeholder.94092.edu. Printing is for personal, private use only. No part of this book may be reproduced or transmitted without publisher's prior permission. Violators will be prosecuted.

		St: White L: Vitreous		
Kernite $Na_2B_4O_6(OH)_2{\cdot}3H_2O$	Monoclinic $2/m$ $a = 15.52$ $b = 9.14$ $c = 6.96$ $\beta = 108.9°$ $Z = 4$ $X \wedge a = +38°$ $Y \wedge c = -19°$, $Z = b$	H: 2.5–3 G: 1.91–1.93 Cl: {100}, {001}pf $\{\bar{2}01\}$ fair Tw: {110} Cl: White St: White L: Vitreous, alters to earthy tincalconite	$n_\alpha = 1.455$ $n_\beta = 1.472$ $n_\gamma = 1.487$ $\delta = 0.032$ Biaxial (−) $2V = 80°$ $r > v$, distinct Colorless	Crystals nearly equant; common as granular masses; may appear fibrous because of intersecting perfect cleavages; found in evaporite deposits from playas and saline lakes
Tincalconite $Na_2B_4O_5(OH)_4{\cdot}3H_2O$	Hexagonal 32 $a = 11.12$ $c = 21.20$ $Z = 6$	H: ?? Soft G: 1.88 Cl: ?? Tw: ?? C: White St: White L: Earthy	$n_\omega = 1.461$ $n_\epsilon = 1.473$ $\delta = 0.013$ Uniaxial (+) Colorless	Forms as an earthy dehydration product on other borates; found in evaporite deposits from playas and saline lakes
Ulexite $NaCaB_5O_6{\cdot}5H_2O$	Triclinic $\bar{1}$ $a = 8.71$ $b = 12.72$ $c = 6.69$ $\alpha = 90.3°$, $\beta = 109.1°$, $\gamma = 105.1°$ $Z = 2$ $X \wedge c = -69°$, $Y \wedge c = +21°$, $Z \sim b$	H: 2.5 G: 1.96 Cl: {010}pf, $\{1\bar{1}0\}$g, {110}pr Tw: {010}, {100} polysynthetic C: White, colorless St: White L: Vitreous, aggregates may be silky	$n_\alpha = 1.491–1.496$ $n_\beta = 1.504–1.506$ $n_\gamma = 1.519–1.520$ $\delta = 0.026$ Biaxial (+) $2V = 73–78°$ Colorless	Crystals are acicular to fibrous parallel to c; may form nodular masses, crusts, compact veins, or loose “cotton balls”; found in evaporite deposits from playas and saline lakes

DO NOT COPY
e48d507df5d1141@placeholder.9409-

Printed by: e48d507df5d1141@placeholder.94092.edu. Printing is for personal, private use only. No part of this book may be reproduced or transmitted without publisher's prior permission. Violators will be prosecuted.

[a] Cl = cleavage (pf = perfect, g = good pr = poor), Tw = twinning, C = color, St = streak, L = luster, ?? = unknown.

Borax, ulexite, and colemanite are the principal sources of boron, which has a variety of industrial uses. The largest use is in the manufacture of glass fiber insulation and borosilicate glass (Pyrex® glassware). Borates are also used in detergents and soap (e.g., Boraxo® brand hand soap), as a flux in metallurgical processes, and in ceramics and wood preservatives. The ^{10}B isotope is a good neutron absorber, so boron is used in nuclear reactor shielding. Borate minerals have been used in the past as antiseptics and food preservatives. Boron currently finds use in a wide range of products including pharmaceuticals, cosmetics, insecticides, and adhesives. Boron carbide is an excellent abrasive. A relatively new application is boron-fiber-reinforced plastic, which is used in aerospace applications to form high-strength panels, structural members, and wing and fuselage surfaces.

DO NOT COPY
e48d507df5d1141@placeholder.9409

Printed by: e48d507df5d1141@placeholder.94092.edu. Printing is for personal, private use only. No part of this book may be reproduced or transmitted without publisher's prior permission. Violators will be prosecuted.

springs and other hydrothermal waters associated with the volcanism presumably carry the boron from these late magmatic liquids to the surface.
Precipitation of borate minerals may be in an apron adjacent to a hot spring or on playa lake beds in response to seasonal evaporation. Borate minerals are typically interbedded with lacustrine sediment and volcanic ash, and may grade laterally into shallow-water lacustrine limestone. Because borate minerals are fairly water soluble, they are not found in wet climates. Notable occurrences include the arid intermontane valleys in southeastern California, Tibet, and Turkey, and in the Andes mountains of Peru, Bolivia, Argentina, and Chile.

Of the 150 or so borates that have been identified, borax, ulexite, colemanite, kernite, and tincalconite are the most common; their properties are listed in Table 17.7. Crystal habits of borax and colemanite are shown in Figure 17.20. Minerals that may be associated with borates in playa and saline lake evaporite deposits include halite, sylvite, gypsum, anhydrite, trona, nahcolite, thenardite, glauberite, polyhalite, and kieserite.

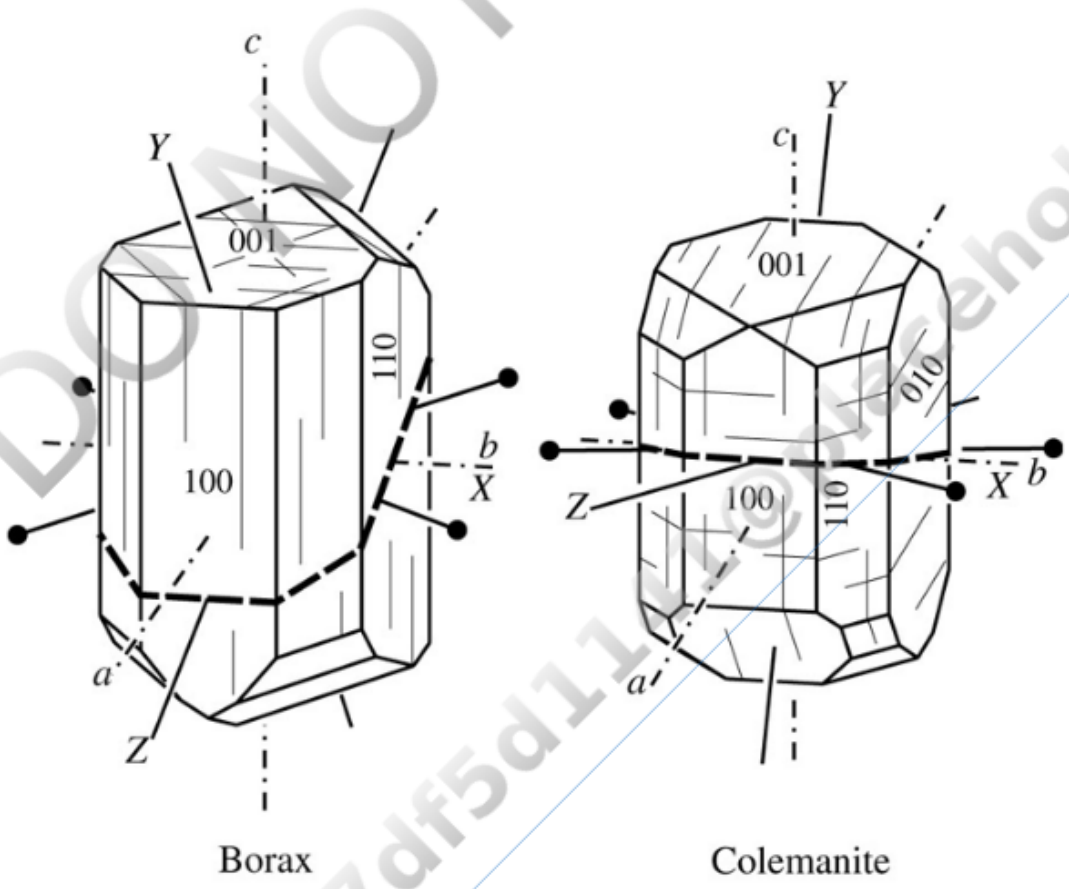

FIGURE 17.20 Crystal habit of borax and colemanite. View larger image

TABLE 17.7 Borate Minerals

Mineral	Unit Cell	Physical Properties[a]	Optical Properties	Comments
Borax	Monoclinic	*H*: 2–2.5	$n_\alpha = 1.447$	Soluble in water.

DO NOT COPY e48d507df5d1141@placeholder.9409

Printed by: e48d507df5d1141@placeholder.94092.edu. Printing is for personal, private use only. No part of this book may be reproduced or transmitted without publisher's prior permission. Violators will be prosecuted.

Borax $Na_2[BO(OH)]_2[BO_2(OH)]_2{\cdot}8H_2O$	Monoclinic $2/m$ $a = 11.86$ $b = 10.67$ $c = 12.20$ $\beta = 106.6°$ $Z = 4$ $Y \wedge c =$ +33° to 36°, $X = b$	H: 2–2.5 G: 1.71 Cl: {l00}pf, {110}g Tw: {100} rare C: White or gray, may be greenish or bluish St: White L: Vitreous	$n_\alpha = 1.447$ $n_\beta = 1.469$ $n_\gamma = 1.472$ $\delta = 0.025$ Biaxial (−) $2V = 39–40°$ $r > v$, strong Colorless	Soluble in water, slightly alkaline taste; crystals stubby prisms with 8-sided cross sections; commonly as granular aggregates; found in saline lake and playa evaporite deposits; readily alters by dehydration to crumbly tincalconite on exposure to air
Colemanite $Ca_2B_6O_{11}{\cdot}5H_2O$	Monoclinic 2/m $a = 8.74$ $b = 11.26$ $c = 6.10$ $\beta = 110.1°$ $Z = 2$ $Y \wedge c =$ −6°, $X = b$	H: 4–4.5 G: 2.42 Cl: {010}pf, {100}g Tw: None reported C: White, colorless, gray, or yellowish St: White L: Vitreous	$n_\alpha = 1.586$ $n_\beta = 1.592$ $n_\gamma = 1.614$ $\delta = 0.028$ Biaxial (+) $2V = 56°$ $r < v$, weak Colorless	Decrepitates (breaks up and makes noise) with heating; crystals stubby prisms; common as granular or cleavable masses; found in evaporite deposits from playas and saline lakes
Kernite $Na_2B_4O_6(OH)_2{\cdot}3H_2O$	Monoclinic $2/m$ $a = 15.52$ $b = 9.14$ $c = 6.96$ $\beta = 108.9°$ $Z = 4$ $X \wedge a =$ +38° $Y \wedge c =$ −19°, $Z = b$	H: 2.5–3 G: 1.91–1.93 Cl: {100}, {001}pf $\{201\}$ fair Tw: {110} Cl: White St: White L: Vitreous, alters to earthy tincalconite	$n_\alpha = 1.455$ $n_\beta = 1.472$ $n_\gamma = 1.487$ $\delta = 0.032$ Biaxial (−) $2V = 80°$ $r > v$, distinct Colorless	Crystals nearly equant; common as granular masses; may appear fibrous because of intersecting perfect cleavages; found in evaporite deposits from playas and saline lakes
Tincalconite	Hexagonal	H: ?? Soft	$n_\omega = 1.461$	Forms as an earthy

DO NOT COPY
e48d507df5d1141@placeholder.9409-

Printed by: e48d507df5d1141@placeholder.94092.edu. Printing is for personal, private use only. No part of this book may be reproduced or transmitted without publisher's prior permission. Violators will be prosecuted.

$Na_2B_4O_5(OH)_4 \cdot 3H_2O$	32 $a = 11.12$ $c = 21.20$ $Z = 6$	G: 1.88 Cl: ?? Tw: ?? C: White St: White L: Earthy	$n_\epsilon = 1.473$ $\delta = 0.013$ Uniaxial (+) Colorless	dehydration product on other borates; found in evaporite deposits from playas and saline lakes
Ulexite $NaCaB_5O_6 \cdot 5H_2O$	Triclinic $\bar{1}$ $a = 8.71$ $b = 12.72$ $c = 6.69$ $\alpha = 90.3°$, $\beta = 109.1°$, $\gamma = 105.1°$ $Z = 2$ $X \wedge c = -69°$, $Y \wedge c = +21°$, $Z \sim b$	H: 2.5 G: 1.96 Cl: {010}pf, $\{1\,\bar{1}0\}$g, {110}pr Tw: {010}, {100} polysynthetic C: White, colorless St: White L: Vitreous, aggregates may be silky	$n_\alpha = 1.491–1.496$ $n_\beta = 1.504–1.506$ $n_\gamma = 1.519–1.520$ $\delta = 0.026$ Biaxial (+) $2V = 73–78°$ Colorless	Crystals are acicular to fibrous parallel to c; may form nodular masses, crusts, compact veins, or loose “cotton balls”; found in evaporite deposits from playas and saline lakes

[a] Cl = cleavage (pf = perfect, g = good pr = poor), Tw = twinning, C = color, St = streak, L = luster, ?? = unknown.

Borax, ulexite, and colemanite are the principal sources of boron, which has a variety of industrial uses. The largest use is in the manufacture of glass fiber insulation and borosilicate glass (Pyrex® glassware). Borates are also used in detergents and soap (e.g., Boraxo® brand hand soap), as a flux in metallurgical processes, and in ceramics and wood preservatives. The ^{10}B isotope is a good neutron absorber, so boron is used in nuclear reactor shielding. Borate minerals have been used in the past as antiseptics and food preservatives. Boron currently finds use in a wide range of products including pharmaceuticals, cosmetics, insecticides, and adhesives. Boron carbide is an excellent abrasive. A relatively new application is boron-fiber-reinforced plastic, which is used in aerospace applications to form high-strength panels, structural members, and wing and fuselage surfaces.

REFERENCES CITED AND SUGGESTIONS FOR ADDITIONAL

DO NOT COPY

Printed by: e48d507df5d1141@placeholder.94092.edu. Printing is for personal, private use only. No part of this book may be reproduced or transmitted without publisher's prior permission. Violators will be prosecuted.

READING

Allaz, J. M., Jercinovic, M. J., and Williams, M. L. 2020. U-Th-Pb_{total} dating of REE-phosphate by electron microprobe: Review and progress. *IOP Conference Series: Materials Science and Engineering* **891**, 1–22.

Alpers, C. N., Jambor, J. L., and Nordstrom, D. K. (eds.). 2000. *Sulfate Minerals—Crystallography, Geochemistry, and Environmental Significance. Reviews in Mineralogy & Geochemistry* **40**, 608 p.

Carlson, W. D. 1980. The calcite–aragonite equilibrium: Effects of Sr substitution and anion orientation disorder. *American Mineralogist* **65**, 1252–1262.

Catlos, E. J., 2013. Generalizations about monazite: Implications for geochronologic studies. *American Mineralogist* **98**, 819–823.

Chang, L. L. Y., Howie, R. A., and Zussman, J. 1996. *Rock-Forming Minerals, Volume 5B: Nonsilicates: Sulfates, Carbonates, Phosphates, Halides*, 2nd ed. The Geological Society, London, 383 p.

Chew, D. M., and Spikings, R. A. 2015. Geochronology and thermochronology using apatite: Time and temperature, lower crust to surface. *Elements* **11**, 189–194.

Friedman, G. M. 1959. Identification of carbonate minerals by staining methods. *Journal of Sedimentary Petrology* **29**, 87–97.

Hardie, L. A. 1967. The gypsum–anhydrite equilibrium at one atmosphere pressure. *American Mineralogist* **52**, 171–200.

Hughes, J. M., 2015. The many facets of apatite. *American Mineralogist* **100**, 1033–1039.

Hughes, J. M., and Rakovan, J. F. 2015. Structurally robust, chemically diverse: Apatite and apatite supergroup minerals. *Elements* **11**, 165–170.

Kennedy, G. C. 1947. Charts for correlation of optical properties with chemical composition of some common rock-forming minerals. *American Mineralogist* **32**, 561–573.

Nasdala, L., Akhmadaliev, S., Burakov, B. E., Chanmuang N. C., and Škoda, R. 2020. The absence of metamictisation in natural monazite. *Scientific Reports* **10**, 14676.

Pasero, M., Kampf, A. R., Ferraris, C., Pekov, I. V., Rakovan, J., and White T. J. 2010. Nomenclature of the apatite supergroup minerals. *European Journal of Mineralogy* **22**, 163–179.

Ravikumar, D., Zhang, D., Keoleian, G., Miller, S., Sick, V., and Li, V. 2021. Carbon dioxide utilization in concrete curing or mixing might not produce a net climate benefit. *Nature Communications* **12**, No. 855, 1–13.

Reeder, R. J. (ed.). 1983. Carbonates: Mineralogy and Chemistry. *Reviews in Mineralogy* **11**, 394 p.

Robbins, L. L., and Blackwelder, P. L. 1992. Biochemical and ultrastructural evidence

DO NOT COPY e48d507df5d1141@placeholder.94092

Printed by: e48d507df5d1141@placeholder.94092.edu. Printing is for personal, private use only. No part of this book may be reproduced or transmitted without publisher's prior permission. Violators will be prosecuted.

Robbins, L. L., and Blackwelder, P. L. 1992. Biochemical and ultrastructural evidence for the origin of whitings: A biologically-induced calcium carbonate precipitation mechanism. *Geology* **20**, 464–468.

Rodriguez-Blanco, J. D., Shaw, S., and Benning, L. G. 2015. A route for the direct crystallization of dolomite. *American Mineralogist* **100**, 1172–1181.

Sánchez-Román, M., Vasconcelos, C., Schmid, T., Dittrich, M., McKenzie, J. A., Zenobi, R., and Rivadeneyra, M. A. 2008. Aerobic microbial dolomite at the nanometer scale: Implications for the geologic record. *Geology* **36**, 879–882.

Spencer, R. J. 2000. Sulfate minerals in evaporite deposits. *Reviews in Mineralogy & Geochemistry* **40**, 173–192.

DO NOT COPY

e48d507df5d1141@placeholder.9409

Printed by: e48d507df5d1141@placeholder.94092.edu. Printing is for personal, private use only. No part of this book may be reproduced or transmitted without publisher's prior permission. Violators will be prosecuted.

LIST OF KEY TERMS

- calcination
- cleavage
- mortar
- portland cement
- quicklime
- rhombohedral carbonate

DO NOT COPY
e48d507df5d1141@placeholder.9409

Printed by: e48d507df5d1141@placeholder.94092.edu. Printing is for personal, private use only. No part of this book may be reproduced or transmitted without publisher's prior permission. Violators will be prosecuted.

CHAPTER 18

Oxides, Hydroxides, and Halides

William D. Nesse
University of Northern Colorado

Graham B. Baird
University of Northern Colorado

DO NOT COPY
e48d507df5d1141@placeholder.9409

Printed by: e48d507df5d1141@placeholder.94092.edu. Printing is for personal, private use only. No part of this book may be reproduced or transmitted without publisher's prior permission. Violators will be prosecuted.

Introduction

The minerals described in this chapter are grouped together because they are constructed with simple anions. Oxygen is the anion in the oxides, hydroxyl (OH^-) anionic groups are found in hydroxide minerals, and halogen elements (Cl^-, F^-, and Br^-) are the anions in the halides. Although it can be argued that hydroxyl groups are complex anions, they behave in crystal structures like simple anions; hence, hydroxides are described here.

DO NOT COPY
e48d507df5d1141@placeholder.9409

Printed by: e48d507df5d1141@placeholder.94092.edu. Printing is for personal, private use only. No part of this book may be reproduced or transmitted without publisher's prior permission. Violators will be prosecuted.

Oxides

The oxides as a group include compounds where cations of one or more metals are combined with oxygen. All of these minerals, except ice, are isodesmic, meaning that they do not contain anionic groups. Rather, each cation–oxygen bond takes less than half of the available −2 charge of oxygen, and the chemical bonding is dominantly ionic. Ice, however, is a molecular crystal.

Most of the minerals in the group have fairly high symmetry, reflecting the fact that their structures are usually based on a systematic packing of the oxygen anions, often in cubic or hexagonal close packing. The cations occupy tetrahedral and octahedral sites between these regularly packed anions. The oxides are conveniently grouped on the basis of the cation to oxygen ratio (Table 18.1).

TABLE 18.1 Oxide Minerals

Mineral	Composition	Mineral	Composition
X_2O		**X_2O_3**	
Cuprite	Cu_2O	Hematite	Fe_2O_3
Ice	H_2O	Corundum	$A1_2O_3$
XO		Ilmenite	$FeTiO_3$
Periclase	MgO		
Zincite	ZnO	**XO_2**	
XY_2O_4		Rutile	TiO_2
Magnetite	$FeFe_2O_4$	Cassiterite	SnO_2
Chromite	$FeCr_2O_4$	Pyrolusite	MnO_2
Spinel	$MgAl_2O_4$	Uraninite	UO_2
Chrysoberyl	$BeAl_2O_4$		

Except for ice, many of the oxide minerals described are widely distributed but are often relatively minor constituents of rocks. The abundance of silicon in most geological environments ensures that most of the oxygen is tied up in silicate minerals. Where geologic concentrations of these minerals occur, they may be mined as sources of metals.

DO NOT COPY e48d507df5d1141@placeholder.9409

Printed by: e48d507df5d1141@placeholder.94092.edu. Printing is for personal, private use only. No part of this book may be reproduced or transmitted without publisher's prior permission. Violators will be prosecuted.

X_2O Group

Cuprite

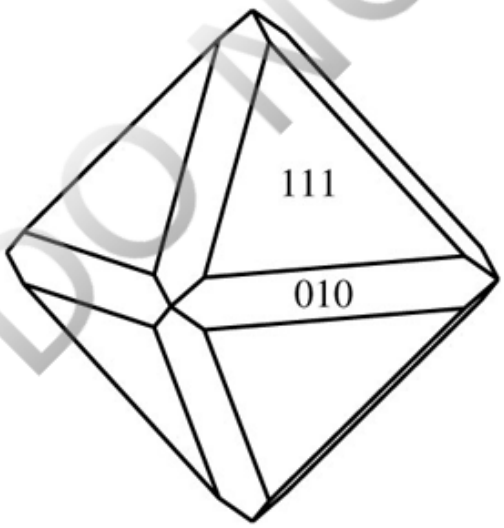

Structure The structure consists of oxygen anions in a simple body-centered cubic arrangement with Cu atoms located in the centers of four of the eight octants (equal-sized cubelets into which a larger cube may be divided; Figure 4.18). Each Cu is therefore coordinated with just two oxygen anions. This somewhat unusual geometry is favored because the bonds are fairly covalent and involve one 4*s* and one 4*p* orbital, which hybridize to form *sp* orbitals that have a linear arrangement.

Composition Most samples are probably close to the ideal composition.

Form and Twinning Crystals are octahedrons, sometimes cubes, dodecahedrons, or combinations. Commonly as massive, granular, or earthy aggregates.

Cleavage {111} fair cleavage. Conchoidal to uneven fracture. Brittle

DO NOT COPY e48d507df5d1141@placeholder.9409

Printed by: e48d507df5d1141@placeholder.94092.edu. Printing is for personal, private use only. No part of this book may be reproduced or transmitted without publisher's prior permission. Violators will be prosecuted.

Cleavage {111} fair cleavage. Conchoidal to uneven fracture. Brittle.

Color Properties

Luster: Submetallic to adamantine.

Color: Ruby-red to deep brownish red or almost black.

Streak: Brownish red.

Color in Thin Section: Red, orange-yellow, or yellow, not pleochroic.

Optical Characteristics

Relief in Thin Section: Very high positive.

Index of Refraction: Isotropic with $n = 2.849$.

Polished Section: Bluish gray. May be anomalously anisotropic with very weak bireflectance and reflection pleochroism, and strong anisotropism with crossed polarizers with blue-gray to olive-green polarization colors. Deep red internal reflections are characteristic.

Alteration Cuprite may be altered to malachite, native copper, or other copper minerals.

Distinguishing Features

Hand Sample: Deep red color is fairly distinctive. Hematite is harder (if coarsely crystalline) and has a lighter red streak. Cinnabar is softer and has a scarlet-red streak.

Thin Section/Grain Mount: Cinnabar is deep red and uniaxial, and hematite is essentially opaque.

Polished Section: Bluish gray color with red internal reflections is characteristic.

Occurrence Cuprite is found in the near-surface oxidized portion of copper-bearing hydrothermal sulfide deposits (Figure 19.3, Table 19.4). It generally is produced by altering and oxidizing primary copper sulfide minerals such as chalcopyrite. Cuprite frequently is associated with iron oxides and hydroxides (limonite), malachite, azurite, native copper, and black tenorite (CuO).

Use Cuprite is an ore mineral for copper, which is used extensively for electrical wiring. Copper also is used in a wide variety of other industrial, commercial, and household products. Copper is alloyed with tin to make bronze.

Ice

H_2O

DO NOT COPY e48d507df5d1141@placeholder.9409

Printed by: e48d507df5d1141@placeholder.94092.edu. Printing is for personal, private use only. No part of this book may be reproduced or transmitted without publisher's prior permission. Violators will be prosecuted.

$$\text{Hexagonal } 6/m\,2/m\,2/m$$

$$a = 4.498 \text{ Å}, \quad c = 7.338 \text{ Å}, \quad Z = 4$$

$$H = 1.5$$

$$G = 0.92$$

$$\text{Uniaxial } (+)$$

$$n_\omega = 1.309$$

$$n_\epsilon = 1.311$$

$$\delta = 0.002$$

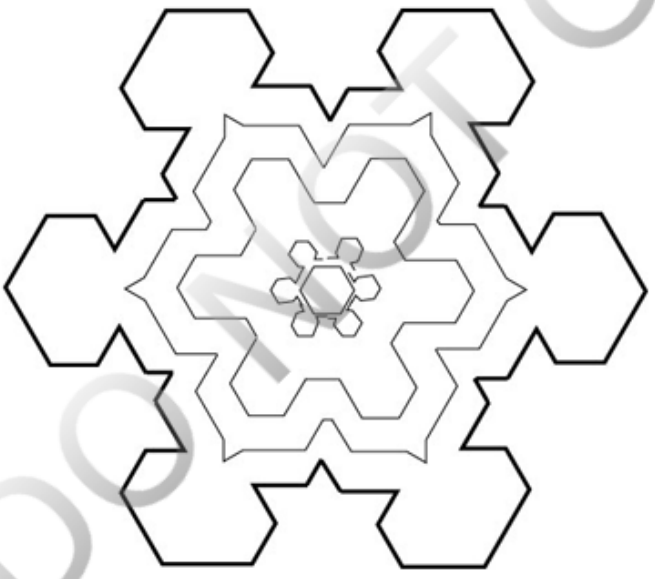

DO NOT COPY

Structure The structure of ice is unusual because ice consists of H_2O molecules that bond together with hydrogen bonds. Each electrically neutral water molecule can be treated as a sphere with a radius of 1.38 Å. The charge distribution is controlled by the location of the positively charged hydrogen nuclei that are located at two of the corners of a tetrahedron within the sphere; the other two corners have negative charge. The water molecules are arranged so that the hydrogen on one molecule points to one of the negatively charged corners of the charge tetrahedron on an adjacent water molecule to provide the hydrogen bond (Figure 18.1). The result is that each water molecule coordinates in tetrahedral fashion with four adjacent water molecules. The three-dimensional structure produced by repeating this pattern is hexagonal. The hydrogen bonding provides weak light absorption at the red end of the spectrum, so large masses of ice, such as in a glacier or iceberg, appear pale blue.

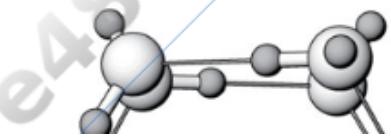

Printed by: e48d507df5d1141@placeholder.94092.edu. Printing is for personal, private use only. No part of this book may be reproduced or transmitted without publisher's prior permission. Violators will be prosecuted.

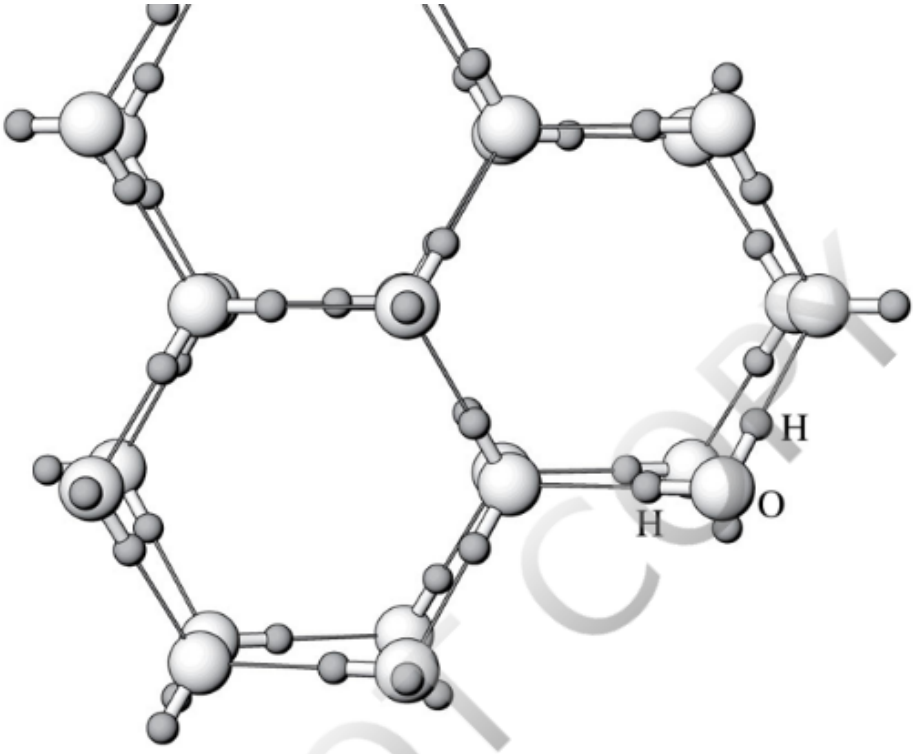

FIGURE 18.1 Ice structure viewed down the *c* axis. Water molecules consisting of one oxygen (large sphere) and two hydrogens (small spheres) are arranged in a hexagonal array. Hydrogen bonds between water molecules are shown with lines. The positions of the H and O are shown accurately, but the sizes of the atoms are reduced. Compare Figure 3.13. View larger image

Composition Most ice is relatively pure, but ice produced by freezing salt water may contain saline fluid inclusions.

Form and Twinning Ice in the form of snow or frost forms eye-catching skeletal crystals with hexagonal symmetry. Glacial ice is a granular aggregate of ice grains, the same as ice cubes from the freezer or the ice on a frozen lake. {001} twins are common and may be produced by deformation.

Cleavage None. Conchoidal fracture. Brittle.

Color Properties

Luster: Vitreous.

Color: Colorless, white, pale blue.

Streak: White.

Optical Characteristics Conventional thin sections and grain mounts are not practical because ice melts at 0°C. However, studying ice with cross-polarized light has been important to understanding how glaciers flow. Glacier ice is also an excellent analog material that provides insights into silicate rock deformation. For petrographic work, the ice is prepared in a similar fashion as standard rock thin sections, but preparation must be done in a cold room (about −10°C) to prevent melting. Ice section are prepared with

DO NOT COPY e48d507df5d1141@placeholder.9409

Printed by: e48d507df5d1141@placeholder.94092.edu. Printing is for personal, private use only. No part of this book may be reproduced or transmitted without publisher's prior permission. Violators will be prosecuted.

be done in a cold room (about −10°C) to prevent melting. Ice section are prepared with large, 10×10 cm glass slides, and sections must be very thick, about 0.4 mm, to accommodate ice's very low birefringence (Langway, 1958). The ice sections are studied in the cold room with a Rigsby apparatus, which is analogous to a petrographic microscope. Glacier ice can even be analyzed with a scanning electron microscope if equipped with a cooled cryostage (e.g., Monz and others, 2021).

Alteration Ice melts at 0°C or may sublimate to form water vapor in the atmosphere.

Distinguishing Features

Hand Sample: Not easily mistaken for any other mineral.

Occurrence Ice forms as a sediment (snow) by precipitation from water vapor in the atmosphere. Snow may subsequently be recrystallized to form glacial ice, which, strictly speaking, is a metamorphic rock. Ice also forms by crystallization from liquid water to form ice on lakes, rivers, and other bodies of water. This ice should be considered an igneous rock. It also acts as a very effective cementing agent in soil in areas where the average temperature drops below freezing. In areas with permafrost, ice in the soil persists year-round.

Use Perhaps its most important use is to cool the drinks that quench the thirst of geologists after long hot days in the field. Ice has been used as a construction material to build dwellings in Arctic regions and supports a major recreational industry (skiing and snowboarding) in many parts of the world. Ice fishing and ice skating would not be possible without it. Ice also poses significant environmental risks when it covers roads and bridges, or when icebergs calved from glaciers endanger shipping. Snow avalanches are a significant threat to life and transportation systems in alpine areas. Glacial ice forms a substantial portion of the world's resource of fresh water, although not one that is readily available for extensive human use. See Box 18.1 for a discussion of how it is used to understand paleoclimate.

BOX 18.1
Paleoclimate

Information regarding past climates can be collected from a number of minerals and rocks. Antarctic glacial ice, for example, contains a record of climate that goes back about a million years. Collected glacial ice cores show annual accumulations of snow and air bubbles. As snow compacts and recrystallizes, the air caught between the crystals of snow as it starts to convert to glacial ice becomes the air bubbles found in the ice. Following ice core collection, the ice is crushed in a lab such that the small samples of ancient air can be collected and analyzed to determine atmospheric composition at the time the snow converted to glacial ice. Of particular interest is how atmospheric CO_2 has changed through time. Also preserved in glacial ice is atmospheric dust (e.g., from volcanoes and deserts) and pollen from vegetation, both

Printed by: e48d507df5d1141@placeholder.94092.edu. Printing is for personal, private use only. No part of this book may be reproduced or transmitted without publisher's prior permission. Violators will be prosecuted.

of which help deduce past climates.

Paleotemperatures can be estimated based on the composition of the oxygen isotopes that make up the H_2O molecules in the ice (Allègre, 2008). Water molecules are made with both a heavier ^{18}O isotope and a lighter, more abundant ^{16}O isotope. The relative amounts of the heavy and light oxygen isotopes in a material can be tracked by its $\delta^{18}O$ (pronounced as "delta O-18") value. The $\delta^{18}O$ compares the $^{18}O/^{16}O$ ratio of a material to a standard of known value, which in this case is the average modern-day $^{18}O/^{16}O$ ratio of seawater (SMOW—standard mean ocean water). In all cases, $\delta^{18}O$ values for a material that is more positive are heavier, with a higher proportion of H_2O having the ^{18}O isotope. More negative $\delta^{18}O$ values are lighter, with a lower proportion of H_2O having the ^{18}O isotope.

There are many processes and factors that control the $\delta^{18}O$ value of ocean water, atmospheric water, glacial ice, and so on. The most important process that controls the $\delta^{18}O$ for polar glacial ice is that the relative amounts of water with ^{18}O vs. ^{16}O evaporating from the ocean surface depend on temperature—the heavier ^{18}O-bearing water evaporates less easily at lower temperatures. If sea-surface temperatures are low, the $\delta^{18}O$ of the water vapor in the atmosphere will be lower than if sea-surface temperatures are high. Snow crystallizing from water vapor in the atmosphere reflects the oxygen isotope composition of the atmosphere, and some of this snow will fall on polar glaciers and be preserved as glacial ice. Therefore, changes in the oxygen isotope composition of ice from successive years of snow accumulation can provide a record of average sea-surface temperatures and changing climate.

The $\delta^{18}O$ value of deep-sea sediments rich with foraminifera shells also provides a record of paleoclimate. Foraminifera ("forams") are single-cell organisms (protists) that form a calcite ($CaCO_3$) shell, or test. When forams grow their calcite tests, they use oxygen from seawater. There are two processes that control the $\delta^{18}O$ value of the test. One is the $\delta^{18}O$ of the ocean water at the time the test was grown. The main controller of the $\delta^{18}O$ of ocean water is sea level. During cold climates, the expansive glaciers across continents have stored enough evaporated water from the oceans to drop sea level by upward of about 120 meters. Though temperature does affect the relative amounts of water with ^{18}O vs. ^{16}O that evaporate (see above), ^{16}O-bearing water always evaporates more easily than ^{18}O water, regardless of the temperature. Therefore, when sea level is low during cold climates and global glaciation, the ocean is relatively enriched in heavy ^{18}O-bearing water and will have a high $\delta^{18}O$ value. Foram tests grown from this ocean water will also have a relatively high $\delta^{18}O$ value. A second process that controls the $\delta^{18}O$ value of the test is that forams vary the amount of ^{18}O taken up for test growth relative to water based on temperature. More ^{18}O is taken up at lower temperature. Fortunately, these processes operate in the same fashion such that high test $\delta^{18}O$ indicates a cold climate.

When forams die, their tests may be deposited on the sea floor and can be preserved as sedimentary rock. Therefore, determination of the $\delta^{18}O$ record from foram tests in deep-sea sediments and sedimentary rock provides a paleoclimate record by tracking sea level, glacier extent, and ocean temperatures. See Zachos and

DO NOT COPY

Printed by: e48d507df5d1141@placeholder.94092.edu. Printing is for personal, private use only. No part of this book may be reproduced or transmitted without publisher's prior permission. Violators will be prosecuted.

record by tracking sea level, glacial extent, and ocean temperatures. See Zachos and others (2001) for more information regarding the paleoclimate record obtained from deep-sea sediments.

Deep-sea sediments accumulate more slowly than glacial ice; therefore, the deep-sea sediment paleoclimate record is of lower resolution than the polar glacial ice record. However, deep-sea sediment provides a substantially longer record than polar glacial ice. Therefore, both polar glacial ice and deep-sea sediment provide important information regarding paleoclimate, depending on the time interval of interest.

See Box 20.1 for more information on how changes in climate are tied to the carbon cycle.

Comments Although not usually thought of as a mineral, ice is a very common mineral that has great geological, meteorological, economic, and social importance.

DO NOT COPY
e48d507df5d1141@placeholder.9409

Printed by: e48d507df5d1141@placeholder.94092.edu. Printing is for personal, private use only. No part of this book may be reproduced or transmitted without publisher's prior permission. Violators will be prosecuted.

XO Group

The XO group members discussed here include the minerals periclase (MgO) and zincite (ZnO), neither of which is common, and other members of this group are even more rare. Their properties are listed in Table 18.2. Periclase is isostructural with NaCl, and zincite has a structure analogous to the wurtzite polymorph of sphalerite (ZnS).

TABLE 18.2 XO Oxide Minerals

Mineral	Unit Cell	Physical Properties[a]	Optical Properties	Comments
Zincite ZnO	Hexagonal $6mm$ $a = 3.249$ $c = 5.205$ $Z = 2$	H: 4 G: 5.68 Cl: {100}pf, {001} parting Tw: {001} C: Orangish yellow to deep red St: Orangish yellow L: Subadamantine	$n_\omega = 2.013$ $n_\epsilon = 2.029$ $\delta = 0.016$ Uniaxial (+) TS: Deep red to yellow PS: Pinkish brown with strong red/yellowish internal reflections	Crystals consist of {101} pyramid, {100} prism, and $\{00\bar{1}\}$ pedion; usually granular; rare except at Franklin, New Jersey
Periclase MgO	Isometric $4/m$ $\bar{3}\,2/m$ $a = 4.213$ $Z = 4$	H: 5.5 G: 3.58 Cl: {100}pf Tw: None C: Colorless, white, or gray; also yellow, brown, or black with inclusions St: White L: Vitreous	$n = 1.735–1.756$ Isotropic Colorless	Cubic crystals rare, usually rounded or irregular grains; found as disseminated grains in metamorphosed limestone and dolostone

[a] Cl = cleavage (pf = perfect), Tw = twinning, C = color, St = streak, L = luster, TS = thin section, PS = polished section.

DO NOT COPY e48d507df5d1141@placeholder.9409

Printed by: e48d507df5d1141@placeholder.94092.edu. Printing is for personal, private use only. No part of this book may be reproduced or transmitted without publisher's prior permission. Violators will be prosecuted.

XY_2O_4 Minerals

Spinel Group

The spinel group of minerals (Table 18.3) crystallizes in the isometric crystal system. The structure (Figure 18.2) is based on cubic close-packed oxygen with X and Y cations in tetrahedral and octahedral coordination sites among the oxygen anions. The unit cell, which is about 8 Å on a side, contains 8 formula units ($Z = 8$) or 8 X cations and 16 Y cations. The X cations are divalent, and the Y cations are either all trivalent or half quadrivalent and half divalent. The unit cell contains 32 octahedral sites and 64 tetrahedral sites. Sixteen of the octahedral sites are occupied, and 8 of the tetrahedral sites are occupied. The two types of spinel structures depend on the distribution of cations between sites.

TABLE 18.3 Spinel Group Minerals

Mineral	Composition	Mineral	Composition
Spinel series		Magnetite series	
Spinel	$MgAl_2O_4$	Magnetite	$FeFe_2O_4$
Hercynite	$FeAl_2O_4$	Magnesioferrite	$MgFe_2O_4$
Gahnite	$ZnAl_2O_4$	Ulvöspinel	$FeFeTiO_4$
Galaxite	$MnAl_2O_4$	Franklinite	$ZnFe_2O_4$
Chromite series		Jacobsite	$MnFe_2O_4$
Chromite	$FeCr_2O_4$	Trevorite	$NiFe_2O_4$
Magnesiochromite	$MgCr_2O_4$	Hausmannite	$MnMn_2O_4$

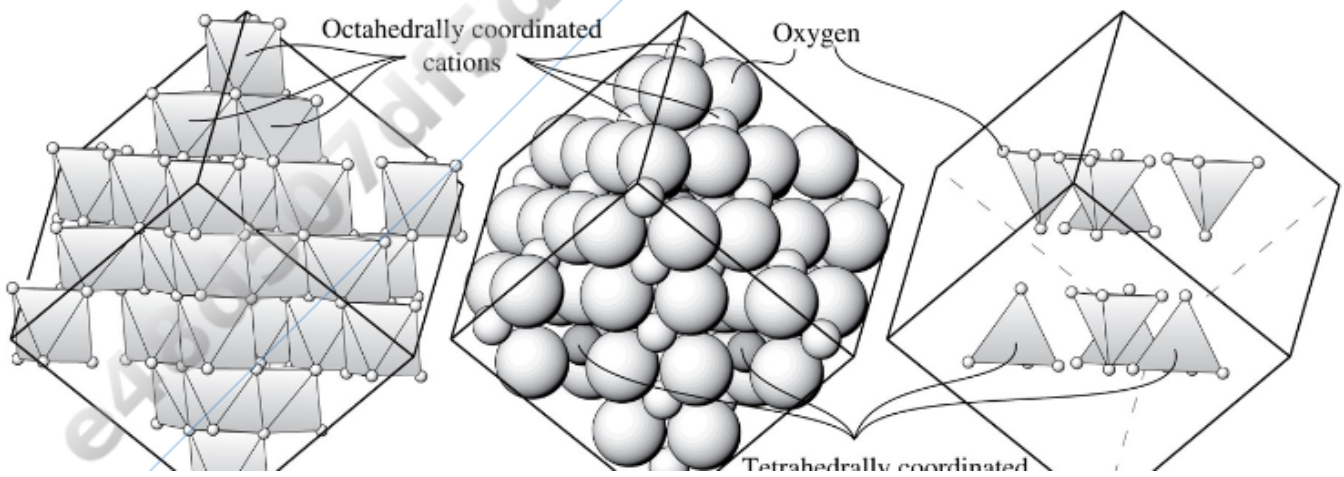

DO NOT COPY e48d507df5d1141@placeholder.9409

Printed by: e48d507df5d1141@placeholder.94092.edu. Printing is for personal, private use only. No part of this book may be reproduced or transmitted without publisher's prior permission. Violators will be prosecuted.

FIGURE 18.2 Spinel structure. Oxygen anions form an approximately cubic close-packed arrangement with layers parallel to {111}, which is horizontal in the illustration. Within each unit cell, cations occupy 8 tetrahedral and 16 octahedral sites between the oxygen layers. All the tetrahedral sites are shown; the octahedral sites shown on the left include both those within the unit cell and additional octahedra that are partially within adjacent unit cells. The cube outlines are slightly larger than the unit cell. The corners of the unit cell are the centers of octahedrally coordinated cations at the corners of the cube. See text for additional discussion. View larger image

The normal spinel structure is displayed by members of the spinel and chromite series. Divalent X cations occupy the 8 tetrahedral (4-fold) coordination sites within the unit cell. Smaller trivalent Y cations occupy the 16 larger octahedral (6-fold) coordination sites. The general formula based on site occupancy is therefore $^{IV}X^{VI}Y_2O_4$, where the roman numerals refer to the coordination number for each cation.

Members of the magnetite series have inverse spinel structures. In magnetite, for example, the unit cell contains 8 Fe^{2+} (the X cations) in octahedral coordination sites. The 16 Fe^{3+} cations (Y cations) are distributed 8 each to tetrahedral sites and octahedral sites. Based on site occupancy, the formula could be written $^{VI}(Fe^{2+}Fe^{3+})^{IV}Fe^{3+}O_4$, or for the general case, $^{VI}X^{VI}Y^{IV}YO_4$.

Both normal and inverse spinel structures place large cations in tetrahedral sites that normally they would not occupy based on size considerations alone (Chapter 3). However, the combination of chemical bonds produced by both structures results in a low-energy configuration that outweighs the ion size considerations.

Of the members of the spinel group, only chromite, magnetite, and Fe/Mg spinel are very common, so they are the only species described in detail here.

Many other minerals and chemical compounds crystallize with the spinel structure and are sometimes referred to as spinel. A particular source of confusion to students is the use of the term *spinel* in reference to high-pressure polymorphs of olivine (e.g., γ-Mg_2SiO_4) that, based on geophysical and experimental studies, should be present in the Earth's mantle. γ-Mg_2SiO_4 has the spinel structure with Si in tetrahedral coordination and Mg in octahedral coordination. Although the cations have the same coordination as in olivine, a different distribution allows the spinel structure to be significantly more dense than olivine. See the section on Olivine in Chapter 16 for more information.

Magnetite

$$FeFe_2O_4 \text{ or } Fe_3O_4$$

Isometric $4/m\,\bar{3}\,2/m$

DO NOT COPY e48d507df5d1141@placeholder.9409

Printed by: e48d507df5d1141@placeholder.94092.edu. Printing is for personal, private use only. No part of this book may be reproduced or transmitted without publisher's prior permission. Violators will be prosecuted.

$$a = 8.396\ \text{Å},\ Z = 8$$

$$H = 5.5 - 6.5$$

$$G = 5.18$$

Opaque

Ferrimagnetic

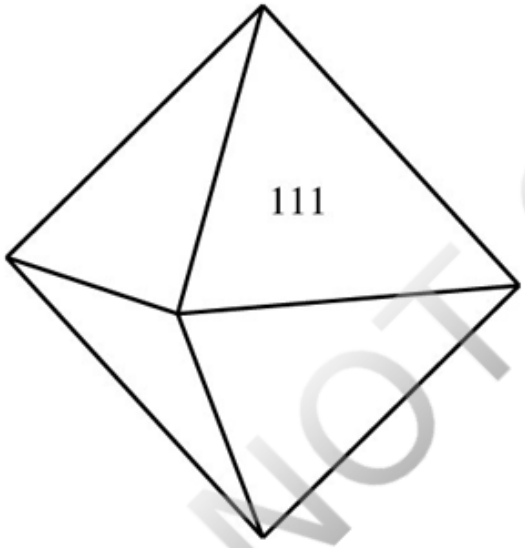

Composition Often the formula is written with the Fe in the octahedral and tetrahedral sites lumped together, which results in a formula of Fe_3O_4. Depending on context, it may be preferable to write the formula with separated sites and include cation valence. Magnetite usually contains some Ti as part of a solid solution series to ulvöspinel, $^{VI}(Fe^{2+}Ti^{4+})^{IV}Fe^{2+}O_4$. The solid solution involves substitution of Ti^{4+} for Fe^{3+} in octahedral sites coupled with substitution of Fe^{2+} for Fe^{3+} in the tetrahedral sites to maintain charge balance. Ti-rich samples are possible only under low-oxidization conditions in which the iron is mostly Fe^{2+}. The availability of oxygen allows the ulvöspinel component of magnetite to be oxidized to form ilmenite and more pure magnetite by the following reaction.

$$3Fe_2^{2+}Ti^{4+}O_4 + 0.5O_2 = 3Fe^{2+}TiO_3 + Fe^{2+}Fec_2^{3+}O_4 \quad \textbf{(18.1)}$$

$$\text{Ulvöspinel} + \text{oxygen} = \text{ilmenite} + \text{magnetite}$$

At a given temperature, oxidation forces the exsolution of ilmenite out of Ti-bearing magnetite, so that the magnetite contains less Ti. At a given oxidation condition, decreasing the temperature accomplishes the same thing. It is quite common to find that magnetite from igneous and metamorphic rocks contains exsolution lamellae of ilmenite produced as a consequence of either cooling or late oxidation of the magnetite in response to changing environmental conditions.

DO NOT COPY

Printed by: e48d507df5d1141@placeholder.94092.edu. Printing is for personal, private use only. No part of this book may be reproduced or transmitted without publisher's prior permission. Violators will be prosecuted.

Ilmenite, however, forms a solid solution series with hematite $\left(Fe_2^{3+}O_3\right)$. The composition of the ilmenite–hematite solid solution is influenced by the reaction of magnetite and oxygen to form hematite.

$$2Fe^{2+}Fe_2^{3+}O_4 + 0.5O_2 = 3Fe_2^{3+}O_3 \quad \textbf{(18.2)}$$
$$\text{Magnetite} + \text{oxygen} = \text{hematite}$$

All other things being equal, oxidation tends to make the ilmenite–hematite solid solution more hematite-rich, provided magnetite is present. This reaction is also temperature sensitive.

The compositions of coexisting magnetite and ilmenite are, therefore, sensitive to both the temperature and the oxidation state. It is therefore possible to analyze coexisting magnetite and ilmenite in an igneous or metamorphic rock to provide information about the chemical environment (oxidation condition) and temperature history of the rock.

Other compositional variation in magnetite includes substitution of Mg^{2+} for Fe^{2+} as part of a continuous solid solution to magnesioferrite ($MgFe_2O_4$) and substitution of some Al^{3+} for Fe^{3+}. Some Mn, Cr, and Ca also may be present.

Form and Twinning Octahedral crystals are common; dodecahedrons are less so. Also granular massive (Figure 18.3) and as isolated anhedral grains. Twinning on {111} (spinel twin) is common, usually forming simple twins, but also multiples.

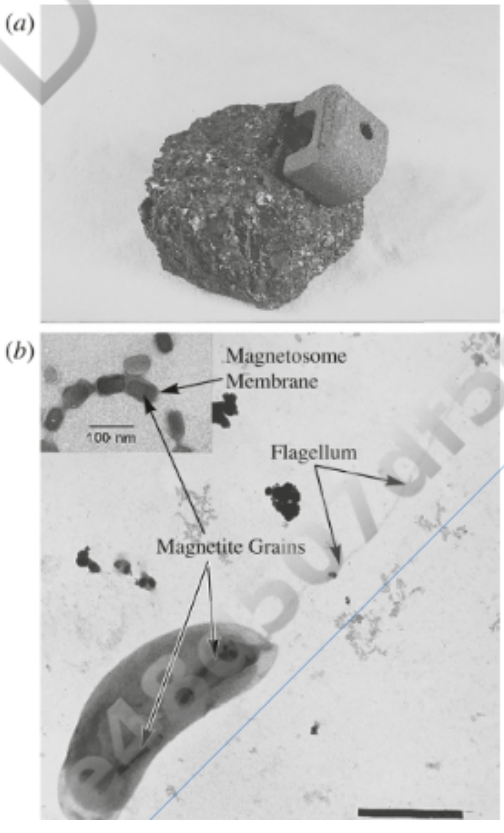

DO NOT COPY

Printed by: e48d507df5d1141@placeholder.94092.edu. Printing is for personal, private use only. No part of this book may be reproduced or transmitted without publisher's prior permission. Violators will be prosecuted.

FIGURE 18.3 Magnetite. (*a*) Massive granular hand sample. (*b*) Transmission electron microscope images (courtesy of D. Bazylinski) of a magnetotactic bacterium (strain MV-1) showing a chain of magnetite grains with a gap in the middle. The cell possesses a single polar flagellum that can be used for propulsion. Inset shows detail of magnetite grains and the magnetosome membrane that surrounds them and anchors them in place. View larger image

Cleavage None, but a parting on {111} may be distinct. Uneven fracture. Brittle.

Color Properties

Luster: Dull metallic to splendent.

Color: Black. Intervalence charge transfer between Fe^{2+} and Fe^{3+} is responsible for absorption of much of the visible light spectrum.

Streak: Black.

Optical Characteristics

Thin Section: Opaque.

Polished Section: Brownish gray (but somewhat variable) without bireflectance or reflection pleochroism. Isotropic.

Alteration Magnetite is readily altered to hematite or goethite and related iron oxides and hydroxides in the weathering environment. The term *martite* is applied to hematite pseudomorphs after magnetite.

Distinguishing Features

Hand Sample: Magnetite is readily attracted by a magnet. The variety lodestone is naturally magnetic and will attract and hold small objects such as paper clips. Ilmenite is similar but is only weakly magnetic. Chromite has a more resinous luster and is not magnetic.

Thin Section/Grain Mount: Difficult to distinguish from other opaque minerals.

Polished Section: Ilmenite is anisotropic, and sphalerite typically displays internal reflections. Magnetite often contains exsolved lamellae of ilmenite or hematite.

Occurrence Magnetite is a very common accessory mineral found in a wide variety of igneous and metamorphic rocks, usually as small euhedral to anhedral grains. Segregations of massive magnetite occur in some mafic magmatic systems. Rarely, Fe-rich magmas can be generated and produce plutons or volcanic features composed almost entirely of magnetite. Examples include the magnetite deposits found in El Laco, Chile, or Kiruna, Sweden, though the origins of such deposits are highly disputed. Skarns,

DO NOT COPY e48d507df5d1141@placeholder.9409

Printed by: e48d507df5d1141@placeholder.94092.edu. Printing is for personal, private use only. No part of this book may be reproduced or transmitted without publisher's prior permission. Violators will be prosecuted.

or contact metamorphosed and metasomatized limestone or dolostone by an adjacent granitic intrusion, may contain large amounts of magnetite associated with diopside, tremolite, garnet, calcite, dolomite, and other calc-silicate minerals. Banded and other iron formations often contain magnetite as a major mineral (see Box 18.2). Magnetite may be concentrated in the heavy mineral fraction of clastic sediments, particularly if the sediments are derived from areas subject to fairly rapid erosion and limited chemical weathering. Once deposited, detrital magnetite may be oxidized to other iron oxides and hydroxides. Magnetite is a significant biomineral (Figure 18.3), and small magnetite grains are commonly found in the cells of many species, including human brains (Chapter 5). In at least some cases, magnetite appears to have biologic uses in orientation (cyanobacteria) and navigation (birds).

DO NOT COPY

BOX 18.2

Banded Iron Formations

Banded iron formations are sedimentary rocks (Figure 18.4) that are a major resource for iron. They are characteristic of the Precambrian, and most were deposited between 3.5 billion and 1.9 billion years ago with a peak at around 2.5 billion years. Trendall (2002) and Klein (2005) provide reviews. Banded iron formations are commonly part of greenstone belts, and the iron-rich layers may be hundreds of meters thick and extend for hundreds of kilometers. The least metamorphosed and deformed units preserve thinly bedded hematite- and magnetite-rich sediment alternating with siltstone, chert, or other material. Other common minerals include siderite, dolomite–ankerite, greenalite, stilpnomelane, riebeckite, and sometimes pyrite. Because modern analogs are lacking, it is difficult to know the primary, prediagenetic, and premetamorphic mineralogy. Possibly it consisted of iron hydroxides [$Fe(OH)_2$, $Fe(OH)_3$], SiO_2 gels, carbonate mud, and poorly defined Fe-silicate and hydrous Na-, K-, and Al-silicate gels.

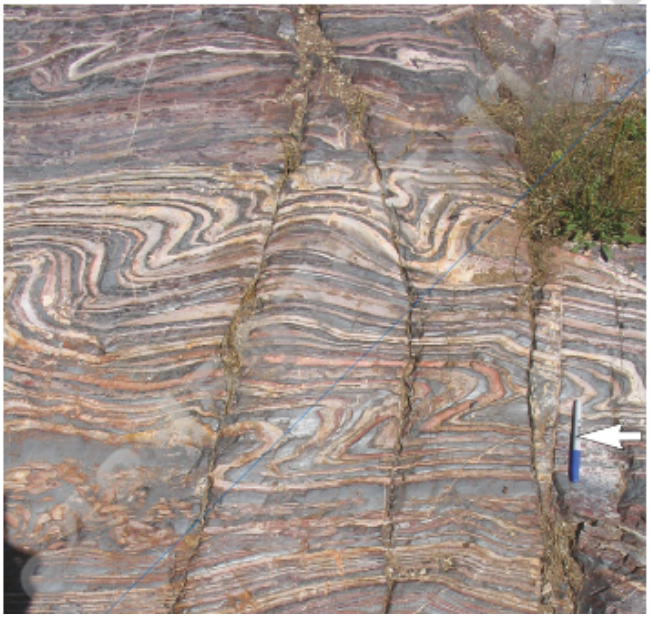

Printed by: e48d507df5d1141@placeholder.94092.edu. Printing is for personal, private use only. No part of this book may be reproduced or transmitted without publisher's prior permission. Violators will be prosecuted.

FIGURE 18.4 The 2.7 Ga Soudan banded iron formation in northeastern Minnesota. The dark layers are dominantly hematite, and the light layers are mostly microcrystalline quartz (jasper). Note the pen at right (*arrow*) for scale. View larger image

The origin of sedimentary iron formations remains a matter of debate. The metamorphism and deformation that most experienced make it quite difficult to reconstruct the environment of deposition. A distinction is often made between banded iron formations and the related granular iron formations. With banded iron formations, the delicate nature of the fine laminations and lack of current-generated sedimentary structures argue for deposition below the maximum depth for wave motion, which is roughly 200 meters. With granular iron formations, whose banding is much coarser and which were mostly deposited after ~2.2 billion years ago, the presence of oolites and other sedimentary structures in some units argues for shallow water. In all cases, there is typically little contribution of clastic sediment to the deposit. It is generally agreed that the iron in the deposits was extracted from anoxic seawater and that the iron probably originated from hydrothermal sources. The association between the peak of banded iron formation generation and the Great Oxidation Event is probably not a coincidence, as it is known that oxygenated waters cannot hold as much iron as anoxic waters. Some authors (e.g., Trendall, 2002; Kronhauser, 2007) have argued that precipitation of the iron oxides, silica, and other material was mediated by microorganisms. It is known that microorganisms are capable of precipitating iron oxide and hydroxide minerals by both biologically induced and biologically controlled processes (Chapter 5). However, a direct biologic origin for banded iron formations is far from universally accepted, and some authors (e.g., Klein, 2005) argue for a purely chemical origin.

Use Magnetite is mined in many locations as an ore of iron from which cast iron and steel are produced. It is also used as a feedstock in the manufacture of other iron-bearing industrial materials. As a mineral, magnetite has some use as a filter media and black pigment. Crushed magnetite has been used as aggregate to make high-density concrete for applications that include nuclear reactors. Magnetite appears in some folk medicine and historical medical treatments, purportedly to help chronic wheezing, tinnitus, cancer, epilepsy, and insomnia; it has even been believed to be an aphrodisiac. An interesting medical research application is to attach very small particles of magnetite to the surfaces of individual cells so that the cells can be manipulated and controlled by applying an external magnetic field (Dobson, 2008).

DO NOT COPY e48d507df5d1141@placeholder.94092

Printed by: e48d507df5d1141@placeholder.94092.edu. Printing is for personal, private use only. No part of this book may be reproduced or transmitted without publisher's prior permission. Violators will be prosecuted.

Comments Microscopic grains of magnetite provided some of the most critical evidence that allowed our concepts of continental drift and plate tectonics to be developed. The key observation is that magnetite can acquire and preserve a magnetic polarity under the influence of an external magnetic field. In a volcanic rock, for example, small grains of magnetite are magnetized parallel to the Earth's magnetic field as the magnetite cools through its Curie temperature (the temperature above which ferrimagnetism is destroyed). Under appropriate conditions, that magnetization will be preserved, and an instrument called a magnetometer allows the direction and magnitude of this "fossil magnetism" to be measured. If the age of the rock is known, perhaps by U–Pb radiometric dating (see Box 5.1), then the Earth's magnetic polarity and the distance and direction to the magnetic poles for that particular time can be deduced. If many samples of different ages are measured, it is possible to determine how the land mass containing the samples moved relative to the Earth's magnetic poles and the sequence of magnetic polarity reversals through time. Paleomagnetic information of this type was some of the most convincing evidence that documented continental drift and helped in the development of the current models of seafloor spreading and plate tectonics.

Chromite

$$FeCr_2O_4$$

Isometric $4 / m \, \bar{3} \, 2 / m$

$$a = 8.38 \text{ Å}, \; Z = 8$$

$$H = 5.5 - 6$$

$$G = 5.09 \text{ (lower with Mg and Al)}$$

Isotropic

$$n = 1.90 - 2.12$$

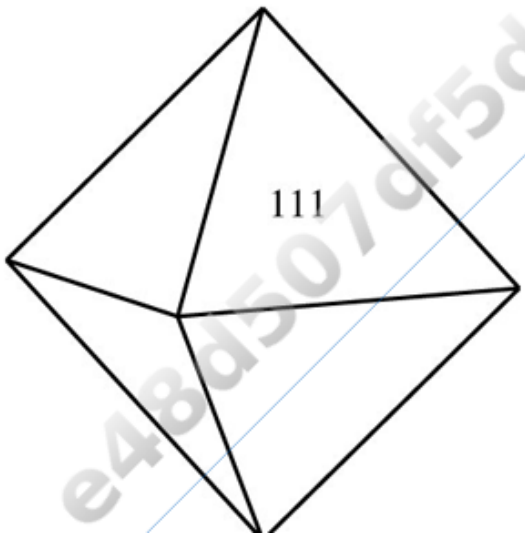

DO NOT COPY
e48d507df5d1141@placeholder.9409

Printed by: e48d507df5d1141@placeholder.94092.edu. Printing is for personal, private use only. No part of this book may be reproduced or transmitted without publisher's prior permission. Violators will be prosecuted.

Composition Chromite forms a continuous solid solution series with magnesiochromite ($MgCr_2O_4$), and substantial Mg is present in most samples. Al, Fe^{3+}, Mn, and Zn may be present, and continuous solid solution to hercynite ($FeAl_2O_4$) is possible.

Form and Twinning Crystals are octahedrons that may be modified by cube faces. Commonly massive granular or as anhedral grains (Figure 2.52f). Simple or multiple twins on {111}, according to the spinel law (Figure 5.22a).

Cleavage None. Parting on {111}. Uneven fracture. Brittle.

Color Properties

Luster: Metallic to somewhat pitchy (black and submetallic).

Color: Black.

Streak: Brown.

Color in Thin Section: Essentially opaque, dark brown on thin edges.

Optical Characteristics

Polished Section: Grayish white to light brown without bireflectance or reflection pleochroism. Usually isotropic, but may show weak anisotropism. Reddish-brown internal reflection common.

Alteration Chromite may alter to limonite and other oxides and hydroxides of Fe, Cr, and Mg, and to Cr-bearing clays.

Distinguishing Features

Hand Sample: Resembles magnetite and ilmenite, but chromite is not magnetic and has a somewhat more resinous luster. Some chromite, however, may have some magnetic character because of intergrown magnetite.

Thin Section/Grain Mount: Difficult to distinguish from other opaque minerals in conventional thin section or grain mount. Some chromite may be transparent and dark brown on thin edges.

Polished Section: Resembles magnetite but is less reflective and has internal reflections.

Occurrence Chromite is found in mafic and ultramafic igneous rocks such as gabbro, peridotite, dunite, and pyroxenite as an accessory mineral. In some cases, masses of chromite may be generated by crystal settling or other magmatic segregation processes in layered mafic intrusions. Chromite may be concentrated in detrital sands in some locations.

DO NOT COPY e48d507df5d1141@placeholder.9409

Printed by: e48d507df5d1141@placeholder.94092.edu. Printing is for personal, private use only. No part of this book may be reproduced or transmitted without publisher's prior permission. Violators will be prosecuted.

Use Chromite is the only ore mineral for Cr. About 70% of world production is alloyed with iron to make stainless steel and other high-strength alloys. Metallic Cr is used to plate steel objects to protect them from corrosion and abrasion, and for decorative purposes. Chromium appears in a wide variety of chemical products used for industrial applications as diverse as tanning leather, printing, catalyzing chemical reactions, preserving wood, and in paints. Chromite also is used to make refractory products for foundries.

Spinel Series

$$\text{Spinel} : \mathrm{MgAl_2O_4}$$

$$\text{Hercynite} : \mathrm{FeAl_2O_4}$$

$$\text{Isometric } 4/m\,\bar{3}\,2/m$$

$$a = 8.103 \text{ Å (spinel)},$$
$$a = 8.135 \text{ Å (hercynite)},$$
$$Z = 8$$

$$H = 7.5 - 8$$

$$G = 3.55 - 4.40 \text{ (higher with Fe)}$$

$$\text{Isotropic}$$

$$n = 1.714 - 1.835$$

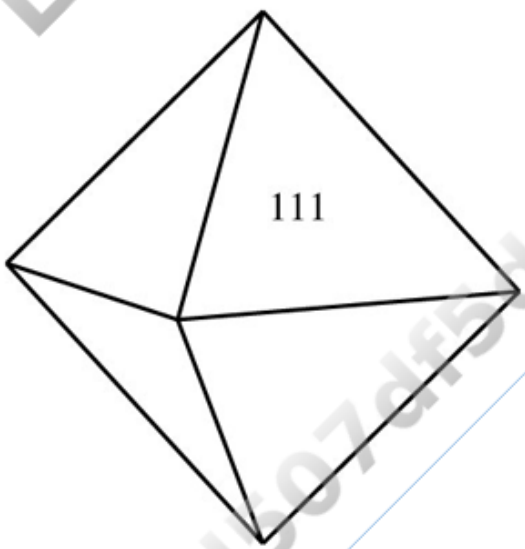

Composition Only common varieties that form a solid solution series between spinel and hercynite are described here. The term *pleonaste* has been applied to compositions intermediate between the Mg and Fe end members. Extensive solid solution is possible to

DO NOT COPY
e48d507df5d1141@placeholder.9409

Printed by: e48d507df5d1141@placeholder.94092.edu. Printing is for personal, private use only. No part of this book may be reproduced or transmitted without publisher's prior permission. Violators will be prosecuted.

galaxite and gahnite (Table 18.3). Chromium may also substitute for Al as part of solid solution to chromite; Cr-bearing spinel has been called picotite.

Form and Twinning Crystals are octahedrons, sometimes modified by cube and dodecahedron faces. Also common as anhedral grains and granular masses. Simple and multiple twins by the spinel law on {111} are common (Figure 5.22a).

Cleavage None, but a parting on {111} may be present. Conchoidal, uneven, to splintery fracture. Brittle.

Color Properties

Luster: Vitreous.

Color: Usually green or blue-green, also colorless, blue, red; darker with Fe content.

Streak: White.

Color in Thin Section: Corresponds with hand-sample color. Not pleochroic.

Optical Characteristics

Relief in Thin Section: Very high positive.

Index of Refraction: Increases systematically with Fe content, from 1.714 for pure spinel to 1.835 for pure hercynite.

Alteration Spinel is relatively resistant in the weathering environment. Alteration to clay or other sheet silicates is possible.

Distinguishing Features

Hand Sample: Crystal habit, hardness, and green color are characteristic. Hercynite-rich samples may resemble magnetite but are not magnetic and have a light streak.

Thin Section/Grain Mount: Isotropic character and strong (usually green or blue-green) color are characteristic. Garnet forms dodecahedrons and is lighter colored.

Occurrence Spinel is a common accessory mineral in aluminous metamorphic rocks associated with andalusite, kyanite, sillimanite, corundum, or cordierite; in contact and regionally metamorphosed limestone and dolostone; and less commonly in granitic pegmatites and hydrothermal veins. Because it is resistant in the weathering environment, it may be found in detrital sediments.

Use Spinel has been used as a gemstone but it does not have significant industrial applications. It has been used in dental ceramics.

Chrysoberyl

DO NOT COPY e48d507df5d1141@placeholder.9409

Printed by: e48d507df5d1141@placeholder.94092.edu. Printing is for personal, private use only. No part of this book may be reproduced or transmitted without publisher's prior permission. Violators will be prosecuted.

Chrysoberyl

Al_2BeO_4

Orthorhombic $2/m\ 2/m\ 2/m$

$a = 5.49$ Å, $b = 9.42$ Å,
$c = 4.43$ Å,

$Z = 4$

$H = 8.5$

$G = 3.68 - 3.75$

Biaxial (+)

$n_\alpha = 1.732 - 1.747$

$n_\beta = 1.734 - 1.749$

$n_\gamma = 1.741 - 1.758$

$\delta = 0.008 - 0.011$

$2V =$ -70° some reports as low as 10°

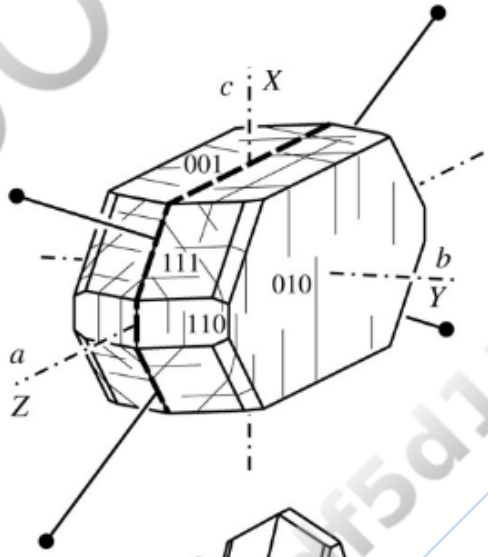

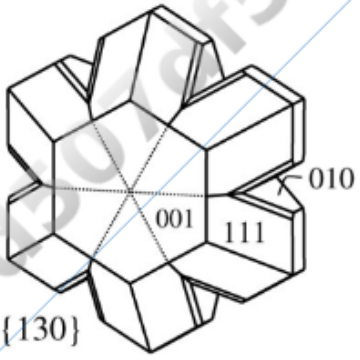

Cyclic twin on {130}

DO NOT COPY
e48d507df5d1141@placeholder.9409

Printed by: e48d507df5d1141@placeholder.94092.edu. Printing is for personal, private use only. No part of this book may be reproduced or transmitted without publisher's prior permission. Violators will be prosecuted.

Structure Chrysoberyl is isostructural with olivine (Figure 16.1). Oxygen forms a slightly distorted hexagonal close-packed arrangement, and Be occupies the tetrahedral sites and Al occupies the octahedral sites.

Composition Up to about 5% Fe^{3+} may substitute for Al^{3+} in octahedral sites. The gem variety alexandrite contains minor Cr^{3+} substituting for Al^{3+}. Mg, Ti, and Ca are reported in some analyses.

Form and Twinning Crystals are usually tabular on (001) with a striation on (001) parallel to the *a* axis. Twinning on {130} is very common and may form simple twins or cyclic twinning may produce pseudohexagonal "sixlings" with reentrants displaying {010} faces or without.

Cleavage {110} good, {010} fair, and {001} poor. Uneven to conchoidal fracture. Brittle.

Color Properties

Luster: Vitreous. Needlelike inclusions and tubelike cavities produce chatoyancy or asterism in the gem variety called cat's eye.

Color: Green, greenish white, greenish yellow, white. Alexandrite is distinctive. The Cr^{3+} produces absorption bands intermediate between those that produce the perception of red in ruby (Figure 6.9) and blue-green in emerald (Figure 15.7) so that the transmission bands in the red and blue-green parts of the spectrum are evenly balanced. When viewed in blue-rich sunlight, our eyes perceive the mineral as blue-green, and when viewed in red-rich incandescent light or a candle flame, our eyes perceive a deep red.

Streak: White.

Color in Thin Section: Colorless.

Pleochroism: Grain mounts may be weakly colored: X = rose-red, Y = orange, Z = green.

Optical Characteristics

Relief in Thin Section: Very high positive.

Optic Orientation: $X = c$, $Y = b$, $Z = a$.

Indices of Refraction and Birefringence: Little variation with compositional changes. Interference colors are a maximum of first-order yellow.

Interference Figure: At room temperature $2V_z$ is between 70° and 10°, $r > v$, weak. With increasing temperature, $2V_z$ gradually decreases to about 0°, $r < v$.

Alteration Chrysoberyl is quite resistant in the weathering environment, so it may appear as detrital grains. It may be altered to sheet silicates such as chlorite and clay.

DO NOT COPY e48d507df5d1141@placeholder.9409

Printed by: e48d507df5d1141@placeholder.94092.edu. Printing is for personal, private use only. No part of this book may be reproduced or transmitted without publisher's prior permission. Violators will be prosecuted.

Distinguishing Features

Hand Sample: Great hardness, crystal habit and twinning, and green color are diagnostic.

Thin Section/Grain Mount: Has very high relief and low birefringence. Corundum, beryl, and tourmaline are uniaxial; the latter two minerals have much lower relief in thin section.

Occurrence Chrysoberyl can occur in granitic pegmatites with quartz, K-feldspar, albite, muscovite, biotite, tourmaline, and beryl. Chrysoberyl is infrequently found in aluminous mica schists and in skarn deposits derived by contact metamorphism of dolostone. Because of its resistance in the weathering environment and relatively high specific gravity, chrysoberyl is a constituent of some placer deposits.

Use The alexandrite and cat's eye varieties are valued as gems. It is a potential source of beryllium, but is not exploited because beryl is far more abundant. Probably because it has been used as a gemstone and is perceived as valuable, chrysoberyl has had historical uses as a treatment for ailments of the pancreas, spleen, and nervous system.

DO NOT COPY
e48d507df5d1141@placeholder.9409

Printed by: e48d507df5d1141@placeholder.94092.edu. Printing is for personal, private use only. No part of this book may be reproduced or transmitted without publisher's prior permission. Violators will be prosecuted.

X_2O_3 Group

The hematite group has the general formula X_2O_3. The common minerals in this group are hematite, corundum, and ilmenite, in which X_2 is , Al_2, and $Fe^{2+}Ti^{4+}$, respectively. All share a common structure based on hexagonally close-packed oxygen anions, with metal cations occupying octahedral sites between the anions (Figure 18.5). For convenience, these minerals can be considered to be constructed of layers of octahedra parallel to {001}. Within each layer, only two-thirds of the octahedra contain cations and the occupied octahedra share two oxygen anions (share edges) with their neighbors. Successive layers of octahedra share a common layer of oxygen anions and are arranged so that occupied octahedra in adjacent layers share three oxygen anions (share a face). Ilmenite differs from both hematite and corundum in that two different cations (Fe^{2+} and Ti^{4+}) are distributed systematically among the octahedral sites.

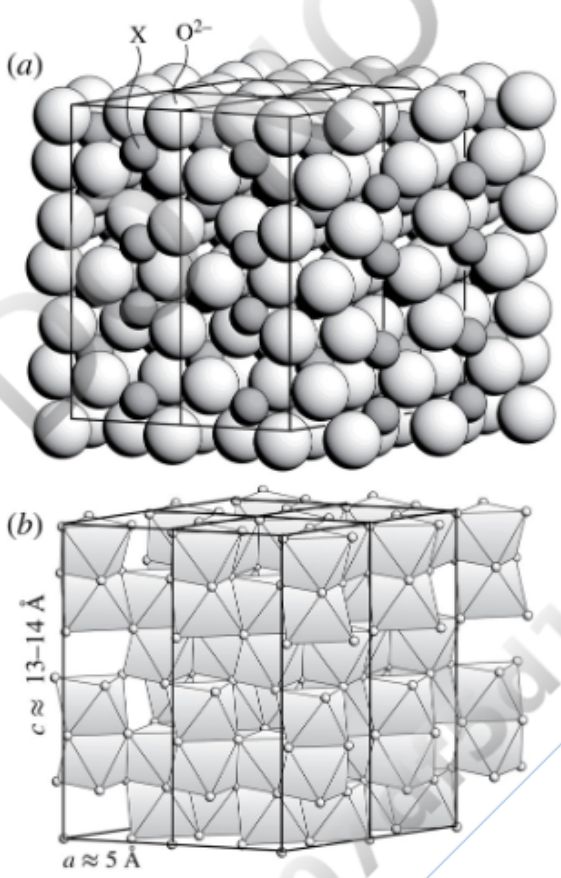

FIGURE 18.5 Structure of the hematite group. (*a*) X cations and O^{2-} anions drawn approximately to scale. The oxygen anions are in an approximately hexagonal close-packed arrangement. The outline of four unit cells is shown. (*b*) Distribution of X octahedra within the structure. View larger image

A full unit cell is constructed of six successive layers of octahedra and is about 13–14 Å

DO NOT COPY e48d507df5d1141@placeholder.9409

Printed by: e48d507df5d1141@placeholder.94092.edu. Printing is for personal, private use only. No part of this book may be reproduced or transmitted without publisher's prior permission. Violators will be prosecuted.

along the *c* axis, with an *a* dimension of about 5 Å. In many references, the Miller indices of crystallographic planes and faces are indexed to a unit cell that has twice the *a* unit cell dimension. In the mineral descriptions that follow, both the unit cell dimensions measured with X-ray diffraction techniques and a unit cell consistent with conventionally assigned Miller indices are provided. As usual, it is important to confirm the crystallographic conventions used when comparing data from different sources.

Hematite

Fe_2O_3

Hexagonal (trigonal) $3\ 2\ /\ m$

$a = 5.038$ Å, $c = 13.772$ Å,
$Z = 6$ ($a = 10.076$ Å,
$c = 13.772$ Å,
$Z = 24$ to be
consistent with Miller
indices)

$H = 5 - 6$ (earthy material may be lower)

$G = 5.25$ if pure, may be less

Opaque

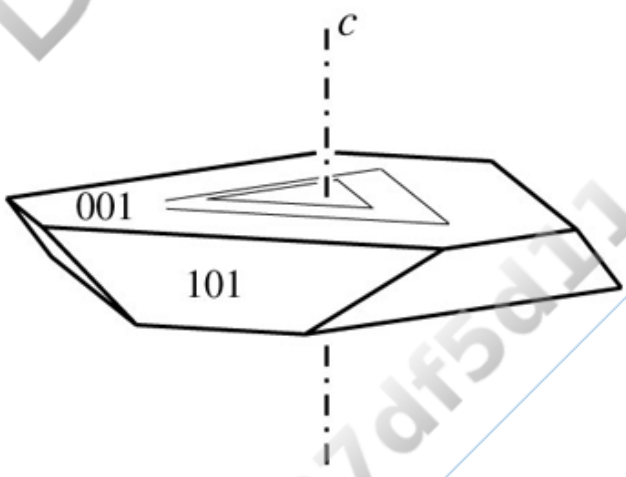

Composition Hematite usually contains some Ti, and above about 1050°C there is complete solid solution between hematite and ilmenite ($FeTiO_3$) that involves substitution of $Fe^{2+}Ti^{4+}$ for $2Fe^{3+}$. Up to about 10% Al can substitute for Fe, as can some Mn.

Form and Twinning Crystals are usually platy with a hexagonal outline and may have triangular markings on the basal pinacoid. Platy grains may form micaceous aggregates.

DO NOT COPY
e48d507df5d1141@placeholder.9409

Printed by: e48d507df5d1141@placeholder.94092.edu. Printing is for personal, private use only. No part of this book may be reproduced or transmitted without publisher's prior permission. Violators will be prosecuted.

Coarsely crystalline material with metallic luster is known as specular hematite. Fine-grained, massive metallic hematite may form oolitic, botryoidal, or rounded shapes with radiating structures (Figure 2.52b and c). Red earthy hematite may be mixed with clay and other minerals, and may form masses or disseminated grains. Twins on {001} and {101} may be lamellar.

Cleavage None, but parting on {001} and {101} may be present. Uneven to subconchoidal fracture. Brittle, elastic in thin laminae.

Color Properties

Luster: Specular hematite variety is metallic. Fine-grained varieties are dull metallic or earthy.

Color: Steel-gray for specular hematite variety; black to dark brown for fine-grained massive metallic variety; dull to bright brownish red for fine-grained earthy samples. The deep red color is produced by charge transfer between O^{2-} and Fe^{3+}.

Streak: Rich red-brown.

Color in Thin Section: Opaque; deep red-brown for very small crystals or thin edges.

Optical Characteristics

Indices of Refraction: Fine grains are uniaxial negative, $n_\omega = 3.15–3.22$, $n_\varepsilon = 2.87–2.94$, $\delta = 0.28$.

Polished Section: Grayish white with bluish tint, weak bireflectance and reflection pleochroism. Deep red internal reflections are common. Distinct anisotropism with gray-blue and gray-yellow polarization colors.

Alteration Hematite may be altered to iron hydroxide minerals. It is stable in the weathering environment and is commonly produced by weathering.

Distinguishing Features

Hand Sample: Fine-grained varieties are distinguished from goethite (and limonite) by a red streak. The streak of cinnabar is more carmine-red, and its specific gravity is higher. Black metallic varieties are distinguished from magnetite and ilmenite by much weaker or no magnetism and red streak.

Thin Section/Grain Mount: The red-brown color on thin edges distinguishes hematite from magnetite, ilmenite, and other likely opaque minerals.

Polished Section: Grayish-white color with red internal reflections and anisotropic character distinguish hematite from magnetite and ilmenite.

Occurrence Hematite is readily produced by weathering or hydrothermal alteration of

DO NOT COPY e48d507df5d1141@placeholder.9409

Printed by: e48d507df5d1141@placeholder.94092.edu. Printing is for personal, private use only. No part of this book may be reproduced or transmitted without publisher's prior permission. Violators will be prosecuted.

iron-bearing minerals in almost any rock type. It is not common as a primary mineral in igneous rocks but may be found in some syenite, trachyte, granite, and rhyolite. Late-stage magmatic processes may alter Fe-bearing minerals or cause the precipitation of hematite from residual fluids. Hematite may be a major mineral in banded iron formations (see Box 18.2), almost all of which are of Precambrian age; associated minerals include magnetite, quartz, carbonates, and various Fe-silicates. The red color of many sediments is due to the presence of disseminated hematite and iron hydroxide minerals; purple-colored sediments may be caused by coarser-grained hematite.

Use Hematite is an important ore of iron and is mined for that purpose in many areas of the world. It is also used as polishing abrasive and as a pigment, such as red ocher, which is widely used by many prehistoric, aboriginal, or indigenous peoples worldwide. Black crystalline material is cut as a gem. Probably because it is red and can be associated with blood, hematite has numerous historical medical uses, most commonly to treat bleeding and blood disorders. To the degree that the iron from hematite is bioavailable in the gut, hematite could potentially be a source of dietary iron, although dietary supplements typically use ferrous sulfate, gluconate, or fumarate for that purpose.

Corundum

$$\mathrm{Al_2O_3}$$

$$\text{Hexagonal (trigonal)} = \bar{3}\ 2/m$$

$$a = 4.75\ \text{Å},\ c = 12.98\ \text{Å},\ Z = 6$$

$$(a = 9.51\ \text{Å},\ c = 12.98\ \text{Å},\ Z = 24 \text{ to be consistent with Miller indices})$$

$$H = 9$$

$$G = 3.98 - 4.02$$

$$\text{Uniaxial } (-)$$

$$n_\omega = 1.766 - 1.794$$

$$n_\epsilon = 1.758 - 1.785$$

$$\delta = 0.008 - 0.009$$

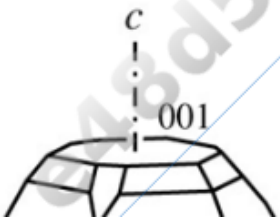

DO NOT COPY
e48d507df5d1141@placeholder.9409

Printed by: e48d507df5d1141@placeholder.94092.edu. Printing is for personal, private use only. No part of this book may be reproduced or transmitted without publisher's prior permission. Violators will be prosecuted.

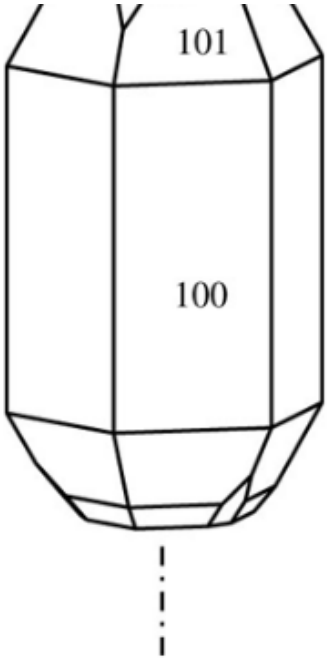

Composition Corundum is usually almost pure Al_2O_3. Blue corundum (sapphire) contains Fe and Ti, red (ruby) contains Cr, and yellow and green varieties contain Fe^{3+} and Fe^{2+}.

Form and Twinning Crystals are usually hexagonal prisms that may taper toward the ends (Figure 18.6). Basal pinacoids may display triangular markings. Crystals may also be tabular on {001}. Also as anhedral grains. Lamellar twins on {101} are common. Simple twins on {101} and {001} are less common.

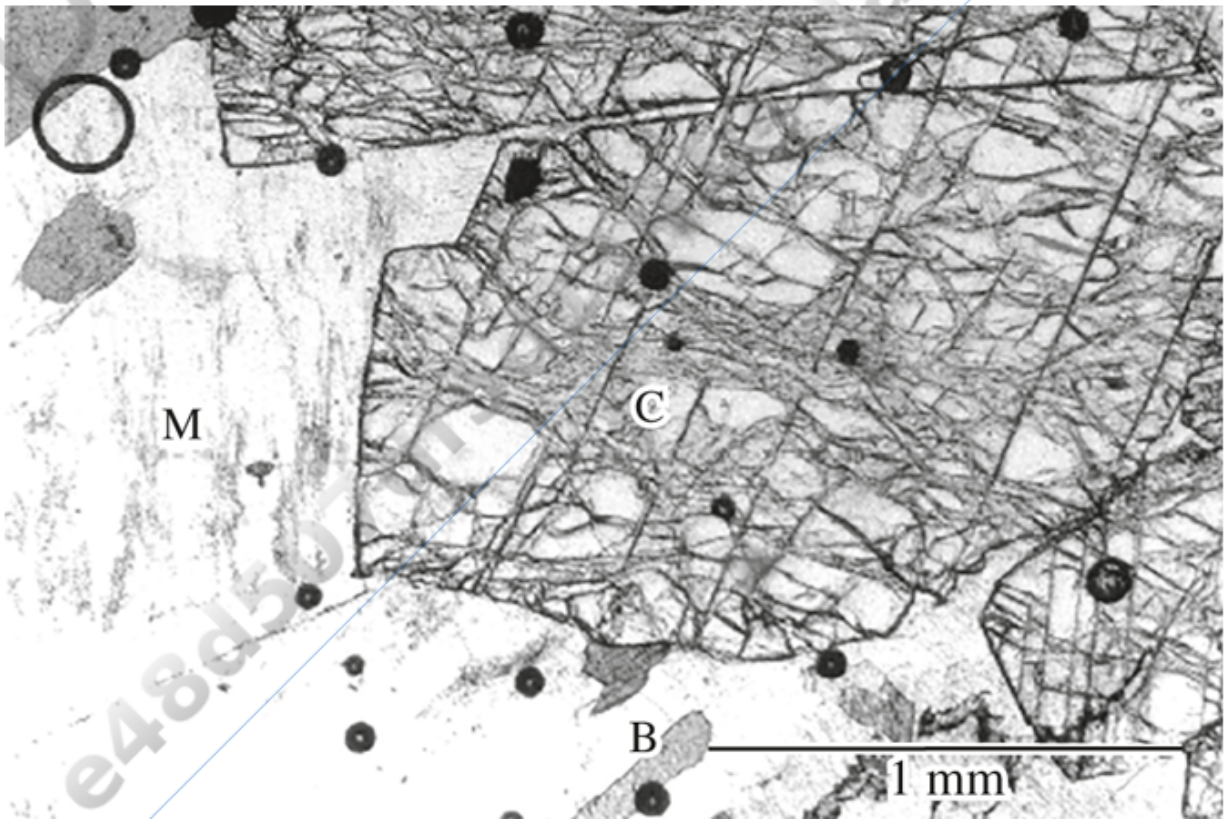

DO NOT COPY

Printed by: e48d507df5d1141@placeholder.94092.edu. Printing is for personal, private use only. No part of this book may be reproduced or transmitted without publisher's prior permission. Violators will be prosecuted.

FIGURE 18.6 Photomicrograph of corundum (C), microcline (M), and small grains of biotite (B) in a thin section of mica schist. Note the rhombohedral parting in the corundum. The small circles are bubbles in the thin section epoxy. Plane light. View larger image

Cleavage None; parting on {101} and {001} is associated with boehmite exsolution lamellae. Uneven to conchoidal fracture. Brittle.

Color Properties

Luster: Vitreous to adamantine.

Color: Most commonly white, gray, or gray-blue; also red (ruby, from Cr^{3+}, Figure 6.9), blue (sapphire, Fe^{2+}–Ti^{4+} intervalence charge transfer), yellow to brown (Fe or color centers), or green.

Streak: White (hardness makes streak difficult to obtain).

Color in Thin Section: Colorless or a pale version of the hand sample color.

Pleochroism: Colored versions are $\omega > \epsilon$.

Other Star sapphire (Figure 6.13) contains fine needles of rutile that exsolved from an originally more Ti-rich corundum. The needles align themselves parallel to the three 2-fold rotation axes at right angles to c and produce a distinct asterism when viewed down the c axis.

Optical Characteristics

Relief in Thin Section: Very high positive.

Optic Orientation: Crystals are length fast, and extinction is parallel to the basal {001} parting.

Indices of Refraction and Birefringence: Pure corundum has indices of refraction $n_\omega = 1.768$, $n_\epsilon = 1.760$. Indices of refraction increase with Fe and Cr content. Interference colors should be first-order gray and white in standard thin sections; but owing to its great hardness, thin sections containing substantial amounts of corundum are almost always thicker than the standard 0.03 mm, and higher-order colors are encountered.

Interference Figure: Basal sections yield uniaxial negative interference figures. Some corundum may be biaxial with $2V_x$ as high as 50° or 60°, perhaps because of twinning.

Alteration Corundum may be altered to fine-grained aggregates of aluminous minerals such as muscovite, margarite, andalusite, sillimanite, kyanite, diaspore, gibbsite, or clay.

Distinguishing Features

DO NOT COPY e48d507df5d1141@placeholder.9409

Printed by: e48d507df5d1141@placeholder.94092.edu. Printing is for personal, private use only. No part of this book may be reproduced or transmitted without publisher's prior permission. Violators will be prosecuted.

Hand Sample: Crystal habit and great hardness are characteristic. Alteration may allow samples to be anomalously soft. Sapphirine [$(Mg,Al)_8(Si,Al)_6O_{20}$], which is an uncommon chain silicate found in aluminous metamorphic rocks, may resemble blue corundum. Sapphirine, however, is monoclinic or triclinic, with fair cleavage on {010} and poor cleavage on {001} and {110}, $H = 7.5$, $G = 3.40–3.58$, crystals are tabular; it is usually light to dark blue; also green, white, red, or yellow.

Thin Section: High relief, low birefringence, and uniaxial character are diagnostic. Twin lamellae are often visible. Great hardness usually makes it difficult to grind thin sections to the standard (0.03 mm) thickness. Sapphirine has similar indices of refraction and birefringence ($n_\alpha = 1.701–1.731$, $n_\beta = 1.703–1.741$, $n_\gamma = 1.705–1.745$, $\delta = 0.005–0.012$), but it is biaxial ($2V_x = 47–114°$) and usually has distinct pleochroism in shades of colorless to blue or pink.

Occurrence In igneous rocks, corundum is infrequently found in Al-rich, Si-poor varieties such as syenite and associated feldspathoidal pegmatites, and is usually associated with feldspars and feldspathoids but not quartz. Al-rich pelitic metamorphic rocks may contain corundum associated with aluminum silicate(s), micas, spinel, and other aluminous minerals. Gem-quality corundum usually is derived from metamorphosed limestone or dolostone; the Al presumably is derived from detrital clay minerals. Other occurrences include metamorphosed bauxite deposits, xenoliths in mafic rocks, and Si-poor hornfels.

Use Corundum is an important gemstone, and high-quality ruby can be more valuable than diamond. The color of natural ruby and sapphire can be improved by various processes, although treated samples have less value than naturally colored stones. Gem-quality corundum can be synthesized but is usually recognized because it lacks the imperfections that are almost always present in natural samples.

The gem varieties of corundum have numerous historical uses in medicine, particularly in the Middle Ages. Presumably because it is red, ruby became associated with treatment of blood and bleeding problems. Other applications included plague, eye problems, bladder and kidney problems, and poisoning. Not surprisingly, there are no modern medicinal uses.

Corundum (emery), long used as an abrasive in sandpaper, grinding wheels, and polishing compounds, is being replaced by more uniform synthetic products (silicon carbide, alumina [synthetic corundum], etc.). Emery also is used as a surface-hardening and nonskid agent in concrete, epoxy coatings, and grouting materials. End uses include pedestrian walkways, steel ship decks, roads, bridges, airport runways, and parking ramps.

Ilmenite

$FeTiO_3$

DO NOT COPY e48d507df5d1141@placeholder.94092-

Printed by: e48d507df5d1141@placeholder.94092.edu. Printing is for personal, private use only. No part of this book may be reproduced or transmitted without publisher's prior permission. Violators will be prosecuted.

Hexagonal (trigonal) $\overline{3}$

$a = 5.089$ Å, $c = 14.09$ Å,
$Z = 6$ ($a = 10.18$ Å,
$c = 14.09$ Å, $Z = 24$
to be consistent with
Miller indices)

$H = 5 - 6$

$G = 4.70 - 4.79$

Opaque

Weakly magnetic

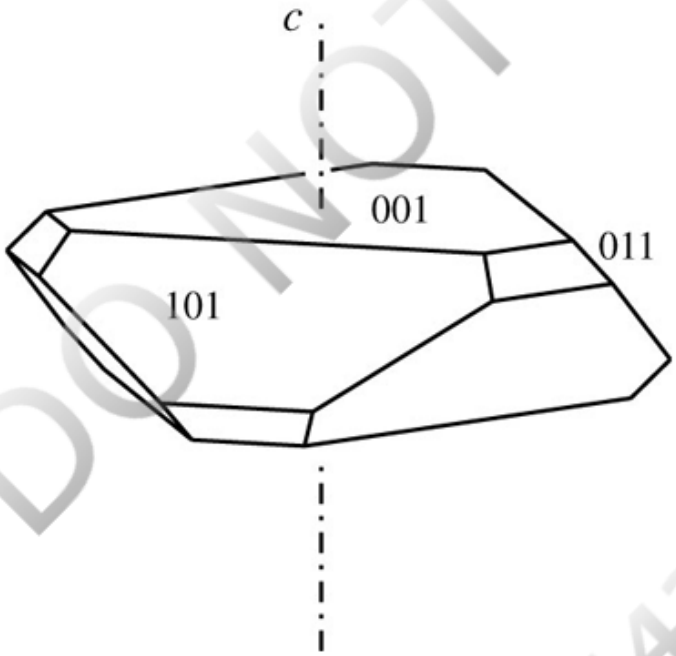

Composition Ilmenite forms a solid solution series with hematite above about 1050°C; most ilmenite contains some Fe^{3+} substituting for $Fe^{2+}Ti^{4+}$. Substantial amounts of Mg and Mn may also substitute for Fe^{2+}.

Form and Twinning Crystals are tabular parallel to {001} with a hexagonal cross section modified by rhombohedral truncations. Also as granular masses and anhedral grains, and common as exsolution lamellae in magnetite. Simple {001} and lamellar {101} twins are common.

Cleavage None, but partings on {001} and {101} may be distinct. Conchoidal to irregular fracture. Brittle.

Color Properties

DO NOT COPY
e48d507df5d1141@placeholder.9409

Printed by: e48d507df5d1141@placeholder.94092.edu. Printing is for personal, private use only. No part of this book may be reproduced or transmitted without publisher's prior permission. Violators will be prosecuted.

Luster: Metallic.

Color: Black.

Streak: Black.

Optical Characteristics

Thin Section: Opaque.

Polished Section: Brownish with a pink or violet tint, distinct bireflectance, and reflection pleochroism. Dark brown internal reflections are rare. Anisotropism is strong in crossed polarizers with gray to brownish-gray polarization colors.

Alteration Ilmenite may be altered to leucoxene, a name applied to a fine-grained yellowish, grayish, or brownish mixture of Ti- and Fe-bearing oxides, hydroxides, and other minerals.

Distinguishing Features

Hand Sample: Distinguished from specular hematite by a black streak and from magnetite by weak magnetism. Pure ilmenite is paramagnetic above −218°C, meaning that it does not behave like a magnet. Ilmenite–hematite solid solutions, however, are weakly magnetic. In addition, most ilmenite, particularly if found in large masses, contains intergrown and exsolved magnetite that contributes to the magnetic behavior.

Thin Section/Grain Mount: Entirely opaque. Hematite may be dark red-brown on thin edges or in small grains. Magnetite crystallizes in octahedrons that yield four- or six-sided cross sections rather than the tabular shapes typical of ilmenite.

Polished Section: Somewhat browner color than either magnetite or hematite. Hematite usually displays red internal reflections.

Occurrence Ilmenite is a common accessory mineral in a wide variety of igneous and metamorphic rocks, either as exsolved lamellae in magnetite grains or as separate grains. Larger masses of ilmenite are typically associated with bodies of gabbro, norite, anorthosite, and related mafic and ultramafic rocks. Detrital sands often contain ilmenite as part of the heavy mineral fraction; it also is a biomineral.

Use Ilmenite is a major ore mineral from which titanium is extracted. Much of the world's economic deposits are alluvial or beach placer deposits. Metallic titanium is similar to aluminum, but has higher strength and greater corrosion resistance. Titanium is also alloyed with iron to make high-strength steel. The major use of titanium is to produce brilliant white pigment (TiO_2) used in paints, plastics, foods, and many other products. Ilmenite is also used as a filter agent in water treatment plants, as a sandblast abrasive, as foundry sand, and as a coating on welding rods.

DO NOT COPY e48d507df5d1141@placeholder.9409

Printed by: e48d507df5d1141@placeholder.94092.edu. Printing is for personal, private use only. No part of this book may be reproduced or transmitted without publisher's prior permission. Violators will be prosecuted.

XO_2 Group

Rutile (TiO_2) and cassiterite (SnO_2) are isostructural and crystallize to form tetragonal crystals. Pyrolusite (MnO_2), which shares the same structure, is included in the discussion of manganese oxide and hydroxide minerals below. The rutile, cassiterite, and pyrolusite structure can be visualized as chains of edge-sharing octahedra that extend parallel to *c* along each corner of the unit cell (Figure 18.7). An additional edge-sharing chain of octahedra extends parallel to *c* in the center of the unit cell and shares corners with and cross-links the chains on the corners.

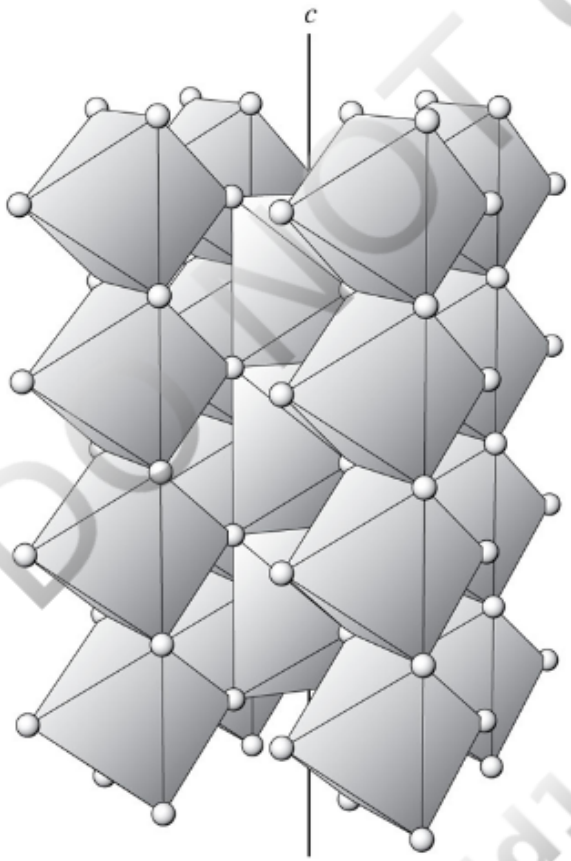

FIGURE 18.7 Rutile, cassiterite, and pyrolusite structure. The Ti^{2+}, Sn^{2+}, or Mn^{2+} cations occupy octahedra that form edge-sharing chains extending parallel to *c* along the corners and center of the unit cell. View larger image

Uraninite is another member of the XO_2 group, but it is isostructural with fluorite (see Figure 18.11) because U is too large to fit into octahedral coordination. In this structure, which is isometric, the anions are arranged in sheets where the anions form a square pattern. Successive sheets are stacked directly on top of each other to form cubic (8-fold) coordination sites. Alternate 8-fold sites are occupied by the cations. This places U cations at the corners and center of the unit cell.

DO NOT COPY e48d507df5d1141@placeholder.9409

Printed by: e48d507df5d1141@placeholder.94092.edu. Printing is for personal, private use only. No part of this book may be reproduced or transmitted without publisher's prior permission. Violators will be prosecuted.

Rutile

$$TiO_2$$

$$\text{Tetragonal } 4/m\,2/m\,2/m$$

$$a = 4.593 \text{ Å},\ c = 2.959 \text{ Å},\ Z = 2$$

$$H = 6 - 6.5$$

$$G = 4.23 - 5.5$$

$$\text{Uniaxial } (+)$$

$$n_\omega = 2.605 - 2.613$$

$$n_\epsilon = 2.899 - 2.901$$

$$\delta = 0.29$$

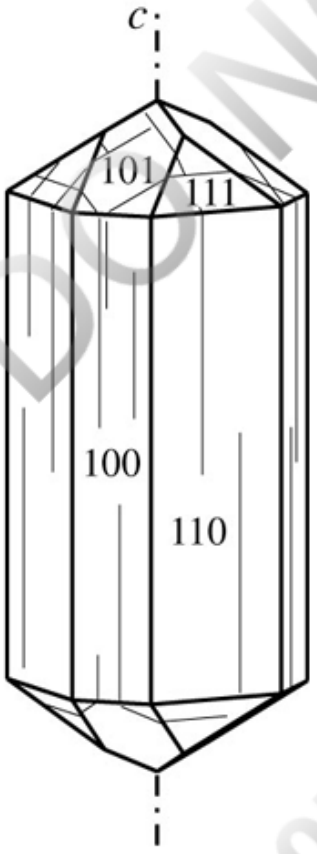

DO NOT COPY
e48d507df5d1141@placeholder.9409

Composition Most rutile is nearly pure TiO_2, but some Fe, Ta, Sn, Nb, Zr, and U may substitute for Ti, and some Cr and V may be present.

Form and Twinning Crystals are elongate tetragonal prisms, often with dipyramidal terminations. Also as anhedral grains or slender, acicular, or fibrous crystals. Contact

Printed by: e48d507df5d1141@placeholder.94092.edu. Printing is for personal, private use only. No part of this book may be reproduced or transmitted without publisher's prior permission. Violators will be prosecuted.

twins on {101} are common and may be elbow shaped or cyclic (Figures 5.21a, 5.24b). Also twins by gliding on {011} and {092}, and rare contact twins on {031}.

Cleavage {110} good, {010} fair, with partings on {092} and {011}. Conchoidal, subconchoidal to uneven fracture. Brittle.

Color Properties

Luster: Metallic to adamantine.

Color: Reddish brown; also black, violet, yellow, or green.

Streak: White.

Color in Thin Section: Yellowish to reddish brown, darker with Fe content.

Pleochroism: Weak, $\epsilon > \omega$.

Optical Characteristics

Relief in Thin Section: Extremely positive.

Optic Orientation: Elongate crystals show parallel extinction and are length slow, but extreme birefringence makes determining sign of elongation in thin section impractical.

Indices of Refraction and Birefringence: Little variation of refractive indices. Birefringence is extreme and yields upper-order white interference colors that are masked by mineral color.

Interference Figure: Basal sections yield uniaxial positive figures with numerous isochromes. May be anomalously biaxial (+) with $2V_z$ up to 10°.

Polished Section: Gray with bluish tint, distinct bireflectance, and reflection pleochroism. Abundant strongly colored internal reflections (white, brown, violet, green, etc.). Strong crossed-polarizer anisotropy, colors often masked by internal reflections.

Alteration Alteration to leucoxene (gray, yellow, or brown mix of Ti- and Fe-oxides and hydroxides and other minerals) is not uncommon. Rutile may form as an alteration product after other Ti-bearing minerals.

Distinguishing Features

Hand Sample: Characterized by adamantine to metallic luster and red-brown color.

Thin Section/Grain Mount: Color, extreme birefringence, extreme relief, and habit are characteristic. Hematite is opaque unless quite thin. Cassiterite is similar but has lower birefringence and refractive indices. Fine fibrous sillimanite has much lower birefringence and is not colored. Anatase and brookite are polymorphs of rutile with similar structure and properties. Both are much rarer than rutile. Anatase is uniaxial

DO NOT COPY

Printed by: e48d507df5d1141@placeholder.94092.edu. Printing is for personal, private use only. No part of this book may be reproduced or transmitted without publisher's prior permission. Violators will be prosecuted.

negative, $n_\omega = 2.561$, $n_\epsilon = 2.488$; brookite is biaxial positive, $n_\alpha = 2.583$, $n_\beta = 2.584$, $n_\gamma = 2.700$, $2V_z = 0$–$30°$.

Polished Section: Abundant internal reflections and twins are characteristic. Cassiterite is similar, but with lower reflectance and is more difficult to polish.

Occurrence Rutile is widely distributed as an accessory mineral in many igneous and metamorphic rocks, but fine grain size may make identification difficult. Because it is fairly stable in the weathering environment, rutile is common in clastic sediments as part of the heavy mineral fraction. In some cases, rutile may be sufficiently abundant to constitute a placer deposit. Fine fibers are not uncommon as inclusions in quartz (rutilated quartz), micas, and other minerals and may give the quartz a silky appearance. Large crystals are generally restricted to pegmatites and to quartz and apatite-bearing veins.

Use Rutile is a significant source of titanium, generally mined from placer deposits. See discussion of ilmenite for additional information. Zirconium content is largely controlled by temperature (Kohn, 2020), so careful determination of Zr content can lead to estimates of rutile and rock (re)crystallization temperatures. Trace U content can be used to date crystallization or cooling of rutile to below its closure temperature of about 500°C via the U–Pb technique (Box 5.1).

Cassiterite

$$SnO_2$$

$$\text{Tetragonal } 4/m\ 2/m\ 2/m$$

$$a = 4.738\ \text{Å},\ c = 3.188\ \text{Å},\ Z = 2$$

$$H = 6 - 7$$

$$G = 6.9 - 7.1$$

$$\text{Uniaxial } (+)$$

$$n_\omega = 1.990 - 2.010$$

$$n_\epsilon = 2.091 - 2.100$$

$$\delta = 0.10 - 0.09$$

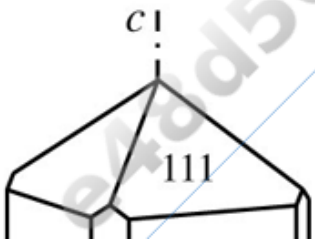

DO NOT COPY
e48d507df5d1141@placeholder.9409

Printed by: e48d507df5d1141@placeholder.94092.edu. Printing is for personal, private use only. No part of this book may be reproduced or transmitted without publisher's prior permission. Violators will be prosecuted.

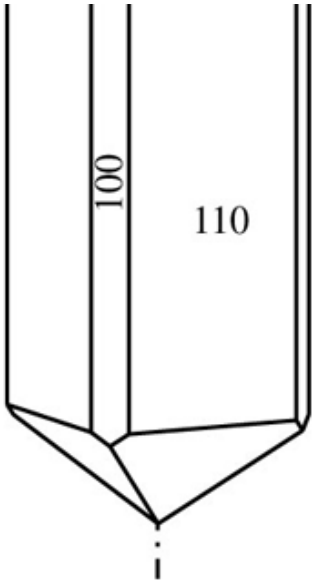

Composition Fe^{3+} is the most common element to substitute for Sn; also some Ti, Nb, and Ta. The variety called wood tin, which forms botryoidal or other rounded shapes with a radiating fibrous structure, often contains intergrown hematite and quartz.

Form and Twinning Crystals are stubby tetragonal prisms with dipyramidal terminations, sometimes elongate prismatic or less commonly pyramidal. Also fine- to coarse-granular massive and in the radially fibrous, concretionary, or botryoidal masses or crusts collectively called wood tin. Contact and penetration twins on {101} are common and may form simple, polysynthetic, or cyclic patterns (Figures 5.21a, 5.24).

Cleavage Fair {100} and poor on {110} and {111} cleavages; also {101} parting. Conchoidal to uneven fracture. Brittle.

Color Properties

Luster: Adamantine to splendent; also earthy.

Color: Yellowish or reddish brown, brownish black; also red, yellow, gray; rarely white.

Streak: Grayish or brownish white.

Color in Thin Section: Distinctly colored in shades of yellow, brown, or red, or greenish; rarely colorless. Color zoning or irregular distribution of color is common. Detrital grains and fragments in grain mount may be nearly opaque.

Pleochroism: Weak to strong, $\omega < \epsilon$.

Optical Characteristics

Relief in Thin Section: Very high positive.

Optic Orientation: Crystals are length slow, but sign of elongation may be difficult to obtain because of extreme birefringence.

DO NOT COPY
e48d507df5d1141@placeholder.9409

Printed by: e48d507df5d1141@placeholder.94092.edu. Printing is for personal, private use only. No part of this book may be reproduced or transmitted without publisher's prior permission. Violators will be prosecuted.

obtain because of extreme birefringence.

Indices of Refraction and Birefringence: Birefringence is extreme; upper-order colors are usually masked by mineral color.

Interference Figure: Uniaxial positive, but some may be anomalously biaxial.

Polished Section: Distinct gray to brownish gray reflection pleochroism with bireflectance and abundant yellow to yellow-brown internal reflections. Distinct crossed polarizers anisotropism with gray polarization colors, often masked by internal reflections.

Alteration Stable in the weathering environment and not readily altered. Cassiterite may be produced by alteration of Sn-bearing sulfide minerals.

Distinguishing Features

Hand Sample: Resembles rutile but with higher specific gravity and more distinctly brown color. Wood tin may resemble goethite and other iron hydroxides but has lighter streak, is harder, and has higher specific gravity.

Thin Section/Grain Mount: Extreme relief and birefringence and distinct color are characteristic. Rutile is quite similar but has even higher birefringence and refractive indices.

Polished Section: Polishes poorly and has numerous internal reflections. Resembles rutile.

Occurrence Cassiterite is not particularly common but may be found in some high-Si granites and granitic pegmatites, and in high-temperature hydrothermal veins associated with wolframite and molybdenite. Skarns developed in carbonate rocks adjacent to granitic intrusions may contain cassiterite. The term *greisen* is applied to metasomatically altered rocks, usually along veins, that contain cassiterite, topaz, tourmaline, muscovite, lepidolite, and fluorite. Wood tin may form by low-temperature colloidal precipitation processes in rhyolitic volcanics, and forms in the near-surface oxidized zone of hydrothermal tin deposits. Because it is stable in the weathering environment, cassiterite may be found in the heavy mineral fraction of detrital sediment and locally may be concentrated to form economic placer deposits.

Use Cassiterite is the principal ore of tin, and most is mined from fluvial and beach placer deposits. One of the principal uses is to manufacture tin-plated steel from which food containers are made. These “tin cans” are economical, and both the tin and steel can be recycled. Plastic, aluminum, and tin-free steel containers have replaced tin-plated cans for many uses. Tin is alloyed with copper to form bronze, and with lead and antimony to form solder used in the electronics industry and plumbing. Tin was one of the earlier metals to be extracted and used by humans.

Uraninite

DO NOT COPY e48d507df5d1141@placeholder.9409

Printed by: e48d507df5d1141@placeholder.94092.edu. Printing is for personal, private use only. No part of this book may be reproduced or transmitted without publisher's prior permission. Violators will be prosecuted.

UO_2

Isometric $4 / m \, \overline{3} \, 2 / m$

$a = 5.468$ Å, $Z = 4$

$H = 5 - 6$

$G = 10.95$ (pure), $6.5 - 10$ (typical)

Opaque except on thin edges

Isotropic

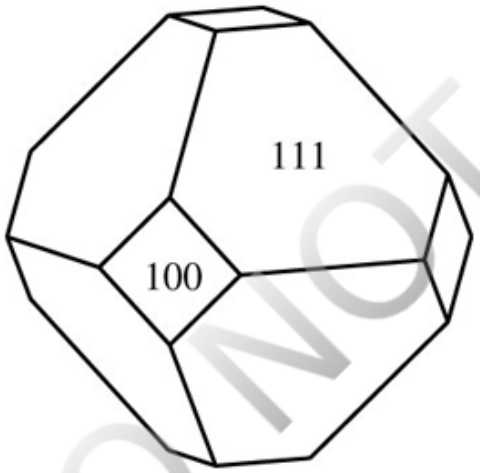

Composition Th may substitute for U to form a continuous solid solution to thorianite (ThO_2). Some U^{6+} is always present. Charge balance is maintained by substituting two U^{6+} for three U^{4+} and leaving sites vacant.

Form and Twinning Crystals are octahedrons with cube and dodecahedron modifications. Also massive granular, or as colloform, botryoidal, or reniform encrustations usually called pitchblende. Rare {111} twins.

Cleavage None; fracture conchoidal to uneven. Brittle.

Color Properties

Luster: Submetallic, pitchy, also earthy.

Color: Steely black or brownish black.

Streak: Brownish black or grayish.

Color in Thin Section: Opaque, dark greenish or yellowish brown on thin edges. Isotropic.

Optical Properties

DO NOT COPY e48d507df5d1141@placeholder.9409

Printed by: e48d507df5d1141@placeholder.94092.edu. Printing is for personal, private use only. No part of this book may be reproduced or transmitted without publisher's prior permission. Violators will be prosecuted.

Polished Section: Gray with brown tint. Isotropic, but some samples may be weakly anisotropic. Dark brown to reddish-brown internal reflections may be seen.

Alteration Uraninite alters easily by oxidation to U_3O_8 and a variety of other U-bearing oxide, carbonate, sulfate, and phosphate minerals, some of which are brightly colored.

Distinguishing Features

Hand Sample: Black color, pitchy luster, and radioactivity are distinctive. Radioactivity can be detected with a Geiger or scintillation counter.

Thin Section/Grain Mount: Because it is essentially opaque, it is not easily identified in conventional thin section.

Polished Section: Similar to magnetite, but the colloform textures are usually different than textures found with magnetite.

Occurrence Uraninite is found in some medium- to high-temperature hydrothermal vein systems, granitic and syenitic pegmatites, and sediment-hosted uranium deposits. The uraninite in sediment-hosted uranium deposits is commonly concentrated at oxidation–reduction fronts. Uranium appears to be moderately soluble in oxygenated water but precipitates if oxygen is removed by oxidation of iron-bearing minerals or organic material. There is growing evidence that microorganisms are actively involved in forming these sediment-hosted deposits (e.g., Min and others, 2005). Because it is well documented that uraninite will precipitate by biologically induced processes on the cell walls of microbes, techniques that use microbes to clean up uranium-contaminated water from mine and mill sites are being developed.

Use Uraninite is mined as a source of uranium, whose principal use is as a fuel for nuclear reactors, which now produce a significant amount of the world's electrical energy.

Comments The uranium and thorium in uraninite are both radioactive. Although casual handling of uraninite samples poses no significant risks, and normal storage cabinets provide shielding from most of the emitted radiation, good practice suggests that some caution is appropriate.

DO NOT COPY e48d507df5d1141@placeholder.9409

Printed by: e48d507df5d1141@placeholder.94092.edu. Printing is for personal, private use only. No part of this book may be reproduced or transmitted without publisher's prior permission. Violators will be prosecuted.

Hydroxides

The hydroxides as a group are very common minerals, with many species produced by the weathering and hydration of other minerals. In most cases these minerals occur as fine-grained aggregates, usually intermixed with other minerals, including the clays, which are produced by weathering or alteration.

The structures of two hydroxides, brucite [$Mg(OH)_2$] and gibbsite [$Al(OH)_3$], are significant because they are commonly used as a starting point for describing the sheet silicates (Chapter 13). In both minerals the OH^- anions are arranged in planes (Figure 18.8a). The cations (Mg or Al) occupy octahedral sites between planes of OH^- to form electrically neutral sheets that are two OH^- planes, or 4.77 Å, thick. Successive octahedral sheets are bonded to each other through weak electrostatic bonds, giving both gibbsite and brucite relatively low hardness.

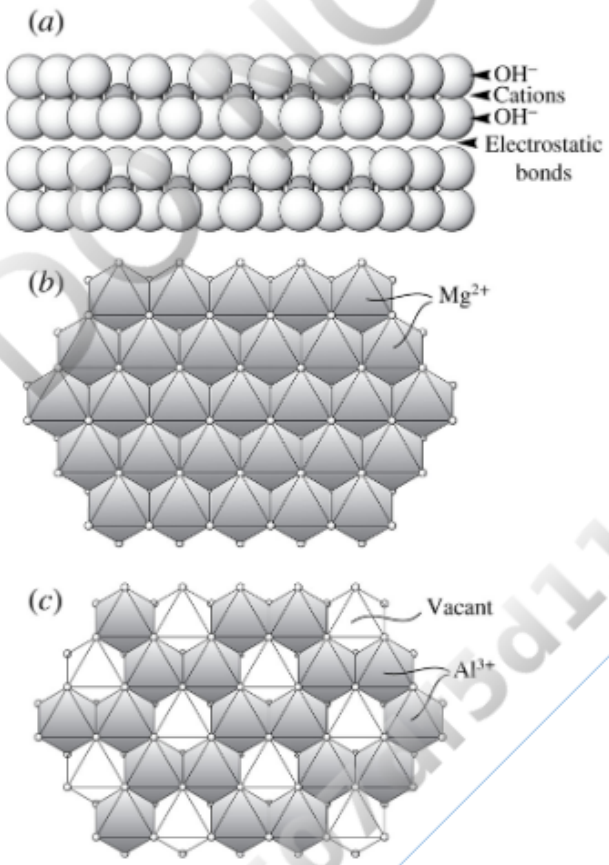

FIGURE 18.8 Brucite and gibbsite structure. (*a*) Octahedral sheets are composed of two layers of OH^- anionic groups with cations in octahedral coordination. (*b*) Plan view of brucite sheet. All octahedral sites (shaded) are occupied by Mg^{2+}. (*c*) Plan view of gibbsite sheet. Only two out of three octahedral sites are occupied by Al^{3+}; the remaining sites are vacant (no shading). View larger image

DO NOT COPY e48d507df5d1141@placeholder.9409

Printed by: e48d507df5d1141@placeholder.94092.edu. Printing is for personal, private use only. No part of this book may be reproduced or transmitted without publisher's prior permission. Violators will be prosecuted.

In the brucite structure (Figure 18.8b), charge balance requires that all the octahedral sites in each sheet be filled with divalent Mg. Because three of three octahedral sites are filled, this structure is sometimes referred to as trioctahedral (see Chapter 13).

In the gibbsite structure (Figure 18.8c), Al^{3+} is the cation. To balance the anion charge, only two Al^{3+} are required, whereas three Mg^{2+} are required in brucite. In the gibbsite structure, therefore, only two-thirds of the octahedral sites are occupied by Al^{3+}; the remaining sites are vacant. Because only two of three octahedral sites are occupied, the gibbsite structure is referred to as dioctahedral (see Chapter 13). Successive octahedral sheets are stacked somewhat differently than in brucite, so gibbsite's unit cell is two octahedral sheets thick, or 9.72 Å.

Brucite

$$\mathrm{Mg(OH)_2}$$

$$\text{Hexagonal (trigonal) } 3\ 2\ /\ m$$

$$a = 3.14\ \text{Å},\ c = 4.77\ \text{Å},\ Z = 1$$

$$H = 2.5$$

$$G = 2.39$$

$$\text{Uniaxial } (+)$$

$$n_\omega = 1.559 - 1.590$$

$$n_\epsilon = 1.580 - 1.600$$

$$\delta = 0.010 - 0.021$$

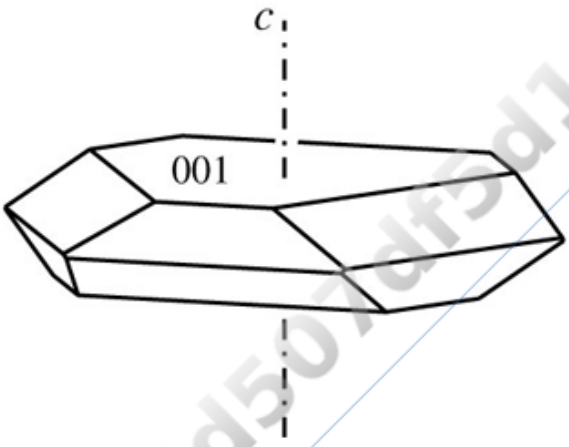

Composition Some Fe^{2+} and limited Mn^{2+} may substitute for Mg.

Form and Twinning Crystals are hexagonal mica-like plates tabular parallel to {001}.

DO NOT COPY
e48d507df5d1141@placeholder.9409

Printed by: e48d507df5d1141@placeholder.94092.edu. Printing is for personal, private use only. No part of this book may be reproduced or transmitted without publisher's prior permission. Violators will be prosecuted.

Form and Twinning Crystals are hexagonal tabular plates flattened parallel to {001}. Usually as foliated or swirled masses and aggregates or granular masses. Fibrous brucite, known as nemalite, is uncommon. No twinning reported.

Cleavage Perfect on {001}.

Color Properties

Luster: Vitreous to pearly or waxy.

Color: White, gray, pale green, brown, or blue.

Streak: White.

Color in Thin Section: Colorless.

Optical Characteristics

Relief in Thin Section: Moderate positive.

Optic Orientation: The trace of cleavage in folia is length fast; fibers are elongate perpendicular to *c* and also are length fast.

Indices of Refraction and Birefringence: Indices of refraction increase with Fe content. First-order interference colors are usually anomalously reddish brown or bluish.

Interference Figure: Cleavage fragments yield centered optic axis figures, but small grain size often precludes obtaining usable figures. Some samples, particularly if fibrous, may be anomalously biaxial with small 2*V*.

Alteration Brucite may alter to hydromagnesite [$3MgCO_3 \cdot Mg(OH)_2 \cdot 3H_2O$] or to other Mg-bearing minerals, including serpentine and periclase.

Distinguishing Features

Hand Sample: Brucite is harder than talc and gypsum and has a less greasy feel than talc; folia are not elastic like those of muscovite. Fibers are not as silky or fine as in chrysotile.

Thin Section/Grain Mount: Both talc and micas are biaxial negative and have higher birefringence; gypsum is biaxial positive. Chlorite and serpentine are usually pale green, length slow, and biaxial. Brucite may be stained to aid in identification (Haines, 1968).

Occurrence Most commonly found in marble, often as an alteration product after periclase. Also found in serpentinite and chlorite schist, usually as small veins, along with talc, magnesite, and other Mg-bearing minerals.

Use Brucite has been quarried for use in refractory materials.

Iron Hydroxide Minerals

DO NOT COPY

Printed by: e48d507df5d1141@placeholder.94092.edu. Printing is for personal, private use only. No part of this book may be reproduced or transmitted without publisher's prior permission. Violators will be prosecuted.

Iron Hydroxide Minerals

The term limonite is generically used for a rock composed of mixtures of various Fe-oxide and hydroxide minerals. The most common of these minerals are goethite and lepidocrocite (Table 18.4). Hematite also may be present, along with clay, quartz/microcrystalline quartz, and other minerals. Fine grain size usually makes identification of the constituent minerals impractical without X-ray diffraction techniques. Despite being officially classified as a rock, it may be treated as a mineral as its physical properties are fairly consistent.

TABLE 18.4 Iron Hydroxide Minerals

Mineral	Unit Cell	Physical Properties[a]	Optical Properties	Comments
Goethite α-FeO(OH)	Orthorhombic 2/*m* 2/*m* 2/*m* $a = 4.60$ $b = 9.96$ $c = 3.02$ $Z = 4$	*H*: 5–5.5 *G*: ~4.3 Cl: {010}pf, {100}f Tw: None reported C: Yellowish brown to red St: Yellowish brown L: Vitreous to earthy Antiferromagnetic, weak ferromagnetic	$n_\alpha = 2.15–2.275$ $n_\beta = 2.22–2.409$ $n_\gamma = 2.23–2.415$ $\delta = 0.138–0.140$ Biaxial (−) $2V = 0–27°$ TS: Yellow, orange-red, brownish orange: $X = b$, $Y = c$, $Z = a$ PS: Gray with bluish tint; bireflectance/pleochroism weak in air; brownish yellow to reddish brown internal reflections; distinct anisotropy, gray-blue, gray-yellow, brownish	Fibrous or acicular parallel to *c*, also granular massive, and disseminated grains; formed by weathering or alteration of Fe-bearing minerals; also in sedimentary iron formations
Lepidocrocite γ-FeO(OH)	Orthorhombic 2/*m* 2/*m* 2/*m* $a = 3.08$ $b = 12.50$ $c = 3.87$ $Z = 4$	*H*: 5 *G*: 4.09 Cl: {010}pf, {100}, {001}f Tw: None reported C: Brown to red St: Orange L: Adamantine to metallic crystals, also earthy	$n_\alpha = 1.94$ $n_\beta = 2.20$ $n_\gamma = 2.51$ $\delta = 0.57$ Biaxial (−) $2V = 83°$ TS: Yellow, orange, red: $Z > Y > X$ PS: Grayish white with weak	Platy parallel to {010} or acicular parallel to *a*; formed by weathering or alteration of Fe-bearing minerals; also in sedimentary iron formations

DO NOT COPY
e48d507df5d1141@placeholder.9409

Printed by: e48d507df5d1141@placeholder.94092.edu. Printing is for personal, private use only. No part of this book may be reproduced or transmitted without publisher's prior permission. Violators will be prosecuted.

		also earthy	to distinct bireflectance/pleochroism; strong gray anisotropy; reddish internal reflections	

[a] Cl = cleavage (pf = perfect f = fair), Tw = twinning, C = color, St = streak, L = luster, TS = thin section, PS = polished section.

Iron oxides and hydroxides are commonly produced by weathering and hydrothermal alteration. What appears to be a yellowish brown or reddish stain in many weathered rocks is very fine-grained goethite, lepidocrocite, hematite, and other minerals produced by the breakdown of biotite, amphibole, pyroxene, magnetite, or other Fe-bearing minerals. Large masses of limonite can be produced by alteration and oxidation of pyrite (FeS_2) in hydrothermal sulfide deposits. Limonite may form pseudomorphs, granular masses, or botryoidal, rounded, or encrusting masses with a radiating internal structure. Intense weathering of Fe-bearing rock may result in the formation of a soil rich in Fe-hydroxide minerals. See the discussion of bauxite below for additional information on how intense weathering can lead to Fe-hydroxide–rich materials.

Both goethite and lepidocrocite are biominerals and have been identified in the radular teeth of chitins. Microbial activity is almost certainly involved in their common occurrence in the near-surface oxidized portions of sulfide mineral deposits.

In hand sample, limonite typically is medium to dark yellowish brown with a dull to earthy luster and has a yellowish brown streak. Hematite, in contrast, has a red streak. Specific gravity is variable (2.7–4.3), as is the hardness (1–5). Limonite usually displays dark shades of red, yellow, or brown in thin section; or it may be nearly opaque. Although goethite and lepidocrocite are both strongly birefringent, that birefringence is not usually displayed because of fine grain size. The index of refraction is high (2.0–2.4).

Aluminum Hydroxide Minerals

Gibbsite, böhmite, and diaspore (Table 18.5) are fairly common minerals in soils. They also may be found in emery deposits or as a weathering or alteration product of corundum, the aluminum silicates, or other Al-rich minerals.

TABLE 18.5 Aluminum Hydroxide Minerals

Mineral	Unit Cell	Physical Properties[a]	Optical Properties	Comments
Gibbsite $Al(OH)_3$	Monoclinic 2/*m* *a* = 8.64 *b* = 5.07	*H*: 2.5–3.5 *G*: 2.4 Cl: {001}	n_α = 1.568–1.578 n_β = 1.568–1.579	Typically occurs as soil constituent produced by weathering or feldspars or other Al-bearing minerals; major mineral in bauxite and also found in some low-

DO NOT COPY e48d507df5d1141@placeholder.9409

Printed by: e48d507df5d1141@placeholder.94092.edu. Printing is for personal, private use only. No part of this book may be reproduced or transmitted without publisher's prior permission. Violators will be prosecuted.

	c = 9.72 β = 94.5° Z = 8	Tw: {001}, {110}, {100}, and [130] C: White, gray, pale pink, green or brown St: White L: Vitreous to earthy	n_γ = 1.587–1.590 δ = 0.019–0.012 Biaxial (+) $2V$ = 0–40° Colorless $X = b$, $Y \wedge a$ = +25 to +35, $Z \wedge c$ = −21 to −30	and also found in some low-temperature hydrothermal environments
Böhmite γ-AlO(OH)	Orthorhombic 2/m 2/m 2/m a = 3.69 b = 12.23 c = 2.86 Z = 4	H: 3.5–4 G: ~3.05 Cl: {010}vg, {100}g C: White St: White L: Vitreous, earthy	n_α = 1.640–1.648 n_β = 1.649–1.657 n_γ = 1.655–1.668 δ = 0.006–0.020 Biaxial (− or +) $2V_x > 80°$ Colorless $X = c$, $Y = b$, $Z = a$	Formed by weathering of aluminous minerals, especially in tropical climates; major constituent of bauxite; also low-temperature hydrothermal alteration of corundum, nepheline, and other aluminous minerals
Diaspore α-AlO(OH)	Orthorhombic 2/m 2/m 2/m a = 4.40 b = 9.42 c = 2.85 Z = 4	H: 6.5–7 G: 3.3–3.5 Cl: {010}g, {110} and {210}f, {100}pr C: White, gray, or various pale shades St: White L: Vitreous, earthy	n_α = 1.682–1.706 n_β = 1.705–1.725 n_γ = 1.730–1.752 δ = 0.04–0.05 Biaxial (+) $2V$ = 84–86° Colorless $X = c$, $Y = b$, $Z = a$	Formed by diagenesis in bauxite deposits and weathering of aluminous minerals; also hydrothermal alteration of aluminous minerals

DO NOT COPY
e48d507df5d1141@placeholder.9409

Printed by: e48d507df5d1141@placeholder.94092.edu. Printing is for personal, private use only. No part of this book may be reproduced or transmitted without publisher's prior permission. Violators will be prosecuted.

[a] Cl = cleavage (vg = very good, g = good, f = fair, pr = poor), Tw = twinning, C = color, St = streak, L = luster.

Bauxite is a rock (Figure 2.52g) that generically refers to a mixture of Al-hydroxide minerals of uncertain identity. It is an analogous term to *limonite* for material that is a mixture of Fe-oxides and hydroxides and *wad* for Fe and Mn hydroxides. Soils rich in Al-hydroxides may be referred to as bauxite as well, but this usage is not preferred.

Bauxite is typically produced in areas subjected to intense weathering, usually in tropical or semitropical climates, and usually contains clay (e.g., kaolin) and Fe-hydroxides. The intense weathering of feldspar and other minerals leaches out and removes the most soluble elements, which include the alkalis (Na and K) and alkaline earth (Mg and Ca) metals, and even Si, thus leaving a material possibly highly enriched in Al and the minerals of gibbsite, diaspore, and/or böhmite. **Laterite** is a generic term for any highly weathered material which has experienced significant leaching, including Si. If the material is cohesive and Al-hydroxide–rich, the specific term *bauxite* can be used; if the material is cohesive and Fe-oxide– and hydroxide-rich, then the term *limonite* can be used.

Karst bauxite deposits are found in solution depressions produced in limestone or dolostone bedrock. The source of the Al that forms karst bauxite is a matter of debate. One explanation is that the Al is derived from silicate minerals carried into karst depressions by wind and water. An alternative source for the aluminum is detrital clay minerals originally dispersed in the carbonate rock that are concentrated by removing the carbonate by dissolution. In either case, the original minerals are intensely weathered and leave behind mostly Al-hydroxide minerals.

As a constituent of soils and other weathering residues, the Al-hydroxide minerals will be indistinguishable from clay and other fine-grained minerals and therefore not identifiable in hand sample or thin section. Bauxite (the rock) may contain pisolitic or other concretionary structures and may be quite cohesive. Except for rare coarse-grained occurrences, X-ray diffraction and scanning electron microscope techniques are required to identify the Al-hydroxide minerals.

Bauxite and related Al-hydroxide–rich laterites are mined as the main ore of Al. Some of the main producers of Al from such sources are Venezuela, China, and Australia.

Manganese Oxide and Hydroxide Minerals

Manganese oxide and hydroxide minerals (Table 18.6) are quite common but typically occur as small grains or fine-grained masses and may be intermixed with each other or with other minerals. Identification by means of conventional hand sample and optical techniques is usually impractical. These minerals are typically black, with a dark streak and a high specific gravity (~4–7). Large crystals are usually fairly hard (5–7); but for most samples, fine grain size usually makes measurement impractical. Earthy masses of

DO NOT COPY e48d507df5d1141@placeholder.9409

Printed by: e48d507df5d1141@placeholder.94092.edu. Printing is for personal, private use only. No part of this book may be reproduced or transmitted without publisher's prior permission. Violators will be prosecuted.

these minerals may be friable and readily leave dark streaks on fingers, clothes, and so on.

TABLE 18.6 Manganese Oxide and Hydroxide Minerals

Mineral	Composition	Occurrence
Birnessite	$Na_{0.5}Mn_2O_4 \cdot 1.5H_2O$	Desert varnish, marine deposits
Braunite	$MnMn_6SiO_{12}$	Hydrothermal, Mn-rich metamorphic rocks, bog deposits, weathering
Coronadite	$PbMn_8O_{16}$	Dendrites, weathering, alteration
Cryptomelane	KMn_8O_{16}	Dendrites, weathering, alteration, marine deposits
Hausmannite	$MnMn_2O_4$	Hydrothermal, metamorphic
Hollandite	$BaMn_8O_{16}$	Dendrites, weathering, alteration
Manganite	$MnO(OH)$	Hydrothermal, bog and marine deposits
Pyrolusite	MnO_2	Bog and marine deposits, alteration product
Romanechite	$(Ba,H_2O)_2Mn_5O_{10}$	Bog and marine deposits, alteration product, dendrites
Todorokite	(Mn,Ca,Na,K) $(Mn,Mg)_6O_{12} \cdot 3H_2O$	Dendrites, weathering, alteration, marine deposits

Wad is a generic term applied to materials that include substantial amounts of Mn-oxide and hydroxide minerals of uncertain identity. Wad has the same relation to Mn-oxides and hydroxides that limonite has to Fe-oxides and hydroxides and that bauxite has to Al-hydroxides.

The environments in which manganese oxide and hydroxide minerals occur include the following.

- **Hydrothermal systems**. Manganite and hausmannite may be primary minerals in some hydrothermal vein systems.
- **Weathering and alteration of Mn minerals.** Primary Mn carbonates, silicates, and oxides (e.g., rhodochrosite, kutnohorite, rhodonite, manganite, hausmannite) may weather or alter to yield pseudomorphs, fine-grained encrusting masses, and disseminated grains of Mn-oxide and hydroxide minerals.
- **Weathering and alteration of other minerals.** Many Fe–Mg minerals (magnetite, biotite, olivine, pyroxene, etc.) contain small amounts of Mn substituting for Fe–Mg in their crystal structure. Weathering of these minerals may release the Mn to form Mn-oxide and hydroxide minerals. The Mn minerals usually will be intermixed with other, more abundant, weathering products.
- **Bog manganese**. Most rocks contain small amounts of Mn that can be released

DO NOT COPY e48d507df5d1141@placeholder.9409

Printed by: e48d507df5d1141@placeholder.94092.edu. Printing is for personal, private use only. No part of this book may be reproduced or transmitted without publisher's prior permission. Violators will be prosecuted.

into aqueous solution by weathering. This manganese may be precipitated in bogs and lake bottoms to form nodules and layers.

- **Ferromanganese nodules**. Some areas of the seafloor, and some freshwater lakes, are littered with nodules that contain substantial amounts of Mn- and Fe-oxide and hydroxide minerals. These minerals are inferred to have precipitated from seawater in a manner similar to bog manganese or from pore water in lake-bed or seafloor sediment. Marine nodules are typically up to 5 or 10 cm across and may be laminated. Recovering the nodules from the seafloor has been proposed, but the process appears to be uneconomic currently. Most manganese is mined from similar marine sediments now exposed on land.
- **Dendrites** (Figure 18.9) are branching mineral growths that precipitate from groundwater onto fracture surfaces. They have often incorrectly been presumed to be pyrolusite. Most dendrites are composed of coronadite, cryptomelane, hollandite, romanechite, or todorokite.
- **Desert varnish** is a red, brown, or black coating that forms on the surface of exposed rocks in desert areas. Similar materials in nonarid climates are given the more generic term *rock varnish*. Desert varnish appears to be composed mostly of air-transported clay particles that are deposited on and adhere to rock surfaces. A mixture of iron and manganese oxide minerals provide the bright coloration. A common Mn mineral in desert varnish is birnessite; pyrolusite is unlikely.

FIGURE 18.9 Dendrites on slab of sandstone. View larger image

The common issue in the formation of bog manganese, ferromanganese nodules, desert varnish, and dendrites is the requirement for some process to selectively extract and concentrate Mn from geologically ordinary environments in which the Mn is present in

Printed by: e48d507df5d1141@placeholder.94092.edu. Printing is for personal, private use only. No part of this book may be reproduced or transmitted without publisher's prior permission. Violators will be prosecuted.

low concentrations. A number of Mn-oxidizing bacteria (e.g., *Metallogenium* spp.) appear to be able to do this quite readily. The details of the biochemistry remain unclear, but these bacteria appear capable of converting Mn^{2+} to Mn^{3+} or Mn^{4+} as part of their metabolic processes and, in the process, cause the precipitation of Mn-oxides and hydroxides from the water with which the bacteria are in contact. The surfaces of the bacteria or associated fungi may serve as convenient nucleation sites for growth of the Mn and Fe minerals. Of course, not all these Mn deposits are necessarily biologically mediated, and not all workers agree that biologic processes are important processes in their formation.

Manganese minerals are mined as the source of Mn, most of which is alloyed with iron to form high-strength steel. Manganese is also used in batteries, paints, fertilizers, and animal feeds. Manganese oxides are used as pigments in the manufacture of bricks.

DO NOT COPY
e48d507df5d1141@placeholder.9409

Printed by: e48d507df5d1141@placeholder.94092.edu. Printing is for personal, private use only. No part of this book may be reproduced or transmitted without publisher's prior permission. Violators will be prosecuted.

Halides

The anion in the halide minerals is one of the halogen elements, Cl, F, Br, and I. These anions are larger than oxygen and have a strong affinity for the electrons needed to complete their outer shell. Therefore, they tend to form strongly ionic compounds with fairly simple structures. Only three halides are common and discussed in detail—halite (NaCl), sylvite (KCl), and fluorite (CaF_2). A few additional halides are listed in Table 18.7.

TABLE 18.7 Less Common Halide Minerals

Mineral	Unit Cell	Physical Properties[a]	Optical Properties	Comments
Carnallite $KMgCl_3 \cdot 6H_2O$	Orthorhombic $2/m\ 2/m\ 2/m$ $a = 16.15$ $b = 22.51$ $c = 9.58$ $Z = 12$	H: 2.5 G: 1.60 Cl: None Tw: ? C: Colorless, white, red with hematite inclusions St: White L: Greasy	$n_\alpha = 1.466$ $n_\beta = 1.474$ $n_\gamma = 1.495$ $\delta = 0.029$ Biaxial (+) $2V = 70°$ Colorless $X = b$, $Y = a$, $Z = c$	Crystals pseudohexagonal dipyramidal; usually massive granular; found in marine evaporite deposits (Box 17.2)
Cryolite Na_3AlF_6	Monoclinic $2/m$ $a = 5.40$ $b = 5.60$ $c = 7.78$ $\beta = 90.2°$ $Z = 2$	H: 2.5 G: 2.97 Cl: None, {001} and {110} parting Tw: {001} and [100] and others C: Colorless, white St: White L: Vitreous to greasy	$n_\alpha = 1.338$ $n_\beta = 1.338$ $n_\gamma = 1.339$ $\delta = 0.001$ Biaxial (+) $2V = 43°$ Colorless $X = b$, $Y \wedge a = +44°$, $Z \wedge c = -44°$	Uncommon cubelike crystals; usually massive, coarse granular; rare mineral from granitic pegmatites; important because it (or synthetic variety) is used in producing aluminum from bauxite
Chlorargyrite AgCl	Isometric $4/m\ 2/m$	H: 2–3 G: 5.5	$n = 2.071$ Colorless	Rare cubic crystals; massive waxy, platy, crusts (horn silver); supergene mineral (see

DO NOT COPY e48d507df5d1141@placeholder.94092

Printed by: e48d507df5d1141@placeholder.94092.edu. Printing is for personal, private use only. No part of this book may be reproduced or transmitted without publisher's prior permission. Violators will be prosecuted.

AgCl	$a = 5.549$ $Z = 4$	G: 5.5 Cl: None, sectile C: Gray, also yellow, greenish brown, colorless; violet-brown on exposure to light L: Resinous	Colorless	silver); supergene mineral (see Chapter 19) in oxidized portion of Ag-bearing hydrothermal sulfide deposits

[a] Cl = cleavage, Tw = twinning, C = color, St = streak, L = luster, ? = unknown.

Halite

$$\mathrm{NaCl}$$

$$\text{Isometric } 4/m\,3\,2/m$$

$$a = 5.639\ \text{Å},\ Z = 4$$

$$H = 2.5$$

$$G = 2.16 - 2.17$$

$$\text{Isotropic}$$

$$n = 1.544$$

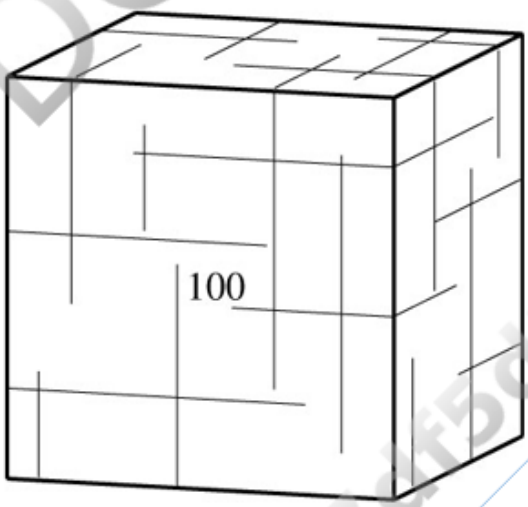

Structure The structure has been described in some detail in Chapters 3 and 4. The Na and Cl ions alternate in rows parallel to the edges of the face-centered cubic unit cell (Figure 18.10). This places the Na in octahedral coordination with Cl in a cubic close packing arrangement.

DO NOT COPY e48d507df5d1141@placeholder.9409

Printed by: e48d507df5d1141@placeholder.94092.edu. Printing is for personal, private use only. No part of this book may be reproduced or transmitted without publisher's prior permission. Violators will be prosecuted.

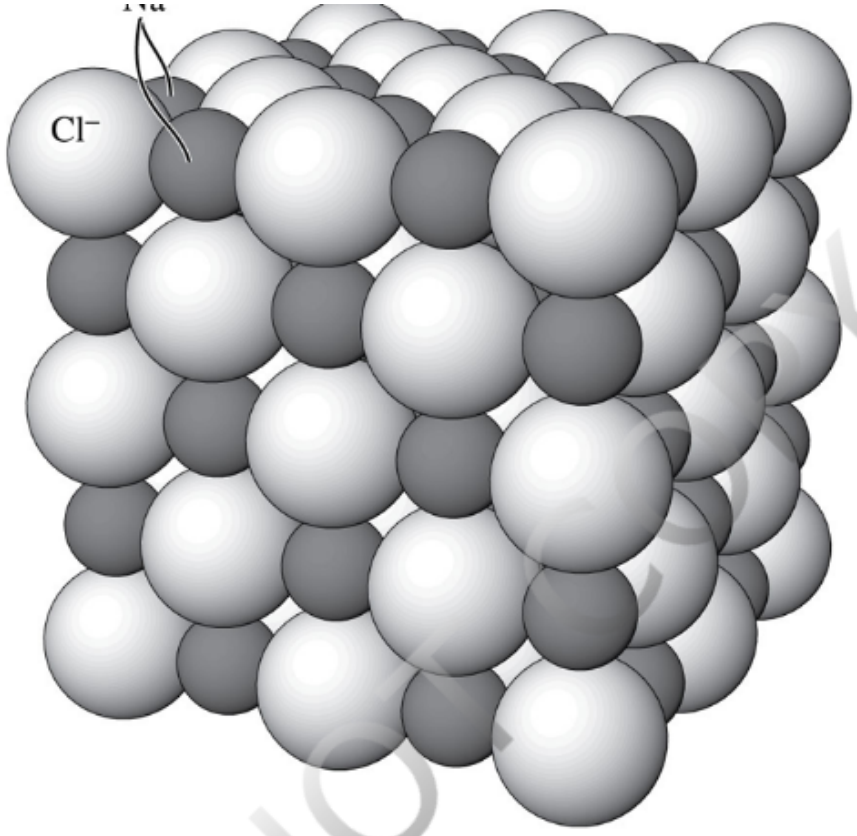

FIGURE 18.10 Halite structure. Each Na^+ coordinates with six Cl^-. View larger image

Composition Halite is usually fairly pure NaCl, with only minor substitution of K for Na. Inclusions of other minerals and saline water are common.

Form and Twinning Crystals are cubes. Rapid crystallization from oversaturated solutions may produce hopper-shaped crystals in which crystal edges and corners grow faster than the centers of crystal faces. Also massive granular. Twinning is not common with natural crystals, but synthetic crystals may twin on {111}.

Cleavage Perfect {001} cubic cleavage. Conchoidal fracture. Brittle.

Color Properties

Luster: Vitreous. May be somewhat greasy on weathered surfaces.

Color: Colorless or white if pure, may be yellow, orange, red, blue, gray, brown, and so on because of lattice imperfections or inclusions. Some samples may fluoresce.

Streak: White.

Color in Thin Section: Colorless.

Optical Characteristics

Relief in Thin Section: Low positive.

DO NOT COPY e48d507df5d1141@placeholder.9409

Printed by: e48d507df5d1141@placeholder.94092.edu. Printing is for personal, private use only. No part of this book may be reproduced or transmitted without publisher's prior permission. Violators will be prosecuted.

Index of Refraction: Intimate intergrowths of halite and sylvite (n = 1.490) may have an intermediate refractive index.

Alteration Easily dissolved in surface or groundwater. Halite is generally not preserved in outcrop except in extremely dry climates.

Distinguishing Features

Hand Sample: Cubic crystal form and cleavage and salty taste are distinctive. Sylvite has a somewhat bitter taste.

Thin Section/Grain Mount: Because it is very soluble, special preparation techniques that do not use water are required if halite is to be preserved in thin sections. The index of refraction for sylvite is less than that of the cements typically used in thin sections, while halite is higher.

Occurrence Halite is an abundant mineral in marine evaporite deposits (Box 17.2) and may form beds up to over 1000 meters thick. Associated minerals include calcite, dolomite, gypsum, anhydrite, and sylvite, along with clay and other clastic material. Halite also may be found in deposits from saline lakes and playas associated with borates, sulfates, and carbonates.

Use Halite (table salt) has been used for dietary purposes since before recorded history. Halite is an important source of dietary sodium and chlorine, though an excess is implicated in hypertension (high blood pressure). It also improves the flavor of food and can serve as a preservative. However, this use accounts for only a small fraction of total salt production. The most important use is as a feedstock in the manufacture of a wide variety of industrial chemicals. Salt is also used in metal processing, tanning and leather treatment, pharmaceuticals, paper manufacturing, and to help keep roads and sidewalks free of ice in the winter. Salt is also used in water softeners for cation exchange; see the zeolite section in Chapter 12 for further discussion.

Production of halite is generally by underground mining, evaporation of natural saline water, or solution mining. Underground mining uses conventional techniques similar in many ways to coal mining. The natural saline water from which salt is produced includes seawater, saline lakes, and natural groundwater brines. The saline water is usually pumped into a shallow pond where the water evaporates, leaving salt and whatever other minerals are in solution. Solution mining involves pumping water through a drill hole into a salt deposit. This water dissolves the salt to form a brine that is then pumped to the surface. The salt is extracted by evaporation of the water, or the brine can be piped directly to an industrial plant where it may be used in various chemical processes.

Halite has a long history of use for medical purposes, and some of those uses continue today. A typical example is gargling with salt water as a treatment for sore throat.

Sylvite

DO NOT COPY e48d507df5d1141@placeholder.94092

Printed by: e48d507df5d1141@placeholder.94092.edu. Printing is for personal, private use only. No part of this book may be reproduced or transmitted without publisher's prior permission. Violators will be prosecuted.

Sylvite

$$KCl$$

Isometric $4 / m \, \overline{3} \, 2 / m$

$$a = 6.293 \text{ Å}, \; Z = 4$$

$$H = 2.5$$

$$G = 1.99$$

Isotropic

$$n = 1.490$$

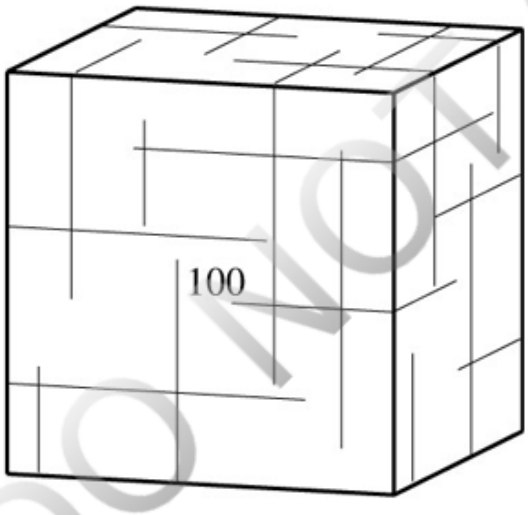

Structure Sylvite is isostructural with halite, with K in place of Na.

Composition Because K^+ and Na^+ have significantly different ionic radii, there is little solid solution between the minerals. Minor amounts of Br may substitute for Cl.

Form and Twinning Crystals are cubes, like halite. Also massive granular. {111} twins are observed in synthetic crystals.

Cleavage Perfect {001} cubic cleavage. Uneven fracture. Brittle. Somewhat sectile.

Color Properties

Luster: Vitreous.

Color: Colorless or white, also grayish, bluish, or yellowish. Iron oxide inclusions may produce an orange or reddish color.

Streak: White.

Color in Thin Section: Colorless.

DO NOT COPY e48d507df5d1141@placeholder.9409

Printed by: e48d507df5d1141@placeholder.94092.edu. Printing is for personal, private use only. No part of this book may be reproduced or transmitted without publisher's prior permission. Violators will be prosecuted.

Optical Characteristics

Relief in Thin Section: Moderate negative.

Index of Refraction: Uncommon submicroscopic mixtures of halite and sylvite may produce indices of refraction intermediate between the two minerals.

Alteration Easily dissolved in surface or groundwater, so sylvite is rarely preserved in outcrop.

Distinguishing Features

Hand Sample: Closely resembles halite in almost every respect but it has a more bitter taste. When scratched with a knife blade, halite yields a white powder, but sylvite, because it is more sectile, yields very little. Granular massive sylvite can sometimes be seen to fill in around cubic crystals of halite, indicating that the halite crystallized first.

Thin Section/Grain Mount: Sylvite is very soluble in water, so it will not be preserved in conventionally made thin sections. Moderate negative relief (in specially prepared thin sections) distinguishes sylvite from halite. The difference in index of refraction measured in grain mount is diagnostic.

Occurrence Sylvite is found in marine evaporite deposits (Box 17.2) but is much less abundant than halite. Precipitation of sylvite from seawater requires substantially more evaporation than halite. Associated minerals include halite, calcite, dolomite, gypsum, anhydrite, and detrital clay, oxide, and other minerals.

Use A small amount of sylvite is used as a salt substitute for those who need to restrict their dietary sodium. The majority of sylvite is mined for use in fertilizer to provide potassium, which is essential for plant growth. Potassium derived from sylvite also finds uses in a wide variety of industrial applications.

Fluorite

$$\mathrm{CaF_2}$$

$$\text{Isometric } 4\,/\,m\,\overline{3}\,2\,/\,m$$

$$a = 5.463\ \text{Å},\ Z = 4$$

$$H = 4$$

$$G = 3.18$$

$$\text{Isotropic}$$

$$n = 1.433 - 1.435$$

DO NOT COPY e48d507df5d1141@placeholder.9409

Printed by: e48d507df5d1141@placeholder.94092.edu. Printing is for personal, private use only. No part of this book may be reproduced or transmitted without publisher's prior permission. Violators will be prosecuted.

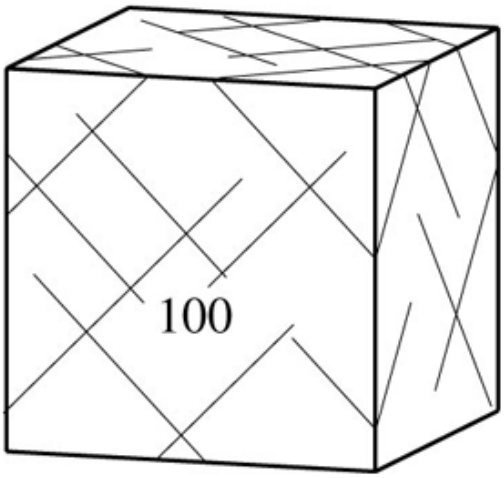

Structure The structure of fluorite (Figure 18.11) consists of layers of F anions in a square arrangement stacked directly on top each other to form cubic (8-fold) coordination sites for the Ca. Alternate 8-fold sites are occupied with Ca such that the cations are located at the corners and center of a cubic lattice.

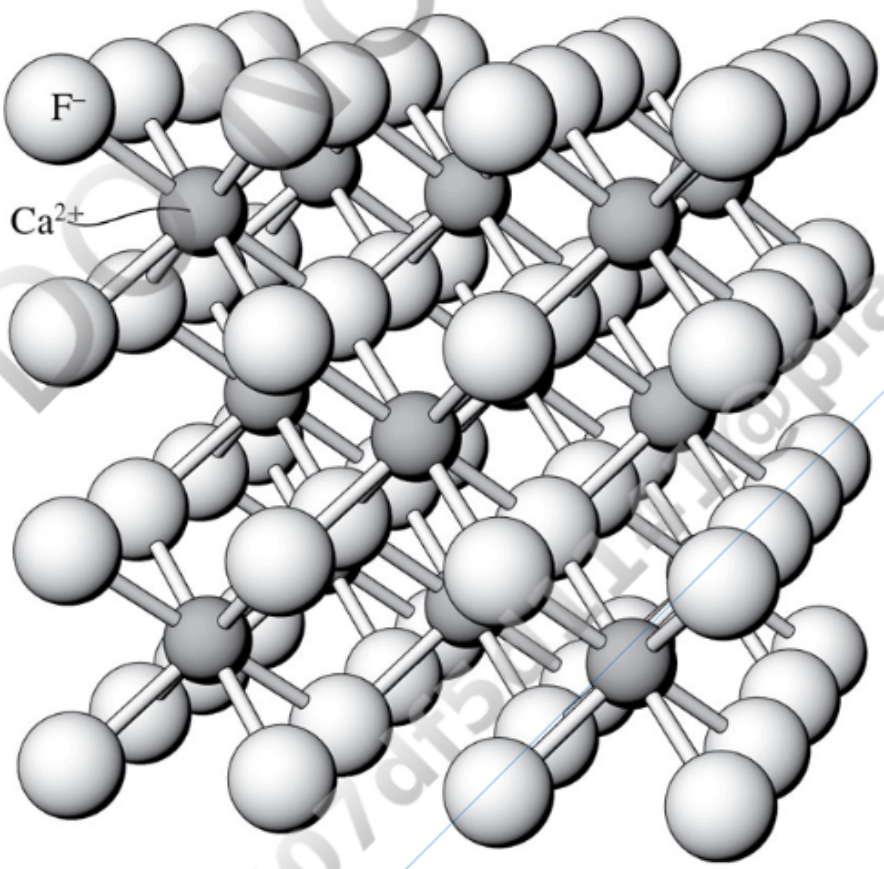

FIGURE 18.11 Fluorite structure. Each Ca^{2+} coordinates with 8 F^-. View larger image

Composition The composition is generally close to the ideal CaF_2. Minor substitution of Sr, Y, or Ce for Ca is possible.

Form and Twinning Crystals are cubes, sometimes modified by {111} octahedron or

Printed by: e48d507df5d1141@placeholder.94092.edu. Printing is for personal, private use only. No part of this book may be reproduced or transmitted without publisher's prior permission. Violators will be prosecuted.

Form and Twinning Crystals are cubes, sometimes modified by {111} octahedron or other forms (Figure 18.12). Also found as granular masses. Penetration twins by rotation on [111] are common.

FIGURE 18.12 Fluorite crystals. Field of view is about 15 cm wide. View larger image

Cleavage Perfect {111} cleavage (four directions) that may produce cleaved octahedrons. Subconchoidal to uneven fracture. Brittle.

Color Properties

Luster: Vitreous.

Color: Commonly colorless, blue, purple, or green, but almost any color is possible. Usually fluoresces in both long- and short-wave UV light, and some varieties are phosphorescent. Color centers are responsible for most of the colors.

Streak: White.

Color in Thin Section: Colorless or pale version of hand sample color. Not pleochroic.

Optical Characteristics

Relief in Thin Section: Moderately low negative.

Index of Refraction: Usually very close to 1.434, but substitution of Y for Ca increases the index to as high as 1.457.

Alteration Pseudomorphs of quartz, clay, Mn minerals, carbonate, and others after fluorite are fairly common.

DO NOT COPY e48d507df5d1141@placeholder.94092

Printed by: e48d507df5d1141@placeholder.94092.edu. Printing is for personal, private use only. No part of this book may be reproduced or transmitted without publisher's prior permission. Violators will be prosecuted.

Distinguishing Features

Hand Sample: Cubic crystals, octahedral cleavage, and hardness are distinctive. Anhedral material may resemble quartz, but is softer and displays cleavage.

Thin Section/Grain Mount: Isotropic character and index of refraction are characteristic.

Occurrence Fluorite is a common mineral in hydrothermal mineral deposits associated with sulfides (pyrite, galena, sphalerite, etc.), carbonates, and barite; it has been found in geodes. Fluorite can be found as a minor mineral in granite, pegmatites, syenite, and greisen. It may occur as veins in carbonate sediments, as detrital grains, or (rarely) as a cement in sandstone. Fluorite is a biomineral, found as very small grains in the gizzard plates of a gastropod (Lowenstam and McConnell, 1968).

Use Given that fluorite forms eye-catching crystals, it is not surprising that it has a number of historical medical uses, including in traditional Chinese medicine, where it has been used for insomnia, anxiety, coughs and wheezing, and for excessive menstrual bleeding.

Fluorite is the principal source of fluorine used in chemical processes. Fluoride compounds are added to drinking water, toothpaste, and mouthwash to help prevent dental cavities. One of the most important uses of fluorite is as a flux in steel-making and other metallurgical processes. Clear fluorite can be used for microscope and telescope lenses.

Chlorofluorocarbon compounds, whose uses include refrigerants in air conditioners and refrigerators, blowing agents in plastic foams, fire extinguishers, solvents and in other industrial applications, are implicated in loss of ozone in the stratosphere and are greenhouse gases. The manufacture and use of these substances are being phased out under the terms of the Montreal Protocol, an international treaty that has been ratified by most nations.

Fluorocarbons are chemically similar to chlorofluorocarbons, but they lack Cl. Many are highly hydrophobic (repel water) and are generally nonreactive. They have wide use as the nonstick surface of cookware, as labware, coatings on rain clothing, in ski waxes, and just about anywhere a slippery or highly water-repellant surface is needed. They additional have medical uses, plus a variety of other specialty uses. However, their use is being banned because some are very strong greenhouse gases, some cause cancer, and they break down so slowly that they are accumulating in the environment.

DO NOT COPY e48d507df5d1141@placeholder.9409

Printed by: e48d507df5d1141@placeholder.94092.edu. Printing is for personal, private use only. No part of this book may be reproduced or transmitted without publisher's prior permission. Violators will be prosecuted.

long- and short-wave UV light, and some varieties are phosphorescent. Color centers are responsible for most of the colors.
Streak: White.

Color in Thin Section: Colorless or pale version of hand sample color. Not pleochroic.

Optical Characteristics

Relief in Thin Section: Moderately low negative.

Index of Refraction: Usually very close to 1.434, but substitution of Y for Ca increases the index to as high as 1.457.

Alteration Pseudomorphs of quartz, clay, Mn minerals, carbonate, and others after fluorite are fairly common.

Distinguishing Features

Hand Sample: Cubic crystals, octahedral cleavage, and hardness are distinctive. Anhedral material may resemble quartz, but is softer and displays cleavage.

Thin Section/Grain Mount: Isotropic character and index of refraction are characteristic.

Occurrence Fluorite is a common mineral in hydrothermal mineral deposits associated with sulfides (pyrite, galena, sphalerite, etc.), carbonates, and barite; it has been found in geodes. Fluorite can be found as a minor mineral in granite, pegmatites, syenite, and greisen. It may occur as veins in carbonate sediments, as detrital grains, or (rarely) as a cement in sandstone. Fluorite is a biomineral, found as very small grains in the gizzard plates of a gastropod (Lowenstam and McConnell, 1968).

Use Given that fluorite forms eye-catching crystals, it is not surprising that it has a number of historical medical uses, including in traditional Chinese medicine, where it has been used for insomnia, anxiety, coughs and wheezing, and for excessive menstrual bleeding.

Fluorite is the principal source of fluorine used in chemical processes. Fluoride compounds are added to drinking water, toothpaste, and mouthwash to help prevent dental cavities. One of the most important uses of fluorite is as a flux in steel-making and other metallurgical processes. Clear fluorite can be used for microscope and telescope lenses.

Chlorofluorocarbon compounds, whose uses include refrigerants in air conditioners and refrigerators, blowing agents in plastic foams, fire extinguishers, solvents and in other industrial applications, are implicated in loss of ozone in the stratosphere and are greenhouse gases. The manufacture and use of these substances are being phased out under the terms of the Montreal Protocol, an international treaty that has been ratified by most nations.

DO NOT COPY e48d507df5d1141@placeholder.94092

Printed by: e48d507df5d1141@placeholder.94092.edu. Printing is for personal, private use only. No part of this book may be reproduced or transmitted without publisher's prior permission. Violators will be prosecuted.

most nations.

Fluorocarbons are chemically similar to chlorofluorocarbons, but they lack Cl. Many are highly hydrophobic (repel water) and are generally nonreactive. They have wide use as the nonstick surface of cookware, as labware, coatings on rain clothing, in ski waxes, and just about anywhere a slippery or highly water-repellant surface is needed. They additional have medical uses, plus a variety of other specialty uses. However, their use is being banned because some are very strong greenhouse gases, some cause cancer, and they break down so slowly that they are accumulating in the environment.

REFERENCES CITED AND SUGGESTIONS FOR ADDITIONAL READING

Allègre, C. A. 2008. *Isotope Geology*. Cambridge University Press, Cambridge, UK, 512 p.

Bentley, W. A., and Humphreys, W. J. 1931. *Snow Crystals*. Dover Publications, New York, 286 p.

Burns, R. G., and Burns, V. M. 1977. Mineralogy, in G. P. Glasby (ed.), *Marine Manganese Deposits*, pp. 185–248. Elsevier, Amsterdam.

Chang, L. L. Y., Howie, R. A., and Zussman, J. 1996. *Rock-Forming Minerals, Volume 5B: Nonsilicates: Sulfates, Carbonates, Phosphates, Halides*, 2nd ed. The Geological Society, London, 383 p.

Dobson, J. 2008. Remote control of cellular behavior with magnetic nanoparticles. *Nature Nanotechnology* **3**, 139–143.

Goresy, A. E., Haggerty, S. E., Huebner, J. S., Lindsley, D. H., and Rumble, D. III. 1976. *Oxide Minerals. Short Course Notes*, Volume 3. Mineralogical Society of America, Washington, DC, 502 p.

Haines, M. 1968. Two staining tests for brucite in marble. *Mineralogical Magazine* **36**, 886–888.

Klein, C. 2005. Some Precambrian banded-iron formations (BIFs) from around the world: Their age, geologic setting, mineralogy, metamorphism, geochemistry and origin. *American Mineralogist* **90**, 1473–1499.

Kohn, M. J. 2020. A refined zirconium-in-rutile thermometer. *American Mineralogist* **105**, 963–971.

Kronhauser, K. 2007. *Introduction to Geomicrobiology*. Blackwell Publishing, Malden, MA, 425 p.

Langway, C. C., Jr. 1958. *Ice Fabrics and the Universal Stage*. U.S. Army Snow, Ice, and Permafrost Research Establishment, Wilmette, IL, 17 p.

Lindsley, D. H. (ed.). 1991. *Oxide Minerals: Petrologic and Magnetic Significance*.

DO NOT COPY e48d507df5d1141@placeholder.94092

Printed by: e48d507df5d1141@placeholder.94092.edu. Printing is for personal, private use only. No part of this book may be reproduced or transmitted without publisher's prior permission. Violators will be prosecuted.

Lindsley, D. H. (ed.). 1991. *Oxide Minerals: Petrologic and Magnetic Significance*. *Reviews in Mineralogy* **25**, 509 p.

Lowenstam, H. A., and McConnell, D. 1968. Biologic precipitation of fluorite. *Science* **162**, 1496–1498.

Min, M., Xuc, H., Chen, J., and Fayek, M. 2005. Evidence of uranium biomineralization in sandstone-hosted roll-front uranium deposits, northwestern China. *Ore Geology Reviews* **26**, 198–206.

Monz, M. E., Hudleston, P. J., Prior, D. J., Michels, Z., Fan, S., Negrini, M., Langhorn, P. J., and Qi, C. 2021. Full crystallographic orientation (c and a axes) of warm, coarse-grained ice in a shear-dominated setting: A case study, Storglaciären, Sweden. *The Cryosphere* **15**, 303–324.

Potter, R. M., and Rossman, G. R. 1979. Mineralogy of manganese dendrites and coatings. *American Mineralogist* **64**, 1219–1226.

Trendall, A. F. 2002. The significance of iron-formation in the Precambrian stratigraphic record, in W. Altermann, and P. L. Corcoran (eds.), *Precambrian Sedimentary Environments: A Modern Approach to Ancient Depositional Systems*, pp. 33–66. Special publication of the International Association of Sedimentologists **33**.

Zachos, J., Pagani, M., Sloan, L., Thomas, E., and Billups, K. 2001. Trends, rhythms, and aberrations in global climate 65 Ma to present. *Science* **292**, No. 5517, 686–693.

DO NOT COPY
e48d507df5d1141@placeholder.9409

Printed by: e48d507df5d1141@placeholder.94092.edu. Printing is for personal, private use only. No part of this book may be reproduced or transmitted without publisher's prior permission. Violators will be prosecuted.

LIST OF KEY TERMS

- bog manganese
- dendrite
- desert varnish
- ferromanganese nodules
- hydrothermal systems
- laterite

DO NOT COPY
e48d507df5d1141@placeholder.9409

Printed by: e48d507df5d1141@placeholder.94092.edu. Printing is for personal, private use only. No part of this book may be reproduced or transmitted without publisher's prior permission. Violators will be prosecuted.

CHAPTER 19
Sulfides and Related Minerals

William D. Nesse
University of Northern Colorado

Graham B. Baird
University of Northern Colorado

DO NOT COPY
e48d507df5d1141@placeholder.9409

Printed by: e48d507df5d1141@placeholder.94092.edu. Printing is for personal, private use only. No part of this book may be reproduced or transmitted without publisher's prior permission. Violators will be prosecuted.

Introduction

The sulfide and related minerals form a large group that includes nearly 600 minerals. Although only a few are abundant, they have great economic value. Metals essential for industrial society extracted from sulfide minerals include copper, zinc, lead, antimony, molybdenum, cobalt, nickel, and silver.

Crystal Chemistry and Classification

A general formula for the sulfides and related minerals can be given as M_pX_r, where *M* is a metal or metalloid such as Fe, Zn, Cu, Pb, Sb, or As. The *X* atoms may be S (for the sulfides), As (for the arsenides), S + As (for the sulfarsenides), or Te (for the tellurides) (Table 19.1).

TABLE 19.1 Common Sulfide and Related Minerals[a]

Sulfides *X* = S	
Acanthite	Ag_2S
Chalcocite	Cu_2S
Galena	PbS
Sphalerite	ZnS
Pyrrhotite	$Fe_{1-x}S$
Pentlandite	$(Fe,Ni)_9S_8$
Cinnabar	HgS
Covellite	CuS
Realgar	AsS
Bismuthinite	Bi_2S_3
Orpiment	As_2S_3
Stibnite	Sb_2S_3
Pyrite	FeS_2
Marcasite	FeS_2
Molybdenite	MoS_2
Chalcopyrite	$CuFeS_2$

DO NOT COPY e48d507df5d1141@placeholder.9409

Printed by: e48d507df5d1141@placeholder.94092.edu. Printing is for personal, private use only. No part of this book may be reproduced or transmitted without publisher's prior permission. Violators will be prosecuted.

Bornite	Cu_5FeS_4
Enargite	Cu_3AsS_4
Pyrargyrite	Ag_3SbS_3
Proustite	Ag_3AsS_3
Tetrahedrite	$(Cu,Fe)_{12}Sb_4S_{13}$
Tennantite	$(Cu,Fe)_{12}As_4S_{13}$
Sulfarsenides X = AsS	
Arsenopyrite	FeAsS
Cobaltite	(Co,Fe)AsS
Arsenides X = As	
Nickeline	NiAs
Skutterudite	$(Co,Ni)As_3$
Tellurides X = Te	
Calaverite	$AuTe_2$
Sylvanite	$(Au,Ag)Te_2$

[a] X = nonmetal element(s) in the general formula M_pX_r.

Chemical bonding in the sulfides is more complex than in the oxides and silicates because sulfur is significantly less electronegative (2.5) than oxygen (3.5). As a consequence, sulfur–metal bonds typically have only about 10–20% ionic character (Table 3.4 and Figure 3.11). Transition metals (Fe, Zn, Cu, Pb, Co, etc.) bond with sulfur by forming molecular bonds (Chapter 3) that share electrons to satisfy the valance requirements of the sulfur. Additional metal–metal molecular bonds may be formed to satisfy remaining valence requirements of the metal atoms. Some of these bonds may have metallic properties.

One of the interesting characteristics of many sulfide minerals is that they are semiconductors (Chapter 3) because the band gap between valence electrons and vacant conduction bands is relatively small (Figure 6.10b). The size of the band gap, molecular bond energies, and details of the light absorption/re-emission characteristics (Chapter 6) control the color properties (Table 19.2).

TABLE 19.2 Band Gap of Selected Sulfide Minerals[a]

Mineral	Band Gap (eV)	Streak Color	Mineral Color	Luster
Arsenopyrite	0.2	Black	Silver	Metallic
Galena	0.42	Black	Black	Metallic

DO NOT COPY e48d507df5d1141@placeholder.9409

Printed by: e48d507df5d1141@placeholder.94092.edu. Printing is for personal, private use only. No part of this book may be reproduced or transmitted without publisher's prior permission. Violators will be prosecuted.

Chalcopyrite	0.53	Black	Yellow	Metallic
Pyrite	0.95	Black	Yellow	Metallic
Bornite	1.0	Black	Bronze	Metallic
Enargite	1.0	Black	Black	Metallic
Chalcocite	1.05	Black	Black	Metallic
Covellite	1.2	Black	Blue	Metallic
Molybdenite	1.3	Black	Black	Metallic
Stibnite	1.7	Black	Black	Metallic
Proustite	2.0	Red	Red	Adamantine
Pyrargyrite	2.0	Red	Red	Adamantine
Cinnabar	2.0	Red	Red	Adamantine
Realgar	2.3	Orange-red	Orange-red	Adamantine
Orpiment	2.7	Yellow	Yellow	Adamantine
Sphalerite	3.7	White	Colorless	Adamantine

[a] See individual mineral descriptions for more detailed descriptions of colors, which are generalized here—shades of dark gray and black = black; all shades of red = red.

Sulfides with a band gap less than 1.7 eV consistently have a black or dark streak and metallic luster because all of the visible spectrum can be absorbed. The reflected light color from smooth surfaces depends on details of absorption/re-emission, as with the metals. The most strongly absorbed wavelengths pass the shortest distance into the mineral and also are the most strongly re-emitted.

Band gaps greater than 1.7 eV allow only light whose energy is greater than the band gap to be absorbed; lower-energy light is not absorbed and is transmitted. These minerals also have an adamantine luster. Proustite, pyrargyrite, and cinnabar are all red because a band gap of 2.0 eV is too high to allow the low-energy, red end of the spectrum to be absorbed, and these wavelengths are therefore observed. Realgar is orangish because it has a band gap of about 2.3 eV, so red and some orange light are not absorbed. Sulfides with a band gap greater than 3.2 eV, such as pure sphalerite, are colorless with a white streak because none of the visible spectrum is absorbed.

The semiconductor properties make sulfides useful in electronic components—the use of galena and pyrite as the “crystals” in early crystal radio sets is probably the earliest use of semiconductors for electronic purposes. Additional uses include the following.

- Small amounts of Cu, Ag, or Mn incorporated in the structure of sphalerite causes it to become electroluminescent. The greenish glow of many old oscilloscopes, radar screens, and similar “green screen” cathode ray tubes was produced by Cu-

DO NOT COPY e48d507df5d1141@placeholder.94092

Printed by: e48d507df5d1141@placeholder.94092.edu. Printing is for personal, private use only. No part of this book may be reproduced or transmitted without publisher's prior permission. Violators will be prosecuted.

doped ZnS.

- Because pyrite has a suitable band gap and high optical absorption, it is a candidate for use as a photovoltaic material in solar cells.
- Transistors can be made from very thin films of molybdenite. Such transistors are useful because of their ability to operate at much higher temperatures (up to 220°C) than conventional Si-based transistors.
- Covellite has potential use in solar cells.
- Cinnabar can be used as a radiation-detector material.

An Internet search of most sulfide minerals will reveal additional examples, although in most cases the material studied is grown in the laboratory.

The sulfides do not lend themselves to an elegant classification, such as the one used successfully for the silicates. Schemes based on metal–sulfur ratios, coordination of metal atoms with sulfur, packing arrangement of the sulfur atoms, cell dimensions, and other variables have been proposed, but none is widely accepted. Classification is complicated because some metalloid elements, particularly As and Sb, can serve either as metals or as nonmetals. The groupings shown in Table 19.1 are based solely on the identity of the nonmetal element(s) in the structure.

Minerals whose composition includes a metal, a metalloid serving the structural role of a metal, and sulfur have been classified as sulfosalts based on chemical notions that have long since been abandoned. The metal is usually Cu, Ag, Bi, or Pb, and the metalloid may be As or Sb. The minerals listed that are conventionally grouped with the sulfosalts are enargite, pyrargyrite, proustite, tetrahedrite, and tennantite.

Of the many hundreds of sulfide and related minerals that have been identified and described, only a handful are routinely encountered. These are described in detail in this chapter. Additional minerals are briefly described in Tables 19.5 and 19.6.

DO NOT COPY e48d507df5d1141@placeholder.9409

Printed by: e48d507df5d1141@placeholder.94092.edu. Printing is for personal, private use only. No part of this book may be reproduced or transmitted without publisher's prior permission. Violators will be prosecuted.

Sulfide Deposits

Hydrothermal Deposits

Although they may be found in a wide variety of geological environments, sulfide and related minerals are characteristic of hydrothermal vein and replacement deposits. These minerals are deposited from hot aqueous solutions in void spaces or by replacement of the rock through which the fluids migrate. The essential features of hydrothermal systems include the following.

- Water: The water may be meteoric (rain, snow), magmatic (originating from magma), metamorphic (released during metamorphism), or connate (trapped in sediment pores).
- Heat: Often provided by an igneous intrusion, but also from burial or proximity to the mantle.
- A source for metals and other elements that will precipitate from the water: The metals, sulfur, and other elements in the water may be derived from a crystallizing magma or may be leached out of a large volume of country rock by the water.
- Migration pathways: Fluids commonly flow through the rocks along faults, fractures, and pore space.
- Precipitation site: Minerals may precipitate either by filling spaces along faults, fractures, and in other voids, or by replacing minerals.

Hydrothermal deposits can be generated in many different geological environments (Pirajno, 2009). Figure 19.1 shows an idealized hydrothermal system with characteristics of a wide variety of different specific types. Commonly, a felsic magma crystallizing at fairly shallow levels within the crust drives the system. The intrusion's country rock may be comagmatic volcanics or other older igneous, sedimentary, or metamorphic rocks. As the magma crystallizes, water and elements that do not easily fit in the crystal structure of quartz, feldspars, and other silicates become concentrated in the late residual fluid. These fluids can migrate into the country rock, where they follow permeable areas such as faults and fractures. As these fluids migrate away from the crystallizing magma, something changes, which could be that they cool, the pressure drops, and/or they encounter chemically reactive rock such as limestone. One or a combination of these changes may trigger precipitation of minerals from the fluid. Precipitated minerals may fill the void space through which the fluids are migrating, or they may react with and replace the country rock.

DO NOT COPY
e48d507df5d1141@placeholder.94092

Printed by: e48d507df5d1141@placeholder.94092.edu. Printing is for personal, private use only. No part of this book may be reproduced or transmitted without publisher's prior permission. Violators will be prosecuted.

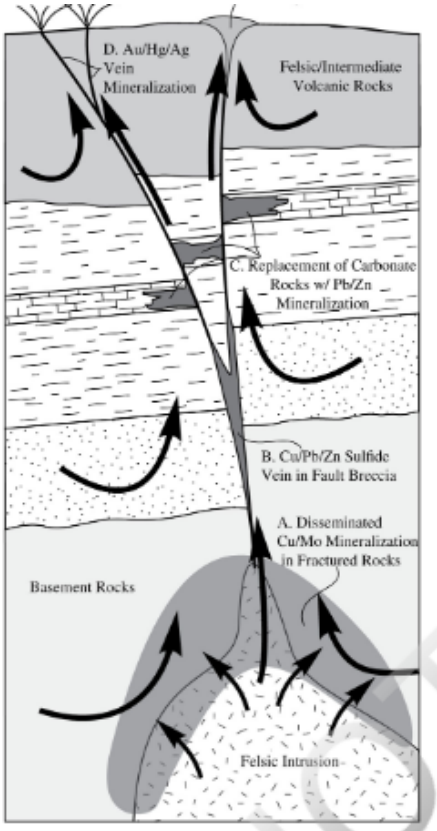

FIGURE 19.1 Schematic hydrothermal system. Hot mineralizing aqueous fluids may evolve from a crystallizing felsic intrusion (*bottom*), or they may be meteoric waters set in motion by the heat from the magma (*large arrows*). Minerals may crystallize in small fractures and among grains of the country rock (A) to form a disseminated deposit. Vein deposits (B) are formed where mineralizing fluids flow along fault or fracture zones. A replacement deposit (C) may be produced if mineralizing fluids interact with a limestone bed. Near-surface mineralization (D), often in volcanic rocks, may form where hydrothermal fluids reach the surface and form hot springs. If the temperature is high enough, hydrothermal fluids can violently flash (convert) to steam near the surface; this may fracture the rock, producing a hydrothermal breccia in which mineralization may occur (E). Many other scenarios are possible. View larger image

Groundwater adjacent to and above the magma chamber will also be heated. Because hot water is less dense than cold, the hot water rises to the surface, and cool water from surrounding areas must flow in to replace the heated water. As long as the intrusion remains hot, it will continue to drive this hydrothermal circulation of water. The surface manifestation of a hydrothermal system may be hot springs and geysers, such as those found in Yellowstone National Park in the United States.

The hydrothermal circulation driven by the heat from the intrusion may itself lead to mineralization. The circulating water can dissolve elements from the rocks it flows through and can dissolve mineralization previously produced from magmatic sources. After transport, this material may be reprecipitated. For some hydrothermal systems, valuable elements are concentrated into a relatively smaller volume of rock such that mining it is economically feasible.

Hydrothermal circulation also can produce extensive alteration of the intrusion and the surrounding rocks. This often produces concentric zoning of alteration, which is most

Printed by: e48d507df5d1141@placeholder.94092.edu. Printing is for personal, private use only. No part of this book may be reproduced or transmitted without publisher's prior permission. Violators will be prosecuted.

surrounding rocks. This often produces concentric zoning of alteration, which is most intense near the intrusion. The alteration mineralogy depends on local conditions. A common pattern consists of an outer zone of propylitic alteration, in turn, surrounding argillic, sericitic, and then potassic alteration zones (Figure 19.2a).

- **Propylitic.** Biotite and hornblende converted to chlorite; plagioclase altered to epidote, chlorite, and carbonates.
- **Argillic.** Extensive development of clay minerals. Plagioclase and mafic minerals are generally completely altered, but some K-feldspar may persist.
- **Sericitic (phyllic).** Fine-grained white mica (sericite) and quartz produced by recrystallization of clay. Pyrite is a common accessory. Original silicates are not preserved.
- **Potassic.** K-feldspar (adularia) crystallized with or without recrystallized biotite and sericite.

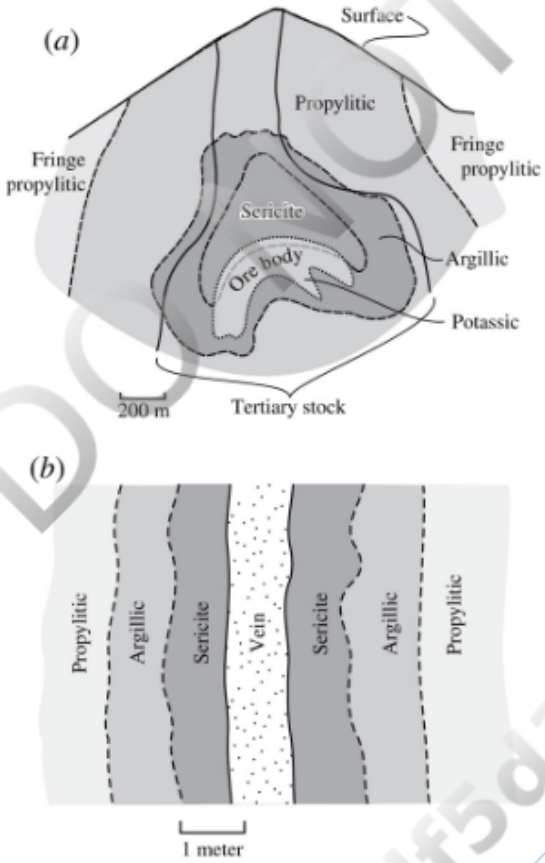

FIGURE 19.2 Hydrothermal alteration. (*a*) Henderson porphyry molybdenum deposit, Colorado. Mineralization is associated with Tertiary felsic intrusions emplaced in Precambrian granite. The molybdenite (MoS_2) in the ore body (>0.3% MoS_2) was deposited with quartz and pyrite in and along abundant fractures in the intrusion. Sericite, argillic, and propylitic alteration form concentric zones. Rocks within the ore body display potassic alteration. The biotite is not completely altered to chlorite in the fringe propylitic zone, which grades outward to unaltered Precambrian granite. Adapted from White and others (1981). (*b*) A similar concentric alteration pattern may be found at a much smaller scale adjacent to a sulfide-bearing vein. View larger image

Alteration may extend up to several kilometers from an intrusion. Similar zones of

DO NOT COPY e48d507df5d1141@placeholder.9409

Printed by: e48d507df5d1141@placeholder.94092.edu. Printing is for personal, private use only. No part of this book may be reproduced or transmitted without publisher's prior permission. Violators will be prosecuted.

Alteration may extend up to several kilometers from an intrusion. Similar zones of alteration may be duplicated at a scale of a few centimeters or meters adjacent to a mineralized vein (Figure 19.2b).

The chemistry of hydrothermal fluids responsible for precipitation of sulfide and other minerals can be deduced from small inclusions of this fluid trapped in minerals as they grow. These fluid inclusions are typically brines rich in NaCl. The presence of Cl^- appears to be important because metals such as Cu, Pb, Zn, Au, and Ag are much more soluble as metal–chloride complexes than they are as simple ions.

The mineralogy found in hydrothermal vein and replacement deposits depends on the temperature and chemistry of the mineralizing fluids, the chemistry of the country rock, pressure, and details of the geological setting. Sulfide minerals may actually constitute only a small fraction of the precipitated minerals; quartz, carbonates, fluorite, sulfates, and others may be the most abundant minerals in many hydrothermal veins. Table 19.3 gives the mineralogy of a number of different types of hydrothermal deposits.

TABLE 19.3 Select Hydrothermal Mineral Assemblages[a]

Deposit Type	Major Minerals	Minor Minerals	Environments
As–Sb sulfide veins	Realgar, orpiment, pyrite, stibnite, quartz, calcite	Chalcopyrite, arsenopyrite, marcasite	Generally low-temperature hydrothermal veins
Hg–sulfide	Cinnabar, pyrite, marcasite	Native mercury, stibnite, sphalerite, pyrrhotite quartz, chalcedony, barite, carbonates, clay	Low-temperature hydrothermal
Epithermal Au–Ag deposits	Gold, gold tellurides, pyrite, proustite, pyrargyrite, stibnite, acanthite, cinnabar, quartz	Galena, sphalerite, chalcopyrite, tetrahedrite–tennantite, silver, carbonates, fluorite, barite, plus others	Shallow hydrothermal systems associated with subaerial volcanism, either in the volcanic rocks or closely adjacent
Porphyry Cu, porphyry Mo deposits	Pyrite, chalcopyrite, molybdenite, bornite	Magnetite, hematite, ilmenite, rutile, enargite, cassiterite, hübnerite, gold, covellite, chalcocite, digenite, native copper	Mineralization in veins and disseminated grains in and adjacent to felsic to intermediate porphyritic intrusions; intrusions and adjacent rock altered in concentric zones
Cu–Pb–Zn–Ag vein and replacement deposits	Pyrite, sphalerite, galena, chalcopyrite, tetrahedrite	Bornite, chalcocite, enargite, argentite, gold, hematite, pyrrhotite, proustite–pyrargyrite	Veins and replacement deposits associated with intermediate to felsic intrusions
Sn–W–Bi veins	Cassiterite, arsenopyrite, wolframite, bismuthinite, pyrite, marcasite, pyrrhotite	Stannite, chalcopyrite, sphalerite, tetrahedrite, pyrargyrite, galena,	Open-space hydrothermal vein filling associated with granitic intrusions

DO NOT COPY e48d507df5d1141@placeholder.94092

Printed by: e48d507df5d1141@placeholder.94092.edu. Printing is for personal, private use only. No part of this book may be reproduced or transmitted without publisher's prior permission. Violators will be prosecuted.

	marcasite, pyrrhotite	pyrargyrite, galena, rutile, gold, molybdenite, bismuth, quartz, tourmaline, apatite, fluorite	
Pb–Zn deposits in carbonate host	Galena, sphalerite, barite, fluorite, pyrite, marcasite, chalcopyrite, calcite, dolomite, quartz, aragonite	Wurtzite, millerite, bornite, covellite, enargite	Deposited in solution voids in or by replacement of dolostone; generally low temperature (<100°C) and not directly associated with intrusions or volcanic activity
Cu–Fe–Pb–Zn volcanogenic massive sulfide (VMS) and sedimentary exhalative (SEDEX)	Pyrite, sphalerite, chalcopyrite, pyrrhotite, galena	Bornite, tetrahedrite, arsenopyrite, marcasite, sulfosalts, cassiterite, plus others	Deposited at or near the sea-floor surface by hydrothermal exhalative activity associated with submarine volcanic activity such as at mid-ocean ridges; may be hosted by volcanic rocks (VMS) or grade laterally into clastic sediments (SEDEX)
Skarn deposits	Magnetite, molybdenite, sphalerite, galena, chalcopyrite, scheelite, wolframite, quartz, calc-silicate minerals (garnet, amphibole, pyroxene, epidote, etc.), carbonates	Pyrrhotite, cassiterite, hematite, gold, sulfosalts	Formed by high-temperature contact metamorphic processes where a silicic magma and fluids metasomatizes surrounding carbonate rocks

[a] See Table 19.4 for minerals formed by supergene alteration.

Supergene Processes

The primary or **hypogene** mineralization produced in a hydrothermal system may be extensively altered when exposed to the near-surface environment (Figure 19.3). Oxygenated groundwater derived from rain or snow will react with pyrite to form iron hydroxides and release the sulfur as sulfuric acid:

$$\text{Pyrite} + \text{oxygen} + \text{water} = \text{goethite} + \text{sulfuric acid}$$
$$4FeS_2 + 15O_2 + 10H_2O = 4FeOOH + 8H_2SO_4 \quad \textbf{(19.1)}$$

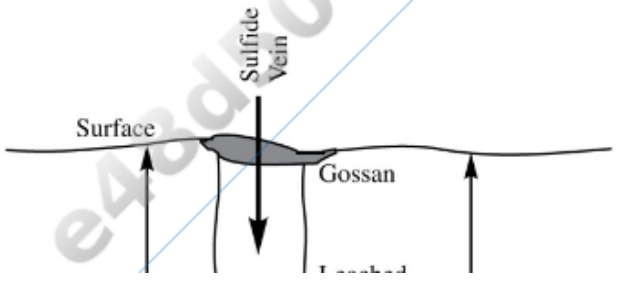

DO NOT COPY e48d507df5d1141@placeholder.94092

Printed by: e48d507df5d1141@placeholder.94092.edu. Printing is for personal, private use only. No part of this book may be reproduced or transmitted without publisher's prior permission. Violators will be prosecuted.

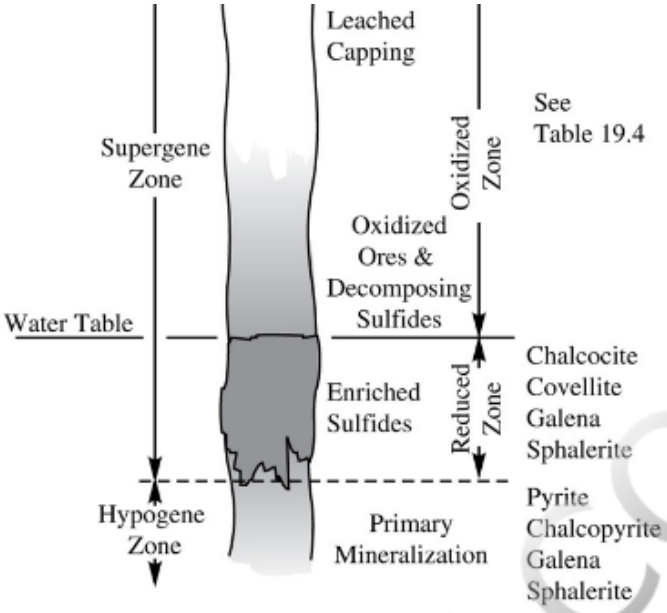

FIGURE 19.3 Supergene enrichment. Meteoric water percolates down through a sulfide-bearing vein. Sulfides are leached out of the near-surface environment, leaving behind a collection of oxide, carbonate, and hydroxide minerals in the oxidized zone. Cu, Pb, Zn, and related elements are largely removed from the leached capping. A gossan, enriched in iron oxides and hydroxides typically derived from alteration of pyrite, may accumulate at the surface as weathering and erosion progress. Sulfide minerals (re)precipitate in the reduced zone, generally below the water table, to form a zone enriched in sulfide minerals. View larger image

A similar reaction of chalcopyrite ($CuFeS_2$) with dissolved atmospheric oxygen and carbon dioxide can produce cuprite (CuO) and siderite ($FeCO_3$):

$$CuFeS_2 + CO_2 + 4O_2 + 2H_2O = CuO + FeCO_3 + 2H_2SO_4 \quad (19.2)$$

The copper carbonates azurite and malachite can be produced by similar reactions. The net result of these and related reactions is to oxidize the metals found in the sulfides to form oxides, hydroxides, carbonates, and sulfates. Because these reactions produce oxygen-bearing minerals at the expense of sulfides, the near-surface zone is often referred to as the oxidized zone. The minerals produced are called **supergene** or secondary minerals. Common supergene minerals found in the oxidized portion of hydrothermal sulfide deposits are listed in Table 19.4.

TABLE 19.4 Common Minerals in the Oxidized Portion of Hydrothermal Sulfide Deposits

Oxides/Hydroxides	Carbonates
Cuprite	Azurite
Goethite	Calcite
Hematite	Cerussite

Printed by: e48d507df5d1141@placeholder.94092.edu. Printing is for personal, private use only. No part of this book may be reproduced or transmitted without publisher's prior permission. Violators will be prosecuted.

Hematite	Cerussite
Lepidocrocite	Dolomite/ankerite
Mn-oxides/hydroxides (Table 18.6)	Malachite
Native elements	Rhodochrosite
Bismuth	Siderite
Copper	Smithsonite
Gold	Sulfates
Silver	Anglesite
Sulfur	Gypsum

Because pyrite is usually the most common sulfide, the oxidized zones of most sulfide deposits are colored yellow and red from the iron oxides and hydroxides derived from it. These minerals are relatively insoluble and may accumulate near the surface to form an encrusting mass called a **gossan**.

The sulfuric acid produced as a byproduct of oxidation reactions dissociates to $2H^+$ and SO_4^{2-} and promotes dissolution of sulfide minerals such as chalcocite (Cu_2S) by reactions such as

$$2Cu_2S + 4H^+ + 2\,SO_4^{2-} + 5O_2 = 4Cu^{2+} + 4\,SO_4^{2-} + 2H_2O. \quad \textbf{(19.3)}$$

When meteoric water carrying dissolved metals and other constituents reaches the water table, it becomes diluted. This commonly triggers precipitation of the metals as sulfides by reversing reactions such as 19.3. Precipitation also can be triggered by reaction of the sulfate solution with sulfide minerals.

$$5\,FeS_2 + 12\,Cu^{2+} + 12SO_4^{2-} + 16H_2O = \text{pyrite}$$
$$6\,Cu_2\,S + 5\,Fe^{2+} + 32H^+ + 16SO_4^{2-} \quad \textbf{(19.4)}$$
$$\text{chalcocite}$$

Pyrite grains in the deeper portions of the supergene alteration zone may therefore serve as host to extensive reprecipitation of copper sulfides in a process called **supergene enrichment**. The zone of concentrated mineralization is commonly at or below the surface of the water table. The sulfide-enriched zone is also referred to as the reduced zone, because the meteoric water, by the time it reaches this level, has no dissolved oxygen left, so it is chemically reducing.

DO NOT COPY e48d507df5d1141@placeholder.94092

Printed by: e48d507df5d1141@placeholder.94092.edu. Printing is for personal, private use only. No part of this book may be reproduced or transmitted without publisher's prior permission. Violators will be prosecuted.

oxygen left, so it is chemically reducing.

Supergene processes cause extensive alteration of the country rock hosting sulfide deposits. Excess acid produced by oxidation of sulfides may be neutralized by reaction with silicates to form clays. A typical reaction involves hydrolysis of K-feldspar ($KAlSi_3O_8$) to form kaolinite [$Al_2Si_2O_5(OH)_4$].

$$2\,KAlSi_3O_8 + 2H^+ + H_2O = Al_2Si_2O_5(OH)_4 + 4SiO_2 + 2K^+ \quad (19.5)$$

Note that this is the same type of reaction that is associated with chemical weathering. The acid released by oxidizing sulfides, however, promotes more intense alteration of silicates to greater depths than is found with weathering.

Microorganisms are directly and indirectly involved in many supergene processes. For example, the bacterium *Thiobacillus ferrooxidans* promotes the oxidation of pyrite (Equation 19.1) because it oxidizes reduced sulfur compounds and ferrous iron to produce sulfuric acid and ferric iron as part of its metabolism (Nordstrom and Southam, 1997). The pyrite (FeS_2) serves as a source of metabolic energy. These biologic processes are not restricted to pyrite—other sulfide minerals also may be involved in microbe metabolism. While the biochemistry may seem exotic, it is not fundamentally different from utilizing reduced carbon and hydrogen in carbohydrates (e.g., common foods such as donuts) as a source of energy and producing H_2O and CO_2 as byproducts that combine to form H_2CO_3, which is carbonic acid.

The same processes can occur in mines and mine waste, where biologic processes accelerate the production of acid (the H_2SO_4 of Equation 19.1) that can pollute waterways. Because microbes can promote dissolution of sulfide minerals, they are increasingly used in processes that extract metals from ores that make them available for modern industry (Rawlings, 2002). Microbes also have become valuable in processes that remove metal contamination from surface waters.

Many sulfides are biominerals (Chapter 5). Of those in Table 19.5, acanthite, orpiment, proustite, and realgar are documented to be biologically induced. Realgar, for example, can be precipitated by the bacterium *Pyrobaculum arsenaticum* at temperatures between 68°C and 100°C (Huber and others, 2000). It is likely that the occurrence of both orpiment and realgar in solfatara fields (areas of volcanic fumarole or vents) may be the result of microbial action.

TABLE 19.5 Less Common Sulfide Minerals

Mineral[a]	Unit Cell	Physical Properties[b]	Optical Properties	Comments
Acanthite Ag_2S	Monoclinic	*H*: 2–2.5	Opaque	Crystals rare,

Printed by: e48d507df5d1141@placeholder.94092.edu. Printing is for personal, private use only. No part of this book may be reproduced or transmitted without publisher's prior permission. Violators will be prosecuted.

	2/*m* *a* = 4.231 *b* = 6.930 *c* = 9.526 *β* = 125.5° *Z* = 4	*G*: 7.22 Cl: f, sectile Tw: $\{\bar{1}11\}$ polysynthetic, {101} contact C: Black St: Black L: Metallic	PS: Light gray ± greenish cast, very weak bireflectance/pleochroism; observable but weak anisotropy	prismatic along *c*; often cube/octahedron pseudomorph after argentite; also dendritic, filiform, massive, or encrusting, and as inclusions in galena; found in hydrothermal systems with pyrargyrite, proustite, silver, and galena
Bismuthinite Bi_2S_3	Orthorhombic 2/*m* 2/*m* 2/*m* *a* = 11.12 *b*= 11.25 *c* = 3.97 *Z* = 4	*H*: 2–2.5 *G*: 6.78 Cl: {010}pf, {100} and {110}f C: Gray to white St: Gray L: Metallic	Opaque PS: White with weak but distinct bireflectance/pleochroism; very strong anisotropy, creamy white/gray-white polarization colors	Stout prismatic to acicular crystals elongate on *c*; usually massive with foliated or fibrous texture; low- or high-temperature hydrothermal veins, VMS/SEDEX deposits, gold veins
Orpiment As_2S_3	Monoclinic 2/*m* *a* = 11.475 *b* = 9.577 *c* = 4.256 *β* = 90.7° *Z* = 4	*H*: 1.5–2 *G*: 3.49 Cl: {010}pf, {100}f, flexible lamellae, somewhat sectile Tw: {100} C: Lemon-yellow to golden or brownish yellow St: Pale lemon-yellow L: Resinous, pearly on cleavage	n_α = 2.4 n_β = 2.8 n_γ = 3.0 δ = 0.6 Biaxial (−) 2*V* = 76°, *r* > *v* strong *X* = *b*, *Z* ∧ *c* = ±2° TS: *Y* = pale yellow, Z = greenish yellow PS: White to gray-white with strong pleochroism; strong anisotropism, masked by yellow to white internal reflection	Crystals tabular to short prismatic; usually foliated or columnar masses, granular or powdery; hydrothermal deposits with lead, silver, gold; almost always associated with realgar

DO NOT COPY
e48d507df5d1141@placeholder.94092-

Printed by: e48d507df5d1141@placeholder.94092.edu. Printing is for personal, private use only. No part of this book may be reproduced or transmitted without publisher's prior permission. Violators will be prosecuted.

		cleavage		
Pentlandite $(Fe,Ni)_9S_8$	Isometric $4/m\ \bar{3}\ 2/m$ $a = 9.928$ $Z = 4$	*H*: 3.5–4 *G*: 4.6–5.0 Cl: None, {111} parting C: Light bronze-yellow St: Light bronze-brown L: Metallic	Opaque PS: Isotropic, creamy white with pinkish or brownish tint	Crystals rare, usually granular masses; found in layered mafic and ultramafic intrusions in thin sulfide-rich layers; usually associated with pyrrhotite, also chalcopyrite and pyrite; mined as a principal source of Ni
Realgar AsS	Monoclinic $2/m$ $a = 9.325$ $b = 13.571$ $c = 6.587$ $\beta = 106.4°$ $Z = 16$	*H*: 1.5–2 *G*: 3.56 Cl: {010}g; $\{\bar{1}01\}$, {110}, {120}, {110}pr Tw: {100} contact C: Red to orange-yellow St: Orange-red to red L: Resinous to greasy	$n_\alpha = 2.538$ $n_\beta = 2.684$ $n_\gamma = 2.704$ $\delta = 0.116$ Biaxial (+) $2V = 39°$, $r > v$ strong $X \wedge c = +11°$, $Y = b$ TS: $X \sim$ colorless, $Y = Z$ pale yellow PS: Dull gray with reddish to bluish pleochroism; strong anisotropism masked by abundant yellowish-red internal reflections	Crystals short, vertically striated prisms; usually coarse to fine granular or encrustating; in hydrothermal deposits with lead, silver, gold; usually associated with orpiment; breaks down to yellow pararealgar (As_4S_4) on exposure to light
Stibnite Sb_2S_3	Orthorhombic $2/m\ 2/m\ 2/m$ $a = 11.229$ $b = 11.310$ $c = 3.839$ $Z = 4$	*H*: 2 *G*: 4.63 Cl: {010}pf; {100}, {110}f Tw: {130}, {120} polysynthetic C: Gray, black, or iridescent tarnish St: Lead-gray	Opaque PS: White to grayish white with strong bireflectance/pleochroism; very strong anisotropy	Crystals (Figure 19.4) stout to elongate prism with complex terminations, may be bent; radiating acicular groups; also columnar, granular, or fine masses; important source of Sb

DO NOT COPY
e48d507df5d1141@placeholder.9409-

Printed by: e48d507df5d1141@placeholder.94092.edu. Printing is for personal, private use only. No part of this book may be reproduced or transmitted without publisher's prior permission. Violators will be prosecuted.

		L: Metallic		
Enargite (ss) Cu_3AsS_4	Orthorhombic *mm*2 $a = 7.407$ $b = 6.436$ $c = 6.154$ $Z = 2$	*H*: 3 *G*: 4.45 Cl: {110}pf, {100} and {010}g Tw: {320} common, penetration C: Grayish black to black St: Grayish black L: Metallic	Opaque PS: Pinkish gray or pinkish brown with bireflectance/pleochroism; strong anisotropism, blue, green, red, orange polarization colors	Crystals tabular on {001} or prismatic with striations parallel to *c*; usually anhedral to subhedral grains and granular masses; found in Cu-bearing hydrothermal deposits; locally an important ore of Cu
Proustite (ss) Ag_3AsS_3	Hexagonal $\bar{3}$ 2/*m* $a = 10.79$ $c = 8.69$ $Z = 6$	*H*: 2–2.5 *G*: 5.57 Cl: {101}g Tw: {104} produces trillings (three cyclic twins), also {101}, {001}, and {012} C: Scarlet-vermilion (darkens with exposure) St: Vermilion L: Adamantine	$n_\omega = 3.088$ $n_\varepsilon = 2.792$ $\delta = 0.296$ Uniaxial (−) TS: Cochineal red to blood red pleochroic PS: Bireflectant/pleochroic white with yellowish tint to bluish gray; strong anisotropy with colors masked by intense scarlet-red internal reflections (stronger than pyrargyrite)	Known as light ruby silver; crystals rhombohedral; commonly massive, compact; late-forming mineral in hydrothermal deposits also in the oxidized/enriched zone; is an important ore mineral of Ag in some deposits; difficult to distinguish from pyrargyrite
Pyrargyrite (ss) Ag_3SbS_3	Hexagonal 3*m* $a = 11.047$ $c = 8.719$ $Z = 6$	*H*: 2.5 *G*: 5.82 Cl: {101}g, {012}pr Tw: {104}complex lamellar, also {101} and [110]	$n_\omega = 3.084$ $n_\varepsilon = 2.881$ $\delta = 0.203$ Uniaxial (−) TS: Deep red PS: Bluish gray, with bireflectance but not pleochroism; strong	Known as dark ruby silver; rare crystals prismatic parallel to *c* with pyramidal terminations; usually compact massive; late-forming mineral in low-temperature hydrothermal

DO NOT COPY
e48d507df5d1141@placeholder.9409-

Printed by: e48d507df5d1141@placeholder.94092.edu. Printing is for personal, private use only. No part of this book may be reproduced or transmitted without publisher's prior permission. Violators will be prosecuted.

		[110] C: Deep red St: Purplish red L: Adamantine	pleochroism; strong anisotropism, color masked by intense carmine-red internal reflections (less than proustite)	hydrothermal veins, also by supergene processes; more common than proustite and an important ore mineral of Ag in some deposits
Tennantite (ss) $(Cu,Fe)_{12}As_4S_{13}$	Isometric $\bar{4}3m$ a = 10.19 Z =2	H: 3–4.5 G: 4.62 Cl: None Tw: [111] axis with {111} twin plane, contact and penetration C: Gray to black St: Black to brown L: Metallic, splendent	Opaque unless very thin PS: Gray with bluish-green tint, isotropic; reddish internal reflections common	Crystals are tetrahedra; also massive, coarse to fine granular, or compact; solid solution to tetrahedrite; hydrothermal veins; tennantite is an important copper mineral in some deposits; also may contain valuable amounts of Ag substituting for Cu, Fe
Tetrahedrite (ss) $(Cu,Fe)_{12}Sb_4S_{13}$	Isometric $\bar{4}3m$ a = 10.23–10.55 (higher with Ag) Z = 2	H: 3–4.5 G: 4.97 Cl: None Tw: [111] axis with {111} twin plane, contact and penetration C: Gray to black St: Reddish brown, black, or dark red L: Metallic	Opaque unless very thin PS: Gray with olive or brownish tint, isotropic; reddish internal reflections uncommon, increasing with As content	Crystals are tetrahedra; also massive, coarse to fine granular or compact; hydrothermal veins; solid solution to tennantite; Ag substitutes for Cu, Fe; important source of Cu and Ag in some deposits

[a] ss = minerals conventionally classified as sulfosalts.

[b] Cl = cleavage (pf = perfect, g = good, f = fair, pr = poor), Tw = twinning, C = color, St = streak, L = luster, TS = thin section, PS = polished section.

DO NOT COPY
e48d507df5d1141@placeholder.9409-

Printed by: e48d507df5d1141@placeholder.94092.edu. Printing is for personal, private use only. No part of this book may be reproduced or transmitted without publisher's prior permission. Violators will be prosecuted.

Sulfide Minerals

Only the more common sulfide minerals are described in detail. Additional sulfides are included in Table 19.5, and stibnite is shown in Figure 19.4.

FIGURE 19.4 Small elongate prismatic crystals of stibnite. View larger image

Sphalerite

Å

DO NOT COPY
e48d507df5d1141@placeholder.9409

Printed by: e48d507df5d1141@placeholder.94092.edu. Printing is for personal, private use only. No part of this book may be reproduced or transmitted without publisher's prior permission. Violators will be prosecuted.

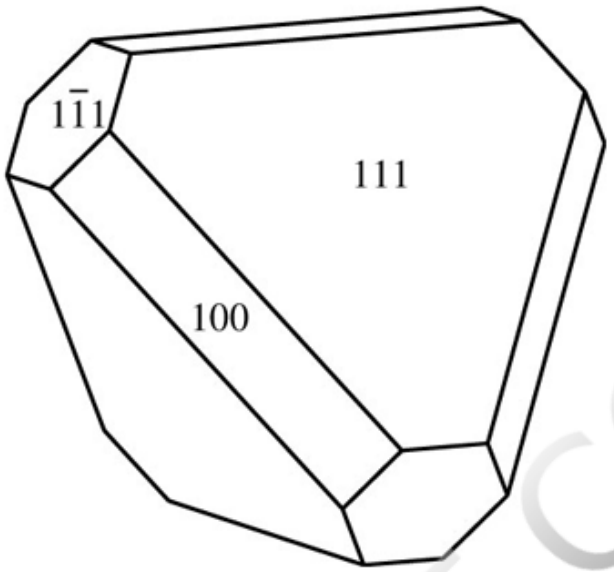

Structure Sulfur is spaced slightly wider than ideal cubic close packing with Zn in tetrahedral sites at the corners and face centers of the unit cell (Figure 19.5). Wurtzite is a polymorph based on hexagonal close packing.

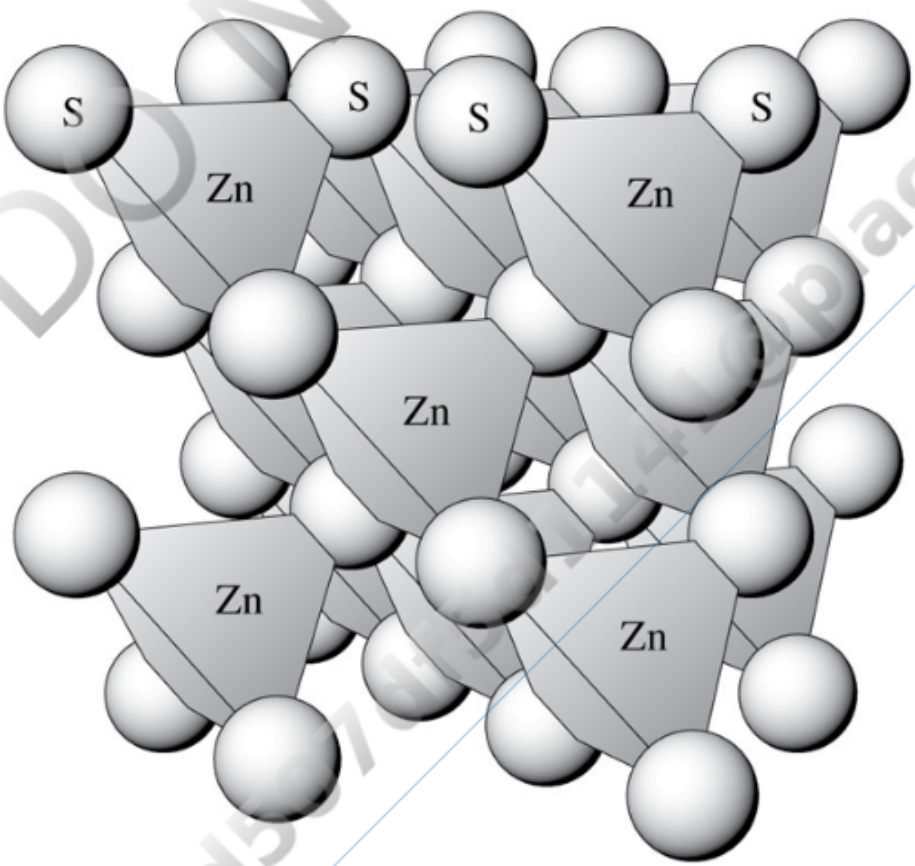

FIGURE 19.5 Structure of sphalerite. Sulfur atoms are arranged in cubic close packing. Zn atoms are positioned in tetrahedral coordination sites that are arranged in rows parallel to the diagonals across each unit cell face. This places Zn at the corners and face centers of the unit cell. Chalcopyrite is similar, but with Cu and Fe occupying alternating tetrahedral sites. View larger image

DO NOT COPY

Printed by: e48d507df5d1141@placeholder.94092.edu. Printing is for personal, private use only. No part of this book may be reproduced or transmitted without publisher's prior permission. Violators will be prosecuted.

image

Composition Over 40% Fe^{2+} may substitute for Zn; higher temperatures are associated with higher Fe content. Small amounts of Cd and Mn also are common. Sphalerite is also called zincblende. *Marmatite* is a term found in the older literature for Fe-rich sphalerite; *black jack* is a miner's term for the same material.

Form and Twinning Tetrahedral crystals are common, often with triangular markings on crystal faces. Other forms include the cube and dodecahedron. Also granular and cleavable masses or forming encrusting aggregates. Twins by rotation on [111] with composition planes ~(111); may be simple or complex.

Cleavage Perfect dodecahedral {011} cleavage (six cleavage directions). Conchoidal fracture. Brittle.

Color Properties

Luster: Resinous, adamantine, to submetallic.

Color: Pale yellow, light brown, brown, black; also red, green, or white. Pure sphalerite is a semiconductor whose band gap is too wide (3.68 eV) to allow any of the visible spectrum to be absorbed, so it is colorless and can be used as a white pigment. Addition of iron causes the color to darken, and cobalt can produce a green color. Higher-energy radiation, including ultraviolet and X-rays, can promote electrons across the band gap and produces fluorescence. Small amounts of Cu, Ag, or Mn incorporated in the structure cause sphalerite to become electroluminescent.

Streak: White to light or medium brown, darker with Fe content.

Color in Thin Section: Colorless, pale yellow, pale brown. Not pleochroic.

Optical Characteristics

Relief in Thin Section: Very high positive.

Index of Refraction: Index of refraction increases with Fe content. Intergrown submicroscopic domains of wurtzite may produce birefringence. Birefringence increases linearly from 0 for 100% sphalerite structure to 0.022 for 100% wurtzite structure. Wurtzite is uniaxial positive $n_\omega = 2.356$, $n_\epsilon = 2.378$, and is similar in appearance to sphalerite.

Polished Section: Gray, sometimes with brown tint, in polished section with yellow, yellowish-brown, or reddish-brown internal reflections.

Alteration Sphalerite may alter to oxides, hydroxides, sulfates, or carbonates of Fe and Zn (limonite, smithsonite, siderite, etc.).

Distinguishing Features

DO NOT COPY e48d507df5d1141@placeholder.9409

Printed by: e48d507df5d1141@placeholder.94092.edu. Printing is for personal, private use only. No part of this book may be reproduced or transmitted without publisher's prior permission. Violators will be prosecuted.

Distinguishing Features

Hand Sample: Distinguished by luster, cleavage, and light streak. Dark varieties may resemble galena (particularly when examined underground with a miner's lamp for illumination) but yields a lighter-colored powder when crushed. It dissolves slowly in dilute HCl, particularly if powdered, and releases H_2S, whose rotten-egg odor is distinctive. Sphalerite is pyroelectric, and some exhibits triboluminescence (i.e., it flashes light when struck).

Thin Section/Grain Mount: Extreme relief, isotropic character, and six cleavage directions are characteristic.

Polished Section: In polished section sphalerite is gray with low reflectance and may display internal reflection.

Occurrence Sphalerite is a common constituent of hydrothermal sulfide deposits. Associated minerals include galena, pyrite, chalcopyrite, pyrrhotite, and other sulfides, along with quartz, carbonates, and sulfates. Sphalerite is found infrequently as an accessory mineral in felsic igneous rocks and in coal beds. Sphalerite may be precipitated by sulfate-reducing bacteria from aqueous solutions that contain less than 1 ppm Zn (Labrenz and others, 2000), suggesting both that bacteria can be used to remove Zn from contaminated surface water and that some low-temperature sphalerite deposits could have been biologically produced.

Use Sphalerite is the most important Zn ore mineral. Zinc is an important industrial metal used to make castings and to plate steel to resist rust. Cast Zn is often referred to as "pot metal." Zinc is alloyed with copper to make brass. Zinc is also an important dietary mineral and is added to fertilizers. Zinc oxide is used in paint, and zinc chloride is used as a soldering flux and as a wood preservative. Sphalerite is used in homeopathic remedies.

Sphalerite is also the most important source of Cd, In, Ga, and Ge. Cadmium is used in batteries and other products. In, Ga, and Ge are used in semiconductors.

Galena

$$\mathrm{PbS}$$

$$\text{Isometric } 4/m\ \bar{3}2/m$$

$$a = 5.936,\ Z = 4$$

$$H = 2.5$$

$$G = 7.58$$

Opaque

DO NOT COPY e48d507df5d1141@placeholder.9409

Printed by: e48d507df5d1141@placeholder.94092.edu. Printing is for personal, private use only. No part of this book may be reproduced or transmitted without publisher's prior permission. Violators will be prosecuted.

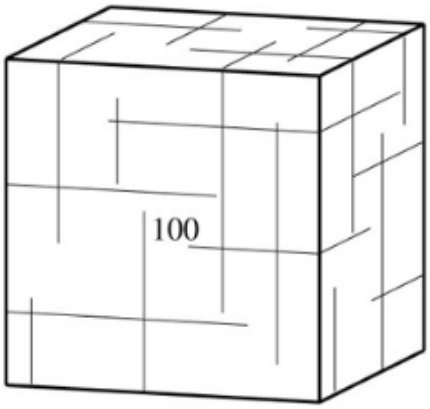

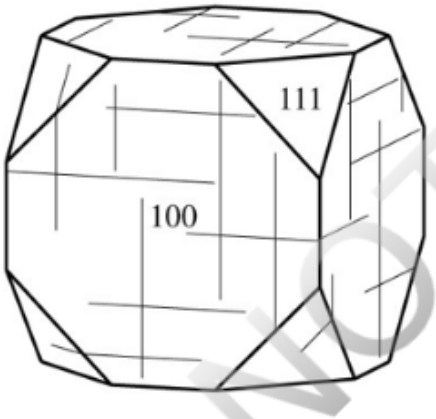

Structure Galena is isostructural with halite. Sulfur is at the corners and face centers of the unit cell, alternating with Pb. The Pb is in octahedral coordination with the S, and vice versa.

Composition Galena is usually fairly pure PbS; some Ag may substitute for Pb, but most of the Ag, As, and Sb reported in analyses is located in small inclusions of acanthite or tetrahedrite.

Form and Twinning Well-formed cubes are common, sometimes modified by octahedron {111} faces (Figure 19.6). Also cleavable masses and coarse to fine aggregates. Twins on {111} may be either contact or penetration; {114} twins are lamellar and may give rise to diagonal striations on cleavage surfaces.

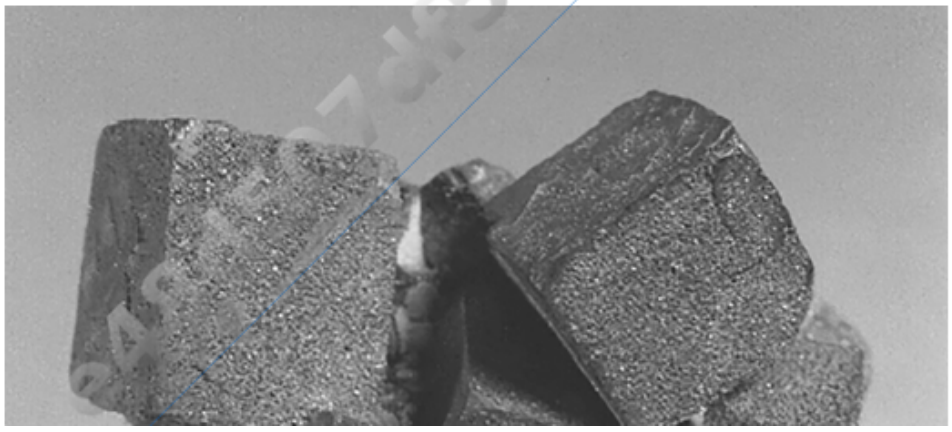

Printed by: e48d507df5d1141@placeholder.94092.edu. Printing is for personal, private use only. No part of this book may be reproduced or transmitted without publisher's prior permission. Violators will be prosecuted.

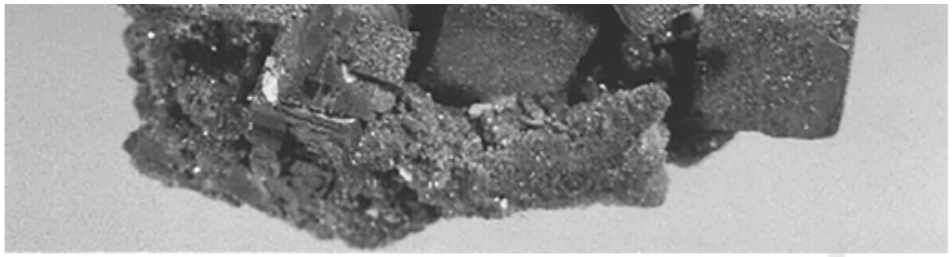

FIGURE 19.6 Galena cubes encrusted with marcasite. View larger image

Cleavage Perfect {001} cubic cleavage similar to halite. Subconchoidal fracture. Brittle.

Color Properties

Luster: Metallic.

Color: Gray/silver. Galena is a semiconductor whose band gap is only 0.42 eV. Visible light has energies above 1.7 eV, so all wavelengths can be absorbed.

Streak: Gray. Galena will barely mark paper.

Optical Characteristics

Thin Section: Opaque.

Polished Section: White, sometimes with pink tint and isotropic.

Alteration Supergene oxidation processes may alter galena to cerussite ($PbCO_3$) or anglesite ($PbSO_4$).

Distinguishing Features

Hand Sample: Gray/silver color and streak, cubic cleavage, metallic luster, and high specific gravity are diagnostic. Dark-colored sphalerite has a light streak.

Thin Section/Grain Mount: Difficult to distinguish from other opaque minerals.

Polished Section: Recognized by white color, moderately high reflectance, and presence of triangular polishing pits.

Occurrence Galena is a very common mineral in hydrothermal sulfide deposits and frequently is associated with sphalerite, pyrite, chalcopyrite, quartz, calcite, fluorite, and/or barite. Galena may be precipitated diagenetically in organic-rich marine sediments both by biologically induced mineralization triggered by sulfate-reducing bacteria and by thermally driven chemistry (Machel, 2001).

Use Galena is the principal ore mineral for Pb and also serves as a significant source of Ag. Lead has a wide range of industrial uses. One familiar to most readers is in lead–acid batteries used in automobiles and elsewhere for a low-cost, durable, and rechargeable power supply. It is also alloyed with Sn and Sb to make electrical solder. In the past, lead

DO NOT COPY e48d507df5d1141@placeholder.9409

Printed by: e48d507df5d1141@placeholder.94092.edu. Printing is for personal, private use only. No part of this book may be reproduced or transmitted without publisher's prior permission. Violators will be prosecuted.

power supply. It is also alloyed with Sn and Sb to make electrical solder. In the past, lead oxide was used in paints, and these paints pose a health hazard. Lead oxide has been used in some areas of the world as a folk remedy for diarrhea. Although it is effective, it also produces possibly debilitating lead poisoning. Galena is used in homeopathic remedies for skin and lung ailments. Since the preparations are extremely dilute, the possibility of lead poisoning is probably minimal, and any benefit likely depends on the placebo effect. Despite its Pb content, galena is touted as a detoxification agent by those who believe in crystal healing.

Pyrrhotite

$$\mathrm{Fe}_{1-x}\mathrm{S}\ (x = 0 \text{ to } 0.13)$$

Monoclinic $2/m$
(pseudohexagonal)

$a = 6.87$ Å, $b = 11.90$ Å,
$c = 22.72$ Å, $\beta = 90.1^\circ$,
$Z = 64$

$$H = 3.5 - 4.5$$

$$G = 4.58 - 4.65$$

Opaque

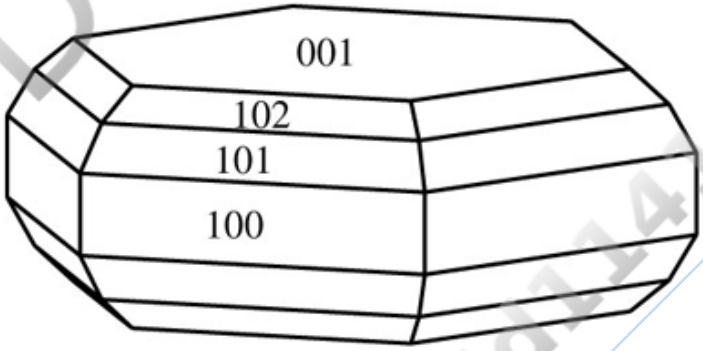

Structure The structure is based on hexagonal close-packed sulfur with Fe occupying octahedral sites between the sulfur layers.

Composition The principal variation is in the iron content with substitution of $2Fe^{3+} + \square$ for $3Fe^{2+}$ ($\square$ represents a vacant site). Chapter 4 describes this type of solid solution in more detail. Up to about 13% of the sites that would hold Fe in the ideal structure may be vacant. Ni, Co, Mn, and Cu may substitute for Fe or may be present in small inclusions of pentlandite [$(Fe,Ni)_9S_8$] or chalcopyrite. Troilite (FeS) is a hexagonal polymorph without significant substitution of Fe^{3+} for Fe^{2+}.

DO NOT COPY
e48d507df5d1141@placeholder.9409

Printed by: e48d507df5d1141@placeholder.94092.edu. Printing is for personal, private use only. No part of this book may be reproduced or transmitted without publisher's prior permission. Violators will be prosecuted.

Form and Twinning Crystals are usually tabular parallel to {001}, also pyramidal or arranged in rosettes. Usually massive granular aggregates. Twinning on {102} may be simple or repeated. (Indexing based on pseudohexagonal symmetry.)

Cleavage None. {001} parting distinct, {102} parting less distinct. Uneven to subconchoidal fracture. Brittle.

Color Properties

Luster: Metallic.

Color: Bronze-yellow with reddish or brownish cast; tarnishes easily, sometimes with iridescence.

Streak: Dark grayish black.

Optical Characteristics

Thin Section: Opaque.

Polished Section: Distinct creamy pinkish-brown to reddish-brown reflectance pleochroism, very strong anisotropism with yellow-gray or grayish-blue polarization colors.

Alteration Pyrrhotite may be replaced by pyrite, marcasite, or other sulfides. Alteration to iron oxides, hydroxides, sulfates, or carbonates is common in the weathering and supergene environments.

Distinguishing Features

Hand Sample: Weakly ferrimagnetic (will attract a magnet), stronger with lower Fe content. Resembles pyrite but has a more bronze color and is softer. Pentlandite, with which it may be associated, is slightly paler, has octahedral parting, is not magnetic, and has a light bronze-brown streak.

Thin Section/Grain Mount: Opaque in thin section.

Polished Section: Light brown color and strong anisotropism. Pentlandite is isotropic.

Occurrence Pyrrhotite is commonly found in both high-temperature hydrothermal sulfide deposits and mafic and ultramafic igneous rocks. Associated sulfides frequently include pyrite, marcasite, chalcopyrite, and pentlandite. Masses found in mafic and ultramafic rock bodies are often interpreted to be formed by immiscible segregation of a sulfide melt from the silicate melt. Pyrrhotite also has been found in pegmatites and contact metamorphic deposits, and troilite is found in meteorites and lunar rocks. Sulfate-reducing bacteria are capable of precipitating pyrrhotite and other iron sulfides.

Use Pyrrhotite has been mined as a source of iron but it is more commonly mined from

DO NOT COPY e48d507df5d1141@placeholder.9409

Printed by: e48d507df5d1141@placeholder.94092.edu. Printing is for personal, private use only. No part of this book may be reproduced or transmitted without publisher's prior permission. Violators will be prosecuted.

mafic intrusion deposits for nickel, copper, and platinum found in associated minerals.

Chalcopyrite

$$CuFeS_2$$

Tetragonal $\bar{4}2m$

$a = 5.281$ Å, $c = 10.401$ Å,
$Z = 4$

$H = 3.5 - 4$

$G = 4.1 - 4.3$

Opaque

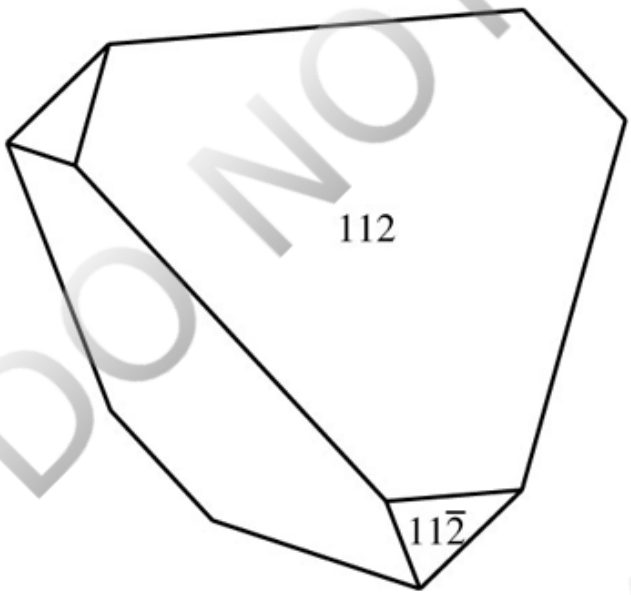

Structure The chalcopyrite structure is equivalent to two stacked sphalerite unit cells parallel to c with Cu and Fe replacing the Zn in an alternating fashion (Figure 19.5). Cu or Fe may occupy additional tetrahedral sites, yielding stoichiometries such as $Cu_9Fe_8S_{16}$ or $Cu_8Fe_{10}S_{16}$. Metallic bonding among the metals evidently allows valence requirements to be satisfied.

Composition Despite similarities in structure, only limited solid solution extends between chalcopyrite and sphalerite. Minor amounts of other elements (Co, Ni, Mn, Sn, As, etc.) may be present, but often are part of small inclusions of other sulfide minerals.

Form and Twinning Crystals are commonly dominated by the {112} disphenoid, which looks like a tetrahedron. The negative disphenoid $\{\bar{1}12\}$ may produce an octahedral habit and a tetragonal prism also may be developed. Lamellar twins on {112}, {102},

DO NOT COPY
e48d507df5d1141@placeholder.9409

Printed by: e48d507df5d1141@placeholder.94092.edu. Printing is for personal, private use only. No part of this book may be reproduced or transmitted without publisher's prior permission. Violators will be prosecuted.

habit and a tetragonal prism also may be developed. Lamellar twins on {112}, {102}, and {110}, deformation twins on {110} and {012}, penetration twin by rotation on [001] with {110} composition plane.

Cleavage Poor on {011} and {111}. Uneven fracture. Brittle.

Color Properties

Luster: Metallic.

Color: Brass-yellow; may be tarnished and iridescent. The band gap is 0.53 eV, so chalcopyrite can absorb all wavelengths and the streak is dark. The re-emitted wavelengths yield a yellow color, similar to pyrite.

Streak: Greenish black.

Optical Characteristics

Thin Section: Opaque.

Polished Section: Yellow with weak reflection pleochroism; high-temperature samples may be strongly pleochroic. Crossed-polarizer anisotropy is weak but distinct, gray-blue to yellow-green.

Alteration Chalcopyrite may alter to other copper sulfides (chalcocite, covellite) or to oxides, sulfates, or carbonates of Fe and Cu (cuprite, malachite, azurite, siderite, limonite, etc.) in the supergene environment. Chrysocolla and turquoise are also alteration products.

Distinguishing Features

Hand Sample: Distinguished from pyrite by lower hardness, different crystal habit, and richer yellow color. Pyrrhotite is less distinctly yellow and is weakly magnetic. Small grains may resemble native gold but are not sectile and yield a greenish-black streak.

Thin Section/Grain Mount: Difficult to distinguish from other opaque minerals.

Polished Section: More distinctly yellow than pyrite and anisotropic.

Occurrence Chalcopyrite is the most common Cu-bearing mineral and is found in many hydrothermal sulfide deposits, often associated with galena, sphalerite, pyrite, and other sulfide minerals. Some mafic igneous rocks may contain chalcopyrite as an accessory mineral, or they may contain segregated masses of sulfides that commonly include pyrrhotite, pentlandite, and chalcopyrite. Chalcopyrite may occur in some sediments without obvious connection to igneous activity. Chalcopyrite is a biomineral (Chapter 5), and it is possible to use bacteria to promote extraction of Cu from it in metallurgical processes.

Use Chalcopyrite is the principal source for Cu. Major deposits are found in many areas

DO NOT COPY e48d507df5d1141@placeholder.9409

Printed by: e48d507df5d1141@placeholder.94092.edu. Printing is for personal, private use only. No part of this book may be reproduced or transmitted without publisher's prior permission. Violators will be prosecuted.

of the world. Some vein deposits are mined, but the majority of Cu production comes from disseminated "porphyry copper" deposits. In these deposits, chalcopyrite and other hydrothermal minerals are deposited in a large volume of rock surrounding a porphyritic felsic intrusion. Open-pit mining on a large scale is generally used to recover the Cu. Industrial uses of Cu are numerous. Perhaps the most important is its use in electrical wires that are required for most of our social, commercial, and industrial infrastructure. Chalcopyrite is another sulfide that appears in homeopathic remedies that likely trigger the placebo effect and whose great dilution probably precludes adverse reactions.

Cinnabar

$$\mathrm{HgS}$$

$$\text{Hexagonal } 32$$

$$a = 4.145 \text{ Å},$$
$$c = 9.496 \text{ Å}, \ Z = 3$$

$$H = 2 - 2.5$$

$$G = 8.18$$

$$\text{Uniaxial } (+)$$

$$n_\omega = 2.91$$

$$n_\epsilon = 3.26$$

$$\delta = 0.35$$

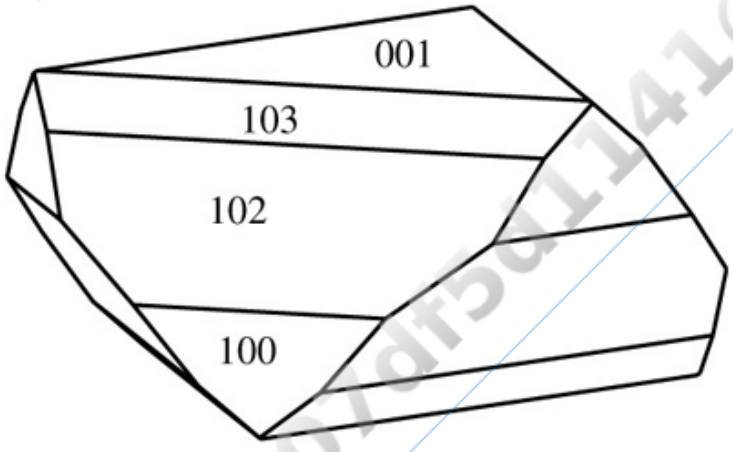

Structure The structure is based on systematic stacking of sheets of S with Hg in octahedral sites. Metacinnabar and hypercinnabar are isometric and hexagonal polymorphs, stable at higher temperatures.

Composition Essentially pure HgS, but some samples may have a deficiency of Hg.

DO NOT COPY
e48d507df5d1141@placeholder.9409

Printed by: e48d507df5d1141@placeholder.94092.edu. Printing is for personal, private use only. No part of this book may be reproduced or transmitted without publisher's prior permission. Violators will be prosecuted.

Form and Twinning Crystals are rhombohedral, thick tabular on {001}, or short prismatic parallel to *c*. Common as fine coatings, crystalline encrustations, granular aggregates, or massive.

Cleavage {100} perfect. Subconchoidal to uneven fracture. Slightly sectile.

Color Properties

Luster: Adamantine, tending to metallic if dark colored.

Color: Carmine-red, brownish red if impure, earthy if fine grained. Cinnabar is a semiconductor whose band gap is 2.0 eV. Incident light whose energy is greater than 2.0 eV (Figure 6.6) will be absorbed and only the red end of the spectrum is transmitted, hence the red color.

Streak: Scarlet-red.

Thin Section: Deep red.

Optical Characteristics

Relief in Thin Section: Very high positive.

Indices of Refraction and Birefringence: Birefringence is extreme, but interference colors will be masked by mineral color.

Polished Section: White with bluish-gray tint, red internal reflections, and distinctly anisotropic with light green polarization colors.

Alteration Cinnabar may weathering to native mercury, montroydite (HgO) (deep red, yellow-brown streak, sectile), or calomel (HgCl) (yellow- or gray-white, yellowish-white streak, sectile, fluoresces brick red in UV light).

Distinguishing Features

Hand Sample: Bright red color and red streak distinguish cinnabar from hematite. Realgar has an orange-red streak and is almost always associated with yellow orpiment. If heated, cinnabar will release mercury, which is toxic. Care should be taken when handling cinnabar to avoid ingestion or inhalation; hands should be washed following contact.

Thin Section/Grain Mount: Deep red color and association.

Polished Section: Similar to proustite, but proustite is not twinned and has no green polarization colors.

Occurrence Found in low-temperature hydrothermal deposits associated with volcanism or shallow intrusions. Associated minerals include pyrite, marcasite, stibnite, chalcedony,

DO NOT COPY e48d507df5d1141@placeholder.9409

Printed by: e48d507df5d1141@placeholder.94092.edu. Printing is for personal, private use only. No part of this book may be reproduced or transmitted without publisher's prior permission. Violators will be prosecuted.

opal, calcite, and dolomite. Some deposits are interpreted to be formed quite near the surface beneath hot springs. Cinnabar may fill fractures or other voids, or replace quartz or other grains in the host rock, as is the case for the world's largest mercury deposit in Almadén, Spain. There cinnabar and native mercury are both found in a weakly metamorphosed quartzite. This deposit has been mined since at least the fourth century BCE and still contains a large resource of easily mined mercury. The mine closed in 2002 because of a ban on mercury mining in Europe.

Use Cinnabar is the principal source for mercury. Mercury is used in fluorescent light bulbs, batteries, electrical switches, thermometers, and various chemical applications.

Cinnabar has numerous historical medical applications including those in Chinese, Tibetan, and Ayurvedic traditional medicine. Liquid mercury and mercury chloride (calomel) have had even more uses. The outbreak of syphilis in Europe in the late fifteenth century triggered a search for cures, and mercury in various forms became one of the standard treatments and remained so until the introduction of antibiotics in the last century. Most medical uses of mercury are now banned in Western countries because of mercury poisoning.

Comments Mercury is volatile, and vapors are quite poisonous. One geochemical technique used in certain mineral exploration programs is to mount analytical equipment in an airplane. The airplane is flown in a systematic pattern over an area of suspected mineralization to sample the air for traces of mercury that may indicate the presence of a hydrothermal deposit.

DO NOT COPY

Pyrite

FeS_2

Isometric $2/m\,\bar{3}$

$a = 5.418$ Å, $Z = 4$

$H = 6 - 6.5$

$G = 5.02$

Opaque

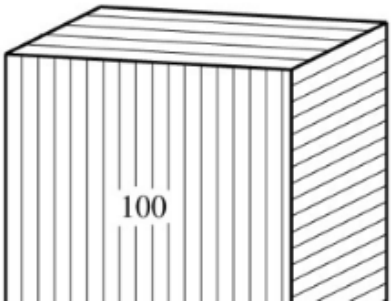

e48d507df5d1141@placeholder.9409

Printed by: e48d507df5d1141@placeholder.94092.edu. Printing is for personal, private use only. No part of this book may be reproduced or transmitted without publisher's prior permission. Violators will be prosecuted.

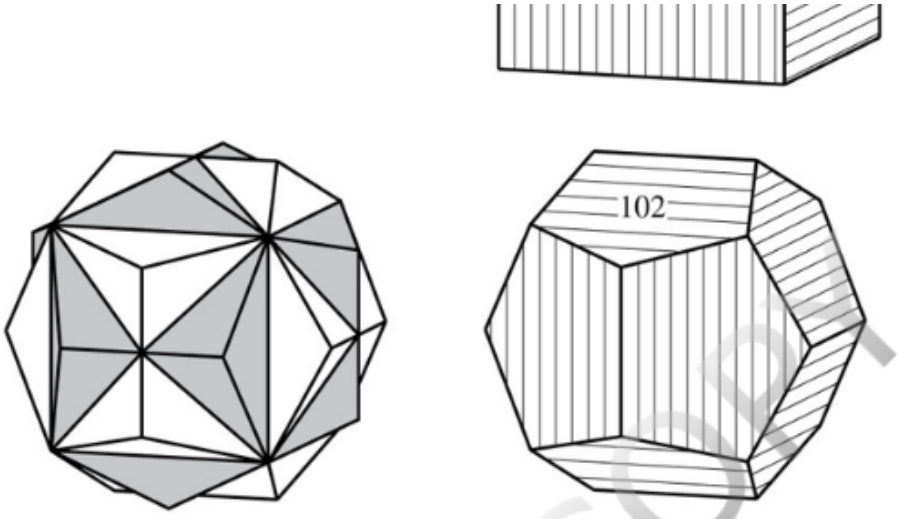

"Iron Cross" Twin

Structure The structure of pyrite (Figure 19.7a) can be derived from halite by replacing the Na with Fe. The sulfur forms covalently bonded S_2 pairs with a combined effective −2 charge that occupy the Cl positions in the halite structure. Each Fe^{+2} coordinates with six S atoms and each S atom bonds with three Fe. Bonding is apparently accomplished by hybridizing the 3*p* and 3*s* orbitals on sulfur to form four sp^3 orbitals. One of these hybrid orbitals is shared with another sulfur to form the S_2 doublet; the remaining three are shared with three iron atoms. The 3*d*, 4*s*, and 4*p* orbitals on each iron are hybridized to form six d^2sp^3 orbitals that are covalently shared with sulfur. Because the covalently bonded S_2 pair is not spherically symmetrical, the symmetry of pyrite is lower than halite. Marcasite is an orthorhombic polymorph of pyrite.

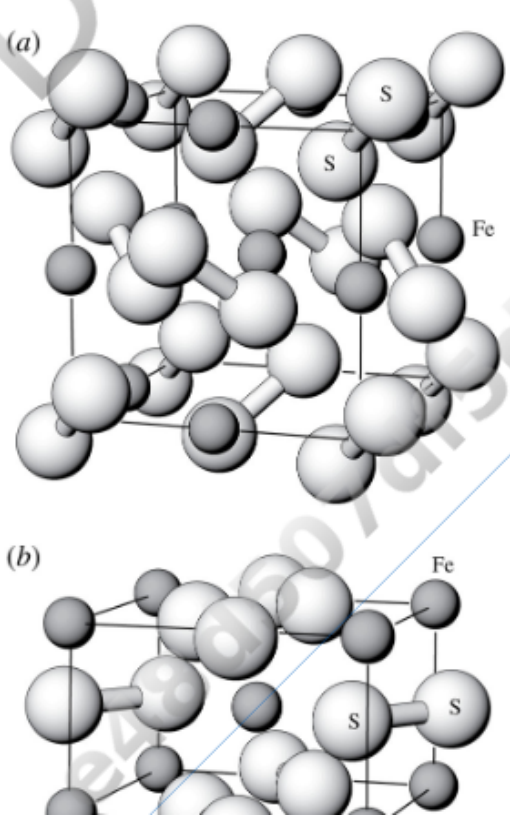

DO NOT COPY e48d507df5d1141@placeholder.94092

Printed by: e48d507df5d1141@placeholder.94092.edu. Printing is for personal, private use only. No part of this book may be reproduced or transmitted without publisher's prior permission. Violators will be prosecuted.

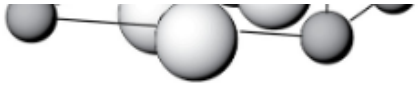

FIGURE 19.7 Structure of iron sulfides. (*a*) The pyrite structure is derived from halite, with Fe in the Na positions and covalently bonded S_2 doublets occupying the Cl positions. (*b*) Marcasite structure. Fe occupies the nodes of a body-centered orthorhombic lattice with covalently bonded S_2 pairs in the center of four unit cell edges parallel to *b* and in the center of the {010} ends of the unit cell. View larger image

Composition Most pyrite is close to the ideal composition. Ni or Co may substitute for Fe in small amounts. Microscopic inclusions of gold or chalcopyrite may be present.

Form and Twinning Cubes {001} and pyritohedrons {102} are characteristic crystals (Figure 19.8). Cube faces are commonly striated, consistent with 3-fold rotational symmetry on the long diagonals through the cube. Octahedral faces are less common and can be striated as well. Commonly massive, fine granular, or encrusting. Sometimes elongate to acicular across the width of thin veins. Twins by rotation on [001], with {110} composition planes, form penetration twins known as "Iron Crosses." Small (1–30 μm) aggregates of pyrite called framboids are common in shale.

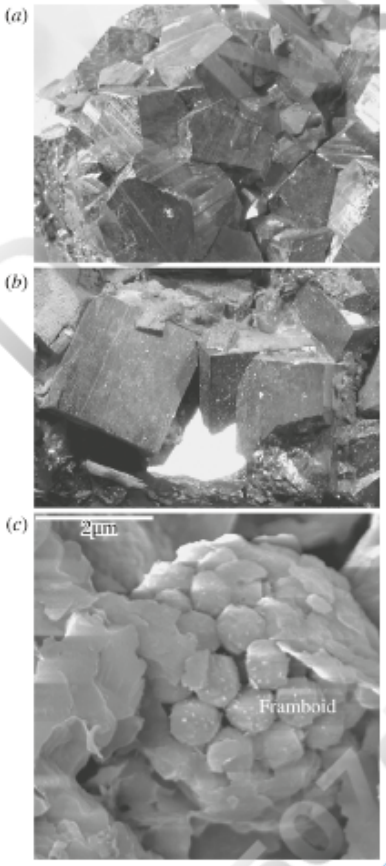

FIGURE 19.8 Pyrite. (*a*) Pyritohedron crystals. Field of view is about 5 cm wide. (*b*) Pyrite cubes with quartz. Field of view is about 2 cm wide. (*c*) Spherical framboid made of numerous equant pyrite grains in clay from Canadian River, Oklahoma, alluvium. The flaky particles are clay minerals. Photo courtesy of G. Breit, U.S. Geological Survey. View larger image

DO NOT COPY e48d507df5d1141@placeholder.9409

Printed by: e48d507df5d1141@placeholder.94092.edu. Printing is for personal, private use only. No part of this book may be reproduced or transmitted without publisher's prior permission. Violators will be prosecuted.

Cleavage A poor cleavage on {001} is usually not observed. Parting on {011} and {111}. Conchoidal to uneven fracture. Brittle.

Color Properties

Luster: Metallic.

Color: Pale brass-yellow, tarnishes darker with iridescence. The color of pyrite was discussed in Chapter 6 (Figure 6.11).

Streak: Greenish black to brownish black.

Optical Characteristics

Thin Section: Opaque.

Polished Section: Creamy white or whitish yellow without bireflectance or pleochroism. May be weakly anisotropic with blue-green to red-orange polarization color.

Alteration Pyrite commonly altered to iron oxides and hydroxides. Pseudomorphs of limonite after pyrite are common. The oxidation of pyrite plays an important role in supergene alteration of hydrothermal sulfide deposits, described earlier.

Distinguishing Features

Hand Sample: Known as "fool's gold" because pyrite routinely is misidentified as gold by the uninitiated (everyone should read Mark Twain's *Roughing It*). Hardness, brittle character, and greenish-black streak are distinctive. Chalcopyrite has a richer yellow color and is softer, and its crystals are typically tetrahedral. Pyrrhotite is softer and brownish bronze. Marcasite has a different crystal habit and somewhat paler color but is otherwise quite similar.

Thin Section/Grain Mount: Difficult to distinguish from other opaque minerals.

Polished Section: Distinguished from marcasite by lack of reflection pleochroism.

Occurrence Pyrite is the most common sulfide mineral, and few hydrothermal deposits lack it. Igneous rocks of almost any composition may contain pyrite as an accessory mineral, and it may form magmatic segregations in some mafic intrusion complexes. Pyrite may be found as an opaque mineral in some metamorphic rocks. Pyrite is common as fine grains in shale, generally precipitated from seawater under reducing conditions. Coal also usually contains some fine pyrite.

Pyrite, one of the best-documented biominerals (Chapter 5), is produced by both biologically induced and biologically controlled processes involving sulfate-reducing bacteria and bacteria that reduce Fe^{3+} to Fe^{2+}. Details of the chemistry remain unclear, but it appears that in some cases the process begins with local precipitation of an amorphous FeS phase that crystallizes to mackinawite (FeS), which subsequently

DO NOT COPY e48d507df5d1141@placeholder.9409

Printed by: e48d507df5d1141@placeholder.94092.edu. Printing is for personal, private use only. No part of this book may be reproduced or transmitted without publisher's prior permission. Violators will be prosecuted.

amorphous FeS phase that crystallizes to mackinawite (FeS), which subsequently combines with additional sulfur or loss of iron to form greigite (Fe_3S_4) and then pyrite. The fact that pyrite may not precipitate directly is a result of unfavorable kinetics compared to the other phases. Whether framboids (Figure 19.8c) are a product of biomineralization is a matter of debate (Pósfi and Dunin-Borkowski, 2006; Konhauser, 2007).

Use Pyrite has been used as a source of iron and sulfur, and is a feedstock in the manufacture of Fe-bearing chemicals. In most cases pyrite is not of economic importance itself, but is often associated with other minerals that have great value, such as chalcopyrite, galena, and sphalerite. Gold is extracted from minute inclusions in pyrite from some deposits. Pyrite has numerous historical medical uses. For example, Agricola (1546, p. 13), in what may be considered the first textbook on mineralogy, includes a section on medical uses of minerals in which he reports that pyrite will "break up gatherings in the body." Other historical uses included treatment of bleeding, gastrointestinal and pulmonary problems, and broken bones.

Comments Pyrite is a mineral with significant environmental impact. Oxygenated surface water that interacts with pyrite oxidizes the iron and releases sulfuric acid (see earlier discussion of supergene processes). Although this process goes on naturally, mining can promote groundwater flow into pyrite-bearing rock and also can provide an easy route to the surface for acidic groundwater. The water issuing from the portals of old mines can be very acidic and can carry substantial amounts of heavy metals, such as lead, in solution. A related problem is the generation of acid when surface water soaks pyrite-bearing mine waste. If discharged into streams, this acidic water may cause substantial changes to the ecosystem and pose a health risk to people. Such acidic waters are often referred to as **acid mine drainage**.

DO NOT COPY e48d507df5d1141@placeholder.9409

Marcasite

FeS_2

Orthorhombic $2/m\ 2/m\ 2/m$

$a = 4.436$ Å, $b = 5.414$ Å,
$c = 3.381$ Å, $Z = 2$

$H = 6 - 6.5$

$G = 4.89$

Opaque

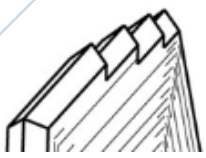

Printed by: e48d507df5d1141@placeholder.94092.edu. Printing is for personal, private use only. No part of this book may be reproduced or transmitted without publisher's prior permission. Violators will be prosecuted.

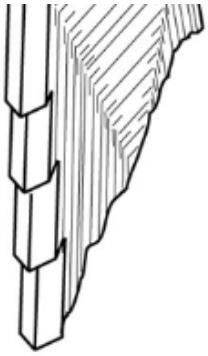

DO NOT COPY

Structure The marcasite structure is based on a body-centered orthorhombic lattice. Fe^{2+} is located at each lattice node and covalently bonded S_2 pairs, with an effective −2 charge, are positioned at the center of each horizontal edge of the unit cell and in the middle of the end {010} faces (Figure 19.7b). This places Fe in octahedral (6-fold) coordination with sulfur, the same as in the pyrite polymorph.

Composition Generally close to the ideal formula. Minor Cu may substitute for Fe, and As for S. Arsenopyrite shares the same structure, but the two minerals exhibit almost no solid solution.

Form and Twinning Crystals are commonly tabular on {010}, less commonly prismatic parallel to *c*; curved faces are common (Figure 19.9). Twins on {101} are common, less common on {011}. Combination of {101} twins and curved faces often produces "cockscomb" or spear-shaped groups. Often forms encrusting, globular, or reniform masses with radiating internal structure and crystals projecting from the surface.

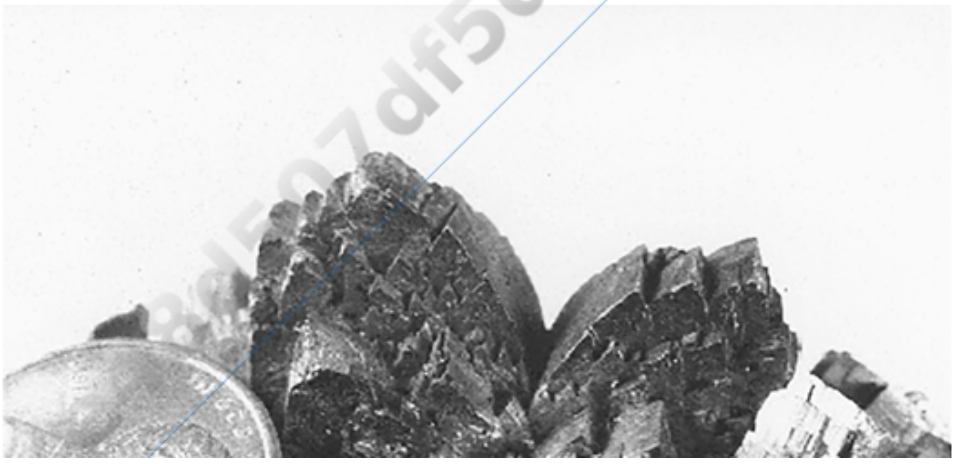

Printed by: e48d507df5d1141@placeholder.94092.edu. Printing is for personal, private use only. No part of this book may be reproduced or transmitted without publisher's prior permission. Violators will be prosecuted.

FIGURE 19.9 Cockscomb crystals of marcasite. View larger image

Cleavage Cleavage on {101} is fair; it also may be a parting. Uneven fracture. Brittle.

Color Properties

Luster: Metallic.

Color: Pale bronze-yellow to almost white, darkening on exposure.

Streak: Grayish black.

Optical Characteristics

Thin Section: Opaque.

Polished Section: Creamy white to yellowish white with greenish and pink hues with reflection pleochroism; strong anisotropy in crossed polarizers, with blue, green-yellow, or purple/violet-gray polarization colors.

Alteration Marcasite is commonly altered to iron hydroxides and sulfates. Limonite pseudomorphs after marcasite are common.

DO NOT COPY
e48d507df5d1141@placeholder.9409

Printed by: e48d507df5d1141@placeholder.94092.edu. Printing is for personal, private use only. No part of this book may be reproduced or transmitted without publisher's prior permission. Violators will be prosecuted.

Distinguishing Features

Hand Sample: Resembles pyrite but has a different crystal habit and is somewhat paler colored if fresh.

Thin Section/Grain Mount: Difficult to distinguish from other opaque minerals.

Polished Section: Pyrite is slightly darker colored and does not display reflection pleochroism with rotation.

Occurrence Marcasite is a common mineral in hydrothermal sulfide deposits, generally formed at fairly low temperatures; it may be produced by supergene processes. Associated minerals commonly include galena and sphalerite. Concretionary masses in shale, limestone, and coal are common. Pseudomorphic replacement of fossils by marcasite may be quite striking. Marcasite may be precipitated by biomineralization processes.

Use Marcasite can be used as a source of sulfur and iron, but is not normally of economic value.

Molybdenite

Å

Å

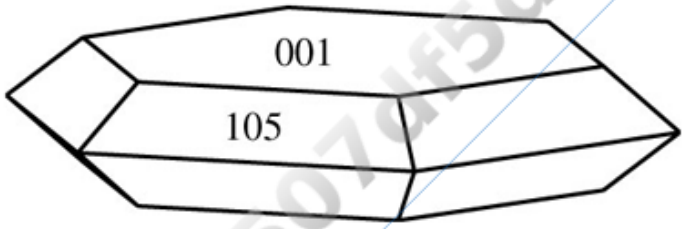

Structure The structure is layered. Each layer consists of two sheets of sulfur atoms with Mo cations in 6-fold coordination sites in between. Successive layers are weakly bonded to each other, producing perfect cleavage on {001}.

Composition Molybdenite is nearly pure MoS_2.

DO NOT COPY e48d507df5d1141@placeholder.9409

Printed by: e48d507df5d1141@placeholder.94092.edu. Printing is for personal, private use only. No part of this book may be reproduced or transmitted without publisher's prior permission. Violators will be prosecuted.

Composition Molybdenite is nearly pure MoS_2.

Form and Twinning Crystals are hexagonal plates or stubby hexagonal prisms. Also scaly and foliated massive. Twins on {001} are reported.

Cleavage Perfect on {001}; folia are inelastic. Greasy feel.

Color Properties

Luster: Metallic.

Color: Dark gray/silver. Molybdenite is a semiconductor with a band gap of 1.29 eV. It therefore is capable of absorbing all of the visible spectrum, hence its dark color and streak. In extremely thin flakes, molybdenite may be translucent pale yellow to deep reddish brown, depending on thickness.

Streak: Bluish gray.

Optical Characteristics

Thin Section: Opaque.

Polished Section: White with bluish tint, with extreme white to gray bireflectance; very strong anisotropy in crossed polarizers, with pinkish white polarization color.

Alteration Molybdenite commonly alters to yellow ferrimolybdite [$Fe_2(MoO_4)_3 \cdot 8H_2O$].

Distinguishing Features

Hand Sample: Most closely resembles graphite but color has a more bluish hue, and the streak on porcelain is somewhat bluish, whereas graphite is black.

Thin Section/Grain Mount: Opaque in thin section.

Polished Section: Habit and white color with strong bireflectance are distinctive. Graphite is similar but less reflective.

Occurrence Found in hydrothermal veins and disseminated deposits. In the largest deposits, such as the Climax and Henderson deposits in Colorado, molybdenite, quartz, pyrite, and other minerals have precipitated in large inverted bowl-shaped volumes of fractured rock over the top of mid-Tertiary felsic intrusions. These deposits are commonly referred to as porphyry “moly” deposits. Molybdenite is found as a minor mineral in porphyry copper deposits that have similar geometries but instead contain copper minerals (e.g., chalcopyrite). Molybdenite is also found in pegmatites and in skarn deposits.

Use Molybdenite is the principal source for molybdenum, which is typically alloyed with iron to make high-strength steel. It is also used in certain lubricants and other chemical products. Molybdenum is an essential nutrient in trace amounts, so small amounts are

DO NOT COPY

Printed by: e48d507df5d1141@placeholder.94092.edu. Printing is for personal, private use only. No part of this book may be reproduced or transmitted without publisher's prior permission. Violators will be prosecuted.

included in fertilizers, animal feeds, and human dietary supplements. High concentrations of molybdenum are toxic.

Bornite

Cu_5FeS_4

Orthorhombic $2/m\ 2/m\ 2/m$
(pseudoisometric)

$a = 10.950$ Å, $b = 21.862$ Å,
$c = 10.950$ Å, $Z = 8$

$H = 3$

$G = 5.06 - 5.08$

Opaque

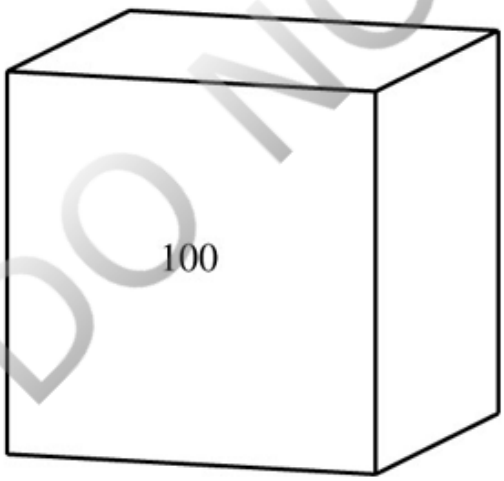

Structure At temperatures above 228°C, the structure is isometric with a unit cell that is about 5.50 Å on an edge. This structure is based on cubic close-packed sulfur atoms, with Cu and Fe atoms randomly distributed into six of the eight tetrahedral sites located in the octants of the cube. With cooling, the Fe and Cu become ordered, so that 5.5 Å subcells, with all eight tetrahedral sites filled, alternate with subcells with only four of the tetrahedral sites filled; symmetry is therefore reduced to orthorhombic.

Composition Substantial variation in the relative amounts of Cu and Fe is possible and solid solution extends toward chalcopyrite ($CuFeS_2$) and digenite (Cu_9S_5). Exsolution of blebs and lamellae of chalcopyrite, digenite, and chalcocite is common.

Form and Twinning Rare crystals are approximately cubic, dodecahedral, or octahedral. Usually massive. Penetration twinning on {111}.

DO NOT COPY e48d507df5d1141@placeholder.9409

Printed by: e48d507df5d1141@placeholder.94092.edu. Printing is for personal, private use only. No part of this book may be reproduced or transmitted without publisher's prior permission. Violators will be prosecuted.

Cleavage Poor {111} cleavage. Uneven to subconchoidal fracture. Brittle.

Color Properties

Luster: Metallic if fresh, iridescent tarnish.

Color: Brownish bronze on fresh surfaces, quickly tarnishes to iridescent purple, blue, and black (hence bornite unofficially is known as peacock ore).

Streak: Grayish black.

Optical Characteristics

Thin Section: Opaque.

Polished Section: Pinkish brown with weak bireflectance and reflection pleochroism; weak but variable anisotropy in crossed polarizers. Tarnishes easily to purple-brown.

Alteration Bornite may alter to chalcocite, chalcopyrite, covellite, cuprite, chrysocolla, malachite, or azurite.

Distinguishing Features

Hand Sample: Brownish-bronze color of fresh surfaces distinguishes bornite from chalcocite and chalcopyrite.

Thin Section/Grain Mount: Difficult to distinguish from other opaque minerals in thin section.

Polished Section: Pinkish-brown color with weak anisotropy is characteristic.

Occurrence Bornite is very common in copper-bearing hydrothermal sulfide deposits, usually as a hypogene (primary) mineral associated with chalcopyrite, chalcocite, covellite, pyrrhotite, and pyrite; less commonly as a supergene mineral in the enriched zone near the water table. It may be found as disseminated grains in mafic igneous rocks and pegmatites.

Use Mined as an ore of copper but it is not as important as chalcopyrite.

Chalcocite

$$Cu_2S$$

$$\text{Monoclinic } 2/m \text{ or } m$$
$$(\text{pseudo-orthorhombic})$$

$$a = 11.82 \text{ Å},\ b = 27.05 \text{ Å},$$
$$c = 13.42 \text{ Å}.\ \beta = 90^\circ.\ Z = 96$$

DO NOT COPY e48d507df5d1141@placeholder.9409

Printed by: e48d507df5d1141@placeholder.94092.edu. Printing is for personal, private use only. No part of this book may be reproduced or transmitted without publisher's prior permission. Violators will be prosecuted.

$c = 13.42$ A, $\beta = 90°$, $Z = 96$

$H = 2.5 - 3$

$G = 5.5 - 5.8$

Opaque

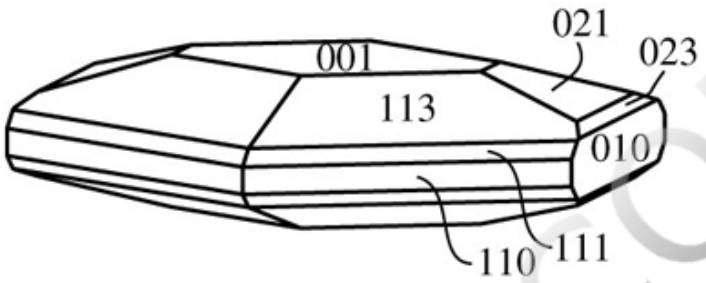

Structure The structure is based on hexagonal close-packed sulfur atoms with copper in triangular coordination with S. Above 103°C, the structure inverts to a hexagonal polymorph. A tetragonal polymorph is stable at high pressures.

Composition The composition is generally close to the ideal formula with only minor substitution of Fe for Cu.

Form and Twinning Rare crystals range from tabular parallel to (001) to short prismatic parallel to *c*. Most common as compact to powdery massive. Common twins on {110} yield pseudohexagonal stellate (star-shaped) forms.

Cleavage Fair on {110}. Conchoidal fracture. Somewhat sectile, brittle if crushed.

Color Properties

Luster: Metallic.

Color: Dark gray.

Streak: Dark gray.

Optical Characteristics

Thin Section: Opaque.

Polished Section: White to grayish white with or without bluish tint with very weak or undiscernible reflectance pleochroism; weak to distinct crossed-polarizer anisotropy with emerald-green to pink polarization colors under intense illumination. Tarnishes easily.

Alteration Chalcocite may be altered to other copper minerals such as covellite, malachite, or azurite.

Distinguishing Features

DO NOT COPY e48d507df5d1141@placeholder.9409

Printed by: e48d507df5d1141@placeholder.94092.edu. Printing is for personal, private use only. No part of this book may be reproduced or transmitted without publisher's prior permission. Violators will be prosecuted.

Hand Sample: Black color with sooty appearance on weathered surfaces and sectile character are distinctive. Bornite is brownish bronze on fresh surfaces.

Thin Section/Grain Mount: Difficult to distinguish from other opaque minerals.

Polished Section: White or bluish-white color and nearly isotropic character are characteristic.

Occurrence Typically found in the supergene-enriched zone of copper-bearing hydrothermal sulfide deposits. Chalcocite, covellite, digenite, djurleite, anilite, and other Cu-bearing sulfides are often intimately intermixed. Like many other sulfides, chalcocite is a biomineral produced by sulfate-reducing bacteria (McNeil and others, 1991).

Use Chalcocite is mined as a source of copper.

Comments A number of closely related minerals with very similar properties include digenite (Cu_9S_5), djurleite ($Cu_{31}S_{16}$), and anilite (Cu_7S_4). A substantial amount of material identified as chalcocite may actually be djurleite. Chalcocite and djurleite are very commonly intergrown.

Covellite

$$CuS$$

$$\text{Hexagonal } 6/m\ 2/m\ 2/m$$

$$a = 3.794 \text{ Å},$$
$$c = 16.341 \text{ Å},\ Z = 6$$

$$H = 1.5 - 2$$

$$G = 4.6 - 4.76$$

Opaque

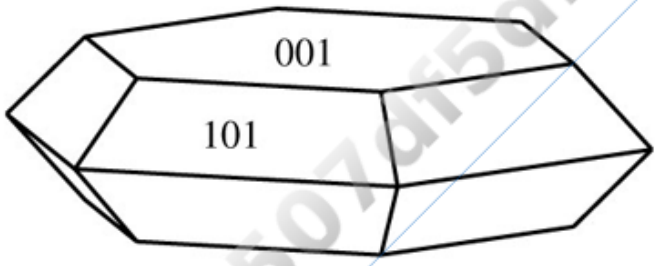

Structure The structure is based on a package of three sheets of sulfur atoms. Some copper is located in triangular coordination within the middle sheet. Additional copper is positioned in tetrahedral sites between the sulfur sheets. The sheets of each three-sulfur-sheet package are weakly bonded to each other through sulfur, producing a perfect

DO NOT COPY
e48d507df5d1141@placeholder.9409

Printed by: e48d507df5d1141@placeholder.94092.edu. Printing is for personal, private use only. No part of this book may be reproduced or transmitted without publisher's prior permission. Violators will be prosecuted.

sheet package are weakly bonded to each other through sulfur, producing a perfect cleavage.

Composition Most covellite is relatively pure CuS. Covellite is the first natural material known to display superconductivity (Di Benedetto and others, 2006).

Form and Twinning Crystals are tabular on {001} with a hexagonal outline and hexagonal markings on the basal pinacoid. Commonly as cleavable or foliated masses, also as rosettes of nearly parallel plates. Twinning is not reported.

Cleavage Perfect on {001} yields thin flexible folia (sheets).

Color Properties

Luster: Submetallic to resinous.

Color: Indigo-blue, sometimes darker; may be iridescent.

Streak: Shiny gray.

Optical Characteristics

Thin Section: Opaque.

Polished Section: Strong reflection pleochroism from indigo-blue with violet tint to bluish white. Extreme anisotropy, red-orange to brownish polarization colors.

Alteration Covellite may be altered to other copper sulfides (chalcocite, digenite, djurleite, bornite, etc.), carbonates (azurite, malachite), oxides (cuprite), and related minerals by hydrothermal and supergene processes.

Distinguishing Features

Hand Sample: Rich blue color and perfect cleavage are distinctive.

Thin Section/Grain Mount: Opaque in thin section.

Polished Section: The distinctive reflection pleochroism in polished section is characteristic.

Occurrence Occurs with other copper sulfides in hydrothermal sulfide deposits. Covellite is most commonly found in zones of supergene enrichment, but also may be a primary mineral. Associated minerals include chalcocite, bornite, chalcopyrite, pyrite, and other copper sulfides. Like many other sulfides, covellite is a biomineral produced by sulfate-reducing bacteria (McNeil and others, 1991).

Use Covellite is mined as copper ore.

DO NOT COPY e48d507df5d1141@placeholder.9409

Printed by: e48d507df5d1141@placeholder.94092.edu. Printing is for personal, private use only. No part of this book may be reproduced or transmitted without publisher's prior permission. Violators will be prosecuted.

Sulfarsenides

The sulfarsenides are minerals in which both sulfur and arsenic serve anion-like roles. Arsenopyrite is the only common sulfarsenide and is described below. Cobaltite is included in Table 19.6 and has a structure similar to pyrite, with Co replacing Fe and As replacing half of the S atoms.

TABLE 19.6 Sulfarsenides, Arsenides, and Tellurides

Mineral	Unit Cell	Physical Properties[a]	Optical Properties	Comments
Sulfarsenides				
Cobaltite CoAsS	Orthorhombic (pseudocubic) *mm*2 $a = 5.582$ $b = 5.582$ $c = 5.582$ $Z = 4$	*H*: 5.5 *G*: 6.33 Cl: {001} cubic, pf Tw: {011}, {111} of cubic habit lamellar C: Silver-white St: Grayish black L: Metallic	Opaque PS: White with pink or violet tint, weak bireflectance/pleochroism; weak anisotropy, blue-gray or brown polarization colors	Same structure as pyrite; crystals cubes or pyritohedrons, uncommon; also granular and compact; hydrothermal vein deposits with other cobalt minerals
Arsenides				
Skutterudite $(Co, Ni)As_{2-3}$	Isometric 2/*m* $a = 8.204$ $Z = 8$	*H*: 5.5–6 *G*: 6.5 Cl: {001}, {111}pf, {011}pr Tw: {112} forms sixlings, also {011} C: Tin-white to silver-gray St: Black	Opaque PS: Creamy white to grayish white, may be zoned; isotropic	Crystals cubic or octahedral, uncommon; massive or dense granular, colloform; high-temperature hydrothermal veins with other Co minerals

DO NOT COPY e48d507df5d1141@placeholder.9409-

Printed by: e48d507df5d1141@placeholder.94092.edu. Printing is for personal, private use only. No part of this book may be reproduced or transmitted without publisher's prior permission. Violators will be prosecuted.

		L: Metallic		
Nickeline NiAs	Hexagonal 6/*m* 2/*m* 2/*m* *a* = 3.602 *c* = 5.009 *Z* = 2	*H*: 5–5.5 *G*: 7.78 Cl: Conchoidal fracture Tw: {101} cyclic C: Pale copper-red, tarnishes gray or blackish St: Pale brownish black L: Metallic	Opaque PS: Strong bireflectance/pleochroism, yellowish pink to brownish pink; very strong anisotropism, yellow, greenish violet-blue, blue-gray polarization colors	Rare crystals tabular on {001} or pyramidal {101}, usually reniform with columnar structure; found with other Ni minerals in segregations ultramafic igneous rocks, also in hydrothermal vein deposits
Tellurides				
Calaverite $AuTe_2$	Monoclinic 2/*m* *a* = 8.76 *b* = 4.41 *c* = 10.15 *β* = 125.2° *Z* = 4	*H*: 2.5–3 *G*: 9.10–9.40 Cl: Uneven to subconchoidal fracture Tw: Common on {110}, also {031}, {111} C: Greenish yellow to silver-white St: Greenish to yellowish gray L: Metallic	Opaque PS: White with weak pleochroism and anisotropy	Rare crystals bladed or lathlike; also massive, granular; low-temperature hydrothermal deposits, less common in higher-temperature deposits
Sylvanite $(Au,Ag)_2Te_4$	Monoclinic 2/*m* *a* = 8.95 *b* = 4.478 *c* = 14.62 *β* = 145.35° *Z* = 2	*H*: 1.5–2 *G*: 8.16 Cl: {010}pf Tw: {100} common: contact, lamellar, penetration (cuneform)	Opaque PS: Bireflectance/pleochroism distinct, creamy white to brownish; strong anisotropism, light bluish gray to dark brown polarization colors	Rare crystals short prismatic on *c* or *b*, also tabular on {100}, also skeletal or bladed; granular; low-temperature and some higher-temperature hydrothermal deposits

DO NOT COPY
e48d507df5d1141@placeholder.9409

Printed by: e48d507df5d1141@placeholder.94092.edu. Printing is for personal, private use only. No part of this book may be reproduced or transmitted without publisher's prior permission. Violators will be prosecuted.

		(cubic form) C: Gray to yellowish silver-white St: Gray to silver-white L: Metallic		deposits

[a] Cl = cleavage (pf = perfect, pr = poor), Tw = twinning, C = color, St = streak, L = luster, PS = polished section.

Arsenopyrite

$$FeAsS$$

$$\text{Monoclinic } 2/m$$

$$\text{(pseudo - orthorhombic)}$$

$$a = 9.568 \text{ Å}, \ b = 5.675 \text{ Å},$$

$$c = 6.433 \text{ Å}, \ \beta = \ - 90^{\circ}, \ Z = 4$$

$$H = 5.5 - 6$$

$$G = 6.07$$

$$\text{Opaque}$$

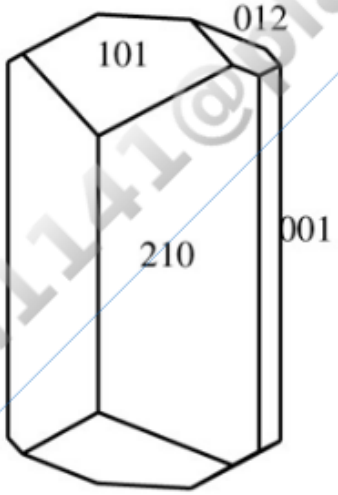

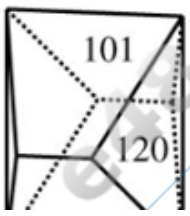

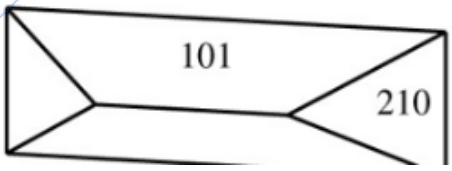

DO NOT COPY
e48d507df5d1141@placeholder.9409

Printed by: e48d507df5d1141@placeholder.94092.edu. Printing is for personal, private use only. No part of this book may be reproduced or transmitted without publisher's prior permission. Violators will be prosecuted.

Structure Arsenopyrite is similar to the marcasite structure, with half of the sulfur atoms replaced by arsenic (Figure 19.7b).

Composition The As:S ratio varies from about 0.9:1.1 to 1.1:0.9. Some Co may substitute for Fe, and solid solution extends to glaucodot [(Co,Fe)AsS]. Bi is reported in some analyses, probably substituting for As.

Form and Twinning Crystals commonly prismatic and elongate on *c*, less commonly on *b*. Also compact, granular, and columnar. Twins are common on {100} and {001}, and produce pseudo-orthorhombic crystals. Twins on {110} yield penetration twins that may be repeated, like marcasite.

Cleavage Fair on {101}, poor on {010}. Uneven fracture. Brittle.

Color Properties

Luster: Metallic.

Color: Silver-white to gray, yellowish tint possible.

Streak: Black.

Optical Characteristics

Thin Section: Opaque.

Polished Section: White with faint yellowish tint and weak reflection pleochroism. Strong anisotropy in crossed polarizers with blue or green polarization colors.

Alteration Alteration products of arsenopyrite include iron oxides, arsenates, and sulfates.

Distinguishing Features

Hand Sample: Emits a garlic odor when crushed. Prismatic habit with rhombic cross sections distinguishes arsenopyrite from cobaltite and skutterudite. Silvery color distinguishes arsenopyrite from pyrite, marcasite, and chalcopyrite.

Thin Section/Grain Mount: Difficult to distinguish from other opaque minerals.

Polished Section: White color, anisotropism, and crystal habit are characteristic.

Occurrence Arsenopyrite is probably the most common arsenic-bearing mineral. It is found in high-temperature hydrothermal vein systems associated with galena, sphalerite, pyrite, chalcopyrite, scheelite, cassiterite, and pyrrhotite. Gold is also commonly associated with arsenopyrite. Infrequent occurrences include pegmatites and gneiss,

DO NOT COPY e48d507df5d1141@placeholder.9409

Printed by: e48d507df5d1141@placeholder.94092.edu. Printing is for personal, private use only. No part of this book may be reproduced or transmitted without publisher's prior permission. Violators will be prosecuted.

schist, and other metamorphic rocks.

Use Potentially a source of As, but most arsenic is obtained from other sulfide minerals as a byproduct of smelting. Arsenic compounds are used in insecticides, pesticides, herbicides, pharmaceuticals, pigments, glass, and fireworks. Metallic As is alloyed with lead for some applications.

DO NOT COPY
e48d507df5d1141@placeholder.9409

Printed by: e48d507df5d1141@placeholder.94092.edu. Printing is for personal, private use only. No part of this book may be reproduced or transmitted without publisher's prior permission. Violators will be prosecuted.

Arsenides

None of the arsenide minerals are particularly common and only skutterudite and nickeline are included in Table 19.6. The structure of nickeline is similar to pyrrhotite with As in hexagonal close packing with Ni in 6-fold coordination sites. Skutterudite has a complex structure that includes covalently bonded As_4 rings with Co and Ni in distorted octahedral sites between the rings.

DO NOT COPY
e48d507df5d1141@placeholder.9409

Printed by: e48d507df5d1141@placeholder.94092.edu. Printing is for personal, private use only. No part of this book may be reproduced or transmitted without publisher's prior permission. Violators will be prosecuted.

Tellurides

The telluride minerals (Table 19.6) have tellurium (Te) as the nonmetal in the structure. They are among the few naturally occurring compounds that include Au as part of the crystal structure. None are common, but they have economic significance as sources of silver and gold. Telluride, a former gold–silver mining town in southwestern Colorado, was named for telluride minerals found elsewhere, but no telluride minerals have been found anywhere near Telluride. It is now largely known as a ski resort town.

DO NOT COPY
e48d507df5d1141@placeholder.9409

Printed by: e48d507df5d1141@placeholder.94092.edu. Printing is for personal, private use only. No part of this book may be reproduced or transmitted without publisher's prior permission. Violators will be prosecuted.

Tellurides

The telluride minerals (Table 19.6) have tellurium (Te) as the nonmetal in the structure. They are among the few naturally occurring compounds that include Au as part of the crystal structure. None are common, but they have economic significance as sources of silver and gold. Telluride, a former gold–silver mining town in southwestern Colorado, was named for telluride minerals found elsewhere, but no telluride minerals have been found anywhere near Telluride. It is now largely known as a ski resort town.

REFERENCES CITED AND SUGGESTIONS FOR ADDITIONAL READING

Agricola, G. 1546. *De natura fossilum*. Translated by M. C. Bandy and J. A. Bandy, 1955. Geological Society of America Special Paper 63, 240 p.

Di Benedetto, F., Borgheresi, M., Caneschi, A., Chastanet, G., Cipriani, C., Gatteschi, D., Pratesi, G., Romanelli, M., and Sessoli, R. 2006. First evidence of natural superconductivity: Covellite. *European Journal of Mineralogy* **18**, 283–287.

Huber, R., Huber, H., and Stetter, K. O. 2000. Towards the ecology of hyperthermophiles: Biotopes, new isolation strategies and novel metabolic properties. *Microbiology Reviews* **24**, 615–623.

Konhauser, K. 2007. *Introduction to Geomicrobiology*. Blackwell, Malden, MA, 425 p.

Labrenz, M., Druschel, G. K., Thomsen-Elbert, T., Gilbert, B., Welch, S. A., Kemer, K. M., Logan, G. A., Summons, R. E., De Stasio, G., Bond, P. L., Lai, B., Kelly, S. D., and Banfield, J. F. 2000. Formation of sphalerite (ZnS) deposits in natural biofilms of sulfate-reducing bacteria. *Science* **290**, 1744–1747.

Machel, H. G. 2001. Bacterial and thermochemical sulfate reduction in diagenetic settings: Old and new insights. *Sedimentary Geology* **140**, 143–175.

McNeil, J. B., Jones, J. M., and Little, B. J. 1991. Mineralogical fingerprints for corrosion processes induced by sulfate reducing bacteria. *NACE Annual Conference, Paper* **580**, 1–16.

Nordstrom, D. K., and Southam, G. 1997. Geomicrobiology of sulfide mineral oxidation. *Reviews in Mineralogy* **35**, 361–390.

Pirajno, F. 2009. *Hydrothermal Processes and Mineral Systems*. Springer Netherlands, Dordrecht, 1250 p.

Pósfi, M., and Dunin-Borkowski, R. E. 2006. Sulfides in biosystems. *Reviews in*

DO NOT COPY e48d507df5d1141@placeholder.9409

Printed by: e48d507df5d1141@placeholder.94092.edu. Printing is for personal, private use only. No part of this book may be reproduced or transmitted without publisher's prior permission. Violators will be prosecuted.

Mineralogy & Geochemistry **61**, 679–714.

Rawlings, D. E. 2002. Heavy metal mining using microbes. *Annual Review of Microbiology* **56**, 65–91.

Ribbe, P. H. 1974. *Sulfide Mineralogy. Short Course Notes*, Volume 1. Mineralogical Society of America, Washington, DC, 281 p.

Ridley, J. 2013. *Ore Deposit Geology*. Cambridge University Press, Cambridge, UK 398 p.

Shuey, R. T. 1975. *Semiconducting Ore Minerals*. Elsevier, Amsterdam, 415 p.

Vaughn, D. J. (ed.). 2006. *Sulfide Mineralogy and Geochemistry. Reviews in Mineralogy & Geochemistry* **61**, 714 p.

White, W. H., Bookstrom, A. A., Kamilli, R. J., Ganster, M. W., Smith R. P., Ranta, D. E., and Steininger, R. C. 1981. Character and origin of Climax-type molybdenum deposits. *Economic Geology* 75th Anniversary volume, 270–316.

DO NOT COPY
e48d507df5d1141@placeholder.9409

Printed by: e48d507df5d1141@placeholder.94092.edu. Printing is for personal, private use only. No part of this book may be reproduced or transmitted without publisher's prior permission. Violators will be prosecuted.

LIST OF KEY TERMS

- acid mine drainage
- gossan
- hypogene
- supergene
- supergene enrichment

DO NOT COPY
e48d507df5d1141@placeholder.9409

Printed by: e48d507df5d1141@placeholder.94092.edu. Printing is for personal, private use only. No part of this book may be reproduced or transmitted without publisher's prior permission. Violators will be prosecuted.

CHAPTER 20
Native Elements

William D. Nesse
University of Northern Colorado

Graham B. Baird
University of Northern Colorado

DO NOT COPY
e48d507df5d1141@placeholder.9409

Printed by: e48d507df5d1141@placeholder.94092.edu. Printing is for personal, private use only. No part of this book may be reproduced or transmitted without publisher's prior permission. Violators will be prosecuted.

Introduction

With the exception of the atmospheric gases (O_2, N_2, etc.), native elements are uncommon in the Earth's crust. Only C, in the form of graphite, constitutes a significant rock-forming mineral. Others, such as gold, silver, copper, and diamond, are rare and valuable. Because they are both rare and very useful, many of the native elements have played a significant role in human history.

It is convenient to group the native elements based on chemical classification as metals, metalloids, and nonmetals. The significant native elements are listed in Table 20.1. Of these, only gold, silver, copper, sulfur, graphite, and diamond are described in detail below. Others are included in Table 20.2.

TABLE 20.1 Native Elements

Metals	Metalloids	Nonmetals
Gold group	Arsenic (As)	Graphite (C)
Copper (Cu)	Bismuth (Bi)	Diamond (C)
Gold (Au)	Antimony (Sb)	Sulfur (S)
Silver (Ag)		
Lead (Pb)		
Platinum group		
Palladium (Pd)		
Platinum (Pt)		
Platiniridium (Pt,Ir)		
Iridosmine (Os,Ir)		
Iron group		
Iron (Fe)		
Kamacite (Fe,Ni)		
Taenite (Ni,Fe)		
Mercury (Hg)		

TABLE 20.2 Properties of Selected Native Elements

Mineral	Unit Cell	Physical	Optical Properties	Comments

DO NOT COPY e48d507df5d1141@placeholder.9409

Printed by: e48d507df5d1141@placeholder.94092.edu. Printing is for personal, private use only. No part of this book may be reproduced or transmitted without publisher's prior permission. Violators will be prosecuted.

		Properties[a]		
Platinum Pt	Isometric 4/*m*3 2/*m* *a* = 3.9231 *Z* = 4	*H*: 4–4.5 *G*: 14–19 Cl: None, hackly fracture, malleable and ductile C: Whitish steel-gray to dark gray St: Whitish steel-gray L: Metallic	Opaque PS: Bluish white and isotropic	Found in selected layers within layered mafic/ultramafic intrusions (e.g., Stillwater complex, Montana; Bushveld, South Africa)
Mercury Hg	Native mercury is a high-density silvery liquid found associated with cinnabar in some hydrothermal mercury deposits; it has very high surface tension and tends not to wet surfaces that it contacts; mercury is highly toxic and can be absorbed through the skin; fumes are also highly toxic, and extreme caution is advised.			
Iron Fe	Isometric 4/*m*3 2/*m* *a* = 2.8644 *Z* = 2	*H*: 4 *G*: 7.3–7.9 Cl: {001} C: Dark gray to black St: Dark gray to black L: Metallic Magnetic	Opaque PS: White and isotropic	Irregular masses and blebs in basalt, carbonaceous sediments, petrified wood, or mixed with limonite and organic matter
Kamacite (Fe,Ni)	Isometric 4/*m*3 2/*m* *a* = ~8.6 *Z* = 54	*H*: 4 *G*: 7.9 C: Gray to black St: Gray L: Metallic Magnetic	Opaque PS: ??	Constituent of iron meteorites with taenite
Taenite (Ni,Fe)	Isometric 4/*m*3 2/*m* *a* = 7.146 *Z* = 32	*H*: 5–5.5 *G*: 7.8–8.22 C: Silver-white to grayish white	Opaque PS: ??	Major constituent of iron meteorites with kamacite

DO NOT COPY

Printed by: e48d507df5d1141@placeholder.94092.edu. Printing is for personal, private use only. No part of this book may be reproduced or transmitted without publisher's prior permission. Violators will be prosecuted.

	$Z = 32$	St: Light gray L: Metallic Magnetic		
Bismuth Bi	Hexagonal $\bar{3}\,2/m$ $a = 4.55$ c = 11.85 $Z = 6$	*H:* 2–2.5 *G*: 9.70–9.83 Cl: {001}pf, {101}g, {104}pr, sectile, brittle C: Silver-white with reddish hue St: Silver-white L: Metallic	Opaque PS: Brilliant creamy white, tarnishes yellow, distinct anisotropism	Crystals rare; usually reticulated, dendritic, foliated, or granular; found in hydrothermal veins
Arsenic As	Hexagonal $\bar{3}\,2/m$ $a = 3.768$ c = 10.574 $Z = 6$	*H*: 3.5 *G*: 5.63–5.78 Cl: {001}pf, {104}f, brittle C: Tin-white tarnishes to dark gray St: Tin-white L: Metallic	Opaque PS: White, tarnishes rapidly; distinctly anisotropic with gray to yellowish gray polarization colors	Crystals rare; usually massive, concentrically layered, reniform; found in hydrothermal veins
Antimony Sb	Hexagonal $\bar{3}\,2/m$ $a = 4.307$ c = 11.273 $Z = 6$	*H*: 3–3.5 *G*: 6.61–6.72 Cl: {001}pf, {101}f, {104}pr, brittle C: Tin-white St: Gray L: Metallic	Opaque PS: White; distinctly anisotropic with yellowish gray, brownish, or bluish gray polarization colors	Crystals rare; usually massive, also lamellar and cleavable, radiating, botryoidal; found in hydrothermal veins

[a] Cl = cleavage (pf = perfect, g = good, f = fair, pr = poor), C = color, St = streak, L = luster, PS = polished section, ?? = unknown.

DO NOT COPY e48d507df5d1141@placeholder.94092

Printed by: e48d507df5d1141@placeholder.94092.edu. Printing is for personal, private use only. No part of this book may be reproduced or transmitted without publisher's prior permission. Violators will be prosecuted.

Metals

The metals are divided into the gold group, the platinum group, and the iron group based on chemistry and structure.

The gold group includes gold, silver, copper, and lead. Lead is by far the least common. The structure of these minerals is simple cubic close packing of the metal atoms (Figure 20.1), which yields a face-centered cubic unit cell. Chemical bonding is strongly metallic and all of these metals are soft, malleable, sectile, good conductors of heat and electricity, and opaque.

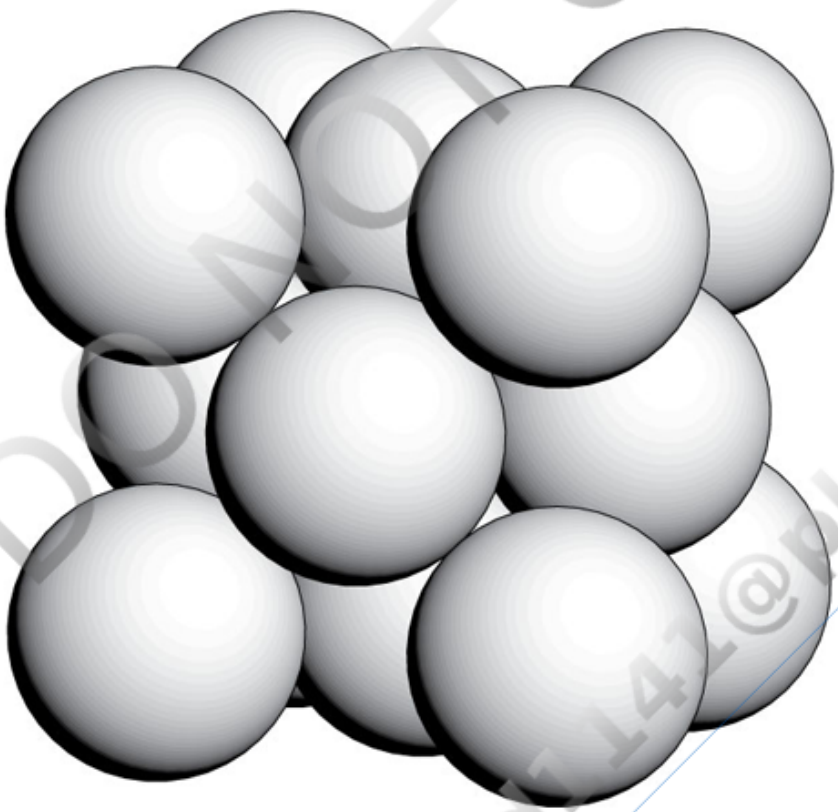

FIGURE 20.1 Many native metals have a cubic close-packed structure with metallic bonding.
View larger image

Substantial solid solution is possible between gold and silver, and between gold and copper. Mercury may also alloy with gold and silver. Mercury's description is included in Table 20.2, though it occurs as a liquid, not a solid.

Members of the platinum group include platinum and palladium, plus rare alloys of iridium–osmium and platinum–iridium. Platinum is the most common (but still quite rare) and is the only one described in Table 20.2. The structure is the same as for gold.

DO NOT COPY e48d507df5d1141@placeholder.9409

Printed by: e48d507df5d1141@placeholder.94092.edu. Printing is for personal, private use only. No part of this book may be reproduced or transmitted without publisher's prior permission. Violators will be prosecuted.

Native iron in terrestrial rocks is found in only a few localities, generally in basalt, carbonaceous sediment, or petrified wood, or mixed with limonite and organic matter. Preservation requires reducing and/or very dry conditions to prevent the iron from oxidizing. Several noted locations are in basalt on the west coast of Greenland, where recent glaciation has provided fresh exposures and where oxidation was limited. The structure of iron is the same as gold (Figure 20.1).

The most familiar occurrence of iron is in the form of Fe–Ni alloys known as kamacite and taenite, which are major constituents of nickel–iron meteorites. Kamacite has the same structure as native iron and contains between 4% and 8% Ni. Kamacite and taenite are often intimately intergrown in a pattern that suggests that they exsolved from a homogeneous phase at higher temperatures. Both minerals are magnetic.

Gold

Au

Isometric $4/m\ 3\ 2/m$

$a = 4.7086$ Å, $Z = 4$

$H = 2.5 - 3$

$G = 19.3$

Opaque

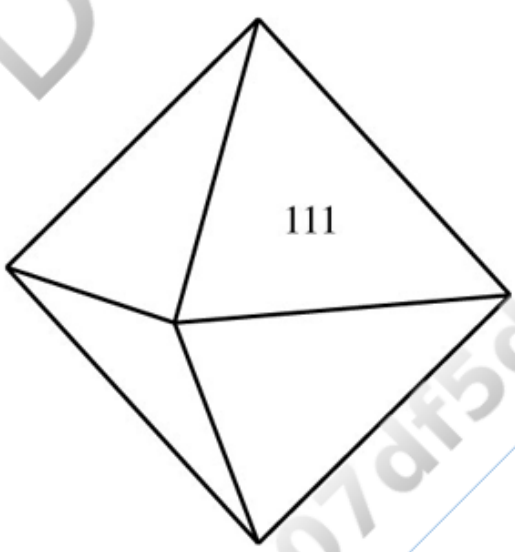

Composition Usually nearly pure Au; some Ag, Cu, or other metals may form an alloy. **Electrum** is the name given to Au–Ag alloys with intermediate compositions.

Form and Twinning Crystals are octahedra, dodecahedra, and cubes, often crude or rounded. Often in reticulated, branching, platy, filiform, spongy, massive, or other masses;

DO NOT COPY e48d507df5d1141@placeholder.9409

Printed by: e48d507df5d1141@placeholder.94092.edu. Printing is for personal, private use only. No part of this book may be reproduced or transmitted without publisher's prior permission. Violators will be prosecuted.

also flakes or scales. Detrital grains are usually flakes or rounded nuggets. Twinning on {111} is common and helps form the complex shapes.

Cleavage None. Malleable and sectile.

Color Properties

Luster: Metallic.

Color: Gold-yellow if pure, lighter with Ag, reddish with Cu.

Streak: Same as color.

Optical Characteristics

Thin Section: Opaque.

Polished Section: Golden yellow and isotropic.

Alteration Gold is very stable in the weathering environment.

Distinguishing Features

Hand Sample: Gold color, gold-yellow streak, and sectility distinguish gold from "fool's gold" (pyrite, chalcopyrite, etc.). Small flakes of weathered biotite may appear golden, particularly if wet, but have much lower specific gravity.

Thin Section/Grain Mount: Difficult to distinguish from other opaque minerals.

Polished Section: Chalcopyrite is somewhat greenish by comparison, and pyrite is somewhat lighter in color, but may be quite similar if fine grained.

Occurrence Most commonly found in hydrothermal sulfide deposits (Table 19.3), either in veins or disseminated through a large volume of rocks. Grains may be quite large (nuggets over a foot across have been found), but more commonly are small to microscopic. It is not uncommon for gold to be found as small inclusions in pyrite or other sulfides. Also found in quartz veins in low-grade metamorphic rocks (greenstones), as an accessory mineral in granitic rocks, and in contact metamorphic rocks. Detrital gold may be concentrated in placer deposits. Gold is a biomineral (Reith and others, 2009). The *Cupriavidus metallidurans* bacterium is capable of extracting gold from dilute solutions and precipitating it as nanoparticles of native gold inside the cell. A number of other microbes are also capable of causing gold to precipitate (Southam and others, 2009). These findings suggest that bacterial processes may be important in concentrating gold in supergene and weathering environments.

Use Gold is valued for its beauty, as an industrial material, and for its monetary value. Since earliest times, people have fashioned gold into ornaments and jewelry. Certainly many readers wear jewelry containing gold. In the form of gold leaf, it has been applied

DO NOT COPY

Printed by: e48d507df5d1141@placeholder.94092.edu. Printing is for personal, private use only. No part of this book may be reproduced or transmitted without publisher's prior permission. Violators will be prosecuted.

to statuary and other ornamental items, and to decorate buildings, such as the "golden dome" of the Colorado state capitol. As coins and bullion, gold has served as a form of monetary exchange. However, its greatest value to society is as an industrial commodity, which only accounts for 10% of its use. Gold is an excellent electrical conductor, does not tarnish or oxidize, and is easily worked. For these reasons it is used in many electronic applications. As mentioned in Chapter 1, gold has historical uses in medicine, presumably because the perception of value produced a belief that it would provide a benefit. Modern applications include dentistry and the use of gold salts in treatment of rheumatoid arthritis.

Comments Like diamonds and other critical minerals, gold can serve as a conflict mineral (see Chapter 1). Gold probably represents humankind's best (and sometimes most troubling) success at recycling. The total amount of gold mined over human history is not large, probably totaling about 200,000 metric tons. All mined gold would fill just a bit over four Olympic-sized swimming pools. Only a relatively small portion of the gold mined since antiquity has been lost. Because of gold's value, people have made extraordinary (and often unethical, immoral, and illegal) efforts to recover gold from graves, ruins, and shipwrecks. The gold in electronic appliances such as computers is routinely recovered with appropriate recycling.

Silver

Ag

Isometric $4/m\,\bar{3}\,2/m$

$a = 4.0862$ Å, $Z = 4$

$H = 2.5 - 3$

$G = 10.1 - 11.1$

Opaque

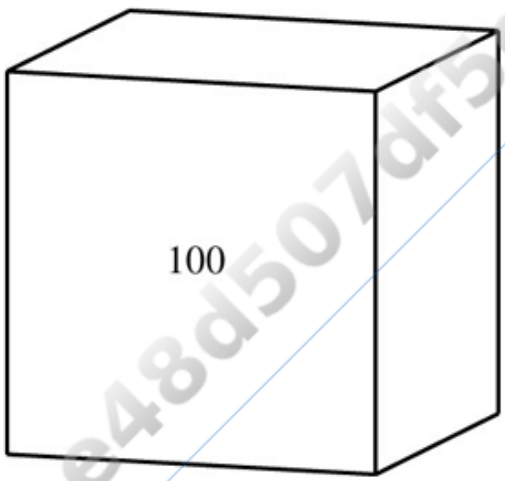

DO NOT COPY
e48d507df5d1141@placeholder.9409

Printed by: e48d507df5d1141@placeholder.94092.edu. Printing is for personal, private use only. No part of this book may be reproduced or transmitted without publisher's prior permission. Violators will be prosecuted.

Composition Often nearly pure Ag, but may contain Au or other metals.

Form and Twinning Crystals uncommon, usually rough cubes, octahedrons, or dodecahedrons; also dendritic or wirelike forms, irregular masses, scales, plates, or fracture fillings. Twins on {111} are common.

Cleavage None. Hackly fracture. Sectile, ductile, and malleable.

Color Properties

Luster: Metallic.

Color: Silvery white (Figure 6.11), often with gray or black tarnish.

Streak: Silvery white.

Optical Characteristics

Thin Section: Opaque.

Polished Section: Bright white with a creamy tint and isotropic.

Alteration Silver is commonly altered to silver sulfide and chloride.

Distinguishing Features

Hand Sample: Silver color with black tarnish and metallic characteristics are distinctive.

Thin Section/Grain Mount: Difficult to distinguish from other opaque minerals.

Polished Section: Extremely high reflectance and tarnish are diagnostic.

Occurrence Most commonly found in the oxidized portion of silver-bearing hydrothermal sulfide deposits; in some cases it also may be a primary mineral (Tables 19.3 and 19.4).

Use Used in jewelry, tableware (knives, forks, spoons, teapots, etc.), coinage (historically), and in many electronic applications. Use in photographic film has decreased markedly with the development of digital photography and X-ray radiography. Quite a few uses take advantage of silver's antimicrobial properties. One example is weaving silver thread into stockings to reduce foot odor. While perhaps unintended, antimicrobial properties benefit silver tableware. Colloidal silver, a solution with tiny suspended silver particles, is a popular ingredient in numerous unproven alternative medicines that claim to improve one's health and well-being. A potential side effect of such ingested solutions is silver poisoning (argyria) in which the skin turns a bluish gray from the buildup of silver compounds.

Copper

DO NOT COPY

Printed by: e48d507df5d1141@placeholder.94092.edu. Printing is for personal, private use only. No part of this book may be reproduced or transmitted without publisher's prior permission. Violators will be prosecuted.

Copper

$$\mathrm{Cu}$$

$$\text{Isometric } 4/m\,\bar{3}\,2/m$$

$$a = 3.615\ \text{Å},\ Z = 4$$

$$H = 2.5 - 3$$

$$G = 8.95$$

Opaque

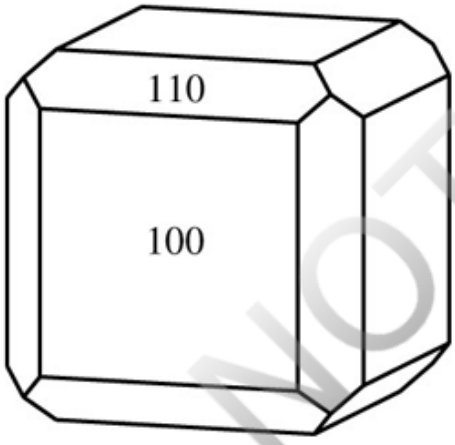

Composition Generally fairly pure, but may contain some Au or other elements.

Form and Twinning Rare crystals are cubic or dodecahedral; usually massive, filiform, or dendritic. Twinning is common on {111}.

Cleavage None. Hackly fracture. Sectile, malleable, and ductile.

Color Properties

Luster: Metallic.

Color: Light rose on fresh surface (Figure 6.11), tarnishes rapidly to copper-red.

Streak: Same as color.

Optical Characteristics

Thin Section: Opaque.

Polished Section: Rose-white and isotropic, tarnishes quickly.

Alteration Copper may be altered to cuprite, copper sulfates, and copper carbonates.

Distinguishing Features

DO NOT COPY
e48d507df5d1141@placeholder.9409

Printed by: e48d507df5d1141@placeholder.94092.edu. Printing is for personal, private use only. No part of this book may be reproduced or transmitted without publisher's prior permission. Violators will be prosecuted.

Hand Sample: Color and metallic characteristics are diagnostic.

Thin Section/Grain Mount: Difficult to distinguish from other opaque minerals.

Polished Section: Color, pink to red tarnish, and association with cuprite are distinctive.

Occurrence Most commonly found associated with mafic volcanic rocks, where it is formed by reaction between Cu-bearing solutions and Fe-bearing minerals. It may fill vesicles, cracks, or other voids. Associated minerals include cuprite, chalcocite, bornite, epidote, calcite, chlorite, and zeolites. A notable occurrence of this type of deposit is on the Keweenaw Peninsula, Michigan. Sediment-hosted occurrences appear to be produced in similar ways. Native copper also may be found in the oxidized zone of Cu-bearing hydrothermal sulfide deposits.

Use Whereas native copper served as main source of Cu early in the development of human civilization, currently, most Cu is extracted from sulfide minerals. The electrical conductivity and relatively low price make copper indispensable as electrical wire and in many industrial and building trade applications. Copper is an excellent antimicrobial agent, and it can be used for surfaces (e.g., doorknobs and countertops in hospitals) where reduction of microbial contamination is desired.

DO NOT COPY
e48d507df5d1141@placeholder.9409

Printed by: e48d507df5d1141@placeholder.94092.edu. Printing is for personal, private use only. No part of this book may be reproduced or transmitted without publisher's prior permission. Violators will be prosecuted.

Metalloids

None of the metalloids are common; their properties are listed in Table 20.2. Bismuth, though typically classified as post-transition metal (Chapter 3), is isostructural with the As and Sb metalloids and it too is part of group 15 on the periodic table, so it included here. As a first approximation, the structure of the metalloid native elements are derived from distorted cubic close packing with one of the diagonals through the cube stretched to yield a rhombohedral lattice. However, the bonding is much more covalent and directional than in the metals. Strong bonds extend only to three closest neighbors, with the result that the sheets of atoms parallel to (001) are corrugated. Weak bonds between sheets produce perfect {001} cleavage.

The native metalloids are typically found in hydrothermal sulfide deposits, as either a primary or secondary mineral. Arsenic is usually associated with barite, cinnabar, realgar, orpiment, stibnite, and galena. Antimony may be associated with silver ores and stibnite, sphalerite, galena, pyrite, and quartz. Bismuth is commonly associated with cobalt, nickel, silver, and tin minerals, and also may be found in pegmatites.

None of the native metalloids are routinely exploited for their metal content; other sources are generally more abundant and economic.

DO NOT COPY e48d507df5d1141@placeholder.9409

Printed by: e48d507df5d1141@placeholder.94092.edu. Printing is for personal, private use only. No part of this book may be reproduced or transmitted without publisher's prior permission. Violators will be prosecuted.

Nonmetals

Sulfur

Å Å
Å

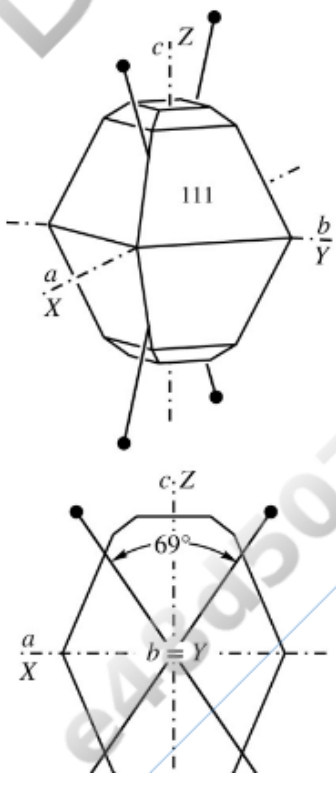

DO NOT COPY
e48d507df5d1141@placeholder.9409

Printed by: e48d507df5d1141@placeholder.94092.edu. Printing is for personal, private use only. No part of this book may be reproduced or transmitted without publisher's prior permission. Violators will be prosecuted.

(010) Section

Structure The structure consists of corrugated rings of eight covalently bonded S atoms forming an S_8 molecule. Each sulfur atom, therefore, shares electrons with two neighbors to satisfy valence requirements. The rings are systematically stacked and held together with van der Waals bonds (Figure 20.2). Three polymorphic varieties are known: α-sulfur, β-sulfur, and γ-sulfur. The latter two are monoclinic. Only orthorhombic α-sulfur is common, and it is described here.

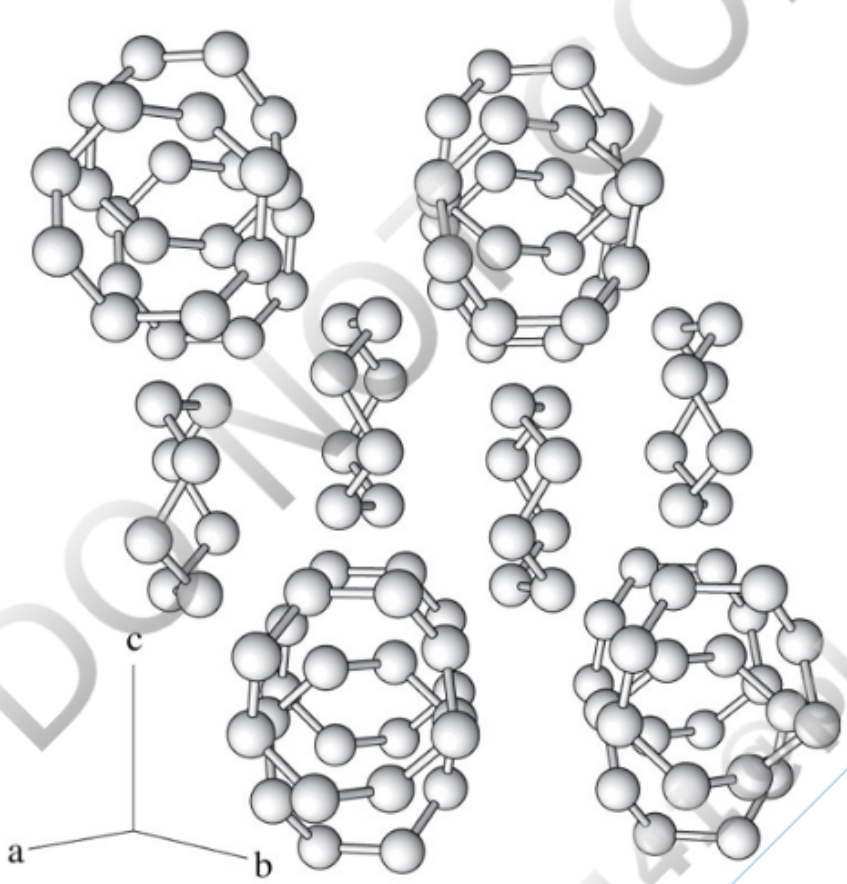

FIGURE 20.2 Structure of native sulfur. Eight-fold rings of covalently bonded sulfur atoms bond laterally through van der Waals bonds. View larger image

Composition Small amounts of Se may substitute for S, but otherwise native sulfur is fairly pure.

Form and Twinning Crystals are pyramidal or tabular, with {111} and {113} dipyramids, {011} prism, and {001} pinacoid the common forms. Commonly as granular masses, or encrusting or reniform forms. Contact twins on {011} are rare.

Cleavage {001} and {110} fair. Conchoidal to uneven fracture. Brittle to somewhat sectile.

Color Properties

DO NOT COPY e48d507df5d1141@placeholder.94092

Printed by: e48d507df5d1141@placeholder.94092.edu. Printing is for personal, private use only. No part of this book may be reproduced or transmitted without publisher's prior permission. Violators will be prosecuted.

Color Properties

Luster: Resinous to greasy.

Color: Yellow to yellowish brown.

Streak: White.

Color in Thin Section: Pale yellow or yellowish gray.

Pleochroism: Weak, from light to darker yellow.

Optical Characteristics

Relief in Thin Section: Extremely positive.

Optic Orientation: $X = a$, $Y = b$, $Z = c$.

Indices of Refraction and Birefringence: Indices do not vary significantly and birefringence is extreme.

Interference Figure: Basal sections yield biaxial positive acute bisectrix figures with numerous isochromes, but extreme birefringence makes interpretation difficult, $r < v$.

Alteration Sulfur may alter to sulfate minerals such as gypsum or anhydrite.

Distinguishing Features

Hand Sample: Yellow color is distinctive. Burns in a candle flame. Orpiment has identifiable cleavage and usually is associated with realgar.

Thin Section/Grain Mount: Extreme relief and birefringence, and limited occurrence are characteristic.

Occurrence Sulfur is found around fumaroles, volcanic vents, and in hot spring deposits associated with recent or active volcanism. The sulfur may precipitate directly from vapors or is produced from bacterial acting on sulfate minerals. Hydrothermal sulfide deposits may also contain native sulfur, usually in the near-surface oxidized zone.

The largest concentrations of sulfur are associated with salt domes of marine evaporite deposits. The evaporites are dominantly halite, but usually contain gypsum, anhydrite, and calcite. Salt domes form because the evaporate minerals are less dense than the overlying rock, such that they will slowly flow upward and take on a diaper shape. During formation, the top of the salt dome may encounter fresh meteoric groundwater within a kilometer of the surface, which dissolves the halite, but other minerals are relatively insoluble. Continuous upward movement of salt from its source and dissolution by groundwater allows a cap of calcite and gypsum to accumulate at the top of a salt dome (Figure 20.3). The cap commonly consists of an outer/upper zone of calcite, transitioning inward to gypsum and then anhydrite. Hydrogen sulfide is produced by anaerobic sulfur-

DO NOT COPY

Printed by: e48d507df5d1141@placeholder.94092.edu. Printing is for personal, private use only. No part of this book may be reproduced or transmitted without publisher's prior permission. Violators will be prosecuted.

reducing bacteria, provided that hydrocarbons (oil/gas) are available, by the following general reaction.

$$CaSO_4 + CH_4(\text{hydrocarbons}) + \text{bacteria} = H_2S + CaCO_3 + H_2O$$

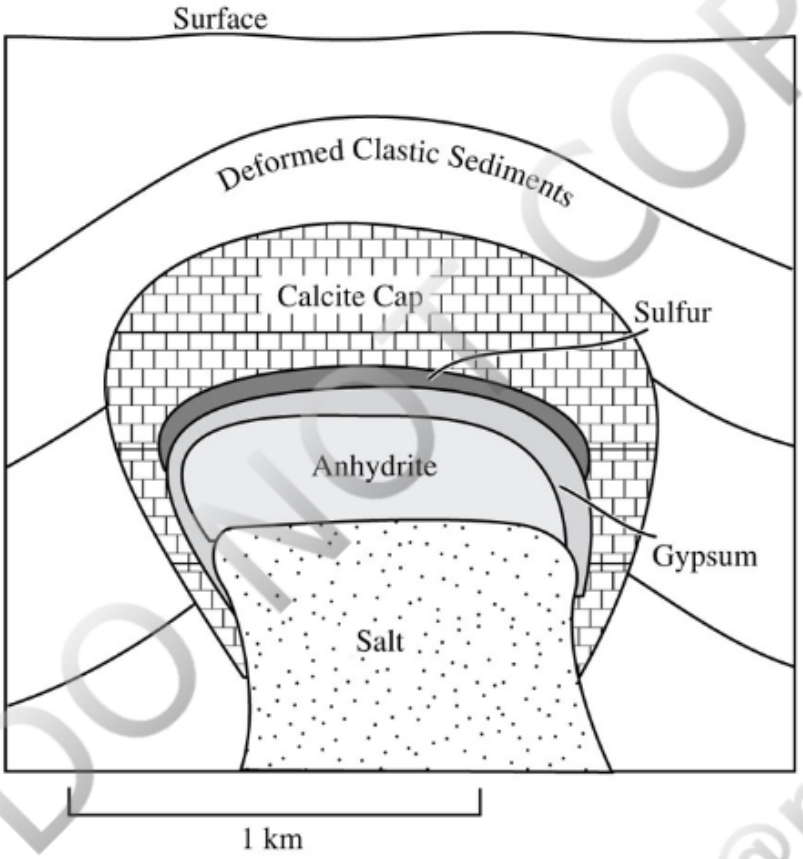

FIGURE 20.3 Schematic cross section through a salt dome showing idealized sequence of cap rock lithologies and location of native sulfur concentrations. View larger image

The hydrogen sulfide is oxidized either by oxygen in the groundwater, hydrocarbons, or other chemical processes to form elemental sulfur.

$$2H_2S + O_2 = 2S + 2H_2O$$

The actual reaction paths are greatly more complicated than presented by these reactions and may additionally involve aerobic bacteria. Because generation of sulfur involves breaking down sulfates and the production of calcite, the sulfur is concentrated at the calcite-sulfate boundary in the cap rock of salt domes. Very fine grains of native sulfur are also found in the cells of certain marine sulfur-oxidizing bacteria (Pasteris, 2001).

DO NOT COPY e48d507df5d1141@placeholder.9409

Printed by: e48d507df5d1141@placeholder.94092.edu. Printing is for personal, private use only. No part of this book may be reproduced or transmitted without publisher's prior permission. Violators will be prosecuted.

Use Sulfur from salt domes is usually extracted by injecting superheated water into the sulfur. The hot water mobilizes the sulfur and both water and sulfur are then pumped to the surface for processing. Sulfur is principally used to manufacture sulfuric acid, which is used to make phosphatic fertilizer, to leach copper from copper ore, and in a wide variety of other chemical processes. Sulfur also is added to soil as a nutrient. A substantial amount of the sulfur used for industrial purposes is derived as a byproduct of extracting metals from sulfide minerals. The use of sulfur for medical purposes goes back thousands of years and some uses continue today. It is an active ingredient in some acne creams, dandruff shampoos, and soaps.

Graphite

$$\mathrm{C}$$

$$\text{Hexagonal } 6/m\,2/m\,2/m$$

$$a = 2.463 \text{ Å},$$
$$c = 6.714 \text{ Å},\ Z = 4$$

$$H = 1 - 2 \text{ (easily marks paper and fingers)}$$

$$G = 2.09 - 2.23$$

Opaque

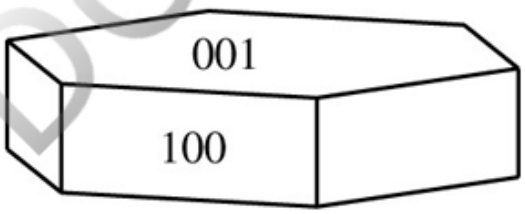

Structure The structure and chemical bonding are described at some length in Chapter 3 (Figure 3.6). Graphite consists of sheets of carbon atoms parallel to {001} that are bonded with both σ and π bonds to satisfy valence requirements. These sheets are bonded to each other with van der Waals bonds.

Composition Nearly pure C.

Form and Twinning Platy hexagonal crystals. Commonly massive, foliated, scaly, granular, or in globular aggregates with radial structure. Twins reported with {111} composition planes, and by rotation on [001]. Twins produced by translation gliding on {*hhl*} may produce triangular markings on the basal pinacoid.

Cleavage Perfect {001} cleavage breaks between sheets of carbon atoms. Folia are flexible. Sectile.

DO NOT COPY e48d507df5d1141@placeholder.9409

Printed by: e48d507df5d1141@placeholder.94092.edu. Printing is for personal, private use only. No part of this book may be reproduced or transmitted without publisher's prior permission. Violators will be prosecuted.

Color Properties

Luster: Dull metallic, may be earthy.

Color: Black.

Streak: Black.

Optical Characteristics

Thin Section: Opaque.

Polished Section: White-gray, sometimes with an orange tint; very strong bireflectance and pleochroism from brownish to nearly black; very strong crossed polarizers anisotropy with straw-yellow to dark brown or violet-gray polarization colors. Basal sections may be nearly isotropic.

Alteration Graphite is not readily altered.

Distinguishing Features

Hand Sample: Black color, greasy feel, and softness are distinctive. Graphite easily marks paper. Molybdenite is similar but not as distinctly black, and has a bluish-gray streak.

Thin Section/Grain Mount: Difficult to distinguish from other opaque minerals.

Polished Section: Anisotropism, extreme pleochroism, and low reflectance are characteristic. Molybdenite has higher reflectance and a pinkish white color.

Occurrence Graphite is a common mineral in pelitic metamorphic rocks such as phyllite, slate, and schist, particularly of Paleozoic and younger age; also found in marble and skarn deposits, and metamorphosed coal beds. It is produced as a result of decomposition of organic material originally deposited in the sediment. Graphite is also found in metamorphic rocks of Precambrian age, either derived from organic material in those rocks or produced by reduction of carbonate layers. Occurrences of graphite in igneous rocks are uncommon but some, either introduced from nearby graphitic sediments or as primary magmatic minerals, have been reported.

Use Most people are familiar with graphite's use as lead of pencils. Graphite is pulverized and mixed with clay and a binder, and then formed into pencil lead. It also is used as a "dry" lubricant in locks or other applications where oil would accumulate dirt and inhibit proper operation. Other uses include automobile brake pads, electrical resistors, gaskets, lubricating oil additive, refractories, and mold-release coating for metal castings.

Comments There are a number of different crystalline materials based on a single sheet of carbon atoms found in the graphite structure. Some of the most commonly discussed are graphene, fullerene, and carbon nanotubes.

DO NOT COPY
e48d507df5d1141@placeholder.9409

Printed by: e48d507df5d1141@placeholder.94092.edu. Printing is for personal, private use only. No part of this book may be reproduced or transmitted without publisher's prior permission. Violators will be prosecuted.

are graphene, fullerene, and carbon nanotubes.

Fullerenes are constructed of a single sheet of periodically bonded (crystalline) carbon that is wrapped into a ball. Fullerenes come in different sizes; some only have 20 carbons (C_{20}), while others are up to several thousand (C_{3996}). The Buckminsterfullerene, or "Buckyball," is perhaps the best known and is shaped like a soccer ball with 60 carbons (C_{60}) arranged in alternating 5 and 6 carbon rings. A carbon nanotube, as the name describes, is a tube of a single sheet of hexagonally bonded carbons. Carbon nanotubes come in different diameters of only a few nanometers. Depending on size, the tubes may be nested inside one another. Graphene is a single sheet of hexagonally bonded carbon. Graphene can be formed easily by simply using a common kitchen blender on a mixture of small graphite particles and water, or by repeatedly exfoliating graphite with standard office adhesive tape.

All these forms of carbon naturally occur, though in very small amounts within, for example, graphitic carbon (Box 20.1). In the last few decades these forms of carbon are receiving considerable attention because of their strength (stronger than diamond in some cases) and electrical and chemical properties. In the future, novel and existing technologies will begin using them or will use them more widely to solve a variety of problems. See Lazzeri and Barreiro (2014) for more information on these materials.

BOX 20.1
Graphitic Carbon

Graphitic carbon is a general term given to solid carbonaceous compounds whose structure is based on 6-fold rings of carbon atoms. It includes coal, kerogen, and graphite, and these materials are important reservoirs of Earth's carbon (Box 20.2). Of these materials, only graphite is crystalline. The carbonaceous material in coal and kerogen lacks long-range order and can be considered amorphous; therefore the term **amorphous carbon** is commonly used. The chemistry of graphitic carbon is relatively simple, consisting mostly of carbon with hydrogen and oxygen in variable amounts. Nitrogen, sulfur, and phosphorous also may be present in trace amounts. Most graphitic carbon in sedimentary rocks is derived from living organisms. Graphitic carbon also can be precipitated from hydrothermal fluids containing C-bearing molecular and ionic species, and it is found in carbonaceous meteorites.

The process by which organic carbonaceous material is converted to graphite (Figure 20.4) can be considered a two-step process—carbonization followed by graphitization. Carbonization occurs during diagenesis as sediments are buried in a sedimentary basin. The large organic molecules in the original organic material are broken ("cracked") into smaller hydrocarbon molecules. With time and temperature, first oil and then gas (mostly methane) are produced and both typically migrate away from their source. The solid residue left after removing oil and gas molecules is progressively enriched in carbon, which forms 6-fold carbon rings. Graphitization occurs when the sediments are subjected to metamorphic conditions and the rings polymerize and rearrange themselves to form continuous sheets of carbon atoms

DO NOT COPY e48d507df5d1141@placeholder.94092

Printed by: e48d507df5d1141@placeholder.94092.edu. Printing is for personal, private use only. No part of this book may be reproduced or transmitted without publisher's prior permission. Violators will be prosecuted.

polymerize and rearrange themselves to form continuous sheets of carbon atoms characteristic of graphite. The process is progressive and a full range of intermediate degrees of crystallinity are found. Raman spectroscopy, an analytical technique that allows the degree of crystallinity to be measured, can be used to estimate metamorphic temperatures. The fractionation of carbon isotopes between graphitic carbon and carbonate minerals also provides a means of estimating metamorphic temperatures.

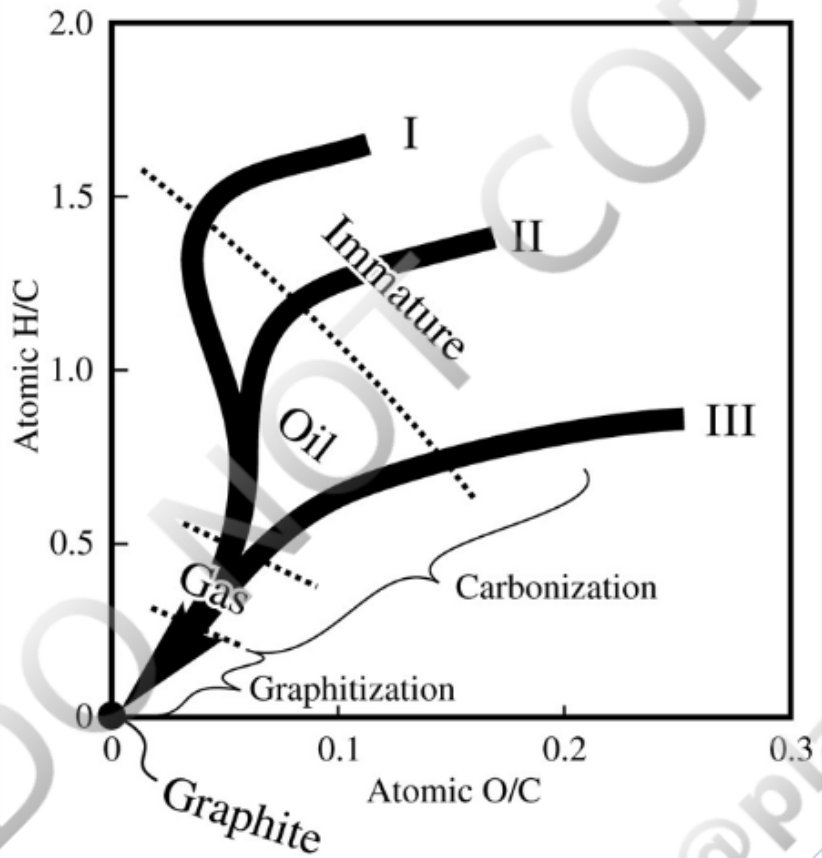

FIGURE 20.4 Van Krevelen diagram showing chemical evolution of organic material derived from lacustrine algae (I), marine microorganisms (II), and terrestrial plants (III) in response to burial and increasing temperatures in sedimentary rocks. During carbonization the O/C and H/C ratios progressively decrease as the organic matter matures and first oil and then gas are extracted. Continued heating under metamorphic conditions causes graphitization as the residual graphitic carbon crystallizes to form graphite. Adapted from Buseck and Beyssac (2014). View larger image

Diamond

C

Isometric $4/m\,\bar{3}\,2/m$

$a = 3.5595$ Å, $Z = 8$

DO NOT COPY e48d507df5d1141@placeholder.9409

Printed by: e48d507df5d1141@placeholder.94092.edu. Printing is for personal, private use only. No part of this book may be reproduced or transmitted without publisher's prior permission. Violators will be prosecuted.

$$a = 3.5595 \text{ Å}, \ Z = 8$$

$$H = 10$$

$$G = 3.511$$

Isotropic

$$n = 2.418$$

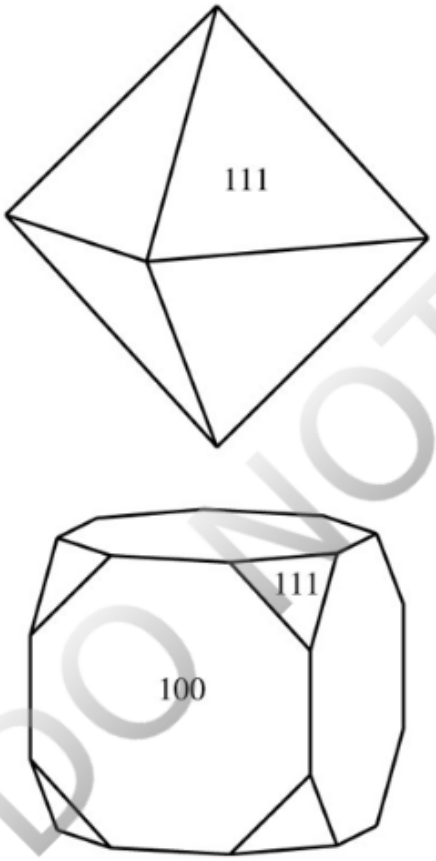

DO NOT COPY
e48d507df5d1141@placeholder.9409

Structure The diamond structure and chemical bonding are described in Chapter 3 (Figure 3.5). Carbon forms hybrid $2sp^3$ orbitals that have a tetrahedral symmetry so that each carbon forms covalent bonds with four other carbon atoms.

Pure diamond is a large band-gap semiconductor with an energy gap of 5.4 eV between the valence and conduction bands (Figure 20.5). Because the energy gap is larger than the energy of visible light, it is transparent and colorless. Trace amounts of nitrogen may substitute for carbon in the structure. Nitrogen has one more $2p$ electron than carbon (Table 3.3) and its energy lies in the diamond band gap, 4 eV below the conduction band. In semiconductor terms, the nitrogen with its extra electron becomes a donor and the diamond becomes an n-type semiconductor. If the concentration of N is around 1 part in 100,000, the energy level represented by those $2p$ electrons spreads out to a band because of the crystal field (Chapter 3) and thermal vibration so that the gap between the top of the nitrogen donor band and the carbon conduction band is just 2.2 eV. This allows violet and blue light to be absorbed by promoting electrons across that energy gap and

Printed by: e48d507df5d1141@placeholder.94092.edu. Printing is for personal, private use only. No part of this book may be reproduced or transmitted without publisher's prior permission. Violators will be prosecuted.

the diamond appears yellow. Yellow diamonds are generally less valuable than clear diamonds. If the nitrogen content is increased to 1 part in 1000, the nitrogen donor band becomes wider and a much rarer green color is produced.

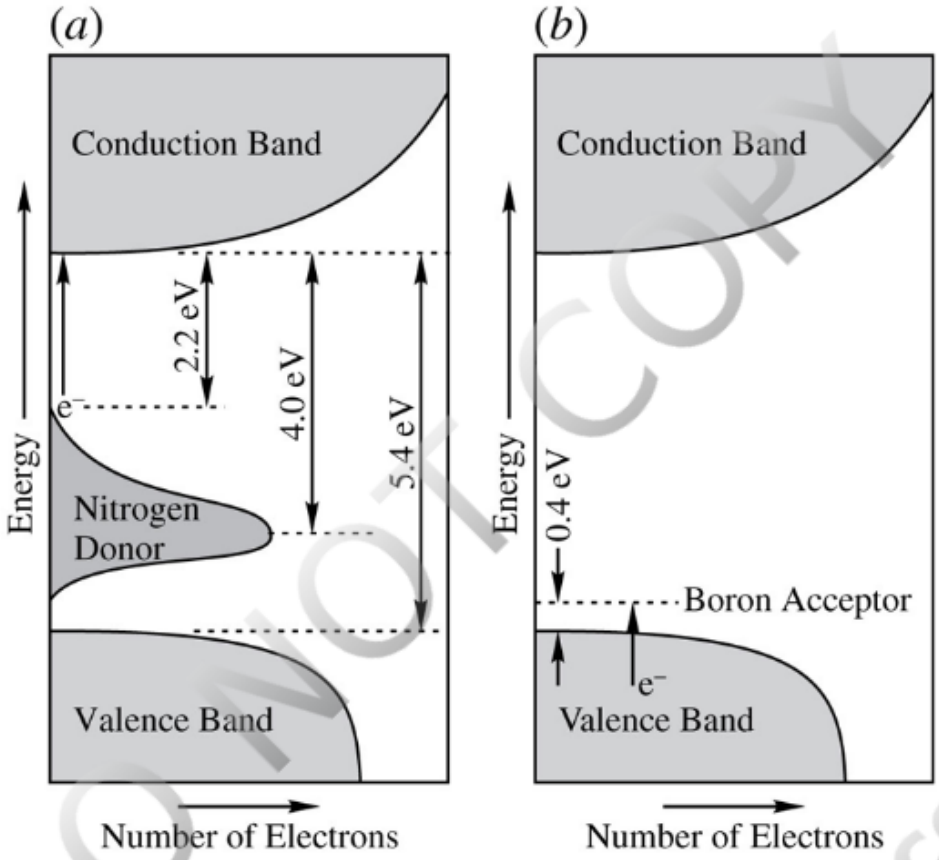

FIGURE 20.5 Color in diamond. (*a*) In pure diamond the band gap between the valence and conduction bands is about 5.4 eV, so visible light (energy between about 1.7 and 3.2 eV) is not absorbed and the mineral is colorless. Small amounts of nitrogen in the structure provide a source of electrons whose energy band is centered about 4 eV below the diamond conduction band. At a concentration of 1 part per 100,000, the top of the nitrogen donor band is just 2.2 eV below the diamond conduction band, so violet and blue light can be absorbed and the diamond appears yellow. (*b*) Trace amounts of boron provide a vacant energy level about 0.4 eV above the diamond valence band. While the entire visible light spectrum can be absorbed, the lower-energy red end of the spectrum is absorbed more strongly than blue, so the diamond appears blue. View larger image

Some diamond may contain trace amounts of boron, which has one less 2*p* electron than carbon. The missing electron represents a *hole* whose energy level is 0.4 eV above the top of the valence band of carbon to which electrons from the valence band can be promoted. In semiconductor terms, the boron represents an electron acceptor and the result is a *p*-type semiconductor. Since the energy gap is small, the entire visible spectrum can be absorbed, although red is more strongly absorbed than blue. If the boron concentration is about 1 to 2 atoms per million carbon atoms, the result is a very attractive blue color, which increases the gem value substantially. Since the boron acceptor level is only 0.4 eV above the valence band, and its energy is spread into a band, normal thermal excitation can promote electrons from the valence band to the boron acceptors, so boron-doped diamond is an electrical conductor. This allows it to be

DO NOT COPY e48d507df5d1141@placeholder.9409

Printed by: e48d507df5d1141@placeholder.94092.edu. Printing is for personal, private use only. No part of this book may be reproduced or transmitted without publisher's prior permission. Violators will be prosecuted.

acceptors, so boron-doped diamond is an electrical conductor. This allows it to be distinguished from diamond whose blue color is artificially produced by irradiation.

The color of some pink diamonds is thought to be associated with defects accompanying deformation lamellae on {111}. Whether this applies to all pink diamonds is unknown (Howell and others, 2015).

Many natural diamonds are brown. The color appears to be the result of C vacancy clusters produced by deformation. Annealing at high temperature and pressure removes the defects. Most brown diamonds are used for industrial purposes, but recent marketing efforts have increased their value as gems and they may be sold as “chocolate diamonds.”

Composition Diamond is nearly pure C.

Form and Twinning Crystals are octahedrons, less commonly cubes or dodecahedrons; faces may be somewhat rounded. Contact or penetration twins on {111}. The term *bort* is used for rounded polycrystalline forms or for diamond without gem value.

Cleavage {111} perfect cleavage. Conchoidal fracture. Brittle.

Color Properties

Luster: Adamantine to greasy.

Color: Gem-quality diamond is colorless, also pale to deep yellow, brown, white, blue-white, or less commonly orange, pink green, blue, red, or black. The term *carbonado* is applied to black or grayish bort. Fluorescent and phosphorescent, also triboelectric.

Streak: White.

Color in Thin Section: Colorless.

Optical Characteristics

Relief in Thin Section: Extremely positive.

Index of Refraction: Gems are cut to take advantage of the very high dispersion of diamond so that incident white light will separate into constituent wavelengths and be reflected to the observer as flashes of different colors known as “fire.”

Comments: Preparation of a thin section of a sample that by chance contains a diamond is difficult because diamond is too hard to be ground or polished with conventional procedures.

Alteration Diamond is very stable in the weathering environment.

Distinguishing Features

Hand Sample: Extreme hardness and crystal habit are distinctive. Synthetic diamond generally lacks internal imperfections. Cubic zirconia is an inexpensive synthetic

DO NOT COPY e48d507df5d1141@placeholder.9409

Printed by: e48d507df5d1141@placeholder.94092.edu. Printing is for personal, private use only. No part of this book may be reproduced or transmitted without publisher's prior permission. Violators will be prosecuted.

generally lacks internal imperfections. Cubic zirconia is an inexpensive synthetic gemstone that resembles diamond but has inferior hardness and lacks internal imperfections.

Thin Section/Grain Mount: Thin sections with large grains generally cannot be made because of the dramatic difference between the hardness of diamond and of other minerals with which it is found. High index of refraction and habit are distinctive in grain mount. Garnet and spinel have lower indices of refraction and are usually colored.

Occurrence Diamond is generally restricted to ultramafic igneous rocks, known as kimberlite, and related peridotite that contain olivine, pyroxene, garnet, magnetite, and phlogopite. Diamond is stable only at pressures found in the Earth's mantle (Figure 4.11), where it is an important reservoir of carbon (Box 20.2). Therefore, diamond found at the surface is usually inferred to have crystallized in the upper mantle and been brought to the surface by violent gas-charged eruption of kimberlite magma. Kimberlite weathers easily and exposures are usually subdued. Diamond exploration often depends on searching for alluvial deposits that contain more abundant minerals, such as chrome diopside, that are part of the kimberlite, and following occurrences of these minerals upstream to their source.

BOX 20.2
The Carbon Cycle

A biogeochemical cycle tracks how an element or chemical compound moves through different components of the Earth system, including the solid Earth, the hydrosphere, biological material, and the atmosphere. One import biogeochemical cycle is the carbon cycle. It has gained significant attention in recent decades because of human-caused cycle changes resulting in the rise of atmospheric CO_2 from about 280 ppm in 1750 to 420 ppm in 2022 (Figure 20.6). As CO_2 is a powerful greenhouse gas that traps heat, this rise is the major driver of present-day global warming and climate change. Average global atmospheric temperatures have risen about 1.2°C (about 2°F) since 1750 (Figure 20.6), which is over 10 times faster than any climate change caused by geologic or natural processes in at least the past million years. The higher temperatures are causing changes in weather patterns, more extreme weather events, and sea-level rise, all of which pose significant challenges for maintaining or trying to achieve a prosperous human society and healthy global ecosystem. Rocks and minerals play a major role in the carbon cycle, and it is critical to understand the cycle in order to identify and implement possible solutions to climate change.

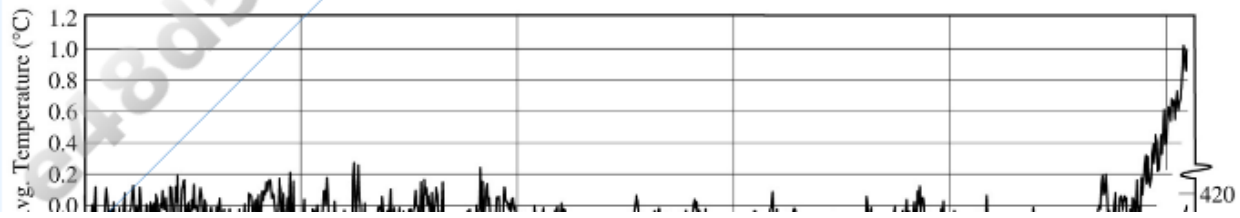

DO NOT COPY

Printed by: e48d507df5d1141@placeholder.94092.edu. Printing is for personal, private use only. No part of this book may be reproduced or transmitted without publisher's prior permission. Violators will be prosecuted.

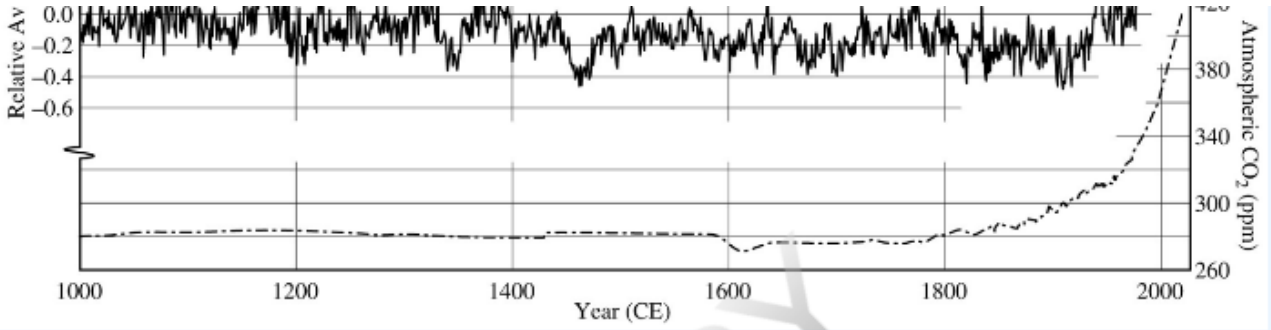

FIGURE 20.6 Change in average global temperature and atmospheric CO_2 over the past 1000 years. Temperature record during 1000–1880 from Mann and others (1999) and during 1880–2020 from NASA.gov. Atmospheric CO_2 during 1000–1996 from MacFarling Meure and others (2006) and during 1996–2020 from NASA.gov. View larger image

Biogeochemical cycles are described by reservoirs, which hold the chemical of interest for some period of time, and fluxes, which is the rate that the chemical moves between the reservoirs. Figure 20.7 depicts a simplified carbon cycle, and Table 20.3 provides the amount of carbon held in various materials found in each of the main reservoirs. Although the Earth's core likely contains large amounts of carbon, it plays essentially no role in carbon cycling for the reservoirs at the Earth's surface, so it will be excluded for simplicity.

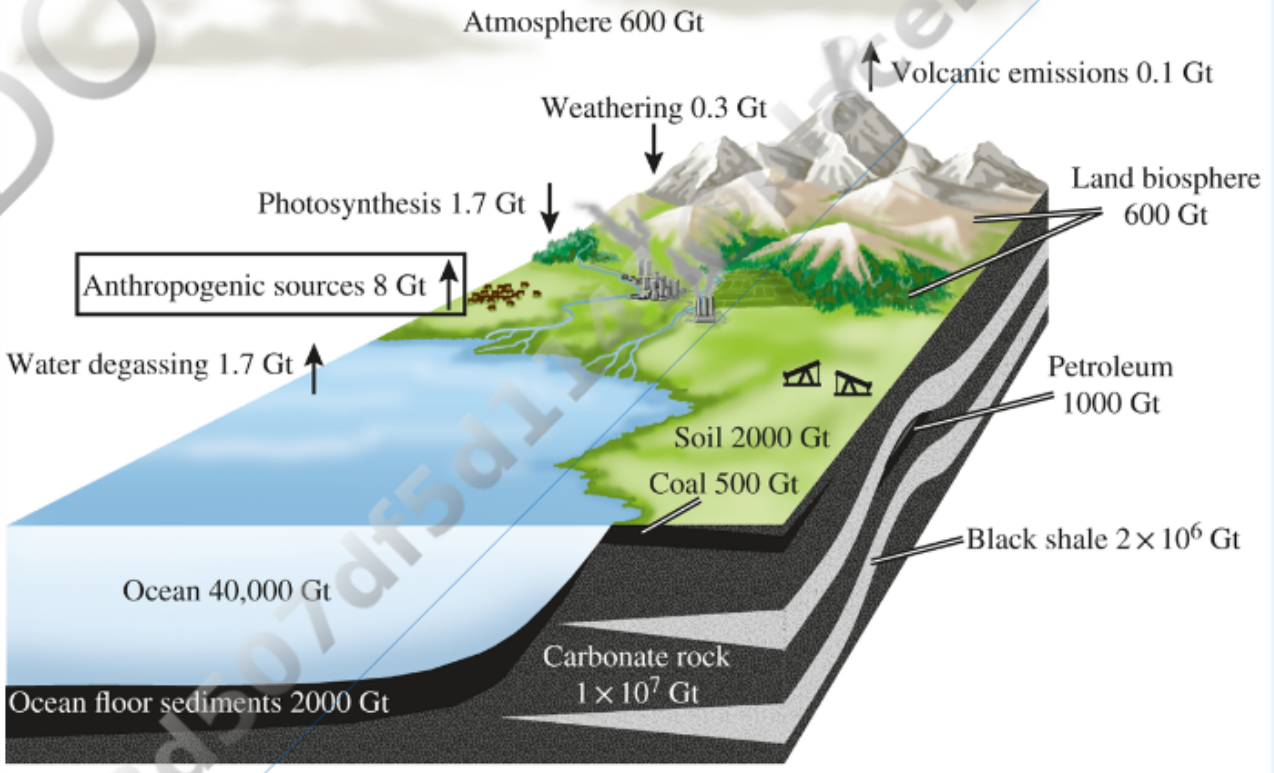

FIGURE 20.7 Schematic diagram of the carbon cycle showing reservoirs and fluxes. Fluxes into and out of the atmosphere are denoted by arrows and are preindustrial revolution values. The current-day anthropogenic contribution of carbon to the atmosphere is highlighted

Printed by: e48d507df5d1141@placeholder.94092.edu. Printing is for personal, private use only. No part of this book may be reproduced or transmitted without publisher's prior permission. Violators will be prosecuted.

by a box. See Table 20.3 and the text for details regarding reservoir and flux values. Figure based on Bowman and Hacker (2020). View larger image

TABLE 20.3 Earth's Carbon Reservoirs[a]

Carbon Reservoir	Gigatons	Carbon-Bearing Material
Atmosphere	600	Mostly CO_2 gas
Ocean	40,000	Dissolved CO_2, carbonic acid (H_2CO_3), bicarbonate (HCO_3^-), and carbonate (CO_3^{2-}); organic compounds, living biomass
Land biosphere	600	Living biomass
Soil	2000	Dead biomass, organic compounds, carbonate minerals
Ocean floor sediment	2000	Dead biomass, organic compounds, carbonate minerals
Crust (detailed below)	1×10^8	See details below for each material
Carbonate rock	1×10^7	Carbonate minerals, mostly as calcite ($CaCO_3$) as part of limestone or marble if metamorphosed
Coal	500	Graphitic carbon; see Box 20.1
Petroleum	1000	Hydrocarbons; see Box 20.1
Other carbon-rich rock	2×10^6	Graphitic carbon commonly in black shales; see Box 20.1; if metamorphosed, graphite is dominant
Mantle	5×10^7	Carbonate minerals, diamond, carbon-bearing fluids/melts, Fe-rich metallic phases

[a] All values rounded to one significant figure; crust carbon and other carbon-rich rocks estimated by values published by NASA.gov, Hunt (1972), Peterson and Depaolo (2007), Clarke and Washington (1924), and Wood et al. (1996); mantle carbon value averaged from Dasgupta and Hirschmann (2010), all other values from IPCC (2013).

Material moves through one reservoir to another by various processes; the most relevant for rocks and minerals include:

- Carbon is stored in the mantle in a variety of phases; in the upper mantle these predominantly include magmas and fluids, carbonate minerals, and diamond (Dasgupta and Hirschmann, 2010). During volcanic eruptions, CO_2 gas is released from mantle melts to the atmosphere.
- CO_2 dissolves in all waters that interact with the atmosphere, resulting in carbonic acid (H_2CO_3):

$$H_2O + CO_2 \rightarrow H_2CO_3 \quad \textbf{(20.1)}$$

Carbonic acid disassociates into a hydrogen ion (H^+) and bicarbonate (HCO_3^-),

DO NOT COPY e48d507df5d1141@placeholder.9409

Printed by: e48d507df5d1141@placeholder.94092.edu. Printing is for personal, private use only. No part of this book may be reproduced or transmitted without publisher's prior permission. Violators will be prosecuted.

Carbonic acid disassociates into a hydrogen ion (H^+) and bicarbonate (HCO_3^-), and bicarbonate can further disassociate in to a hydrogen ion and carbonate (CO_3^{2-}):

$$H_2CO_3 \rightarrow H^+ + HCO_3^- \quad \textbf{(20.2)}$$

$$HCO_3^- \rightarrow H^+ + CO_3^{2-} \quad \textbf{(20.3)}$$

Water with the hydrogen ions (from Equations 20.2 and 20.3) can chemically weather silicate minerals. There are many possible weathering reactions (see Chapters 11 and 13 and Box 16.1), but the weathering of anorthite ($CaAl_2Si_2O_8$) produces kaolinite [$Al_2Si_2O_5(OH)_4$] and dissolved calcium ions (Ca^{2+}):

$$CaAl_2Si_2O_8 + 2H^+ + H_2O \rightarrow Al_2Si_2O_5(OH)_4 + Ca^{2+} \quad \textbf{(20.4)}$$

The calcium ions released by Equation 20.4 can combine with the carbonate formed by equation 20.3 to result in the mineral calcite ($CaCO_3$).

$$Ca^{2+} + CO_3^{2-} \rightarrow CaCO_3 \quad \textbf{(20.5)}$$

This reaction may occur inorganically or it may be driven by organisms (Chapter 17), some of this calcite can become part of the crust, commonly as part of limestone deposited in an ocean setting. Limestone and related rocks represent the largest reservoir of carbon in the crust (Table 20.3).

- Photosynthesis by plants and bacteria converts atmospheric CO_2, or atmospheric CO_2 dissolved in water, into biomass (plant/animal flesh). In ocean environments, some of this biomass, mostly plankton, may become part of ocean sediment and ultimately a sedimentary rock. In this setting, shales are the most common noncarbonate sedimentary rock that can contain high concentrations of carbon. Such shales are often black because of the presence of the organic carbon and contain the second-largest amount of carbon in the crust. If appropriate conditions exist, the carbon goes through carbonization (Box 20.1) and petroleum (oil and natural gas) is produced. If the petroleum is appropriately trapped and concentrated in the crust, it may be extracted as a fuel source. In swamp environments, thick accumulations of predominantly plant biomass may form and be converted to coal through burial. If a layer of coal is thick enough and of appropriate quality, it too can be extracted as a

DO NOT COPY

Printed by: e48d507df5d1141@placeholder.94092.edu. Printing is for personal, private use only. No part of this book may be reproduced or transmitted without publisher's prior permission. Violators will be prosecuted.

coal is thick enough and of appropriate quality, it too can be extracted as a fuel source. Coal and petroleum hold a relatively small proportion of the carbon in the crust.

- Subduction of carbon-bearing rocks returns carbon to the mantle, completing the cycle.

It is important to recognize that all carbon in the crust, whether it is part of carbonate rocks and minerals, petroleum, coal, or carbon-rich shale, originates as CO_2 gas in the atmosphere and that hundreds and thousands of millions of years of natural processes slowly built these reservoirs.

A discussion of carbon fluxes into and out of the atmosphere (IPCC, 2013) is needed to understand how human activity has caused rapid changes in the carbon cycle. Volcanism adds about 0.1 gigaton (Gt) of carbon to the atmosphere a year, while silicate rock weathering removes about 0.3 Gt of carbon from the atmosphere a year. Outside of human-caused cycle changes, oceans and fresh water naturally give off about 1.7 Gt per year of carbon. On land, organism respiration and natural fire, which add CO_2 to the atmosphere, are offset by photosynthesis, which results in about 1.7 Gt of net carbon removed from the atmosphere. The astute reader will recognize that these fluxes result in a 0.2 Gt per year imbalance of atmospheric CO_2 fluxes. The fluxes should balance because prior to about 1750, atmospheric CO_2 concentrations were consistent during the previous hundreds of years (Figure 20.6). This discrepancy is caused by minor amounts of uncertainty in the fluxes and rounding errors.

The most obvious way that humans have impacted the carbon cycle is that since the Industrial Revolution, starting around 1750, the burning of fossil fuel (oil, natural gas, and coal) became the major energy source for society. Burning of any fossil fuel emits CO_2 (and water) to the atmosphere, as shown by the following combustion reactions for coal (as pure carbon), natural gas (methane—CH_4), and gasoline refined from oil (mostly hexane—C_6H_{14}):

$$C + O_2 \rightarrow CO_2 \quad \textbf{(20.6)}$$

$$CH_4 + 2O_2 \rightarrow 2H_2O + CO_2 \quad \textbf{(20.7)}$$

$$2C_6H_{14} + 19O_2 \rightarrow 14H_2O + 12CO_2 \quad \textbf{(20.8)}$$

Another important human-caused source of atmospheric CO_2 is the production of cement and concrete (Chapter 17), which begins with the heating of, most typically, calcite, until it breaks down and releases CO_2. This is called calcination and is generalized by the following reaction:

DO NOT COPY e48d507df5d1141@placeholder.9409-

Printed by: e48d507df5d1141@placeholder.94092.edu. Printing is for personal, private use only. No part of this book may be reproduced or transmitted without publisher's prior permission. Violators will be prosecuted.

$$CaCO_3 \rightarrow CaO + CO_2 \quad \textbf{(20.9)}$$

Collectively, the burning of fossil fuels and calcite calcination add about 8 Gt of carbon a year to the atmosphere in the form of CO_2. This flux of carbon into the atmosphere is much larger than any natural source of CO_2 and is over 100 times the amount of atmospheric CO_2 added by volcanoes per year. Fossil fuel combustion and calcite calcination (Equations 20.6–20.9) very rapidly return carbon stored in the rock record to the atmosphere, which natural processes took hundreds of millions of years to remove.

In response to the increase in atmospheric CO_2, both the land biosphere and ocean environments now take up more CO_2 through increased photosynthesis and oceanic CO_2 uptake. The latter is a major contributor to a variety of problematic changes in the oceans and is a contributing cause of coral reef whitening events and coral death (e.g., Barker and Ridgwell, 2012). Despite the increased uptake of CO_2 on land, the land environment is capable of taking up even more, but land use changes by agriculture and deforestation limit this ability. Regardless, the increased uptake of CO_2 by the land biosphere and oceans only offset about half of all human-produced CO_2 and explains why atmospheric CO_2 is rapidly increasing and is driving global warming. The IPCC (2013) report can be consulted for more detail regarding the carbon cycle and global warming. See Box 18.1 for more information covering some of the techniques used to determine the global temperature and atmospheric CO_2 record, and Box 16.1, which discusses how enhanced rock weathering is one method capable of decreasing atmospheric CO_2 from human sources.

While quite rare, diamonds are fairly widely distributed over the Earth; notable occurrences in the United States include Murfreesboro, Arkansas, and at the Colorado–Wyoming border near Cheyenne, Wyoming. Over a third of the world's production (over 100 million carats per year) comes from Australia. Other major producers include Zaire, Botswana, Russia, and South Africa.

Extremely small diamond grains have been reported from ultra-high-pressure metamorphic rocks formed at great depth in the Earth's mantle (see also coesite, Chapter 12), and nanometer-scale diamond has reportedly been produced by radioactive bombardment of coal. Graphite has been converted to diamond by the transient high pressures from meteoritic impacts.

A process to make synthetic diamond was developed in the 1950s and is used to make diamond for industrial purposes. Synthetic diamond production is over three times the amount mined.

Use Because of a very successful marketing effort that has stretched over many decades, diamond is considered an extremely desirable gemstone. The most valuable stones have a

Printed by: e48d507df5d1141@placeholder.94092.edu. Printing is for personal, private use only. No part of this book may be reproduced or transmitted without publisher's prior permission. Violators will be prosecuted.

blue-white color. Traces of yellow color, inclusions, or other imperfections detract from the value. See Chapter 1 for information regarding "blood diamonds."

Over half of natural diamond production and most synthetic diamonds are used for industrial purposes. The most important use is in cutting tools and as an abrasive and polishing material. Diamonds appear in cutting tools as diverse as rock saws and drills, surgical instruments, and knives to cut frozen fish. Diamonds find their way into fingernail files, sharpening stones for woodworkers, and polishing paste for polishing rock thin sections and eyeglass lenses. Diamonds are also used in diamond anvil cells, an apparatus that squeezes material between two diamond tips only 200 microns in diameter. When squeezed, the material between the diamond tips routinely experiences upward of 2000 kbar, which is the pressure of the Earth's core. Much higher pressures are also possible and provide a unique way to study planet interiors. Diamond's transparency allows direct observation of the high-pressure material using a variety of electromagnetic radiations, including visible light and X-rays.

Diamond has a long history of use for medical purposes, probably because it triggers the placebo effect. Pliny the Elder (see Chapter 1), reports that "adamas overcomes and neutralizes poisons, dispels delirium and banishes groundless perturbations of the mind." Whether the adamas to which Pliny refers is actually diamond is open to question, but beliefs that diamond could cure ailments were commonplace.

DO NOT COPY
e48d507df5d1141@placeholder.9409

Printed by: e48d507df5d1141@placeholder.94092.edu. Printing is for personal, private use only. No part of this book may be reproduced or transmitted without publisher's prior permission. Violators will be prosecuted.

surface is usually inferred to have crystallized in the upper mantle and been brought to the surface by violent gas-charged eruption of kimberlite magma. Kimberlite weathers easily and exposures are usually subdued. Diamond exploration often depends on searching for alluvial deposits that contain more abundant minerals, such as chrome diopside, that are part of the kimberlite, and following occurrences of these minerals upstream to their source.

BOX 20.2
The Carbon Cycle

A biogeochemical cycle tracks how an element or chemical compound moves through different components of the Earth system, including the solid Earth, the hydrosphere, biological material, and the atmosphere. One import biogeochemical cycle is the carbon cycle. It has gained significant attention in recent decades because of human-caused cycle changes resulting in the rise of atmospheric CO_2 from about 280 ppm in 1750 to 420 ppm in 2022 (Figure 20.6). As CO_2 is a powerful greenhouse gas that traps heat, this rise is the major driver of present-day global warming and climate change. Average global atmospheric temperatures have risen about 1.2°C (about 2°F) since 1750 (Figure 20.6), which is over 10 times faster than any climate change caused by geologic or natural processes in at least the past million years. The higher temperatures are causing changes in weather patterns, more extreme weather events, and sea-level rise, all of which pose significant challenges for maintaining or trying to achieve a prosperous human society and healthy global ecosystem. Rocks and minerals play a major role in the carbon cycle, and it is critical to understand the cycle in order to identify and implement possible solutions to climate change.

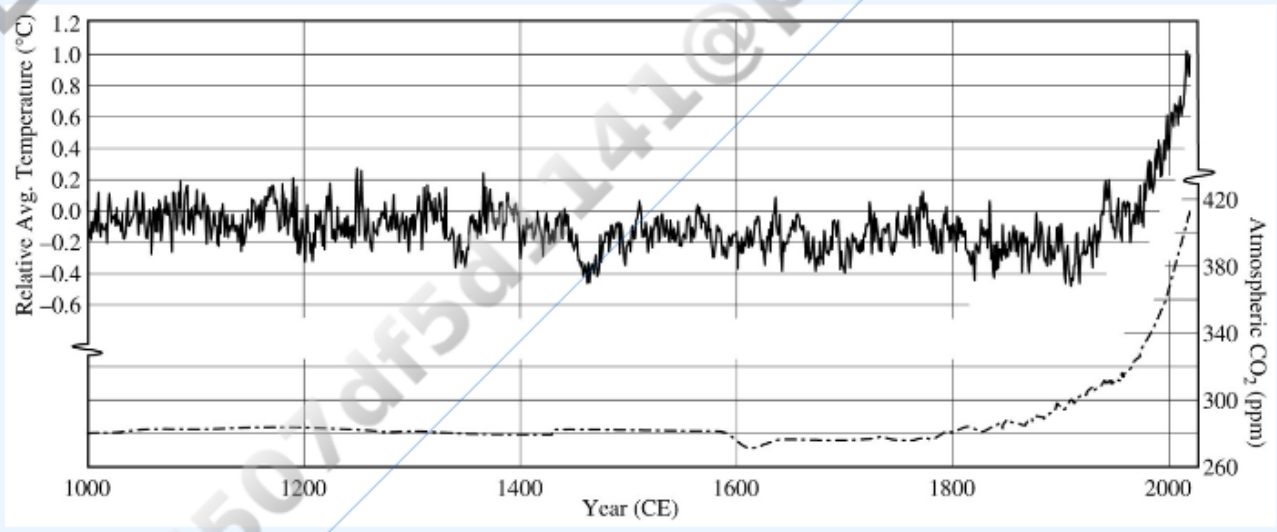

FIGURE 20.6 Change in average global temperature and atmospheric CO_2 over the past 1000 years. Temperature record during 1000–1880 from Mann and others (1999) and during 1880–2020 from NASA.gov. Atmospheric CO_2 during 1000–1996 from MacFarling Meure and others (2006) and during 1996–2020 from NASA.gov. View larger image

DO NOT COPY

Printed by: e48d507df5d1141@placeholder.94092.edu. Printing is for personal, private use only. No part of this book may be reproduced or transmitted without publisher's prior permission. Violators will be prosecuted.

Biogeochemical cycles are described by reservoirs, which hold the chemical of interest for some period of time, and fluxes, which is the rate that the chemical moves between the reservoirs. Figure 20.7 depicts a simplified carbon cycle, and Table 20.3 provides the amount of carbon held in various materials found in each of the main reservoirs. Although the Earth's core likely contains large amounts of carbon, it plays essentially no role in carbon cycling for the reservoirs at the Earth's surface, so it will be excluded for simplicity.

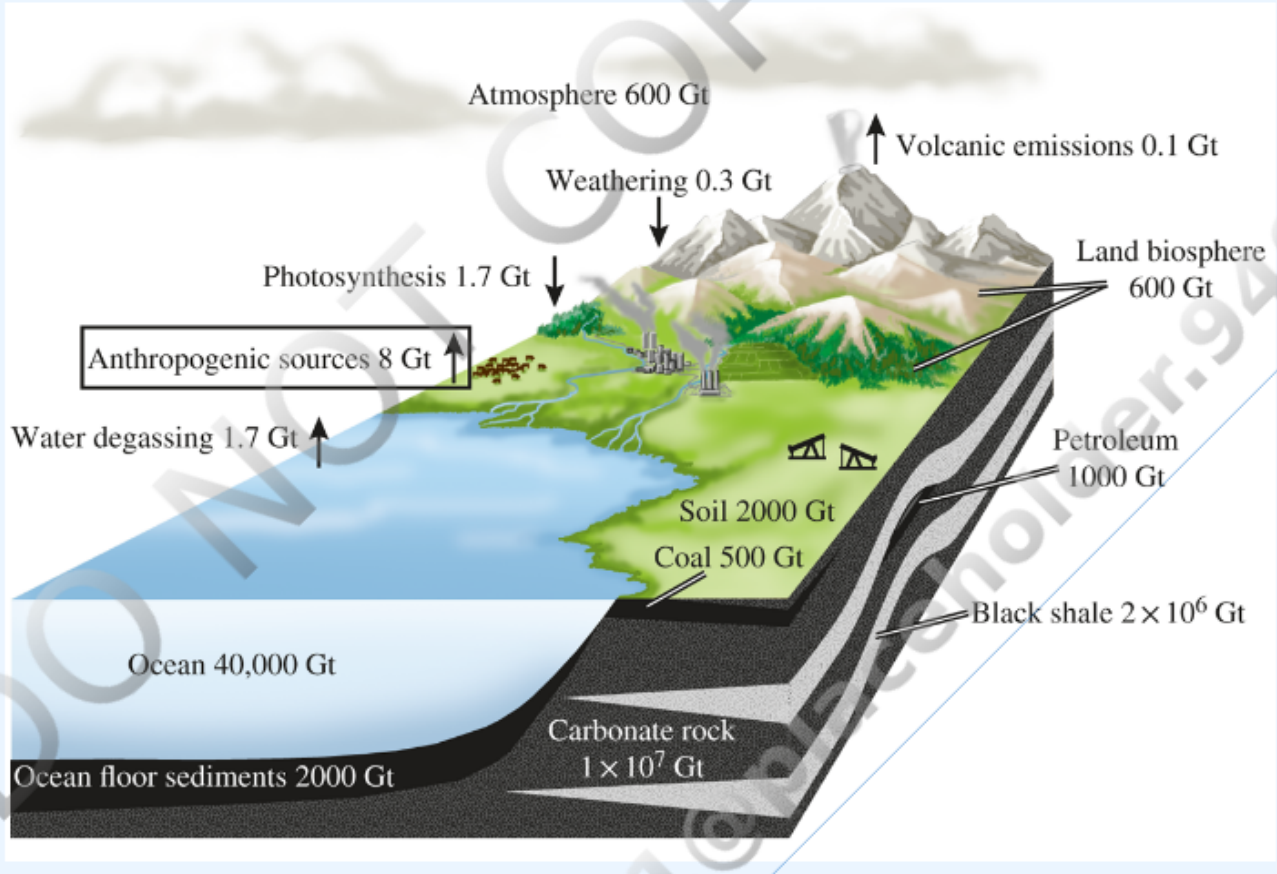

FIGURE 20.7 Schematic diagram of the carbon cycle showing reservoirs and fluxes. Fluxes into and out of the atmosphere are denoted by arrows and are preindustrial revolution values. The current-day anthropogenic contribution of carbon to the atmosphere is highlighted by a box. See Table 20.3 and the text for details regarding reservoir and flux values. Figure based on Bowman and Hacker (2020). View larger image

TABLE 20.3 Earth's Carbon Reservoirs[a]

Carbon Reservoir	Gigatons	Carbon-Bearing Material
Atmosphere	600	Mostly CO_2 gas
Ocean	40,000	Dissolved CO_2, carbonic acid (H_2CO_3), bicarbonate (HCO_3^-), and carbonate (CO_3^{2-}); organic compounds, living biomass
Land biosphere	600	Living biomass
Soil	2000	Dead biomass, organic compounds, carbonate minerals

Printed by: e48d507df5d1141@placeholder.94092.edu. Printing is for personal, private use only. No part of this book may be reproduced or transmitted without publisher's prior permission. Violators will be prosecuted.

Soil	2000	Dead biomass, organic compounds, carbonate minerals
Ocean floor sediment	2000	Dead biomass, organic compounds, carbonate minerals
Crust (detailed below)	1×10^{8}	See details below for each material
Carbonate rock	1×10^{7}	Carbonate minerals, mostly as calcite ($CaCO_3$) as part of limestone or marble if metamorphosed
Coal	500	Graphitic carbon; see Box 20.1
Petroleum	1000	Hydrocarbons; see Box 20.1
Other carbon-rich rock	2×10^{6}	Graphitic carbon commonly in black shales; see Box 20.1; if metamorphosed, graphite is dominant
Mantle	5×10^{7}	Carbonate minerals, diamond, carbon-bearing fluids/melts, Fe-rich metallic phases

[a] All values rounded to one significant figure; crust carbon and other carbon-rich rocks estimated by values published by NASA.gov, Hunt (1972), Peterson and Depaolo (2007), Clarke and Washington (1924), and Wood et al. (1996); mantle carbon value averaged from Dasgupta and Hirschmann (2010), all other values from IPCC (2013).

Material moves through one reservoir to another by various processes; the most relevant for rocks and minerals include:

- Carbon is stored in the mantle in a variety of phases; in the upper mantle these predominantly include magmas and fluids, carbonate minerals, and diamond (Dasgupta and Hirschmann, 2010). During volcanic eruptions, CO_2 gas is released from mantle melts to the atmosphere.
- CO_2 dissolves in all waters that interact with the atmosphere, resulting in carbonic acid (H_2CO_3):

$$H_2O + CO_2 \rightarrow H_2CO_3 \quad \textbf{(20.1)}$$

Carbonic acid disassociates into a hydrogen ion (H^+) and bicarbonate (HCO_3^-), and bicarbonate can further disassociate in to a hydrogen ion and carbonate (CO_3^{2-}):

$$H_2CO_3 \rightarrow H^+ + HCO_3^- \quad \textbf{(20.2)}$$

$$HCO_3^- \rightarrow H^+ + CO_3^{2-} \quad \textbf{(20.3)}$$

Water with the hydrogen ions (from Equations 20.2 and 20.3) can chemically weather silicate minerals. There are many possible weathering reactions (see

DO NOT COPY e48d507df5d1141@placeholder.9409-

Printed by: e48d507df5d1141@placeholder.94092.edu. Printing is for personal, private use only. No part of this book may be reproduced or transmitted without publisher's prior permission. Violators will be prosecuted.

weather silicate minerals. There are many possible weathering reactions (see Chapters 11 and 13 and Box 16.1), but the weathering of anorthite ($CaAl_2Si_2O_8$) produces kaolinite [$Al_2Si_2O_5(OH)_4$] and dissolved calcium ions (Ca^{2+}):

$$CaAl_2Si_2O_8 + 2H^+ + H_2O \rightarrow Al_2Si_2O_5(OH)_4 + Ca^{2+} \quad \textbf{(20.4)}$$

The calcium ions released by Equation 20.4 can combine with the carbonate formed by equation 20.3 to result in the mineral calcite ($CaCO_3$).

$$Ca^{2+} + CO_3^{2-} \rightarrow CaCO_3 \quad \textbf{(20.5)}$$

This reaction may occur inorganically or it may be driven by organisms (Chapter 17), some of this calcite can become part of the crust, commonly as part of limestone deposited in an ocean setting. Limestone and related rocks represent the largest reservoir of carbon in the crust (Table 20.3).

- Photosynthesis by plants and bacteria converts atmospheric CO_2, or atmospheric CO_2 dissolved in water, into biomass (plant/animal flesh). In ocean environments, some of this biomass, mostly plankton, may become part of ocean sediment and ultimately a sedimentary rock. In this setting, shales are the most common noncarbonate sedimentary rock that can contain high concentrations of carbon. Such shales are often black because of the presence of the organic carbon and contain the second-largest amount of carbon in the crust. If appropriate conditions exist, the carbon goes through carbonization (Box 20.1) and petroleum (oil and natural gas) is produced. If the petroleum is appropriately trapped and concentrated in the crust, it may be extracted as a fuel source. In swamp environments, thick accumulations of predominantly plant biomass may form and be converted to coal through burial. If a layer of coal is thick enough and of appropriate quality, it too can be extracted as a fuel source. Coal and petroleum hold a relatively small proportion of the carbon in the crust.
- Subduction of carbon-bearing rocks returns carbon to the mantle, completing the cycle.

It is important to recognize that all carbon in the crust, whether it is part of carbonate rocks and minerals, petroleum, coal, or carbon-rich shale, originates as CO_2 gas in the atmosphere and that hundreds and thousands of millions of years of natural processes slowly built these reservoirs.

A discussion of carbon fluxes into and out of the atmosphere (IPCC, 2013) is needed to understand how human activity has caused rapid changes in the carbon cycle. Volcanism adds about 0.1 gigaton (Gt) of carbon to the atmosphere a year,

DO NOT COPY

Printed by: e48d507df5d1141@placeholder.94092.edu. Printing is for personal, private use only. No part of this book may be reproduced or transmitted without publisher's prior permission. Violators will be prosecuted.

cycle. Volcanism adds about 0.1 gigaton (Gt) of carbon to the atmosphere a year, while silicate rock weathering removes about 0.3 Gt of carbon from the atmosphere a year. Outside of human-caused cycle changes, oceans and fresh water naturally give off about 1.7 Gt per year of carbon. On land, organism respiration and natural fire, which add CO_2 to the atmosphere, are offset by photosynthesis, which results in about 1.7 Gt of net carbon removed from the atmosphere. The astute reader will recognize that these fluxes result in a 0.2 Gt per year imbalance of atmospheric CO_2 fluxes. The fluxes should balance because prior to about 1750, atmospheric CO_2 concentrations were consistent during the previous hundreds of years (Figure 20.6). This discrepancy is caused by minor amounts of uncertainty in the fluxes and rounding errors.

The most obvious way that humans have impacted the carbon cycle is that since the Industrial Revolution, starting around 1750, the burning of fossil fuel (oil, natural gas, and coal) became the major energy source for society. Burning of any fossil fuel emits CO_2 (and water) to the atmosphere, as shown by the following combustion reactions for coal (as pure carbon), natural gas (methane—CH_4), and gasoline refined from oil (mostly hexane—C_6H_{14}):

$$\mathrm{C} + \mathrm{O_2} \rightarrow \mathrm{CO_2} \tag{20.6}$$

$$\mathrm{CH_4} + 2\mathrm{O_2} \rightarrow 2\mathrm{H_2O} + \mathrm{CO_2} \tag{20.7}$$

$$2\mathrm{C_6H_{14}} + 19\mathrm{O_2} \rightarrow 14\mathrm{H_2O} + 12\mathrm{CO_2} \tag{20.8}$$

Another important human-caused source of atmospheric CO_2 is the production of cement and concrete (Chapter 17), which begins with the heating of, most typically, calcite, until it breaks down and releases CO_2. This is called calcination and is generalized by the following reaction:

$$\mathrm{CaCO_3} \rightarrow \mathrm{CaO} + \mathrm{CO_2} \tag{20.9}$$

Collectively, the burning of fossil fuels and calcite calcination add about 8 Gt of carbon a year to the atmosphere in the form of CO_2. This flux of carbon into the atmosphere is much larger than any natural source of CO_2 and is over 100 times the amount of atmospheric CO_2 added by volcanoes per year. Fossil fuel combustion and calcite calcination (Equations 20.6–20.9) very rapidly return carbon stored in the rock record to the atmosphere, which natural processes took hundreds of millions of years to remove.

In response to the increase in atmospheric CO_2, both the land biosphere and ocean environments now take up more CO_2 through increased photosynthesis and

DO NOT COPY e48d507df5d1141@placeholder.9409

Printed by: e48d507df5d1141@placeholder.94092.edu. Printing is for personal, private use only. No part of this book may be reproduced or transmitted without publisher's prior permission. Violators will be prosecuted.

ocean environments now take up more CO_2 through increased photosynthesis and oceanic CO_2 uptake. The latter is a major contributor to a variety of problematic changes in the oceans and is a contributing cause of coral reef whitening events and coral death (e.g., Barker and Ridgwell, 2012). Despite the increased uptake of CO_2 on land, the land environment is capable of taking up even more, but land use changes by agriculture and deforestation limit this ability. Regardless, the increased uptake of CO_2 by the land biosphere and oceans only offset about half of all human-produced CO_2 and explains why atmospheric CO_2 is rapidly increasing and is driving global warming. The IPCC (2013) report can be consulted for more detail regarding the carbon cycle and global warming. See Box 18.1 for more information covering some of the techniques used to determine the global temperature and atmospheric CO_2 record, and Box 16.1, which discusses how enhanced rock weathering is one method capable of decreasing atmospheric CO_2 from human sources.

While quite rare, diamonds are fairly widely distributed over the Earth; notable occurrences in the United States include Murfreesboro, Arkansas, and at the Colorado–Wyoming border near Cheyenne, Wyoming. Over a third of the world's production (over 100 million carats per year) comes from Australia. Other major producers include Zaire, Botswana, Russia, and South Africa.

Extremely small diamond grains have been reported from ultra-high-pressure metamorphic rocks formed at great depth in the Earth's mantle (see also coesite, Chapter 12), and nanometer-scale diamond has reportedly been produced by radioactive bombardment of coal. Graphite has been converted to diamond by the transient high pressures from meteoritic impacts.

A process to make synthetic diamond was developed in the 1950s and is used to make diamond for industrial purposes. Synthetic diamond production is over three times the amount mined.

Use Because of a very successful marketing effort that has stretched over many decades, diamond is considered an extremely desirable gemstone. The most valuable stones have a blue-white color. Traces of yellow color, inclusions, or other imperfections detract from the value. See Chapter 1 for information regarding "blood diamonds."

Over half of natural diamond production and most synthetic diamonds are used for industrial purposes. The most important use is in cutting tools and as an abrasive and polishing material. Diamonds appear in cutting tools as diverse as rock saws and drills, surgical instruments, and knives to cut frozen fish. Diamonds find their way into fingernail files, sharpening stones for woodworkers, and polishing paste for polishing rock thin sections and eyeglass lenses. Diamonds are also used in diamond anvil cells, an apparatus that squeezes material between two diamond tips only 200 microns in diameter. When squeezed, the material between the diamond tips routinely experiences upward of 2000 kbar, which is the pressure of the Earth's core. Much higher pressures are also possible and provide a unique way to study planet interiors. Diamond's

DO NOT COPY e48d507df5d1141@placeholder.94092

Printed by: e48d507df5d1141@placeholder.94092.edu. Printing is for personal, private use only. No part of this book may be reproduced or transmitted without publisher's prior permission. Violators will be prosecuted.

are also possible and provide a unique way to study planet interiors. Diamond's transparency allows direct observation of the high-pressure material using a variety of electromagnetic radiations, including visible light and X-rays.

Diamond has a long history of use for medical purposes, probably because it triggers the placebo effect. Pliny the Elder (see Chapter 1), reports that "adamas overcomes and neutralizes poisons, dispels delirium and banishes groundless perturbations of the mind." Whether the adamas to which Pliny refers is actually diamond is open to question, but beliefs that diamond could cure ailments were commonplace.

REFERENCES CITED AND SUGGESTIONS FOR ADDITIONAL READING

Barker, S., and Ridgwell, A. 2012. Ocean acidification. *Nature Education Knowledge* **3**, No. 10, 21.

Beyssac, O., and Rumble, D. 2014. Graphitic carbon: A ubiquitous, diverse, and useful geomaterial. *Elements* **10**, 415–420.

Bowman, W. D., and Hacker, S. D. 2020. *Ecology*, 5th ed. Oxford University Press, New York, 744 p.

Buseck, P. R., and Beyssac, O. 2014. From organic matter to graphite: Graphitization. *Elements* **10**, 421–426.

Clarke, F. W., and Washington, H. S. 1924. *The Composition of the Earth's Crust*. United States Geological Survey Professional Paper 127.

Dasgupta, R., and Hirschmann, M. M. 2010. The deep carbon cycle and melting in Earth's interior. *Earth and Planetary Science Letters* **298**, 1–13.

Field, J. E. (ed.). 1992. *The Properties of Natural and Synthetic Diamond*. Academic Press, London, 710 p.

Howell, D., Fisher, D., Piazolo, S., Griffin, W. L., and Sibley, S. J. 2015. Pink color in type I diamonds: Is deformation twinning the cause? *American Mineralogist* **100**, 1518–1527.

Hunt, J. M. 1972. Distribution of carbon in crust of Earth. *AAPG Bulletin* **56**, 2273–2277.

IPCC, 2013: *Climate Change 2013: The Physical Science Basis. Contribution of Working Group I to the Fifth Assessment Report of the Intergovernmental Panel on Climate Change* [Stocker, T.F., D. Qin, G.-K. Plattner, M. Tignor, S.K. Allen, J. Boschung, A. Nauels, Y. Xia, V. Bex and P.M. Midgley (eds.)]. Cambridge University Press, Cambridge, United Kingdom and New York, NY, USA, 1535 pp.

Johnston, D. T. 2010. Touring the biogeochemical landscape of a sulfur-fueled world. *Elements* **6**, 101–106.

DO NOT COPY e48d507df5d1141@placeholder.9409

Printed by: e48d507df5d1141@placeholder.94092.edu. Printing is for personal, private use only. No part of this book may be reproduced or transmitted without publisher's prior permission. Violators will be prosecuted.

Lazzeri, M., and Barreiro, A. 2014. Carbon-based nanoscience. *Elements* **10**, 447–452.

Liddicoat, R. T. 1989. *Handbook of Gem Identification*, 12th ed. Gemological Institute of America, Santa Monica, CA, 364 p.

MacFarling Meure, C., Etheridge, D., Trudinger, C., Steele, P., Langenfelds, R., van Ommen, T., Smith, A., and Elkins, J. 2006. Law Dome CO_2, CH_4 and N_2O ice core records extended to 2000 years BP. *Geophysical Research Letters* **33**, No. 14, 1–4.

Mann, M. E., Bradley, R. S., and Hughes, M. K. 1999. Northern Hemisphere temperatures during the past millennium: Inferences, uncertainties, and limitations. *Geophysical Research Letters* **26**, No. 6, 759–762.

Pasteris, J. D. 2001. Raman spectroscopic and laser scanning confocal microscopic analysis of sulfur in living sulfur-precipitating marine bacteria. *Chemical Geology* **180**, 3–18.

Peterson, B. T., and Depaolo, D. J., 2007. Mass and composition of the continental crust estimated using the CRUST2.0 model. *Eos, Transactions, American Geophysical Union* **88**, No. 52, 1161.

Reith, F., Etschmann, B., Grosse, C., Moors, H., Benotmane, M. A., Monsieurs, P., Grass, G., Doonan, C., Vogt, S., Lai, B., Martinez-Driado, G., George, G. N., Nies, D. H., Mergeay, M., Pring, A., Southam, G., and Brugger, J. 2009. Mechanisms of gold biomineralization in the bacterium *Cupriavidus metallidurans. Proceedings of the National Academy of Science* **106**, 17757–17762.

Southam, G., Lengke, J. F., Fairbrother, L., and Reith, F. 2009. The biogeochemistry of gold. *Elements* **5**, 303–307.

Wood, B. J., Pawley, A., and Frost, D. R. 1996. Water and carbon in the Earth's mantle. *Philosophical Transactions of the Royal Society A: Mathematical, Physical and Engineering Sciences* **354**, No. 1711, 1495–1511.

DO NOT COPY
e48d507df5d1141@placeholder.9409

Printed by: e48d507df5d1141@placeholder.94092.edu. Printing is for personal, private use only. No part of this book may be reproduced or transmitted without publisher's prior permission. Violators will be prosecuted.

LIST OF KEY TERMS

amorphous

DO NOT COPY
e48d507df5d1141@placeholder.9409

Printed by: e48d507df5d1141@placeholder.94092.edu. Printing is for personal, private use only. No part of this book may be reproduced or transmitted without publisher's prior permission. Violators will be prosecuted.

APPENDIX A

Effective Ionic Radii of the Elements

William D. Nesse
University of Northern Colorado

Graham B. Baird
University of Northern Colorado

DO NOT COPY
e48d507df5d1141@placeholder.9409

Element	Atomic No.	Coordination Number				
		III	IV[a]	VI[a]	VIII	XII
Ac^{3+}	89			1.26		
Ag^{1+}	47		1.14 (sq)	1.29	1.42	
Ag^{2+}			0.93 (sq)	1.08		
Ag^{3+}			0.81 (sq)	0.89		
Al^{3+}	13		0.53	0.68		
As^{3+}	33			0.72		
As^{5+}			0.475	0.60		
At^{7+}	85			0.76		
Au^{1+}	79			1.51		
Au^{3+}			0.82 (sq)	0.99		
Au^{5+}				0.71		
B^{3+}	5	0.15	0.25	0.41		
Ba^{2+}	56			1.49	1.56	1.75

Printed by: e48d507df5d1141@placeholder.94092.edu. Printing is for personal, private use only. No part of this book may be reproduced or transmitted without publisher's prior permission. Violators will be prosecuted.

Be^{2+}	4	0.30	0.41	0.59		
Bi^{3+}	83			1.17	1.31	
Bi^{5+}				0.91		
Br^{1-}	35			1.82		
Br^{3+}			0.73 (sq)			
Br^{5+}		0.45				
Br^{7+}			0.39	0.53		
C^{4+}	6	0.06	0.29	0.30		
Ca^{2+}	20			1.14	1.26	1.40
Cd^{2+}	48		0.92	1.09	1.24	1.45
Ce^{3+}	58			1.15	1.28	1.48
Ce^{4+}				1.01	1.11	1.28
Cl^{1-}	17			1.67		
Cl^{5+}		0.26				
Cl^{7+}			0.22	0.41		
Co^{2+}	27		0.72 (hs)	0.79 (ls) 0.85 (hs)	1.04	
Co^{3+}				0.685 (ls) 0.75 (hs)		
Co^{4+}			0.54	0.67 (hs)		
Cr^{2+}	24			0.87 (ls) 0.94 (hs)		
Cr^{3+}				0.76		
Cr^{4+}			0.55	0.69		
Cr^{5+}			0.485	0.63	0.71	
Cr^{6+}			0.40	0.58		
Cs^{1+}	55			1.81	1.88	2.02

DO NOT COPY
e48d507df5d1141@placeholder.9409-

Printed by: e48d507df5d1141@placeholder.94092.edu. Printing is for personal, private use only. No part of this book may be reproduced or transmitted without publisher's prior permission. Violators will be prosecuted.

Cu^{1+}	29		0.74	0.91		
Cu^{2+}			0.71	0.87		
Cu^{3+}				0.68		
Dy^{2+}	66			1.21	1.33	
Dy^{3+}				1.05	1.17	
Er^{3+}	68			1.03	1.14	
Eu^{2+}	63			1.31	1.39	
Eu^{3+}				1.09	1.21	
F^{1-}	9	1.16	1.17	1.19		
F^{7+}				0.22		
Fe^{2+}	26		0.77	0.75 (ls) 0.92 (hs)	1.06	
Fe^{3+}			0.63	0.69 (ls) 0.79 (hs)	0.92	
Fe^{4+}				0.73		
Fe^{6+}			0.39			
Fr^{1+}	87			1.94		
Ga^{3+}	31		0.61	0.76		
Gd^{3+}	64			1.08	1.19	
Ge^{2+}	32			0.87		
Ge^{4+}			0.53	0.67		
H^{1+}	1	−0.24 (I), −0.04(II)				
Hf^{4+}	72		0.72	0.85	0.97	
Hg^{1+}	80	1.11		1.33		
Hg^{2+}			1.10	1.16	1.28	
Ho^{3+}	67			1.04	1.16	
I^{1-}	53			2.06		

DO NOT COPY
e48d507df5d1141@placeholder.9409

Printed by: e48d507df5d1141@placeholder.94092.edu. Printing is for personal, private use only. No part of this book may be reproduced or transmitted without publisher's prior permission. Violators will be prosecuted.

I^{5+}		0.58		1.09		
I^{7+}			0.56	0.67		
In^{3+}	49		0.76	0.94	1.06	
Ir^{3+}	77			0.82		
Ir^{4+}				0.765		
Ir^{5+}				0.71		
K^{1+}	19		1.51	1.52	1.65	1.78
La^{3+}	57			1.17	1.30	1.50
Li^{1+}	3		0.73	0.90	1.06	
Lu^{3+}	71			1.00	1.12	
Mg^{2+}	12		0.71	0.86	1.03	
Mn^{2+}	25		0.80 (hs)	0.97 (hs) 0.81 (ls)	1.10	
Mn^{3+}				0.79 (hs) 0.72 (ls)		
Mn^{4+}			0.53	0.67		
Mn^{5+}			0.47			
Mn^{6+}			0.395			
Mn^{7+}			0.39	0.60		
Mo^{3+}	42			0.83		
Mo^{4+}				0.79		
Mo^{5+}			0.60	0.75		
Mo^{6+}			0.55	0.73		
N^{3-}	7		1.32			
N^{3+}				0.30		
N^{5+}		0.044	0.27			
Na^{1+}	11		1.13	1.16	1.32	1.53

DO NOT COPY e48d507df5d1141@placeholder.9409

Printed by: e48d507df5d1141@placeholder.94092.edu. Printing is for personal, private use only. No part of this book may be reproduced or transmitted without publisher's prior permission. Violators will be prosecuted.

Nb^{3+}	41			0.86		
Nb^{4+}				0.82	0.93	
Nb^{5+}			0.62	0.78	0.88	
Nd^{2+}	60				1.43	
Nd^{3+}				1.12	1.25	1.41
Ni^{2+}	28		0.69	0.83		
Ni^{3+}				0.70 (ls) 074 (hs)		
Ni^{4+}				0.62		
O^{2-}	8	1.22	1.24	1.26	1.28	
OH^{1-}		1.20	1.21	1.23		
Os^{4+}	76			0.77		
Os^{5+}				0.72		
Os^{6+}				0.69		
Os^{7+}				0.67		
Os^{8+}			0.53			
P^{3+}	15			0.58		
P^{5+}			0.31	0.52		
Pa^{3+}	91			1.18		
Pa^{4+}				1.04	1.15	
Pa^{5+}				0.92	1.05	
Pb^{2+}	82		1.12	1.33	1.43	1.63
Pb^{4+}			0.79	0.92	1.08	
Pd^{2+}	46		0.78	1.0		
Pd^{3+}				0.90		
Pd^{4+}				0.76		
Pm^{3+}	61			1.11	1.23	

DO NOT COPY
e48d507df5d1141@placeholder.9409

Printed by: e48d507df5d1141@placeholder.94092.edu. Printing is for personal, private use only. No part of this book may be reproduced or transmitted without publisher's prior permission. Violators will be prosecuted.

Po^{4+}	84			1.08	1.22	
Po^{6+}				0.81		
Pr^{3+}	59			1.13	1.27	
Pr^{4+}				0.99	1.10	
Pt^{2+}	78		0.74	0.94		
Pt^{4+}				0.77		
Pt^{5+}				0.71		
Ra^{2+}	88				1.62	1.84
Rb^{1+}	37			1.66	1.75	1.86
Re^{4+}	75			0.77		
Re^{5+}				0.72		
Re^{6+}				0.69		
Re^{7+}			0.52	0.67		
Rh^{3+}	45			0.81		
Rh^{4+}				0.74		
Rh^{5+}				0.69		
Ru^{3+}	44			0.82		
Ru^{4+}				0.76		
Ru^{5+}				0.71		
Ru^{7+}				0.52		
Ru^{8+}				0.50		
S^{2-}	16			1.70		
S^{4+}				0.51		
S^{6+}			0.26	0.43		
Sb^{3+}	51		0.90	0.90		
Sb^{5+}				0.74		
Sc^{3+}	21			0.89	1.01	

DO NOT COPY e48d507df5d1141@placeholder.9409-

Printed by: e48d507df5d1141@placeholder.94092.edu. Printing is for personal, private use only. No part of this book may be reproduced or transmitted without publisher's prior permission. Violators will be prosecuted.

Se^{2-}	34			1.84		
Se^{4+}				0.64		
Se^{6+}			0.42	0.56		
Si^{4+}	14		0.40	0.54		
Sm^{2+}	62				1.41	
Sm^{3+}				1.10	1.22	1.38
Sn^{4+}	50		0.69	0.83	0.95	
Sr^{2+}	38			1.32	1.40	1.58
Ta^{3+}	73			0.86		
Ta^{4+}				0.82		
Ta^{5+}				0.78	0.88	
Tb^{3+}	65			1.06	1.18	
Tb^{4+}				0.90	1.02	
Tc^{4+}	43			0.79		
Tc^{5+}				0.74		
Tc^{7+}			0.51	0.70		
Te^{2-}	52			2.07		
Te^{4+}		0.66	0.80	1.11		
Te^{6+}			0.57	0.70		
Th^{4+}	90			1.08	1.19	1.35
Ti^{2+}	22			1.00		
Ti^{3+}				0.81		
Ti^{4+}			0.56	0.75	0.88	
Tl^{1+}	81			1.64	1.73	1.84
Tl^{3+}			0.89	1.03	1.12	
Tm^{2+}	69			1.17		

DO NOT COPY
e48d507df5d1141@placeholder.9409

Printed by: e48d507df5d1141@placeholder.94092.edu. Printing is for personal, private use only. No part of this book may be reproduced or transmitted without publisher's prior permission. Violators will be prosecuted.

Tm^{3+}				1.02	1.13	
U^{3+}	92			1.17		
U^{4+}				1.03	1.14	1.31
U^{5+}				0.90		
U^{6+}			0.66	0.87	1.00	
V^{2+}	23			0.93		
V^{3+}				0.78		
V^{4+}				0.72	0.86	
V^{5+}			0.50	0.68		
W^{4+}	74			0.80		
W^{5+}				0.76		
W^{6+}			0.56	0.74		
Xe^{8+}	54		0.54	0.62		
Y^{3+}	39			1.04	1.16	
Yb^{2+}	70			1.16	1.28	
Yb^{3+}				1.01	1.13	
Zn^{2+}	30		0.74	0.88	1.04	
Zr^{4+}	40		0.73	0.86	0.98	

[a] sq = square coordination, hs = high spin, ls = low spin.

Source: Data from Shannon, R. D. l976. Revised effective ionic radii and systematic studies of interatomic distances in halides and chalcogenides. Acta Crystallographica 32, 751–767.

DO NOT COPY
e48d507df5d1141@placeholder.9409

Printed by: e48d507df5d1141@placeholder.94092.edu. Printing is for personal, private use only. No part of this book may be reproduced or transmitted without publisher's prior permission. Violators will be prosecuted.

APPENDIX B

Determinative Tables

William D. Nesse
University of Northern Colorado

Graham B. Baird
University of Northern Colorado

DO NOT COPY

TABLE B.1 Determinative Table for Nonmetallic Minerals with White, Gray, or Other Pale-Colored Streak[a]

Color	Hardness			
	<3	3-5	5-7	>7
Cleavage Not Prominent				
Colorless, white, gray	**Ice** **Bauxite** Carnallite Chlorargyrite Cryolite Gibbsite Tincalconite *Wulfenite*	**Apatite** **Bauxite** **Zeolites** Böhmite Gibbsite *Wulfenite*	**Apatite** **Chalcedony** **Chert** **Cordierite** **Cristobalite** **Leucite** **Nepheline** **Opal** **Quartz** **Scapolite** **Tridymite** **Zeolites** Analcime Datolite	**Beryl** **Chalcedony** **Chert** **Cordierite** **Corundum** **Quartz** **Tridymite** **Zircon** Diamond ***Spinel*** *Sapphirine*

Printed by: e48d507df5d1141@placeholder.94092.edu. Printing is for personal, private use only. No part of this book may be reproduced or transmitted without publisher's prior permission. Violators will be prosecuted.

			Diaspore Melilite Monticellite ***Garnet*** ***Sodalite***	
Red, pink, orange, yellow	**Sulfur** Wulfenite *Chlorargyrite*	**Apatite** Pyromorphite Wulfenite	**Apatite** **Garnet** **Monazite** Chondrodite Melilite Vesuvianite ***Chalcedony*** ***Opal*** ***Quartz*** ***Sodalite*** ***Tourmaline*** *Monticellite* *Axinite* *Cassiterite*	***Beryl*** ***Chalcedony*** ***Corundum*** ***Quartz*** ***Spinel*** ***Tourmaline*** ***Zircon*** *Sapphirine*
Blue	Chrysocolla	**Apatite** **Azurite** Chrysocolla	**Apatite** **Opal** **Sodalite** **Turquoise** ***Cordierite*** ***Quartz*** ***Tourmaline***	**Beryl** **Corundum** Dumortierite Sapphirine ***Cordierite*** ***Quartz*** ***Spinel*** ***Tourmaline***
Green	Chrysocolla Gibbsite	**Malachite** **Serpentine** Chrysocolla Gibbsite	**Garnet** **Olivine** **Opal** **Tourmaline**	**Beryl** **Spinel** ***Corundum*** ***Quartz***

DO NOT COPY e48d507df5d1141@placeholder.9409-

Printed by: e48d507df5d1141@placeholder.94092.edu. Printing is for personal, private use only. No part of this book may be reproduced or transmitted without publisher's prior permission. Violators will be prosecuted.

			Pyromorphite ***Apatite***	**Turquoise** Datolite ***Apatite*** ***Quartz*** ***Sodalite*** *Chondrodite* *Melilite* *Monticellite* *Vesuvianite*	***Tourmaline*** ***Zircon*** *Sapphirine*
Tan, brown		**Bauxite** Chlorargyrite Gibbsite	**Bauxite** Gibbsite Pyromorphite ***Apatite***	**Chalcedony** **Garnet** Allanite Cassiterite Chondrodite Melilite Monazite Vesuvianite ***Chert*** ***Apatite*** ***Opal*** ***Quartz*** ***Tourmaline***	**Staurolite** **Zircon** ***Quartz*** ***Tourmaline***
Black				**Tourmaline** Cassiterite ***Garnet*** ***Quartz***	**Tourmaline** ***Quartz***
Minerals with Cleavage[b]					
Colorless, white, gray	One cleavage	**Clay** **Muscovite** **Pyrophyllite**	**Aragonite** **Zeolites** Alunite	**Clinozoisite** **Sillimanite** **Zeolites**	**Sillimanite** **Topaz**

DO NOT COPY e48d507df5d1141@placeholder.9409-

Printed by: e48d507df5d1141@placeholder.94092.edu. Printing is for personal, private use only. No part of this book may be reproduced or transmitted without publisher's prior permission. Violators will be prosecuted.

		Talc Borax Brucite Epsomite Glauberite Paragonite Thenardite Trona Ulexite ***Serpentine*** *Gibbsite* *Lepidolite*	Apophyllite Böhmite Chabazite Clinoptilolite Clintonite Colemanite Gibbsite Heulandite Margarite Polyhalite Stilbite Witherite ***Serpentine*** *Lepidolite*	**Zoisite** ***Chloritoid*** *Axinite* *Prehnite*	
	Two cleavages	Kernite Nahcolite	**Wollastonite** **Zeolites** Cerussite Colemanite Lithiophilite Natrolite Pectolite Strontianite Thomsonite	**Adularia** **Andalusite** **Jadeite** **Kyanite** **Lawsonite** **Microcline** **Orthoclase** **Plagioclase** **Sanidine**	**Andalusite** Chrysoberyl
			Wavellite Xenotime	**Scapolite** **Spodumene** **Tremolite** **Zeolites** Amblygonite Anorthoclase Natrolite Pectolite	

DO NOT COPY
e48d507df5d1141@placeholder.9409

Printed by: e48d507df5d1141@placeholder.94092.edu. Printing is for personal, private use only. No part of this book may be reproduced or transmitted without publisher's prior permission. Violators will be prosecuted.

				Thomsonite ***Orthoamphibole*** ***Orthopyroxene*** ***Titanite***	
	Three or more cleavages	**Barite** **Calcite** **Gypsum** **Halite** Sylvite	**Anhydrite** **Barite** **Calcite** **Dolomite** **Fluorite** **Magnesite** **Scapolite** **Zeolites** Ankerite Celestine Kieserite Kutnohorite Laumontite Smithsonite Scheelite *Apophyllite*	**Zeolites** Cancrinite Periclase Scheelite	Diamond
Red, pink, orange, yellow	One cleavage	**Phlogopite** Glauberite Lepidolite Thenardite ***Pyrophyllite*** *Epsomite*	Lepidolite ***Anhydrite*** ***Zeolites*** *Alunite* *Apophyllite* *Chabazite* *Clintonite* *Heulandite* *Margarite* *Polyhalite* *Stilbite*	Monazite Piemontite ***Sillimanite*** *Prehnite* *Axinite*	***Sillimanite*** ***Topaz***

DO NOT COPY
e48d507df5d1141@placeholder.9409

Printed by: e48d507df5d1141@placeholder.94092.edu. Printing is for personal, private use only. No part of this book may be reproduced or transmitted without publisher's prior permission. Violators will be prosecuted.

			Stilbite		
	Two cleavages		Lithiophilite ***Zeolites*** *Natrolite* *Strontianite* *Thomsonite* *Wavellite* *Xenotime*	**Microcline** **Orthoclase** Rhodonite Thulite ***Adularia*** ***Andalusite*** ***Plagioclase*** ***Spodumene*** ***Titanite*** *Amblygonite* *Anorthoclase* *Natrolite* *Thomsonite*	***Andalusite***
	Three or more cleavages	Sylvite ***Barite*** ***Gypsum***	**Rhodochrosite** Kutnohorite ***Barite*** ***Dolomite*** ***Magnesite*** ***Sphalerite***	Cancrinite Scapolite *Kieserite* *Scheelite*	Diamond
			Zeolites *Ankerite* *Celestine* *Laumontite* *Smithsonite*		
Blue	One cleavage	Lepidolite ***Pyrophyllite*** *Brucite*	Lepidolite ***Zeolites***	***Sillimanite***	Dumortierite ***Sillimanite*** ***Topaz***
	Two cleavages		**Azurite** Triphylite ***Zeolites***	**Na amphiboles** **Kyanite** ***Andalusite***	***Andalusite***

DO NOT COPY
e48d507df5d1141@placeholder.9409-

Printed by: e48d507df5d1141@placeholder.94092.edu. Printing is for personal, private use only. No part of this book may be reproduced or transmitted without publisher's prior permission. Violators will be prosecuted.

				Jadeite ***Microcline*** ***Plagioclase*** ***Scapolite*** ***Spodumene***	
	Three or more cleavages	***Barite***	**Anhydrite** **Fluorite** Celestine Smithsonite ***Barite*** ***Zeolites***		*Diamond*
Green	One cleavage	**Chlorite** **Glauconite** **Pyrophyllite** **Serpentine** **Talc** *Brucite* *Epsomite* *Gibbsite*	**Serpentine** Antlerite Clintonite Margarite Stilpnomelane ***Zeolites*** *Apophyllite* *Gibbsite*	**Chloritoid** **Clinozoisite** **Epidote** **Pumpellyite** **Zoisite** Prehnite	***Topaz***
	Two cleavages		**Malachite** Triphylite Wavellite ***Zeolites*** ***Wollastonite*** *Xenotime*	**Aegirine** **Aegirine-augite** **Ca-clinoamphibole** **Ca-clinopyroxene** **Cummingtonite** **Grunerite** **Jadeite** **Omphacite** **Scapolite** ***Kyanite*** ***Lawsonite***	**Chrysoberyl**

DO NOT COPY
e48d507df5d1141@placeholder.9409-

Printed by: e48d507df5d1141@placeholder.94092.edu. Printing is for personal, private use only. No part of this book may be reproduced or transmitted without publisher's prior permission. Violators will be prosecuted.

				Microcline ***Orthopyroxene*** ***Pigeonite*** ***Plagioclase*** ***Rutile*** ***Spodumene*** ***Titanite*** *Amblygonite* *Anorthoclase*	
	Three or more cleavages		**Fluorite** Smithsonite ***Barite*** ***Sphalerite*** ***Zeolites*** *Celestine* *Strontianite*		
Tan, brown	One cleavage	**Biotite** **Clay** Brucite ***Talc*** *Thenardite* *Trona*	Clintonite Lithiophylite Stilpnomelane ***Zeolites*** *Stilbite* *Witherite*	**Sillimanite** Allanite Axinite Monazite ***Pumpellyite***	**Sillimanite** **Topaz**
	Two cleavages		Lithiophilite Xenotime ***Zeolites*** *Thomsonite* *Wavellite*	**Cummingtonite** **Grunerite** **Orthoamphibole** **Orthopyroxene** **Pigeonite** **Rutile** **Titanite** Amblygonite	

DO NOT COPY e48d507df5d1141@placeholder.9409-

Printed by: e48d507df5d1141@placeholder.94092.edu. Printing is for personal, private use only. No part of this book may be reproduced or transmitted without publisher's prior permission. Violators will be prosecuted.

				Aegirine ***Aegirine-augite*** ***Ca-clinoamphiboles*** ***Na-Ca-clinoamphibole***	
	Three or more cleavages	**Barite** ***Gypsum***	**Dolomite** **Siderite** **Sphalerite** Ankerite Smithsonite ***Barite*** ***Magnesite*** ***Rhodochrosite*** ***Zeolites*** *Celestine* *Scheelite* *Strontianite* *Laumontite*		Diamond
Black	One cleavage	**Biotite**	Stilpnomelane	Allanite ***Epidote*** ***Pumpellyite*** *Piemontite*	
	Two cleavages			**Aegirine** **Aegirine-augite** **Ca-clinoamphibole** **Ca-clinopyroxene** **Na-Ca-clinoamphibole** **Pigeonite** ***Na-clinoamphibole***	

DO NOT COPY
e48d507df5d1141@placeholder.9409

Printed by: e48d507df5d1141@placeholder.94092.edu. Printing is for personal, private use only. No part of this book may be reproduced or transmitted without publisher's prior permission. Violators will be prosecuted.

				Orthopyroxene ***Titanite***	
	Three or more cleavages		**Sphalerite**		Diamond

[a] **Bold roman type**: Common properties for common minerals
Normal roman type: Common properties for less common minerals
Bold italic type: Less common properties for common minerals
Normal italic type: Less common properties for less common minerals

[b] Only prominent or well-developed cleavage. Cleavable minerals may not display possible cleavages depending on how the sample has been broken and grain size.

TABLE B.2 Non metallic Minerals with Distinctly Colored Streak

	Hardness		
Color of Streak	**<3**	**3–5**	**5–7**
Red, Reddish brown	Cinnabar Proustite Pyrargyrite Realgar	Cuprite Hematite	
Orange		Lepidocrocite	Lepidocrocite
Yellow	Autunite Carnotite Orpiment	Zincite	
Brown, Yellowish brown		Limonite Goethite	Goethite
Black		Mn Oxides and Hydroxides	Uraninite

TABLE B.3 Minerals with Metallic and Submetallic Luster

Color	Hardness		
	<3	**3–5**	**5–7**
Cleavage Not Prominent			
Silver	Calaverite Silver	Platinum	Taenite

DO NOT COPY e48d507df5d1141@placeholder.9409

Printed by: e48d507df5d1141@placeholder.94092.edu. Printing is for personal, private use only. No part of this book may be reproduced or transmitted without publisher's prior permission. Violators will be prosecuted.

Yellow, brassy yellow, gold	Calaverite Gold	Chalcopyrite Pentlandite	Marcasite Pyrite
Red, rose	Copper	Cuprite	Nickeline
Blue	Bornite (tarnished)		
Brown	Bornite		
Black	Acanthite Chalcocite	Antimony Iron Pyrrhotite Tennantite Tetrahedrite	Chromite Hematite Ilmenite Magnetite
Minerals with Cleavage			
Silver	Bismuth Bismuthinite Sylvanite	Antimony Arsenic	Arsenopyrite Cobaltite Skutterudite
Yellow, brassy yellow, gold	Orpiment		
Red	Cinnabar Proustite Pyrargyrite Realgar		Lepidocrocite
Blue	Covellite		
Green			Rutile
Brown		Lepidocrocite Sphalerite Wolframite	Lepidocrocite Rutile
Black, gray	Bismuthinite Enargite Galena Graphite Molybdenite Stibnite	Arsenic (tarnished) Enargite Sphalerite Uraninite Wolframite	Rutile

DO NOT COPY
e48d507df5d1141@placeholder.9409

Printed by: e48d507df5d1141@placeholder.94092.edu. Printing is for personal, private use only. No part of this book may be reproduced or transmitted without publisher's prior permission. Violators will be prosecuted.

	Sylvanite		

TABLE B.4 Specific Gravity

G	Mineral
0.92	Ice
1.0–2.6	Palygorskite
1.60	Carnallite
1.68	Epsomite
1.71	Borax
1.88	Tincalconite
1.91–1.93	Kernite
1.96	Ulexite
1.99	Sylvite
2.00–2.25	Opal
2.0–2.5	Sepiolite
2.05–2.20	Chabazite
2.07	Sulfur
2.09–2.23	Graphite
2.11–2.13	Trona
2.16	Clinoptilolite
2.16–2.17	Halite
2.16–2.21	Nahcolite
2.19	Stilbite
2.20	Heulandite
2.25	Analcime
2.25	Natrolite
2.27	Tridymite
2.27–2.33	Sodalite

DO NOT COPY e48d507df5d1141@placeholder.9409

Printed by: e48d507df5d1141@placeholder.94092.edu. Printing is for personal, private use only. No part of this book may be reproduced or transmitted without publisher's prior permission. Violators will be prosecuted.

2.3	Laumontite
2.30–2.37	Gypsum
2.32–2.36	Cristobalite
2.32–2.37	Wavellite
2.33–2.37	Apophyllite
2.35	Thomsonite
2.39	Brucite
2.4–2.95	Glauconite
2.4	Gibbsite
2.42	Colemanite
2.45–2.50	Leucite
2.50–2.78	Scapolite
2.53–2.78	Cordierite
2.54–2.63	Adularia
2.54–2.63	Microcline
2.54–2.63	Orthoclase
2.54–2.63	Sanidine
2.54–2.64	Anorthoclase
2.55–2.65	Serpentine
2.55–2.67	Nepheline
2.57	Kieserite
2.57–2.64	Chalcedony
2.57–2.64	Chert
2.58–2.83	Talc
2.59–2.96	Stilpnomelane
2.6–2.8	Turquoise
2.6–2.9	Alunite
2.60–2.76	Plagioclase

DO NOT COPY
e48d507df5d1141@placeholder.9409

Printed by: e48d507df5d1141@placeholder.94092.edu. Printing is for personal, private use only. No part of this book may be reproduced or transmitted without publisher's prior permission. Violators will be prosecuted.

2.6–2.9	Clay
2.6–3.3	Chlorite
2.63–2.97	Beryl
2.65–2.90	Pyrophyllite
2.65	Quartz
2.67	Thenardite
2.7–3.3	Biotite
2.71	Calcite
2.75–2.85	Glauberite
2.77–2.88	Muscovite
2.78	Polyhalite
2.8–2.9	Lepidolite
2.80–2.95	Prehnite
2.85	Paragonite
2.85–3.57	Orthoamphibole
2.86–2.90	Pectolite
2.86–2.93	Dolomite
2.86–3.09	Wollastonite
2.9–3.0	Anhydrite
2.90–3.22	Tourmaline
2.93–3.10	Ankerite
2.94–2.95	Aragonite
2.94–3.07	Melilite
2.96–3.00	Datolite
2.97	Cryolite
2.98	Magnesite
2.99–3.08	Margarite
2.99–3.48	Tremolite–Ferro-actinolite

DO NOT COPY
e48d507df5d1141@placeholder.9409

Printed by: e48d507df5d1141@placeholder.94092.edu. Printing is for personal, private use only. No part of this book may be reproduced or transmitted without publisher's prior permission. Violators will be prosecuted.

3.0–3.1	Amblygonite
3.0–3.1	Clintonite
3.0–3.57	Gedrite
3.02–3.59	Hornblende
3.03–3.23	Spodumene
3.03–3.27	Monticellite
3.05	Böhmite
3.05–3.12	Lawsonite
3.05–3.50	Glaucophane-Riebeckite
3.1–3.2	Autunite
3.1–3.35	Apatite
3.10–3.60	Cummingtonite–Grunerite
3.1–4.2	Garnet
3.12	Kutnohorite
3.13–3.16	Andalusite
3.15–3.37	Zoisite
3.16–3.25	Pumpellyite
3.16–3.26	Chondrodite
3.16–3.43	Omphacite
3.17–3.46	Pigeonite
3.18	Fluorite
3.18–3.43	Axinite
3.19–3.56	Ca-clinopyroxene
3.21–3.38	Clinozoisite
3.21–3.41	Dumortierite
3.21–3.96	Orthopyroxene
3.22–4.39	Olivine
3.23–3.27	Sillimanite

DO NOT COPY
e48d507df5d1141@placeholder.9409

Printed by: e48d507df5d1141@placeholder.94092.edu. Printing is for personal, private use only. No part of this book may be reproduced or transmitted without publisher's prior permission. Violators will be prosecuted.

3.24–3.43	Jadeite
3.3–3.5	Diaspore
3.32–3.34	Vesuvianite
3.34–3.58	Lithiophilite–Triphylite
3.38–3.49	Epidote
3.38–3.61	Piemontite
3.40–3.60	Aegirine/Aegirine-augite
3.4–4.2	Allanite
3.46–3.80	Chloritoid
3.48–3.60	Titanite
3.49	Orpiment
3.49–3.57	Topaz
3.51	Diamond
3.53–3.67	Kyanite
3.55–4.40	Spinel
3.56	Realgar
3.57–3.76	Rhodonite
3.58	Periclase
3.68–3.75	Chrysoberyl
3.70	Rhodochrosite
3.74–3.83	Staurolite
3.75	Strontianite
3.77	Azurite
3.88–3.94	Antlerite
3.9–4.05	Malachite
3.9–4.1	Sphalerite
3.96	Celestine
3.96	Siderite

DO NOT COPY e48d507df5d1141@placeholder.9409

Printed by: e48d507df5d1141@placeholder.94092.edu. Printing is for personal, private use only. No part of this book may be reproduced or transmitted without publisher's prior permission. Violators will be prosecuted.

3.98–4.02	Corundum
4–7	Mn oxides
4.09	Lepidocrocite
4.1–4.3	Chalcopyrite
4.23–5.5	Rutile
4.29–4.32	Witherite
4.3	Goethite
4.30–4.45	Smithsonite
4.3–5.1	Xenotime
4.45	Enargite
4.5	Barite
4.58–4.65	Pyrrhotite
4.6–4.76	Covellite
4.6–5.0	Pentlandite
4.62	Tennantite
4.62–4.73	Molybdenite
4.63	Stibnite
4.68	Zircon
4.70–4.79	Ilmenite
4.7–5.0	Carnotite
4.89	Marcasite
4.97	Tetrahedrite
5.0–5.3	Monazite
5.02	Pyrite
5.06–5.08	Bornite
5.09	Chromite
5.18	Magnetite
5.25	Hematite

DO NOT COPY e48d507df5d1141@placeholder.9409

Printed by: e48d507df5d1141@placeholder.94092.edu. Printing is for personal, private use only. No part of this book may be reproduced or transmitted without publisher's prior permission. Violators will be prosecuted.

5.5	Chlorargyrite
5.5–5.8	Chalcocite
5.57	Proustite
5.63–5.78	Arsenic
5.68	Zincite
5.82	Pyrargyrite
5.9–6.1	Scheelite
6.07	Arsenopyrite
6.14	Cuprite
6.33	Cobaltite
6.5	Skutterudite
6.5–7.0	Wulfenite
6.5–10.95	Uraninite
6.55	Cerussite
6.61–6.72	Antimony
6.78	Bismuthinite
6.9–7.1	Cassiterite
7.04	Pyromorphite
7.1–7.5	Wolframite
7.22	Acanthite
7.3–7.9	Iron
7.58	Galena
7.78	Nickeline
7.8–8.22	Taenite
7.9	Kamacite
8.16	Sylvanite
8.18	Cinnabar
8.95	Copper
9.10–9.40	Calaverite

DO NOT COPY
e48d507df5d1141@placeholder.9409

Printed by: e48d507df5d1141@placeholder.94092.edu. Printing is for personal, private use only. No part of this book may be reproduced or transmitted without publisher's prior permission. Violators will be prosecuted.

9.10–9.40	Calaverite
9.7–9.83	Bismuth
10.1–11.1	Silver
14–19	Platinum
19.3	Gold

TABLE B.5 Minerals That May Fluoresce[a]

Aragonite	Halite
Autunite	Nahcolite
Calcite	Opal
Chondrodite	Scapolite
Datolite	Scheelite
Diamond	Sodalite
Fluorite	Wollastonite

[a] Over 700 minerals may fluoresce under certain conditions. See fluomin.org for a complete list. Only those that consistently fluoresce are listed here.

TABLE B.6 Selected Minerals That Are Ferromagnetic and Ferrimagnetic

Mineral	Formula	Nature of Magnetism
Magnetite	Fe_3O_4	Ferrimagnetic
Hematite	Fe_2O_3	Weak ferrimagnetic
Maghemite	Fe_2O_3	Ferrimagnetic
Ilmenite	$FeTiO_3$	Ferrimagnetic[a]
Pyrrhotite	$Fe_{1-x}S$	Ferrimagnetic
Goethite	FeOOH	Antiferromagnetic, weak ferromagnetic
Native iron	Fe	Ferromagnetic
Kamacite	(Fe,Ni)	Ferromagnetic
Taenite	(Ni,Fe)	Ferromagnetic

[a] Ferrimagnetic because of inclusions of magnetite, antiferromagnetic below −183°C.

Source: Adapted from Harrison, R. J., and Feinberg, J. M. 2009. Mineral magnetism: Providing new insights into geoscience processes. Elements 5, 29–215.

TABLE B.7 Minerals That Effervesce in Dilute HCl

DO NOT COPY

Printed by: e48d507df5d1141@placeholder.94092.edu. Printing is for personal, private use only. No part of this book may be reproduced or transmitted without publisher's prior permission. Violators will be prosecuted.

Without Powdering	Only if Powdered
Aragonite	Ankerite
Azurite	Dolomite
Calcite	Kutnohorite
Cerussite	Magnesite
Malachite	Rhodochrosite
Nahcolite	Siderite
Strontianite Trona	
Witherite	
Smithsonite	

TABLE B.8 Color of Minerals in Thin Section and Grain Mount

Colorless and Gray		Pink and Red	Yellow	Green	Blue and Violet	Tan an Brown
Isotropic						
Analcime	Ice	Garnet	Garnet	Chlorite	Sodalite	Chloro
Chlorargyrite	Leucite	Cuprite	Collophane	Chlorophaeite	Spinel	Garnet
Chlorite	Opal	Spinel	Cuprite	Serpentine	Fluorite	Colloph
Clay	Periclase		Spinel	Garnet		Chromi
Collophane	Sodalite		Sphalerite	Spinel		Clay
Diamond	Sphalerite					Opal
Fluorite	Spinel					Sphaler
Garnet	Sylvite					
Halite						
Uniaxial (−)						
Ankerite	Magnesite	Corundum	Autunite	Biotite	Corundum	Ankerit
Apatite	Melilite	Hematite	Collophane	Chlorite	Tourmaline	Biotite
Apophyllite	Nepheline	Proustite	Siderite	Glauconite		Colloph
Beryl	Phlogopite	Pyrargyrite	Stilpnomelane	Stilpnomelane		Dolomit
Calcite	Pyromorphite	Rhodochrosite	Tourmaline	Tourmaline		Hemati

DO NOT COPY e48d507df5d1141@placeholder.9409

Printed by: e48d507df5d1141@placeholder.94092.edu. Printing is for personal, private use only. No part of this book may be reproduced or transmitted without publisher's prior permission. Violators will be prosecuted.

Cancrinite	Rhodochrosite	Tourmaline	Vesuvianite	Vesuvianite		Siderite
Chabazite	Scapolite		Wulfenite			Stilpnor
Corundum	Siderite					Tourma
Cristobalite	Scheelite					
Dolomite	Smithsonite					
Kalsilite	Tourmaline					
Kutnohorite	Vesuvianite					
Uniaxial (+)						
Alunite	Melilite	Cassiterite	Cassiterite	Cassiterite		Cassite
Apophyllite	Quartz	Cinnabar	Rutile	Chlorite		Chalced
Brucite	Scheelite	Rutile	Xenotime	Chloritoid		Rutile
Cassiterite	Tincalconite	Zincite	Vesuvianite			Xenotin
Chabazite	Xenotime		Zincite			Zircon
Chalcedony	Zircon					
Leucite						
Biaxial (−)						
Adularia	Axinite	Andalusite	Andalusite	Aegirine	Axinite	Aegirin
Allanite	Böhmite	Goethite	Anthophyllite	Actinolite	Dumortierite	Allanite
Amblygonite	Borax	Lepidocrocite	Axinite	Aegirine–Augite	Glaucophane	Anthop
Andalusite	Cerussite	Lepidolite	Carnotite	Allanite	Kyanite	Biotite
Anorthoclase	Chabazite	Lithiophilite	Goethite	Biotite	Riebeckite	Clay
Anthophyllite	Chlorite	Orthopyroxene	Lepidocrocite	Chlorite	Sapphirine	Clinton
Aragonite	Chloritoid	Oxyhornblende	Olivine	Chloritoid		Cummi
Biaxial (−)						
Clay	Nahcolite	Piemontite	Orpiment	Cummingtonite		Gedrite
Clinoptilolite	Olivine	Sapphirine	Pumpellyite	Datolite		Goethit
Clintonite	Orthoclase	Triphylite	Stilpnomelane	Epidote		Gruneri

DO NOT COPY e48d507df5d1141@placeholder.9409

Printed by: e48d507df5d1141@placeholder.94092.edu. Printing is for personal, private use only. No part of this book may be reproduced or transmitted without publisher's prior permission. Violators will be prosecuted.

Cordierite	Orthopyroxene			Ferro-actinolite		Hornbl
Cummingtonite	Palygorskite			Glauconite		Iddings
Datolite	Phlogopite			Grunerite		Lepidoc
Epidote	Plagioclase			Hornblende		Na–Ca-amphib
Epsomite	Polyhalite			Jadeite		Orthopy
Glauberite	Pyrophyllite			Malachite		Oxyhor
Glaucophane	Sanidine			Na–Ca-amphibole		Pumpel
Grunerite	Sapphirine			Orthopyroxene		Stilpno
Jadeite	Sepiolite			Pumpellyite		
Kernite	Serpentine			Serpentine		
Kyanite	Stilbite			Stilpnomelane		
Laumontite	Strontianite					
Lepidolite	Talc					
Lithiophilite	Tremolite					
Margarite	Triphylite					
Microcline	Trona					
Monticellite	Witherite					
Muscovite	Wollastonite					
Na–Ca-amphibole						
Biaxial (+)						
Allanite	Lawsonite	Lithiophilite	Anthophyllite	Aegirine	Azurite	Aegirin
Anhydrite	Pumpellyite	Orthopyroxene	Chondrodite	Aegirine–Augite	Riebeckite	Aegirin Augite
Anthophyllite	Lithiophilite	Piemontite	Monazite	Allanite	Sapphirine	Allanite
Barite	Monazite	Rhodonite	Pumpellyite	Antlerite	Turquoise	Anthop
Böhmite	Natrolite	Sapphirine	Realgar	Ca-clinopyroxene	Wavellite	Ca-clinopy

DO NOT COPY e48d507df5d1141@placeholder.9409

Printed by: e48d507df5d1141@placeholder.94092.edu. Printing is for personal, private use only. No part of this book may be reproduced or transmitted without publisher's prior permission. Violators will be prosecuted.

Ca-clinopyroxene	Olivine	Thulite	Sillimanite	Chlorite		Clay
Carnallite	Omphacite	Triphylite	Staurolite	Chloritoid		Cummi
Celestine	Orthopyroxene		Sulfur	Cummingtonite		Gedrite
Chabazite	Pectolite		Titanite	Grunerite		Gruneri
Chloritoid	Pigeonite		Wolframite	Hornblende		Iddings
Chondrodite	Plagioclase			Jadeite		Orthopy
Chrysoberyl	Prehnite			Lawsonite		Pigeoni
Clay	Pumpellyite			Omphacite		Pumpel
Clinoptilolite	Rhodonite			Orthopyroxene		Sillima
Clinozoisite	Sapphirine			Pigeonite		Staurol
Colemanite	Sillimanite			Pumpellyite		Titanite
Cordierite	Spodumene			Turquoise		Wavelli
Cryolite	Thenardite			Wavellite		Wolfran
Cummingtonite	Thomsonite			Wolframite		
Diaspore	Titanite					
Gibbsite	Topaz					
Grunerite	Tridymite					
Gypsum	Triphylite					
Heulandite	Ulexite					
Jadeite	Wavellite					
Kieserite	Zoisite					

TABLE B.9

DO NOT COPY e48d507df5d1141@placeholder.9409

Printed by: e48d507df5d1141@placeholder.94092.edu. Printing is for personal, private use only. No part of this book may be reproduced or transmitted without publisher's prior permission. Violators will be prosecuted.

Indices of Refraction of Isotropic Minerals

Mineral	n
Opal	1.43–1.46
Fluorite	1.433–1.435
Analcime	1.479–1.493
Sodalite	1.483–1.487
Sylvite	1.490
Halite	1.544
Spinel	1.714–1.835
Garnet	1.714–1.890
Periclase	1.735–1.756
Chromite	1.90–2.12
Chlorargyrite	2.071
Sphalerite	2.37–2.50
Diamond	2.418
Cuprite	2.849

TABLE B.10 Indices of Refraction of Uniaxial Minerals

Mineral	n_ω	$n\varepsilon$
Uniaxial (−)		
Chabazite	1.462–1.515	1.460–1.513
Cristobalite	1.486–1.488	1.482–1.484
Cancrinite	1.507–1.528	1.495–1.503
Nepheline	1.529–1.546	1.526–1.544
Apophyllite	1.531–1.542	1.533–1.543
Scapolite	1.532–1.607	1.522–1.571
Kalsilite	1.540	1.535
Beryl	1.560–1.610	1.557–1.599

DO NOT COPY e48d507df5d1141@placeholder.9409

Printed by: e48d507df5d1141@placeholder.94092.edu. Printing is for personal, private use only. No part of this book may be reproduced or transmitted without publisher's prior permission. Violators will be prosecuted.

Stilpnomelane	1.576–1.745	1.543–1.634
Autunite	1.577	1.554
Apatite	1.629–1.667	1.624–1.666
Melilite	1.629–1.699	1.616–1.661
Tourmaline	1.631–1.698	1.610–1.675
Calcite	1.658	1.486
Dolomite	1.679–1.690	1.500–1.510
Ankerite	1.690–1.750	1.510–1.548
Magnesite	1.700	1.509
Vesuvianite	1.703–1.752	1.700–1.746
Kutnohorite	1.727	1.535
Corundum	1.766–1.794	1.758–1.785
Rhodochrosite	1.816	1.597
Smithsonite	1.850	1.625
Siderite	1.875	1.635
Pyromorphite	2.058	2.048
Wulfenite	2.405	2.283
Anatase	2.561	2.488
Pyrargyrite	3.084	2.881
Proustite	3.088	2.792
Uniaxial (+)		
Ice	1.309	1.311
Chabazite	1.460–1.513	1.462–1.515
Tincalconite	1.461	1.473
Leucite	1.508–1.511	1.509–1.511
Chalcedony	1.53–1.544	1.53–1.553
Apophyllite	1.531–1.542	1.533–1.543
Quartz	1.544	1.553

DO NOT COPY
e48d507df5d1141@placeholder.9409

Printed by: e48d507df5d1141@placeholder.94092.edu. Printing is for personal, private use only. No part of this book may be reproduced or transmitted without publisher's prior permission. Violators will be prosecuted.

Brucite	1.559–1.590	1.580–1.600
Alunite	1.568–1.585	1.590–1.601
Melilite	1.629–1.669	1.616–1.661
Xenotime	1.690–1.724	1.760–1.827
Zircon	1.920–1.960	1.967–2.015
Scheelite	1.921	1.938
Cassiterite	1.990–2.010	2.091–2.100
Zincite	2.013	2.029
Rutile	2.605–2.613	2.899–2.901
Cinnabar	2.91	3.26

TABLE B.11 Indices of Refraction of Biaxial Negative Minerals Arranged in Order of Increasing n_β

Mineral	n_β	n_α	n_γ	$2V_x(^\circ)$
Epsomite	1.455	1.432	1.461	52
Chabazite	1.462–1.515	1.460–1.513	1.462–1.515	0–30
Borax	1.469	1.447	1.472	39–40
Kernite	1.472	1.455	1.487	80
Stilbite	1.489–1.507	1.482–1.500	1.493–1.513	30–49
Trona	1.494	1.416	1.542	75
Smectite	1.50–1.64	1.48–1.61	1.50–1.64	Small
Nahcolite	1.503	1.377	1.583	75
Laumontite	1.512–1.524	1.502–1.514	1.514–1.525	25–47
Adularia	1.518–1.530	1.514–1.526	1.521–1.533	Variable
Microcline	1.518–1.530	1.514–1.526	1.521–1.533	65–88
Orthoclase	1.518–1.530	1.514–1.526	1.521–1.533	40–70
Sanidine	1.518–1.530	1.514–1.526	1.521–1.533	0–47
Anorthoclase	1.524–1.534	1.519–1.529	1.527–1.536	42–52
Sepiolite	n.d.	1.515–1.520	1.525–1.529	0–50

DO NOT COPY e48d507df5d1141@placeholder.9409-

Printed by: e48d507df5d1141@placeholder.94092.edu. Printing is for personal, private use only. No part of this book may be reproduced or transmitted without publisher's prior permission. Violators will be prosecuted.

Sepiolite	n.d.	1.515–1.520	1.525–1.529	0–50
Palygorskite	1.530–1.546	1.522–1.528	1.533–1.548	30–61
Vermiculite	1.530–1.583	1.520–1.564	1.530–1.583	0–18
Serpentine	1.530–1.603	1.529–1.595	1.537–1.604	20–50
Plagioclase	1.531–1.585	1.527–1.577	1.534–1.590	45–90
Cordierite	1.532–1.574	1.527–1.566	1.537–1.578	35–90
Glauberite	1.535	1.515	1.536	7
Biotite	1.548–1.696	1.522–1.625	1.549–1.696	0–25
Chlorite	1.55–1.69	1.55–1.67	1.55–1.69	0–40
Kaolinite	1.559–1.596	1.553–1.565	1.560–1.570	24–50
Polyhalite	1.562	1.547	1.567	62–70
Illite	1.57–1.61	1.54–1.61	1.57–1.61	<10
Talc	1.575–1.599	1.538–1.554	1.575–1.60	20–30
Stilpnomelane	1.576–1.745	1.543–1.634	1.576–1.745	~0
Muscovite	1.582–1.615	1.552–1.576	1.587–1.618	28–47
Pyrophyllite	1.586–1.589	1.552–1.556	1.596–1.601	53–62
Amblygonite	1.587–1.610	1.575–1.595	1.590–1.622	50–90
Paragonite	1.594–1.609	1.564–1.580	1.594–1.618	0–40
Chrysocolla	1.597	1.575–1.585	1.598–1.635	?
Chondrodite	1.602–1.635	1.592–1.617	1.621–1.646	50–85
Anthophyllite	1.602–1.670	1.587–1.660	1.613–1.680	65–90
Glauconite	1.61–1.64	1.59–1.61	1.61–1.64	0–20
Hornblende	1.61–1.71	1.60–1.70	1.62–1.73	35–90
Tremolite–Ferro-actinolite	1.612–1.697	1.599–1.688	1.622–1.705	62–88
Glaucophane–Riebeckite	1.612–1.711	1.594–1.701	1.618–1.71	70–90
Richterite	1.615–1.700	1.605–1.685	1.622–1.712	64–87
Arfvedsonite–Eckermannite	1.625–1.709	1.612–1.700	1.630–1.710	0–90
Wollastonite	1.628–1.652	1.616–1.645	1.631–1.656	36–60
Andalusite	1.634–1.645	1.629–1.640	1.638–1.650	71–88

DO NOT COPY
e48d507df5d1141@placeholder.9409-

Printed by: e48d507df5d1141@placeholder.94092.edu. Printing is for personal, private use only. No part of this book may be reproduced or transmitted without publisher's prior permission. Violators will be prosecuted.

Andalusite	1.634–1.645	1.629–1.640	1.638–1.650	71–88
Gedrite	1.635–1.710	1.627–1.694	1.644–1.722	72–90
Cummingtonite–Grunerite	1.638–1.709	1.630–1.696	1.655–1.729	82–90
Margarite	1.642–1.648	1.630–1.638	1.644–1.650	40–67
Jadeite	1.645–1.684	1.640–1.681	1.652–1.692	84–90
Monticellite	1.648–1.664	1.638–1.654	1.650–1.674	69–88
Datolite	1.649–1.654	1.622–1.626	1.666–1.670	72–75
Böhmite	1.649–1.657	1.640–1.648	1.655–1.668	80–90
Olivine	1.651–1.869	1.635–1.827	1.670–1.879	46–90
Orthopyroxene	1.653–1.770	1.649–1.768	1.657–1.788	50–90
Clintonite	1.655–1.662	1.643–1.648	1.655–1.663	0–33
Katophorite	1.658–1.688	1.639–1.681	1.660–1.690	0–70
Strontianite	1.663–1.686	1.517–1.525	1.667–1.690	7–10
Pumpellyite	1.670–1.720	1.665–1.710	1.683–1.726	70–90
Witherite	1.676	1.529	1.677	16
Lithiophilite–Triphylite	1.677–1.710	1.670–1.705	1.684–1.720	0–90
Aragonite	1.680	1.530	1.685	18
Dumortierite	1.684–1.722	1.659–1.686	1.686–1.723	13–55
Kaersutite	1.690–1.741	1.670–1.707	1.700–1.772	66–84
Allanite	1.700–1.857	1.690–1.813	1.706–1.891	40–90
Chloritoid	1.708–1.734	1.705–1.730	1.712–1.740	55–88
Aegirine/Aegirine–augite	1.710–1.820	1.700–1.776	1.730–1.836	60–90
Kyanite	1.719–1.725	1.710–1.718	1.724–1.734	78–84
Epidote	1.725–1.784	1.715–1.751	1.734–1.797	64–90
Piemontite	1.740–1.807	1.730–1.794	1.762–1.829	74–90
Malachite	1.875	1.655	1.909	43
Carnotite	1.90–2.06	1.75–1.78	1.92–2.08	43–60
Cerussite	2.074	1.803	2.076	9
Lepidocrocite	2.20	1.94	2.51	83

DO NOT COPY
e48d507df5d1141@placeholder.9409-

Printed by: e48d507df5d1141@placeholder.94092.edu. Printing is for personal, private use only. No part of this book may be reproduced or transmitted without publisher's prior permission. Violators will be prosecuted.

Lepidocrocite	2.20	1.94	2.51	83
Goethite	2.22–2.409	2.15–2.275	2.23–2.415	0–27
Orpiment	2.8	2.4	3.0	76

TABLE B.12 Indices of Refraction of Biaxial Positive Minerals Arranged in Order of Increasing n_β

Mineral	n_β	n_α	n_γ	$2V_z(°)$
Cryolite	1.338	1.338	1.339	43
Chabazite	1.460–1.515	1.460–1.513	1.462–1.515	0–30
Tridymite	1.470–1.484	1.468–1.482	1474–1.486	40–90
Carnallite	1.474	1.466	1.495	70
Thenardite	1.475	1.469	1.484	83
Natrolite	1.476–1.491	1.473–1.490	1.485–1.502	0–64
Heulandite	1.487–1.507	1.487–1.505	1.488–1.515	0–70
Ulexite	1.504–1.506	1.491–1.496	1.519–1.520	73–78
Thomsonite	1.513–1.533	1.497–1.530	1.518–1.544	41–75
Gypsum	1.522–1.526	1.519–1.521	1.529–1.531	58
Wavellite	1.526–1.543	1.518–1.535	1.545–1.561	72
Plagioclase	1.531–1.585	1.527–1.577	1.534–1.590	75–90
Cordierite	1.532–1.574	1.527–1.560	1.537–1.578	74–90
Kieserite	1.533	1.520	1.584	55
Natroapophyllite	1.538	1.536	1.544	32
Chlorite	1.55–1.69	1.55–1.67	1.55–1.69	0–60
Gibbsite	1.568–1.579	1.568–1.578	1.587–1.590	0–40
Anhydrite	1.574–1.579	1.569–1.574	1.609–1.618	42–44
Colemanite	1.592	1.586	1.614	56
Anthophyllite	1.602–1.670	1.587–1.660	1.613–1.680	58–90
Pectolite	1.603–1.615	1.592–1.610	1.630–1.645	50–63
Topaz	1.609–1.637	1.606–1.635	1.616–1.644	44–68
Hornblende	1.61–1.71	1.60–1.70	1.62–1.73	50–90

DO NOT COPY e48d507df5d1141@placeholder.9409

Printed by: e48d507df5d1141@placeholder.94092.edu. Printing is for personal, private use only. No part of this book may be reproduced or transmitted without publisher's prior permission. Violators will be prosecuted.

Hornblende	1.61–1.71	1.60–1.70	1.62–1.73	50–90
Glaucophane–Riebeckite	1.612–1.711	1.594–1.701	1.618–1.717	0–90
Prehnite	1.615–1.647	1.610–1.637	1.632–1.670	64–70
Turquoise	1.62	1.61	1.65	40
Celestine	1.623	1.621	1.630	50
Arfvedsonite–Eckermannite	1.625–1.709	1.612–1.700	1.630–1.710	80–90
Gedrite	1.635–1.710	1.627–1.694	1.644–1.722	47–90
Barite	1.636–1.639	1.634–1.637	1.646–1.649	36–40
Cummingtonite–Grunerite	1.638–1.709	1.630–1.696	1.655–1.729	65–90
Jadeite	1.645–1.684	1.640–1.681	1.652–1.692	60–90
Böhmite	1.649–1.657	1.640–1.648	1.655–1.668	80–90
Olivine	1.651–1.869	1.635–1.827	1.670–1.879	82–90
Orthopyroxene	1.653–1.770	1.649–1.768	1.657–1.788	48–90
Spodumene	1.655–1.671	1.648–1.668	1.662–1.682	58–68
Sillimanite	1.657–1.662	1.653–1.661	1.672–1.683	20–30
Omphacite	1.670–1.712	1.662–1.701	1.685–1.723	56–84
Pumpellyite	1.670–1.720	1.665–1.710	1.683–1.726	7–90
Lawsonite	1.672–1.675	1.663–1.665	1.682–1.686	76–87
Ca-clinopyroxene	1.672–1.753	1.664–1.745	1.694–1.771	25–70
Lithiophilite–Triphylite	1.677–1.710	1.670–1.705	1.684–1.720	0–90
Pigeonite	1.684–1.732	1.682–1.732	1.705–1.757	0–32
Zoisite	1.688–1.710	1.685–1.705	1.697–1.725	0–69
Allanite	1.700–1.857	1.690–1.813	1.706–1.891	57–90
Diaspore	1.705–1.725	1.682–1.706	1.730–1.752	84–86
Clinozoisite	1.707–1.725	1.703–1.715	1.709–1.734	14–90
Chloritoid	1.708–1.734	1.705–1.730	1.712–1.740	36–72
Aegirine/Aegirine-augite	1.710–1.820	1.700–1.776	1.730–1.836	70–90
Rhodonite	1.715–1.739	1.711–1.734	1.724–1.748	63–87
Chrysoberyl	1.734–1.749	1.732–1.747	1.741–1.758	70

DO NOT COPY
e48d507df5d1141@placeholder.94092

Printed by: e48d507df5d1141@placeholder.94092.edu. Printing is for personal, private use only. No part of this book may be reproduced or transmitted without publisher's prior permission. Violators will be prosecuted.

Chrysoberyl	1.734–1.749	1.732–1.747	1.741–1.758	70
Antlerite	1.738	1.726	1.789	53
Staurolite	1.740–1.754	1.736–1.747	1.745–1.762	80–90
Piemontite	1.740–1.807	1.730–1.794	1.762–1.829	64–90
Azurite	1.756	1.730	1.836	68
Monazite	1.778–1.801	1.772–1.800	1.823–1.860	6–26
Titanite	1.870–2.034	1.843–1.950	1.943–2.110	17–40
Sulfur	2.038	1.958	2.245	69
Wolframite	2.22–2.40	2.17–2.31	2.30–2.46	73–79
Brookite	2.584	2.583	2.700	0–30
Realgar	2.684	2.538	2.704	39

TABLE B.13 Minerals That Produce Pleochroic Halos in Surrounding Minerals

Allanite
Zircon
Xenotime
Monazite
Titanite

TABLE B.14 Colors Exhibited by Opaque Minerals in Polished Section Viewed in Air

Dominant Color	Isotropic or Weakly Anisotropic	Anisotropic
Distinctly Colored		
Blue	Chalcocite	Covellite[a]
Yellow	Gold	Chalcopyrite[a]
Red/Brown	Bornite, copper	
Pink/Purple/Violet	Bornite, copper	
Slightly Colored		
Blue	Tetrahedrite	Hematite,[b] cuprite,[b] cinnabar,[a, b] proustite,[a, b] pyrargyrite[a, b]

DO NOT COPY e48d507df5d1141@placeholder.9409-

Printed by: e48d507df5d1141@placeholder.94092.edu. Printing is for personal, private use only. No part of this book may be reproduced or transmitted without publisher's prior permission. Violators will be prosecuted.

Green	Tetrahedrite, acanthite	
Yellow	Pyrite, pentlandite	Marcasite,[a] nickeline[a]
Red/Brown	Magnetite	Pyrrhotite,[a] ilmenite,[a] enargite[a]
Pink/Purple/Violet	Cobaltite	Nickeline[a]
Not Significantly Colored[c]		
Reflectance > Pyrite	Skutterudite, silver	Arsenopyrite, bismuth, antimony, arsenic, calaverite, sylvanite[a]
Reflectance < Pyrite, ≥ Galena	Galena	Pyrargyrite,[a, b] bismuthinite,[a] stibnite[a]
Reflectance < Galena, > Magnetite	Tetrahedrite, realgar[b], tennantite[b]	Hematite,[b] Acanthite,[a] enargite,[b] orpiment,[a, b] realgar,[a, b] molybdenite,[a] pyrolusite
Reflectance < Magnetite	Chromite,[b] sphalerite[b]	Scheelite,[b] cassiterite,[a, b] lepidocrocite,[b] goethite,[b] zincite,[b] uraninite,[b] wolframite,[b] rutile,[a, b] graphite[a]

[a] These minerals display bireflectance and/or reflection pleochroism.

[b] These minerals can display internal reflection.

[c] Pyrite has reflectance of 51.5%, galena 43.1%, and magnetite 20%.

TABLE B.15 Opaque or Nearly Opaque Minerals That Display Internal Reflections with Reflected Light

Predominant Internal Reflection Color	Mineral
Yellow	Cassiterite, goethite, orpiment, rutile, sphalerite
Brown	Cassiterite, chromite, realgar, rutile, sphalerite, uraninite (rare), wolframite
Red	Cinnabar, cuprite, goethite, hematite, lepidocrocite, proustite, pyrargyrite, rutile, sphalerite, stibnite, tennantite
White/Colorless	Cassiterite, orpiment, rutile, scheelite, sphalerite, plus many silicates and carbonates

DO NOT COPY e48d507df5d1141@placeholder.9409-

Printed by: e48d507df5d1141@placeholder.94092.edu. Printing is for personal, private use only. No part of this book may be reproduced or transmitted without publisher's prior permission. Violators will be prosecuted.

APPENDIX C

Mineral Associations

William D. Nesse
University of Northern Colorado

Graham B. Baird
University of Northern Colorado

DO NOT COPY e48d507df5d1141@placeholder.9409

TABLE C.1 Mineralogy of Common Igneous Rocks

Rock Type	Common or Essential Minerals	Additional Likely Minerals	Accessory Minerals	
Felsic (granite, granodiorite, rhyolite, rhyodacite, etc.)	Quartz Plagioclase (albite or oligoclase) K-feldspar	Muscovite Biotite Hornblende	Zircon Apatite Fe–Ti oxides Epidote Allanite Titanite Rutile	Sillimanite Tourmaline Garnet Topaz Xenotime Monazite Spinel Fluorite
Granitic pegmatite	Quartz Plagioclase (albite) K-feldspar Muscovite Biotite	Tourmaline Beryl Lepidolite Spodumene Amblygonite	Zircon Apatite Fe–Ti oxides Allanite Garnet	Chrysoberyl Rare earth minerals
Intermediate (diorite, andesite, dacite)	Plagioclase (andesine) Hornblende	Quartz Biotite Muscovite	Zircon Fe–Ti oxides Epidote	

Printed by: e48d507df5d1141@placeholder.94092.edu. Printing is for personal, private use only. No part of this book may be reproduced or transmitted without publisher's prior permission. Violators will be prosecuted.

		Muscovite Orthopyroxene Clinopyroxene	Epidote Apatite Allanite	
Mafic (basalt, gabbro, norite, peridotite)	Plagioclase (labradorite or bytownite) Clinopyroxene Orthopyroxene Olivine	Hornblende Biotite	Fe–Ti oxides Chromite Apatite Spinel	
Alkalic and Si-deficient (syenite, phonolite)	K-feldspar Plagioclase (albite–andesine) Nepheline Sodalite Leucite	Na-pyroxene Na-Ca-pyroxene Na-amphibole Na-Ca-amphibole Biotite Muscovite Olivine Melilite Vesuvianite	Fe–Ti oxides Epidote Apatite Rare earth minerals	

TABLE C.2 Mineralogy of Sedimentary Rocks

Clastic	Carbonate	Evaporite[a]
Quartz	Calcite	Calcite
K-feldspar	Dolomite	Dolomite
Plagioclase	Clay	Gypsum
Clay	Glauconite	Anhydrite
Chalcedony	Clastic material	Halite
Calcite	Skeletal remains	Sylvite
Muscovite	Chert	Sulfur
Biotite		Chalcedony
Glauconite		Clastic material
Hematite		Borates
Zeolites		

DO NOT COPY e48d507df5d1141@placeholder.9409

Printed by: e48d507df5d1141@placeholder.94092.edu. Printing is for personal, private use only. No part of this book may be reproduced or transmitted without publisher's prior permission. Violators will be prosecuted.

Plus many more		
Heavy mineral content may be diagnostic of provenance		

[a] See also Table 17.3.

TABLE C.3 Mineralogy of Common Metamorphic Rocks

Rock Type	Common Minerals		Accessory Minerals
Pelitic to psammitic (metamorphosed shale to quartz-rich sandstone; includes slate, phyllite, mica schist, hornfels, quartzite)	Quartz Plagioclase (albite–andesine) Muscovite Biotite Chlorite Chloritoid Cordierite Staurolite	Garnet Andalusite Sillimanite Kyanite K-feldspar	Apatite Fe–Ti oxides Graphite Epidote group Tourmaline Sapphirine Zircon
Mafic (metamorphosed mafic igneous rocks and sediments derived therefrom)	Plagioclase (andesine, labradorite) Orthoamphibole Ca-clinoamphibole Low-Ca-clinoamphibole Ca-clinopyroxene Cordierite Epidote group Garnet Biotite Chlorite Titanite Omphacite		Apatite Zircon Fe–Ti oxides Spinel
Carbonate (metamorphosed limestone, dolostone, and other calcareous sediments)	Calcite Aragonite	Talc Scapolite	Titanite Graphite

DO NOT COPY e48d507df5d1141@placeholder.9409-

Printed by: e48d507df5d1141@placeholder.94092.edu. Printing is for personal, private use only. No part of this book may be reproduced or transmitted without publisher's prior permission. Violators will be prosecuted.

	Dolomite Quartz Wollastonite Ca-clinoamphibole Ca–Na-clinoamphibole Olivine Garnet Ca-clinopyroxene Biotite Epidote group Brucite Periclase	Humite group Monticellite Vesuvianite	Periclase Corundum Fe–Ti oxides
Blueschist and related (metamorphosed graywacke and shale: high pressure/low temperature)	Quartz Plagioclase Muscovite Biotite Chlorite Lawsonite Pumpellyite Sodic amphibole Sodic-calcic amphibole Garnet Jadeite Omphacite Calcite Aragonite	Titanite Serpentine Epidote group Zeolites	Prehnite Apatite Zircon Fe–Ti oxides
Granitic gneiss (metamorphosed arkosic sediments, granite, rhyolite, etc.)	Quartz Plagioclase K-feldspar Biotite		Apatite Epidote Garnet Zircon

DO NOT COPY
e48d507df5d1141@placeholder.9409

Printed by: e48d507df5d1141@placeholder.94092.edu. Printing is for personal, private use only. No part of this book may be reproduced or transmitted without publisher's prior permission. Violators will be prosecuted.

	Biotite Orthopyroxene Cordierite		Zircon Allanite Fe–Ti oxides Sapphirine

TABLE C.4 Mineralogy of Hydrothermal Sulfide Deposits

Hypogene (Primary) Minerals		Minerals Produced by Supergene Alteration	Hydrothermal Alteration
Sulfides and Related	Oxides	Azurite	Adularia
Acanthite	Magnetite	Calcite	Albite
Arsenopyrite	Cassiterite	Chrysocolla	Alunite
Bornite	Other Related	Clay	Biotite
Chalcopyrite	Sulfantimonides	Copper	Chlorite
Cinnabar	Sulfarsenides	Cuprite	Clay
Covellite	Tellurides of Au and Ag	Dolomite	Epidote
Enargite	Tungstates	Goethite	Muscovite
Galena	Molybdates	Gypsum	Sulfur
Molybdenite		Hematite	
Pentlandite	Gangue	Hemimorphite	
Pyrite	Ankerite	Malachite	
Pyrrhotite	Barite	Rhodochrosite	
Sphalerite	Calcite	Smithsonite	
Tennantite	Dolomite	Sulfur	
Tetrahedrite	Quartz	Turquoise	
	Rhodochrosite		
Native Elements Gold Mercury	Rhodenite Siderite	Plus other oxides or carbonates of cations in primary minerals.	

DO NOT COPY e48d507df5d1141@placeholder.9409-

Printed by: e48d507df5d1141@placeholder.94092.edu. Printing is for personal, private use only. No part of this book may be reproduced or transmitted without publisher's prior permission. Violators will be prosecuted.

Silver		Sulfides of the primary mineral cations may also be reprecipitated in the vicinity of the water table or elsewhere.	

DO NOT COPY
e48d507df5d1141@placeholder.9409

Printed by: e48d507df5d1141@placeholder.94092.edu. Printing is for personal, private use only. No part of this book may be reproduced or transmitted without publisher's prior permission. Violators will be prosecuted.

Glossary

William D. Nesse
University of Northern Colorado

Graham B. Baird
University of Northern Colorado

DO NOT COPY

ϵ ray See extraordinary ray.

ω ray See ordinary ray.

2-fold coordination A cation being bonded to two anions.

$2E$ See apparent optic angle.

$2V$ angle See apparent optic angle.

$2V_x$ The angle between the optic axes bisected by the X axis.

$2V_z$ The angle between the optic axes bisected by the Z axis.

3-fold coordination A cation being bonded to three anions.

4-fold coordination A cation being bonded to four anions.

6-fold coordination A cation being bonded to six anions.

8-fold coordination A cation being bonded to eight anions.

12-fold coordination A cation being bonded to 12 anions.

32 point groups There are 32 unique set of three-dimensional symmetry operations, each one comprises one of the 32 point groups.

^{14}C radiometric dating A radiometric dating technique that uses the radioactive decay of ^{14}C to determine geologic time. It generally can be applied only to carbon-bearing materials less than 50,000 years old. It is also called radiocarbon dating.

^{40}Ar/^{39}Ar radiometric dating A radiometric dating technique that uses the radioactive decay of ^{40}K into ^{40}Ar to determine geologic time. ^{40}K is not measured directly; its concentration is determined by analyzing for ^{39}Ar. ^{39}Ar is produced by neutron irradiation

Printed by: e48d507df5d1141@placeholder.94092.edu. Printing is for personal, private use only. No part of this book may be reproduced or transmitted without publisher's prior permission. Violators will be prosecuted.

of some of the ^{39}K also present in the mineral, which has a known ratio to ^{40}K. The technique could be applied to any K-bearing mineral and generally is best at constraining the timing of when the mineral last cooled to below about 520°C to 220°C, depending on the mineral.

accessory mineral A mineral found in a rock not required to be present given the rock name (e.g., granite). If abundance is sufficient, the accessory mineral name can be used to modified the rock name (e.g., biotite granite); otherwise, the mineral may be referred to a trace accessory mineral.

accessory plates Polarizing plates that are added to the optical path of the petrographic microscope. They are used to assist with measuring a variety of optical properties. Also called compensator plates.

acicular A mineral grain shape that is very elongate and rod-shaped.

acid mine drainage Waters exiting mines which have interacted with pyrite and other sulfide minerals resulting in a very low pH. If the same interaction occurs naturally, it is called acid rock drainage.

actinide series Elements with atomic numbers 89–103.

activation energy The energy needed for a chemical reaction to occur.

acute bisectrix The axis that bisects the acute optic angle.

acute bisectrix interference figure An interference figure that includes the acute bisectrix.

aggregate Sand and gravel used as building material.

albite twinning Feldspar twinning with {010} as a twin plane. Albite twinning produces striations seen on the cleavage surfaces of plagioclase feldspars.

alkali metals Group 1 elements on the periodic table, not including H. Also referred to as the alkalis.

alkaline earth metals Group 2 elements on the periodic table.

alkalis Group 1 elements on the periodic table, not including H. Also referred to as the alkalis.

allochromatic Describes minerals with highly variable color.

alloy A mixture of different metals.

alpha decay Radioactive decay where the unstable atom ejects an alpha particle, which is the nucleus of a helium atom (^{4}He).

alteration Any chemical or mineralogical change to a mineral that occurs after it

DO NOT COPY e48d507df5d1141@placeholder.94092

Printed by: e48d507df5d1141@placeholder.94092.edu. Printing is for personal, private use only. No part of this book may be reproduced or transmitted without publisher's prior permission. Violators will be prosecuted.

alteration Any chemical or mineralogical change to a mineral that occurs after it crystallized. Alteration is most commonly recognized as weathering or other low-temperature changes, but not exclusively.

aluminosilicate polymorph Kyanite, andalusite, and sillimanite.

aluminum silicate polymorphs Kyanite, andalusite, and sillimanite.

amorphous Describes a material with atoms that lack long-range atomic order or a crystalline structure. Also called non-crystalline.

amygdules Vesicles filled with secondary minerals.

analyzer The polarizer of a petrographic microscope located between the objective lens and the oculars.

angular aperture The angle of the cone of light that can enter a microscope objective lens.

angular momentum quantum number A value that distinguishes atomic subshells of different shapes. It is denoted by l and has values between 0 and n − 1, where n indicates the shell (e.g., K shell has n = 1).

anhedral Describes a mineral grain that displays no crystal faces.

anhydrous Describes a mineral without OH^- in its chemical formula.

anion A negatively charged atom (ion).

anisodesmic bonding Bonding where some anion–cation bonds take more than half of the anion charge.

annealing A mineral grain recrystallizing, or rearranging its bonding, to remove dislocations or other imperfections.

annealing temperature The temperature above which a mineral can recrystallize to remove dislocations or other imperfections.

anomalous interference colors Interference colors not shown on the interference color chart.

antiferromagnetism A special case of ferrimagnetism in which antiparallel spins completely cancel to yield zero net magnetic moment.

antiperthite An exsolved feldspar where the host is albite and the exsolution lamellae are K-feldspar.

antiperthitic Describes an exsolved feldspar where the host is albite and the exsolution lamellae are K-feldspar.

DO NOT COPY

Printed by: e48d507df5d1141@placeholder.94092.edu. Printing is for personal, private use only. No part of this book may be reproduced or transmitted without publisher's prior permission. Violators will be prosecuted.

antiphase domain boundary Planar defect in a crystal where the crystals on either side of the planar defect are related to each other by a simple translation.

antiphase domain The part of a crystal on one side of an antiphase domain boundary.

antirapakivi A feldspar texture where the core of a feldspar grain is plagioclase while the rim is alkali feldspar.

aperture diaphragm An iris diaphragm in the substage assembly of the petrographic microscope that controls the image contrast.

apparent optic angle The angle between the refracted optic axes; it is referred to as $2E$.

arenite Sandstone with less than 15% matrix.

argillaceous Describes a soillike odor that may be produced by wetted clay minerals.

asbestiform The fibrous habit that some asbestos minerals may have.

asbestos Chrysotile, tremolite, actinolite, anthophyllite, riebeckite, and cummingtonite–grunerite minerals with an asbestiform habit, used as an industrial product.

ash glass Vesicle-filled, slaglike glass created by burning coal beds that melt the surrounding rock.

assimilation Addition of material from the country rock to a magma.

asterism Star-shaped light reflectance from a mineral caused by fine fibrous parallel inclusions.

atomic mass The mass of an atom divided by one-twelfth the mass of a ^{12}C atom.

atomic mass number The mass of an atom divided by one-twelfth the mass of a ^{12}C atom.

atomic number (Z) The number of protons within an element.

atomic radius The effective radius of an uncharged atom.

atomic weight The weighted average of the atomic masses of the isotopes of an element.

auxiliary condensing lens A lens part of the substage assembly of a petrographic microscope that, when placed in the optical path, provides conoscopic illumination, or strongly converging light, which is needed for producing interference figures.

axial intercept The distance from the origin where a crystal face, when extended, crosses the crystal axes.

axial ratio The ratio of the unit cell dimensions found by dividing each unit cell dimension by the b unit cell dimension.

DO NOT COPY

Printed by: e48d507df5d1141@placeholder.94092.edu. Printing is for personal, private use only. No part of this book may be reproduced or transmitted without publisher's prior permission. Violators will be prosecuted.

dimension by the b unit cell dimension.

background X-rays of random energy and wavelength produced when an electron beam interacts with a sample. Also called the continuous spectrum. Can also more generally refer to any signal detected by analytical instrumentation from which no meaningful information can be extracted.

backscattered electrons Beam electrons that have been deflected by the atoms of the sample through one or more interactions. Scanning electron microscope images produced by backscattered electrons show contrast (brightness vs. darkness) strongly controlled by the average atomic number of the sample (bright indicates high average atomic number).

band gap The energy difference between a bonded atom's valence band and conduction band.

band theory A theory that describes a bonded atom's orbitals and the electrons in those orbitals as having specific energies.

banded A rock texture with layers of minerals with different color or texture.

basal Describes a crystallographic plane that is at an angle to the *c* axis and parallel to the *a* and *b* axes; it is denoted by (001) using Miller indices.

Becke line The bright line that appears adjacent to a grain boundary when placed slightly out of focus with the petrographic microscope. Behavior of the Becke line indicates relative index of refraction compared to neighboring materials.

bentonite A rock or sediment containing abundant swelling clays; bentonite beds are often formed by alteration of volcanic ash layers.

Bertrand lens A small, removable lens positioned just below the ocular; it is one petrographic microscope component needed to produce interference figures.

beta decay Radioactive decay where a neutron in an unstable atom breaks down into a proton and an electron; the electron (beta particle) is ejected from the atom along with an antineutrino.

biaxial Describes having two optic axes. Orthorhombic, monoclinic, and triclinic crystal system minerals are biaxial.

binary minimum The point that represents the lowest temperature melt possible on a temperature–composition (T–X) phase diagram where the solidus and liquidus are not influenced by exsolution.

biologically controlled mineralization The growth of minerals controlled by biology that serve some physiological purpose.

biologically induced mineralization Mineral precipitation resulting from an

DO NOT COPY

Printed by: e48d507df5d1141@placeholder.94092.edu. Printing is for personal, private use only. No part of this book may be reproduced or transmitted without publisher's prior permission. Violators will be prosecuted.

organism's interaction with the surrounding aqueous environment or as a byproduct of metabolic activity.

bio-mediation Using plants and bacteria to improve the engineering properties of weak soils unsuitable for construction.

biomineralization Mineral growth induced by organisms.

biominerals Any mineral or mineraloid produced by biomineralization.

biomining Mining where organisms are used to help extract the metal of interest from the ore.

bio-remediation Using plants and bacteria to remove unwanted chemicals from the environment.

bird's-eye extinction The speckled appearance that typically muscovite and biotite display when near extinction in cross-polarized light.

birefringence The difference in the index of refraction between the slow ray and the fast ray.

bisectrix dispersion Variation in the orientation of the indicatrix; also called indicatrix dispersion.

bladed Describes a crystal shape similar to the shape of a knife blade.

body-centered (I) A unit cell with nodes at its corners and center.

body-centered cubic packing A crystal structure where atoms are placed at the nodes of a body-centered cubic unit cell.

bog manganese A manganese deposit formed by precipitation on bog and lake bottoms.

Bøggild intergrowth A microscopic plagioclase exsolution texture that forms between about An_{46} and An_{60} compositions.

Bohr magnetic moment A magnetic field produced by unpaired electrons in an orbital.

bond length The distance between the nuclei of two bonded atoms. It is the sum of the effective radius of each atom.

botryoidal Describes a crystal habit where the mineral forms a mass that looks like a bunch of grapes.

Bragg equation The mathematical formula that describes the geometry necessary for an X-ray to be diffracted by a crystal.

Bragg reflection indices A labelling method for reflections within an X-ray diffraction pattern. They are related to Miller indices by the integer *n*, which indicates the order of

DO NOT COPY

Printed by: e48d507df5d1141@placeholder.94092.edu. Printing is for personal, private use only. No part of this book may be reproduced or transmitted without publisher's prior permission. Violators will be prosecuted.

pattern. They are related to Miller indices by the integer n, which indicates the order of the reflection.

Bragg's law The mathematical formula that describes the geometry necessary for an X-ray to be diffracted by a crystal.

Bravais lattices The 14 different ways lattice nodes can be arranged into the unit cells of the six crystal systems.

bulk chemical analysis The chemical analysis of a whole rock or multi-mineral sample.

bulk composition The chemistry of a whole rock or multi-mineral sample.

Burgers vector The direction and magnitude of displacement of a crystal structure caused by a dislocation.

Bxa The axis that bisects the acute optic angle.

Bxo The axis (either *Z* or *X*) that bisects the obtuse angle between the optic axes.

calcination Breaking down a mineral into a metal oxide and other volatiles using high heat. It is most commonly used in reference to the specific case of breaking down calcite in this way, which results in CaO (quicklime) and CO_2.

calories A unit of energy. One calorie is the amount of heat energy required to change the temperature of 1 g of water from 15°C to 16°C.

capillary Describes a crystal shape that is the most elongate possible, even longer and thinner than fibrous.

Carlsbad-albite method A technique that uses the extinction patterns of Carlsbad and albite twins to determine plagioclase composition.

cathodoluminescence (CL) The visible light emitted from a sample caused by the interaction with an electron beam.

cations A positively charged atom (ion).

center symmetry Symmetry where crystal features projected through the crystal's origin have identical features equidistant from the origin on opposite sides of the crystal.

center (C) Refers to any unit mesh or unit cell with a lattice node at the center of the unit mesh or unit cell.

centered rectangle (C) Unit mesh with nodes at the corners of a rectangle and an additional node at the center of the rectangle.

chain silicates The silicate minerals where silicon tetrahedrons are bonded together in such a way as to result in long chains of silicon tetrahedrons one or two tetrahedrons wide within the crystal structure.

DO NOT COPY e48d507df5d1141@placeholder.9409

Printed by: e48d507df5d1141@placeholder.94092.edu. Printing is for personal, private use only. No part of this book may be reproduced or transmitted without publisher's prior permission. Violators will be prosecuted.

characteristic X-Ray A fluoresced X-Ray from an element produced by an electron dropping in energy from a higher- to lower-energy orbital. Such X-Rays have energy (and wavelength) controlled by the energy difference between the two orbitals involved and are thus characteristic of the element that produced it.

characteristic X-ray spectrum all the characteristic X-rays emitted by a sample.

charge transfer transition Also known as molecular orbital transition and intervalence charge transfer; occurs when a valence electron is promoted to higher energy levels on an adjacent ion. This absorbs the electromagnetic radiation that caused the promotion.

chatoyancy Having a chatoyant optical character.

chatoyant Describes a mineral or material with the optical character of reflecting light in a way similar to a cat's eye. Tiger's eye is the best common example.

chemical weathering Weathering process where minerals are chemically broken down due to interactions with surfaced waters.

chromophore element Element within a mineral that absorbs various wavelengths of visible light, producing the particular color of a mineral.

circular section A section through the indicatrix normal to an optic axis.

clay Depending on context, a sediment that becomes plastic when mixed with water, a particular sediment size of less than about 0.004 mm in diameter, or a group of particular hydrous sheet silicate minerals.

clay-sized Describes sediment size of less than about 0.004 mm in diameter.

claystone A clastic sedimentary rock predominantly made of clay-sized sediment.

cleavage The physical property whereby a mineral can break along regular flat planes controlled by variation in bond strength within the crystal structure.

cleavage form The collection of cleavage planes related by the point group symmetry of the mineral.

cleavage plane A specific plane produced by cleavage.

closed form A crystal form that is completely enclosed.

closure temperature The temperature below which diffusion is slow enough that a daughter is retained within a mineral grain.

coccolithophores Unicellular phytoplankton that produce calcite shells called coccoliths.

coccoliths The calcite shells produced by unicellular phytoplankton called

DO NOT COPY

Printed by: e48d507df5d1141@placeholder.94092.edu. Printing is for personal, private use only. No part of this book may be reproduced or transmitted without publisher's prior permission. Violators will be prosecuted.

coccoliths The calcite shells produced by unicellular phytoplankton called coccolithophores.

colloform A crystal habit where a mineral aggregate forms rounded radiating masses.

color A mineral physical property that is the color of the mineral.

color centers Mislocated electrons in the crystal structure that absorb some wavelength of light and are responsible for partially controlling the color of a mineral.

columnar Describes column-shaped crystals.

compensator plates Polarizing plates that are added to the optical path of the petrographic microscope. They are used to assist with measuring a variety of optical properties.

composition The chemical makeup of a rock or of a mineral.

composition plane A flat rational crystallographic plane along which a twin occurs.

composition surface A rational crystallographic plane along which a twin occurs that is not flat.

compositional maturity The degree to which sediment lacks both feldspar and lithic fragments or other easily weathered materials.

conchoidal Describes a smooth, curved fracture surface.

condensing lens A lens in the substage assembly of the petrographic microscope that focuses orthoscopic light, which has parallel light rays, onto the sample.

conduction band Outer electron orbitals not normally occupied if the atom is in the ground state; if electrons are excited to the conduction band, they are free to move throughout the material, which results in electric conductivity of the material.

conductor A material that easily conducts electricity.

conflict mineral A mineral that is mined to obtain profits to fund war or repressive regimes.

conoscopic illumination Sample illumination in the petrographic microscope that uses strongly converging light.

contact metamorphism Metamorphism driven by heat from nearby hot igneous rocks or magma.

contact twins A twin composition plane where the twinned segments do not appear to be intergrown.

continental flood basalts Great quantities of basaltic magma that erupted over very short geological time periods.

DO NOT COPY
e48d507df5d1141@placeholder.9409

Printed by: e48d507df5d1141@placeholder.94092.edu. Printing is for personal, private use only. No part of this book may be reproduced or transmitted without publisher's prior permission. Violators will be prosecuted.

short geological time periods.

continuous solid solution series A solid solution series where all intermediate compositions between end members are possible.

complete solid solution series A solid solution series where all intermediate compositions between end members are possible.

continuous spectrum X-rays of random energy and wavelength produced when an electron beam interacts with a sample. Can also more generally refer to any signal detected by analytical instrumentation from which no meaningful information can be extracted.

converse piezoelectric effect Deformation of a crystal produced by application of a voltage to the crystal. Also called electrostriction.

coordination number The number of anions surrounding and bonded to a cation.

coordination polyhedron The shape produced by the arrangement of anions surrounding and bonded to a cation.

core The center part of a mineral grain.

country rock The rock surrounding a magma chamber or pluton.

coupled substitution Solid solution due to interchanging two cations for two other cations with different charge; the total charge of each cation couple is the same, so charge balance is maintained.

covalent bonding Atomic bonding where electrons are shared between the bonded atoms.

critical angle The angle of light incidence that yields an angle of refraction of 90°.

critical growth radius The minimum size of a crystal embryo needed for the crystal to not be resorbed back into the melt.

critical mineral A mineral that contain a metal required for some current technology.

Crossed refers to polarizers that are 90 degrees to each other.

crossed bisectrix dispersion The acute bisectrix being parallel to the *b* axis.

crossed polarizers On the petrographic microscope, the sample is viewed with the upper polarizer inserted; thus the image is created using cross-polarized light.

cryptoperthite An exsolved alkali feldspar where the albite lamellae are sub-microscopic and cannot be seen with a petrographic microscope.

crystal A mineral sample with at least some crystal faces; sometimes also refers to a

DO NOT COPY e48d507df5d1141@placeholder.9409

Printed by: e48d507df5d1141@placeholder.94092.edu. Printing is for personal, private use only. No part of this book may be reproduced or transmitted without publisher's prior permission. Violators will be prosecuted.

mineral grain.

crystal axes Three intersecting axes applied to a crystal or crystal structure that provides a reference frame to the crystal or crystal structure.

crystal class The crystal form or set of forms for a particular point group.

crystal face Smooth crystal surfaces controlled by the crystal structure and produced during growth.

crystal family Analogous to crystal system, but used when the trigonal and hexagonal are recognized as separate crystal systems. Both are lumped together into the hexagonal crystal family. A more precise definition requires a discussion of space groups.

crystal field The negatively charged electric field produced by the anions in a crystal structure.

crystal field splitting Bound cations and anions causing the 3*d* subshells to change their energy slightly.

crystal field theory A theory that explains how *d* orbital energies change with bonding, which leads to an explanation of, for example, how some light is absorbed by a mineral, leading to its color.

crystal form The collection of crystal faces that make up a crystal.

crystal habit A description of the way mineral grains are shaped and intergrown in an aggregate.

crystal lattice The grid of nodes that shows how the atomic structure gets repeated in three dimensions according to the crystal's symmetry.

crystal structure The particular repeating arrangement of atoms within a crystalline material.

crystal system A collection of similar unit cell shapes and symmetry. Generally, mineralogists identify six crystal systems: isometric (or cubic), tetragonal, orthorhombic, monoclinic, triclinic, and hexagonal. Some, however, identify seven crystal systems when a trigonal crystal system is separated from the hexagonal system.

crystalline solid Any solid with a crystalline structure.

crystallization The process that forms a new grain of a mineral.

crystallographic direction A particular orientation within a crystal, typically identified by Miller indices.

cubic A crystal system with a cube-shaped unit cell.

cubic closest packing One way for similar-sized atoms to be packed and bonded

DO NOT COPY e48d507df5d1141@placeholder.9409

Printed by: e48d507df5d1141@placeholder.94092.edu. Printing is for personal, private use only. No part of this book may be reproduced or transmitted without publisher's prior permission. Violators will be prosecuted.

cubic closest packing One way for similar-sized atoms to be packed and bonded together. It is produced by ABC stacking and results in a face-centered cubic lattice.

cubic coordination Eight anions being bonded to a cation, resulting in a cube coordination polyhedron.

cumulate An igneous rock produced by the accumulation of crystals on the floor of a magma chamber.

Curie temperature The temperature above which ferrimagnetism is destroyed.

cyclic twin Multiple twins in which composition surfaces are not parallel, possibly resulting in a twinned crystal that circles back on itself.

daughter New element or isotope produced by the decay, or radioactive breakdown, of a parent atom.

decay The radioactive breakdown of an unstable element or isotope.

decompression melting Melting of a rock induced by a reduction of the lithostatic pressure acting on the rock or the pressure due to the weight of the overlying rock.

deform Change in shape.

dendrite Manganese oxide or hydroxide mineral with a tree-like shape that crystallized on a rock fracture surface.

dendritic Describes a crystal habit in which a crystal aggregate has a branching form somewhat like a tree.

density Mass per unit volume.

desert varnish A red, brown, or black coating that forms on the surface of exposed rocks in desert areas; the coating is mostly Fe- and/or Mn-bearing minerals and clay.

desiccant A material used to remove humidity.

detection limit The minimum amount of an element that must be present to allow a precise analysis.

detrital Describes mineral grains in sediment or a sedimentary rock that originated from another rock.

devitrification The breakdown of an amorphous material into a crystalline material.

diagenesis The lithification of sediments into rock, plus other chemical and physical changes to the sediment or rock that might occur because of burial, interactions with water in the material, and microbial activity.

diamagnetic Magnetic behavior in which the material repels a magnetic field.

DO NOT COPY
e48d507df5d1141@placeholder.9409

Printed by: e48d507df5d1141@placeholder.94092.edu. Printing is for personal, private use only. No part of this book may be reproduced or transmitted without publisher's prior permission. Violators will be prosecuted.

diamond Various definitions depending on use, one definition includes the unit mesh with a diamond shape.

diffusion The movement of matter or energy from regions of relatively high concentration to regions of relatively low concentration.

dihedron A crystal form of two nonparallel faces. Also known as a dome if the two faces are related only by a mirror plane or as a sphenoid if the two faces are related by a 2-fold rotation axis.

dimensional stone Rock used to build structures.

dioctahedral Describes an octahedral sheet of metal cations between two OH^- layers where two-thirds of the octahedral sites are occupied by metal cations.

dipyramid A crystal form where both ends of the crystal terminate with a total of 6, 8, 12, 16, or 24 faces.

discontinuous solid solution series A solid solution series where only a limited range of compositions between the end members is possible.

disilicates The silicate minerals where only two silicon tetrahedrons are bonded together within the crystal structure.

dislocation line A line of broken bonds within a crystal structure.

dispersion Different wavelengths of light being refracted differently.

displacive polymorphism The crystal structure of polymorphs being related by a simple distortion of the crystal structure.

disseminated Describes grains of a relatively low abundance mineral that are isolated from each other and evenly scattered throughout a rock or ore body.

dome A crystal form of two nonparallel faces related by a mirror plane.

double refraction Light traveling through a material being split into two rays at right angles to each other, each with a different velocity.

drusy An encrustation or coating of euhedral crystals around other minerals.

***d*-spacing** The spacing between neighboring planes of atoms.

dynamic recrystallization Recrystallization during deformation.

edge dislocation A dislocation with a Burgers vector that is perpendicular to the dislocation line.

EDS Abbreviation for “energy-dispersive X-ray spectrometer.”

DO NOT COPY e48d507df5d1141@placeholder.9409

Printed by: e48d507df5d1141@placeholder.94092.edu. Printing is for personal, private use only. No part of this book may be reproduced or transmitted without publisher's prior permission. Violators will be prosecuted.

effective radius The radius of an atom or ion if it were to behave like a hard sphere. Effective radius is controlled by valence and coordination number.

electromagnetic radiation Wave energy in the form of long electric waves, radio waves, microwaves, infrared light, visible light, ultraviolet rays, X-rays, gamma rays, and cosmic rays.

electron A negatively charged subatomic particle found in the orbitals of atoms.

electron capture A type of radioactive decay where an electron is captured by the nucleus so that a proton is converted to a neutron.

electron color centers An electron being trapped in a vacancy in the crystal structure that can absorb light and impart a color to the mineral.

electron microprobe An electron beam instrument used to image and quantitatively chemically analyze minerals or other materials.

electron probe microanalyzer An electron beam instrument used to image and quantitatively chemically analyze minerals or other materials.

electron spin Also known as the spin quantum number, the last of the four quantum numbers describing the state of an electron.

electronegativity A measure of the tendency of an element to gain or lose electrons.

electrostatic valence bond A method of determining bond strength. The electrostatic valence bond is equal to the cation charge divided by its coordination number.

electrostriction Deformation of a crystal produced by application of a voltage to the crystal.

elongate Describes a crystal or grain shape that is long and narrow.

embryo The initial cluster of atoms of a new mineral grain; same as a nucleus in this context.

end member A chemical formula that represents one of the mixing components in a solid solution series.

Energy a quantitative measure of the ability to do work. It has SI units of joules.

energy-dispersive X-ray spectrometer A device that detects characteristic X-rays and uses their energies (in kiloelectron volts—keV) and intensities (typically in counts per second—cps) to allow chemical analysis of a sample. They are found in, for example, handheld X-ray fluorescence spectrometers, scanning electron microscopes, and electron microprobes.

epitaxial nucleation Crystallization of a new mineral grain beginning on the surface of a

DO NOT COPY e48d507df5d1141@placeholder.9409

Printed by: e48d507df5d1141@placeholder.94092.edu. Printing is for personal, private use only. No part of this book may be reproduced or transmitted without publisher's prior permission. Violators will be prosecuted.

epitaxial nucleation Crystallization of a new mineral grain beginning on the surface of a previously existing mineral grain.

EPMA Abbreviation for "electron probe micro-analyzer"; more typically referred to an electron microprobe, or microprobe for short.

equant A crystal or grain shape that has approximately equal length radii in all orientations; or, more simply, a crystal or grain shape that is approximately spherical or cube shaped.

equilibrium In the context of chemical reactions, equilibrium is the condition where the phases present in a system and their compositions represent the lowest-energy configuration for the state of the system. This conditions is therefore stable and will not change over time.

equilibrium crystallization During crystallization from a melt, the crystals and melt maintain proportions and compositions that are in equilibrium with each other and the state of the system.

equilibrium melting During melting of a rock, the crystals and melt maintain proportions and compositions that are in equilibrium with each other and the state of the system.

euhedral Describes a mineral grain that displays well-formed crystal faces.

eutectic On a binary (two component) temperature-composition (T-*X*) phase diagram, the temperature and composition of the melt in equilibrium with two different solids. The eutectic liquid is the lowest temperature melt possible for any mixture of the two components.

eutectic composition The composition of the eutectic, which is the melt in equilibrium with two different solids. The eutectic liquid is the lowest temperature melt possible for any mixture of the two components.

eutectic temperature The temperature of the eutectic, which is the melt in equilibrium with two different solids. The eutectic liquid is the lowest temperature melt possible for any mixture of the two components.

exsolution A solid solution mineral unmixing, forming lamellae, which are rich in one end member, and the host, which is rich in the other end member.

extinct Using cross-polarized light with the petrographic microscope, the orientation of the fast and slow rays of an anisotropic mineral being parallel to the lower- and upper-polarizers, which results in the mineral grain transmitting no light (it appears black).

extinction angle When a grain is extinct, the angle between the long axis of the grain or of a prominent cleavage with respect to the north-south direction of the microscope image.

DO NOT COPY e48d507df5d1141@placeholder.9409

Printed by: e48d507df5d1141@placeholder.94092.edu. Printing is for personal, private use only. No part of this book may be reproduced or transmitted without publisher's prior permission. Violators will be prosecuted.

extraordinary ray Also called an ϵ ray, light refracted through an anisotropic mineral where the ray path and wave normal are not parallel.

face-centered (C) A unit cell with nodes at its corners and additional nodes in the center of two opposite sides of the unit cell.

face-centered (F) A unit cell with nodes at its corners and additional nodes in the center of all unit cell sides.

fair A cleavage-quality term indicating that the cleavage surface does not reflect light well because of its roughness.

fast ray For anisotropic minerals, the refracted ray of light with lower index of refraction and greater velocity.

ferric iron Trivalent iron, or Fe^{3+}.

ferrimagnetism Magnetic behavior where the material maintains a magnetic field which cannot be influenced by external magnetic fields.

ferromagnetism Magnetic behavior where the material maintains a magnetic field, but the details of the magnetism can be changed by external magnetic fields.

ferromanganese nodules Iron and manganese oxide and hydroxide minerals shaped as nodules that are found on the seafloor and bottom of some freshwater lakes.

ferrous iron Divalent iron, or Fe^{2+}.

fibrous Describes a crystal shape that is very elongate and shaped like a fiber.

field notebook A notebook used to record information collected in the field or outside at study sites.

filiform Describes a crystal shape that is very elongate and shaped like a filament.

Fink search method One method of systematically analyzing a powder X-ray diffraction pattern to identify the mineral that produced the pattern.

first-order red plate A petrographic microscope accessory plate that retards the slow wave by either 537 or 550 nm.

first-order reflection The reflection in an X-ray diffraction pattern where the integer n in the Bragg equation is 1.

fission A method of decay of an unstable nuclide where the nuclide breaks apart into two nuclei of approximately equal mass. If fission occurs in a crystal, the two nuclei produced by fission tear through the crystal structure, leaving a track of damage.

fission track The line of damaged crystal structure resulting from the nuclei produced

Printed by: e48d507df5d1141@placeholder.94092.edu. Printing is for personal, private use only. No part of this book may be reproduced or transmitted without publisher's prior permission. Violators will be prosecuted.

fission track The line of damaged crystal structure resulting from the nuclei produced by fission traveling through the mineral grain.

fission track dating A geochronology technique that uses the ratio of parent atoms that are able to produce fission tracks to the number of tracks present to determine the amount of time since the material cooled to below the material's annealing temperature.

flash figure An interference figure produced when the grain is oriented with an optic axis parallel to the microscope stage.

fluorescence Light produced by a material of a different wavelength than the incident electromagnetic radiation causing the light production. Fluorescence stops immediately upon removal of the electromagnetic radiation that causes the light production.

flux melting Melting of a rock caused by the addition of another material, such as water or some other volatile.

foliated Describes having aligned inequant minerals, including platy or micaceous minerals.

foliation A rock texture that approximates a plane or surface produced by having aligned inequant minerals or alternating layers of lighter- and darker-colored minerals.

foraminifera Unicellular protists found most typically in marine environments that produce calcite shells called tests. They are called "forams" for short.

formula units per unit cell The number of chemical formulas found in the unit cell of a mineral. Designated by Z in the mineral descriptions in Part 3 of this text.

fourth-order reflection The reflection in an X-ray diffraction pattern where the integer n in the Bragg equation is 4.

fractional crystallization Crystallization of a magma occurring under conditions where the crystals and melt are unable to stay in equilibrium.

fractional melting Partial melting of a rock occurring under conditions where the crystals and melt are unable to stay in equilibrium. This often occurs because the melt produced is removed from the rock melting.

fractionation series A sequence of compositionally diverse magmas produced by fractional crystallization.

fracture The physical property of a mineral breaking along irregular surfaces.

fracture surface Irregular broken surfaces on a mineral sample.

framework silicates The silicate minerals where oxygens of the silicon tetrahedrons are shared between multiple other silicon tetrahedrons in a three-dimensional pattern.

Frantz Isodynamic Magnetic Separator Instrument used to separate mineral grains

DO NOT COPY e48d507df5d1141@placeholder.9409

Printed by: e48d507df5d1141@placeholder.94092.edu. Printing is for personal, private use only. No part of this book may be reproduced or transmitted without publisher's prior permission. Violators will be prosecuted.

Frantz Isodynamic Magnetic Separator Instrument used to separate mineral grains based on their magnetic properties.

Frantz Magnetic Barrier Separator A more precise version of the Frantz Isodynamic Magnetic Separator.

free working distance On the petrographic microscope, the distance between the end of the lens and the top of the sample.

Frenkel defect A mislocation defect in a crystal structure where a cation (or anion) is moved from its normal position to an alternative site that normally is not occupied.

frequency For waves, the number of peak or troughs that pass a point per unit of time.

fulgurite Glass produced from lightning striking soil or rock.

full-wave plate A petrographic microscope accessory plate that retards the slow wave by either 537 or 550 nm.

fuse Melt a material and quench it, or quickly cool it so that it solidifies it into a glass.

gangue The economically worthless minerals in an ore deposit.

geochronology The study of "earth-time" that places absolute time constraints on geologic events.

geologically ephemeral elements Elements with sufficiently short half-lives that they exist on earth only in very small quantities as the product of radioactive decay of some other element.

Gibbs free energy of formation The energy difference between the elements in their standard states (e.g., 298 K and 1 atm pressure) and the elements when bonded to form a mineral at a particular temperature and pressure.

Gibbs free energy A particular measure of a system's energy that is useful for determining whether a system is in equilibrium or whether a chemical reaction will proceed.

glide A symmetry operation that is the combination of a specific translation with a reflection across a mirror plane called the glide plane.

glide plane The plane along which a glide symmetry operation occurs.

globular Radiating aggregates of elongate mineral grains or crystals in roughly spherical masses.

gneissic foliation A metamorphic rock foliation defined by alternating layers of lighter- and darker-colored minerals; also called gneissic layering.

good A cleavage-quality term indicating that the cleavage surface reflects light well but

DO NOT COPY e48d507df5d1141@placeholder.9409

Printed by: e48d507df5d1141@placeholder.94092.edu. Printing is for personal, private use only. No part of this book may be reproduced or transmitted without publisher's prior permission. Violators will be prosecuted.

not perfectly because of its slight roughness.

gossan Insoluble iron oxides and hydroxides that accumulate near the surface of a pyrite-bearing ore deposit, produced by interactions with surface waters (supergene processes).

grain boundary The edge of a mineral grain or crystal. Grain boundaries may be crystal faces, fracture surfaces, or cleavage surfaces, or the contact between adjacent grains within a rock.

grain mounts Individual mineral grains placed on a microscope slide with or without immersion oil and a coverslip. Permanent ground mounts are made by casting the grains in epoxy.

granophyric Describes a mineral texture composed of vermicular (wormlike) intergrowths of quartz with feldspar.

granular Describes a texture composed of intergrown grains of equant shape and uniform size.

graphic Describes a mineral texture composed of large alkali feldspar grains with triangular to irregular quartz inclusions.

groundmass Usually, the finer-grained material that surrounds larger grains (phenocrysts) in igneous rocks. Also called the matrix.

gypsum plate A petrographic microscope accessory plate that retards the slow wave by about 147 nm.

hackly Describes the roughness of a fracture surface. Hackly is intermediate between irregular (moderately rough) and splintery (very rough).

half-life The time it takes one-half of the parent atoms to decay to daughter atoms.

halogens Elements in group 17 on the periodic table.

Hanawalt method One method of systematically analyzing a powder X-ray diffraction pattern to identify the mineral that produced the pattern.

hardness A physical property that measures a mineral's resistance to scratching.

heavy minerals Minerals with a specific gravity greater than that of quartz, clay, or the feldspars. Usually refers to the minerals found in clastic sediments.

heft A simple method to estimate the relative specific gravity of two similarly sized samples. Heft is tested by gently shaking the two samples in the hand to get a sense of their relative weights.

Hermann-Mauguin A notation used to list the symmetry of a point group.

hexagonal A unit mesh constructed of hexagons. Also, a crystal system with a unit cell

DO NOT COPY e48d507df5d1141@placeholder.9409

Printed by: e48d507df5d1141@placeholder.94092.edu. Printing is for personal, private use only. No part of this book may be reproduced or transmitted without publisher's prior permission. Violators will be prosecuted.

hexagonal A unit mesh constructed of hexagons. Also, a crystal system with a unit cell that has a 3-fold or 6-fold rotation axis parallel to the *c* axis.

hexagonal Bravais lattice A Bravais lattice with the angle between the *a* and *b* axes equaling 120°.

hexagonal closest packing One way for similar-sized atoms to be packed and bonded together. It is produced by AB stacking of close-packed layers.

high relief Having a large difference in the index of refraction of a grain and a surrounding material. High relief is identified by grains appearing to stand out in three dimensions using plane-polarized light with the petrographic microscope. In this view, grain boundaries and cleavage and fracture surfaces will appear distinctly dark.

high spin Ions with minimum pairing of electrons in the *d* orbitals.

high-eye-point oculars Microscope oculars designed for used with eyeglasses.

high-grade Describes the relatively high pressures and temperatures that a metamorphic rock experienced during metamorphism. Can also refer to ore that is particularly rich in the mineral or element of interest.

hole color center Color that occurs in crystals that have had an electron ejected from an oxygen by high-energy radiation; the missing electron allow the orbital energy levels of the oxygen to absorb some wavelengths of light such that it imparts a color to the mineral.

horizontal dispersion Dispersion produced when the obtuse bisectrix is parallel to the *b* axis.

Huttenlocher A microscopic plagioclase exsolution texture that forms between about An_{65} and An_{85} compositions.

hybrid orbitals Electron orbitals that are a combination of two different orbitals. Most common is the hybridization of $2s$ and $2p$ orbitals to form sp^3 orbitals.

hydrogen bond the atomic bonding found in ice, the bond is produced by the attraction between the negatively and positively charged sides of polar water molecules.

hydrothermal metamorphism Metamorphism produced by the flow of hot aqueous solutions into and through rocks.

hydrothermal systems A system of circulating hot aqueous solutions driven by nearby hot rocks or a magma chamber; can generate large areas of hydrothermally metamorphosed rocks and possibly ore deposits.

hypogene The primary or original ore produced by a hydrothermal system that has subsequently been altered by supergene processes.

DO NOT COPY e48d507df5d1141@placeholder.9409

Printed by: e48d507df5d1141@placeholder.94092.edu. Printing is for personal, private use only. No part of this book may be reproduced or transmitted without publisher's prior permission. Violators will be prosecuted.

idiochromatic Minerals with a coloring produced by the chromophore (color-producing) elements required to be in the mineral.

igneous rock A rock formed by the crystallization and/or solidification of magma (melted rock).

immersion method A method of determining the indices of refraction of a mineral grain by immersion in oils of a variety of known index of refraction and using the Becke line method.

immersion oil Oil that generally has a known index of refraction and is used as part of grain mounts in order to determine the index of refraction of an unknown mineral.

impact melt Melt produced by a meteorite impact. Small masses of glass solidified from such melt are called tektites.

incandescent A material that emits visible light as a consequence of it being heated.

inclined dispersion Dispersion observed in a particular interference figure, produced when the optic normal (*Y*) is parallel to the *b* axis.

inclined extinction Describes a mineral grain being extinct in cross-polarized light and the cleavage or long axis of the grain being at some angle to either north-south or east-west in the image.

inclusion A mineral grain, pocket of melt, or pocket of aqueous fluid found within a larger mineral grain. Generally, inclusions are formed as the larger mineral grows and engulfs the material that becomes the inclusion.

incomplete solid solution series A solid solution series where only a limited range of compositions between the end members is possible.

incongruent melting A rock partially melting and the formed melt having a different composition than of the melting rock. Typically the melt is more felsic (higher in silica) than the melting rock.

indentation hardness A particular type of mineral hardness measured by placing a plunger with a carefully machined tip of diamond or other hard material in contact with a polished mineral surface and applying a constant load.

index mineral A mineral that indicates the relative metamorphic grade of a rock.

index of refraction The ratio of the velocity of light in a vacuum to its velocity in the mineral.

indicatrix dispersion The acute bisectrix being parallel to the *b* axis.

industrial minerals Minerals used by society for their physical or chemical properties.

DO NOT COPY e48d507df5d1141@placeholder.9409

Printed by: e48d507df5d1141@placeholder.94092.edu. Printing is for personal, private use only. No part of this book may be reproduced or transmitted without publisher's prior permission. Violators will be prosecuted.

insulators Materials that do not conduct electricity.

integrated intensity The area of the peak associated with an X-ray diffraction reflection on a diffraction pattern.

interference color chart A chart that displays the interference colors based on birefringence or retardation and sample thickness. See Plate 1. Also known as the Michel-Lévy chart.

interference colors The colors produced by anisotropic minerals in cross-polarized light. They are best viewed with a petrographic microscope.

interference figure The image produced by a petrographic microscope when the auxiliary condensing lens and Bertrand lens are introduced to the optical path.

intergrown Describes grains with interlocking grain boundaries resulting from simultaneous growth.

interlayer In sheet silicates, the space between layers of bonded octahedral and tetrahedral sheets.

intermolecular bonds Atomic bonds produced by asymmetric charge distribution; hydrogen and Van der Waals bonding are specific types.

interstitial defects A type of crystal defect where foreign atoms occupy sites that do not normally exist in the crystal.

interstitial solid solution Solid solution resulting from adding varying amounts of ions into sites that are normally vacant.

inversion symmetry Symmetry where crystal features projected through the crystal's origin have identical features equidistant from the origin on opposite sides of the crystal.

ionic bonding An atomic bond formed by the transfer of an electron from the cation to the anion. The opposite charges of the cation and anion leads to their attraction and bonding.

ionic radius The radius of an ion in a crystal structure if it were to behave like a hard sphere. Effective radius is controlled by valence and coordination number.

iridescence Light reflected from a material that changes color depending on sample orientation.

irregular Describes the roughness of a fracture surface. Irregular is the least rough.

isochromes The pattern of interference colors found in an interference figure. A band of the same color within in this pattern is an isochrome.

isodesmic bonding Bonding where each bond is the same strength.

DO NOT COPY e48d507df5d1141@placeholder.9409

Printed by: e48d507df5d1141@placeholder.94092.edu. Printing is for personal, private use only. No part of this book may be reproduced or transmitted without publisher's prior permission. Violators will be prosecuted.

isograd A line mapped across a metamorphic terrane presumed to be a line of constant metamorphic grade. Typically isograds are mapped as the first appearance of index minerals when moving to higher metamorphic grade. In such cases, isograds should more appropriately be called mineral zone boundaries.

isogyres The dark bands found in interference figures.

isometric A crystal system with a cube-shaped unit cell.

isometric Bravais lattices A Bravais lattice with a cube-shaped unit cell.

isostructural Describes minerals with different composition but the same crystal structure.

isostructural group A group of minerals that are isostructural but are also related chemically by having the same anion or anionic group.

Jolly balance An instrument used to determine the specific gravity of small samples.

joule A unit of energy.

kimberlite An ultramafic igneous rock in which diamond may be found.

labradorescence The iridescence of Ca-rich plagioclase.

lamellae Thin layers. In minerals, lamellae may be produced by exsolution or by polysynthetic twinning.

lamellar Describes rock or mineral texture composed of thin layers.

lanthanide series Elements with atomic numbers of 57–71.

laterite Generic term for any highly weathered material which has experienced significant removal of water-soluble elements, including Si.

lattice node A point within a crystal structure surrounded by identical collection of atoms. Also, the point of intersection between lattice lines.

lattice line Edges of unit cells are constructed of lattice lines; other symmetrically equivalent lines exist within the crystal structure and can be considered to be lattice lines and intersect at lattice nodes.

law of Bravais A law that states that common crystal faces are parallel to lattice planes that have high lattice-node density.

law of constancy of interfacial angles A law that states that the angles between equivalent faces on crystals of the same mineral are the same. Also called Steno's law.

law of Haüy A law that states that crystal faces intercept crystal axes with unit cell

DO NOT COPY

Printed by: e48d507df5d1141@placeholder.94092.edu. Printing is for personal, private use only. No part of this book may be reproduced or transmitted without publisher's prior permission. Violators will be prosecuted.

coordinates of whole numbers.

layer repeat distance The thickness of the package of layers that is repeated in the sheet silicate.

layered mafic intrusion A large mafic body found within continental crust where fractional crystallization results in the formation of distinct layers as sequentially different assemblages of crystals settle on to the magma chamber floor.

length fast The fast ray vibrates approximately parallel to the length of an elongate mineral.

length slow The slow ray vibrates approximately parallel to the length of an elongate mineral.

lever rule A method for determining proportions of phases in equilibrium by analyzing component lengths of tie lines on phase diagrams.

light ray Using the particle theory for light, the path followed by a photon, or the propagation direction of light energy.

line defect A line in a crystal structure where the crystal structure is imperfect and atoms are not properly bonded to neighboring atoms.

linear coordination A cation being bonded to two anions and the three ions being aligned into a line; the polyhedron resulting from 2-fold coordination.

liquidus A line on a phase diagram that represents the composition of the liquid in equilibrium with crystals at a specific temperature.

low relief Having a small difference in the index of refraction of a grain and a surrounding material. Low relief is identified by grains not appearing to stand above or below neighboring material using plane-polarized light with the petrographic microscope. In this view, grain boundaries and cleavage and fracture surfaces are difficult to identify, as they are not distinctly dark.

low spin Describes ions with maximum pairing of electrons in the *d* orbitals.

lower polarizer On a petrographic microscope, the polarizer located in the substage assembly.

low-grade Describes the relatively low pressures and temperatures that a metamorphic rock experienced during metamorphism. Can also refer to ore that is poor in the mineral or element of interest.

luminescence A phenomenon in which a material absorbs one form of energy and then re-emits the energy as visible light.

luster Mineral physical property that is a measure of the amount of light reflected from

DO NOT COPY e48d507df5d1141@placeholder.9409

Printed by: e48d507df5d1141@placeholder.94092.edu. Printing is for personal, private use only. No part of this book may be reproduced or transmitted without publisher's prior permission. Violators will be prosecuted.

luster Mineral physical property that is a measure of the amount of light reflected from the surface of the mineral. A variety of descriptor terms are used to indicate a mineral's luster, including *metallic*, *vitreous*, *dull*, etc.

magma Liquid or molten rock.

magma mingling Occurs when magmas of different composition occur in the same magma chamber but are immiscible, that is, they cannot mix and remain separate.

magma mixing Occurs when magmas of different composition mix and produce a magma with a composition intermediate between the two initials magmas.

magmatic differentiation The changing of a magma composition due to fractional crystallization, magma mixing, and assimilation.

magnetic Attracted to a magnet.

magnetic quantum number One of the four quantum numbers describing the state of an electron. The magnetic quantum number distinguishes among different electron orbitals.

magnetic susceptibility The strength of the magnetism produced by the application of an external magnetic field.

mammillary Describes overlapping colloform masses that have smooth rounded forms.

marl A sedimentary rock with approximately equal proportions of clay and carbonate.

mass number The sum of the number of neutrons and protons in an isotope.

mass spectrometry An analytical technique that determines the abundance of different mass nuclides within a sample. The abundance of different nuclides could be used to determine the chemistry of the sample, the ratio of various specific isotopes from which geologic dates can be determined, or what various geologic processes or conditions might have been (such as past climates).

massive An aggregate of mineral grains without distinctive form or crystal faces. Can also refer to a rock without a foliation.

medium-grade Describes the moderate pressures and temperatures that a metamorphic rock experienced during metamorphism.

melatope In an interference figure, the point where two isogyres cross.

mesodesmic bonding Bonding where the anion-cation bonds take exactly half of the anion charge.

mesoperthite An alkali feldspar texture where lamellae and host are in approximately the same proportion and are not easily distinguished.

DO NOT COPY
e48d507df5d1141@placeholder.9409

Printed by: e48d507df5d1141@placeholder.94092.edu. Printing is for personal, private use only. No part of this book may be reproduced or transmitted without publisher's prior permission. Violators will be prosecuted.

metallic Describes having some property similar to a metal or a material that contains a metal. It could refer to a luster that looks like a metal, a type of bond, a type of ore, etc.

metallic bonding A type of covalent bonding in which the valence electrons are not associated with just two nuclei but are free to move from atom to atom throughout the crystal structure.

metalloids Elements that have properties shared between those of metals and non-metals; most commonly these include B, Si, Ge, As, Sb, and Te.

metamict A mineral grain that is amorphous because radiation from radioactive decay has destroyed the crystal structure.

metamorphic facies A set of minerals commonly found in metamorphosed mafic rocks and partly controlled by the temperature–pressure conditions of metamorphism.

metamorphic reaction A chemical reaction that occurs between minerals and fluids during metamorphism.

metamorphic rock A rock formed by metamorphism, which is the change in a rock's mineralogy and texture due to various conditions of pressure, temperature, and/or the introduction of fluids.

metasomatism The change in bulk composition of a rock during metamorphism due to the introduction of fluids.

metastable Describes the condition of a state being stable despite a lower-energy configuration being possible; ideally the system would change to reach the lower-energy state, but the activation energy needed for that change is not available.

mica plate A petrographic microscope accessory plate that retards the slow wave by about 147 nm.

micaceous Describes a crystal shape that is very flat and thin.

Michel-Lévy chart A chart that displays the interference colors based on birefringence or retardation and sample thickness. Also called the interference color chart. See Plate 1.

Michel-Lévy method A technique that uses the extinction patterns of albite twins to determine plagioclase composition.

microperthite An exsolved alkali feldspar where the albite lamellae cannot be seen in hand sample but can be seen with a petrographic microscope.

Miller index A three-digit notation that allows individual crystal faces and crystallographic planes and directions to be identified and described numerically.

Miller-Bravais index A four-digit notation that allows crystallographic planes and directions to be identified and described numerically for the hexagonal crystal system.

DO NOT COPY

Printed by: e48d507df5d1141@placeholder.94092.edu. Printing is for personal, private use only. No part of this book may be reproduced or transmitted without publisher's prior permission. Violators will be prosecuted.

directions to be identified and described numerically for the hexagonal crystal system.

mineral A naturally occurring crystalline solid.

mineral assemblage All the minerals in a rock; usually it is used in reference to metamorphic rocks.

mineral grain An individual crystal of a mineral, regardless of the nature of the external surfaces of the crystal.

mineral group A set of minerals with the same basic structure but different compositions.

mineral series Two or more minerals among which there is a range of chemical compositions related by solid solution.

mineral species A specific composition and crystal structure for a mineral.

mineral variety A mineral with an identified specific set of physical properties that are variable for that mineral, including color, habit, or other properties.

mineral zone A region of metamorphic rock with the same set of index minerals.

mineral zone boundary A line that separates metamorphic rocks with one set of index minerals from rocks with a different set of index minerals.

mineraloid Mineral-like materials that lack crystalline structure.

mining The extraction of material from the Earth that will be processed to extract resources needed for society.

modal mineralogy The volume percent of each mineral in a rock.

moderate relief Intermediate between high relief and low relief.

Mohs scale of hardness A 1–10 scale of hardness with 1 being soft and 10 being hard; common minerals are assigned to each number as a reference material.

molecular bonds Atomic bonds produced by asymmetric charge distribution; hydrogen and Van der Waals bonding are specific types.

monochromatic light Light of a single wavelength or color.

monoclinic A crystal system with a unit cell that has only either a 2-fold rotation axis, or a single mirror, or both.

monoclinic Bravais lattices A Bravais lattice where the angle between the *a* and *c* axes is not 90°.

mortar A building material used to bind brick and rocks together. It is often made from portland cement, which is produced by the calcination of a calcite-bearing rock, typically

DO NOT COPY e48d507df5d1141@placeholder.9409

Printed by: e48d507df5d1141@placeholder.94092.edu. Printing is for personal, private use only. No part of this book may be reproduced or transmitted without publisher's prior permission. Violators will be prosecuted.

portland cement, which is produced by the calcination of a calcite-bearing rock, typically with shale.

mud rock A generic term for all sedimentary rocks composed of over 75% mud-sized particles, including silt- and clay-sized particles.

mudstone A sedimentary rock that does not split easily into layers and is composed of over 75% mud-sized particles, including silt- and clay-sized particles.

multiple twins Three or more segments repeated by the same twin law.

myrmekite Mineral texture composed of vermicular (wormlike) intergrowth quartz in sodic plagioclase.

naturally occurring Formed by natural processes without human intervention.

negative elongation The fast ray vibrates approximately parallel to the length of an elongate mineral.

negative relief The relief resulting from a mineral having an index of refraction lower than that of the surrounding material.

neutron A subatomic particle with no charge found in the nuclei of atoms.

Nicols A lens that polarizes the light that travels through it or restricts the light to vibrate in a single plane.

no extinction angle An equant mineral grain without visible cleavage is said to have no extinction angle.

noble gases Elements in group 18 on the periodic table.

noble-gas core The inner-shell electron configuration of an element that is identical to the electron configuration of a noble gas.

non-crystalline Describes a material with atoms that lack long-range atomic order or a crystalline structure. Also called amorphous.

nonmetallic A large group of luster descriptors encompassing all lusters that do not look like metal. Also describes a mineral that does not look like metal.

nonmetal Elements that are not metal-like, including H, C, N, O, P, S, and Se, plus the halogens and noble gases.

nonuniform bond strength Strength of anion-cation bonding that is variable throughout a crystal structure.

normative mineralogy The collection of minerals that could possibly be created from the bulk chemistry, given certain assumptions concerning distribution of elements among the minerals.

DO NOT COPY

Printed by: e48d507df5d1141@placeholder.94092.edu. Printing is for personal, private use only. No part of this book may be reproduced or transmitted without publisher's prior permission. Violators will be prosecuted.

nuclei The nucleus of an atom.

numerical aperture A measure of the size of the cone of light that an objective lens of a petrographic microscope can accommodate.

objective lens The lens of a petrographic microscope that provides the primary magnification and is located directly above the thin section sample.

oblique Describes a plane lattice and unit mesh where the lengths of the two sides are unequal and the angles between the sides are not 90°.

obsidian A mineraloid formed from the quick cooling of magma or lava.

obtuse bisectrix The axis (either Z or X) that bisects the obtuse angle between the optic axes.

octahedral coordination Six-fold coordination that results in an octahedral coordinating polyhedron.

ocular The eyepiece or the lens that a microscope user looks through to see the sample image.

off-center figure An interference figure where the melatope is not in the center of the image.

off-center optic axis figure An interference figure where the melatope is visible but not in the center of the image.

omission solid solution A solid solution controlled by the addition of a cation of higher charge with a vacancy.

ON Abbreviation for optic normal, which is the axis perpendicular to the optic plane.

one-wavelength plate A petrographic microscope accessory plate that retards the slow wave by either 537 or 550 nm.

oolitic Describes roughly spherical mineral grains of a few millimeters in diameter formed of concentric layers.

opaque Describes a material that does not transmit light.

open form A crystal form that is not completely enclosed.

ophiolites A complete package of ocean sediments, oceanic crust, and the underlying mantle that has been thrust onto continental crust during convergent plate tectonics.

optic axis A direction within anisotropic materials where light is not split into two rays.

optic axis dispersion Variation in the size of the $2V$ angle.

DO NOT COPY e48d507df5d1141@placeholder.9409

Printed by: e48d507df5d1141@placeholder.94092.edu. Printing is for personal, private use only. No part of this book may be reproduced or transmitted without publisher's prior permission. Violators will be prosecuted.

optic normal The axis perpendicular to the optic plane.

optic normal interference figure An interference figure produced when the grain is oriented with an optic axis parallel to the microscope stage.

optic orientation The angular relationship between the indicatrix axes and crystal axes.

optic plane The plane that contains both optic axes.

optic sign Describes the shape of the indicatrix.

optical character Describes whether a mineral is optically uniaxial or biaxial and its optic sign.

optical indicatrix A geometric figure that shows the index of refraction and vibration direction for light passing in any direction through a material.

optically anisotropic Describes light behaving differently depending on its direction through the material, which results in interference colors and other optical phenomena.

optically biaxial Two optic axes exist.

optically isotropic Light behaves the same in all direction through the material, and thus no light is transmitted in cross-polarized light.

optically negative For uniaxial minerals, n_ϵ is less than n_ω and thus the extraordinary rays are fast rays; for biaxial minerals, the acute bisectrix is the Z axis.

optically neutral For biaxial minerals, the mineral is optically neither positive nor negative.

optically positive For uniaxial minerals, n_ϵ is greater than n_ω and the extraordinary rays are slow rays; for biaxial minerals, the acute bisectrix is the X axis.

optically uniaxial Only one optic axis exists.

orbitals Regions around an atom's nucleus where the electrons reside.

Orders refers to separating a continuum into hierarchy or repeating similar pattern.

order-disorder polymorphism Polymorphism controlled by differences in the cation distribution within different structural sites, which results in minor changes to the crystal structure.

ordinary ray The light ray that travels through an anisotropic material with a parallel ray path and wave normal.

ore Any material extracted from the Earth that can be processed to obtain a specific mineral and/or metal of value.

DO NOT COPY e48d507df5d1141@placeholder.9409

Printed by: e48d507df5d1141@placeholder.94092.edu. Printing is for personal, private use only. No part of this book may be reproduced or transmitted without publisher's prior permission. Violators will be prosecuted.

oriented sample A rock or mineral sample that has been marked with registration lines that allow the sample to be reoriented exactly as it was where collected.

origin The intersection of crystal axes.

orthorhombic Describes a crystal system with a unit cell having either three 2-fold rotation axes or two mirrors and a 2-fold rotation axis.

orthorhombic Bravais lattices A Bravais lattice where the angles between all crystal axes are 90° and none of the lengths of the axes are equal.

orthoscopic illumination Light where all rays are ideally parallel.

orthosilicates Silicate minerals where the silicon tetrahedrons are isolated and not linked with any other silicon tetrahedrons.

oxidation state The charge of an ion.

packing index A measure of how tightly the atoms are arranged in a crystal structure. It uses the ratio of the total volume of the atoms in the unit cell based on their ionic radii to the volume of the unit cell.

parallel dispersion Dispersion produced when the obtuse bisectrix is parallel to the *b* axis.

parallel extinction A mineral grain being extinct in cross-polarized light and the cleavage or long axis of the grain being either north-south or east-west in the image.

paramagnetism The property of minerals that are not noticeably attracted to a handheld magnet but become weakly magnetic when placed in a strong magnetic field.

paramorph A pseudomorph where the replacing mineral is a polymorph of the replaced mineral.

parent A radioactive element or isotope. Parents break down to daughter atoms upon radioactive decay.

partial melting Refers to most rocks only melting partially when melted.

parting A physical property where minerals can break along regular flat planes that are not controlled by planes of weak bonds (as they are for cleavage); the parting is caused by twinning or exsolution lamellae, if present.

Pauli exclusion principle The principle that no two electrons in an atom can have the same four quantum numbers.

Pauling's rules Five guidelines that explain details regarding crystal structures.

peak Signal detected by an analytical instrument that stands above the background.

DO NOT COPY e48d507df5d1141@placeholder.9409

Printed by: e48d507df5d1141@placeholder.94092.edu. Printing is for personal, private use only. No part of this book may be reproduced or transmitted without publisher's prior permission. Violators will be prosecuted.

peak Signal detected by an analytical instrument that stands above the background.

peak height intensity In a powder diffraction pattern or a characteristic X-ray spectrum, the height of any peaks above background, usually in counts per second.

peak metamorphic conditions The highest-grade conditions recorded by a metamorphic rock, which is typically the highest temperature conditions.

peak overlap In a powder diffraction pattern or a characteristic X-ray spectrum, the overlap of the approximately bell-shaped normal curves that make up each peak in the spectrum. That is, X-ray intensity does not return to background before the next peak is encountered along the spectrum.

peak pressure The highest pressure conditions, corresponding to the greatest depth a metamorphic rock experienced during its metamorphic history.

peak temperature The highest temperature conditions a metamorphic rock experienced during its metamorphic history.

pedion A crystal form of a single crystal face with no geometrically equivalent face elsewhere on the crystal

pelite A metamorphic rock with a mud rock protolith.

penetration twins Twin segments that appear to be intergrown.

perfect A cleavage-quality term indicating that the cleavage surface reflects light perfectly because is it very flat and smooth.

pericline twinning Twinning in the feldspars that occurs by rotation along the *b* axis.

periodic table An arrangement of the elements based on atomic number and electron configuration.

peristerite A microscopic plagioclase exsolution texture that forms between about An_2 and An_{17} compositions.

perthite An alkali feldspar that has exsolved such that it is composed of albite lamellae with a K-feldspar host.

perthitic texture The texture of perthite, which is an alkali feldspar that has exsolved such that it is composed of albite lamellae with a K-feldspar host.

petrographic microscope A microscope that uses polarizing light transmitted through rock and mineral samples such that their optical properties and textures can be studied. Typical samples are 30 microns thick and are mounted on a microscope slide called a thin section.

phase A physically separable material in a system; phases include different minerals, fluids such as melt or aqueous fluids, plus gases and glasses.

DO NOT COPY
e48d507df5d1141@placeholder.9409

Printed by: e48d507df5d1141@placeholder.94092.edu. Printing is for personal, private use only. No part of this book may be reproduced or transmitted without publisher's prior permission. Violators will be prosecuted.

fluids such as melt or aqueous fluids, plus gases and glasses.

phase diagrams A diagram that displays which phase(s) represents the lowest energy configuration for a given set of conditions.

phenocryst A distinctly large grain in an igneous rock.

phosphorescence Light produced by a material of a wavelength different than the incident electromagnetic radiation causing the light production. Phosphorescence continues for some period of time following removal of the electromagnetic radiation that causes the light production.

photograph An important type of pictorial data collected when doing field work.

photoluminescence Light emitted by a material in response to being exposed to visible or ultraviolet light.

photon The elementary particle that makes up light rays.

phyllosilicate The silicate minerals where silicon tetrahedrons are bonded together in such a way as to result in sheets of silicon tetrahedrons within the crystal structure. Same as sheet silicate.

physical properties Measurable properties of minerals that can be used to identify a sample. These include habit, color, luster, streak, hardness, specific gravity, cleavage, fracture, etc.

physical weathering Rock and mineral weathering caused by breaking or grinding of the rock and mineral grains.

pi bond A type of chemical bond where electrons are shared laterally across $2p_z$ orbitals.

piezoelectric Describes the property of generating a voltage when deformed.

pinacoid Crystal form of two parallel faces on opposite sides of the crystal related by inversion or a mirror.

pisolitic Describes roughly spherical mineral grains of about a centimeter in diameter formed of concentric layers.

placer deposit An ore deposit of high concentration of a dense mineral in clastic sediments and sedimentary rocks formed through the selective transport and deposition of sediment.

planar defect A mismatch of the crystal structure across a surface; includes grain boundaries, stacking faults, and antiphase domain boundaries.

plane lattice A series of nodes produced by repeating and translating the nodes along two different vectors.

DO NOT COPY e48d507df5d1141@placeholder.94092

Printed by: e48d507df5d1141@placeholder.94092.edu. Printing is for personal, private use only. No part of this book may be reproduced or transmitted without publisher's prior permission. Violators will be prosecuted.

plane light Only plane-polarized light from the lower polarizer being used to form the image viewed on a petrographic microscope.

plane polarized Light is polarized by a single polarizer; see **plane light**.

platy A crystal shape that approximates that of a plate.

play of color Light reflected from a material that changes color depending on sample orientation, also called **iridescence**.

pleochroic Describes a mineral that changes color in plane-polarized light with rotation under the petrographic microscope.

pleochroic halos A halo of disrupted crystal structure around an inclusion or neighboring grain containing radioactive elements. The halo may appear discolored or pleochroic in plane light. Also called radiohalos or radiation damage halos.

plumose Radiating aggregate of platy or micaceous minerals.

poikilitic An igneous rock texture where relatively large crystals (oikocrysts) have abundant inclusions of associated minerals.

point defects Crystal defects consisting of vacant sites, atoms out of their correct position, extraneous atoms, or substituted atoms.

point group One of 32 different complete three-dimensional combinations of symmetry for a crystal or crystal structure.

point symmetry The symmetry of a pattern with respect to a point—all symmetry operations must extent through that point.

polarizer A lens that polarizes the light that travels through it or restricts the light to vibrate in a single plane.

polarizing film A thin layer that polarizes light.

polarizing light microscope A microscope that uses polarizing light to image the sample.

polymerize To repeatedly bond together a chemical unit to form a more complex chemical structure.

polychromatic light Light that consists of more than one wavelength.

polymorphic forms Different structures of a given chemical compound.

polymorphic group A set of different minerals with different structures that have same chemical composition.

polymorphism The ability of a chemical compound to form more than one structure.

DO NOT COPY e48d507df5d1141@placeholder.94092

Printed by: e48d507df5d1141@placeholder.94092.edu. Printing is for personal, private use only. No part of this book may be reproduced or transmitted without publisher's prior permission. Violators will be prosecuted.

polymorphism The ability of a chemical compound to form more than one structure.

polymorphs Different structures of a given chemical compound.

polysynthetic twins Repeated twins of the same twin law on parallel composition planes; often this results in thin, sheetlike twin segments.

polytypism The ability of layered silicates to have different layer stacking patterns.

poor A cleavage-quality term indicating that the cleavage surface is very rough and does not reflect light well.

porphyritic Describes igneous rock where two distinct grain sizes are present, including large, often euhedral grains called phenocrysts, which are surrounded by a finer-grained groundmass or matrix.

porphyroblast A relatively large, metamorphically grown grain in a metamorphic rock.

portland cement An important ingredient in building materials such as mortar and concrete. It is produced by the calcination of a calcite-bearing rock, typically with shale.

positive elongation The slow ray vibrates approximately parallel to the length of an elongate mineral.

positive relief The relief resulting from a mineral having an index of refraction higher than that of the surrounding material.

positron decay Radioactive decay where a proton in an unstable atom breaks down into a neutron and a positron and a neutrino; the latter are ejected from the atom.

potash A general name for any K-bearing, water-soluble materials; generally used as a fertilizer.

powder diffraction file A compilation by the International Centre for Diffraction Data of X-ray diffraction data.

powder X-ray diffraction A technique that obtains X-ray diffraction patterns using powdered samples.

primitive A type of unit mesh or unit cell with nodes only at its corners.

principal indices of refraction For biaxial materials, the three indices of refraction needed to define the indicatrix; generally they are identified by n_α, n_β, and n_γ and include the fastest and slowest axes.

principal quantum number (n) An integer that denotes the shell within which an electron resides within an atom.

Principal sections planes through the optical indicatrix that include two of the principal indices of refraction.

DO NOT COPY e48d507df5d1141@placeholder.94092

Printed by: e48d507df5d1141@placeholder.94092.edu. Printing is for personal, private use only. No part of this book may be reproduced or transmitted without publisher's prior permission. Violators will be prosecuted.

prism (O) A crystal form consisting of a collection of 3, 4, 6, 8, or 12 faces that intersects in a set of mutually parallel edges forming a tube.

prismatic Describes a crystal form or a crystal that is dominated by prism crystal faces. Can also describe cleavages that are parallel to the prism crystal form.

products In a chemical reaction, the phases produced by the reaction.

prograde metamorphism The metamorphic changes that occur during the prograde metamorphic path, where pressure and temperature are both increasing.

prograde path The part of the metamorphic history of a rock where pressure and temperature are both increasing.

protolith What a metamorphic rock once was prior to metamorphism; sometimes called the parent rock.

proton A subatomic particle with a positive charge found in the nuclei of atoms.

provenance The source of sediment for a clastic sedimentary rock.

psammite A metamorphic rock with a protolith intermediate between sandstone and mudstone.

pseudomorphism One mineral being replaced by one or more minerals that retain the external form of the original mineral.

pseudo-noble-gas core An electron configuration that consists of a noble gas core plus an entirely filled *d* and/or *f* subshell.

pseudotachylite A glass produced by frictional melting along a fault zone.

pycnometer A small flask fitted with a stopper that contains a fine hole, used for determining the specific gravity of small samples.

pyramid A crystal form consisting of a collection of 3, 4, 6, 8, or 12 non-parallel faces that intersect at a point.

pyroelectric Describes the property of a material where a change in temperature causes displacement of positive and negative charges and the development of a voltage.

qualitative analysis Chemical analysis that determines the presence or absence of particular elements.

quantitative analysis Chemical analysis that determines the precise abundance of particular elements.

quarter-wave A petrographic microscope accessory plate that retards the slow wave by about 147 nm.

DO NOT COPY
e48d507df5d1141@placeholder.9409

Printed by: e48d507df5d1141@placeholder.94092.edu. Printing is for personal, private use only. No part of this book may be reproduced or transmitted without publisher's prior permission. Violators will be prosecuted.

about 147 nm.

quarter-wavelength plate A petrographic microscope accessory plate that retards the slow wave by about 147 nm.

quartz wedge A petrographic microscope accessory plate that consists of a wedge-shaped piece of quartz.

quartz-sensitive tint A petrographic microscope accessory plate that retards the slow wave by either 537 or 550 nm.

quasicrystals Materials with an ordered structure that have rotational symmetry but lack translational symmetry.

quenching Rapidly cooling a material such that the high-temperature form is retained and does not change to the form expected for lower temperatures (or pressures).

quicklime Calcium oxide (CaO), typically formed by calcination of Ca-bearing minerals; it is used in mortar and other building materials.

radiating Describes a crystal habit where elongate minerals angle outward from a central point.

radiocarbon dating A radiometric dating technique that uses the radioactive decay of ^{14}C to determine geologic time. It generally can be applied only to carbon-bearing materials less than 50,000 years old. It is also called ^{14}C radiometric dating.

radiometric dating A geochronology technique that uses radioactive isotope decay to determine the timing of a geologic event.

radius ratio The cation radius divided by the anion radius.

rapakivi A feldspar texture found in igneous rocks consisting of grains with alkali feldspar cores and sodic plagioclase rims.

rare earth elements Y, Sc, and the lanthanide series of elements (La through Lu).

reactants In a chemical reaction, the phases required for a chemical reaction to occur.

reconstructive polymorphism Polymorphism where the crystal structures have a different bonding arrangement.

recrystallization A process that occurs during metamorphism where grains of a mineral already present in the rock change their shape or composition (if possible) or break down to create new grains of the same mineral.

rectangle Specific unit mesh shaped like a rectangle.

REE Abbreviation for “rare earth element(s).”

DO NOT COPY
e48d507df5d1141@placeholder.94092

Printed by: e48d507df5d1141@placeholder.94092.edu. Printing is for personal, private use only. No part of this book may be reproduced or transmitted without publisher's prior permission. Violators will be prosecuted.

reflected Describes a light ray interacting with a surface when the angle of incidence is equal to the angle of reflection.

reflection A symmetry operation where the pattern on one side of a line or a plane is a mirror image of the pattern on the other.

refracted Describes a light ray passing through the boundary between materials that is bent based on the index of refraction of the two materials as described by Snell's law.

refractometry Any method that allows measurement of the indices of refraction.

refractory Describes a material with a very high melting point.

regional metamorphism Metamorphism of large volumes of rocks that usually occurs in orogenic belts.

relief The degree to which a material appears to stand out in three dimensions relative to surrounding materials when using plane-polarized light with the petrographic microscope.

remnant magnetism The magnetism of a rock that is representative of the Earth's magnetic field at the time the rock formed.

reniform Describes a kidney-shaped crystal habit of a colloform mass.

retardation The amount the slow wave is behind or out of phase with the fast ray, usually reported in nanometers.

reticle markings Markings in ocular lenses that indicate orientation or scale.

reticulated Describes a crystal habit of intergrown crystals in an open framework.

retrograde metamorphism The metamorphic changes that occur during the retrograde metamorphic path, where pressure and temperature are both decreasing.

retrograde path The part of the metamorphic history of a rock where pressure and temperature are both decreasing.

rhombohedral carbonate Any carbonate mineral in the trigonal division of the hexagonal crystal system. This includes the calcite and dolomite groups.

rhombohedron A crystal form consisting of six faces, each of which is rhomb-shaped.

rim The outer portion of a mineral grain.

ring silicates The silicate minerals where two oxygens of the silicon tetrahedrons are shared between two other silicon tetrahedrons, forming a ring shape.

rock A naturally occurring solid cohesive aggregate of mineral grains and/or mineraloids.

DO NOT COPY e48d507df5d1141@placeholder.9409

Printed by: e48d507df5d1141@placeholder.94092.edu. Printing is for personal, private use only. No part of this book may be reproduced or transmitted without publisher's prior permission. Violators will be prosecuted.

rock cycle A description of the processes involved in changing one rock type (igneous, sedimentary, or metamorphic) into the same or another rock type.

rotation Symmetry operation where a motif is exactly repeated by a specific angle about an axis.

rotoinversion A compound symmetry operation that involves both rotation and inversion.

rotoinversion axis The line along which a rotoinversion symmetry operation occurs.

sample A portion of material used for study of that material.

scalenohedron A crystal form consisting of 8 or 12 faces, each of which is a scalene triangle.

scaly Describes a crystal habit where the grain shape is flat and thin.

scanning electron microscope An electron-beam instrument used to image and qualitatively or semi-quantitatively chemically analyze minerals or other materials.

schiller Same as iridescence, which is light reflected from a material that changes color depending on sample orientation, or chatoyance, which is when a material reflects light in a way similar to a cat's eye.

schistosity Foliation produced by alignment of inequant minerals.

Schottky defect A vacancy defect in a crystal structure.

screw A compound symmetry operation that involves translation and rotation.

screw axis An axis about which rotation and translation symmetry occurs.

screw dislocation A dislocation with a Burgers vector that is parallel to the dislocation line.

secondary electrons Electrons dislodged from a sample atom's orbitals by an electron beam.

second-order reflection Reflection in an X-ray diffraction pattern where the integer n in the Bragg equation is 2.

sediment The weathered remains of rocks.

sedimentary rock A rock composed of sediment.

SEM Abbreviation for "scanning electron microscope."

semiconductor A material with a small band gap between the valence band and conduction band.

DO NOT COPY
e48d507df5d1141@placeholder.9409

Printed by: e48d507df5d1141@placeholder.94092.edu. Printing is for personal, private use only. No part of this book may be reproduced or transmitted without publisher's prior permission. Violators will be prosecuted.

semi-quantitative Describes chemical analysis that determines the abundance of particular elements, but the precision of the analysis is not good.

shale A sedimentary rock that is composed of dominantly clay-sized grains and is fissile, or breaks easily approximately parallel to bedding.

sheet silicates The silicate minerals where three oxygens of the silicon tetrahedrons are shared with three other silicon tetrahedrons, which all align in a plane, resulting in a sheet.

shells Different electron orbitals (*K*, *L*, *M*, *N*, ...).

sigma bonds Covalent bonds formed by aligned overlap of sp^3 hybrid orbitals.

sign of elongation The relative orientation of the fast and slow rays relative to the long axis of a mineral grain. Can be described as length fast, where the fast ray vibrates approximately parallel to the length of an elongate mineral, or length slow, where the slow ray vibrates approximately parallel to the length of an elongate mineral.

silicon tetrahedron A tetrahedron polyhedron resulting from a silicon cation bonded to four oxygen anions.

siltstone A sedimentary rock composed dominantly of silt-sized sediment.

simple substitution solid solution Solid solution resulting from substituting cations with identical charges.

simple twins A twin composed of just two twin segments.

single-crystal X-ray diffraction A technique that obtains X-ray diffraction patterns using a sample composed of a single crystal.

skeletal Describes a crystal habit where crystals have both euhedral faces and voids.

sketch A line drawing that highlights important observations, often created when doing field work and recorded in a field notebook.

slaty cleavage Schistosity where the grain size is too small to be seen.

slip system The crystallographic plane and slip direction along which dislocations move.

slow ray For anisotropic minerals, the refracted ray of light with a higher index of refraction and slower velocity.

smell A mineral physical property that is the smell of the mineral.

Snell's law A law that describes the amount a light ray is bent when it passes from one material to another; mathematically it is the ratio of the sine of the angle of incidence to the sine of the angle of refraction, which is equal to the ratio of the index of refraction of

DO NOT COPY e48d507df5d1141@placeholder.9409

Printed by: e48d507df5d1141@placeholder.94092.edu. Printing is for personal, private use only. No part of this book may be reproduced or transmitted without publisher's prior permission. Violators will be prosecuted.

the second material to the index of refraction of the first material.

solid solution Mineral compositional variation due to more than one element being found within specific crystal structural sites.

solid solution series The range of compositions produced by solid solution in a given mineral.

solidus A line on a phase diagram that represents the composition of the solid in equilibrium with melt at a specific temperature.

solute A material that dissolves within a liquid solvent.

solvent A liquid material within which a solute dissolves.

solvus A line on a phase diagram that defines the temperature–pressure field where two separate minerals represent the lowest-energy configuration rather than a single homogeneous solid.

space group A crystal structure symmetry defined by the combination of point symmetry and translational symmetry.

space lattice The three-dimensional lattice created by node repetition in three dimensions.

specific gravity The density of a material divided by the density of water at 4°C.

sphenoid A crystal form of two nonparallel faces where the two faces are related by a 2-fold rotation axis.

spherulite A sphere-shaped radiating mass of crystals produced by glass devitrification.

spin quantum number The quantum number that distinguishes between different electrons within the same orbital; possible values are $+\frac{1}{2}$ and $-\frac{1}{2}$.

spin state The amount of pairing of electrons in the *d* orbitals for an ion.

splendent Describes metallic luster, where more than about 50% of the light is reflected from a mineral.

splintery Describes a very rough fracture surface.

spongy Describes a rounded intergrowth pattern.

square Unit mesh with a square shape.

stability The relative degree to which a system may spontaneously change to a new configuration. Stable configurations have low energy.

stable mineral assemblage The collection of minerals in a rock whose aggregate free

DO NOT COPY e48d507df5d1141@placeholder.9409

Printed by: e48d507df5d1141@placeholder.94092.edu. Printing is for personal, private use only. No part of this book may be reproduced or transmitted without publisher's prior permission. Violators will be prosecuted.

stable mineral assemblage The collection of minerals in a rock whose aggregate has energy of formation is the lowest of all the possible mineral combinations that might be made from the chemical elements in the rock for a particular pressure and temperature condition.

stacking faults Planar defect in a crystal where a layered mineral structure contains a layer that is out of sequence or position.

stage The part of an instrument where a sample is placed for study.

stage goniometer The component of a stage that allows the stage angle to be determined.

stage micrometer A microscope slide on which a millimeter scale has been etched; allows scale calibration of ocular reticles.

standard A material with known characteristics or chemistry, etc. used to calibrate analytical instruments.

Steno's law A law that states that the angles between equivalent faces on crystals of the same mineral are the same. Also called the **law of constancy of interfacial angles**.

streak A mineral physical property that constitutes the color of a powdered sample; sample powdering is most commonly done by rubbing the sample on a streak plate.

streak plate An unglazed white porcelain tile used to determine a mineral's streak.

stress Force per area applied to an object.

stromatolites Fine laminations in limestone, typically in dome shapes, generated by microbial mats of cyanobacteria.

structure Usually refers to the crystal structure, which is the particular repeating arrangement of atoms within a crystalline material.

stubby Describes the crystal habit of a grain shape that is short and wide.

subhedral Describes a mineral grain that displays some well-formed crystal faces.

submetallic Describes luster of a mineral that reflects light well but somewhat less than that needed to be called metallic luster.

subshells Different orbitals within an electron shell; subshells are typically identified by *s*, *p*, *d*, etc.

substitution defect An ion that substitutes for one of the normally present ions in the ideal or pure crystal structure.

substitution solid solution Solid solution due to interchanging one cation for another in a structural site.

DO NOT COPY e48d507df5d1141@placeholder.9409

Printed by: e48d507df5d1141@placeholder.94092.edu. Printing is for personal, private use only. No part of this book may be reproduced or transmitted without publisher's prior permission. Violators will be prosecuted.

supergene enrichment Zones of enriched ore created by supergene processes.

supergene The area that has been affected by supergene processes, also can be used as a modifying term to indicate that the origin of something is by supergene processes.

symmetrical extinction The extinction angles (EA_1 and EA_2) as measured from the two cleavages or crystal faces to the same vibration direction being the same.

symmetry symbols Symbols used to indicate symmetry operations.

symplectite A texture that is composed of wormlike intergrowths of two or more minerals.

synthetic mineral A human-made material that otherwise fits the definition of a mineral.

tabular A crystal shape that approximates the shape of a book or tabletop.

taste A mineral physical property that is the taste of the mineral.

tektite Small mass of glass created by a meteorite impact.

TEM Abbreviation for "transmission electron microscope."

tenacity A mineral physical property that refers to the behavior of minerals when deformed or broken. Terms used to describe a mineral's tenacity include *brittle*, *malleable*, *elastic*, etc.

tetragonal A crystal system with a unit cell with a single 4-fold rotation or rotoinversion axis.

tetragonal Bravais lattices A Bravais lattice where the angles between all crystal axes are 90° and two of the lengths of the axes are equal.

tetrahedral coordination -fold coordination that results in a tetrahedron coordinating polyhedron.

tetrahedron A crystal form consisting of four triangular faces.

texture The pattern that mineral grains make. Textural terms may describe a rock's grain size, alignment, and so on; the size or shape of individual mineral grains; or how two mineral are intergrown.

thermochronology Radiometric dating techniques that provide the timing of cooling.

thermoluminescent A material that emits visible light as a consequence of it being heated. Also called **incandescent**.

thin section A thin slice, typically 30 microns thick, of rock or mineral mounted on a microscope slide. They are initially studied with a petrographic microscope, but they may

DO NOT COPY e48d507df5d1141@placeholder.9409

Printed by: e48d507df5d1141@placeholder.94092.edu. Printing is for personal, private use only. No part of this book may be reproduced or transmitted without publisher's prior permission. Violators will be prosecuted.

serve as the sample for analysis by other instrumentation as well.

third-order reflection Reflection in an X-ray diffraction pattern where the integer n in the Bragg equation is 3.

tie-line A line on a phase diagram that connects two phases in equilibrium.

total internal reflection A light ray being completely reflected by the boundary between two materials because of the particular angle of incidence and the index of refraction of each material.

T-P loop The complete history of changes in temperature (T) and pressure (P) for a metamorphic rock during one metamorphic event.

transition metals Metals in groups 3 through 12 on the periodic table.

translational symmetry The symmetry created by repeating a node or motif along a vector of fixed length and direction.

transmission electron microscope An electron-beam instrument that transmits the beam through an ultra-thin sample. It can be used to determine crystal structure of materials.

transparent Describes the optical property of a material where objects viewed through the material are clearly seen.

trapezohedron A crystal form consisting of 6, 8, or 12 faces, each of which is a trapezoid.

triangular coordination A cation being bonded to three anions forming a triangle.

triboluminescence Having the property of giving light off when struck, crushed, scratched, or rubbed.

triclinic A crystal system with a unit cell with 1-fold rotation with or without inversion.

triclinic Bravais lattice A Bravais lattice where the angles between all crystal axes are different and not 90°, and no axes lengths are equal.

trioctahedral Describes an octahedral sheet of metal cations between two OH^- layers where all of the octahedral sites are occupied by metal cations.

twin law The detailed description of the relationship of the crystal orientation across a twin composition plane.

twin operation A specific symmetry operation, including reflection, rotation, and inversion, that produces a twin.

twinning The symmetrical intergrowth, or intertwining, of two or more crystal segments of the same mineral

DO NOT COPY

Printed by: e48d507df5d1141@placeholder.94092.edu. Printing is for personal, private use only. No part of this book may be reproduced or transmitted without publisher's prior permission. Violators will be prosecuted.

of the same mineral.

type sample A sample of something that is the first described example of that specific thing.

undulatory extinction A mineral grain exhibiting extinction in an irregular or wavy pattern because of a bent, twisted, or strained crystal structure.

undulose extinction A mineral grain exhibiting extinction in an irregular or wavy pattern because of a bent, twisted, or strained crystal structure.

uniaxial Having one optic axis. Tetragonal and hexagonal crystal system minerals are uniaxial.

unit cell For a Bravais lattice, the volume outlined by lattice nodes that is stacked repeatedly via only translation to create the entire crystal lattice. Within the unit cell is the smallest collection of bonded atoms that retains all the properties of the mineral.

unit face The crystal face that intercepts the crystal axes at values equal to one unit cell; therefore, the (111) crystal face.

unit mesh The two-dimensional shape produced by simple translation of a node using two vectors. Repetition of the unit mesh in two dimensions generals a plane lattice.

unit mesh axes The vectors that make up the edges of a unit mesh.

U-Pb radiometric dating A geochronology technique that uses the breakdown of ^{238}U and ^{235}U to ^{206}Pb and ^{207}Pb, respectively, to determine the timing of a geologic event.

(U-Th)/He radiometric dating A radiometric dating technique that uses the radioactive decay of U and Th into He to determine geologic time. It can be applied to any U- and Th-bearing mineral and generally is best at constraining the timing that a mineral last cooled to below about 200°C or lower, depending on the mineral.

upper polarizer The polarizer of a petrographic microscope located between the objective lens and the oculars.

valence The charge of an ion.

valence band The outermost orbitals occupied by electrons if the atom is in the ground state.

valence electrons Electrons within subshells that are not entirely filled.

Van der Waals bonding Bonding resulting from asymmetrical charge distribution.

velocity Distance per time.

vernier A particular type of scale that allows very precise measurements of distance or angle.

DO NOT COPY e48d507df5d1141@placeholder.9409

Printed by: e48d507df5d1141@placeholder.94092.edu. Printing is for personal, private use only. No part of this book may be reproduced or transmitted without publisher's prior permission. Violators will be prosecuted.

angle.

Vickers hardness A particular type of indentation hardness that uses a pyramid-shaped indenter with a square cross section.

wackes Sandstones with 15–75% matrix.

wave front A surface that connects the same points on adjacent waves.

wave normal The line perpendicular to the wave front.

wavelength The distance between neighboring peaks (or troughs) of a wave.

wavelength-dispersive X-ray spectrometer A device that separates characteristic X-rays based on their wavelength and detects each of their intensities (typically in counts per second—cps) to allow precise quantitative chemical analysis of a sample. They are found in, for example, X-ray fluorescence spectrometers and electron microprobes.

WDS Abbreviation for "wavelength-dispersive X-ray spectrometer."

work-hardening When a crystalline material experiences ductile deformed and the stress needed to continue deformation increases.

xenocryst Foreign crystals introduced into a magma from the surrounding country rock.

X-ray chemical map An image collect by either EDS or WDS where brightness reflects the intensity of a characteristic X-ray from a particular element from across an area.

X-ray diffractometer An instrument that uses X-ray diffraction to produce a diffraction pattern, from which a mineral may be identified or the structure of an unknown crystalline material may be determined.

X-ray fluorescence spectrometer An instrument that uses X-rays to produce characteristic X-rays from elements within a sample. The characteristic X-rays are analyzed by energy-dispersive X-ray spectrometers and/or wavelength-dispersive X-ray spectrometer to provide a semi-quantitative or quantitative chemical analysis of the sample.

X-rays Electromagnetic waves with wavelength of about 0.01 to 10 nanometers.

XRD Abbreviation for "X-ray diffractometer."

XRF Abbreviation for "X-ray fluorescence spectrometer."

zone A region of a mineral with similar orientation and/or composition; also a collection of crystal faces, all of which are parallel to a common line called a zone axis.

zone axis A region of a mineral with similar orientation and/or composition; also a collection of crystal faces, all of which are parallel to a common line called a zone.

zoned crystals Mineral grains with a variation in the composition across the sample

DO NOT COPY e48d507df5d1141@placeholder.94092

Printed by: e48d507df5d1141@placeholder.94092.edu. Printing is for personal, private use only. No part of this book may be reproduced or transmitted without publisher's prior permission. Violators will be prosecuted.

Mineral and Mineraloid Index

DO NOT COPY e48d507df5d1141@placeholder.9409

Bold type refers to full mineral descriptions.

Abelsonite 124

Acanthite 124, 459, 463–64, 468, 504, 506, 513, 517

Acmite 342

Actinolite 231, 262, 302, 311, 338, 342, 351, **352–59**, 371, 505, 507, 511

Adularia 278, 281, 288, **289**, **293**, 461, **500–1**, **505**, **507**, **510**, **517**

Aegirine 335, **336–38**, **342–46**, **359**, 502–8, 511–12

Aegirine-augite 335, **336–38**, **342–45**, **359**, 502

Agate 274

Alabaster **419–20**

Albite 5, 87–88, **99–101**, **106**, 113, **116–17**, 199, 262–63, 276, **278–87**, **290–94**, 300, **330–31**, 336, 344, 346, 361, 366, 370, 373, 429, 442, 515–17

Alexandrite 442

Alkali feldspar 55, 92, 99–100, 116, 199, 229, 245, 267, **276–81**, **284**, **288–95**, 336

Allanite 363–64, **367–69**, 427, 500, 503, 505, 507–8, 511–17

Almandine 379, **382–84**

α-quartz 84–85

Aluminosilicate polymorphs 387

Aluminum hydroxide minerals **451–52**

Aluminum silicates 95–96, 252, 261, **378**, **386–97**, 445

Alunite 418, 500–1, 505, 507, 510, 517

Amazonite 141, **290**

Amblygonite 319, **432**, 501–7, 511, 515

Amethyst **141–42**, 269, 271

Ammonium phosphate 124

Amorphous carbon 485

Amosite 311, **355–56**

Amphibole group **349–61**

Analbite 279

Printed by: e48d507df5d1141@placeholder.94092.edu. Printing is for personal, private use only. No part of this book may be reproduced or transmitted without publisher's prior permission. Violators will be prosecuted.

Analbite 279

Analcime 295–300, 344, 499, 505, 507, 509

Anatase 124, 396

Andalusite 83, 95–96, 105, 131, 139, 198, 236, 255, 259, 262, 264, 320, 339, 366, 370, **374–75**, 379, **386–93**, 425, 442, 445, 500–2, 505, 507, 511, 516

Andesine 276, 280, 282, 284, 287

Andradite 379, **382–84**

Anhydrite 82, 255, 416, **417–22**, 431, **455–56**, 484, 501–2, 505, 508, 512, 516

Anilite 476

Ankerite 401, 402, 404, **409–10**, 440, 464, 501–9, 517

Annite 316

Anorthite 5, 87–88, 96–98, 106–7, **276–80**, 282, **284–87**, 488

Anorthoclase 276, 288, **289–90**, **293**

Anthophyllite 311, 313, 351, **352–55**, 374–75, 507–8, 511–12

Antigorite 257, **308–10**, 357, 381

Antimony **448–49**, 459, 479–80, 483, 504, 506, 513

Antiperthite 117, 280

Antlerite 418, 502, 505, 508, 513

Apatite 10, 46, 105, 116–21, 124, 126, 133, 255, 366, 373, 377, 384, 390, 423, **424–26**, 429, 447, 463, 499–500, 505, 507, 509, 515–17

Aphthitalite 124

Apophyllite **331–32**

Aquamarine **372–73**

Aragonite 4, 117, 124, 125, 344, **400–5**, **410–14**, 416, 463, 500, 505–7, 511, 516–17

Aragonite group 400, 401, 404, **410–14**

Ardealite 124

Arsenic 8, 55, 148, **476–80**, 483, 504, 506, 513

Arsenopyrite 225, 429, 459–60, 463, 473, **476–78**, 504, 506, 513, 517

Atacamite 124

Augite 139, 244, **335–45**, 352, 359, 380, 502–3, 505, 507–8, 511–12

Autunite 423, 504–9

Axinite 371

Azurite 401, 414, **415**, 434, 462, 464, 469, **475–76**, 499, 502, 505, 507–8, 513, 517

Bakhchisaraitsevite 124

DO NOT COPY e48d507df5d1141@placeholder.9409

Printed by: e48d507df5d1141@placeholder.94092.edu. Printing is for personal, private use only. No part of this book may be reproduced or transmitted without publisher's prior permission. Violators will be prosecuted.

Bakhchisaraitsevite 124

banded iron 439–40

Barite 50, 124, 275, 409, 413, **417–19**, **421–23**, 457, 463, 468, 483, 501–5, 508, 512, 517

Bauxite 6, 50, 295, 313, 445, **451–52**, 454, 499–500

Bentonite 328

Beryl 46, 88, 124, 141, 202, 241–42, 248, **269–70**, 319, 346, 363, 371, **372–75**, 425, 433, **442–43**, 499–509, 512, 515

β-quartz 84–85

Biotite 88, 92, 108, 116–17, 120, 122, 139, 197–98, 217, 221, 225, 229, 242, **244–47**, 249–52, 255, 257, **260–64**, 295, 306–7, **314–25**, **330–31**, **338–43**, 353, 356, 359, 367, **368–69**, 373, 375, 377, **384–88**, **393–96**, 427, 442, 444, **461–62**, 481, 503, 505, 507, 510, 515–17

Bismuth 53, 329, 459, 463–64, 479–80, 483, 504, 506, 513

Black jack 466

Böhmite 126, 499–500, 505, 507–8, 511–12

Borates 86, 400, 416, 426, **430–32**, 455, 516

Borax 416, **430–31**, 500, 505, 507, 510

Bornite 142, 459–60, 463, **474–76**, 482, 504, 506, 513, 517

Bort 487

Braunite 453

Bronzite 338

Brookite 447, 513

Brucite **304**, 307, 310, 313, 398, 449, **450**, 500, 502–3, 505, 507, 510, 516

Brushite 124

Bustamite 348

Bytownite 276, 280, 515

Calaverite 459, 477, 504, 506, 513

Calcic-clinamphibole 242, 244, **351–57**, **502–3**, 516

Calcic clinopyroxene 302, 335–36, 338, **341**, 352, 355

Calcite 4–5, 9–11, 45, 79, 83, 92, 112, **114–17**, 121, 124, **125–27**, 133, 135, 142, 148, 155, 158, **166–70**, 255, 257, 260, 263, 283, **295–96**, 302, 310, 313, 317, 319, **330–32**, 338, 342, 344, 347, 349, 357, 371, 381, 382, 384, 398, 400, **401–12**, 416, **419–24**, 436, 439, **455–56**, 463–64, 468, 470, 482, 484, 489–90, **501**, 505–7, 509, 516–17

Calcite group 5, 45, 83, **400–2**

Calcium pyrophosphate dihydrate 124, 25

DO NOT COPY e48d507df5d1141@placeholder.9409

Printed by: e48d507df5d1141@placeholder.94092.edu. Printing is for personal, private use only. No part of this book may be reproduced or transmitted without publisher's prior permission. Violators will be prosecuted.

Calcium pyrophosphate dihydrate 124–25

Calomel 8, **470–71**

Ca malate 124

Cancrinite 295–96

Carbonado 487

Carbonate-apatite 124, 126, **424–25**

Carbonate minerals 11, 125, 148, 195, 233, 259, 263, 270, **400–1**, 402, 407, 410, **414–16**, 457, 485, 488, 490

Carnallite 416, 454, 499, 505, 508, 512

Carnotite 423, 504–5, 507, 511

Carpathite 124

Cassiterite 423, 429, 433, **446–48**, 463, 478, 499–500, 506–7, 510, 513–14, 517

Ca tartrate 124

Cat's eye 442

Celadonite 319–20, 325

Celestine 413, 418–19, 422, 501–3, 505, 508, 512

Cerussite 124, 401–2, 410, 413, 464, 468, 500, 506–7, 511

Chabazite 297–300, 512

Chalcedonite 273–74

Chalcedony 50, **269–70**, 273–74, 332, 407, 463, 470, **499–500**, 505, 507, 510, 516

Chalcocite 124, 459–64, 469, **475–76**, 482, 504, 506, 513

Chalcocyanite 415

Chalcopyrite 6, 44, 124, 142, 415, 429, 434, 459, 460–67, **468–78**, 481, 504–5, 513, 517

Chamosite 321

Chert 126, 253, 256, 270, 273–75, 407, 440, **499–500**, 505, 516

Chiastolite 374, 388, **389–90**

Chlorapatite 424–25

Chlorite 125, 199, 242, 257, **260–64**, 302, 306, **307–13**, 315, 317, 320, **321–32**, **340–44**, **354–59**, 361, **367–71**, **374–76**, 381, 384, 388, 390, **392–95**, 442, 450, 461–62, 482, **502**, 505, 507–8, 510, 512, 516–17

Chloritoid 242, 263, **320–21**, 363, 375, 378–79, 388, **393–95**, **500**, **502**, 505, 507–8, 511–12, 516

Chlorophaeite 381, 507

Chondrodite 398, 499–500, 505–6, 508, 511

DO NOT COPY e48d507df5d1141@placeholder.9409

Printed by: e48d507df5d1141@placeholder.94092.edu. Printing is for personal, private use only. No part of this book may be reproduced or transmitted without publisher's prior permission. Violators will be prosecuted.

Chromite 50, 135, 310, 433, 437, 439, **440–41**, 504–9, 513–15

Chrysoberyl 433, **442–43**, 500, **502**, 505, 508, 512, 515

Chrysocolla **332**, 428, 469, 475, 499–500, 511, 517

Chrysotile 8, 257, **308–10**, 311–12, 347, 357, 361, 381, 450

Cinnabar 140, 434, 444, **459–60**, 463, **470–71**, 480, 483, 504, 506–7, 510, 513–14, 517

Citrine 269

Clay minerals 9, 11, 69, 85, 92–93, 110, 125, 148, 205, 242, **253–55**, 261, 295, **313–29**, 332, 338, 373, 445, 452, 461, 472

Cleavelandite 282

Clinoamphibole 242, 244, **351–58**, 502–3, 516

Clinochlor 321

Clinohumite 398

Clinoptilolite 298, **300–1**, 500, 505, 508

Clinopyroxene 197, 217, 221, 242, **244–46**, 247, 262, 296, 302, **335–42**, 345, 352, 355, 381, 396, **502–3**, 505, 508, 512, 515–16

Clinozoisite **363–71**, **500**, **502**, 505, 508, 512

Cintonite 242, 306, 307, **321**, 500–8, 511

Cobaltite 459, 476–78, 504, 506, 513

Coesite 83, 491

Colemanite 416, 430, 431, 500, 505, 508, 512

Collophane **424–25**, 507

Copper 4, 6, 8, 10, 67–68, 75, 109, 127, 133, 140, 146, 202–3, 232, 332, 373, **414–15**, 428, 434, 448, 459, **462–76**, 477, 479, **482–84**, 504, 506, 513, 517

Cordierite 242, 252, 261, 263, **269–70**, 284, 302, 353, **355–56**, 363, 371, **373–75**, 386, 388, 390, 393, 427, 442, **499**, 505, 508, 510, 512, 516–17

Coronadite 453

Corundum 5, 10, 88, 133, 135–36, 139, 142, 314, 320, 374, 377, 395, 433, **442–45**, 451–52, **499–500**, 505, 507, 509, 516

Coumbite 7

Covellite 124, 459, 460, 463, 464, 469, 475, **476**, 504–5, 513, 517

Cristobalite 83, 242, **267–68**, **272–75**, **499**, 505, 507, 509

Crocidolite 271, 311, **360–61**

Crossite 359

Cryolite 454, 499, 505, 508, 512

DO NOT COPY e48d507df5d1141@placeholder.94092

Printed by: e48d507df5d1141@placeholder.94092.edu. Printing is for personal, private use only. No part of this book may be reproduced or transmitted without publisher's prior permission. Violators will be prosecuted.

Cryptomelane 453

Cummingtonite 311, 351–54, **355–60**, **502–8**, 511–12

Cuprite 91, 414, **433–34**, 462, 464, 469, **475–76**, 482, 504, 506–7, 509, 513–14, 517

Cystine 124

Dahllite 424

Dataolite 371, 398, 499–500, 505–6, 508, 511

Decagonite 29

Diammonium calcium phosphate 124

Diamond 6–7, 10, 15–16, 18, 29, 63–64, 67, 76, 83, 84, 95, 105, 131, 133–34, 137, **140–41**, 233, 268, **354–58**, 390, 395, 397, 430, 445, 479, 481, **486–87**, 488–91, 499, 501–9

Diaspore 445, 451–52, 499, 505, 508, 512

Dickite 324

Digenite 463, **475–76**

Diopside 89, 96–97, 244, 302, **335–38**, **341–42**, **345–47**, 352, 357, 381, 384, 398, 405, 410, 429, 439, 491

Disilicates 242–44, **363–67**

Djurleite 476

Dogtooth spar 403

Dolomite 11, 45, 124–25, 148, 257, 260, 263, 310, 313, 338, 342, 347, 357, 377, 381, 384, 398, 400, **401–11**, 416, 419, **421–22**, 439, 440, **455–56**, 463–64, 470, **501**, **503**, 505, 507, 509, 516–17

Dolomite group 400–9

Dolostone 406

Dravite 376–77

Dumortierite 269, 398, 499, 502, 505, 507, 511

Earlandite 124

Eastonite 316

Edenite 358–59

Elbaite 376

Emerald 372–73, 377, 442

Enargite 459–60, 463, 465, 504–5, 513, 517

Enstatite 90, 227, 334–9, 381

Epidote 242, 244, **255**, 257, 260, 262, **263–64**, 283, 302, 317, **330–31**, 338, **342–43**, 357, 361, **363–69**, 371, 378, 381, 384, 387, 405, 426, 437, 461, 463, 482, **502–3**, 505, 508, 511, 515–17

DO NOT COPY e48d507df5d1141@placeholder.9409

Printed by: e48d507df5d1141@placeholder.94092.edu. Printing is for personal, private use only. No part of this book may be reproduced or transmitted without publisher's prior permission. Violators will be prosecuted.

508, 511, 515–17

Epidote group 242, 263, 283, **330–31**, 338, 347, 357, 361, **363–71**, 378, 381, 426, 516–17

Epsomite 124, 416, 418, 500–2, 505, 508, 510

Erionite 298, **300–1**, 510

Eucryptite 346

Eulite 338

Fayalite 87, 89–90, 98, 132, 244, **378–81**

Feldspar 11, 55, 76, 85, 87, 92, 94, 99–101, **112–17**, 120, 123, 141, **142–43**, 146, 199, 229, 233, 237, **241–49**, 250, **253–57**, **260–61**, 263–64, **267–70**, **294–95**, 302, **314–15**, 319, 326, 336, 339, 343, 346, 373, **375–76**, 388, 442, 445, 451, 461, 463, 515–17

Feldspar group 276–93

Ferberite 429

Ferric iron 59

Ferrihydrite 124–25

Ferrimolybdite 474

Ferro-actinolite 231, 351–52, **356–59**, 505, 508, 511

Ferro-edenite 358

Ferrohornblende 352, 358

Ferrohypersthene 338

Ferropargasite 358

Ferrosilite 90, 227, **335–39**

Ferrotschermakite 358

Ferrous iron 59

Fibrolite 390–91

Flint 274, 369, 427

Fluorapaphyllite 331

Fluorapatite 424–25

Fluorite 10, 62, 124, **133–34**, 141, 190, 209, 275, 296, 397, 408, 409, 422, 429, **447–48**, 454, **456–57**, 462–63, 468, **501–2**, 505–7, 509, 515

Forsterite 80, 87–90, 98–99, 132, 267, 310, 342, 357, **378–81**, 382, 398

Francolite 124, 424

Gahnite 437, 441

Galaxite 437, 441

DO NOT COPY e48d507df5d1141@placeholder.9409

Printed by: e48d507df5d1141@placeholder.94092.edu. Printing is for personal, private use only. No part of this book may be reproduced or transmitted without publisher's prior permission. Violators will be prosecuted.

Galena 6, 50, 68, 83, 124, 140, 146, 196, 223, 413, 422, 457, 459–60, 463–64, **467–68**, 470, **473–74**, 478, 483, 504, 506, 513, 517

Garnet 6, 108, 117, 198, 242, 248, 252, 255, 257, **260–63**, 264, 273, 296, 302, 331, 339, **342–45**, **355–57**, 361, 369, 375, **378–85**, 388, **390–95**, 405, 410, 425, 429, 439, 442, 463, 487, **499–500**, 505, 507, 509, 515–17

Gedrite 351–52, **354–55**, 505, 508, 511–12

Gibbsite 304, 326, 445, **449–51**, 452, 499–500, 502, 505, 508, 512

Glauberite 416, 418, 431, 500–1, 505, 508, 510

Glaucodot 477

Glauconite 314, **319–25**, **502**, 505, 507–8, 511, 516

Glaucophane 257, 262, 330, **344–45**, 351–53, **359–61**, 370–71, 388, 395, 412, 505, 507–8, 511–12

Glushinskite 124

Goethite 124, 199, 255, 271

Gold 3, 6, 8, 67, 75, 125, 127, 137, 140, 216, 235, 241, 317, 397, 463–65, **470–81**, 504, 506, 513, 517

Grandite 382–84

Graphite 63–64, 67, 69, 83–84, 91, 95, 131, 142, 148, 398, 474, 479, **484–86**, 490–91, 504–5, 513, 516

Greenalite 440

Greigite 124, **126**, **472**

Grossular 342, 347, 379, **381–84**, 398

Grunerite 311, 351–52, **355–56**, **502–3**, 505, 508, 511–12

Guanine 124

Gypsum 10, 50, 112, 124, 133, 142, 157, **164–66**, 255, 286, 314, 317, 406, 415–16, **417–22**, 431, 450, **455–56**, 464, 484, **501**, **503**, 505, 508, 512, 516–17

Hafnon 385

Halite 11, 61–64, 67, 82–83, **104–5**, 133, 144, 148, 204, 211, 401, 416, **418**, 419, 421, 431, **454–56**, 468, 471, 484, 500, **501**, 505–10, 516

Halloysite 324

Hannayite 124

Hartite 124

Hastingsite 358

Hausmannite 437, 452, 453

Haüyne 296

DO NOT COPY e48d507df5d1141@placeholder.9409

Printed by: e48d507df5d1141@placeholder.94092.edu. Printing is for personal, private use only. No part of this book may be reproduced or transmitted without publisher's prior permission. Violators will be prosecuted.

Hazenite 124

Hectorite 346

Hedenbergite 335–36, 341, 352

Hematite 6, 50, 103, 123, 135, 139, **141–50**, 271, 310, 319, 408, 429, 433–34, **438–39**, 440, **443–48**, 451, 454, 463–64, 470, 504, 506–7, 513–17

Hercynite 437, **440–41**

Heulandite 297–300, 500–1, 505, 508, 512

Hexahydrite 124

Hieratite 124

High albite 279

High quartz 84–85

Hoganite 124

Hollandite 453

Hornblende 120, 139, 173, 199, 242, 244, 246, 252, 255, 257, 262, 302, 315, 317, 322, **336–43**, 351, **352–59**, 361, 367, **368–69**, **376–77**, 381, 384, 386, 396, 426, 461, 505, 507–8, 511–12, 515

Hübnerite 429, 463

Humite 398, 516

Hydrocerussite 124

Hydrogrossular 382–84

Hydromagnesite 450

Hydrotroilite 124

Hydroxide minerals 125, 255, 409, 433, 440, 446, **450–53**, 464

Hydroxyapophyllite 331

Hydroxylapatite 424–25

Hypercinnabar 470

Ice 68, 83, 95, 433, **434**, 435–36, 455, 499, 505, 507, 510

Iceland spar 403

Icosahedrite 29

Iddingsite 380–81, 508

Idrialite 124

Illite 314, 319, **323–27**, 510

Imenite 6, 124–25, 135, 144, 145, 221, 255, 433, **438–47**, 463, 504–6, 513

Indialite 277

DO NOT COPY e48d507df5d1141@placeholder.9409

Printed by: e48d507df5d1141@placeholder.94092.edu. Printing is for personal, private use only. No part of this book may be reproduced or transmitted without publisher's prior permission. Violators will be prosecuted.

Indicolite 377

Iolite 246, 326, 375, 505, 508, 510

Iridosmine 479

Iron 3, 6–8, 55, 59–61, 66, 71–72, 75, 88, 113, **122–25**, 132, 141, 144–45, **219–21**, 229, 244, 255, 275, **310–12**, **317–23**, 327, 330, 335–36, **339–40**, 351, **356–57**, **360–61**, 365, **367–68**, **371–72**, 381, 384, 393, **404–12**, 429, 434, **438–41**, **444–55**, **462–64**, **467–74**, **478–81**, 504, 506

Iron hydroxide materials 125, 255, 381, 444, **450**, 451

Jade 6, 344, 357

Jadeite 6, **335–36**, 338, 342, **343–45**, 361, 370, 388, 500, 502, 505, 508, 511–12, 517

Jarosite 124

Jasper **141–42**, 274, 440

Kaersutite 361, 511

Kalsilite 294, 507, 509

Kamacite 479–80, 506

Kanonaite 388

Kaolinite 8, 125, 254, **306–7**, **310–13**, **323–29**, 463, 488, 510

Kataphorite 361, 511

Kernite 416, 430, 431, 500, 505, 508, 510

K-feldspar 11, 85, 87, 94, 99–101, 112, **115–17**, 120, 123, 141, 146, 199, 229, 233, 242, **244–48**, 249–50, **254–56**, **260–64**, 267, 272, 276, **277–81**, **289–95**, 319, 326, 343, 346, 373, 388, 442, 461, 463, 515–17

Kieserite 416, 418, 431, 501, 505, 508, 512

Kimberlite 84, 342, 487, 491

Kratochvilite 124

Kutnohorite 401–2, 404, **408–9**, 453, 501, 505, 507, 509

Kyanite 83, 95–96, 131, 133, **255**, 257, 259, 262–63, 345, 375, 379, **386–93**, 442, 445, **500**, **502**, 505, 507–8, 511, 516

Labradorite 276, 280, 282, 284, 515–16

Lansfordite 124

Lapis lazuli 6, 296

Laumontite 262, 298, 300, 501–3, 505, 508, 510

Lawsonite 242, 262, 331, **344–45**, 361, 365, **369–71**, 378, **387–88**, 412, 500, 502, 505, 508, 512, 517

Lazurite 139, 296

DO NOT COPY e48d507df5d1141@placeholder.9409

Printed by: e48d507df5d1141@placeholder.94092.edu. Printing is for personal, private use only. No part of this book may be reproduced or transmitted without publisher's prior permission. Violators will be prosecuted.

Lead 4, 6, 8, 53, 69, 84, 131, 402, 448, 459, 465, 468, 473, **478–79**, 486

Lepidocrocite 124, 139, 199, 248, **314–15**, **318–19**, 346, 376, 448, 451, 464, 500–8, 511, 513, 515

Lepidolite 139, 248, **314–15**, **318–19**, 346, 376, 448, 500–2, 505, 507–8, 515

Leucite **113–15**, 242, 245, 247, 267, 293, **295–96**, 499, 505, 507, 510, **515**

Leucoxene 396, **446–47**

Limonite 125, 319, 423, 426, 434, 441, 444, **450–52**, 467, 469, **472–73**, 479–80, 504

Limestone 406

Lindbergite 124

Lithiophilite 318, 423, 500–8, 511–12

Lithium 59, 132, 219, 235, 248, 314, 319, 335, 346, 350, 416

Lizardite **308–10**

Lodestone 439

Low albite 279, 282

Low quartz 85

Lussatine 272, 275

Lussatite 272, 275

Lutecite 274

Mackinawite 124, 472

Maghemite 124, 126, 506

Magnesiochromite 437, 440

Magnesioferite 437, 438

Magnesiohornblende 352, 358

Magnesite 5, 83, 124–25, 310, 313, 401–4, **406–8**, 416, 450, 501, 503, 505, 507, 509

Magnesium 65, 124, 132, 244, 335–36, 351, **360–61**, 410

Magnetite 6, 55, 103, **123–26**, 135, 139, 144, **145–46**, 196, 236, 255, 257, 260, **309–10**, 313, 356, 429, 433, 437, **438–41**, 444, 446, 449, **451–52**, 463, 487, 504, 506, 513, 517

Malachite 401, **414–15**, 434, 462, 464, 469, **475–76**, 500, 502, 505, 507–8, 511, 517

Manganese 8, 71, 124–25, 320, 404, 446, **452–53**, 457

Manganite 452–53

Marcasite 83, 124, 135, 459, 463, **468–74**, **477–78**, 504–5, 513

Margarite 242, 306, 307, **320–21**, 445, 500–2, 505, 508, 511

Marialite 301

DO NOT COPY e48d507df5d1141@placeholder.9409

Printed by: e48d507df5d1141@placeholder.94092.edu. Printing is for personal, private use only. No part of this book may be reproduced or transmitted without publisher's prior permission. Violators will be prosecuted.

Marmatite 466

Martite 439

Meioite 301–2

Melanterite 124

Melilite 366, 499–500, 505, 507, 509–10, 515

Mercury 8, 148, 463, **470–71**, 479, 480, 517

Mesolite 298

Mesoperthite 117, 280

Metacinnabar 470

Mica 314–21

Microcline 41, 83, 85, 115, 257, 269, 270, 276, **278–81**, 284, 288, **289–94**, 444, **500–2**, 505, 508, 510

Microlite 284, 293, 295

Milky quartz 142, 269

Millerite 124, 463

Minium 8

Minnesotaite 312–13

Moganite 268, 273–74

Molybdates 86, 400, **428–29**, 517

Molybdenite 6, 220, 429, 448, 459–63, **474–75**, **485–86**, 504, 513, 515, 517

Monalbite 279

Monazite 7, 119–20, 255, 369, 424, **426–28**, 499–501, 503, 505, 508, 513, 515

Monetite 124

Monohydrocalcite 124

Monosodium urate monohydrate 124

Montasite 355–56

Monticellite 398, 499–500, 505, 508, 511, 516

Montmorillonite 8, 254, 328

Montroydite 470

Moolooite 125

Mordenite 298, **300–1**

Morganite 372–73

Mullite 388

DO NOT COPY e48d507df5d1141@placeholder.9409

Printed by: e48d507df5d1141@placeholder.94092.edu. Printing is for personal, private use only. No part of this book may be reproduced or transmitted without publisher's prior permission. Violators will be prosecuted.

Muscovite 92, 94, 120, 164, 180, 242, 244, **246–47**, 249–50, 252, 255, 257, **260–61**, 263–64, 306–7, **312–22**, 325, 330, 370, **374–75**, 384, 388, 391, 393, 395, 442, 445, 448, 450, 500, 505, 508, 511, 515–17

Nacrite 324, 502

Nahcolite 402, 416, 431, 500, 505–10

Natroapophyllite **331–32**, 512

Natrolite 297–301, 349, 500–1, 505, 508, 512

Nemalite 450

Nepheline 46, 242, 244, 245, 247, 267, **293–96**, 302, 317, 338, **343–44**, 349, 361, 366, 373, 405, 425, 452, 499, 505, 507, 509, 515

Nephrite 6, 344, 357

Nesquehonite 124

Nickeline 459, 477, 478, 504, 506, 513

Norbergite 398

Nosean 296

Octocalcium phosphate 124

Oligoclase 276, 280, 284, 287, 515

Olivine 3, 5, 73–74, 87–90, 98–99, 106, 122, 132, 135, **144–45**, 146, 199, 217, 221, 242, **244–52**, 255, 257, 260, 263, 267, 309–10, 313, **336–42**, 352, 368, **378–81**, 382, 398, 405, 437, 442, 452, 487, 500, 505, 507–8, 511–12, 515–16

Omphacite 257, 262, 335, **342–45**, 388, 502, 505, 508, 512, 516–17

Oolite 49, 407, 409, 440

Opal 4, 6, 125, 142, **269–76**, 291, 332, 404, 407, 419, 470, **499–500**, 505–7, 509

Orpiment 124, 459–60, 463–65, 470, **483–84**, 504–5, 508, 511, 513–14

Orthoamphibole 242, **351–56**, 375, 501, 503, 505, 516

Orthoclase 10, 83, 133, 269, **276–80**, **288–94**, 375, 500–2, 505, 507, 510

Orthoferrosilite 338

Orthopyroxene 217, 219, 221, 242, 244, **246–47**, 262, **335–41**, 352, 381, 390, 501–8, 511–12, 515, 517

Orthosilicates **242–44**, 249, **378–99**

Ottrelite 394

Oxide minerals 409, 415, **433–39**

Oxybiotite 316

Oxyhornblende **358–59**, 507–8

Pyroxite 125

DO NOT COPY e48d507df5d1141@placeholder.9409

Printed by: e48d507df5d1141@placeholder.94092.edu. Printing is for personal, private use only. No part of this book may be reproduced or transmitted without publisher's prior permission. Violators will be prosecuted.

Paceite 125

Palladium 479

Palygorskite 326, 329, 505, 508, 510

Paragonite 314–16, 320, 500, 505, 511

Pargasite 358–59

Peacock ore 475

Pearceite 124

Pectolite 332, 347, **348–49**, 500–1, 505, 508, 512

Pentlandite 6, 365, 459, **468–70**, 504–5, 513, 517

Periclase 407, 433, 436, 450, 501, 505, 507, 509, 516

Perovskite 81

Perthite 117

Phengite 314, 316

Phillipsite 298–300

Phlogopite 307, 312, **315–17**, 321, 398, 487, 501, 507–8

Phosphate minerals 424–28, 449

Picotite 441

Piemontite 139, 366, **367–68**, 501, 503, 505, 508, 511, 513

Pigeonite 111, **335–42**, 352, **502–3**, 508, 512

Pinite 269, 284, **374–75**

Pitchblende 449

Plagioclase 5, 41, 87–88, 92, 96, 106–7, **111–13**, 116, 123, 175, 197, 199, 217, 221, 229, 233, 242, 244, **245–57**, 261–63, 267–70, **276–96**, **301–2**, 315, 320, 336, 339, **344–46**, **355–56**, 366, 370, **374–75**, 381, 384, 388, 396, 405, 461, **500–2**, 505, 508, 510, 512, 515–17

Platiniridium 479

Platinum 252, 469, 479–80, 504, 506

Pleonaste 441

Polyhalite 416, 418, 431, 500–1, 505, 508, 510

Polylithionite 318

Potassium feldspar *see* Alkali feldspar

Powellite 429

Prehnite 262, 265, **330–32**, 371, 500–2, 505, 508, 512, 517

Proustite 124, **459–60**, 463–66, 470, 504, 506–7, 509, 513–14

DO NOT COPY e48d507df5d1141@placeholder.9409

Printed by: e48d507df5d1141@placeholder.94092.edu. Printing is for personal, private use only. No part of this book may be reproduced or transmitted without publisher's prior permission. Violators will be prosecuted.

Pseudoleucite 295

Pseudowollastonite 347

Pumpellyite 242, 262, 265, **330–31**, 361, 365, 368, **370–71**, 378, 387, 412, 502–3, 505, 508, 511–12, 517

Pyralspite **382–84**

Pyrargyrite **459–60**, 463–66, 504, 506–7, 509, 513–14

Pyrite 4, 6, 9, 29, 37, 44, 46, 83, 93, 113, 117, 124, 125, 135, 140, 142, **146–48**, 196, 216, 225, 255, 275, 296, 410, **414–15**, 422, 429, 434, 440, 451, 457, 459, **460–78**, 481, 483, 504–6, 513, 517

Pyrolusite 348, 433, 446, 453, 513

Pyromorphite 423, 499–500, 506–7, 509

Pyrope 379, **382–84**, 388

Pyrophyllite 8, 242, 283, 306–7, 312, **313–15**, 323, **500–2**, 505, 508, 511

Pyroxene 6, 28, 41, 76, 89–90, 96, 106, 111, 115, 117, 122, 135, 143, 175, 197, 217, 219, 221, 225, **226–27**, 242, **244–55**, 257, **260–63**, 284, **295–96**, 302, 309–10, 313, **346–61**, 381, 390, 396, 451, 453, 463, 487, **501–3**, 505, 507–8, 511–12, 515–17

Pyroxene group **344–45**

Pyroxenoids **334–35**, **346–48**

Pyroxmangite 348

Pyrrhotite 88, 124–25, 398, 429, 459, 463, 465, 467, **468–72**, 475, 478, 504–6, 513, 517

Quartz 3, 8–12, 26, 28, 38–40, 45, 50, 67, 68, 83, 84–85, 92–94, 102, 108, 116, 123, 126, 133, **141–44**, **147–48**, **161–64**, 196, 198, **205–9**, 212, 229, **232–33**, 237, **241–57**, **260–63**, **267–75**, 281, 284, **290–95**, 302, **311–19**, **322–26**, 332, **343–48**, 353, 356, **360–61**, **373–77**, 381, 384–85, **386–90**, **394–98**, 404, 408, **409–10**, **419–22**, 425, 429, 440, 442, 444, **447–48**, 451, 457, **461–62**, 463, **468–74**, 481, 483, **499–500**, 505, 507, 510, 515–17

Quartzine 273–74

Realgar 124, **459–60**, 463–65, 470, **483–84**, 504–5, 508, 513–14

Rhodochrosite 5, 83, 124, 348, 401–4, **406–9**, 452, 464, 501, 503, 505, 507, 509, 517

Rhodonite **347–48**, 409, 452, 501, 505, 508, 512

Rhombohedral carbonates **401–10**, 413

Richterite 311, 351, 357, 361, 511

Riebeckite 311, 342, 351–352, **359–61**, 440, 505, 507–8, 511–12

Ring silicates 145, **242–43**, 257, **260–61**, 334, 363, **371–75**, 381

Rock crystal 269, 290, 386, 398, 448

Romanechite 453

DO NOT COPY

Printed by: e48d507df5d1141@placeholder.94092.edu. Printing is for personal, private use only. No part of this book may be reproduced or transmitted without publisher's prior permission. Violators will be prosecuted.

Rose quartz 142, 269, 398

Rubellite 377

Ruby 5–6, 139, 143, 433, 442, **444–45**, 465

Rutile 6, **112–13**, 135, 142, 255, 386, 391, **427–28**, 433, **445–48**, 463, **502–5**, 507, 510, 513–15

Sandstone 253–57, 261, 270–75, 315, 324, 366, 422, 428, 453, 457, 516

Sanidine 42, 83, 85, 108, 269, 276, **278–80**, 288, **289–96**, **500**, 505, 508, 510

Sapphire 5–6, 139, 142, **444–45**

Sapphirine **445**, 499–500, 507–8, 516–17

Satin spar 142, 419

Sausserite 283

Scapolite 44, 242, 263, 267, 283, **301–2**, **499–502**, 505–7, 509, 516

Scheelite 6, 429, 463, 478, 501, 503, 506–7, 510, 513–14

Schorl 172, **376–77**

Schwertmannite 124

Scolecite 298, 300

Selenite 419

Sepiolite 326, 505, 508, 510

Sericite 199, 283, **291–93**, 302, **314–17**, 366, 372, 376, **390–97**, 461–62

Serpentine 68, 242, 257, 306–7, **308–13**, **322–24**, **339–41**, **355–56**, 381, 425, 450, **500**, **502**, 505, 507–8, 510, 517

Siderite 5, 83, 124, 401–4, **406–12**, 428, 440, 462, 464, 467, 469, **503**, 505, 507, 509, 517

Siderophyllite 316

Silicate group 242, 244, **267–73**, 274–75, 424

Sillimanite 83, 94–96, 105, 255, 259, 262–64, 355, 375, 379, **386–92**, 425, 442, 445, 447, **500–3**, 505, 508, 512, 515–16

Silver 67, 75, 127, 140, 454, 459, 460, 463–66, **478–83**, 504, 506, 513, 517

Skutterudite 459, 477, 478, 504, 506, 513

Smectite 125, 323, **324–29**, 346, 349, 510

Smithsonite 5, 83, 401–2, 464, 467, 501–3, 505, 507, 509, 517

Smoky quartz 141, 269

Sodalite 242, 245, 247, 267, **293–96**, 360, **499–500**, 505–7, 509, 515

Sodic-calcic clinoamphibole 352

DO NOT COPY e48d507df5d1141@placeholder.9409

Printed by: e48d507df5d1141@placeholder.94092.edu. Printing is for personal, private use only. No part of this book may be reproduced or transmitted without publisher's prior permission. Violators will be prosecuted.

Sodic-calcic clinoamphibole 352

Sodic-calcic clinopyroxene 335, 338

Sodic clinoamphibole 351–52

Sodic clinopyroxene 335, 338, 352

Sodium urate 124–25

Specular hematite 443–44, 446

Spessartine 379, **382–84**

Sphalerite 6, 50, 124, 148, 396, 408, 422, 429, 436, 439, 457–64, **466–70**, **473–74**, 478, 481, **501–3**, 504–5, 507, 509, 513–14, 517

Spinel 112, 113, 135, 381, 384, 398, 433, **437–42**, 445, 487, 499–500, 505, 507, 509, 515–16

Spinel group 113, **437–41**

Spinel series 437, 441

Spodumene 248, 319, 335, 338, **345–46**, **501–2**, 505, 508, 512, 515

Staurolite 111, 113, 242, 255, **260–63**, 264, 355, 363, **374–75**, **378–79**, **387–96**, 426, 500, 505, 508, 513, 516

Steatite 312

Stevensite 349

Stibnite 459–60, 463–65, 467, 470, 483, 504–5, 513–14

Stilbite 297–300, 500–3, 505, 508, 510

Stilpnomelane 317, **329–30**, 440, 502–3, 505, 507–11

Stishovite 83, 264, **267–68**

Stolzite 439

Strontianite 83, 124–25, 401, 410, **413–14**, 500–3, 505, 507–8, 511

Struvite 124

Sulfate minerals 417–24, 484

Sulfur 61, 67, 71, 82, 88, 125, 127, 139, 148, 220, 254, 296, **405–6**, 410, 417, **420–21**, **450–63**, **466–68**, **471–77**, 479, **483–84**, 485, **499**, 505, 508, 513, 516–17

Sylvanite 459, 477, 504, 506, 513

Sylvite 11, 148, 416, 419, 454, **455–56**, 501, 505, 507, 509, 516

Taenite 479–80, 504, 506

Talc 10, 69, 133, **212–13**, 242, 263, 306–7, 310–11, **312–13**, 315, 321, 323, **339–40**, **355–57**, 375, 381, 450, 462, **500**, **502–3**, 505, 508, 511, 516

Tantalite 7

Tantalum 7

DO NOT COPY e48d507df5d1141@placeholder.9409

Printed by: e48d507df5d1141@placeholder.94092.edu. Printing is for personal, private use only. No part of this book may be reproduced or transmitted without publisher's prior permission. Violators will be prosecuted.

Tantalum 7

Tawmanite 367

Tennantite 459–60, 463, 466, 504–5, 513–14, 517

Tenorite 247, 415, 434

Tephroite 379

Tetrahedrite 459–60, 463, 466, 468, 504–5, 513, 517

Thenardite 416–17, 431, 500–1, 503, 505, 508, 512

Thomsonite 297–300, 500–1, 503, 505, 508, 512

Thorianite 449

Thulite 365–66, 501, 508

Tiger's eye 271, **360–61**

Tincalconite 417, 430–31, 499, 505, 507, 510

Titanian augite 341

Titanite 119–20, 135, 242, 244, 255, 302, 353, 370, 378–79, 386, **395–96**, **426–28**, **501–3**, 505, 508, 513, 515–17

Todorokite 124, 453

Topaz 10, 43, 133, 141, **147**, 242, 273, 314, 319, **377–79**, **396–97**, 425, 429, 448, **500–3**, 505, 508, 512, 515

Tourmaline 6, 45, 104, 135, 147, 172, 242, 248, 255, 319, 346, 361, 363, 371, 373, **375–77**, 393, 425, **429–30**, 442, 499–500, 505, 507, 509, 515–16

Tremolite 231, 311, 313, 331, 338, 342, 344, **346–47**, 351–53, **356–59**, 361, 381, 384, 391, 398, 405, 410, 429, 439, **501**, 505, 508, 511

Tricalcium phosphate 124

Tridymite 83, 94, 242, **267–68**, **271–75**, 294, **499**, 505, 508, 512

Trilithionite 318

Triphylite 423, 502, 505, 508, 511–12

Troilite 124, **468–69**

Trona 402, 416, 431, 500, 503, 505, 507–8, 510

Tschermakite 358–59

Tungstates 86, **132–33**, **235–36**, 400, **428–30**, 517

Turquoise 332, **424–25**, **428**, 469, **499–500**, 505, 508, 512, 517

Ugrandite 382

Ulexite 416, 430–31, 500, 505, 508, 512

Ulvöspinel 437, 438

Uralite **241**, **42**, 357, 359

DO NOT COPY e48d507df5d1141@placeholder.9409

Printed by: e48d507df5d1141@placeholder.94092.edu. Printing is for personal, private use only. No part of this book may be reproduced or transmitted without publisher's prior permission. Violators will be prosecuted.

Uralite **341–42**, 357, 359

Uraninite 124, 433, 447, **449**, 504, 506, 513

Urea 125

Uicite 125

Uvarovite 382

Vanadates 86, 382, 423, 424, 426

Vaterite 124

Vermiculite 311, 317, **323–25**, 327, 510

Vesuvianite 366, 371, 499–500, 505, 507, 509, 515–16

Vivianite 124

Wad 451–52

Wairakite 262, 298

Wavellite 423, 501–3, 505, 508, 512

Whewellite 125

White mica 283, 314, **315**, 461

Whitlockite 124

Witherite 148, 401, 410, **412–13**, 422, 500, 503, 505, 507–8, 511

Wolframite 6, 429, 448, 463, 504, 506, 508, 513–14

Wollastonite 90, 227, 257, 260, **331–32**, 335, 342, **346–49**, 357, 384, 391, 398, 405, 429, **500**, **502**, 505–6, 508, 511, 516

Wood tin 448

Wulfenite 429–30, 499, 506–7, 509

Wurtzite 124, 436, 463, **466–67**

Xenotime 386, 424, 426, **427–28**, 501–3, 505, 507, 510, 513, 515

Zeolites 9, 205, 242, 255, 262, 265, 267, 283, 295–302, 323, 329, **331–32**, 349, 455, 482, **499–503**, 516–17

Zincblende 466

Zincite 46, 433, 436, 504, 506–7, 510, 513

Zircon 4, 6, 8, 44, 105, **117–22**, 218, 234, 241–42, **255**, 283, 317, **374–75**, 378–79, **385–86**, **426–28**, 447, 487, 499–500, 505, 507, 510, 513, 515–17

Zoisite 255, 262, 344, 363–64, **365–71**, 425, **500**, 502, 505, 508, 512

DO NOT COPY
e48d507df5d1141@placeholder.9409

Printed by: e48d507df5d1141@placeholder.94092.edu. Printing is for personal, private use only. No part of this book may be reproduced or transmitted without publisher's prior permission. Violators will be prosecuted.

Subject Index

2V angle 171, 186–88

Absorption
- carbonates and 404, 408
- color and 137
- crystallography and 209
- of light 137–40, 143, 153, 161, 209, 404, 408, 434, 439, 442, 459–60
- optical mineralogy and 153, 161
- oxides and 434, 439, 442
- physical properties and 137–40, 143
- sulfides and 459–60

Accessory minerals 245

Accessory plates 157, 164–66

Acer saccharum 315

Acicular crystals 48

Acids
- carbonates and 403–6, 410, 414–15
- chemical analysis and 214, 219, 224
- mineral growth and 118–21, 125, 127
- native elements and 484, 488, 490–91
- physical properties and 9–11, 131, 148
- silicates and 254, 269, 301, 348, 382
- study strategies and 232, 234
- sulfates and 421
- sulfides and 462–64, 468, 473

Actinide series 55

Activation energy 93–95, 102–3, 125, 143

Acute bisectrix interference figures 171, 180–81

Aerometers 235

Aggregates
- as building material 6
- carbonates and 410

DO NOT COPY e48d507df5d1141@placeholder.9409

Printed by: e48d507df5d1141@placeholder.94092.edu. Printing is for personal, private use only. No part of this book may be reproduced or transmitted without publisher's prior permission. Violators will be prosecuted.

carbonates and 410
crystallography and 48–49
mineral growth and 92, 94, 117
oxides and 434, 439
silicates and 271, 283, 287, 290, 310, 374, 381, 396
Agricola, Georgius (Georg Bauer) 4
Albite twinning 113, 199, 278, 280–87, 290–94
Alkali metals 55
Alkaline earth metals 55
Allochromatic color 142
Alloys 66
Alpha decay 117
Al/Si order-disorder 277–78
Aluminum avoidance principle 279, 294
American Mineralogist journal 5, 12
Ammonia beccarri 126
Amorphous minerals 3
Amygdules 331
Analyzer 156
Angular momentum quantum number 54
Anhedral faces 48
Anions 58
Anisodesmic bonding 79–80, 82
Anistropic minerals
double refraction and 158–59
fast/slow vibration directions and 165
interference and 159–66
polychromatic illumination 161–62
Annealing 109, 120–21
Anomalous interference colors 162
Antiferromagnetism 143, 145–46
Antiphase domains 110–11
Antirapakivi texture 281
Aperture diaphragm 155

DO NOT COPY
e48d507df5d1141@placeholder.9409

Printed by: e48d507df5d1141@placeholder.94092.edu. Printing is for personal, private use only. No part of this book may be reproduced or transmitted without publisher's prior permission. Violators will be prosecuted.

Apparent optic angle 186–88

Arenites 253

Argillic sulfides 461

Arsenides 478

Asbestiform 311–13

Asbestos

- banning of 8, 311
- cancer and 8, 313, 333
- habit of 311
- silicates and 271, 301, 310–13, 333, 347, 355–57, 361
- substitutes for 271

Ash glass 4

Assimilation 51, 250–51

Asterism 142

Atomic mass 52

Atomic mass number 52, 117–18

Atomic number 52

Atomic radius 69–71, 493–98

Atomic weight 52

Auxiliary condensing lens 155

Axial intercepts 33

Axial ratio 33

Background 202

Backscattered electrons 218

Band gap 65, 140

Band theory 138–40

- Basal pedions 41

Basalt 61, 123, 252, 299

Baveno twinning 281–83, 290–92

Becke line method 190–91

Bertrand lens 156–57

Berzelius, J. J. 4

Beta decay 117–18

Biaxial indicatrix 170–72

DO NOT COPY e48d507df5d1141@placeholder.9409

Printed by: e48d507df5d1141@placeholder.94092.edu. Printing is for personal, private use only. No part of this book may be reproduced or transmitted without publisher's prior permission. Violators will be prosecuted.

Biaxial indicatrix 170–72

Biaxial interference figures
- acute bisectrix 180–81
- determining 2V and 186–88
- dispersion effects and 188–89
- obtuse bisectrix 182–83
- off-center 183
- optic axes and 182
- optic normal (flash) 183
- optic sign and 185–86

Biaxial minerals 173, 193–94

Binary diagrams 89–90

Binary minimum 99

Binary systems 96–101

Biologically controlled mineralization 123, 125–26

Biologically induced mineralization 123–25

Biomediation 127

Biomineralization 123–26

Biominerals 4

Biomining 127

Bioremediation 127

Bird's eye extinction 317

Bireflectance 194

Birefringence 159, 163

Bisectrix dispersion 188

Bladed crystals 48

Body-centered cubic packing 75

Böggild intergrowths 280

Bohr magnetic moment 143

Bond length 69

Borates 428–30

Born repulsion 62

Bowen's Reaction Series 123, 249

Bragg reflection indices 207–8

Bragg's Law 204

DO NOT COPY
e48d507df5d1141@placeholder.9409

Printed by: e48d507df5d1141@placeholder.94092.edu. Printing is for personal, private use only. No part of this book may be reproduced or transmitted without publisher's prior permission. Violators will be prosecuted.

Bragg's Law 204

Bragg, W. H. 5

Bragg, W. L. 5

Bravais lattices
- crystallography and 14–21, 24, 28
- crystal systems and 17–21
- hexagonal 19
- isometric 21
- Law of Bravais and 29
- monoclinic 18
- orthorhombic 18–19
- tetragonal 19–20

Breccia 253, 332, 461

Brittleness
- carbonates and 404–15
- halides and 454–56
- ionic bonding and 62
- mineral growth and 122
- native elements and 480, 483, 487
- oxides and 433–4, 438–49
- phosphates and 425–28
- silicates and 269–72, 275, 283, 290–96, 301, 307, 320–21, 339–42, 345, 347–48, 354–60, 365–76, 379, 383, 385, 390–94, 397
- sulfates and 419–22
- sulfides and 466–69, 472–77

Bulk chemical analysis 244

Bulk composition 93

Burgers vector 109

Bxa 171

Bxo 171, 185

Calcidiscus leptoporus 126

Calcination 405

Calc-silicates 263

Calomel 8

Calories 94

Canadian Mineralogist journal 12

DO NOT COPY e48d507df5d1141@placeholder.9409

Printed by: e48d507df5d1141@placeholder.94092.edu. Printing is for personal, private use only. No part of this book may be reproduced or transmitted without publisher's prior permission. Violators will be prosecuted.

Canadian Mineralogist journal 12

Cancer 8, 271, 301, 311, 313, 439, 457

Capillary crystals 48

Carbonates

- aggregates and 410
- cleavage and 402–15
- color and 402, 404–16
- diffraction and 403, 412
- fracture and 404–15
- gems and 412, 487
- habit and 403, 412, 414
- hardness and 404, 407
- inversion and 412
- light and 404, 408, 411
- luster and 404–15
- mass and 405
- OH-bearing 414–17
- optical mineralogy and 404–15
- ores and 407–10, 413–15
- point groups and 401
- polarized light and 404, 407–8
- reflection and 407
- refraction and 404–15
- rhombohedral 401–10
- rotation and 404–13
- shape and 406, 409, 412
- specific gravity and 404, 407–8, 410–13
- streak and 404, 406–15
- structure of 400–1
- symmetry and 401, 404, 407–8, 410, 413
- twinning and 402–3, 406–15
- unit cells and 401–3, 411
- X-rays and 403, 412, 414
- zones and 402, 404, 406, 409, 412

Carbon cycle 488–91

Carbon sequestration 283

Carcinogens 271

DO NOT COPY
e48d507df5d1141@placeholder.9409

Printed by: e48d507df5d1141@placeholder.94092.edu. Printing is for personal, private use only. No part of this book may be reproduced or transmitted without publisher's prior permission. Violators will be prosecuted.

Carlsbad twinning
mineral growth and 112–13
optical mineralogy and 199
silicates and 269, 281–87, 290, 291–92, 303
Cathodoluminescence 215, 218, 233, 385
Cation coordination 78–79
Cation lines 109
Cations 58
Cell intercepts 30–32
Chain silicates 242
amphibole group 349–61
igneous 336–38
metamorphic 338
optical mineralogy and 336, 339–49, 352–61
pyroxene group 334–46
pyroxenoids 346–49
sedimentary 338
twinning and 338–48, 354–60
Characteristic X-rays spectrum 203
Charge transfer transitions 138–39
Chatoyancy 142, 280
Chemical analysis
analytical instrumentation for 214–27
bulk 244
cleavage and 228–29
conventions in reporting 225–26
conversion to structural formulas 226–27
crystal form and 216
diffraction and 215–16, 219, 223
electron beam instruments 214
light and 214–23, 233–34
major elements 225
mass spectrometry and 224–25
mineral grain and 216, 218, 221, 224–25
mining and 224
periodic table of the elements and 226

DO NOT COPY
e48d507df5d1141@placeholder.9409

Printed by: e48d507df5d1141@placeholder.94092.edu. Printing is for personal, private use only. No part of this book may be reproduced or transmitted without publisher's prior permission. Violators will be prosecuted.

radiation types 216–23
shape and 223
spectrometers and 215–25
trace elements 225–26
wet chemical 214
X-rays and 214–24, 227
zones and 214

Chemical bonding
asymmetric charge distribution and 68–69
conductors and 67–68
covalent 62–64, 76–81
hydrogen 68–69
insulators and 67–68
ionic 61–62
metallic 64–66, 74–76
semiconductors and 67–68
valence dependent 61–67
van der Waals 69

Chemical pretreatment 327

Chemical weathering 92

Chemical zoning
mineral growth and 106, 119
optical mineralogy and 175
silicates and 233, 282, 285, 369, 373, 376, 380, 384

Chitons 126

Chlorobium ferroxidans 125

Chromophore elements 138

Circular sections 167, 171

Claystone 253

Cleavage
carbonates and 402–15
chemical analysis and 228–29
crystal chemistry and 62
crystallography and 3, 6, 14–15, 30, 33–34, 41–42, 49, 205, 209
crystal structure and 83
determinative tables and 499–504

DO NOT COPY
e48d507df5d1141@placeholder.9409

Printed by: e48d507df5d1141@placeholder.94092.edu. Printing is for personal, private use only. No part of this book may be reproduced or transmitted without publisher's prior permission. Violators will be prosecuted.

fair 11, 134–35
fracture and 6, 110, *see also* Fracture
good 11, 134–35
halides and 454–56
hardness and 4, 9, 131, 133, 158, 195, 232, 269, 283, 289, 317, 341–46, 357, 359, 392, 397, 404, 419–21, 427, 445, 457
hydroxides and 450–53
mineral growth and 110–14
molybdates and 428–30
native elements and 481–87
optical mineralogy and 158, 167–68, 173–77, 195–200
oxides and 433–49
perfect 10, 134–35
phosphates and 424–28
poor 11, 134–35
silicates and 254, 256–57, 269–72, 275, 283–85, 289–304, 310–23, 330–35, 338–61, 365–98
slaty 256–57
study strategies and 231–32
sulfates and 417–24
sulfides and 465–77
symmetry and 3, 15, 41–42, 83, 133–34, 174–77, 304, 370, 390, 404, 407–10, 413, 422
tungstates and 428–30
Cleavage form 134
Cleavage planes 134
Cloizeaux, Alfred Des 5
Closed form 35
Closest packing 74
Closure temperature 119–20
Coccolithophores 126
Coccoliths 126
Cold field emission electron gun 211
Color
allochromatic 142
band theory and 138–40
borates and 428–30
carbonates and 402, 404–16

DO NOT COPY
e48d507df5d1141@placeholder.9409

Printed by: e48d507df5d1141@placeholder.94092.edu. Printing is for personal, private use only. No part of this book may be reproduced or transmitted without publisher's prior permission. Violators will be prosecuted.

carbonates and 402, 404–16
charge transfer transitions and 138–39
consistency of 142
crystal chemistry and 67, 214, 218, 223
crystal field theory and 138–39
crystallography and 49
crystal structure and 84, 86
determinative tables and 499–504, 507–8, 513–14
extinction angle and 173–75
halides and 454–57
hydroxides and 449–54
idiochromatic 142
interference figures and 173–75
iridescence and 142
luminescence and 119, 131, 137, 142–43, 215, 218, 233, 385, 460, 467
luster and 6, 9, 11, 131, 136–43, 154, 158, 195, 232, 238, 294, 297, 312, 315–16, 332, 339, 344, 348, 369, 381, 393, 428, 446–49, 459–60, 467–70, 475, 485, 487
from mechanical causes 141–42
mineral growth and 106, 122–25
molybdates and 428–30
native elements and 479–91
optical mineralogy and 153–200
oxides and 433–49
perception of 136–37
phosphates and 424–28
physical properties and 5–11, 131, 136–43
pleochroism and 172–73, 194
sign of elongation and 173–75
silicates and 244, 255, 257, 264, 269–76, 283–302, 310–98
streak and 9–11, *see also* Streak
study strategies and 232–33, 238
sulfates and 417–24
sulfides and 459–78
tungstates and 428–30
Color centers 138, 141
Columnar crystals 48
Commission on Isotropic Abundances and Atomic Weights 52
Commission on New Minerals, Nomenclature and Classification 5

DO NOT COPY
e48d507df5d1141@placeholder.9409

Printed by: e48d507df5d1141@placeholder.94092.edu. Printing is for personal, private use only. No part of this book may be reproduced or transmitted without publisher's prior permission. Violators will be prosecuted.

Commission on New Minerals, Nomenclature and Classification 5

Compensator plates 157

Complete solid solution series 87–88

Compositional maturity 255

Composition plane 112

Composition surface 112

Condensing lens 155

Conduction band 65, 139

Conductors 67–68, 146–47

Conflict minerals 7

Conglomerates 253

Conoscopic illumination 156

Constancy of interfacial angles 4

Contact metamorphism 263

Contact twins 112

Continental collision 252

Continental cratons 256

Continuous solid solution series 87–88

Continuous spectrum X-rays 202

Converse piezoelectric effect 147

Coordination number 71, 76

Coordination polyhedron 76

Coordination principle 76–79

Coulomb's law 62

Coupled substitution 87–88

Covalent bonding 62–64

Critical angle 154

Critical growth radius 102

Critical minerals 7

Crossed polarizers 156

Crushing 234

Cryptoperthite 280

Crystal axes

assigning 24

DO NOT COPY e48d507df5d1141@placeholder.9409

Printed by: e48d507df5d1141@placeholder.94092.edu. Printing is for personal, private use only. No part of this book may be reproduced or transmitted without publisher's prior permission. Violators will be prosecuted.

assigning 24
crystal faces and 9, 17, 21–22, 29–34, 41, 46–48, 231, 283, 353
inconsistencies in 238
indices and 31–33
isometric system and 46
monoclinic system and 41
optical mineralogy and 171–72, 175, 188
origin and 17
orthorhombic system and 42
point groups and 25
reflection and 21, 210
silicates and 283, 289
sulfates and 419, 422
tetragonal system and 43
triclinic system and 40–41
unit cells and 14–20, 25, 29–34, 41–42, 46–47, 114, 167, 210, 419
Crystal chemistry
abundance of elements and 60–61
asymmetric charge distribution and 68–69
chemical bonding and 61–69
cleavage and 62
color and 67, 214, 218, 223
conductors and 67–68
density and 61
diffraction and 69
electronegativity and 59
hardness and 63–64
insulators and 67–68
lattices and 67
light and 52, 55, 58, 68
magnetism and 54–55
nature of elements and 52–59
periodic table and 52–55, 59, 70
polarized light and 69
shape and 54, 69, 71
size of atoms and 69–72
sulfides and 459–60
symmetry and 62–63, 66–69

DO NOT COPY
e48d507df5d1141@placeholder.9409

Printed by: e48d507df5d1141@placeholder.94092.edu. Printing is for personal, private use only. No part of this book may be reproduced or transmitted without publisher's prior permission. Violators will be prosecuted.

symmetry and 62–63, 66–69
unit cells and 68
valence-related bonding and 61–67
X-rays and 69–70
Crystal class
crystal forms and 40–47
nomenclature of 14
Crystal faces
anhedral 48
crystal axes and 9, 17, 21–22, 29–34, 41, 46–48, 231, 283, 353
crystal form and 35–40
euhedral 48
Law of Bravais and 29
Law of Haüy and 29
Miller index and 14, 30–35, 40, 111–12, 134–35, 207, 231, 354
subhedral 48
Crystal family 27
Crystal field splitting 138
Crystal field theory 138–39
Crystal forms
chemical analysis and 216
closed 35
combining 38
crystal class and 40–47
crystal faces and 35–40
enantiomorphous 38–40
halides and 455
isometric 35–37
mineral growth and 95, 105
negative 40
nomenclature of 14
nonisometric 37–38
open 35
physical properties and 134–35
positive 40
silicates and 377
study strategies and 229

DO NOT COPY
e48d507df5d1141@placeholder.9409

Printed by: e48d507df5d1141@placeholder.94092.edu. Printing is for personal, private use only. No part of this book may be reproduced or transmitted without publisher's prior permission. Violators will be prosecuted.

Crystalline solids 3–4

Crystallization 92

Crystallographic directions 14, 34–35, 194, 200

Crystallography

- aggregates and 48–49
- analytical instrumentation for 201–13
- angle measurement and 26
- cleavage and 3, 6, 14–15, 30, 33–34, 41–42, 49, 205, 209
- color and 49
- density and 29–30
- diffraction and 15, 17, 24, 201–12
- error sources and 209
- fracture and 48
- habit and 5, 9, 14, 42, 46, 48–50
- inversion and 14, 21–27, 30, 37, 39–40, 43, 46–47
- lattices and 14–24, 28–30, 34–35, 42, 204, 208
- light and 32, 48, 201, 203–4
- mass and 52, 61
- Miller index and 14, 30–35, 40, 207
- mineral grain and 14, 48–49
- mining and 211
- nomenclature for 14
- ore and 49
- point groups and 14, 24–28, 35, 37–48
- polarized light and 217
- reflection and 14, 21, 28, 36–37, 204–11
- refraction and 204
- relative abundance estimation and 209–10
- rotation and 14, 21–29, 32, 37, 40–43, 48
- shape and 14–22, 29, 37–38, 41, 48–49, 207
- space groups and 27–29
- symmetry and 14–29, 35–48, 205–6
- transmission electron microscopy and 211–13
- unit cells and 14–21, 24–25, 29–34, 40–42, 46–47, 207, 210
- X-rays and 15, 17, 24, 201–12
- zones and 14, 17, 25, 34–35, 40–41, 48

Crystal structure

DO NOT COPY e48d507df5d1141@placeholder.9409

Printed by: e48d507df5d1141@placeholder.94092.edu. Printing is for personal, private use only. No part of this book may be reproduced or transmitted without publisher's prior permission. Violators will be prosecuted.

bond strength 79–80
cleavage and 83
color and 84, 86
composition variation and 86–88
controls of 73–83
coordination principle and 76–79
covalent bonding and 76
density and 76, 83, 90
electrostatic valency principle 79–80
graphic representation and 89–90
habit and 83
illustrating 73
inversion and 84–85
ionic bonding and 76–81
isostructural minerals 83
lattices and 75–76, 85
light and 77, 79
metallic bonding and 74–76
mineral classification and 85–86
mineral formulas and 89–91
molecular controls and 83
Pauling's Rules and 76, 81–83, 86–87
periodic table of the elements and 75
point groups and 83
polymorphism and 83–85
principle of parsimony and 81
shape and 73, 76, 83, 85
sharing polyhedral elements and 80–81
solid solutions and 86–88
sphere packing and 74–75
symmetry and 79–85
unit cells and 73–74, 76, 82–86, 90–91
Crystal systems 210
Bravais lattices and 17–21
combining forms and 38
Hermann-Maugin symbols and 23
hexagonal 17, 31–33, 43–46, 79

DO NOT COPY
e48d507df5d1141@placeholder.9409

Printed by: e48d507df5d1141@placeholder.94092.edu. Printing is for personal, private use only. No part of this book may be reproduced or transmitted without publisher's prior permission. Violators will be prosecuted.

isometric (cubic) 17, 46–48, 79
lattices and 14–20, 24, 29, 43, 109
mineral growth and 113
monoclinic 17, 41
nonisometric forms and 37
optical mineralogy and 151, 153, 158–59, 170, 194
orthorhombic 17, 42
oxides and 437
physical properties and 134, 148
point groups and 24–27
reflection and 21
silicates and 268, 298, 366, 371, 398
Steno's Law and 26
study strategies and 231–32
tetragonal 17, 43, 79
triclinic 17, 40–41
Cubic closest packing 74–75
Cubic coordination 78
Cupriavidus metallidurans 481
Curie temperature 145
Cyclic twin 113
Dana, James D. 5
Dana's Manual of Mineralogy (Dana) 12
Dana system 86
Decay 117–22
Decompression melting 251
Deformation 109
Deformation twinning 114
Democratic Republic of Congo (DRC) 7
Dendrites 453
Density
composition and 131–32
controls on 131–32
crystal chemistry and 61
crystallography and 29–30
crystal structure and 76, 83, 90

DO NOT COPY e48d507df5d1141@placeholder.9409

Printed by: e48d507df5d1141@placeholder.94092.edu. Printing is for personal, private use only. No part of this book may be reproduced or transmitted without publisher's prior permission. Violators will be prosecuted.

crystal structure and 76, 83, 90
defined 131
energy levels and 140
heft and 133
light and 136
mineral growth and 95, 107, 109, 118, 122
native elements and 480
optical mineralogy and 152–53, 168
oxides and 439
separation and 235–36
silicates and 247, 258, 317
specific gravity and 10, 131
study strategies and 9–10, 234–36
sulfates and 423
Desert varnish 453
Desiccants 300
Detection limits 221
Determinative tables
cleavage and 499–504
color and 499–504, 507–8, 513–14
grain mount and 507–8
hardness and 499–504
index of refraction 509–13
light and 514
luster and 504
magnetism and 506
opaque minerals 513–14
reflection and 513–14
refraction and 509–10, 512
specific gravity and 505–6
streak and 504
Detrital grains 92
Diagenesis 253
Diamagnetism 142–43
Diffraction 3, 5, 11
carbonates and 403, 412
chemical analysis and 215–16, 219, 223

DO NOT COPY
e48d507df5d1141@placeholder.9409

Printed by: e48d507df5d1141@placeholder.94092.edu. Printing is for personal, private use only. No part of this book may be reproduced or transmitted without publisher's prior permission. Violators will be prosecuted.

chemical analysis and 210–16, 219, 223
crystal chemistry and 69
crystallography and 15, 17, 24, 201–12
hydroxides and 451–52
mineral growth and 122
optical mineralogy and 158
oxides and 443
phosphates and 426
physical properties and 142
silicates and 274–75, 279–80, 297, 304, 310–14, 318, 322–24, 327, 347, 350, 369, 371
study strategies and 231–34, 237
Diffusion 98–99
Dihedrons 37
Dimensional stone 6
Dioctahedral sheets 304
Dipyramids 37
Discontinuous solid solution series 87–88
Disilicates 242
classification 363–65
optical mineralogy and 365–71
twinning and 365–70
Dispersion 154, 188–91
Dome 37
Double refraction 158–59
D-spacing 204
Dynamic recrystallization 259–60
Earthquakes 3–4, 381
Edge dislocations 109
Effective radius 69–71, 493–98
Elasticity 134
hydroxides and 450
oxides and 443
silicates and 312–18, 322, 354
sulfates and 419
sulfides and 474
Electrical conductivity 146–47

DO NOT COPY
e48d507df5d1141@placeholder.9409

Printed by: e48d507df5d1141@placeholder.94092.edu. Printing is for personal, private use only. No part of this book may be reproduced or transmitted without publisher's prior permission. Violators will be prosecuted.

Electrical conductivity 116–17

Electricity 146–48

Electromagnetic radiation 136

Electron capture 118

Electron color centers 140

Electronegativity 59–60, 65–68, 71, 74, 459

Electron microprobe 214

Electron probe microanalyzer (EPMA) 214–16, 219, 223, 233–34

Electrons

- backscattered 218
- capture decay 117
- crystal chemistry and 52–55
- promotion 137, 143
- secondary 216–18

Electron spin 143

Electrostatic valence bond 79–80

Electrostatic valency principle 79–80

Electrostriction 147

Elongate crystals 48

End members 87–88

Energy 93

Energy-dispersive X-ray spectrometers (EDS) 219–21

Epitaxial nucleation 103

Equant crystals 48

Equilibrium 94

Equilibrium crystallization 96

Equilibrium melting 97–98

Euhedral faces 48

European Journal of Mineralogy 12

Eutectic composition 97

Eutectic temperature 97

Evaporites 415–16

Exsolution 87, 115–17

Extinction 163–64, 268–69, 315

DO NOT COPY e48d507df5d1141@placeholder.9409

Printed by: e48d507df5d1141@placeholder.94092.edu. Printing is for personal, private use only. No part of this book may be reproduced or transmitted without publisher's prior permission. Violators will be prosecuted.

Extinction angle 173–75

Extraordinary rays 167–68

Fast rays 159

Felsic silicates 244

Felted masses 50, 298, 344

Fenitization 343

Ferrimagnetism 143, 145–46

Ferromagnetism 143, 145

Fibrous crystals 48

Field notebook 228

Field study 228–30

Filiform crystals 48

Fink search method 208

First-order red plate 164

First-order reflection 204

Fission tracks 118, 121

Flash figures 178–80, 183

Fluorescence 143

Flux melting 251

Focusing mechanism 157

Foliation 256

Foraminifera 126

Formula units 91

Fourth-order reflection 204

Fractional crystallization 106, 250–51

Fractional melting 248, 250

Fractionation series 251

Fracture 6–8

- carbonates and 404–15
- conchoidal 10, 269, 283
- crystallography and 48
- hackly 10
- halides and 454–56
- hydroxides and 453

DO NOT COPY
e48d507df5d1141@placeholder.9409

Printed by: e48d507df5d1141@placeholder.94092.edu. Printing is for personal, private use only. No part of this book may be reproduced or transmitted without publisher's prior permission. Violators will be prosecuted.

hydroxides and 453
irregular 10
mineral growth and 108, 110, 119
native elements and 480–83, 487
optical mineralogy and 195–96
oxides and 433–34, 438, 441–49
phosphates and 425–28
physical properties and 9–11, 131, 133, 135–36
silicates and 263, 269, 271, 275, 283, 290–95, 301, 331–32, 339–48, 354, 357–60, 365–69, 372–76, 379–85, 390–93, 397–98
splintery 10
study strategies and 228–29, 232
sulfates and 421–22
sulfides and 461, 466–77
Fracture surfaces 135
Framboids 472–73
Framework silicates 242
feldspar group 276–94
feldspathoids 293–96
open structure of 267
optical mineralogy and 269–75, 283–86, 289–97, 300, 302
silica group 267–76
twinning and 268–72, 275, 278–86, 289–96, 301
zerolite group 296–301
Frantz Isodynamic Magnetic Separator 236–37
Frantz Magnetic Barrier Separator 237
Frenkel defects 108–9
Frequency 151
Fresnel equation 153–54
Full-wave plate 164
Gabbro
chemical analysis and 217, 220–21
mineral associations and 515
oxides and 441, 446
silicates and 244–47, 251, 261, 264, 270, 284, 317, 336–39, 342, 356, 359, 370
Gems
carbonates and 412

DO NOT COPY
e48d507df5d1141@placeholder.9409

Printed by: e48d507df5d1141@placeholder.94092.edu. Printing is for personal, private use only. No part of this book may be reproduced or transmitted without publisher's prior permission. Violators will be prosecuted.

carbonates and 412
color and 6
luster and 6
mineral variety and 5
native elements and 487
oxides and 442, 444–45
physical properties and 139, 141
as protection 8
reconstructive polymorphisms and 84
silicates and 271, 275, 331–32, 366, 368, 373, 375, 381
society and 6
synthetic 6
Geobacter metallireducens 125
Geochronology 118–21
Geologically ephemeral elements 53
Geomicrobiology 4
Gibbs free energy 94
Gibbs free energy of formation 94
Glide planes 28–29, 114
Glycolating 328
Gneissic roliation 257
Gossan 462
Grain boundaries 110
Grain mount
determinative tables 507–8
optical mineralogy and 150, 195, 196
study strategies and 233
Grain size 148
carbonates and 414
chemical analysis and 223
crystallography and 209
determinative tables and 503
hydroxides and 450–52
mineral growth and 102–3, 115
optical mineralogy and 157, 195–96
oxides and 447

DO NOT COPY
e48d507df5d1141@placeholder.9409

Printed by: e48d507df5d1141@placeholder.94092.edu. Printing is for personal, private use only. No part of this book may be reproduced or transmitted without publisher's prior permission. Violators will be prosecuted.

phosphates and 425, 427–28
silicates and 246–48, 253–56, 259–61, 273–74, 297, 300, 310, 319, 322–23, 367, 382, 385
study strategies and 229–34
Grain washing 235
Granite 92, 230
Granophyric intergrowths 281
Graphic intergrowths 281
Gypsum plate 164
Habit
borates and 421
carbonates and 403, 412, 414
crystallography and 5, 9, 14, 42, 46, 48–50
crystal structure and 83
forms of 48–50
molybdates and 429
native elements and 487
optical mineralogy and 177, 195, 197
oxides and 441–42, 445, 447
phosphates and 425–28
silicates and 268, 272–73, 288–98, 304, 309–12, 315–21, 324, 327, 332, 347, 356–59, 362, 366, 371–74, 377, 384–86, 390–93, 396–98
study strategies and 228, 232
sulfates and 418–19
sulfides and 469–74, 477–78
tungstates and 429
Half-life 117
Halides
cleavage and 454–56
crystal form and 455
fracture and 454–56
lattices and 454, 456
light and 454, 457
luster and 454–56
mass and 462
mining and 455
optical mineralogy and 454–57

DO NOT COPY
e48d507df5d1141@placeholder.9409

Printed by: e48d507df5d1141@placeholder.94092.edu. Printing is for personal, private use only. No part of this book may be reproduced or transmitted without publisher's prior permission. Violators will be prosecuted.

optical mineralogy and 191–97
refraction and 454–57
rotation and 456
shape and 454
streak and 454–57
twinning and 454–56
unit cells and 454
zones and 457
Halogens 55
Hanawalt search method 208
Handbook of Mineralogy (Anthony, et al) 12
Hand lens 9
Hardness
carbonates and 404, 407
cleavage and 4, 9, 131, 133, 158, 195, 232, 269, 283, 289, 317, 341–46, 357, 359, 392, 397, 404, 419–21, 427, 445, 457
crystal chemistry and 63–64
defined 10
determinative tables and 499–504
hydroxides and 451, 457
indentation 134
measurement of 133–34
Moh's scale of 133–34
native elements and 487
optical mineralogy and 158, 195
oxides and 441–42, 445
phosphates and 425–29
silicates and 255, 269, 275, 283, 289, 297, 301, 307–8, 317, 320, 322, 332, 341–46, 357, 359, 373–74, 384–87, 390–93, 396–97
streak and 9, 131, 142, 195, 232, 297
study strategies and 231–32, 238
sulfates and 419, 421
sulfides and 470, 472
Vickers 134
Haüy, René Juste 4
Hexagonal closest packing 74–75
Heating 327–28

DO NOT COPY
e48d507df5d1141@placeholder.9409

Printed by: e48d507df5d1141@placeholder.94092.edu. Printing is for personal, private use only. No part of this book may be reproduced or transmitted without publisher's prior permission. Violators will be prosecuted.

Heavy minerals 255
Heft 10, 133, 232
Henry II, King of France 8
Hermann-Mauguin symbols 23–25, 42–46
Heterogeneous nucleation 103
High-grade metamorphic rock 93
High relief 189–90
High spin 71–72
Hippocrates 8
Hole color centers 141
Homogeneous nucleation 101–3
Horizontal dispersion 189
Hornfels 257, 262, 265, 315, 317, 356, 375, 387, 445, 516
Hot spots 251–53
Hund's Rule 145
Huttenlocher intergrowths 280
Hydrogen bonding 68–69
Hydrothermal deposits 460–64, 517
Hydrothermal metamorphism 263
Hydroxides
aluminum 451–52
cleavage and 450–53
color and 449–54, 454–57
dendrites 453
desert varnish and 453
diffraction and 451–52
fracture and 453
hardness and 451, 457
iron 450–51
laterite and 451–52
luster and 450–54
manganese 452–53
mineral grain and 452
optical mineralogy and 450–52
ores and 452

DO NOT COPY
e48d507df5d1141@placeholder.9409

Printed by: e48d507df5d1141@placeholder.94092.edu. Printing is for personal, private use only. No part of this book may be reproduced or transmitted without publisher's prior permission. Violators will be prosecuted.

radioactivity and 117–22
reflection and 451
refraction and 450–51
specific gravity and 451–52
streak and 450–54
twinning and 450–52
unit cells and 450–52
X-rays and 451–52
Hypogene processes 462
Idiochromatic color 142
Igneous rock 92
chain silicates and 336–38
continental collision and 252
hot spots and 251–53
intracontinental rifting and 252–53
magmatic processes and 251
mid-ocean ridges and 251
mineral associations and 515
mineral growth and 92
oceanic hot spots and 251
silicates and 244–53
subduction zones and 251–52
Illite group 325
Illuminator 155
Immersion method 189
Immersion oil 150
Impact melts 4
Impurity defects 108–9
Inclined dispersion 189
Incline extinction 174
Inclusions 106–7
Incomplete solid solution series 87–88
Incongruent melting 248, 250
Intracontinental rifting 252–53
Indentation hardness 134

DO NOT COPY
e48d507df5d1141@placeholder.9409

Printed by: e48d507df5d1141@placeholder.94092.edu. Printing is for personal, private use only. No part of this book may be reproduced or transmitted without publisher's prior permission. Violators will be prosecuted.

Index minerals 262

Index of refraction

- Becke line method and 190–91
- biaxial minerals and 193–94
- determinative tables and 509–13
- dispersion effects and 191
- immersion method and 189–90
- refractometry and 193
- relief and 189–90
- uniaxial minerals and 193

Indicatrix dispersion 188

Industrial minerals 241

Insulators 67–68

Integrated intensity 206–7

Interference

- accessory plates and 164–66
- anisotropic minerals and 159–66
- birefringence and 159, 163
- extinction and 163–64
- monochromatic illumination and 159–62
- order of 166

Interference color chart 161–63

Interference figures

- biaxial 180–89
- determining 2V 186–88
- dispersion effects and 188–89
- obtuse bisectrix 182–83
- off-center 177–78, 183–85
- optical mineralogy and 173–75
- optic axis 176–77, 182
- optic normal (flash) 178–80, 183
- optic sign determination and 180, 185–88
- uniaxial 176–80

Interlayer 304

Intermolecular bonds 68–69

International Agency for Research on Cancer 271

DO NOT COPY
e48d507df5d1141@placeholder.9409

Printed by: e48d507df5d1141@placeholder.94092.edu. Printing is for personal, private use only. No part of this book may be reproduced or transmitted without publisher's prior permission. Violators will be prosecuted.

International Agency for Research on Cancer 271
International Centre for Diffraction Data 207–8
International Mineralogical Association 5
International Union of Pure and Applied Chemistry 53
Interstitial defects 108
Interstitial solid solutions 87–88
Intervalence charge transfer 139, 376, 391, 439, 445
Intraplate volcanic centers 251
Inversion
  carbonates and 412
  crystallography and 14, 21–27, 30, 37–40, 43, 46–47
  crystal structure and 84–85
  mineral growth and 111–12
  physical properties and 147–48, 172
  rotoinversion axes and 22
  silicates and 272
  symmetry and 14, 21–27, 40, 43, 46, 84, 85, 111, 147–48, 172
Ionic bonding 61–62
  coordination principle 76–79
  crystal structure and 76–81
  electrostatic valency principle 79–80
  principle of parsimony 81
  sharing polyhedral elements and 80–81
Ionic radii 69–71, 493–98
Ions
  anions 58–59
  cations 58–59
  electronegativity and 59
  formation of 58–59
  valance and 58–59
Iridescence 142, 280
Island arc 252, 264–65
Isochromes 175–76
Isodesmic bonding 79
Isograd boundaries 262
Isogyres 175–76

DO NOT COPY
e48d507df5d1141@placeholder.9409

Printed by: e48d507df5d1141@placeholder.94092.edu. Printing is for personal, private use only. No part of this book may be reproduced or transmitted without publisher's prior permission. Violators will be prosecuted.

Isogyres 178–79

Isomorphism 83

Isostructural minerals 83

Isotopes
- borates and 431
- carbonates and 405
- chemical analysis and 220, 224–25
- crystal chemistry and 52–53
- mineral growth and 117–21
- native elements and 485
- oxides and 435–36
- silicates and 301, 384, 386

Isotropic indicatrix 166–67

Isotropic minerals
- index of refraction and 193
- optical mineralogy and 157–58, 172, 192
- refractometry and 193

Isotypism 83

Jolly balance 132

Joules 94

Labradorescence 280

Lamellae 112–13

Lanthanide series 55

Laterite 451–52

Lattices
- Bravais 14–21, 24, 28
- crystal chemistry and 67
- crystallography and 14–24, 28–30, 34–35, 42, 204, 208
- crystal structure and 75–76
- crystal systems and 14–21, 24, 29, 43, 109
- cubic 17, 19, 21, 29, 62, 75–76, 272, 456, 483
- diamond 15–18
- halides and 454, 456
- hexagonal 15–24, 29, 75
- lines 15
- mineral growth and 105–10, 114–15, 118
- nodes 15, 21, 28, 30, 34, 35, 75, 76, 105, 109, 473

DO NOT COPY
e48d507df5d1141@placeholder.9409

Printed by: e48d507df5d1141@placeholder.94092.edu. Printing is for personal, private use only. No part of this book may be reproduced or transmitted without publisher's prior permission. Violators will be prosecuted.

nodes 15–21, 28–30, 34–35, 75–76, 105, 109, 473
oblique 15–18
orthorhombic 17–19, 109
physical properties and 145, 148
plane 15–21
primitive unit meshes and 16
rectangular 15–19, 105
silicates and 259, 268, 272, 278, 302, 371
space 16–17, 105
square 15–16, 19–22
sulfides and 471, 473, 483
tetragonal 17, 19, 21, 24, 28, 43, 272
Law of Bravais 29
Law of Constancy of Interfacial Angles 26
Law of Haüy 29
Layered mafic intrusions 252–53
Layer repeat distance 306
Lepispheres 274–75
Lever rule 97
Light
absorption 137–40, 143, 153, 161, 209, 404, 408, 434, 439, 442, 459–60
anisotropic materials and 158–66
carbonates and 404, 408, 411
chemical analysis and 214–23, 233–34
crystal chemistry and 52, 55, 58, 68
crystallography and 32, 48, 201, 203–4
crystal structure and 77, 79
density and 136
determinative tables and 514
diffraction and 3, *see also* Diffraction
dispersion and 154
electromagnetic radiation and 136
extinction angle and 173–75
frequency 151
halides and 454, 457
incandescent 143, 201, 429, 442
interaction with matter 152–54

DO NOT COPY
e48d507df5d1141@placeholder.9409

Printed by: e48d507df5d1141@placeholder.94092.edu. Printing is for personal, private use only. No part of this book may be reproduced or transmitted without publisher's prior permission. Violators will be prosecuted.

interaction with matter 152–54
interference figures and 173–75
isotropic materials and 157–58
luminescence and 119, 131, 137, 142–43, 215, 218, 233, 385, 460, 467
mineral growth and 95, 108, 121
monochromatic 136
native elements and 486–87, 491
opaque minerals and 152
optical indicatrix and 158–66
optically anisotropic 151–53
optically isotropic 151–53
optical mineralogy and 150–200
oxides and 434–35, 439, 442–45
perception of 136–37
petrograpic microscope and 154–57
phosphates and 425–26, 428
photons 136, 150–51, 204
physical properties and 4, 9–11, 131–43
plane 108, 152, 156–59, 164, 167–68, 172–73, 189, 194–200, 217, 270, 285, 291, 292, 309, 353, 367, 370, 374, 376, 380, 384–85, 389, 393–97, 403, 421, 425, 444
pleochroism and 172–73
polarized 4, 6, 69, 106, 108, 150–52, 154–56, *see also* Polarized light
polychromatic 136
reflection and 150, *see also* Reflection
refraction and 106, 185–200, *see also* Refraction
sign of elongation and 173–75
silicates and 270, 275, 280–301, 305, 308–9, 323, 345, 353, 367, 374, 376, 380, 384–89, 393–4, 396–98
streak and 131, *see also* Streak
sulfates and 421, 423
sulfides and 459–60, 465, 468, 470–71
transparent materials and 152
tungstates and 429
ultraviolet (UV) 136, 143, 233, 301, 345, 385, 404, 411, 423, 429, 457, 467, 470
velocity 151
wavelength 151
wave normal 151
Light ray 151

DO NOT COPY
e48d507df5d1141@placeholder.9409

Printed by: e48d507df5d1141@placeholder.94092.edu. Printing is for personal, private use only. No part of this book may be reproduced or transmitted without publisher's prior permission. Violators will be prosecuted.

Linear coordination 78

Line defects 107–10

Liquidus 96

Lithostatic pressure 95, 258

Lodestone 439

Lower polarizer 155

Low-grade metamorphic rock 258

Low-microcline polymorphism 85

Low relief 189–90

Low spin 71–72

Luminescence

- cathodoluminescence 215, 218, 233, 385
- electroluminescence 460, 467
- light and 119, 131, 137, 142–43, 215, 218, 233, 385, 460, 467
- mineral growth and 119
- photoluminescence 143
- thermoluminescence 143, 385
- triboluminescence 142–43

Luster

- carbonates and 404–15
- color and 6, 9, 11, 131, 136–43, 154, 158, 195, 232, 238, 294, 297, 312, 315–16, 332, 339, 344, 348, 369, 381, 393, 428, 446–49, 459–60, 467–70, 475, 485, 487
- determinative tables and 504
- earthy 137
- gems and 6
- halides and 454–56
- hydroxides and 450–54
- metallic 11, 137
- native elements and 481–87
- nonmetallic 11, 137
- optical mineralogy and 153–54, 158, 195
- oxides and 433–49
- pearly 137
- phosphates and 425–28
- physical properties and 131, 136–43
- resinous 137

DO NOT COPY e48d507df5d1141@placeholder.9409

Printed by: e48d507df5d1141@placeholder.94092.edu. Printing is for personal, private use only. No part of this book may be reproduced or transmitted without publisher's prior permission. Violators will be prosecuted.

silicates and 257, 269, 271–75, 283, 290–301, 310–23, 330–32, 339–48, 354–60, 365–85, 390–97
silky 137, 142
splendent 137
study strategies and 232, 238
submetallic 137
sulfates and 419–22
sulfides and 459–60, 467–76
vitreous 137
Mafic silicates 244, 252–53
Magma 92
Magma mixing 250–51
Magmatic differentiation 250
Magmatic processes
assimilation 51
basalt and 61, 123, 252, 299
Bowen's reaction series and 249
fractional crystallization 250–51
igneous environments and 251
magma mixing 250–51
melting 248, 250
Magnetic quantum number 54
Magnetic susceptibility 145
Magnetism
antiferromagnetism 143, 145–46
Bohr magnetic moment and 143
crystal chemistry and 54–55
Curie temperature and 145
determinative tables and 506
diamagnetism 142–43
electron spin and 143
ferrimagnetism 143, 145–46
ferromagnetism 143, 145
mineral growth and 125
oxides and 439, 444, 446
paramagnetism 143, 145
physical properties and 6–11, 131, 143–46

DO NOT COPY
e48d507df5d1141@placeholder.9409

Printed by: e48d507df5d1141@placeholder.94092.edu. Printing is for personal, private use only. No part of this book may be reproduced or transmitted without publisher's prior permission. Violators will be prosecuted.

physical properties and 6–11, 131, 143–46
quantum 54
remnant 146
separation 236–37
spin quantum number and 143
Magnetotactic bacteria 438
Malleability 66, 76, 134, 479–82
Manebach twinning 281–83, 290–92
Mass 10
atomic mass number 52, 117–18
carbonates and 405
chemical analysis and 214, 224–25
crystal chemistry and 52, 61
density and 9, *see also* Density
dependent properties and 131–33, 147
halides and 462
mineral growth and 117–21
optical mineralogy and 150
oxides and 439
phosphates and 425
silicates and 267, 273, 328, 350, 389
specific gravity and 9, *see also* Specific gravity
Mass number 52
Mass spectrometry 214, 224–25, 350
Maximum-microcline polymorphism 85
Mechanical cohesion 133–36
Medium-grade metamorphic rock 93
Melatope 176
Melting 248, 250–51
Mesodesmic bonding 79–80
Metallic bonding 64–66, 74–76, 139
Metallic luster 11, 137
Metallogenium spp. 453
Metalloids 55
Metamict 4, 122
Metamorphic facies 261

DO NOT COPY
e48d507df5d1141@placeholder.9409

Printed by: e48d507df5d1141@placeholder.94092.edu. Printing is for personal, private use only. No part of this book may be reproduced or transmitted without publisher's prior permission. Violators will be prosecuted.

Metamorphic facies 261

Metamorphic reactions 92

Metamorphic rock 92–93

- chain silicates and 338
- environments for 263–66
- high-grade 258
- low-grade 258
- medium-grade 258
- mineral assemblage and 260–63
- mineral associations and 516–17
- pelitic 261–62
- processes of 259–61
- psammitic 261–62
- silicates and 256–65
- variables in 258–59

Metasomatism 260

Metastability 93–94

Mica plate 164

Michel-Lévy Chart 161

Michel-Lévy method 285–86

Microperthite 280

Mie scattering 275

Miller-Bravais indices 32–33

Miller index

- assigning 33–34
- crystal faces and 14, 30–35, 40, 111–12, 134–35, 207, 231, 354
- crystallography and 14, 30–35, 40, 207
- determining 33
- mineral growth and 111–12
- physical properties and 134–35
- silicates and 354
- study strategies and 231

Mineralogical Society of America 12

Mindat.org 12

Mineral assemblage 260–63

Mineral associations 237, 515–17

DO NOT COPY
e48d507df5d1141@placeholder.9409

Printed by: e48d507df5d1141@placeholder.94092.edu. Printing is for personal, private use only. No part of this book may be reproduced or transmitted without publisher's prior permission. Violators will be prosecuted.

Mineral associations 237, 315–17

Mineral grain 6
- banded 49
- botryoidal 49
- boundaries and 110
- chemical analysis and 216, 218, 221, 224–25
- colloform 49
- crystallography and 14, 48–49
- dendritic 49
- detrital 92
- disseminated 49
- drusy 49
- foliated 48
- globular 49
- granular 48
- hydroxides and 452
- intergrown 48
- lamellar 49
- mammillary 49
- massive 49
- micaceous 48
- mineral growth and 92, 94, 101–2, 106–15
- oolitic 49
- optical mineralogy and 150, 159–66, 169, 174–78, 182, 189–91, 196
- parallel 48
- phosphates and 425, 427
- physical properties and 132, 137
- pisolitic 49
- platy 48
- plumose 48
- prismatic 49
- radiating 48
- reniform 49
- reticulated 49
- scaly 48
- silicates and 253–54, 259, 323, 338
- skeletal 49
- stubby 48

DO NOT COPY
e48d507df5d1141@placeholder.9409

Printed by: e48d507df5d1141@placeholder.94092.edu. Printing is for personal, private use only. No part of this book may be reproduced or transmitted without publisher's prior permission. Violators will be prosecuted.

study strategies and 228, 234–37

Mineral group 5

Mineral growth

aggregates and 92, 94, 117

applications for 127

binary systems 96–101

biomineralization and 123–26

cleavage and 110–14

color and 106, 122–25

crystal form and 95, 105

crystal growth and 103–7

crystal systems and 113

density and 95, 107, 109, 118, 122

diffraction and 122

evolution and 122–23

fracture and 108, 110

igneous rock and 92

inversion and 111–12

lattices and 105–10, 114–15, 118

light and 95, 108, 121

luminescence and 119

magnetism and 125

mass and 117–21

Miller index and 111–12

mineral grain and 92, 94, 101–2, 106–15

nucleation and 101–3

ores and 127

phase diagrams and 95–101

point groups and 105

polarized light and 106, 108

postcrystallization processes and 114–22

rate of 103–5

reactions and 94–95

reflection and 111–14

refraction and 106, 122

rotation and 111–13

shape and 92, 108–9, 113–14, 117, 121

DO NOT COPY e48d507df5d1141@placeholder.9409

Printed by: e48d507df5d1141@placeholder.94092.edu. Printing is for personal, private use only. No part of this book may be reproduced or transmitted without publisher's prior permission. Violators will be prosecuted.

stability and 93–95
structural defects and 107–11
symmetry and 111–15
twinning and 111–14
unit cells and 105, 114–15
X-rays and 122
zones and 105–6, 118–19, 122, 125–27
Mineral identification tactics 232–34
Mineralogical Magazine 12
Mineralogical Society of America 5
Mineraloids 4
Minerals
accessory 245
amorphous 3
biominerals 4
classification of 85–86
compositional variation in 86–89
conflict 7
critical resources of 7
crystalline solids 3–4
formulas 89–91
gems 6, *see also* Gems
general references for 11–12
health and 8
heavy 255
industrial 241
medical uses of 8–9
nomenclature for 5–6
naturally occurring 3
non-crystalline 3
physical properties and 9–11, *see also* Physical properties
radioactivity and 117–22
society and 6–9
synthetic 3
tactics for identification 195–200
use of term 3
value of 7

DO NOT COPY
e48d507df5d1141@placeholder.9409

Printed by: e48d507df5d1141@placeholder.94092.edu. Printing is for personal, private use only. No part of this book may be reproduced or transmitted without publisher's prior permission. Violators will be prosecuted.

values of 7

Mineral separation 234–36

Mineral series 5

Mineral shape *see* Shape

Minerals species 5

Mineral variety 5

Mineral zone boundaries 262

Mining
- chemical analysis and 224
- crystallography and 49, 211
- halides and 455
- natural resources and 4, 6–7, 10
- ores and 4, 6–7, 127, 234
- silicates and 271, 311, 356, 384
- study strategies and 234
- sulfates and 420
- sulfides and 461, 470–71, 473, 478

Modal mineralogy 246

Moderate dispersion 188

Moderate relief 189–90

Moh's scale of hardness 133–34

Molecular bonds 68–69

Molecular sieve 300

Molybdates
- cleavage and 428–30
- color and 428–30
- habit and 429
- optical mineralogy and 429
- ores and 429
- refraction and 429–30
- twinning and 429
- unit cells and 429

Monochromatic light 136

Mortar 405

Mud rock 253

Mudstone 253

DO NOT COPY e48d507df5d1141@placeholder.9409

Printed by: e48d507df5d1141@placeholder.94092.edu. Printing is for personal, private use only. No part of this book may be reproduced or transmitted without publisher's prior permission. Violators will be prosecuted.

Mudstone 253

Multiple twins 112

Myrmekite 281

Native elements
- cleavage and 481–87
- color and 479–91
- density and 480
- fracture and 480–83, 487
- habit and 487
- hardness and 487
- light and 486–87, 491
- luster and 481–87
- metalloids 483
- metals 479–82
- nonmetals 483–91
- optical mineralogy and 480–87
- ores 483–84
- periodic table of the elements and 483
- polarized light and 480, 485
- rotation and 485
- shape and 481, 484, 486
- specific gravity and 481
- streak and 481–87
- symmetry and 486
- twinning and 481–87
- unit cells and 479–80
- X-rays and 482, 491
- zones and 482, 484

Naturally occurring minerals 3–4

Natural resources 4, 6–7, 10

Néel temperature 145

Negative front pedions 41

Neutrons 52

Nicol prism 4–5, 155

Noble-gas core 55

Non-crystalline minerals 3

Nonmetallic luster 11, 127

DO NOT COPY
e48d507df5d1141@placeholder.9409

Printed by: e48d507df5d1141@placeholder.94092.edu. Printing is for personal, private use only. No part of this book may be reproduced or transmitted without publisher's prior permission. Violators will be prosecuted.

Nonmetallic luster 11, 137

Nonmetals 55

Nonuniform bonding 82

Nonuniform bond strength 79–80

Normative mineralogy 246

Nucleation 101–3

Numerical aperture 156

Objective lenses 156

Obsidian 4

Obtuse bisectrix 171, 182–83

Oceanic hot spots 251

Ocean ridge 251–52, 264–65, 371, 463

Octahedral coordination 78

Oculars 157

Off-center interference figures 183–84

Off-center optic axis figure 177–78

Omission solid solutions 87–88

One-wavelength plate 164

On Stones (Theophrastus) 4

Opaque minerals 152, 513–14

Open form 35

Optical character 159

Optical indicatrix

- biaxial 170–72
- isotropic 166–67
- uniaxial 167–70

Optically anisotropic light 151–53

Optically biaxial minerals 159

Optically isotropic light 151–53

Optically negative minerals 171

Optically neutral minerals 171

Optically positive minerals 171

Optically uniaxial minerals 167

Optical mineralogy

DO NOT COPY e48d507df5d1141@placeholder.9409

Printed by: e48d507df5d1141@placeholder.94092.edu. Printing is for personal, private use only. No part of this book may be reproduced or transmitted without publisher's prior permission. Violators will be prosecuted.

Optical mineralogy
anisotropic materials and 158–66
borates and 430
carbonates and 404–15
chain silicates and 336, 339–49, 352–61
cleavage and 158, 167–68, 173–77, 195–200
color and 153–200
crystal axes and 171–72, 175, 188
crystal systems and 151, 153, 158–59, 170, 194
density and 152–53, 168
diffraction and 158
disilicates and 365–71
dispersion and 154
extinction angle and 173–75
fracture and 195–96
framework silicates and 269–75, 283–86, 289–97, 300, 302
habit and 177, 195, 197
halides and 454–57
hardness and 158, 195
hydroxides and 450–52
identification tactics and 195–200
interference figures and 173–75
isotropic materials and 157–58
light and 150–200
luster and 153–54, 158, 195
mass and 150
mineral grain and 150, 159–66, 169, 174–78, 182, 189–91, 196
molybdates and 429
native elements and 480–87
opaque minerals and 152
ores and 196
orthosilicates and 379–81, 384–85, 390–98
oxides and 434–36, 439–49
petrographic microscope and 154–57, 195–200
phosphates and 425–28
pleochroism and 172–73
polarization and 150–69, 172–75, 178, 193–200
reflection and 150, 153–54, 161, 170, 190–91, 194–95, 196

DO NOT COPY
e48d507df5d1141@placeholder.9409

Printed by: e48d507df5d1141@placeholder.94092.edu. Printing is for personal, private use only. No part of this book may be reproduced or transmitted without publisher's prior permission. Violators will be prosecuted.

refraction and 150, 153–59, 162–63, 166–73, 176, 185–200
ring silicates and 373–76
rotation and 156, 163–66, 171–76, 179–89, 193–97
shape and 158, 161, 166–67, 170, 176, 181, 183, 197
sheet silicates and 304, 310–23, 327, 330–32
sign of elongation and 173–75
specific gravity and 195
streak and 195
sulfates and 418–23
sulfides and 460, 464–77
symmetry and 153, 166–67, 171–78, 189, 193
tactics for identification 195–200
transparent materials and 152
tungstates and 429
unit cells and 166–67, 170
X-rays and 158
zones and 175, 199
Optic angle 171, 181, 186–87, 231, 284, 340
Optic axes
anisotropic minerals and 159
biaxial 159
extinction and 163–64
inconsistencies in 238
indicatrix and 166–72
interference figures and 176–77, 182
off-center 177–78
study strategies and 238
uniaxial 159
Optic axis dispersion 188
Optic normal (flash) figure 178–80, 183
Optic normal (ON) minerals 171
Optic orientation 171–72
Optic plane 171
Optic sign 164, 168–69, 180, 185–88
Opx 217, 221, 335, 338–39, 342
Orbitals 54

DO NOT COPY
e1a4d507df5d1141@placeholder.9409

Printed by: e48d507df5d1141@placeholder.94092.edu. Printing is for personal, private use only. No part of this book may be reproduced or transmitted without publisher's prior permission. Violators will be prosecuted.

Ordering
crystal structure and 85
mineral growth and 114–15
physical properties and 145
silicates and 277–81, 289, 292, 383
Orders 161
Ordinary rays 167–68
Ores 3
carbonates 407–10, 413–15
crystallography and 49
hydroxides 452
metallic 4
mineral growth and 127
mining of 4, 6–7, 127, 234
molybdates 429
native elements 483–84
optical mineralogy and 196
oxides 431, 434, 439, 441, 444, 446, 448
silicates 241, 270–71, 332, 396
study strategies and 234
sulfates 422
sulfides 462–68, 475–76
tungstates and 429
Oriented samples 230
Origin 17
Orogenic belt 256, 263, 265
Orthoscopic illumination 155
Orthosilicates 242
additional 398
aluminum silicates 386–87
carbon sequestration 283
enhanced rock weathering and 382
optical mineralogy and 379–81, 384–85, 390–98
placer deposits and 386
sphenes 396
structure of 378

DO NOT COPY
e48d507df5d1141@placeholder.9409

Printed by: e48d507df5d1141@placeholder.94092.edu. Printing is for personal, private use only. No part of this book may be reproduced or transmitted without publisher's prior permission. Violators will be prosecuted.

twinning and 379, 381, 383, 385, 389–97
Oxidation state 58, 71
Oxides
aggregates and 434, 439
cleavage and 433–49
color and 433–49
crystal systems and 437
density and 439
diffraction and 443
fracture and 433–34, 438, 441–49
gems and 442, 444–45
habit and 441–42, 445, 447
hardness and 441–42, 445
light and 434–35, 439, 442–45
luster and 433–49
magnetism and 439, 444, 446
mass and 439
optical mineralogy and 434–36, 439–49
ores and 431, 434, 439, 441, 444, 446, 448
polarized light and 434–35, 444–48
reflection and 434, 436, 439–41, 444, 446–49
refraction and 434, 441–48
rotation and 445
shape and 443, 446–48
specific gravity and 442, 444, 448
streak and 434, 439–449
symmetry and 433–34
twinning and 433–34, 436, 438, 440–49
unit cells and 436–437, 443, 446–47
XO group 436
XO_2 group 446–49
X_2O group 433–36
X_2O_3 group 443–46
X-rays and 443
XY_2O_4 group 437–43
zones and 448
Packing index 131

DO NOT COPY
e48d507df5d1141@placeholder.9409

Printed by: e48d507df5d1141@placeholder.94092.edu. Printing is for personal, private use only. No part of this book may be reproduced or transmitted without publisher's prior permission. Violators will be prosecuted.

Paleoclimate 435–36

Paleomagnetism 439

Pallasites 123

Parallel dispersion 189

Parallel extinction 174

Paramagnetism 143, 145

Paramorphs 117

Parent atoms 117

Particle-size separation 327

Parting 135–36

Pauli exclusion principle 53

Pauling, Linus 59

Pauling's Rules
- crystal structure and 76, 81–83, 86–87
- silicates and 242, 378

Peak height intensity 206–7

Peak metamorphic conditions 259

Peak overlap 203

Peak pressure 259

Peaks 203

Peak temperature 259

Pedions 37, 41

Pelites 261–62

Pelotherapy 328–29

Penetration twins 112

Penrose tiling 29

Pericline twinning 278, 281–85, 290–94

Periodic table of the elements
- chemical analysis and 226
- crystal chemistry and 52–53, 55, 59, 70
- crystal structure and 75
- native elements and 483
- rare earth elements 7

Perthitic texture 117, 280

DO NOT COPY
e48d507df5d1141@placeholder.9409

Printed by: e48d507df5d1141@placeholder.94092.edu. Printing is for personal, private use only. No part of this book may be reproduced or transmitted without publisher's prior permission. Violators will be prosecuted.

Perthitic texture 117, 280

Petrographic microscope
- grain mount and 195, 196
- parts of 154–57
- reflection and 196
- thin section analysis and 196–200

Phase diagrams 95–102

Phosphates 424–29

Phosphorescence 143

Photographs 228

Photoluminescence 143

Photons 136, 150–51, 204

Phyllic sulfides 461

Physical properties
- band theory and 138–40
- brittleness 62, *see also* Brittleness
- charge transfer transitions and 138–39
- cleavage 9, 131, *see also* Cleavage
- color 5–6, 9–11, 131, 136–43
- crystal field theory and 138–39
- crystal form and 134–35
- crystal systems and 134, 148
- density 9–10, *see also* Density
- diffraction and 142
- electrical 146–48
- fracture 9–11, 131, 133, 135–36
- gems and 139, 141
- grain size 148, *see also* Grain size
- hard lens and 9
- hardness 4, *see also* Hardness
- heft 10, 133, 232
- inversion and 147–48, 172
- lattices and 145, 148
- light 4, 9–11, 131–43
- luminescence 119, 131, 137, 142–43, 215, 218, 233, 385, 460, 467
- luster 131, 136–43
- magnetism 6–8, 9–11, 131, 143–46

DO NOT COPY
e48d507df5d1141@placeholder.9409

Printed by: e48d507df5d1141@placeholder.94092.edu. Printing is for personal, private use only. No part of this book may be reproduced or transmitted without publisher's prior permission. Violators will be prosecuted.

malleability 66, 76, 134, 479–82
- mass-dependent 131–33
- mass 9, *see also* Mass
- mechanical cohesion 133–36
- Miller index 134–35
- mineral grain 132, 137
- miscellaneous 148
- parting 135–36
- point groups and 133–34, 147–48
- reflection and 137, 140
- refraction and 136–37
- rotation and 142, 148
- shape 9, *see also* Shape
- smell 9, 11, 148, 232
- specific gravity 10, *see also* Specific gravity
- study strategies for 9–11
- symmetry 133–34, 142, 147–48
- taste 9, 11, 131, 148, 402, 413, 418, 430, 455–56
- tenacity 134
- unit cells and 131, 134
- X-rays and 136
- Physical weathering 92
- Pi bonds 64
- Piezoelectricity 147
- Pinacoids 37
- Placebo effect 8
- Placer deposits 386
- Planar defects 107, 110–11
- Plane lattices 15–21
- Play of color 142
- Pleochroic halos 122
- Pleochroism 172–73, 194
- Pleural plaque 311
- Pliny the Elder 4, 8
- Plutonic rocks
  - crystal structure and 85
  - mineral growth and 102
  - silicates and 245–47, 252, 256, 278–81, 284, 286, 291, 294–96, 340, 379–80

DO NOT COPY e48d507df5d1141@placeholder.9409

Printed by: e48d507df5d1141@placeholder.94092.edu. Printing is for personal, private use only. No part of this book may be reproduced or transmitted without publisher's prior permission. Violators will be prosecuted.

- Poikilitic grains 301
- Point defects 107–8
- Point groups
  - 32 elements for 24–25
  - carbonates and 401
  - crystallography and 14, 24–28, 35, 37–48
  - crystal structure and 83
  - crystal systems and 26–27
  - mineral growth and 105
  - physical properties and 133–34, 147–48
  - silicates and 268, 323
  - study strategies and 231
- Poitiers, Diane de 8
- Polarized light
  - anisotropism and 194–95
  - carbonates and 404, 407–8
  - crystal chemistry and 69
  - crystallography and 217
  - isotropism and 194–95
  - mineral growth and 106, 108
  - native elements and 480, 485
  - Nicol prism and 4–5
  - optical mineralogy and 150–69, 172–75, 178, 193–200
  - oxides and 434–35, 444–48
  - petrographic microscope and 154–57
  - phosphates and 425, 427
  - physical properties and 4, 6
  - plane 151
  - reflection and 194–95
  - silicates and 270, 273, 280–86, 291, 309–10, 316, 321, 330, 353–54, 360–61, 376–77, 393
  - sulfides and 464–65, 469–77
- Polarizing film 151–52
- Polishing 233
- Polychromatic illumination 161–62
- Polychromatic light 136
- Polyhedral element sharing 80–81
- Polymerization 242

DO NOT COPY e48d507df5d1141@placeholder.9409

Printed by: e48d507df5d1141@placeholder.94092.edu. Printing is for personal, private use only. No part of this book may be reproduced or transmitted without publisher's prior permission. Violators will be prosecuted.

- Polymorphic forms 83
- Polymorphism 83–85
- Polysynthetic twins 112
- Polytypism 84–85, 308
- Porphyroblasts 102–3
- Portland cement 328, 405, 410, 420–21
- Positive front pedions 41
- Positive relief 189–90
- Positron decay 118
- Postcrystallization processes
  - exsolution 115–17
  - mineral growth and 114–22
  - ordering 115
  - radioactivity and 117–22
  - recrystallization 115
  - twinning 115
- Potassic sulfides 461
- Powder Diffraction File (PDF) 207
- Powder X-ray diffraction
  - Bragg reflection indices and 207–8
  - composition estimation and 210
  - data reduction and 206–7
  - error sources and 209
  - instrumental output and 205–6
  - integrated intensity and 206–7
  - mineral identification and 208–9
  - mixed samples and 209
  - relative abundance estimation and 209–10
  - sample preparation and 205
- Principal quantum number 53
- Principal sections 167
- Principle of parsimony 81
- Prisms 37
- Products 94
- Prograde metamorphism 259
- Prograde path 259
- Propylitic sulfides 461
- Protolith 92, 93

DO NOT COPY
e48d507df5d1141@placeholder.9409

Printed by: e48d507df5d1141@placeholder.94092.edu. Printing is for personal, private use only. No part of this book may be reproduced or transmitted without publisher's prior permission. Violators will be prosecuted.

- Protons 52
- Provenance 256
- Psammites 261–62
- Pseudomorphism 117
- Pseudo-noble-gas core 55
- Pseudotachylite 4
- Pycnometer 132
- Pyramids 37
- *Pyrobaculum arsenaticum* 464
- Pyroelectricity 147–48

Qualitative analysis 219

Quarter-wave 164

Quarter-wavelength plate 164

Quartz-sensitive tint 164

Quartz wedge 161

Quasicrystals 29

Quenching 279

Quicklime 405, 420

Radioactivity 117–22

Radiometric dating 118–21

Radius ratio 76

Raman spectroscopy 485

Rapakivi texture 281

Rare earth elements (REE) 7, 55

Reactants 94

Recrystallization 92, 115, 259–60

Reflection

anisotropism and 194–95

bireflectance and 194

carbonates and 407

crossed polarizers and 194–95

crystal axes and 21, 210

crystallography and 14, 21, 28, 36–37, 204–11

crystal systems and 21

determinative tables and 513–14

first-order 204

DO NOT COPY e48d507df5d1141@placeholder.9409

Printed by: e48d507df5d1141@placeholder.94092.edu. Printing is for personal, private use only. No part of this book may be reproduced or transmitted without publisher's prior permission. Violators will be prosecuted.

first-order 204
fourth-order 204
hydroxides and 451
identification and 233
internal 154, 190–91, 195, 196, 434, 436, 439, 441, 513–14
isotropism and 194–95
mineral growth and 111–14
optical mineralogy and 150, 153–54, 161, 170, 190–91, 194–95, 196
oxides and 434, 436, 439–41, 444, 446–49
petrographic microscope and 196
physical properties and 137, 140
plane-polarized light and 194
pleochroism and 194
polished sample identification and 196
refraction and 153–54
second-order 204
silicates and 269, 278, 281–82, 304
sulfides and 465–77
symmetry and 14, 21, 28, 36, 111–14, 278
third-order 204
total internal 154
X-rays and 204–5
Refraction
carbonates and 404–15
critical angle for 154
crystallography and 204
determinative tables and 509–10, 512
double 158–59
Fresnel equation and 153–54
halides and 454–57
hydroxides and 450–51
index of 153, 189–94, 509–13
mineral growth and 106, 122
molybdates and 429–30
optical mineralogy and 150, 153–59, 162–63, 166–73, 176, 185–200
oxides and 434, 441–48
phosphates and 425–28
physical properties and 136–37

DO NOT COPY
e48d507df5d1141@placeholder.9409

Printed by: e48d507df5d1141@placeholder.94092.edu. Printing is for personal, private use only. No part of this book may be reproduced or transmitted without publisher's prior permission. Violators will be prosecuted.

physical properties and 326–27
reflection and 153–54
silicates and 269–75, 283–86, 289–97, 300, 302, 310–22, 328, 330–32, 339–49, 354–60, 365–77, 380–98
Snell's law and 153
study strategies and 231
sulfates and 419, 421–22
sulfides and 467, 470, 484–87
tungstates and 429–30
Refractometry
Becke line method and 190–91
biaxial minerals and 193–94
dispersion effects and 191
immersion method and 189
isotropic minerals and 193
practical considerations in 191–92
relief and 189–90
thin sections and 192–93
uniaxial minerals and 193
Regional metamorphism 263
Relief 189–90
Remnant magnetism 146
Retardation 159
Reticle markings 157
Retrograde metamorphism 259
Retrograde path 259
Reviews in Mineralogy & Geochemistry series 12
Rhombohedrons 37
Ring silicates 242, 377
classification 371
optical mineralogy and 373–76
twinning and 372–76
Rock cycle 92
Rock-Forming Minerals (Deer, et al) 11–12
Rocks 92
Rotation
nesosilicates and 404–12

DO NOT COPY
e48d507df5d1141@placeholder.9409

Printed by: e48d507df5d1141@placeholder.94092.edu. Printing is for personal, private use only. No part of this book may be reproduced or transmitted without publisher's prior permission. Violators will be prosecuted.

carbonates and 404–13
crystallography and 14, 21–29, 32, 37, 40–43, 48
halides and 456
mineral growth and 111–13
native elements and 485
optical mineralogy and 156, 163–66, 171–76, 179–89, 193–97
oxides and 445
physical properties and 142, 148
rotation and 14, 21–29, 32, 37, 40–43, 48
silicates and 268–69, 278–82, 286, 314–15, 318, 330, 376
sulfides and 466, 469–74
symmetry and 14, 21–29, 40–43, 48, 111–13, 148, 189, 268, 471
Rotoinversion axes 22
Salt domes 484
Sample collection 228–30
Scalenohedrons 37
Scanning electron microscope (SEM) 214–16, 219, 223, 233–34
Schiller 280
Schistocity 256
Schottky defects 107–9
Screw axes 28–29
Screw dislocations 103, 109
Secondary electrons 216–18
Secondary ion mass spectrometry (SIMS) 224–25
Second-order reflection 204
Second setting 41
Sedimentary rock 92–93
arenites 253
chain silicates and 338
claystone 253
compositional maturity and 255
diagenesis and 253
environments for 256
mineral associations and 516
mud rock 253
mudstone 253

DO NOT COPY
e48d507df5d1141@placeholder.9409

Printed by: e48d507df5d1141@placeholder.94092.edu. Printing is for personal, private use only. No part of this book may be reproduced or transmitted without publisher's prior permission. Violators will be prosecuted.

mudstone 253
shale 253
silicates and 253–56
siltstone 253
wackes 253
Sediments 92
Semiconductors 67–68, 139
Sensitive high-resolution ion microprobe (SHRIMP) 224
Sericitic sulfides 461
Shale 253
Shape
carbonates and 406, 409, 412
chemical analysis and 223
coordination polyhedra and 139
crystal axes and 9, *see also* Crystal axes
crystal chemistry and 54, 69, 71
crystallography and 14–22, 29, 37–38, 41, 48–49, 207
crystal structure and 73, 76, 83, 85
habit and 14, *see also* Habit
halides and 454
indentation hardness and 134
mineral growth and 92, 108–9, 113–14, 117, 121
mineral variety and 5
native elements and 481, 484, 486
optical mineralogy and 158, 161, 166–67, 170, 176, 181, 183, 196
oxides and 443, 446–48
silicates and 247, 255, 259, 269, 271, 292, 296–97, 301, 304–5, 308, 316–17, 323, 329, 350, 354–58, 371, 374–75, 383, 388–97
study strategies and 232, 234
sulfates and 419
sulfides and 473–75
symmetry and 9–10, 14, 16, 21–22, 29, 85, 166–67, 271, 304
Sheet silicates 242
classification of 304–8
clay minerals 323–29
dioctahedral 304
interlayer 304

DO NOT COPY
e48d507df5d1141@placeholder.9409

Printed by: e48d507df5d1141@placeholder.94092.edu. Printing is for personal, private use only. No part of this book may be reproduced or transmitted without publisher's prior permission. Violators will be prosecuted.

layer repeat distance and 306
optical mineralogy and 304, 310–23, 327, 330–32
other 329–32
polytypism and 308
TO structures 305–12
TOT structures 312–14
TOT+C structures 314–21
TOT+O structures 321–23
trioctahedral 304
twinning and 309, 312–23, 329–32
Shells 53, 56–58
Shewanella putrefaciens 125
Side pedion 41
Sieving 235
Sigma bonds 63–64
Sign of elongation 164, 173–75
Silicates
aggregates and 271, 283, 287, 290, 310, 374, 381, 396
Bowen's reaction series and 249
brittleness and 269–72, 275, 283, 290–96, 301, 307, 320–21, 339–42, 345, 347–48, 354–60, 365–76, 379, 383, 385, 390–94, 397
calc 263
chain 242, 334–61
chemical formulas and 244
classification of 241–43
clastic sedimentary rocks 253–56
cleavage and 254–57, 269–72, 275, 283–85, 289–304, 310–23, 330–35, 338–61, 365–98
color and 244, 255, 257, 264, 269–76, 283–302, 310–98
crystal axes and 283, 289
crystal form and 377
crystal systems and 268, 298, 366, 371, 398
density and 247, 258, 317
diffraction and 274–75, 279–80, 297, 304, 310–14, 318, 322–24, 327, 347, 350, 369, 371
disilicates 242, 363–71
fracture and 263, 269, 271, 275, 283, 290–95, 301, 331–32, 339–48, 354, 357–60, 365–69, 372–76, 379–85, 390–93, 397–98

DO NOT COPY
e48d507df5d1141@placeholder.9409

Printed by: e48d507df5d1141@placeholder.94092.edu. Printing is for personal, private use only. No part of this book may be reproduced or transmitted without publisher's prior permission. Violators will be prosecuted.

framework 242, 267–302
gems and 271, 275, 331–32, 366, 368, 373, 375, 381
habit and 268, 272–73, 288–98, 304, 309, 311–12, 315–21, 324, 327, 332, 347, 356–59, 362, 366, 371–74, 377, 384–86, 390–93, 396–98
hardness and 255, 269, 275, 283, 289, 297, 301, 307–8, 317, 320, 322, 332, 341–46, 357, 359, 373–74, 384–87, 390–93, 396–97
hot spots and 251–53
igneous rock and 244–53
industrial minerals and 241
inversion and 272
lattices and 259, 268, 272, 278, 302, 371
light and 270, 275, 280–301, 305, 308–9, 323, 345, 353, 367, 374, 376, 380, 384–89, 393–4, 396–98
luster and 257, 269, 271–75, 283, 290–301, 310–23, 330–32, 339–48, 354–60, 365–85, 390–97
mafic vs. felsic 244
magmatic processes and 248–53
mass and 267, 273, 328, 350, 389
metamorphic rocks and 256–65
Miller index and 354
mineral grain and 253–54, 259, 323, 338
mining and 271, 311, 356, 384
ores and 241, 270–71, 332, 396
orthosilicates 242, 378–98
Pauling's Rules and 242, 378
point groups and 268, 323
polarization and 270, 273, 280–86, 291, 309–10, 316, 321, 330, 353–54, 360–61, 376–77, 393
reflection and 269, 278, 281–82, 304
refraction and 269–75, 283–86, 289–97, 300, 302, 310–22, 328, 330–32, 339–49, 354–60, 365–77, 380–98
ring 242
rotation and 268–69, 278–82, 286, 314–15, 318, 330, 376
shape and 247, 255, 259, 269, 271, 292, 296–97, 301, 304–5, 308, 316–17, 323, 329, 350, 354–58, 371, 374–75, 383, 388–97
sheet 242, 304–32
specific gravity and 255, 267–69, 274–75, 294, 297, 339, 373, 380, 384, 387, 397
streak and 269–72, 275, 283, 290–97, 301, 310–23, 330–32, 339, 349, 354–60, 365–70, 373–76, 379, 384–85, 390–97

DO NOT COPY
e48d507df5d1141@placeholder.9409

Printed by: e48d507df5d1141@placeholder.94092.edu. Printing is for personal, private use only. No part of this book may be reproduced or transmitted without publisher's prior permission. Violators will be prosecuted.

373–76, 379, 384–85, 390–97
structure 241–43
symmetry and 268–72, 289–90, 293, 295, 304, 308, 335, 339, 351, 364, 370–80, 383–84, 390
unit cells and 269, 304, 306–8, 313–14, 316, 325, 334, 339, 346, 354, 364, 365, 380
X-rays and 273–74, 279–80, 290, 297, 304, 310–15, 318, 322–24, 327, 347, 350, 358, 369, 371, 373
zones and 247–48, 251–52, 259, 262–65, 272, 282, 285, 297, 336–38, 345, 375, 377, 379, 381
Silicon tetrahedron 80
Silicosis 8, 271, 311
Siltstone 253
Simple substitution solid solution 87
Simple twins 112
Single component systems 95
Single crystal X-ray diffractometer 205, 210–11
Sketches 228
Slip system 109
Slow rays 159
Smell 9, 11, 148, 232
Snell's law 153
Solid solutions 86–87
Solidus 96
Solutes 86
Solvents 86
Solvus 99
Sorby, Henry Clifton 5
Space groups 27–29
Specific gravity 9
carbonates and 404, 407–8, 410–13
composition and 131–32
controls on 131–32
defined 131
density and 10, 131
determinative tables and 505–6
hydroxides and 451–52

DO NOT COPY
e48d507df5d1141@placeholder.9409

Printed by: e48d507df5d1141@placeholder.94092.edu. Printing is for personal, private use only. No part of this book may be reproduced or transmitted without publisher's prior permission. Violators will be prosecuted.

hydroxides and 451–52
Jolly balance and 132
measurement of 132–33
native elements and 481
optical mineralogy and 195
oxides and 442, 444, 448
packing index and 131
phosphates and 426
pycnometer and 132
silicates and 255, 267–69, 274–75, 294, 297, 339, 373, 380, 384, 387, 397
study strategies and 231–32, 238
sulfates and 419, 421–22
sulfides and 468
Spectrometers 233
chemical analysis and 215–25
mineral growth and 119–20
Sphene 396
Sphere packing 74–75
Spherulites 292
Spin quantum number 54–55, 143
Spin state 71–72
Splendent luster 137
Sporosarcina pasteurii 127
Stability 93–95
Stable mineral assemblage 94
Stacking faults 110
Standards 219
Staphylococcus aureus 415
State goniometer 156
State micrometer 157
Steno's Law 26
Stensen, Niels (Nicholas Steno) 4
Streak 10–11
carbonates and 404, 406–15
determinative tables and 504
halides and 454–57

DO NOT COPY
e48d507df5d1141@placeholder.9409

Printed by: e48d507df5d1141@placeholder.94092.edu. Printing is for personal, private use only. No part of this book may be reproduced or transmitted without publisher's prior permission. Violators will be prosecuted.

halides and 454–57
hardness and 9, 131, 142, 195, 232, 297
hydroxides and 450–54
native elements and 481–87
optical mineralogy and 195
oxides and 434, 439–49
phosphates and 425–28
silicates and 269–72, 275, 283, 290–97, 301, 310–23, 330–32, 339, 349, 354–60, 365–70, 373–76, 379, 384–85, 390–97
study strategies and 232
sulfates and 419–22
sulfides and 459–60, 467–77
use of 142
Streak plate 142
Stress 109
Stromatolites 125
Strong dispersion 188
Strunz-Nickel system 86
Stucco 420
Study strategies
alteration and 238
cleavage and 231–32
color and 232–33, 238
costs and 237
crystal form and 229
crystal systems and 231–32
data presentation 231
density and 234–36
diffraction and 231–34, 237
field study 228–30
fracture and 228–29, 232
habit and 228, 232
hard lens and 9
hardness and 231–32, 238
identification tactics 232–34
insufficient data and 237
luster and 232, 238

DO NOT COPY
e48d507df5d1141@placeholder.9409

Printed by: e48d507df5d1141@placeholder.94092.edu. Printing is for personal, private use only. No part of this book may be reproduced or transmitted without publisher's prior permission. Violators will be prosecuted.

Miller index and 231
mineral grain and 228, 234–37
mining and 234
mixtures and 238
optic axes and 238
ores and 234
photographs and 228
physical properties and 9–11
point groups and 231
refraction and 231
sample collection 228–30
shape and 232, 234
sketches and 228
specific gravity and 231–32, 238
streak and 232
symmetry and 232
unit cells and 231
X-rays and 231–34, 237–38
Subduction zones 251–52
Subhedral faces 48
Submetallic luster 137
Subshells 54, 56–58
Substitution defects 108
Substitution solid solutions 87–88
Sulfarsenides 476–78
Sulfates
cleavage and 417–24
color and 417–24
crystal axes and 419, 422
density and 423
fracture and 421–22
habit and 418–19
hardness and 419–21
light and 421, 423
luster and 419–22
mining and 420

DO NOT COPY
e48d507df5d1141@placeholder.9409

Printed by: e48d507df5d1141@placeholder.94092.edu. Printing is for personal, private use only. No part of this book may be reproduced or transmitted without publisher's prior permission. Violators will be prosecuted.

optical mineralogy and 418–23
ores and 422
refraction and 419, 421–22
shape and 419
specific gravity and 419, 421–22
streak and 419–22
symmetry and 419, 422
twinning and 418–23
unit cells and 418–19, 423
X-rays and 424
zones and 420, 423, 461–65, 476–77

Sulfides
argillic 461
classification of 459–60
cleavage and 465–77
color and 459–78
common minerals of 464–76
crystal chemistry of 459–60
deposits of 460–64
fracture and 461, 466–77
habit and 469–74, 477–78
hardness and 470, 472
lattices and 471, 473, 483
light and 459–60, 465, 468, 470–71
luster and 459–60, 467–76
mineral associations and 517
mining and 461, 470–71, 473, 478
optical mineralogy and 460, 464–77
ores and 462–68, 475–76
phyllic 461
polarized light and 464–65, 469–77
propylitic 461
reflection and 465–77
refraction and 467, 470, 484–87
rotation and 466, 469–74
sericitic 461
shape and 473–75
specific gravity and 468

DO NOT COPY
e48d507df5d1141@placeholder.9409

Printed by: e48d507df5d1141@placeholder.94092.edu. Printing is for personal, private use only. No part of this book may be reproduced or transmitted without publisher's prior permission. Violators will be prosecuted.

specific gravity and 468
streak and 459–60, 467–77
supergene processes and 462–64
symmetry and 469, 471, 475
twinning and 466–77
unit cells and 464–74, 477
X-rays and 467

Sulfosalts 124, 460, 463, 466

Supergene processes 462–64

Surface energy 96, 101–5, 115, 259

Swelling soils 69, 328

Symmetrical extinction 174

Symmetry
carbonates and 401, 404, 407–8, 410, 413
center 21–26, 38, 40–41, 375–76
cleavage and 3, 15, 41–42, 83, 133–34, 174–77, 304, 370, 390, 404, 407–10, 413, 422
compound operations and 22
crystal axes and 9, *see also* Crystal axes
crystal chemistry and 62–63, 66–69
crystallography and 14–29, 35–48, 205–6
crystal structure and 79–85
Hermann-Mauguin 23–25, 42–46
inversion 14, 21–24, 27, 40, 43, 46, 84, 85, 111, 147–48, 172
mineral growth and 111–15
native elements and 486
notation for 22–24
optical mineralogy and 153, 166–67, 171–78, 189, 193
oxides and 433–34
physical properties and 133–34, 142, 147–48
point 9, 14, 21, 21–28, 35, 37–46, 48, 133–34, 142, 147, 268, 272, 375, 380
reflection and 14, 21, 28, 36, 111–14, 278
rotation 14, 21–29, 40–43, 48, 111–13, 148, 189, 268, 471
shape and 9–10, 14, 16, 21–22, 29, 85, 166–67, 271, 304
silicates and 268–72, 278–82, 289–90, 293, 295, 304, 308, 335, 339, 351, 364, 370, 372–78, 380, 383–84, 390
space groups and 27–29
study strategies and 232

DO NOT COPY
e48d507df5d1141@placeholder.9409

Printed by: e48d507df5d1141@placeholder.94092.edu. Printing is for personal, private use only. No part of this book may be reproduced or transmitted without publisher's prior permission. Violators will be prosecuted.

sulfates and 419, 422
sulfides and 469, 471, 475
symmetry and 14–29, 35–48
translational 14–28, 29
unit cells and 14, *see also* Unit cells
Symmetry symbols 22–24
Synchrotrons 201
Synthetic minerals 3
Tabular crystals 48
Taste
borates and 430
carbonates and 402, 413
halides and 455–56
physical properties and 9, 11, 131, 148, 402, 413, 418, 430, 455–56
sulfates and 418
Tektites 4
Tellurides 478
Tenacity 134
Ternary diagrams 89–90, 256, 351
Tetrahedrons 37–38
Texture 256
Theophrastus 4
Thermochronology 120
Thermoluminescence 143
Thin sections 150, 192–93, 199–200, 233
Thiobacillus ferrooxidans 463
Third-order reflection 204
Tie-lines 96
Total internal reflection 154
T-P loop 259
Transformation twinning 113–14
Transition metals 55
Transmission electron microscopy 211–13
Transparent minerals 152

DO NOT COPY
e48d507df5d1141@placeholder.9409

Printed by: e48d507df5d1141@placeholder.94092.edu. Printing is for personal, private use only. No part of this book may be reproduced or transmitted without publisher's prior permission. Violators will be prosecuted.

Trapezohedrons 37

Triangular coordination 78

Triboluminescence 142–43

Trioctahedral sheets 304

Tungstates 428–30

Twain, Mark 472

Twin law 111

Twinning 114

- albite 113, 199, 278, 280–87, 290–94
- Baveno 281, 281–83, 290–92
- borates and 430
- carbonates and 402–3, 406–15
- Carlsbad 112–13, 199, 269, 281–87, 290–93, 303
- chain silicates and 338–48, 354–60
- disilicates and 365–70
- framework silicates and 268–72, 275, 278–86, 289–96, 301
- halides and 454–56
- hydroxides and 450–52
- Manebach 281–83, 290–92
- molybdates and 429
- native elements and 481–87
- orthosilicates and 379, 381, 383, 385, 389–97
- oxides and 433–34, 436, 438, 440–49
- pericline 278, 281–85, 290–94
- phosphates and 424, 426–28
- postcrystallization processes and 115
- ring silicates and 372–76
- sheet silicates and 309, 312–23, 329–32
- sulfates and 418–23
- sulfides and 466, 468–77
- tungstates and 429

Twin operation 111

Type samples 5

Uncompahgre Ute Native Americans 142–43

Undulose extinction 175, 268–69

Uniaxial indicatrix 167–70

DO NOT COPY e48d507df5d1141@placeholder.9409

Printed by: e48d507df5d1141@placeholder.94092.edu. Printing is for personal, private use only. No part of this book may be reproduced or transmitted without publisher's prior permission. Violators will be prosecuted.

Uniaxial minerals 172, 193

Uniaxial optic axis interference figure 176–77

Uniform bonding 79–82

Unit cells

- body-centered 17
- borates and 430
- carbonates and 401–3, 411
- crystal axes and 14–20, 25, 29–34, 41–42, 46–47, 114, 167, 210, 419
- crystal chemistry and 68
- crystallography and 14–21, 24–25, 29–34, 40–42, 46–47, 207, 210
- crystal structure and 73–74, 76, 82–86, 90–91
- face-centered 17
- formula units and 91
- halides and 454
- Haüy and 4
- hydroxides and 450–52
- mineral formulas and 90–91
- mineral growth and 105, 114–15
- molybdates and 429
- native elements and 479–80
- optical mineralogy and 166–67, 170
- oxides and 436–37, 443, 446–47
- physical properties and 131, 134
- silicates and 269, 304–8, 313–16, 325, 334, 339, 346, 354, 364–65, 380
- study strategies and 231
- sulfates and 418–19, 423
- sulfides and 464–74, 477
- tungstates and 429
- X-rays and 210

Unit face 34

Unit mesh axes 15–18, 21

Upper polarizer 156

Valence 58

Valence band 65, 139

Valence-related bonding

- conductors and 67–68

DO NOT COPY
e48d507df5d1141@placeholder.9409

Printed by: e48d507df5d1141@placeholder.94092.edu. Printing is for personal, private use only. No part of this book may be reproduced or transmitted without publisher's prior permission. Violators will be prosecuted.

covalent 62–64
insulators and 67–68
ionic 61–62
metallic 64–66
relation among 66–67
semiconductors and 67–68
Van der Waals bonding 68–69
Van Kreveken diagram 485
Velocity 151
Vernier 156
Vesuvius 4
Vibration directions 165, 176–77
Vickers hardness 134
Volcanic glass 4, 92, 272, 275, 292
Von Laue, Max 5
Wackes 253
Wad 452
Wave front 151–53, 166–69, 204
Wavelength 151
Wavelength-dispersive X-ray spectrometers (WDS) 219–21
Wave normal 151
Weak dispersion 188
Werner, G. 4
Wet chemical techniques 214
Work-harden metals 109
XO group 436
XO_2 group 446–49
X_2O group 433–36
X_2O_3 group 443–46
X-ray chemical maps 221–23
X-ray fluorescence 214, 223–24
X-rays 5
background and 202
Bragg's Law and 204

DO NOT COPY
e48d507df5d1141@placeholder.9409

Printed by: e48d507df5d1141@placeholder.94092.edu. Printing is for personal, private use only. No part of this book may be reproduced or transmitted without publisher's prior permission. Violators will be prosecuted.

Bragg's Law and 204
carbonates and 403, 412, 414
characteristic 203, 218–19
chemical analysis and 214–23, 227
continuous spectrum 202
crystal chemistry and 69–70
crystallography and 15, 17, 24, 201–12
crystal structure and 5
detection of 203–4
differentiation of 204–5
diffraction of 3, 5, *see also* Diffraction
energy-dispersive spectrometers 219
generation of 201–3
hydroxides and 451–52
mineral growth and 122
monochromatic 203
native elements and 482, 491
optical mineralogy and 158
oxides and 443
peak and 203, 206–7
phosphates and 426–27
physical properties and 136
powder 205–10
reflection and 204–5
silicates and 273–74, 279–80, 290, 297, 304, 310–15, 318, 322–24, 327, 347, 350, 358, 369, 371, 373
single crystal 205, 210–11
study strategies and 231–34, 237–38
sulfates and 424
sulfides and 467
transmission electron microscopy and 211–13
unit cells and 210
von Laue and 5
wavelength-dispersive spectrometers 219–21
XY_2O_4 group 437–43
Zones
axis 34–35
borates and 430

DO NOT COPY
e48d507df5d1141@placeholder.9409

Printed by: e48d507df5d1141@placeholder.94092.edu. Printing is for personal, private use only. No part of this book may be reproduced or transmitted without publisher's prior permission. Violators will be prosecuted.

carbonates and 402, 404, 406, 409, 412
chemical analysis and 214
crystallography and 14, 17, 25, 34–35, 40–41, 48
halides and 457
mineral growth and 105–6, 118–19, 122, 125–27
native elements and 482, 484
optical mineralogy and 175, 199
oxides and 448
silicates and 247–48, 251–52, 259, 262–65, 272, 282, 285, 297, 336–38, 345, 375, 377, 379, 381
sulfates and 420, 423, 461–65, 476–77

DO NOT COPY
e48d507df5d1141@placeholder.9409

Printed by: e48d507df5d1141@placeholder.94092.edu. Printing is for personal, private use only. No part of this book may be reproduced or transmitted without publisher's prior permission. Violators will be prosecuted.

List of Illustrations

Part One Crystallography and Crystal Chemistry

Chapter 1 Introduction

Figure 1.1 Simple representations that compare the highly organized atoms in a...

Figure 1.2 Mineralogy tools and use. (*a*) Basic tools used...

Chapter 2 Crystallography

Figure 2.1 Simple translation to form a plane lattice. (*a*)...

Figure 2.2 Plane lattices and unit meshes. (*a*) Five different...

Figure 2.3 Plane lattices and unit meshes in everyday life. (*a*...

Figure 2.4 Space lattice. (*a*) A plane lattice with axes *a*

Figure 2.5 Triclinic Bravais lattice. An oblique plane lattice is repeated by...

Figure 2.6 Bravais lattices produced by translation of a rectangle plane lattice where

Figure 2.7 Bravais lattices produced by translation of a centered rectangle (diamond)...

Figure 2.8 Bravais lattices produced by translation of a hexagonal plane lattice. (

Figure 2.9 Bravais lattices produced by translation of a square plane lattice...

Figure 2.10 The 14 Bravais lattices define six different three-dimensional volumes (

Figure 2.11 Symmetry by a mirror (*m*) plane or reflection....

Figure 2.12 Rotational symmetry. (*a*) Four-fold rotation. The full crystal...

Figure 2.13 Inversion. (*a*) Crystal with inversion. Points *h, i, j*

Figure 2.14 Rotoinversion. See text for discussion. (*a*) One-fold rotoinversion...

Figure 2.15 This orthorhombic crystal has center symmetry (*i*), three...

Figure 2.16 The 10 two-dimension point groups.

Figure 2.17 Contact goniometer. (*a*) The base of the goniometer...

DO NOT COPY
e48d507df5d1141@placeholder.9409

Printed by: e48d507df5d1141@placeholder.94092.edu. Printing is for personal, private use only. No part of this book may be reproduced or transmitted without publisher's prior permission. Violators will be prosecuted.

Figure 2.18 Determining crystal symmetry. (*a*) Mirrors split the crystal...

Figure 2.19 Glide symmetry. (*a*) Footprints repeated by a translation *t*

Figure 2.20 Screw axis. A 3-fold screw axis is shown. In quartz,...

Figure 2.22 Primitive monoclinic lattice. Prominent crystal faces are parallel to rational...

Figure 2.23 Miller index. (*a*) Face *t*, when extended,...

Figure 2.24 Miller indices for all visible faces on the crystal shown in

Figure 2.25 Miller indices in the hexagonal crystal system. (*a*)...

Figure 2.26 Miller–Bravais indices in the hexagonal crystal system. (*a*)...

Figure 2.27 Calculating the Miller index for face *x* on an...

Figure 2.28 Crystallographic planes are assigned the same Miller index as the...

Figure 2.29 Assigning Miller indices by inspection. See text for discussion.

Figure 2.30 Crystallographic directions. Crystallographic direction [111] (line *p*) goes through...

Figure 2.31 Crystal zone. The (110), $\left(1\bar{1}0\right)$, $\left(\bar{1}10\right)$, and $\left(\bar{1}\bar{1}0\right)$ faces constitute a [001]...

Figure 2.32 Crystal forms are produced by a repetition of crystal faces...

Figure 2.33 Crystal forms in the isometric system.

Figure 2.21 (*a*) A synthetic pentagonal dodecahedron quasicrystal of Ho-Mg-Zn...

Figure 2.34 Crystal forms in the nonisometric crystal systems. (*a*)...

Figure 2.35 Crystal forms in the nonisometric crystal systems: prisms, pyramids, and...

Figure 2.36 Crystal forms in the nonisometric crystal systems: trapezohedrons, scalenohedrons, rhombohedrons,...

Figure 2.37 Enantiomorphous forms and crystals. (*a*) The right-handed {211}...

Figure 2.38 Positive and negative forms. (*a*) Tetrahedrons. (*b*...

Figure 2.39 Forms in the triclinic crystal system. (*a*) A...

Figure 2.40 Monoclinic crystals. The views down the *b* axis show that the

Figure 2.41 Orthorhombic crystals. Note how the (111), (110), and $\left(001\right)$ faces...

Figure 2.42 Tetragonal crystals. (*a*) 4/*m* scapolite crystal...

DO NOT COPY
e48d507df5d1141@placeholder.9409

Printed by: e48d507df5d1141@placeholder.94092.edu. Printing is for personal, private use only. No part of this book may be reproduced or transmitted without publisher's prior permission. Violators will be prosecuted.

Figure 2.43 Crystals in the hexagonal crystal system, trigonal division. (*a*...

Figure 2.44 Crystals in the hexagonal crystal system, hexagonal division. (*a*...

Figure 2.45 $2\ /\ m\ \bar{3}$point group. (*a*) Three 2-fold axes are parallel...

Figure 2.46 $\bar{4}3m$point group. (*a*) Crystal axes (*a*, *b*, *c*

Figure 2.47 Symmetry elements in the $\bar{4}/m\ \bar{3}\ 2\ /m$ point group. (*a*) Three...

Figure 2.48 Various combinations of {001} cube (white), {011} dodecahedron (light), and...

Figure 2.49 Degree to which crystal faces are well developed. (*a*...

Figure 2.50 Nomenclature for describing the habit of individual mineral grains as...

Figure 2.51 Patterns of mineral growth. (*a*) Elongate minerals can...

Figure 2.52 Habits of crystalline masses. (*a*) Drusy encrustation of...

Chapter 3 Crystal Chemistry

Figure 3.1 Geometry of orbitals in the *s*, *p*, and *d* ...

Figure 3.2 Relative energy level of electron subshells. Electrons fill subshells in...

Figure 3.3 Common oxidation states of elements 1 through 38.

Figure 3.4 Ionic bonding between Na^+ and Cl^-. (*a*

Figure 3.5 Formation of carbon covalent sigma (σ) bonds in...

Figure 3.6 Formation of covalent σ and π bonds with carbon...

Figure 3.7 Hybrid orbitals. Each consists of a large and small lobe (

Figure 3.8 Energy bands form when atoms are brought into close proximity. (

Figure 3.9 Range of bond character (shaded) found in valance-dependent bonding. Continuous...

Figure 3.10 Conceptual model of ionic and covalent bonding. (*a*)...

Figure 3.11 Curve showing the relationship between difference in electronegativity and degree...

Figure 3.12 Band energies. Valence bands (VB) filled with electrons are shaded;...

Figure 3.13 Hydrogen bonding. (*a*) Ice. A polar H_2...

Figure 3.14 Van der Waals bonding. Sheets of carbon are bonded internally by

DO NOT COPY
e48d507df5d1141@placeholder.9409

Printed by: e48d507df5d1141@placeholder.94092.edu. Printing is for personal, private use only. No part of this book may be reproduced or transmitted without publisher's prior permission. Violators will be prosecuted.

Figure 3.15 Bond length and effective radius. (*a*) Close-packed metal...

Figure 3.16 Effective atomic radii for the elements. The lanthanide and actinide...

Figure 3.17 Effective radii as a function of oxidation state (charge) for...

Figure 3.18 Effective ionic radii of the common cations as a function...

Figure 3.19 Spin configuration in Fe^{3+}. (*a*) Low...

Chapter 4 Crystal Structure

Figure 4.1 Illustration of olivine (Mg_2SiO_4) crystal structure...

Figure 4.2 Closest packing of spheres. (*a*) Close-packed layer of...

Figure 4.3 Body-centered cubic packing. (*a*) Body-centered lattice (left)...

Figure 4.4 Coordination polyhedra. Anions with radius R_a are shown...

Figure 4.5 Tetrahedral and octahedral sites in close-packed structures. A layer of...

Figure 4.6 Anisodesmic carbonate (CO_3^{2-}) group. Each O–C bond...

Figure 4.7 Mesodesmic silicon tetrahedra. (*a*) Si–O bonds occupy 1...

Figure 4.8 Sharing anions between polyhedra. (*a*) Sharing a single...

Figure 4.9 NaCl structure. (*a*) Layers of Cl^- ...

Figure 4.10 Anhydrite structure. Isolated SO_4^{2-} groups are bonded...

Figure 4.11 Diamond and graphite stability fields (Day, 2012). The...

Figure 4.12 Structures of *β*-quartz and *α*-quartz (compare Figure 2.20...

Figure 4.13 Order–disorder in K-feldspar ($KAlSi_3O_8$) polymorphs. (

Figure 4.14 Polytypism involves different patterns of stacking identical sheets. The symbols...

Figure 4.15 Solid solution. (*a*) Simple substitution in olivine, whose...

Figure 4.16 Binary diagrams of olivine. (*a*) The end members,...

Figure 4.17 Pyroxene ternary diagram. The end members enstatite (En, Mg_2Si

Figure 4.18 Cuprite structure and unit cell. Oxygen occupy the corners and...

Chapter 5 Mineral Growth

Figure 5.1 The rock cycle. The rock cycle fundamentally involves mineralogical changes...

Figure 5.2 Stability. A book 2 meters above the floor is unstable...

Figure 5.3 Aluminum silicate stability. (*a*) Schematic illustration of Gibbs...

DO NOT COPY e48d507df5d1141@placeholder.9409

Printed by: e48d507df5d1141@placeholder.94092.edu. Printing is for personal, private use only. No part of this book may be reproduced or transmitted without publisher's prior permission. Violators will be prosecuted.

Figure 5.4 Crystallization in the system diopside (Di)–anorthite (An) at 1 atm...

Figure 5.5 Lever rule. Given the bulk composition and a tie-line *qrs*

Figure 5.6 Olivine crystallization at 1 atm pressure. After Bowen and Schairer (1935)

Figure 5.7 Alkali feldspar crystallization. (*a*) The system at 1.96...

Figure 5.8 Formation of crystal embryo from a melt. (*a*)...

Figure 5.9 Epitaxial growth. Hematite crystal (shaded) may nucleate and grow on...

Figure 5.10 Growth on a crystal face. (*a*) Adding a...

Figure 5.11 Slow-growing faces become larger. (*a*) The {111}...

Figure 5.12 Growth rates of crystal faces are inversely proportional to interplanar (

Figure 5.13 Photomicrograph of a thin section (see Chapter 7) showing...

Figure 5.14 Plagioclase phase diagram at 5 kbar water pressure. Adapted from ...

Figure 5.15 Examples of inclusions. (*a*) Fracture surface of a...

Figure 5.16 Point defects. (*a*) Schottky defects. A missing cation...

Figure 5.17 Slip system in a crystal lattice. Slip occurs on a...

Figure 5.18 Dislocations. The Burgers vector *b* is defined by completing...

Figure 5.19 Unless terminated at the edge of a crystal, a dislocation...

Figure 5.20 Antiphase boundary in pigeonite $(Mg,Fe,Ca)_2Si_2O$

Figure 5.21 Symmetry operations in twinning. (*a*) Twinning by reflection...

Figure 5.22 Contact twins. (*a*) Octahedron of spinel twinned by...

Figure 5.23 Penetration twins. (*a*) Pyrite “Iron Cross” twin by...

Figure 5.24 Multiple twins. (*a*) Polysynthetic twinning in plagioclase by...

Figure 5.25 Transformation twinning in leucite. (*a*) The unit cell...

Figure 5.26 Deformation twinning in calcite can be produced by glide on...

Figure 5.27 Recrystallization. (*a*) Recrystallization allows irregular grain boundaries to...

Figure 5.28 Exsolution in alkali feldspar. (*a*) The solvus for...

Figure 5.29 Each dark feature is an aggregate of biotite grains in...

Figure 5.30 Cross section through a zircon crystal imaged with cathodoluminescence to...

Figure 5.31 Transmitted-light image of etched fission tracks in apatite. The

DO NOT COPY
e48d507df5d1141@placeholder.9409

Printed by: e48d507df5d1141@placeholder.94092.edu. Printing is for personal, private use only. No part of this book may be reproduced or transmitted without publisher's prior permission. Violators will be prosecuted.

fission...

Figure 5.32 Photomicrograph of a thin section of mica schist showing dark...

Figure 5.33 Coccoliths and foraminifera. (*a*) A combination coccosphere of...

Part Two Mineral Properties, Study, and Identification

Chapter 6 Physical Properties of Minerals

Figure 6.1 Specific gravity of olivine. The dotted line assumes a linear...

Figure 6.2 Apparatus to measure specific gravity. (*a*) Jolly balance;...

Figure 6.3 Variation of mineral hardness with direction. (*a*) Kyanite....

Figure 6.4 Approximate range of Vickers indentation hardness (shaded) as a function...

Figure 6.5 Cleavage. (*a*) Isometric {001} cleavage (cubic). (*b*...

Figure 6.6 The electromagnetic spectrum. Visible light, with wavelengths (λ)...

Figure 6.7 Absorption of electromagnetic radiation. (*a*) Electromagnetic radiation, whose...

Figure 6.8 Crystal field splitting. (*a*) All five *d* orbitals (

Figure 6.9 Light absorption in ruby. (*a*) Light with energies...

Figure 6.10 Band theory. (*a*) Valence bands and conduction bands...

Figure 6.11 Reflectivity of metals and semiconductors. The most strongly absorbed wavelengths...

Figure 6.12 Color centers. (*a*) Electron color center. A F^-

Figure 6.13 Photograph of star sapphire whose long dimension is 8 mm....

Figure 6.14 Magnetism. See text for discussion. (*a*) Diamagnetism in...

Figure 6.15 Electrical conductivity σ ($ohm^{-1}meter^{-1}$) of selected...

Figure 6.16 Piezoelectricity. (*a*) A silicon tetrahedron consists of a Si

Chapter 7 Optical Mineralogy

Figure 7.1 Sample preparations for the petrographic microscope. (*a*) Grain...

Figure 7.2 Electromagnetic radiation. (*a*) Electric and magnetic components of...

Figure 7.3 Vector resolution of light waves. (*a*) Waves *A* and

Figure 7.4 Polarized light. (*a*) Unpolarized light vibrates in all...

Figure 7.5 Light entering a mineral slows down and the wavelength (λ

DO NOT COPY e48d507df5d1141@placeholder.94092

Printed by: e48d507df5d1141@placeholder.94092.edu. Printing is for personal, private use only. No part of this book may be reproduced or transmitted without publisher's prior permission. Violators will be prosecuted.

Figure 7.5 Light entering a mineral slows down and the wavelength (λ)

Figure 7.6 Reflection and refraction. (*a*) Reflection from a smooth...

Figure 7.7 Critical angle and total internal reflection. Some of the light...

Figure 7.8 Dispersion. (*a*) White light is spread into its...

Figure 7.9 The petrographic microscope. Photo courtesy of Nikon Instruments Inc., Melville,...

Figure 7.10 Objective lens. (*a*) Typical objective lens markings. P...

Figure 7.11 Calibration of an ocular micrometer scale. Fifty divisions of the...

Figure 7.12 Cleavage in isometric minerals as seen in grain mount. (*a*

Figure 7.13 Double refraction of calcite. (*a*) Cleavage rhomb of...

Figure 7.14 Development of retardation. Light entering the mineral with thickness *d* ...

Figure 7.15 Interference at the upper polarizer with monochromatic light. (*a*...

Figure 7.16 Interference pattern formed with a quartz wedge in monochromatic light. (

Plate 1 Interference Color Chart.

Figure 7.17 Formation of interference colors with polychromatic light. (*a*)...

Figure 7.18 Use of the interference color chart (Plate 1)....

Figure 7.19 Extinction. (*a*) When the vibration directions of a...

Figure 7.20 Compensation with an accessory plate. (*a*) Typical gypsum...

Figure 7.21 Determining slow and fast ray vibration directions between crossed polarizers. (

Figure 7.22 Optical indicatrix. (*a*) The indicatrix is constructed by...

Figure 7.23 Uniaxial indicatrix. The circular section and a principal section are...

Figure 7.24 Ordinary and extraordinary rays. Light incident at right angles to...

Figure 7.25 Behavior of uniaxial minerals in orthoscopic illumination. The optic axis...

Figure 7.26 Calcite indicatrix construction. The ϵ' ray path is found...

Figure 7.27 Biaxial indicatrix. (*a*) The indices n_α, n_β

Figure 7.28 Relationship between crystal axes and indicatrix axes. The optic planes...

DO NOT COPY
e48d507df5d1141@placeholder.9409

Printed by: e48d507df5d1141@placeholder.94092.edu. Printing is for personal, private use only. No part of this book may be reproduced or transmitted without publisher's prior permission. Violators will be prosecuted.

Figure 7.29 Behavior of biaxial minerals in orthoscopic illumination. (*a*)...

Figure 7.30 Pleochroism is seen in plane light. (*a*) The...

Figure 7.31 Measurement of extinction angle and sign of elongation. Polarizers are...

Figure 7.32 Categories of extinction. All grains are in extinction orientations. (*a*

Figure 7.33 Extinction in a typical tetragonal mineral. (*a*) Mineral...

Figure 7.34 Extinction in monoclinic minerals. (*a*) Crystal habit showing...

Figure 7.35 Uniaxial optic axis interference figure.

Figure 7.36 Formation of uniaxial isochromes. (*a*) Light following path...

Figure 7.37 Formation of isogyres. (*a*) Vibration directions for light...

Figure 7.38 Off-center uniaxial interference figures. (*a*) Off-center optic...

Figure 7.39 Uniaxial optic normal (flash) figure. The optic axis is parallel...

Figure 7.40 Determining optic sign in a uniaxial optic axis interference figure. (

Figure 7.41 Biaxial acute bisectrix interference figure. The melatopes (M) mark the...

Figure 7.42 Formation of biaxial isochromes. Light following the optic axes emerges...

Figure 7.43 Formation of biaxial isogyres. (*a*) Vibration directions for...

Figure 7.44 Biaxial optic axis interference figure. (*a*) $2V$...

Figure 7.45 Obtuse bisectrix interference figure. (*a*) Pattern of vibration...

Figure 7.46 Optic normal (flash) interference figure. The optic normal (ON) emerges...

Figure 7.47 Biaxial interference figure for randomly oriented grain. As the stage...

Figure 7.48 Determining optic sign in acute bisectrix interference figures. The trace...

Figure 7.49 Determining optic sign with an optic axis figure. The trace...

Figure 7.50 $2E$ versus $2V$. The angle between the...

Figure 7.51 Rapid estimation of $2V$ based on separation of...

Figure 7.52 Isogyre curvature in biaxial optic axis interference figures with the...

Figure 7.53 Optic axis dispersion: M_v and M_r are...

Figure 7.54 Formation of relief in grain mount. If indices of refraction...

DO NOT COPY
e48d507df5d1141@placeholder.9409

Printed by: e48d507df5d1141@placeholder.94092.edu. Printing is for personal, private use only. No part of this book may be reproduced or transmitted without publisher's prior permission. Violators will be prosecuted.

Figure 7.55 High, moderate, and low relief.

Figure 7.56 The Becke line. (*Left*) Microscope focused on a...

Figure 7.57 Formation of the Becke line by the lens effect. Light...

Figure 7.58 Formation of the Becke line by internal reflection at vertical...

Figure 7.59 Movement of the Becke line as the stage is lowered....

Figure 7.60 Formation of colored Becke lines. Immersion oil typically has higher...

Plate 2 Birefringence vs. Average Index of Refraction.

Figure 7.61 Photomicrographs highlighting various optical properties and features seen in thin...

Figure 7.62 Relief and isotropic vs. anisotropic optical properties. (*a*)...

Figure 7.63 Photomicrographs highlighting various optical properties and features seen in thin...

Chapter 8 Analytical Instrumentation and Techniques I: Crystallography

Figure 8.1 X-ray diffractometer. The principal components are an X-ray tube, sample...

Figure 8.2 X-ray tube. The cathode filament is heated so that it...

Figure 8.3 X-ray spectra. (*a*) Intensity of X-rays emitted...

Figure 8.4 Diffraction from parallel planes of atoms (atoms not shown where...

Figure 8.5 Sample holders for routine powder diffraction work. (*a*)...

Figure 8.6 Collection of a powder diffraction pattern for quartz. (*a*...

Figure 8.7 Recording data from the diffraction pattern: 2θ is...

Figure 8.8 Powder Diffraction File. The three *d* values [d (Å)]...

Figure 8.9 Single crystal X-ray diffraction. (*a*) Main components...

Figure 8.10 Transmission electron microscope. (*a*) A typical transmission electron...

Figure 8.11 Example images collected by a transmission electron microscope. (*a*...

Chapter 9 Analytical Instrumentation and Techniques II: Chemical Analysis of Minerals

Figure 9.1 Electron microprobes and scanning electron microscopes. (*a*) An...

Figure 9.2 Scanning electron microscope and electron microprobe samples and chamber interior. (

DO NOT COPY e48d507df5d1141@placeholder.9409

Printed by: e48d507df5d1141@placeholder.94092.edu. Printing is for personal, private use only. No part of this book may be reproduced or transmitted without publisher's prior permission. Violators will be prosecuted.

and chamber interior. (

Figure 9.3 Secondary electron image of pyrite grains from alluvium of the...

Figure 9.4 Excitation volume within a scanning electron microscope or electron microprobe...

Figure 9.5 Hand sample to thin section and scanning electron microscope/electron microprobe...

Figure 9.6 Cathodoluminescence image of a zircon grain. The grain was extracted...

Figure 9.7 Energy-dispersive X-ray spectra from orthopyroxene; compare with Figure 9.8

Figure 9.8 Wavelength-dispersive X-ray spectra for the same orthopyroxene analyzed by energy-dispersive...

Figure 9.9 Comparison of energy-dispersive (EDS) and wavelength-dispersive (WDS) scans on molybdenite....

Figure 9.10 X-ray chemical maps. Maps cover the same area as shown in

Figure 9.11 X-ray fluorescence spectrometer. Background and characteristic X-rays from the X-ray...

Figure 9.12 Handheld X-ray fluorescence spectrometer analyzing a sample of galena (PbS)....

Figure 9.13 Schematic of typical mass spectrometer magnet and detector. A single...

Chapter 10 Strategies for Study

Figure 10.1 Example outcrop description entry in a field notebook. Only the...

Figure 10.2 Photograph of the outcrop described by field notes and the...

Figure 10.3 Sample collection directly from the outcrop aided by a hammer...

Figure 10.4 Collected sample. The sample description is recorded in the field...

Figure 10.5 Presentation of mineral data.

Figure 10.6 Crushing tools. (*a*) Piston-type percussion steel mortar and...

Figure 10.7 Sieve used with small samples. On the left is a...

Figure 10.8 Shaker table. For this type of table, sample is added...

Figure 10.9 Separatory funnel setup.

Figure 10.10 Frantz® Magnetic Barrier Laboratory Separator. The closely related Frantz®

DO NOT COPY e48d507df5d1141@placeholder.9409

Printed by: e48d507df5d1141@placeholder.94092.edu. Printing is for personal, private use only. No part of this book may be reproduced or transmitted without publisher's prior permission. Violators will be prosecuted.

Part Three Mineral Descriptions

Chapter 11 Silicates

Figure 11.1 A silicon tetrahedron consists of four O^{2-} forming...

Figure 11.2 Silicate structures. (*a*) Orthosilicates. The basic building block...

Figure 11.3 Classification of igneous rocks. Classification is based on the relative...

Figure 11.4 Chemical classification of volcanic rocks based on weight percent of SiO

Figure 11.5 Classification of plutonic igneous rocks lacking significant amounts of quartz,...

Figure 11.6 This small pegmatite dike (*top*) that has intruded...

Figure 11.7 Bowen's reaction series simplified and connected to mineral melting and...

Figure 11.8 Classification of sandstones based on quartz, feldspar (K-feldspar + plagioclase),...

Figure 11.9 Mineralogy of framework grains in sandstone derived from different tectonic...

Figure 11.10 Generalized temperature and pressure loop for a rock buried by...

Figure 11.11 Metamorphic grade and facies boundaries. Stability fields of the aluminum...

Figure 11.12 Metamorphic zones in Proterozoic pelitic/psammitic metamorphic rocks (no shading) of...

Figure 11.13 T–P conditions found in different tectonic environments. Adapted from Spear (1993)

Chapter 12 Framework Silicates

Figure 12.1 Stability fields of the silica minerals. Adapted from Griffen (1992).

Figure 12.2 Quartz structure viewed down the *c* axis. A unit...

Figure 12.3 Quartz. (*a*) Rounded quartz (left) phenocryst in rhyodacite....

Figure 12.4 Opal microstructure. (*a*) Randomly packed spheres of silica...

Figure 12.5 Simplified composition range of common feldspar; see text for details. (

Figure 12.6 Idealized feldspar structure: T_1 and T_2 refer...

Figure 12.7 Ordering of Al and Si in tetrahedral sites in the...

DO NOT COPY
e48d507df5d1141@placeholder.9409

Printed by: e48d507df5d1141@placeholder.94092.edu. Printing is for personal, private use only. No part of this book may be reproduced or transmitted without publisher's prior permission. Violators will be prosecuted.

Figure 12.8 Arrangement of oxygen anions about K^+ in sanidine...

Figure 12.9 Perthitic exsolution. (*a*) Hand sample. Thin netlike or...

Figure 12.10 Quartz–feldspar intergrowths. (*a*) Myrmekite (My) consists of irregular...

Figure 12.11 Common twins in the feldspars. (*a*) Albite twins...

Figure 12.12 Plagioclase in thin section. Cross-polarized light. (*a*)...

Figure 12.13 Optical properties of low (plutonic) and high (volcanic) plagioclase. Adapted from

Figure 12.14 Index of refraction of the fast ray (n'_α

Figure 12.15 Michel-Lévy method. Extinction angles a_1 and a_2 ...

Figure 12.16 Diagram for use with the Michel-Lévy method. The maximum extinction...

Figure 12.17 Carlsbad–albite method. (*a*) Grain with twin lamellae N–S...

Figure 12.18 Diagrams for use with the Carlsbad–albite method. Solid lines are...

Figure 12.19 Variation of $2V_x$ and indices of refraction...

Figure 12.20 Alkali feldspar. (*a*) Perthitic microcline crystals with quartz...

Figure 12.21 Photomicrograph of nepheline (N) in thin section with plagioclase (P)...

Figure 12.22 Typical zeolite structure. Heulandite viewed down the *c* axis....

Figure 12.23 Scanning electron microscope images of zeolites from altered basaltic tuff,...

Chapter 13 Sheet Silicates

Figure 13.1 Sheet silicate sheets and layers. (*a*) An octahedral (

Figure 13.2 Schematic plan view of trioctahedral and dioctahedral sheets. (*a*...

Figure 13.3 Schematic sheet silicate unit structures. Dioctahedral minerals are indicated with...

Figure 13.4 Polytypism in the micas. (*a*) In a *TOT* ...

Figure 13.5 Serpentine structures. All are based on dioctahedral *TO* layers. (*a*

Figure 13.6 Serpentine. (*a*) Hand sample in which veins of...

Figure 13.7 Muscovite. (*a*) Muscovite “book” with [310] twin from...

Figure 13.8 Compositional range of common biotite (shaded). Adapted

DO NOT COPY
e48d507df5d1141@placeholder.94092

Printed by: e48d507df5d1141@placeholder.94092.edu. Printing is for personal, private use only. No part of this book may be reproduced or transmitted without publisher's prior permission. Violators will be prosecuted.

from Deer and...

Figure 13.9 Biotite. (*a*) Foliated biotite grains in mica schist....

Figure 13.10 Lepidolite composition. The common range is shown with the shaded area.

Figure 13.11 Glauconite pellets (G) with rounded quartz (Q) grains and elongate...

Figure 13.12 Chlorite. (*a*) Foliated chlorite grains (C) with biotite...

Figure 13.13 SEM images of clay minerals. (*a*) Kaolinite platelets...

Figure 13.14 Clay mineral structure. Refer also to Figures 13.1 and 13.3...

Figure 13.15 Clay mineralogy in selected size fractions of Miocene–Oligocene sediment in...

Figure 13.16 Idealized structure of stilpnomelane. Some tetrahedra point outward from the *TOT*

Figure 13.17 Stilpnomelane grains in a stilpnomelane schist.

Chapter 14 Chain Silicates

Figure 14.1 Pyroxene structure. (*a*) Top and end views of...

Figure 14.2 Pyroxene classification; see text for details. (*a*) Calcic...

Figure 14.3 Photomicrographs of pyroxene in thin section. (*a*) Anhedral...

Figure 14.4 Exsolution lamellae may be responsible for partings in pyroxene. (*a*

Figure 14.5 Optical properties, specific gravity, and unit cell dimensions of orthopyroxene....

Figure 14.6 Variation of optical properties of aegirine and aegirine–augite with Fe^{3+}

Figure 14.7 Chain structure of pyroxenes and pyroxenoids. (*a*) Pyroxenes...

Figure 14.8 Photograph of radiating masses of pectolite. Field of view is...

Figure 14.9 Amphibole structure. (*a*) Top and end views of...

Figure 14.10 Fe–Mg–Ca amphiboles; common compositions are shown with shading. Decimal numbers...

Figure 14.11 Common amphiboles. (*a*) Hornblende in outcrop. (*left*...

Figure 14.12 Optical properties of cummingtonite–grunerite. Data from Winchell (1938), Deer and...

Figure 14.13 Composition and variation of n_γ for the sodic...

Chapter 15 Disilicates and Ring Silicates

Figure 15.1 Structural elements in disilicates and ring silicates. (*a*)...

DO NOT COPY e48d507df5d1141@placeholder.9409

Printed by: e48d507df5d1141@placeholder.94092.edu. Printing is for personal, private use only. No part of this book may be reproduced or transmitted without publisher's prior permission. Violators will be prosecuted.

Figure 15.2 Structure of the epidote group. See text for additional discussion. (

Figure 15.3 Epidote. (*a*) Euhedral 2 cm crystal. (*b*...

Figure 15.4 Optical properties of clinozoisite–epidote. Compiled from Johnston (1949), Deer and...

Figure 15.5 Photomicrograph of thin section of glaucophane schist with lawsonite (L),...

Figure 15.6 Structure of beryl. (*a*) Side and top view...

Figure 15.7 Beryl crystal from a granitic pegmatite.

Figure 15.8 Photomicrograph of thin section of anthophyllite–cordierite gneiss showing cordierite (C)...

Figure 15.9 Tourmaline structure consisting of tetrahedral rings, triangular groups of octahedra...

Figure 15.10 Tourmaline. (*a*) Elongate crystals with fractures roughly perpendicular...

Chapter 16 Orthosilicates

Figure 16.1 Olivine structure. (*a*) Oxygen anions form a somewhat...

Figure 16.2 Specific gravity, $d_{(130)}$, and optical properties of olivine.

Figure 16.3 Olivine phenocryst (O) in basaltic dike. Note the alteration to...

Figure 16.4 Garnet structure. Isolated silicon tetrahedra share single oxygen anions with...

Figure 16.5 Garnet. (*a*) 2-cm garnet crystal in mica schist. (

Figure 16.6 Photomicrograph of a thin section of granite showing a small...

Figure 16.7 Structure of the aluminum silicates. (*a*) Andalusite. Edge-sharing...

Figure 16.8 Aluminum silicate stability fields. From Hemingway and others (1991).

Figure 16.9 Aluminum silicates in mica schist. (*a*) Blocky andalusite...

Figure 16.10 Sieved (inclusion filled) staurolite porphyroblast (St) with porphyroblasts of garnet...

Figure 16.11 Chloritoid structure. Octahedral layer I contains Al^{3+} sandwiched...

Figure 16.12 Photomicrograph of chloritoid in a thin section of schist. Plane light.

Figure 16.13 Photomicrograph of subhedral to anhedral titanite (T) grains with hornblende...

DO NOT COPY
e48d507df5d1141@placeholder.9409

Printed by: e48d507df5d1141@placeholder.94092.edu. Printing is for personal, private use only. No part of this book may be reproduced or transmitted without publisher's prior permission. Violators will be prosecuted.

Figure 16.14 Topaz. (*a*) Topaz crystal. (*b*) Photomicrograph...

Chapter 17 Carbonates, Sulfates, Phosphates, Tungstates, Molybdates, and Borates

Figure 17.1 CO_3^{2-} anionic groups. A carbon cation is...

Figure 17.2 Structure of the rhombohedral carbonates. O^{2-} anions at...

Figure 17.3 Calcite. (*a*) Calcite crystals. Field of view is...

Figure 17.4 Twins in rhombohedral carbonates. (*a*) Lamellar {012} twins...

Figure 17.5 Index of refraction n_ω in the rhombohedral carbonates. After ...

Figure 17.11 A view of Desert Peak across Bonneville Salt Flats, a...

Figure 17.6 The Alma King, at 16.5 cm across, is perhaps the...

Figure 17.7 Dolomite. (*a*) Dolomite crystals. Note the curved crystal...

Figure 17.8 Aragonite structure. Triangular CO_3^{2-} groups are arranged...

Figure 17.9 Aragonite crystals.

Figure 17.10 Temperature–pressure stability fields of calcite and aragonite. After Carlson (1980).

Figure 17.12 Structure of sulfate minerals. SO_4^{2-} groups are...

Figure 17.13 Gypsum. (*a*) Selenite with a swallowtail twin, U.S....

Figure 17.14 Stability of gypsum and anhydrite at 1 atm. Decreasing activity...

Figure 17.15 Photomicrograph of a thin section of bedded anhydrite. Plane light.

Figure 17.16 Barite. (*a*) Intergrown platy barite crystals with mammillary...

Figure 17.17 Structure of apatite viewed down the *c* axis. The...

Figure 17.18 Photomicrograph of apatite in thin section.

Figure 17.19 Crystal habit of wolframite, wulfenite, and scheelite.

Figure 17.20 Crystal habit of borax and colemanite.

Chapter 18 Oxides, Hydroxides, and Halides

Figure 18.1 Ice structure viewed down the *c* axis. Water molecules...

Figure 18.2 Spinel structure. Oxygen anions form an approximately cubic close-packed arrangement...

Figure 18.3 Magnetite. (*a*) Massive granular hand sample. (*b*...

Figure 18.4 The 2.7 Ga Soudan banded iron formation in northeastern Minnesota....

Figure 18.5 Structure of the hematite group. (*a*) X cations...

DO NOT COPY

Printed by: e48d507df5d1141@placeholder.94092.edu. Printing is for personal, private use only. No part of this book may be reproduced or transmitted without publisher's prior permission. Violators will be prosecuted.

Figure 18.5 Structure of the hematite group. (*a*) X cations...

Figure 18.6 Photomicrograph of corundum (C), microcline (M), and small grains of...

Figure 18.7 Rutile, cassiterite, and pyrolusite structure. The Ti^{2+}, Sn^{2+}...

Figure 18.8 Brucite and gibbsite structure. (*a*) Octahedral sheets are...

Figure 18.9 Dendrites on slab of sandstone.

Figure 18.10 Halite structure. Each Na^{+} coordinates with six Cl^{-}.

Figure 18.11 Fluorite structure. Each Ca^{2+} coordinates with 8 F^{-}.

Figure 18.12 Fluorite crystals. Field of view is about 15 cm wide.

Chapter 19 Sulfides and Related Minerals

Figure 19.1 Schematic hydrothermal system. Hot mineralizing aqueous fluids may evolve from...

Figure 19.2 Hydrothermal alteration. (*a*) Henderson porphyry molybdenum deposit, Colorado,...

Figure 19.3 Supergene enrichment. Meteoric water percolates down through a sulfide-bearing vein....

Figure 19.4 Small elongate prismatic crystals of stibnite.

Figure 19.5 Structure of sphalerite. Sulfur atoms are arranged in cubic close...

Figure 19.6 Galena cubes encrusted with marcasite.

Figure 19.7 Structure of iron sulfides. (*a*) The pyrite structure...

Figure 19.8 Pyrite. (*a*) Pyritohedron crystals. Field of view is...

Figure 19.9 Cockscomb crystals of marcasite.

Chapter 20 Native Elements

Figure 20.1 Many native metals have a cubic close-packed structure with metallic bonding.

Figure 20.2 Structure of native sulfur. Eight-fold rings of covalently bonded sulfur...

Figure 20.3 Schematic cross section through a salt dome showing idealized sequence...

Figure 20.4 Van Krevelen diagram showing chemical evolution of organic material derived...

Figure 20.5 Color in diamond. (*a*) In pure diamond the...

Figure 20.6 Change in average global temperature and atmospheric CO_2 ...

Figure 20.7 Schematic diagram of the carbon cycle showing reservoirs and

DO NOT COPY
e48d507df5d1141@placeholder.94092

Printed by: e48d507df5d1141@placeholder.94092.edu. Printing is for personal, private use only. No part of this book may be reproduced or transmitted without publisher's prior permission. Violators will be prosecuted.

List of Tables

Part One Crystallography and Crystal Chemistry

Chapter 1 Introduction

Table 1.1 Select Metals and Some Minerals from Which They Are Extracted

Table 1.2 Iron Ore Production in 1937 in Select Countries

Table 1.3 Mohs Scale of Hardness

Chapter 2 Crystallography

Table 2.1 Nomenclature for Symmetry Elements

Table 2.2 The 32 Point Groups[a]

Table 2.3 Percentage of Minerals in Each Crystal System and Point Group

Table 2.4 Alternative Crystal System Nomenclature

Table 2.5 Enantiomorphous Forms (Figures 2.33, 2.36, and 2.37) and the Point Groups in Which They Occur

Table 2.6 Forms Found in the Point Groups and Crystal Classes of the Triclinic, Monoclinic, and Orthorhombic Crystal Systems[a]

Table 2.7 Forms Found in the Point Groups and Crystal Classes of the Tetragonal Crystal System[a]

Table 2.8 Forms Found in the Crystal Classes and Point Groups of the Hexagonal Crystal System[a]

Table 2.9 Forms Found in the Crystal Classes and Point Groups of the Isometric Crystal System[a]

Chapter 3 Crystal Chemistry

Table 3.1 The Principal Atomic Particles

Table 3.2 Relationship among Quantum Numbers[a]

Table 3.3 Electron Configuration of Uncharged Atoms[a]

Table 3.4 Electronegativity of the First 38 Elements in Their Most Common Oxidation State(s)

Table 3.5 Abundance of the Elements in the Earth's Crust[a]

Table 3.6 The Eight Most Abundant Elements in the Earth's Crust

Chapter 4 Crystal Structure

DO NOT COPY e48d507df5d1141@placeholder.9409

Printed by: e48d507df5d1141@placeholder.94092.edu. Printing is for personal, private use only. No part of this book may be reproduced or transmitted without publisher's prior permission. Violators will be prosecuted.

Chapter 4 Crystal Structure

Table 4.1 Radius Ratio for Common Coordination Geometries

Table 4.2 Cation Sizes for Common Coordination Polyhedra When Coordinating with O^{2-} (~1.26 Å)

Table 4.3 Calcite Isostructural Group[a]

Table 4.4 Common Polymorphic Mineral Groups

Table 4.5 Chemical Classification of Minerals

Table 4.6 Charge Balance Calculation for Diopside ($CaMgSi_2O_6$)

Chapter 5 Mineral Growth

Table 5.1 Selected Radioactive Isotopes Found in Common Minerals

Table 5.2 Approximate Closure and Annealing Temperatures (°C) of Some Minerals and Isotopic Systems[a]

Table 5.3 Biominerals

Part Two Mineral Properties, Study, and Identification

Chapter 6 Physical Properties of Minerals

Table 6.1 Heavy Liquids

Table 6.2 Mohs Scale of Hardness

Table 6.3 Tenacity

Table 6.4 Fracture

Table 6.5 Common Minerals in Which Partings Have Been Associated with Twin Planes

Table 6.6 Varieties of Nonmetallic Luster

Table 6.7 Minerals with Color Centers

Table 6.8 The 20 Piezoelectric Point Groups and 10 Pyroelectric Point Groups[a]

Chapter 7 Optical Mineralogy

Table 7.1 $2V$ angle ($2V_{max}$) for Melatopes at the Edge of the Field of View for Different Values of n_β and Numerical Apertures of 0.65 and 0.85

Table 7.2 Becke Line Relationships When the Microscope Stage Is Lowered

Chapter 8 Analytical Instrumentation and Techniques I: Crystallography

Table 8.1 Characteristic Wavelengths (Å) of Metals Commonly Used as Targets in X-ray Tubes[a]

Table 8.2 Data Reduction from X-Ray Diffraction Pattern Shown in Figure 8.6[a]

DO NOT COPY e48d507df5d1141@placeholder.9409

Printed by: e48d507df5d1141@placeholder.94092.edu. Printing is for personal, private use only. No part of this book may be reproduced or transmitted without publisher's prior permission. Violators will be prosecuted.

Table 8.3 Relation between d_{hkl} and Unit Cell Parameters[a]

Chapter 9 Analytical Instrumentation and Techniques II: Chemical Analysis of Minerals

Table 9.1 Preferred Characteristic X-Rays Used for Quantitative Analysis of Elements Found in Common Minerals[a]

Table 9.2 Wavelength-Dispersive Quantitative Analysis of Minerals in a Gabbro Sample (Figure 9.5)[a]

Table 9.3 Chemical Analysis of a Biotite Sample

Table 9.4 Typical Trace Element Analysis of a Pyroxene

Table 9.5 Recalculation of a Pyroxene Analysis

Table 9.6 Molecular Weight of Common Oxide Species

Chapter 10 Strategies for Study

Table 10.1 Sieve Openings

Part Three Mineral Descriptions

Chapter 11 Silicates

Table 11.1 Silicate Classification[a]

Table 11.2 Common Silicate Minerals

Table 11.3 Silicate Chemical Formulas Using the General Formula (Equation 11.1)

Table 11.4 Criteria to Distinguish between Diorite and Gabbro or Related Rocks (Figure 11.3)[a]

Table 11.5 Bowen's Reaction Series Mineral Commonality in Igneous Rocks[a]

Table 11.6 Simplified Classification of Clastic Sedimentary Rocks

Table 11.7 Heavy Minerals Commonly Found in Clastic Sediments[a]

Table 11.8 Sedimentary Environments

Table 11.9 Classification of Common Metamorphic Rocks

Table 11.10 Lithostatic Pressure Produced by Different Rock Types

Table 11.11 Mineralogy of Metamorphic Facies for Mafic Rocks

Table 11.12 Typical Mineral Zones in Pelitic Rocks[a]

Chapter 12 Framework Silicates

Table 12.1 Common Framework Silicate Minerals[a]

Table 12.2 Silica Polymorphs

Table 12.3 Quartz Varieties

DO NOT COPY e48d507df5d1141@placeholder.9409

Printed by: e48d507df5d1141@placeholder.94092.edu. Printing is for personal, private use only. No part of this book may be reproduced or transmitted without publisher's prior permission. Violators will be prosecuted.

Table 12.4 Modes of Al:Si Ordering in Tetrahedral Sites in the Feldspars[a]

Table 12.5 Plagioclase Composition in Common Igneous Rock Types

Table 12.6 Physical Properties of Selected Zeolite Minerals

Table 12.7 Optical Properties of Selected Zeolites

Chapter 13 Sheet Silicates

Table 13.1 Common Sheet Silicate Minerals

Table 13.2 Properties of Clay Minerals

Table 13.3 Properties of Palygorskite and Sepiolite

Table 13.4 Clay Mineral Identification[a]

Chapter 14 Chain Silicates

Table 14.1 Pyroxene Classification[a]

Table 14.2 Abbreviated Amphibole Classification of Four Common Amphiboles with Examples, Based on the General Formula $A_{0-1}B_2C_5T_8O_{22}W_2$[a]

Table 14.3 Simple Substitutions in the Amphiboles

Table 14.4 Selected Coupled Substitution Schemes in Clinoamphiboles

Table 14.5 Properties of Less Common Amphiboles[a]

Chapter 15 Disilicates and Ring Silicates

Table 15.1 Epidote Group Minerals[a]

Table 15.2 Properties of Less Common Disilicates and Ring Silicates

Table 15.3 Properties of Axinite

Chapter 16 Orthosilicates

Table 16.1 Common Orthosilicate Minerals[a]

Table 16.2 Garnet

Table 16.3 Application of Zircon to Geologic Problems

Table 16.4 Pleochroism in Sillimanite[a]

Table 16.5 Properties of Less Common Orthosilicates

Chapter 17 Carbonates, Sulfates, Phosphates, Tungstates, Molybdates, and Borates

Table 17.1 Major Groups of Carbonate Minerals

Table 17.2 Properties of Less Common Carbonate Minerals

Table 17.3 Select Minerals Formed in Evaporite Deposits

Table 17.4 Properties of Less Common Sulfate Minerals[a]

Table 17.5 Less Common Phosphate and Vanadate Minerals

DO NOT COPY e48d507df5d1141@placeholder.9409

Printed by: e48d507df5d1141@placeholder.94092.edu. Printing is for personal, private use only. No part of this book may be reproduced or transmitted without publisher's prior permission. Violators will be prosecuted.

Table 17.5 Less Common Phosphate and Vanadate Minerals

Table 17.6 Tungstates and Molybdates

Table 17.7 Borate Minerals

Chapter 18 Oxides, Hydroxides, and Halides

Table 18.1 Oxide Minerals

Table 18.2 XO Oxide Minerals

Table 18.3 Spinel Group Minerals

Table 18.4 Iron Hydroxide Minerals

Table 18.5 Aluminum Hydroxide Minerals

Table 18.6 Manganese Oxide and Hydroxide Minerals

Table 18.7 Less Common Halide Minerals

Chapter 19 Sulfides and Related Minerals

Table 19.1 Common Sulfide and Related Minerals[a]

Table 19.2 Band Gap of Selected Sulfide Minerals[a]

Table 19.3 Select Hydrothermal Mineral Assemblages[a]

Table 19.4 Common Minerals in the Oxidized Portion of Hydrothermal Sulfide Deposits

Table 19.5 Less Common Sulfide Minerals

Table 19.6 Sulfarsenides, Arsenides, and Tellurides

Chapter 20 Native Elements

Table 20.1 Native Elements

Table 20.2 Properties of Selected Native Elements

Table 20.3 Earth's Carbon Reservoirs[a]

Appendix B Determinative Tables

Table B.1 Determinative Table for Nonmetallic Minerals with White, Gray, or Other Pale-Colored Streak[a]

Table B.2 Non metallic Minerals with Distinctly Colored Streak

Table B.3 Minerals with Metallic and Submetallic Luster

Table B.4 Specific Gravity

Table B.5 Minerals That May Fluoresce[a]

Table B.6 Selected Minerals That Are Ferromagnetic and Ferrimagnetic

Table B.7 Minerals That Effervesce in Dilute HCl

Table B.8 Color of Minerals in Thin Section and Grain Mount

Table B.9 Indices of Refraction of Isotropic Minerals

DO NOT COPY

Printed by: e48d507df5d1141@placeholder.94092.edu. Printing is for personal, private use only. No part of this book may be reproduced or transmitted without publisher's prior permission. Violators will be prosecuted.

Table B.9 Indices of Refraction of Isotropic Minerals

Table B.10 Indices of Refraction of Uniaxial Minerals

Table B.11 Indices of Refraction of Biaxial Negative Minerals Arranged in Order of Increasing n_β

Table B.12 Indices of Refraction of Biaxial Positive Minerals Arranged in Order of Increasing n_β

Table B.13 Minerals That Produce Pleochroic Halos in Surrounding Minerals

Table B.14 Colors Exhibited by Opaque Minerals in Polished Section Viewed in Air

Table B.15 Opaque or Nearly Opaque Minerals That Display Internal Reflections with Reflected Light

Appendix C Mineral Associations

Table C.1 Mineralogy of Common Igneous Rocks

Table C.2 Mineralogy of Sedimentary Rocks

Table C.3 Mineralogy of Common Metamorphic Rocks

Table C.4 Mineralogy of Hydrothermal Sulfide Deposits

DO NOT COPY

e48d507df5d1141@placeholder.9409

Printed by: e48d507df5d1141@placeholder.94092.edu. Printing is for personal, private use only. No part of this book may be reproduced or transmitted without publisher's prior permission. Violators will be prosecuted.

Images

This section includes full-size versions of all labelled images from the book, organized by chapter or module. Links provided with the images will return you to the location in the main text where the image appears. The full-size images in this section can also be accessed from their locations in the main text.

DO NOT COPY
e48d507df5d1141@placeholder.9409

Printed by: e48d507df5d1141@placeholder.94092.edu. Printing is for personal, private use only. No part of this book may be reproduced or transmitted without publisher's prior permission. Violators will be prosecuted.

Chapter 1 Introduction

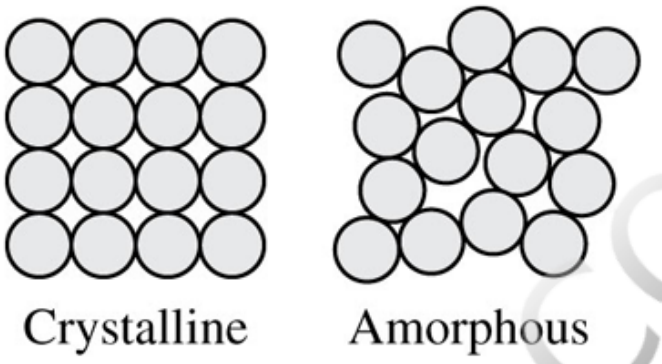

FIGURE 1.1 Simple representations that compare the highly organized atoms in a crystalline material to the relatively disorganized atomic arrangement found in an amorphous material. Back to text

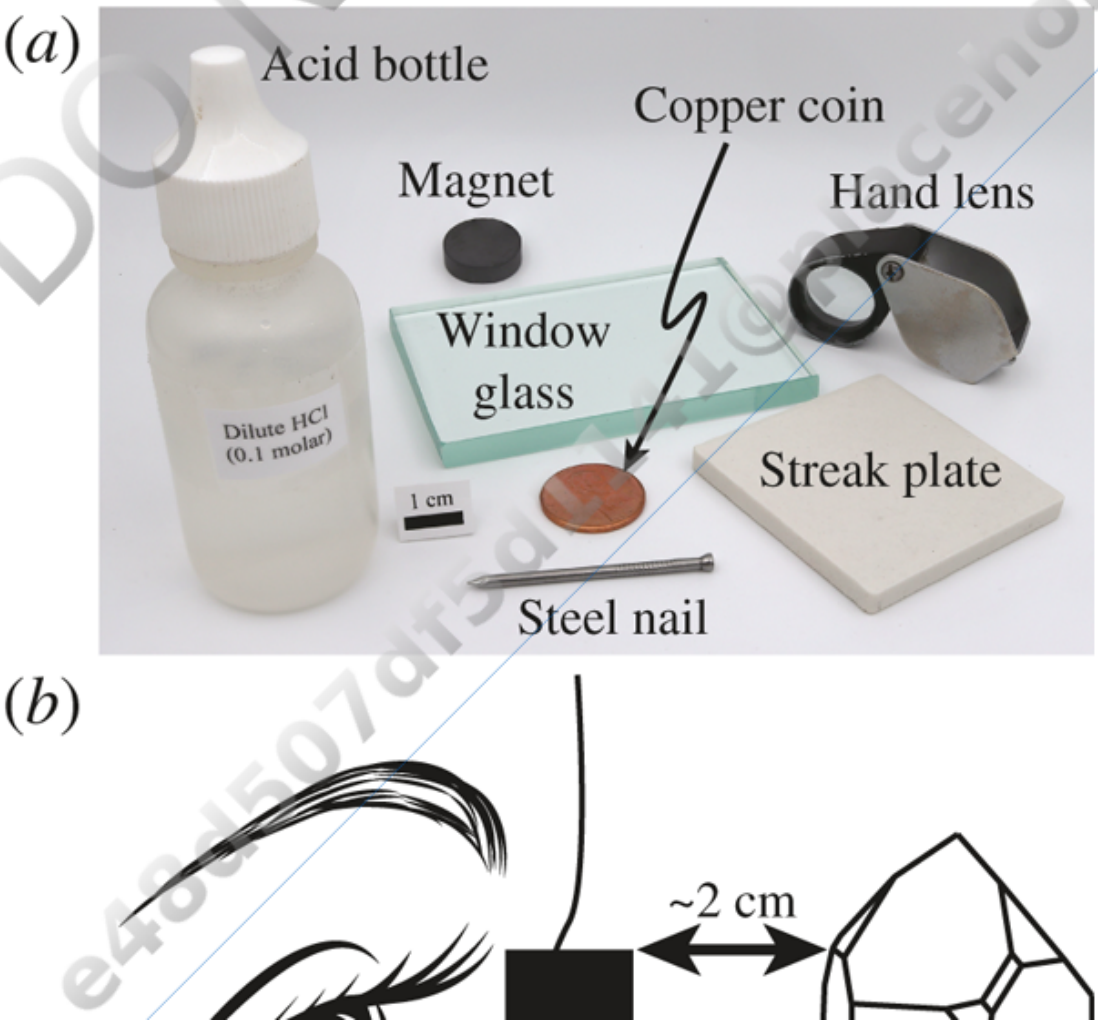

DO NOT COPY

Printed by: e48d507df5d1141@placeholder.94092.edu. Printing is for personal, private use only. No part of this book may be reproduced or transmitted without publisher's prior permission. Violators will be prosecuted.

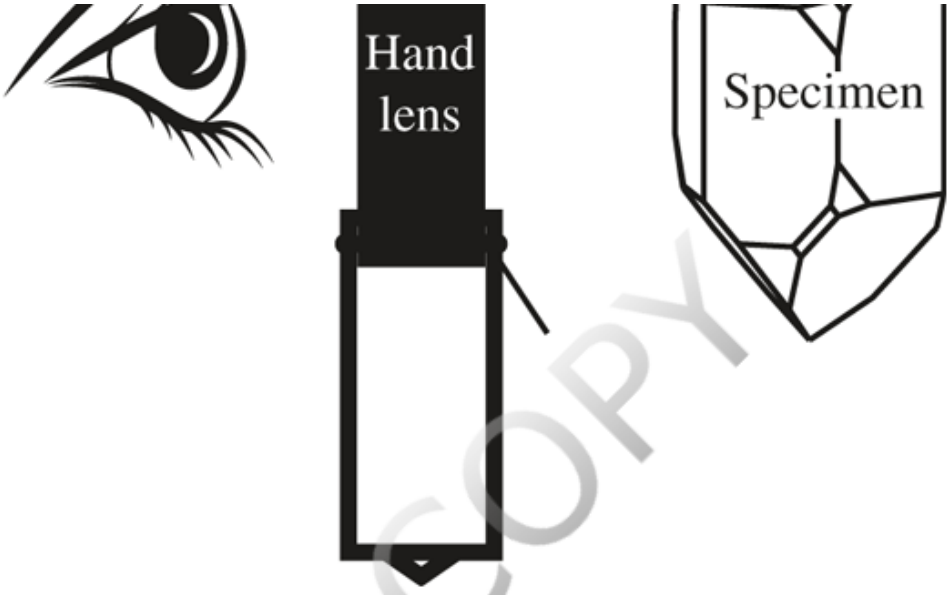

FIGURE 1.2 Mineralogy tools and use. (*a*) Basic tools used in mineral identification. (*b*) Proper use of typical 10× hand lens. Back to text

DO NOT COPY
e48d507df5d1141@placeholder.9409

Printed by: e48d507df5d1141@placeholder.94092.edu. Printing is for personal, private use only. No part of this book may be reproduced or transmitted without publisher's prior permission. Violators will be prosecuted.

Chapter 2 Crystallography

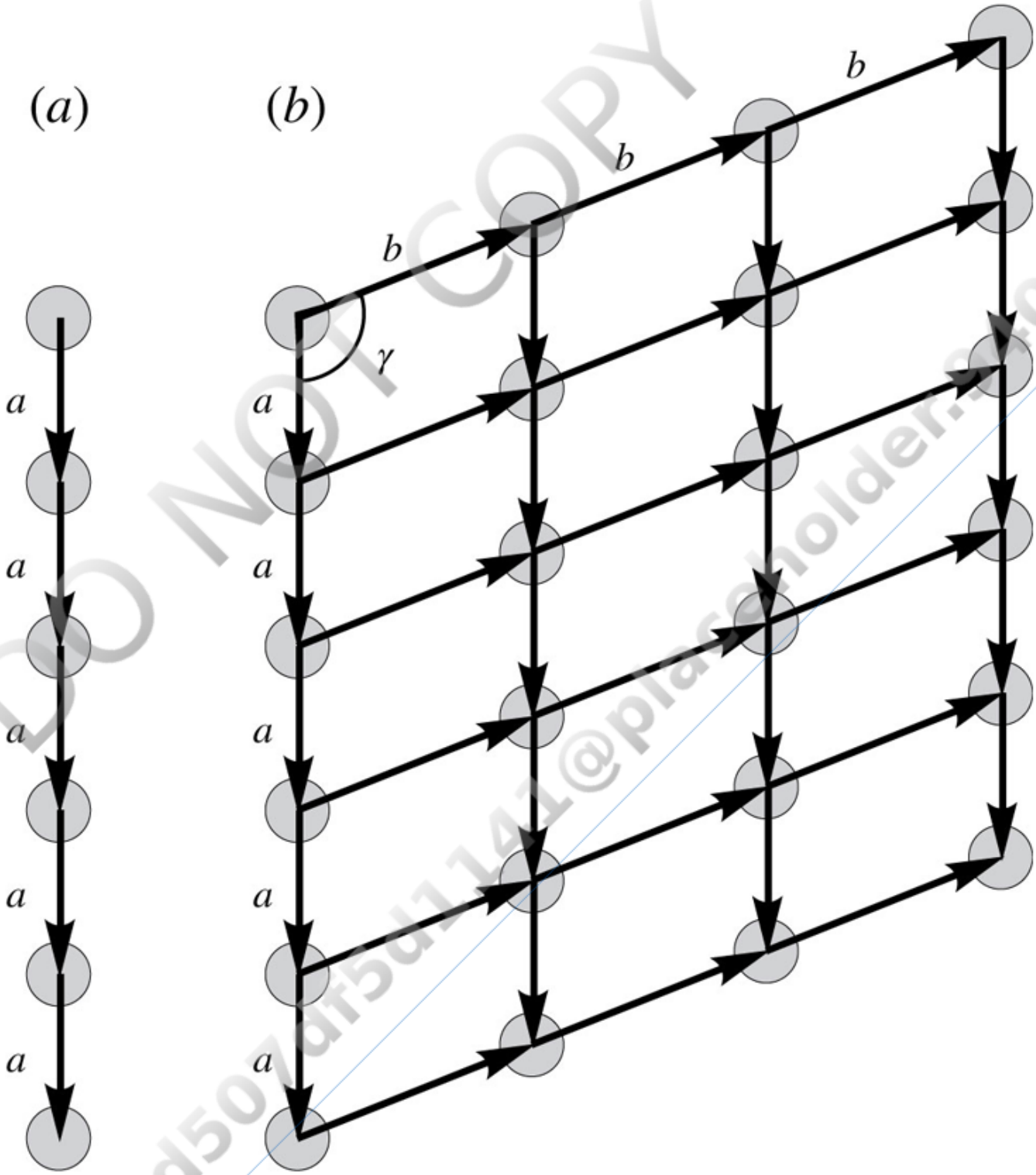

FIGURE 2.1 Simple translation to form a plane lattice. (*a*) A dot is repeated by translation distance *a* toward the bottom of the page. (*b*) Repeated translation of these dots, distance *b* at angle γ, produces a two-dimensional plane lattice. The dots represent the lattice nodes. Back to text

DO NOT COPY
e48d507df5d1141@placeholder.94092

Printed by: e48d507df5d1141@placeholder.94092.edu. Printing is for personal, private use only. No part of this book may be reproduced or transmitted without publisher's prior permission. Violators will be prosecuted.

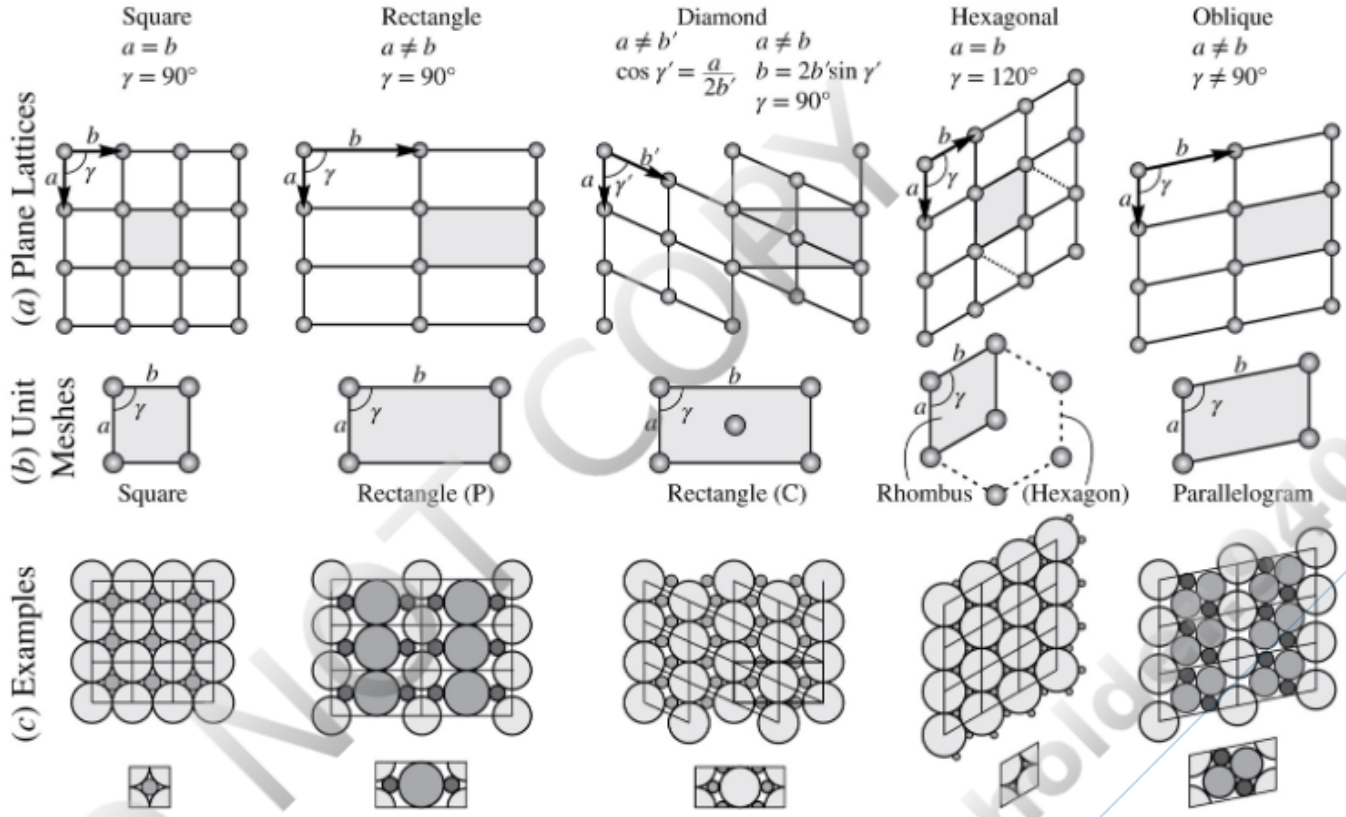

FIGURE 2.2 Plane lattices and unit meshes. (*a*) Five different plane lattices can be produced by combinations of translation in two directions. The unit meshes are shaded. (*b*) Unit meshes for the five plane lattices. A rectangle unit mesh can be used for both the rectangle and diamond plane lattice; the only difference is that the unit mesh for the diamond lattice has an additional lattice node at its center. If desired, a hexagon unit mesh (dashed lines) can be used with the hexagonal plane lattice, but the rhombus is simpler. (*c*) Examples of how hypothetical two-dimensional "atoms" might be arranged in the five plane lattices. A single unit mesh is shown below each lattice. Back to text

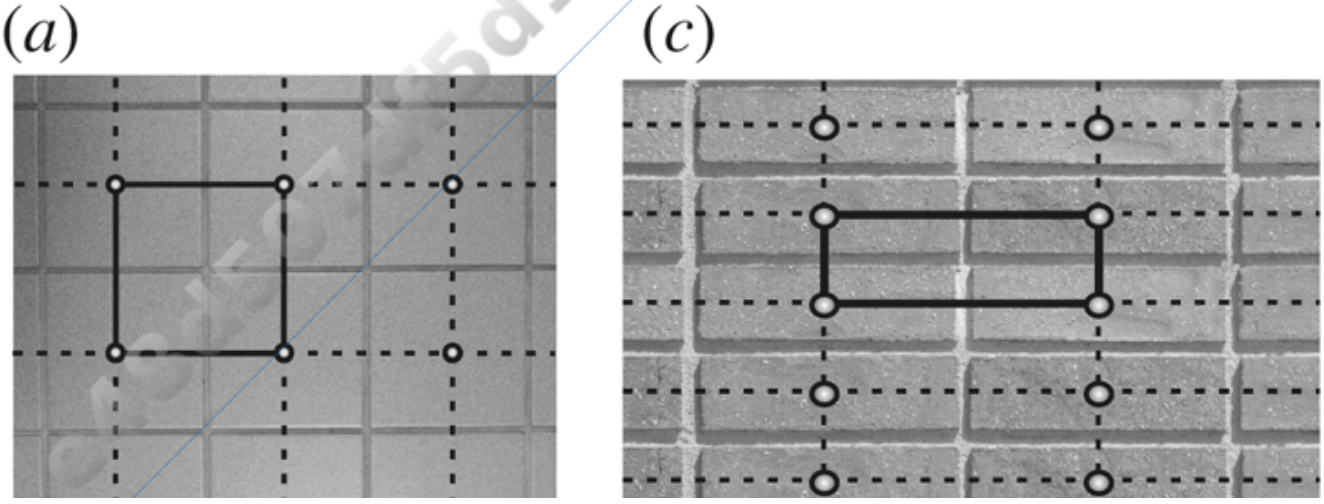

Printed by: e48d507df5d1141@placeholder.94092.edu. Printing is for personal, private use only. No part of this book may be reproduced or transmitted without publisher's prior permission. Violators will be prosecuted.

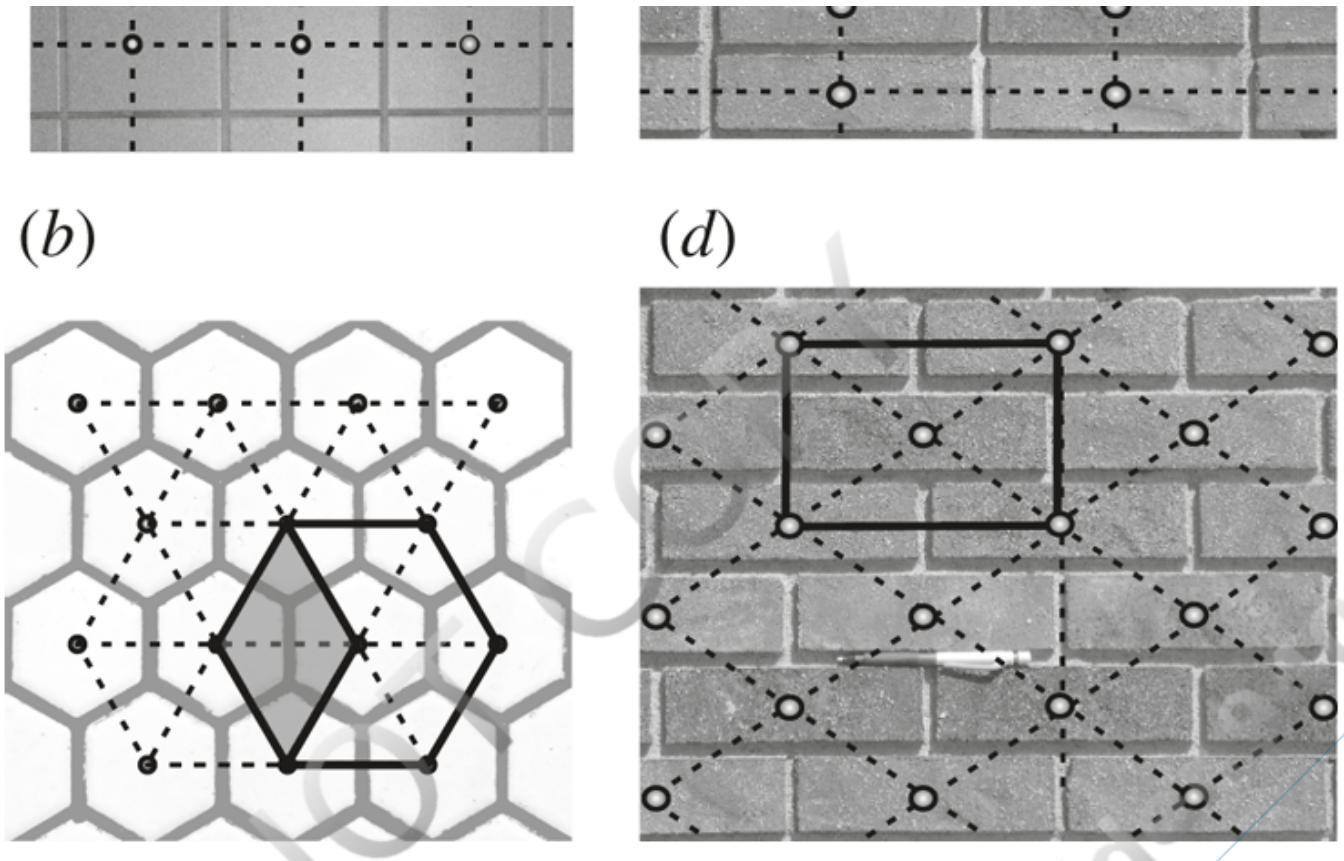

FIGURE 2.3 Plane lattices and unit meshes in everyday life. (*a*) Square ceramic tile laid in a square lattice. (*b*) Hexagonal ceramic tile laid in a hexagonal lattice. The rhombic unit mesh includes pieces sufficient to make one tile if the tile parts within the unit mesh are rearranged. (*c*) Rectangular bricks laid in a rectangular lattice. The unit mesh contains one brick. (*d*) Rectangular bricks laid in a centered rectangular (diamond) lattice. The unit mesh contains pieces sufficient to make two bricks. Back to text

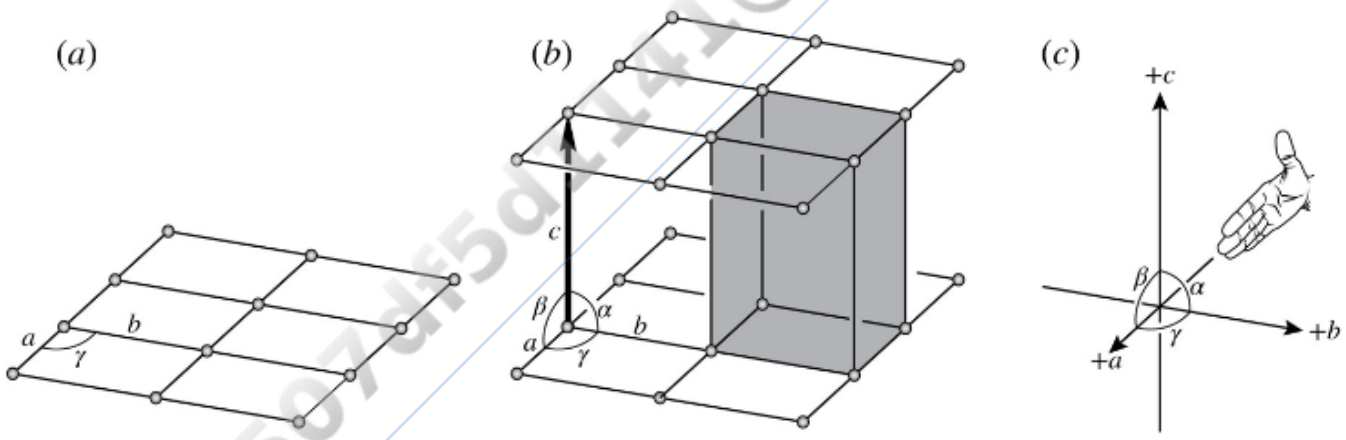

FIGURE 2.4 Space lattice. (*a*) A plane lattice with axes *a* and *b* at angle *γ*. (*b*) Translation of the lattice distance *c* at angles *α* and *β* to form a repeating pattern of lattice nodes in three dimensions. A unit cell (shaded) is the volume outlined by lattice nodes. (*c*) Crystal axes *a*, *b*, and *c* are parallel to the edges of the unit cell at angles *α*, *β*, and *γ*. A flattened right hand can be used to ensure the positive ends of the crystal axes are correctly positioned relatively to each other. Back to text

Printed by: e48d507df5d1141@placeholder.94092.edu. Printing is for personal, private use only. No part of this book may be reproduced or transmitted without publisher's prior permission. Violators will be prosecuted.

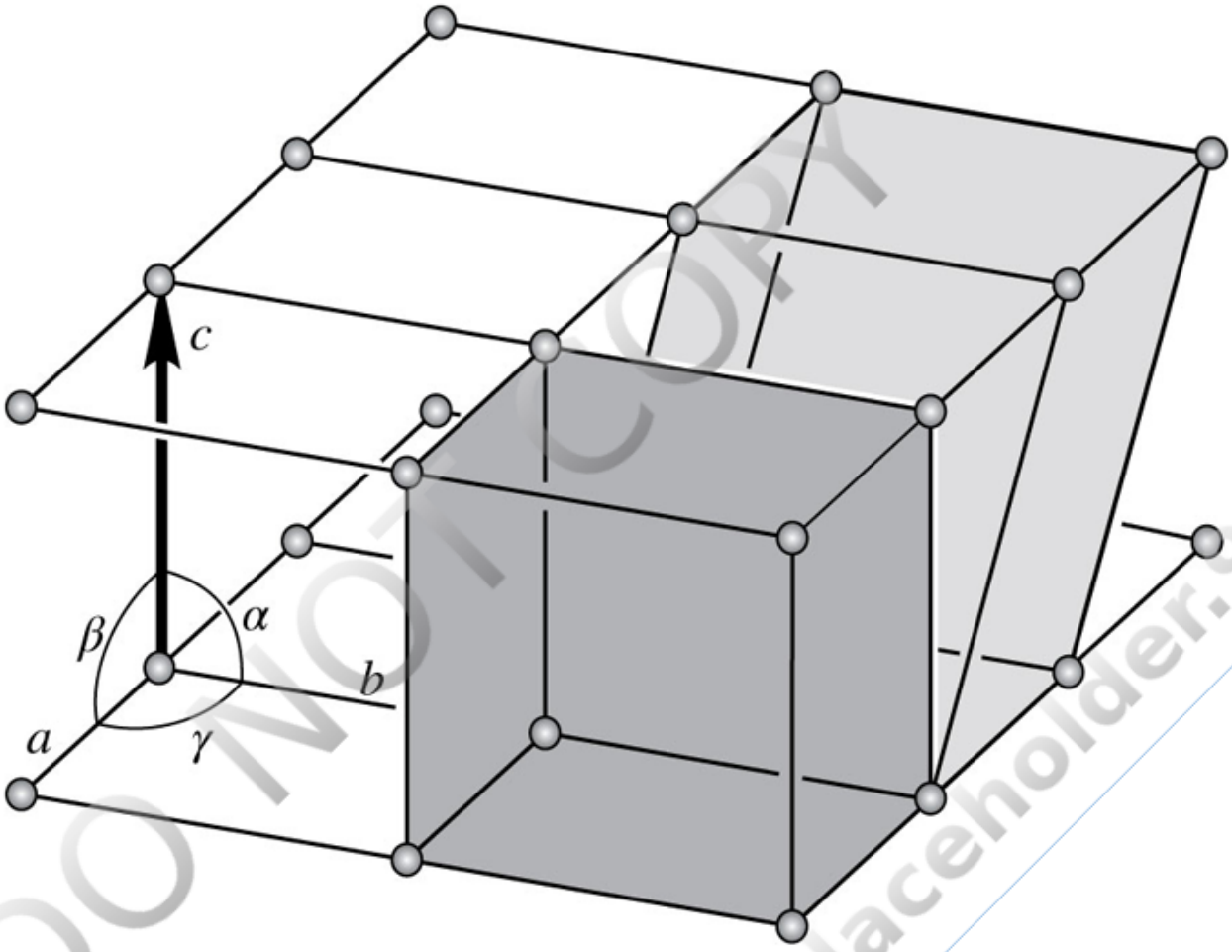

FIGURE 2.5 Triclinic Bravais lattice. An oblique plane lattice is repeated by translation distance c so that the α and β angles are not equal to 90°. Light and dark shading show two unit cell choices. Generally, the unit cell with angles closer to 90° is used, but crystal morphology and/or convenience in describing the crystal structure may dictate that a different unit cell is chosen. Back to text

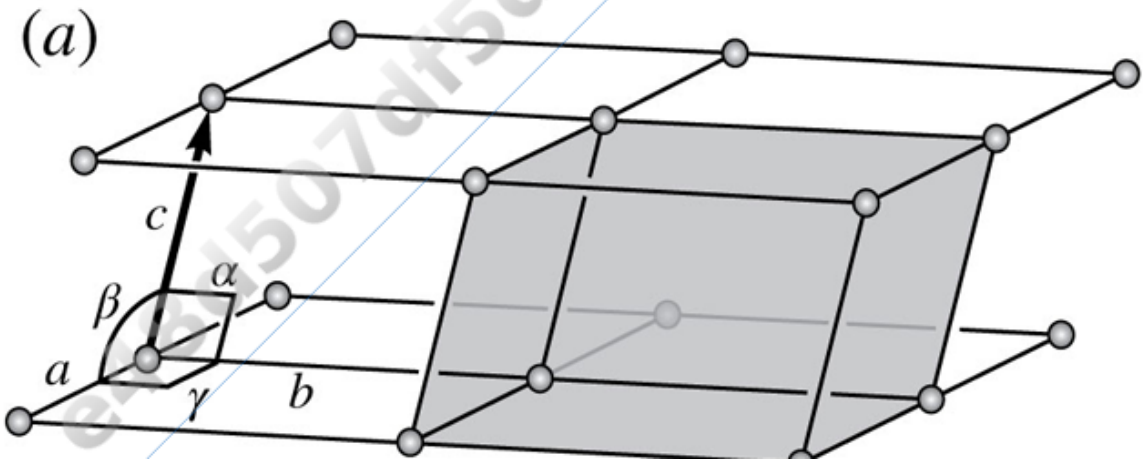

DO NOT COPY
e48d507df5d1141@placeholder.9409

Printed by: e48d507df5d1141@placeholder.94092.edu. Printing is for personal, private use only. No part of this book may be reproduced or transmitted without publisher's prior permission. Violators will be prosecuted.

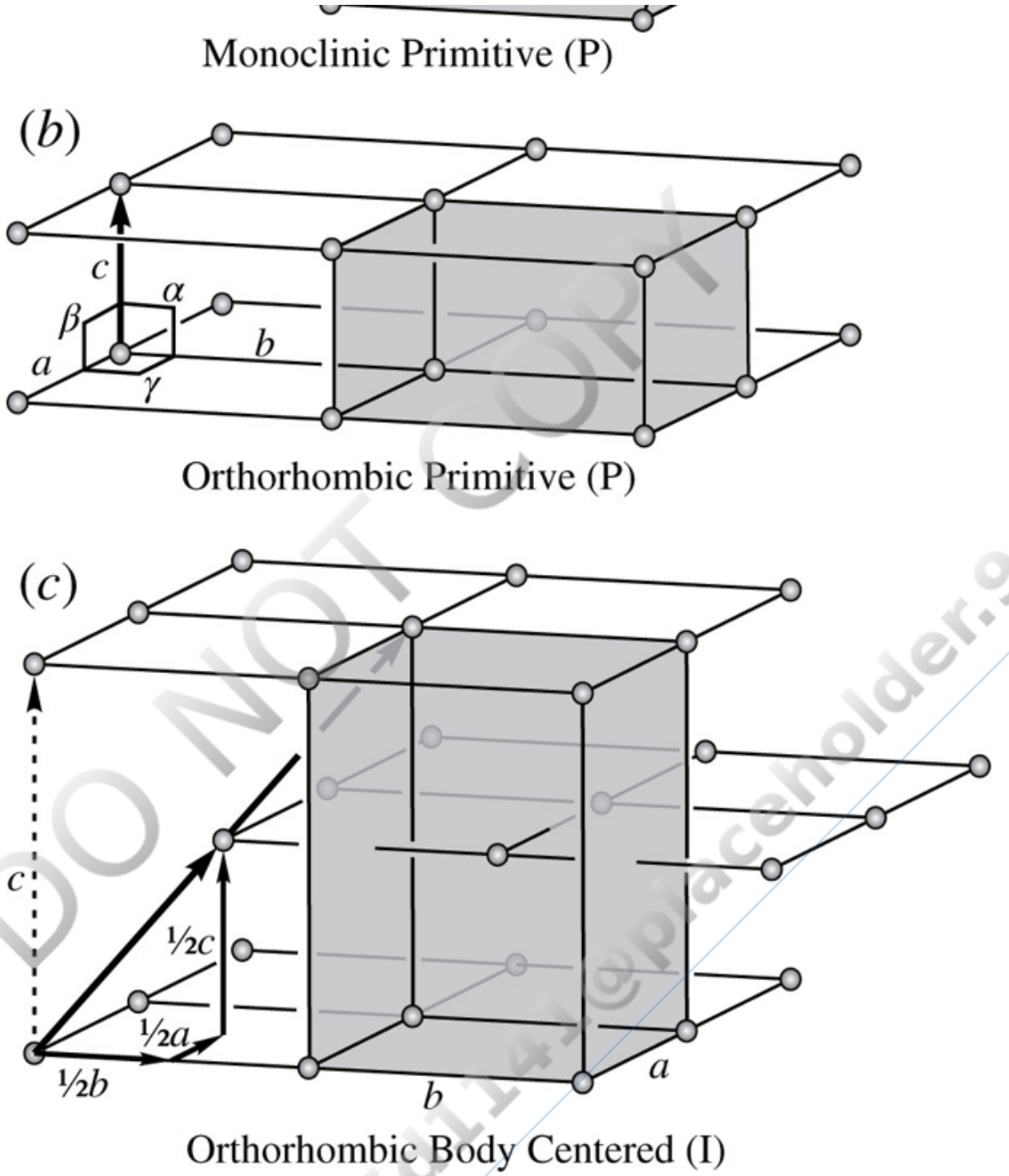

FIGURE 2.6 Bravais lattices produced by translation of a rectangle plane lattice where *a* and *b* are different lengths and angle $\gamma = 90°$. (*a*) Primitive (P) monoclinic lattice produced by translation distance *c* so angles $\alpha = 90°$ and $\beta > 90°$. (*b*) Primitive (P) orthorhombic lattice produced by translation distance *c* so that angles α and β are 90°. (*c*) Translation ½ *b* to the right, ½ *a* back, and ½ *c* up produces a body-centered orthorhombic (I) lattice. Back to text

DO NOT COPY
e48d507df5d1141@placeholder.9409

Printed by: e48d507df5d1141@placeholder.94092.edu. Printing is for personal, private use only. No part of this book may be reproduced or transmitted without publisher's prior permission. Violators will be prosecuted.

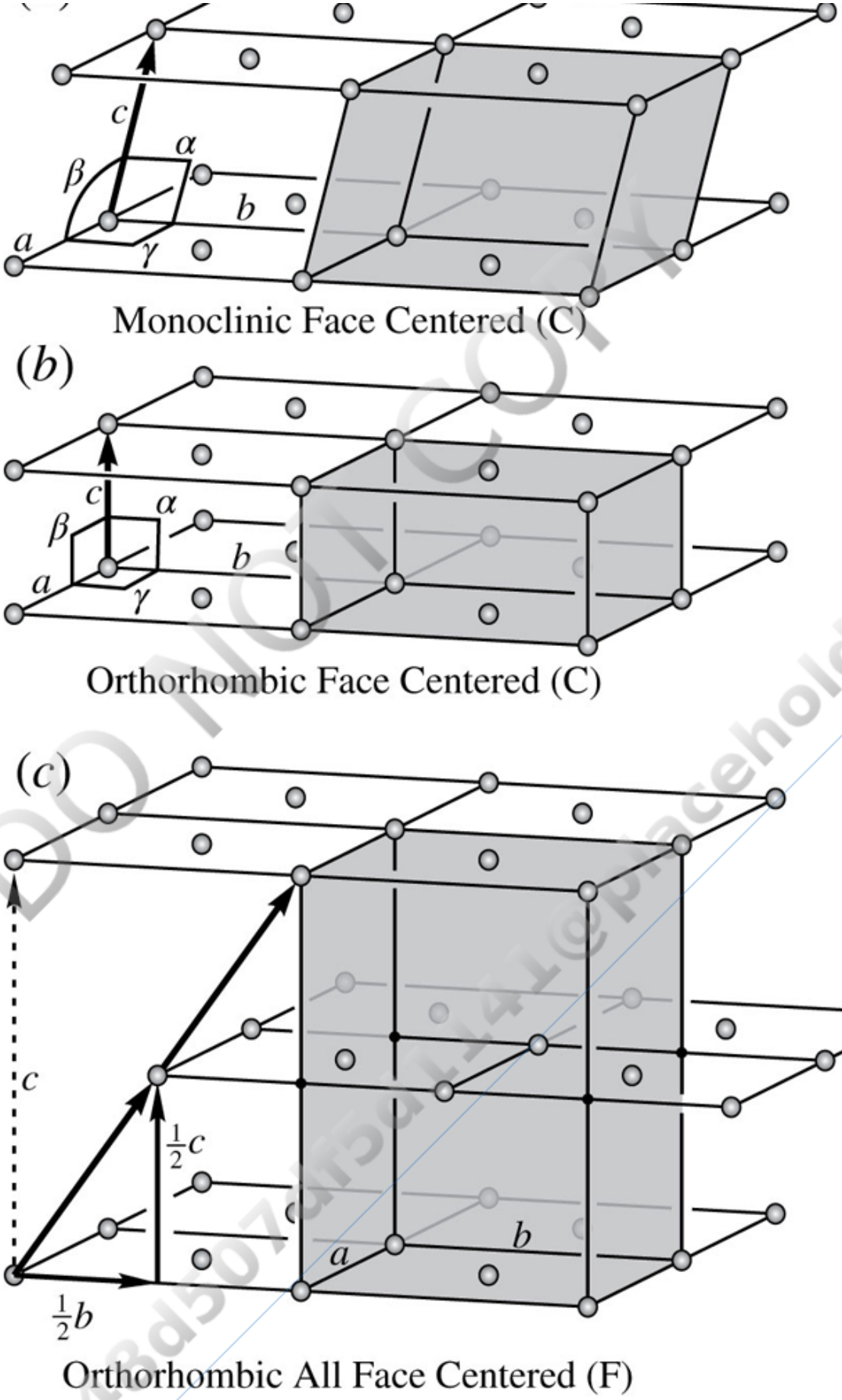

FIGURE 2.7 Bravais lattices produced by translation of a centered rectangle (diamond) plane lattice where a and b are different lengths and $\gamma = 90°$. (a) Translation distance c so that $\alpha = 90°$ and

Printed by: e48d507df5d1141@placeholder.94092.edu. Printing is for personal, private use only. No part of this book may be reproduced or transmitted without publisher's prior permission. Violators will be prosecuted.

lattice where *a* and *b* are different lengths and $\gamma = 90°$. (*a*) Translation distance *c* so that $\alpha = 90°$ and $\beta > 90°$ yields a face-centered (C) monoclinic lattice. (*b*) Translation distance *c* so that $\alpha = \beta = 90°$ produces a face-centered (C) orthorhombic lattice. (*c*) Translation ½ *b* to the right and ½ *c* up produces an all face-centered (F) orthorhombic lattice. Back to text

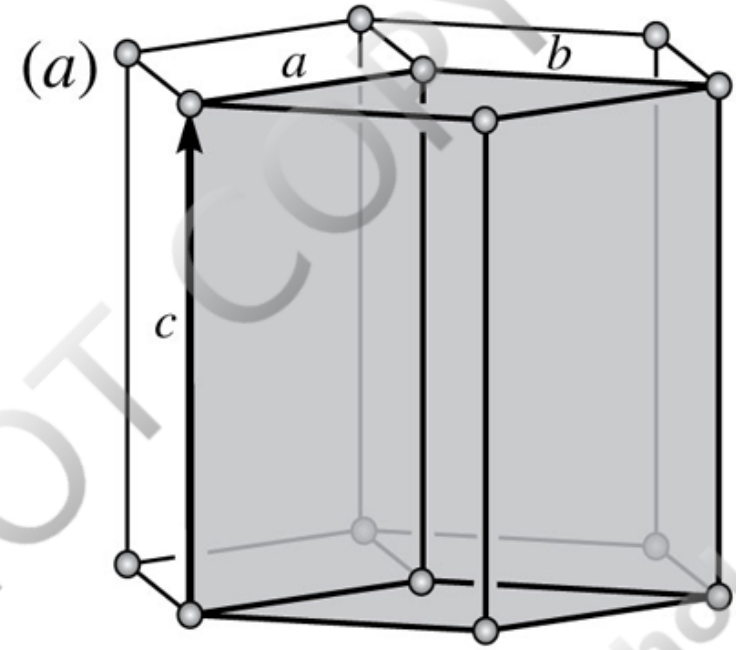

Hexagonal (P)

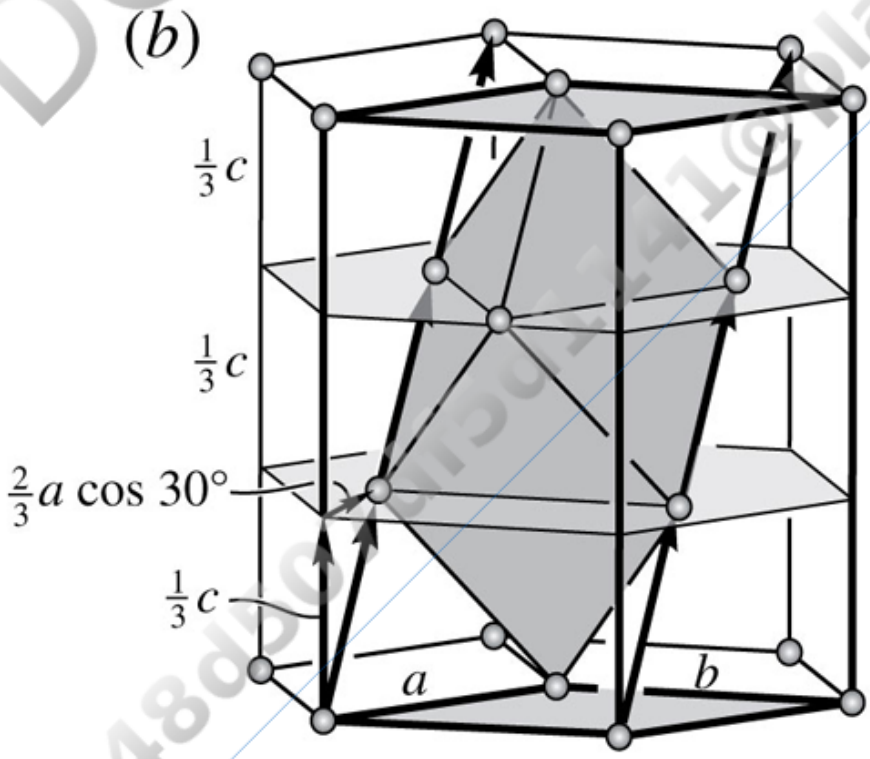

Rhombohedral (R)

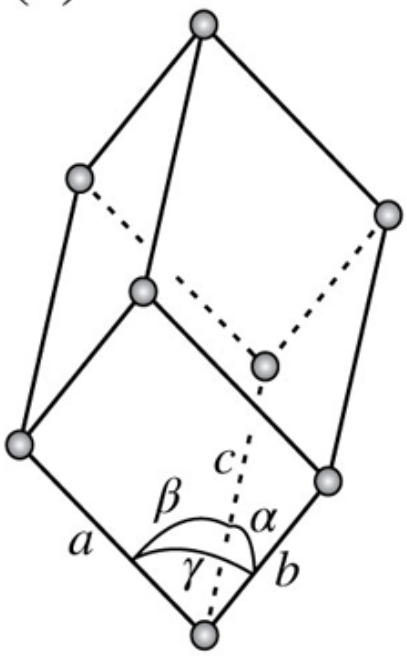

Rhombohedral (R)

DO NOT COPY
e48d507df5d1141@placeholder.9409

Printed by: e48d507df5d1141@placeholder.94092.edu. Printing is for personal, private use only. No part of this book may be reproduced or transmitted without publisher's prior permission. Violators will be prosecuted.

FIGURE 2.8 Bravais lattices produced by translation of a hexagonal plane lattice. (*a*) Vertical translation by distance *c* produces a primitive hexagonal (P) lattice. The simplest unit cell is shaded. (*b*) Translation ⅓ *c* up and ⅔ *a* cos 30° back at right angles to the *b* axis produces a rhombohedral (R) lattice. The translation vector is parallel to two edges of the rhombohedron defined by the lattice nodes as shown. A unit cell that is the same as the primitive hexagonal lattice is shown with heavy lines and shading on the top and bottom. (*c*) A unit cell and crystal axes also can be defined by the edges of the rhombohedron ($a = b = c$, $\alpha = \beta = \gamma \neq 90°$), but this unit cell is almost never used. Back to text

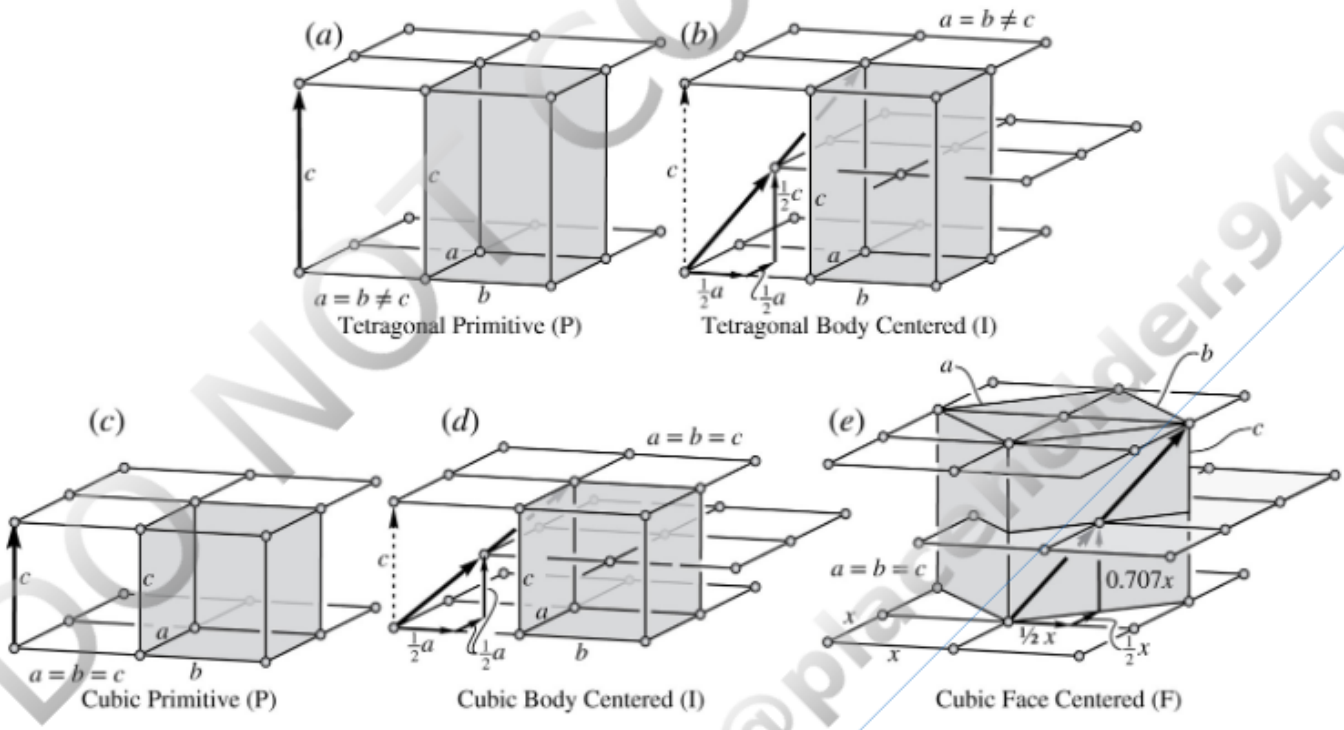

FIGURE 2.9 Bravais lattices produced by translation of a square plane lattice whose dimensions are $a = b$. (*a*) Vertical translation distance $c \neq a$ produces a primitive (P) tetragonal lattice. (*b*) Translation ½ *a* right, ½ *a* back, and ½ *c* up where $c \neq a$ produces a body-centered (I) tetragonal lattice. (*c*) Vertical translation distance $c = a$ yields a primitive (P) cubic (isometric) lattice. (*d*) Translation ½ *a* right, ½ *a* back, and ½ *a* up yields a body-centered (I) cubic lattice. (*e*) Given a square lattice whose dimensions are *x*, translation ½ *x* to the right, ½ *x* back, and 0.707 *x* up produces a face-centered (F) cubic lattice whose unit cell outline is at 45° to the lattice edges of the original plane lattice. Back to text

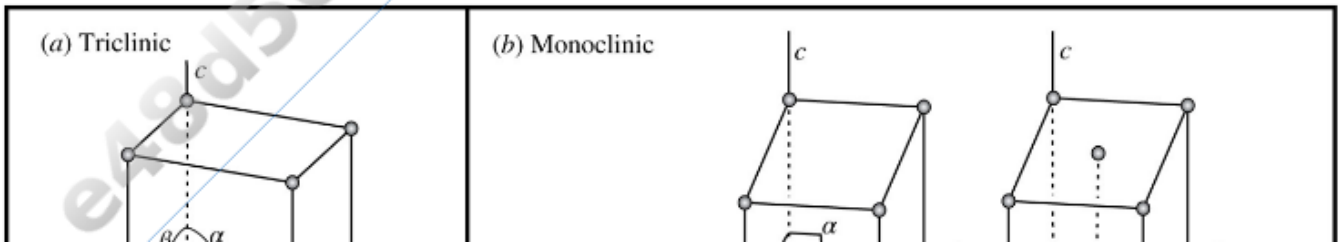

DO NOT COPY e48d507df5d1141@placeholder.9409

Printed by: e48d507df5d1141@placeholder.94092.edu. Printing is for personal, private use only. No part of this book may be reproduced or transmitted without publisher's prior permission. Violators will be prosecuted.

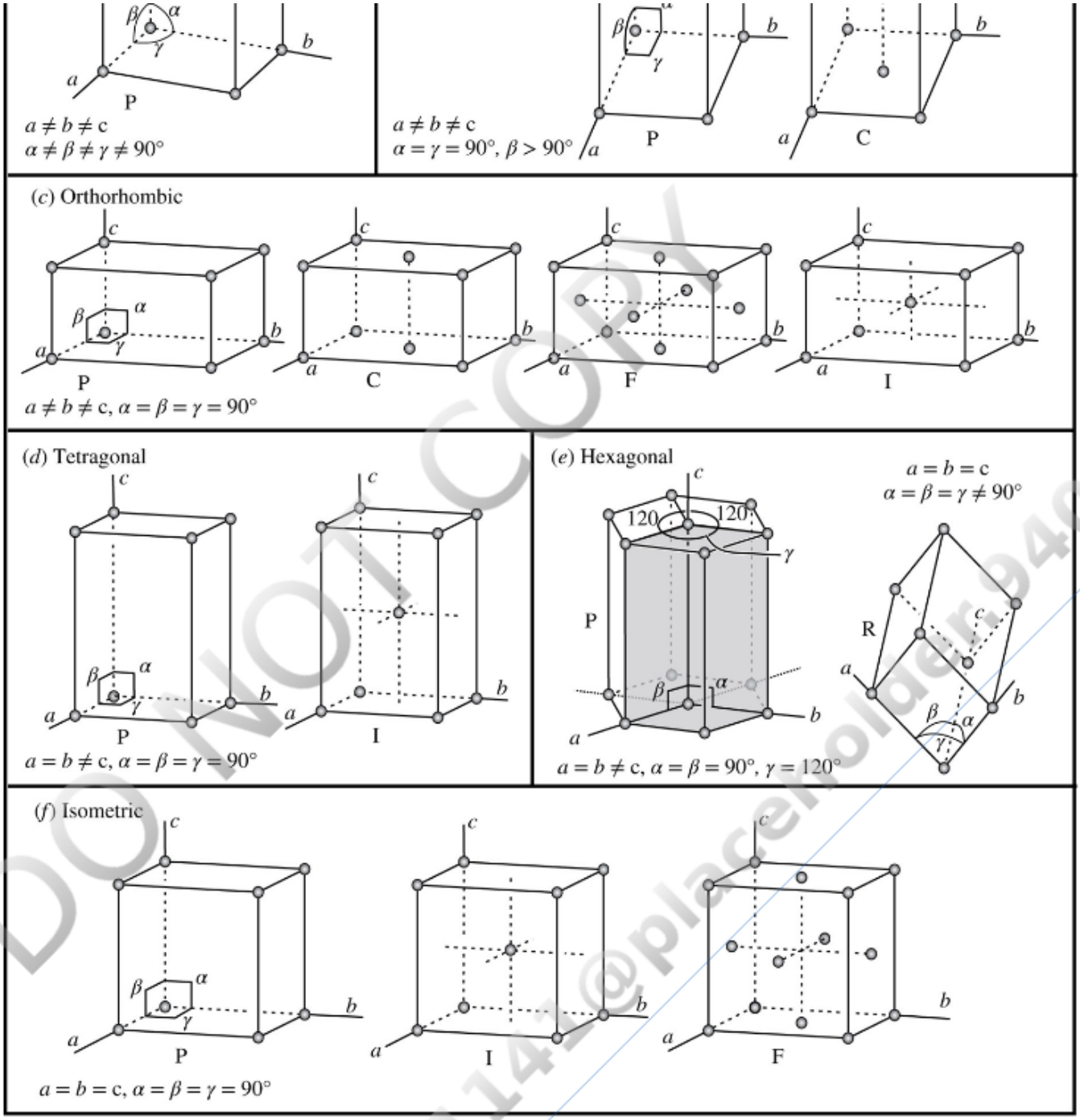

FIGURE 2.10 The 14 Bravais lattices define six different three-dimensional volumes (*a*–*f*) that correspond to the unit cells of the six crystal systems. The lengths of the three unit cell axes are *a*, *b*, and *c*, and the angles between them are α, β, and γ. In the notations, the $\neq$ sign indicates that equality of the axis lengths or angles is not required, although occasionally equality may occur by chance. The hexagonal (R) lattice shown in (*e*) is based on the rhombohedral axes shown in Figure 2.8c. A unit cell with the same geometry as the hexagonal (P) lattice shown in Figure 2.8a is far more commonly used. Back to text

DO NOT COPY
e48d507df5d1141@placeholder.9409

Printed by: e48d507df5d1141@placeholder.94092.edu. Printing is for personal, private use only. No part of this book may be reproduced or transmitted without publisher's prior permission. Violators will be prosecuted.

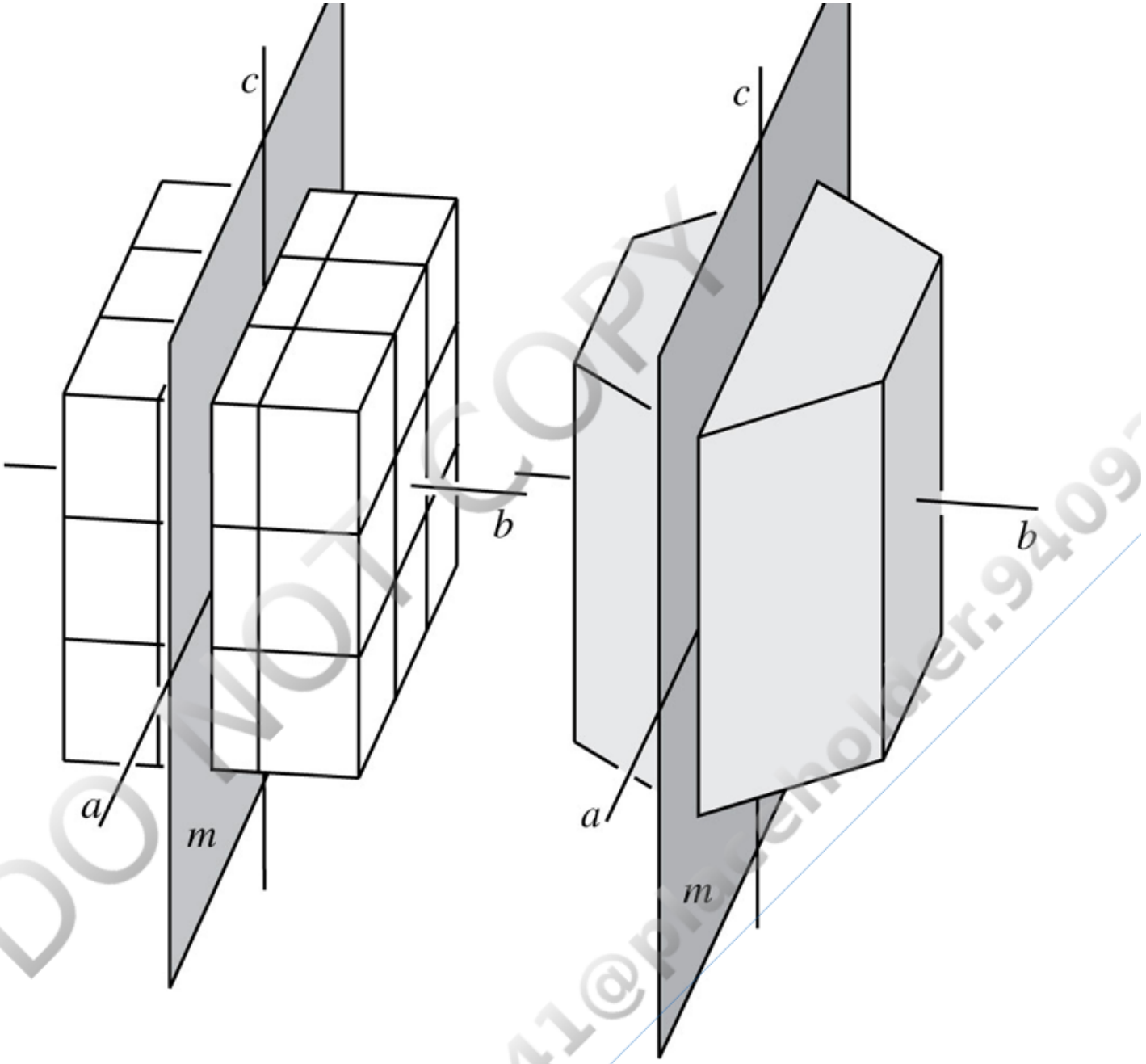

FIGURE 2.11 Symmetry by a mirror (*m*) plane or reflection. The mirror plane operates on the lattice, structure, and crystal faces of the mineral. Back to text

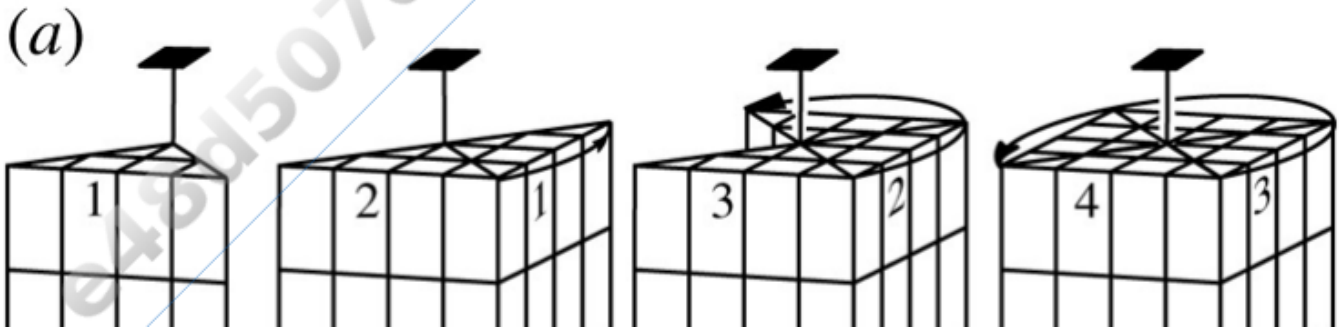

DO NOT COPY
e48d507df5d1141@placeholder.9409

Printed by: e48d507df5d1141@placeholder.94092.edu. Printing is for personal, private use only. No part of this book may be reproduced or transmitted without publisher's prior permission. Violators will be prosecuted.

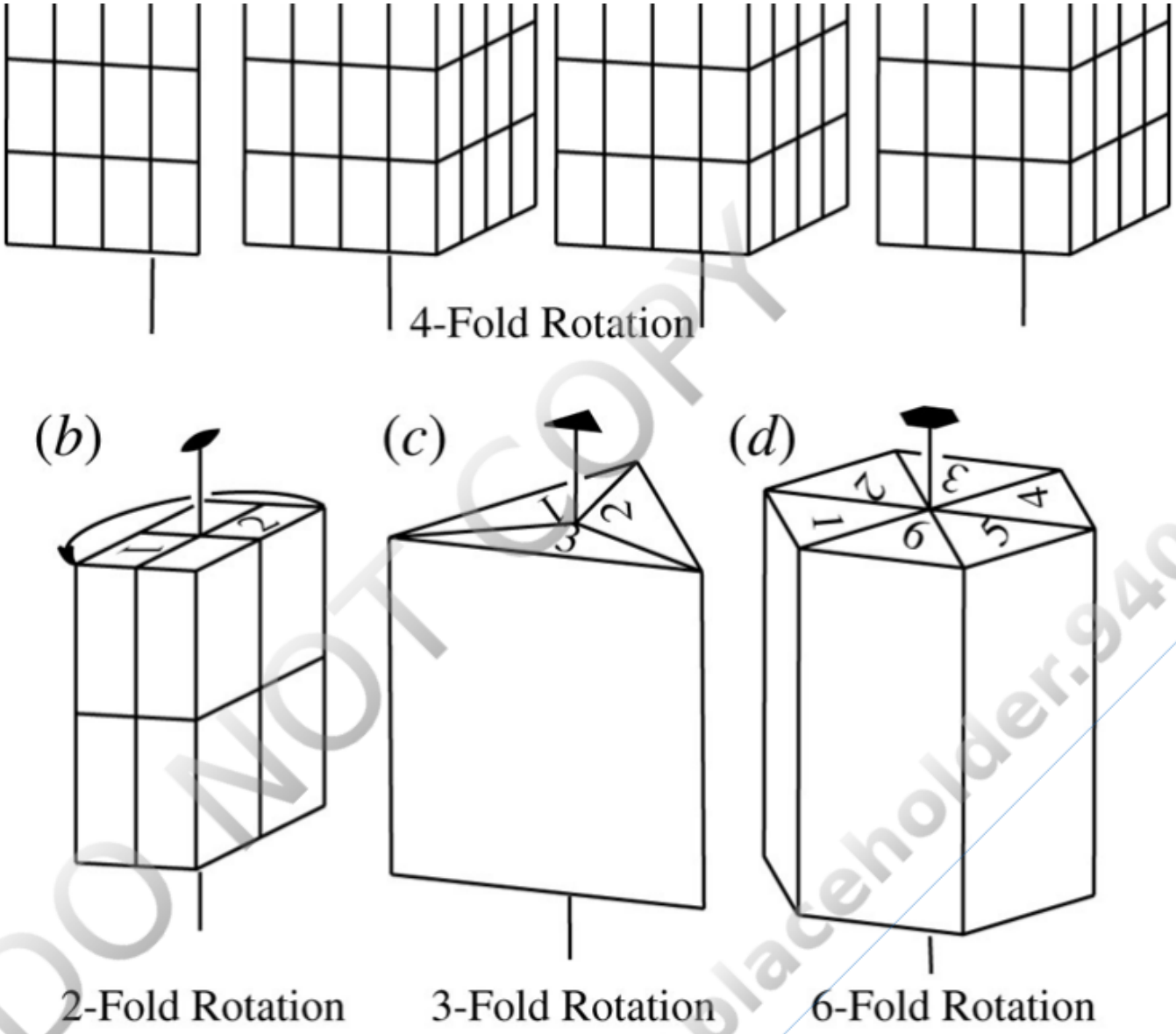

FIGURE 2.12 Rotational symmetry. (*a*) Four-fold rotation. The full crystal can be produced by repeating four wedge-shaped motifs by rotations of 90° about the rotation axis. (*b*) Two-fold rotation. The lattice and crystal faces are repeated every 180°. (*c*) Three-fold rotation. The lattice and crystal faces are repeated every 120°. (*d*) Six-fold rotation. The lattice and crystal faces are repeated every 60°. Note that different symbols label the rotation axes and include a lemon (A_2), a triangle (A_3), a square (A_4), and a hexagon (A_6). Back to text

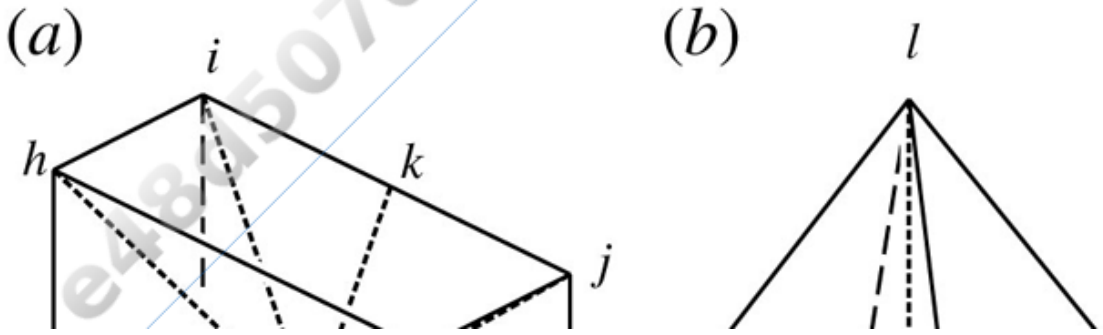

DO NOT COPY
e48d507df5d1141@placeholder.9409

Printed by: e48d507df5d1141@placeholder.94092.edu. Printing is for personal, private use only. No part of this book may be reproduced or transmitted without publisher's prior permission. Violators will be prosecuted.

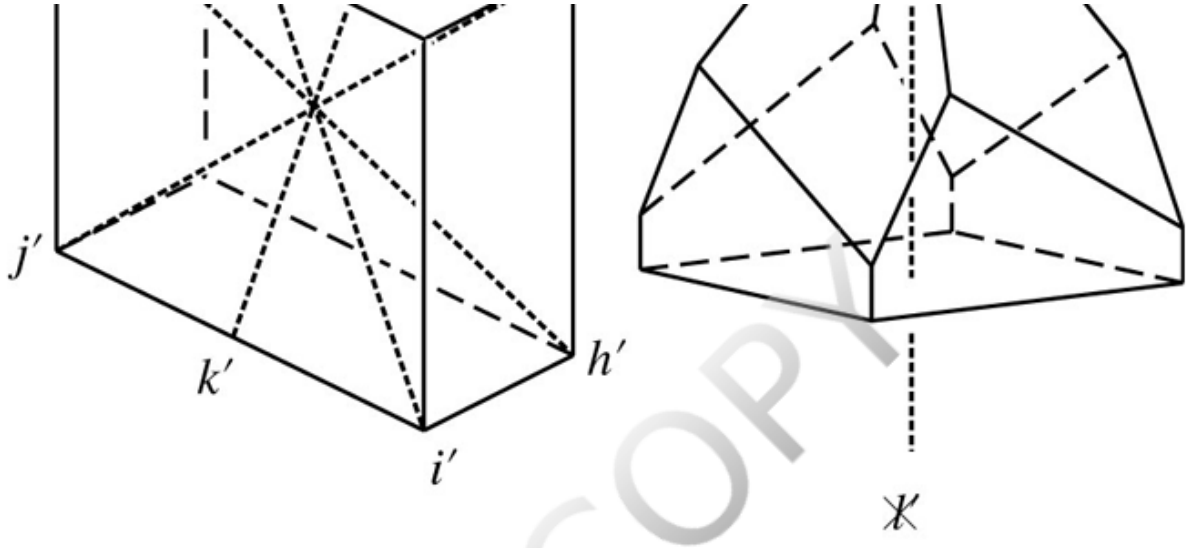

FIGURE 2.13 Inversion. (*a*) Crystal with inversion. Points *h*, *i*, *j*, and *k* all have equivalent points *h*′, *i*′, *j*′, and *k*′ on the opposite side of the crystal. (*b*) Crystal without inversion. Points such as the *l* are not duplicated on the opposite side of the crystal (hence *l* is crossed out). Back to text

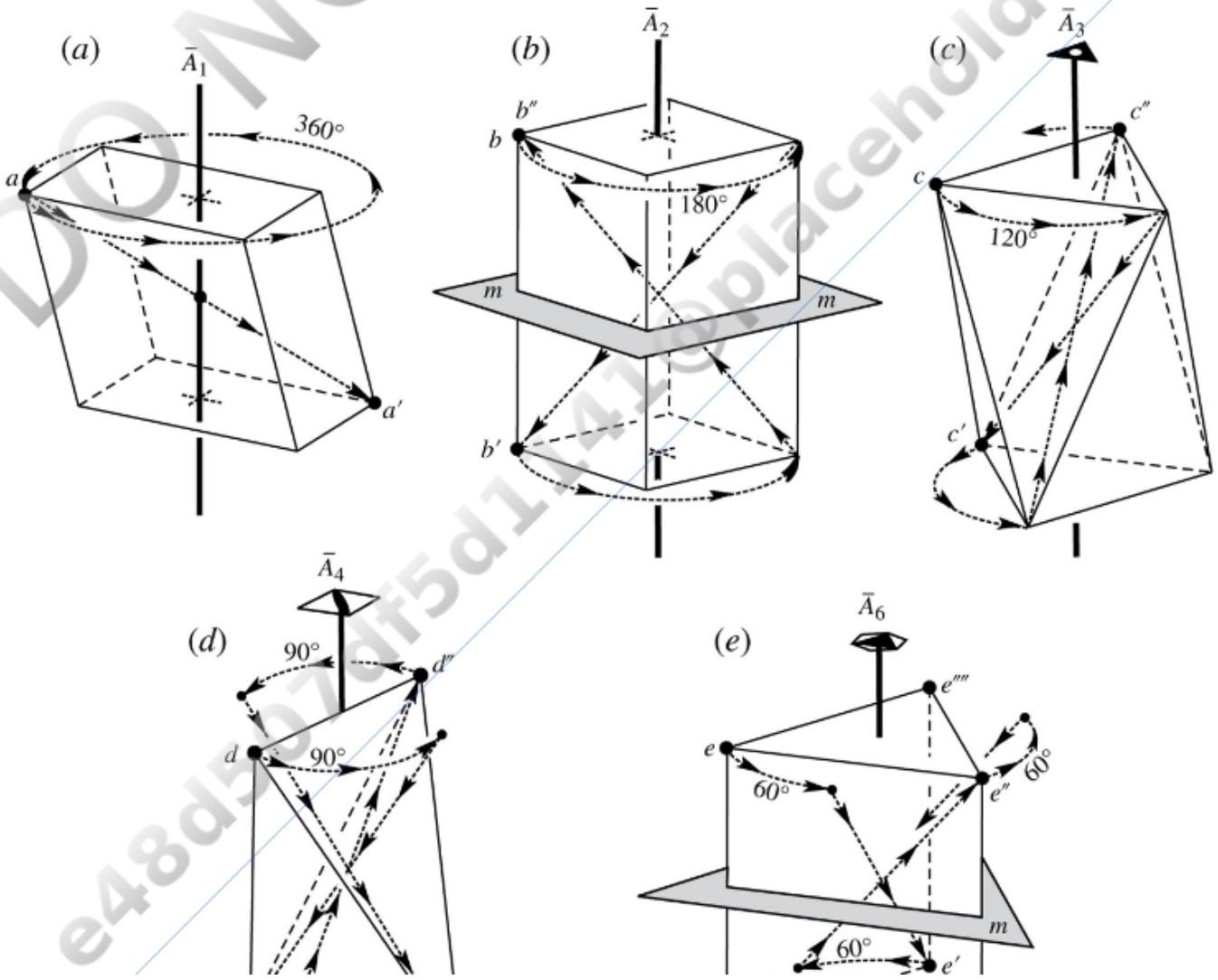

DO NOT COPY e48d507df5d1141@placeholder.9409

Printed by: e48d507df5d1141@placeholder.94092.edu. Printing is for personal, private use only. No part of this book may be reproduced or transmitted without publisher's prior permission. Violators will be prosecuted.

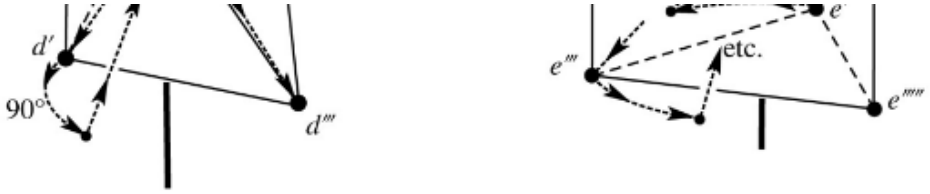

FIGURE 2.14 Rotoinversion. See text for discussion. (*a*) One-fold rotoinversion equals a simple inversion. (*b*) Two-fold rotoinversion is the same as a mirror at right angles to the rotation axis. (*c*) Three-fold rotoinversion is equivalent to a simple 3-fold rotation and inversion. (*d*) Four-fold rotoinversion is not replicated by other simpler symmetry operations. (*e*) Six-fold rotoinversion is equivalent to 3-fold rotation with a mirror at right angles. Back to text

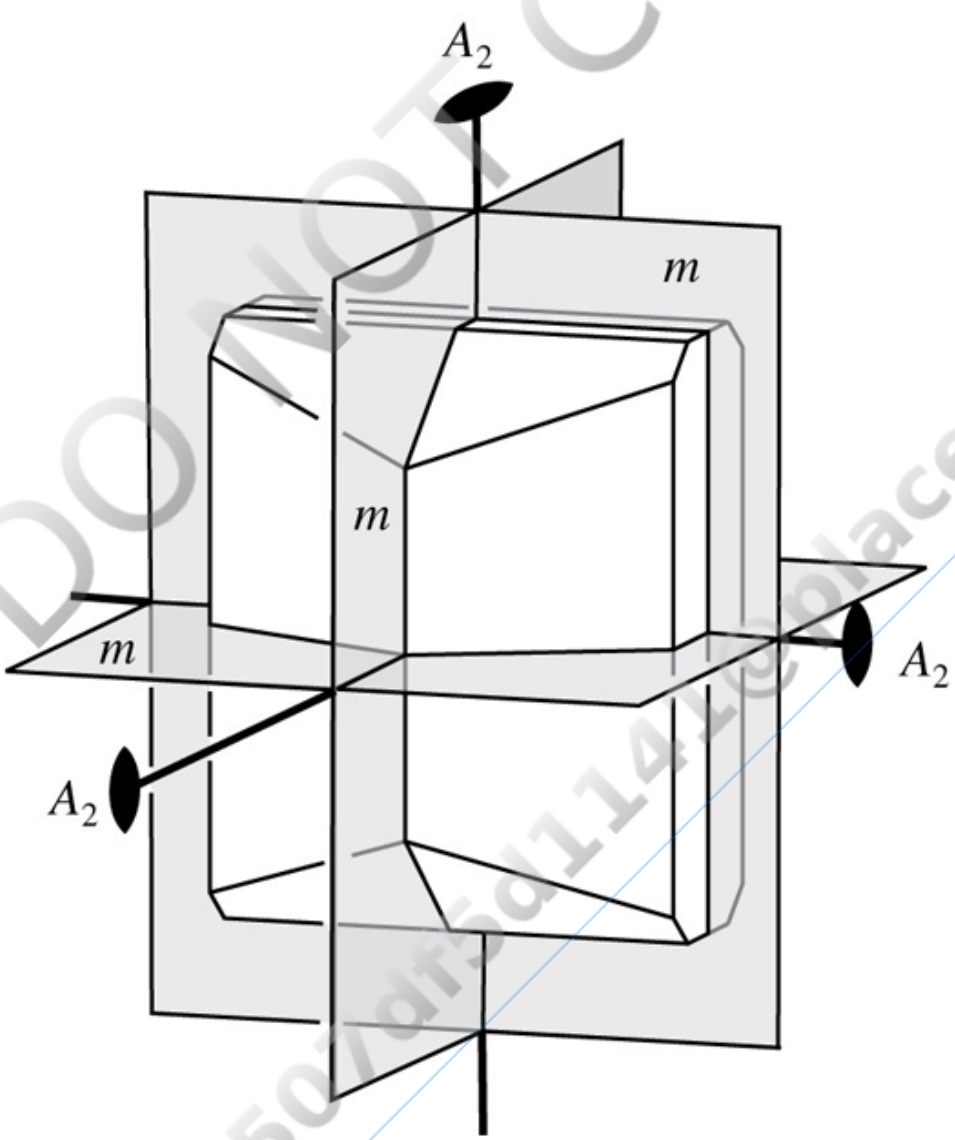

FIGURE 2.15 This orthorhombic crystal has center symmetry (*i*), three 2-fold axes ($3A_2$), and three mirrors ($3m$). Back to text

DO NOT COPY
e48d507df5d1141@placeholder.9409

Printed by: e48d507df5d1141@placeholder.94092.edu. Printing is for personal, private use only. No part of this book may be reproduced or transmitted without publisher's prior permission. Violators will be prosecuted.

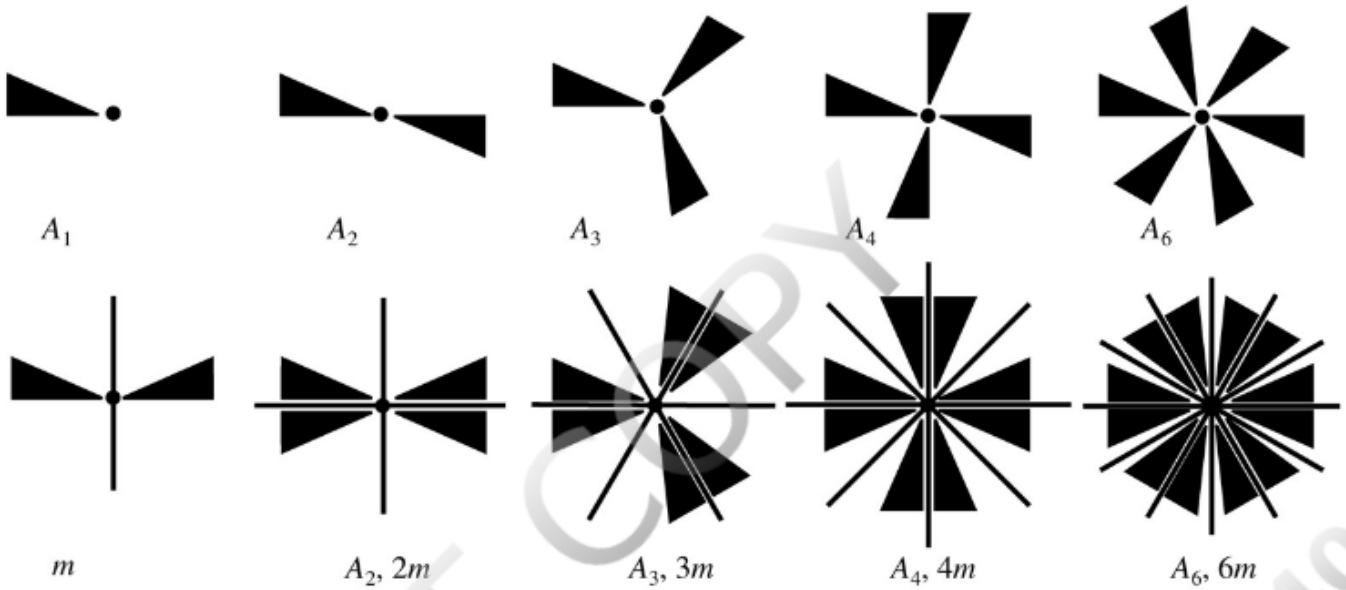

FIGURE 2.16 The 10 two-dimension point groups. Back to text

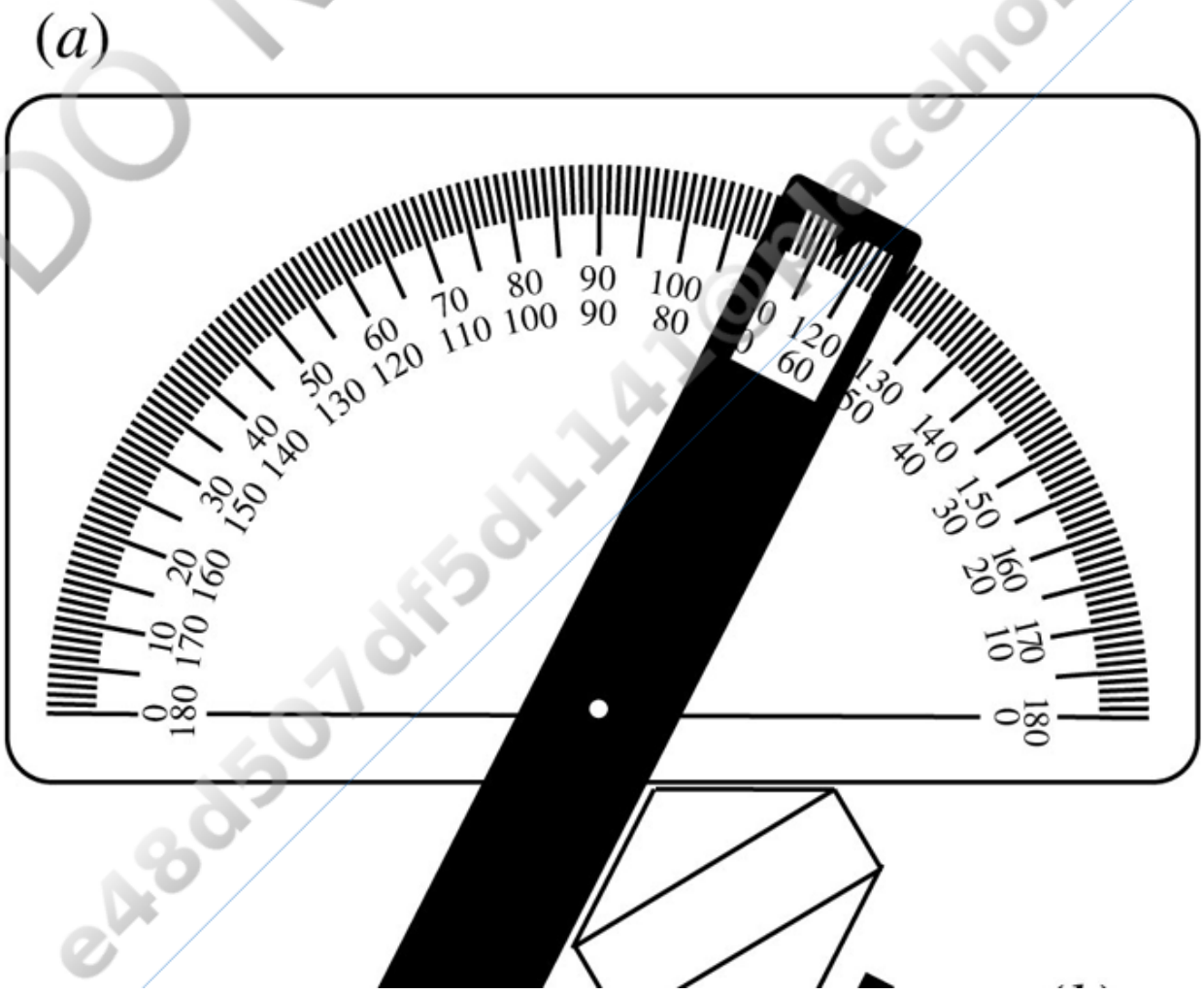

DO NOT COPY
e48d507df5d1141@placeholder.9409

Printed by: e48d507df5d1141@placeholder.94092.edu. Printing is for personal, private use only. No part of this book may be reproduced or transmitted without publisher's prior permission. Violators will be prosecuted.

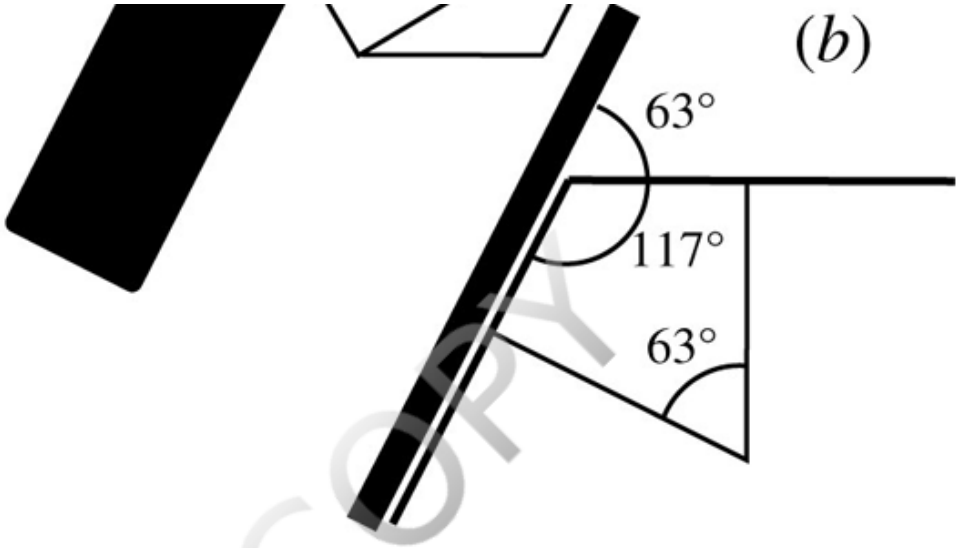

FIGURE 2.17 Contact goniometer. (*a*) The base of the goniometer is placed on one crystal face, and the cursor (movable arm) is aligned with the adjacent face. The edge between the faces must be perpendicular to the plane of the goniometer. The internal angle between the faces is read from the scale. (*b*) The internal angle (63°) is the angle between lines at right angles to the crystal faces.
Back to text

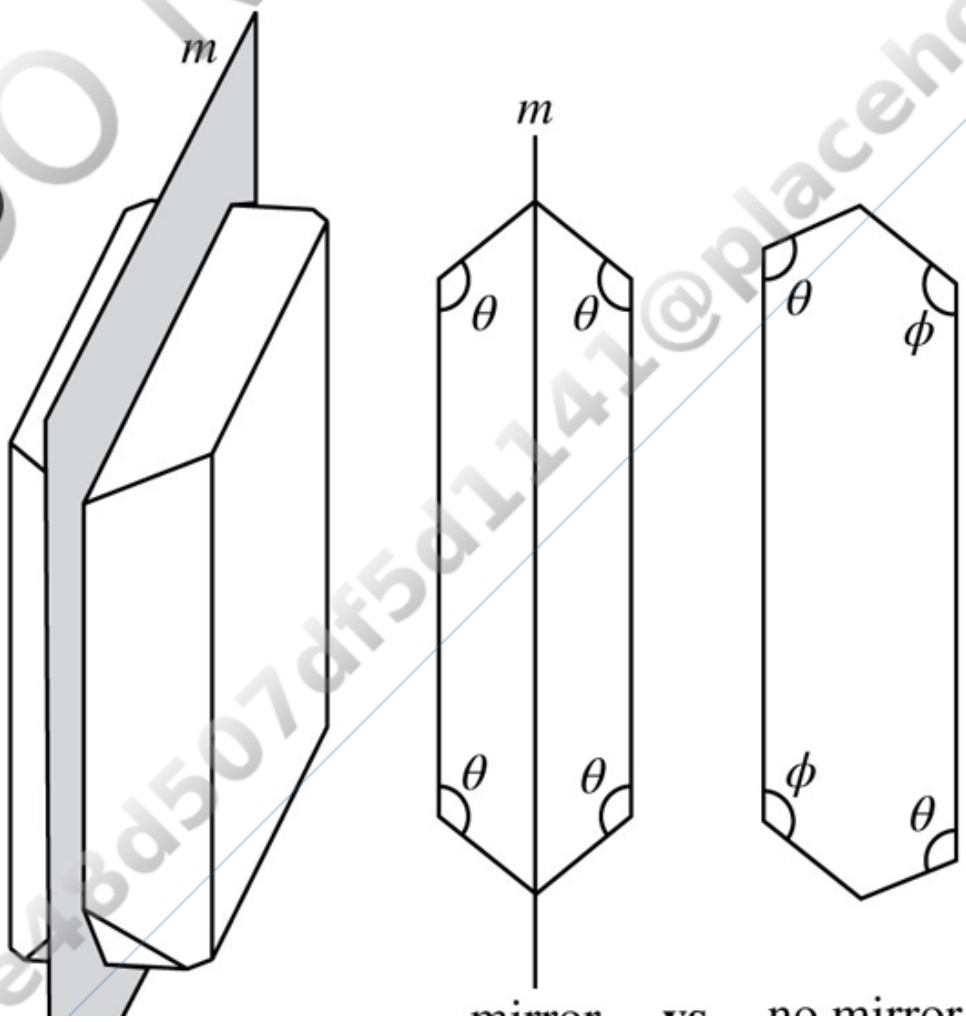

DO NOT COPY
e48d507df5d1141@placeholder.9409

Printed by: e48d507df5d1141@placeholder.94092.edu. Printing is for personal, private use only. No part of this book may be reproduced or transmitted without publisher's prior permission. Violators will be prosecuted.

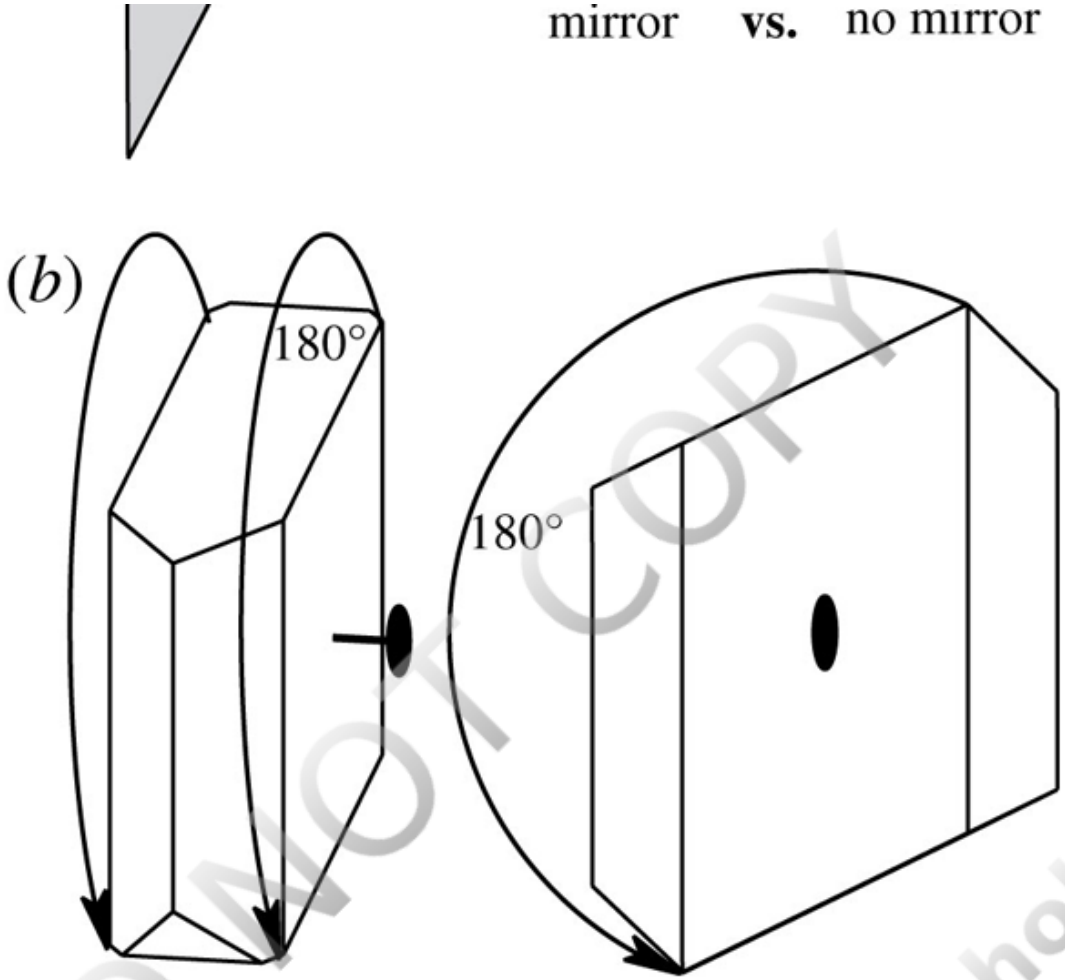

FIGURE 2.18 Determining crystal symmetry. (*a*) Mirrors split the crystal into two mirror images. Angles on opposite sides of the mirror are the same. (*b*) Rotations repeat the same collection of faces every 60°, 90°, 120°, or 180° of rotation (A_6, A_4, A_3, A_2). A 2-fold rotation is shown. Back to text

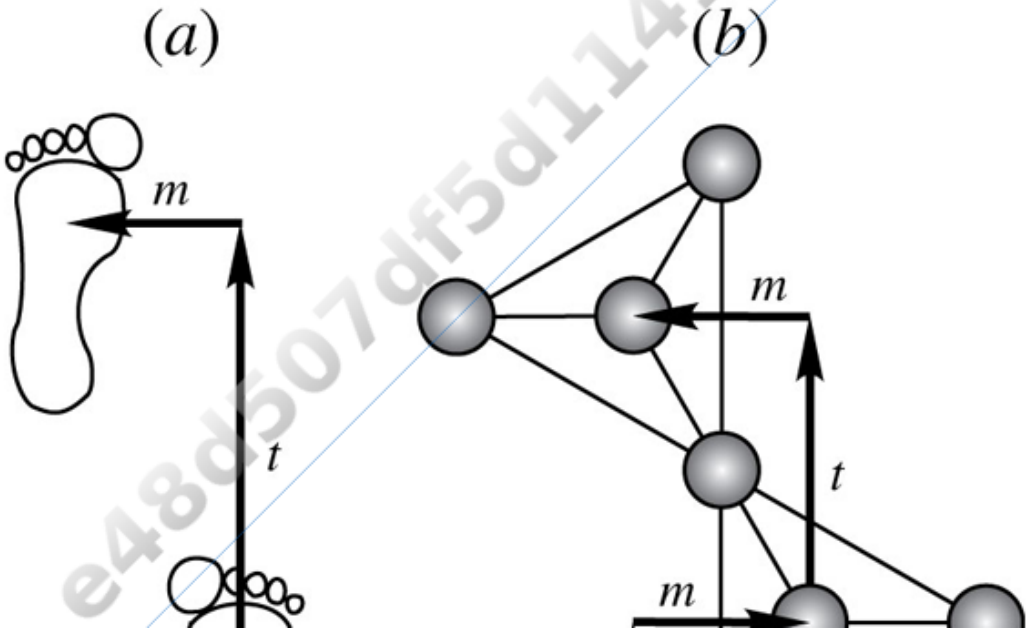

DO NOT COPY
e48d507df5d1141@placeholder.9409

Printed by: e48d507df5d1141@placeholder.94092.edu. Printing is for personal, private use only. No part of this book may be reproduced or transmitted without publisher's prior permission. Violators will be prosecuted.

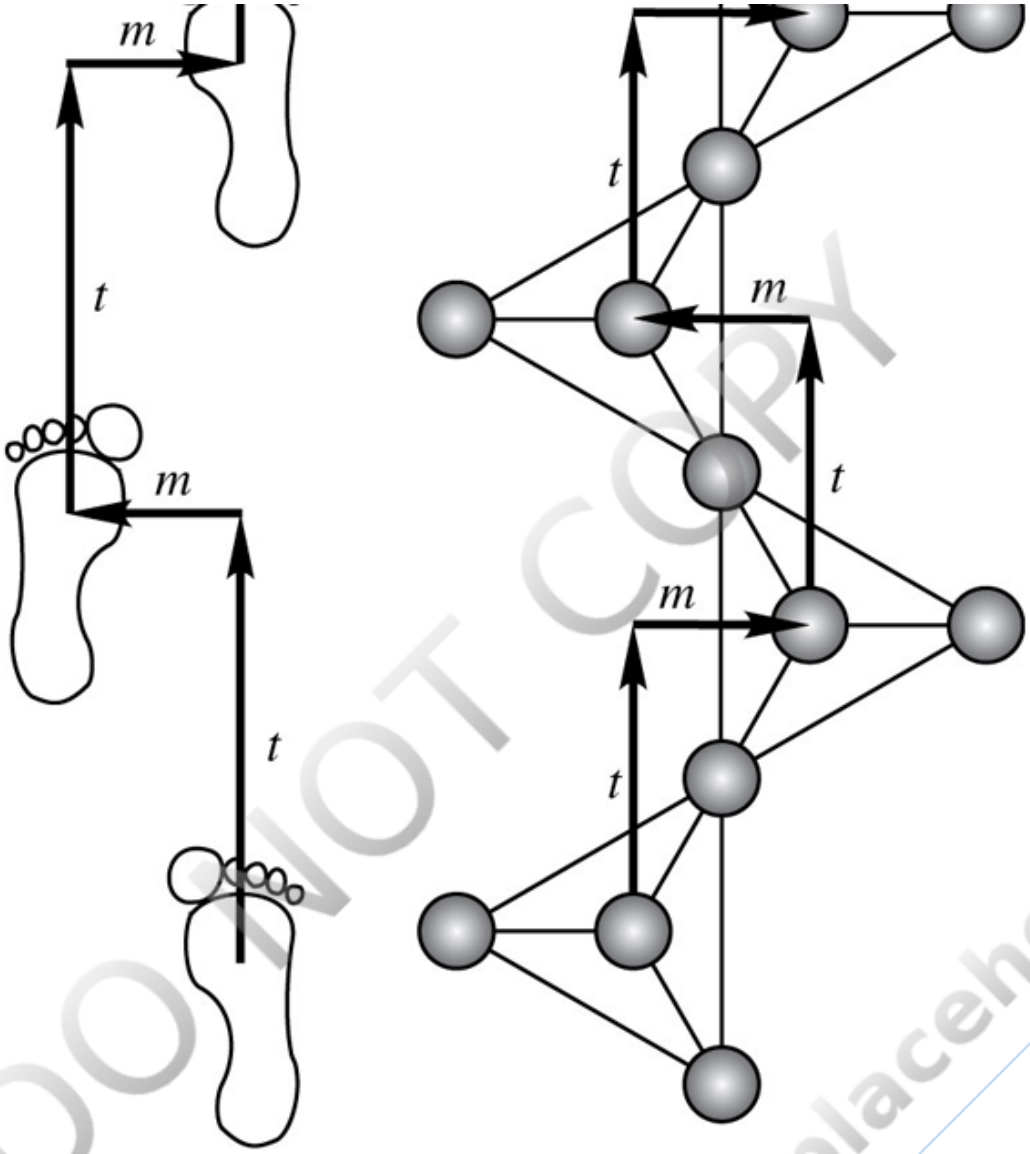

FIGURE 2.19 Glide symmetry. (*a*) Footprints repeated by a translation *t* and reflection *m*. (*b*) Chain of silicon tetrahedra (single silicon, hidden, surrounded by four oxygen ions) produced by translation *t* followed by reflection *m*. Back to text

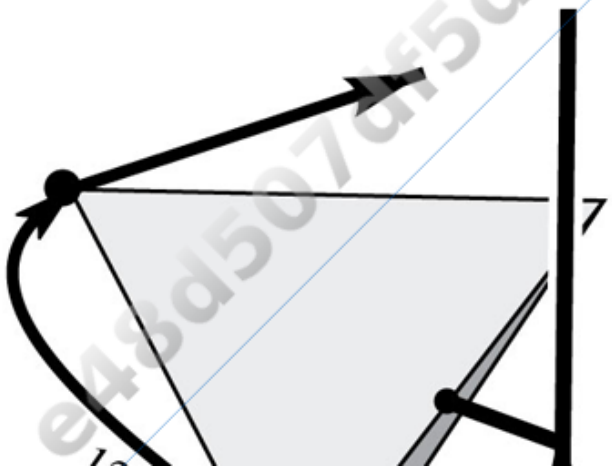

DO NOT COPY
e48d507df5d1141@placeholder.9409

Printed by: e48d507df5d1141@placeholder.94092.edu. Printing is for personal, private use only. No part of this book may be reproduced or transmitted without publisher's prior permission. Violators will be prosecuted.

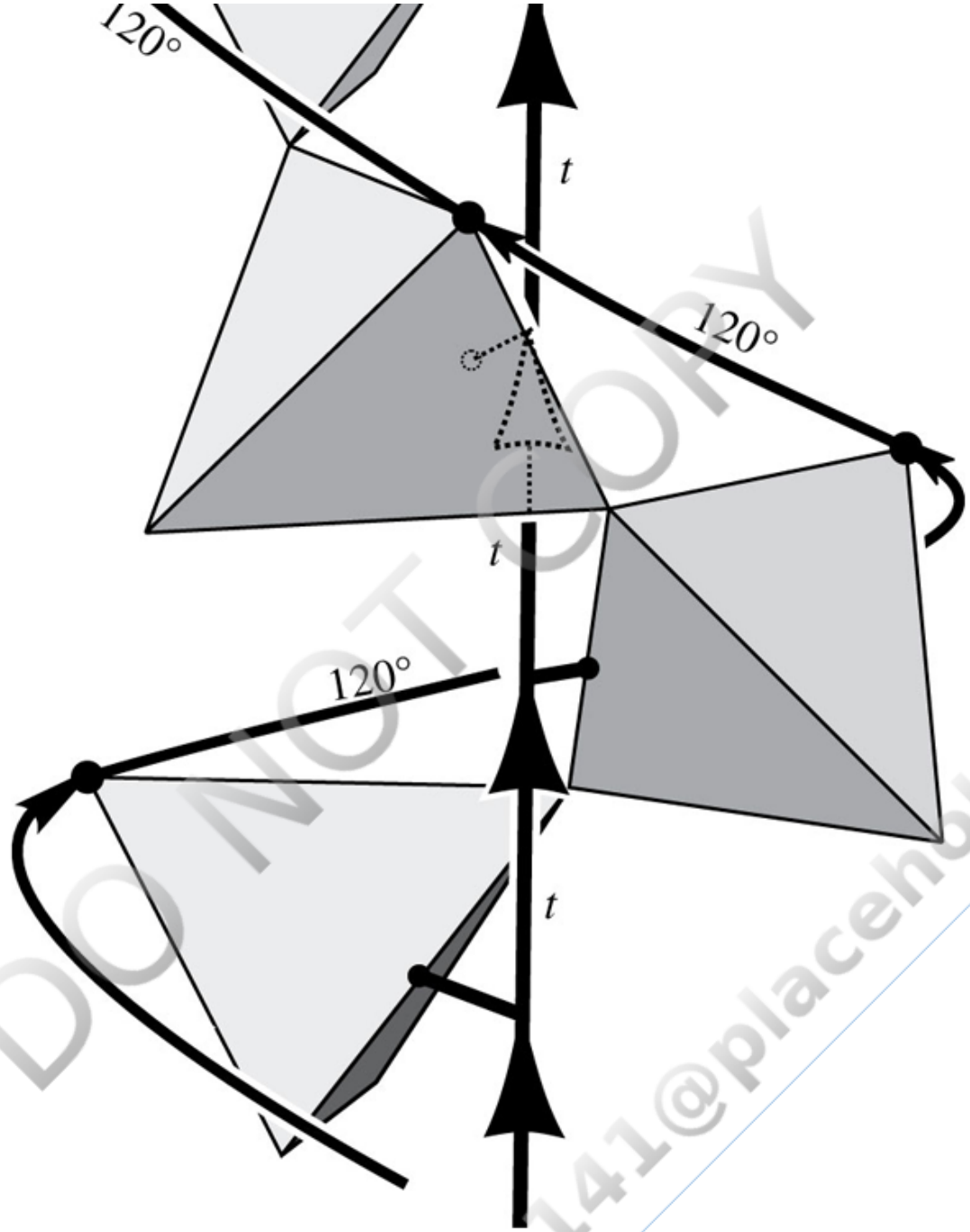

FIGURE 2.20 Screw axis. A 3-fold screw axis is shown. In quartz, a silicon tetrahedron is translated distance *t* and rotated 120° in spiral-staircase fashion to form a helix of tetrahedra extending along the *c* axis. Screw axes may also be 2-fold, 4-fold, or 6-fold. Back to text

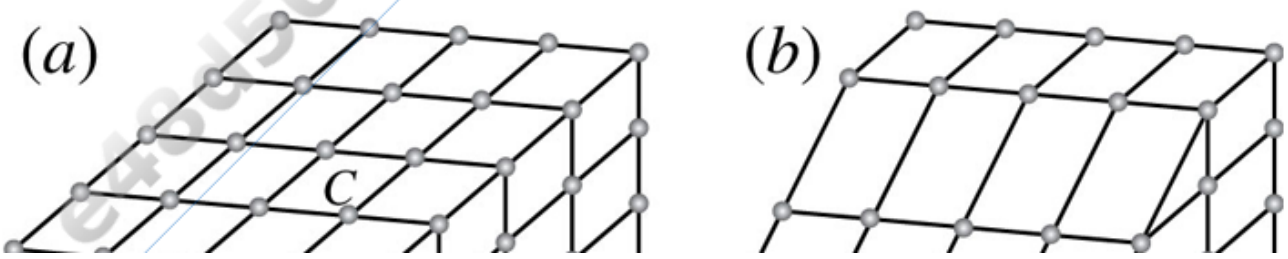

DO NOT COPY
e48d507df5d1141@placeholder.9409

Printed by: e48d507df5d1141@placeholder.94092.edu. Printing is for personal, private use only. No part of this book may be reproduced or transmitted without publisher's prior permission. Violators will be prosecuted.

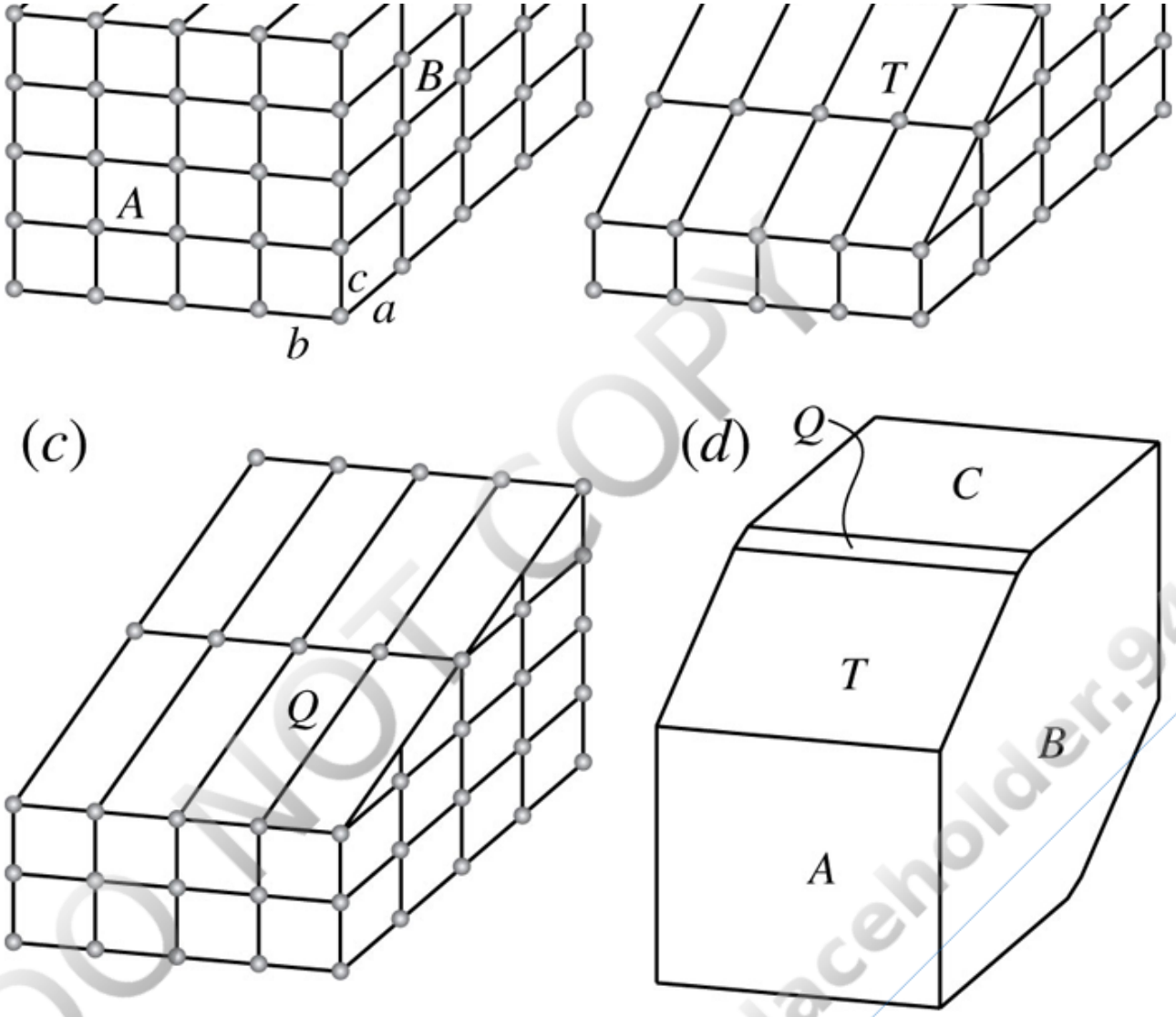

FIGURE 2.22 Primitive monoclinic lattice. Prominent crystal faces are parallel to rational planes in the lattice that have high density of lattice nodes. (*a*) Planes *A*, *B*, and *C* are parallel to the faces of the unit cell, have high lattice-node density, and are likely crystal faces. (*b*) Plane *T* has fairly high lattice-node density and is a likely crystal face. (*c*) Plane *Q* has low lattice-node density and is not a prominent crystal face. (*d*) A simple crystal with these faces. Back to text

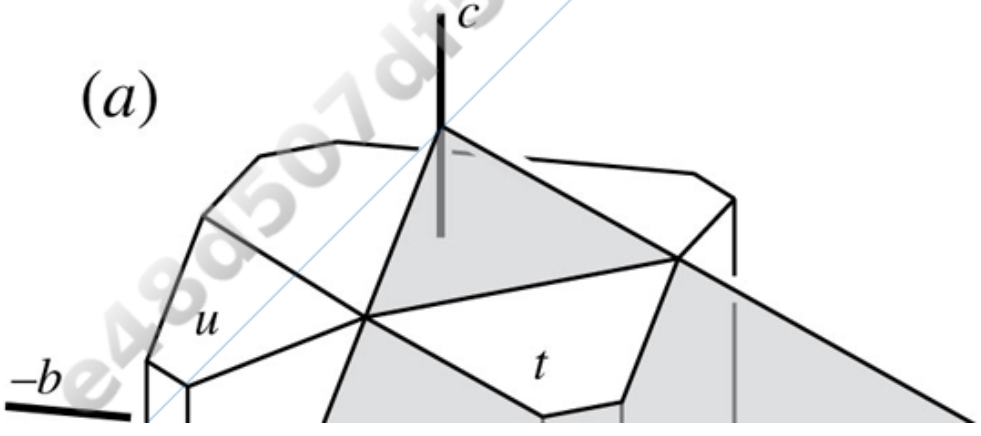

DO NOT COPY
e48d507df5d1141@placeholder.9409

Printed by: e48d507df5d1141@placeholder.94092.edu. Printing is for personal, private use only. No part of this book may be reproduced or transmitted without publisher's prior permission. Violators will be prosecuted.

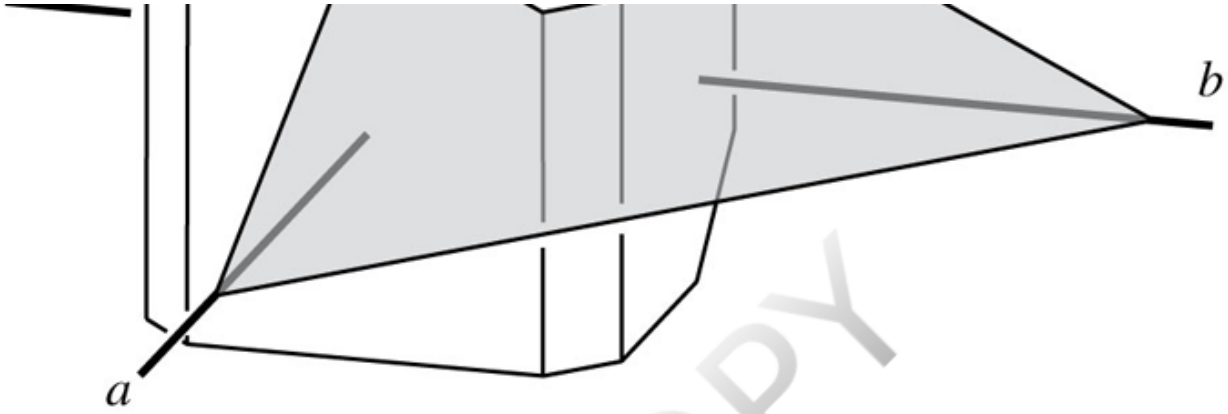

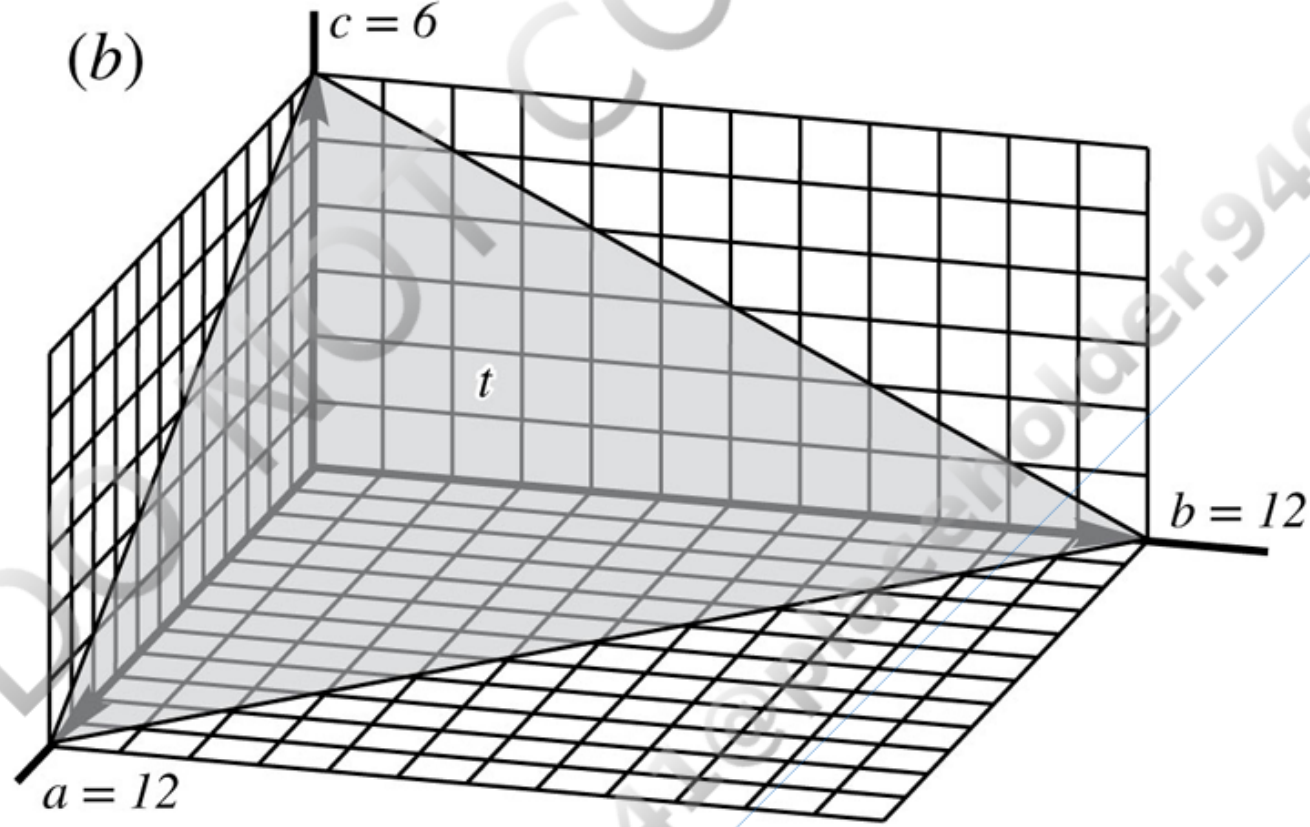

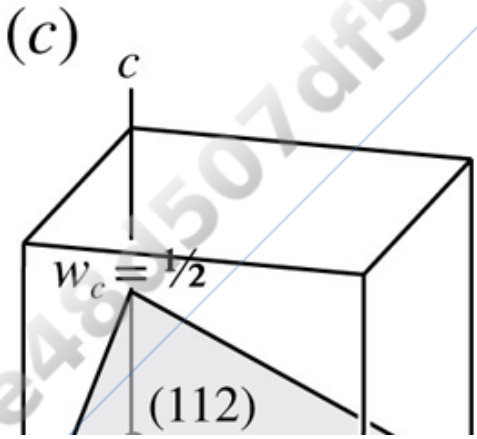

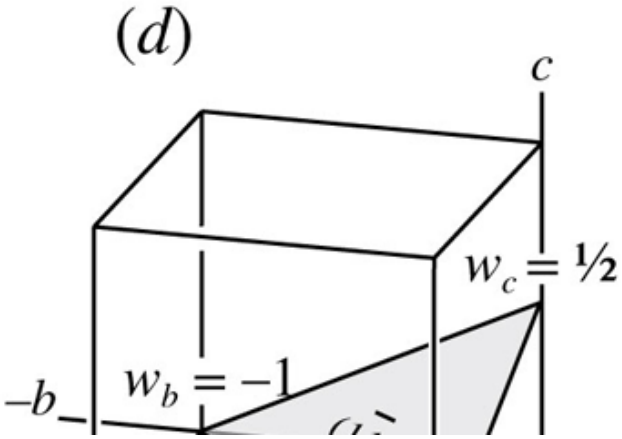

DO NOT COPY
e48d507df5d1141@placeholder.9409

Printed by: e48d507df5d1141@placeholder.94092.edu. Printing is for personal, private use only. No part of this book may be reproduced or transmitted without publisher's prior permission. Violators will be prosecuted.

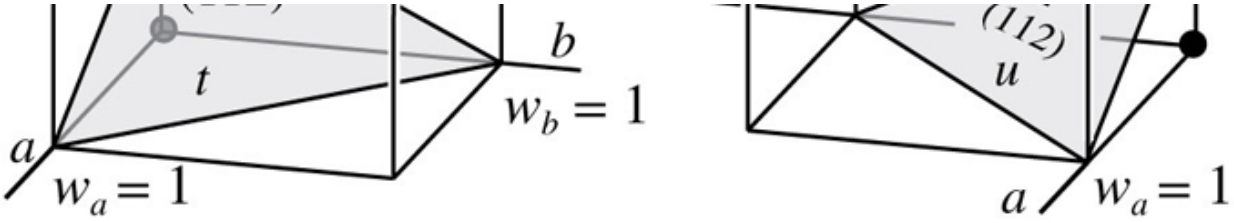

FIGURE 2.23 Miller index. (*a*) Face *t*, when extended, intersects the positive ends of all three crystal axes. (*b*) Face *t* cuts through the lattice so that it intersects the *a* and *b* crystal axes at the same number of unit cells from the origin (12 in this case) and intersects the *c* crystal axis at half that number (six). (*c*) When referenced to a single unit cell, face *t* intersects the crystal axes so that $w_a = 1$, $w_b = 1$, and $w_c = ½$. Fraction inversion results in a (112) Miller index label for this plane. (*d*) Face *u*, which intersects the negative end of *b*, intersects the crystal axes of a single unit cell at $w_a = 1$, $w_b = -1$, and $w_c = ½$. Fraction inversion results in a $(1\bar{1}2)$ Miller index label for this plane. See text for discussion. Back to text

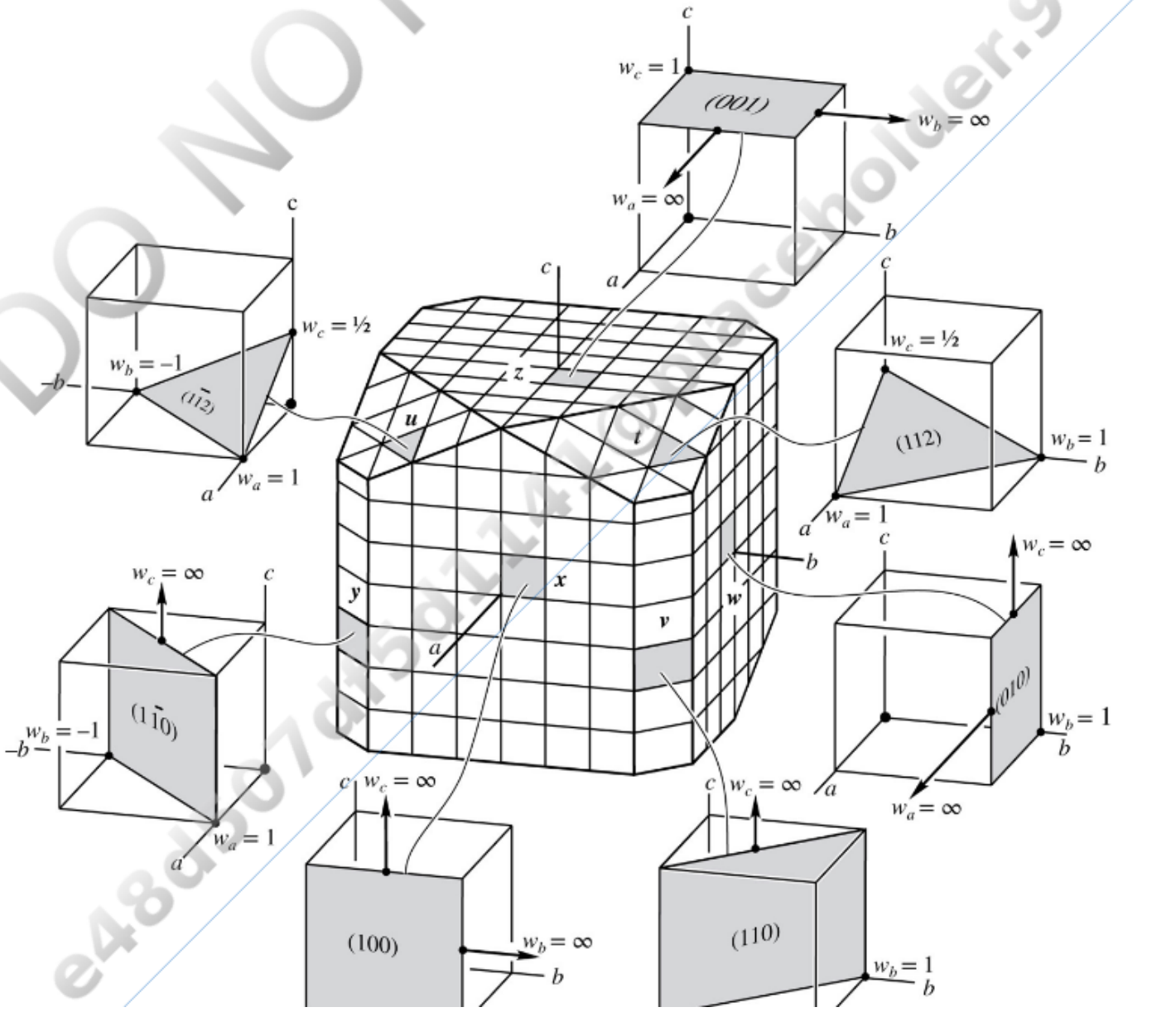

DO NOT COPY
e48d507df5d1141@placeholder.9409

Printed by: e48d507df5d1141@placeholder.94092.edu. Printing is for personal, private use only. No part of this book may be reproduced or transmitted without publisher's prior permission. Violators will be prosecuted.

FIGURE 2.24 Miller indices for all visible faces on the crystal shown in Figure 2.23. The traces of unit cells are sketched on the crystal. See text for discussion. Back to text

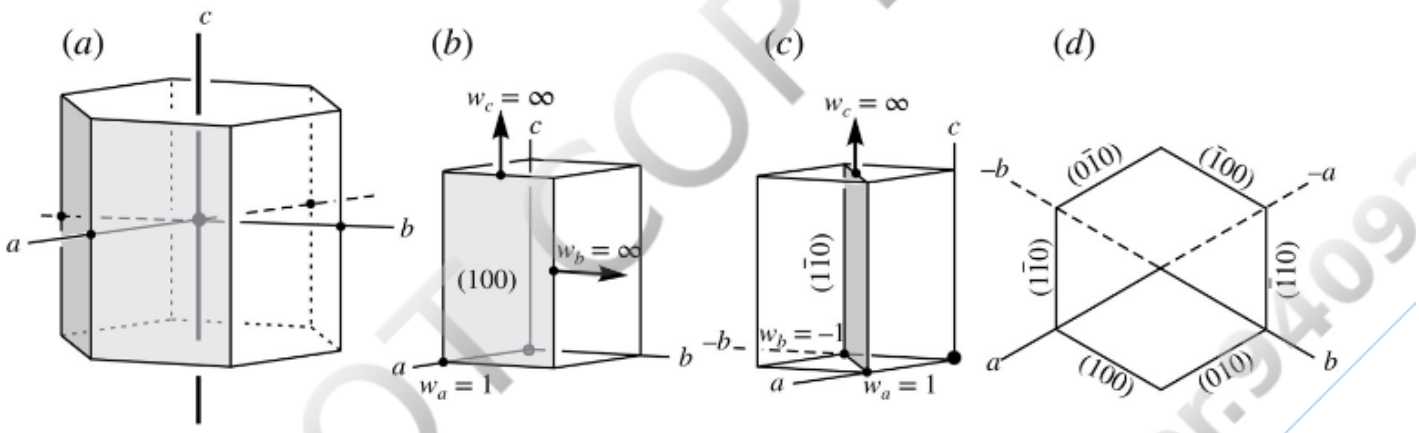

FIGURE 2.25 Miller indices in the hexagonal crystal system. (*a*) Hexagonal crystal with *a*, *b*, and *c* crystal axes. (*b*) Relation of light-shaded face to the unit cell. Based on unit cell intercepts, the Miller index is (100). (*c*) Relation of the dark-shaded face to a unit cell. Based on unit cell intercepts, the Miller index is $\left(1\,\bar{1}0\right)$. (*d*) View down the *c* axis with the Miller indices for all vertical faces shown. Back to text

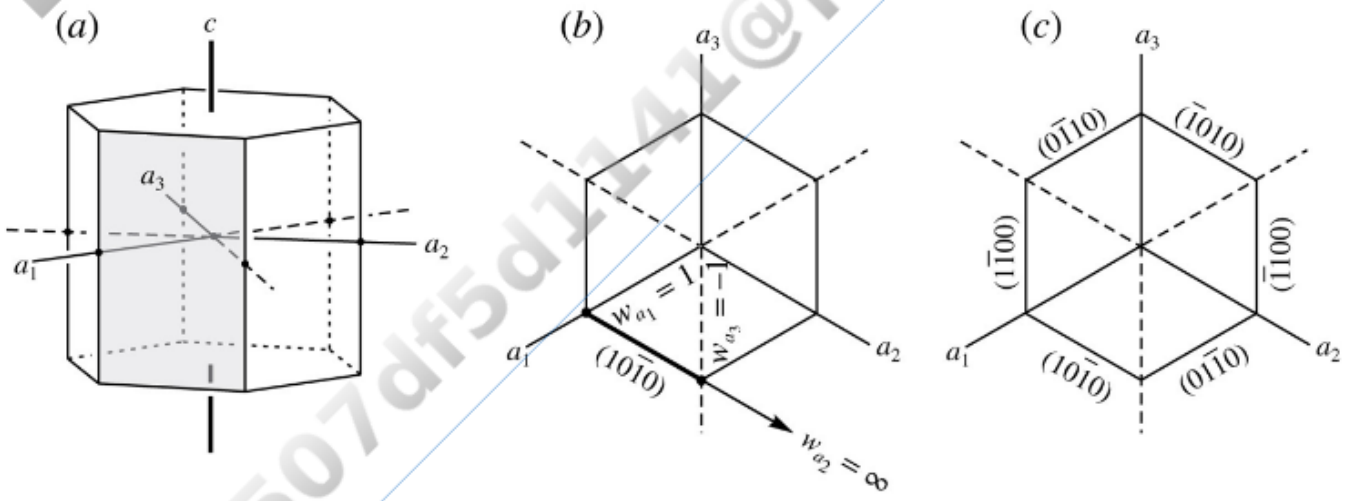

FIGURE 2.26 Miller–Bravais indices in the hexagonal crystal system. (*a*) Hexagonal crystal with a_1, a_2, a_3, and *c* crystal axes. The *a* axes are parallel to 2-fold rotation axes and are 120° from each other. The shaded face cuts the a_1 and $-a_3$ axes and is parallel to a_2 and *c*. (*b*) Top view of the unit cell showing the unit cell intercepts that yield a Miller–Bravais index of $\left(10\bar{1}0\right)$. (*c*) Top view of the crystal showing the Miller–Bravais indices for all the vertical faces. The top and bottom faces are

DO NOT COPY
e48d507df5d1141@placeholder.9409

Printed by: e48d507df5d1141@placeholder.94092.edu. Printing is for personal, private use only. No part of this book may be reproduced or transmitted without publisher's prior permission. Violators will be prosecuted.

crystal showing the Miller–Bravais indices for all the vertical faces. The top and bottom faces are (0001) and $\left(000\bar{1}\right)$, respectively. See text for discussion. Back to text

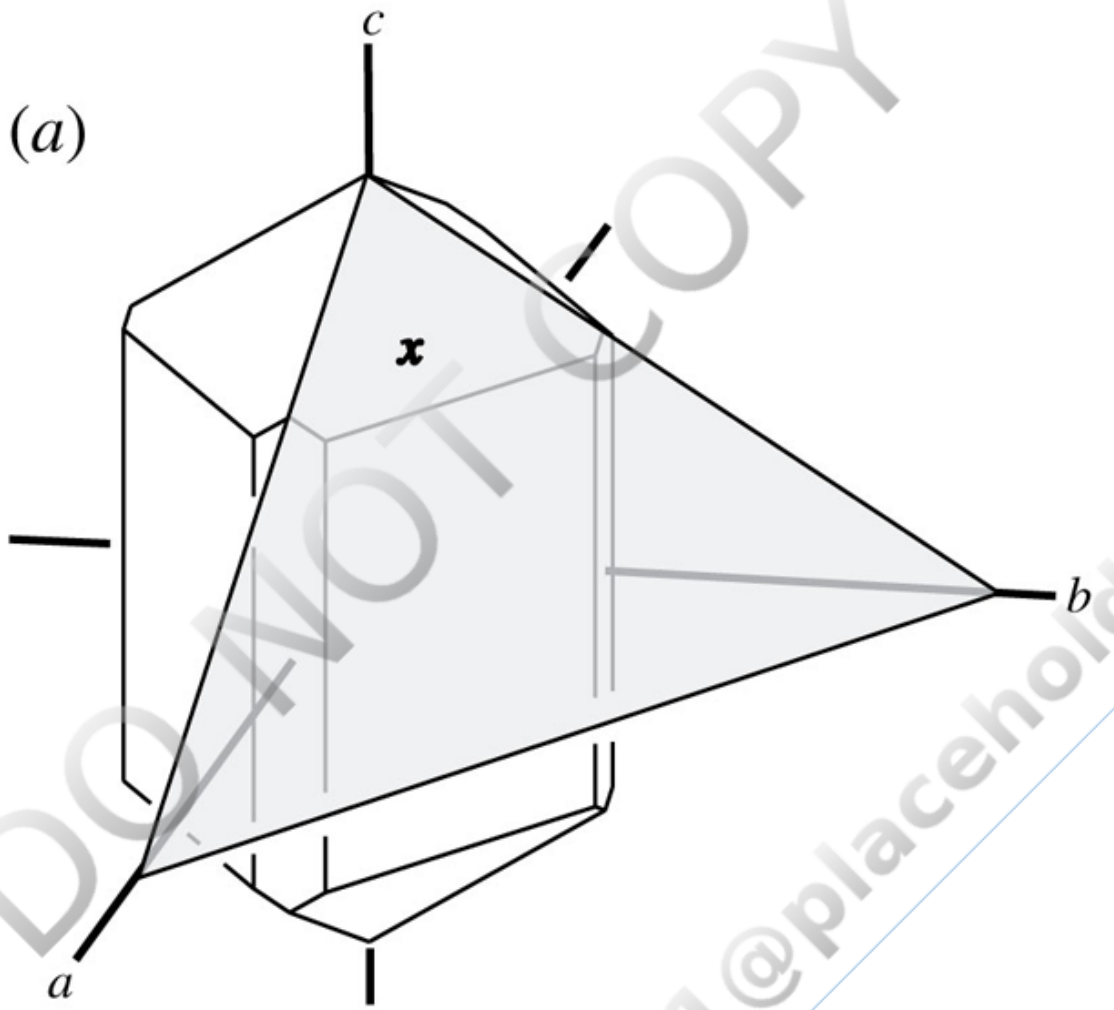

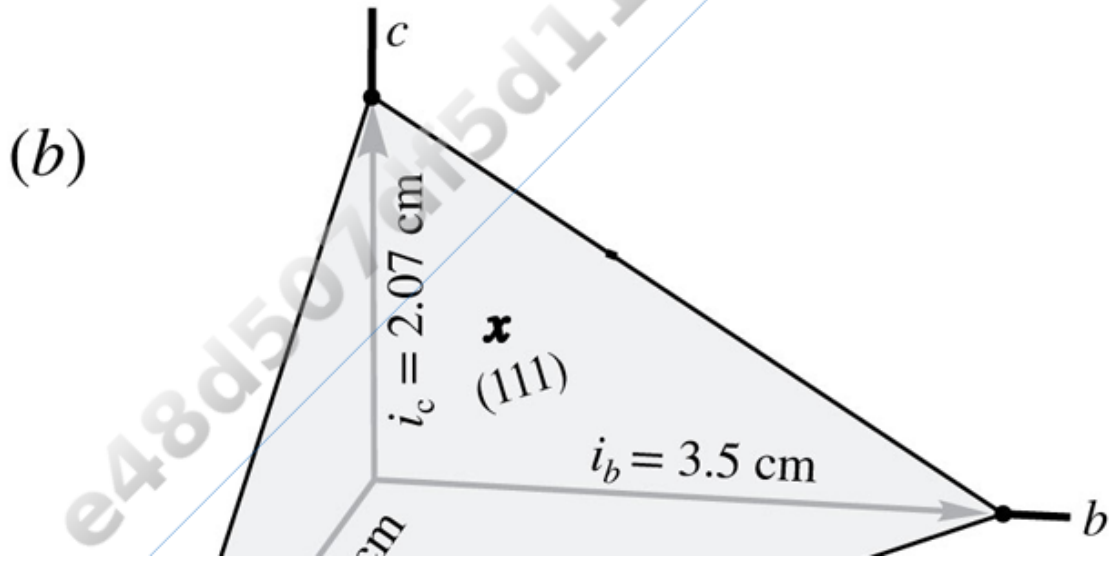

DO NOT COPY
e48d507df5d1141@placeholder.9409

Printed by: e48d507df5d1141@placeholder.94092.edu. Printing is for personal, private use only. No part of this book may be reproduced or transmitted without publisher's prior permission. Violators will be prosecuted.

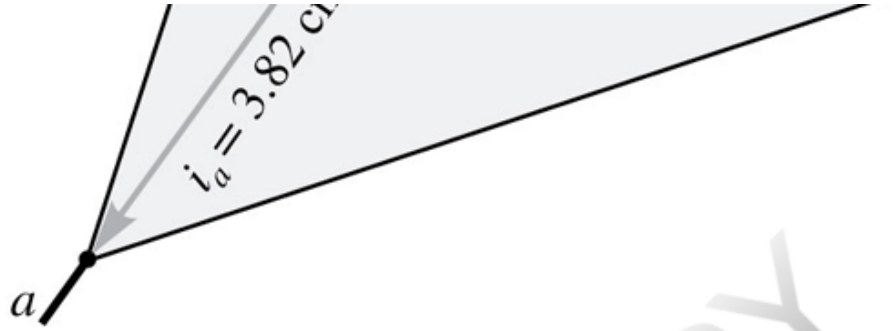

FIGURE 2.27 Calculating the Miller index for face *x* on an augite crystal. (*a*) Face *x* is extended out until it intersects all three crystal axes, as shown by the shaded plane. (*b*) The dimensions of these intersections measured from the center of the crystal are i_a = 3.82 cm, i_b = 3.5 cm, and i_c = 2.07 cm. The Miller index for this face is (111). See text for discussion. Back to text

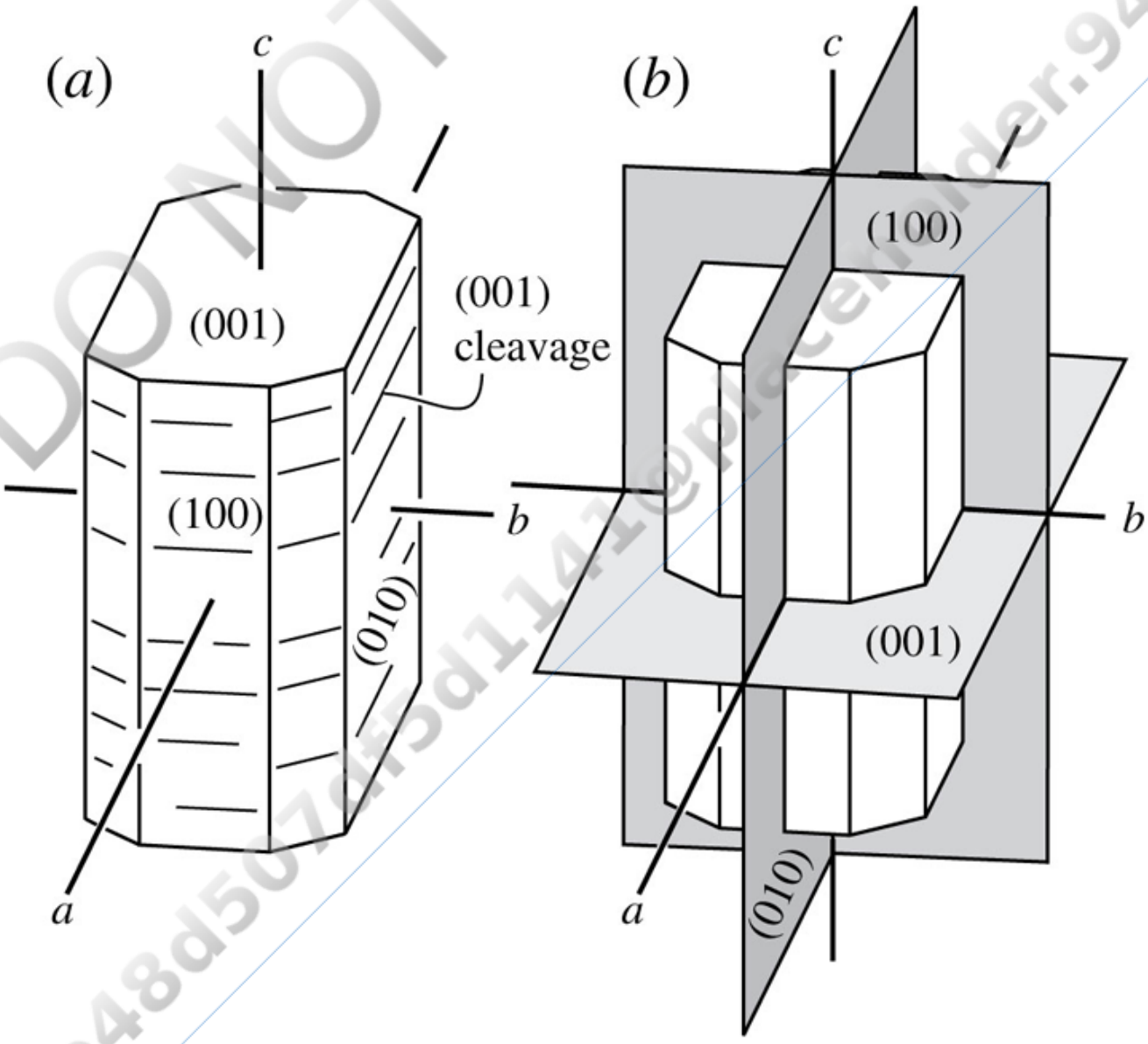

FIGURE 2.28 Crystallographic planes are assigned the same Miller index as the crystal face to

Printed by: e48d507df5d1141@placeholder.94092.edu. Printing is for personal, private use only. No part of this book may be reproduced or transmitted without publisher's prior permission. Violators will be prosecuted.

FIGURE 2.28 Crystallographic planes are assigned the same Miller index as the crystal face to which they are parallel. (*a*) A cleavage (shown with thin lines) parallel to the (001) crystal face is identified as a (001) cleavage. (*b*) The three principal crystallographic planes are parallel to the surfaces of the unit cell and the (100), (010), and (001) crystal faces. They therefore have Miller indices of (100), (010), and (001). Back to text

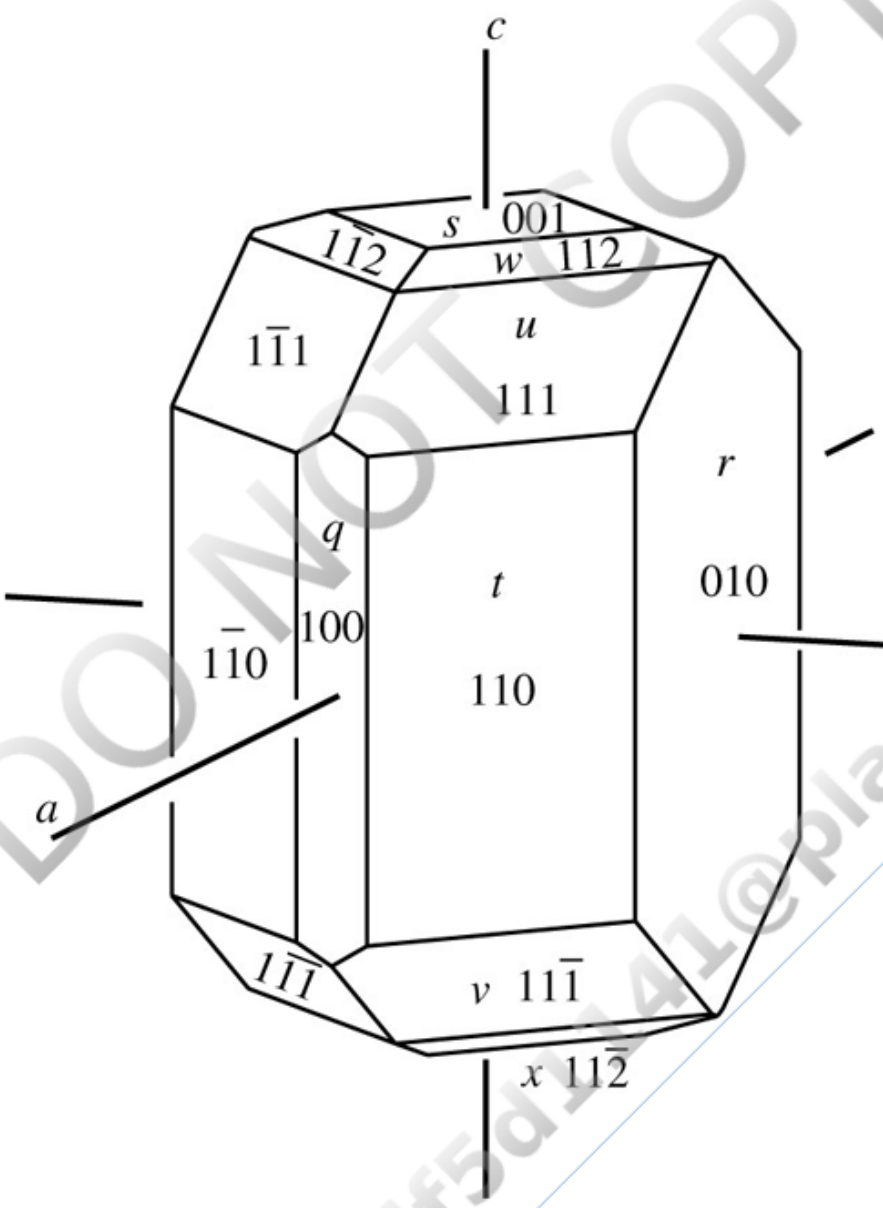

FIGURE 2.29 Assigning Miller indices by inspection. See text for discussion. Back to text

DO NOT COPY
e48d507df5d1141@placeholder.9409

= [001]

= [111]

Printed by: e48d507df5d1141@placeholder.94092.edu. Printing is for personal, private use only. No part of this book may be reproduced or transmitted without publisher's prior permission. Violators will be prosecuted.

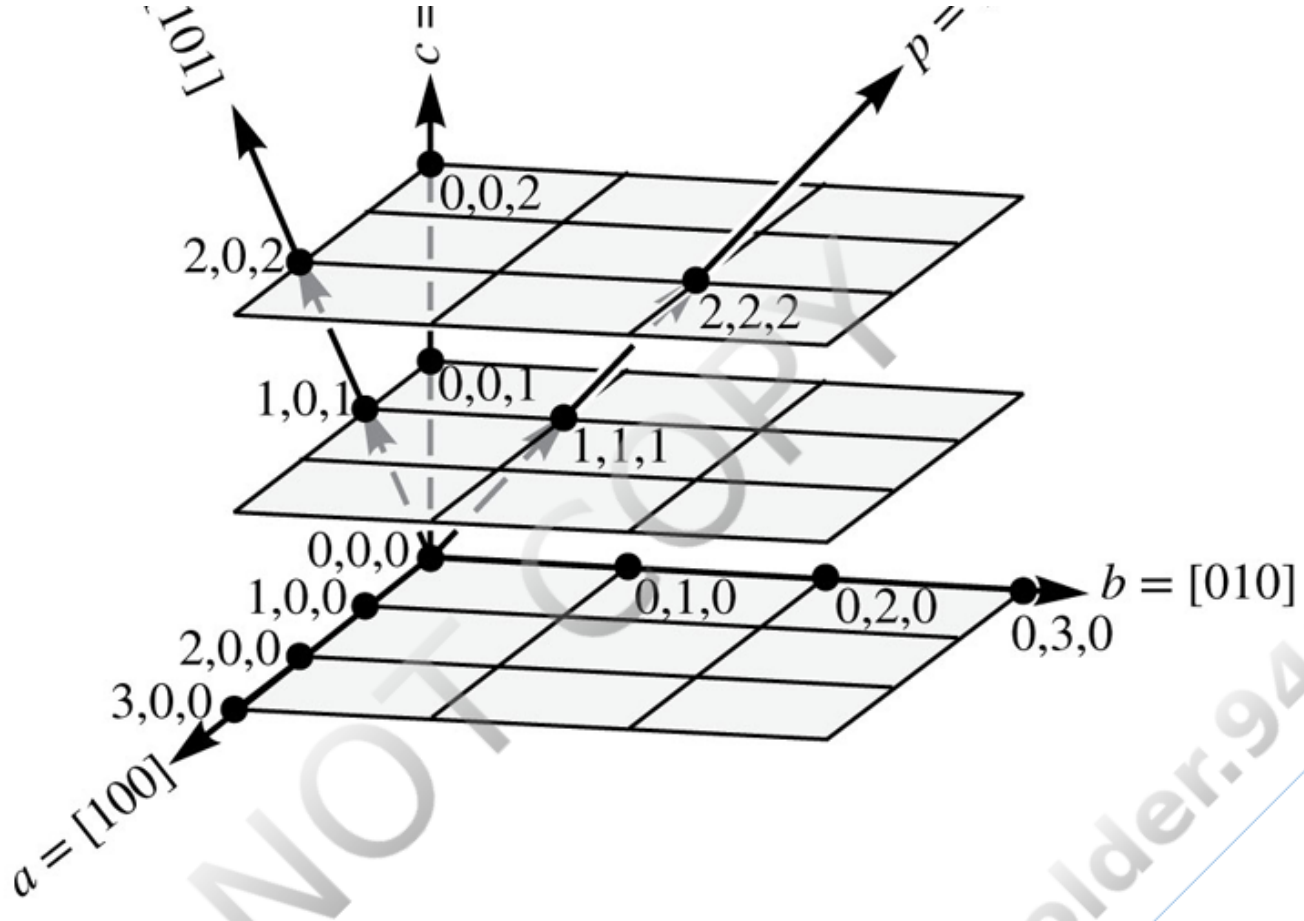

FIGURE 2.30 Crystallographic directions. Crystallographic direction [111] (line *p*) goes through lattice nodes 1,1,1 and 2,2,2, and so forth. Direction [101] (*q*) goes through lattice nodes 1,0,1 and 2,0,2. The three crystal axes *a*, *b*, and *c* are the [100], [010], and [001] crystallographic directions.
Back to text

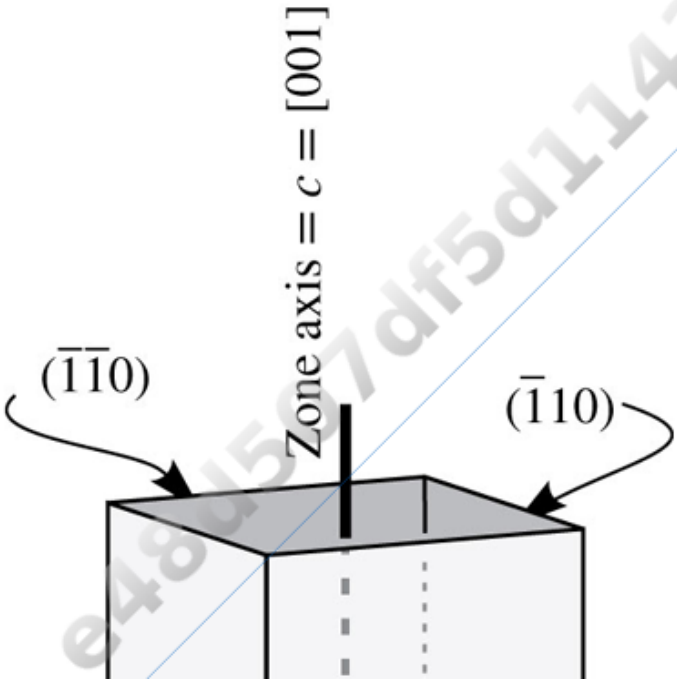

DO NOT COPY
e48d507df5d1141@placeholder.9409

Printed by: e48d507df5d1141@placeholder.94092.edu. Printing is for personal, private use only. No part of this book may be reproduced or transmitted without publisher's prior permission. Violators will be prosecuted.

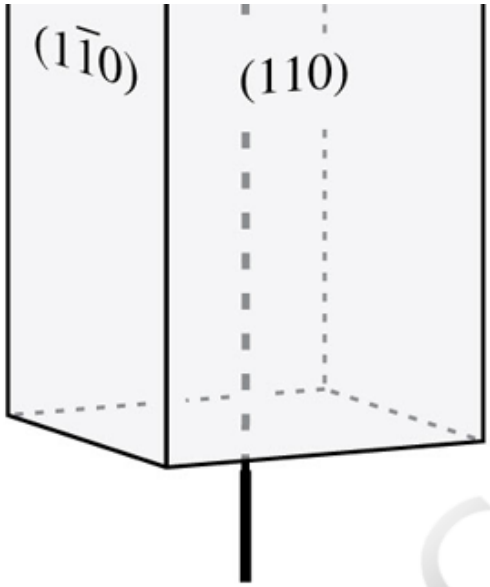

FIGURE 2.31 Crystal zone. The (110), $(1\bar{1}0)$, $(\bar{1}10)$, and $(\bar{1}\bar{1}0)$ faces constitute a [001] zone because they intersect in edges parallel to [001] (the *c* axis), which is the zone axis. Back to text

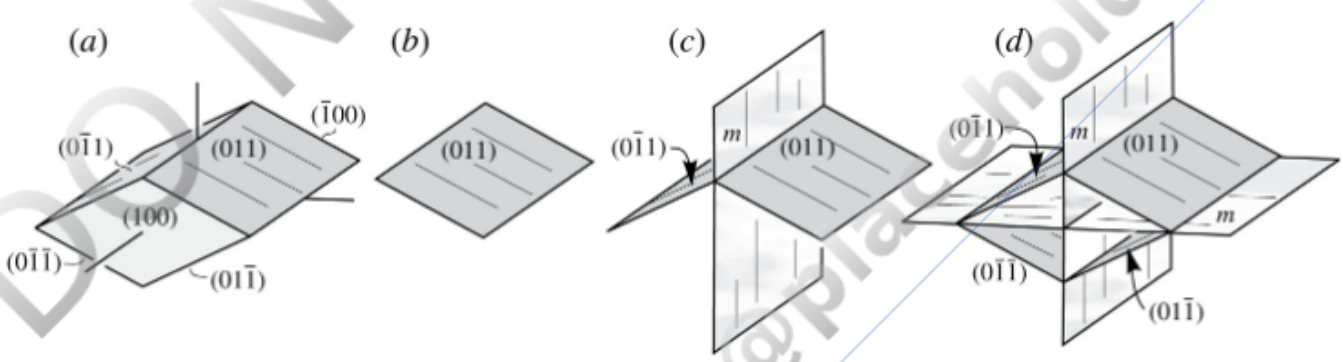

FIGURE 2.32 Crystal forms are produced by a repetition of crystal faces by symmetry operations. (*a*) A simple orthorhombic crystal. (*b*) The (011) face. (*c*) The $(0\bar{1}1)$ face is produced by reflection on the vertical mirror (*m*). (*d*) A horizontal mirror produces the $(01\bar{1})$ and $(0\bar{1}\bar{1})$ faces to complete the four faces of the {011} rhombic prism. Back to text

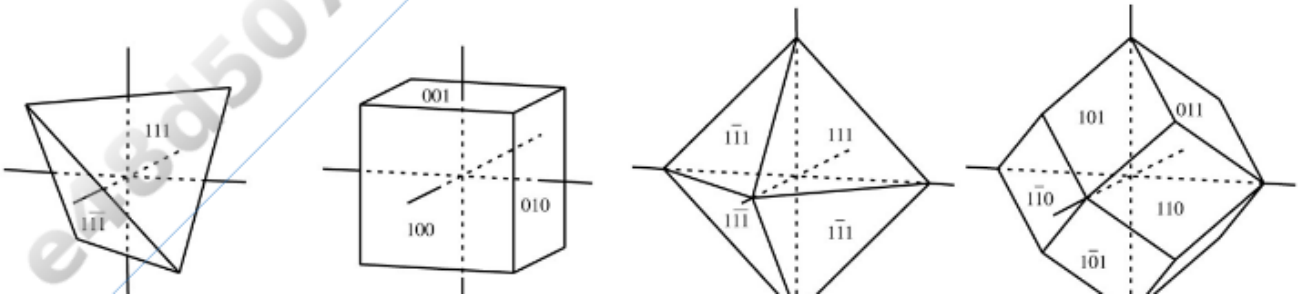

Printed by: e48d507df5d1141@placeholder.94092.edu. Printing is for personal, private use only. No part of this book may be reproduced or transmitted without publisher's prior permission. Violators will be prosecuted.

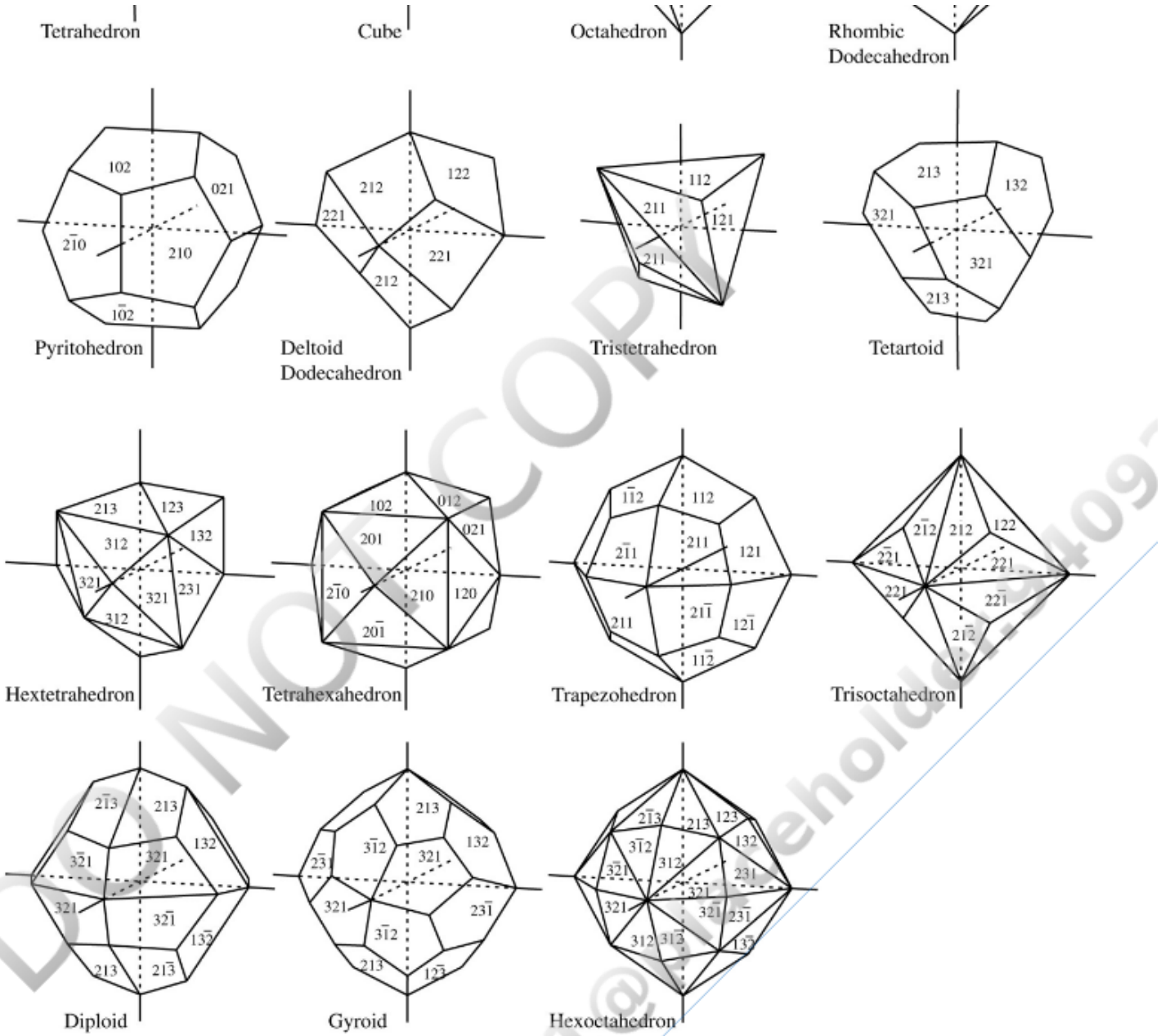

FIGURE 2.33 Crystal forms in the isometric system. Back to text

(*a*)

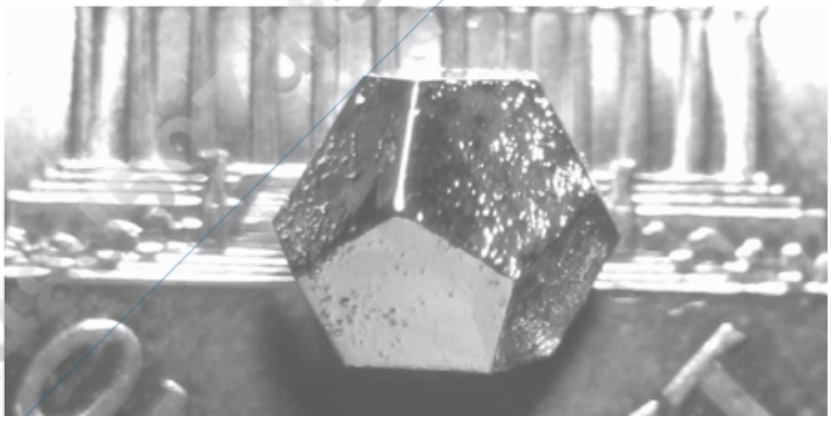

Printed by: e48d507df5d1141@placeholder.94092.edu. Printing is for personal, private use only. No part of this book may be reproduced or transmitted without publisher's prior permission. Violators will be prosecuted.

(*b*)

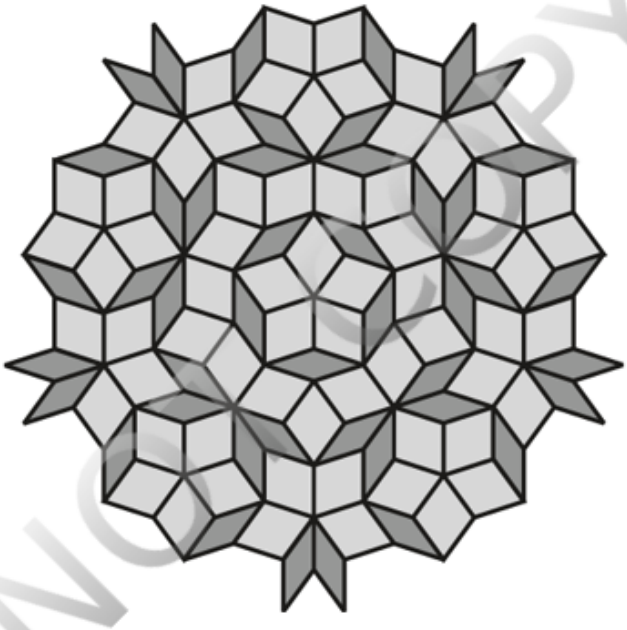

FIGURE 2.21 (*a*) A synthetic pentagonal dodecahedron quasicrystal of Ho-Mg-Zn resting on a penny coin. Unlike pyrite, which has a similar appearance, the faces of the pentagonal dodecahedron are regular pentagons, revealing the pentagonal (5-fold) rotational symmetry. Photo courtesy of Dr. Paul Canfield, Ames Laboratory, U.S. Department of Energy. (*b*) Penrose tiling using two different diamond-shaped tiles to produce pentagonal symmetry. While the pattern is systematic, it lacks translational symmetry. Photo courtesy of Dr. Paul Canfield, Ames Laboratory, U.S. Department of Energy. Back to text

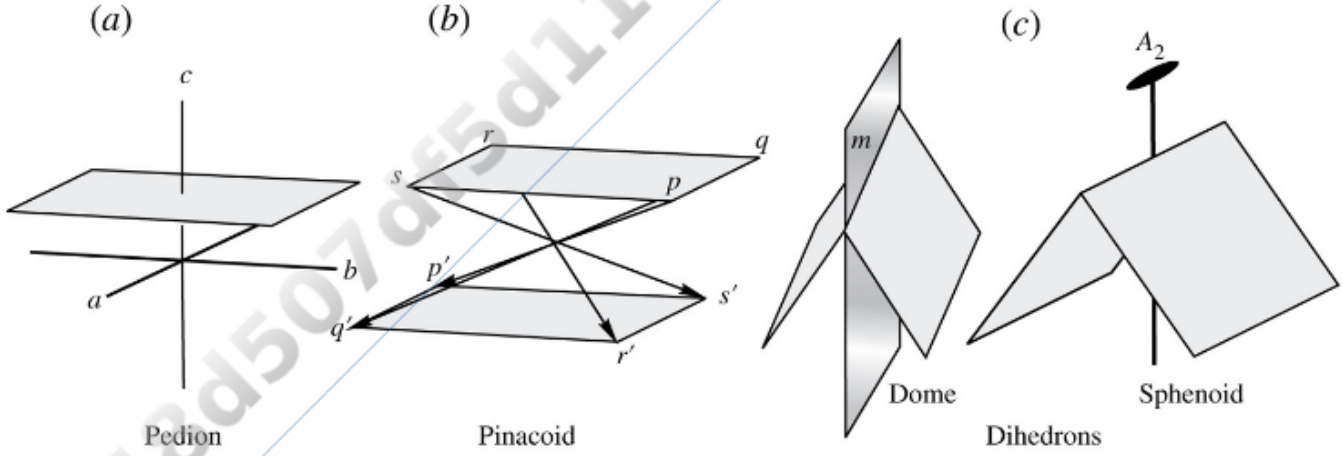

FIGURE 2.34 Crystal forms in the nonisometric crystal systems. (*a*) Pedion. (*b*) Pinacoid. (*c*) Dihedrons (dome and sphenoid). Back to text

Printed by: e48d507df5d1141@placeholder.94092.edu. Printing is for personal, private use only. No part of this book may be reproduced or transmitted without publisher's prior permission. Violators will be prosecuted.

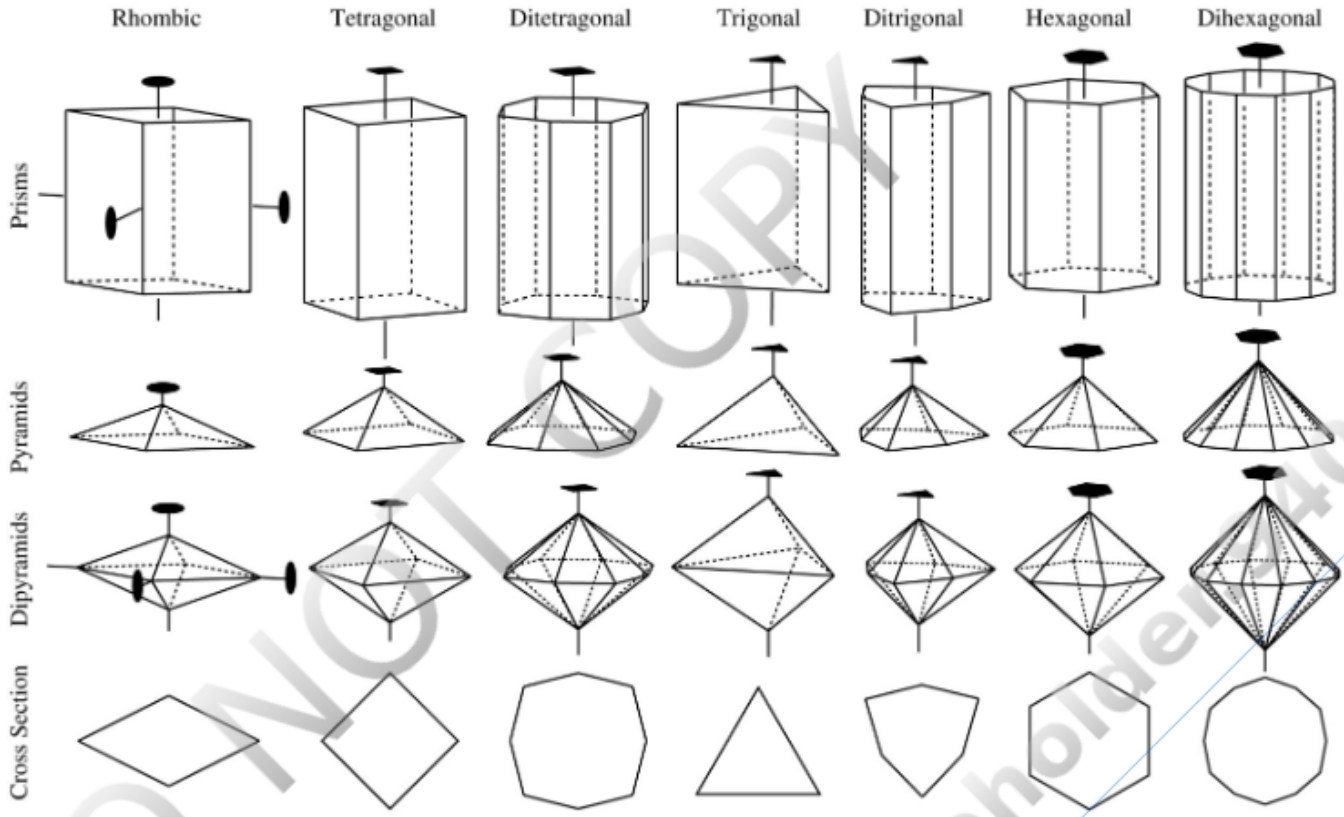

FIGURE 2.35 Crystal forms in the nonisometric crystal systems: prisms, pyramids, and dipyramids. Each form is modified by the name of the cross section shape (hexagonal prism, tetragonal pyramid, ditrigonal dipyramid, etc.). Back to text

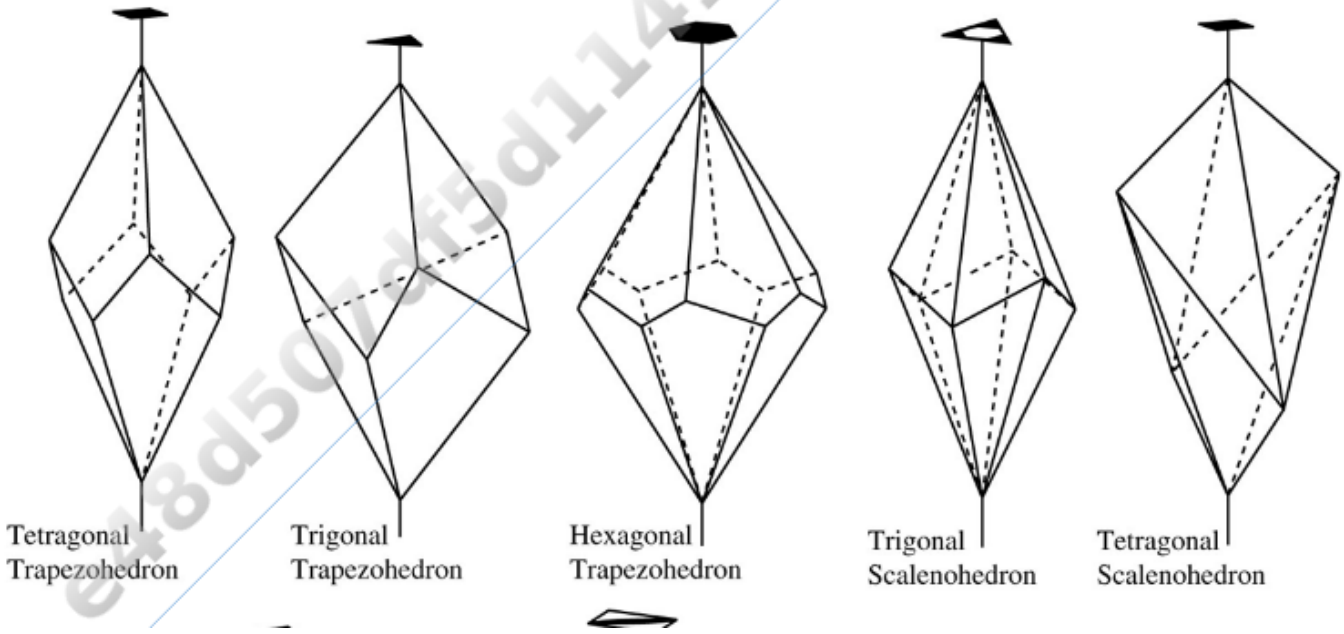

DO NOT COPY e48d507df5d1141@placeholder.94092

Printed by: e48d507df5d1141@placeholder.94092.edu. Printing is for personal, private use only. No part of this book may be reproduced or transmitted without publisher's prior permission. Violators will be prosecuted.

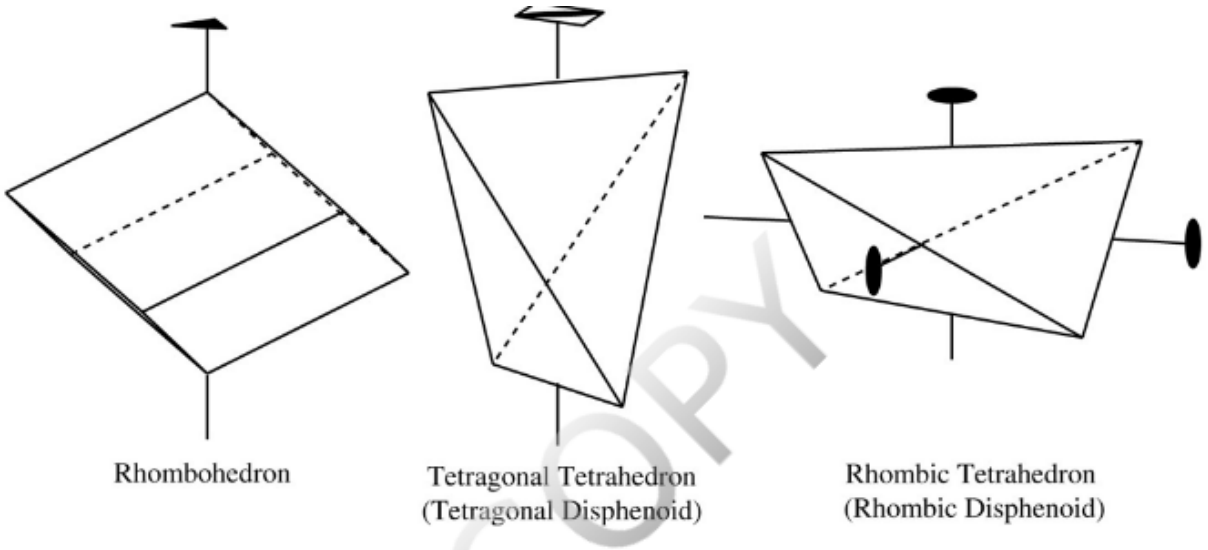

FIGURE 2.36 Crystal forms in the nonisometric crystal systems: trapezohedrons, scalenohedrons, rhombohedrons, and tetrahedrons (rhombic and tetragonal). Tetragonal trapezohedrons have 8 faces, 4 each on the top and bottom. Trigonal trapezohedrons have 6 faces, 3 each on the top and bottom. Both positive and negative forms are possible, as shown later (Figure 2.38). Hexagonal trapezohedrons have 12 faces, 6 each on the top and bottom. Back to text

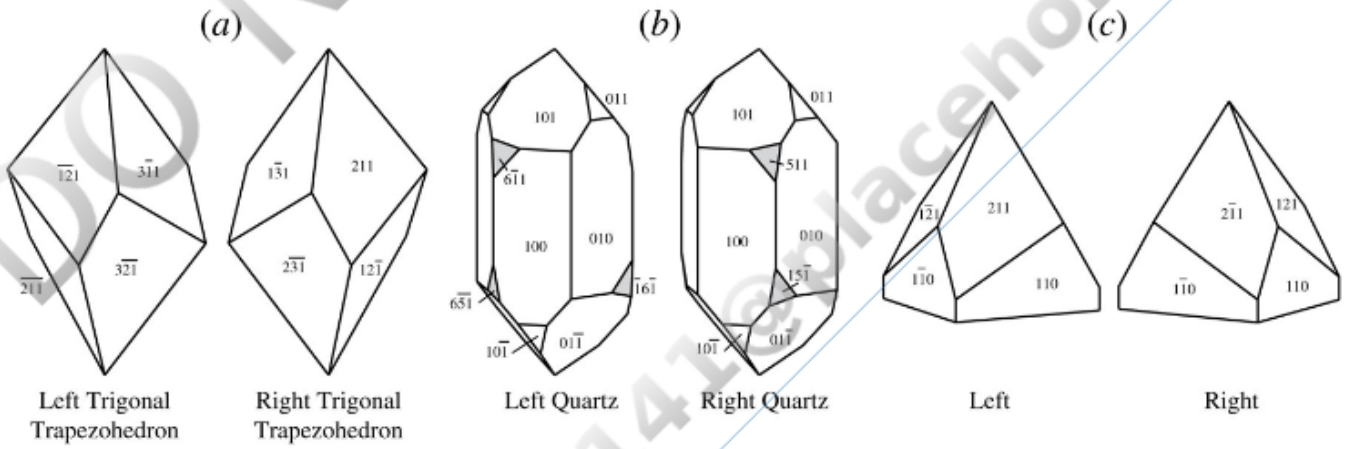

FIGURE 2.37 Enantiomorphous forms and crystals. (*a*) The right-handed {211} and left-handed $\{3\bar{1}1\}$ trigonal trapezohedron lack center or mirrors. (*b*) The right {511} and left $\{6\bar{1}1\}$ trigonal trapezohedron (small shaded faces) on right- and left-handed quartz. (*c*) Right- and left-handed crystals in the 4 point group. The {211} and $\{2\bar{1}1\}$ pyramids are not themselves enantiomorphous, but when combined with the {110} prism and $\{00\bar{1}\}$ pedion, they form right- and left-handed crystals. Back to text

(a)

Printed by: e48d507df5d1141@placeholder.94092.edu. Printing is for personal, private use only. No part of this book may be reproduced or transmitted without publisher's prior permission. Violators will be prosecuted.

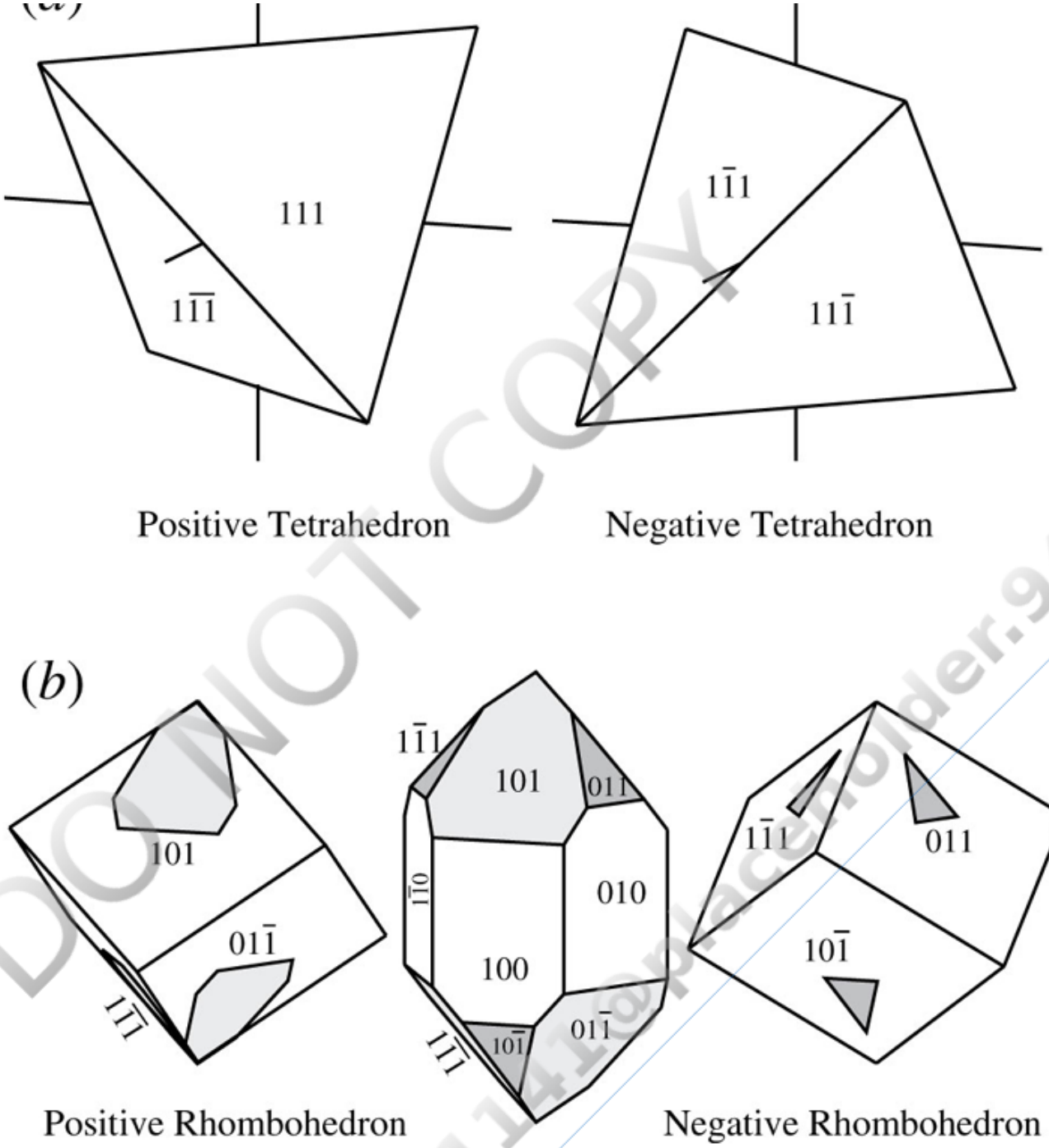

FIGURE 2.38 Positive and negative forms. (*a*) Tetrahedrons. (*b*) Quartz crystal with both positive {101} and negative {011} unit rhombohedrons. Back to text

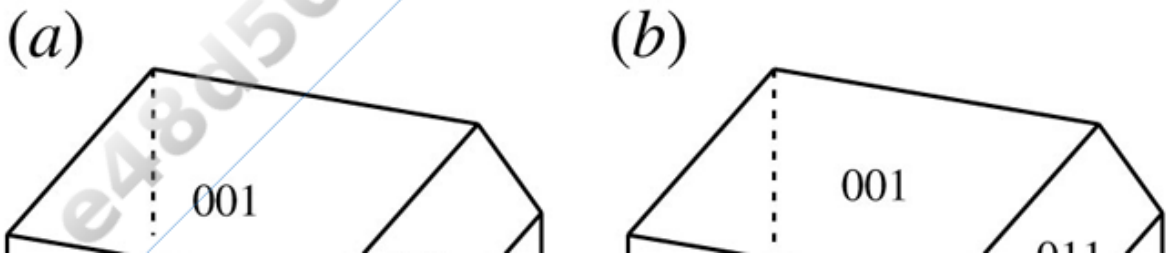

DO NOT COPY
e48d507df5d1141@placeholder.9409

Printed by: e48d507df5d1141@placeholder.94092.edu. Printing is for personal, private use only. No part of this book may be reproduced or transmitted without publisher's prior permission. Violators will be prosecuted.

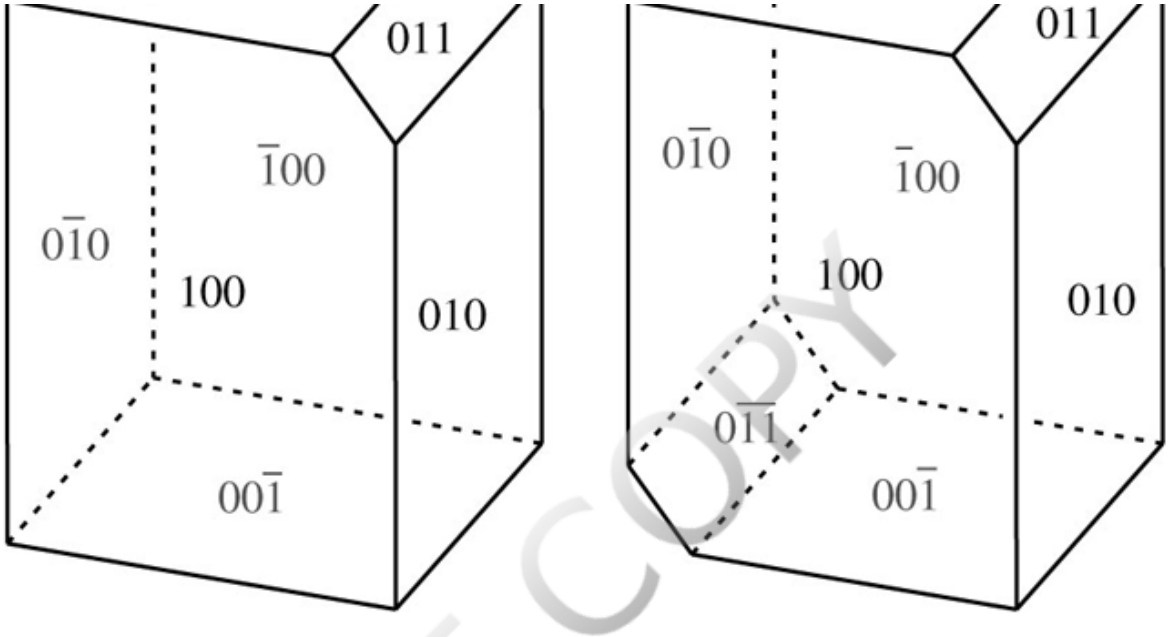

FIGURE 2.39 Forms in the triclinic crystal system. (*a*) A pedial class crystal of the 1 point group consisting of {100}, $\{\bar{1}00\}$, {010}, $\{0\,\bar{1}0\}$, {001}, $\{00\,\bar{1}\}$, and {011} pedions. Note the lack of center symmetry. (*b*) A pinacoidal class crystal of the $\bar{1}$ point group consisting of {100}, {010}, {001}, and {011} pinacoids. Back to text

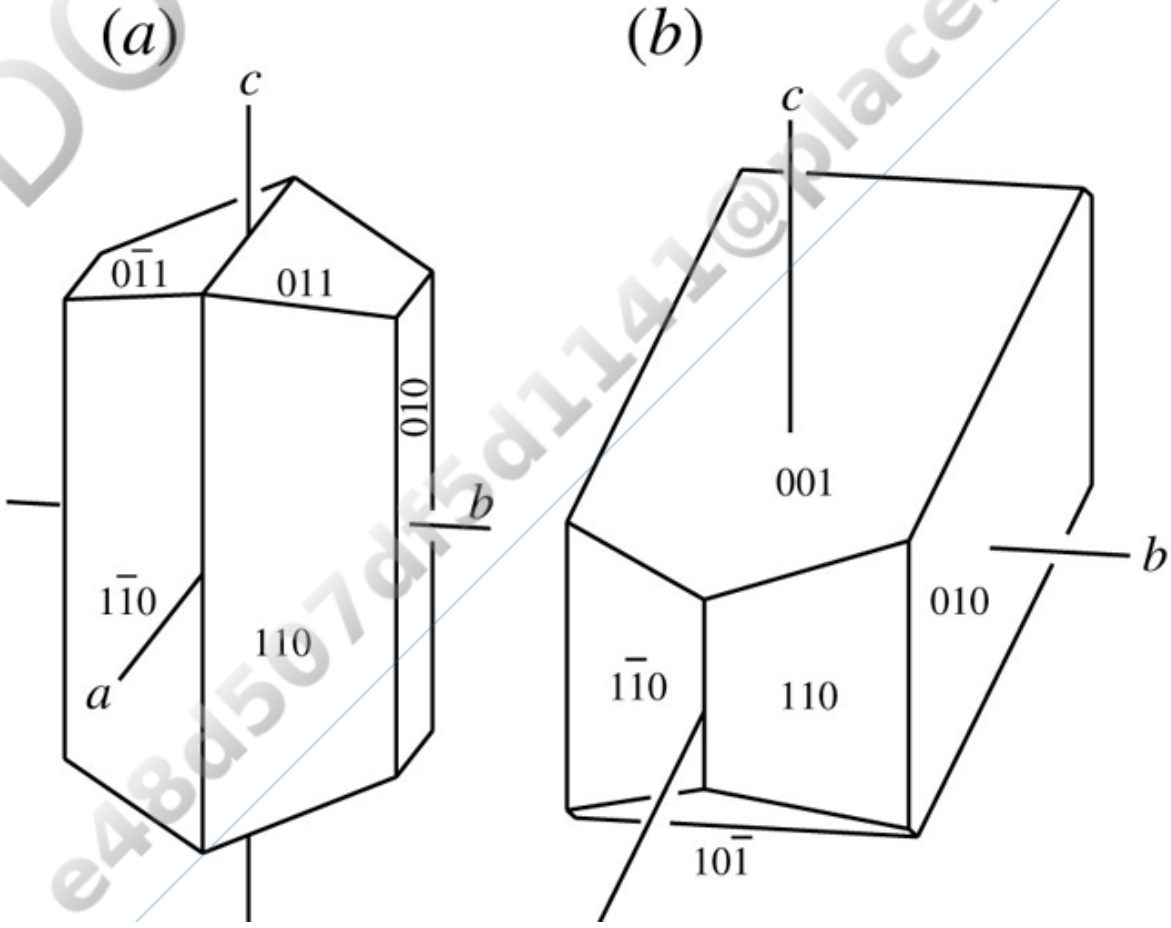

DO NOT COPY
e48d507df5d1141@placeholder.9409

Printed by: e48d507df5d1141@placeholder.94092.edu. Printing is for personal, private use only. No part of this book may be reproduced or transmitted without publisher's prior permission. Violators will be prosecuted.

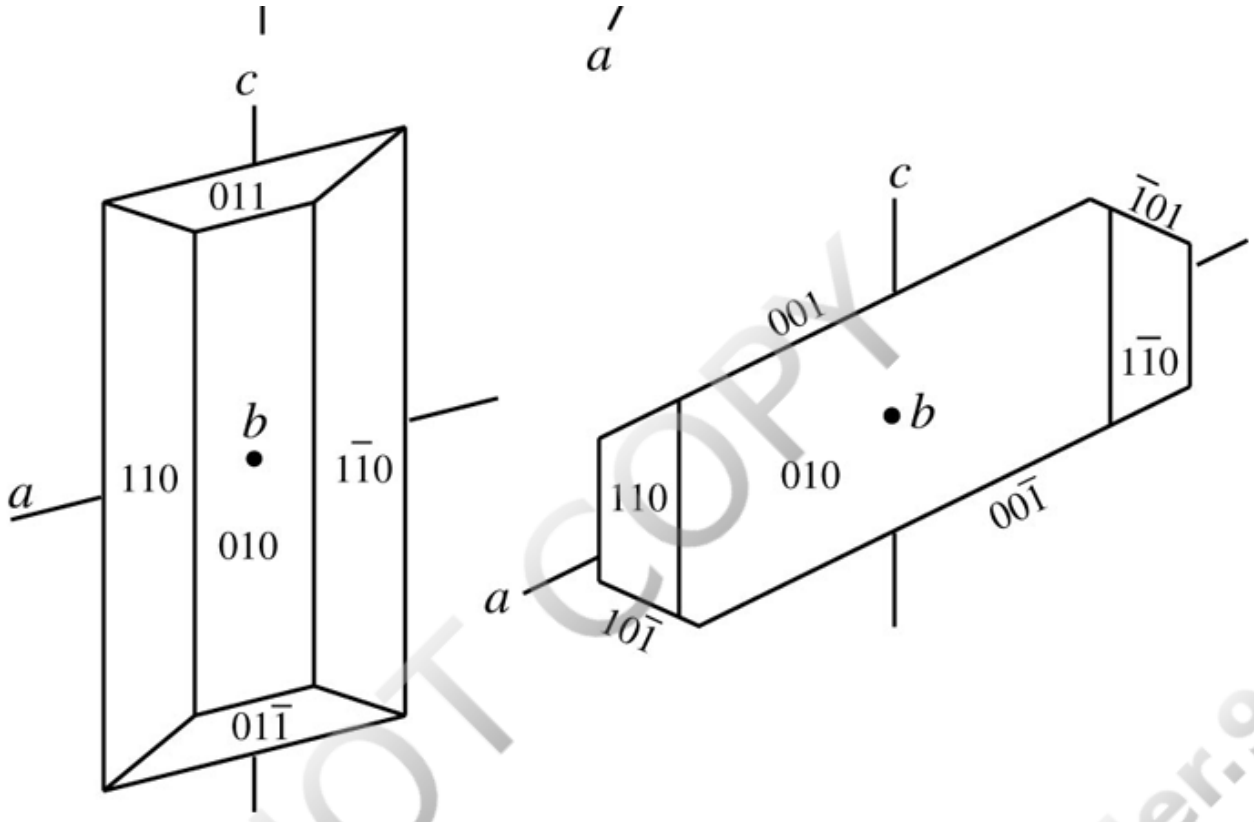

FIGURE 2.40 Monoclinic crystals. The views down the *b* axis show that the *a* and *c* axes are not at right angles. (*a*) 2/*m* point group amphibole crystal with a side {010} pinacoid and {110} and {011} prisms. (*b*) 2/*m* point group sanidine crystal with side {010}, basal {001}, and $\{10\bar{1}\}$ pinacoids; and {110} prism. Back to text

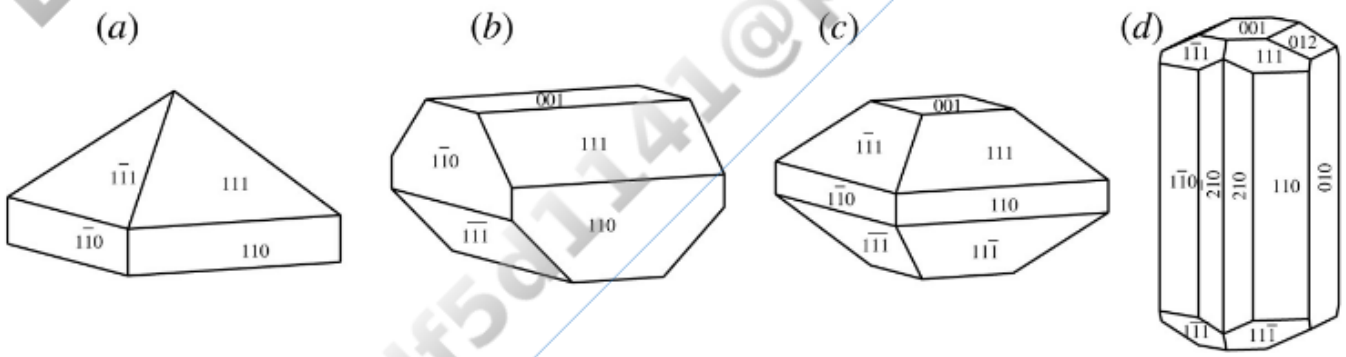

FIGURE 2.41 Orthorhombic crystals. Note how the (111), (110), and $(00\bar{1})$ faces are duplicated to produce different forms based on the symmetry content. (*a*) *mm*2 point group crystal with a {110} rhombic prism, $\{00\bar{1}\}$ bottom pedion, and {111} rhombic pyramid. (*b*) 222 point group crystal with {111} rhombic tetrahedron (disphenoid), {110} rhombic prism, and {001} pinacoid. (*c*) 2/*m* 2/*m* 2/*m* point group crystal with a {001} pinacoid, {110} rhombic prism, and {111} rhombic dipyramid. (*d*) 2/*m* 2/*m* 2/*m* topaz crystal with {010} and {001} pinacoids; {110}, {210}, and {012} rhombic prisms, and {111} rhombic dipyramid. Back to text

DO NOT COPY
e48d507df5d1141@placeholder.9409

Printed by: e48d507df5d1141@placeholder.94092.edu. Printing is for personal, private use only. No part of this book may be reproduced or transmitted without publisher's prior permission. Violators will be prosecuted.

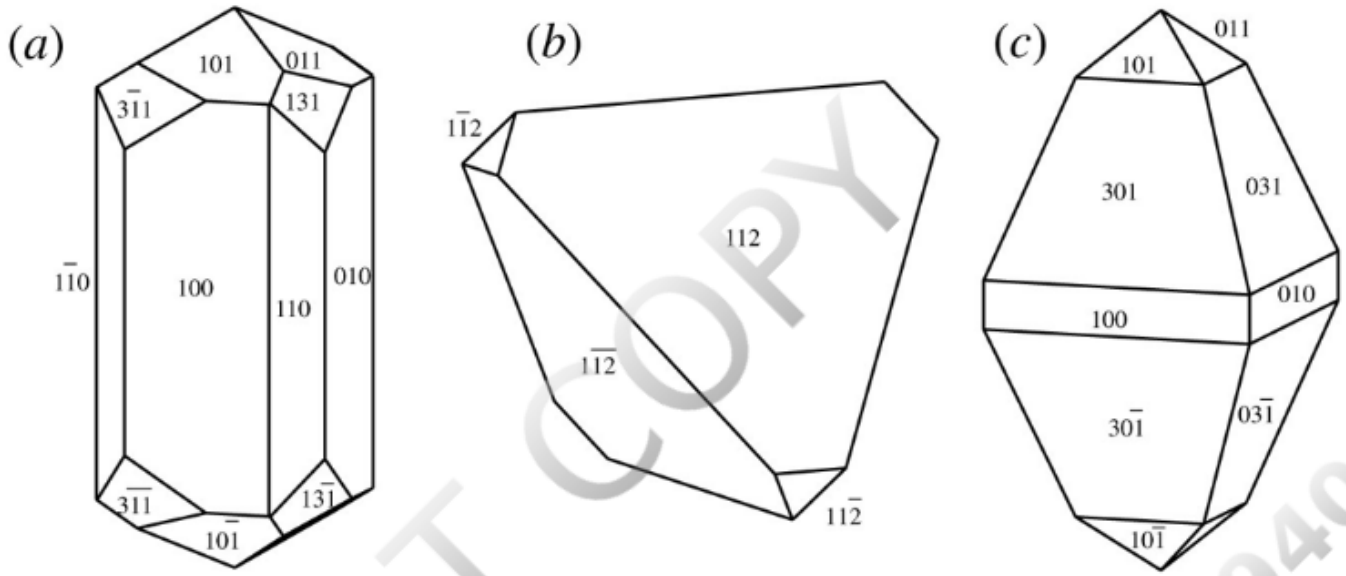

FIGURE 2.42 Tetragonal crystals. (*a*) 4/*m* scapolite crystal with {100} and {110} prisms, and {011} and {131} dipyramids. (*b*) $\bar{4}2m$ chalcopyrite crystal consisting of a positive {112} tetragonal tetrahedron (disphenoid) and a negative $\left\{1\ \bar{1}2\right\}$ tetragonal tetrahedron (smaller faces). (*c*) 4/*m* 2/*m* 2/*m* zircon crystal with {100} prism and {011} and {031} dipyramids. Back to text

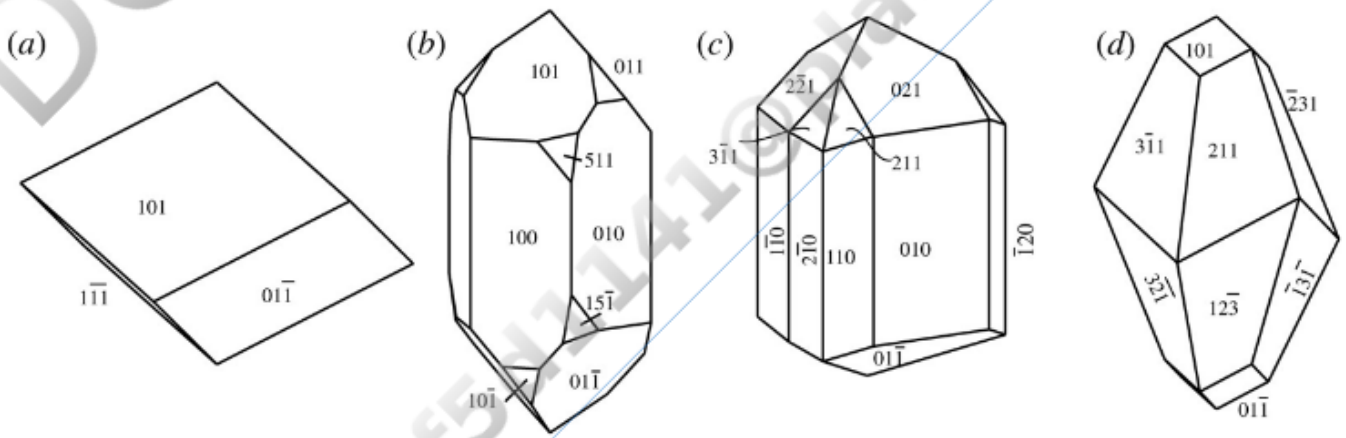

FIGURE 2.43 Crystals in the hexagonal crystal system, trigonal division. (*a*) Dolomite {101} rhombohedron in the $\bar{3}$ point group. The lack of vertical mirrors is not obvious based on these crystal faces. (*b*) 32 point group. Right-handed quartz with {100} prism, positive {101} and negative {011} rhombohedrons, and {511} trigonal scalenohedron. (*c*) 3*m* point group. Tourmaline with {021} trigonal pyramid and {211} ditrigonal pyramid on top, {110} and {010} prisms in the middle, and $\left\{01\ \bar{1}\right\}$ trigonal pyramid on the bottom. (*d*) $\bar{3}2m$ point group. Calcite crystal with {211} scalenohedron and {101} positive rhombohedron. Back to text

DO NOT COPY
e48d507df5d1141@placeholder.9409

Printed by: e48d507df5d1141@placeholder.94092.edu. Printing is for personal, private use only. No part of this book may be reproduced or transmitted without publisher's prior permission. Violators will be prosecuted.

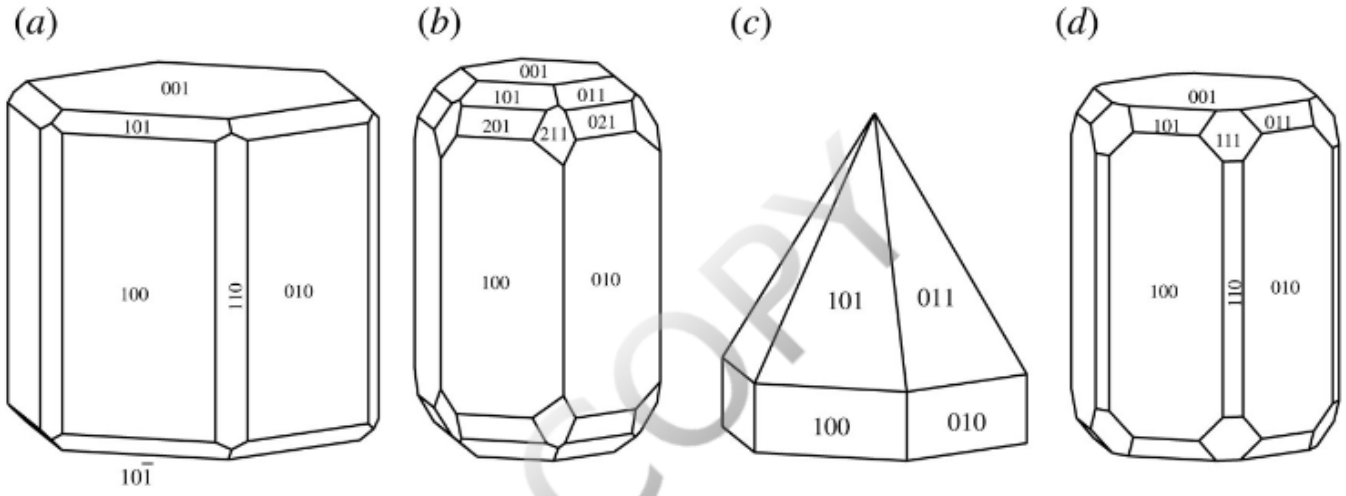

FIGURE 2.44 Crystals in the hexagonal crystal system, hexagonal division. (*a*) Nepheline (6 point group) crystals are rare, composed of {100} and {110} prisms, upper {101} and lower $\left\{10\bar{1}\right\}$ pyramids, and top {001} and bottom $\left\{00\bar{1}\right\}$ pedions. The crystal habit appears to have higher symmetry than the nepheline actually possesses. (*b*) 6/*m* apatite crystal composed of {100} prism; {101}, {201}, {211} dipyramids; and {001} pinacoid. Only the {211} dipyramid indicates that the symmetry is 6/*m*. (*c*) 6*mm* zincite crystal consists of {100} prism, {101} pyramid, and $\left\{00\bar{1}\right\}$ pedion. (*d*) 6/*m* 2/*m* 2/*m* beryl crystal with {100} and {110} prisms, {101} and {111} dipyramids, and {001} pinacoid. Back to text

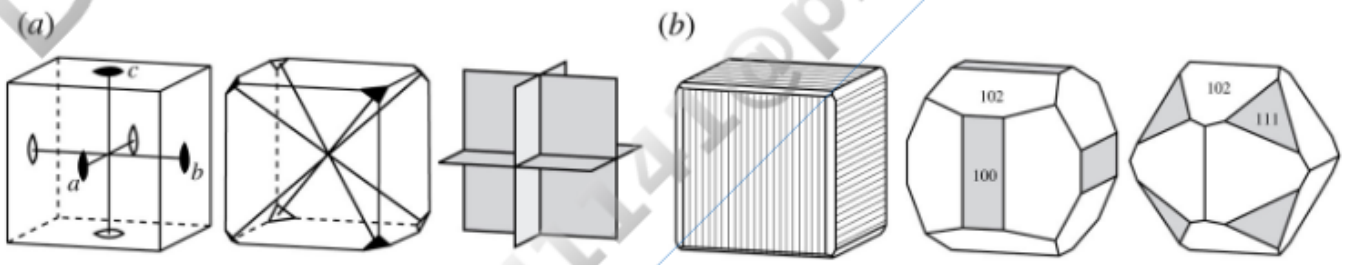

FIGURE 2.45 $2\,/\,m\,\bar{3}$ point group. (*a*) Three 2-fold axes are parallel to the crystal axes, four 3-fold axes are parallel to the long diagonals through the unit cell, and three mirror planes are parallel to the cube faces. (*b*) Striations on pyrite cube (left) are produced by interaction between the shaded cube {001} and pyritohedron {102} faces (center). Shaded octahedron {111} faces modify a pyritohedron (right). Not shown, but striations are also commonly found on pyritohedron and octahedron faces. Back to text

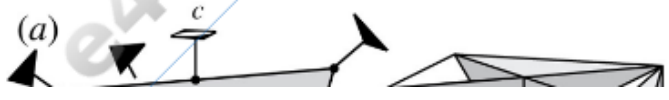

DO NOT COPY

Printed by: e48d507df5d1141@placeholder.94092.edu. Printing is for personal, private use only. No part of this book may be reproduced or transmitted without publisher's prior permission. Violators will be prosecuted.

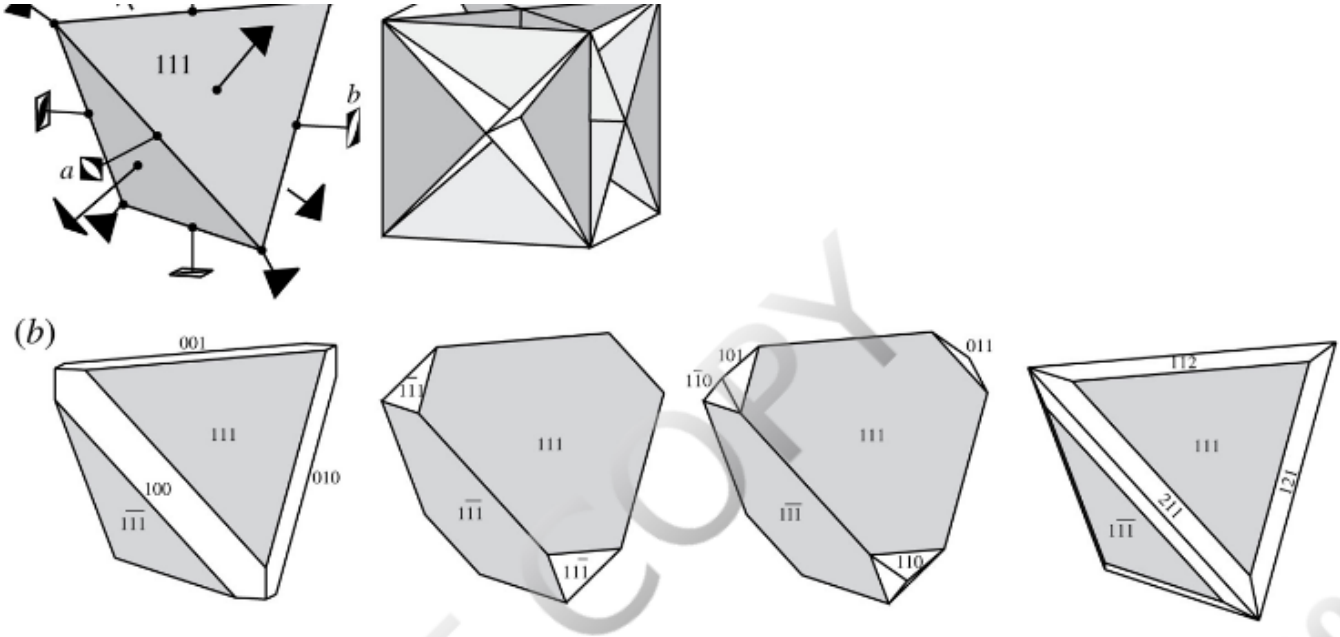

FIGURE 2.46 $\bar{4}3m$ point group. (*a*) Crystal axes (*a*, *b*, *c*) are parallel to the three 4-fold rotoinversion axes. Four 3-fold axes are parallel to the long diagonals through the cube and perpendicular to the tetrahedron crystal faces. Six mirrors are parallel to the body diagonals through the cubic unit cell. (*b*) Tetrahedrons {111} (dark) combined with (left to right) cube {001}, negative tetrahedron $\{1\bar{1}1\}$, dodecahedron {011}, and tristetrahedron {121}. Back to text

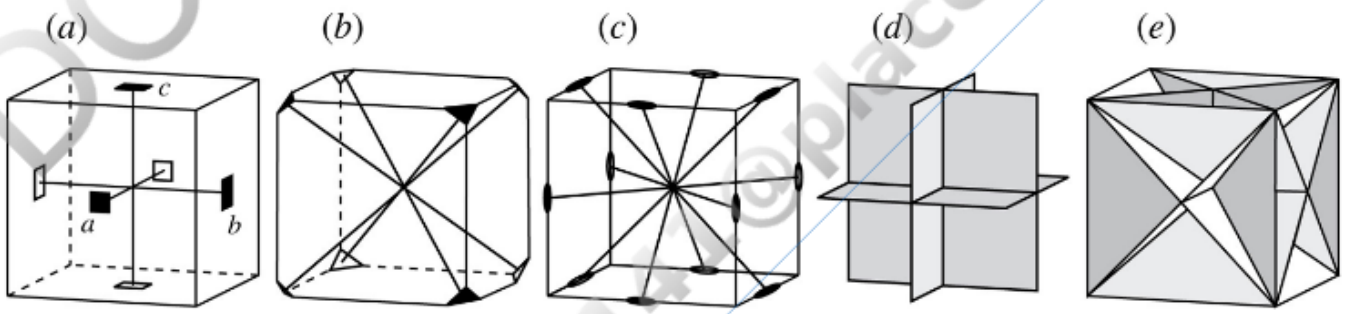

FIGURE 2.47 Symmetry elements in the $\bar{4}/m\,\bar{3}\,2/m$ point group. (*a*) Three 4-fold rotation axes are parallel to the three crystal axes. (*b*) Four 3-fold axes are parallel to the long diagonals through the cube. (*c*) Six 2-fold axes are parallel to edge-to-edge diagonals. (*d*) Three mirrors are parallel to cube faces. (*e*) Six mirrors are parallel to diagonals through the cube. Back to text

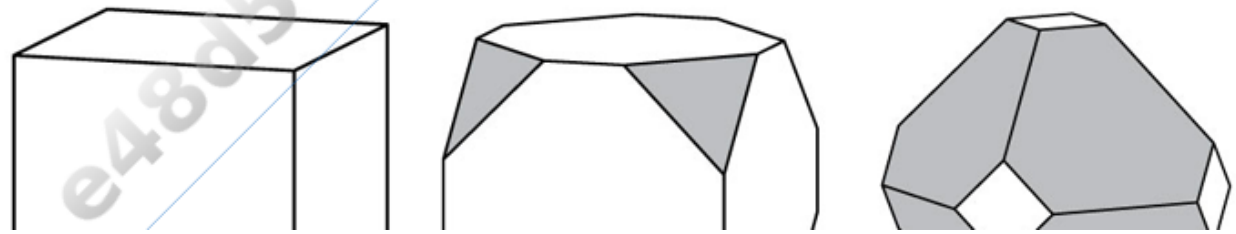

Printed by: e48d507df5d1141@placeholder.94092.edu. Printing is for personal, private use only. No part of this book may be reproduced or transmitted without publisher's prior permission. Violators will be prosecuted.

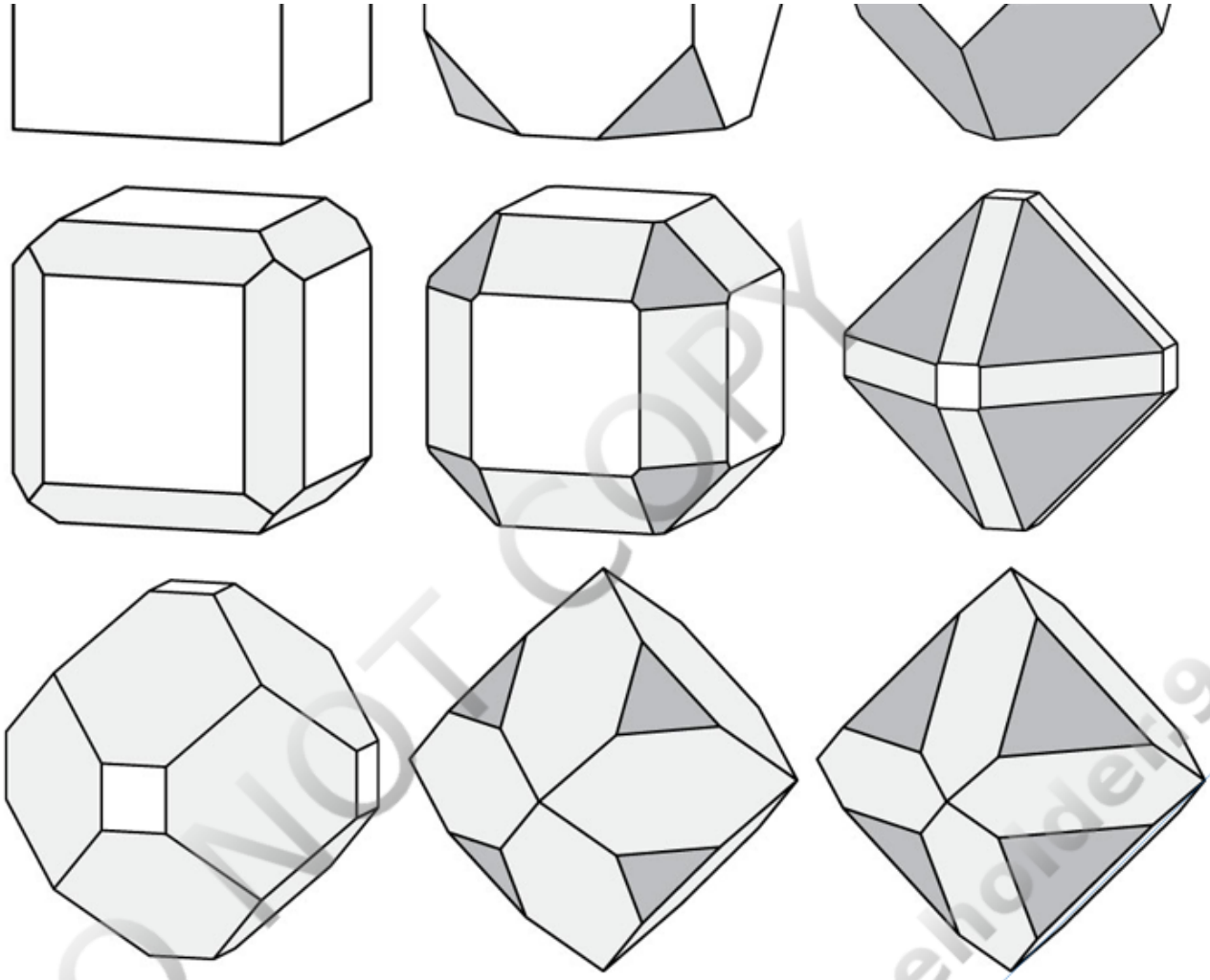

FIGURE 2.48 Various combinations of {001} cube (white), {011} dodecahedron (light), and {111} octahedron (dark) in the $\overline{4}/m\,\overline{3}\,2/m$ point group. See Table 2.9 and Figure 2.33 for additional forms that may appear. Back to text

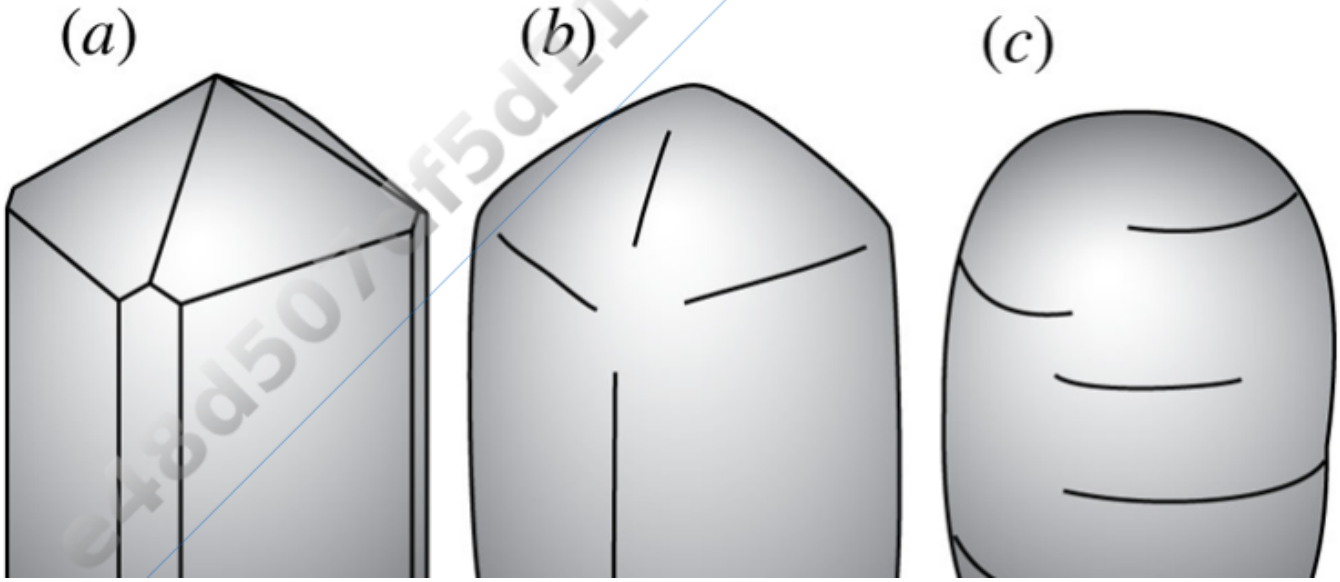

DO NOT COPY
e48d507df5d1141@placeholder.9409

Printed by: e48d507df5d1141@placeholder.94092.edu. Printing is for personal, private use only. No part of this book may be reproduced or transmitted without publisher's prior permission. Violators will be prosecuted.

FIGURE 2.49 Degree to which crystal faces are well developed. (*a*) Euhedral. (*b*) Subhedral. (*c*) Anhedral. Back to text

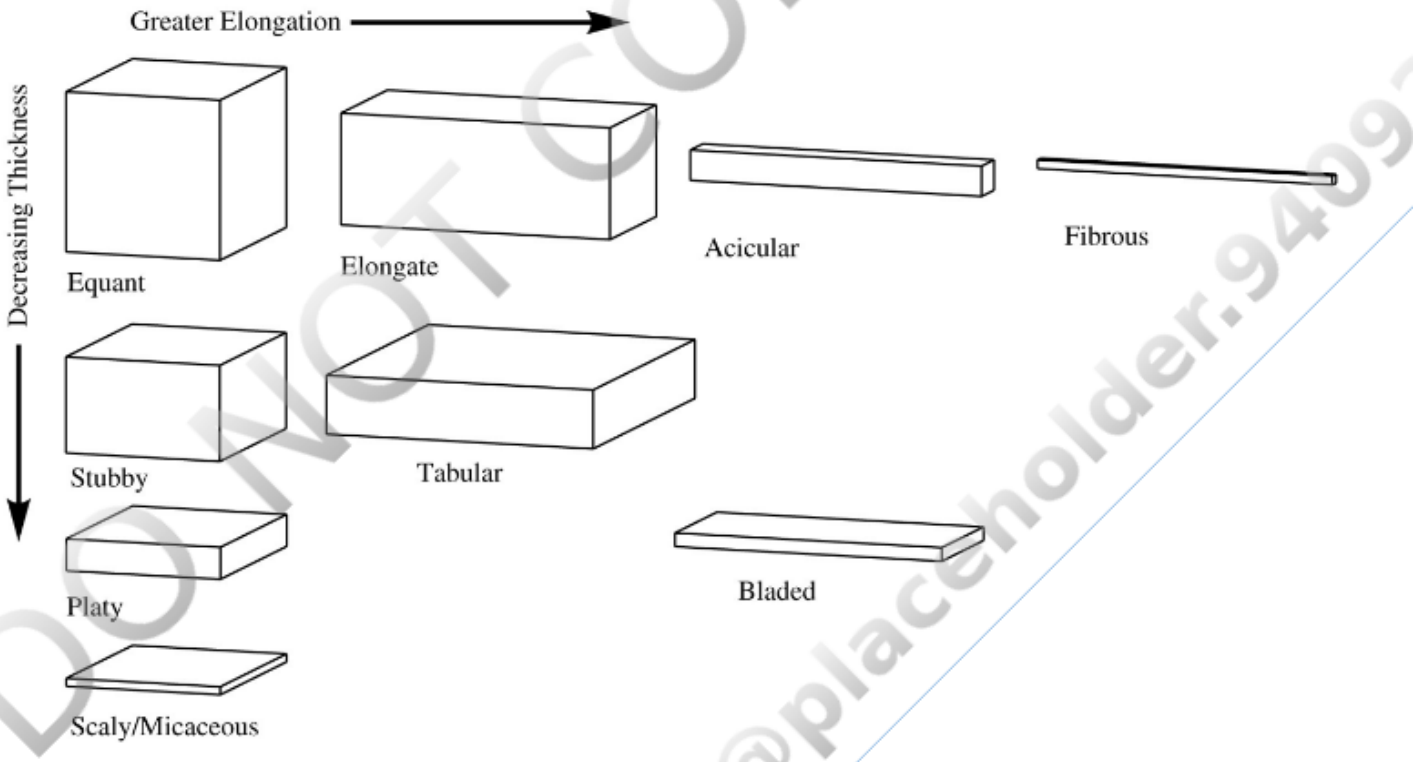

FIGURE 2.50 Nomenclature for describing the habit of individual mineral grains as a function of relative dimensions. Back to text

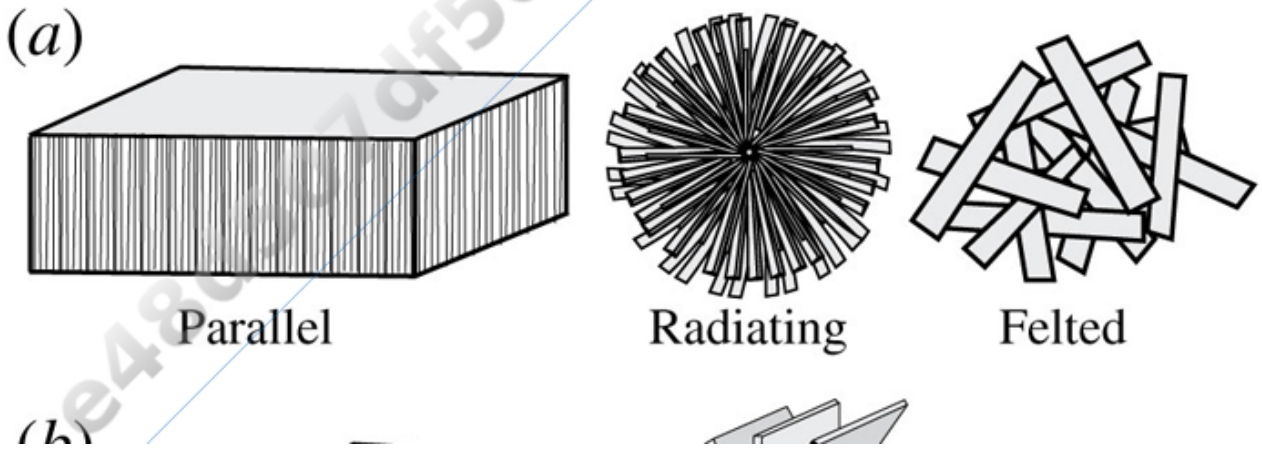

DO NOT COPY
e48d507df5d1141@placeholder.9409

Printed by: e48d507df5d1141@placeholder.94092.edu. Printing is for personal, private use only. No part of this book may be reproduced or transmitted without publisher's prior permission. Violators will be prosecuted.

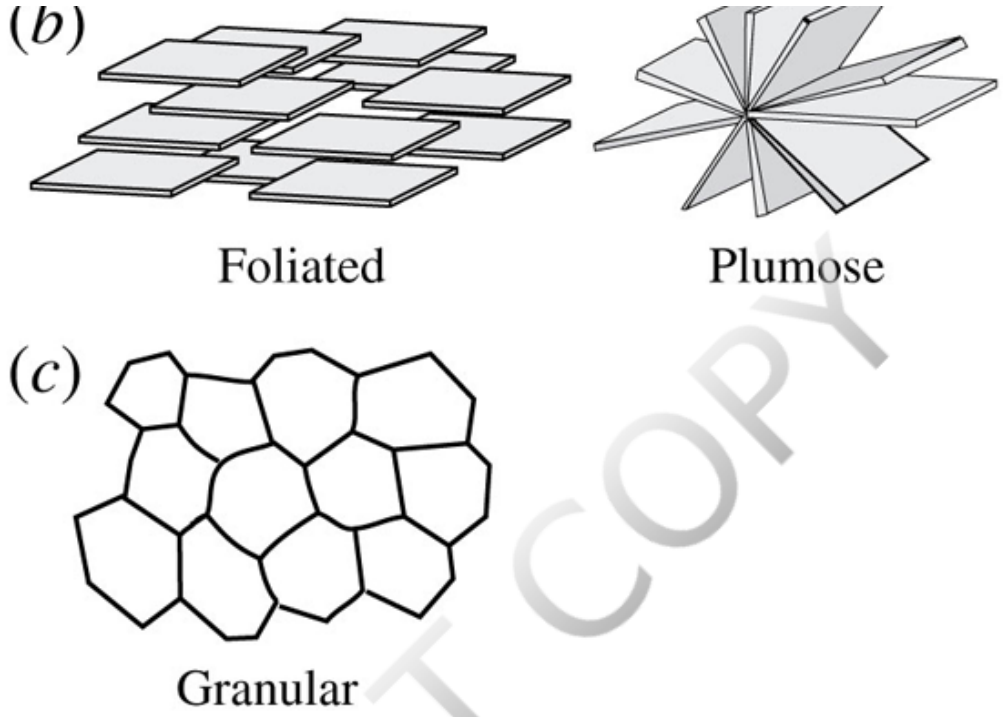

FIGURE 2.51 Patterns of mineral growth. (*a*) Elongate minerals can form parallel, radiating, or felted masses. (*b*) Platy or micaceous minerals can form foliated or plumose arrangements. (*c*) Equant minerals can form fine- to coarse-grained granular masses. Back to text

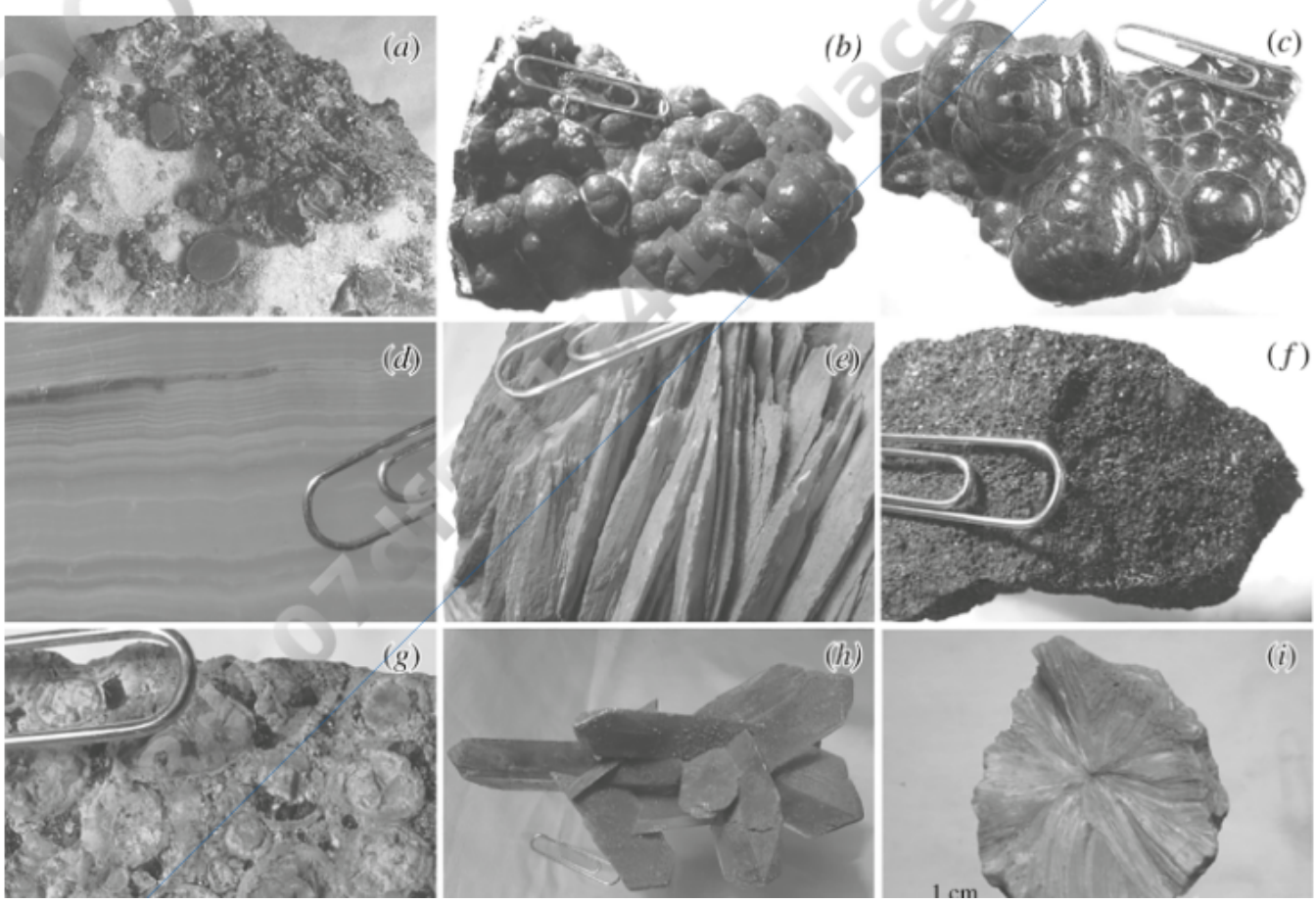

DO NOT COPY

Printed by: e48d507df5d1141@placeholder.94092.edu. Printing is for personal, private use only. No part of this book may be reproduced or transmitted without publisher's prior permission. Violators will be prosecuted.

Chapter 3 Crystal Chemistry

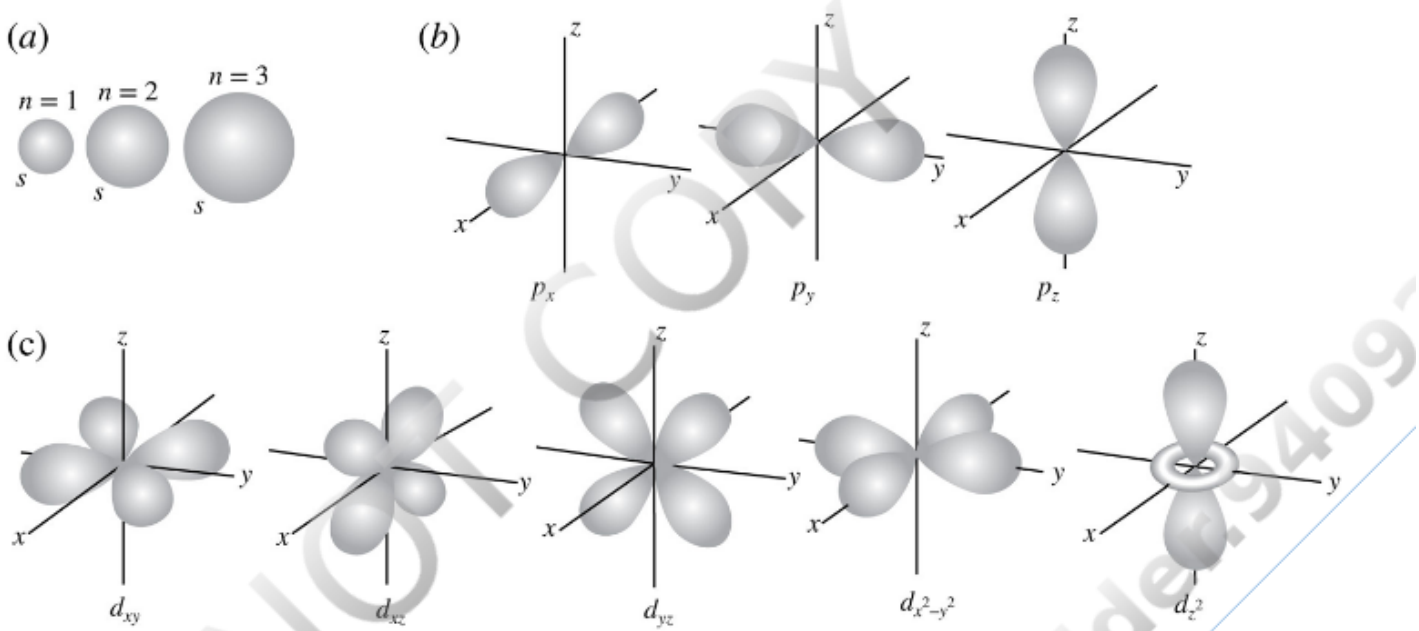

FIGURE 3.1 Geometry of orbitals in the *s*, *p*, and *d* subshells. Orbitals represent the volume around a nucleus in which an electron is most probably located. (*a*) Orbitals in the *s* subshells are spherical in all shells. (*b*) The *p* subshell contains three different bilobate orbitals oriented along orthogonal *x*, *y*, and *z* axes. (*c*) The *d* subshell contains five orbitals. The d_{xy}, d_{xz}, and d_{yz} orbitals are quadralobate and lie in the *xy*, *xz*, and *yz* planes, respectively, so that they bisect the angles between the orthogonal axes. The orbital forms a quadralobate shape with lobes aligned along the *x* and *y* axes. The orbital forms a torus with a bilobate shape aligned along the *z* axis. Back to text

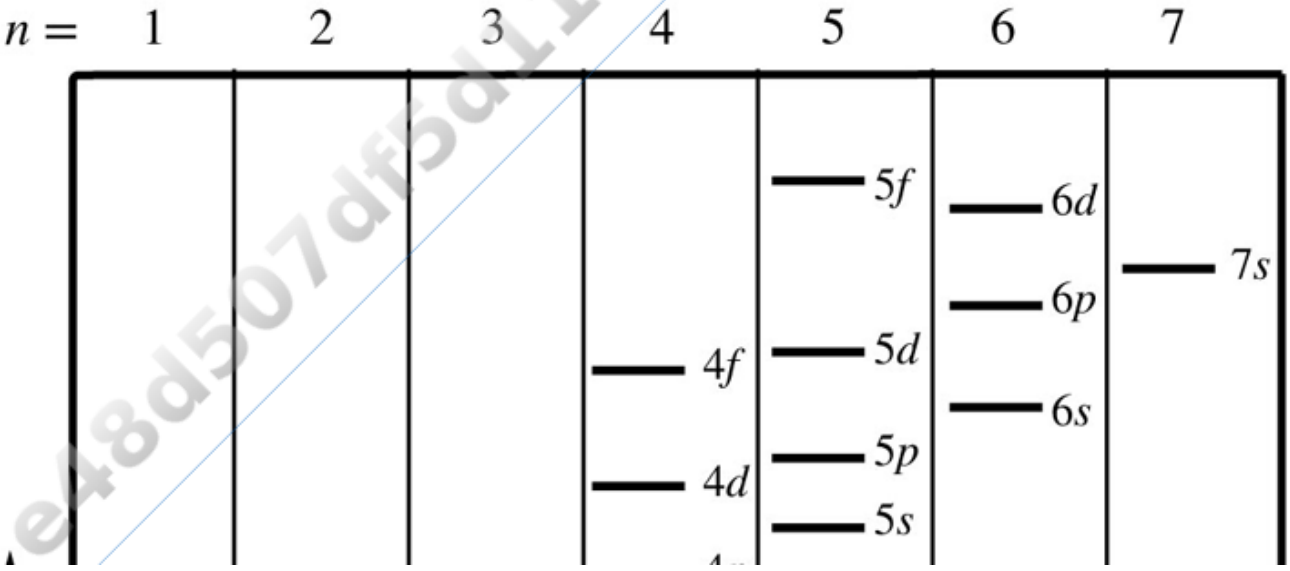

DO NOT COPY e48d507df5d1141@placeholder.94092

Printed by: e48d507df5d1141@placeholder.94092.edu. Printing is for personal, private use only. No part of this book may be reproduced or transmitted without publisher's prior permission. Violators will be prosecuted.

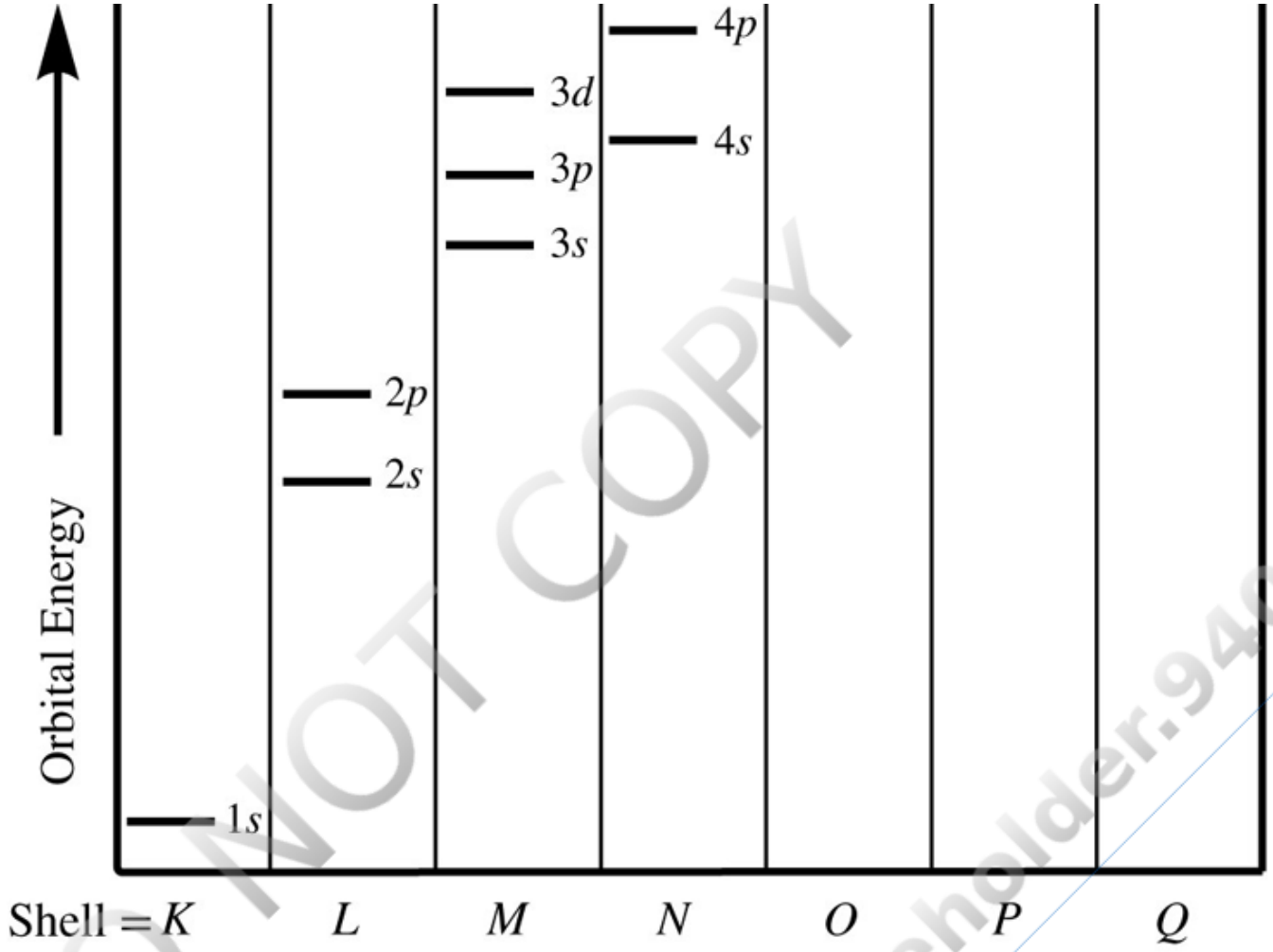

FIGURE 3.2 Relative energy level of electron subshells. Electrons fill subshells in order of increasing energy level (compare to Table 3.3). Back to text

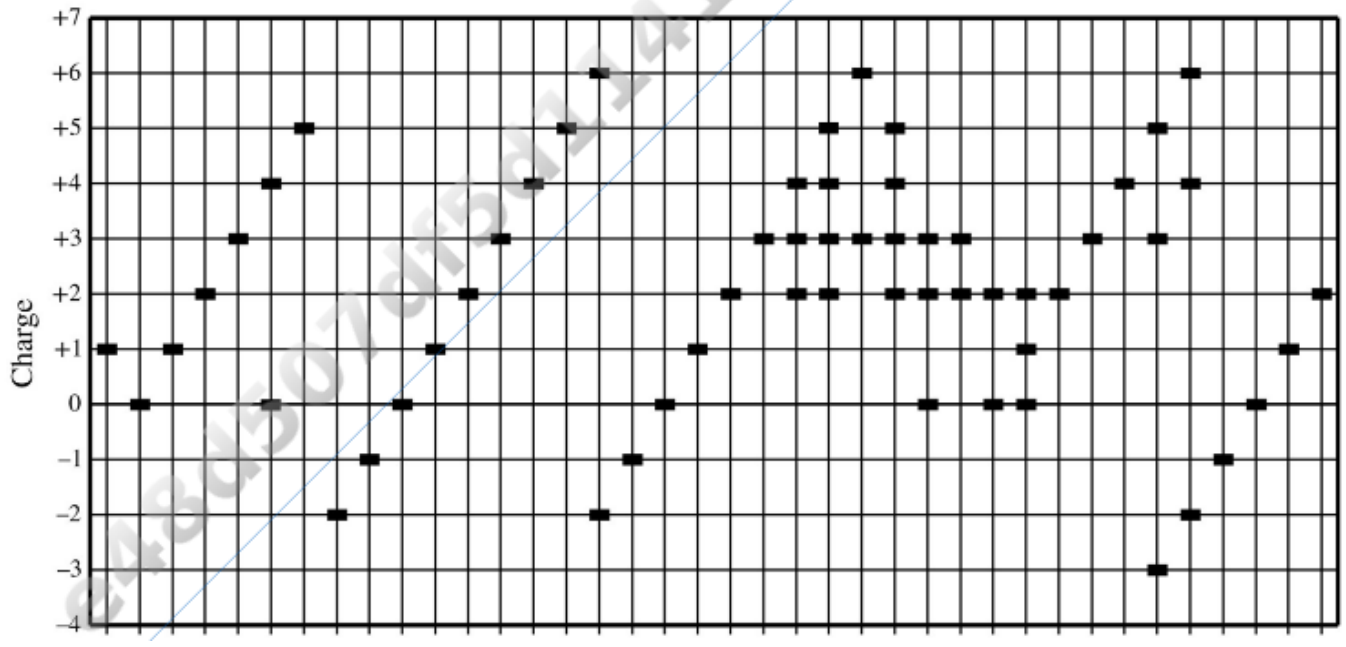

DO NOT COPY
e48d507df5d1141@placeholder.9409

Printed by: e48d507df5d1141@placeholder.94092.edu. Printing is for personal, private use only. No part of this book may be reproduced or transmitted without publisher's prior permission. Violators will be prosecuted.

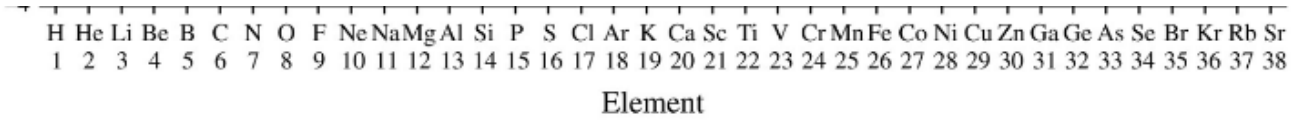

FIGURE 3.3 Common oxidation states of elements 1 through 38. Back to text

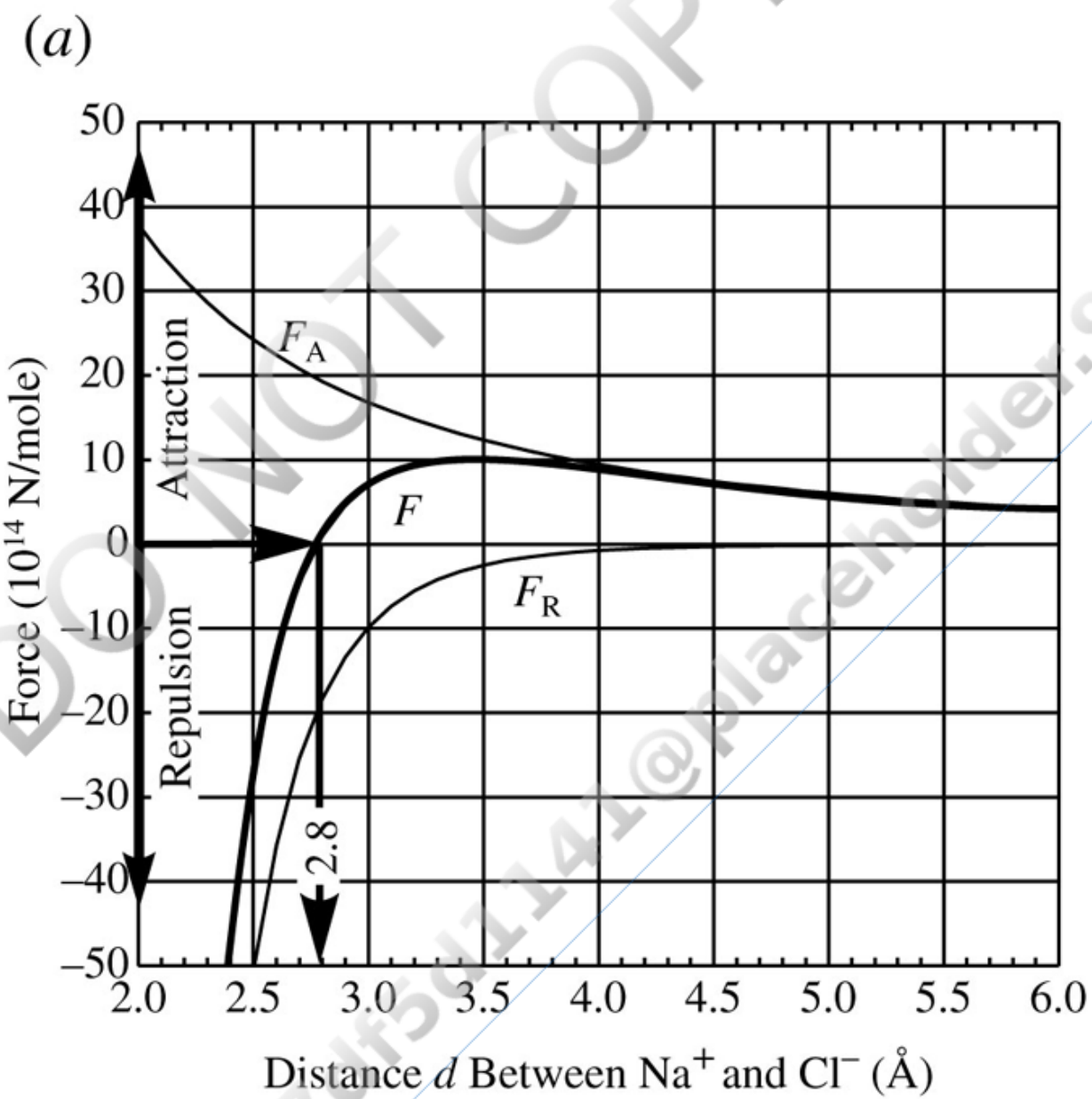

DO NOT COPY
e48d507df5d1141@placeholder.9409

Printed by: e48d507df5d1141@placeholder.94092.edu. Printing is for personal, private use only. No part of this book may be reproduced or transmitted without publisher's prior permission. Violators will be prosecuted.

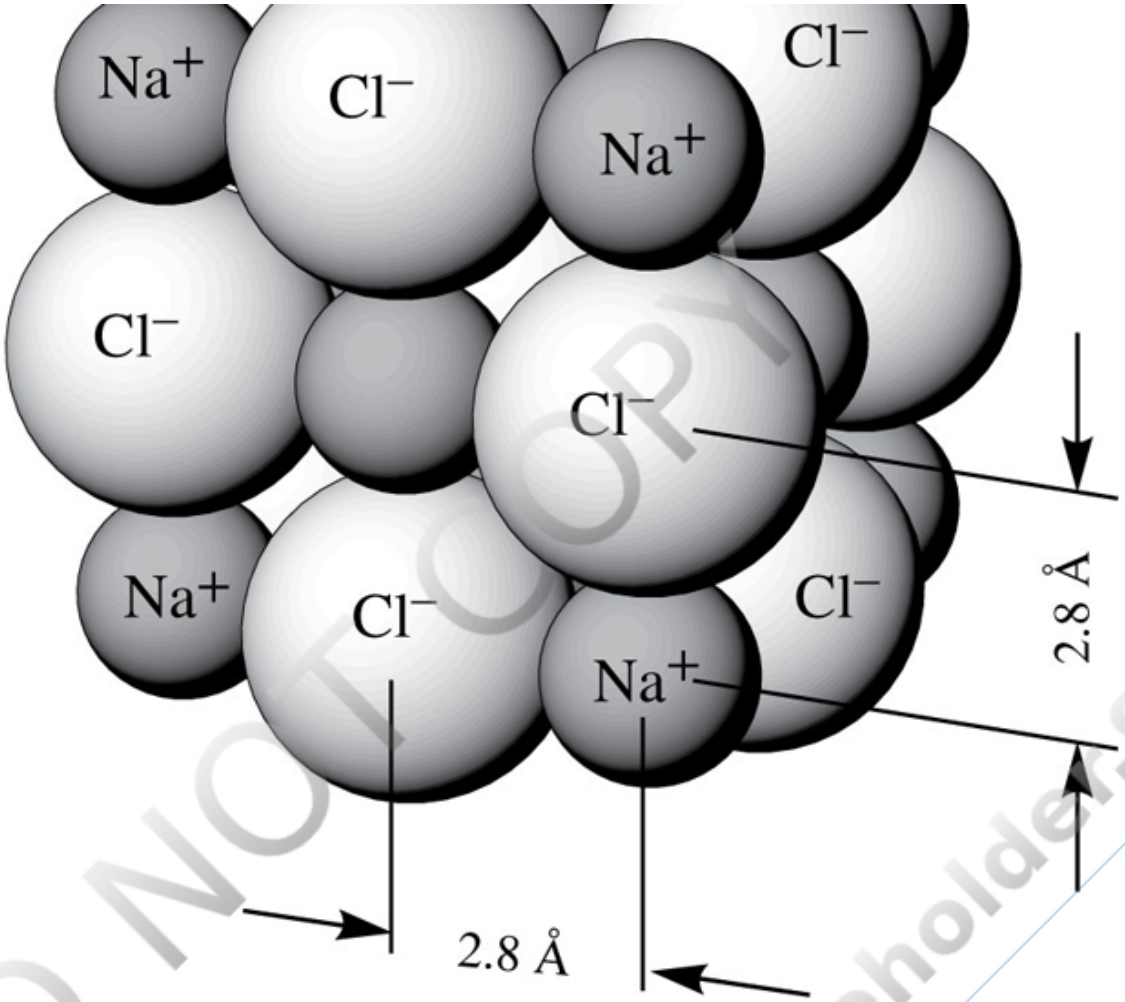

FIGURE 3.4 Ionic bonding between Na^+ and Cl^-. (*a*) The attractive F_A and repulsive F_R forces between Na^+ and Cl^- ions. The net force F is zero when the centers of the ions are at a distance of about 2.8 Å. At greater distances there is a net attraction and at a smaller distance a net repulsion. (*b*) Na^+ and Cl^- ions pack together in a face-centered cubic lattice with a spacing of about 2.8 Å.
Back to text

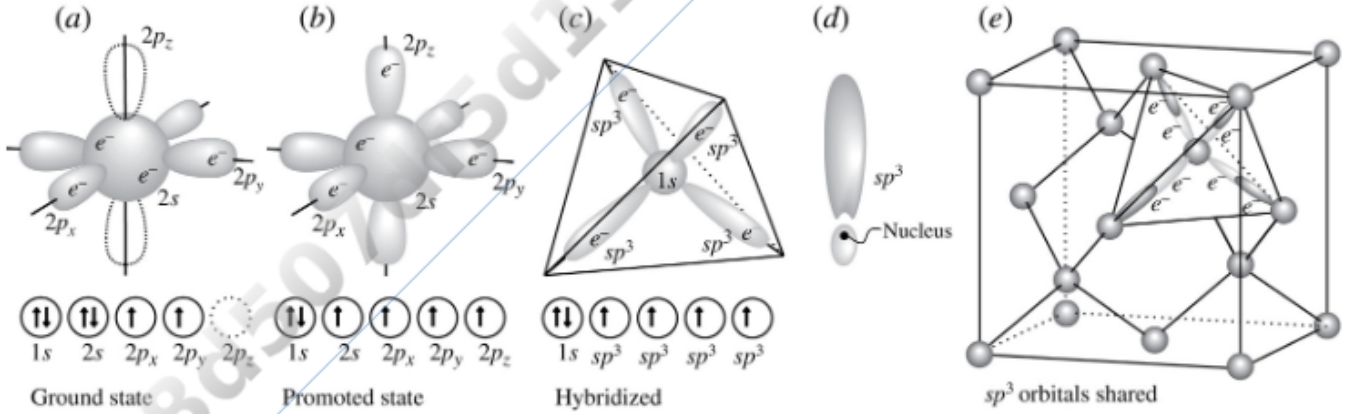

FIGURE 3.5 Formation of carbon covalent sigma (σ) bonds in diamond. (*a*) Ground-state electron configuration of carbon. The 2*s* orbital contains two electrons, the $2p_x$ and $2p_y$ orbitals each contain one electron, and the $2p_z$ orbital is vacant. (*b*) One electron from the 2*s* orbital is promoted to the

Printed by: e48d507df5d1141@placeholder.94092.edu. Printing is for personal, private use only. No part of this book may be reproduced or transmitted without publisher's prior permission. Violators will be prosecuted.

one electron, and the $2p_z$ orbital is vacant. (*b*) One electron from the 2*s* orbital is promoted to the $2p_z$ orbital so that four orbitals are partially filled. (*c*) Hybridization of the half-filled orbitals into four identical sp^3 orbitals arranged to point to the corners of a tetrahedron. (*d*) Each sp^3 orbital consists of a large lobe with a small lobe on the opposite side of the nucleus. The small lobes are not shown in (*c*). (*e*) Bonding of carbon atoms in diamond by sharing electrons between hybridized $2sp^3$ orbitals on adjacent atoms. Four pairs of overlapping sp^3 orbitals reaching a carbon atom are shown; similar bonds occur along each of the solid lines. The small lobes are omitted for clarity. Back to text

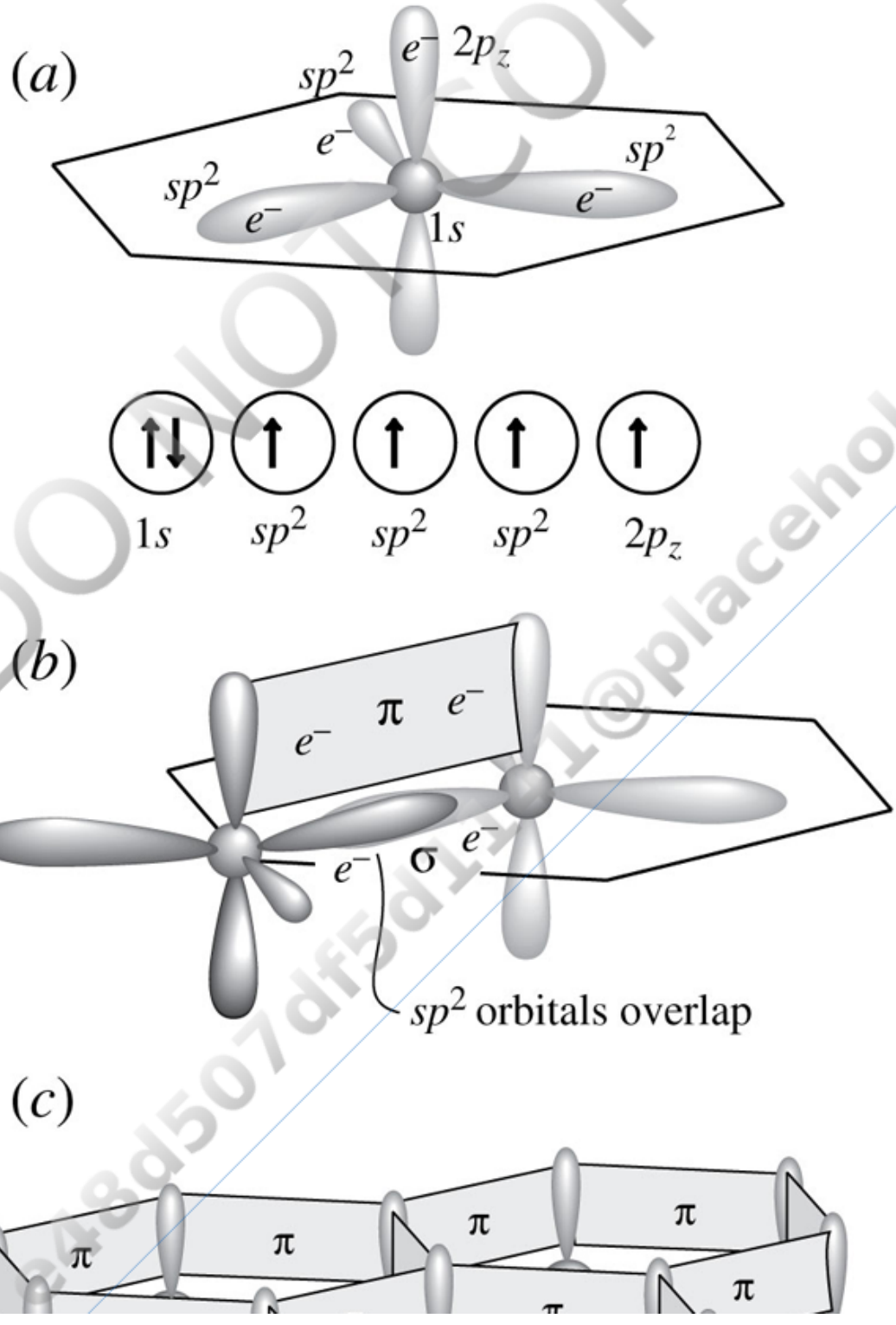

DO NOT COPY e48d507df5d1141@placeholder.94092

Printed by: e48d507df5d1141@placeholder.94092.edu. Printing is for personal, private use only. No part of this book may be reproduced or transmitted without publisher's prior permission. Violators will be prosecuted.

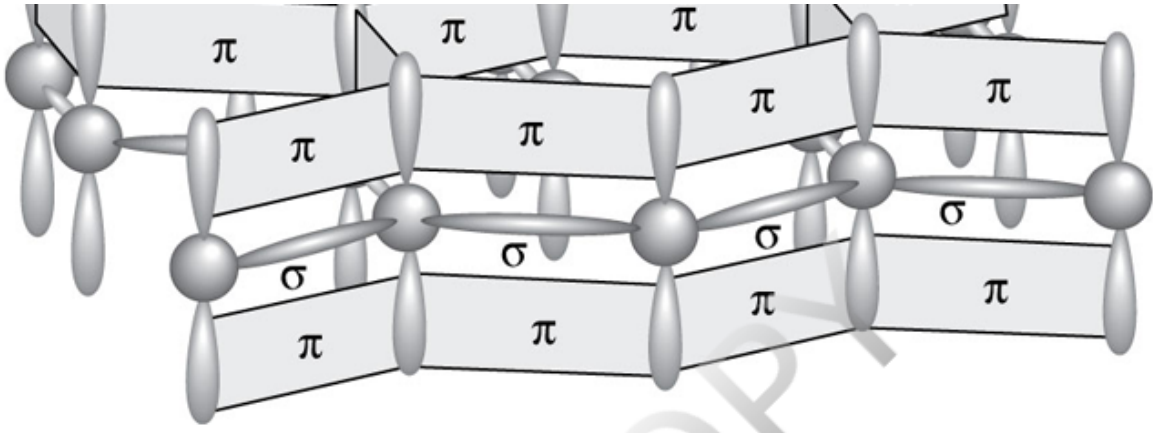

FIGURE 3.6 Formation of covalent σ and π bonds with carbon in graphite. The ground and promoted states of carbon are shown in Figure 3.5a and b. (*a*) Hybridization of orbitals forms three sp^2 orbitals with the $2p_z$ orbital at right angles. (*b*) σ Bonds form by sharing electrons between sp^2 orbitals from adjacent C atoms. π Bonds are formed by sharing electrons laterally between the $2p_z$ orbitals. (*c*) Carbon bonds to form continuous sheets. The π bonds form on both the top and bottom of the sheet, but only those in the front are shown on the bottom. Back to text

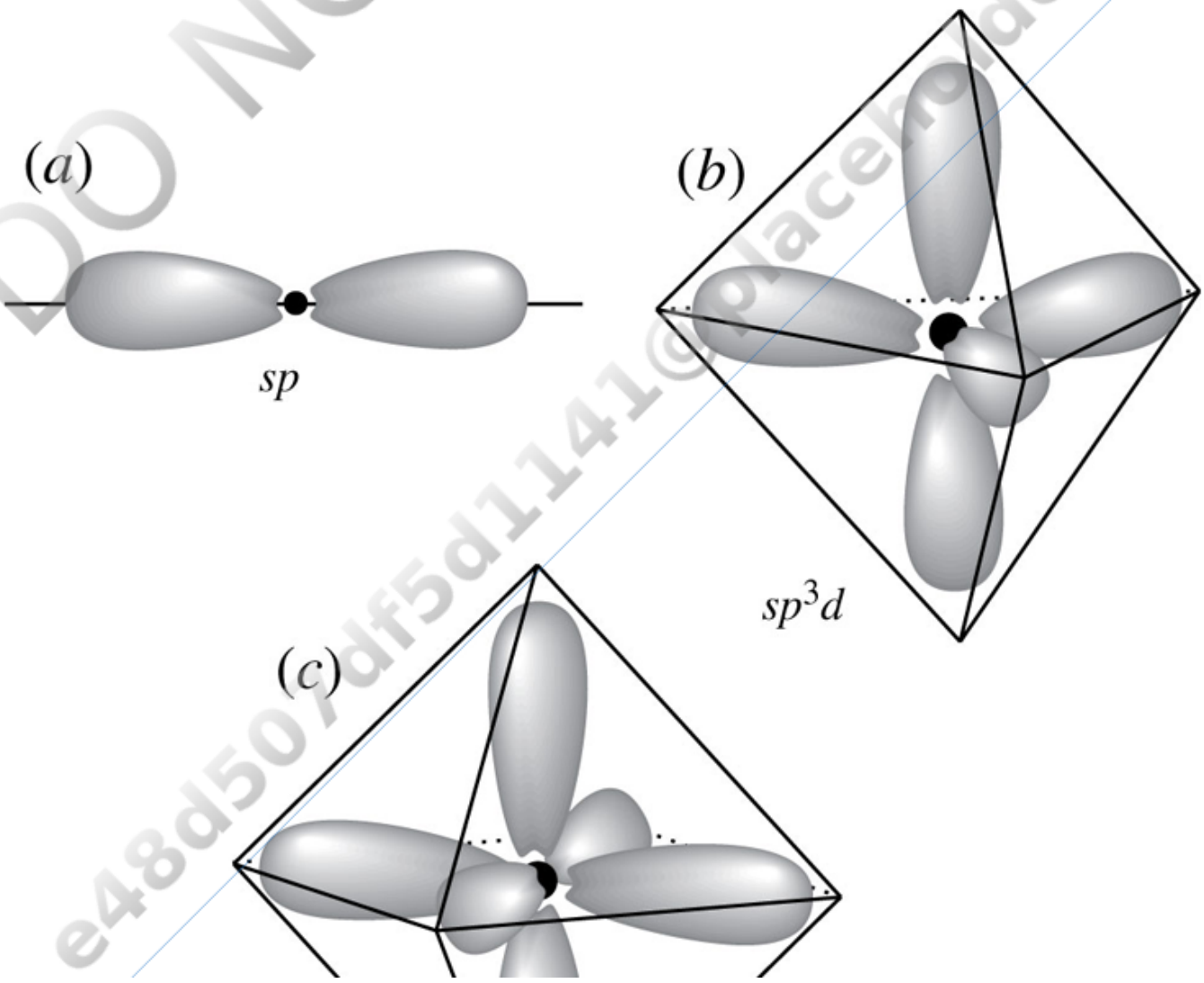

DO NOT COPY
e48d507df5d1141@placeholder.9409

Printed by: e48d507df5d1141@placeholder.94092.edu. Printing is for personal, private use only. No part of this book may be reproduced or transmitted without publisher's prior permission. Violators will be prosecuted.

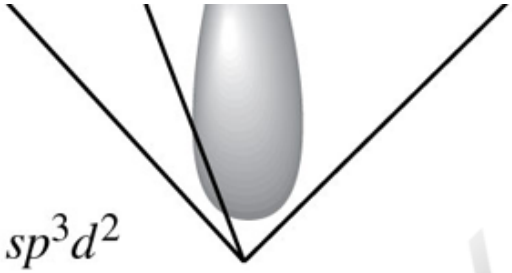

FIGURE 3.7 Hybrid orbitals. Each consists of a large and small lobe (Figure 3.5d); only the large lobe is shown. (*a*) Hybrid *sp* orbital formed from an *s* orbital and a single *p* orbital. (*b*) Hybrid sp^3d orbitals formed from an *s*, three *p*, and a *d* orbital. (*c*) Hybrid sp^3d^2 orbitals formed from an *s*, three *p*, and two *d* orbitals. Back to text

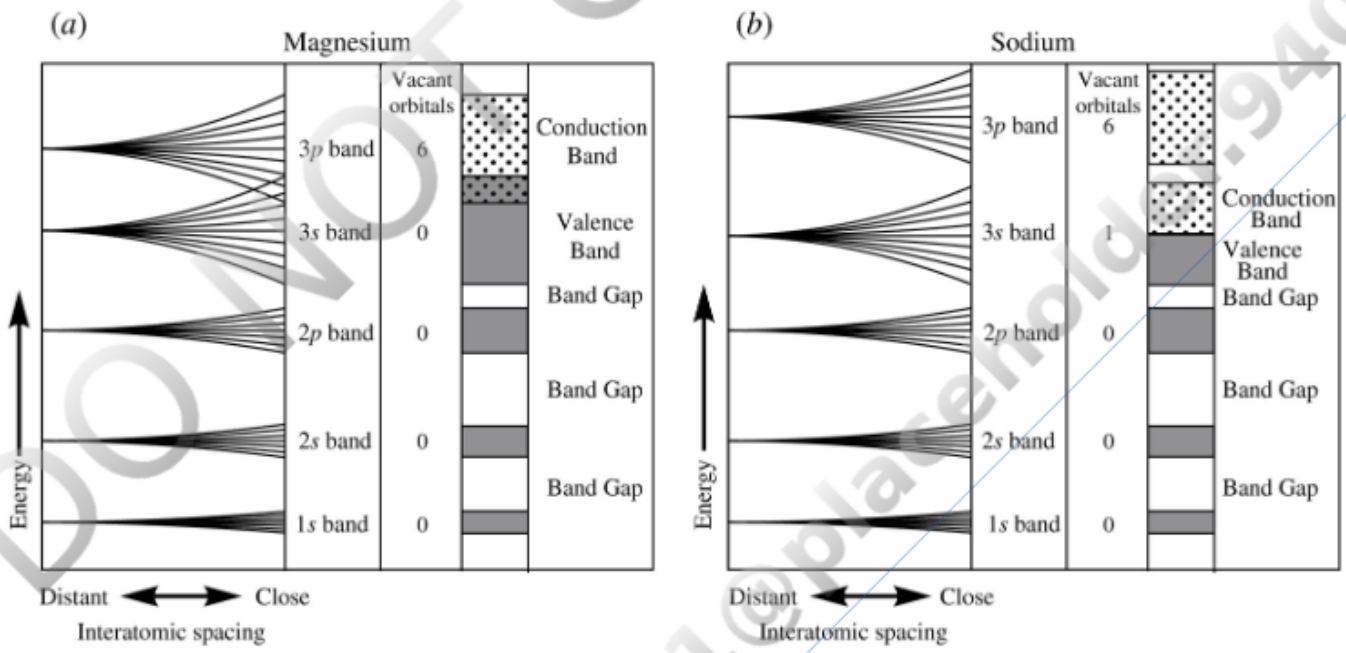

FIGURE 3.8 Energy bands form when atoms are brought into close proximity. (*a*) Magnesium. Energy levels of the 3*s* and 3*p* subshells spread into bands that overlap. Electrons from the 3*s* subshell (the valence band) can move into unoccupied energy levels of the 3*p* subshell and therefore move freely throughout the structure. (*b*) Sodium. Energy levels of electrons in the 3*s* subshell spread into a band when sodium atoms are packed together to form sodium metal but do not overlap with other bands. However, orbitals in the 3*s* subshell are only half-filled, so electrons can move into vacant energy levels and therefore move freely throughout the structure. The 3*s* subshell serves as both the valence and conduction bands. Back to text

DO NOT COPY
e48d507df5d1141@placeholder.9409

Printed by: e48d507df5d1141@placeholder.94092.edu. Printing is for personal, private use only. No part of this book may be reproduced or transmitted without publisher's prior permission. Violators will be prosecuted.

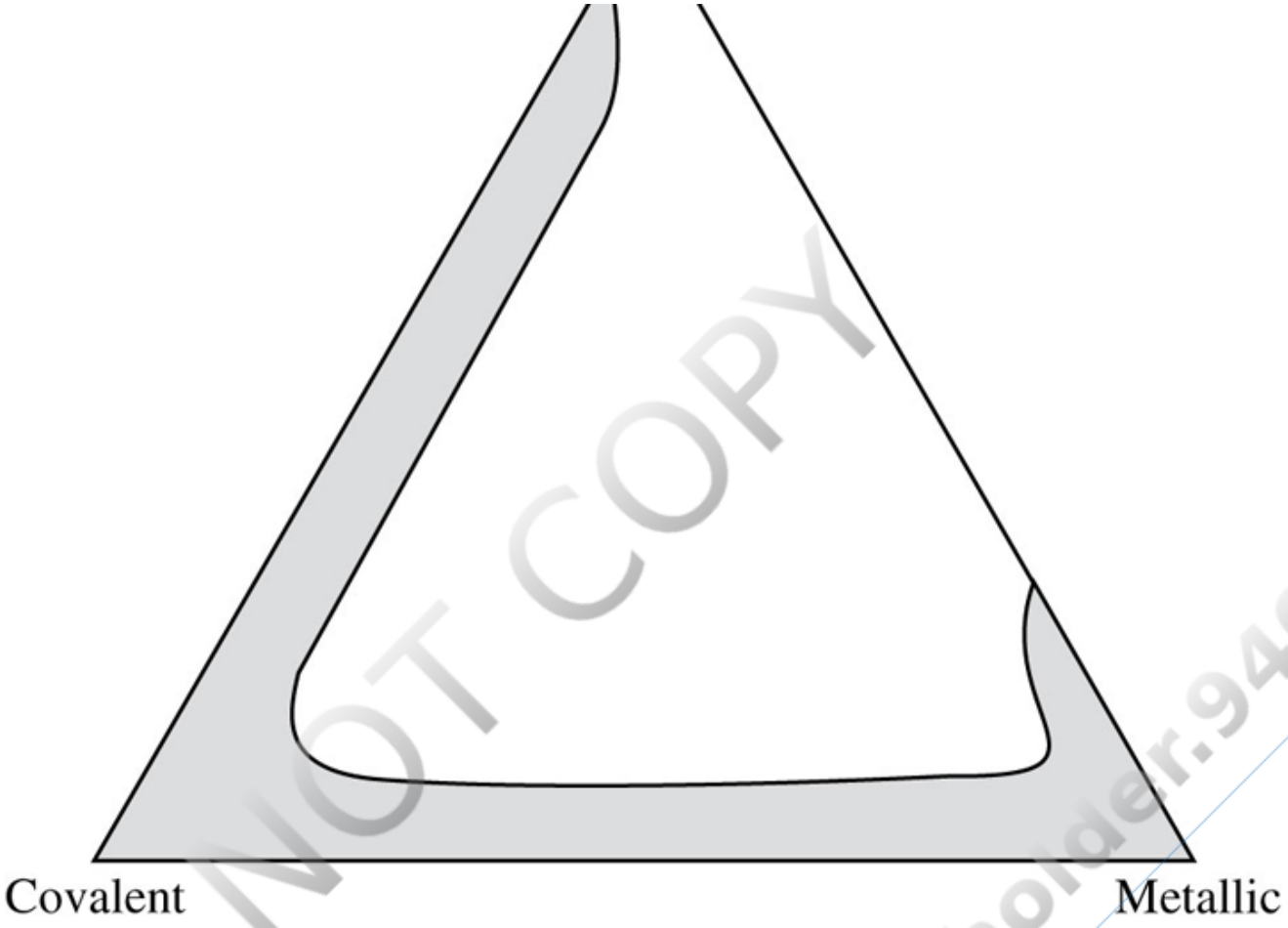

FIGURE 3.9 Range of bond character (shaded) found in valance-dependent bonding. Continuous variation exists between ionic and covalent bonds and between covalent and metallic bonds. Limited ionic character is found in metallic bonds between different metals. Back to text

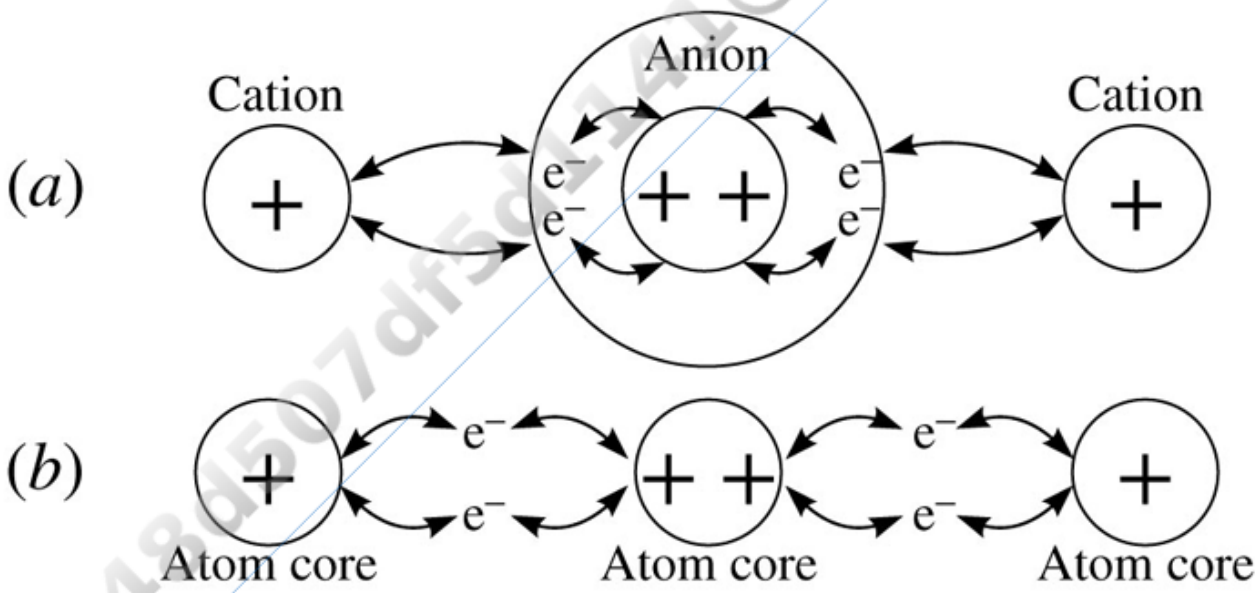

FIGURE 3.10 Conceptual model of ionic and covalent bonding. (*a*) Ionic bonding. A valence electron from each monovalent cation pairs with a valence electron from a divalent anion to satisfy

Printed by: e48d507df5d1141@placeholder.94092.edu. Printing is for personal, private use only. No part of this book may be reproduced or transmitted without publisher's prior permission. Violators will be prosecuted.

electron from each monovalent cation pairs with a valence electron from a divalent anion to satisfy valence requirements—the bonding electrons reside on the anion. Bonding is achieved because the positively charged cations are attracted to the negative charge of the valence electrons in the anion. (*b*) Covalent bonding. The bonding electron pairs are located, at least on average, between the atoms, and the atom cores each get a net positive charge. The positively charged core of each atom is attracted to the concentration of shared electrons in the space between them. In the general case where bonding is intermediate between the ionic and covalent, the average position of the valence electrons can be considered to be intermediate between being centered on the anion and being centered halfway between atoms. Adapted from Brown (2002). Back to text

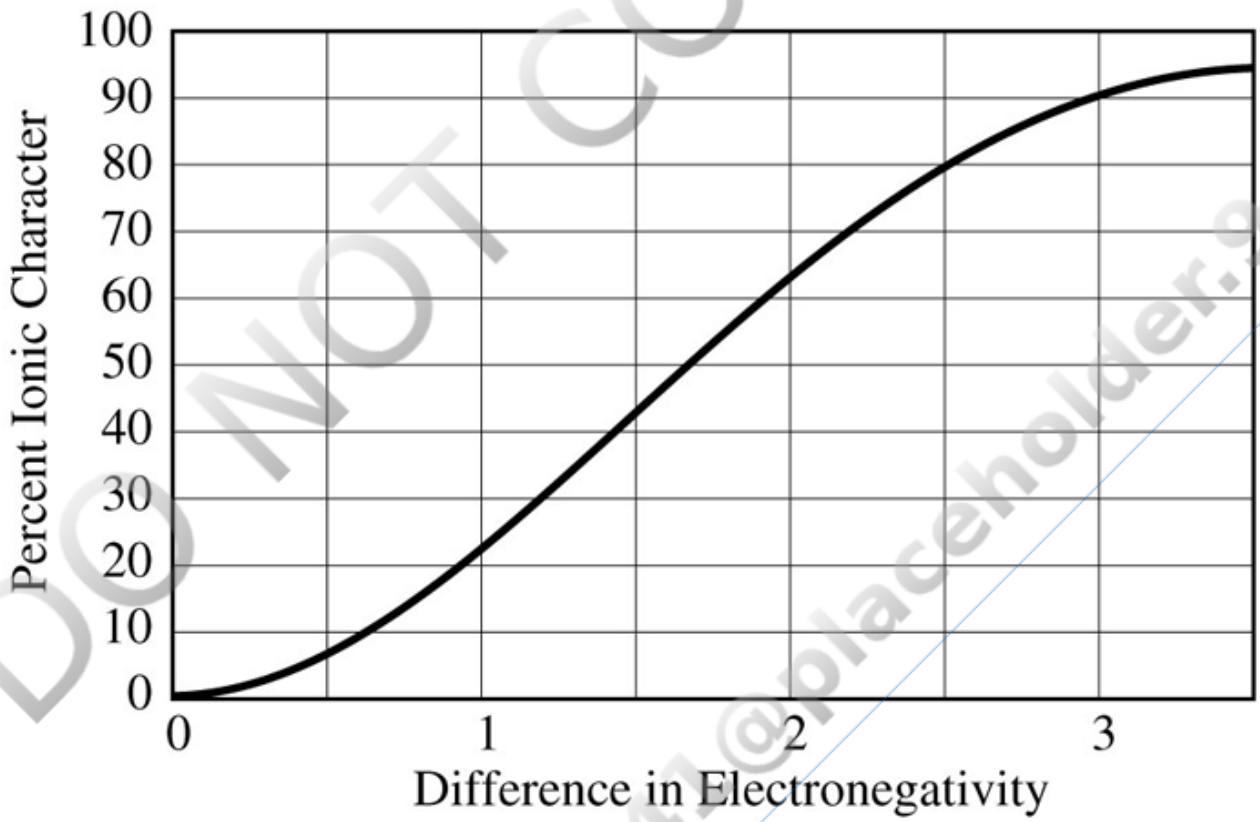

FIGURE 3.11 Curve showing the relationship between difference in electronegativity and degree of ionic character. See Table 3.4 for values of electronegativity. Back to text

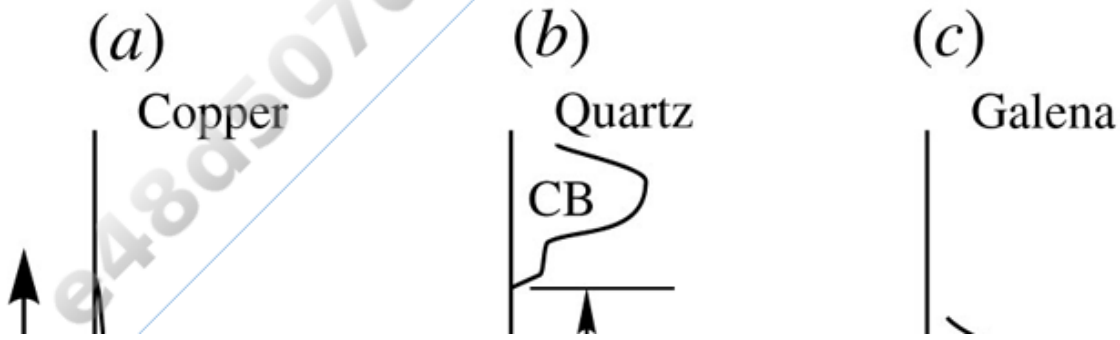

DO NOT COPY
e48d507df5d1141@placeholder.9409

Printed by: e48d507df5d1141@placeholder.94092.edu. Printing is for personal, private use only. No part of this book may be reproduced or transmitted without publisher's prior permission. Violators will be prosecuted.

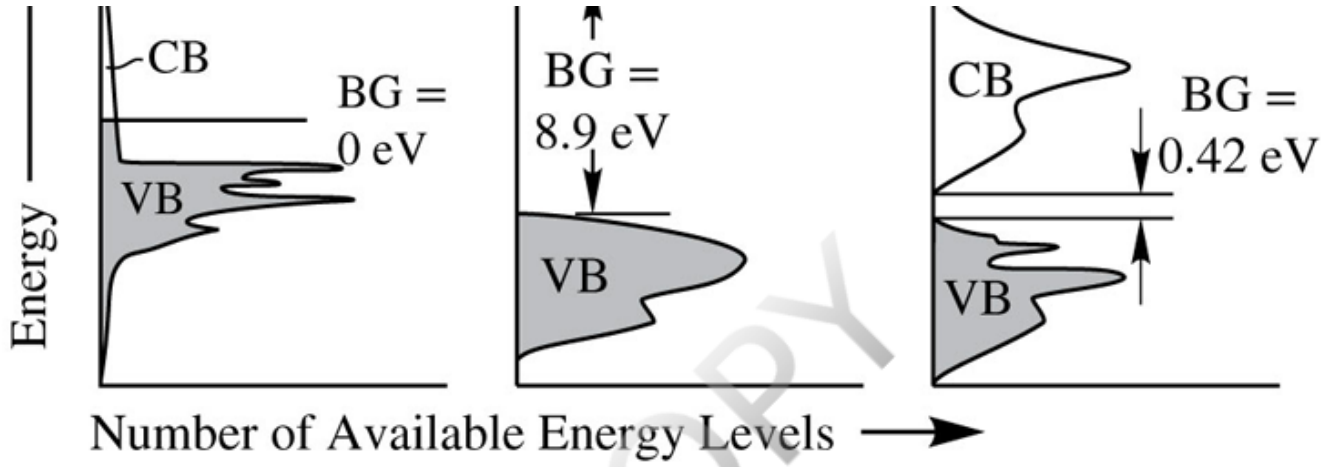

FIGURE 3.12 Band energies. Valence bands (VB) filled with electrons are shaded; the unfilled conduction bands (CB) are unshaded. (*a*) Conductor. No band gap (BG) is present between the valence and conduction bands of copper (Janak and others, 1975). (*b*) Insulator. A band gap of ~8.9 eV is present between the valence and conduction bands of quartz (Garvie and others, 2000). (*c*) Semiconductor. A band gap of only 0.42 eV is present between the valence and conduction bands of galena (Walsh, 2011). Back to text

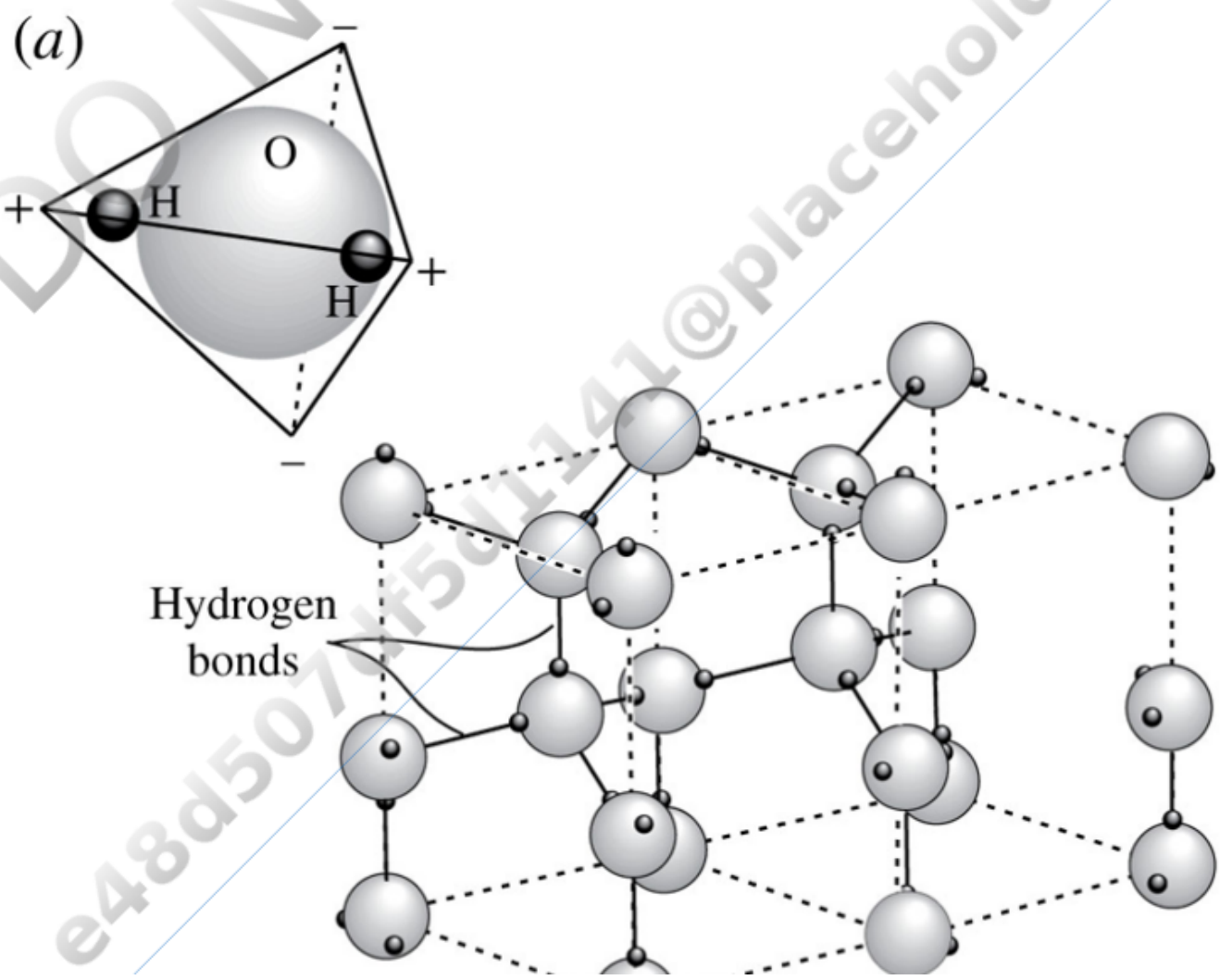

DO NOT COPY
e48d507df5d1141@placeholder.9409

Printed by: e48d507df5d1141@placeholder.94092.edu. Printing is for personal, private use only. No part of this book may be reproduced or transmitted without publisher's prior permission. Violators will be prosecuted.

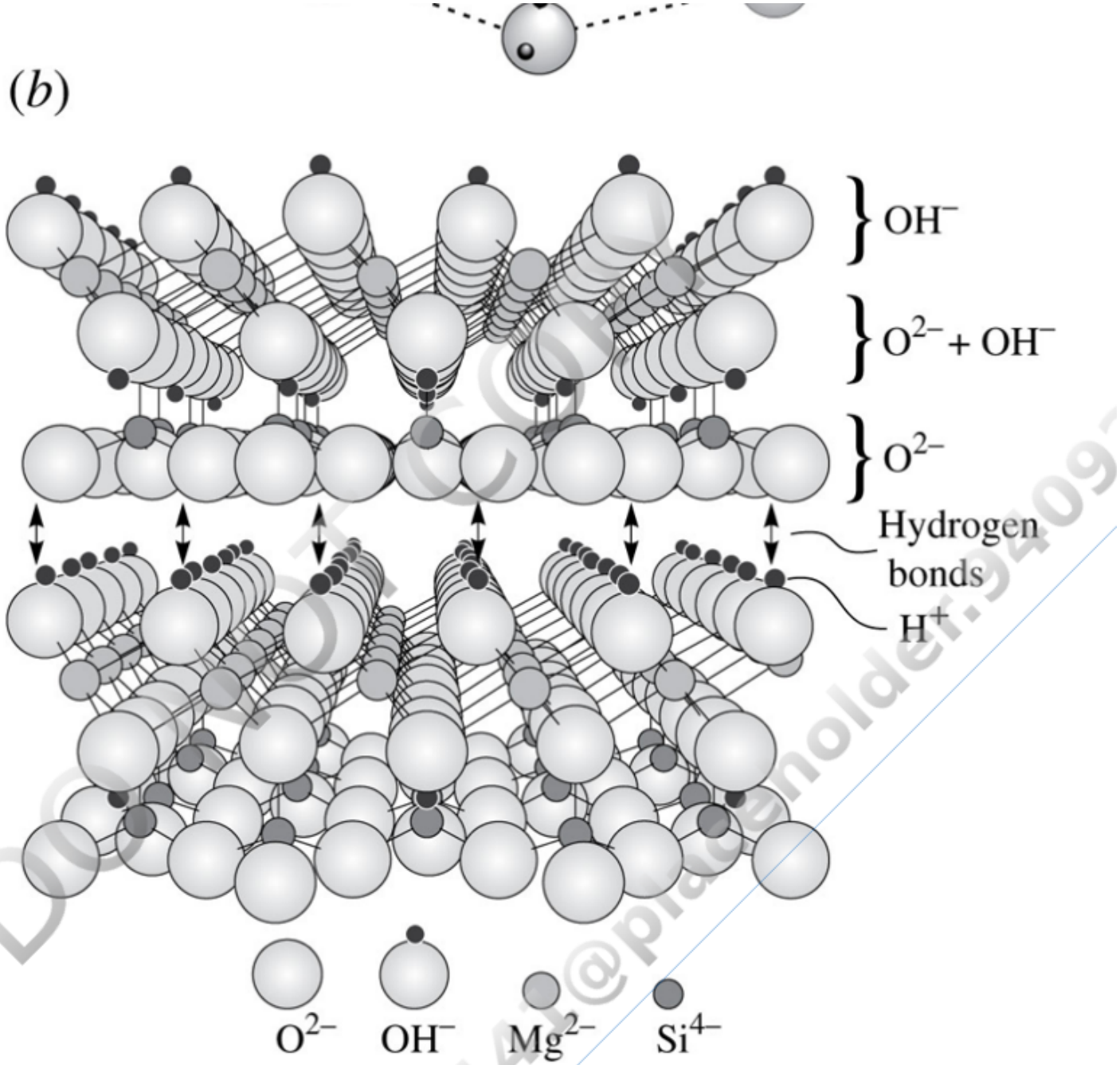

FIGURE 3.13 Hydrogen bonding. (*a*) Ice. A polar H_2O molecule is formed by covalent/ionic bonds between H and O using the 2*p* orbitals in the O. The O has greater claim on the electrons, so the H consists of little more than its positively charged nucleus, a single proton. Charge is tetrahedrally distributed—positive at the H^+ ions and negative at nodes on the opposite side of the oxygen. Each negative node on the molecule is attracted to a positive node (an H^+ ion) on an adjacent H_2O molecule to form a hydrogen bond that holds the water molecules together. Two unit cells are outlined with dashed lines. (*b*) Serpentine. The structure consists of layers made of three planes of O^{2-} and OH^- which bond with Mg^{2-} and Si^{4+} in the interstices to satisfy all valence requirements. Adjacent layers bond to each other because positively charged H^+ on the top surface of one layer face the negatively charged O^{2-} on the bottom of the adjacent layer. The opposite charges attract, producing a hydrogen bond. Back to text

Printed by: e48d507df5d1141@placeholder.94092.edu. Printing is for personal, private use only. No part of this book may be reproduced or transmitted without publisher's prior permission. Violators will be prosecuted.

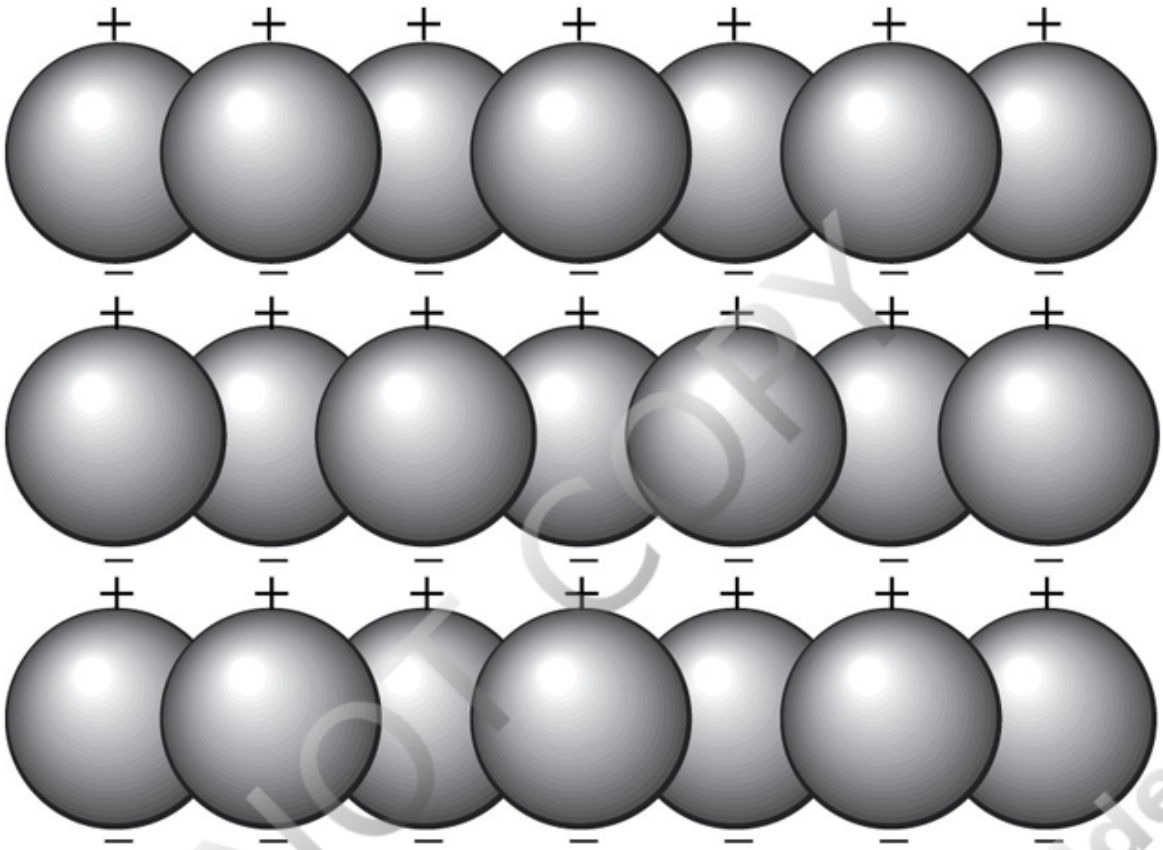

FIGURE 3.14 Van der Waals bonding. Sheets of carbon are bonded internally by π and σ covalent bonds (Figure 3.6). At any instant, more negatively charged electrons are on one side of a sheet than the other, producing a polarization. The polarization of one sheet produces a similar polarization in its neighbors. Van der Waals bonds are produced by the weak electrostatic attraction between the opposite charges on the surfaces of adjacent sheets at any instant. Back to text

DO NOT COPY e48d507df5d1141@placeholder.9409

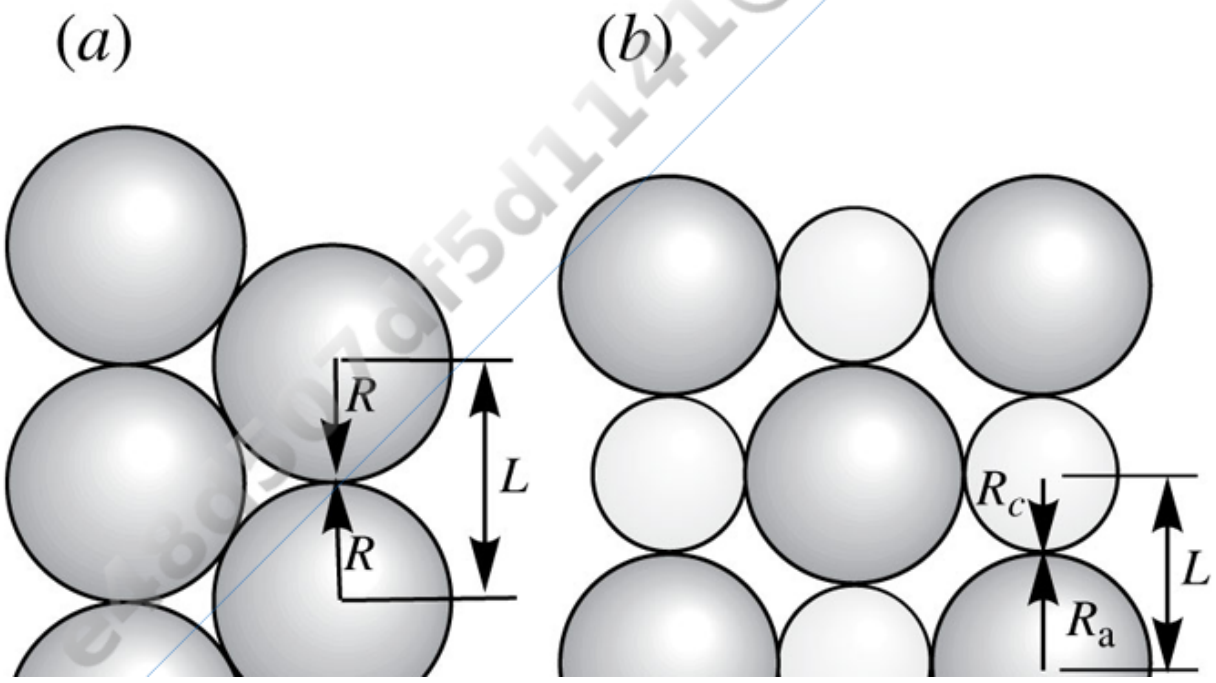

Printed by: e48d507df5d1141@placeholder.94092.edu. Printing is for personal, private use only. No part of this book may be reproduced or transmitted without publisher's prior permission. Violators will be prosecuted.

FIGURE 3.15 Bond length and effective radius. (*a*) Close-packed metal atoms of uniform size. The bond length (L) is twice the effective atomic radius R. (*b*) Anions and cations of different size. The bond length (L) is the sum of the effective ionic radii of the cation (R_c) and anion (R_a). Back to text

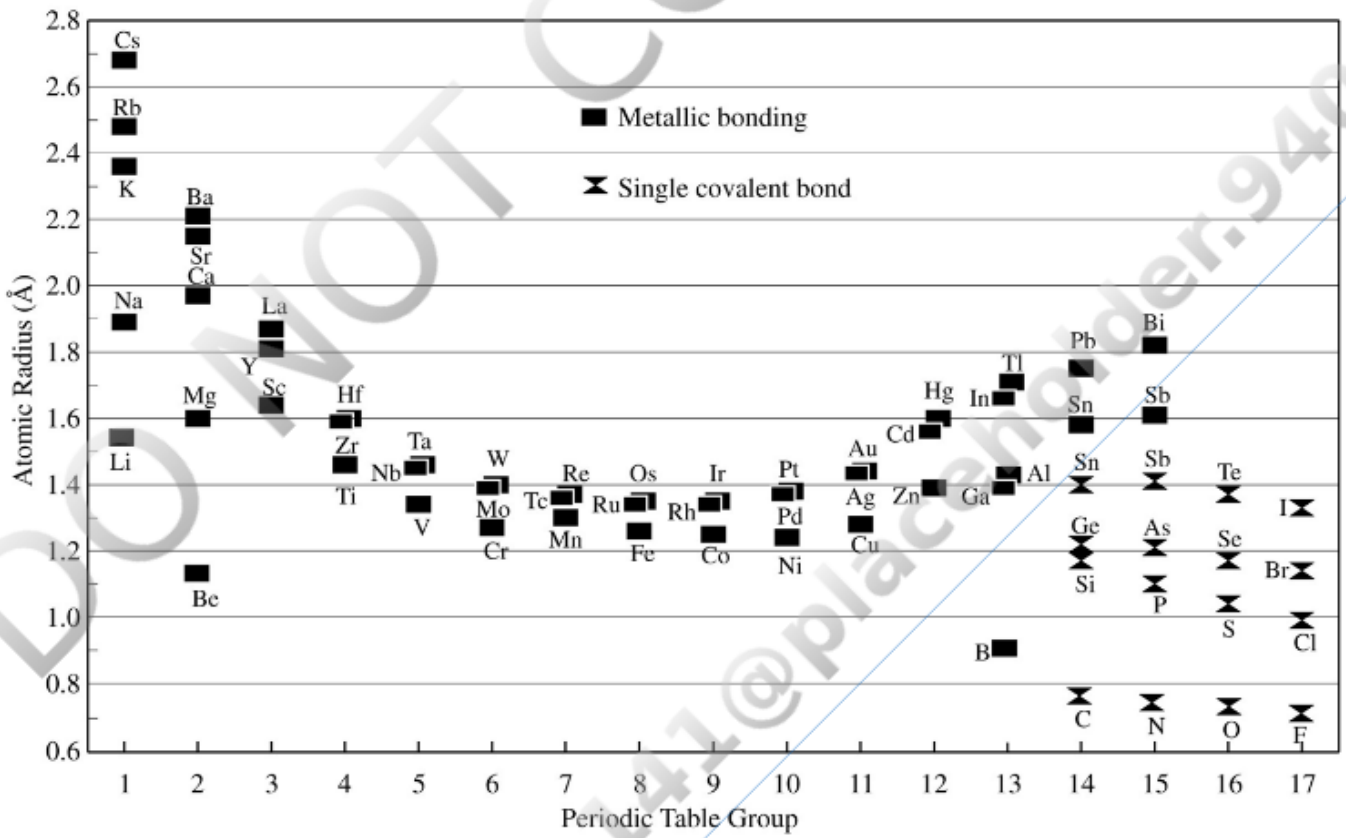

FIGURE 3.16 Effective atomic radii for the elements. The lanthanide and actinide series and noble gases are omitted. Elements with metallic bonding are closely packed and in contact with 12 other atoms. Elements that do not form metallic bonds are shown for a single covalent bond. Data from Zhdanov (1965). Back to text

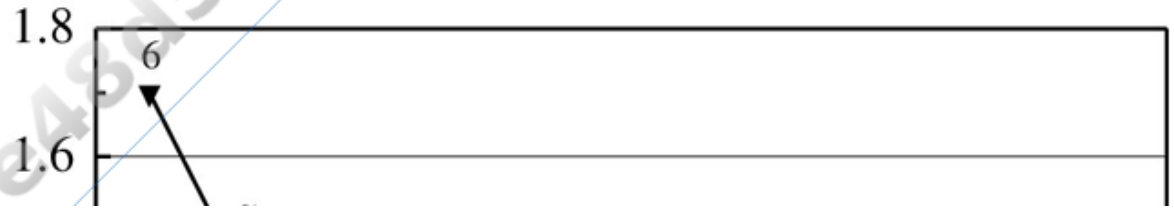

DO NOT COPY
e48d507df5d1141@placeholder.9409

Printed by: e48d507df5d1141@placeholder.94092.edu. Printing is for personal, private use only. No part of this book may be reproduced or transmitted without publisher's prior permission. Violators will be prosecuted.

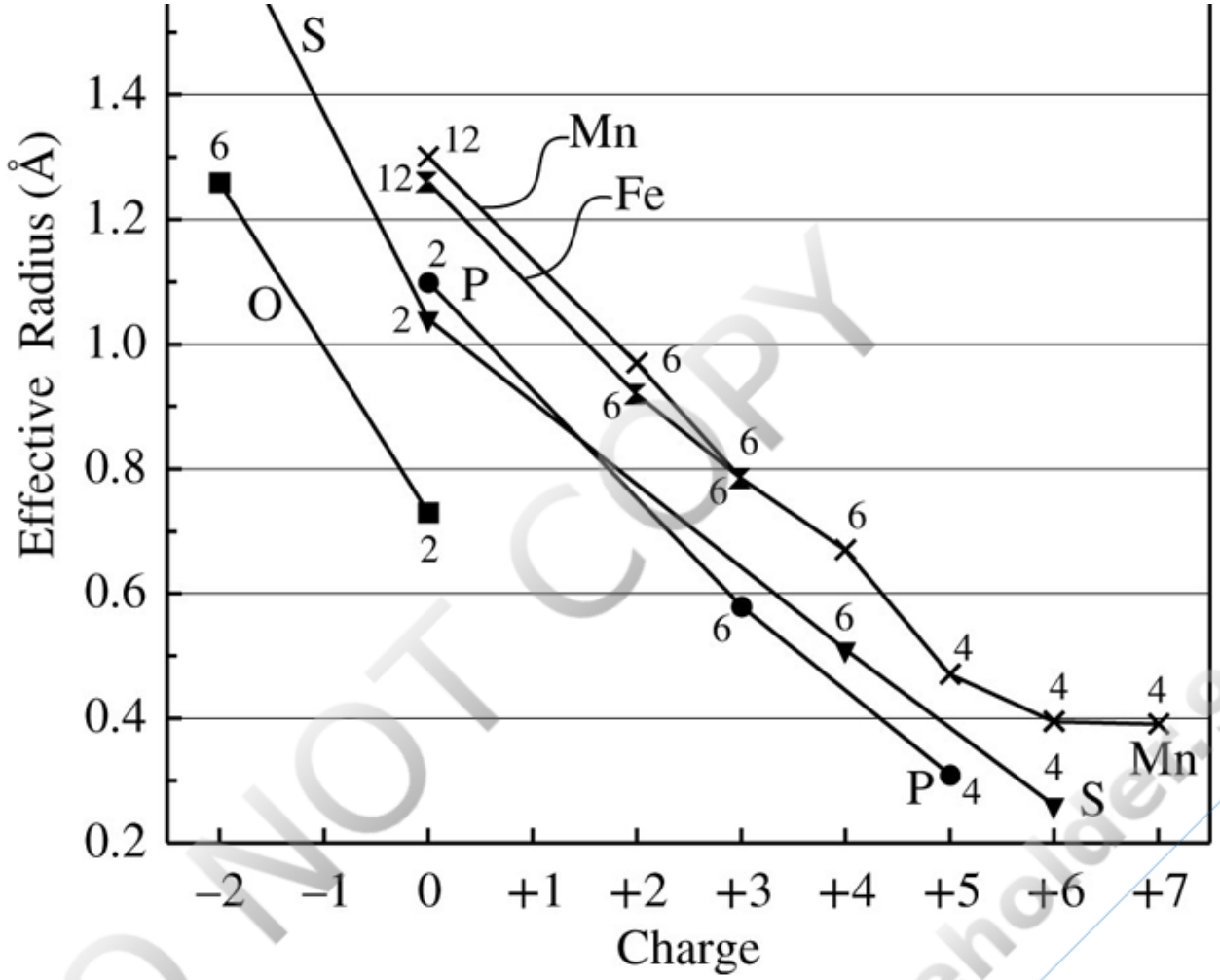

FIGURE 3.17 Effective radii as a function of oxidation state (charge) for oxygen (O), sulfur (S), phosphorus (P), manganese (Mn), and iron (Fe), elements that occur in different oxidation states. The coordination number is indicated by each symbol. Data from Appendix A and Figure 3.16. Back to text

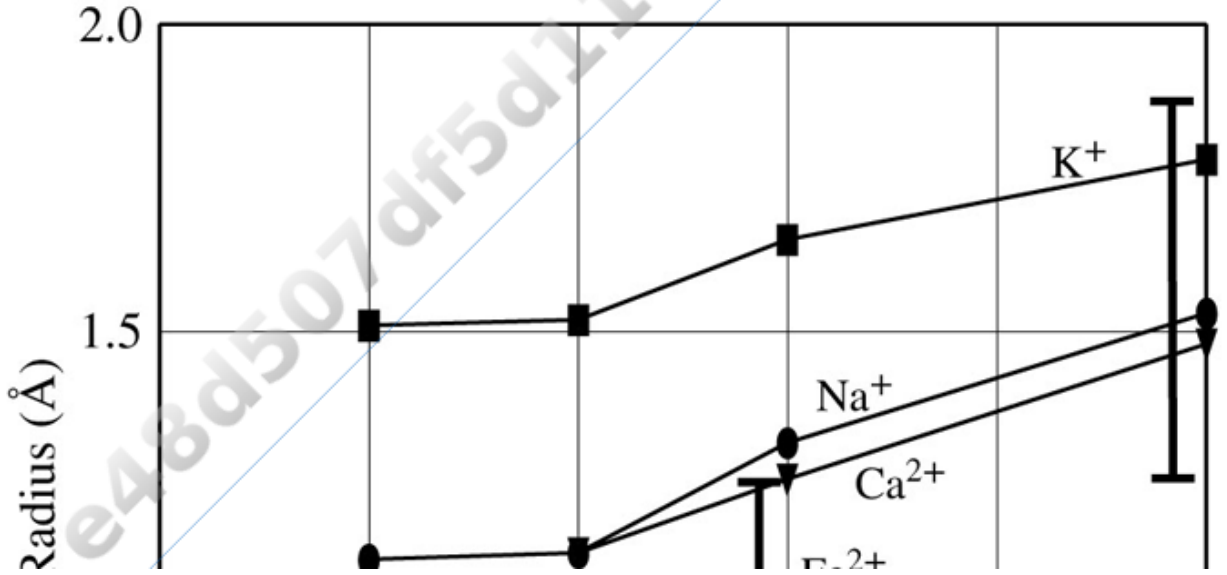

DO NOT COPY
e48d507df5d1141@placeholder.9409

Printed by: e48d507df5d1141@placeholder.94092.edu. Printing is for personal, private use only. No part of this book may be reproduced or transmitted without publisher's prior permission. Violators will be prosecuted.

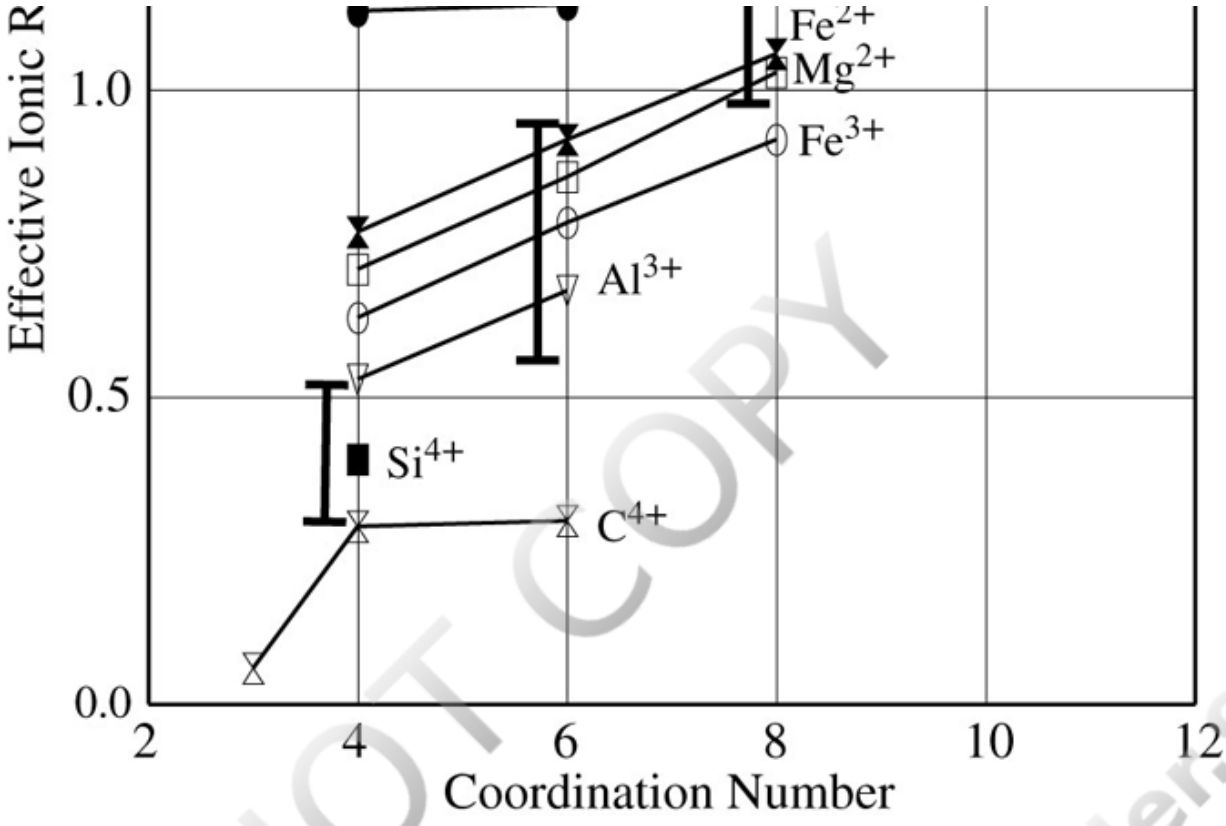

FIGURE 3.18 Effective ionic radii of the common cations as a function of coordination number. The normal ranges of cation sizes that will fit into 4-, 6-, 8-, and 12-fold coordination with oxygen are shown by bars (compare Table 4.1). Data from Appendix A. Back to text

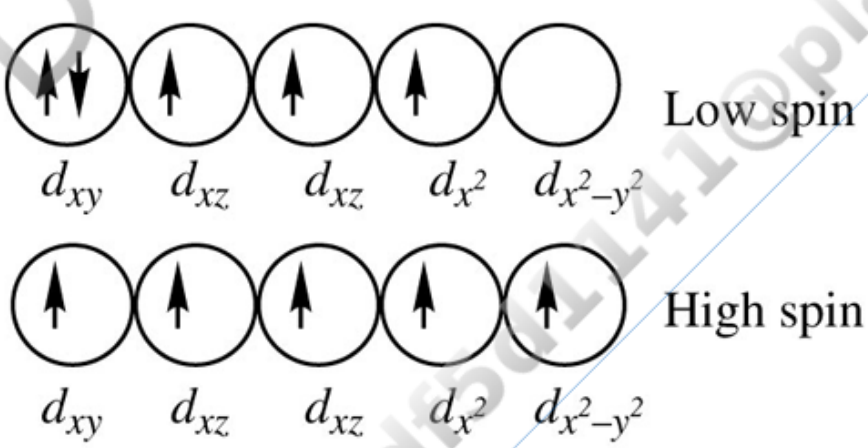

FIGURE 3.19 Spin configuration in Fe^{3+}. (*a*) Low spin. Electrons are paired in the d_{xy} orbital even though the $3d_{x^2-y^2}$ orbital is vacant. (*b*) High spin. No electrons are paired in the orbitals. Back to text

DO NOT COPY
e48d507df5d1141@placeholder.9409

Printed by: e48d507df5d1141@placeholder.94092.edu. Printing is for personal, private use only. No part of this book may be reproduced or transmitted without publisher's prior permission. Violators will be prosecuted.

Chapter 4 Crystal Structure

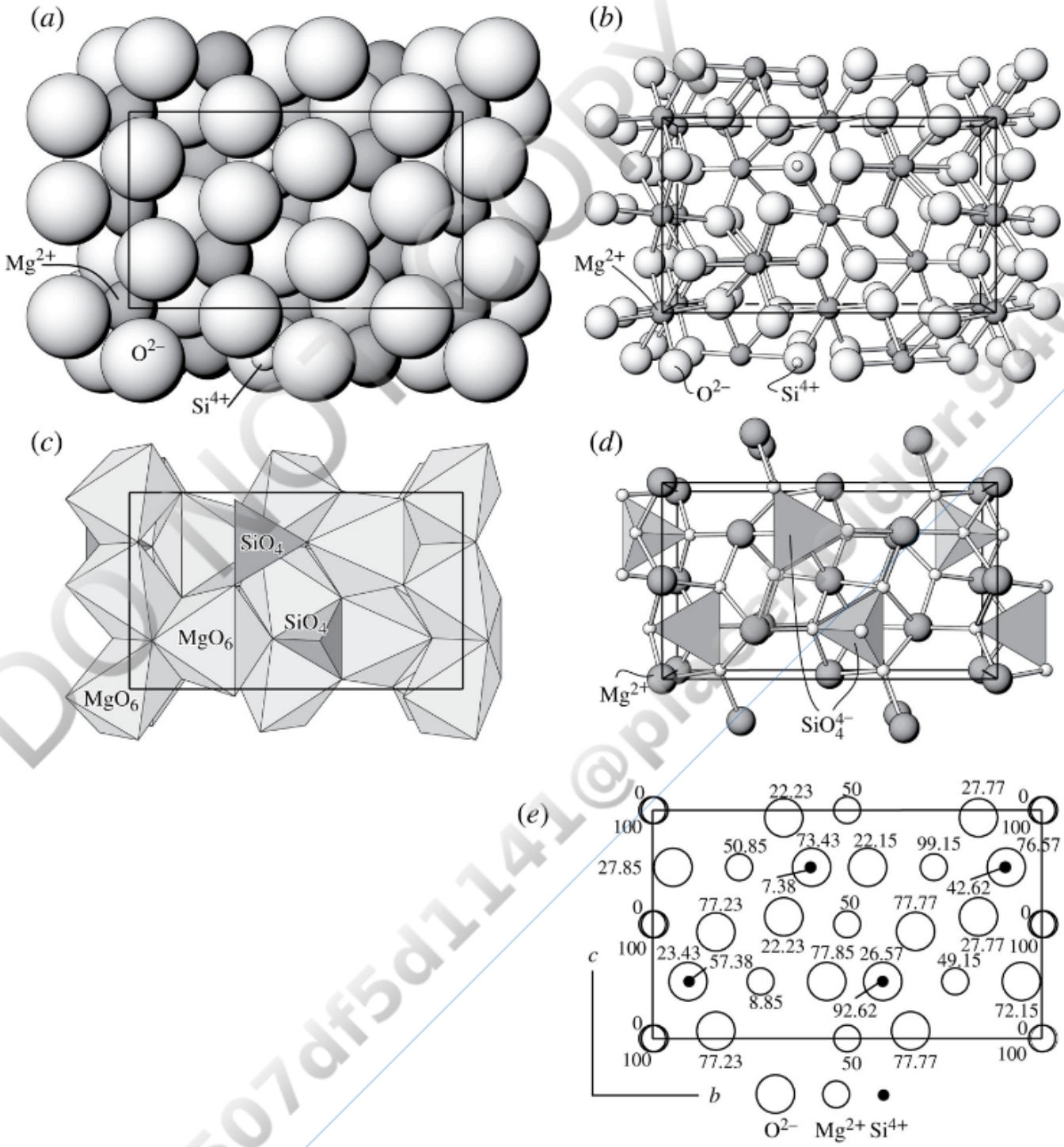

FIGURE 4.1 Illustration of olivine (Mg_2SiO_4) crystal structure viewed down the *a* axis. Each unit cell is outlined. (*a*) Scaled spheres: O^{2-} Mg^{2+}, and Si^{4+} are large, medium, and small spheres, respectively. (*b*) Ball-and-stick. Sphere size is reduced and the sticks represent bonding. (*c*) Polyhedral. Only the polyhedral framework is shown. The Si^{4+} and Mg^{2+} cations are inferred to be at the centers of the tetrahedra (dark) and octahedra (light), respectively. Oxygen anions are inferred to be at the corners of the polyhedra. (*d*) Hybrid model using both polyhedra and ball-and-stick. O^{2-} are

Printed by: e48d507df5d1141@placeholder.94092.edu. Printing is for personal, private use only. No part of this book may be reproduced or transmitted without publisher's prior permission. Violators will be prosecuted.

be at the corners of the polyhedra. (*d*) Hybrid model using both polyhedra and ball-and-stick. O are shown as small spheres at corners of the tetrahedra. (*e*) "Mapped" structure. The height of the ions above the back surface of the unit cell is given as a percentage of the *a* unit cell dimension. The outlines of the Mg^{2+} at the corners of the unit cell are offset slightly so that all atoms are visible. Back to text

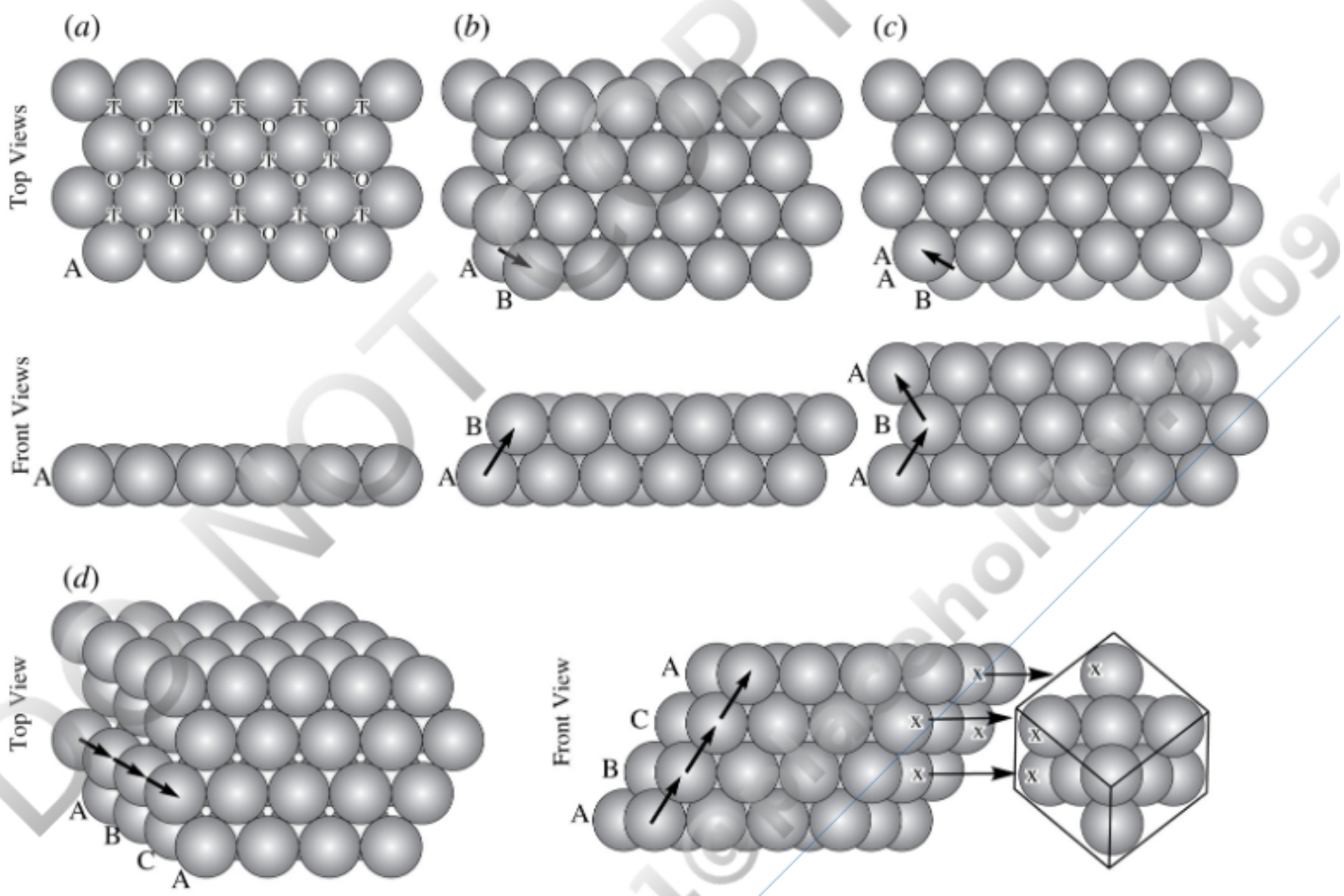

FIGURE 4.2 Closest packing of spheres. (*a*) Close-packed layer of spheres (A). Each sphere is in contact with six neighbors. The T and O sites that will be formed when the B layer is placed on top of A are indicated. (*b*) Second layer of spheres (B) stacked on top of the first so that the spheres nestle into the T sites. The T site is surrounded by four spheres and the O sites are surrounded by six spheres. (*c*) Hexagonal close packing is produced when a third layer is stacked directly above the first. The layers of spheres therefore alternate ABAB ... and are parallel to the (001) plane in the hexagonal lattice. (*d*) Cubic close packing of spheres. Instead of shifting back and forth between two positions, each successive layer is shifted in the same direction. The first two layers of spheres (A and B) are the same as with hexagonal close packing. The C layer is shifted in the same direction as B, so the C spheres are directly above the O sites in the A layer. An additional shift in the same direction places the spheres in the top layer (A) directly above those in the initial A layer. The layers of spheres therefore alternate ABCABC ... and are parallel to the (111) plane in a face-centered cubic lattice. The spheres marked *x* define the corners on one face of the cube. Back to text

Printed by: e48d507df5d1141@placeholder.94092.edu. Printing is for personal, private use only. No part of this book may be reproduced or transmitted without publisher's prior permission. Violators will be prosecuted.

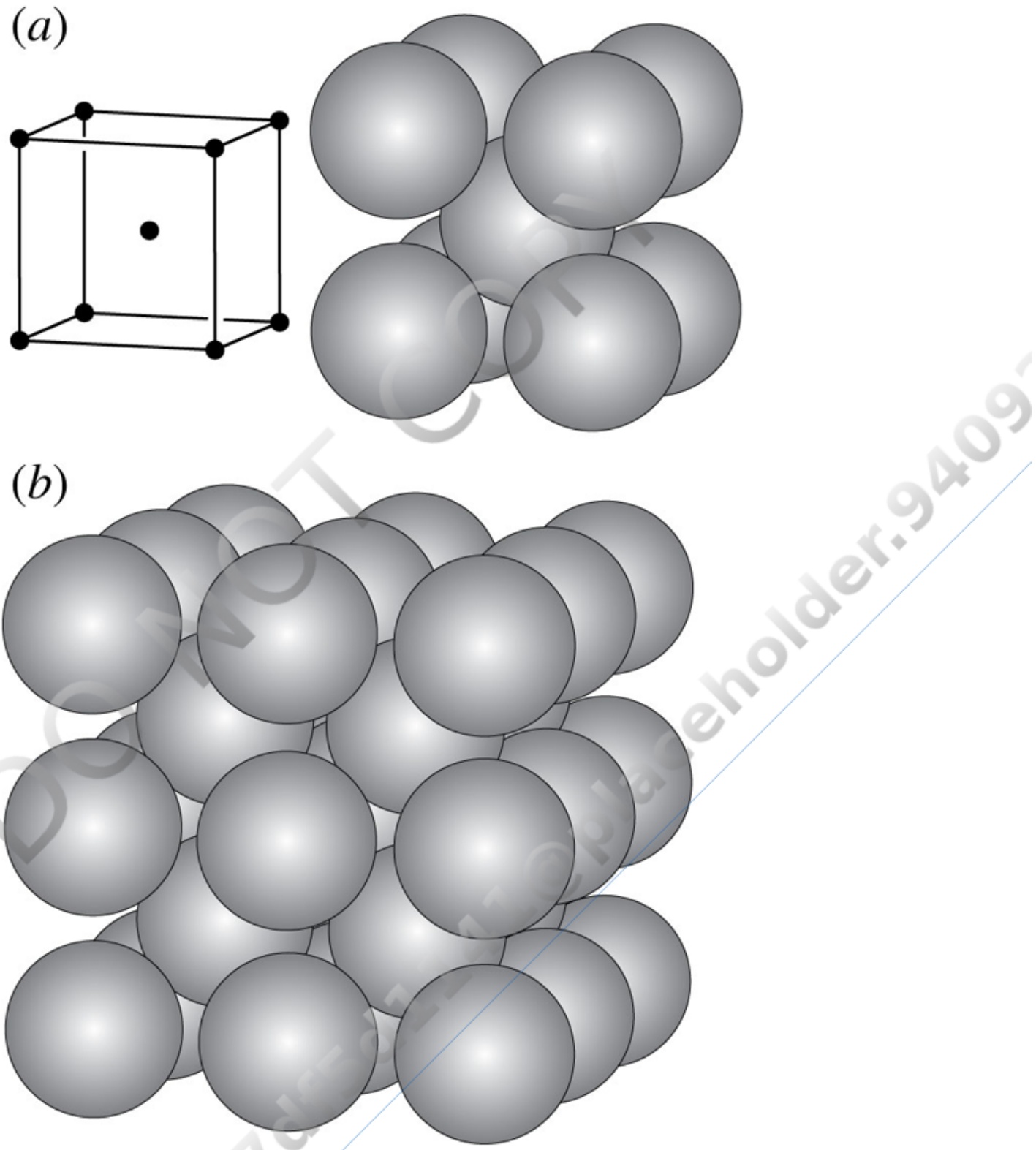

FIGURE 4.3 Body-centered cubic packing. (*a*) Body-centered lattice (left) and with atoms at each lattice node (right). (*b*) Eight unit cells. Each sphere is in contact with eight neighbors. Back to text

Printed by: e48d507df5d1141@placeholder.94092.edu. Printing is for personal, private use only. No part of this book may be reproduced or transmitted without publisher's prior permission. Violators will be prosecuted.

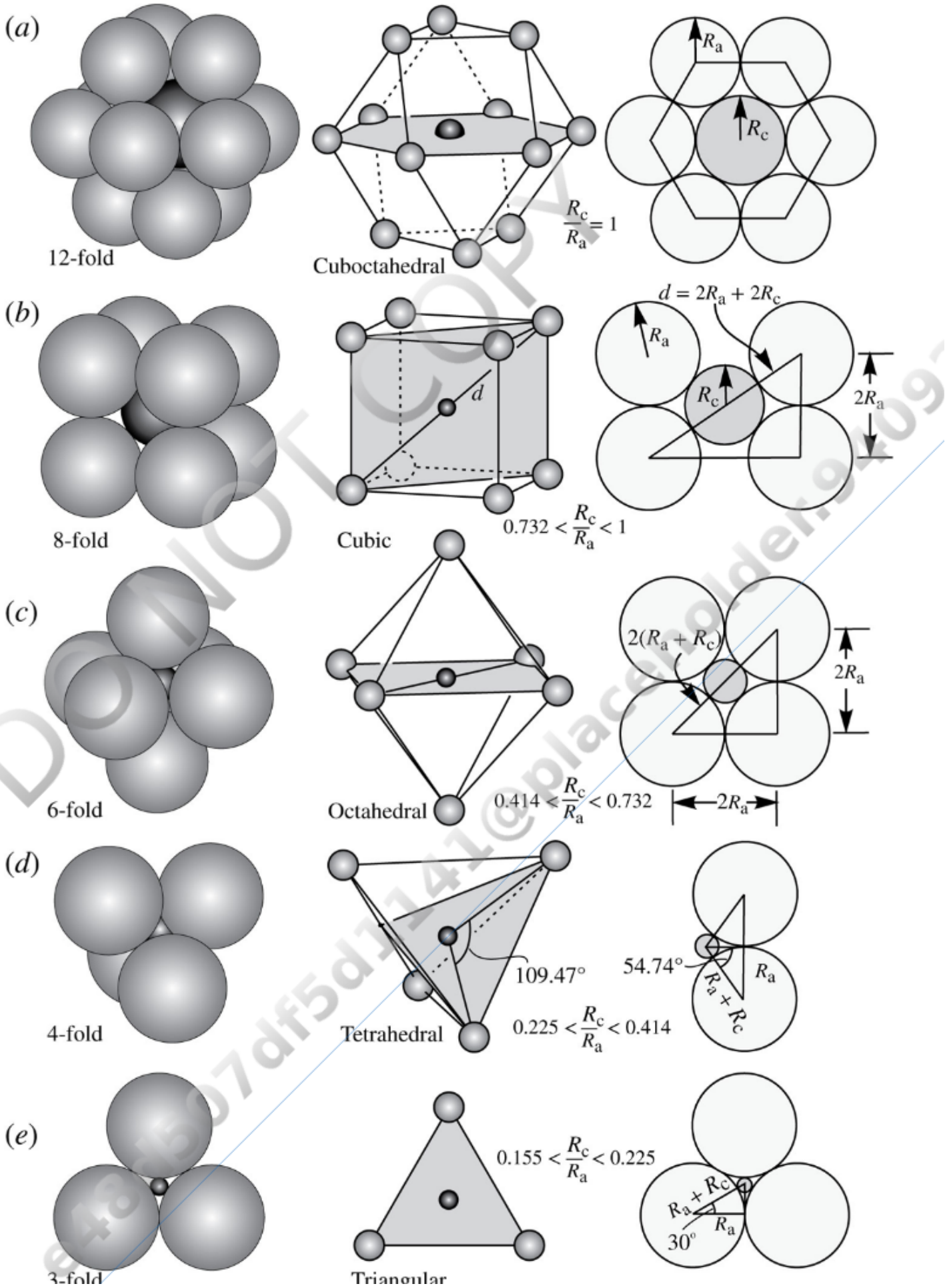

Printed by: e48d507df5d1141@placeholder.94092.edu. Printing is for personal, private use only. No part of this book may be reproduced or transmitted without publisher's prior permission. Violators will be prosecuted.

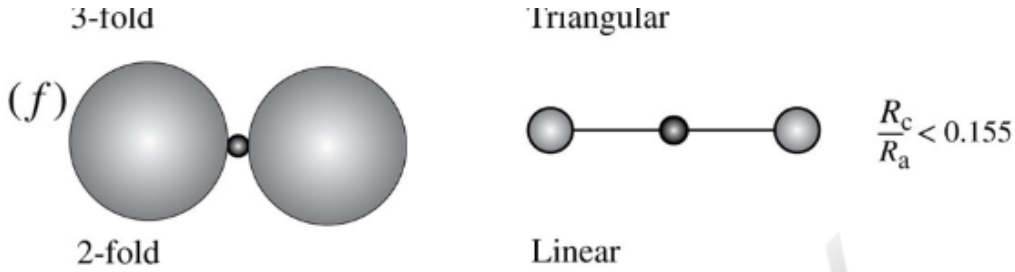

FIGURE 4.4 Coordination polyhedra. Anions with radius R_a are shown with light shading, and cations with radius R_c are dark. Left view shows cation and anions as scaled spheres. Center view shows the coordination polyhedra. Right view shows the plane through the polyhedron (shaded in center view) from which the radius ratio is calculated. See text for additional discussion. (*a*) 12-fold coordination (based on cubic closest packing), or cuboctahedral, coordination as shown. (*b*) 8-fold, or cubic, coordination. (*c*) 6-fold, or octahedral, coordination. (*d*) 4-fold, or tetrahedral, coordination. (*e*) 3-fold, or triangular, coordination. (*f*) 2-fold, or linear, coordination. Back to text

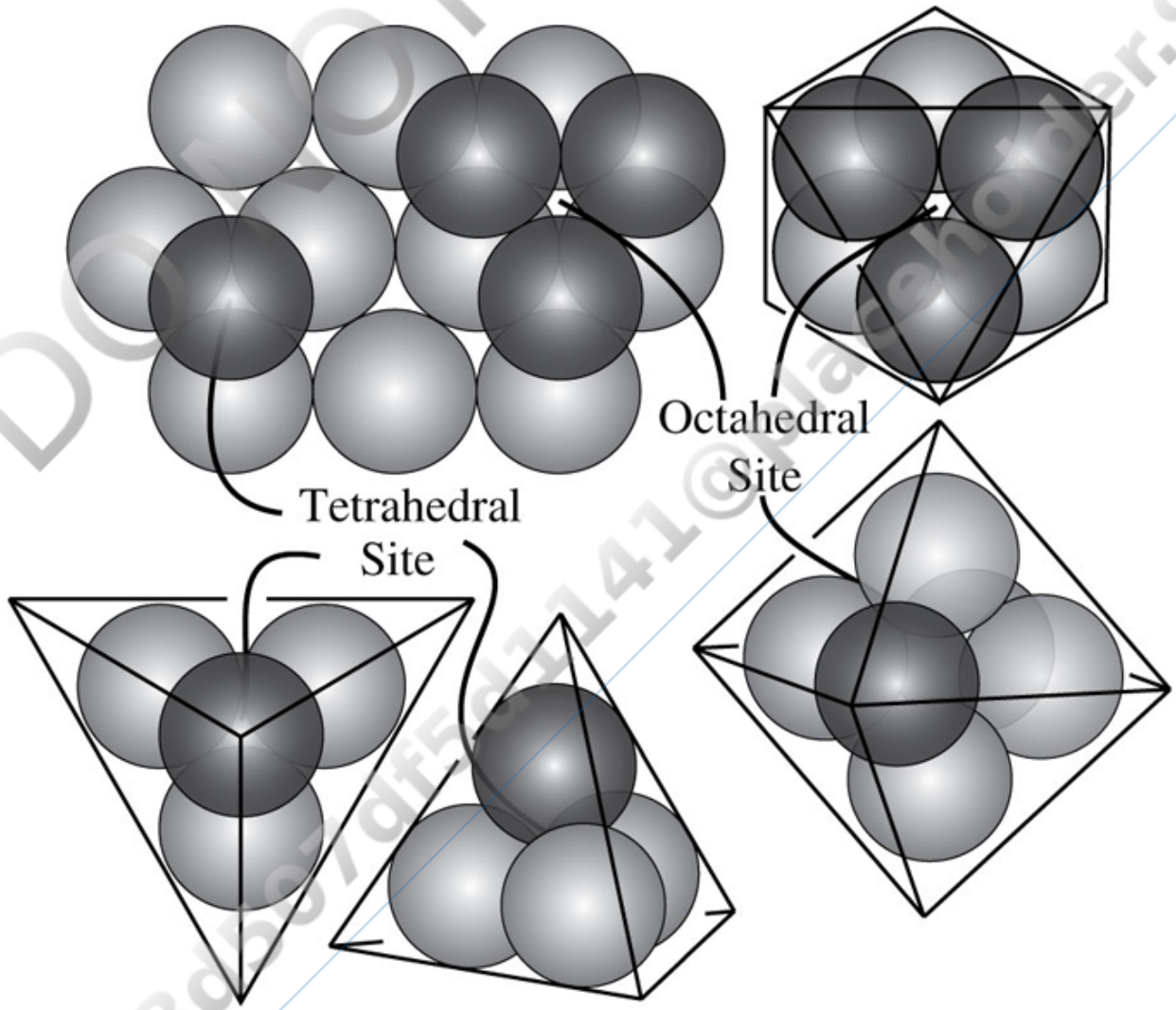

FIGURE 4.5 Tetrahedral and octahedral sites in close-packed structures. A layer of anions (light) is shown with just four anions from an adjacent layer (dark). Tetrahedral, or 4-fold, coordination sites are formed where an anion from one layer nestles into the hollow formed by three anions from the

Printed by: e48d507df5d1141@placeholder.94092.edu. Printing is for personal, private use only. No part of this book may be reproduced or transmitted without publisher's prior permission. Violators will be prosecuted.

next layer. The tetrahedral site is the little opening hidden in the middle of the four anions. Octahedral, or 6-fold, coordination sites are formed where three anions from one layer nestle into three from the next. Compare Figure 4.2a, where all the tetrahedral and octahedral sites between two layers of anions are identified. Back to text

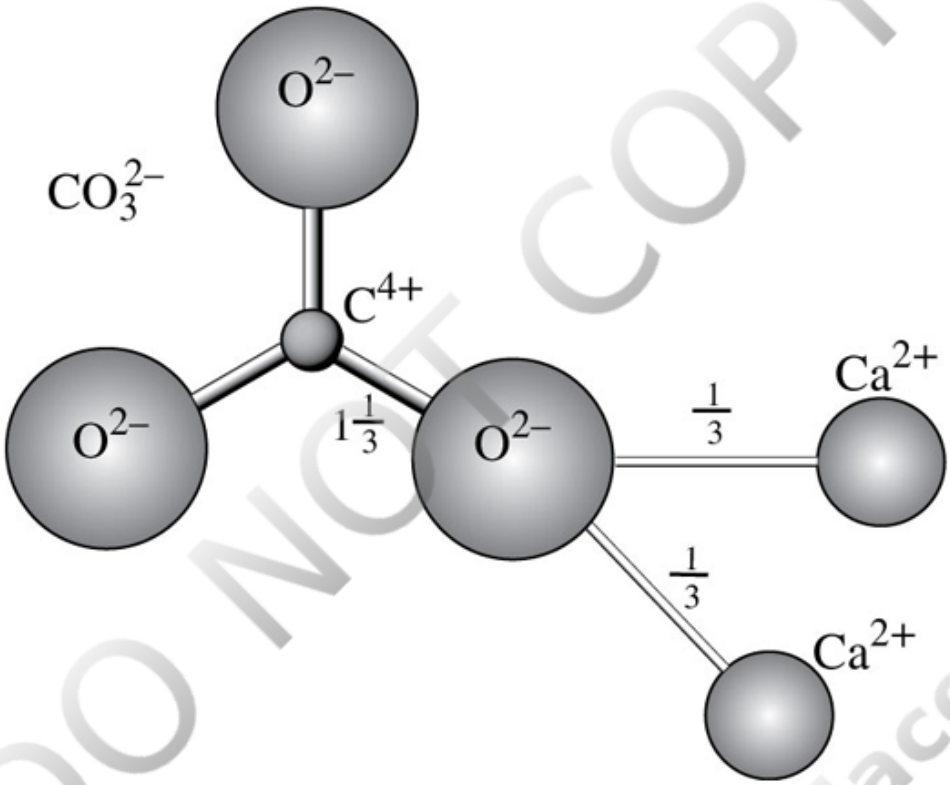

FIGURE 4.6 Anisodesmic carbonate (CO_3^{2-}) group. Each O–C bond occupies 1.33 of the available −2 charge on oxygen; only two-thirds of a charge on the oxygen is available to bond with other cations, such as Ca^{2+}. Back to text

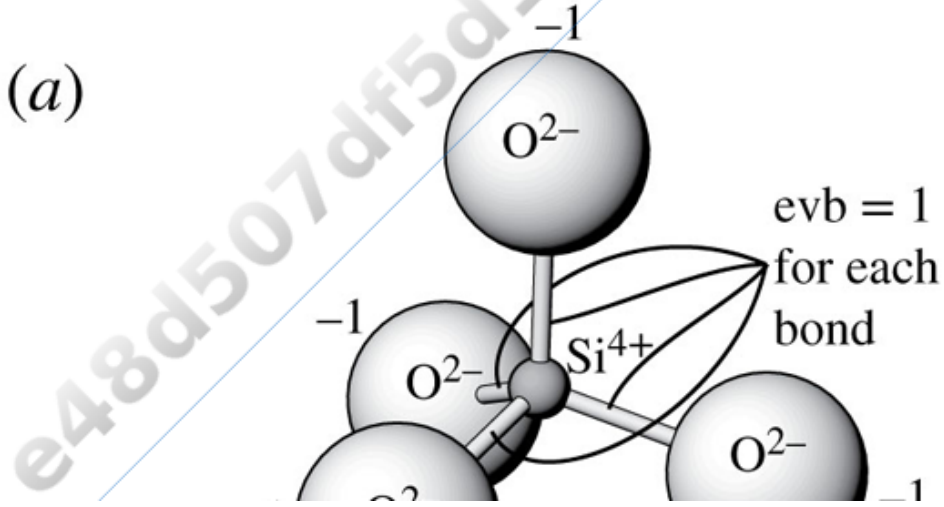

DO NOT COPY
e48d507df5d1141@placeholder.9409

Printed by: e48d507df5d1141@placeholder.94092.edu. Printing is for personal, private use only. No part of this book may be reproduced or transmitted without publisher's prior permission. Violators will be prosecuted.

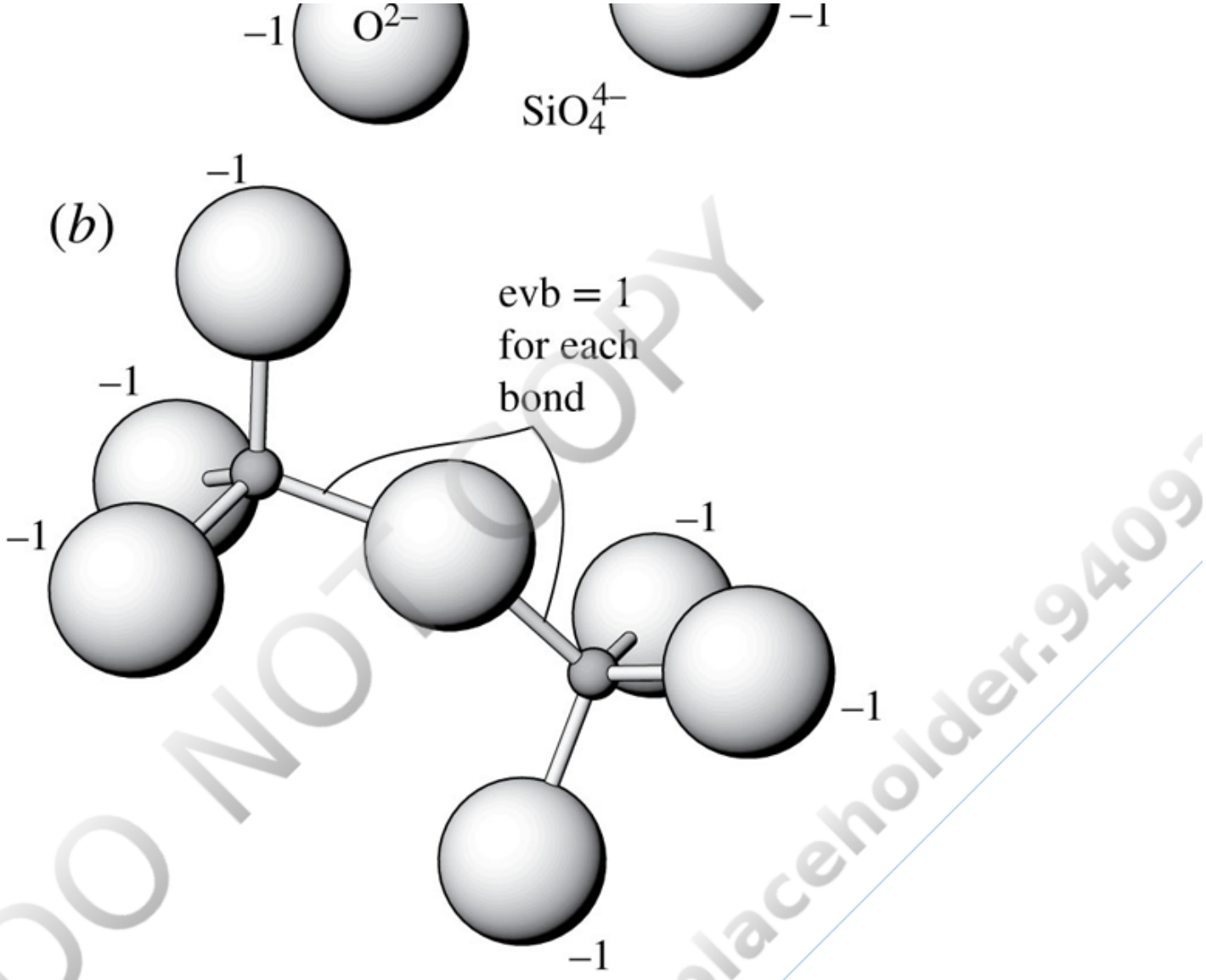

FIGURE 4.7 Mesodesmic silicon tetrahedra. (*a*) Si–O bonds occupy 1 (evb = 1) of the available −2 charge on oxygen, which is left with a net −1 charge unsatisfied. (*b*) Each oxygen can therefore bond to another Si^{4+} so that the oxygen anion is equally shared between silicon tetrahedra. A silicon tetrahedron may share one, two, three, or all four of its oxygen anions with adjacent tetrahedra.
Back to text

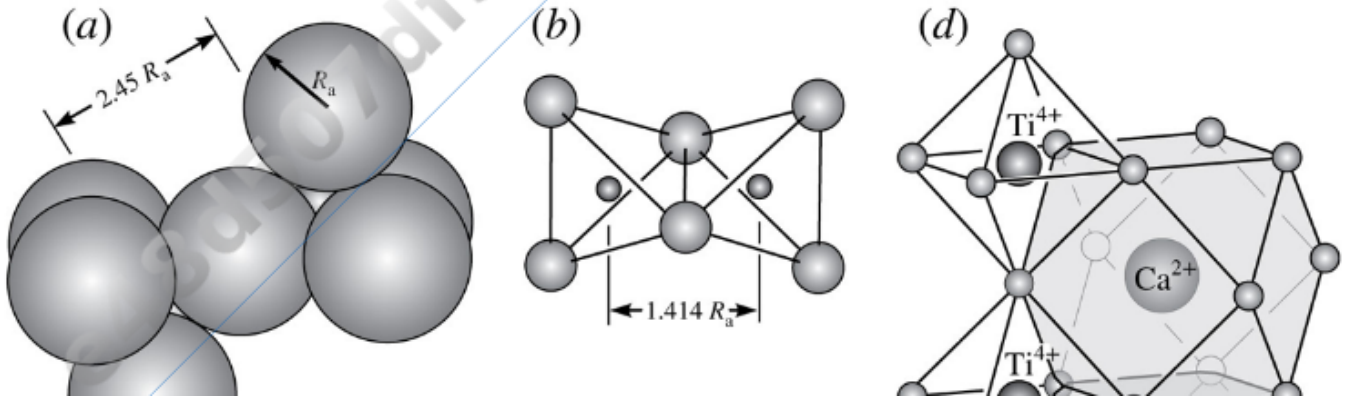

DO NOT COPY
3d507df5d1141@placeholder.9409

Printed by: e48d507df5d1141@placeholder.94092.edu. Printing is for personal, private use only. No part of this book may be reproduced or transmitted without publisher's prior permission. Violators will be prosecuted.

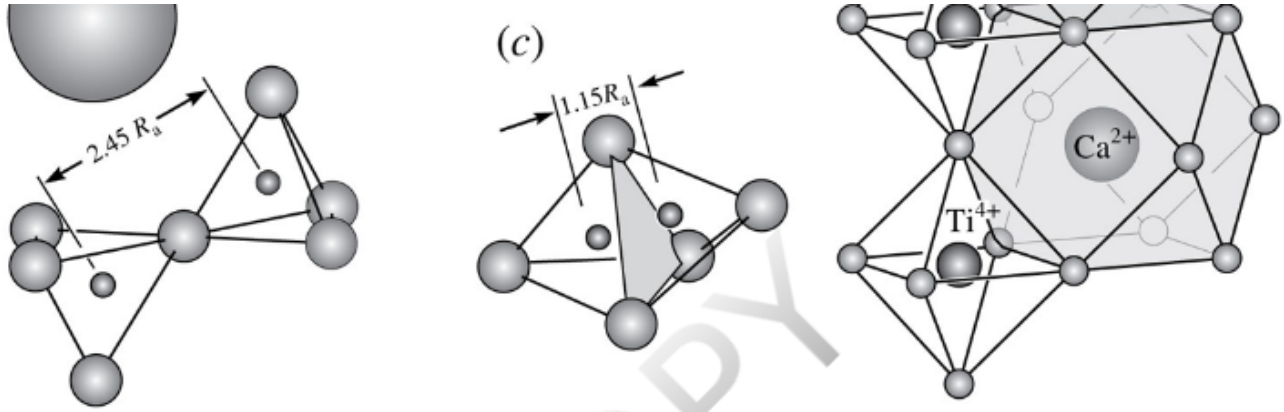

FIGURE 4.8 Sharing anions between polyhedra. (*a*) Sharing a single anion (a corner) between tetrahedra keeps the positively charged cations at a maximum distance. The upper diagram shows the anions (large) and cations (small) to scale. The lower diagram reduces the ion size to allow the tetrahedral coordination polyhedra to be more easily seen. The cations are 2.45R_a apart where R_a is the radius of the anion. (*b*) Sharing two anions (an edge) places the cations 1.414R_a apart. (*c*) Sharing three anions (a face, shaded) places the cations 1.15R_a apart. (*d*) In perovskite ($CaTiO_3$), the Ti^{4+} occupies octahedra that share only a single oxygen (small spheres), and Ca^{2+} occupies cuboctahedra that share four oxygen anions on common faces. Back to text

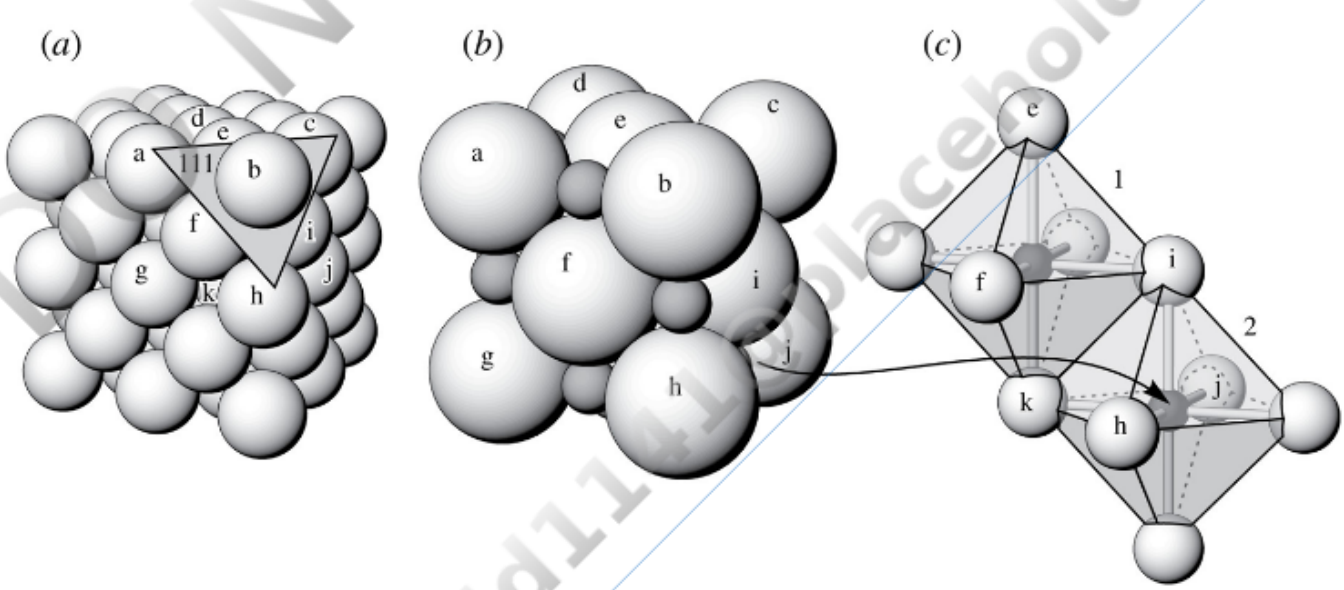

FIGURE 4.9 NaCl structure. (*a*) Layers of Cl^- anions are arranged parallel to the (111) crystallographic plane. (*b*) One unit cell showing Na^+ (dark spheres) in octahedral interstices between the Cl^-. (*c*) Octahedron 1 is formed by the Cl^- on the center of each face of the unit cell (the ions are shown at a reduced size). Octahedron 2 surrounds the Na^+ on the bottom right edge of the unit cell and includes Cl^- from adjacent unit cells. The octahedra share an edge. Back to text

Printed by: e48d507df5d1141@placeholder.94092.edu. Printing is for personal, private use only. No part of this book may be reproduced or transmitted without publisher's prior permission. Violators will be prosecuted.

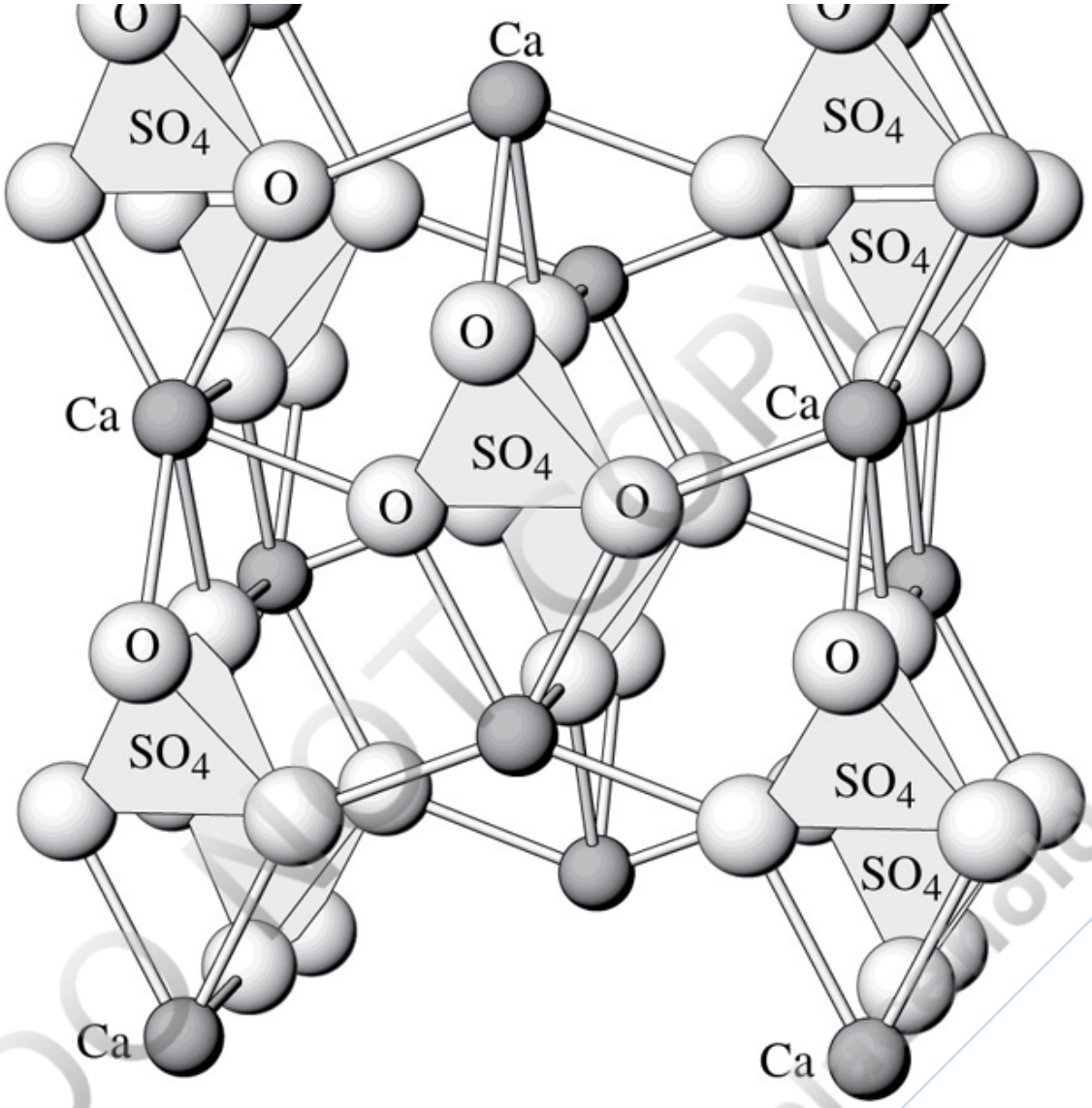

FIGURE 4.10 Anhydrite structure. Isolated SO_4^{2-} groups are bonded laterally through Ca^{2+} (dark spheres). Back to text

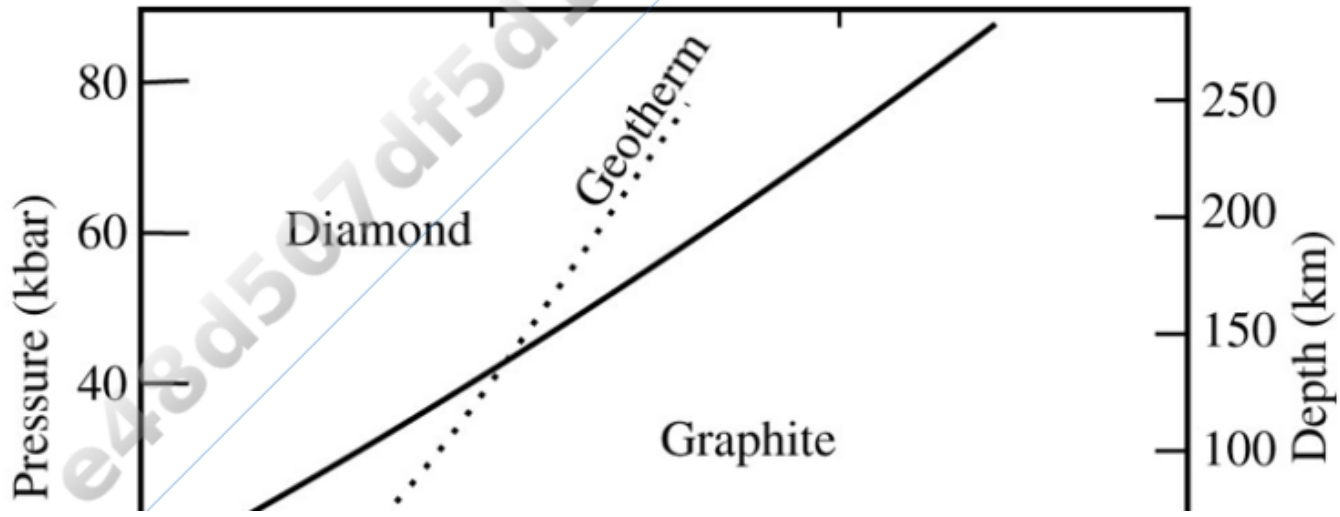

Printed by: e48d507df5d1141@placeholder.94092.edu. Printing is for personal, private use only. No part of this book may be reproduced or transmitted without publisher's prior permission. Violators will be prosecuted.

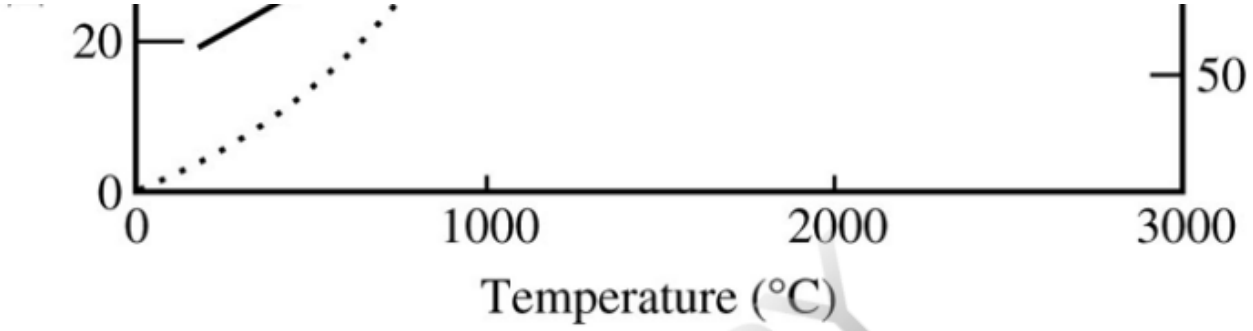

FIGURE 4.11 Diamond and graphite stability fields (Day, 2012). The geotherm tracks how pressure and temperature change with increasing depth; in this case it is shown for the rocks beneath continental shields. For this geothermal gradient, diamond is stable only at pressures greater than ~40 kilobars, which corresponds to a depth of about 125 km in the Earth's mantle. Back to text

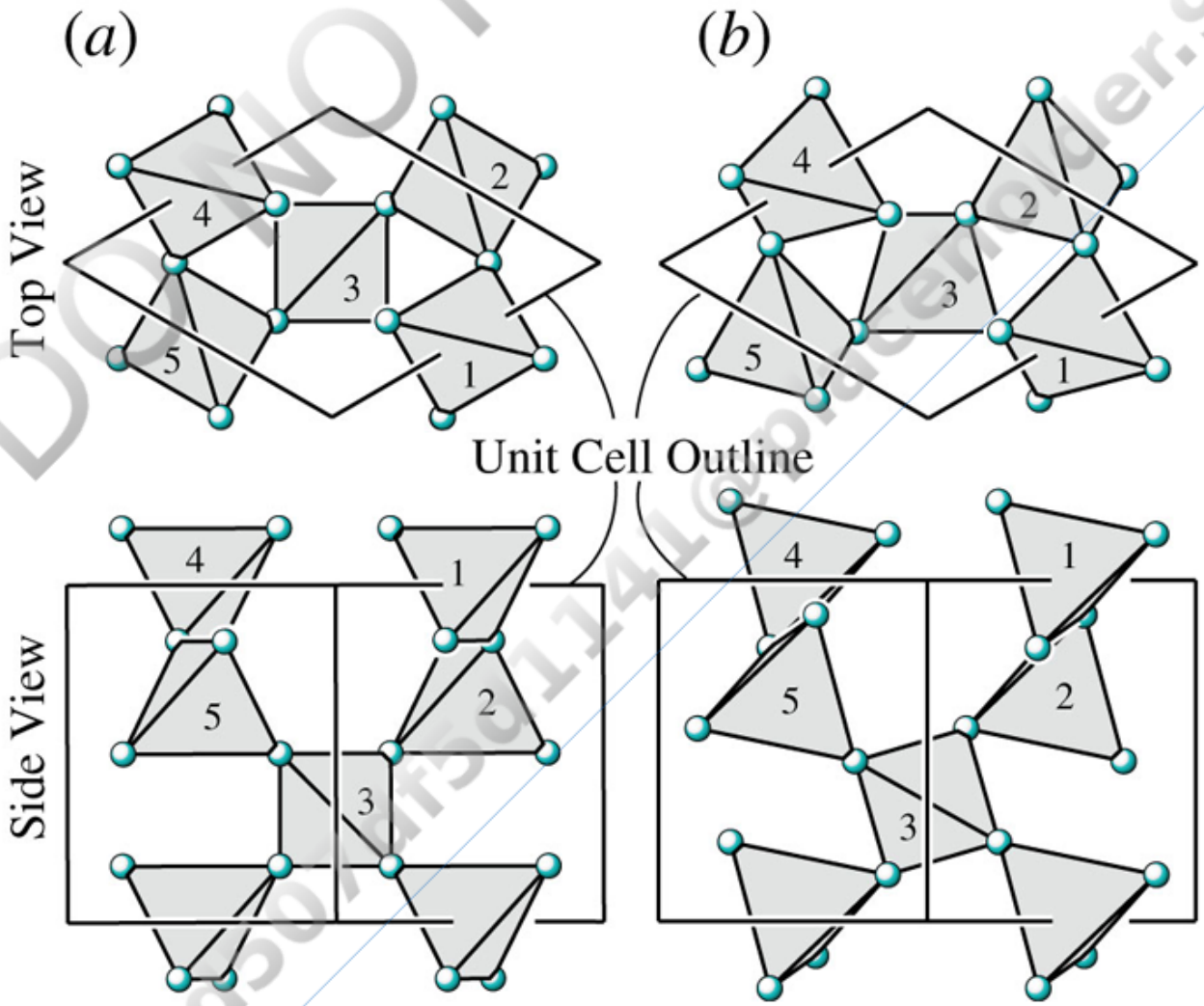

FIGURE 4.12 Structures of β-quartz and α-quartz (compare Figure 2.20). The top view looks down the *c* axis; the bottom view is from the side. The unit cell is outlined. (*a*) β-Quartz is the high-temperature polymorph. (*b*) α-Quartz is the low-temperature polymorph. The inversion from β-quartz to α-quartz is accomplished by a distortion that reduces the symmetry. Back to text

Printed by: e48d507df5d1141@placeholder.94092.edu. Printing is for personal, private use only. No part of this book may be reproduced or transmitted without publisher's prior permission. Violators will be prosecuted.

to α-quartz is accomplished by a distortion that reduces the symmetry. Back to text

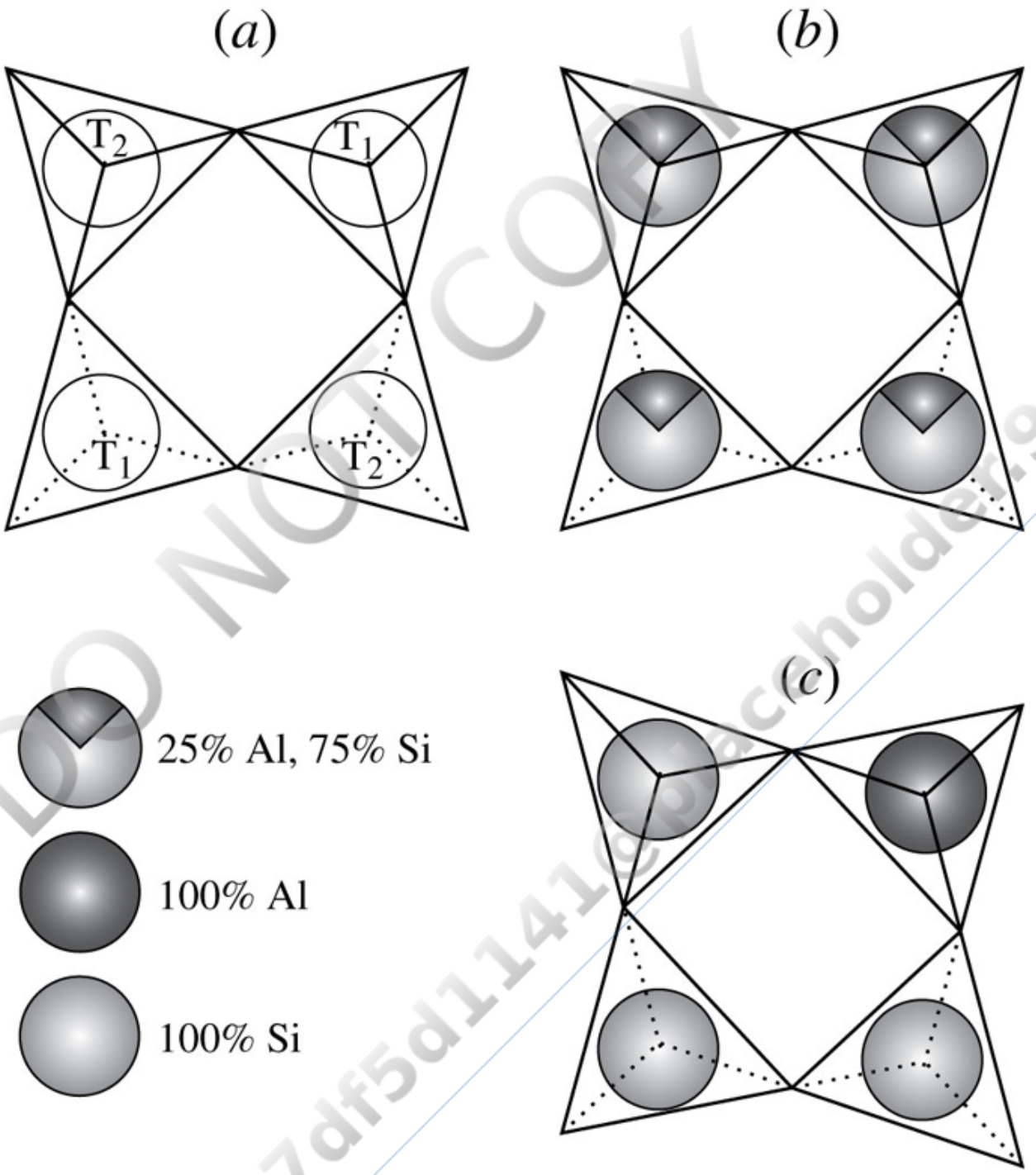

FIGURE 4.13 Order–disorder in K-feldspar ($KAlSi_3O_8$) polymorphs. (*a*) Schematic view of two up-pointing and two down-pointing tetrahedra that contain the three Si and one Al per formula unit. Two tetrahedra are T_1 sites and two are T_2 sites. (*b*) High sanidine. Al is equally likely to be in any of the four sites, so on average each contains 25 percent Al. (*c*) Maximum microcline: Al is preferentially placed in one T_1 site; Si occupies the other three sites, producing a distortion to the structure. Back to text

DO NOT COPY e48d507df5d1141@placeholder.9409

Printed by: e48d507df5d1141@placeholder.94092.edu. Printing is for personal, private use only. No part of this book may be reproduced or transmitted without publisher's prior permission. Violators will be prosecuted.

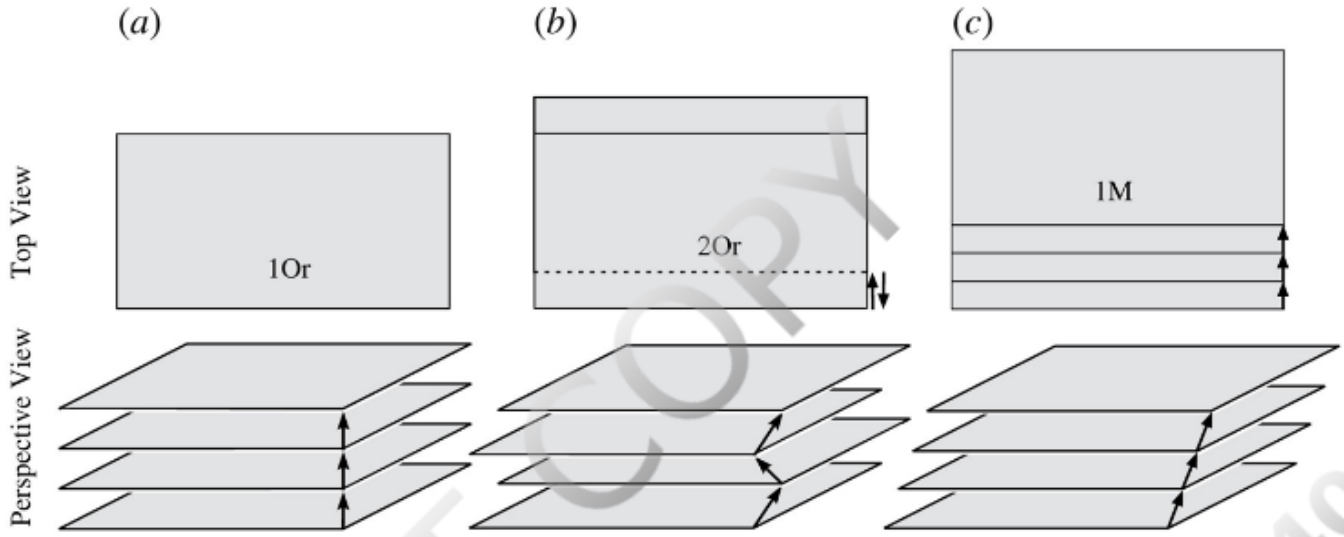

FIGURE 4.14 Polytypism involves different patterns of stacking identical sheets. The symbols used here are adapted from those used in the sheet silicates. The number in the symbol indicates the number of layers per unit cell, and the letters indicate the crystal system that results (Or = orthorhombic, M = monoclinic). (*a*) 1Or polytype with a single stacking vector at right angles to the sheets. (*b*) 2Or polytype with two stacking vectors with opposite senses. (*c*) 1M polytype with a single stacking vector at an angle to the sheets. Back to text

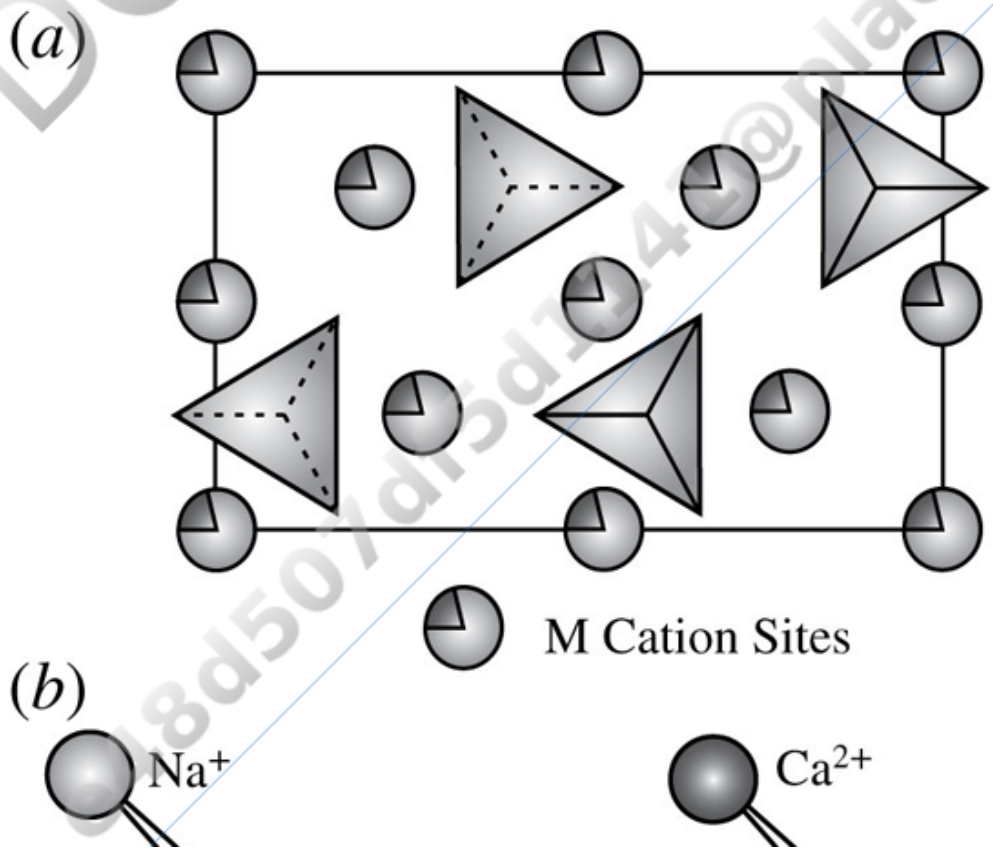

DO NOT COPY

Printed by: e48d507df5d1141@placeholder.94092.edu. Printing is for personal, private use only. No part of this book may be reproduced or transmitted without publisher's prior permission. Violators will be prosecuted.

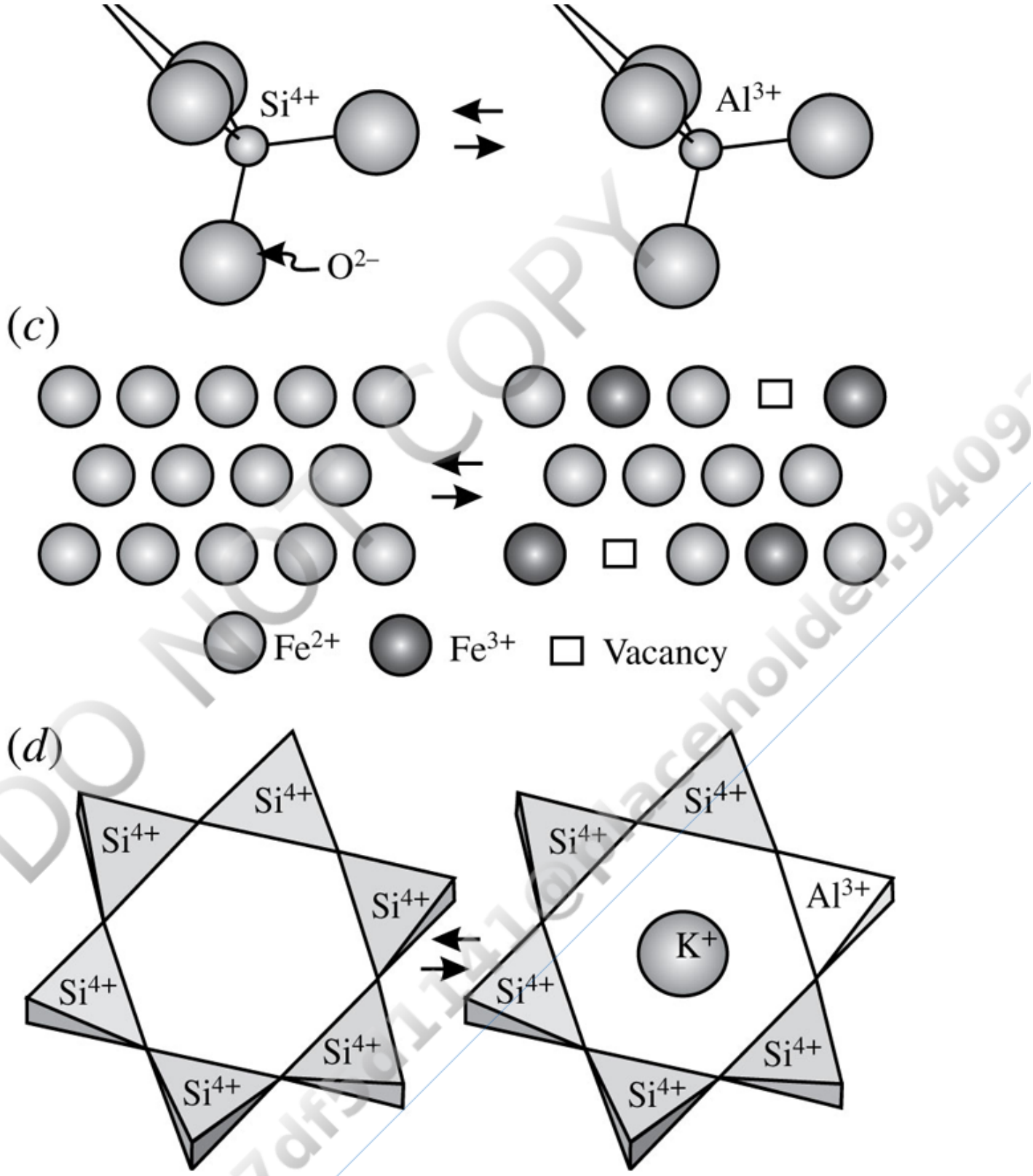

FIGURE 4.15 Solid solution. (*a*) Simple substitution in olivine, whose structure is viewed down the *a* axis. The octahedral M sites between tetrahedra may be occupied by either Mg^{2+} or Fe^{2+}. The shaded wedge shown on each M cation graphically indicates the percentage of the M sites that are occupied by Fe^{2+} (22 percent in this case). (*b*) Coupled substitution in plagioclase shown schematically. To maintain charge balance, substitution of Ca^{2+} for Na^{+} is balanced by substitution of Al^{3+} for Si^{4+}. (*c*) Omission substitution of $3Fe^{2+} \Leftrightarrow 2Fe^{3+} + \square$ in pyrrhotite shown schematically. (*d*) Interstitial ionic substitution in beryl. Insertion of large monovalent cations (K^{+}, Na^{+}, Rb^{+}, etc.) in the open channelways defined by the rings of silicon tetrahedra is balanced by substitution of Al^{3+} for

Printed by: e48d507df5d1141@placeholder.94092.edu. Printing is for personal, private use only. No part of this book may be reproduced or transmitted without publisher's prior permission. Violators will be prosecuted.

Si^{4+} in the tetrahedra. Back to text

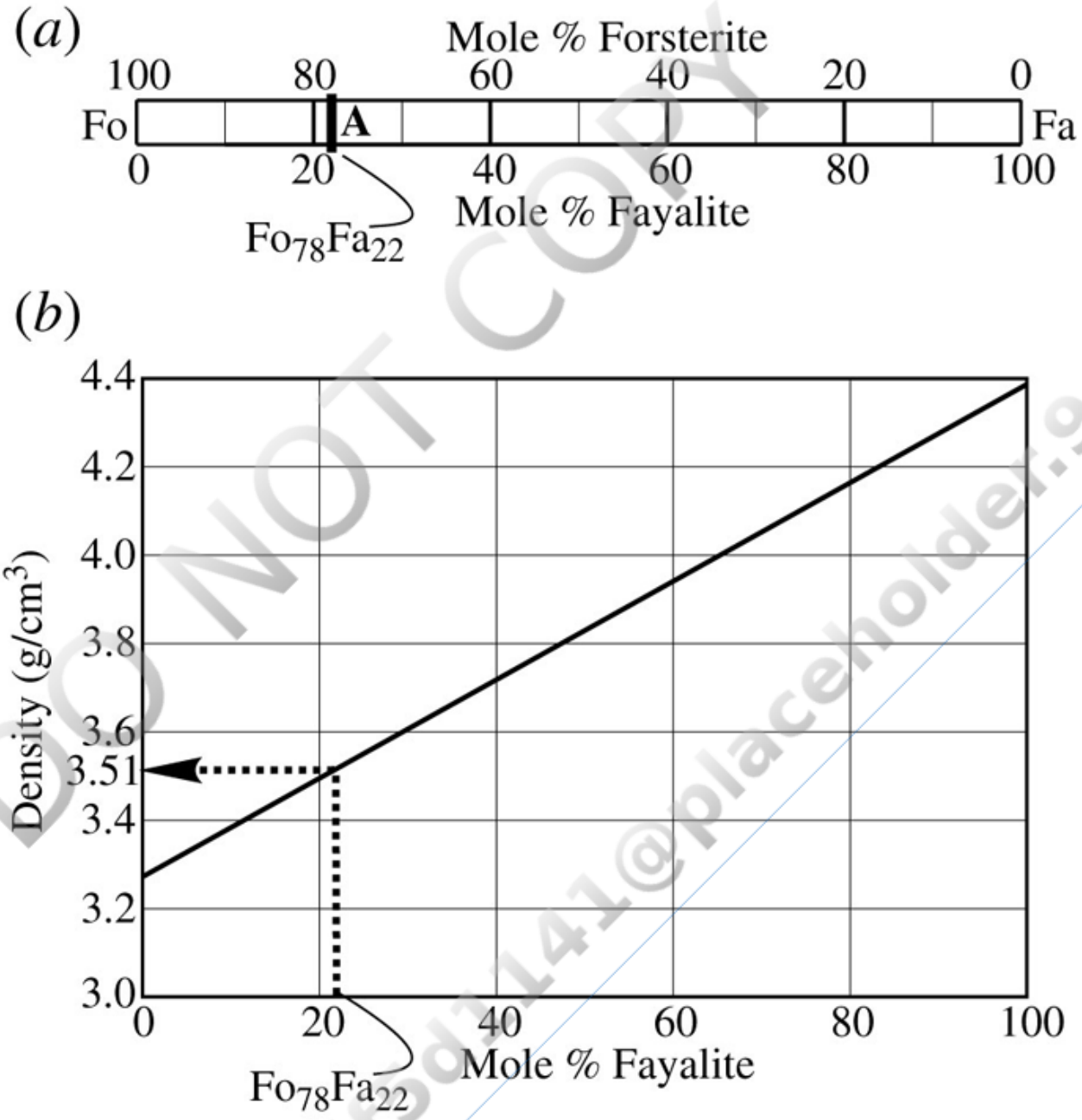

FIGURE 4.16 Binary diagrams of olivine. (*a*) The end members, forsterite (Mg_2SiO_4) and fayalite (Fe_2SiO_4), are plotted at the ends of a line. The scale is mole percent of the end members. Point A indicates a composition with 22 percent fayalite and 78 percent forsterite ($Fo_{78}Fa_{22}$). (*b*) Use of a binary composition diagram to illustrate the variation of density as a function of composition in olivine. Olivine A has a density of 3.51 g/cm^3. Back to text

DO NOT COPY
e48d507df5d1141@placeholder.9409

Printed by: e48d507df5d1141@placeholder.94092.edu. Printing is for personal, private use only. No part of this book may be reproduced or transmitted without publisher's prior permission. Violators will be prosecuted.

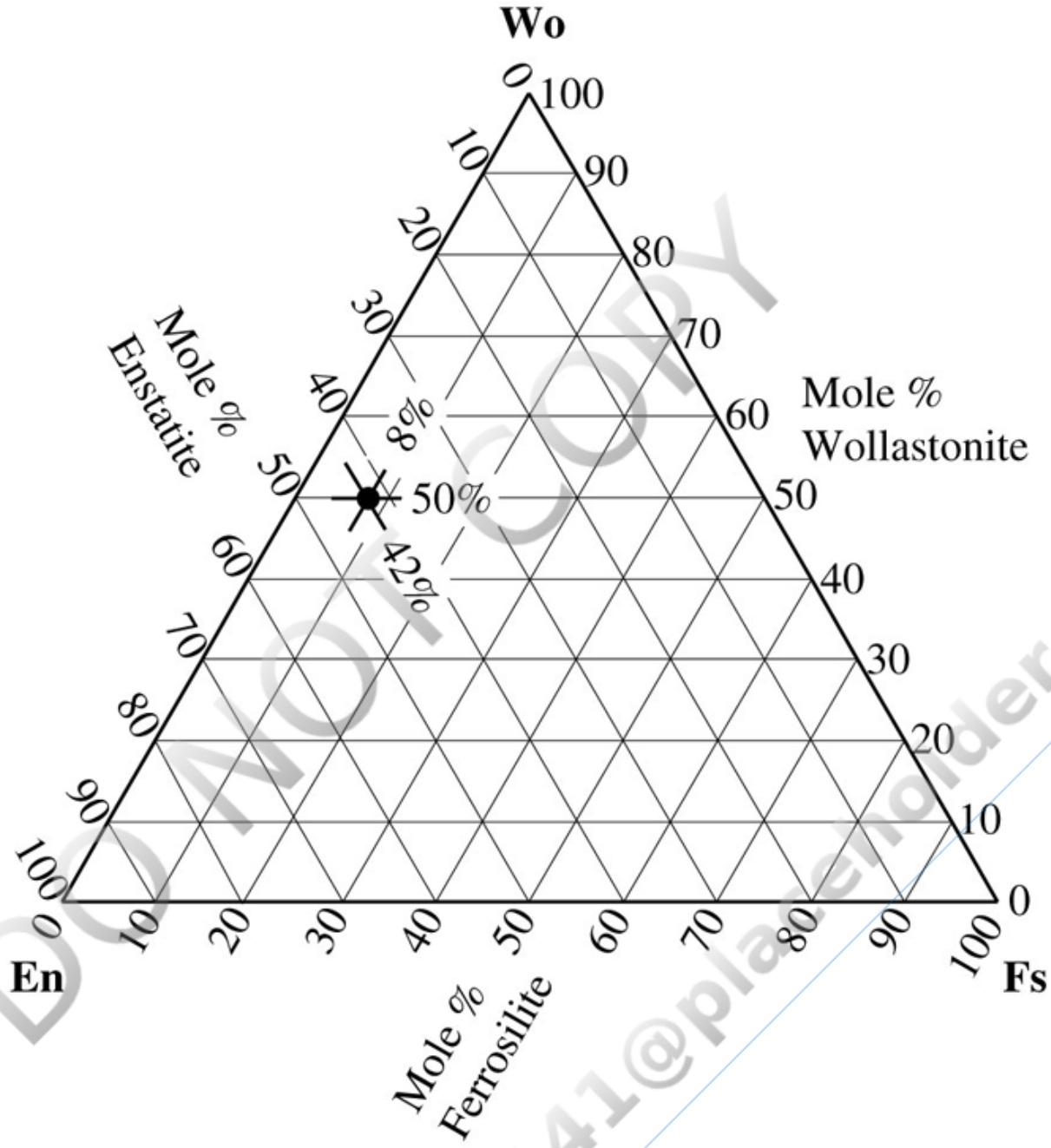

FIGURE 4.17 Pyroxene ternary diagram. The end members enstatite (En, $Mg_2Si_2O_6$), ferrosilite (Fs, $Fe_2Si_2O_6$), and wollastonite (Wo, $Ca_2Si_2O_6$) are plotted at the corners of a triangle. Three sets of lines on the diagram as labeled allow compositions to be plotted. The composition $En_{42}Fs_8Wo_{50}$ is plotted where the 50 percent Wo line intersects the 8 percent Fs and 42 percent En lines. Back to text

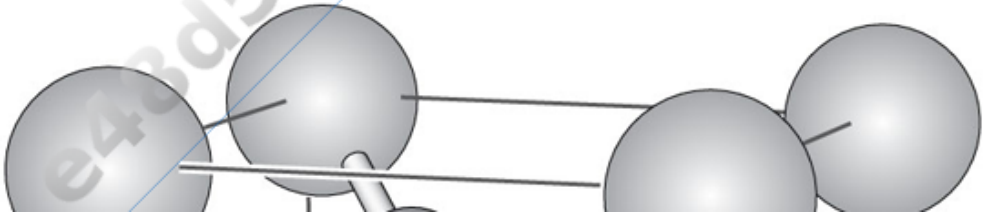

Printed by: e48d507df5d1141@placeholder.94092.edu. Printing is for personal, private use only. No part of this book may be reproduced or transmitted without publisher's prior permission. Violators will be prosecuted.

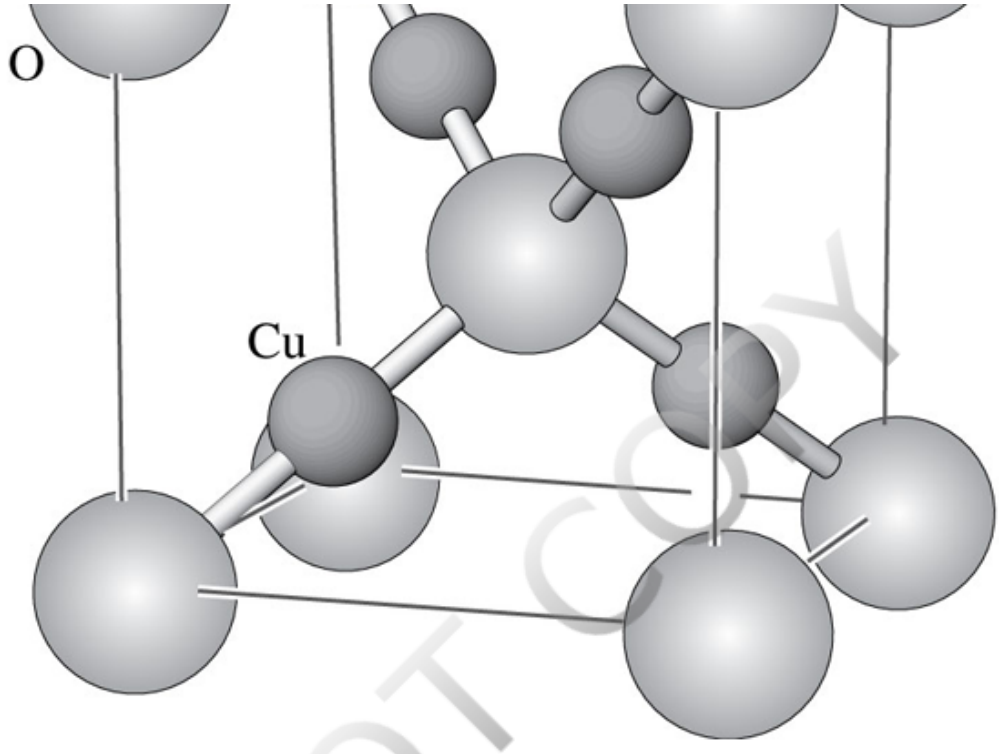

FIGURE 4.18 Cuprite structure and unit cell. Oxygen occupy the corners and center of the unit cell; Cu occupies four of the eight cube octants, or the eight smaller cubes into which any larger cube can be divided. Back to text

DO NOT COPY
e48d507df5d1141@placeholder.9409

Printed by: e48d507df5d1141@placeholder.94092.edu. Printing is for personal, private use only. No part of this book may be reproduced or transmitted without publisher's prior permission. Violators will be prosecuted.

Chapter 5 Mineral Growth

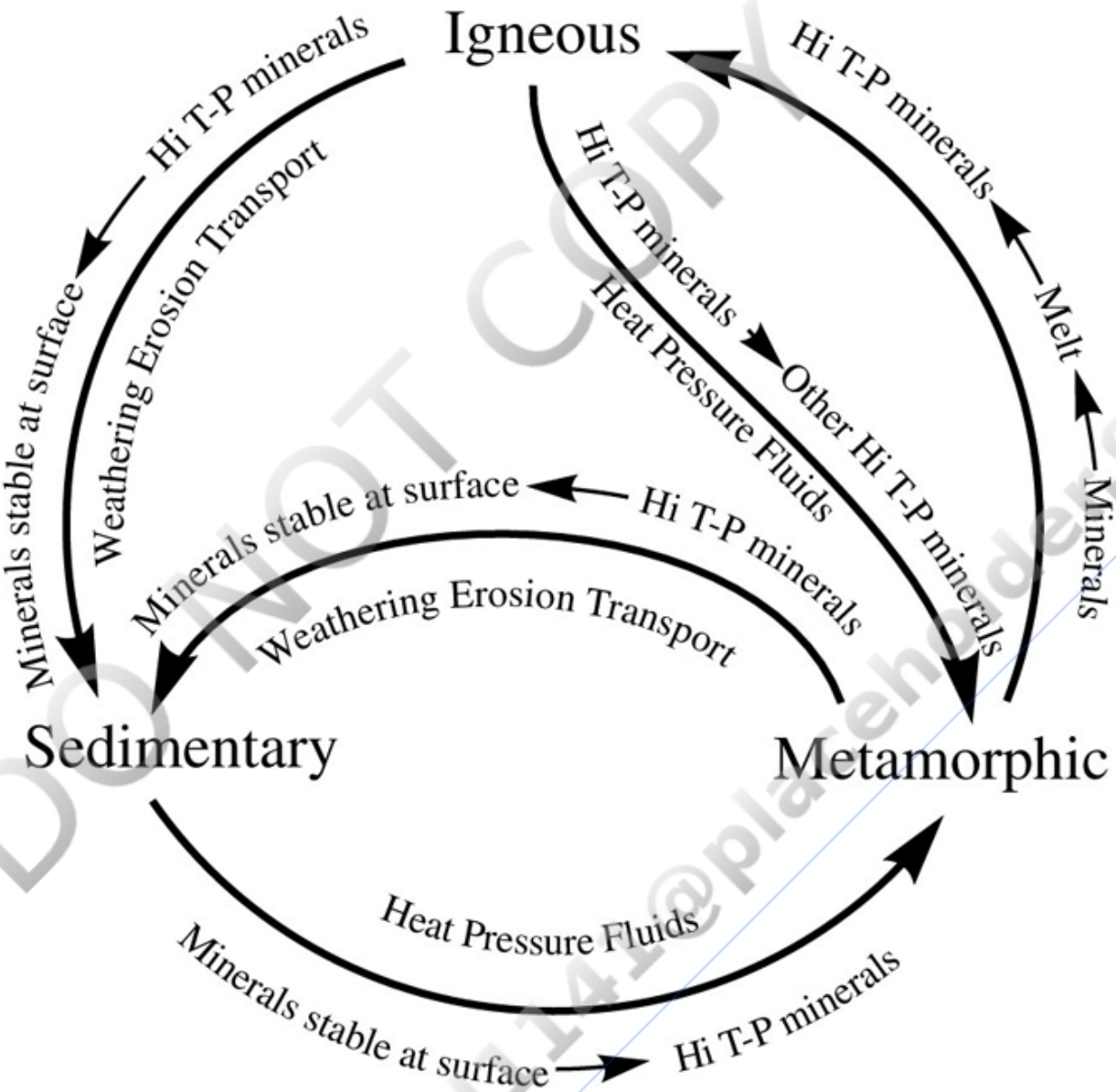

FIGURE 5.1 The rock cycle. The rock cycle fundamentally involves mineralogical changes in response to different temperature–pressure (T–P) and fluid conditions. Back to text

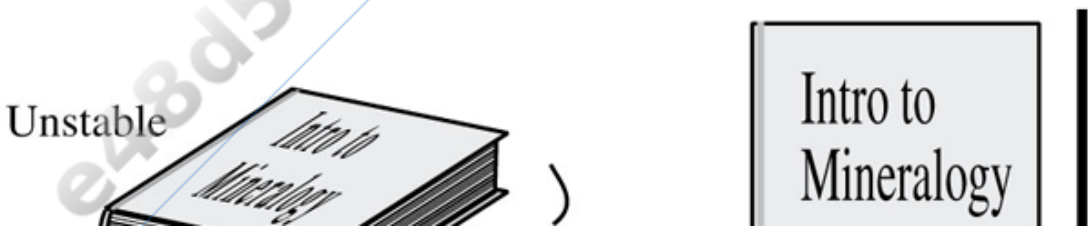

Printed by: e48d507df5d1141@placeholder.94092.edu. Printing is for personal, private use only. No part of this book may be reproduced or transmitted without publisher's prior permission. Violators will be prosecuted.

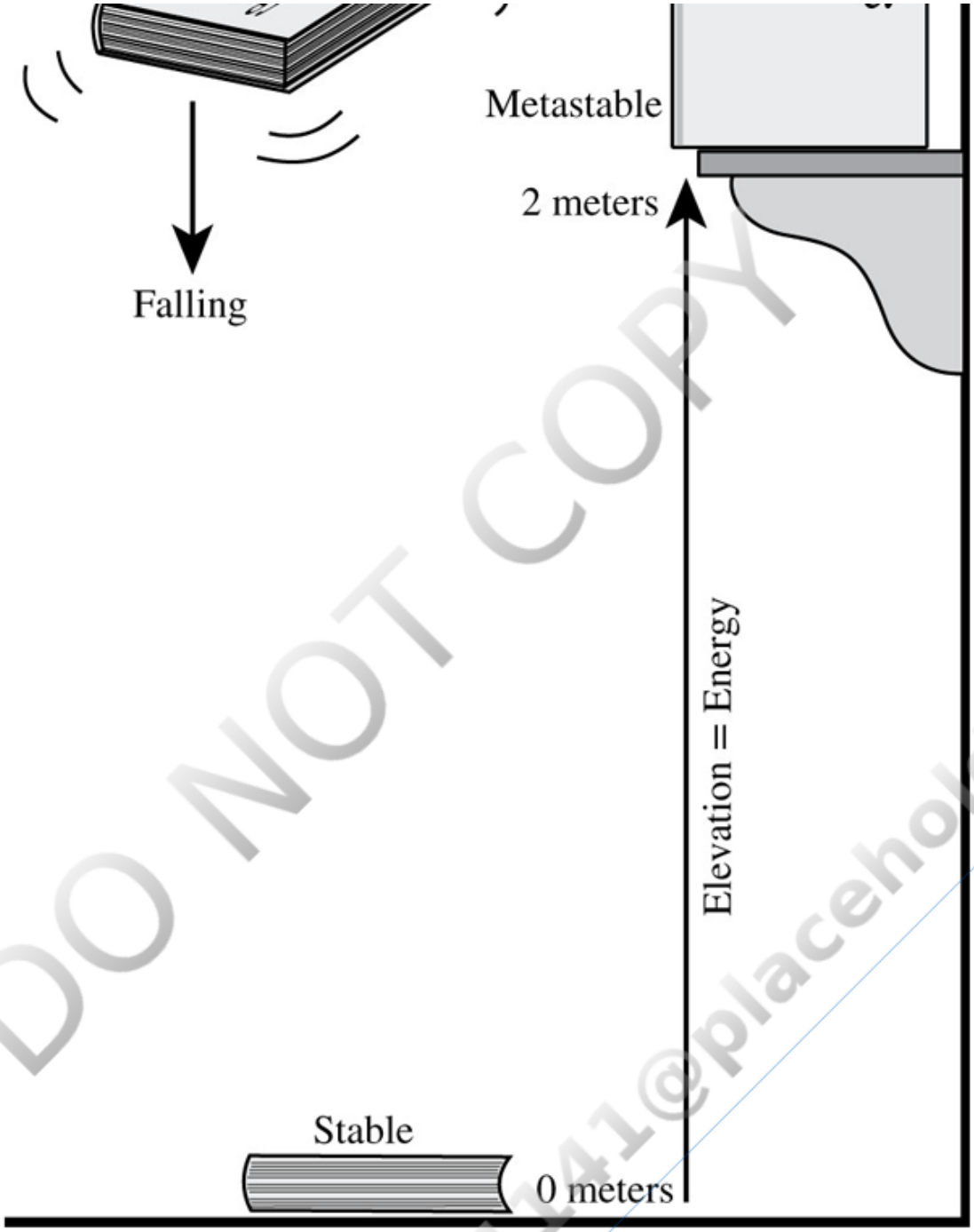

FIGURE 5.2 Stability. A book 2 meters above the floor is unstable relative to a position on the floor. If unrestrained (left, unstable book), the book will spontaneously fall to the floor. The book on the shelf is metastable relative to a position on the floor. While the floor represents a lower-energy position, activation energy, or a push of the book off the shelf, is required to allow the book to reach the low-energy floor. Back to text

DO NOT COPY
e48d507df5d1141@placeholder.9409

Printed by: e48d507df5d1141@placeholder.94092.edu. Printing is for personal, private use only. No part of this book may be reproduced or transmitted without publisher's prior permission. Violators will be prosecuted.

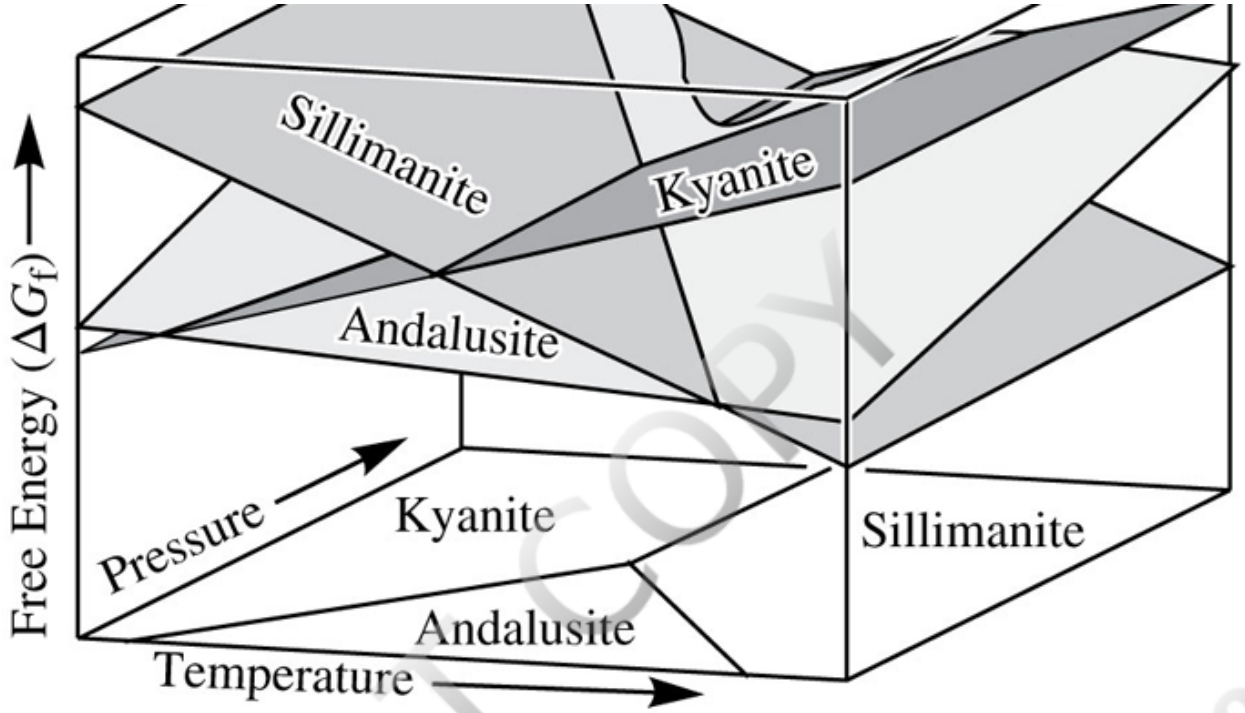

(*b*)

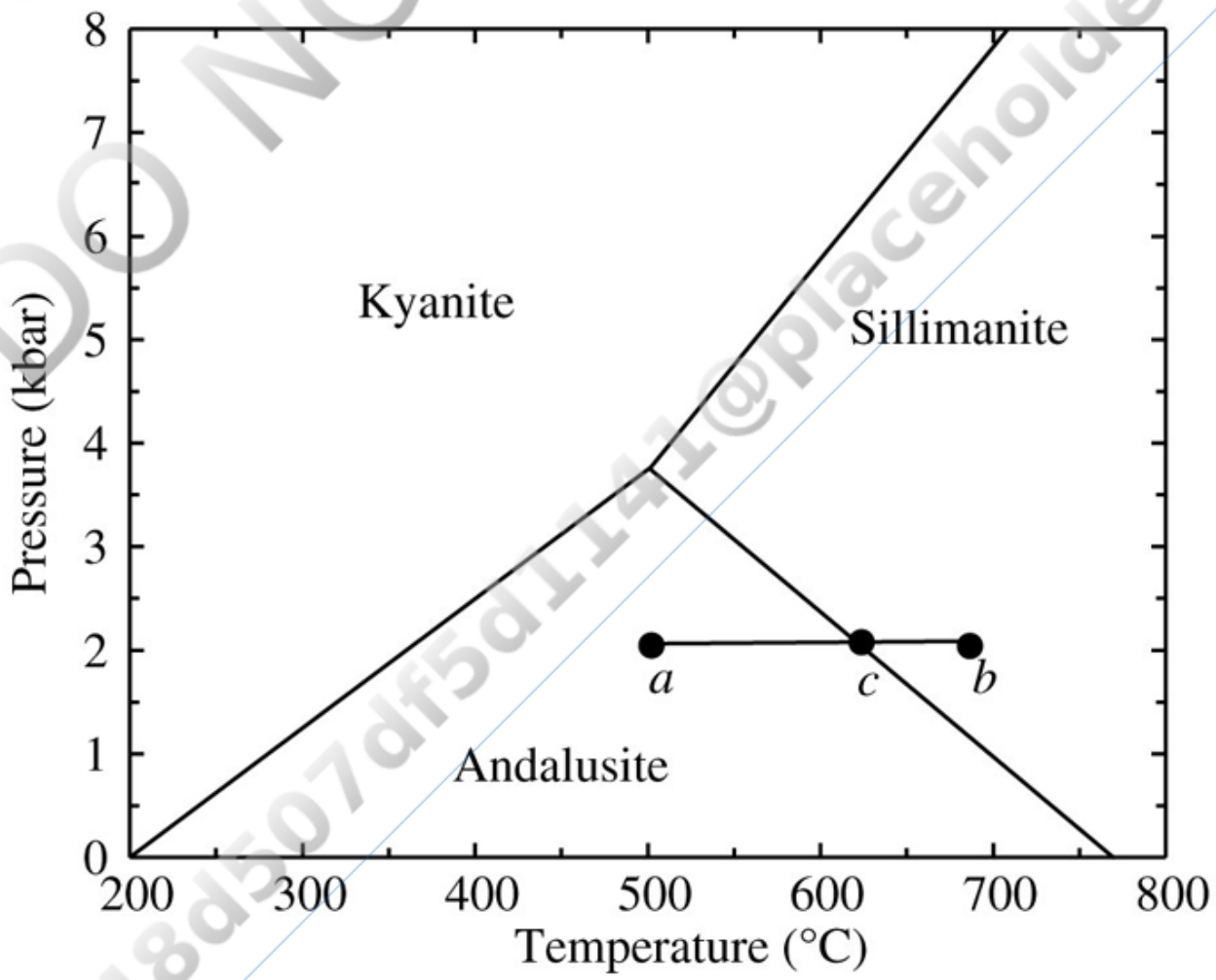

FIGURE 5.3 Aluminum silicate stability. (*a*) Schematic illustration of Gibbs free energy of formation of andalusite (light), sillimanite (intermediate), and kyanite (dark) as a function of pressure

DO NOT COPY
e48d507df5d1141@placeholder.9409

Printed by: e48d507df5d1141@placeholder.94092.edu. Printing is for personal, private use only. No part of this book may be reproduced or transmitted without publisher's prior permission. Violators will be prosecuted.

and temperature. The mineral with the lowest free energy at a specific T–P condition is the stable phase at those conditions. (*b*) T–P stability fields of the aluminum silicates. See text for discussion. Adapted from Hemingway and others (1991). Back to text

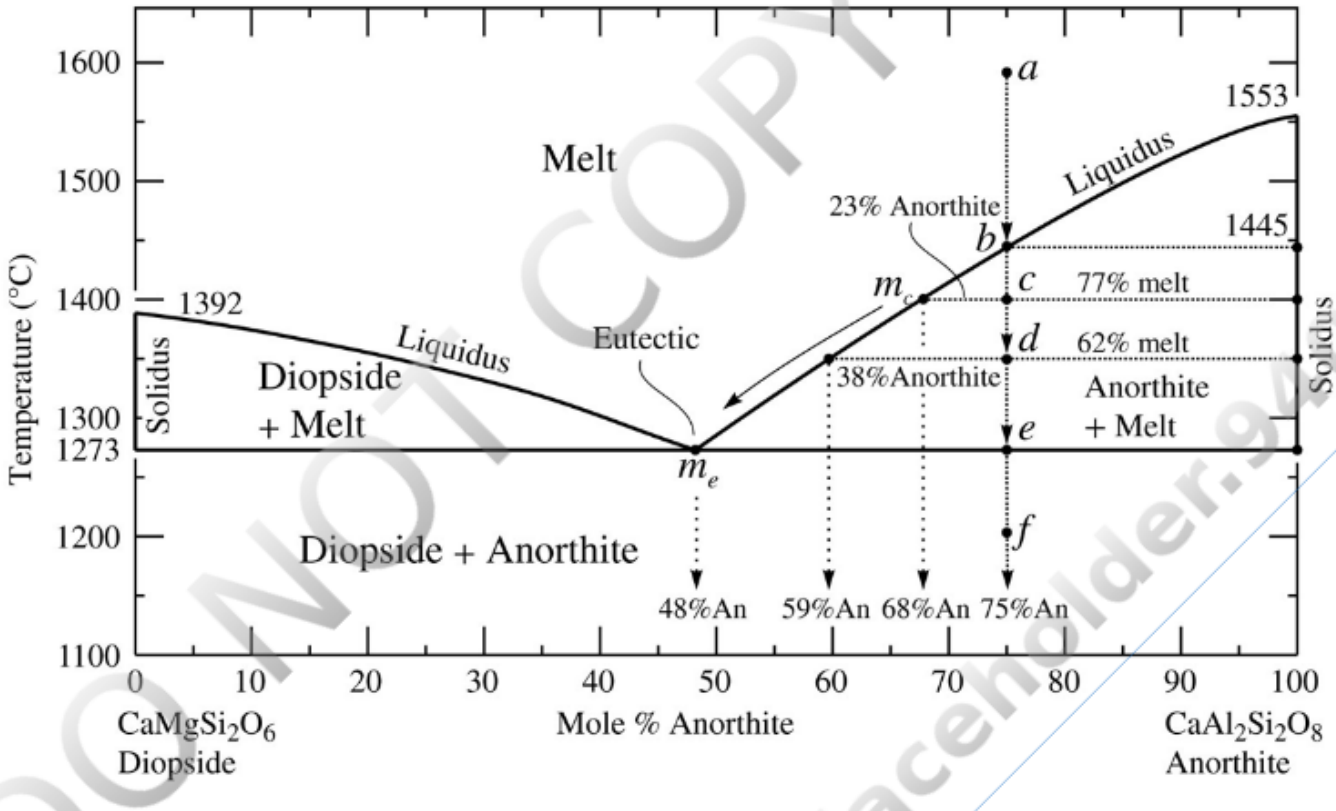

FIGURE 5.4 Crystallization in the system diopside (Di)–anorthite (An) at 1 atm pressure. After Osborn (1942). See text for discussion. Back to text

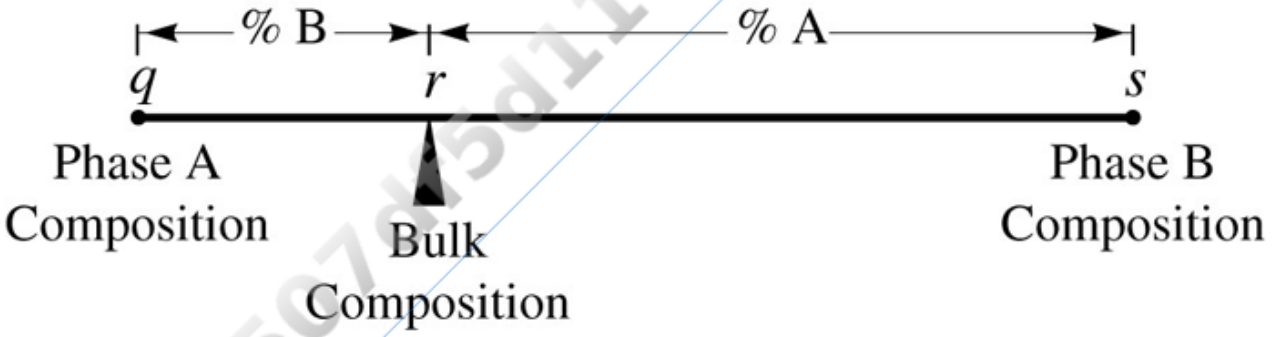

FIGURE 5.5 Lever rule. Given the bulk composition and a tie-line *qrs* between the compositions of phase A and phase B, the relative amounts of A and B are given by the relative lengths of the two line segments: %A = *rs/qs* and %B = *qr/qs*. Back to text

DO NOT COPY
e48d507df5d1141@placeholder.9409-

Printed by: e48d507df5d1141@placeholder.94092.edu. Printing is for personal, private use only. No part of this book may be reproduced or transmitted without publisher's prior permission. Violators will be prosecuted.

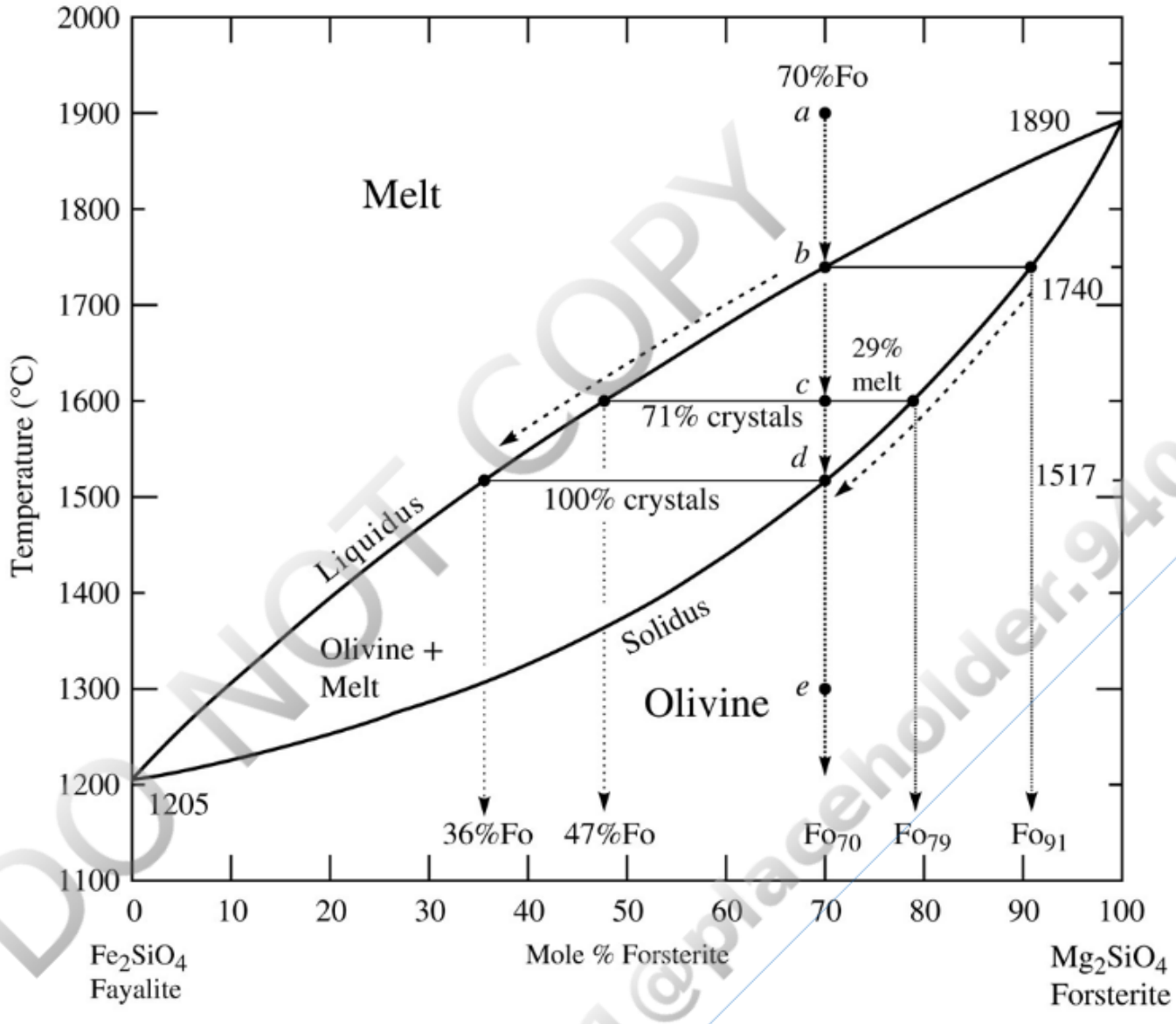

FIGURE 5.6 Olivine crystallization at 1 atm pressure. After Bowen and Schairer (1935). See text for discussion. Back to text

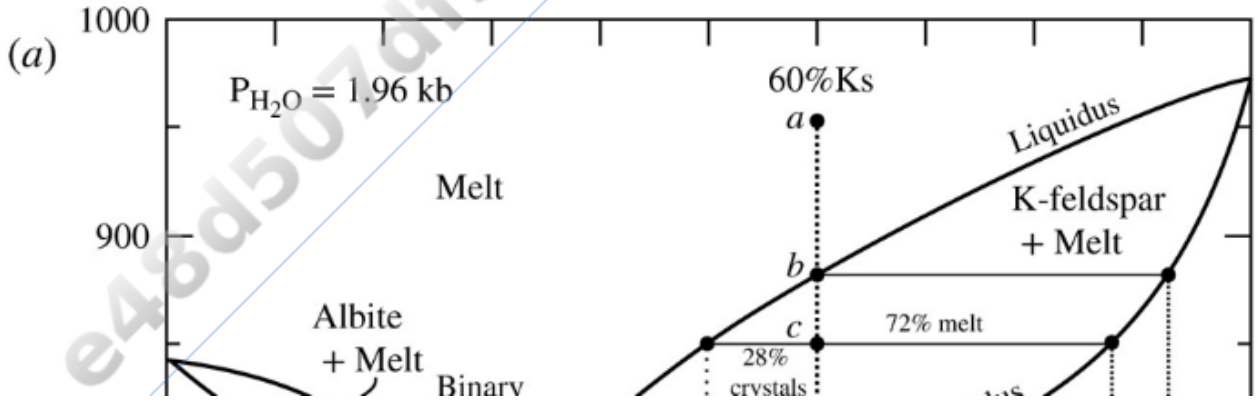

DO NOT COPY
e48d507df5d1141@placeholder.9409-

https://print.vitalsource.com/requests/GM7Nq1ZS0WtoausAQTDB/c...

Printed by: e48d507df5d1141@placeholder.94092.edu. Printing is for personal, private use only. No part of this book may be reproduced or transmitted without publisher's prior permission. Violators will be prosecuted.

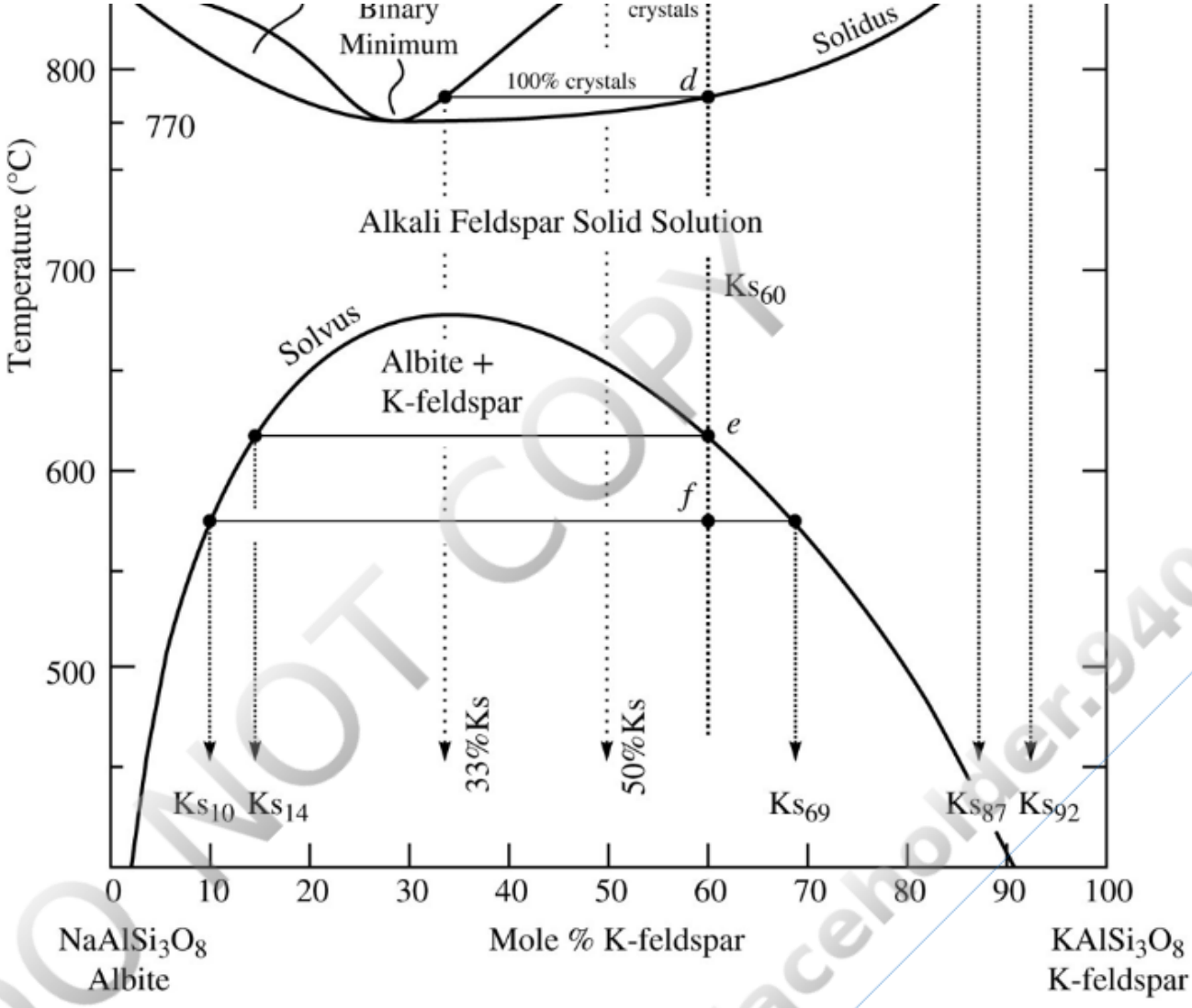

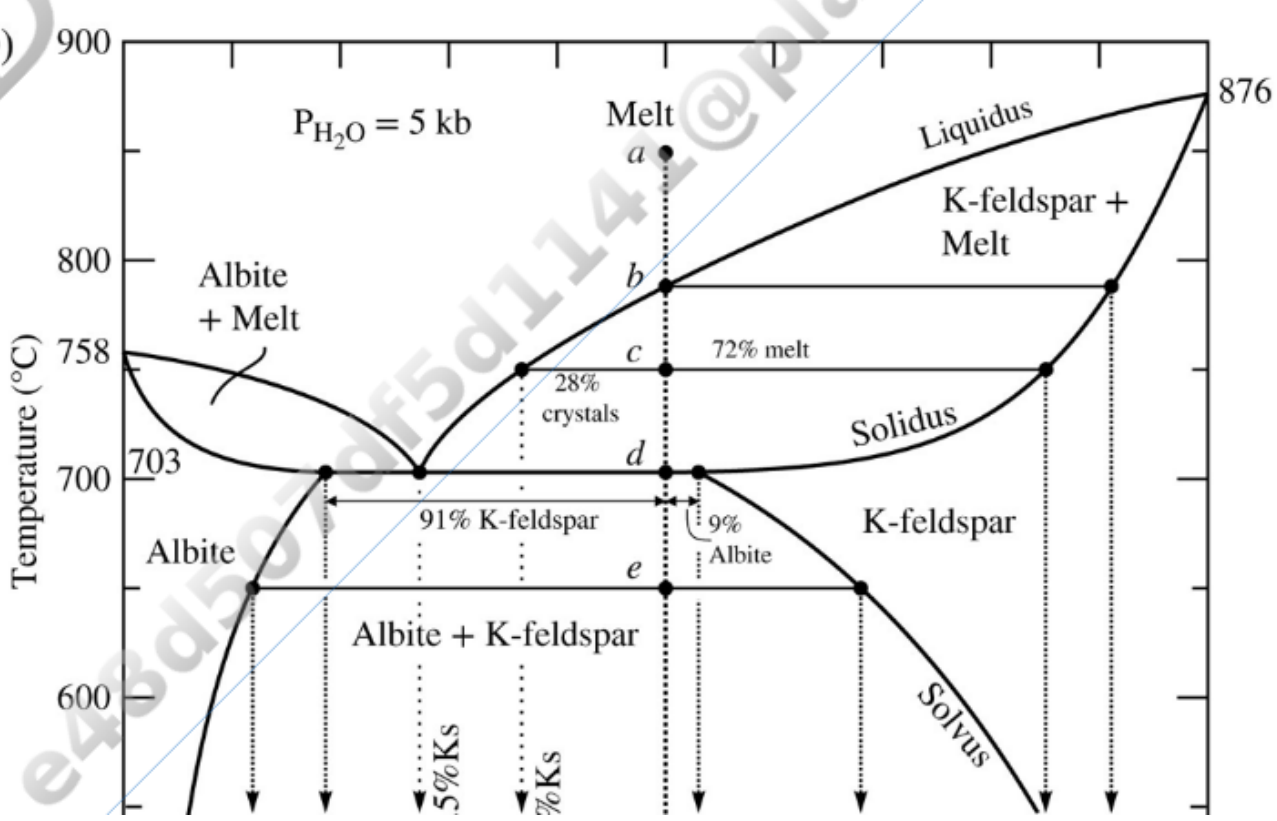

DO NOT COPY
e48d507df5d1141@placeholder.9409

Printed by: e48d507df5d1141@placeholder.94092.edu. Printing is for personal, private use only. No part of this book may be reproduced or transmitted without publisher's prior permission. Violators will be prosecuted.

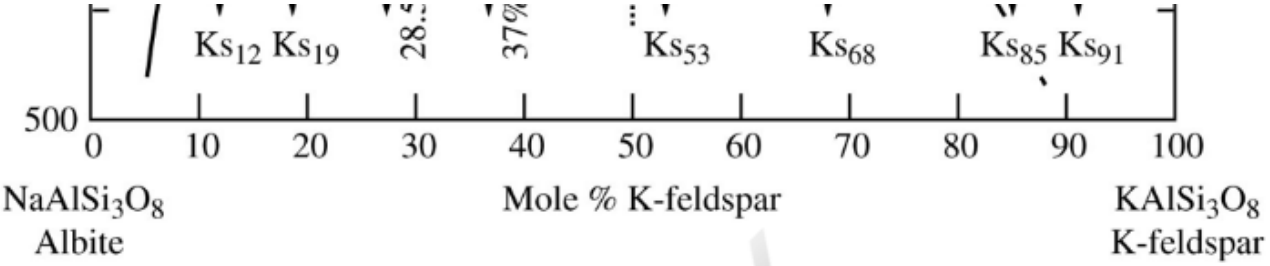

FIGURE 5.7 Alkali feldspar crystallization. (*a*) The system at 1.96 kbar water pressure (after Bowen and Tuttle, 1950; the solvus is from Thompson and Waldbaum, 1969). (*b*) The system at 5 kbar water pressure (Morse, 1970). See text for discussion. Back to text

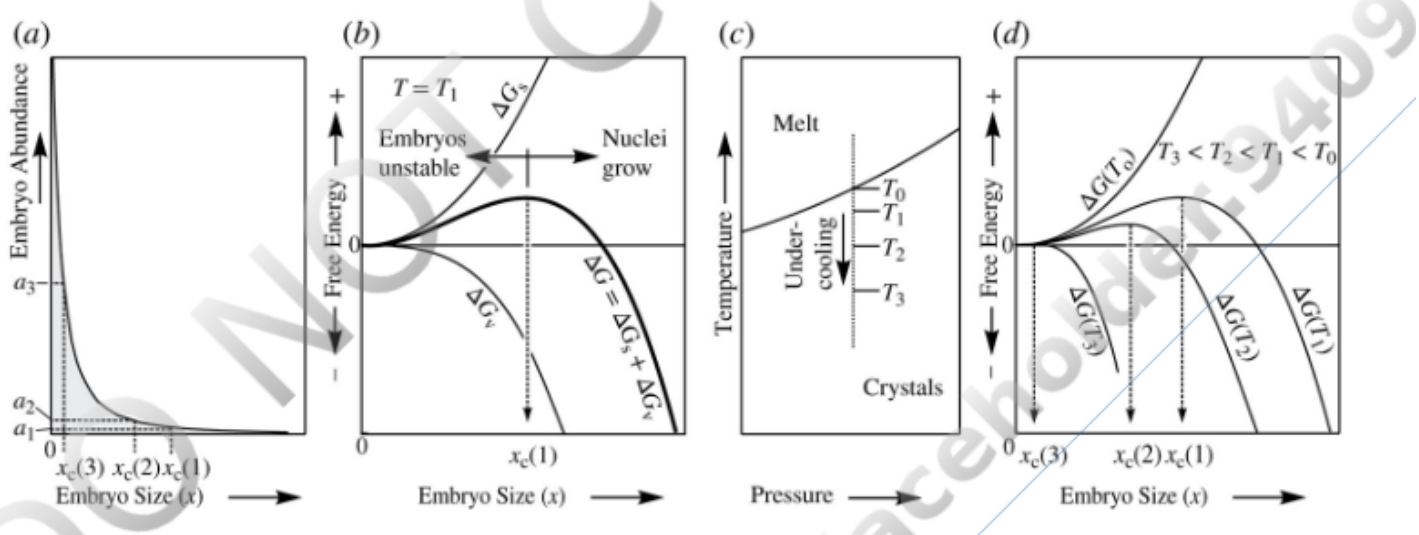

FIGURE 5.8 Formation of crystal embryo from a melt. (*a*) Abundance of different-sized crystal embryos in melt. Small embryos are much more abundant than large embryos. (*b*) The Gibbs free energy of formation ΔG of crystal embryos is the sum of the surface energy ΔG_S and ΔG_V. Only embryos larger than the critical growth radius x_c are stable with respect to the melt; additional growth reduces the energy level. Crystal embryos smaller than x_c will be resorbed spontaneously by the melt because they represent a higher-energy configuration than melt, and additional growth involves an increase in energy. (*c*) Schematic T–P plot of mineral stability with different degrees of undercooling T_0, T_1, T_2, and T_3. (*d*) The critical growth radius for different degrees of undercooling. See text for discussion. Back to text

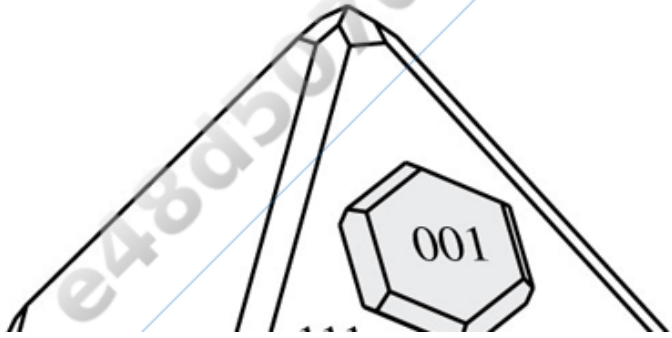

Printed by: e48d507df5d1141@placeholder.94092.edu. Printing is for personal, private use only. No part of this book may be reproduced or transmitted without publisher's prior permission. Violators will be prosecuted.

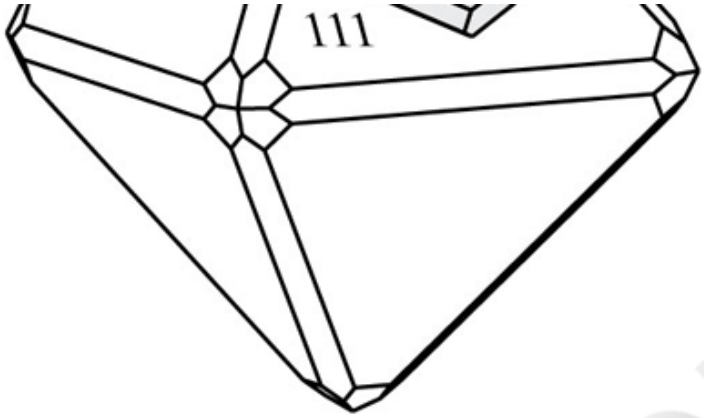

FIGURE 5.9 Epitaxial growth. Hematite crystal (shaded) may nucleate and grow on the (111) face of magnetite. See text for discussion. Back to text

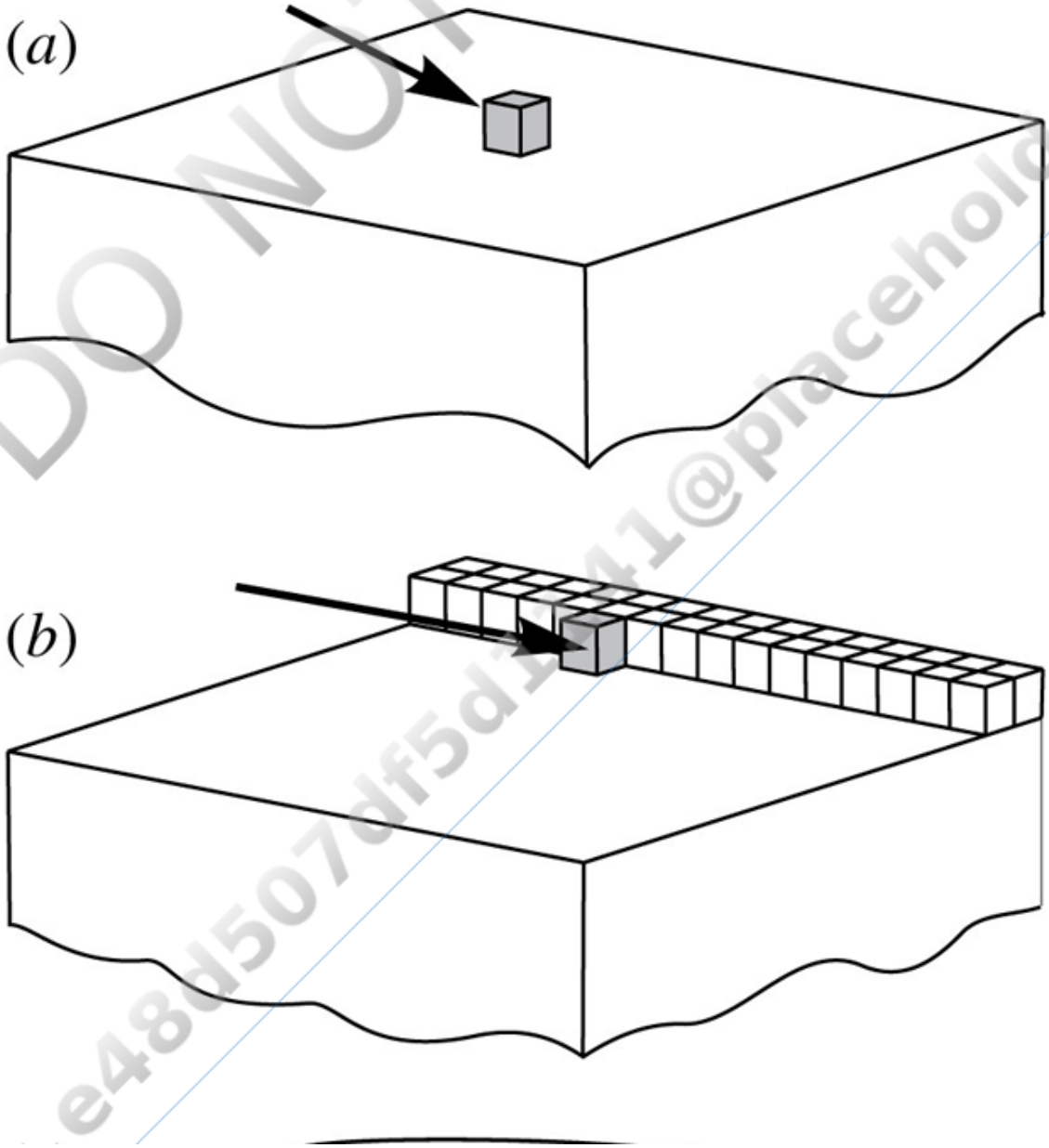

DO NOT COPY
e48d507df5d1141@placeholder.9409

Printed by: e48d507df5d1141@placeholder.94092.edu. Printing is for personal, private use only. No part of this book may be reproduced or transmitted without publisher's prior permission. Violators will be prosecuted.

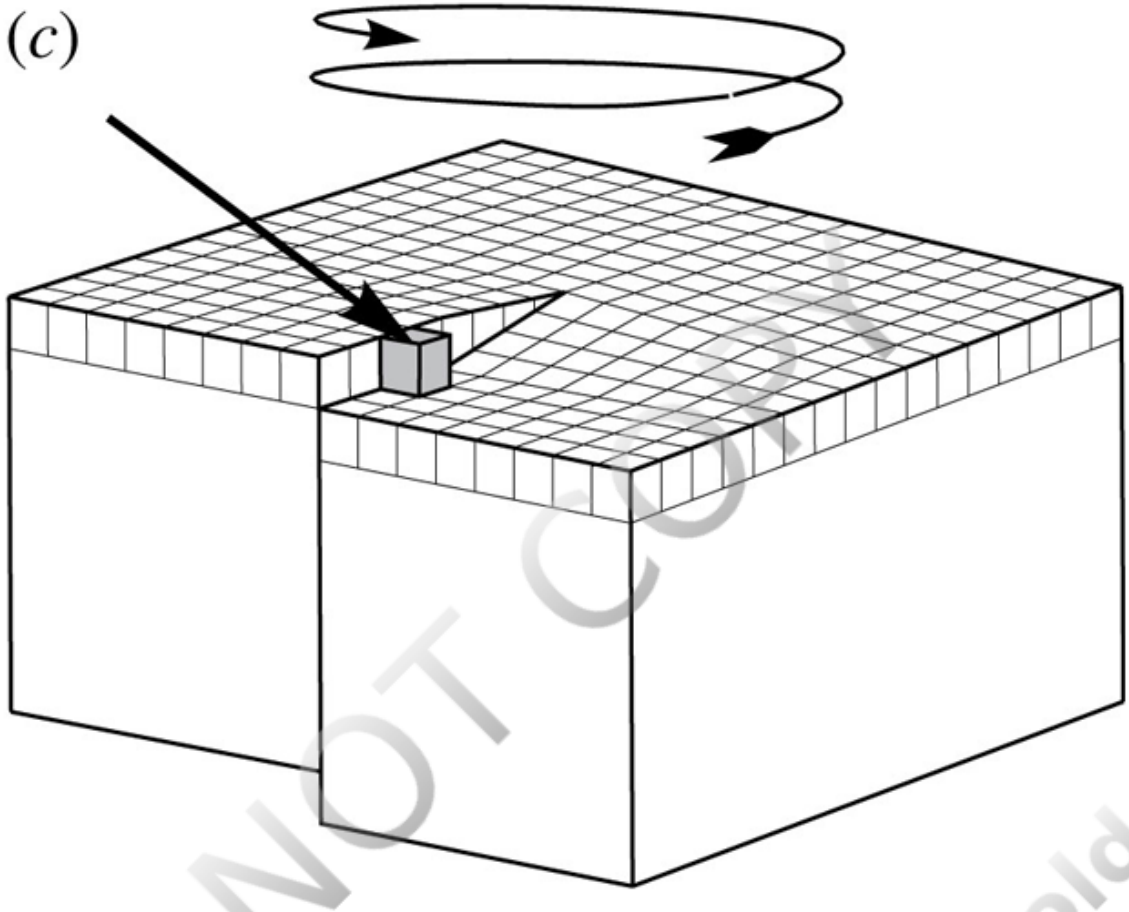

FIGURE 5.10 Growth on a crystal face. (*a*) Adding a new growth unit to a crystal face is energetically difficult because the new unit stands proud of the surface and has many unsatisfied chemical bonds. (*b*) Adding a new growth unit along the edge of a partially completed layer is easier because more chemical bonds are satisfied. (*c*) Growth on a screw dislocation ensures that an edge always remains available for growth. The crystal grows by adding a continuous spiraling layer. Back to text

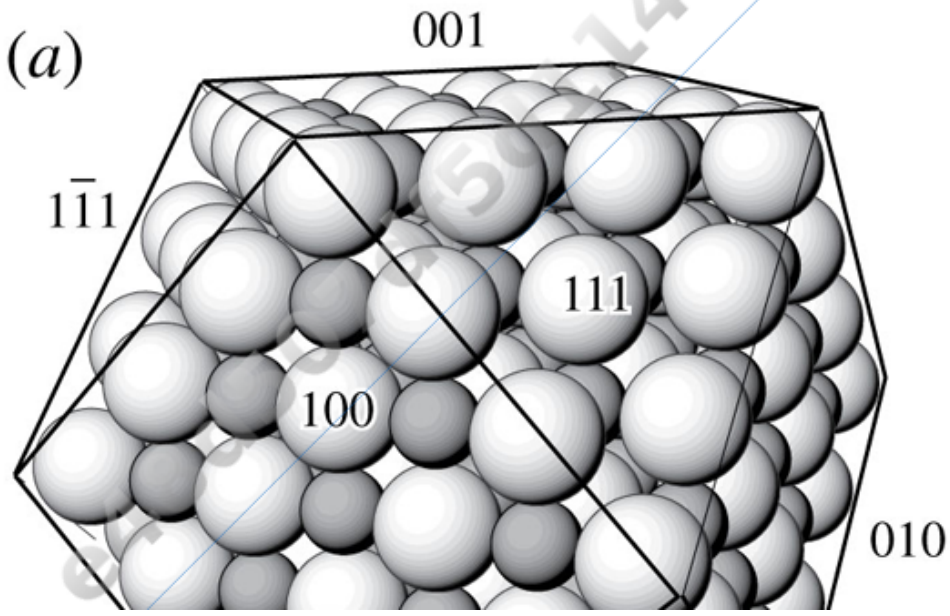

Printed by: e48d507df5d1141@placeholder.94092.edu. Printing is for personal, private use only. No part of this book may be reproduced or transmitted without publisher's prior permission. Violators will be prosecuted.

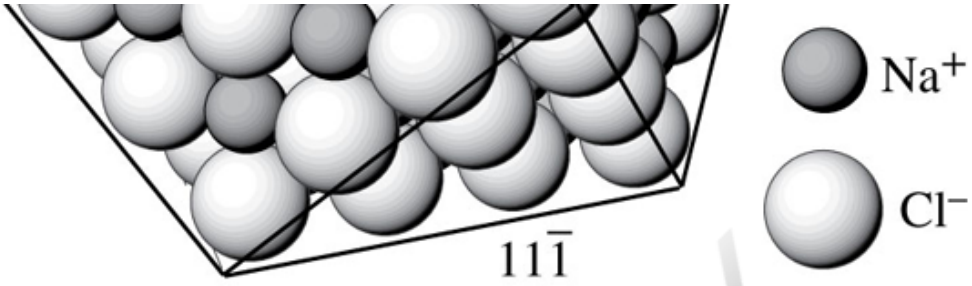

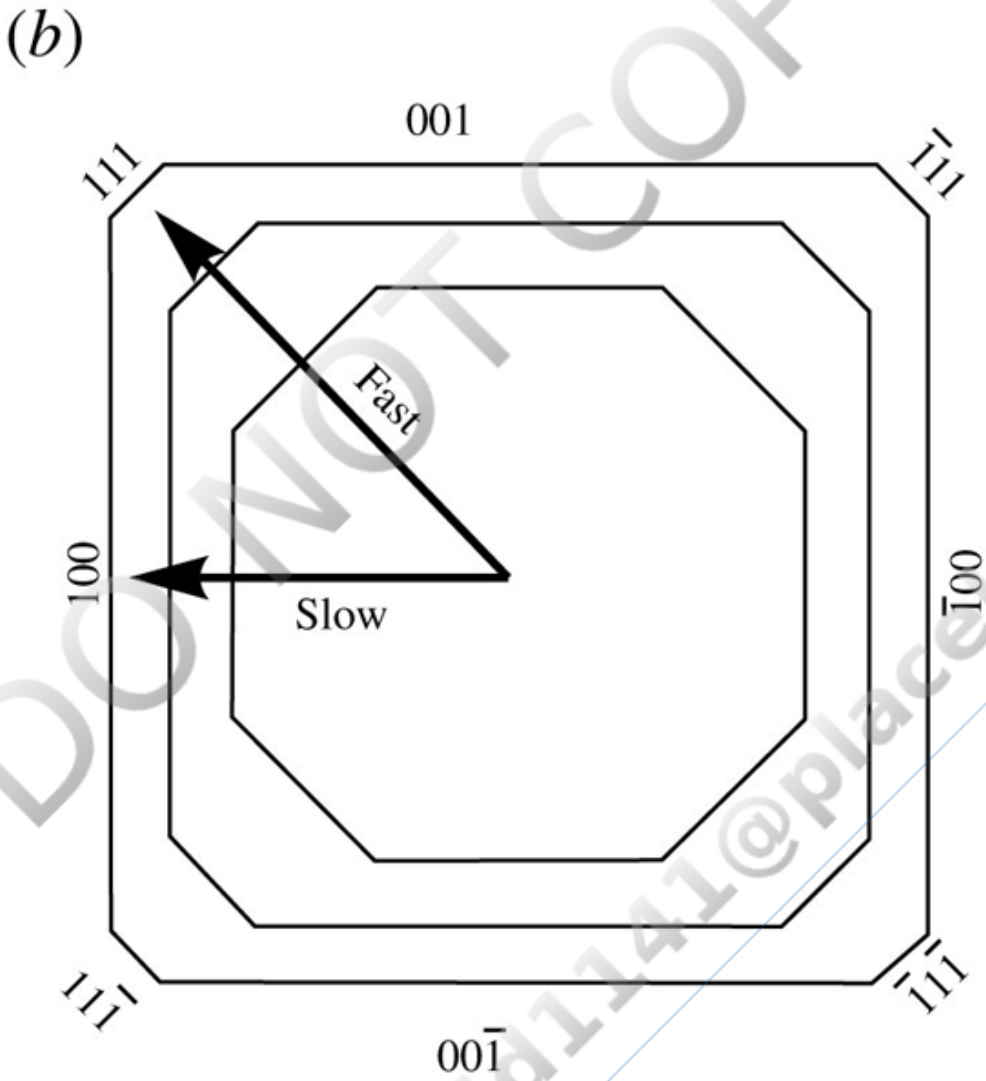

FIGURE 5.11 Slow-growing faces become larger. (*a*) The {111} crystal faces of halite are covered with either all Na^+ or all Cl^- and have a high net charge and high surface energy, which strongly attracts successive layers of Na^+ and Cl^- on such faces to produce high growth rates. The {001} faces have equal numbers of Na^+ and Cl^- with a relatively low charge and low surface energy leading to slow growth rates. (*b*) Section through the halite crystal showing {001} and {111} faces. Because growth rate on the {111} faces is higher than on the slow-growing {100} faces, the {111} faces will "grow" out of existence. Back to text

DO NOT COPY
e48d507df5d1141@placeholder.9409

Printed by: e48d507df5d1141@placeholder.94092.edu. Printing is for personal, private use only. No part of this book may be reproduced or transmitted without publisher's prior permission. Violators will be prosecuted.

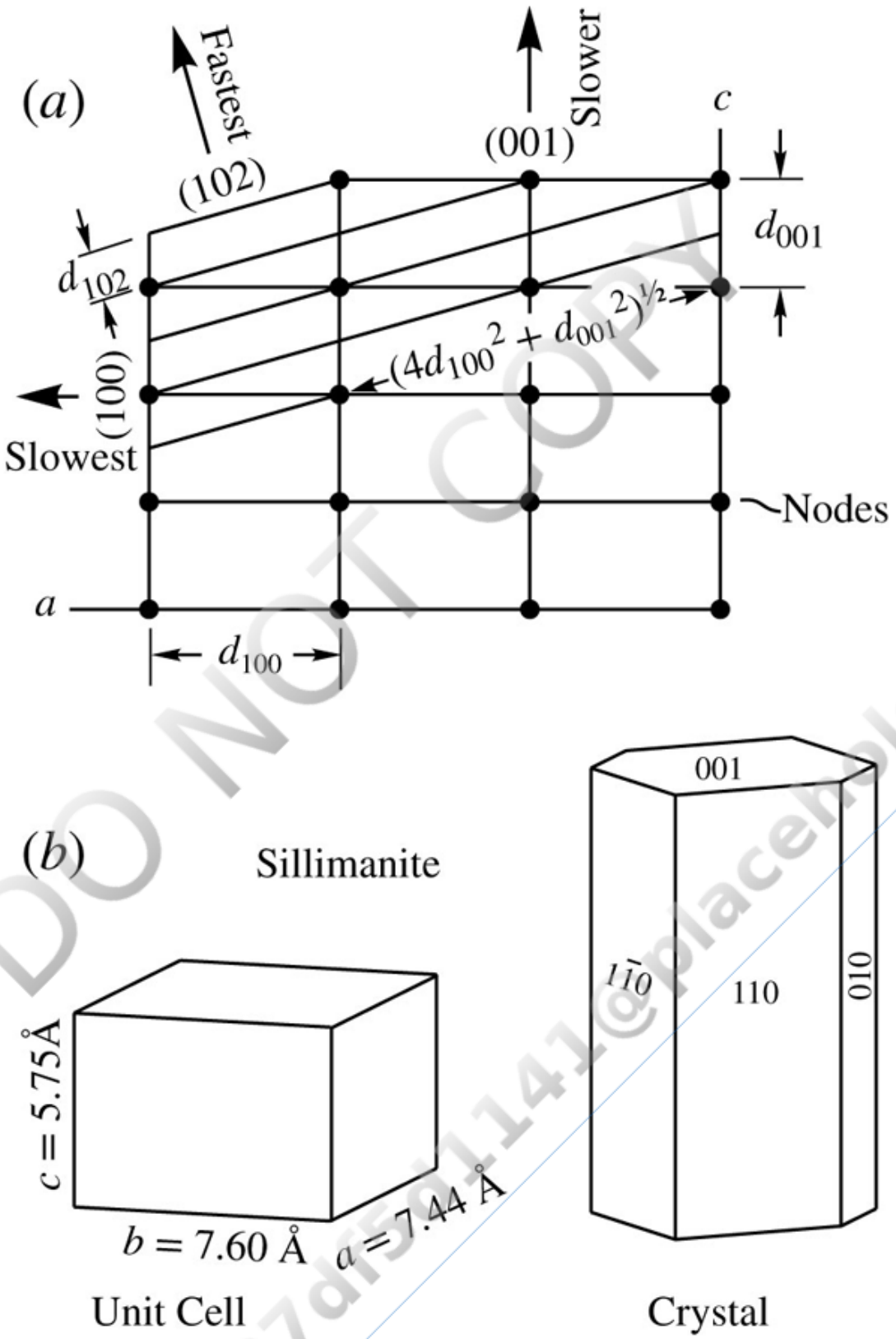

FIGURE 5.12 Growth rates of crystal faces are inversely proportional to interplanar (d) spacing. (a) Growth is fastest normal to the (102) face, slower normal to the (001) face, and slowest normal to the (100) face because $d_{102} < d_{001} < d_{100}$. Crystals should therefore be elongate parallel to the c axis, and the {102} faces should be small or nonexistent. (b) Sillimanite. The c unit cell dimension is smallest, so crystals are elongate parallel to the c axis. Back to text

DO NOT COPY e48d507df5d1141@placeholder.9409

Printed by: e48d507df5d1141@placeholder.94092.edu. Printing is for personal, private use only. No part of this book may be reproduced or transmitted without publisher's prior permission. Violators will be prosecuted.

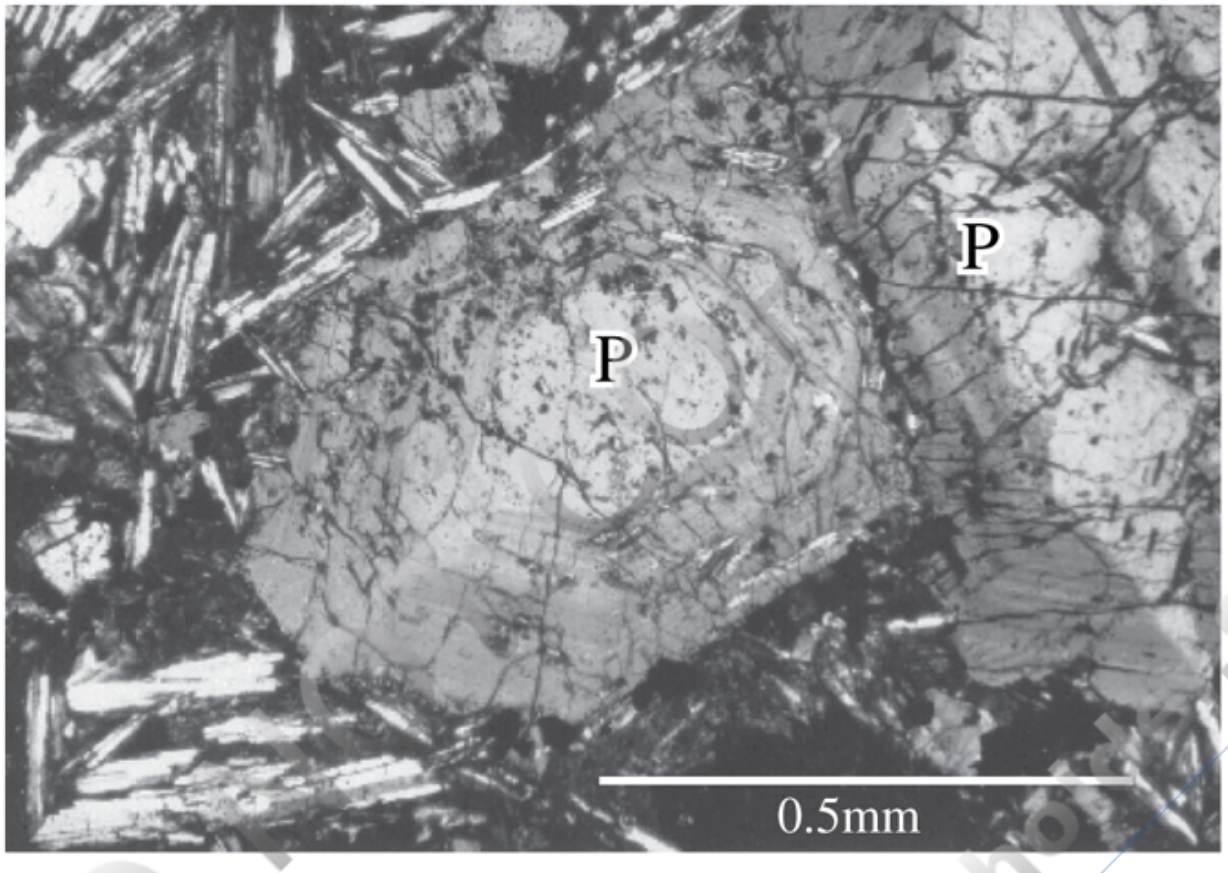

FIGURE 5.13 Photomicrograph of a thin section (see Chapter 7) showing zoned crystals of pyroxene (P) (crossed polarizers). The chemical zoning is indicated by a change in the color from the center of crystals to the rim. The slender crystals are plagioclase. See also Figure 12.12 for zoned plagioclase. Back to text

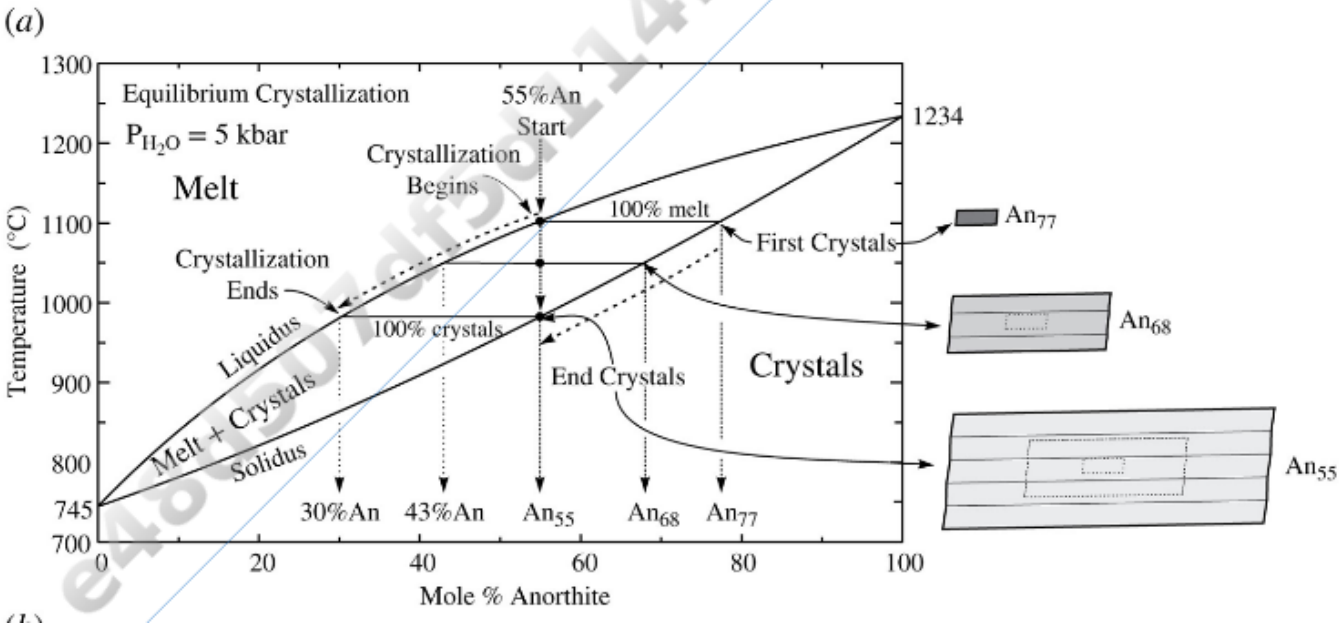

Printed by: e48d507df5d1141@placeholder.94092.edu. Printing is for personal, private use only. No part of this book may be reproduced or transmitted without publisher's prior permission. Violators will be prosecuted.

(*b*)

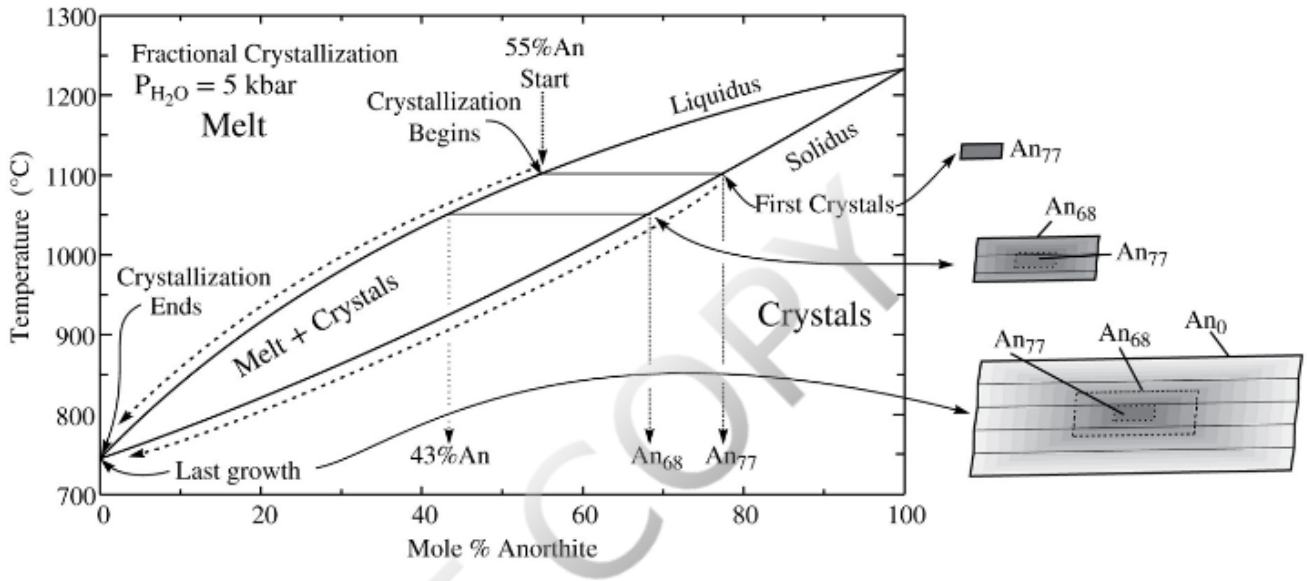

FIGURE 5.14 Plagioclase phase diagram at 5 kbar water pressure. Adapted from Yoder and others (1957). (*a*) Equilibrium crystallization. (*b*) Fractional crystallization. See text for discussion. Back to text

(*a*)

(*b*)

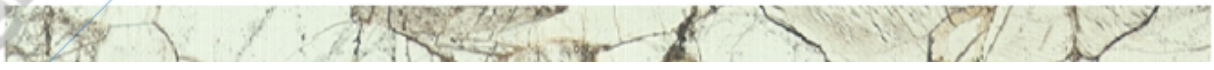

DO NOT COPY

Printed by: e48d507df5d1141@placeholder.94092.edu. Printing is for personal, private use only. No part of this book may be reproduced or transmitted without publisher's prior permission. Violators will be prosecuted.

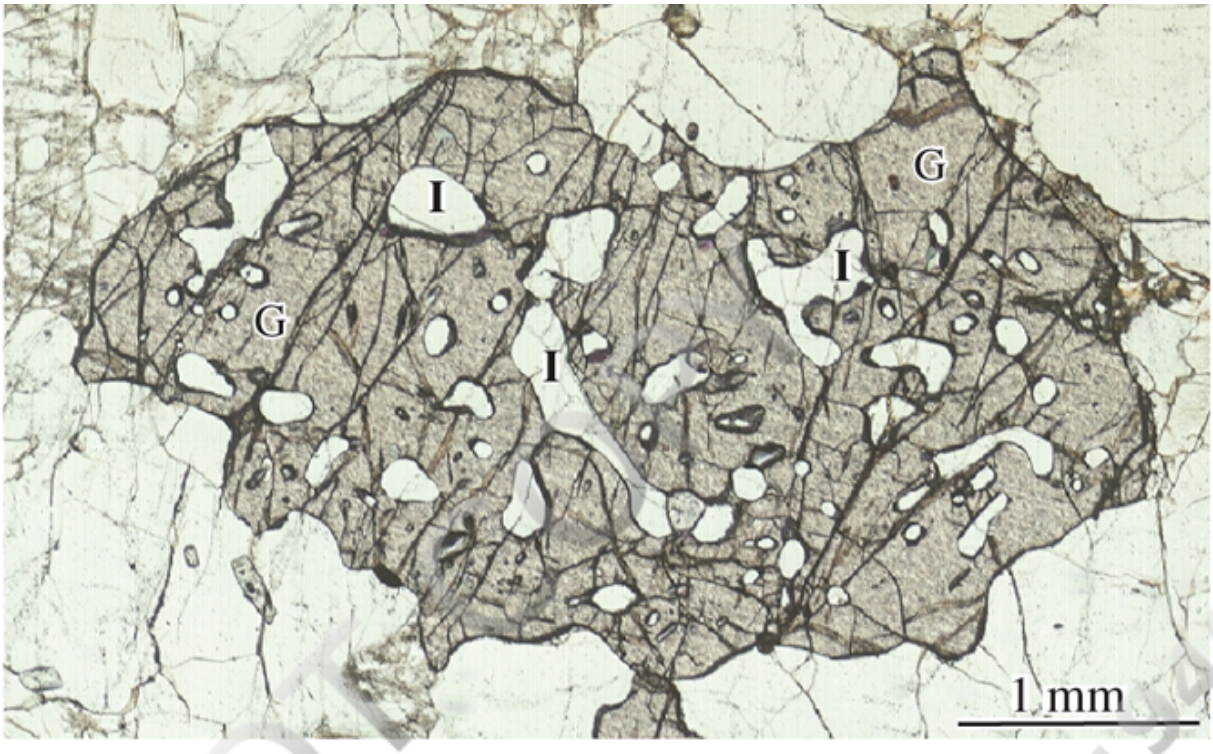

FIGURE 5.15 Examples of inclusions. (*a*) Fracture surface of a sanidine crystal as viewed through the hand lens. Four relatively large black biotite inclusions are in the image's center. Small black flecks elsewhere in the image are also biotite inclusions. (*b*) Photomicrograph of a thin section showing an anhedral garnet (G) with many irregularly shaped inclusions (I) of mostly quartz. Only three inclusions are labeled. Plane-polarized light. Back to text

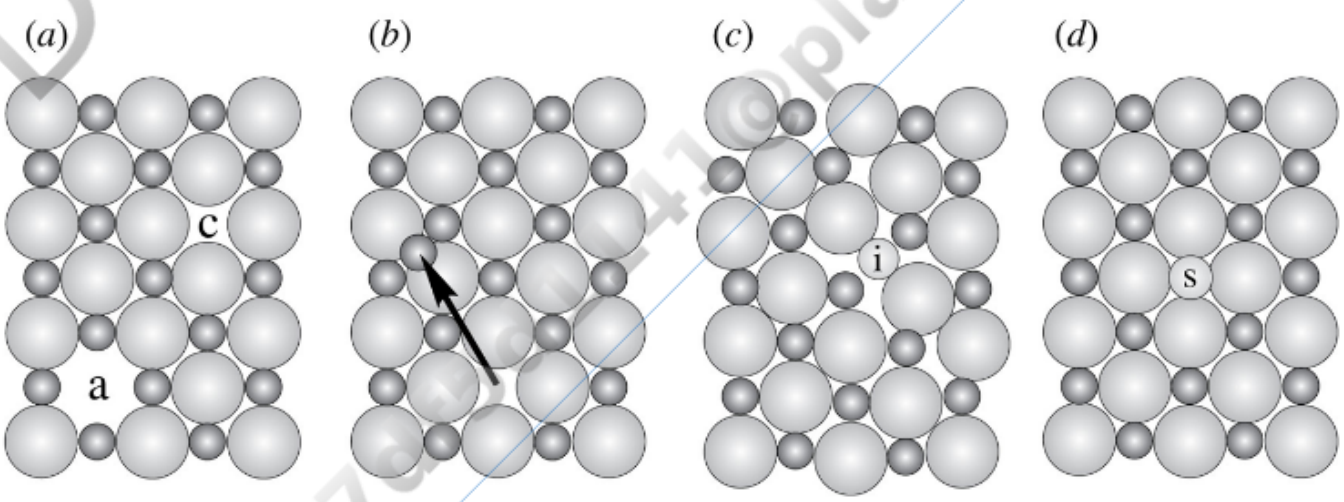

FIGURE 5.16 Point defects. (*a*) Schottky defects. A missing cation (c) is balanced by a missing anion (a). (*b*) Frenkel defects. A cation, missing from its normal structural site, is located elsewhere in the structure (arrow). (*c*) Interstitial defect. A foreign cation is located in the structure (i), presumably charge balanced elsewhere. (*d*) Substitution defect. A foreign cation (s) substitutes for a cation normally in the structure. Back to text

Printed by: e48d507df5d1141@placeholder.94092.edu. Printing is for personal, private use only. No part of this book may be reproduced or transmitted without publisher's prior permission. Violators will be prosecuted.

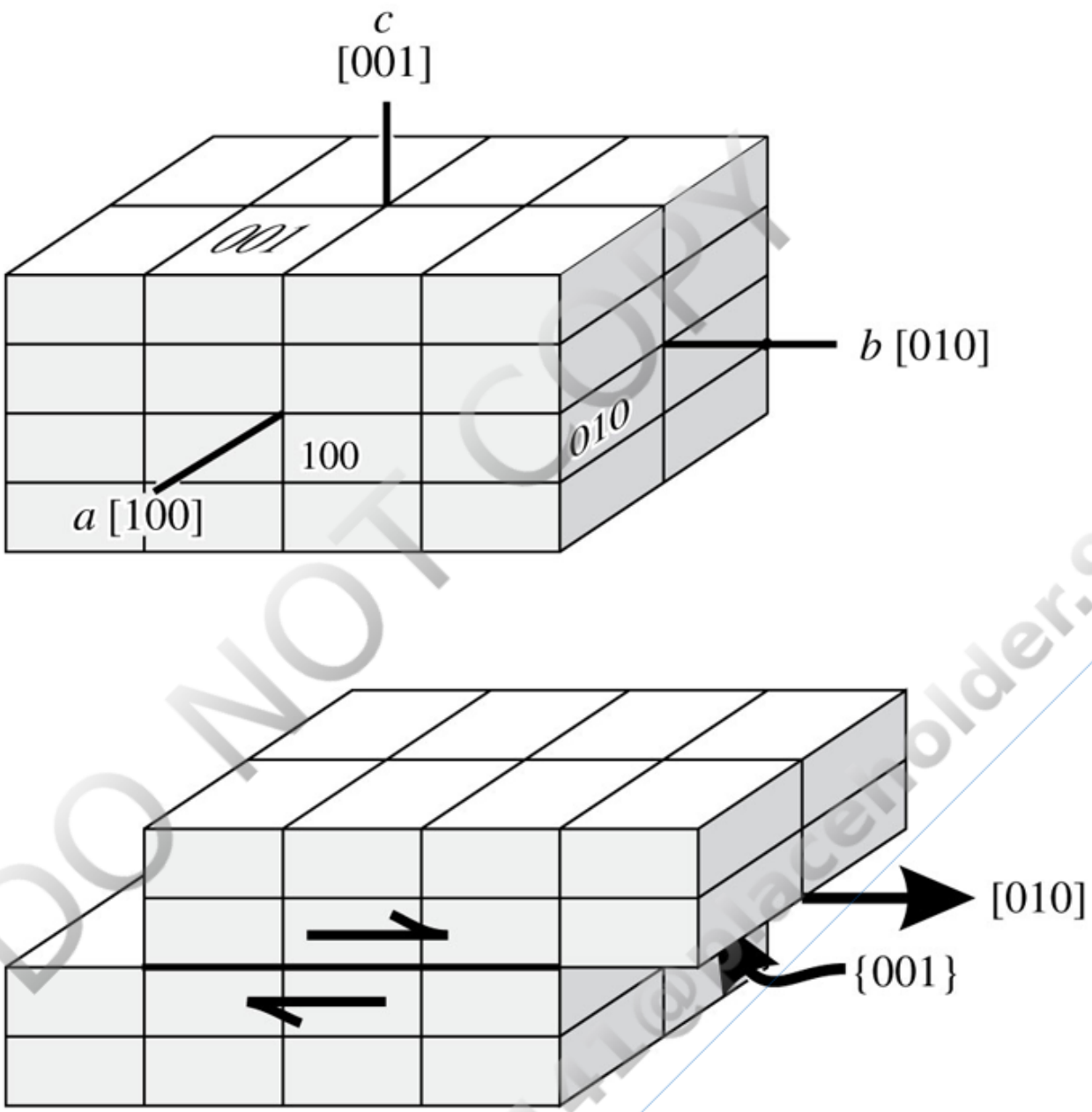

FIGURE 5.17 Slip system in a crystal lattice. Slip occurs on a crystal plane parallel to (001) and in a direction parallel to [010] (the *b* axis), so the slip system is {001}[010]. Back to text

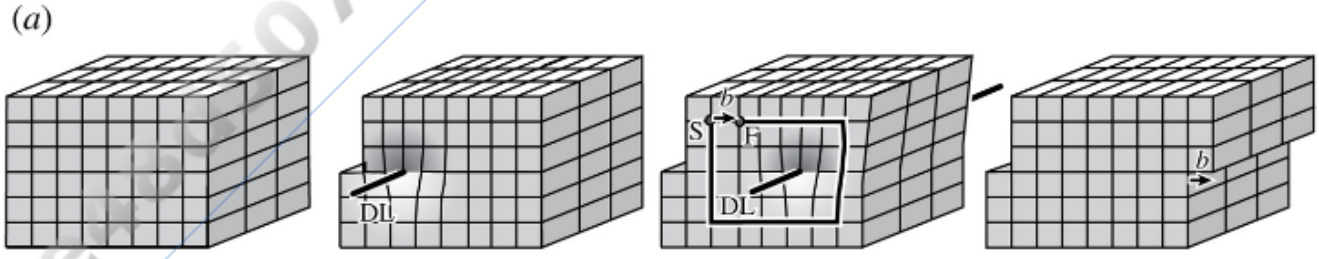

Printed by: e48d507df5d1141@placeholder.94092.edu. Printing is for personal, private use only. No part of this book may be reproduced or transmitted without publisher's prior permission. Violators will be prosecuted.

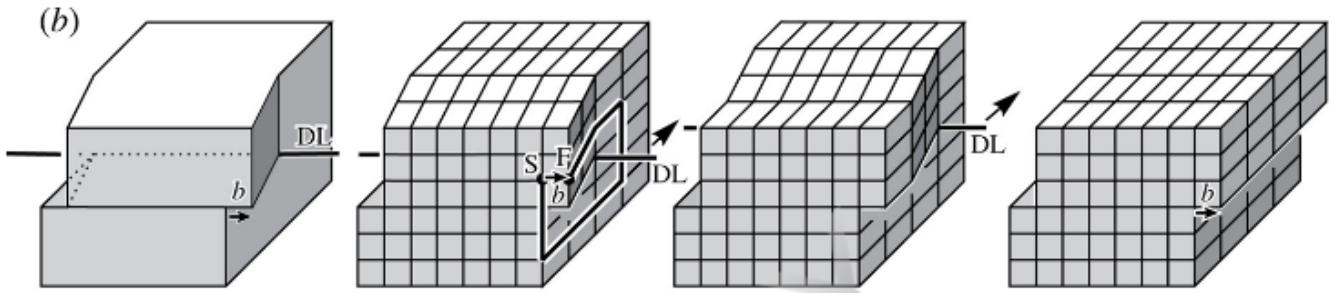

FIGURE 5.18 Dislocations. The Burgers vector *b* is defined by completing a Burgers circuit. Start at lattice position S and make a box around the dislocation, counting the same number of lattice units in opposite directions, to reach finish position F. Vector *b* between S and F is the Burgers vector. (*a*) An edge dislocation is produced by deforming the crystal as shown. The dislocation line (DL) is perpendicular to the Burgers vector and moves to the right (parallel to the Burgers vector) as deformation progresses. When the dislocation line exits the crystal on the right, the top segment of the crystal is offset relative to the bottom by a distance equal to the Burgers vector. (*b*) Screw dislocation. The dislocation line is parallel to the Burgers vector and moves to the back (perpendicular to the Burgers vector) as deformation progresses. When the dislocation line exits the crystal to the back, the top of the crystal is offset relative to the bottom by a distance equal to the Burgers vector. Back to text

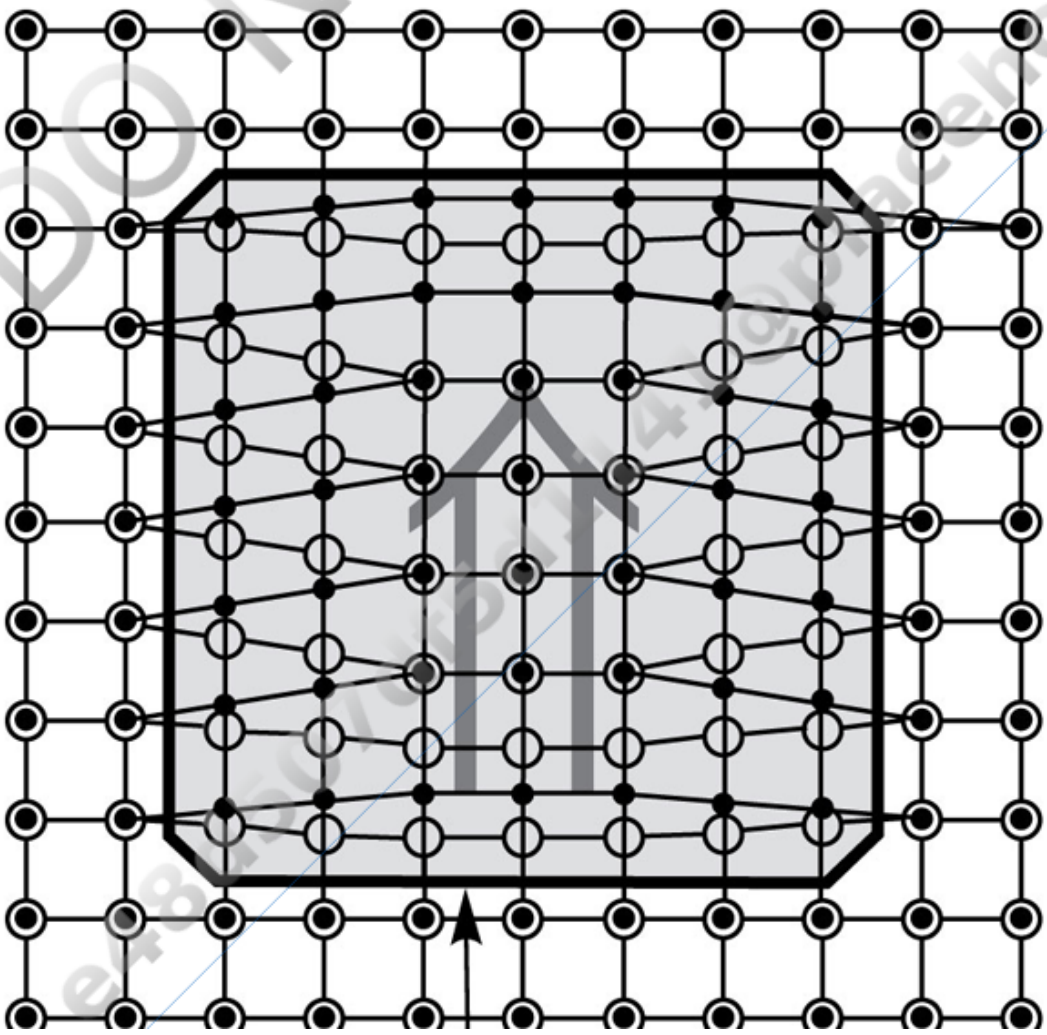

DO NOT COPY

Printed by: e48d507df5d1141@placeholder.94092.edu. Printing is for personal, private use only. No part of this book may be reproduced or transmitted without publisher's prior permission. Violators will be prosecuted.

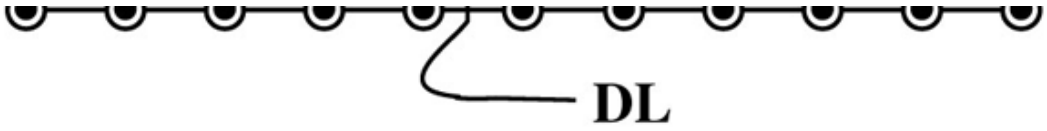

FIGURE 5.19 Unless terminated at the edge of a crystal, a dislocation line (DL) forms a continuous loop outlining a surface, equivalent to a fault, with movement parallel to the Burgers vector. The "fault surface" (shaded) between the lower layer of circles and upper layer of solid dots is bounded by screw dislocations on the sides and edge dislocations at the top and bottom. Back to text

DO NOT COPY

(a)

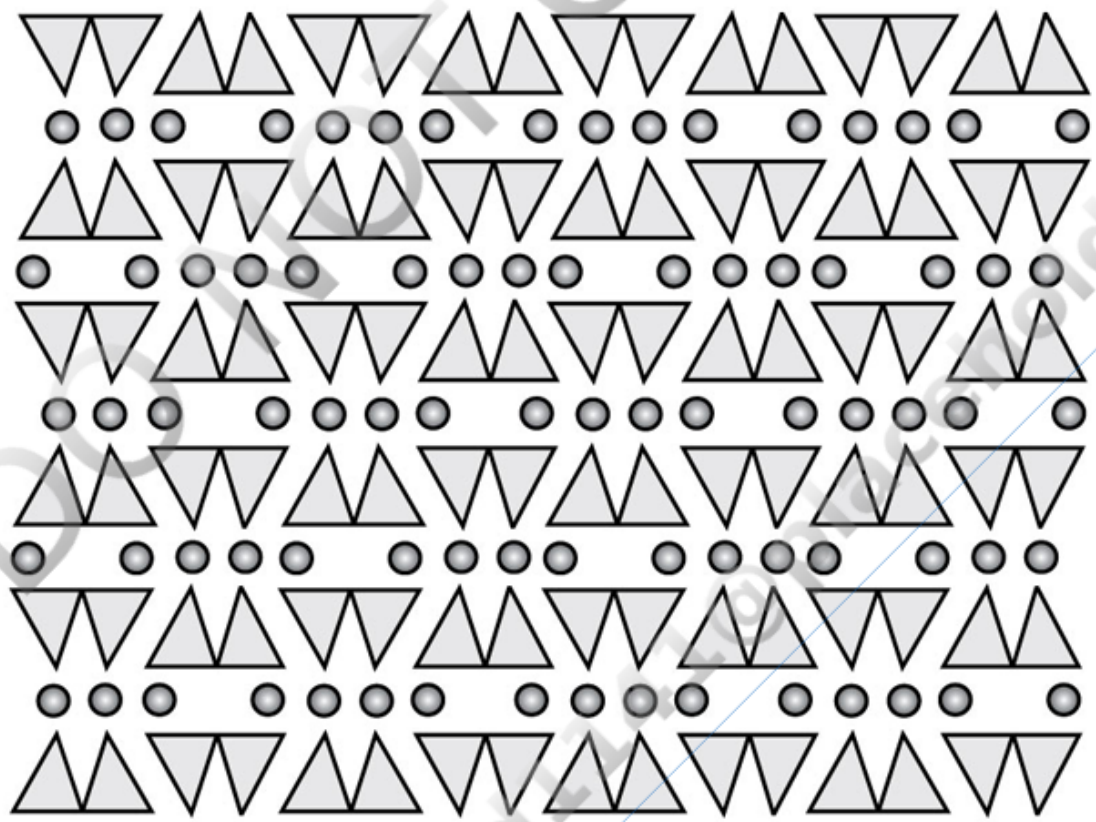

(b)

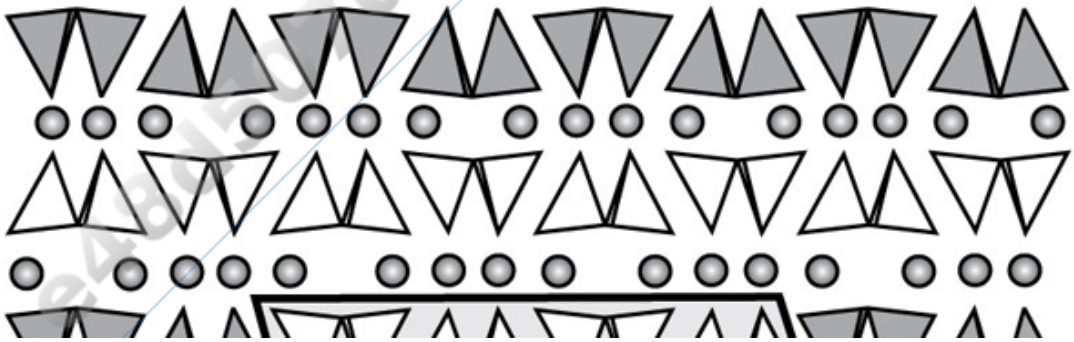

Printed by: e48d507df5d1141@placeholder.94092.edu. Printing is for personal, private use only. No part of this book may be reproduced or transmitted without publisher's prior permission. Violators will be prosecuted.

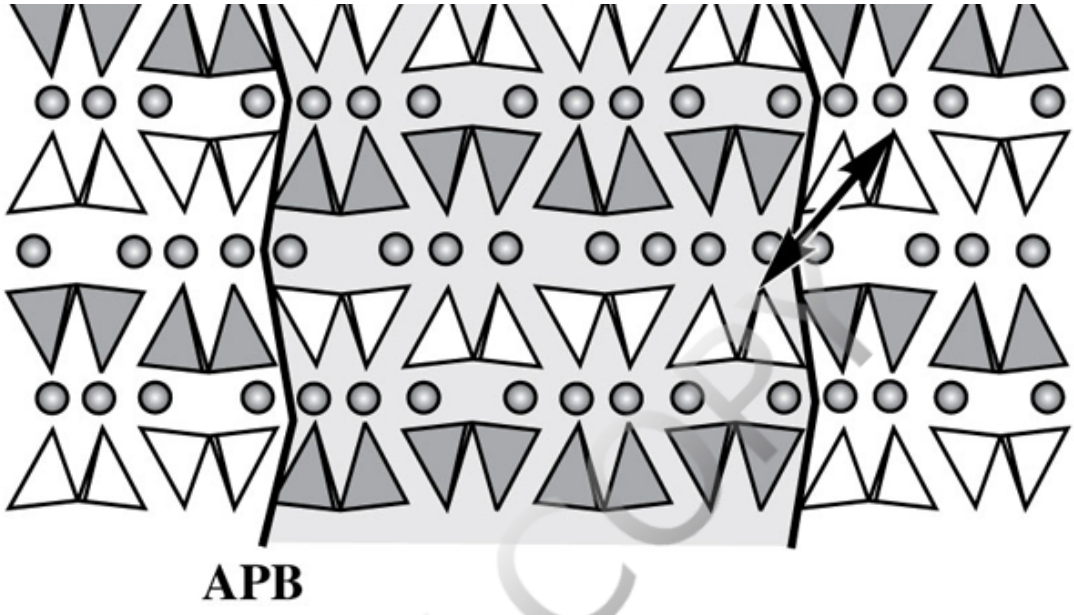

FIGURE 5.20 Antiphase boundary in pigeonite $(Mg,Fe,Ca)_2Si_2O_6$. (*a*) The high-temperature structure consists of chains of silicon tetrahedra extending in and out of the page. The chains are bonded to each other through the Mg, Fe, and Ca (circles). (*b*) Upon cooling, the chains distort, with alternate layers of chains kinking inward (darker) and outward (lighter). The pattern of kinking in one part of the crystal may differ from that in adjacent parts, resulting in the formation of an antiphase domain (shaded) bounded by an antiphase boundary (APB). The antiphase domain is related to the surrounding crystal by a translation (arrow). Back to text

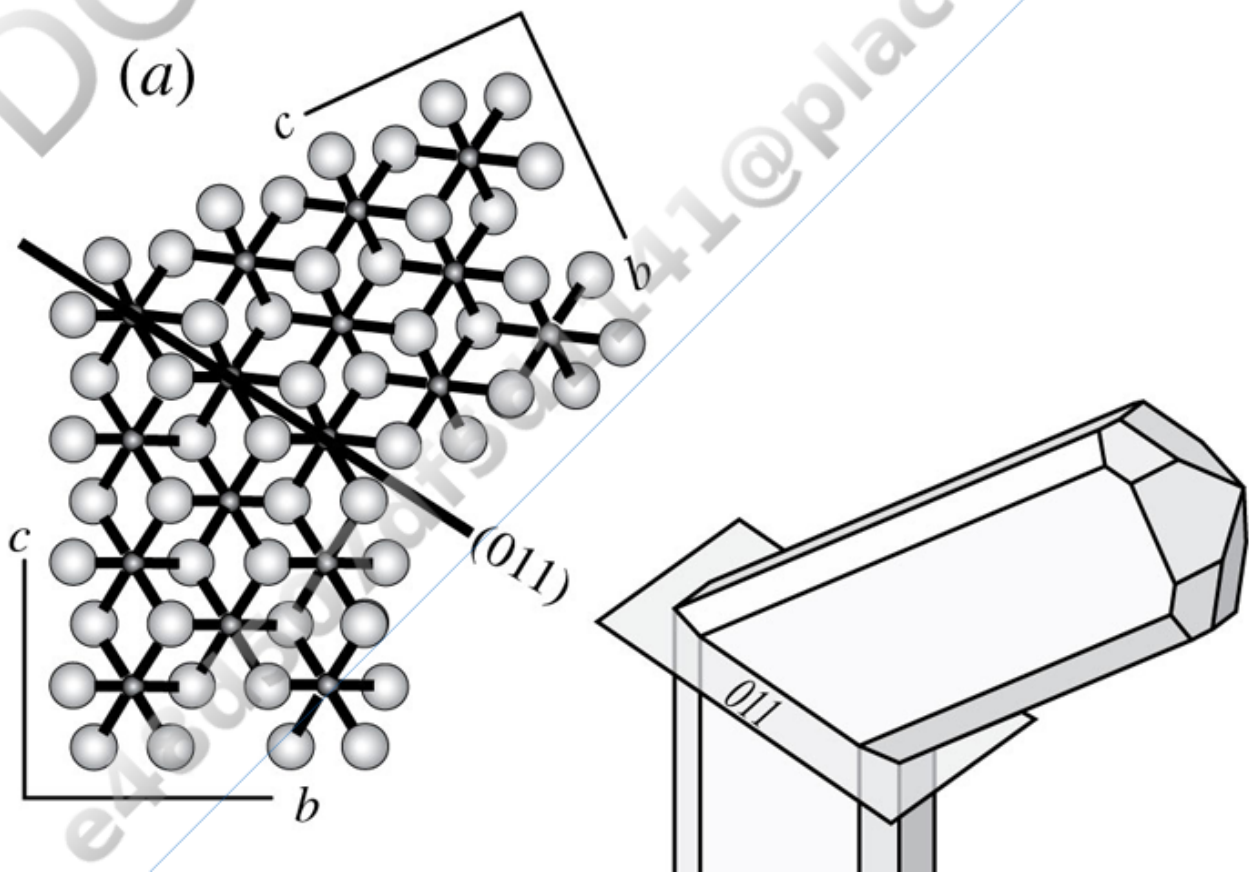

DO NOT COPY
e48d507df5d1141@placeholder.94092

Printed by: e48d507df5d1141@placeholder.94092.edu. Printing is for personal, private use only. No part of this book may be reproduced or transmitted without publisher's prior permission. Violators will be prosecuted.

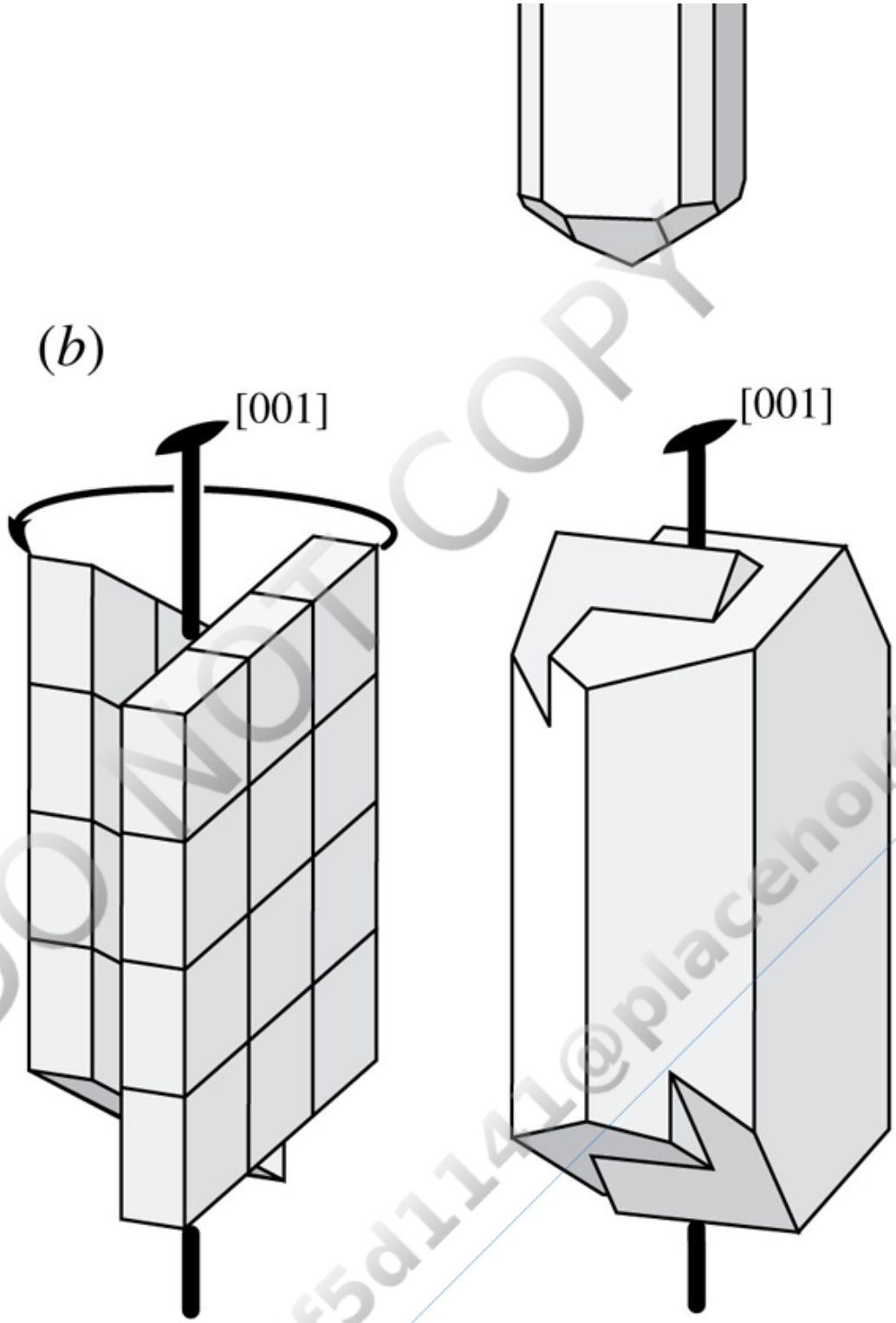

FIGURE 5.21 Symmetry operations in twinning. (*a*) Twinning by reflection on {011} in rutile. (*b*) Twinning by rotation on [001] in K-feldspar to produce a Carlsbad twin. Back to text

DO NOT COPY
e48d507df5d1141@placeholder.9409

(a)

Printed by: e48d507df5d1141@placeholder.94092.edu. Printing is for personal, private use only. No part of this book may be reproduced or transmitted without publisher's prior permission. Violators will be prosecuted.

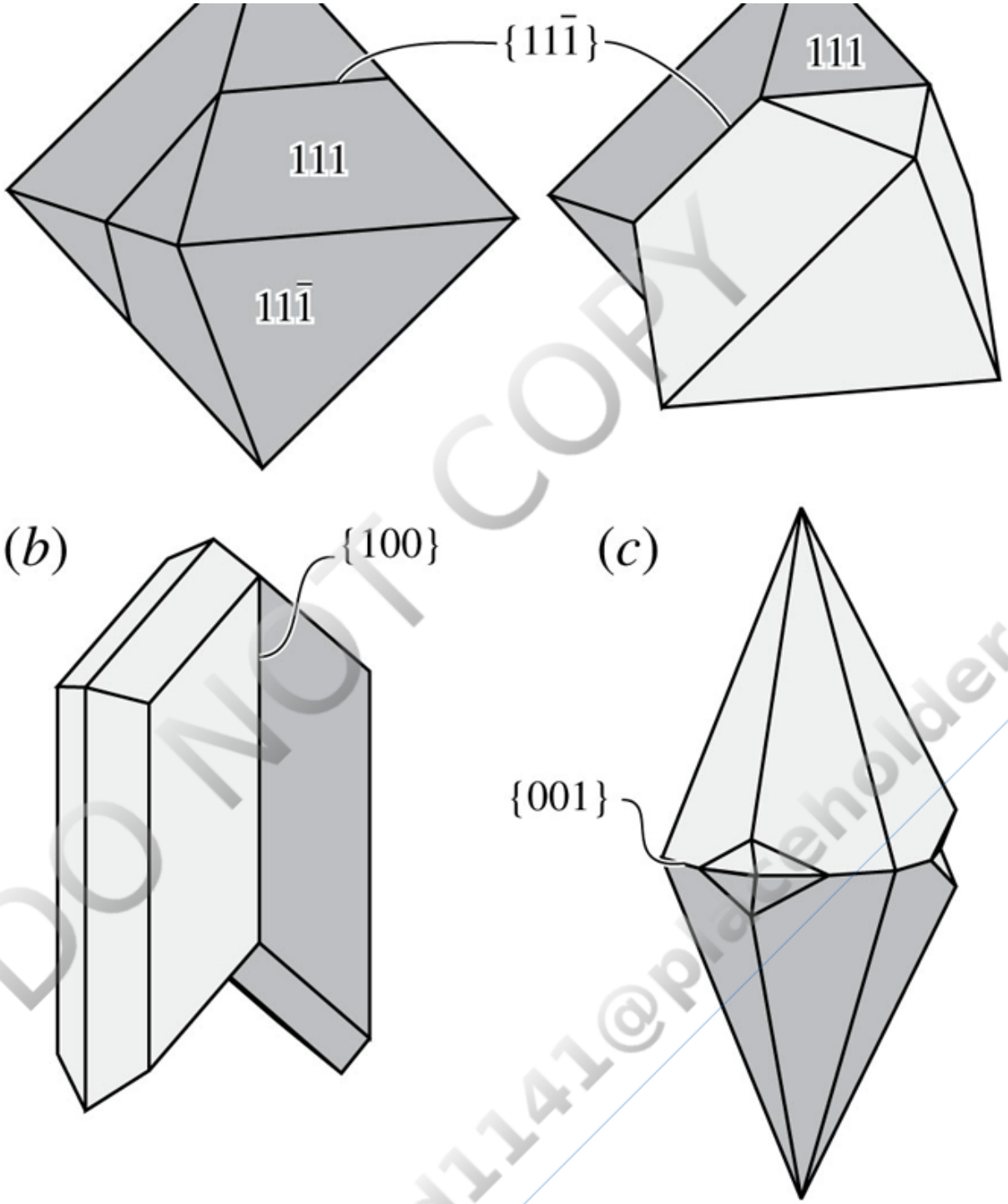

FIGURE 5.22 Contact twins. (*a*) Octahedron of spinel twinned by reflection on $\{11\,\bar{1}\}$ (spinel law). (*b*) Gypsum twinned by reflection on {100}. (*c*) Calcite twin with {001} composition plane.
Back to text

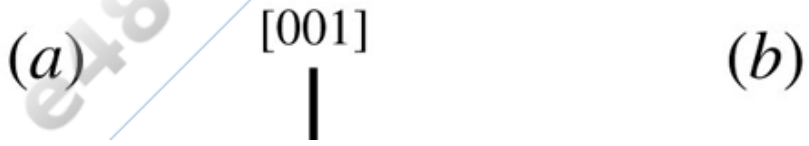

DO NOT COPY
e48d507df5d1141@placeholder.9409

Printed by: e48d507df5d1141@placeholder.94092.edu. Printing is for personal, private use only. No part of this book may be reproduced or transmitted without publisher's prior permission. Violators will be prosecuted.

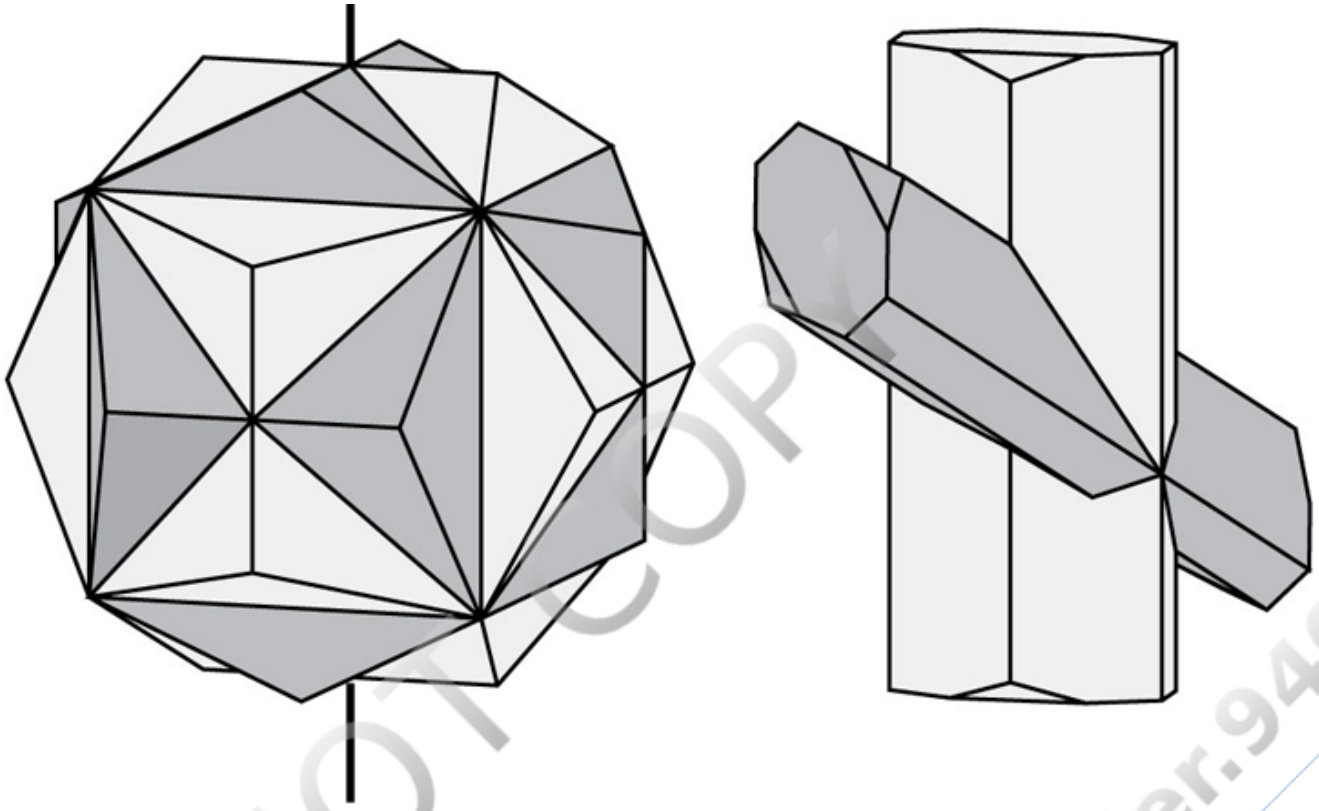

FIGURE 5.23 Penetration twins. (*a*) Pyrite "Iron Cross" twin by 90° rotation on [001]. (*b*) Staurolite twin by reflection on {231}. Back to text

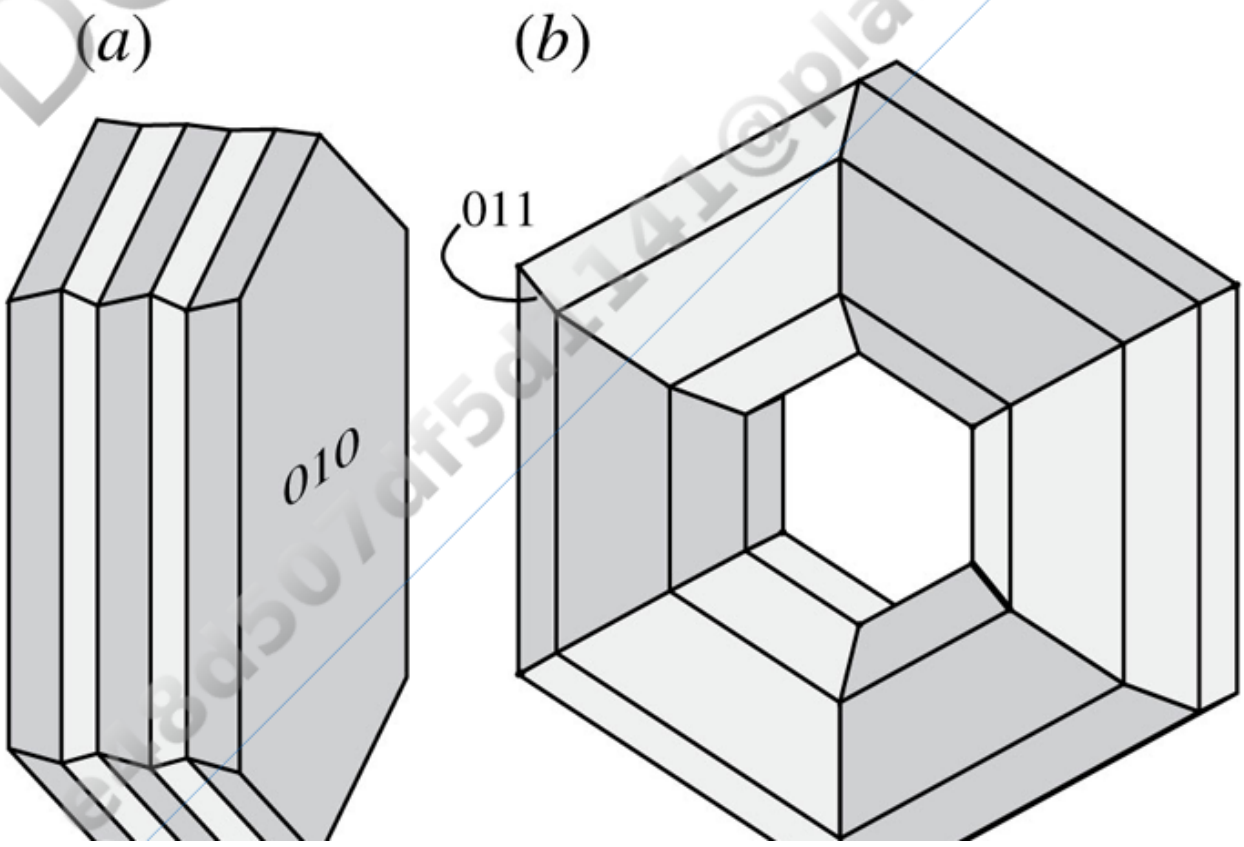

DO NOT COPY
e48d507df5d1141@placeholder.9409

Printed by: e48d507df5d1141@placeholder.94092.edu. Printing is for personal, private use only. No part of this book may be reproduced or transmitted without publisher's prior permission. Violators will be prosecuted.

FIGURE 5.24 Multiple twins. (*a*) Polysynthetic twinning in plagioclase by repeated reflection on {010}. These twins are known as albite twins. (*b*) Cyclic twinning in rutile by repeated reflection on {011}. Back to text

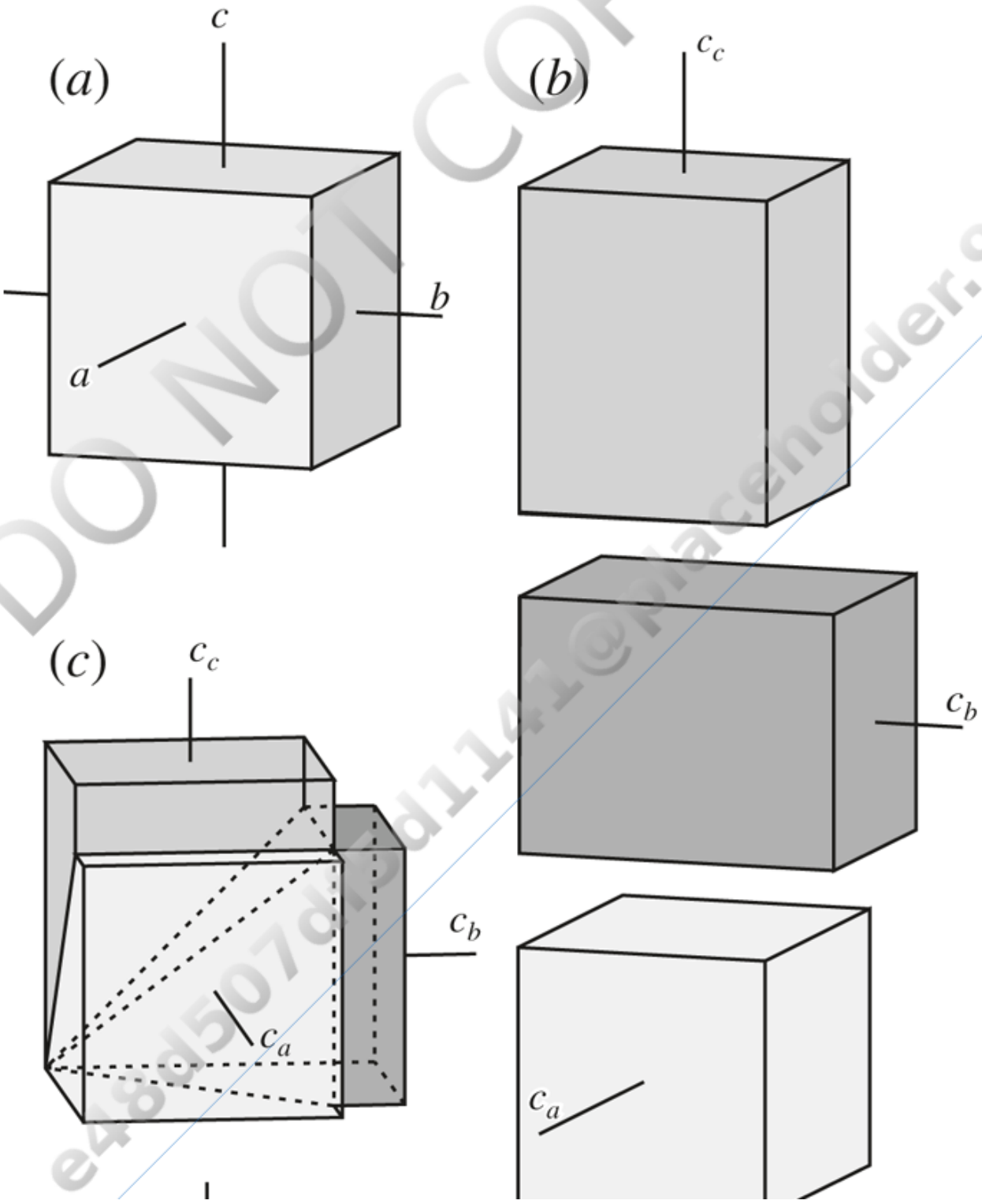

DO NOT COPY
e48d507df5d1141@placeholder.9409

Printed by: e48d507df5d1141@placeholder.94092.edu. Printing is for personal, private use only. No part of this book may be reproduced or transmitted without publisher's prior permission. Violators will be prosecuted.

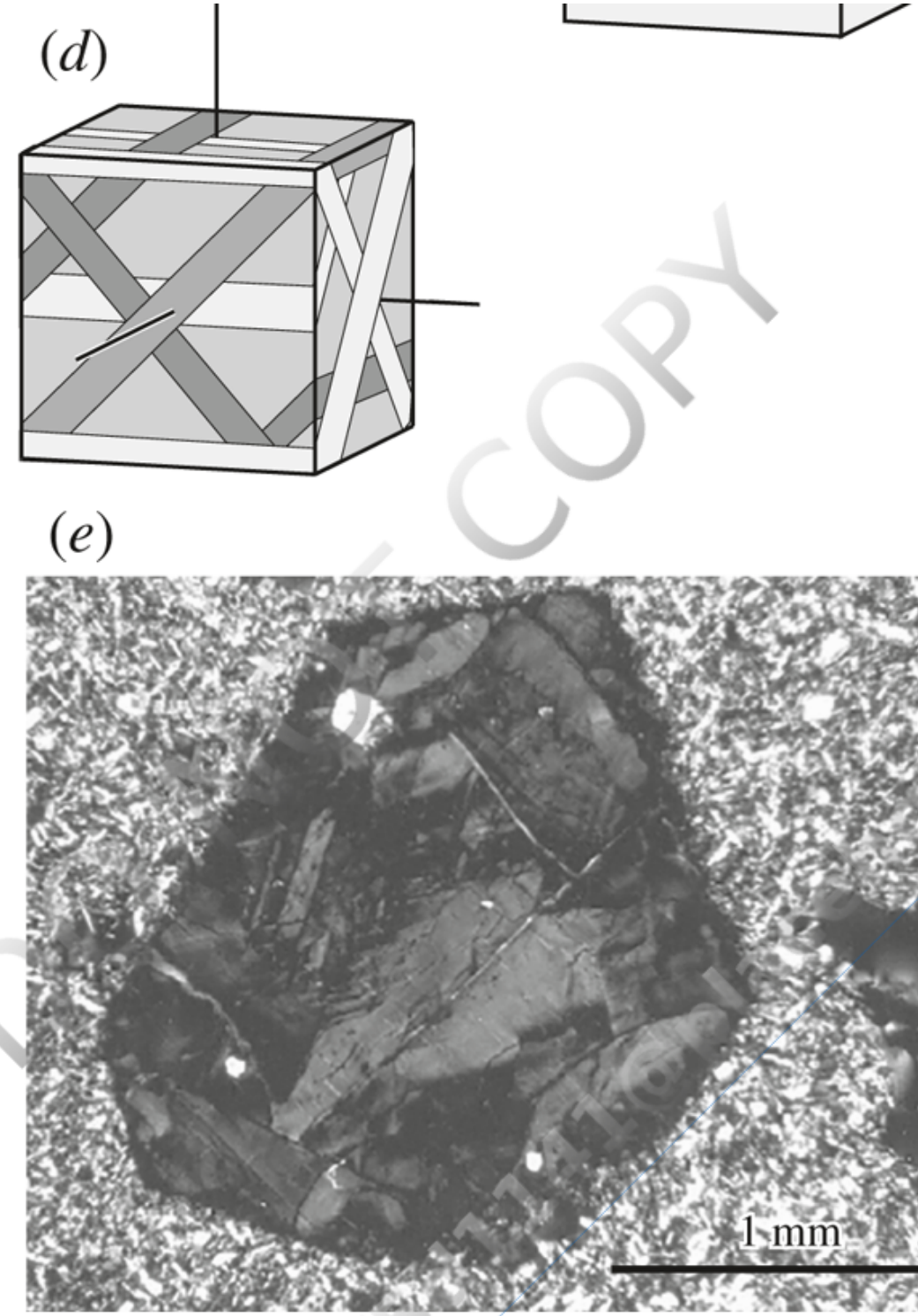

FIGURE 5.25 Transformation twinning in leucite. (*a*) The unit cell is isometric ($a = b = c$) at temperatures above 665°C. (*b*) Below 665°C the symmetry transforms to tetragonal ($a = b < c$). The tetragonal *c* axis could be parallel to either the *a*, *b*, or *c* axis (c_a, c_b, c_c) of the original crystal. When the transformation occurs, different parts of the crystal assume each of the three possible orientations. Dimensions are exaggerated. (*c*) The three orientations are related by reflection on the {101} dodecahedral faces. (*d*) Twinned crystals contain lamellae in each of the three different orientations. (*e*) Photomicrograph of a leucite phenocryst showing twin lamellae related to each other by reflection on {101}. Back to text

Printed by: e48d507df5d1141@placeholder.94092.edu. Printing is for personal, private use only. No part of this book may be reproduced or transmitted without publisher's prior permission. Violators will be prosecuted.

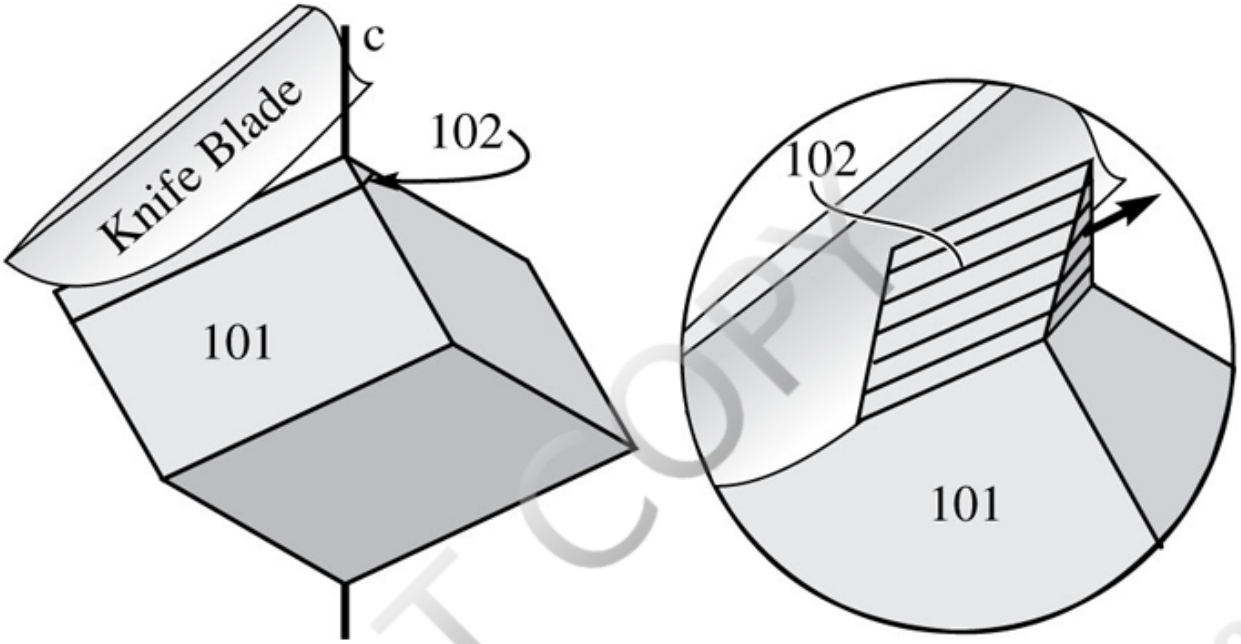

FIGURE 5.26 Deformation twinning in calcite can be produced by glide on {102} crystallographic planes. Such twinning could be artificially produced by deformation from a knife blade. Back to text

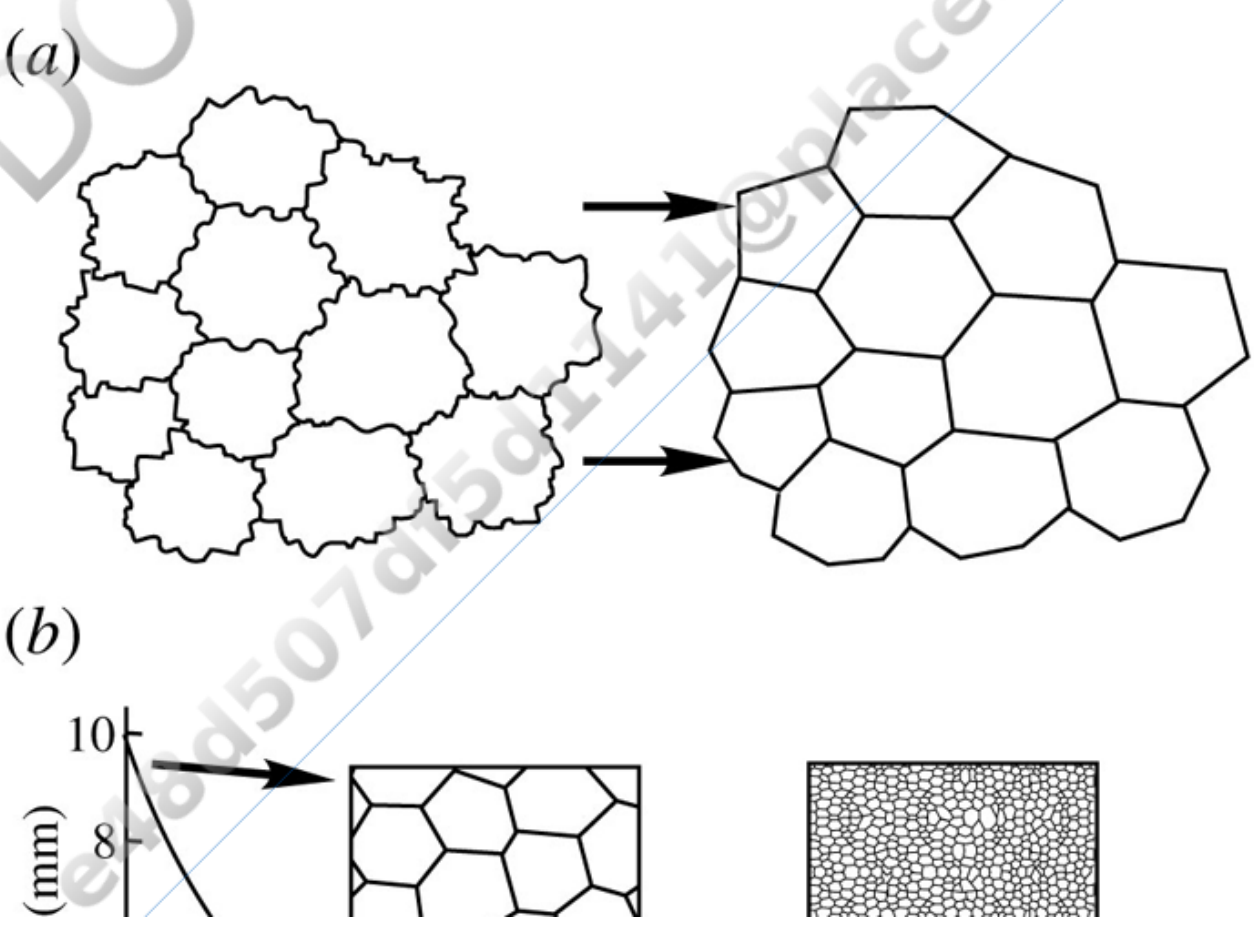

DO NOT COPY
e48d507df5d1141@placeholder.9409

https://print.vitalsource.com/requests/GM7Nq1ZS0WtoausAQTDB/c...

Printed by: e48d507df5d1141@placeholder.94092.edu. Printing is for personal, private use only. No part of this book may be reproduced or transmitted without publisher's prior permission. Violators will be prosecuted.

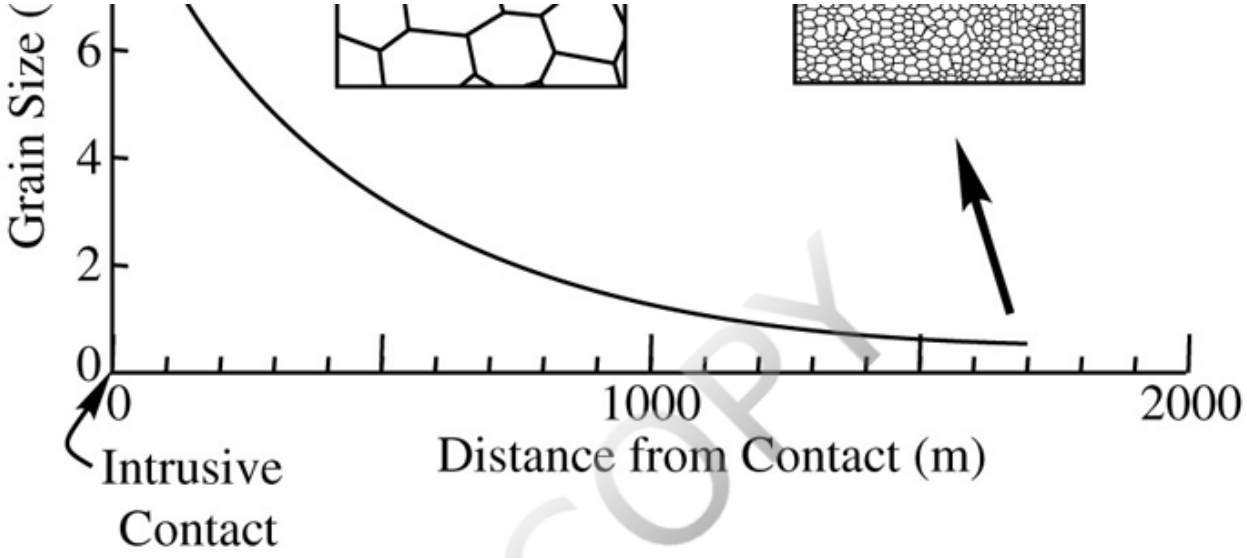

FIGURE 5.27 Recrystallization. (*a*) Recrystallization allows irregular grain boundaries to become smooth, reducing surface energy. (*b*) Average grain size of calcite in marble in a contact metamorphic aureole increases systematically toward the intrusion. Adapted from Grigor'ev (1965). Increase in grain size reduces mineral surface area and surface energy. Back to text

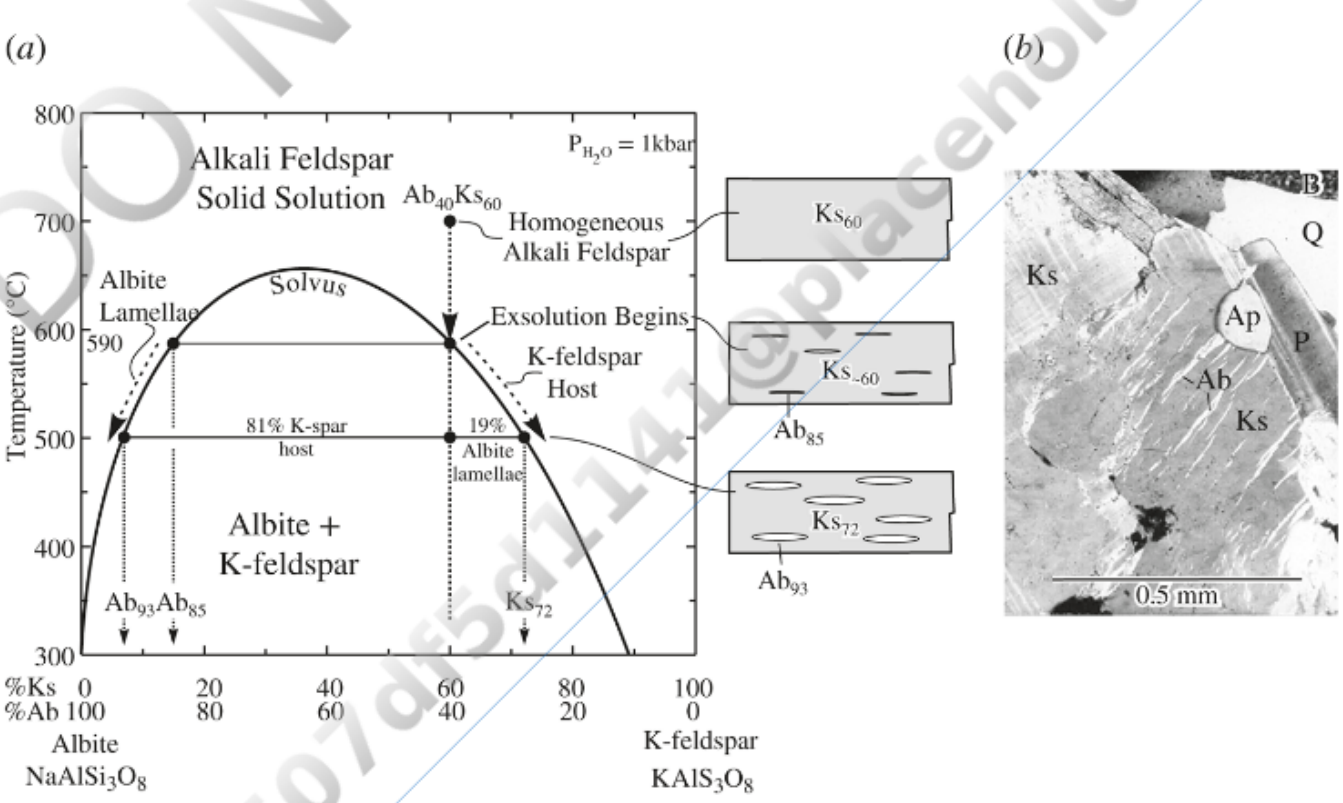

FIGURE 5.28 Exsolution in alkali feldspar. (*a*) The solvus for alkali feldspar. See text for discussion. Adapted from Smith and Parsons (1974). (*b*) Photomicrograph of a thin section of perthitic K-feldspar (Ks, center) with exsolution lamellae of albite (Ab) that extend NE–SW. Plagioclase (P), quartz (Q), apatite (Ap), and biotite (B) are also present. Back to text

DO NOT COPY
e48d507df5d1141@placeholder.9409

Printed by: e48d507df5d1141@placeholder.94092.edu. Printing is for personal, private use only. No part of this book may be reproduced or transmitted without publisher's prior permission. Violators will be prosecuted.

FIGURE 5.29 Each dark feature is an aggregate of biotite grains in the shape of dodecahedrons. These biotite after garnet pseudomorphs formed when biotite replaced garnet as a result of metamorphic reactions. Rock thin sections reveal that in the cores of some biotite pseudomorphs some garnet is preserved. Back to text

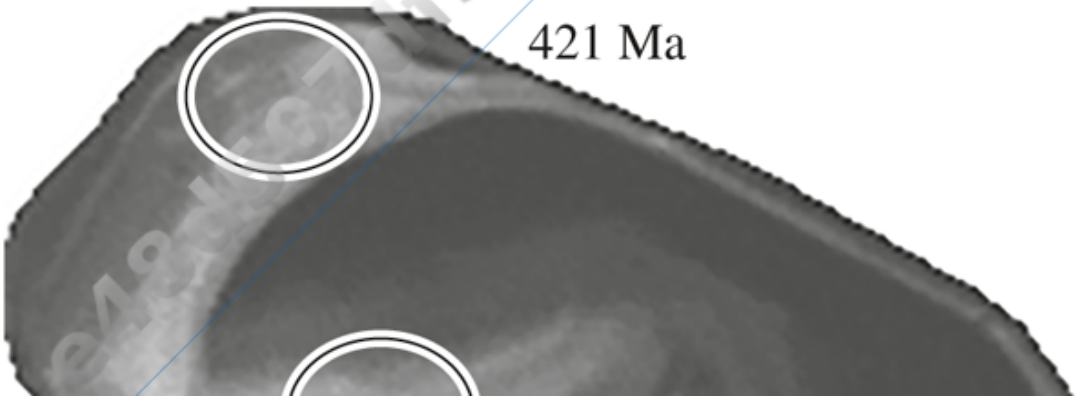

Printed by: e48d507df5d1141@placeholder.94092.edu. Printing is for personal, private use only. No part of this book may be reproduced or transmitted without publisher's prior permission. Violators will be prosecuted.

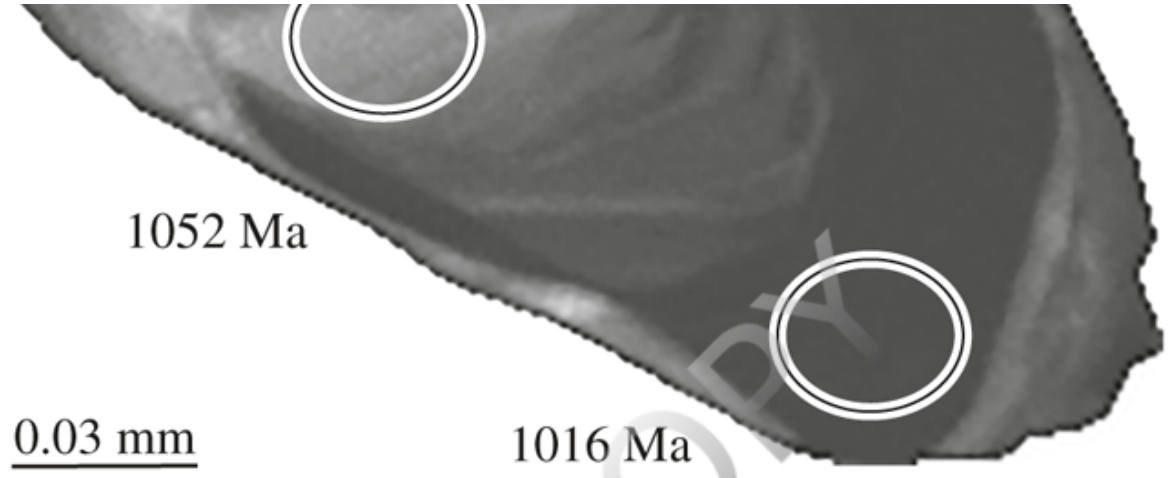

FIGURE 5.30 Cross section through a zircon crystal imaged with cathodoluminescence to highlight chemical zoning (Chapter 9). Ellipses represent spots dated by U-Pb isotopic analysis by a secondary ion mass spectrometer; the age of each spot is provided. An interpretation based on zoning characteristics is that crystallization from a magma at about 1052 Ma (millions of years before present) produced the core of the zircon, metamorphism at about 1016 Ma resulted in additional zircon growth, and lastly, the zircon grain again was placed in a crystallizing magma resulting in the growth of the rim at about 421 Ma. Back to text

DO NOT COPY

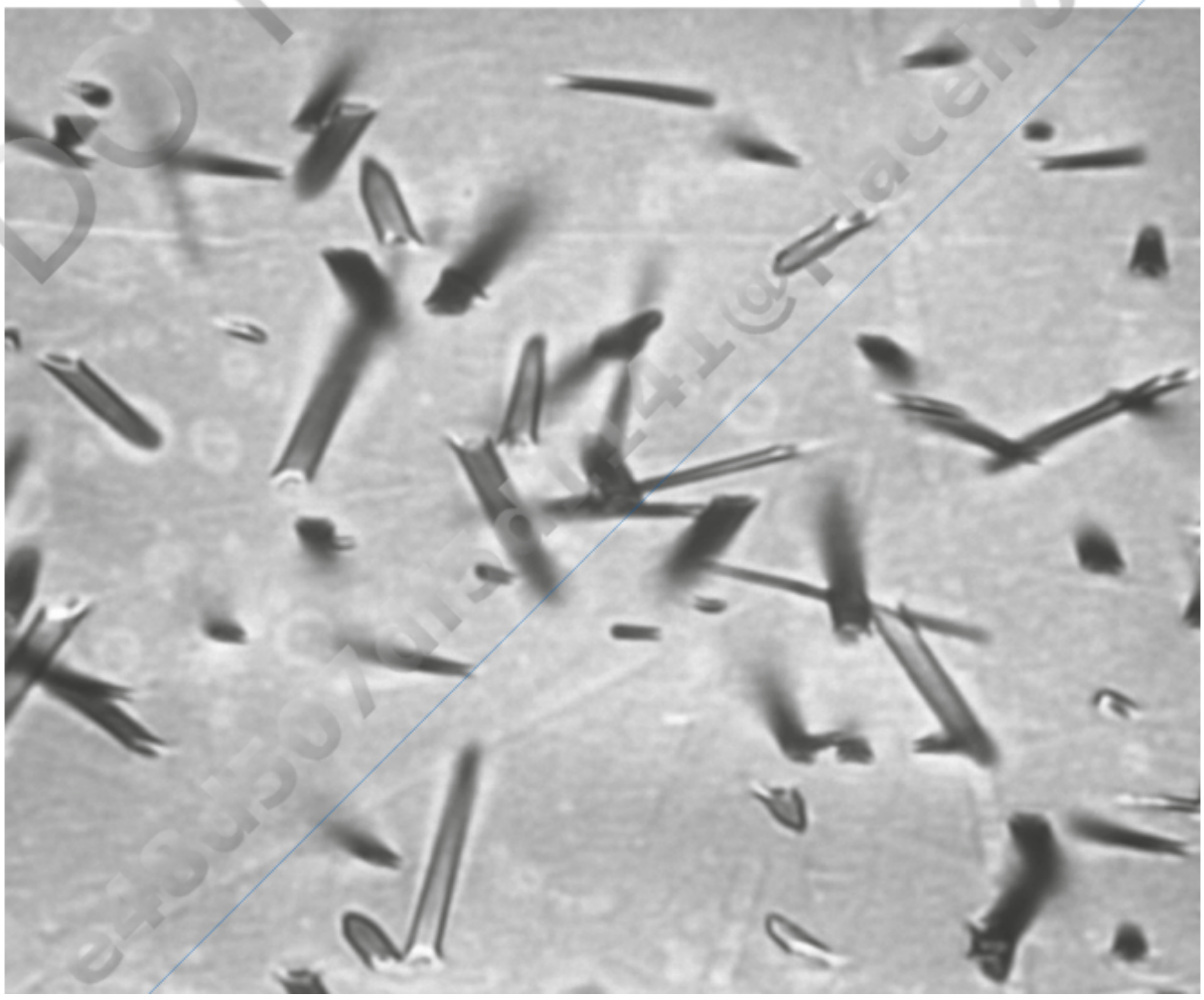

Printed by: e48d507df5d1141@placeholder.94092.edu. Printing is for personal, private use only. No part of this book may be reproduced or transmitted without publisher's prior permission. Violators will be prosecuted.

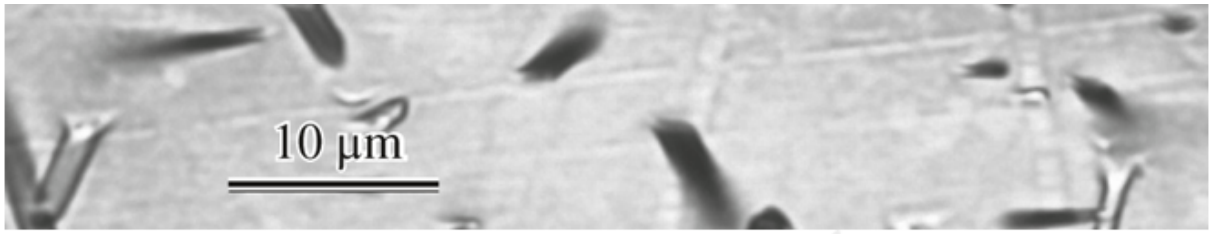

FIGURE 5.31 Transmitted-light image of etched fission tracks in apatite. The fission tracks are the randomly oriented dark features. The appearance of each fission track is controlled by its length and orientation relative to the polished grain surface. Short tracks or tracks nearly perpendicular to the surface appear as relatively small elliptical shapes; long tracks and tracks more parallel to the surface are elongate and may have a lighter central region. Image courtesy of Andrew Gleadow, University of Melbourne, Australia. Back to text

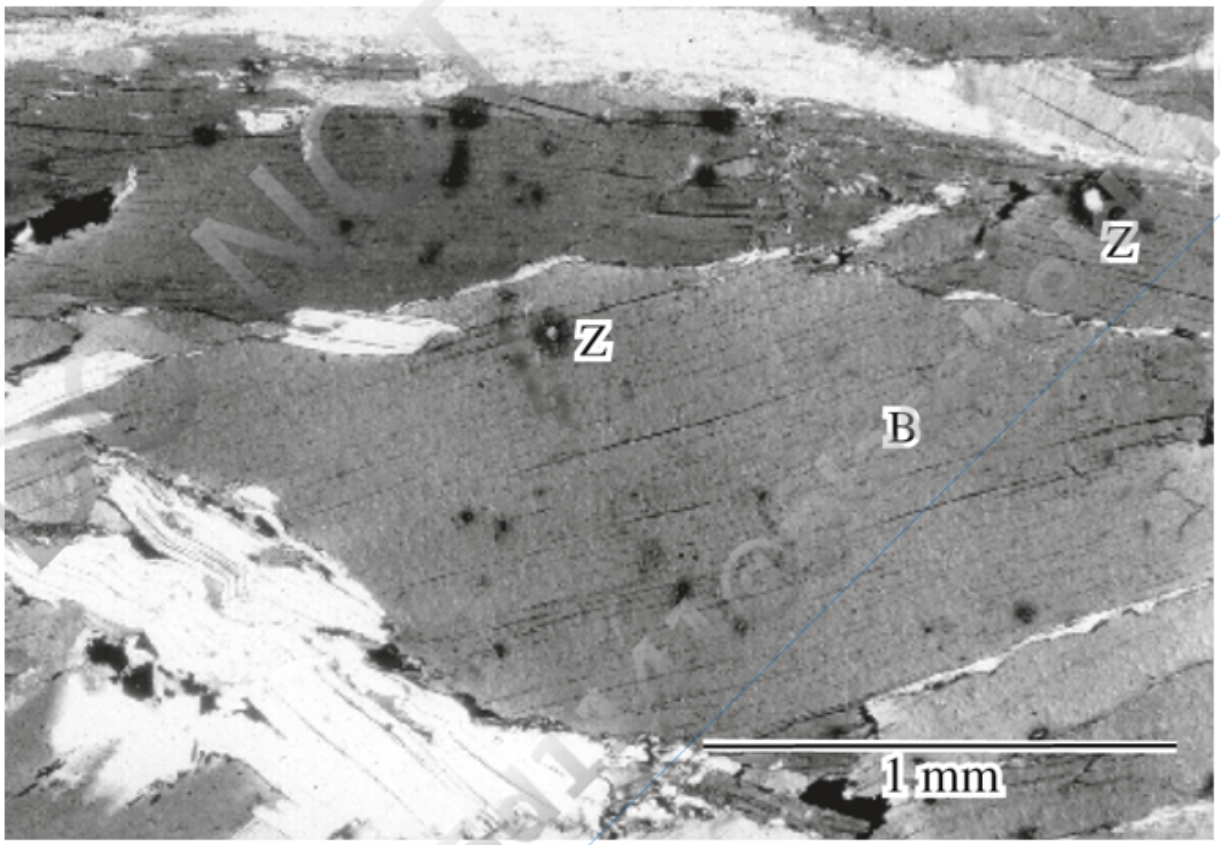

FIGURE 5.32 Photomicrograph of a thin section of mica schist showing dark pleochroic halos around radioactive zircon (Z) inclusions in biotite (B). Back to text

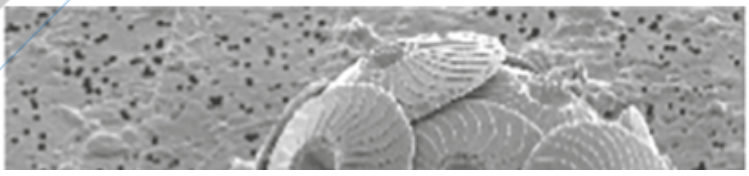

Printed by: e48d507df5d1141@placeholder.94092.edu. Printing is for personal, private use only. No part of this book may be reproduced or transmitted without publisher's prior permission. Violators will be prosecuted.

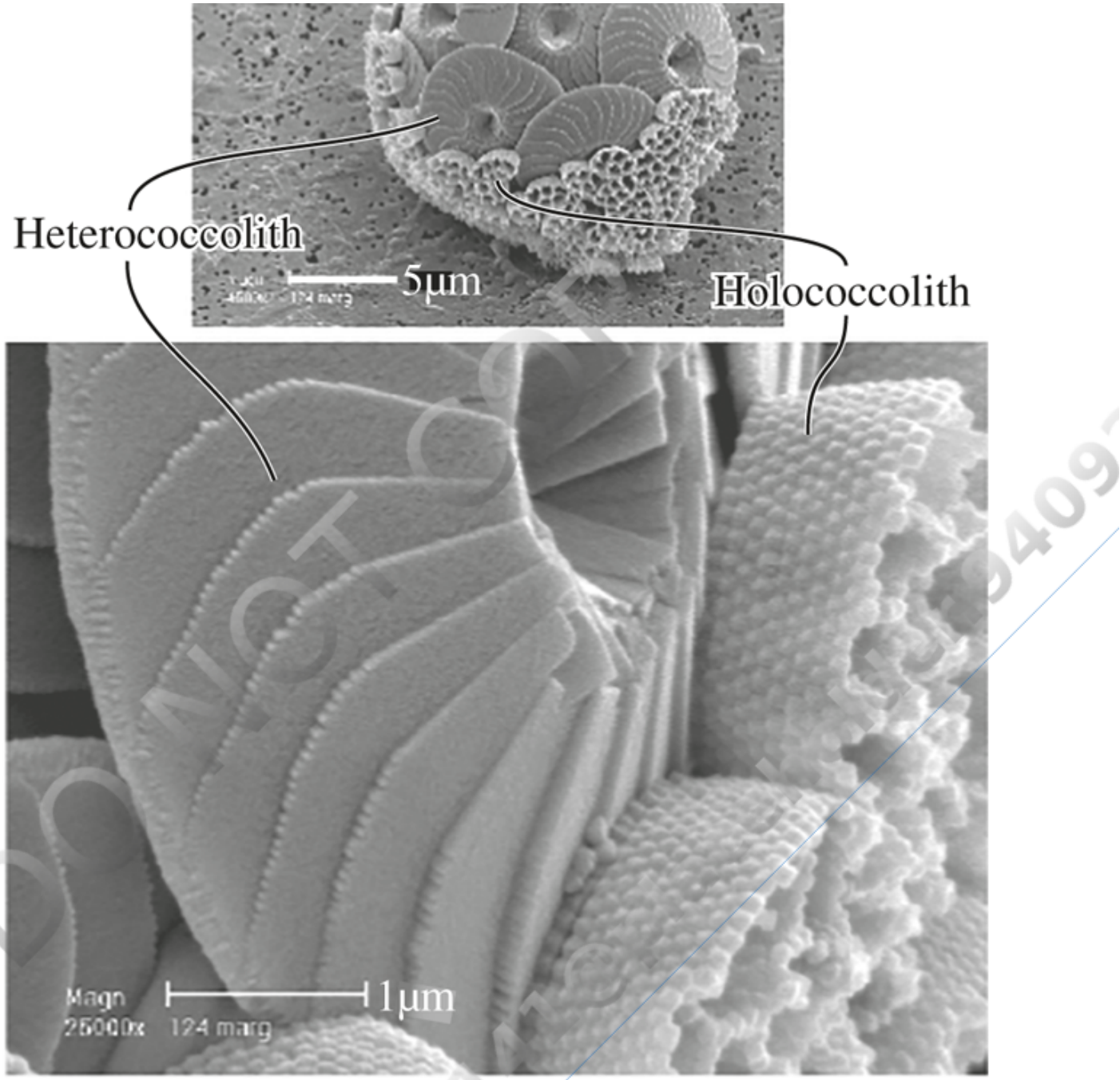

(*b*)

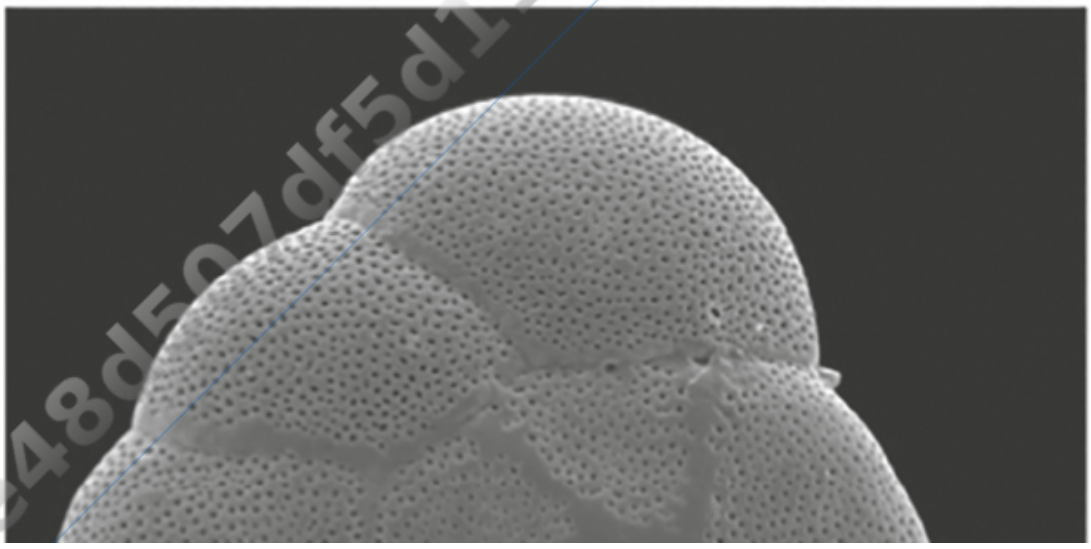

Printed by: e48d507df5d1141@placeholder.94092.edu. Printing is for personal, private use only. No part of this book may be reproduced or transmitted without publisher's prior permission. Violators will be prosecuted.

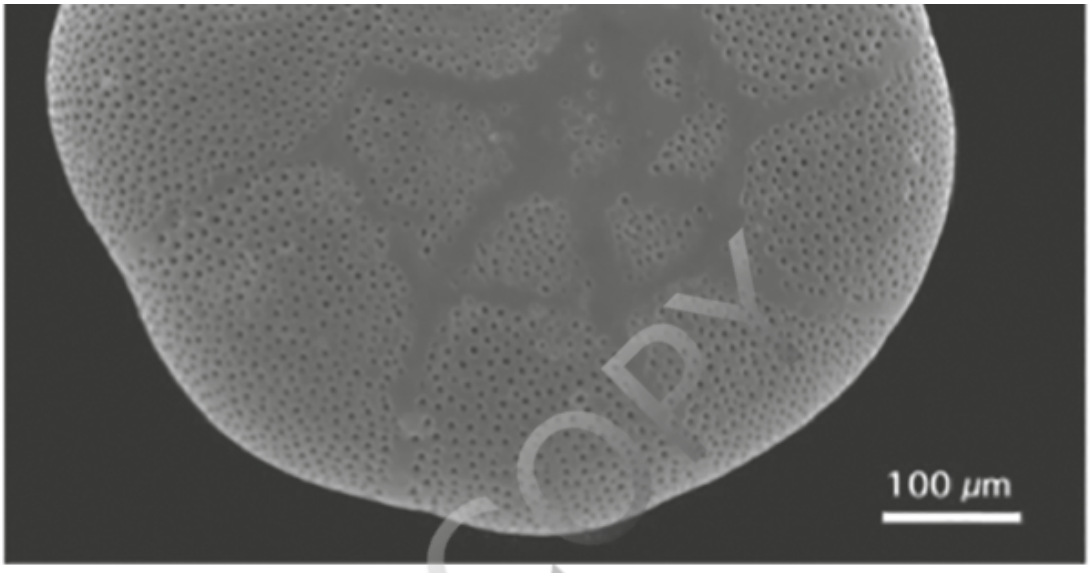

FIGURE 5.33 Coccoliths and foraminifera. (*a*) A combination coccosphere of the coccolithophore *Calcidiscus leptoporus* sp. *quadriperforatus*. Heterococcoliths and holococcoliths are formed during different phases of coccolithophore growth. Each of the individual plates in a heterococcolith consists of a single calcite crystal. Holococcoliths are made of numerous granules, each of which is a single calcite crystal. It is rare to find coccospheres with both heterococcoliths and holococcoliths. Images © Jeremy Young and Markus Geisen, The Natural History Museum London, and used by permission. (*b*) The foraminifera *Ammonia beccarii* (Thomas, E., Gapoichenko, T., Varekamp, J. C., Mecray, E. L., and Buchholtz ten Brink, J. R. 2000. Maps of benthic foraminiferal distribution and environmental changes in Long Island Sound between 1940s and 1990s. U.S. Geological Survey Open File Report OF00-304.). Back to text

DO NOT COPY
e48d507df5d1141@placeholder.94092

Printed by: e48d507df5d1141@placeholder.94092.edu. Printing is for personal, private use only. No part of this book may be reproduced or transmitted without publisher's prior permission. Violators will be prosecuted.

Chapter 6 Physical Properties of Minerals

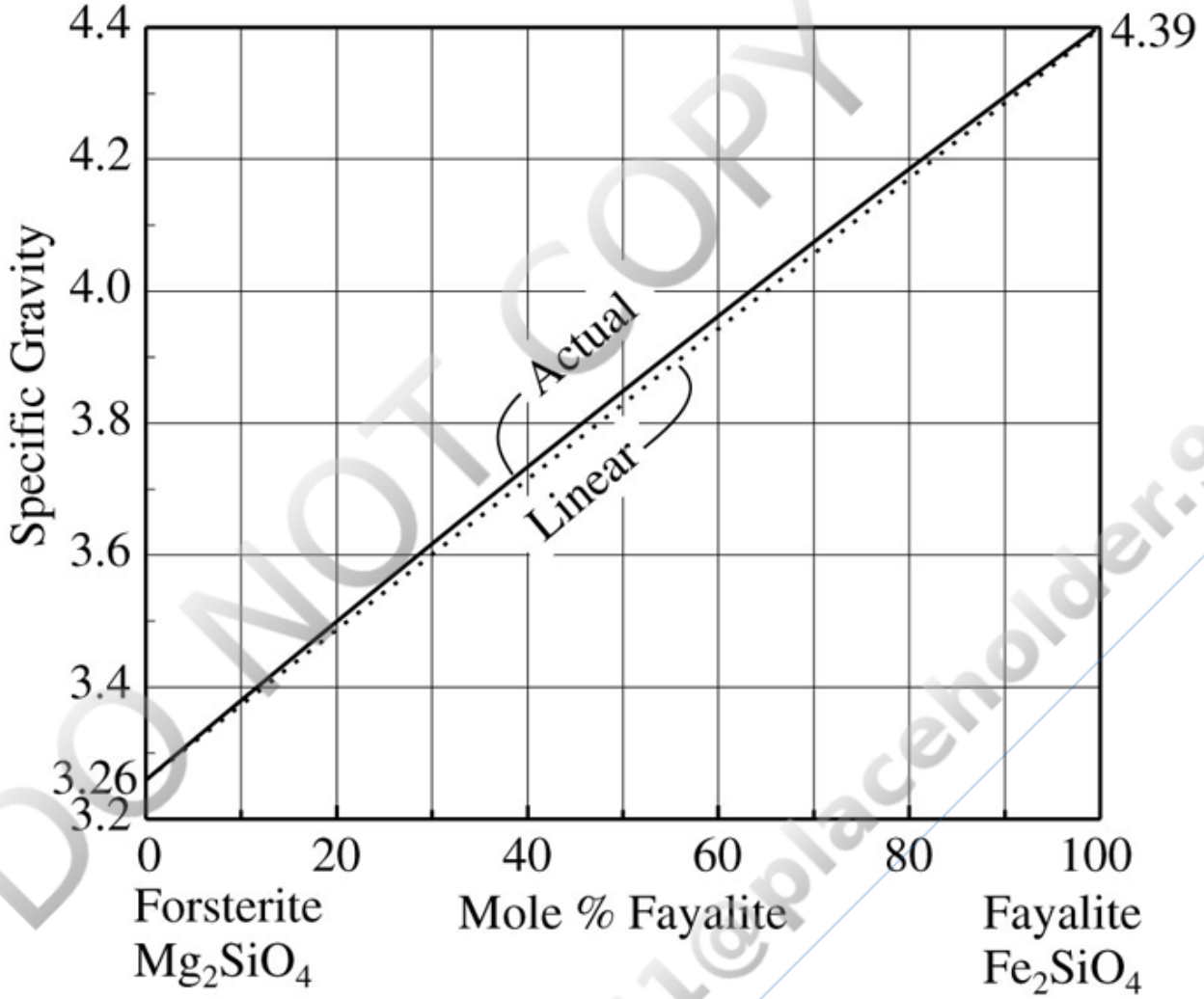

FIGURE 6.1 Specific gravity of olivine. The dotted line assumes a linear variation in specific gravity between 3.26 for forsterite (Mg_2SiO_4) and 4.39 for fayalite (Fe_2SiO_4). The solid line is the actual specific gravity for intermediate compositions. Back to text

(*a*)

DO NOT COPY
e48d507df5d1141@placeholder.9409

Printed by: e48d507df5d1141@placeholder.94092.edu. Printing is for personal, private use only. No part of this book may be reproduced or transmitted without publisher's prior permission. Violators will be prosecuted.

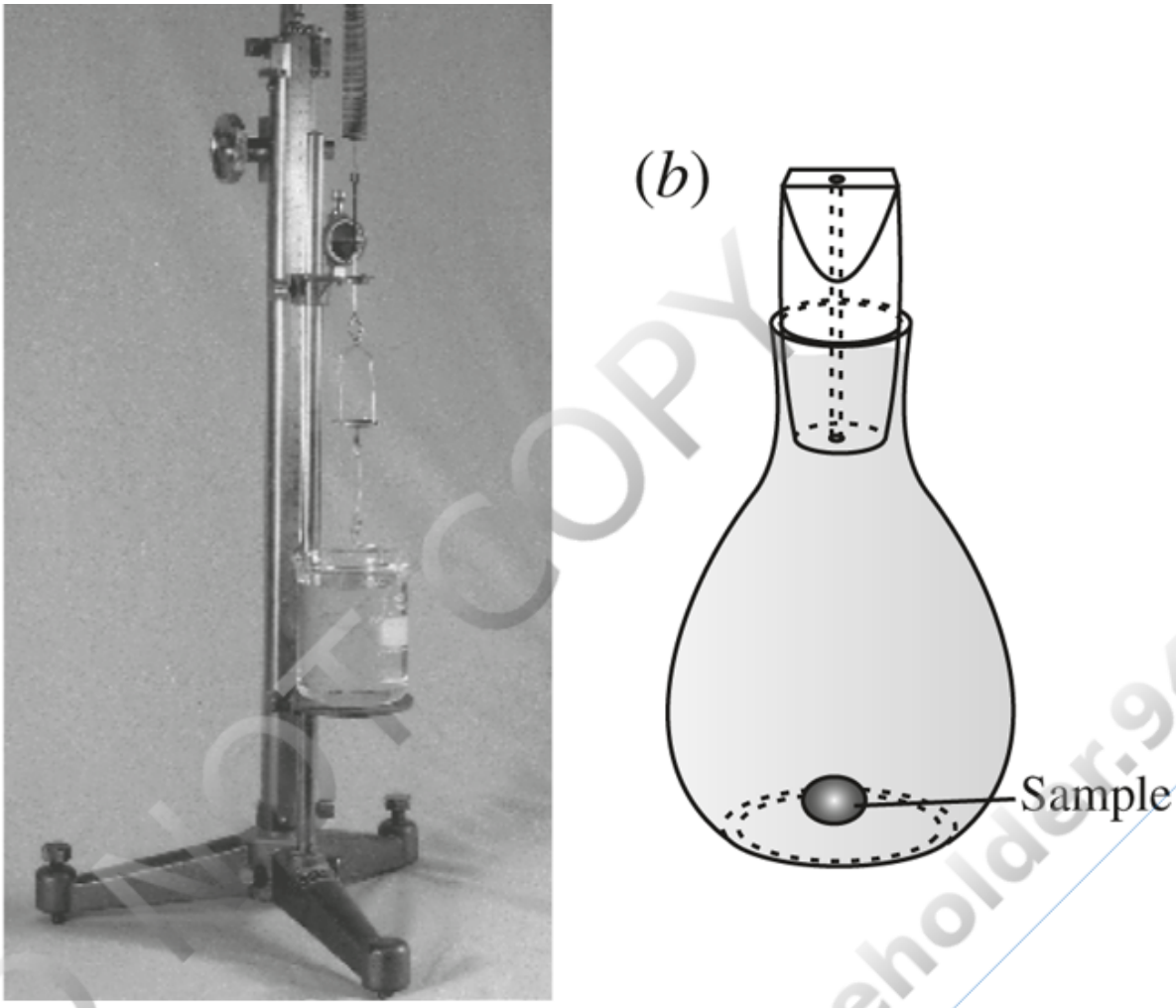

FIGURE 6.2 Apparatus to measure specific gravity. (*a*) Jolly balance; a sample of a mineral is weighed first in the upper pan and then in the lower pan, which is suspended in water. (*b*) Pycnometer. Back to text

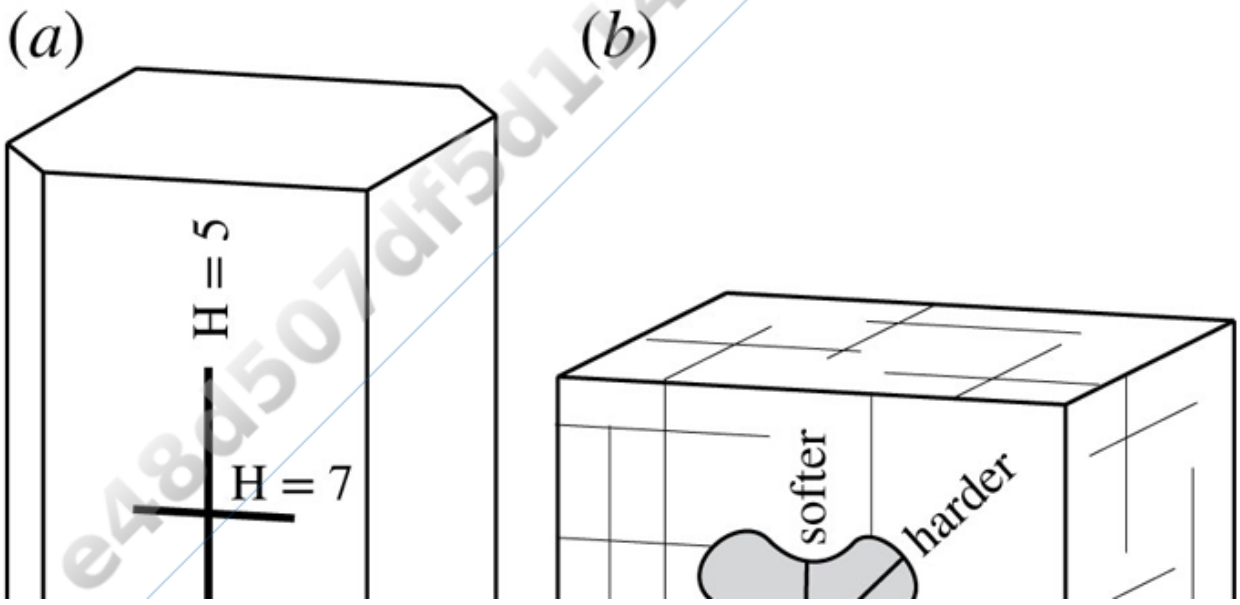

DO NOT COPY
e48d507df5d1141@placeholder.9409

Printed by: e48d507df5d1141@placeholder.94092.edu. Printing is for personal, private use only. No part of this book may be reproduced or transmitted without publisher's prior permission. Violators will be prosecuted.

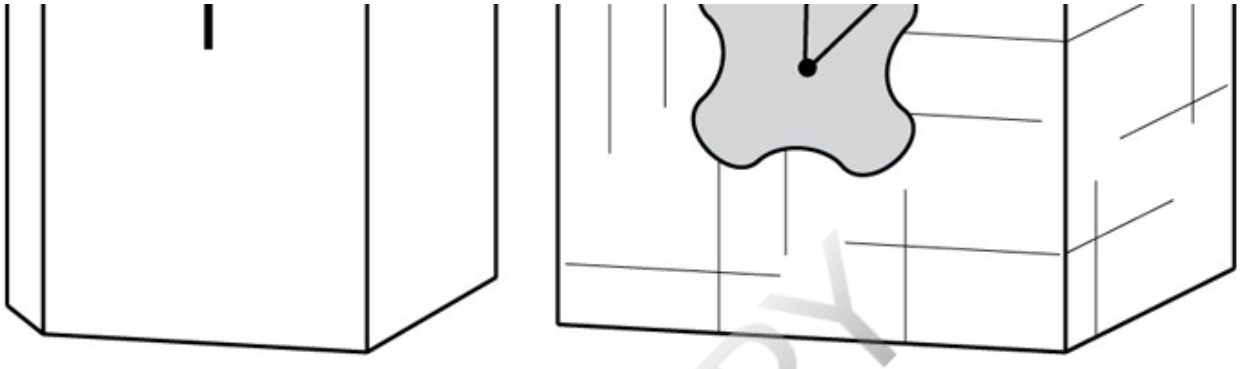

FIGURE 6.3 Variation of mineral hardness with direction. (*a*) Kyanite. Scratch hardness parallel to the length of crystals is 5 and at right angles is 7. (*b*) Halite. Scratch hardness parallel to the trace of cleavage is slightly less than hardness, at 45°. The length of a line drawn from the central dot to the edge of the shaded figure schematically shows the hardness parallel to that line. Back to text

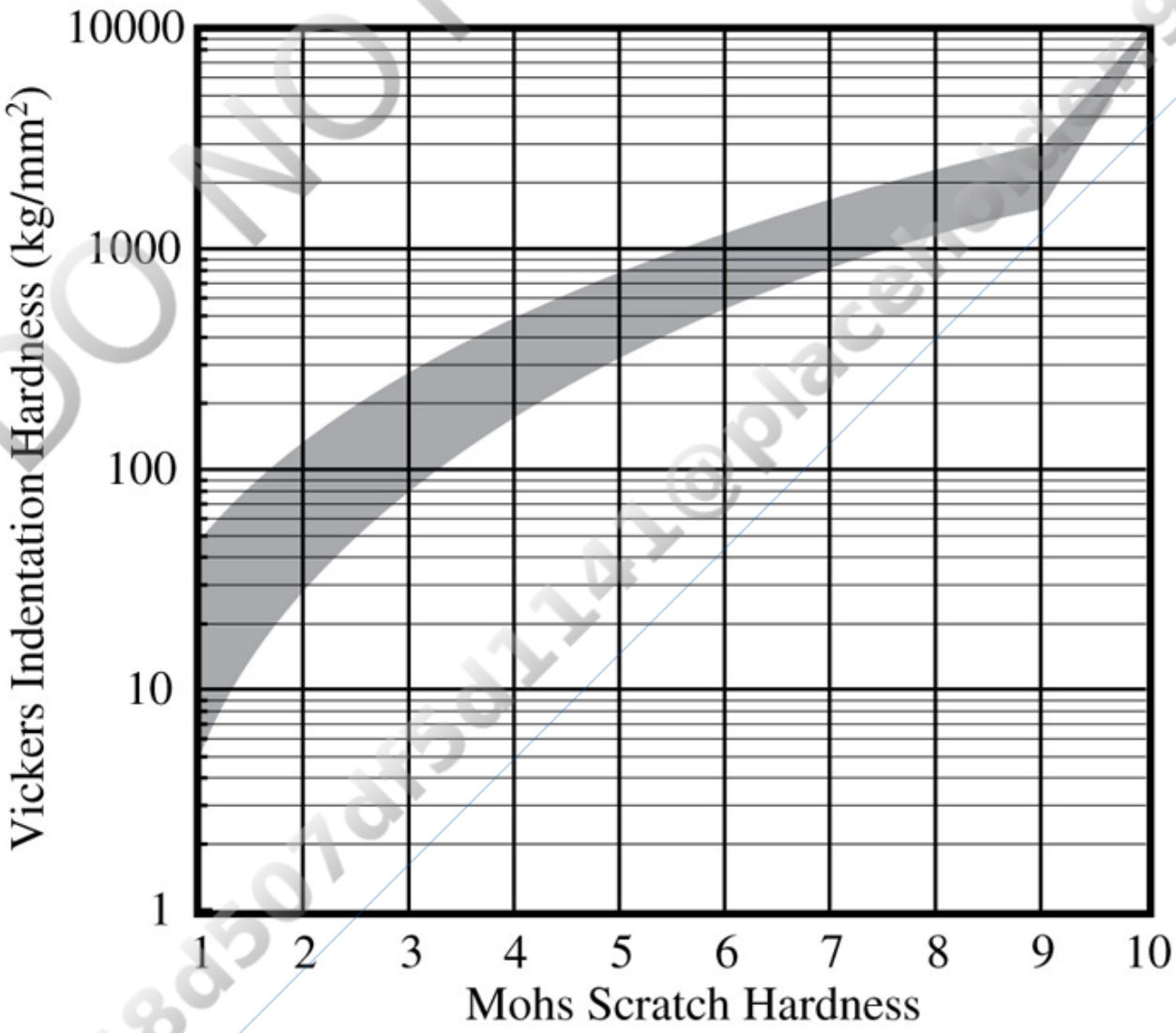

FIGURE 6.4 Approximate range of Vickers indentation hardness (shaded) as a function of Mohs scratch hardness. Back to text

DO NOT COPY
e48d507df5d1141@placeholder.9409

Printed by: e48d507df5d1141@placeholder.94092.edu. Printing is for personal, private use only. No part of this book may be reproduced or transmitted without publisher's prior permission. Violators will be prosecuted.

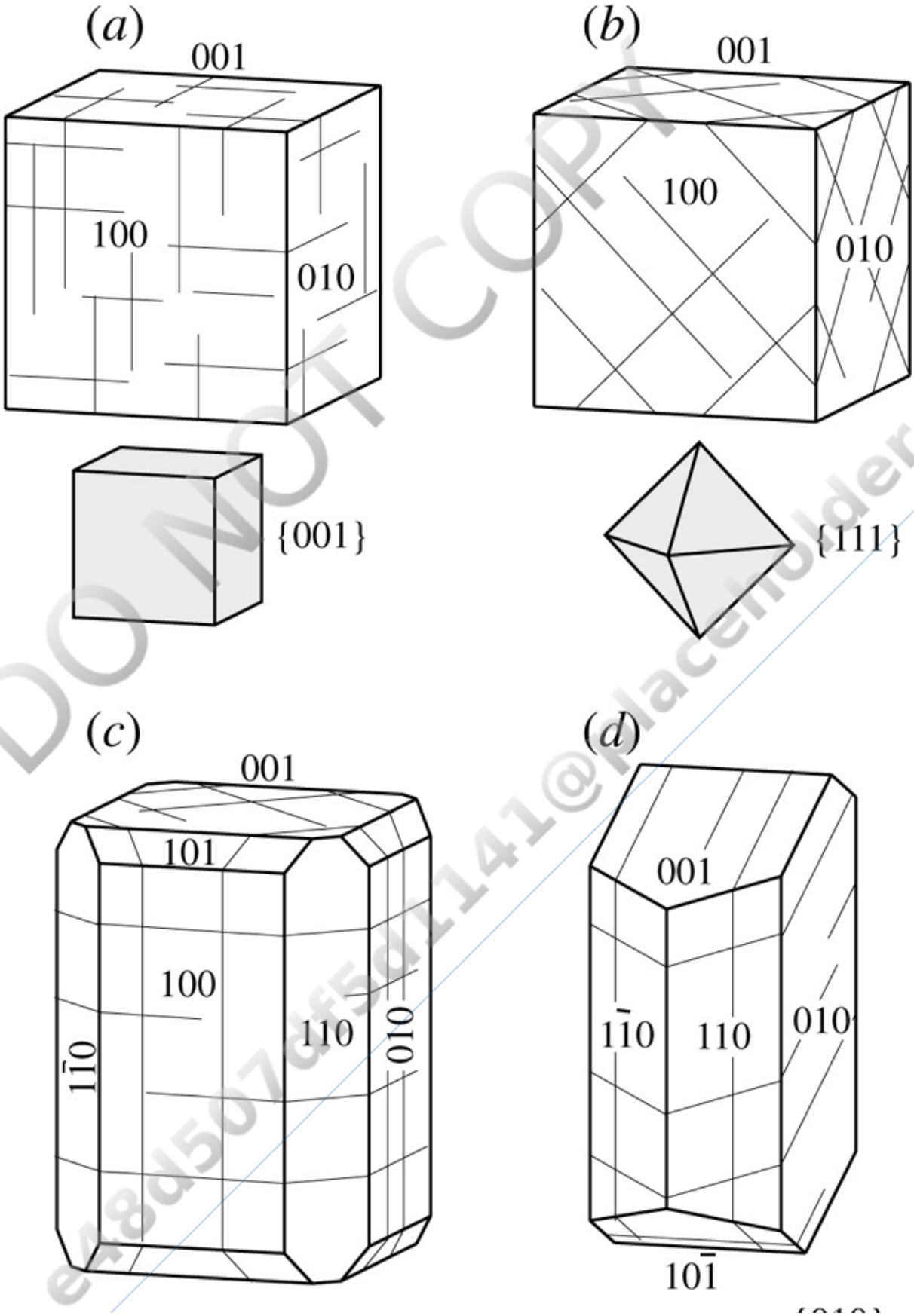

DO NOT COPY
e48d507df5d1141@placeholder.9409

Printed by: e48d507df5d1141@placeholder.94092.edu. Printing is for personal, private use only. No part of this book may be reproduced or transmitted without publisher's prior permission. Violators will be prosecuted.

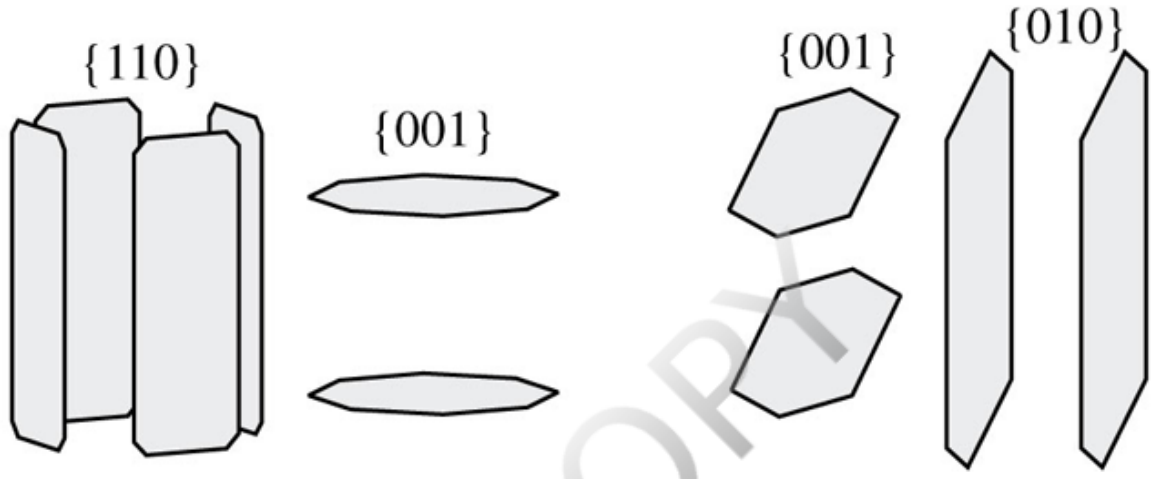

FIGURE 6.5 Cleavage. (*a*) Isometric {001} cleavage (cubic). (*b*) Isometric {111} cleavage (octahedral). (*c*) Tetrahedral {110} (prism) and {001} (pinacoid) cleavage. (*d*) Monoclinic {001} (pinacoid) and {010} (pinacoid) cleavage. Back to text

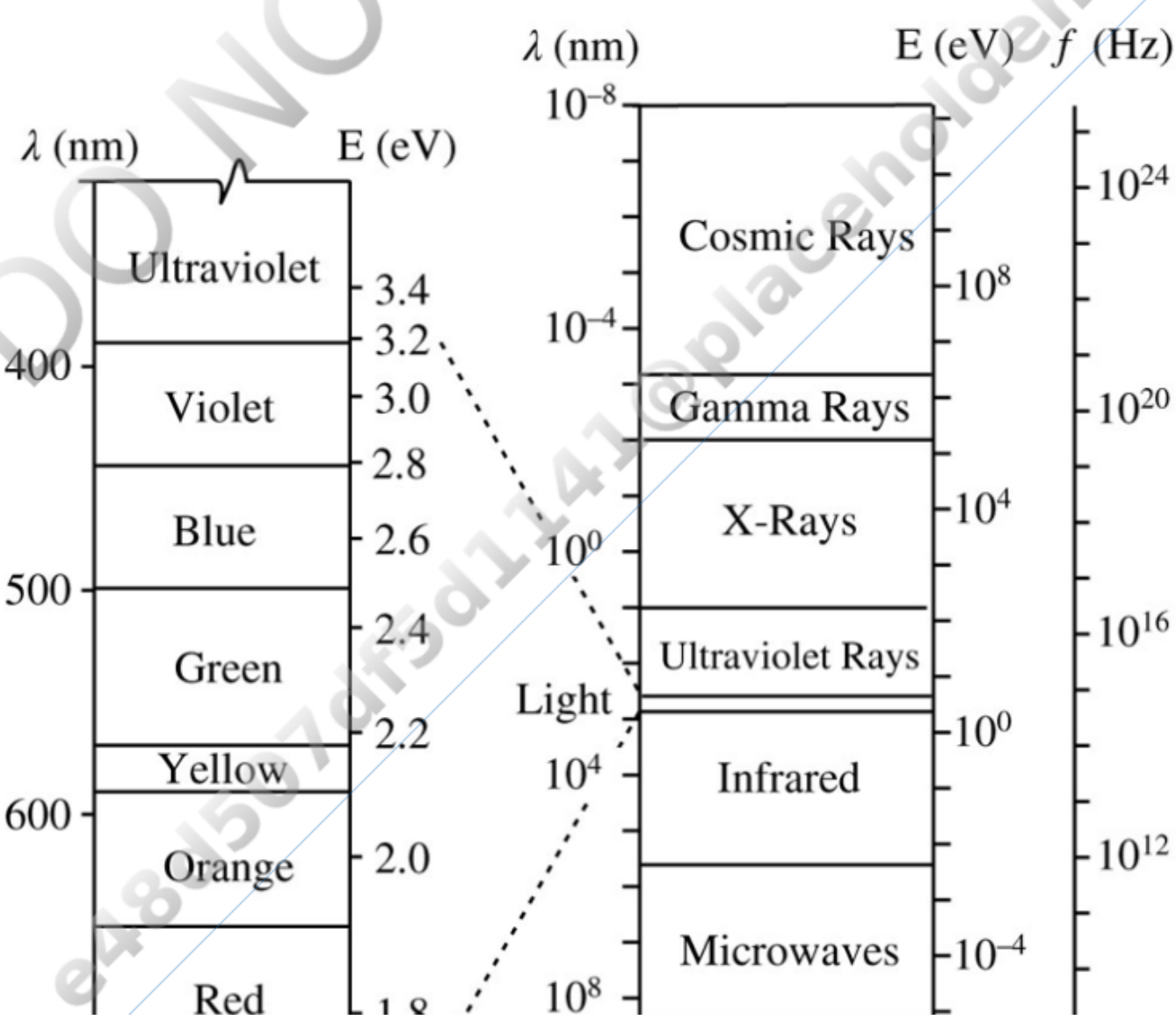

DO NOT COPY
e48d507df5d1141@placeholder.9409

Printed by: e48d507df5d1141@placeholder.94092.edu. Printing is for personal, private use only. No part of this book may be reproduced or transmitted without publisher's prior permission. Violators will be prosecuted.

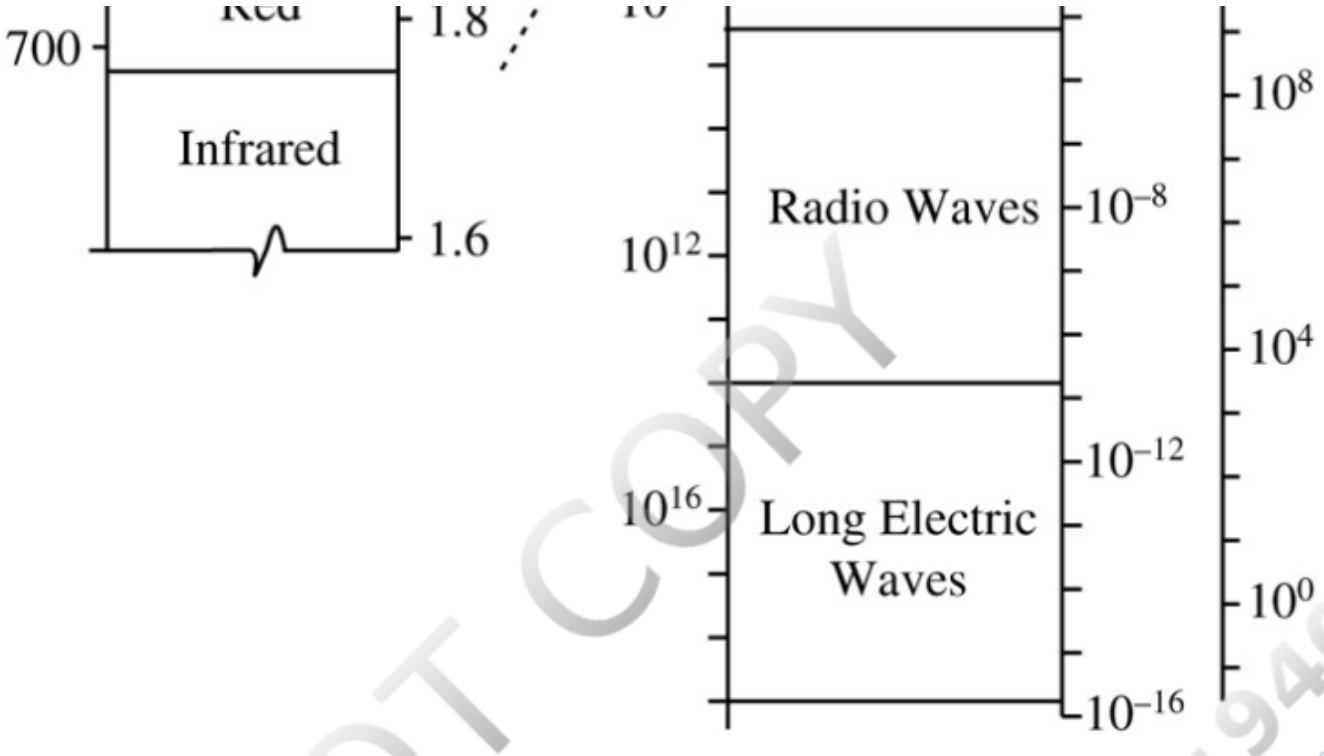

FIGURE 6.6 The electromagnetic spectrum. Visible light, with wavelengths (λ) between about 400 and 700 nm and energy (E) between about 1.8 and 3.2 electron volts (eV), is a small part of the spectrum. The frequency (f) in Hertz also is shown. Back to text

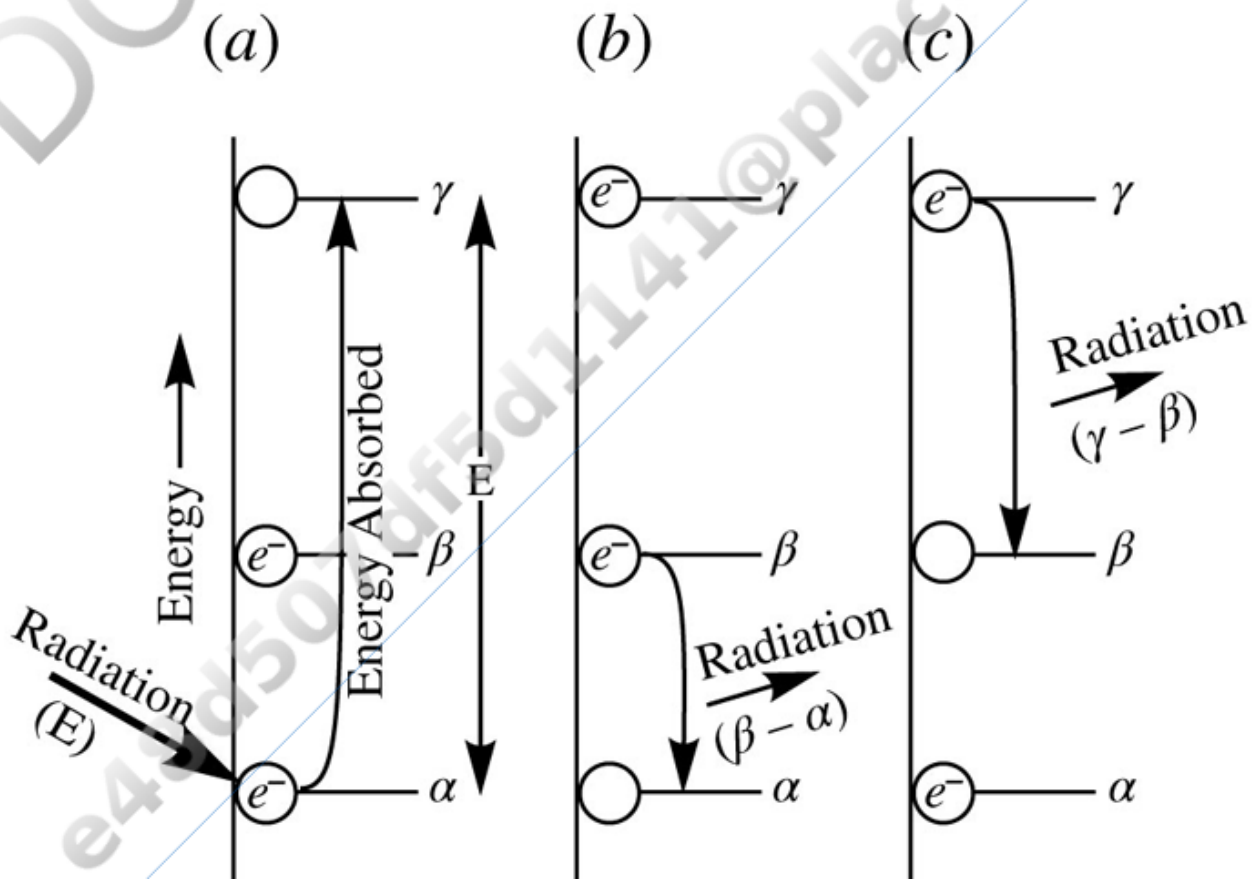

DO NOT COPY
e48d507df5d1141@placeholder.9409

Printed by: e48d507df5d1141@placeholder.94092.edu. Printing is for personal, private use only. No part of this book may be reproduced or transmitted without publisher's prior permission. Violators will be prosecuted.

FIGURE 6.7 Absorption of electromagnetic radiation. (*a*) Electromagnetic radiation, whose energy level is *E*, excites an electron in its base energy level, *α*. If the electron can be promoted to an open energy level *γ* where the difference between *γ* and *α* is equal to *E*, the electromagnetic radiation energy will be absorbed. (*b*) An electron whose base energy level is *β* may drop into the now-vacant *α* level, releasing electromagnetic radiation whose energy is *β* − *α*. (*c*) The high-energy *γ* electron now can drop into the lower-energy *β* level, releasing electromagnetic radiation whose energy is equal to *γ* − *β*. Back to text

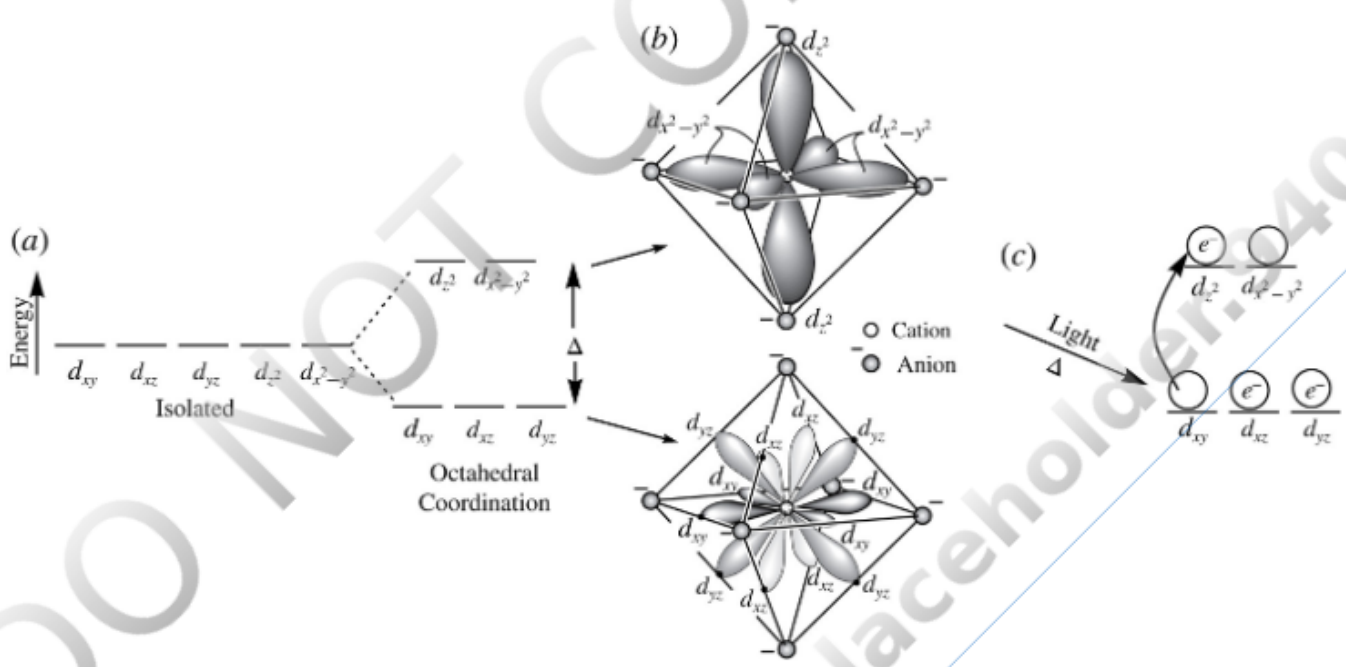

FIGURE 6.8 Crystal field splitting. (*a*) All five *d* orbitals (d_{xy}, d_{xz}, d_{yz}, d_{z^2}, and $d_{(x^2-y^2)}$) are identical in energy in an isolated transition metal cation (left). Compare with Figure 3.1. When placed in regular octahedral coordination with six anions, the *d* orbitals are split into two energy levels with an energy difference = *Δ*. (*b*) The d_{z^2} and $d_{(x^2-y^2)}$ orbitals are directed toward the position of the anions (top) and are forced to have higher energy because the negative charges of the anions repel the electrons. The d_{xy}, d_{xz}, and d_{yz} orbitals are directed between the anions (bottom), and have lower energy. (*c*) If incident electromagnetic energy has energy equal to *Δ*, it can be absorbed by promoting a lower-energy electron into a vacant higher-energy position. Back to text

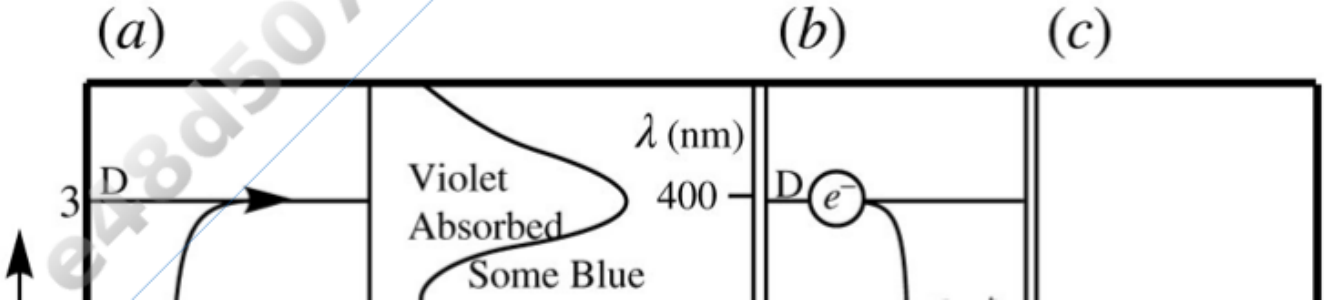

Printed by: e48d507df5d1141@placeholder.94092.edu. Printing is for personal, private use only. No part of this book may be reproduced or transmitted without publisher's prior permission. Violators will be prosecuted.

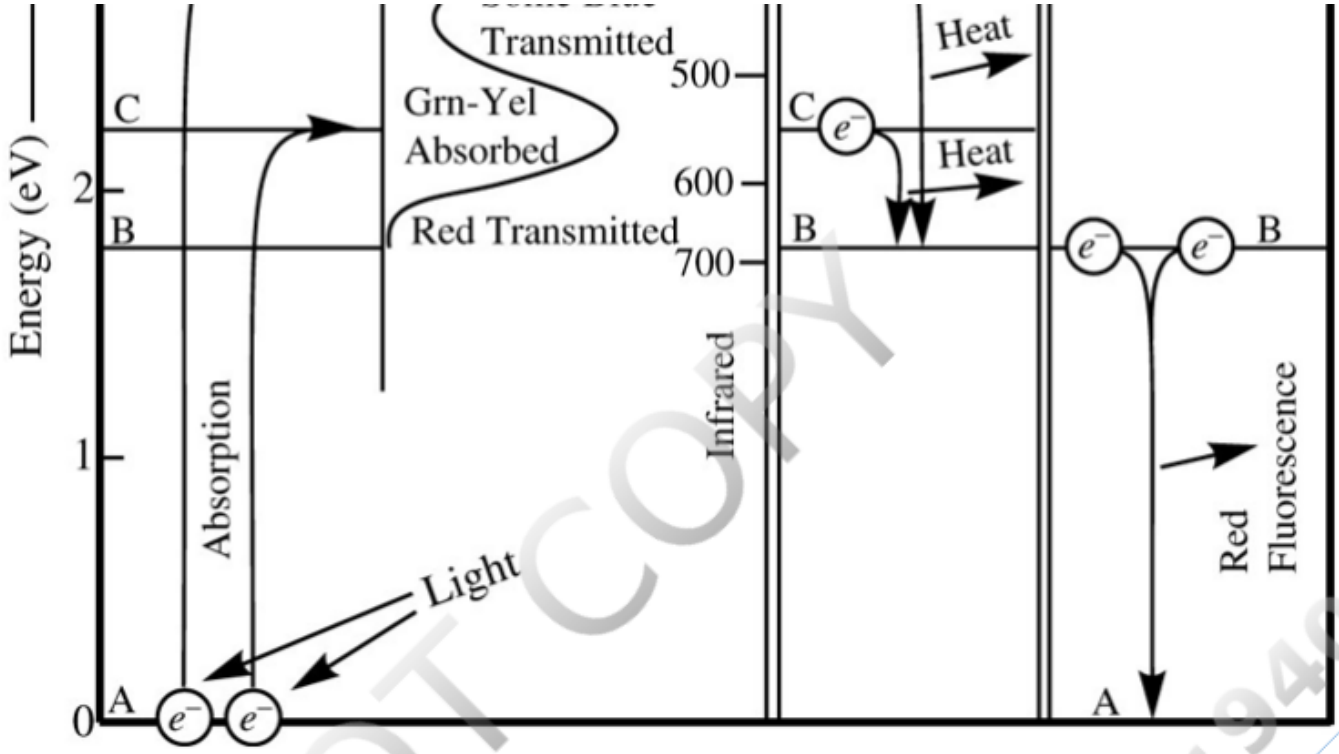

FIGURE 6.9 Light absorption in ruby. (*a*) Light with energies of about 2.23 eV and 3.0 eV can be absorbed by promoting electrons from their ground state (A) to energy levels C and D produced by crystal field splitting of Cr^{3+}. When the electrons return to their ground states, they do so by stages. (*b*) Electrons promoted to C and D fall back to the vacant B level with emission of heat. (*c*) Electrons from the B level subsequently return to A with emission of red light. Adapted from Nassau (2001).
Back to text

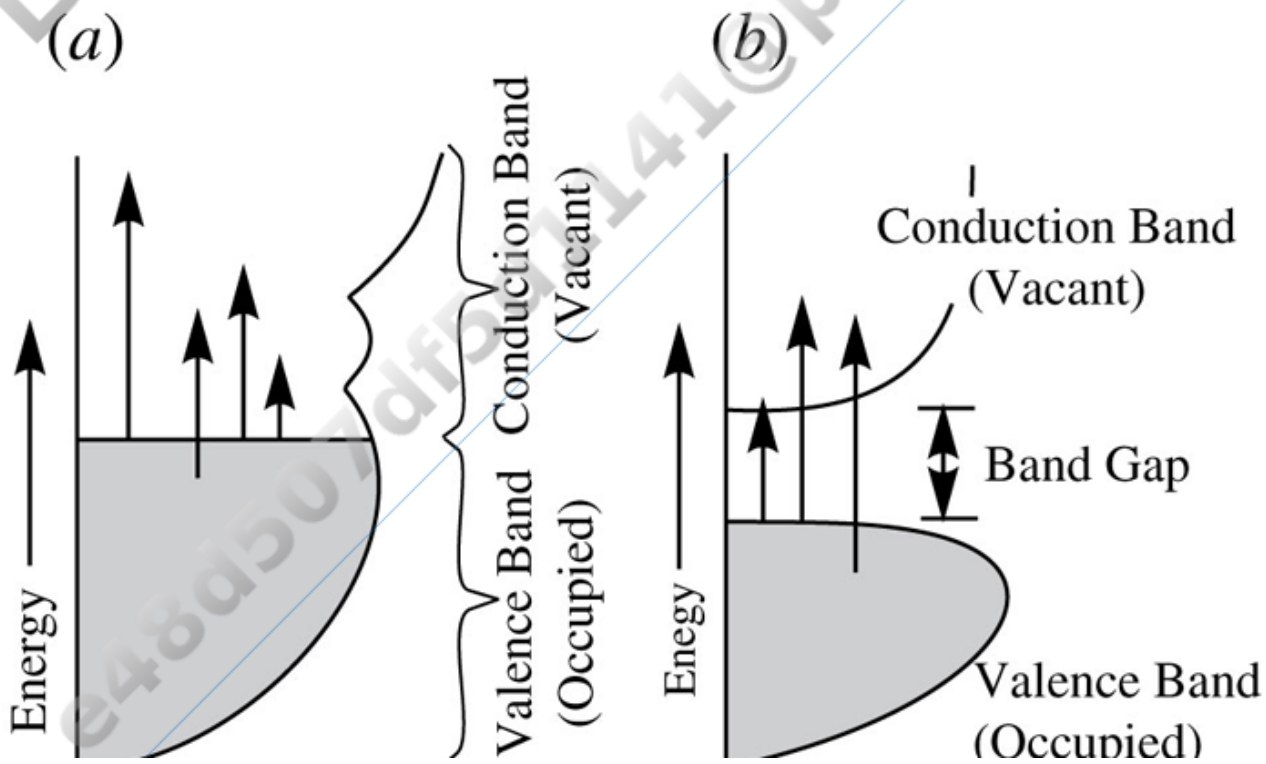

Printed by: e48d507df5d1141@placeholder.94092.edu. Printing is for personal, private use only. No part of this book may be reproduced or transmitted without publisher's prior permission. Violators will be prosecuted.

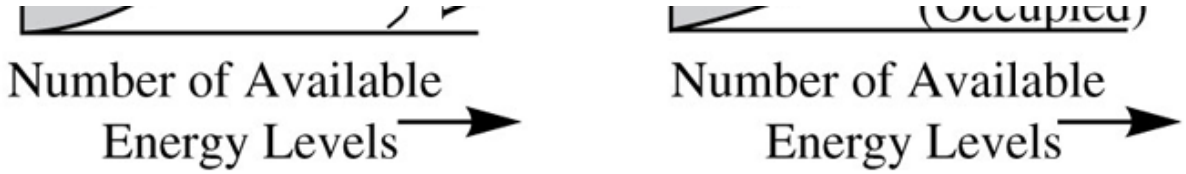

FIGURE 6.10 Band theory. (*a*) Valence bands and conduction bands do not have an energy gap between them with metallic bonding. All light is absorbed because a continuum of energy levels is available to which electrons in the valence band can be promoted. The light that is emitted as electrons return to their base energy state determines the mineral color. The emitted light is perceived as being reflected. (*b*) In semiconductors, an energy gap exists between the valence band and the conduction band. Light whose energy is greater than the band gap can be absorbed by promoting valence electrons into the conduction band. Back to text

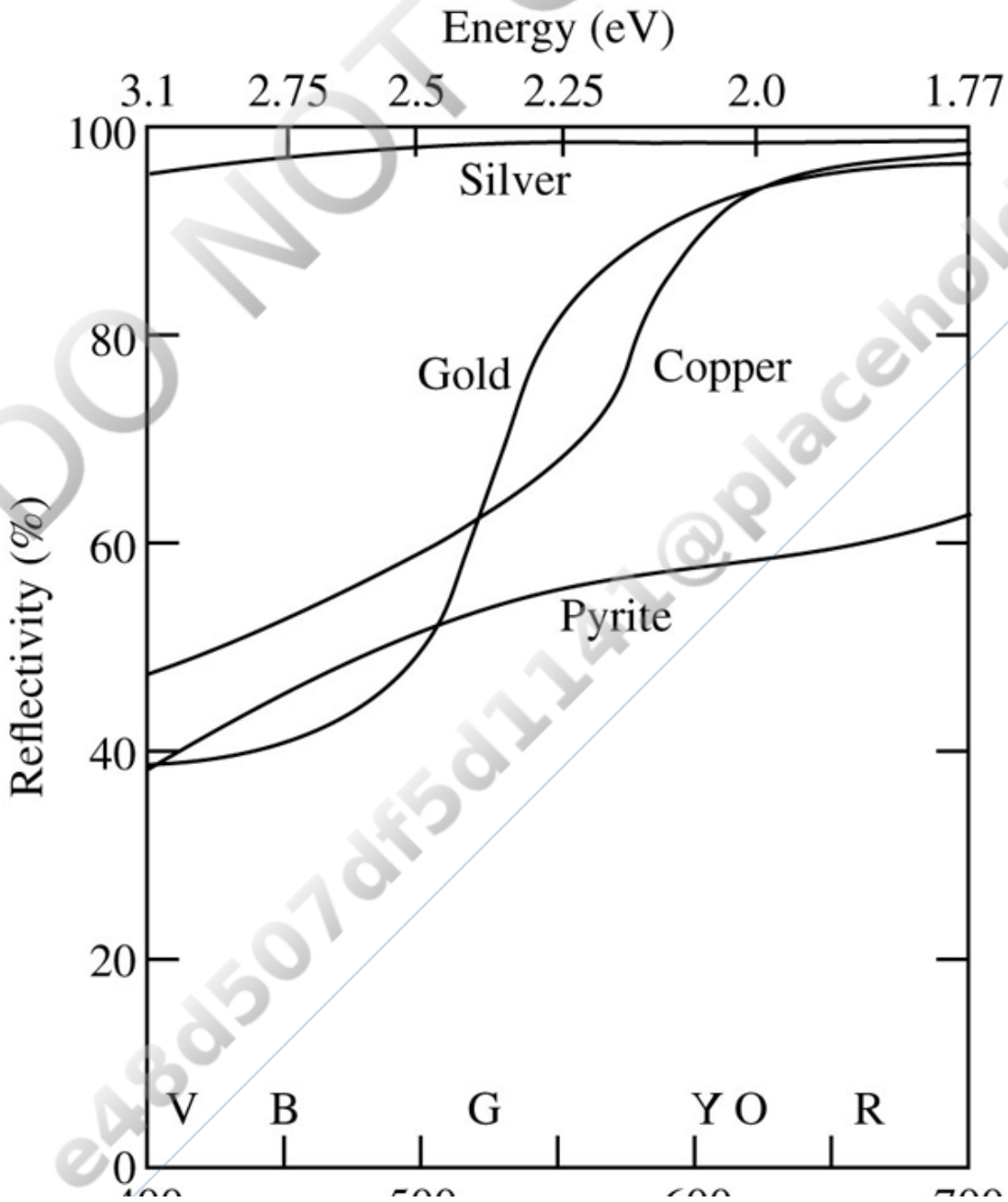

DO NOT COPY
e48d507df5d1141@placeholder.9409

Printed by: e48d507df5d1141@placeholder.94092.edu. Printing is for personal, private use only. No part of this book may be reproduced or transmitted without publisher's prior permission. Violators will be prosecuted.

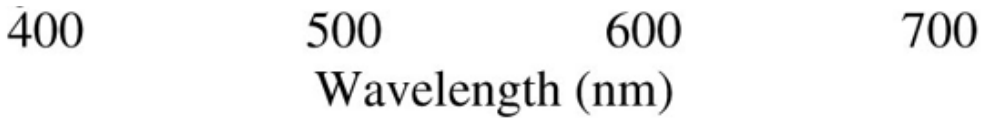

FIGURE 6.11 Reflectivity of metals and semiconductors. The most strongly absorbed wavelengths also are most strongly re-emitted. Silver absorbs and re-emits the visible spectrum with more than 95 percent efficiency. Gold and copper absorb and re-emit the red end of the spectrum more efficiently than the blue-violet end of the spectrum. Pyrite, which is a semiconductor, also has stronger absorption and re-emission at the red end of the spectrum and hence has a color similar to gold in hand sample. Back to text

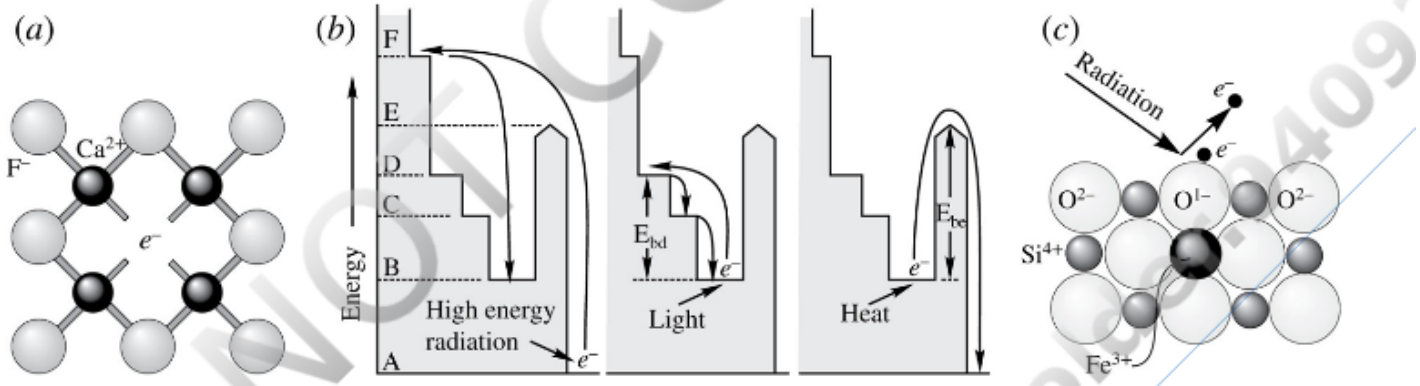

FIGURE 6.12 Color centers. (*a*) Electron color center. A F^- anion in fluorite is missing and the vacancy is occupied by an electron. (*b*) Electron color center energy structure. See text for details. (*c*) Hole color center in amethyst. See text for details. (Adapted from Nassau, 2001.) Back to text

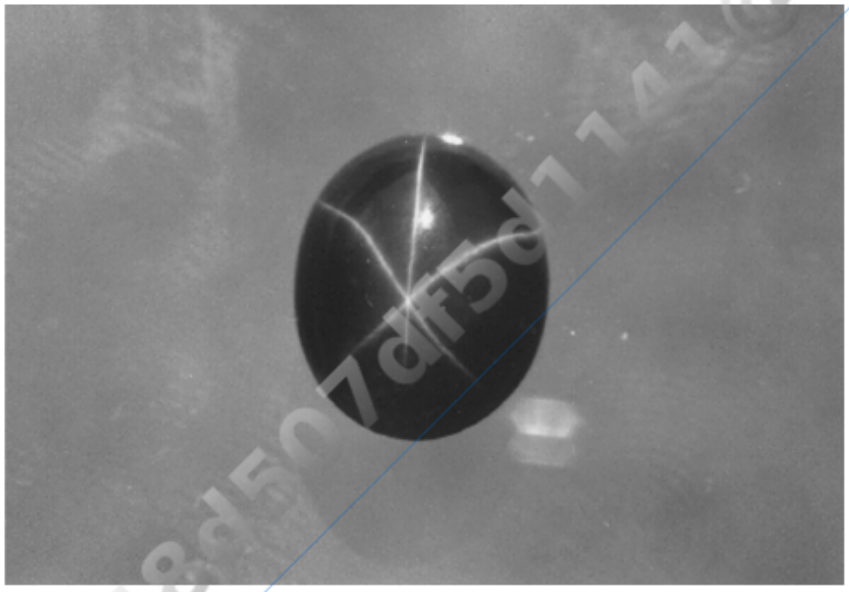

FIGURE 6.13 Photograph of star sapphire whose long dimension is 8 mm. The star pattern is due to numerous fibrous rutile (TiO_2) inclusions parallel to the hexagonally arranged 2-fold rotation axes in the host corundum. Back to text

Printed by: e48d507df5d1141@placeholder.94092.edu. Printing is for personal, private use only. No part of this book may be reproduced or transmitted without publisher's prior permission. Violators will be prosecuted.

axes in the host corundum. Back to text

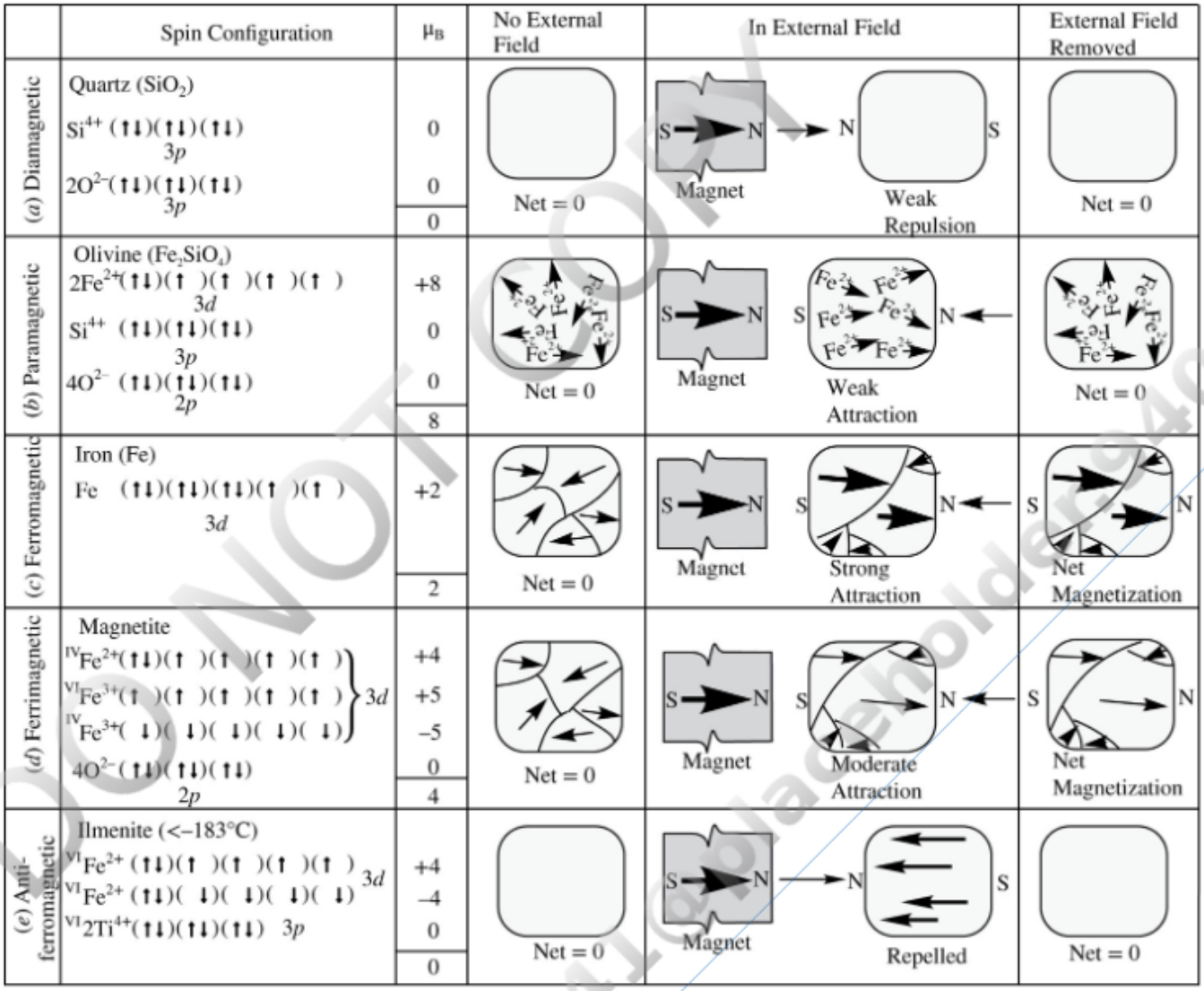

FIGURE 6.14 Magnetism. See text for discussion. (*a*) Diamagnetism in quartz. Neither Si^{4+} nor O^{2-} has unpaired electrons, so neither has a Bohr magnetic moment μ_B. (*b*) Paramagnetism in olivine. The Fe^{2+} has a net Bohr magnetic moment; but in the absence of an external magnetic field, the orientations are random. (*c*) Ferromagnetism in native iron. Each iron atom has two unpaired electrons and a Bohr magnetic moment of 2. Domains within the mineral have uniform magnetic orientation. (*d*) Ferrimagnetism in magnetite. The $^{IV}Fe^{2+}$ has a net magnetic moment and causes the magnetite to have ferromagnetic properties. (*e*) Antiferromagnetism in ilmenite below −183°C. Fe^{2+} in adjacent sites have antiparallel spins. Net magnetic moments cancel. Antiferromagnetic materials are repelled by a magnet. Back to text

(a) 1×10^{8}

https://print.vitalsource.com/requests/GM7Nq1ZS0WtoausAQTDB/c...

Printed by: e48d507df5d1141@placeholder.94092.edu. Printing is for personal, private use only. No part of this book may be reproduced or transmitted without publisher's prior permission. Violators will be prosecuted.

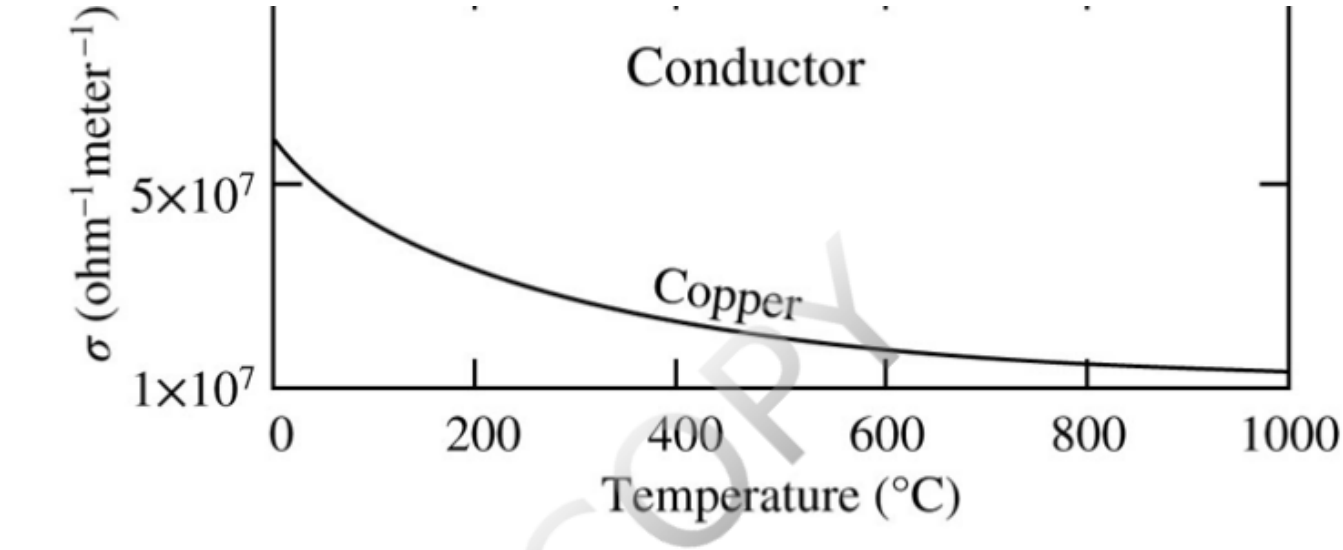

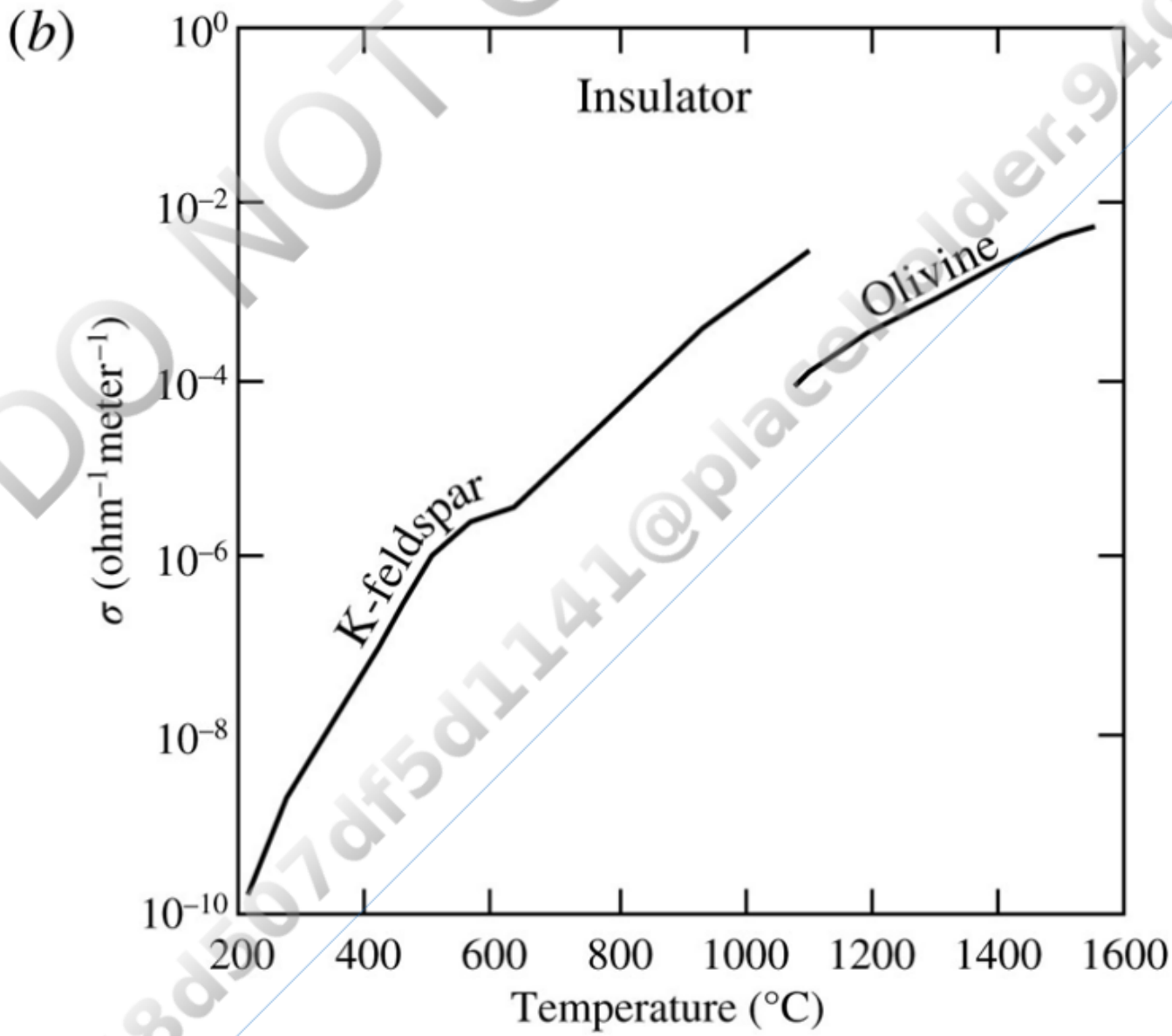

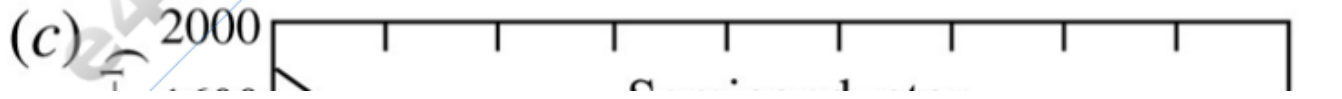

DO NOT COPY
e48d507df5d1141@placeholder.9409

Printed by: e48d507df5d1141@placeholder.94092.edu. Printing is for personal, private use only. No part of this book may be reproduced or transmitted without publisher's prior permission. Violators will be prosecuted.

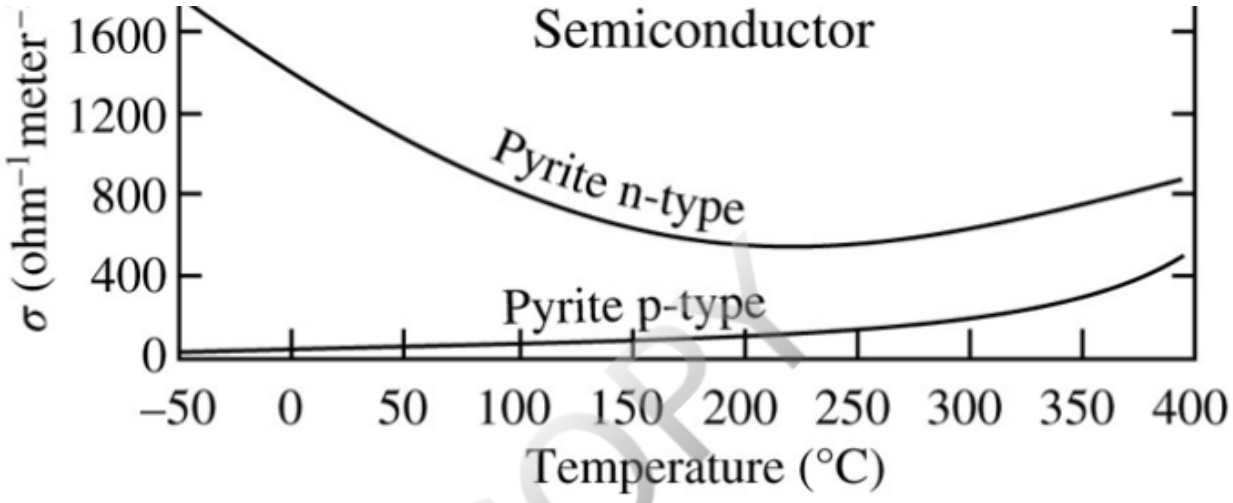

FIGURE 6.15 Electrical conductivity σ (ohm^{-1}meter^{-1}) of selected minerals. (*a*) Copper. (*b*) K-feldspar (Guseinov and Gargatsev, 2002) and olivine at 70 kbar pressure (Yousheng and others 1998). (*c*) Two samples of pyrite (Marinage, 1954). Pyrite may form both n-type and p-type semiconductors depending on details of the chemical composition. Back to text

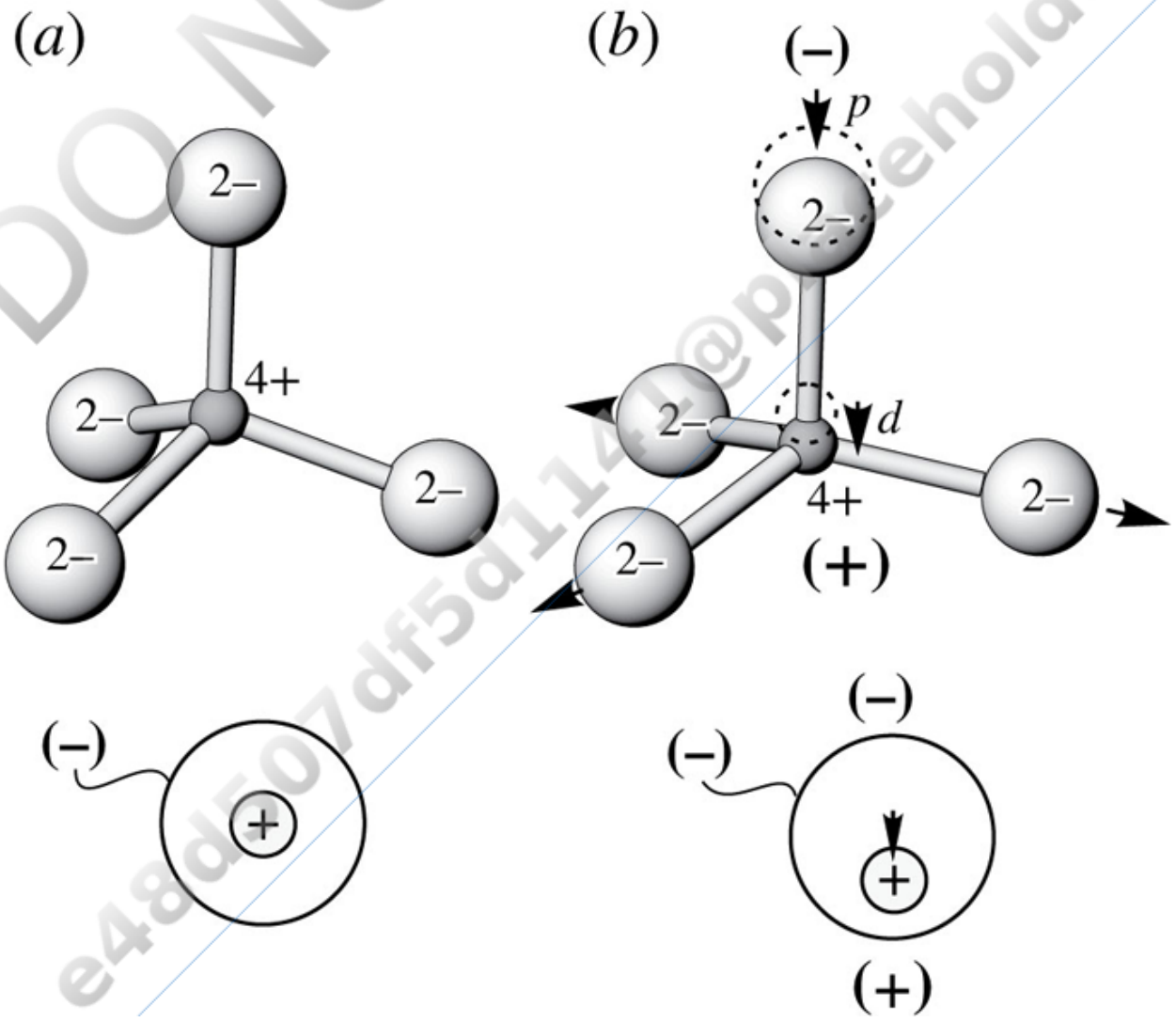

DO NOT COPY
e48d507df5d1141@placeholder.9409

Printed by: e48d507df5d1141@placeholder.94092.edu. Printing is for personal, private use only. No part of this book may be reproduced or transmitted without publisher's prior permission. Violators will be prosecuted.

FIGURE 6.16 Piezoelectricity. (*a*) A silicon tetrahedron consists of a Si^{4+} centered within four O^{2-}. The positive charge is centered within the negative charge, as shown schematically with the two circles below. (*b*) If deformed by pressing downward at *p*, an O^{2-} and the Si^{4+} are moved downward distance *d* and the O^{2-} on the base are spread outward. Because only one O^{2-} moves down, the center of the positive charge on the Si^{4+} is moved downward relative to the center of mass of the negative charge on the four O^{2-}. This charge displacement produces a voltage, positive on the bottom, negative on top. Back to text

DO NOT COPY
e48d507df5d1141@placeholder.9409

Printed by: e48d507df5d1141@placeholder.94092.edu. Printing is for personal, private use only. No part of this book may be reproduced or transmitted without publisher's prior permission. Violators will be prosecuted.

Chapter 7 Optical Mineralogy

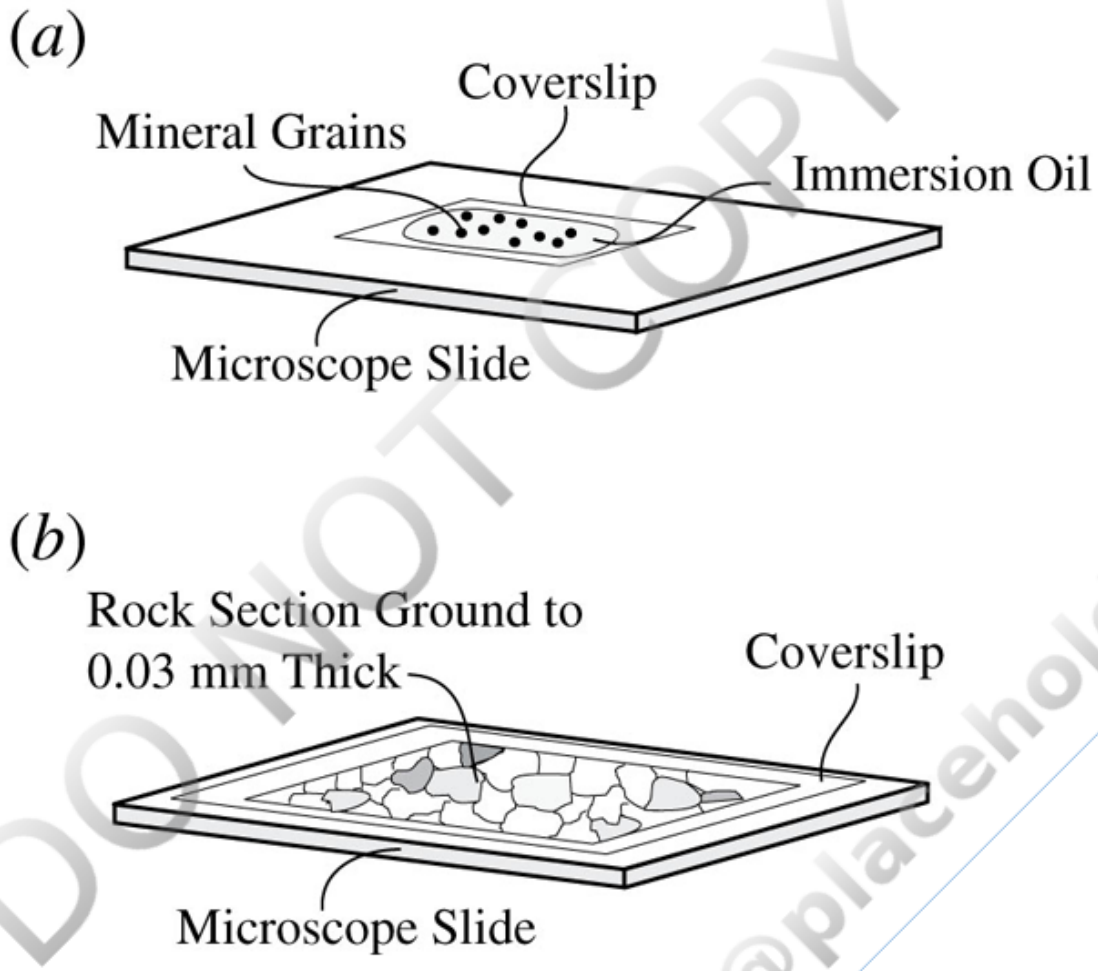

FIGURE 7.1 Sample preparations for the petrographic microscope. (*a*) Grain mount. (*b*) Thin section. Back to text

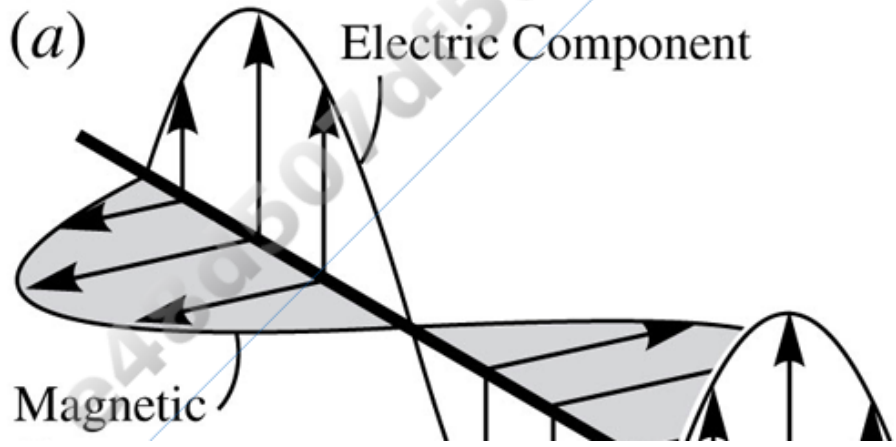

Printed by: e48d507df5d1141@placeholder.94092.edu. Printing is for personal, private use only. No part of this book may be reproduced or transmitted without publisher's prior permission. Violators will be prosecuted.

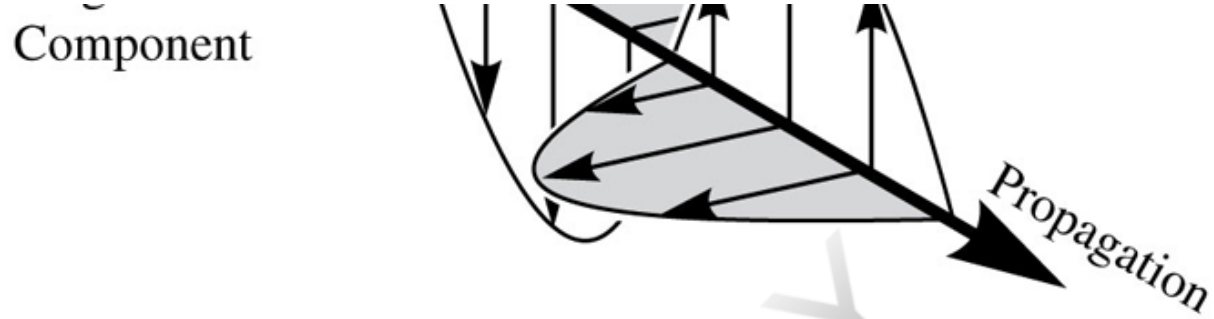

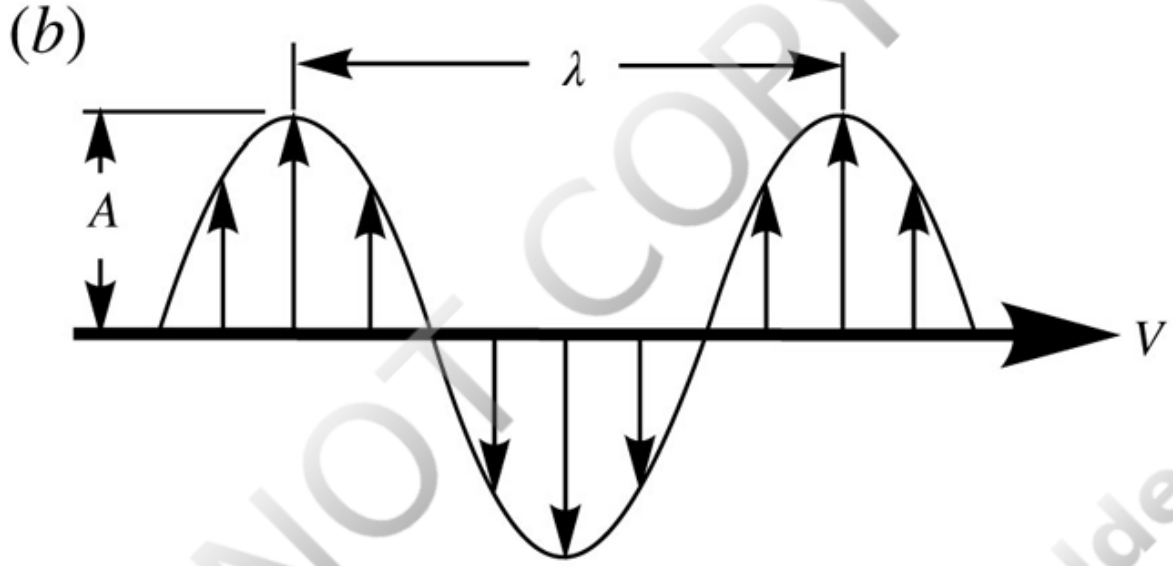

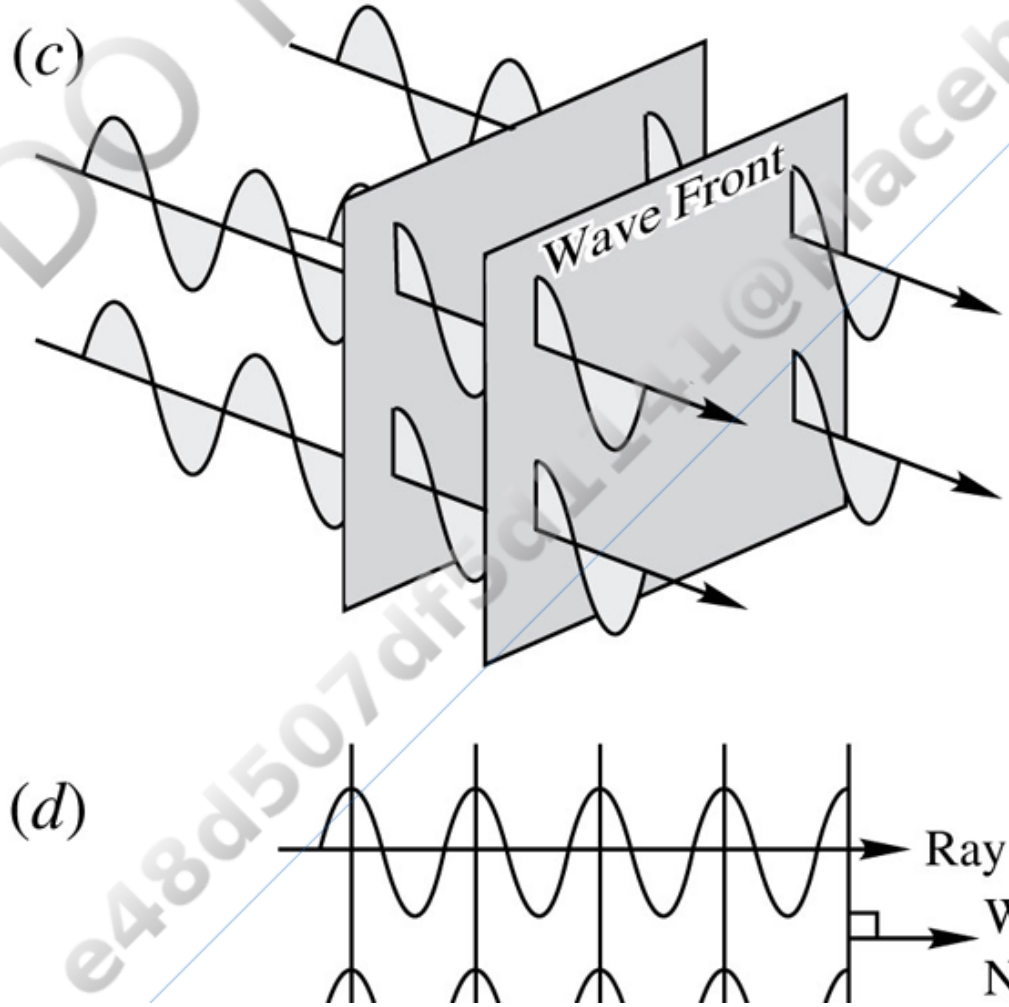

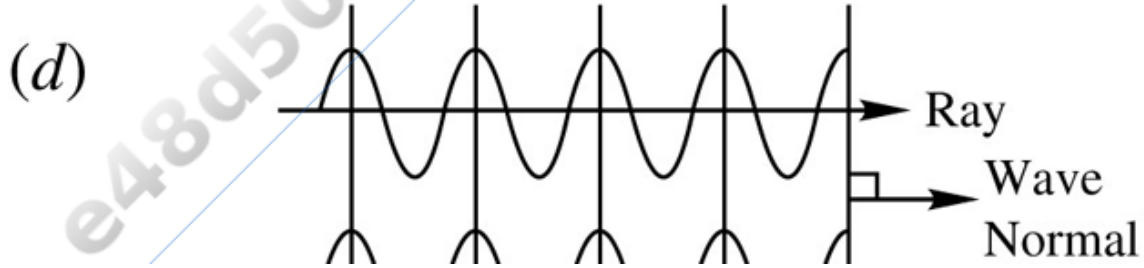

DO NOT COPY
e48d507df5d1141@placeholder.9409

Printed by: e48d507df5d1141@placeholder.94092.edu. Printing is for personal, private use only. No part of this book may be reproduced or transmitted without publisher's prior permission. Violators will be prosecuted.

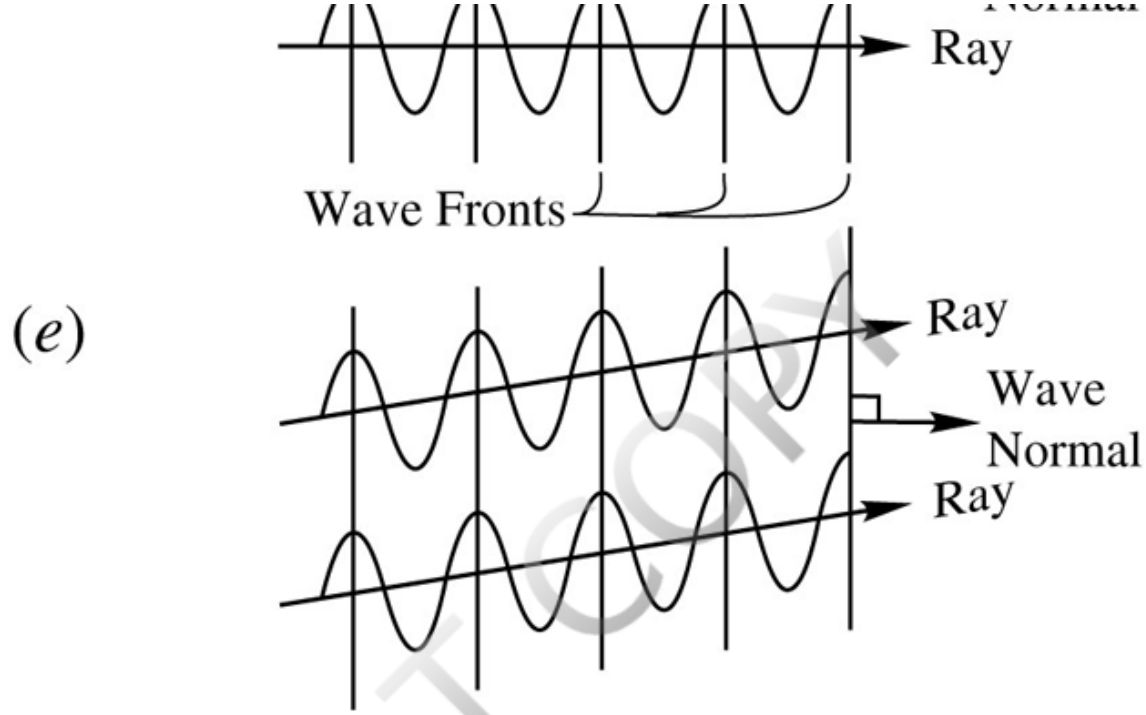

FIGURE 7.2 Electromagnetic radiation. (*a*) Electric and magnetic components of electromagnetic radiation vibrate perpendicular to the direction of propagation or travel. (*b*) Wave nomenclature. The wave travels to the right with velocity *V*. The wavelength (λ) is the distance between successive wave crests. Frequency (*f*) is the number of wave crests that pass some point per second, expressed in units of cycles per second, or hertz (Hz). Brightness of the light is proportional to the square of the amplitude (*A*). (*c*) Wave fronts connect equivalent points on adjacent waves. (*d*) In isotropic materials, the wave normal and ray directions are parallel. (*e*) In anisotropic materials, wave normal and ray directions are not parallel except for certain directions.
Back to text

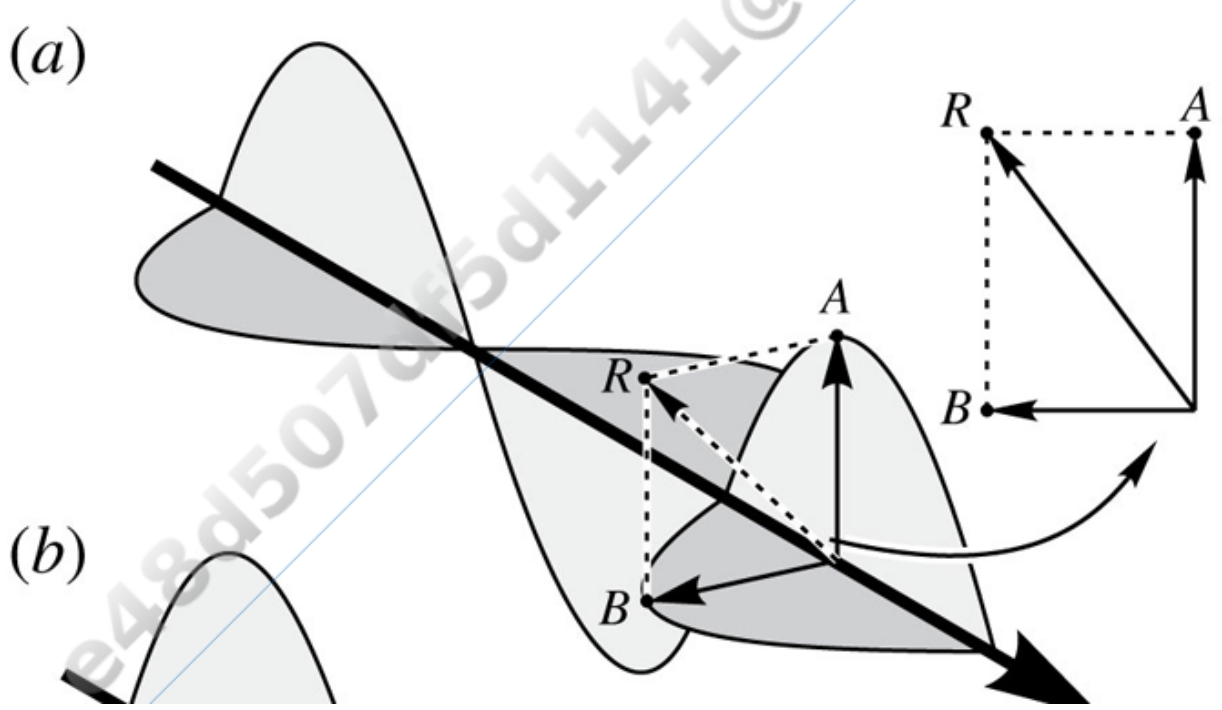

Printed by: e48d507df5d1141@placeholder.94092.edu. Printing is for personal, private use only. No part of this book may be reproduced or transmitted without publisher's prior permission. Violators will be prosecuted.

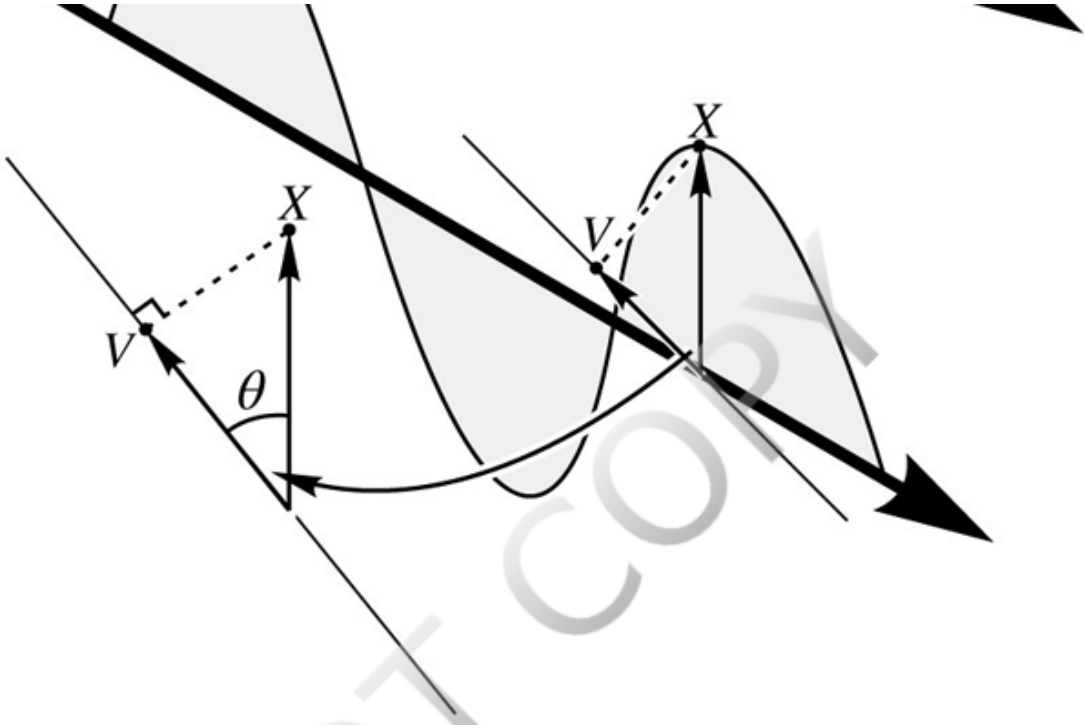

FIGURE 7.3 Vector resolution of light waves. (*a*) Waves *A* and *B* form resultant *R*. (*b*) A component *V* of wave *X* can be resolved in a new direction at angle *θ* from *X*. Back to text

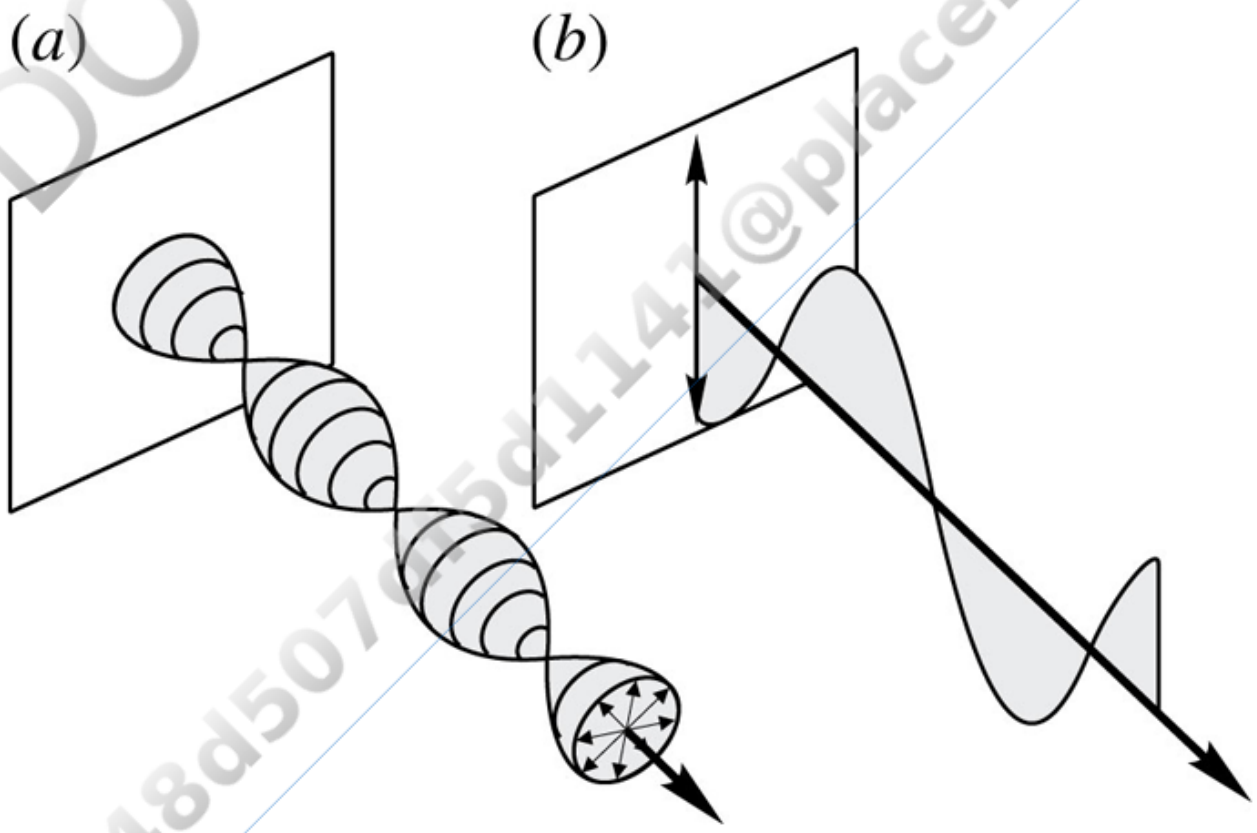

FIGURE 7.4 Polarized light. (*a*) Unpolarized light vibrates in all directions at right angles to the direction of propagation. (*b*) Plane-polarized light. The electric vector vibrates in a single plane. Back

DO NOT COPY
e48d507df5d1141@placeholder.9409

Printed by: e48d507df5d1141@placeholder.94092.edu. Printing is for personal, private use only. No part of this book may be reproduced or transmitted without publisher's prior permission. Violators will be prosecuted.

direction of propagation. (*b*) Plane-polarized light. The electric vector vibrates in a single plane. Back to text

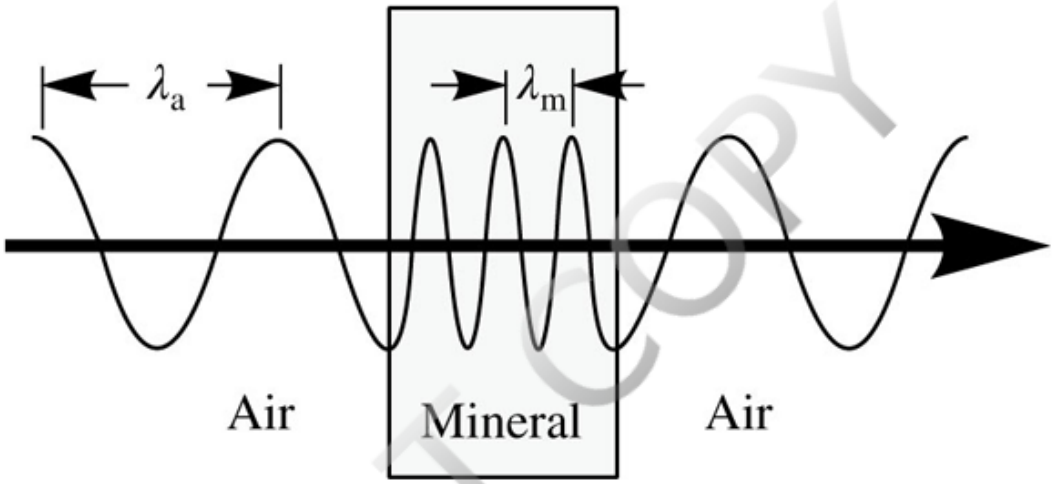

FIGURE 7.5 Light entering a mineral slows down and the wavelength (λ) decreases. Back to text

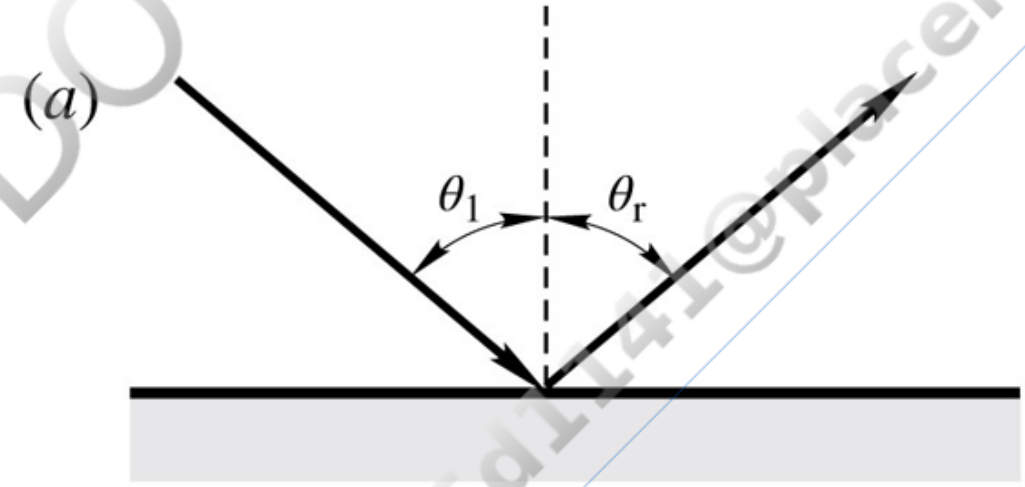

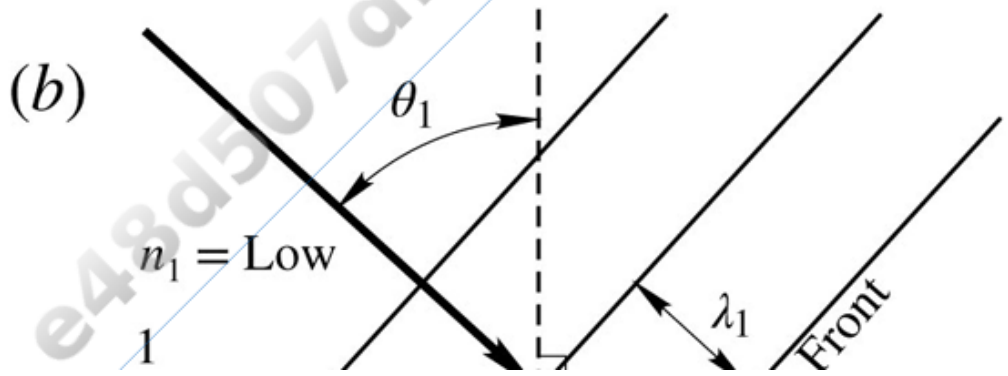

DO NOT COPY
e48d507df5d1141@placeholder.9409

Printed by: e48d507df5d1141@placeholder.94092.edu. Printing is for personal, private use only. No part of this book may be reproduced or transmitted without publisher's prior permission. Violators will be prosecuted.

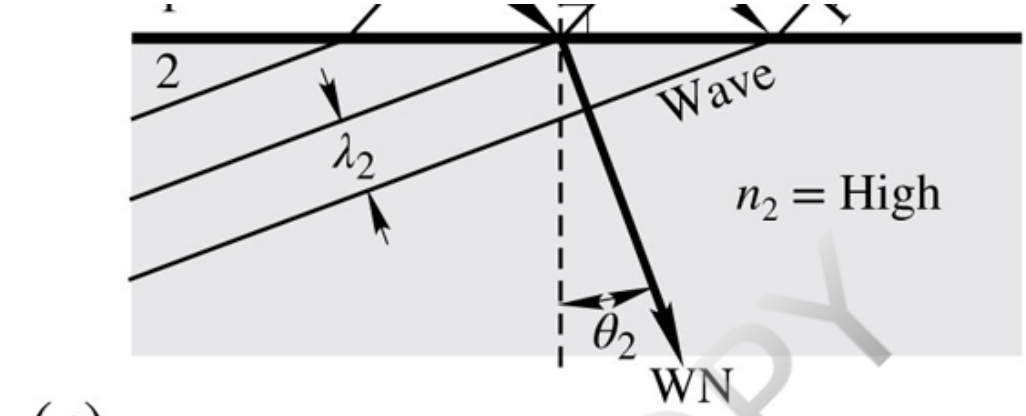

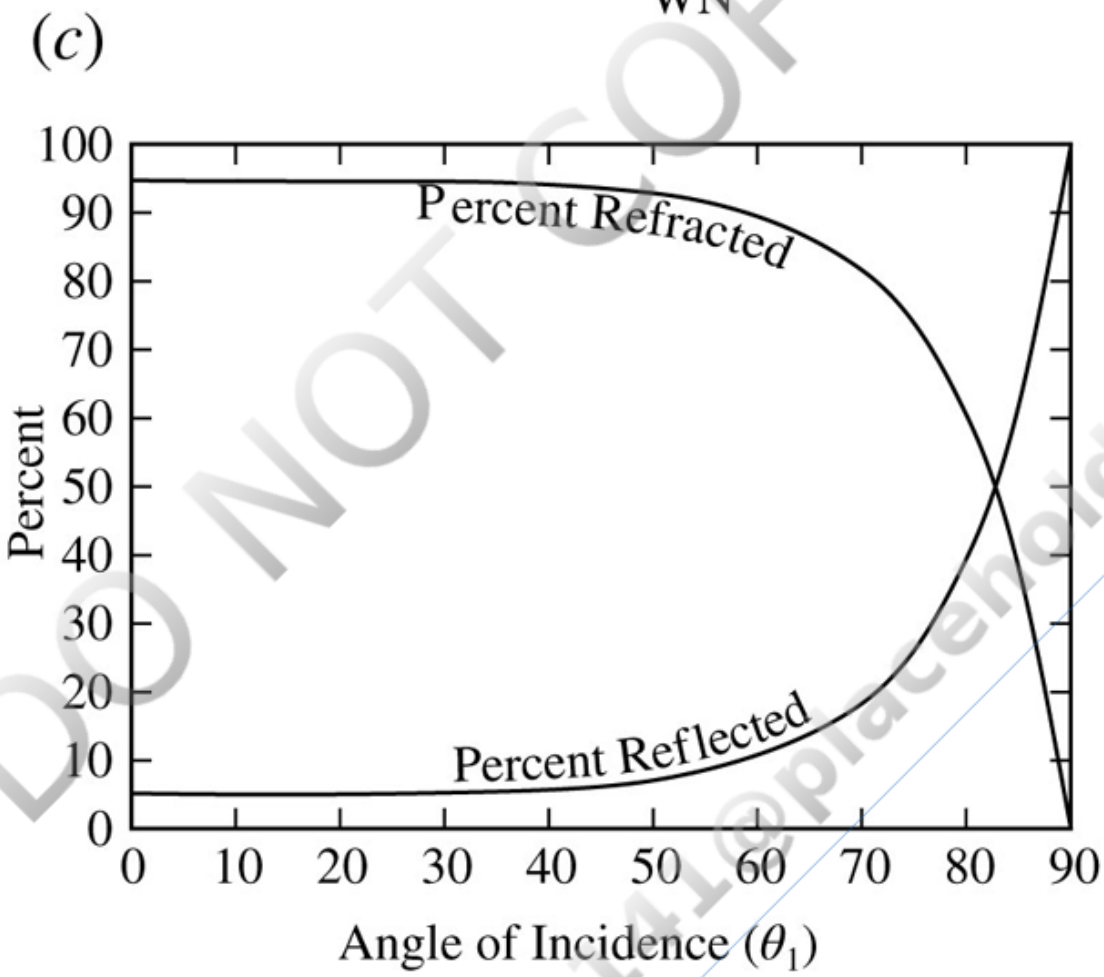

FIGURE 7.6 Reflection and refraction. (*a*) Reflection from a smooth surface. The angles of incidence (θ_1) and reflection (θ_r) are identical. (*b*) Refraction. Wave fronts one wavelength apart and the wave normal (WN) are shown for light passing from material 1 (n_1 = low index of refraction, higher velocity) to material 2 (n_2 = high index of refraction, low velocity). The wave fronts and wave normal bend at the interface because the wavelength λ_2 in the low-velocity material is shorter than the wavelength in the high-velocity material. (*c*) Relative amount of light coming from air ($n = 1$) that is reflected and refracted from the surface of a material with $n = 1.55$ as a function of the angle of incidence. Back to text

Printed by: e48d507df5d1141@placeholder.94092.edu. Printing is for personal, private use only. No part of this book may be reproduced or transmitted without publisher's prior permission. Violators will be prosecuted.

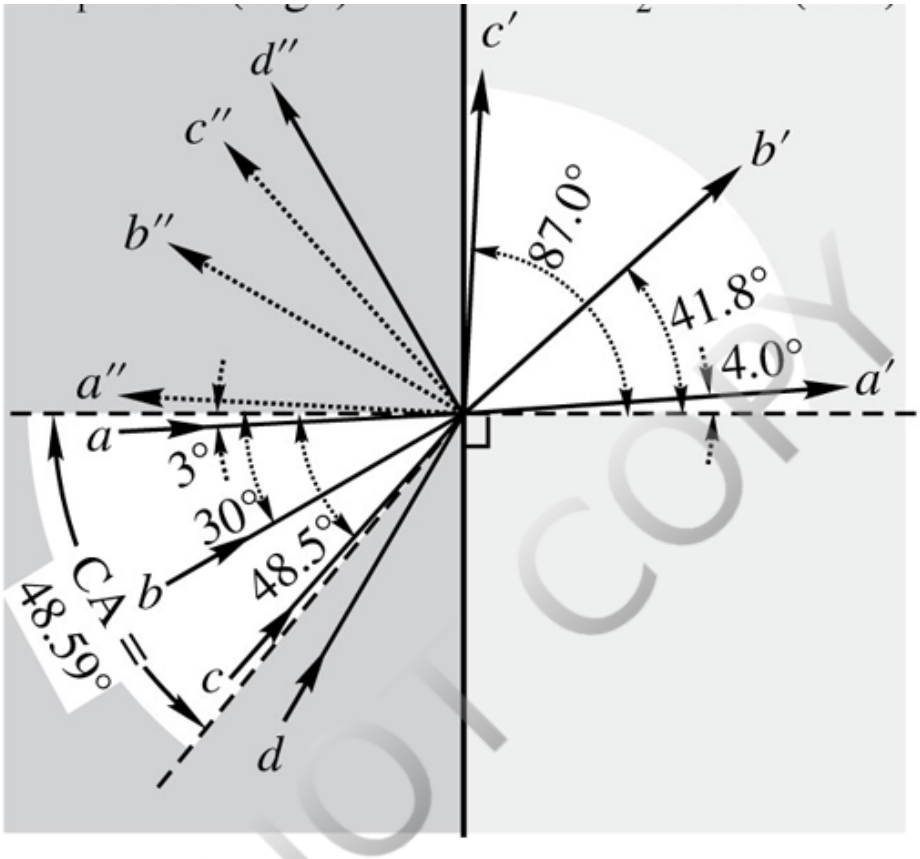

FIGURE 7.7 Critical angle and total internal reflection. Some of the light following wave normals *a*, *b*, and *c* in material 1 ($n_1 = 2.0$) is refracted into material 2 ($n_2 = 1.5$) to *a*′, *b*′, and *c*′. The angles of incidence are 3°, 30°, and 48.5°, and angles of refraction are 4.0°, 41.8°, and 87.0°, respectively, in this case. Wave normal *d*, with an angle of incidence greater than the critical angle (CA = 48.59°), is completely reflected at the boundary to *d*″. Portions of wave normals *a*, *b*, and *c* are reflected to *a*″, *b*″, and *c*″, as shown with dotted lines. The amount of reflection increases from *a* to *c* and is 100 percent for angles of incidence greater than the critical angle (Figure 7.6). Back to text

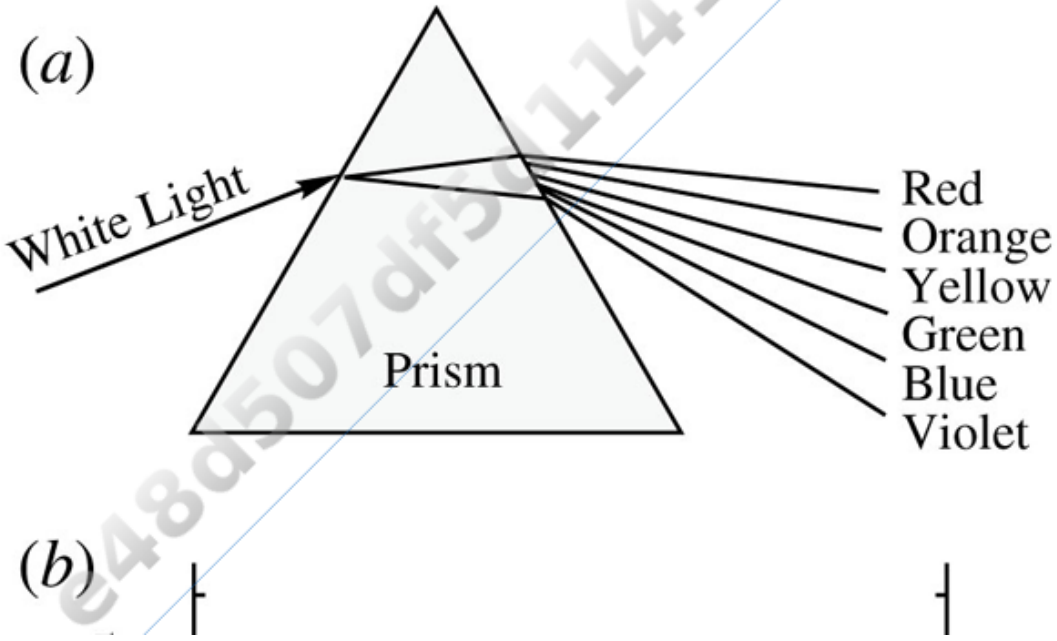

DO NOT COPY
e48d507df5d1141@placeholder.9409

Printed by: e48d507df5d1141@placeholder.94092.edu. Printing is for personal, private use only. No part of this book may be reproduced or transmitted without publisher's prior permission. Violators will be prosecuted.

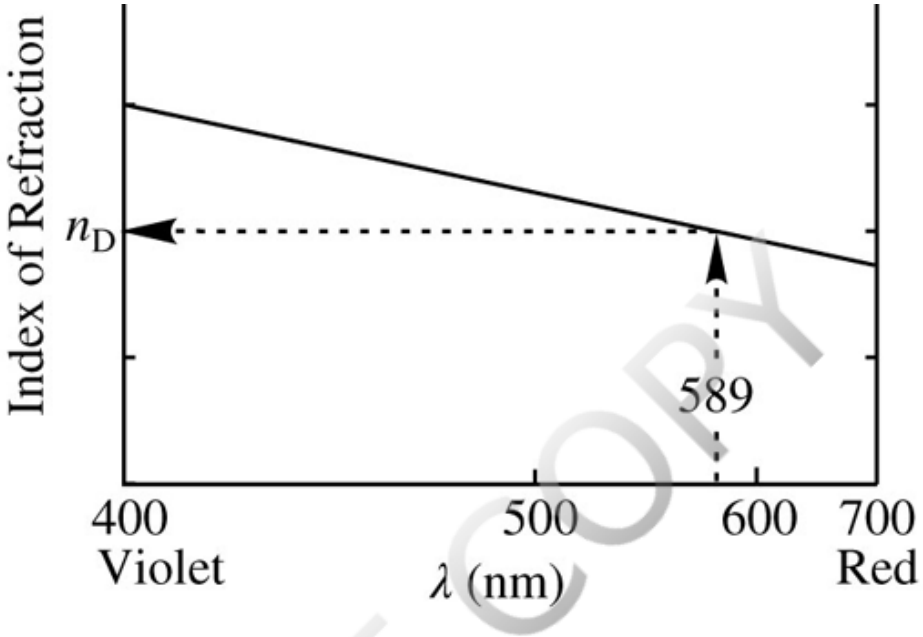

FIGURE 7.8 Dispersion. (*a*) White light is spread into its spectral colors when passed through a prism because the index of refraction for violet light is higher than for red light. (*b*) Normal dispersion of the refractive indices. Index of refraction decreases with increasing wavelength. Strongly colored minerals may display abnormal dispersion of the refractive indices (index of refraction increases with increasing wavelength) for wavelengths that are strongly absorbed by the mineral. Back to text

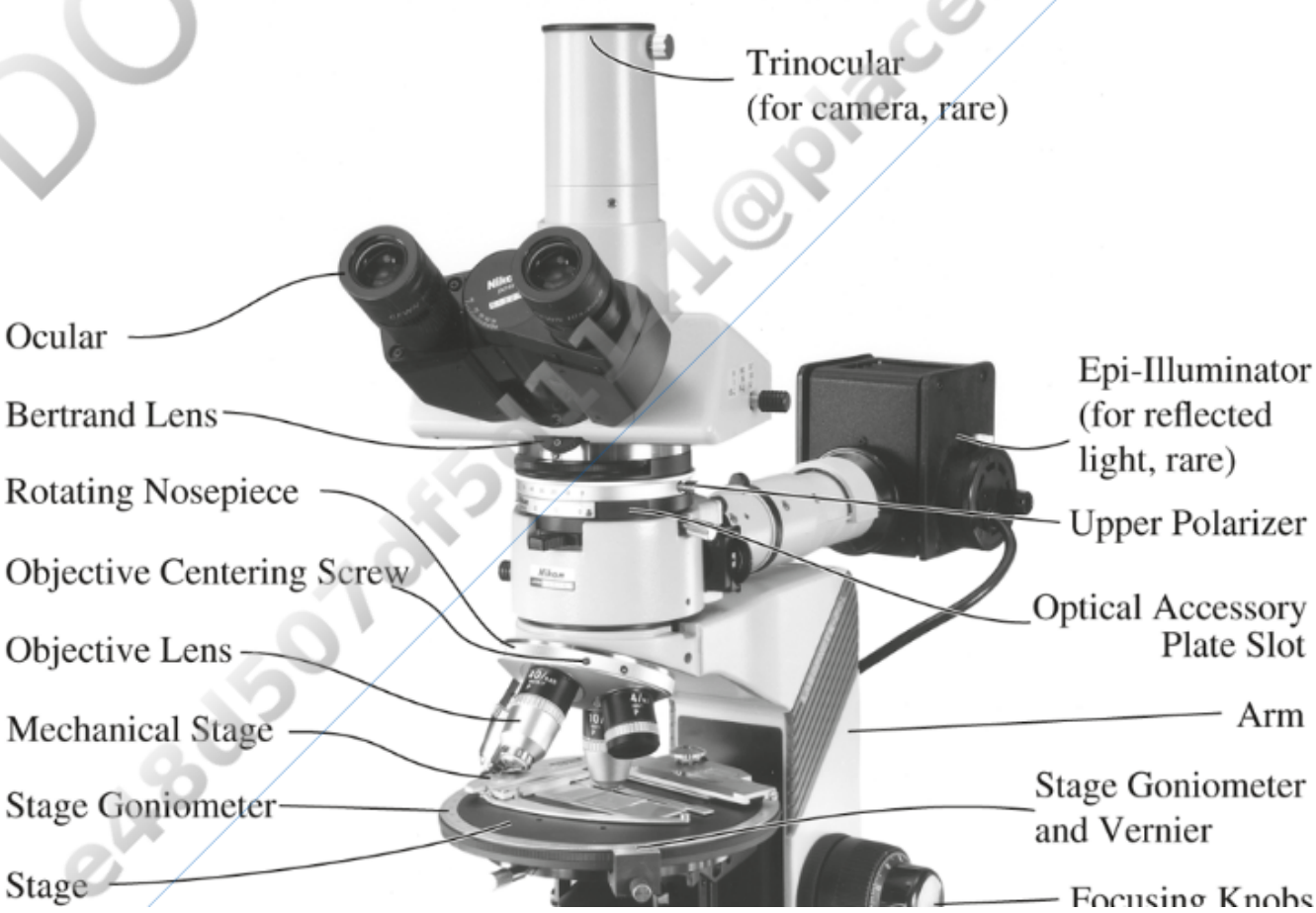

DO NOT COPY

Printed by: e48d507df5d1141@placeholder.94092.edu. Printing is for personal, private use only. No part of this book may be reproduced or transmitted without publisher's prior permission. Violators will be prosecuted.

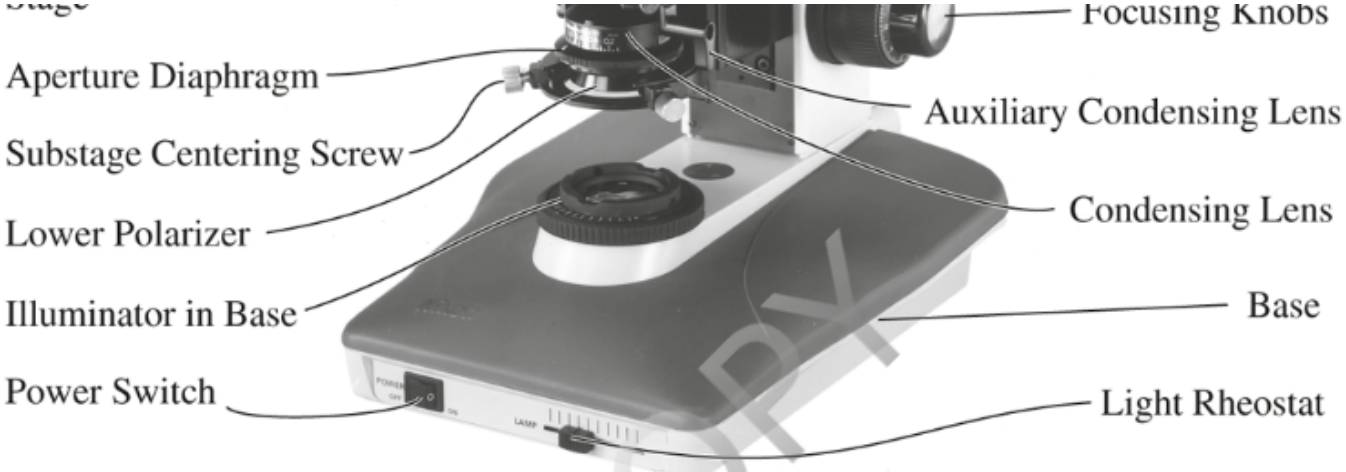

FIGURE 7.9 The petrographic microscope. Photo courtesy of Nikon Instruments Inc., Melville, New York. Back to text

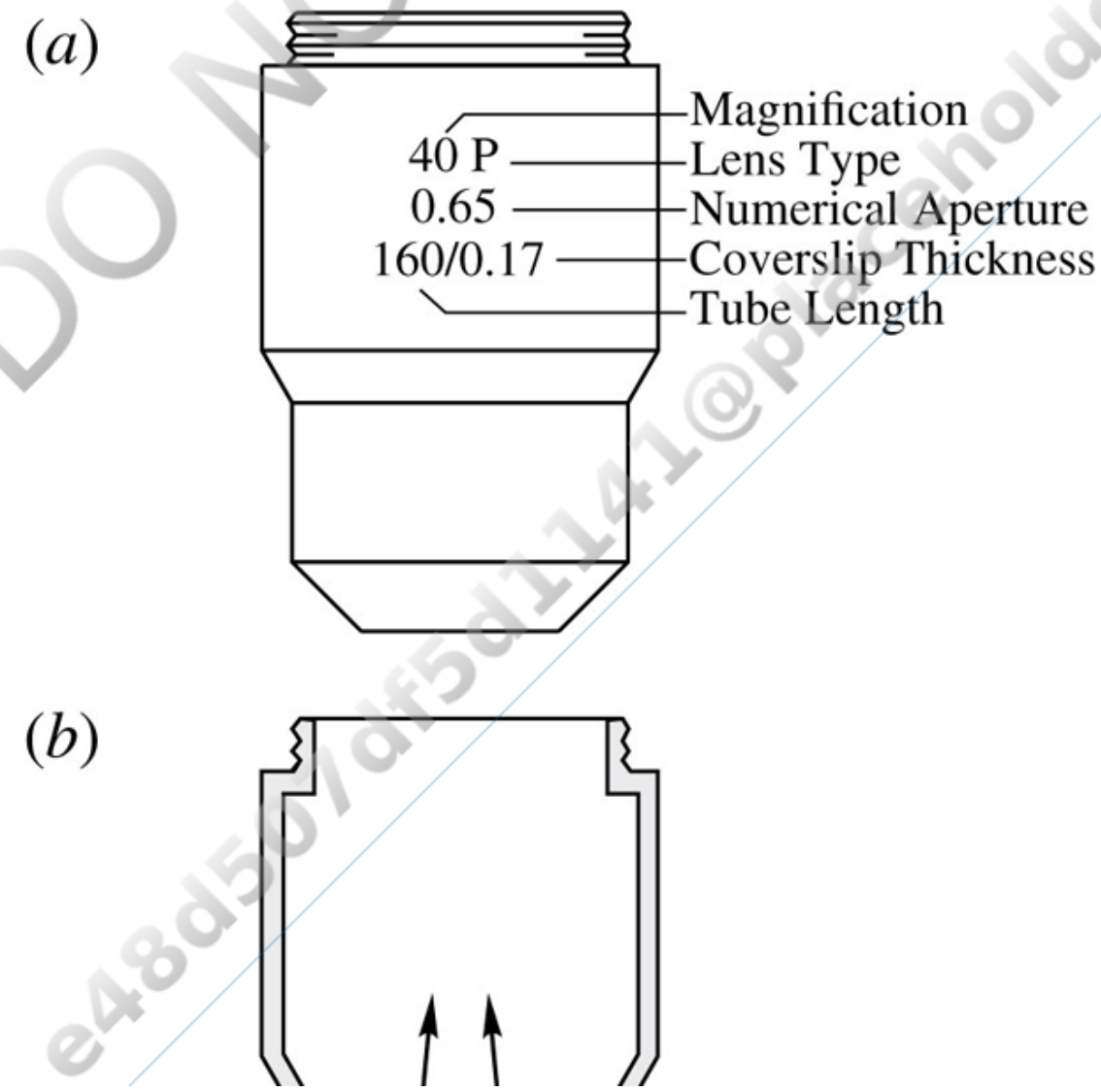

DO NOT COPY
e48d507df5d1141@placeholder.9409

Printed by: e48d507df5d1141@placeholder.94092.edu. Printing is for personal, private use only. No part of this book may be reproduced or transmitted without publisher's prior permission. Violators will be prosecuted.

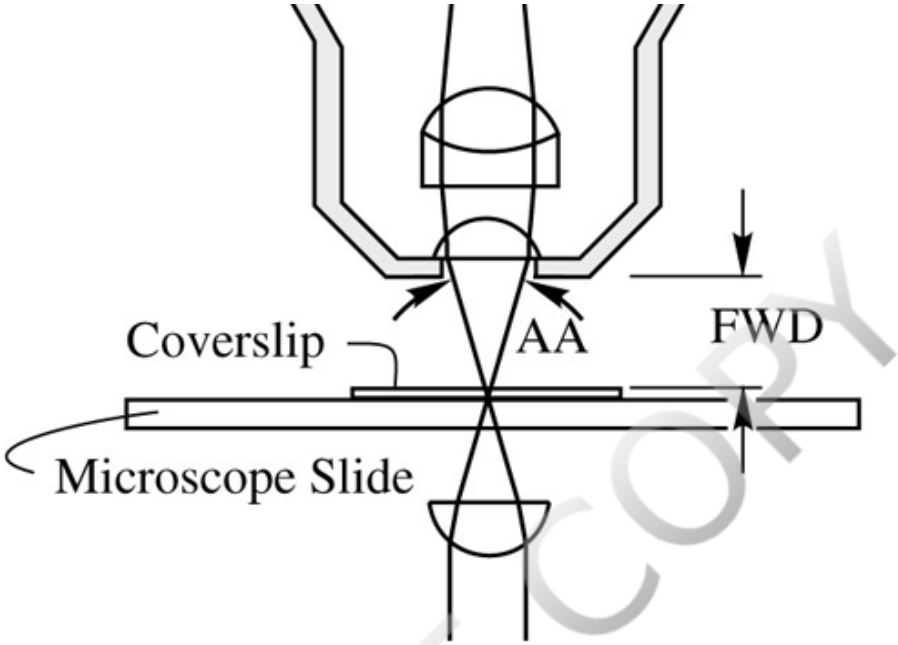

FIGURE 7.10 Objective lens. (*a*) Typical objective lens markings. P indicates that the lens is intended for use with polarized light. (*b*) The free working distance (FWD) is the distance between the end of the lens and top of the sample. Angular aperture (AA) is the size of the cone in degrees of light that the lens can accept. Back to text

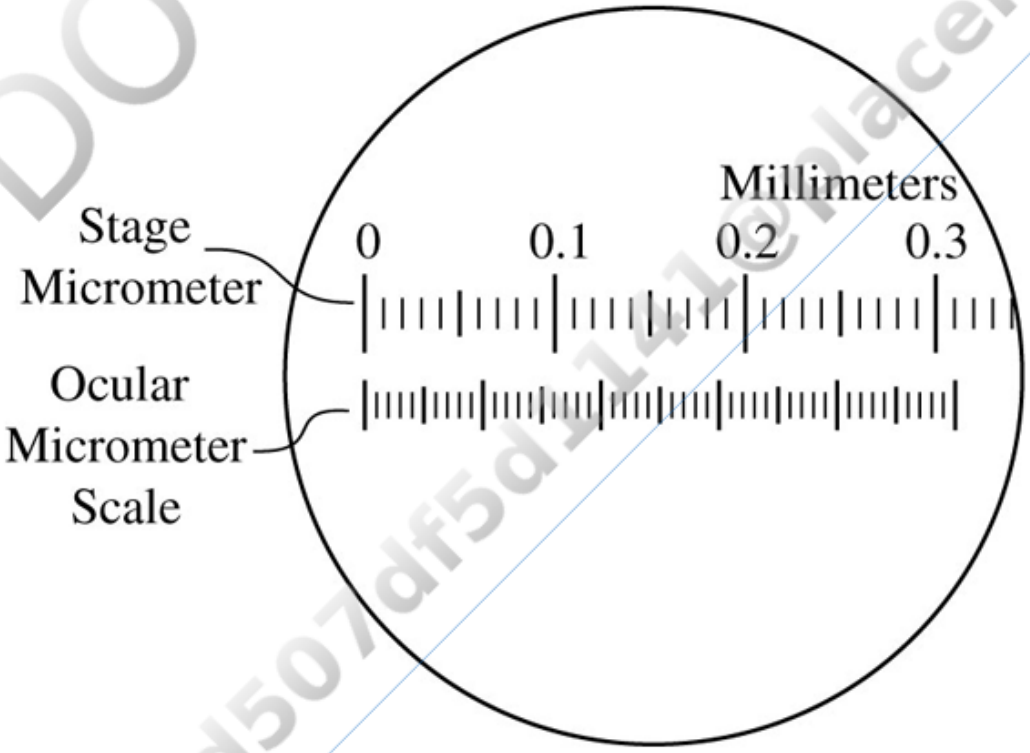

FIGURE 7.11 Calibration of an ocular micrometer scale. Fifty divisions of the ocular micrometer scale (bottom scale) equals 0.31 mm on the stage micrometer. Each ocular micrometer division must therefore equal 0.0062 mm. A separate calibration must be made for each objective lens. Back to text

DO NOT COPY
e48d507df5d1141@placeholder.94092

Printed by: e48d507df5d1141@placeholder.94092.edu. Printing is for personal, private use only. No part of this book may be reproduced or transmitted without publisher's prior permission. Violators will be prosecuted.

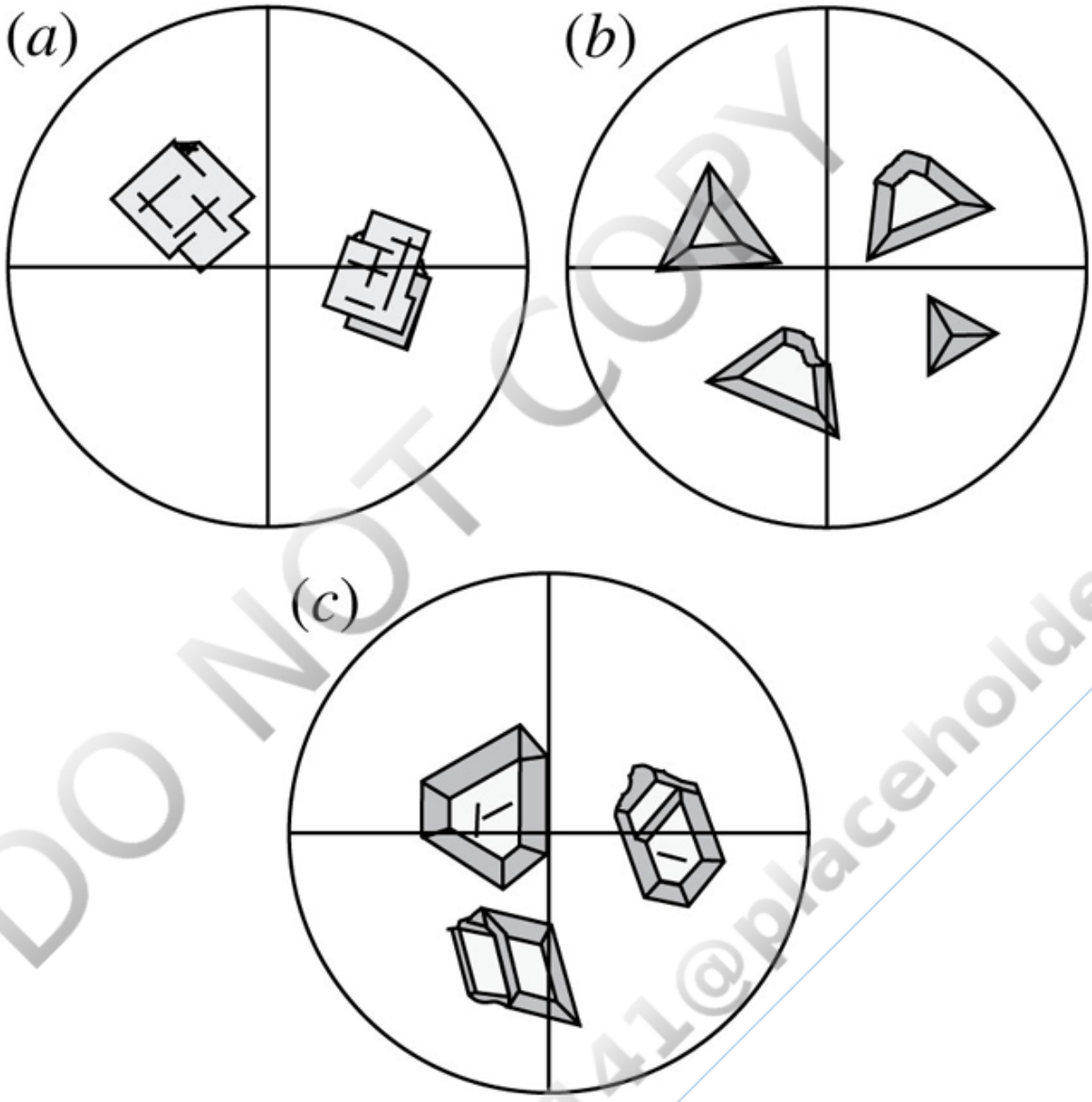

FIGURE 7.12 Cleavage in isometric minerals as seen in grain mount. (*a*) Cubic {001} cleavage. (*b*) Octahedral {111} cleavage. (*c*) Dodecahedral {011} cleavage. Back to text

(a)

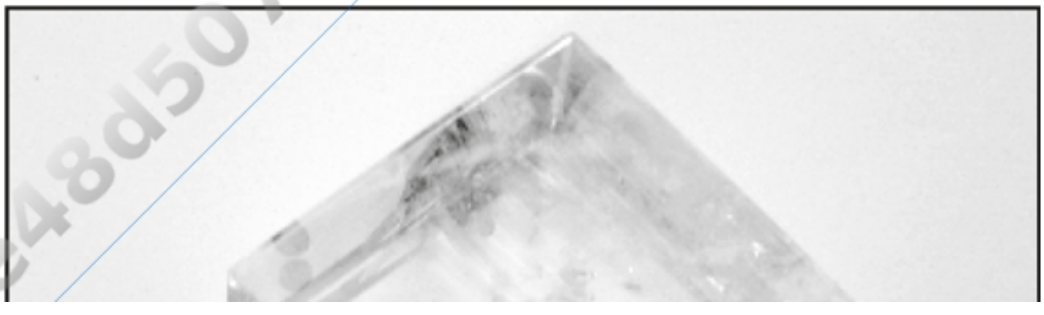

DO NOT COPY
e48d507df5d1141@placeholder.9409

Printed by: e48d507df5d1141@placeholder.94092.edu. Printing is for personal, private use only. No part of this book may be reproduced or transmitted without publisher's prior permission. Violators will be prosecuted.

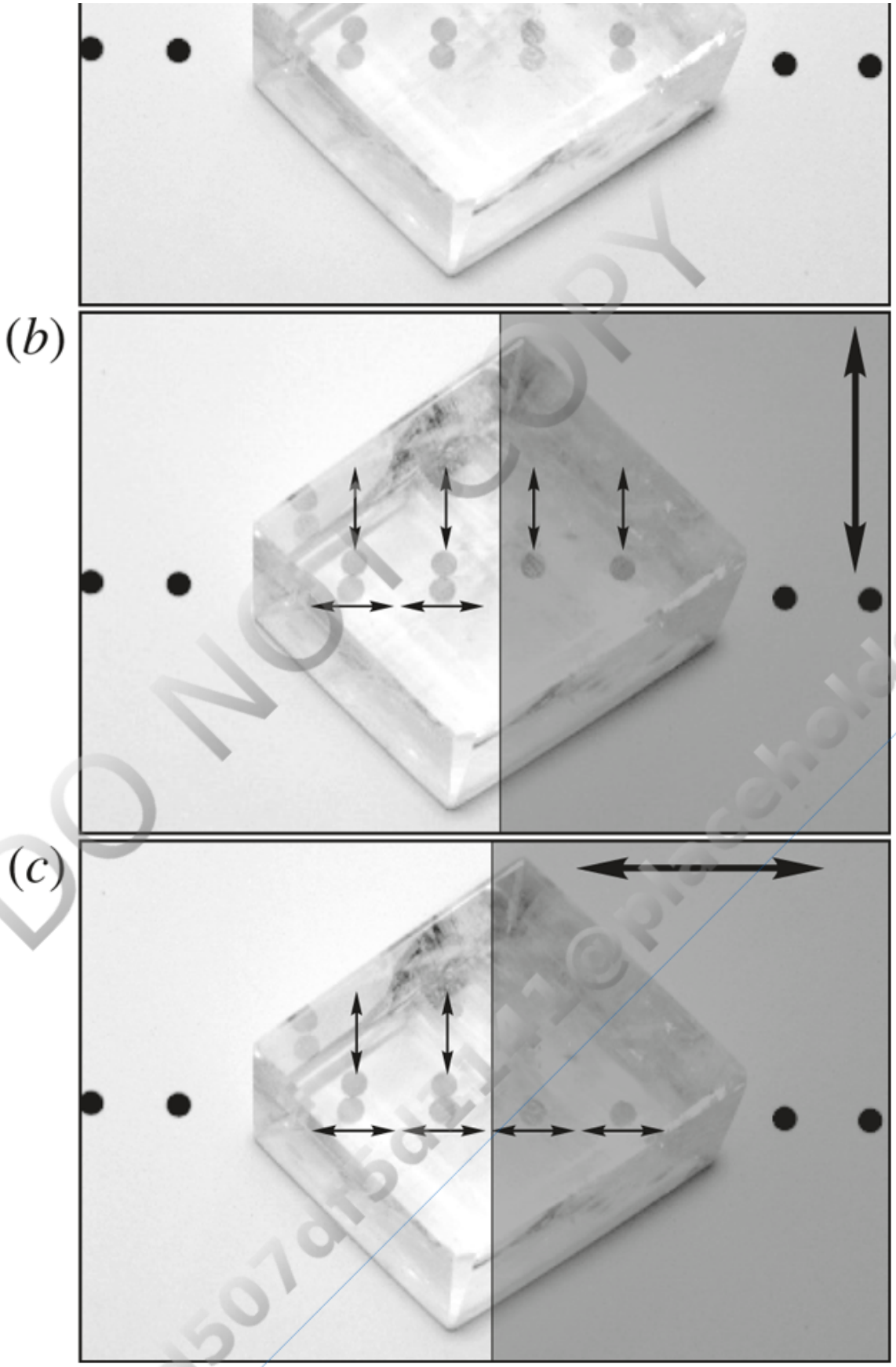

FIGURE 7.13 Double refraction of calcite. (*a*) Cleavage rhomb of clear calcite on a row of dots. Two images are produced because the light is split into two rays that vibrate at right angles to each other. (*b*) A polarizing film, whose vibration direction is parallel to the short diagonal of the rhomb, transmits one set of dots but absorbs the other. (*c*) The polarizing film is rotated 90°. The first set of dots is now absorbed, but the other is transmitted. In intermediate orientations, both sets of dots are

Printed by: e48d507df5d1141@placeholder.94092.edu. Printing is for personal, private use only. No part of this book may be reproduced or transmitted without publisher's prior permission. Violators will be prosecuted.

dots is now absorbed, but the other is transmitted. In intermediate orientations, both sets of dots are visible but darker. Back to text

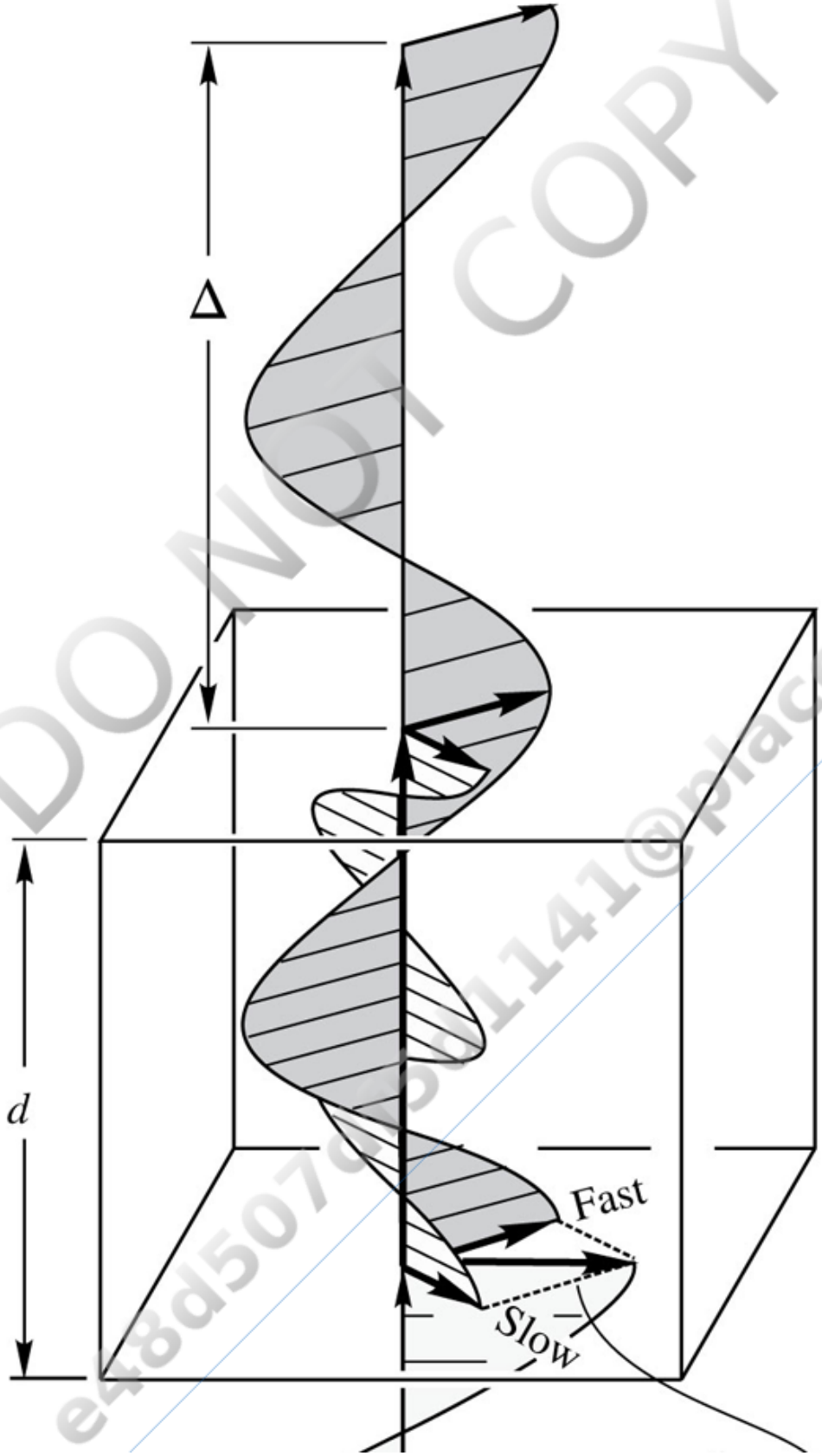

DO NOT COPY
e48d507df5d1141@placeholder.9409

Printed by: e48d507df5d1141@placeholder.94092.edu. Printing is for personal, private use only. No part of this book may be reproduced or transmitted without publisher's prior permission. Violators will be prosecuted.

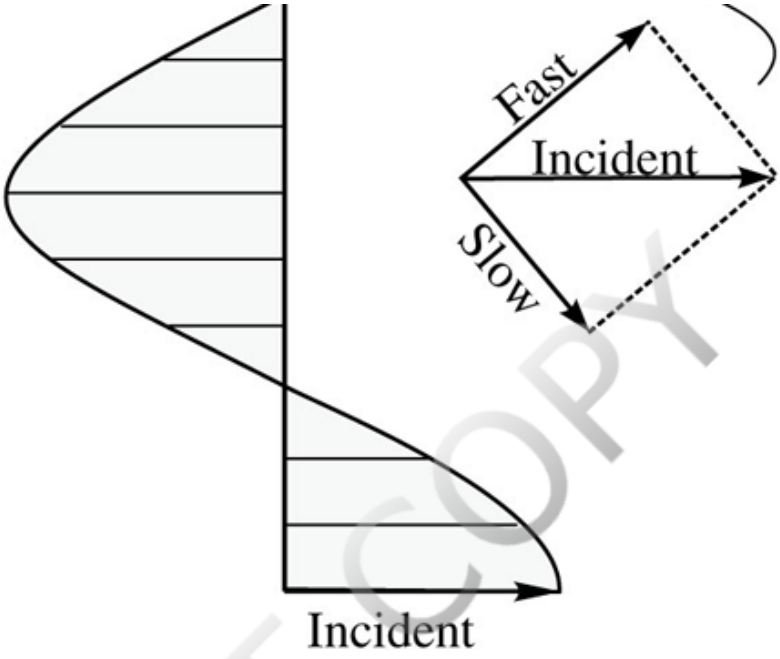

FIGURE 7.14 Development of retardation. Light entering the mineral with thickness *d* is split into slow and fast rays. In the time it takes the slow ray to pass through the mineral, the fast ray has passed through the mineral and traveled an additional distance Δ, which is the retardation. Back to text

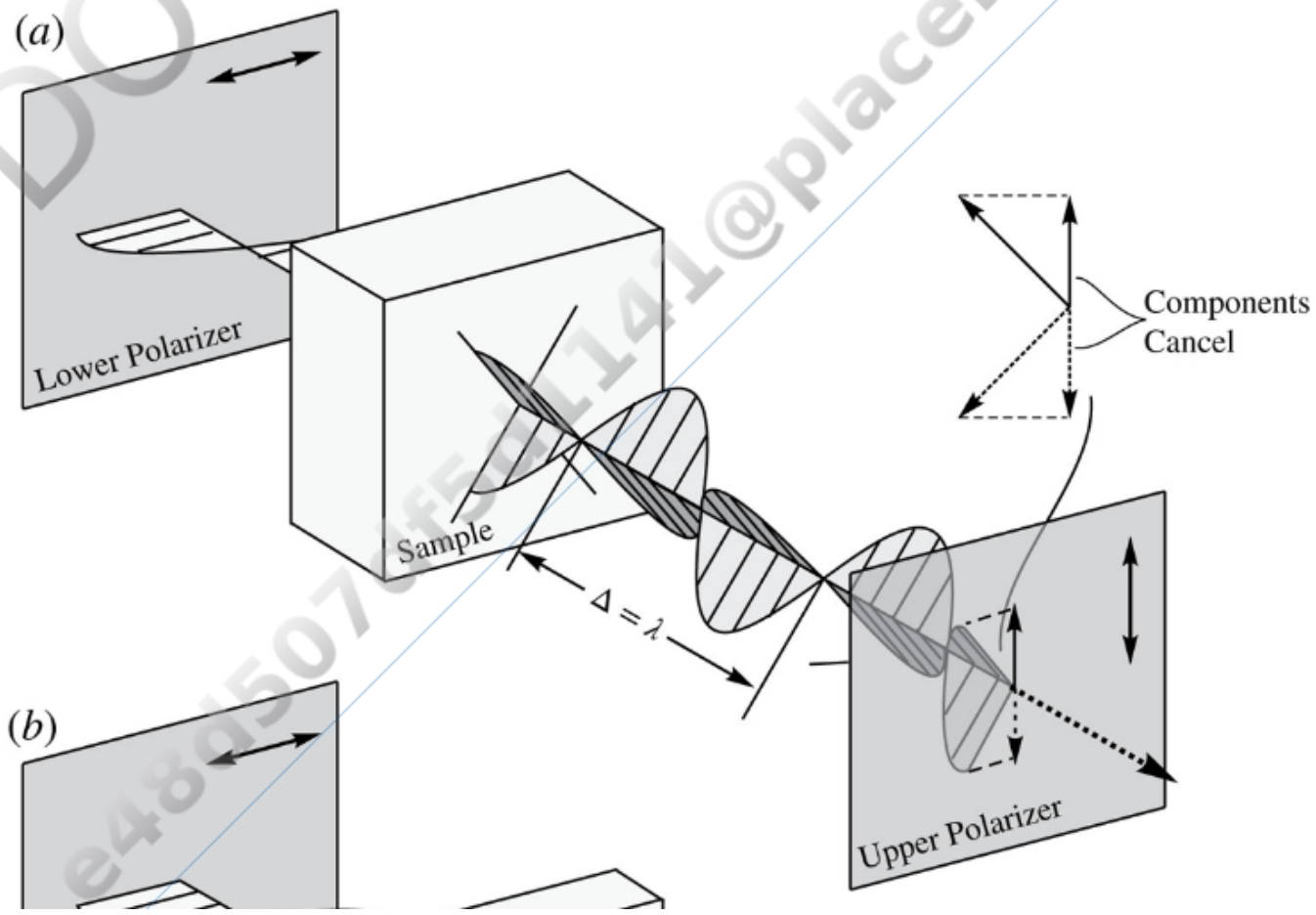

DO NOT COPY
e48d507df5d1141@placeholder.9409

Printed by: e48d507df5d1141@placeholder.94092.edu. Printing is for personal, private use only. No part of this book may be reproduced or transmitted without publisher's prior permission. Violators will be prosecuted.

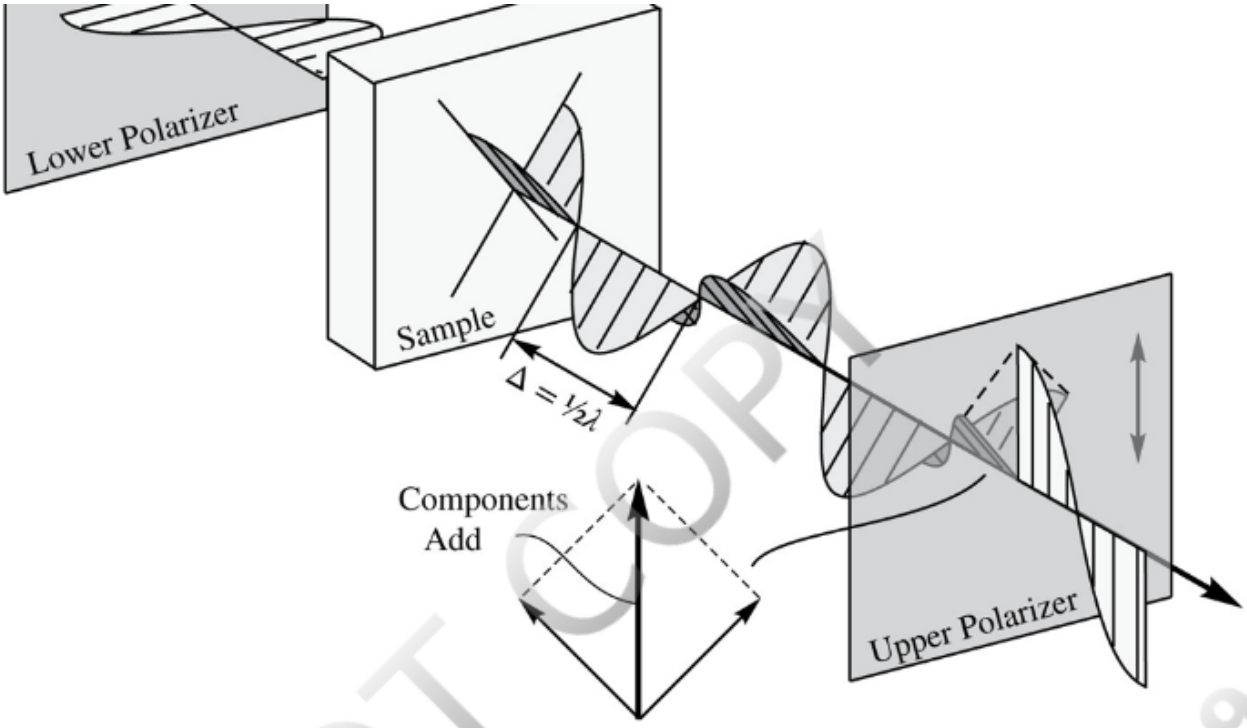

FIGURE 7.15 Interference at the upper polarizer with monochromatic light. (*a*) The retardation (Δ) is one wavelength. Vector components of the two rays resolved into the vibration direction of the upper polarizer are in opposite directions, so they cancel. No light passes and the mineral appears dark. (*b*) The retardation is one-half wavelength. Vector components of the two waves resolved into the vibration direction of the upper polarizer are in the same direction, so they constructively interfere. Light passes the upper polarizer, and the mineral appears bright. Back to text

DO NOT COPY

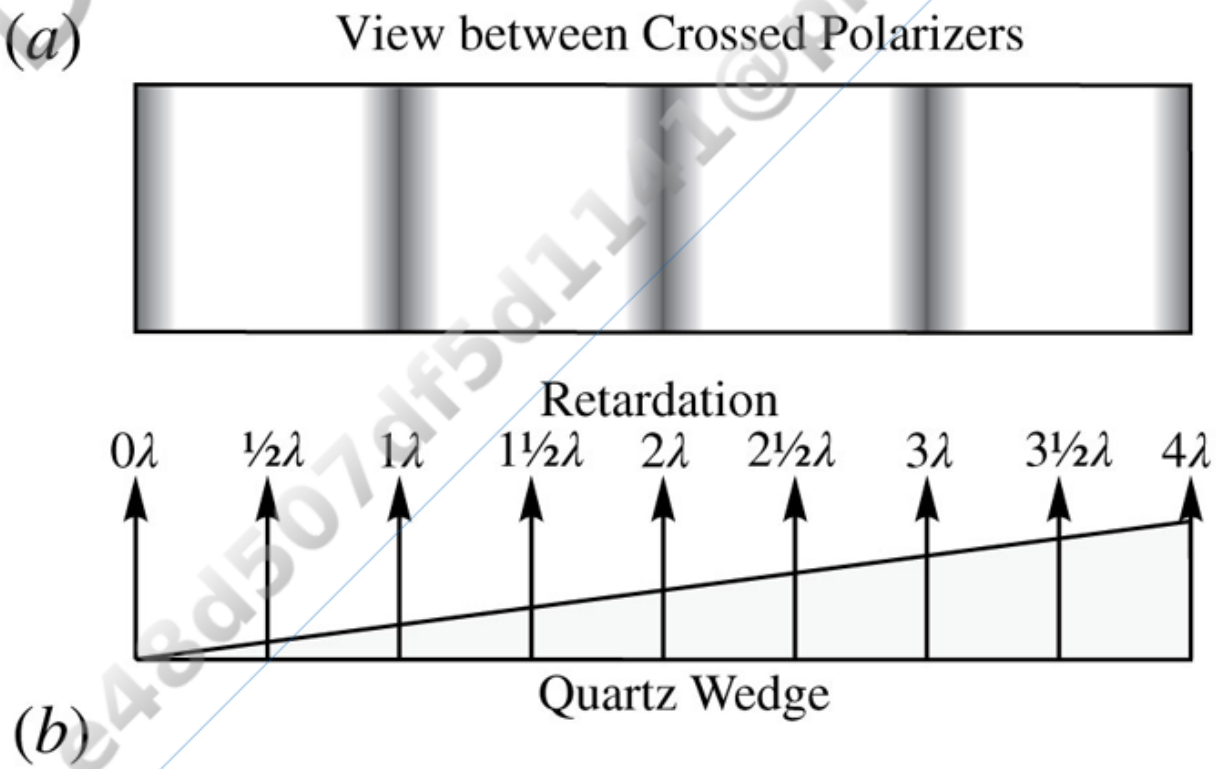

Printed by: e48d507df5d1141@placeholder.94092.edu. Printing is for personal, private use only. No part of this book may be reproduced or transmitted without publisher's prior permission. Violators will be prosecuted.

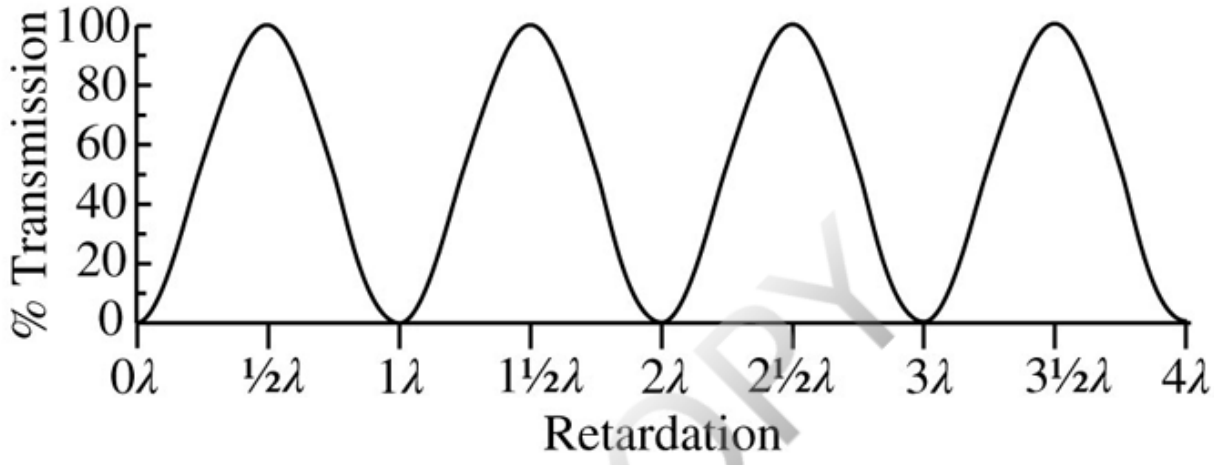

FIGURE 7.16 Interference pattern formed with a quartz wedge in monochromatic light. (*a*) Where retardation is an integer number of wavelengths, slow and fast rays destructively interfere at the upper polarizer and a dark band results. Where retardation is *i* + ½ wavelengths, the two rays constructively interfere and light passes with maximum intensity. (*b*) Percentage transmission of light by the upper polarizer, assuming ideal optical conditions. Computed from Equation 7.11. Back to text

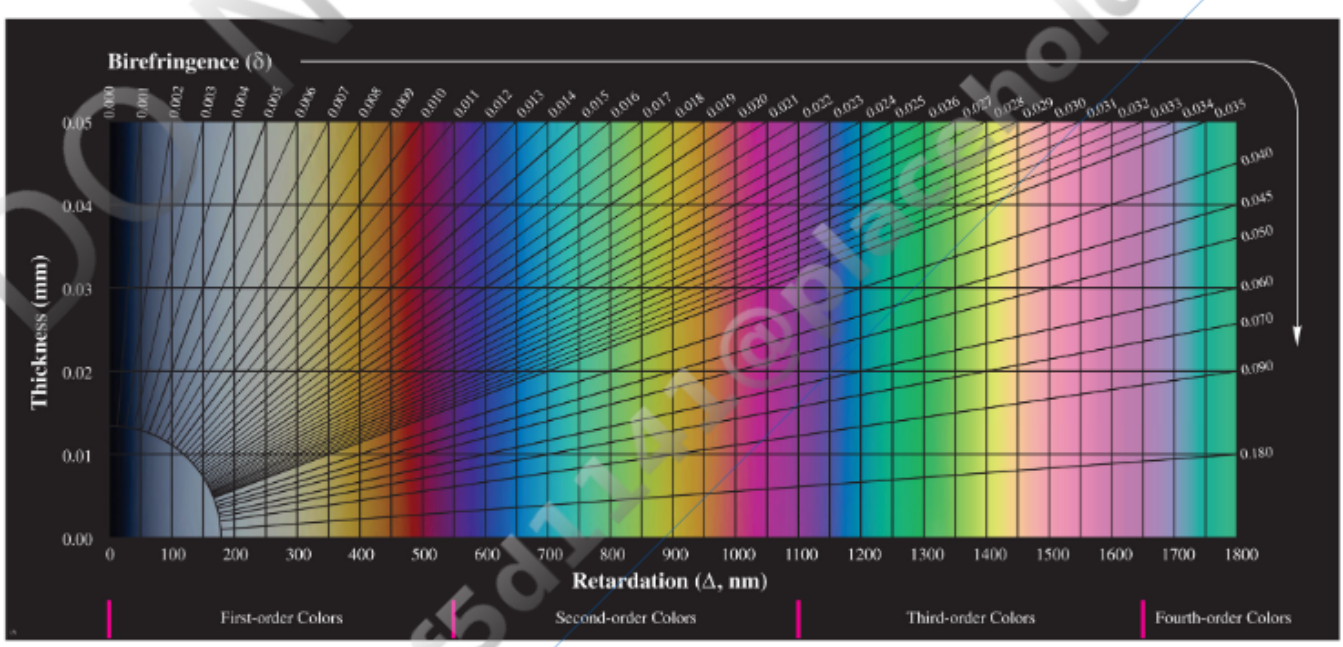

PLATE 1 Interference Color Chart. Back to text

Printed by: e48d507df5d1141@placeholder.94092.edu. Printing is for personal, private use only. No part of this book may be reproduced or transmitted without publisher's prior permission. Violators will be prosecuted.

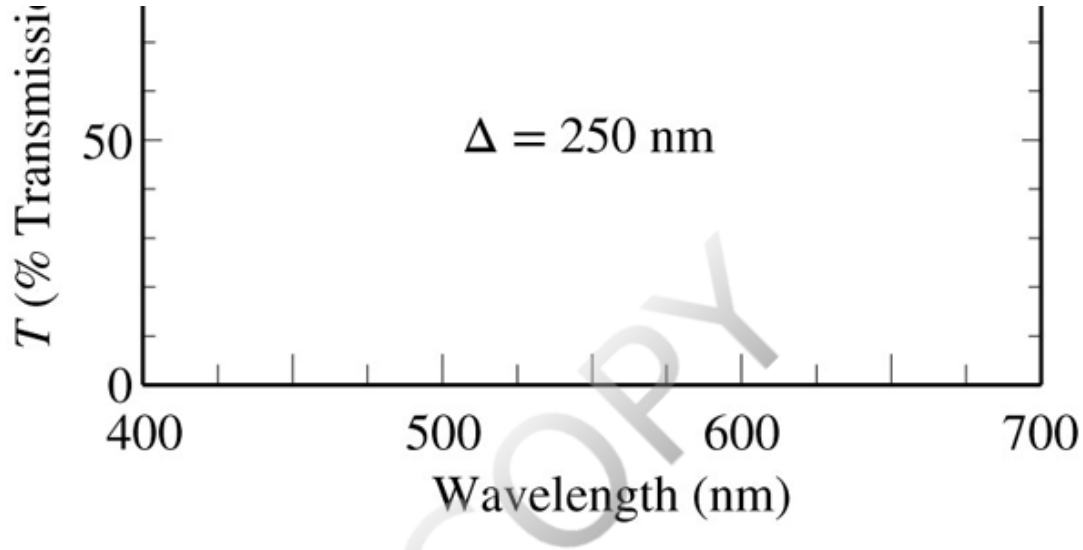

(b)

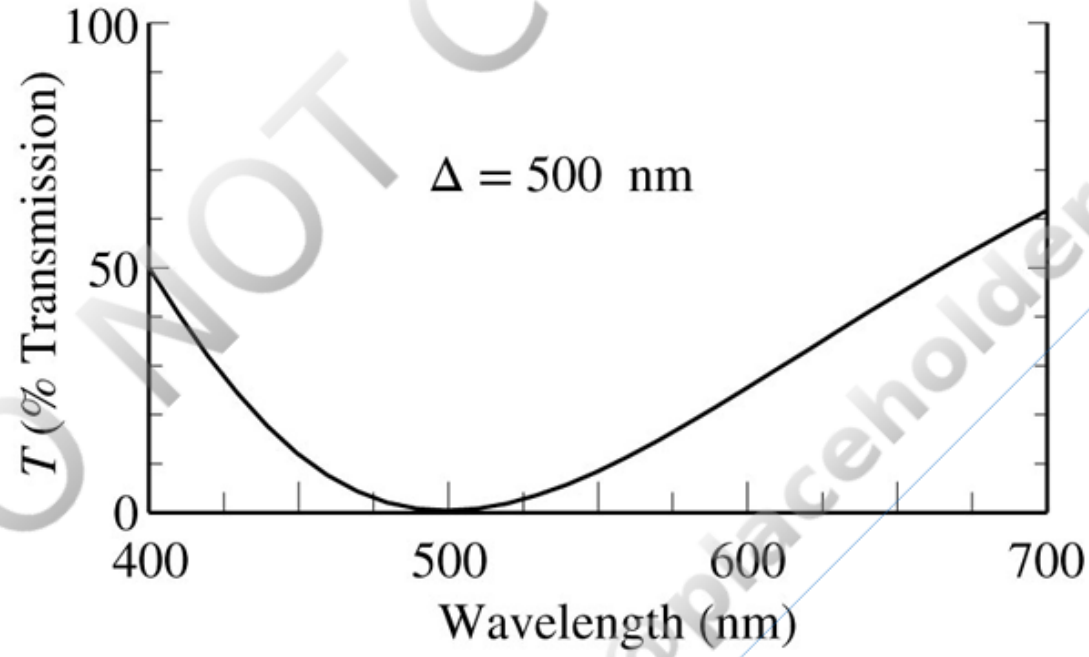

(c)

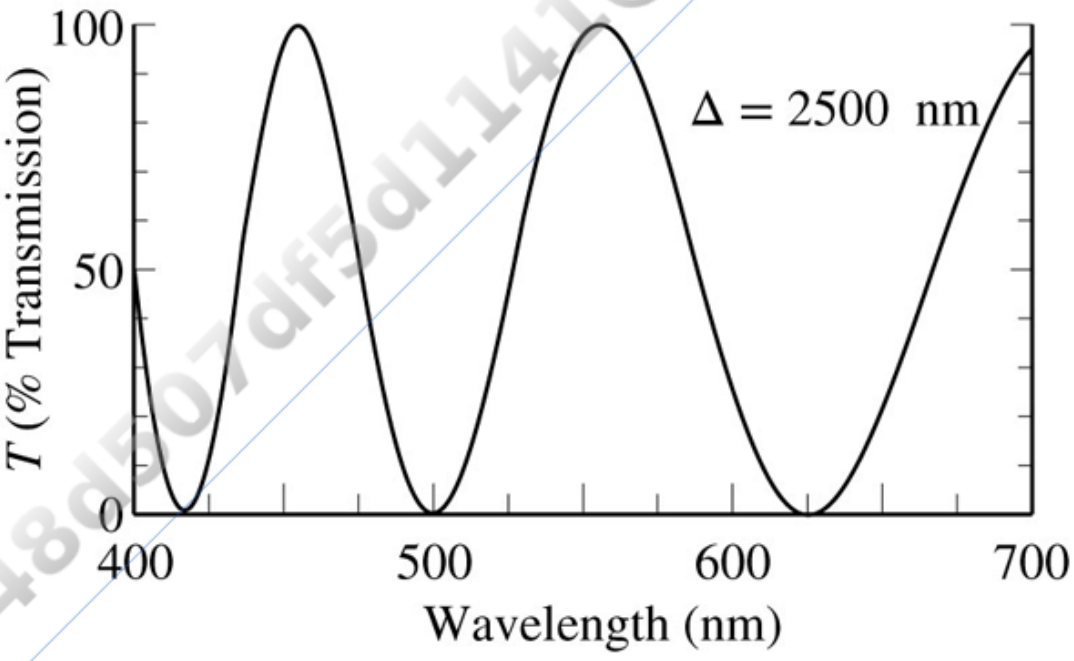

DO NOT COPY
e48d507df5d1141@placeholder.9409

Printed by: e48d507df5d1141@placeholder.94092.edu. Printing is for personal, private use only. No part of this book may be reproduced or transmitted without publisher's prior permission. Violators will be prosecuted.

FIGURE 7.17 Formation of interference colors with polychromatic light. (*a*) Retardation for all wavelengths is 250 nm. Slow and fast rays are largely out of phase for all wavelengths, so over 80 percent of all wavelengths pass the upper polarizer to form a first-order white interference color. (*b*) Retardation for all wavelengths is 500 nm. Portions of the violet and red ends of the spectrum are transmitted and 500 nm light is entirely canceled, producing a color perceived as first-order red. (*c*) Retardation for all wavelengths is 2500 nm. Wavelengths around 417, 500, and 625 nm are canceled, and wavelengths near 455, 555, and 714 nm are passed with maximum intensity. This combination of transmitted light is perceived as an upper-order creamy white. Back to text

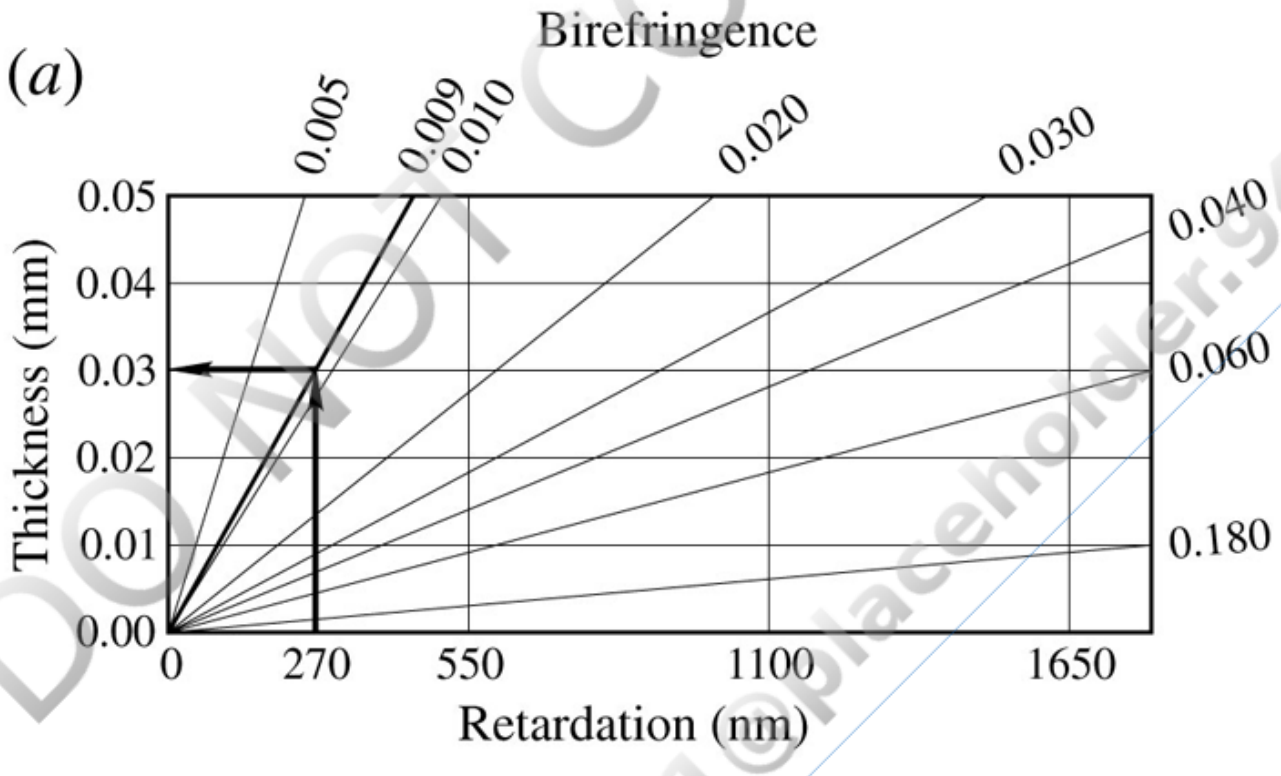

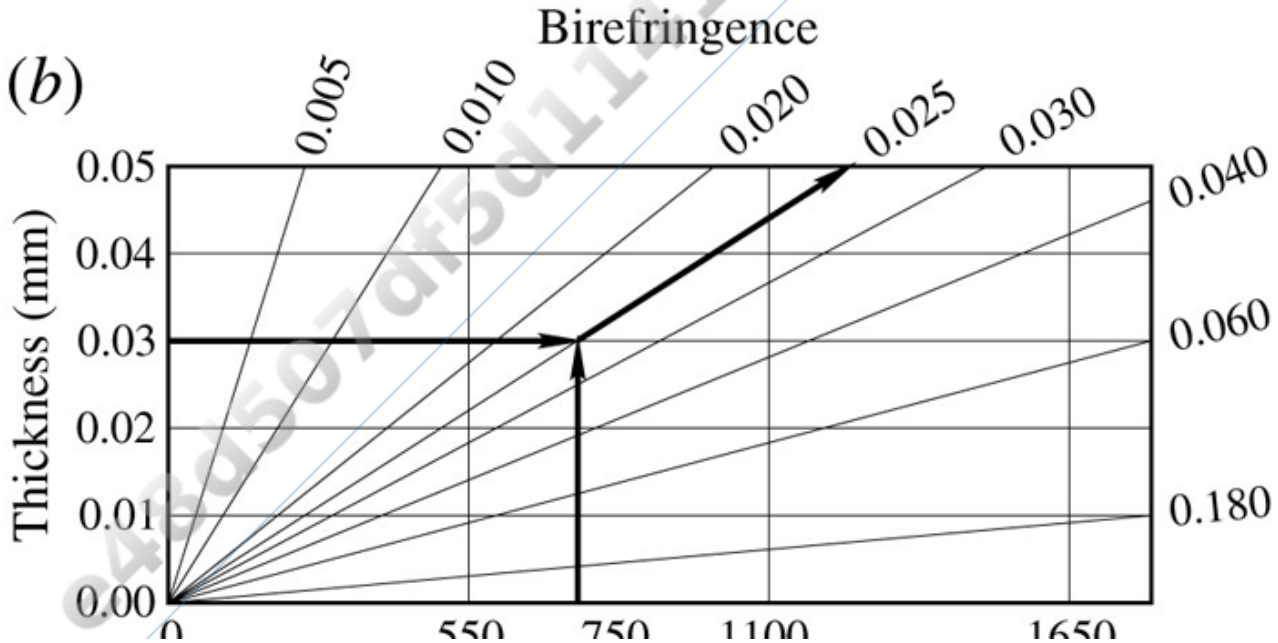

DO NOT COPY

Printed by: e48d507df5d1141@placeholder.94092.edu. Printing is for personal, private use only. No part of this book may be reproduced or transmitted without publisher's prior permission. Violators will be prosecuted.

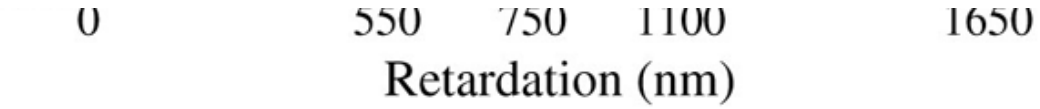

FIGURE 7.18 Use of the interference color chart (Plate 1). Horizontal lines indicate thickness, diagonal lines are for birefringence, and vertical lines indicate retardation (interference color). (*a*) Thickness is indicated by the horizontal line that goes through the point where birefringence and interference color intersect. (*b*) Birefringence is indicated by the diagonal line that goes through the intersection of interference color (retardation) and thickness. Back to text

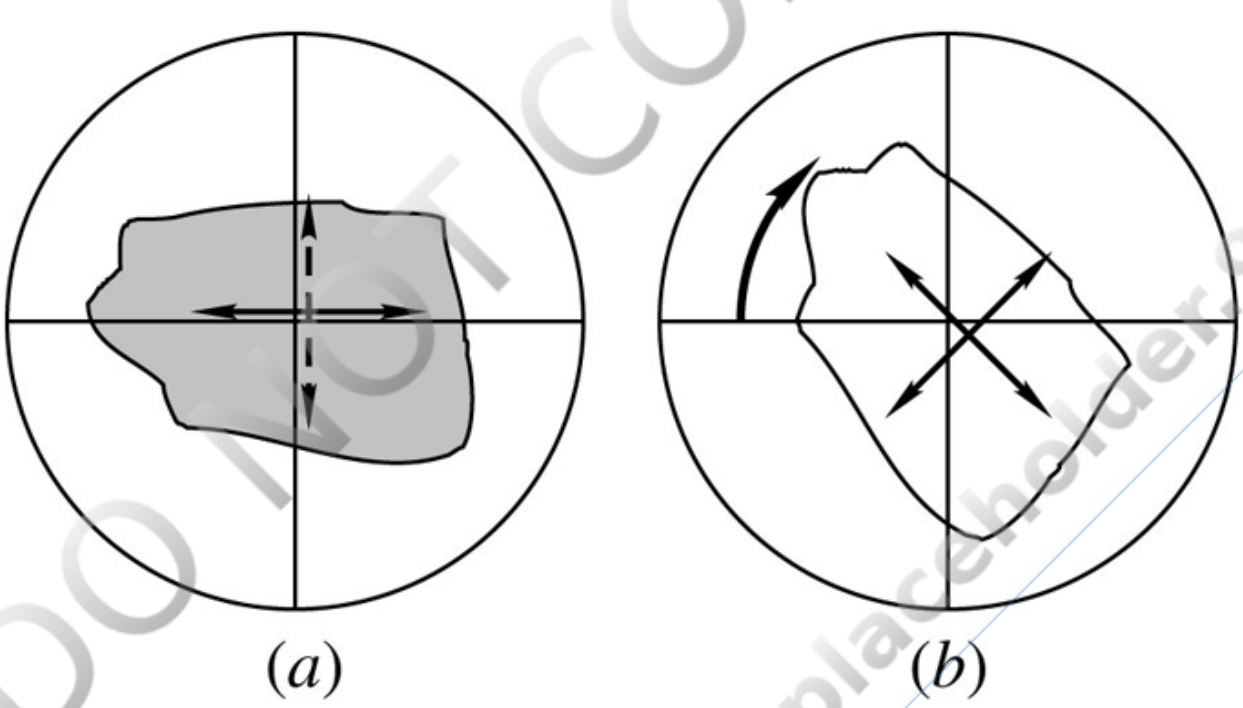

FIGURE 7.19 Extinction. (*a*) When the vibration directions of a mineral grain are parallel to the vibration directions of the lower and upper polarizer, the mineral is dark or extinct between crossed polarizers. (*b*) If the stage is rotated so that the mineral's vibration directions are not parallel to the polarizers, vector components of both rays may be resolved into the N–S vibration of the upper polarizer so that they may interfere to form interference colors. Back to text

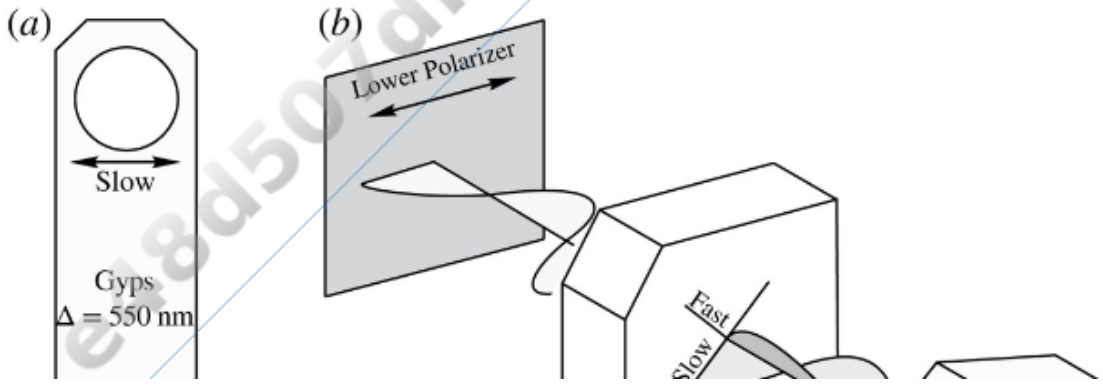

Printed by: e48d507df5d1141@placeholder.94092.edu. Printing is for personal, private use only. No part of this book may be reproduced or transmitted without publisher's prior permission. Violators will be prosecuted.

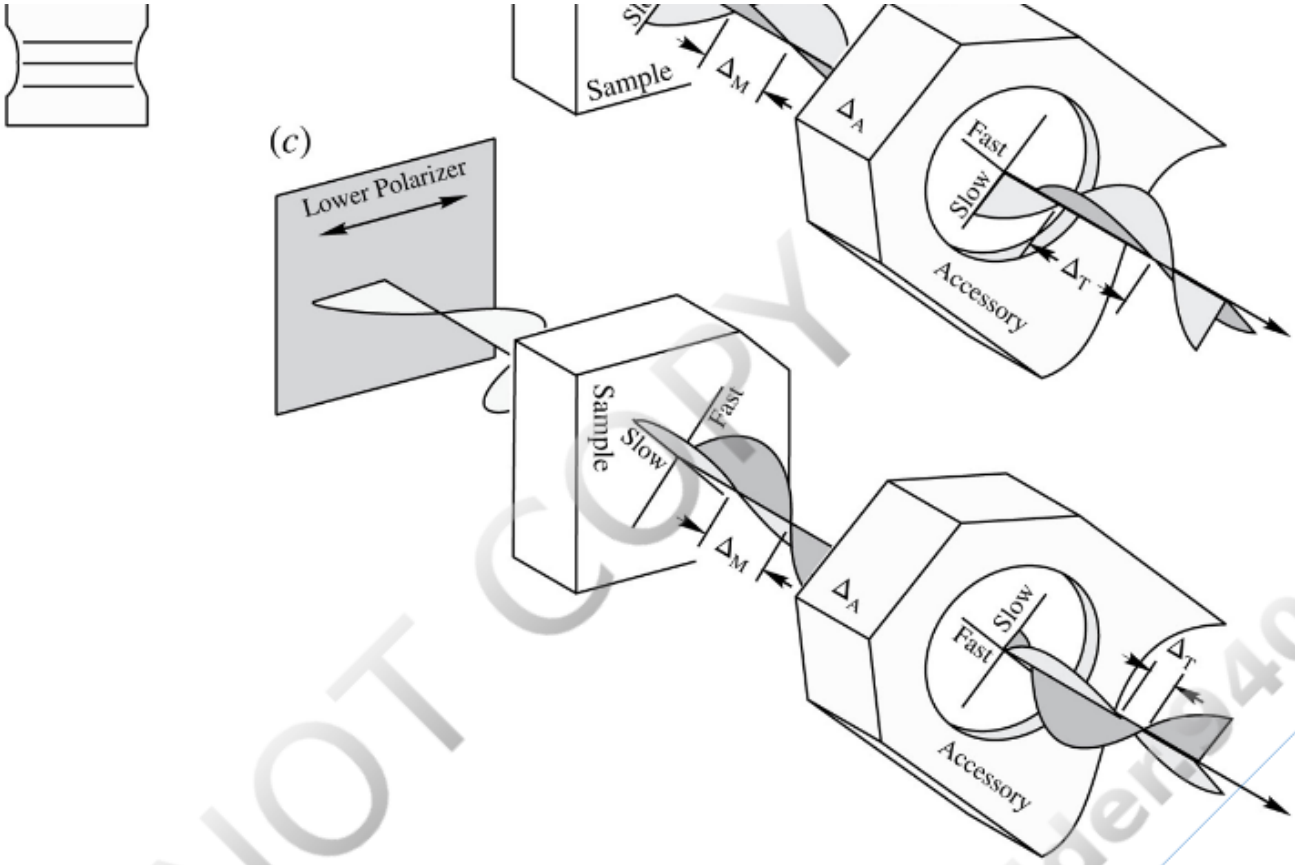

FIGURE 7.20 Compensation with an accessory plate. (*a*) Typical gypsum plate. The optical element produces a retardation Δ_A = 550 nm. The slow vibration direction is as indicated. (*b*) The mineral sample, which produces a retardation = Δ_M, is oriented so that its slow and fast ray vibration directions coincide with those of the accessory plate. The total retardation produced by sample and accessory is Δ_T, which equals $\Delta_M + \Delta_A$. (*c*) The sample is rotated so that its slow ray vibration is parallel to the fast ray vibration direction in the accessory plate. The total retardation is Δ_T, which equals $|\Delta_M - \Delta_A|$. Back to text

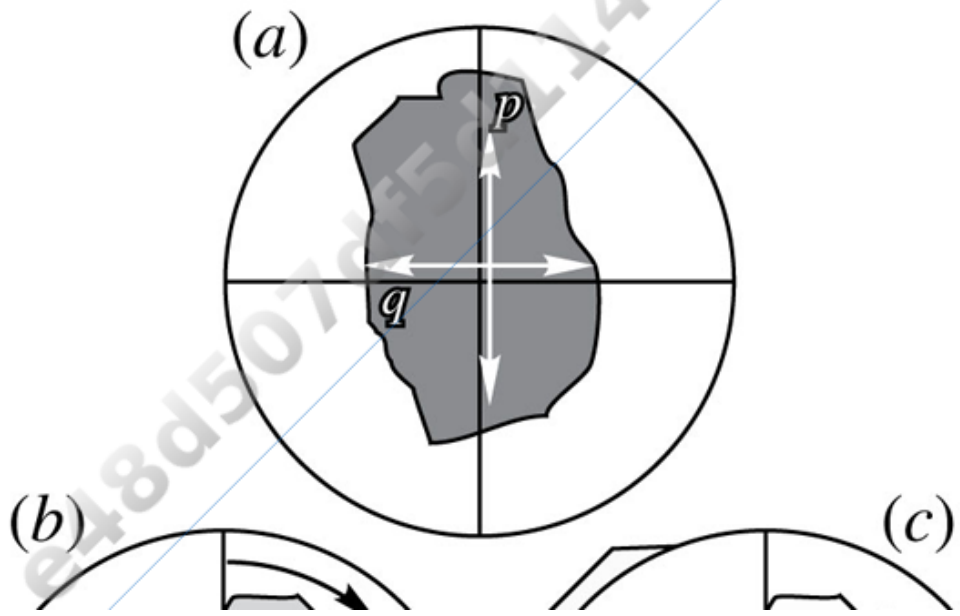

Printed by: e48d507df5d1141@placeholder.94092.edu. Printing is for personal, private use only. No part of this book may be reproduced or transmitted without publisher's prior permission. Violators will be prosecuted.

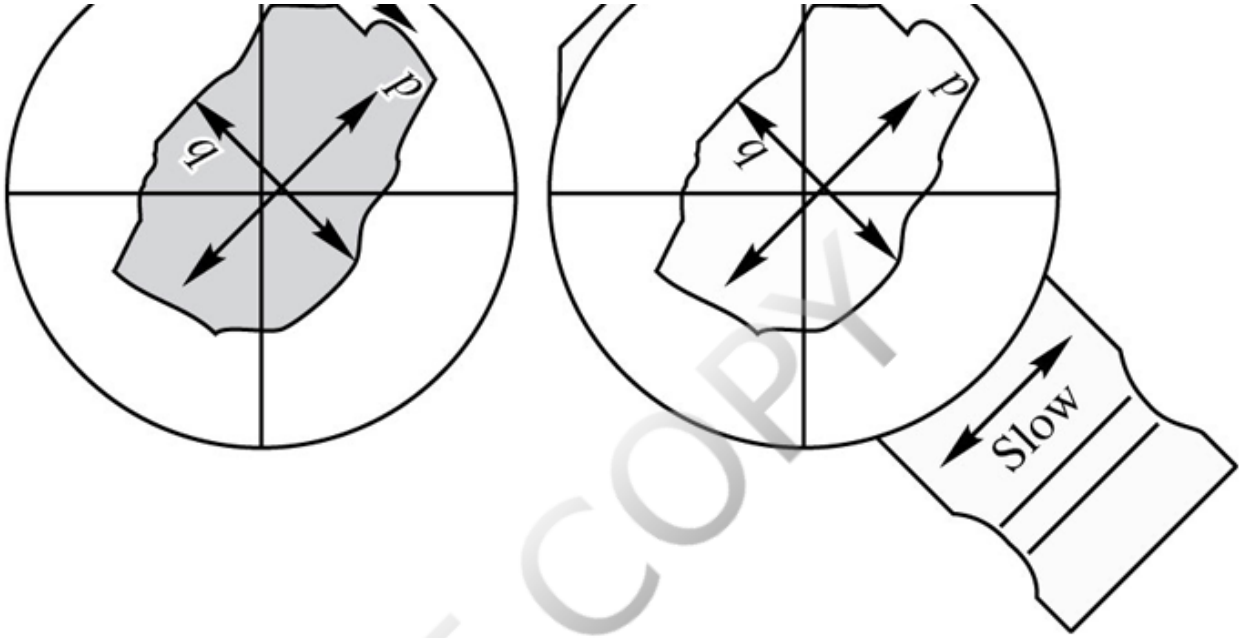

FIGURE 7.21 Determining slow and fast ray vibration directions between crossed polarizers. (*a*) Mineral grain at extinction between crossed polarizers. Vibration directions *p* and *q* in the mineral are N–S and E–W. (*b*) Mineral grain rotated 45° clockwise so that vibration direction *p* is NE–SW. (*c*) Accessory plate inserted. If retardation and interference colors add, *p* is the slow ray vibration direction; if retardations subtract, *p* is the fast ray vibration direction. Back to text

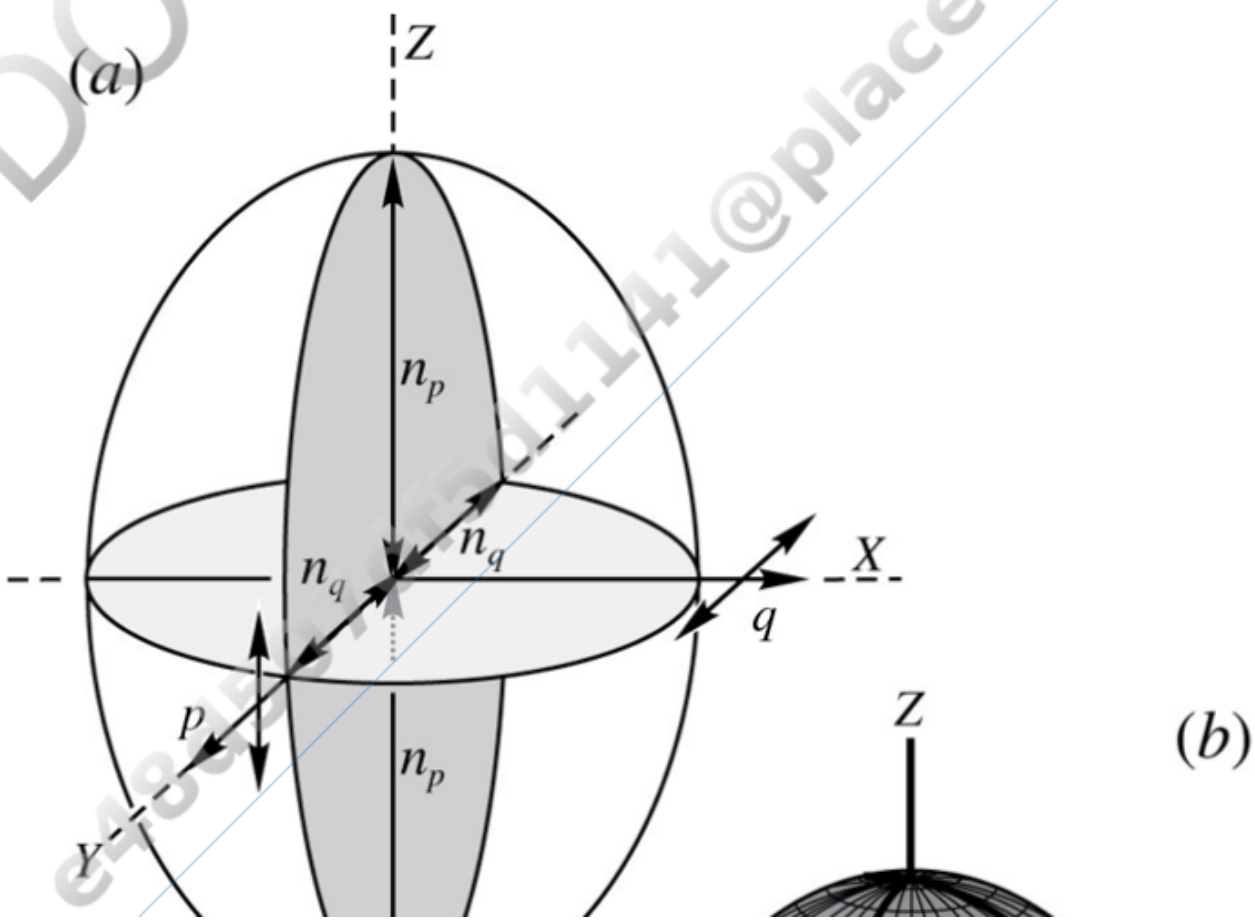

DO NOT COPY

Printed by: e48d507df5d1141@placeholder.94092.edu. Printing is for personal, private use only. No part of this book may be reproduced or transmitted without publisher's prior permission. Violators will be prosecuted.

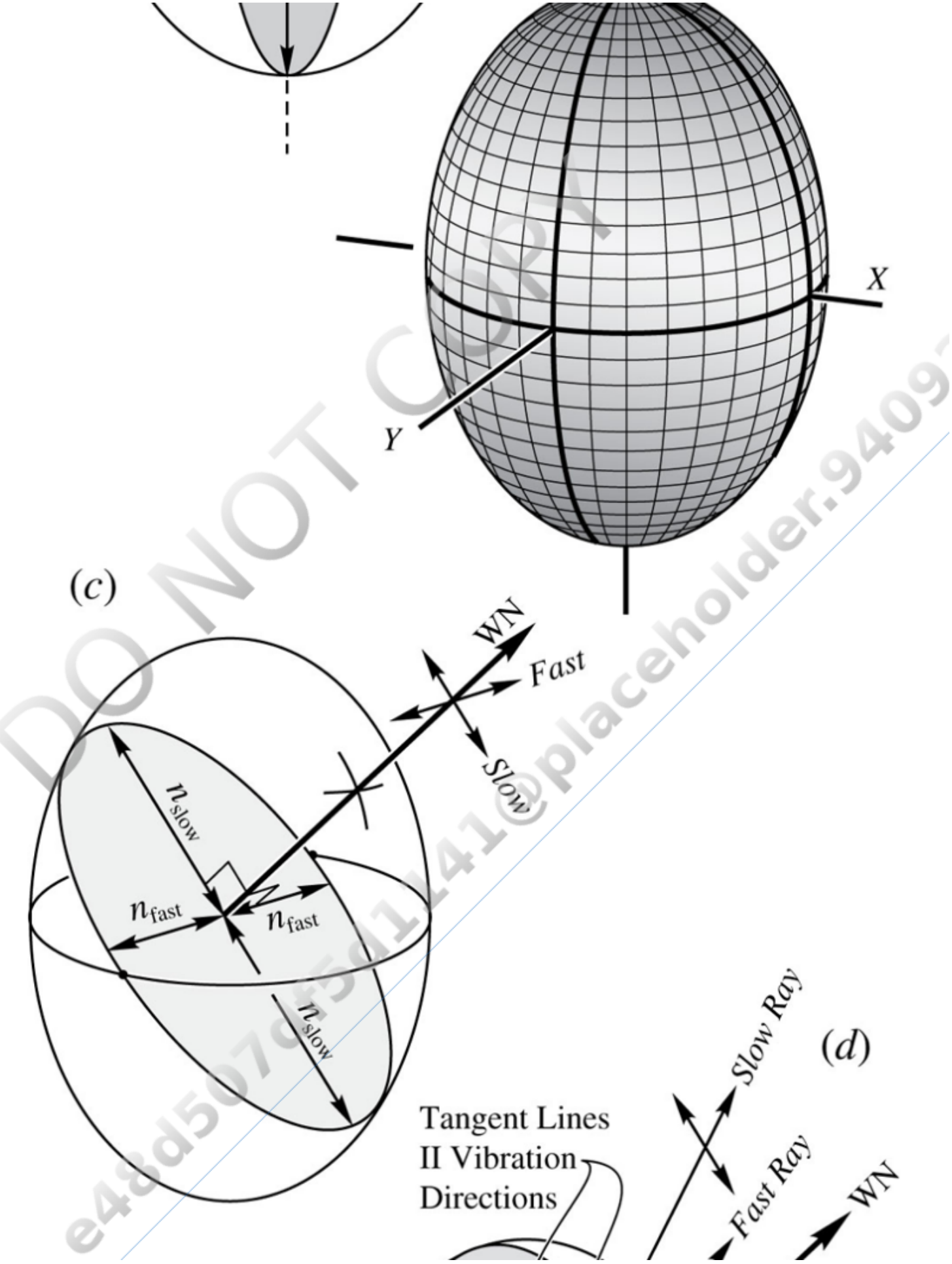

DO NOT COPY
e48d507df5d1141@placeholder.9409

Printed by: e48d507df5d1141@placeholder.94092.edu. Printing is for personal, private use only. No part of this book may be reproduced or transmitted without publisher's prior permission. Violators will be prosecuted.

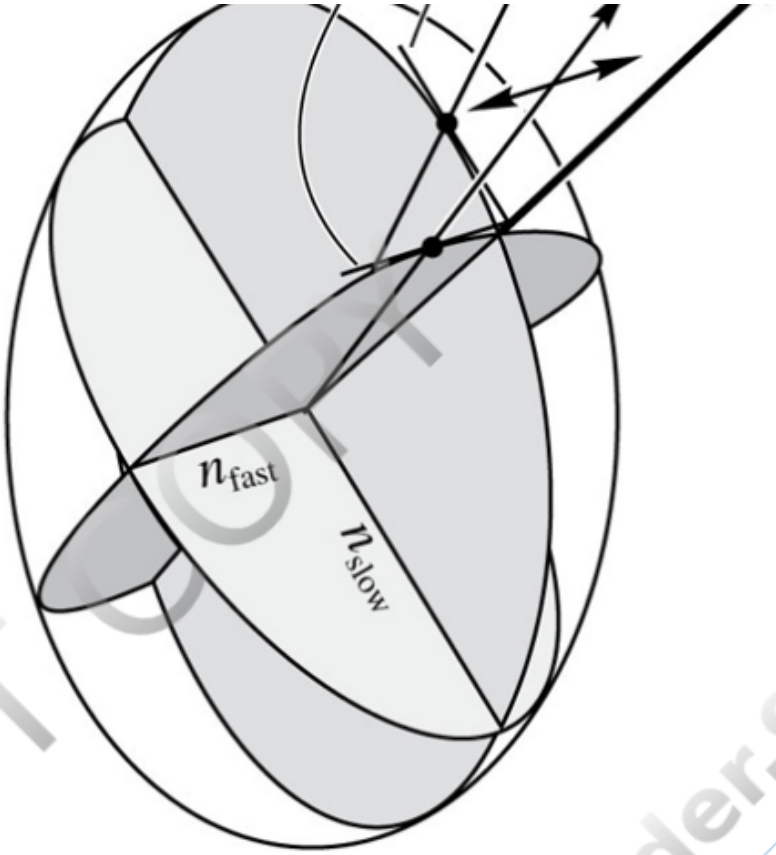

FIGURE 7.22 Optical indicatrix. (*a*) The indicatrix is constructed by plotting indices of refraction as radii parallel to the vibration direction of the light. Wave normal *p*, propagating along *Y*, vibrates parallel to the *Z* axis, so its index of refraction (n_p) is plotted as radii along *Z*. Wave normal *q*, propagating along *X*, vibrates parallel to *Y* so its index of refraction (n_q) is plotted as radii along *Y*. (*b*) The indicatrix is an ellipsoid whose shape depends on the mineral symmetry. (*c*) An indicatrix showing a wave normal direction (WN) along which the light propagates. An elliptical section through the indicatrix perpendicular to the wave normal is parallel to the wave front. The long axis of this elliptical section is parallel to the slow ray vibration direction, and the radius parallel to this direction is equal to the slow ray index of refraction (n_{slow}). The short axis of the elliptical section is parallel to the fast ray vibration direction, and the radius parallel to this direction is equal to the fast ray index of refraction (n_{fast}) (*d*) Ray paths are determined by constructing tangents to the indicatrix as shown.
Back to text

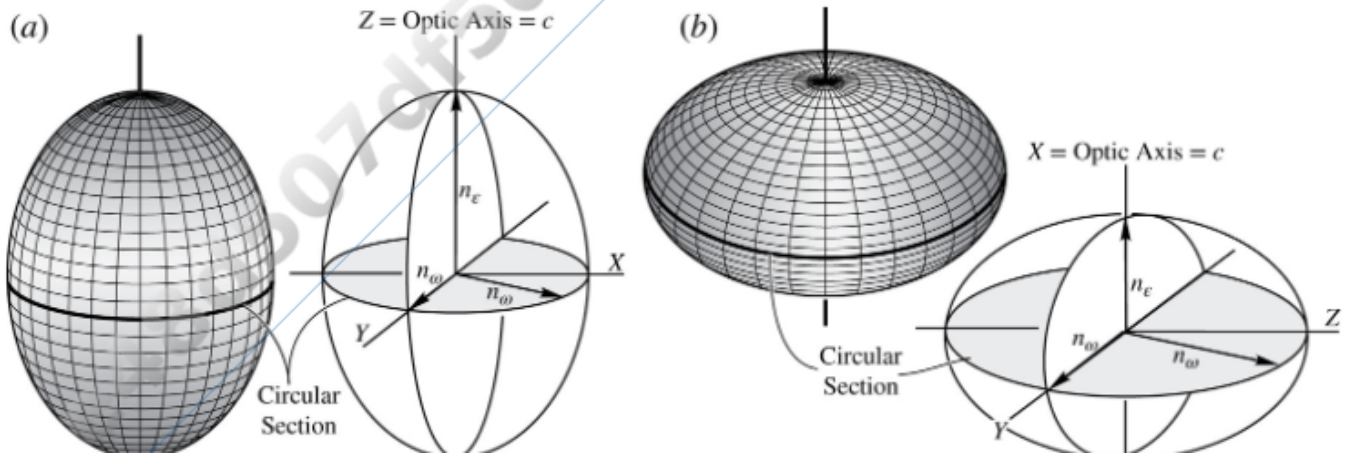

Printed by: e48d507df5d1141@placeholder.94092.edu. Printing is for personal, private use only. No part of this book may be reproduced or transmitted without publisher's prior permission. Violators will be prosecuted.

FIGURE 7.23 Uniaxial indicatrix. The circular section and a principal section are shown for each indicatrix. *X*, *Y*, and *Z* axes are included to be consistent with the convention used in biaxial minerals. (*a*) Uniaxial positive. The indicatrix is a prolate spheroid (elongated spheroid) whose axes are n_ϵ and n_ω where $n_\epsilon > n_\omega$. (*b*) Uniaxial negative. The indicatrix is an oblate spheroid (flattened spheroid) whose axes are n_ϵ and n_ω where $n_\epsilon < n_\omega$. Back to text

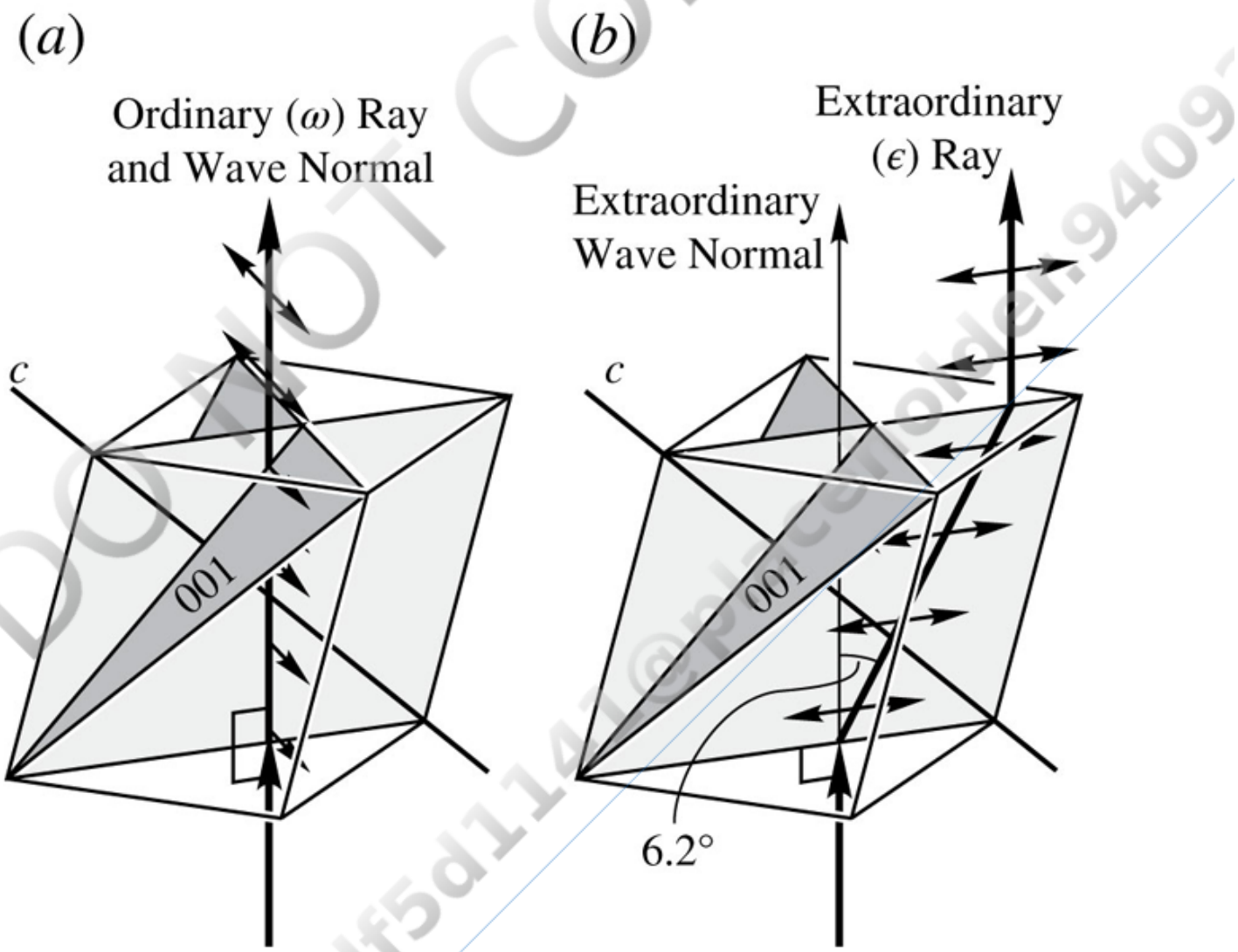

FIGURE 7.24 Ordinary and extraordinary rays. Light incident at right angles to the bottom surface of a calcite rhomb is split into two rays (Figure 7.13). (*a*) The vibration vector of ordinary ω rays is always parallel to (001) planes, and the wave normal and ray direction coincide. If the calcite rhomb is rotated about a vertical axis, the image composed of ordinary rays (ω) remains stationary. (*b*) The extraordinary (ϵ') ray direction diverges from its wave normal, and its vibration direction lies in a plane (light shading) containing the *c* axis and the two rays. If the calcite rhomb is rotated, the position of the extraordinary ray image rotates about the ordinary ray image. Back to text

DO NOT COPY
e48d507df5d1141@placeholder.9409

Printed by: e48d507df5d1141@placeholder.94092.edu. Printing is for personal, private use only. No part of this book may be reproduced or transmitted without publisher's prior permission. Violators will be prosecuted.

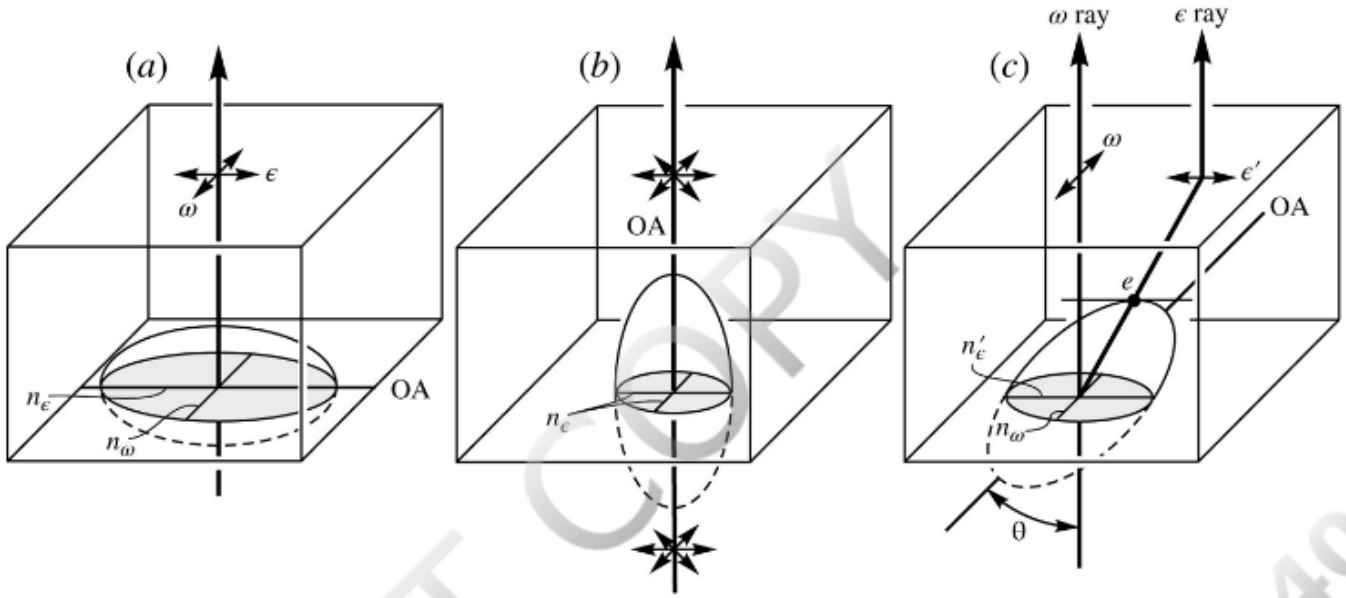

FIGURE 7.25 Behavior of uniaxial minerals in orthoscopic illumination. The optic axis is labeled OA. (*a*) Mineral grain oriented with the optic axis horizontal. The section through the indicatrix is a principal section with axes n_ω and n_ϵ. The mineral displays maximum birefringence and interference color. (*b*) Mineral grain oriented with the optic axis vertical. The section through the indicatrix is the circular section; all light passes as ordinary ray and preserves its original vibration direction. This grain displays zero birefringence and behaves like an isotropic mineral. (*c*) Mineral grain with a random orientation. The section through the indicatrix is an ellipse whose axes are n_ω and n'_ϵ. Birefringence is intermediate and the ω and ϵ' rays diverge. Back to text

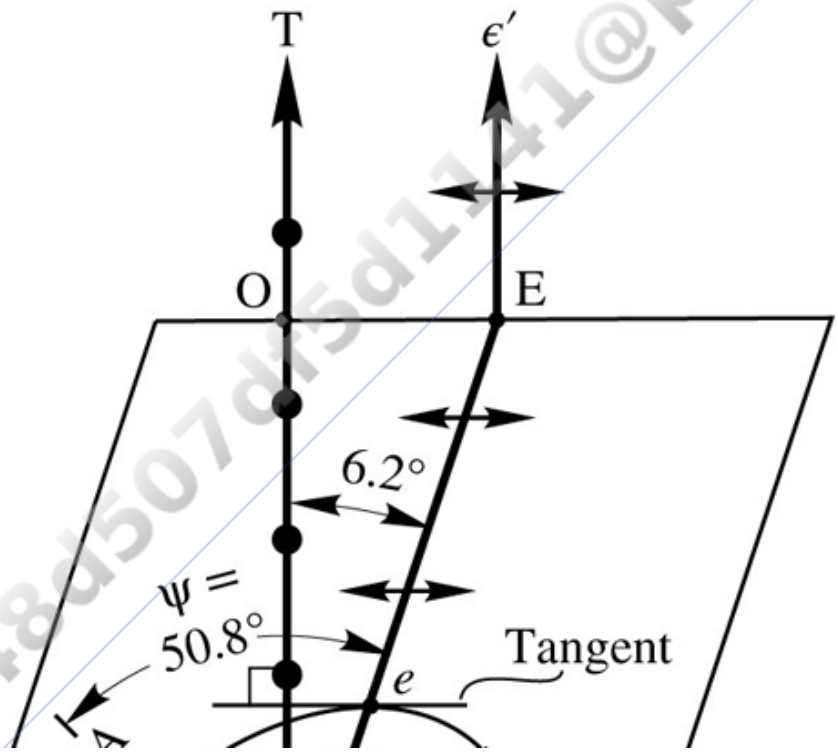

DO NOT COPY
e48d507df5d1141@placeholder.9409

Printed by: e48d507df5d1141@placeholder.94092.edu. Printing is for personal, private use only. No part of this book may be reproduced or transmitted without publisher's prior permission. Violators will be prosecuted.

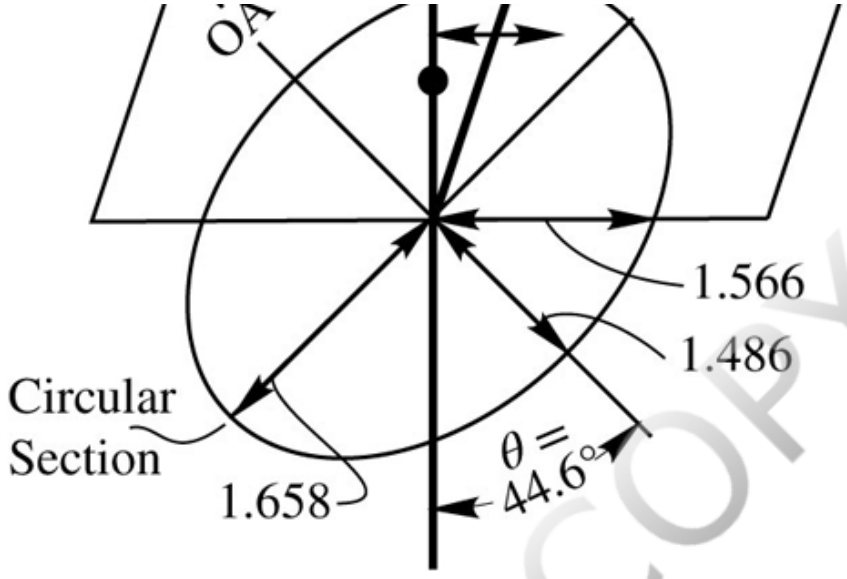

FIGURE 7.26 Calcite indicatrix construction. The ϵ' ray path is found by constructing a tangent to the indicatrix parallel to the ϵ' ray vibration direction at point *e*. The extraordinary image, which follows the ray, emerges from the top of the rhomb at *E*. A similar tangent for the ordinary ray (not shown in and out of the page) yields an ordinary ray path that coincides with the wave normal so the ordinary ray emerges at *O*. The dimensions of the indicatrix are not drawn to scale. Back to text

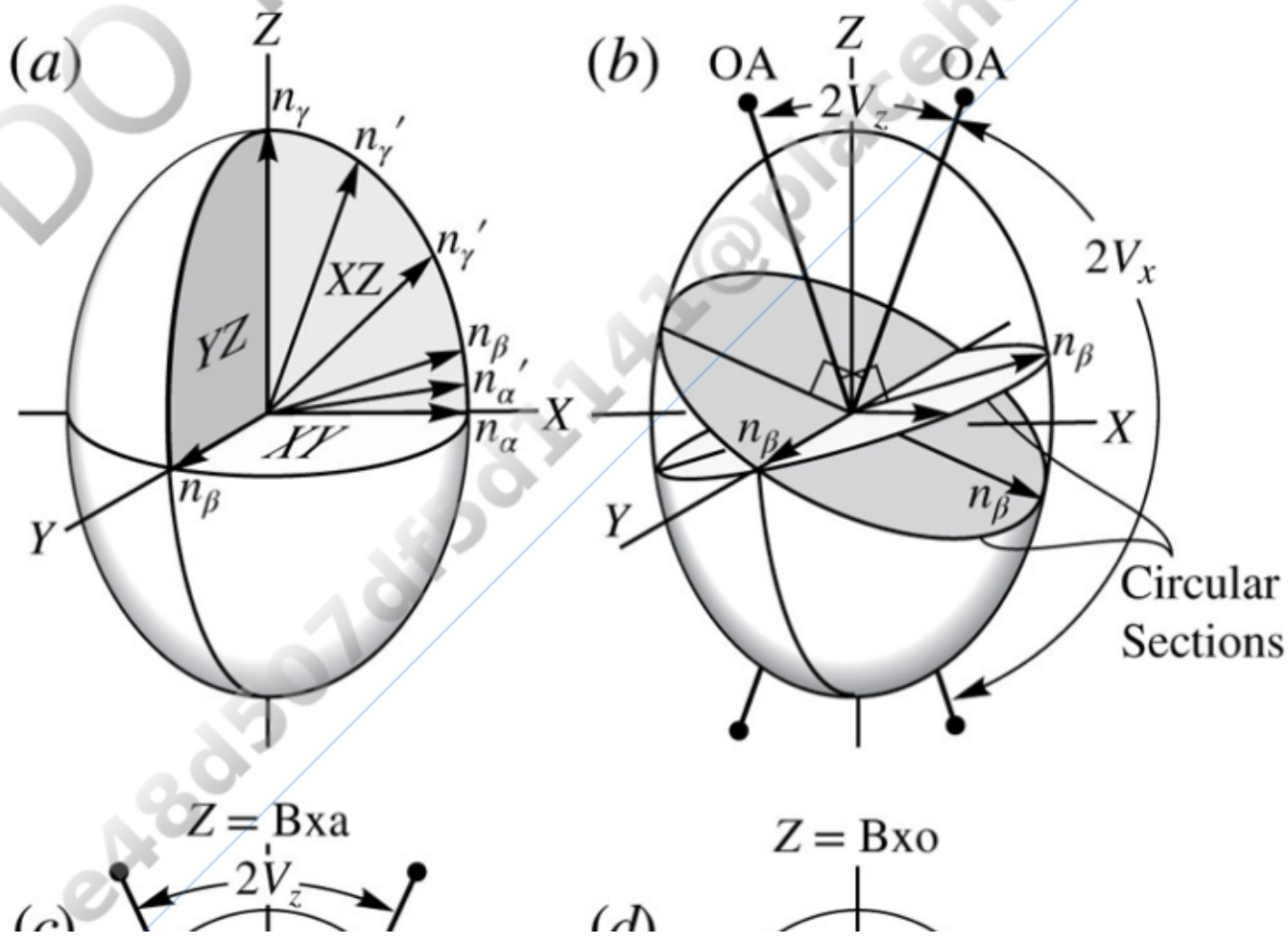

Printed by: e48d507df5d1141@placeholder.94092.edu. Printing is for personal, private use only. No part of this book may be reproduced or transmitted without publisher's prior permission. Violators will be prosecuted.

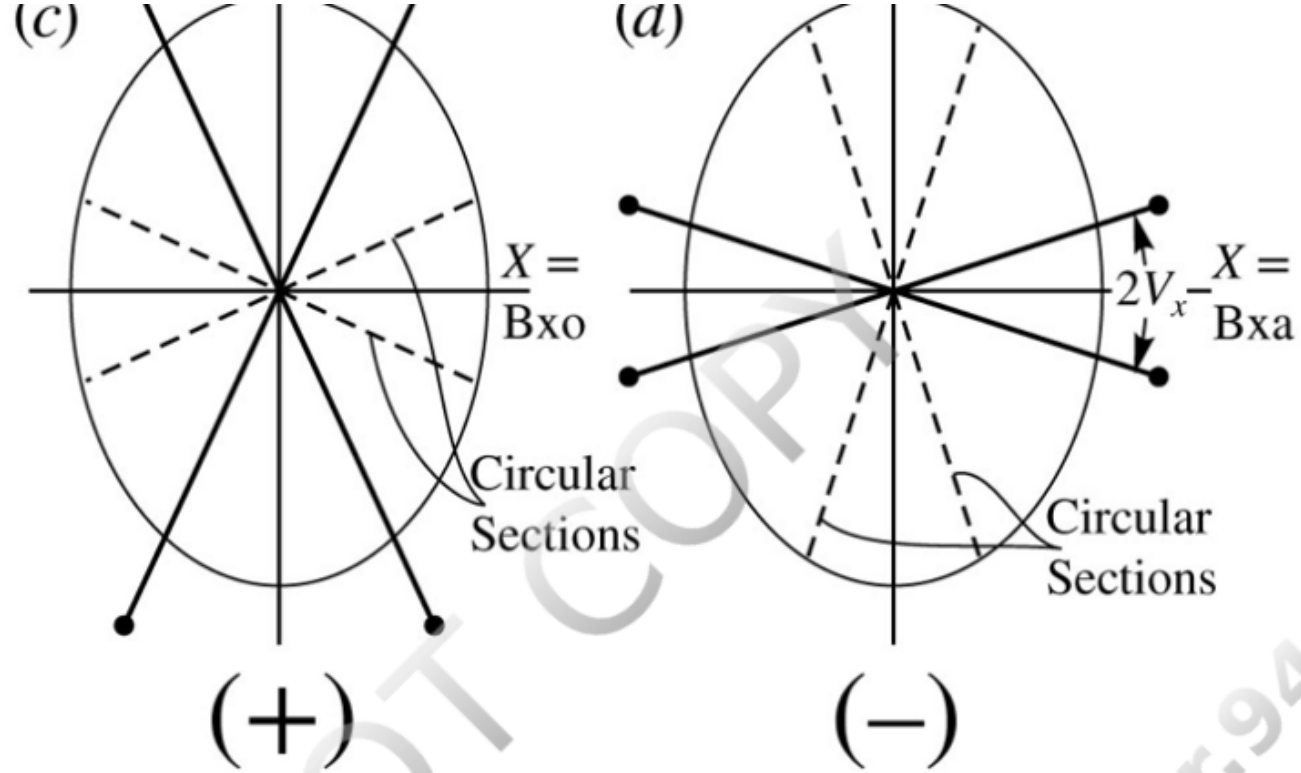

FIGURE 7.27 Biaxial indicatrix. (*a*) The indices n_α, n_β, and n_γ are plotted along the *X*, *Y*, and *Z* axes, respectively. Principal sections are the *XY*, *XZ*, and *YZ* planes. Within the *XZ* plane, radii of the ellipse vary from n_α to n_γ with certain radii equal to n_β. (*b*) Circular sections have radius n_β. The optic axes (OA) are perpendicular to the circular sections and lie in the *XZ*, or optic, plane. (*c*) Optic plane of a biaxial positive indicatrix. (*d*) Optic plane of a biaxial negative indicatrix. Back to text

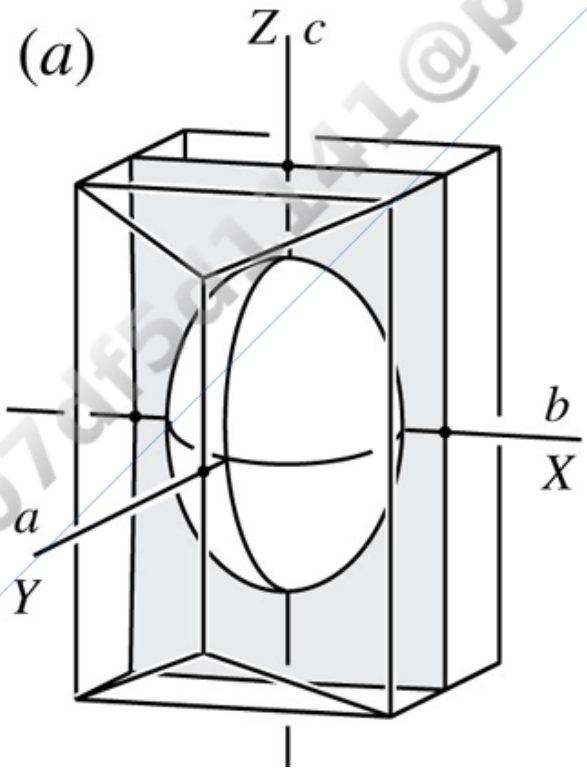

DO NOT COPY
e48d507df5d1141@placeholder.9409

Printed by: e48d507df5d1141@placeholder.94092.edu. Printing is for personal, private use only. No part of this book may be reproduced or transmitted without publisher's prior permission. Violators will be prosecuted.

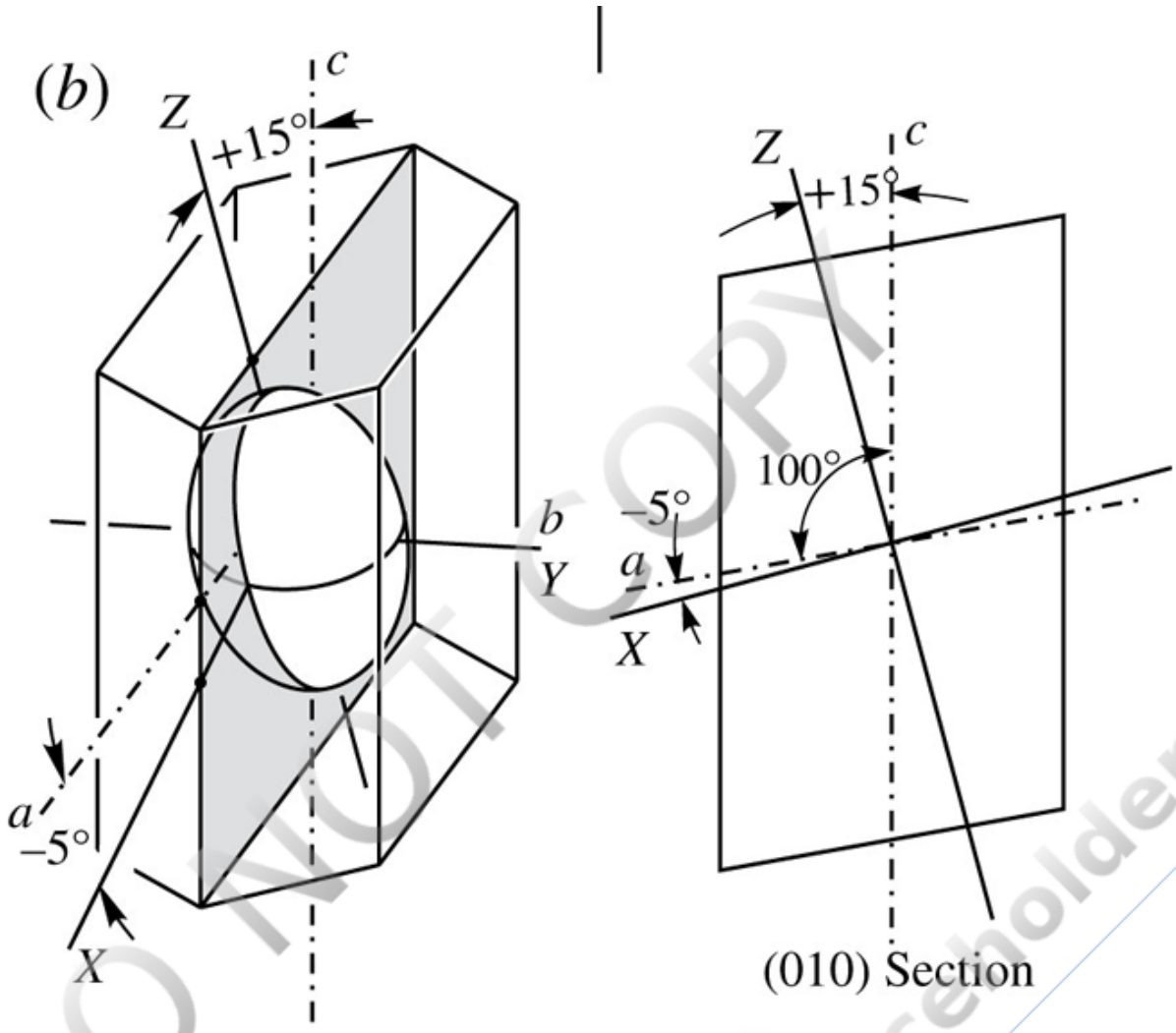

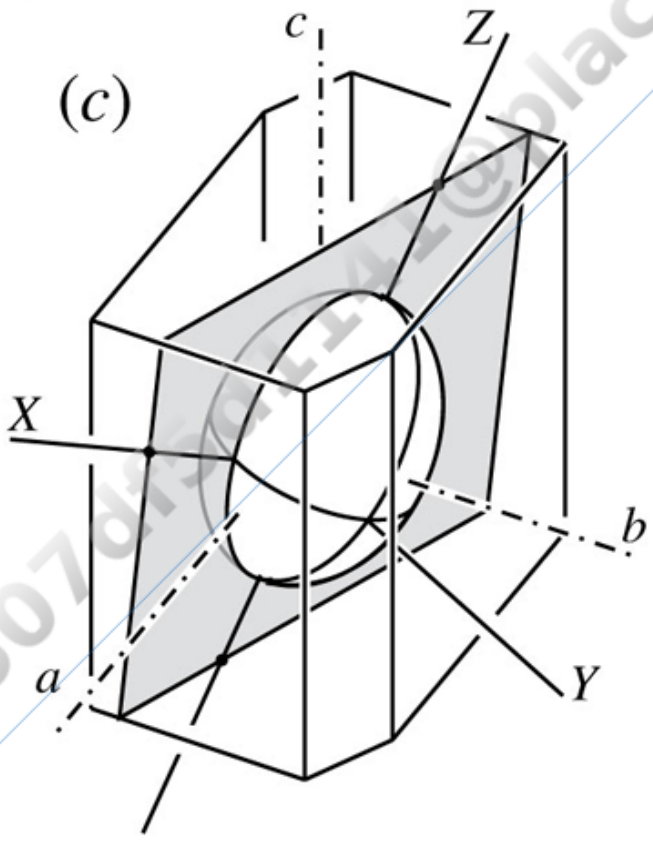

DO NOT COPY
e48d507df5d1141@placeholder.9409

Printed by: e48d507df5d1141@placeholder.94092.edu. Printing is for personal, private use only. No part of this book may be reproduced or transmitted without publisher's prior permission. Violators will be prosecuted.

FIGURE 7.28 Relationship between crystal axes and indicatrix axes. The optic planes are shaded. (*a*) Orthorhombic. Crystal axes and indicatrix axes coincide. In this case the optic orientation is $X = b$, $Y = a$, $Z = c$. (*b*) Monoclinic. The *b* crystal axis coincides with one of the indicatrix axes. The other axes do not coincide except by chance. In this case the $X \wedge a = -5°$, $Y = b$, $Z \wedge c = +15°$. (*b*) Triclinic. None of the crystal axes coincide with indicatrix axes except by chance. Back to text

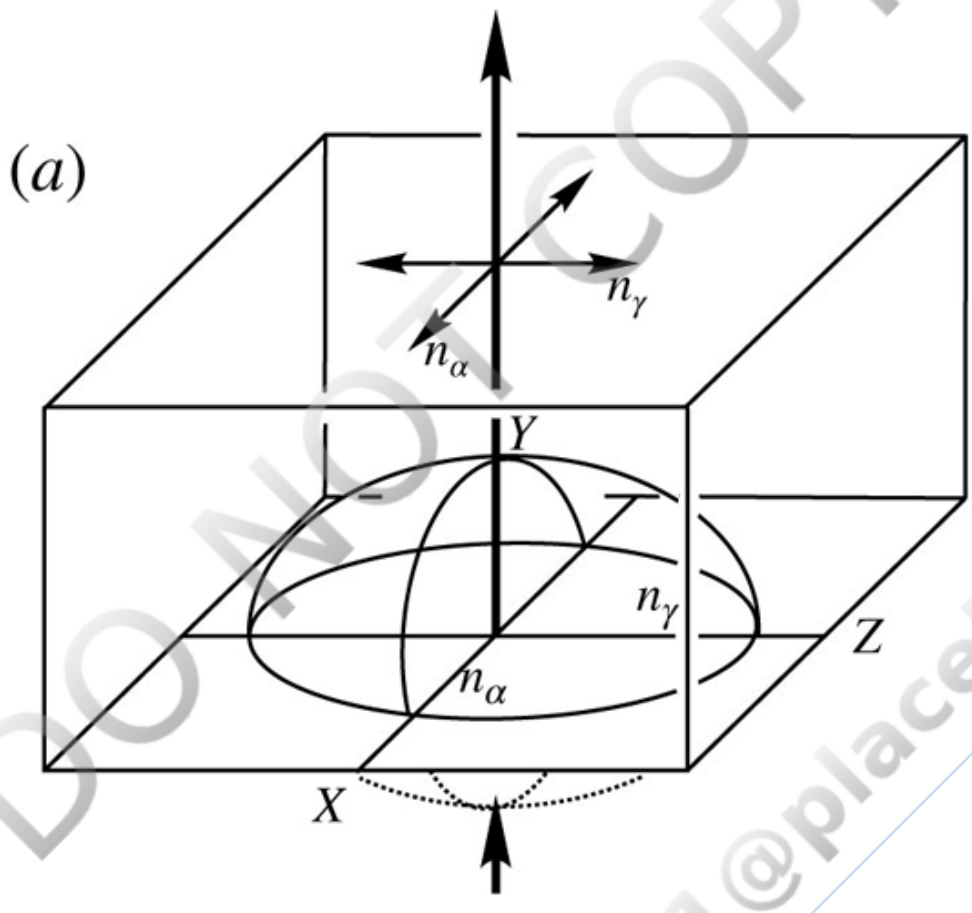

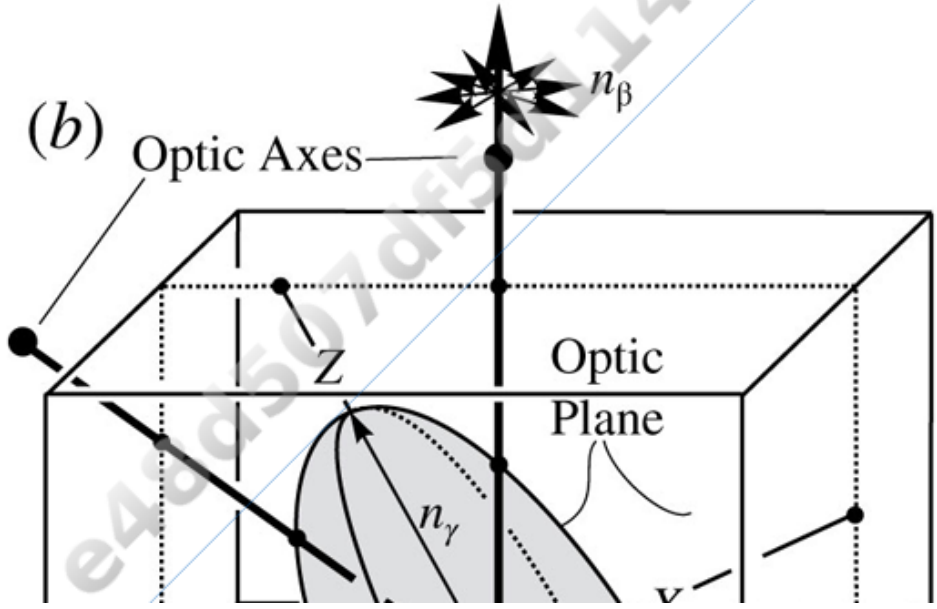

DO NOT COPY
e48d507df5d1141@placeholder.9409

Printed by: e48d507df5d1141@placeholder.94092.edu. Printing is for personal, private use only. No part of this book may be reproduced or transmitted without publisher's prior permission. Violators will be prosecuted.

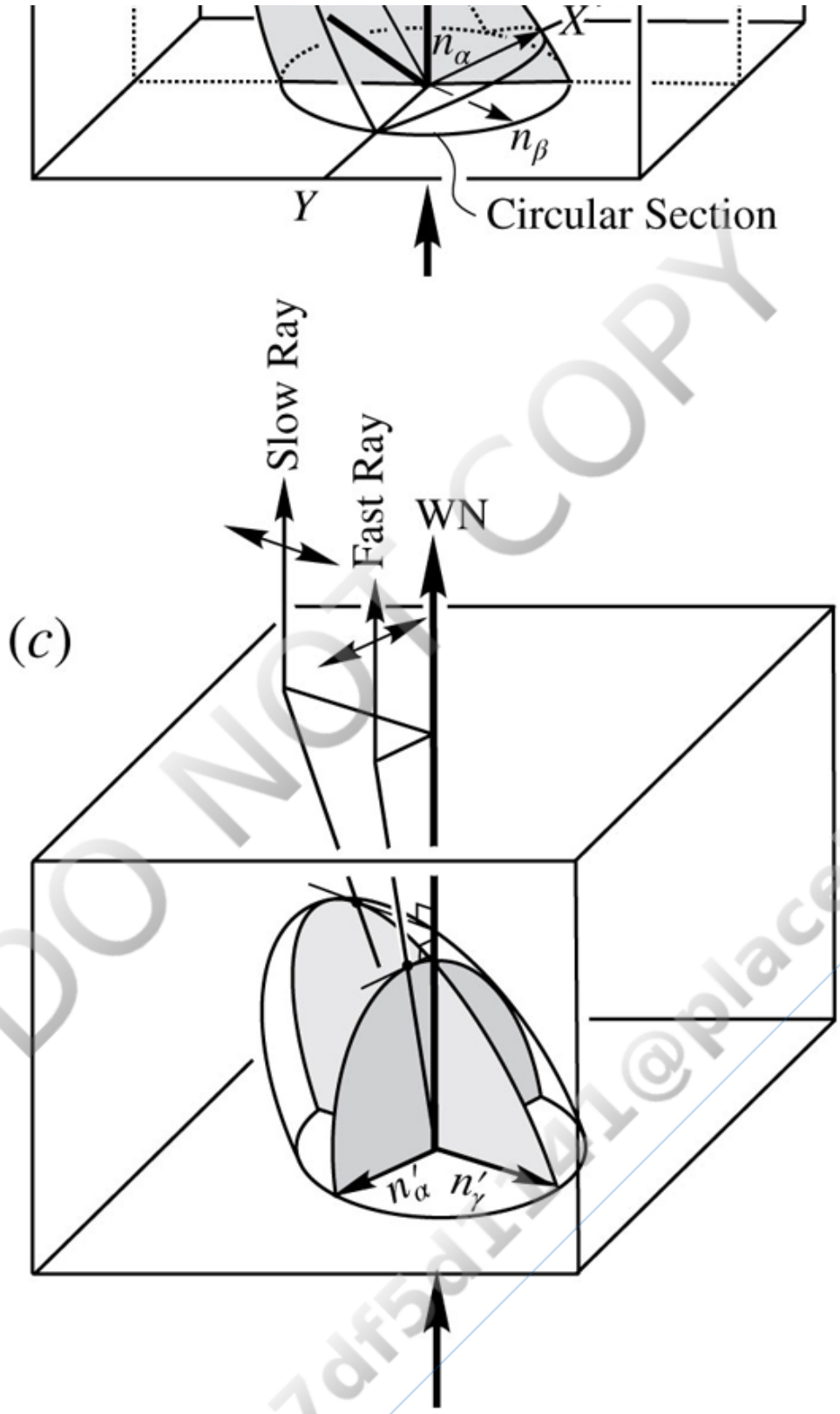

FIGURE 7.29 Behavior of biaxial minerals in orthoscopic illumination. (*a*) Optic normal (*Y*) vertical. Axes of the indicatrix section are *X* and *Z*, indices of refraction are n_α and n_γ, and birefringence is maximum. The slow ray vibrates parallel to *Z* and the fast ray vibrates parallel to *X*. (*b*) Optic axis vertical. The indicatrix section is a circle with radius n_β, birefringence is zero, and the mineral would be dark between crossed polarizers. (*c*) Random orientation. The indicatrix section yields indices of refraction n'_α and n'_γ and vibration directions as shown. Because n'_α is greater than n_α and n'_γ is less than n'_γ, birefringence is intermediate. Ray paths for both the slow and fast rays diverge from the wave normal, so both slow and fast rays are extraordinary. Back to text

DO NOT COPY
e48d507df5d1141@placeholder.9409

Printed by: e48d507df5d1141@placeholder.94092.edu. Printing is for personal, private use only. No part of this book may be reproduced or transmitted without publisher's prior permission. Violators will be prosecuted.

diverge from the wave normal, so both slow and fast rays are extraordinary. Back to text

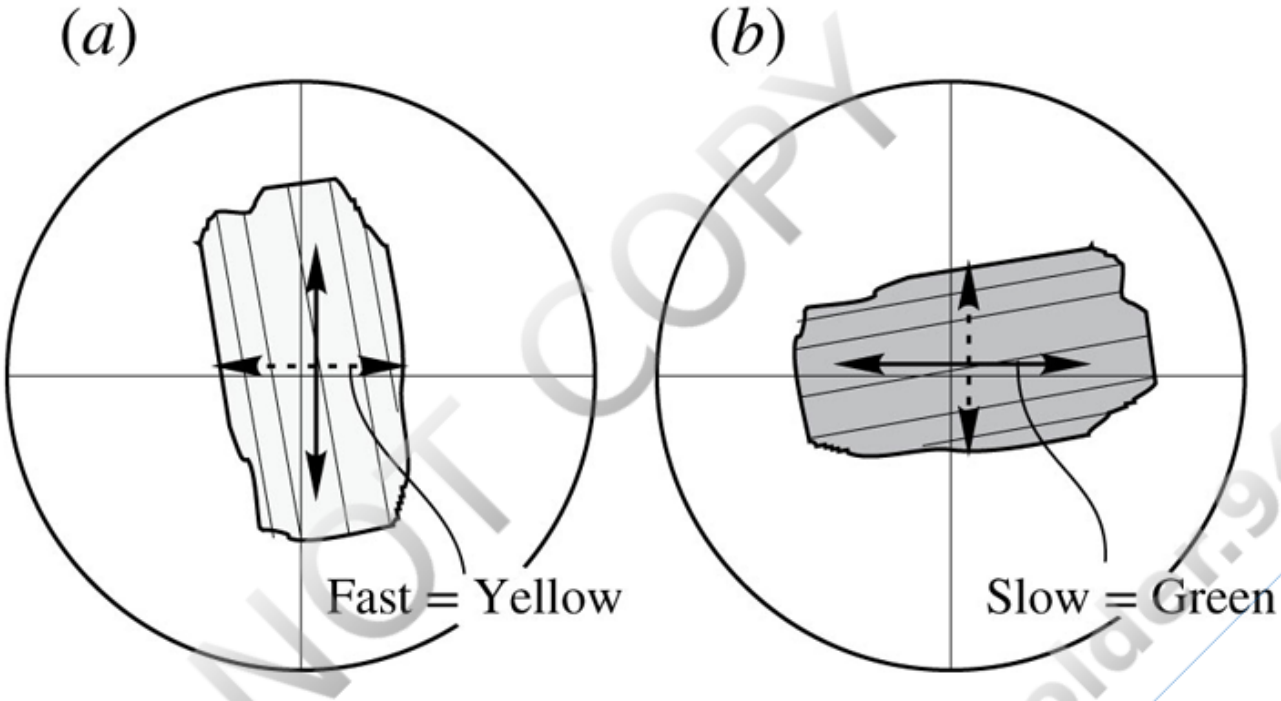

FIGURE 7.30 Pleochroism is seen in plane light. (*a*) The fast ray is yellow. When its vibration direction is parallel to the lower polarizer (E–W), the mineral is yellow. (*b*) The slow ray is green. When its vibration direction is parallel to the lower polarizer, the mineral appears green. In intermediate positions, both rays come through the mineral and color is intermediate. Back to text

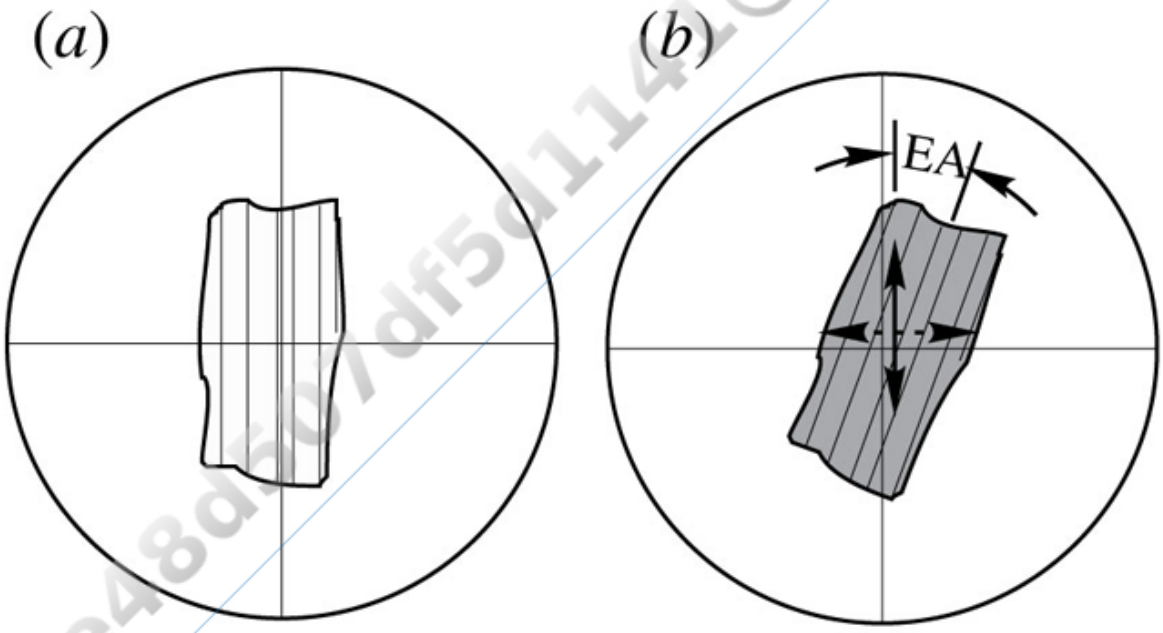

DO NOT COPY
e48d507df5d1141@placeholder.9409

Printed by: e48d507df5d1141@placeholder.94092.edu. Printing is for personal, private use only. No part of this book may be reproduced or transmitted without publisher's prior permission. Violators will be prosecuted.

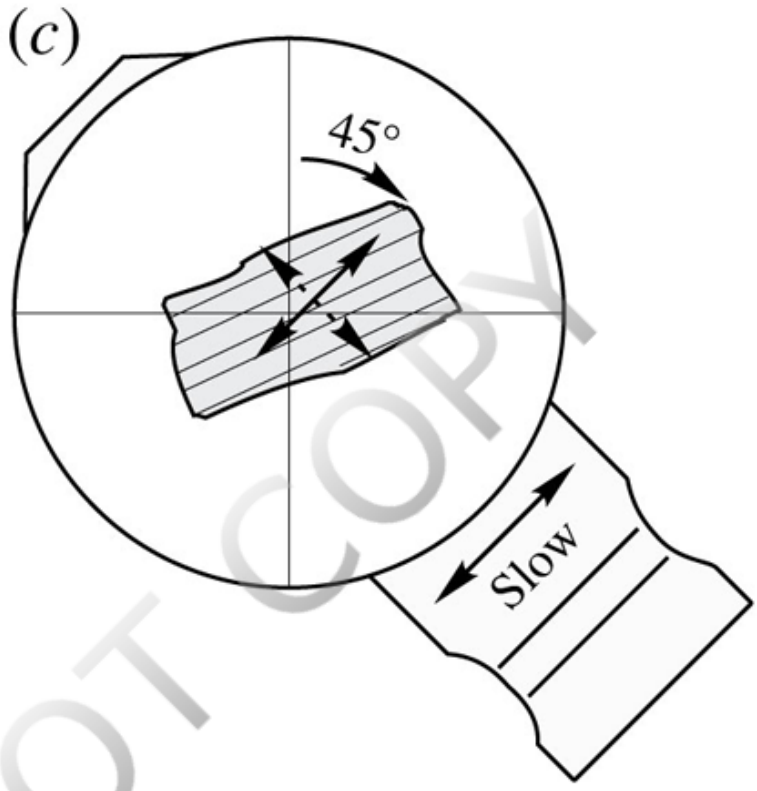

FIGURE 7.31 Measurement of extinction angle and sign of elongation. Polarizers are crossed. (*a*) Grain oriented so that cleavage or length is parallel to the N–S crosshair. (*b*) Stage rotated so the grain is extinct and one vibration direction is parallel to the N–S crosshair. The extinction angle (EA) is the angle through which the stage was rotated to go from (*a*) to (*b*). (*c*) Stage rotated 45° clockwise to place the vibration direction nearest the mineral length parallel to NE–SW. Insert the accessory plate. If retardations add, the mineral is length slow; if retardations cancel, the mineral is length fast. Back to text

DO NOT COPY

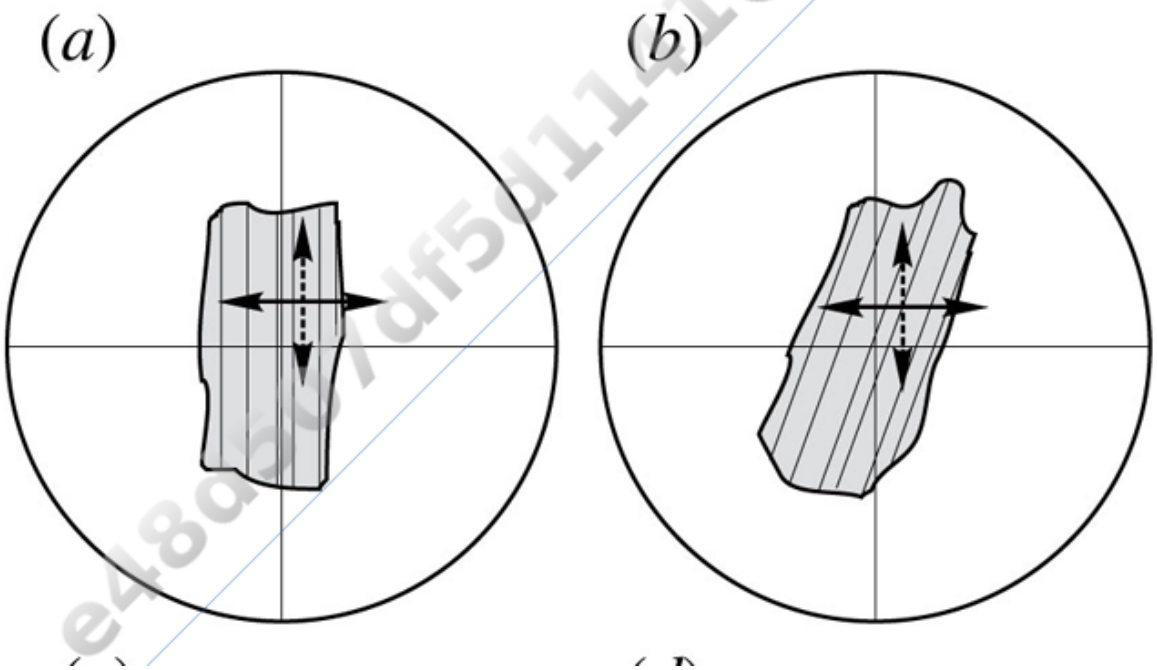

Printed by: e48d507df5d1141@placeholder.94092.edu. Printing is for personal, private use only. No part of this book may be reproduced or transmitted without publisher's prior permission. Violators will be prosecuted.

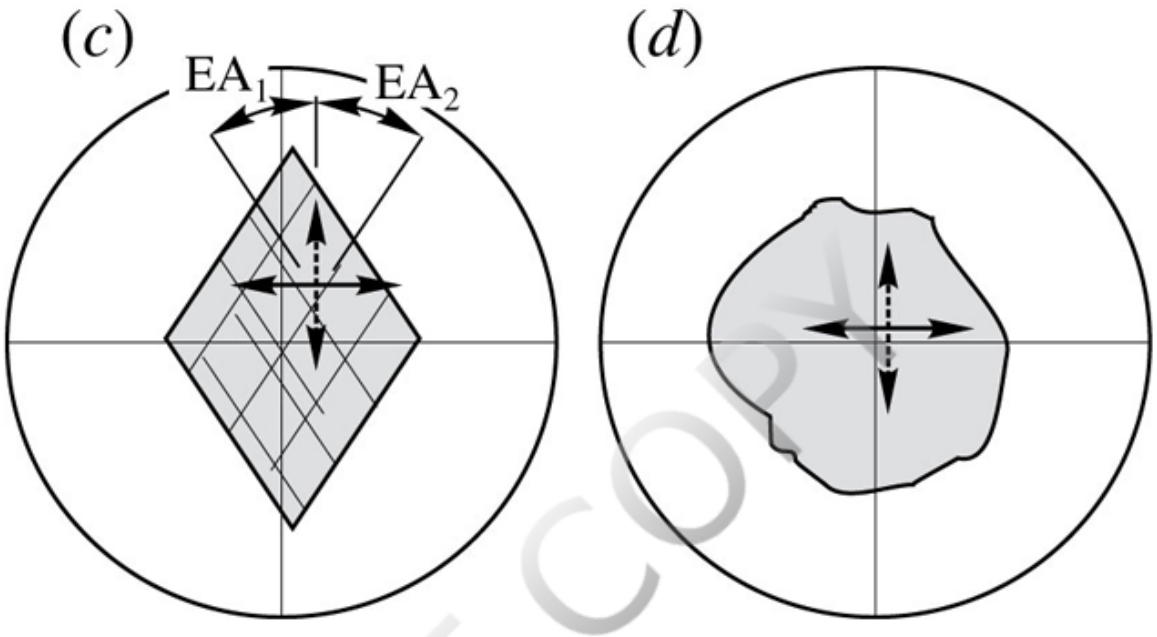

FIGURE 7.32 Categories of extinction. All grains are in extinction orientations. (*a*) Parallel extinction. The grain is extinct when the trace of cleavage or length is parallel to a crosshair. (*b*) Inclined extinction. The grain is extinct when the cleavage or length is at an angle to a crosshair. (*c*) Symmetrical extinction. Extinction angles EA_1 and EA_2 measured to the two cleavages are the same. (*d*) No extinction angle. The grain lacks cleavage or elongation from which to measure an extinction angle. Back to text

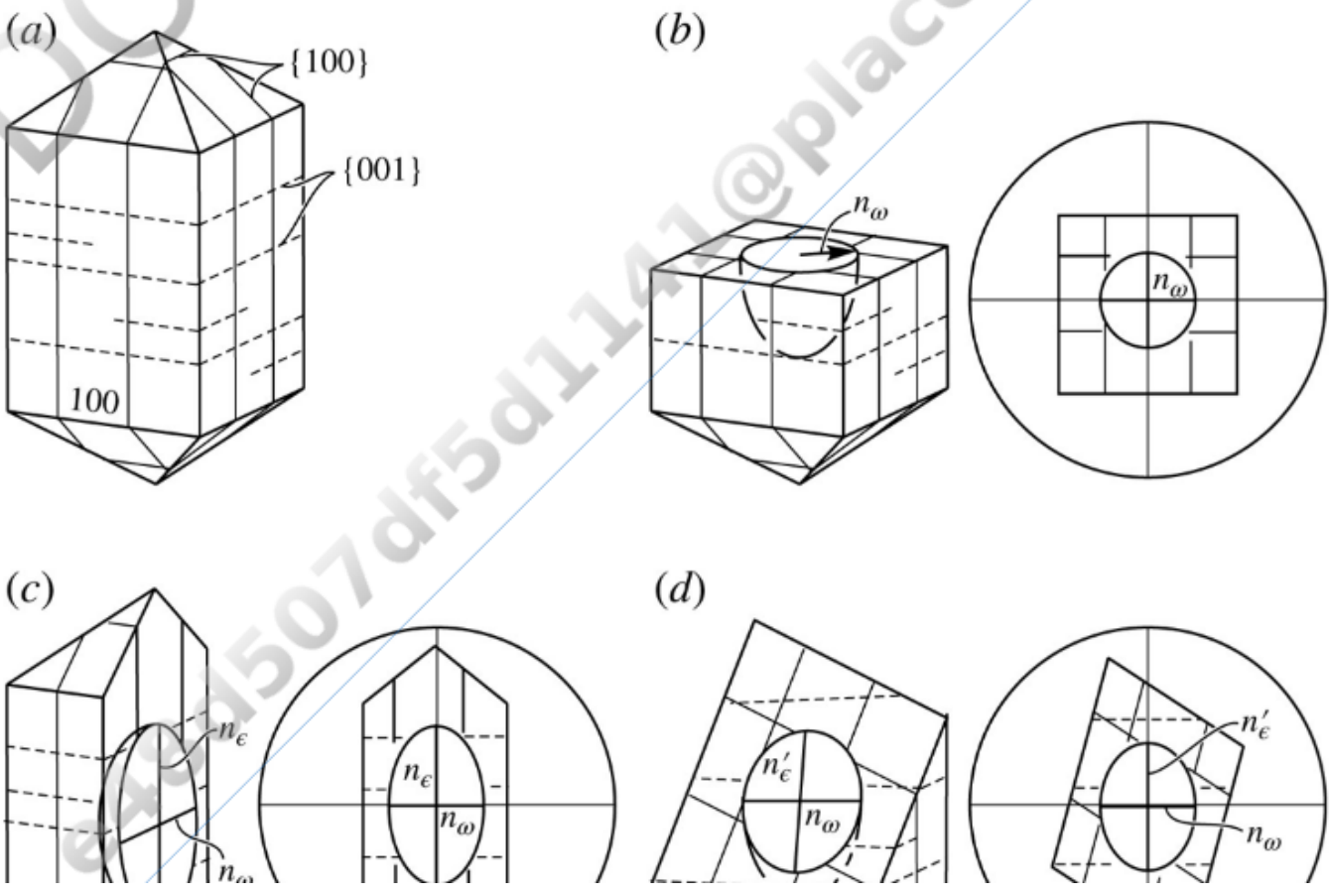

DO NOT COPY e48d507df5d1141@placeholder.94092

Printed by: e48d507df5d1141@placeholder.94092.edu. Printing is for personal, private use only. No part of this book may be reproduced or transmitted without publisher's prior permission. Violators will be prosecuted.

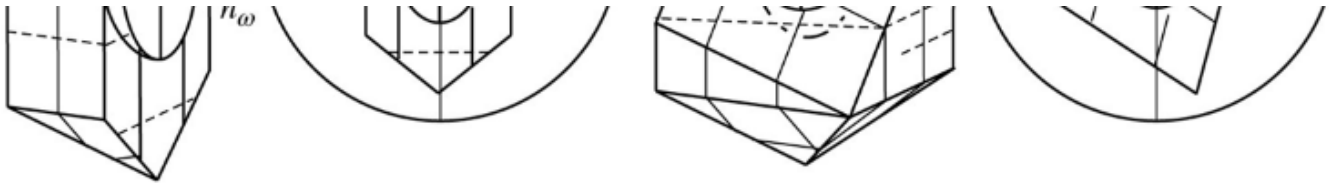

FIGURE 7.33 Extinction in a typical tetragonal mineral. (*a*) Mineral showing traces of pinacoid {001} (dashed) and prismatic {100} (solid) cleavages. (*b*) Mineral resting on the {001} cleavage with the optic axis vertical. The indicatrix section is circular, so all light passes as ordinary rays. The mineral behaves like an isotropic mineral and remains extinct with stage rotation. (*c*) Mineral oriented with optic axis horizontal. The indicatrix section is a principal section, so indices of refraction are n_ω and n_ϵ, and retardation is maximum. Extinction is parallel to the traces of both {001} and {100} cleavage. (*d*) A random cut yields a parallelogram-shaped section. Birefringence is intermediate, and extinction is parallel to the trace of {001} and inclined to the traces of the {100} cleavages. Back to text

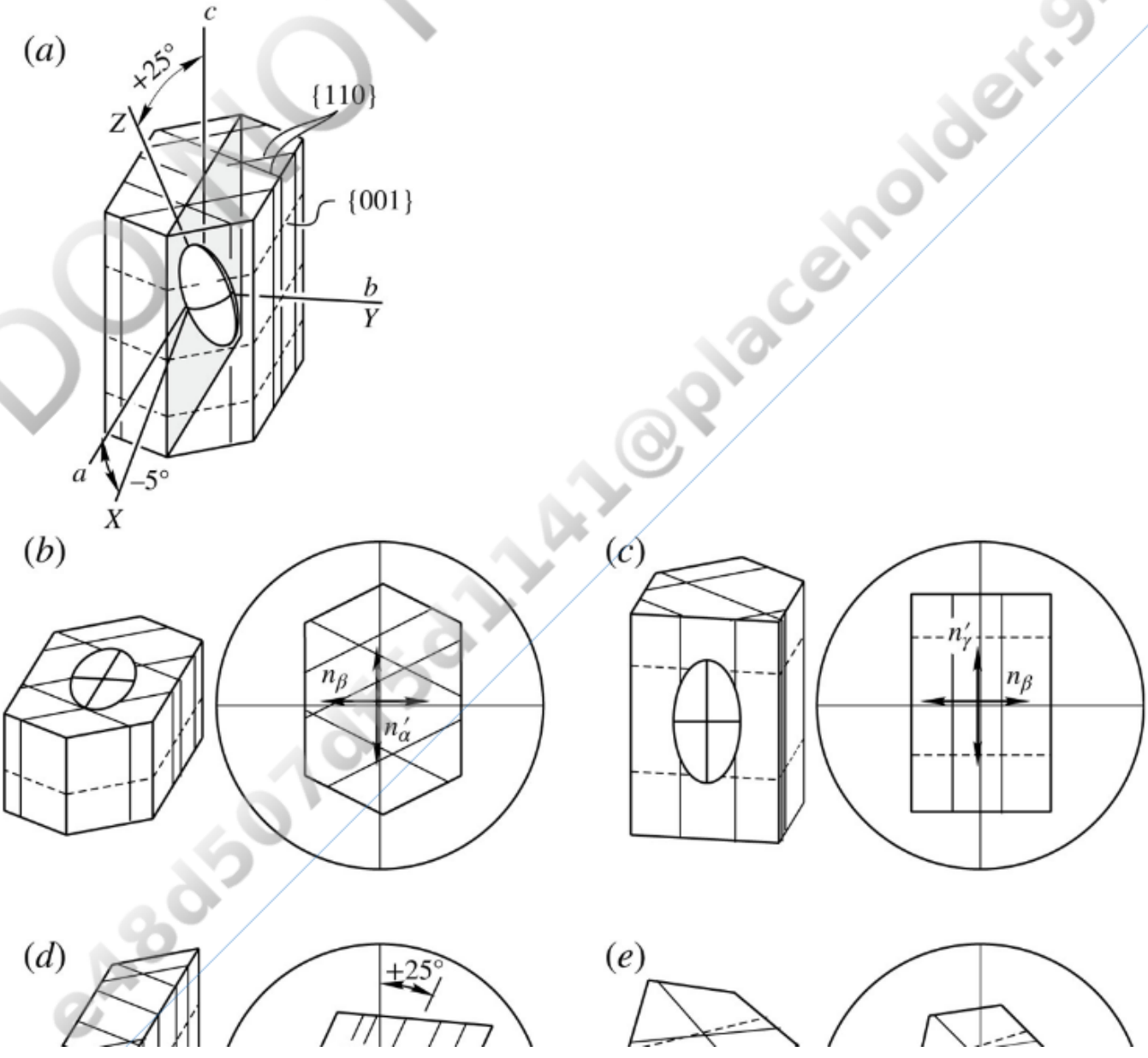

DO NOT COPY e48d507df5d1141@placeholder.9409

Printed by: e48d507df5d1141@placeholder.94092.edu. Printing is for personal, private use only. No part of this book may be reproduced or transmitted without publisher's prior permission. Violators will be prosecuted.

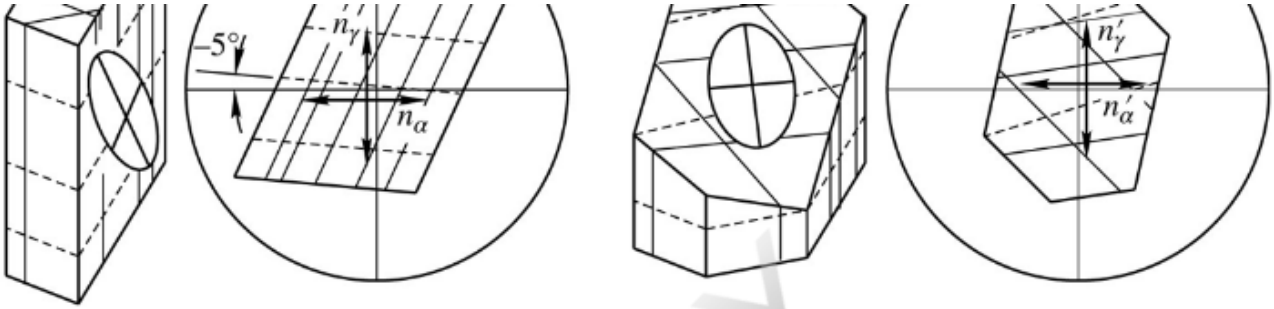

FIGURE 7.34 Extinction in monoclinic minerals. (*a*) Crystal habit showing trace of prismatic {110} (solid lines) and pinacoidal {001} (dashed lines) cleavages. The indicatrix orientation is $Y = b$, $Z \wedge c = +25°$, $X \wedge a = -5°$. (*b*) Fragment resting on the {001} cleavage. Extinction is symmetrical. (*c*) Section parallel to {100} shows parallel extinction to the trace of both cleavages. (*d*) Section parallel to {010} displays maximum retardation. Extinction is 25° (the $Z \wedge c$ angle) measured to the trace of the {110} cleavage and 5° (the $X \wedge a$ angle) measured to the trace of the {001} cleavage. (*e*) Random section: inclined extinction to all cleavage traces. Back to text

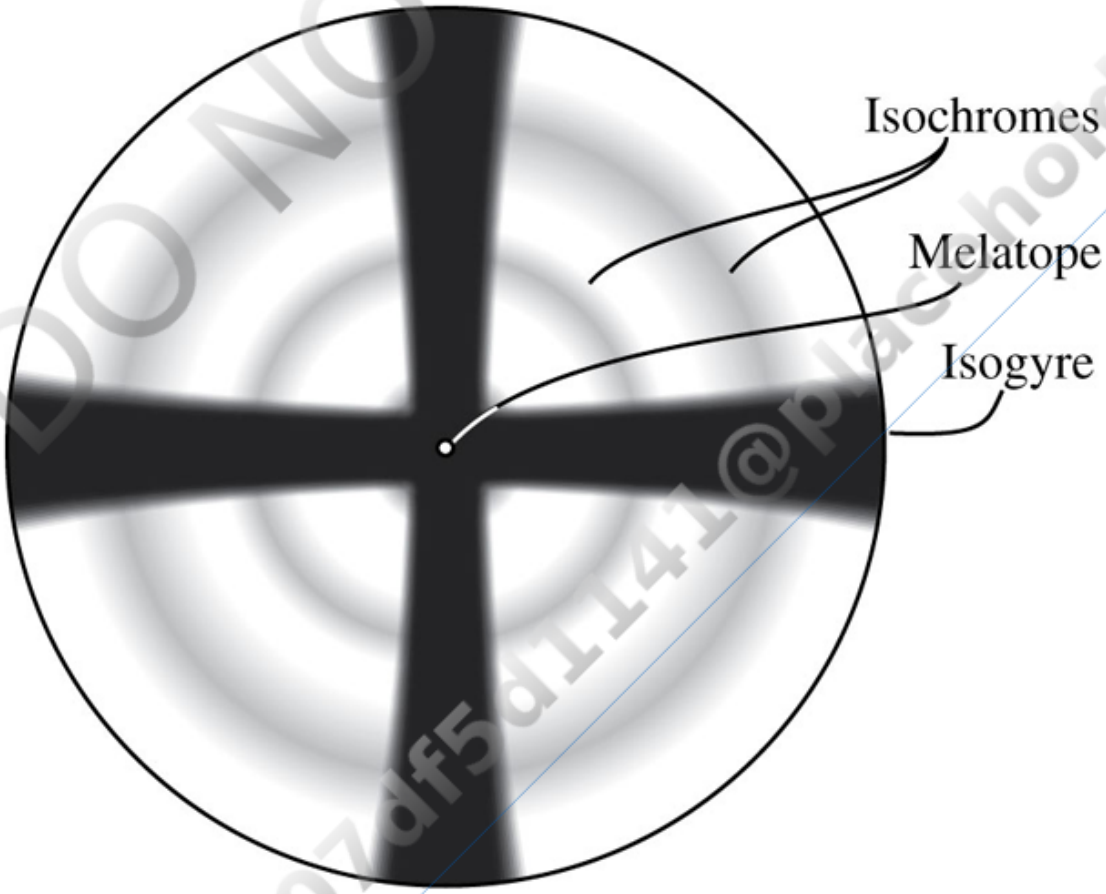

FIGURE 7.35 Uniaxial optic axis interference figure. Back to text

(*b*)

DO NOT COPY
e48d507df5d1141@placeholder.9409

Printed by: e48d507df5d1141@placeholder.94092.edu. Printing is for personal, private use only. No part of this book may be reproduced or transmitted without publisher's prior permission. Violators will be prosecuted.

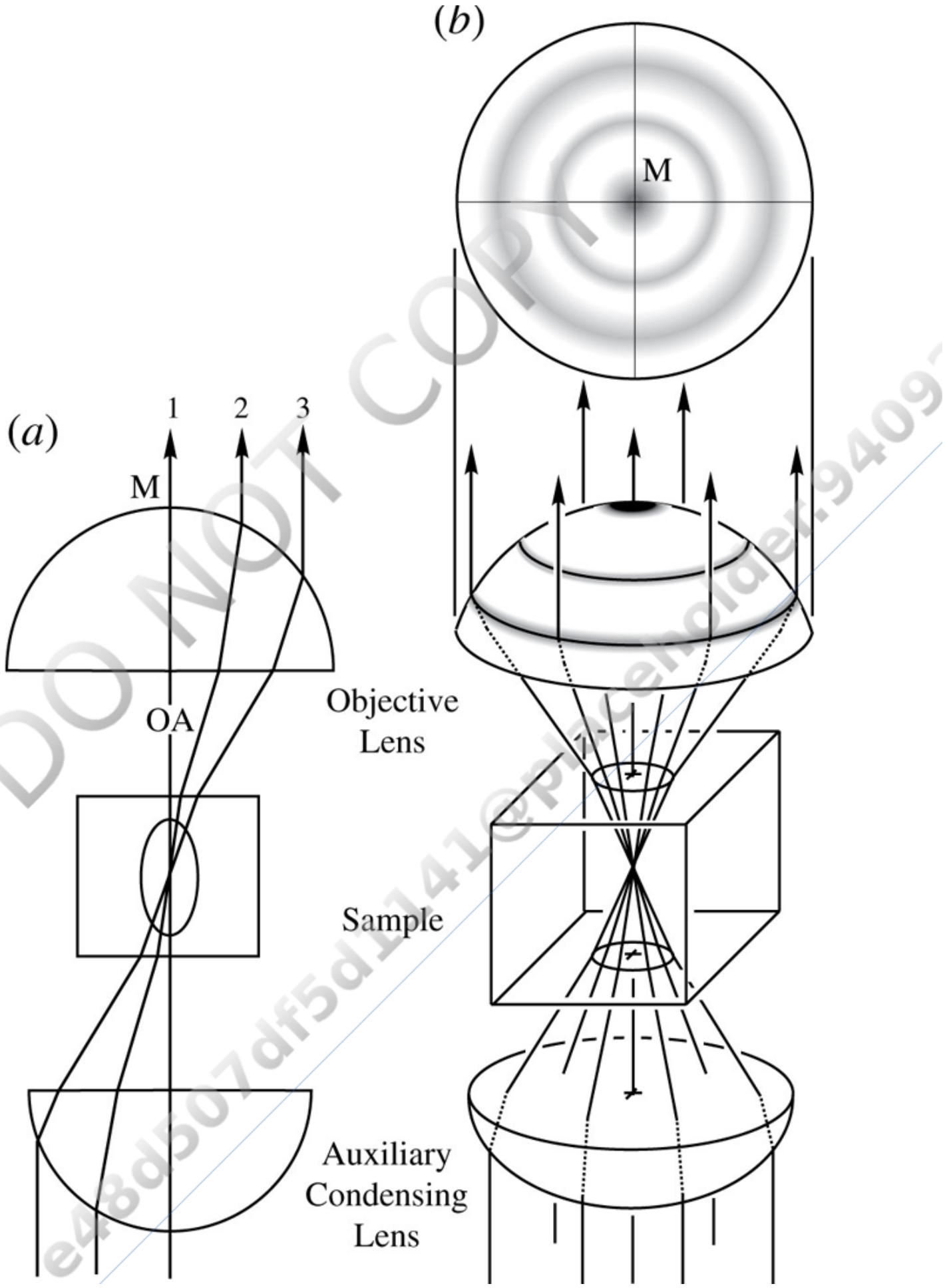

DO NOT COPY
e48d507df5d1141@placeholder.9409

Printed by: e48d507df5d1141@placeholder.94092.edu. Printing is for personal, private use only. No part of this book may be reproduced or transmitted without publisher's prior permission. Violators will be prosecuted.

FIGURE 7.36 Formation of uniaxial isochromes. (*a*) Light following path 1, which emerges at the melatope (M), experiences zero retardation because it follows the optic axis (OA). Paths 2 and 3 produce progressively higher retardation because both birefringence and path length through the sample increase as the inclination of the path to the optic axis increases. (*b*) Optical properties are symmetric about the optic axis, so rings of equal retardation are produced about the melatope. Back to text

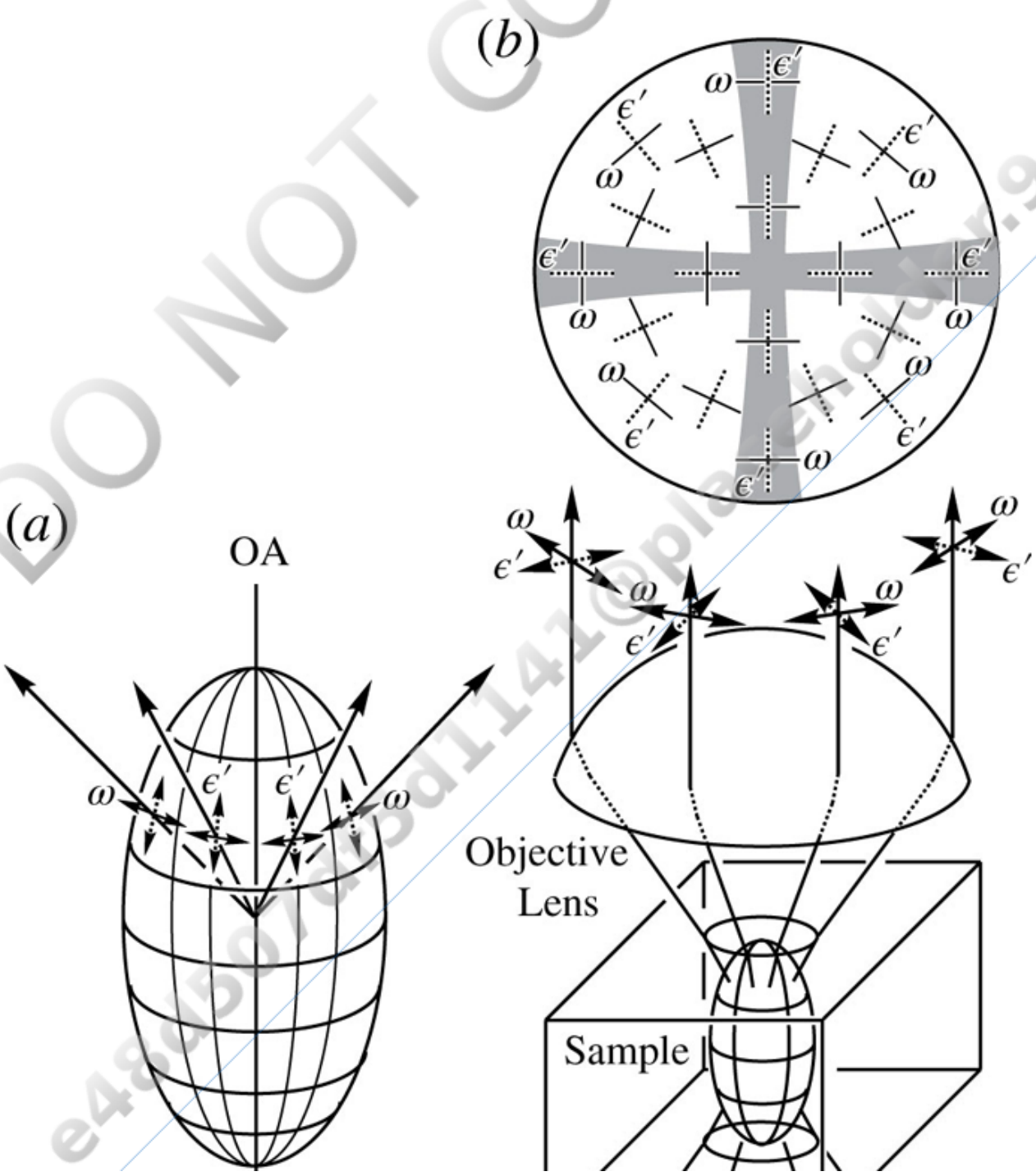

DO NOT COPY

Printed by: e48d507df5d1141@placeholder.94092.edu. Printing is for personal, private use only. No part of this book may be reproduced or transmitted without publisher's prior permission. Violators will be prosecuted.

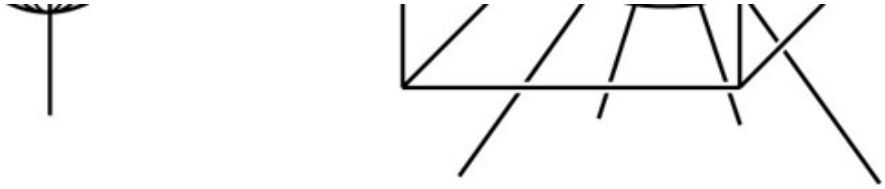

FIGURE 7.37 Formation of isogyres. (*a*) Vibration directions for light emerging from the center of a uniaxial indicatrix. Ordinary (ω) rays vibrate parallel to lines of latitude and extraordinary (ϵ') rays vibrate parallel to lines of longitude. (*b*) Strongly convergent light that passes through a mineral whose optic axis is vertical exits with a vibration pattern that is symmetric about the melatope. Extraordinary rays (ϵ') vibrate parallel to radial lines (similar to lines of longitude as seen from above), and ordinary rays (ω) vibrate tangent to the circular isochromes (similar to lines of latitude as seen from above). Isogyres form between crossed polarizers where vibration directions in the figure are parallel to the vibration directions of the lower and upper polarizers. They are areas of extinction. Back to text

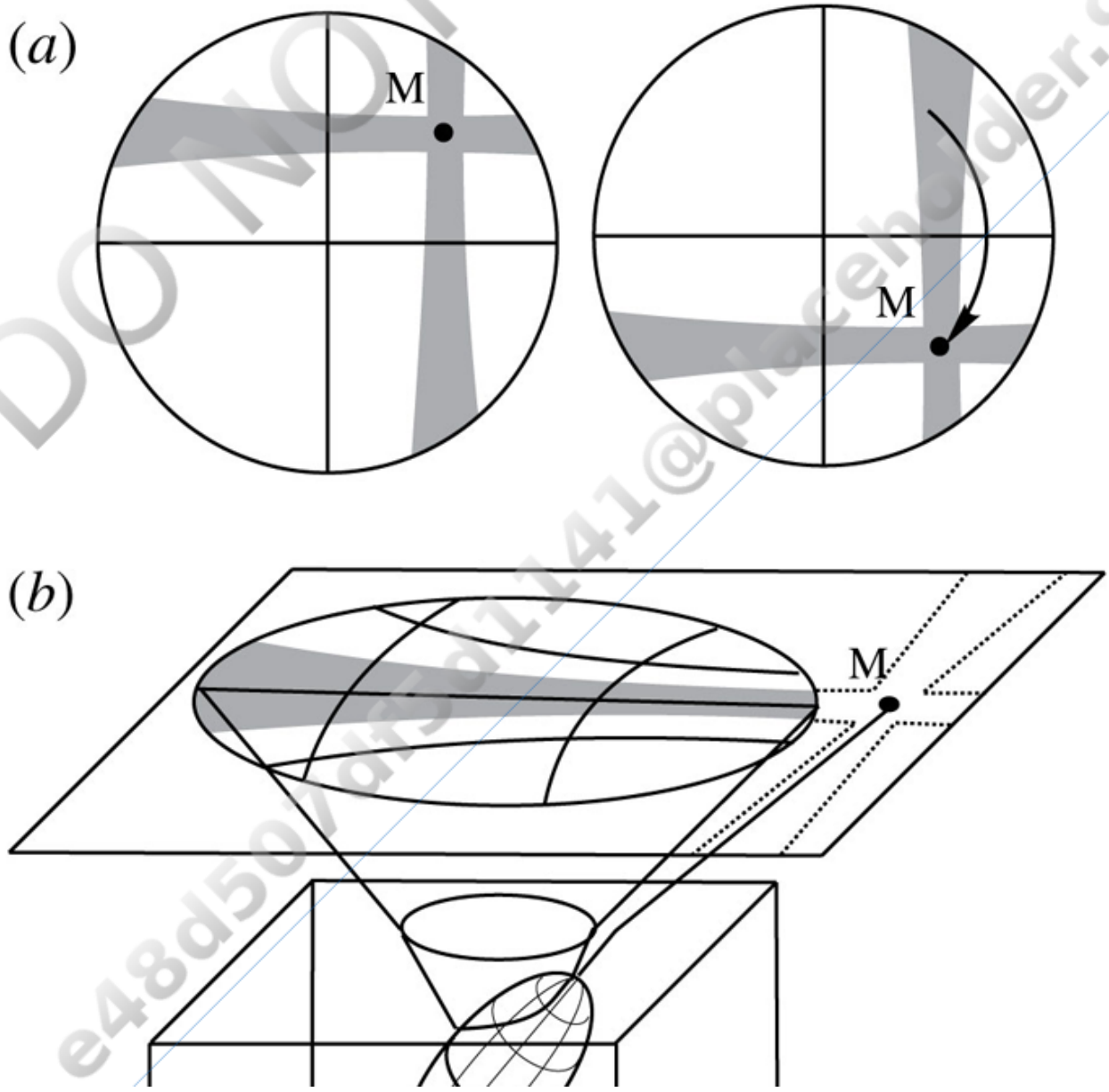

DO NOT COPY
e48d507df5d1141@placeholder.9409

Printed by: e48d507df5d1141@placeholder.94092.edu. Printing is for personal, private use only. No part of this book may be reproduced or transmitted without publisher's prior permission. Violators will be prosecuted.

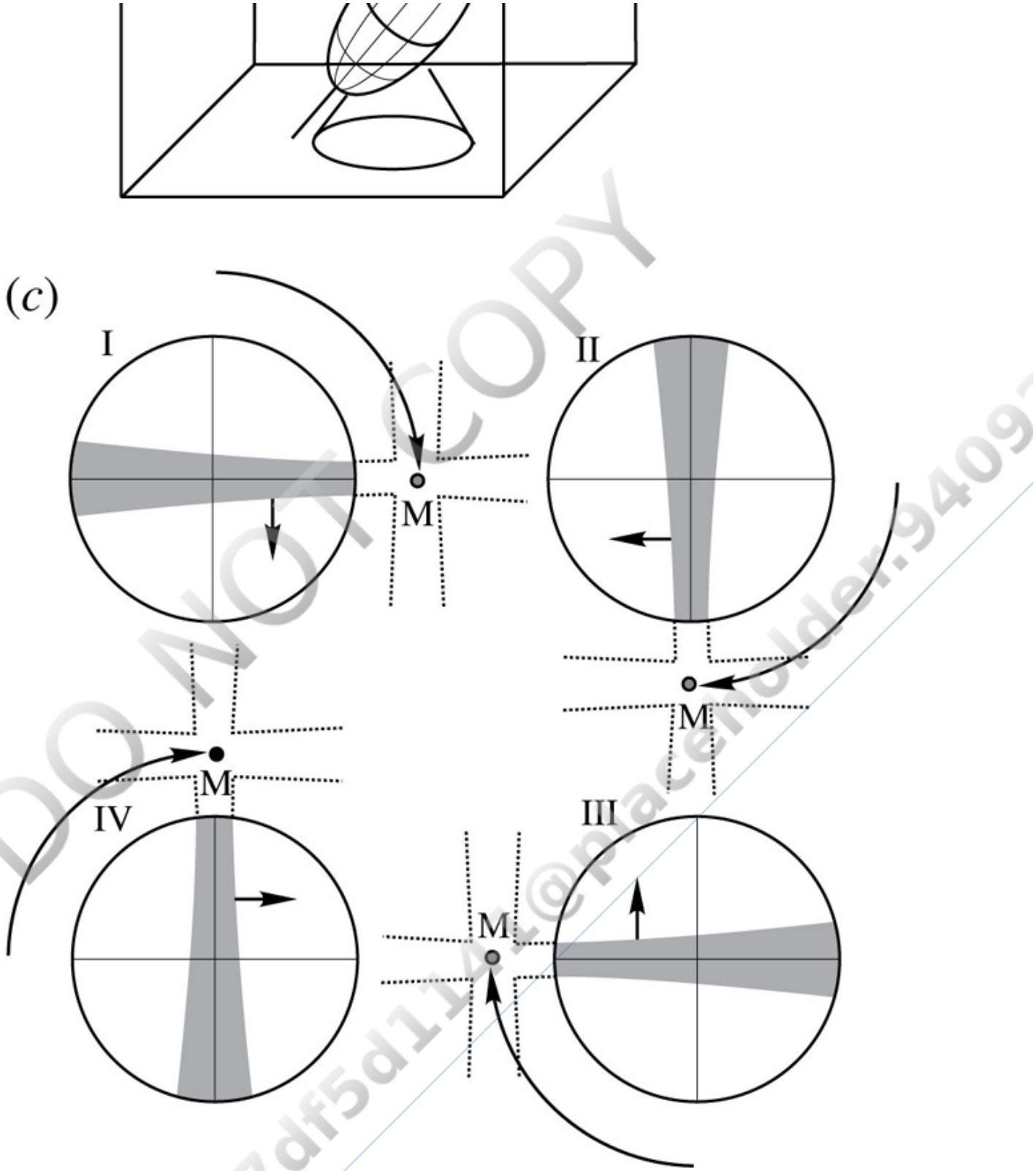

FIGURE 7.38 Off-center uniaxial interference figures. (*a*) Off-center optic axis figure. As the stage is rotated, the melatope sweeps around the field of view. Isogyres and isochromes remain centered on the melatope and the isogyres retain their essential N–S and E–W orientations. (*b*) Mineral sample with optic axis more than 30° from vertical. The melatope is out of the field of view. (*c*) Stage rotation causes isogyre arms to sweep across the field of view in sequence. The thin end of an isogyre arm points to the melatope. Back to text

DO NOT COPY
e48d507df5d1141@placeholder.9409

Printed by: e48d507df5d1141@placeholder.94092.edu. Printing is for personal, private use only. No part of this book may be reproduced or transmitted without publisher's prior permission. Violators will be prosecuted.

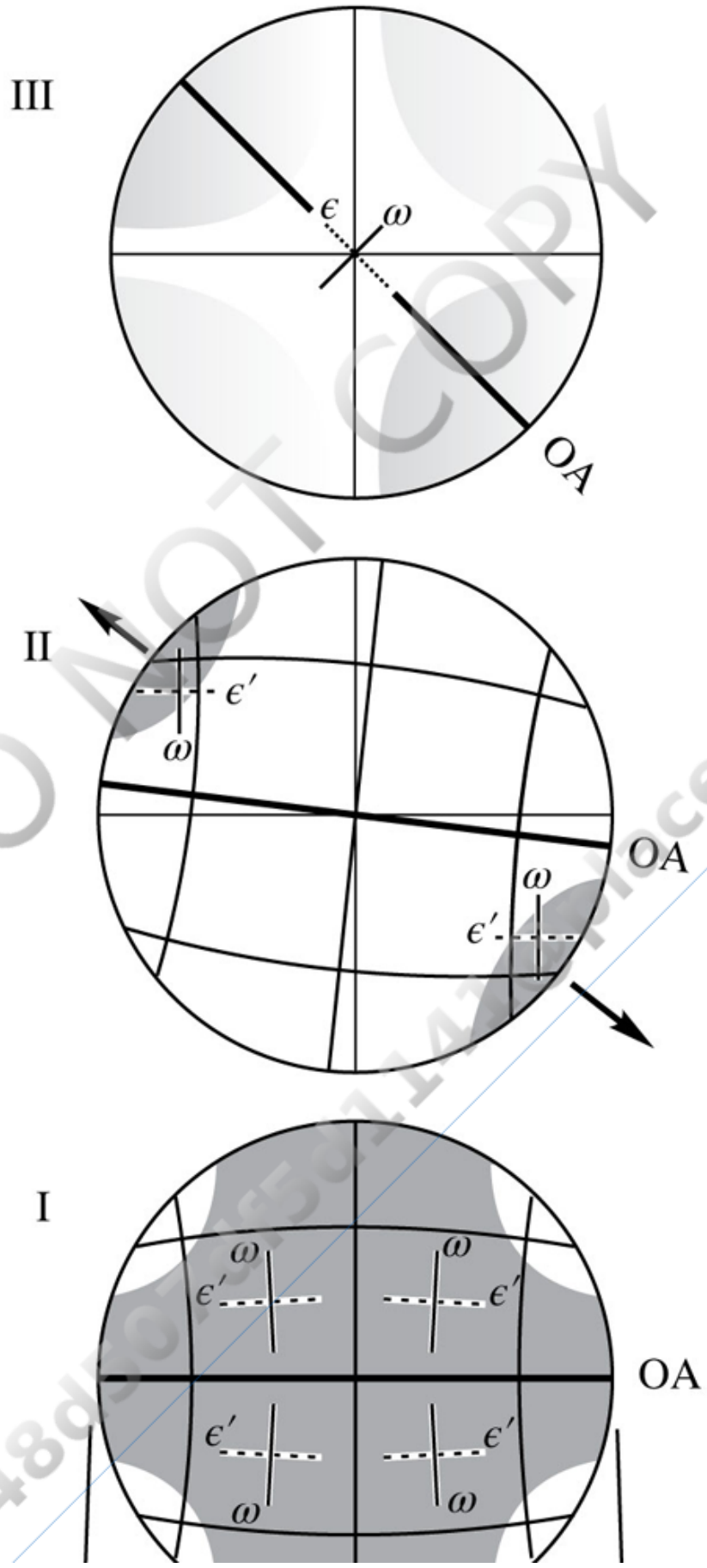

DO NOT COPY

Printed by: e48d507df5d1141@placeholder.94092.edu. Printing is for personal, private use only. No part of this book may be reproduced or transmitted without publisher's prior permission. Violators will be prosecuted.

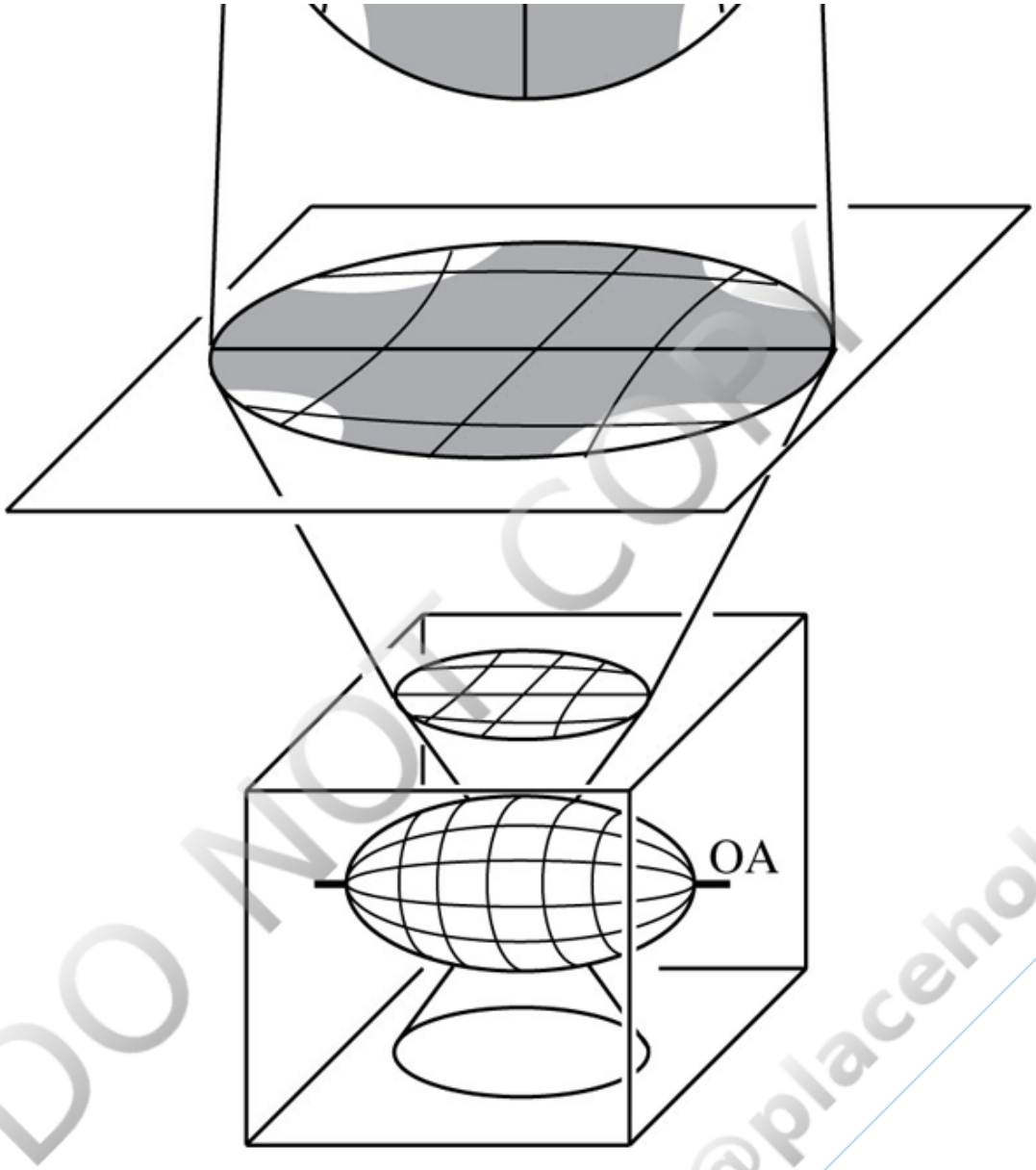

FIGURE 7.39 Uniaxial optic normal (flash) figure. The optic axis is parallel to the microscope stage. Vibration directions in the figure are derived as shown in Figure 7.37. In view I, the optic axis is exactly E–W. The isogyre is a broad, fuzzy cross because vibration directions of ω and ϵ' rays in all but the outer parts of the four quadrants are parallel to the lower and upper polarizers. In view II, the stage has been rotated a few degrees clockwise. The isogyres quickly split and exit the field of view from the quadrants into which the optic axis (OA) is being rotated (isochromes are not shown). View III shows the figure with the optic axis NW–SE. Diffuse isochromes are concave outward. The retardation decreases outward toward the NW and SE and increases outward toward the NE and SW.
Back to text

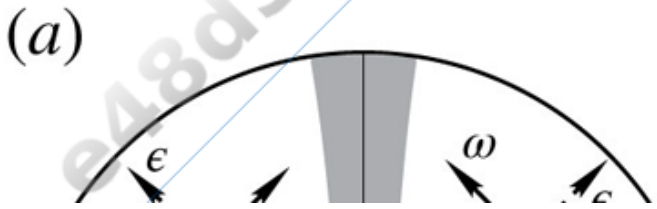

DO NOT COPY
e48d507df5d1141@placeholder.9409

Printed by: e48d507df5d1141@placeholder.94092.edu. Printing is for personal, private use only. No part of this book may be reproduced or transmitted without publisher's prior permission. Violators will be prosecuted.

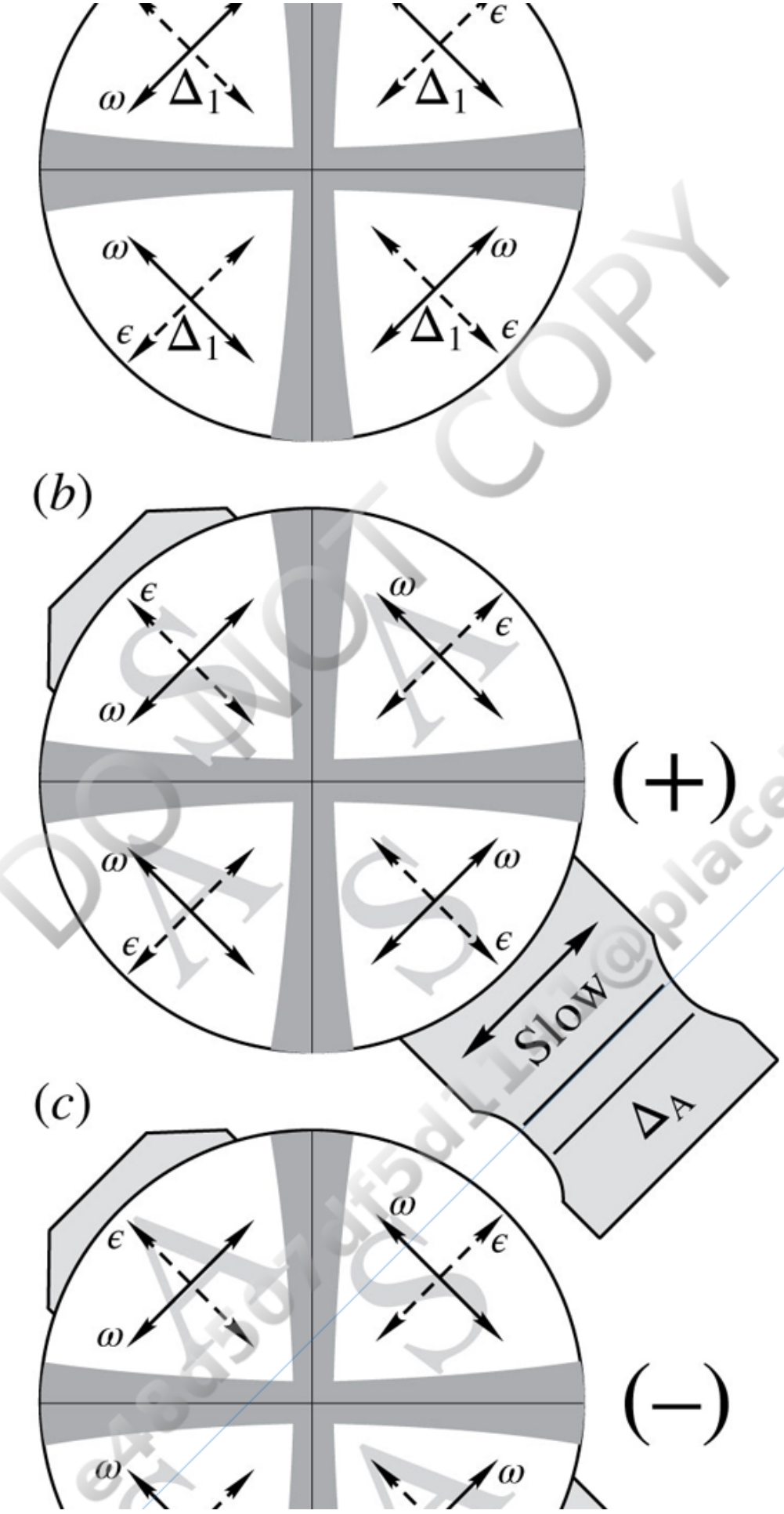

DO NOT COPY
e48d507df5d1141@placeholder.9409

Printed by: e48d507df5d1141@placeholder.94092.edu. Printing is for personal, private use only. No part of this book may be reproduced or transmitted without publisher's prior permission. Violators will be prosecuted.

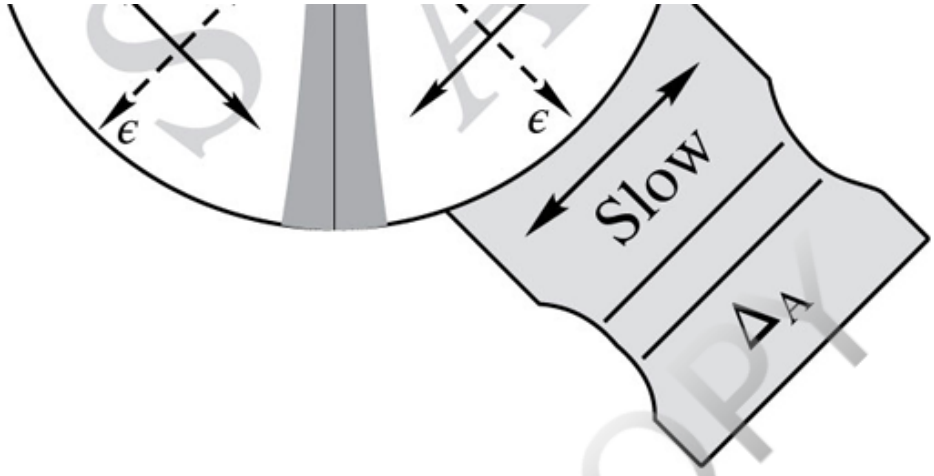

FIGURE 7.40 Determining optic sign in a uniaxial optic axis interference figure. (*a*) Retardation Δ_1 is displayed in the four quadrants and the vibration directions of ordinary (ω) and extraordinary (ϵ) rays are shown. When an accessory plate with retardation Δ_A (slow NE–SW) is inserted, retardations in two quadrants will add (A) to become $\Delta_1 + \Delta_A$, and retardations in the other two quadrants will subtract (S) to become $|\Delta_1 - \Delta_A|$. (*b*) Optically positive. (*c*) Optically negative. Back to text

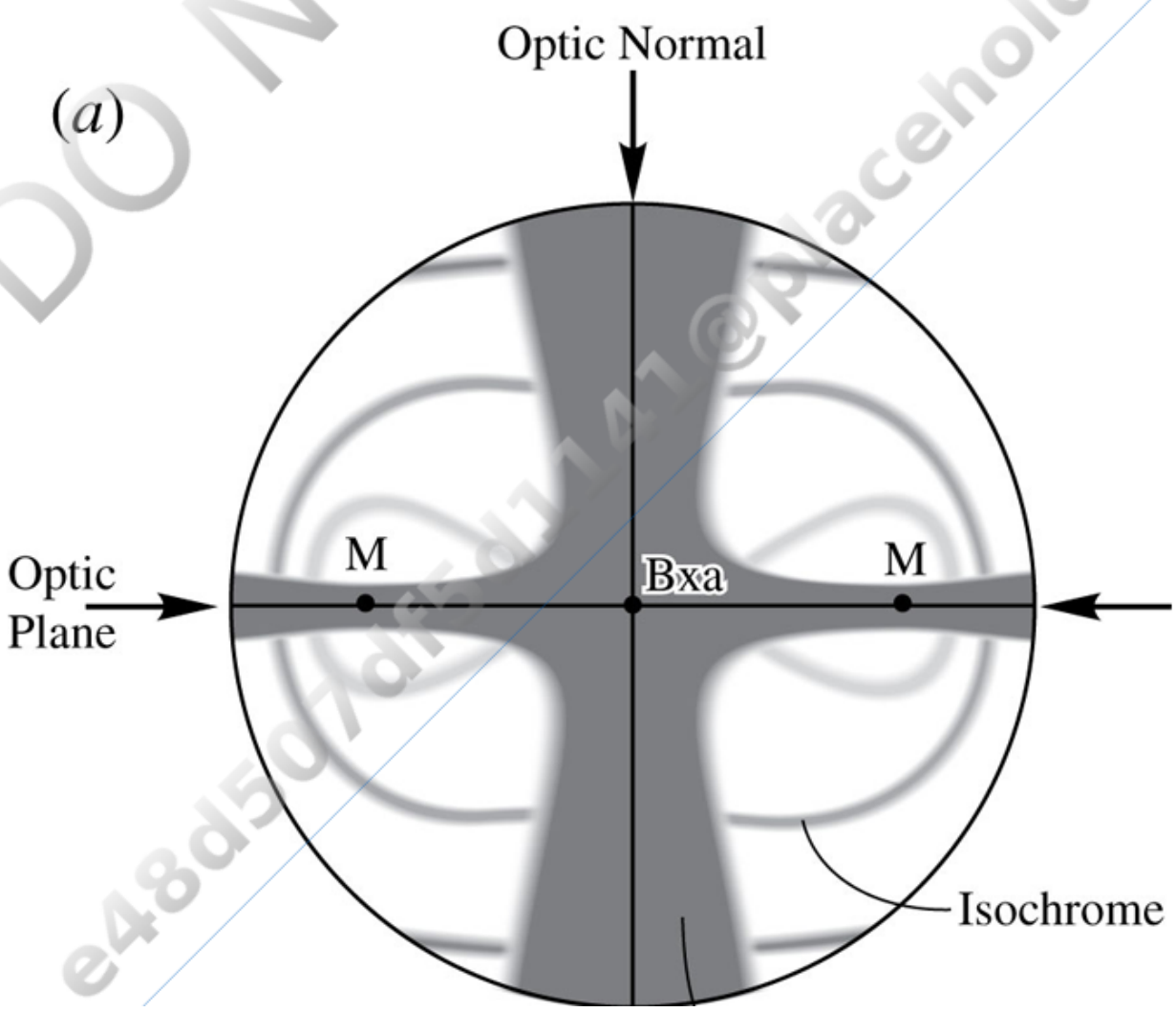

DO NOT COPY
e48d507df5d1141@placeholder.9409

Printed by: e48d507df5d1141@placeholder.94092.edu. Printing is for personal, private use only. No part of this book may be reproduced or transmitted without publisher's prior permission. Violators will be prosecuted.

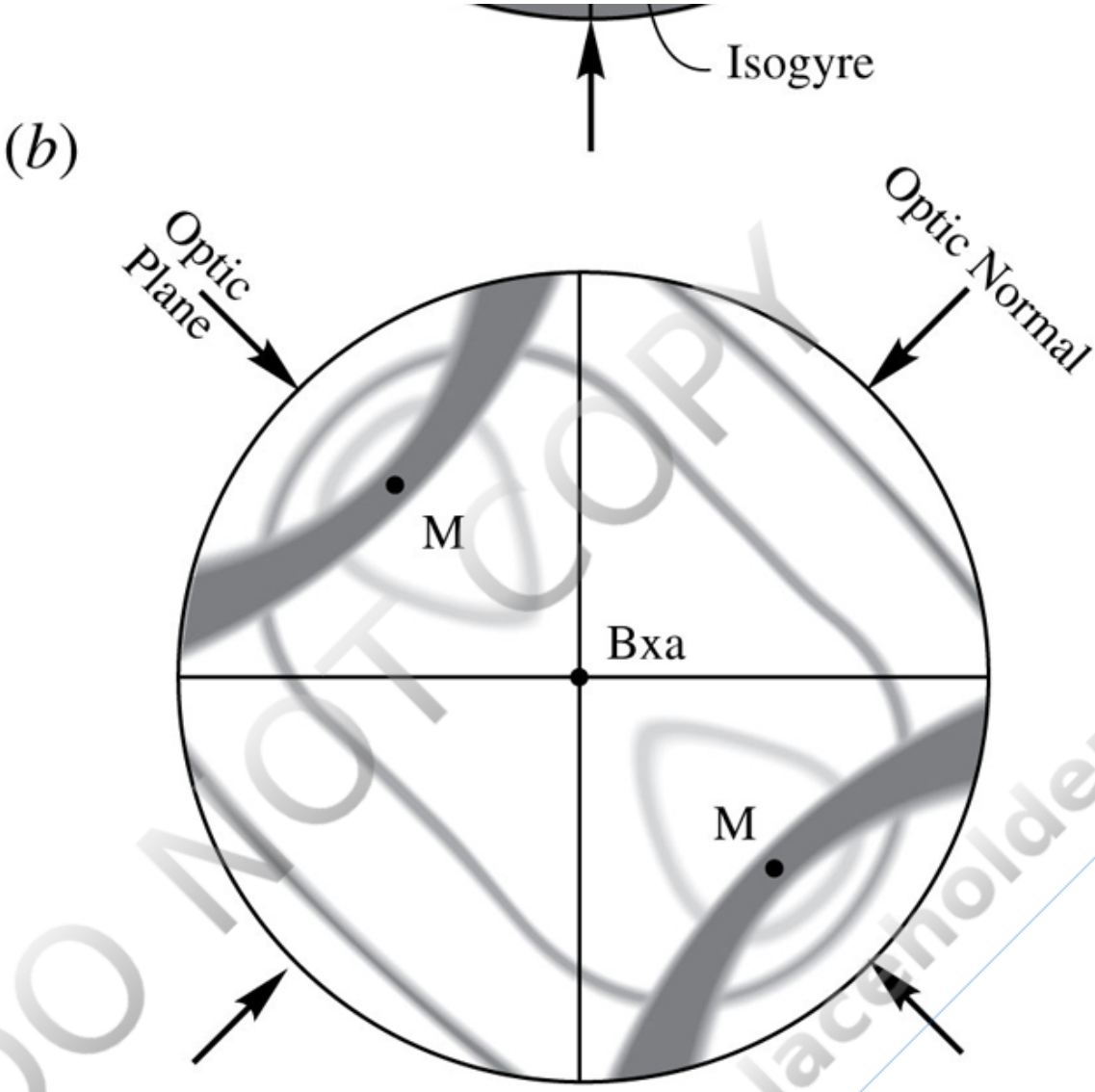

FIGURE 7.41 Biaxial acute bisectrix interference figure. The melatopes (M) mark the points of emergence of the optic axes, and the acute bisectrix (Bxa) is in the center of the field of view. Isochromes form an oval or figure-eight pattern centered on the melatopes. The isogyre pattern depends on stage rotation. (*a*) The isogyres form a cross-shaped pattern when the trace of the optic plane is oriented E–W. (*b*) Optic plane rotated to a 45° position. With rotation from (*a*) to (*b*), the isogyres split and move across the field of view to form the two arc-shaped segments centered on the melatopes. Back to text

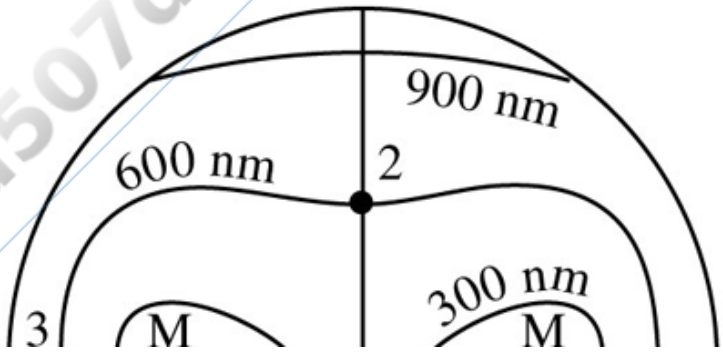

DO NOT COPY
e48d507df5d1141@placeholder.9409

Printed by: e48d507df5d1141@placeholder.94092.edu. Printing is for personal, private use only. No part of this book may be reproduced or transmitted without publisher's prior permission. Violators will be prosecuted.

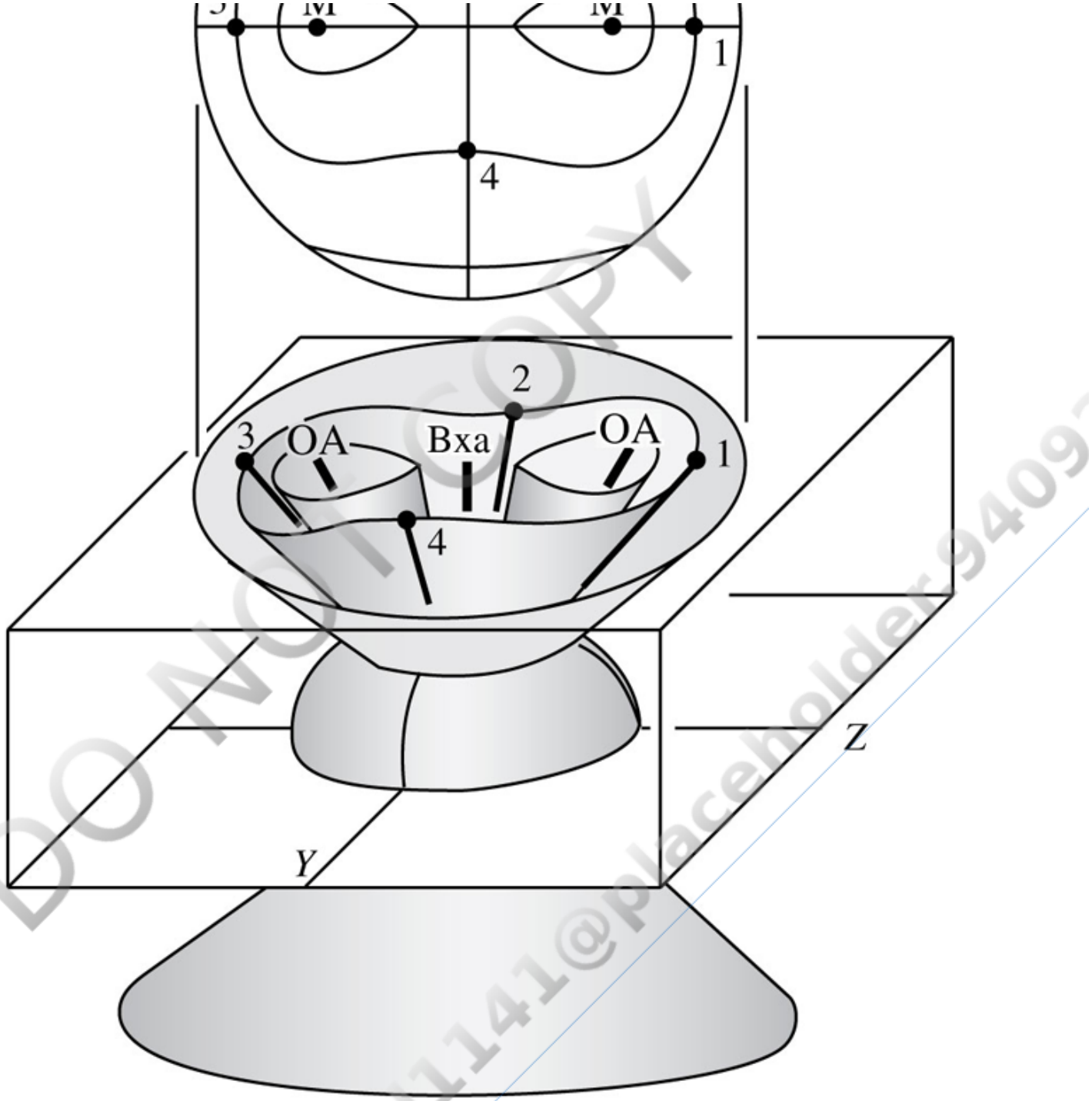

FIGURE 7.42 Formation of biaxial isochromes. Light following the optic axes emerges at the melatopes (M) with zero retardation. Light following paths within the flattened cone outlined by rays 1, 2, 3, and 4 develops the same retardation by the time each ray has exited the top of the mineral. Light inclined further from the optic axes develops greater retardation, and light following paths inclined less to the optic axes develops less. Isochromes are formed in the interference figure along bands of equal retardation. Back to text

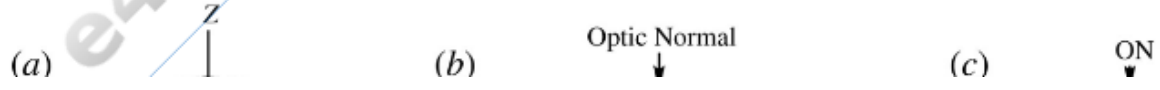

Printed by: e48d507df5d1141@placeholder.94092.edu. Printing is for personal, private use only. No part of this book may be reproduced or transmitted without publisher's prior permission. Violators will be prosecuted.

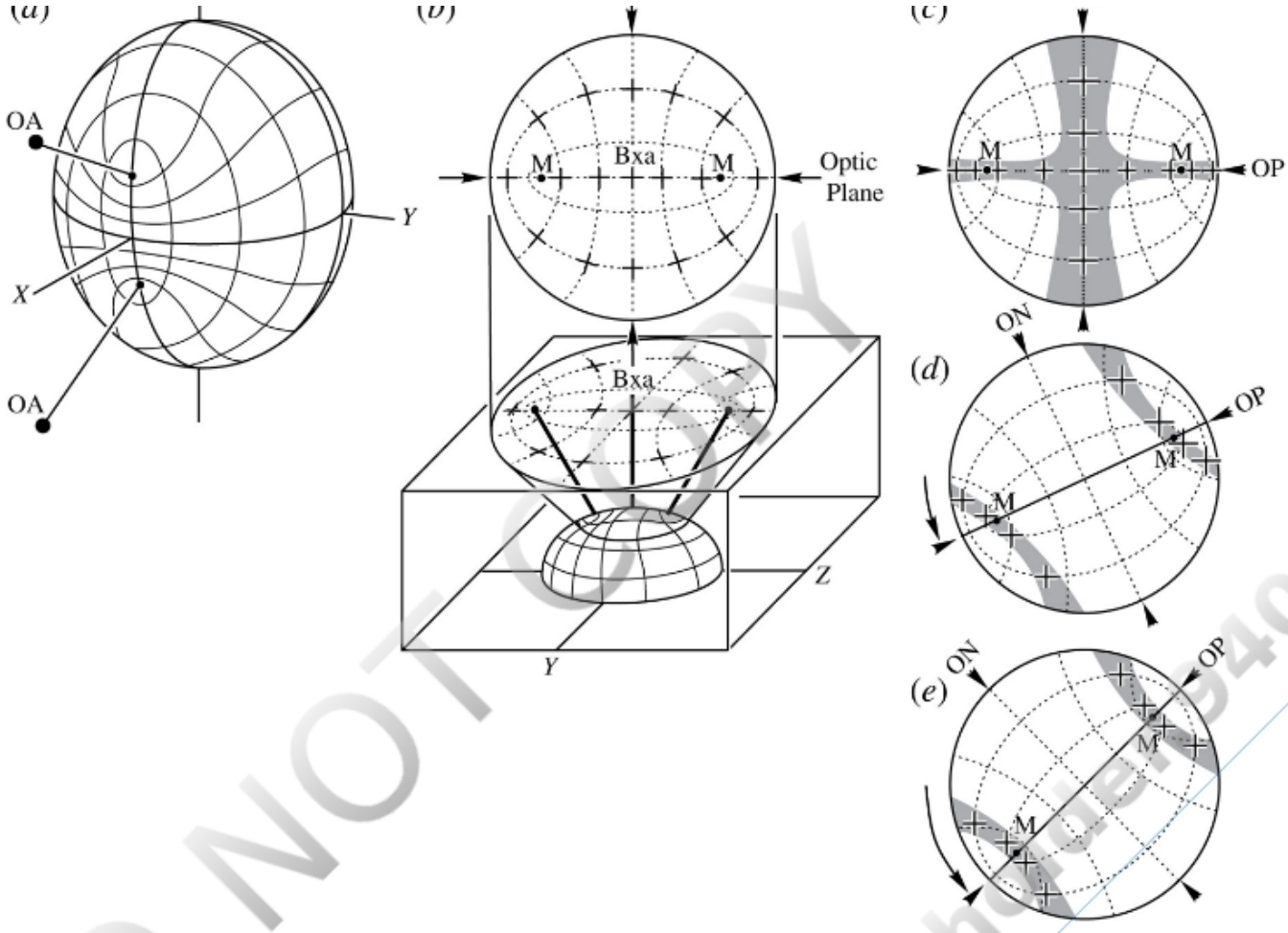

FIGURE 7.43 Formation of biaxial isogyres. (*a*) Vibration directions for all paths emerging from the biaxial indicatrix are determined as described in Figure 7.22 and are projected onto the indicatrix. (*b*) Vibration directions for a number of light paths have been projected onto the upper surface of the mineral grain and are shown in the interference figure. Isogyres are areas of extinction where vibration directions in the interference figure are N–S and E–W. (*c*) Optic plane oriented E–W. The isogyres form a cross that is wider along the trace of the optic normal (ON) and is thin at the melatopes (M). (*d*) With a few degrees of stage rotation, the isogyres split into two segments that pivot about the position of the melatopes. (*e*) Optic plane NE–SW. Isogyres form hyperbolas centered on the melatopes. Back to text

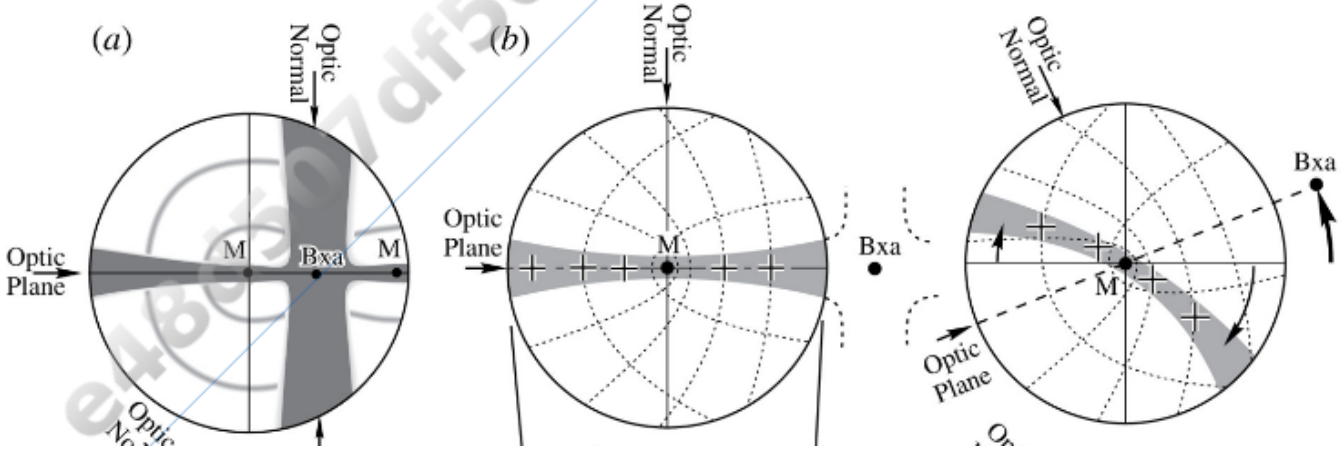

Printed by: e48d507df5d1141@placeholder.94092.edu. Printing is for personal, private use only. No part of this book may be reproduced or transmitted without publisher's prior permission. Violators will be prosecuted.

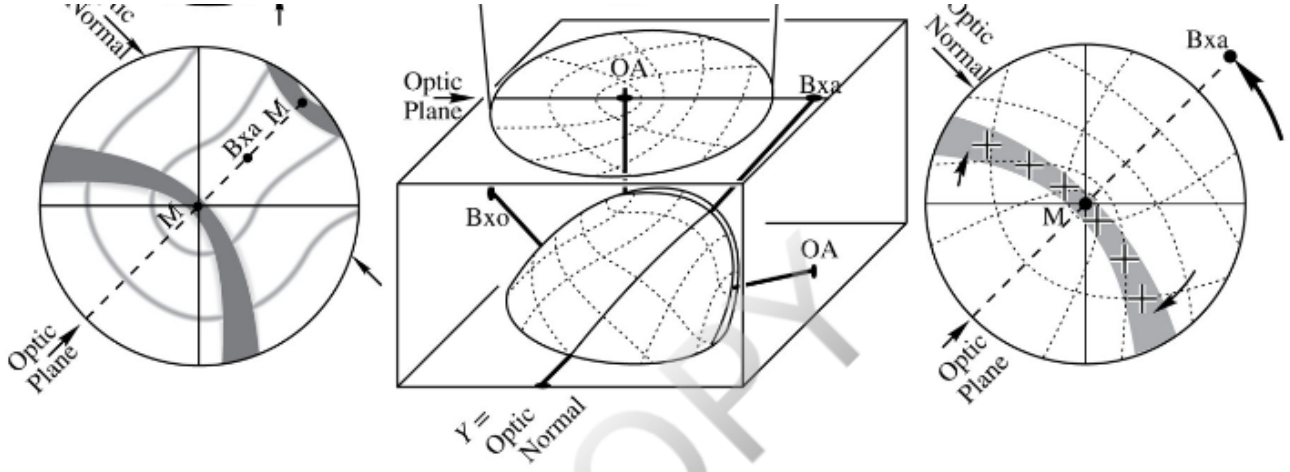

FIGURE 7.44 Biaxial optic axis interference figure. (*a*) 2*V* less than about 30°. The second melatope is in the field of view, and the figure looks like an off-center acute bisectrix figure. Isochromes are shown. (*b*) Larger 2*V*. The second melatope is out of the field of view. The dashed lines show vibration directions; isochromes are not shown. The view on the left shows the indicatrix orientation and interference figure with the optic plane oriented E–W. The views on the right show the isogyre motion as the stage is rotated counterclockwise. Note that isogyres pivot in a sense opposite to the stage rotation direction. Back to text

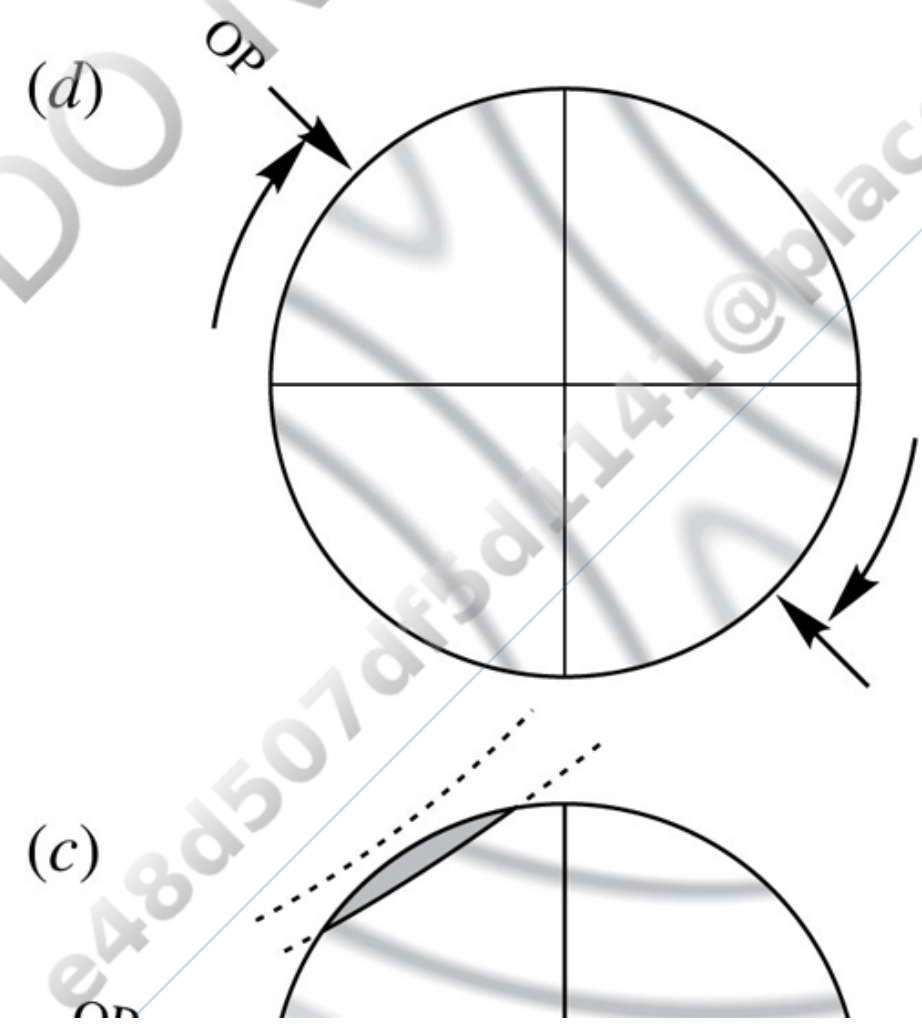

DO NOT COPY
e48d507df5d1141@placeholder.9409

Printed by: e48d507df5d1141@placeholder.94092.edu. Printing is for personal, private use only. No part of this book may be reproduced or transmitted without publisher's prior permission. Violators will be prosecuted.

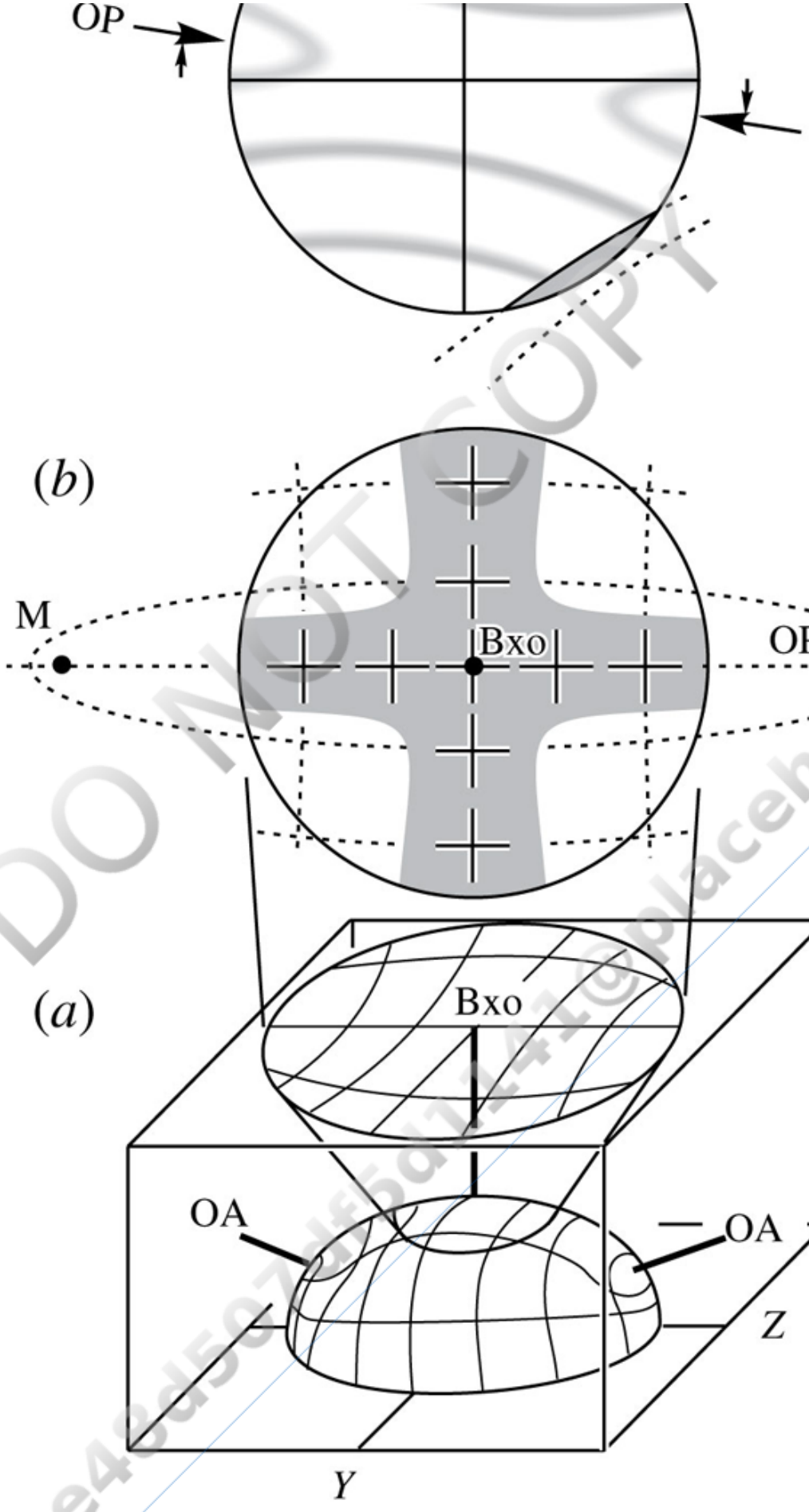

DO NOT COPY
e48d507df5d1141@placeholder.9409

Printed by: e48d507df5d1141@placeholder.94092.edu. Printing is for personal, private use only. No part of this book may be reproduced or transmitted without publisher's prior permission. Violators will be prosecuted.

FIGURE 7.45 Obtuse bisectrix interference figure. (*a*) Pattern of vibration directions in the interference figure. (*b*) With the optic plane E–W, the isogyres form a broad cross. Melatopes are well out of the field of view. Compare with the acute bisectrix figure in Figure 7.41. (*c*) Less than ~15° of stage rotation causes the isogyres to exit the field of view. The pattern of isochromes is similar to that formed in an acute bisectrix figure. (*d*) With the optic plane in a 45° position, the field is occupied only by isochromes. Back to text

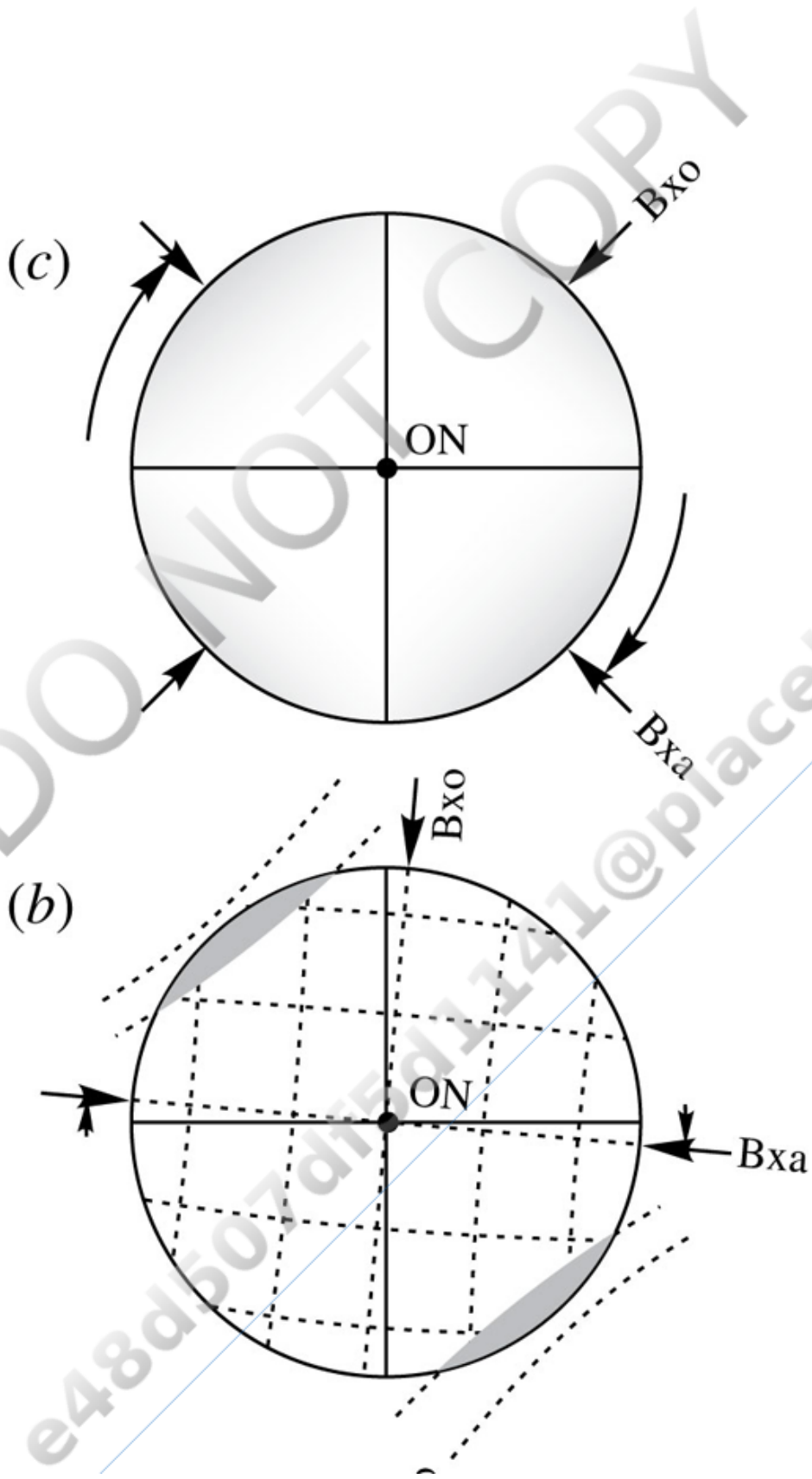

DO NOT COPY
e48d507df5d1141@placeholder.9409

Printed by: e48d507df5d1141@placeholder.94092.edu. Printing is for personal, private use only. No part of this book may be reproduced or transmitted without publisher's prior permission. Violators will be prosecuted.

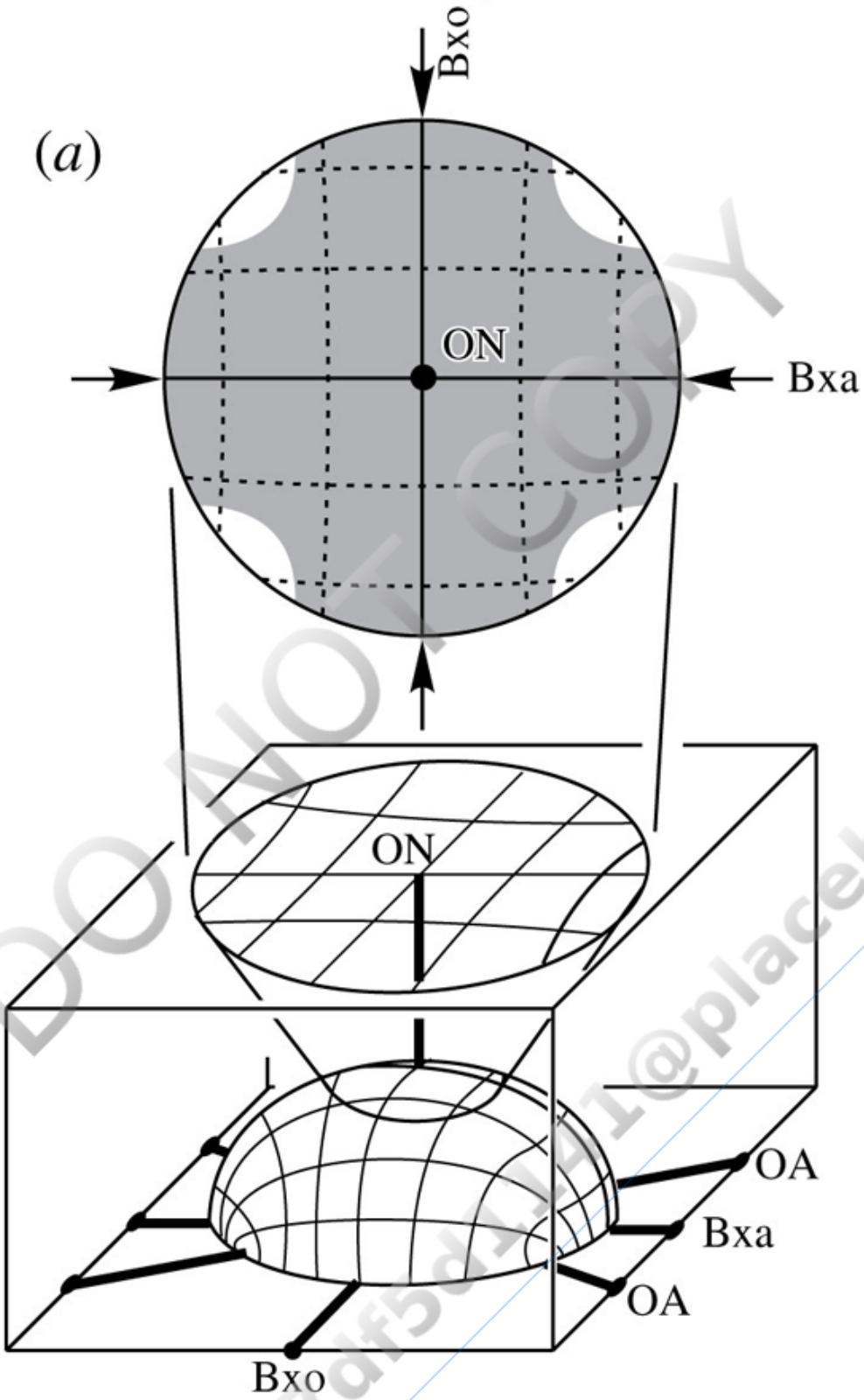

FIGURE 7.46 Optic normal (flash) interference figure. The optic normal (ON) emerges in the center of the figure. (*a*) With the Bxa and Bxo E–W and N–S, the field is occupied by a broad fuzzy cross. Only the outer edges of the four quadrants are not extinct. (*b*) Isogyres split and exit the field with a few degrees of stage rotation. The isogyres exit from the quadrants into which the trace of the Bxa is being rotated. (*c*). Isochrome pattern. No isogyres are present with traces of the Bxo and Bxa in 45° positions. The interference color in the middle of the figure is the same as that displayed by the grain in orthoscopic illumination. Colors increase outward in all four quadrants. Back to text

DO NOT COPY e48d507df5d1141@placeholder.9409

Printed by: e48d507df5d1141@placeholder.94092.edu. Printing is for personal, private use only. No part of this book may be reproduced or transmitted without publisher's prior permission. Violators will be prosecuted.

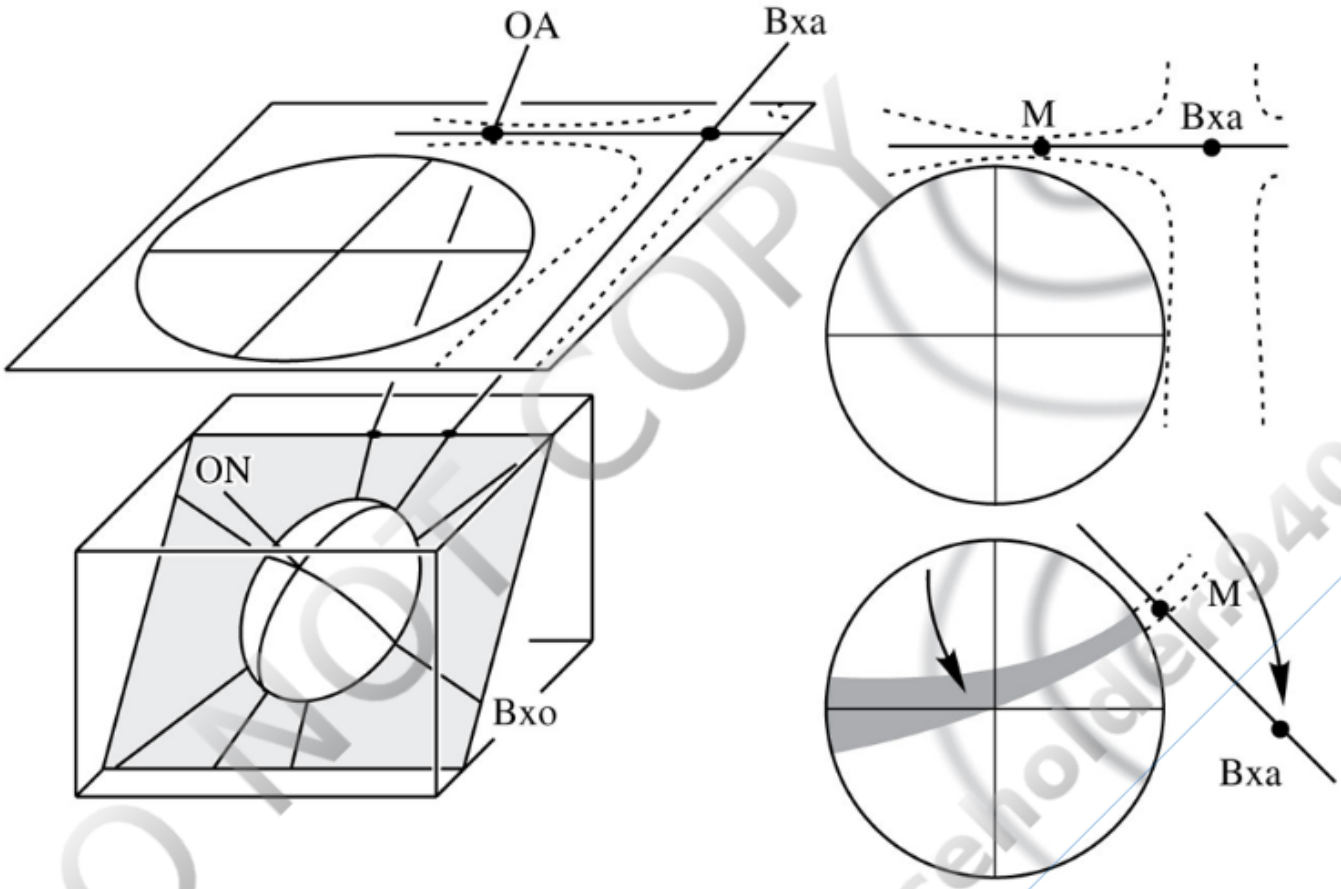

FIGURE 7.47 Biaxial interference figure for randomly oriented grain. As the stage is rotated, isogyres sweep sequentially across the field but are not parallel to the crosshairs. Back to text

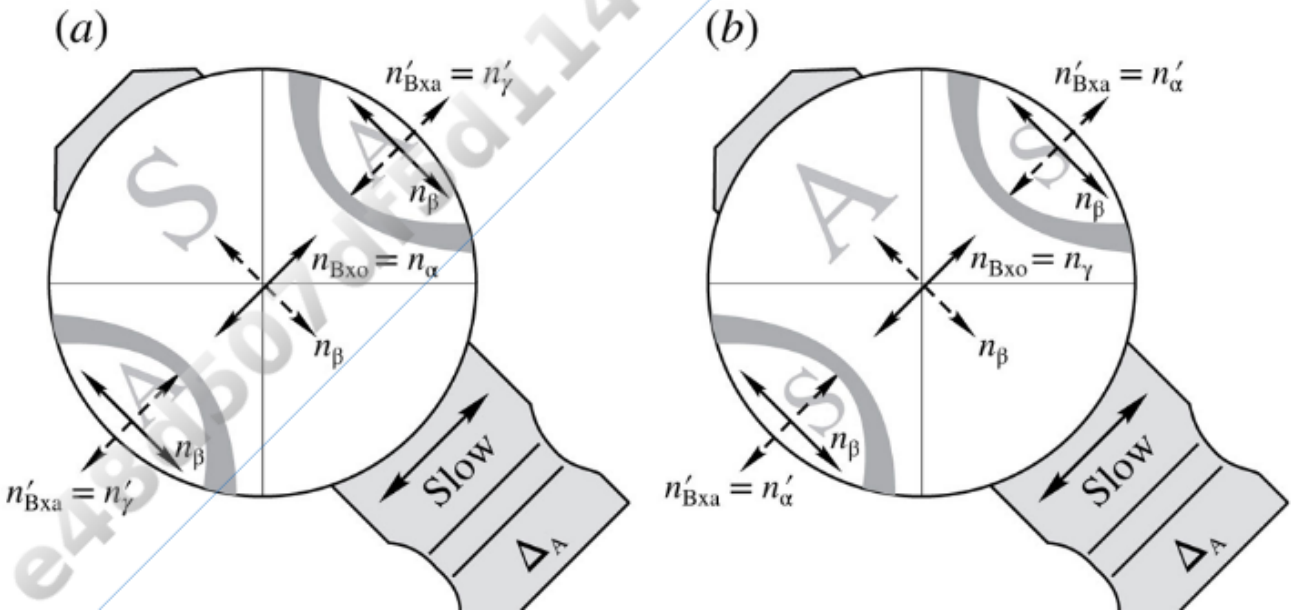

Printed by: e48d507df5d1141@placeholder.94092.edu. Printing is for personal, private use only. No part of this book may be reproduced or transmitted without publisher's prior permission. Violators will be prosecuted.

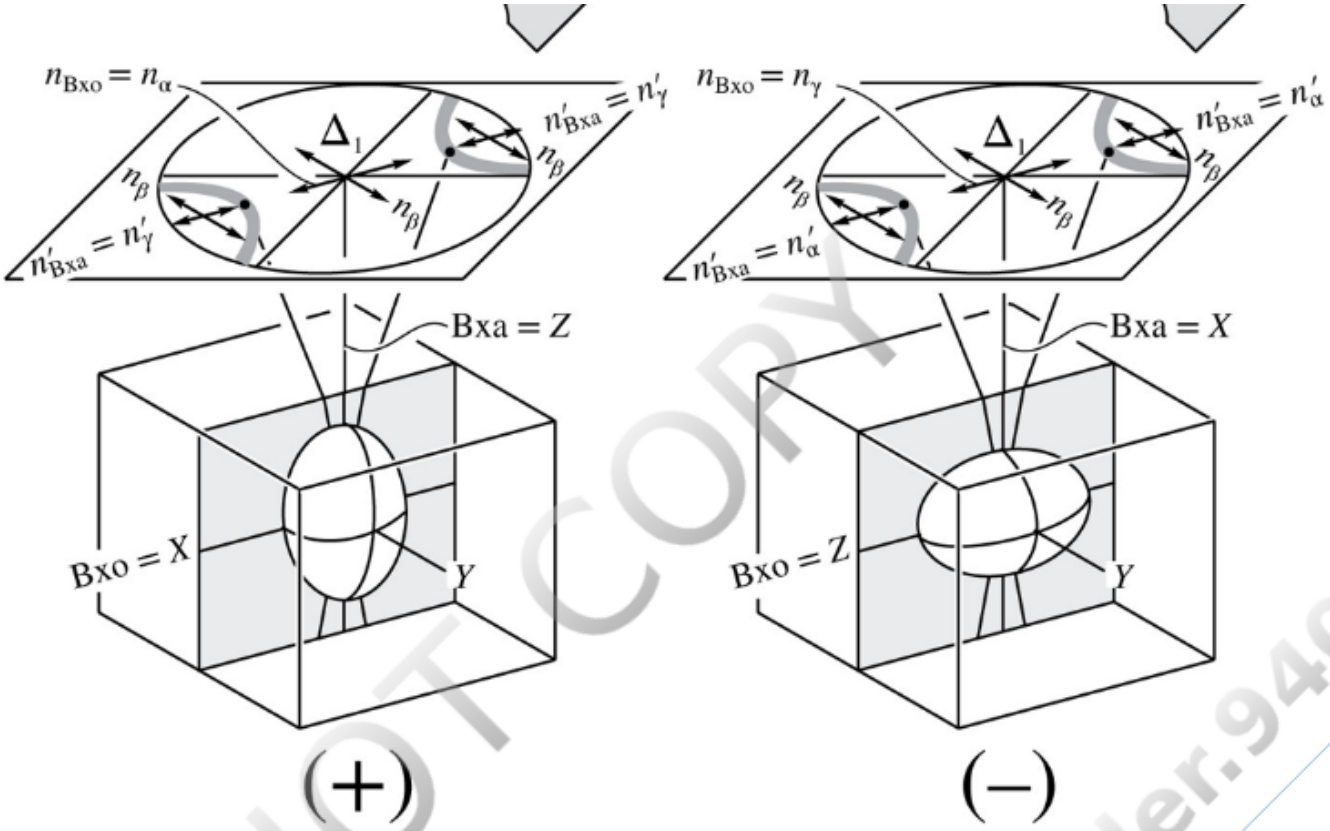

FIGURE 7.48 Determining optic sign in acute bisectrix interference figures. The trace of the optic plane is NE–SW. In the center of the field of view, the retardation is Δ_1, and the NW–SE ray vibrates parallel to the optic normal *Y* and has index of refraction n_β. Insert an accessory plate with retardation Δ_A (slow NE–SW) and note the change in interference color. (If the optic plane is NW–SE, the color changes are reversed.) (*a*) Optically positive. The ray vibrating NE–SW in the center of the figure vibrates parallel to *X* = Bxo, has index of refraction n_α, and is the fast ray compared to n_β, so retardations subtract to become $|\Delta_1 - \Delta_A|$. Outside the isogyres, the ray vibrating NE–SW has index of refraction n'_γ, which is the slow ray compared to n_β, so retardations add. (*b*) Optically negative. The ray vibrating NE–SW in the center of the figure vibrates parallel to *Z* = Bxo, has index of refraction n_γ, and is the slow ray compared to n_β, so retardations add to become $\Delta_1 + \Delta_A$. Outside the isogyres, the ray vibrating NE–SW has index of refraction n'_α, which is the fast ray compared to n_β, so retardations subtract. Back to text

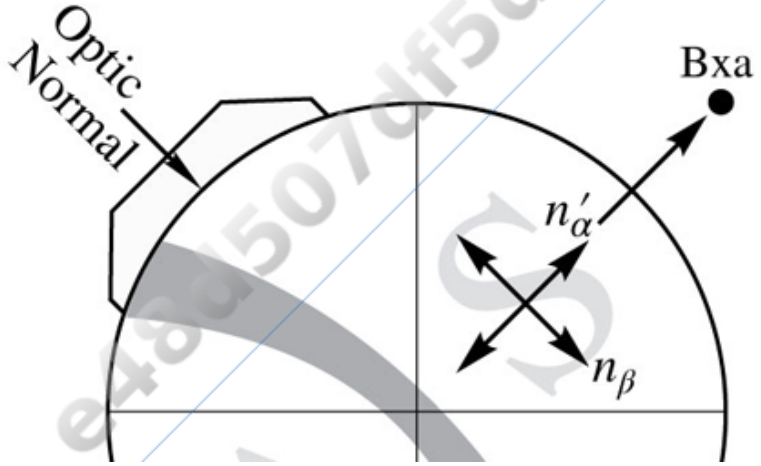

Printed by: e48d507df5d1141@placeholder.94092.edu. Printing is for personal, private use only. No part of this book may be reproduced or transmitted without publisher's prior permission. Violators will be prosecuted.

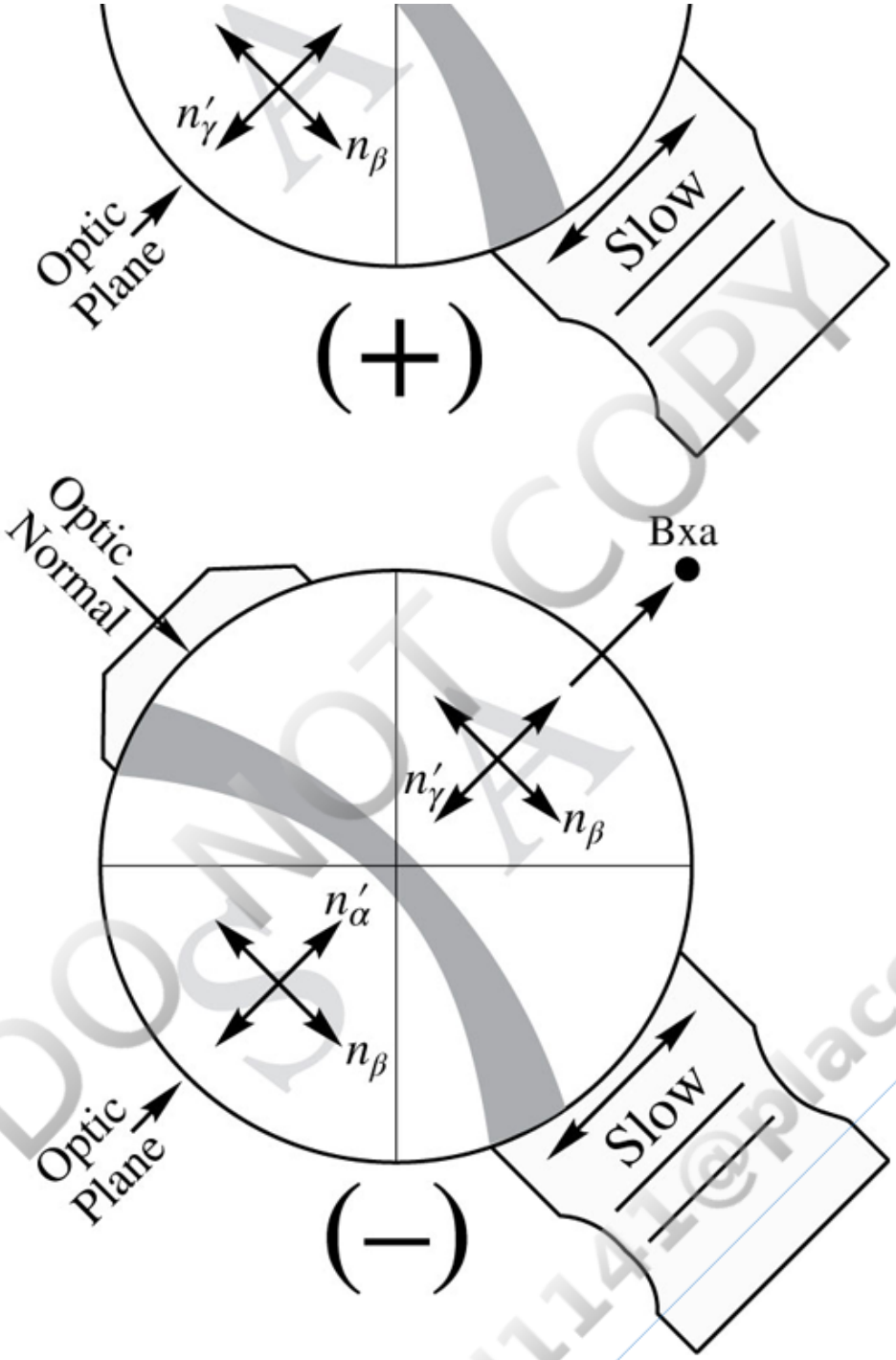

FIGURE 7.49 Determining optic sign with an optic axis figure. The trace of the optic plane is parallel to the slow ray vibration direction in the accessory plate. Retardations subtract (S) on the convex side of the isogyre for optically positive minerals and add (A) for negative. If the optic plane is oriented NW–SE, the color changes are reversed. Back to text

DO NOT COPY
e48d507df5d1141@placeholder.9409

Printed by: e48d507df5d1141@placeholder.94092.edu. Printing is for personal, private use only. No part of this book may be reproduced or transmitted without publisher's prior permission. Violators will be prosecuted.

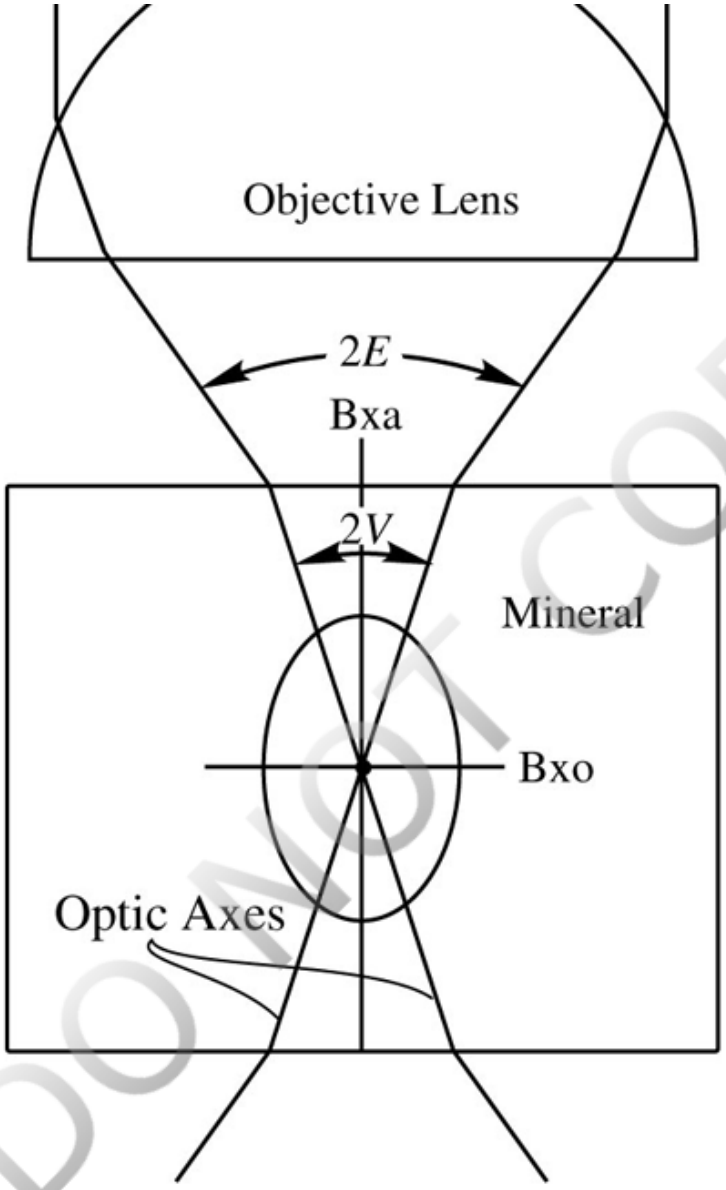

FIGURE 7.50 2*E* versus 2*V*. The angle between the optic axes is 2*V* within the mineral. Light following the optic axes is refracted as it exits the mineral to form the apparent optic angle 2*E*. The position of the melatopes in an acute bisectrix interference figure depends on the value of 2*E*. Back to text

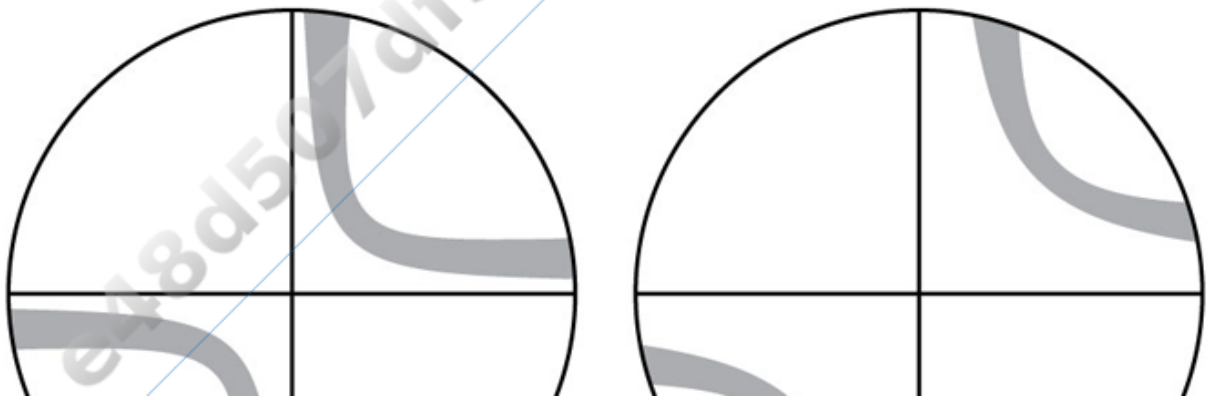

DO NOT COPY

Printed by: e48d507df5d1141@placeholder.94092.edu. Printing is for personal, private use only. No part of this book may be reproduced or transmitted without publisher's prior permission. Violators will be prosecuted.

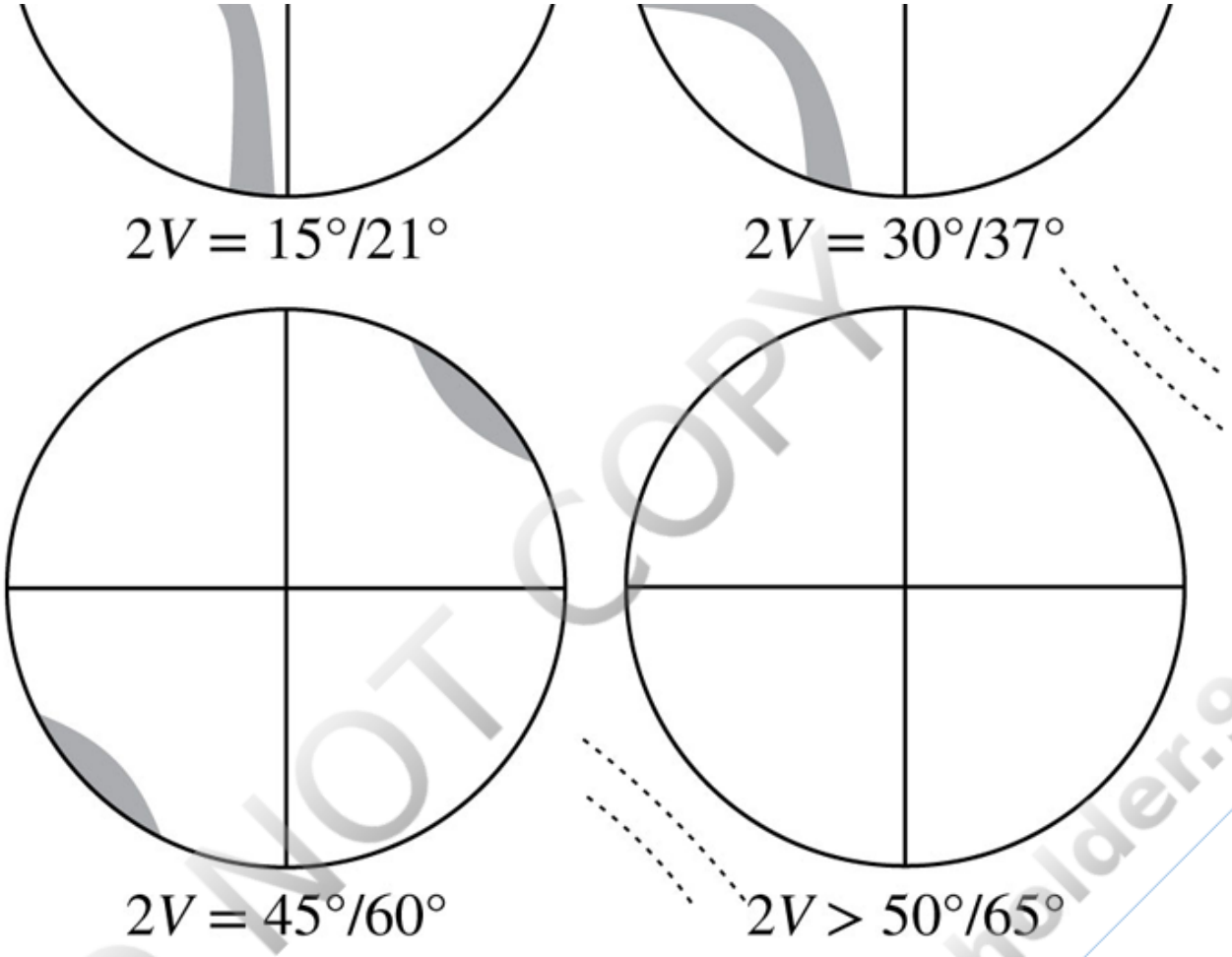

FIGURE 7.51 Rapid estimation of $2V$ based on separation of isogyres in acute bisectrix interference figures. The positions of the isogyres are shown for $n_\beta = 1.60$. Two values of $2V$ are given, the first for objective lenses with NA = 0.65, the second for NA = 0.85. Back to text

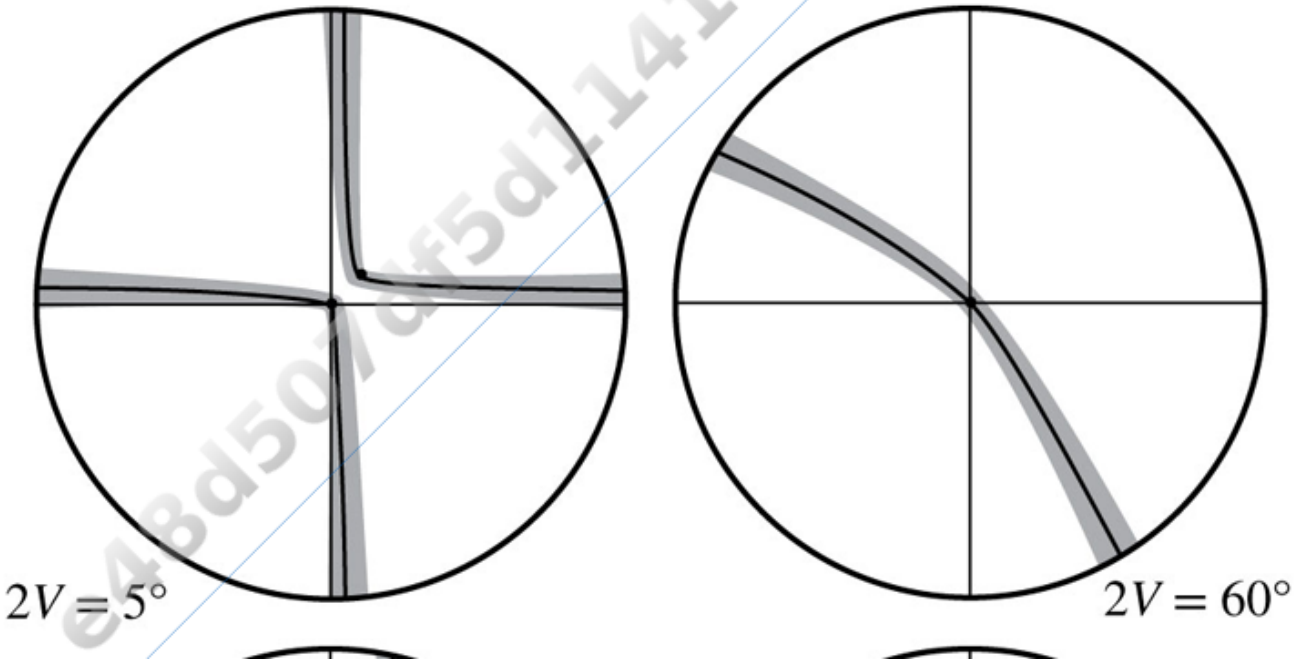

DO NOT COPY
e48d507df5d1141@placeholder.9409

Printed by: e48d507df5d1141@placeholder.94092.edu. Printing is for personal, private use only. No part of this book may be reproduced or transmitted without publisher's prior permission. Violators will be prosecuted.

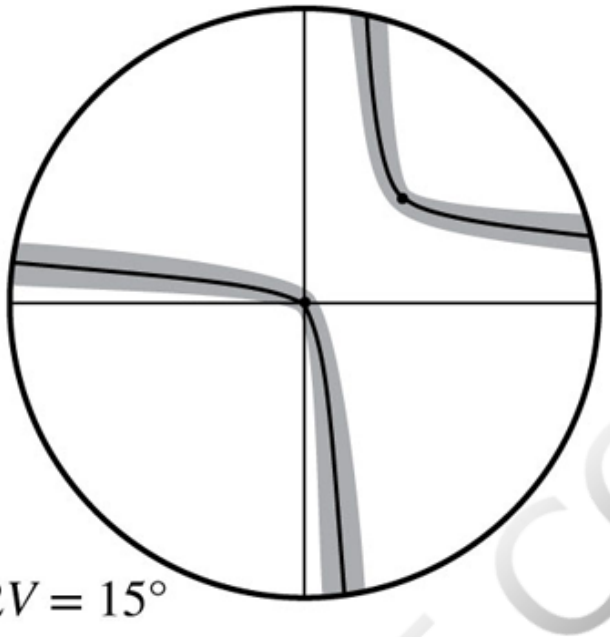

$2V = 15°$

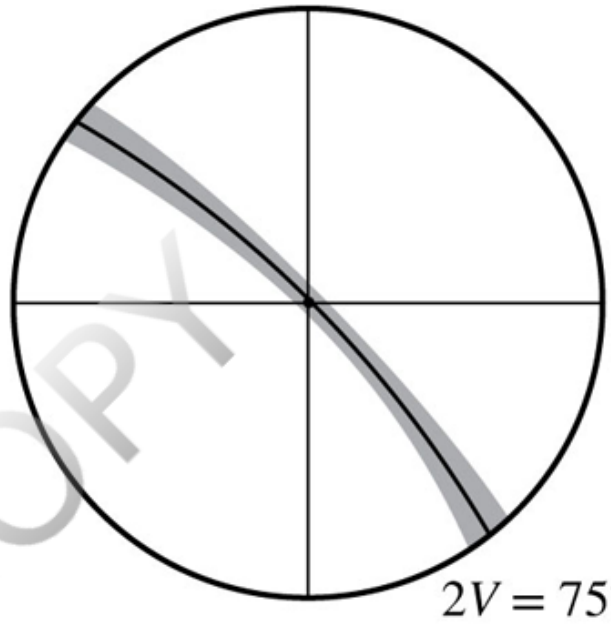

$2V = 75°$

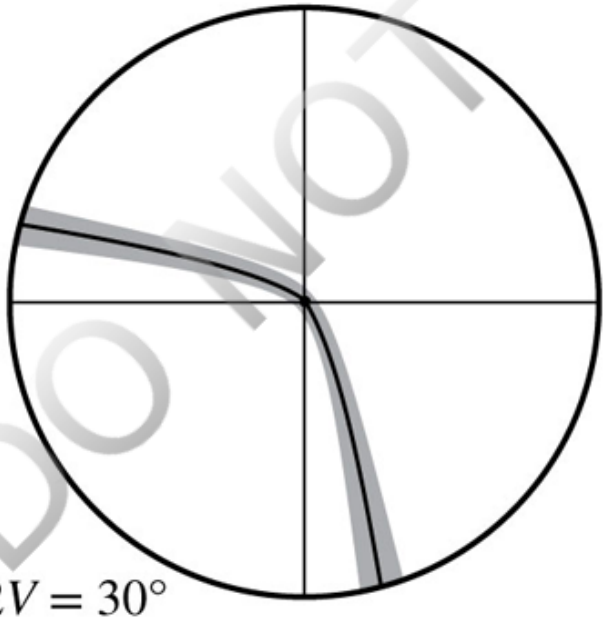

$2V = 30°$

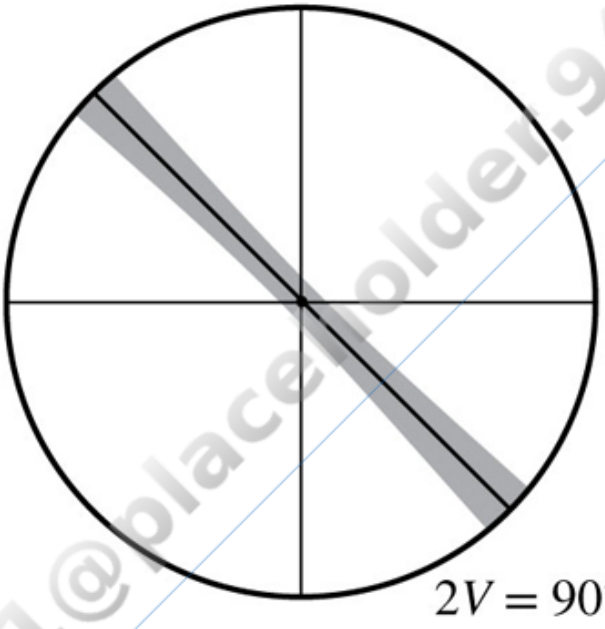

$2V = 90°$

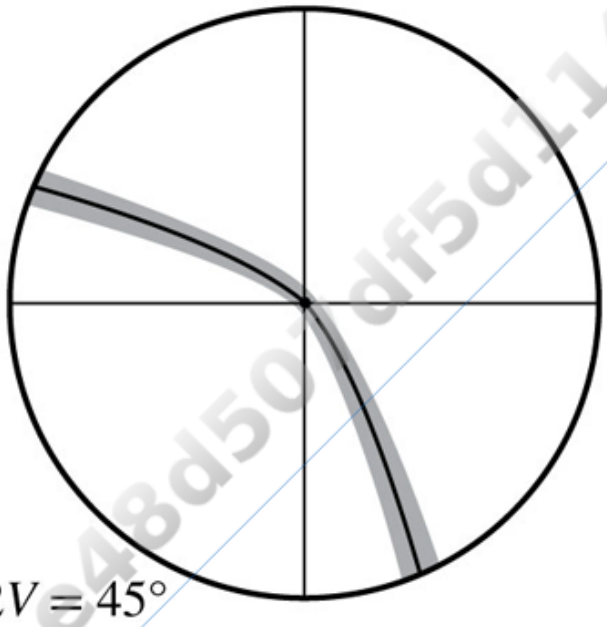

$2V = 45°$

DO NOT COPY
e48d507df5d1141@placeholder.9409

Printed by: e48d507df5d1141@placeholder.94092.edu. Printing is for personal, private use only. No part of this book may be reproduced or transmitted without publisher's prior permission. Violators will be prosecuted.

FIGURE 7.52 Isogyre curvature in biaxial optic axis interference figures with the optic plane aligned NE–SW. The geometry shown here assumes $n_\beta = 1.60$ and NA = 0.65 but will work for $NA_1 = 0.85$ and other values of n_β with little loss of accuracy. Compare Figure 7.51. Back to text

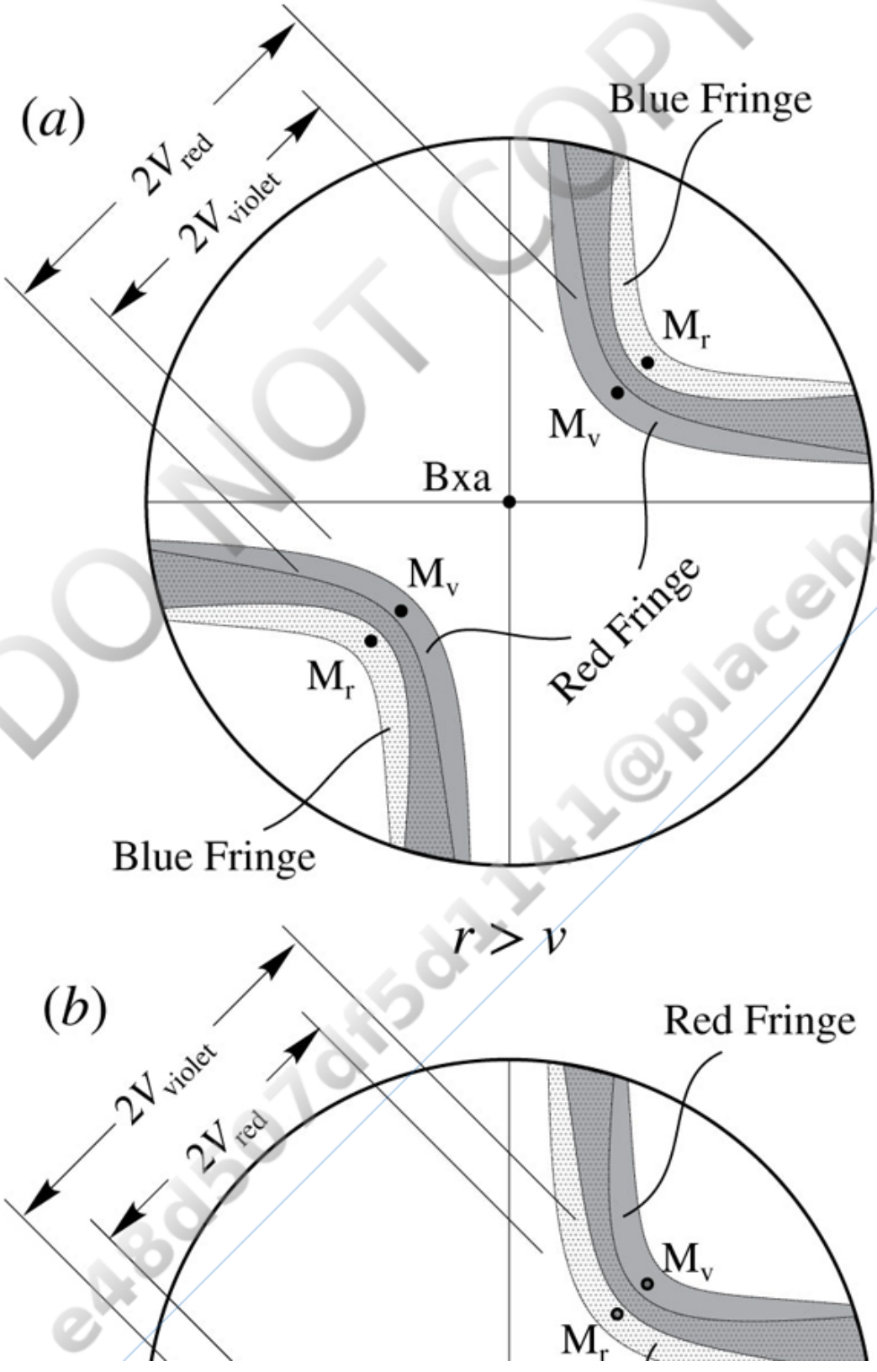

DO NOT COPY
e48d507df5d1141@placeholder.9409

Printed by: e48d507df5d1141@placeholder.94092.edu. Printing is for personal, private use only. No part of this book may be reproduced or transmitted without publisher's prior permission. Violators will be prosecuted.

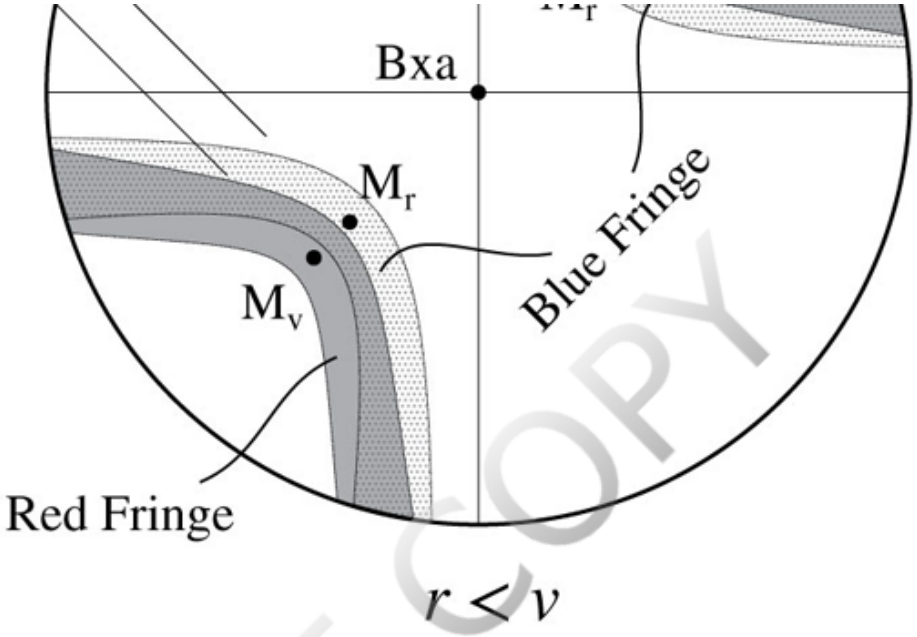

FIGURE 7.53 Optic axis dispersion: M_v and M_r are the melatopes for violet and red light, respectively. The isogyre for violet light (shaded) marks the area where no violet light comes through. The isogyre for red light (stippled) marks the area where no red light comes through. Red fringes are therefore produced where blue and violet light are lacking, and the blue fringe is produced where red light is lacking. The areas of overlap represent the normal isogyres. (*a*) $2V$ for red light is greater than $2V$ for violet light ($r > v$). (*b*) $2V$ for red light is less than $2V$ for violet light ($r < v$). The widths of the colored fringes are exaggerated here. Back to text

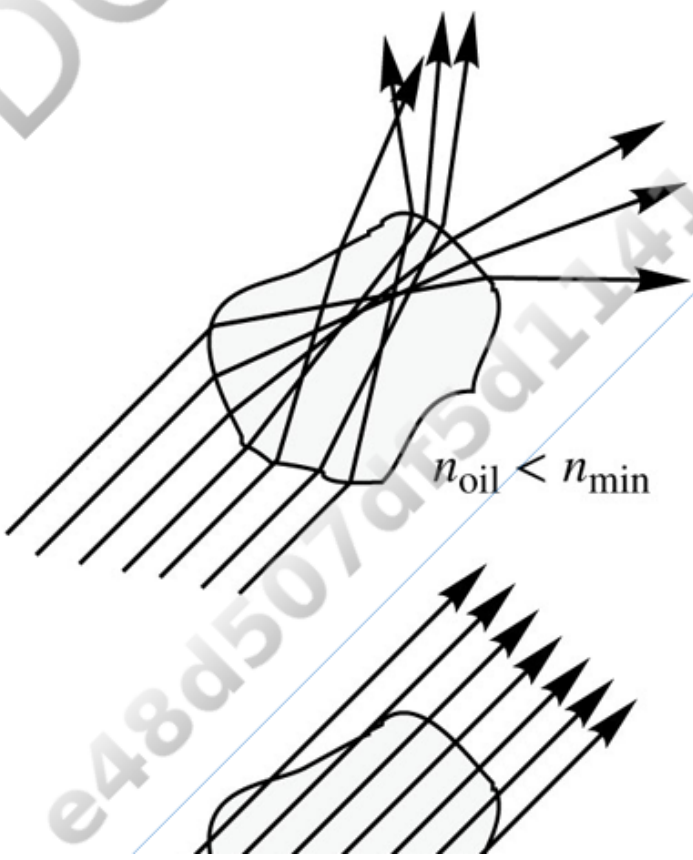

DO NOT COPY
e48d507df5d1141@placeholder.9409

Printed by: e48d507df5d1141@placeholder.94092.edu. Printing is for personal, private use only. No part of this book may be reproduced or transmitted without publisher's prior permission. Violators will be prosecuted.

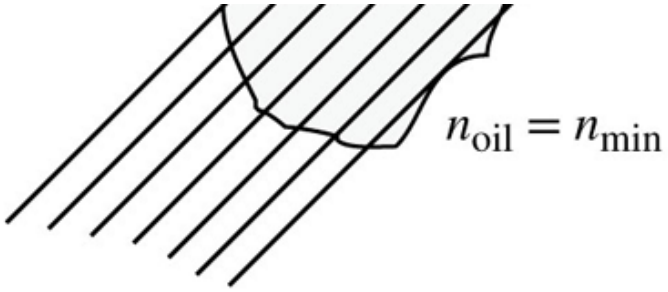

FIGURE 7.54 Formation of relief in grain mount. If indices of refraction of oil and mineral are different, light is refracted at the mineral–oil boundary and the grain stands out. If the indices of refraction are the same, light passes the mineral–oil boundary without refraction and the mineral grain does not stand out. Back to text

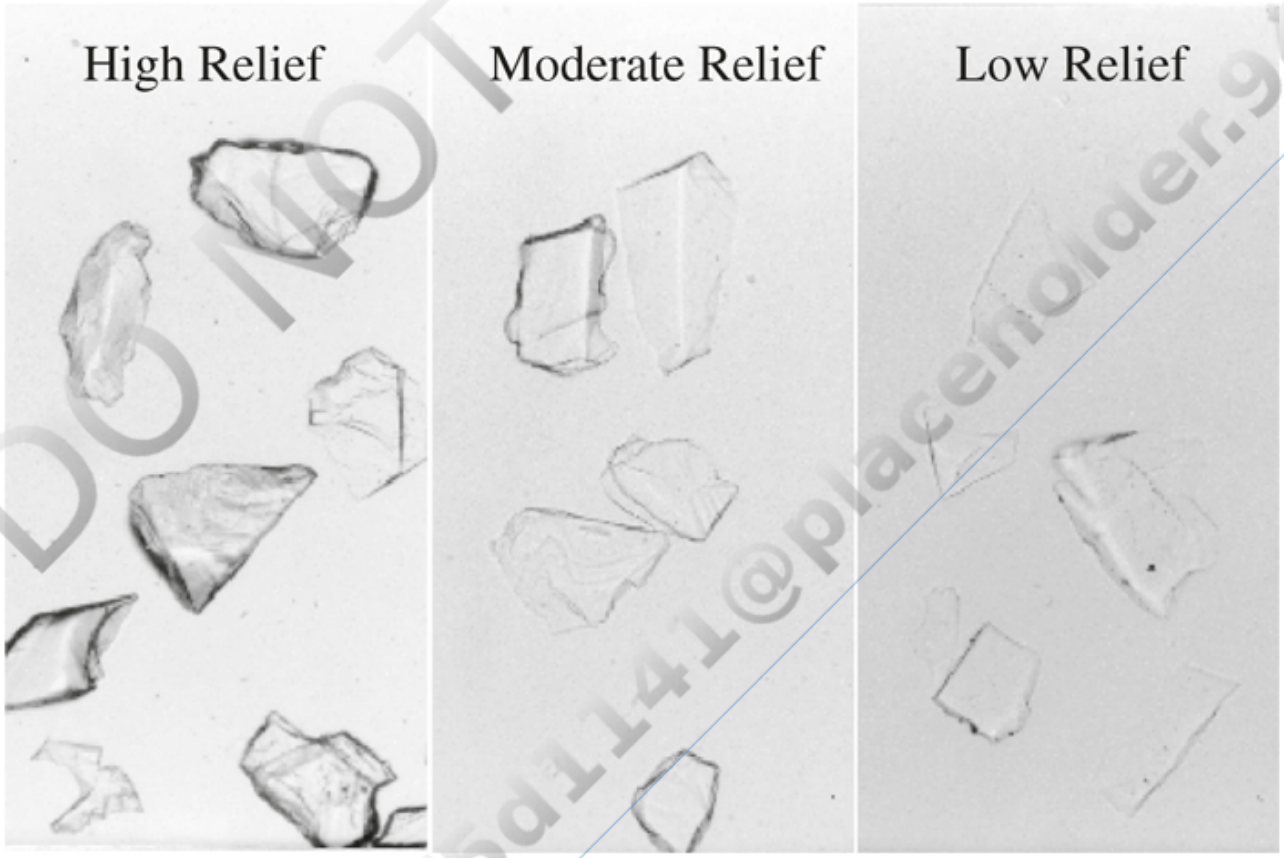

FIGURE 7.55 High, moderate, and low relief. Back to text

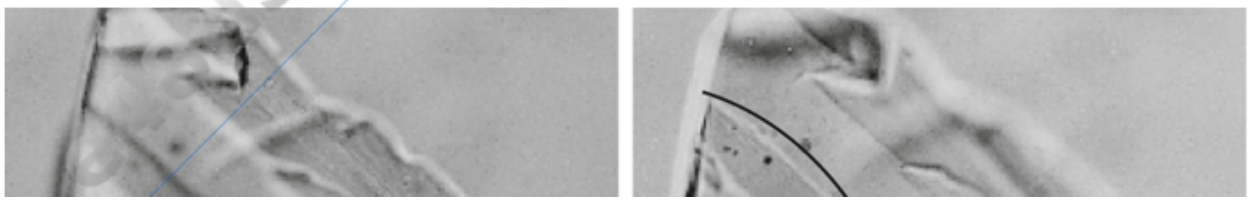

DO NOT COPY
e48d507df5d1141@placeholder.9409

Printed by: e48d507df5d1141@placeholder.94092.edu. Printing is for personal, private use only. No part of this book may be reproduced or transmitted without publisher's prior permission. Violators will be prosecuted.

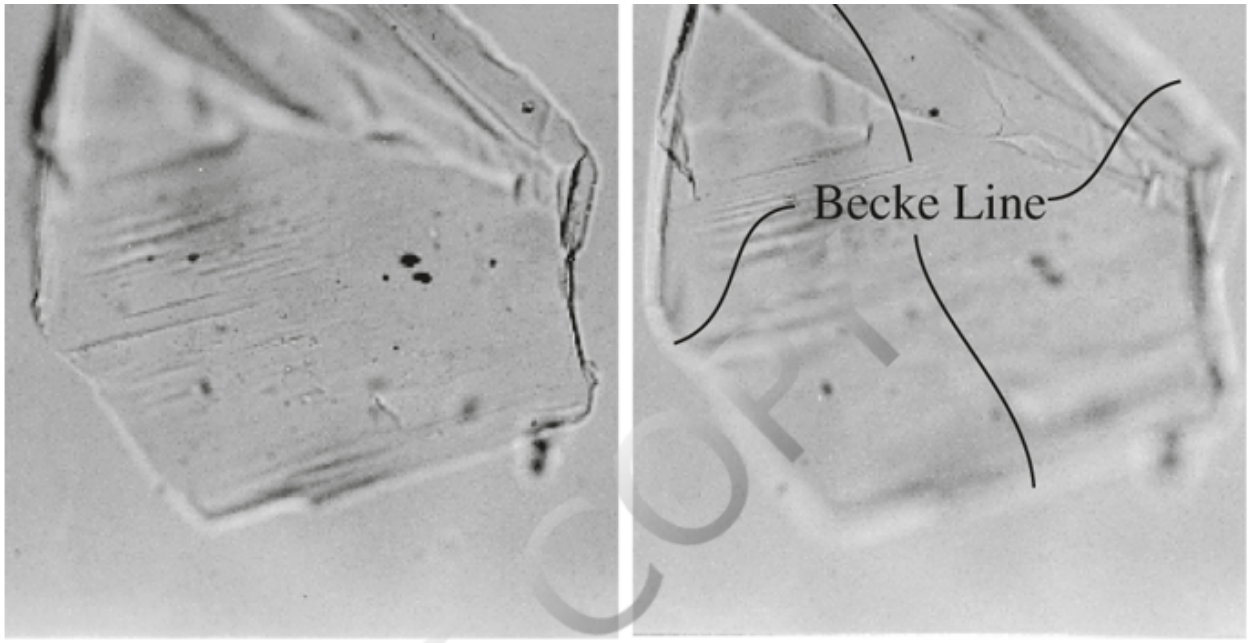

FIGURE 7.56 The Becke line. (*Left*) Microscope focused on a grain of fluorite that shows moderate relief. (*Right*) Microscope stage lowered. The Becke line is a thin band of light that moves into the medium with the higher index of refraction, which in this case is the immersion oil. Back to text

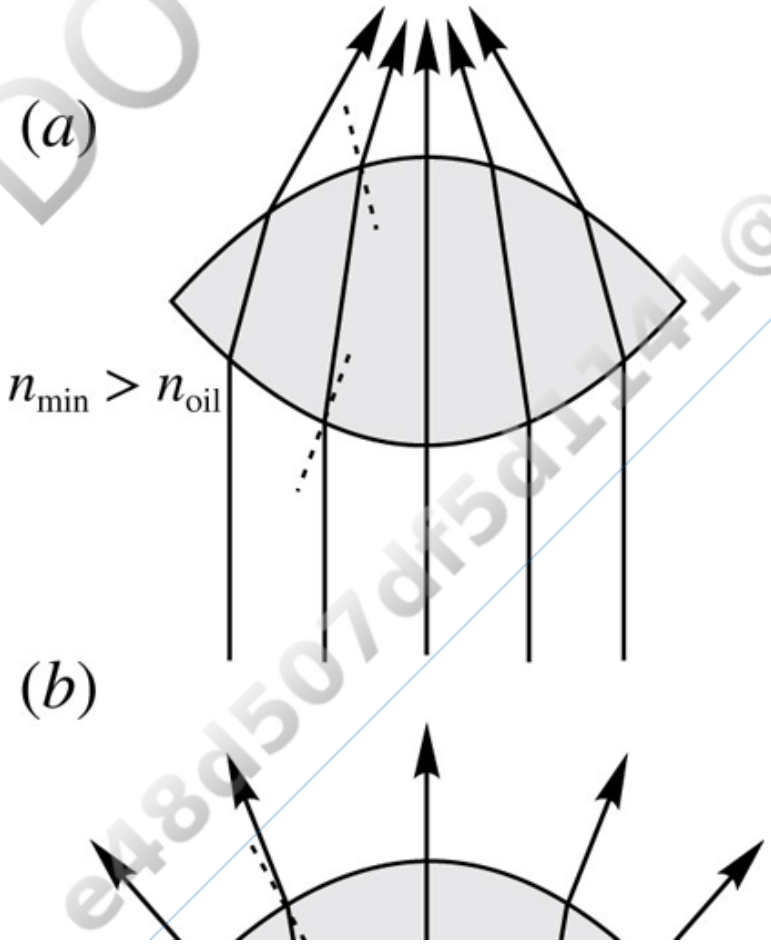

DO NOT COPY
e48d507df5d1141@placeholder.9409

Printed by: e48d507df5d1141@placeholder.94092.edu. Printing is for personal, private use only. No part of this book may be reproduced or transmitted without publisher's prior permission. Violators will be prosecuted.

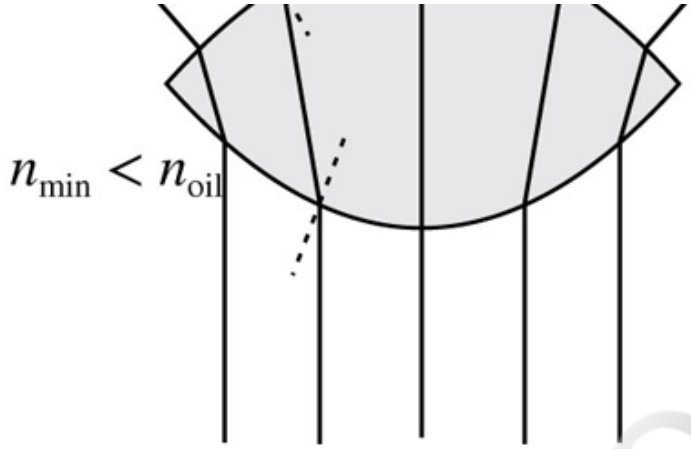

FIGURE 7.57 Formation of the Becke line by the lens effect. Light is refracted toward the normal on passing into a material with higher index of refraction and away from the normal when passing into a material with lower index of refraction as predicted by Snell's law (Equation 7.5). (*a*) $n_{mineral} > n_{oil}$. The grain acts as a crude converging lens, concentrating light above the mineral. (*b*) $n_{mineral} < n_{oil}$. The grain acts as a crude diverging lens, refracting light away from the center of the grain.
Back to text

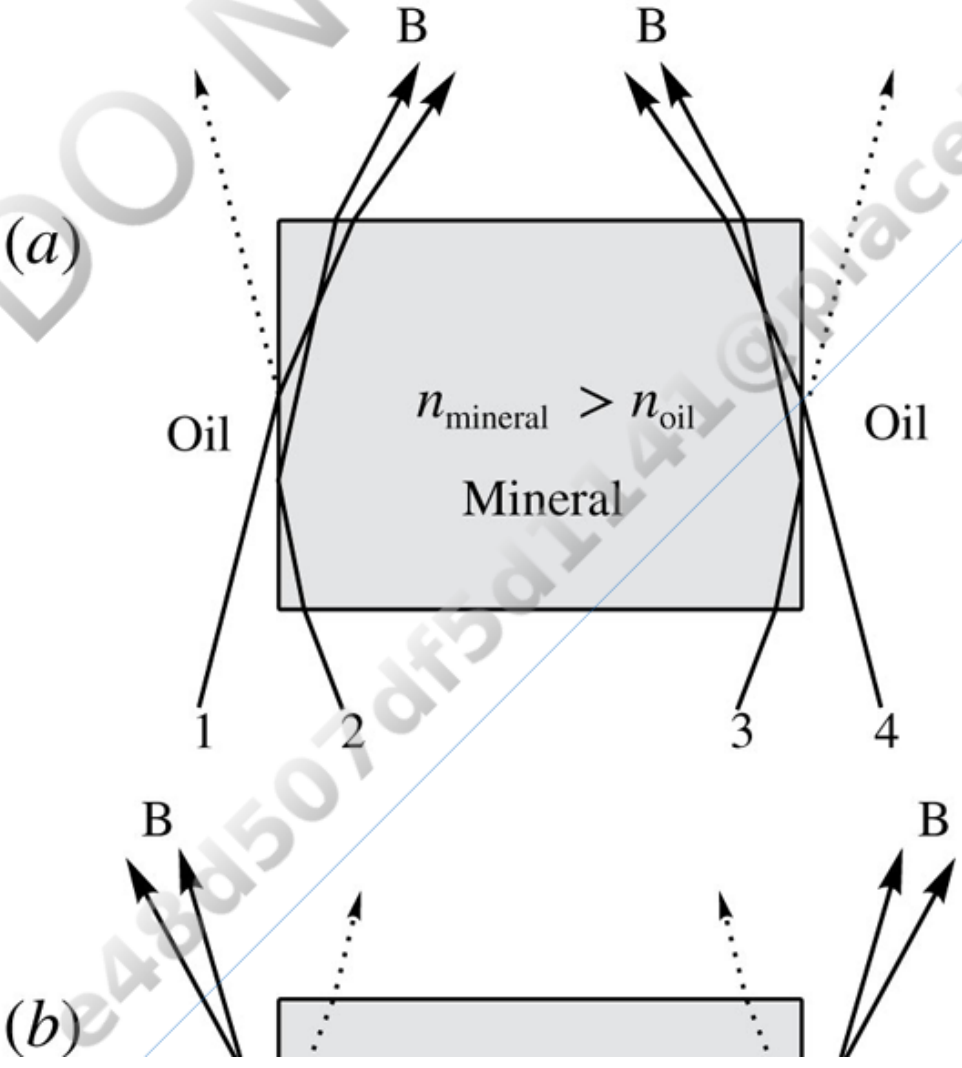

DO NOT COPY
e48d507df5d1141@placeholder.9409

Printed by: e48d507df5d1141@placeholder.94092.edu. Printing is for personal, private use only. No part of this book may be reproduced or transmitted without publisher's prior permission. Violators will be prosecuted.

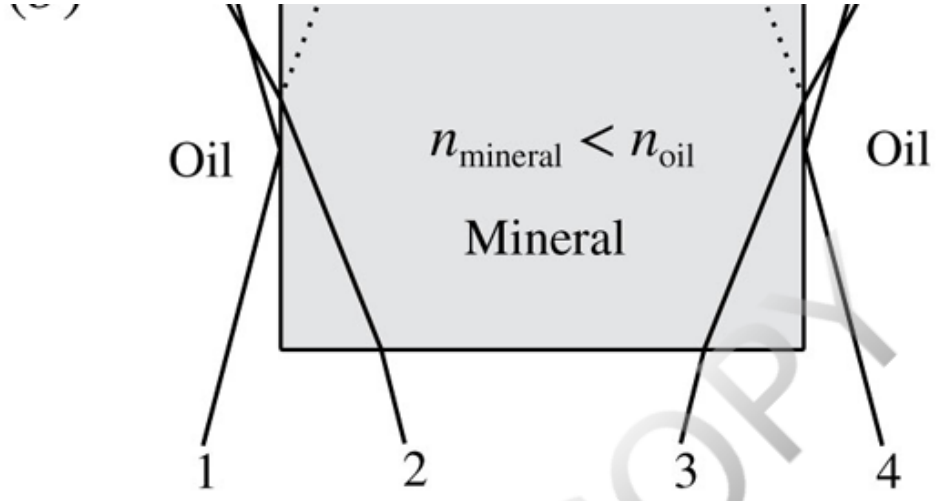

FIGURE 7.58 Formation of the Becke line by internal reflection at vertical grain boundaries. The Becke line (B) consists of a concentration of light above the mineral–oil boundary in the material with the higher index of refraction. (*a*) $n_{minerals} > n_{oil}$. Some of rays 1 and 4 are reflected (dotted lines) at the vertical mineral boundary, and some are refracted into the mineral (shaded) even for shallow angles of incidence (compare Figure 7.6c). Rays 2 and 3 strike the mineral–oil interface at greater than the critical angle and are internally reflected in the mineral (compare Figure 7.7). (*b*) $n_{mineral} < n_{oil}$. Rays 1 and 4 strike the vertical mineral–oil boundary at greater than the critical angle and are totally reflected back into the oil. Some of rays 2 and 3 are refracted into the oil. Back to text

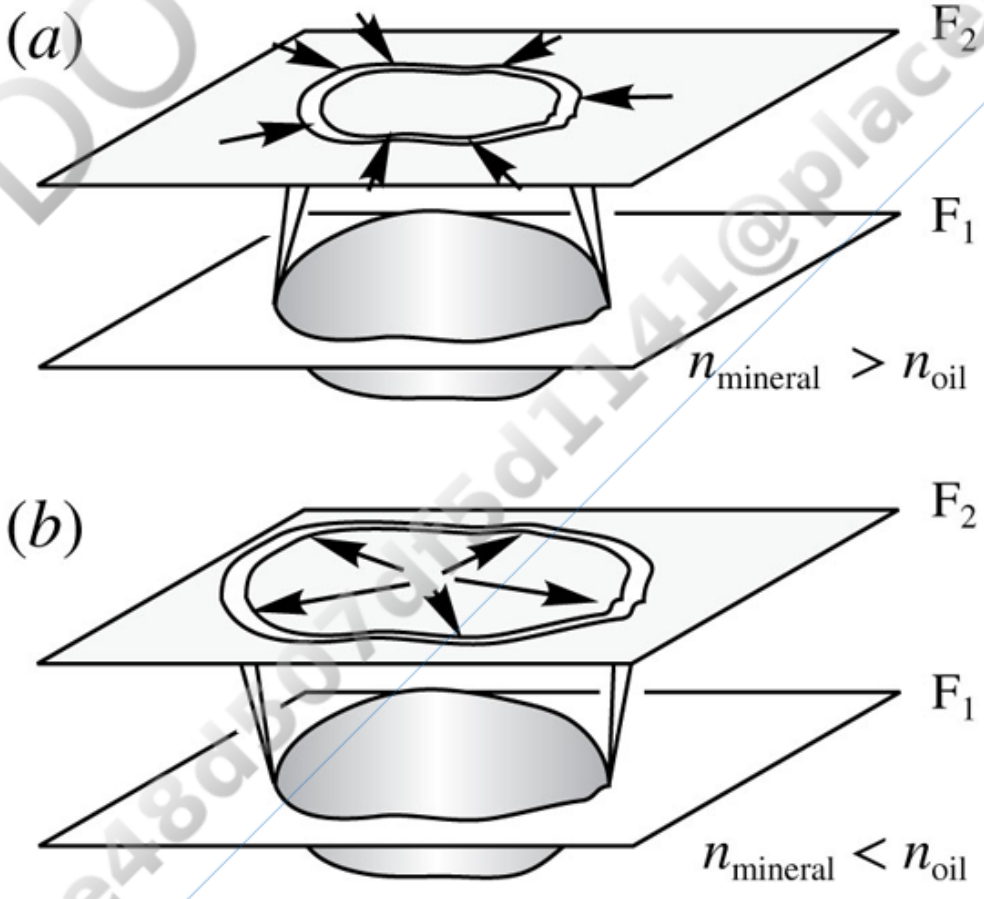

FIGURE 7.59 Movement of the Becke line as the stage is lowered. The Becke line may be

Printed by: e48d507df5d1141@placeholder.94092.edu. Printing is for personal, private use only. No part of this book may be reproduced or transmitted without publisher's prior permission. Violators will be prosecuted.

FIGURE 7.59 Movement of the Becke line as the stage is lowered. The Becke line may be considered to consist of a cone of light that extends upward from the mineral grain. If $n_{mineral} > n_{oil}$, the cone converges upward, and if $n_{mineral} < n_{oil}$, the cone diverges upward. If the stage is lowered, the plane of focus goes from F_1 to F_2 and the Becke line appears to move toward the material with the higher index of refraction. (*a*) $n_{mineral} > n_{oil}$. (*b*) $n_{mineral} < n_{oil}$. Back to text

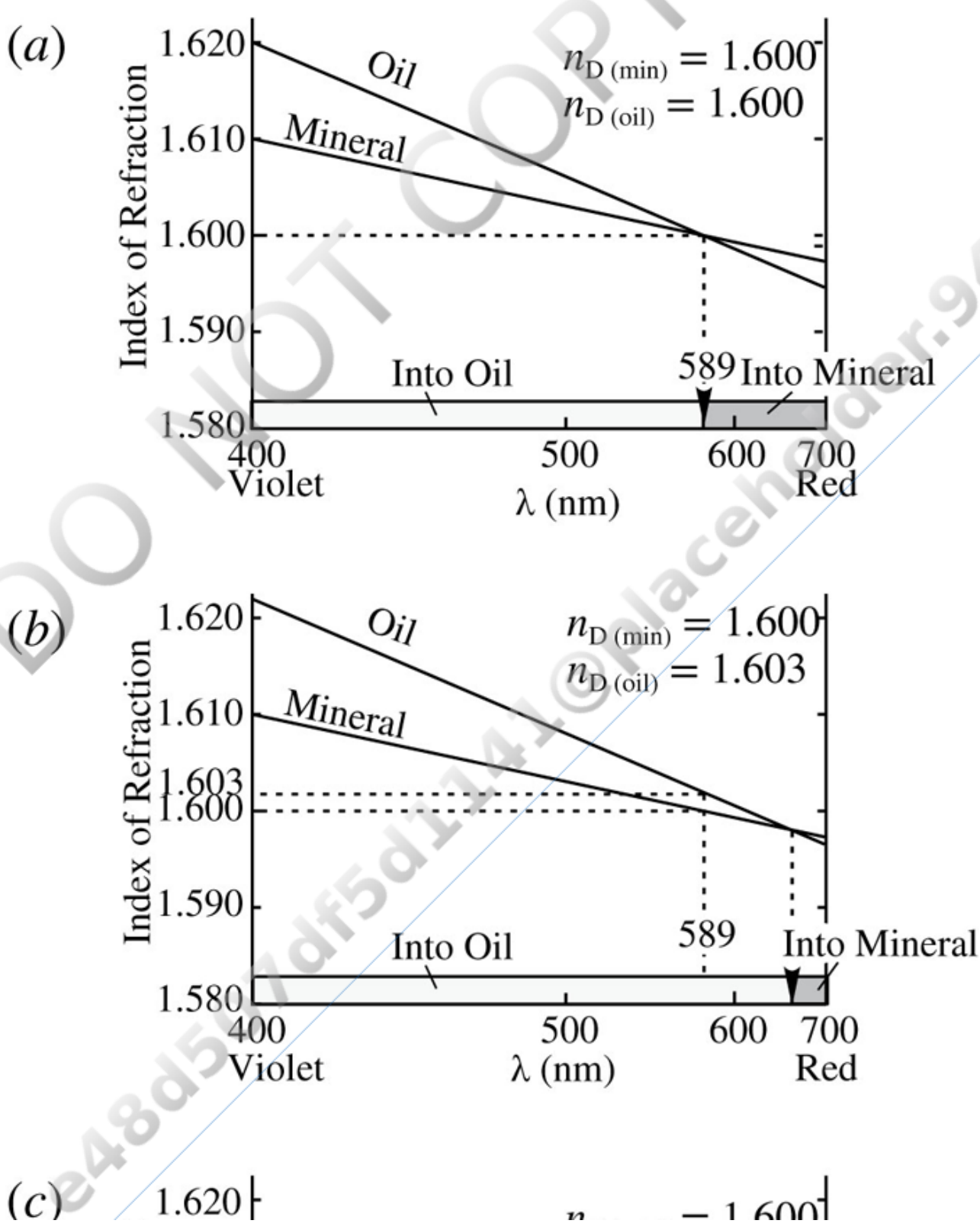

DO NOT COPY

Printed by: e48d507df5d1141@placeholder.94092.edu. Printing is for personal, private use only. No part of this book may be reproduced or transmitted without publisher's prior permission. Violators will be prosecuted.

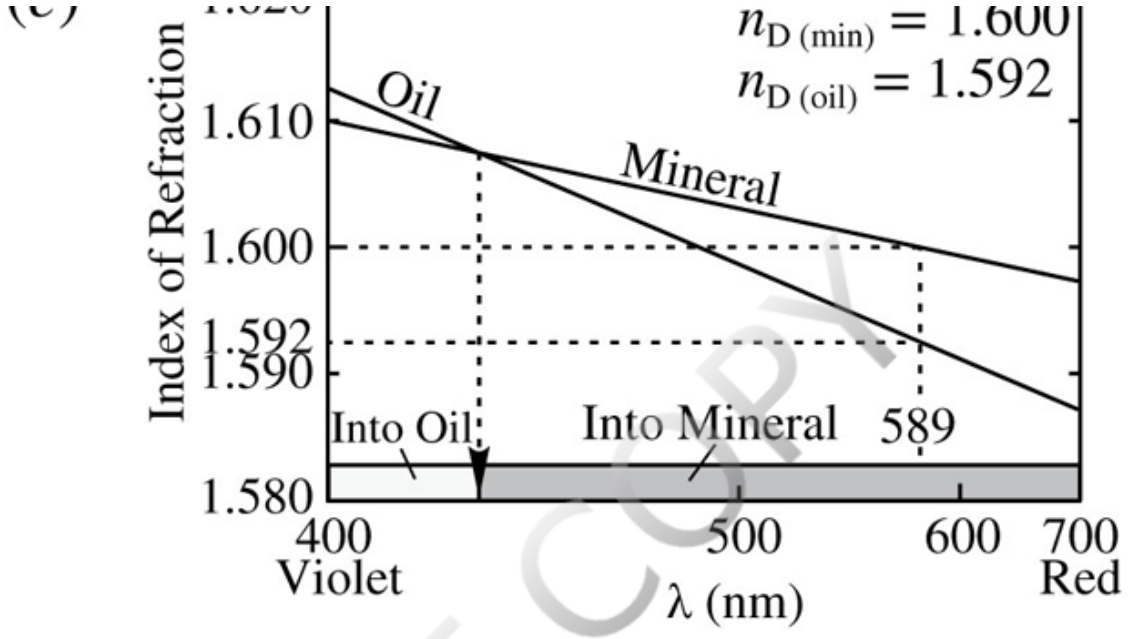

FIGURE 7.60 Formation of colored Becke lines. Immersion oil typically has higher dispersion than minerals. (*a*) Indices of refraction of oil and mineral matched at light whose wavelength is 589 nm. The mineral has higher index of refraction for longer wavelengths, so these wavelengths, perceived as yellowish orange, go into the mineral as the stage is lowered. The immersion oil has higher index of refraction for shorter wavelengths, and this bluish light forms a Becke line that goes into the oil. (*b*) Indices of oil and mineral are matched near the red end of the spectrum. The mineral has higher index of refraction for red light, and the oil for all other wavelengths, perceived as bluish white. When the stage is lowered, a red Becke line moves into the mineral, and bluish white into the oil. (*c*) Indices of oil and mineral match near the blue end of the spectrum. The oil has higher index of refraction for blue and violet light, the mineral for the rest of the spectrum. When the stage is lowered, a blue-violet Becke line moves into the oil, and yellowish white into the mineral. Back to text

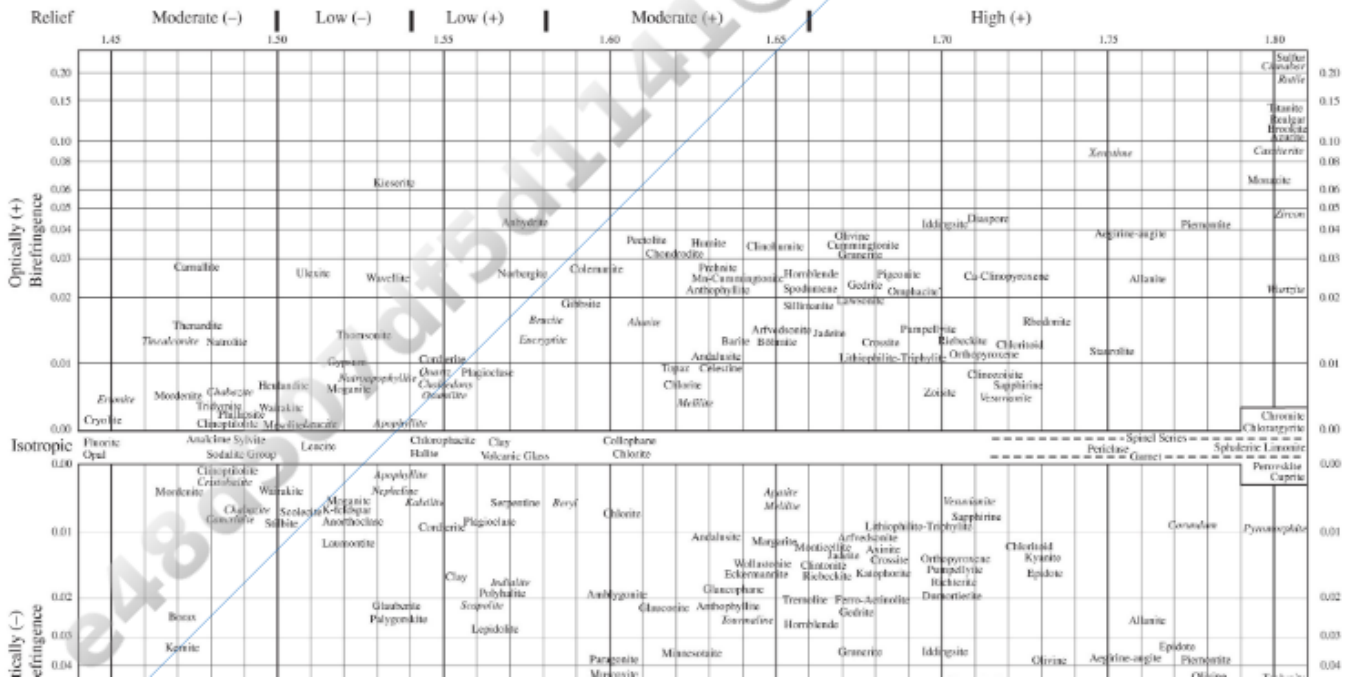

Printed by: e48d507df5d1141@placeholder.94092.edu. Printing is for personal, private use only. No part of this book may be reproduced or transmitted without publisher's prior permission. Violators will be prosecuted.

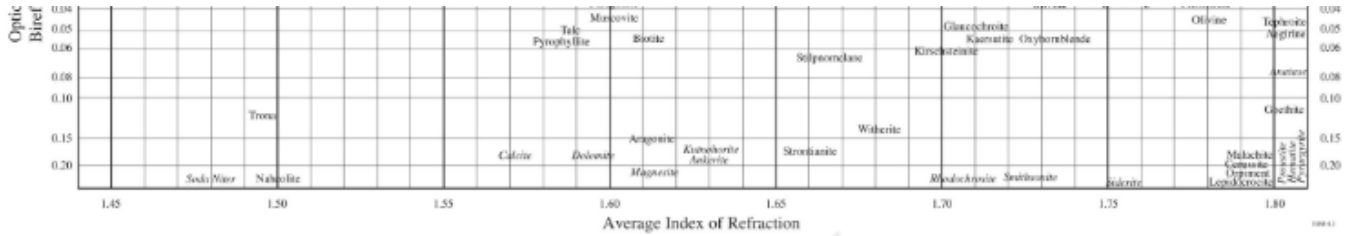

PLATE 2 Birefringence vs. Average Index of Refraction. Back to text

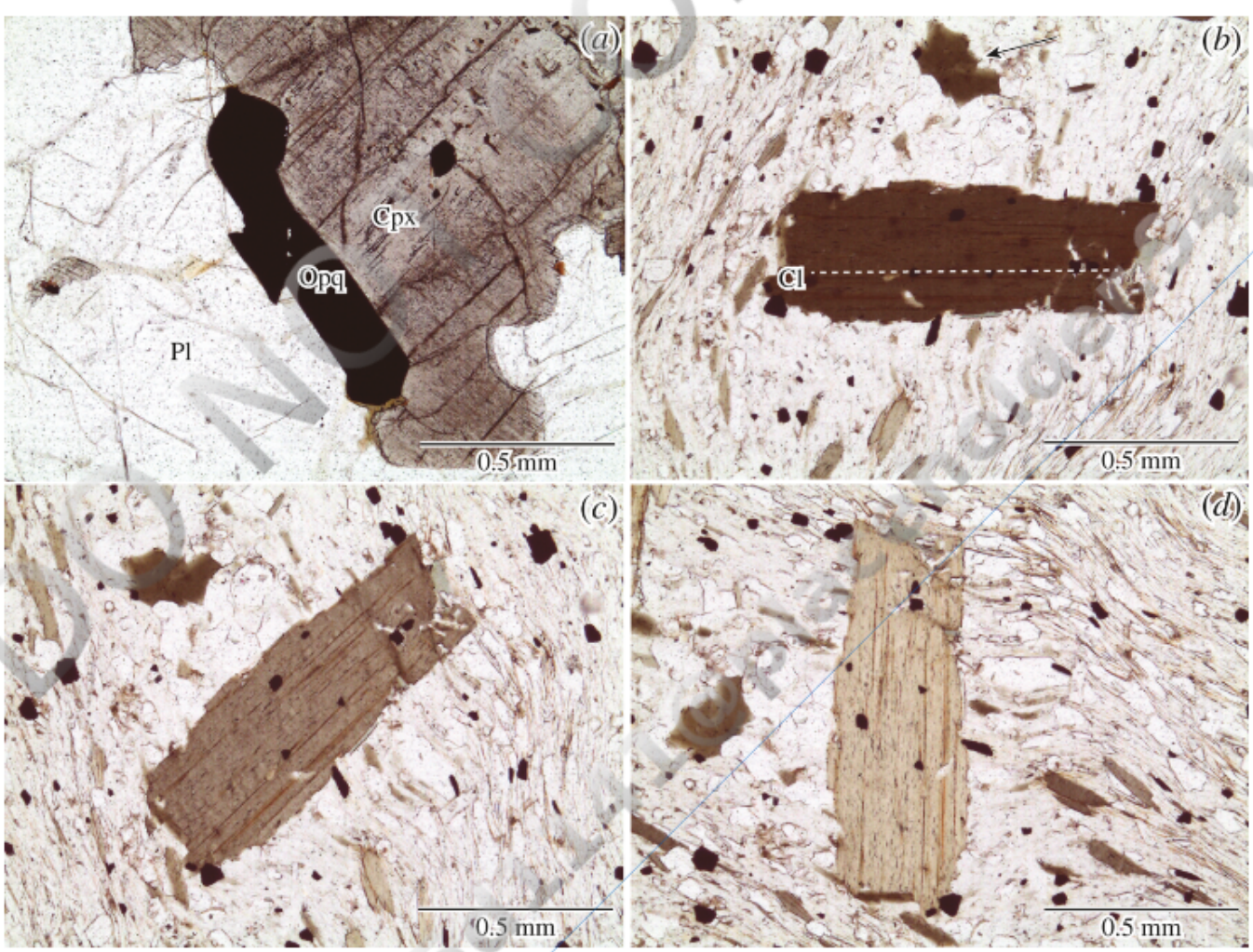

FIGURE 7.61 Photomicrographs highlighting various optical properties and features seen in thin section. (*a*) Mineral color (plane-polarized light). Plagioclase (Pl) is colorless, clinopyroxene (cpx) is colored, and the mineral that transmits no light (appears black) is said to be opaque (Opq). (*b*) (*c*) (*d*) Pleochroism in biotite (plane-polarized light). For most petrographic microscopes, if biotite cleavage (Cl) is horizontal, biotite displays a dark color; during a 90° rotation the color changes to a light version of the dark color. Some pleochroic minerals can change to a different color entirely with rotation and do not just cycle between light and dark versions of the same color. Arrow marks biotite grain viewed nearly down the *c* axis as indicated by no visible cleavage. This grain does not show pleochroism, emphasizing how optical properties vary with grain orientation. Back to text

Printed by: e48d507df5d1141@placeholder.94092.edu. Printing is for personal, private use only. No part of this book may be reproduced or transmitted without publisher's prior permission. Violators will be prosecuted.

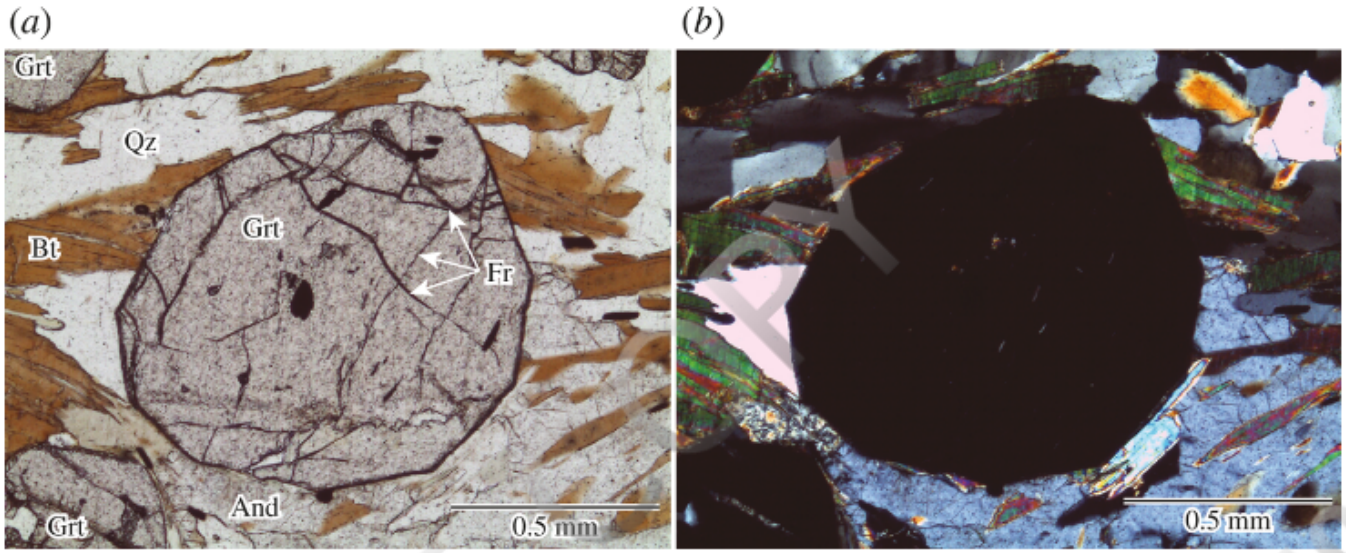

FIGURE 7.62 Relief and isotropic vs. anisotropic optical properties. (*a*) Plane-polarized light. Garnet (Grt) displays high relief, emphasized by its dark euhedral grain boundaries and dark fractures (Fr). Andalusite (And) and biotite (Bt) are moderate relief, and quartz (Qz) is low relief. (*b*) Cross-polarized light of the same area shown in (*a*). Garnet is isotropic, so it is black between crossed polarizers, no matter the orientation. Andalusite, biotite, and quartz all display interference colors.
Back to text

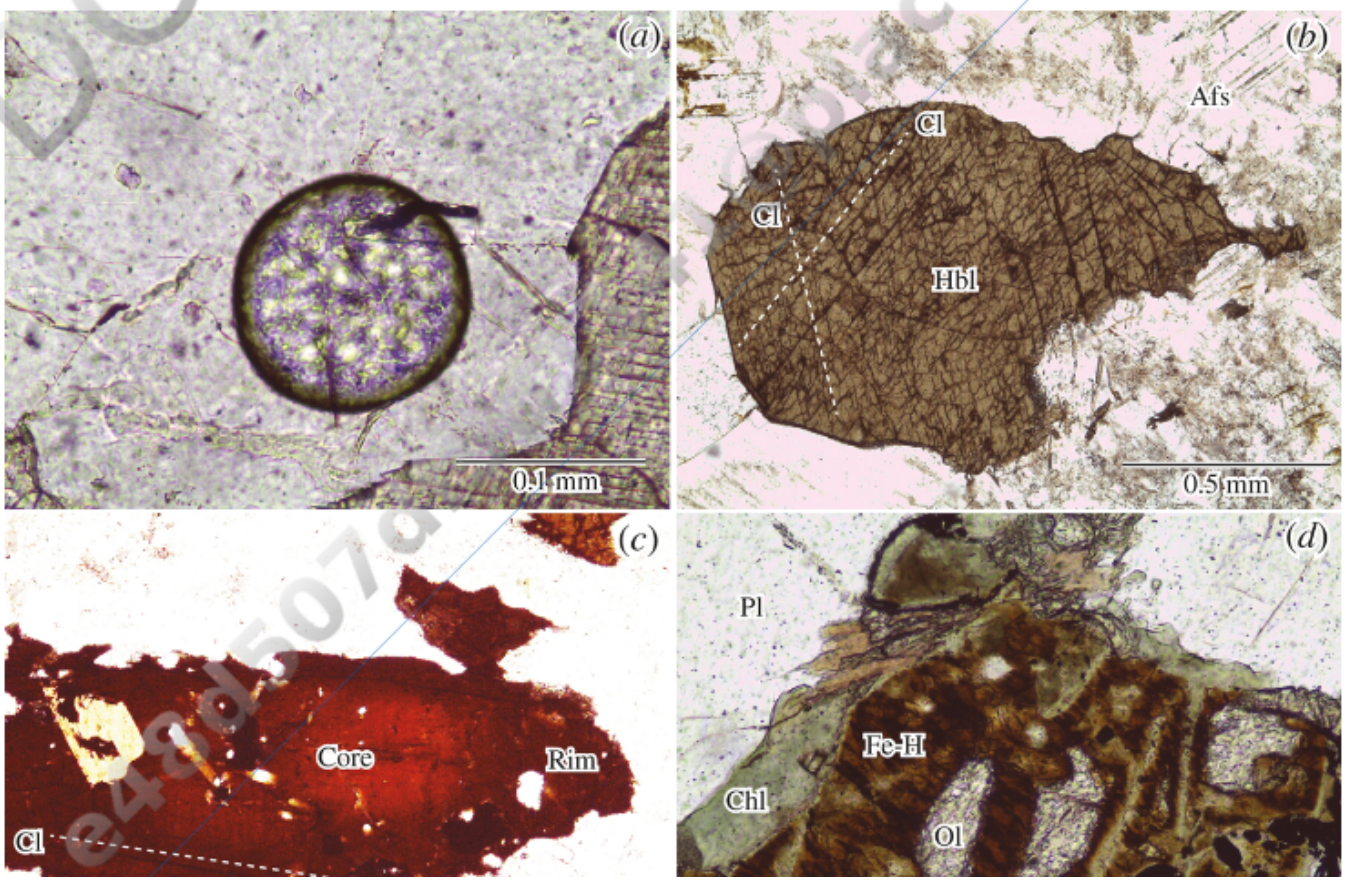

Printed by: e48d507df5d1141@placeholder.94092.edu. Printing is for personal, private use only. No part of this book may be reproduced or transmitted without publisher's prior permission. Violators will be prosecuted.

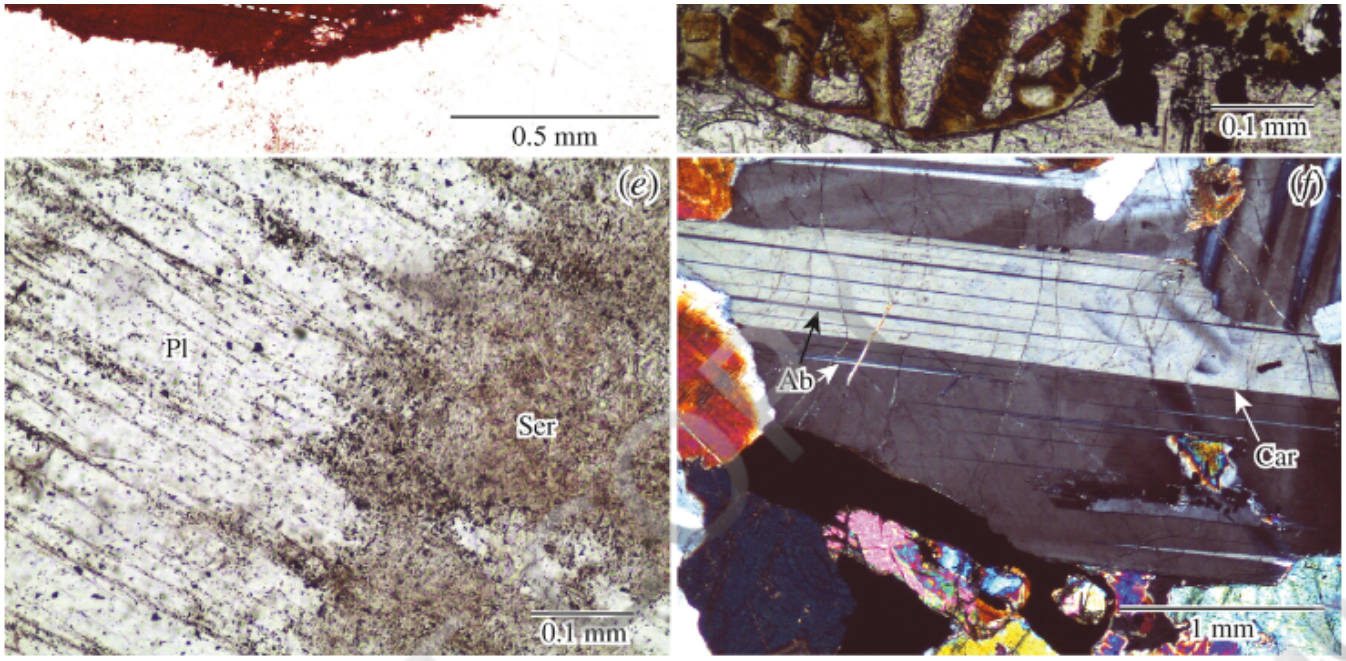

FIGURE 7.63 Photomicrographs highlighting various optical properties and features seen in thin section. (*a*) Circular, high-relief air bubble in thin section epoxy (plane-polarized light). (*b*) High-relief hornblende (Hbl) grain surrounded by alkali feldspar (Afs). The view is nearly down the *c* axis of the hornblende grain, so the angle between the two cleavages (Cl) is close to the true 56° and 124° (plane-polarized light). Compare with (*c*). (*c*) The colored hornblende grain has its *c* axis parallel to the plane of the thin section, so only one cleavage (Cl) is visible (plane-polarized light). Compare with (*b*). The hornblende is also zoned with a lighter-colored core surrounded by a darker rim. (*d*) An olivine grain (Ol) partially altered to Fe-hydroxides (Fe-H, probably goethite and/or lepidocrocite) and chlorite (Chl). Alteration pattern suggests factures helped facilitate alteration. Plagioclase (Pl) surrounds the altered olivine grain. Plane-polarized light. (*e*) Plagioclase (Pl) altered to sericite (Ser). Cleavage planes are accentuated by sericite alteration. Plane-polarized light. (*f*) Cross-polarized light image of two types of twinning in plagioclase. Carlsbad twin composition surface (Car) cuts the grain in approximately half such that at this orientation, half the grain is near extinction and the other half is not. Closely spaced composition surfaces of albite twins (Ab) produce thin zones that are either extinct or not. Back to text

DO NOT COPY e48d507df5d1141@placeholder.94092-

Printed by: e48d507df5d1141@placeholder.94092.edu. Printing is for personal, private use only. No part of this book may be reproduced or transmitted without publisher's prior permission. Violators will be prosecuted.

Chapter 8 Analytical Instrumentation and Techniques I: Crystallography

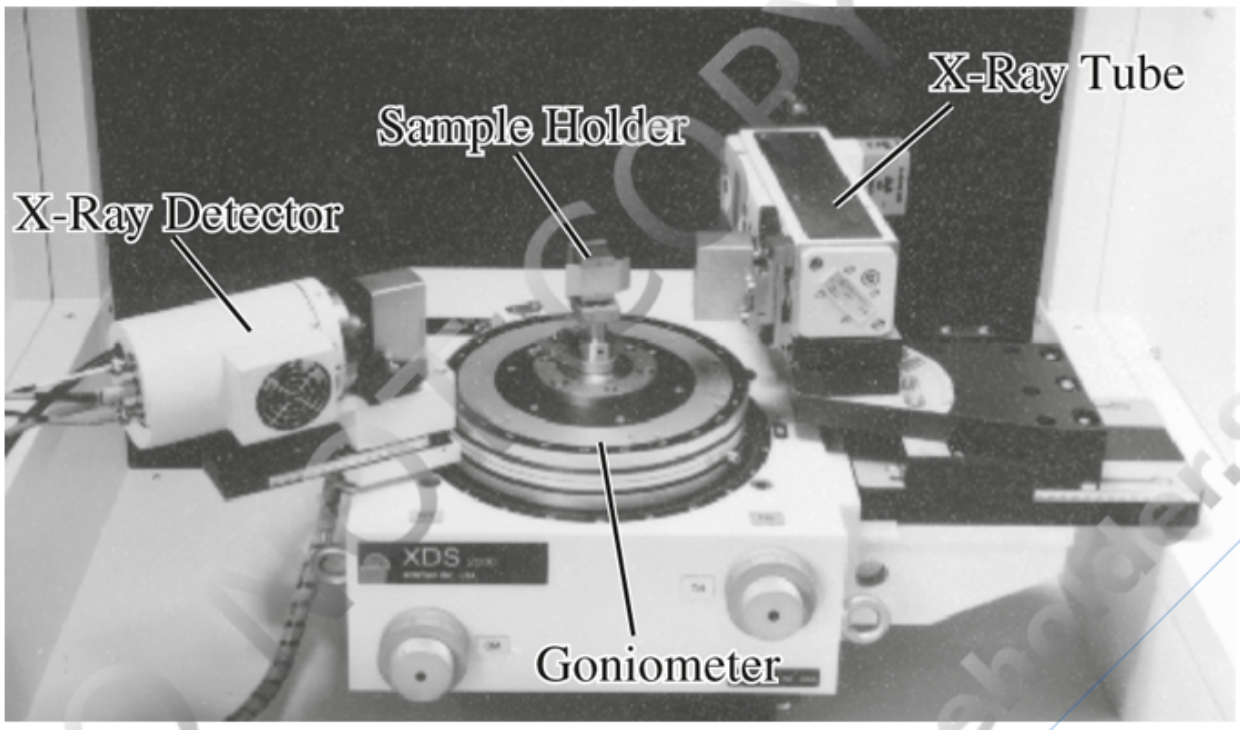

FIGURE 8.1 X-ray diffractometer. The principal components are an X-ray tube, sample holder, and an X-ray detector. X-rays are produced in the X-ray tube and directed to the sample on the holder; the X-ray detector then records the X-rays after they interacted with the sample. Sample and detector are mounted on the goniometer, which allows both to be synchronously rotated through angles θ and 2θ, respectively. Additional components include power supplies, controls, and electronics to allow the output of the detector to be recorded and displayed. Because X-rays can be very hazardous, an enclosure, shields, and other safety devices (not shown) are provided to prevent the operator from being exposed to X-rays. Photo courtesy of Scintag, Inc. Back to text

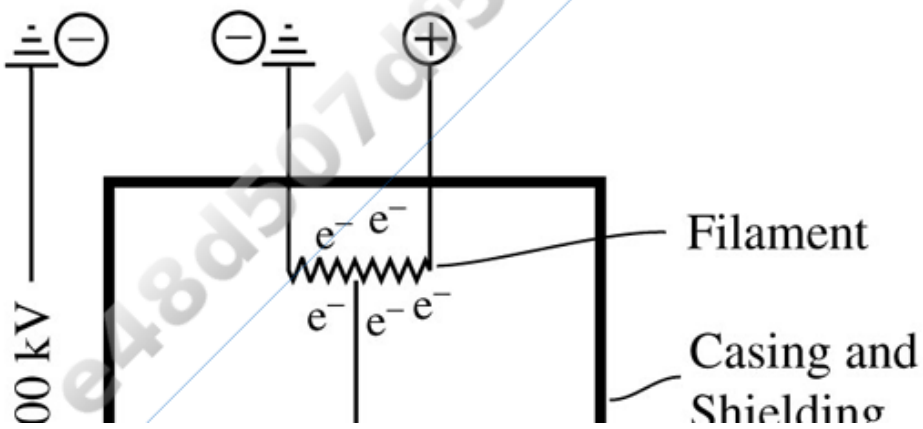

Printed by: e48d507df5d1141@placeholder.94092.edu. Printing is for personal, private use only. No part of this book may be reproduced or transmitted without publisher's prior permission. Violators will be prosecuted.

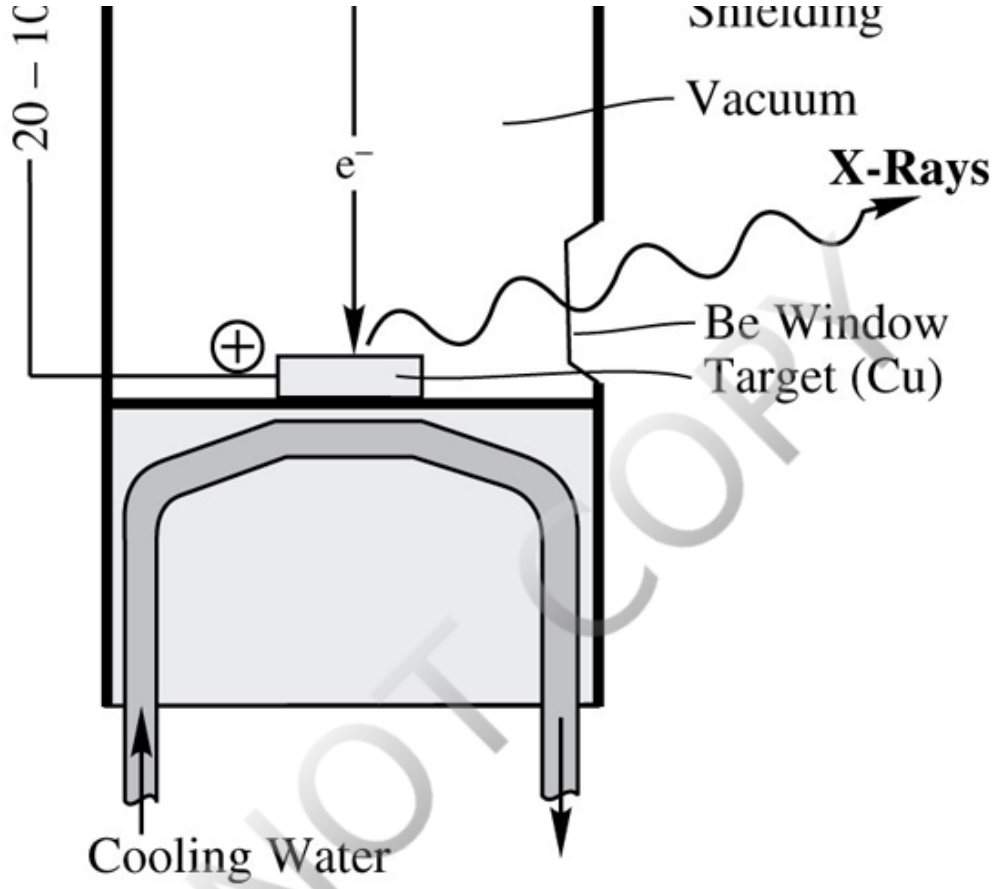

FIGURE 8.2 X-ray tube. The cathode filament is heated so that it emits electrons. A voltage of 20 to 100 kV is maintained between the filament and the target (the anode) to accelerate the electrons as a beam toward the target. When these high-energy electrons strike atoms in the target, X-rays are generated and exit through a thin beryllium window in the tube. The target is most commonly copper or molybdenum. Back to text

DO NOT COPY
e48d507df5d1141@placeholder.9409

(*a*)

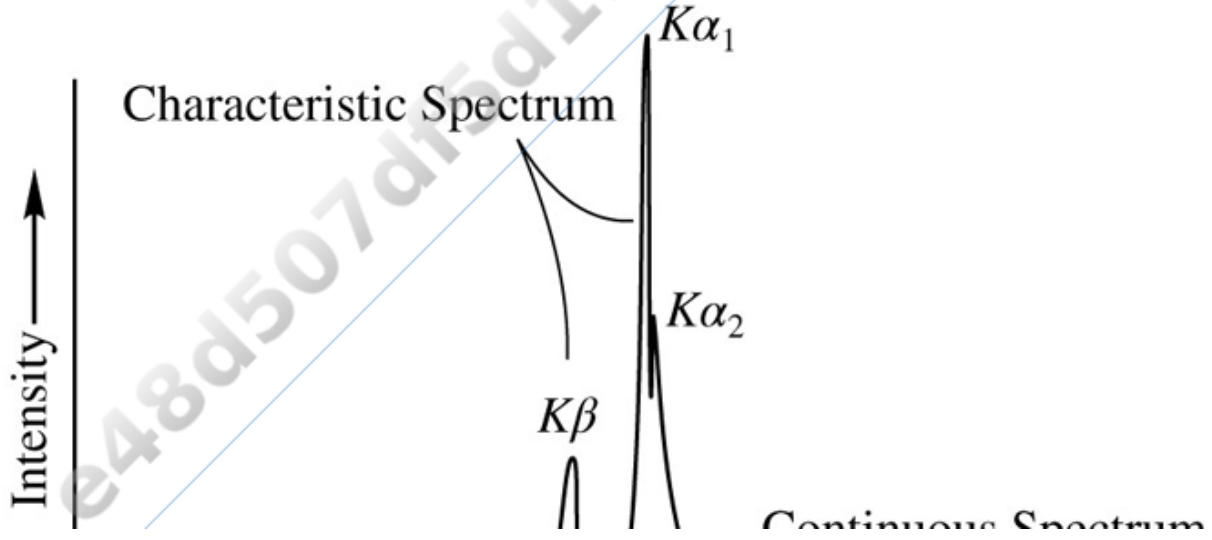

Printed by: e48d507df5d1141@placeholder.94092.edu. Printing is for personal, private use only. No part of this book may be reproduced or transmitted without publisher's prior permission. Violators will be prosecuted.

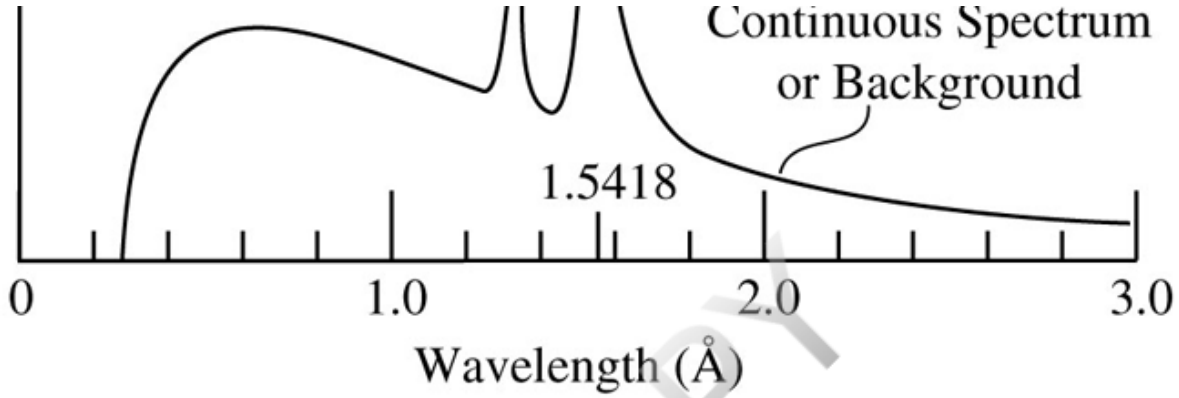

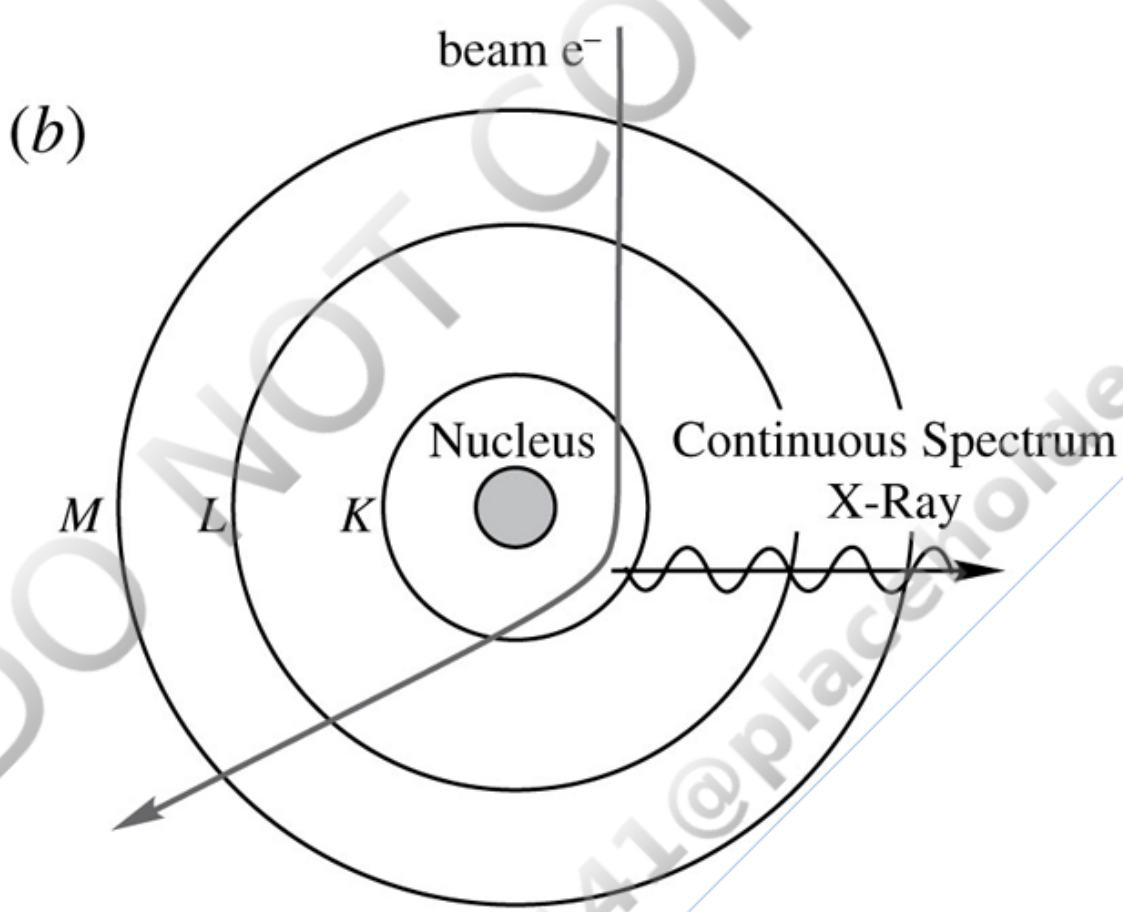

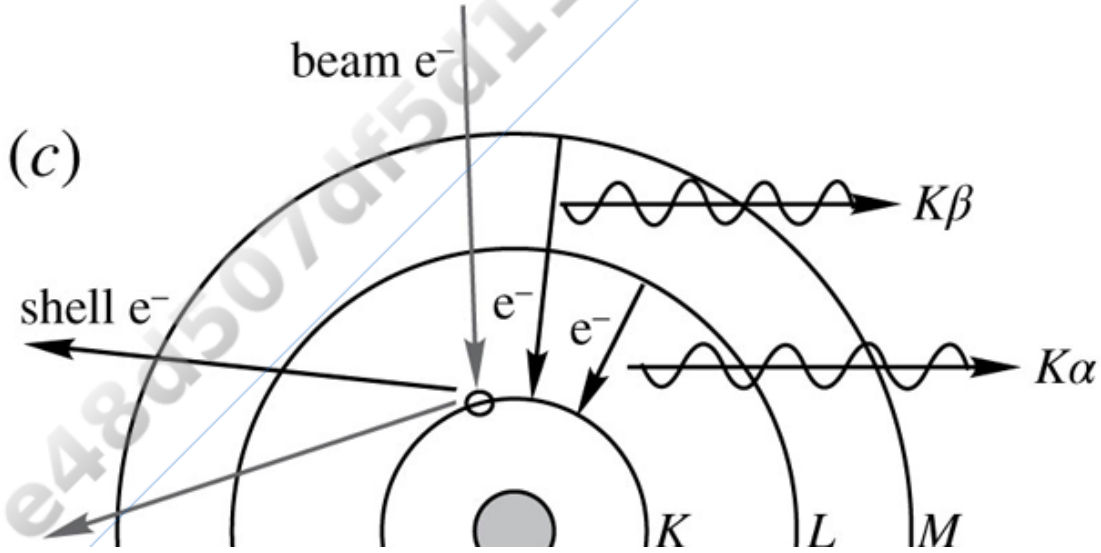

DO NOT COPY
e48d507df5d1141@placeholder.9409

Printed by: e48d507df5d1141@placeholder.94092.edu. Printing is for personal, private use only. No part of this book may be reproduced or transmitted without publisher's prior permission. Violators will be prosecuted.

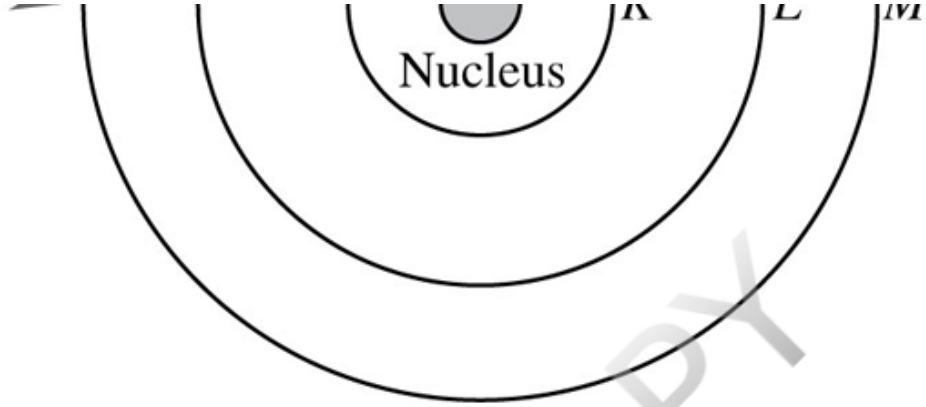

FIGURE 8.3 X-ray spectra. (*a*) Intensity of X-rays emitted by a copper target operated at 50 kV. The characteristic X-ray spectrum (peaks) is superimposed on the continuous spectrum. (*b*) Beam electron deflection (scattering) by a nucleus in the target results in the emission of a continuous spectrum X-ray. (*c*) The characteristic X-ray spectrum is produced when electrons are dislodged from the *K* shell (or other inner shells) and electrons from outer shells drop in energy to occupy the vacancy. Back to text

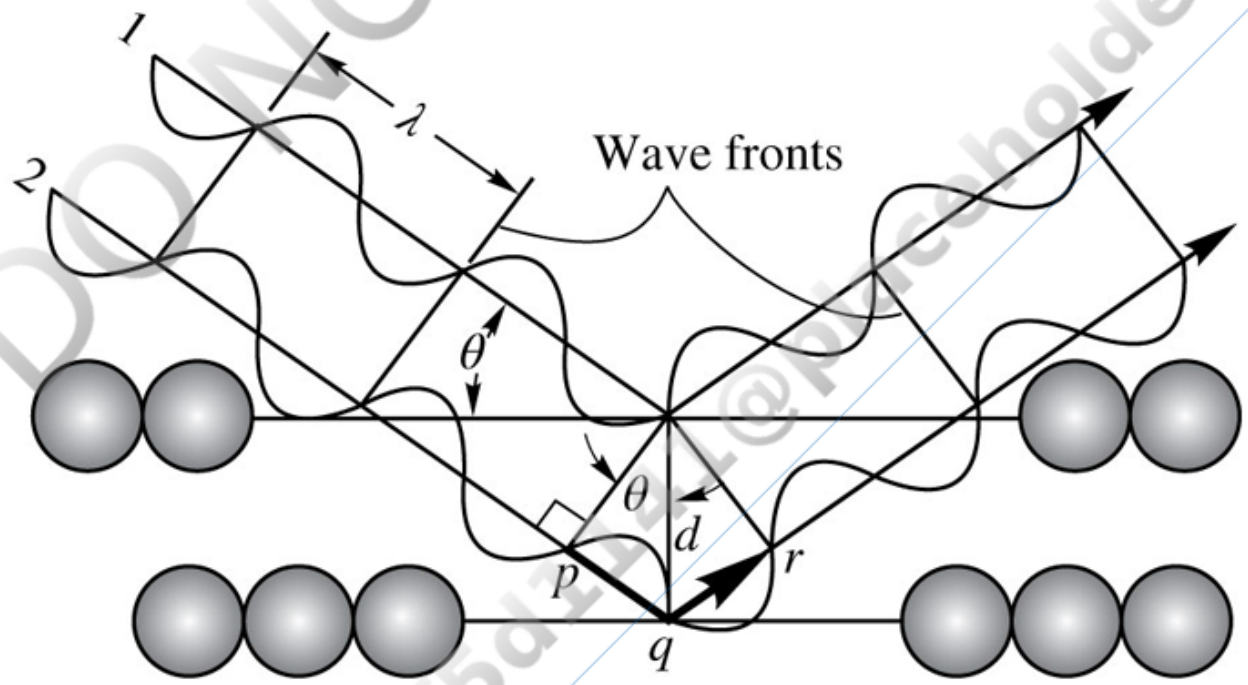

FIGURE 8.4 Diffraction from parallel planes of atoms (atoms not shown where the X-ray rays are drawn). Rays 1 and 2 interact with layers of atoms that are distance *d* apart. Constructive interference ("reflection") of the X-rays diffracted from these layers is possible only if the angle of incidence θ is such that the distance *pqr* is an integer number of wavelengths. Back to text

Printed by: e48d507df5d1141@placeholder.94092.edu. Printing is for personal, private use only. No part of this book may be reproduced or transmitted without publisher's prior permission. Violators will be prosecuted.

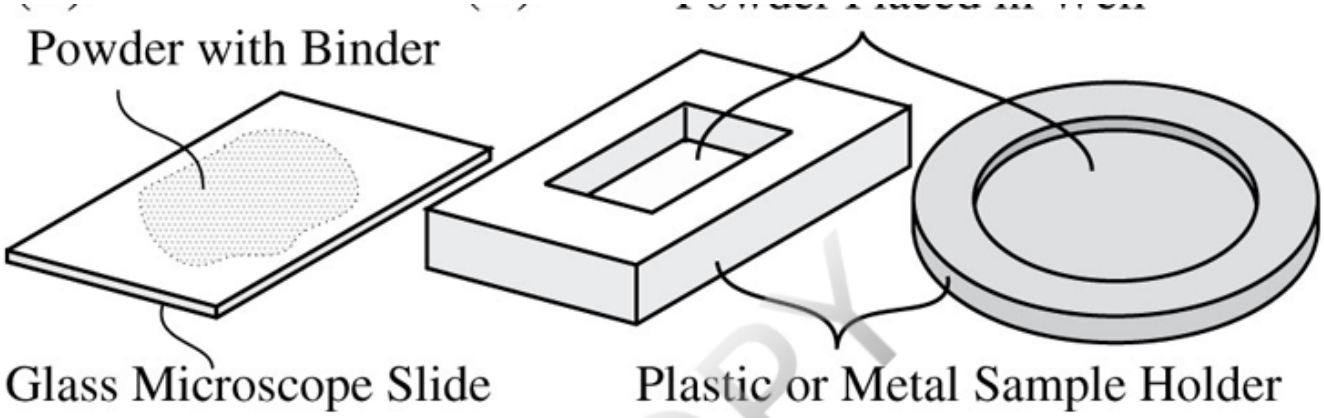

FIGURE 8.5 Sample holders for routine powder diffraction work. (*a*) Mineral powder adhered to a 26 × 47 mm glass microscope slide. (*b*) Powder is placed into the well of a plastic or metal mount. Sample holders of other types may be used, depending on the design of the instrument. Many instruments have a sample stage that allows multiple samples to be loaded and run sequentially.
Back to text

DO NOT COPY
e48d507df5d1141@placeholder.9409

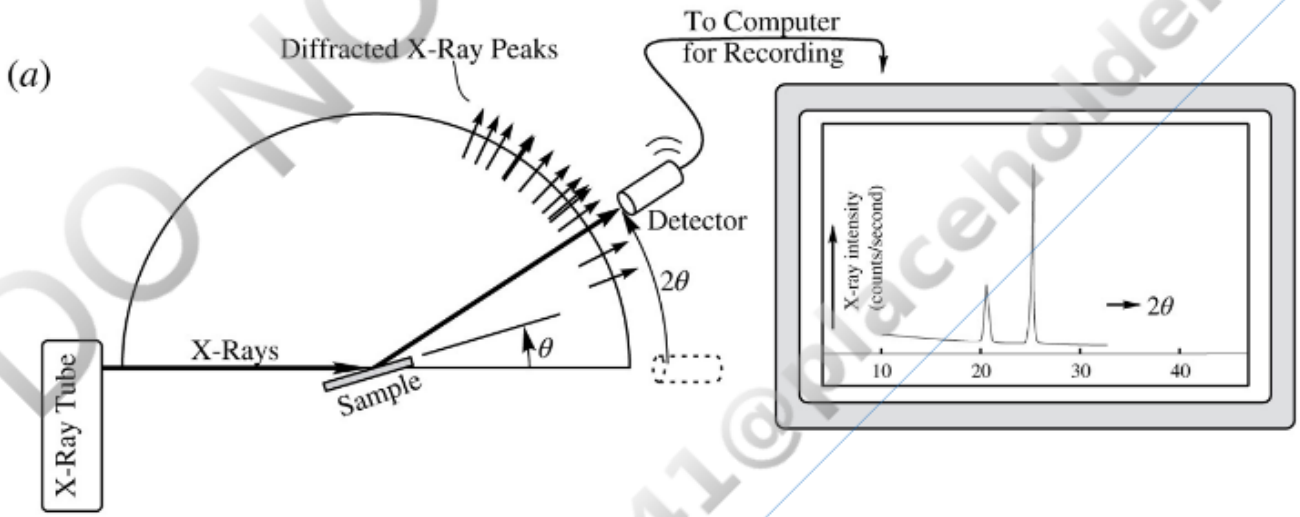

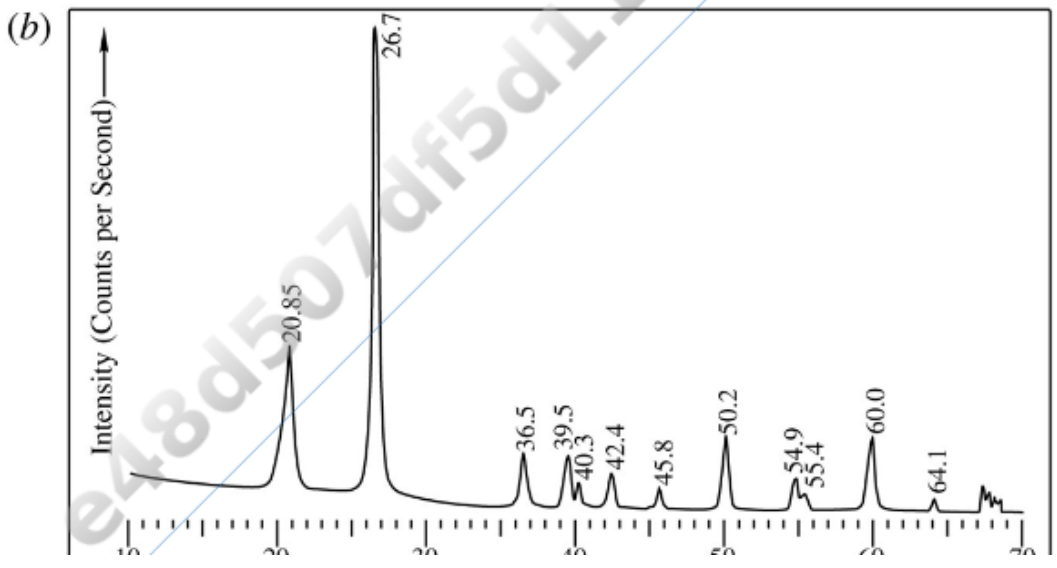

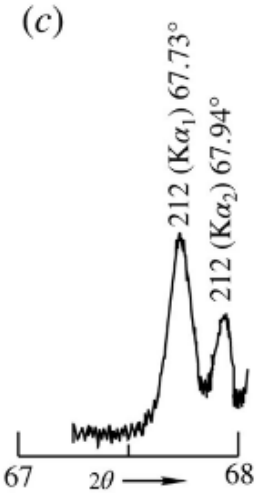

Printed by: e48d507df5d1141@placeholder.94092.edu. Printing is for personal, private use only. No part of this book may be reproduced or transmitted without publisher's prior permission. Violators will be prosecuted.

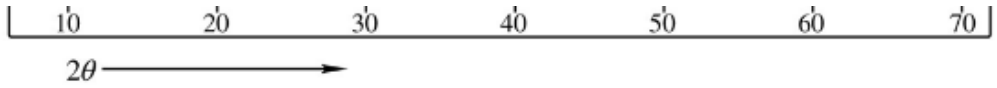

FIGURE 8.6 Collection of a powder diffraction pattern for quartz. (*a*) As the detector moves through its range of 2θ, the sample moves through angle θ, and the intensity of the diffracted X-rays is recorded as a line plot in a computer and displayed on a screen. Each reflection from the mineral is recorded as a peak on the screen at its 2θ position. (*b*) On the output X-ray profile, the horizontal axis is the 2θ angle, and the vertical scale is the intensity of diffracted X-rays, usually in terms of counts per second (cps). (*c*) Because $K\overline{\alpha}$ radiation consists of two different peaks, $K\alpha_1$ and $K\alpha_2$, each atomic plane actually produces two reflections. The peak for the $K\alpha_1$ wavelength has higher intensity than that of Kα_2. At small values of 2θ, the $K\alpha_2$ reflection may show as a slight bulge on the side of the diffraction peak created by the larger $K\alpha_1$ peak. At larger 2θ, the peaks can be distinguished. The $K\alpha_2$ peak will be on the larger 2θ side of the $K\alpha_1$ peak, as is shown for reflections from the {212} plane in quartz. Back to text

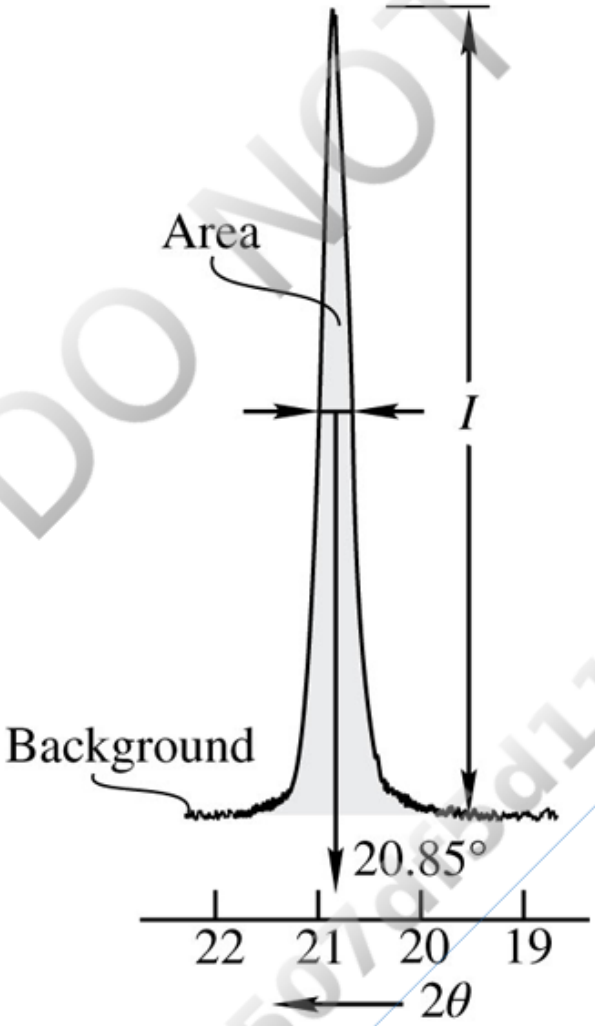

FIGURE 8.7 Recording data from the diffraction pattern: 2θ is taken as the center of the peak measured halfway from the base to the peak. Peak height (*I*) is the height of the peak above the background level. Integrated peak height is less commonly used and is the area of the peak (shaded). Back to text

DO NOT COPY
e48d507df5d1141@placeholder.9409

Printed by: e48d507df5d1141@placeholder.94092.edu. Printing is for personal, private use only. No part of this book may be reproduced or transmitted without publisher's prior permission. Violators will be prosecuted.

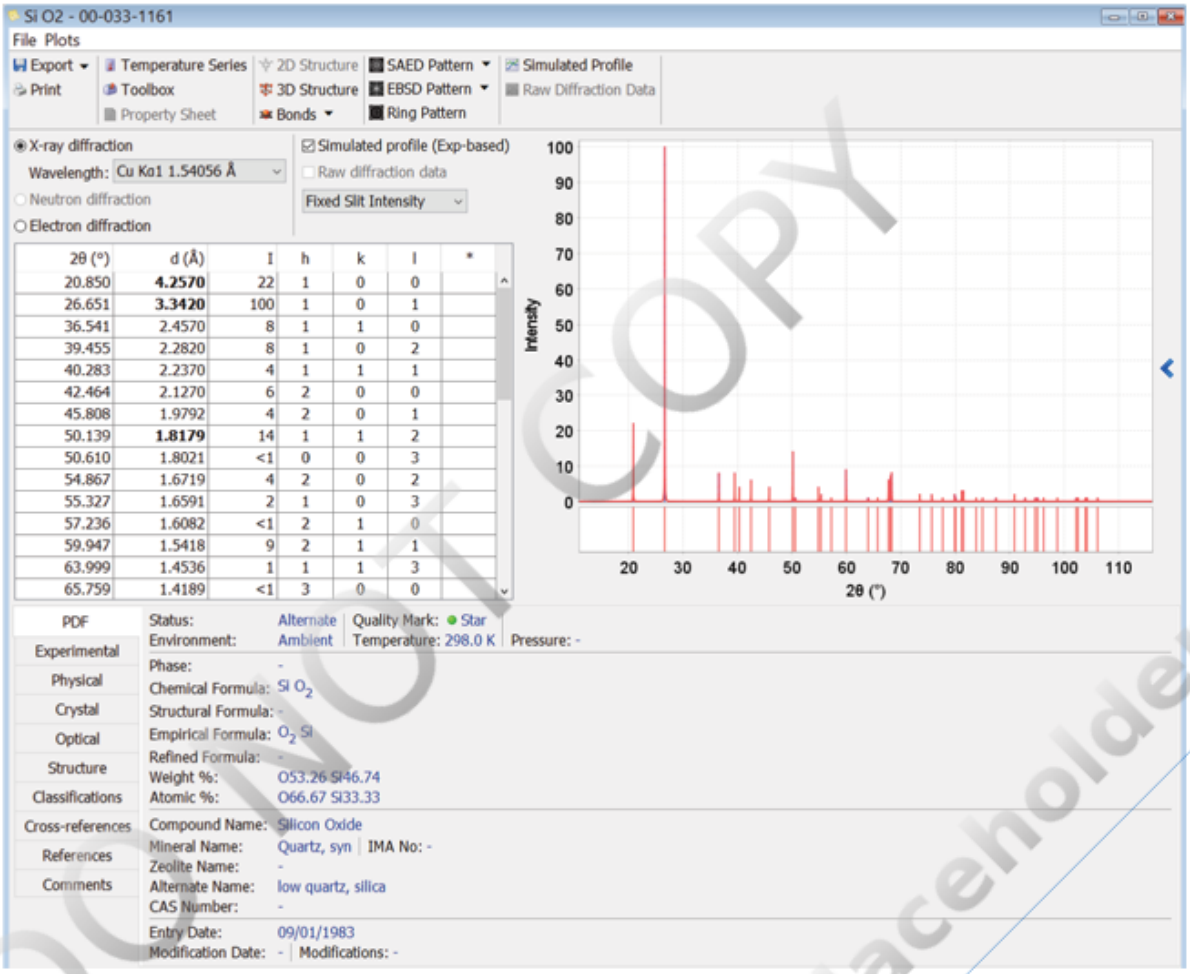

FIGURE 8.8 Powder Diffraction File. The three *d* values [d (Å)] in bold are for the three most intense peaks. Below this on the left side are the reference(s) from which the data was taken, crystallographic data, optical and physical property data, and additional information. The columns on the right include relative intensity (I, which is $I/I_1 \times 100$) and Bragg reflection index for the crystal plane producing the reflection (h, k, and l). These data are listed in order of decreasing *d*-spacing and increasing 2θ. © Joint Committee on Powder Diffraction Standards—International Centre for Diffraction Data.
Back to text

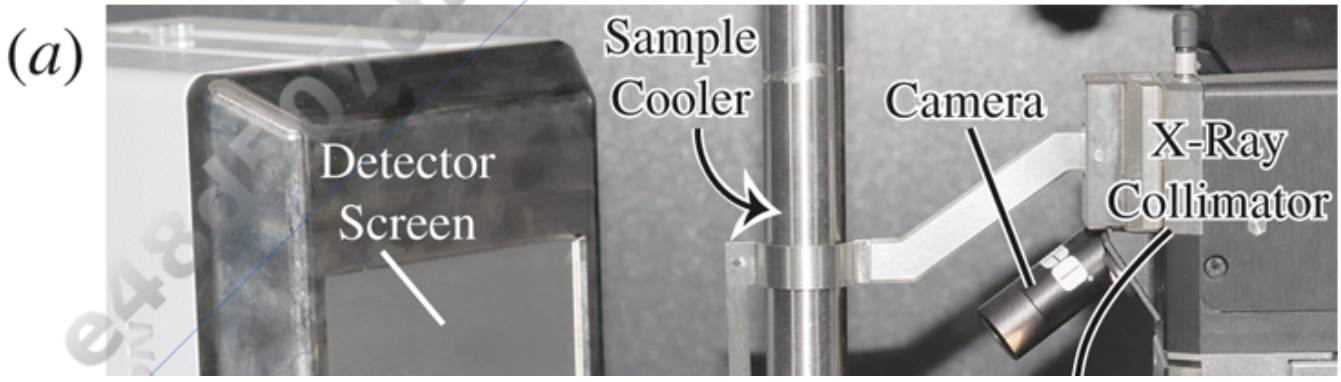

Printed by: e48d507df5d1141@placeholder.94092.edu. Printing is for personal, private use only. No part of this book may be reproduced or transmitted without publisher's prior permission. Violators will be prosecuted.

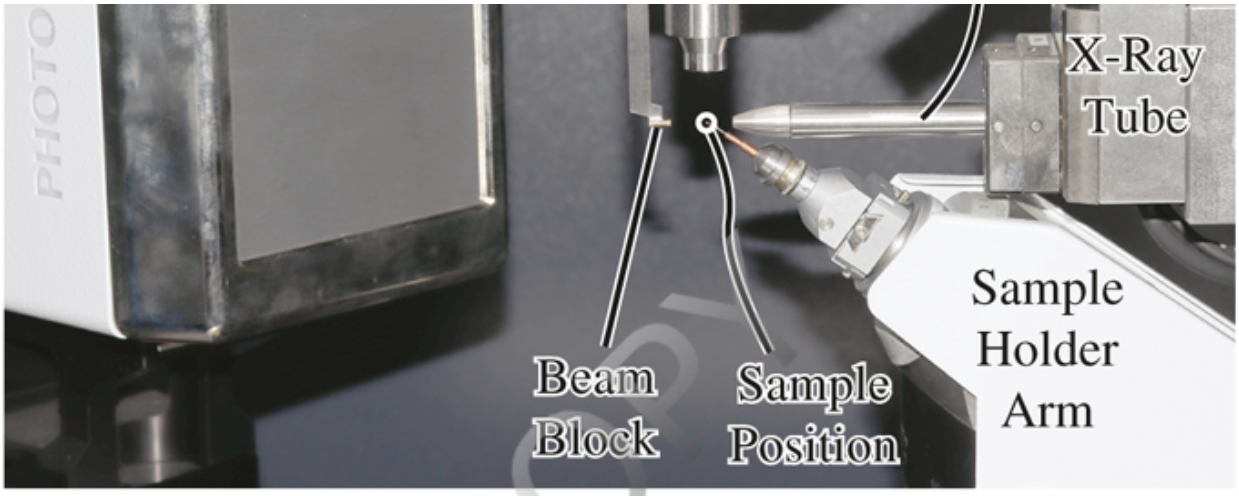

(*b*)

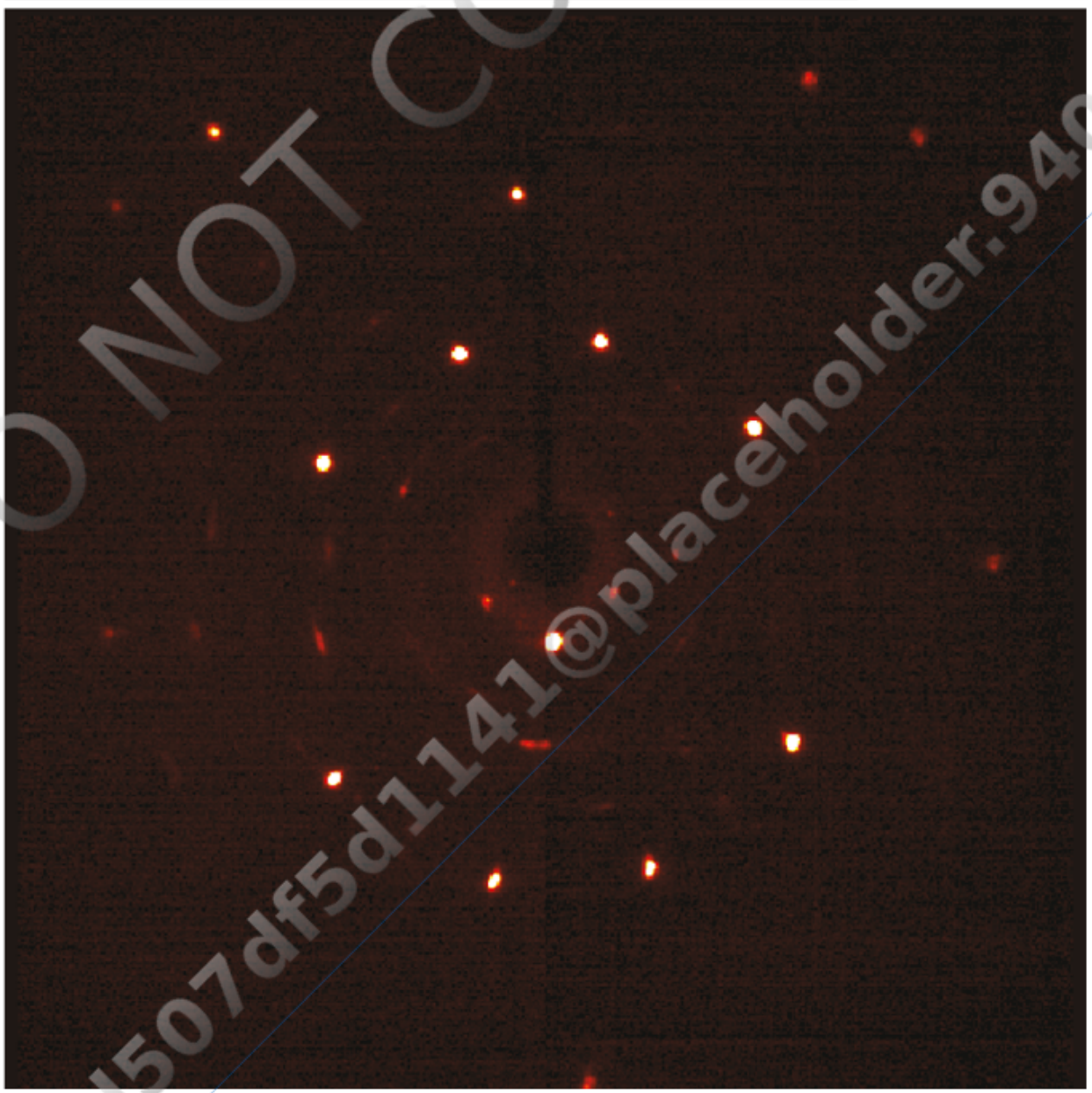

DO NOT COPY
e48d507df5d1141@placeholder.9409

FIGURE 8.9 Single crystal X-ray diffraction. (*a*) Main components of a single crystal X-ray diffractometer. The instrument is a Bruker D8 QUEST at the University of Northern Colorado. The camera ensures the sample is properly positioned, and the sample cooler allows study of *d*-space changes with changing temperature. See text for details. (*b*) Example diffraction pattern from a potassium iodide crystal, which is isostructural with halite (NaCl). Bright spots are Bragg reflections

Printed by: e48d507df5d1141@placeholder.94092.edu. Printing is for personal, private use only. No part of this book may be reproduced or transmitted without publisher's prior permission. Violators will be prosecuted.

potassium iodide crystal, which is isostructural with halite (NaCl). Bright spots are Bragg reflections from particular planes of atoms. Back to text

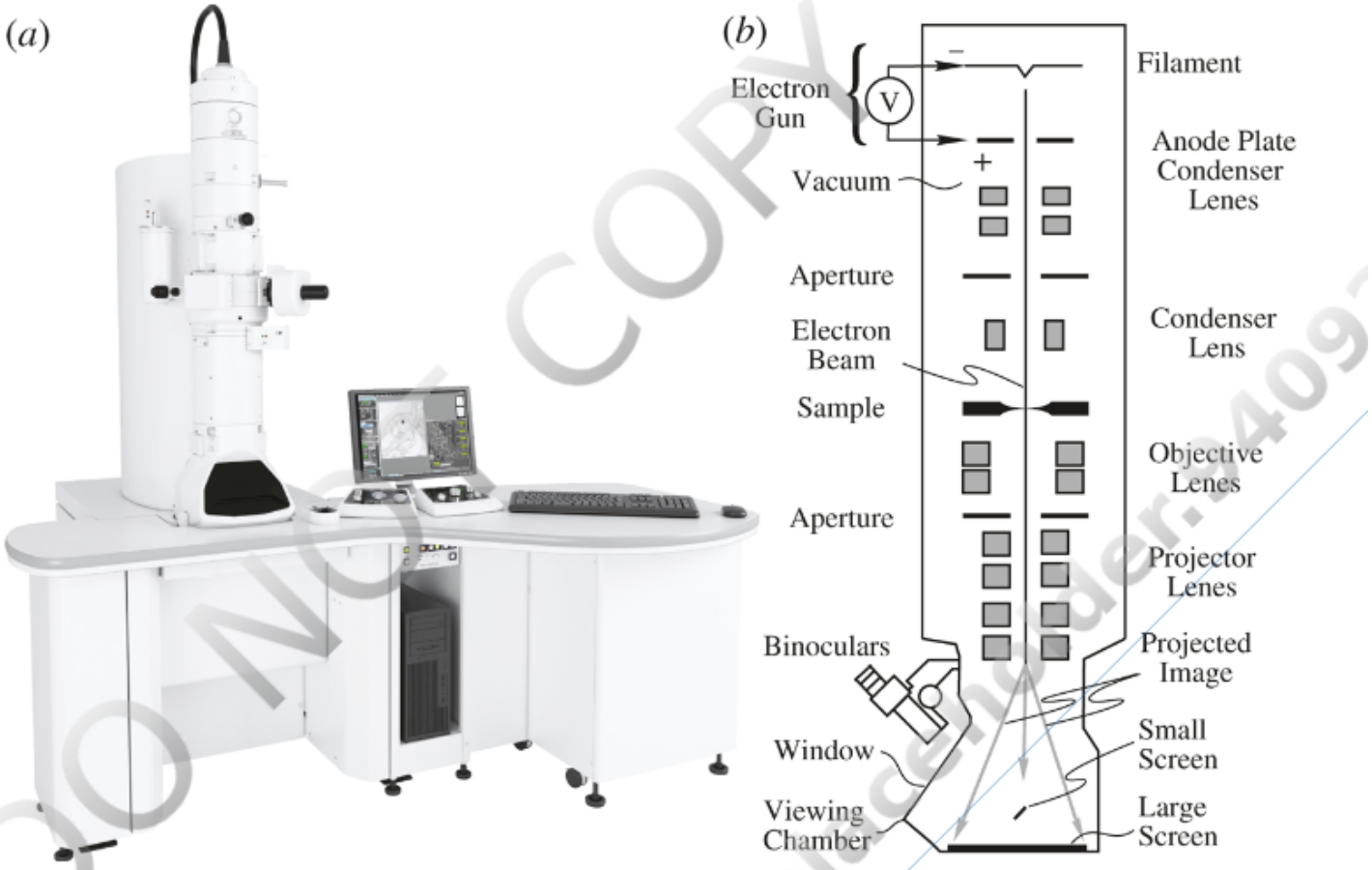

FIGURE 8.10 Transmission electron microscope. (*a*) A typical transmission electron microscope. Image courtesy of JEOL USA. (*b*) Schematic diagram showing the major components of a transmission electron microscope column, shown in the upper-left portion of (*a*). Image courtesy of JEOL USA. Back to text

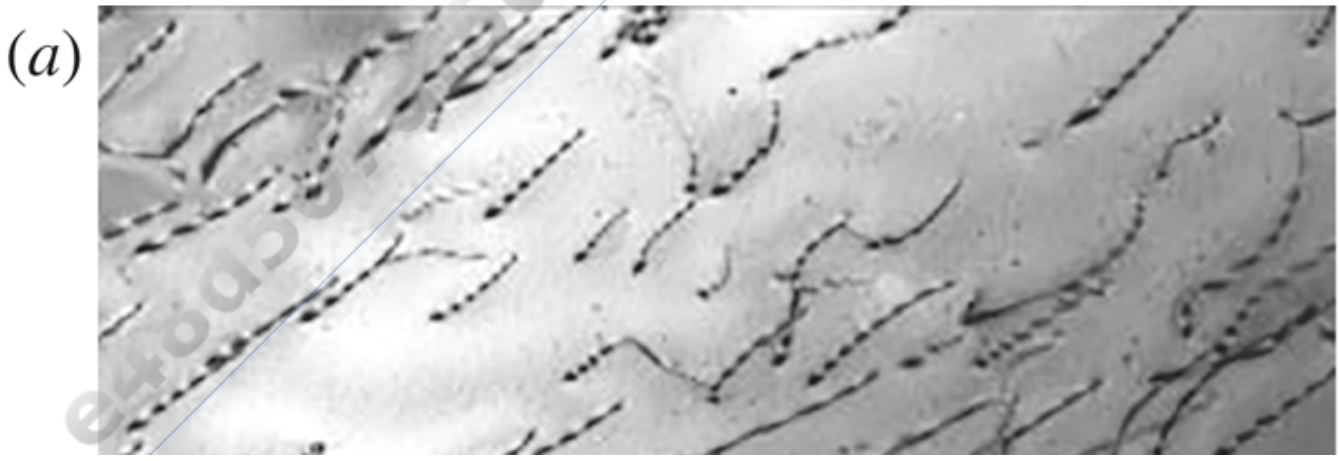

DO NOT COPY
e48d507df5d1141@placeholder.94092

Printed by: e48d507df5d1141@placeholder.94092.edu. Printing is for personal, private use only. No part of this book may be reproduced or transmitted without publisher's prior permission. Violators will be prosecuted.

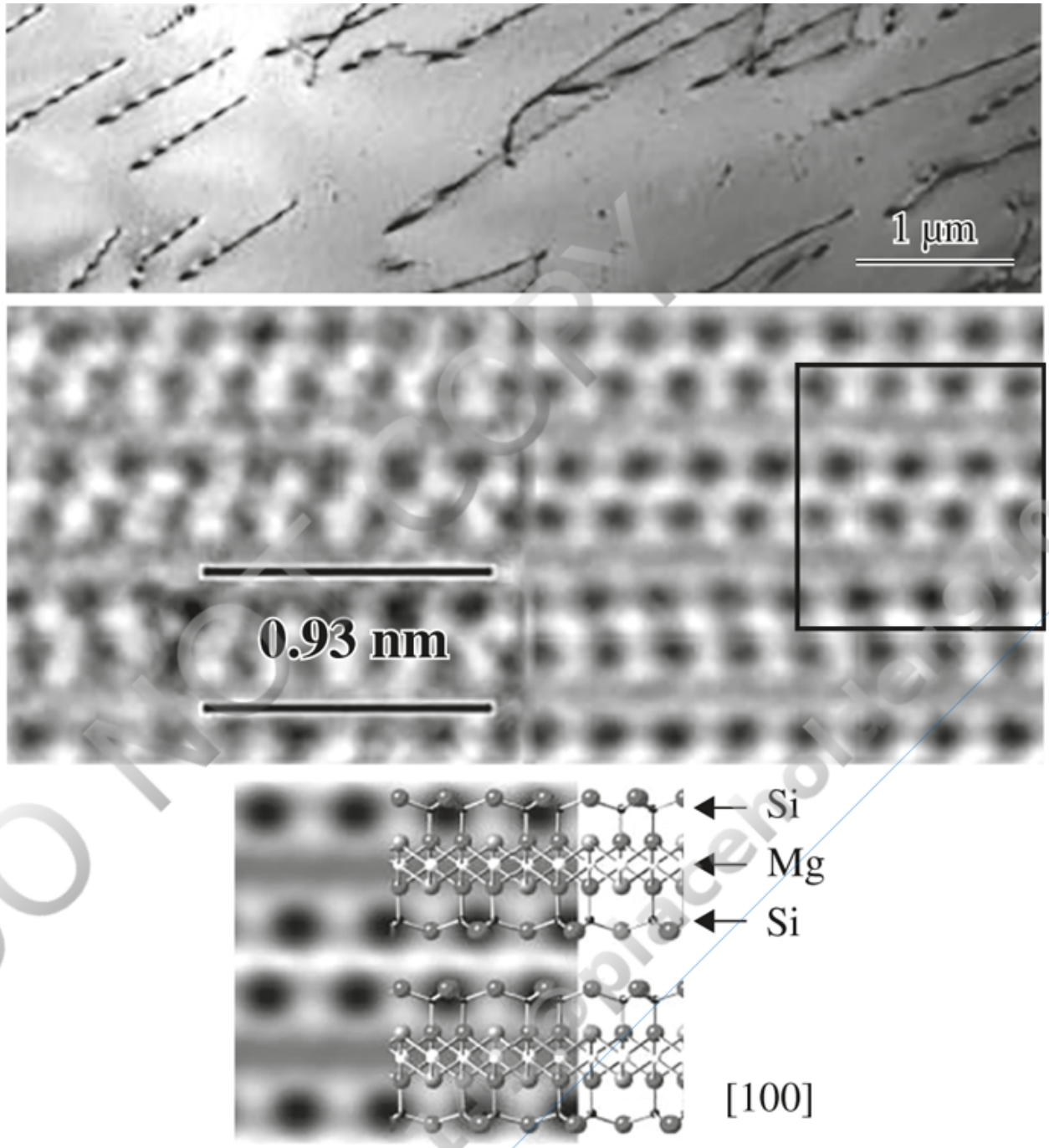

FIGURE 8.11 Example images collected by a transmission electron microscope. (*a*) Bright-field image of quartz; dislocations (Chapter 5) appear as the black lines (© Morales, L. F. G., Mainprice, D., Lloyd, G. E., and Law, R. D., 2011, Crystal fabric development and slip systems in a quartz mylonite: an approach via transmission electron microscopy and viscoplastic self-consistent modelling, in Prior, D. J., Rutter, E. H. and Tatham, D. J. (eds) Deformation Mechanisms, Rheology and Tectonics: Microstructures, Mechanics and Anisotropy. Geological Society, London, Special Publications, 360, 151–174). (*b*) High-resolution phase-contrast transmission electron microscope image of talc. At the upper left is the raw image; at the upper right is a filtered image. A computer simulation produced the lower image with the incident electrons in the [100] direction. Note that the computer simulation matches the image within the box in the upper right; therefore atom locations within the crystal structure as shown can be connected to the phase-contrast image (Kogure, T., Kameda, J., Matsui, T., and Miyawaki, R. 2006. Stacking structure in disordered talc: Interpretation of its X-ray diffraction pattern by using pattern simulation and high-resolution transmission electron microscopy. American Mineralogist 91). Back to text

Printed by: e48d507df5d1141@placeholder.94092.edu. Printing is for personal, private use only. No part of this book may be reproduced or transmitted without publisher's prior permission. Violators will be prosecuted.

Chapter 9 Analytical Instrumentation and Techniques II: Chemical Analysis of Minerals

DO NOT COPY

(a)

(b)

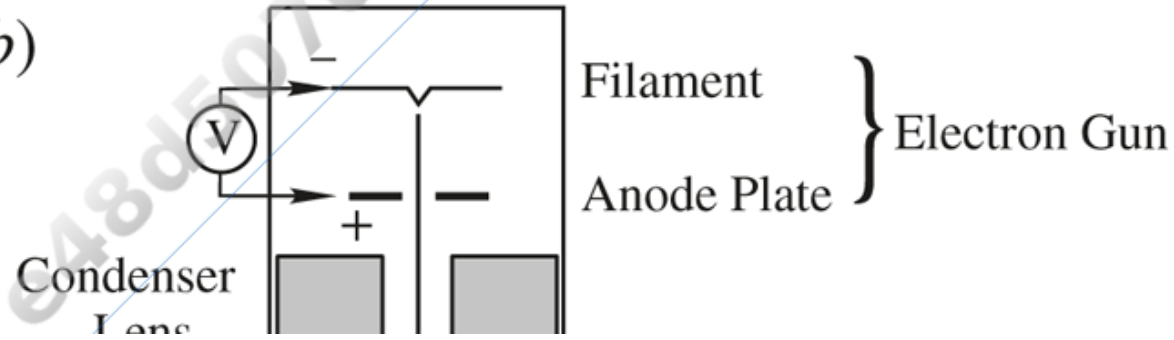

Printed by: e48d507df5d1141@placeholder.94092.edu. Printing is for personal, private use only. No part of this book may be reproduced or transmitted without publisher's prior permission. Violators will be prosecuted.

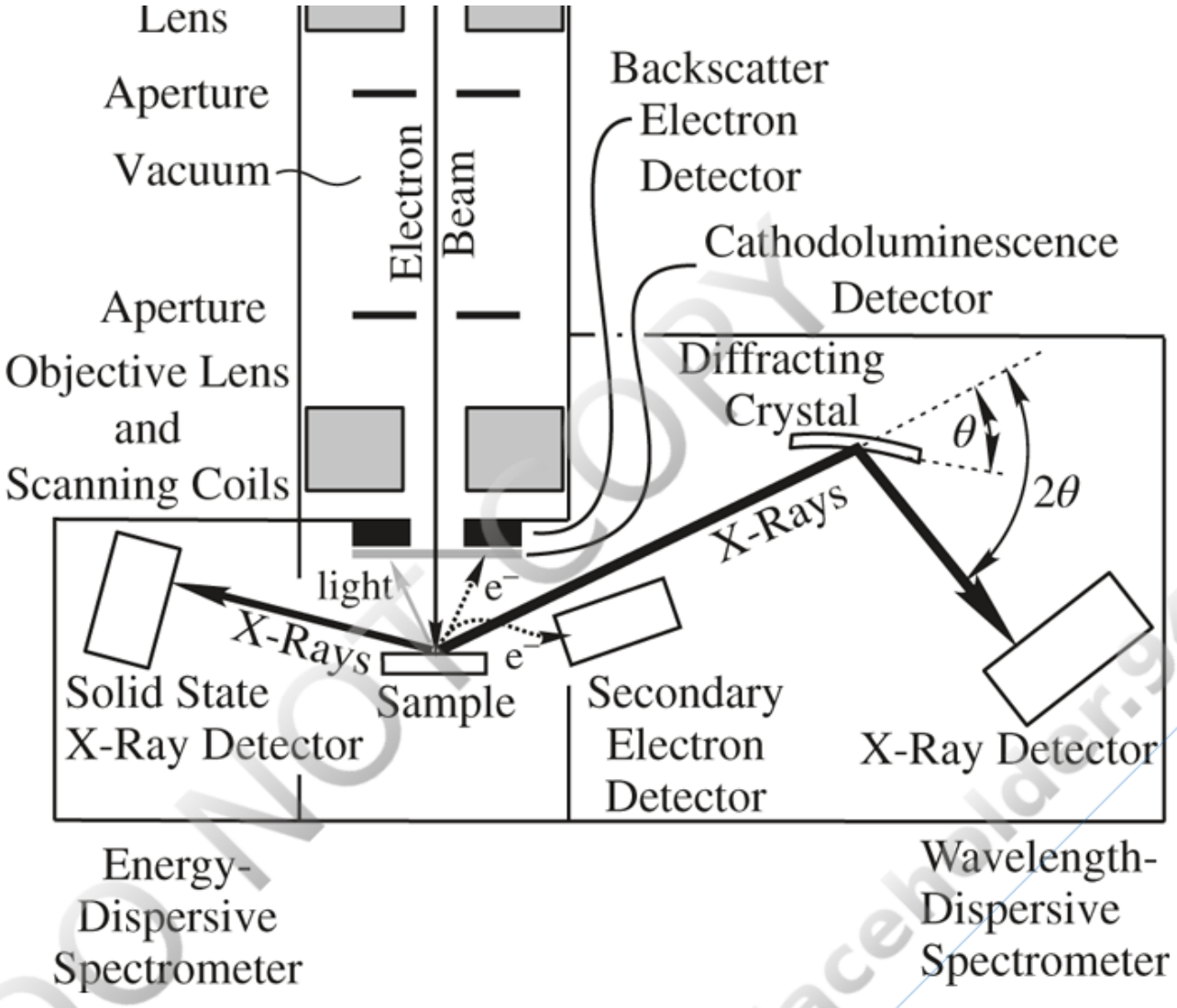

FIGURE 9.1 Electron microprobes and scanning electron microscopes. (*a*) An electron microprobe. Scanning electron microscopes look very similar. Image courtesy of JEOL USA. (*b*) Schematic diagram showing the major components of both electron microprobes and scanning electron microscopes. See text for additional discussion. Back to text

(*a*)

Printed by: e48d507df5d1141@placeholder.94092.edu. Printing is for personal, private use only. No part of this book may be reproduced or transmitted without publisher's prior permission. Violators will be prosecuted.

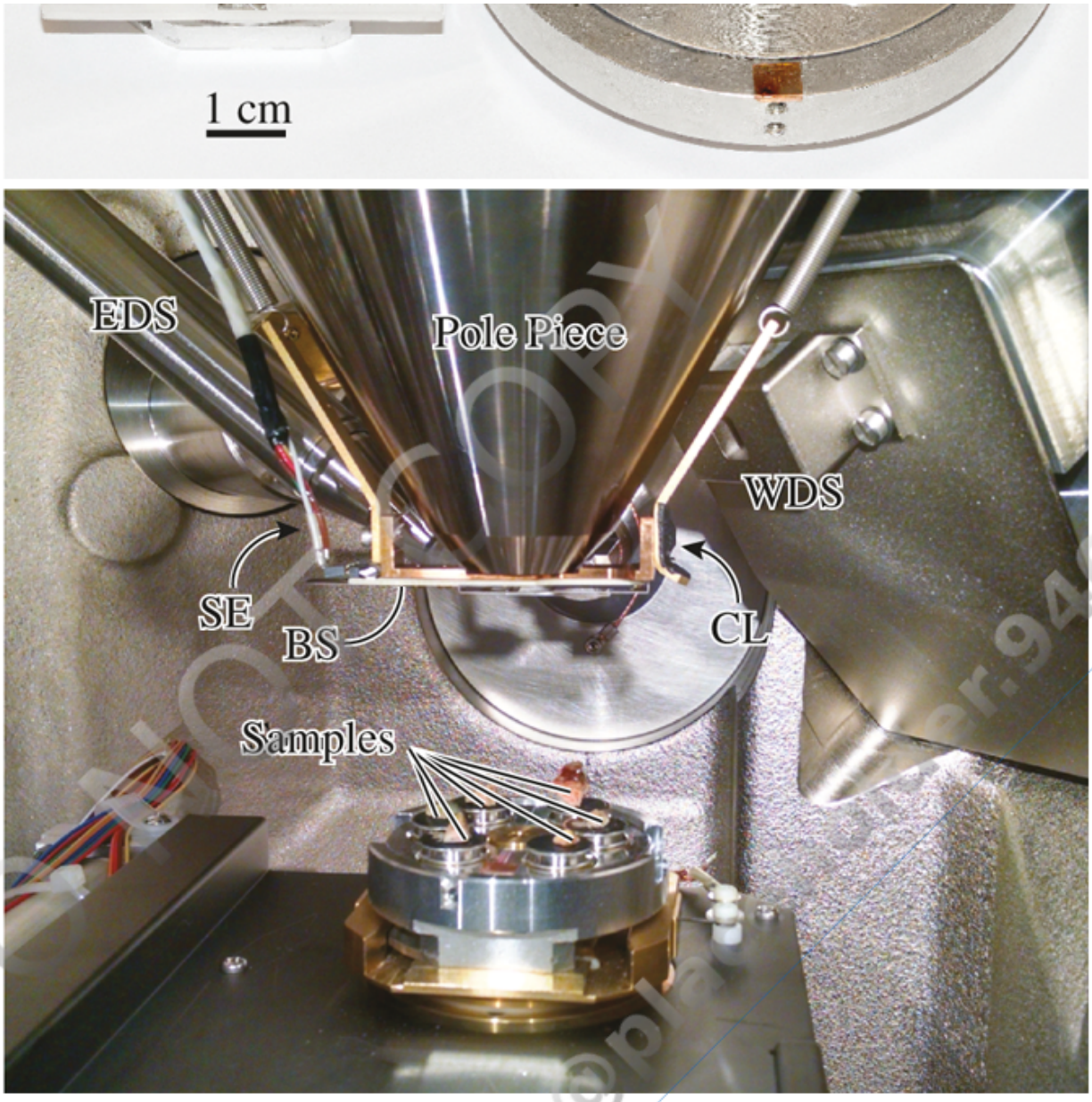

FIGURE 9.2 Scanning electron microscope and electron microprobe samples and chamber interior. (*a*) Polished samples mounted on a sample holder. On the left are two thin sections; on the right are rock fragments mounted in epoxy. The thin, about 15-nanometer, carbon coat on samples tint the samples a light gray. Here, samples are held to the holders with conductive tape. (*b*) Sample chamber. Six samples are on the stage, which will be raised to be about 1–2 cm from the pole piece for imaging and analysis. BS—Backscatter electron detector; SE—secondary electron detector (behind pole piece); EDS—energy-dispersive spectrometer; WDS—wavelength-dispersive spectrometer; CL—cathodoluminescence detector (behind pole piece). The sample chamber is evacuated by a vacuum pump after samples are loaded. Back to text

Printed by: e48d507df5d1141@placeholder.94092.edu. Printing is for personal, private use only. No part of this book may be reproduced or transmitted without publisher's prior permission. Violators will be prosecuted.

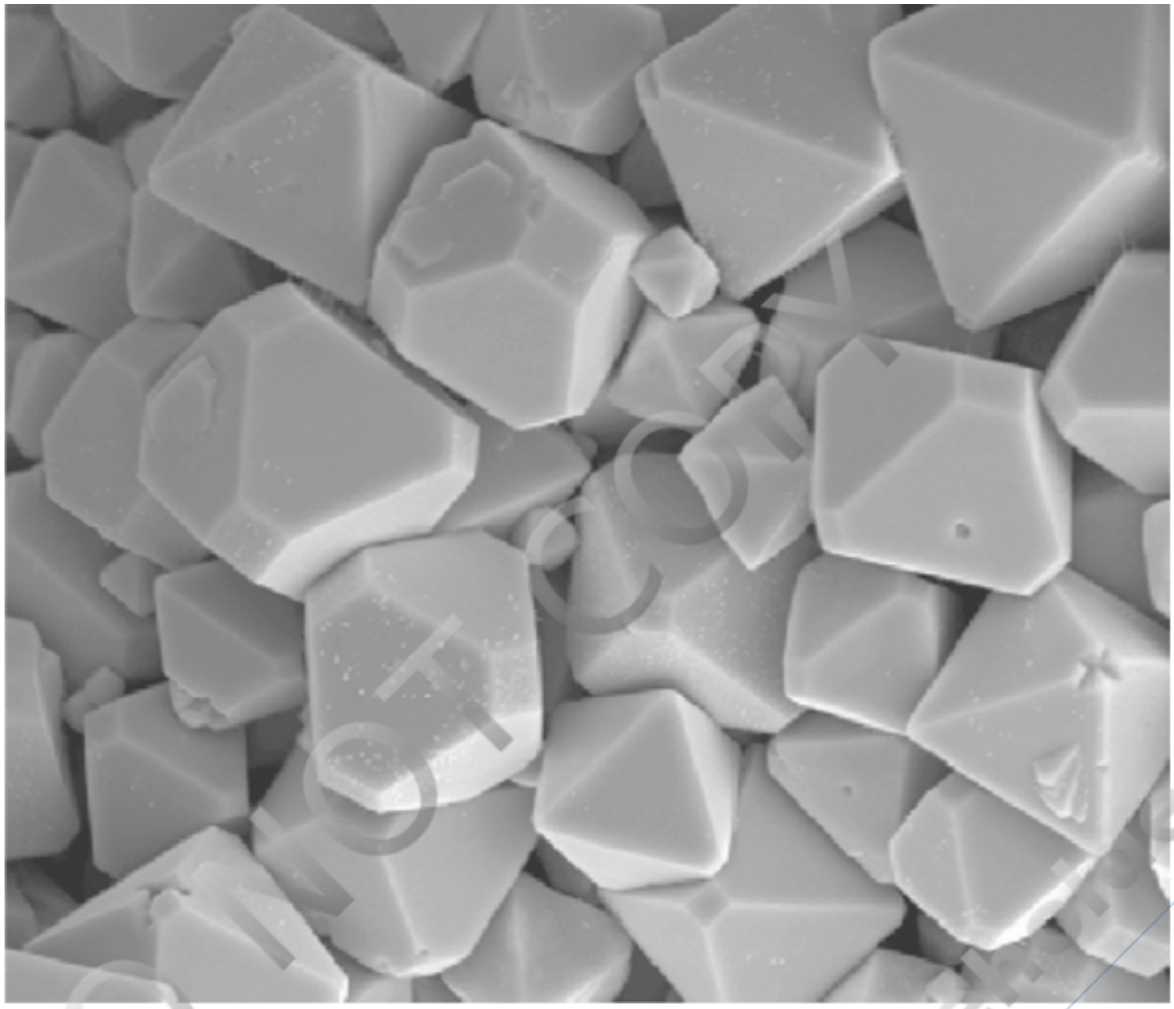

FIGURE 9.3 Secondary electron image of pyrite grains from alluvium of the Canadian River, Oklahoma. The loose grains of this sample allow crystal form to be studied. Most of the crystals are octahedrons or octahedrons modified by cubes. © George N. Breit, Michele L.W. Tuttle, Isabelle M. Cozzarelli, Scott C. Christenson, Jeanne B. Jaeschke, David L. Fey, and Cyrus J. Berry 2005. Results of Chemical and Isotopic Analyses of Sediment and Water from Alluvium of the Canadian River near a Closed Municipal Landfill, Norman, Oklahoma. U.S. Geological Survey. Back to text

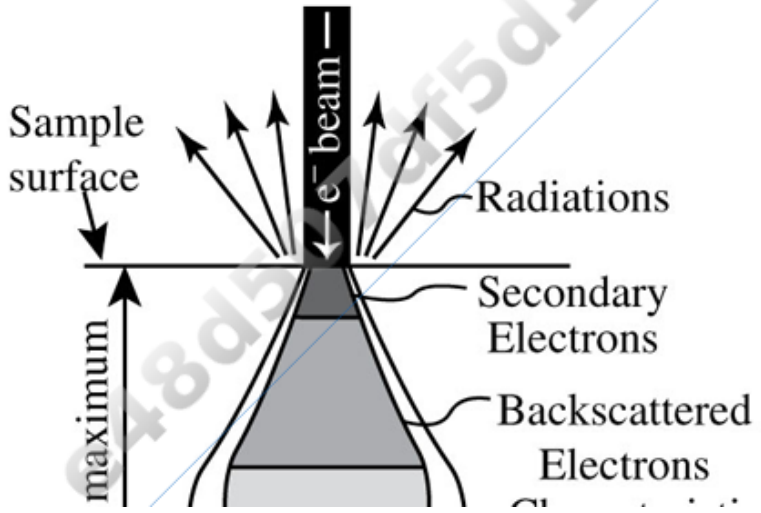

Printed by: e48d507df5d1141@placeholder.94092.edu. Printing is for personal, private use only. No part of this book may be reproduced or transmitted without publisher's prior permission. Violators will be prosecuted.

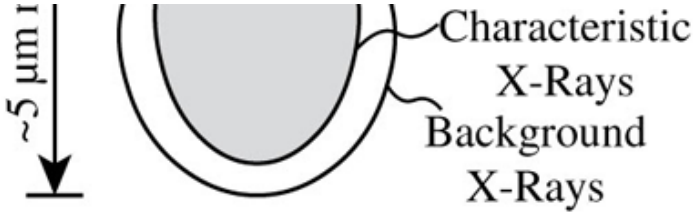

FIGURE 9.4 Excitation volume within a scanning electron microscope or electron microprobe sample showing the approximate extent within that volume from which some of the radiations originate. Size of the excitation volume depends on the instrumental operating conditions and the nature of the sample. For most typical operating conditions and geologic samples, the excitation volume extends to a maximum depth of about 5 µm. Back to text

DO NOT COPY

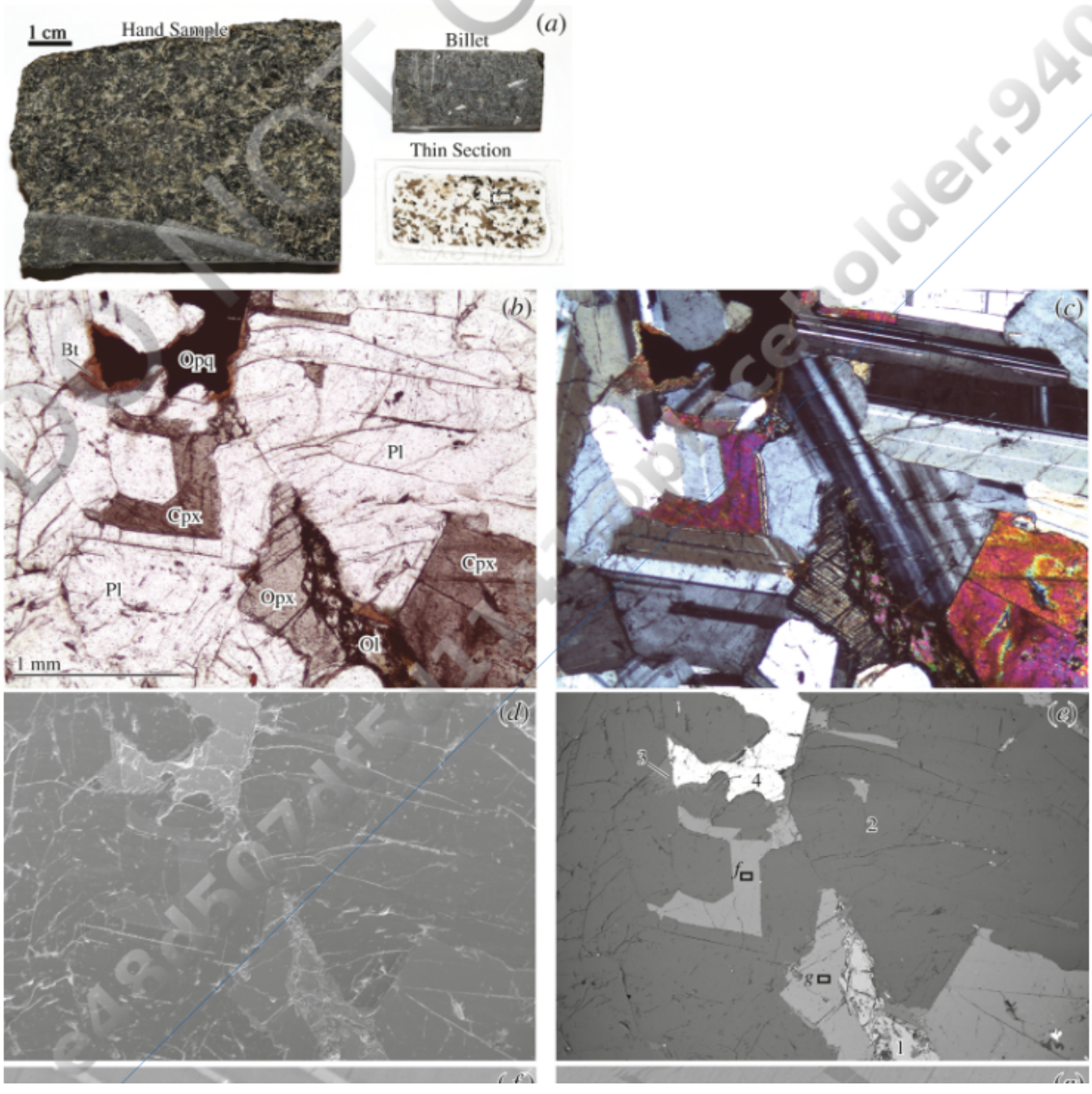

Printed by: e48d507df5d1141@placeholder.94092.edu. Printing is for personal, private use only. No part of this book may be reproduced or transmitted without publisher's prior permission. Violators will be prosecuted.

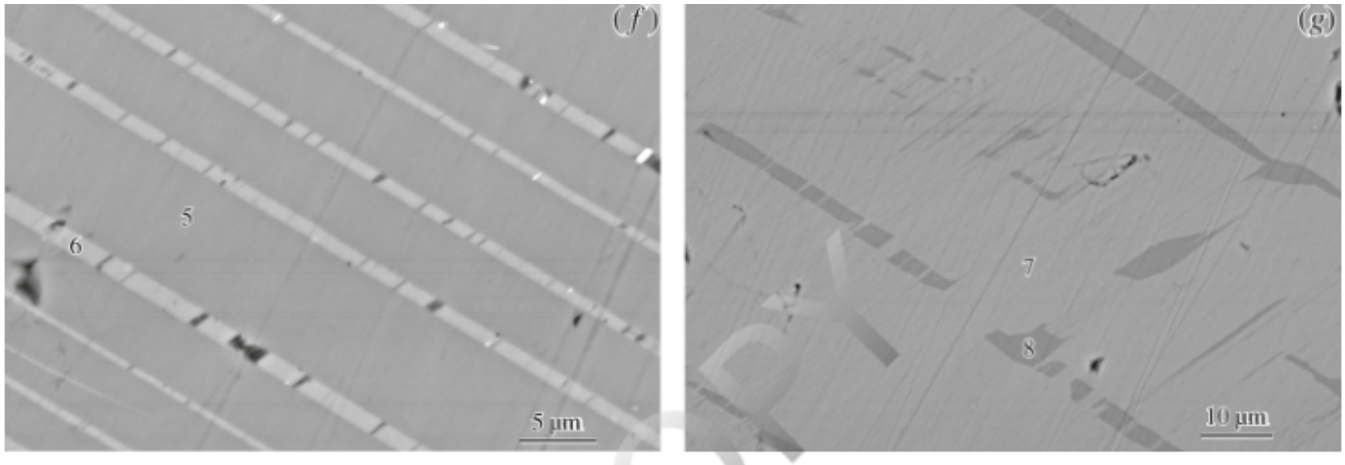

FIGURE 9.5 Hand sample to thin section and scanning electron microscope/electron microprobe analysis. (*a*) Hand sample and thin section of a gabbro sample. (*b*) Plane-polarized light image of the box shown on the thin section in (*a*). The major minerals are plagioclase (Pl), clinopyroxene (Cpx), orthopyroxene (Opx), olivine (Ol), biotite (Bt), and an opaque mineral (Opq). The opaque mineral will be revealed to be ilmenite (Ilm) with chemical analysis. (*c*) Cross-polarized light image of (*b*). (*d*) Secondary electron image of (*b*); the cracks and pits that persist after polishing are highlighted by light edges, but average atomic number of different minerals does affect the intensity of secondary electrons somewhat (brighter from higher average atomic number). (*e*) Backscattered electron image (BEI) of (*b*); cracks and pits are less obvious compared to (*d*) and appear as black features. Average atomic number of minerals controls the brightness of minerals strongly; plagioclase has the lowest average atomic number and lowest brightness of all minerals in the image. Numbers are the location of wavelength-dispersive spectrometer (WDS) analysis (results are shown in Table 9.2). Boxes are shown in (*f*) and (*g*). (*f*) BEI close-up of clinopyroxene that reveals orthopyroxene exsolution lamellae (bright) not easily observable in other images shown. The numbers are locations of WDS analysis (results are shown in Table 9.2). (*g*) BEI close-up of orthopyroxene that highlights the clinopyroxene exsolution lamellae (dark), which are also observable in (*c*). The numbers are locations of WDS analysis (results are shown in Table 9.2). Back to text

FIGURE 9.6 Cathodoluminescence image of a zircon grain. The grain was extracted from the

Printed by: e48d507df5d1141@placeholder.94092.edu. Printing is for personal, private use only. No part of this book may be reproduced or transmitted without publisher's prior permission. Violators will be prosecuted.

host rock, mounted in epoxy, and ground and polished so that a cross section through the center of the grain could be imaged. Zircon zoning patterns, controlled by slight changes in chemistry, are often only observable by cathodoluminescence and are key information used for interpreting the origin and history of the grain (Box 5.1). This grain has a dark core surrounded by oscillatory zoning. Back to text

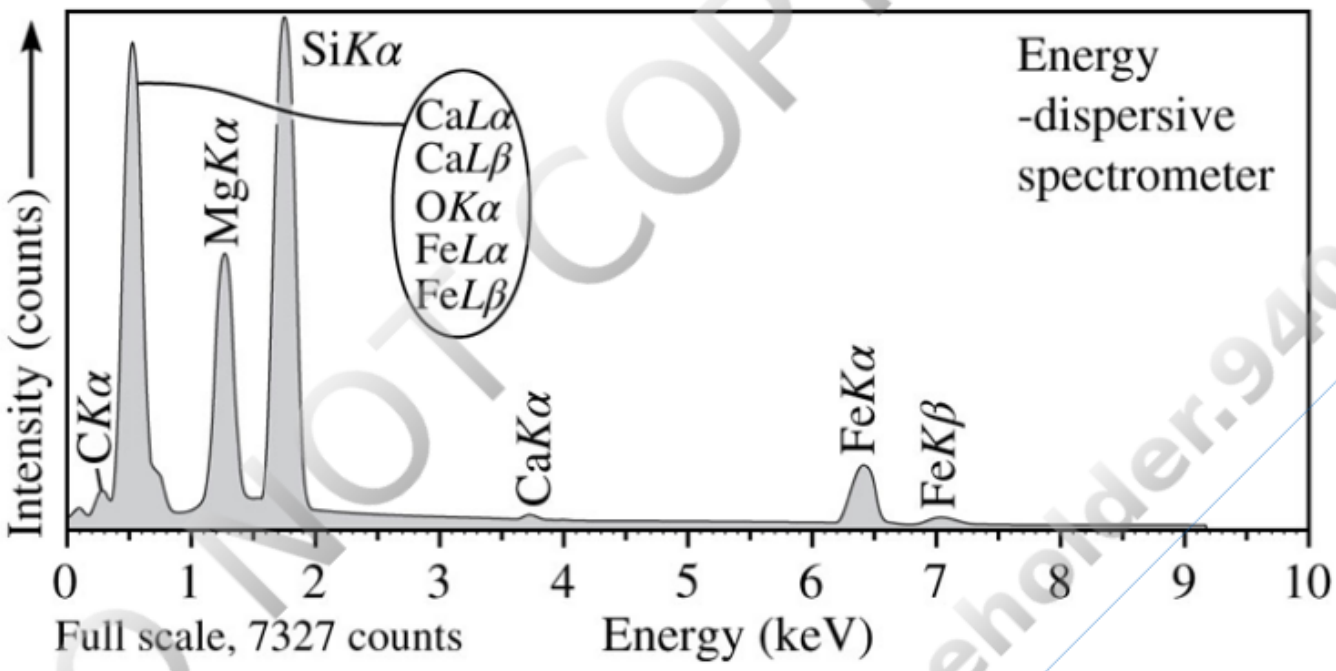

FIGURE 9.7 Energy-dispersive X-ray spectra from orthopyroxene; compare with Figure 9.8. Note that Al was not detected by the energy-dispersive spectrometer, and that the peak at about 0.5 keV includes characteristic spectra from oxygen, iron, and calcium. The small carbon *Kα* peak is from the carbon coating on the sample. Back to text

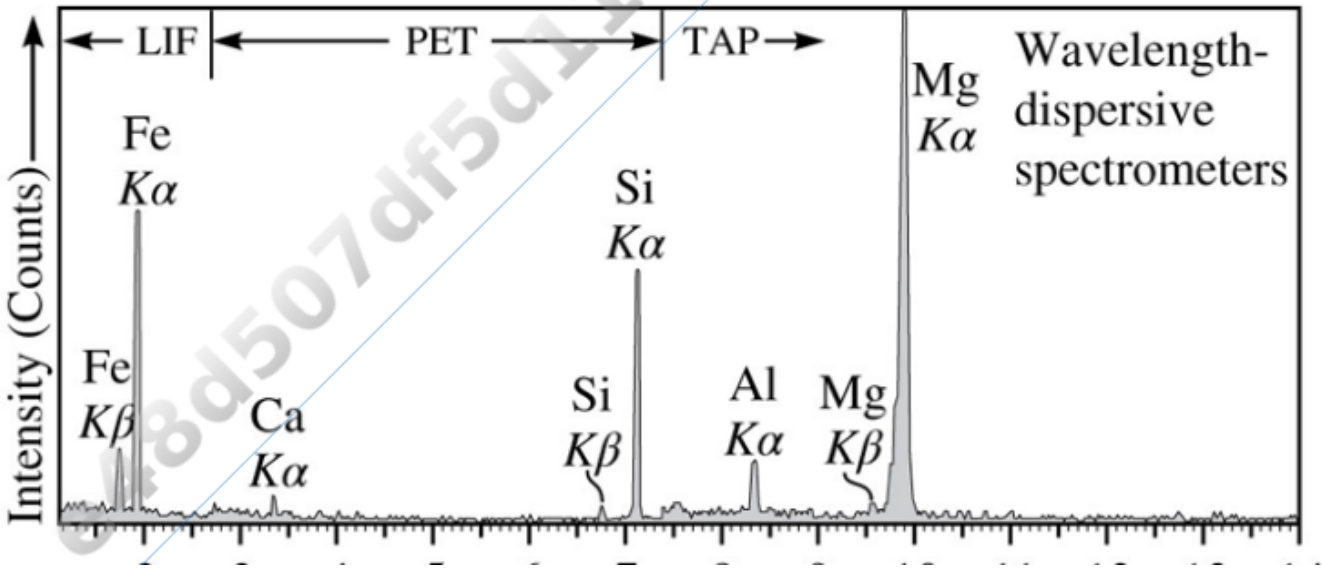

DO NOT COPY
e48d507df5d1141@placeholder.9409

Printed by: e48d507df5d1141@placeholder.94092.edu. Printing is for personal, private use only. No part of this book may be reproduced or transmitted without publisher's prior permission. Violators will be prosecuted.

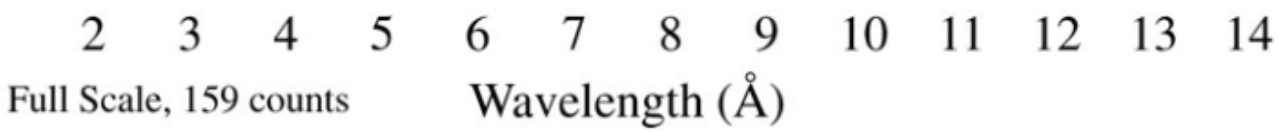

FIGURE 9.8 Wavelength-dispersive X-ray spectra for the same orthopyroxene analyzed by energy-dispersive spectrometry and presented in Figure 9.7. The wavelength ranges of the different diffracting crystals are indicated (LIF—lithium fluoride, PET—pentaerythritol, TAP—thallium acid pthalate). Note that this spectrometer is more sensitive and is able to more easily detect Al. Back to text

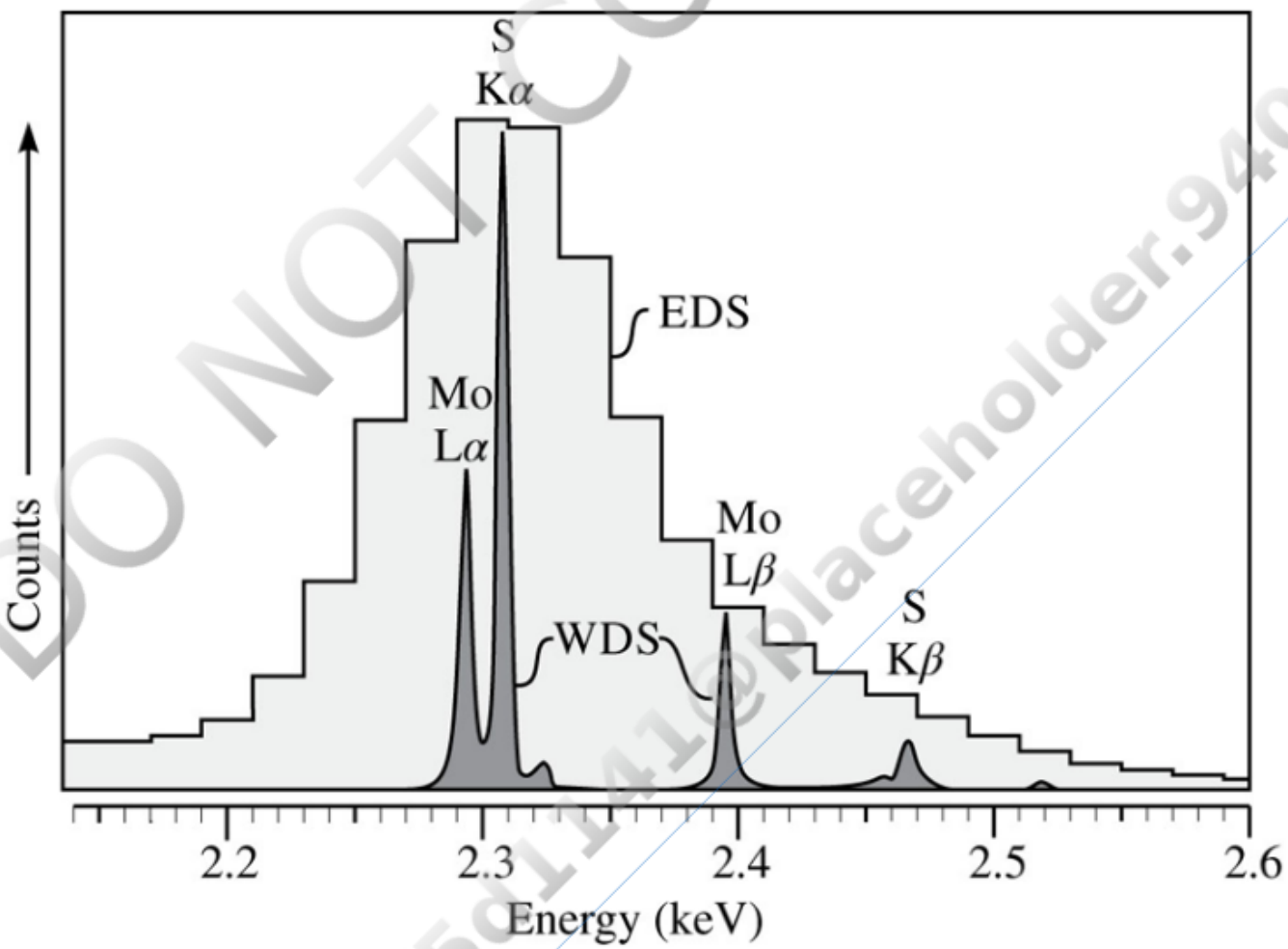

FIGURE 9.9 Comparison of energy-dispersive (EDS) and wavelength-dispersive (WDS) scans on molybdenite. The energy-dispersive spectrometer merges all the peaks for sulfur and molybdenum into a single broad peak that does not allow the two elements to be distinguished. The wavelength-dispersive spectrometer clearly distinguishes each peak of the characteristic spectra. Back to text

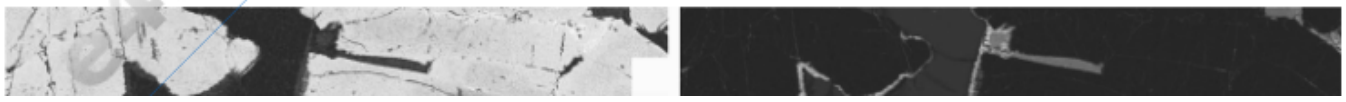

DO NOT COPY
e48d507df5d1141@placeholder.9409

Printed by: e48d507df5d1141@placeholder.94092.edu. Printing is for personal, private use only. No part of this book may be reproduced or transmitted without publisher's prior permission. Violators will be prosecuted.

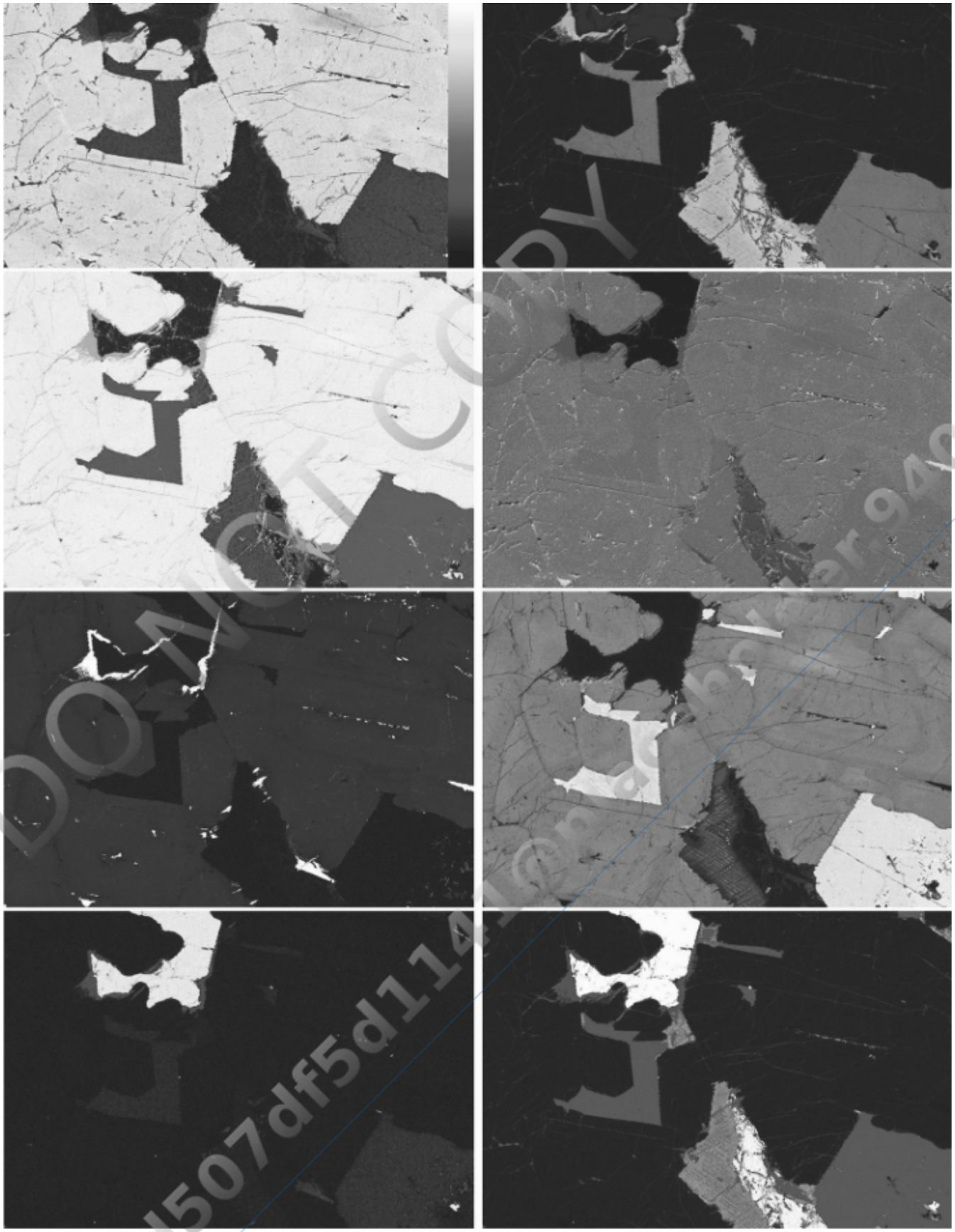

FIGURE 9.10 X-ray chemical maps. Maps cover the same area as shown in Figure 9.5b–e. For all maps, brighter indicates higher relative concentration of the element as labeled. Brightness of images has been scaled to highlight features. Note that minerals with high concentration of particular elements matches the quantitative analysis (Table 9.2). Back to text

Printed by: e48d507df5d1141@placeholder.94092.edu. Printing is for personal, private use only. No part of this book may be reproduced or transmitted without publisher's prior permission. Violators will be prosecuted.

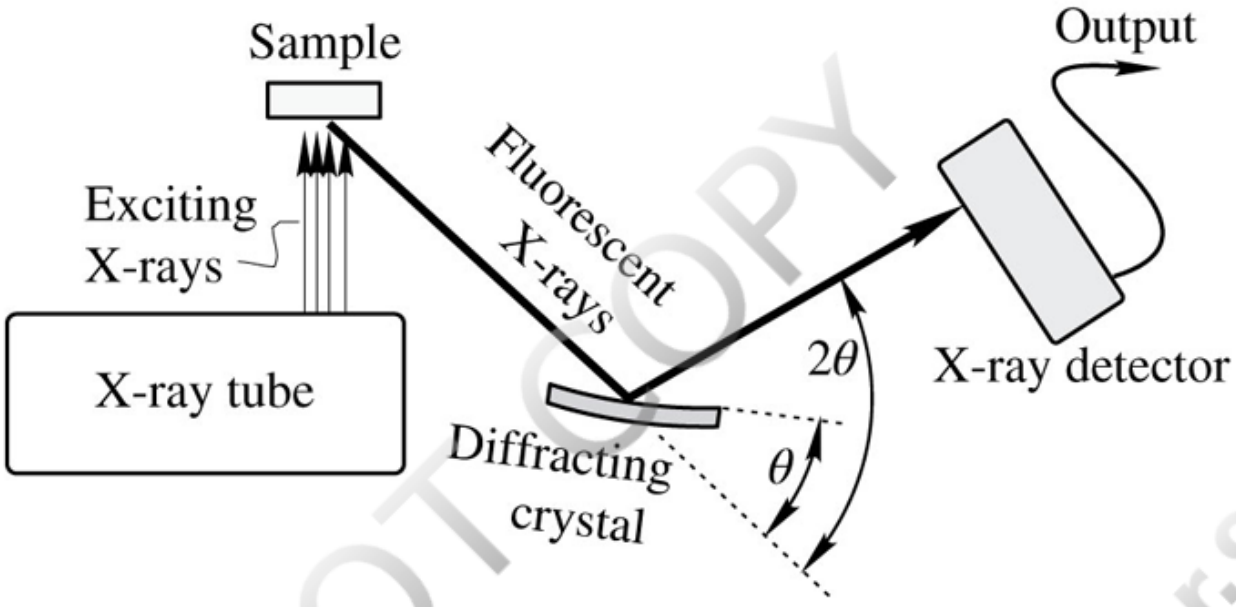

FIGURE 9.11 X-ray fluorescence spectrometer. Background and characteristic X-rays from the X-ray tube cause elements in the sample to generate their characteristic X-rays. Chemical analysis is done by either wavelength- or energy-dispersive spectrometers; here a wavelength-dispersive spectrometer is shown. Back to text

DO NOT COPY

Printed by: e48d507df5d1141@placeholder.94092.edu. Printing is for personal, private use only. No part of this book may be reproduced or transmitted without publisher's prior permission. Violators will be prosecuted.

FIGURE 9.12 Handheld X-ray fluorescence spectrometer analyzing a sample of galena (PbS). The instrument is the Bruker Tracer 5 owned by the University of Northern Colorado. Back to text

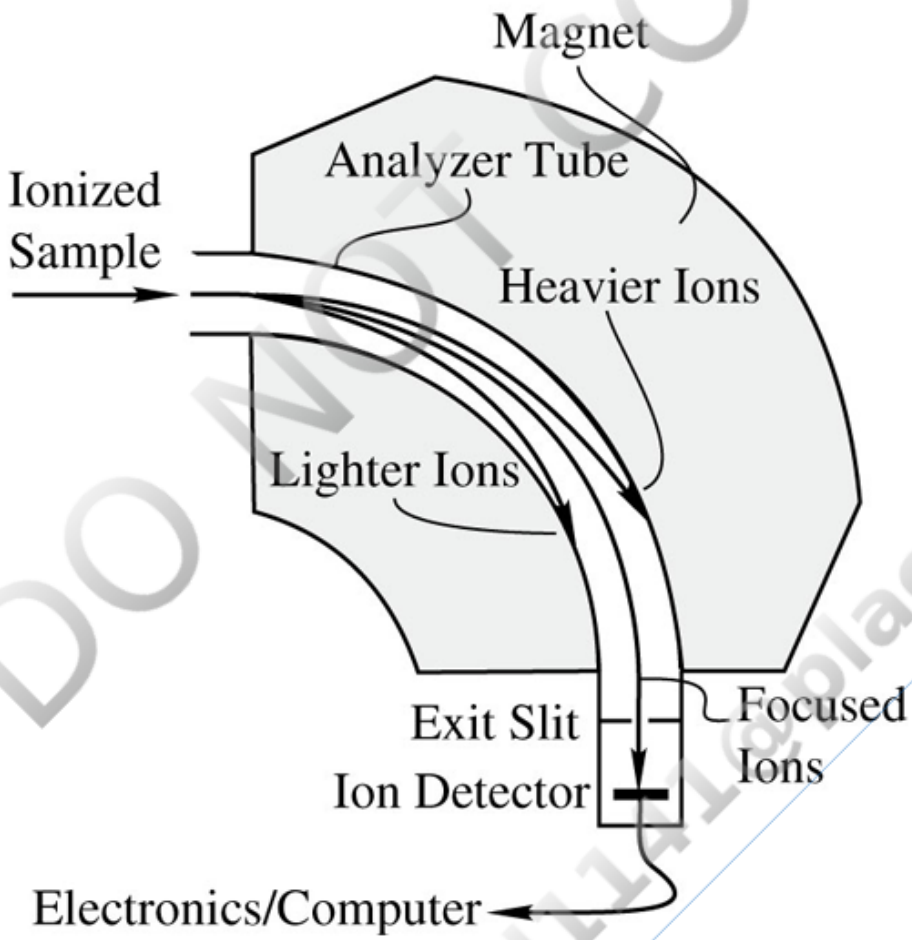

FIGURE 9.13 Schematic of typical mass spectrometer magnet and detector. A single collector mass spectrometer is depicted. Back to text

DO NOT COPY
e48d507df5d1141@placeholder.9409

Printed by: e48d507df5d1141@placeholder.94092.edu. Printing is for personal, private use only. No part of this book may be reproduced or transmitted without publisher's prior permission. Violators will be prosecuted.

Chapter 10 Strategies for Study

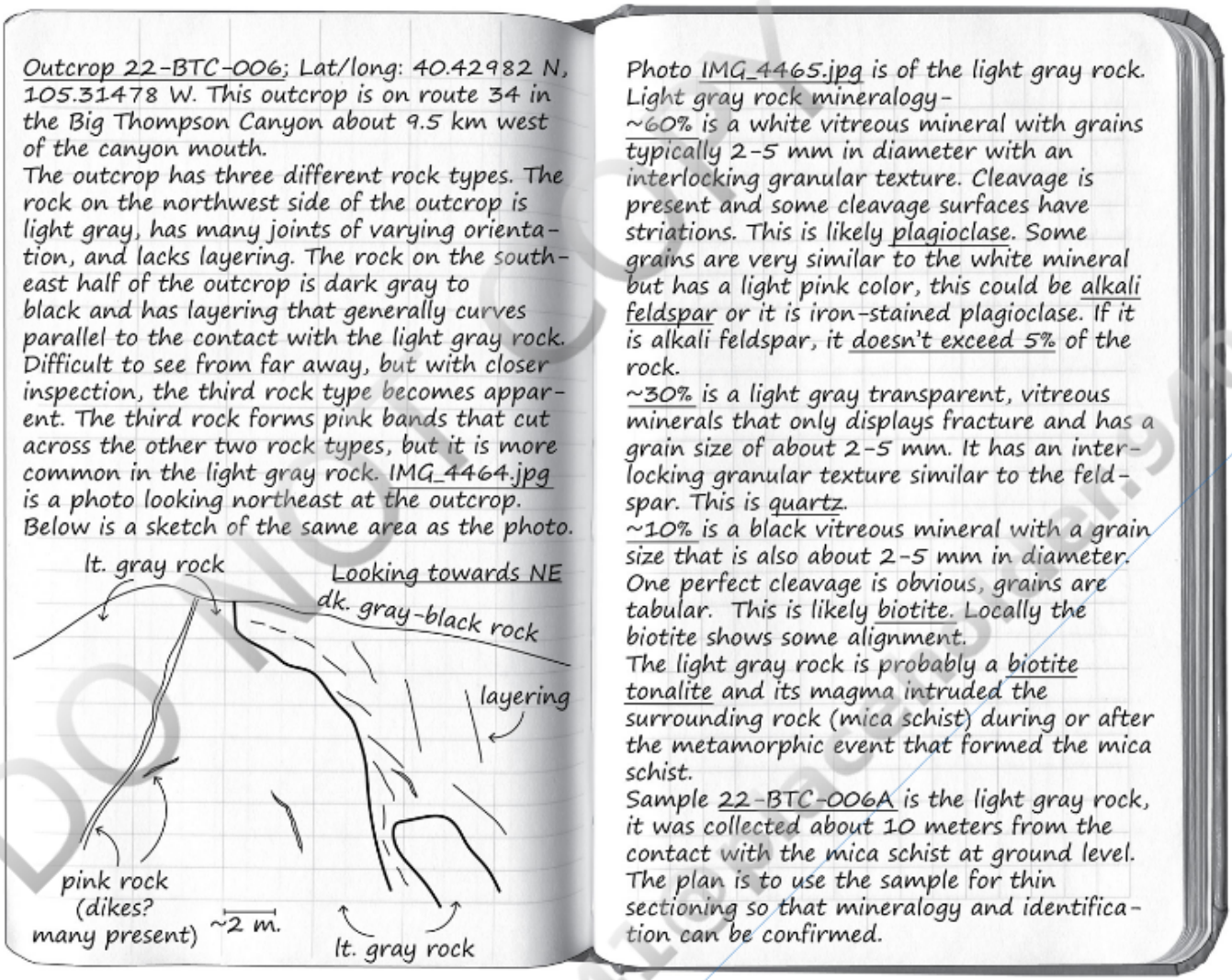

FIGURE 10.1 Example outcrop description entry in a field notebook. Only the notes that cover the outcrop general description and the light gray rock are shown. Underlining can be used to highlight important components, such as photographs, collected samples, and key observations. Figure 10.2 provides a photograph of the outcrop. Figure 10.4 is a photograph of the collected sample. Back to text

Printed by: e48d507df5d1141@placeholder.94092.edu. Printing is for personal, private use only. No part of this book may be reproduced or transmitted without publisher's prior permission. Violators will be prosecuted.

FIGURE 10.2 Photograph of the outcrop described by field notes and the sketch in Figure 10.1. Road marker in the lower right, about 1.5 meters tall, provides scale. Back to text

DO NOT COPY e48d507df5d1141@placeholder.94092

Printed by: e48d507df5d1141@placeholder.94092.edu. Printing is for personal, private use only. No part of this book may be reproduced or transmitted without publisher's prior permission. Violators will be prosecuted.

FIGURE 10.3 Sample collection directly from the outcrop aided by a hammer and chisel. Back to text

FIGURE 10.4 Collected sample. The sample description is recorded in the field notes (Figure 10.1) and on the bag label. Samples should be marked with a label using a permanent marker, shown for scale (14 cm). Canvas bags (shown) are often used to hold samples, but any sturdy bag or box can be used. Back to text

Printed by: e48d507df5d1141@placeholder.94092.edu. Printing is for personal, private use only. No part of this book may be reproduced or transmitted without publisher's prior permission. Violators will be prosecuted.

TREMOLITE - FERRO-ACTINOLITE — Mineral Name or Mineral Series Name

$Ca_2(Mg,Fe)_5Si_8O_{22}(OH)_2$ — Chemical Formula

Monoclinic 2/*m* — Crystal System and Point Group

$a = 9.84–10.02$Å, $b = 18.05–18.20$ Å, $c = 5.29–5.31$Å, $\beta = 104.8–104.6°$ — Unit Cell Dimensions

$Z = 2$ — Formula Units per Unit Cell (Z)

$H = 5 – 6$ — Hardness (H)

$G = 2.99 – 3.48$ — Specific Gravity (G)

Biaxial (–) — Optical Class and Sign

$n_\alpha = 1.599–1.688$

$n_\beta = 1.612–1.697$ — Indices of Refraction

$n_\gamma = 1.622–1.705$

$\delta = 0.027–0.017$ — Birefringence (δ)

$2V_x = 62–88$ — Optic Angle ($2V_x$)

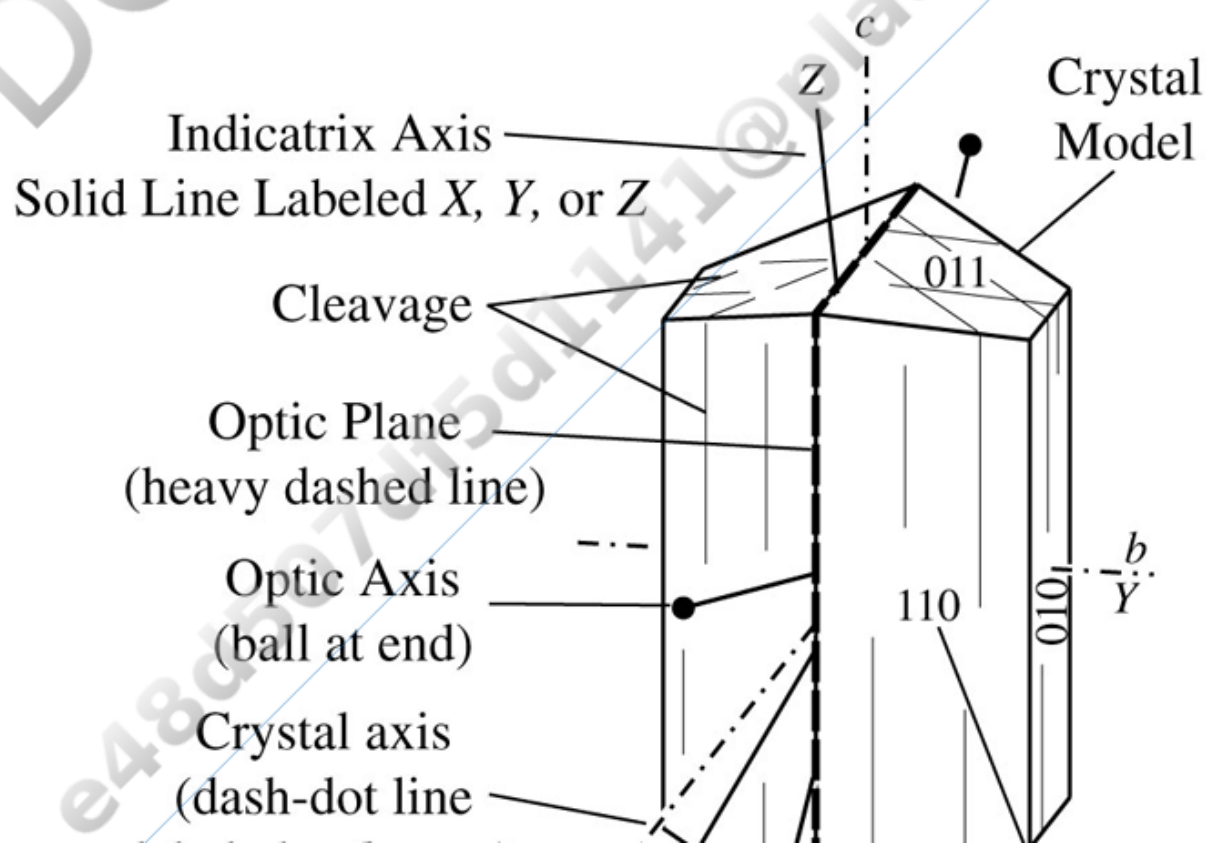

DO NOT COPY

Printed by: e48d507df5d1141@placeholder.94092.edu. Printing is for personal, private use only. No part of this book may be reproduced or transmitted without publisher's prior permission. Violators will be prosecuted.

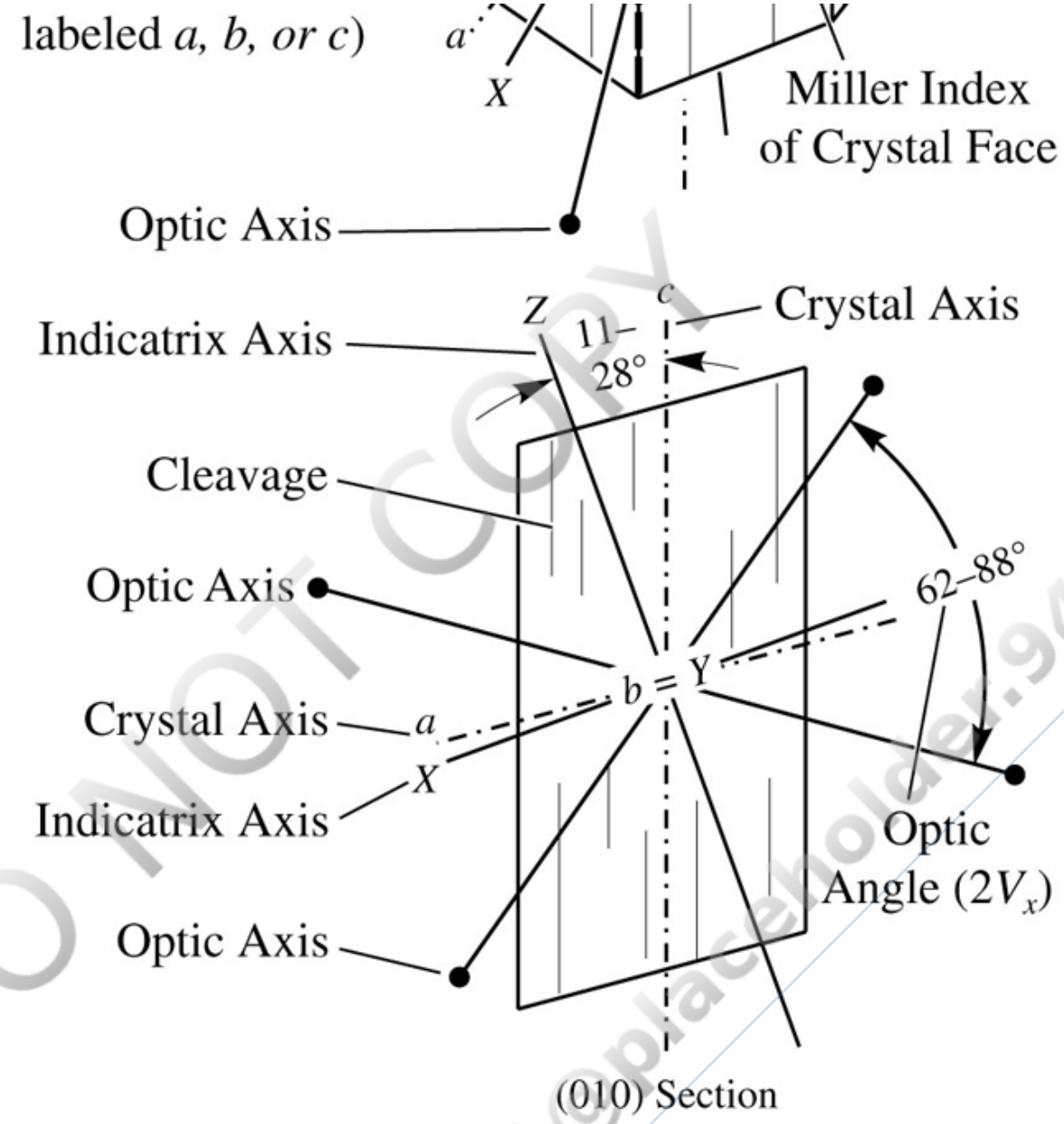

FIGURE 10.5 Presentation of mineral data. Back to text

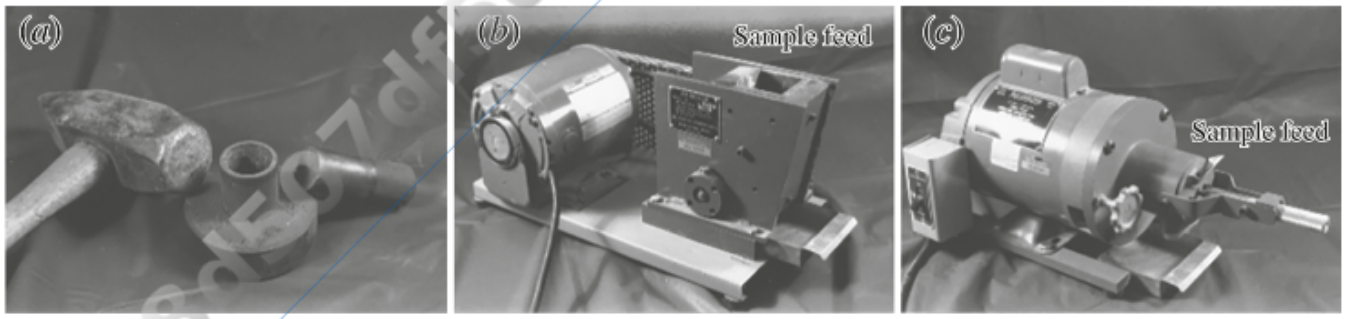

FIGURE 10.6 Crushing tools. (*a*) Piston-type percussion steel mortar and pestle. The mortar accepts samples upward of about 2 cm in diameter. The sample is crushed by placing the pestle on top of the sample in the mortar and tapping the pestle down against the sample with a hammer. (*b*)

Printed by: e48d507df5d1141@placeholder.94092.edu. Printing is for personal, private use only. No part of this book may be reproduced or transmitted without publisher's prior permission. Violators will be prosecuted.

top of the sample in the mortar and tapping the pestle down against the sample with a hammer. (*b*) Laboratory jaw crusher. This relatively small jaw crusher accepts samples upward of about 2 cm in diameter; larger version can crush samples upward of tens of decimeters in diameter. A jaw crusher crushes samples by moving a plate toward and away an immovable plate, similar to the motion of jaws of a feeding animal. (*c*) Rotary mill. The sample is fed into the chute and is crushed between rotating plates. This small mill accepts samples upward of about 5 mm in diameter; larger versions can crush samples upward of 1–2 cm in diameter. Back to text

FIGURE 10.7 Sieve used with small samples. On the left is a sieve, constructed of a brass ring with brass wire mesh that only allows grains of a certain size to pass. Usually two sieves of different sizes are stacked (larger size on top) with a lid and base (on right). Sample is added to the top sieve in the stack, the lid is placed, and the whole stack is shaken until no more sample passes through the sieves. Back to text

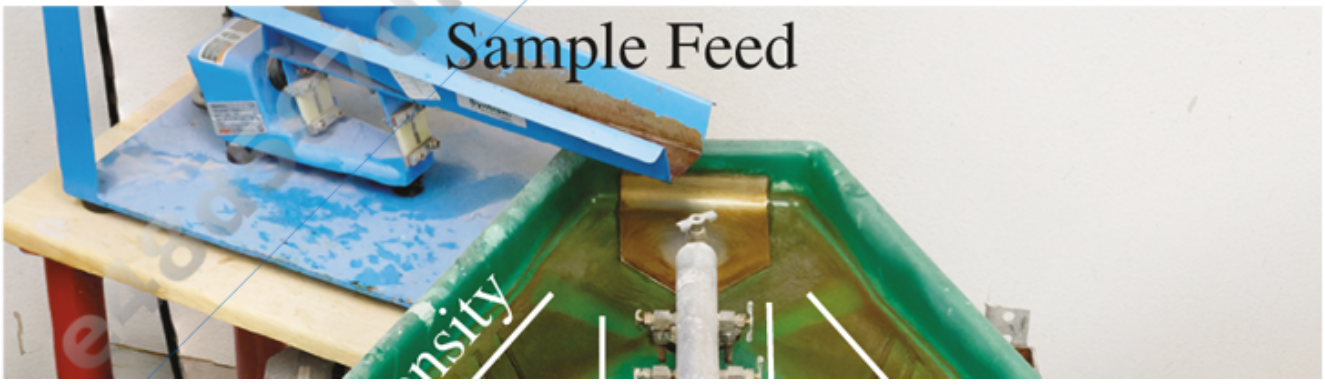

Printed by: e48d507df5d1141@placeholder.94092.edu. Printing is for personal, private use only. No part of this book may be reproduced or transmitted without publisher's prior permission. Violators will be prosecuted.

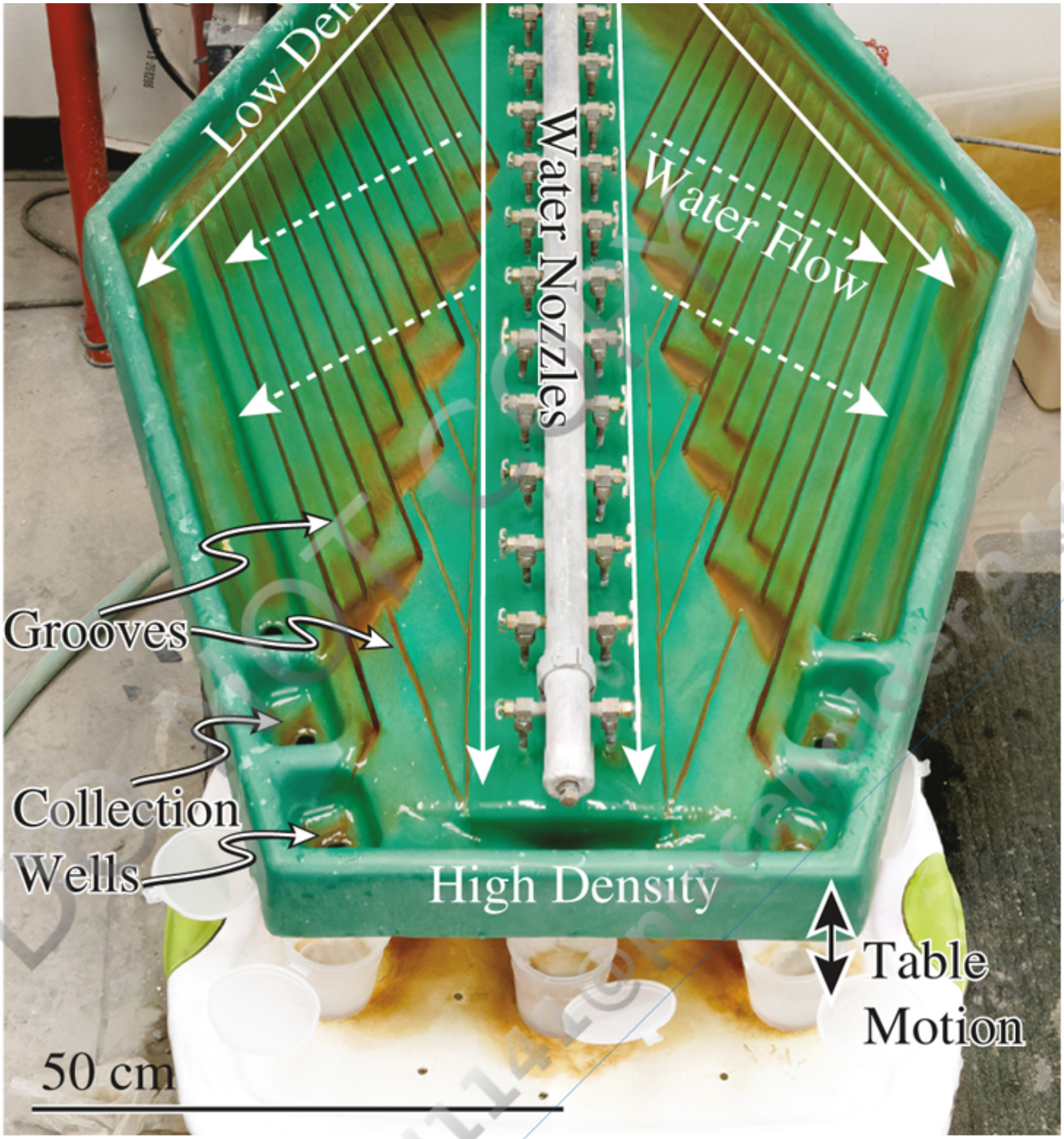

FIGURE 10.8 Shaker table. For this type of table, sample is added to the table at the top of the image by a feed hopper, and water from water nozzles along the table center washes lighter grains to the side while the table shakes back and forth. Dense grains are caught in grooves and are directed to the collection wells at the bottom of the table. Back to text

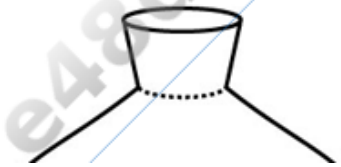

Printed by: e48d507df5d1141@placeholder.94092.edu. Printing is for personal, private use only. No part of this book may be reproduced or transmitted without publisher's prior permission. Violators will be prosecuted.

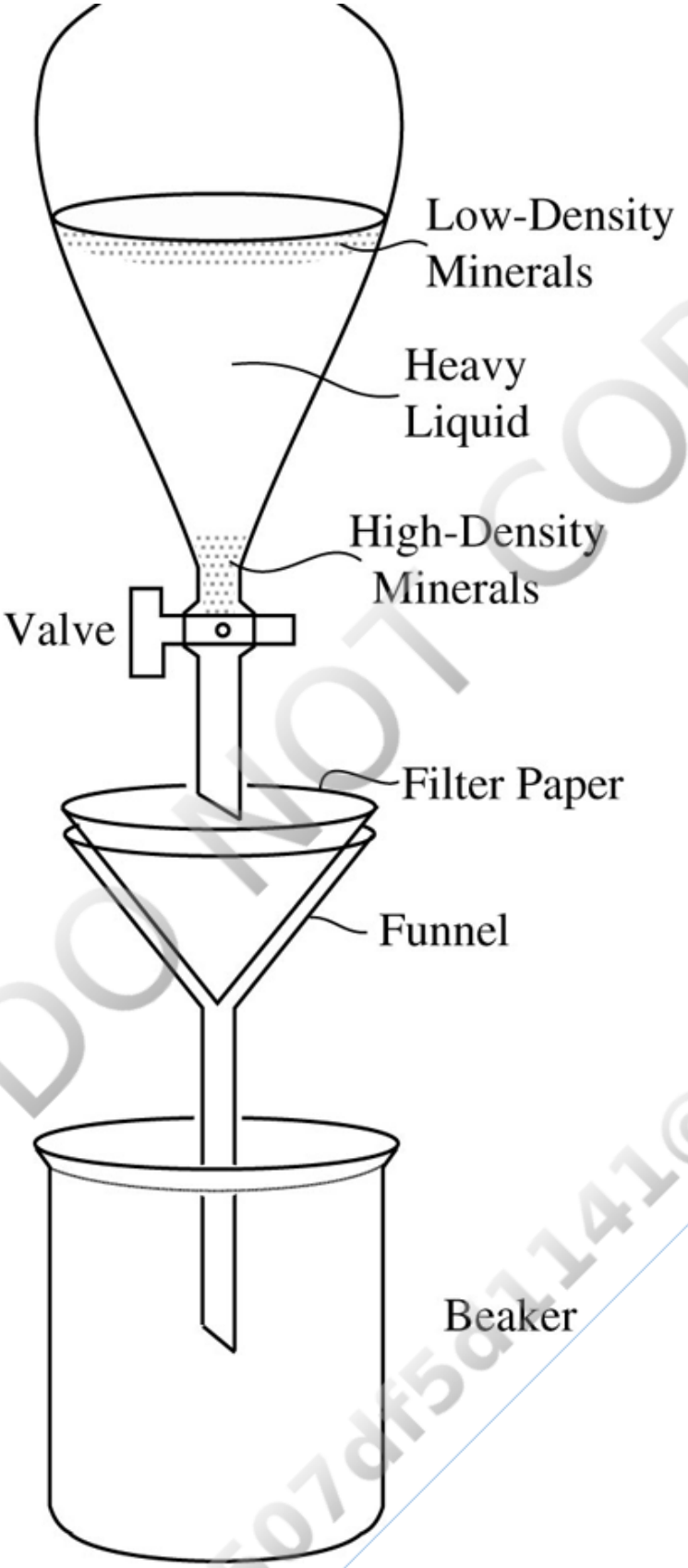

FIGURE 10.9 Separatory funnel setup. Back to text

DO NOT COPY
e48d507df5d1141@placeholder.9409

Printed by: e48d507df5d1141@placeholder.94092.edu. Printing is for personal, private use only. No part of this book may be reproduced or transmitted without publisher's prior permission. Violators will be prosecuted.

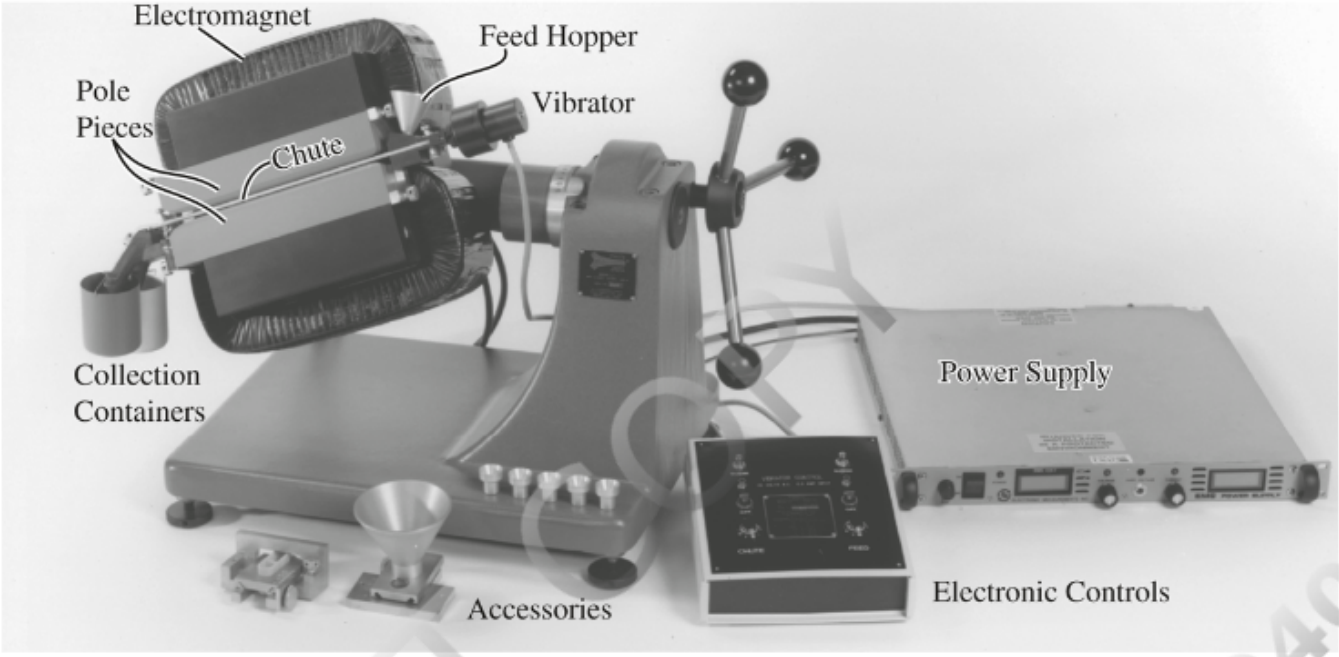

FIGURE 10.10 Frantz® Magnetic Barrier Laboratory Separator. The closely related Frantz® Magnetic Barrier Laboratory Separator provides improved capabilities and appears much similar but with a different feed hopper and chute. Photo courtesy of S. G. Frantz Company. Back to text

DO NOT COPY e48d507df5d1141@placeholder.94092

Printed by: e48d507df5d1141@placeholder.94092.edu. Printing is for personal, private use only. No part of this book may be reproduced or transmitted without publisher's prior permission. Violators will be prosecuted.

Chapter 11 Silicates

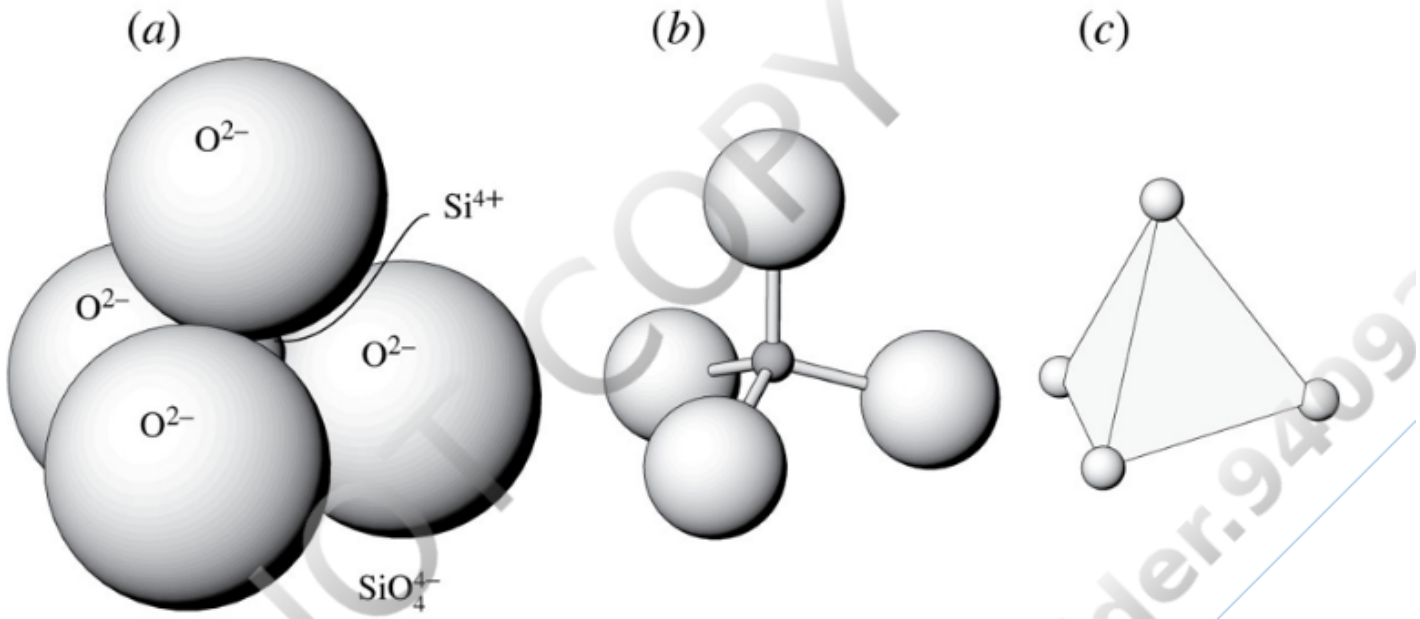

FIGURE 11.1 A silicon tetrahedron consists of four O^{2-} forming a tetrahedral coordination polyhedron around a Si^{4+}. (*a*) Silicon and oxygen as scaled spheres. (*b*) Ball-and-stick representation with silicon and oxygen sizes reduced by half. (*c*) Oxygen anions shown as small spheres at corners of tetrahedron. Back to text

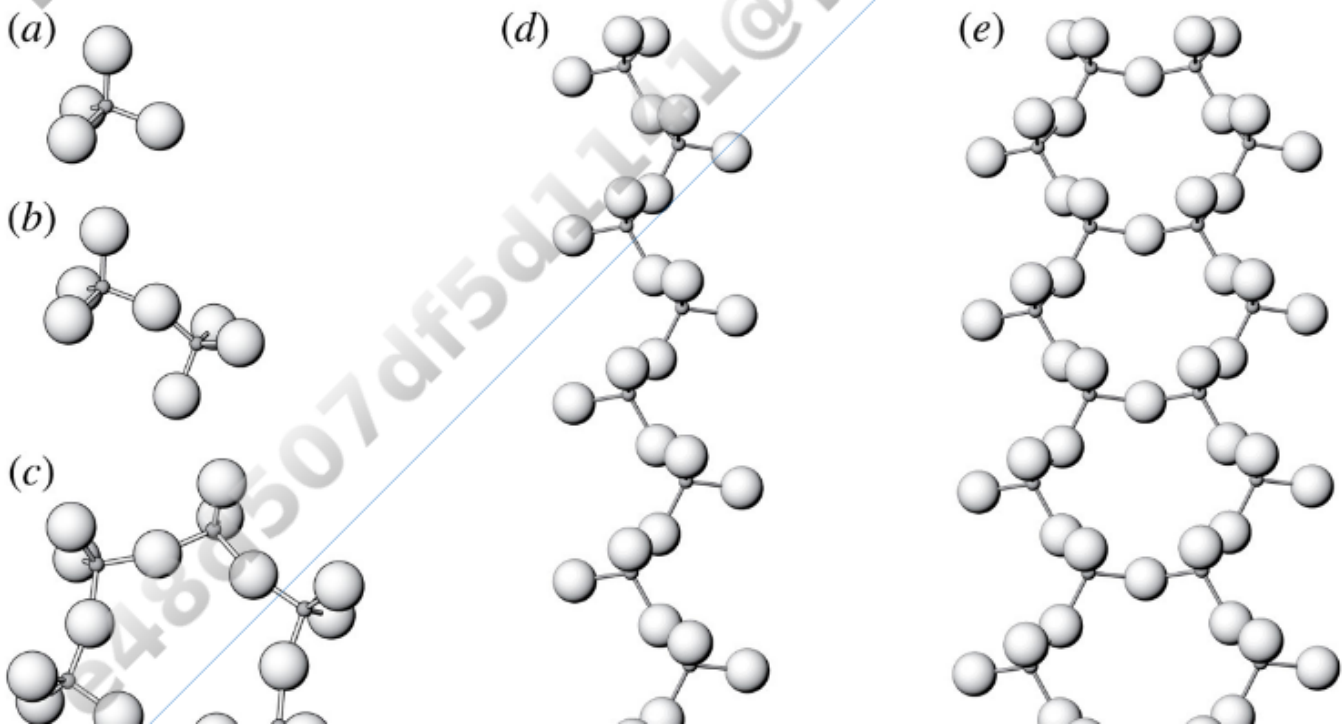

DO NOT COPY e48d507df5d1141@placeholder.9409

Printed by: e48d507df5d1141@placeholder.94092.edu. Printing is for personal, private use only. No part of this book may be reproduced or transmitted without publisher's prior permission. Violators will be prosecuted.

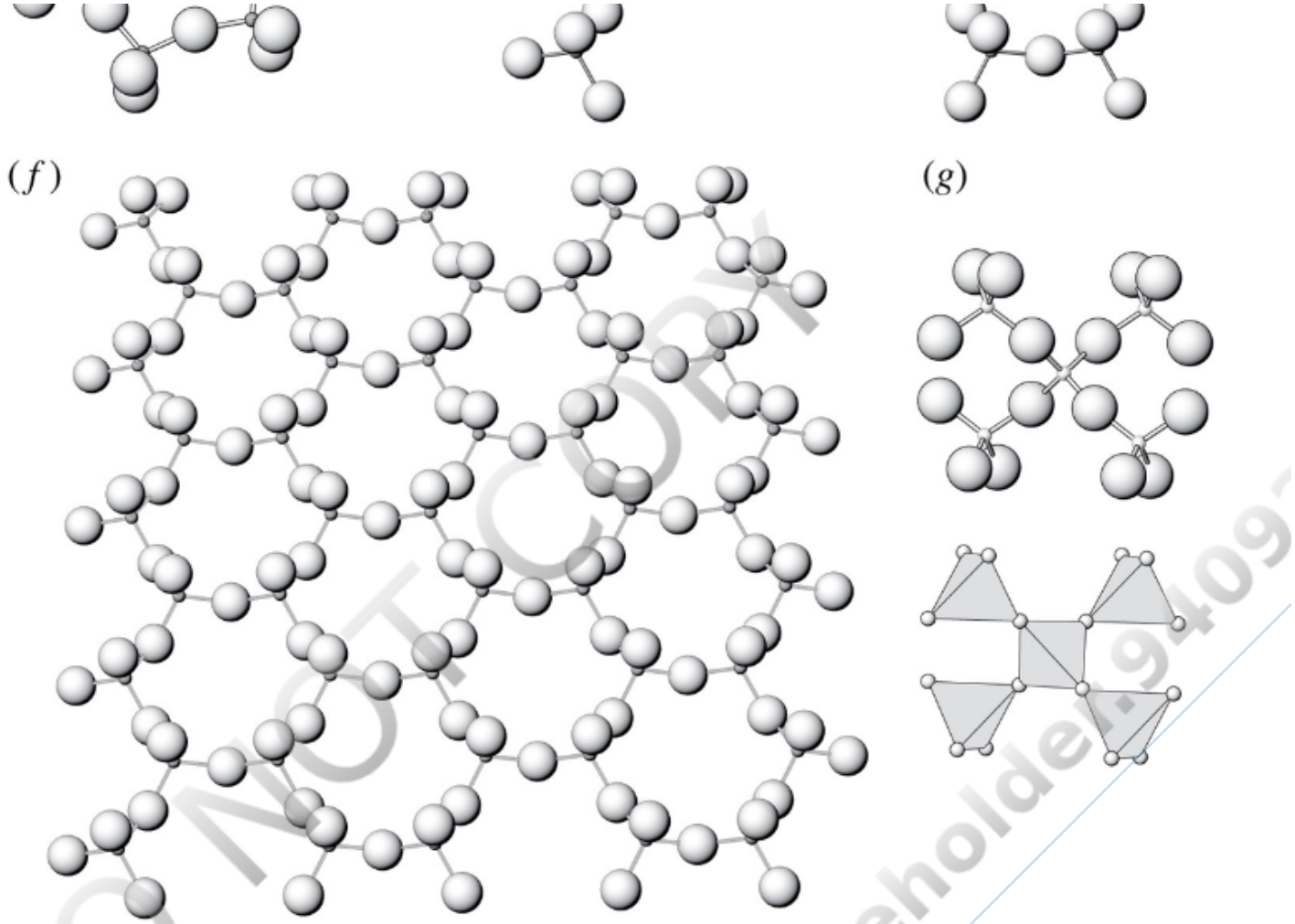

FIGURE 11.2 Silicate structures. (*a*) Orthosilicates. The basic building block is a single tetrahedron. (*b*) Disilicates. A single oxygen is shared between two tetrahedra. (*c*) Ring silicates. Tetrahedra share two oxygen each to form rings. (*d*) Single-chain silicates. Two oxygen are shared per tetrahedron. (*e*) Double-chain silicates. Tetrahedra share two and/or three oxygens. (*f*) Sheet silicates. Three oxygen per tetrahedron are shared to form continuous sheets. (*g*) Framework silicates. All four oxygens on the central tetrahedron are shared with adjacent tetrahedra, as shown in the ball-and-stick and polyhedra diagrams. While not shown, the oxygens in the outer four tetrahedra are shared with additional tetrahedra to form a three-dimensional framework. Back to text

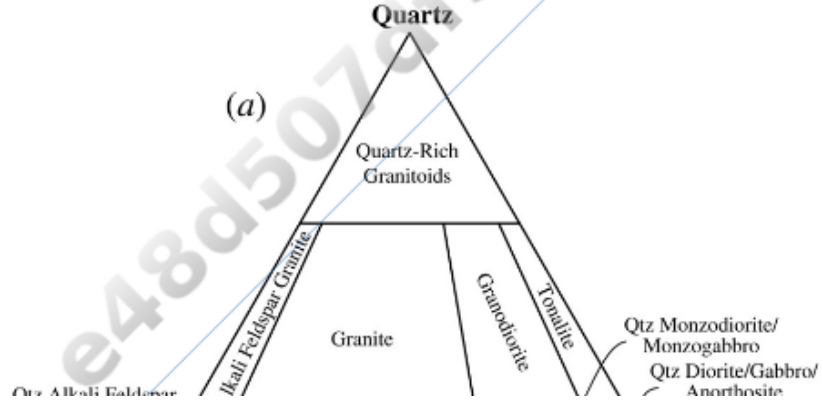

Printed by: e48d507df5d1141@placeholder.94092.edu. Printing is for personal, private use only. No part of this book may be reproduced or transmitted without publisher's prior permission. Violators will be prosecuted.

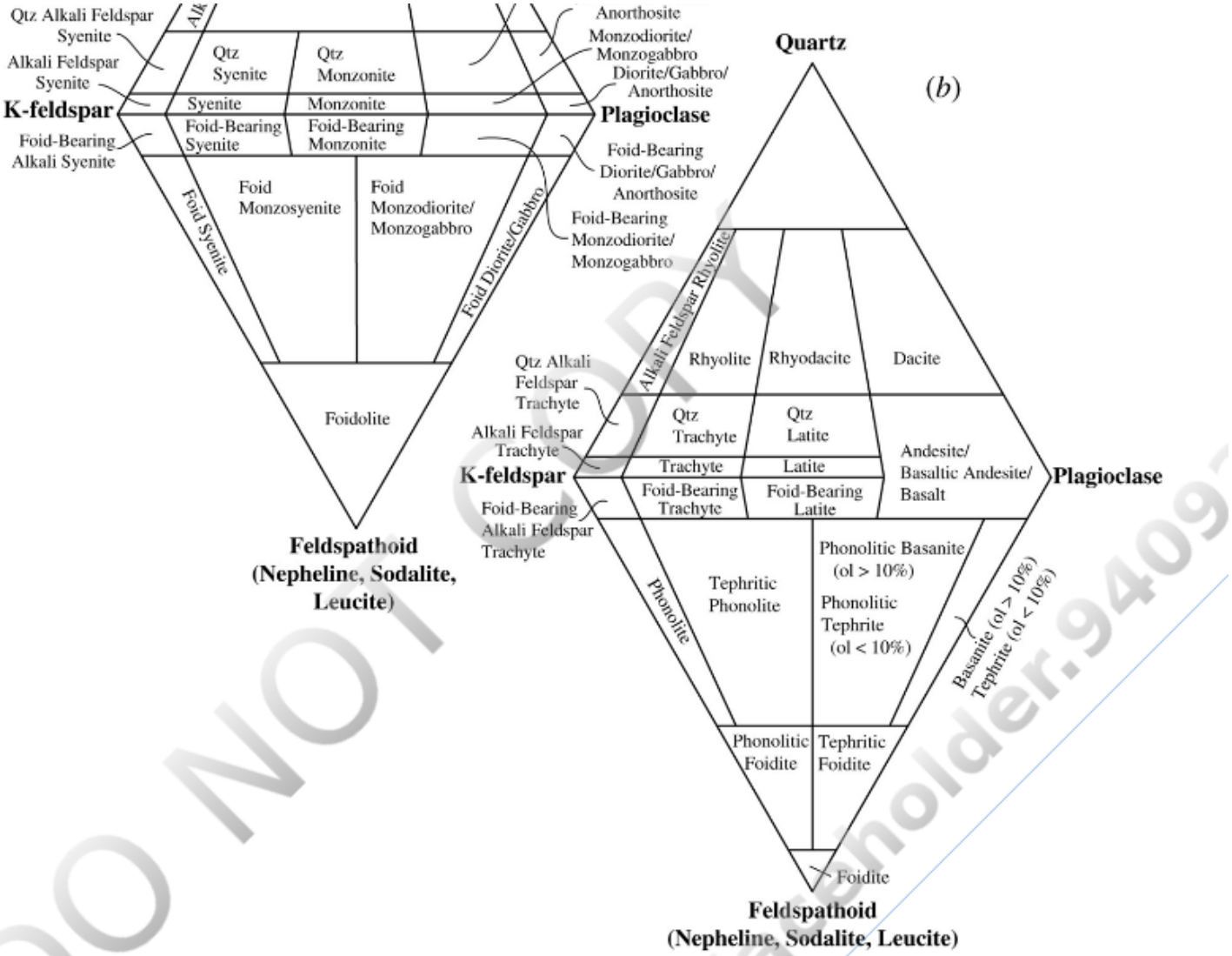

FIGURE 11.3 Classification of igneous rocks. Classification is based on the relative amounts (volume percentages) of quartz, K-feldspar, plagioclase, and feldspathoids (nepheline, sodalite, leucite). Other minerals are ignored. (*a*) Plutonic rocks. (*b*) Volcanic rocks. Adapted from Streckheisen (1976) and Le Maitre and others (2002). Back to text

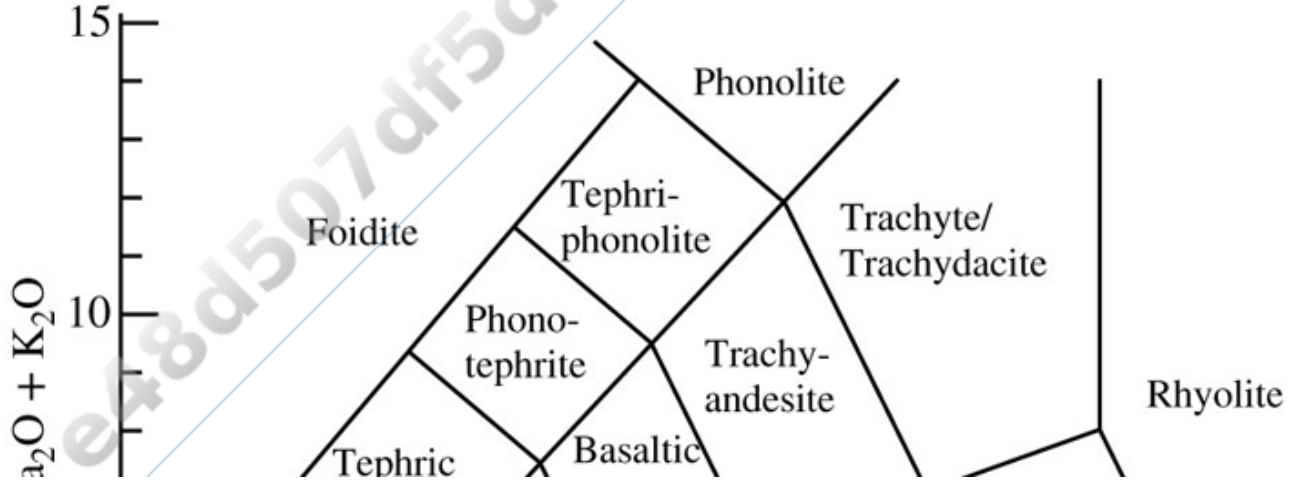

DO NOT COPY e48d507df5d1141@placeholder.9409

Printed by: e48d507df5d1141@placeholder.94092.edu. Printing is for personal, private use only. No part of this book may be reproduced or transmitted without publisher's prior permission. Violators will be prosecuted.

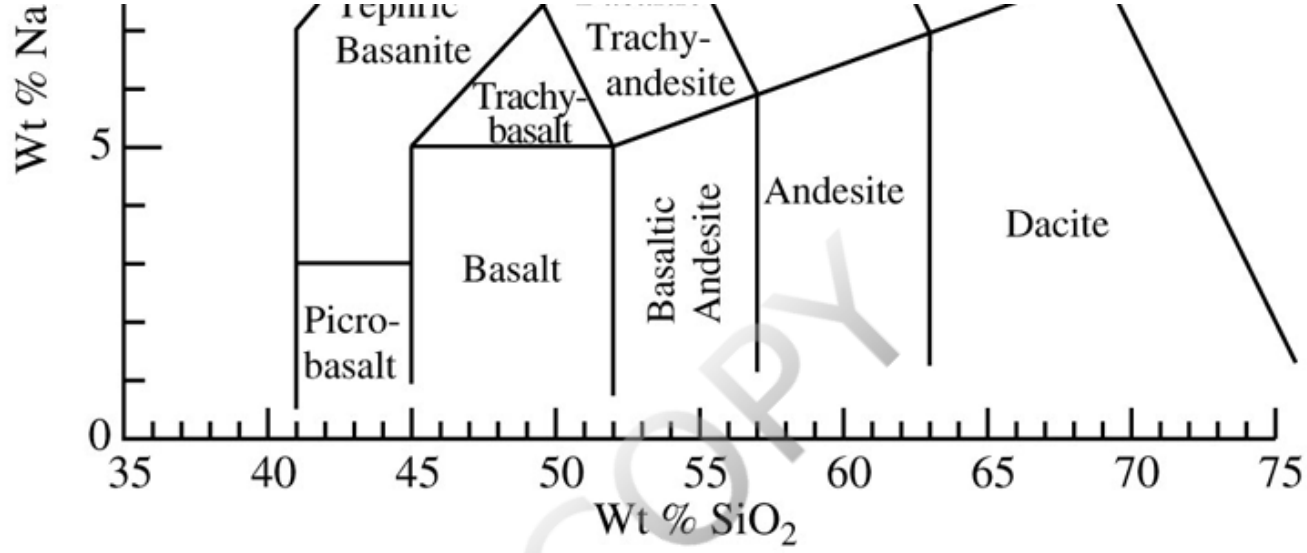

FIGURE 11.4 Chemical classification of volcanic rocks based on weight percent of SiO_2 and $Na_2O + K_2O$. Based upon Le Bas and others (1986). Back to text

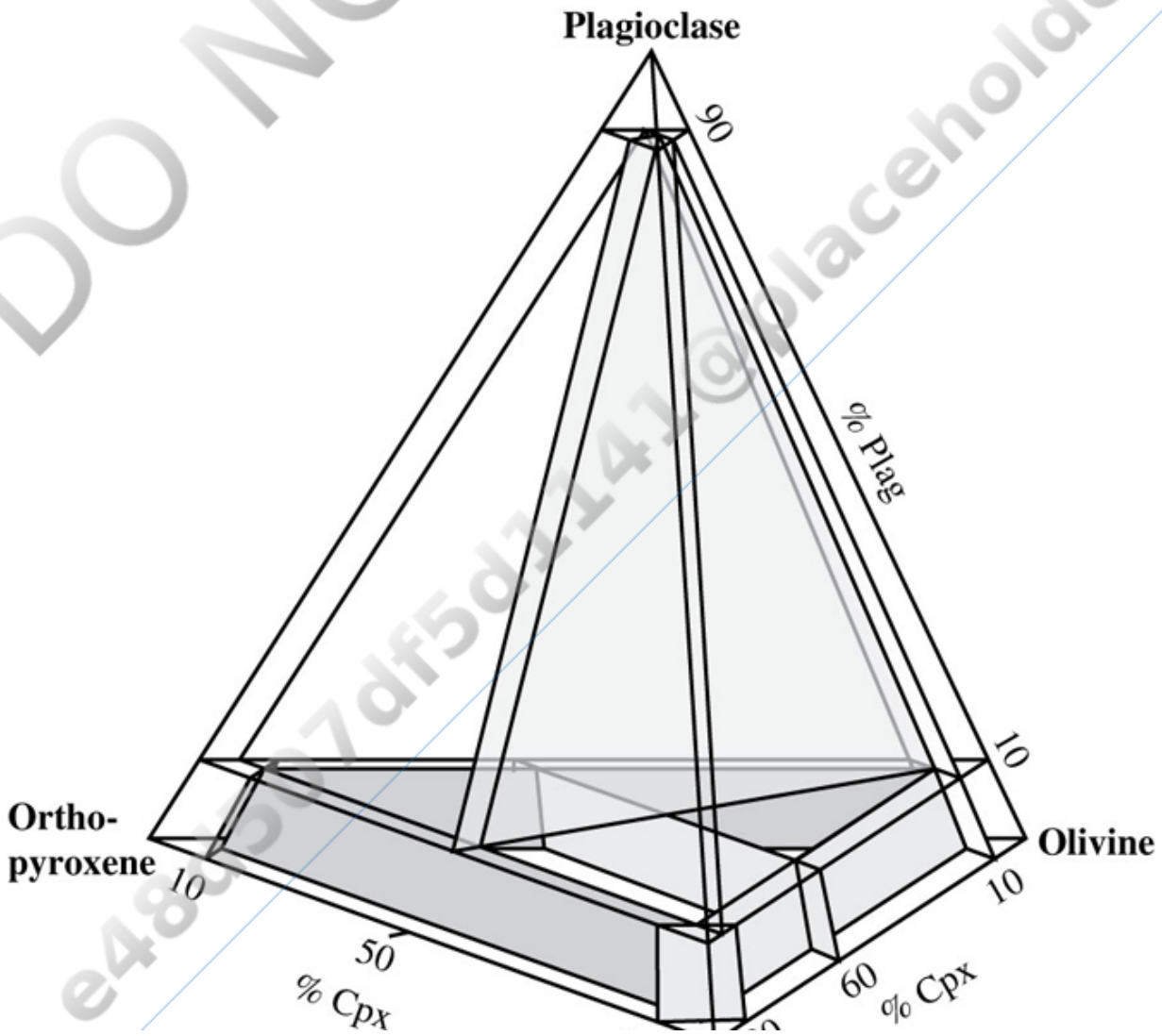

DO NOT COPY
e48d507df5d1141@placeholder.9409

Printed by: e48d507df5d1141@placeholder.94092.edu. Printing is for personal, private use only. No part of this book may be reproduced or transmitted without publisher's prior permission. Violators will be prosecuted.

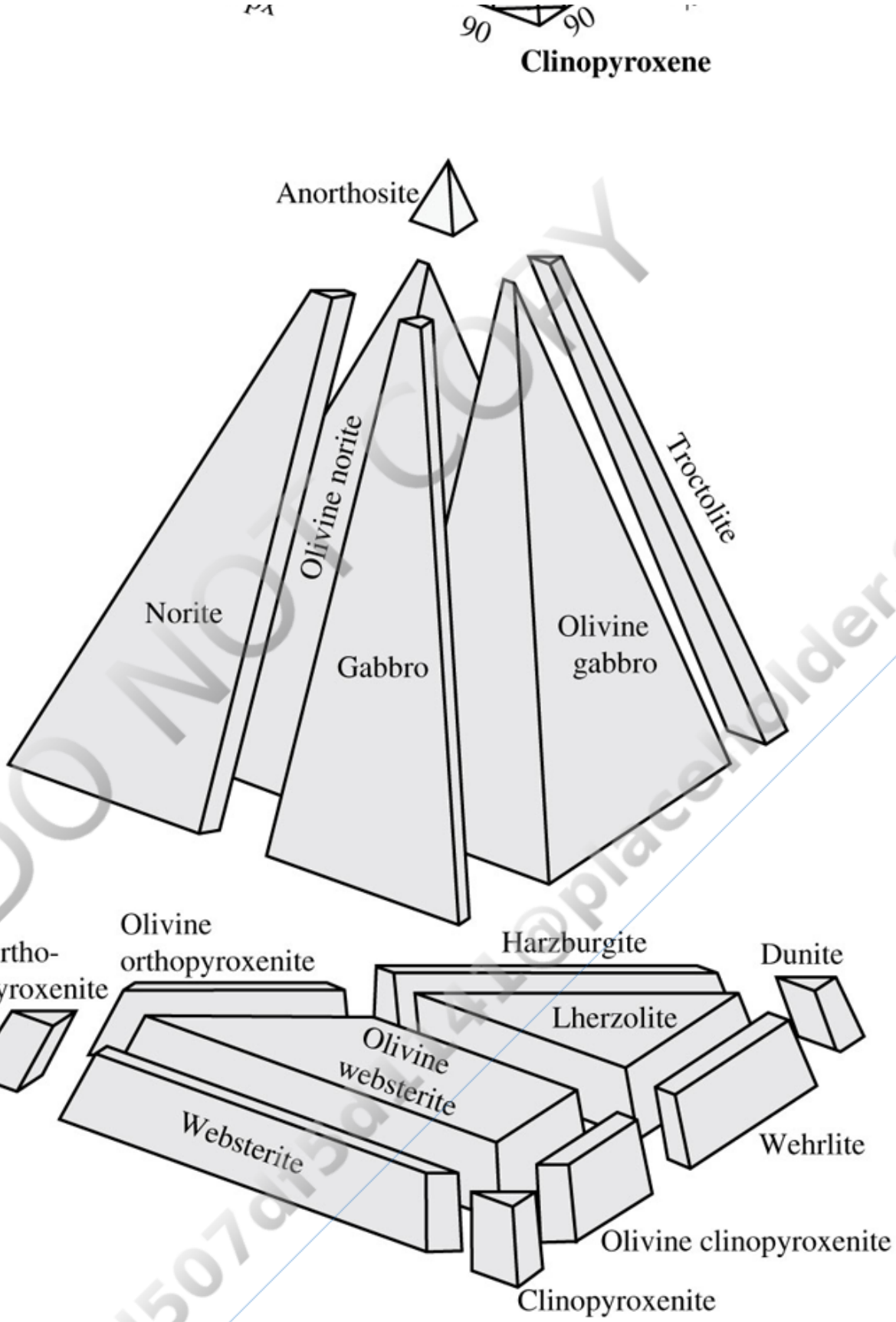

FIGURE 11.5 Classification of plutonic igneous rocks lacking significant amounts of quartz, K-feldspar, or feldspathoids. Adapted from Streckheisen (1976) and Le Maitre and others (2002). Back to text

DO NOT COPY
e4d507df5d1141@placeholder.9409

Printed by: e48d507df5d1141@placeholder.94092.edu. Printing is for personal, private use only. No part of this book may be reproduced or transmitted without publisher's prior permission. Violators will be prosecuted.

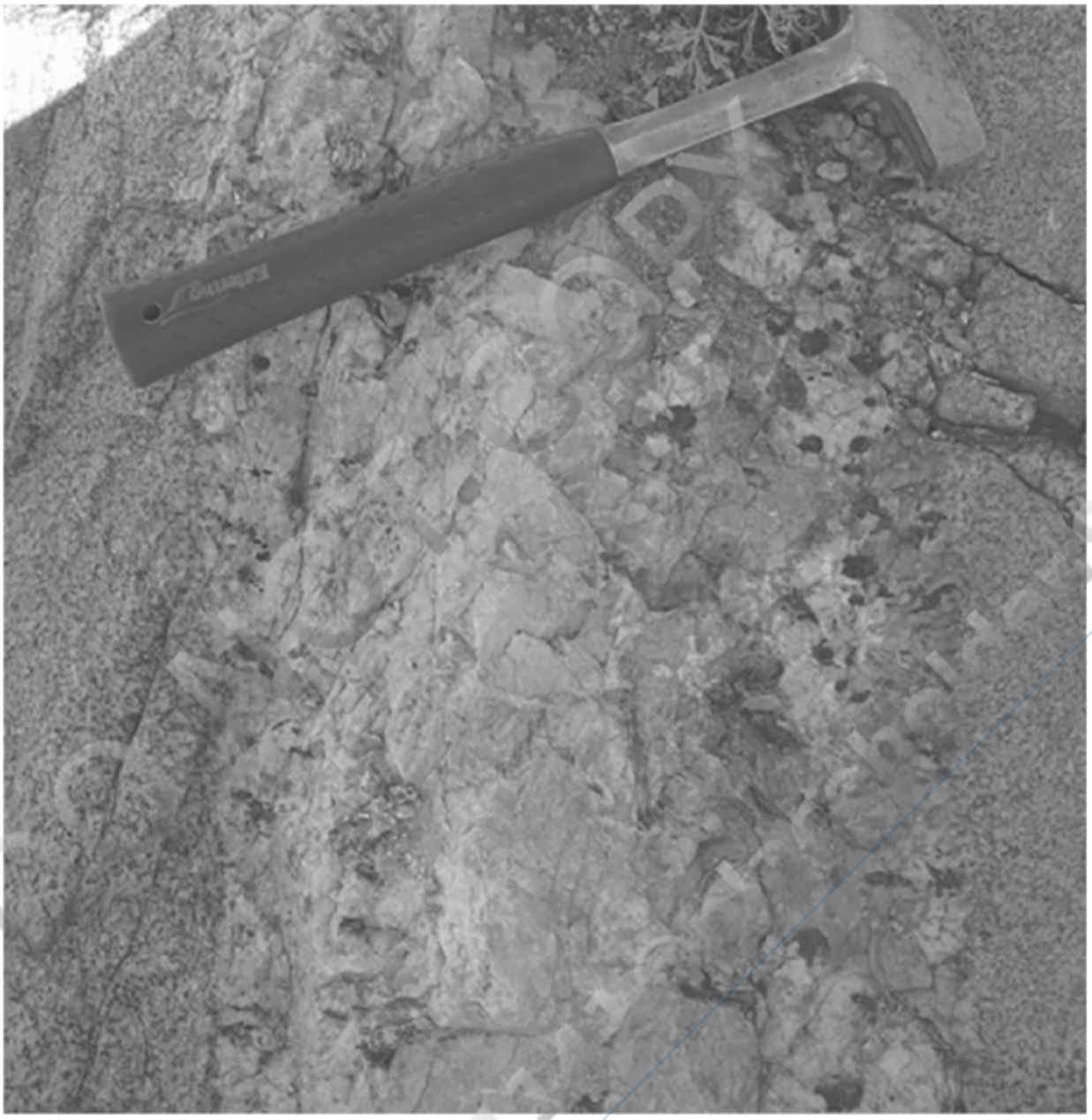

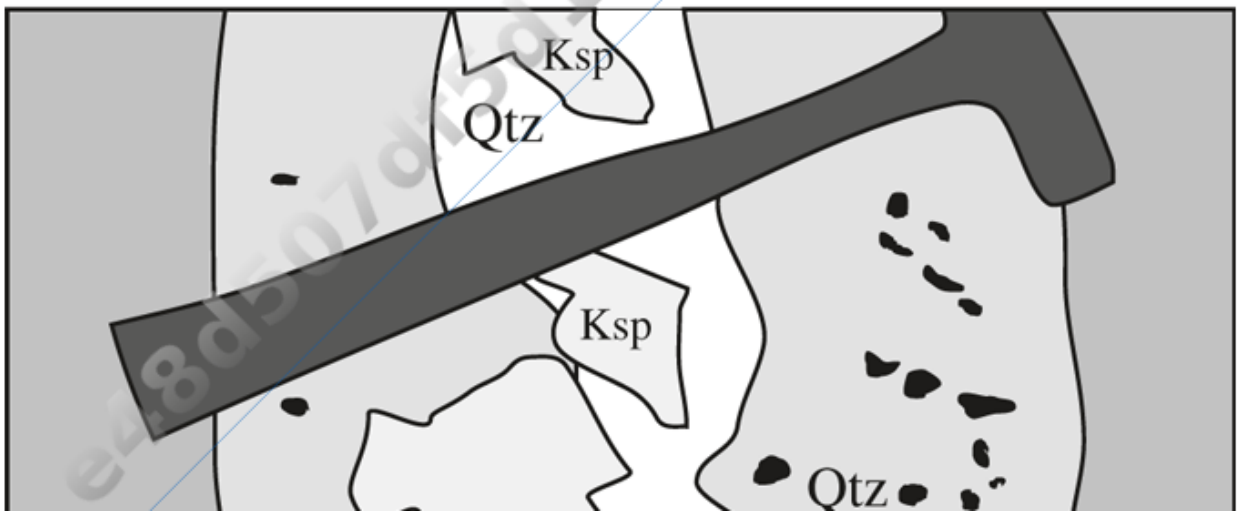

Printed by: e48d507df5d1141@placeholder.94092.edu. Printing is for personal, private use only. No part of this book may be reproduced or transmitted without publisher's prior permission. Violators will be prosecuted.

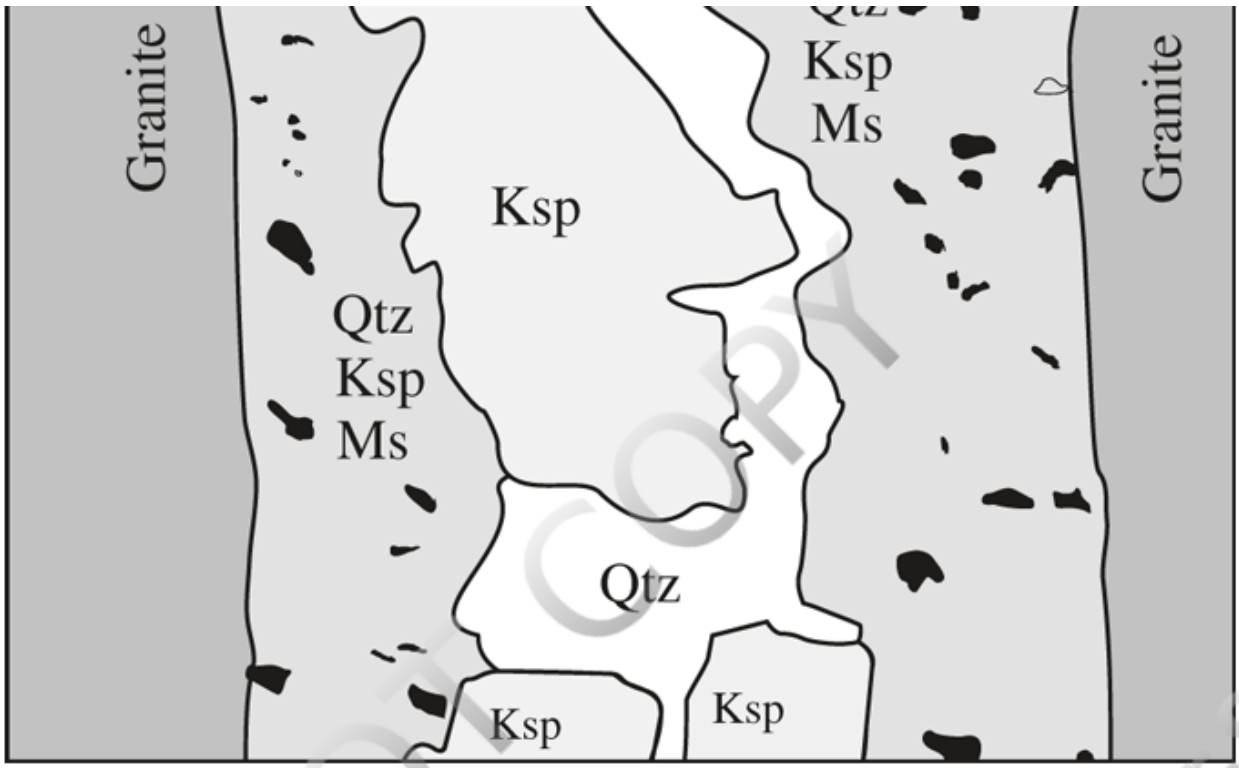

FIGURE 11.6 This small pegmatite dike (*top*) that has intruded Precambrian granite is compositionally zoned. The outer zones consist of intergrown quartz (Qtz), K-feldspar (Ksp), and muscovite (Ms) with scattered tourmaline grains (black). The central zone consists of large K-feldspar grains (some are euhedral) and large masses of quartz. The mineral zoning documents the sequence of crystallization of the magma from the margin of the intrusion to the center. The sketch at the bottom shows the major components. Back to text

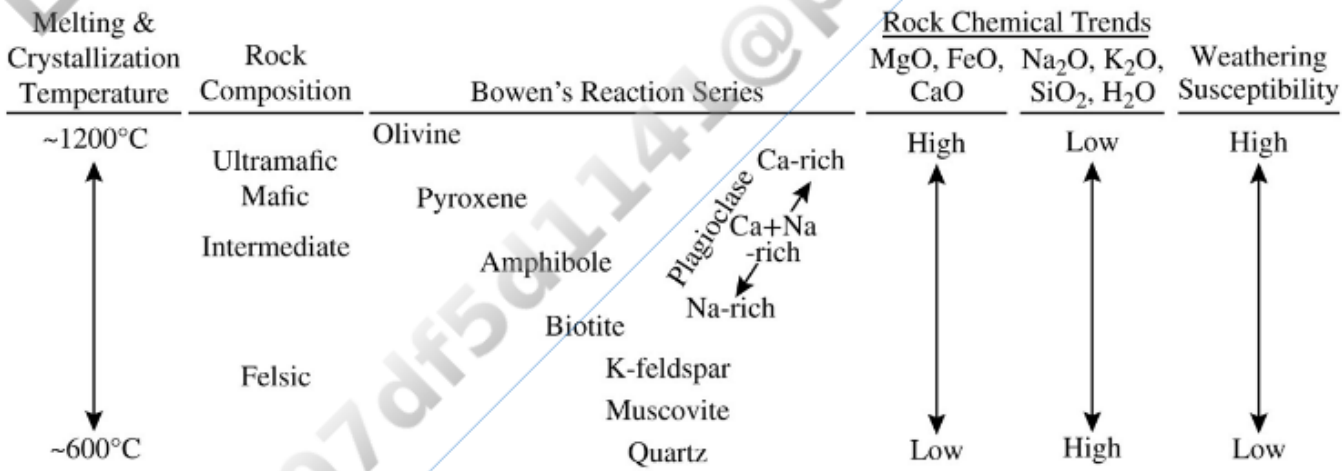

FIGURE 11.7 Bowen's reaction series simplified and connected to mineral melting and crystallization temperatures, rock chemical trends, and mineral weathering susceptibilities. Back to text

Printed by: e48d507df5d1141@placeholder.94092.edu. Printing is for personal, private use only. No part of this book may be reproduced or transmitted without publisher's prior permission. Violators will be prosecuted.

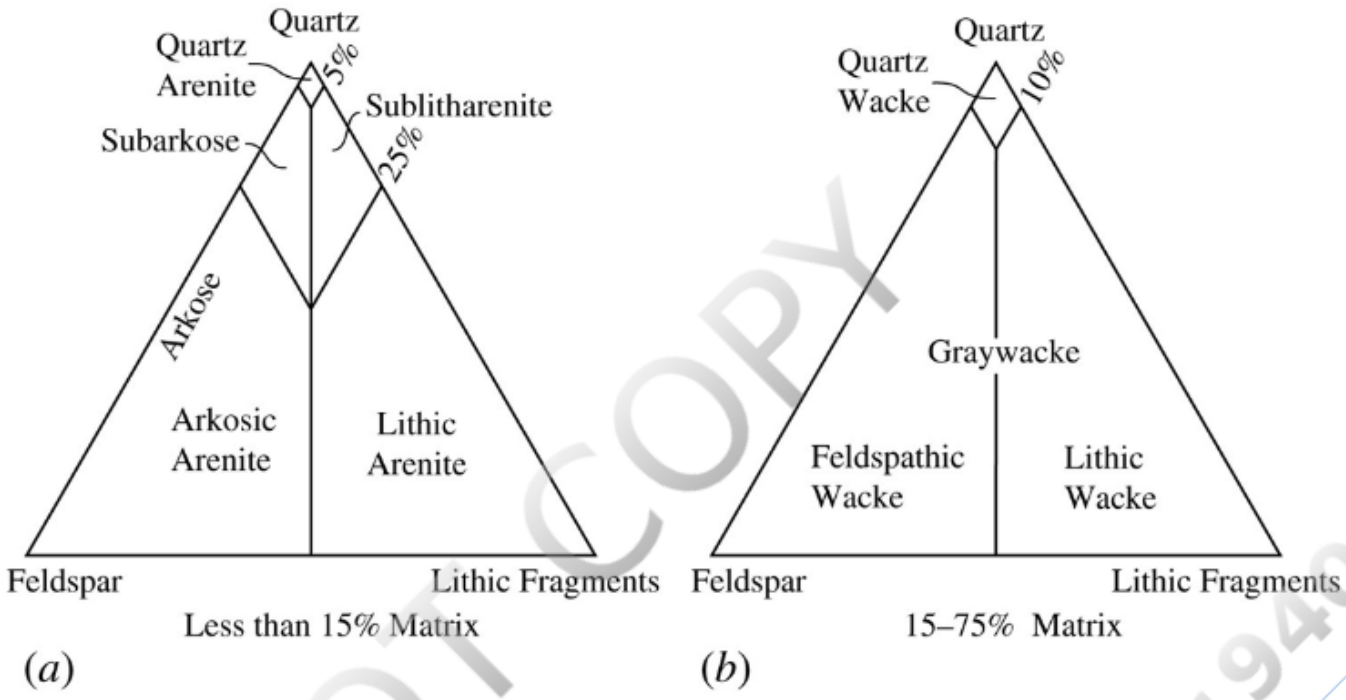

FIGURE 11.8 Classification of sandstones based on quartz, feldspar (K-feldspar + plagioclase), and lithic fragment content of the sand-sized particles. (*a*) *Arenites* have less than 15 percent matrix material (clay, fine quartz, etc.). *Arkose* is a common term for rocks with mostly quartz and feldspar grains. (*b*) *Wackes* have 15 percent or more matrix material. *Graywacke* is a more generic term applied to wackes with substantial amounts of quartz, feldspar, and lithic fragments. Modified from Dott (1964). Back to text

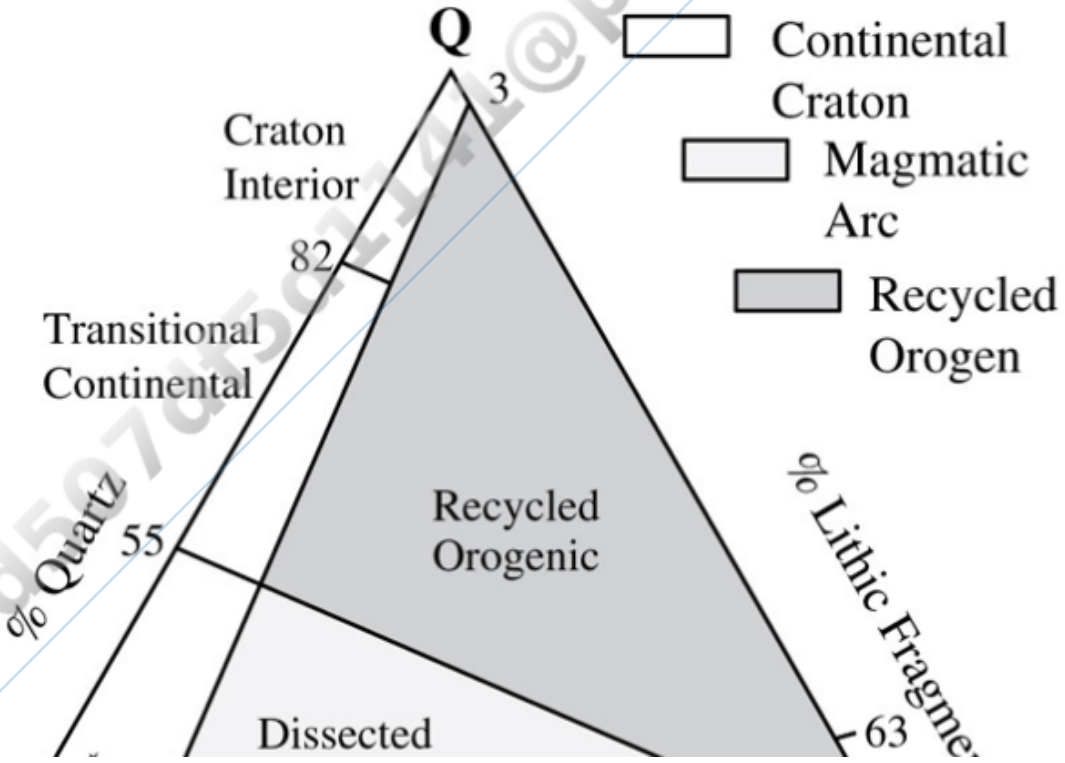

DO NOT COPY

Printed by: e48d507df5d1141@placeholder.94092.edu. Printing is for personal, private use only. No part of this book may be reproduced or transmitted without publisher's prior permission. Violators will be prosecuted.

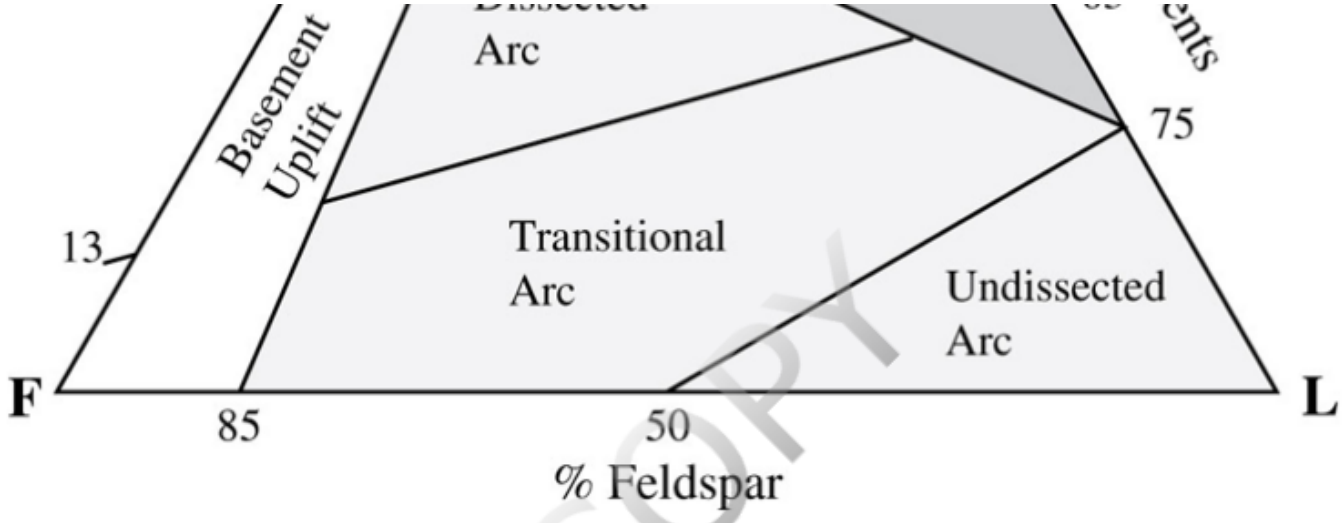

FIGURE 11.9 Mineralogy of framework grains in sandstone derived from different tectonic settings. Q=quartz, F=feldspar, L=lithic fragments. Adapted from Dickinson and others (1983). See text for additional discussion. Back to text

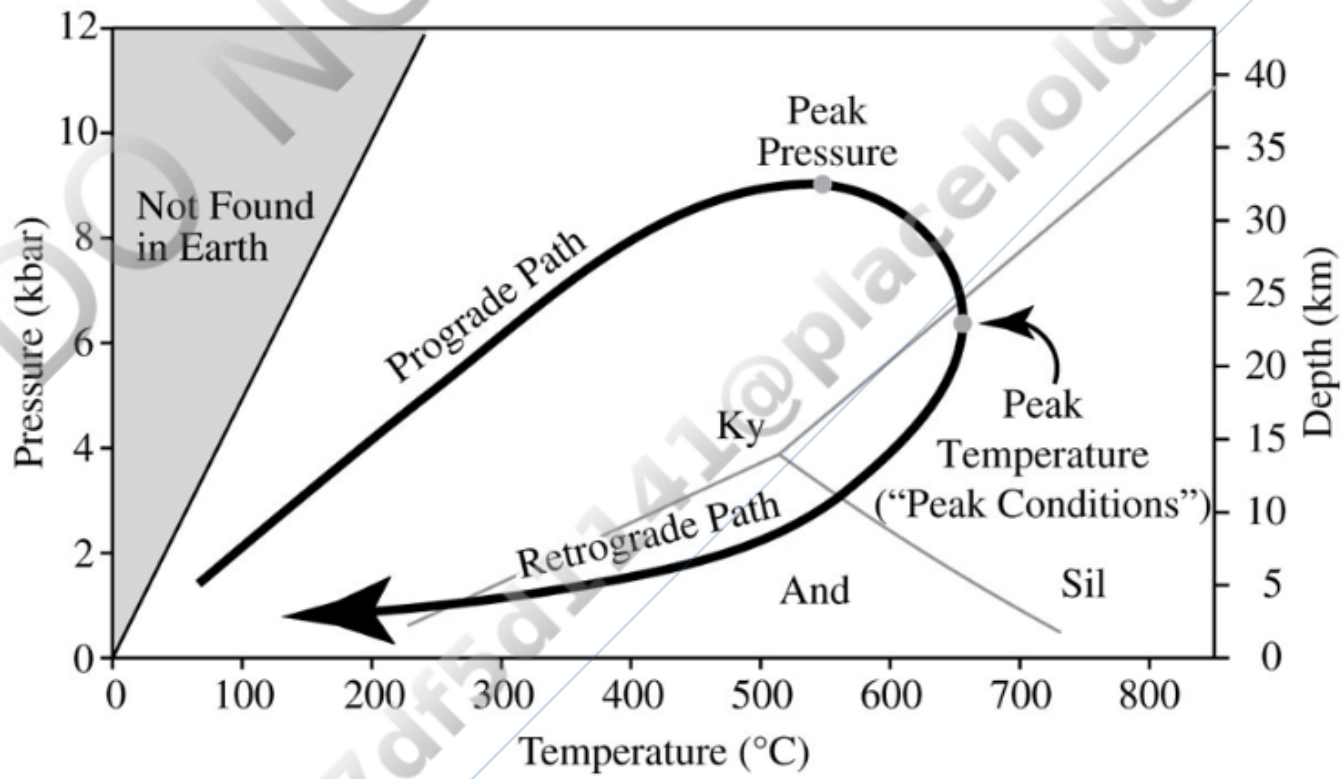

FIGURE 11.10 Generalized temperature and pressure loop for a rock buried by convergent tectonics and brought back to the surface by erosion. Important components of the loop are labeled. Stability fields of the aluminum silicates (Al_2SiO_5: andalusite [And], sillimanite [Sil], and kyanite [Ky]) are shown for reference. Back to text

Printed by: e48d507df5d1141@placeholder.94092.edu. Printing is for personal, private use only. No part of this book may be reproduced or transmitted without publisher's prior permission. Violators will be prosecuted.

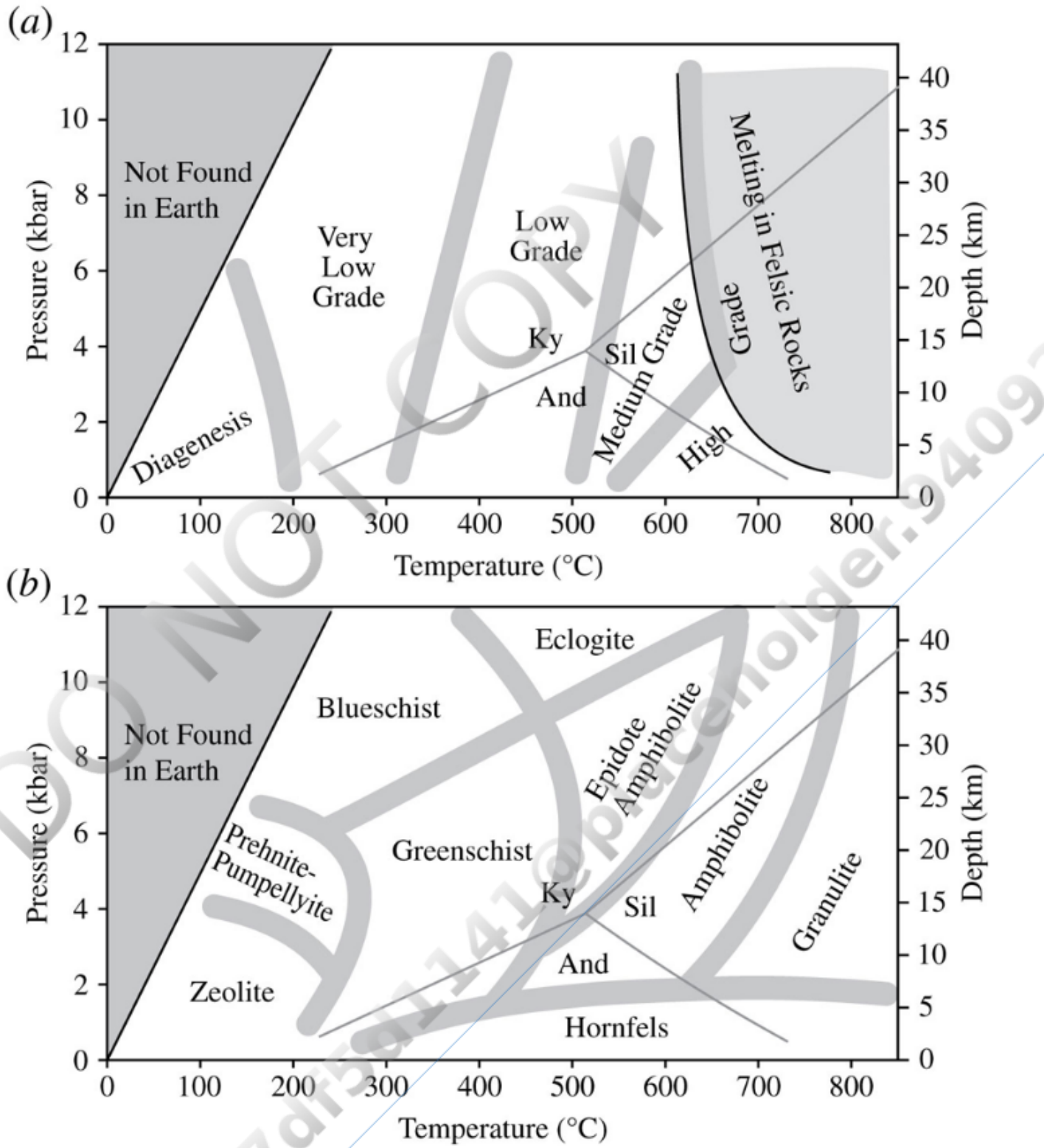

FIGURE 11.11 Metamorphic grade and facies boundaries. Stability fields of the aluminum silicates (Al_2SiO_5: andalusite [And], sillimanite [Sil], and kyanite [Ky]) are shown for reference. (*a*) Metamorphic grade, adapted from Winkler (1976). (*b*) Approximate temperature–pressure fields of the nine principal metamorphic facies. Adapted from Spear (1993) and Winter (2010). Back to text

Printed by: e48d507df5d1141@placeholder.94092.edu. Printing is for personal, private use only. No part of this book may be reproduced or transmitted without publisher's prior permission. Violators will be prosecuted.

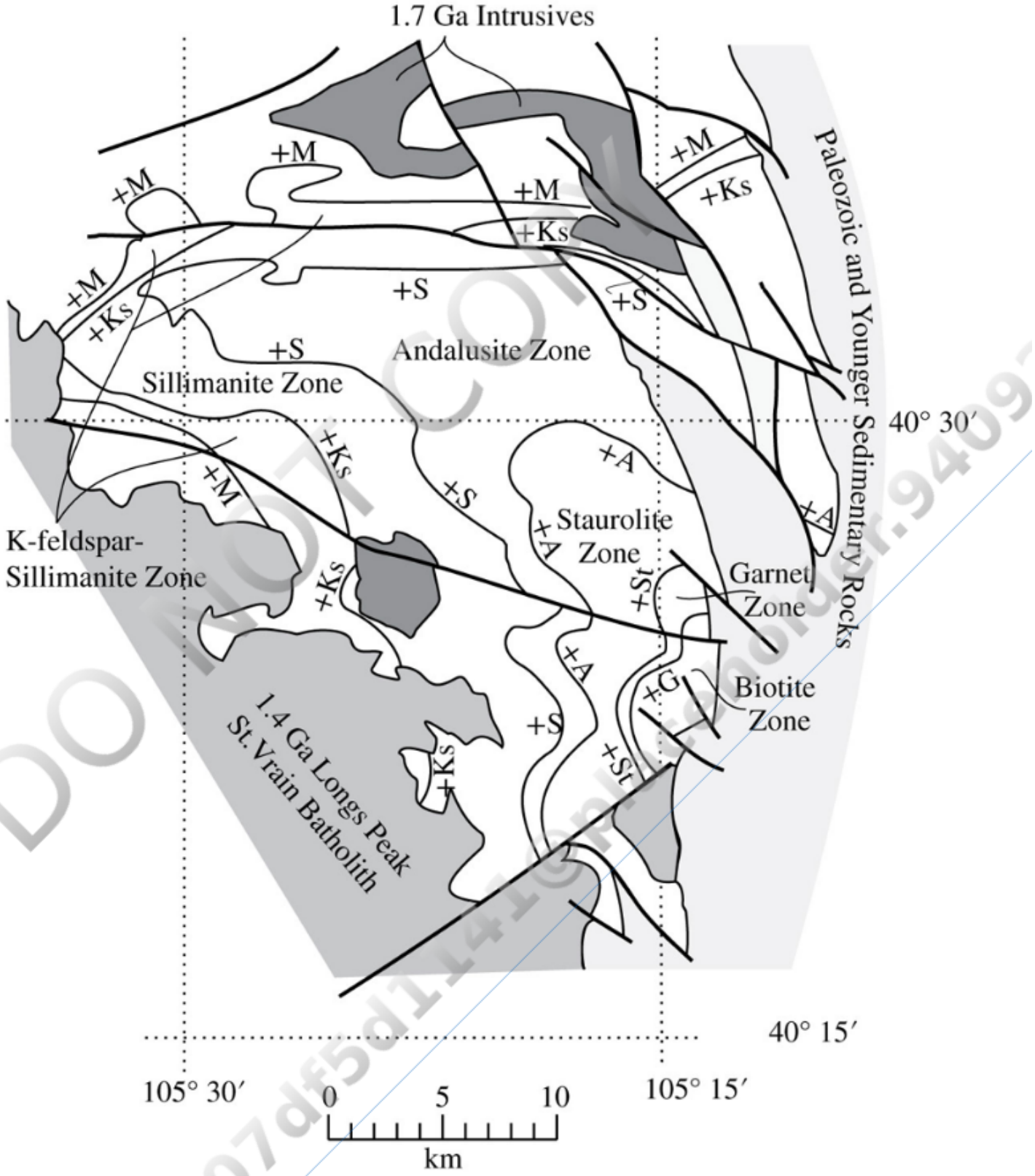

FIGURE 11.12 Metamorphic zones in Proterozoic pelitic/psammitic metamorphic rocks (no shading) of the northeastern Front Range, Colorado. The lowest-grade, biotite-zone rocks are in the southeastern part of the area. Chlorite-zone rocks are not exposed. Mapped mineral zone boundaries include garnet-in (+G), staurolite-in (+St), andalusite-in (+A), sillimanite-in (+S), and K-feldspar + sillimanite-in (+Ks). Rocks on the high-grade side of the +M boundary were partially melted during metamorphism and are migmatites. The sillimanite boundary is associated with the loss of andalusite, and the K-feldspar boundary is associated with the loss of muscovite (though muscovite

Printed by: e48d507df5d1141@placeholder.94092.edu. Printing is for personal, private use only. No part of this book may be reproduced or transmitted without publisher's prior permission. Violators will be prosecuted.

andalusite, and the K-feldspar boundary is associated with the loss of muscovite (though muscovite produced during retrograde metamorphism may exist). Faults and shear zones are shown with heavy lines. Back to text

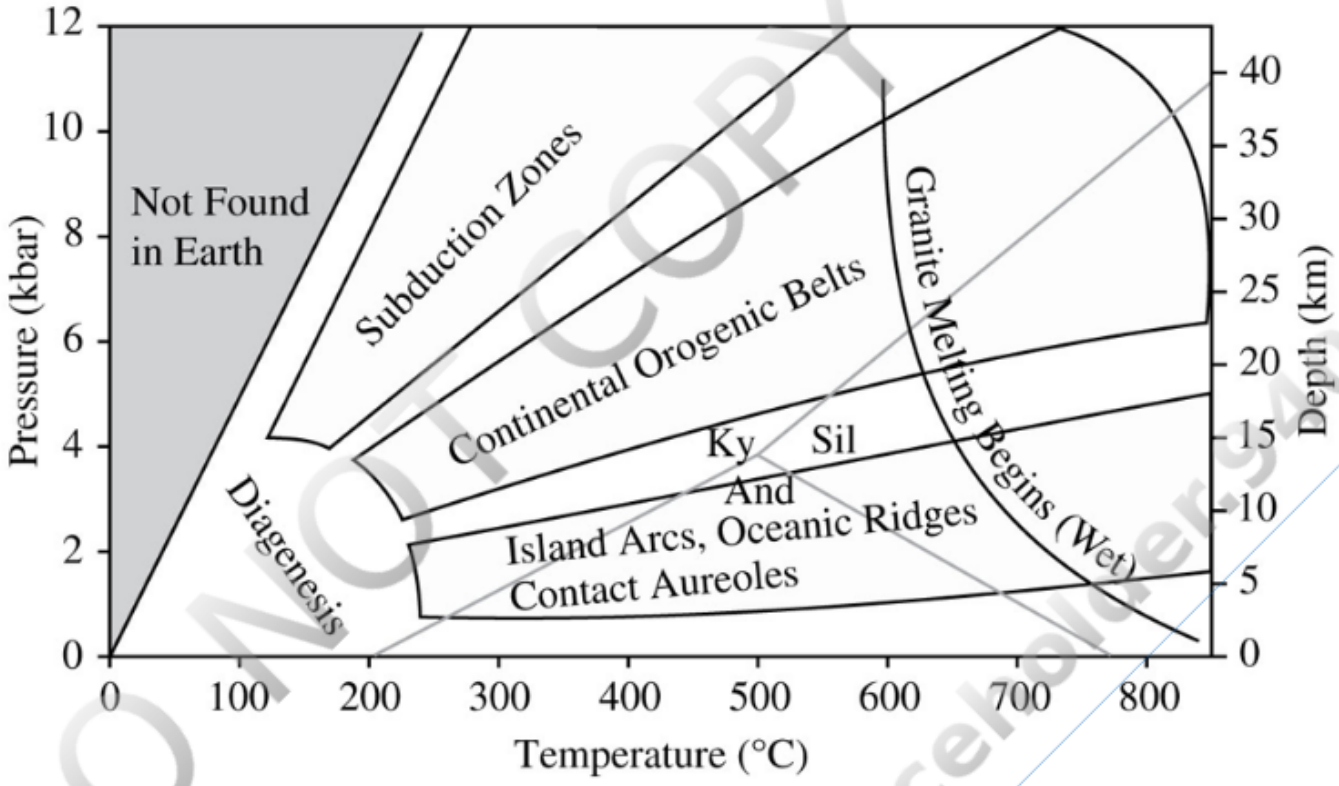

FIGURE 11.13 T–P conditions found in different tectonic environments. Adapted from Spear (1993). Back to text

DO NOT COPY
e48d507df5d1141@placeholder.9409

Printed by: e48d507df5d1141@placeholder.94092.edu. Printing is for personal, private use only. No part of this book may be reproduced or transmitted without publisher's prior permission. Violators will be prosecuted.

Chapter 12 Framework Silicates

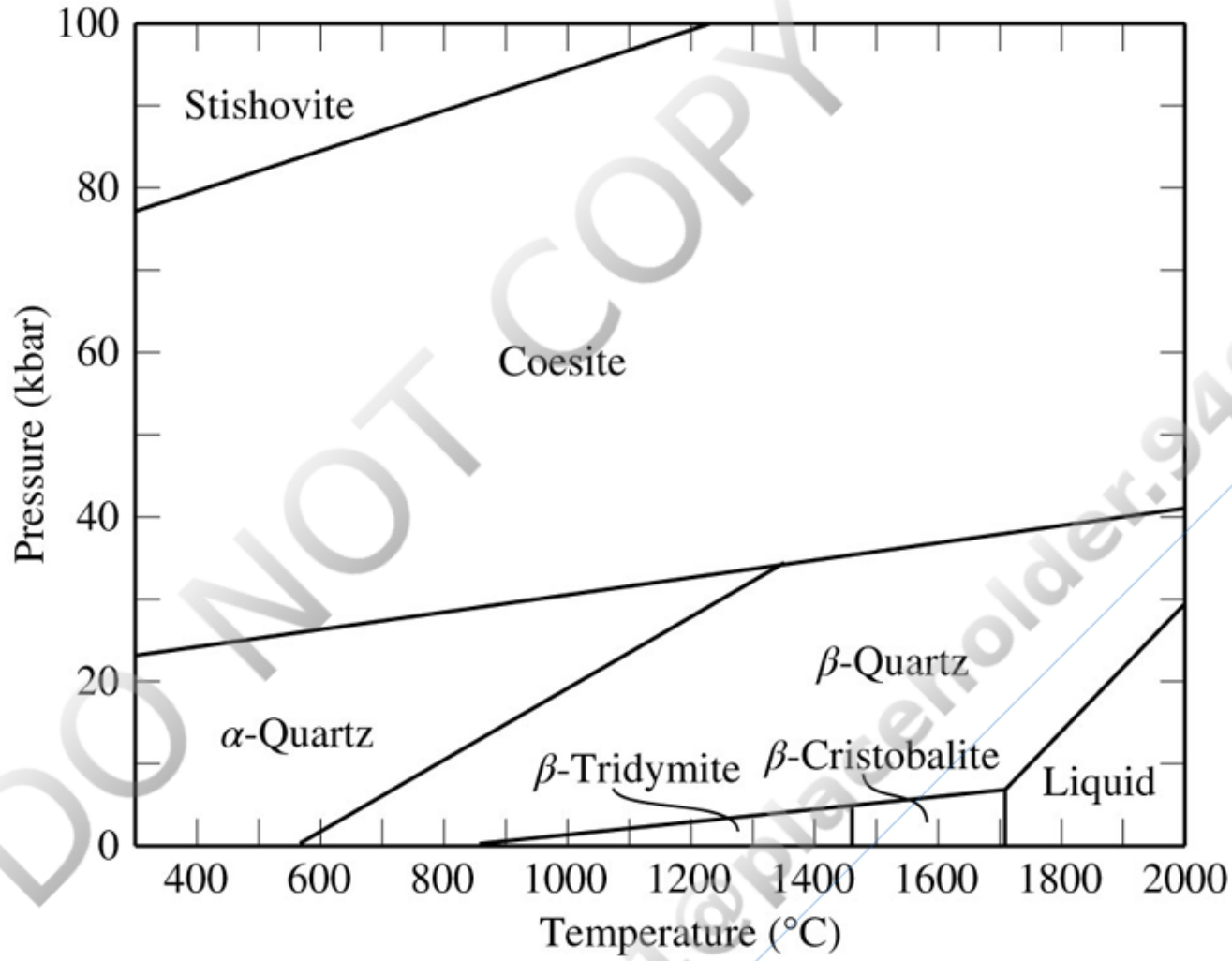

FIGURE 12.1 Stability fields of the silica minerals. Adapted from Griffen (1992). Back to text

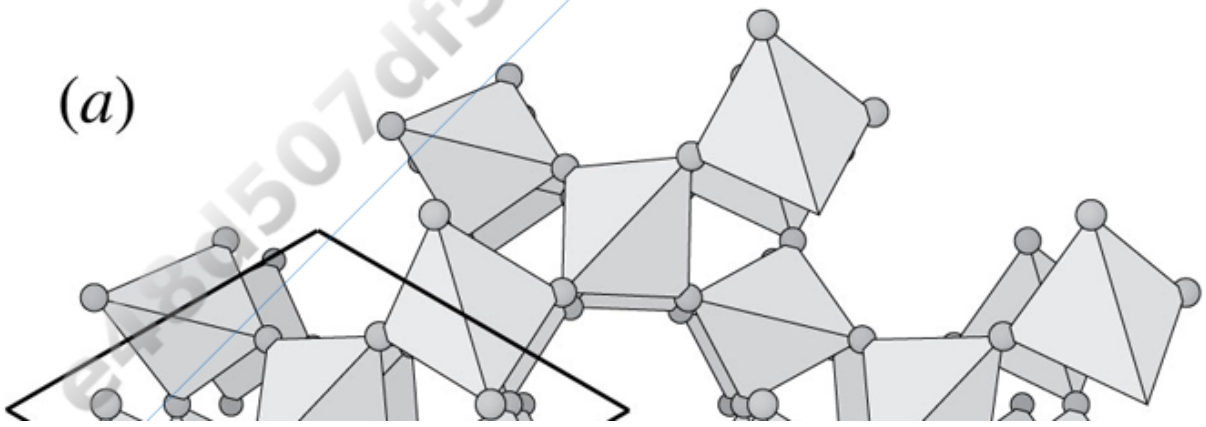

DO NOT COPY

Printed by: e48d507df5d1141@placeholder.94092.edu. Printing is for personal, private use only. No part of this book may be reproduced or transmitted without publisher's prior permission. Violators will be prosecuted.

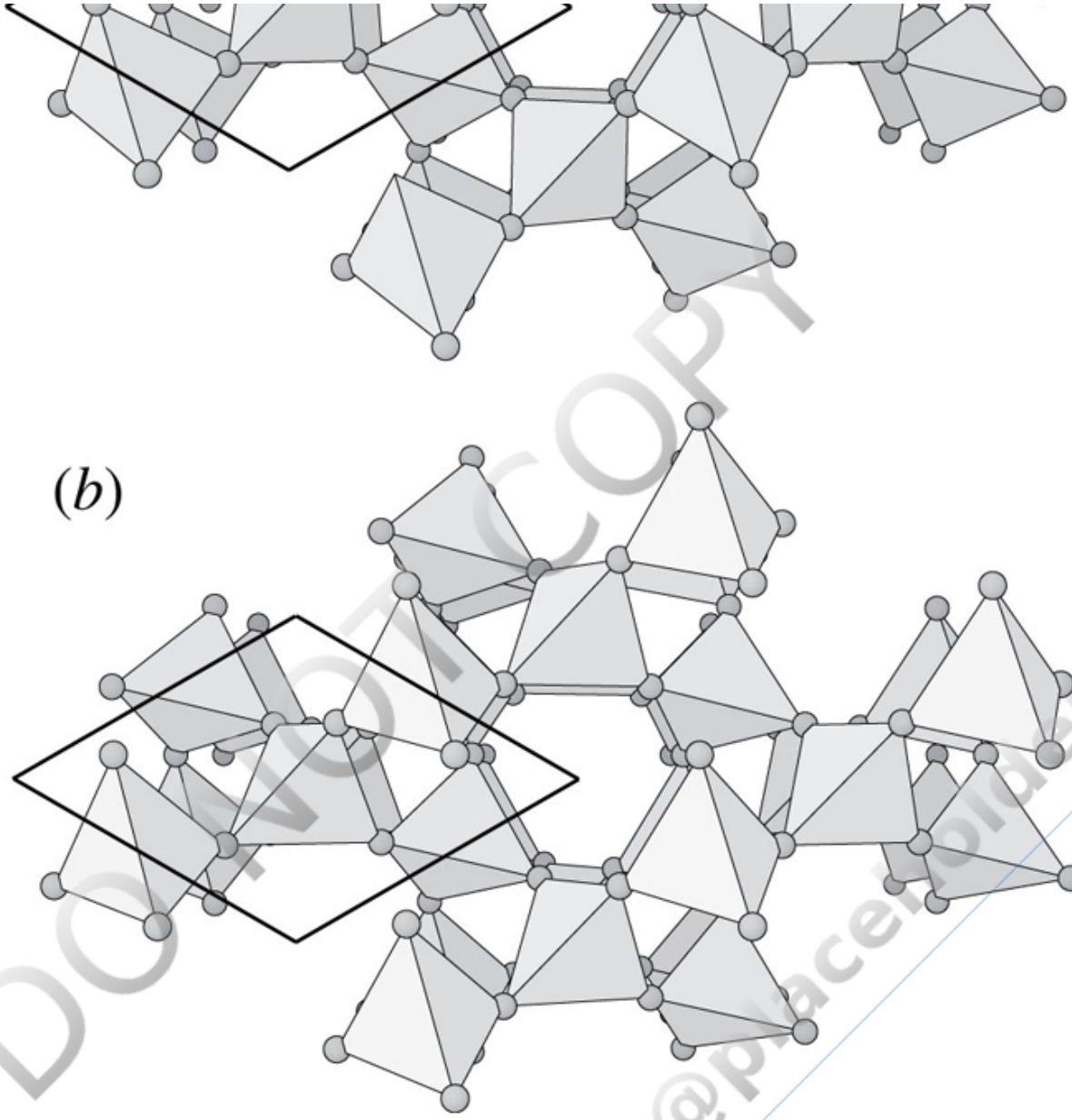

FIGURE 12.2 Quartz structure viewed down the *c* axis. A unit cell outline is shown. Silica tetrahedra link together to form spirals that extend parallel to the *c* axis (Figure 4.12). (*a*) *β*-quartz. The spirals produce hexagonal symmetry. (*b*) *α*-quartz. The structure is distorted, reducing symmetry to 3-fold. Back to text

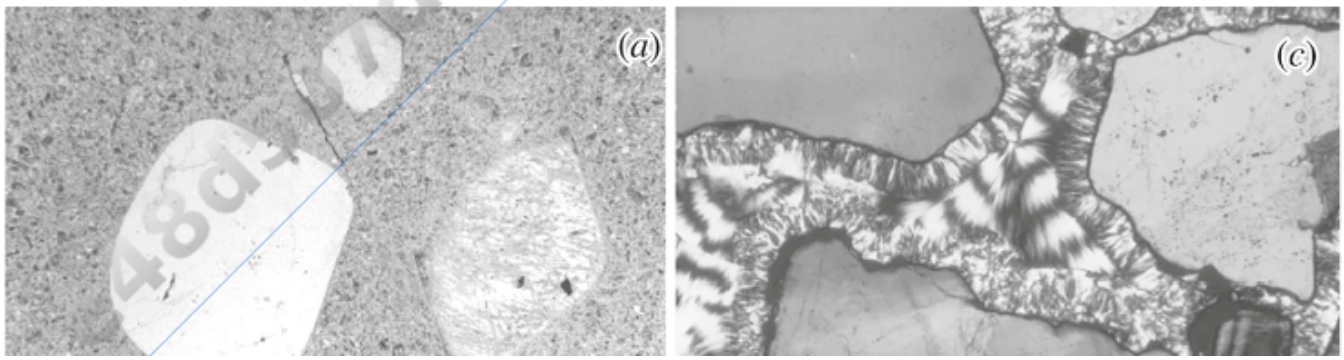

DO NOT COPY

Printed by: e48d507df5d1141@placeholder.94092.edu. Printing is for personal, private use only. No part of this book may be reproduced or transmitted without publisher's prior permission. Violators will be prosecuted.

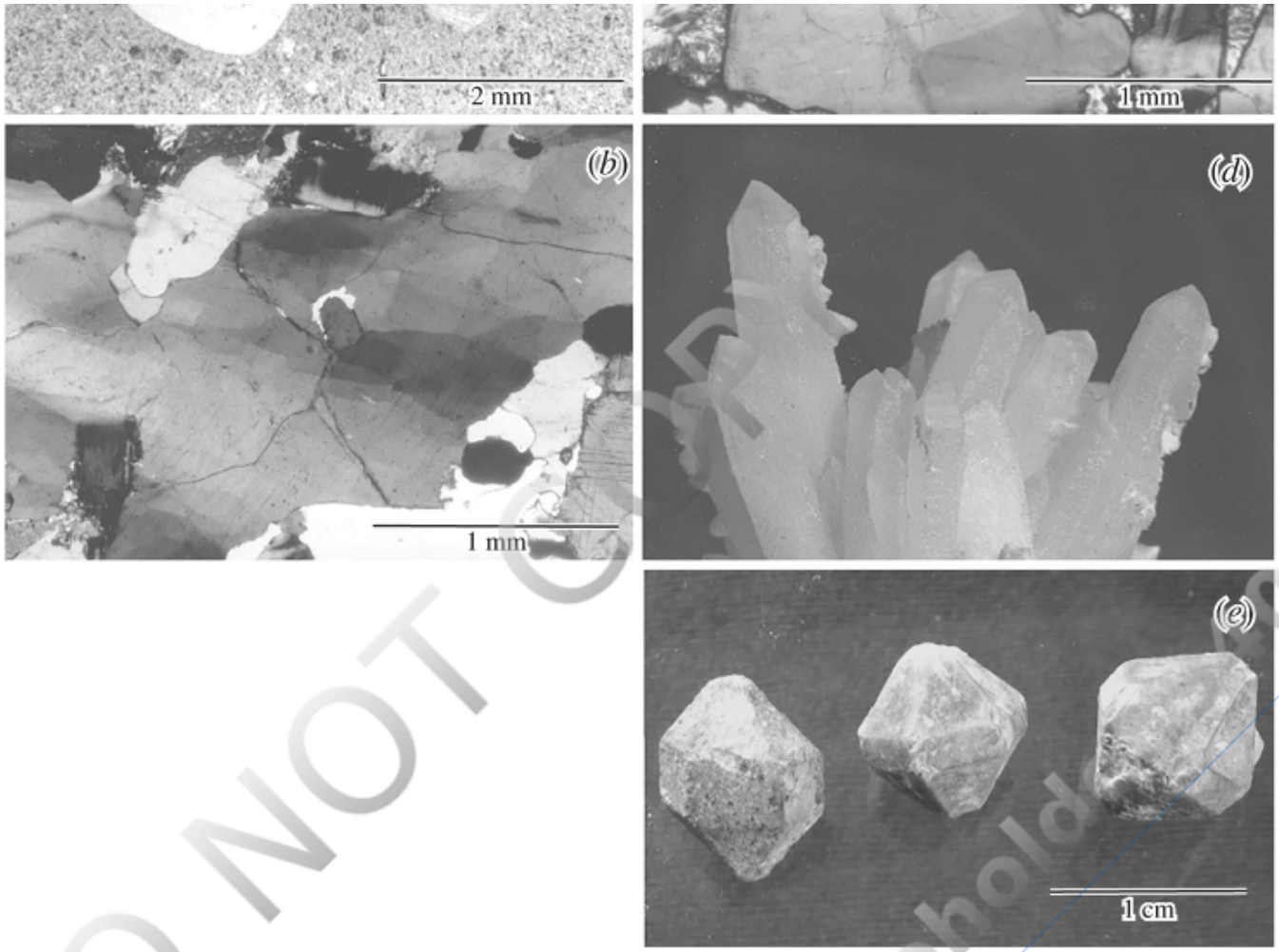

FIGURE 12.3 Quartz. (*a*) Rounded quartz (left) phenocryst in rhyodacite. The other phenocrysts are altered plagioclase. Plane light. (*b*) Undulatory anhedral quartz in deformed granite. Crossed polarizers. (*c*) Feathery-appearing chalcedony cementing quartz and microcline grains in a sandstone. Crossed polarizers. (*d*) Quartz crystals. Field of view is about 10 cm wide. (*e*) *β*-quartz crystals (now *α*-quartz). Back to text

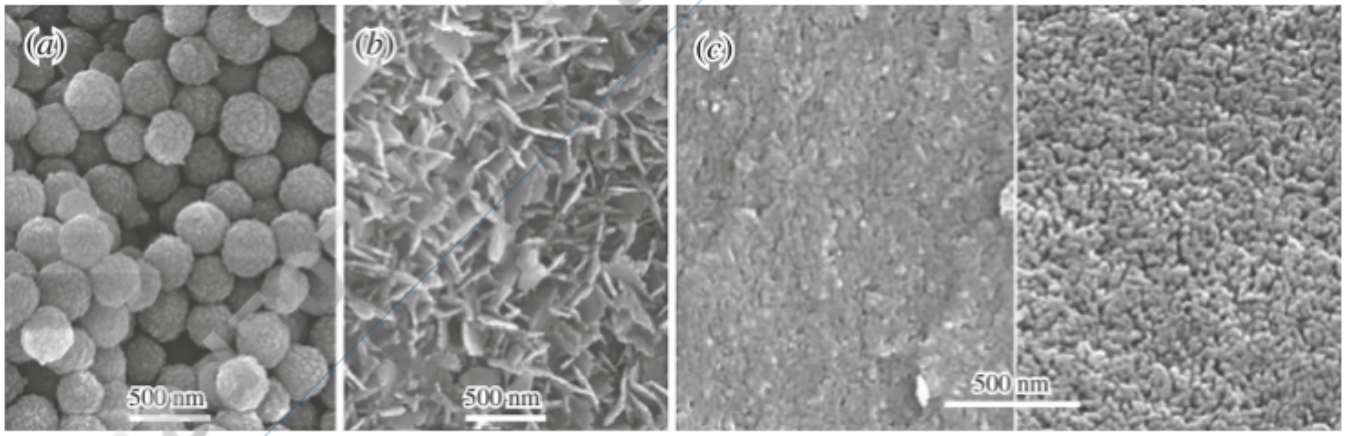

FIGURE 12.4 Opal microstructure. (*a*) Randomly packed spheres of silica in common white opal-A. Spheres may have a concentric or radial structure. In opal-CT, similar spheres made of

Printed by: e48d507df5d1141@placeholder.94092.edu. Printing is for personal, private use only. No part of this book may be reproduced or transmitted without publisher's prior permission. Violators will be prosecuted.

cristobalite/tridymite nanoparticles and platelets are called lepispheres. (*b*) Opal-CT made of random platelets, each roughly 25 nm × 300 nm. Each platelet is made of numerous ~25 nm nanograins of cristobalite/tridymite. (*c*) Opal-CT (fire opal). The left image shows a freshly broken surface. If etched with HF (right image), the structure consisting of randomly packed nanoparticles of cristobalite/tridymite is revealed. © Dr. Eloïse Gaillou / Nantes Université. Back to text

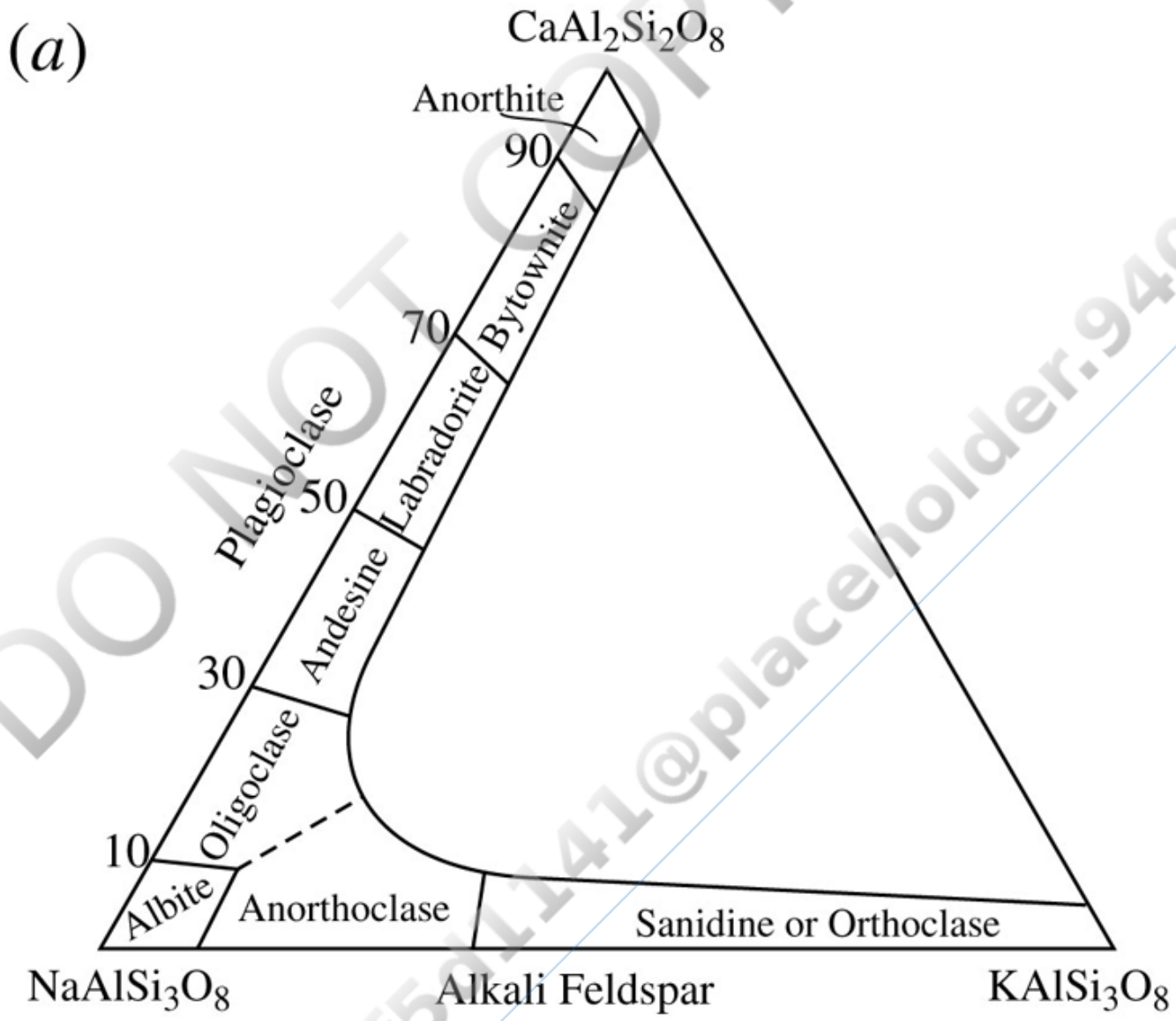

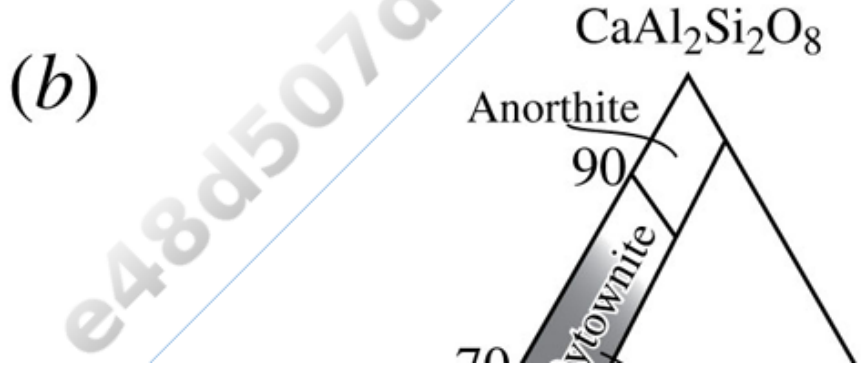

DO NOT COPY
e48d507df5d1141@placeholder.9409

Printed by: e48d507df5d1141@placeholder.94092.edu. Printing is for personal, private use only. No part of this book may be reproduced or transmitted without publisher's prior permission. Violators will be prosecuted.

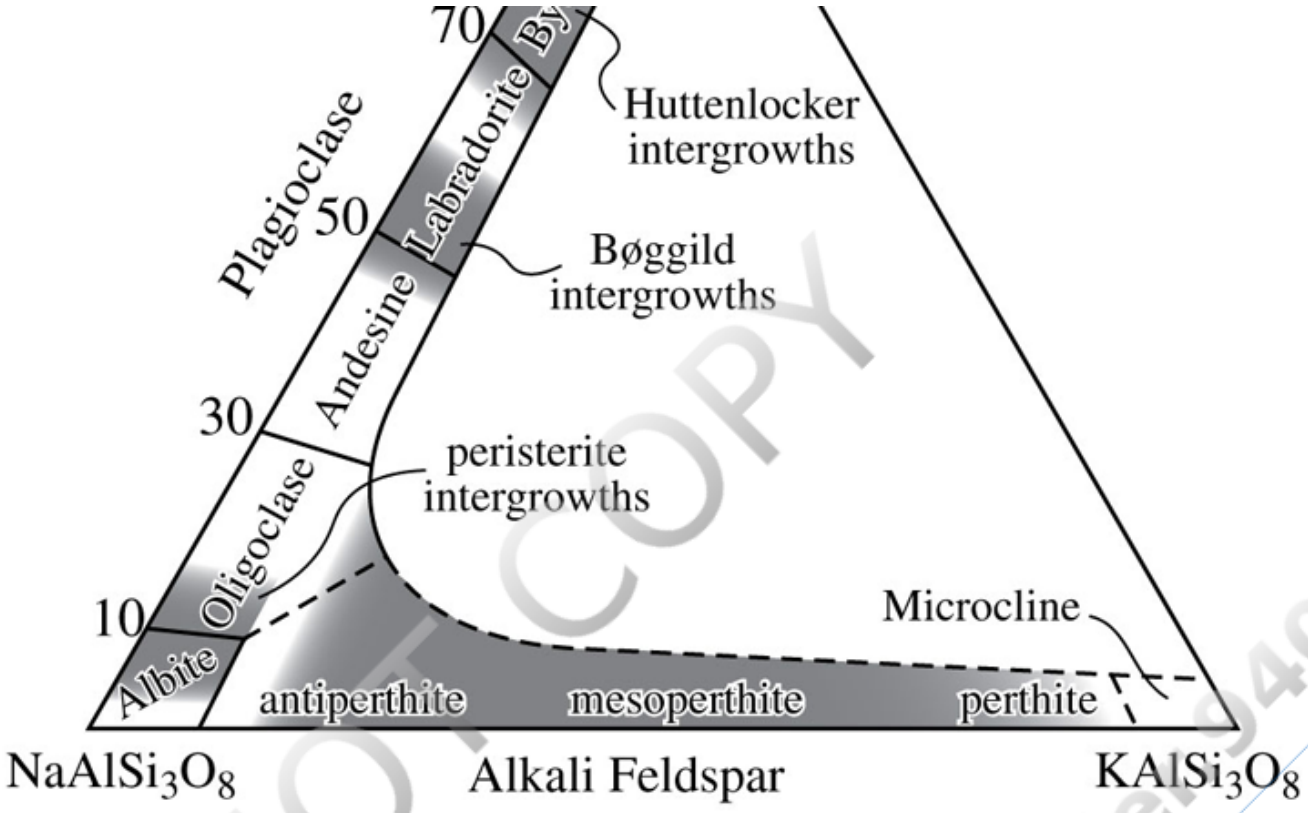

FIGURE 12.5 Simplified composition range of common feldspar; see text for details. (*a*) At high temperature there is continuous solid solution for both plagioclase and the alkali feldspars. (*b*) With slow cooling, exsolution occurs across multiple feldspar compositions (shaded regions). Plagioclase intergrowths are submicroscopic and are only visible with a transmission electron microscope. High-temperature alkali feldspars exsolve to form antiperthite, mesoperthite, or perthite, depending on composition. For these, exsolution lamellae are typically visible in thin section or perhaps hand sample. Exsolution composition ranges are approximate. Back to text

DO NOT COPY
e48d507df5d1141@placeholder.94092

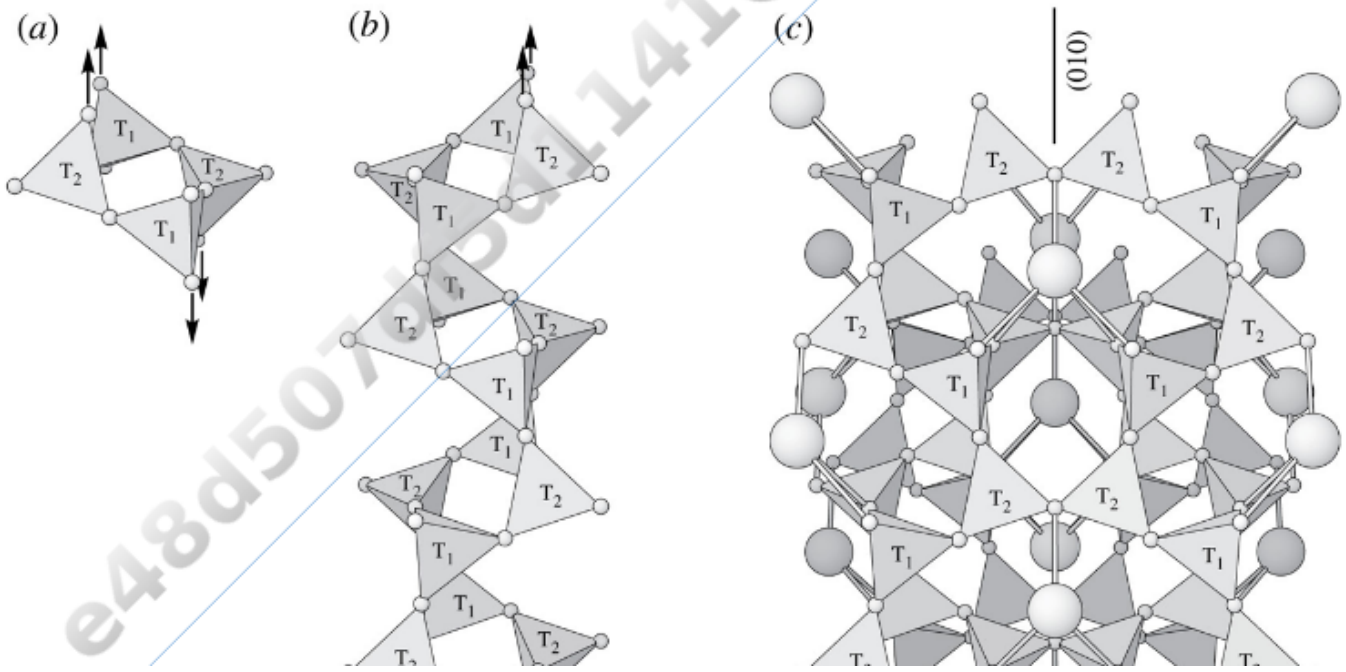

Printed by: e48d507df5d1141@placeholder.94092.edu. Printing is for personal, private use only. No part of this book may be reproduced or transmitted without publisher's prior permission. Violators will be prosecuted.

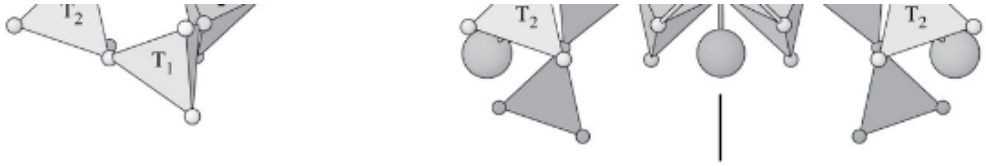

FIGURE 12.6 Idealized feldspar structure: T_1 and T_2 refer to different tetrahedral sites. View is perpendicular to the (001) plane; the same view is used in Figure 12.7. (*a*) Four-member ring of silicon tetrahedra containing two nonequivalent tetrahedral sites, T_1 and T_2. (*b*) The four-member rings share O^{2-} anions to form a crankshaft-like chain of silicon tetrahedra extending parallel to *a*. (*c*) Chains are cross-linked by sharing the remaining oxygen anions on each tetrahedron to form large coordination sites occupied by Ca^{2+}, Na^{+}, or K^{+} (large spheres). Back to text

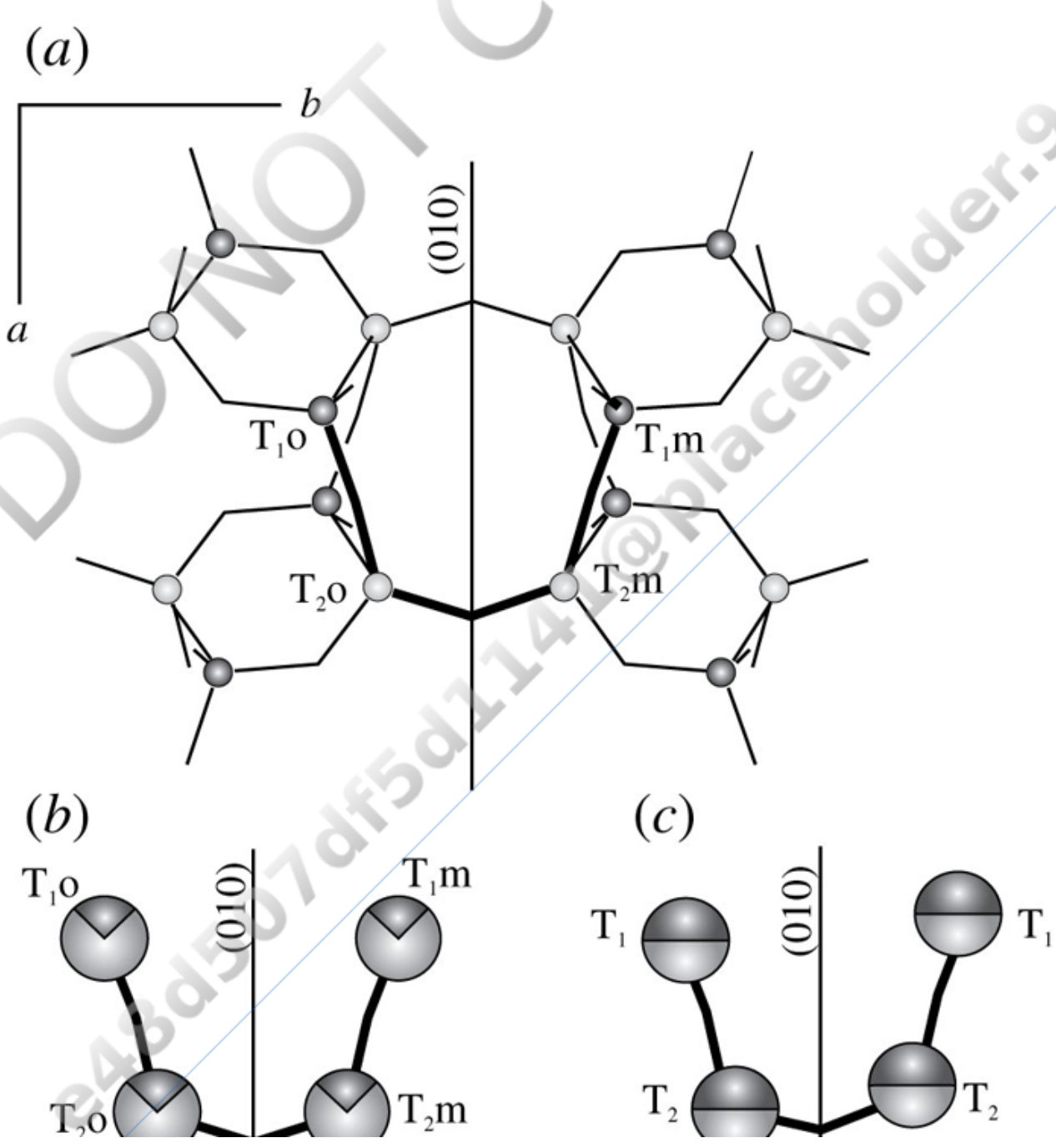

DO NOT COPY
e48d507df5d1141@placeholder.9409

Printed by: e48d507df5d1141@placeholder.94092.edu. Printing is for personal, private use only. No part of this book may be reproduced or transmitted without publisher's prior permission. Violators will be prosecuted.

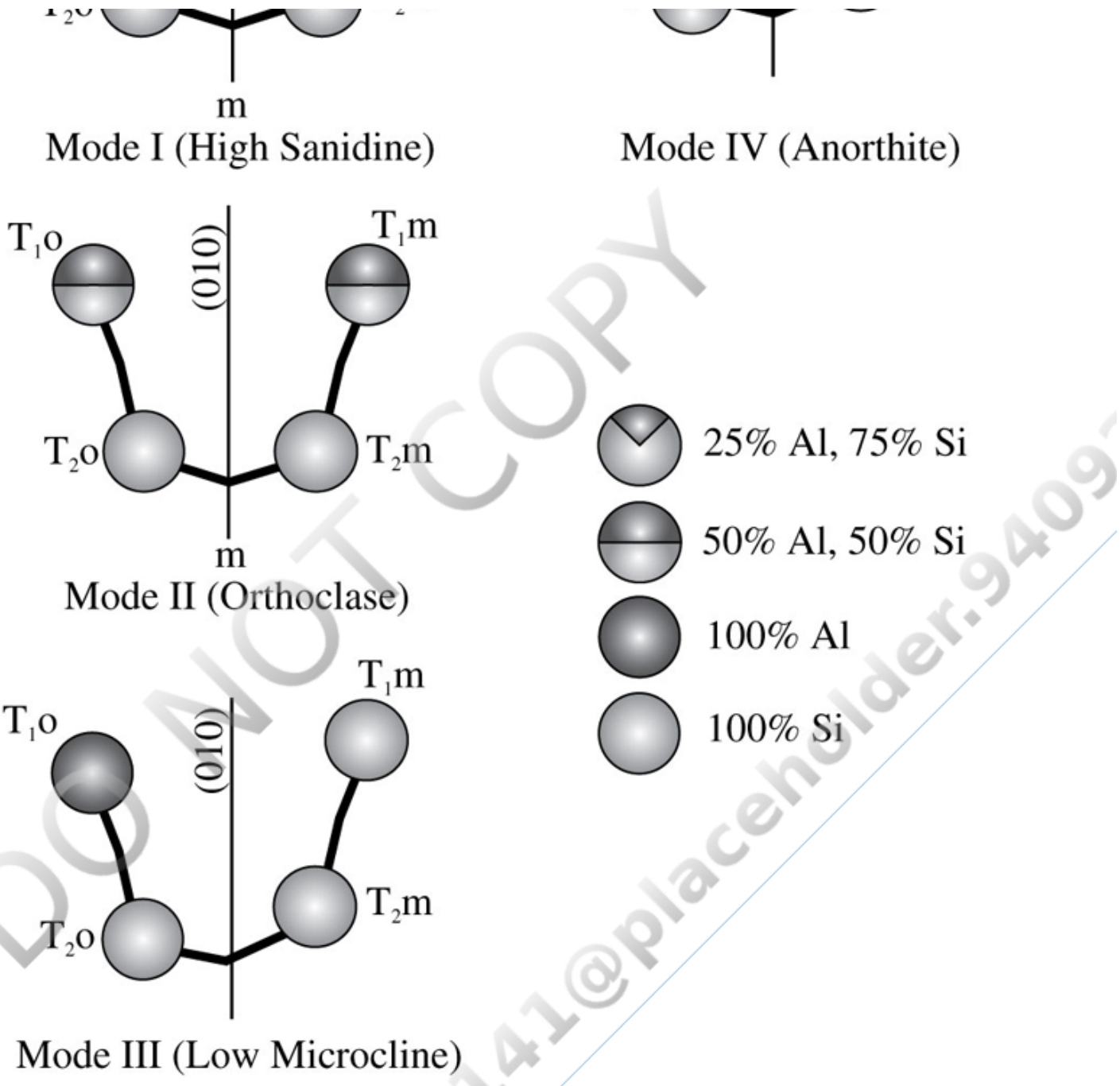

FIGURE 12.7 Ordering of Al and Si in tetrahedral sites in the feldspars. (*a*) Sketch showing the location of the T_1 (dark spheres) and T_2 (light spheres) cations within tetrahedra. The "o" and "m" identify sites on opposite sides of the (010) plane. Compare with Figure 12.6c. (*b*) Alkali feldspars, which have an Al:Si ratio of 1:3. In Mode I ordering, Al and Si are randomly distributed in the T_1 and T_2 sites so 25 percent of each site is occupied by Al^{3+} and a mirror plane exists parallel to {010}. The "o" and "m" sites are structurally identical. In Mode II ordering, the T_1 sites are half occupied by Al and half by Si. The T_2 sites contain only Si. This ordering preserves the {010} mirror, so the "o" and "m" sites are structurally identical and orthoclase is ideally monoclinic. In Mode III ordering, all of the Al is in the T_1o site, and the T_1m, T_2o, and T_2m sites contain only Si^{4+}. The {010} mirror is destroyed, and the "o" and "m" sites are structurally different. The structure distorts slightly, and symmetry is reduced to triclinic. (*c*) Anorthite, in which the Al:Si ratio is 2:2. Al and Si occupy alternating tetrahedral sites, so T_1 and T_2 sites are occupied, on average, with half Al and half Si. See text for additional discussion. Back to text

DO NOT COPY
e48d507df5d1141@placeholder.9409

Printed by: e48d507df5d1141@placeholder.94092.edu. Printing is for personal, private use only. No part of this book may be reproduced or transmitted without publisher's prior permission. Violators will be prosecuted.

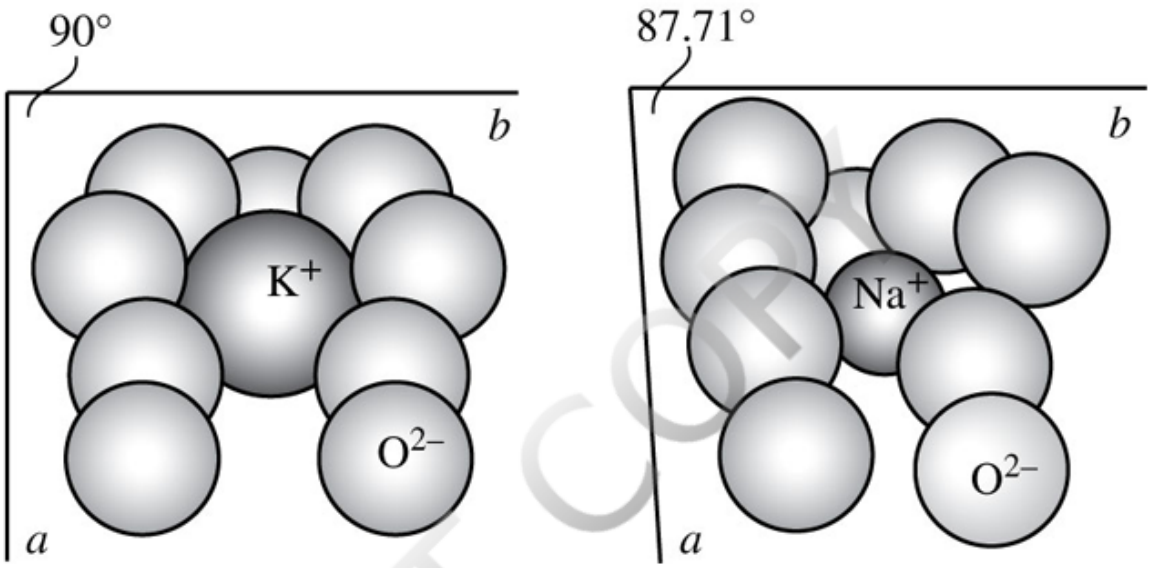

FIGURE 12.8 Arrangement of oxygen anions about K^+ in sanidine (left) and the distorted or collapsed arrangement around Na^+ in albite (right). The angle between the *a* and *b* axes in sanidine is 90°, allowing for monoclinic symmetry. In the albite structure $\gamma = 87.71°$, so symmetry is reduced to triclinic. Only at high temperatures is the vibrational energy of Na^+ in albite sufficient to keep the "cage" in which it resides from collapsing. Back to text

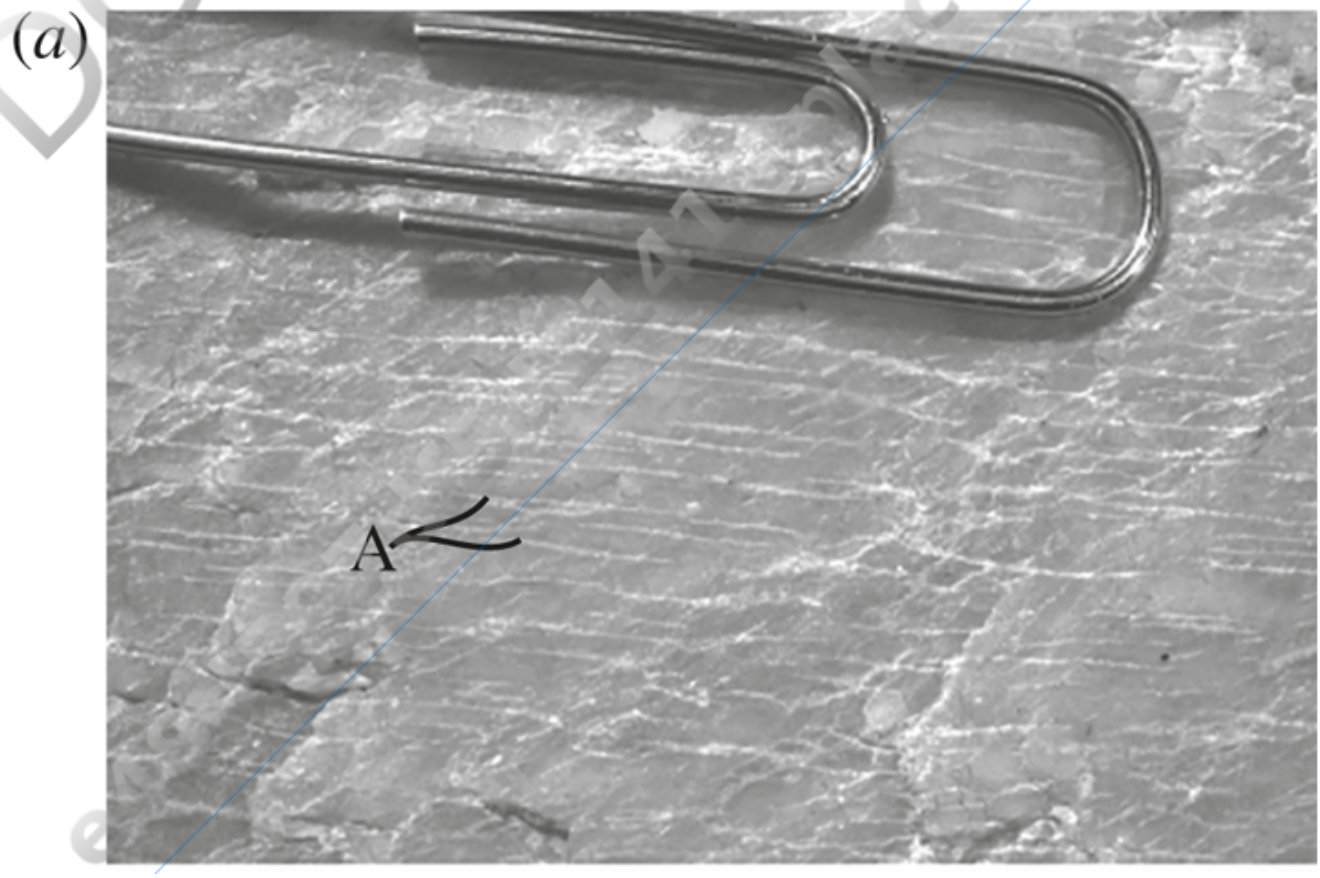

Printed by: e48d507df5d1141@placeholder.94092.edu. Printing is for personal, private use only. No part of this book may be reproduced or transmitted without publisher's prior permission. Violators will be prosecuted.

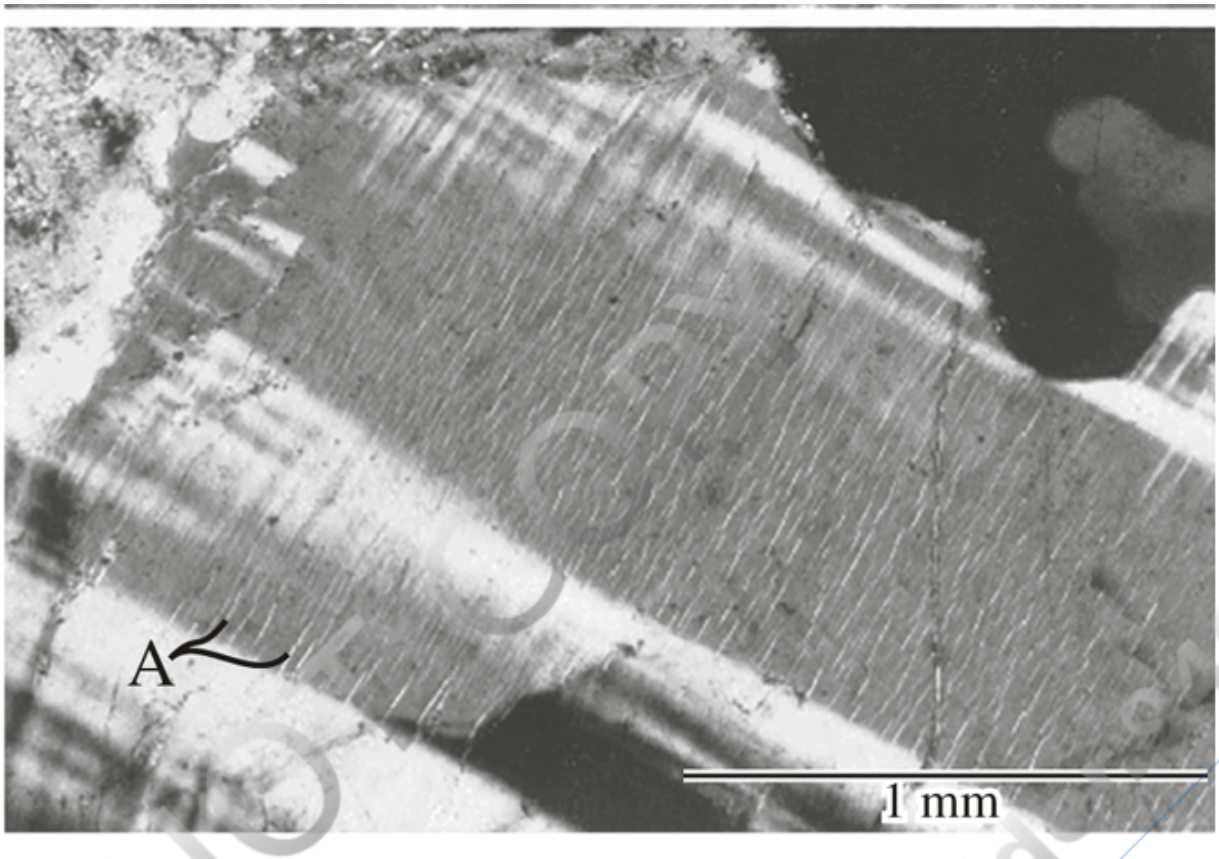

FIGURE 12.9 Perthitic exsolution. (*a*) Hand sample. Thin netlike or branching layers of albite (A) in microcline extend roughly parallel to the paper clip. (*b*) Thin section. Light thin irregular blebs (inclusions) of albite extending NE are visible in microcline (crossed polarizers). The sample also displays "tartan plaid" twinning, with relatively thick twin lamellae with diffuse borders extending NW–SE and NE–SW (cf. Figure 12.20b). Back to text

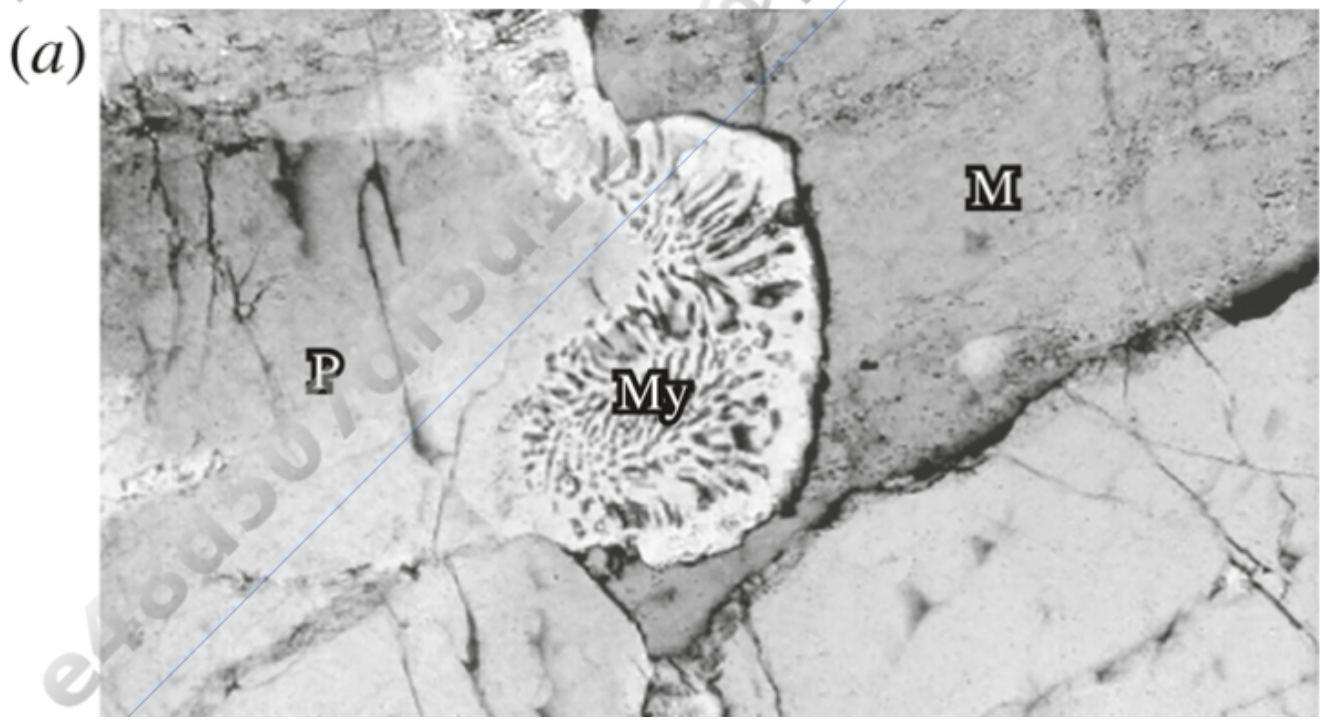

Printed by: e48d507df5d1141@placeholder.94092.edu. Printing is for personal, private use only. No part of this book may be reproduced or transmitted without publisher's prior permission. Violators will be prosecuted.

(b)

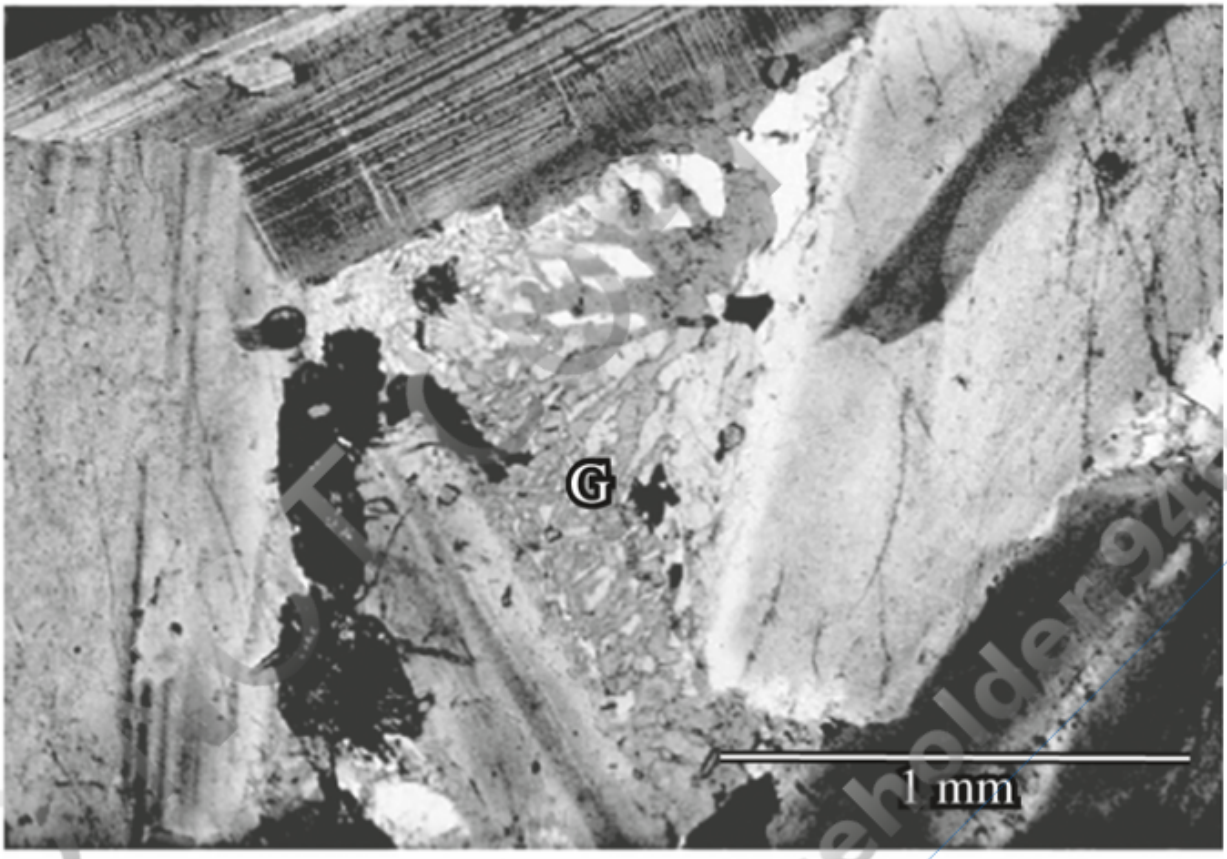

(c)

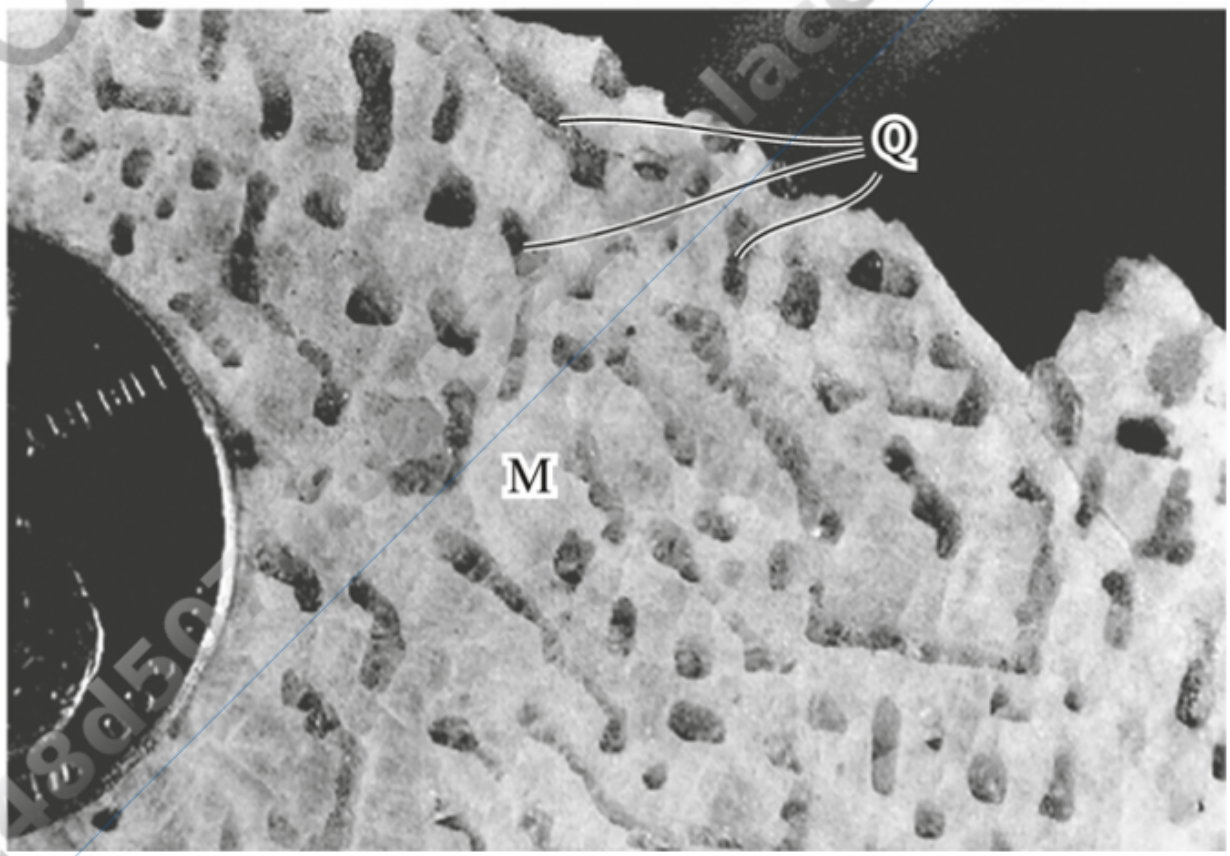

Printed by: e48d507df5d1141@placeholder.94092.edu. Printing is for personal, private use only. No part of this book may be reproduced or transmitted without publisher's prior permission. Violators will be prosecuted.

FIGURE 12.10 Quartz–feldspar intergrowths. (*a*) Myrmekite (My) consists of irregular quartz grains (dark) in plagioclase (light) seen at the contact between plagioclase (P) and microcline (M). Crossed polarizers. (*b*) Granophyre (G) in the space between plagioclase laths in norite. Crossed polarizers. (*c*) Graphic intergrowth of quartz (Q) and microcline (M) from a pegmatite. Back to text

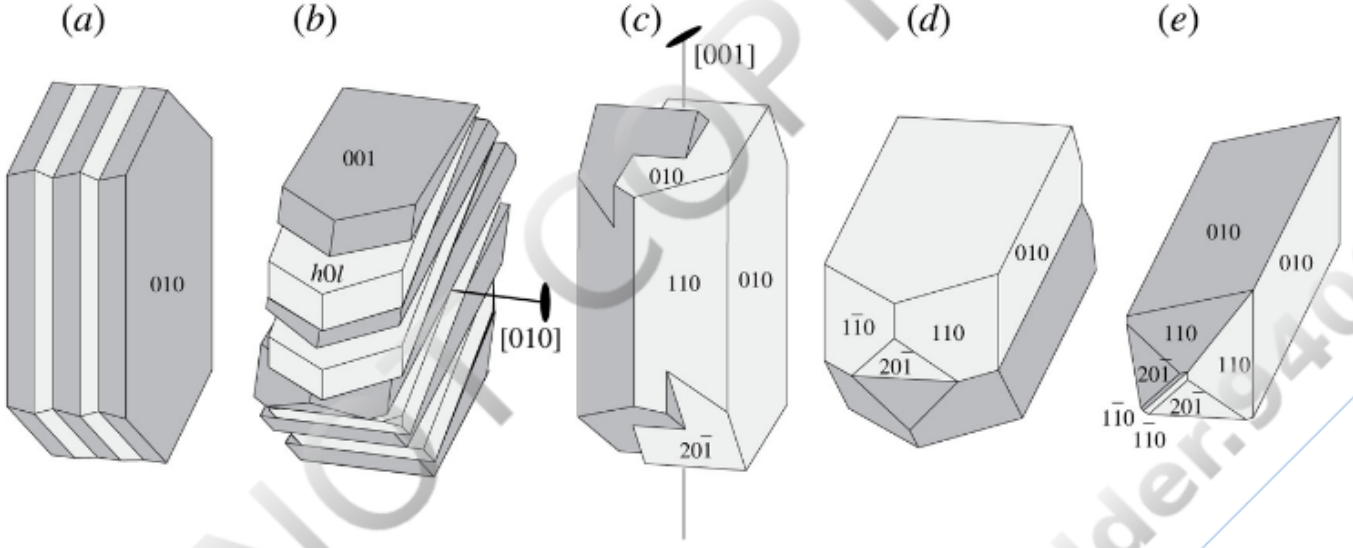

FIGURE 12.11 Common twins in the feldspars. (*a*) Albite twins on {010}. (*b*) Pericline twins produced by rotation on [010]. (*c*) Carlsbad twins produced by rotation on [001]. (*d*) Manebach twins by reflection on {001}. (*e*) Baveno twins produced by reflection on {021}. In the triclinic varieties, twinning is also possible on $\{0\bar{2}1\}$. Back to text

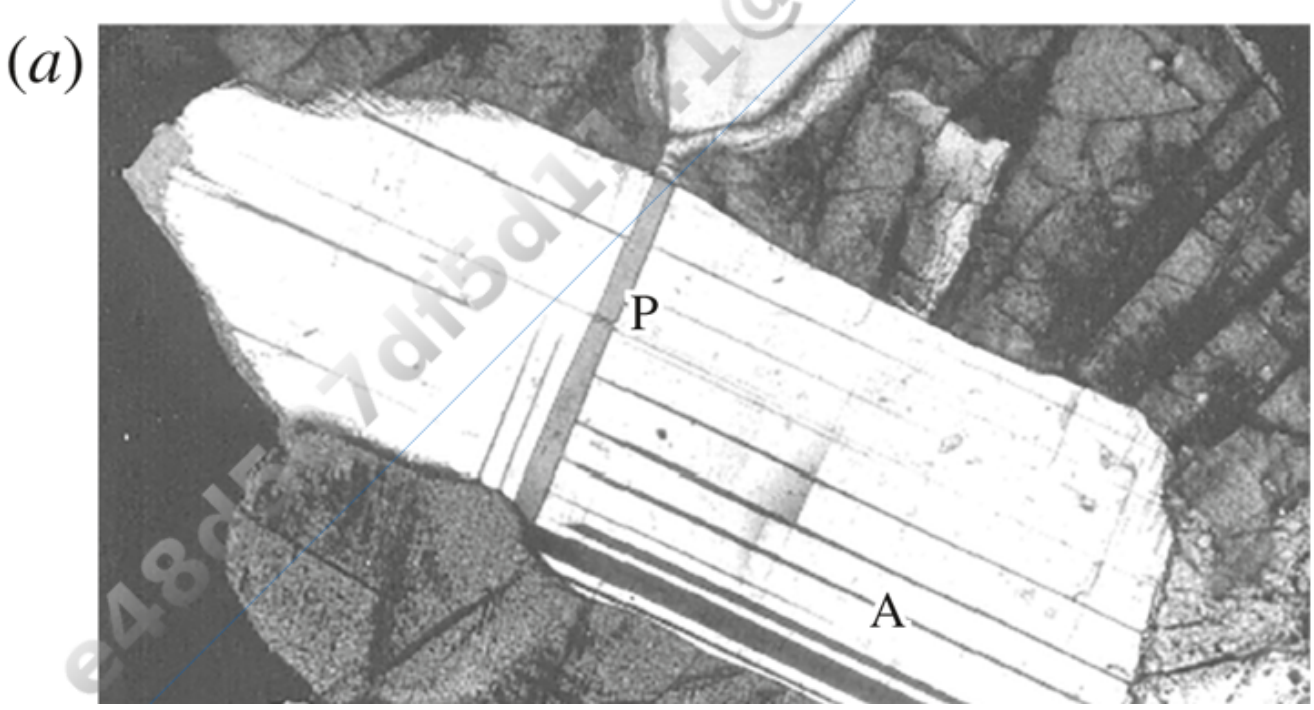

Printed by: e48d507df5d1141@placeholder.94092.edu. Printing is for personal, private use only. No part of this book may be reproduced or transmitted without publisher's prior permission. Violators will be prosecuted.

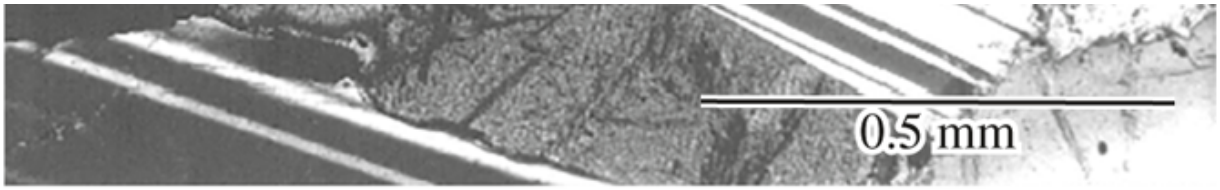

(b)

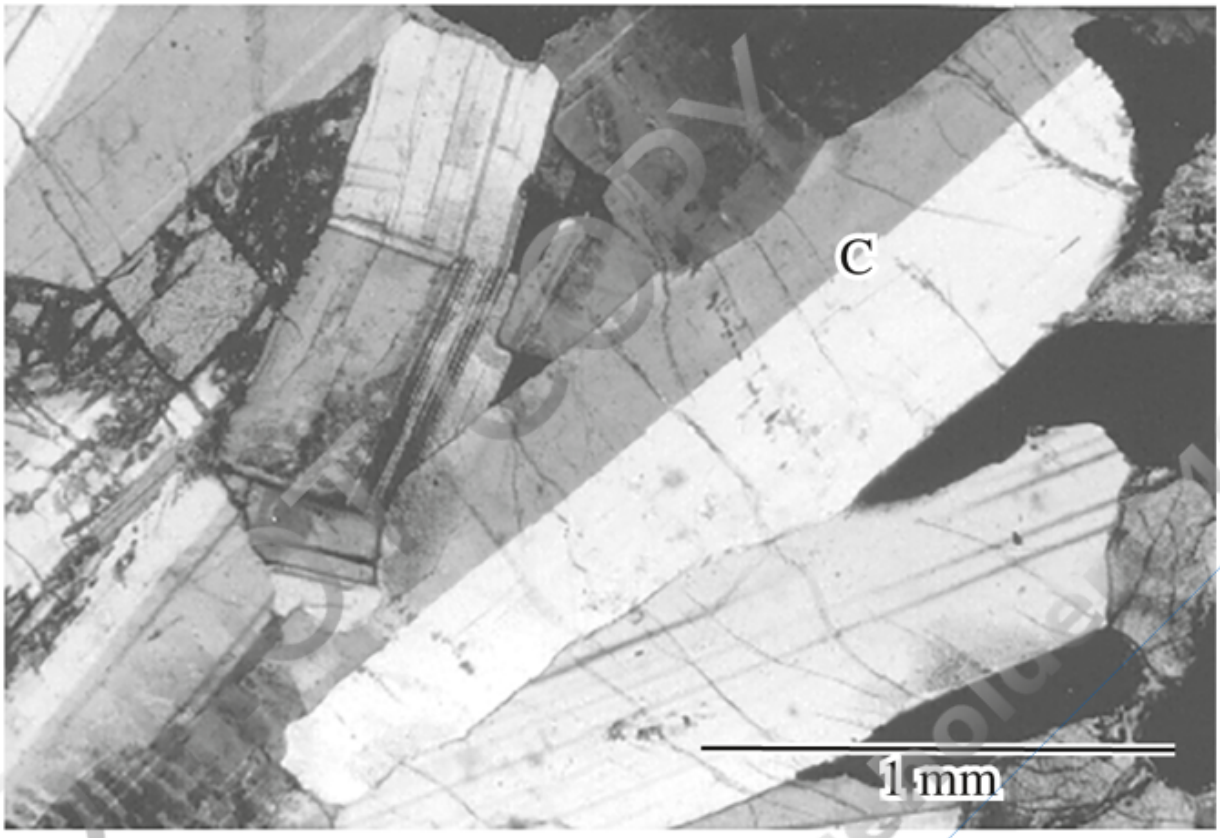

(c)

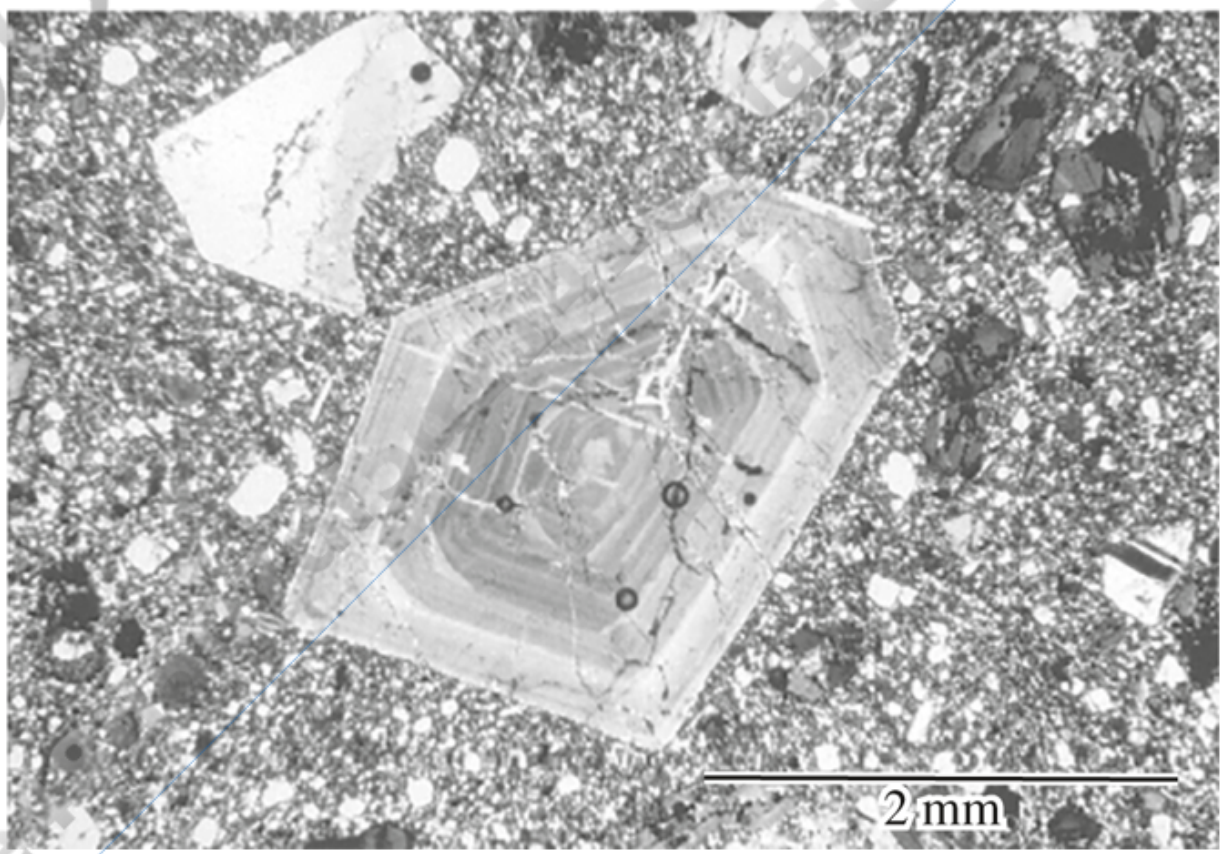

Printed by: e48d507df5d1141@placeholder.94092.edu. Printing is for personal, private use only. No part of this book may be reproduced or transmitted without publisher's prior permission. Violators will be prosecuted.

FIGURE 12.12 Plagioclase in thin section. Cross-polarized light. (*a*) Albite twin lamellae (A) extend NW–SE, and pericline twin lamellae (P) extend NE–SW. (*b*) Large grain in the center displays a Carlsbad twin (C) that divides the grain into right and left portions. (*c*) Phenocryst with oscillatory zoning. Back to text

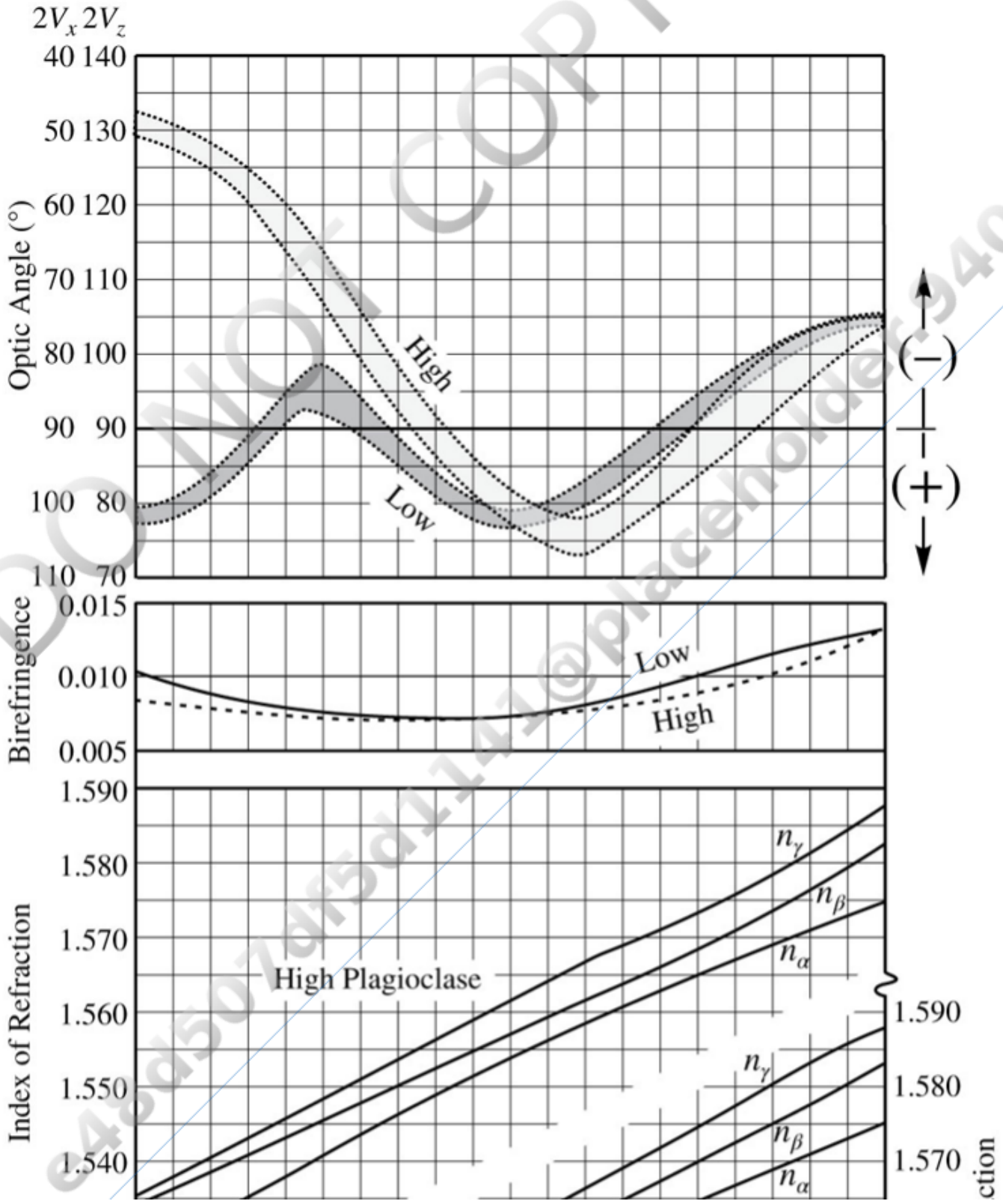

DO NOT COPY
e48d507df5d1141@placeholder.9409

Printed by: e48d507df5d1141@placeholder.94092.edu. Printing is for personal, private use only. No part of this book may be reproduced or transmitted without publisher's prior permission. Violators will be prosecuted.

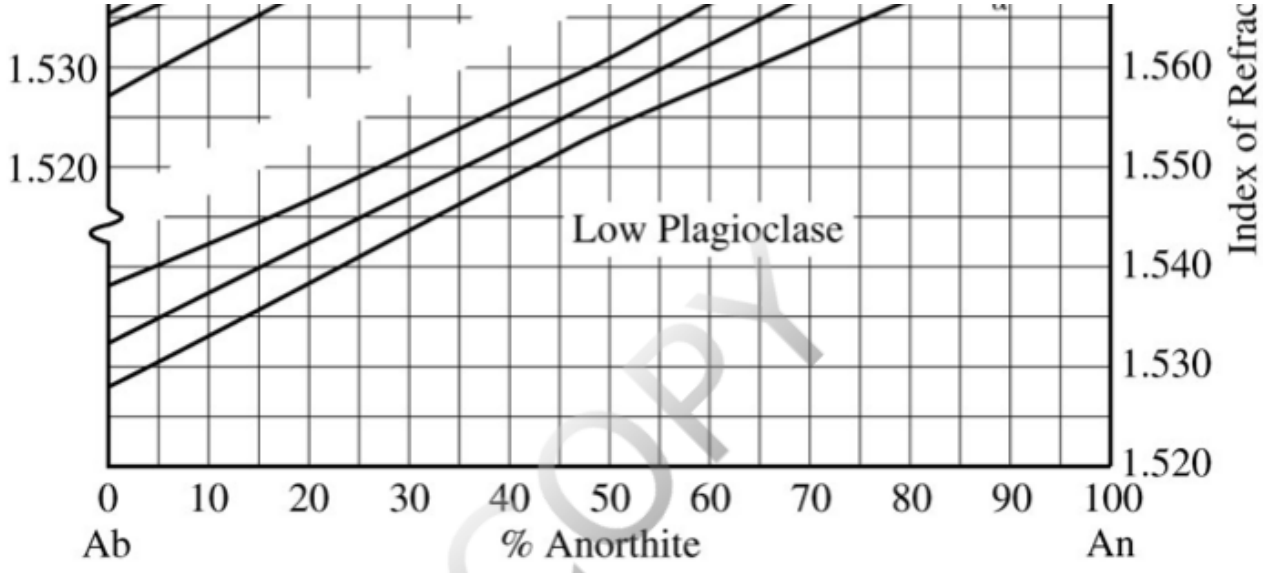

FIGURE 12.13 Optical properties of low (plutonic) and high (volcanic) plagioclase. Adapted from Smith (1958) and Burri and others (1967). Back to text

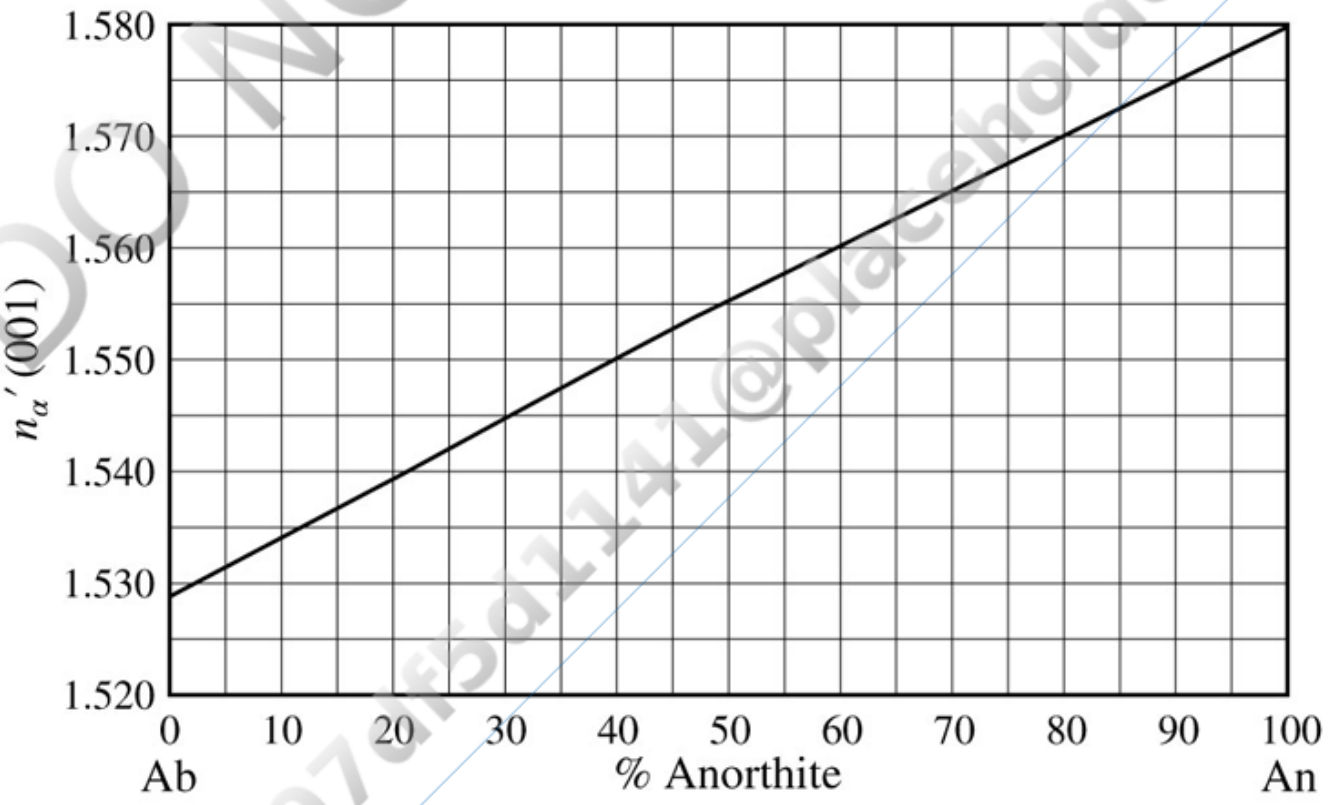

FIGURE 12.14 Index of refraction of the fast ray (n'_α) for plagioclase fragments lying on cleavages. The diagram is constructed for fragments on (001) cleavage surfaces but also may be used for fragments on (010) cleavage surfaces. After Morse (1968). Back to text

DO NOT COPY
e48d507df5d1141@placeholder.9409

Printed by: e48d507df5d1141@placeholder.94092.edu. Printing is for personal, private use only. No part of this book may be reproduced or transmitted without publisher's prior permission. Violators will be prosecuted.

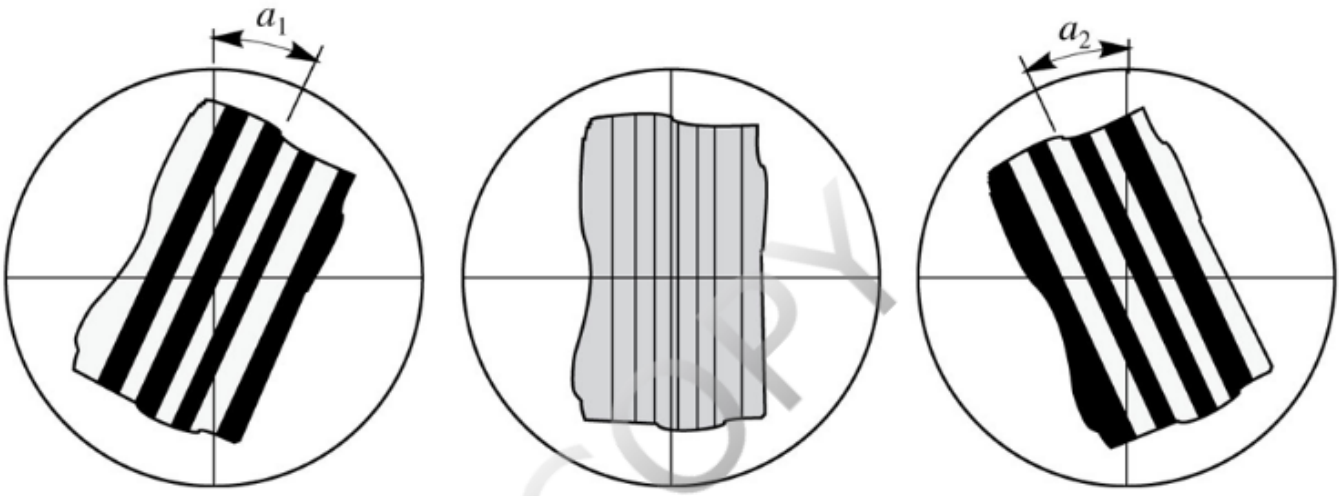

FIGURE 12.15 Michel-Lévy method. Extinction angles a_1 and a_2 are measured to the fast ray vibration direction in their respective sets of albite twin lamellae. The two angles are averaged. A half-dozen or more grains are measured, and the largest average extinction angle is used to estimate the plagioclase composition from Figure 12.16. Back to text

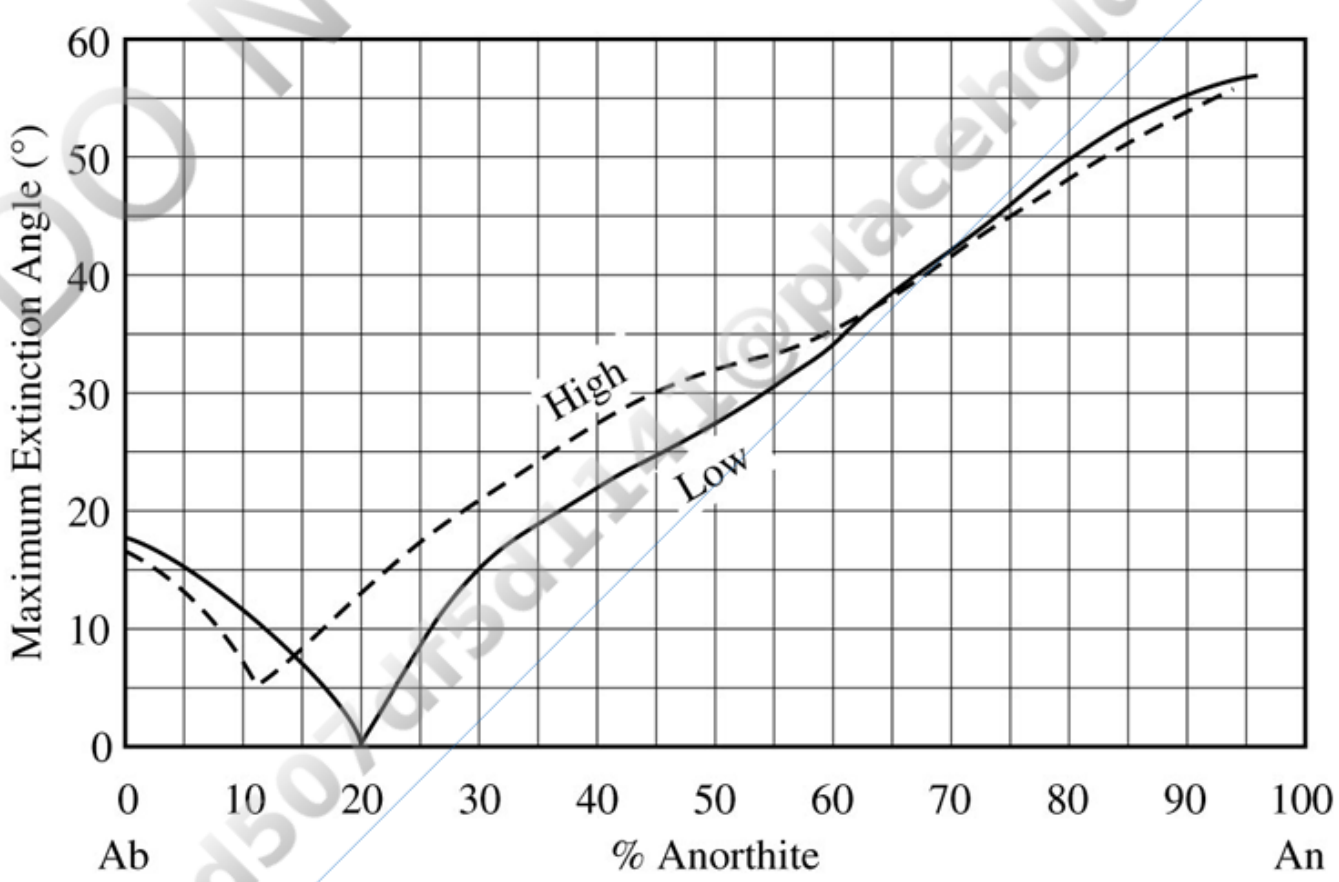

FIGURE 12.16 Diagram for use with the Michel-Lévy method. The maximum extinction angle to albite twin lamellae in sections cut perpendicular to {010} is plotted on the vertical axis; composition is the horizontal axis. The dashed curve is for high (volcanic) plagioclase, and the solid curve for low (plutonic) plagioclase. See text for additional discussion. Based on curves of Tobi and

Printed by: e48d507df5d1141@placeholder.94092.edu. Printing is for personal, private use only. No part of this book may be reproduced or transmitted without publisher's prior permission. Violators will be prosecuted.

curve for low (platonic) plagioclase. See text for additional discussion. Based on curves of Tobi and Kroll (1975). Back to text

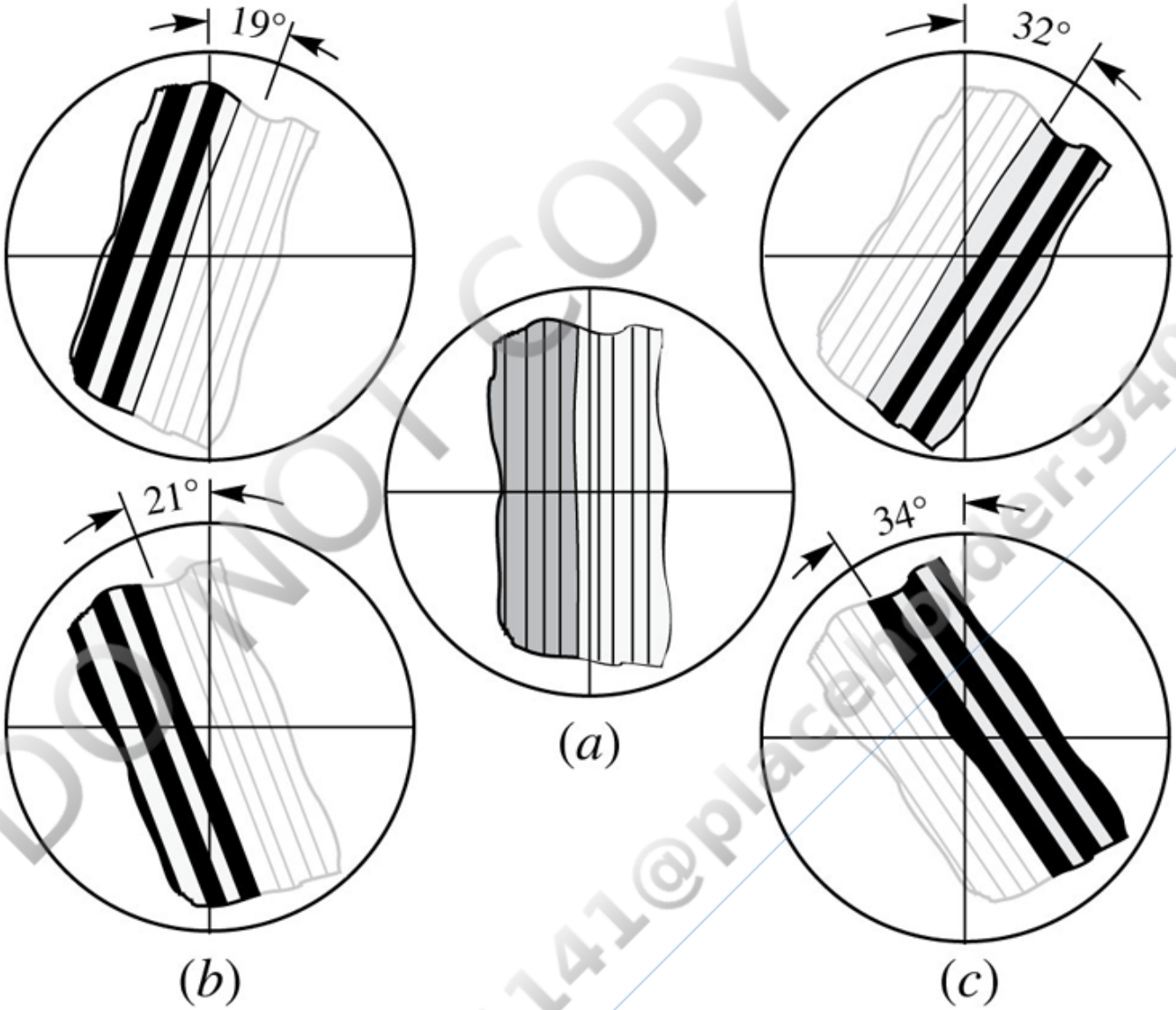

FIGURE 12.17 Carlsbad–albite method. (*a*) Grain with twin lamellae N–S between crossed polarizers. The two sides of the Carlsbad twin show different colors, but the albite lamellae within each side are uniform. (*b*) Extinction angles measured to the fast ray vibration direction in the albite lamellae on the left side of the Carlsbad twin. The average extinction angle in this case is 20°. (*c*) Extinction angles measured to the fast ray vibration direction in the albite lamellae on the right side of the Carlsbad twin. The average extinction angle in this case is 33°. The composition of the plagioclase (An_{60}) is determined from Figure 12.18a. Back to text

DO NOT COPY e48d507df5d1141@placeholder.9409

(a) Extinction Angles (°)

15 10 5 0 5 10 15 20 25 30 35

Printed by: e48d507df5d1141@placeholder.94092.edu. Printing is for personal, private use only. No part of this book may be reproduced or transmitted without publisher's prior permission. Violators will be prosecuted.

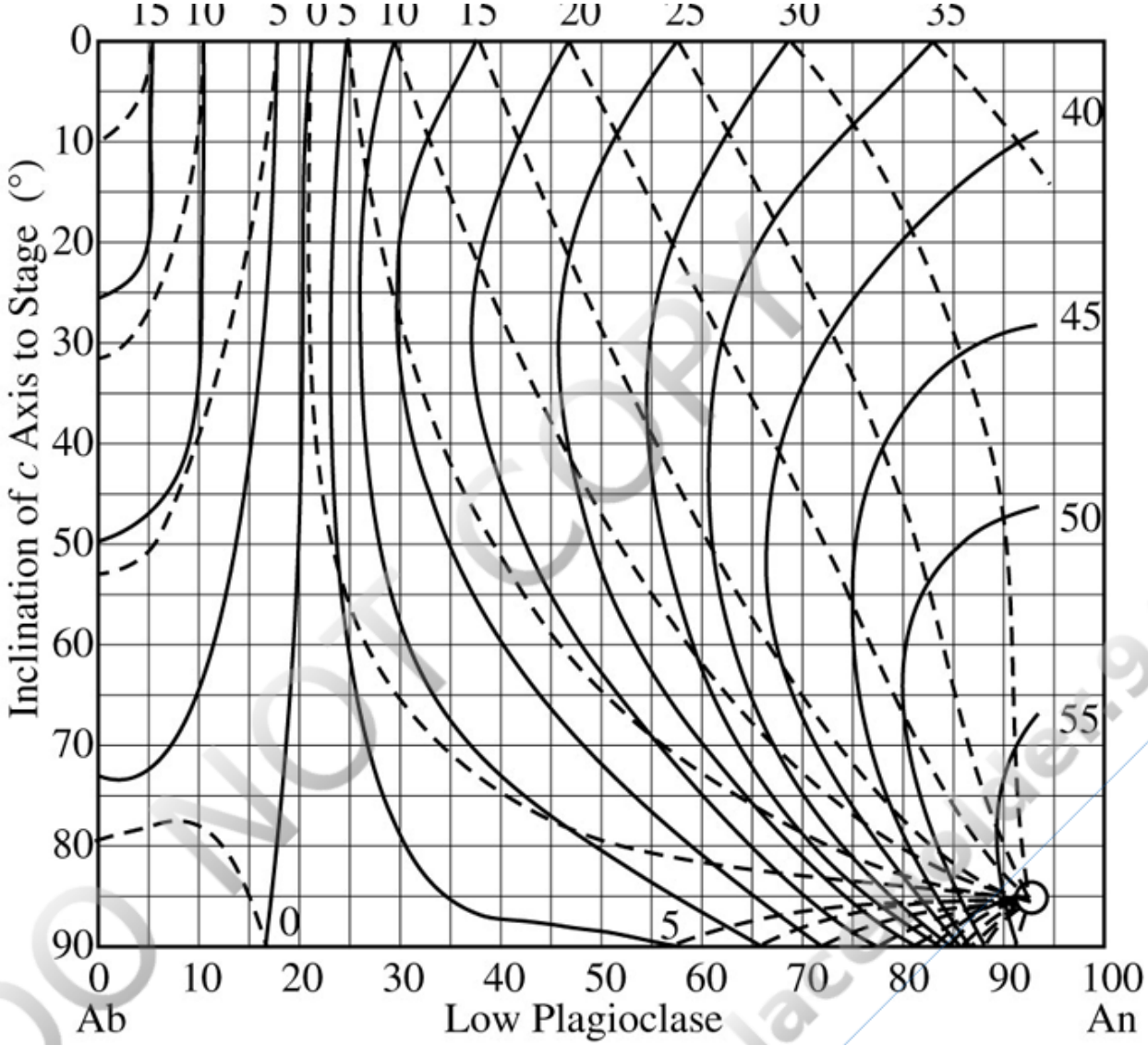

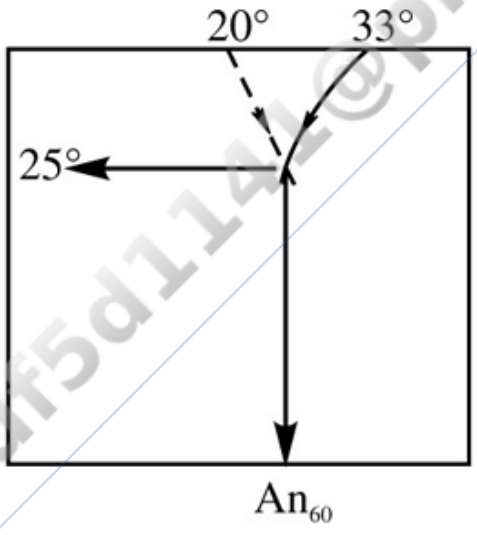

(b)

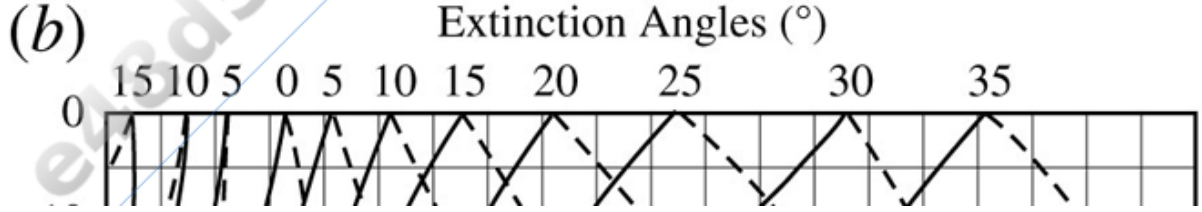

Printed by: e48d507df5d1141@placeholder.94092.edu. Printing is for personal, private use only. No part of this book may be reproduced or transmitted without publisher's prior permission. Violators will be prosecuted.

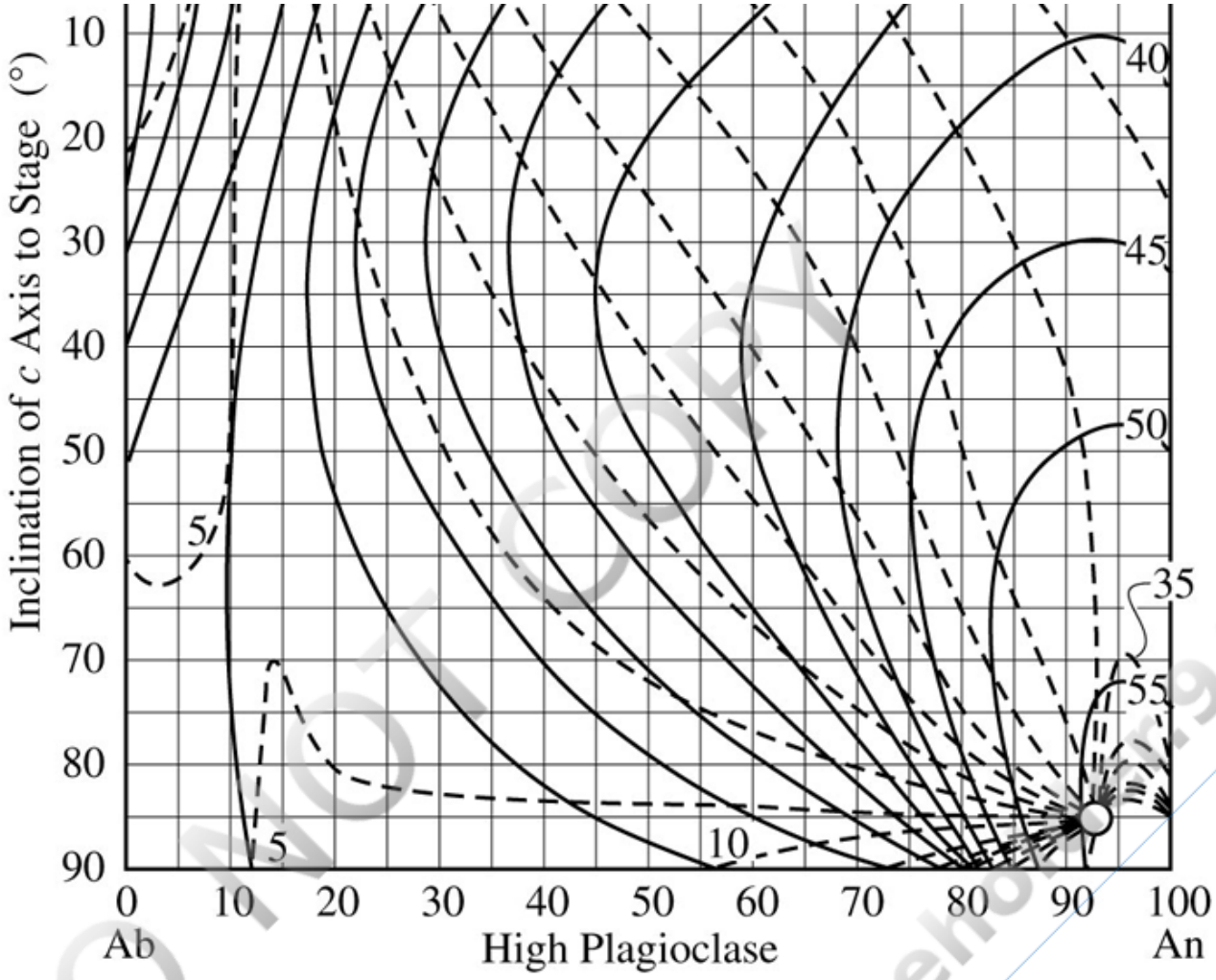

FIGURE 12.18 Diagrams for use with the Carlsbad–albite method. Solid lines are for the larger extinction angle, and dashed lines for the smaller extinction angle (Figure 12.17). See text for additional discussion. (*a*) Low plagioclase. A composition of An_{60} is indicated for a smaller extinction angle of 20° and a larger angle of 33°, and the *c* axis of the grain is inclined 25° from the microscope stage. (*b*) High plagioclase. From Tobi and Kroll (1975). Back to text

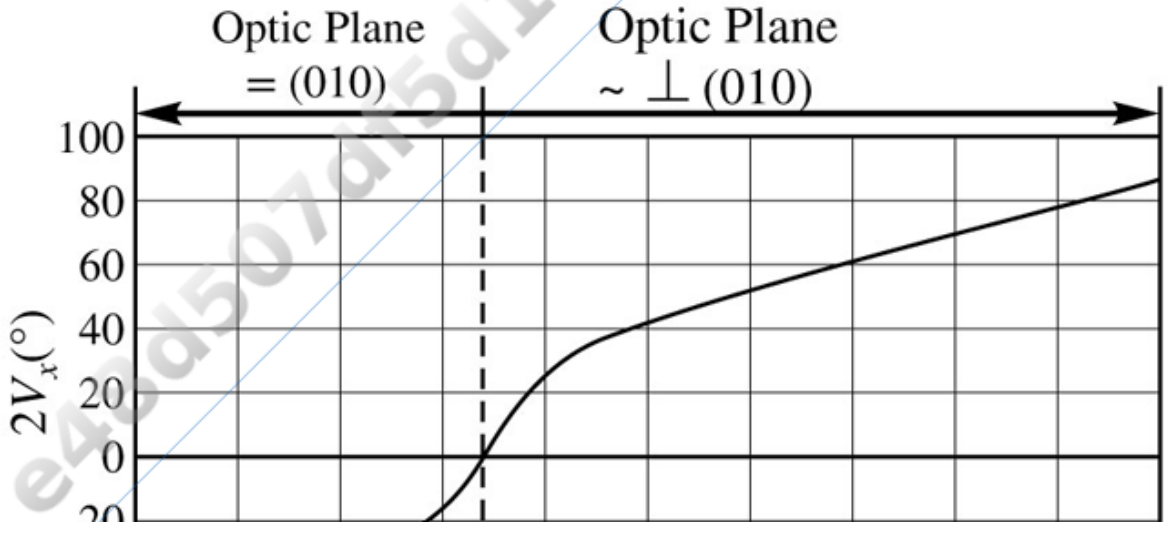

Printed by: e48d507df5d1141@placeholder.94092.edu. Printing is for personal, private use only. No part of this book may be reproduced or transmitted without publisher's prior permission. Violators will be prosecuted.

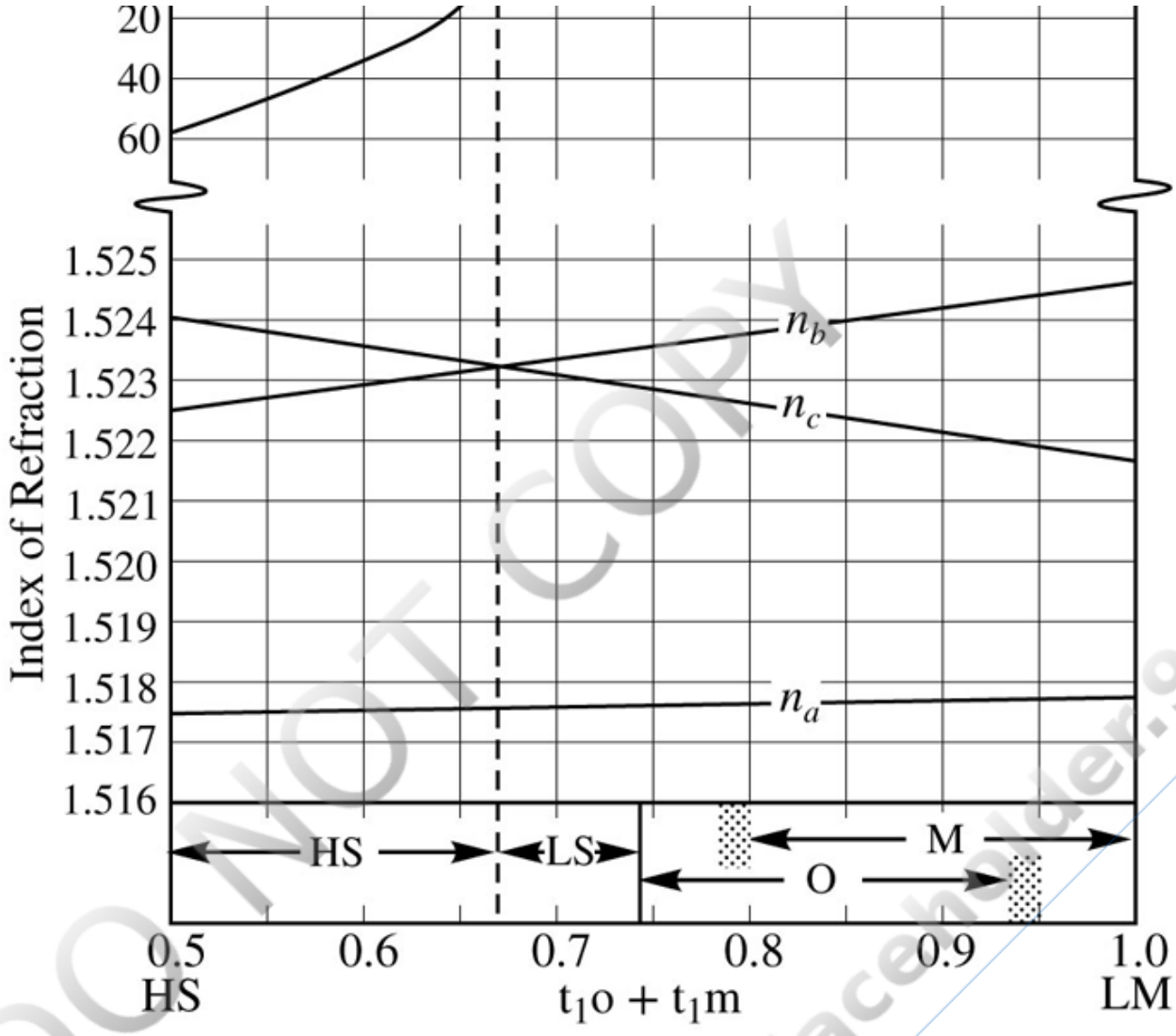

FIGURE 12.19 Variation of $2V_x$ and indices of refraction for common alkali feldspar as a function of the degree of Si–Al order. The occupancies of Al in the T_1o and T_1m tetrahedral sites are t_1o and t_1m, respectively. If Al and Si are randomly distributed among the tetrahedral sites, as in high sanidine (HS), then one-quarter of the T_1o and one-quarter of the T_1m sites are filled with Al: $t_1o + t_1m = 0.50$. If all Al is in the T_1o site, then $t_1o + t_1m = 1.00$ as in low microcline (LM). The principal indices of refraction n_a, n_b, and n_c are for light vibrating most nearly parallel to the *a*, *b*, and *c* crystal axes, respectively. The approximate ranges of high sanidine (HS), low sanidine (LS), orthoclase (O), and microcline (M) are indicated. After Su and others (1984). Back to text

(*a*)

DO NOT COPY

Printed by: e48d507df5d1141@placeholder.94092.edu. Printing is for personal, private use only. No part of this book may be reproduced or transmitted without publisher's prior permission. Violators will be prosecuted.

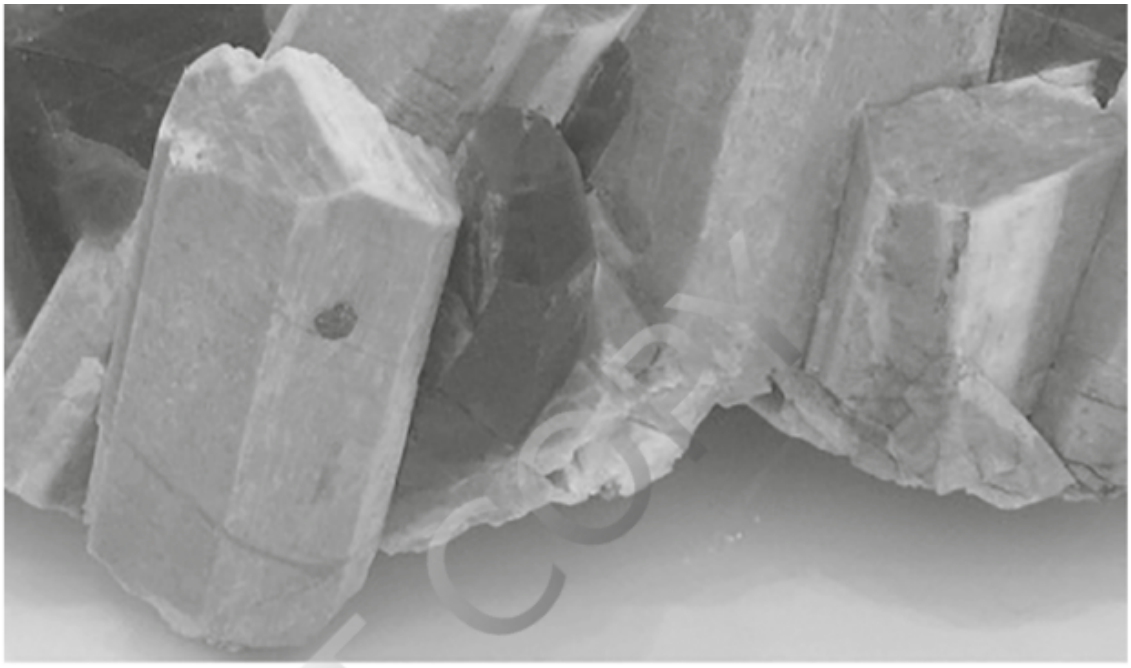

(*b*)

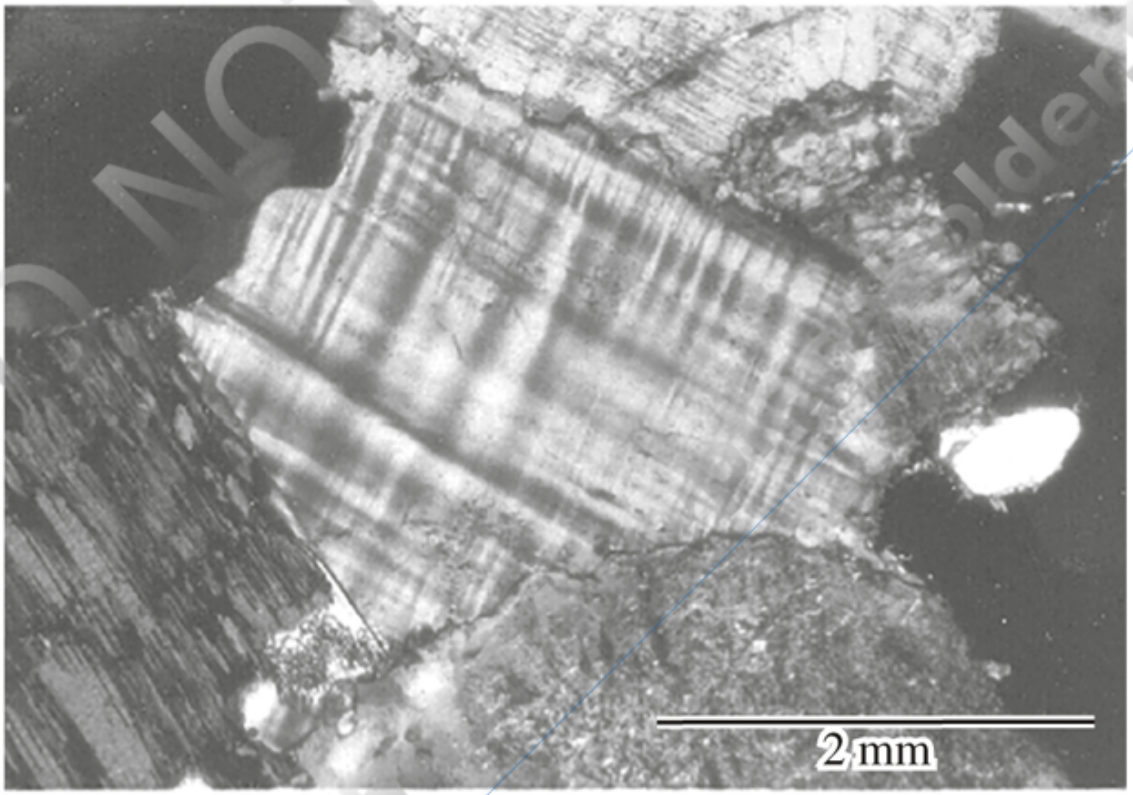

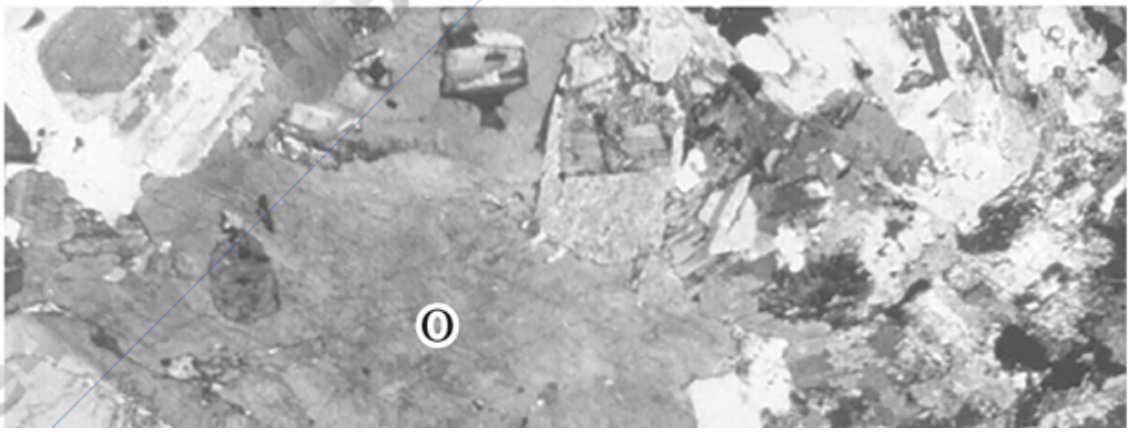

Printed by: e48d507df5d1141@placeholder.94092.edu. Printing is for personal, private use only. No part of this book may be reproduced or transmitted without publisher's prior permission. Violators will be prosecuted.

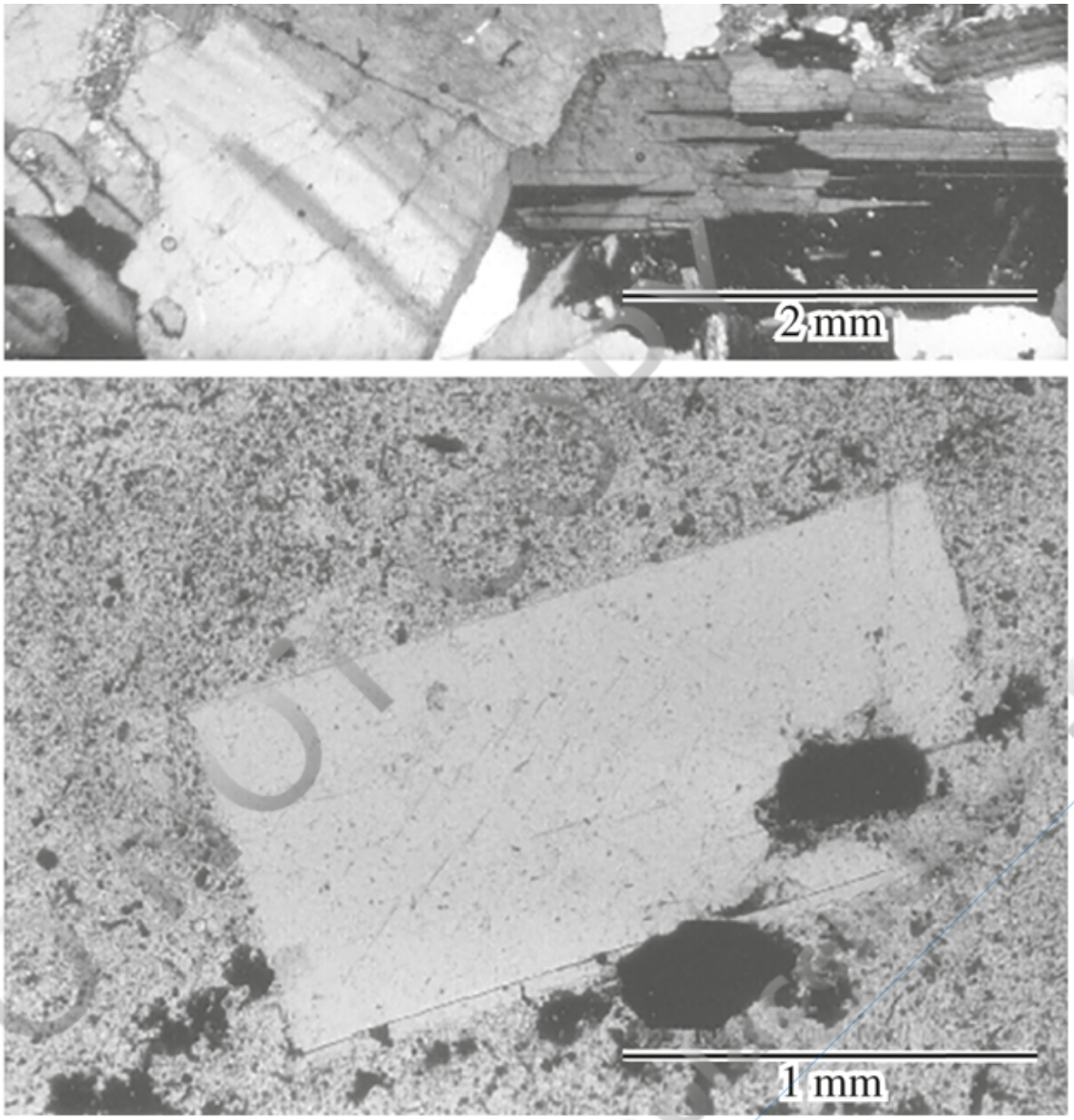

FIGURE 12.20 Alkali feldspar. (*a*) Perthitic microcline crystals with quartz (dark). (*b*) Photomicrographs. (*Top*) Thin section of granite showing microcline with "tartan plaid" albite and pericline twinning. Crossed polarizers. (*Middle*) Orthoclase (O) in granite. Crossed polarizers. (*Bottom*) Sanidine phenocryst in rhyolite. Plane light. Back to text

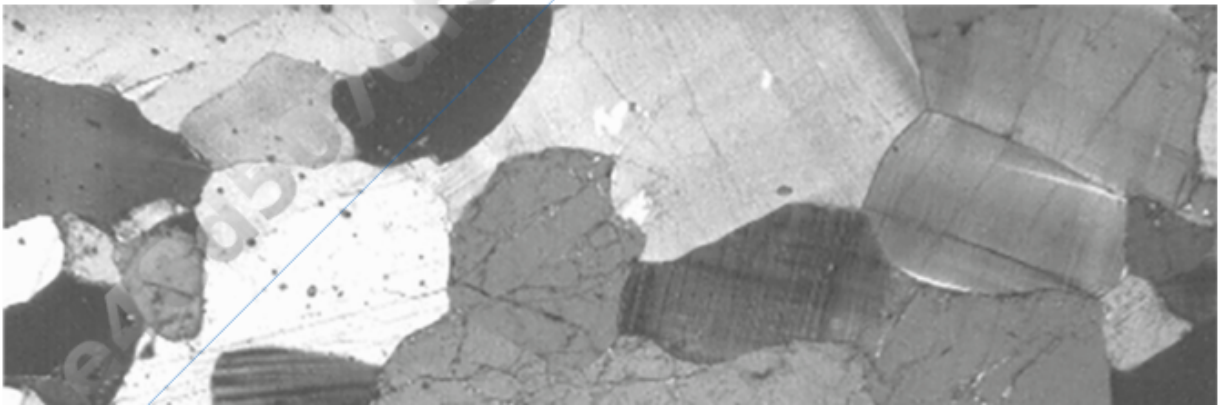

Printed by: e48d507df5d1141@placeholder.94092.edu. Printing is for personal, private use only. No part of this book may be reproduced or transmitted without publisher's prior permission. Violators will be prosecuted.

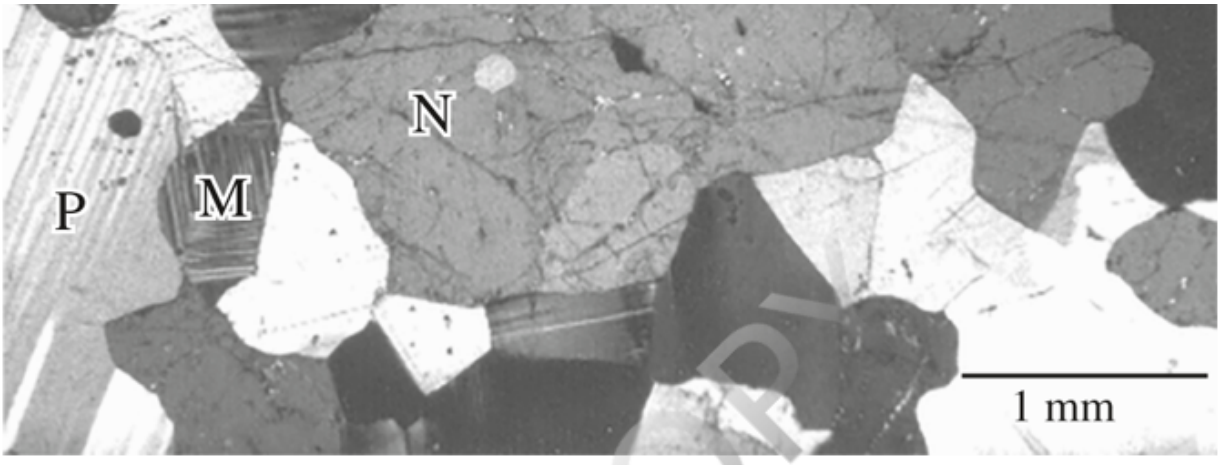

FIGURE 12.21 Photomicrograph of nepheline (N) in thin section with plagioclase (P) and microcline (M) in nepheline syenite. Crossed polarizers. Back to text

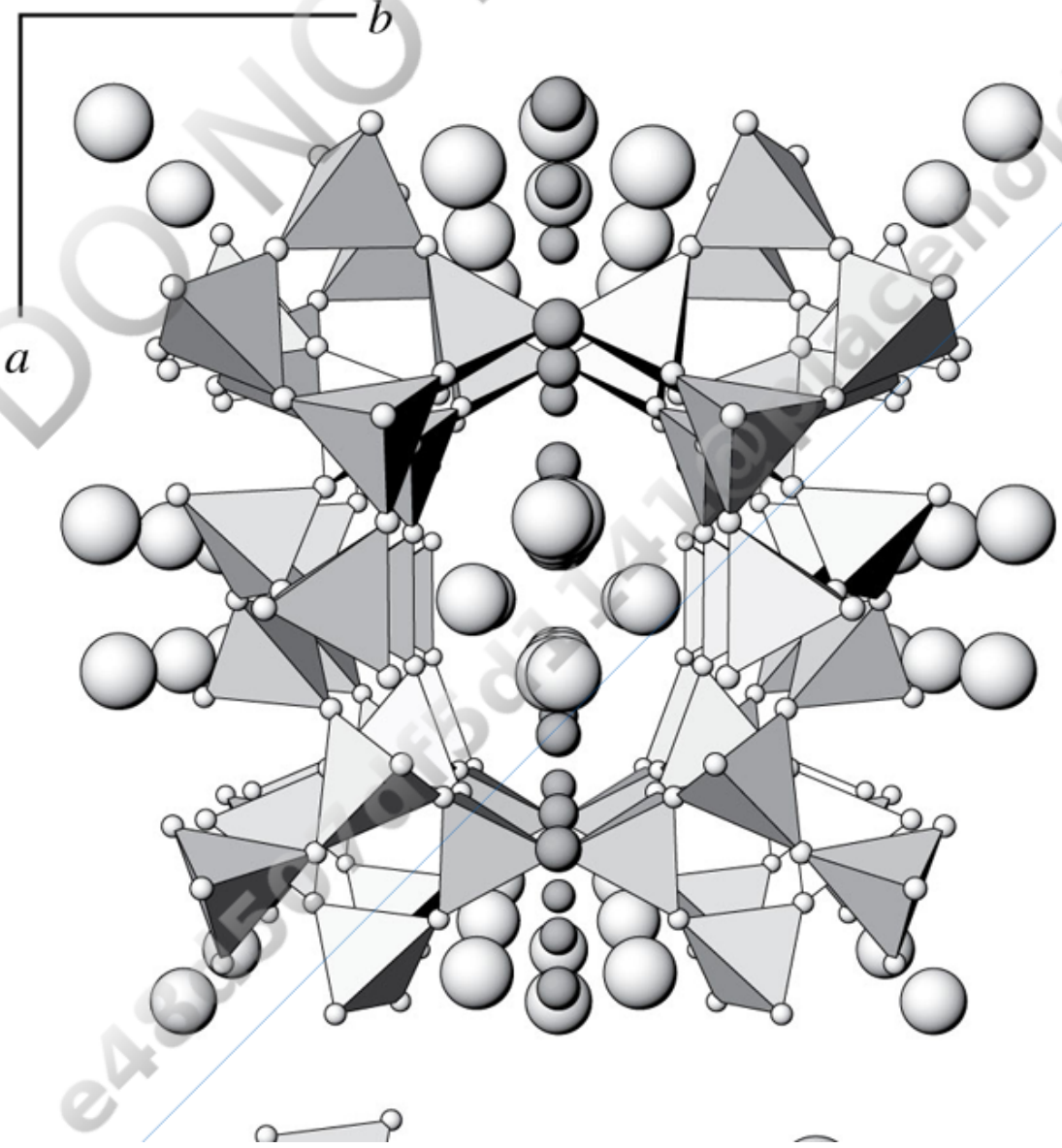

DO NOT COPY

Printed by: e48d507df5d1141@placeholder.94092.edu. Printing is for personal, private use only. No part of this book may be reproduced or transmitted without publisher's prior permission. Violators will be prosecuted.

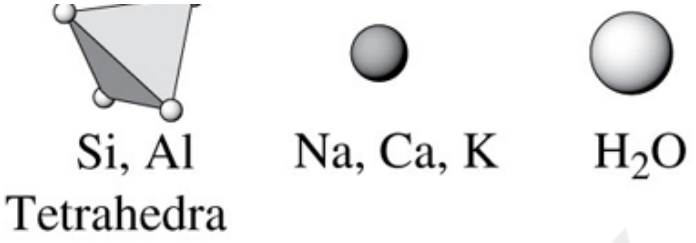

FIGURE 12.22 Typical zeolite structure. Heulandite viewed down the *c* axis. The open channels provide space for water molecules and mono- and divalent cations. Structural data from Gunter and others (1994). Back to text

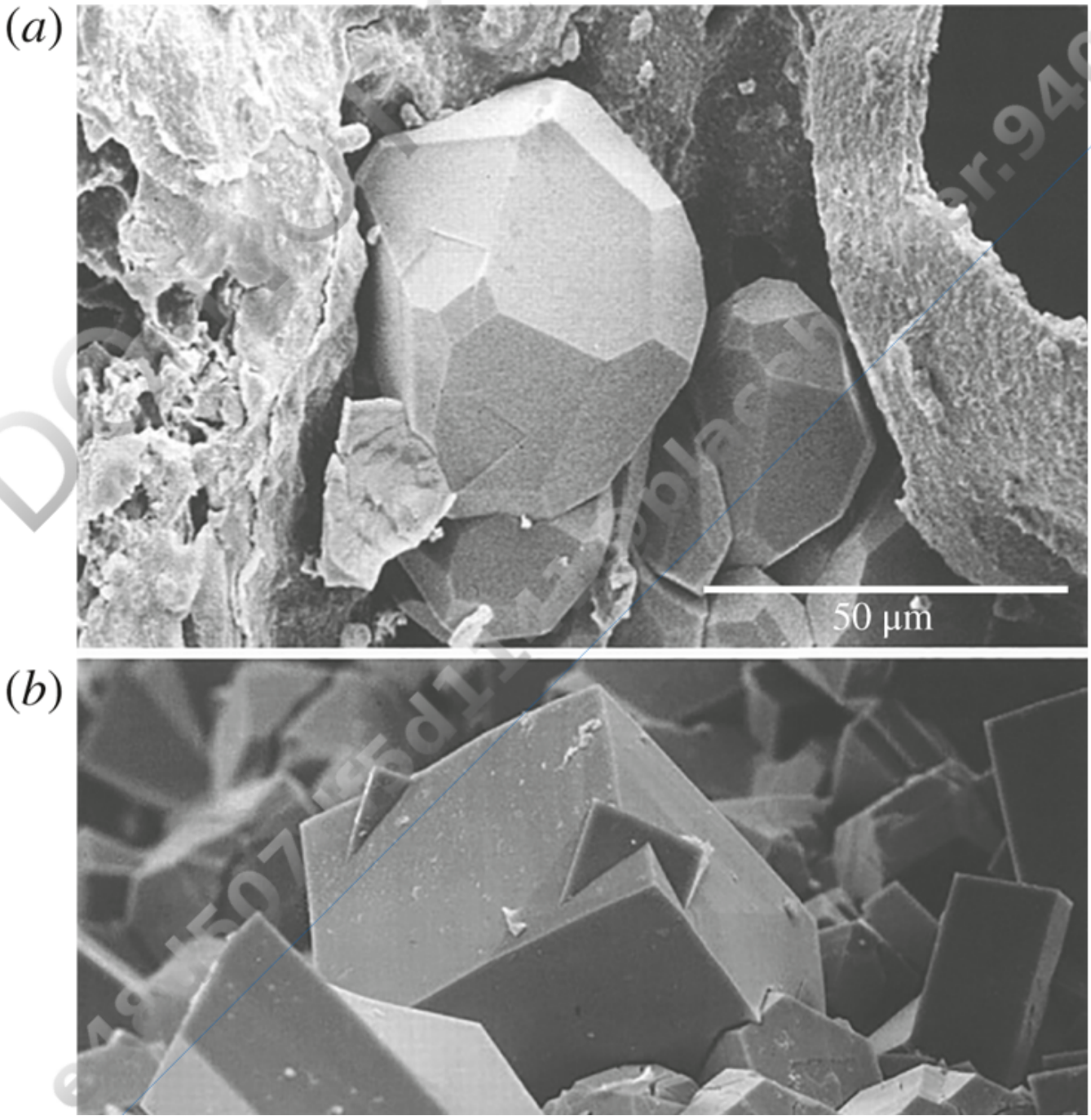

Printed by: e48d507df5d1141@placeholder.94092.edu. Printing is for personal, private use only. No part of this book may be reproduced or transmitted without publisher's prior permission. Violators will be prosecuted.

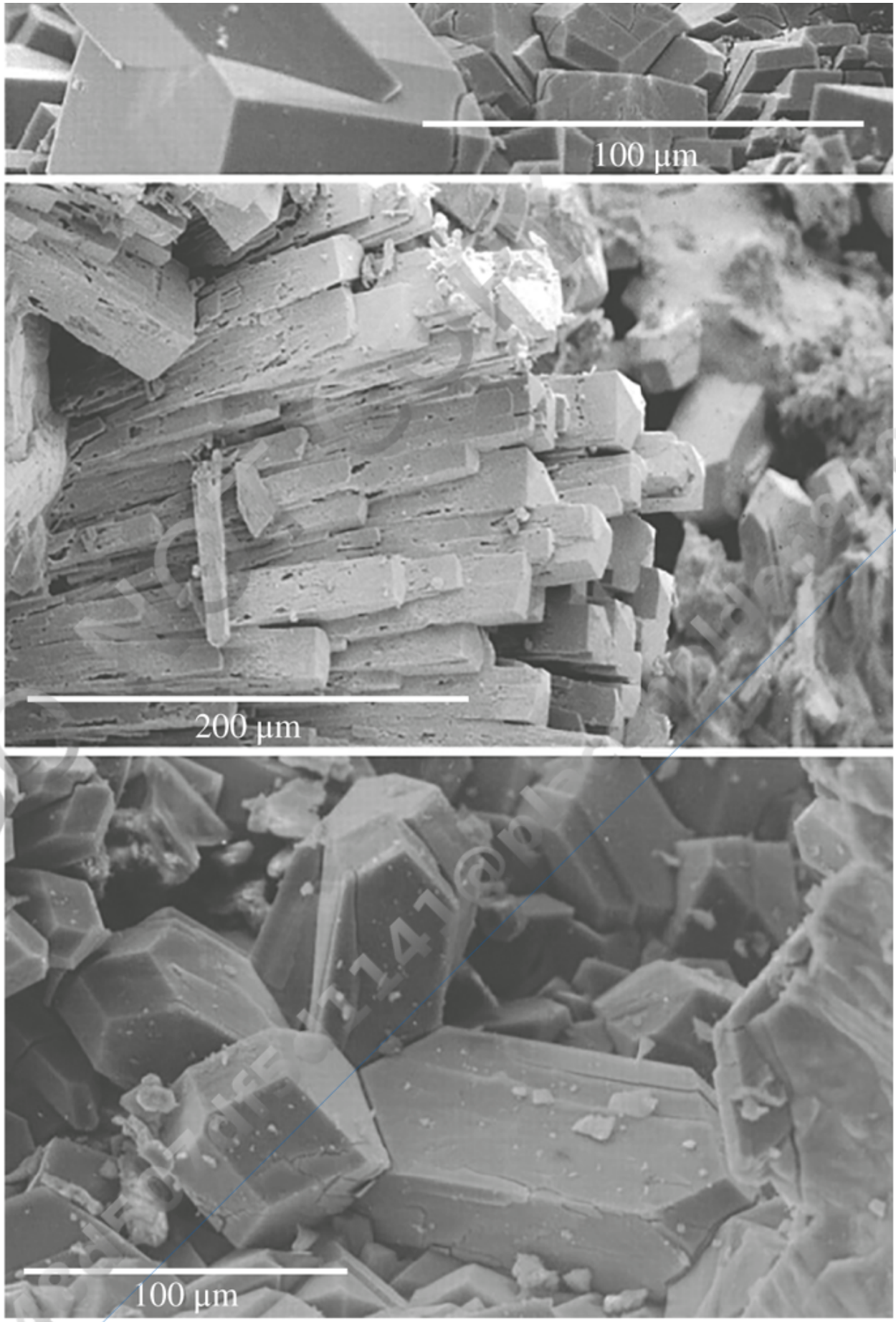

FIGURE 12.23 Scanning electron microscope images of zeolites from altered basaltic tuff,

Printed by: e48d507df5d1141@placeholder.94092.edu. Printing is for personal, private use only. No part of this book may be reproduced or transmitted without publisher's prior permission. Violators will be prosecuted.

Chapter 13 Sheet Silicates

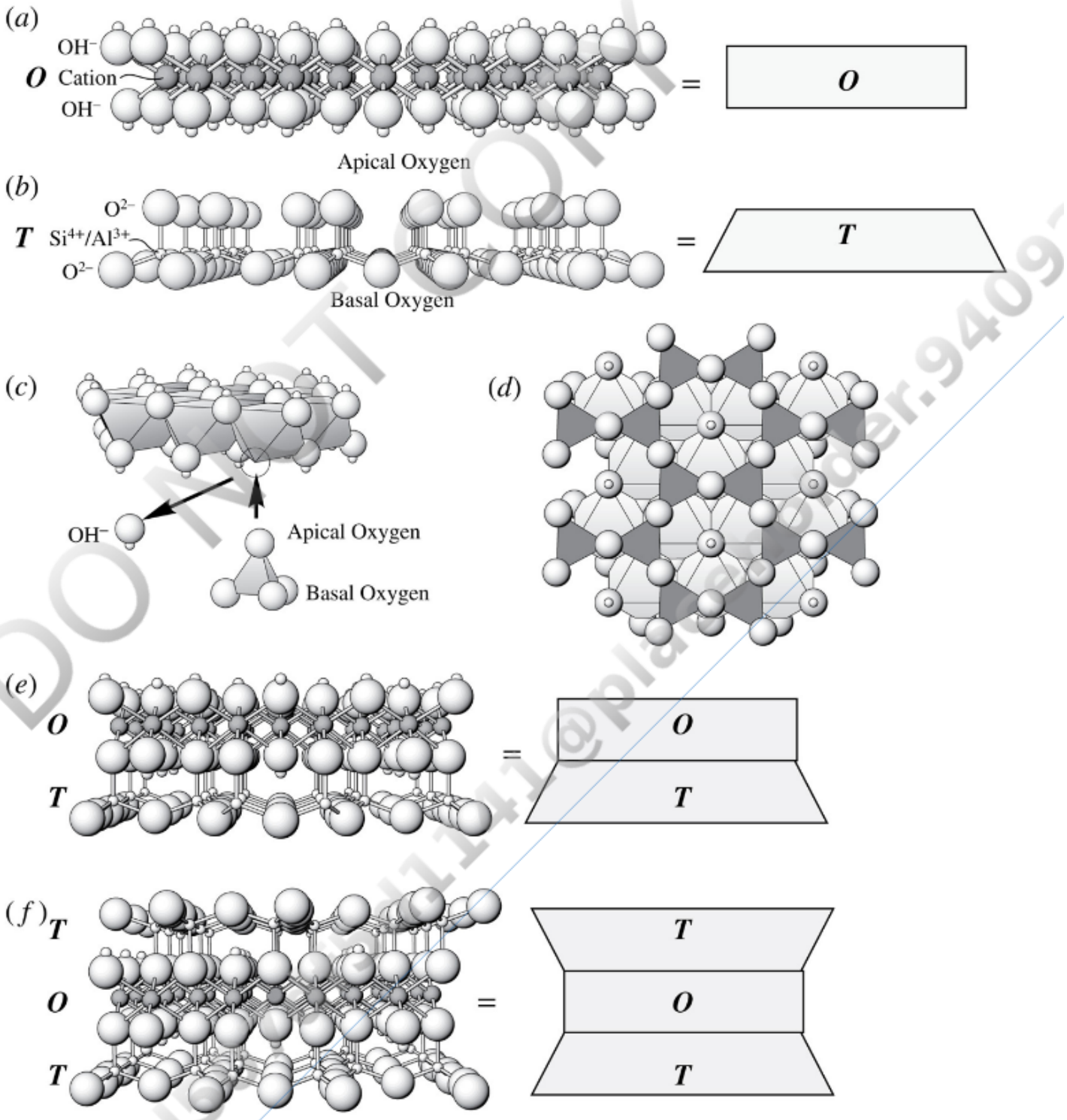

FIGURE 13.1 Sheet silicate sheets and layers. (*a*) An octahedral (*O*) sheet consists of two close-packed planes of OH^- with di- or trivalent cations occupying octahedral sites in between. The side view of an octahedral sheet is schematically represented by a rectangle. (*b*) A tetrahedral (*T*) sheet commonly consists of Si or Al tetrahedra; each tetrahedra shares three oxygen atoms with neighboring tetrahedra to form a continuous hexagonal mesh (cf. Figure 11.2f). The side view of a

Printed by: e48d507df5d1141@placeholder.94092.edu. Printing is for personal, private use only. No part of this book may be reproduced or transmitted without publisher's prior permission. Violators will be prosecuted.

neighboring tetrahedra to form a continuous hexagonal mesh (cf. Figure 11.2f). The side view of a tetrahedral sheet is schematically represented by a trapezoid. (*c*) Combining a tetrahedral sheet with an octahedral sheet requires that an octahedral sheet OH^- is replaced by the apical oxygen of each tetrahedron. (*d*) Sheet-perpendicular view of a tetrahedral sheet combined with an octahedral sheet. The apical oxygens on the tetrahedra (dark shading) point away from the viewer and substitute for OH^- on the top of the octahedral sheet. The octahedra are shown with light shading. Note the openings formed in the center of the hexagonal rings of tetrahedra. (*e*) Side view of the bonded tetrahedral-octahedral sheets, forming a 1:1 or *TO* layer that is three layers of O^{2-}/OH^- thick. (*f*) Two tetrahedral sheets may bond on opposite sides of an octahedral sheet to form a 2:1 or *TOT* layer that is four layers of O^{2-}/OH^- thick. Back to text

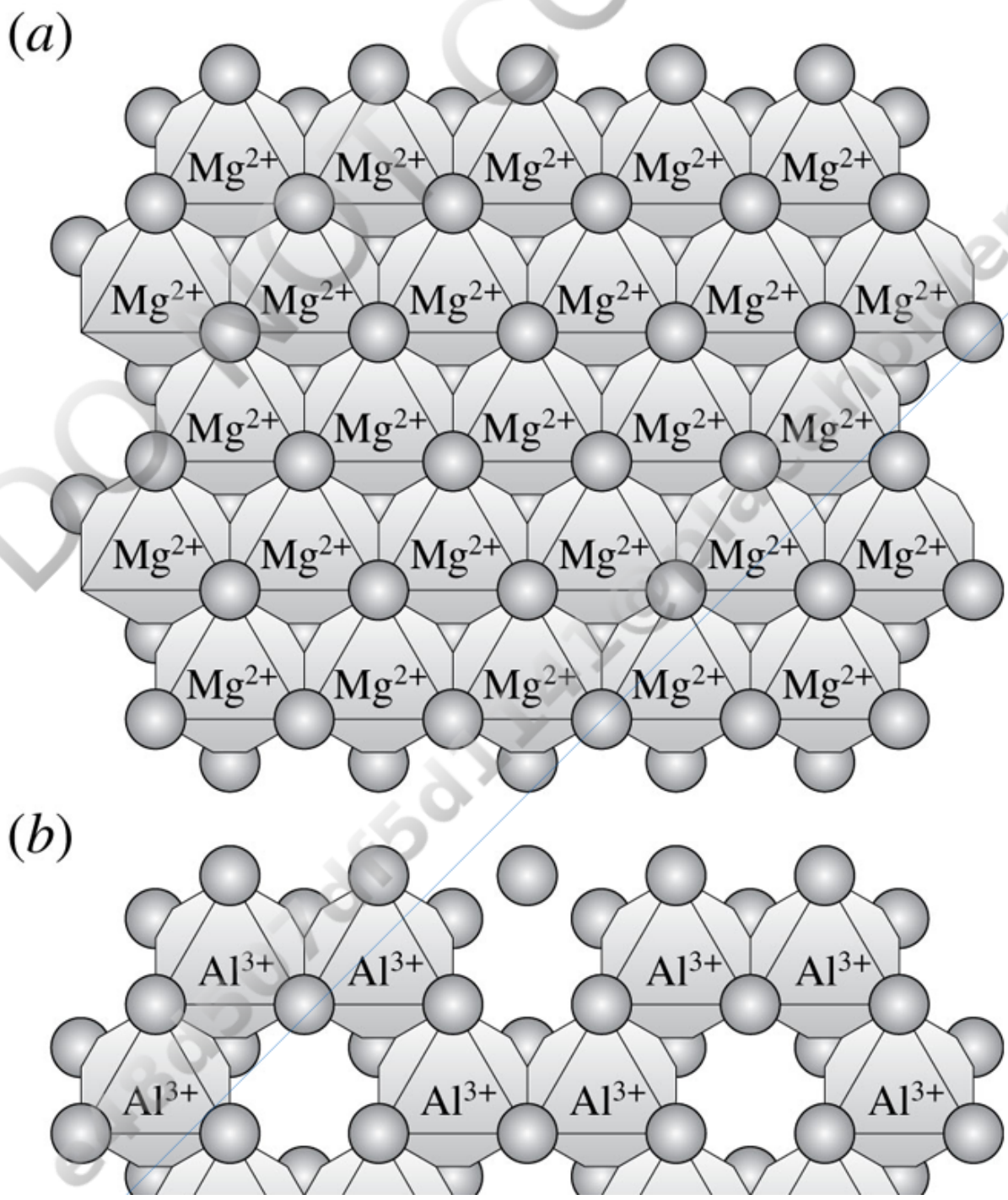

DO NOT COPY

Printed by: e48d507df5d1141@placeholder.94092.edu. Printing is for personal, private use only. No part of this book may be reproduced or transmitted without publisher's prior permission. Violators will be prosecuted.

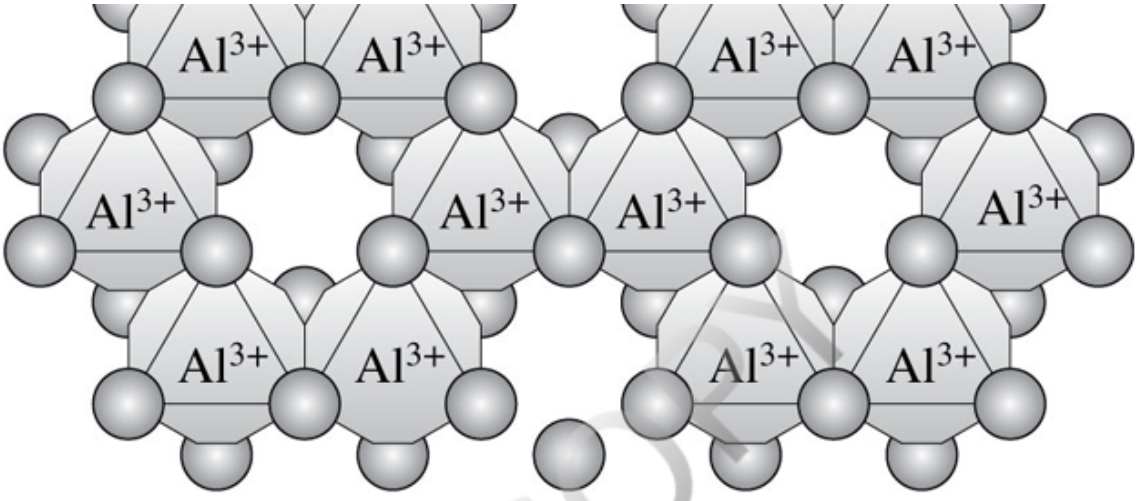

FIGURE 13.2 Schematic plan view of trioctahedral and dioctahedral sheets. (*a*) Trioctahedral. Divalent cations (usually Mg^{2+} or Fe^{2+}) occupy all (three out of three) octahedral sites. (*b*) Dioctahedral. Trivalent cations (usually Al^{3+}) occupy two-thirds of the potential octahedral sites.
Back to text

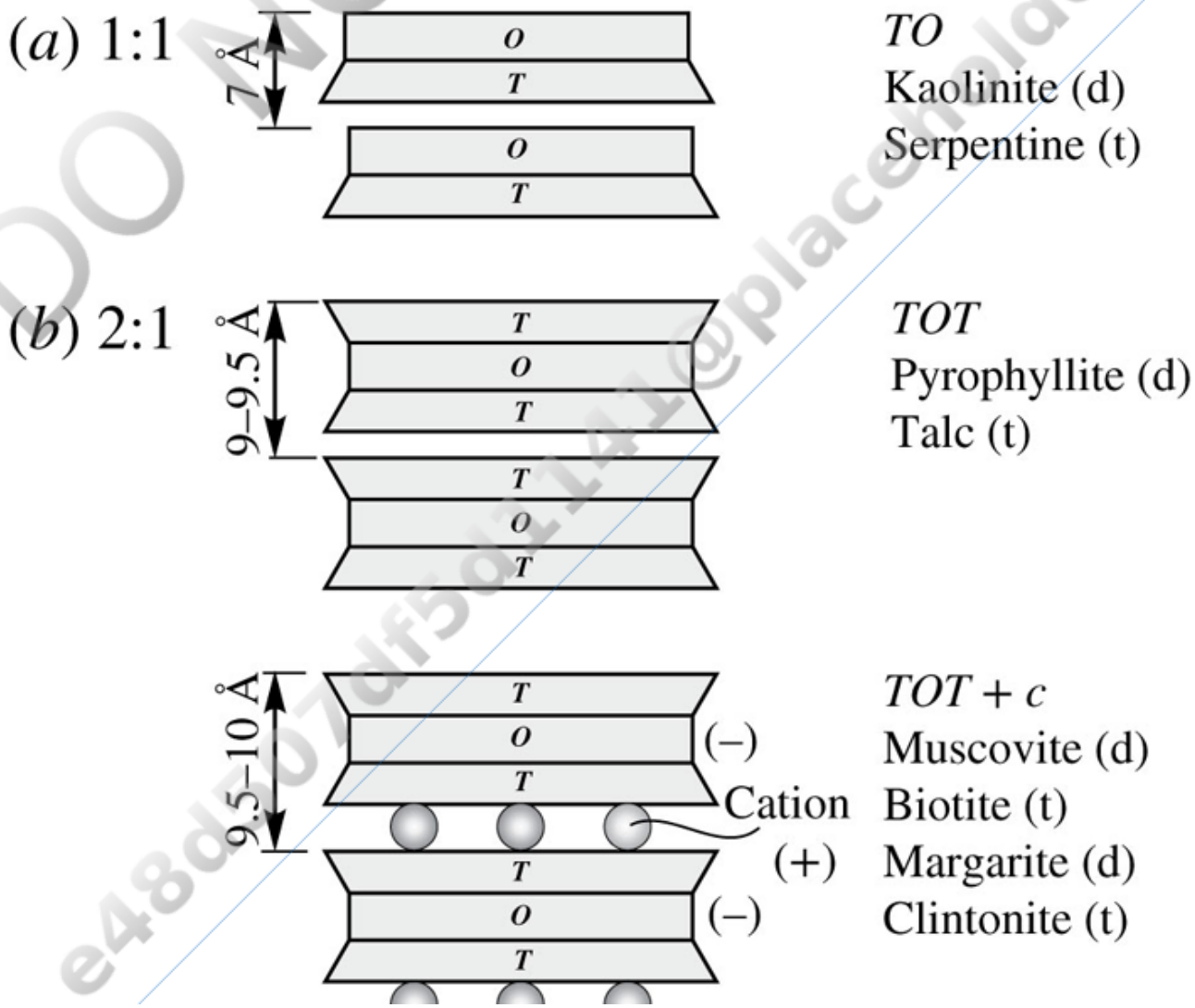

DO NOT COPY
e48d507df5d1141@placeholder.9409

Printed by: e48d507df5d1141@placeholder.94092.edu. Printing is for personal, private use only. No part of this book may be reproduced or transmitted without publisher's prior permission. Violators will be prosecuted.

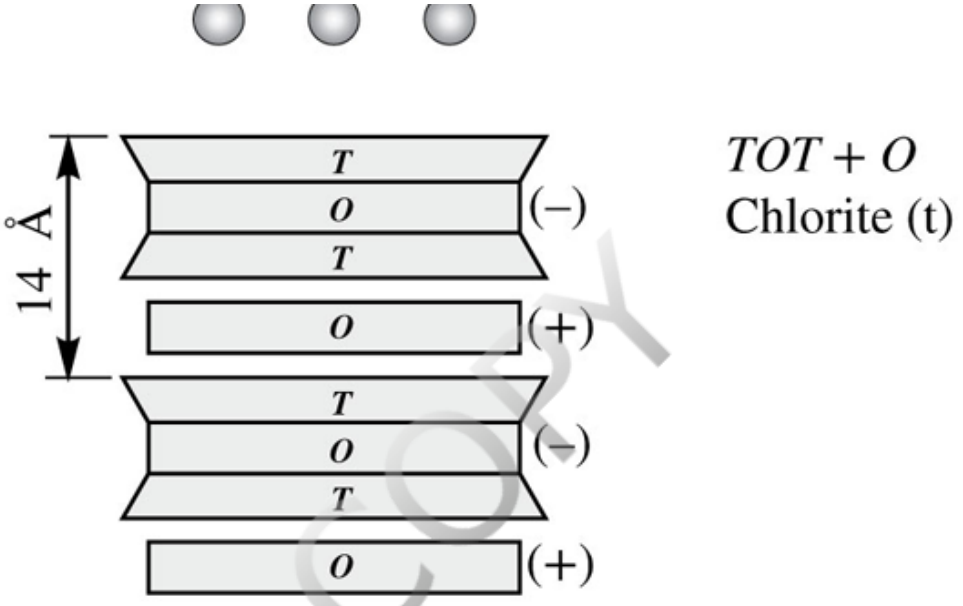

FIGURE 13.3 Schematic sheet silicate unit structures. Dioctahedral minerals are indicated with (d) and trioctahedral with (t). (*a*) 1:1 layer silicates. *TO* layers are bonded to each other with weak electrostatic bonds. (*b*) 2:1 layer silicates. Successive uncharged *TOT* layers are bonded together with weak electrostatic bonds (*TOT*, top). *TOT* layers with a net negative charge are bonded through interlayer cations (*TOT* + *c*, middle) or through *O* sheets with a net positive charge (*TOT* + *O*, bottom). Back to text

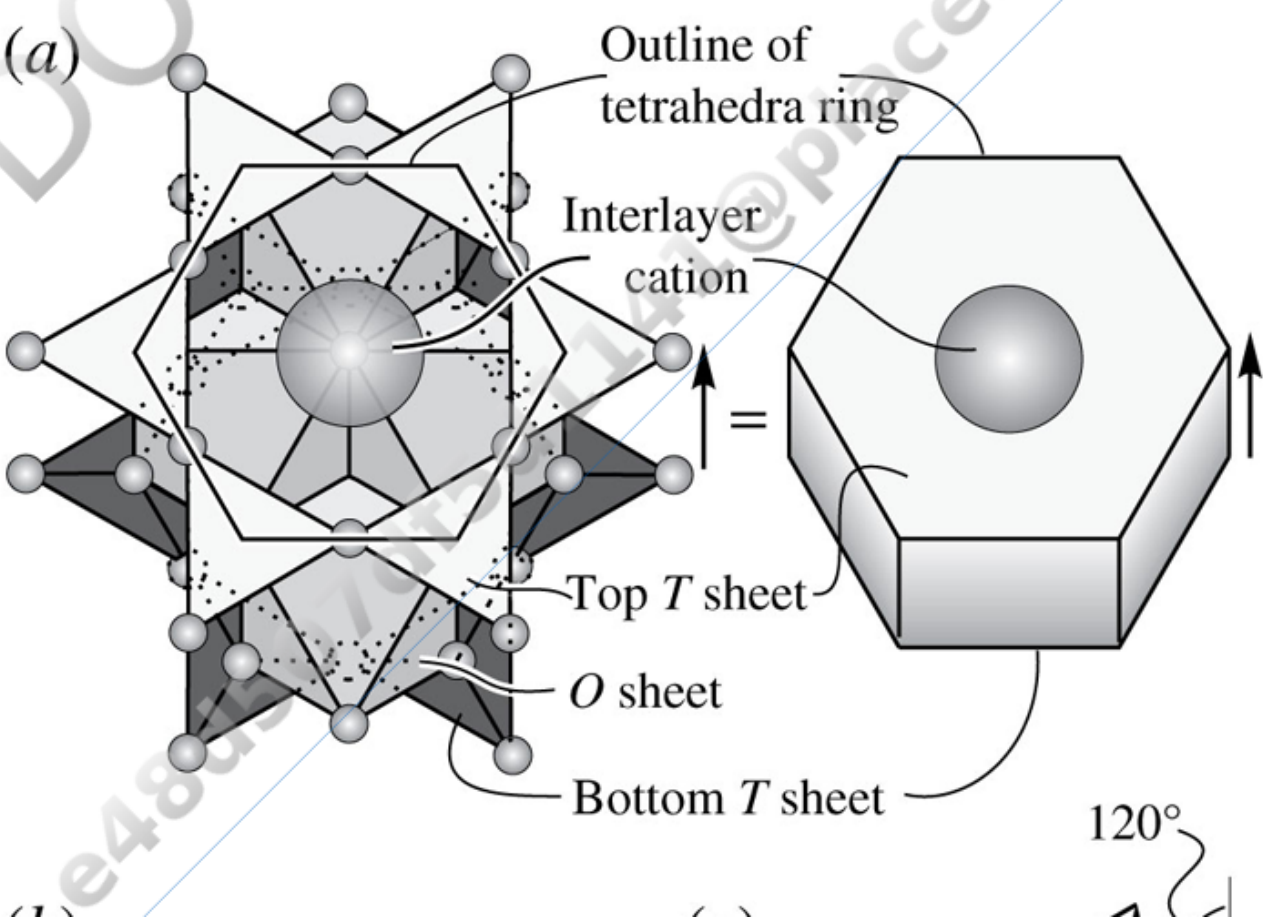

DO NOT COPY

Printed by: e48d507df5d1141@placeholder.94092.edu. Printing is for personal, private use only. No part of this book may be reproduced or transmitted without publisher's prior permission. Violators will be prosecuted.

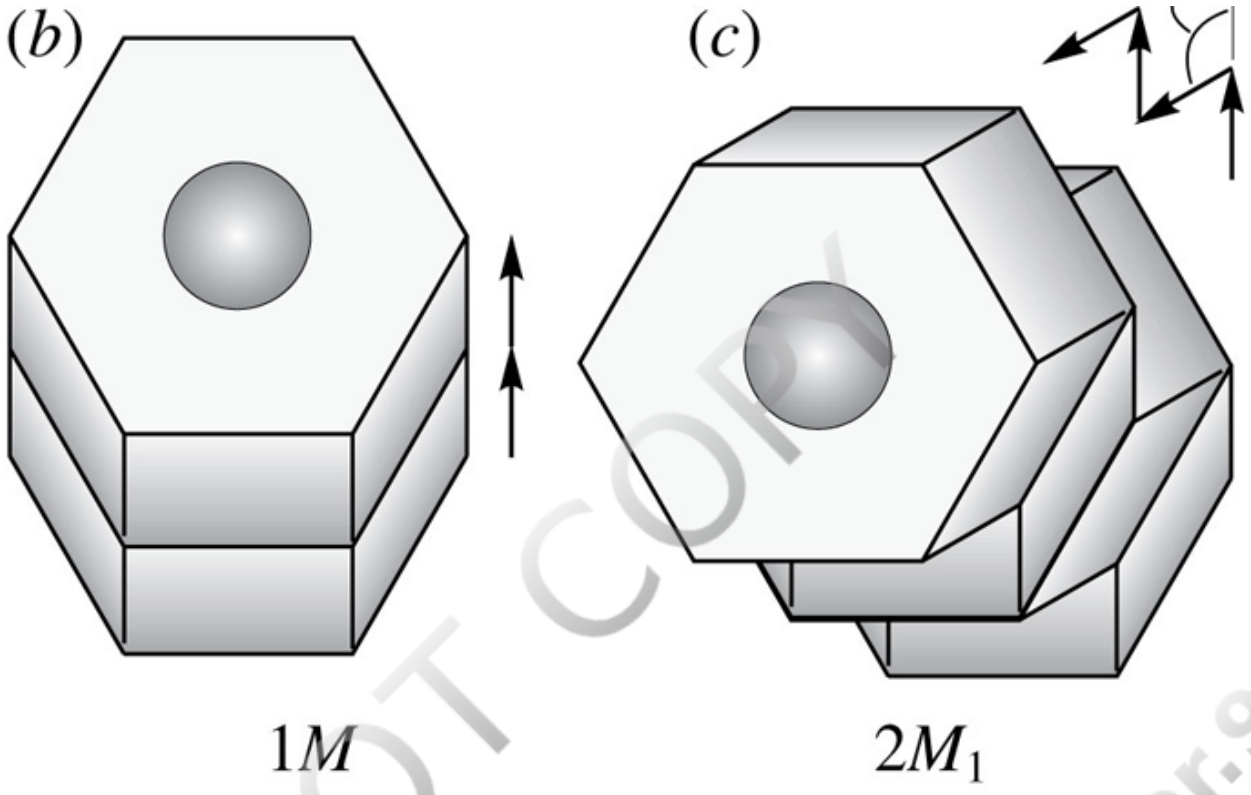

FIGURE 13.4 Polytypism in the micas. (*a*) In a *TOT* layer, the top *T* sheet must be offset relative to the bottom *T* sheet. Four octahedra from the octahedral sheet (*O*) are shown with a single ring of tetrahedra from the tetrahedral (*T*) sheets on the top (light shading) and bottom (dark shading). Adjacent *TOT* layers are aligned to each other by the interlayer cation that fits in the center of the tetrahedra rings. The shape on the right schematically represents the position of the tetrahedra rings on bottom and top. (*b*) 1*M* polytype. Adjacent *TOT* layers have the same direction of offset. (*c*) $2M_1$ polytype. The offset direction in adjacent *TOT* layers is at 120°, and the repeat distance is two layers.
Back to text

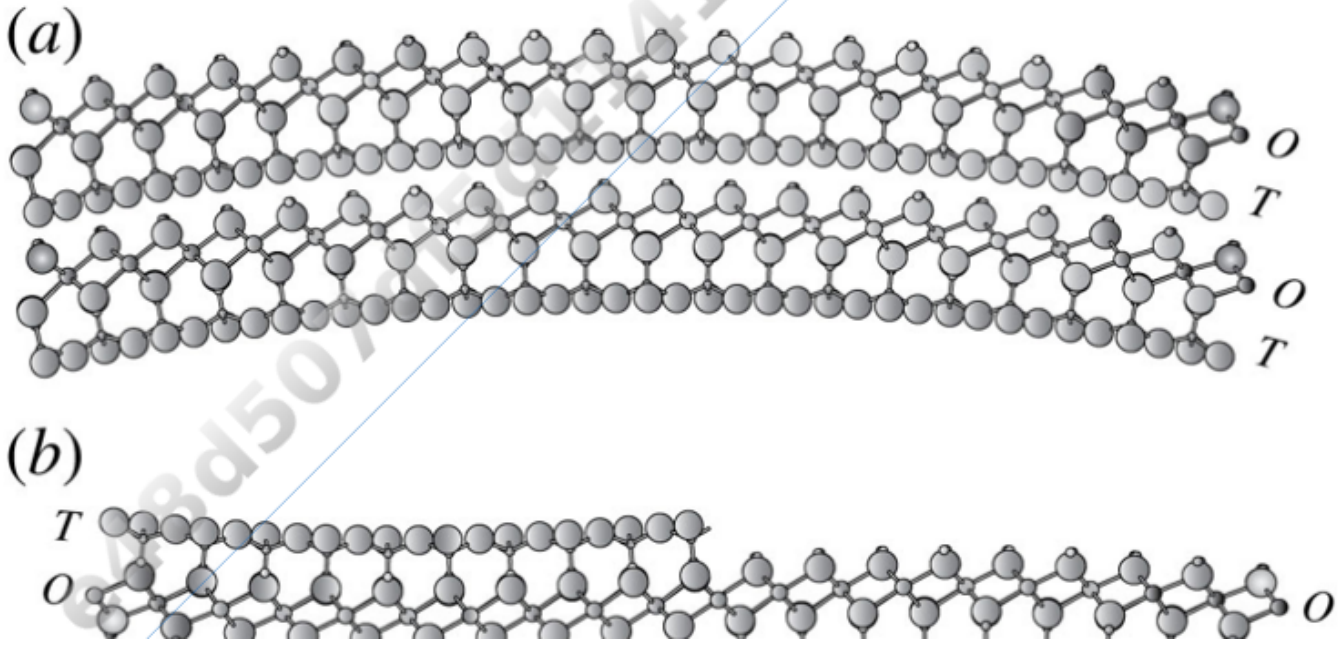

Printed by: e48d507df5d1141@placeholder.94092.edu. Printing is for personal, private use only. No part of this book may be reproduced or transmitted without publisher's prior permission. Violators will be prosecuted.

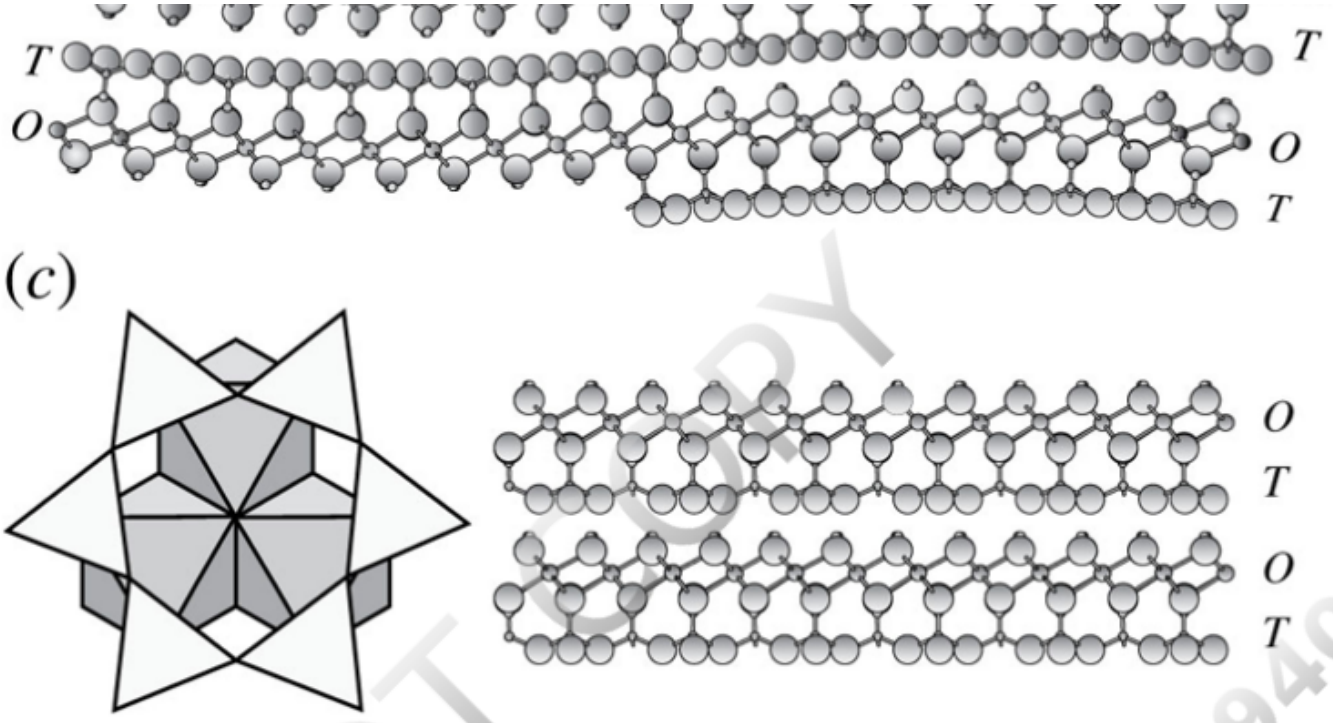

FIGURE 13.5 Serpentine structures. All are based on dioctahedral *TO* layers. (*a*) Chrysotile. Mismatch in the lateral dimensions of *T* and *O* sheets is accommodated by curving the *TO* layers so that they curve into fibers as they grow. (*b*) Antigorite. Continuous *TO* sheets contain reversals in the tetrahedra-facing direction. (*c*) Lizardite. The tetrahedra mesh (light shading) is distorted from its ideal hexagonal geometry to match the dimensions of the octahedral sheet. *TO* layers are relatively flat. Back to text

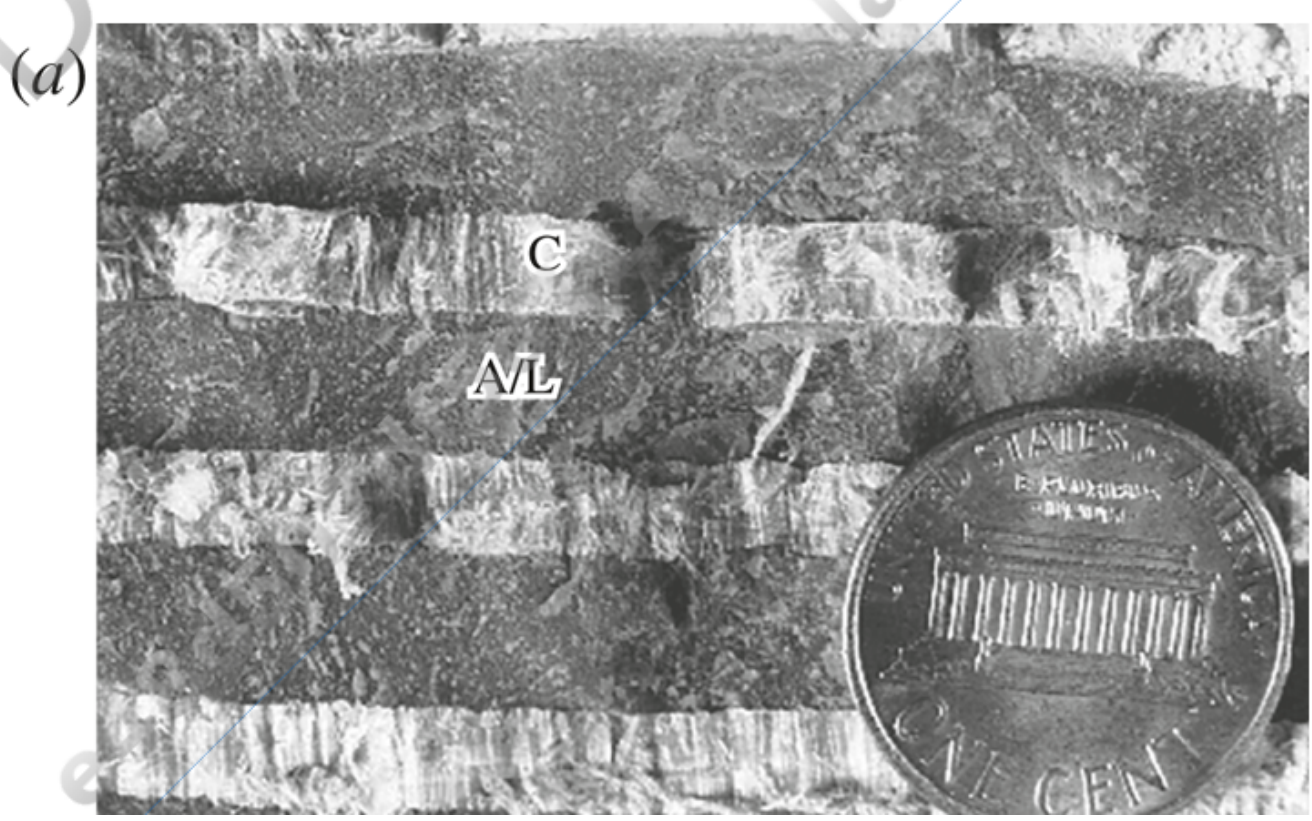

Printed by: e48d507df5d1141@placeholder.94092.edu. Printing is for personal, private use only. No part of this book may be reproduced or transmitted without publisher's prior permission. Violators will be prosecuted.

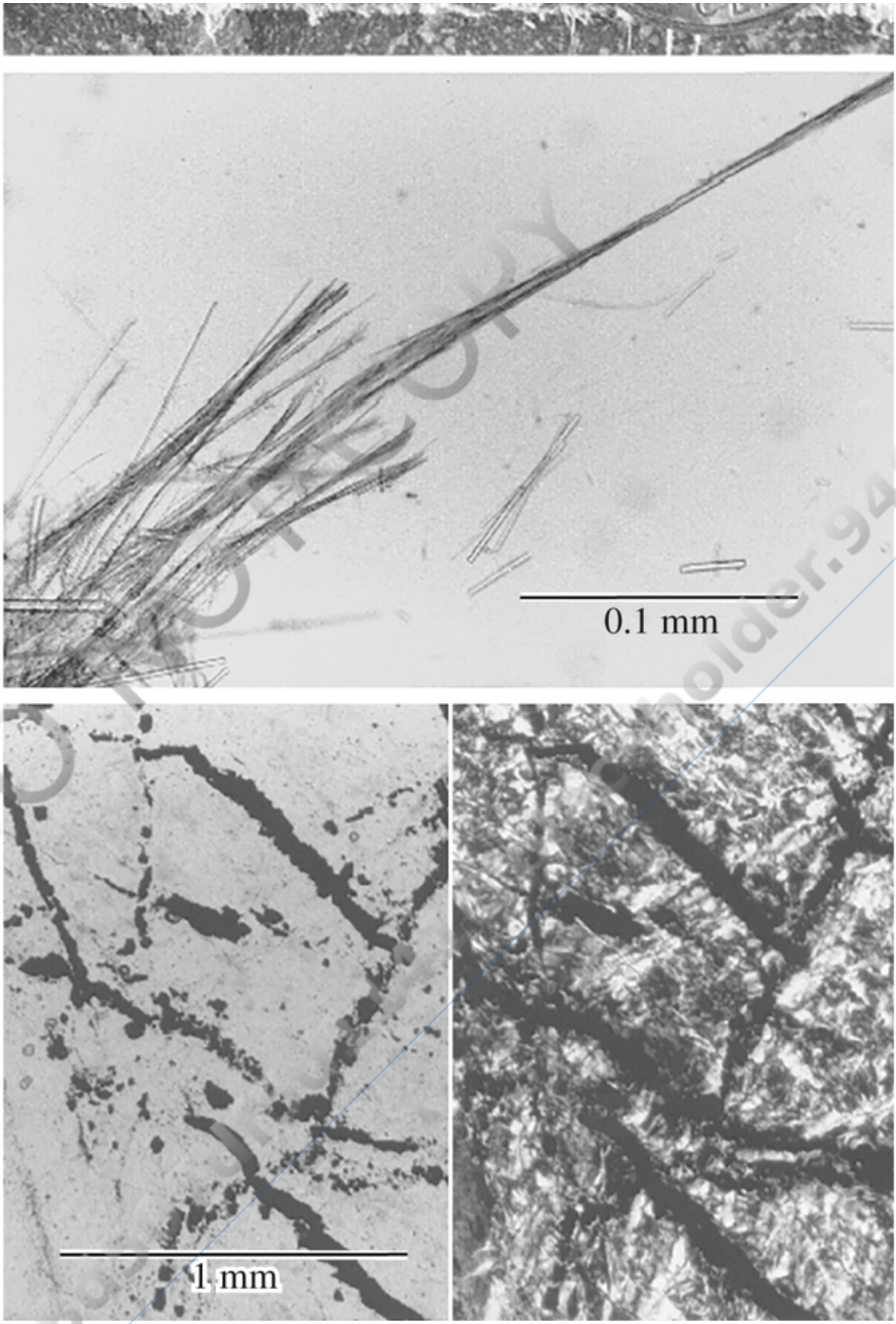

FIGURE 13.6 Serpentine. (*a*) Hand sample in which veins of cross-fiber chrysotile (C) alternate with antigorite/lizardite (A/L). (*b*) Fibers of chrysotile in grain mount. (*c*) Thin section of antigorite/lizardite. Plane light (*left*) and crossed polarizers (*right*). Note the abundance of opaque

Printed by: e48d507df5d1141@placeholder.94092.edu. Printing is for personal, private use only. No part of this book may be reproduced or transmitted without publisher's prior permission. Violators will be prosecuted.

antigorite/lizardite. Plane light (*left*) and crossed polarizers (*right*). Note the abundance of opaque magnetite inclusions derived from Fe in the olivine and pyroxene that were altered to form the serpentine. Back to text

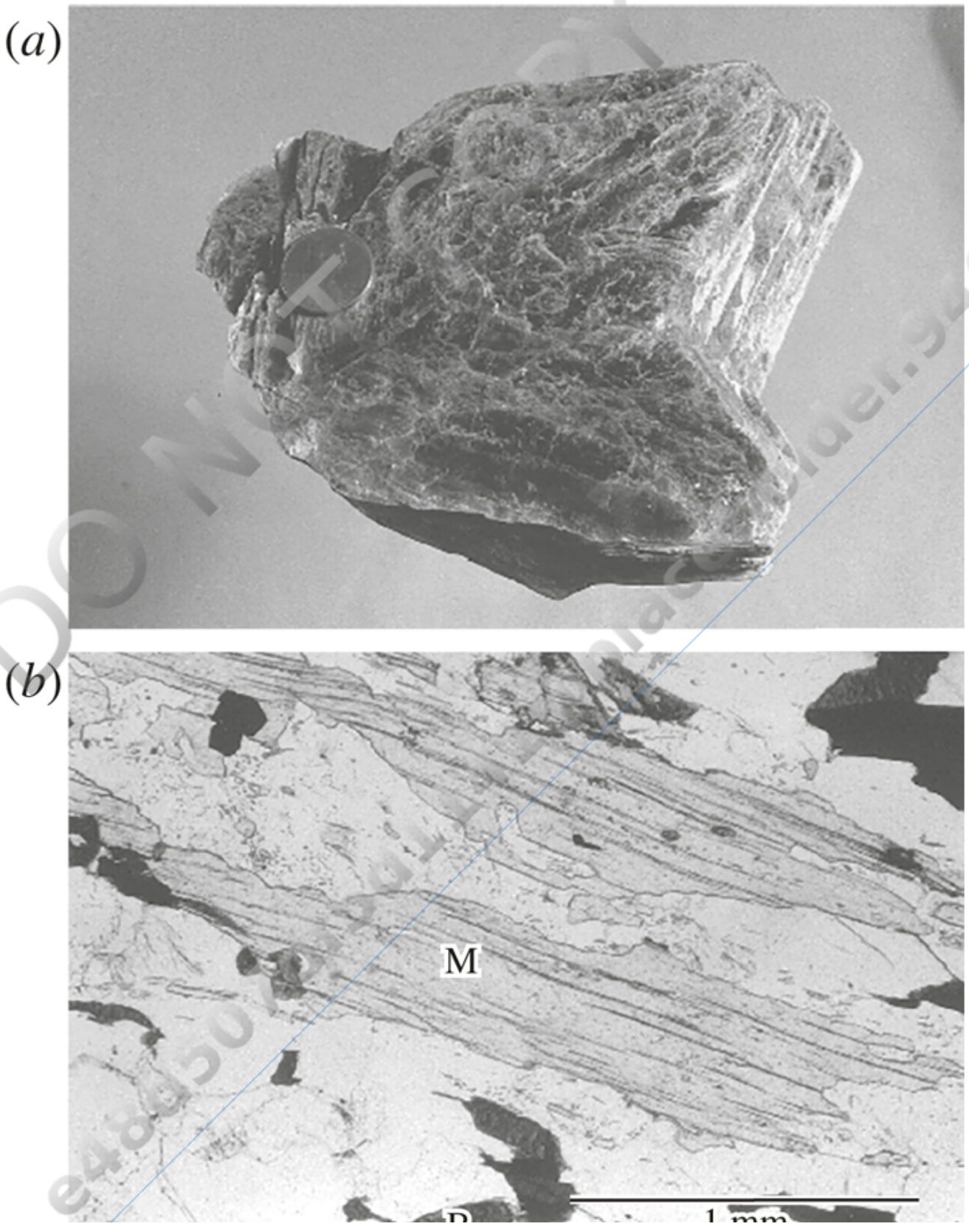

Printed by: e48d507df5d1141@placeholder.94092.edu. Printing is for personal, private use only. No part of this book may be reproduced or transmitted without publisher's prior permission. Violators will be prosecuted.

FIGURE 13.7 Muscovite. (*a*) Muscovite "book" with [310] twin from a granitic pegmatite. (*b*) Photomicrograph of muscovite (M) with dark biotite (B) and colorless quartz in a mica schist. Back to text

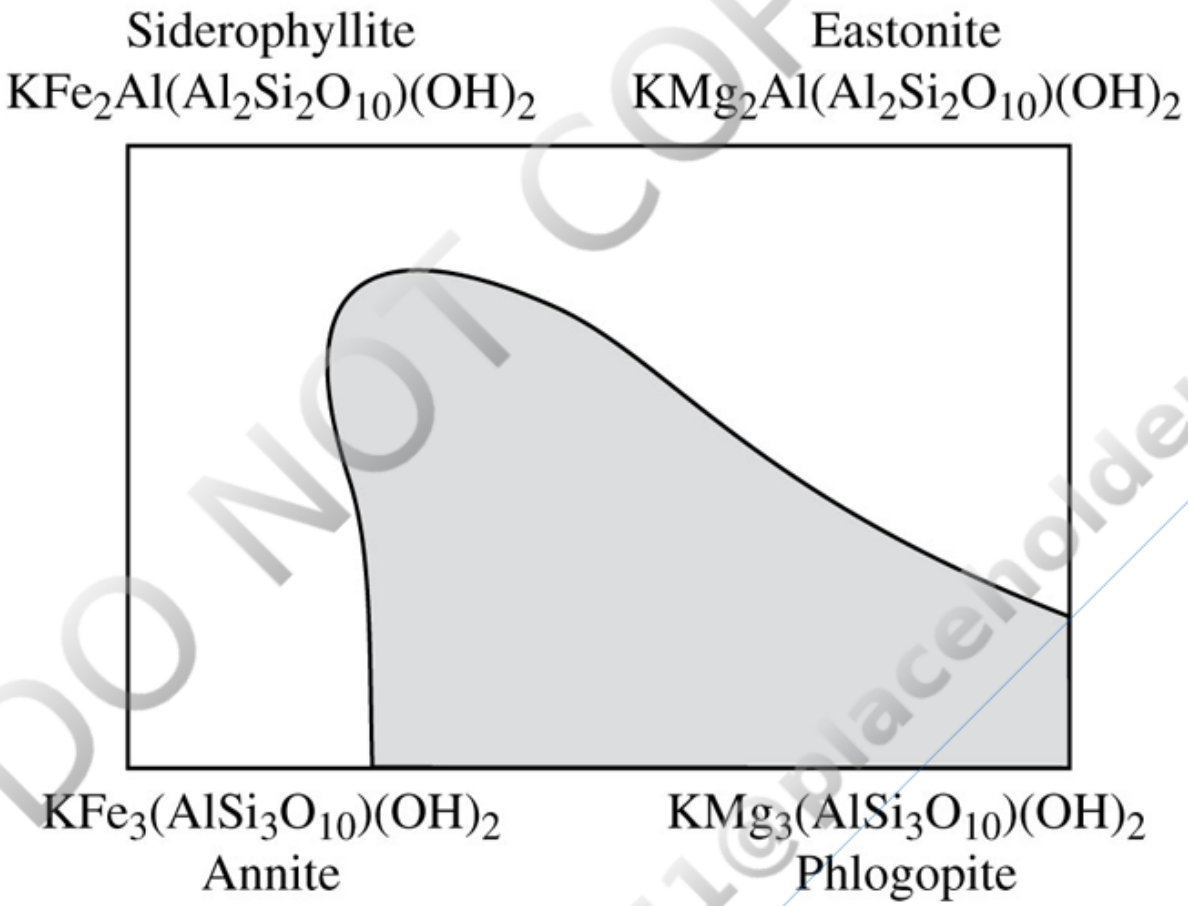

FIGURE 13.8 Compositional range of common biotite (shaded). Adapted from Deer and others (1992). Back to text

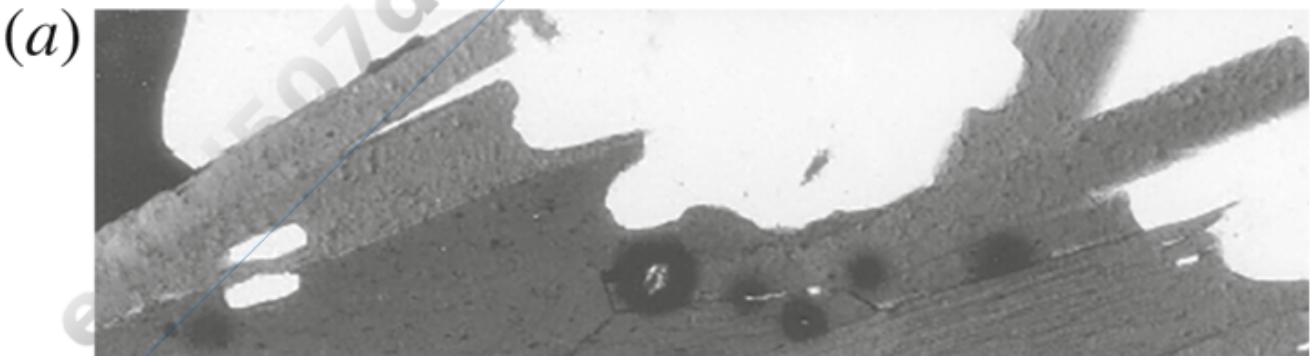

DO NOT COPY

Printed by: e48d507df5d1141@placeholder.94092.edu. Printing is for personal, private use only. No part of this book may be reproduced or transmitted without publisher's prior permission. Violators will be prosecuted.

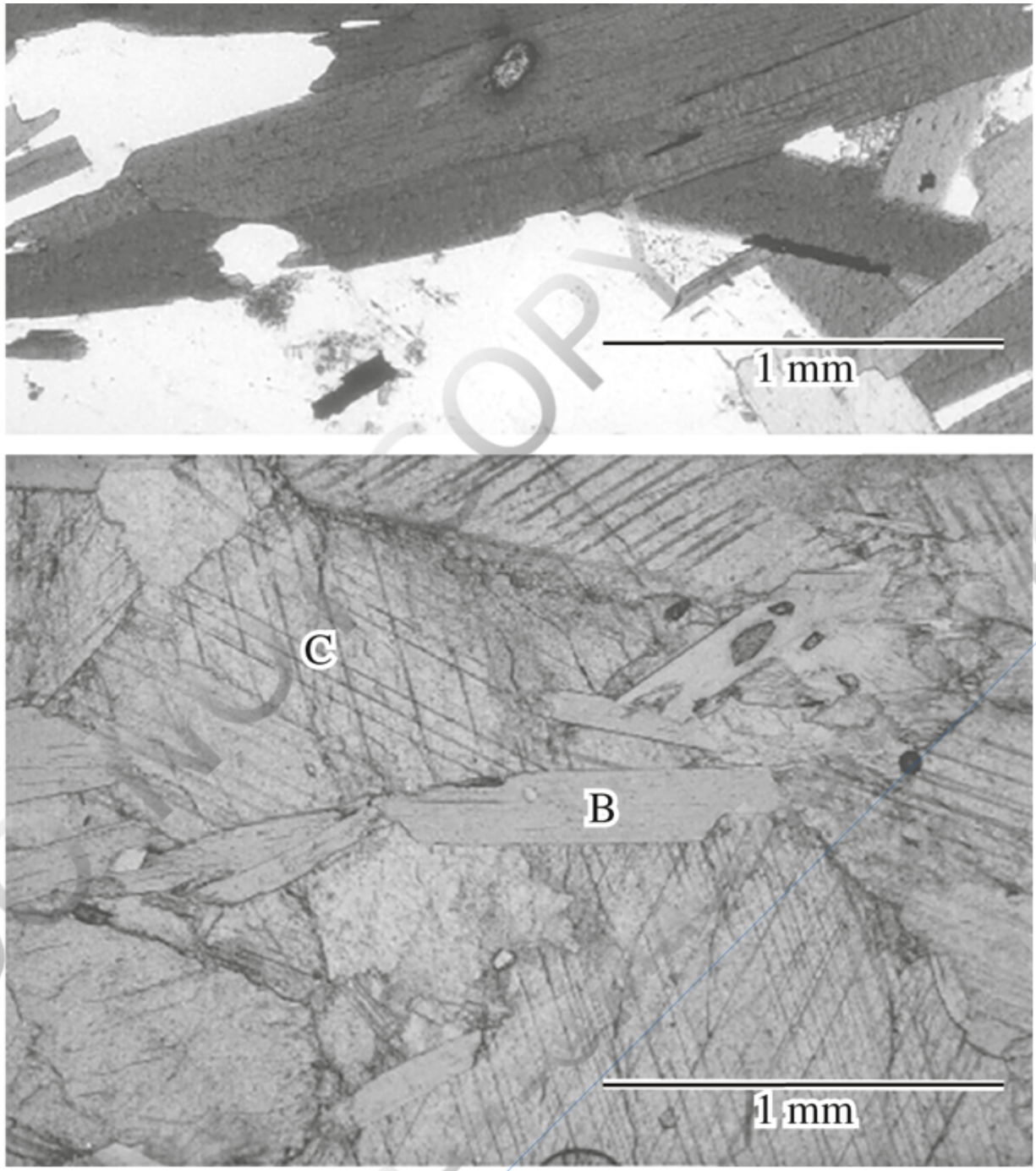

FIGURE 13.9 Biotite. (*a*) Foliated biotite grains in mica schist. Note the dark pleochroic halos around radioactive inclusions. (*b*) Pale grains of phlogopite-rich biotite (B) with calcite (C) in marble.
Back to text

Muscovite

$KAl_2AlSi_3O_{10}(OH)_2$

Printed by: e48d507df5d1141@placeholder.94092.edu. Printing is for personal, private use only. No part of this book may be reproduced or transmitted without publisher's prior permission. Violators will be prosecuted.

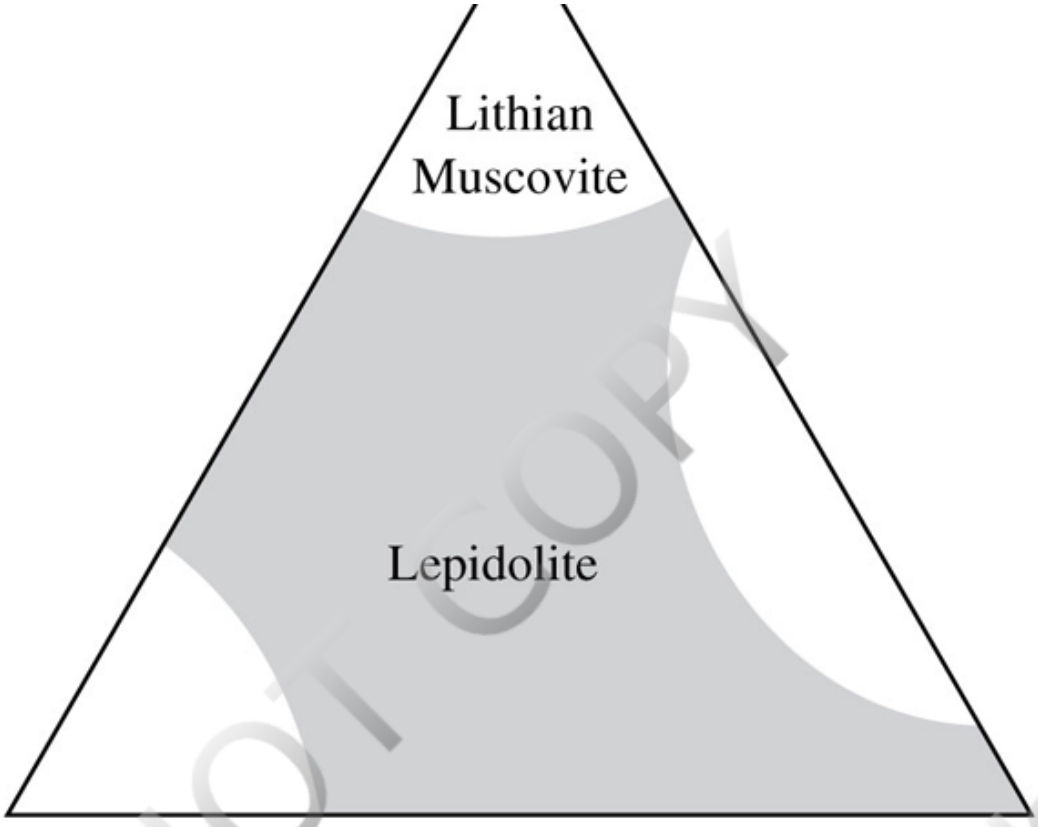

FIGURE 13.10 Lepidolite composition. The common range is shown with the shaded area. Back to text

DO NOT COPY

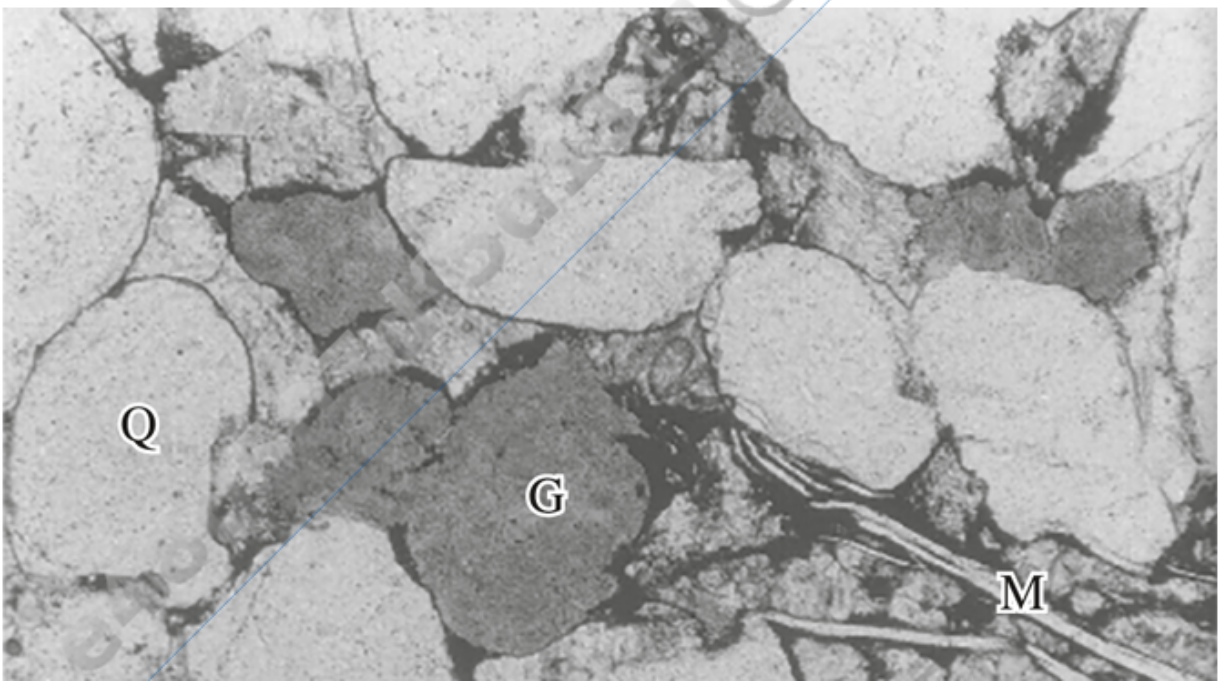

Printed by: e48d507df5d1141@placeholder.94092.edu. Printing is for personal, private use only. No part of this book may be reproduced or transmitted without publisher's prior permission. Violators will be prosecuted.

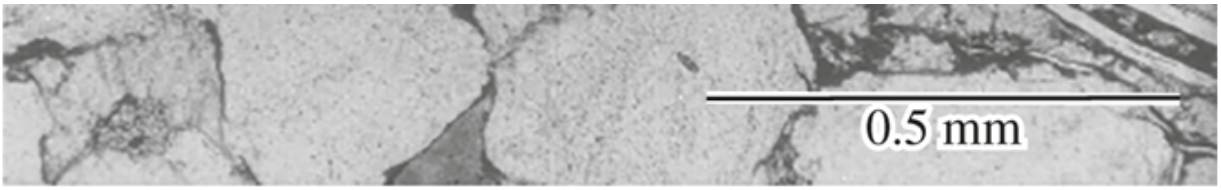

FIGURE 13.11 Glauconite pellets (G) with rounded quartz (Q) grains and elongate detrital muscovite (M). Calcite forms the cement between grains, and the opaque mineral is hematite. Back to text

DO NOT COPY

(a)

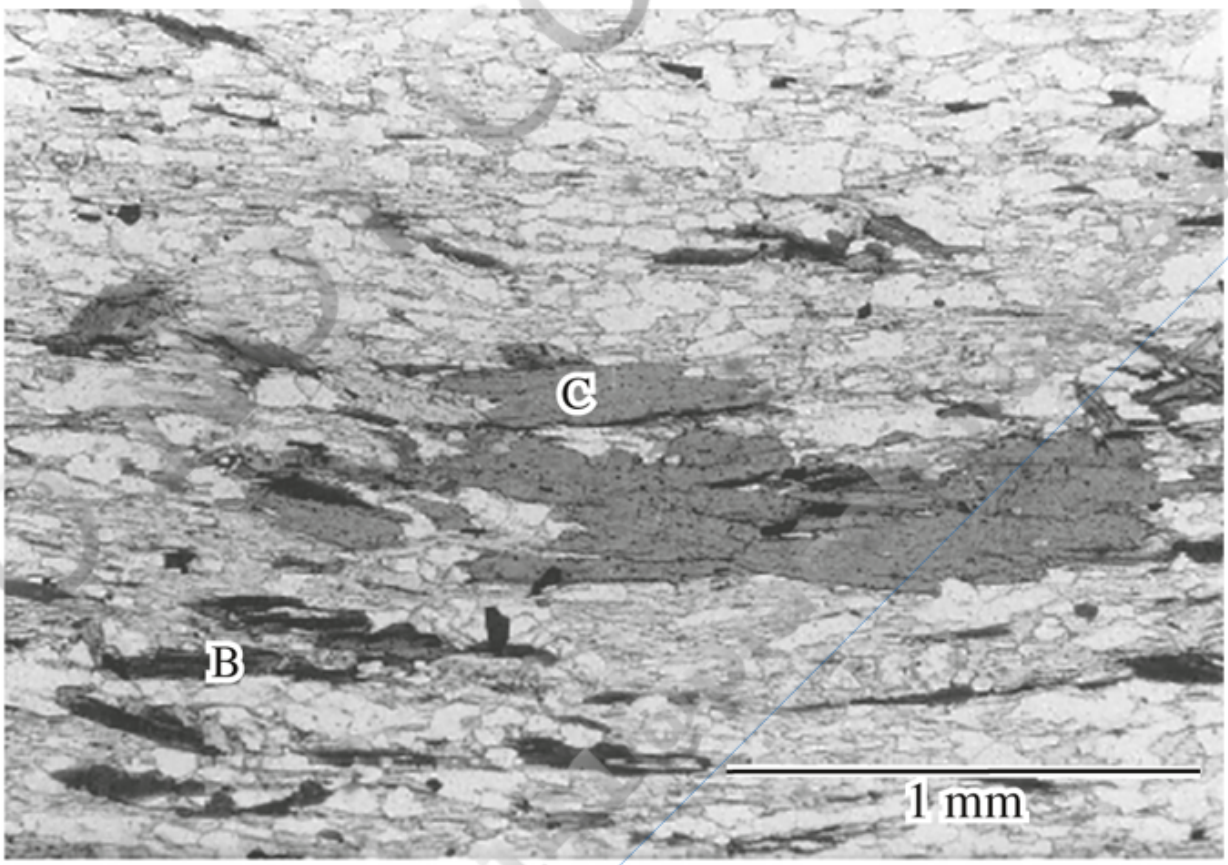

(b)

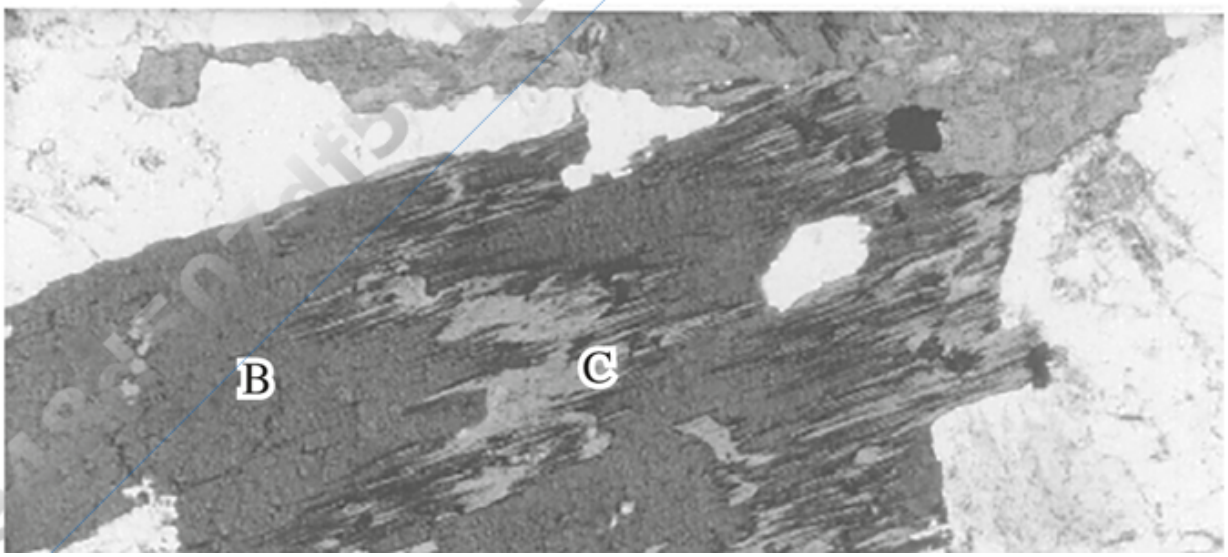

Printed by: e48d507df5d1141@placeholder.94092.edu. Printing is for personal, private use only. No part of this book may be reproduced or transmitted without publisher's prior permission. Violators will be prosecuted.

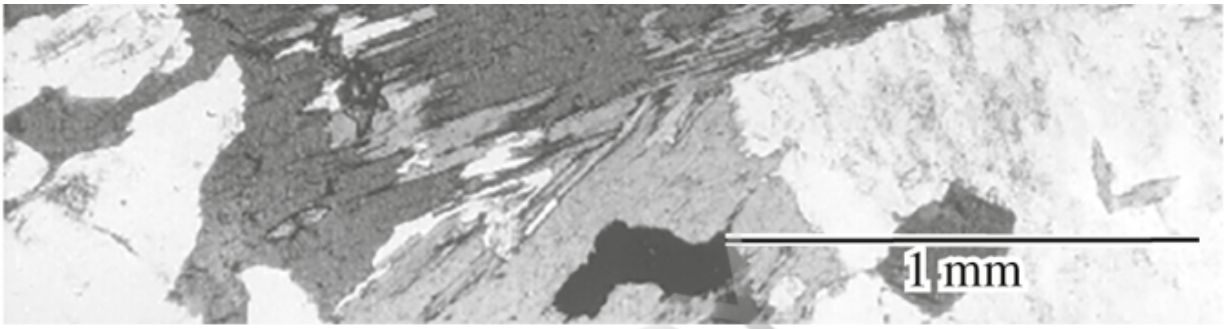

FIGURE 13.12 Chlorite. (*a*) Foliated chlorite grains (C) with biotite (B) in a thin section of moderately low-grade pelitic schist. The finer-grained matrix includes scaly chlorite and muscovite, and clear quartz. (*b*) Chlorite (C) alteration along cleavage traces in biotite (B) in a thin section of granodiorite. Back to text

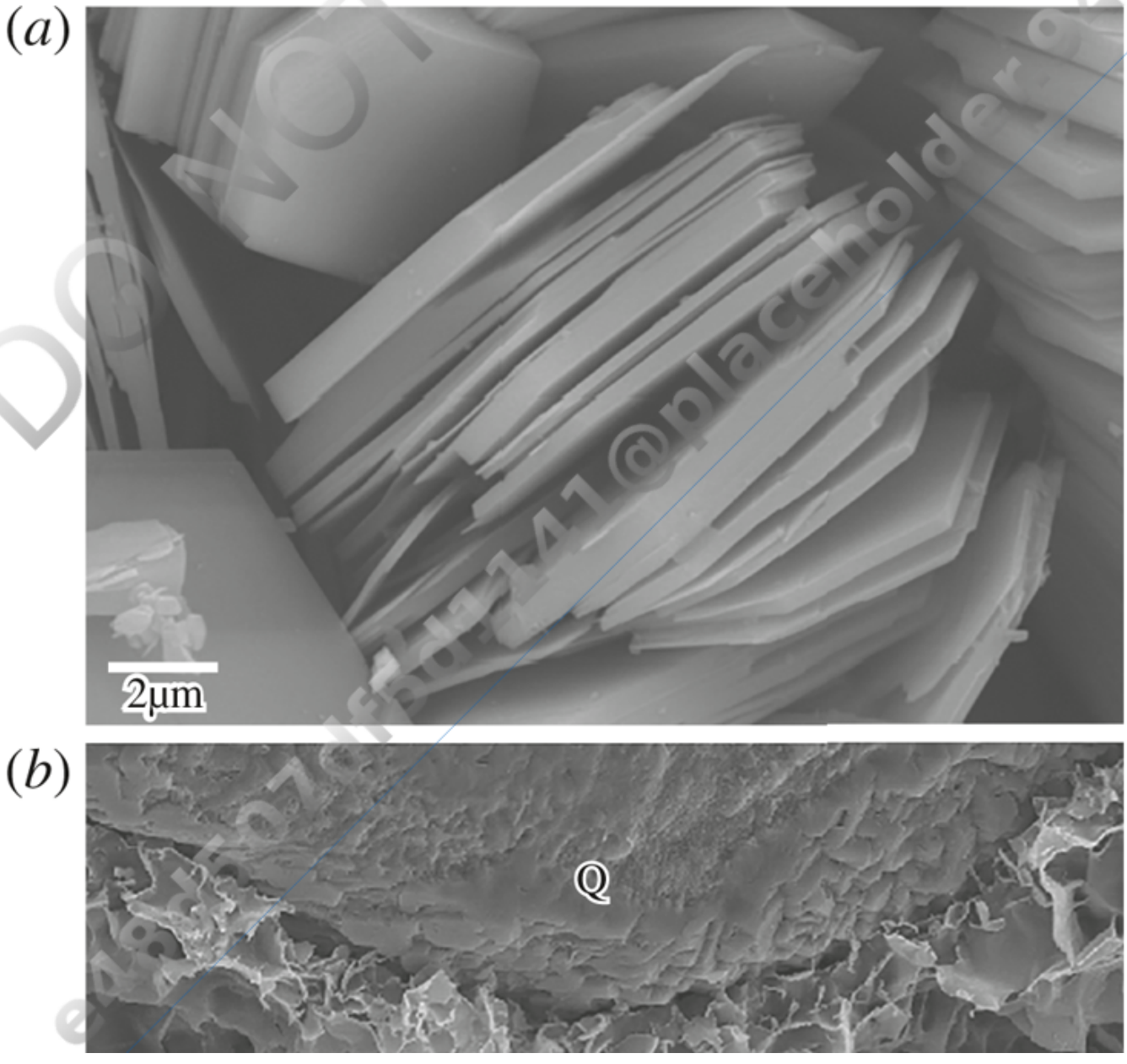

DO NOT COPY

Printed by: e48d507df5d1141@placeholder.94092.edu. Printing is for personal, private use only. No part of this book may be reproduced or transmitted without publisher's prior permission. Violators will be prosecuted.

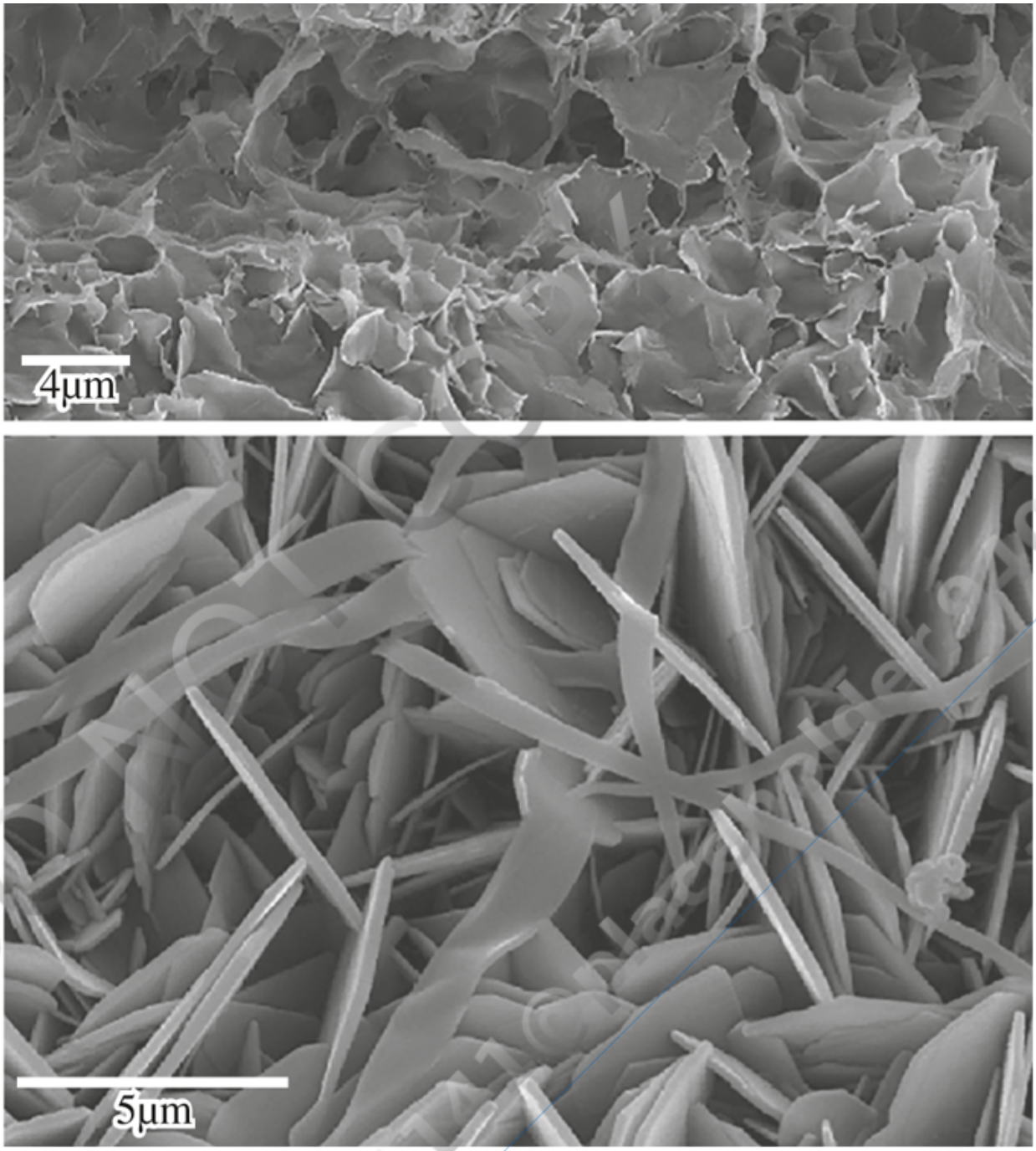

FIGURE 13.13 SEM images of clay minerals. (*a*) Kaolinite platelets in Jurassic sandstone, North Sea. (*b*) Dioctahedral smectite lining pores in Ordovician sandstone, Oman. The grain at top is quartz (Q). (*c*) Pseudohexagonal platelets of chlorite intergrown with ribbons of illite; Garn Formation, North Sea. Images courtesy of Evelyn Delbos, The James Hutton Institute, and reproduced from the "Images of Clay Archive" of the Mineralogical Society of Great Britain & Ireland and The Clay Minerals Society. Used by permission. Back to text

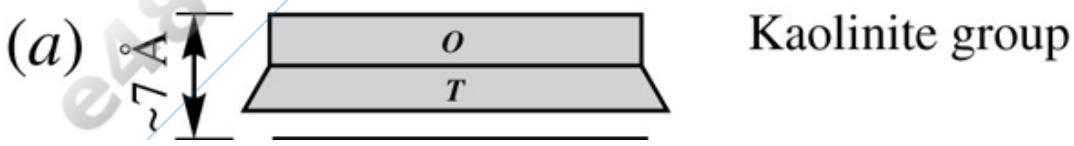

Printed by: e48d507df5d1141@placeholder.94092.edu. Printing is for personal, private use only. No part of this book may be reproduced or transmitted without publisher's prior permission. Violators will be prosecuted.

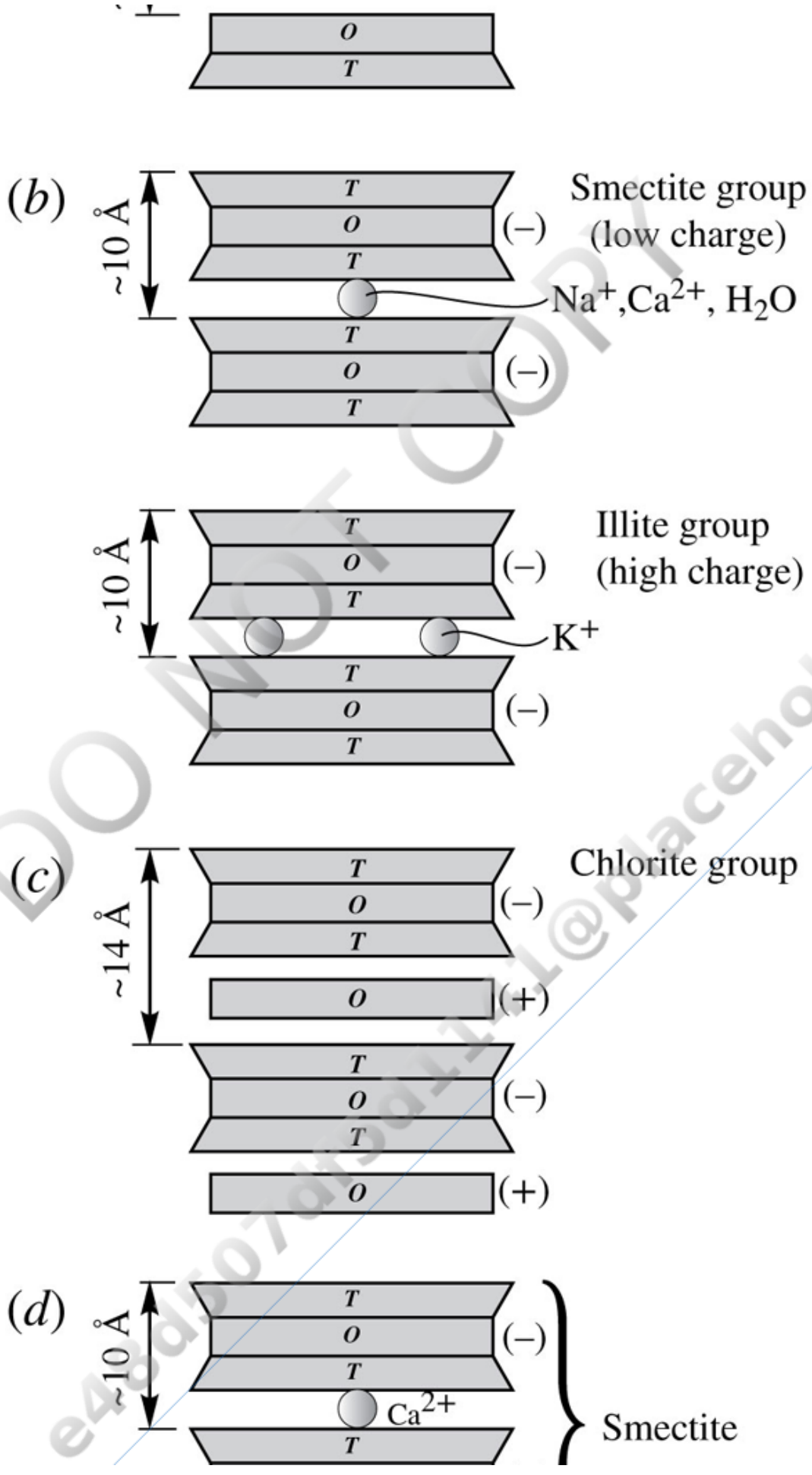

DO NOT COPY
e48d507df5d1141@placeholder.9409

Printed by: e48d507df5d1141@placeholder.94092.edu. Printing is for personal, private use only. No part of this book may be reproduced or transmitted without publisher's prior permission. Violators will be prosecuted.

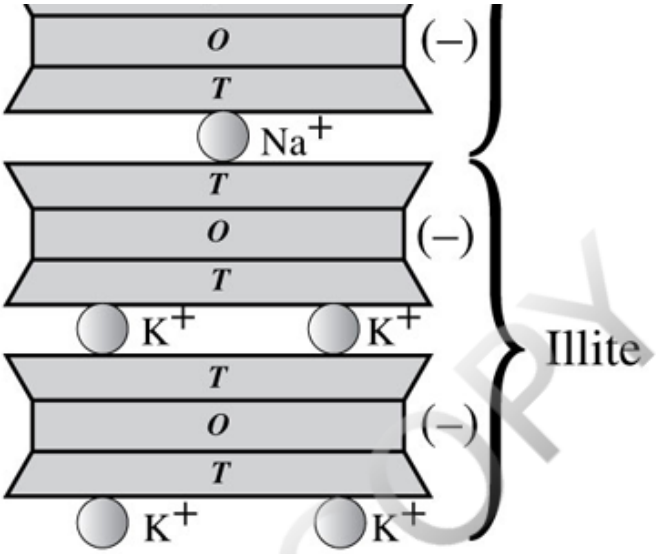

FIGURE 13.14 Clay mineral structure. Refer also to Figures 13.1 and 13.3. (*a*) 7 Å clays have 1:1 or *TO* structures. (*b*) 10 Å clays have 2:1 or *TOT* + *c* structures. The *TOT* layers in the smectite group have a relatively low charge and require fewer Na^+ or Ca^{2+} cations in the interlayer sites. In the illite group, *TOT* layers have a higher negative charge and require more cations in the interlayer sites to maintain charge balance. (*c*) 14 Å clays have the chlorite structure in which octahedral sheets with a positive charge occupy the interlayer between negatively charged *TOT* layers. (*d*) A common mixed-layer clay contains both smectite and illite layers. Back to text

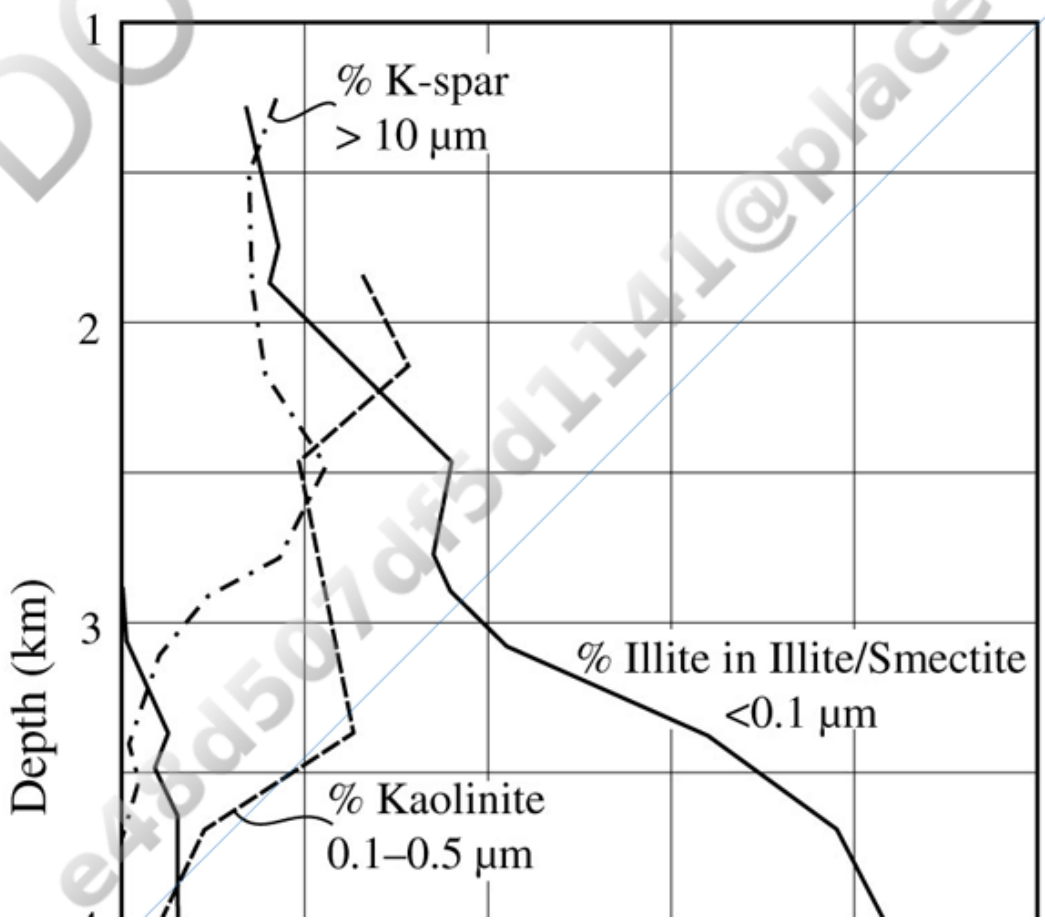

DO NOT COPY
e48d507df5d1141@placeholder.94092

Printed by: e48d507df5d1141@placeholder.94092.edu. Printing is for personal, private use only. No part of this book may be reproduced or transmitted without publisher's prior permission. Violators will be prosecuted.

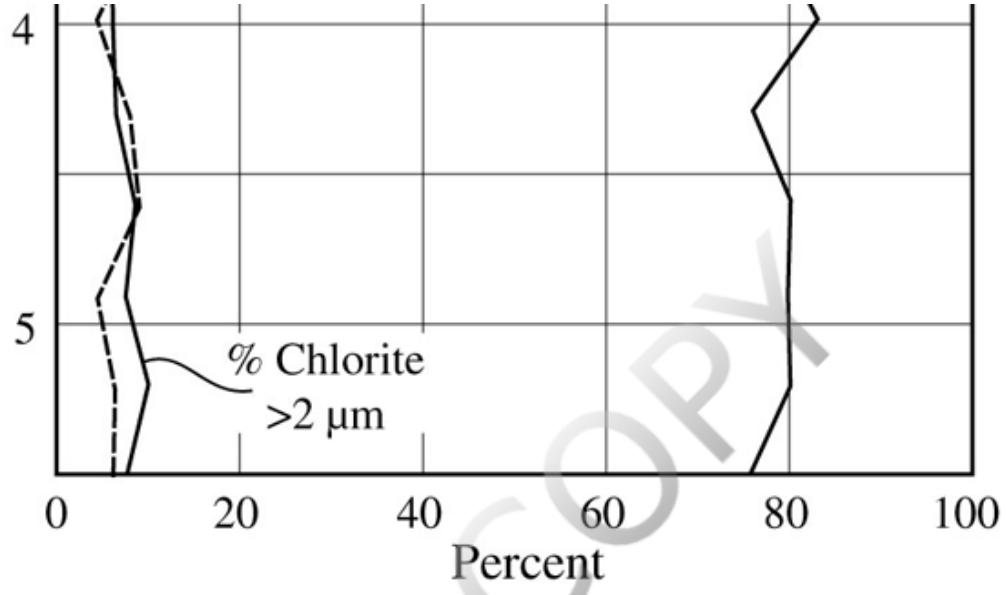

FIGURE 13.15 Clay mineralogy in selected size fractions of Miocene–Oligocene sediment in the Gulf Coast of the United States. See text for additional discussion. Adapted from Hower and others (1976). Back to text

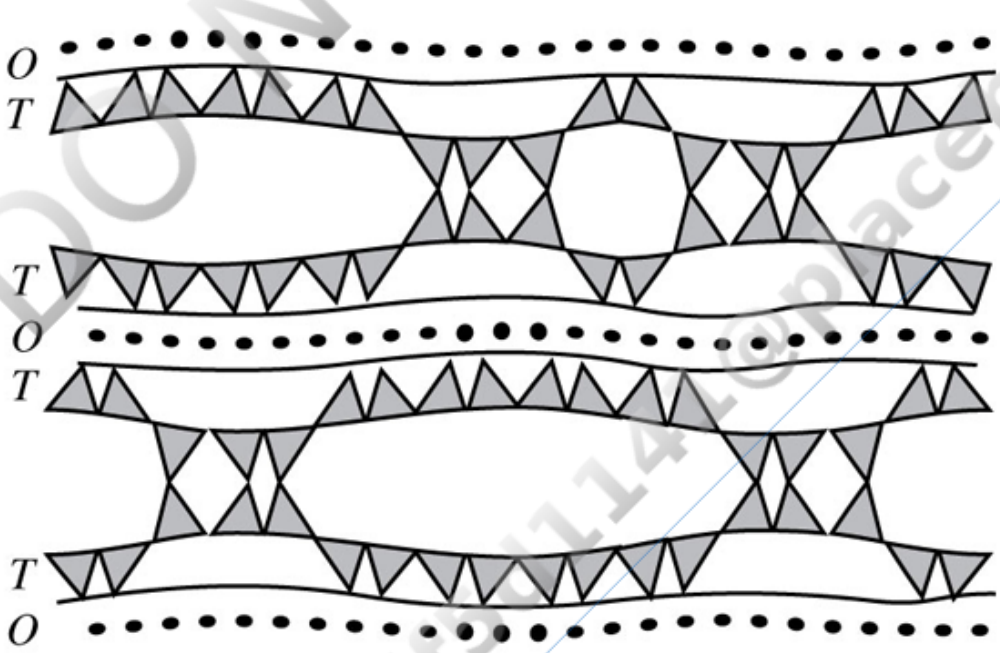

FIGURE 13.16 Idealized structure of stilpnomelane. Some tetrahedra point outward from the *TOT* layers and share oxygen anions with similar tetrahedra from adjacent *TOT* layers. Adapted from Guggenheim and Eggleton (1987). Back to text

Printed by: e48d507df5d1141@placeholder.94092.edu. Printing is for personal, private use only. No part of this book may be reproduced or transmitted without publisher's prior permission. Violators will be prosecuted.

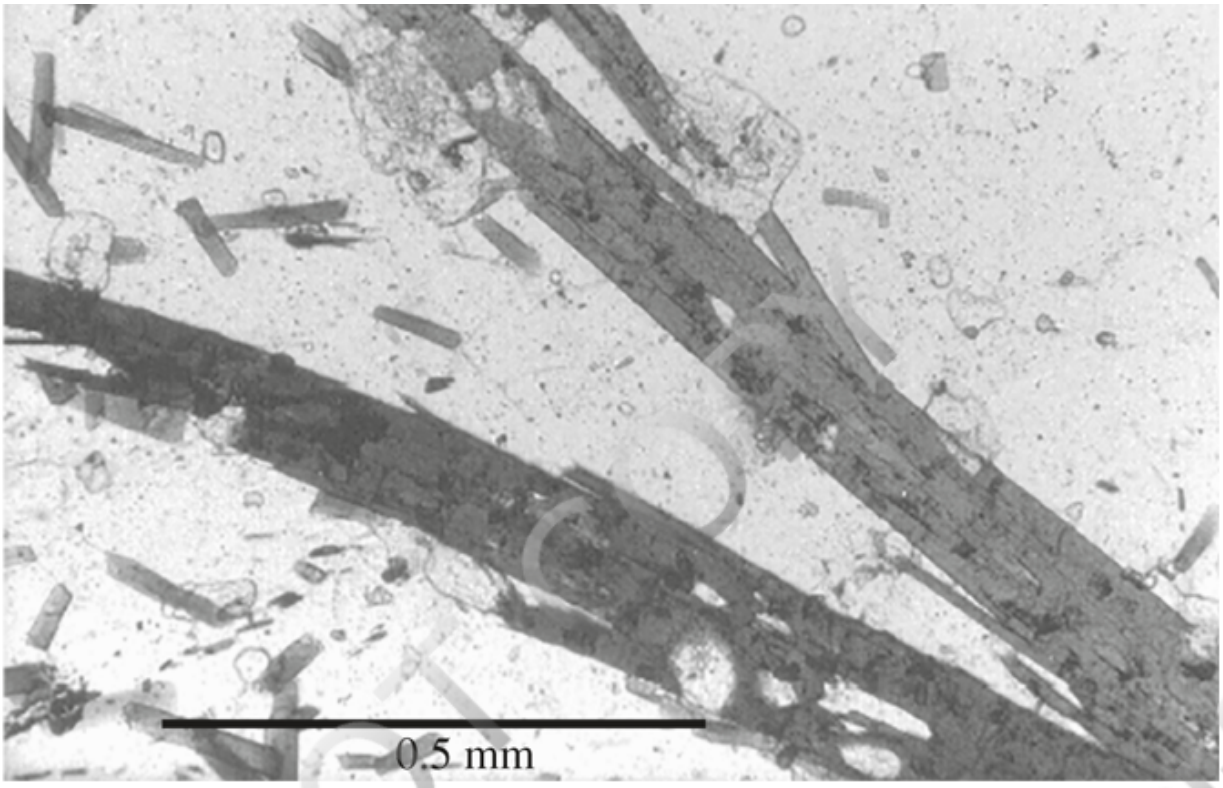

FIGURE 13.17 Stilpnomelane grains in a stilpnomelane schist. Back to text

DO NOT COPY
e48d507df5d1141@placeholder.9409

Printed by: e48d507df5d1141@placeholder.94092.edu. Printing is for personal, private use only. No part of this book may be reproduced or transmitted without publisher's prior permission. Violators will be prosecuted.

Chapter 14 Chain Silicates

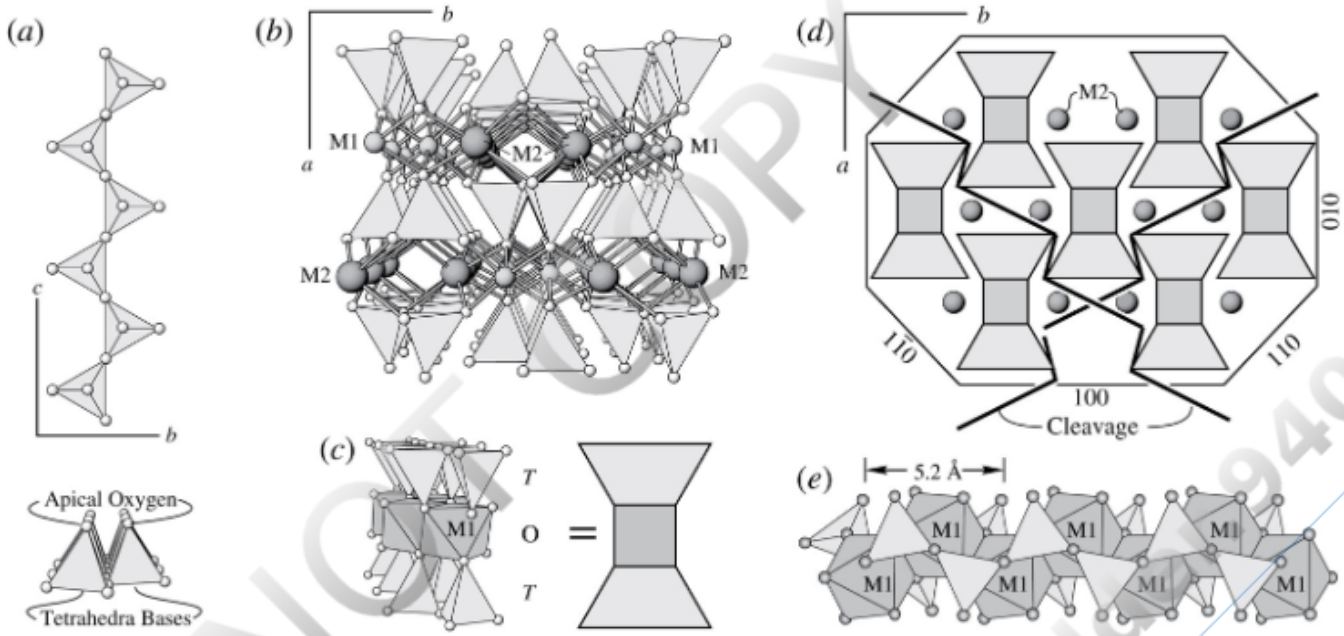

FIGURE 14.1 Pyroxene structure. (*a*) Top and end views of an idealized single chain of silicon tetrahedra. (*b*) Chains are stacked in alternating fashion to form 6-fold coordinated M1 sites between the unshared apical oxygens of the tetrahedra and 6- to 8-fold coordinated M2 sites between the bases. (*c*) Two chains and the intervening octahedral M1 sites form a structural *TOT* "I-beam." (*d*) View similar to (*b*) but with I-beams shown. Cleavage at about 87° and 93° between the I-beams is parallel to the {110} faces in the monoclinic unit cell. (*e*) In pyroxenes, the tetrahedra chains are typically kinked, rather than straight, as shown in this top view of an enstatite *TOT* I-beam. The repeat distance along chains is two tetrahedra at about 5.2 Å. Compare with Figure 14.7a. Back to text

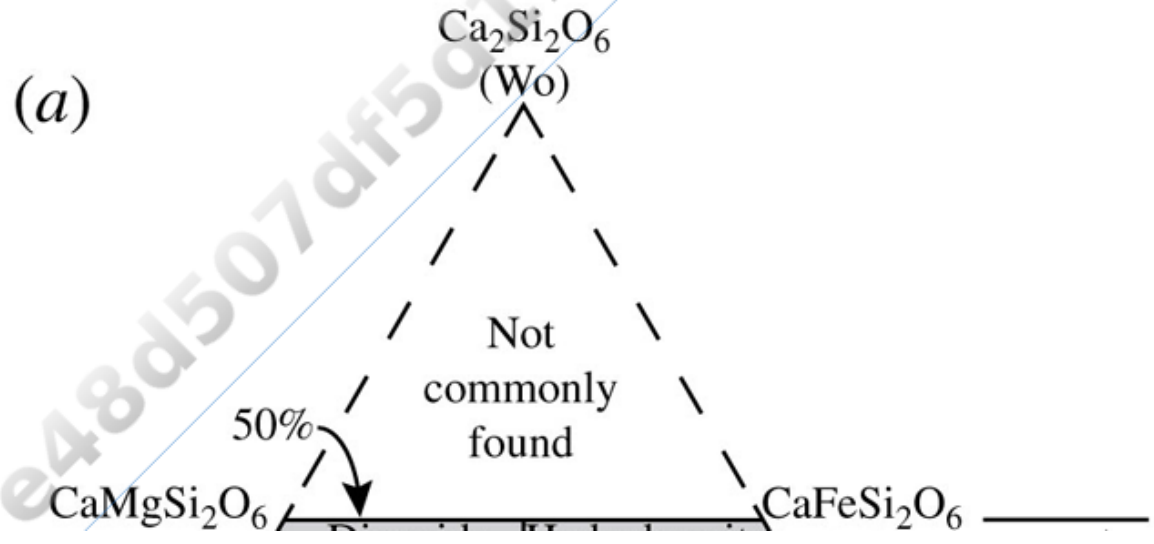

DO NOT COPY e48d507df5d1141@placeholder.94092

Printed by: e48d507df5d1141@placeholder.94092.edu. Printing is for personal, private use only. No part of this book may be reproduced or transmitted without publisher's prior permission. Violators will be prosecuted.

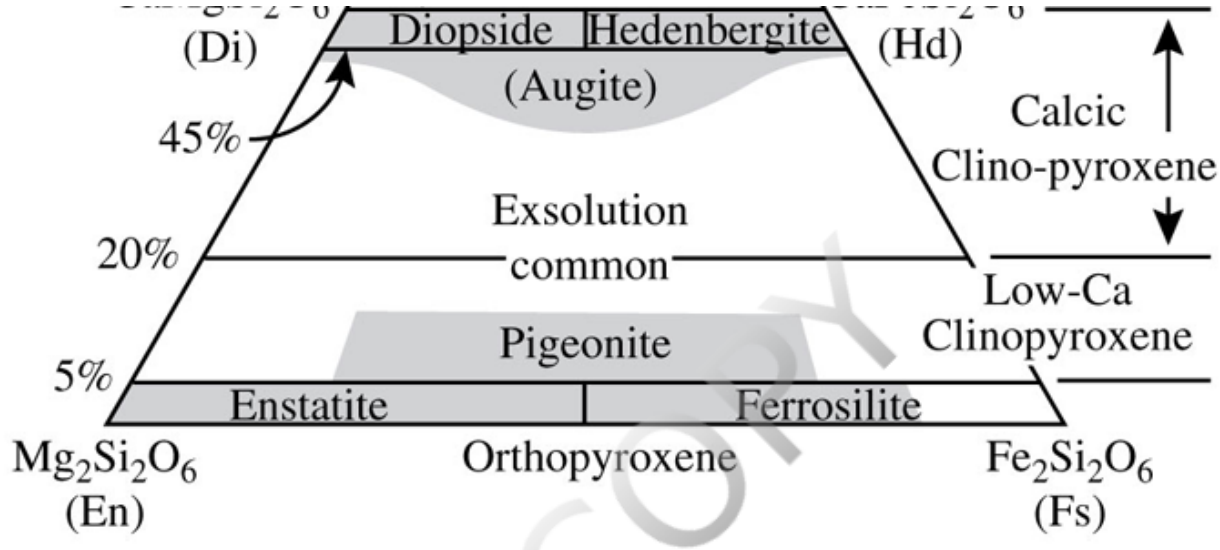

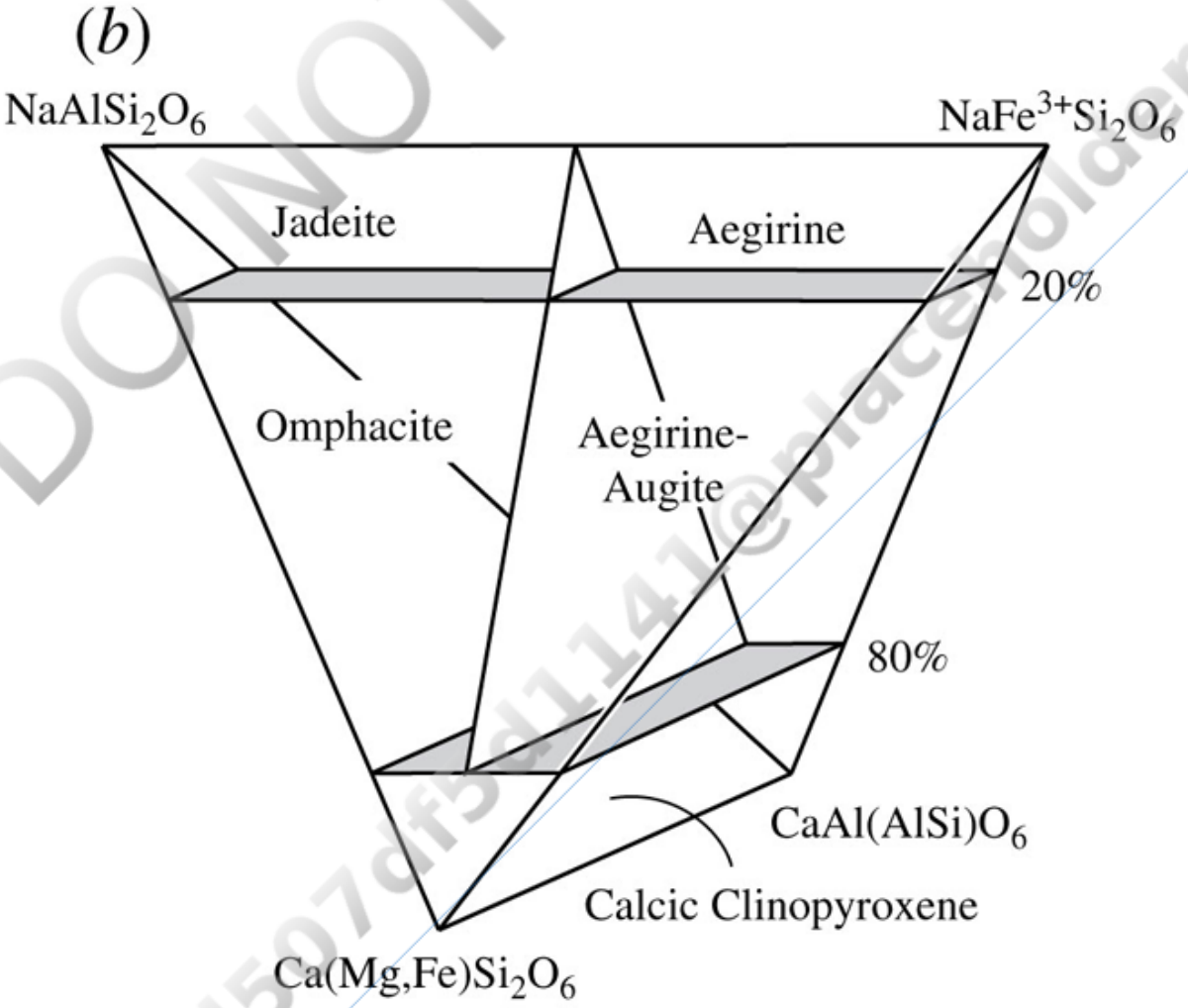

FIGURE 14.2 Pyroxene classification; see text for details. (*a*) Calcic and iron–magnesium pyroxenes. The percentages on the left side refer to the amount of Ca relative to Fe + Mg + Ca. The common compositions are shaded. (*b*) Sodic and sodic–calcic pyroxenes. Back to text

DO NOT COPY
e48d507df5d1141@placeholder.9409

Printed by: e48d507df5d1141@placeholder.94092.edu. Printing is for personal, private use only. No part of this book may be reproduced or transmitted without publisher's prior permission. Violators will be prosecuted.

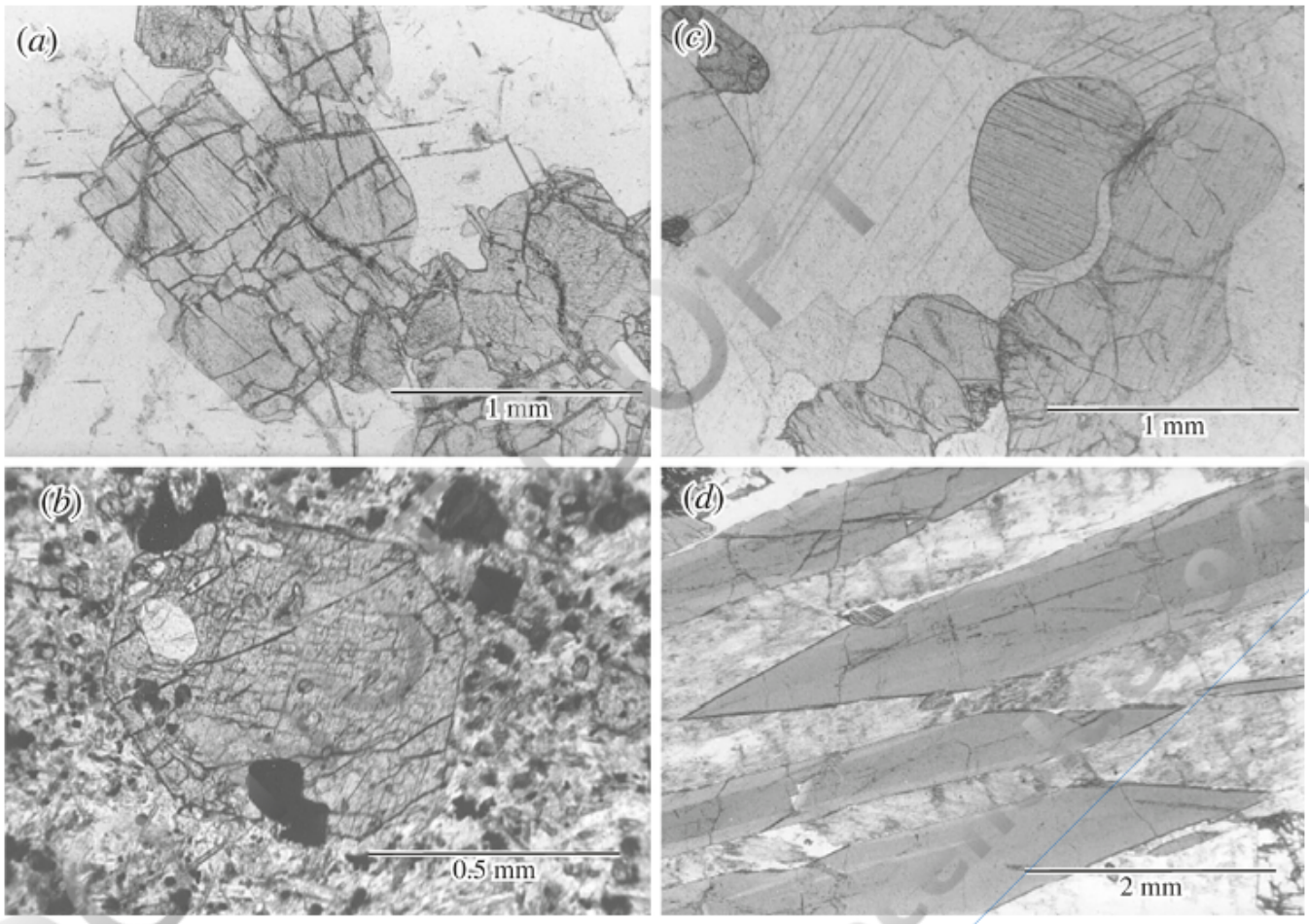

FIGURE 14.3 Photomicrographs of pyroxene in thin section. (*a*) Anhedral orthopyroxene in norite. (*b*) Euhedral augite phenocryst in basalt. (*c*) Rounded diopside in marble. (*d*) Zoned aegirine in syenite. Back to text

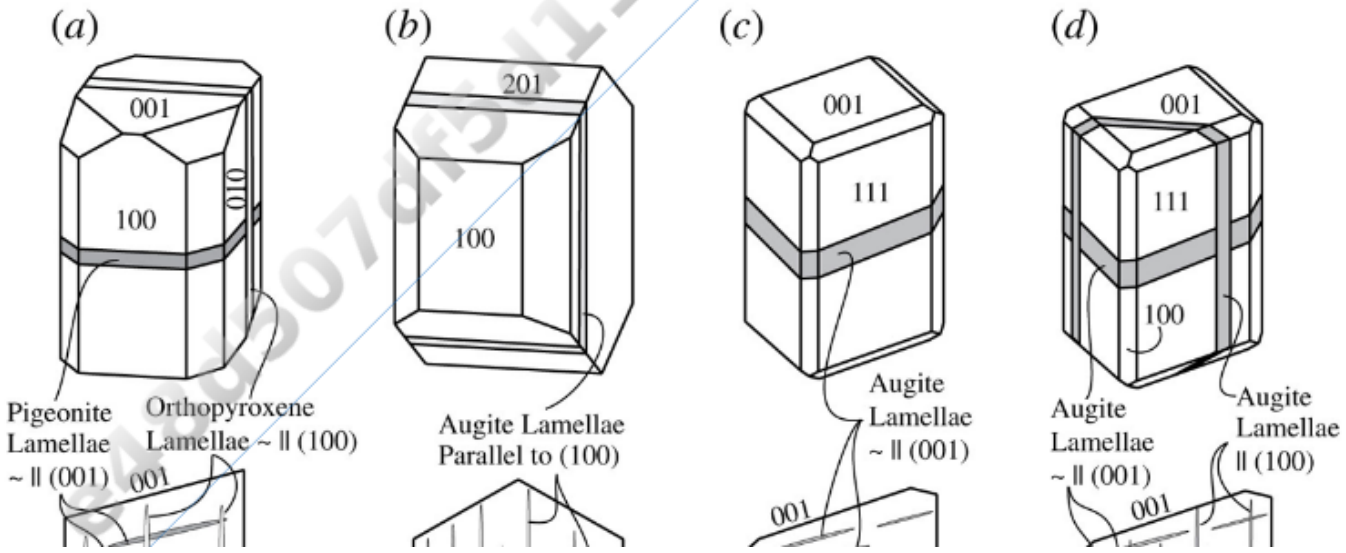

Printed by: e48d507df5d1141@placeholder.94092.edu. Printing is for personal, private use only. No part of this book may be reproduced or transmitted without publisher's prior permission. Violators will be prosecuted.

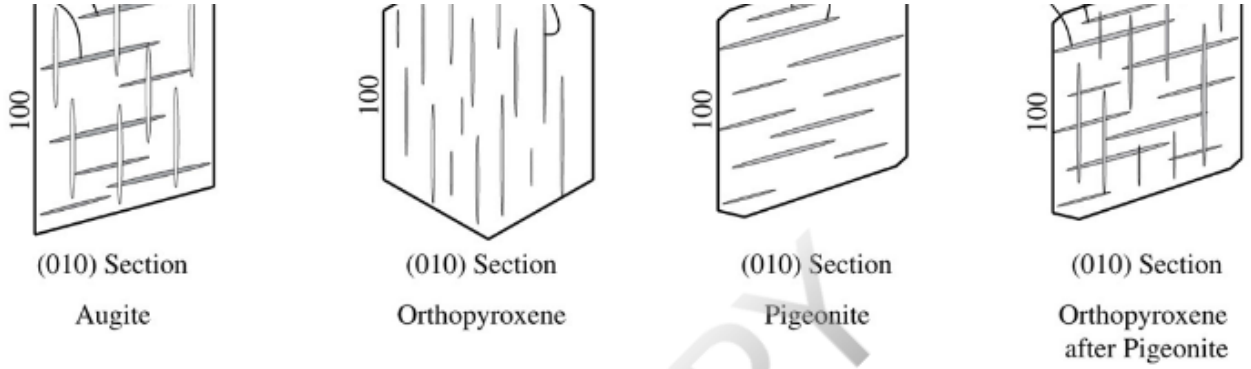

FIGURE 14.4 Exsolution lamellae may be responsible for partings in pyroxene. (*a*) Augite. Pigeonite may exsolve as lamellae roughly parallel to (001); the exact orientation depends on composition and temperature. The pigeonite converts to orthopyroxene with slow cooling. Primary orthopyroxene lamellae may exsolve parallel to (100). (*b*) Primary orthopyroxene. Lamellae of augite develop parallel to (100) of the orthopyroxene. (*c*) Pigeonite. Augite lamellae may exsolve roughly parallel to (001). The exact orientation depends on temperature and composition. (*d*) Orthopyroxene converted from pigeonite (inverted pigeonite). Unless cooled rapidly, pigeonite converts to orthopyroxene. The (001) lamellae of augite in the original pigeonite are preserved, and additional lamellae of augite develop parallel to (100) of the orthopyroxene. Back to text

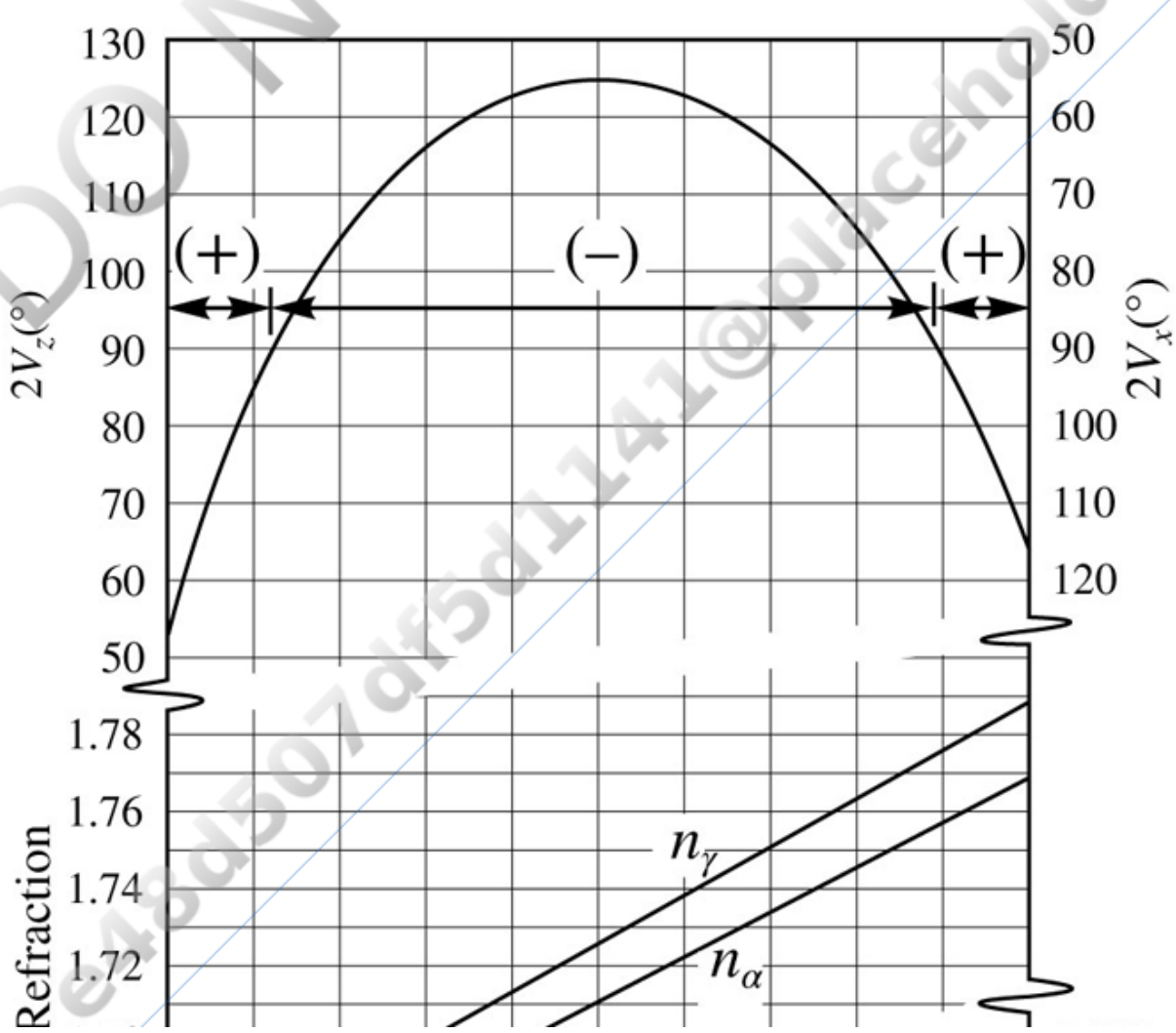

DO NOT COPY
e48d507df5d1141@placeholder.9409

Printed by: e48d507df5d1141@placeholder.94092.edu. Printing is for personal, private use only. No part of this book may be reproduced or transmitted without publisher's prior permission. Violators will be prosecuted.

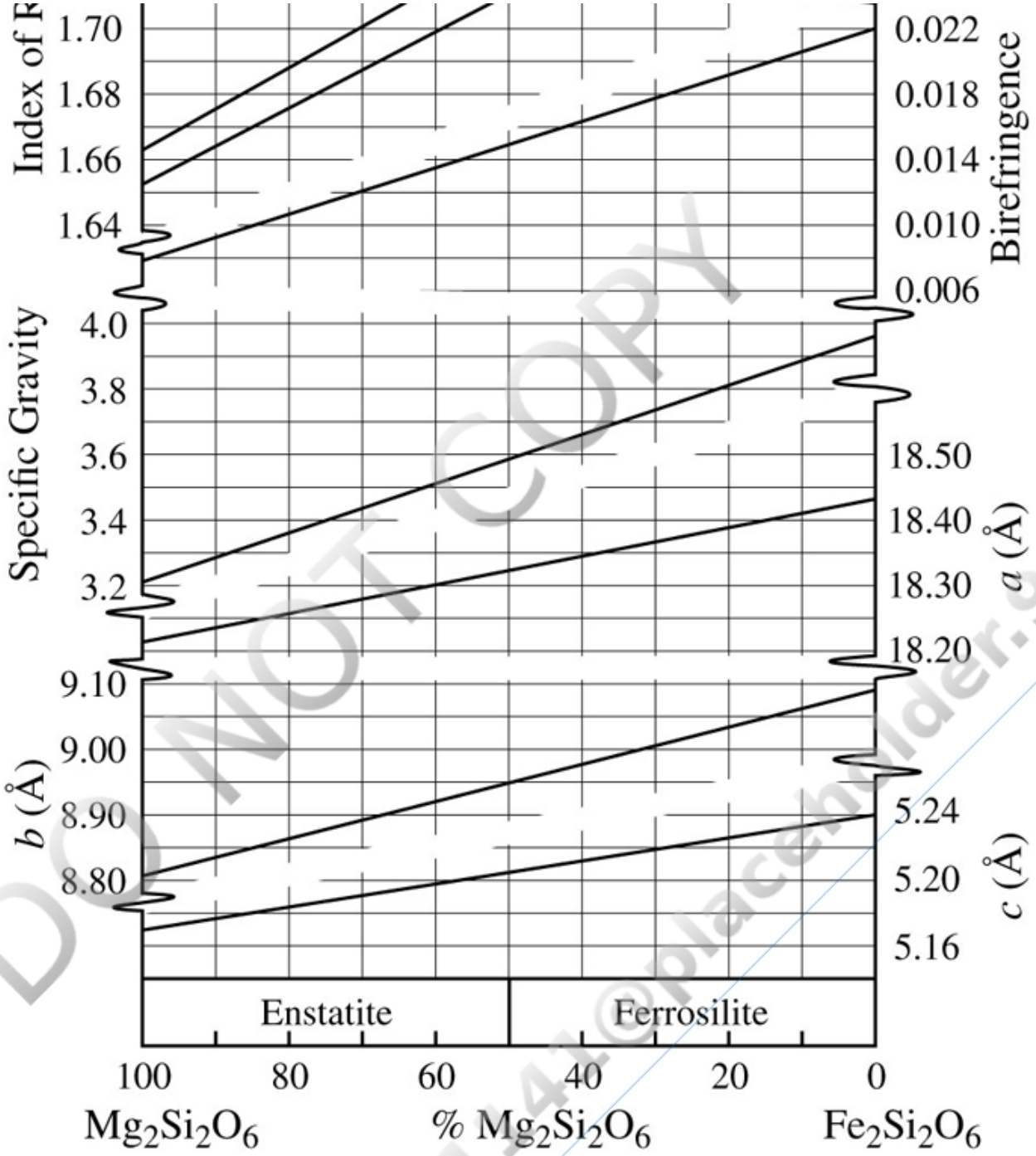

FIGURE 14.5 Optical properties, specific gravity, and unit cell dimensions of orthopyroxene. Adapted from Leake (1968), Jaffe and others (1975, 1978), and Deer and others (1978). Back to text

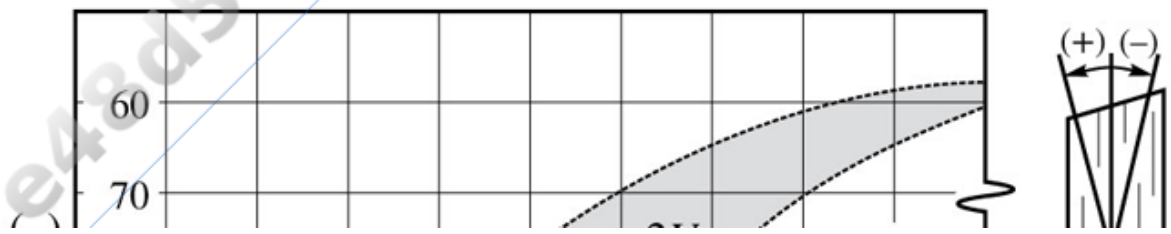

Printed by: e48d507df5d1141@placeholder.94092.edu. Printing is for personal, private use only. No part of this book may be reproduced or transmitted without publisher's prior permission. Violators will be prosecuted.

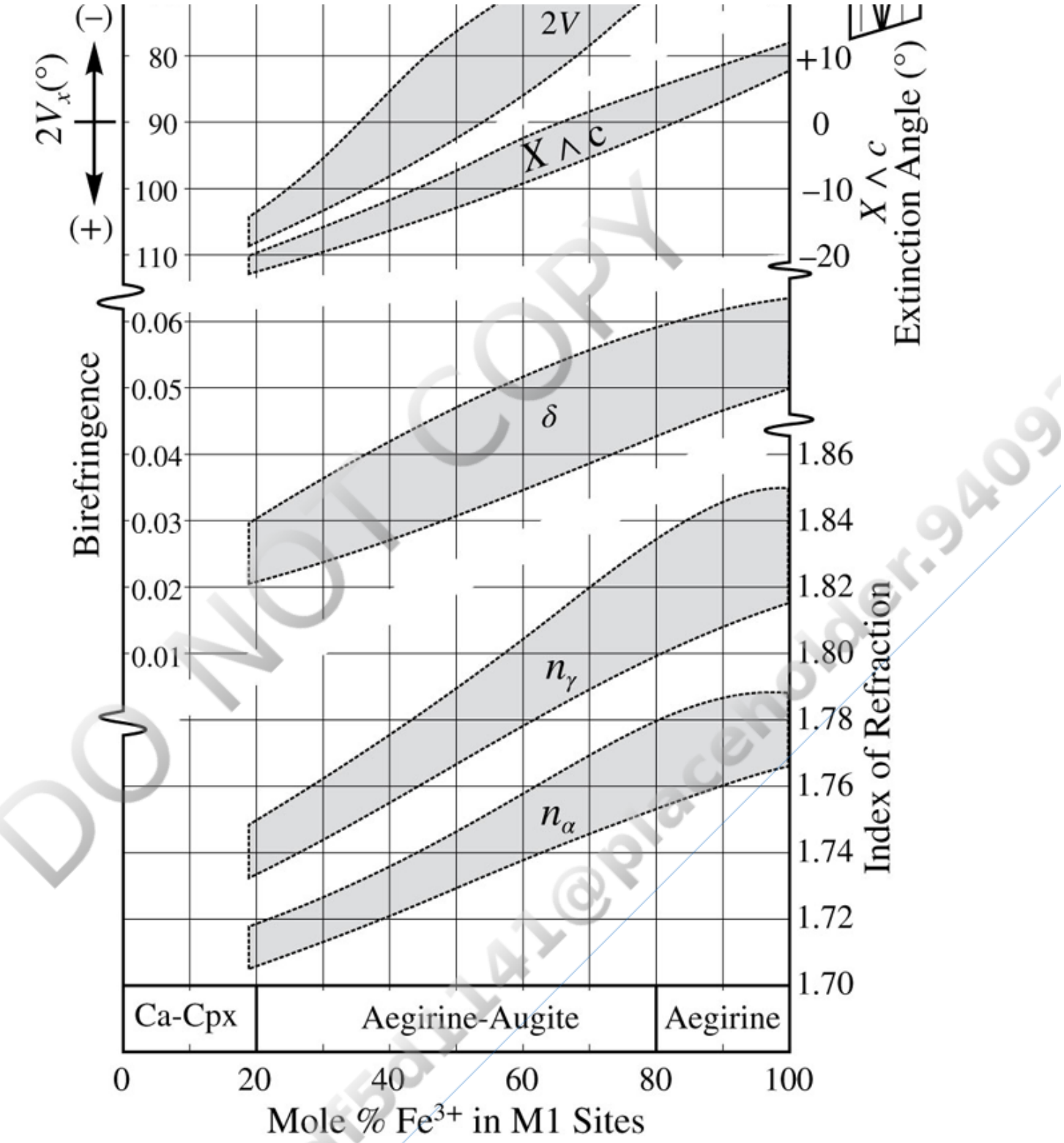

FIGURE 14.6 Variation of optical properties of aegirine and aegirine–augite with Fe^{3+} content. Data from Larsen (1942), Sabine (1950), Nolan (1969), and Deer and others (1978). Back to text

DO NOT COPY
e48d507df5d1141@placeholder.9409

(a) (b)

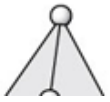

Printed by: e48d507df5d1141@placeholder.94092.edu. Printing is for personal, private use only. No part of this book may be reproduced or transmitted without publisher's prior permission. Violators will be prosecuted.

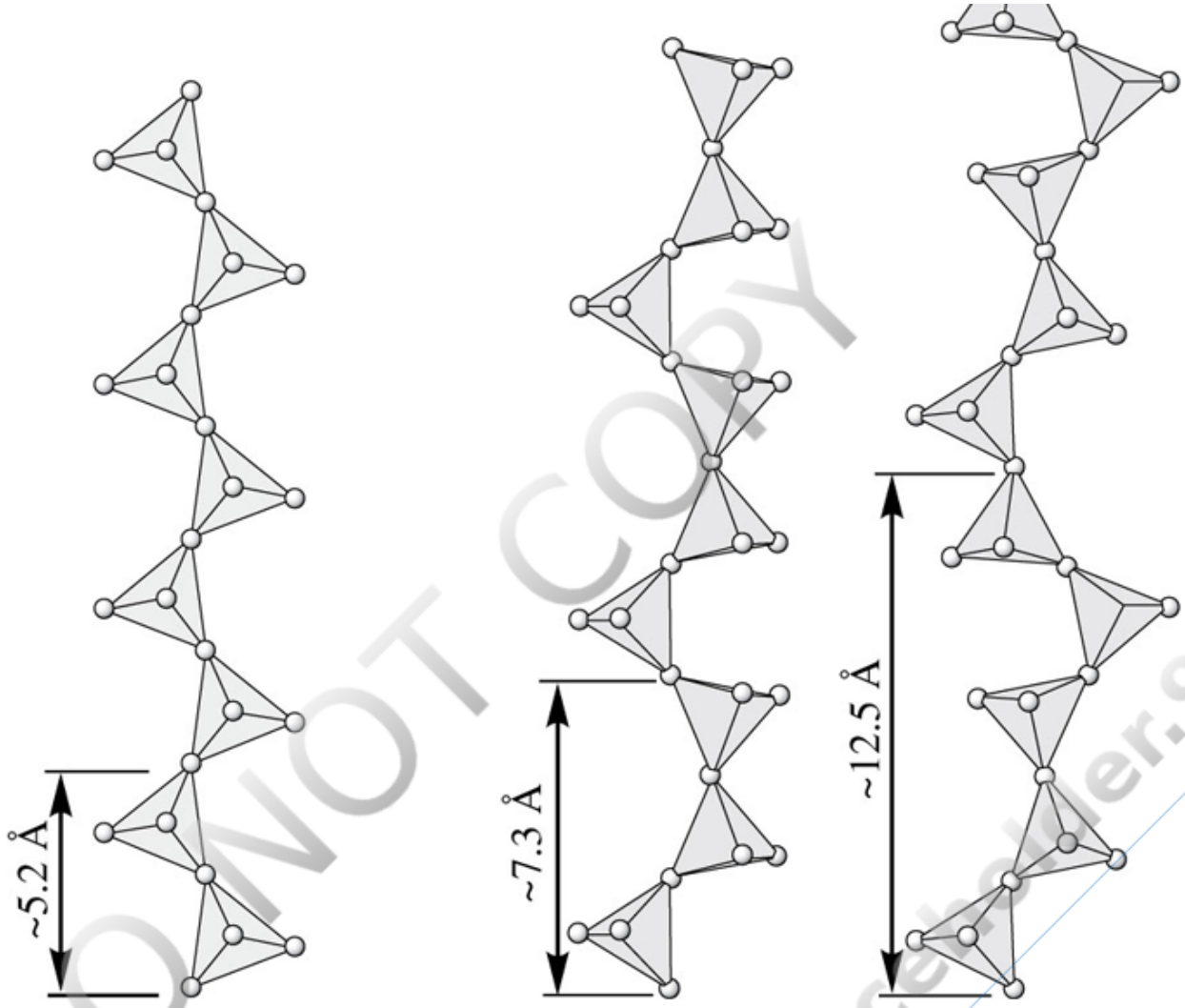

FIGURE 14.7 Chain structure of pyroxenes and pyroxenoids. (*a*) Pyroxenes have a repeat of two silicon tetrahedra at a distance of about 5.2 Å. Diopside is shown here, compare with enstatite in Figure 14.1e. (*b*) Pyroxenoids have a repeat of three or more tetrahedra. Cations in distorted octahedral coordination tie chains together as in the pyroxenes. Wollastonite (*left*) has a repeat of three silicon tetrahedra at a distance of about 7.3 Å. Rhodenite (*right*) has a repeat of five silicon tetrahedra at about 12.5 Å. Back to text

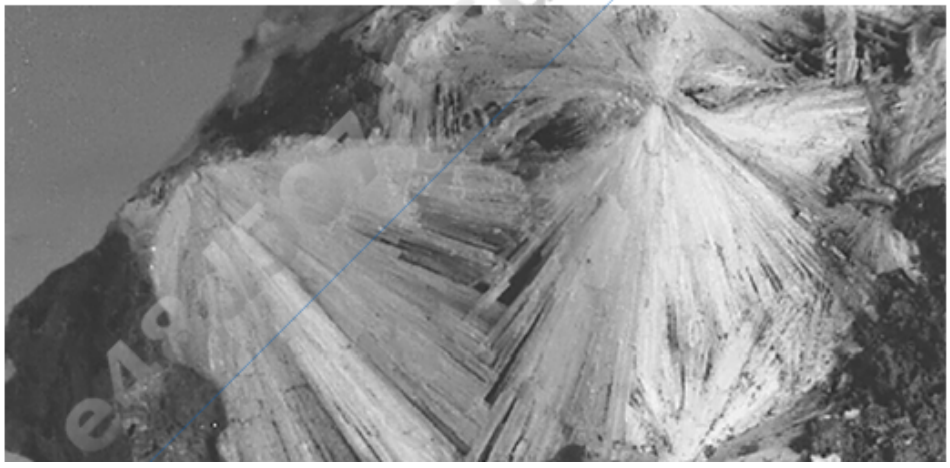

Printed by: e48d507df5d1141@placeholder.94092.edu. Printing is for personal, private use only. No part of this book may be reproduced or transmitted without publisher's prior permission. Violators will be prosecuted.

FIGURE 14.8 Photograph of radiating masses of pectolite. Field of view is about 10 cm wide. Back to text

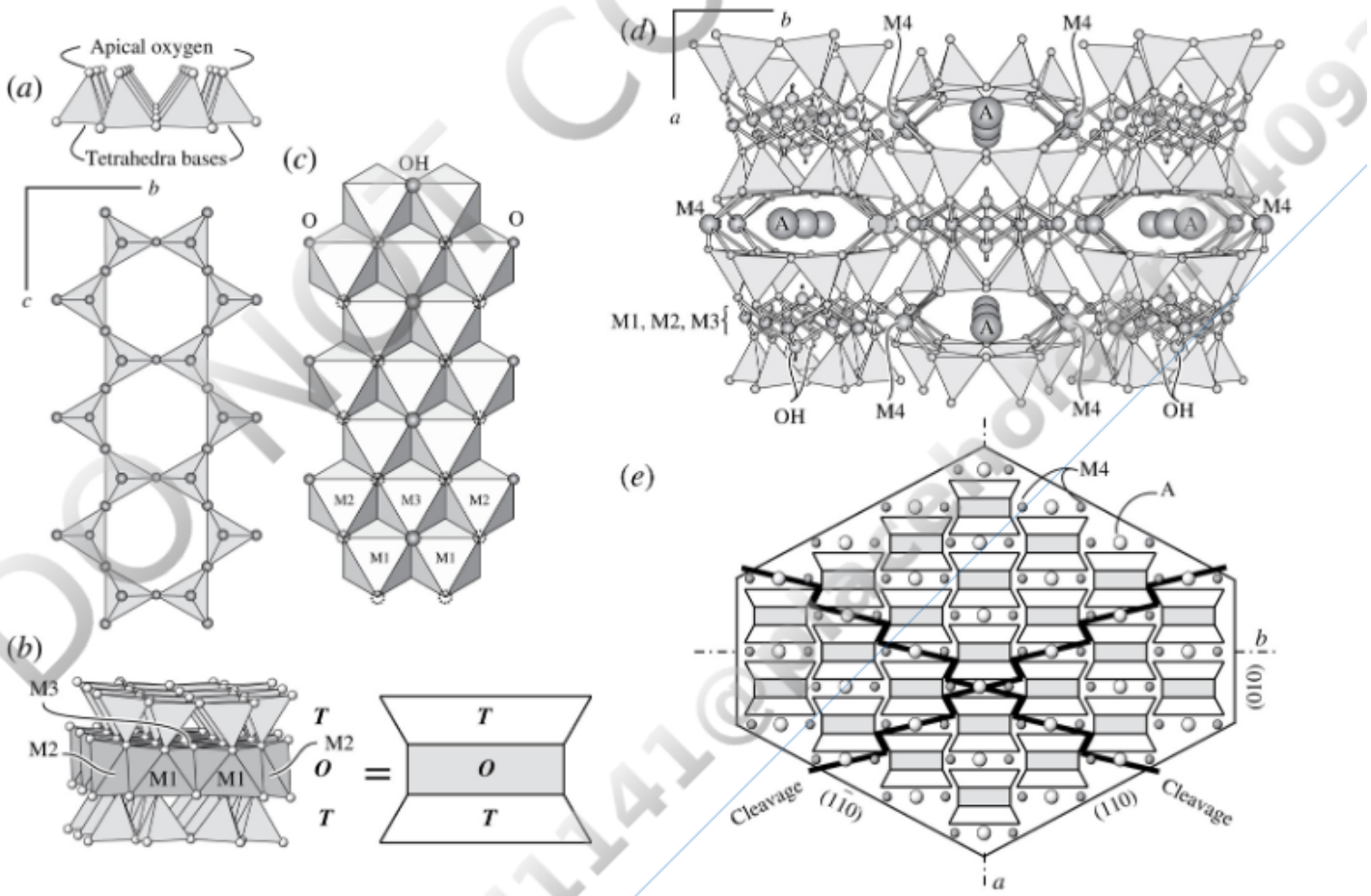

FIGURE 14.9 Amphibole structure. (*a*) Top and end views of an idealized double chain of tetrahedra. (*b*) Two chains of tetrahedra (*T*) are arranged facing each other forming octahedral (*O*) M1, M2, and M3 sites in between. The cross-section shape of this *TOT* strip, or I-beam, is shown to the right. (*c*) Top view of the octahedral layer showing distribution of M1, M2, and M3 sites. O and OH that are not shared with a tetrahedral chain are shown as filled spheres on the top surface of the octahedrons. O that are shared with a tetrahedral chain are shown as dotted circles. (*d*) *TOT* strips extend parallel to the *c* axis and are stacked in the *a* direction to produce M4 and A sites between the bases of the tetrahedra. The M1, M2, and M3 cations are shown, rather than their coordination polyhedra. (*e*) View down the *c* axis showing the arrangement of *TOT* strips (I-beams) and their relation to the typical amphibole cross section. Cleavage between chains parallel to (110) and $(1\bar{1}0)$ is at about 56° and 124°. Back to text

Printed by: e48d507df5d1141@placeholder.94092.edu. Printing is for personal, private use only. No part of this book may be reproduced or transmitted without publisher's prior permission. Violators will be prosecuted.

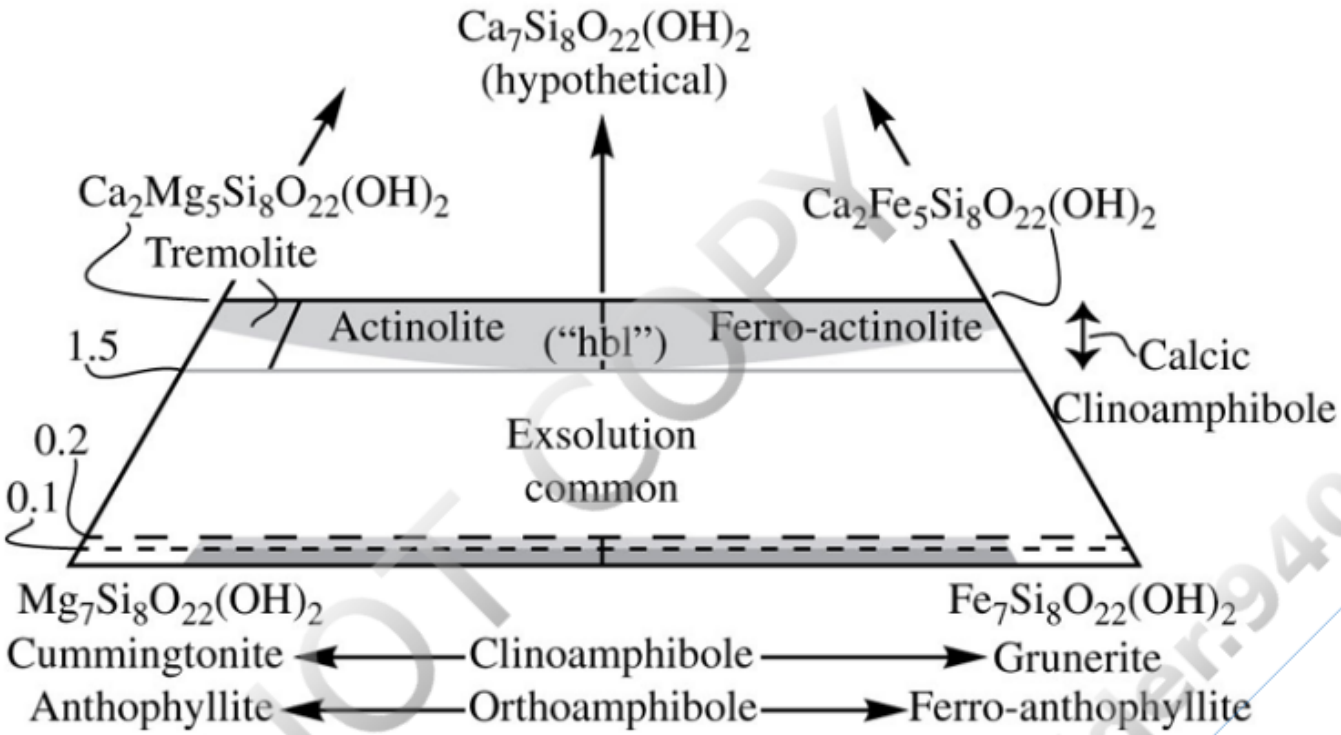

FIGURE 14.10 Fe–Mg–Ca amphiboles; common compositions are shown with shading. Decimal numbers on the left side mark various Ca compositions in atoms per formula units. ("hbl") is the approximate composition of some minerals often informally identified as hornblende, but such minerals often contain appreciable Al, Na, K, and Fe^{3+}, so they do not strictly lie in the plane of this composition diagram. See text for details. Back to text

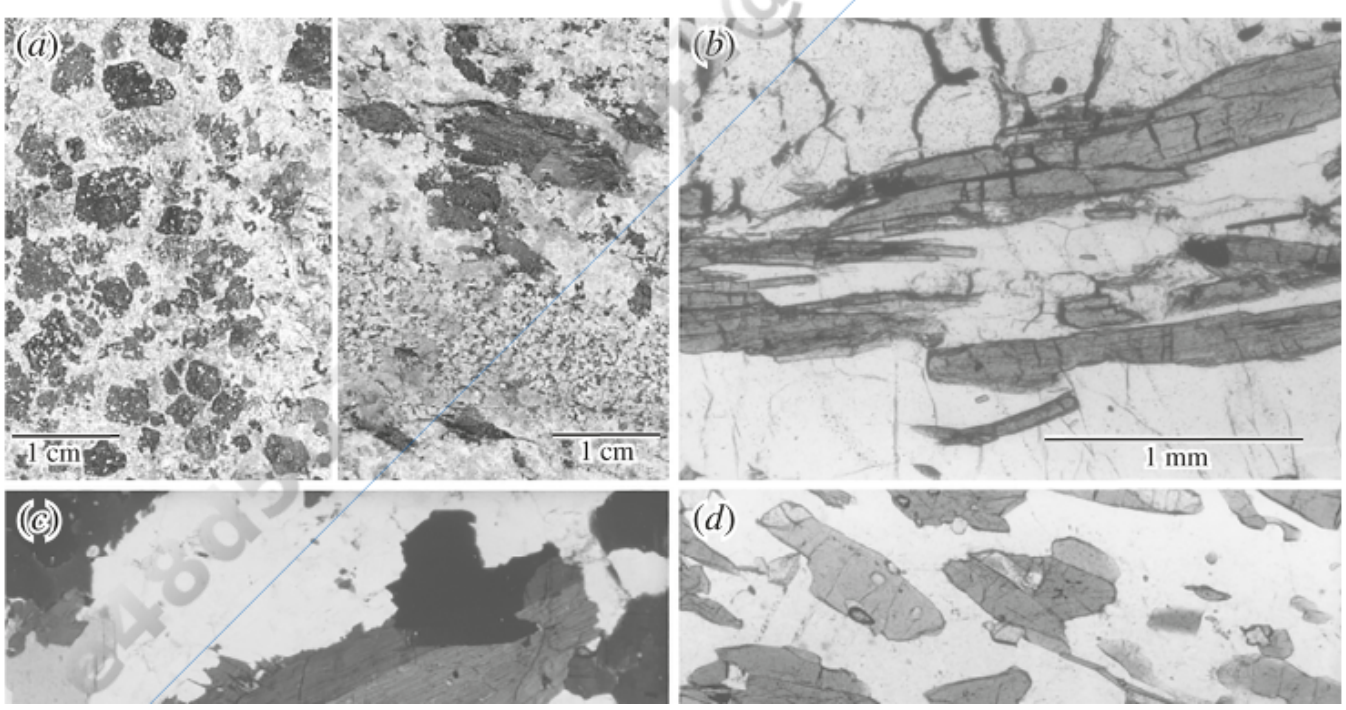

Printed by: e48d507df5d1141@placeholder.94092.edu. Printing is for personal, private use only. No part of this book may be reproduced or transmitted without publisher's prior permission. Violators will be prosecuted.

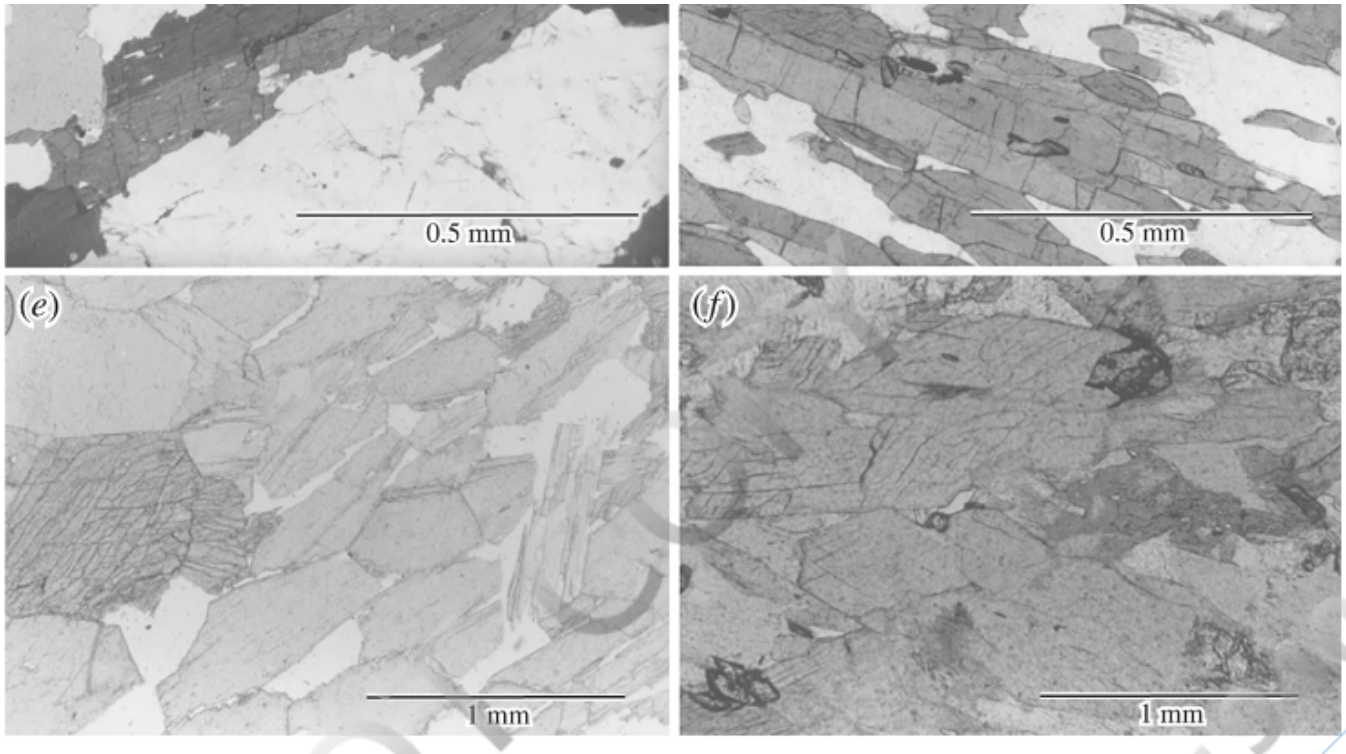

FIGURE 14.11 Common amphiboles. (*a*) Hornblende in outcrop. (*left*) Most grains are subhedral to euhedral with *c* axes parallel to the view direction; some grains display {110} and {010} crystal faces defining an irregular hexagon. (*right*) Grain *c* axes are parallel to the image. (*b*) Plane-polarized light photomicrograph of anthophyllite with cloudy cordierite (*top*) and quartz. (*c*) Plane-polarized light photomicrograph of hornblende in granodiorite. Note the twin. (*d*) Plane-polarized light photomicrograph of hornblende in amphibolite. (*e*) Plane-polarized light photomicrograph of tremolite in marble. Note that the grain on the left edge of the image is oriented with its *c* axis parallel to the view direction and clearly displays the 56° and 124° {110} cleavages. (*f*) Plane-polarized light photomicrograph of glaucophane in glaucophane schist. The small high-relief grains at the lower left and upper right are titanite. Back to text

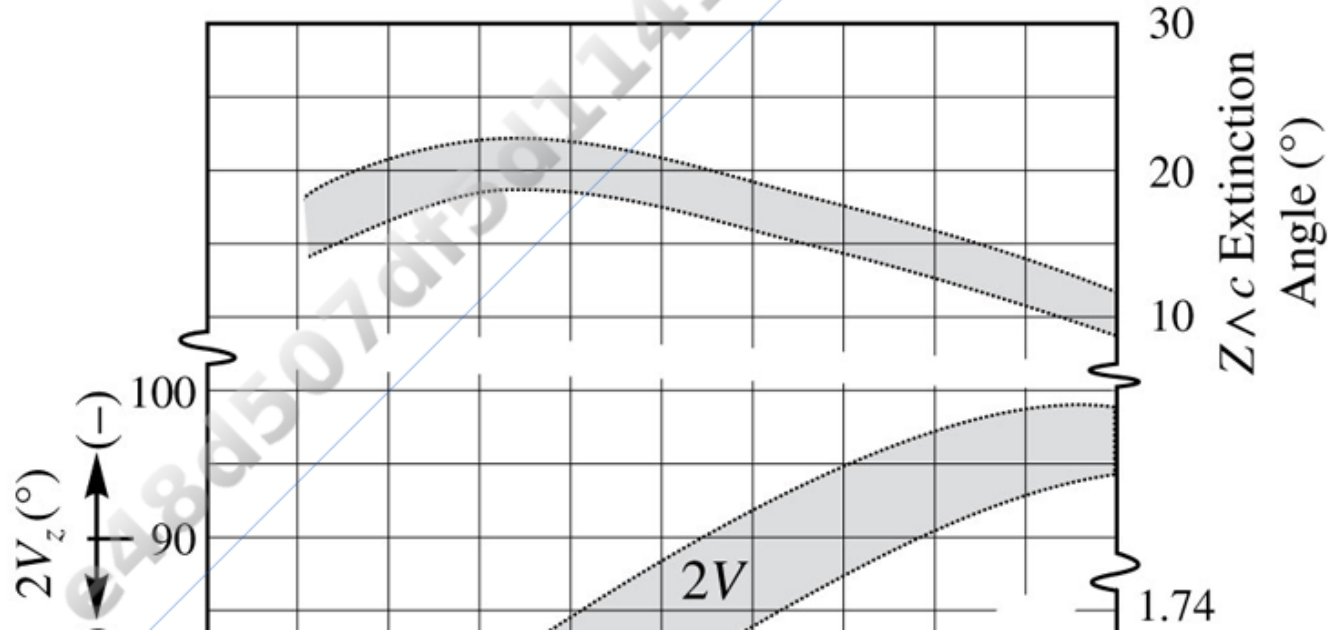

Printed by: e48d507df5d1141@placeholder.94092.edu. Printing is for personal, private use only. No part of this book may be reproduced or transmitted without publisher's prior permission. Violators will be prosecuted.

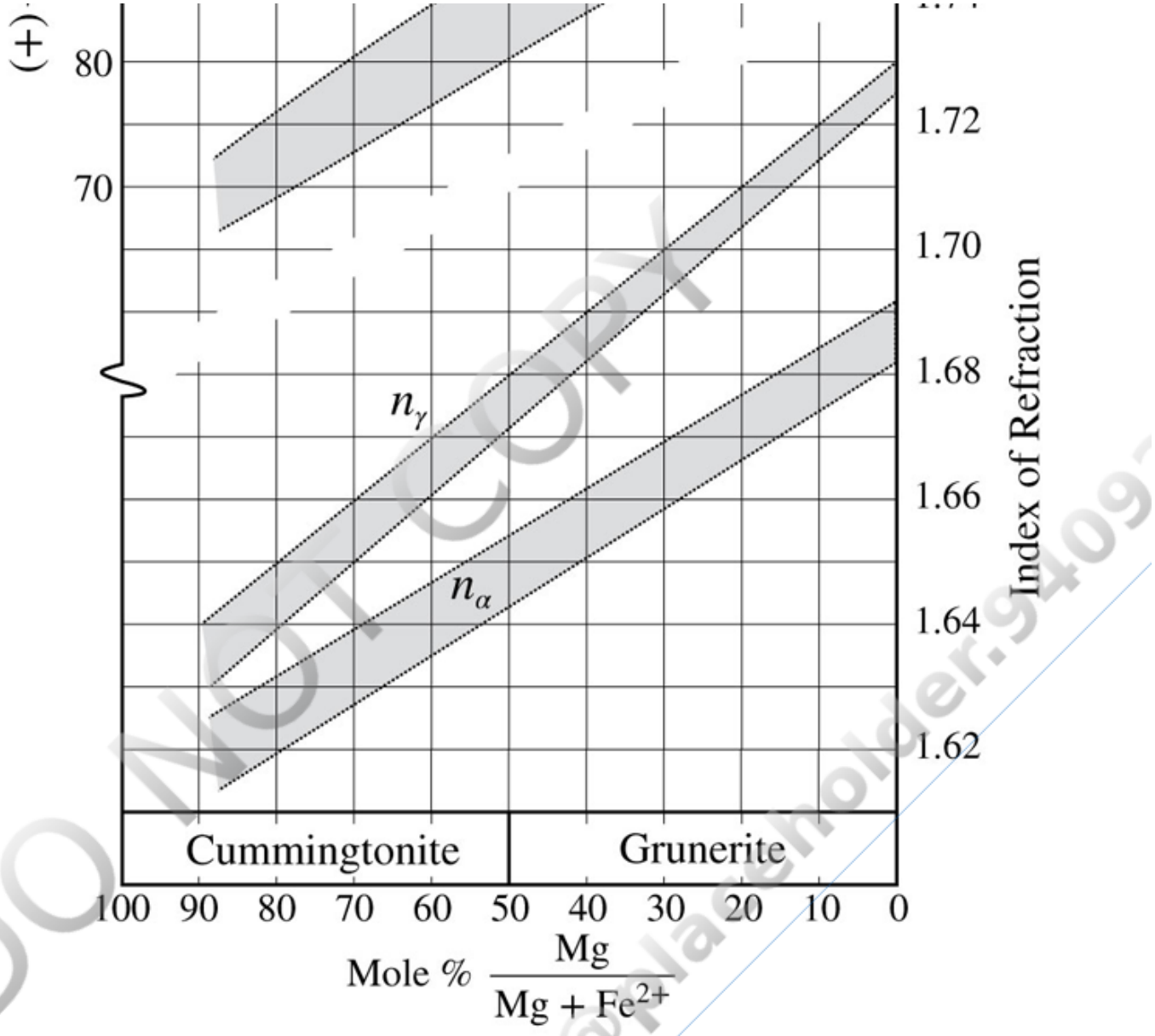

FIGURE 14.12 Optical properties of cummingtonite–grunerite. Data from Winchell (1938), Deer and others (1963, 1997), and Klein (1964). Back to text

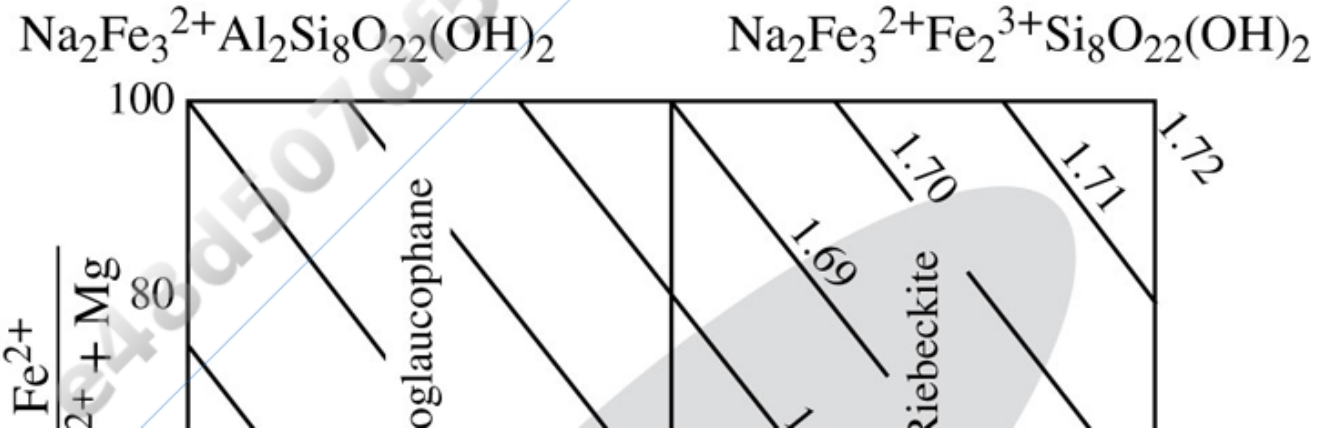

Printed by: e48d507df5d1141@placeholder.94092.edu. Printing is for personal, private use only. No part of this book may be reproduced or transmitted without publisher's prior permission. Violators will be prosecuted.

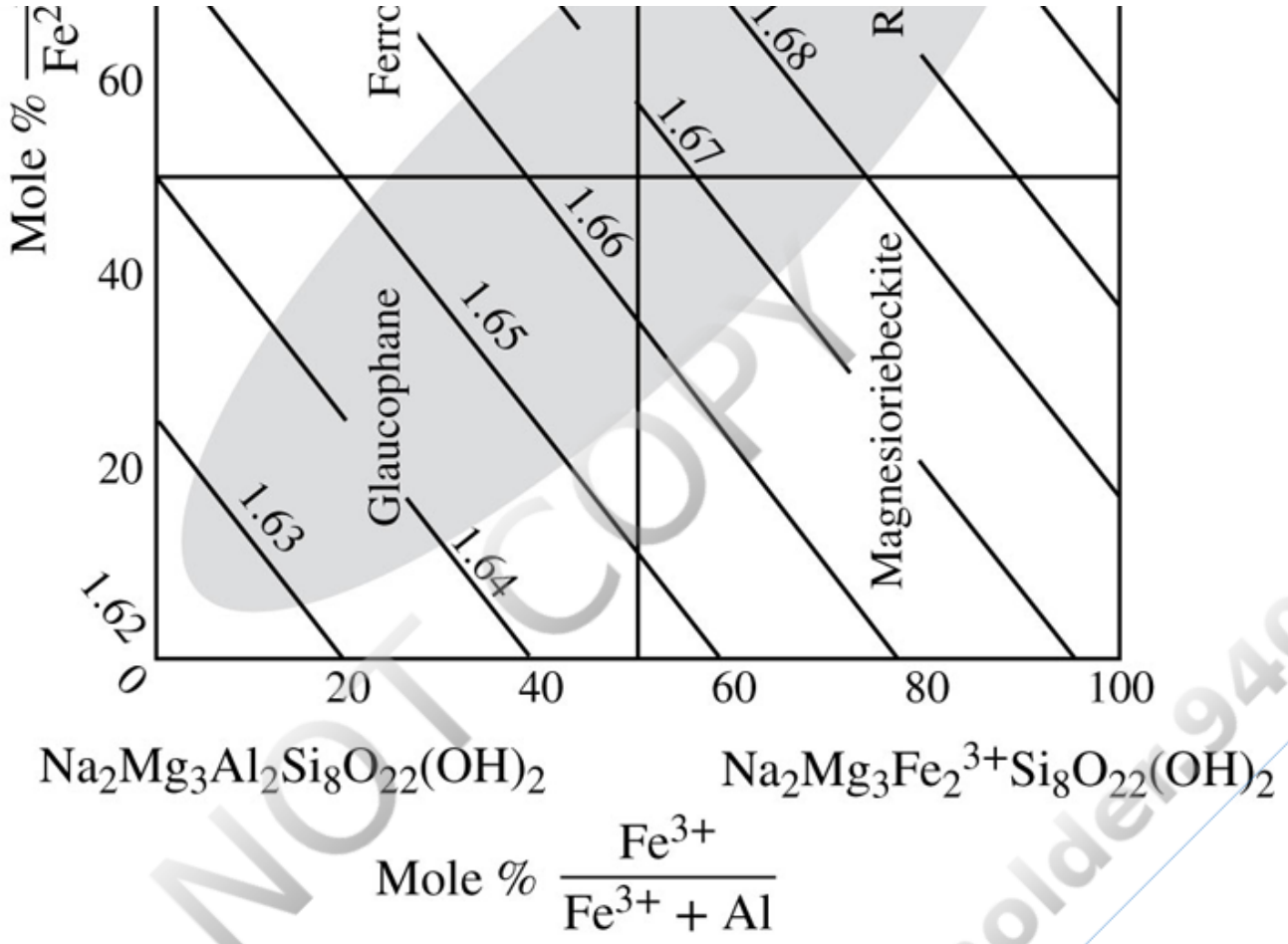

FIGURE 14.13 Composition and variation of n_γ for the sodic amphiboles. Compositions found in blueschist and related rocks fall in the shaded field extending from glaucophane to riebeckite. Compositions found in metamorphosed iron formations and alkalic igneous rocks usually fall in the riebeckite and magnesio-riebeckite fields. Data from Deer and others (1963), Borg (1967), Coleman and Papike (1968), and Ernst and Wai (1970). Back to text

DO NOT COPY
e48d507df5d1141@placeholder.94092

Printed by: e48d507df5d1141@placeholder.94092.edu. Printing is for personal, private use only. No part of this book may be reproduced or transmitted without publisher's prior permission. Violators will be prosecuted.

Chapter 15 Disilicates and Ring Silicates

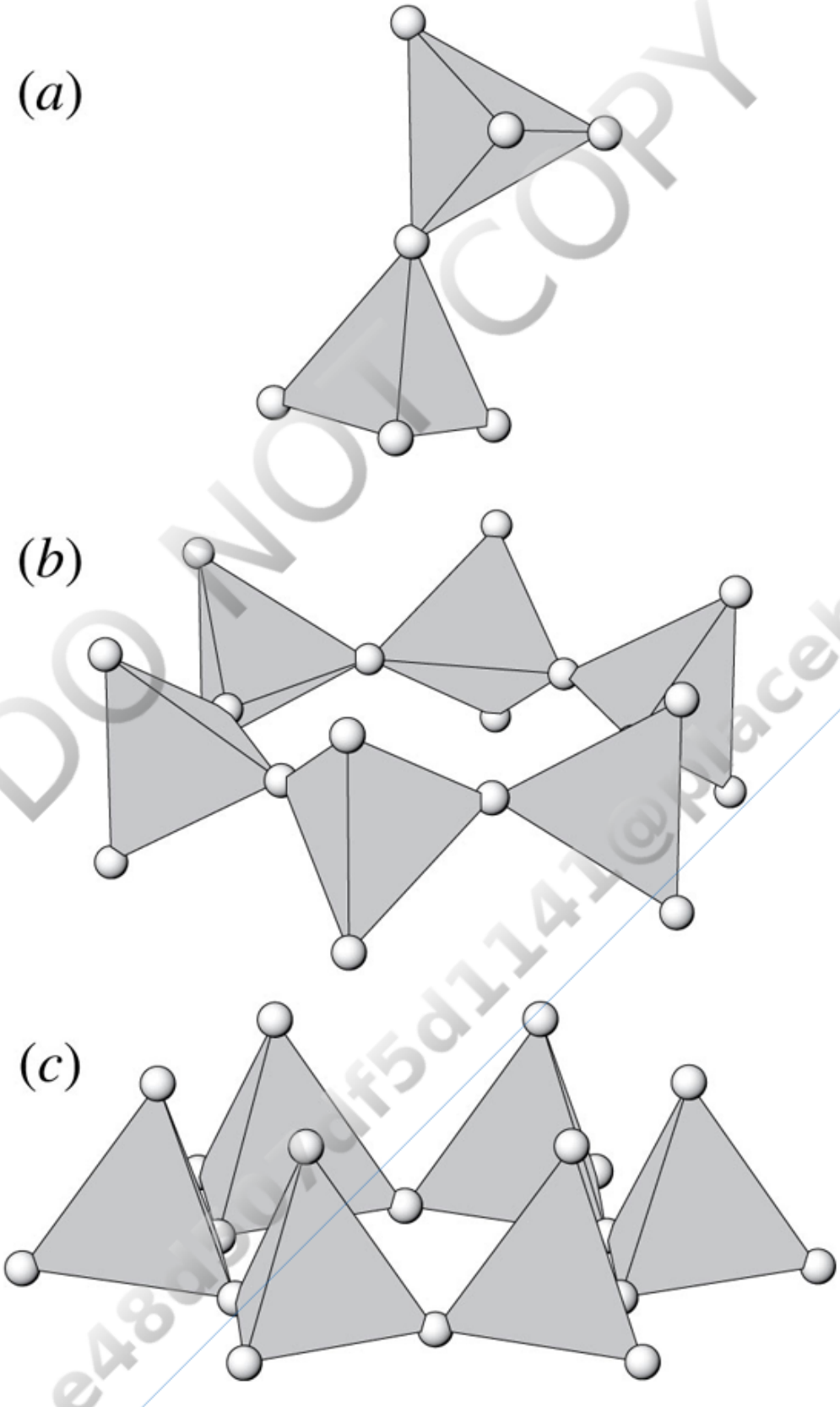

DO NOT COPY
e48d507df5d1141@placeholder.9409

FIGURE 15.1 Structural elements in disilicates and ring silicates. (a) Double silicon tetrahedra

Printed by: e48d507df5d1141@placeholder.94092.edu. Printing is for personal, private use only. No part of this book may be reproduced or transmitted without publisher's prior permission. Violators will be prosecuted.

FIGURE 15.1 Structural elements in disilicates and ring silicates. (*a*) Double silicon tetrahedra. (*b*) Six-member tetrahedral ring found in beryl and cordierite. (*c*) Six-member tetrahedral ring found in tourmaline. Back to text

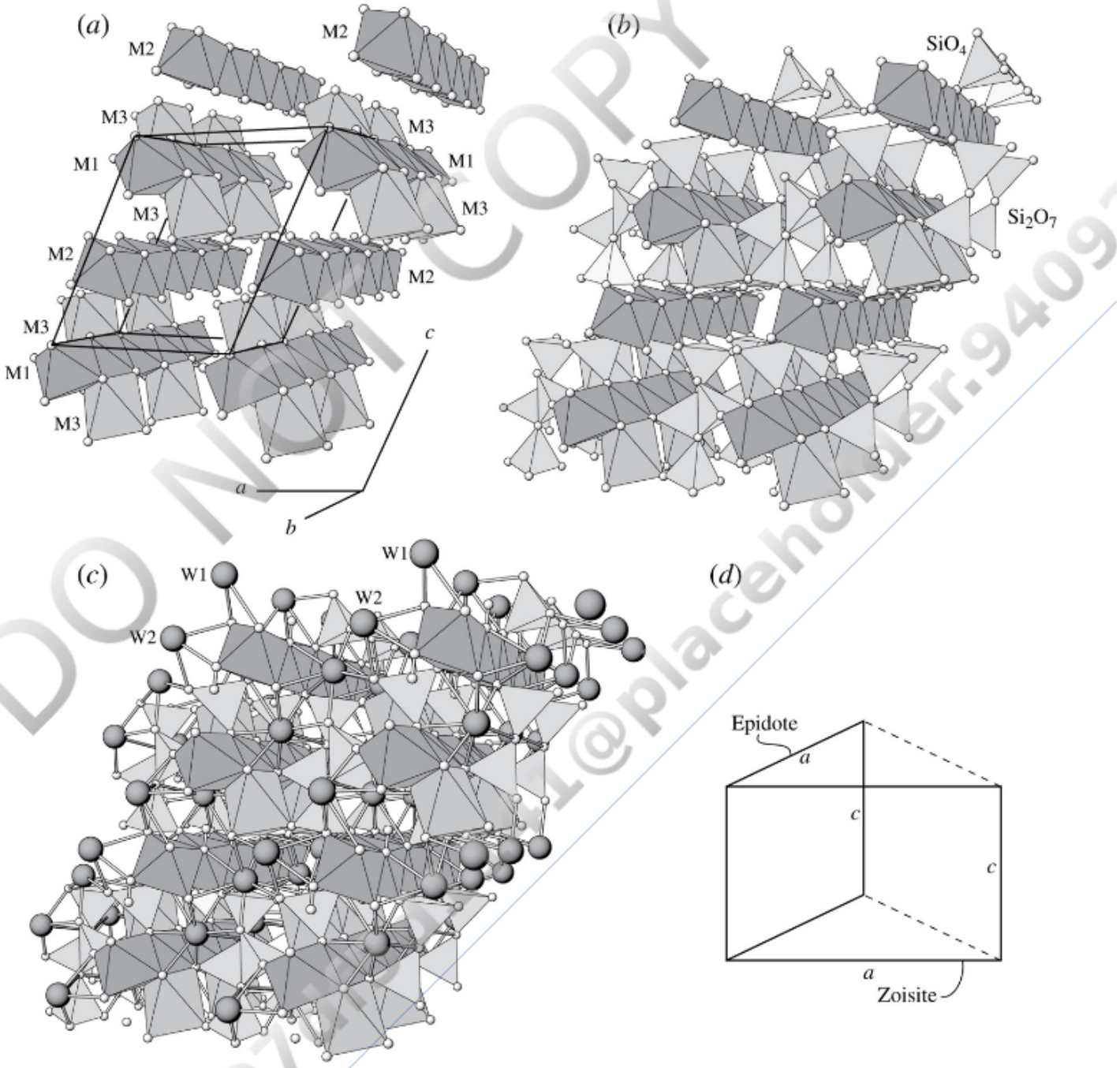

FIGURE 15.2 Structure of the epidote group. See text for additional discussion. (*a*) Chains of octahedra extend parallel to *b*. The outline of one unit cell is shown. M2 octahedra form simple chains; M1 octahedra form chains with M3 octahedra on alternate sides. (*b*) Same image as (*a*), but additionally with silicon tetrahedra. Single and double silicon tetrahedra cross-link the octahedral chains. (*c*) Same image as (*b*), but with W cations added. Large W1 and W2 cations in 7- to 11-fold coordination occupy interstices between octahedra and tetrahedra. (*d*) The orthorhombic zoisite unit cell is related to the monoclinic epidote unit cell by a twinlike doubling of the epidote unit cell along *a*. View is looking down the *b* axis. Back to text

Printed by: e48d507df5d1141@placeholder.94092.edu. Printing is for personal, private use only. No part of this book may be reproduced or transmitted without publisher's prior permission. Violators will be prosecuted.

a. View is looking down the *b* axis. Back to text

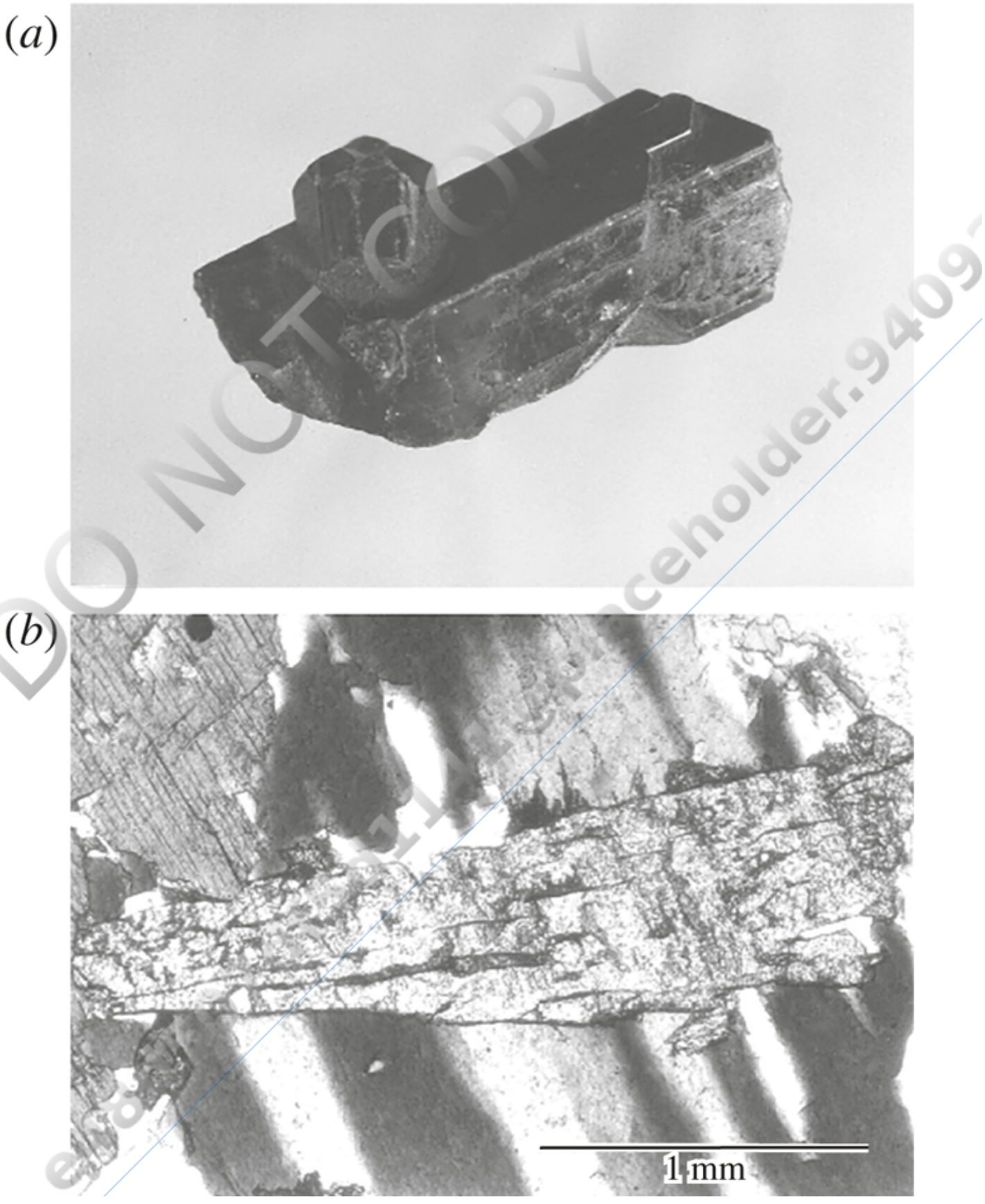

DO NOT COPY

Printed by: e48d507df5d1141@placeholder.94092.edu. Printing is for personal, private use only. No part of this book may be reproduced or transmitted without publisher's prior permission. Violators will be prosecuted.

FIGURE 15.3 Epidote. (*a*) Euhedral 2 cm crystal. (*b*) Photomicrograph of a thin section of granodiorite showing of epidote (*center*) enclosed in biotite that is partially replaced by chlorite. Hornblende is at the upper left (plane light). Back to text

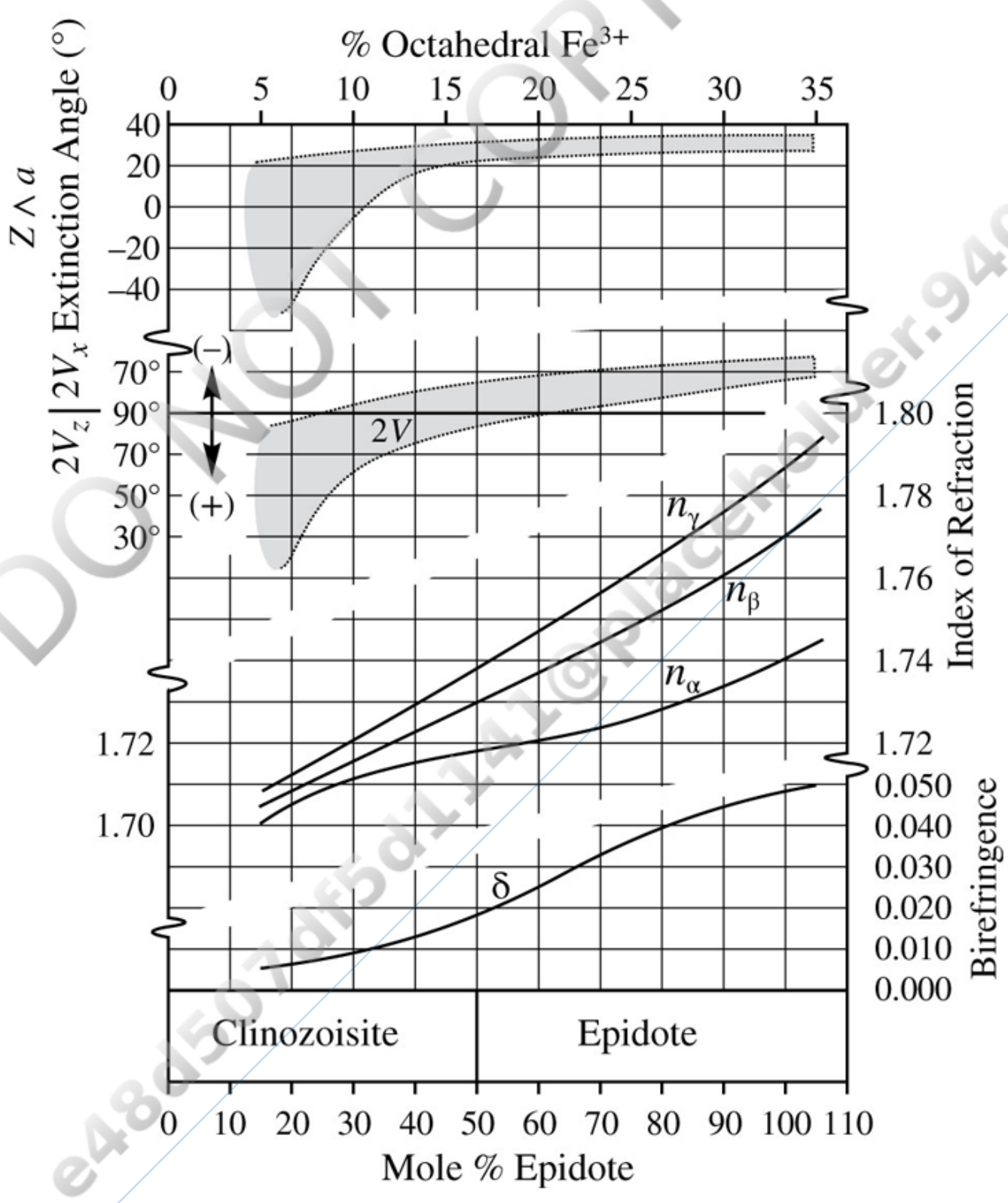

DO NOT COPY
e48d507df5d1141@placeholder.9409

Printed by: e48d507df5d1141@placeholder.94092.edu. Printing is for personal, private use only. No part of this book may be reproduced or transmitted without publisher's prior permission. Violators will be prosecuted.

FIGURE 15.4 Optical properties of clinozoisite–epidote. Compiled from Johnston (1949), Deer and others (1962), Myer (1965), Strens (1966), and Hormann and Raith (1971), with modifications after Franz and Liebscher (2004). Indices of refraction and birefringence have some scatter about the lines shown. Back to text

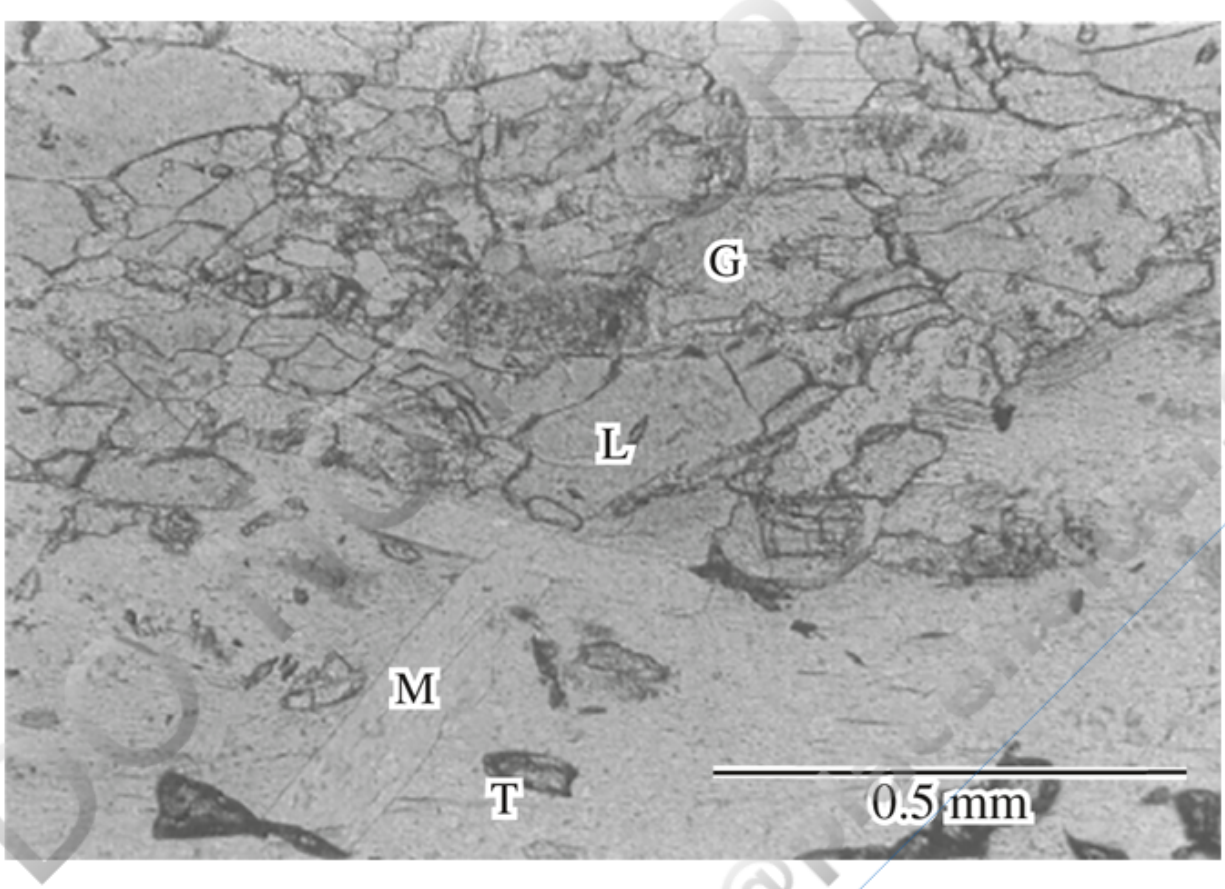

FIGURE 15.5 Photomicrograph of thin section of glaucophane schist with lawsonite (L), phengitic muscovite (M), glaucophane (G), and high-relief titanite (T) in plane light. Back to text

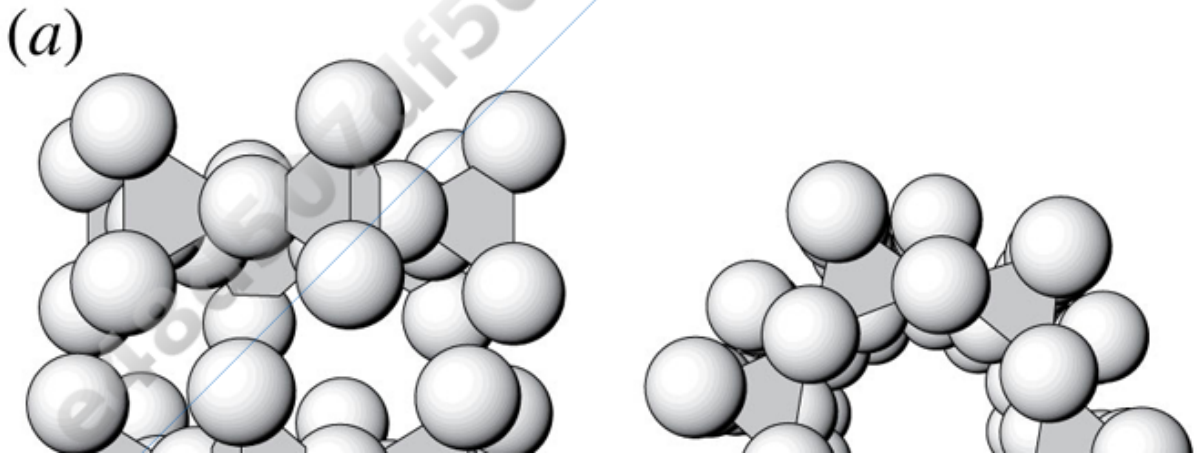

Printed by: e48d507df5d1141@placeholder.94092.edu. Printing is for personal, private use only. No part of this book may be reproduced or transmitted without publisher's prior permission. Violators will be prosecuted.

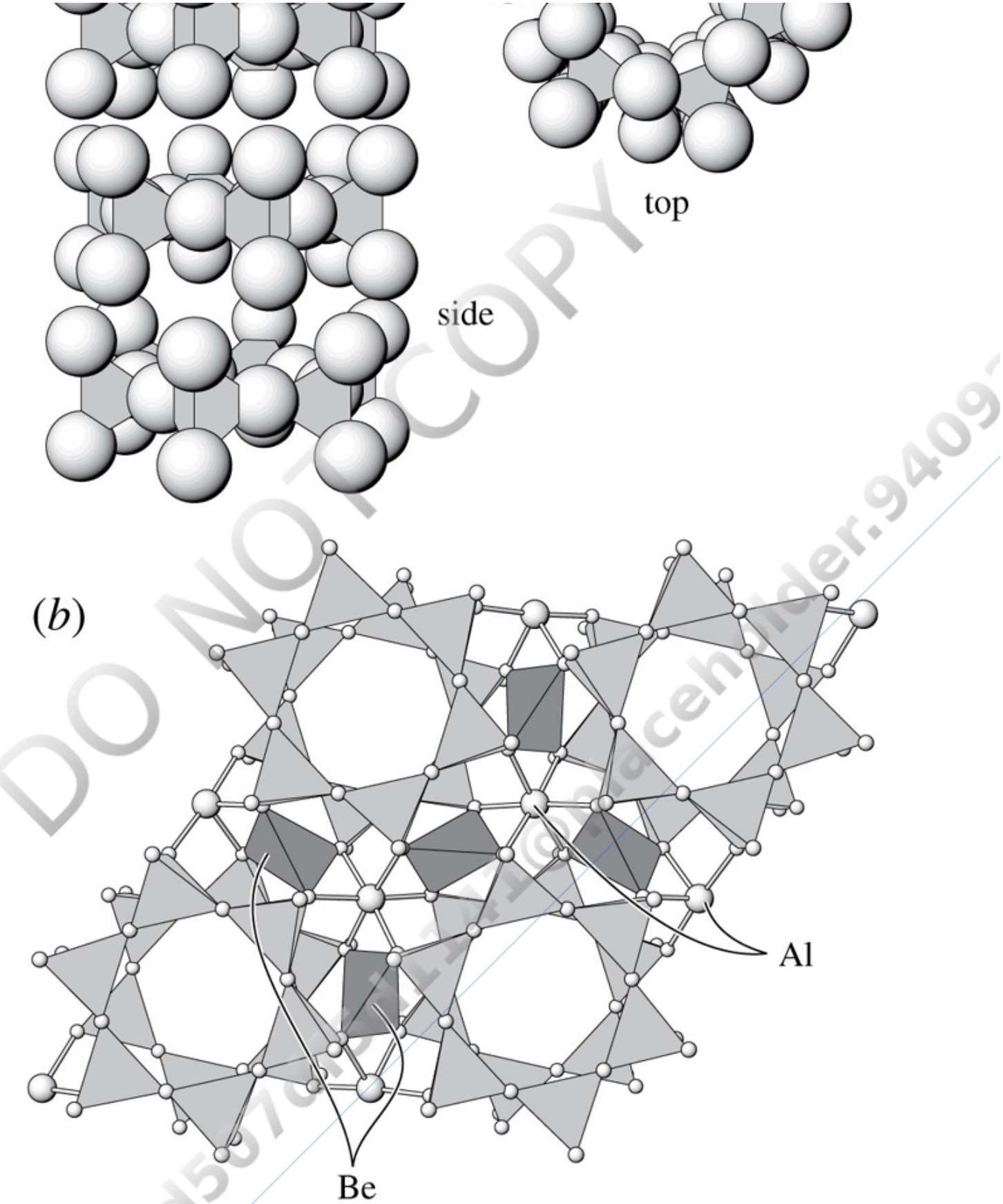

FIGURE 15.6 Structure of beryl. (*a*) Side and top view of column structure. The oxygen anions are drawn at about 70% of full size. (*b*) Columns of tetrahedral rings are cross-linked through Be in tetrahedral coordination (dark tetrahedra) and through Al in octahedral coordination. View down the *c* axis, with oxygen anions drawn as small spheres. Back to text

Printed by: e48d507df5d1141@placeholder.94092.edu. Printing is for personal, private use only. No part of this book may be reproduced or transmitted without publisher's prior permission. Violators will be prosecuted.

FIGURE 15.7 Beryl crystal from a granitic pegmatite. Back to text

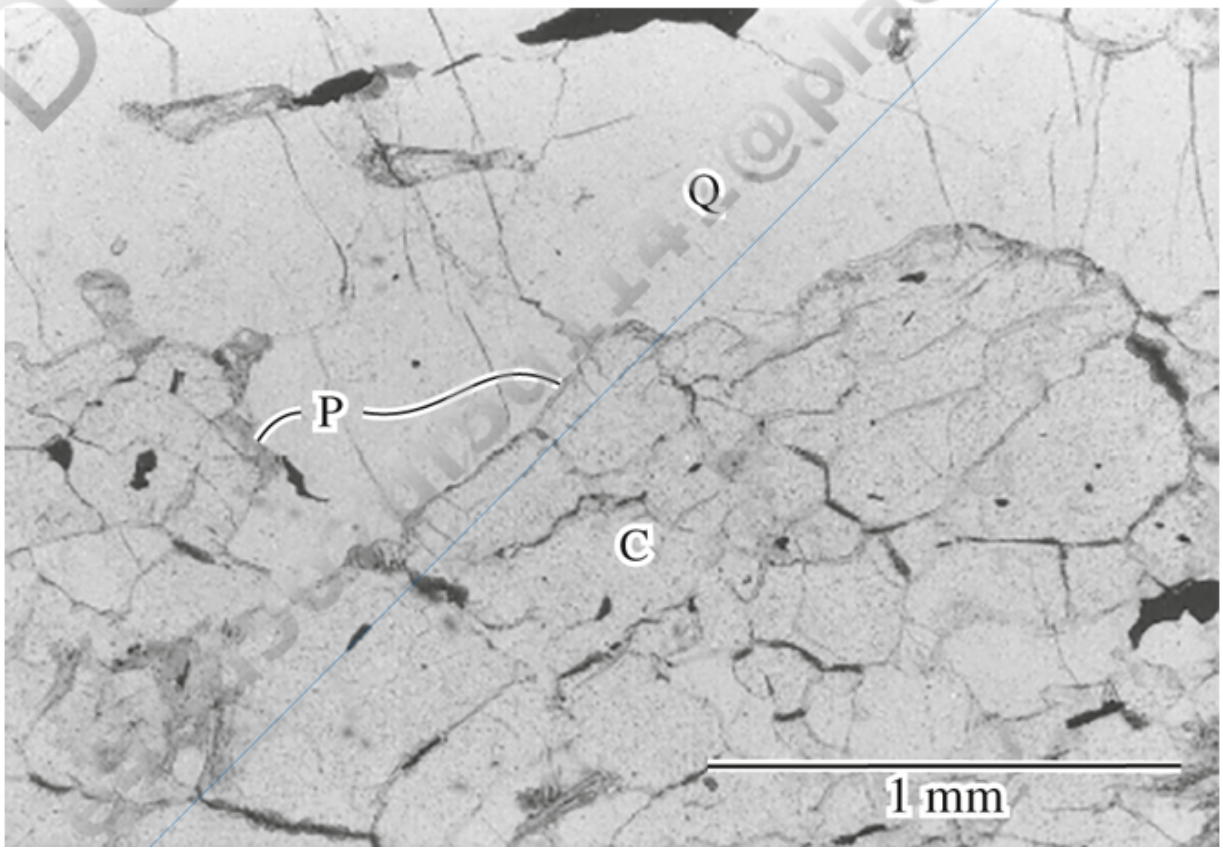

DO NOT COPY

Printed by: e48d507df5d1141@placeholder.94092.edu. Printing is for personal, private use only. No part of this book may be reproduced or transmitted without publisher's prior permission. Violators will be prosecuted.

FIGURE 15.8 Photomicrograph of thin section of anthophyllite–cordierite gneiss showing cordierite (C) and quartz (Q) in plane light. Note that the cordierite has minor pinite (P) alteration at the edge of grains and is slightly cloudy because of fine opaque inclusions. Back to text

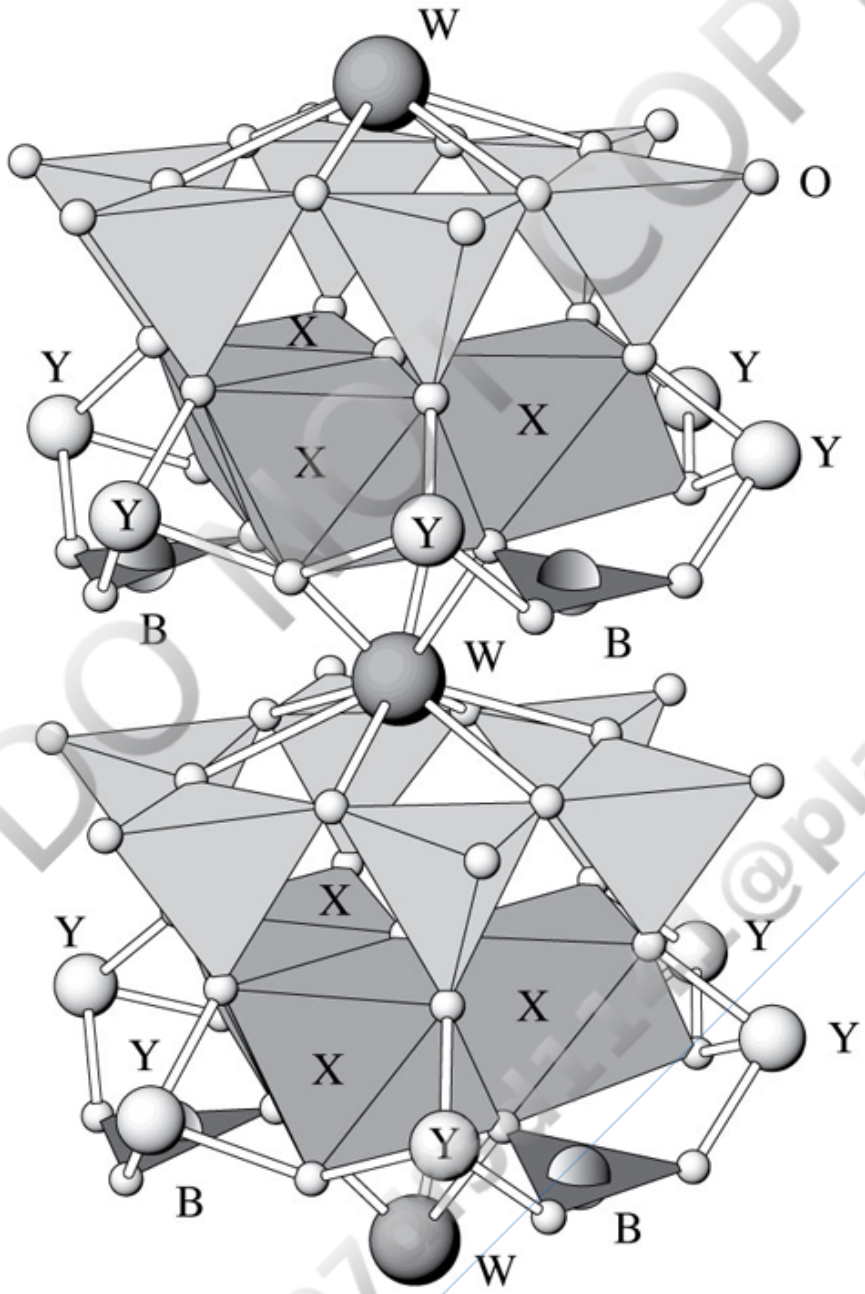

FIGURE 15.9 Tourmaline structure consisting of tetrahedral rings, triangular groups of octahedra (X), and large cation sites (W) along the axis of the column. Boron (B) is situated in triangular coordination along the edges of the columns. Columns are stacked adjacent to each other and are cross-linked through octahedrally coordinated Y cations. Back to text

DO NOT COPY e48d507df5d1141@placeholder.94092

Printed by: e48d507df5d1141@placeholder.94092.edu. Printing is for personal, private use only. No part of this book may be reproduced or transmitted without publisher's prior permission. Violators will be prosecuted.

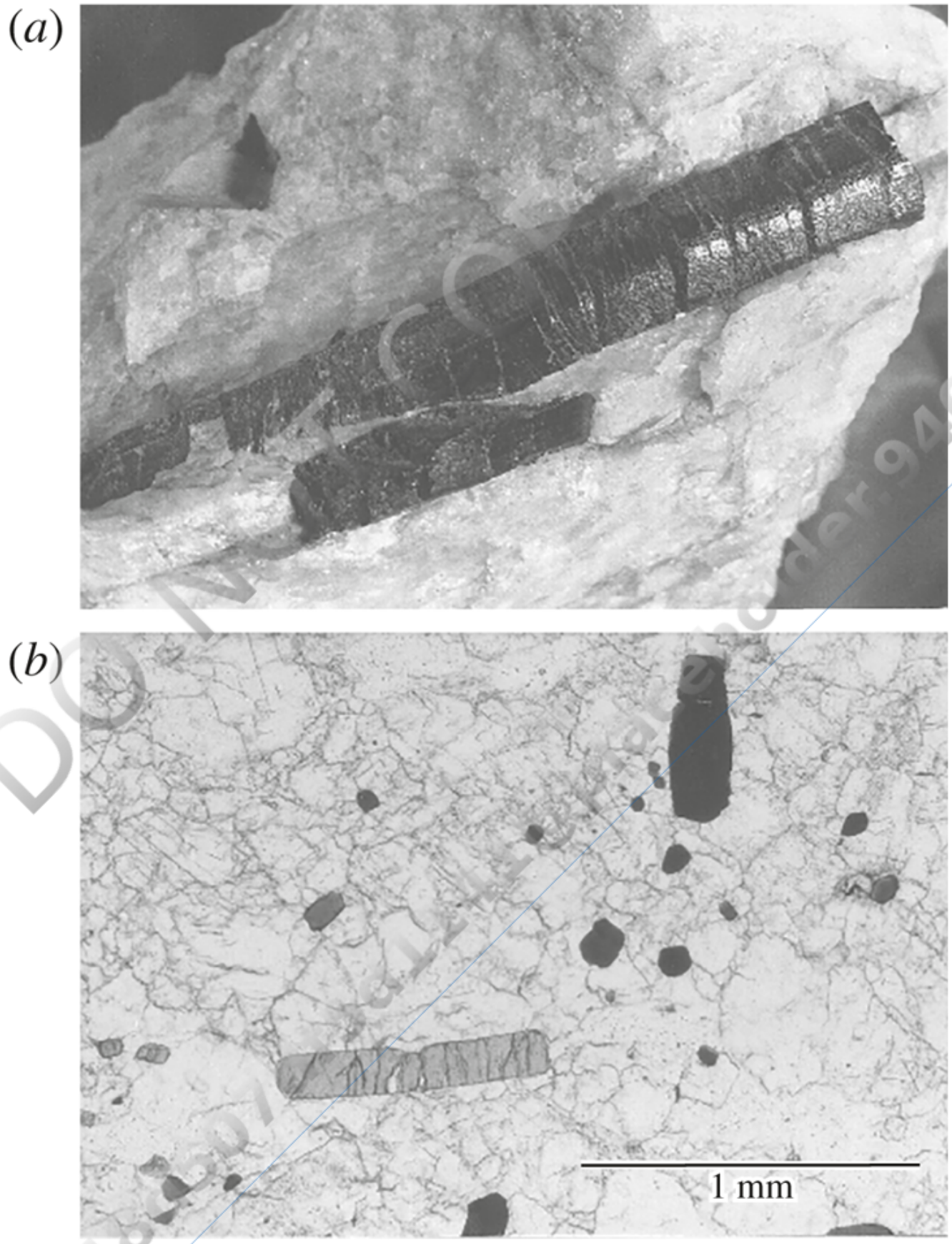

FIGURE 15.10 Tourmaline. (*a*) Elongate crystals with fractures roughly perpendicular to the length, found in a felsic pegmatite. The field of view is about 20 cm wide. (*b*) Thin section showing tourmaline crystals in a metaquartzite in plane light. The ordinary ray is dark and extraordinary ray is

Printed by: e48d507df5d1141@placeholder.94092.edu. Printing is for personal, private use only. No part of this book may be reproduced or transmitted without publisher's prior permission. Violators will be prosecuted.

Chapter 16 Orthosilicates

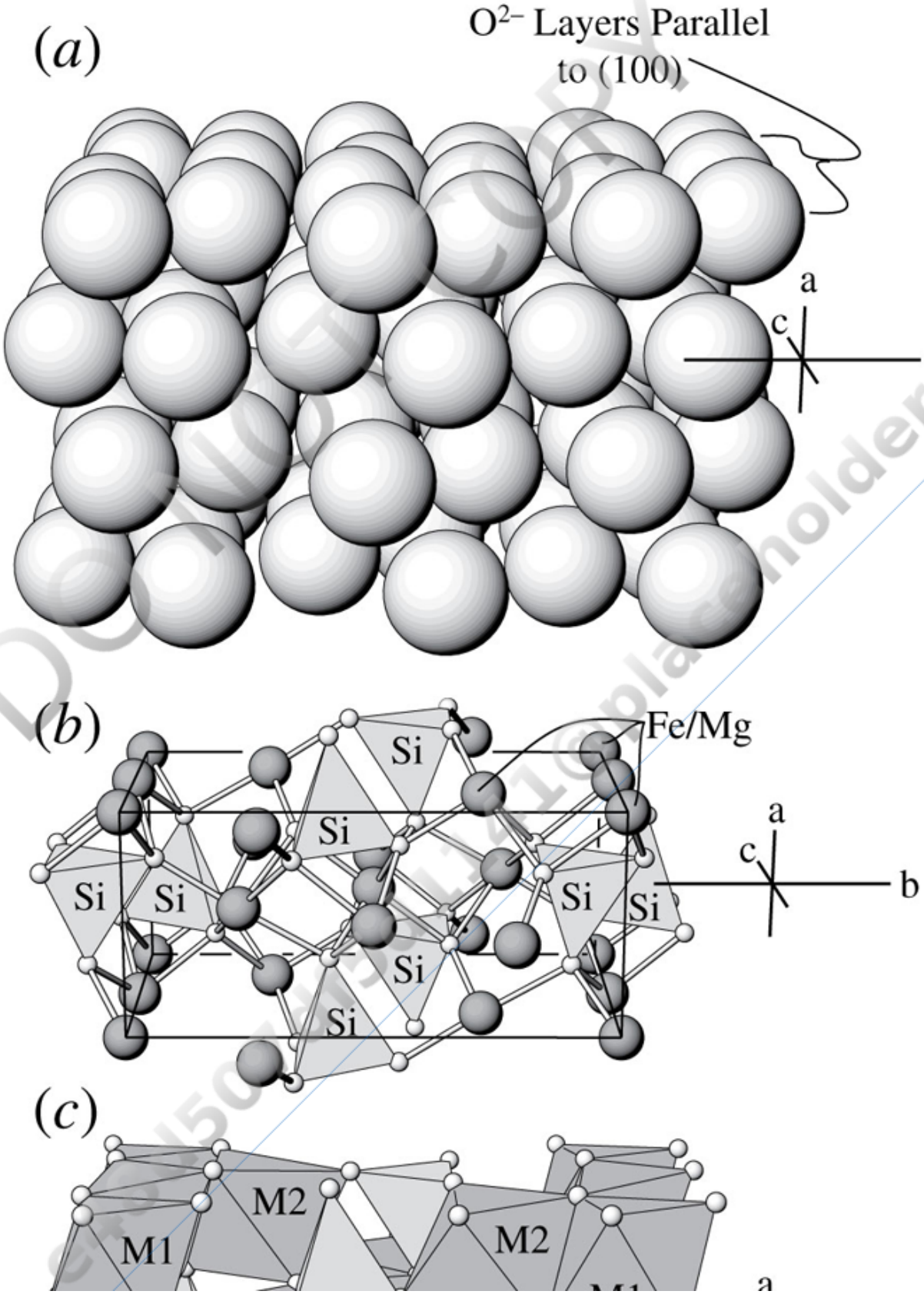

Printed by: e48d507df5d1141@placeholder.94092.edu. Printing is for personal, private use only. No part of this book may be reproduced or transmitted without publisher's prior permission. Violators will be prosecuted.

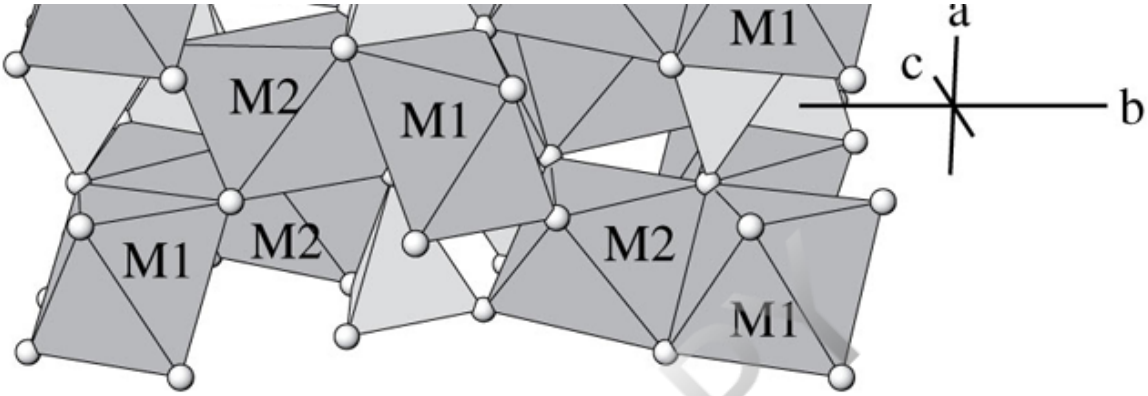

FIGURE 16.1 Olivine structure. (*a*) Oxygen anions form a somewhat loose and distorted hexagonal close-packed array with layers parallel to (100). The distortion reduces symmetry to orthorhombic. (*b*) Silicon tetrahedra point alternately up and down relative to the {100} plane and are tied laterally through Mg/Fe cations in octahedral coordination. Oxygen anions are shown as the smallest spheres; some of the oxygen anions shown in (*a*) have been omitted. The unit cell is shown. (*c*) M1 octahedral sites form edge-sharing chains that extend parallel to the *c* axis. M2 sites are attached to the sides of the M1 chains. All of the oxygen anions shown in (*a*) appear here as small spheres. See also Figure 4.1. Back to text

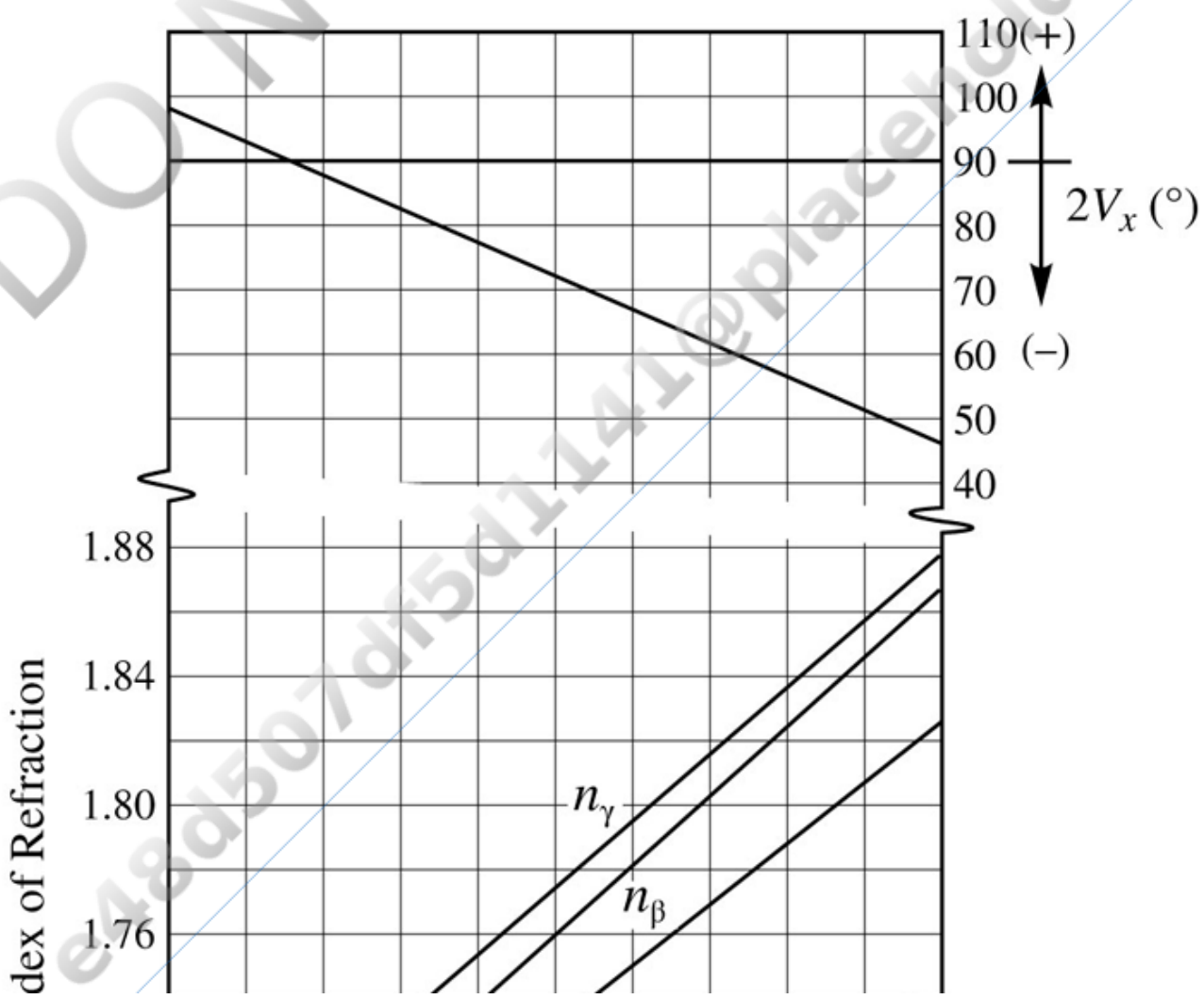

DO NOT COPY
e48d507df5d1141@placeholder.9409

Printed by: e48d507df5d1141@placeholder.94092.edu. Printing is for personal, private use only. No part of this book may be reproduced or transmitted without publisher's prior permission. Violators will be prosecuted.

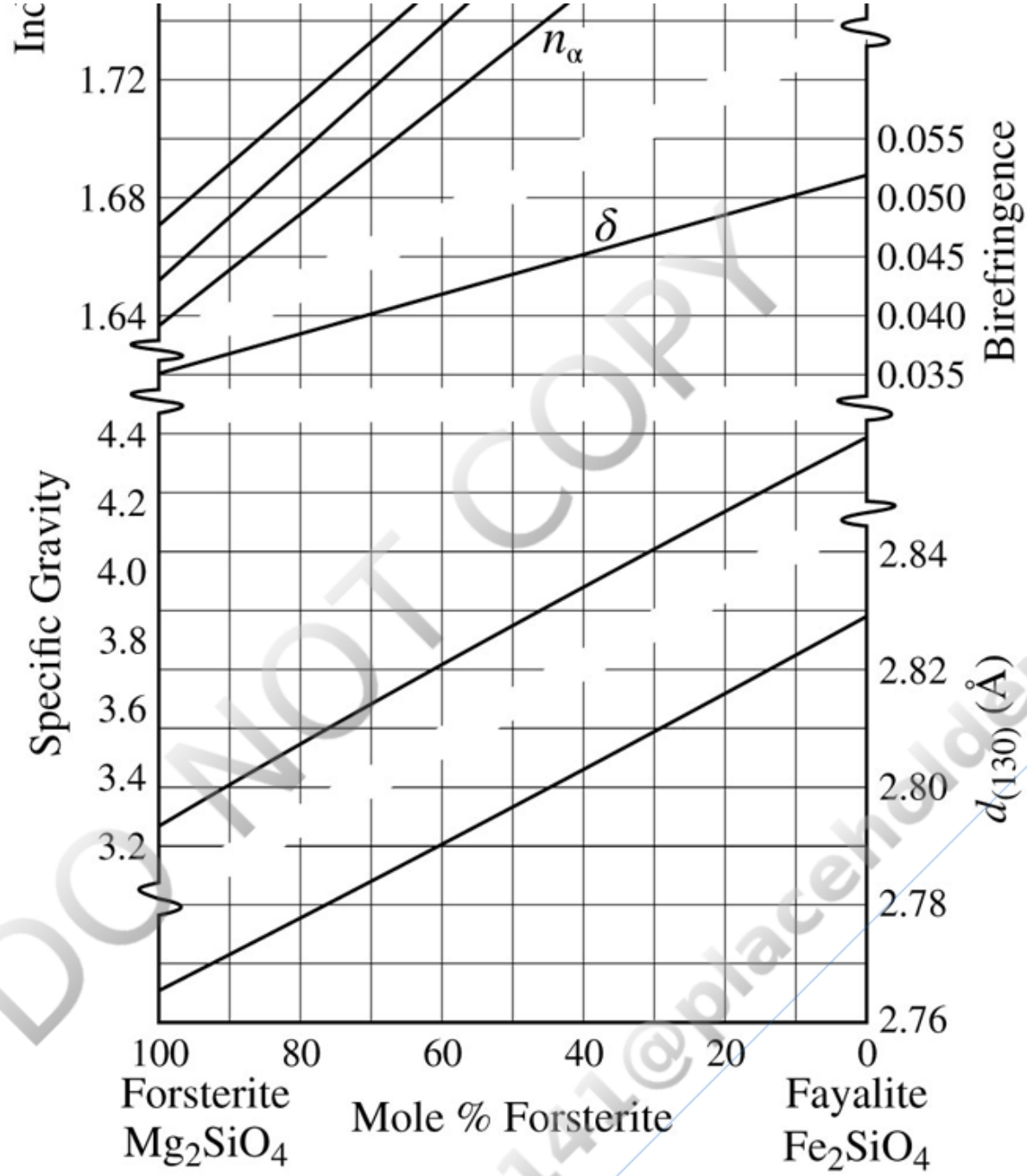

FIGURE 16.2 Specific gravity, $d_{(130)}$, and optical properties of olivine. Back to text

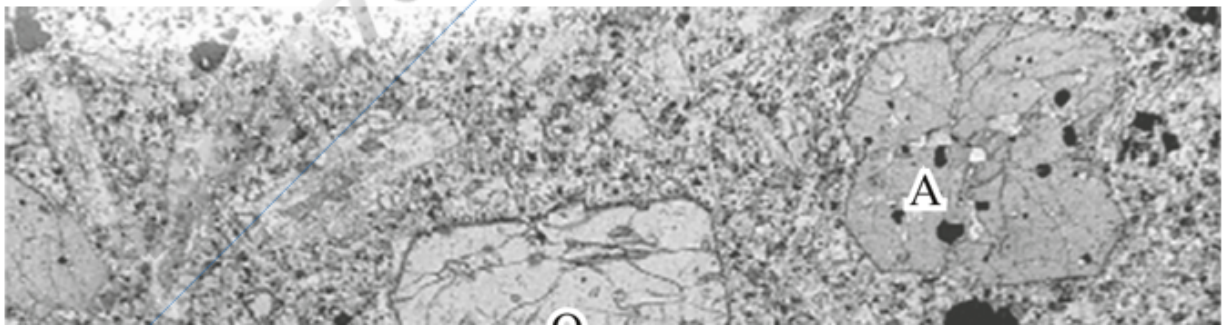

DO NOT COPY

Printed by: e48d507df5d1141@placeholder.94092.edu. Printing is for personal, private use only. No part of this book may be reproduced or transmitted without publisher's prior permission. Violators will be prosecuted.

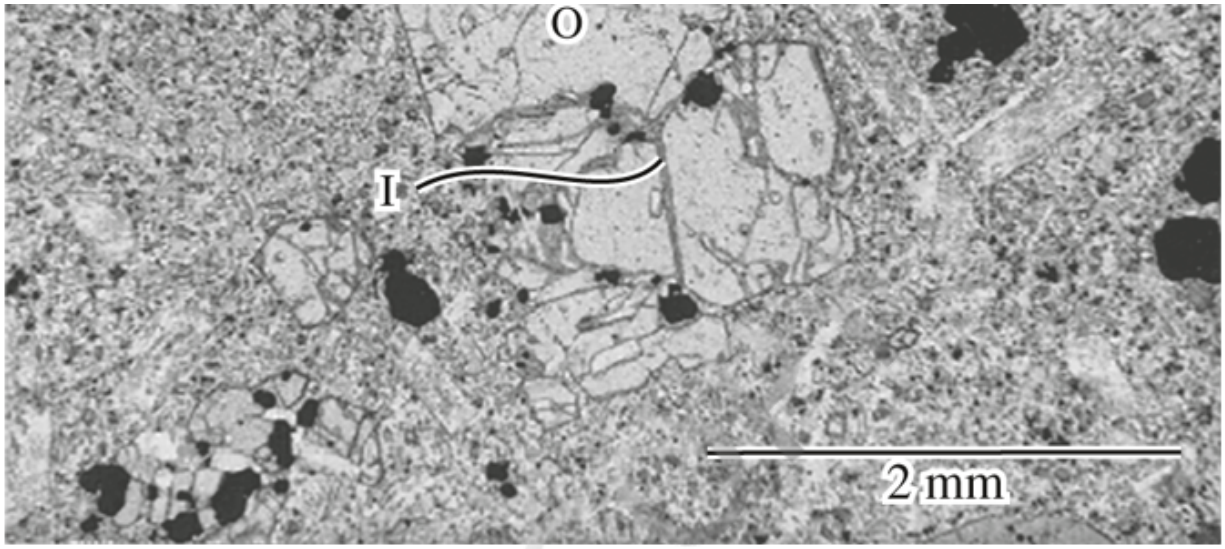

FIGURE 16.3 Olivine phenocryst (O) in basaltic dike. Note the alteration to iddingsite (I) along grain boundaries and cracks (cf. Figure 7.63d). The phenocryst at the upper right is augite (A). Plane light. Back to text

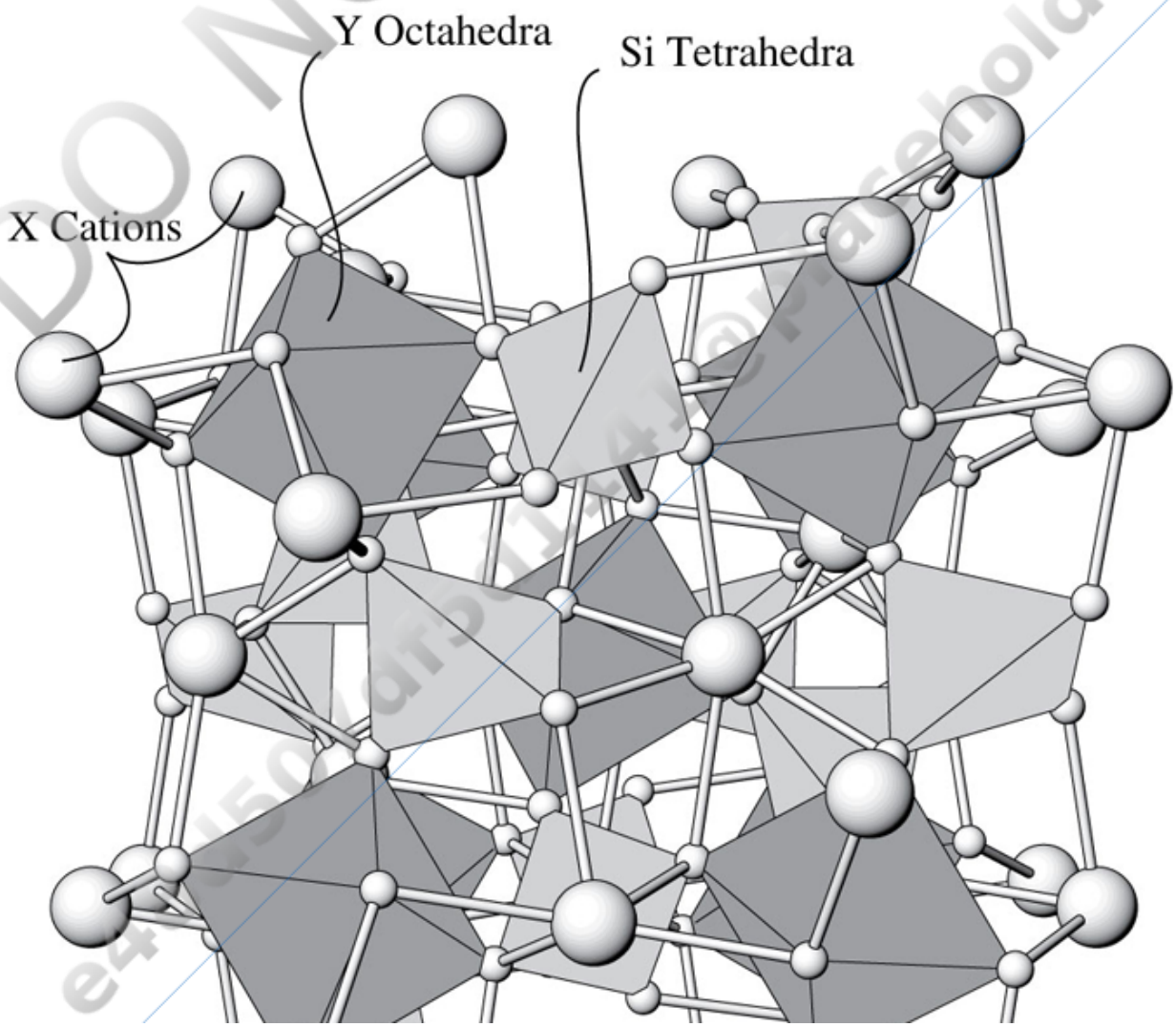

DO NOT C

Printed by: e48d507df5d1141@placeholder.94092.edu. Printing is for personal, private use only. No part of this book may be reproduced or transmitted without publisher's prior permission. Violators will be prosecuted.

FIGURE 16.4 Garnet structure. Isolated silicon tetrahedra share single oxygen anions with Y cations in 6-fold coordination. The spaces between are distorted 8-fold sites occupied by the larger X cations. Back to text

DO NOT COPY

(a)

(b)

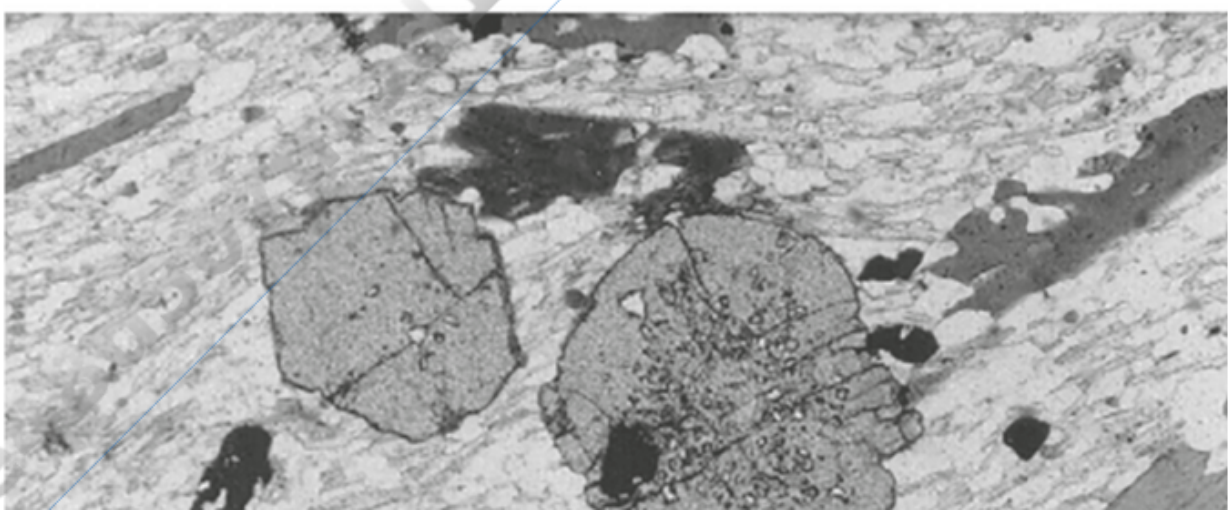

Printed by: e48d507df5d1141@placeholder.94092.edu. Printing is for personal, private use only. No part of this book may be reproduced or transmitted without publisher's prior permission. Violators will be prosecuted.

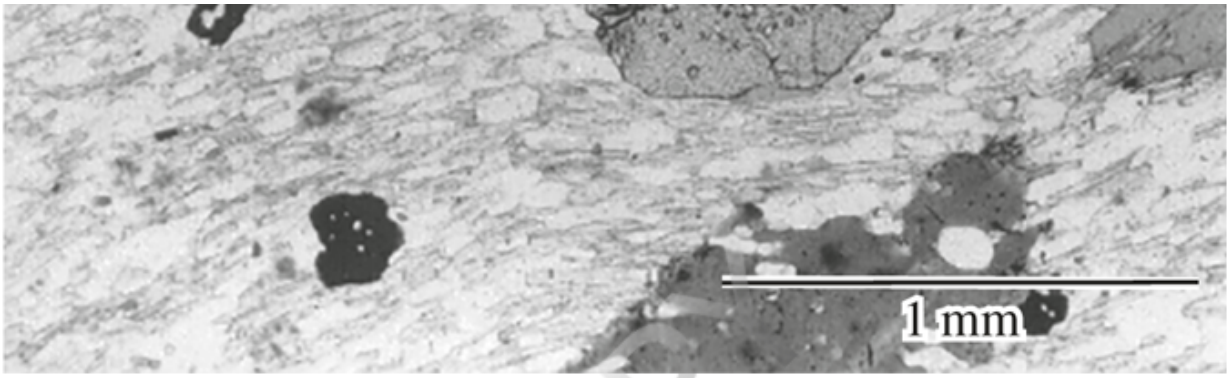

FIGURE 16.5 Garnet. (*a*) 2-cm garnet crystal in mica schist. (*b*) Photomicrograph of garnet porphyroblasts in mica schist. The larger dark grains are biotite, and the finer grains in the groundmass are quartz, plagioclase, muscovite, and chlorite. Plane light. Back to text

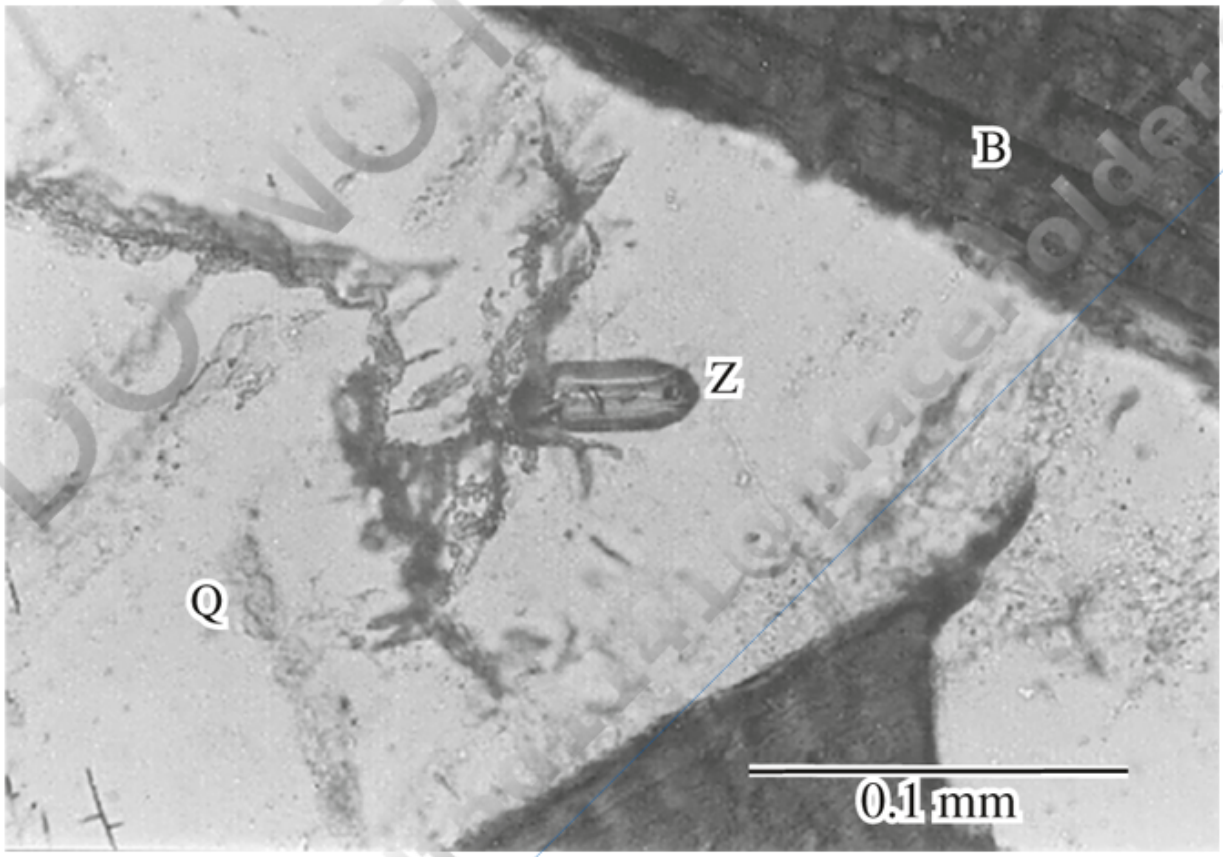

FIGURE 16.6 Photomicrograph of a thin section of granite showing a small zircon crystal (Z) in quartz (Q). The dark mineral is biotite (B). Plane light. Back to text

Printed by: e48d507df5d1141@placeholder.94092.edu. Printing is for personal, private use only. No part of this book may be reproduced or transmitted without publisher's prior permission. Violators will be prosecuted.

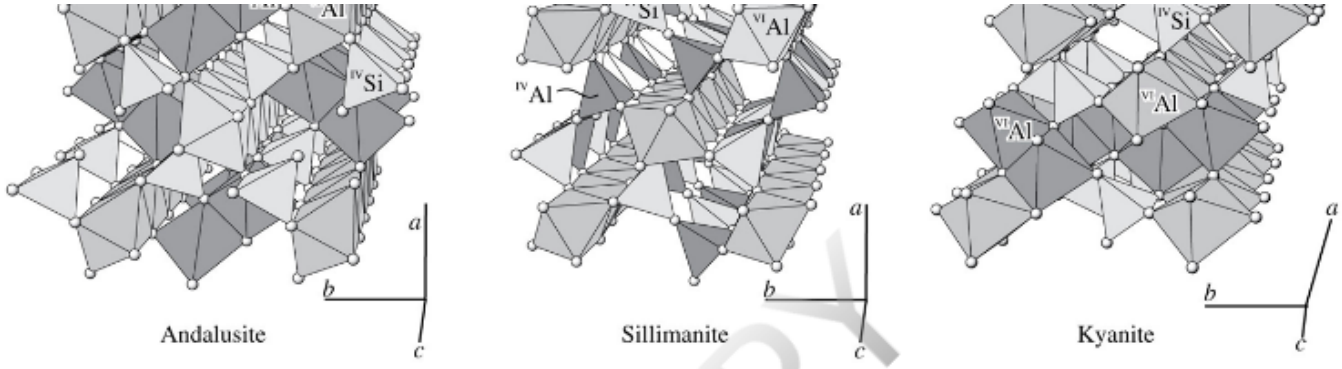

FIGURE 16.7 Structure of the aluminum silicates. (*a*) Andalusite. Edge-sharing chains of $^{VI}Al^{3+}$ octahedra (medium shading) extend parallel to *c* and are bonded laterally through pairs of $^{V}Al^{3+}$ in irregular 5-fold coordination (dark), and single $^{IV}Si^{4+}$ tetrahedra (light). (*b*) Sillimanite. Edge-sharing chains of $^{VI}Al^{3+}$ octahedra (medium shading) extend parallel to *c* and are bonded laterally through alternating $^{IV}Al^{3+}$ (dark) and $^{IV}Si^{4+}$ (light) tetrahedra. (*c*) Kyanite. Straight chains of $^{VI}Al^{3+}$ octahedra (medium shading) extend parallel to *c* and are bonded laterally through zigzag chains of $^{VI}Al^{3+}$ octahedra (dark) and $^{IV}Si^{4+}$ (light) in tetrahedral coordination. Back to text

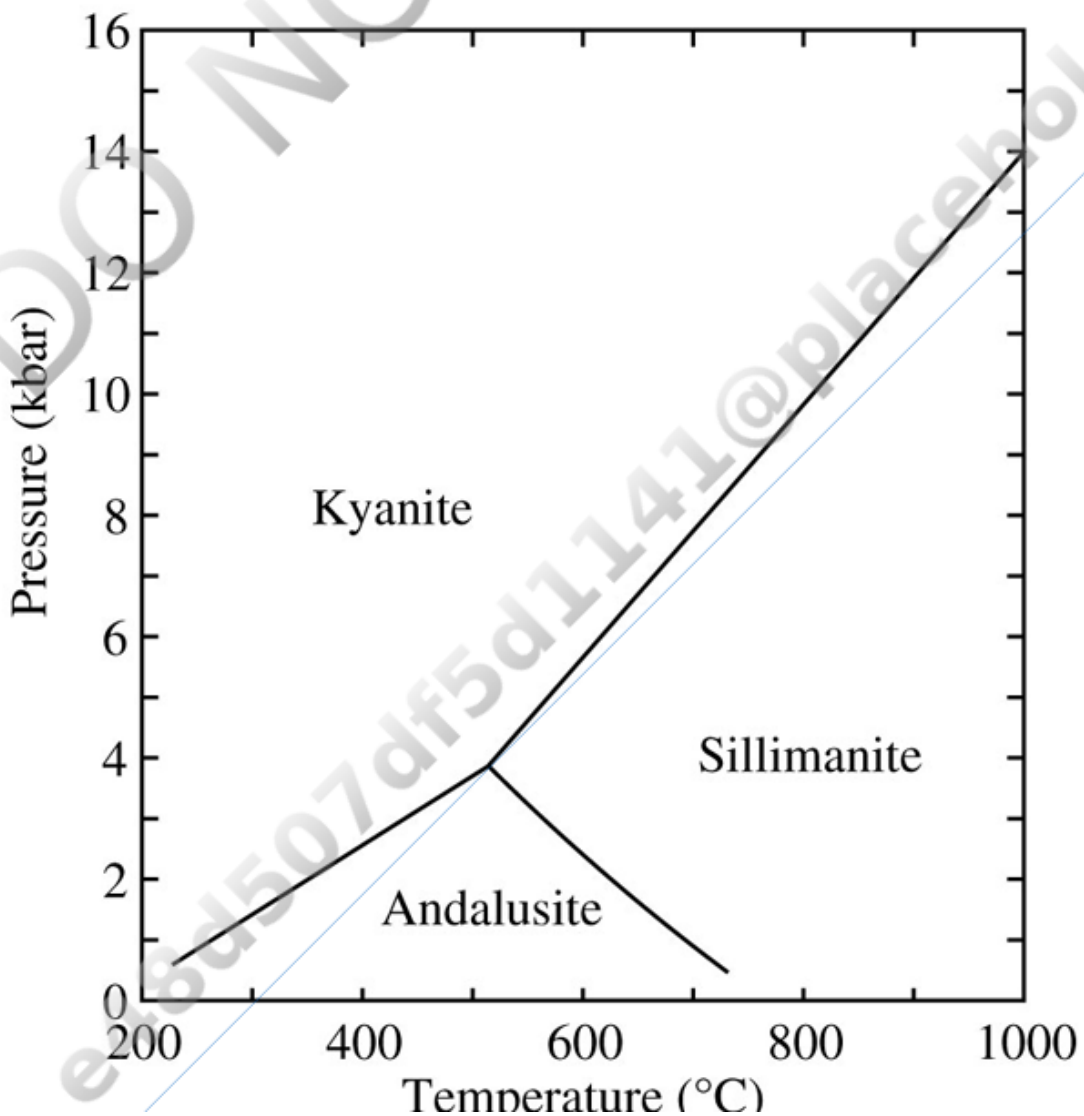

DO NOT COPY
e48d507df5d1141@placeholder.9409

Printed by: e48d507df5d1141@placeholder.94092.edu. Printing is for personal, private use only. No part of this book may be reproduced or transmitted without publisher's prior permission. Violators will be prosecuted.

Temperature (°C)

FIGURE 16.8 Aluminum silicate stability fields. From Hemingway and others (1991). Back to text

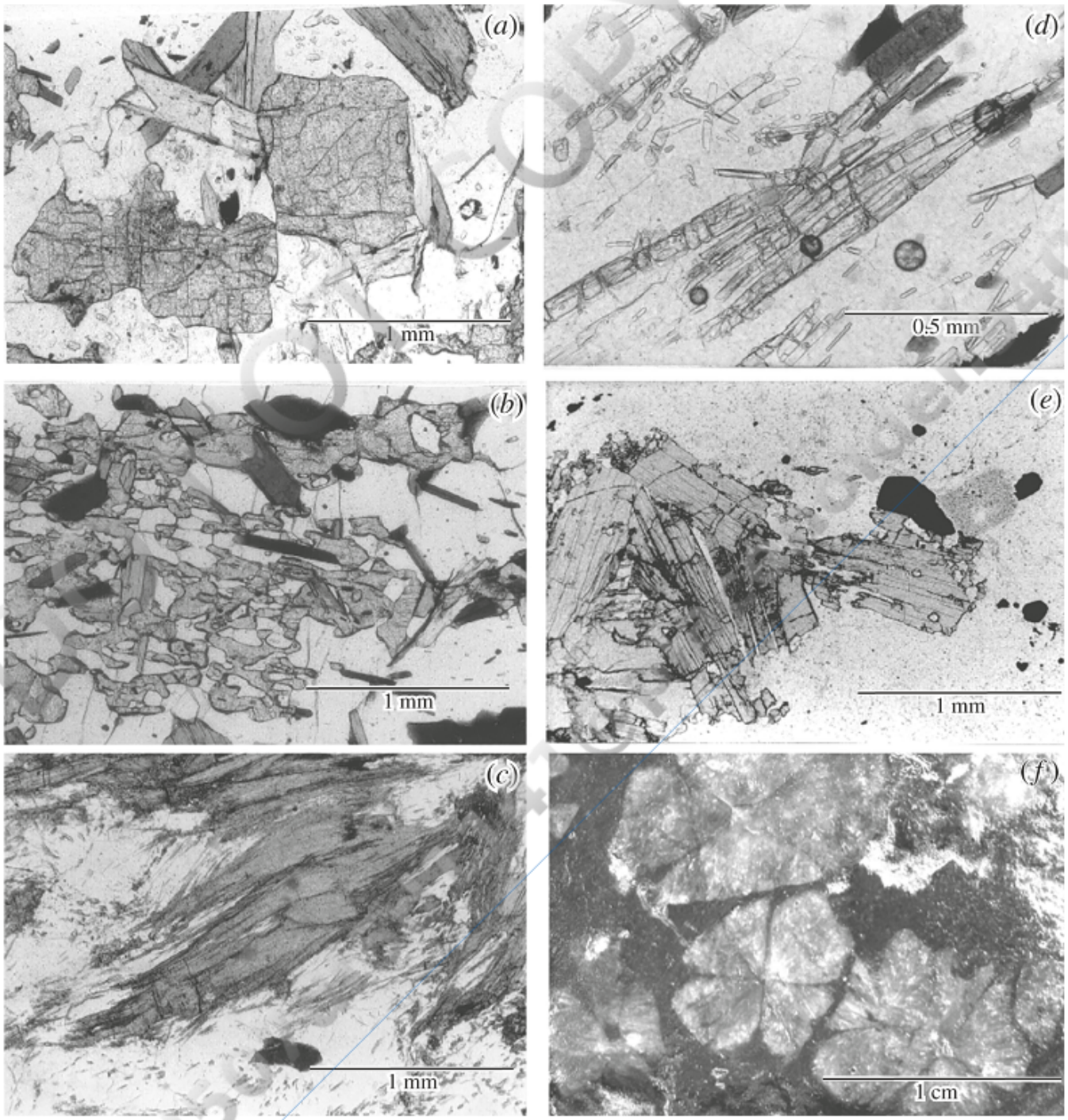

FIGURE 16.9 Aluminum silicates in mica schist. (*a*) Blocky andalusite crystal in thin section. (*b*) Strongly sieved (inclusion-rich) andalusite porphyroblast (high relief) in thin section. (*c*) Fibrolitic sillimanite mass in thin section. (*d*) Elongate prismatic crystals of sillimanite in thin section. (*e*) Bladed kyanite in thin section. (*f*) Hand sample showing cross-shaped pattern of inclusions in basal sections of chiastolite. All thin sections plane light. Back to text

Printed by: e48d507df5d1141@placeholder.94092.edu. Printing is for personal, private use only. No part of this book may be reproduced or transmitted without publisher's prior permission. Violators will be prosecuted.

sections of chiastolite. All thin sections plane light. Back to text

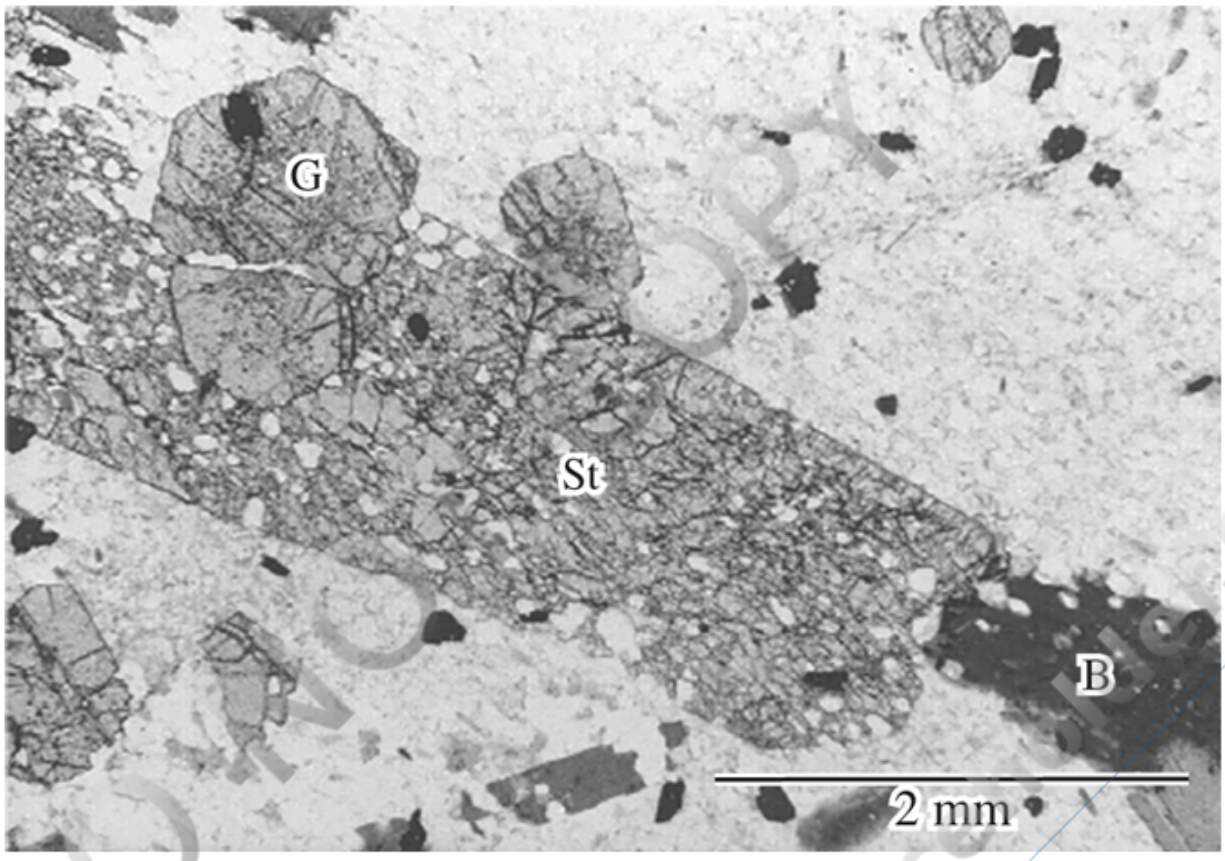

FIGURE 16.10 Sieved (inclusion filled) staurolite porphyroblast (St) with porphyroblasts of garnet (G) and biotite (B) in thin section of mica schist. Plane light. Back to text

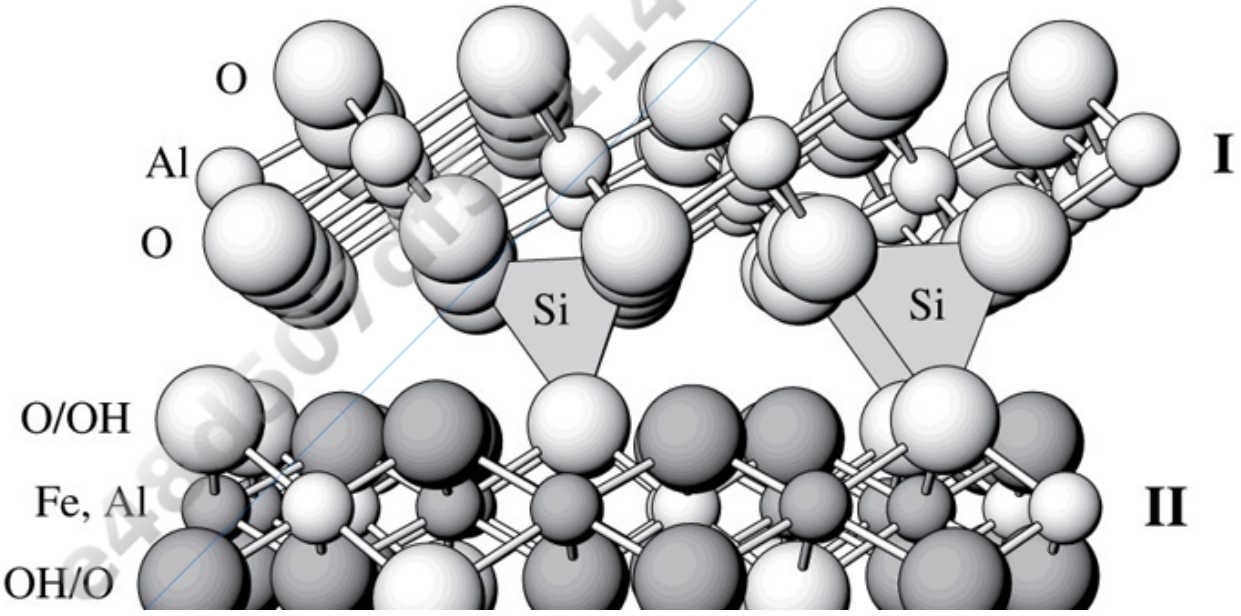

Printed by: e48d507df5d1141@placeholder.94092.edu. Printing is for personal, private use only. No part of this book may be reproduced or transmitted without publisher's prior permission. Violators will be prosecuted.

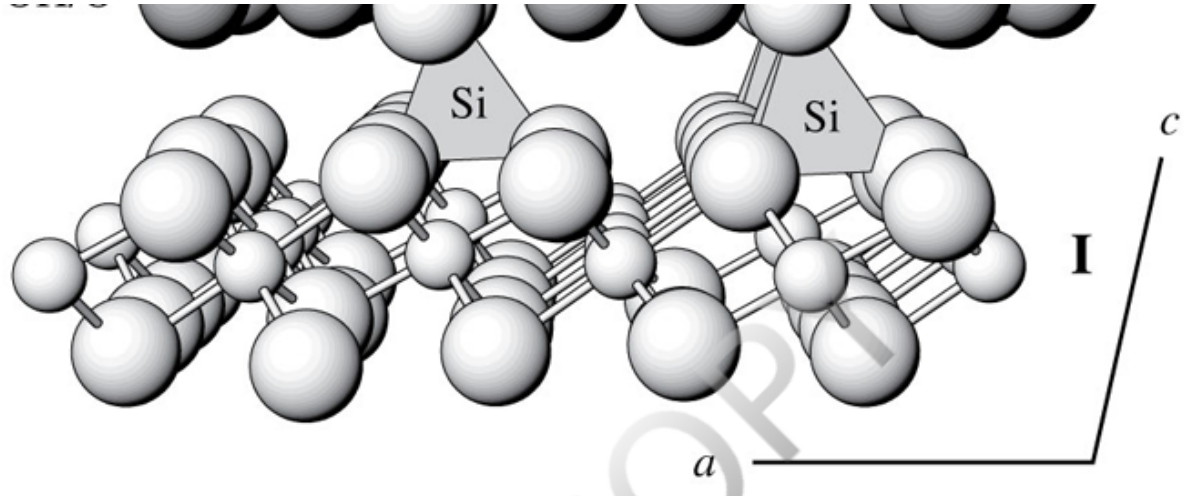

FIGURE 16.11 Chloritoid structure. Octahedral layer I contains Al^{3+} sandwiched between two sheets of O. Octahedral layer II contains Fe^{2+} (small dark spheres) and Al^{3+} sandwiched between sheets of O and OH (large dark spheres). Si^{4+} occupies isolated tetrahedral sites between alternating layers I and II. Back to text

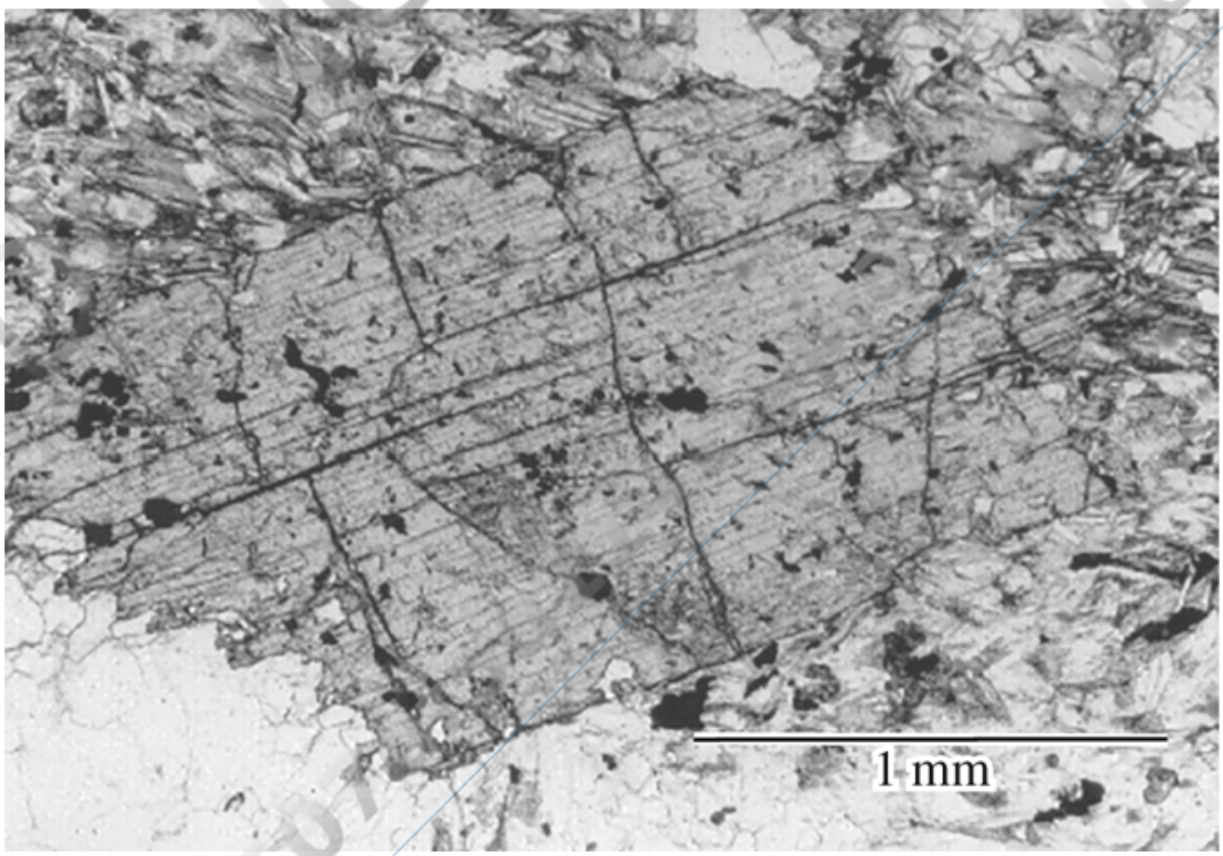

FIGURE 16.12 Photomicrograph of chloritoid in a thin section of schist. Plane light. Back to text

Printed by: e48d507df5d1141@placeholder.94092.edu. Printing is for personal, private use only. No part of this book may be reproduced or transmitted without publisher's prior permission. Violators will be prosecuted.

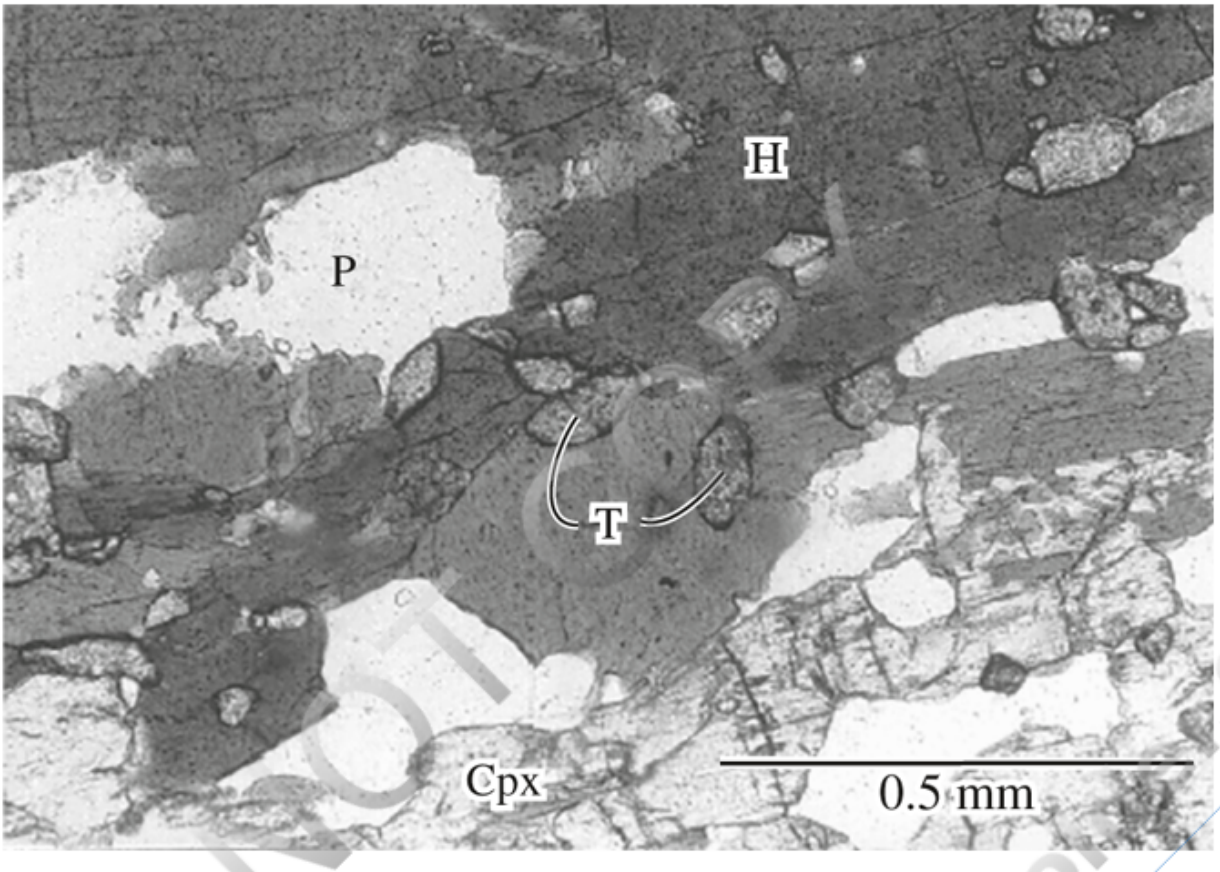

FIGURE 16.13 Photomicrograph of subhedral to anhedral titanite (T) grains with hornblende (H), plagioclase (P), and Ca-clinopyroxene (Cpx) in a thin section of an amphibolite. Plane light. Back to text

(*a*)

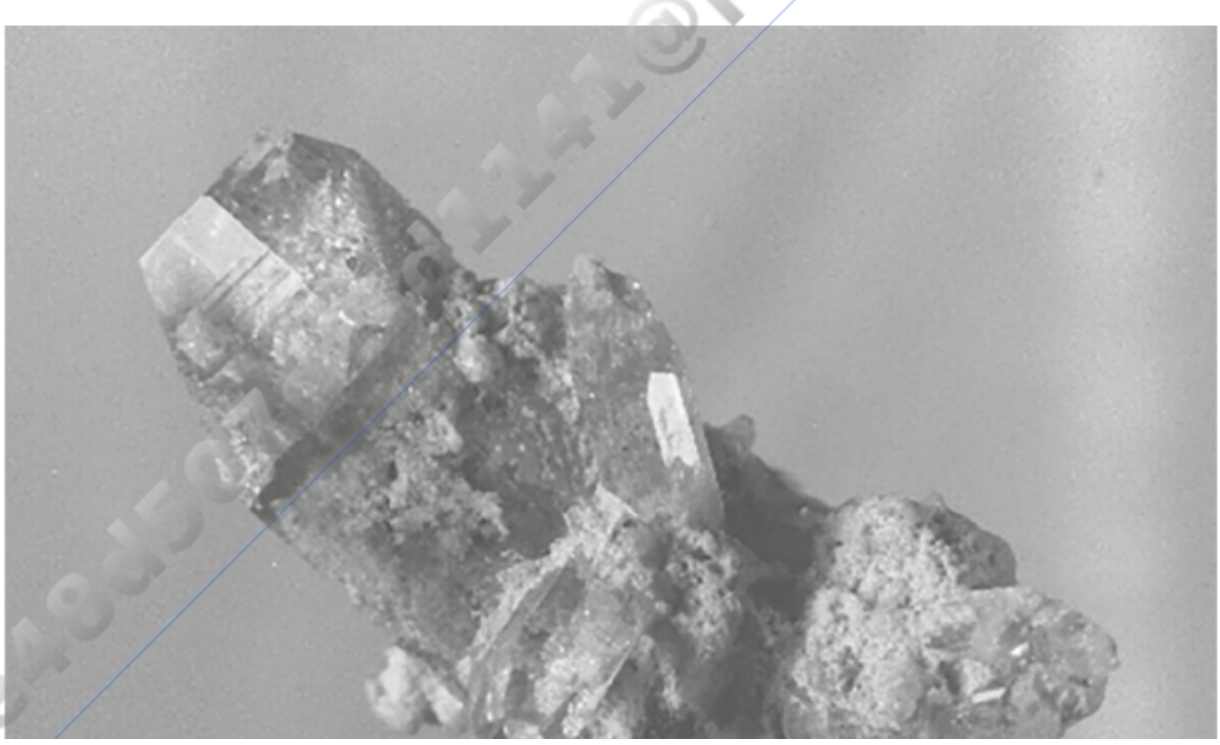

Printed by: e48d507df5d1141@placeholder.94092.edu. Printing is for personal, private use only. No part of this book may be reproduced or transmitted without publisher's prior permission. Violators will be prosecuted.

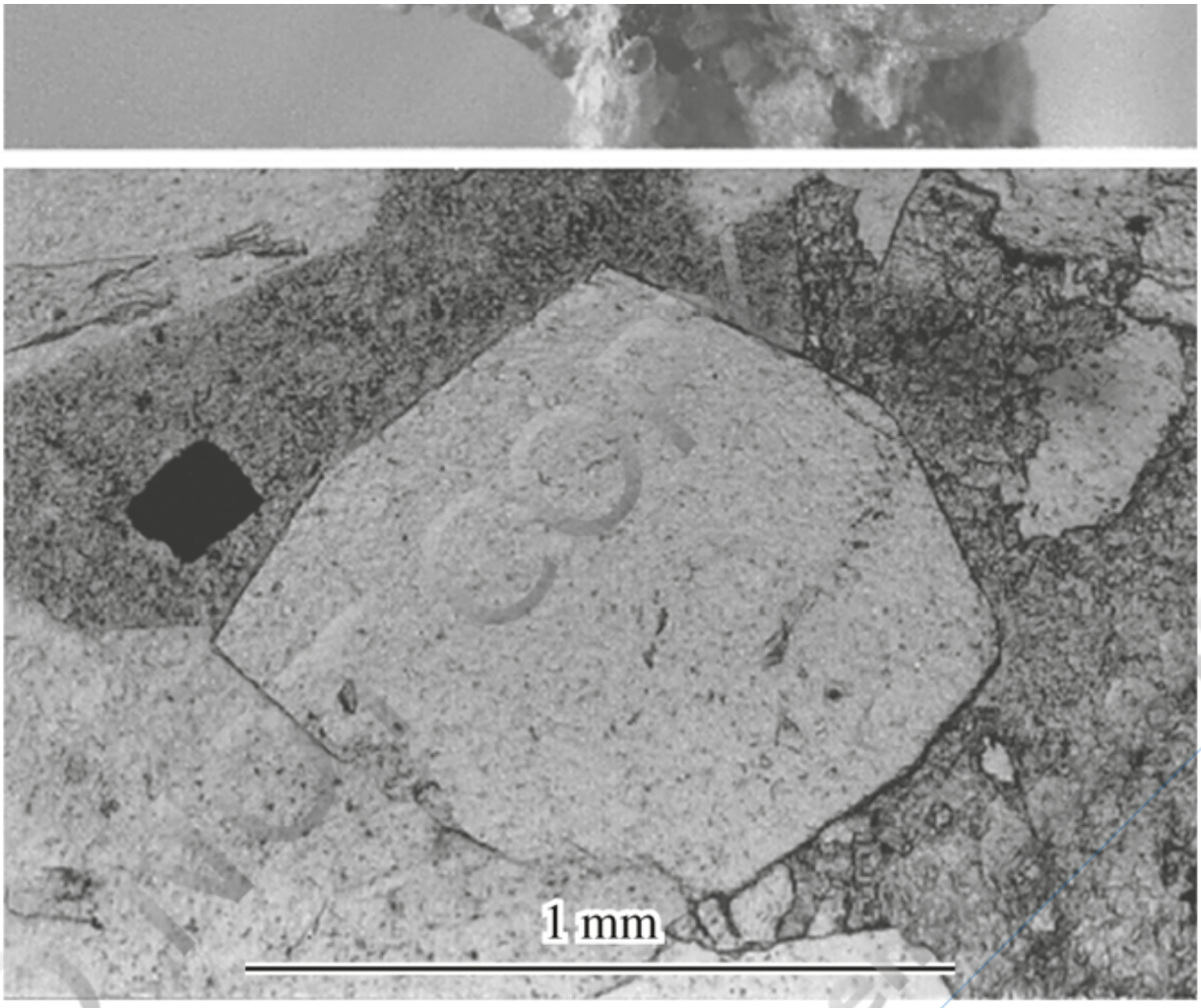

FIGURE 16.14 Topaz. (*a*) Topaz crystal. (*b*) Photomicrograph of basal section of topaz in thin section. Plane light. Back to text

e48d507df5d1141@placeholder.94092.edu

Printed by: e48d507df5d1141@placeholder.94092.edu. Printing is for personal, private use only. No part of this book may be reproduced or transmitted without publisher's prior permission. Violators will be prosecuted.

Chapter 17 Carbonates, Sulfates, Phosphates, Tungstates, Molybdates, and Borates

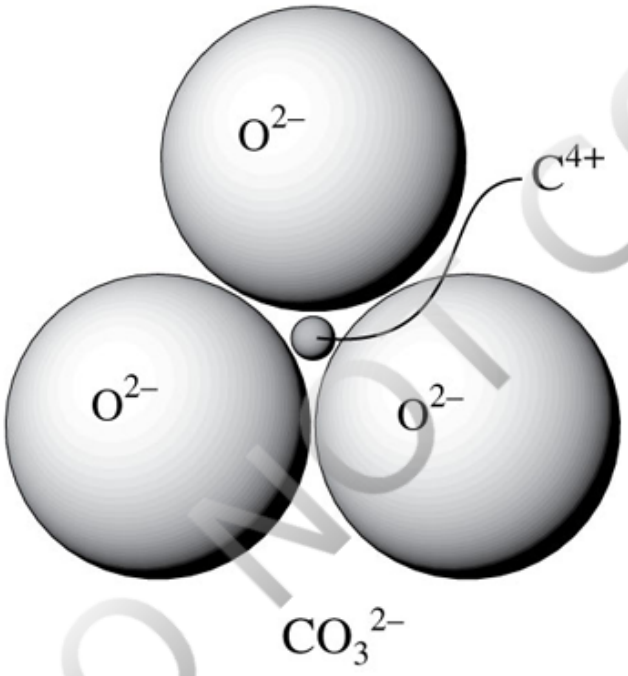

FIGURE 17.1 CO_3^{2-} anionic groups. A carbon cation is situated at the center of three oxygen anions. Back to text

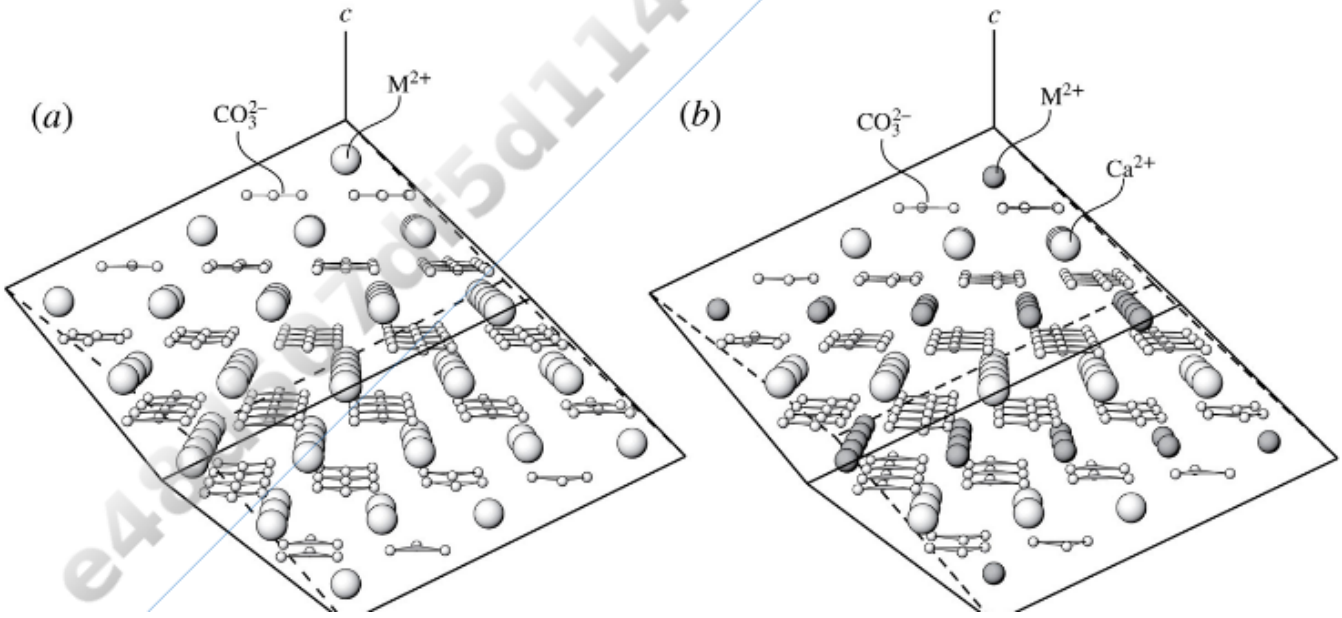

DO NOT COPY e48d507df5d1141@placeholder.9409

Printed by: e48d507df5d1141@placeholder.94092.edu. Printing is for personal, private use only. No part of this book may be reproduced or transmitted without publisher's prior permission. Violators will be prosecuted.

FIGURE 17.2 Structure of the rhombohedral carbonates. O^{2-} anions at the corners of triangular CO_3^{2-} groups are shown as small spheres. (*a*) In the calcite structure, CO_3 groups form sheets parallel to {001} separated by octahedrally coordinated cations (M^{2+} = Ca, Mg, Mn, Fe, or Zn). Note that the direction the CO_3 groups "point" alternates every other sheet. (*b*) In the dolomite structure, layers of larger Ca cations alternate with layers of smaller metal cations (M^{2+} = Mg, Fe, or Mn). Back to text

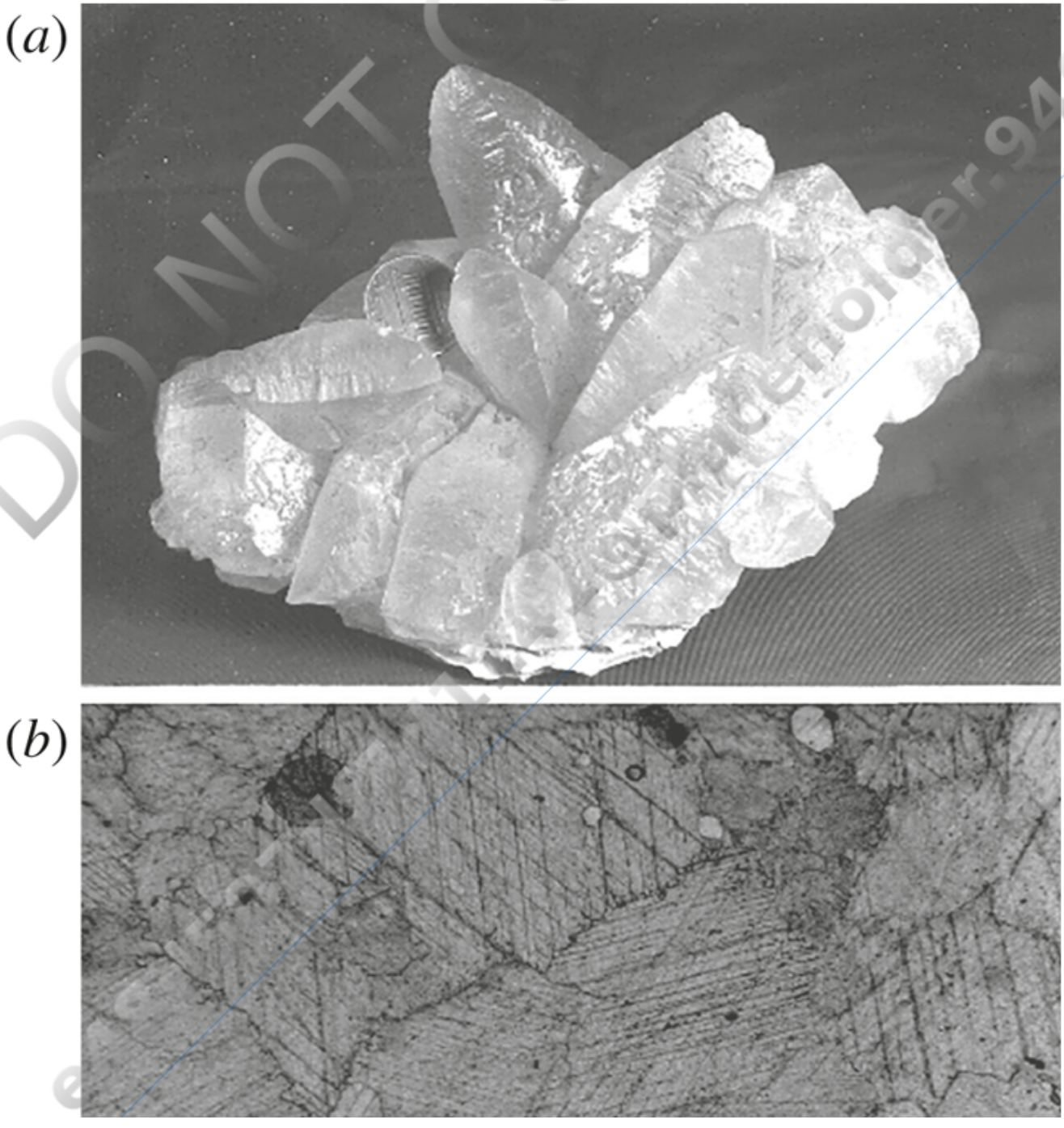

DO NOT COPY

Printed by: e48d507df5d1141@placeholder.94092.edu. Printing is for personal, private use only. No part of this book may be reproduced or transmitted without publisher's prior permission. Violators will be prosecuted.

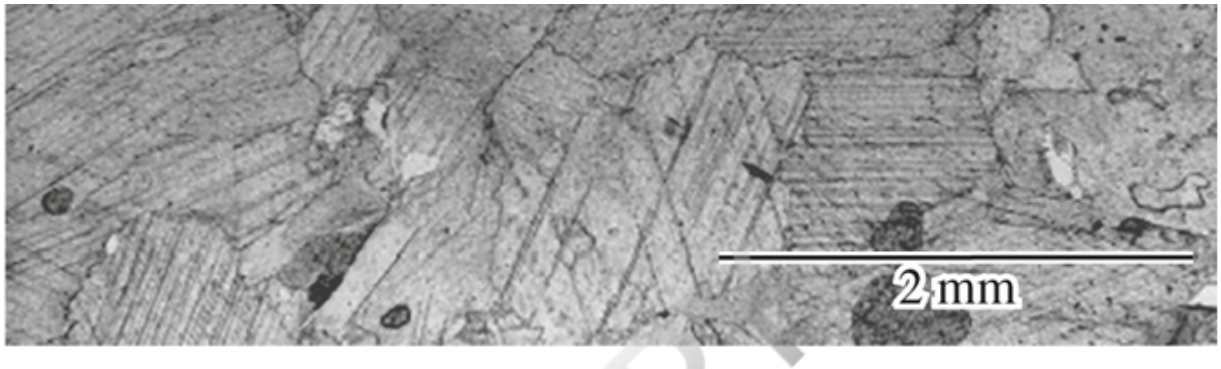

FIGURE 17.3 Calcite. (*a*) Calcite crystals. Field of view is about 20 cm wide. (*b*) Photomicrograph of calcite in marble. Plane light. Back to text

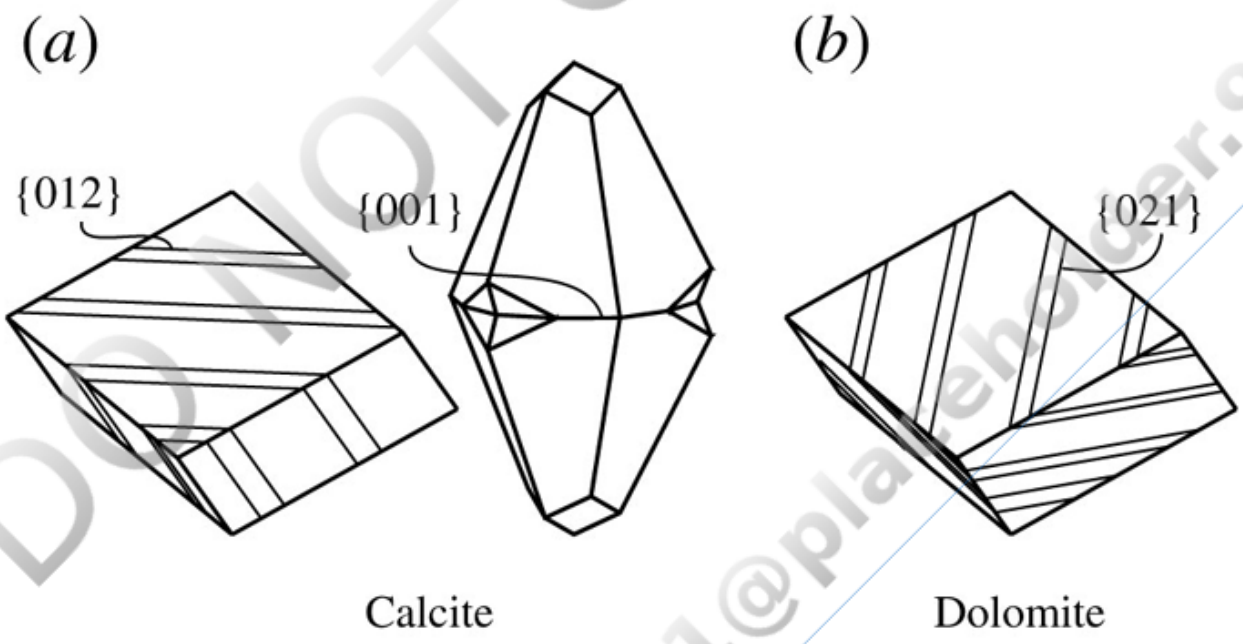

FIGURE 17.4 Twins in rhombohedral carbonates. (*a*) Lamellar {012} twins may be parallel to rhomb face edges or parallel to the long diagonal. Simple {001} twins may form distinctive crystals. (*b*) Dolomite. Lamellar {021} twins may be parallel to either the short or the long diagonal between rhombohedral cleavage traces. Back to text

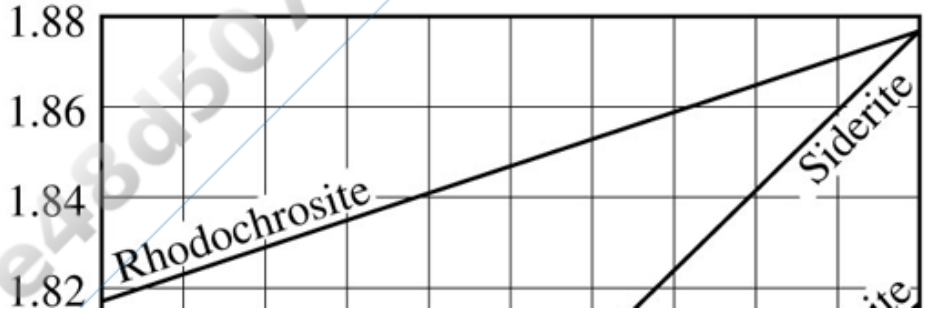

Printed by: e48d507df5d1141@placeholder.94092.edu. Printing is for personal, private use only. No part of this book may be reproduced or transmitted without publisher's prior permission. Violators will be prosecuted.

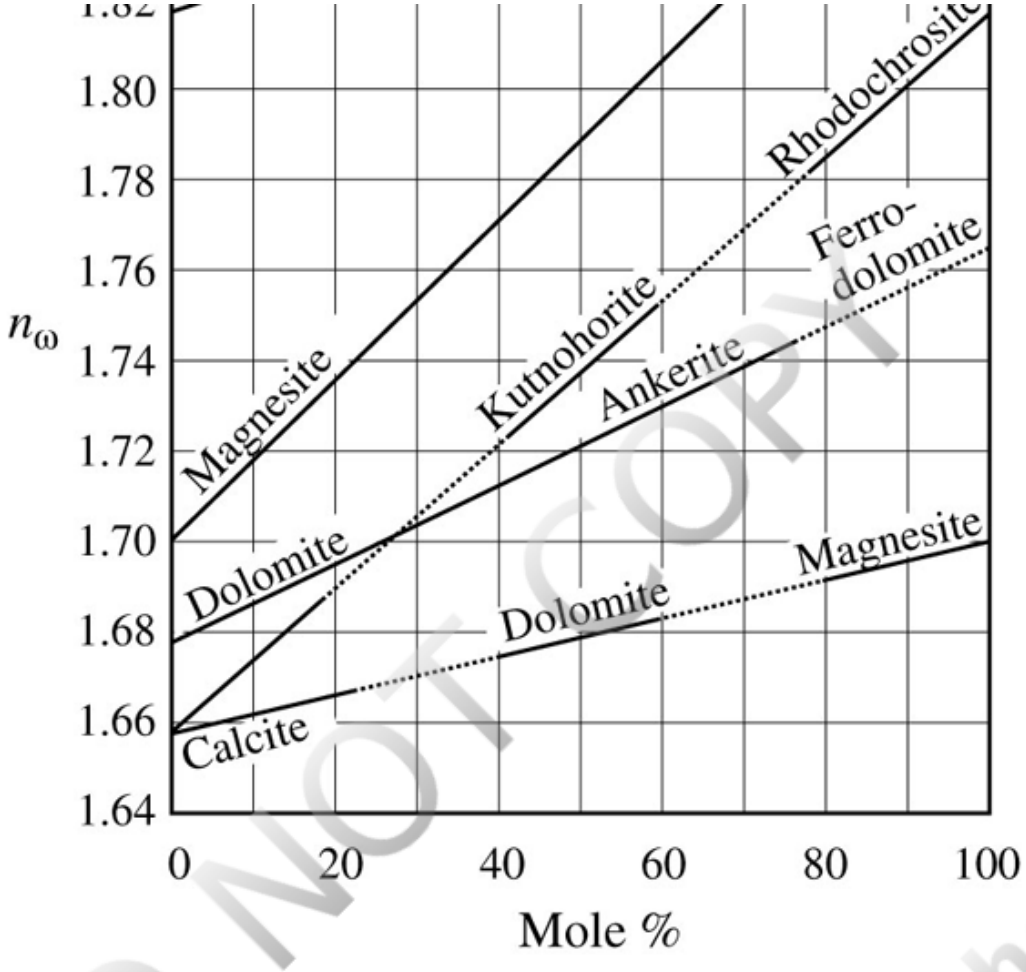

FIGURE 17.5 Index of refraction n_ω in the rhombohedral carbonates. After Kennedy (1947).
Back to text

FIGURE 17.11 A view of Desert Peak across Bonneville Salt Flats, a playa in western Utah.
Back to text

DO NOT COPY e48d507df5d1141@placeholder.9409

Printed by: e48d507df5d1141@placeholder.94092.edu. Printing is for personal, private use only. No part of this book may be reproduced or transmitted without publisher's prior permission. Violators will be prosecuted.

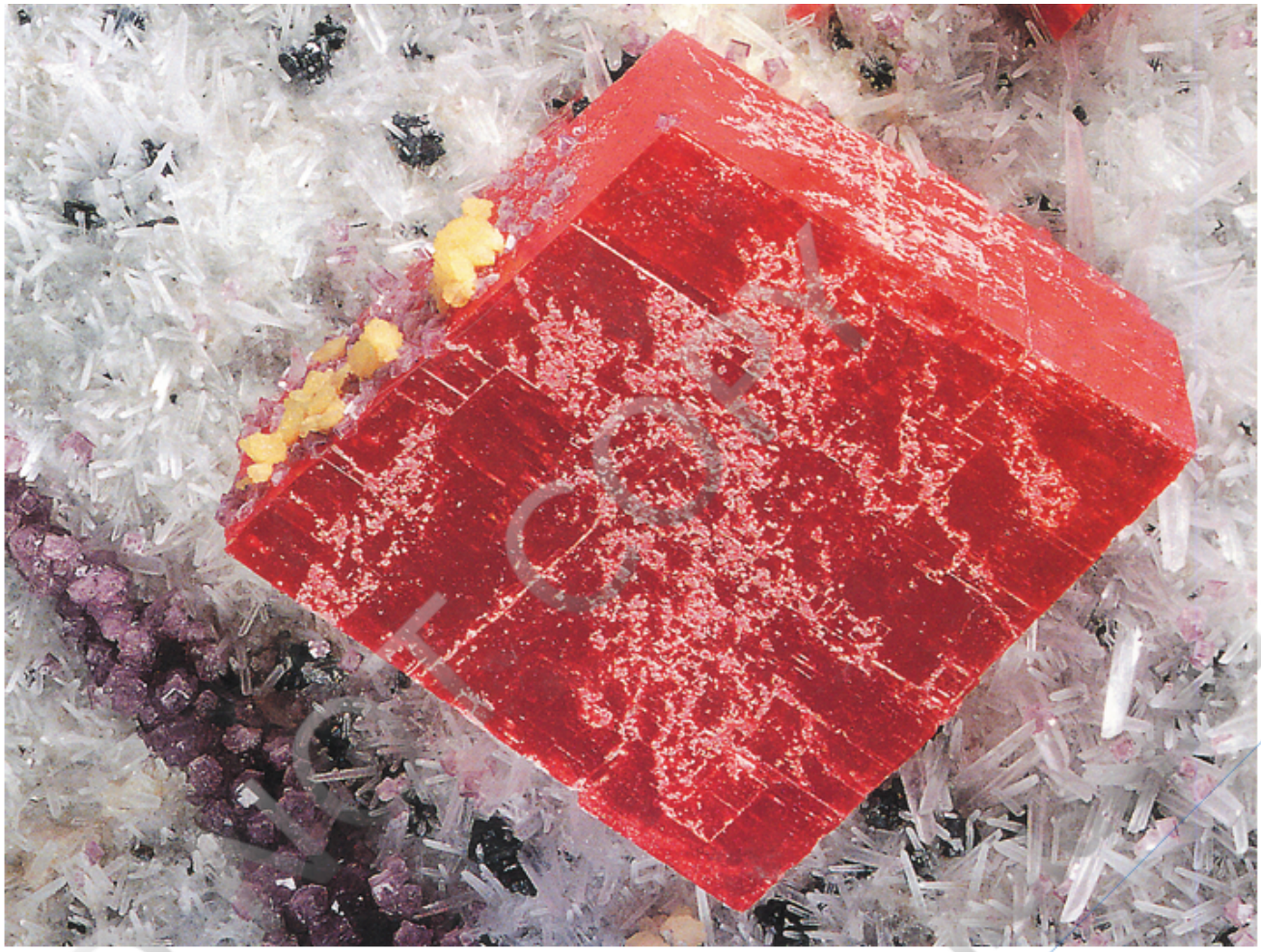

FIGURE 17.6 The Alma King, at 16.5 cm across, is perhaps the largest rhodochrosite crystal in a collection. It is from the Sweethome Mine, Park County, Colorado. The acicular white crystals are quartz, the dark grains are sphalerite, and the equant crystals (lower left) are fluorite. © Denver Museum of Nature and Science. Back to text

(a)

Printed by: e48d507df5d1141@placeholder.94092.edu. Printing is for personal, private use only. No part of this book may be reproduced or transmitted without publisher's prior permission. Violators will be prosecuted.

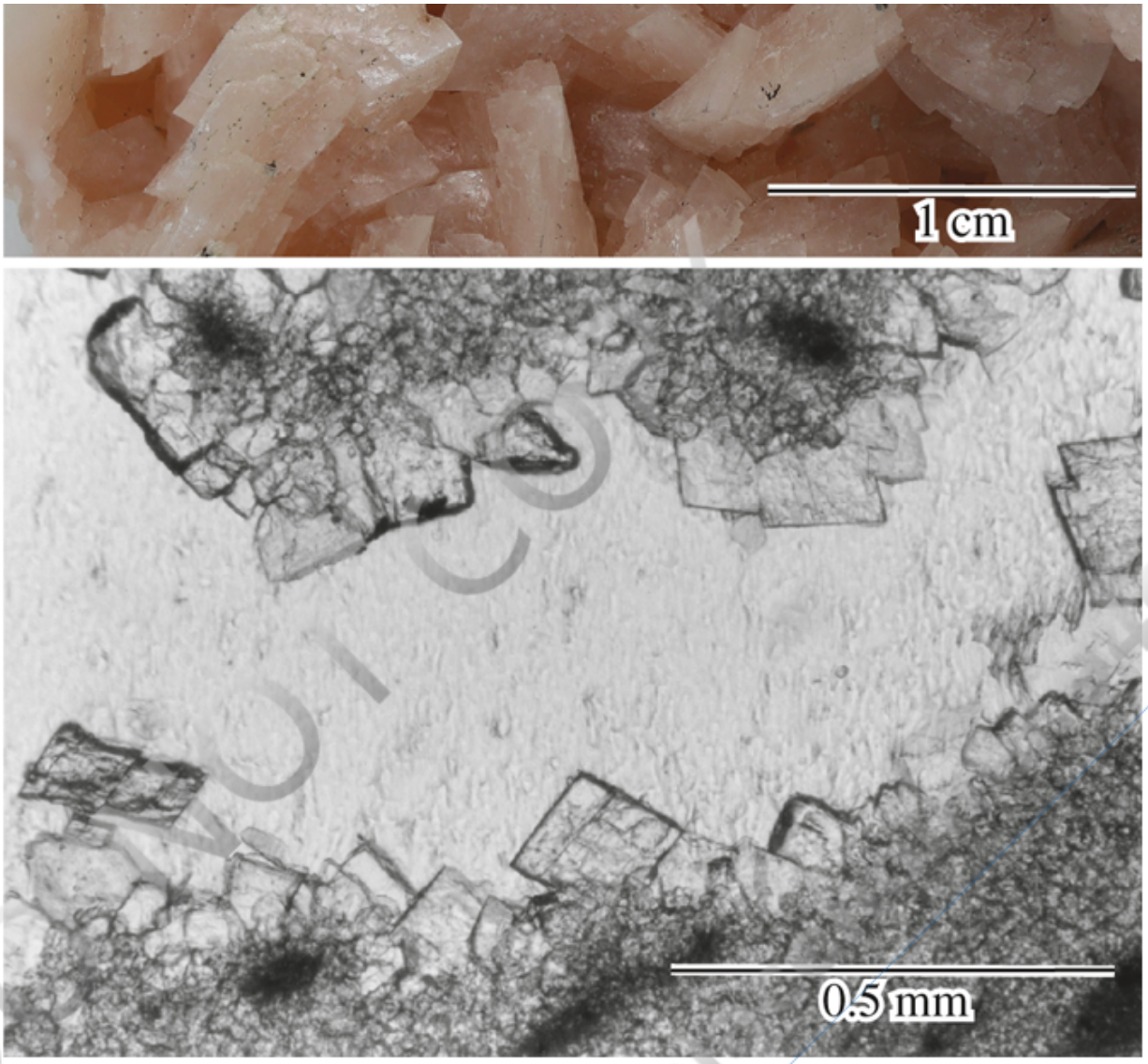

FIGURE 17.7 Dolomite. (*a*) Dolomite crystals. Note the curved crystal faces (arrows). (*b*) Photomicrograph showing dolomite rhombs lining a void in a thin section of limestone. Back to text

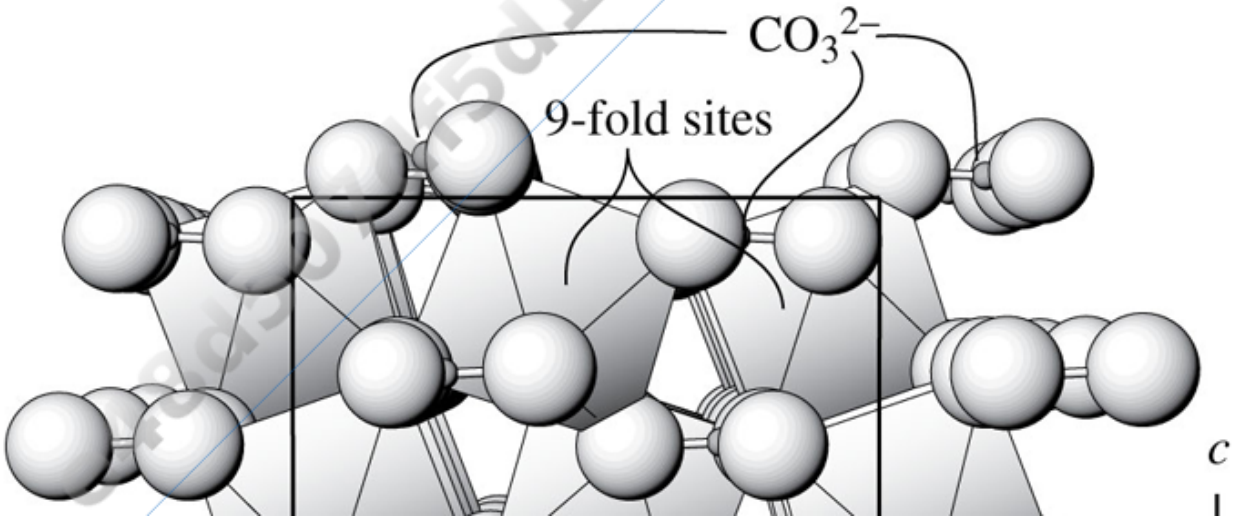

Printed by: e48d507df5d1141@placeholder.94092.edu. Printing is for personal, private use only. No part of this book may be reproduced or transmitted without publisher's prior permission. Violators will be prosecuted.

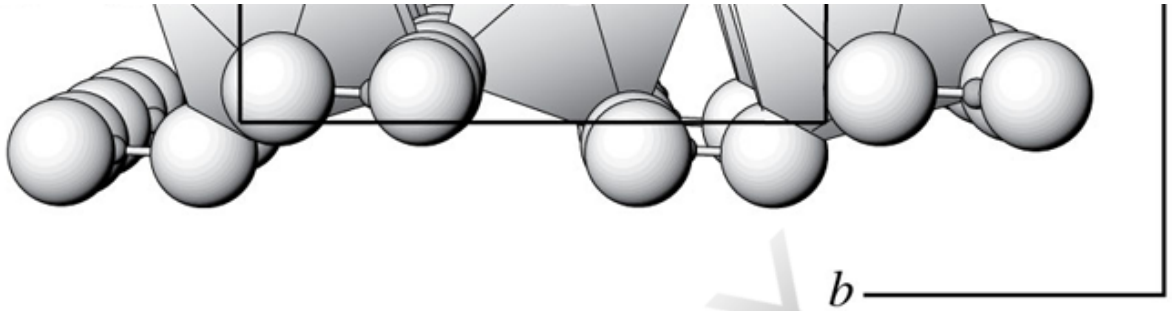

FIGURE 17.8 Aragonite structure. Triangular CO_3^{2-} groups are arranged in rows parallel to *a* (into the page). Oxygen anions are shown as larger spheres and carbon cations as small spheres. Large cations such as Ca^{2+}, Ba^{2+}, Sr^{2+}, or Pb^{2+} occupy 9-fold coordination sites between the CO_3^{2-} groups. A unit cell is outlined. Back to text

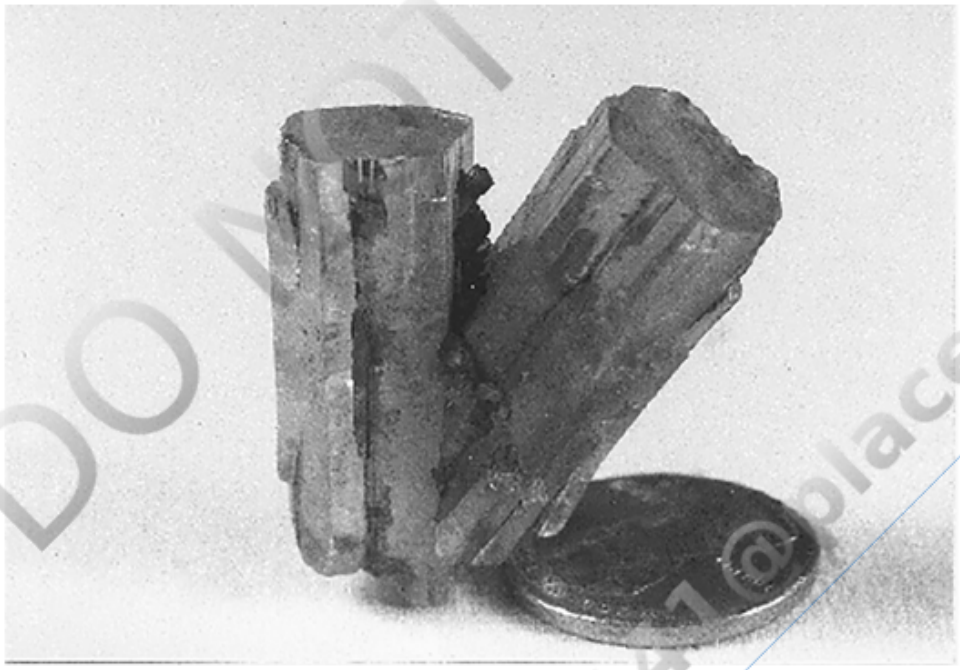

FIGURE 17.9 Aragonite crystals. Back to text

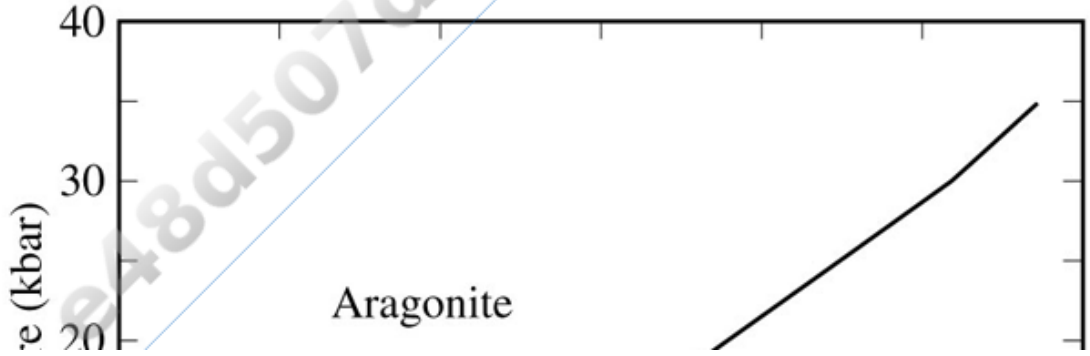

DO NOT COPY e48d507df5d1141@placeholder.9409

Printed by: e48d507df5d1141@placeholder.94092.edu. Printing is for personal, private use only. No part of this book may be reproduced or transmitted without publisher's prior permission. Violators will be prosecuted.

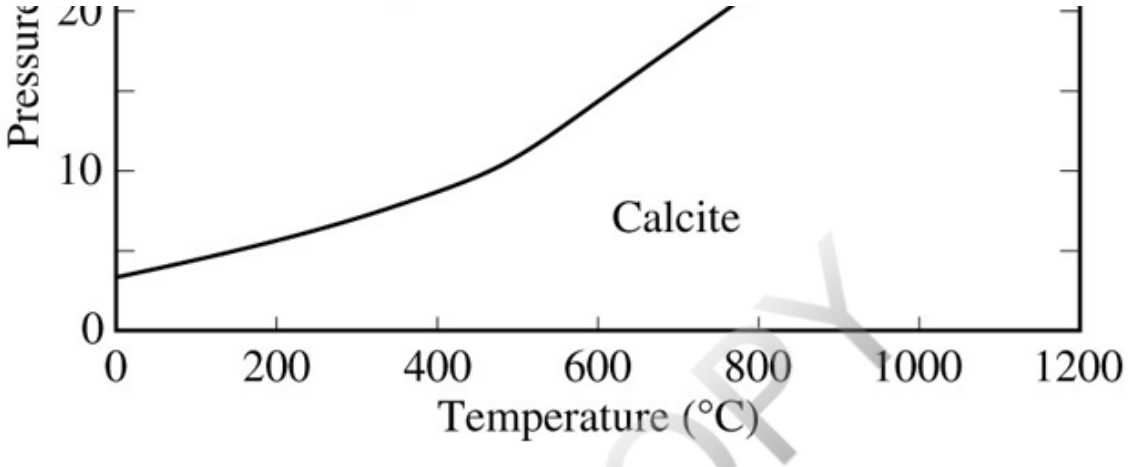

FIGURE 17.10 Temperature–pressure stability fields of calcite and aragonite. After Carlson (1980). Back to text

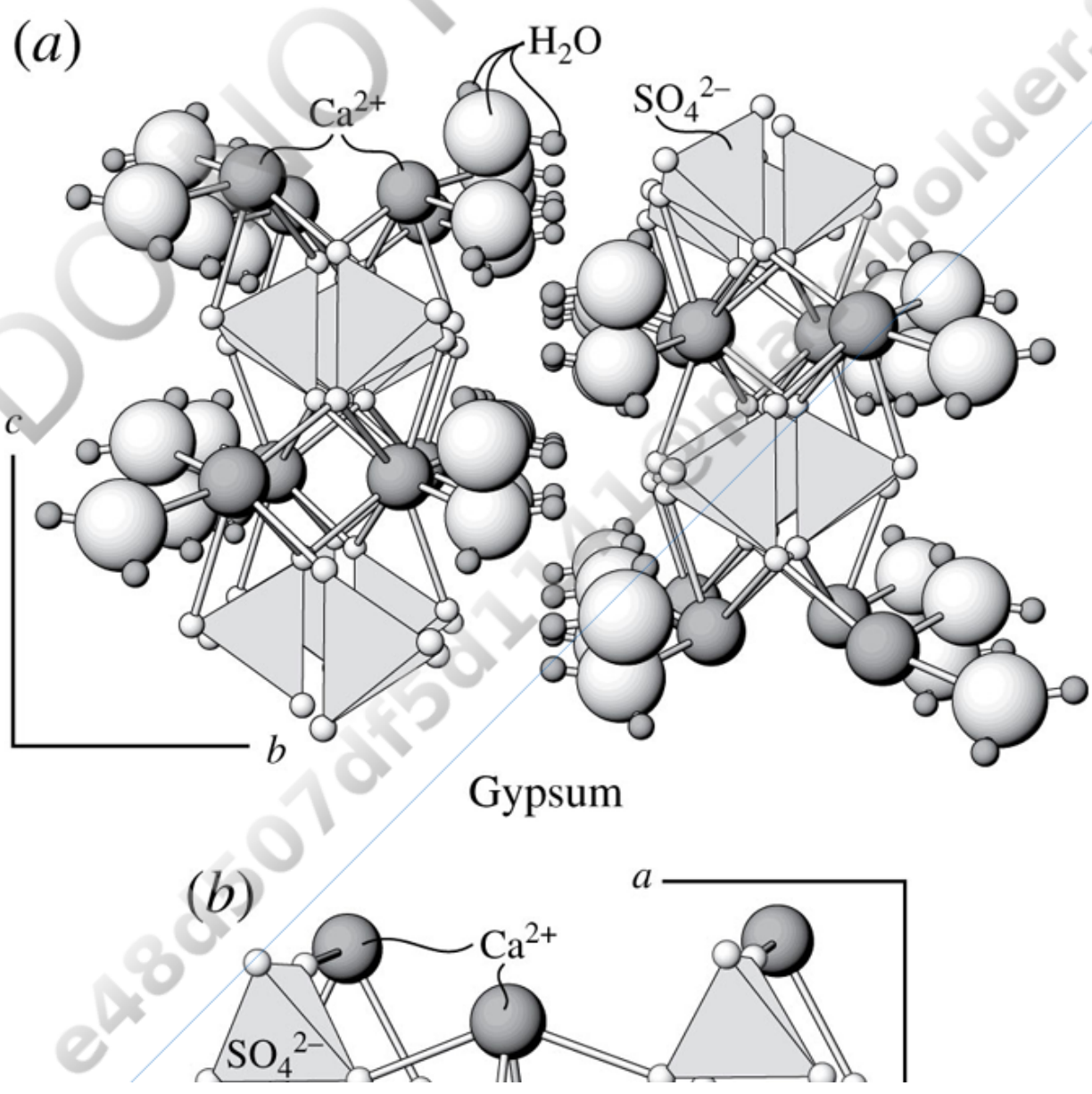

DO NOT COPY

Printed by: e48d507df5d1141@placeholder.94092.edu. Printing is for personal, private use only. No part of this book may be reproduced or transmitted without publisher's prior permission. Violators will be prosecuted.

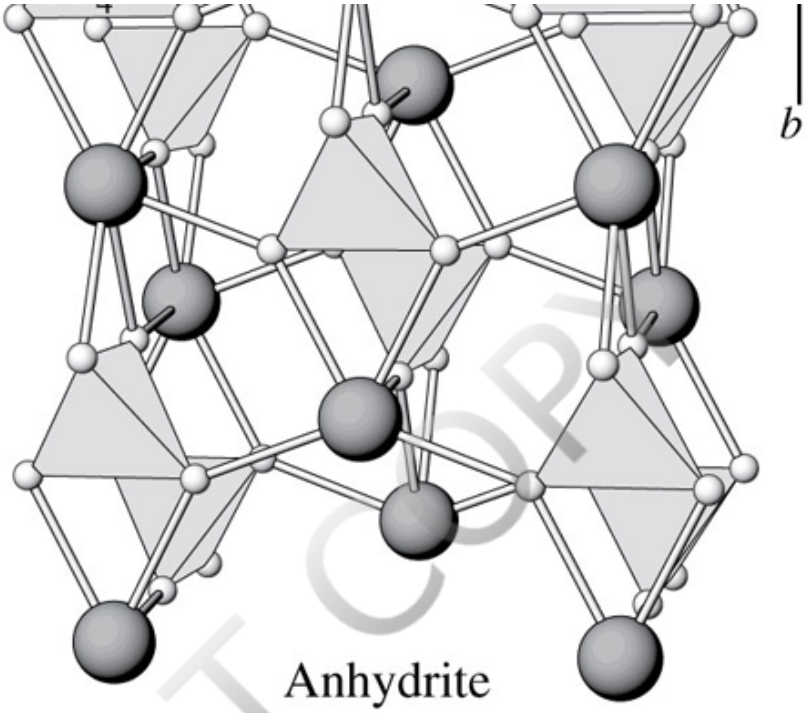

Anhydrite

(c)

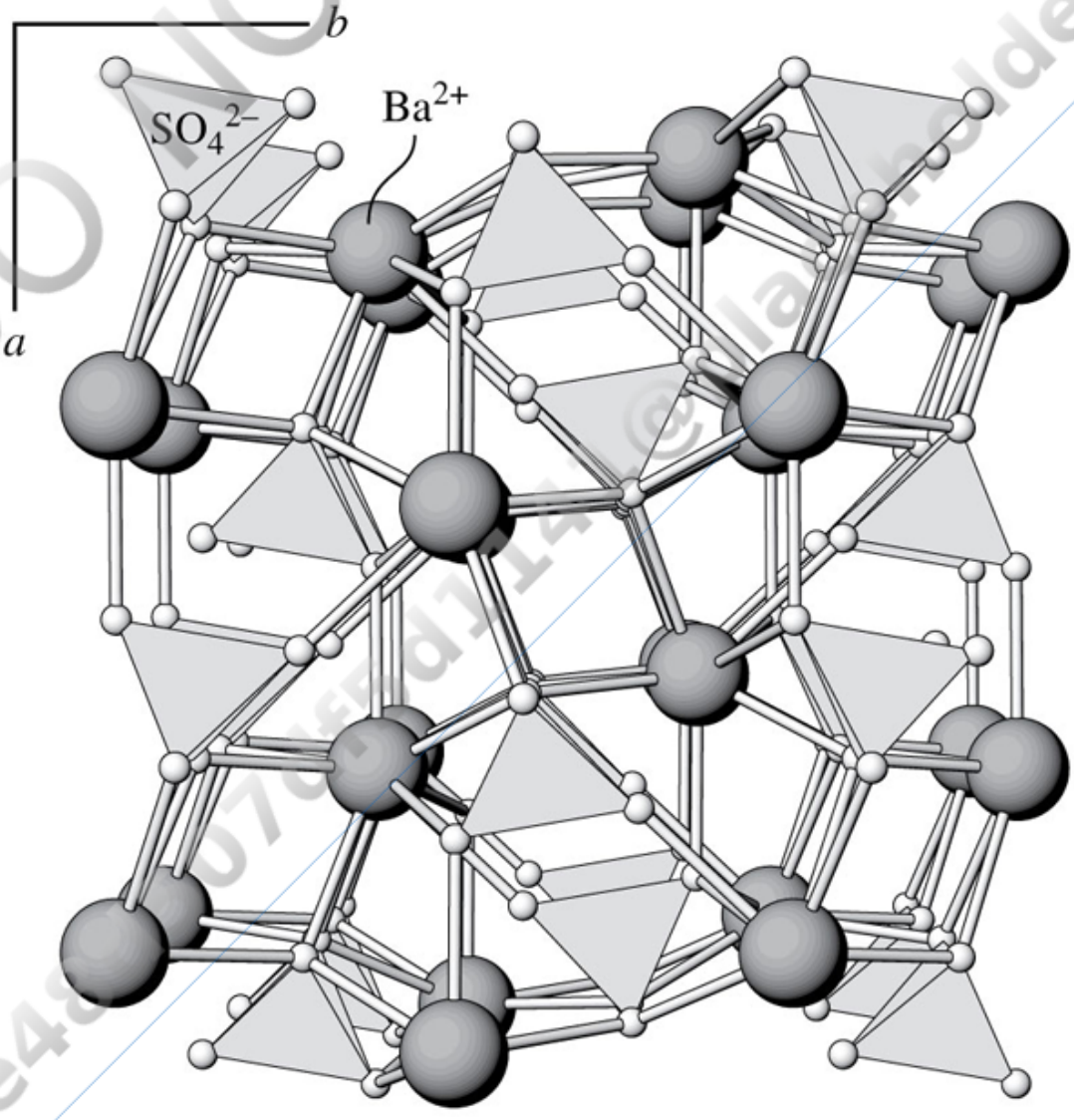

DO NOT COPY

Printed by: e48d507df5d1141@placeholder.94092.edu. Printing is for personal, private use only. No part of this book may be reproduced or transmitted without publisher's prior permission. Violators will be prosecuted.

Barite

FIGURE 17.12 Structure of sulfate minerals. SO_4^{2-} groups are shown with oxygen anions as light-colored small spheres. (*a*) Gypsum viewed down the *a* axis. Cleavage on {010} splits along the layers of water molecules on the sides of the $CaSO_4$ layers. Hydrogen is shown as small dark spheres. (*b*) Anhydrite viewed down the *c* axis. (*c*) Barite viewed down the *c* axis. Back to text

(*a*)

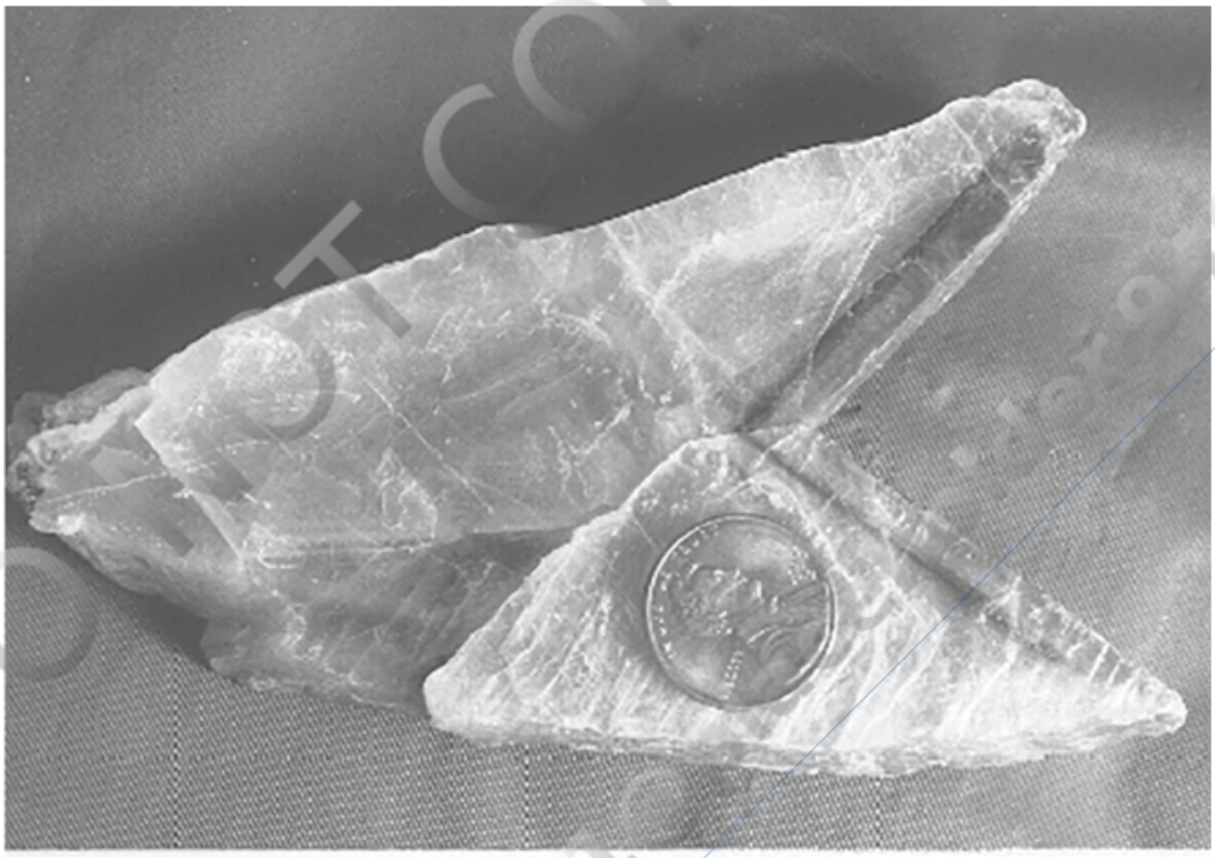

(*b*)

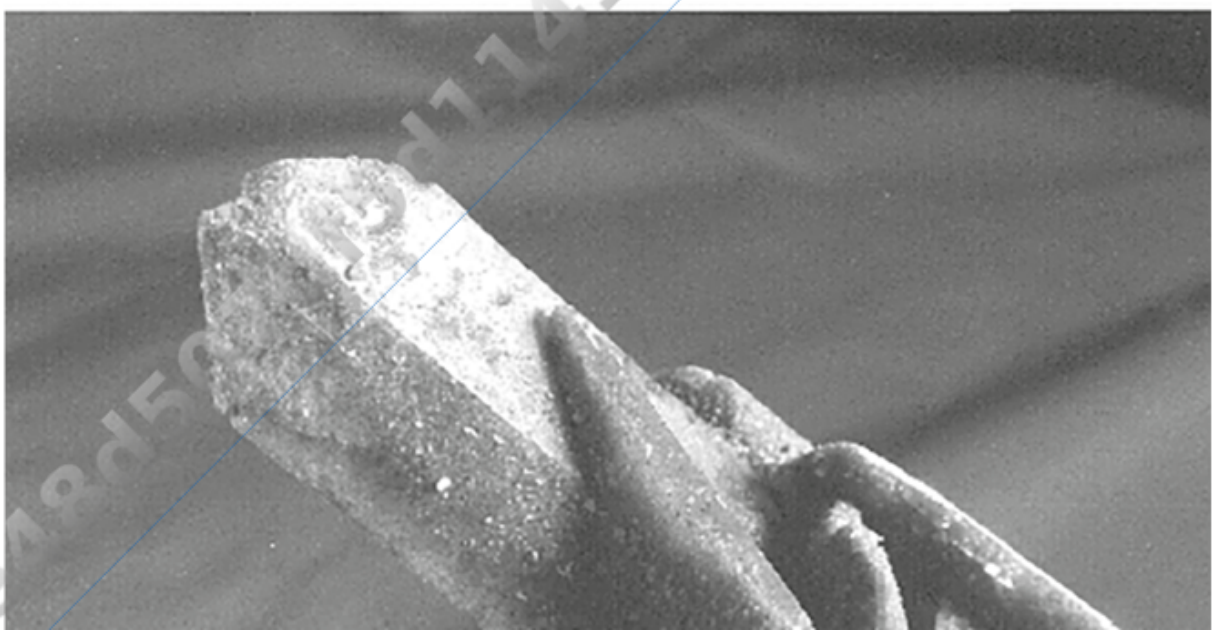

DO NOT COPY

Printed by: e48d507df5d1141@placeholder.94092.edu. Printing is for personal, private use only. No part of this book may be reproduced or transmitted without publisher's prior permission. Violators will be prosecuted.

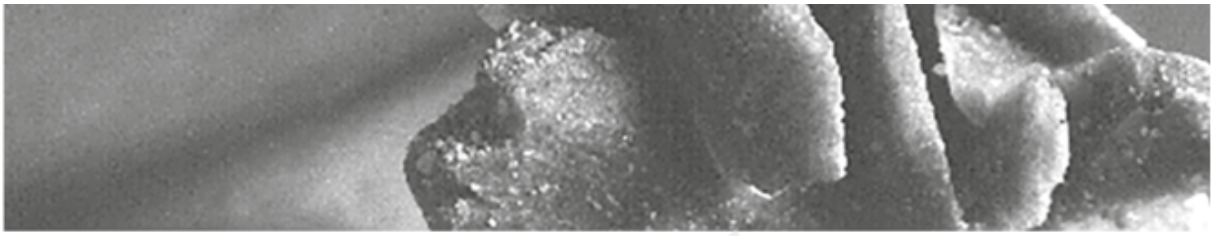

FIGURE 17.13 Gypsum. (*a*) Selenite with a swallowtail twin. U.S. penny is about 2 cm in diameter. (*b*) Bladed crystals. Field of view is about 10 cm across. Back to text

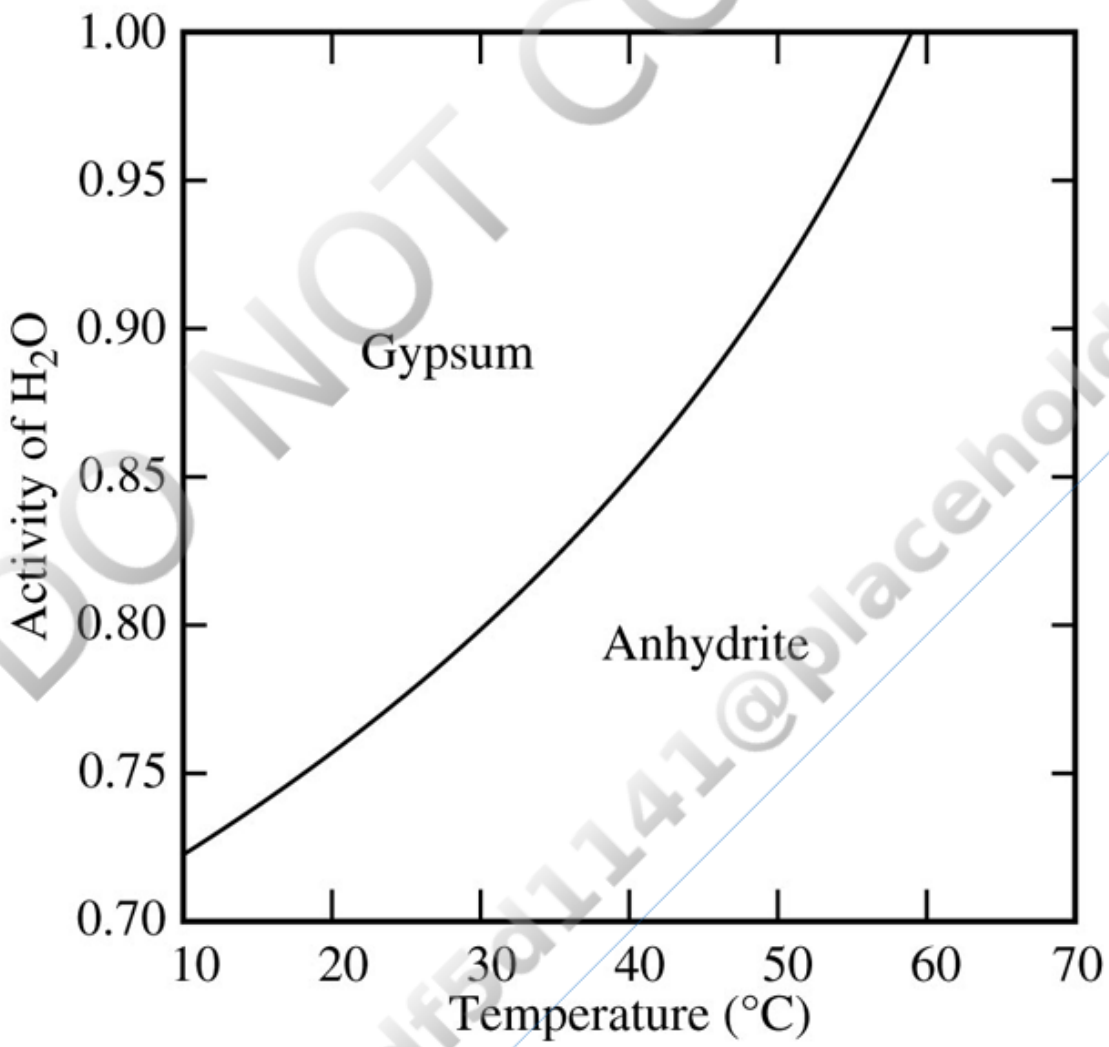

FIGURE 17.14 Stability of gypsum and anhydrite at 1 atm. Decreasing activity of water is produced by increasing salinity. © Hardie, L. A. (1967). The gypsum-anhydrite equilibrium at one atmosphere pressure, American Mineralogist, Volume 52. Back to text

DO NOT COPY
e48d507df5d1141@placeholder.9409

Printed by: e48d507df5d1141@placeholder.94092.edu. Printing is for personal, private use only. No part of this book may be reproduced or transmitted without publisher's prior permission. Violators will be prosecuted.

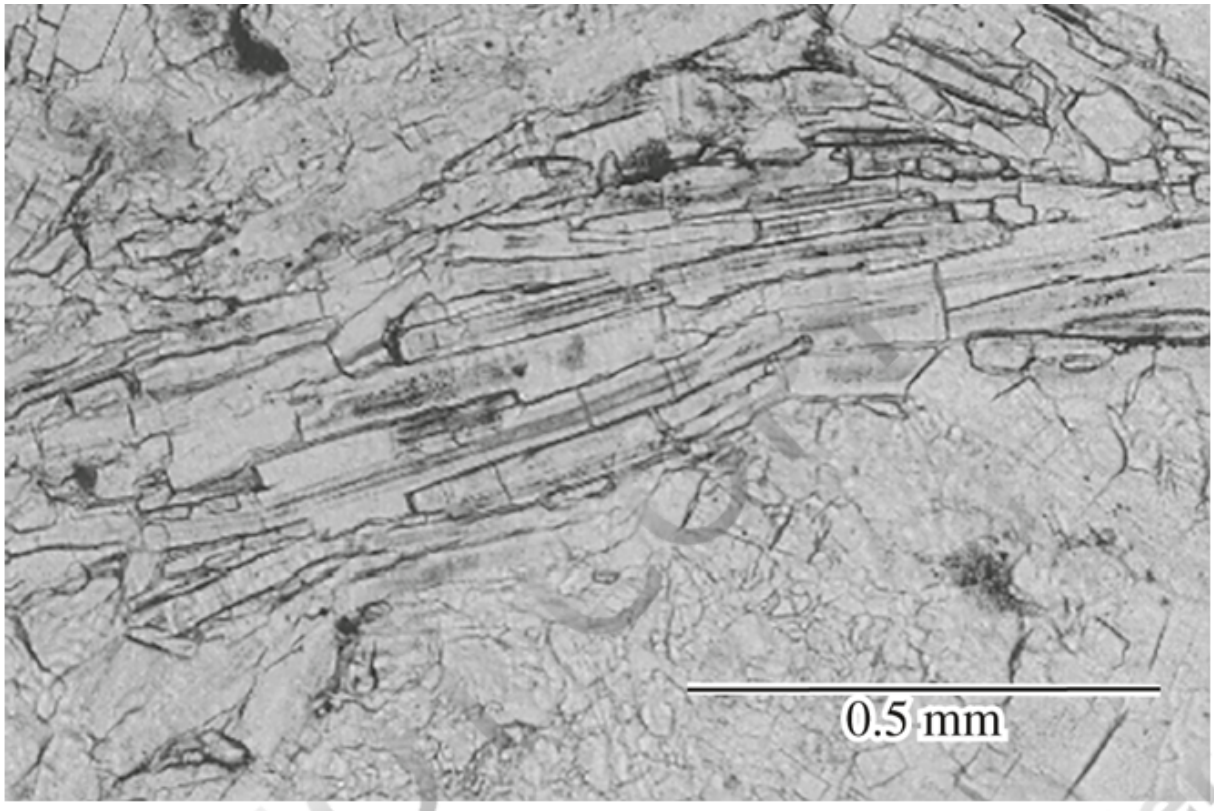

FIGURE 17.15 Photomicrograph of a thin section of bedded anhydrite. Plane light. Back to text

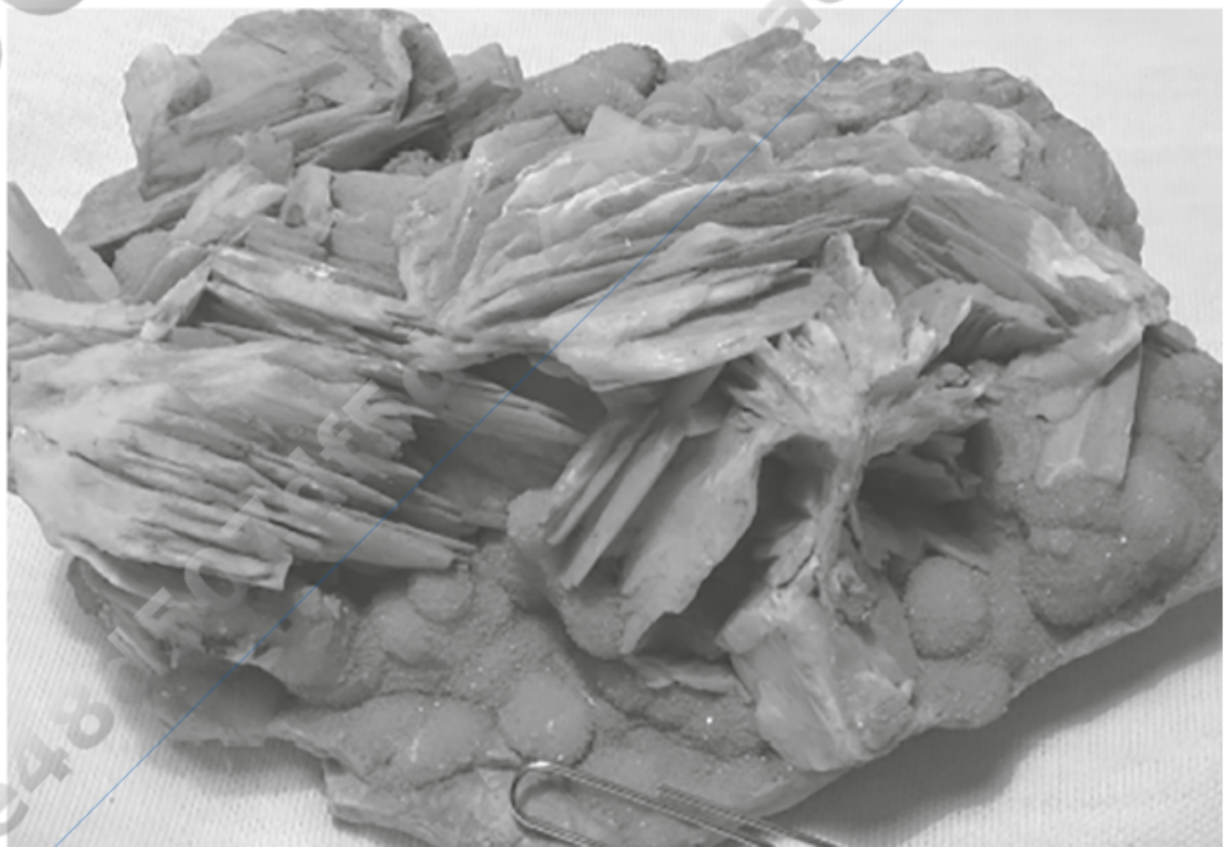

Printed by: e48d507df5d1141@placeholder.94092.edu. Printing is for personal, private use only. No part of this book may be reproduced or transmitted without publisher's prior permission. Violators will be prosecuted.

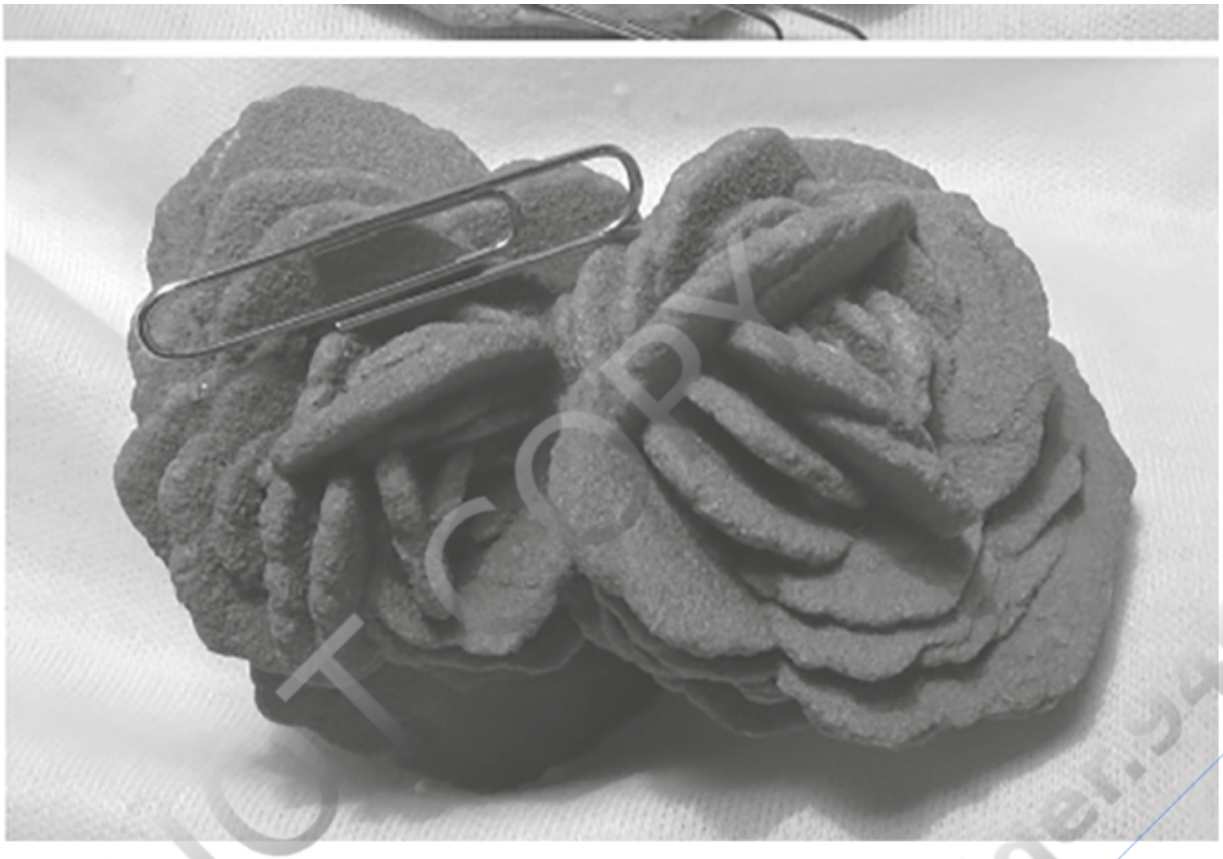

FIGURE 17.16 Barite. (*a*) Intergrown platy barite crystals with mammillary masses of quartz (near paper clip). Width of paper clip is about 7 mm. (*b*) Two intergrown barite roses that formed as concretionary masses in sedimentary rocks. Width of paper clip is about 7 mm. Back to text

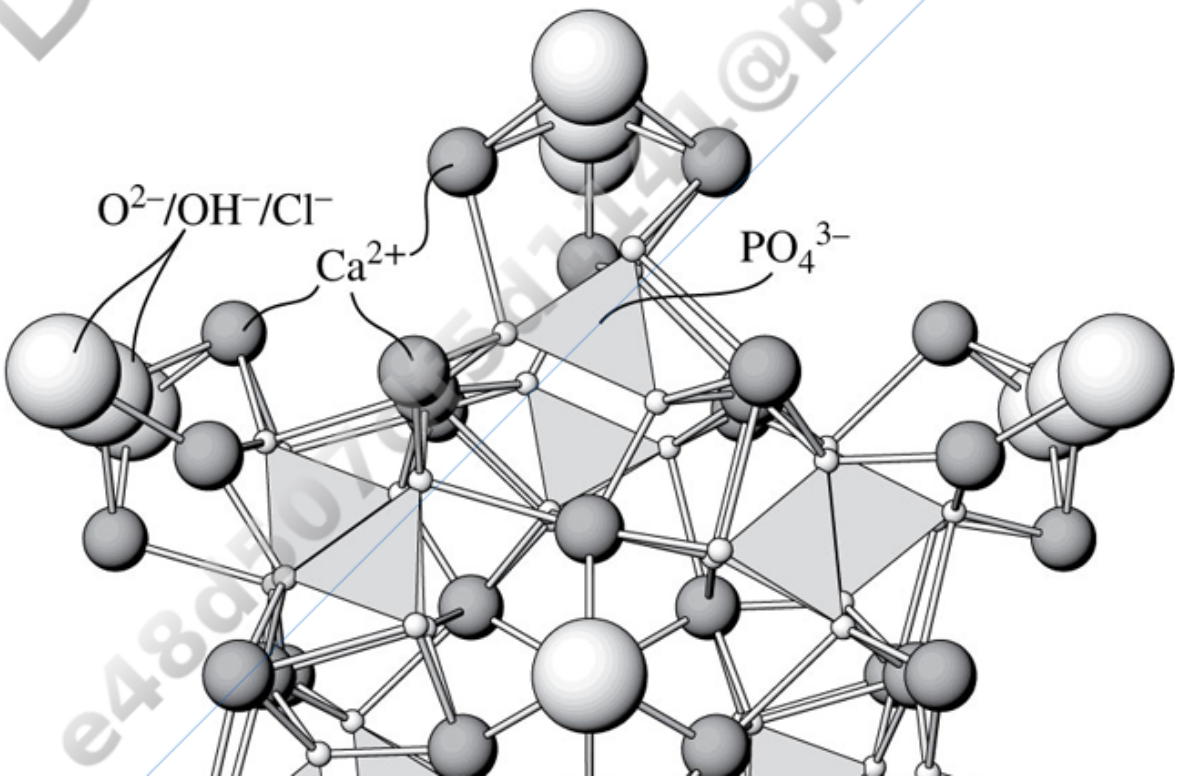

Printed by: e48d507df5d1141@placeholder.94092.edu. Printing is for personal, private use only. No part of this book may be reproduced or transmitted without publisher's prior permission. Violators will be prosecuted.

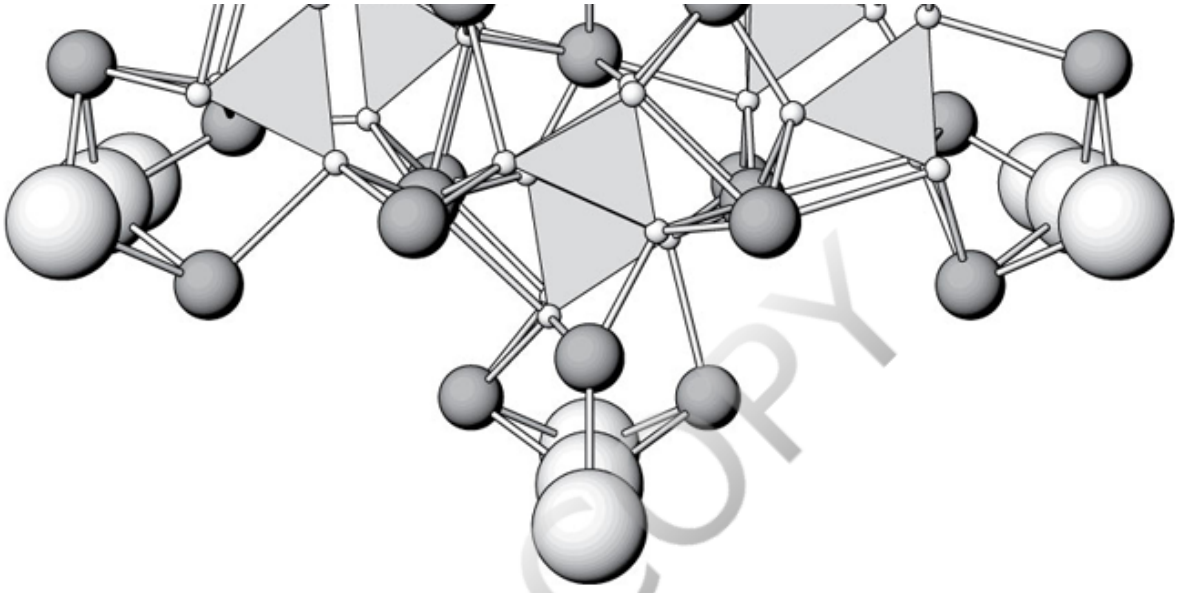

FIGURE 17.17 Structure of apatite viewed down the *c* axis. The hexagonal symmetry is evident. Back to text

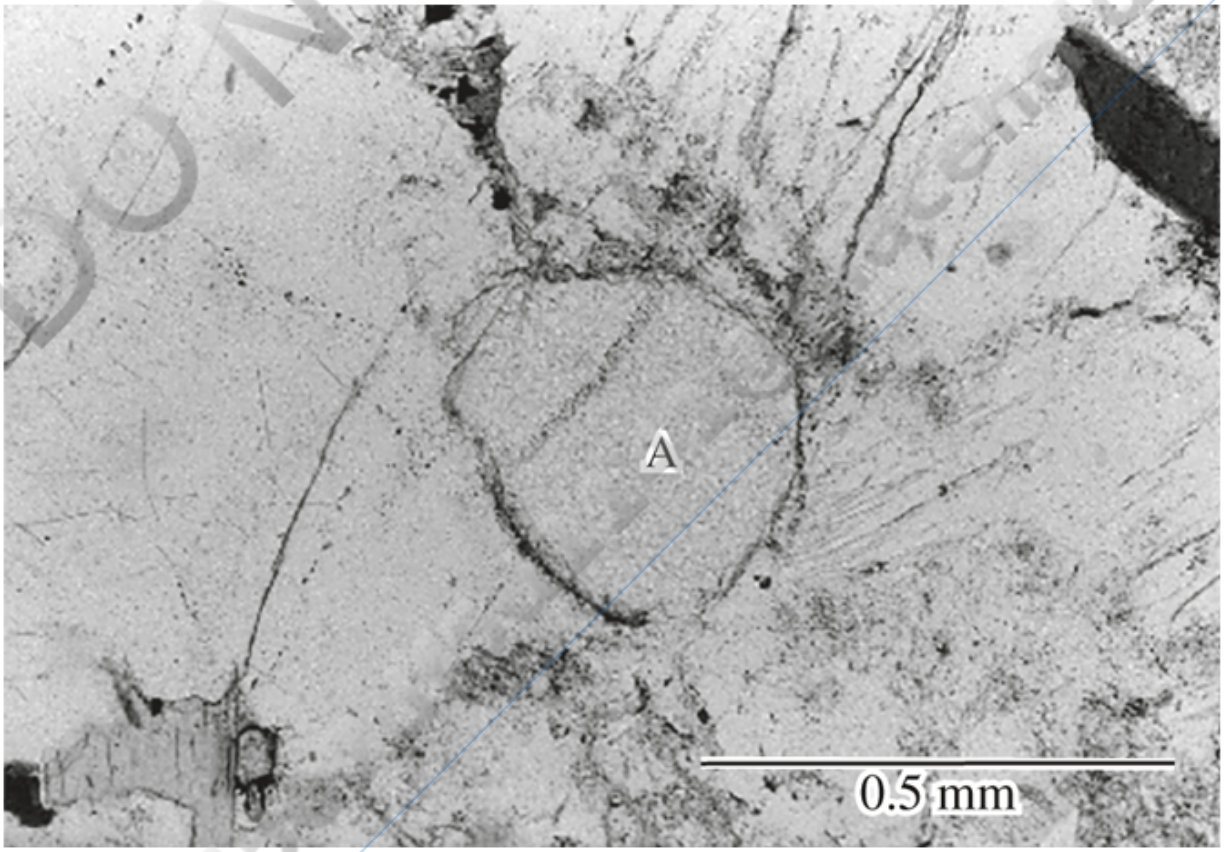

FIGURE 17.18 Photomicrograph of apatite in thin section. Back to text

DO NOT COPY

Printed by: e48d507df5d1141@placeholder.94092.edu. Printing is for personal, private use only. No part of this book may be reproduced or transmitted without publisher's prior permission. Violators will be prosecuted.

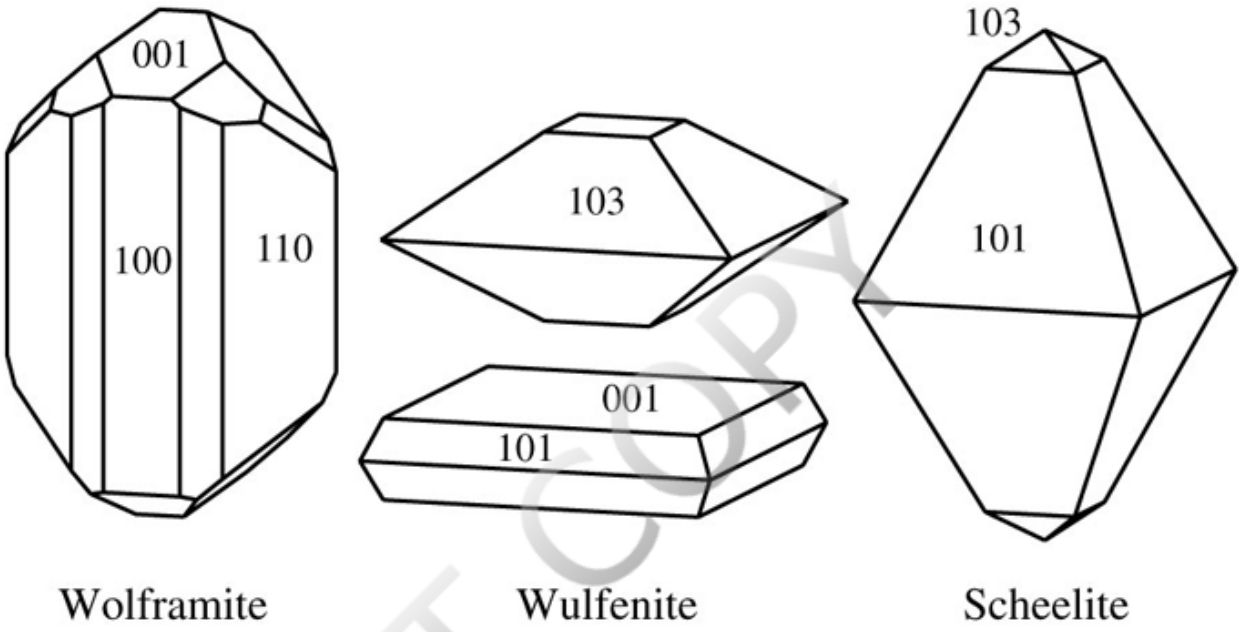

FIGURE 17.19 Crystal habit of wolframite, wulfenite, and scheelite. Back to text

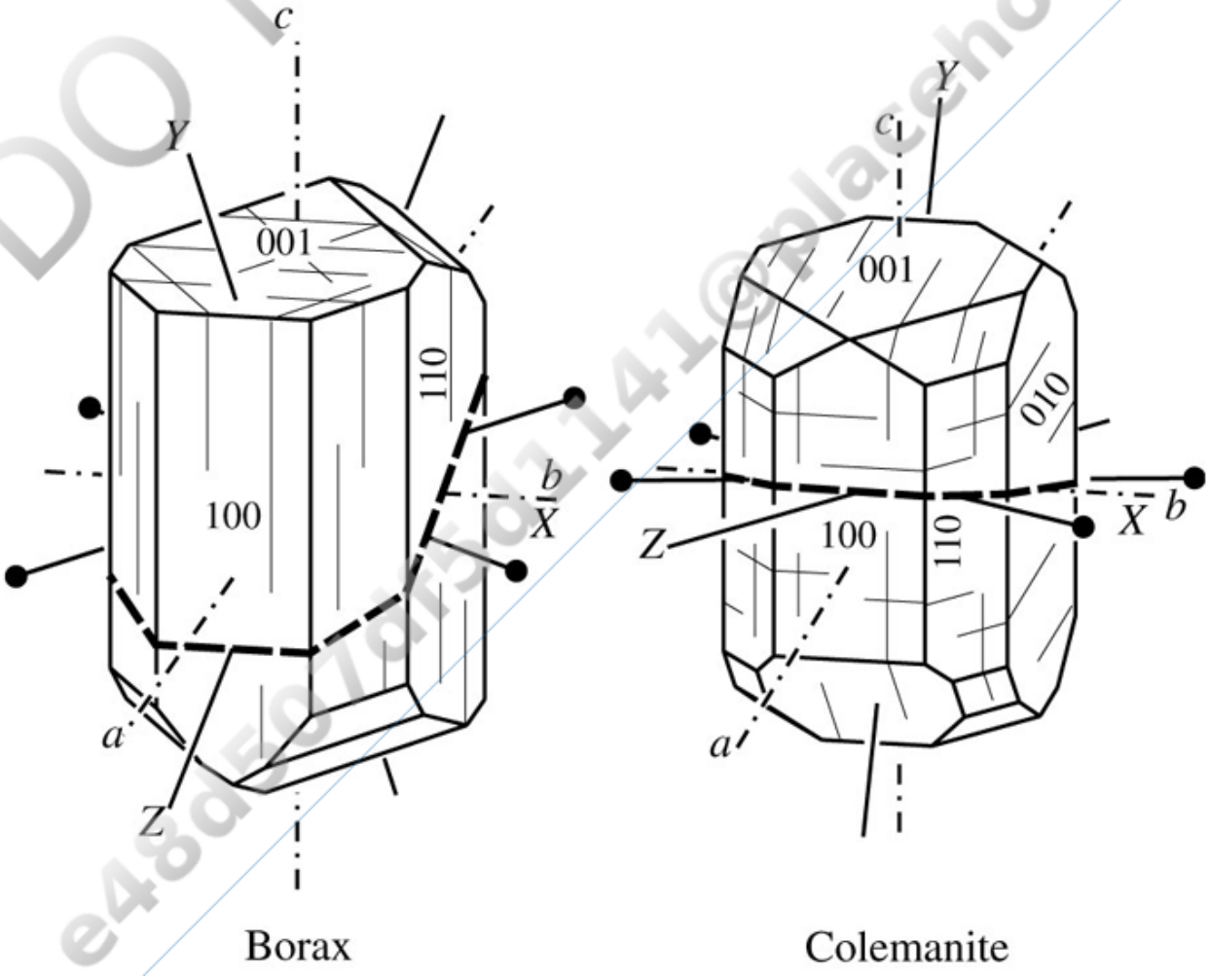

DO NOT COPY
e48d507df5d1141@placeholder.9409

Printed by: e48d507df5d1141@placeholder.94092.edu. Printing is for personal, private use only. No part of this book may be reproduced or transmitted without publisher's prior permission. Violators will be prosecuted.

Chapter 18 Oxides, Hydroxides, and Halides

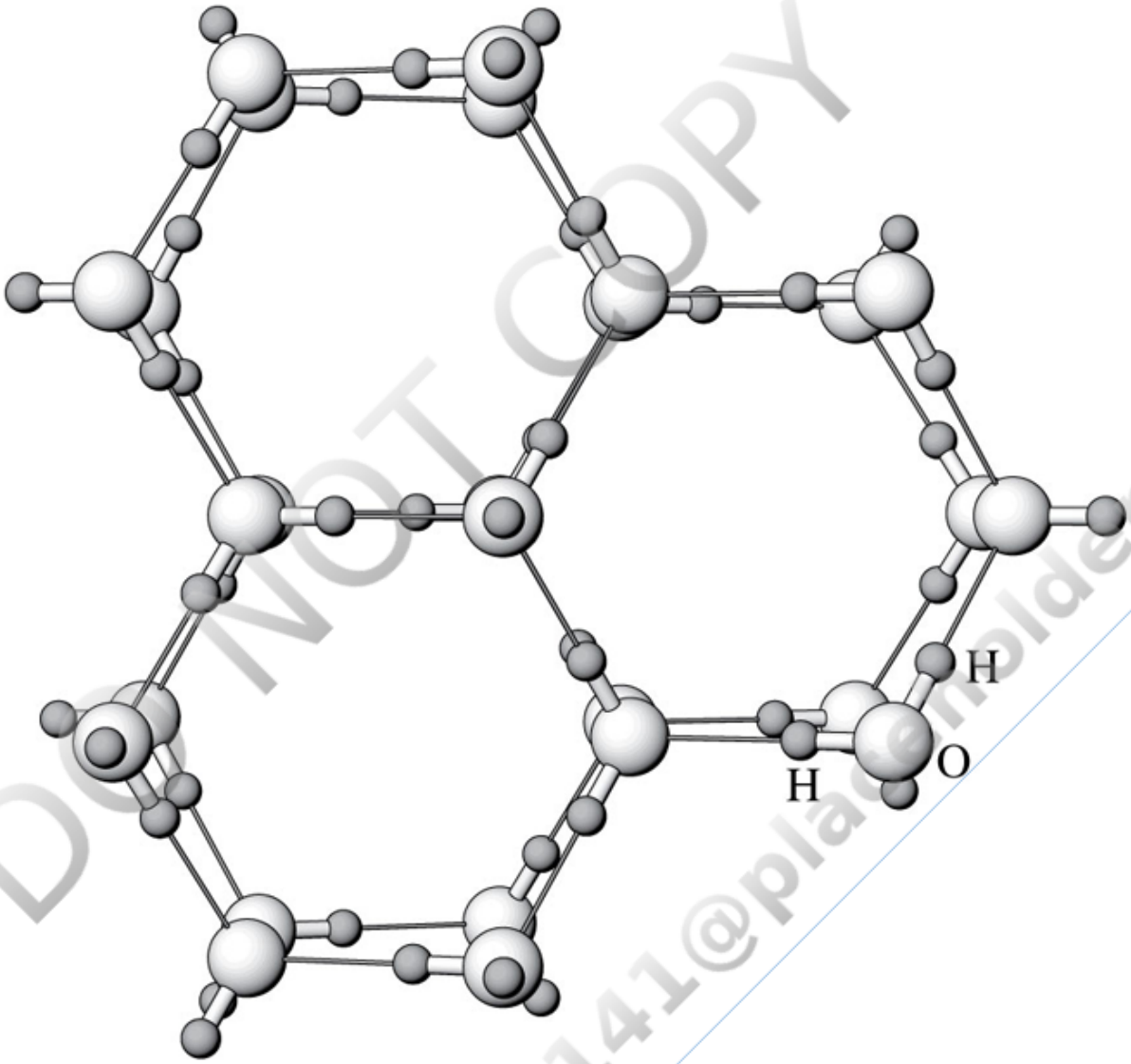

FIGURE 18.1 Ice structure viewed down the *c* axis. Water molecules consisting of one oxygen (large sphere) and two hydrogens (small spheres) are arranged in a hexagonal array. Hydrogen bonds between water molecules are shown with lines. The positions of the H and O are shown accurately, but the sizes of the atoms are reduced. Compare Figure 3.13. Back to text

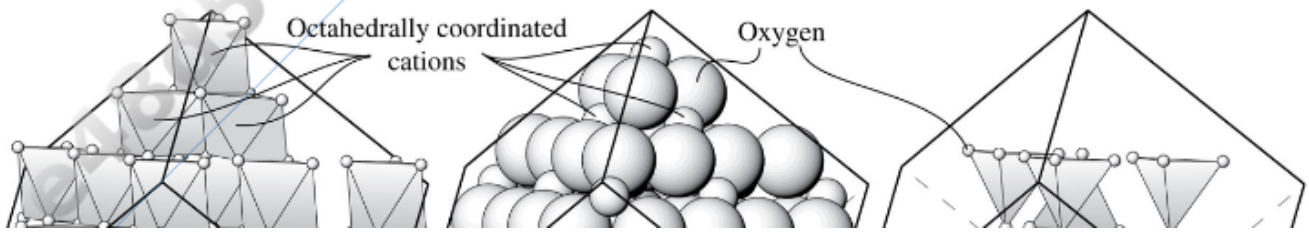

DO NOT COPY e48d507df5d1141@placeholder.9409

Printed by: e48d507df5d1141@placeholder.94092.edu. Printing is for personal, private use only. No part of this book may be reproduced or transmitted without publisher's prior permission. Violators will be prosecuted.

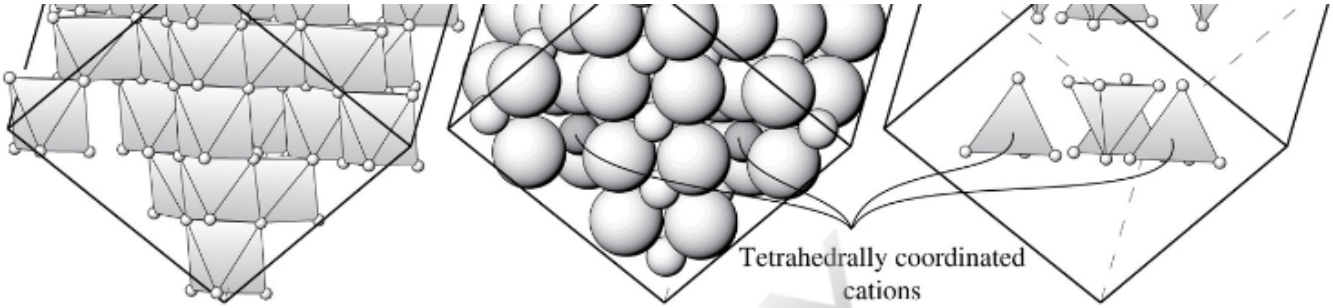

FIGURE 18.2 Spinel structure. Oxygen anions form an approximately cubic close-packed arrangement with layers parallel to {111}, which is horizontal in the illustration. Within each unit cell, cations occupy 8 tetrahedral and 16 octahedral sites between the oxygen layers. All the tetrahedral sites are shown; the octahedral sites shown on the left include both those within the unit cell and additional octahedra that are partially within adjacent unit cells. The cube outlines are slightly larger than the unit cell. The corners of the unit cell are the centers of octahedrally coordinated cations at the corners of the cube. See text for additional discussion. Back to text

DO NOT COPY

(*a*)

(*b*)

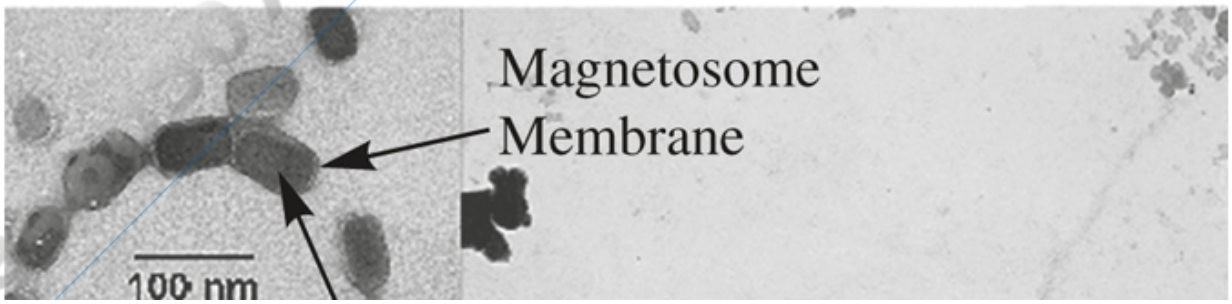

Printed by: e48d507df5d1141@placeholder.94092.edu. Printing is for personal, private use only. No part of this book may be reproduced or transmitted without publisher's prior permission. Violators will be prosecuted.

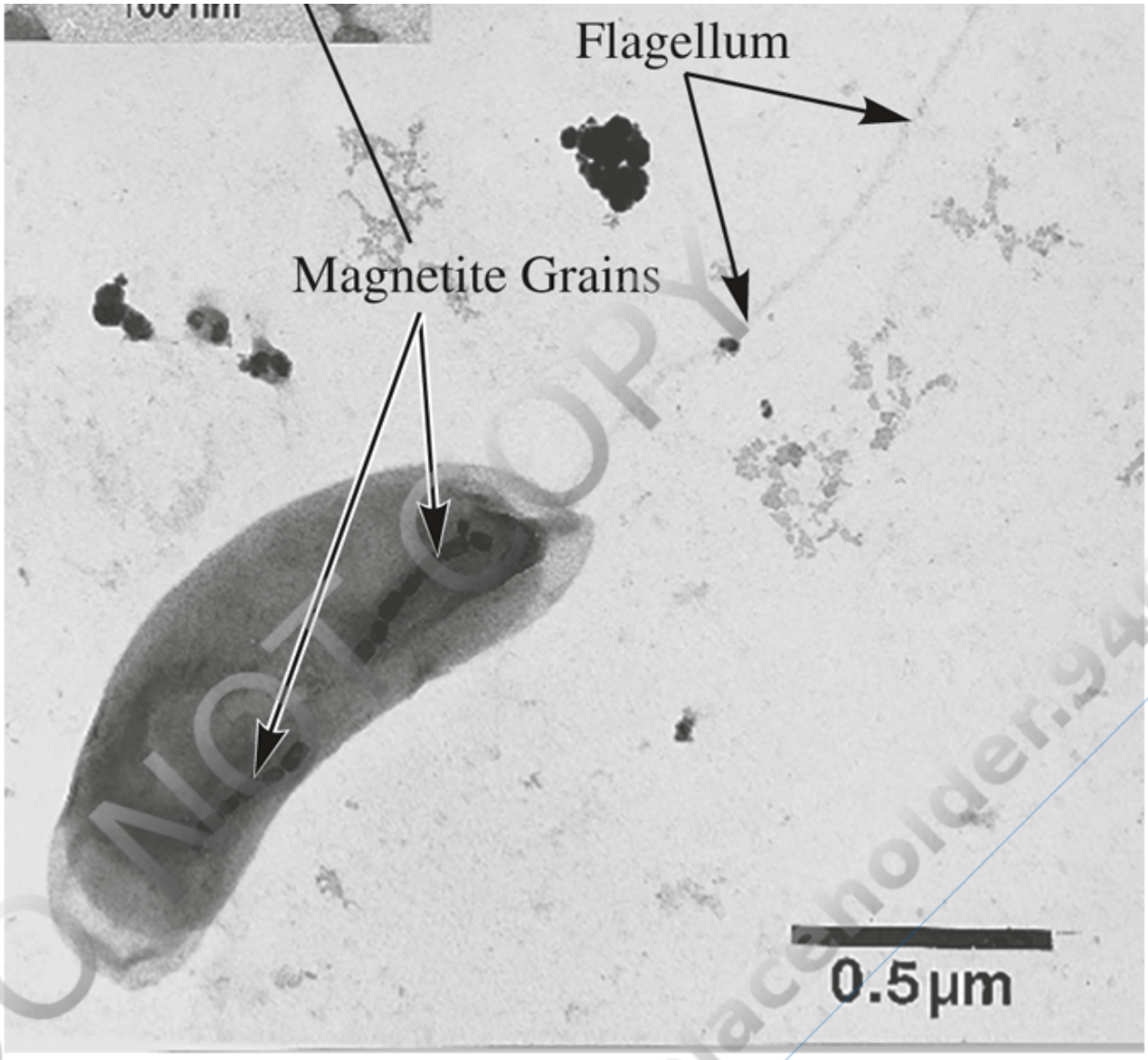

FIGURE 18.3 Magnetite. (*a*) Massive granular hand sample. (*b*) Transmission electron microscope images (courtesy of D. Bazylinski) of a magnetotactic bacterium (strain MV-1) showing a chain of magnetite grains with a gap in the middle. The cell possesses a single polar flagellum that can be used for propulsion. Inset shows detail of magnetite grains and the magnetosome membrane that surrounds them and anchors them in place. Back to text

Printed by: e48d507df5d1141@placeholder.94092.edu. Printing is for personal, private use only. No part of this book may be reproduced or transmitted without publisher's prior permission. Violators will be prosecuted.

FIGURE 18.4 The 2.7 Ga Soudan banded iron formation in northeastern Minnesota. The dark layers are dominantly hematite, and the light layers are mostly microcrystalline quartz (jasper). Note the pen at right (*arrow*) for scale. Back to text

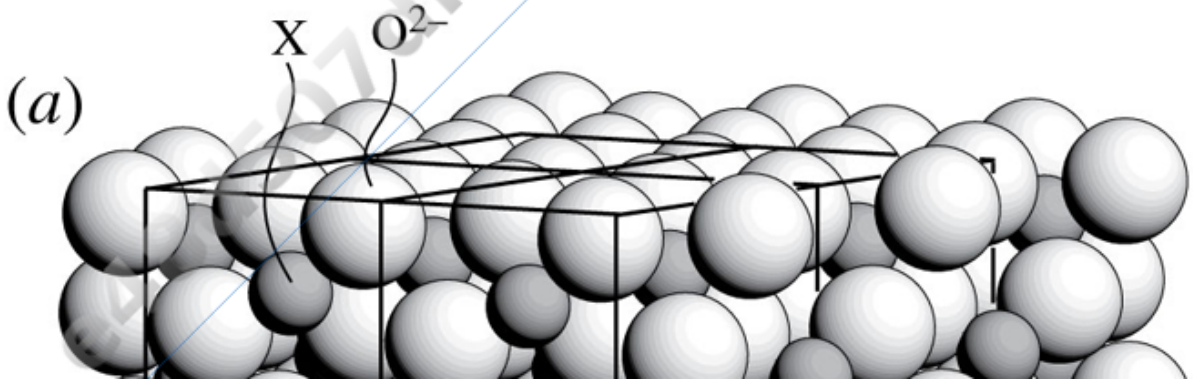

Printed by: e48d507df5d1141@placeholder.94092.edu. Printing is for personal, private use only. No part of this book may be reproduced or transmitted without publisher's prior permission. Violators will be prosecuted.

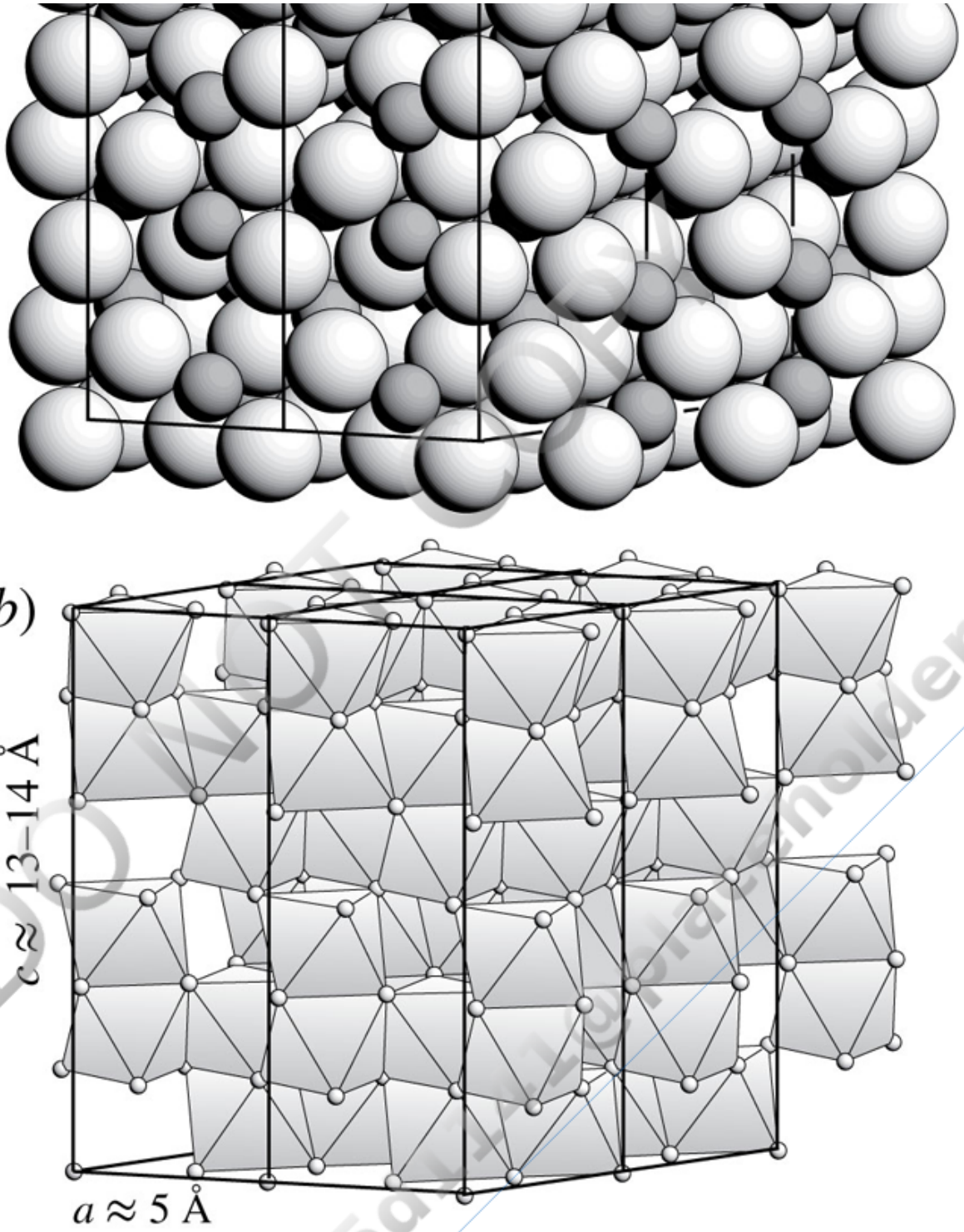

FIGURE 18.5 Structure of the hematite group. (*a*) X cations and O^{2-} anions drawn approximately to scale. The oxygen anions are in an approximately hexagonal close-packed arrangement. The outline of four unit cells is shown. (*b*) Distribution of X octahedra within the structure. Back to text

Printed by: e48d507df5d1141@placeholder.94092.edu. Printing is for personal, private use only. No part of this book may be reproduced or transmitted without publisher's prior permission. Violators will be prosecuted.

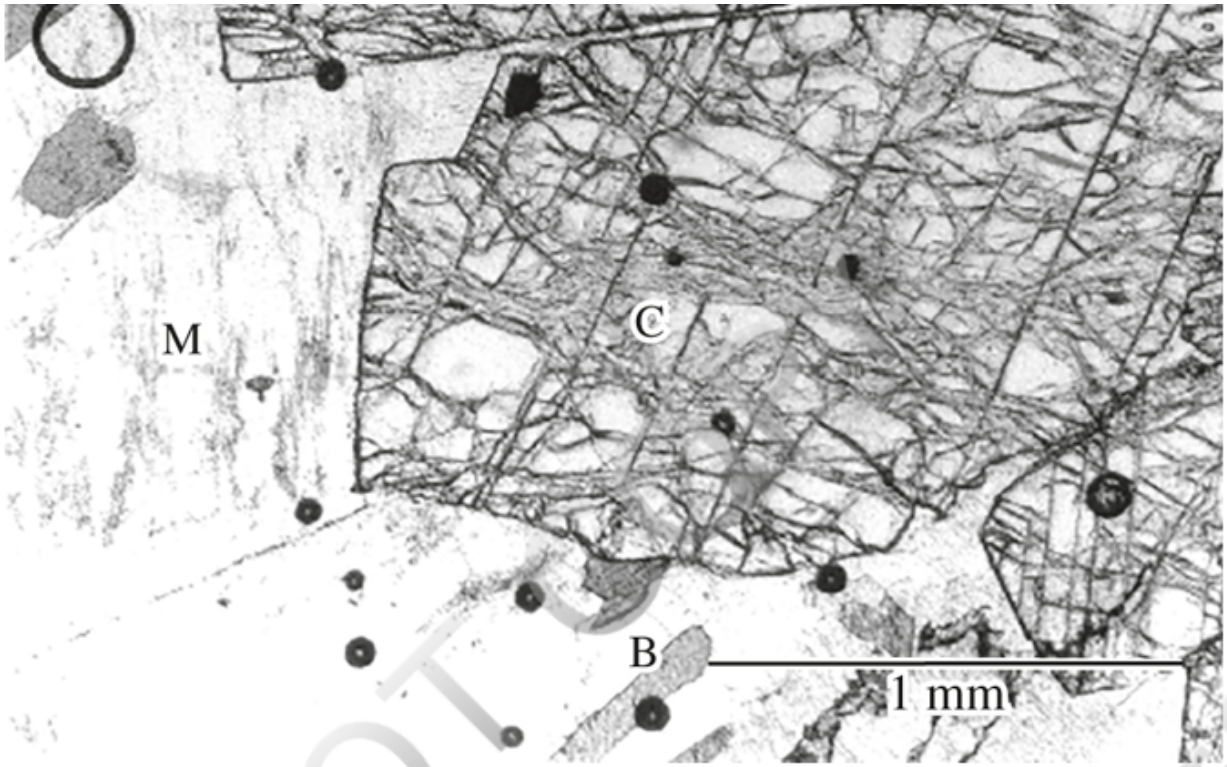

FIGURE 18.6 Photomicrograph of corundum (C), microcline (M), and small grains of biotite (B) in a thin section of mica schist. Note the rhombohedral parting in the corundum. The small circles are bubbles in the thin section epoxy. Plane light. Back to text

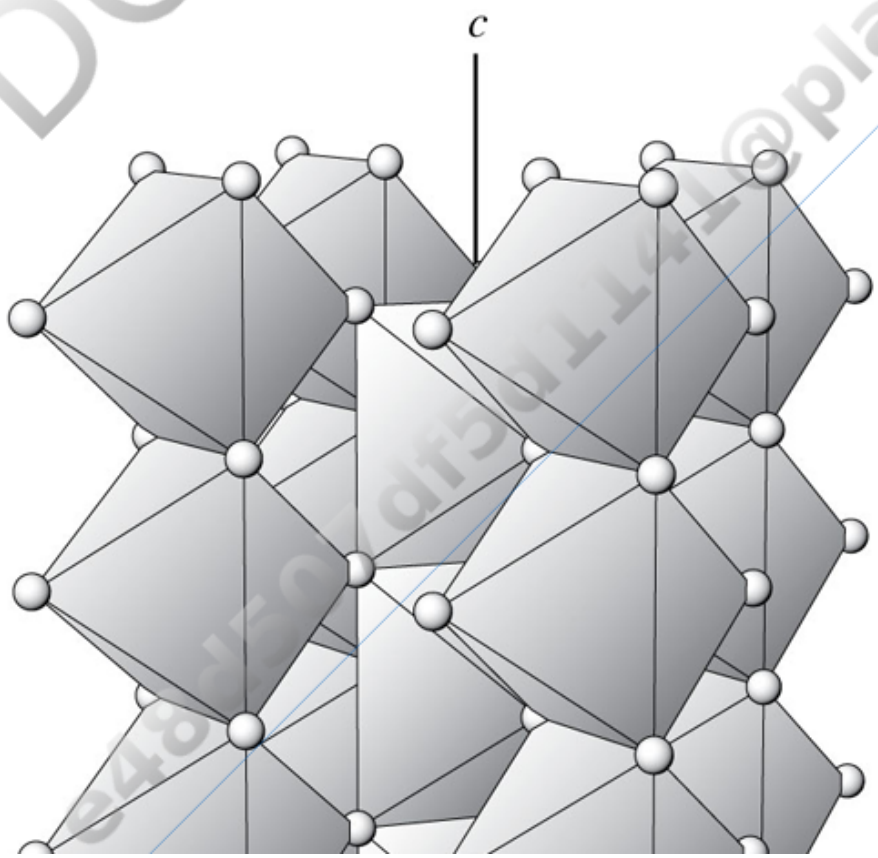

DO NOT COPY e48d507df5d1141@placeholder.94092

Printed by: e48d507df5d1141@placeholder.94092.edu. Printing is for personal, private use only. No part of this book may be reproduced or transmitted without publisher's prior permission. Violators will be prosecuted.

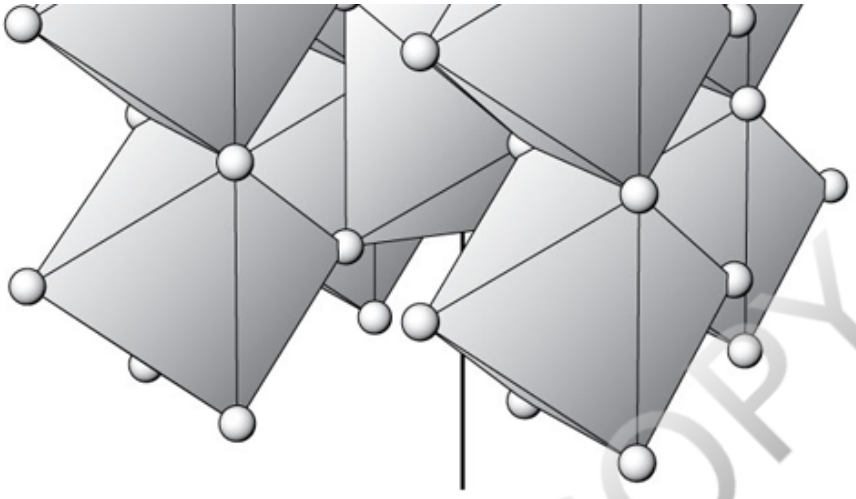

FIGURE 18.7 Rutile, cassiterite, and pyrolusite structure. The Ti^{2+}, Sn^{2+}, or Mn^{2+} cations occupy octahedra that form edge-sharing chains extending parallel to *c* along the corners and center of the unit cell. Back to text

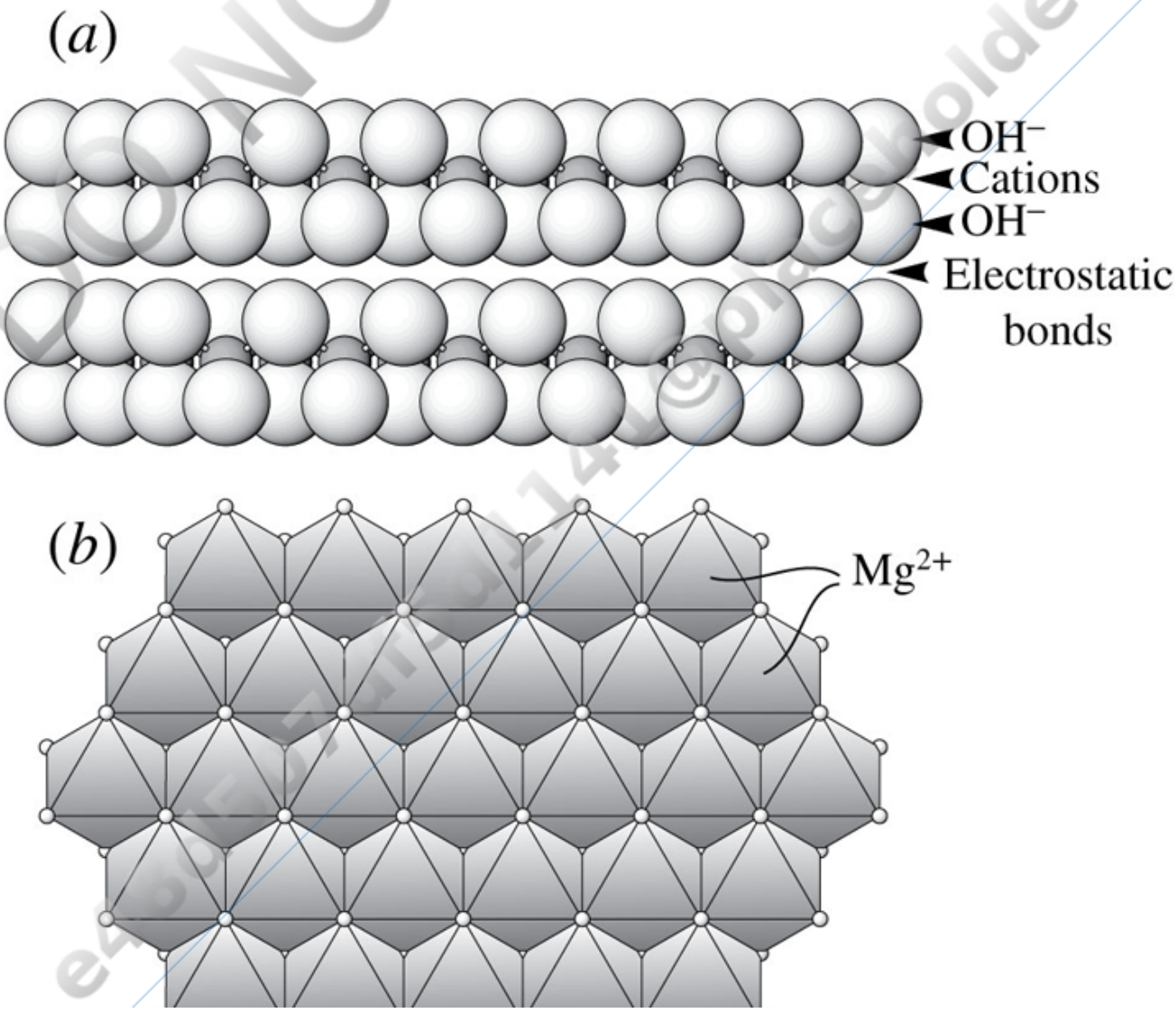

DO NOT COPY

Printed by: e48d507df5d1141@placeholder.94092.edu. Printing is for personal, private use only. No part of this book may be reproduced or transmitted without publisher's prior permission. Violators will be prosecuted.

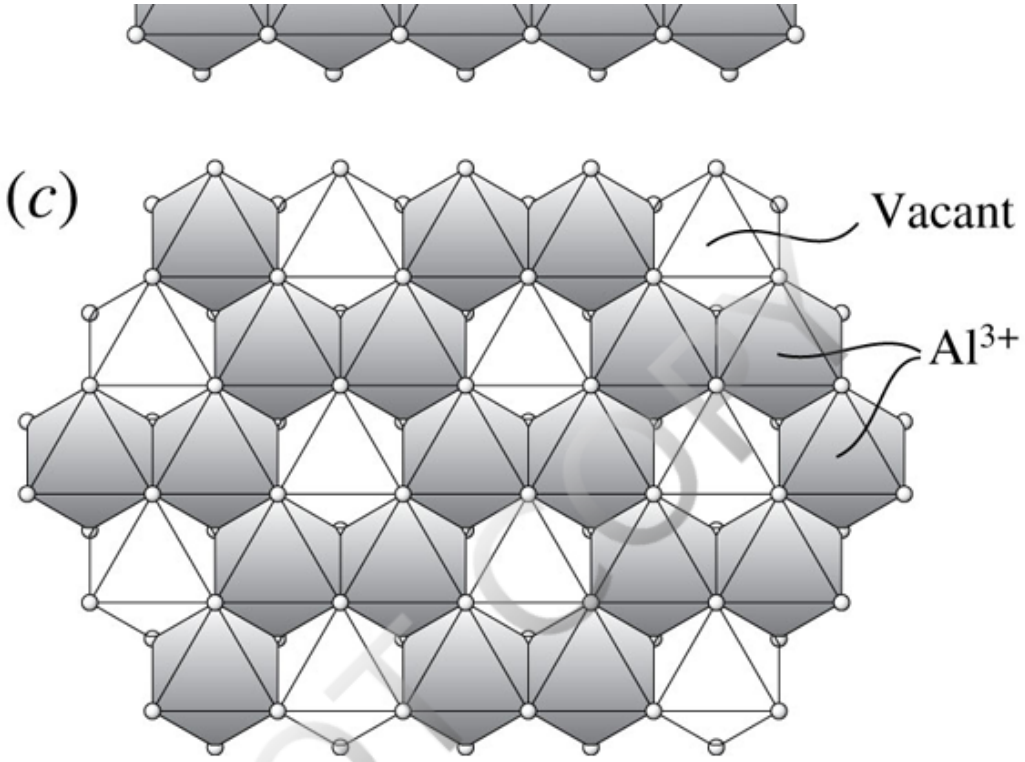

FIGURE 18.8 Brucite and gibbsite structure. (*a*) Octahedral sheets are composed of two layers of OH^- anionic groups with cations in octahedral coordination. (*b*) Plan view of brucite sheet. All octahedral sites (shaded) are occupied by Mg^{2+}. (*c*) Plan view of gibbsite sheet. Only two out of three octahedral sites are occupied by Al^{3+}; the remaining sites are vacant (no shading). Back to text

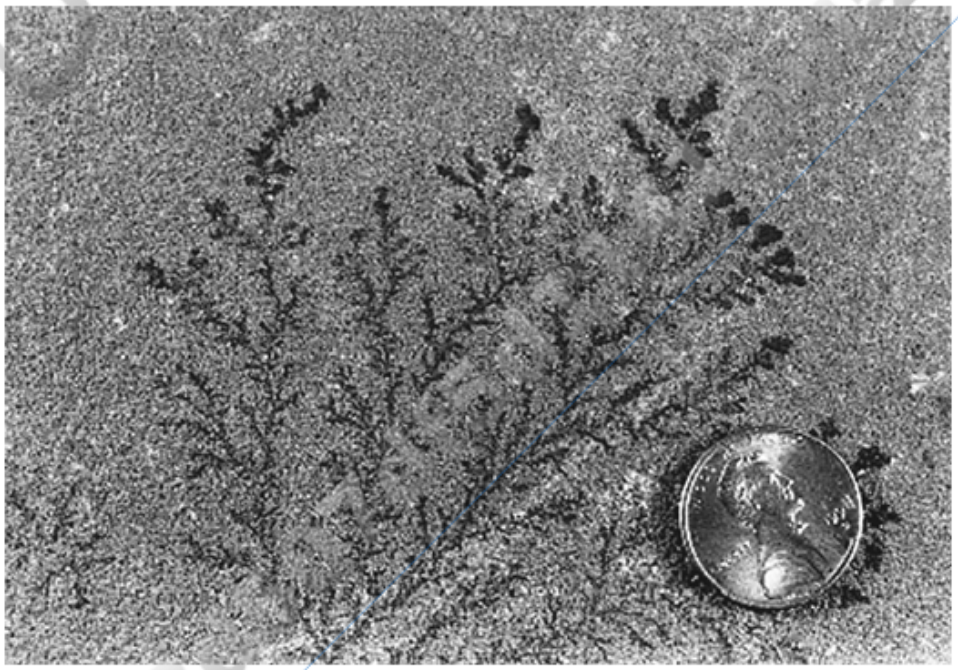

FIGURE 18.9 Dendrites on slab of sandstone. Back to text

Printed by: e48d507df5d1141@placeholder.94092.edu. Printing is for personal, private use only. No part of this book may be reproduced or transmitted without publisher's prior permission. Violators will be prosecuted.

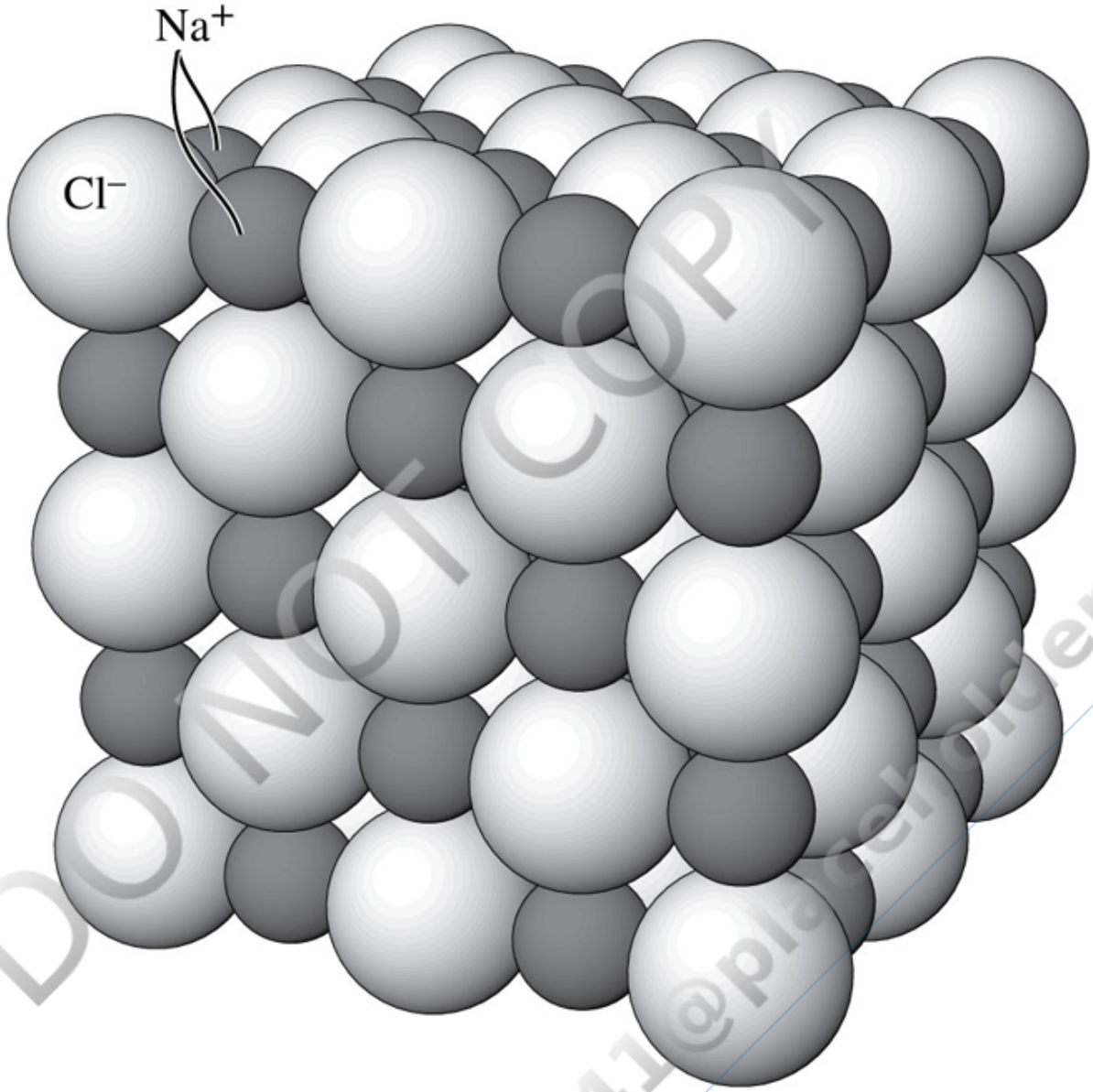

FIGURE 18.10 Halite structure. Each Na^+ coordinates with six Cl^-. Back to text

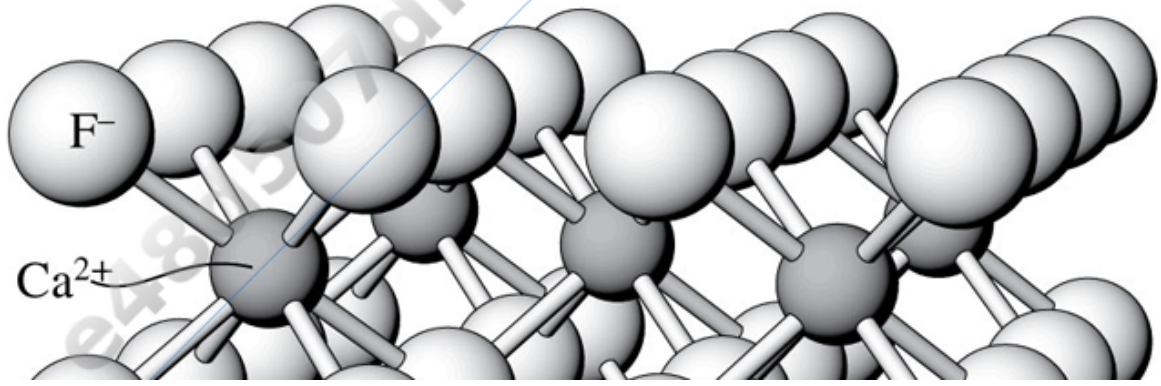

DO NOT COPY

Printed by: e48d507df5d1141@placeholder.94092.edu. Printing is for personal, private use only. No part of this book may be reproduced or transmitted without publisher's prior permission. Violators will be prosecuted.

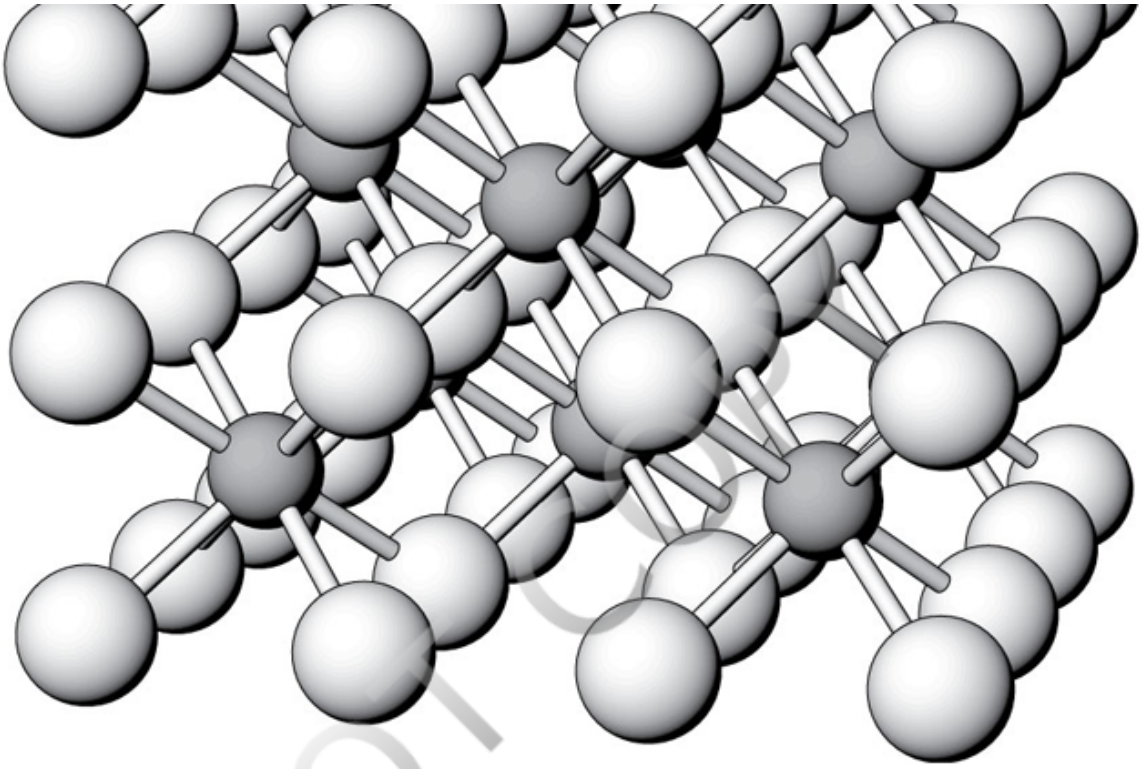

FIGURE 18.11 Fluorite structure. Each Ca^{2+} coordinates with 8 F^{-}. Back to text

FIGURE 18.12 Fluorite crystals. Field of view is about 15 cm wide. Back to text

DO NOT COPY e48d507df5d1141@placeholder.94092

Printed by: e48d507df5d1141@placeholder.94092.edu. Printing is for personal, private use only. No part of this book may be reproduced or transmitted without publisher's prior permission. Violators will be prosecuted.

Chapter 19 Sulfides and Related Minerals

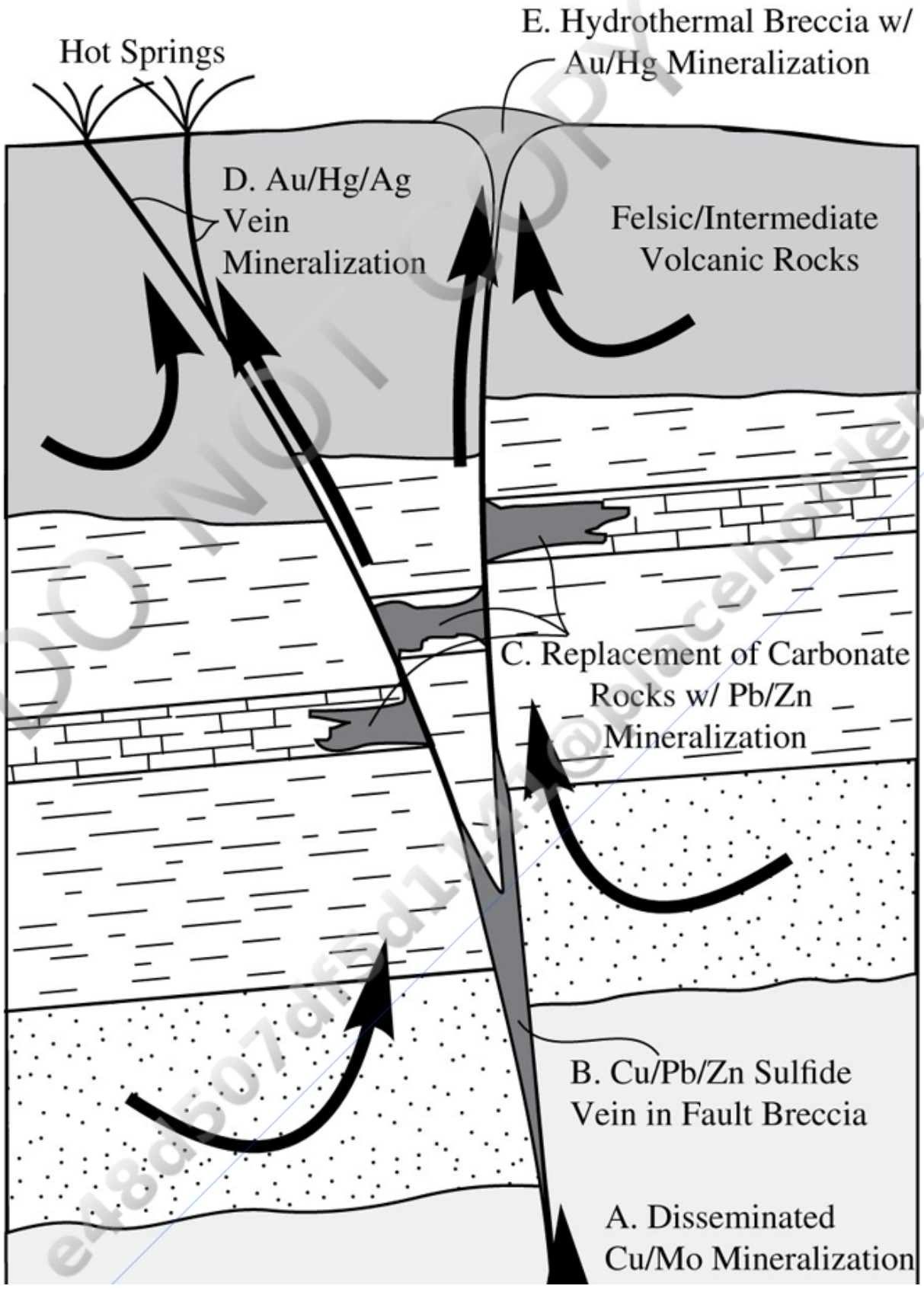

DO NOT COPY

Printed by: e48d507df5d1141@placeholder.94092.edu. Printing is for personal, private use only. No part of this book may be reproduced or transmitted without publisher's prior permission. Violators will be prosecuted.

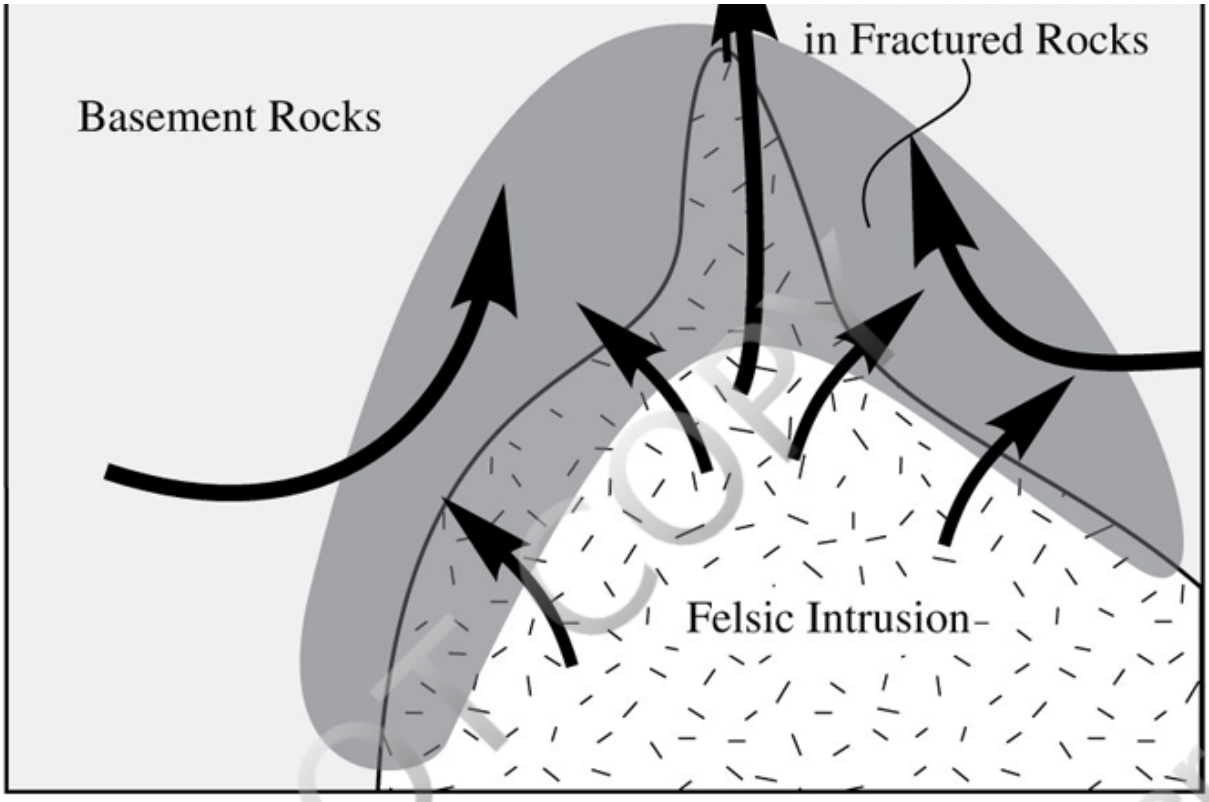

FIGURE 19.1 Schematic hydrothermal system. Hot mineralizing aqueous fluids may evolve from a crystallizing felsic intrusion (*bottom*), or they may be meteoric waters set in motion by the heat from the magma (*large arrows*). Minerals may crystallize in small fractures and among grains of the country rock (A) to form a disseminated deposit. Vein deposits (B) are formed where mineralizing fluids flow along fault or fracture zones. A replacement deposit (C) may be produced if mineralizing fluids interact with a limestone bed. Near-surface mineralization (D), often in volcanic rocks, may form where hydrothermal fluids reach the surface and form hot springs. If the temperature is high enough, hydrothermal fluids can violently flash (convert) to steam near the surface; this may fracture the rock, producing a hydrothermal breccia in which mineralization may occur (E). Many other scenarios are possible. Back to text

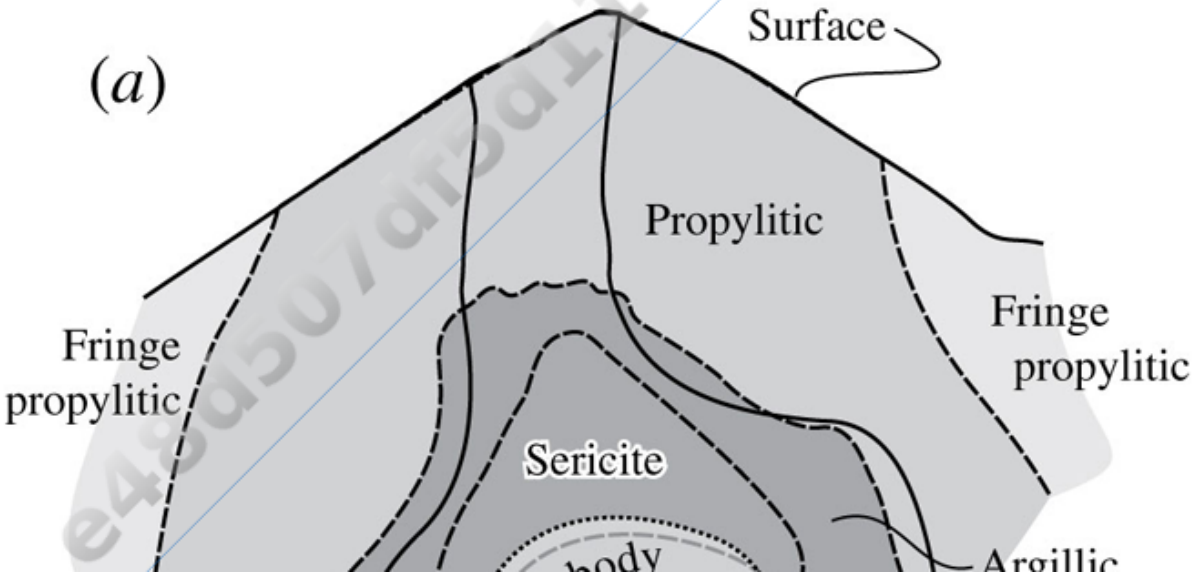

DO NOT COPY e48d507df5d1141@placeholder.9409

Printed by: e48d507df5d1141@placeholder.94092.edu. Printing is for personal, private use only. No part of this book may be reproduced or transmitted without publisher's prior permission. Violators will be prosecuted.

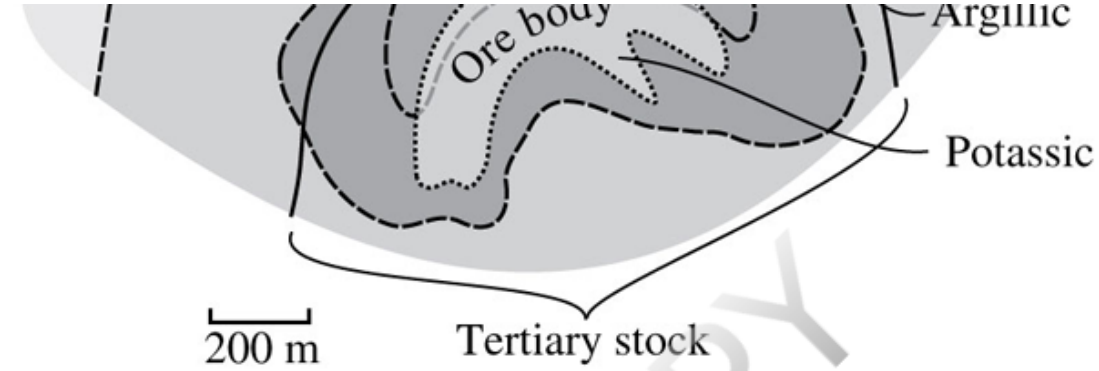

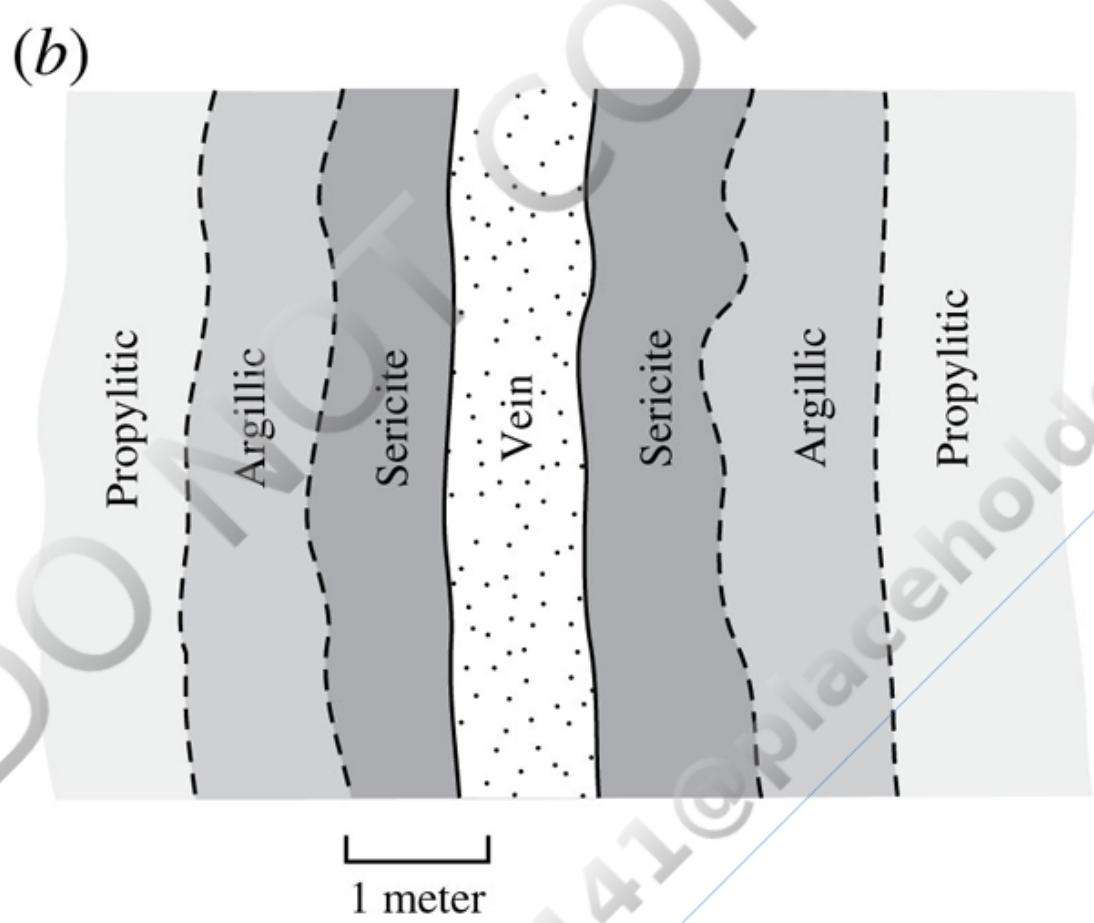

FIGURE 19.2 Hydrothermal alteration. (*a*) Henderson porphyry molybdenum deposit, Colorado. Mineralization is associated with Tertiary felsic intrusions emplaced in Precambrian granite. The molybdenite (MoS_2) in the ore body (>0.3% MoS_2) was deposited with quartz and pyrite in and along abundant fractures in the intrusion. Sericite, argillic, and propylitic alteration form concentric zones. Rocks within the ore body display potassic alteration. The biotite is not completely altered to chlorite in the fringe propylitic zone, which grades outward to unaltered Precambrian granite. Adapted from White and others (1981). (*b*) A similar concentric alteration pattern may be found at a much smaller scale adjacent to a sulfide-bearing vein. Back to text

DO NOT COPY
e48d507df5d1141@placeholder.9409

Printed by: e48d507df5d1141@placeholder.94092.edu. Printing is for personal, private use only. No part of this book may be reproduced or transmitted without publisher's prior permission. Violators will be prosecuted.

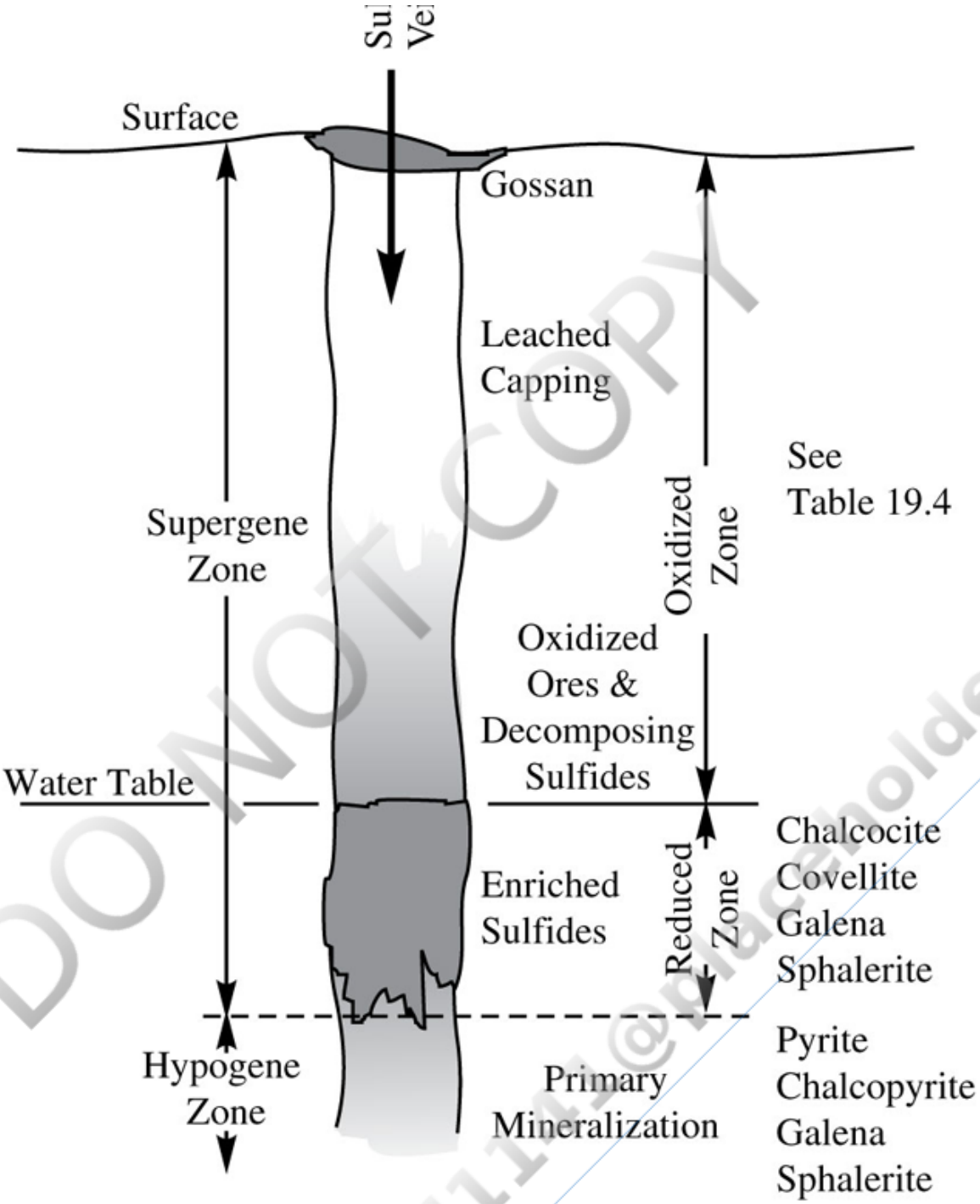

FIGURE 19.3 Supergene enrichment. Meteoric water percolates down through a sulfide-bearing vein. Sulfides are leached out of the near-surface environment, leaving behind a collection of oxide, carbonate, and hydroxide minerals in the oxidized zone. Cu, Pb, Zn, and related elements are largely removed from the leached capping. A gossan, enriched in iron oxides and hydroxides typically derived from alteration of pyrite, may accumulate at the surface as weathering and erosion progress. Sulfide minerals (re)precipitate in the reduced zone, generally below the water table, to form a zone enriched in sulfide minerals. Back to text

Printed by: e48d507df5d1141@placeholder.94092.edu. Printing is for personal, private use only. No part of this book may be reproduced or transmitted without publisher's prior permission. Violators will be prosecuted.

FIGURE 19.4 Small elongate prismatic crystals of stibnite. Back to text

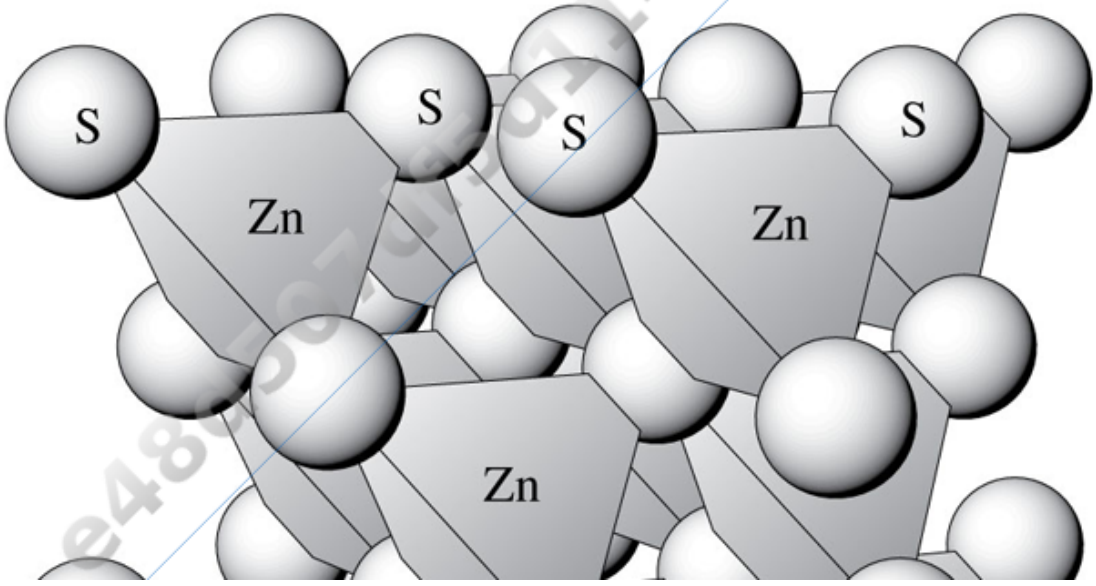

DO NOT COPY

Printed by: e48d507df5d1141@placeholder.94092.edu. Printing is for personal, private use only. No part of this book may be reproduced or transmitted without publisher's prior permission. Violators will be prosecuted.

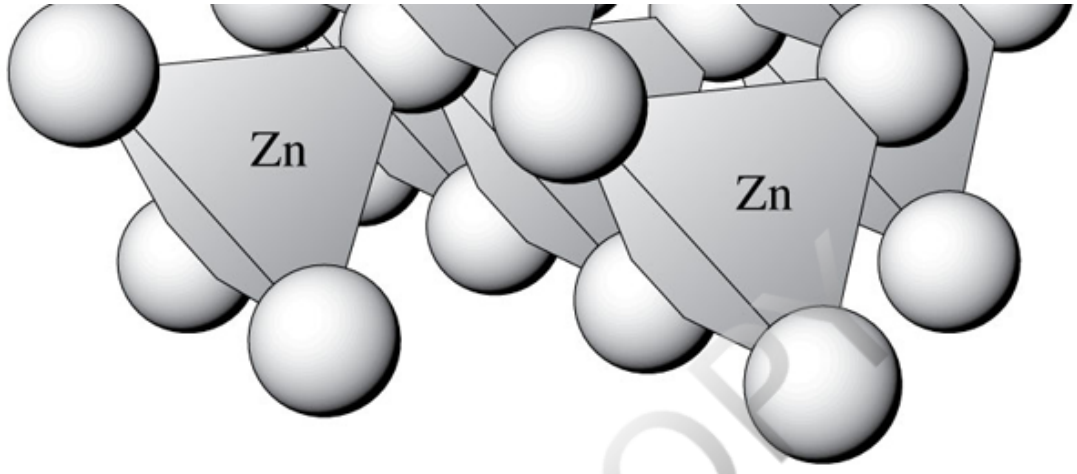

FIGURE 19.5 Structure of sphalerite. Sulfur atoms are arranged in cubic close packing. Zn atoms are positioned in tetrahedral coordination sites that are arranged in rows parallel to the diagonals across each unit cell face. This places Zn at the corners and face centers of the unit cell. Chalcopyrite is similar, but with Cu and Fe occupying alternating tetrahedral sites. Back to text

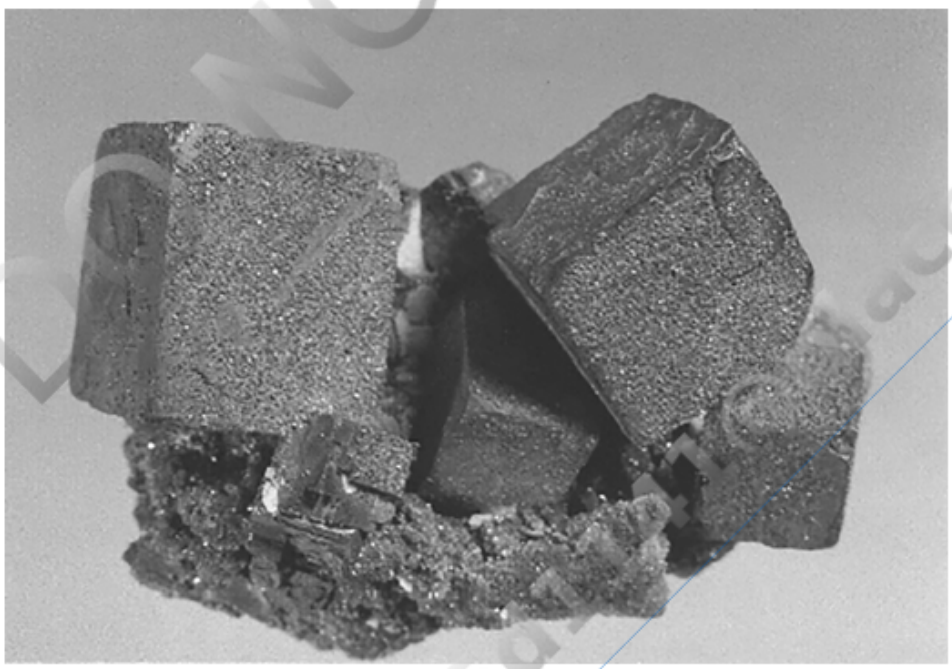

FIGURE 19.6 Galena cubes encrusted with marcasite. Back to text

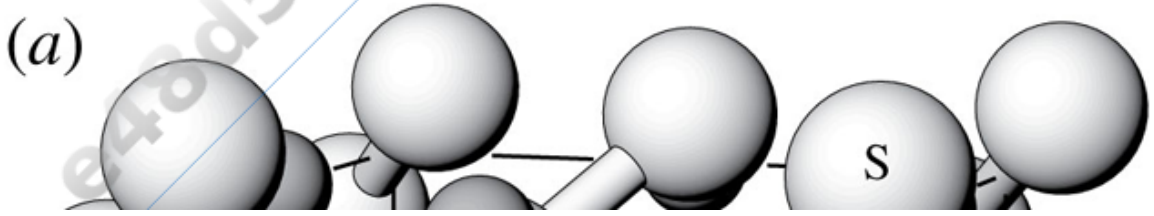

DO NOT COPY e48d507df5d1141@placeholder.94092

Printed by: e48d507df5d1141@placeholder.94092.edu. Printing is for personal, private use only. No part of this book may be reproduced or transmitted without publisher's prior permission. Violators will be prosecuted.

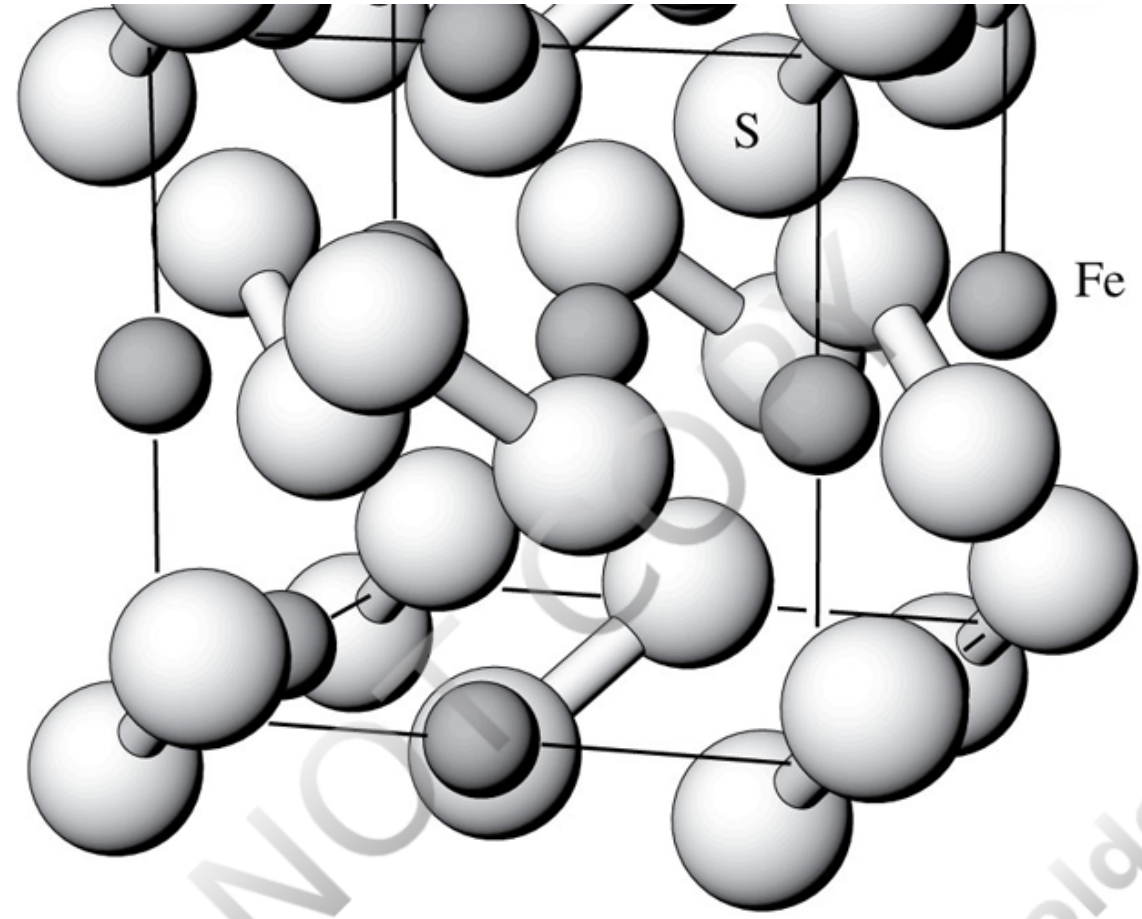

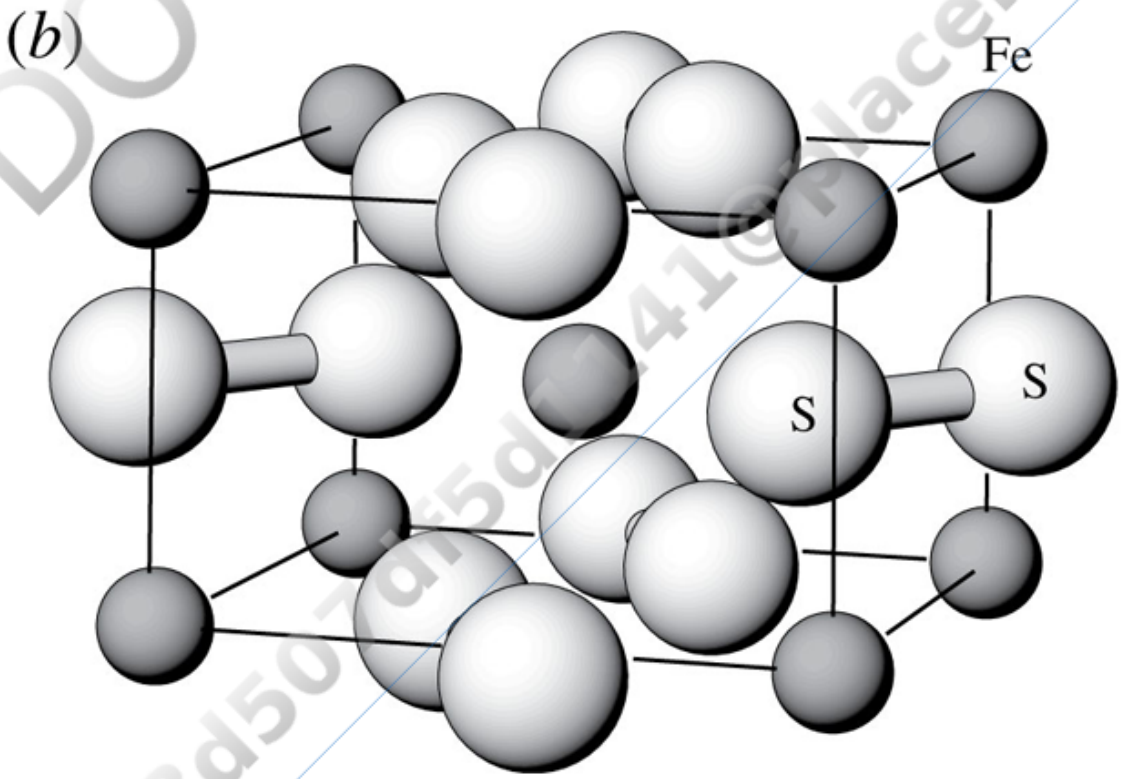

FIGURE 19.7 Structure of iron sulfides. (*a*) The pyrite structure is derived from halite, with Fe in the Na positions and covalently bonded S_2 doublets occupying the Cl positions. (*b*) Marcasite structure. Fe occupies the nodes of a body-centered orthorhombic lattice with covalently bonded S_2 pairs in the center of four unit cell edges parallel to *b* and in the center of the {010} ends of the unit

Printed by: e48d507df5d1141@placeholder.94092.edu. Printing is for personal, private use only. No part of this book may be reproduced or transmitted without publisher's prior permission. Violators will be prosecuted.

pairs in the center of four unit cell edges parallel to *b* and in the center of the {010} ends of the unit cell. Back to text

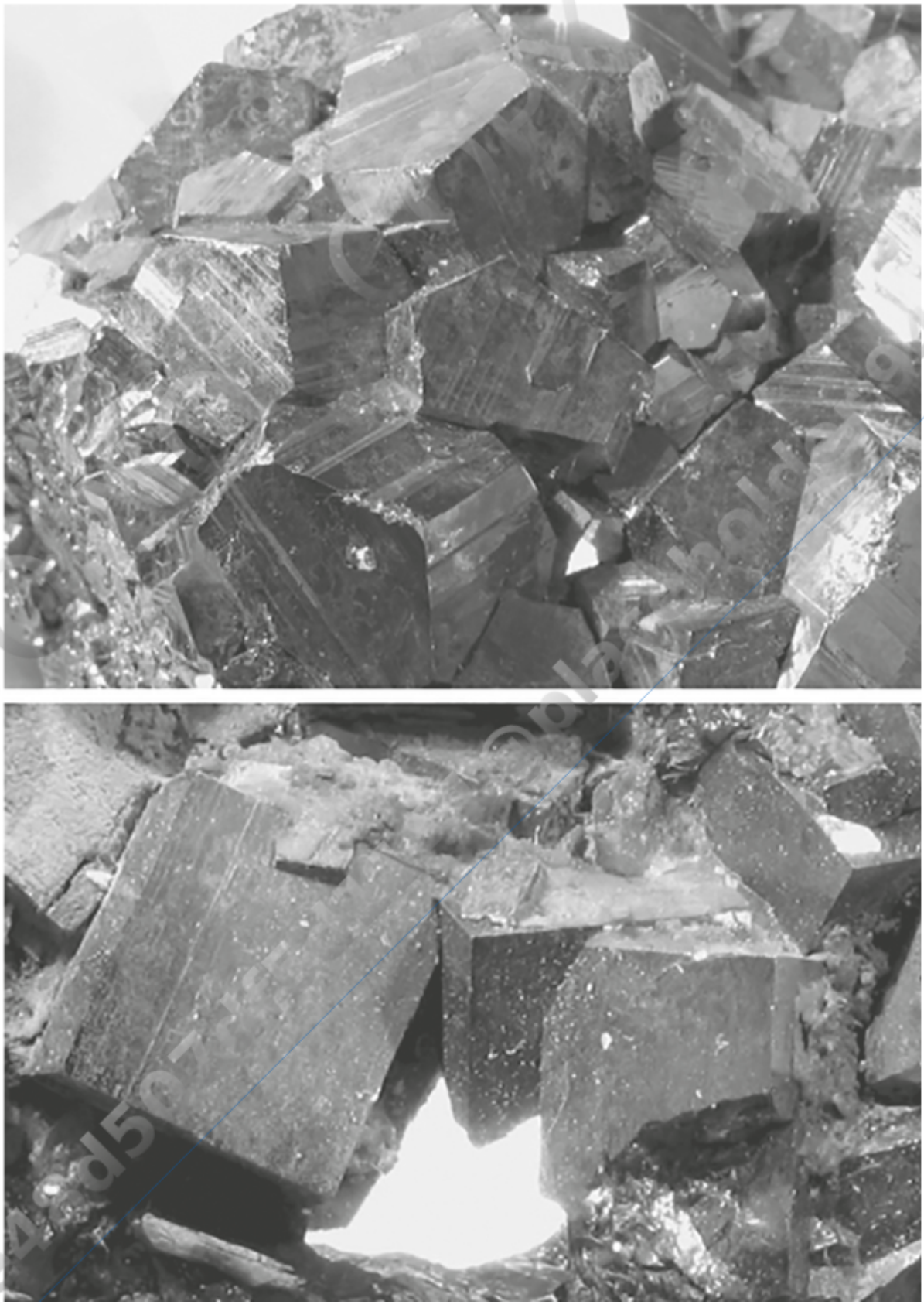

Printed by: e48d507df5d1141@placeholder.94092.edu. Printing is for personal, private use only. No part of this book may be reproduced or transmitted without publisher's prior permission. Violators will be prosecuted.

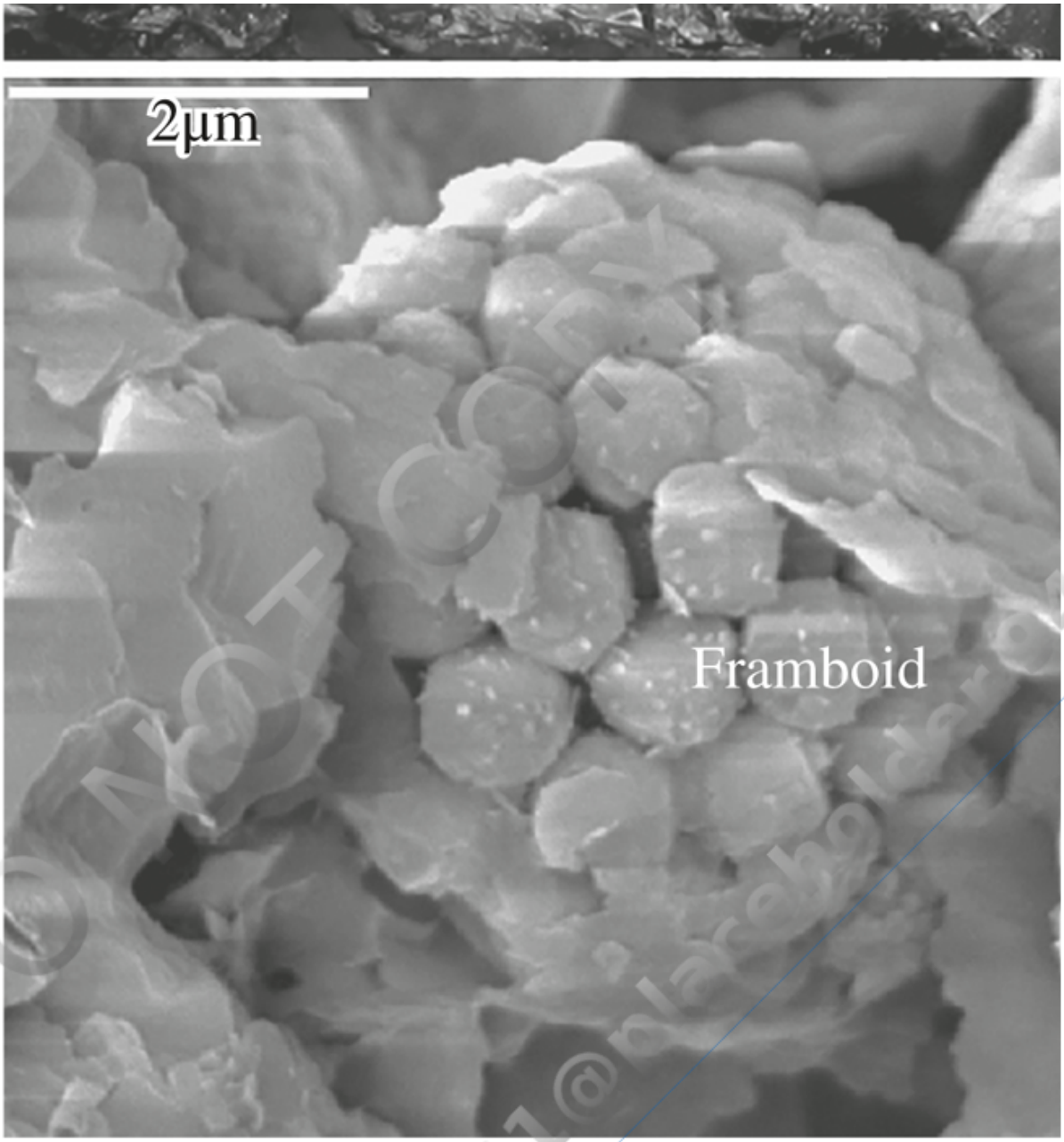

FIGURE 19.8 Pyrite. (*a*) Pyritohedron crystals. Field of view is about 5 cm wide. (*b*) Pyrite cubes with quartz. Field of view is about 2 cm wide. (*c*) Spherical framboid made of numerous equant pyrite grains in clay from Canadian River, Oklahoma, alluvium. The flaky particles are clay minerals. Photo courtesy of G. Breit, U.S. Geological Survey. Back to text

Printed by: e48d507df5d1141@placeholder.94092.edu. Printing is for personal, private use only. No part of this book may be reproduced or transmitted without publisher's prior permission. Violators will be prosecuted.

FIGURE 19.9 Cockscomb crystals of marcasite. Back to text

DO NOT COPY
e48d507df5d1141@placeholder.9409

Printed by: e48d507df5d1141@placeholder.94092.edu. Printing is for personal, private use only. No part of this book may be reproduced or transmitted without publisher's prior permission. Violators will be prosecuted.

Chapter 20 Native Elements

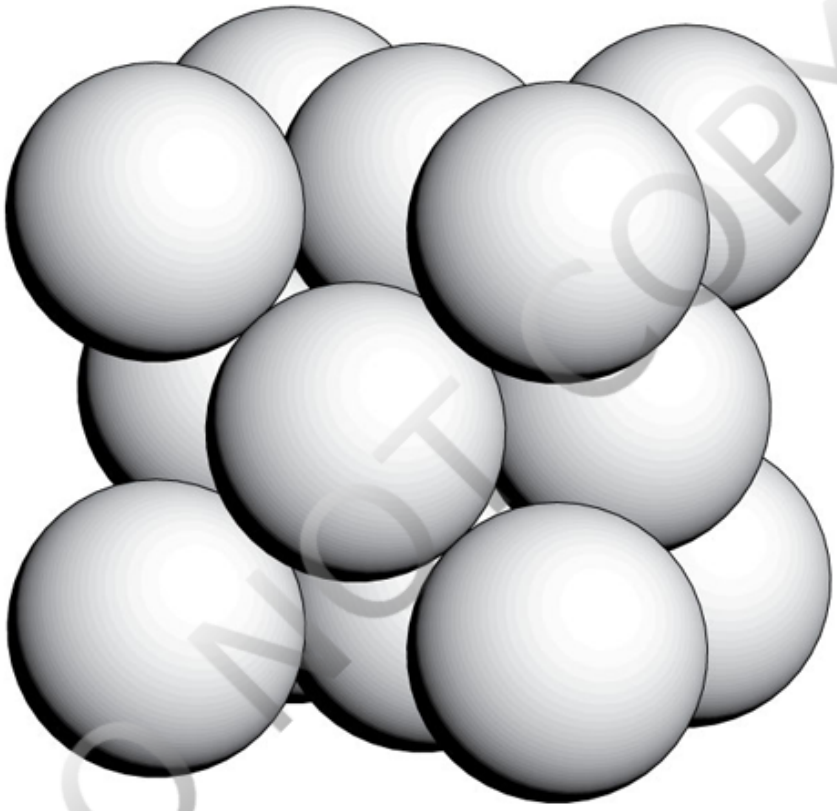

FIGURE 20.1 Many native metals have a cubic close-packed structure with metallic bonding.
Back to text

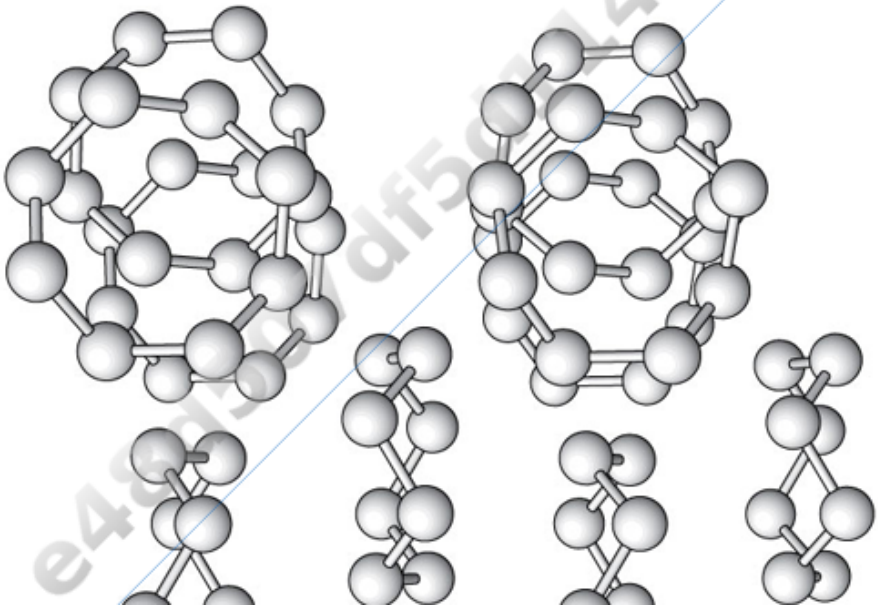

DO NOT COPY e48d507df5d1141@placeholder.9409

Printed by: e48d507df5d1141@placeholder.94092.edu. Printing is for personal, private use only. No part of this book may be reproduced or transmitted without publisher's prior permission. Violators will be prosecuted.

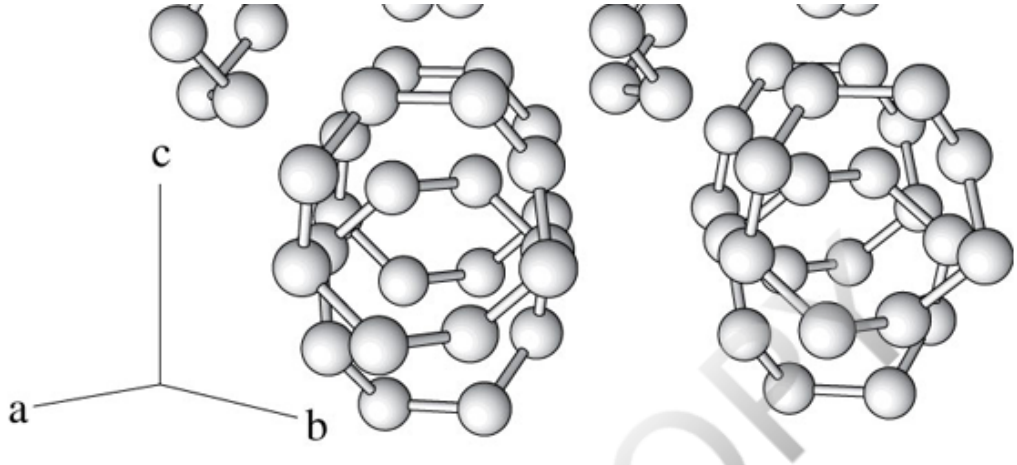

FIGURE 20.2 Structure of native sulfur. Eight-fold rings of covalently bonded sulfur atoms bond laterally through van der Waals bonds. Back to text

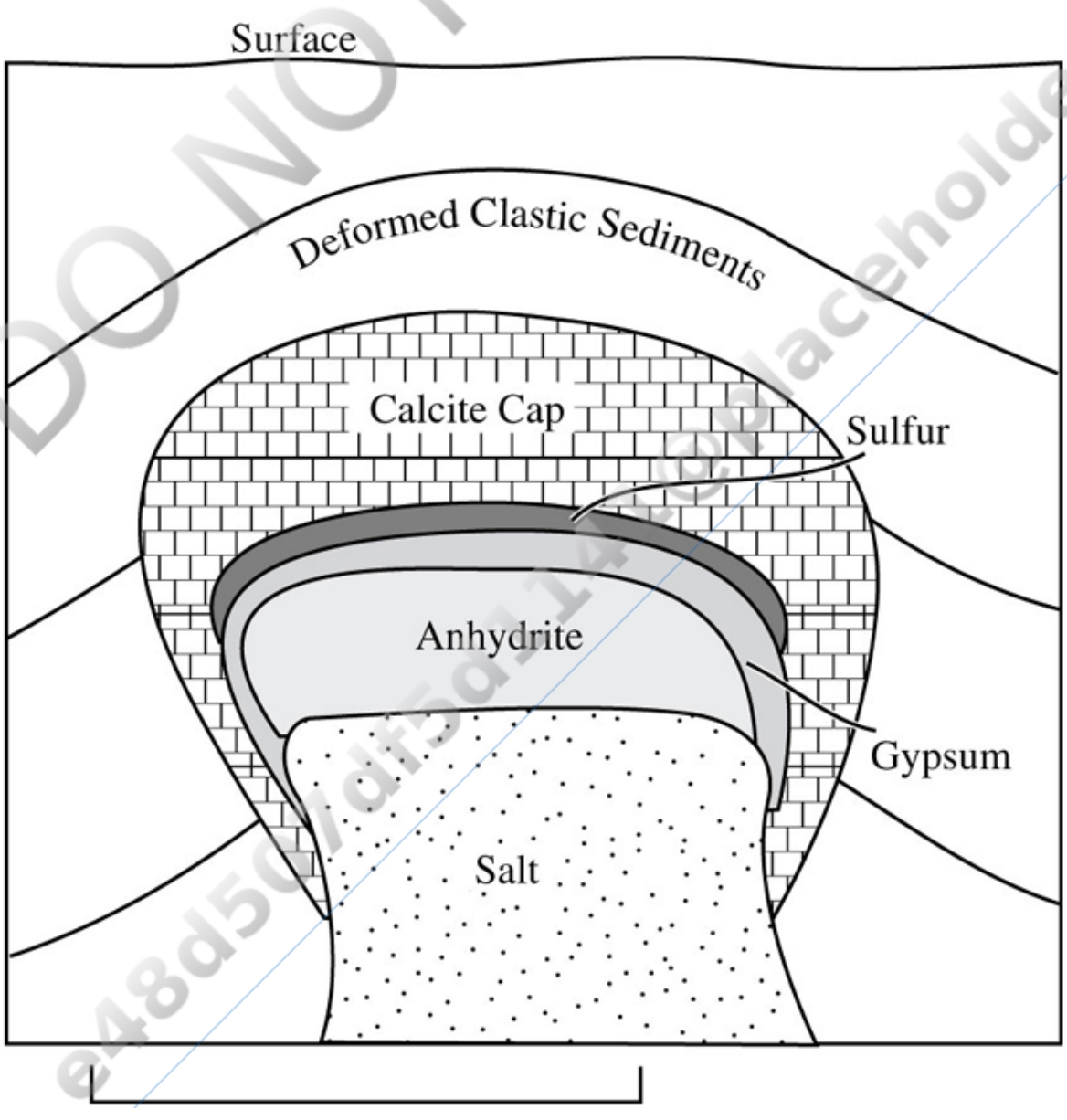

DO NOT COPY
e48d507df5d1141@placeholder.9409

Printed by: e48d507df5d1141@placeholder.94092.edu. Printing is for personal, private use only. No part of this book may be reproduced or transmitted without publisher's prior permission. Violators will be prosecuted.

1 km

FIGURE 20.3 Schematic cross section through a salt dome showing idealized sequence of cap rock lithologies and location of native sulfur concentrations. Back to text

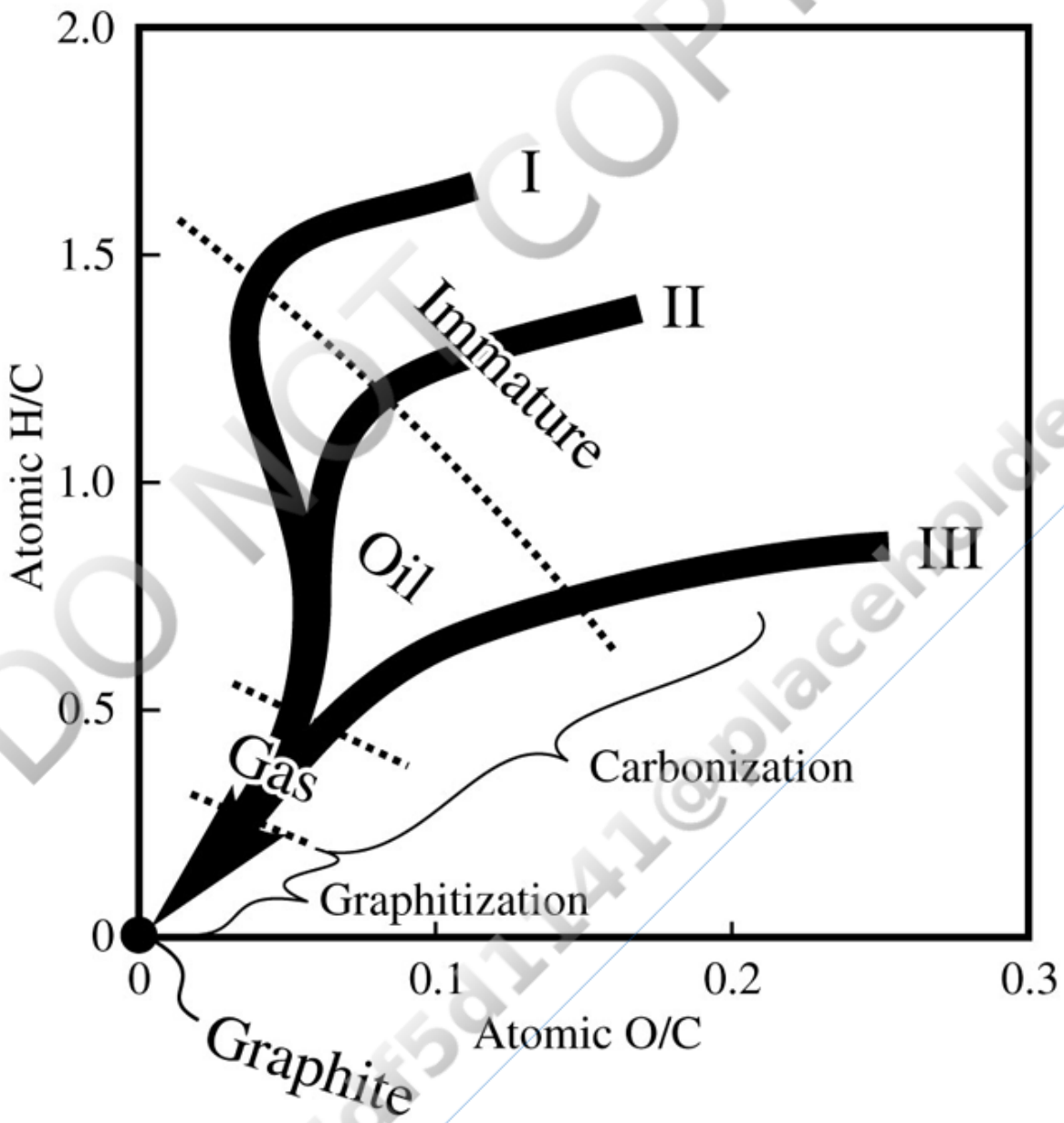

FIGURE 20.4 Van Krevelen diagram showing chemical evolution of organic material derived from lacustrine algae (I), marine microorganisms (II), and terrestrial plants (III) in response to burial and increasing temperatures in sedimentary rocks. During carbonization the O/C and H/C ratios progressively decrease as the organic matter matures and first oil and then gas are extracted. Continued heating under metamorphic conditions causes graphitization as the residual graphitic carbon crystallizes to form graphite. Adapted from Buseck and Beyssac (2014). Back to text

DO NOT COPY
e48d507df5d1141@placeholder.9409

Printed by: e48d507df5d1141@placeholder.94092.edu. Printing is for personal, private use only. No part of this book may be reproduced or transmitted without publisher's prior permission. Violators will be prosecuted.

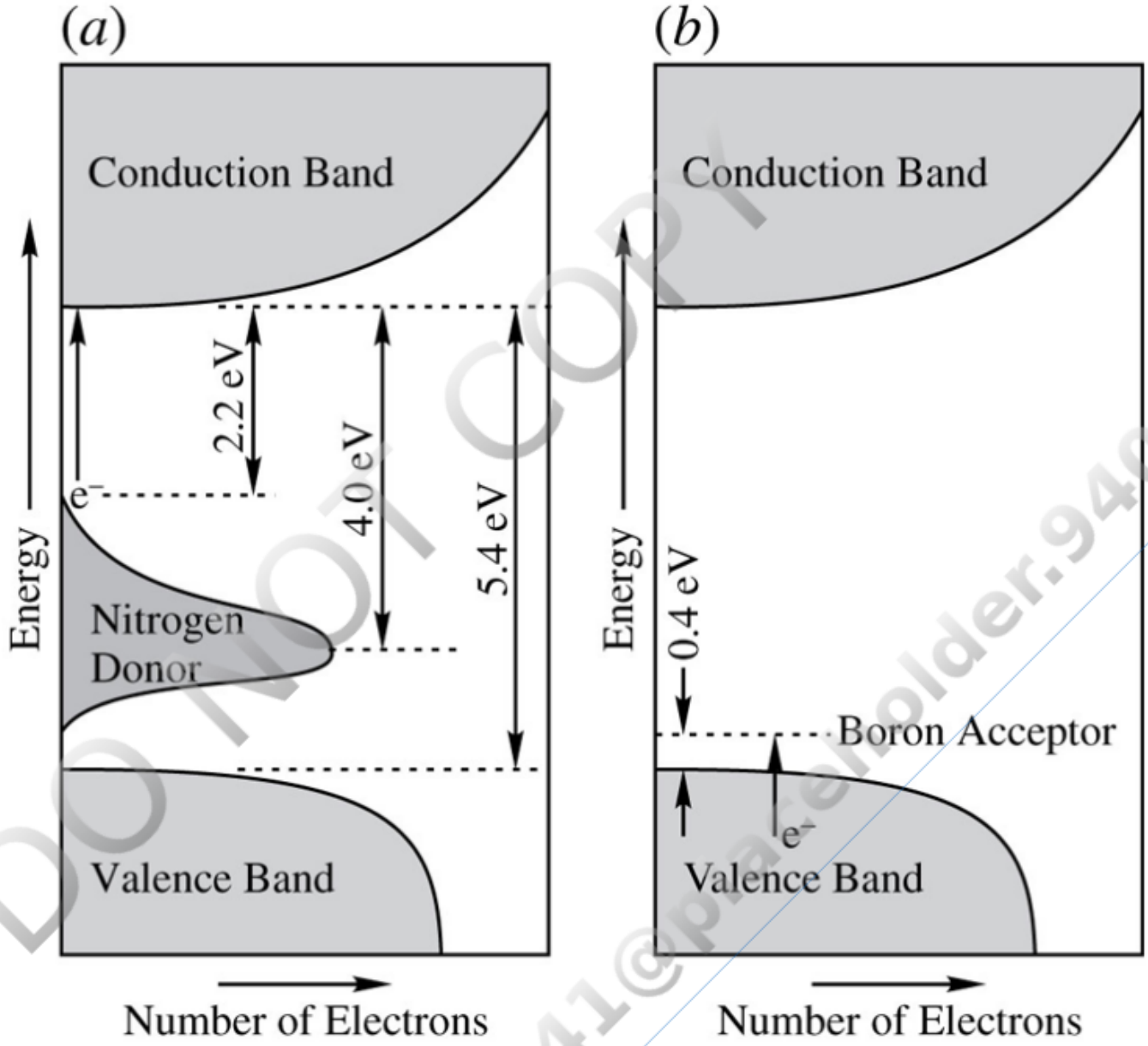

FIGURE 20.5 Color in diamond. (*a*) In pure diamond the band gap between the valence and conduction bands is about 5.4 eV, so visible light (energy between about 1.7 and 3.2 eV) is not absorbed and the mineral is colorless. Small amounts of nitrogen in the structure provide a source of electrons whose energy band is centered about 4 eV below the diamond conduction band. At a concentration of 1 part per 100,000, the top of the nitrogen donor band is just 2.2 eV below the diamond conduction band, so violet and blue light can be absorbed and the diamond appears yellow. (*b*) Trace amounts of boron provide a vacant energy level about 0.4 eV above the diamond valence band. While the entire visible light spectrum can be absorbed, the lower-energy red end of the spectrum is absorbed more strongly than blue, so the diamond appears blue. Back to text

Printed by: e48d507df5d1141@placeholder.94092.edu. Printing is for personal, private use only. No part of this book may be reproduced or transmitted without publisher's prior permission. Violators will be prosecuted.

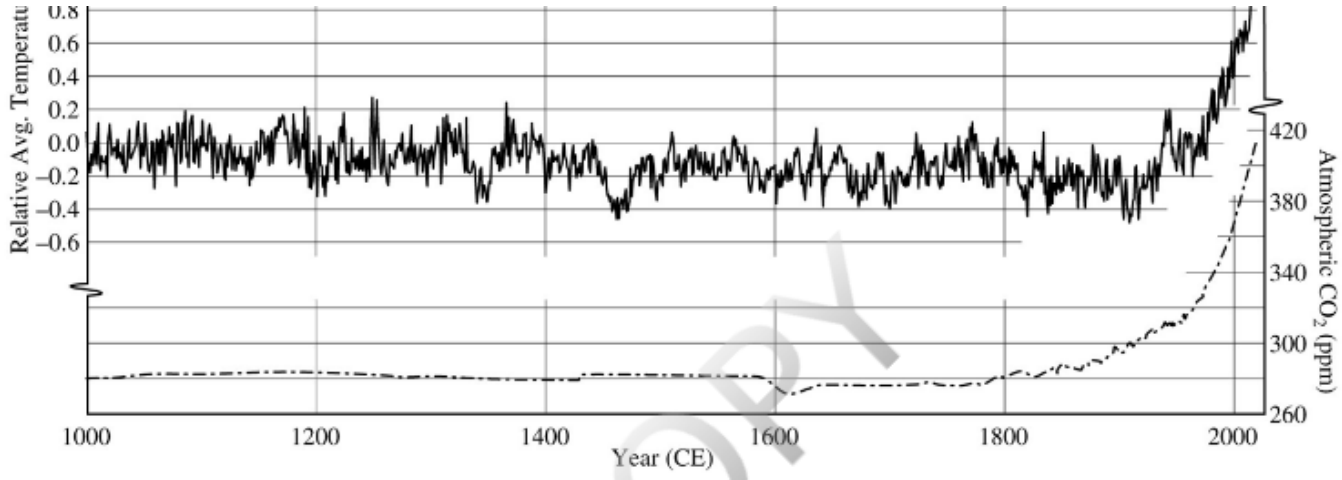

FIGURE 20.6 Change in average global temperature and atmospheric CO_2 over the past 1000 years. Temperature record during 1000–1880 from Mann and others (1999) and during 1880–2020 from NASA.gov. Atmospheric CO_2 during 1000–1996 from MacFarling Meure and others (2006) and during 1996–2020 from NASA.gov. Back to text

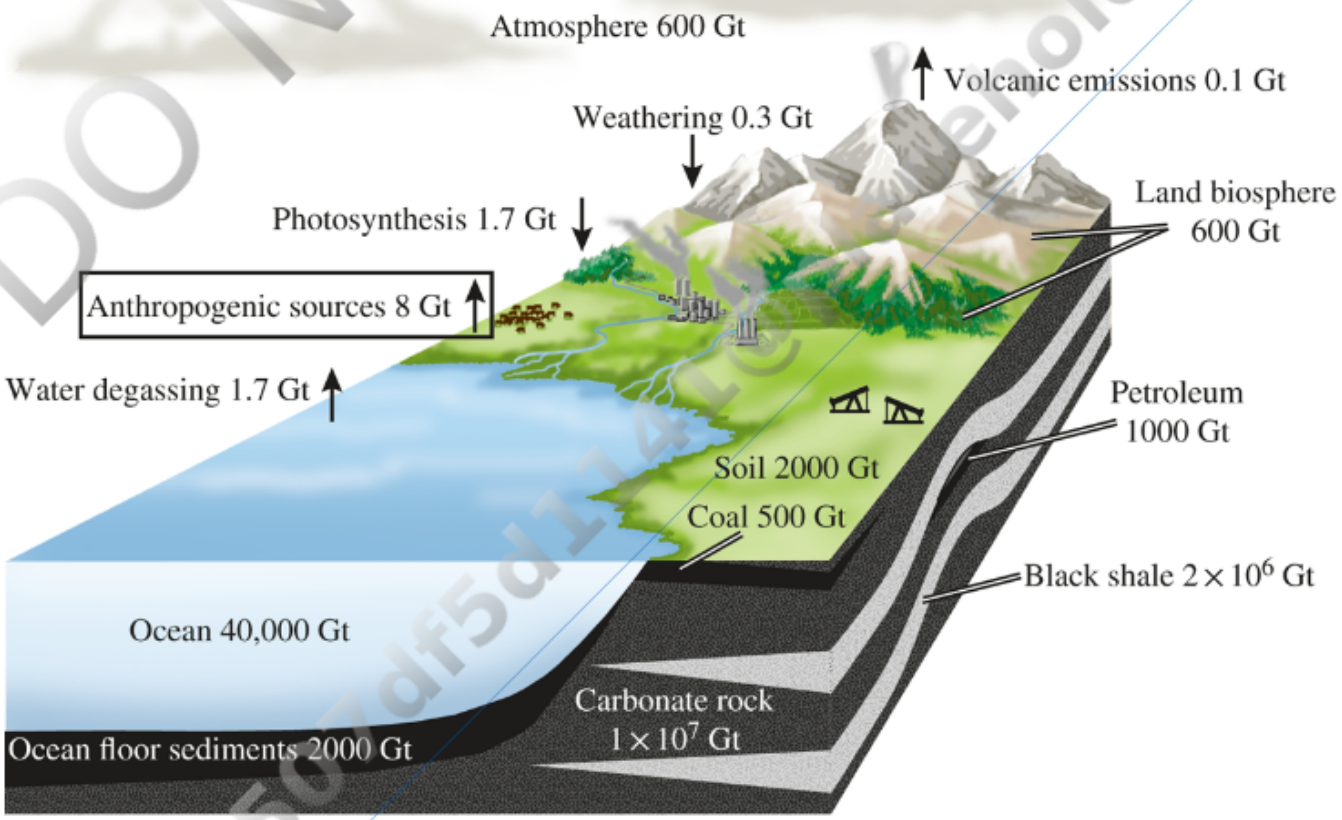

FIGURE 20.7 Schematic diagram of the carbon cycle showing reservoirs and fluxes. Fluxes into and out of the atmosphere are denoted by arrows and are preindustrial revolution values. The current-day anthropogenic contribution of carbon to the atmosphere is highlighted by a box. See Table 20.3 and the text for details regarding reservoir and flux values. Figure based on Bowman and Hacker (2020). Back to text